The Program for the Fourth North American Congress on Biomechanics

The Thirty Second Annual Conference of the American Society of Biomechanics

and

The Fifteenth Biennial Conference of the Canadian Society for Biomechanics / Société Canadienne de Biomécanique

NORTH AMERICAN CONGRESS ON BIOMECHANICS

NACOB

Ann Arbor, MI, U.S.A. August 5-9, 2008

SPONSORS

We gratefully acknowledge the generous financial support of the following companies and institutions:

SILVER

Johnson & Johnson, Inc.

Liberty Mutual Insurance Company

The Mathworks

BRONZE

Exponent, Inc.

Ford Motor Company

Co-Sponsors

Delsys, Inc.

Elsevier / Saunders / Mosby

Human Kinetics

Northern Digital, Inc.

North American Congress on Biomechanics

2008

August 5 - 9
Ann Arbor, Michigan

The Program for the Fourth North American Congress on Biomechanics

The joint meeting of

The 32nd Annual Conference of the American Society of Biomechanics (ASB)

and

The 15th Biennial Conference of the Canadian Society for Biomechanics (CSB)/

Société Canadienne de Biomécanique (SCB)

Ann Arbor, Michigan, USA

2

LIST OF CONTENTS

The Executive Boards which have governed the American Society of Biomechanics (ASB) and the Canadian Society for Biomechanics (CSB) over the past year included the following members:

NACOB	**ASB** **2007 - 2008**	**CSB** **2007 - 2008**

Conference Co-Chairs

Meeting Chair
James A. Ashton-Miller (ASB)
University of Michigan

Scientific Program Co-Chair
Richard E. Hughes (ASB)
University of Michigan

Scientific Program Co-Chair
David Andrews (CSB)
   University of Windsor

President
Rodger Kram
University of Colorado,

Past-President
Kenton Kaufman
Mayo Clinic

President-Elect
Irene Davis
University of Delaware

Secretary/Treasurer
Paul DeVita
East Carolina University,

Program Chair
Richard E. Hughes
The University of Michigan,

Program Chair-Elect
Steve McCaw
Illinois State University

Meeting Chair
James A. Ashton-Miller
The University of Michigan

Membership Chair
Max Kurz
The University of Houston,

Education Committee Chair
Nick Stergiou
University of Nebraska –

Communications Committee Chair
Andy Karduna, Ph.D.
University of Oregon,

Newsletter Editor
Michelle Sabick, Ph.D.
Boise State University

Student Representative
Katie Bieryla
Virginia Tech

President
Jack Callaghan
University of Waterloo

Past-President
Stephen Prentice
University of Waterloo

Secretary-Treasurer
Wayne Albert
University of New Brunswick

Conference Chair
David Andrews
University of Windsor

Members Affairs & Secretariat
Jennifer Durkin
University of Waterloo

Communications Officer
Peter Keir
McMaster University

Members-at-Large

Kevin Deluzio
Dalhousie University

Sylvie Nadeau
University de Montréal

Wayne Albert

Student Representatives

Doug Bourne
University of Calgary

Steven L. Fischer
University of Waterloo

LIST AND LOCATION OF EXHIBITORS
All Exhibits are on the second floor of the Michigan League, Central Campus, University of Michigan, Ann Arbor

Company	Representative	Address	Booth	Room
AMTI	Bruce White	Waltham, MA, U.S.A.	6	Ballroom
GAITRite	Michael Rowling	Havertown, PA, U.S.A.	7	Ballroom
Anybody Technology	Arne Kiis	Aalborg Oest, Denmark	20	Vandenberg
Bertec Corporation	Jeff Sobotka	Columbus, OH, U.S.A.	13	Hussey
Bio Logic Engineering	Neil, Chuck, Walt Cole	Dexter, MI, U.S.A.	8	Ballroom
C-Motion, Inc	John Kiser	Germantown, MD, U.S.A.	19	Vandenberg
Cleveland Medical Devices, Inc.	Maureen Phillips	Cleveland, OH, U.S.A.	23	Ballroom
Delsys Inc	Devi Bheemappa	Boston, MA, U.S.A.	11	Hussey
Elsevier/Saunders/Mosby	Tom Vokal	Washington, MI, U.S.A.	3	Ballroom
Human Kinetics	Loarn Robertson	Champaign, IL, U.S.A.	21	Vandenberg
Innovative Sports Training, Inc	Mona Bhuta	Chicago, IL, U.S.A.	4	Ballroom
Innovision Systems, Inc.	Victoria Berger	Columbiaville, MI, U.S.A.	18	Vandenberg
Kistler Instrument Corp	Paul Bussman	Amherst, NY, U.S.A.	9	Ballroom
Materialise, Inc.	Michael Lawrenchuck	Ann Arbor, MI, U.S.A.	12	Hussey
Motion Analysis, In.	Phil Hagerman	Santa Rosa, CA, U.S.A.	10	Ballroom
Motion Lab Systems	Chris LeBlanc	Baton Rouge, LA, U.S.A.	15	Hussey
Noraxon U.S.A., Inc	Todd Shewman	Scottsdale, AZ, U.S.A.	1	Ballroom
Northern Digital, Inc	Bob Bordignon	Waterloo, ON, CANADA	5	Ballroom
Novel Electronics	Maria Pasquale	St. Paul, MN, U.S.A.	14	Hussey
PhoeniX Technologies	Prasad Nair	Burnaby, BC, Canada	24	Ballroom
Qualisys, Inc.	Daniel India	Charlotte, NC, U.S.A.	17	Vandenberg
Tekscan, Inc.	John Guarino	South Boston, MA, U.S.A.	2	Ballroom
The Mathworks	Etham Woodruff	Natick, MA, U.S.A.	22	Vandenberg
Vicon, Inc.	George Miller	Centennial, CO, U.S.A.	16	Hussey

ACKNOWLEDGEMENTS

The Organizing Committee of the Fourth North American Congress on Biomechanics acknowledges the generous support of the following institutions, colleges, schools, departments, centers and laboratories:

University of Michigan

University of Michigan Office of the Vice-President for Research
University of Michigan College of Engineering
University of Michigan Medical School
University of Michigan Dental School
University of Michigan Division of Kinesiology

University of Michigan Department of Mechanical Engineering
University of Michigan Department of Biomedical Engineering
University of Michigan Department of Obstetrics and Gynecology
University of Michigan Department of Orthopedic Surgery
University of Michigan Department of Physical Medicine and Rehabilitation

University of Michigan Institute of Gerontology
University of Michigan Transportation Institute

University of Michigan Center for Ergonomics
University of Michigan Injury Prevention and Rehabilitation Center
University of Michigan Biomechanics Research Laboratory
University of Michigan Humosim Laboratory
University of Michigan Orthopedic Research Laboratories
University of Michigan Orthotics and Prosthetics Center

University of Windsor

University of Windsor Faculty of Human Kinetics
VP Research at the University of Windsor

The American Society of Biomechanics

The Canadian Society for Biomechanics

The International Society of Biomechanics

National Institute of Biomedical Imaging and Bioengineering (via an R13 grant to support the attendance of for minority and women students)

6

Thanks to the following individuals for giving of their time and expertise

ASB Awards Committees (Chair: Ken Kaufman)
   Borelli & Hay Awards: Tom Brown ▪ Irene Davis ▪ Rodger Kram ▪ Bill Marras ▪ Ron Zernicke
   Post-Doctoral Scientist Award: Melissa Gross ▪ Ted Gross ▪ Mont Hubbard ▪ Maury Nussbaum ▪ A Joseph Threlkeld
   Pre-Doctoral Scientist Award: Joan Bechtold ▪ Jesus Dapena ▪ Mark Grabiner ▪ Rick Lieber ▪ Mark Redfern
   Journal of Biomechanics Award Finalists: Tom Buchanan ▪ Frank Buczek ▪ Raki Cham (Finalists) ▪ Max Donelan ▪ David Gabriel (Initial Screening) ▪ Phil Martin
   Clinical Biomechanics Award Finalists: Kai-Nan An ▪ Roger Enoka ▪ Richard Hughes ▪ Todd Royer ▪ Zev Rymer
   Travel: Don Anderson ▪ Irene Davis ▪ Gary Heise ▪ Roger Kram ▪ Mark McMulkin

CSB Awards Committee
   NDI New Investigator Awards Committee (CSB): Sandi Spaulding (Chair) ▪ Jim Dickey ▪ Pierre Gervais ▪ Sylvain Grenier ▪ Anne Moore

NACOB Awards Committees
   Delsys Recognition Award: Michael Agnew ▪ Jack Dennerlein ▪ Clark Dickerson ▪ Peter Johnson.
   NCAA Award: Benno Nigg ▪ Melissa Gross ▪ Scott McLean

NACOB Program Committee: Steve Abramowitch ▪ Alaa Ahmed ▪ Wayne Albert ▪ David Andrews (Co-Chair) ▪ Nadia Azar ▪ Joan Bechtold ▪ Michael Bey ▪ Thomas Brown ▪ Sachin Budhabhatti ▪ Graham Caldwell ▪ Jack Callaghan ▪ Young-Hui Chang ▪ Li-Shan Chou ▪ Pat Costigan ▪ Trey Crisco ▪ Margot Damaser ▪ Richard Debski ▪ Kevin Deluzio ▪ Jules Dewald ▪ Clark Dickerson ▪ Yasin Dhaher ▪ Max Donelan ▪ Jennifer Durkin ▪ Tammy Eger ▪ John Elias ▪ Glenn Fleisig ▪ Steve Goldstein ▪ Joseph Hamill ▪ Roger Haut ▪ Tammy Haut Donahue ▪ Walter Herzog ▪ Jill Higgenson ▪ Katherine Holzbaur ▪ Elizabeth Hsiao-Wecksler ▪ Richard Hughes (Co-Chair) ▪ Devin Jindrich ▪ Andy Karduna ▪ Peter Keir ▪ David Kohn ▪ Cheryl Kozey ▪ John Kozey ▪ Zong-Min Li ▪ Richard Lieber ▪ Steve McCaw ▪ Craig McGowan ▪ Mark McMulkin ▪ Jill McNitt-Gray ▪ Clare Milner ▪ Benno Nigg ▪ Maury Nussbaum ▪ David Pearsall ▪ Steve Piazza ▪ Jim Potvin ▪ Steve Prentice ▪ Francois Prince ▪ Mark Redfern ▪ Shirley Rietdyk ▪ Stacie Ringleb ▪ Gord Robertson ▪ Jason Scibek ▪ Darren Stefanyshyn ▪ Darryl Thelen ▪ Samual Ward ▪ Paul Weinhold ▪ Jason Wening ▪ Bing Yu ▪ Xudong Zhang ▪ Ron Zernicke

NACOB Tutorials: Kai-Nan An ▪ Qingshan (Frank) Chen ▪ Zachary J. Domire ▪ Scott Delp ▪ Steve Goldstein ▪ Art Kuo ▪ Mark Redfern ▪ David Vaillancourt ▪ Ron Zernicke

Assistants to the NACOB Meeting Chair: Sarah Ilkhani ▪ Mark Gordon

Assistants to the NACOB Program Chairs: Robyn Bertram ▪ Timothy Burkhart ▪ Chris Gatti ▪ Sylvia Steffani ▪ Edward Sihler ▪ Paula van Wyk

NACOB Web Site and Management: Dejun Jing

NACOB Graphics Design: Lindsay Ashton-Miller ▪ Youkeun Oh

NACOB Conference Organization: Cheryl Miller ▪ Nicole Miller ▪ Sue Schaefgen ▪ Bill Vlisides

Tuesday, August 5, 2008

	Tutorials	Lab Tours
< 8:00 am	**Registration (Michigan League Building)**	
8:15 – 8:45 am	**Bus From Michigan League to Computer Science Engineering (CSE) on North Campus**	
8:45 – 10:15 am	**I:** Arthur Kuo **Location:** Computer Science Engineering (CSE 1690) **Dynamic Walking: Analytical and Computational Methods** **II:** Scott Delp **Location:** Computer Science Engineering (CSE 1670) **OpenSim Workshop**	**Lab Tours I** **(Details on Website)**
10:45 – 12:30 pm	**I:** Arthur Kuo **Location:** Computer Science Engineering (CSE 1690) **Dynamic Walking: Analytical and Computational Methods** **II:** Scott Delp **Location:** Computer Science Engineering (CSE 1670) **OpenSim Workshop**	**Lab Tours II** **(Details on Website)**
1:30 – 3:00 pm	**I:** Arthur Kuo **Location:** Computer Science Engineering (CSE 1690) **Dynamic Walking: Analytical and Computational Methods** **III:** Kai-Nan (Andy) An, Qingshan (Frank) Chen, Zachary J. Domire **Location:** Modern Languages Building (MLB 1200 Auditorium 3) **MR Elastography and its Applications on Characterization of Skeletal Muscle** **IV:** David Vaillancourt **Location**: Rackham Ampitheatre (Rackham Building, 4th floor) **Structural and Functional Neuroimaging in Humans**	**Lab Tours III** **(Details on Website)**
3:30 – 5:00 pm	**I:** Arthur Kuo **Location:** Computer Science Engineering (CSE 1690) **Dynamic Walking: Analytical and Computational Methods** **V:** Ron Zernicke **Location:** Modern Languages Building (MLB 1200 Auditorium 3) **Successful Grant Writing in Canada** **VI:** Mark Redfern and Steve Goldstein **Location**: Kraus Natural Science Building Auditorium, Room 2140 **Successful Grant Writing in the USA**	**Lab Tours IV** **(Details on Website)**

5:30 - 7:00 pm: Opening Reception and Vendor Exhibits (Michigan League)
7:00 - 8:30: ASB and CSB Executive Board Meetings (Zanzibar Restaurant)

Wednesday, August 6, 2008

< 8:00 am   **Coffee at Vendor Exhibits (Michigan League)**

8:00
Keynote Lecture I
Location: Rackham Auditorium

On the Challenge of Vaginal Birth
John O.L. DeLancey, M.D.
University of Michigan

9:00   **Coffee at Vendor Exhibits (Michigan League)**

9:15
Borelli Award Lecture (ASB)
Location: Rackham Auditorium

Why Bones Bend but Don't Break: What Cement Lines, Floyd Landis and Laundry Detergent Have in Common
David B. Burr
Indiana University

10:15   **Coffee at Vendor Exhibits (Michigan League)**

10:45
ASB Awards Session
Location: Rackham Auditorium

10:45   Young Scientist Pre-Doctoral Award Winner
Post-Hibernation Black Bears (Ursus Americanus) do not Demonstrate Cortical Bone Loss Compared to Pre-Hibernation Bears Despite 6 Months of Disuse (#10)
Meghan McGee
Michigan Technological University

11:00   Young Scientist Post-Doctoral Award Winner
Architectural and In Vivo Analyses Demonstrate the Unique Stabilizing Function of the Lumbar Multifidus Muscle (#582)
Sam Ward
University of California-San Diego

11:15   Clinical Biomechanics Award Finalists
Effect of Hip Protectors and Body Mass Index on Pressure Distribution During a Fall on the Hip (#573)
Woochol Joseph Choi
Simon Fraser University

11:30   **Co-Activation Differences in Lower Limb Muscles Between Asymptomatic Controls and Those with Varying Degrees of Knee Osteoarthritis During Walking** (#388)
Cheryl Hubley-Kozey
Dalhousie University

11:45   Journal of Biomechanics Award Finalists
A 3-D Finite Element Model of Anterior Vaginal Wall Support for Evaluating Mechanisms Underlying Cystocele Formation (#497)
Luyun Chen
University of Michigan

12:00   **Kinematics of a Walking Spinal Cord: Insights from a Novel Isolated Spinal Cord-Hindlimb Preparation**
(#330)
Heather Hayes
Georgia Tech/Emory University

12:15 - 1:30 pm: **Box Lunch at Vendor Exhibit (Michigan League)**
Women in Biomechanics Lunch (Rackham Assembly Hall, 4th Floor)

<u>NOTES</u>

Wednesday, August 6, 2008

Scientific Sessions

Automobile Safety (ASB/CSB Symposium)	**Motor Control I (Podium Session 1)**
Wednesday, August 6: 1:30 - 3:00 pm	Wednesday, August 6: 1:30 - 3:00 pm
Location: MLB 1200 AUD 3	Location: MLB 1400 AUD 4
Session chair: Larry Schneider	Session chairs: Stephen Scott, Scott Selbie

Protection for Elderly Occupants

Effects of Occupant Age on Injury Outcome in Motor-Vehicle Crashes
Jonathan Rupp
University of Michigan Transportation Research Institute

Fragility, Frailty, and the Biomechanics of Aging
Richard Kent
University of Virginia

Evaluating Occupant Protection for Elderly Rear-Seat Passengers in Frontal Crash Testing
Suzanne Tylko
Transport Canada

Belt Donning and Belt Fit for Elderly Drivers
Matthew Reed or Stephanie Huang
University of Michigan Transportation Research Institute

1:30   **Stability of Multi-Finger Prehension Synergy: Exploration With Transcranial Magnetic Stimulation** (#326)
Xun Niu, Vladimir Zatsiorsky & Mark Latash
The Pennsylvania State University

1:45   **Flexible Representations of Dynamics are Used in Object Manipulation** (#561)
Alaa Ahmed, Daniel Wolpert & Randall Flanagan
University of Cambridge

2:00   **Altered Reflex Modulation to Changes in Mechanical Environment Following Stroke** (#484)
Randy Trumbower, James Finley, Jonathan Shemmell & Eric Perreault
Northwestern University & Rehabilitation Institute of Chicago

2:15   ***Deterioration of Kinematic and Muscle Performance and Associated Cortical Activity Related to Increased Shoulder Abduction Drive in Chronic Hemiparetic Stroke** (#252)
Albert Chen, Jun Yao, Ana Maria Acosta & Julius Dewald
Northwestern University

       *Delsys Award Finalist

2:30   **A New Methodology for the Assessment of Movement Repeatability in Functional Upper Limb Tasks** (#97)
Sibylle Thies, Phil Tresadern, Laurence Kenney, Dave Howard & Yannis Goulermas
University of Salford, Centre for Rehabilitation and Human Performance Research

2:45   **Synergies Hierarchies During Accurate Rotations Tasks** (#451)
Wei Zhang, Vladimir Zatsiorsky & Mark Latash
The Pennsylvania State University

3:00 - 3:30 pm: Coffee at Vendor Exhibits (Michigan League)

Wednesday, August 6, 2008

Scientific Sessions

Methods/Instrumentation I (Podium Session 2)	**Knee I (Podium Session 3)**
Wednesday, August 6: 1:30 - 3:00 pm	Wednesday, August 6: 1:30 - 3:00 pm
Location: Rackham Amphitheatre	Location: Mendelsohn Theatre
Session chairs: Jim Dickey, Tom Jenkyn	Session chairs: Kevin Deluzio, Katherine Boyer

1:30 **Development of a Fiber-Optic Force Sensing Glove to Provide Clinical BiomechanicsMeasurements** (#527)
David Nuckley, David Linders & Wei-chih Wang
University of Minnesota

1:30 **Biomechanical Modeling to Predict the Risk of Developing Painful Knee OA** (#130)
Krishna Iyer, Donald Anderson, Jennifer Baker, James Torner, Thomas Brown & Neil Segal
University of Iowa

1:45 **Dynamic Pressure Mapping of the Head-Helmet Interface** (#208)
Ryan Ouckama & David Pearsall
McGill University

1:45 **Mechanisms Underlying Reductions in Knee Extension Strength in Knee Osteoarthritis** (#43)
Tamika Heiden, David Lloyd & Tim Ackland
University of Western Australia

2:00 **Development and Validation of a Versatile Intra-Articular Pressure Sensing Array** (#540)
Judson Welcher, John Popovich, Thomas Hedman & Wafa Tawackoli
University of Southern California-Los Angeles

2:00 **Knee-Joint Loading Variability During Gait Does Not Differ Between Individuals With and Without Knee Osteoarthritis** (#245)
Todd Royer, Jeremy Crenshaw, Joaquin Barrios & Irene Davis
University of Delaware

2:15 **Ground Reaction Forces During Running Can be Estimated From Insole Pressure Measurements by Considering Whole Body Dynamics** (#27)
Elizabeth Chumanov, Christian Remy & Darryl Thelen
University of Wisconsin-Madison

2:15 **Tibiofemoral Contact Pressures and Osteochondral Microtrauma From ACL Rupture via Hyperextension and Joint Compression** (#231)
Eric Meyer, Timothy Baumer & Roger Haut
Michigan State University

2:30 **A Technique for Optimizing the Center of Pressure and Kinetic Data Obtained From a Split-Belt Instrumented Treadmill** (#117)
Saryn Goldberg, Thomas Kepple & Steven Stanhope
Hofstra University

2:30 **An Innovative Method to Analyze the Chondrocyte Response to Mechanical Injury Both Temporally and Spatially** (#123)
Daniel McCabe, Nicholas Stroud, Douglas Pedersen & James Martin
University of Iowa

2:45 **Virtual Forceplate: Predicting Ground Reaction Forces During Single Leg Hopping Using Only Kinematic Measurements** (#218)
Alison Sheets, Stefano Corazza & Thomas Andriacchi
Stanford University

2:45 **Walking Exercise Differently Alters the Metabolic Activity of Bone in the Knee Measured With 18F-Fluoride PET/CT Between Healthy and Osteoarthritic Knees** (#246)
Seungbum Koo, Andrew Quon, David Clark, Garry Gold & Thomas Andriacchi
Stanford University

3:00 - 3:30 pm: Coffee at Vendor Exhibits (Michigan League)

Wednesday, August 6, 2008

Scientific Sessions

Spine I (Podium Session 4) Wednesday, August 6: 3:30 - 5:00 pm Location: MLB 1200 AUD 3 Session chairs: Kermit Davis, John Kozey	**Aging I (Podium Session 6)** Wednesday, August 6: 3:30 - 5:00 pm Location: MLB 1400 AUD 4 Session chairs: Jonathan Dingwell, Mike Pavol

3:30   **Comparing Uniaxial and Biaxial Strain Responses of the Porcine Annulus Fibrosus** (#405)
Diane Gregory & Jack Callaghan
University of Waterloo

3:30   **The Challenge of Monitoring Activity Level in the Elderly** (#590)
Jonathan Rylander, Katherine Boyer, Thomas Andriacchi & Gary Beaupre
VA Palo Alto

3:45   **A Finite Element Study of the Effect of Cross-Shear on Wear of the Prodisc Total Disc Replacement** (#72)
Curt Goreham-Voss & Thomas Brown
University of Iowa

3:45   **Physical Activity for Maintaining Healthy Bone Denisty With Aging** (#142)
Katherine Boyer, Jonathan Rylander, B. Jenny Kiratli, Tom Andriacchi & Gary Beaupre
Stanford University

4:00   **In Vivo Compressive Stresses in the Intervertebral Disc** (#227)
Donita Bylski-Austrow, David Glos, Frank Sauser, Alvin Crawford & Eric Wall
Cincinnati Children's Hospital Medical Center

4:00   **On the Predicted Buckling Behavior of the Human Upper Extremity Under Impulsive End-Loading: Age and Gender Effects** (#136)
Yunju Lee & James Ashton-Miller
University of Michigan

4:15   **Biomechanical Analysis of the Lumbar Spine on the Facet Joint Force and Intradiscal Pressure: A Realistic Finite Element Study** (#343)
Hsuan-Teh Hu, Ruey-Mo Lin, Ching-Sung Kuo, Po-Chun Lin, Zheng-Cheng Zhong, Mu-Lin Hsieh & Kuo-Yuan Huang
National Cheng Kung University

4:15   **Age-Associated Dopaminergic Influences on Foot-Tapping and Temporal Gait Parameters in Healthy Older Adults** (#372)
Chris Bogan, Nicolaas Bohnen, Robert Koeppe, K. Frey, Roger Albin & Martijn Muller
University of Michigan

4:30   **Implementation of Facet Joints in a Detailed Musculoskeletal Lumbar Spine Model Based on Inverse Dynamics** (#352)
Mark de Zee, Peter Mikkelsen, Christian Wong & Erik B. Simonsen
Aalborg University

4:30   **Age Related Changes in Postural Muscle Responses With Increasing Perturbations to the Upper Back** (#448)
Luis Rosado, Christopher Hasson, Richard Van Emmerik & Graham Caldwell
University of Massachusetts Amherst

4:45   **The Use of Artificial Neural Networks as a Data Reduction Approach In Determining Cumulative Exposures** (#331)
Robert Parkinson & Jack Callaghan
University of Waterloo

4:45   **Strategies for Balance Maintenance During Sit-to-Stand Movement in Elderly People** (#19)
Masahiro Fujimoto, Shintaro Beppu, Kazuya Okubo, Toru Fujii & Li-Shan Chou
University of Oregon

5:00 - 7:00 pm: Poster Session I and Vendor Exhibits (Michigan League)
6:30 - 8:00 pm: ISB Student Travel Grants Session (Rackham Assembly Hall, 4ᵗʰ Floor)
7:00 - later: Night on the Town (Buses Circulate Between Campus Downtown and Hotels)

Wednesday, August 6, 2008

Scientific Sessions

Bone (Podium Session 7)	Sport I (Podium Session 5)
Wednesday, August 6: 3:30 - 5:00 pm	Wednesday, August 6: 3:30 - 5:00 pm
Location: Rackham Amphitheatre	Location: Mendelsohn Theatre
Session chairs: Ron Zernicke, Gregory Wohl	Session chairs: Robin Queen, Thorsten Sterzing

3:30 **Ultrastructural Disorder in D_2O-Equilibrated Bone Tissue Studied by Polarized Raman Spectroscopy-Implications for Biomechanics** (#474)
Mekhala Raghavan, Michael Morris, Nadder Sahar & David Kohn
University of Michigan

3:30 **Football Playing Surface Components May Affect Lower Extremity Injury Risk** (#37)
Mark Villwock, Eric Meyer, John Powell, Amy Fouty & Roger Haut
Michigan State University

3:45 **Femur Bone Mass and Bone Geometry After Spinal Cord Injury** (#512)
Gail Forrest, Thomas Beck, Chris Cirnigliaro, Arvind Ramanujam, Steven Kirshblum, William Bauman, John Mores & Susan Harkema
Koessler Medical Rehabilitation Research and Education Center

3:45 **Effects of Gender on Kinematics of the Hip, Knee, and Ankle in Unanticipated Droplandings of Adolescent Soccer Players** (#299)
Michelle Sabick, Seth Kuhlman, Ronald Pfeiffer, Benjamin Cooper, David Clark & Kevin Shea
Boise State University

4:00 **Structural Properties of Trabecular Cores from Femoral Heads** (#455)
Sylvana Garcia-Rodriguez, Meghan Crookshank, Norma MacIntyre, Mark Harrison, Everett Smith, Rick Sellens & Heide-Lynn Ploeg
University of Wisconsin-Madison

4:00 **Comparison of Landing Biomechanics Between Male and Female Professional Dancers** (#36)
Karl Orishimo, Ian Kremenic, Marijeanne Liederbach, Evangelos Pappas & Marshall Hagins
Nicholas Institute of Sports Medicine and Athletic Trauma

4:15 **Dietary Effects on Bone Mechanical Properties and Molecular Markers** (#203)
Caeley Lorincz, Raylene Reimer & Ronald Zernicke
University of Calgary

4:15 **Determination of the Optimal Seat Position That Maximizes Average Crank Power: A Theoretical Study** (#485)
Jeffery Rankin & Richard Neptune
The University of Texas at Austin

4:30 **Determination of Calcaneal Bone Strain During Simulated Walking With Cadaver Legs** (#288)
Lawrence Noble, Dong-gil Lee, Robb Colbrunn, Ton van den Bogert, Peter Cavanagh & Brian Davis
Cleveland Clinic Foundation

4:30 **Predictors of Scoring Accuracy: Ice Hockey Wrist Shot Mechanics** (#54)
Yannick Paquette, David Pearsall, Rene Turcotte & Ken Covo
McGill University

4:45 **The Effect of Varying the Density-Modulus Relationship Used to Apply Material Properties in a Finite Element Model of the Distal Ulna** (#66)
Rebecca Austman, Jaques Milner, David Holdsworth & Cynthia Dunning
The University of Western Ontario

4:45 **Sources of Forward Ball Velocity in a Pitched Baseball** (#86)
Gordon Alderink, Thomas Kepple, Karen Lohmann Siegel, Alexander Razzook & Steven Stanhope
Grand Valley State University

5:00 - 7:00 pm: Poster Session I and Vendor Exhibits (Michigan League)
6:30 - 8:00 pm: ISB Student Travel Grants Session (Rackham Assembly Hall, 4th Floor)
7:00 - later: Night on the Town (Buses Circulate Between Campus Downtown and Hotels)

Wednesday, August 6, 2008

Poster Session I
Location: Michigan League
Time: 5:00 - 7:00 pm

2nd Floor
Room: Michigan Ballroom (Posters 1-74: Gait, Posture & Balance, Motor Control, Lower Extremity)

1) **The Impact of Medial Plantar Flexor Dysfunction on Mid Foot Joint Pressures** (#114)
Dong-gil Lee, Robb Colbrunn, Antonie van den Bogert, Peter Cavanagh & Brian Davis
Cleveland Clinic Foundation, Cleveland State University

2) **Differences in Correlations of Anterior-Posterior Ground Reaction Forces With Paretic and Control Leg Gait Variables** (#222)
Carrie Peterson, Richard Neptune & Steven Kautz
University of Texas at Austin

3) **Effects of Asymmetric Ankle Plantarflexor Recruitment on Post-Stroke Walking: A 3D Simulation Study** (#183)
Ming Xiao & Jill Higginson
University of Delaware

4) **Analysis of Amputee Gait Using Center-of-Mass Velocity** (#498)
Peter Gabriel Adamczyk, Michael Orendurff, Joseph Czerniecki, Ava Segal, Hannah Sutton, Glenn Klute & Art Kuo
University of Michigan

5) **Effects of Down Syndrome on Mediolateral Motion During Walking at Different Speeds** (#442)
Stamatis Agiovlasitis, Michael Pavol, Jeffrey McCubbin & Joonkoo Yun
University of Illinois at Urbana-Champaign

6) **Objective Evaluation of Ankle Foot Orthotics for Ambulatory Function in Hemiplegic Gait** (#578)
Karen Nolan, Mathew Yarossi, Krupa Savalia, Howard Hillstrom & Elie Elovic
Koessler Medical Rehabilitation Research and Education Center

7) **Are Asymmetries in Joint Kinetics Related to Limb Dominance?** (#311)
Matthew Seeley, Brian Umberger & Robert Shapiro
Brigham Young University

8) **Dual Task Performance in a Healthy Young Adult Population: Results From a Symmetric Manipulation of Task Complexity and Articulation** (#56)
Albert Armieri, Jeffrey Holmes, Alexandrea Gow, Tanu Sharma, Sandi Spaulding, Mary Jenkins & Andrew Johnson
The University of Western Ontario

9) **Analysis of the Effects of Stilts Walking on Joint Moments in Low Extremities** (#73)
John Wu, Sharon Chiou & Christopher Pan
National Institute for Occupational Safety and Health (NIOSH)

10) **The Effect of Unloader Braces on Knee Loads During Gait** (#403)
Kristin Whitney, Ian Jones, Trevor Birmingham & Thomas Jenkyn
The University of Western Ontario

11) **Kinetic Characteristics of Barefoot Running** (#82)
Julia Freedman, Janet Dufek & John Mercer
University of Tennessee

12) **Selection of Double Support Duration in a Compliant Walking Model** (#581)
Shawn O'Connor & Arthur Kuo
University of Michigan

13) **A Robotic Cadaveric Flatfoot Simulation of Stance Phase** (#515)
Lyle Jackson, Patrick Aubin, Matthew Cowley, Bruce Sangeorzan & William Ledoux
VA Puget Sound

14) **Vertical Stiffness During the Double Support Period of Walking** (#558)
John Rebula, Shawn O'Connor & Arthur Kuo
University of Michigan

15) **Evaluation of a Human Foot Placement Model** (#223)
Matthew Millard, Derek Wight, John McPhee, Eric Kubica & David Wang
University of Waterloo

16) **Treatment Insight From Subject-Based Simulation of Crouch Gait** (#543)
Ajay Seth, May Liu, Michael Schwartz, Frank Anderson & Scott Delp
Stanford University

17) **Reducing Residual Forces and Moments in a Three-Dimensional Simulation of Running** (#535)
Samuel Hamner, Chand John, Frank Anderson, Jill Higginson & Scott Delp
Stanford University

18) **Stability and Adaptability of Passivity-Based Bipedal Locomotion With Flat Feet and Ankle Compliance** (#363)
Qining Wang, Yan Huang, Long Wang & Dongjiao Lv
Peking University

19) **Increased Inertial Forces Reduces Locomotive Stability** (#413)
Christopher Arellano, Daniel O'Connor, Melissa Scott-Pandorf, Charles Layne & Max Kurz
University of Houston

20) **Locomotor Initiation: Influence of Chronic Ankle Instability** (#433)
Chris Hass, Erik Wikstrom, Kimberly Fournier, Amruta Inamdar & Mark Bishop
University of Florida

21) **Walking Step Width During the Transition Between Level and Sloped Surfaces** (#488)
Nori Okita & Jinger Gottschall
The Pennsylvania State University

23) **Effects of Varying Surface Inclines and Suit Pressure: Implications on Space Suit Design** (#50)
Kurt Clowers, Timothy Clark, Lauren Harvill, Richard Morency & Sudhakar Rajulu
MEI Technologies, Inc, National Aeronautics and Space Administration (NASA)

24) **Increased Exposure to an Obstacle Crossing Task Decreased Toe Elevation at Obstacle Crossing, but not Estimation of Obstacle Height** (#371)
Chris Rhea, Julia Drifmeyer & Shirley Rietdyk
Purdue University

25) **Adaptations and Aftereffects of Muscle Activation Patterns and Foot Kinematics Following Passive Swing Phase Assistance** (#340)
Montakan Thajchayapong, Brian Schmit & T. George Hornby
Northwestern University

16

26) **Detection of Gait Imbalance Using the Extrapolated Center of Mass** (#138)
Vipul Lugade, Sue Ewers, Chu-Jui Chen, Sujitra Boonyong, Patima Silsupadol & Li-Shan Chou
University of Oregon

27) **Contribution of Joint Torque Coordination to Vertical Force Stabilization During Human Locomotion is Speed Dependent** (#440)
Jasper Yen, Arick Auyang & Young-Hui Chang
Georgia Institute of Technology

28) **Stepping Tasks That Require Greater Executive Control Induce Multiple Postural Adjustments** (#444)
Joseph Lacko, Mark Redfern, Joseph Furman & Patrick Sparto
University of Pittsburgh

29) **Effects of a Subtalar Strapped Wedge on Knee Dynamics During Gait in Younger and Older Adults** (#426)
Kristian O'Connor, Nandina Hill, Barbara Hart & Jennifer Earl
University of Wisconsin-Milwaukee

30) **Implications of Alternate Stair Descent Strategies on Knee Biomechanics: Backwards Descent is Less Demanding** (#278)
Tyler Cluff & D. Gordon Robertson
University of Ottawa

31) **A Parametric Approach for Estimating a Range of Physiological Tibiofemoral Contact Force During Gait** (#589)
Sean Scanlan, Darryl D'Lima, Clifford Colwell & Thomas Andriacchi
Stanford University

32) **The Relationship Between Hip and Knee Kinematics to the Knee Adduction Moment in Asymptomatic Individuals With Genu Varum** (#119)
Joaquin Barrios & Irene Davis
University of Delaware

33) **Disease Severity Influences Patient Response to Variable-Stiffness Walking Shoe After One Year of Wear** (#32)
Jennifer Erhart, Nicholas Giori & Thomas Andriacchi
Stanford University

34) **Angular Momentum Primitives as Gait Invariants** (#244)
Bradford Bennett, Shawn Russell & Mark Abel
University of Virginia

35) **Induced Lower Extremity Vascular Occlusion Affects Gait Variability** (#197)
Sara Myers, Iraklis Pipinos, Jason Johanning & Nick Stergiou
University of Nebraska at Omaha

36) **Gait Variability is Reduced by Sub-Threshold Vibrations to the Feet** (#270)
Hyun Gu Kang, Andrew Galica, Attila Priplata, Olga Starobinets, Susan D'Andrea, James Collins & Lewis Lipsitz
Hebrew SeniorLife, Harvard Medical School

37) **Effects of Walking Speed on Step Width and Step Length Variability** (#276)
Daniel Peterson & Philip Martin
Pennsylvania State University

38) **The Effect of Stride-Length Changes on Triceps Surae Excitation During Walking** (#120)
David Sanderson, Ryan Cawsey, Scott Apperely & Julia Wilkes
University of British Columbia

39) **Maximum Allowable Force on a Safety Harness Cable to Discriminate a Successful From a Failed Balance Recovery** (#490)
Marc-Andre Cyr & Cecile Smeesters
Universite de Sherbrooke

40) **Correlation Between Postural Sway During Quiet Standing and Balance Recovery After Small Perturbations** (#84)
Sara Matrangola, Michael Madigan, Bradley Davidson & Maury Nussbaum
Virginia Polytechnic Institute and State University

41) **Effects of Obesity on Balance in Response to Small Postural Perturbations** (#264)
Emily Miller, Michael Madigan & Sara Matrangola
Virginia Polytechnic Institute and State University

42) **The Effects of Reflex Delays on Postural Control During Unstable Seated Balance** (#262)
N. Peter Reeves, Jacek Cholewicki & Kumpati Narendra
Michigan State University

43) **Postural Control During Quiet Standing in Patients With a Total Hip Arthroplasty or a Hip Resurfacing** (#416)
Vicky Bouffard, Marc Therrien, Martin Lavigne, Pascal-Andre Venditolli & Francois Prince
Marie Enfant Rehabilitation Centre, University of Montreal, Maisoneuve-Rosemont Hospital

44) **Effect of Proprioceptive and Visual Perturbations on Postural Control About the Vertical Axis in Quiet Standing** (#361)
Marlene Beaulieu, Martin Simoneau, Georges Dalleau, Charles-Hilaire Rivard & Paul Allard
Universite de Montreal,Sainte-Justine Hospital

45) **Effects of Lumbar Extensor Fatigue on Postural Control Assessed With Fractal Analysis** (#79)
Sunwook Kim, Maury Nussbaum & Michael Madigan
Virginia Tech University

46) **Performance Measures That Influence the Most the Ability to Recover Balance to Avoid a Fall** (#495)
Alessandro Telonio & Cecile Smeesters
Universite de Sherbrooke

47) **The Role of Knee Extensor Strength in Landing Phase Characteristics of a Balance-Restoring Step Response** (#192)
Gregory King & Carl Luchies
University of Missouri-Kansas City

48) **Trip-Recovery Strategies of a Transfemoral Amputee** (#257)
Jeremy Crenshaw, Kenton Kaufman & Mark Grabiner
University of Illinois at Chicago

49) **Gait and Balance Comparisons Between Leather and Rubber Boots in Professional Firefighters** (#379)
Chip Wade, Ryan Garten, Scott Breloff & Ed Acevedo
Auburn University

50) **The Acute Effects of Chronic Trekking Pole Use on Static and Dynamic Balance** (#113)
Julianne Abendroth-Smith, Victoria Swigart & Michael Bohne
Willamette University

51) **The Influence of Height and Edge Proximity on Balance and Reaction Time** (#526)
Wendi Weimar, John Garner, Brian Campbell & Paul St. Onge
Auburn University

52) Dynamical Models of Repeated Goal-Directed Movements (#410)
Joby John & Joseph Cusumano
The Pennsylvania State University

53) Inverse Piano Technique for Studying Finger Interaction During Pressing Tasks (#90)
Joel Martin, Mark Latash & Vladimir Zatsiorsky
The Pennsylvania State University

54) Grasping Force Magnitude Affects the Force Sharing Pattern in Multi-Finger Prehension (#327)
Xun Niu, Mark Latash & Vladimir Zatsiorsky
The Pennsylvania State University

55) Hierarchical Synergies in Bimanual Prehension (#224)
Stacey Gorniak, Vladimir Zatsiorksy & Mark Latash
The Pennsylvania State University

56) Grasping a Handle With Constant External Torque and Variable Load (#194)
Jason Friedman, Mark Latash & Vladimir Zatsiorsky
The Pennsylvania State University

57) Evidence for Goal Equivalent Control in Treadmill Walking (#550)
Joseph Cusumano, Joby John & Jonathan Dingwell
The Pennsylvania State University

58) Interjoint Compensation Stabilizes Leg Length and Orientation During Human Locomotion (#191)
Arick Auyang, Jasper Yen & Young-Hui Chang
Georgia Institute of Technology

59) Neuromechanics of Muscle Synergies During Cycling (#205)
James Wakeling & Tamara Horn
Simon Fraser University

60) Frequency Influences the Regularity of the Structural Variations Present in the Leg Swing Kinematics (#445)
Vladimir Ivkovic & Max Kurz
University of Houston

61) Flexor and Extensor Contributions to the Joint Moment During Stair Ascent for Healthy Subjects and Those With Knee OA (#503)
Joseph Gardinier & Kurt Manal
University of Delaware

62) The Effects of Local Vibration on a Joystick Pursuit-Task (#398)
Joseph Soltys, John Keighley & Sara Wilson
University of Kansas

63) ACL Reconstruction Affects Lower Extremity Energy Absorption More Than Task Diversion During One Leg Landings (#415)
Marissa Link & Steven McCaw
Illinois State University

64) The Effect of a Linear In-Flight Perturbation on Landing Biomechanics (#565)
Scott Arnett, Yang-Chieh Fu, Ryan Thompson, Petur Sigurdsson & Kathy Simpson
Western Kentucky University

65) Patellar Tendinopathy Alters the Distribution of Lower Extremity Joint Effort During Hopping (#251)
Richard Souza, Shruti Arya, Christine Pollard, George Salem & Kornelia Kulig
University of Southern California

66) Duration of Pronation Period During Ground Contact in Heel-to-Toe Running (#23)
Jens Heidenfelder, Thorsten Sterzing, David Schreiter & Thomas Milani
Chemnitz University of Technology

67) Gender Differences of 2-Point Touch Sensitivity Thresholds of the Human Foot (#156)
Sabrina Kunde, Thorsten Sterzing & Thomas Milani
Chemnitz University of Technology

68) The Influence of Time Interval Between Loadings on Heel Pad Properties (#476)
Daniel Gales & John Challis
The Pennsylvania State University

69) The Dynamic Quadriceps Angle: A Comparison of Persons With and Without Patellofemoral Pain (#323)
Yu-Jen Chen & Christopher Powers
University of Southern California

70) Developing a Cumulative Loading Measure for the Knee: Examining Test-Retest Reliability (#65)
Shawn Robbins, Gareth Jones, Trevor Birmingham, Jack Callaghan & Monica Maly
University of Western Ontario

71) A Comparison Between Two Systems for the Quantification of Lower Extremity Kinematic Gait Data (#342)
Andrew Kraszewski, Sherry Backus, Rebecca Zifchock, Mark Lenhoff & Howard Hillstrom
Hospital for Special Surgery

72) Computer Simulation of Internal Structural Loading: Application to Overuse Running Injuries (#491)
Ross Miller & Joseph Hamill
University of Massachusetts-Amherst

73) Effects of Stilts Walking on Musculoskeletal Loading in Low Extremities (#75)
John Wu, Sharon Chiou & Christopher Pan
National Institute for Occupational Safety and Health (NIOSH)

74) Predicting Patient Function and Joint Loading Post-Total Knee Replacement Using Muscle Activation Patterns (#16)
Gillian Hatfield, Cheryl Hubley-Kozey & Michael Dunbar
Dalhousie University

2nd Floor
Room: Vandenberg (Posters 75-90: Lower Extremity, Methods/Instrumentation, Comparative)

75) Biomechanical Testing of the Shear Modulating Diabetic Insoles: An Engineering Perspective (#286)
Dan Lanctot, David Armstrong, Manish Bharara & Ryan Crews
Rosaline Franklin University of Medicine & Science

76) Hyperspectral Imaging to Assess and Predict Diabetic Foot Ulcers (#284)
Samantha Keevey, Brian Davis, Byron Hoogwerf, Emile Mohler, Elizabeth Medinilla, Marie Neverov, Aksone Nouvong & Kevin Schomacker
Lerner Research Institute, Cleveland Clinic

77) Meniscal Motion During the Gait Cycle (#591)
Nathan Netravali, Seungbum Koo, Brian Hargreaves, Nicholas Giori & Thomas Andriacchi
Stanford University

78) Markerless Versus Marker-Based Motion Capture: A Comparison of Measured Joint Centers (#592)
Katherine Steele, Stefano Corazza, Sean Scanlan, Alison Sheets & Thomas Andriacchi
Stanford University

79) Validation of Walkway Slip Resistance Measurements: A Gait Based Approach (#139)
Christopher Powers, Mark Blanchette, John Brault, Jim Flynn & Gunter Siegmund
University of Southern California

80) Validation of Windows for Examining Kinematics of the Foot With Respect to the Shoe Using a Multi-Segmented Foot Model (#464)
Rebecca Shultz, Trevor Birmingham & Thomas Jenkyn
The University of Western Ontario

81) A MR-Compatible Loading Device for Dynamically Imaging Shortening and Lengthening Muscle Contractions (#397)
Christopher Westphal, Amy Silder & Darryl Thelen
University of Wisconsin-Madison

82) Evaluation of Footswitches to Detect Heel Contact (#180)
Jennica Roche, Daniel Steed & Mark Redfern
University of Pittsburgh

83) A Novel Technique to Determine Gravitational and Passive Joint Torques From Dynomometer-Measured Passive Torque Data (#214)
Dennis Anderson, Michael Madigan & Maury Nussbaum
Virginia Polytechnic and State University

84) Can Between-Day Kinematic Reliability be Improved? (#104)
Brian Noehren & Irene Davis
University of Delaware

85) Development of an Apparatus to Produce High Impact Extremity Loading With an Application in the Lower Leg (#145)
Cheryl Quenneville, Gillian Fraser & Cynthia Dunning
The University of Western Ontario

86) An Objective Evaluation of Segmented Foot Models Using Robotic Dynamic Activity Simulator (#229)
Nori Okita, Steven Meyers, John Challis & Neil Sharkey
The Pennsylvania State University

87) Three Dimensional Kinematics and Kinetics of the Center of Mass of the Cat During Walking on a Narrow Walkway (#421)
Brad Farrell, Irina Beloozerova & Boris Prilutsky
Georgia Institute of Technology

88) Experimental Study of the Deformation and Flexibility of Insect Wings (#333)
Xiaolin Wang, Afzal Khan, Lingxiao Zheng & Rajat Mittal
George Washington University

89) **Inverse Dynamic Analysis of the Stifle Joint in Labrador Retrievers With Cranial Cruciate Ligament Deficiency** (#566)
Chantal Ragetly, Dominique Griffon, Jason Thomas, Ayman Mostafa & Elizabeth Hsiao-Wecksler
University of Illinois

90) **Non Invasive Determination of Body Segment Parameters in Labrador Retrievers** (#564)
Chantal Ragetly, Dominique Griffon, Jason Thomas, Ayman Mostafa, David Schaeffer, Gerald Pijanowski & Elizabeth Hsiao-Wecksler
University of Illinois

2nd Floor
Room: Hussey (Posters 91-106: Ergonomics)

91) **Comparison of Strength Between Pregnant and Non-Pregnant Women** (#216)
Genevieve Dumas, Karine Charpentier, Mei Wang & Andrew Leger
Queen's University

92) **Upper Body Posture During Tree Planting Work** (#115)
Tegan Upjohn, Peter Keir & Genevieve Dumas
Queen's University

93) **A Three-Dimensional Model to Examine the Effects of Posture on Carpal Tunnel Size and Shape** (#186)
Jeremy Mogk & Peter Keir
Rehabilitation Institute of Chicago

94) **Predicting Female Arm Strength From Hand Location** (#99)
Christopher Freeman & Jim Potvin
University of Windsor

95) **Astronaut Rotational Motion During Simulated Microgravity** (#83)
Leia Stirling, Dava Newman & Karen Willcox
Massachusetts Institute of Technology

96) **Evaluation of Physical Stress During Hand Gestures for Human Machine Interaction** (#368)
Razie Riemer, Adi Ronen, Helman Stern & Yael Edan
Ben Gurion University of the Negev

97) **Lateral Reaching From Fixed Ladders** (#291)
Justin Young, Hogene Kim, Chuck Woolley, Tom Armstrong & James Ashton-Miller
University of Michigan

98) **Hand Load Contributions to Cervical Spine Compression Forces** (#172)
Adam Pickens & Jeff Woldstad
Texas Tech University

99) **Manual Patient Transfer Training: Student Nurse Perceptions** (#127)
Paula van Wyk, David Andrews & Patricia Weir
University of Windsor

100) **Trade-Off Between Lift Rate and Box Weight: A Spine Load Perspective** (#585)
Susan Kotowski, Kermit Davis & William Marras
University of Cincinnati

101) **The Effect of Starting Location on Posture During a Fine Assembly Part Insertion Task** (#137)
Sean Abdulla & Anne Moore
York University

102) **Modeling Time Varying Moment Profiles Determined From Automotive Assembly Workers Using a First Order System Response** (#391)
Steven Fischer, Wayne Albert & Jack Callaghan
University of Waterloo

103) **Preferred Position and Associated Forces for Lower Back Support in Vehicle and Office Seating Environments** (#266)
Zahid Rampurawala & Tamara Reid-Bush
Michigan State University

104) **Children's Postural Habits While Working at Computer Workstations** (#521)
Carol Murphy, Joan Stevenson & Mohammad Abdoli
Queens University

105) **Minimising Trunk Angle Prediction Errors Associated With Field Goniometry by Utilizing a Subject Specific Calibration of Planar Leg Movements in Seated Drivers** (#106)
Robert Jack & Michele Oliver
University of Guelph

106) **Biomechanical and Physiologic Cost of Body Armor** (#583)
Leif Hasselquist, Carolyn Bensel, Brian Corner, Karen Gregorczyk & Jeffrey Schiffman
Natick Soldier Research, Development, and Engineering Center

3rd Floor
Room: Room 'D' (Posters 107-121: Computational Modeling, Injury)

107) **Differences Between Joint Work and Muscle Fiber Work During Steady-State Walking** (#108)
Kotaro Sasaki, Richard Neptune & Steven Kautz
University of Texas at Austin

108) **Independent Effects of Weight and Mass on Plantar Flexor Muscle Function: A Comparative Modeling and Simulation Study** (#469)
Craig McGowan, Rodger Kram & Richard Neptune
University of Texas at Austin

109) **A Preliminary Study on Musculoskeletal Finite Element Model With Accurate Muscle Moment Arms in Human Elbow** (#153)
Hideyuki Kimpara, Takahiko Sugiyama, Chikara Nagai, Kyuengbo Min, Yuko Nakahira & Masami Iwamoto
Toyota Central R&D Labs., Inc.

110) **Comparison of Computational and Experimental Results for Femur Fracture Risk Following Double-Bundle ACL Reconstruction** (#132)
Madelyn O'Farrell, Osmar Lopes Jr., Yonsik Yoo, Freddie Fu & Patrick Smolinski
University of Pittsburgh

111) **Development of a Semi-Automated Method for Generation of Hexahedral Femoral Cartilage Meshes From MRI** (#187)
Mark Baldwin, Joseph Langenderfer & Paul Rullkoetter
University of Denver

113) **Effect of Ageing and Arterial Stenosis on Ventricular-Arterial Coupling: A Computational Model Study** (#6)
Fuyou Liang, Shu Takagi, Ryutaro Himeno & Hao Liu
RIKEN

114) **Effect of Ankle Instability on the Load Bearing Characteristics of the Ankle-Foot Structure During Touchdown** (#260)
Jason Tak-Man Cheung, Victor Valderrabano, Scott Landry & Benno Nigg
University of Calgary

115) **Liquid Plug Dynamics in Microfluidic Flexible Channels: A Small Airway Model** (#499)
Ying Zheng, Hideki Fujioka, Yusuke Torisawa, Shuichi Takayama & James Grotberg
University of Michigan

116) **Elastic Rod Model for Protein Mediated DNA Looping** (#500)
Todd Lillian, Sachin Goyal, Edgar Meyhofer & Noel Perkins
University of Michigan

117) **Head Angular Acceleration Pulse Characteristics Affect Behavioral Outcomes Following Mild Diffuse Brain Injury** (#131)
Brian Stemper, Ronald Fijalkowski, Thomas Gennarelli, Narayan Yoganandan & Frank Pintar
Medical College of Wisconsin

118) **The Effects of Muscle Tension on Human Biomechanical Response and Perceived Impact Intensity** (#240)
Felix Tsui & Matthew Pain
Loughborough University

119) **Design of Low Stiffness Floors for Preventing Hip Fractures in High Risk Environments: Comparison of Force Attenuation and Influence on Balance** (#555)
Andrew Laing & Stephen Robinovitch
Simon Fraser University

120) **A Preliminary Study: Tracking 3D Kinematics of the Goat Knee Joint In-Vivo** (#341)
Daniel Miranda, Michael Rainbow, Beth Brainerd & Braden Fleming
Brown University

121) **Tibiofemoral Contact Pressures and Osteochondral Microtrauma During ACL Rupture Due to Excessive Compressive Loading and Internal Tibia Torsion** (#212)
Eric Meyer, Timothy Baumer & Roger Haut
Michigan State University

3rd Floor
Room: Henderson (Posters 123-146: Bone, Cartilage, Tendon/Ligament, Muscle)

123) **Numerical Model of Bone Remodelling Sensitive to Loading Frequency** (#62)
Etienne Malachanne, Franck Jourdan & David Dureisseix
University Montpellier 2

124) **Lacunocanalicular Fluid Flow and Regulation of Basic Multicellular Unit Activity** (#34)
Grant Goulet, David Cooper, Dennis Coombe, Robert Martinuzzi & Ronald Zernicke
University of Calgary

125) **Differences in Bone Morphology in Male Rats Selectively Bred for High or Low Aerobic Capacity** (#71)
Sarah Manske, Russell Hepple, Lauren Koch, Steven Britton, Steven Boyd & Ronald Zernicke
University of Calgary

126) **Effect of Treadmill Exercise in Tibiae of Ovariectomized Rats: A Biomechanical Analysis** (#217)
Patricia Bloes, Ariane Zamarioli, Antonio Shimano, Priscila Simoes, Jose Volpon, Luis Pereira & Francisco Mazzocato
University of Sao Paulo

127) **Experimental and Finite Element Investigations of the Press-Fit Fixation of a Bone Implant Interface in the Distal Femur** (#460)
Travis Burgers & Heidi Ploeg
University of Wisconsin-Madison

128) **Structural Properties of Fourth-Generation Composite Femurs and Tibias** (#12)
Anneliese Heiner
University of Iowa

129) **Achilles Tendon Injury: Predisposing Factors in Men Between 30 and 50 Years of Age** (#549)
Kathryn Antle & David Hawkins
University of California-Davis

130) **Tendinopathy Alters Mechanical Properties of the Achilles Tendon** (#481)
Shruti Arya & Kornelia Kulig
University of Southern California

131) **Mechanical Characteristics of Native Tendon Slices for Tissue Engineering Scaffold** (#308)
Ting-Wu Qin, Chun-Feng Zhao, Yu-Long Sun, Scott Steinmann, Peter Amadio & Kai-Nan An
Mayo Clinic, West China Hospital, Sichuan University

132) **Measurement of Elbow Medial Ulnar Collateral Ligament Strain: Choice of Reference Length Reduces Interspecimen Variability** (#382)
Laurel Kuxhaus, Florian Thomines, Angela Flamm, Patrick Schimoler, Mandy Brogdon, Jeffrey Vipperman, Patrick DeMeo & Mark Carl Miller
University of Pittsburgh

133) **Automated Mankin Scoring of Osteoarthritis Severity in Rabbits** (#364)
Richard Amendola, James Martin, Gail Kurriger, Farshid Moussavi-Harami, Thomas Brown & Douglas Pedersen
University of Iowa

134) **Pulling a Fast One: Mechanical Response of Articular Cartilage to High Frequency Loading** (#325)
Matt Szarko & John Bertram
University of Calgary

135) **A Technique for Calculating and Mapping Focal Cartilage Thickness** (#335)
William Anderst, Eric Thorhauer & Scott Tashman
University of Pittsburgh

136) **In-Vitro Investigation of Meniscal Movement Using Medical Imaging** (#411)
Maeghan Innes, Mark Hurtig, David Holdsworth & Karen Gordon
University of Guelph

137) **Subject-Specific Force-Length Parameters of the Ankle Plantarflexors in Young Adults** (#309)
Ross Miller, Christopher Hasson & Graham Caldwell
University of Massachusetts-Amherst

138) **Predicting Quadriceps Fatigue During Electrically Stimulated Non-Isometric Contractions** (#317)
Susan Marion, Maury Hull & Anthony Wexler
University of California-Davis

139) **Long-Term Morphological and Functional Changes Following an Acute Hamstring Strain Injury** (#406)
Amy Silder, Darryl Thelen, Michael Tuite & Bryan Heiderscheit
University of Wisconsin-Madison

140) **Force and Excursion Demands of Rotator Cuff Muscles During Abduction** (#67)
James Otis, Matthew Hansen, Jared Johnson, Frank Cordasco, Edward Craig & Russell Warren
The SHRI-CORE Biomechanics Lab

141) **An Experimental Model of Dilated Cardiomyopathy** (#574)
Audree McKenzie & Walter Herzog
University of Calgary

142) **Estimating the Appropriate Sample Size for the Determination of Optimal Fiber Length** (#437)
Benjamin Infantolino & John Challis
The Pennsylvania State University

143) **A Surface EMG Study of Healthy Jaw Function** (#414)
Steph Forrester, Matthew Pain, Andy Toy & Ron Presswood
Loughborough University

144) **Actively Generated Force and Stiffness Transmission Through Layers of the Rat Abdominal Wall** (#168)
Stephen Brown & Stuart McGill
University of Waterloo

145) **The Steps of Muscle Myosin II** (#189)
Ashi Mehta & Walter Herzog
University of Calgary

146) **Modelling the Effect of Brownian Motion on the Amount of Backwards Steps in the Classical Three-Beads Laser Trap Setup for Actin-Myosin Interaction** (#42)
Gudrun Schappacher-Tilp & Walter Herzog
University of Calgary

3rd Floor
Room: Koessler (Posters 147-166: Sport Science, Memorial Posters)

147) **The Effects of Leg Dominance on Knee Joint Kinetics During Cutting** (#302)
Szu-Ping Lee, John Chow & Mark Tillman
University of Florida, University of Southern California

148) **Quantifying the Planarity of the Field Hockey Hit** (#401)
Alexander Willmott & Jesus Dapena
Indiana University

149) **Effects of Ice Hockey Facial Protectors on Response Time** (#128)
Patrick Dowler & David Pearsall
McGill University

150) **Portable Strain Measurement System for Ice Hockey Sticks** (#418)
Patrick Magee, Phil Dixon, TJ Stidwill, David Pearsall, Rene Turcotte & Ken Covo
McGill University

151) **A Comparison Between Three Downswings for the Moy to Support and Giant on Parallel Bars in Men's Gymnastics** (#468)

Pierre Gervais, Pierre Baudin, Toshiyuki Fujihara & Tom Wu
University of Alberta

152) **Kinematic Comparison of Circles in Cross Support and Circles in Side Support** (#200)
Toshiyuki Fujihara & Pierre Gervais
University of Alberta

153) **Does Midsole Deformation Reflect Rearfoot Motion During Running? A Multiple Regression Approach to Evaluate Pronation by Hall Sensors** (#167)
Thomas Milani, Torsten Brauner, Thorsten Sterzing & Doris Oriwol
Chemnitz University of Technology

154) **Soccer Shoes Reduce Foot Sensitivity Compared to Barefoot for External Vibration Stimuli** (#29)
Thorsten Sterzing, Sabrina Kunde, Franziska Scholz & Thomas Milani
Chemnitz University of Technology

155) **Effects of Footwear on Plantar Foot Sensitivity are Frequency Dependent: A Study With Formula 1 Footwear** (#96)
Gunther Schlee, Thorsten Sterzing & Thomas Milani
Chemnitz University of Technology

156) **Different Approach Techniques in Volleyball Spike** (#171)
Claas Kuhlmann, Karen Roemer & Thomas Milani
Chemnitz University of Technology

157) **Reliability of Joint Angle Movements During Rock Climbing** (#359)
Paris Malin, Shinya Abe, Randall Jensen & Phillip Watts
Northern Michigan University

158) **Compression Apparel Effects on Soft Tissue Vibrations** (#211)
Aurel Coza & Benno Nigg
University of Calgary

159) **Tennis Serve Analysis Using on-the-field Markerless Motion Capture** (#587)
Stefano Corazza, Alison Sheets, Geoff Abrams, Marc Safran & Thomas Andriacchi
Stanford University

160) **Lower-Back Compressive Forces During Drop Landings** (#501)
Christopher Sorensen, W. Brent Edwards, Brett Sealine, Jason Gillette & Timothy Derrick
Iowa State University

161) **Comparison of Moment-Angle Profile of Elbow Flexors-Extensors in Elite Young Overhead Athletes** (#402)
Maria Elissavet Nikolaidou & Konstantinos Boudolos
National and Kapodistrian University of Athens

162) **The Influence of Rate of Muscle Activation on the Neural Adaptations to Resistance Exercise** (#482)
Clayton Peterson, Michel Ladouceur & Warren Darling
University of Iowa

163) **Muscle Activation Correlates With Vibration Intensity Measured During Alpine Skiing** (#234)
Peter Federolf, Benno Nigg, Vinzenz von Tscharner, Martin Gimpl & Erich Mueller
University of Calgary

164) **Comparison of Stopping Tasks Used to Assess ACL Injury Risk** (#467)
Mukta Joshi, Joshua Weinhandl & Kristian O'Connor
University of Wisconsin-Milwaukee

165) **Memorial Poster:** James J. Stone

166) **Memorial Poster:** Yuli Toshev

<u>NOTES</u>

Thursday, August 7, 2008

< 8:00 am	**Coffee at Vendor Exhibits (Michigan League)**

8:00

Keynote Lecture II
Location: Rackham Auditorium

Locomoting in a Turbulent World
Mimi A.R. Koehl
University of California-Berkeley

9:00   **Coffee at Vendor Exhibits (Michigan League)**

9:15

CSB Career Award
Location: Rackham Auditorium

Biomechanicz in Three Acts
Ronald F. Zernicke
University of Michigan

10:15   **Coffee at Vendor Exhibits (Michigan League)**

10:30

NDI New Investigator Awards Session (CSB)
Location: Rackham Auditorium

10:30   <u>Masters Award Finalists</u>
Force Enhancement Reaches a Plateau at Critical Stretch Magnitudes (#523)
Brandon Hisey
University of Calgary

10:41   **Strength Training of the Quadriceps Muscles Following ACL Transection: Effects on Strength and Joint Integrity** (#35)
Eva Szabo
University of Calgary

10:52   **Changes in Passive Muscle Properties of Cerebral Palsy Patients** (#436)
Megan Yaraskavitch
University of Calgary

11:03   <u>Doctorate Award Finalists</u>
Mechanical Loading of In Situ Chondrocytes in Their Native Environment (#384)
Sang-Kuy Han
University of Calgary

11:14   **Shortening-Induced Force Depression is Primarily Caused by Cross-Bridges in Strongly Bound States** (#15)
Eun-Jeong Lee
University of Calgary

11:25   **Skeletal Muscle Myofibrils Fail at Different Forces but Similar Sarcomere Lengths for Active and Passive Stretching** (#250)
Tim Leonard
University of Calgary

11:36   <u>Post Doctorate Award Finalists</u>
Force Depression in Single Myofibrils and Sarcomeres (#89)
Venus Joumaa
University of Calgary

11:47   **Evaluation of a Dynamic Load Sharing Approach for the Lower Extremity** (#285)
Martijn Klein Horseman
University of Twente, University of Calgary

11:58   **Residual Force Enhancement in Maximal Voluntary Contractions of Human Dorsi Flexors** (#40)
Markus Tilp
University of Calgary

12:15 - 1:30 pm: **Box Lunch at Vendor Exhibit (Michigan League)**
CSB Annual General Meeting (MLB 1400 AUD 4)
Free Matlab Tutorial (1420 MLB)

<u>NOTES</u>

Thursday, August 7, 2008

Scientific Sessions

Occupational Biomechanics (CSB Symposium)	Computational Modeling I (Podium Session 8)
Thursday, August 7: 1:30 - 3:00 pm Location: MLB 1200 AUD 3 Session chair: Jack Callaghan	Thursday, August 7: 1:30 - 3:00 pm Location: MLB 1400 AUD 4 Session chairs: Michael Hahn, Ton van den Bogert

Occupational Evaluations Using Advanced Biomechanical Models: Circumventing Workplace Barriers Through Simulation

Making Digital Human Models More 'Human': Focusing on the Shoulder
Clark Dickerson
University of Waterloo

Industrial Vehicle Design: Understanding the Interplay Between Vision, Vibration, and Posture - Simulation Can Help
Tammy Eger
Laurentian University

Can we Perform Valid Ergonomic Assessments on Automotive Assembly Tasks that Don't Even Exist Yet?
Jim Potvin
McMaster University

Bring the Lab to Work - An Examination of Data Reduction Approaches to Document Spine Loading
Robert Parkinson
University of Waterloo

1:30 Finite Element Modeling of Intraneural Ganglion Cysts of the Common Peroneal Nerve (#159)
Shreehari Elangovan, Gregory Odegard, Duane Morrow & Robert Spinner
Michigan Technological University

1:45 A Finite Element Micromechanical Model of Muscle to Explore the Role of Intramuscular Connective Tissue (#428)
Bahar Sharafi & Silvia Blemker
University of Virginia

2:00 Finite Element Modelling and Analysis of Custom Foot Orthotics (#370)
Lieselle Trinidad, Sundar Krishnamurty, Ryan Chang & Joseph Hamill
University of Massachusetts-Amherst

2:15 Simple Models of Drop Jumps: Evaluating a Model Against the Subject Specific Group of Models From Which it was Developed (#206)
Matthew Pain & Stephanie Forrester
Loughborough University

2:30 Determination of Subject-Specific Mechanical Properties of Individual Ankle Joint Muscles (#548)
Christopher Hasson, Ross Miller & Graham Caldwell
University of Massachusetts-Amherst

2:45 Subject Specific Anatomic Parameters Improve Moment Predictions of an EMG-Driven Knee Joint Model (#305)
Liang-Ching Tsai, John Popovich, Mark Lyle & Christopher Powers
University of Southern California

3:00 - 3:30 pm: Coffee at Vendor Exhibits (Michigan League)

Thursday, August 7, 2008

Scientific Sessions

Orthopaedics I (Podium Session 9) Thursday, August 7: 1:30 - 3:00 pm Location: Rackham Amphitheatre Session chairs: Michelle Sabick, Xudong Zhang	**Gait I (Podium Session 10)** Thursday, August 7: 1:30 - 3:00 pm Location: Mendelsohn Theatre Session chairs: Scott White, Chris McGibbon

1:30   **Deformability of the Carpal Tunnel With and Without the Transverse Carpal Ligament** (#263)
Kai-Hua Xiu, Joo-Han Kim & Zong-Ming Li
University of Pittsburgh

1:45   **Comparing the Fixation of a Novel Hollow Screw Versus a Conventional Solid Screw in Human Sacra Under Cyclic Loading** (#68)
Stewart McLachlin, Brendon Beaton, Marlis Sabo, Kevin Gurr, Steward Bailey, Chris Bailey & Cynthia Dunning
The University of Western Ontario

2:00   **Influence of Posterior Cruciate Ligament Treatment on Quadriceps Demand in TKR: A Computer Simulation Study** (#522)
Michael Hast, Ryan Landon & Stephen Piazza
The Pennsylvania State University

2:15   **An In-Vivo Examination of the Effect of Femoral Tunnel Placement During ACL Reconstruction on Tibial Rotation** (#20)
Stavros Ristanis, Eleftheria Siarava, Nick Stergiou & Anastasios Georgoulis
University of Ioannina Medical Center

2:30   **An Association Between Preoperative Gait Patterns and Postoperative Total Knee Implant Migration** (#373)
David Wilson, Janie Astephen, Michael Dunbar & Kevin Deluzio
Dalhousie University, University of Cape Town

2:45   **In-Vivo Measurement of Tibiotalar Joint Motion: Accuracy Assessment and Preliminary Results** (#25)
Sukhinder Bilkhu, Stephanie Kline, Mitch Mager, Jason Davis, Richard Needleman & Michael Bey
Henry Ford Hospital

1:30   **Regulation of Mechanical Energy Generated During Walking in Healthy Children** (#393)
Brian Umberger, Sam Augsburger, JoAnne Resig, Donna Oeffinger, Robert Shapiro & Chester Tylkowski
University of Massachusetts-Amhurst

1:45   **Joint Powers but not Joint Torques Discriminate Highly Mobile and Functional Old From Young Adults** (#546)
Paul DeVita, Patrick Rider, Ben Long, Ken Steinweg, Allison Gruber, Stan Solnik & Tibor Hortobagyi
East Carolina University

2:00   **Energetics and Biomechanics of Walker Assisted Gait** (#2)
Jonathon Priebe & Rodger Kram
University of Colorado

2:15   **Elastic Energy and Optimal Stride Frequency in Running: The Effects of Uphill and Downhill** (#193)
Kristine Snyder & Claire Farley
University of Colorado

2:30   **A Comparison Between Sloped and Level Surface Gait Initiation** (#486)
Scott Breloff, Dwight Waddell & Chip Wade
University of Mississippi

2:45   **Gait Dynamics on a Cross-Slope Walking Surface** (#271)
Phil Dixon & David Pearsall
McGill University

3:00 - 3:30 pm: Coffee at Vendor Exhibits (Michigan League)

Thursday, August 7, 2008

Scientific Sessions

Ergonomics I (Podium Session 14)	**Posture & Balance I (Podium Session 12)**
Thursday, August 7: 3:30 - 5:00 pm	Thursday, August 7: 3:30 - 5:00 pm
Location: MLB 1200 AUD 3	Location: MLB 1400 AUD 4
Session chairs: Tammy Eger, Michele Oliver	Session chairs: Shirley Rietdyk, Jeffrey Haddad

3:30 — **Proactive Ergonomic Analyses With Digital Human Modeling: A Validation Study of Percent Capable Values** (#101)
Jim Potvin, James Chiang, Monica Jones, Brian McInnes & Allison Stephens
McMaster University

3:30 — **The Effect of Parkinson's Disease on the Step Response to a Backwards Pull: Center of Pressure** (#297)
Molly McVey, Antonis Stylianou, Carl W Luchies, Michael Haines, Kelly Lyons & Rajesh Pahwa
The University of Kansas

3:45 — **Vertical Ground Reaction Forces and Center of Pressure Excursion During Two-Hand Push Exertions** (#432)
Suzanne Hoffman, Matthew Reed & Don Chaffin
General Motors

3:45 — **Repeated Exposure to Small Postural Perturbations Leads to Improvements in Balance Recovery** (#165)
Kathleen Bieryla, Bradley Davidson & Michael Madigan
Virginia Polytechnic and State University

4:00 — **The Effect of Drywall Stilts on the Control of Quiet Standing** (#376)
Jeremy Noble, Jonathan Singer, Kaitlin Gallagher & Stephen Prentice
University of Waterloo

4:00 — **Loss of Complexity in Balance Dynamics During Quiet Standing and Dual-Task: A Marker of Frailty in Elderly People** (#273)
Hyun Gu Kang, Madalena Costa, Olga Starobinets, Ary Goldberger, Chung-Kang Peng, Dan Kiely, Adrienne Cupples & Lewis Lipsitz
Hebrew SeniorLife and Harvard Medical School

4:15 — **The Effectiveness and User-Acceptability of a Personal Lift Assist Device (PLAD) in Reducing Erector Spinae Demand Associated With an Automotive Assembly Task** (#190)
Ryan Graham, Joan Stevenson, Michael Agnew & Mohammad Abdoli-Eramaki
Queen's University

4:15 — **Do Vestibular Inputs Trigger Upper Body Responses During a Slip?** (#387)
Kurt Beschorner, Mark Redfern, Peter Sandrian & Rakie Cham
University of Pittsburgh

4:30 — **Effects of the Seat Armrest and Assistive Devices on Lumbar Kinetics During Dependent Transfers on an Aircraft** (#458)
Kristof Kipp & Michael Pavol
Oregon State University

4:30 — **Recovery of Postural Sway After Static Stretch of the Ankle Joint** (#149)
Tomoaki Iwata, Akinori Nagano & Zhi-wei Luo
Kobe University

4:45 — **Gender and Passive Tissue Responses to Prolonged Sitting in an Automobile Seat** (#347)
Diana De Carvalho & Jack Callaghan
University of Waterloo

4:45 — **The Effects of Walking Speed and Surface on Dynamic Stability in Young Adults With Unilateral Trans-Tibial Amputations** (#429)
Shawn Scott, Jonathan Dingwell & Jason Wilken
University of Texas

5:15 - 6:15 pm: Buses to Henry Ford Museum (Pick up at Michigan League South Entrance)
6:15 - 8:45 pm: Strolling Banquet: Henry Ford Museum (Dearborn)
8:45 - 10:00 pm: Buses from Henry Ford Museum to Hotels, Downtown and Central Campus

Thursday, August 7, 2008

Scientific Sessions

Muscle I (Podium Session 13) Thursday, August 7: 3:30 - 5:00 pm Location: Rackham Amphitheatre Session chairs: Stephen Piazza, Silvia Salinas Blemker	**Sport II (Podium Session 11)** Thursday, August 7: 3:30 - 5:00 pm Location: Mendelsohn Theatre Session chairs: Glenn Fleisig, Dave Fortenbaugh

3:30 **How is Sarcomere Length Affected by the Procedures for Intraoperative Measurements Using Laser Diffraction?** (#477)
Huub Maas, Jeremy Eagles, Thomas Sandercock & Wendy Murray
Northwestern University

3:30 **Effect of Ability on Freestyle Swimbench Stroke Characteristics** (#140)
Tracy Spigelman, Tim Uhl, David Mullineaux, Thomas Cunningham, Scott Mair & Robert Shapiro
University of Kentucky

3:45 **The Force-Length Relationship of the Cat Soleus Muscle** (#202)
Marco Aurelio Vaz, Cintia de la Rocha Freitas, Tim Leonard & Walter Herzog
Federal University of Rio Grande Do Sul

3:45 **Timing and Velocity of Shoulder and Hip Horizontal Rotation in Novice and Skilled Golfers** (#201)
Isao Okuda, Junji Shinohara & Charles Armstrong
University of New England

4:00 **Muscle Excursion Scales With Normalized Fiber Length in a Rabbit Model** (#336)
Taylor Winters, Mitsuhiko Takahashi, Richard Lieber & Samuel Ward
University of California-San Diego

4:00 **Technique Differences Among Male and Female Intermediate Hurdlers and Steeplechasers** (#242)
Laurence Bollschweiler, Iain Hunter, Brent Feland & Ty Hopkins
Brigham Young University

4:15 **Deletion of Nebulin Alters the Length-Tension Properties of Neonatal Skeletal Muscle** (#18)
David Gokhin, Jianlin Zhang, Ju Chen & Richard Lieber
University of California-San Diego

4:15 **Joint Coupling of the Rearfoot and Knee in Runners With Patellofemoral Pain Syndrome During a Prolonged Run** (#133)
Tracy Dierks & Irene Davis
Indiana University

4:30 **Automated Method for Tracking Change in Muscle Fascicle Length for Ultrasound Images** (#332)
Manku Rana & James Wakeling
Simon Fraser University

4:30 **Relationship Between Mechanical, Biomechanical and Perceptual Parameters of Cushioning Properties in Running Shoes** (#152)
Julia Augustijn, Thorsten Sterzing & Thomas L. Milani
Chemnitz University of Technology

4:45 **Assessment of Immobilized Muscle Using MRE** (#63)
Takayuki Muraki, Zachary Domire, Qingshan Chen, Matthew Mccullough & Kai-Nan An
Mayo Clinic

4:45 **Football Shoe Designs May Affect Lower Extremity Injury Risk** (#38)
Mark Villwock, Eric Meyer, John Powell, Amy Fouty & Roger Haut
Michigan State University

5:15 - 6:15 pm: Buses to Henry Ford Museum (Pick up at Michigan League South Entrance)
6:15 - 8:45 pm: Strolling Banquet: Henry Ford Museum (Dearborn)
8:45 - 10:00 pm: Buses from Henry Ford Museum to Hotels, Downtown and Central Campus

Friday, August 8, 2008

< 8:00 am	**Coffee at Vendor Exhibits (Michigan League)**
8:00	**Keynote Lecture III** Location: Rackham Auditorium

The 3 Bs of Motor Control: Behavior, Brains and Biomechanics
Steve Scott
Queen's University

9:00	**Coffee at Vendor Exhibits (Michigan League)**
9:15	**Hay Award (ASB)** Location: Rackham Auditorium

From Biomechanics to Motor Control – From 1973 to 2008
Vladimir M. Zatsiorsky
The Pennsylvania State University

10:15 – 10:45 am	**Coffee at Vendor Exhibits (Michigan League)**

NOTES

<u>NOTES</u>

Friday, August 8, 2008

Scientific Sessions

Aftab Patla Symposium (CSB Career Award)	Motor Control II (Podium Session 15)
Friday, August 8: 10:45 am – 12:15 pm	Friday, August 8: 10:45 am – 12:15 pm
Location: MLB 1200 AUD 3	Location: MLB 1400 AUD 4
Session chair: Stephen Prentice	Session chairs: Jules Dewald, Albert Chen

Silly Walks and Other Insights to the Control of Locomotion. Celebrating the Contribution of Aftab Patla

Just Walk Normally, Adapting to Changing Circumstances
Stephen Prentice
University of Waterloo

Compensatory Responses to Perturbations During Rhythmic Movements in Human Subjects
Marc Bélanger
Université du Québec à Montréal

Evaluating Adaptation and Avoidance in Clinical Motion: Concepts Learned From Aftab
Sandi Spaulding
The University of Western Ontario

Aftab Patla's Perspective on Stability: Four Legs Good, Two Legs Bad
Shirley Rietdyk
Purdue University

Watch Where You're Walking: How Aftab Saw Vision Guiding Locomotion
Michael Cinelli
Wilfrid Laurier University

10:45 **Neuromechanical Representations of Leg Orientation and Length Control are Preferentially Conserved After Peripheral Nerve Injury During Cat Locomotion** (#435)
Young-Hui Chang, Arick Auyang, John Scholz & Richard Nichols
Georgia Institute of Technology

11:00 **Neuromuscular Contribution of the Leg Flexor Muscles to Knee Joint Stiffness Following a Sudden Leg Perturbation** (#147)
Joel Cort & Jim Potvin
McMaster University

11:15 **Proprioceptive Sensitivity in Constrained and Unconstrained Degrees of Freedom** (#456)
Martha Cammarata & Yasin Dhaher
Northwestern University

11:30 **The Influence of Increasing Steady-State Walking Speed on Muscle Coordination in Below-Knee Amputees** (#450)
Nicholas Fey, Anne Silverman, Albert Portillo, Gail Walden, Gordon Bosker & Richard Neptune
The University of Texas at Austin

11:45 **Decreased Stability of Multisegmental Postural Coordination in ACL-Injured Female Athletes** (#483)
Adam Kiefer, Kevin Ford, Mark Paterno, Gregory Myer, Michael Riley, Kevin Shockley & Timothy Hewett
University of Cincinnati

12:00 **A Simple, Anatomically Based Correction to the Conventional Ankle Joint Center** (#110)
Dustin Bruening, Ashlie Crewe & Frank Buczek
University of Delaware, Shriners Hospitals for Children

12:15 - 1:30 pm: **Box Lunch at Vendor Exhibit (Michigan League)**
ASB Annual Business Meeting (MLB 1400 AUD 4)
Free Matlab Tutorial (1420 MLB)

Friday, August 8, 2008

Scientific Sessions

Methods/Instrumentation II (Podium Session 16) Friday, August 8: 10:45 am – 12:15 pm Location: Rackham Amphitheatre Session chairs: Stacie Ringleb, Kristin Zhao	**Shoulder (Podium Session 17)** Friday, August 8: 10:45 am – 12:15 pm Location: Mendelsohn Theatre Session chairs: Wendy Murray, Maury Nussbaum

10:45 **A Comparison of Musculoskeletal Model Predictions of Muscle Strain With Dynamic MRI Measures** (#408)
Amy Silder, Scott Reeder & Darryl Thelen
University of Wisconsin-Madison

10:45 **Unconstrained Shoulder Joint Position Sense Does not Change With Body Orientation** (#568)
Jason Chapman, David Suprak & Andrew Karduna
University of Oregon

11:00 **Rectus Femoris Moment Arms Estimated Over a Large Range of Motion From Real-Time MRI** (#441)
Niccolo Fiorentino, Jonathan Lin, Mike Guttman, Elliot McVeigh & Silvia Blemker
University of Virginia

11:00 **The Relationship Between Glenoid Inclination and In-Vivo Glenohumeral Joint Motion During Shoulder Abduction** (#14)
Jennifer Bishop, Stephanie Kline, Kristopher Aalderink & Michael Bey
Henry Ford Hospital

11:15 **Automatic Extraction of Distal Femur Articular Geometric Measures From 3D Surface Data** (#248)
Kang Li, Scott Tashman, Christopher Harner & Xudong Zhang
University of Pittsburgh

11:15 **A Multi-Subject Evaluation of Uncertainty in Anatomical Landmark Location on Shoulder Kinematic Description** (#185)
Joseph Langenderfer, Paul Rullkoetter & Peter Laz
Central Michigan University

11:30 **Dynamics Analysis of Ankle, Knee and Hip Joint in Sagittal Plane Using a Wearable Sensor System** (#439)
Rencheng Zheng, Tao Liu, Yoshio Inoue, Kyoko Shibata & Kun Liu
Kochi University of Technology

11:30 **Muscle Activity in Various Overhead Work Postures** (#394)
Steven Fischer, Jaclyn Chopp & Clark Dickerson
University of Waterloo

11:45 **A Novel Ambulatory Device for Continuous 24-H Monitoring of Physical Activity in Daily Life** (#586)
Bijan Najafi, James Wrobel & David Armstrong
Rosalind Franklin University of Medicine and Science

11:45 **Muscle Contributions to Joint Stability in the Anatomical Shoulder** (#349)
David Ackland & Marcus Pandy
University of Melbourne

12:00 **Quantifying and Predicting Elevation Angle Error Using Tri-Axial Accelerometer During Dynamic Motion** (#238)
Tal Amasay & Andrew Karduna
University of Oregon

12:00 **3-D Strength Surfaces of Shoulder Internal and External Rotation** (#374)
Gary Pierce & Laura Frey-Law
University of Iowa

12:15 - 1:30 pm: **Box Lunch at Vendor Exhibit (Michigan League)**
ASB Annual Business Meeting (MLB 1400 AUD 4)
Free Matlab Tutorial (1420 MLB)

Friday, August 8, 2008

Scientific Sessions

Rehabilitation (Podium Session 20) Friday, August 8: 1:30 - 3:00 pm Location: MLB 1200 AUD 3 Session chairs: Sylvie Nadeau, Dany Gagnon	**Computational Modeling II (Podium Session 19)** Friday, August 8: 1:30 - 3:00 pm Location: MLB 1400 AUD 4 Session chairs: Darryl Thelen, Jeff Reinbolt

1:30   **Virtual Reality in Stroke Rehabilitation** (#235)
Martha Walker, Stacie Ringleb, George Maihafer, Jessica Crouch, Nigel Tierney, Bonnie Van Lunen, Gianluca De Leo, Jean Shelton, Robert Walker & Hector Garcia
Old Dominion University

1:30   **A Practical Model of the Muscle/Tendon Moment Arms in a Thumb** (#76)
John Wu, Kai-Nan An & Robert Cutlip
National Institute for Occupational Safety and Health (NIOSH)

1:45   **Limited Assistance Practice Increases Active Dorsiflexion Range of Motion in the Impaired Ankle of Stroke Subjects** (#577)
Kari Danek, Brent Gillespie, Daniel Ferris, Jessy Grizzle & James Patton
University of Michigan

1:45   **Creation of the Geometry for a Finite Element Model of the Wrist Under Loaded and Unloaded Conditions** (#449)
Charlotte Curtis, Robert Dony, Michele Oliver, Anne Agur, David Salonen & Vincent Lo
University of Guelph

2:00   **Effects of Ankle Stretching on Passive and Active Muscle-Tendon Properties of Plantar Flexors in Stroke** (#493)
Fan Gao & Li-Qun Zhang
Northwestern University

2:00   **Refinements of Moment-Based Cost Functions Improve Prediction of Experimental Moment Profiles in Cycling** (#289)
Herman van Werkhoven, Joseph Sommer & Philip Martin
The Pennsylvania Sate University

2:15   **Bilateral Lower Limb Force Production in Individuals With Post-Stroke Hemiparesis** (#81)
Ann Simon, Brian Kelly & Daniel Ferris
University of Michigan

2:15   **Real-Time Estimation of Muscle Forces From Inverse Dynamics** (#198)
Antonie van den Bogert, Thomas Geijtenbeek & Oshri Even-Zohar
Cleveland Clinic Foundation

2:30   **Improved Locomotion in Human SCI Through Motor Adaptation** (#346)
Ming Wu, T. George Hornby, W. Zev Rymer & Brian Schmit
Rehabilitation Institute of Chicago, Northwestern University

2:30   ***An EMG-Driven Forward Simulation of Single Support Phase During Gait** (#400)
Qi Shao & Thomas Buchanan
University of Delaware

*Delsys Award Winner

2:45   **Influence of Wheelchair Suspension on Seat Forces and Head Accelerations During Curb Descent Landings** (#344)
Philip Requejo, Jill McNitt-Gray & Henryk Flashner
Rancho Los Amigos National Rehabilitation Center

2:45   **Toward a Minimal Input Model for Joint Moment Estimation During Gait** (#269)
Michael Hahn
Montana State University

3:00 - 3:30 pm: Coffee at Vendor Exhibits (Michigan League)

Friday, August 8, 2008

Scientific Sessions

Cartilage (Podium Session 18) Friday, August 8: 1:30 - 3:00 pm Location: Rackham Amphitheatre Session chairs: John Elias, Li-Qun Zhang	**Gait II (Podium Session 21)** Friday, August 8: 1:30 - 3:00 pm Location: Mendelsohn Theatre Session chairs: Clare Milner, Brandi Row

1:30 **Frictional Properties of Intact Mutant PRG4 Mouse Knee Articular Cartilage** (#518)
Elizabeth Drewniak, Michael Rainbow, Gregory Jay, Braden Fleming & Joseph Crisco
Brown University

1:45 **Quantifying Meniscal Volume and Articular Cartilage Thickness in Patients Treated With Partial Meniscectomy** (#55)
Megan Bowers, Glenn Tung, Heidi Oksendahl, Michael Hulstyn, Paul Fadale & Braden Fleming
Brown University

2:00 **Cartilage Cell Viability After Submaximal and Maximal Muscle Loading With and Without Impact Loading** (#375)
Douglas Bourne, John Matyas, Ken Muldrew & Walter Herzog
University of Calgary

2:15 **Elucidating the Relationship Between Residual Incongruities, Elevated Contact Stresses, and Cartilage Degeneration in Fractures of the Tibial Plafond** (#134)
Thaddeus Thomas, Chris Van Hofwegen, Donald Anderson, J.L. Marsh & Thomas Brown
University of Iowa

2:30 **Correlation Between Focal Cartilage Thickness and Femur Cartilage Contact Regions During Running** (#489)
William Anderst, Eric Thorhauer & Scott Tashman
University of Pittsburgh

2:45 **The Adduction Moment During Walking is Correlated With Cartilage Thickness Ratio in Younger Male Subjects** (#588)
Chris Dyrby, Jessica Asay, Seungbum Koo & Thomas Andriacchi
Stanford University

1:30 **Strategies for Walking on a Laterally Oscillating Treadmill** (#265)
Brian Peters, Rachel Brady & Jacob Bloomberg
Wyle Laboratories

1:45 **Dynamic Stability of Walking During Anterior-Posterior and Medio-Lateral Support Surface and Visual Field Translations** (#430)
Patricia McAndrew, Jonathan Dingwell & Jason Wilken
University of Texas

2:00 **Direction-Dependent Weighting of Vision for Balance During Walking** (#557)
Shawn O'Connor & Arthur Kuo
University of Michigan

2:15 **Effects of Long-Duration Space Flight on Toe Clearance During Treadmill Walking** (#295)
Chris Miller, Brian Peters, Rachel Brady, Ajitkumar Mulavara, Jason Richards, Matthew Hayat & Jacob Bloomberg
Wyle Laboratories

2:30 **Locomotion Stability in Simulated Martian Gravity: Insights on the Influence of Load Location** (#354)
Melissa Scott-Pandorf, Dan O'Connor, Charles Layne, Kresimir Josic & Max Kurz
University of Houston

2:45 **Predictive Simulation of Gait at Low Gravity Using Direct Collocation** (#78)
Marko Ackermann & Antonie van den Bogert
Cleveland Clinic Foundation

3:00 - 3:30 pm: Coffee at Vendor Exhibits (Michigan League)

Friday, August 8, 2008

Scientific Sessions

Ergonomics II (Podium Session 23)	Aging II (Podium Session 22)
Friday, August 8: 3:30 - 5:00 pm	Friday, August 8: 3:30 - 5:00 pm
Location: MLB 1200 AUD 3	Location: MLB 1400 AUD 4
Session chairs: Clark Dickerson, Joan Stevenson	Session chairs: Sibylle Thies, Alaa Ahmed

3:30 **Biomechanical Analysis of Opening Glass Jars: Using Kinematics to Inform Design** (#225)
Joseph Fair, Tamara Reid Bush & Laura Bix
Michigan State University

3:30 **Postural Control During a Standing Turning Task in Young and Older Adults** (#524)
Jennifer Baird & Richard Van Emmerik
University of Massachusetts-Amherst

3:45 **Overhead Grasp Capability for Typical Ladder Handholds** (#294)
Justin Young, Michael Sackllah, Chuck Woolley, Tom Armstrong & James Ashton-Miller
University of Michigan

3:45 **Change of Postural Feedback Gain Scaling by Aging** (#151)
Seyoung Kim, Fay Horak & Sukyung Park
KAIST

4:00 **Learning Effects of Simultaneous Grip and Shoulder Exertion on Muscle Activity** (#298)
Joanne Hodder & Peter Keir
McMaster University

4:00 **Stability of Superior Segments During Gait in Older Adults** (#279)
Hyun Gu Kang & Jonathan Dingwell
Hebrew SeniorLife, Harvard Medical School

4:15 **Constrained Handgripping Reduces Maximal Arm Strength and Muscle Activation of the Upper Extremities** (#230)
Martin Smets, Potvin Jim & Peter Keir
McMaster University

4:15 **Can Thinking be Hazardous to Your Balance? The Effects of Cognition on Postural Stability in Older Adults** (#389)
Jeffrey Haddad, Winona Snapp-Childs, Richard Van Emmerik & Matthew Davidson
Purdue University

4:30 **The Effect of the Object Distance on Hand Movement During Reach-to-Grasp Tasks** (#507)
Sungchan Bae & Thomas Armstrong
University of Michigan

4:30 **Age-Related Changes in the Neuromuscular Coordination of Human Walking** (#116)
Anne Schmitz, Amy Silder, Bryan Heiderscheit, Jane Mahoney & Darryl Thelen
University of Wisconsin- Madison

4:45 **Vibration Transmissibility of Multi-Body Segments in Reach Movements Under Whole-Body Vibration Exposure** (#103)
Heon-Jeong Kim & Bernard Martin
University of Michigan

4:45 **Walking Speed, Leg Strength, Range of Motion, and Dynamic Stability in the Gait of Healthy Older Adults** (#281)
Hyun Gu Kang & Jonathan Dingwell
Hebrew SeniorLife, Harvard Medical School

5:00 - 7:00 pm: Poster Session II (Michigan League)
6:30 - 8:00 pm: Student Mentoring Session (Rackham Assembly Hall, 4th Floor)
7:00 - later: Night on the Town (Buses Circulate Between Campus Downtown and Hotels)

Friday, August 8, 2008

Scientific Sessions

Tendon & Ligament (Podium Session 24)	Lower Extremity (Podium Session 25)
Friday, August 8: 3:30 - 5:00 pm Location: Rackham Amphitheatre Session chairs: John Wu, Zong-Ming Li	Friday, August 8: 3:30 - 5:00 pm Location: Mendelsohn Theatre Session chairs: Graham Caldwell, Brian Umberger

3:30 — **Native Ulnar Collateral Ligament Strain Under a Rehabilitation Protocol** (#124)
Ramon Ruberte Thiele, Geoffrey Bernas, Karen Kinnaman, Bruce Miller & James Carpenter
University of Michigan

3:45 — **Achilles Tendon Moment Arms via a Hybrid Method Using Motion Analysis and Ultrasound: In Vivo Estimations in Male Subjects** (#210)
Justin Cowder, Thomas Buchanan & Kurt Manal
University of Delaware

4:00 — **Use of Ultrasound to Dynamically Evaluate Achilles Tendon Mechanical Properties in Stroke** (#454)
Heng Zhao & Li-Qun Zhang
Northwestern University, Rehabilitation Institute of Chicago

4:15 — **In Vivo Evaluation of The Stiffness of the Healing Human Patellar Tendon** (#49)
Hsin-Yi Liu, R. Alex Creighton, Troy Blackburn, Darin Padua & Paul Weinhold
University of North Carolina at Chapel Hill

4:30 — **Forces in Anterior Cruciate Ligament During Simulated Weight-Bearing Flexion With Anterior and Internal Rotational Tibial Load** (#170)
Jia-Hsuan Lo, Otto Muller, Markus Wunschel, Steffen Bauer & Nikolaus Wulker
University of Tuebingen

4:45 — **Effects of Cyclic Stretch on Behavior of Tenocytes Seeded in Acellular Tendon Scaffolds** (#312)
Ting-Wu Qin, Cheng-Jun Liu, Zhi-Ming Yang, Chun-Feng Zhao, Yu-Long Sun & Kai-Nan An
West China Hospital, Sichuan University, University, Mayo Clinic

3:30 — **Differences in Hamstring Mechanics Between Shortening and Lengthening Contractions Revealed by Dynamic MRI** (#407)
Amy Silder, Christopher Westphal, Scott Reeder & Darryl Thelen
University of Wisconsin-Madison

3:45 — **The Influence of Muscle Activation-Deactivation Dynamics on the Chainring Shape That Maximizes Average Crank Power** (#334)
Jeffery Rankin & Richard Neptune
The University of Texas at Austin

4:00 — **Validation of Agonist and Antagonist Muscle Force Estimation During Jumping at Three Different Effort Levels** (#157)
Kevin Ford, Antonie van den Bogert, Gregory Myer, Robert Shapiro & Timothy Hewett
Cincinnati Children's Hospital, University of Kentucky

4:15 — **The Effects of Mid-Air Adjustments on Knee Joint Loading When Landing From a Jump** (#409)
Guan Tan & Timothy Derrick
Iowa State University

4:30 — **Gender Comparisons Between Unilateral and Bilateral Landings** (#390)
Joshua Weinhandl, Mukta Joshi & Kristian O'Connor
University of Wisconsin-Milwaukee

4:45 — **Internal Femoral Forces and Moments During Running: Implications for Stress Fracture Development** (#17)
W. Brent Edwards, Jason Gillette, Joshua Thomas & Timothy Derrick
Iowa State University

5:00 - 7:00 pm: Poster Session II (Michigan League)
6:30 - 8:00 pm: Student Mentoring Session (Rackham Assembly Hall, 4th Floor)
7:00 - later: Night on the Town (Buses Circulate Between Campus Downtown and Hotels)

Friday, August 8, 2008

Poster Session II
Location: Michigan League
Time: 5:00 - 7:00 pm

2nd Floor
Room: Michigan Ballroom (Posters 167-240: Gait, Posture & Balance, Methods/Instrumentation,
Lower Extremity)

167) **Differences in Lower Extremity Coordination in High- Compared to Low-Arched Female Athletes During Running** (#510)
Douglas Powell, Songning Zhang, Clare Milner, Benjamin Long & Matt Bice
University of Texas of the Permian Basin

168) **Effect of Neutral Trial on Dynamic Foot Kinematics** (#462)
Rebecca Shultz & Thomas Jenkyn
The University of Western Ontario

169) **Foot Kinematics During Barefoot Running and Cutting** (#466)
Rebecca Shultz & Thomas Jenkyn
The University of Western Ontario

170) **Does Restraining Arm Motion Alter Ground Reaction Forces During Running?** (#256)
Ross Miller, Graham Caldwell, Richard Van Emmerik, Joseph Hamill & Brian Umberger
University of Massachusetts-Amherst

171) **Relationship Between Static Arch Stiffness and Medial-Longitudinal Arch Behavior During Walking** (#494)
Pedro Rodrigues, Trampas TenBroek, Alan Tomasko & Joseph Hamill
University of Massachusetts-Amherst

172) **Trunk Bend and Twist Coordination in Runners With Low Back Pain** (#274)
Joseph Seay, Richard van Emmerik & Joseph Hamill
University of Massachusetts-Amherst

173) **Invariant Ankle Moment Patterns With Plantar Flexor Assistance From a Powered Ankle Orthosis** (#560)
Cara Lewis, Pei-Chun Kao & Daniel Ferris
University of Michigan

174) **Motor Response During Unexpectedly Reduced Plantar Flexor Torque Provided by a Powered Orthosis During Walking** (#571)
Pei-Chun Kao, Cara Lewis & Daniel Ferris
University of Michigan

175) **Gait Characteristics of the Centre of Pressure in Sub-Acute Stroke Patients** (#237)
Amanda Chisholm, Stephen Perry & William McIlroy
University of Toronto, Toronto Rehabilitation Institute

176) **Influence of Incremental Increases in Orthotic Height on Dynamic Stability in Functional Flatfooted Individuals** (#417)
Stephen Perry & Kelly Goodwin
Wilfrid Laurier University

177) Lower Extremity Kinematic Effects of Medial Arch Support Among Functionally Flatfooted Individuals (#107)
E. Anne Cunningham & Stephen Perry
Wilfrid Laurier University

178) Tracking Gait Asymmetries During Rehabilitation Using Regions of Deviation Measures: A Case Study (#443)
K. Alex Shorter, John Polk, Karl Rosengren & Elizabeth Hsiao-Wecksler
University of Illinois at Urbana-Champaign

179) Changes in Kinetic and Kinematic Gait Parameters due to Firefighting Air Bottle Configuration (#579)
Kiwon Park, Pilwon Hur, Karl Rosengren, Gavin Horn & Elizabeth Hsiao-Wecksler
University of Illinois at Urbana-Champaign

180) Comparison of Variability Between Overground and Treadmill Running (#122)
Rebecca Fellin & Irene Davis
University of Delaware

181) A 3-D Kinematic Comparison Between Single-Belt and Split-Belt Treadmill Walking (#386)
Allison Altman, Michael Pohl, Joaquin Barrios & Irene Davis
University of Delaware

182) Calculation of Vertical Load Rates in the Absence of Vertical Impact Peaks (#434)
Richard Willy, Michael Pohl & Irene Davis
University of Delaware

183) High Energetic Cost of Sudden Center-of-pressure Advancement During Human Walking (#567)
Peter Gabriel Adamczyk & Arthur Kuo
University of Michigan

184) Gravitational Effects Upon Locomotion Posture (#472)
John DeWitt, Jason Bentley, W. Brent Edwards, Gail Perusek & Sergey Samorezov
Wyle's Life Sciences Group

185) Walking Stability Analysis of Brace and FES-Based Interventions for Multiple Sclerosis (#478)
Vanessa Everding, Anirban Dutta & Elizabeth Hardin
Case Western Reserve University; Cleveland FES Center, Cleveland VAMC

186) Determination of Pronation Parameters by Midsole Deformation is Independent of Running Velocity (#22)
Torsten Brauner, Thomas Milani, Thorsten Sterzing & Doris Oriwol
Chemnitz University of Technology

187) Matching Performance of a Hybrid Gait Recognition Solution (#475)
Adam Fullenkamp & James Richards
University of Delaware

188) Crossover and Free Moment During Running (#538)
Stacey Meardon & Timothy Derrick
Iowa State University

189) Effect of Speed on Emotion-Related Kinematics During Walking (#547)
Rebecca Edgeworth, Brendan Keen, Elizabeth Crane & Melissa Gross
University of Michigan

44

190) **Changes in Wheeling Kinematics After 8 Weeks of Pushrim-Activated Power-Assisted Wheelchair Use** (#423)
Mark Tillman, John Chow, Kim Fournier, Srikant Vallabhajosula, Peter Giacobbi Jr., Frederick Dietrich, Sandra Hubbard & Charles Levy
University of Florida

191) **A Neuro-Muscoloskeletal Model for Testing Bipedal Locomotor Control Hypotheses** (#378)
Jeremy Noble & Stephen Prentice
University of Waterloo

192) **Fluctuation of EMG Patterns at Multiple Walking Speeds** (#275)
Hyun Gu Kang & Jonathan Dingwell
Hebrew SeniorLife, Harvard Medical School

193) **Conflict Resolution Task Effects on Gait Balance After a Concussion** (#258)
Robert Catena, Paul van Donkelaar & Li-Shan Chou
University of Oregon

194) **Lower Extremity Mechanical Work Explains Interindividual Variability of Running Economy** (#249)
Gary Heise, Jeremy Smith & Philip Martin
University of Northern Colorado

195) **Des Moines University Foot Model: Reliability and Case Report** (#209)
Vassilios Vardaxis, Greg Iwaasa, Phillip Hasler & James Mahoney
Des Moines University

196) **Effects of Optic Flow When Spontaneously Accelerating Towards the Walk-to-Run Transition** (#158)
Kristof De Smet, Philippe Malcolm, Veerle Segers, Matthieu Lenoir & Dirk De Clercq
Ghent University

197) **Three-Dimensional Analysis of the Trajectory of the Ankle While Running** (#148)
Thomas Cunningham, Tim Uhl, Robert Shapiro & Carl Mattacola
University of Kentucky

198) **Stability Margin During Gait: Identifying Balance Impairment in the Elderly** (#121)
Vipul Lugade, Sue Ewers, Chu Jui Chen, Sujitra Boonyong, Patima Silsupadol & Li-Shan Chou
University of Oregon

199) **Trunk Lean as a Mechanism to Reduce the Knee Joint Loading in Patients With Knee Osteoarthritis** (#576)
Heather Linley, Elizabeth Sled, Elsie Culham & Kevin Deluzio
Queen's University

200) **Measurement of Dynamic Muscle Function via Electrical Stimulation Synchronized to the Gait Cycle** (#290)
Antonio Hernandez & Darryl Thelen
University of Wisconsin-Madison

201) **Determinants for Direction of Obstacle Avoidance During Goal-Directed Locomotion** (#554)
Michael Cinelli & William Warren
Brown University

202) **Changes of Arm Movements in Dual Task Condition on Different Walking Environment in Healthy Young Adults** (#41)
Yao-Cheng Hsieh & Chiung-Yu Cho
National Cheng Kung University

203) **Multivariate Conservative Gait Pattern in Diabetes** (#21)
James Wrobel, Ryan Crews & John Connolly
Rosalind Franklin University of Medicine and Science

204) **Constraints to Overground Walking Velocity Elicited Decreased Within Subjects Gait Variability** (#473)
Adam Fullenkamp & James Richards
University of Delaware

205) **Initial Electromechanical Reaction to Rearward Perturbation** (#487)
Nitin Moholkar, Venkata Gade, Jerome Allen & W. Thomas Edwards
Koessler Medical Rehabilitation Research & Education Center

206) **Effects of Obesity on Single Step Balance Recovery From a Forward Fall** (#219)
Michael Whitley, Michael Madigan & Kevin Davy
Virginia Polytechnic and State University

207) **Pre and Post Assessment of Normal Pressure Hydrocephalus Patients Using a Head Mounted Accelerometer** (#328)
Brandy Wozniak, Stephen Dombrowski, Brian Davis & Mark Luciano
Cleveland Clinic

208) **Postural Balance During One Leg Standing in Patients With Total Hip Arthroplasty and Surface Replacement Arthroplasty** (#351)
Marc Therrien, Julie Nantel, Martin Lavigne, Pascal-Andre Vendittoli, & Francois Prince
Marie Enfant Rehabilitation Center

209) **Physical Assistance Can be Detrimental to Learning Walking Balance** (#559)
Antoinette Domingo & Daniel Ferris
University of Michigan

210) **Determining Biomechanical Properties of Falls Using an Adult Anthropometric Dummy** (#320)
Daniel Steed, Jennica Roche & Mark Redfern
University of Pittsburgh

211) **Sensory Integration for Visually Induced Roll Tilt Perception** (#356)
Heewon Park & Sukyung Park
KAIST

212) **Step to Step Variation in Step Width Suggests a Link to Variations in Trunk Kinematics** (#259)
Christopher Hurt, Karrie Hamstra-Wright, Noah Rosenblatt, Karen Troy & Mark Grabiner
University of Illinois at Chicago

213) **Perception of Weight-Bearing Distribution During Sit-to-Stand Tasks in Hemiparetic and Healthy Individuals** (#126)
Anabele Briere, Selena Lauziere, Denis Gravel & Sylvie Nadeau
Universite de Montreal

214) **Effect of the Boston Brace on Standing Balance in Adolescent Idiopathic Scoliosis** (#150)
Heydar Sadeghi & Paul Allard
Tarbiat Moallem University

215) **Poor Glucose Control is Related to Reduced Balance Control in Adults With Type II Diabetes** (#505)
Brandi Row, Kathleen Knutzen, Lorrie Brilla, Jeanne Freeman, Ying Li & Billie Lindsey
Western Washington University

216) **Gender Differences in Postural Control Strategies During Prolonged Standing** (#318)
Erika Nelson-Wong, Diane Gregory, David Winter & Jack Callaghan
University of Waterloo

217) **Estimating the Moment of Inertia of the Human Body as a Single Link Inverted Pendulum Model** (#575)
Pilwon Hur & Elizabeth Hsiao-Wecksler
University of Illinois at Urbana-Champaign

218) **Using Vicon to Determine the Area and Volume of Body Segments** (#427)
Idafe Perez Jimenez
Loughborough University

219) **Manual Segmentation of DXA Scan Images Results in Reliable Upper and Lower Extremity Tissue Mass Estimates** (#304)
Timothy Burkhart, Katherine Arthurs & David Andrews
University of Windsor

220) **Measuring In-Vivo Humeral Head Translation Using Fluoroscopy: A Comparison of Static and Dynamic Positioning** (#268)
Jun San Juan & Andrew Karduna
University or Oregon

221) **Radiosteerometric Analysis (RSA) Calibration Accuracy is Unaffected by Non-Orthogonal Images** (#196)
Angela Kedgley & Thomas Jenkyn
The University of Western Ontario

222) **Development of a Laser Reflectance System to Measure the Cross-Sectional Area of Soft Tissue** (#339)
Gabriel Pokhai, Karen Gordon & Michele Oliver
University of Guelph

223) **Calculation Method Affects Tibial Acceleration Slope Values** (#5)
Adriana Holmes, Nikki Nolte & David Andrews
University of Waterloo

224) **A Unifying Approach to Determine the Number of Padding Points When Digitally Filtering Kinematic Data** (#31)
Samuel Howarth & Jack Callaghan
University of Waterloo

225) **Longitudinal Strain Estimation in Muscles, Tendons, and other Incompressible Generalized Cylinders** (#479)
Qi Wei & Dinesh Pai
University of British Columbia, Rutgers University

226) **Analysis of the Internal Stresses in USS I Pedicle Screws Using the Photoelasticity** (#64)
Sarah Fakhouri, Ariane Zamarioli, Antonio Carlos Shimano, Cleudmar Amaral Araujo, Helton Defino, Patricia Silva & Otavio Terra
University of Sao Paulo

227) **The Influence of Noise and Time Series Length on Two Common Measures of Entropy** (#357)
Tobin Silver, Chris Rhea, Breanna Studenka, Joong Hyun Ryu, Charmayne Mary Lee Hughes & Jeffrey Haddad
Purdue University

228) **The Comparison of Supinated and Pronated Foot in Ground Reaction Forces Attenuation During Single Leg Drop-Landing** (#58)
Ali Abbasi, Heydar Sadeghi & Mehdi Khaleghi
Tarbiat Moallem University of Tehran

229) Gender Differences in Peak Vertical Ground Reaction Force and Rate of Loading During Stop-Jump Task (#57)
Ali Abbasi, Heydar Sadeghi & Mehdi Khaleghi
Tarbiat Moallem University of Tehran

230) Dynamic Foot Mobility in High and Low Arched Individuals (#177)
Andrew Barnes, Jonathan Wheat & Clare Milner
Sheffield Hallam University

231) Quantification Using Fluoroscopic RSA of Syndesmotic Motion in the Intact State and Following Simulation of High Ankle Sprain (#111)
Angela Kedgley & Thomas Jenkyn
The University of Western Ontario

232) Bilateral Intermittent Claudication Affects Joint Powers During Gait (#51)
Panagiotis Koutakis, Sara Myers, Jason Johanning, Iraklis Pipinos & Nick Stergiou
University of Nebraska at Omaha

233) Biomechanical Changes During Prolonged Running (#195)
Lisa Stirling, Vincent Von Tscharner, Seong Hoon Kim & Benno Nigg
University of Calgary

234) Impact Attenuation Through Human Body During Heel-Toe Running With Different Cushioning Shoes (#292)
Yongkoo Lee, Martijn Klein Horsman & Benno Nigg
University of Calgary

235) Quadriceps EMG During Weighted Knee Extension Following Total Knee Arthroplasty (#367)
Jeannette Byrne & Stephen Prentice
Memorial University of Newfoundland

236) How Does Isolated Gastronemius Contracture Affect Plantar Pressure in Neurologically Healthy Subjects? (#207)
Nicole Chimera, Michael Castro & Kurt Manal
University of Delaware

237) Minimal Foot Clearance in Stair Descent: Application of a Simple, Robust Empirical Methodology (#280)
Tyler Cluff & D. Gordon E. Robertson
University of Ottawa

238) Motor Unit Discharge During Steady Isometric Contractions With the Dorsiflexor Muscles (#293)
Mark Jesunathadas, Malgorzata Klass, Jacques Duchateau & Roger Enoka
University of Colorado

239) An Ankle Orthosis With a Subtalar Locking System is More Effective in Restricting Passive and Active Ankle Kinematics (#85)
Songning Zhang, Michael Wortley, Qingjian Chen, Julia Freedman & Casey Riley
The University of Tennessee

240) Subject-Specific Changes in Knee Loading in Response to an Unstable Shoe Intervention (#310)
Katerina Blazek, Katherine Boyer & Thomas Andriacchi
Stanford University

2nd Floor
Room: Vandenberg (Posters 241-256: Lower Extremity, Sport Science)

241) **The Relationship Between Knee Valgus When Squatting and During Vertical Jump Takeoff and Landing** (#531)
Mostafa Afifi, Kristinn Heinrichs & Richard Hinrichs
Arizona State University

242) **Association Between 30sec Maximal Tethered Swimming and Swimming Performance in Front Crawl** (#380)
Pedro Morouco, Susana Soares, Joao Paulo Vilas-Boas & Ricardo Fernandes
University of Porto, Polytechnic Institute of Leiria, Portuguese Swimming Federation

243) **Influence of Cadence, Power Output and Hypoxia on the Joint Powers and Muscle Excitation During Cycling** (#184)
David Sanderson, Guillaume Mornieux, Jordan Guenette & Bill Sheel
University of British Columbia

244) **Total Kinetic Energy Production of Body Segments is Different Between Racing and Training Pace in Elite Olympic Rowers** (#112)
Daniel Bechard, Angela Kedgley, Volker Nolte & Thomas Jenkyn
The University of Western Ontario

245) **Kinematic Analysis on Influence of an Extra Weight in Horizontal Arm Swing** (#542)
Young-Kwan Kim & Richard Hinrichs
Arizona State University

246) **Arm Swing of Volleyball Spike Jump Performance Between Advanced and Recreational Female Players** (#306)
ChengTu Hsieh & Gary Heise
University of Texas, Pan American

247) **Effects of an Unstable Shoe Construction in Low Speed Running** (#143)
Katherine Boyer, Katerina Blazek & Tom Andriacchi
Stanford University

248) **The Association of Foot Print Parameters and Running Training Level/Event Focus** (#70)
Jeanna Fascione, Ryan Crews & James Wrobel
Rosalind Franklin University of Medicine and Science

249) **The Effectiveness of an Unstable Shoe on Golf Performance and a Reduction of Low Back Pain** (#88)
Elysia Davis, Benno Nigg, David Lindsay & Carolyn Emery
University of Calgary

250) **Plantar Loading Differences Between Racing Flats and Training Shoes at a Self-Selected Running Speed** (#8)
Robin Queen, Jordan Yoder, Johannes Wiegerinck, Jennifer Boyd, Alicia Abbey & James Nunley
Duke University Medical Center

251) **Hip Kinematics During Three Soccer Kicking Tasks** (#39)
Robin Queen, Brian Charnock & William Garrett
Duke University Medical Center

252) **A Quantitative Analysis of Joint Phasing and Efficiency in the Olympic Clean** (#154)
Justin Byers, Tom Wu & Pierre Gervais
University of Alberta

253) Two-Dimensional Sequential Analysis of the Underhand Softball Pitch (#461)
John Garner, Wendi Weimar & Nels Madsen
University of Mississippi

254) Head Motion During Baseball Pitching (#46)
Dave Fortenbaugh, Glenn Fleisig, Shouchen Dun & James Andrews
American Sports Medicine Institute

255) The Comparison of Kinetics and Kinematics Among Different Types of Resistance Training (#141)
Hsiang-Hsin Wang, Tzyy-Yuan Shiang & Chuan-Show Chen
Taiwan Sport University

256) Ground Reaction Forces in Skateboarding: The Ollie (#319)
Matthew Nevitt, Jeremy Determan, Joseph Cox & Edward Frederick
Sole Technology Institute

2nd Floor
Room: Hussey (Posters 257-272: Rehabilitation, Aging)

257) Contribution of Active Dorsiflexion to Toe Clearance in Transtibial Amputees: A Case Study (#254)
Noah Rosenblatt, Jeremy Crenshaw, Jason Wenning & Mark Grabiner
University of Illinois

258) Muscular Demands During Prosthetic Leg Swing Increase due to Increased Interactions Among Segments (#220)
Jeremy Smith & Philip Martin
University of Northern Colorado

259) Shape Memory Alloys, an Alternative Actuation Method for Orthosis Devices (#517)
Ehsan Tarkesh Esfahani, Mohammad Elahinia, Mohamed Hefzy & Charles Armstrong
University of Toledo

260) The Influence of Trans-Tibial Prostheses' Mechanical Properties on the Performance of the Amputee (#360)
Matthew Major, Martin Twiste, Laurence Kenney & David Howard
University of Salford

261) Neural Coupling Between the Upper and Lower Limbs in Individuals With Incomplete Spinal Cord Injury (#420)
Helen Huang & Daniel Ferris
University of Michigan

262) Temporal Changes in Motor Impairments and Gait Function Post Stroke (#239)
Theresa Hayes Cruz & Yasin Dhaher
Northwestern University, Rehabilitation Institute of Chicago

263) Mechanisms Underlying Increased Walking Speed After Rehabilitation in Persons With Post-Stroke Hemiparesis (#125)
Jessica Allen, Mark Bowden, Steven Kautz & Richard Neptune
University of Texas

264) Effects of Muscle Vibration on Control of Finger Movements Following Stroke (#45)
Bing-Shiang Yang
National Chiao Tung University

265) **Anthropometric Parameters in the Elderly: A DXA-Based Study** (#166)
April Chambers, Jean McCrory, Alison Sukits & Rakie Cham
University of Pittsburgh

266) **Examination of Joint Work During Walking in Older Adults** (#160)
Cory Christiansen & Gary Heise
University of Colorado

267) **Effects of Aging on Gait Initiation When Combined With a Change of Direction** (#26)
Evelyn Anaka & Philippe Corbeil
Universite Laval

268) **The Effect of Dual Task And Proprioceptive Stimulation on Stepping Ability for Fallers and Nonfallers** (#59)
Chiung-Yu Cho & Li-Ping Hsiao
National Cheng Kung University

269) **Perceptuo-Sensory, Cognitive and Sensory-Motor Characteristics That Influence the Ability to Recover Balance to Avoid a Fall** (#492)
Alessandro Telonio, Helene Corriveau & Cecile Smeesters
Universite de Sherbrooke

270) **Effect of Age and Target Length on the Speed-Accuracy Trade-Off of Center of Pressure Movements Near the Anterior Margin of the Base of Support in Standing** (#580)
Manuel Hernandez, James Ashton-Miller & Neil Alexander
University of Michigan

271) **Postural Stability in Individuals With Normal and Low Bone Mineral Density** (#385)
Chip Wade, Andrea Johnson, Scott Breloff & M. Allison Ford
Auburn University

272) **Effects of A 6-Month Yoga Program on Scapular Posturing in Older Adults With Hyperkyphosis** (#28)
Man-Ying Wang, Abbie Ferris, Gail Greendale & George Salem
University of Southern California

3rd Floor
Room: Room 'D' (Posters 273-288: Orthopaedics, Upper Extremity)

273) **A Test Method for the Fatigue Testing of Tibial Intramedullary Nails Using Segment Constructs** (#176)
J. Craig Fryman, Balz Mueri, Barbara Kralovic & Roger Kenyon
Zimmer, Inc.

274) **Cadaveric Measurement of Impact Force on Total Hip Arthroplasty Surgical Instrumentation** (#173)
Cristina West & J. Craig Fryman
Zimmer, Inc.

275) **Assessment of Motion of Long-Stemmed Tibial Implant** (#369)
Jill Schmidt & Heidi-Lynn Ploeg
University of Wisconsin-Madison

276) **Subtalar Joint Kinetics During Standing and Walking** (#530)
Tara Sulewski, Tamara Cohen, Gregory Lewis & Stephen Piazza
The Pennsylvania State University

277) Scratching Vulnerability of Conventional vs. Highly Crosslinked Polyethylene Liners With Embedded Third Body Particles (#87)
Anneliese Heiner & Thomas Brown
University of Iowa

278) Hand Approach Velocity and Impact Force During Manual Wheelchair Propulsion (#534)
Shashank Raina, Jill McNitt-Gray & Philip Requejo
University Of Southern California

279) Moment Arms of the Muscles Crossing the Anatomical Shoulder (#348)
David Ackland & Marcus Pandy
University of Melbourne

281) Asymmetric Tonic Neck Reflexes Induced Changes in Joint Torque Generation in the Hemiparetic Upper Extremity: Preliminary Results (#480)
Jules Dewald, Mike Ellis & Thierry Keller
Northwestern University

282) Separability of Individuals With Non-Specific Arm Pain From Asymptomatic Subjects Using EMG Spike Shape Analysis (#233)
Kristina Calder, David Gabriel & Linda McLean
Queen's University

284) Neuromuscular Activation in the Wrist During Isometric Contractions (#215)
Sarah Eby & Michael Hahn
Montana State University

285) Flexor Tendon and Median Nerve Excursion in Healthy and Self-Identified Symptomatic Wrists (#272)
Melanie Lopes & Peter Keir
York University

286) Segmentation of Computed Tomography Data and Creation of a Three-Dimensional Representation of the Wrist (#213)
Vincent Lo, Michele Oliver, Robert Dony, Anne Agur & David Salonen
University of Guelph

287) Upper Extremity Soft and Rigid Tissue Mass Prediction Using Segment Anthropometric Measures and DXA (#93)
Katherine Arthurs, Timothy Burkhart & David Andrews
University of Windsor

288) Three-Dimensional Endpoint Force Production of Muscles in the Extended Thumb: Possible Evidence for a Translational Degree of Freedom at the Base Joint That Dramatically Affects Force Production (#528)
Joseph Towles & Vincent Hentz
Rehabilitation Institute of Chicago

3rd Floor
Room: Henderson (Posters 289-312: Computational Modeling, Clinical)

289) Computational Modelling of Peri-Implant Bone Healing Considering Cell-Biomaterial Interactions (#33)
Nadia Amor, Liesbet Geris, Jos Vander Sloten & Hans Vanoosterwyck
Katholieke Universiteit Leuven

290) Numerical Modeling of Age Related Remodelling of Thoracic Aorta and Mechanical Stress Consequences (#60)
Hanieh Niroomand oscuii, Mohammad Tafazzoli-Shadpour & Farzan Ghalichi
Sahand University of Technology

291) Static Optimization of Muscle Forces During Drop Landings: A Comparison of Cost Functions (#447)
W. Brent Edwards, Brett Sealine, Ross Miller, Jason Gillette & Timothy Derrick
Iowa State University

292) Neuromuscular Biomechanics Simulation Ontology (#163)
Anders Sandholm & Daniel Thalmann
Swiss Federal Institute of Technology

293) A Forward Bio-Dynamic Model for a Three-Segment Open-Chain System: An Application to Multi-Fingered Hand Movement (#241)
Kang Li & Xudong Zhang
University of Illinois, University of Pittsburgh

294) Moment-Generating Capacity of Tendons in Finger Movements: Evaluation of the Tendon Moment Arms Obtained From the Excursion Method (#529)
Sang Wook Lee & Derek Kamper
Rehabilitation Institute of Chicago

295) Muscle Force Estimates for Walking Using an EMG-Driven Musculoskeletal Model of the Knee are Reliable Within and Between Days (#453)
Kurt Manal, Lynn Snyder-Mackler, Michael Axe & Thomas Buchanan
University of Delaware

296) A Proportional Derivative Controller for Planar Human Arm Movement Using Functional Electrical Stimulation (#199)
Kathleen Jagodnik, Robert Kirsch & Antonie van den Bogert
Case Western Reserve University; Lerner Research Institute

297) Image-Based Mesh Generation and its Role Within Computational Biomechanics (#350)
Philippe Young, Terry Beresford-West & Frank Murphy
University of Exeter

298) Biomechanical Simulation of a Greater Trochanter Fixation System (#355)
Kajsa Duke, G.Yves Laflamme & Yvan Petit
Ecole de Technologie Superieure, Hopital du Sacre-Coeur Montreal

299) Blood Flow and Oxygen Level Characterization of the Forearm With Changes in Normal and Shear Load (#161)
Abinand Anbazhagan Manorama, Seungik Baek & Tamara Reid Bush
Michigan State University

300) Is Upper Extremity Loading Symmetric During Weight-Relief Lifts Performed by Individuals With Spinal Cord Injury? (#511)
Dany Gagnon, Sylvie Nadeau, France Piotte & Luc Noreau
Universite de Montreal

301) The Effectiveness of Wrist Guards for Reducing Wrist and Elbow Accelerations Following Simulated Forward Falls (#92)
Timothy Burkhart & David Andrews
University of Windsor

302) **Ground Reaction Forces Recorded Underneath Hands During Sitting Pivot Transfers in Individuals With Spinal Cord Injury** (#509)
Dany Gagnon, Sylvie Nadeau, France Piotte, Luc Noreau & Denis Gravel
Universite de Montreal

303) **Comparison of Muscle Activity During Common Lower Extremity Rehabilitation Exercises** (#569)
Sabrina Silver, Cara Lewis & Riann Palmieri-Smith
University of Michigan

304) **Electromyography Evaluation of Manual Muscle Tests** (#329)
Rebecca Brookham, Clark Dickerson & Linda McLean
University of Waterloo

305) **Efficiency of Step-to-Step Transition Work in Hemiparetic Gait** (#537)
Daniel Hewson, Arrlann Christie, Janice Eng & Max Donelan
Simon Fraser University

306) **The Relationship Between Static Arch Height and Arch Stiffness** (#179)
Andrew Barnes, Jonathan Wheat & Clare Milner
Sheffield Hallam University

307) **Does Decompressive Spinal Surgery for Older Patients With Cervical Myelopathy Improve Gait on Flat and Irregular Surfaces?** (#545)
Fatima Makhzoum, Janet Kemp, James Ashton-Miller & Frank La Marca
University of Michigan

308) **Dynamic Stability of the Parkinsonian Gait** (#404)
Christopher Arellano, Ashley Hickerson, Melissa Scott-Pandorf, Vladimir Ivkovic & Max Kurz
University of Houston

309) **Levodopa Influences the Regularity of the Ankle Joint Kinematics in Individuals With Parkinsons Disease** (#396)
Max Kurz, Ashley Hickerson, Chris Arellano, J. G. Gabriel Hou & Eugene Lai
University of Houston

310) **The Relationship Between Interjoint Coordination During Gait and Strength, Spasticity and Selective Voluntary Motor Control in Children With Spastic Diplegic Cerebral Palsy** (#243)
Evan Goldberg, Loretta Staudt, Marcia Greenberg, William Oppenheim & Eileen Fowler
University of California-Los Angeles

311) **Coordination Pattern in Children With Spastic Diplegia: Pre-Operative and 1 and 5-Years Post-Operative** (#399)
Elizabeth Russell, George Gorton, Peter Masso, Richard Van Emmerik & Joseph Hamill
University Of Massachusetst-Amherst

312) **Resistance Training Alters Joint Powers in Multiple Sclerosis Patients** (#175)
Jessie Huisinga, Mary Filipi & Nicholas Stergiou
University of Nebraska at Omaha

3rd Floor
Room: Koessler (Posters 313-331: Spine, Ergonomics)

313) **Tyramine-Based Hyaluronan Hydrogels for Nucleus Pulposus Replacement: Characterization by Magnetic Resonance Imaging** (#135)
Ediuska Laurens, Aniq Darr, William Montgomery, Lars Gilbertson, Peter Zahos, Carl Winalski, Erika Schneider, Amit Vasanji & Anthony Calabro
Cleveland Clinic Foundation, Cleveland State University

314) **Disc Height Reduction is a Better Predictor of Cervical Disc Degeneration Progression Than Reduction in the Area of Nucleus Pulposus: A Finite Element Analysis** (#532)
Mozammil Hussain & Rodger Tepe
Logan University

315) **Comparison of Anterior 3-Hole Plate and Paired/Single Anterior Cages for Anterior Lumbar Interbody Fusion** (#69)
Ethan Daley, Ramon Ruberte-Thiele, Gregory Poulter, Steven Goldstein & Gregory Graziano
University of Michigan

316) **Reproducibility of Kinematical Variables Describing Head and Neck Movement-A 3D Movement Analysis Using the Finite Helical Axis Method** (#44)
Helena Grip & Fredrik Ohberg
University Hospital of Umea

317) **Spinal Stiffness Measures do not Change With Chiropractic Manipulation Even With Clinical Improvement** (#282)
Edward Owens, David Wilder, M. Ram Gudavalli, James DeVocht & William Meeker
Palmer Center for Chiropractic Research

318) **The Effect of Gender on Abdominal Muscle Activation in Response to an Asymmetrical Leg Loading Task in Healthy Adults** (#105)
Melissa McKeon, Sarah Gordon & Cheryl Hubley-Kozey
Dalhousie University

319) **Gender Responses to Sitting in Automobile and Office Seats-Influence of Hip and Hamstring Flexibility on Seated Postures** (#30)
Tyson Beach, Katherine McDonald, Stephanie Coke & Jack Callaghan
University of Waterloo

320) **Line of Sight and Driving Posture Evaluation: What an Operator Cannot See Influences Driving Posture** (#446)
Tammy Eger, Alison Godwin, Sylvain Grenier & Jack Callaghan
Laurentian University

321) **Validation of an Instrumented Handrail Stairway System** (#459)
Matija Radovic, Nicholas Hanson, Palav Deka & Shing-yen Chen
University of Nebraska at Omaha

322) **A Biomechanical Investigation of the Forces Applied to Lift Truck Steering Wheels: Effects of Posture, Gender and Steering Forces on Cumulative Low Back Loading** (#508)
Sylvain Grenier, Aaron Kocielek & Tammy Eger
Laurentian University

323) **Modeling Muscle Fatigue for Multiple Joints** (#412)
Ting Xia & Laura Frey Law
University of Iowa

324) **Lumbar Spine Movement and Pain During Prolonged Seated Work** (#162)
Nadine Dunk & Jack Callaghan
University of Waterloo

325) **The Effect of External Loads on Whole Body Discomfort** (#77)
Seokhee Na, Min Chung, Dohyung Kee & Maury Nussbaum
Virginia Tech

326) **Changes in Thoracolumbar Kinematics and Centre of Pressures While Performing a Lifting and Lowering Task** (#465)
Carolyn Duncan, Scott MacKinnon & Wayne Albert
Memorial University of Newfoundland

327) **A Comparison of the Repeatability of Submaximal and Maximal Methods Commonly Employed for Normalization of the Erector Spinae Muscles in the Thoracic and Lumbar Region** (#381)
Jennie Jackson, Niall O'Brien, Patrick Dempsey & Jack Callaghan
University of Waterloo

328) **Effects of Load and Frequency on Muscle Activity in a Repetitive Upper Extremity Task** (#287)
Melissa Brown & Peter Keir
McMaster University

329) **Video Evaluation of Distal Upper Extremity Posture** (#300)
Aaron Kociolek & Peter Keir
McMaster University

330) **The Effects of Task Rotation on Muscle Activity and Fatigue** (#313)
Michael Holmes, Kia Sanei & Peter Keir
McMaster University

331) **A Comparison of the Kinematics of Ladder Climbing Using Rungs vs. Side Rails** (#552)
Hogene Kim, Justin Young, Chuck Woolley, Tom Armstrong & James Ashton-Miller
University of Michigan

Saturday, August 9, 2008

< 8:00 am	**Coffee (Michigan League)**
8:00	**ISB Keynote Lecture** Location: Rackham Auditorium

Low Back Injury: From Workplace to Lab and Back
Jaap van Dieën
Vrije Universiteit Amsterdam

9:00 – 9:30 am	**Coffee (Michigan League)**

NOTES

<u>NOTES</u>

Saturday, August 9, 2008

Scientific Sessions

Injury (Podium Session 28) Saturday, August 9: 9:30 - 11:00 am Location: MLB 1200 AUD 3 Session chairs: David Pearsall, Scott McLean	**Posture & Balance II (Podium Session 27)** Saturday, August 9: 9:30 - 11:00 am Location: MLB 1400 AUD 4 Session chairs: Stephen Prentice, Stephen Perry

9:30   **ACL Rupture is an In Vivo Impact Model** (#362)
Douglas Pedersen, Daniel Thedens, James Martin, Sirisha Tadimalla, Prem Ramakrishnan & Annunziato Amendola
University of Iowa

9:30   **Effects of Seated Whole-Body Vibration on Seated Postural Sway** (#181)
Gregory Slota, Kevin Granata & Michael Madigan
Virginia Polytechnic and State University

9:45   **Gender Differences During a Run to Cut Task on Surfaces With Different Friction Interactions: Implications for ACL Injury Risk** (#118)
Ariel Dowling, Stefano Corazza, Todd Alamin, Ajit Chaudhari & Thomas Andriacchi
Stanford University

9:45   **Can Children Control Their Joint Variability in Standing While Confronting a Perturbation of Tendon Vibration?** (#255)
Jianhua (Jerry) Wu, Sandra McKay & Rosa Angulo-Barroso
Georgia State University

10:00   **Tibiofemoral Moments of Force and Co-Stabilization: Revisiting the Non-Contact Mechanism of Anterior Cruciate Ligament Injury** (#324)
Jeffery Podraza & Scott White
University at Buffalo, Daemen College

10:00   **Vibrotactile Tilt Feedback Reduces Mediolateral Tilt in Vestibulopathic Subjects During Locomotor Tasks** (#519)
Kathleen Sienko, Kennyn Statler, Lars Oddsson & Conrad Wall
University of Michigan

10:15   **Shear Thickening Fluid Based Protective Foam Padding** (#563)
Sarah Trager, Norman Wagner & Buz Swanik
University of Delaware

10:15   **Self-Selected Transition Between Movement Patterns on a Moving Platform** (#424)
Venkata Gade, Nitin Moholkar, Jerome Allen & W. Thomas Edwards
Koessler Medical Rehabilitation Research & Education Center

10:30   **Modifying Landing Mat Material Properties to Reduce Injuries in Gymnastics Landings** (#9)
Chris Mills, Matthew Pain & Maurice Yeadon
University of Exeter

10:30   **Moving Environments and Their Effects on Thoracolumbar Kinematics and Centre of Pressure When Performing Stationary Tasks** (#470)
Carolyn Duncan, Scott MacKinnon & Wayne Albert
Memorial University of Newfoundland

10:45   **A Model to Determine the Effect of Multiple Subconcussive Impacts in the Rat** (#572)
Erin Hanlon & Cynthia Bir
Wayne State University

10:45   **The Relationship Between Center of Pressure Displacement and Estimated Instability of Dancers and Non-Dancers While in a Moving Room** (#452)
Leigh Schanfein & Shirley Rietdyk
Purdue University

11:00 - 11:30 am: Coffee (Michigan League)

Saturday, August 9, 2008

Scientific Sessions

Muscle II (Podium Session 29)	Pelvis (Podium Session 26)
Saturday, August 9: 9:30 - 11:00 am	Saturday, August 9: 9:30 - 11:00 am
Location: Rackham Amphitheatre	Location: Mendelsohn Theatre
Session chairs: Joe Langenderfer, Sam Ward	Session chairs: Lennox Hoyte, Daniel Simkins

9:30   **A Mathematical Model of Force Transmission by Desmin in Skeletal Muscle** (#314)
Gretchen Meyer, Miklos Kellermeyer, Samuel Ward & Richard Lieber
University of California-San Diego

9:30   **How Different Maternal Volitional Pushing Profiles Affect the Duration of the Second Stage of Labor: A 3-D Visco-Hyperelastic Finite Element Model** (#570)
Dejun Jing, James Ashton-Miller & John DeLancey
University of Michigan

9:45   **Development of Sarcomere Length Non-Uniformity During Lengthening Contractions of Permeabilized Single Muscle Fibers From Rat** (#471)
Appaji Panchangam, Dennis Claflin, Mark Palmer & John Faulkner
University of Michigan

9:45   ***Fundamental Biopotential Analysis for Quantification of Pudendal Nerve Injury Recovery** (#307)
Bradley Gill, Hai-Hong Jiang, Jonathan Glaab, Paul Zaszczuryski & Margot Damaser
Cleveland Clinic

*Delsys Award Finalist

10:00   **In Vivo Sarcomere Length and Fiber Tension Measurements** (#544)
Yi-Ning Wu, Yupeng Ren & Li-Qun Zhang
Rehabilitation Institute of Chicago, Northwestern University

10:00   **Visco-Hyperelastic Properties of the Pelvic Floor Muscles in Healthy Women** (#562)
Dejun Jing, Kuo-Cheng Lien, James Ashton-Miller & John DeLancey
University of Michigan

10:15   **In Vivo Skeletal Muscle Fibre Function During Cycling** (#422)
Neal Austin, Tim Keren, Chris Wieland & Walter Herzog
University of Calgary

10:15   **Determining the Biomechanical Properties of Nulliparous and Parous Vaginal Tissue** (#457)
Andrew Feola, Keisha Jones, Pam Moalli & Steven Abramowitch
University of Pittsburgh

10:30   **Muscle Activation Timing Influences Muscle-Tendon Mechanical Performance During Cyclic Contractions** (#551)
Gregory Sawicki, Emanuel Azizi & Thomas Roberts
Brown University

10:30   **Role of Pelvic Floor Muscle in Urinary Continence During a Stress to the Bladder: An Electrophysiological and Biomechanical Evaluation on Female Rats** (#146)
Hai-Hong Jiang, Levilester Salcedo, A. Marc Gustilo-Ashby , Bo Song & Margot Damaser
Cleveland Clinic

10:45   **Differences in Gastrocnemius Architecture Between Sprinters and Non-Sprinters: Implications for Muscle Function** (#525)
Sabrina Lee & Stephen Piazza
The Pennsylvania State University

10:45   **Biomechanical Relationships Between Urodynamic Pressures During Cough and Valsalva in Normal and Stress Incontinent Women** (#53)
Thomas Spirka, Kimberly Kenton, Robert Butler, Margot Damaser & Linda Brubaker
Cleveland Clinic

11:00 - 11:30 am: Coffee (Michigan League)

Saturday, August 9, 2008

Scientific Sessions

Spine II (Podium Session 30)	**Knee II (Podium Session 32)**
Saturday, August 9: 11:30 am - 1:00 pm	Saturday, August 9: 11:30 am - 1:00 pm
Location: MLB 1200 AUD 3	Location: MLB 1400 AUD 4
Session chairs: Jacek Cholewicki, Jaap van Dieën	Session chairs: Ajit Chaudhari, Nick Stergiou

11:30   **Intervertebral Neural Foramina Deformation Due to Two Types of Repetitive Combined Loading** (#514)
Janessa Drake & Jack Callaghan
University of Windsor

11:30   **Biomechanical Mechanisms of Knee Osteoarthritis** (#102)
Janie Astephen, Kevin Deluzio, Graham Caldwell, Michael Dunbar & Cheryl Hubley-Kozey
Dalhousie University, University of Cape Town

11:45   **Continuous Motion Monitoring of the Cervical Spine** (#377)
Andrew Sterling, Daniel Cobian, Paul Anderson & Bryan Heiderscheit
University of Wisconsin-Madison

11:45   **Comparison of Three Dimensional Patellofemoral Joint Reaction Forces in Persons With and Without Patellofemoral Pain** (#322)
Yu-Jen Chen & Christopher Powers
University of Southern California

12:00   **Head and Neck Kinematics During Horizontal and Combined Horizontal/Vertical Low Velocity Whiplash-Like Perturbations** (#584)
Loriann Hynes & James Dickey
University of Guelph

12:00   **Changes in Patellofemoral Contact Pressure Caused by Imbalance of the Knee Extensor Muscles** (#502)
Andrew Sawatsky, Doug Bourne, Azim Jinha & Walter Herzog
University of Calgary

12:15   **Biomechanical Properties of the Cervical Facet Joint Capsule in an In-Vivo Caprine Model** (#597)
Nadia Azar, Chaoyang Chen, Srinivasu Kallakuri & John Cavanaugh
University of Windsor

12:15   **Improving VMO Function Unloads Lateral Cartilage Within the Patellofemoral Joint** (#24)
John Elias, Srianjana Kilambi, Derek Goerke & Andrew Cosgarea
Medical Education and Research Institute of Colorado

12:30   **Changes in Natural Frequency of the Trunk With Exposure to Seated Whole-Body Vibration** (#182)
Gregory Slota & Michael Madigan
Virginia Polytechnic and State University

12:30   **Knee Joint Relative Motion During ACL Rupture by Internal Tibial Torsion or Tibiofemoral Compression** (#232)
Eric Meyer, Timothy Baumer & Roger Haut
Michigan State University

12:45   **Ultrasound Analysis of In-Vivo Connective Tissue Deformations of the Human Abdominal Wall** (#169)
Stephen Brown & Stuart McGill
University of Waterloo

12:45   **Validation of the Computational Knee Joint Model Under High Compressive Loading Conditions** (#504)
Bhushan Borotikar & Antonie van den Bogert
Cleveland Clinic

1:00 - 1:30 pm: Box Lunch (Michigan League)

Saturday, August 9, 2008

Scientific Sessions

Orthopaedics II (Podium Session 33)	Gait III (Podium Session 31)
Saturday, August 9: 11:30 am - 1:00 pm	Saturday, August 9: 11:30 am - 1:00 pm
Location: Rackham Amphitheatre	Location: Mendelsohn Theatre
Session chairs: Tom Brown, Richard Hughes	Session chairs: Elizabeth Hsiao-Wecksler, Max Kurz

11:30 — **Prediction of Fracture Load and Initiation Location of Acetabular Fractures by Means of Nonlinear FEM - A Feasibility Study** (#395)
Peter Vaitl, Vickie Shim, Joerg Boehme, Roland Huelse, Ian Anderson & Chistoph Josten
University of Leipzig

11:30 — **Feedback Driven Locomotor Adaptation in a Human Spinal Cord Injury Population** (#316)
Keith Gordon, Ming Wu, Jennifer Kahn & Brian Schmit
Rehabilitation Institute of Chicago

11:45 — **Comparison of Asia-Specific Sliding Intramedullary Hip Screw, Intramedullary Fixed Angle Hip Screw, and Sliding Hip Screw Plate Using Photoelastic Analyses** (#1)
Fumihiro Yoshimine, Jacob Cartner, Steve Summy & Zane Hartsell
Tokyo Metropolitan Ohkubo Hospital

9:45 — **Can we Assume That the Individuals With Incomplete Spinal Cord Injury Have a Symmetrical Gait Pattern?** (#338)
Sylvie Nadeau, Hugues Barbeau, Christiane Garneau & Cyril Duclos
Universite de Montreal

12:00 — **Bone Strains Associated With Femoral Neck Fracture Following Hip Resurfacing** (#52)
Jason Long, Thomas Santner & Donald Bartel
Cornell University

10:00 — **Compensatory Gait Movements Post Stroke: The Influence of Synergies** (#236)
Theresa Hayes Cruz & Yasin Dhaher
Northwestern University, Rehabilitation Institute of Chicago

12:15 — **Knee Mechanics While Walking on Different Surfaces After Total Knee Replacement** (#253)
Clare Milner & Michael Smith
University of Tennessee

10:15 — **Kinematic and Kinetic Changes During Gait Before and After Botulinum Toxin A Treatment in Chronic Stroke** (#315)
Alison Novak, Stephen Bagg & Brenda Brouwer
Queen's University

12:30 — **Changes in In-Vivo Glenohumeral Joint Contact Patterns and Clinical Outcomes From 3 to 12 Months After Rotator Cuff Repair** (#74)
Stephanie Kline, Roger Zauel, Terrence Lock & Michael Bey
Henry Ford Hospital

10:30 — **Compensatory Mechanisms in Below-Knee Amputee Gait in Response to Increasing Steady-State Walking Speeds** (#80)
Anne Silverman, Nicholas Fey, Alberto Portillo, J. Gail Walden, Gordon Bosker & Richard Neptune
The University of Texas at Austin

12:45 — **Chemical Structure Effects on Bone Response To Mechanical Load** (#13)
Peizhi Zhu, Jiadi Xu, Michael Morris, Nadder Sahar, David Kohn, Ayyalusamy Ramamoorthy & Mary Tecklenburg
University of Michigan

10:45 — **Transition Work in Simulated Pathological Walking** (#541)
Caroline Soo & J. Maxwell (Max) Donelan
Simon Fraser University

1:00 - 1:30 pm: Box Lunch (Michigan League)

Saturday, August 9, 2008

1:30 –
2:30 pm

Running Energetics and Biomechanics of Oscar Pistorius: A Case Study (Symposium)
Location: Rackham Auditorium
Chair: Daniel Ferris

Introduction
Hugh Herr
Massachusetts Institute of Technology

Background: Transtibial Amputee Running Physiology
Mary Beth Brown
Georgia Tech University

Metabolic Running Economy
Alena Grabowski
Massachusetts Institute of Technology

Physiological and Mechanical Determinants of all-out Sprint Performances
Matt Bundle
University of Wyoming

Leg Mechanical Energetics
Craig McGowan
University of Texas at Austin

Panel Discussion Including Audience Questions
Rodger Kram (*University of Colorado at Boulder*)
Hugh Herr (*Massachusetts Institute of Technology*)
Mary Beth Brown *(Georgia Tech University)*
Alena Grabowski *(Massachusetts Institute of Technology)*
Matt Bundle *(University of Wyoming)*
Craig McGowan *(University of Texas at Austin)*

2:30 –
3:00 pm

Awards and Closing Ceremonies
Location: Rackham Auditorium

3:00 - 4:45 pm: ASB Executive Board Meeting (Room 4, Michigan League)

NOTES

Index

(includes registrants as of 7/16/08)

6th World Congress on Biomechanics

2010 @ SINGAPORE

August 1 - 6, 2010

Contact Person:
James Goh
Chair, WCB2010
Email: wcb2010@inmeet.com.sg

VISIT OUR WEBSITE:

www.wcb2010.org

Jointly Organised by
Biomedical Engineering Society (Singapore)
Global Enterprise for Micro-Mechanics and Molecular Medicine (GEM4)
National University of Singapore

Endorsed by
World Council of Biomechanics

2008 North American Congress on Biomechanics • University of Michigan, Ann Arbor • 'Program-At-A-Glance'

Tuesday, 8/5-2008

- **<8 AM** — Registration @ League Bldg
- **8:15-8:30** — Bus from League Bldg
- **8:30-8:45** — to CSE on North Campus
- **Tutorial / Lab** — I - Kuo (CSE 1690); II - Delp (CSE 1670); Tours I
- **Tutorial / Lab** — ASB Awards Session; I - Kuo (CSE 1690); II - Delp (CSE 1670); Tours II
- **Lunch on Your Own** — Free Materialise Inc. Tutorial & Pizza (Kalamazoo Room, League)
- **Tutorials / Lab** — I - Kuo (CSE 1690); III - An (MLB 1200 Aud 3); IV-Vaillancourt (Rackham); Tours III; Amphitheater
- **Tutorials / Lab** — I - Kuo (CSE 1690); V - Zernicke (MLB 1200); VI - Redfern & Goldstein (Kraus Nat. Sci. Auditorium, Room 2140); Tours IV
- **ISB Student Travel Grants** (Rackham Assembly Hall, 4th Floor)
- **OPENING RECEPTION & VENDOR EXHIBITS** (Michigan League)
- ASB; CSB; Executive; Board; Mtg (Zanzibar Restaurant)
- **Night on the Town** (Buses circulate between campus downtown, and hotels)

Wednesday, 8/6-2008

- Coffee at Vendor Exhibits (League)
- **Keynote Lecture 1** — John O.L. DeLancey, M.D. "On the Challenge of Vaginal Birth" (Rackham Auditorium)
- **Borelli Award (ASB)** "Why Bones Bend But Don't Break: ..." David B. Burr, Ph.D. (Rackham Auditorium)
- Coffee at Vendor Exhibits (League)
- **ASB Awards Session** — Post-Doc Awardee: Sam Ward (UCSD); Pre-Doc Awardee: Meghan McGee (MTU); J Biomech Award Finalists: Luyun Chen (U-M) & Heather Hayes (GT/EU); Clinical Biomechanics Award Finalists: Cheryl Hubley-Kozey (Dalhousie U) & Woochol Choi (SFU) (Rackham Auditorium)
- Box Lunch at Vendor Exhibits (League)
- **Women in Biomechanics Lunch** (Rackham 4th Floor Assembly Hall)

Motor Control 1	Methods & Instrumentation I	Knee I	Sport I
Auto Safety Symposium (ASB/CSB); Spine I	Aging 1	Bone	Ergonomics I; Posture & Balance I
Podium 1	Podium 2	Podium 3	Podium 5
Podium 4	Podium 6	Podium 7	Podium...
MLB 4 / MLB 3	Rackham Amph	Rackham Amph	Mendelsohn

- Coffee at Vendor Exhibits (League)
- **POSTER SESSION I and VENDOR EXHIBITS** (Michigan League)
- **ISB Student Travel Grants** (Rackham Assembly Hall, 4th Floor)
- **Night on the Town** (Buses circulate between campus downtown, and hotels)

Thursday, 8/7-2008

- Coffee at Vendor Exhibits (League)
- **Keynote Lecture II** — Mimi A.R. Koehl, Ph.D. "Locomoting in a Turbulent World" (Rackham Auditorium)
- **CSB Career Award** "Biomechanicz in Three Acts" Ronald F. Zernicke, Ph.D. (Rackham Auditorium)
- Coffee at Vendor Exhibits (League)
- **NDI New Investigator Awards (CSB)** (MS, Pre and Post-doc) (Rackham Auditorium)
- Box Lunch at Vendor Exhibits (League)
- **CSB Annual General Meeting** (Room: MLB 4); Free Matlab Tutorial (Room: 1420 MLB)

Computational Modeling I	Orthopaedics I	Gait I
Occupational Biomechanics Symposium (CSB); Muscle I	Posture & Balance I	Sport II
Podium 8	Podium 9	Podium 10
Podium 12 / Podium 14	Podium 13	Podium 11
MLB 4 / MLB 3	Rackham Amph	Mendelsohn

- Coffee at Vendor Exhibits (League)
- **Buses to The Henry Ford Museum** (Pick-up from Michigan League's South Entrance Door) (en route)
- **STROLLING BANQUET at The Henry Ford Museum** (Dearborn)
- **Buses from The Henry Ford Museum** (Drop off at hotels, downtown & central campus)

Friday, 8/8-2008

- Coffee at Vendor Exhibits (League)
- **Keynote Lecture III** — Steve Scott, Ph.D. "The 3 B's of Motor Control: Behavior, Brains and Biomechanics" (Rackham Auditorium)
- **Hay Award (ASB)** "From Biomechanics to Motor Control - From 1973 To 2008. From Biomechanics to Motor Control - From 1973 to 2008" Vladimir M. Zatsiorsky, Ph.D. (Rackham Auditorium)
- Coffee at Vendor Exhibits (League)

Aftab Patla Symposium (CSB)	Motor Control II	Methods & Instrumentation II	Shoulder
Rehabilitation	Computational Modeling II	Cartilage	Gait II
Podium 15	Podium 16	Podium 17	
Podium 20 / Podium 19	Podium 18	Podium 21	
MLB 4 / MLB 3	Rackham Amph	Mendelsohn	

Aging II	Tendon & Ligament	Lower Extremity	Ergonomics II
Podium 22	Podium 24	Podium 25	Podium 23
MLB 4 / MLB 3	Rackham Amph	Mendelsohn	

- Box Lunch at Vendor Exhibits (League)
- **ASB Annual Business Meeting** (Room: MLB 4); Free Matlab Tutorial (Room: 1420 MLB)
- Coffee at Vendor Exhibits League
- **Student Mentoring Session** (Rackham Assembly Hall, 4th Floor)
- **POSTER SESSION II** (Michigan League)
- **Night on the Town** (Buses circulate between campus downtown, and hotels)

Saturday, 8/9-2008

- Coffee (League)
- **ISB Keynote Lecture** — Jaap van Dieën, Ph.D. "Low Back Injury: From Workplace to Lab and Back" (Rackham Auditorium)
- Coffee (League)

Injury	Posture & Balance II	Muscle II	Pelvis
Spine II	Knee II	Orthopedics II	Gait III
Podium 28	Podium 27	Podium 29	Podium 26
Podium 30	Podium 32	Podium 33	Podium 31
MLB 3	MLB 4	Rackham Amph	Mendelsohn

- Coffee (League)
- **Running Energetics and Biomechanics of Oscar Pistorius: A Case Study (Symposium)** (Rackham Auditorium)
- Box Lunch (League)
- **Awards & Closing Ceremony** (Rackham Auditorium)
- ASB Executive Board Mtg (Room 4) (League)

COMPARISON OF ASIA-SPECIFIC SLIDING INTRAMEDULLARY HIP SCREW, INTRAMEDULLARY FIXED ANGLE HIP SCREW, AND SLIDING HIP SCREW PLATE USING PHOTOELASTIC ANALYSES

[1]Yoshimine, F; [2]Cartner, J; [2]Summy, S; [2]Hartsell, Z

[1]Tokyo Metropolitan Ohkubo Hospital, Tokyo, Japan
[2]Smith & Nephew, Inc., Memphis, TN, USA
Jacob.Cartner@smithnephew.com

INTRODUCTION

Sliding intramedullary hip screws, intramedullary fixed angle hip screws, and sliding hip screw plates have been successful in treating intertrochanteric hip fractures. While sliding intramedullary hip screws may be preferred for unstable intertrochanteric fractures, sliding hip screw plates remain the preferred treatment for most stable intertrochanteric fractures (Baumgaertner *et al*, 1998). It is thought that the sliding intramedullary hip screw used with a centering sleeve behaves similar to the sliding hip screw plate, but it is not proven that this sliding intramedullary hip screw provides a clinical or biomechanical advantage over the fixed angle hip screw without a sleeve. The purpose of this study was to investigate the load distribution on the femur when treating unstable intertrochanteric fractures with sliding intramedullary hip screws, intramedullary fixed angle hip screws, and sliding hip screw plates. Specifically, we chose hip screws that are designed for the Asian population.

METHODS

Medium composite femora (Pacific Research Laboratories, Vashon, WA, USA) were used to simulate an Asian adult femur. Each femur was potted with 0º of flexion and 20º of adduction in a custom base fixture. This 20º force angle is representative of one legged stance during gait. One femur was tested intact in order to serve as a control; one femur was implanted with an Asian IMHS nail with a centering

sleeve and sliding hip screw, (IMHS-A, Smith and Nephew, Memphis, TN, USA); one femur was implanted with an IMHS-A and subtrochanteric screw [a Gamma-type nail] (Smith and Nephew, Memphis, TN, USA); one femur was implanted with a titanium sliding hip screw plate (CHS Ti Classic, Smith and Nephew, Memphis, TN, USA). A four-part unstable intertrochanteric fracture was created in each implanted femur (Figure 1).

Figure 1: Four part unstable intertrochanteric fracture.

After implantation, PhotoStress coating (Vishay Intertechnology, Malvern, PA, USA) was applied to each femur. Prior to loading, low-viscosity lubricant was applied to the lag screw in each construct to simulate *in vivo* sliding conditions. Each specimen was loaded and held in axial compression at 0, 600, 1200, and 1800 N. As the specimens were each loaded, the resulting strains produced proportional optical effects in the photoelastic coating. When viewed with a reflection polaroscope, isochromatic fringes correspond to the stress distribution on the surface of the femur. Color images were

obtained at each load, and the fringe patterns were noted.

RESULTS

Both the sliding IMHS-A and CHS exhibited localized stress near the fracture at the medial cortex, which extended distally into the diaphysis. This similar medial stress distribution was seen in the intact bone. The Gamma-type nail depicted a very localized high stress area just distal to the fracture in the medial cortex, which did not extend into the diaphysis. These observations were independent of load (Figure 2).
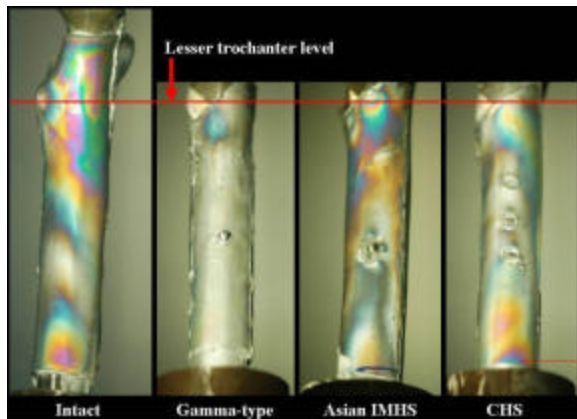
Figure 2: Medial View of Stress Distribution at 1800 N load. (blue represents region of highest strain)

DISCUSSION

Photoelastic analyses showed differences between sliding IMHS-A and CHS versus the Gamma-type nail. The sliding capabilities of the IMHS and CHS allowed for the transfer of compressive load through the fracture contact surface, indicating that the IMHS and CHS are effective load sharing devices. The Gamma-type nail showed a high localized stress distribution with no extension into the diaphysis, which seemed to be caused by varus bending of the proximal fragment, in which the medial fracture site acted as a fulcrum. Such resistance to sliding for the Gamma-type

nail is likely attributed to its rigid behavior during one legged stance of gait. The sliding IMHS and CHS load sharing phenomenon may lead to decreased cut-out, hasten fracture healing, and increase overall fracture fixation strength. The new visual method shown through this testing indicated clear advantages of load sharing (sliding IMHS and CHS) over load bearing (subtrochanteric Gamma-type nail) devices as compared to intact bone.

REFERENCES

Baumgaertner *et al*. Intramedullary Versus Extramedullary Fixation for the Treatment of Intertrochanteric Hip Fractures. *CORR* 348:87-94, 1998.

ENERGETICS AND BIOMECHANICS OF WALKER ASSISTED GAIT

Jonathon R. Priebe and Rodger Kram

Locomotion Laboratory, Department of Integrative Physiology
University of Colorado, Boulder, CO, USA
E-mail: Priebe@colorado.edu   Web: www.colorado.edu/intphys/research/locomotion.html

INTRODUCTION

Nearly 4 million Americans use a "walker" to aid with ambulation. Four-wheeled (4W) and two-wheeled (2W) walkers are pushed from behind and involve a normal bipedal (BP) walking pattern. In contrast, a four-footed (4F) walker must be lifted completely off the ground and requires a special type of walking pattern (gait) referred to as "step-to" (ST). ST walking requires the user to step forward with one foot and then step-to the same position with the other foot.

Previous research report that using a 4F walker increases energetic cost by 212%, but did not offer any biomechanical explanation for the elevated cost (Holder et al., 1993; Foley et al., 1996).

The purpose of this study was to investigate the energetic cost and kinematics of walking unassisted and with three different walkers. We tested two hypotheses: 1) At a fixed speed, walking with a 4F walker, using a ST gait is metabolically more expensive than walking unassisted or with a 2W or 4W walker. 2) The greater cost of using a 4F walker is due to the slower walking speed, cost of lifting the walker, and a disabled inverted-pendulum energy exchange mechanism associated with the step-to gait.

METHODS

Ten (5M, 5F) young, healthy, adult subjects volunteered. We trained the subjects to walk with the three walkers and the ST gait. After training, we measured preferred walking speed (PWS) with each device and unassisted.

The experimental protocol consisted of eight trials: 1. standing, 2. BP at 1.25 m/s, 3. BP at 0.30 m/s, 4. 2W walker BP at 0.30 m/s, 5. 4W walker BP at 0.30 m/s, 6. 4F walker ST at 0.30 m/s, 7. ST unassisted at 0.30 m/s, 8. repeated lifting of 4F walker.

We measured metabolic rate using expired gas analysis. Net metabolic rate = exercise - standing. For the ST trial without walker, subjects matched their step-step-pause pattern to the rhythm used with the 4F walker. The 4F walker lifting trial consisted of lifting the walker forward, with a pause and then backward followed by another pause, matched to the same timing as the 4F walker trial.

We used repeated-measures ANOVA and Tukey post-hoc test with a criterion of $p < 0.05$.

RESULTS AND DISCUSSION

The net metabolic cost for subjects walking with the 4F walker at 0.30m/s was "only" 84% greater than bipedal (BP) walking at the same speed ($p<.001$). Metabolic cost with the 4W and 2W walkers was just 3% and 10% greater than BP walking at the same speed; respectively ($p<.001$; Figure 1).
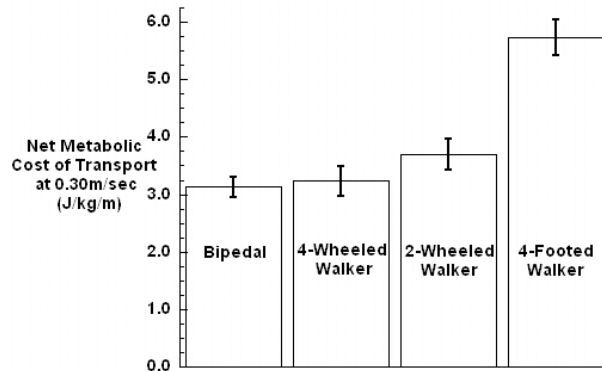
Figure 1: Mean values ± SEM.

Net metabolic power for walking at 0.30 m/s with the 4F walker was not statistically different from the combined metabolic rates for ST walking at 0.30 m/s plus the cost of 4F walker lifting (p=.25, Figure 2).
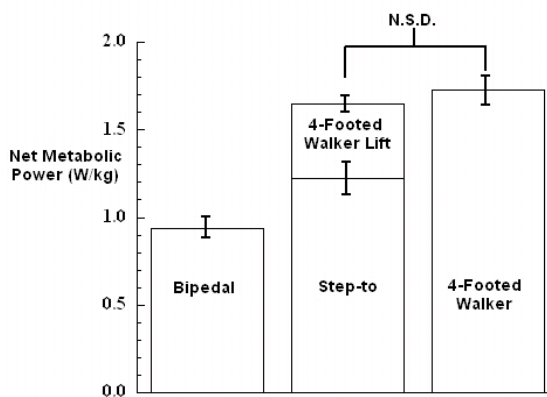

Figure 2: Mean values ± SEM..

Our findings suggest that three principle factors contribute to the greatly elevated metabolic cost of using a 4F walker: slow speed, lifting, and the step-to gait.

The 4F walker involves a dramatically slower preferred walking speed (4F 0.35m/s vs. BP 1.52m/s). The metabolic cost of bipedal walking at 0.30m/s increased metabolic cost per distance by 73% compared to walking bipedally at 1.25m/s.

Lifting the 4F walker comprised 25% of the metabolic rate when using the 4F walker. Reducing the weight of 4F walkers could help mitigate the elevated cost of using these walkers.

The 4F walker requires the user to employ a ST gait. At 0.30m/s, ST walking unassisted was 29% more expensive than BP unassisted.

Using a 4F walker is an aerobically challenging task for elderly people. Using a 4F walker requires 90% of $\dot{V}O_2$ max in 85 year old community dwelling females, which is comparable to elite marathon runners.

Future walker designs should combat the three major problems we have identified. Ideally, such devices should provide the stability of a 4F walker, but allow the users to walk bipedally at a normal speed with no lifting required.

SUMMARY/CONCLUSIONS
Three principle factors contribute to the greatly elevated metabolic cost of using a 4F walker: slow speed, lifting the walker, and the step-to gait.

REFERENCES

Holder, C.G., Haskvitz, E.M., Weltman, A. (1993). Journal of Orthopaedic and Sports Physical Therapy. **18**, 537-542.

Foley, M.P., Prax, B., Crowell, R., and Boone, T. (1996). Physical Therapy. **76**, 1313-1319.

CALCULATION METHOD AFFECTS TIBIAL ACCELERATION SLOPE VALUES

Adriana M. Holmes[1], Nikki L. Nolte[2] and David M. Andrews[2]

[1]Department of Kinesiology, University of Waterloo, Waterloo, ON, Canada
[2]Department of Kinesiology, University of Windsor, Windsor, ON, Canada,
dandrews@uwindsor.ca

INTRODUCTION

Considerable variability in tibial acceleration slope (AS) values, and different interpretations of injury risk based on these values, have been reported in the literature. Variability in AS values may be due, at least in part, to variations in the method used to quantify slope from the acceleration waveforms (Flynn et al., 2004; Holmes & Andrews, 2006; Lafortune & Lake, 1995; Lafortune et al., 1996). Therefore, the purpose of this study was to quantify differences in AS magnitudes determined using end points at various percentage ranges between impact and peak tibial acceleration (PA), as a function of either amplitude or time.

METHODS AND PROCEDURES

Tibial accelerations were recorded at the tibial tuberosity from 10 male and 10 female participants (21.8 ± 2.9 years) during 24 unshod heel impacts using a human pendulum apparatus. AS was calculated as the slope between two end points described by percentages, as a function of the PA amplitude ($AS_{Amplitude}$) or the time to PA (AS_{Time}) (Figure 1). Nine percentage ranges were tested from 5-95% (widest range) to 45-55% (narrowest range) at 5% increments.

RESULTS

The magnitudes of $AS_{Amplitude}$ values were larger and more sensitive to changes in percentage range than AS_{Time} values derived from the same impact data (p=0.00). The $AS_{Amplitude}$ magnitudes increased consistently across all ranges, and levelled off at the narrowest ranges, from 35-65% to 45-55%; while all AS_{Time} magnitudes narrower than 5-95% were statistically the same (Figure 2).
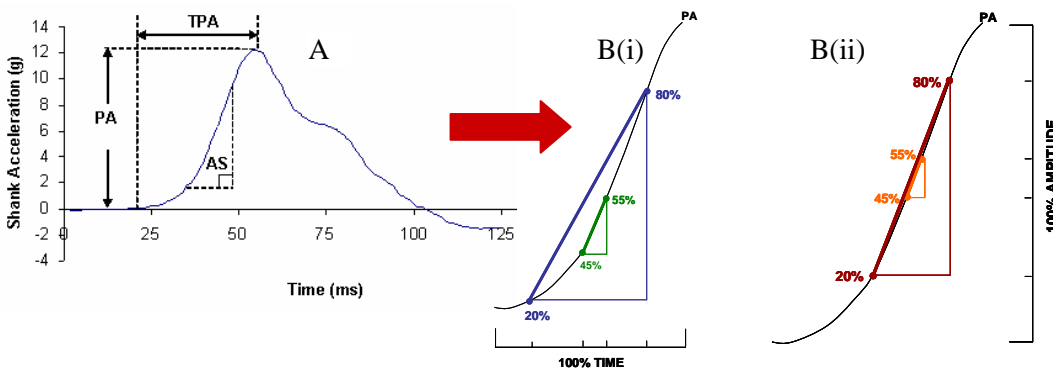

Figure 1. A) Tibial acceleration waveform with Peak Tibial Acceleration (PA), Time to Peak Tibial Acceleration (TPA), and Acceleration Slope (AS) highlighted. B) Sample Ranges for Acceleration Slope (AS) calculations as a function of (i) time and (ii) amplitude.
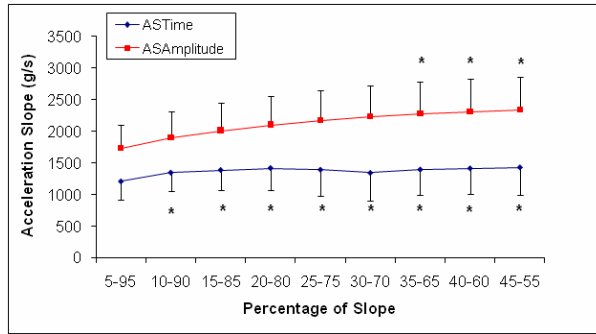
Figure 2. Acceleration Slope (AS) calculated as a function of amplitude (AS$_{Amplitude}$) or time (AS$_{Time}$). * = Statistically the same.

DISCUSSION

When characterizing tibial acceleration waveforms, a decision must be made regarding what portion of the waveform most appropriately describes the acceleration slope. Most authors have assessed the linear portion of the acceleration waveform, yet major inconsistencies in methods of quantifying slope have been reported (Flynn et al., 2004; Holmes & Andrews, 2006; Lafortune & Lake, 1995; Lafortune et al., 1996).

The current study has shown that AS$_{Amplitude}$ values were significantly higher and more sensitive to changes in percentage range than AS$_{Time}$ values derived from the same impact data. Despite differences in magnitude and variability, AS values calculated by both methods fell within the range of those previously reported in the literature (Table 1).

Magnitudes of AS are highly dependent on the method used to calculate them. Researchers are encouraged to carefully consider the choice of method when calculating AS following impact, so that equivalent comparisons and assessments of injury risk across studies can be made.

REFERENCES

Flynn, J.M. et al. (2004). *Clinical Biomechanics,* 19(7): 726-732.
Holmes, A.M. & Andrews, D.M. (2006). *J. Applied Biomechanics,* 22(4): 275-284.
Lafortune, M.A. & Lake, M.J. (1995). *J. Biomechanics,* 28(9) : 1111-1114.
Lafortune, M.A. et al. (1996). *J. Biomechanics,* 29(12): 1523-1529.

ACKNOWLEDGEMENTS

Table 1. Comparison of the Acceleration Slope Means (± Standard Deviations) across studies in the literature that used similar methodologies.

Reference	Slope Method Used	Acceleration Slope (g/s)
Current Study	Amplitude	2121 (463)
Current Study	Time	1374 (375)
Holmes & Andrews (2006)	Amplitude	1563 (614)
Flynn et al. (2004)	Time	2742 (1426)
Lafortune & Lake (1995)	Amplitude	671 (220)
Lafortune et al. (1996)	Amplitude	1150 (930)

EFFECT OF AGEING AND ARTERIAL STENOSIS ON VENTRICULAR-ARTERIAL COUPLING: A COMPUTATIONAL MODEL STUDY

Fuyou Liang[1], Shu Takagi[1], Ryotaro Himeno[1], Hao Liu[2]

[1]Research Program for Computational Science, RIKEN, Wako, Japan,
fyliang@riken.jp, takagish@riken.jp, himeno@riken.jp
[2]Graduate School of Engineering, Chiba University, Chiba Shi, Japan,
hliu@faculty.chba-u.jp

INTRODUCTION

The performance of the left ventricle (LV) is determined directly by its intrinsic properties (myocardial contractility and heart rate), and is regulated indirectly by the preload, and the afterload. In particular, the coupling between the left ventricle and the arterial system (VA coupling) was considered to have considerable influence both on the mechanical performance and on the biological remodeling of the coupled VA system. The VA coupling problems are most frequently pointed to in the context of ageing and hypertension. Ageing and hypertension lead to degenerated arterial remodeling featured by stiffness, which results in later and higher systolic pressure and wider pulse pressure that might in turn stimulate the remodeling of the LV. Typically, the LV adapts to confront higher and later systolic pressure by both hypertrophy and ventricular systolic stiffening (David A. Kass, 2005). As a result of the remodeling in both, AV coupling will be further altered to impair the cardiovascular reserve function.

VA coupling may also be affected by arterial stenoses which induce changes both in the magnitude of the afterload and in the pattern of wave propagation in the arterial system. So far, stenoses have generally been considered to have significant influences on local and downstream hemodynamics; the effects on far upstream hemodynamics and VA coupling were rarely addressed.

In this study, we develop a multi-scale model of the CVS, by coupling a one-dimensional (1D) model of the arterial system with a lumped parameter model (0D model) of the remainder. The multi-scale model is in a closed-loop form, which affords us a useful tool for investigating the interrelationship between cardiac indices and preload/afterload. With the model, we investigate the effects of ageing and arterial stenoses on VA coupling.
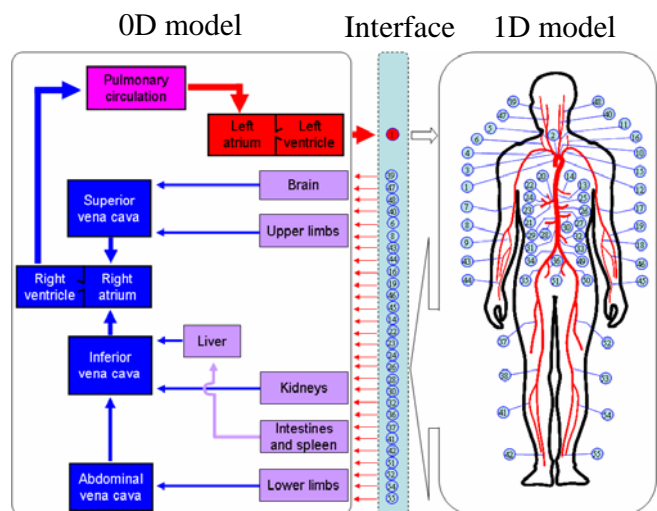

Figure 1. Schematic description of multi-scale modeling of the cardiovascular system

METHODS

The 55 largest arteries in the arterial system are described by a 1D model, and the remaining peripheral vascular systems, the heart and the pulmonary circulation are represented by a 0D model. The two models

are then coupled numerically to form a closed-loop system as shown in figure 1.

0-1D coupling computation is implemented at the aortic inlet and the distal ends of the 27 arteries through numerical iteration to reach continuity of mass and pressure between the two models.
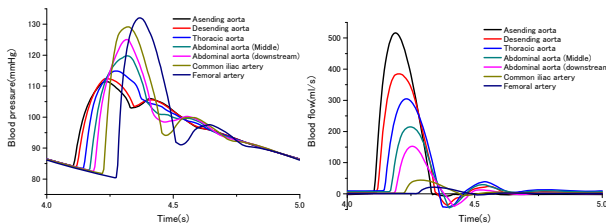

Figure 3. Effects of ageing on aortic pressure (left) and on P-V relationship of the LV

Figure 2. Simulated arterial pressure (left), and flow (right) waveforms

RESULTS

Figure 2 shows the simulated pressure and flow waveforms at several typical locations in the arterial system of a young adult. The simulations well reproduce the essential characteristics of arterial wave transmission in the arterial system. The systolic pressure increases away from the heart, towards the periphery, while the mean pressure decreases. Differently from the pressure waves, the flow waves show decreasing peaks and mean values along the aorta. In particular, in early diastole, strong retrograde flow appears downstream of the abdominal aorta.

The effects of ageing are studied for three representative ages: 20, 55 and 70 years old, respectively. Figure 3 shows the effects of ageing on the ascending aortic pressure and on the P-V relationship of the LV. It is evident that the systolic pressures of the elderly are much higher than the young adult, which is considered to result from the early arrival of the reflected waves at the LV due to the increased wave propagation speed in the arterial system in the elderly with arterial stiffening. The P-V relationships of the LV

Figure 4. Effects of stenoses on aortic pressure (left) and on P-V relationship of the LV (right).

indicate the higher oxygen consumption while smaller stroke volume in the elderly than in the young adult.

The effects of stenoses located in the abdominal aorta and the femoral artery are compared. The ascending aortic pressures and the P-V relationships of the LV simulated for the two 90% (occlusion ratio) stenoses are plotted in figure 4. The femoral arterial stenosis seems to only affect the diastolic pressure in the ascending aorta with no significant influence on the P-V relationship, while the aortic stenosis induces considerable changes in the ascending aortic pressure over a cardiac duration and deterioration of the LV performance characterized by early closure of the aortic valve and abrupt increase in LV pressure in late systole.

REFERENCES

Kass DA (2005). *Hypertension*, 46:1-9

ACKNOWLEDGEMENTS

PLANTAR LOADING DIFFERENCES BETWEEN RACING FLATS AND TRAINING SHOES AT A SELF-SELECTED RUNNING SPEED.

Robin M. Queen PhD[1,3], Jordan C. Yoder[1,2], Johannes I. Wiegerinck[1,4], Jennifer Boyd, BS[1,5], Alicia N Abbey, BS, ATC[1,3], James A. Nunley MD[3],

[1]Michael W. Krzyzewski Human Performance Lab, [2]Pratt School of Engineering, [3]Orthopaedic Surgery Duke University Medical Center, Durham, NC, USA
[4]Academic Medical Center, University of Amsterdam, Netherlands
[5]College of Engineering, North Carolina State University, Raleigh, NC, USA
Contact: robin.queen@duke.edu, http://klab.surgery.duke.edu

INTRODUCTION

Recently racing flats have been gaining popularity as not only competitive racing shoes, but also as shoes used for daily training. This switch from standard training shoes to racing flats does not come without consequence. Racing flats have less cushioning and support as well as being a lighter weight shoe than training shoes. It has been suggested that a decrease in cushioning could lead to an increase in plantar pressure, which has been linked to an increased risk of lower leg injuries. (McKenzie, et al, 1985, Nigg, et al, 2003, Eils, et al, 2004) The purpose of this study was to determine the effect of two different types of running shoes on plantar pressure while running at a self-selected speed.

METHODS AND PROCEDURES

Using the Pedar-X in-shoe system, plantar pressure data was collected for 17 male and 20 female subjects who run at least 10 miles per week and ranged in age from 18-29. The subjects completed 7 acceptable trials at a self-selected pace while wearing both a training shoe (Nike Air Pegasus) as well as a racing flat (Nike Zoom Katana IV) (Figure 1). The peak pressure, maximum force, contact area, and contact time were calculated for each shoe type.

Training Shoe   Racing Flat

Figure 1: Running Shoes Used for Testing

The foot was divided into eight regions (rearfoot, medial midfoot, lateral midfoot, medial forefoot, middle forefoot, lateral forefoot, hallux, and lesser toes) in order to determine the difference in loading in each of these foot regions. Maximum force was normalized to body weight, while contact area was normalized to the size of the insole that was used during testing. The data was analyzed using a paired t-test after determining that no significant differences existed in the running speed between the two shoe conditions ($\alpha=0.05$).

RESULTS

Subjects had a mean height of 1.699 ± 0.068 m, mean weight of 63.0 ± 8.3 kg, were 22.9 ± 3.0 years old and ran an average of 29.7 ± 18.0 miles per week. Subjects demonstrated significantly greater total foot peak pressure (p=0.019) and total foot maximum force (p=0.001) while wearing the racing flats. Peak pressure was significantly increased

beneath the medial (p=0.005), middle (p=0.008), and lateral (p<0.0001) forefoot regions as well as beneath the lateral (p=0.014) midfoot and the hallux (p=0.002) in the racing flats when compared to the training shoes (Figure 2). Similarly, significant increases in maximum force were found in the lateral forefoot (p<0.0001), hallux (p=0.001), and lesser toes (p<0.001) in the racing flats. Contact area was significantly increased in the lateral forefoot (p=0.029) in the racing flats. However, contact area was significantly decreased in the medial forefoot (p=0.048). Total foot contact time was not significantly different between the two shoe types.
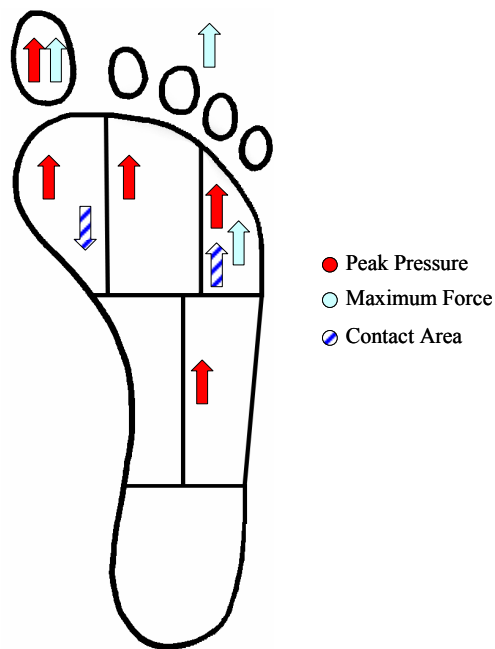
Figure 2: Plantar Loading Differences between the Racing Flats and Trainers.

DISCUSSION

Runners wearing racing flats experienced greater peak pressures and maximum forces in various regions of the foot. Based on the results of this study the

increase in pressure and force in the racing flats could indicate a potential increase in injury risk when running in a racing flat. These results indicate that racing flats should be reserved for competition as the distance and time in the shoe is much shorter, which could decrease the risk of injury. Future work should include an analysis of three-dimensional lower extremity kinematics and kinetics in order to understand any differences that might result from running in these different types of shoes.

SUMMARY

Increased plantar pressure and maximum force in the forefoot regions could be a potential risk factor for overuse injuries when running in racing flats. Therefore, the results of this study indicate the importance of not running long distances in a racing flat in order to avoid increased loads.

REFERENCES

McKenzie DC, et al. (1985) Sports Med. 2(5):334-47.
Nigg BM, et al. (2003) J Biomech. 36(4):569-75.
Eils, E., et al. (2004) AJSM 33:140-145.

ACKNOWLEDGEMENTS

MODIFYING LANDING MAT MATERIAL PROPERTIES TO REDUCE INJURIES IN GYMNASTICS LANDINGS

Chris Mills[1], Matthew T. G. Pain[2] and Maurice R. Yeadon [2]

[1]School of Sport and Health Sciences, University of Exeter, St. Luke's Campus, Exeter, UK, EX1 2LU, chris.mills@exeter.ac.uk
[2]School of Sport and Exercise Sciences, Loughborough University, Ashby Road, Loughborough, UK, LE11 3TU.

INTRODUCTION

Many sporting activities, from running to Artistic Gymnastics, involve a landing component. Several factors may contribute to the frequency and severity of injuries during landing including body position at the instant of touchdown, performance execution and the landing surface (McNitt-Gray, 2000).

In Artistic Gymnastics the landing mat is standardised by the international governing body (F.I.G.) and the standards are based upon the need to establish uniformity of the equipment used during competition rather than purely musculo-skeletal issues (McNitt-Gray, 2000). A better landing mat may exist that could reduce injury risk whilst allowing the gymnast to maintain a landing technique that minimises landing deductions.

The aim of this study is to determine the material properties of a landing mat that minimise internal loading and external forces experienced by the gymnast during landing.

METHODS AND PROCEDURES

A subject-specific 7 link planar model representing the gymnast was constructed using visualNastran 4D (Figure 1). This model has previously been successfully evaluated against gymnast landings (Mills et al., 2008).
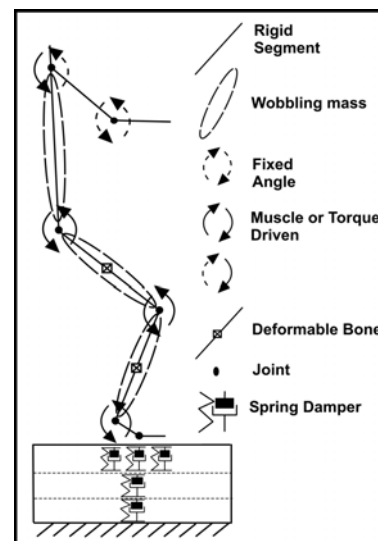
Figure 1. Simulation model of the landing mat and the gymnast.

The competition landing mat's material properties were based upon rigid body impact tests performed independently (Pain et al., 2005). The landing mat model was based upon a multi-layer spring-damper design and evaluated using the independent impact tests (Mills et al., 2006). This 6 parameter landing mat model combined sufficient detail allowing the modification of the stiffness and damping parameters for each of the independent layers of the mat.

The stiffness and damping characteristics for each layer of the mat were optimised using a Simplex algorithm to minimise the GRFs. Since the muscle activation histories remained unchanged from the model evaluation any decrease in external GRFs may also result in decreased internal loading.

RESULTS

Optimisation of the six landing mat parameters resulted in the peak vertical (Figure 2) and horizontal ground reaction force being reduced.
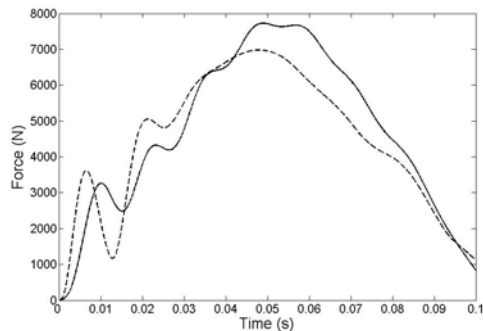
Figure 2. VGRF after optimisation of landing mat properties (Solid line = matching simulation, dashed line = opt simulation).

This reduction in peak GRFs was also accompanied by a decrease in peak shank (Figure 3) and femur bone bending moments.
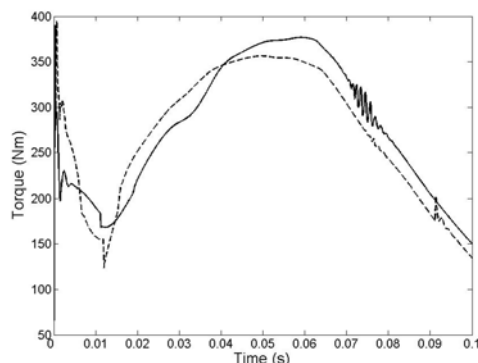
Figure 3. Shank bone bending moments during landing. (Solid line = matching simulation, dashed line = optimised simulation).

The optimisation of the landing mat parameters were characterised by minimal changes to the landing mat's stiffness (<0.5%) but increased damping (272%).

DISCUSSION

The most significant finding of this study was that modifying the material properties of the competition landing mat could reduce the peak GRFs and internal loading on the gymnast during landing. A reduction in forces on and inside the musculo-skeletal system could help to reduce the injury risk associated with landing (McNitt-Gray et al., 2000).

The increased damping in the optimised mat may alter the physical recovery of the mat to its original shape. This may also compromise the stability and therefore affect the recovery of balance of the gymnast. A finite element model could help to reproduce the surface area deformation seen in the impact tests (Pain et al., 2005). It is also possible that increased damping may cause increased initial foot contact forces. The use of a thin, soft additional layer to reduce this potential foot problem needs investigating.

The solution found here is likely to be a local minima, near to the original F.I.G. competition mat and although this may be a shortcoming of the study in methodological terms it does not affect the major finding.

Local solutions may also be more useful from an applied point of view as a true global solution may require very different manufacturing processes to construct the landing mat. The local minimum solution means that minor manufacturing changes to the material properties of the mat would result in the gymnast experiencing reduced internal loading forces.

REFERENCES

Mills et al., (2008). *J of Biomech*, 41, 621-628.

Mills et al., (2006). *J of App Biomech*, 22, 103-111.

Pain et al., (2005). *Med Sci. Sports & Exerc*, 37, 1754-1760.

McNitt-Gray, J. L. (2000). *Encyclopaedia of Sports Medicine: Biomechanics in Sports*. IOC, Blackwell Science, pp.523-549.

POST-HIBERNATION BLACK BEARS (URSUS AMERICANUS) DO NOT DEMONSTRATE CORTICAL BONE LOSS COMPARED TO PRE-HIBERNATION BEARS DESPITE 6 MONTHS OF DISUSE

Meghan E. McGee[1], Lindsay N. Barlow[1], Kirsten J. Simoni[1], Samantha J. Wojda[1], Janene Auger[2], Hal L. Black[2], Seth W. Donahue[1]

[1] Department of Biomedical Engineering, Michigan Technological University, Houghton, MI, USA, swdonahu@mtu.edu
[2] Department of Integrative Biology, Brigham Young University, Provo, UT, USA

INTRODUCTION

Disuse typically causes unbalanced bone remodeling which leads to bone loss and reduced bone strength (Li et al., 2005). However, previous studies suggest that bears are able to prevent bone loss during disuse associated with hibernation. Cortical bone geometry and strength are preserved in hibernating grizzly bears, and interestingly, intracortical porosity is lower and mineral content is higher in hibernating compared to active grizzly bears (McGee et al., 2008). However, previous sample sizes were small (n = 4 bears in each season), limiting the conclusions that could be drawn from the data regarding the effects of hibernation on bear cortical bone structure and strength. Here we investigated bone properties in a large sample of pre- and post-hibernation black bears to comprehensively determine the effects of hibernation on bear cortical bone.

METHODS AND PROCEDURES

One femur was obtained from each of 65 black bears (*Ursus americanus*) killed during the fall and spring hunting seasons in Utah; 18 were from female bears (mean age = 8.4 ± 5.5 yrs) and 47 were from male bears (mean age = 5.6 ± 3.6 yrs). Age and sex distributions were comparable between seasons. Post-hibernation bears had remobilized following 6 months of disuse for approximately 1-4 weeks.

Bones were loaded to failure in three-point bending, after which the midshaft of the diaphysis was reconstructed and embedded in methyl methacrylate. Midshaft cross-sections were exposed with a diamond saw and digitized with a digital camera. Bone geometrical properties including moments of inertia about the mediolateral and anteroposterior axes (I_{ML} and I_{AP}, respectively), maximum moment of inertia (I_{max}), periosteal, cortical, and endosteal bone areas (Ps.Ar, Ct.Ar, and Es.Ar, respectively), and endosteal area fraction (Es.Ar/Ps.Ar) were calculated with Scion Image (Frederick, MD) and a custom macro. Beam theory was used to calculate whole bone ultimate stress (σ_U), energy to failure (U), and modulus of toughness (u). Diaphyseal segments proximal to the reconstructed midshaft were used to quantify ash fraction (a measure of mineral content). Sections of the diaphysis distal to the reconstructed midshaft were histologically processed for a sampling of bears from each season (n = 13 pre-hibernation and 16 post-hibernation). Slides were prepared with basic fuchsin and were used to quantify intracortical porosity at 40x magnification. Bone properties were compared between pre- and post-hibernation bears with ANCOVA, treating age as the covariate. Males and females were pooled for statistical analyses since group distributions were similar.

RESULTS

There were no differences in bone geometrical properties between pre- and post-hibernation bears (p > 0.458). A representative plot is shown in Figure 1.
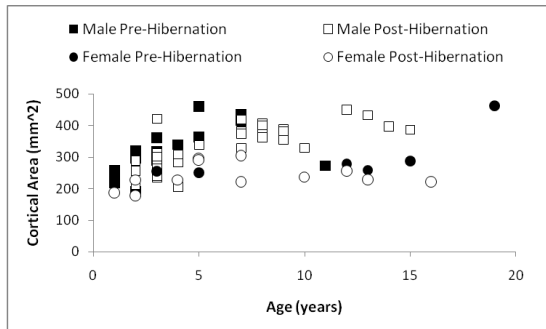

Figure 1. Cortical area was not different between fall and spring bears (p = 0.699)

There were no differences in bone mechanical properties or ash fraction between pre- and post-hibernation bears (Table 1). Intracortical porosity was significantly lower (p = 0.044) in post- compared to pre-hibernation bears (Table 1).

Property	Pre-hib	Post-hib	Pre- vs. Post-ANCOVA p-value
σ_U (MPa)	238 (42)	233 (27)	0.519
U (J)	46 (15)	43 (16)	0.500
u (mJ/mm^3)	6.1 (1.5)	5.5 (1.6)	0.261
ash fraction	0.694 (0.011)	0.696 (0.010)	0.797
porosity (%)	6.2 (2.6)	4.7 (1.8)	0.044

Table 1. Means & standard deviations for cortical bone properties in pre- and post-hibernation bears.

DISCUSSION

In most animals, disuse causes bone loss because bone remodeling processes become imbalanced. In contrast, post-hibernation black bears did not demonstrate bone loss compared to pre-hibernation bears, since bone geometrical, mechanical, and mineral properties were not different, and porosity was significantly lower in the post-hibernation bears. This is likely because hibernating bears experience decreased, but balanced, intracortical remodeling (McGee et al., 2008), which would contribute to the preservation of cortical bone structure and decrease in bone porosity during hibernation. The decrease in bone remodeling activity during hibernation may be a result of energy conservation and recycling mechanisms used to survive prolonged periods of famine. The results of this study are in agreement with our previous findings in hibernating and active grizzly bears (McGee et al., 2008) and another study which showed that bone cross-sectional area of the forelimb is not different in pre- and post-hibernation black bears (Pardy et al., 2004). The mechanism which prevents bone loss in bears may lead to the development of treatments (e.g., novel PTH peptides) for human osteoporoses. For example, we found bear PTH 1-34 promotes greater anti-apoptotic gene expression in osteoblasts than human PTH 1-34.

REFERENCES

Li CY et al. (2005). *JBMR,* 20: 117-124.

McGee ME et al., (2008). *Bone,* 42: 396-404.

Pardy CK et al., (2004). *J Zool Lond*, 263: 359-364.

ACKNOWLEDGEMENTS

STRUCTURAL PROPERTIES OF FOURTH-GENERATION COMPOSITE FEMURS AND TIBIAS

Anneliese Heiner

Department of Orthopaedics and Rehabilitation, Department of Biomedical Engineering, University of Iowa, Iowa City, IA, USA, anneliese-heiner@uiowa.edu

INTRODUCTION

Composite replicate femurs and tibias (Sawbones, Pacific Research Laboratories, Inc., Vashon, WA) are widely used in orthopaedic research, and have undergone several design changes since their introduction in 1987. Fourth-generation composite bones, the latest design, have the same geometries as the third-generation bones, but the cortical bone analogue material was changed to increase fracture and fatigue resistance, tensile and compressive properties, thermal stability, and moisture resistance (Pacific Research Laboratories, Inc., 2007). The purpose of this study was to measure the structural properties of this latest design of composite femurs and tibias from Pacific Research Laboratories, Inc. This was done to confirm that these composite bones still had structural properties that were in the range of those for natural human bones.

METHODS AND PROCEDURES

Six medium fourth-generation composite femurs (model 3403) and six medium fourth-generation composite tibias (model 3401) were tested under bending, axial, and torsional loading in an MTS 858 Bionix materials testing machine (MTS Systems Corp., Eden Prairie, MN). The research design is described in detail in earlier studies by the author (Heiner and Brown, 2001; Heiner and Brown, 2003) and is outlined only briefly here. Bending was applied through a 4-point bending fixture, with 62 mm between successive contact points. Each bone was bent in two directions, anterior surface in tension

and lateral surface in tension. Loading was between 50 N and 500 N at 0.025 mm/sec. For axial testing, the femurs and tibias were distally potted to depths of approximately 8 cm and 6 cm, respectively. The composite bones were aligned using a rigid, centrally-located rod, which went up into the bones' intramedullary shaft. The femurs were oriented in 11° of adduction from the vertical, and the tibias were oriented vertically. The bones were loaded through a platen that conformed to the femoral head or tibial condyles, and connected to the MTS machine through a ball joint and x-y table in series. The ball joint location utilized on the load platen was that for which axial stiffness was the highest. Compression was between 60 N and 600 N, at 60 N/sec. Strain distribution along the proximal-medial diaphysis was measured for three of the femurs with five unidirectional strain gages (Measurements Group, Inc., Raleigh, NC). For torsional testing, the femurs and tibias were proximally and distally potted with Cerrobend to depths of approximately 8 cm and 6 cm, respectively. The bones were oriented vertically, and otherwise aligned as described for axial testing. The bones were constrained in all other degrees of freedom except for axial motion, which was allowed to float during the testing. Torsional loading was applied such that the proximal ends of the bones rotated internally. Loading was between 0.5 Nm and 7.5 Nm at 0.25 deg/sec. Setup variability was determined by completely disassembling the set-up then retesting one bone for each loading mode.

RESULTS

Property	Bone Type	Femur	Tibia	Units
Flexural	Natural	317 (23%)	233 (30%)	Nm^2
Rigidity,	3rd gen	210 (7.2%)	209 (7.2%)	
AT	4th gen	241 (4.5%)	199 (5.0%)	
Flexural	Natural	290 (42%)	205 (23%)	Nm^2
Rigidity,	3rd gen	239 (5.6%)	131 (2.0%)	
LT	4th gen	273 (5.8%)	146 (3.5%)	
Axial	Natural	2.48 (25%)	NA	N/μm
Stiffness	3rd gen	1.47 (12%)	7.80 (5.6%)	
	4th gen	1.86 (7.5%)	7.48 (9.3%)	
Torsional	Natural	4.41 (37%)	2.42 (33%)	Nm^2/
Rigidity	3rd gen	2.15 (10%)	1.69 (7.9%)	deg
	4th gen	3.21 (2.6%)	1.93 (3.6%)	

Table 1. Structural properties of natural (Heiner and Brown, 2003), medium third-generation (3rd gen) composite, and medium fourth-generation (4th gen) composite femurs and tibias (average and coefficient of variation, n=6). AT = anterior surface in tension; LT = lateral surface in tension.

Strain gage location	Natural	3rd gen	4th gen
Highest	633 (28%)	1193 (2%)	708 (10%)
2nd highest	454 (38%)	930 (8%)	703 (8%)
Middle	376 (38%)	582 (13%)	504 (7%)
2nd lowest	182 (32%)	248 (22%)	259 (17%)
Lowest	36 (213%)	-61 (62%)	44 (88%)

Table 2. Compressive strain (με) on natural (Heiner and Brown, 2003), medium third-generation (3rd gen) composite, and medium fourth-generation (4th gen) composite femoral proximal-medial shafts (average and coefficient of variation, n=3), at 600 N of compression. Strain gages were equally spaced from the level of the lesser trochanter ("Highest") to the middle of the shaft ("Lowest").

DISCUSSION

The fourth-generation composite bones had average stiffnesses and strains that were for the most part closer to those values measured for the natural bones, than were the third-generation composite bones in comparison to natural bones (all measurements by the same author). (Natural tibia axial stiffness results were not reported, because of unacceptably high setup variability indicating exceptional difficulty in obtaining proper bone alignment (Heiner and Brown, 2003); this complication was also reported by Cristofolini and Viceconti (2000).) For the stiffness tests, variability between the specimens was less than 10% for all cases, and setup variability, calculated as the percent change between a test and re-test on the same specimen (with re-potting, when applicable), was less than 6% for all cases. The inter-specimen variability of the fourth-generation composite bones was much less than that of the natural bones; other studies have reported this as well (Cristofolini et al., 1996; Cristofolini and Viceconti, 2000; Heiner and Brown, 2001; Heiner and Brown, 2003).

SUMMARY

The structural properties of Pacific Research Laboratory's fourth-generation composite femurs and tibias are in the range of those for natural human bones.

REFERENCES

Cristofolini, L and Viceconti, M (2000). *J Biomech* 33:279-288.
Cristofolini, L et al. (1996). *J Biomech* 29:525-535.
Heiner, AD and Brown, TD (2001). *J Biomech* 34:773-782.
Heiner, AD and Brown, TD (2003). *Trans 29th SFB* 26:702.
Pacific Research Laboratories, Inc. (2007). Informational handout.

ACKNOWLEDGEMENTS

Chemical Structure Effects on Bone Response to Mechanical Loading

Peizhi Zhu[1], Jiadi Xu[1], Michael D. Morris[1], Nadder Sahar[2], David H. Kohn[2], Ayyalusamy Ramamoorthy[1], Mary Tecklenburg[3]

[1] Department of Chemistry, University of Michigan, Ann Arbor, MI, 48109
[2] School of Dentistry, University of Michigan, MI, 48109
[3] Department of Chemistry, Central Michigan University, Mount Pleasant, MI 48859

INTRODUCTION

Solid state nuclear magnetic resonance (SSNMR) spectroscopy is a powerful tool for studying high-resolution structural changes in a wide variety of materials, including materials subjected to high pressure (Redfern, 2000). We show that SSNMR can probe load-induced changes in the chemical structure of bone mineral and bone matrix. We use magic angle spinning NMR spectroscopy (MAS-NMR) and a specially designed load cell, to probe changes in the ion spacings of bovine cortical bone mineral in response to compressive loads in the MPa region.

METHODS AND PROCEDURES

For these studies, ^{31}P NMR of bone mineral phosphate was investigated. All NMR experiments were performed on a Chemagnetics/Varian 400MHz solid-state NMR spectrometer equipped with a 5mm double tuned MAS probe. The spin-echo pulse sequence outlined in figure 1 was used. A purpose-built cell was used to apply known loads to the tissue specimens. The cell was constructed entirely from ceramics. Loads were applied with a torque wrench.
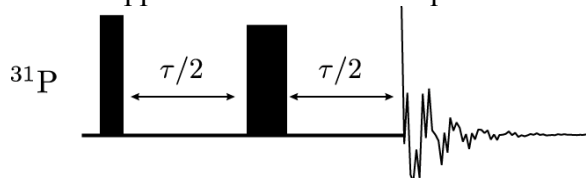
Figure 1. Spin-echo pulse sequence to measure ^{31}P isotropic chemical shifts from bone specimens under MAS. The first and second solid blocks are 90 and 180 degree RF pulses.
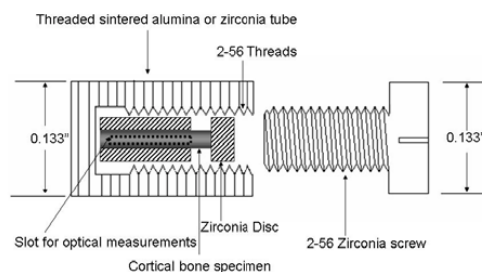
Figure 2. NMR cell to apply a high pressure load with a torque wrench. The cell fits into a standard MAS rotor. The slot is for optical measurements of strain.

RESULTS

In our first proof of principle experiments we were able to load the tissue only to about 1.1 MPa. The limitation was failure of the ceramic NMR cell. Our initial tests of new ceramics confirm that we can reach about 4 MPa with no other changes. Further changes in the cell design should allow us to reach loads in the 8-10 MPa range.

We observed that the resonance frequency of phosphate was independent of load (Figure 3). Our earlier experiments were performed at a low spinning frequency, resulting in the spinning side bands shown in the figure. The intensity of spinning side bands increases linearly with the load (Figure 4). The reason for this observation is that homonuclear and heteronuclear dipolar coupling constants, which measure the interaction between

adjacent atoms or ions, increase linearly with the inverse cube of spacing, i.e. with the inverse of volume. The scaling is the same for pressure-induced volume changes. Thus, the slope of the curve is directly proportional to the decrease in mineral volume accompanying the load. The same linear change with pressure is expected for any effect that depends linearly on the dipolar coupling.
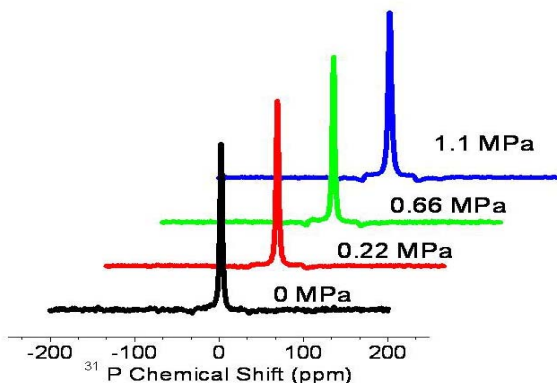
Figure 3. ^{31}P NMR spectra of bone mineral as a function of compressive load. Applied pressures are included. Intensity of spinning side bands increase with pressure.
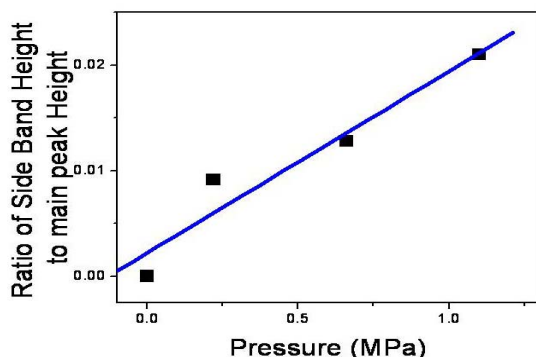
Figure 4. Spinning side band intensity of bone mineral ^{31}P resonance scales linearly (R^2=0.97) with the compressive load.

DISCUSSION

No observed changes in the isotropic and anisotropic chemical shift values of ^{31}P nuclei under the compressive load suggest that the chemical environment of the phosphate group in the bone sample is unaltered. However, bone samples under pressure showed a significant increase in the intensity of spinning sidebands, suggesting that dipolar couplings are not completely suppressed by the MAS speed. This observation is most likely due to the pressure-induced decrease in the distance between dipolar coupled nuclei. As with most minerals, loads in the MPa range changes ion spacings, but does not deform covalent bonds.

Most importantly, these results demonstrate that a wide variety of biomechanical NMR studies of bone are possible. In particular, any effect that results in a linear dependence of dipolar coupling constants will be amenable to relatively straightforward interpretation.

SUMMARY

Solid-state MAS-NMR can be used to measure atomistic-level changes in the chemical structure of bone tissue caused by mechanical load. Where NMR techniques that use dipolar coupling are employed, linear dependences on pressure are expected and spacing between ions in matrix or between nuclei in bone collagen can be measured directly.

REFERENCES

Redfern SAT et al (2000). *Transformation Processes in Minerals (Reviews in Mineralogy and Geochemistry)*, Vol 39 .

ACKNOWLEDGEMENTS

THE RELATIONSHIP BETWEEN GLENOID INCLINATION AND IN-VIVO GLENOHUMERAL JOINT MOTION DURING SHOULDER ABDUCTION

Jennifer L Bishop[1], Stephanie K Kline[1], Kristopher J Aalderink[2], and Michael J Bey[1]

[1]Henry Ford Hospital, Bone and Joint Center, Detroit, MI, USA
[2] Henry Ford Hospital, Department of Orthopaedic Surgery, Detroit, MI, USA
jbishop2@ hfhs.org

INTRODUCTION

Rotator cuff injuries are common, leading to pain, loss of function, and medical expense. The etiology of rotator cuff injuries is not well understood, but cadaveric studies have shown that glenoid inclination (i.e., the extent to which the glenoid is tipped superiorly relative to the scapula) may be associated with rotator cuff tears and superior translation of the humerus (Konrad et al., 2006; Wong et al., 2003). However, the relationship between glenoid inclination and superior translation of the humerus has not been determined under in-vivo conditions. The objectives of this study were to: 1) compare glenoid inclination between the repaired and contralateral shoulders of patients undergoing unilateral rotator cuff repair, and 2) quantify the relationship between glenoid inclination and in-vivo superior translation of the humerus relative to the scapula. We hypothesized that glenoid inclination would be greater in the repaired shoulder and that there would be a significant association between glenoid inclination and superior translation of the humerus during shoulder abduction.

METHODS AND PROCEDURES

Following IRB approval, 21 subjects (14 male; age: 63 ± 11.4) were enrolled. Each subject underwent arthroscopic surgery to repair an isolated supraspinatus tendon tear 3-4 months prior to this study. The contralateral shoulder of each subject was asymptomatic.

Subjects were positioned with their shoulder centered in a biplane x-ray system (Tashman and Anderst, 2003). X-ray images were acquired at 60 Hz while subjects abducted their shoulder in the frontal plane from full adduction to $\sim 120°$ of abduction. Three trials from each shoulder were recorded.

Following testing, bilateral CT images of the humerus and scapula were acquired. The humerus and scapula were segmented and reconstructed into 3D bone models. Using these models, glenoid inclination was measured using landmarks reported by Hughes and colleagues (2003) (Figure 1).
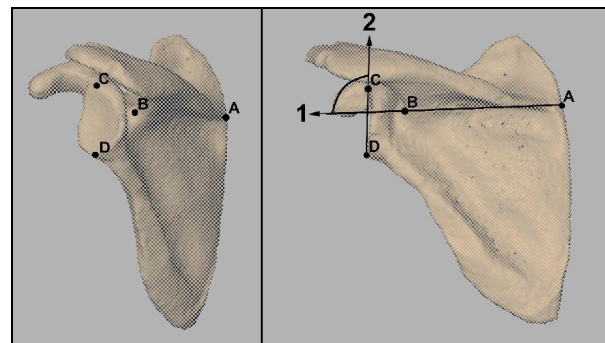
Figure 1. Glenoid inclination is the angle between lines 1 and 2. Line 1 connects (A) the scapular spine's intersection with the medial border, and (B) the spinoglenoid notch. Line 2 connects (C) superior most and (D) inferior most points on the glenoid rim.

The 3D positions of the humerus and scapula were measured from the biplane x-ray images using an accurate (± 0.4 mm, $\pm 0.5°$) model-based tracking technique (Bey et al., 2006). Superior/inferior (S/I) translation of the humeral head center (HHC) relative to the scapula was quantified in terms of: S/I translation range (HHC RANGE), S/I translation from the adducted starting position to full abduction (HHC ABD), and maximum superior translation relative to the adducted starting position (HHC MAX).

As an alternative measure of joint motion, glenohumeral joint contact patterns were calculated using a technique that combined joint motion measured from the biplane x-ray images with the CT based bone models (Anderst and Tashman, 2003). The contact center location was determined by calculating the centroid of the closest 200 mm^2 region of contact between the articulating surfaces of the humerus and glenoid. The 3D coordinates of this contact center location were expressed relative to the scapula. S/I translation of the contact center (CC) was quantified in terms of: S/I translation range (CC RANGE), S/I translation from the adducted starting position to full abduction (CC ABD), and maximum superior translation relative to the adducted starting position (CC MAX).

A paired t-test assessed the effect of shoulder condition (repaired vs. contralateral) on glenoid inclination. The association between glenoid inclination and the six measures of glenohumeral joint translation was assessed for only the contralateral shoulder with linear regression and a correlation coefficient. Significance was set at $p < 0.05$.

RESULTS

Glenoid inclination was an average of 1.6 ± 3.3° lower in the repaired shoulder than in the contralateral shoulder ($p = 0.04$). The study failed to detect any statistically significant association between glenoid inclination and the six measures of joint translation (Table 1).

S/I Translation Outcome Measure	Correlation Coefficient (r)	P value
HHC RANGE	-0.25	0.30
HHC ABD	-0.25	0.30
HHC MAX	0.02	0.95
CC RANGE	-0.10	0.67
CC ABD	-0.22	0.37
CC MAX	-0.16	0.50

Table 1. Correlation and regression results between glenoid inclination and kinematics.

DISCUSSION

Previous research has reported that rotator cuff tears are associated with greater glenoid inclination (Hughes et al., 2003; Tetrault et al, 2004). In contrast, the current study indicates that glenoid inclination of the repaired shoulder is *lower* than the contralateral shoulder. It is possible that this discrepancy is due, in part, to differences in measurement technique. In fact, Kandemir and colleagues (2006) found a significant difference between 2D and 3D measurements of this angle.

Previous cadaver studies showed a decrease in superior translation as glenoid inclination decreased (Wong et al., 2003; Konrad et al., 2006). Contrary to these findings, the current study failed to detect any statistically significant association between glenoid inclination and the six measures of superior humeral translation. One potential explanation for this discrepancy is that previous research was based on cadaveric studies that cannot accurately simulate in-vivo muscle and joint forces. Moreover, it seems overly simplistic to expect that glenohumeral joint motion is influenced by a single anatomic factor such as glenoid inclination. In summary, this study failed to support the theory that glenoid inclination is the primary etiologic factor responsible for superior humeral translation and the development of rotator cuff tears.

REFERENCES

Anderst, WJ and Tashman, S (2003). *J Biomech,* 36:1291-9.
Bey MJ et al. (2006). *J Biomech Eng* 128:604-9.
Hughes RE et al. (2003). *CORR*, 407:86-91.
Kandemir U et al. (2006). *JBJS*, 88-B:1105-9.
Konrad GG et al. (2006). *Clin Biomech,* 21:942-9.
Tashman, S and Anderst, WJ (2003). *J Biomech Eng* 125:238-45.
Tetrault P et al. (2004). JOR 22(1):202-7.
Wong et al (2003). *JSES* 12(4):360-4.

Shortening-induced force depression is primarily caused by cross-bridges in strongly bound states

Eun-Jeong Lee and Walter Herzog

Human Performance Lab, Faculty of Kinesiology, University of Calgary, Calgary, AB, Canada,
ejlee@kin.ucalgary.ca

INTRODUCTION

Force depression has been defined as the decrease in steady-state isometric force following shortening of an active muscle compared to the steady-state force obtained for purely isometric contractions at the corresponding length (Edman *et al.*, 1993). In previous studies, force depression has been shown to depend on the force and magnitude (and thus the work) of shortening (Herzog and Leonard, 1997), and has been associated with a decrease in stiffness in single fiber preparations (Sugi and Tsuchiya, 1988). Therefore, force depression has been thought to be associated with a decrease in the proportion of attached cross-bridges which might be caused by an inhibition of cross-bridge attachment following shortening contractions (Maréchal and Plaghki, 1979). However, it is not clear if all cross-bridges contribute to force depression equally, or if force depression affects specific states in the cross-bridge cycle.

The purpose of this study was to investigate if force depression affects so-called weakly and strongly bound cross-bridges to the same degree. Specifically, we hypothesized that active muscle shortening inhibits cross-bridge binding to the same degree for all cross-bridge states. In order to address this specific hypothesis, tests were performed with normal fibers and fibers exposed to 2,3-butanedione monoxime (BDM) which biases cross-bridges towards the weakly bound state. If our hypothesis is correct, then the amount of force depression relative to the isometric reference values and decrease in stiffness should be the same for the fibers in normal Ringer's and the experimental BDM solution.

METHODS AND PROCEDURES

Single fibers (n = 9) were dissected from frog lumbrical muscles and suspended between a motor arm and a force transducer inside an experimental chamber. Isometric reference contractions were performed at a length corresponding to the length following the shortening step in the experimental contractions (i.e., optimal length in this study). Test contractions consisted of an isometric contraction that was immediately followed by active shortening with magnitudes of 10 or 15% of the optimal length at a speed of 13% optimal length/s. Each contraction lasted 5s and stiffness was measured using a quick stretch (1% optimal length over 1ms) just before deactivation. Experiments were performed in Ringer's solution (pH=7.2), and following that were repeated after exposure to 7.5mM BDM. Force depression was measured as the median of force over a 0.3s period starting 4.5s following the onset of activation. Force was normalized to fiber cross-sectional area and stiffness was calculated by dividing force by elongation.

RESULTS AND DISCUSSION

Average isometric force decreased by 42% and stiffness by 25% when fibers were exposed to BDM. The absolute amount of force depression was decreased while the relative amount was the same in the BDM exposed (10.7%) compared to the normal fibers (12.3%; Fig.1, table1). The absolute

amount of force depression was strongly correlated to the work performed by the fibers during shortening for both the BDM exposed and normal fibers (Fig. 2, $p\sim0$).
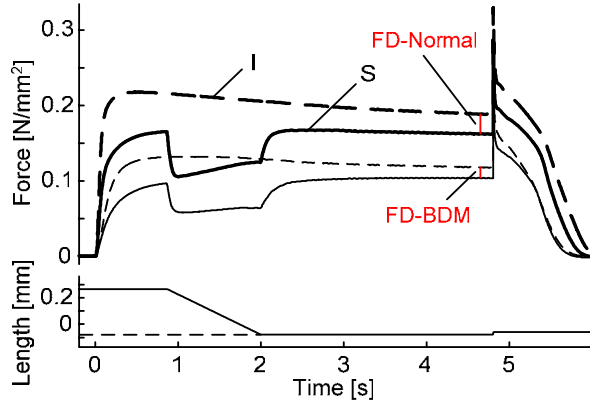

Figure 1. Raw force (top) and change in length (bottom) time histories of active shortening (solid, S) and isometric reference contractions at the corresponding final length (dashed, I) in normal (thick) and BDM (thin) conditions. Force depression with normal (FD-Normal) and BDM exposed fiber (FD-BDM) are indicated in red.
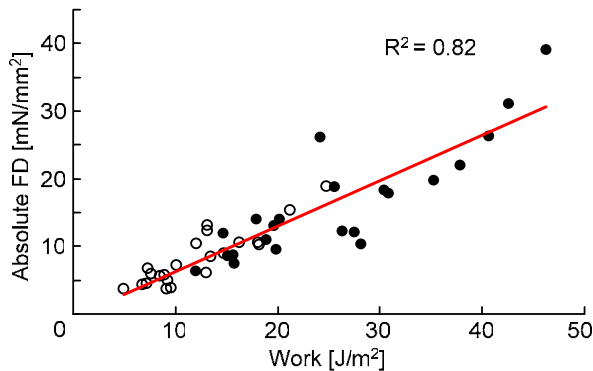

Figure 2. Work vs. absolute force depression with normal (●) and BDM (○) exposed fibers.

The average decrease in stiffness was smaller in the BDM exposed fibers (6.7%) than the normal fibers (16.8%; table1). The results of this study confirm previous findings in that force depression was strongly correlated to the amount of work performed during active muscle shortening and that force depression was nearly proportional to the decrease in stiffness in fibers exposed to normal conditions. New to the literature is the result that force depression in fibers biased towards weakly bound cross-bridge states (BDM) showed the same amount of relative force depression as normal fibers but had a much reduced decrease in stiffness. These results support the idea that force depression through active muscle shortening is primarily produced by cross-bridges in the strongly bound states while cross-bridges in the weakly bound states are unaffected.

CONCLUSIONS

From the results of this study we conclude that active muscle shortening affects cross-bridges in different ways depending on their states. Strongly bound cross-bridges are inhibited and so contribute to the observed force depression, while weakly bound cross-bridges remain largely unaffected.

REFERENCES

Edman, KAP et al. (1993). *J Physiol,* 466:535-552.
Herzog, W and Leonard, TR (1997). *J Biomech,* 30(9):865-872.
Marechal, G and Plaghki, L (1979). *J Gen Physiol,* 73:453-467.
Sugi, H and Tsuchiya, T (1988). *J Physiol,* 407:215-229.

ACKNOWLEDGEMENTS

Table 1. Force (relative and absolute) and stiffness depression (mean±SE, * sig. level, $p<.01$).

Condition	Relative FD [%]*	Absolute FD [mN/mm^2]*	Stiffness Depression [%]*
Normal	12.3 ± 1.0	16.3 ± 1.8	16.8 ± 1.2
BDM	10.7 ± 0.8	8.2 ± 0.9	6.7 ± 1.1

PREDICTING PATIENT FUNCTION AND JOINT LOADING POST-TOTAL KNEE REPLACEMENT USING MUSCLE ACTIVATION PATTERNS

Gillian Hatfield[1], Cheryl Hubley-Kozey[1,2], Michael Dunbar[3].
Schools of Physiotherapy[1], Biomedical Engineering,[2] and the Department of Surgery[3], Dalhousie University, Halifax, NS, Canada. Email: GHatfield@dal.ca

INTRODUCTION

Knee osteoarthritis (OA) is a leading cause of chronic disability, resulting in huge economic costs (Sharma et al. 2006). The prevalence of OA is expected to increase in North America as the population ages, resulting in increased demand for total knee replacements (TKR) (Sharma et al. 2006, Health Canada 2003).

Better functional outcomes after TKR surgery have been linked to higher pre-operative functional scores (Lingard et al. 2004) and quadriceps strength (Mizner, 2005), but these studies did not examine the change in function. Given that muscle activation patterns are altered in those with severe knee OA (Hubley-Kozey et. al., 2008), this study aimed to examine the relationship between pre-TKR muscle activation patterns and changes in objective measures of function (velocity) and knee joint loading (knee adduction moment). We hypothesized that pre-TKR electromyographic (EMG) patterns could predict changes between pre-and post-TKR walking velocity and knee adduction moment (KAM).

METHODS AND PROCEDURES

Forty-five participants (65 ± 7 years of age) with severe knee OA were tested within one week prior to TKR surgery, and one year post-TKR surgery. After standard skin preparation Ag/AgCl surface electrodes (0.79 mm) were placed in line with the muscle fibres of the lateral (LG) and medial gastrocnemius (MG), rectus femoris (RF), vastus lateralis (VL), vastus medialis (VM), and lateral (LH) and medial hamstrings (LH).

EMG signals from an eight channel surface EMG system (AMT-8™ Bortec, Inc., Calgary, Alberta) were collected at 1000 Hz. Three-dimensional motion (Optotrak™) and ground reaction forces (AMTI™) were also collected while the participants walked at their self-selected velocity. After the walking trials, maximum voluntary isometric contraction (MVIC) exercises were completed for amplitude normalization. The EMG signals were full-wave rectified, low pass filtered at 6 Hz then amplitude normalized to MVIC. The KAM was calculated using an inverse dynamics and was amplitude normalized to body mass. The EMG and moment waveforms were time normalized to 100% of the gait cycle.

Pattern recognition techniques determined the principal amplitude and shape characteristics in the EMG and KAM waveforms. Principal components (PC) were extracted which explained over 95% of the variance, and PC *scores* were calculated for each subject's original waveforms. These *scores* for each PC were then used in the statistical analyses.

Paired Student's t-tests ($\alpha = 0.05$) were used to detect significant pre to post-TKR differences in the gait velocity and knee adduction moment PC *scores*. Step-wise regression models ($\alpha = 0.1$) determined which pre-TKR EMG PCs best predicted pre to post-TKR changes in gait velocity and the KAM PC *scores*.

RESULTS

The mean gait velocity significantly increased from 0.93 to 1.09 m/s (p<0.001). Three PC *scores* explained 36% of the variance in the change. Prolonged activation of the LH (Figure 1, PC2, 17%) and high activity of the RF in stance (PC3, 13%) were positively correlated with the change in gait velocity. High MG amplitude (PC1, 6%) was negatively correlated with the change.
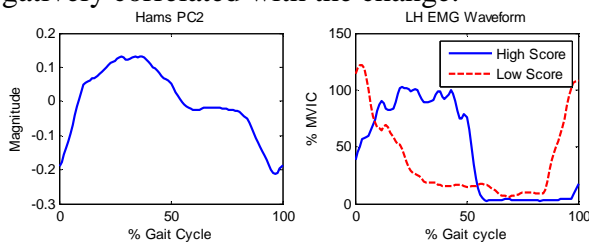

Figure 1: Left: PC2 for the hamstrings, capturing prolonged activation. Right: Waveforms for two participants with high and low *scores* for PC2.

The first two PCs for the KAM explained 97% of the variance in waveforms. PC1 captured the overall magnitude, and PC2 captured the magnitude of the KAM during mid-stance. There was no significant difference in PC1 *scores* from pre to post-TKR (p>0.05). The PC2 *scores* significantly decreased (p=0.002), showing a decrease in the magnitude of the mid-stance KAM. Five PC *scores* explained 58% of the variance in the change in midstance loading (PC2). Similar to velocity, prolonged LH activation (PC2) explained 31% of variance, and high RF activity in stance (PC3) explained 8%.

DISCUSSION

Prolonged LH activation (PC2) was the greatest predictor of changes in velocity and loading. This PC has been reported for participants with severe knee OA and is associated with antagonist co-activation (Hubley-Kozey et al. 2008). The KAM PCs from this study are similar to those in the literature for participants with knee OA

(Landry et al. 2007). As the KAM has been linked to medial compartment loading (Schnitzer et al, 1993), a change in the magnitude of the midstance moment (PC2) may indicate reduced loading of the joint.

These results provide evidence that patients with more typical EMG profiles have less improvement in objective measures of function and loading post-TKR, whereas those with altered profiles have greater objective improvement. This contrasts previous studies linking higher pre-TKR function to higher post-TKR function (Lingard et al. 2004, Mizner, 2005).

SUMMARY

Pre-TKR EMG patterns predicted pre- to post-TKR changes in gait velocity and the KAM during mid-stance. Participants with greater alterations pre-TKR have a greater improvement in function, and a greater decrease in medial compartment joint loading post-TKR. Potential implications of these results are in triaging surgical waiting lists and in pre-operative management.

REFERENCES

Health Canada (2003). *Arthritis in Canada.* Ottawa: Health Canada.
Hubley-Kozey et al. (2008). *Clin Biomech* **23**,71-80.
Landry S et al. (2007) *J Biomech.***40**,1754-1761
Lingard E et al. (2004). *J Bone Joint Surg Am.* **86,** 2179-2186.
Mizner R et al. (2005). *J Rheumatol* **32,** 1533-1539
Schnitzer et el. (1993). *Arthritis Rheum* **41**,1233-1240
Sharma L et al. (2006). *Curr Opin Rheumatol* **18**, 147-156

ACKNOWLEDGEMENTS

INTERNAL FEMORAL FORCES AND MOMENTS DURING RUNNING: IMPLICATIONS FOR STRESS FRACTURE DEVELOPMENT

W. Brent Edwards [1], Jason C. Gillette [1] Joshua M. Thomas [2], and Timothy R. Derrick [1]

[1] Department of Kinesiology, Iowa State University, Ames, IA, USA
[2] Human Performance and Wellness Department, Trinity International University, Deerfield, IL, USA
E-mail: edwards9@iastate.edu   Web: www.kin.hs.iastate.edu

INTRODUCTION

Femoral stress fractures are among the most serious of overuse injuries. Certain femoral stress fractures have a tendency to displace and require surgical fixation (Visuri et al., 1988). Bone damage resulting from the fracture itself, as well as perioperative trauma can lead to avascular necrosis, osteoarthritis, and in some instances permanent handicap (Visuri et al., 1988).

In long-distance runners and military recruits femoral stress fractures commonly occur at the neck, medial proximal-shaft, and distal-shaft (Hershman et al., 1990; McBryde, 1985; Niva et al., 2005). The purpose of this study was to determine if the internal femoral forces and moments during running are associated with common sites of femoral stress fractures.

METHODS

Ten experienced male runners were recruited for this study (age 22.2 ± 3.2 yrs, height 1.8 ± 0.1 m, mass 69.8 ± 6.5 kg). Motion-capture (120 Hz) and force platform data (1200 Hz) were collected while subjects ran at their preferred running speed (4.4 ± 0.5 m/s). Kinematics of the thigh, leg, and foot were calculated and inverse dynamics were used to obtain joint reaction forces and joint moments at the hip, knee, and ankle.

Kinematic data were imported into a scaled SIMM 4.0 model to obtain maximal dynamic muscle forces, muscle moment arms, and muscle orientations at each 1% of stance. Static optimization was used to calculate individual muscle forces. The cost function to be minimized was the sum of squared muscle stresses. The optimization was constrained so that the resulting hip, knee, and ankle moments (hip flex/ext, abd/add, introt/extrot; knee flex/ext; ankle flex/ext) equaled experimental data.

Joint contact forces at the hip and knee were calculated as the sum of reaction force and muscle forces crossing the joint. Patella-femoral contact force was calculated as the resultant of the quadriceps and patella ligament forces. Internal femoral forces and moments were calculated at 11 equidistant points along a centroid path in accordance with Duda et al. (1997). Point 1 corresponded to the femoral neck and point 11 corresponded to the femoral condyle (Figure 1). The peak internal femoral loads were calculated and averaged across subjects.

Figure 1. Reference frames for femur points

RESULTS

The mean peak loads were as follows: anterior-posterior (AP) shear, -7.47 BW at point 11 (posterior); axial force, -11.40 BW at point 11 (compression); medial-lateral (ML) shear, -3.75 BW at point 1 (medial);
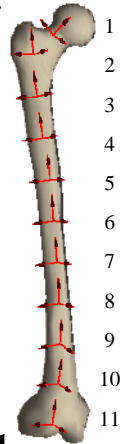
AP moment, -0.42 BWm at point 2 (medial-surface compression); torsional moment, -0.20 BWm at point 11 (external rotation); ML moment, -0.44 BWm at point 11 (anterior-surface compression) (Figure 2).

DISCUSSION

Our results suggest that frequently cited locations of femoral stress fracture can be explained biomechanically. The femoral neck is subjected to large ML shear forces. Although, axial forces and bending moments at the neck were not larger than those experienced by the rest of the femur, peak magnitudes occurred during the impact phase and were associated with a high rate of loading. The largest bending moments about the AP axis were observed at the proximal femur. The direction of this moment, combined with the axial compressive force would place the largest normal stress on the medial proximal-shaft. The largest AP shear forces, compressive axial forces, ML bending moments, and torsional moments were observed at the

distal-shaft. Overtime, these types of combined loads may pose a threat to skeletal integrity at these three locations.

SUMMARY

The mechanical loading environment of the femur appears to explain well the locations of femur stress fracture cited in the literature. As each of the three locations experience a relatively unique loading environment, several different mechanisms may be responsible for the development of femoral stress fracture.

REFERENCES

Duda GN (1997). *J. Biomech*, 30:933-941.
Hershman EB et al. (1990). *Clin Sport Med*, 9:111-119.
McBryde AM (1985). *Clin Sport Med,* 4:737-752.
Niva MH et al. (2005). *J Bone Joint Surg,* 87-B:1385-1390.
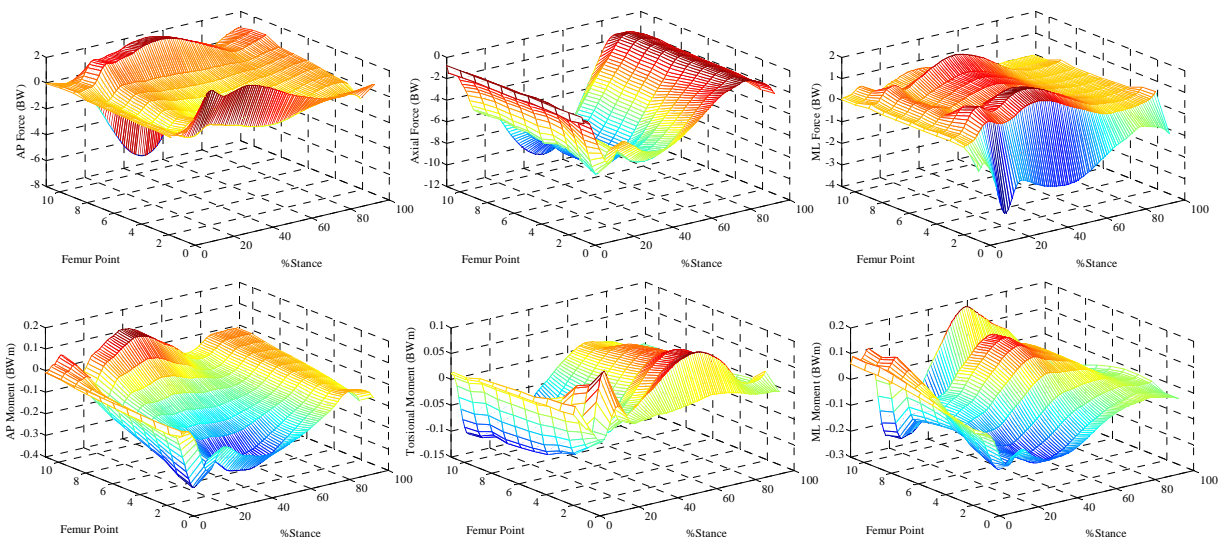Visuri T et al. (1988). *J Traum,* 28:1562-1569

Figure 2. Group ensemble internal forces and moments at the femur. Positive internal forces correspond to anterior shear, tension, and lateral shear. Positive internal moments correspond to lateral-surface compression, internal-rotation torsion, and posterior-surface compression.

DELETION OF NEBULIN ALTERS THE LENGTH-TENSION PROPERTIES OF NEONATAL SKELETAL MUSCLE

David S. Gokhin[1], Jianlin Zhang[2], Ju Chen[2], Richard L. Lieber[1]

[1]Departments of Bioengineering and Orthopaedic Surgery, [2]Department of Medicine, University of California-San Diego and Veterans Affairs Medical Center, La Jolla, CA 92093 USA
Email: rlieber@ucsd.edu, Web: http://muscle.ucsd.edu

INTRODUCTION

The magnitude of isometric stress production by skeletal muscle is predicted by the sliding filament theory and is described as the length-tension curve (LTC). The LTC is sensitive to actin thin filament length. As thin filament length increases, the shallow portion of the ascending limb of the LTC widens due to an increased domain of thin filament double-overlap. This results in an overall widening and rightward shift of the LTC (Granzier et al., 1991).

Nebulin is a large, rod-like protein (500-900 kDa) believed to act as a thin filament "ruler" that specifies thin filament length during sarcomere assembly (McElhinny et al., 2003). Nebulin-knockout (NKO) mice have thin filaments up to 25% shorter than wild-type (WT) mice, exhibit rapid postnatal myofibrillar degeneration, and die after about 1-2 postnatal weeks (Bang et al., 2006). Sliding filament theory predicts an altered LTC in NKO muscle. Therefore, the goal of this project was to test this prediction and better understand the role of nebulin *in vivo* by subjecting neonatal NKO and WT muscles to a series of functional physiological assays.

METHODS

Bilateral bone-tendon-muscle-tendon units associated with the gastrocnemius (GN) muscle from WT and NKO mice were used at postnatal days 1 (P1) and 7 (P7). Fatigue responses and LTCs were measured only at P1 to minimize the confounding effect of postnatal degeneration in NKO muscle.

Isometric contractions. GN muscles were transferred to a custom muscle-testing chamber filled with Ringer solution. Tendons were secured with silk suture. Slack muscle length (L_m) was measured using an eyepiece crosshair reticule. Fiber length (L_f) was computed as $0.46L_m$, where 0.46 is the characteristic L_f:L_m ratio for the mouse GN. The GN underwent maximal isometric stimulation using a 400-ms train of 0.3-ms pulses delivered at 100 Hz. Isometric force was measured 3 times with 2 min between contractions. After testing, GN muscles were weighed. Isometric stress was estimated by normalizing maximum isometric force to GN physiological cross-sectional area.

Fatigue responses. A series of 10 isometric contractions (Iso1-Iso10) was imposed at slack length. Fatigue was defined as a reduction in isometric stress production across the isometric exercise bout.

LTCs. Isometric contractions were imposed at slack length and then at a series of muscle lengths $\pm 0.2L_f$, $\pm 0.4L_f$, $\pm 0.6L_f$, $\pm 0.8L_f$, and $\pm L_f$ from slack length. Isometric stress was normalized to maximum isometric stress (to compute the fraction of peak tension), and muscle length was normalized to slack length (to compute relative muscle length). The fraction of peak tension was then plotted as a function of relative muscle length, and parabolic regression was applied. An applet

written in MATLAB computed the optimum relative muscle length (L_{opt}) and full-width at half-maximum (FWHM) of each parabola.

Statistics. Comparisons were made using the unpaired Student's t-test. Data are shown as mean±SEM, and significance was $P<0.05$.

RESULTS

The isometric stress produced by the WT GN increased ~2-fold from P1 to P7, whereas the stress produced by the NKO GN deteriorated by ~75% from P1 to P7, consistent with severe myopathy in NKO mice (Fig. 1).
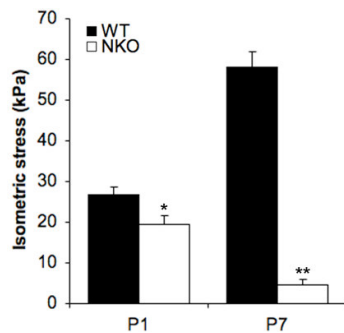
Figure 1. Isometric stress production in WT and NKO GN at P1 and P7. *, $P<0.05$; **, $P<10^{-7}$ compared to WT.

During 10 cyclic isometric contractions, the NKO GN consistently generated less stress than WT (Fig. 2). The WT GN exhibited no decline in stress production, whereas the NKO GN exhibited a ~20% decline (-0.5±0.9 kPa vs. -5.6±1.7 kPa, $P<0.05$).
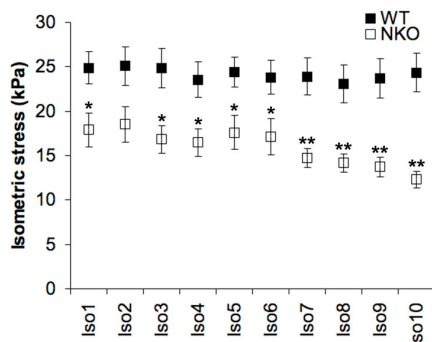
Figure 2. Fatigue responses of WT and NKO GN. *, $P<0.05$; **, $P<0.01$ compared to WT.

The LTC of the NKO GN was narrower than the WT GN and shifted leftward, consistent with shorter thin filaments (Fig. 3). Parabolic regression analysis of the LTCs verified these observations quantitatively, with reduced L_{opt} and FWHM in the NKO GN (Table 1).
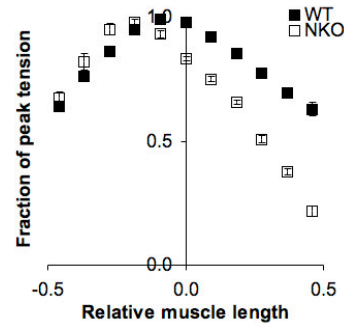
Figure 3. LTCs of WT and NKO GN at P1.

Parameter	WT	NKO
L_{opt}	-0.025±0.008	-0.160±0.014**
FWHM	1.10±0.02	1.02±0.02*

Table 1. Parabolic regression analysis of LTCs. *, $P<0.01$; **, $P<10^{-5}$ compared to WT.

DISCUSSION

These data confirm the severe functional consequences of nebulin deletion in skeletal muscle. The LTC of the NKO GN was consistent with reduced thin filament length. Future work will use site-specific mutagenesis to tease apart the particular *in vivo* functions of individual nebulin protein domains.

REFERENCES

Bang ML et al. (2006). *J Cell Biol*, 173:905-916

Granzier HL et al. (1991). *Am J Physiol*, 260:C1060-C1070.

McElhinny AS et al. (2003). *Trends Cardiovasc Med*, 13:195-201.

ACKNOWLEDGEMENTS

STRATEGIES FOR BALANCE MAINTENANCE DURING SIT-TO-STAND MOVEMENT IN ELDERLY PEOPLE

Masahiro Fujimoto[1,2], Shintaro Beppu[1], Kazuya Okubo[1], Toru Fujii[1] and Li-Shan Chou[2]

[1] Department of Mechanical Engineering, Doshisha University, Kyoto, JAPAN
[2] Department of Human Physiology, University of Oregon, Eugene, Oregon, USA,
Email: chou@uoregon.edu, Web: http://biomechanics.uoregon.edu/MAL/index.html

INTRODUCTION

Sit-to-stand (STS) movement is one of the daily activities that the elderly feel anxiety of falling (Tinetti et al., 1990). It requires a precise shifting of the center of mass (COM) to maintain balance. In addition, it demands significant muscular power at the knee, which depends on the COM position and acceleration. The COM acceleration also determines dynamic limits of balance control. Therefore, COM position and its acceleration are important factors governing STS movement. The objectives of this study were to investigate balance control during STS and to identify the differences in strategies for STS in terms of COM position and acceleration between elderly people with and without difficulty in STS in order to reveal underlying causes of the difficulty. Applying a concept of dynamic stability area (DSA), the relationship between the COM and the DSA was investigated.

METHODS AND PROCEDURES

Ten subjects participated in this study: 6 young males (Young (NORM), mean age = 22.7±1.2 years) and 4 elderly people (with 2 having difficulty in STS, Elderly (DIFF), and 2 healthy elderly, Elderly (NORM); mean age = 80.5±3.5 and 81.0±1.4 years, respectively). All subjects were asked to stand up from a 40 cm high chair as they normally do. Each subject performed 5 trials. Motion data was captured with a motion analysis system (Motion Analysis Corp.). Markers were placed on the subject's bony landmarks

according to Helen Hayes marker set (Kabada et al, 1990), as well as the estimated position of the hip joint and the fifth metatarsal bone. Two forceplates (AMTI) were used to collect floor reaction forces (FRF) for the calculation of center of pressure (COP). Net joint moments acting at the ankle, knee, and hip were estimated with inverse dynamics using a rigid link model defined by markers. The DSA was derived based on an inverted pendulum model (Fig.1; Mourey et al, 2000):

$$X_h - A\ddot{X} \leq X \leq X_t - A\ddot{X} \qquad (1)$$

where X indicates the COM position in the antero-posterior (A-P) direction, $\ddot{X}$ indicates its acceleration, and $A = l/g$. X_h and X_t indicate the heel and toe position, respectively. The relationship when $\ddot{X}$ is zero defines the static stability area (SSA), the area within the base of support.

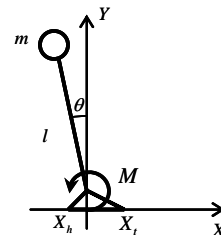**Figure 1.** Model of simple inverted pendulum

RESULTS AND DISCUSSION

The relationship between the COM position and its acceleration (both were normalized to the foot length) at the instant of seat-off is shown in Fig.2. The area between 0 and 100 indicates the SSA, and the area within two solid lines indicates the DSA. All but three trials preformed by Young (NORM) and Elderly (NORM) were located in the DSA

region, whereas all trials preformed by Elderly (DIFF) were located within the SSA. Elderly (DIFF) were found to stand up with a greater trunk forward bending angle than Elderly (NORM) and Young (NORM) (51.2±5.3, 24.0±5.2, and 21.1±5.2 deg from vertical line, respectively) and with a smaller COM acceleration than Elderly (NORM) and Young (NORM), which allow them to control the COM motion within the SSA.
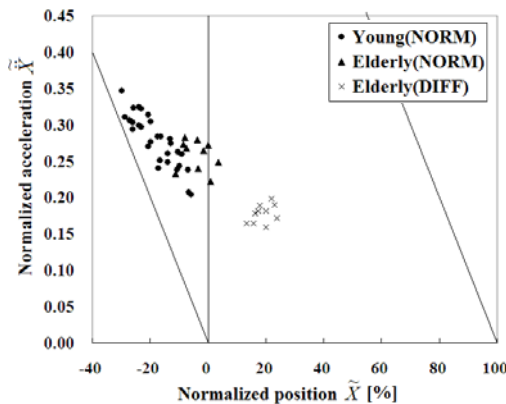
Figure 2. Relationship between normalized COM position and acceleration at the instant of seat-off.

Elderly (DIFF) were further found to demonstrate greater hip and ankle joint moments and a smaller knee joint moment at seat-off when compared to those of the healthy groups (Fig.3). Furthermore, the A-P COP displacement of Elderly (DIFF) was higher than those of Elderly (NORM) and Young (NORM) (Fig.4).
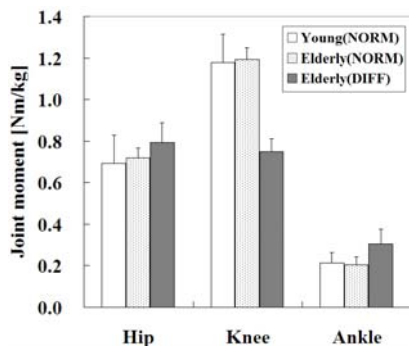
Figure 3. Joint moments at the instant of seat-off. The values were averaged for both legs and normalized by their body weight.

It is reasonable to expect that Elderly (DIFF) bent their trunk forward at seat-off to shift the COM to a more anterior position and achieve a more statically balanced posture, which results in a shorter moment arm for the knee joint.
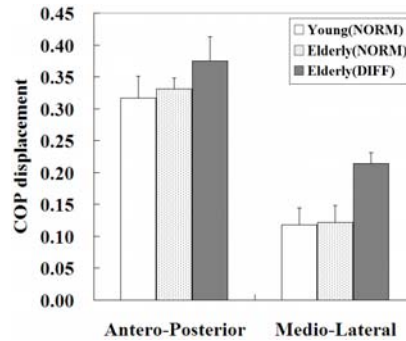
Figure 4. COP displacement in the antero-posterior and medio-lateral directions.

SUMMARY

Findings from this study suggest that elderly people having difficulty in STS have to carefully perform the task with a controlled COM position and acceleration that ensures a static stability (located in the SSA). A strategy of bending the trunk further forward was identified, which allows the Elderly (DIFF) to maintain the COM motion within the SSA and decreases the muscle demand at the knee.

REFERENCES

Tinetti, M.E., et al. (1990),
    J.Gerontol. Psychol. Sci., 45-6, 239-243.
Kadaba, M. P., et al. (1990),
    J. Orthop. Res., 8, 383-392.
Mourey, F., et al. (2000),
    J.Gerontol. Bio. Sci., 55A-9, B425-B431.

ACKNOWLEDGEMENTS

AN IN-VIVO EXAMINATION OF THE EFFECT OF FEMORAL TUNNEL PLACEMENT DURING ACL RECONSTRUCTION ON TIBIAL ROTATION

[1]Stavros Ristanis, [1]Eleftheria Siarava, [2]Nick Stergiou and [1]Anastasios D. Georgoulis

[1]Orthopaedic Sports Medicine Center, University of Ioannina Medical Center, Ioannina, Greece
[2]HPER Biomechanics Laboratory, University of Nebraska at Omaha, Omaha, USA
URL: http://biomech.unomaha.edu; nstergiou@unomaha.edu

INTRODUCTION

Our recent in-vivo studies have demonstrated abnormal tibial rotation after ACL reconstruction during high demanding activities [Ristanis et al, 2006; Stergiou et al, 2007]. In-vitro studies have supported these findings and examined possible causes for this phenomenon such as the effects of the ACL graft's configuration and placement at the knee [Woo et al, 2002]. They reported that the inability of the ACL reconstructed knee to control rotational loads probably occurs because the commonly used single-bundle surgical procedure places the femoral bone tunnel at the so-called 11 o'clock position for the right knee. This placement replicates the origin of the anteromedial bundle of the ACL, but not the posterolateral bundle, which is important for knee stabilization against rotational loads. Thus, it has been proposed that a more horizontal placement of the graft can address abnormal tibial rotation after an ACL reconstruction. However, this proposition has not been tested with in-vivo studies that can identify how rotational kinematics is affected. Our goal was to investigate the effect of femoral tunnel placement, at (a) laterally and more horizontally at the 10 o'clock position and (b) at the standard 11 o'clock, on tibial rotation after ACL reconstruction with a bone-patellar tendon-bone (BPTB) graft.

METHODS AND PROCEDURES

Twenty patients who underwent an ACL reconstruction with a BPTB graft were randomly assigned in two groups (Group A and B). Group A consisted of ten patients that the femoral tunnel was placed at 10 o'clock, while group B of ten patients where the femoral tunnel was placed at the 11 o'clock. Ten healthy matched subjects formed the control group. Kinematic data were collected (50Hz) with an 8-camera optoelectronic system, while the subjects performed two activities: (1) descend from a stairway and subsequent pivoting, and (2) land from a platform and subsequent pivoting. After foot contact from the descend or the landing, the subjects were instructed to pivot on the landing (ipsilateral) leg at 90º and walk away. Pivoting was performed on both legs. To better analyze our kinematic data, we had a simultaneous recording of the signal describing the key events of the patient's gait cycle with inline foot switches. To further validate our procedures, an additional trial was recorded with the subject in the anatomical position, which was used as the reference for the calculation of the anatomical angles. Based on our hypothesis, the dependent variable examined was the range of motion of tibial rotation during the pivoting period of the two tasks. The selection of the range of motion as the dependent variable eliminated possible errors reported in the literature that used absolute measures (i.e. maximum). A one-way ANOVA was performed on the group means to identify differences between Groups A and B, and the healthy control. Post-hoc analysis was

performed if significant differences were identified. Paired t-tests were performed within the two groups to compare the ACL reconstructed leg with the intact.
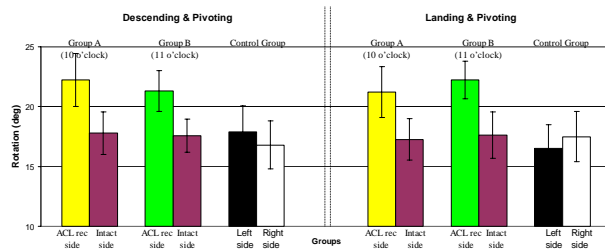

Figure 1. Group means and SDs for range of motion of tibial rotation during the evaluation period for both activities.

RESULTS

Negative Lachman and pivot shift tests, along with KT-1000 results, indicated that the knee joint stability was regained. The one-way ANOVA showed the existence of significant differences among the groups in both examined activities [(F=6.918; p=0.003) for landing and pivoting and (F=8.948; p=0.001) for descending stairs and pivoting] (Fig. 1). The post-hoc comparisons revealed a) significantly more tibial rotation in the ACL reconstructed leg in both groups and for both activities as compared to the control, b) significantly more tibial rotation in the ACL reconstructed leg within both groups and for both activities as compared with the intact leg c) no significant differences for the ACL reconstructed leg between the two groups.

DISCUSSION

Our results refuted the hypothesis that a more horizontal placement of the femoral tunnel of the BPTB graft during an ACL reconstruction will restore the increased tibial rotation found during dynamic activities that produce higher rotational loads at the knee. It seems that a single-bundle ACL reconstruction placed at either the 10 or 11 o'clock position can not

fully restore the complex structure of the ACL and adequately resist dynamic rotational loading. Our results are also supported by an in-vitro investigation by Loh et al [Loh et al, 2003] where it was found that neither femoral tunnel position could completely restore the kinematics and the in situ forces to the level of the intact knee. An alternative solution could be to reconstruct the two bundles separately. Actually, several surgeons have started in the last few years to perform double-bundle reconstructions in order to replicate the exact anatomy of the ACL and solve the problem of abnormal rotational kinematics that also seems to correlate with the initiation of knee degeneration [Asano et al, 2004]. So far only in-vitro studies have reported results of this reconstruction which are very encouraging [Yagi et al, 2007]. However, the superiority of this procedure in restoring abnormal tibial rotation during dynamic activities has not been investigated in-vivo. Furthermore, our results need to be verified for other grafts such as the quadrupled semitendinosus/ gracilis tendon graft.

REFERENCES

Ristanis S et al. (2006). *CJSM,* 16(2):111-6.
Stergiou N et al. (2007). *Sports Med,* 37(7): 601-13.
Woo SL et al. (2002). *JBJS Am,* 84(A): 907-914.
Loh JC et al. (2003). *Arthroscopy,* 19(3): 297-304
Asano H et al. (2004). *Arthroscopy,* 20(5): 474-481
Yagi M et al. (2007). *CORR,* 454(1): 100-7

ACKNOWLEDGEMENTS

MULTIVARIATE CONSERVATIVE GAIT PATTERN IN DIABETES

James S. Wrobel, DPM, MS[1]; Ryan Crews, MS[1]; and John Connolly, DPM[2]

[1]Center for Lower Extremity Ambulatory Research at Scholl College of Podiatric Medicine, Rosalind Franklin University of Medicine and Science, North Chicago, Illinois, USA, james.wrobel@rosalindfranklin.edu; http://diabeticfootonline.com
[2]VAM&ROC White River Junction, Vermont, USA

INTRODUCTION

Patients with diabetes and peripheral neuropathy (DMPN) exhibit gait instability. While appearing trivial, gait unsteadiness demonstrated a strong association with depressive symptoms. Fearful walkers adopt a slower walking speed, shorter stride length, and longer double support time than fearless walkers. Similar gait patterns have been described in patients with diabetes and DMPN patients. While intuition suggests patients with diabetes adopt a more conservative gait pattern to make them feel more stable, they remain at higher risk for falls. A recent study accounted for multiple domains of falls and diabetes, gait, and balance remained as significant independent predictors in the final model.(Maurer, Burcham et al. 2005) The purpose of this study is to use a multivariate approach to describe the conservative gait pattern in diabetes patients.

METHODS AND PROCEDURES

This study took place from July 2000 to May 2001 at the Veterans Affairs Medical and Regional Office Center, White River Junction, VT. Male patients with diabetes without a history of foot surgery were asked to enroll. Two examiners were trained to assure standardization of exam techniques. Inter-rater reliability of ankle and 1st metatarsal phalangeal joint (1st MPJ) motion was 0.71 and 0.95 respectively. Apropulsive gait was defined visually by the absence of ankle plantarflexion during the propulsive phase of gait. Maximum peak plantar pressures were measured using the F-Scan mat system, version 4.12F (Tekscan, Boston, MA) using the average of five steps. The sampling frequency was 50 Hz. For univariate analyses, Fisher's Exact Test was used for dichotomous data and oneway analysis of variance for continuous data. The multivariate model was built using a forward stepwise logistic regression. Of the 152 patients, 40 patients exhibited the conservative gait pattern. Based on this, we nominated 4 *A Priori* covariates for our regression model.(age, neuropathy, and range of motion at the ankle and 1st MPJ)

RESULTS

Patients with the conservative gait pattern had lower walking speed and decreased stride length compared to normal gait.(0.68 m/s v. 0.91 m/s, $p=0.0000$; 1.04 m v. 1.24 m, $p=0.0000$) Age, neuropathy, and Romberg's sign were significantly higher; and ankle mobility was significantly lower in the conservative gait pattern group.(Table) In the multivariate analysis; age, ankle joint mobility, and callus were retained in the final model. This model described 17% of the variance. In a stepwise fashion, age described 8.2% of the variance. Ankle joint mobility and callus described 3.4% and 1.4% of the variance respectively.

DISCUSSION

The prevalence of conservative gait in our cohort of elderly diabetic veterans was 26%. Thinking that neuropathy would lead to fearful walking, we were surprised that neuropathy was not retained in the model. We were equally surprised that Romberg's

sign was not retained as this may represent more advanced neuropathy. These findings are also supported by Mueller and colleagues.(Mueller, Minor et al. 1994) Our approach addressed invited commentary to Mueller et al. suggesting that neuropathy-free and patients not affected by foot ulcer treatment be included. Our study has limitations. The cross-sectional design and secondary analyses make causal attribution problematic. Neuropathy definitions were coarse. This study has clinical implications for callus care and exercise training in this population. (Richardson, Sandman et al. 2001; Balducci, Iacobellis et al. 2006)

SUMMARY

The results of our multivariate analysis of conservative gait in diabetes patients suggest that benefits previously observed from exercise training DMPN patients might be from increased ankle mobility or strengthening rather than reversal of lost sensory afferent deficits.

References

Balducci, S., G. Iacobellis, et al. (2006). "Exercise training can modify the natural history of diabetic peripheral neuropathy." J Diabetes Complications **20**(4): 216-23.

Maurer, M. S., J. Burcham, et al. (2005). "Diabetes mellitus is associated with an increased risk of falls in elderly residents of a long-term care facility." J Gerontol A Biol Sci Med Sci **60**(9): 1157-62.

Mueller, M. J., S. D. Minor, et al. (1994). "Differences in the gait characteristics of patients with diabetes and peripheral neuropathy compared with age-matched controls." Phys Ther **74**(4): 299-308; discussion 309-13.

Richardson, J. K., D. Sandman, et al. (2001). "A focused exercise regimen improves clinical measures of balance in patients with peripheral neuropathy." Arch Phys Med Rehabil **82**(2): 205-9.

Descriptive characteristics	Conservative Gait	Normal Gait	p-value
N	40	264	
Age (mean yrs)	73.1	66.2	0.0000
Insulin (% yes)	36	28	0.3450
HgbA1c (%)	7.89	7.64	0.2896
DM Duration (mean yrs)	9.5	10.1	0.7272
Smoking History(% yes)	92	82	0.1126
Height (mean inches)	68.5	68.4	0.9505
Weight (mean lbs)	212	211	0.8497
1st MPJ ROM (mean degrees)	12.1	14.2	0.1344
Bunion deformity (% yes)	18	17	1.0000
Hammer toe (% yes)	51	37	0.1142
Non-palpable pulse (% yes)	59	43	0.0599
Monofilament insensitivity (%)	46	27	0.0223
Absent joint position sense (%)	5	2.6	0.3450
Ankle ROM (mean degrees)	3.6	5.6	0.0059
Callus (% yes)	49	36	0.0793
Fat pad atrophy (% yes)	31.4	47.1	0.1158
Stride length (mean meters)	1.04	1.24	0.0000
Walking speed (mean m/s)	0.68	0.91	0.0000
Peak Pressure (kg/cm^2)	3.81	3.87	0.7449

DETERMINATION OF PRONATION PARAMETERS BY MIDSOLE DEFORMATION IS INDEPENDENT OF RUNNING VELOCITY

Torsten Brauner, Thomas L. Milani, Thorsten Sterzing, Doris Oriwol

Department of Human Locomotion, Chemnitz University of Technology, Chemnitz, Germany
torsten.brauner@phil.tu-chemnitz.de

INTRODUCTION

Since rearfoot motion is discussed to be related to overuse injuries in running its analysis has become mandatory in running studies. Various direct (motion analysis systems) and indirect (electrogoniometers) measurement devices have been used to determine rearfoot motion parameters. Recently, two innovative indirect systems have been developed based on the findings of Hennig & Milani (2000). They found a load shift in the rearfoot area from lateral to medial during early ground contact. This load shift can be identified by usage of discrete pressure sensors under the heel (Brauner et al., 2008) or by measuring local midsole deformations by use of Hall sensors (Milani et al., 2008). Both strategies require the calculation of an algorithm to determine maximum pronation and pronation velocity. However, rearfoot motion (Nigg, 1987), impact forces, and pressure distribution (Hennig & Milani, 2000) depend on running velocity. Usage of pressure distribution to determine rearfoot motion has been shown to be reasonable independent of running velocity (Brauner et al., 2008). The goal of this study is to analyze the effect of different running velocities on rearfoot motion calculation from local midsole deformations.

METHODS AND PROCEDURES

13 male (25.0yrs $\pm$2.8, 71.5kg $\pm$7.8) runners took part in the testing. All subjects were familiar with the laboratory testing conditions and categorized as heel-toe runners. Running velocity conditions were 2.9, 3.2, 3.5, 3.8, and 4.1m/s ($\pm$0.1). Speeds were controlled by three photoelectric barriers and executed in randomized order. Subjects performed five repetitive trials for each velocity condition on a runway across an integrated KISTLER force plate (9287BA). All subjects used an EVA test shoe with 10 Hall sensors placed within the EVA midsole around the heel cup (Milani et al., 2008). Deformation data were collected and post processed according to Milani et al. (2008). As additional reference an electrogoniometer was used to measure pronation (TPR_{Gonio}) and maximum pronation velocity (MPV_{Gonio}) (Milani & Hennig, 1995). To calculate pronation (TPR_{Hall}) and maximum pronation velocity (MPV_{Hall}) the necessary algorithms were determined for the running velocity of 3.5m/s and then applied to the deformation data of the other velocity conditions. For statistical validation of the algorithms, Pearson's correlation coefficients were calculated by correlating goniometer pronation values with the pronation values determined by the Hall sensors.

RESULTS

In accordance to the literature, TPR_{Gonio}, MPV_{Gonio}, impact force, and tibial acceleration increased highly significantly with increased running velocity (p<0.001). TPR_{Hall} and MPV_{Hall} data showed similar patterns (Figure 1).
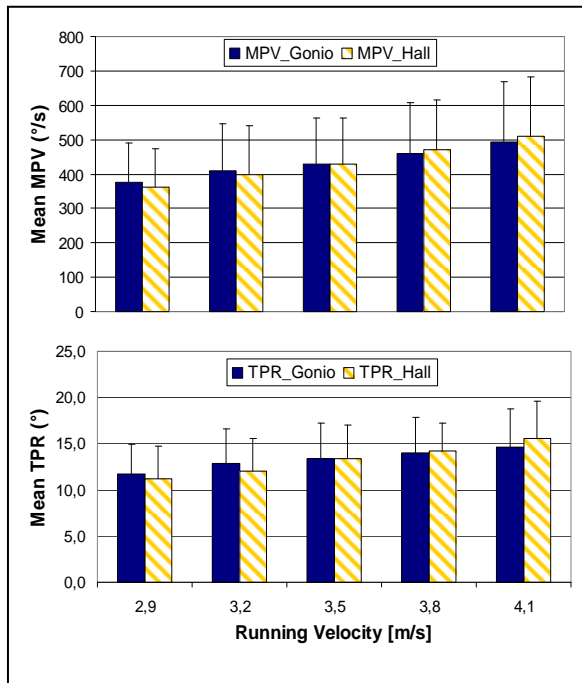
Figure 1: Velocity dependency of TPR and MPV determined by goniometer and Hall sensors (n=13)

Correlation coefficients calculated by comparing goniometer and Hall sensor data at different running velocities confirm this observation (Table 1).

Parameter	Velocity Ranges (m/s)			
	2.9 (±0.1)	3.2 (±0.1)	3.8 (±0.1)	4.1 (±0.1)
MPV	0.857	0.861	0.825	0.794
TPR	0.820	0.846	0.793	0.666

Table 1: Coefficient of correlation of rearfoot motion determined by goniometer and Hall sensors (n=13)

DISCUSSION

The algorithms to calculate TPR and MPV using local midsole deformations developed by Milani et al. (2008) proved to be also valid at changing shock parameters due to different running velocities. Hennig &

Milani (2000) observed that higher running velocities lead to higher local loading peaks. However, they also showed that these peaks occur earlier in time. This reciprocal behaviour facilitates the determination of pronation parameters by deformation values at different running velocities, since maximum deformation peaks and the corresponding times to maximum deformation are used in the algorithm to calculate rearfoot motion.

SUMMARY

Considering the velocity range of recreational heel-toe running (2.7 - 4.2m/s), midsole deformation can be used to calculate rearfoot motion parameters such as pronation and maximum pronation velocity in a modified EVA shoe. Additional data of midsole deformations of the forefoot might improve the algorithm at higher running speeds.

REFERENCES

Brauner, T et al. (2008). Submitted to *ESM 2008,* Dundee, Scotland.
Hennig, EM & Milani, TL (2000). *Sportverletz Sportschaden.* 14: 90-97.
Milani, TL et al. (2008). Submitted to *NACOB*, Ann Arbor, Michigan, USA.
Nigg, B et al. (1987). *J. Biomech.* 10: 951-959.

ACKNOWLEDGEMENTS

DURATION OF PRONATION PERIOD DURING GROUND CONTACT IN HEEL-TO-TOE RUNNING

Jens Heidenfelder, Thorsten Sterzing, David Schreiter, Thomas L. Milani

Department of Human Locomotion, Chemnitz University of Technology, Chemnitz, Germany,
jens.heidenfelder@phil.tu-chemnitz.de

INTRODUCTION

Pronation may be considerably influenced by footwear (Bates et al. 1979). Therefore, different shoe constructions are built to control rearfoot motion and protect against excessive pronation and high pronation velocities. Hintermann et al. (1994) reported that excessive pronation and induced tibial rotation might lead to overuse injuries. However, duration times of maximum pronation were not yet in the focus of investigations. Longer duration may result in prolonged loading of the achilles and the patella tendon and might therefore be the cause of running-related overuse injuries. Thus, the goal of the study was to investigate duration times of peak pronation in different shoe conditions.

METHODS AND PROCEDURES

Twenty male and injury-free recreational runners (age: 24.8 ± 2.5 years, height: 177.7 ± 5.8 cm, weight: 72.2 ± 6.9 kg) participated in this study. Running speed was set to 3.5 m/s (± 0.1). Data of each subject was collected for a total of five trials over a Kistler force platform. Three running shoes of the categories cushioning (CU), motion control (MC), and low profile (LP) were used. Pronation and supination was measured with an electrogoniometer (Milani et al. 1995) during ground contact time (GCT).
A digital filter was applied to the rearfoot motion (RF-motion) data before traditional parameters were calculated, such as total pronation (TPR), maximum supination angle at foot strike (MSA), maximum pronation (MPA) as well as maximum pronation velocity (MPV).

To determine pronation duration a new parameter was defined describing subjects' individual total pronation (Fig.1). Two relative levels, 80% (DTP80) and 90% (DTP90) of total pronation were analyzed. Finally, the analyzed parameters were normalized to individual ground contact time to get the relative pronation duration in percentage of ground contact time: RDTP80 and RDTP90, respectively.
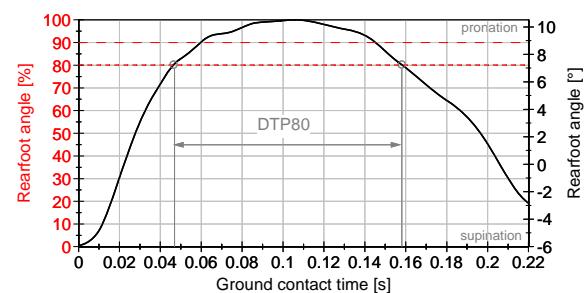
Figure 1: Definition of pronation duration during stance phase

To compare the effect of different shoe conditions, means of five repetitive trials were calculated and analyzed by using repeated measures ANOVA and Post-Hoc tests according to Fisher's LSD. Cluster analysis was performed to identify different pronation duration groups among subjects.

RESULTS

shoe	MSA [°]	MPA [°]	TPR [°]	DTP80 [ms]	DTP90 [ms]
CU	-4.6 (2.6)	8.5 (2.8)	13.1 (2.9)	108 (27)	66 (32)
MC	-4.0 (2.5)	7.5 (2.6)	11.5 (2.7)	116 (37)	73 (36)
LP	-5.8 (2.3)	7.1 (2.5)	12.9 (3.1)	99 (32)	68 (33)
p	<0.01	<0.01	<0.01	=0.10	=0.52

Table 2: mean (SD) of RF-motion parameters

Regarding the traditional rearfoot parameters in running highly significant differences between shoe conditions could be observed.

For all shoe conditions no significant differences were found for RDTP80 as well as RTDP90 (Fig. 2). Furthermore, positive correlation coefficients were found for these parameters (MC: r=0.74, LP: r=0.97, CU: r=0.66).
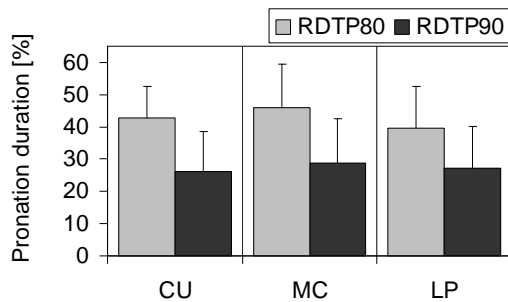
Figure 2: Pronation duration at 80% (90%) of subject's individual total pronation rate

Since the general pattern of pronation duration is not different for RDTP80 and RDTP90 only RDTP80 values are dicussed in further analysis. High interindividual variability is present for the duration time. RDTP80 ranges from 13% up to 71% of ground contact time. Across all shoe conditions subjects reached DTP80 after $42(\pm11.5)$ ms and stayed for a mean period of $108(\pm32.5)$ ms in this position. Cluster analysis with average linkage between groups results in three clusters (Tab. 1).

cluster	1	2	3
range	< 35%	35 - 50%	> 50%
n	3	15	2
Ø (SD)	23.9 (4.4)	44.7 (4.1)	57.4 (3.0)

**Table 1:** cluster analysis for RDTP80 across subjects for mean of shoes (n=20)

The majority of the cases (n=15) is grouped in Cluster 2 in a range of 35% to 50% of RDTP80.
No correlations were found between RDTP80 (RDTP90) and traditional rearfoot motion parameters.

DISCUSSION

The average duration pronation period (>80%) starts directly after impact peak and is present until the middle of take off phase after active peak of the vertical ground reaction force during heel-to-toe running. Traditional rearfoot motion parameters were analyzed to be highly significant different between shoe conditions. No significant difference was found between shoe conditions comparing the parameters relative duration of total pronation (80% and 90%). Therefore, these parameters seem to be independent from shoe construction and traditional rearfoot motion parameters. As pronation duration also considers pronation when the heel has already left the ground, modifications of the heel area between shoe conditions most likely have only minor effects on this parameter. Positive correlations between RDTP80 and RDTP90 show that one parameter is sufficient for a general discussion.

SUMMARY

Pronation duration of 80% and 90% was analyzed as a new distance running parameter. For complete assessment of pronation behaviour it seems to be important to discuss also the duration next to the maximum pronation angle and total pronation. In further studies, the relationship between pronation duration and running-related injuries should be investigated. Also, anthropometrical data like foot type and lower extremity alignment should be considered with respect to pronation duration.

REFERENCES

Bates BT et al. (1979). *Am J Sports Med*, 6: 338-342.
Hintermann B et al. (1994). *Clin Biomech*, 9: 349-355.
Milani TL et al. (1995). *J Appl Biom,* 11: 117-187.

ACKNOWLEDGEMENTS

IMPROVING VMO FUNCTION UNLOADS LATERAL CARTILAGE WITHIN THE PATELLOFEMORAL JOINT

John Elias[1], Srianjana Kilambi[1], Derek Goerke[1] and Andrew Cosgarea[2]

[1]Medical Education and Research Institute of Colorado, Colorado Springs, CO, USA,
elias@meric.info
[2]Department of Orthopaedic Surgery, Johns Hopkins University, Baltimore, MD, USA

INTRODUCTION

Patellofemoral pain is commonly attributed to lateral malalignment, which can lead to overloading of the lateral cartilage and subsequent areas of degeneration, or lesions. Impaired function of the vastus medialis obliquus (VMO), as either weakness or delayed activation, is believed to contribute to lateral malalignment. Although physical therapy regimens commonly focus on improving VMO function, the biomechanical benefit of improved VMO function has yet to be established. The current hypothesis is that improving VMO function will unload lateral cartilage, both when the cartilage is intact and in the presence of a lateral lesion.

METHODS AND PROCEDURES

Ten cadaveric knees were tested in vitro to characterize the influence of VMO function on patellofemoral loading. Each knee was secured to a testing frame with the femur horizontal. Loads were applied to represent the VMO, the vastus lateralis (VL), and the combination of the vastus intermedius, the vastus medialis longus, and the rectus femoris (VI/VML/RF). Loading cables connected to dead weights over pulleys were clamped to the quadriceps muscles at their insertion sites on the patella, with the anatomic orientations of the VMO, VL and VI/VML/RF reproduced on the testing frame.

The quadriceps muscles were loaded to represent a normal quadriceps force distribution, a weak VMO and a VMO with delayed activation. Previously published muscle extension moments for patients with pain and normal subjects (Makhsous et al., 2004; Zhang et al., 2003) were input into a computational model (Elias and Cosgarea, 2007) to determine the force applied by each muscle for each case. For the normal quadriceps force distribution, 420 N, 116 N, and 60 N were applied through the VI/VML/RF, the VL and the VMO, respectively. For the weak VMO, the applied forces were 432 N, 127 N and 27 N, respectively. The delayed activation case used the same forces as the weak case, except with no force applied by the VMO. All loading conditions were applied at 40°, 60° and 80° of flexion. All tests were repeated after removing the cartilage within a radius of 6 mm from a point at the approximate center of the lateral facet of the patella.

Patellofemoral forces and pressures were measured using a calibrated sensor (K-Scan, Tekscan, Boston, MA). The lateral joint capsule was sectioned to insert the sensor. For each test, with the sensor loaded, the patellar ridge was palpated on the sensor. The maximum lateral and medial pressure and the percentage of the total force applied to the lateral cartilage were quantified. At each flexion angle, a two level repeated measures ANOVA showed if creating a lesion or varying the loading condition significantly ($p < 0.05$) influenced the output. A Student-Newman-Keuls test was used for comparisons between individual loading cases.

RESULTS

Increasing the force applied by the VMO unloaded lateral cartilage. The lateral force percentage varied significantly between all loading cases at each flexion angle (Fig. 1). Increasing the VMO force decreased the maximum lateral pressure (Fig. 2) and increased the maximum medial pressure (Fig. 3), with significant differences noted at each flexion angle. Creating a lateral lesion significantly increased the maximum lateral pressure at 60° and 80° of flexion.

DISCUSSION

For intact cartilage, restoring a normal VMO force lowered the maximum lateral pressure to the same level as the maximum medial pressure. For an increase in the VMO force, the increase in the maximum medial pressure was more consistent than the decrease in the maximum lateral pressure due to a slight increase in the total force as the VMO force was increased. Creating a lateral lesion increased the maximum lateral pressure at 60° and 80°. At 40°, the area of contact tended to be distal to the lesion. The decrease in the maximum lateral pressure as the VMO force increased was not more consistent when a lesion was present, although the average decrease tended to be larger due to the elevated pressure caused by the lesion.

SUMMARY

The current results indicate that eliminating VMO weakness and a delay in VMO activation can reduce pressure applied to overloaded cartilage. Improving VMO function can be particularly beneficial when overloading has led to lateral cartilage lesions.

REFERENCES

Elias J, Cosgarea A. (2007). *Sports Med Arthrosc*, 15: 89-94.
Makhsous M, et al. (2004). *Med Sci Sports Exerc*, 36: 1768-75.
Zhang LQ, et al. (2003). *J Orthop Res,* 21: 565-71.

ACKNOWLEDGEMENTS
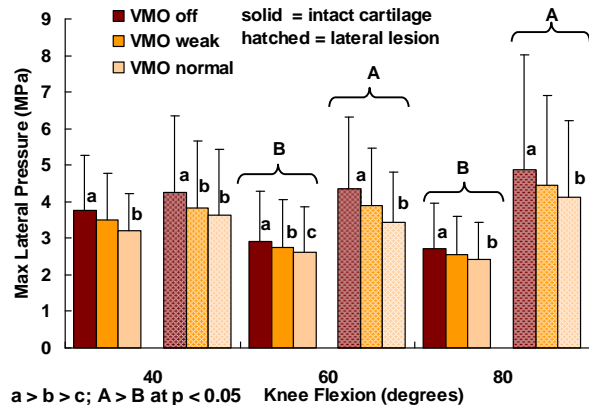
Figure 2: Average peak lateral pressure.

Figure 3: Average peak medial pressure.
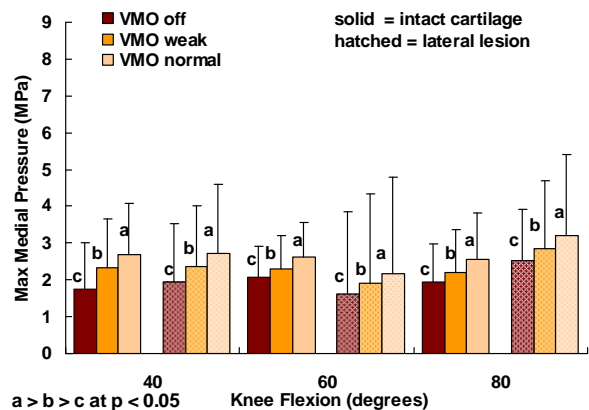

Figure 1. Average (± standard deviation) lateral force percentage for all tests.

IN-VIVO MEASUREMENT OF TIBIOTALAR JOINT MOTION: ACCURACY ASSESSMENT AND PRELIMINARY RESULTS

Sukhinder K. Bilkhu[1], Stephanie K. Kline[1], Mitch J. Mager[1], Jason J. Davis[2], Richard L. Needleman[2], Michael J. Bey[1]

[1]Bone & Joint Center, [2]Department of Orthopaedic Surgery, Henry Ford Hospital, 2799 W. Grand Blvd, Detroit, MI 48202, USA, sbilkhu1@hfhs.org

INTRODUCTION

Adult acquired flatfoot deformity (AAFD) is a chronic debilitating foot and ankle condition that is very common. It is often caused by posterior tibial tendon dysfunction, where the tendon no longer supports the navicular, causing a collapsed arch. AAFD is believed to cause a shift in tibiotalar joint contact patterns and eventually lead to arthritis. The ability to accurately measure foot and ankle motion and, in particular, tibiotalar joint contact patterns is critical to understanding the etiology and treatment of AAFD. The objectives of this study were to: 1) assess the accuracy of a model-based tracking technique for measuring in-vivo foot and ankle motion and 2) demonstrate the application of this technique by quantifying tibiotalar joint contact patterns.

METHODS AND PROCEDURES

In-Vitro Accuracy Assessment: To assess the accuracy of our technique for measuring in-vivo foot and ankle motion, a matched pair of fresh-frozen cadaveric lower legs was thawed to room temperature. Under flouroscopic guidance, three 1.6 mm diameter tantalum beads were inserted in both the tibia and talus. Biplane x-ray images were acquired as the specimen was manually moved to simulate plantarflexion, dorsiflexion and tibial rotation. Each trial was 2 seconds in duration, the biplane x-ray images were collected at 120 Hz, and 18 total trials were collected (2 specimens, 3 trials per motion). Following testing, CT images of the entire foot and ankle complex were acquired. The talus and tibia were manually segmented from surrounding tissues and reconstructed into 3D specimen-specific bone models.

The positions of the tibia and talus were tracked from the biplane x-ray images using a previously described model-based tracking technique (Bey 2006). Briefly, this method tracks the 3D position and orientation of each bone based on its 3D shape and density. For comparison, the position of each bone was also determined from the biplane x-ray images by tracking the implanted tantalum beads with an accurate (±0.1 mm) dynamic radiostereometric analysis (RSA) technique (Tashman 2003). These RSA data were used as the "gold standard" for this comparison. Accuracy of the model-based tracking technique was measured by comparing the 3D bead positions determined with model-based tracking to the 3D bead positions determined with dynamic RSA. Specifically, accuracy was quantified by calculating the RMS error between the two measurement techniques.

In-Vivo Human Testing: To demonstrate the utility of this measurement technique, we then tracked the position and orientation of the tibia and talus during gait from two male subjects. The subjects included one with no history of foot or ankle injury (i.e., a normal subject) and one with a clinical diagnosis of AAFD. The normal subject was tested once and the AAFD subject was tested twice: once with an arch-support orthotic in his shoe and

once without the orthotic. Each subject walked at a comfortable speed with their right foot centered in the biplane x-ray system's imaging field during the stance phase of the gait cycle. Following testing, CT scans of the entire foot/ankle complex were acquired for both subjects. 3D bone models of the tibia and talus were reconstructed from the CT images. The positions of the tibia and talus were then determined from the biplane x-ray images using model-based tracking.

Tibiotalar joint contact patterns were determined using a previously reported technique that combines the joint motion measured from the biplane x-ray images with the CT-based bone models (Anderst 2003). Specifically, this technique calculated the distance between the articulating surfaces of the tibia and talus at each frame of data. Tibiotalar joint contact was defined as occurring in those regions where the tibiotalar joint space was ≤ 2 mm. After defining an anatomical coordinate system for the talus with an axis bisecting the talar dome into medial and lateral aspects, we calculated a distance-weighted distribution of medial/lateral joint contact.

RESULTS

There was excellent agreement between the model-based tracking and dynamic RSA techniques. Specifically, the RMS error between the two measurement techniques was ±0.7 mm for both the tibia and talus.

The joint contact patterns demonstrated that the normal subject had a higher percentage of contact on the medial portion of the talar dome. In contrast, the AAFD subject experienced a more even distribution of contact between medial and lateral portions of the talar dome. This distribution of contact shifted slightly more medially with the addition of the orthotic (Figure 1, Table 1).
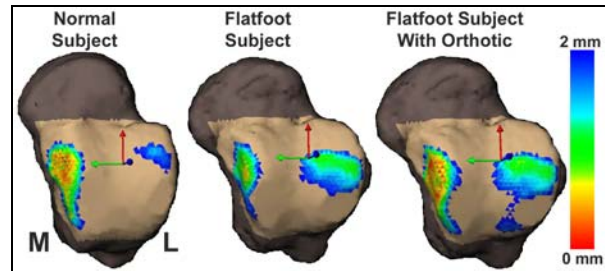
Figure 1. Tibiotalar joint contact patterns during the midstance phase of gait for a normal subject, flatfoot subject, and flatfoot subject with an orthotic. M=medial, L=lateral.

Condition	Medial	Lateral
Normal	83.2%	16.8%
Flat Foot	49.8%	50.2%
Flat Foot w/Orthotic	54.1%	45.9%

Table 1. Contact distribution between medial and lateral portions of the tibiotalar joint.

DISCUSSION

This study assessed the accuracy and demonstrated the utility of a technique for measuring in-vivo tibiotalar joint motion. The study indicated that the model-based tracking technique can measure the motion of the tibia and talus to an accuracy of within ± 0.7 mm. An analysis of the tibiotalar joint contact patterns suggests that this technique is sensitive to identifying subtle differences in joint mechanics between subjects. Future research will use this experimental approach to characterize joint contact patterns at the tibiotalar, talonavicular and subtalar joints. These data will be used to assess the etiology and treatment of AAFD and to improve upon the design of total ankle joint replacements.

REFERENCES

Anderst, W. J. and S. Tashman (2003). *Journal of Biomechanics* 36: 1291-1299.
Bey, M.J., R. Zauel, et al. (2006). *J Biomech Eng* 128(4): 604-9.
Tashman, S. and W. Anderst (2003). *J Biomech Eng* 125(2): 238-45.

EFFECTS OF AGING ON GAIT INITIATION WHEN COMBINED WITH A CHANGE OF DIRECTION

Evelyn Anaka[1-2] and Philippe Corbeil[1-3]

[1] Division de kinésiologie, Université Laval, Québec, Canada; [2] Unité de recherche en gériatrie de l'Université Laval (URGUL); [3] Centre d'excellence sur le vieillissement de Québec; Email : Philippe.Corbeil@kin.msp.ulaval.ca

INTRODUCTION

Gait initiation (GI) is the transition between quiet stance and steady state gait. Typically, when gait is initiated straight ahead, the body's net center of foot pressure (COP), which starts centered between the feet just anterior to the malleolus, first moves posteriorly towards the limb which will take the first step (swing limb), then shifts laterally towards the stance limb and finally anteriorly as the first step is taken (Mann et al. 1979). With this pattern, two main objectives of GI are fulfilled; the swing limb is unloaded to take the first step and the body's center of mass (COM) is accelerated anteriorly (Breniere et al. 1987).

It has been proposed that, for young adults (YA), the postural adjustments prior to the start of GI are modulated to generate the propulsive forces required to orient the COM displacement towards the desired direction of gait progression (Anaka and Corbeil 2007) as well as to reach the intended gait speed by the end of the first step (Breniere et al. 1987).

It has been shown that in older adults (OA), the COP's posterior shift at the start of GI generates less COM forward momentum then in YA (Polcyn et al. 1998). In addition, compared to YA, healthy OA take a shorter first step during GI (Mbourou et al. 2003).

The aim of this current study is to identify whether OA use the same strategies as YA to initiate gait towards different directions.

METHODS AND PROCEDURES

Healthy adults, aged 20 to 30 and 65 to 75 years old, initiated gait with their right (swing) limb towards five directions (-40°, -20°, 0°, 20° and 40°) at a normal and fast self-selected walking speed. When gait is initiated towards the positive directions, the swing limb is on the desired side of gait. When gait is initiated towards the negative directions, the swing limb is on the opposite side of the desired gait and the swing and stance limbs cross during the first step.

Participants initiated gait from an AMTI force platform embedded into a 5m walkway at an auditory start signal. At the start of each trial, participants were told which angle to position themselves in and looked straight ahead at the corresponding sign indicating the angle. Ground reaction forces as well as full body kinematics were recorded.

Speed conditions were blocked, the order alternated between participants, and starting angles were presented randomly. Each participant completed eight trials per condition for a total of 80 trials.

The medio-lateral (ML) and anterio-posterior (AP) COP coordinates, relative to the participant at the start of each trial were analysed at three events; A) the furthest lateral displacement towards the swing limb; B) the change from predominant lateral shift to predominant anterior shift of the COP; C) the position of the COP just prior to swing heel strike. The speed and direction of COM velocity, relative to the desired direction of gait, will be analysed at the same three events. The position and orientation of the first step will also be analysed.

Results were analysed using a mixed-design ANOVA, with Angle and Speed as within factors and Age as between factor. A post-hoc analysis (Tukey) was preformed for all significant effects (α=0.05).

RESULTS

Preliminary results show that both YA (n=7) and OA (n=5) modify their COP trajectory with regards to the desired direction of gait.

The ML position of the COP at event A is further towards the swing limb when gait is initiated towards a negative direction and more medial when gait is initiated towards a positive direction for both YA and OA (Ps<0.001).

The AP position of the COP at event A has a significant Angle/Speed interaction (P<0.001). For both YA and OA, the COP at event A is more posterior at the fast speed (Ps<0.001) except at the -40° condition. In addition, the COP at event A at the positive starting angles is less posterior than the 0° condition for both

YA and OA at both speed conditions (P<0.05).

DISCUSSION

Preliminary results show that GI combined with a change in direction is associated with a modulation of the postural adjustments prior to the start of movement. Further analysis of COM velocity as well as the position and orientation of the foot at the first step, will provide insight on the organisation of GI. This data will indicate whether OA use the same GI strategies as YA when GI is combined to a change in direction.

SUMMARY

In both young and older adults postural adjustments are modulated in order to initiate gait towards the desired direction of progression.

REFERENCES

Anaka and Corbeil. ISPGR, Burlington (VT), 2007.
Breniere et al. (1987). J Mot Behav **19**(1): 62-76.
Mann et al. (1979). J Bone Joint Surg Am **61**(2): 232-9.
Mbourou et al. (2003). Gerontology **49**(1): 21-6.
Polcyn et al. (1998). Arch Phys Med Rehabil **79**(12): 1582-9.

ACKNOWLEDGEMENTS

Ground Reaction Forces during Running can be Estimated from Insole Pressure Measurements by Considering Whole Body Dynamics

Elizabeth S. Chumanov[1], Christian D. Remy[1], and Darryl G. Thelen[1]

[1]Department of Mechanical Engineering, University of Wisconsin-Madison Madison, WI
E-mail: easchmerr@wisc.edu Web: Web: www.engr.wisc.edu/groups/nmbl/

INTRODUCTION

Insole pressure sensors allow one to gauge the pressure distribution on the foot, in addition to the net center of pressure (COP) and vertical force (Chesnin et al. 2000). However, current insoles do not provide measures of shear force, which means that traditional biomechanical analyses of joint and muscle loads cannot be conducted. Kuo (1998) showed that center of pressure information may be sufficient to estimate shear forces when a least squares inverse dynamics (LSID) approach is used. We have extended these ideas to generate least squares forward dynamic (LSFD) simulations of locomotion that are dynamically consistent over time (Remy et al. 2008). The objective of this study was to evaluate the accuracy of using insole pressure data together with LSFD to estimate ground reactions during running.

METHODS

Five healthy young adults (25 ±2 yrs, 68.9 ±6.8 kg, 172 ±5 cm) were tested. Ground reactions (1000 Hz) were recorded while each subject ran at two speeds (preferred, fast) over a fixed force plate (AMTI), with three repeated trials performed for each speed. Pressure sensitive insoles (99 capacitive sensors per insole, Novel Inc.) were used to record the pressure distribution (100 Hz) on the bottom of the feet during all trials. Whole body kinematics (200 Hz) were simultaneously recorded using a motion capture system (Fig. 1a).

(a)   (b)
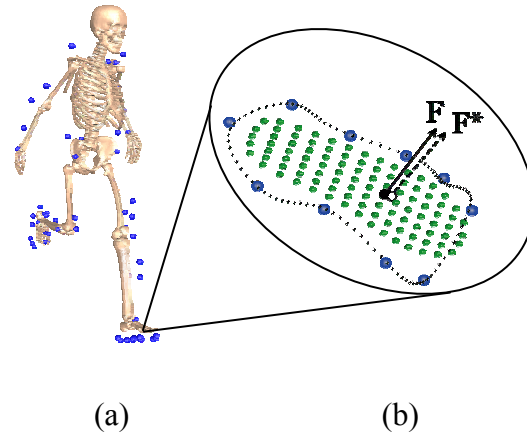
Figure 1: a) Whole body kinematics. b) LSFD estimates of the ground reaction force, **F***, were compared with forceplate measures, **F**.

Ten markers located around the periphery of the shoe were used to track the insole sensor positions. At each frame, a natural cubic spline through the 10 markers was used to infer the positions of 100 virtual markers around the shoe (Fig. 1b). Each subject performed a standing static calibration trial in which he/she stood one-legged on a forceplate while voluntarily shifting the center of pressure. This data was used to determine a linear transformation from the ground to the insole reference frame that minimized differences between the insole and forceplate COP trajectories. During running trials, piecewise affine transformations applied to the 100 virtual markers were then used to determine the position of each insole sensor. Sensor positions and pressure measurements were subsequently used to estimate the center of pressure and net vertical force on each foot (Chumanov et al. 2007).

We used then LSFD to estimate the ground reactions through the stance phase of running. At each time step, a least squares solution of the equations of motion of a 27 degree of freedom whole body model was performed. Specifically, we solved for joint accelerations and ground reactions that acted at the insole center of pressure, while minimizing the discrepancy between estimated and measured accelerations. Estimated accelerations were then numerically integrated to obtain the resulting joint velocities and positions. Optimization was employed to determine a set of initial velocities and positions that produced a forward simulation that was consistent with measured marker kinematics (Remy et al. 2008)

RESULTS
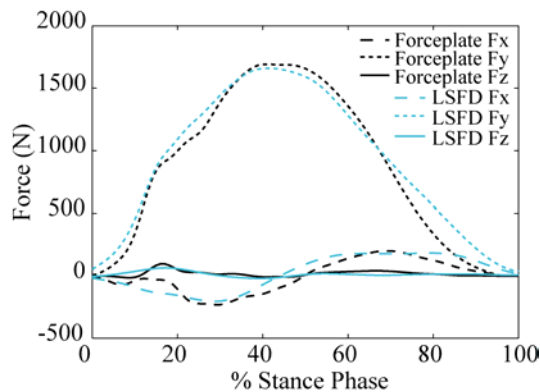
Figure 2: LSFD estimates of the ground reactions derived from the insole pressure data agree well with forceplate measures

The insole sensor tracking algorithm generated COP trajectories that were within 10 mm of forceplate measures for all trials.

Root mean square (RMS) errors in the estimated shear forces averaged from 5-8 N in the medio-lateral direction and from 10-15 N in the anterior-posterior directions (Table 1). These errors are less than 8% of the peak force measured in these directions (Fig. 2). The largest error in shear force estimates tended to occurr at heel contact and toe-off, which may results from deviations in the insole COP position at those portions of stance.

DISCUSSION

We have demonstrated that least squares forward dynamics can be used together with insole pressure data to obtain reasonably accurate estimates of ground reactions during running. This advance could facilitate the use of insoles to analyze joint and muscle mechanics during running on un-instrumented surfaces or treadmills.

REFERENCES

Chesnin, KJ, et al. (2000). *Gait Posture* 12, 128-133.
Chumanov, et.al. (2007). Conference abstract, *Am Society of Biomech*, Stanford, CA.
Kuo, AD. (1998). *J Biomech Eng* 120, 148-159.
Remy, CD, et al. (2008). *J Biomech Eng*, in press.

ACKNOWLEDGEMENTS

Table 1. RMS errors (mean (sd)) for measured COP and estimated forces.

	COPx (mm)	COPz (mm)	A-P (Fx, N)	Vertical (Fy, N)	M-L (Fz, N)
Preferred Run	8.2 (4.9)	4.6 (1.2)	10.4 (7.2)	15.6 (7.1)	5.0 (1.8)
Fast Run	5.5 (1.1)	1.8 (1.0)	15.3 (7.2)	22.8 (5.6)	8.4 (3.2)

EFFECTS OF A 6-MONTH YOGA PROGRAM ON SCAPULAR POSTURING IN OLDER ADULTS WITH HYPERKYPHOSIS

Man-Ying wang[1], Abbie E. Ferris[1], Gail A. Greendale[2] and George J. Salem[1]

[1]Division of Biokinesiology and Physical Therapy, University of Southern California,
Los Angeles, California, USA, mwang@usc.edu
[2]Division of Geriatrics, University of California at Los Angeles, Los Angeles, California, USA
URL: http://pt.usc.edu/labs/mbrl

INTRODUCTION

Hyperkyphosis, or an increased thoracic curvature, is a common posture syndrome in older adults. This excessive curvature is related to decreased functional capacity, including rising from a chair, bending and reaching (Ryan, 1997; Kado, 2005). These functional capabilities, however, were improved by Yoga intervention (Greendale, 2002). Scapular posture is also affected by thoracic curvature (Kebaetse, 1999 and Finley, 2003); yet it is unknown if Yoga intervention may improve scapular posturing, especially in older subjects diagnosed with hyperkyphosis. The purpose of this study was to quantify the change in scapular posturing during static (sitting and standing) and dynamic (walking) tasks, following completion of a 6-month Yoga program.

METHODS AND PROCEDURES

Eighteen older adults (75.4 ± 7.3 yrs) with hyperkyphosis ($52.2^o \pm 9.4^o$) participated in this study. Hyperkyphosis was defined by Debrunner kyphotic angle greater than 40 degrees. At baseline, subjects were instrumented for motion analysis with reflective markers placed on the spinous process of the 7th cervical vertebra (C7), sternal notch (St), and bilateral acromion processes (RA, LA). They were then asked to perform 4 tasks: 1) quiet-standing, 2) normal walking, 3) fast walking, and 4) sitting, in a randomized order, while recorded by an 8-camera motion analysis system (Vicon 612,

Oxford, UK). Following the baseline measurement, subjects participated in a Hatha yoga program, 3 times per week for 24 weeks. The program focused on poses intended to improve strength, increase flexibility, and restore upright posture. Motion analysis was repeated after 6 months. Scapular posturing was quantified by protraction index, calculated by the following formula, where a greater value indicates greater protracted scapular posturing.

Protraction Index *= [(distance from C7 to RA) + (distance from C7 to LA)] / [(distance from St to RA) + (distance from St to LA)]*

Paired t-tests were used to test the difference in protraction index between baseline and 6-month follow-up. Since walking is a dynamic task and the protraction index varies with gait cycle, the maximum, minimum, and averaged protraction index during a complete gait cycle were obtained. The difference between maximum and minimum was also calculated as a measure of scapular excursion.

RESULTS

Statistical results demonstrated significant improvements (2.9%)of scapular posturing in the static sitting condition after 6 months of yoga intervention ($p < 0.05$) (Table 1). A similar trend of a decrease in protraction index was also observed during static standing, but did not reach statistical significance ($p = 0.059$). During dynamic walking, the subject's scapulae were statistically significantly less protracted

during the maximum protracted phase for both normal (p < 0.05) and fast (p < 0.05) walking, following the yoga intervention. However, no significant differences were found during the minimum protracted phase of gait. The average protraction index of the entire gait cycle decreased significantly during normal walking (p < 0.05) but only decreased at a borderline significant level during fast walking (p = 0.053). The overall excursion of the protraction index during gait decreased significantly after the 6-month yoga intervention for both fast and normal walking. This is primarily due to the significantly less protracted posture during the maximum protracted phase and relatively unchanged posture during the minimum protracted phase after the yoga intervention.

DISCUSSION AND SUMMERY

Findings of this study suggest that the 6-month yoga program improved scapular posturing, to a less protracted position, during both static and dynamic conditions. The scapulae were also more stable, as indicated by a significantly decreased scapular excursion, during both normal and fast walking. Abnormal scapular positioning may decrease the subacromial space and consequently increase the risk of impingement syndromes (Lukasiewics, 1999; Michner, 2003). This study demonstrated that the yoga intervention effectively improved scapular posturing in older adults with hyperkyphosis.

REFERENCES

Finley MA and Lee RY (2003). *Arch Phys Med Rehabil,* 84:563-8.
Greendale GA et al (2002). *Am J Public Health,* 92:1611-4.
Kado DM et al (2005). *J Gerontol: Med Sci,* 60:633-7.
Kebaetse M et al (1999). *Arch. Phys. Med. Rehabil,* 80: 945-50.
Lukasiewicz AC et al (1999). *J Orthop Sports Phys Ther,* 29:574-83.
Michner LA et al (2003). *Clin Biomech,* 18:369-79.
Ryan SD and Fried LP (1997). *J Am Geriatr Soc,* 45:1479-86.

ACKNOWLEDGEMENTS

Table 1. Protraction index during static sitting, static standing, normal walking and fast walking

	Baseline	Follow-up	P-value
Static Sitting	1.068 (0.049)	1.037 (0.065)	0.001
Static Standing	1.051 (0.048)	1.040 (0.059)	0.059
Normal Walking			
Maximum	1.037 (0.043)	1.017 (0.051)	0.014
Minimum	1.020 (0.042)	1.022 (0.052)	0.685
Average	1.028 (0.043)	1.011 (0.052)	0.020
Change	0.017 (0.006)	0.012 (0.005)	0.005
Fast Walking			
Maximum	1.043 (0.044)	1.029 (0.046)	0.026
Minimum	1.015 (0.042)	1.009 (0.052)	0.197
Average	1.030 (0.043)	1.019 (0.048)	0.053
Change	0.028 (0.010)	0.021 (0.014)	0.035

Mean (SD)

SOCCER SHOES REDUCE FOOT SENSITIVITY COMPARED TO BAREFOOT FOR EXTERNAL VIBRATION STIMULI

Thorsten Sterzing, Sabrina Kunde, Franziska Scholz, Thomas L. Milani

Department of Human Locomotion, Chemnitz University of Technology, Chemnitz, Germany,
thorsten.sterzing@phil.tu-chemnitz.de

INTRODUCTION

The human foot as a sensory organ uses tactile stimuli from its environment to adapt motor performance. Touch pressure and vibration stimuli are recognized by Merkel, Meissner, and Pacini skin mechanoreceptors. A sensitivity mapping for touch pressure and vibration stimuli showed different sensitivity levels of the numerous anatomical locations of the foot (Sterzing et al., 2006). Regarding motor performance, plantar foot sensitivity supports balance tasks (Perry et al., 2000). Foot sensitivity is likely to be decreased in athletes performing shod sports compared to athletes performing unshod sports (Schlee et al., 2007). This indicates the necessity to consider the role of footwear with respect to foot sensitivity in sports performance.

For soccer players ball sensing is an important shoe property (Sterzing et al., 2007). Soccer shoes act as artificial interfaces between the foot and the ball. They need to protect the player's foot but should also allow optimal ball handling, thereby supporting technical skills of the players. Sensory information is a crucial input variable for ball handling. Thus, the purpose of this study was to examine vibration sensitivity of the foot in different soccer shoe models compared to barefoot.

METHODS AND PROCEDURES

15 experienced soccer players took part in the study (game experience: 15,0±3,9 years; age: 23,8±2,7 years; height: 175,5±3,9 cm; weight: 70,9±6,1 kg). Four shoe conditions and the barefoot condition were included in the test: Puma King (PKT), Puma V-Konstrukt (PVK), Puma V1 (PV1), Nike Mercurial Vapor (NMV), and Barefoot (BAR). Whereas PKT (3,8mm) and PVK (3,9mm) have rather thick shoe upper materials and a relatively wide forefoot fit, PV1 (1,4mm) and NMV (2,2mm) have rather thin shoe upper materials and a relatively narrow forefoot fit (Figure 1).
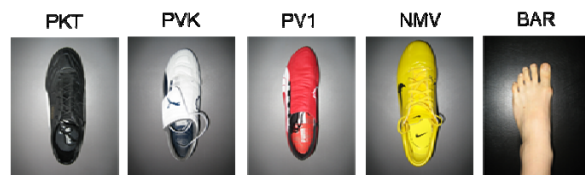
Figure 1: Foot/shoe conditions

Vibration sensitivity was measured at four anatomical locations of the shoe/foot:
- MM-I   medial metatarsal head I
- DM-I   dorsal metatarsal head I
- DM-V   dorsal metatarsal head V
- LM-V   lateral metatarsal head V

These locations are important for accurate passing, receiving and handling of the ball. Measurements were performed with a Horwell Neurothesiometer (Scientific Laboratory Supplies Ltd., Nottingham, UK) at a frequency of 100Hz. Vibration amplitude was increased until subjects perceived the stimulus. In the shod conditions the anatomical locations were palpated through the shoe and marked for each subject individually prior to the testing. Five repetitive trials were performed per anatomical location and foot/shoe condition. For statistical analysis mean values of the three most homogenous trials (CoV) were calculated. A repeated measures ANOVA and

Post-Hoc tests according to Fishers' PLSD were performed to identify differences between the foot/shoe conditions and between anatomical locations.

RESULTS

Mean barefoot vibration sensitivity of the four anatomical locations of the foot is lower than mean shod sensitivity of all tested shoe conditions ($p < 0,01$). Among the shoe conditions there were no statistically different vibration thresholds (Figure 2). Lower vibration thresholds of barefoot compared to shod conditions are present for all examined anatomical locations ($p < 0,01$).
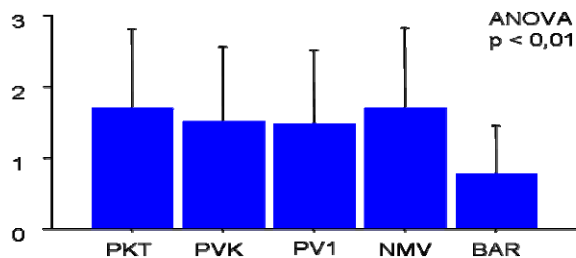

Figure 2: Shoe/foot vibration thresholds [µm]

The medial metatarsal head I is the least sensitive anatomical location whereas the lateral metatarsal head V is the most sensitive anatomical location when wearing soccer shoes ($p < 0,01$). Shoe means are presented in Figure 3.
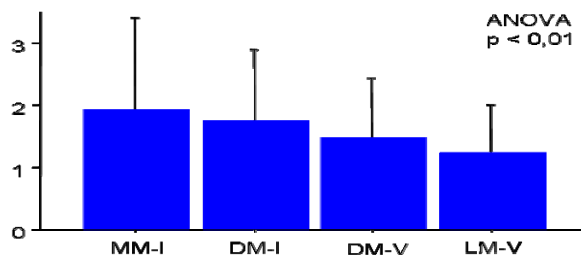

Figure 3: Shod vibration thresholds of anatomical locations [µm]

DISCUSSION

The transfer quality of external vibration stimuli to the foot via artificial interfaces like soccer shoes is likely to be dependent on the type and thickness of the shoe upper material. Also, an anatomically rather tight or wide fit of the shoe may have an effect. In this study these factors potentially cancel out with respect to shoe discrimination. To solidly investigate these ideas, a systematically designed variety of shoes needs to be built in order to isolatedly examine the addressed aspects. Vibration sensitivity at the metatarsal head I is lower than at the metatarsal head V when wearing soccer shoes. As most ball handling actions are performed with the inside and the inner instep of the shoe/foot this creates a margin for shoe improvement.

SUMMARY

Soccer shoes reduce vibration sensitivity with respect to external stimuli compared to barefoot. Differences between soccer shoes with regard to transfer quality of external vibration stimuli to the foot were not found. In this study this might be due to the relatively low number of subjects with respect to natural high variability of sensitivity measurements and negative interaction of shoe properties. In general, the influence of foot sensitivity level on ball handling skills of players is not yet determined and thus needs to be investigated.

REFERENCES

Perry, S. et al. (2000). *Brain Research,* 877: 401-406.

Prätorius B. et al. (2004). *Proceedings 13. Conference of the Canadian Society for Biomechanics*, Halifax, NS, Canada.

Schlee, G. et al. (2007). *25. Symposium of the International Society of Biomechanics in Sports,* Ouro Preto, Brazil.

Sterzing T. et al. (2006). 7. dvs-Symposium, Bad Sassendorf, Germany.

Sterzing, T. et al. (2007). *Orthopädie Technik,* 9: 646-655.

GENDER RESPONSES TO SITTING IN AUTOMOBILE AND OFFICE SEATS – INFLUENCE OF HIP AND HAMSTRING FLEXIBILITY ON SEATED POSTURES

Tyson A.C. Beach, Katherine A. McDonald, Stephanie K. Coke, Jack P. Callaghan
Department of Kinesiology, University of Waterloo, Waterloo, ON, Canada,
callagha@uwaterloo.ca

INTRODUCTION

Sustained lumbar spine flexion, characteristic of both office (Beach et al., 2005) and automobile (Harrison et al., 2000) sitting, is considered an important factor in hypothesized LBP-generating mechanisms. Consequently, understanding factors that influence lumbar flexion in these seated exposures may be used to help those who experience LBP while seated. The purpose of this study was to examine the influence of gender and hip/hamstring flexibility on lumbo-pelvic postures adopted when performing laboratory-simulated computer work and automobile driving.

METHODS AND PROCEDURES

Ten female and 9 male university student volunteers were exposed to 10 minutes each of the abovementioned sitting conditions. Accelerometers, taped to the skin over the sacrum and L1 spinous process, were used as inclinometers (c.f., Hansson et al., 2001) to characterize sagittal lumbo-pelvic postures while sitting. ANOVAs (general linear model) with one within-subject factor (sitting condition) and one between-subject factor (gender) were used to compare lumbo-pelvic postures. Correlation analyses were performed between lumbo-pelvic postures and various measures of hip and hamstring flexibility. $P < 0.05$ was considered to be statistically significant.

RESULTS

When driving, females displayed 9.8 degrees more posterior pelvic tilt ($P = 0.0329$) and 10.5 degrees more lumbar flexion ($P = 0.0116$) than males with respect to their lumbo-pelvic alignments in upright standing. When performing seated computer work, it was males who experienced greater posterior pelvic tilt ($P = 0.0048$) (Figs. 1 and 2).
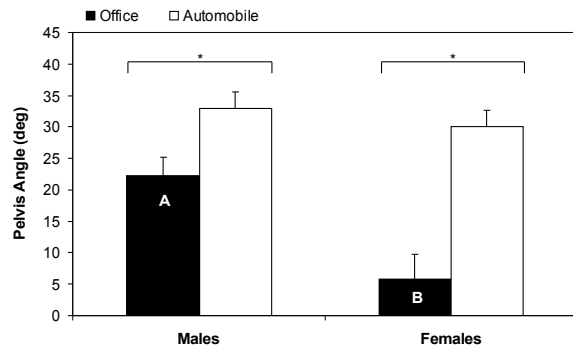

Fig. 1. Mean (SEM) posterior pelvic tilt angles during sitting. "A" and "B" indicate that posterior pelvic tilt angles were significantly different between genders during office chair sitting.
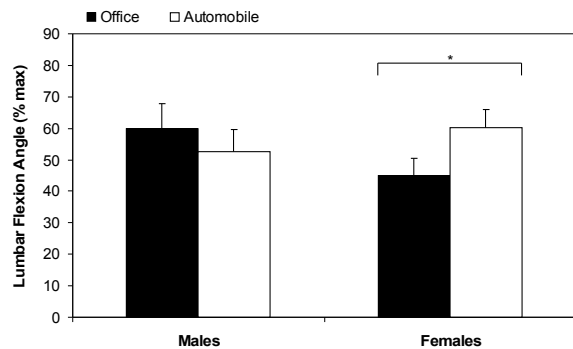

Fig. 2. Mean (SEM) lumbar flexion angles during sitting.

Results of flexibility tests are summarized in Table 1.

Table 1. Summary of flexibility test results. Mean (SEM) values are provided. Larger magnitudes represent greater flexibility.

	Hip Flexibility, deg	Hamstring Flexibility, deg	Sit-and-Reach, cm
Females	107 (3.9)	251.9 (6.6)	34.5 (2.4)
Males	97.2 (3.4)	239.8 (1.4)	24.9 (2.6)
p-value	0.0725	0.1020	0.0132*

* indicates that female flexibility was significantly greater than that of males.

Individuals who exhibited greater posterior pelvic tilt in office chair sitting, typically males, were those with less hip (r = –0.5484; $P = 0.0150$) and less hamstring (r = –0.4690; $P = 0.0496$) flexibility (Fig. 3). Individuals with greater hip flexibility, typically females, adopted lumbar flexion postures closer to their voluntary end-range while driving (r = 0.5709; $P = 0.0107$) (Fig. 4).
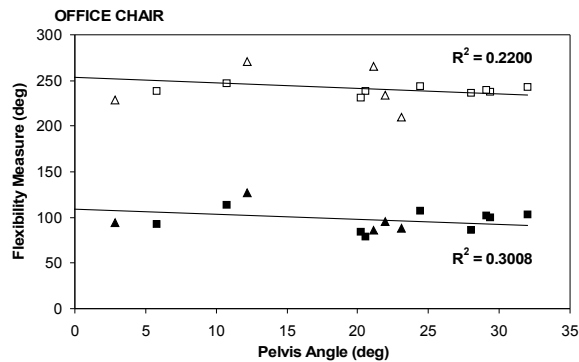
Fig. 3. Relationship between pelvic tilt angles in office chair sitting and hip (■ males; ▲ females) and hamstring (□ males; △ females) flexibility. Positive (negative) pelvic tilt angles represent posterior (anterior) rotation with respect to vertical.

DISCUSSION

The results of this study suggest that individuals with lower hip and hamstring flexibility experience greater posterior pelvic tilt in office chair sitting, but more lumbar spine flexion in automobile driving. Given that differences existed between males and females with respect to various indices of hip and hamstring flexibility, it is possible that gender-based differences observed in seated lumbo-pelvic postures were related to these inherent differences in flexibility between the sexes.

CONCLUSIONS

The findings of this study suggest that strategies to prevent LBP associated with sitting depend on both individual characteristics and the type of seated exposure. With apparent increases in sedentary occupational and recreational activities, more studies are warranted to determine if gender-based postural differences in sitting are related to other anthropometric differences, or if improving hip and specifically hamstring flexibility would be associated with different seated lumbo-pelvic postures.

Fig. 4. Relationship between hamstring flexibility and lumbar flexion postures in automobile driving (■ males; ▲ females).

REFERENCES

Beach TAC, et al. (2005). *Spine J*, 5: 145-154.

Harrison DD, et al. (2000). *J Manipulative Physiol Ther*, 23: 37-47.

Hansson GÅ, et al. (2001). *Med Biol Eng Comput*, 39: 405-413.

A UNIFYING APPROACH TO DETERMINE THE NUMBER OF PADDING POINTS WHEN DIGITALLY FILTERING KINEMATIC DATA

Samuel J. Howarth and Jack P. Callaghan

Department of Kinesiology, University of Waterloo, Waterloo, ON, Canada,
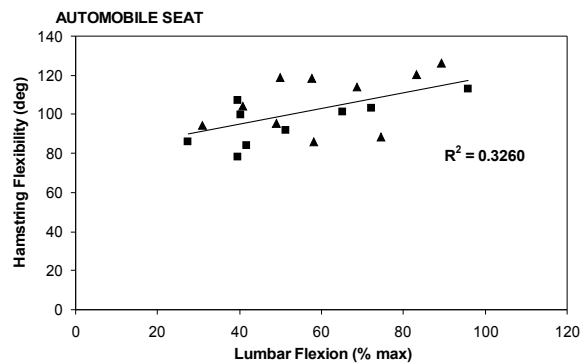sjhowart@uwaterloo.ca

INTRODUCTION

Signal sampling frequency and the low-pass digital filter cutoff frequency are factors that may influence the minimum number of padding points when applied to digital filtering of kinematic data that are often omitted from data processing descriptions. Amplitude distortion in response to a step input before converging on the true value of the input is a characteristic of the underdamped and recursive Butterworth filter (Robertson and Dowling, 2003). Due to this period of amplitude distortion, it is important to either collect data records of durations beyond the events of interest or add points to the beginning and end of data records to reduce amplitude distortion caused by the filtering process. The purpose of this investigation was to determine the influence that the ratio between filter cutoff frequency and signal sampling frequency (f_c/f_s) has on the minimum number of required padding points using 3 different extrapolation techniques.

METHODS

Two kinematic recordings, each 30 seconds in length, representing signals with high and low deterministic variation were obtained from a previous investigation (Beach et al., in press). Signals from the original investigation were sampled at a frequency of 64 Hz. Kinematic data were resampled at frequencies from 40-128 Hz at intervals of 1 Hz while the low-pass filter cutoff frequency was varied from 2-10 Hz at intervals of 0.5 Hz. This generated a set of 1513 combinations of filter cutoff and signal sampling frequency. Prior to filtering, a window of data was removed from the resampled kinematic signals between 4.65 and 10.93 seconds. This section of data served as the test signal. Padding points were incrementally added to the beginning of the test signal with three different techniques (first order polynomial, third order polynomial, and data reflection) until 2 seconds of padding points had been added to the test signal. The test signals were then dual-pass filtered using a 2nd order low-pass digital Butterworth filter.

Each resampled 30 seconds record was filtered using the identical digital filter as the corresponding test signal. The identical duration was removed from the resampled and filtered 30 seconds record and served as the criterion signal. Padding points were removed from the filtered test signal and the root mean square difference (RMSD) between the filtered test and criterion signals was calculated during the first second of data for each increment in the number of padding points. This produced an RMSD that was a function, R(p), of the number of padding points. The minimum number of padding points for a combination of sampling and cutoff frequency was defined as the number of padding points required to attain a constant RMSD or steady state defined by R′(p) = R″(p) = 0.

RESULTS

The RMSD between the filtered test and criterion signals exhibited an oscillatory pattern that achieved a steady state response. A non-linearly decreasing power-law relationship was observed between the minimum number of padding points and f_c/f_s (Table 1).

Method	α	β	R^2
1st order	2.538	-0.748	0.937
3rd order	1.706	-0.985	0.873
Reflection	2.584	-0.804	0.912

Table 1 – Curve fit coefficients relating the number of padding points (P) to the ratio between the cutoff frequency and the sample frequency (f_c/f_s) for the kinematic signal with larger deterministic variation. The general equation used for the power-law curve fit was $P\left(\dfrac{f_c}{f_s}\right) = \alpha\left(\dfrac{f_c}{f_s}\right)^{\beta}$.

Padding points that were added beyond the determined minimum did not change the RMSD. The signal with larger deterministic variation required more padding points than the signal with minimal variation.
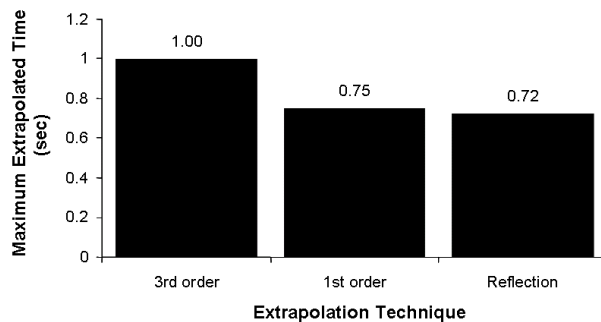
Figure 1 – Maximum extrapolated time for each of the three extrapolation techniques.

The largest extrapolated duration to produce a constant RMSD was 1 second (Figure 1).

DISCUSSION

As a general criterion, we suggest a minimum duration of one second of data be extrapolated for all kinematic recordings prior to digital filtering. This is based on the result that one second was the maximum extrapolated time, for all 1513 combinations of sampling and filter cutoff frequencies, across each of the three extrapolation techniques. A more suitable alternative to data extrapolation is to collect an extra second of superfluous data at the beginning and end of the desired sample period that can be removed following digital filtering. Adding excessive padding points beyond the determined minimum did not increase nor decrease the discrepancy between the filtered test and criterion signals which implies that overestimation of the minimum number of padding points is not detrimental to error determination.

SUMMARY

The current work extends previously published padding point criterions (Smith, 1989) by demonstrating that sampling and cutoff frequency will both affect the minimum number of padding points to be added prior to digital filtering. It is suggested that a minimum of 1 second of extraneous data be used when using a low pass recursive digital filter to remove noise from kinematic data.

REFERENCES

Beach, TAC et al. (in press). *Hum Mov Sci*.
Robertson DGE and Dowling JJ (2003). *J Elect Kines*, 13: 569-73.
Smith, G (1989). *J Biomech* 22: 967-71.

DISEASE SEVERITY INFLUENCES PATIENT RESPONSE TO VARIABLE-STIFFNESS WALKING SHOE AFTER ONE YEAR OF WEAR

Jennifer C. Erhart [1,2], Nicholas J. Giori [1,2,3], and Thomas P. Andriacchi [1,2,3]

[1] Department of Mechanical Engineering, Stanford University, Stanford, CA, USA
[2] Bone and Joint Center, Palo Alto VA, Palo Alto, CA, USA
[3] Department of Orthopedic Surgery, Stanford University, Stanford, CA, USA
E-mail: jerhart@stanford.edu   Web: www.stanford.edu/group/biomotion

INTRODUCTION

Many studies have reported the effectiveness of footwear modifications using laterally-wedged insoles (Kerrigan et al. 2002, Toda et al. 2004) and, more recently, variable-stiffness soles (Erhart et al. 2007) in patients with medial compartment knee osteoarthritis (OA) in reducing the adduction moment at the knee. The adduction moment is known to be associated with the progression (Miyazaki et al. 2002) and treatment outcome (Andriacchi et al. 1994) of medial compartment knee OA. Studies of clinical effects with lateral wedges, however, have shown mixed reports on improvement (Baker et al. 2007, Tohyama et al. 1991) and it is possible that OA severity may affect clinical outcome (Sasaki and Yasuda 1987, Shimada et al. 2006).

The purpose of this study was to test the hypothesis that the severity of OA in patients with medial compartment knee osteoarthritis will influence the reduction in the knee adduction moment and the reduction in pain and improvement in function after 12 months of wearing a variable-stiffness shoe, while no differences will be related to severity for patients wearing a control shoe for 12 months.

METHODS AND PROCEDURES

The data was obtained from 49 patients with radiographically diagnosed (Kellgren-Lawrence grade ≥ 1) medial compartment knee OA. At an initial visit, subjects were randomly assigned to either a uniform stiffness control shoe (n=23) or a variable-stiffness intervention shoe (n=26) to wear as their main walking shoe for 1 year. Subjects were blinded as to their shoe type. The intervention shoe had a lateral heel sole stiffness 2.3 times greater than the medial heel, and lateral forefoot sole stiffness 3 times greater than the medial forefoot, with the medial sole stiffness comparable to the stiffness of the control shoe. Both intervention and control subjects were divided into 2 groups based on OA severity: less severe (KL ≤ 2) and more severe (KL >2). Demographic data is provided in Table 1. If patients were affected bilaterally, their more severely affected side was used for analysis. Subjects participated in the study after giving written consent in accordance with the Institutional Review Board.

Table 1: Demographic data of patients

Group	Severity	Male	Female	Age (yrs)	Height (m)	Mass (kg)
Intervention	KL ≤ 2	7	6	60.0 (7.4)	1.67 (0.07)	73.2 (14.9)
	KL > 2	7	6	66.8 (3.7)	1.70 (0.09)	87.1 (13.8)
Control	KL ≤ 2	4	9	57.8 (9.9)	1.68 (0.10)	73.0 (10.0)
	KL > 2	6	4	64.0 (9.3)	1.71 (0.07)	82.7 (12.9)

Subjects completed WOMAC functional improvement-based ratings specific to OA to assess pain and function (Bellamy et al. 1988) at the baseline and 12 month time points. At the 12 month time point, subjects performed 3 walking trials at a self-selected normal speed in their personal walking shoe (comfortable walking shoe used by patient) and their study shoe (control or intervention). Kinematic and kinetic data were collected using an 8-camera optoelectronic motion capture system. External inter-segmental forces and moments were calculated for the lower limb using previously described methods (Andriacchi et

al. 2004). The first peak knee adduction moment was calculated for each trial. Average values for each shoe and subject were determined for each subject's more affected leg. Paired two-tailed Student's T-tests ($\alpha = 0.05$) were used to compare the different shoes and to compare the WOMAC ratings between the baseline and 12 month time points.

RESULTS

The knee adduction moment of the less severe intervention group (KL $\leq$ 2) was significantly reduced with the variable-stiffness shoes versus the subjects' own personal walking shoes after 12 months of wear (7.6%, p=0.001). These subjects also had a significant reduction in total WOMAC score, with an average absolute reduction of 40 points, translating to a 56% reduction from baseline (p=0.01). There was no statistically significant reduction in WOMAC score in the intervention shoe subjects with more severe OA (KL >2), and no significant reduction in knee adduction moment. For both the less severe (p=0.03) and more severe (p=0.01) control shoe groups, there were increases in knee adduction moment, 3.8% and 7.9%, respectively, with the control shoe versus the subjects' own personal shoes after 12 months of wear. There was no change in total WOMAC score in patients with the control shoe regardless of Kellgren-Lawrence grade.

DISCUSSION

The use of a variable-stiffness intervention shoe successfully reduced the knee adduction moment in less severe patients after 12 months of wear, supporting our hypothesis. This reduction in knee adduction moment was accompanied by a reduction in pain and improvement in function in this group. These results were not seen in the more severe intervention patients or in the control groups. These results demonstrate the usefulness of the intervention shoe in early osteoarthritis, both in reducing pain and improving function and in possibly slowing the rate of progression of the disease by lowering the adduction moment at the knee.

SUMMARY

The results of this study help to clarify which subjects may benefit the greatest from a footwear intervention. The data supports the recommendation for use of the variable-stiffness sole intervention shoe in subjects with early medial compartment osteoarthritis (KL $\leq$ 2).

REFERENCES

Andriacchi TP et al. (1994) *Orthop Clin North Am* 14:289-295.

Andriacchi TP et al. In *Basic Orthopaedic Biomechanics*, 3rd ed., 91-121, 2004.

Baker K et al. (2007) *Arth Rheum* 56:1198-1203.

Bellamy N et al. (1988) *J Rheumatol* 15:1833-1840.

Erhart JC et al. (2007). *54th Meeting of the ORS*

Kerrrigan DC et al. (2002). *Arch Phys Med Rehabil*, 83:889-893.

Miyazaki T et al. (2002) *Ann Rheum Dis* **61**, 617-622.

Sasaki T and Yasuda K. (1987). *Clin Orthop* 221:181-187.

Shimada S et al. (2006). *Arch Phys Med Rehabil* 87:1436-1441.

Toda Y et al. (2004). *Arch Phys Med Rehabil* 85:673-677.

Tohyama H et al. (1991). *Int Orthop* 15:31-33.

COMPUTATIONAL MODELLING OF PERI-IMPLANT BONE HEALING CONSIDERING CELL-BIOMATERIAL INTERACTIONS

Nadia Amor[1], Liesbet Geris, Jos Vander Sloten and Hans Van Oosterwyck[2]

Division of Biomechanics and Engineering Design, Department of Mechanical Engineering,
K.U.Leuven, Leuven, Belgium
[1]PhD currently in progress, nadia.amor@mech.kuleuven.be
[2]Professor, hans.vanoosterwyck@mech.kuleuven.be
http://www.mech.kuleuven.be/bmgo/

INTRODUCTION

Surface characteristics of a biomaterial, such as topography (roughness) and chemical composition, are important determinants of bone healing around endosseous implants. A better understanding of the complexity of the *in vivo* cellular responses involved in peri-implant healing may contribute to improving implant design. Mathematical models may help to unravel this complexity.

As peri-implant healing recapitulates some of the processes, encountered during fracture healing, a mathematical model, originally developed for fracture healing (Bailón-Plaza and van der Meulen, 2001), can be used as a model for peri-implant healing as well. However, the influence of a biomaterial surface on cell response should be considered. The aim of this study was to demonstrate that this model can predict peri-implant healing, as seen in a selected experimental study (Berglundh et al., 2003), and that, by (implicitly) taking into account the cell-biomaterial interactions, the agreement between experimental data and simulations can be improved.

METHODS AND PROCEDURES

The mathematical model of Bailón-Plaza and van der Meulen (2001), which accounts for intramembraneous and endochondral ossification during fracture healing, was used

for peri-implant healing. The system is represented by the following equations:

$$\partial c_m / \partial t = \text{div} \left[D_m(\boldsymbol{c}) \text{grad } c_m - c_m \sum f_i(\boldsymbol{c}) \text{ grad } \boldsymbol{c}_i \right] + f_0(c_m, \boldsymbol{c})$$
$$\partial \boldsymbol{c} / \partial t = D \Delta \boldsymbol{c} + g(c_m, \boldsymbol{c}), \tag{1}$$

where c_m is the density of the mesenchymal stem cells and $\boldsymbol{c}$ a vector of five densities or concentrations of osteoblasts (c_b), chondrocytes (c_c), bone extracellular matrix (m_b), combined connective/cartilage ECM matrix (m_c), and an osteogenic (g_b) and a chondrogenic (g_c) growth factors respectively. The diffusion coefficients are noted by $D_m(\boldsymbol{c})$ and D, $f_i(\boldsymbol{c})$ represents a taxis coefficient (i=1 to 6) and $f_0(c_m, \boldsymbol{c})$ and $g(c_m, \boldsymbol{c})$ represent the reaction terms. Initially, the model parameters were taken from previous work (Geris et al., 2006). This model was applied to simulate early healing around an unloaded oral implant for an *in vivo* experiment, reported in (Berglundh, Abrahamsson et al., 2003). A geometrical domain representative for the inner part of the implant thread (wound compartment) was defined for the simulations. For symmetry reasons, only one half of this part was considered (Figure 1). Initial and boundary conditions were adequately applied to simulate healing processes reflecting direct (bidirectional) bone formation using a finite volume code. In a first analysis (case A), parameter values (Table 1) accounting for cell proliferation rate, osteoblast differentiation rate and growth
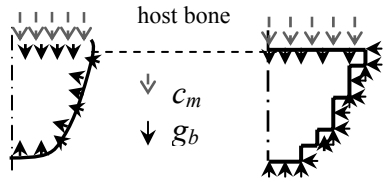
Figure 1. Wound domain and boundary conditions.

factor production rate were uniform for the entire model domain Values were established that led to an optimal correspondence between the experimental findings (Berglundh, et al., 2003) and model simulations. It is known from in vitro experiments that proliferation, differentiation and growth factor production can be modulated by surface characteristics (Boyan et al., 1999). Therefore, in a second analysis (case B), different parameter values were applied in the vicinity of the implant surface (2.5-7.5 μm wide zone), compared to the rest of the wound domain. In this way, cell-biomaterial surface interactions could be implicitly taken into account in the model.

Variable	Case A	Case B
Proliferation	50%	47.5%
Differentiation	150%	225%
Growth factor synthesis	171%	205.2%

Table 1. Rate parameters (% with respect to fracture healing model, Geris et al. 2006) for case A (entire wound domain) and B (at implant surface).

RESULTS

The spatio-temporal evolution of bone matrix density (Figure 2) was corroborated to the *in vivo* experiment (Berglundh et al., 2003) for both cases A and B. The evolution over time of the osteogenic growth factor concentration was more realistic for case B, which, for case A, tended towards zero at the end of the healing period (28 days).
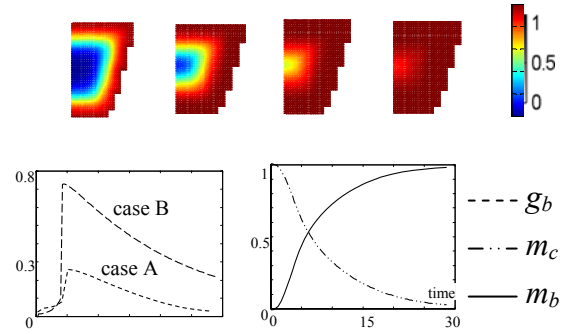
Figure 2. Top: bone density distribution (x0.1g/ml; case B) for 1, 2, 3 & 4 weeks post implantation. Bottom: temporal evolution of osteogenic growth factor concentration g_b (left; x100ng/ml, case A & B) and matrix density (right; case B) of connective tissue m_c (x0.01g/ml) and bone m_b (x0.1g/ml).

DISCUSSION

In this study, space-dependent model parameters were considered to implicitly take into account cell-biomaterial interactions. This led to more realistic predictions of the evolution of the osteogenic growth factor concentration. Future work will involve a more mechanistic treatment of cell-biomaterial interactions.

REFERENCES

Bailón-Plaza A et al. (2001). *J Theor Biol*, 212: 191-9.

Berglundh T et al. (2003). *Clin Oral Impl Res*, 14:251-262.

Boyan B et al. (1999). *Biomaterials*, 20:2305-2310.

Geris L et al. (2006). *Med Biol Eng Comput*, 44:280-289.

ACKNOWLEDGEMENTS

LACUNOCANALICULAR FLUID FLOW AND REGULATION OF BASIC MULTICELLULAR UNIT ACTIVITY

[1]Grant C. Goulet, [2]David M.L. Cooper, [3]Dennis Coombe,
[1]Robert Martinuzzi, and [1,4]Ronald F. Zernicke

[1]Schulich School of Engineering, University of Calgary,
Calgary, AB, Canada, gcgoulet@ucalgary.ca
[2]College of Medicine - Anatomy and Cell Biology, University of Saskatchewan,
Saskatoon, SK, Canada
[3]Computer Modelling Group, Ltd., Calgary, AB, Canada
[4]Orthopaedic Surgery, Kinesiology, and Biomedical Engineering, University of Michigan,
Ann Arbor, MI, USA, zernicke@med.umich.edu

INTRODUCTION

Human bone is continuously regenerated through remodelling, in which discrete packets of bone are replaced while maintaining a constant geometry (Parfitt, 1994). The process of remodelling is carried out by a complex mediator mechanism called the Basic Multicellular Unit (BMU) (Frost, 1990). In cortical bone, BMUs proceed by osteonal tunneling, during which osteoclasts excavate a canal that is subsequently refilled by osteoblasts (Smit and Burger, 2000). Current theories suggest that coordinated cellular activities associated with BMU remodelling are strain and fluid-flow regulated (Burger et al., 2003; Smit and Burger, 2000; Smit et al., 2002). Theoretical models to examine cortical remodelling have focused on idealized views of BMU forms. In reality, BMU morphology varies and includes unidirectional, bidirectional, and branched forms (Cooper et al., 2006) (Figure 1).

PURPOSE

The purpose of this study was to examine remodelling theories in relation to complex BMU forms observed in secondary bone.
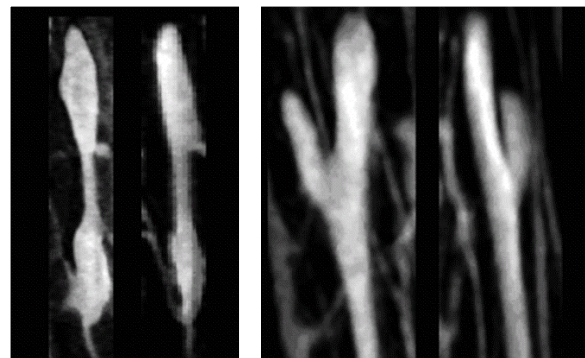
Figure 1. Micro-computed tomography images of bidirectional (left) and branched (right) BMU morphologies (Cooper et al., 2006).

METHODS

Computational models were developed in STARS, a coupled finite difference fluid flow and finite element mechanics simulator (Computer Modelling Group, Ltd., Calgary, AB, Canada). One idealized model and two geometrically accurate (unidirectional and branched canal forms) generated from three-dimensional micro-computed tomography image data were analyzed. Models were subjected to physiologically relevant axial compressive loads, which induced pressure-driven fluid flow through the simulated lacunocanalicular porosity.

RESULTS

Upon loading, fluid flowed from the high-pressure bone matrix into the low-pressure resorption space. Consistent with previous models, the idealized form had reduced longitudinal normal strain directly in front of the cutting cone where osteoclasts are activated, and increased strain behind the cutting cone where osteoclasts are inhibited. The unidirectional canal model also displayed decreased strain in front of the cutting cone, although strain behind the cone increased minimally, relative to the idealized case. Similarly, the geometrically accurate branched model demonstrated strain reduction in front of both cutting cones and minimally increased strain behind the cones. Fluid stasis has been implicated as a regulating mechanism in BMU activity, whereby decreased osteocytic stimulation results in reduced production of nitric oxide, inducing apoptosis, which subsequently signals the recruitment of osteoclasts. In all three BMU models, regions of relative fluid stasis were observed in front of the cutting cones (Figure 2). Branched morphology also displayed significant strain reduction and fluid stasis above the fork in the canal, where it divided into two distinct resorption spaces.
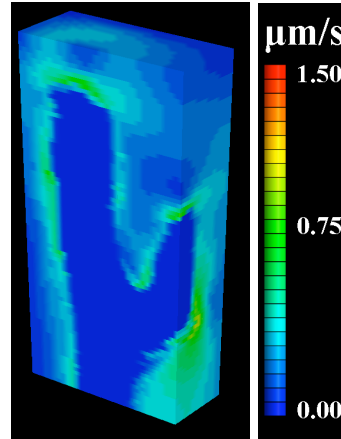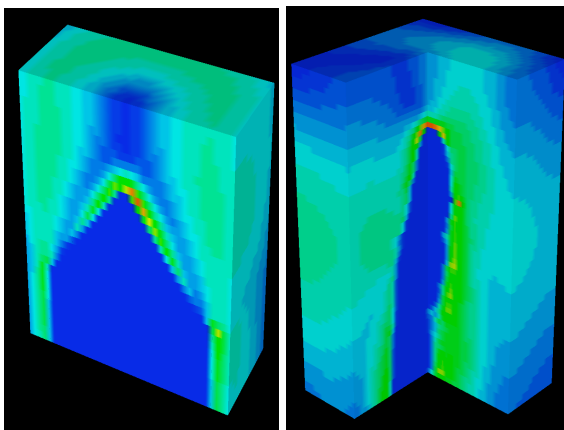
Figure 2. Three-dimensional sectioned views of idealized (lower left), unidirectional (lower right), and branched (left) BMU fluid velocity magnitude distributions.

CONCLUSIONS

If strain and fluid flow play a central role in coordinating BMU activity, inter-branch strain shielding and reduced fluid flow suggested that the region between resorption spaces would also be prone to osteocyte apoptosis and osteoclastic activity, effectively eliminating the branched structure. Therefore, strain and related fluid flow may not explain complex canal geometries. Consequently, further investigation is required to elucidate the underlying mechanisms involved in cortical bone remodelling.

REFERENCES

Burger et al. (2003). *J Biomech*, 36:1453-9.
Cooper et al. (2006). *Anat Rec A*, 288:806-16.
Frost (1990). *Anat Rec*, 226:414-22.
Parfitt (1994). *J Cell Biochem*, 55:273-286.
Smit and Burger (2000). *J Bone Miner Res*, 15:301-7.
Smit et al. (2002). *J Bone Miner Res*, 17:2021-9.

ACKNOWLEDGEMENTS

STRENGTH TRAINING OF THE QUADRICEPS MUSCLES FOLLOWING ACL TRANSECTION: EFFECTS ON STRENTH AND JOINT INTEGRITY

Eva Szabo[1], Ruth Seerattan[2], Tim Leonard[2] and Walter Herzog[2]

[1]Biomedical Engineering, University of Calgary, Calgary, AB, Canada, eszabo@kin.ucalgary.ca
[2]Department of Kinesiology, University of Calgary, Calgary, AB, Canada

INTRODUCTION

The quadriceps muscles have a complex role following injury to the anterior cruciate ligament (ACL) and in the development of osteoarthritis (OA). High correlations have been found between quadriceps strength and joint function in ACL deficient subjects (Keays et al., 2003). Similarly, quadriceps strength training has been shown to promote function in subjects with knee OA (Huang et al., 2003). However, there are two major complicating factors. First, quadriceps weakness in ACL deficient subjects often persists despite rehabilitation (Arrangio et al., 1997). Second, intense exercise has been shown to accelerate the development of OA in the knee (Appleton et al., 2007).

In this study, we asked two main questions: (i) could an aggressive strength training protocol eliminate quadriceps weakness in ACL deficient subjects? And (ii) what effect would this training protocol have on the articular cartilage of the knee?

METHODS AND PROCEDURES

New Zealand White rabbits underwent unilateral ACL transection and were divided into two groups: trained (n = 12) and untrained (n = 4). For one month, the untrained animals were allowed to recover while the trained animals underwent one of two strength training protocols 3 days a week. Both protocols used electrical stimulation of the quadriceps of anaesthetized rabbits. Each session in the first protocol, maximal training (n = 6), included 5 sets of 10 maximal contractions. Contractions were 0.5 seconds with 0.5 seconds between contractions in a set and 2 minutes between sets. Each session in the second protocol, 20% training (n = 6), consisted of a single maximal contraction followed by a 15 minute set of contractions at 20% of the force produced in the maximal contraction. Voltage and frequency were monitored and altered continuously to maintain the force at 20% of maximal throughout the testing period. Contractions in this protocol were 0.5 seconds with 1.5 seconds between contractions.

One month after ACL transection surgery, the quadriceps strength of both hind limbs was measured using electrical stimulation of the femoral nerve. Rabbits were then sacrificed, the quadriceps muscles were weighed and the knees were prepared for histological analysis.

For histological analysis of the cartilage, knees were separated into six areas: the medial and lateral tibia, the medial and lateral femoral condyles, the femoral groove and the patella. Each area was evaluated separately using the Mankin scoring system (Mankin et al., 1971).

RESULTS

Rabbits in the maximal training group showed increased force production over the course of the exercise sessions. Nonetheless, in the terminal experiment they showed persistent weakness and atrophy on the ACL deficient side compared to the contralateral side

(Figure 1). Further, there were no significant differences between strengths or percent weakness and atrophy between maximally trained and untrained rabbits (Figure 2). Maximal training group rabbits did, however, have a greater body weight normalized quadriceps mass.

In contrast to the maximal training group, 20% training group rabbits showed a balance in quadriceps strength between experimental and contralateral hind limbs following the four week training protocol (Figure 1).

For untrained and maximally trained rabbits, cartilage condition was significantly worse in specific areas of ACL deficient relative to contralateral knees. Also, in the areas with the worst signs of OA, OA was significantly worse in maximally trained compared to untrained rabbits. Histological analysis of the 20% trained group is ongoing; however, based on initial inspection, the ACL deficient knees had more signs of OA than contralateral knees.
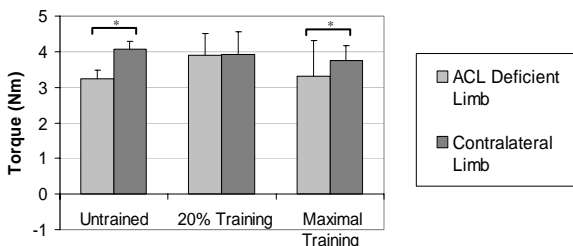
Figure 1: Torques produced in terminal experiments.
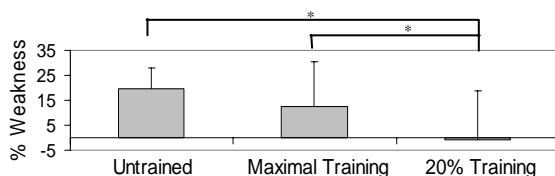
Figure 2: Percent weakness of the animals.

DISCUSSION

Despite an apparent improvement during the training sessions, the maximal training protocol was unable to eliminate side-to-side differences in strength in ACL deficient rabbits (Figure 1). A contralateral training effect likely contributed to this result, as the trained rabbits tended to have a greater quadriceps mass relative to their body weight than the untrained rabbits. The 20 % training protocol, however, did successfully eliminate side-to-side differences.

Further, both training protocols appeared to have a detrimental effect on the cartilage of the knee beyond that of ACL transection alone.

SUMMARY

In unilaterally ACL deficient rabbits, a strength training protocol involving sets of maximal contractions was unable to eliminate side-to-side differences in strength, whereas a protocol involving longer periods of repeated sub-maximal contractions was successful in eliminating these side-to-side differences. Both types of exercise had a detrimental effect on cartilage integrity. Therefore, we conclude that although some strength training might be beneficial for avoiding quadriceps atrophy and loss of strength, the protocols used here resulted in an increased rate of OA development.

REFERENCES
Appleton, CTG et al. (2007) *Arthritis Res Ther* 9: R13.
Arangio, GA et al. (1997) *J Orthop Sports Phys Ther*, 26: 238-243.
Huang, MH et al. (2003) *Semin Arthritis Rheum* 32: 398 – 406.
Keays, SL at al. (2003) *J Orthop Res*, 21: 231–237.
Mankin, HJ et al. (1971) *J Bone Joint Surg Am,* 53: 523-537.

COMPARISON OF LANDING BIOMECHANICS BETWEEN MALE AND FEMALE PROFESSIONAL DANCERS

Karl Orishimo[1], Ian Kremenic[1], Marijeanne Liederbach[2], Evangelos Pappas[3], Marshall Hagins[3]

[1]Nicholas Institute of Sports Medicine and Athletic Trauma, New York, NY, karl@nismat.org
[2]Harkness Center for Dance Injuries, NYU Hospital for Joint Diseases, New York, NY
[3]Long Island University, Division of Physical Therapy, Brooklyn, NY

INTRODUCTION

The gender disparity in the incidence of non-contact anterior cruciate ligament (ACL) injuries among athletes has been well documented. (Ireland, 1999) Studies of landing activities have revealed gender differences in lower extremity biomechanics that may place female athletes at increased relative risk. (Hewett et al, 2005) By contrast, the gender disparity in the incidence of ACL injuries among elite ballet and modern dancers is much less apparent, even though the activity is laden with jumping and landing activities. (Liederbach, in press) The low incidence of ACL injuries in dancers of both sexes coupled with the fact that they receive intensive training in jumping and landing from a young age seems to suggest that technique and training may play a more prominent role in the commonly-reported disparity in ACL injuries than gender-specific anatomical or hormonal factors. There is little research comparing landing biomechanics of male and female dancers. The purpose of this study was to compare lower extremity kinematics and kinetics during single-leg drop-landings between male and female professional dancers. Our hypothesis was that no difference in lower extremity biomechanics would exist between men and women dancers.

METHODS AND PROCEDURES

Twenty-nine professional dancers (14M, 15F) performed single-leg drop-landings from a 30 cm platform onto a force plate. Each landing was defined from initial contact with the force plate to peak knee flexion achieved during each trial. Kinematic data were recorded using eight Eagle cameras (Motion Analysis Corp.) and 22 reflective markers. Ground reaction forces were recorded with an OR6-5 force platform (AMTI). Sagittal and frontal plane angles and moments (internal) were calculated for the ankle, knee and hip. Total support moment (TSM) was calculated by adding sagittal plane moments at each joint throughout each trial. (Winter, 1980) Two separate MANOVAs were used to compare joint kinematics and kinetics between men and women. A t-test was used for TSM. The a level was set a priori at 0.05.

RESULTS

There were no gender differences in joint kinetics (p=0.462) (Table 1), kinematics (p=0.056) (Table 2), or TSM (p=0.618) (Figure 1).
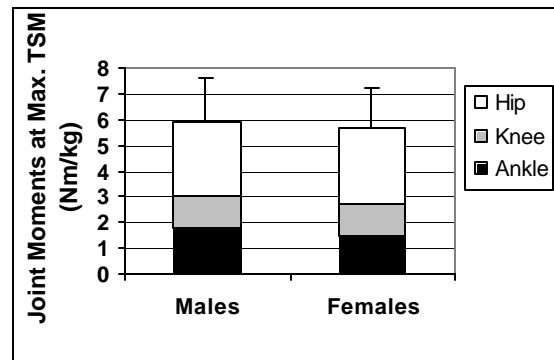

Figure 1. Joint contributions to maximum total support moment

DISCUSSION

Lower extremity kinematics and kinetics were not different between male and female dancers during this landing task. Maximum TSM and distribution of that moment among joints were also not different, indicating the demands placed on the lower extremity were similar between genders. These results are in contrast to previous studies indicating that landing biomechanics between male and female athletes are different. (Ford et al, 2006; Kernozek et al, 2005) We speculate that the extensive landing training provided to both male and female dancers from an early age may contribute to the lack of gender related landing differences.

SUMMARY

In contrast to previous research comparing landing biomechanics between male and female athletes of similar training background and skill level, our study found no difference in lower extremity kinetics and kinematics between male and female professional dancers. These results indicate that the gender disparity among athletes in the incidence of ACL injuries may be the result of an experience and training disparity rather than purely gender.

REFERENCES

Ford, KR et al.(2006).*Clin Biomech* 21: 33-40
Hewett, TE et al.(2005).*Am J Sport Med* 33: 492-501
Ireland ML.(1999).*J Athl Train* 34: 150-154
Kernozek, TW et al. (2005) *Med Sci Sport Exerc* 37: 1003-1012
Liederbach M et al.(2008). *Am J Sport Med* In press
Winter DA.(1980). *J Biomech* 13: 923-92

Table 1. Comparison of knee and hip kinematics between male and female dancers

Joint Angles (?)	Knee Flexion (+)	Knee Abduction (+)	Hip Flexion (+)	Hip Adduction (+)
Initial Contact				
Males	1.5 (6.3)	- 0.2 (2.4)	- 3.6 (10.0)	- 10.3 (4.9)
Females	4.2 (4.0)	- 1.7 (3.8)	8.1 (7.9)	- 13.9 (5.1)
Max. Knee Flexion				
Males	61.8 (10.3)	- 2.8 (5.0)	21.3 (15.0)	3.9 (5.6)
Females	60.5 (5.8)	-3.4 (11.2)	32.2 (10.3)	1.2 (5.2)
Range of Motion				
Males	60.3 (6.8)	8.5 (4.4)	25.4 (7.4)	15.5 (4.2)
Females	56.3 (4.8)	11.3 (5.8)	24.3 (5.8)	16.2 (5.1)

Table 2. Comparison of knee and hip kinetics between male and female dancers

Joint Moments (Nm/kg)	Knee Extension (+)	Knee Adduction (+)	Hip Extension (+)	Hip Abduction (+)
Initial Contact				
Males	- 0.4 (0.1)	0.02 (0.09)	- 2.8 (3.4)	- 0.2 (0.1)
Females	- 0.5 (0.2)	- 0.01 (0.14)	- 2.4 (3.5)	- 0.3 (0.5)
Max. Knee Flexion				
Males	1.7 (0.4)	- 0.5 (0.3)	0.9 (0.6)	1.2 (0.4)
Females	1.4 (0.5)	- 0.4 (0.3)	1.2 (0.8)	0.9 (0.5)
Maximum during Landing				
Males	3.1 (0.7)	- 1.8 (0.4)	4.0 (1.2)	3.1 (0.9)
Females	3.3 (0.8)	- 1.6 (0.4)	4.3 (1.5)	3.0 (1.0)

FOOTBALL PLAYING SURFACE COMPONENTS MAY AFFECT LOWER EXTREMITY INJURY RISK

Mark R Villwock, Eric G Meyer, John W Powell, Amy J Fouty, Roger C Haut

Michigan State University, East Lansing, MI, USA
E-mail: haut@msu.edu, Web: www.obl.msu.edu

INTRODUCTION

Injuries to the lower extremity are among the most frequent injuries in all levels of sports and often account for more than 50% of reported injuries (Fernandez et al., 2007). While translational friction is necessary for high-level performance during any athletic contest, it is generally accepted that excessive rotational friction results in high forces being transmitted to vulnerable anatomic structures which may then precipitate ankle and knee injuries.

Although the torsional friction of shoe-surface interfaces has been documented, it has been limited by non-portable testing equipment (Cawley et al., 2006), forefoot only cleat engagement with the surface and small compressive loads (Lambson et al., 1996; Livesay et al., 2006), and an inadequate representation of modern day artificial turfs used in football (Cawley et al., 2003; Torg et al., 1974).

In the current study a mobile testing apparatus was developed to measure the torque produced at the shoe/surface interface on sixteen surface systems. It was hypothesized that the size and structure of the infill would affect the rotational resistance of cleated shoes.

METHODS

The testing method conformed to the ASTM standard method for traction characteristics of an athletic shoe-surface interface (F2333). A static compressive load of 1000N and a dynamic 90° external rotation were applied to shoes mounted on a rigid footform.

Additionally, a compliant ankle joint was developed to better represent the *in vivo* loading at the shoe-surface interface.

Ten cleated football shoes were tested across 16 surfaces (Figure 1). Five trials were conducted on fresh sections of turf resulting in a total n=50 for each surface. Peak torques were compared for various shoe-surface interfaces with an ANOVA and SNK post-hoc tests, when appropriate. An additional two-way ANOVA of the GameDay surfaces was performed to determine the effect of infill and surface fiber structure.
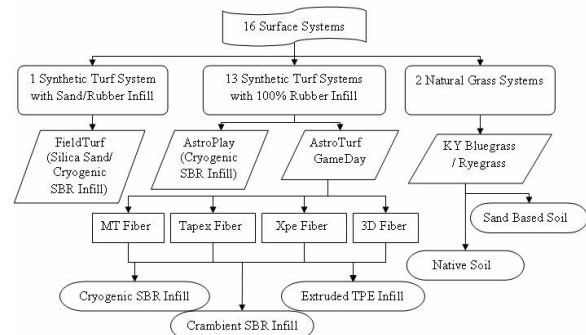
Figure 1: Description of the test matrix.

RESULTS AND DISCUSSION

Peak torques were significantly affected by playing surface (Figure 2). FieldTurf and the native soil natural grass system produced significantly different torques than all other surfaces. This was in agreement with the trend in a comparable study performed by Livesay et al (2006). In the GameDay analyses, all three infills were found to be significantly different from one another. The highest torques were associated with the cryogenic SBR infill. This infill consisted

of fine crumb rubber particles capable of packing into a dense structure thought to increase a cleated shoe's resistance to rotation. The lowest torques were associated with the extruded infill, a larger rounded cylindrical particle made of TPE, incapable of packing as tight as the cryogenically processed infill. The open structure of the extruded infill layer was thought to reduce the frictional resistance.

The GameDay analyses also indicated significant differences in peak torque for fiber structure in the GameDay 3D surface. This was the only fiber structure which consisted of a nylon root zone. The nylon root zone leads to a reduction in the amount of infill required for a stable system, which may lower the compactness of the infill layer. This may limit cleat contact with the infill, thereby lowering the peak torque.

Similarly, the highest mean torque, seen in the FieldTurf system, may be due to the cryogenically processed rubber embedded in a fiber layout constructed with a gauge length of 3/4". The gauge length is the distance between rows of fiber on the artificial surface, and it was 3/8" on all other tested synthetic surfaces. A greater gauge length may lead to more cleat penetration into the infill and in the case of a densely compacted infill, higher torques.

SUMMARY/CONCLUSIONS

Generation of excessive torque at the shoe-surface interface was a factor of both the infill particle size and fiber spacing. The peak torques measured in the current study exceed injury levels based on cadaveric studies (Hirsch and Lewis, 1965). However, muscle stiffness has been shown to protect the lower extremity at similar torques (Shoemaker, 1988). Future studies using a more biofidelic ankle may help establish relationships between shoe-surface

interfaces and the potential for ankle injury. Additionally, epidemiological studies of shoe and surface injury rates will be important for validating the injury risk potential of various shoe-surface interfaces.
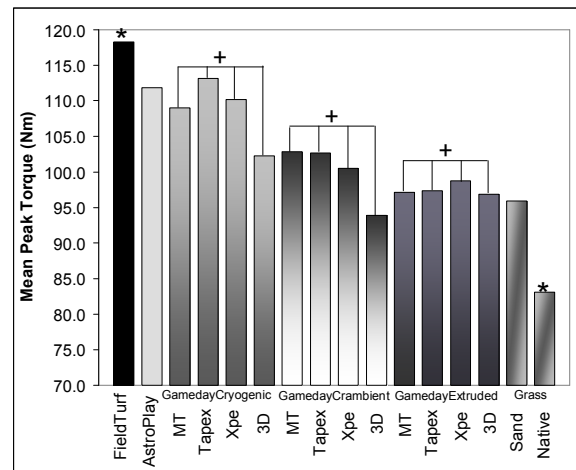
Figure 2: Mean peak torques
* significantly different from all systems.
+ significantly different from other infills.
 (+ from GameDay analyses)

REFERENCES

Cawley, P.W. et al. (2003). *Foot Ankle Int*, **24**(7), 551-556.
Fernandez, W.G. et al. (2007). *Academic Emergency Medicine*, **14**(7), 641-645.
Hirsch, C., Lewis, J. (1965). *Acta Orthop Scand*, **36**(4), 408-417
Lambson, R.B. et al. (1996). *Am J Sports Med*, **24**(2), 155-159.
Livesay, G.A. et al. (2006). *Am J Sports Med*, **34**(3), 415-422.
Shoemaker, S.C. et al. (1988). *Clin Orthop Relat Res*, **228**, 164-170
Torg, J.S. et al. (1974). *J Sports Med*, **2**(5), 261-269.

ACKNOWLEDGEMENTS

FOOTBALL SHOE DESIGNS MAY AFFECT LOWER EXTREMITY INJURY RISK

Mark R Villwock, Eric G Meyer, John W Powell, Amy J Fouty, Roger C Haut

Michigan State University, East Lansing, MI, USA
E-mail: haut@msu.edu, Web: www.obl.msu.edu

INTRODUCTION

High torsional friction between football shoes and the playing surface yields a potential for injury to the lower extremity (Torg et al., 1974). A study on the effect of four cleat designs on ACL injury rates determined that the cleat category with the highest torsional moment was associated with an ACL injury rate 3.4 times higher than all other cleat designs combined (Lambson et al., 1996).

Although the torsional friction of shoe-surface interfaces has been documented, it has been limited by non-portable testing equipment (Cawley et al., 2003), a small number of cleated shoes (Livesay et al., 2006), and forefoot only cleat engagement with small compressive loads (Lambson et al., 1996; Livesay et al., 2006).

The current study developed a mobile testing apparatus to measure the torque produced at the shoe/surface interface and the relative shoe rotation for ten football shoes representing five cleat design categories. It was hypothesized that shoes with numerous and/or large cleats around the peripheral margin of the sole would have higher torsional resistance than shoes with fewer or smaller cleats on the periphery.

METHODS

The testing method conformed to the ASTM standard method for traction characteristics of an athletic shoe-surface interface (F2333). A static compressive load of 1000N and a dynamic 90° external rotation were applied to shoes mounted on a rigid footform.

Additionally, a compliant ankle joint was developed to better represent the *in vivo* loading scenario at the shoe-surface interface.

Ten football shoes (Figure 1) were tested on sixteen surfaces, (14 infill based synthetic surfaces and 2 natural grass plots). Five trials were conducted on fresh sections of turf resulting in a total n=80 for each shoe. Rotational interface stiffness was computed as the slope of the torque versus shoe rotation plot between the onset of the test and 75% of peak torque. Peak torque and rotational interface stiffness were compared between shoe models and groups using an ANOVA followed by SNK post-hoc tests, when appropriate.

12 Stud Peripheral Molded Cleats		Edge Molded Blades			Hybrid (15+) Molded Cleats		7 Stud Replaceable Cleats		Turf Molded Nubs
Nike	Adidas	Nike	Adidas	Adidas	Nike	Adidas	Nike	Adidas	Adidas
Bladell TD	Scorch 7 Fly	Vapor Jet TD	Scorch TRX	Corner Blitz 7 MD	Air Zoom Superbad FT	Grid Iron	Air Zoom Blade D	Quickslant D	Turf Hog LE
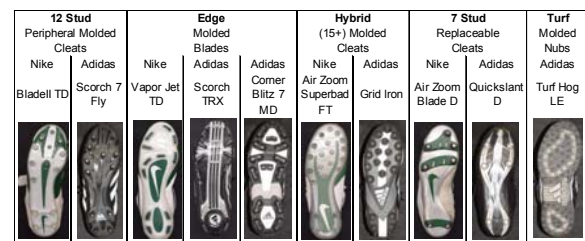
Figure 1: Description of tested shoes.

RESULTS AND DISCUSSION

Peak torques were significantly affected by the model and cleat design of the football shoe (Figure 2). The cleat group category with perimeter cleats (12 Stud and Edge) produced the highest torques in this study, comparable to the results of Lambson et al. (1996). Additionally, Blade II, a member of the 12 stud group, resulted in a significantly higher mean torque than the other perimeter cleat models. This may be due to the increased cleat length on this shoe, similar to

a previously documented relationship between cleat length and peak torque (Torg, 1974).

The highest rotational stiffnesses (Blitz and Grid Iron) were associated with large rubber cleats, and perhaps more importantly, the most rigid uppers and soles (Table 1). By comparison, the shoe with the lowest stiffness (Superbad) had a relatively pliable upper and sole, making it more capable of rotating on the rigid footform. This caused the leading edge of the shoe to dig into the ground and create a "snowplow" effect with the infill material. This gradual buildup of infill posed an additional source of torsional resistance that occurred after breakaway. This increase in rotation before reaching peak torque resulted in a lower stiffness for this particular shoe.

Livesay et al (2006) measured the rotational interface stiffness of different shoe-surface combinations, but only using forefoot cleats rigidly mounted on a plate. The results of the present study indicate that rotational interface stiffness of whole shoes may be a function of shoe fit as well as its ability to resist rotation about the mid-foot.

Table 1: Mean stiffness (Nm/deg).
* significantly different from all models.

12 Stud		Edge			Hybrid		7 Stud		Turf
Bladell	7Fly	Vapor	TRX	Blitz	Superbad	GridIron	BladeD	Qslant	TurfHog
3.2	3.3	3.1	2.9	4.0*	2.2*	3.9*	3.0	2.9	3.0

SUMMARY/CONCLUSIONS

Generation of excessive torque at the shoe-surface interface was a product of the cleat shape, length, and layout. The peak torques measured in the current study exceeded injury levels based on cadaveric studies (Hirsch and Lewis, 1965). However, muscle stiffness has been shown to protect the lower extremity at similar torques (Shoemaker, 1988). Future studies, using a more biofidelic ankle, may help establish

relationships between shoe-surface interfaces and the potential for ankle injury. Additionally, epidemiological studies of shoe and surface injury rates will be important for validating the predicted injury risk for various shoe-surface interfaces.
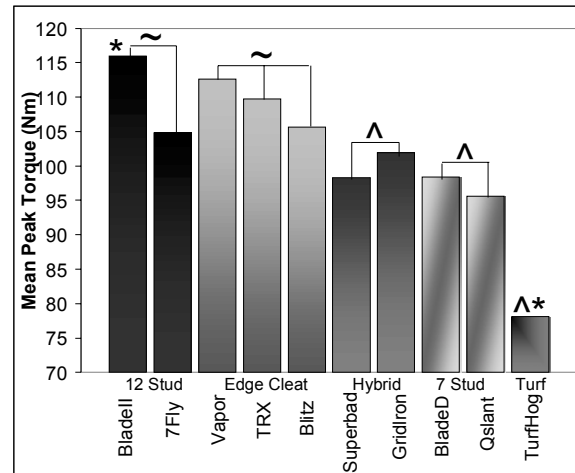
Figure 2: Peak torques for all shoe models
* significantly different from all models,
^ significantly different from all groups,
~ significantly different from Hybrid, 7 Stud, and Turf groups.

REFERENCES

Cawley, P.W. et al. (2003). *Foot Ankle Int*, **24**(7), 551-556.

Hirsch, C., Lewis, J. (1965). *Acta Orthop Scand*, **36**(4), 408-417

Lambson, R.B. et al. (1996). *Am J Sports Med*, **24**(2), 155-159.

Livesay, G.A. et al. (2006). *Am J Sports Med*, **34**(3), 415-422.

Shoemaker, S.C. et al. (1988). *Clin Orthop Relat Res*, **228**, 164-170

Torg, J.S. et al. (1974). *J Sports Med*, **2**(5), 261-269.

ACKNOWLEDGEMENTS

HIP KINEMATICS DURING THREE SOCCER KICKING TASKS

Robin M. Queen PhD[1,2], Brian L. Charnock, AB[1], William E. Garrett, Jr, MD, PhD[2]

[1]Michael W. Krzyzewski Human Performance Lab, [2]Orthopaedic Surgery Duke University
Medical Center, Durham, NC, USA
Contact: robin.queen@duke.edu, http://klab.surgery.duke.edu

INTRODUCTION

Groin injuries have been reported to account for between 5% and 13% of all soccer injuries, however, they result in a substantial loss of time from both practice and competition.(Gilmore, 1998; Wong and Hong, 2005) Groin injuries are most prevalent in sports involving repetitive kicking motions such as soccer, rugby and Australian Rules football, and are most predominant in males.(Gilmore, 1998; Karlsson, et al, 1994) Potential risk factors for groin injuries are thought to be previous strains, direct trauma, overuse and muscular imbalance between the abdominal muscles and adductors. (Gilmore, 1998). Therefore, the purpose of this study was to determine the differences in hip and knee kinematics of the kicking leg during three different kicking tasks in order to determine which kicking task put a player at the greatest risk for a groin injury.

METHODS AND PROCEDURES

Thirteen male, division one soccer players (mean age 20.7 ± 2.8 years, mean height 1.8 ± .08 m, mean weight 78.2 ± 9.7 kg) were tested using an 8 camera motion capture system collecting at 240 Hz (Motion Analysis, Santa Rosa, CA). All subjects were currently active at least 3 times per week, had no previous history of chronic groin pain, and no lower extremity or abdominal injuries in the previous 6 months. The ball used was an official size and weight Nike Geo (Nike, Inc,

Beaverton, OR). Subjects wore Nike Air Pegasus running shoes to minimize variability due to footwear. Subjects were asked to perform 7 acceptable trials for each of the following kicking tasks (direct shots at maximal effort, a pass with the medial side of the foot, and a crossing pass aiming at the top corner of the goal opposite their kicking foot) (Figure 1).
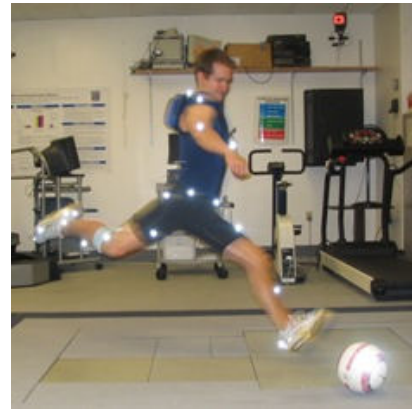
Figure 1: Subject set-up used for testing.

For each subject, 5 of the 7 collected trials were randomly selected for reduction. The swing phase for data reduction was defined as the time from toe off of the kicking foot until ball contact with the kicking foot and the data were normalized to 100% of the swing phase with toe off being zero percent and ball contact being 100%. The peak hip angles for external rotation (ER), abduction (ABD) and extension (EXT) were determined as well as the timing of each of these peaks as a percentage of the swing phase. In addition, peak knee flexion (FLEX) angle as well peak knee flexion timing and

contralateral heel strike (plant leg) were recorded as a percentage of the swing phase using OrthoTrak v6.3.4c (Motion Analysis Corporation, Santa Rosa, CA). The data was analyzed using a series of 1 X 3 repeated measures ANOVAs with Tukey's Post-hoc testing to determine statistical differences between the three kicking types ($\alpha = 0.05$).

RESULTS

Significant differences existed between the three kick types for peak hip ER, peak hip ABD, peak hip EXT, and peak knee FLEX (Figure 2). Peak hip ABD timing was significantly different between all three kick types. Peak hip ABD happens first during the pass followed by the cross and finally the shot. Peak hip EXT timing was significantly different between the pass and shot, with peak hip EXT happening first during the pass.

Kicking Leg Joint Angles for Three Kick Types

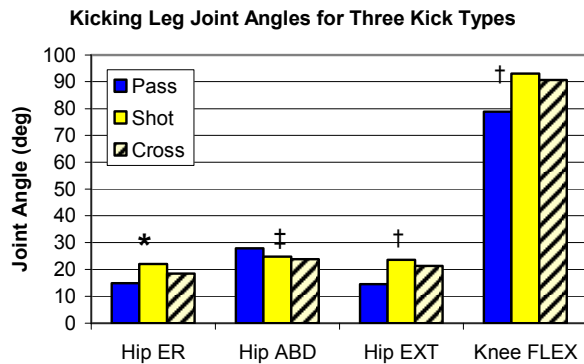**Figure 2:** Peak joint angles of the kicking leg during three kicking tasks. (*significant difference between 3 kick types, ‡ significant difference between pass and cross, † significant difference between pass and shot and between pass and cross)

In addition, peak hip EXT was significantly different between the pass and cross, with peak hip EXT happening first during the pass. Finally, contralateral foot strike (plant foot strike) was significantly different between the three kick types with foot strike happening first during the pass followed by the cross then the shot.

DISCUSSION

Previous literature has most often examined the in-step pass or shot in terms of describing the biomechanics of the task. However, this study aimed at understanding the differences between three different kicking tasks that are used during the game of soccer. Based on the results of this study it appears that the shooting task could potentially be the most dangerous when considering injury risk factors for the groin. Peak ER, peak EXT and peak knee flexion were all significantly greater during the shooting task when compared to the other kicking tasks. The fact that peak hip ABD was greatest during the passing task could be the result of contacting the ball with the instep of the foot as opposed to the laces as is done during the other two tasks.

SUMMARY

Future work examining potential groin injuries during soccer should be performed during a shooting task as this is the task that appears to put the adductors under the most stress during kicking. Future work should include some musculoskeletal modeling to determine the length of the adductors during these three kicking tasks.

REFERENCES

Gilmore J. (1998) *Clin Sports Med*. **17**:787-93.
Wong P and Hong Y. (2005) *Br J Sports Med*. **39**:473-82.
Karlsson J, et al. (1994) *Sports Medicine*. **17**(2):141-148.

Residual force enhancement in maximal voluntary contractions of human dorsi flexors

Markus Tilp, Simon Steib, Gudrun Schappacher-Tilp and Walter Herzog

Human Performance Laboratory, The University of Calgary, Faculty of Kinesiology 2500 University Drive NW Alberta, Calgary, Canada T2N IN4, mtilp@kin.ucalgary.ca

INTRODUCTION

When an activated muscle is stretched, the force during stretch exceeds the isometric force at the corresponding muscle length. In the steady state phase following the stretch, there is a remnant increase in force called "residual force enhancement" (RFE). RFE has been observed at different structural levels (ranging from myofibrils to human muscles), across activation levels (stimulated, sub- and maximal voluntary contractions), and on the entire force-length relationship (ascending and descending limb, plateau). Several mechanisms have been suggested to explain this phenomenon but no generally accepted explanation has been found (Herzog, 2004). In voluntary activated human muscles, different results have been found. Lee & Herzog (2002) reported RFE in maximal activated m. adductor pollicis, Pinniger & Cresswell (2007) observed RFE during submaximal voluntary contractions in the plantar- and dorsiflexion groups, while Hahn et al. (2007) did not find RFE in human quadriceps femoris. This study was aimed at investigating RFE under different stretch conditions to identify the possible reasons for the discrepancies in results reported in the literature. We hypothesized that RFE might be abolished in human voluntary contractions following great stretch magnitudes or fast stretch speeds.

METHODS AND PROCEDURES

Ten subjects (5 male, 5 female; 29 (9) years, 177 (11) cm, 71 (14) kg) participated in this study which was approved by the local Ethics Committee. Subjects were seated on a dynamometer (Biodex®, System 3) with their test leg horizontally extended. The backrest was set to 155 degrees to allow for a comfortable sitting position. The flexion-extension axis of the ankle was carefully aligned with the axis of the dynamometer and the ankle securely attached to the footplate with inelastic strapping. Knee and hip were fixed to the dynamometer chair with inelastic strapping. Ankle torque, angle and angular velocity as well as EMG from the tibialis anterior (TA) and medial gastrocnemius (MG) were recorded at 1,000 Hz. Fascicle lengths of TA were measured with ultrasound imaging.
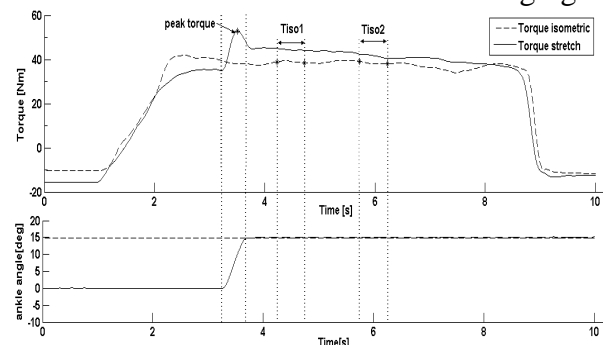
Figure 1. Ankle joint torque and angle as a function of time for an isometric reference contraction and an isometric contraction following stretch.

After a warm up, subjects performed isometric contractions with induced stretches from 0 (sole of the foot perpendicular to tibia) to 15 and from 0 to 30º plantar flexion. The stretches were performed at angular velocities of 10 and 45º/s in random order. Isometric reference contractions at the final stretch position preceded each test contraction. To evaluate possible RFE, we compared the

mean torque values of the isometric reference and the stretch test contractions at 0.5-1.0s ($T_{iso}1$) and 2.0-2.5s ($T_{iso}2$) following stretch (Fig.1). Differences were evaluated at a level of significance of 0.05 using paired t-tests (Bonferroni-Holmes corrected). Normalized mean values were analyzed using repeated measures ANOVA.

RESULTS

Peak torques during stretch did not occur at the end of the stretch and were always greater than the isometric reference torques (Fig. 1). Force following stretch was significantly greater than the isometric reference force at both times of evaluation and for both stretch magnitudes and stretch speeds. Residual force enhancement was greater at 0.5-1.0 than 2.0-2.5s. Stretch amplitude and angular velocity did not significantly influence RFE.

$T_{iso}1$		
Velocity/amplitude	15 deg	30 deg
10 deg/s	112 (10)	114 (10)
45 deg/s	112(10)	115 (10)
$T_{iso}2$		
10 deg/s	110 (10)	109 (14)
45 deg/s	106 (11)	108 (11)

Table 1. $T_{iso}1$ and $T_{iso}2$ torques normalized to isometric reference in %. Data are means (SD). n=10

The mean EMG values (rms 500ms) of TA during stretch exceeded the mean values observed during the isometric reference contractions for all stretch conditions (104-107 % of isometric). For the 0.5-1.0s evaluation period, mean EMG values were greater for all but one (30º and 45º/s) condition (105-107 vs. 97 % of isometric).

DISCUSSION

The aim of this study was to measure RFE for different stretch conditions of human TA activated by maximal voluntary effort. In accordance with Hahn et al. (2007), peak torques did not occur at the end of the stretch. Since we observed a decrease of EMG after peak torques had been achieved, it appears that muscle inhibition may have caused this result. Contrary to Hahn et al. (2007), but in accordance with Lee & Herzog (2002) and Pinniger & Cresswell (2007), we observed significant RFE in voluntary activated human muscles. We must reject the hypothesis that RFE is abolished by long stretch magnitudes or high speeds of muscle stretch during voluntary contractions, and thus cannot explain the discrepancies regarding RFE in the literature with differences in stretch conditions. Possibly, RFE in human muscles depends on muscle size, or might be masked by changes in activation that cannot be observed by surface EMG recordings. Comparisons of RFE at different times following stretch show that the residual force enhancement decreases with time, at least for the short time (2500ms) evaluated here.

SUMMARY

Residual force enhancement was observed for maximal voluntary contractions of the dorsi flexors at 0.5-1.0s and 2.0- 2.5s following stretch. EMG activity was greater during and after stretch compared to isometric. Stretch amplitude and velocity did not significantly affect the amount of RFE. The contradictory results in the literature remain unexplained.

REFERENCES

Hahn, D. et al. (2007). *Eur J Appl Physiol 100:* 701-709.

Herzog, W. (2004). *Hum Mov Sci 23:* 591 – 604.

Lee, HD and Herzog, W. (2002). *J Physiol 545:* 321-330.

Pinniger, GJ and Cresswell, AG. (2007). *J Appl Physiol 102:* 18-25.

CHANGES OF ARM MOVEMENTS IN DUAL TASK CONDITION ON DIFFERENT WALKING ENVIRONMENT IN HEALTHY YOUNG ADULTS

Yao-Cheng Hsieh, Chiung-Yu Cho

Department of Physical Therapy, Medical College, National Cheng Kung University
Email: cycho@mail.ncku.edu.tw

INTRODUCTION

Most of the previous studies investigated dual task effects on gait performance. Few of them focused on changes of arm movements. However, arms movement seems to play an important role to regulate balance control during walking. The purpose of this study was to investigate whether dual task paradigm would influence upper extremity movement during walking. Furthermore, we would like to examine the effect of different walking surfaces on dual task gait.

METHODS AND PROCEDURES

We recruited fifteen healthy young adults. All participants were asked to perform both walking task alone (single-task condition) and in combination with cognitive task while walking (dual-task condition). In the single task condition, each subject was asked to walk on soft foam and hard floor separately. In the dual task condition, subjects were asked to perform stroop test and digit span test while walking. Three dimensional relative angles of shoulder, elbow and lumbersacral joint; Absolute angle of pelvis and trunk were used as outcome measures. Also, we would compare the gait parameters and cognitive task performance between different conditions. Multivariate Analysis of Covariance (MANCOVA) was used to compare movement amplitude of joint angle among different walking conditions and groups. Velocity was considered as a covariance.

RESULTS

In the preliminary results, we included thirteen healthy young adults (age 23 ± 1.96 years). Compared with single task condition, young adults significantly decreased walking velocity (p=0.034) (Fig1) and step length (p=0.01), along with nearly significant increased stance time (p=0.061) in the dual task condition. But there was no significant difference in the movement amplitude of joint angle between different tasks.

Compared with hard floor condition, young adults significantly decreased walking velocity (p=0.034) (Fig1) and swing time (p=0.001), along with significantly increased step length (p=0.029), stance time (p<0.001), and movement amplitude of left shoulder flex/ext (p=0.026) abd/add (p=0.025), elbow flex/ext (p<0.035) varus/valgus (p<0.005) in the soft floor. Trunk/pelvis three dimensional movements (p<0.001) and lumbersacral joint A/P IR/ER movements (p<0.001) also significantly increased in the soft floor condition. There was no significant interaction between task and floor factors (p>0.1). For the cognitive task performance, only stroop test (1Hz) significantly decreased its scoring in the hard floor condition compared to the baseline performance (p=0.043).
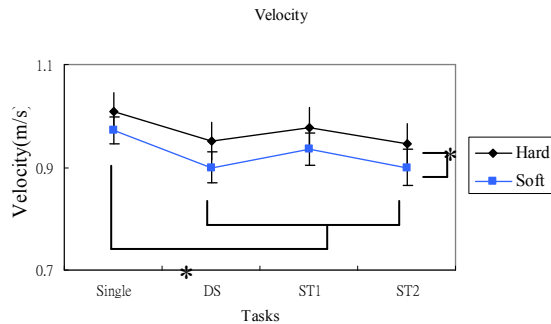
Fig 1. Walking velocity between different tasks and floors. (DS= digit span test, ST1= stroop test 1word/s, ST2= stroop test 1word/2s)

DISCUSSION

Preliminary results show that the dual task effects on our healthy young adults were mainly on the gait performance, but not on upper extremity movements. Since our young adults seemed to cope with dual task condition well, two tasks might not overload the central resources, and thus only provoked small interferences on the gait performance. Changes of gait patterns in the dual task condition were similar to previous studies. In the soft floor condition, healthy young adults change their movement pattern to cope with the challenging environment. They walked slower and increased joint movement amplitude to compensate for this situation.

SUMMARY

Healthy young adults change their gait pattern but not upper extremity movement to compensate the dual task condition. When confronting with soft foam challenging environment, young adults used a more conservative and protective strategy to compensate for this situation.

REFERENCES

Van Emmerik, R. E. A.et al (2005). Age-related changes in upper body adaptation to walking speed in human locomotion. *Gait Posture, 22*(3), 233-239.

Woollacott, M., & Shumway-Cook, A. (2002). Attention and the control of posture and gait: a review of an emerging area of research. *Gait Posture, 16*(1), 1-14.

Modelling the effect of Brownian motion on the amount of Backwards steps in the Classical Three-beads Laser Trap Setup for Actin-Myosin Interaction

Gudrun Schappacher-Tilp, Walter Herzog

Human Performance Laboratory, The University of Calgary, Faculty of Kinesiology 2500 University Drive NW Alberta, Calgary, Canada T2N IN4, gschappacher@kin.ucalgary.ca

INTRODUCTION

The properties of force and displacement of a single myosin molecule interacting with an actin filament attached between two optically trapped beads have been studied for more than a decade (Finer et al, 1994). According to the cross-bridge theory, the interaction between myosin and actin is governed by a deterministic process and the myosin molecule pulls the actin filament in one specific direction only (Huxley, 1957, Huxley and Simmons, 1971)

However, studies of single myosin-actin interactions have shown that cross-bridges pull actin filaments not only in a preferred but also in the opposite direction, thereby performing what is typically referred to as backward steps (e.g. Molloy et al, 1995). In a recent study, Jinha et al. (unpublished observations) found up to 30% backward steps, which is much greater than the average of about 10% of backward steps previously reported in these types of experiments. One possible explanation for this phenomenon could be, that due to the relatively soft laser trap setup used in Jinha's study (k_t=0.005 pN/nm) the Brownian motion acting on the actin filament has huge effects.

The aim of this study is to investigate, whether backwards steps could be explained by a cross-bridge model strictly based on Huxley's assumptions (Huxley, 1957), but incorporating large perturbations that are caused by Brownian motion, as observed in single cross-bridge-actin interactions.

METHODS AND PROCEDURES

We developed a mathematical model of the classical three-bead laser trap setup introduced by Finer et al. (1994, see Fig. 1). Briefly, this setup consists of two micron-sized beads attached to the ends of an actin filament. The beads are controlled by lasers for manipulation as well as for force and step size measurements. A heavy meromyosin (working part of a cross-bridge) is placed on a third bead fixed on a surface.
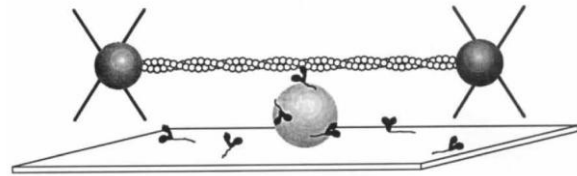
Figure 1. (Finer et al., 1994) Schematic diagram of two optical traps focused on beads which are attached to a single actin filament. The filament is held near a single heavy meromyosin molecule attached to a third bead.

The mathematical model is based on stochastic differential equations, the attachment and detachment rates of a single myosin are retrieved from the classical Huxley model (Huxley, 1957). This structure leads to coupled Fokker-Planck equations. If no analytical solution of the model can be found, a stable numerical algorithm will be used for analysing the model.

Different parameters for the laser trap stiffness are taken into account, since they influence Brownian motion which is a powerful force on the molecular level. The behaviour of a Brownian particle in a potential can be approximated by the

Boltzmann distribution, which describes the particle's steady state. The density function in Fig. 2 describes the influence of Brownian motion on the movement of the actin filament.

Figure 2. The density functions of Boltzmann distributions with different parameters for the trap stiffness. Further relevant parameters are: Boltzmann's constant ($k_B = 1.38065 \cdot 10^{-23}$ J/K), viscous damping coefficient 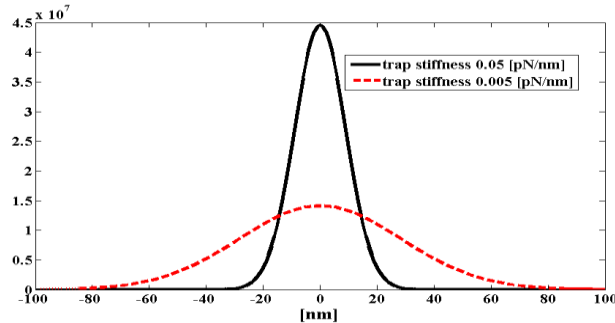on both beads attached to the actin filament ($b = 2 \cdot 10^{-8}$ N·s·m^{-1}) as well as the temperature (T = 290.15 °K).

The probability of a movement of the actin filament exceeding 10 nm is around 26 % for a trap stiffness of 0.05 pN/nm, whereas the same probability for a trap stiffness lowered by a factor of ten is approximately 72 %. We hypothesize that this dramatic change has an important and non-negligible effect on the attachment and detachment behaviour of cross-bridges.

DISCUSSION

Many approaches aimed at modelling the displacements of an optically trapped actin filament and its interaction with a myosin molecule have been published. Some of these models are based on the classical cross-bridge theory (Huxley, 1957). Backward steps in these models are accomplished with attachment rate functions that allow for such events a priori (e.g. Smith, 1998). Other approaches are based on stochastic models in which actin-myosin interactions are defined by Brownian ratchets in which directed motion is achieved by exposing cross-bridges to switching potentials (e.g. Shimakawa et al., 2003).

In contrast to these approaches we suggest that backward steps can be explained by Brownian motion as a perturbation on the actin filament in a three bead laser trap setup (Figure 1) while maintaining rate functions for single myosin interactions converging to the classical, deterministic cross-bridge rate functions (Huxley, 1957) for large numbers of actin-myosin interactions.

SUMMARY

Studies on single cross-bridge interaction with an optically trapped actin filament report a significant number of "backward" steps. This result appears in contradiction with the classic cross-bridge theory. However, Brownian motion is a powerful force on the molecular level and is directly related to the laser trap stiffness. Therefore, we suggest, that the number of backward steps is directly related to the stiffness of the laser trap: the greater the stiffness, the smaller the Brownian motion and the less the percentage of backward steps. In order to demonstrate this relationship, we developed a model derived from the attachment and detachment rate functions of the classical cross-bridge model that incorporates Brownian noise as a function of trap stiffness.

REFERENCES

Finer, J.T., et.al. (1994). *Nature,* 368:113-119

Huxley, A.F., (1957), *Prog Biophys Biophys Chem.,* 7: 255-318

Huxley, A.F., Simmons, R.M., (1971), *Nature.* 233:533-538

Molloy, J.E., et.al. (1995), *Nature,* 378: 209-212

Shimokawa, T., et al. (2003), *BioSystems,* 71:179-187

Smith, D.A., (1997), *Biophysical Journal,* 75:2996-3007

MECHANISMS UNDERLYING REDUCTIONS IN KNEE EXTENSION STRENGTH IN KNEE OSTEOARTHRITIS

Tamika Heiden, Dr David Lloyd, and Professor Tim Ackland

School of Sport Science, Exercise and Health, University of Western Australia, Perth, WA, Australia, dlloyd@cyllene.uwa.edu.au

INTRODUCTION

Quadriceps weakness (inferred from knee extension strength) is a common symptom in individuals with knee osteoarthritis (OA) (Hurley et al, 1998). Knee OA patients have deficiencies of 10-60% during maximal voluntary isometric extension (MVIE) compared with healthy age matched controls (Pap and Machner, 2004). Three factors thought to be responsible for this are 1) disuse atrophy, 2) quadriceps muscle inhibition (QMI), and 3) antagonist muscle co-contraction (ACC).

QMI in knee OA has been measured using the burst super-imposition technique (a train of pulses) or the twitch interpolation technique (a single pulse). The former method is preferred when examining QMI at high force levels (Stackhouse et al, 2000). With sufficient practice, motivation, feedback and rest knee OA patients showed no difference to controls in voluntary activation levels, and disuse atrophy was suggested as the likely cause of quadriceps weakness (Lewek et al, 2004). However, they did not measure ACC and, therefore, could not eliminate this as a cause for the apparent quadriceps weakness.

Knee muscle co-contraction occurs to improve movement efficiency, protect joints (Kellis, 1998) and decrease anterior shear forces (Kingma et al, 2004). Small amounts of ACC (10%) occur in MVIE trials of healthy adults (Busse et al, 2006). Since knee OA patients increase ACC during walking, possibly due to pain (Hubley-Kozey et al 2008), it is possible that abnormal ACC levels could decrease apparent knee extension strength in knee OA patients.

Therefore the purpose of this study was to examine the quadriceps strength, QMI and ACC during MVIE of knee OA patients.

METHODS AND PROCEDURES

Fifty-two patients (age 65.5 ± 7.6 years, height 1.70 ± 0.09 m, mass 81.4 ± 14.2 kg) previously diagnosed with OA and twenty-seven controls (age 64.9 ± 5.3 years, height 1.70 ± 0.09 m, mass 71.2 ± 13.2 kg) were recruited for this study. Exclusion criteria included previous ankle, knee, hip or back injuries and neurological conditions affecting motor function. This study was approved by the University of Western Australia Ethics Review Board.

Electromyographic (EMG) data were recorded from the rectus femoris (RF), vastus lateralis (VL), vastus medialis (VM), biceps femoris (BF) and semimembranosus (SM) using a tripolar configuration and an inter-electrode distance of 25 mm.

Strength was measured using a Biodex Isokinetic dynamometer with the knee and hip flexed to 90°. After familiarization subjects performed three maximum isometric trials of the quadriceps and hamstring muscle groups, each lasting approximately 4 seconds followed by a 2 minute rest period. Verbal encouragement and visual feedback was provided. The strongest measured trial was used for analysis.

QMI was measured with the use of a burst superimposition technique in which a supramaximal burst of electrical stimulation was superimposed on a MVIE trial. QMI values were calculated using central activation ratio (CAR), the ratio of volitional force and peak force with stimulus. All data were sampled simultaneously at 2000Hz.

Differences between patients and controls for each variable were examined using unpaired t-tests, significance was set at $p<0.01$.

RESULTS

Normalised (for body mass) knee extension strength of the OA group was significantly lower 1.50 ± 0.62 Nm.kg^{-1} than the control group 1.90 ± 0.48 Nm.kg^{-1} ($p = 0.005$).

The mean CAR values were 0.942 ± 0.041 and 0.952 ± 0.033 for the OA and control groups respectively and no significant difference existed between the groups ($p = 0.267$).

The co-contraction ratio of the quadriceps to hamstrings was 0.78 ± 0.12 for OA and 0.74 ± 0.17 for controls and was also not significantly different ($p = 0.205$).

DISCUSSION

These results demonstrate reduced MVIE strength in the absence of excessive ACC or QMI in OA patients compared with age matched controls.

Knee OA patients in this study had 22% less quadriceps strength compared with age matched controls. These findings are in agreement with previous finding of 24% strength reductions in OA patients compared to controls (Lewek et al, 2004).
The average voluntary quadriceps activation of healthy older controls in MVIE has been reported at 93% (Newham et al, 2001 &

Lewek et al, 2004). Both OA patients and controls in the current study had 94% activation, signifying healthy activation levels.

ACC of the hamstrings during MVIE trials has been reported between 12- 20% in young healthy subjects (Kubo et al, 2004) and up to 40% in healthy older women (Macaluso et al, 2002). ACC did not differ between the controls and patients in this study with values of 26% and 22% respectively, and were well within the normal values for healthy adults.

SUMMARY

The reductions in quadriceps strength seen in knee OA patients are not due to QMI or ACC, leaving disuse atrophy as a likely cause for quadriceps weakness in knee OA patients.

REFERENCES

Busse ME et al. (2006). *J Neuroeng Rehabil*, 3: 26-32.

Hubley-Kozey CL et al. (2008), *Clin Biomech,* 23: 71-80.

Hurley MV et al. (1998). *Curr.Opin. Rheumatol,*10: 246-250.

Kellis, E. (1998). *Sports Med*, 25: 37-62.

Kingma I et al. (2004). *J Electromyography Kinesiol*, 14: 307-315.

Kubo K et al. (2004). *Eur J Appl Physiol*, 91: 349-352.

Lewek MD et al. (2004). *J Orthopaed Res*, 22: 110-115.

Macaluso A et al. (2002). *Muscle Nerve*, 25: 858-863.

Newham DJ and Hsiao SF. (2001). *Disabil Rehabil,* 23:379-386

Pap, G and Machner, A (2004). *J Orthop Res,* 22: 96-103.

Stackhouse SK et al. (2000). *Muscle Nerve*, 23: 1706-1712.

Reproducibility of kinematical variables describing head and neck movement – A 3D movement analysis using the Finite Helical Axis Method

Helena Grip,[1] Fredrik Öhberg[1]

[1] Biomedical Engineering & Informatics, University Hospital of Umeå, Umeå, Sweden
E-mail: Helena.grip@vll.se

INTRODUCTION

The finite helical axis method (Spoor and Veldpaus, 1980) is an illustrative way to describe the combined rotation and translation of composite joint segments, such as the cervical spine. The head rotation relative the upper body is described with the helical rotation angle; θ, around the moving helical axis (described by position vector $\mathbf{c}$ and direction vector $\mathbf{n}$). The helical axis ("axis of motion") visualize on which level the rotation occurs. It relates to the composite movement of all cervical vertebrae and migrates during head movement (Winters, 1993). The helical rotation angle is well defined for small rotations, while error in axis direction and position are inversely proportional to the rotation magnitude (Woltring, 1985). This may affect the reliability of finite helical axis variables.

The aim of this pilot study was to investigate the reproducibility of head movement variables derived with the finite helical axis method (Grip, 2007) in a group of healthy volunteers.

METHODS

A task, including fast head rotations, was performed by 6 healthy young adults. The movement task was performed twice by each subject, with one week between each performance. The subject sat on a chair and a board with arrows was placed one meter in front of the subject. Fast maximal movements of flexion, extension and side rotations (left and right), were performed immediately after an arrow on the board (showing the direction) was illuminated. The movement was performed as fast as possible to a comfortable extent.

Movements were registered at 120 Hz with an optical movement capture system that included five cameras (Qualisys Medical AB®, Gothenburg, Sweden). In total, 10 retro-reflective markers were placed on the head and upper torso: four in a rigid cluster configuration on the head, one on the suprasternal notch, three on a rigid plate on the back, and one on each shoulder. The subject was seated relative to the lab coordinate frame, the X axis was transverse (along the shoulders), Y axis was anterior-posterior and Z-axis was vertical.

Data analysis was performed off-line using MATLAB® (The MathWorks Inc., Natick, MA, USA) and SPSS (version 11.0.1). The coordinate data were filtered with a 2nd order low-pass Butterworth filter, cut-off frequency 6 Hz. Head rotation was calculated relative initial head position. The maximal range of movement (ROM) and mean velocity were then calculated. The direction vector at 80% of ROM, $\mathbf{n}_{ref}$, was derived. The finite helical axis variables ($\mathbf{c}$ and $\mathbf{n}$) were estimated for each time frame using a dynamic moving window ($\Delta\theta = 4°$) and were filtered with the same filter as above The 3D angle between finite position of $\mathbf{n}$ and $\mathbf{n}_{ref}$; called ω, described the change

in axis direction. The center of rotation; **CR**, was defined as the intersection of the different finite axes; and was calculated for combined flexion/ extension and combined right/left side rotations. The trajectory of **c**, **CR** and ω was averaged over consecutive rotation levels (0-15°, 15-30°, 30-45°, 45-60°).

All variables described above were averaged from 5 repetitions on the day of measurement, and the test-retest reliability was estimated as follows: The effect from day (n=2) on ROM, mean head velocity, **CR**, mean ω and mean **c** was studied using a 2×1 repeated-measures ANOVA design. The effect from day (n=2) and rotation level (m=4; 0-15°, 15-30°, 30-45°, 45-60°) was studied for **CR**, ω and **c** using a 2×3 repeated-measures ANOVA design.

RESULTS AND DISCUSSION

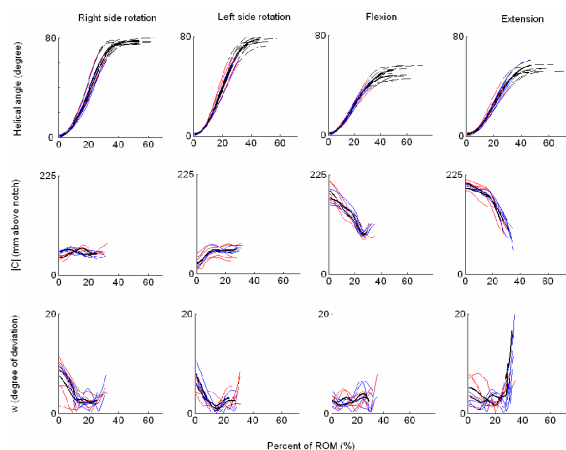Head movement curves were repeatable, as illustrated in Figure 1.

Figure 1: Repeated measurements for one subject from day 1 (red lines), and day 2 (blue lines) together with mean curves for each day (thick black lines). Angle of rotation (θ, on the top), axis position (**c,** in the middle) and 3D angle of **n** (ω, on the bottom); are illustrated for four movement directions; right, left, flexion and extension.

Repeated-measures ANOVA showed no significant effects from day of measurement on any of the derived variables (p = 0.11 to p = 0.99). A downward migration of **c** and **CR** was significant during flexion and extension, as well as lateral migration of **CR** during side rotation and extension (no interactions with day of measurement). A significant increase of ω towards the end of the movements was also observed.

SUMMARY/CONCLUSIONS

Estimates of ROM, head velocity, **CR**, ω and **c** were repeatable. The use of a moving window of 4° and a low-pass filtering when calculating finite positions of **n** and **c** may have increased the reliability.

The downward migration of the axis (Figure 1, middle row) was probably related to an increased curvature of the neck during flexion and extension as well as greater contributions from the lower cervical spine vertebrae towards the end of the side rotations. The change of ω for all movement directions (Figure 1, bottom row) was probably related to an increased amount of lateral bending towards the end of the movement.

REFERENCES

Spoor, C.W., Veldpaus, F.E., (1980). *J Biomech,* 13(4):391-3

Grip, H. et al, (2007). *J Clinical Biomech,* 22(8):865-73

Winters, J.M. et al (1993). *Spine*, 18 (9):1178-85

Woltring, H.J. et al (1985). *J Biomech,* 18(5):379-8

EFFECTS OF MUSCLE VIBRATION ON CONTROL OF FINGER MOVEMENTS FOLLOWING STROKE

Bing-Shiang Yang

Assistant Professor, Department of Mechanical Engineering and Brain Research Center,
National Chiao Tung University, Hsinchu, Taiwan, bsyang@mail.nctu.edu.tw

INTRODUCTION

Stroke is the leading cause of long-term disability. Hand dysfunction, primarily contributed by lack of finger independency or muscle selectivity, is the most common impairment in stroke survivors (Lang and Schieber, 2004; Nakayama et al., 1994). Muscle vibration to hand or wrist muscles can selectively modulate corticomotor excitability in unimpaired individuals (e.g. Kossev et al., 2001; Rosenkranz and Rothwell, 2003) and individuals following chronic stroke (Yang et al., 2006). A small-amplitude muscle vibration can enhances the excitability of a selective motor pathway controlling stroke-affected hand muscle while inhibiting (or providing no change to) the pathways controlling neighbouring same-hand muscles, though there are large inter-subject variations of vibration-induced modulations in corticomotor excitability (Yang et al., 2006). If this vibration-induced neurophysiological changes reflects in the control of finger movements, it would be a useful tool for improving independent control of finger movements. The purpose of this study is to examine the corresponding changes in active finger independency to the vibration-induced neurophysiological modulations in the stroke-affected sensorimotor functions.

METHODS

Ten stroke subjects (aged 55-75 yrs; 2-12 yrs post stroke) have been tested so far. Each subject was/will be tested in two set of experiments:

Neurophysiological Evaluation. The protocol is similar to our previous study (Yang et al., 2006). Muscle vibration (MV) was delivered to the rested muscle belly of individual hand muscles, bilateral abductor pollicis brevis (APB), first dorsal interosseus (FDI), or abductor digiti minimi (ADM), by an electromechanical vibrator (ET-132-203, Labworks Inc., California, USA) with a 7-mm diameter probe. The vibration frequency was set at 80 Hz and the amplitude adjusted to be just below each subject's threshold for perceiving an illusory movement or tonic vibration reflex. The excitability of contralaterally descending motor pathways was assessed by transcranial magnetic stimulation (TMS, Magstim 200, Magstim, Dyfed, UK). 120%-resting motor threshold TMS stimuli were used to elicit motor-evoked potentials (MEPs) in APB, FDI and ADM muscles in the stroke-affected hand, recorded using surface electromyography (EMG, AMT-4, Bertec Biomedical, Alberta, Canada), without and during vibration to one of the six hand muscles.

This set of experiment was used to identify the vibration location(s)/muscle(s) at which vibration provided facilitation to one of the three investigated motor pathways and inhibition or no change to the other two pathways, according to the MEP amplitudes measured from the target muscles. This identified vibration location was then used for the biomechanical study (described below).

Biomechanical Study. While the same-type vibration as used in Neurophysiological Evaluation was applied to the above identified location, subjects were instructed to move the individual finger in the direction (abduction) which the agonist muscle pathway was facilitated during vibration. The same EMG measurements were conducted as in Neurophysiological Evaluation. Kinematics of the thumb, index and little finger of the stroke-affected hand were recorded at 100 Hz using accelerometers. An *individuation index* and an *index of selective activation* were calculated to quantify the individuation of finger control and selectivity of muscle activation (Lang and Schieber, 2004).

RESULTS AND DISCUSSION

For every tested subject, MV to at least one location significantly modified corticomotor excitability (p<0.05). Subject-specific vibration-induced corticomotor excitability modulations were also identified. Figure 1 shows example data from one subject. For this subject, vibration to either stroke-affected APB (p<0.001) or FDI (p<0.05) provided differential modulations to the three tested motor pathways, e.g. MV to FDI facilitated MEPs in APB but provided no change to MEPs in FDI or ADM.

The observed MV-induced modulations in the Neurophysiological Evaluation also reflected in the control of finger movements. While APB was instructed to ab/adduct repeatedly, the *individuation index* of thumb and *selective activation* of APB (not shown) were higher during MV to FDI that that without MV (Figure 1).

SUMMARY

Individual muscle vibration could selectively modulate corticomotor excitability and active control of finger movements in individual

following chronic stroke. Vibration might be a useful tool for stroke hand rehabilitation to promote more independent finger movements.
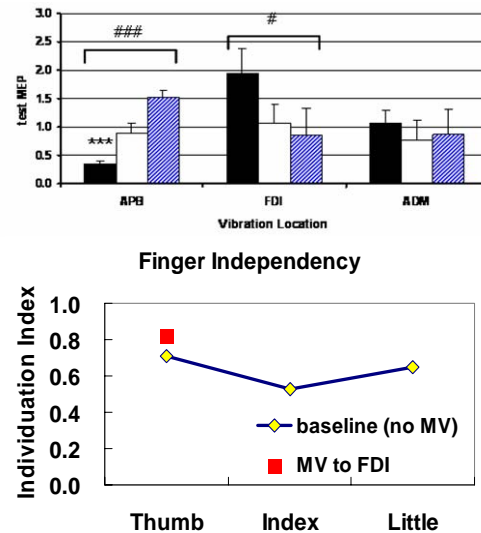

Figure 1. Example data of one subject. Means of ten MEPs (normalized by MEPs of each muscle without vibration) in the stroke-affect hand muscles during vibration to three different locations (top); *individuation index* of instructed ab/adductions of different fingers without vibration (no MV) and with MV to FDI (bottom).

REFERENCES

Kossev, A, et al. (2001). *Clin Neurophysio*, 112:453-456.

Lang, CE and Schieber, MH (2004). *J Neurophysio*, 91:1722-1733.

Nakayama, H, et al. (1994). *Arch Phys Med and Rehab*, 75:394-398.

Rosenkranz, K and Rothwell, JC (2003). *J Physio*, 551:649-660.

Yang, B-S, et al. (2006). *Soc for Neurosci Ann Meeting*, Atalanta, Georgia, USA.

ACKNOWLEDGEMENTS

HEAD MOTION DURING BASEBALL PITCHING

Dave Fortenbaugh, Glenn S. Fleisig, Shouchen Dun, James R. Andrews

American Sports Medicine Institute, Birmingham, AL, USA
E-mail: davef@asmi.org

INTRODUCTION

Coaching literature has suggested that limiting head movement is a key to pitching accuracy (Winkin et al., 2001). The movement of the head during pitching has not been well documented (Dun et al., 2006), and no studies have linked head movement to the ability to throw strikes. The purpose of this study was to quantify the movement of the head during pitching and determine if a relationship exists between head movement and pitch accuracy.

METHODS

Current collegiate and professional pitchers (N=43) volunteered to participate in this study. Subjects were 22 ± 3 years old, with an average height and mass of 191 ± 6 cm and 94 ± 10 kg, respectively. All subjects were healthy enough to pitch competitively. Each subject completed an informed consent form prior to testing.

An eight-camera Eagle 4 motion capture system (Motion Analysis Corp., Santa Rosa, CA) tracked reflective markers that had been placed on anatomical landmarks of the subject's body (Barrentine et. al.,1998; Dillman et. al., 2002). The subject was also fitted with a hat that contained four markers (front, top, rear, and lateral offset) to track the head movement specifically for this study. After completing a normal warm-up routine, a preliminary static trial was collected to define a neutral position for the head. Then, the subject pitched 10 fastballs from an indoor pitching mound with maximal effort towards a strike zone target located 18.4 m away from the rubber. A researcher logged each pitch's location.

Local, orthogonal coordinate frames were created in order to calculate movement in reference to the global frame (see Figure 1). Global x-axis rotation was called lateral head tilt with positive rotation towards the throwing shoulder. Global y-axis rotation was called forward head tilt with positive rotation looking upwards. Global z-axis rotation was called head rotation with positive rotation towards the non-throwing shoulder.

Figure 1. Global and local coordinate frames for the head and trunk.

For each pitch, the head's orientation among the three axes with respect to the global frame was recorded at four discrete events of the pitch sequence: foot contact (FC), maximum external rotation of the shoulder (MER), ball release (BR), and maximum internal rotation of the shoulder (MIR). Two separate data analyses were performed based on available data. In the first analysis, subjects were classified into accuracy groups by the number of strikes thrown out of 10: very accurate (9 or 10), somewhat

accurate (7 or 8), or not accurate (6 or less). Using five randomly selected pitches per subject, MANOVAs were used to compare the subjects' head orientation by accuracy group at each of the events and over the range of events. In the second analysis, MANOVAs were used to compare the head's orientation within each pitcher at each of the events for three balls versus three strikes. For all tests, $\alpha = .05$.

RESULTS

The head's range of motion from FC to MIR was $33° \pm 2°$ of lateral head tilt, $15° \pm 2°$ of forward head tilt, and $37° \pm 2°$ of head rotation. Analyzing pitchers by accuracy group, significant differences were seen only in lateral head tilt at FC, forward head tilt at FC and MIR, and head rotation in the FC-to-MIR range of motion (Table 1). Analyzing within pitcher, no significant differences were found in head orientation at any event.

Variable	Very Accurate	Somewhat Accurate	Not Accurate
FC – Lat. Tilt (deg)	8(2)[*]	12(2)[+]	1(2)[*+]
FC – For. Tilt (deg)	20(2)[*+]	13(2)[*]	14(2)[+]
MIR – For. Tilt (deg)	32(3)	24(3)[*]	34(2)[*]
Range – Rotation (deg)	32(3)[*]	44(3)[*]	36(3)

Table 1. Means (SDs) by accuracy group for significantly different variables. [*+] Post-hoc differences between groups.

DISCUSSION

While the head motion was further quantified by having a larger sample than previous research (Dun et.al., 2006), it was surprising that, contrary to the coaching literature that preaches maintaining a steady head to improve control (Winkin et al., 2001), few differences were seen between the most accurate and the least accurate pitchers and within individual pitchers. Moreover, no practical differences or logical trends were seen; the magnitude of the differences was at most $8°$ to $10°$, and there was no discernible progression from the most accurate to the least accurate pitchers. Two limitations to this study may have led to this result and should be the focus of future research. First, pitch location could have been better differentiated (e.g. inside balls, strikes, and outside balls) in order to determine a relationship between head movement and accuracy. Second, since pitching is an open-loop action, it may be that by the time of FC the mind and body have already determined the location to which they want the ball to be delivered. In this case, the motions recorded in this study are more probably a consequence of the other, more rapidly moving body parts and an anticipation of viewing the result of the pitch. Perhaps an analysis of head motion in the earlier phases in the delivery may correlate more strongly with accuracy.

REFERENCES

Barrentine, SW et al. (1998) *JOSPT*, 28: 405-15.
Dillman, CJ et al. (2002) *JOSPT*, 18: 403-8
Dun, S et al. (2006) *ASB Conf. Proceeding*
Winkin, J et al. (2001) *Baseball Skills & Drills*. Champaign: Human Kinetics

INVESTIGATING THE EFFECT OF CONTROLLING FOR WALKING VELOCITY: AN ELECTROMYOGRAPHIC ANALYSIS OF THE LOWER EXTERMITY DURING GAIT IN KNEE OSTEOARTHRITIS

Derek Rutherford[1], Cheryl Hubley-Kozey[1,2] and William Stanish[3].

[1]School of Biomedical Engineering, Dalhousie University, Halifax, NS, Canada. djr@dal.ca
[2]School of Physiotherapy, Dalhousie University, Halifax, NS, Canada
[3]Department of Surgery, Dalhousie University, Halifax, NS, Canada.

INTRODUCTION

Investigating neuromuscular control and recruitment strategies during gait in individuals with knee osteoarthritis (OA) is relatively novel. Differential, medial/lateral muscle group activation is important for understanding of these factors in individuals with knee OA (Hubley-Kozey et al. 2006, Lewek et al 2004). Despite these findings, determining if these features of differential activation are characteristic of individuals with a certain severity of knee OA or an artifact of differing spatial and temporal gait characteristics remains fundamental.

The purpose of this gait study was to investigate the overall magnitude of the electromyogram (EMG) of seven lower extremity muscles while controlling for velocity in asymptomatic individuals (ASY), those with mild to moderate knee OA (MOA) and individuals with severe knee OA (SOA) using principal component analysis (PCA).

METHODS AND PROCEDURES

Fifteen ASY, 16 MOA (classified by Kellgren-Lawrence I-III, and functional assessments) and 16 subjects with SOA (tested within one week of total knee replacement surgery) were selected from a large group of individuals who had all completed prior gait analysis. All subjects provided written informed consent. Participants with self-selected gait velocity greater than one m/s from each group were selected. After appropriate skin preparation procedures, circular Ag/AgCl bipolar skin surface electrodes (interelectrode distance 20mm) were affixed over the lateral gastrocnemius (LG), medial gastrocnemius (MG), vastus lateralis (VL),vastus medialis (VM), rectus femoris (RF), lateral hamstring (LH) and medial hamstring (MH). At least five walking trials were completed where subjects ambulated at their self-selected velocity. Signals were collected at 1000 Hz using an AMT-8™ (Bortec, Inc., Calgary, Alberta) EMG measurement system. Time normalization was determined from three-dimensional motion and ground reaction force data. All EMG waveforms were corrected for subject bias, full wave rectified, low pass filtered (Butterworth, zero lag, 6Hz), time normalized to represent 100% of the gait cycle and amplitude normalized to the respective MVIC activity.

PCA, a multivariate statistical technique was employed (Hubley-Kozey et al. 2006) to extract the waveform features from each muscle group that explained the variance in the overall magnitude of the EMG signal. *PC-Scores* were computed for each original EMG waveform. Analysis of variance models were used to test for group and muscle main effects and interactions. Bonferonni post hoc adjustments were used to test significance at alpha = 0.05.

Group	N	Age (years)	BMI (kg/m^2)	Velocity (m/s)	Stride Length (m)
ASY	15	56 ± 5*	25.1 ± 3.5*	1.19 ± 0.06	1.33 ± 0.08
MOA	16	64 ± 7	31.1 ± 3.9	1.18 ± 0.09	1.35 ± 0.09
SOA	16	67 ± 9	31.0 ± 4.6	1.14 ± 0.12	1.33 ± 0.11

Table 1: Demographics and Spatial Temporal Gait Characteristics (Mean ± SD) [* (A) sig. < (M) & (S)]

RESULTS

Demographic and spatial/temporal gait characteristics are shown in table 1. For each muscle group, principal component (pattern) one (PC1) captured the overall magnitude of the waveforms, explaining 63%, 70% and 56% of the variance in the calf, quadriceps and hamstring waveforms respectively. There were no group differences in the overall magnitude of VL, VM and RF ($p>0.05$).
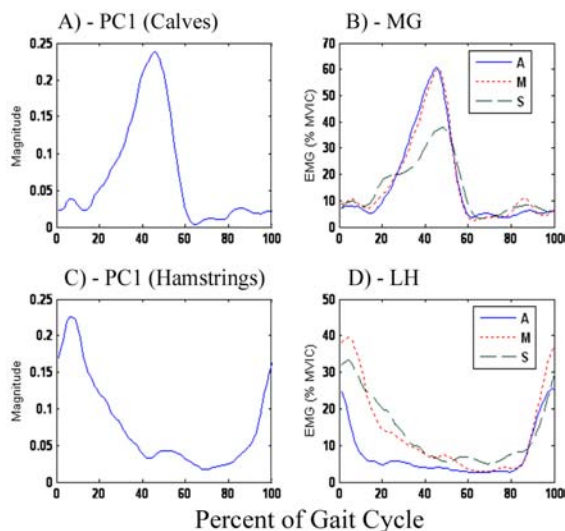

Figure 1: PC1 and ensemble averaged waveforms for MG (A & B) and LH (C & D).

For the ASY group, the overall MG magnitude was greater than LG ($p=0.01$). This was not found in the MOA ($p=0.08$) or (SOA) ($p=1.00$) group. No group differences were found in the overall magnitude of the LG ($p=1.00$). The overall magnitude of the MG was reduced in the SOA group compared to ASY and MOA ($p<0.05$). The overall magnitude of LH was greater than the MH for all groups ($p<0.05$). The magnitude of the LH and MH was greater

for the MOA and SOA groups compared to the ASY group ($p<0.001$) (Fig. 1D).

DISCUSSION

In the severe OA group, the reduction in MG activity may indicate that a mechanism to reduce medial joint loading is occurring despite a similar velocity between groups. The magnitude differences in hamstring EMG are consistent with previous literature implying that greater antagonist hamstring activation is occurring during the gait cycle in those with knee OA. These findings also suggest, that the lateral muscles are activated to a greater degree than medial muscles, a possible mechanism to reduce medial joint loading.

SUMMARY

This study provides evidence that differences in the magnitude of myoelectric activity during gait occur based on the presence and severity of knee OA and that these differences are occurring independent of gait velocity. Overall, the reduction in MG magnitude unique to the SOA subjects and an increased magnitude of LH in both groups with knee OA are consistent with a strategy to reduce medial knee joint loading.

REFERENCES

Hubley-Kozey C.L et al. (2006)
   J. Electro Kinesio 16, 365-378.
Lewek M.D et al. (2004)
   Osteoarthritis Cartilage 12, 745-751.

ACKNOWLEDGEMENTS

AN ELECTROMYOGRAPHIC ANALYSIS OF ALTERING
FOOT PROGRESSION ANGLE DURING GAIT

Derek Rutherford[1], Cheryl Hubley-Kozey[1,2]

[1]School of Biomedical Engineering, Dalhousie University, Halifax, NS, Canada. djr@dal.ca
[2] School of Physiotherapy, Dalhousie University, Halifax, NS, Canada

INTRODUCTION

Toe out gait has been shown to reduce the medial compartment loading environment during gait. This affect has been quantified through knee adduction moment analysis (Guo et al. 2007). The loading environment of the knee joint can also be affected by subsequent muscle forces experienced during gait. Differential activation is important to the understanding of neuromuscular control strategies and joint loading mechanisms (Hubley-Kozey et al. 2006, Lewek et al 2004). While many studies support that toe out gait affects the knee adduction moment, to our knowledge no study has evaluated the neuromuscular demands of this modification in any population.

The purpose of this study was to investigate the overall magnitude of the electromyogram (EMG) of eight lower extremity muscles during neutral and toe out gait in a healthy adult population using principal component analysis (PCA).

METHODS AND PROCEDURES

Twenty-two volunteers (13 females and 9 males) between the ages of 35 and 60 ($\bar{x}$ 46.7 and SD 7.6) years participated in this study. All subjects gave written informed consent. After appropriate skin preparation procedures, bipolar skin surface electrodes (Ag/AgCl-interelectrode distance 20mm) were placed over the lateral gastrocnemius (LG), medial gastrocnemius (MG), vastus lateralis (VL), vastus medialis (VM), rectus femoris (RF), lateral hamstring (LH) medial hamstring (MH) and gluteus medius (GM). Subjects completed at least five trials of toe out walking (TO) and five trials of neutral walking (N) at their self-selected speed. Criteria for toe out gait included a foot progression angle at least 10 degrees greater than neutral and velocity within 0.1 m/s. Maximal voluntary isometric contraction (MVIC) exercises were completed for normalization purposes. Three-dimensional motion and ground reaction force data were recorded during gait for foot progression angle calculations and waveform time normalization. The myoelectric signals were collected at 1000 Hz using an AMT-8™ (Bortec, Inc., Calgary, Alberta) EMG measurement system. All of the EMG waveforms were corrected for subject bias, full wave rectified, low pass filtered (Butterworth, zero lag, 6Hz), amplitude normalized to MVIC and time normalized to represent 100% of the gait cycle.

PCA was used to extract the waveform feature from each muscle group that explained the variance in the overall magnitude of the EMG signal (Hubley-Kozey et al. 2006). *PC-Scores* were computed for each original EMG waveform. Repeated measures ANOVA models were used to test for walking condition and muscle main effects and interactions. Bonferonni post hoc adjustments were used to test significance at alpha = 0.05.

RESULTS

Foot progression angle was significantly different between conditions (5 ± 4.5 degrees (N) and 21.5 ± 4.5 degrees (TO)) (p<0.05). Self-selected velocity was not different between conditions (1.46 ± 0.14 m/s (N) and 1.47 ± 0.15 m/s (TO)) (P>0.05). For each muscle group, principal component one captured the overall magnitude of the waveforms, explaining 60%, 66% , 67% and 62% of the variance in the calf, quadriceps, hamstrings and gluteus medius waveforms respectively. A significant condition main effect was not found for any of the muscles (p>0.05). The ensemble averaged EMG waveforms, separated by condition, for each of the eight muscles are shown in figure 1.

DISCUSSION

Principal EMG patterns for these muscles, except gluteus medius have been described in the literature (Hubley-Kozey et al 2006). Principal component one for Gluteus Medius is shown in figure 2. The overall magnitude and principal shape of the myoelectric activity did not differ between subjects walking in neutral alignment and during the adoption of a toe out gait. This finding suggests that knee joint loading cannot be expected to increase as a result of increased muscle forces during toe out gait.
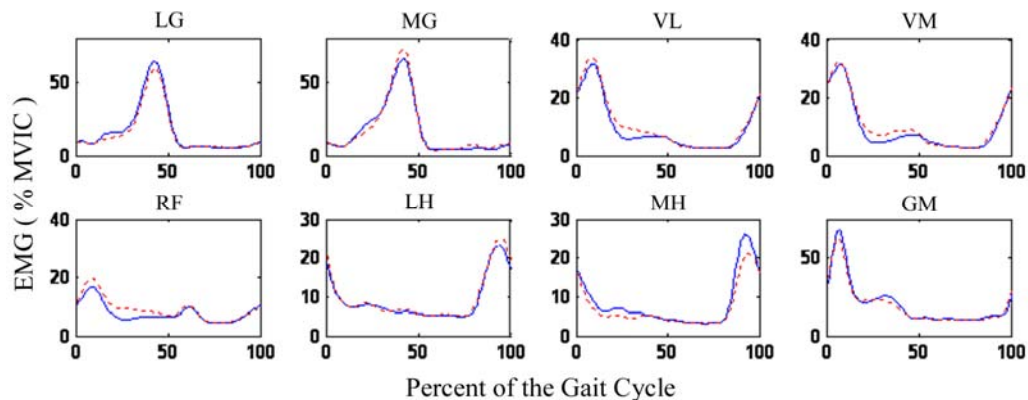

Figure 2: PC1 for Gluteus Medius

SUMMARY

Where other studies have focused on the kinetics of gait, these findings suggest that this gait modification does not alter the myoelectric activity of the major muscle groups in the lower extremity of asymptomatic subjects that have potential to influence knee joint loading. Toe out gait, a strategy to reduce medial knee joint loads, requires further electromyographic testing in patients with knee osteoarthritis.

REFERENCES

Guo M. et al. (2007)
    Gait and Posture 26, 436-441.
Hubley-Kozey C.L et al. (2006)
    J. Electro Kinesio **16**, 365-378.
Lewek M.D et al. (2004)
    Osteoarthritis Cartilage **12**, 745-751.

ACKNOWLEDGMENTS

Figure 1: Ensemble averaged waveforms for the eight lower extremity muscles. Solid line (Neutral Walking (N)), Dashed line (Toe out walking (TO)).
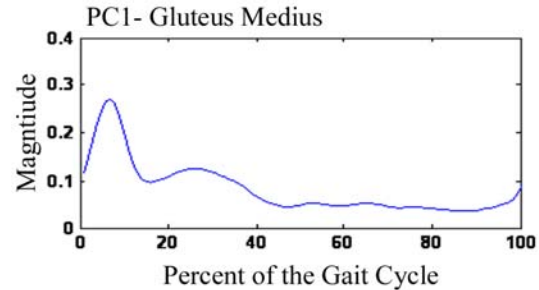
IN VIVO EVALUATION OF THE STIFFNESS OF THE HEALING HUMAN PATELLAR TENDON

Hsin-Yi Liu; R. Alex Creighton; Troy Blackburn; Darin Padua; Paul Weinhold

Human Movement Science Program, Depts. of Orthopaedics and Exercise and Sports Science
University of North Carolina, Chapel Hill, NC, hsinliu@med.unc.edu

INTRODUCTION

Tendon injuries are common among athletes as well as the general population. However, the success of current tendon repair and rehabilitation protocols remains controversial due to the subjective content of clinical assessments of recovery. Tendon mechanical properties have been considered the "gold standard" in evaluating the healing of tendon, but these measures have not been convenient to record *in vivo* due to the invasive nature of conventional mechanical testing. Recently, an *in vivo* ultrasonography technique has been applied in human subjects to detect the change in mechanical properties of healthy tendon with altered loading (Reeves et al., 2003). The objective of this study was to assess the capability of this technique to track the change in stiffness in the healing human patellar tendon.

METHODS AND PROCEDURES

Eight subjects undergoing anterior cruciate ligament reconstruction with a patellar tendon autograft were enrolled in the study as well as 8 healthy matched-control subjects. Surgical subjects had their patellar tendon stiffness evaluated at 2, and 6 months after surgery while control subjects were evaluated at 0 and 4 months after enrollment. Surgical subjects were evaluated for both knees (surgical and contralateral) while the control subjects were evaluated for only the knee that matched to the same side of the matched surgical knee. Each subject performed 6 trials of an isometric maximal contraction of knee extensors at 90° of knee flexion while knee torque was measured on a muscle strength system. During the task, an ultrasonic transducer was alternately used to track the displacement of the inferior border of the patella or distal insertion of the patellar tendon. Hamstrings EMG was monitored during the extension task and was used to account for the counter torque provided by this muscle group. The knee torque, EMG, and ultrasonic video data were initiated and sampled simultaneously. The cross-sectional area and the original length of the patellar tendon were measured from ultrasonic images. The displacements at the tendon insertions were computed using a pattern matching algorithm based on the normalized cross-correlation function and used to estimate the tendon deformation. The deformation at the tibial insertion at the same loading level was adjusted to the deformation at the patellar insertion. Tendon force was computed from the knee torque data and estimates of the patellar tendon moment arm. The force-deformation curve of the tendon was fitted with a nonlinear function and the tangential stiffness was evaluated at an equivalent load across paired subjects and time points. A normalized stiffness was computed as the stiffness multiplied by the ratio of tendon length to area. Subjects filled out a Visual Analog Scale (VAS), Activity Rating Scale (ARS), and International Knee Documentation Subjective Knee Form (IKDC) at each time point. A paired sign-rank test was performed to examine if the outcome measures changed with healing time.

RESULTS

The average time from injury to surgery for the surgical subjects was 49.5 days (range: 20~99). During the second testing session, the tangent stiffness of the surgical tendons relative to the contralateral tendons at the first visit increased from ~63% to ~74%; however, the difference was not significant (P=0.74) (Figure 1). The normalized tendon stiffness of the surgical tendons relative to the contralateral tendons at the first visit increased from ~58% to ~88% (P=0.25) (Table1). For the surgical knee, the max knee torque, IKDC, and ARS scores significantly improved with time and tendon area and VAS decreased with time (Table 1). No difference with time was found in any of outcome measures for the control subjects.

	Surgical		
Parameter	2 month	6 month	Pvalue
Knee torque	547 ± 228	1088 ± 403 *	0.008
Tendon area	119 ± 15	100 ± 26 *	0.039
IKDC	26.7 ± 22.5	47.3 ± 28.4 *	0.008
VAS	3.93 ± 2.40	2.26 ± 1.42 *	0.016
ARS	0.13 ± 0.35	8.38 ± 5.42 *	0.016
Normalized Stiffness	0.57 ± 0.25	0.86 ± 0.68	0.250

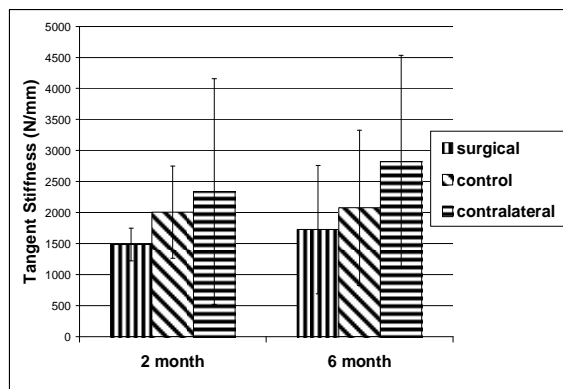**Table 1.** Outcome measures for surgical knee at the two visits (Mean $\pm$ SD)

Figure 1. Tangent stiffness of the three groups during the two visits. (Mean $\pm$ SD)

DISCUSSION

A priori power analysis was performed to determine the required sample size based on the data of previous animal studies (Ng et al., 1995; Atkinson et al., 1998) and our pilot studies. However, because of the smaller increase and larger variation in stiffness properties of the healing tendons, we were unable to detect a significant change in tendon stiffness during the 4 month time frame. This was despite significant improvements in max knee torque, VAS, ARS, and IKDC scores for the surgical subjects. These contrasting results suggest functional activity level and symptoms should not be used as the only indication for tendon healing as they may allow for the healing tendon to be put at risk of re-injury. Our results suggest a larger time frame or sample size may be needed to observe the healing effects on human tendon stiffness properties. It is possible that subjects who maintained a relative sedentary life style after the surgery may have prevented increases in the tendon stiffness.

Limitations of the study include: 1. The more lateral placement of the US transducer in the surgical knees may increase the probability of misalignment of the ultrasound scan with the line of action of the tendon and thus cause an increase in variation of the data. 2. In order to normalize to the weakest subject and time point, we did not include the data from the higher force region, which may have decreased the chance for us to see a difference in the tangential stiffness across time and between groups. Future studies may have to evaluate stiffness properties using a relative force level approach and use a larger sample size and/or time frame to confirm the healing effects on the stiffness properties of human tendon.

REFERENCES

Atkinson TS et al. (1998). *J Surg Res* 79: 25-30.
Ng GY et al. (1995). *J OrthopRes* 13: 602-8.
Reeves ND et al. (2003). *J Physiol (Lond)* 548: 971-81.

EFFECTS OF VARYING SURFACE INCLINES AND SUIT PRESSURE; IMPLICATIONS ON SPACE SUIT DESIGN

Kurt Clowers[1], Timothy Clark[1], Lauren Harvill[2], Richard Morency[3], and Sudhakar Rajulu[3]

[1]MEI Technologies, Inc, Anthropometry & Biomechanics Facility, National Aeronautics and Space Administration (NASA), Houston, TX, kurt.g.clowers@nasa.gov
[2]Lockheed Martin, Anthropometry & Biomechanics Facility, National Aeronautics and Space Administration (NASA), Houston, TX
[3]Anthropometry & Biomechanics Facility, National Aeronautics and Space Administration (NASA), Houston, TX,

INTRODUCTION

Suited human performance studies in reduced gravity environments to date included limited observations from Apollo Lunar surface Extravehicular Activities (EVA) and from previous studies conducted in partial gravity simulation environments. The Constellation Program EVA Systems Project office has initiated a series of tests to develop design requirements for the next generation Lunar EVA suit. Theses studies are conducted in the Space Vehicle Mock-Up Facility (SVMF) at Johnson Space Center from which the results will provide recommendations for suit weight, mass, center of gravity, pressure, and suit kinematic constraints that optimize human performance in partial gravity environments.

METHODS AND PROCEDURES

All studies at the SVMF used a pneumatic cylinder servo controlled to result in a constant simulated gravitational offloading throughout the subject's motion. All subjects donned the Mark III (MKIII) technology demonstrator suit. A gimbal support structure attached to the end of the lifting actuator supported a suited subject and allowed for the pitch, roll, and yaw rotational degrees-of-freedom during movement. Six astronauts approved by NASA JSC Committee for the Protection of Human Subjects walked at 10, 20, and 30 percent inclines on a VacuMed treadmill instrumented with four strain gauge force plates (1000 Hz, AMTI, Watertown, MA) that recorded the ground reaction forces (GRF) and moments. Three-dimensional trajectories of 65 retro-reflective markers placed at approximate landmarks on the MKIII suit were digitized (100 Hz, Vicon, Oxford, UK) to determine the displacement of the segments of the suit. This information was used for subsequent analysis to describe the kinematics of the MKIII suit during treadmill ambulation at varying suit pressures. Each astronaut completed each ambulation trial for 30 gait cycles at 5 different suit pressures: 1.0, 3.0, 4.3, 5.0 and 6.5 psi. Each astronaut was offloaded $5/6^{th}$ the combined suit plus body weight.

RESULTS

Peak vertical ground reaction force (GRF) data were normalized to $1/6^{th}$ each astronauts' lunar suited body weight (LSBW- body weight plus the 265lb MKIII suit). This method was chosen since the specific aim of the study was to determine the effects of different suit pressures in lunar gravity rather than Earth gravity. There was little change in the magnitude of the average peak vertical

GRF while walking up inclines or with changing pressure (Table 1). Knee flexion at initial contact increased with an increase in incline (Figure 1). Varying suit pressures did not affect the knee joint angular displacement across the gait cycle. Cadence increased as incline increased, but no clear trends were observed with increased pressure (Figure 2).

Table 1. Average peak vertical GRF normalized LSBW at varying pressures.

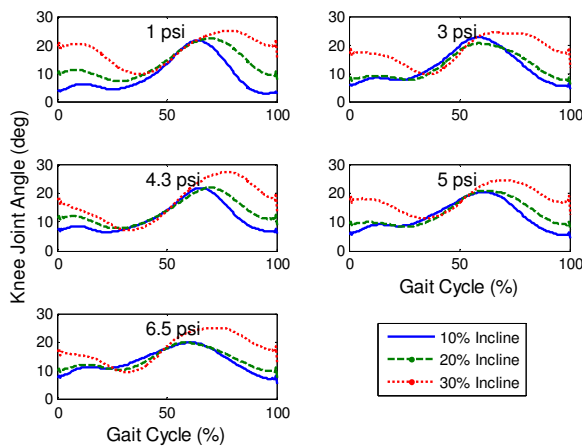| Incline	1.0psi	3.0psi	4.3psi	5.0psi	6.5psi
10 %	1.8	1.8	1.8	2.0	2.0
20 %	1.9	1.9	1.9	2.0	2.0
30 %	1.8	1.9	1.8	2.0	1.8

Figure 1. Average knee joint kinematics normalized against time and averaged between subjects.
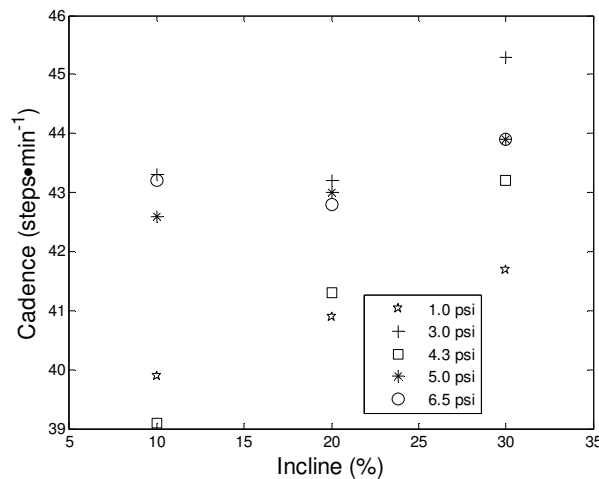

Figure 2. Cadence averaged between subjects.

DISCUSSION

The GRF data revealed minimal change across different varying inclines or across different suit pressures. The GRF analysis with this normalization scheme can be used to help quantify the amount of loading applied to the musculoskeletal system during EVA locomotion. This information can be further used to develop an exercise protocol to complement this loading as a result of an EVA. The increase in joint angle as incline increases can be attributed to raising and lowering of the body with uphill walking. A.S. McIntosh et al. (2006) reported decreases in cadence with increasing inclines in normal un-suited treadmill walking. They speculated that their findings may have been a result of a short walkway which did not allow for a steady gait pattern. One possible explanation for the differences in our findings is the subjects achieved steady gait after which 30 gait cycles were collected. Further the subjects were wearing a 265 lb space suit which was off-loaded to simulate lunar gravity. While in fact the subjects may have "weighed" less, the mass and inertia characteristics of the subject and suit remained unchanged. Hence, with increasing inclines they may have needed to take more frequent steps to compensate for the suit.

SUMMARY

This study showed walking on an incline while wearing the MKIII requires greater knee joint motion but there is no effect from varying the suit pressure. This is particularly important for design requirements for the next generation Lunar EVA suit.

REFERENCES

McIntosh, AS et al. (2006). *J Biomechanics,* 39: 2491-2502.

BILATERAL INTERMITTENT CLAUDICATION AFFECTS JOINT POWERS DURING GAIT

Panagiotis Koutakis[1], Sara A. Myers[1], Jason M. Johanning[2,3], Iraklis Pipinos[2,3] and Nick Stergiou[1,2]

[1]HPER Biomechanics Lab, University of Nebraska at Omaha, Omaha, NE
[2]Department of Surgery, University of Nebraska Medical Center, Omaha, NE
[3]Veterans Affairs Medical Center, Omaha, NE, USA
pkoutakis@mail.unomaha.edu; URL: http://biomech.unomaha.edu

INTRODUCTION

Peripheral arterial disease (PAD) affects over 10 million people in US and is a manifestation of atherosclerosis leading to decreased blood flow to the legs. Claudication is the primary PAD symptom resulting in a cramping pain in the legs that significantly limits the ability of these patients to walk resulting in significant disability. Our previous work suggested that ground reaction forces, joint kinematics, and joint moments are altered in patients with unilateral PAD as compared to controls (Scott-Pandorf et al, 2007; Chen et al, 2008). These gait alterations are present even before the onset of claudication and variably worsen with the onset of claudication pain. The present investigation extends this previous research work to the evaluation of joint powers in patients with bilateral PAD. We hypothesized that the joint powers of these patients will be different compared to healthy matched controls and that they would become worse after the onset of claudication pain.

METHODS AND PROCEDURES

Thirteen (age: 64.46 ± 8.47 years) patients with bilateral PAD and ten healthy gender-height-age matched (age: 67.23 ± 12.67 years) controls walked on a 10 meter walkway over an embedded Kistler force platform while kinetics and kinematics were recorded using a Motion Analysis system. Five trials were captured for each leg during pain free PAD-PF (prior to claudication onset) and pain induced PAD-P (after claudication onset) conditions. The PAD-PF condition was acquired first. During this condition, rest periods were required between trials. Then, claudication was induced by having patients walk on a treadmill set at 10% grade and 0.67 m/s until the onset of pain. At this point the patients were moved immediately back to the walkway, where the PAD-P condition was collected with no rest between trials. Hip, knee, and ankle joint powers were calculated from the ground reaction forces and kinematics during the stance phase. The maximum power absorption and generation were identified for the hip, knee, and ankle joints. T-tests were used to compare the PAD-PF and PAD-P conditions to the healthy controls, and between the PAD-PF to PAD-P conditions.

RESULTS

Patients in both PAD-PF and PAD-P conditions showed significantly ($p < 0.05$) less power generation at the ankle at terminal stance, less power generation at the knee at midstance and less power generation at the hip at early stance, as compared to controls (Fig. 1). In the PAD-P condition, patients showed significantly less power generation at the ankle at terminal stance, less power absorption at the knee at late stance and more power generation at the hip at late stance, as compared to the PAD-PF condition.

DISCUSSION

Our data demonstrate that PAD patients have insufficient ankle muscular strength to push off during late stance and this weakness worsens after onset of claudication pain. The current findings may be the result of the myopathy and neuropathy described in PAD limbs at the cellular level due to chronic and repetitive ischemia (Pipinos et al, 2008). The combined changes observed in the three joints provide a better understanding for the instability of the PAD patients. Several of these alterations (such as the reduction of knee power generation and the joint power redistribution after onset of claudication) but not all (reduced hip power generation at early stance) are similar to those observed in elderly individuals (DeVita et al, 2000 and Kerrigan et al, 1998). The similarity of the aging and PAD gait may be attributed to a similar neuromuscular deterioration in the lower limbs or heretofore unrecognized incidence of PAD in the elderly population. Such an association makes further evaluation of gait in elderly patients with and without PAD extremely important, and is the object of research work currently in progress in our laboratory. Furthermore, we are also exploring what adaptations are present in unilateral PAD patients (only one leg with atherosclerotic occlusions) and patients with unifocal and multifocal disease. This research will provide the foundation for the development and evaluation of the treatment methodologies currently used for PAD.

REFERENCES

Chen CJ et al. (2008). *Submitted J Biomech*
DeVita, P and Hortobagyi, T (2000). *J Appl Physiol,* 88: 1804-1811.
Kerrigan CD et al. (1998). *Arch Phys Med Rehabil,* 79: 317-322.
Pipinos II et al. (2008). *Vasc Endovascular Surg,* 41: 481-9.
Scott-Pandorf MM et al. (2007). *J Vascul Surg,* 46: 491-9.
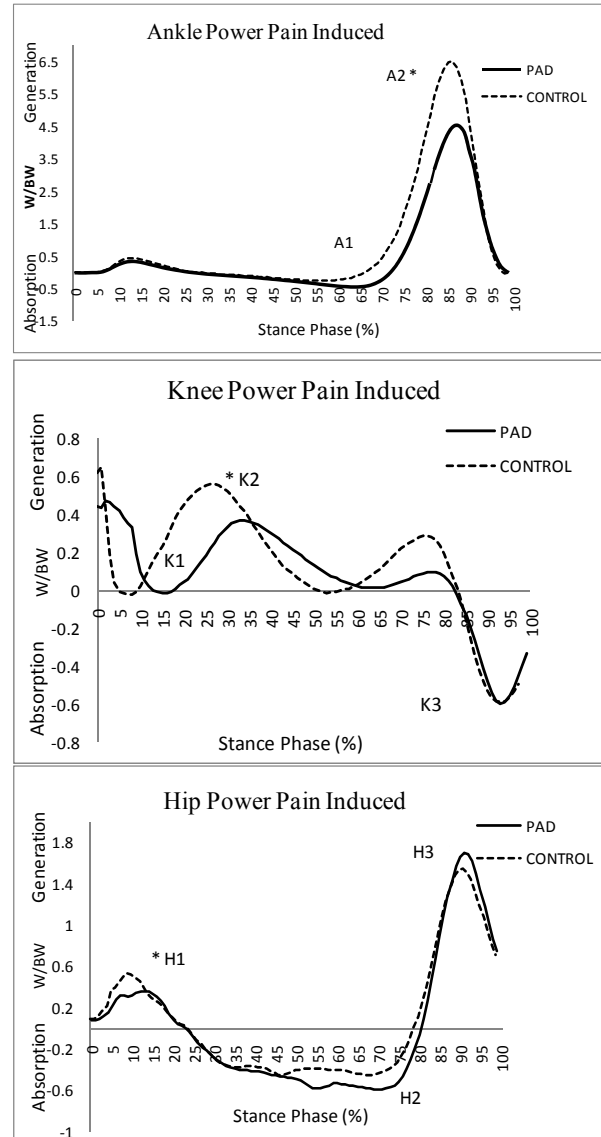
ACKNOWLEDGEMENTS

Figure 1. Mean ensemble joint power curves for the ankle, knee and hip for the Controls and the PAD group in the pain condition.

BONE STRAINS ASSOCIATED WITH FEMORAL NECK FRACTURE FOLLOWING HIP RESURFACING

Jason P. Long[1], Thomas J. Santner[2], and Donald L. Bartel[1]

[1]Cornell University, Ithaca, NY; [2]Ohio State University, Columbus, OH
E-mail: jpl38@cornell.edu

INTRODUCTION

The primary mode of short-term failure for hip resurfacing systems is femoral neck fracture (Shimmin, 2005). While some of these fractures are associated with neck notching, or cutting into the neck with an external reamer, others occur in the absence of intrasurgical notching (Anglin, 2007). In such cases, large magnitude bone strains near the implant rim may lead to a region of damage accumulation and eventual short-term fatigue fracture of the femoral neck.

The structural performance of hip resurfacing systems is a function of design (stem loading and implant fixation) and environmental (bone structure, bone stiffness, and joint loading) variables (Chang, 1999). The combination of these variables differs from individual to individual and within the same individual over time. While analysis of a large number of design and environmental variables has traditionally been computationally expensive using the finite element (FE) method, an inexpensive stochastic predictor can improve efficiency (Santner, 2003).

To better understand short-term neck fracture, we used FE analyses in conjunction with an inexpensive predictor function to: 1) determine design and environmental variables that cause an increase in strain magnitude near the implant rim following resurfacing, 2) identify variables that lead to large bone strain magnitudes near the implant rim.

METHODS

Finite element models of the proximal femur were created from computed tomography (CT) scans for intact (pre-op) and resurfaced (immediate post-op) cases. The bone-implant system consisted of the surgically-altered bone, cement mantle, and implant. Bone material properties were assigned element by element using relationships between CT number, apparent density, and elastic modulus (Rho, 1993). Head and abductor loads applied to the models were based upon telemetric implant and gait data (Bergmann, 1993 & 2001). The structural response of the FE models was analyzed as a function of design (stem-hole geometry, shell fixation, and stem friction coefficient) and environmental (bone, bone material stiffness, head load direction, head load magnitude, and abductor load magnitude) variables.
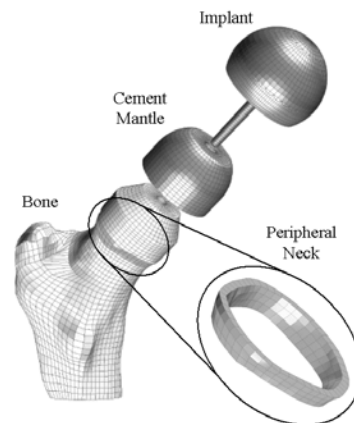

Figure 1: An exploded view of a resurfaced finite element model showing the peripheral neck near the implant rim.

From the FE models, max. and min. principal strains were calculated within the peripheral bone near the implant rim (see Fig 1). The FE models were analyzed at a total of 110 "training sites" throughout the design and environmental variable space to generate the stochastic predictor functions. The predictor functions were then used to analyze the effect of 2000 combinations of the design and environmental variables on strains in the intact and resurfaced models. Sensitivity analysis was done to identify the variables that lead to large magnitude bone strains.

RESULTS

The min. principal strains in the peripheral neck were substantially higher in magnitude and had more variance than the max. principal strains. Additionally, the min. principal strains increased in magnitude by approximately 25% after resurfacing, but only when the implant shell was bonded to the cement mantle (see Fig 2). In some cases, the min. principal strain exceeded 0.35% in magnitude after resurfacing, while the max. principal strains never exceeded 0.15% strain.
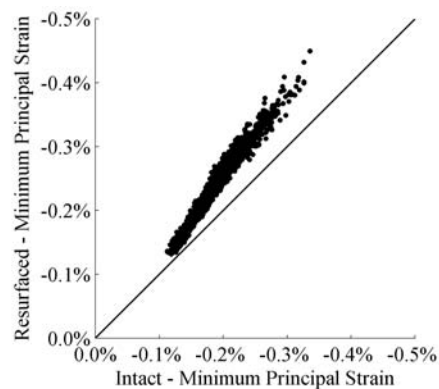

Figure 2: Predicted strains above the bisecting line indicate an increase in strain magnitude after resurfacing.

Bone material stiffness and head load magnitude contributed the most to the variance in min. principal strain, explaining 67% and 23% of the variation, respectively. The highest magnitude strains were primarily associated with low bone material stiffness and high head load magnitude.

DISCUSSION

Resurfacing increased the min. principal strains within the femoral neck near the implant rim by approximately 25% compared to the intact bones. Low bone material stiffness and high head load magnitude were the primary variables that contributed to large magnitude strains. In some cases the min. principal strains exceeded 0.35% in magnitude, indicating a possibility of damage accumulation in the femoral neck due to fatigue loading (Moore and Gibson, 2003). Short-term neck fracture after hip resurfacing may be associated with bone damage accumulation, which is a failure mechanism similar to stress fractures suffered by competitive athletes and military recruits (Burr, 1997).

REFERENCES

Anglin C et al. (2007). *CORR*, 465: 71-79
Bergmann G et al. (1993). *J Biomech*, 26: 969-990
Bergmann G et al. (2001). *J Biomech*, 34: 859-871
Burr D et al. (1997). *JBMR*, 12: 6-15
Chang P et al. (1999). *J Biomech Eng*, 121: 304-310
Moore and Gibson (2003). *J Biomech Eng*, 125: 761-768
Rho J et al. (1993). *J Biomech*, 26: 111-119
Santner T et al. (2003). *The Design and Analysis of Computer Experiments*. NY, Springer
Shimmin A et al. (2005). *Orthop Clin N Am*, 36: 187-193

BIOMECHANICAL RELATIONSHIPS BETWEEN URODYNAMIC PRESSURES DURING COUGH AND VALSALVA IN NORMAL AND STRESS INCONTINENT WOMEN

Thomas Spirka,[1] Kimberly Kenton,[2] Robert S. Butler,[3] Margot S. Damaser,[1,4] and Linda Brubaker[2]

[1]Dept. of Biomedical Engineering, Cleveland Clinic, Cleveland, OH, damasem@ccf.org;
[2]Division of Female Pelvic Medicine & Reconstructive Surgery, Loyola University, Chicago, IL;
[3]Dept of Quantitative Health Sciences Cleveland Clinic, Cleveland, OH;
[4]Research Service, Louis Stokes VA Medical Center, Cleveland, OH

INTRODUCTION & OBJECTIVES

Stress urinary incontinence (SUI) is a common health problem among American women (Norton 2006). Symptoms include the complaint of involuntary leakage of urine on effort or exertion, or on sneezing or coughing. When these symptoms are confirmed with the urodynamic finding of urodynamic stress incontinence (transurethral leakage in the absence of a bladder contraction), the condition of SUI is diagnosed (Abrams 2002). Improved understanding of the relationship between abdominal, vesical and urethral pressures may help us better evaluate and treat SUI. Therefore the primary objective of this study was to quantify the biomechanical relationships between these pressures. In addition, we sought to determine how demographics such as age and SUI continence status affect these relationships.

METHODS

Using an IRB-approved, NIH funded protocol, standardized urodynamic data, including vesical, abdominal, and urethral pressures, were acquired from 2 groups of women: (1) *continent women* had no incontinence symptoms or urodynamic findings; (2) *stress incontinent women* had SUI symptoms and confirmatory urodynamic stress incontinence. Urodynamic pressure data including abdominal, vesical and urethral pressure were obtained during cough and valsalva manoeuvres at 0.2 second intervals at maximum cystometric capacity. Phase plots were generated for each event by plotting abdominal pressure (pabd) versus vesical pressure (pves), vesical pressure versus urethral pressure (pura) and pabd versus pura. A least squares method of linear regression was used to fit a trend line to the phase plots. The coefficients of correlation and determination were calculated for each phase plot in order to establish if the compared variables were mathematically associated and to what extent the variables were dependent. The repeat measures mixed models method was then used to determine the statistical significance of age, continence status, type of event (cough/valsalva) and the volume of urine contained in the bladder at the time of event on the pabd/pura ratio (APUP) and the pves/pura ratio (VPUP) during a cough or valsalva. $P<0.05$ indicated a significant difference. A VPUP greater than 1 indicates that pves exceeded pura at least once during the event. Predictive models were developed for each of the two ratios, relating both the APUP and VPUP ratio to the variables listed above.

RESULTS

The urodynamic data of 11 continent and 8 stress incontinent women were analyzed. The

results obtained from the linear regression analysis of the pressure phase plots is summarized in Table 1.

	Slope	R	R^2
Pabd vs. Pves	0.93 (0.13)	0.99 (0.06)	0.98 (0.09)
Pves vs. Pura	1.22 (0.32)	0.93 (0.07)	0.87 (0.12)
Pabd vs. Pura	1.13 (0.35)	0.92 (0.09)	0.85 (0.15)

Table 1: Summary of linear regression results: Data is listed in the form of mean (standard deviation). (R = Coefficient of Correlation; R^2=Coefficient of Determination; Pabd = abdominal pressure; Pves = vesical pressure; Pura = urethral pressure)

The linear regression results show a strong mathematical association and dependence between abdominal, vesical and urethral pressure as evidenced by R and R^2 values not significantly different from unity.

The following predictive equations were generated for APUP and VPUP.

Equation 1:
APUP = 0.75 – 0.08E – 0.28C-0.00035V + 0.017A – 0.0068t

Equation 2:
VPUP = 0.95 + 0.001E – 0.346C – 0.00024V + 0.11A – 0.0082t

E = type of event (Cough =1; Valsalva = 0); C = continence status (Continent = 1; Stress Incontinent = 0); V = volume of urine contained in bladder during event; A = age; t = time in tenths of a second from start of event

Statistical results indicated that SUI subjects were significantly older (47$\pm$2.6 years) than continent subjects (39$\pm$ 2.6 years; P<0.05).

The APUP ratio was found to be significantly dependent on age and continence status (P<0.05) while the VPUP ratio was only significantly dependent on continence status (P<0.05) but did contain a trend toward significance with age (P=0.09).

DISCUSSION

Abdominal, vesical and urethral pressures are all strongly and mathematically related to one another. The fact that the slope of the trend lines for all pressure relationships was not significantly different from 1 indicates that abdominal pressure is completely transmitted to both the bladder and the urethra.

APUP and VPUP ratios are biomechanical variables that are predictive of continence status. The decrease in the APUP ratio with increasing age suggests that the urethral pressure that women generate in response to increased abdominal pressure decreases with age in both continent and incontinent women. This finding is consistent with the findings of other studies that have reported the link between the reduction of striated muscle fibres in the external urethral sphincter and age (Perucchini 2002 & DeLancey 2007).

REFERENCES

Abrams, P et al (2002) *Am J Obstet Gynecol* 187:116-126

DeLancey, J and Ashton-Miller, J (2007) *Ann. N.Y. Acad. Sci 1101:266-296*

Norton, P and Brubaker, L (2006). *Lancet* 367:57-67.

Perucchini, D et al (2002). *Am J Obstet Gynecol* 186:351-355.

PREDICTORS OF SCORING ACCURACY: ICE HOCKEY WRIST SHOT MECHANICS

Yannick M.-Paquette[1], David J. Pearsall[1] , René A. Turcotte[1] , Ken Covo[2]

[1]Department of Kinesiology and Physical Education, Mcgill University, Montréal, QC, Canada,
yannick.michaud-paquette@mail.mcgill.ca, david.pearsall@mcgill.ca, rene.turcotte@mcgill.ca
[2]Nike Bauer Hockey Inc, St-Jerome, QC, Canada
URL: http://icehockeyscience.mcgill.ca

INTRODUCTION

In the sport of ice hockey the stick is used to control and shooting the puck (hard rubber cylindrical disk) while points gained by scoring (i.e. putting the puck in opposing team's net The wrist shot is generally accepted as a more accurate technique for puck projection[1]. There has been little attempt to compare the stick behavior with the performance outcome during shooting. In throwing or striking tasks, the projection angle and velocity release are crucial for the accuracy outcome [2,3,4]. The purpose of this study is to identify the kinematics patterns of the ice hockey stick from a wrist shot that correspond to the accuracy of puck trajectory.

METHODS AND PROCEDURES

A total of twenty five male subjects ranging in skill participated in this study. Each subjects executed 10 successful wrist shots on four targets (Figure 1). All subjects were performing shots standing with their skates on low friction synthetic polymer surface (to simulate ice). Reflective markers (14mm diameter) were attached on the ice hockey stick and puck. Performances were evaluated by simultaneously recording the movements of the stick's shaft and blade and of the puck with a 6 six cameras infra-red based motion capture (Vicon®) system (240 Hz). These data were used to calculate stick and puck velocities, shaft flexion angles and a series of gross blade projection angles (see Table 1) measured with respect to the blade

local coordinate system, in order to quantify the behavior of the ice hockey stick during the execution of the stationary wrist shot.
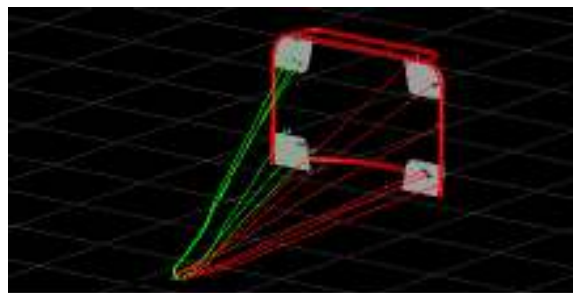

Figure 1: Hockey net with the four different targets and the corners identification relative to the subject shooting side (RH – Right handed, LH – Left handed)

The coordinates of the center of all four targets were used to obtain the vertical (Z-dis) and horizontal (Y-dis) RMS of every shot according to the puck's intercept point with the net's plane. Multiple regression analysis was used with the release parameters to predict accuracy score.

Table 1 Calculated release parameters and their abbreviations

Shaft bend (θ_{SB})	Yaw at release (Ψ_r)
Blade velocity (v_h)	Pitch at release (Φr)
Puck release velocity (v_{p-r})	Roll at release (βr)
Puck spin (ω_p)	Delta Yaw ($\Delta\Psi$)
Time of puck contact (Ct)	Delta Pitch ($\Delta\Phi$)
Puck contact distance (Cd)	Delta Roll ($\Delta\beta$)

RESULTS AND DISCUSSION

With regards to the accuracy scores by target, a height main effect was observed regardless of players caliber (p>0.05) for top and bottom corners accuracy scores (65% and 45% respectively). Similarly, when

considering the variables of shooting precision Y-dis, Z-dis and radial distances were found to be significantly different between the bottom and top corners (p>0.05). The radial RMS from the center of the targets was greater for the top targets primarily due to the larger vertical variance (Z-dis).

For the bottom corners, the principal predictors of accuracy were the blade's heel velocity (km/h) and the position of the puck relative to the blade heel. These derived regression equations explained 36% and 40% of the variance in overall accuracy for BC and BI respectively. For the top corners, six parameters were found to be significant predictors of accuracy: puck release velocity (v_{p-r}), blade heel velocity (v_h), shaft bend (θ), release roll (β) and changes in blade orientation angles: $\Delta\Phi$ and $\Delta\Psi$. These six parameters explained 76% of the accuracy variance for both TC and TI. The results indicate that accurate shooters tended to alter release parameters (puck release orientation and velocity), loading mechanics and blade orientation to achieve proper puck trajectory.

Relative to coaching terms, taking a wrist shot at one of the top targets will require the shooter to "scoop" under the puck (i.e. moving the blade under the puck to permit application of a vertical force component to the puck) in order to lift it and provide the optimal puck's velocity vector to intercept the target window. Therefore, a substantial amount of change in the pitch angle ($\Delta\Phi$) throughout the contact phase In addition to the "scoop" mechanism, the wrist shot is characterized by a rapid "flick" during the end contact phase between the blade and puck. This descriptive term "flick" corresponds to the fast change in blade orientation ($\Delta\Phi$ and $\Delta\Psi$) and concurrent stick bend recoil ($\Delta\theta$).
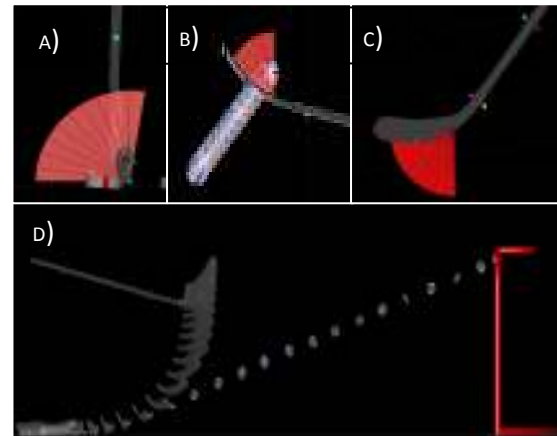

Figure 2. 3-D visualization of the calculated pitch (A), yaw (B) and roll (C) angles. 3-D reconstruction of a top corner wrist shot (D).

SUMMARY

This study has provided a unique insight into the ice hockey stick usage associated with accuracy of stationary wrist shots. As such these findings provoke a series of additional research questions (e.g. the role of the whole body kinematics associated with stick behavior) relevant to design engineers, as well as coaches and athletes.

REFERENCES

Pearsall, DJ et al., (1999), Sports Engineering. 2, 3-11

Martin TA et al., (2001), J Neurophysiol. May;85(5):2298-302

Button C et al., (2003), Res Q Exerc Sport. 2003 Sep;74(3):257-69

Williams KR and Sih BL, (2002), Sports Engineering 5 (2), 65–80.

QUANTIFYING MENISCAL VOLUME AND ARTICULAR CARTILAGE THICKNESS IN PATIENTS TREATED WITH PARTIAL MENISCECTOMY

Bowers ME, Tung GA, Oksendahl HL, Hulstyn MJ, Fadale PD, Fleming BC
Dept. of Orthopaedics, Warren Alpert Medical School of Brown University, Providence, RI
E-mail: Braden_Fleming@brown.edu

INTRODUCTION

Meniscal injuries may place the knee at risk of osteoarthritis (OA) by disrupting its load-bearing capabilities. Partial resection is routinely performed to alleviate symptomatic meniscal tears. While the volume of meniscal tissue removed likely contributes to functional loss, it is unknown whether there is a critical amount of meniscal tissue that can be removed without diminishing the structure's chondroprotective function. The use of quantitative MRI to measure meniscal volume and articular cartilage thickness has been validated *ex vivo* (Bowers et al., 2007; 2008). The purpose of this study was to evaluate the reliability of these techniques to quantify meniscal volume and articular cartilage thickness *in vivo*, before and after surgery, in patients treated with partial meniscectomy. We expected significant reductions in the volume of the resected menisci following surgery (Fig 1), but did not expect any volume change in the uninjured menisci, or in cartilage thickness, over the 1-month study interval.

METHODS

MR Imaging: After IRB approval and informed consent were obtained, 4 human subjects' injured knees (2 right, 2 left) were imaged on a 3T scanner (Siemens Trio, Erlangen, Germany), using a surface coil, prior to partial meniscectomy (2 medial, 2 lateral) and 1 month after surgery. The T2*-weighted 3D-CISS (constructive interference in the steady state) sequence (1mm slices) was used to image the menisci (Bowers et al., 2007), and the T1-weighted WE-3D FLASH sequence (1.5mm slices) was used to image articular cartilage (Eckstein et al., 2004; Bowers et al., 2008).

Segmentation Technique: The femoral and tibial articular cartilage structures of each knee were manually segmented in the sagittal plane and reconstructed using commercial software (Mimics 9.11; Materialise, Ann Arbor, MI). Similarly, the menisci were manually segmented in both the sagittal and coronal planes. 3D voxel models were generated and wrapped with a triangular mesh to create a virtual solid model of each structure (Fig 1).

Meniscal Volume: The volume of each 3D meniscal model was calculated by surface integration. The uninjured menisci served as repeated normals.

Articular Cartilage Thickness: Cartilage thickness measurements were performed on load-bearing regions of interest (ROIs). A cylinder was fit to the bone-cartilage interface of the 3D femoral cartilage model. A line was drawn from a distinctive notch on the lateral condyle to the center of the cylinder. Each femoral condyle was divided from the notch point toward the posterior aspect of the femur to create 6 femoral ROIs (3 medial, 3 lateral) (Fig. 2a). Two ROIs (1 medial, 1 lateral) were defined on the cartilage regions of the tibial 3D model. The inertial axes of the medial compartment and the centroid of each compartment were calculated with MATLAB (The Mathworks, Inc., Natick MA, USA). The calculated inertial axes were projected onto the centroid of each tibial compartment to determine ROI orientation (Fig. 2b). The

mean thickness of each cartilage patch was calculated with a closest point algorithm using MATLAB (Bowers et al., 2008).

Statistical Analysis: Two-way repeated measures analyses of variance were performed to compare meniscal volume in response to surgical time point (pre-operative vs. post-operative) and meniscus (injured vs. uninjured). Pair-wise comparisons were made with the Holm-Sidak test. One-way repeated measures analyses of variance were performed in each cartilage ROI to compare pre-operative and post-operative cartilage thickness values.
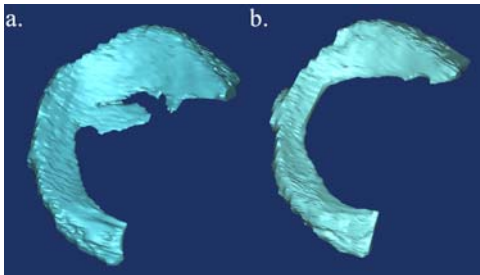

Figure 1: MR-based 3D models of a medial meniscus with a flap tear, (a) before and (b) after partial meniscectomy.
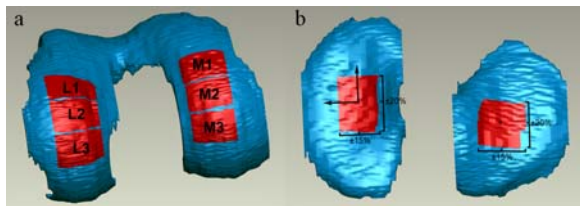

Figure 2: (a) Femoral ROIs. "L" and "M" denote lateral and medial. Regions 1-3 denote the areas divided from the notch toward the posterior femur. (b) Tibial ROIs were centered about the centroid of each condyle.

RESULTS

The pre-operative mean volume of the injured menisci was significantly greater than the post-operative volume (p=0.003), and there was no significant difference between the pre-operative and post-operative mean volumes of the uninjured menisci (p>0.88; Figure 3). There was no

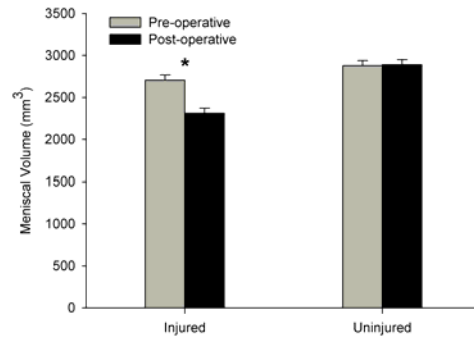significant difference between the pre-operative and post-operative mean thickness of any cartilage ROI (p>0.33).

Figure 3: Mean volumes (mm^3) of the injured and uninjured menisci, before and after partial meniscectomy. * denotes a statistically significant difference in volume.

DISCUSSION

Our data demonstrate that the described segmentation techniques are able to quantify meniscal volume and articular cartilage thickness *in vivo* in patients treated with partial meniscectomy. Although a relatively small sample size was studied (n=4), statistically significant differences were seen between pre-operative and post-operative volumes of the resected menisci (p=0.003); no significant differences were seen in the uninjured menisci, or in any cartilage ROI, before and after partial meniscectomy. This approach may offer a novel means of studying the relationship between the volume of meniscal tissue removed during partial meniscectomy and subsequent changes in articular cartilage thickness.

REFERENCES

Bowers (2007). *J Biomech*, **40**:2811-2815.
Bowers (2008). *Osteoarthritis Cartilage*, EPub [PMID: 17933559].
Eckstein (2004). *Methods Molec Med*, **101**:191-218.

ACKNOWLEDGEMENTS

Dual Task Performance in a Healthy Young Adult Population: Results from a Symmetric Manipulation of Task Complexity and Articulation

Albert Armieri[1,*], Jeffrey D. Holmes[2], Alexandrea K. Gow[1], Tanu Sharma[1], Sandi J. Spaulding, Mary E. Jenkins[3], and Andrew M. Johnson[4]

[1] Health and Rehabilitation Sciences, The University of Western Ontario, London, ON
[2] School of Occupational Therapy, The University of Western Ontario, London, ON
[3] Clinical Neurological Sciences, The University of Western Ontario, London, ON
[4] Bachelor of Health Sciences Program, The University of Western Ontario, London, ON
* Tel: (519) 661-2111 x88997, Email: aarmieri@uwo.ca

INTRODUCTION

The ability to execute and maintain gait, while performing simultaneous cognitive, verbal, or motor tasks is presumably beneficial in a multitude of ways (e.g., walking while talking). Gait performed concurrently with a secondary task is termed 'dual-tasking' and it is well-documented that simultaneous task performance can result in cognitive or motoric interference. Dual-task interference typically results in a decrement within gait performance, as well as impairment of performance on the secondary task (Woolacott & Shumway-Cook, 2002). Due to the fact that most cognitive secondary tasks involve a substantial articulation component (i.e., they involve speaking aloud), it is important to identify the extent to which this factor interacts with the cognitive complexity of the task (Bloem et al., 2001; Dault, Yardley, & Frank, 2003; Pellecchia, 2003; Yardley, Gardner, Leadbetter, & Lavie, 1999).

The goal of this project, therefore, was to manipulate both complexity and articulation within a single working memory task, in order to examine the respective impact of these factors on continuous gait parameters.

METHODS AND PROCEDURES

Fourteen healthy young adults (3 men and 11 women) were recruited from a pool of students at the University of Western Ontario (age: $M = 22.14$, $SD = 2.28$). Participants were asked to memorize a random, non-repeating, sequence of 3, 5, or 7 digits. Articulation was manipulated by either having participants rehearse the digits aloud, or rehearse the digits silently during the performance of the gait task. For the gait task, participants were asked to walk down a 20-foot instrumented walkway (GAITRite). Articulation (i.e., articulation versus no articulation) was completely crossed with complexity (i.e., 3, 5, and 7 digits), and participants were asked to perform three trials within each experimental block. Experimental blocks were randomized for each participant.

RESULTS

Data were analyzed using 3x2 (complexity and articulation) multivariate analyses of variance. Temporal properties of gait (velocity, cadence, step time, swing time, and stance time) were evaluated separately from spatial properties of gait (step length, stride length, and base of support). Descriptives for all spatial-temporal measures are presented in Table 1.

The multivariate analysis of the temporal properties demonstrated a statistically significant interaction term [$F(10,46)=4.42$, $p < .05$]. This multivariate effect was further evaluated at the univariate level, and all temporal measures demonstrated a statistically significant interaction effect. The means of each variable were parsed by evaluating the simple main effect of articulation at complexity, and these post-hoc evaluations consistently demonstrated that articulation had a greater effect at higher levels of complexity.

The multivariate analysis of the spatial properties demonstrated a statistically significant main effect for both complexity [$F(6,50)=2.39$, $p < .05$] and articulation [$F(3,11)=7.44$, $p < .05$], but no significant effect was demonstrated for the interaction between these factors. Univariate analysis revealed that step length and stride length showed a statistically significant main effect for both complexity and articulation, but neither of these variables demonstrated a statistically significant interaction effect. Post hoc analysis of these significant main effects suggested that articulation constrains the spatial properties of gait, and also suggested that these spatial parameters became significantly smaller with each successive level of complexity.

DISCUSSION

Overall these results suggest that articulation produces a substantive change in the spatial and temporal properties of gait, above and beyond the effects of memory demands. This is particularly important when one considers the nature of most cognitive secondary tasks (i.e., the fact that most include some auditory verbal content). While the etiology of this effect cannot be explicitly evaluated within the present paradigm, it is possible that this effect may be due to the respiratory demands of articulation, or it may also be due to the increased cognitive complexity of the task, due to the addition of a verbal component. Future research should focus on the dissociation of these articulation effects on the spatial-temporal properties of gait.

REFERENCES

Dault, M.C., Yardley, L., & Frank, J.S. (2003). *Cognitive Brain Research, 16(3),* 434-440.

Pellecchia, G.L. (2003). *Gait & Posture, 18(1),* 29-34.

Woollacott, M., & Shumway-Cook, A. (2002). *Gait & Posture, 16(1)*, 1-14.

Yardley, L., Gardner, M., Leadbetter, A., & Lavie, N. (1999). *Neuroreport, 10(2),* 215-219.

Table 1: Means (and standard deviations) across all conditions.

	LC/NA	LC/A	MC/NA	MC/A	HC/NA	HC/A
Velocity	144.0 (10.7)	139.2 (10.9)	145.4 (11.0)	138.1 (12.0)	140.4 (11.1)	128.3 (13.5)
Cadence	119.5 (7.3)	116.3 (6.1)	120.2 (7.3)	116.0 (7.4)	117.9 (8.5)	109.3 (8.6)
Step Time	0.5 (.03)	0.5 (0.03)	0.5 (0.03)	0.5 (0.03)	0.5 (0.04)	0.6 (0.04)
Swing Time	0.4 (.03)	0.4 (0.02)	0.4 (0.02)	0.4 (0.03)	0.4 (0.03)	0.4 (0.04)
Stance Time	0.6 (.04)	0.6 (0.04)	0.6 (0.04)	0.6 (0.04)	0.6 (0.04)	0.7 (0.05)
Step Length	72.5 (6.4)	72.0 (6.3)	72.75(6.03)	71.5 (6.0)	71.7 (6.0)	70.5 (6.1)
Stride Length	145.3 (12.9)	144.2 (12.5)	145.8 (12.1)	143.1 (11.8)	143.7 (11.8)	141.2 (12.0)
Base of Support	10.0 (3.2)	9.8 (4.3)	10.6 (3.0)	10.3 (3.3)	10.1 (3.2)	10.2 (3.2)

Notes: LC=low complexity; MC=medium complexity; HC=high complexity; NA=no articulation; A=articulation

GENDER DIFFERENCES IN PEAK VERTICAL GROUND REACTION FORCE AND RATE OF LOADING DURING STOP-JUMP TASK

Ali Abbasi[1], Heydar Sadeghi[2] and Mehdi Khaleghi[3]

[1]Master in Sport Biomechanics, Physical Education and Sport Sciences, Iran,
abbasi.bio@gmail.com
[2]Associate professor, department of physical education and sport sciences, Tarbiat Moallem University, Tehran, Iran.
[3]Master in Corrective Exercises and Sport Injuries, Physical Education and Sport Sciences, Iran.

INTRODUCTION

Females have been found to have eight time higher anterior cruciate ligament (ACL) injuries incidence compared to males participating in the same sport activities (Boden & Dean, 2000). It is further reported that 70% of these injuries occur during landing from a jump (Boden & Dean, 2000). Supposing that one of the possible implications for high knee injuries in females is imposed impact forces on their lower extremities during landing, the purpose of this study was to examine gender differences in peak vertical ground reaction forces (VGRF) and rate of loading (ROL) during stop-jump task.

METODS AND PROCEDURES

44 healthy (22 males, weight of 75.89±3.22 kg, height of 177.84±4.52 Cm, age of 24±3 years, and 22 females, weight of 64±2.85 kg, height of 164±5.58 Cm, and age of 22±2 years) participated in this study. 50% of maximum high jump of subjects calculated. Subjects were asked to jump from the distance of 70 Cm from force plate with two legs and after touching the sign of 50% of high jump, landing on center of force plate with preferred leg. We determined (VGRF) as the peak vertical force (N) recorded during landing, normalized for body weight (N), and expressed as a multiple of body weight (BW). ROL was calculated as the normalized peak vertical force divided by the time to peak force.

$$ ROL = \left[\frac{peakFz(N)/BW(N)}{t} \right] = \frac{BW}{ms} $$

Multivariate analysis of variance (MANOVA) was used to compare peak VGRF and ROL between two groups at the p level of 0.05.

RESULTS

Significant differences found between males and females ($F_{1,41}$=5.627, Wilks' Lambda = 0.372, P≤0.05). This differences was attributed to differences in ROL, while no significant differences have been found between two groups in peak VGRF ($F_{1,42}$ = 2.818, P > 0.05). Mean force-time curve for males and females have presented in figure 1.
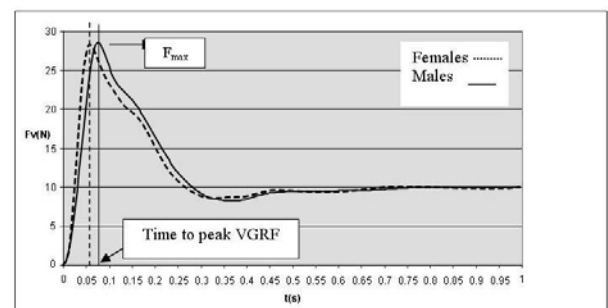

Figure1: force-time curve for males and females during landing

As it is seen in figure 1, the mean of peak VGRF are adequate between two groups,

but females reach to peak VGRF 20% faster than males. It results in 15.85% increase in ROL in females than males and this difference is significant at p level of 0.05.

The mean and standard deviation of peak VGRF and ROL for males and females and the results of MANOVA presented in the table of 1.

parameter	groups	mean±Sd.	$F_{1,42}$	P
Peak GRF (N)	males	29.80±4.30	2.818	0.101
	Females	28.40±4.90		
ROL (N/s)	males	403.20±98.50	5.627	0.022*
	Females	479.10±113.30		

Table 1: mean and Std. peak VGRF and ROL of males and females.* significant at p level of 0.05

DISCUSSION

The purpose of this study was to examine gender differences in peak VGRF and ROL during jump-landing task. With respect to the results, increase the ROL in females can increase the knee ROL secondary, and subsequently increase the probability of knee injuries, especially ACL in females than males. Increasing the ROL in females might be explained with respect to differences in landing pattern and neuromuscular control.

Past research has reported that females had significantly lese knee flexion at contact to same male athletes (Lephart & Ferris, 2002; Decker & Torry, 2003). This situation decreases their ability to attenuation forces imposed to their body (Boden & Dean, 2000). Researchers suggested that the more extension in joints during touching the toes with ground, the less time to dissipate the impact and the more impact of GRF and ROL imposed to their body (Boden & Dean, 2000; Hewett & Stroupe, 1996; Lephart & Ferris, 2002). This increase in ROL can impose stress on the soft tissues of the knee, especially ACL and injure this structure. it is, Also, suggested that the impact of GRF imposed to the body during activities can be dissipated by eccentric activity of the lower extremities muscles (Coventry & O'Conner, 2006). It is possible that

females have less neuromuscular response than males to dissipate the load during landing. Previous studies demonstrated that females may benefit from neuromuscular training programs that are designed to decrease GRF (Hewett & Stroupe, 1996). Neuromuscular training can increase proprioception and muscle strength in females and secondary their ability to absorb the shock of GRF and ROL. It is possible that females' muscles have reduced ability to absorb the impact during contact with ground.

SUMMERY

ROL significantly difference between males and females participated in this study. One possible reason for higher expectation on non-contact ACL injuries in females compared to males can be considered as result of high ROL imposed to their lower extremities during landing. To reduce the risk of knee injuries, it seems to be suggested to focusing on neuromuscular training and landing strategies in females' athletes.

REFERENCES

Boden, BP, Dean, GS, Feagin, JA, Garrett, WE (2000). Mechanisms of anterior cruciate ligament injury. *Orthopedics*, 23:573-78.
Coventry, E, O'Conner, KM, Hart, BA, Earl, JE, Ebersole, KT (2006). The effect of lower extremity fatigue on shock attenuation during single-leg landing. *Clin Biomech*, 21(10): 1090-1097.
Decker, MJ, Torry, MR, Wyland, DJ, Sterett, WI, Steadman, JR (2003). Gender differences in lower extremity kinematics, kinetics and energy absorption during landing. *Clin Biomech*, 18(7):662-669.
Hewett, TE, Stroupe, AL, Nance, TA, Noyes, FR (1996). Plyometric training in female athletes decreased impact forces and increased hamstring torques. *Am J Sports Med*, 24(6):765-73.
Lephart, SM, Ferris, MC, Riemann, BL, Myers, JB, Fu, FH (2002). Gender differences in strength and lower extremity kinematics during landing. *Clin Orthop*, (401):162-69.

THE COMPARISON OF SUPINATED AND PRONATED FOOT IN GROUND REACTION FORCES ATTENUATION DURING SINGLE LEG DROP-LANDING

Ali Abbasi[1], Heydar Sadeghi[2] and Mehdi Khaleghi[3]

[1]Master in Sport Biomechanics, Physical Education and Sport Sciences, Iran,
abbasi.bio@gmail.com
[2]Associate Professor, Department of Physical Education and Sport Sciences, Tarbiat Moallem University, Tehran, Iran.
[3]Master in Corrective Exercises and Sport Injuries, Physical Education and Sport Sciences, Iran.

INTRODUCTION

Since the foot is the interface with the ground during activities such as gait, running, landing, structural changes may cause compensatory malalignment and, consequently, mechanical deviations of the entire lower extremity (Williams, McClay, 2001). Supposing that excessive pronation and supination can result in differences in Vertical ground reaction forces (VGRF) and rate of loading (ROL) imposed on lower extremities and consequently injury in the lower extremities, this study accomplished to comparison of peak VGRF and ROL between supinated and pronated and normal foot during single drop-landing.

METODS AND PROCEDURES

30 students from department of physical education and sport science having the weight of 75.27±4.70 kg, height of 176.50±5.30 cm and age of 23±3 yrs participated in this study. Subjects were grouped (n= 10 per group) on the basis of weight bearing navicular drop (ND) (supinated, < 5mm; neutral, 5-10 mm; pronators, >10 mm) (Cote, Brunet, 2005). The subjects positioned barefoot on a box 0.3 m above the landing surface in barefoot situation. Subjects landed on force plate, while the force plate served as the landing surface that placed on the floor 15 cm in front of the box. The vertical ground reaction force (VGRF) determined as the peak vertical force (N) recorded during landing. Data normalized according to body weight (N), and expressed as a multiple of body weight (×BW). Rate of loading (ROL) was calculated as the normalized peak vertical force divided by the time to peak force.

$$ROL = \left[\frac{peakFz(N)/BW(N)}{t} \right] = \frac{BW}{ms}$$

Multivariate analysis of variance used to compare Peak VGRF and ROL between three groups (at the p level of 0.05).

RESULTS

The results of applying MANOVA shown significant differences between three groups of supinated, pronated, and normal ($F_{2,22}$=15.553, Wilks' Lambda = 0.370, P≤0.05). The differences in three groups was due to differences in ROL between them, while differences in VGRF was not significant ($F_{2,22}$ = 2.632, P >0.05).
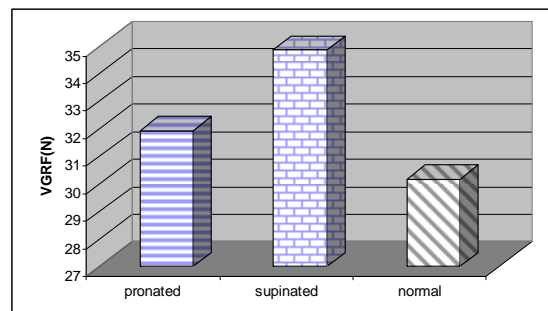

Figure 1: mean and Std. for peak VGRF in supinated, pronated and normal groups

Peak VGRF and ROL in three groups are presented in Figure 1 and Figure 2 respectively. Peak GRF in the supinated group was 14% more than two other groups, though it was not significant. ROL in the supinated group was 28% more than normal group and 31% more than pronated group.
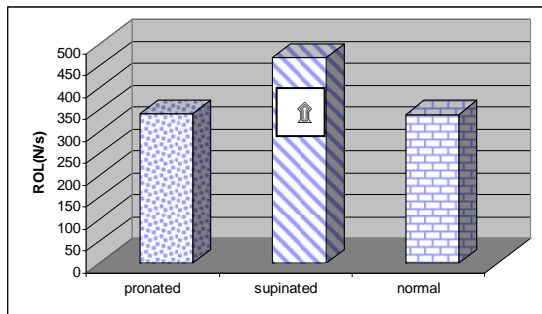

Figure 2: mean and Std. for ROL in supinated, pronated and normal groups, ⇑ significant differences.

The mean and standard deviation of VGRF and ROL and the results of MANOVA in table 1.

Parameter	Groups	Mean±Std.	$F_{2,22}$	P
Peak VGRF (N)	pronated	30.20±4.60	2.632	0.097
	Supinated	34.80±5.50		
	normal	30.10±2.60		
ROL (N/s)	pronated	327.60±31.90	15.553	0.000*
	Supinated	468±93		
	normal	338.20±13.20		

Table 1: mean and Std. for peak VGRF, ROL in supinated, pronated and normal groups, *significant at p level of 0.05

DISCUSSION

The purpose of this study was to examine the differences of maximum VGRF and ROL between supinated and pronated and normal foot during single drop-landing. The supinated group has more ROL during landing in comparison of two other groups. The possible reason for increase of ROL in supinated group can be attributed to the shortening of invertors' foot muscles of in these groups and decrease the ability of these muscles to control pronation of the foot during landing. Williams and McClay (2001) reported that persons with supinated foot are susceptible for knee and shank injuries, because of

increase in ROL. Although previous studies have focused on foot deformities and impact forces on gait and running, this study done during single leg drop-landing, the results for ROL in supinated foot is similar to them. It can be explained that increase of ROL in supinated foot secondary can increase the shank and knee ROL during landing and pose these subjects at risk of knee and shank injuries. Neely (1998) reported that pronation unlocks the midtarsal joint and depresses the medial longitudinal arch of the foot, allowing the foot to become flexible and absorb shock during weight bearing. But with regards to our finding, no significant differences seen in ROL between pronated foot groups with normal groups. The probable reason for it can be attributed to the differences in landing and running mechanics. Ground contact during heel-toe running is normally initiated with the rear foot, whereas ground contact during landing is normally initiated with forefoot. Landing from a jump can involve forces that are 2 to 12 times more than body weight whereas heel-toe running at 4.5 m/s produces forces that are 2.8 times the body weight; yet specific variables affecting the impact forces of the 2 activities have not been clearly distinguished.

SUMMERY

These results suggest that supinated and pronated foot is associated with specific lower extremity kinetics. Differences in these parameters may subsequently lead to differences in injury patterns in supinated and pronated foot in athletes.

REFERENCES

Cote, KP, et al. (2005). Effect of pronated and supinated foot postures on static and dynamic postural stability. *J Athl Train*, 40(1):41-46.
Neely, FG. (1998). Biomechanical risk factors for exercise-related lower limb injuries. *Sports Med*, 26:395–413.
Williams, DS, et al. (2001). Lower extremity kinematics and kinetics differences in runners with high and low arches. *J Appl Biomech*, 17:153-163.

THE EFFECT OF DUAL TASK AND PROPRIOCEPTIVE STIMULATION ON STEPPING ABILITY FOR FALLERS AND NONFALLERS

Chiung-Yu Cho, Li Ping Hsiao
Department of Physical Therapy, Medical College, National Cheng Kung University
Email: cycho@mail.ncku.edu.tw

INTRODUCTION

Normal aging is usually demonstrated on changes in the sensory, neurological and musculoskeletal systems. These changes might affect balance and gait, even related to elder's falls. Balance control and gait might be affected by another task performed concurrently. However, few studies have investigated the effect of dual task on the stepping ability for the old adults as well as fallers. Whether proprioceptive stimulation could improve the ability to cope with the dual task challenge has not been explored. The purpose of this study was to explore whether dual task would affect the gait initiation ability differently in a group healthy old adults and a group of old adults with fall experiences. Moreover, whether an externally applied proprioceptive stimulation produced by weight would affect the stability of the stepping ability was also investigated.

METHODS AND PROCEDURES

We would like to recruit 30 older adults from the Tainan, Taiwan. A dual task paradigm (motor and cognitive tasks) was used in the current study. For the motor task, all participants were asked to perform three times of anterior, lateral, and posterior stepping tasks using their normal walking speed. Cognitive task was backward counting by 7. There were four experimental conditions including: single task, dual task, single task with weight, and dual task with weight. ANOVA with repeated measures was used for data analysis. Significant level was set at $p<0.05$.

RESULTS

In the preliminary results, twenty two older adults (fallers' age: 76.3±5.6; non-fallers'age: 74.8±7.9) were recruited, including 11 normal elderly and 11 fallers. Compared with the single task condition, stance (P<0.001), swing time (P<0.001), and its variability (P<0.001) increased significantly for the dual task condition. Besides, step length decreased under the dual task condition (P=0.001). Comparing the difference between fallers and non-fallers, fallers had longer stance time (P=0.036) and shorter step width (P=0.038). Stance time decreased while we added weight on subjects' leg (P=0.004).

Although adding weight to the dominant leg decreased the stance and swing time variability; it did not reach significant level. Compared with baseline data, the speed of cognitive tasks was slower, it almost reached the significant level ($P=0.051$). The accuracy of cognitive task decreased significantly under the dual task condition ($P=0.031$).
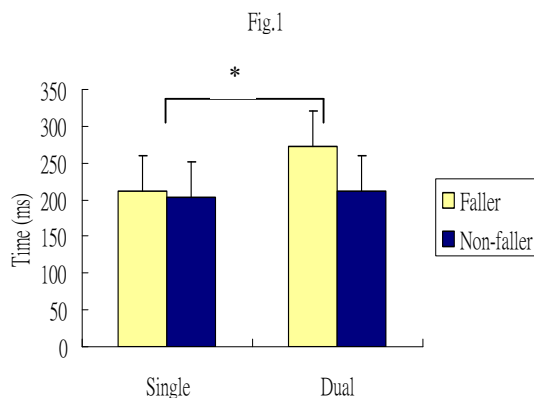

Fig.1

Fig 1. Stance time between two task conditions and two groups.

DISCUSSION

All of the subjects had longer stance, swing time and larger variability under the dual task condition. Due to limited attentional resource, subjects slowed down their stepping speed for the dual task trials. Also, slower stepping speed might cause larger variability for the dual task trials. Our subjects decreased their step length for the dual task condition which might be due to they were afraid of falls and dared not to step out.

Fallers had longer stance time and

shorter step width compared to non-fallers. Fallers used longer stance time to maintain their balance. On the other hand, shorter step width might reduce their base of support, fallers might be easier to experience fall compared to non-fallers.

Stance time decreased while we added weight on subject's leg. The adding weight provided a downward force (proprioceptive stimulation), therefore subjects tended to step down their legs sooner. Subjects did not decrease their stance and swing time variability significantly which was probably due to large variance among subjects. Also, the amount of weight might not be sufficient to cause the change of motor control pattern.

SUMMARY

Subjects increased the stance time for the dual task trials, especially for fallers. Fallers tended to use a more conservative pattern such as increase of stance time to cope with the dual task trials. Proprioceptive stimulation might be effective to decrease variability of gait parameters but dose should be re-considered.

REFERENCE

Melzer, I. & Oddsson, L. I. (2004). The effect of a cognitive task on voluntary step execution in healthy elderly and young individuals. *J Am Geriatr Soc,* **52,** 1255-62.

NUMERICAL MODELING OF AGE RELATED REMODELLING OF THORACIC AORTA AND MECHANICAL STRESS COSEQUENCES

Hanieh Niroomand Oscuii[1], Mohammad Tafazzoli-Shadpour[2] and Farzan Ghalichi[3]

[1]Biomedical Engineering Group, Sahand University of Technology, Tabriz, Iran, niroomand@sut.ac.ir
[2]Faculty of Biomedical Engineering, Amirkabir University of Technology (Tehran Polytechnic), Tehran, Iran, tafazoli@aut.ac.ir
[3]Biomedical Engineering Group, Sahand University of Technology, Tabriz, Iran, fghalichi@sut.ac.ir

INTRODUCTION

Experimental observations have shown that changes in physical and mechanical environments of arteries result in remodeling of arterial structure. Two major determinants of arterial remodeling are arterial wall circumferential stress caused by blood pressure and wall shear stress caused by blood flow defining the adaptive algorithms introduced by different studies (Taber (1998)). Different arteries undergo various patterns of remodeling due to their levels of shear and circumferential stresses for the optimum adaptation to situations such as aging and hypertension. Aging causes thickening of the arterial wall especially the media which is the major pressure bearing component. The age related changes are more obvious in aorta and other central elastic arteries by dilating and becoming tortuous. In addition to increase of luminal diameter arterial wall stiffens with age (O'Rourke and Nichols (2005)). Since both hemodynamic shear stress due to blood flow and wall circumferential stress caused by blood pressure contribute to the arterial remodeling, computational modeling based on the fluid-solid interaction (FSI) method might be of importance in quantitative analysis of remodeling (Niroomand Oscuii et. al. (2007)). In this study effects of mechanical factors in arterial remodeling are analyzed with assumption of constant flow during aging to meet the metabolic requirements of tissues. Models of young, hypertensive without remodeling and aged human subjects are developed using loose coupling FSI methods to study effects of remodeling and its limitations on mechanical stresses and their phase angles.

METHODS AND PROCEDURES

Three dimensional models of thoracic aorta as an elastic artery are analyzed for young and old human subjects using loose coupling FSI method. Boundary conditions include pulsatile pressure and flow waves. Three sets of models are developed indicating young thoracic aorta, un-remodeled thoracic aorta with aged blood pressure conditions (hypertensive), and age related remodeled thoracic aorta to investigate effects of remodeling on optimizing mechanical stresses. Mechanical properties, geometrical dimensions and boundary condition of young and old thoracic aortas are obtained from previous published experimental data (O'Rourke and Nichols (2005)). The resultant hemodynamic wall shear stress (WSS), wall circumferential stress (WCS) and the stress phase shift (SPA) between them are obtained for three sets of models and compared to analyze effects of remodeling on limited optimization of mechanical stress values.

RESULTS

Figure 1 shows the resultant wall circumferential stress waves for three FSI models on the innermost part of arterial wall, i.e. intima. Results show significant decrease in maximum and mean value of WCS wave by external hypertrophic remodeling. Such process significantly decreases possibility of endothelial injury despite structural changes such as elastin damage, calcification and loss of residual stress.
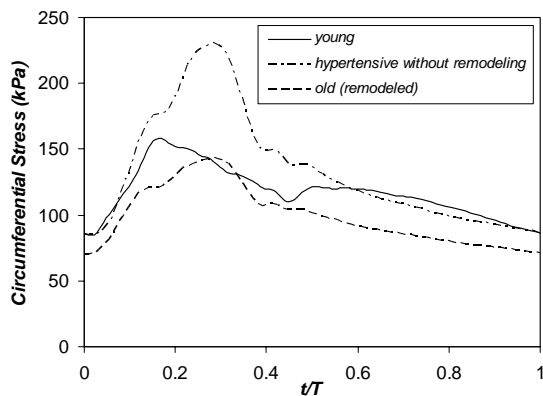

Figure 1. Wall circumferential stress waves in three models.

Figure 2 shows resultant WSS waves for three models. Results show overall reduction of average WSS, maximum WSS and WSS amplitude values by remodeling. Increase in internal diameter and decrease of pressure gradient are major causes of decrease in WSS related parameters. Results show that decrease in WSS values for remodeled artery compared to arterial wall without remodeling is a remodeling related improved parameter for minimizing possibility of endothelial injury with age. The fundamental harmonic of stress phase angle of young and old models are signified in Figure 3. Results show overall increase of SPA by remodeling. Experimental published data have shown that the increase in SPA triggers further release of prostacylin and cell proliferation which is essential for external hypertrophic remodeling.
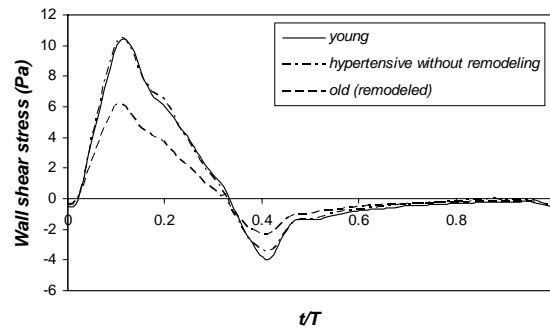

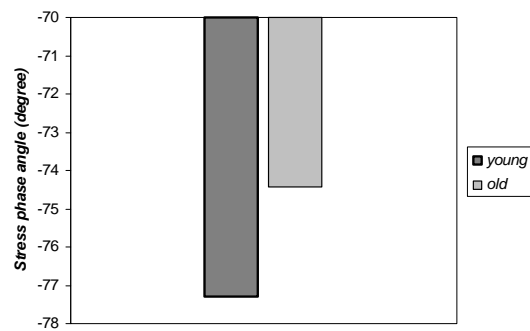**Figure 2.** Wall shear stress waves in three models.

Figure 3. The fundamental harmonic of stress phase angle.

DISCUSSION

It can be concluded that remodeling of thoracic aorta with external hypertrophic mechanism provides an improved level of stresses at the interface of blood with the arterial wall. The increased value of stress phase angle determines elevation of prostacylin that is required for development of endothelium on increased intimal area due to external hypertrophic remodeling.

REFERENCES

Taber, LA (1998). *J Biomech Eng,* 120(3):348-54.

O'Rourke, MF and Nichols, WW (2005). *Hypertension,* 45:652-658.

Niroomand Oscuii, H, et. al. (2007). *American Journal of Applied Sciences,* 4(8): 516-524.

NUMERICAL MODEL OF BONE REMODELLING SENSITIVE TO LOADING FREQUENCY

Etienne Malachanne, Franck Jourdan, David Dureisseix

LMGC, CNRS/University Montpellier 2, Montpellier, France
malachanne@lmgc.univ-montp2.fr

INTRODUCTION

Fluid movement is considered as an important factor in bone remodelling (Kafka, 1993), (Li et al., 1987). Moreover some works relate the sensitivity of bone adaptation to the load frequency (Qin et al., 2003), (Warden and Turner, 2004). Our work proposes a numerical model of bone adaptation based on poroelasticity theory, which takes loading frequency into account through the movement of interstitial fluid.

METHODS AND PROCEDURES

Poroelasticity theory is used to consider the complex structure of bone and interactions between fluid phases and solid phases. The classical saturated poroelastic model involves independent conservation laws for the solid part and the fluid part, and coupled constitutive relations such as:

$$\underline{\underline{\sigma}} = D\underline{\underline{\varepsilon}} - bp\underline{\underline{I}}$$

$$q = \frac{1}{Q}\dot{p} + bTr\underline{\underline{\varepsilon}}$$

$$\underline{W} = H \, \underline{grad} \, p$$

where $\underline{\underline{\sigma}}$ and $\underline{\underline{\varepsilon}}$ are the stress and strain tensors, D is the Hooke tensor, b the Biot coefficient equal to 0.18 (Smit et al., 2002), p the interstitial pressure, $\underline{\underline{I}}$ the identity matrix, q is the rate of fluid accumulation in the representative elementary volume, Q is the biot modulus equal to 14.56×10^9 Pa (Smit et al., 2002), $\underline{W}$ is the opposite of Darcy speed and H the hydraulic permeability of cortical bone equal to $1.1 \times 10^{-13} \, \mathrm{m^4 N^{-1} s^{-1}}$

(Malachanne et al., 2008). The proposed remodelling law, relying on poroelasticity theory, comes from the "Stanford law" (Beaupré et al., 1990). The daily stress level is here defined as:

$$\psi = \frac{1}{T}\sum_i T_i \overline{\sigma}_i g(\|W\|, \|\Gamma\|) \qquad (1)$$

where T is the duration of one day, T_i the duration of the loading type i over one day, $\overline{\sigma}_i$ the average stress of loading type i, and $g(\|W\|, \|\Gamma\|)$ a function of Darcy velocity and Darcy acceleration:

$$g(\|W\|, \|\Gamma\|) = 1 + \frac{a}{2\pi\|W\|}\|\Gamma\|$$

The value of parameter 'a' was deduced from experimental studies (Warden and Turner, 2004) with a = 4s. Parameter ψ contains the load history of one day; for each type of loading it takes into account load amplitude and duration, as well as frequency through Darcy velocity and Darcy acceleration. A reference daily stress level ψ_{ref} is defined as (1) with the loading level necessary to maintain cortical bone. Remodelling law is defined as:

$$\dot{r} = \begin{cases} c(\psi - \psi_{ref}) + cw & \text{if} \quad (\psi - \psi_{ref}) < -w \\ c(\psi - \psi_{ref}) - cw & \text{if} \quad (\psi - \psi_{ref}) > w \\ 0 & \text{if} \quad -w < \psi - \psi_{ref} < w \end{cases}$$

where $\dot{r}$ is the rate of remodelling which depends on bone specific mass through the relationship:

$\dot{\rho} = \dot{r}S_v\rho_t$ with S_v defined as a specific surface (Martin, 1984) and $\rho_t = 1.9 \mathrm{g/cm^3}$ the

density of fully mineralized tissue. As proposed in (Beaupré et al., 1990), w is equal to 10% of ψ_{ref} and c is here equal to $2 \times 10^{-10}\,\mathrm{m\,Pa^{-1}day^{-1}}$. A limitation of bone increase is applied at around 30%, assuming that after this threshold, $\psi = \psi_{ref}$.

RESULTS

Relying on experimental works (Qin et al., 2003), a finite element model was built. An axisymetric mesh of a turkey ulna was performed and low amplitude and high frequency fluid pressure signal (8000 Pa, 20Hz) applied on $\partial_1 \Omega$, 10 min a day during 28 days. Initial bone mass was about 0.5 g/cm^3. Figure 1 shows the distribution of bone mass density (in g/cm^3) after 28 days of this loading.
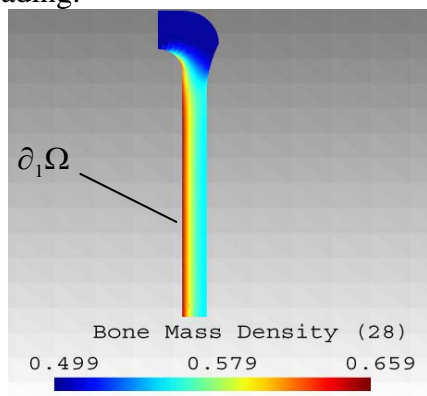

Figure 1. Bone Mass Density (in g/cm^3)

Figure 2 shows gain of mean bone mass density after 28 days of loading versus increasing frequencies. Gain of bone mass increases with a stabilization around 20 Hz.
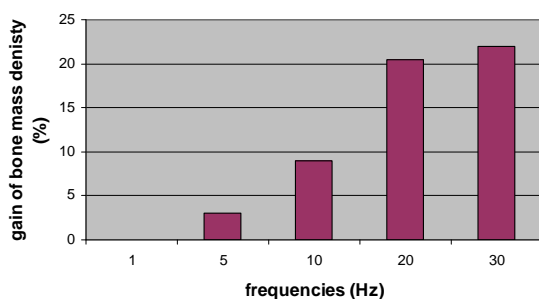

Figure 2. Bone mass gain vs frequencies

DISCUSSION

In the work of (Qin et al., 2003), after 10 min per day of low amplitude and high frequency pressure signal applied on turkey ulna during 28 days, a significant mean bone mass gain (18%) was achieved. The work of (Warden and Turner, 2004) on mice ulna has shown a relationship between load frequency and bone adaptation. Our numerical model depends on bone internal pressure and frequency, integrated to the remodelling law through Darcy velocity and Darcy acceleration. With a gain of mean bone mass density near 20%, the numerical results agree with (Qin et al., 2003). Figure 2 also shows a dependency between frequency and remodelling bone. So this model takes into account the effects of fluid movement on bone remodelling.

SUMMARY

A model of bone remodelling was proposed, based on poroelasticity theory, considering loading frequency through fluid movement.

REFERENCES

Beaupré GS et al. (1990). *J Orthop Research,* 8 :651-661.
Beaupré GS et al. (1990). *J Orthop Research,* 8 :662-670.
Kafka V (1993). *J Biomech,* 26:761-762.
Li G et al. (1987). *Microvasc Res,* 34: 302-310.
Malachanne E et al. (2008). *J Biomech,* 41 :721-725.
Martin RB (1984). *Crit Rev In Biomed Eng,* 10:179-222.
Qin Y-X et al. (2003). *J Biomech,* 36:1427-1437.
Smit TH et al. (2002). *J Biomech,* 35:829-835.
Warden SJ and Turner CH (2004). *Bone,* 34:261-270.

ASSESSMENT OF IMMOBILIZED MUSCLE USING MRE

Takayuki Muraki, Zachary J. Domire, Qingshan Chen, Matthew B. Mccullough, Kai-Nan An

Biomechanics Laboratory, Division of Orthopedic Research, Mayo Clinic
College of Medicine, Rochester, MN, USA, an.kainan@mayo.edu
URL: http://mayoresearch.mayo.edu/mayo/research/biomechanics/

INTRODUCTION

Joint immobilization often results in contracture (Chesworth and Vavndervoort, 1995). Muscle and articular structures both contribute to this (Trudel and Uhtoff, 2000). Magnetic Resonance Elastography (MRE) is a possible method to assess the contributions of individual muscles.

MRE is a novel imaging technique that allows measurement of tissue shear modulus in vivo (Muthupillai et al, 1995). In this technique a small amplitude shear wave is induced in a tissue. At the same time a motion-sensitizing gradient synchronized to the shear wave is applied. From this process a phase shift can be measured using phase-contrast MRI. The displacement at each voxel can be directly calculated from this phase shift and the shear wave can be imaged as it moves through the tissue.

The purpose of this study is to determine the feasibility of using magnetic resonance elastography (MRE) to non-invasively measuring shear stiffness of muscle following immobilization.

METHODS AND PROCEDURES

Six pairs of dog forelimbs were harvested for this study following 42 days of one forelimb immobilization in a maximally flexed position. The biceps from each limb was tested using MRE. All procedures were approved by the Institutional Animal Care and Use Committee.

Specimens were prepared for the MRE testing by mounting them onto a custom-made acrylic jig capable of adjusting the elbow joint angle and immobilizing the shoulder joint. The MRE measurement was conducted in 1.5T scanner (Signa, General Electric, Fairfield, CT). Vibration was applied to the distal muscle belly at 175 Hz, generating shear waves propagating along the length of the muscle. The immobilized specimen was scanned with a maximally extended elbow. The control specimen was scanned in two positions: the joint angle matching the extended position in the immobilized limb and full extension. Maximum extension in both specimens was defined as the joint angle that produced a torque of 0.6 Nm. Muscle belly lengths were measured in each position.

Before stiffness inversion the data was phase unwrapped and a directional filter was applied (Manduca et al., 2001). Shear modulus was calculated at each voxel by determining the phase gradient for a small window around each point (Manduca et al., 2001). The magnitude of the shear modulus within the muscle was calculated as the mean value for each voxel within a central region of the muscle.

Following MRE scans the biceps was removed and a slack length (SL) was measured. This length was defined as the muscle belly length when the muscle was stretched with a force of 1N. The muscle mass and volume were then measured.

Muscle cross sectional area (CSA) was calculated by dividing muscle volume by SL.

A repeat measures analysis of variance with Tukey post-hoc tests was performed to test for difference between means. The significance was set as 0.05.

RESULTS

The immobilized muscles showed significant atrophy, reduction in muscle SL, and reduced range of motion (Table 1). The shear modulus of the immobilized muscles was significantly higher than the control when scanned at matching angles. The muscle lengths were similar between limbs when measured at the same angle. When comparing modulus at maximum joint angle, the control muscle was much stiffer (Table 2).

	Control	Immobilized
Mass(g)*	31.7 ± 3.9	24.1 ± 2.4
CSA(mm^2)*	234.2 ± 32	190.8 ± 20
SL(mm)*	126.4 ± 3.6	121.2 ± 0.4
Ext Angle(º)*	120 ± 11.5	96.5 ± 16.2

Table 1. Muscle size parameters and maximum elbow extension. *$p<0.05$

DISCUSSION

When comparing specimens at the same joint angle, the immobilized muscle was far stiffer. While muscle lengths were similar at this joint angle, this was a larger change in length from SL in immobilized muscle. This difference can likely be explained by a loss of muscle sarcomeres as a result of immobilization (Tabary et al 1972) and length-tension relationship of passive muscle (Ramsey and Street, 1940).

When comparing specimens at maximal joint extension, the control muscle was stiffer. In this position the control muscle had a longer absolute muscle length, but the differences from SL were similar between specimens. This difference is possibly due to a loss of collagen associated with disuse (Takala and Virtanen 2000).

SUMMARY

MRE demonstrated to detect differences between immobilized and control muscle. These differences depend on the joint angle selected for comparison and are likely the result of a combination of loss of sarcomeres and muscle collagen.

REFERENCES

Chesworth B.M., Vandervoort A.A. (1995). *Phys Ther,* 75:253-61.
Manduca, A., et al. (2001). *Med Image Anal,* 5(4):237-54.
Muthupillai, R. et al. (1995). *Science,* 269: 1854-7.
Ramsey R.W., Street S.F. (1940). *J Cell Comp Physiol* 15:11-34.
Tabary J.C. et al. (1972). *J Phys* 224:231-44.
Takala T. E., Virtanen P. (2000). *Scand J Med Sci Sports* 10:321-5.
Trudel G., Uhthoff H. K. (2000). *Arch Phys Med Rehabil* 81: 6-13.

	Disuse extended	Control matching disuse	Control extended
Shear modulus (kPa)*	77.3 ± 13.4	30.0 ± 27.7	107.9 ± 20.0
Length (mm)	128.1 ± 4.8	127.4 ± 4.0	132.1 ± 2.8

Table 2. Shear modulus and muscle length for each testing condition. *$p<0.05$

ANALYSIS OF THE INTERNAL STRESSES IN USS I PEDICLE SCREWS USING THE PHOTOELASTICITY

Sarah Fakher Fakhouri[1], Ariane Zamarioli[1], Antônio Carlos Shimano[1], Cleudmar Amaral Araújo[2], Helton L. A. Defino[1], Patricia Silva[1] and Otávio Terra[1]

[1]Department of Biomechanics, Medicine and Rehabilitation of the Locomotor Apparatus of Faculty of Medicine of Ribeirão Preto of University of São Paulo
[2]School of Mechanical Engineering of Federal University of Uberlândia
http://www.fmrp.usp/bioengenharia

INTRODUCTION

The treatment of the spinal deformities, degenerative diseases, injuries and tumors of the vertebral spine usually require the internal fixation system (Vaccaro et al., 1995; Matuoka and Basile Júnior, 2002). The screw is one of the anchorage elements of the vertebral fixation system. The performance and the properties of the mechanical function of these systems are directly correlated to the fixation quality of the screws into the bone (Benzel, 2001; Law, Tencer and Anderson, 1993). The stability failure of the vertebral fixation system may be correlated to the mechanical failure of the screw or to the failure in the interface between the bone tissue and the implant. This bone-screw interface is undergone to a pullout strength that may cause instability of the fixation system (Lastra and Benzel, 2003). In this case, the photoelasticity technique is an important tool to develop comparative studies about this topic. The photoelasticity has been noticeable in the techniques available for determine and evaluate the stress distribution in the structural systems. It is an experimental technique that allows a fast qualitative and quantitative analysis of the internal stresses of the materials by mean of the observation of the optic effects. The photoelasticity studies the physical effects of the light due the tension or deformation actions in the transparent elastic bodies (Doyle and Phillips, 1978; Hirokawa, Yamamoto and Kawada, 1998; Rubo and Souza, 2001).

METHODS AND PROCEDURES

To the development of this study we used stainless steel screws of 6 and 7 mm of external diameter and 50 mm of length. Eight photoelastic models made by flexible photoelastic epoxy resin (Polipox) were produced by a screwed acrylic mould. The models had 58 mm of width and 12 mm of thickness.

The screws were inserted into the photoelastic models at 30 mm of deep. The models were divided into two groups according to their external diameters. The first group was consisted by the 6 mm screws and, the second group by the 7 mm screw. A load of 0.75 Kgf was used to the quantitative analysis of the shear stress. In this analysis we observed the internal stress by means of the fringe orders of each photoelastic model. The shear stresses were evaluated via a 19 selected points, along the screws body.

The Tardy compensation method was used to calculate the shear stress. The data were statistically analyzed by the ANOVA method. The level of significance was set at 5% ($p \leq 0.05$).

RESULTS

According to the analysis performed, the mean shear stress was (9.20 ± 3.12) KPa for 6 mm screw and (8.19 ± 2.89) KPa for 7 mm screw. Based on these data, we found a significant statistical difference between the two groups ($p < 0,001$). The 6

mm screw reached higher shear stress values than the 7 mm screw, according to the behaviour of the curves shear stress versus analyzed points (Figure 1).
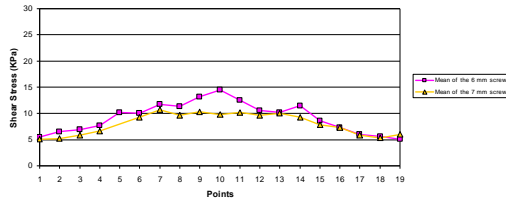

Figure 1. Mean of the shear stress of 6 and 7 mm screws.

DISCUSSION

The data from our study show that the highest concentration of the shear stress occurred at the tip of the screws when they were undergone to pullout strength. The fringe orders grew helicoidally, based on the shape of the screws. The 6 mm screw is probably the most susceptible to the pullout because it reached the highest values of shear stress and due to their measurements and geometry. This information may help the surgeons to make the most adequate choice of the pedicle screw for the spine fixation.

REFERENCES

Vaccaro AR et al. (1995). *J Bone and Joint Surg [Am]*, 77: 1200-06.
Matuoka, CM and Basile Júnior, R (2002). *Acta Ortopédica Brasileira,* 10: 25-34.
Law et al. (1993). *Spine*, 18: 2438-43.
Benzel EC (2001). New York.
Lastra J and Benzel CE (2003). St. Louis, Mosby.
Doyle JF and Phillips JW (1978). *Manual on Experimental Stress Analysis. Society for Experimental Mechanics*.
Hirokawa S et al. (1998). *IEEE Transactions on Rehabilitation Engineering*, 6:300-308.
Rubo JH and Souza EAC (2001). *Revista Faculdade de Odontologia de Bauru*, 9: 97-103.

DEVELOPING A CUMULATIVE LOADING MEASURE FOR THE KNEE: EXAMINING TEST-RETEST RELIABILITY

Shawn Robbins[1], Gareth Jones[2], Trevor Birmingham[1], Jack P. Callaghan[3] and Monica Maly[1]
[1]School of Physical Therapy, University of Western Ontario, London, ON, Canada,
smrobbin@uwo.ca
[2]Human Kinetics, University of British Columbia Okanagan, Kelowna, BC, Canada
[3]Department of Kinesiology, University of Waterloo, Waterloo, ON, Canada

INTRODUCTION

The peak external knee adduction moment (PKAM) is a validated proxy for the maximum medial knee load during gait. The PKAM predicts knee osteoarthritis (OA) progression (Miyazaki et al., 2002), but does not explain variance in mobility or disability measures in subjects with knee OA (Maly et al., 2006). This poor relationship may reflect that the PKAM represents a single loading exposure event, while cartilage deformation varies in a time-dependent manner (Sharma et al., 2007). As an alternative, a cumulative knee load (CKL) measure could represent the total exposure to knee loading during daily activity. CKL would incorporate the repetitive nature of walking and might be better related to mobility or disability in patients with knee OA. The purpose of this study was to develop a measure of CKL and determine its test-retest reliability in healthy subjects.

METHODS AND PROCEDURES

CKL was calculated for 12 healthy subjects (mean age 31±6 years; 6 women, 6 men) on two occasions. One knee was randomly selected for each subject. The CKL was calculated as the product of the stance phase external knee adduction moment impulse and the mean step counts accumulated per day by each subject. The external knee adduction moment was calculated for 5 walking trials at a self-selected speed using a 3-dimensional motion analysis system (Motion Analysis Corporation, CA, U.S.A.) and force plate (Advanced Mechanical Technology Inc., FL, U.S.A.). The impulse was calculated as the integrated positive values of the external knee adduction moment curve (Figure 1) during stance phase. Subject total daily step counts were collected using a waist-born unidimensional accelerometer (GT1M ActiGraph, Florida, U.S.A.). Subjects wore the accelerometer over their randomly selected leg for 7 days, during waking hours. All measurements were repeated after 2 weeks on the same leg, producing 2 estimates of CKL for each subject. The test-retest reliability of the CKL measure, external knee adduction impulse and mean step counts per day were determined using intraclass correlation coefficients (ICC) (2,1) with 95% confidence intervals (CI). The standard error of the measurement (SEM) was also calculated for the CKL.
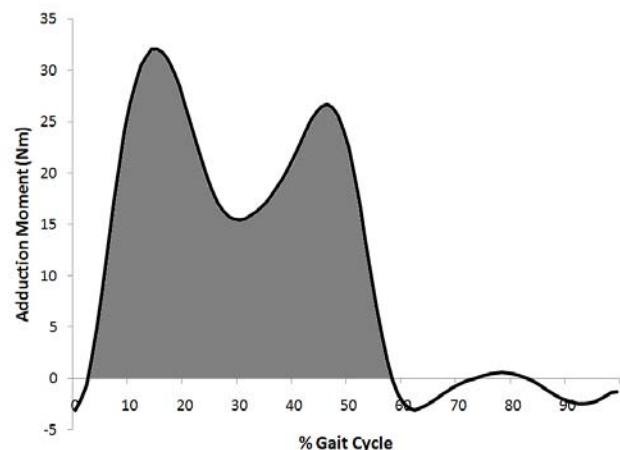

Figure 1. A representative graph of the external knee adduction moment during level walking for a subject (one trial only). The impulse was calculated from the integration of the grey shaded area.

RESULTS

Table 1 provides the means and standard deviations for the external knee adduction impulse, mean step counts per day and CKL measures on both occasions. The CKL measure [ICC(2,1)=0.91; CI 0.73 to 0.97], adduction impulse [ICC(2,1)=0.92, CI 0.76 to 0.98] and step counts per day [ICC(2,1)=0.88; CI 0.62 to 0.96] all demonstrated excellent test-retest reliability. A graph of the CKL on occasion 1 versus occasion 2 (Figure 2) also revealed good agreement with most of the points near the line of perfect agreement. The SEM for the CKL was 1.15 MNm*s. A large range of CKL per day between subjects was noted. For example, across subjects the CKL varied from 1.06 to 16.73 MNm*s on occasion 1 and from 1.22 to 12.80 MNm*s on occasion 2.

Variable	Occasion 1	Occasion 2
Adduction impulse (Nm*s)	557.69 (316.62)	538.80 (257.54)
Step counts per day	8507 (2901)	8581 (3203)
CKL (MNm*s)	5.12 (4.40)	4.66 (3.11)

Table 1. Means and (standard deviations) of the different measures.
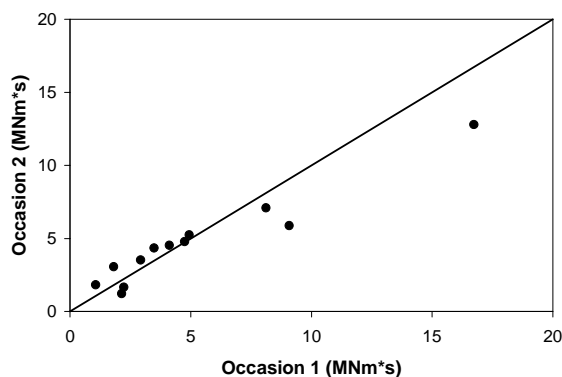

Figure 2. A comparison of the CKL on occasion 1 and occasion 2. The diagonal line represents perfect agreement.

DISCUSSION

The CKL demonstrated excellent test-retest reliability. The CKL represents the total exposure to medial compartment load by incorporating estimates of medial knee loading during stance and the repetitive nature of walking during day-to-day physical activity. Though no other studies were found to compare our cumulative load data for the knee, previous work has evaluated the knee adduction impulse. Values of the external knee adduction moment impulse found in this study were similar to data previously reported (Thorp et al., 2007). Step counts were highly variable between subjects and as a result, a large variance between subjects was noted in the CKL measure. Further studies are required to determine CKL reliability and validity in a larger sample. Future work is planned for determining the utility of CKL in explaining variance in mobility, performance, disability and pain in patients with knee OA.

SUMMARY

The CKL is a promising measure that demonstrated excellent test-retest reliability. Further studies should examine the measure in different patient populations.

REFERENCES

Maly, MR et al. (2006). *Clin Biomech,* 21:1051-1059.

Miyazaki, T et al. (2002). *Ann Rheum Dis,* 61: 617-611.

Sharma, G et al. (2007). *Clin Biomech,* 22: 248-255.

Thorp, LE et al. (2007). *Arthritis Rheum,* 57: 1254-1260.

ACKNOWLEDGEMENTS

THE EFFECT OF VARYING THE DENSITY-MODULUS RELATIONSHIP USED TO APPLY MATERIAL PROPERTIES IN A FINITE ELEMENT MODEL OF THE DISTAL ULNA

Rebecca L. Austman[1], Jaques S. Milner[2], David W. Holdsworth[2], Cynthia E. Dunning[1]

[1]The Jack McBain Biomechanical Testing Laboratory, Department of Mechanical and Materials Engineering, The University of Western Ontario, London, Ontario, Canada, cdunning@uwo.ca
[2]Imaging Research Laboratories, Robarts Research Institute, London, Ontario, Canada

INTRODUCTION

One challenge in developing biomechanical Finite Element (FE) models is the assignment of accurate bone material properties. Many recent studies have developed subject-specific FE models, where material properties of bone are assigned by converting density (ρ) information derived from Computed Tomography (CT) scans to elastic modulus (E). The ρ-E relationship can have a great effect on FE results (Schileo et al., 2007); however, few studies have directly compared the use of the various reported equations, and none in a model of the distal ulna. Therefore, the purpose of this study was to apply six different ρ-E equations from the literature to subject-specific FE models of distal ulna, and compare the strain results to those previously found experimentally using strain gauges.

METHODS AND PROCEDURES

The experimental methodology has been published in detail (Austman et al., 2007) and is described briefly here. The proximal ends of eight fresh-frozen cadaveric ulnae were cemented in a custom-designed jig. A 20N force was applied to the distal articular surface via a materials testing machine (Instron 8872, Canton, MA, USA). Each ulna was instrumented with 12 uniaxial strain gauges, applied in pairs to the medial and lateral surfaces, at six locations along its length. The gauge pairs were wired into six Wheatstone half-bridges to measure bending strains during loading.

A MicroCT scanner with isotropic 152μm voxel spacing (eXplore Ultra, GE Healthcare, London, Canada) was used to scan each of the eight bones both prior to and following experimental testing. The post-testing scans were necessary to record the exact locations of the strain gauges. A triangular surface mesh was created for each native bone using the FEA module of Mimics (Materialise, Leuven, Belgium), then imported into Abaqus (Simula, Providence, USA) and converted into 2nd order tetrahedral meshes. Material properties were mapped to each element via custom-written software that converted ρ into E using a user-defined equation and averaged the E values of the voxels within the element. Six ρ-E relationships from the literature (Carter and Hayes, 1977; Keller, 1994; Lotz et al., 1990; Lotz et al., 1991; Morgan et al., 2003; Snyder and Schneider, 1991; Wirtz et al., 2000) were trialed in each bone, resulting in 48 models. Boundary conditions and loads mimicked the experimental set-up.

The strain values from the model's surface elements representing the strain-gauged areas were averaged. The absolute values of the strain output for the medial and lateral locations were averaged for comparison to experimental results since the Wheatstone bridges output only one strain value per gauge pair. The percent error between the model and experimental results from the six gauge locations were calculated, and averaged to provide an overall value for each ρ-E relationship in every specimen. The root mean square error (RMSE) for all gauge

locations and specimens combined was also calculated for each ρ-E relationship.

RESULTS

The percent error found using each ρ-E relationship for every specimen, and the RMSE for all specimens combined are shown in Table 1. The lowest error for each specimen is highlighted. Three specimens matched experimental values most closely by using the Carter & Hayes (1977) equation (which tended to over-estimate), and 5 were matched most closely using the Morgan et al. (2003) equation (which tended to under-estimate). Overall, the Morgan et al. (2003) equation resulted in the lowest average percent error and the lowest RMSE.

Bone	Carter & Hayes	Wirtz et al.	Morgan et al.	Keller	Snyder & Schneider	Lotz et al.
1	10.8	43.2	-25.5	33.7	20.8	68.6
2	10.0	42.7	-24.1	34.3	21.6	68.8
3	79.7	131.1	1.6	103.7	79.8	149.6
4	45.7	90.6	-8.5	72.0	53.3	95.1
5	42.0	83.5	-9.4	68.1	50.8	106.6
6	27.8	66.7	-16.3	52.5	37.3	86.6
7	8.4	43.2	-24.8	35.4	22.3	75.1
8	27.1	61.1	-16.0	52.7	37.6	88.5
Avg (%)	31.4	70.3	-15.4	56.6	40.4	92.4
RMSE (με)	99.3	194.0	62.1	153.6	112.5	242.8

Table 1. Percent errors for each bone and ρ-E relationship, and the RMSE (in microstrain, με) for all specimens combined.

DISCUSSION

Proper development of subject-specific FE models requires care during multiple model steps including geometry extraction, meshing, material assignment, and assigning boundary conditions. The selection of an appropriate ρ-E relationship is one area that has received little attention in the literature, and this study was undertaken to address this void. In a recent similar study conducted on the human femur, Schileo et al. (2007) concluded that a femur-specific relationship between ρ and E was required for accurate results. As no such data were available in the literature for the human ulna, the present investigation focused on using equations that were derived from data using multiple bone sites.

This study focused only on bending strains, as the distal ulna has been shown to receive primarily bending loads (Gordon et al., 2006). Other loading modes may produce different results; however, Schileo et al. (2007) found no effect of loading case between their experimental and FE predicted strains.

The current results showed the Morgan et al. (2003) relationship tended to underestimate the bone strains by an average of 15%, and the Carter & Hayes (1977) equation tended to overestimate by an average of 31%. This suggests that the ideal ρ-E relationship for the ulna might lie somewhere between these two equations, and will be the subject of future investigations.

REFERENCES

Austman RL et al. (2007). *J Hand Surg [Am]*, 32:848-854.

Carter DR and Hayes WC (1977). *J Bone Joint Surg [Am],* 59:954-962.

Gordon KD et al. (2006). *J Biomech*, 39: 1335-1341.

Keller TS (1994). *J Biomech*, 27:1159-1168

Lotz JC et al. (1990). *J Comput Assist Tomogr*, 14:107-114.

Lotz JC et al. (1991). *J Biomech*, 24:317-329.

Morgan EF et al. (2003). *J Biomech*, 36:897-904.

Schileo E et al. (2007). *J Biomech*, 40:2982-2989.

Snyder SM and Schneider E (1991). *J Orthop Research*, 9:422-431.

Wirtz DC et al. (2000). *J Biomech*, 33:1325-1330.

FORCE AND EXCURSION DEMANDS OF ROTATOR CUFF MUSCLES DURING ABDUCTION

James C Otis[1], Matthew L Hansen[1], Jared S Johnson[2], Frank A Cordasco[3], Edward V Craig[3], Russell F Warren[3]

[1] The SHRI-CORE Biomechanics Lab, Sun City West, AZ, james_c_otis@sbcglobal.net, matthew.hansen@thecoreinstitute.com

[2]UCLA Department of Orthopaedic Surgery; [3]Hospital for Special Surgery, NY, NY

INTRODUCTION

Injuries to the rotator cuff and surgical procedures such as cuff repair, arthroplasty, and muscle transfer may alter the resting and operating lengths of the rotator cuff muscles. Consequently, these muscles may no longer possess the necessary excursion and force-generating capacity to perform their essential functions in stabilizing and moving the glenohumeral joint. To optimize shoulder function, treatment should aim to re-establish the normal length-tension relationship. It was hypothesized that during scapular plane abduction each rotator cuff muscle has distinctive force and excursion demands. The objective of this study was to identify the force and excursion demands of the rotator cuff during abduction and to compare these demands with the maximum available forces.

METHODS AND PROCEDURES

A unique cadaver model with simulated neuromuscular control was used. This shoulder controller replicated in vivo glenohumeral kinematics by utilizing active position and orientation feedback control algorithms. Stepper motors (Industrial Devices Corporation, Salem, NH) connected to the rotator cuff tendons and deltoid insertions mimicked the actions of the deltoid and cuff muscles. Force transducers measured the forces generated by each stepper motor. An electromagnetic three-dimensional space tracking device (FASTRAK, Polhemus Inc., Colchester, VT) was used to track glenohumeral position and calculate muscle excursion. Five cadaver glenohumeral joint specimens (mean age 64.2 years) were tested in open-chain scapular plane abduction from 10° to 80° with the full mass of the upper extremity simulated.

RESULTS

Two patterns of excursion were observed in the five rotator cuff regions investigated (Table 1). The inferior cuff (teres minor and inferior subscapularis) demonstrated nearly isometric behavior. The middle cuff (infraspinatus and superior subscapularis) and the supraspinatus demonstrated concentric behavior, with the supraspinatus exhibiting nearly twice the excursion of the middle cuff muscles. The greatest forces were seen in the posterior cuff.

	Max Exc (mm)	Max For (N)	Abd MA (mm)
Supra	31 ± 2	38 ± 14	26.0
Sup Sub	16 ± 4	38 ± 14	13.0
Inf Sub	2 ± 3	38 ± 14	1.6
Infra	21 ± 3	43 ± 13	17.2
Ter Min	-4 ± 4	44 ± 12	2.9

Table 1. Mean (± 1 SD) max excursion and max force for rotator cuff muscles through 10° - 80° abduction arc. The abduction moment arms of the individual muscles were calculated from linear regression line slopes.
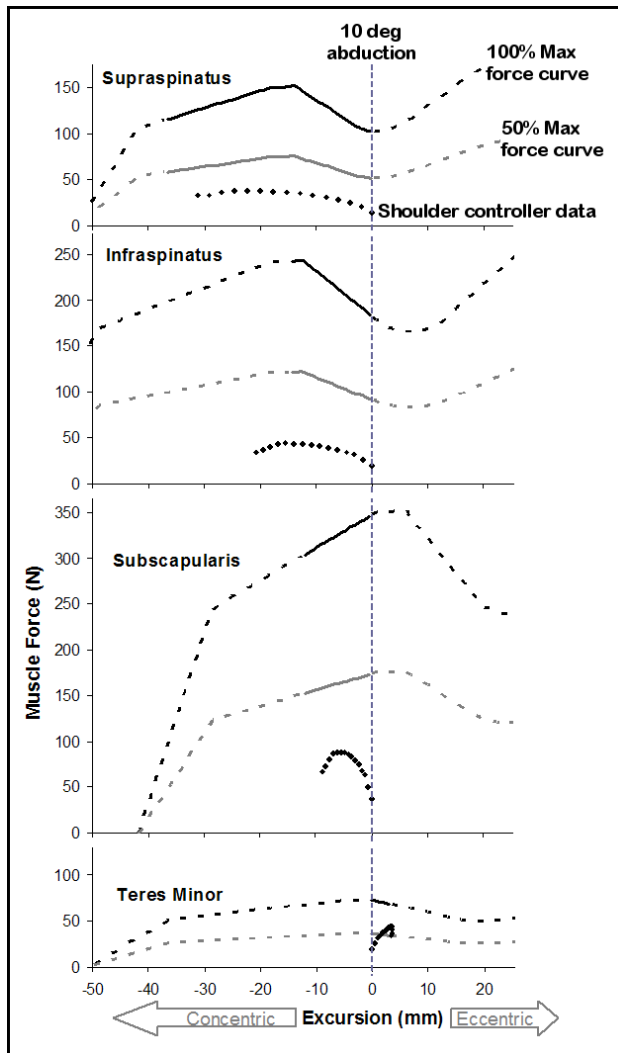
Figure 1. Comparison of experimental data from our shoulder controller experiments, max force available from Ward et al (2006), and 50% max force available. The shoulder controller data are shown for 10° to 80° of scapular abduction. Regions corresponding to 10° to 80° of abduction for the max force curves are solid lines. The vertical dashed line is the reference excursion position with the glenohumeral joint in 10° abduction.

Figure 1 shows the muscle force requirements for scapular plane abduction versus excursion from our study. Also shown is the maximum muscle force available as a function of muscle length based upon the work of Ward et al (2006). For these figures, measurements for

the superior and inferior subscapularis were combined. The force demands for all cuff muscles were below the 50% max force curves with the exception of teres minor whose demand was approximately 65% max.

DISCUSSION

The isometric function and small abduction moment arms of teres minor and the inferior subscapularis indicate their role is that of stabilizers during abduction. This role is distinct from that of the infraspinatus and superior subscapularis which have relatively larger abduction moment arms and function concentrically. Figure 1 illustrates that the inherent length-tension properties of the rotator cuff muscles are well suited to the force and excursion demands placed upon them. It is notable that the teres minor does not have as great a safety margin as do the other muscles. This may indicate that the teres minor is particularly vulnerable to alterations in force and excursion demands that may result from cuff injury or surgical technique. These results highlight the specialized roles of the individual rotator cuff muscles and provide guidance for rehabilitation, surgical decision-making, and prosthesis design. These results highlight the specialized roles of the individual rotator cuff muscles and provide guidance for rehabilitation, surgical decision-making, and prosthesis design.

REFERENCES

Ward, SR et al. (2006). *Clin Orthop Relat Res*, 448: 157-163.

ACKNOWLEDGEMENTS

COMPARING THE FIXATION OF A NOVEL HOLLOW SCREW VERSUS A CONVENTIONAL SOLID SCREW IN HUMAN SACRA UNDER CYCLIC LOADING.

Stewart D. McLachlin[1], Brendon J.B. Beaton[1], Marlis T. Sabo[2], Kevin R. Gurr[2], Stewart I. Bailey[2], Chris S. Bailey[2], and Cynthia E. Dunning[1]

[1] The Jack McBain Biomechanical Testing Laboratory, Department of Mechanical & Materials Engineering, The University of Western Ontario, London, Ontario, Canada, cdunning@uwo.ca
[2] Orthopaedic Spine Program, Department of Surgery, London Health Sciences Centre, The University of Western Ontario, London, Ontario, Canada

INTRODUCTION

Pedicle screw loosening in the sacrum is a significant mode of failure for lumbosacral fusions, particularly in long constructs (Carlson *et al.*, 1992). The success of this procedure depends, in part, on the initial stability of the mechanical construct within bone. Currently, solid pedicle screws are the standard instrumentation used in the sacrum; however, use of a hollow screw has been proposed. The hollow screw increases contact area with the surrounding bone, both on the outer and inner surface of the screw, and thus may potentially improve fixation within the trabecular bone of the first sacral (S1) pedicle.

The purpose of this study was to determine if a hollow screw would be more resistant to loosening than a solid pedicle screw in the S1 pedicle under cyclic loading.

METHODS AND PROCEDURES

Seven fresh-frozen cadaveric sacra (mean age: 72 ± 4 years) were thawed and stripped of soft tissue. In each specimen, a solid 7.5 x 35 mm Xia® monoaxial titanium screw (Stryker Spine, Allendale, NJ) was placed in one S1 pedicle and a 12 x 34 mm MACS-TL HMA® (hollow monoaxial) titanium screw was inserted contralaterally. Insertion was performed under fluoroscopic guidance and the initial screw purchase was visualized using Computed Tomography (CT).
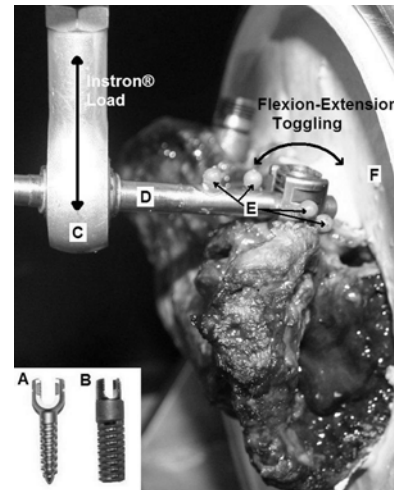

Figure 1. INSET: (A) Solid Screw, (B) Hollow Screw. APPARATUS: (C) Ball joint connected to the actuator of the Instron® materials testing machine, (D) Connecting rod between ball joint and screw, (E) Optical tracking beads, and (F) Sacrum potted within Denstone™ cement, with endplate exposed.

Each sacrum was potted in a custom-designed fixture. A standard fusion connecting rod was secured to both the screw and via a ball joint to the actuator of a materials testing machine (Instron 8872, Canton, MA) (Figure 1). Using load control, an alternating tension-compression load was applied in a sinusoidal pattern (frequency = 1Hz) to the connecting rod, such that the screw was subject to flexion and extension bending moments. Flexion moments started at 0.5 Nm (*i.e.* non-destructive level) for the first 1000 cycles, and increased by 0.5 Nm every 1000 cycles until the screw had visibly failed. Extension moments were maintained at 0.5 Nm

throughout testing. Beads fixed to the rod and the sacrum were used to record screw rotation (flexion) relative to bone at 7.5 Hz using custom optical tracking software (Camera: Sony DFW-SX910, Japan; Software: Labview Vision Acquistion, National Instruments, TX). CT scans were repeated following experimental testing. Both the magnitude of the applied flexion moment and the number of loading cycles to cause loosening were analyzed using two-way repeated measures ANOVAs with post-hoc Student-Newman-Keuls tests ($\alpha=0.05$).

RESULTS

Loading of each screw continued until gross screw loosening was evident by visual inspection. It was determined post-hoc that visible failure corresponded to an average of 6° of screw flexion, by examining a graph of screw rotation versus time for each specimen. Relative performances of the two screws were therefore compared at both 3° and 6° of rotation.
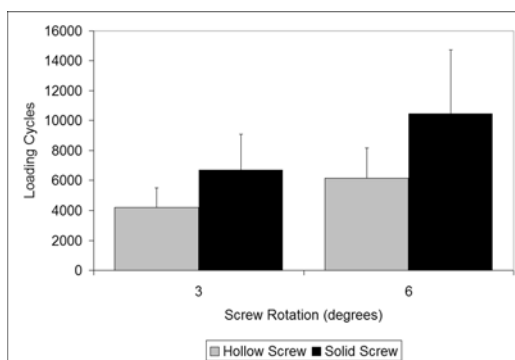
Figure 2. Loading cycles required to reach both 3° and 6° of screw rotation.

Overall, the hollow screw required fewer loading cycles (p=0.004) (Figure 2) and less applied moment (p=0.003) to achieve the same magnitude of screw rotation as the solid screw. Post-loading CT scans showed the hollow screw tended to cut through trabecular bone, with a central core of bone remaining

within screw, while the solid screw 'swept away' interior trabecular bone.

DISCUSSION

Sacral screw loosening continues to be a clinical problem due to the large cyclic bending moments applied at the screw-bone interface in the sacrum. Altering existing screw designs could improve fixation between the bone and screw in the early post-operative period, allowing a better chance for successful fusion. The *in-vitro* nature of this study is indicative of the initial fixation strength available in the bone-screw interface.

A previous study has shown the hollow screw to provide comparable results to bicortical fixation in an axial pullout test when used from an anterior approach in other vertebral bodies (Schramm *et al.*, 2003). Subjected to cyclic flexion-extension loading in the present model, however, the hollow screw proved to be less effective at resisting screw loosening. The current findings are supported by the work of Ferguson *et al.* (2002) who also found the hollow screw to be ineffective under cyclic conditions in thoraculumbar vertebrae, which they attributed to cancellous bone cut-out.

SUMMARY

The novel hollow screw was less resistant to loosening when compared to a conventional solid pedicle screw in this sacral model under cyclic loading.

REFERENCES

Carlson GD et al. (1992). *Spine*, 17: S196-203.
Ferguson SJ et al. (2002). *Eur Spine J*, 11: 527-34.
Schramm M et al. (2003). *Biomed. Technik (Berl)*, 48: 356-61.

COMPARISON OF ANTERIOR 3-HOLE PLATE AND PAIRED/SINGLE ANTERIOR CAGES FOR ANTERIOR LUMBAR INTERBODY FUSION

Daley, ELH[1]; Ruberte Thiele, RA[1]; Poulter, GT[2]; Goldstein, SA[1]; Graziano, GP[1]

[1]University of Michigan, Ann Arbor, MI
[2]University of California San Francisco, San Francisco, CA

INTRODUCTION

Anterior Lumbar Interbody Fusion (ALIF) is an effective treatment for degenerative disc disease and other debilitating spine conditions. Posterior instrumentation is a well-established means of promoting spine fusion, but often requires two surgical exposures. The use of anterior devices has the advantage of one fewer approach, which can reduce patient morbidity.

This study assessed the performance of three newer anterior ALIF devices in restoring spine stability in vitro using an established bovine spine model. To our knowledge, no prior in vitro study has compared the combination of a 3-hole anterior screw-plate (Pyramid, Sofamor Danek, Memphis, TN) with paired titanium threaded and single PEEK non-treaded anterior cages (LT and Perimeter respectively, Sofamor Danek, Memphis, TN).

MATERIALS AND METHODS

13 one-level lumbar motion segments from 2 year-old calves were cleaned of soft tissues and potted in poly(methyl methacrylate) (PMMA) (Ortho-Jet, Lang Dental MFG. Co. Inc., Wheeling, IL). A custom-built, electrohydraulic device provided pure, load-controlled moments about the axial, flexion/extension and lateral anatomic orientations (Figure 1).
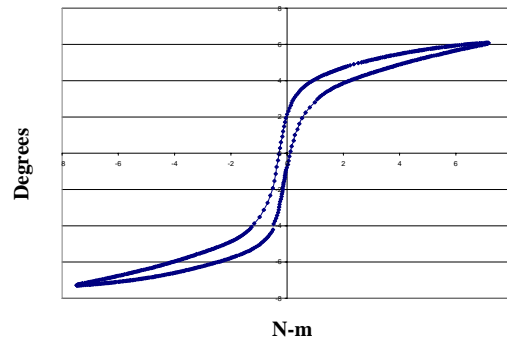

Figure 1: Typical angle vs. moment plot.

Loading began with four +/- 7.5N-m pre-cycles applied at a rate of +/- 0.5 N-m/sec followed by one +/- 7.5 N-m cycle at +/- 0.5 N-m/sec. Test order was randomized. Data were normalized to intact specimen values and the results pooled into four groups (LT, Per, LT+Pyr, Per+Pyr) per test orientation (n $\geq$ 5). Range of motion (ROM) was defined as angular displacement between the + and - 7.5 N-m peaks, and neutral zone (NZ) as that between the + and - loading phases at 0 N-m. Stiffness (in N/degree) was the mean inverse of the slopes at the +/- peaks of the angle versus moment plot (calculated from a least squares fit of the data points 1 N-m from each peak). Data was analyzed using one-way ANOVA with Tukey *post-hoc* test (SPSS Inc. Chicago, IL). A p-value of $\leq$ 0.05 was considered significant. Outliers $>+/- 1.5 \sigma$ from the means were removed.

RESULTS

ANOVA comparisons are summarized in Tables 1-3 (below).

	LT			Per			LT+Pyr			Per+Pyr		
	A	F	L	A	F	L	A	F	L	A	F	L
LT				+	+	+	+	**+**	+	+	**+**	+
Per	-	-	-				+	**+**	-	+	**+**	-
LT+Pyr	-	**-**	-	-	**-**	+				+	-	+
Per+Pyr	-	**-**	-	-	**-**	+	-	+	-			

Table 1: Range of motion (ROM) ANOVA results, row vs. column. A = axial, F = flexion/extension, L = lateral. "+" where row value > column value, "-" where row value < column value. Bold for p<= 0.05.

	LT			Per			LT+Pyr			Per+Pyr		
	A	F	L	A	F	L	A	F	L	A	F	L
LT				+	+	+	+	**+**	-	+	**+**	+
Per	-	-	-				+	+	-	+	+	+
LT+Pyr	-	**-**	+	-	-	+				+	+	+
Per+Pyr	-	**-**	-	-	-	-	-	-	-			

Table 2: Neutral zone (NZ) ANOVA results, row vs. column. A = axial, F = flexion/extension, L = lateral. "+" where row value > column value, "-" where row value < column value. Bold for p<= 0.05.

	LT			Per			LT+Pyr			Per+Pyr		
	A	F	L	A	F	L	A	F	L	A	F	L
LT				+	**+**	**+**	-	-	-	+	+	+
Per	-	**-**	**-**				-	**-**	**-**	+	-	-
LT+Pyr	+	+	+	+	**+**	**+**				+	**+**	**+**
Per+Pyr	-	-	-	-	+	+	-	**-**	**-**			

Table 3: Stiffness ANOVA results, row vs. column. A = axial, F = flexion/extension, L = lateral. "+" where row value > column value, "-" where row value < column value. Bold for p<= 0.05.

Overall, axial ROMs were roughly equal to 1.00 (no change from intact) while lateral ROMs and NZs were less than 1.00. Normalized LT ROM was 1.38. In axial NZ all mean values exceeded 1.00.

Axial stiffness for all groups exceeded 1.00. In lateral stiffness, LT and LT+Pyr exceeded 1.00. In flexion/extension, all groups but the Perimeter had a mean stiffness greater than 1.00.

Despite the addition of the Pyramid plate, the Per+Pyr and LT+Pyr groups had no statistical advantage in axial ROM, NZ, and stiffness and lateral ROM and NZ. Interestingly, the LT cage showed similar flexion/extension and lateral stiffness to the Per+Pyr group (though at the cost of increased flex/ex ROM and NZ). The LT+Pyr group had greater flex/ex and lateral stiffness compared to the Per+Pyr group, but similar ROMs and NZs.

DISCUSSION

Contrary to the view that posterior instrumentation is needed to provide adequate stability during ALIF, our data show that the LT+Pyr group consistently provided intact-like performance with improved ROMs, NZs and stiffnesses. Prior studies have asserted that there are no significant variations in the stability provided by different anterior cages. However, the paired, threaded LT cages offered significantly improved flex/ext and lateral stiffness over the single Perimeter cage. Thus, our results suggest that anterior cage design can affect performance.

Last, our results reinforce the view that cages alone do not lend the compromised spine "intact-like" stability, and may require the addition of an anterior plate for optimal effectiveness.

REFERENCES

Beaubien BP et al. (2005). *Spine*, 16:1846-1851.
Bozkus H et al. (2004). *Spine*, 29:635-641.
Gerber M et al. (2006). *Spine*, 31:762-768.
Madan SS et al. (2003). *European Spine Journal*.
Oda I et al. (2000). *Spine*, 18:2303-2311.
Oxland TR et al. (2000). *European Spine Journal*. 9:S95-S101.
Wilke HJ et al. (1998). *European Spine Journal*, 7:148-154.

THE ASSOCIATION OF FOOT PRINT PARAMETERS AND RUNNING TRAINING LEVEL/EVENT FOCUS

Jeanna Fascione[1] Ryan Crews[1] and James Wrobel[1]

[1] Center for Lower Extremity Ambulatory Research at Scholl College of Podiatric Medicine, Rosalind Franklin University of Medicine and Science, North Chicago, Illinois, USA, james.wrobel@rosalindfranklin.edu, URL: www.diabetic-foot.net

INTRODUCTION

Individual's footprint parameters differ, and are often assessed for injury status. Presently, no study has considered competitive runners' footprints in relation to running competition level (CL) and event focus (EF).

Structural and functional changes occur as different physical demands are applied. Measurements used to assess footprints include: truncated arch index (TAI), arch index (AI), Chippaux-Smirak index (CSI), and Staheli arch index (SAI). These changes are inferred through the evaluation of footprints as the medial longitudinal arch has been found to correlate with footprint measurements. (Queen, 2007) Limited studies have focused on musculoskeletal adaptations as sport specific change. This investigation's purpose is to describe the associations between footprint measurements, CL, and EF.

METHODS AND PROCEDURES

100 competitive runners were recruited through local college and high school track and cross-country coaching staffs. (Table 1).

	Mean	SD
Age (yr)	19.13	2.07
Height (m)	1.71	.10
Weight (kg)	61.44	9.80
BMI (kg/m^2)	20.90	2.04
Women (N=57) 55 %		

Table 1. Baseline Characteristics.

Static weight bearing right footprints were taken by pedograph. The measurements are demonstrated in Figures 1. EF was assigned as sprinter, middle distance, or distance.
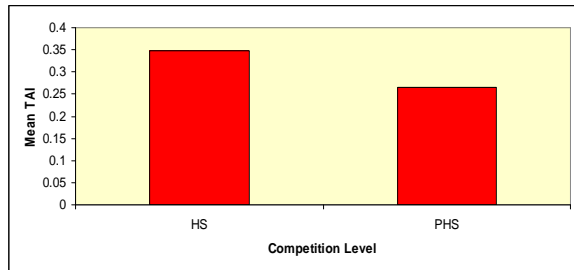

TAI	AI	CSI	SAI
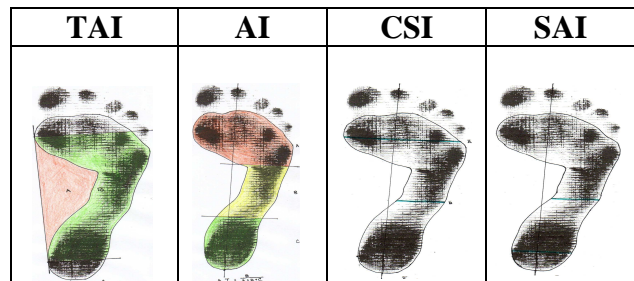
Figure 1. TAI is the non contact to truncated contact area. AI is the mid-foot contact area to entire contact area ratio, excluding the toes. CSI is the forefoot toe midfoot width ratio. SAI is the mid-foot to hind-foot width ratio.

Further calculation using PictZar-Calibrated Digital Measurements version 4.02 was utilized to determine linear and area footprint measurements. ANOVA was used to assess footprint measurements with competition level. A Mixed Linear Models Analysis was used to assess footprint measurement's association with event focus.
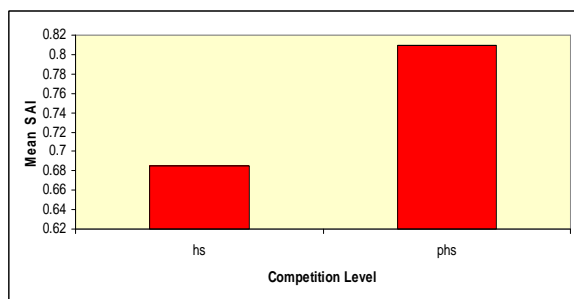
RESULTS

PHS runners had significantly decreased TAI [0.27 ($\pm$0.10) versus 0.35 ($\pm$0.14)], increased AI [0.30 ($\pm$0.03) versus 0.27 ($\pm$0.04)], p = 0.000], and increased SAI [0.81 ($\pm$0.15) versus 0.69 ($\pm$0.16)], p = 0.01. (Graphs 1-3). Event focus was not shown to be associated with any of the footprint measurements.

Graph 1. CL & TAI Association.
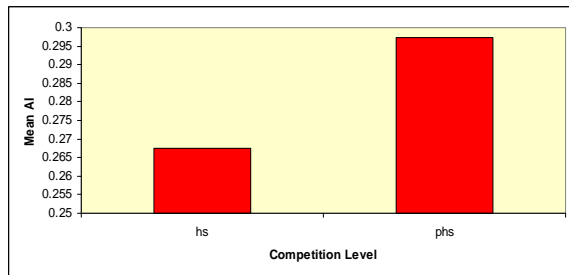
Graph 2. CL & AI Association.

Graph 3. CL & SAI Association.

DISCUSSION

An association exists between running CL and footprint measurements. TAI, AI, CSI, and SAI differed with competitive HS and PHS runners. These trends indicate an increased midfoot surface contact, potentially reflective of training induced lowered arches. The outcome of this potential remodeling is unknown at this time.

Adaptations may occur according to different applied demands. Sport specific adaptations have been suggested with lowered arches in elite gymnasts and competitive runners (Aydog, 2005) (Fascione, 2005). The sprint gait involves contacting the ground with the ball of the foot followed by forceful forward propulsion. In comparison, the distance gait involves a heel-to-toe foot strike (Adelaar, 1986). Faster velocities result in increased leg stiffness and different biomechanics (Butler, 2003). Additionally, different running speeds are associated with different vertical force impact peaks, medio-lateral force patterns, and anterior-posterior braking force curves (Nilsson, 1989). These findings suggest a potential anatomical accommodation in response to prolonged training, or different biomechanics.

SUMMARY

Such associations may represent physical characteristics associated with a competitive advantage or consequences of extensive training. Should future work show this adaptation to be problematic, additional research will be required to assess the feasibility to limit or prevent these adaptations through orthotics, training modifications, or other modalities.

REFERENCES

Adelaar, RS (1986). *The American Journal of Sports Medicine*, 14: 497-500.
Aydog, S et al (2005). *British Journal of Sports Medicine*, 39: http://bjsm.bmj.com, 8/5/07.
Butler, R et al (2003). *Clinical Biomechanics*, 18: 511-517.
Fascione, J et al (2005). *Medicine and Science in Sports and Exercise*, 37: S153.
Nilsson, J and Thorstensson, A (1989) *Acta Physiol Scand*, 136: 217-227.
Queen, R et al (2007). *Foot & Ankle International,* 28: 456-462.

ACKNOWLEDGEMENTS

DIFFERENCES IN BONE MORPHOLOGY IN MALE RATS SELECTIVELY BRED FOR HIGH OR LOW AEROBIC CAPACITY

Sarah L Manske[1], Russell T Hepple[1], Lauren G Koch[2], Steven L Britton[2], Steven K Boyd[1], and Ronald F Zernicke[1,3]

[1]Faculty of Kinesiology, University of Calgary, Calgary, Alberta, Canada, smanske@ucalgary.ca
[2]Department of Physical Medicine & Rehabilitation, University of Michigan, Ann Arbor, Michigan, USA, [3]Departments of Orthopaedic Surgery, Kinesiology and Biomedical Engineering, University of Michigan, Ann Arbor, Michigan, USA, zernicke@med.umich.edu

INTRODUCTION

Aerobic capacity reflects multiple genetic and environmental factors. A large-scale selective breeding program was initiated to develop two lines of rats with enhanced or reduced aerobic capacity (Koch and Britton, 2001). A founder stock of 96 male and 96 female genetically heterozygous N:NIH rats were tested for intrinsic (i.e., untrained) treadmill running capacity to exhaustion. The maximal distance run was used to choose the 13 highest and 13 lowest capacity rats for each sex, which were mated using outbred rotational breeding at subsequent generations. Selection produced differences in body weight such that the low line became increasingly heavier and the high line increasingly lighter at each generation. After 11 generations, the animals bred as high capacity runners (HCR) ran 347% greater treadmill distance than the animals bred as low capacity runners (LCR) (Koch and Britton, 2001), and adaptations for oxygen utilization occurred predominantly in the peripheral skeletal muscles (Howlett et al., 2003).

Areal BMD and section modulus in young women have been positively associated with aerobic capacity (Lloyd et al., 2002), however such an analysis in humans can not differentiate clearly between genetic and environmental effects. The selective bred model allows us to elucidate the genetic influences of inherent aerobic capacity, body mass, and muscle mass on skeletal health independent of environmental factors, such as exercise training effects. A previous analysis found that 4-month old Generation 17 male LCR rats exhibited improved bone morphology compared with HCR rats (Sharkey et al., 2006). Nonetheless, most of the between-group differences were negated after adjusting for body mass. We were interested in determining whether these same relations existed after adjusting for muscle mass, and in a slightly older age group. Thus, the purpose of the study was to determine whether high aerobic capacity can elicit improved bone structure relative to body weight and muscle weight in the absence of exercise training.

METHODS AND PROCEDURES

Twelve male rats selectively bred for high (HCR, n = 7) and low (LCR, n = 5) running capacity were obtained at 10 – 12 months of age from Generation 19. After sacrifice, the animals were weighed (body mass) and the muscles of the posterior compartment (muscle mass: gastrocnemius, soleus, and plantaris) were dissected and weighed.

The right tibia was extracted and scanned by micro-computed tomography (μCT40, Scanco Medical) at the proximal and mid-diaphyseal regions of the tibia (20 μm isotropic voxel size) for trabecular and cortical bone analyses, respectively. Variables of interest in the proximal region included bone volume (BV), total volume (TV), bone volume ratio (BV/TV), trabecular thickness (Tb.Th), number (Tb.N), and separation (Tb.S). Variables of interest in the mid-diaphyseal

region included cortical cross-sectional area (C.Ar), cortical thickness (Ct.Th), maximal cross-sectional moment of inertia (Imax), and polar moment of inertia (J). Independent t-tests were performed to evaluate differences between HCR and LCR rats. Analyses of covariance (ANCOVAs) were performed with body mass or muscle mass as covariates to determine whether differences between groups were attributable to size differences.

RESULTS

Before adjusting for body or muscle mass, LCR rats tended to have improved bone structure compared with HCR rats (Table 1). These trends were significant for most measures of cortical morphology (Figure 1) and bone size in the proximal tibia, but not for trabecular architecture. Many of these differences remained significant after adjusting for body or muscle mass. For all measures except BV/TV, the estimated marginal means for LCR rats were greater than for HCR rats.

	HCR (n = 7)	LCR (n = 5)
Body mass (g)	389.2 ± 36.3[1]	541.6 ± 77.6
Mus mass (g)	2.31 ± 0.14[1]	2.94 ± 0.30
Length (mm)	43.0 ± 0.7	44.0 ± 2.0
Trabecular Architecture in Proximal Tibia		
TV (mm^3)	16.4 ± 0.6[1,2]	9.2 ± 1.3
BV (mm^3)	3.0 ± 0.7[1,2]	4.6 ± 1.3
BV/TV (%)	18.5 ± 4.2	23.8 ± 5.6
Tb.Th (mm)	0.09 ± 0.01	0.10 ± 0.02
Tb.N (mm^{-1})	3.29 ± 0.36	3.58 ± 0.12
Tb.Sp (mm)	0.30 ± 0.04	0.26 ± 0.01
Cortical Morphology in Tibia Mid-Diaphysis		
C.Ar (mm^2)	4.41 ± 0.38[1,2]	5.65 ± 0.74
C.Th (mm)	0.73 ± 0.03	0.74 ± 0.01
Imax (mm^4)	2.89 ± 0.59[1,2]	5.34 ± 1.86
J (mm^4)	4.49 ± 0.80[1,2]	7.76 ± 2.35

Table 1. Differences between young male HCR and LCR rats. [1]indicates HCR significantly less than LCR at $p < 0.05$ for t-test. [2]indicates HCR significantly less than LCR at $p < 0.05$ after adjusting for body mass or posterior muscle mass in an ANCOVA.
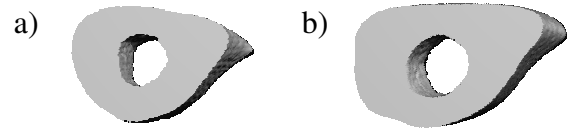

Figure 1. Representative µCT images of mid-diaphyseal cortical bone in a) HCR and b) LCR rats.

DISCUSSION

The results differ from those of Sharkey et al. (2006) who found that scaling effects could explain the differences between groups. As these rats were older (10-12 months) than the rats previously studied (4 months), the magnitude of the difference between groups may increase with age. The greater estimated marginal means for LCR than HCR rats suggested that male LCR rats had enhanced bone size beyond which were accounted for by body mass or muscle mass alone. The results of this study will be combined with an examination of the effects of aging on the relation between aerobic capacity and skeletal health.

SUMMARY

Exercise training may be required to elicit enhanced bone structure in animals with inherently high aerobic capacity.

REFERENCES

Howlett RA, et al. (2003). *J Appl Physiol* 94(4): 1682-8.
Koch LG and Britton SL (2001). *Physiol Genomics* 5(1): 45-52.
Lloyd T, et al. (2002). *Bone* 30(2): 416-21.
Sharkey NA, et al. (2006). Transactions of the ORS, Chicago, IL.

ACKNOWLEDGEMENTS

A FINITE ELEMENT STUDY OF THE EFFECT OF CROSS-SHEAR ON WEAR OF THE PRODISC TOTAL DISC REPLACEMENT

Curtis Goreham-Voss[1*] and Thomas Brown[1]

[1]Orthopaedic Biomechanics Laboratory, University of Iowa, Iowa City, IA, USA,
*curtis-voss@uiowa.edu

INTRODUCTION

Polyethylene wear in a total disc replacement (TDR) is a substantial clinical concern and design consideration. Due to the expense and time involved in long-term preclinical laboratory wear testing, numerical simulations incorporating the Archard wear formulation have emerged as a practical, efficient complement that yields reasonable results (Maxian et al., 1996). Recent laboratory testing has suggested that numerical simulations may achieve more accuracy by replacing the constant wear coefficient with a wear coefficient that is dependent on cross-shear (Kang et al., 2008). In this study, cross-shear is implemented in a long-term numerical simulation of the Prodisc TDR. The effect of cross-shear is investigated by comparing two loading profiles that produce differing levels of cross-shear.

METHODS AND PROCEDURES

A finite element (FE) model of a Prodisc lumbar TDR was created in ABAQUS (Figure 1). The polyethylene insert was modeled as linear elastic, with a modulus of 1,400 MPa and a Poisson's ratio of 0.3. The (CoCr) superior endplate and inferior side of the poly insert were treated as rigid surfaces. The rigid surfaces were controlled through forces and displacements applied to reference points located at the implant's center of rotation. The insert was meshed with 2,048 8-node quadrilateral elements. The contact surface was assigned a friction coefficient of 0.08. The rotations and loading prescribed by

the recent ISO draft standard (ISO/DIS 18192-1) for disc prosthesis wear tests were applied via time-dependent amplitudes within a single ABAQUS step. Rotational inputs were applied to the insert undersurface, while the axial load was applied to the superior endplate. All translational degrees of freedom for the undersurface of the UHMWPE insert were constrained, as were all rotational degrees of freedom for the superior endplate.
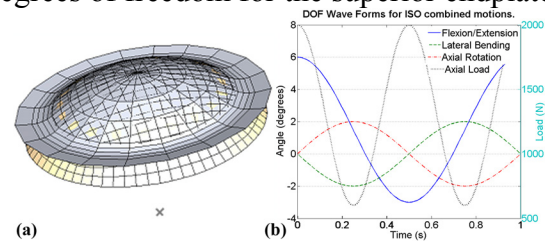

Figure 1. (a)FE model, and (b) loading input for Prodisc wear simulation.

Wear was incorporated through user-defined adaptive meshing. Linear wear depths for each node were defined in the subroutine UMESHMOTION, according to the Archard wear formulation,

$$w = k(CS)*\sigma*d \qquad (1)$$

where w is the linear wear depth, $k(CS)$ is the wear coefficient as a function of cross-shear ratio (CS), σ is the contact pressure, and d is the sliding distance. The wear coefficient curve was based on the power law described by Kang et al. (2008), scaled (to account for the respective differences in bearing surface tribology) so as to recover wear rates comparable to Prodisc-L data reported by Rawlinson et al. (2007).

Calculation of the cross-shear ratio requires specifying a principal molecular orientation

(PMO) of the polymer chains. For this study, the polymer chains were assumed to align in the direction of the dominant frictional work. Therefore, the PMO was defined as the orientation that would minimize the amount of work perpendicular to the PMO. The cross-shear ratio (CS) could then be defined as the ratio of the work performed in a direction perpendicular to the PMO ($W_\perp$) to the total frictional work (W_{tot}):

$$CS = \frac{W_\perp}{W_{tot}} \qquad (2)$$

To test the effect of cross-shear on a long-term wear simulation, two variants of otherwise similar loading were applied to the implant. Both variants used the rotations and loadings of the ISO standard. In one simulation, the rotations were applied as recommended for 10 million cycles, resulting in a crossing motion that generated significant cross-shear. In a second simulation, the rotational inputs were separated and applied individually (a testing variant included in the current ASTM guidance document), each for 10 million cycles, resulting in three concatenated sequences of virtually uni-directional motion with very low cross-shear.

RESULTS

Figure 2 shows the cross-shear throughout one motion cycle under the combined motions input, with the relative position of a typical node on its motion locus shown in red. Low cross-shear is seen as the implant moves in a long sweep along the AP direction and high cross-shear is seen during the short crossing motions in the ML direction.
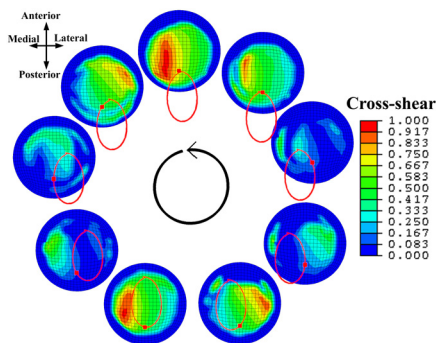
Figure 2. Cross-shear on the insert during one motion cycle.

Wear results for 10 million cycles (mc) under the two input conditions were compared in terms of maximum linear wear depth, total volumetric wear, and wear rate (Table 1).

Simulation	Max Linear Wear (mm)	Vol. Wear (mm^3)	Wear Rate (mg/mc)
Combined	0.636	120.02	10.71
Separated	0.382	56.04	0.67 (f/e)
			2.79 (lat)
			1.10 (rot)

Table 1. Wear measures for combined and separated motion simulations.

DISCUSSION

The order-of-magnitude difference in wear rates shows the importance of cross-shear in polyethylene wear. Under otherwise similar conditions, the presence of cross-shear predicated a dramatic increase in wear rates over primarily unidirectional motion. Linear wear depths were not affected as strongly. A disproportionally high fraction of the wear in the separated-motion model occurred in the first few cycles after changing the rotational input, during which there was brief, but very high, cross-shear. Future applications of this model will be useful for evaluating the wear testing guidelines, and perturbations thereof, put forth for consensus standards.

REFERENCES

Maxian, TA et al. (1996). *J Orthop Res.,* 14:668-675.

Kang, L et al. (2008). *J Biomech.*, 41:340-346.

Rawlinson, JJ et al. (2007). *J Neurosurg Spine.* 7:165-173

ACKNOWLEDGEMENTS

ANALYSIS OF THE EFFECTS OF STILTS WALKING ON JOINT MOMENTS IN LOW EXTREMITIES

John Z. Wu, Sharon S. Chiou, and Christopher S. Pan
National Institute for Occupational Safety and Health
Morgantown, West Virginia, USA

INTRODUCTION

Stilts are commonly used at construction sites for many tasks, such as taping and sanding on ceiling or upper half of a wall (Fig. 1). Some epidemiological studies indicate that the use of stilts may place workers at increased risk for knee injuries or may increase the likelihood of trips and falls (Schneider and Susi, 1994). However, it is not clear whether the use of stilts during walking will increase musculoskeletal loading, thereby increasing the risk of musculoskeletal injuries in the lower limbs. In the present study, we developed an inverse dynamic model of stilts walking to investigate the effects of this activity on the joint moments in the lower limbs.

METHODS AND PROCEDURES

The stilts-walking model was developed using the commercial musculoskeletal simulation software AnyBody (version 2.0, Anybody Technology, Aalborg, Denmark) by modifying its existing three-dimensional gait model (Gait3D). The 3D gait model (Gait3D) includes only the lower body, i.e., two legs and pelvis. The hip, knee, and ankle joints are considered to have 3 DOFs (degree of freedom) (external/internal rotation, abduction/adduction, and extension/flexion), 1 DOF (extension/flexion), and 2 DOFs (plantar/dosiflexsion and eversion/inversion), respectively.

Four healthy construction workers participated in the study. Subjects walked without or with stilts through a 12-meter straight path. When walking on the stilts, the subjects were elevated by 0.61 m from the floor. A total of 18 reflective spherical markers were placed on the lower extremities of the subjects at the anatomical landmarks, as suggested by Vaughan et al. (1999). For the tests with stilts walking, three additional motion markers were placed on each stilt (Fig. 1). The marker kinematics data were collected at 60 Hz using a six-camera system (Peak Performance Technologies Inc., Englewood, CO, USA). Two force platforms (Type 9287 and 9287A, Kistler Instrument Corp., Amherst, NY, USA) embedded in the walkway were used to measure ground reaction forces at a frequency of 600 Hz.
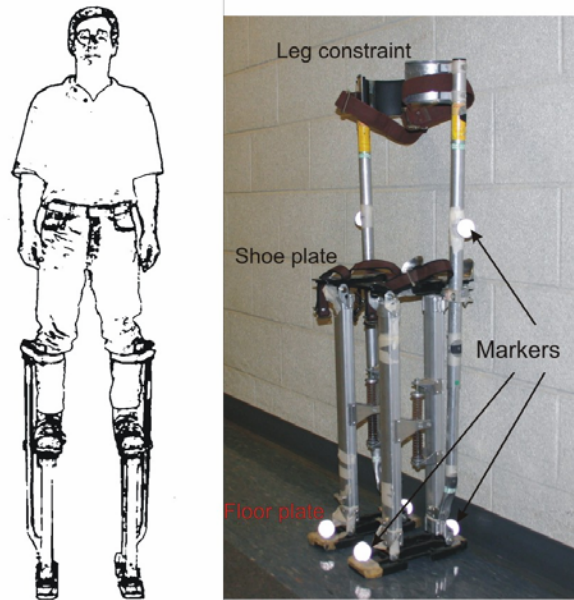

Figure 1: A construction worker walking on stilts (Left). Typical stilts used in constructions are made of aluminium (Right).

The simulations were performed using an inverse dynamic approach. The model was driven by the motion markers; and the ground reaction forces were applied as boundary conditions. The simulations were performed by applying universal joint muscles on each

joint. The obtained generalized muscle ``force'' in the simulations were the joint moments.

RESULTS
The predicted time-histories of the joint moments in the sagittal plane for stilts walking are compared with those for normal walk in Fig. 2. The joint moments shown in the figures were normalized by dividing the computed values with the body mass of the subject (in kg). The maximal joint moment was found in the ankle flexional motion and reaches a magnitude of approximately 1.5 Nm/kg at peak. It is seen that the use of stilts caused the peak flexion/extension joint moment to increase by approximately 25% in knee while to decrease by approximately 15% in ankle. The stilts use is found not to cause significant changes of the peak flexional joint moment in the hip.

DISCUSSION
A comparison of the patterns of the joint moment during swing phase indicates that the joint moments for the normal walking become zero immediately after the completion of the walk stance while those for the stilts walking oscillate for one cycle (Fig. 2). These oscillations of the joint moments are caused by the mass inertia effects of the stilts; the legs have to apply extra force to initiate and stop the motion of the stilts at the stance-swing transition and terminal swing, respectively. The mass of a stilt is approximately equivalent to that of a thigh and twice that of a shank (Vaughan et al., 1999). Since the mass in the thigh and shank is approximately evenly distributed in a cylindrical section with a length of about 0.4 m, while the mass in the stilt is unevenly distributed in a slim structure with a length of 1.02 m, the mass moments of inertia of a stilt around its lateral axes are estimated to be around ten times those of the thigh and shank.

SUMMARY
In the current study, we have analyzed the joint moment and muscle forces in the lower extremities during stilts walking and theoretically evaluated the effects of the stilts use on the joint moments.

REFERENCES
Vaughan, C., Davis, B., O'Connor, J. (1999). Dynamics of Human Gait. Cape Town, Kiboho Publishers.
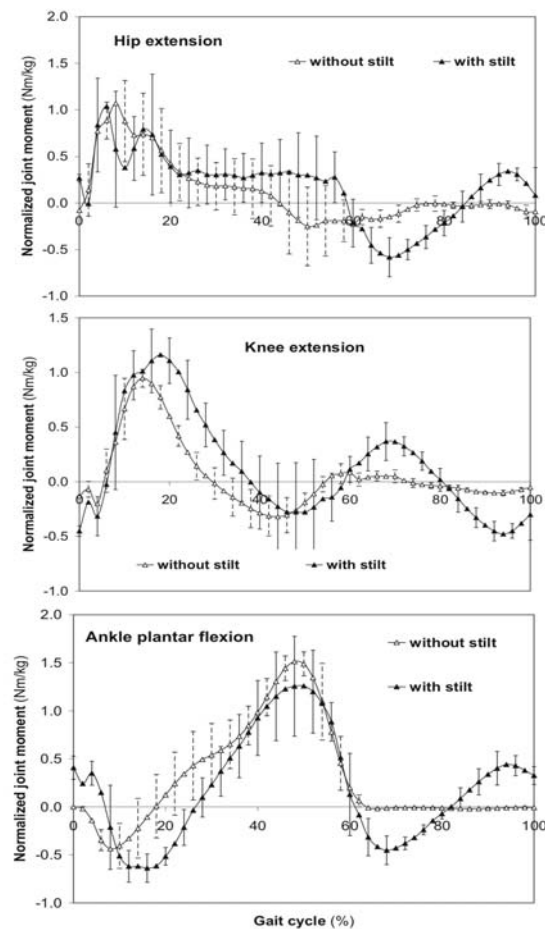Schneider, S., Susi, P. (1994). Am Ind Hyg Assoc J, 55 (7), 635-49.

Disclaimers

Figure 2: Comparison of the predicted moments in hip, knee, and ankle joints for stilts walking with those in normal walking.

CHANGES IN IN-VIVO GLENOHUMERAL JOINT CONTACT PATTERNS AND CLINICAL OUTCOMES FROM 3 TO 12 MONTHS AFTER ROTATOR CUFF REPAIR

Stephanie K. Kline[1], Roger Zauel[1], Terrence R. Lock[2], Michael J. Bey[1]

[1]Bone and Joint Center, [2]Dept of Orthopaedic Surgery, Henry Ford Hospital, 2799 W. Grand Blvd., Detroit, MI 48202, USA, sbrock2@hfhs.org

INTRODUCTION

Rotator cuff tears are common and have a significant impact on comfort, function, and medical expense. Treatment strategies rely implicitly on the belief that restoring normal joint mechanics is necessary to obtain a satisfactory clinical result. However, it is unknown if rotator cuff repair restores normal joint mechanics, or if changes in joint mechanics are associated with clinical outcomes. Thus, the purpose of this study was to quantify in-vivo glenohumeral joint mechanics and clinical outcomes in patients following rotator cuff repair.

METHODS AND PROCEDURES

Following IRB approval and informed consent, 12 subjects (age: 62 ± 12) enrolled in the study. Each subject had undergone surgical repair of a full-thickness supraspinatus tendon only rotator cuff tear. The contralateral shoulder of each subject was asymptomatic. Subjects were tested at 3 and 12 months post-surgery. At each visit, biplane x-ray images were collected at 60 Hz during coronal plane abduction from full adduction to approximately 120° (Tashman 2003). Images were collected for three trials of each shoulder. In addition, clinical outcomes were assessed with the Western Ontario Rotator Cuff (WORC) Index and maximum isometric shoulder strength was measured during abduction, elevation, internal rotation, and external rotation. Repaired shoulder strength was expressed as a percentage of contralateral shoulder strength.

Following testing, CT scans of the humerus and scapula of both shoulders were obtained and 3D bone models were created (Mimics V11.11, Materialise, Ann Arbor, MI). Anatomical landmarks were identified on the bone models to produce coordinate systems for the humerus and scapula. The 3D position of the humerus and scapula were tracked from the biplane x-ray images using an accurate (±0.4mm, ±0.5°) model-based tracking technique (Bey et al, 2006).

Glenohumeral joint contact patterns were measured using a technique that combines joint motion measured from biplane x-ray images with the CT-based bone models (Anderst, 2003). This technique first calculated the distance between the articulating surfaces of the humerus and glenoid, and then calculated the centroid of a $200mm^2$ region of contact between the joint surfaces. This contact center position was normalized relative to the glenoid dimensions and expressed in the superior/inferior (S/I) and anterior/posterior (A/P) directions of the scapula coordinate system. This position was averaged over the tested range of motion to produce an average contact center position for each trial.

A two-way ANOVA assessed the effects of shoulder condition (repaired, contralateral) and time post-surgery (3 months, 12 months) on the average S/I and A/P contact center positions. A one-way ANOVA assessed the effect of time post-surgery on the WORC Index and normalized shoulder strength.

RESULTS

At 3 and 12 months post-surgery, the S/I contact center position was significantly higher on the glenoid in the repaired shoulders than in the contralateral shoulders (p<0.04, Fig. 1). No significant difference was detected from 3 to 12 months post-surgery in the S/I contact center position of either shoulder (p>0.82, Fig. 1). No significant differences were detected in the A/P contact center position between shoulders or over time (p>0.19, Fig. 1).
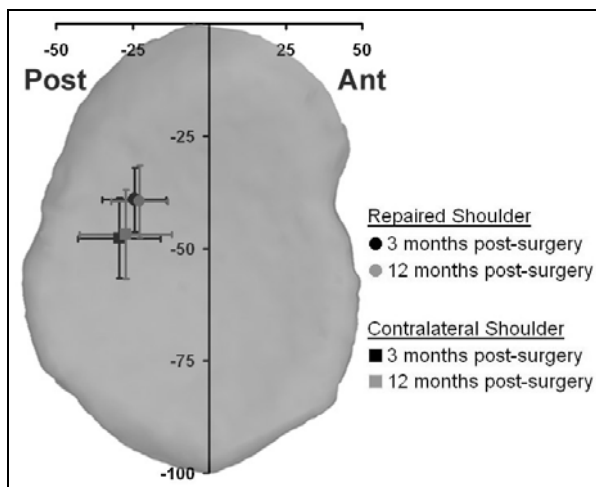

Figure 1. Average contact center position is shown superimposed on a typical glenoid for repaired (●) and contralateral (■) shoulders. The contact center's S/I position was significantly different between shoulders at 3 and 12 months post-surgery (p<0.04). No significant differences in A/P contact center location were detected.

Despite the lack of differences over time in glenohumeral joint contact patterns, both shoulder strength and the patients' quality of life improved from 3 to 12 months post-surgery. Specifically, internal rotation and external rotation strength both increased significantly (p<0.04, Fig. 2) from 3 to 12 months post-surgery. Similarly, there were significant improvements in the WORC Index from 3 to 12 months post-surgery (p<0.01).
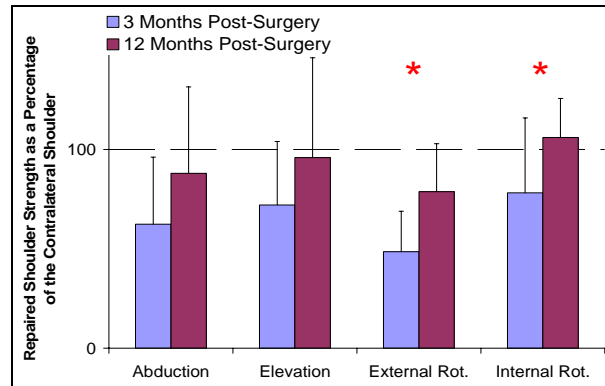
Figure 2. Strength of the repaired shoulder (expressed as a percentage of the contralateral shoulder) increased over time. *p<0.05.

DISCUSSION

This study failed to detect significant changes in glenohumeral joint contact patterns from 3 to 12 months post-surgery, but demonstrated improvements in both quality of life and shoulder strength over time. These findings suggest that restoring normal glenohumeral joint mechanics may not be necessary in order to achieve a satisfactory clinical outcome.

It is interesting that at 12 months post-surgery the humerus remained positioned more superiorly on the glenoid in the repaired shoulder than in the contralateral shoulder. However, it is unclear if this finding represents an etiologic factor associated with the development of the injury or a persistent transient effect due to surgery. On-going research in our laboratory is addressing this question. Future plans include the recruitment of additional subjects and data collection through 24 months post-surgery.

REFERENCES

Anderst, WJ and Tashman, S (2003). *J Biomech*, 36: 1291-99.
Bey, MJ et al. (2006). *J Biomech Eng*, 128(4):604-9.
Tashman, S and Anderst, W (2003). *J Biomech Eng*, 125(2):238-45.

EFFECTS OF STILTS WALKING ON MUSCULOSKELETAL LOADING IN LOW EXTREMITIES

John Z. Wu*, Sharon S. Chiou, and Christopher S. Pan
National Institute for Occupational Safety and Health
Morgantown, West Virginia, USA. *E-mail: jwu@cdc.gov

INTRODUCTION

Stilts are commonly used at construction sites to raise the workers to a higher level above ground to increase the efficiency for many tasks. Some epidemiological studies indicate that the use of stilts may place workers at increased risk for knee injuries or may increase the likelihood of trips and falls (Schneider and Susi, 1994). However, no biomechanical analysis has been performed to examine the effects of the stilts walking on the musculoskeletal loading. In the current study, we hypothesize that the use of stilts in walking will increase the musculoskeletal loadings in the lower limbs.

METHODS AND PROCEDURES

The stilts-walking model was developed using the commercial musculoskeletal simulation software AnyBody (version 2.0, Anybody Technology, Aalborg, Denmark) by modifying its existing three-dimensional gait model (Gait3D) (Fig. 1). The 3D gait model (Gait3D) includes only the lower body, i.e., two legs and pelvis. The gait model includes a total of 70 muscles -- 35 muscles on each leg. The muscles were simulated by a "classical" three-element muscle model, consisting of a Hill-type contractile element, a parallel elastic element, and a serial elastic element. The recruitment of the muscle forces was calculated by using a min/max optimization procedure in AnyBody, in which the maximal normalized muscle force was minimized. The simulations were performed using an inverse dynamic approach. The model was driven by the motion markers; and the ground reaction forces were applied as boundary conditions.

Four healthy construction workers participated in the study. Subjects walked without or with stilts through a 12-meter straight path. When walking on the stilts, the subjects were elevated by 0.61 m from the floor. A total of 18 reflective spherical markers were placed on the lower extremities of the subjects at the anatomical landmarks, as suggested by Vaughan et al. (1999). For the tests with stilts walking, three additional motion markers were placed on each stilt. The marker kinematics data were collected at 60 Hz using a six-camera system (Peak Performance Technologies Inc., Englewood, CO, USA). Two force platforms (Type 9287 and 9287A, Kistler Instrument Corp., Amherst, NY, USA) embedded in the walkway were used to measure ground reaction forces at a frequency of 600 Hz.
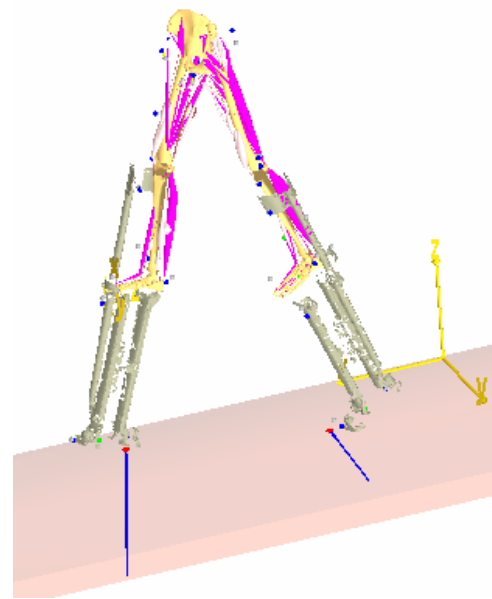

Figure 1: Modeling of stilts walking using commercial software package AnyBody.

RESULTS

The time-histories of the normalized muscle force for eight muscle groups are depicted in Fig. 2. The predicted muscle forces are normalized by their maximal isometric forces in these figures. GAS, GMEDP, and GMEDA muscles are relatively heavily loaded during the normal waling; the peak normalized forces in these muscles are predicted to be around 0.4-0.6. The RF muscle group is least loaded, the normalized muscle force reaches merely 0.16 at peak during the normal walking. The use of stilts induced substantial increases of the peak normalized muscle force in RF and SOL muscles (180% and 35%, respectively). The peak normalized muscle forces in VAS, GMAX, and GMEDA increased by approximately 6%, 9%, and 19%, respectively, due to the stilts use. The peak normalized muscle force in GAS decreased by approximately 49%, while those in HAMS and GMEDP decreased by approximately 29% and 20%, respectively, due to the stilts use.

DISCUSSION

The use of stilts is found to influence force distributions among the muscles. Our simulations indicated that, for the eight muscles groups analyzed, the forces in five muscle groups are increased while those in three muscle groups are decreased due to the stilts use. The increases in muscle loading during the stilts walking may speed the muscle fatigue of the workers, influencing the postural balance.

SUMMARY

Our simulations suggested that the use of stilts may potentially cause an increase in loadings in five of eight major muscle groups in the lower extremities. Most remarkable is the force in RF muscle, which was found to increase 1.8 times for the stilts walking compared to that for the normal walking.

REFERENCES

Vaughan, C., Davis, B., O'Connor, J. (1999). Dynamics of Human Gait. Cape Town, Kiboho Publishers.
Schneider, S., Susi, P. (1994). Am Ind Hyg Assoc J, 55 (7), 635-49.

Disclaimers
The findings and conclusions in this report are those of the authors and do not necessarily represent the views of the National Institute for Occupational Safety and Health.
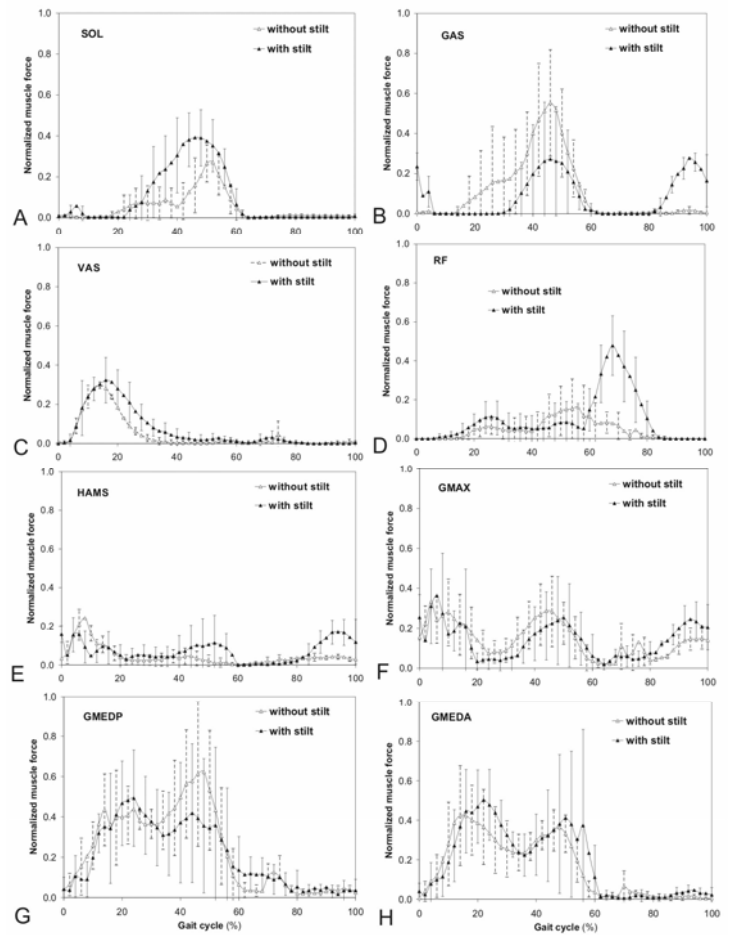

Figure 2: Comparison of the normalized forces in eight muscles or muscle groups for stilts walking with those for normal walking during one gait cycle. A: SOL (soleus), B: GAS (gastrocnemius), C: VAS (vastii: vastus lateralis/medialis/intermedius), D: RF (rectus femoris), E: HAMS (hamstring), F: GMAX (gluteus maximus), G: GMEDP (posterior gluteus minimus/medius), and H: GMEDA (anterior gluteus minimus/medius).

A PRACTICAL MODEL OF THE MUSCLE/TENDON MOMENT ARMS IN A THUMB

John Z Wu[1][*], Kai-Nan An[2], and Robert G. Cutlip[1]
[1] National Institute for Occupational Safety and Health, Morgantown, WV, USA
[2] Mayo Clinic College of Medicine, Rochester, MN, USA
*E-mail: jwu@cdc.gov

INTRODUCTION

Many occupation-related hand injuries are associated with excessive loadings in the tendons and muscles in the fingers. A biomechanical model of a thumb can be used to explore the mechanical loadings in the musculoskeletal system in the finger, which cannot be measured in vivo. One of the technical difficulties for the development of such a model is the correct description of the kinematics of the thumb joint motions (Valero-Cuevas et al., 2003). The previous thumb models (e.g., Valero-Cuevas et al., 2003) are formulated analytically/numerically and are not convenient for the researchers to solve practical problems. The purpose of the current study is to develop a practical kinematical thumb model using the commercial software Anybody (Anybody Technology, Aalborg, Denmark), which includes the real micro-CT-scans of the bony sections and realistic tendon/muscle attachments on the bones.

METHODS AND PROCEDURES

The thumb is modeled as a linkage system, consisting of a fixed trapezium, a metacarpal bone, a proximal and distal phalanx (Fig. 1). The IP joint is considered as a hinge (1 DOF) while MP and CMC are considered as universal joints (2 DOFs). The dimensional scale of the thumb model is consistent with An et al. (1979). Nine muscles were included in the proposed model: FPL, EPL, EPB, APL, FPB, APB, ADPt, ADPo, and OPP. In order to better visualize the muscle/tendon attachment locations and to guide the muscle/tendon during the movements, the real

3D bony section meshes were implemented into the thumb model. The predicted muscle/tendon excursions and moment arms were compared with the experimental data by Smutz et al. (1998). Initially, the attachment locations of the tendons from the normative model (An et al., 1979) were applied. The attachment locations were then adjusted for the model predictions to match the muscle moment arms measured experimentally by Smutz et al. (1998). The excursions of each individual muscle/tendon were first calculated from the model. The moment arms of the muscles/tendons corresponding to a particular joint were then derived by differentiating the excursions with respect to that joint rotation.
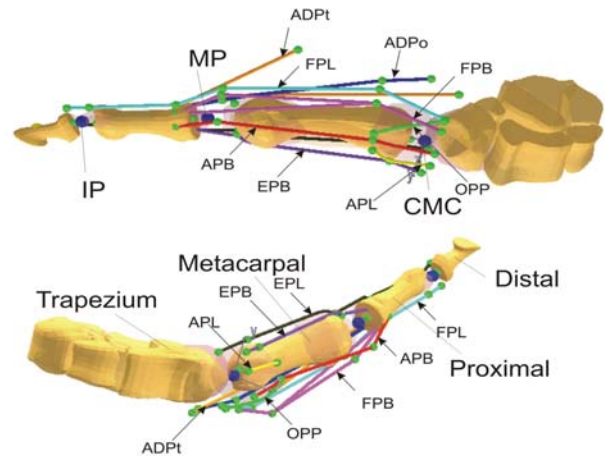

Figure 1: Schematics of the proposed thumb model developed using AnyBody.

RESULTS

The variations of the muscle/tendon moment arm as a function of the angular motions of the IP, MP, and CMC joints were calculated and compared with the experimental data (results
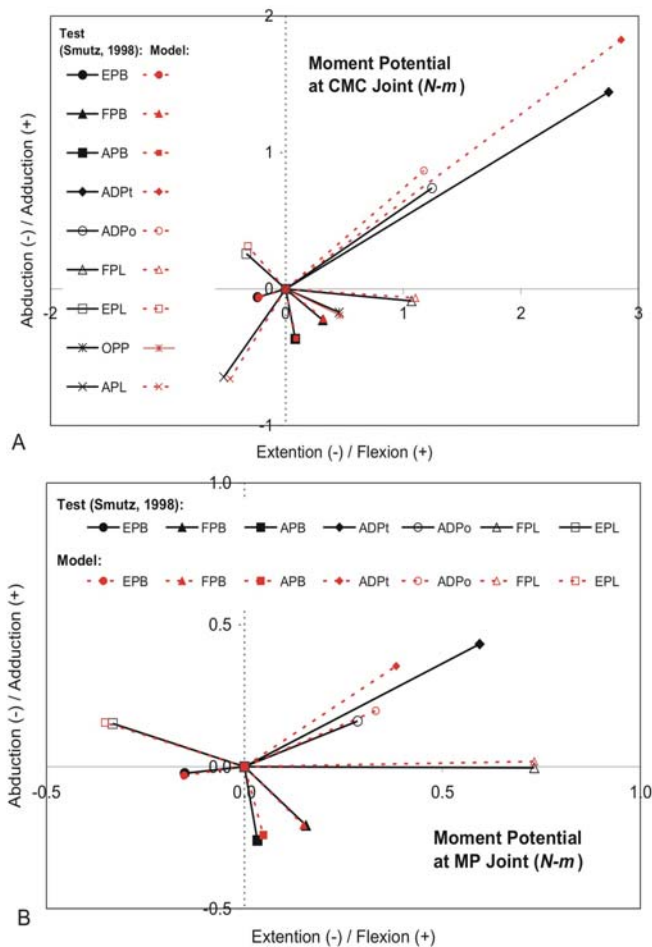
Figure 2: The predicted muscle/tendon moment potentials in CMC (A) and MP (B) joints compared with the experimental data by Smutz et al. (1998).

not shown). The calculated moment potentials of the MP and CMC joints using the current model were compared with the experimental data in Fig. 2. The muscle moment potentials were constructed using the averaged moment arms multiplied by their corresponding maximal isometric forces, which were evaluated by multiplying the physiological cross-sectional area (PCSA) by a specific muscle strength (35 N/cm^2). The diagrams illustrate the magnitude and direction of the maximal muscle moment that can be generated in each muscle.

DISCUSSION

Except the ADPo muscle for both MP and CMC joint motions, all other calculated muscle moment arm potentials agree well with the experimental data. The abductor pollicis muscle has a large PCSA and is attached to the metacarpal bone and proximal phalanx in a region; however, it is modeled as a string and attached to the bony sections at points in the biomechanical model. The difference between the finger anatomies and model representations may contribute to the difference between experimental data and the theoretical predictions.

SUMMARY

In the present study, we proposed a universal model to simulate the muscle/tendon excursions and moment arms in a thumb using the commercial software AnyBody. One of the important features of the proposed model over the previous studies is that the proposed approach can include the realistic bony geometries, such that the mechanical consequence of the variations in the attachment locations of the muscles/tendons can be investigated.

REFERENCES

An, K.N., Chao, E.Y., Cooney, W.P., Linscheid, R. L. (1979). *J Biomech*, 12(10):775–88.

Smutz WP, Kongsayreepong A, Hughes RE, Niebur G, Cooney WP, An KN. (1998). J Biomech, 31(6):565-70.

Valero-Cuevas FJ, Johanson ME, Towles JD (2003). *J Biomech*, 36 (7):1019–30.

DISCLAIMER

The findings and conclusions in this report are those of the authors and do not necessarily represent the views of the *National Institute for Occupational Safety and Health*

THE EFFECT OF EXTERNAL LOADS ON WHOLE BODY DISCOMFORT

Seokhee Na[1], Min K. Chung[2], Dohyung Kee[3], and Maury A. Nussbaum[1]

[1]Department of Industrial and Systems Engineering,
Virginia Tech, Blacksburg, VA, US, seokhee@vt.edu
[2]Department of Industrial and Management Engineering, Postech, Pohang, Korea
[3]Department of Industrial and Systems Engineering, Keimyung University, Dae-gu, Korea

INTRODUCTION

Awkward postures have been identified as risk factors for work-related musculoskeletal disorders. Perceptual responses (i.e. discomfort) to such postures are one approach to assessing risk, and reduction of discomfort may lead to a reduction in risk. (Nag, 1991, Putz-Anderson et al., 1993). Several observational methods have been presented to assess postural workload based on experimental data (Chung et al., 2005, Kee, and Karwowski, 2001), yet these are limited in that they did not consider an external load. The objective of this study was to evaluate and quantify the effects of an external load on postural discomfort, with a longer-term goal to develop an observational ergonomic method that accounts for an external load.

METHODS AND PROCEDURES

Eight healthy male adults participated in the experiment. Independent variables were hand height and horizontal distance, and external load. Experimental postures were defined by hand position, using two relative parameters: the percentage of shoulder height and the percentage of the arm reach. Arm reach (AR) was defined as the maximum horizontal distance measured from the tip of the middle finger to dorsum of the thorax. Shoulder height (SH) was measured as the vertical distance from the floor to the acromion in the upright position. Using these parameters, all combinations of four levels of hand height (40, 70, 100, and 120% of SH) and four levels of

hand distance (0, 40, 70, and 100% of AR) were tested (Figure 1), along with three levels of external load mass (0, 1.5kg, 3kg). These levels of the independent variables were intended to span a wide range of actual occupational tasks. The dependent variable was perceived whole body discomfort, rated on a scale from 0 to 100.
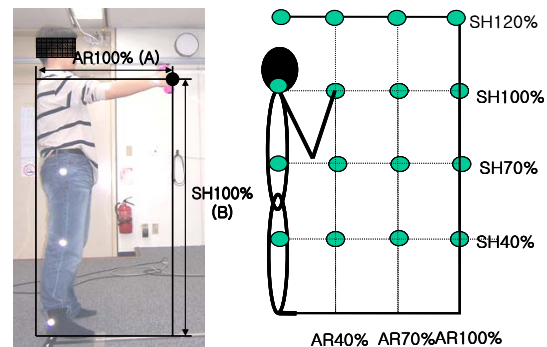

Figure 1. Experimental Postures

A within-subject design was used, with experimental conditions presented in a random order for each participant. The participant was asked to assume the experimental postures as naturally as possible and maintain each posture for 60 seconds. After this, a rating of perceived discomfort was provided.

RESULTS

Simple linear regression analyses were performed for each of the 16 experimental hand positions to investigate the effect of external load in each posture. Qualitative inspection of the data indicated that such linear models were appropriate. For all 16

postures, the slope (relating discomfort to load magnitude) was significant (i.e. >0) using a criterion of $p<0.05$. A substantial proportion of the variance in discomfort scores was explained by load magnitude. Coefficients of determination (R^2) were at least 0.64, except for AR 0, SH 40% (0.22) and AR 40%, SH 40% (0.34).

Quantification and classification of the effect of external load was determined by grouping the postures using the slope data and categorizing the characteristics of postures in each group. Table 1 shows *post-hoc* (SNK) groupings of the slopes obtained in each posture. The 16 postures could be classified roughly into three groups (divided by bold horizontal lines in Table 1).

Table 1. SNK results of the slope ($\alpha=0.05$)

Hand distance	Hand height	Slope	SNK Results
AR 70%	SH 100%	24.46	
AR 70%	SH 70%	21.67	
AR 100%	SH 100%	21.17	
AR 70%	SH 120%	20.42	
AR 40%	SH 120%	19.88	
AR 100%	SH 70%	18.08	
AR 100%	SH 120%	17.84	
AR 40%	SH 70%	16.75	
AR 100%	SH 40%	15.59	
AR 0%	SH 120%	15.54	
AR 70%	SH 40%	14.17	
AR 40%	SH 100%	14.17	
AR 0%	SH 70%	10.83	
AR 0%	SH 100%	8.5	
AR 40%	SH 40%	7.63	
AR 0%	SH 40%	7.04	

DISCUSSION

Postural discomfort was measured to quantify the effects of an external load in a variety of postures. Regression analyses were conducted to quantify the relationship between external load and discomfort. External loads had a linear effect on discomfort in wide range of postures, and in general a close relationship was found between these.

Classifying the effect of load is needed in order to develop an observational ergonomic method that accounts for an external load. While distinct effects of load were found in the 16 postures studied, these effects could be classified into three groups although there was overlap among these. Practical usage was also considered to classify the effect of load. The classification used in any observational method needs to be easy to determine visually and also have a minimum number of groups for users in real work environments (Chung et al., 2005).

There is some level of consistency within each postural group, and differences evident between the groups. Postures included in the first group were those with substantial forward reach and an elevated hand position. Those in the third group had minimal forward reach and mid-range hand height. Hand positions of the second group were between those in the first and the third group.

Our longer-term goal is to develop an observational tool for task assessment that accounts for an external load. The results obtained here will be one of the main components of this tool.

REFERENCES

Chung, MK et al. (2005). *Ergonomics*, 48, 5, 492-505.

Kee, D and Karwowski, W (2001). *Applied Ergonomics*, 32,357-366.

Nag, PK (1991). *Applied Ergonomics*, 22, 185-188.

Putz-Anderson, V and Galinsky, TL (1993). *Int. J of Industrial Eng.*, 11, 19-28.

PREDICTIVE SIMULATION OF GAIT AT LOW GRAVITY USING DIRECT COLLOCATION

Marko Ackermann and Antonie J. van den Bogert

Department of Biomedical Engineering, Cleveland Clinic Foundation, Cleveland, OH, USA,
ackermm2@ccf.org, bogerta@ccf.org

INTRODUCTION

Predictive simulations of gait have several applications that range from prostheses design to planning of surgical interventions. The conventional approach to solve the optimal neuromuscular control problem is represented by the work of Anderson and Pandy (2001). However, the overwhelming computational cost arising from the necessity of multiple numerical integrations of the system differential equations prevents its wider use.

Direct collocation (DC) is an alternative approach that reduces the computational burden by avoiding forward simulation. It also allows straightforward inclusion of task-related boundary conditions such as periodicity and forward movement. DC has been used in aeronautics and aerospace engineering (Betts, 1998) and was first employed to solve a neuromuscular optimization problem by Kaplan and Heegaard (2001). Here we use direct collocation to generate predictive simulations of gait in different gravitational environments.

METHODS AND PROCEDURES

The musculoskeletal model used is described elsewhere (Gerritsen et al., 1998) and is composed of seven segments actuated by eight Hill-type muscle models at each leg. The model has 50 state variables in x: 9 generalized coordinates, 9 generalized velocities, 16 muscle contractile element lengths, and 16 muscle activations. The interaction between ground and feet is modeled by means of 10 spring-damper elements distributed along the foot sole. The dynamics of the model is described as

$$\dot{x} = f(x,u), \qquad (1)$$

where u is the vector of neural excitations to the muscles. Assuming symmetry, the period of half a gait cycle is divided into n nodes, resulting in discretized time histories of the states and the neural excitations. The differential equations (1) are transformed into a set of algebraic constraints by a finite difference scheme, with additional periodic boundary conditions, as

$$x_k - x_{k-1} = f(x_k, u_k)\Delta t. \qquad (2)$$

A cost function that quantifies muscle "effort" is adopted as

$$J = \frac{1}{(n-1)\sum V_i} \sum_{i=1}^{16} V_i \sum_{k=1}^{n-1} a_{i,k}^2, \qquad (3)$$

where $a_{i,k}$ is the ith muscle activation at node k, and V_i is volume of muscle i. The SNOPT optimization code (http://www.tomlab.biz) was used to minimize cost function (3), while requiring (2) to be satisfied.

RESULTS

Figure 1 shows predicted gait cycles for the four simulated scenarios: Earth (g=9.8m/s^2) at 1.1m/s; Mars (g=3.72 m/s^2) at 1.1m/s, Moon (g=1.63m/s^2) at 1.1 and 2.0 m/s, with n=50.
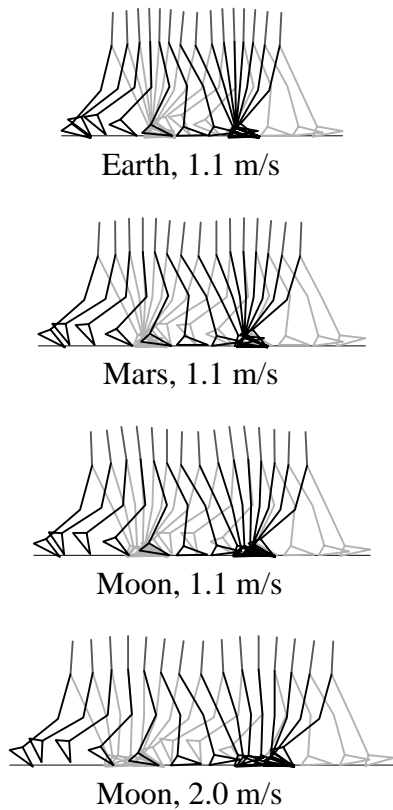
Figure 1. Predicted whole gait cycles for different speed and gravity conditions.
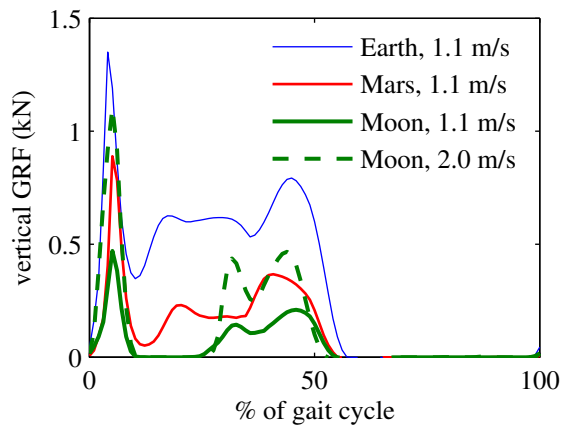

Figure 2. Ground reaction forces for the gait predictions shown in Figure 1.

Figure 2 shows the vertical ground reaction forces for the same conditions.

DISCUSSION

Normal-looking walking is predicted on Earth at 1.1 m/s. However, some details are different from typical normal gait, including a straight-leg pattern in the stance phase and high impact forces after heel-strike. These deviations will be the focus of future investigation by the authors.

On Mars, walking is predicted as the more "efficient" locomotion strategy at 1.1 m/s, although with significantly lower ground reaction forces than the occurring in walking on the Earth at the same speed. Reducing gravity to Moon levels further decreased predicted ground reaction forces and revealed an extra flight phase in the first half of the gait cycle, suggesting that skipping is a more "efficient" locomotion strategy than walking at 1.1 m/s and 2.0 m/s. This is consistent with the locomotion strategy favoured by astronauts from the Apollo Missions (Minetti, 1998). The extra flight phase may allow muscles to work more efficiently by increasing step length and decreasing cadence.

REFERENCES

Anderson, FC and Pandy, MG (2001*). J Biomech*, 34:153-63.
Betts, JT (1998). *J Guid Control Dynam*, 21:193-207.
Gerritsen, KGM et al. (1998). *Motor Control*, 2:206-20.
Kaplan, ML and Heegaard, JH (2001). *J Biomech*, 34:1077-83.
Minetti, AE (1998). *Proc R Soc Lond B*, 265:1227-35.

ACKNOWLEDGEMENTS

EFFECTS OF LUMBAR EXTENSOR FATIGUE ON POSTURAL CONTROL ASSESSED WITH FRACTAL ANALYSIS

Sunwook Kim[1], Maury A. Nussbaum[1] and Michael L. Madigan[2]

[1]Department of Industrial and Systems Engineering, sunwook@vt.edu, nussbaum@vt.edu
[2]Department of Engineering Science and Mechanics, Virginia Tech, Blacksburg, USA

INTRODUCTION

A decrement in the control of quiet upright stance has been reported with fatigue of the lumbar extensors (e.g., Davidson et al., 2004; Madigan et al., 2006). In these and related studies, descriptive measures based on center of pressure (COP) were employed to quantify changes in postural control. COP dynamics, however, appear to have fractal characteristics (Collins & De Luca, 1995; Duarte & Zatsiorsky, 2000). As such, fractal methods may help to describe the complexity of the postural control system (Eke et al., 2002). In this study, we assessed the effects of lumbar extensor muscle fatigue on postural control during quiet upright stance using both a fractal analysis and traditional descriptive COP-based measures.

METHODS AND PROCEDURES

Thirty-two healthy individuals (16 older and 16 young) from the university and local community participated in the study. Mean (SD) age, stature and body mass were 20.9 (1.7) yr, 171.1 (6.8) cm and 67.3 (12) kg for young participants; and 63.2 (5.5) yr, 167.8 (10.6) cm and 77.6 (17.8) kg for older participants. All provided informed consent following the procedure approved by the Virginia Tech Institutional Review Board.

Each experimental session consisted of three stages following an initial warm-up and practice. Within each stage, trials of quiet-upright stance were performed. There were three pre-fatigue trials, followed by fatiguing exercise, and 11 post-fatigue sway trials (over a 30-min period). During stance trials, participants stood as still as possible on a force platform (AMTI, Watertown, MA) while barefoot with their eyes closed, arms at side and feet together. Triaxial ground reaction forces and moments were sample at 100 Hz for 75 s, and the first 10 s and the last 5 s were removed. COP trajectories were obtained in the anterior-posterior (AP) and the medial-lateral (ML) direction and were demeaned in their respective directions.

Fatigue was induced using a dynamometer (Biodex 3 Pro, NY). Participants performed sub-maximal isotonic lumbar exertions (60% of their maximum voluntary contractions) at a pace of 12 repetition/min throughout a range of motion (ROM) of 45 degrees. This exercise was terminated when participants failed to perform exertions over the entire ROM in three consecutive attempts.

As proposed by Eke et al. (2000), the Hurst exponent ($\hat{H}$) was estimated by first classifying each COP trajectory in the AP and ML directions using bridge detrended scaled window variance (bdSWV) analysis with the signal summation conversion. Based on the classification, either dispersional, bdSWV, or detrended fluctuation analysis was applied to the COP trajectory to obtain $\hat{H}$. Four descriptive COP-based measures were also obtained: COP mean velocity (MV), 95% confidence ellipse area (EA95), and mean power frequency (MPF_{AP} and MPF_{ML}). These descriptive measures were normalized using individual anthropometric data (Hof, 1996).

Two-way ANOVAs were performed to determine the effects of age (Older vs. Young) and fatigue condition (Baseline vs. Fatigued vs. Recovered) on the dependent measures. Means of measures obtained in the last three post-fatigue sway trials (20, 25 and 30 min) were used to represent a 'recovered' condition. Significant effects were followed by post-hoc analyses (Tukey HSD), and statistical significance was determined at p < .05.

RESULTS

Fatigue had a significant effect on $\hat{H}_{AP}$, which was highest in the recovered condition. Main and interactive effects of age and fatigue were found on $\hat{H}_{ML}$ (Figure 1).
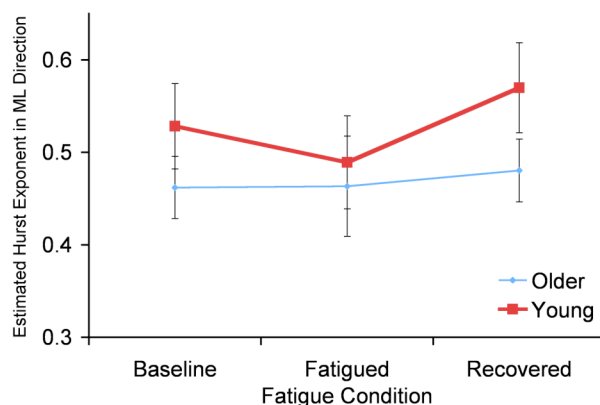
Figure 1. Main and interactive effects of age and fatigue on $\hat{H}_{ML}$. Error bars indicated two standard errors (SE).

Fatigue and age x fatigue interaction effects were found for MV; MV values significantly increased in the fatigued condition, but only for young participants. Fatigue effects were also found on EA95, MPF_{AP} and MPF_{ML}, with larger values found in the fatigued condition.

DISCUSSION

Young participants demonstrated a slight persistence of COP increments in the ML direction in both the baseline and recovered conditions ($\hat{H}_{ML} > .5$), while older participants had a slight anti-persistence of COP increments ($\hat{H}_{ML} < .5$). Changes in $\hat{H}_{ML}$ and MV with fatigue were found only for young participants, which may be related to postural adaptations reported among young people (Madigan et al., 2006). Specifically, lumbar extensor fatigue caused a slight forward lean and an increase in variability of lower extremity joint angle and angular velocity in this group. Older participants may not have adopted such postural adaptations or employed different adaptations.

Descriptive COP-based measures returned to baseline values over ~25 minutes of recovery, comparable to the results in Yaggie and McGregor (2002). Of interest, however, is that $\hat{H}_{AP}$ values increased post-fatigue. It may be that alterations of the postural control system induced by lumbar extensor muscle fatigue were not fully recovered, or that different strategies were adopted. Further study is needed to understand the relationship between postural changes (joint kinematics) and changes in $\hat{H}$ during quiet upright stance with localized muscle fatigue.

REFERENCES

Collins, JJ and De Luca, CJ (1995). *Chaos*, 5:57-63.
Davidson BS et al. (2004). *Eur J Appl Physiol,* 93:183-189.
Duarte, M and Zatsiorsky, VM (2000). *Neurosci Lett*, 283:173-176.
Eke A et al. (2000). *Eur J Physiol*, 439:403-415.
Eke A et al. (2002). *Physiol Meas*, 23:R1-R38.
Hof AL, (1996). *Gait & Posutre*, 4:222-223.
Madigan ML et al. (2006). *Hum Mov Sci*, 25:788-799.
Yaggie, JA and McGregor, SJ (2002). *Arch Phys Med Rehabil*, 83:224-228.

COMPENSATORY MECHANISMS IN BELOW-KNEE AMPUTEE GAIT IN RESPONSE TO INCREASING STEADY-STATE WALKING SPEEDS.

A. K. Silverman[1], N. P. Fey[1], A. A. Portillo[2], J. G. Walden[2], G. Bosker[3], and R. R. Neptune[1]

[1]Department of Mechanical Engineering, The University of Texas at Austin, Austin, TX
(asilverman@mail.utexas.edu)
[2]Physical Medicine & Rehabilitation Service, Audie L. Murphy VA Hospital, San Antonio, TX
[3]Department of Rehabilitation Medicine, University of Texas Health Science Center,
San Antonio, TX

INTRODUCTION

Below-knee amputee walking is often characterized by bilateral asymmetry (Arya et al., 1995; Sanderson and Martin, 1997) such as increased intact leg loading, which can lead to a higher risk of developing musculoskeletal disorders in the intact leg (e.g., Lemaire and Fisher, 1994). Much of this asymmetry is due to the functional loss of the ankle plantar flexors, which have been shown to be critical in providing body support, forward propulsion, and leg swing initiation during normal walking (e.g., Neptune et al., 2004). Thus, significant compensatory mechanisms are necessary to fulfill the role of the lost ankle muscles. However, it is not clear if these compensatory mechanisms remain invariant with changes in task demands, such as walking over a wide range of walking speeds.

Since walking at faster speeds requires greater propulsion, it may be expected that amputees depend more on the intact leg for propulsion with increasing speed. We hypothesized that GRF asymmetry between the intact and residual legs would increase with walking speed. To test this hypothesis, we examined the braking and propulsive impulses and impulse ratios, as well as joint kinetics to identify how amputees modulate propulsion with increasing speed.

METHODS AND PROCEDURES

Kinematic and kinetic data were collected from 14 amputees and 10 control subjects at four walking speeds: 0.6, 0.9, 1.2 and 1.5 m/s. Kinematic data were captured using a motion capture system (Vicon, Oxford Metrics) while GRFs were collected using four force plates (Advanced Mechanical Technology, Inc.) imbedded in a 10-m walkway. Average speed was measured with two infrared timing gates at each end of the walkway. The kinematic and kinetic data were processed in Visual 3D (C-Motion, Inc.). Propulsive and braking GRF impulses were calculated as the positive and negative time-integral of the anterior/posterior (A/P) GRF, respectively. The impulse ratio was calculated as a measure of loading asymmetry. For the amputee subjects, the propulsive and braking impulse ratios were computed as the residual leg impulse divided by the intact leg impulse. In control subjects, the impulse ratios were computed as the left leg impulse divided by the right leg impulse. Positive and negative joint work was determined as the time-integral of the joint power.

Statistical analyses included three, two-factor, repeated measures ANOVAs for the impulse and work calculations. A one-factor repeated measures ANOVA was used for the impulse ratios. When significant differences were found, Bonferroni pairwise comparisons were used to determine which values were significantly different ($p \leq 0.05$).

RESULTS

Both the intact and control legs generated significantly more propulsion than the residual leg at every speed ($p < 0.001$). The

amputee propulsive impulse ratio at 0.9 m/s was significantly different than at 1.2 and 1.5 m/s (p≤0.025), but a clear increasing or decreasing trend was not observed. The residual leg had significantly less braking than the control subjects at the three highest speeds (p≤0.050; Fig. 1). Neither the amputee nor control braking impulse ratio significantly changed with walking speed.
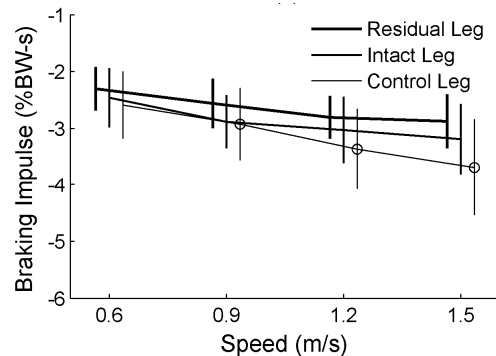

Figure 1. Residual, intact and control braking impulses. '○' indicates a significant difference with the residual leg.

In general, positive and negative joint work increased with increasing speed for all three leg conditions. The residual leg positive hip work was significantly greater than the control subjects at the three highest speeds (p≤0.016). The intact leg positive hip work was significantly greater than the control subjects as well, but only at the two highest speeds (p≤0.040). Residual positive knee work was significantly less than the intact leg (0.6, 1.2, and 1.5 m/s; p≤0.001) and control subjects (1.2 and 1.5 m/s; p≤0.003). Positive joint work at the residual ankle was significantly less than the intact leg and control subjects (p<0.001).

DISCUSSION

Our hypothesis that the intact leg would generate a greater portion of the necessary propulsion as walking speed increased was not supported, as the propulsive impulse ratio did not decrease with speed. This shows that the residual leg can effectively modulate

propulsion when varying task demands are placed on the body.

As walking speed increased, the residual leg reduced residual braking and increased positive hip work. It's likely that the residual hip extensors act to provide propulsion in early stance, thus reducing the net braking impulse. The hip extensors have been shown to provide propulsion in simulations of able-bodied walking (Neptune et al., 2004), and so may be used in the absence of the ankle plantar flexors. The reduced knee work observed also supports this conclusion, as the biarticular hip extensor (hamstring) muscles would act to provide a knee flexor moment, and therefore reduce the net knee extensor moment during this period.

SUMMARY

Amputee subjects maintained their initial loading asymmetry as walking speed increased. The most prominent compensatory mechanism was increased positive hip work in early stance, which led to reduced residual braking. Rehabilitation strategies that increase the residual hip extensor output may help to improve loading asymmetry in amputee walking.

REFERENCES

Arya, AP, et al. (1995). *Prosthet Orthot Int,* 19:37-45.
Lemaire, ED and Fisher, FR (1994). *Arch Phys Med Rehabil,* 75:1094-9.
Neptune, RR, et al. (2004). *Gait Posture,* 19:194-205.
Sanderson, DJ and Martin, PE (1997). *Gait Posture,* 6:126-136.

ACKNOWLEDGEMENTS

BILATERAL LOWER LIMB FORCE PRODUCTION IN INDIVIDUALS WITH POST-STROKE HEMIPARESIS

Ann M. Simon[1], Brian M. Kelly[2], and Daniel P. Ferris[1,2,3]

[1]Department of Biomedical Engineering, [2]Department of Physical Medicine and Rehabilitation, [3]Department of Movement Science, University of Michigan, Ann Arbor, MI, USA
E-mail: asimon@umich.edu

INTRODUCTION

Stroke-induced hemiparesis affects patients' abilities to gauge force production in their limbs. These individuals' inability to understand their limitations in producing appropriate force levels with their paretic limb affects their mobility and transfers (e.g. standing from a seated position). A mismatch between expected force production and actual force production in these situations can have serious implications on safety. Previous studies that have examined upper limb force production and perception suggests that individuals with hemiparesis use a sense of effort, more than proprioceptive feedback, to gauge force production in their upper limbs (Gandevia and McCloskey 1977, Bertrand et. al. 2004, Mercier et. al. 2004).

We investigated post-stroke individuals force production in their lower limbs during isometric and isotonic movements to determine if stroke subjects primarily rely on sense of effort for gauging force. Results from these experiments will provide insight into whether or not control of force in stroke subjects is the same for static and dynamic movements. We hypothesized that hemiparetic subjects attempting to produce equal forces in their lower limbs would generate equal percentages of their bilateral maximum voluntary strength rather than equal absolute limb forces during both types of movement.

METHODS

Eight subjects with stroke-induced hemiparesis performed isometric lower limb extensions on an exercise machine (Figure 1).
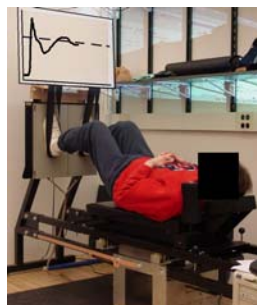

Figure 1. Leg press exercise machine.

For all trials, we recorded individual limb forces from a dual force plate. We measured subjects' strength of bilateral, non-paretic limb, and paretic limb maximum voluntary contractions (MVC) for both isometric and isokinetic movements.

In Experiment 1, subjects were asked to exert an isometric force using their non-paretic limb equal to 35% of the paretic limb peak force during bilateral isometric MVC condition. Subjects received visual force feedback of only the target and non-paretic limb force. When subjects reach the target force level, they began applying force with the paretic limb and verbally signaled to the experimenter when they believed they had matched forces in both lower limbs.

In Experiment 2, subjects performed lower limb extensions against a constant (isotonic) resistance equal to 80% of the paretic limb peak force during bilateral isokinetic MVC testing. We instructed subjects to push equally with their feet.

For all trials we calculated the average force applied by each limb during the extension movement. We normalized foot forces to each limbs' bilateral MVC. We used a repeated measures ANOVA and Tukey-Kramer
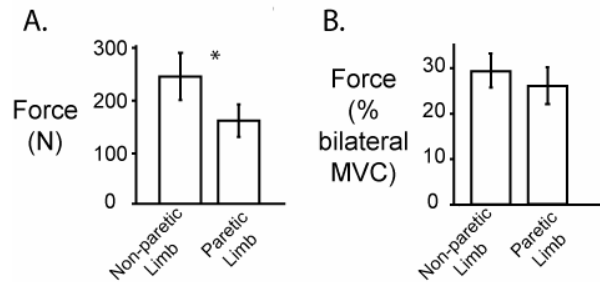
Figure 2. Experiment 1 average isometric lower limb force for all subjects. A) Absolute forces show significant differences between limbs. B) Forces normalized to bilateral MVC show no significant differences between limbs. Error bars are standard error of mean.
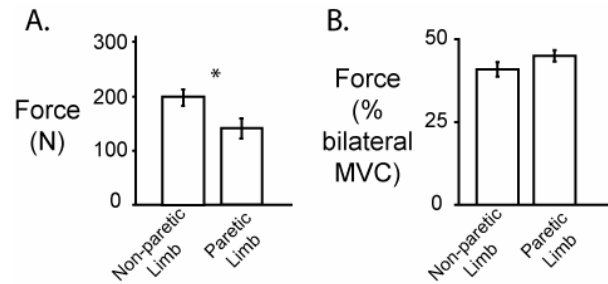

Figure 3. Experiment 2 average isotonic lower limb force for all subjects. A) Absolute forces show significant differences between limbs. B) Forces normalized to bilateral MVC show no significant differences between limbs. Error bars are standard error of mean.

hoc tests to determine if there were differences between limbs.

RESULTS

During the isometric force matching trials of Experiment 1, subjects consistently produced significantly less absolute force in the paretic limb than the non-paretic limb (ANOVA: $P < 0.0001$) (Figure 2). Normalizing force to each limbs' bilateral isometric MVC force showed no significant differences (ANOVA: $P = 0.11$). There was only an 11.3% difference between normalized limb force as compared to a 34.5% difference between absolute limb force.

In Experiment 2 when subjects were attempting to produce equal forces during isotonic lower limb extensions, they produced significantly less absolute force in the paretic limb than the non-paretic limb (ANOVA: $P = 0.01$) (Figure 3). Normalizing force magnitudes to each limbs' bilateral isokinetic maximum strength revealed no significant differences between limbs (ANOVA: $P = 0.17$). There was only a 10.0% difference between normalized limb force as compared to a 29.3% difference between absolute limb force.

DISCUSSION

The results supported our hypothesis that for isometric and isotonic conditions hemiparetic subjects relied primarily on sense of effort, rather than proprioceptive feedback, for gauging lower limb force production. Individuals with post-stroke hemiparesis did not produce equal lower limb forces even though the target forces were set to levels below the paretic limbs' bilateral strength capabilities. The results for Experiments 1 and 2 indicate that bilateral lower limb force production in stroke subjects is similar for isometric and isotonic contractions. This outcome is important because it extends the findings to force production during dynamic movements that are functionally relevant for activities of daily living. Our findings about the importance of sense of effort in post-stroke individuals suggests that lower limb rehabilitation therapies need to not only train strength in the paretic limb but also to train patients to recalibrate their force scaling abilities.

REFERENCES

Bertrand, AM et. al. (2004). *J Neurophysiol*, **91**(4), 1579-85.
Mercier C et. al. (2004). *Exp Brain Res*, **157**(1), 324-42.
Gandevia, SC, McCloskey, DI (1977). *Brain* **100**(2), 345-54.

ACKNOWLEDGEMENTS

KINETIC CHARACTERISTICS OF BAREFOOT RUNNING

Julia A. Freedman, M.S.[1], Janet S. Dufek, Ph.D.[2], John A. Mercer, Ph.D.[2]

[1]University of Tennessee, Knoxville, Knoxville, TN, USA
[2]University of Nevada, Las Vegas, Las Vegas, NV, USA
Email: jfreedm2@utk.edu

INTRODUCTION

In spite of extensive research, as well as advances in shoe development, runners continue to be injured at similar rate to those of 25 years ago [1, 2]. It has been hypothesized that shoes may actually contribute to injury rates by blocking plantar sensory information [3]. Preliminary research has shown that the kinetics and kinematics during running barefoot are different from running in shoes, yet this research has constrained runners to a heel-toe running pattern both barefoot and in shoes [4].

Therefore the purpose of this study was to compare impact characteristics between barefoot and shod running when footstrike is not constrained as well as to compare impact characteristics of barefoot running with a heel-toe running pattern to barefoot running with no constraints on footstrike.

It was hypothesized that: 1) runners would have a flatter foot position when running barefoot without instructions, 2) there would be an increase in the loading rate and peak leg acceleration of barefoot running compared to running in shoes, 3) there would be an increase in the loading rate and peak leg acceleration from barefoot running without instruction to barefoot heel-toe running, and 4) stride length would be shorter in barefoot running than shod running.

METHODS

Subjects (n=10; 22.5 ± 3.1 yrs; 170.3 ± 6.8 cm; 66.7 ± 10.5 kg) who ran at least 10 miles per week were recruited to participate in this study. Subjects were instrumented with seven 25mm reflective markers (Laterally: lateral maleolous, fifth metatarsal head and base; Medially: medial malleolous, first metatarsal head and base; and a shared heel marker), as well as a piezoelectric uniaxial accelerometer (1000 Hz; Piezoeletronics) attached distally to the medial side of the right tibia.

Subjects were instructed to complete 10 successful trials in each of three conditions: 1) Shod, no instructions on footstrike, 2) Barefoot (BF) no instructions on footstrike, and 3) BF heel-toe instructions (BFHT). A successful trial had the subject run across a 10 m indoor runway contacting a force platform (Kistler; 1080 Hz), which was installed in the center of the runway, with their right foot without altering their stride, as well as maintaining a running velocity of 3.83 m/s ($\pm 5\%$). Velocity was monitored utilizing two photocell timing lights. Three-dimensional kinematics were collected (120 Hz) to capture the position of the foot and ankle (Vicon Corp., V4.6.142).

Dependant variables of ground reaction force impact peak (F1), peak leg acceleration (PkLeg), stride length, loading rate and ground contact index (GCI, a measure of the position of the foot at the time of ground contact as determined by the slope of the

markers) were compared across running conditions using repeated measures ANOVA.

RESULTS

PkLeg was influenced by running condition: Shod PkLeg < BF PkLeg (p<0.05); BF PkLeg was not different from BFHT; Shod PkLeg < BFHT PkLeg (p=0.0002). Loading rate (LR) was influenced by running condition: Shod LR < BF LR (p<0.001); BF LR <BFHT LR (p<0.05); Shod LR < BFHT LR (p<0.0001). F1 was not influenced by running condition (p=0.051).

Ground Reaction Force Characteristics

Running Condition	Impact Peak (F1) (BW)	Loading Rate (BW/s)	LgPk (g)
SHOD	2.00 ± 0.32	61.8 ± 12.3	7.36 ± 1.8
BF	2.25 ± 0.35	248.4 ± 90.1 *	18.09 ± 8.4 *
BFHT	2.11 ± 0.36	315.7 ± 67.9 *^	18.31 ± 5.9 *

* Significantly Different (p<0.05) from Shod
^ Significantly Different (p<0.05) from BF

Table 1. Impact Characteristics (Mean ± SD).

Stride length was not influenced by running condition (p=0.09). GCI was influenced by running condition: Shod GCI > BF GCI (p<0.05); BFHT GCI > BF GCI (p<0.05); Shod GCI > BFHT GCI (p=0.0001).

DISCUSSION

This investigation confirms that, as observed in previous research [4], kinetic characteristics of barefoot running are different from shod running. As hypothesized, runners selected a flatter foot position when running barefoot without instruction and there was an increase in the loading rate from shod to BF to BFHT running. PkLeg increased between Shod and BF but did not change between BF and BFHT. Lastly, the hypothesis that stride length would be shorter during barefoot running was not supported by the data collected in this investigation.

Although some differences in impact characteristics were observed (e.g. loading rate), other impact characteristics (e.g. F1 and PkLeg) did not differ across all conditions. This observation seems to suggest that while GCI affected impact values, its influence was less than that of the change observed between BF and shod conditions.

It is not clear why F1 did not change across conditions. Perhaps runners made subtle changes in running behavior to optimize impact that are not characterized by stride length. Alternatively, F1 during BF running may not represent the same kinetic event as during shod running. Future research is needed to investigate injury rates in BF runners to determine whether or not there are benefits in reducing the risk of overuse injury by running in bare feet.

REFERENCES
[1]Hreljac A., *Med Sci Sports Exerc* **36**, 845-849, 2004.
[2]James S.L., et al., *Am J Sports Med* **6**, 40-50, 1978.
[3]Robbins S.E., Gouw, G.J., *Med Sci Sports Exerc* **23**, 217-224, 1991.
[4]De Wit B., et al., *J Biomech* **33**, 269-278, 2000.

ASTRONAUT ROTATIONAL MOTION DURING SIMULATED MICROGRAVITY

Leia Stirling, Dava Newman, and Karen Willcox

Department of Aeronautics and Astronautics, Massachusetts Institute of Technology, Cambridge, MA
Email: leia@mit.edu

INTRODUCTION

In order to reduce astronaut adaptation time and provide a safety countermeasure during extravehicular activity (EVA), this research effort investigates astronaut reorientation. Even though astronauts undergo hundreds of hours of training, the strategies for locomotion and orientation in a reduced gravity environment are not specifically prescribed. The problem of self-rotation, which is a human-body rotation without external torques, has been previously studied to determine its feasibility (Kulwicki et al., 1962; Scher and Kane, 1969; Parin and Gazenko, 1975). Since astronauts are not familiar with reorienting without external forces, they are unlikely to develop self-rotation techniques naturally. The goal of the current study was to experimentally examine the effects of rotation training. Understanding self-rotation will help develop an astronaut motion-training program and could contribute to safety countermeasures during EVA.

METHODS AND PROCEDURES

This study adhered to MIT's Committee On the Use of Human Experimental Subjects and the participants gave their written informed consent to participate. There were 20 volunteer subjects (10 male, 10 female) with a mean age of 23.6 ± 3.5. The experiments used a suspension and harness system, with the subjects in three different configurations allowing rotations about each body axis. Subjects performed a series of rotations about the body axes in both the counterclockwise and clockwise directions. A total of 48 rotations were performed by each subject, with an equal number of counterclockwise and clockwise rotations. The subjects were placed in one of two groups, minimally and fully trained. Prior to performing the experiment, the subjects went through a training program based on their group. The minimally trained group received a theoretical description of momentum conservation, while the fully trained group was additionally provided with descriptions and videos of strategies for rotating about all three body axes (Figure 1).
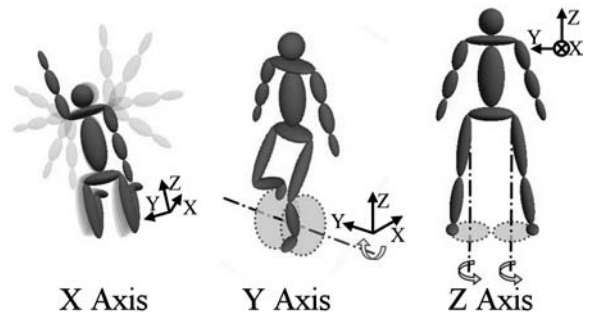

Figure 1. Recommended methods for single-axis rotations for the fully trained group.

Experimental measures included a subject coordination score, video data, a motion usability score (modified Cooper-Harper), a fatigue rating, and a cognitive workload measure (NASA-TLX).

RESULTS AND DISCUSSION

In this study it was observed that fully trained subjects had a better initial performance time than the minimally trained groups for Y and Z axis rotations ($p < 0.0005$ and $p = 0.027$, respectively). All subjects in the fully trained group showed typical learning curves, with

the highest performance time during the first trial. However, five of the ten minimally trained subjects showed an increase in performance time over the first few trials. This was due to a misconception of the feature in their technique that produced the rotation. When steady state performance times were analyzed, a statistically significant difference was only found for counter-clockwise Y rotations ($p = 0.006$). The steady state analysis was performed with 19 of the 20 subjects, as one minimally trained subject never reached a steady state for rotations about Y. For an emergency EVA scenario, it is important to examine the first attempt of each motion (Figure 2). While all fully trained subjects completed the rotation in the allotted time, not all minimally trained subjects could. If this were an emergency scenario, an untrained astronaut would have significant difficulty rotating about Y.
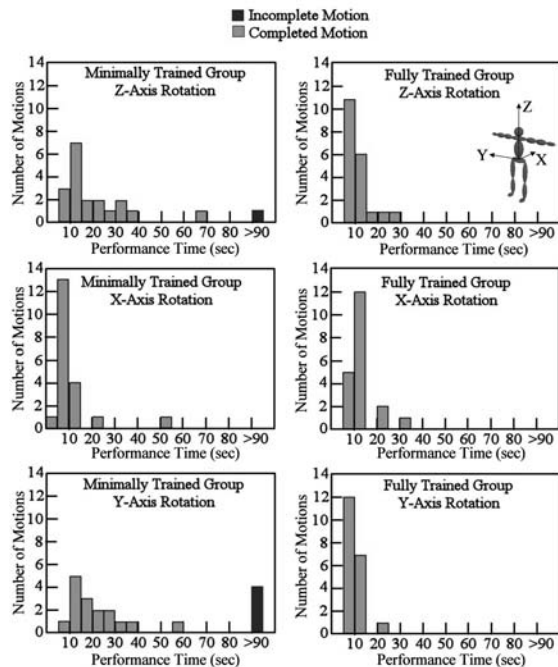
Figure 2. The distribution of performance times for the first trial for each axis (n = 20).

The motions developed by the minimally trained subjects for rotations about X were greatly affected by the suspension system. This group tended to use leg motions that achieved the net rotation, but would have yielded off-axis motions in true microgravity. The trained group performed the recommended strategy that yielded planar motions, but took longer to perform, thus yielding similarities in performance time.

For the minimally trained group, the Y rotations had the highest workload when compared to the other two axes. However, for the fully trained group, the X rotations were perceived as most difficult. Significant differences in the workload between groups were seen in Y and Z rotations ($p = 0.002$ and 0.023, respectively).

In the development of motion strategies, it is important to understand their usability. The modified Cooper-Harper rating and the NASA TLX implemented in this study have been beneficial in showing perceived difficulty of a motion. We have shown that certain axes are easier to rotate about than others and that trained subjects have an easier time performing the body rotations than those that have not been trained. This study has provided groundwork for the development of an astronaut motion control training program.

REFERENCES

Kulwicki, P et al. (1962). AMRL-TDR-62-129.

Parin, V and Gazenko, O (1975). NASA TTF-16105

Scher M and Kane, T (1969). NASA CR-108930.

ACKNOWLEDGEMENTS

CORRELATION BETWEEN POSTURAL SWAY DURING QUIET STANDING AND BALANCE RECOVERY AFTER SMALL PERTURBATIONS

Sara L. Matrangola[1], Michael L. Madigan[1], Bradley S. Davidson[2], Maury A. Nussbaum[1]

[1] Virginia Polytechnic Institute and State University, Blacksburg, VA, USA
[2] University of Colorado Health Science Center, Denver, CO, USA
E-mail: smatrang@vt.edu, Web: http://www.biomechanics.esm.vt.edu/

INTRODUCTION

Previous studies have found minimal correlation between postural steadiness during quiet standing and recovery of balance from a perturbation (Owings, Pavol et al. 2000; Mackey and Robinovitch 2005). These results may reflect differences in the governing postural control mechanisms involved in these two tasks. These studies, however, used relatively large perturbations that significantly challenged the postural control system in order to maintain balance. Investigating small perturbation in this regard may provide insight as to how the postural control system adapts to different tasks and difficult levels.

The goal of the current study was to determine correlations between commonly used postural sway measures during quiet standing and measures of recovery from a small postural perturbation. We hypothesized that stronger correlations would exist with small perturbations as opposed to large perturbations used in previous studies (Mackey and Robinovitch 2005). We also hypothesized that there will be a difference in these correlations between young and older adults, which may indicate differences in the flexibility of the postural control system to adapt to different tasks.

METHODS

Thirty subjects including 16 young (19.4 ± 1.4 years) and 14 older (62.2 ± 5.1 years) participated in the study. Each age group was comprised equally of males and females. Two tasks were performed by each subject: quiet standing and perturbation trials. For all tasks, subjects stood on two force platforms with one foot on each platform. Force platform data were sampled at 1000 Hz (Bertec Corporation, Columbus, OH) and center of pressure was calculated.

During quiet standing trials, subjects were instructed to stand as still as possible with their feet together, eyes closed, and hands at their sides for 60 seconds. Subjects performed three trials.

During perturbation trials, subjects were instructed to stand with their eyes closed and hands behind their back. A ballistic pendulum was used to apply an anteriorly-directed impulse of 6.5 N-s just inferior to the scapula. This perturbation was small enough that a step was not required to maintain balance. Subjects performed six trials.

Six quiet standing and six perturbation variables were calculated from center of pressure data. The quiet standing variables consisted of 50% power frequency (MFreqQS), maximum distance (MaxDQS), mean distance (MeanQS), mean velocity (MeanVelQS), maximum velocity (MaxVelQS) and estimated time to support boundary (TTBQS). The perturbation variables consisted of maximum distance (MaxDP), time to maximum displacement

(TTM), maximum velocity (MaxVelP), time to maximum velocity (TTMVelP), estimated time to the support boundary (TTBP), and time to return to within 20% of the relative displacement (Ret20P).

The coefficient of determination (r^2) was found from correlations between all quiet standing variables and all perturbation variables. A Wilcoxon Rank-Sum test was used to analyze differences in r^2 values between age groups.

RESULTS AND DISCUSSION

Statistically significant correlations were found between some quiet standing and perturbation variables (Table 1). These moderate correlations suggest that the postural control system may employ some of the same control mechanisms in response to a small perturbation as during quiet standing.

Quiet Standing	Perturbation	Age Group	r^2
TTB	TTMVel	Young	0.53
MaxVel	TTMVel	Young	0.52
MeanVel	TTB	Old	0.44
MeanVel	TTMVel	Young	0.42
MaxVel	TTB	Old	0.41
MaxVel	MaxD	Old	0.39
MeanVel	MaxD	Old	0.34

Table 1. Statistically significant quiet standing and perturbation coefficients of determination.

There was no difference in r^2 values between quiet standing and perturbation variables across age groups (p=0.175). A qualitative comparison between the r^2 values of the present study and those presented by Mackey et al. (2005) showed that measures from small perturbations tended to have higher correlations with quiet standing than measures from large perturbations. This may indicate more similar postural control mechanisms between quiet standing and small perturbations compared to large perturbations.

A p-value of 0.175 between age groups suggests no age-related difference in the adaptability of the postural control system between quiet standing and the perturbations used here.

SUMMARY/CONCLUSIONS

Moderate correlations were found between quiet standing and perturbation variables. These results suggest that the governing strategies of the postural control system for maintaining balance and recovering balance do share some similarities. Future studies should investigate a range of perturbation magnitudes to more clearly understand how the postural control system adapts from quiet standing to perturbations.

REFERENCES

Mackey, D. C. and S. N. Robinovitch (2005). *Clin Biomech* 20(8): 776-83.
Owings, T. M., M. J. Pavol, et al. (2000). *J Am Geriatr Soc* 48(1): 42-50.

ACKNOWLEDGEMENTS

This work is dedicated to the memory of Dr. Kevin P. Granata, who was tragically killed on April 16th, 2007 at Virginia Tech.

AN ANKLE ORTHOSIS WITH A SUBTALAR LOCKING SYSTEM IS MORE EFFECTIVE IN RESTRICTING PASSIVE AND ACTIVE ANKLE KINEMATICS

Songning Zhang, Michael Wortley, Qingjian Chen, Julia Freedman and Casey Riley
Biomechanics/Sports Medicine Lab, The University of Tennessee, Knoxville, TN, USA
email: szhang@utk.edu web: web.utk.edu/~Esals/resources/biomechanics_laboratory.html

INTRODUCTION

The ankle joint is the most injured joint during sports participation (Arendt 1995, Garrick 1988, Hootman 2007). Ankle braces are superior to adhesive ankle taping in restricting ankle inversion and eversion range of motion (ROM). Ankle orthoses have also been shown to be effective in reducing ankle inversion injuries. Efficacy of ankle orthoses is often assessed by comparing reduction of inversion ROM in a passive setting as well as peak inversion angle and ROM in an inversion drop test, between braced and unbraced movements (Alt 1999, Cordova 1998, De Clercq 1997, Lohrer 1999). Therefore, the objective of this study was to examine the effectiveness of a new semi-rigid ankle orthosis with a subtalar joint locking mechanism in restricting ankle inversion motion during passive and dynamic movements.

METHODS

Ten female (age: 24.8 ± 3.6 yrs, height: 1.65 ± 0.06 m, mass: 57.9 ± 5.8 kg) and ten male subjects (age: 24.4 ± 3.7 yrs, height: 1.75 ± 0.07 m, mass: 73.4 ± 15.7 kg) with no current ankle injury and no history of major lower extremity injuries participated in the study. A seven-camera motion analysis system (240 Hz, Vicon Motion Analysis Inc., UK) was used to obtain the three-dimensional (3D) kinematics during the test. Reflective anatomical and tracking markers were placed on foot, ankle, leg, knee, thigh and pelvis of the right side of the body to obtain 3D kinematics. An electrogoniometer was placed around the posterior side of the heel and leg of the subject to measure passive inversion and eversion range of motion of the ankle joint in wearing no brace (NB), a semi-rigid Element ankle brace with a calcaneal and subtalar locking system (AB1, DeRoyal), a semi-rigid Functional ankle brace with a hinge joint (AB2, DeRoyal), and a soft ASO lace-up ankle brace (AB3, Medical Specialties). The participant performed five ankle inversion drop trials of 30º in each of four conditions on a customized inversion drop platform: wearing no brace, AB1, AB2 and AB3.

A one-way repeated measures ANOVA was used to evaluate differences among the brace conditions on selected variables ($p < 0.05$) with post hoc comparisons conducted to detect specific differences among the braces using a Bonforroni adjustment (SPSS, Inc.).

RESULTS

The statistical results showed that the inversion ROMs for three braces were significantly reduced compared to no brace (Figure 1). Furthermore, AB1 had smaller ROMs than the other two braces and the ROMs for AB3 were significantly smaller than AB2.

During the inversion drop test, the right leg was dropped to invert the ankle soon after the foot touches the ground. The ankle inversion movement during the test shows two distinctive peak angles, with first and smaller peak occurring soon after the release of the trap door prior to its contact with

ground, and a second and greater peak occurring at around 330 ms after the door release.

For the inversion drop test, the ANOVA results showed that the peak inversion angle after contact for the three braces were all significantly reduced than that of no brace (Table 1). The inversion ROM was also significantly reduced in all three braces compared to the no brace. The peak inversion velocity was also significantly reduced by wearing an AB1 and AB2 brace (Table 1).
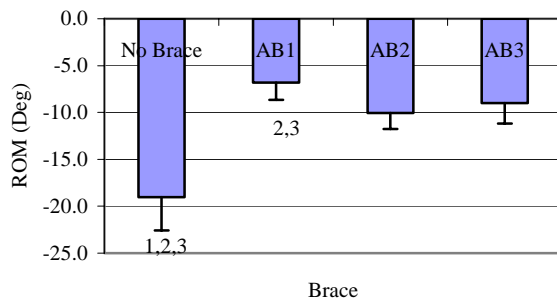

Figure 1. Mean and standard deviation of passive inversion ROM. [1] – significantly different from AB1, [2] – significantly different from AB2, and [3] – significantly different from AB3.

Cond	Max_Inv (deg)	Max_Inv_Vel (deg/s)
NB	26.1 ± 6.7 [1,2,3]	236.8 ± 75.2 [1,2]
AB1	13.7 ± 8.2	146.9 ± 84.3
AB2	17.1 ± 8.9	183.1 ± 94.5
AB3	18.7 ± 11.0	188.5 ± 110.2

Table 1. Average selected ankle kinematic variables of ankle inversion drop: Mean ± SD. [1]: significantly different from AB1, [2]: significantly different from AB2, [3]: significantly different from AB3.

DISCUSSION

The effectiveness of the three ankle braces is evident with reductions of inversion ROM of 70%, 49% and 61% for AB1, AB2 and AB3 respectively. The efficacy of the braces was further demonstrated in the kinematic behaviors during the inversion drop test. The peak inversion angle in the inversion drop test showed reductions of 48%, 34% and 28% for AB1, AB2 and AB3, respectively, compared to the no brace condition. For the ROM, reductions of 35%, 17% and 21% were seen for these braces. The reduction for the peak inversion velocity showed similar trends with 38%, 23% and 20% reduction for the same braces. The Element (AB1) was most effective, showing a greater reduction (more control) on peak inversion (13%), inversion ROM (18%), and peak inversion velocity (15%) than Functional Ankle brace (AB2) and ASO brace (AB3).

SUMMARY

In summary, the Element ankle brace with a subtalar locking system is most effective in restricting inversion motion during the passive and dynamic tests.

REFERENCES

Alt, W., et al. (1999). *Foot Ankle Int,* **20**, 238-245.
Arendt, E. and Dick, R. (1995). *Am J Sports Med,* **23**, 694-701.
Cordova, M. L., et al. (1998). *Med Sci Sports Exerc,* **30**, 1363-1370.
De Clercq, D. L. (1997). *Int J Sports Med,* **18**, 222-228.
Garrick, J. G. and Requa, R. K. (1988). *Clin Sports Med,* **7**, 29-36.
Hootman, J. M., et al. (2007). *J Athl Train,* **42**, 311-319.
Lohrer, H., et al. (1999). *Am J Sports Med,* **27**, 69-75.

ACKNOWLEDGEMENTS

SOURCES OF FORWARD BALL VELOCITY IN A PITCHED BASEBALL

Gordon Alderink[1], Thomas Kepple[2], Karen Lohmann Siegel[4], Alexander Razzook[5] & Steven Stanhope[2,3]

[1]Grand Valley State University, College of Health Professions, Grand Rapids, MI,
aldering@gvsu.edu

University of Delaware, [2]Departments of Health, Nutrition Exercise Sciences and [3]Mechanical Engineering Newark, DE

[4]Agency for Healthcare Research and Quality, Rockville, MD

[5]Physical Disabilities Branch, National Institutes of Health, Bethesda, MD

INTRODUCTION

During a baseball pitch, the dependence of ball velocity on muscle/joint actions has been inferred (Toyoshima et al., Stodden et al., 2001, Stodden et al., 2005), but not measured directly. Recent advances (Anderson et al., 2004, Goldberg et al., 2004) in musculoskeletal modeling have included the development of techniques that can directly determine the contribution of muscle groups to joint or segment velocities associated with locomotion. This approach (induced velocity analysis) is ideal for studying whole body and upper extremity motions where there is an easily measured goal, such as maximizing ball velocity during pitching. Our purpose was to study high level adolescent pitchers to determine how joint torques, gravity and velocity effects (centripetal/ coriolis) contribute to the forward velocity of a baseball at release.

METHODS AND PROCEDURES

Kinematic and kinetic data were collected from six elite high school male baseball pitchers (mean height = 1.86m, mean weight = 83.9kg) who had no history of arm injury and were able to throw at least 80 mph under game conditions. During testing the subjects threw a straight overhand pitch from the windup on flat ground. Data were collected using a 7-camera Vicon 612 motion capture system (250 Hz) and three AMTI force platforms (1000 Hz). One representative pitch per subject was analyzed from the last instant of zero ball velocity to ball release.

The 14 segment biomechanical model included feet, legs, thighs, a pelvis, a combined thorax-abdomen-head, arms, forearms and hands. The hips and shoulders were modeled as 3 DOF ball and socket joints. The thorax-abdomen-head segment was connected to the proximal end of the pelvis using a ball and socket joint (waist). The knees and wrists were modeled as revolute joints allowing flexion/extension. The elbows and ankles were modeled as 2 DOF universal joints; the elbow allowed flexion/extension and pronation/supination and the ankle allowed dorsi/plantar flexion and inversion/eversion. The pelvis served as the model's root segment and was free to rotate and translate relative to ground.

Visual3D software (C-Motion, Inc.) computed the kinematics and kinetic input for the model. The model was implemented in Visual3D as a dynamic link library built using SD/Fast (PTC Software) software. At each video sample, the model was positioned based on the pelvis and joint kinematic data. Gravity and all velocities were set to zero. The joint torques were turned on, one at a time, to determine the forward acceleration imparted on the ball by that torque. The forward acceleration due to gravity was determined by setting all torques to zero and

setting gravity to 9.81 m/s^2. Finally, the centripetal/coriolis effects were determined by setting all torques and gravity to zero and driving the model using the velocities as measured by the motion capture system.

The induced velocity from each source was obtained by calculating the area under each induced acceleration curves. The model was validated by comparing the total induced velocity of the ball computed by the model with the forward velocity of the ball obtained from a radar gun.

RESULTS

Net ball velocity at release determined by the model was 64.5 mph, which was comparable to that recorded by the radar gun (73.8 mph). The induced velocity analysis (Table 1) indicated that acceleration produced by the velocity of the segments (centripetal/coriolis), made the largest contribution to ball velocity (57.8%). In the pitching arm, the shoulder was found to generate forward ball velocity (31.0%) in the period of rapid acceleration just prior to release while the elbow torque tended to increase forward velocity (18.1%) during cocking phase of the pitch. Gravity, the lower extremity joint moments, and wrist joint moment made either small or negative direct contributions to ball velocity.

DISCUSSION

Toyoshima et al. (1974) inferred that the trunk and lower extremity accounted for almost 50% of ball velocity, whereas Stodden et al. (2001, 2005) concluded that ball velocity increased with increases in elbow

flexion torque, elbow and shoulder joint forces, and increases in pelvic and upper torso velocity. Results from the induced velocity analysis indicate that the largest contributions came from the centripetal and coriolis effects. The study also found that the lower extremities were unlikely to make a direct contribution to ball velocity while the muscles crossing the shoulder and elbow did indeed make significant contributions.

SUMMARY

Induced velocity analysis has shown that centripetal/coriolis accelerations are the largest contributor to forward ball velocity. It is hoped that decomposing the centripetal/coriolis accelerations back to the muscular sources will further clarify anatomically relevant sources that indirectly contribute to forward ball velocity.

ACKNOWLEDGEMENTS

REFERENCES

Anderson, FC et al. (2004). J Biomech, 37, 731-737.
Goldberg, SR et al. (2004). J Biomech, 37, 1189-1196.
Stodden DF et al. (2001), J Appl Biomech, 17, 164-172.
Stodden DF et al. (2005), J Appl Biomech, 21, 44-56.
Toyoshima S. (1974), Biomechanics IV. Baltimore: University Park Press, pp. 169-174.

	lower extremities	waist	shoulder	elbow	wrist	gravity	centripetal/ coriolis
Mean%	-1.3	1.3	31.0	18.1	-6.9	0.0	57.8

Table 1. Mean (n=6) sources of ball velocity as percentages of total induced forward velocities.

SCRATCHING VULNERABILITY OF CONVENTIONAL VS. HIGHLY CROSSLINKED POLYETHYLENE LINERS WITH EMBEDDED THIRD BODY PARTICLES

Anneliese Heiner[1,2], Thomas Brown[1,2]

[1]Department of Orthopaedics and Rehabilitation, [2]Department of Biomedical Engineering, University of Iowa, Iowa City, IA, USA, anneliese-heiner@uiowa.edu

INTRODUCTION

In total joint arthroplasty, third body particle migration into the bearing space results in accelerated wear. Laboratory tests of polyethylene against metal have demonstrated that scratching of the metal surface and dramatically increased polyethylene wear can occur after the introduction of third body particles into the lubricant fluid, and third body particles embedded in polyethylene acetabular components are a well-documented finding in THA retrieval studies.

For hip simulator testing of metal-on-polyethylene THA implants, under clean conditions HXPE acetabular liners wear less than conventional polyethylene (CPE) liners (McKellop et al., 1999). However, it is possible that this wear advantage of HXPE may be reduced when third bodies are present; HXPE has reduced fatigue strength and reduced strain-to-failure as compared to CPE, which may make HXPE more susceptible to damage from local asperities (such as scratches from third bodies) on the metal counterface.

The hypothesis of this study was that liner vulnerability to scratching from heads roughened by third bodies is only mildly reduced for HXPE, as opposed to CPE. The third bodies were embedded into the liners under controlled, reproducible conditions.

METHODS AND PROCEDURES

Six CPE and six HXPE 28mm acetabular liners were each embedded with five CoCrMo beads (F-75 alloy) measuring $300 - 320$ μm diameter (Figure 1). One bead was embedded where an earlier FEA had determined to be a maximally problematic site for third body particle embedment to accelerate liner wear through roughening of the femoral head counterface (Lundberg et al., 2006). The other four beads were embedded on a 10 mm diameter circle centered about that location.

a)   b)
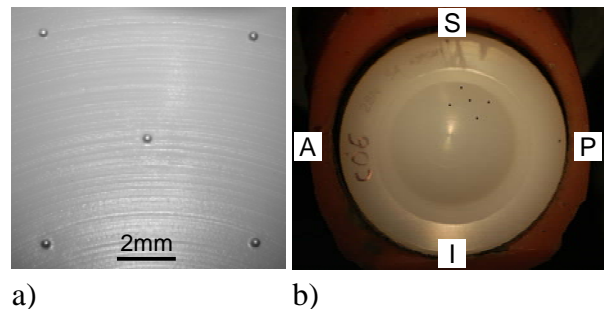
Figure 1. Third body beads embedded in acetabular liner: a) close-up and b) bead positions during testing (bead appearance enhanced and not to scale).

Each liner was run for 10,000 level walking cycles in a joint motion simulator, articulating against an Orthochrome femoral head. The heads and liners were then photographed and qualitatively evaluated for severity of scratch damage. An experienced orthopaedic surgeon rank-ordered the pictures of the liners for scratch severity.

RESULTS

The femoral heads each had five scratch families, which corresponded to the five embedded beads on their respective liners (Figure 2a). The damage to the acetabular liners included macroscopically-visible scratches (Figures 2b&c).
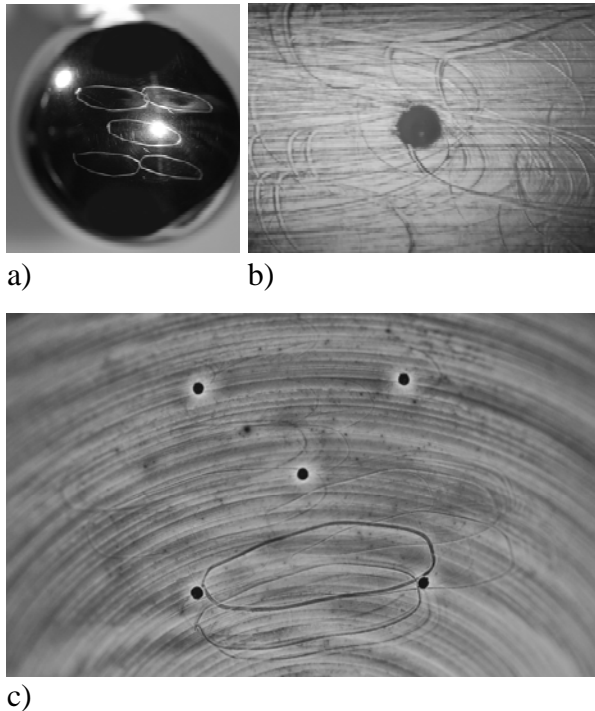

a)   b)

c)

Figure 2. Scratches resulting from third bodies embedded in the liner: a) femoral head (white spots are light reflections), b) close-up of acetabular liner, around one of the embedded beads, and c) acetabular liner, around all five embedded beads.

The rank-order of the CPE (C) and HXPE (X) acetabular liners, from most to least scratched, was: X C X X X X C C C C X C.

DISCUSSION

The HXPE liners did not offer appreciable protection against severe scratching induced by large embedded third body particles, as compared to the CPE liners; in fact, the HXPE liners were generally more scratched than the CPE ones. This severe scratching occurred within a very short test period.

Many hip simulator studies have indicated that under third body conditions, HXPE liners wear less than CPE liners. However, the third body challenge in such work has involved either very small particles suspended in the lubricant fluid, or heterogeneous particle embedment in explanted liners. While remelting of HXPE liners removes small scratches, indicative of plastic deformation rather than wear (Muratoglu et al., 2005), remelting recovery of more severe surface damage is much less complete (Lazzarini et al., 2007), ostensibly because of material loss. The relative dominance of plastic deformation vs. material loss in scratching from large third body particles merits further investigation.

SUMMARY

Under controlled conditions of third body embedment, HXPE liners were more vulnerable to scratching than were CPE liners.

REFERENCES

Lazzarini, AM et al. (2007). *Clin Orthop Relat Res* 465:128-132.
Lundberg, HJ et al. (2006). *J Biomech* 39(7):1208-1216.
McKellop, H et al. (1999). *J Orthop Res* 17(2):157-167.
Muratoglu, OK et al. (2005). *Clin Orthop Relat Res* 438:158-164.

ACKNOWLEDGEMENTS

THE EFFECTIVENESS OF AN UNSTABLE SHOE ON GOLF PERFORMANCE AND A REDUCTION OF LOW BACK PAIN

Elysia M. Davis[1], Benno M. Nigg[1], David Lindsay[2], and Carolyn Emery[2]

[1]Human Performance Laboratory, Faculty of Kinesiology, University of Calgary, Calgary, AB, Canada, edavis@kin.ucalgary.ca
[2]Sport Medicine Center, Faculty of Kinesiology, University of Calgary, Calgary, AB, Canada

INTRODUCTION

Improvements in golf performance can be accomplished through improved technique, better equipment, enhanced physiological capabilities or a combination of these factors (Doan et al., 2006).One of the limiting factors is injury, which in the case of golf is often related to low back pain (McCarroll, 1996). Reducing such pain would likely result in enhanced performance. There is anecdotal evidence that using an unstable shoe reduces low back pain (personal communication). However, the effects of unstable shoes on performance, balance and low back pain are not known.

Therefore, the objectives of this study were to assess the effects of unstable sandals on (a) golf performance, (b) static and dynamic balance and (c) reduction of pain in golfers with undiagnosed low back pain

METHODS AND PROCEDURES

The six week repeated measures randomized controlled trial study was performed with 37 male golfers (20 in the control and 17 in the intervention group) with moderate low back pain (minimum rating of 3 on a 10 point scale). Their golf performance, balance and low back pain, were assessed at baseline and at six weeks. Motion analysis of their swing, timed balance scores and visual analog scales (VAS) for pain were used to asses the effect of the unstable shoes. Results within group and between groups were compared through a group mean comparison test.

Figure 1. Picture of the unstable MBT-Sandal used as shoe intervention in this study.

RESULTS

(1) There was no significant change in performance between the intervention and control group in any of the ten variables measuring golf performance.
(2) There was no significant change between groups in the static or dynamic balance times.
(3) There was a significant difference between groups in perceived low back pain scores for the in lab measurement on a VAS ($t = -2.02$, $P = 0.0515$) and a trend of a between group difference in the last recorded pain score immediately after playing golf ($t = -1.95$, $P = 0.0609$).
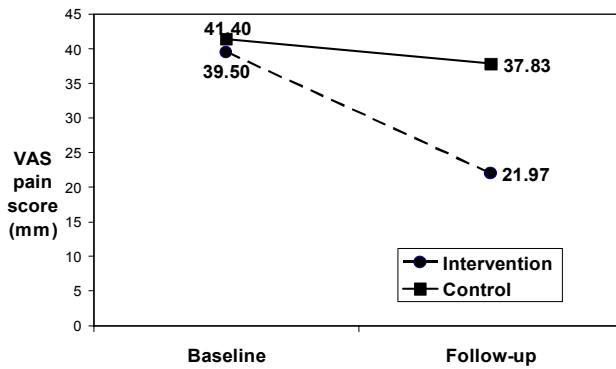
Figure 2. Illustration of the visual analog scale (VAS) results for the test (●) and the control (■) group for the baseline and the follow-up measurements

DISCUSSION

Performance: It was speculated that the initial impact of introducing an unstable shoe to a golf swing would have a negative effect on golf performance. However, a reduction of performance between the stable and unstable shoe condition was not seen at baseline for power (club head speed, ball speed, and ball carry) or consistency (path and impact variability) variables. There was no change in golf performance due to playing golf for six weeks for the control group and for the unstable shoe group. This suggests that the golf related mechanics do not change when using an unstable shoe condition in this population of golfers (handicap < 15). It may be that the swing is more controlled in an unstable condition, which would compensate for the instability. In addition, not only the performance variables but also their standard deviations were not influenced by the unstable shoe condition.

Low back pain: There were two separate reports of perceived low back pain during this experiment. The first was a baseline and final indication of perceived low back pain filled out in the laboratory prior to the completion of the last motion analysis protocol. From this measurement there was a significant reduction in self-reported low back pain in the intervention group where the average pain score decreased by almost half (17.5 mm on a 100mm continuous scale), and no change in the control group (a reduction in the group average of 3.6 mm). The second measure of low back pain was filled out after every round of 18 holes of golf in a log book. The comparison was made by looking at the first and last recorded entries of perceived pain in the log book. These differences were not significant, but showed a trend in the same direction as the lab assessments with the final assessment lower than the initial one.

SUMMARY

The results of this study suggest that the unstable shoe has the potential to reduce perceived lower back pain in golfers. The reduction of lower back pain is expected to start relatively soon after starting to use the shoes. They may even be more pronounced if the unstable shoes would be used during the actual golf games. Adding an element of instability did not negatively affect golf performance. However, the potentially positive effects of an unstable shoe as a training device need further study.

REFERENCES

Doan BK et al. (2006). Effects of physical conditioning on intercollegiate golfer performance. *J Strength Cond Res*. 20(1).

McCarroll JR. (1996) The frequency of golf injuries. *Clin Sports Med*. 15(1):1-7.

FORCE DEPRESSION IN SINGLE MYOFIBRILS AND SARCOMERES

Venus Joumaa[1] and Walter Herzog[1]
[1]Human Performance Laboratory, University of Calgary, Calgary, Canada
vjoumaa@kin.ucalgary.ca ; walter@kin.ucalgary.ca

INTRODUCTION

It is well accepted that the steady-state isometric force following shortening of an activated muscle is smaller than the corresponding steady-state force obtained for a purely isometric contraction at the corresponding length (Abbott and Aubert, 1952; Marechal and Plaghki, 1979; Herzog & Leonard, 1997). This phenomenon is referred to as force depression.

Despite an abundance of experimental observations, the origin of force depression is still a matter of debate. One of the hypotheses proposed to explain force depression is sarcomere length non-uniformity (Edman et al., 1993; Morgan et al., 2000). According to this hypothesis, during shortening on the descending limb of the force-length relationship, sarcomeres are assumed to shorten by different amounts because of instability. Some sarcomeres shorten a slight amount, whereas others shorten more than average; these sarcomeres may shorten to a degree that places them on the ascending limb of the force-length relationship. This behaviour leads to a situation in which the tension produced is smaller than that produced at the corresponding length during an isometric contraction in which sarcomere lengths are assumed to be relatively uniform.

The aim of this study was to investigate this hypothesis by testing force depression in single myofibrils and tracking at the same time the changes in individual sarcomere lengths. If the sarcomere length non-uniformity hypothesis was true, and force depression was caused by sarcomere length non-uniformity exclusively, the following predictions should hold: (i) myofibrils should show force depression, (ii) there should be an increase in sarcomere length non-uniformity after shortening, and (iii) force depression should not be observed in individual sarcomeres.

METHODS AND PROCEDURES

Myofibrils isolated from rabbit psoas muscle were fixed to a glass needle and a motor at one end and to a nanolever at the other end, allowing for length changes and force measurements, respectively. The striation pattern of myofibrils was projected onto a linear photodiode array for determination of individual sarcomere lengths.

Myofibrils (n=11) were activated at an average sarcomere length (SL) of 2.8µm and then shortened at a speed of 0.1µm/s/sarcomere to an average SL of 2.4µm. Myofibrils were then held isometrically for 1min, and then deactivated. After a rest period of 5 mins, myofibrils were reactivated at the final SL of 2.4µm in order to obtain an isometric reference force. Forces were normalized by myofibril cross-sectional area and expressed as stress (nN/µm²).

Force depression for a myofibril was defined as the difference in the steady-state isometric force following shortening, and the purely isometric reference contraction at 2.4µm sarcomere length.

Since myofibrils are formed of sarcomeres arranged in series, measuring the force at the end of a myofibril gives the instantaneous

force in each sarcomere; and therefore, by measuring individual sarcomere lengths, we can determine force depression for individual sarcomeres.

RESULTS AND DISCUSSION

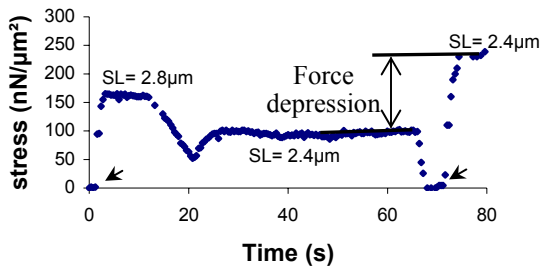All eleven myofibrils showed force depression averaging 31.0±3.9% of the isometric reference force (figure 1).

Figure 1. Myofibril response when activated at an average SL of 2.8μm, then shortened to an average SL of 2.4μm, deactivated, then activated. Arrows indicate the activation time.

This result indicates that the origin of force depression must be within the sarcomeric structure. In order to test if force depression might be caused by the development of sarcomere length non-uniformities, we tracked sarcomere lengths prior to, during and after myofibril shortening. According to the sarcomere length non-uniformity theory, we would expect an increase in the sarcomere length distribution after shortening and an abolishment of force depression in individual sarcomeres. However, this was not the case. First, sarcomere lengths after shortening were non-uniform (the standard deviation (SD) of the sarcomere lengths was 0.10μm) but this non-uniformity was not greater than the non uniformity observed before shortening (SD= 0.12μm; figure 2), or the non-uniformity obtained at 2.4μm after the purely isometric reference force (SD= 0.11μm). Second, all individual sarcomeres (n=60) showed force depression ranging from 6.1% to 54.3%.
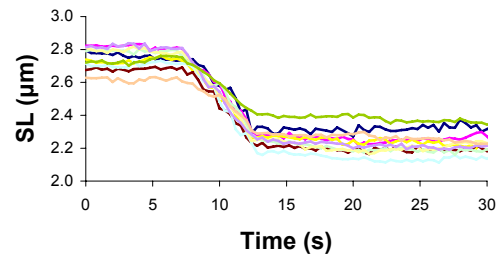
Figure 2. Sarcomere lengths prior to, during and after shortening from a typical myofibril.

This result suggests that force depression cannot be explained by the sarcomere length non-uniformities. Changes in the kinetics of cross bridges leading to a decrease in the force produced per cross bridge or the number of attached cross-bridges should be considered. It has been proposed (Marechal and Plaghki, 1979) that shortening might induce an inhibition of cross-bridge attachment in the newly formed overlap zone and therefore resulting in a decrease in the number of attached cross-bridges and force.

CONCLUSION

Force depression does not depend on sarcomere length non-uniformity, but rather seems an inherent property of the molecular mechanism underlying contraction.

REFERENCES

Abbott, BC and Aubert, XM (1952). *J. Physiol* 117:77-86.

Edman K et al. (1993). *J Physiol* 466:535-552.

Herzog, W and Leonard, TR (1997). *J Biomech* 30:865-872.

Marechal, G and Plaghki, L (1979). *J Gen Physiol* 73:453-467.

Morgan DL et al. (2000). *J Physiol* 522:503-513.

ACKNOWLEDGEMENTS

Inverse Piano Technique for Studying Finger Interaction During Pressing Tasks

Joel R. Martin, Mark L. Latash, and Vladimir M. Zatsiorsky
Department of Kinesiology, The Pennsylvania State University, University Park
Email: jrm496@psu.edu

Introduction

When a person moves or presses with an individual finger other fingers also produce a force (Kilbreath and Gandevia 1994; Li et al. 2004; Zatsiorsky et al. 2000). Several factors are known to contribute to this response: (1) peripheral mechanical coupling, (2) multi-digit motor units, and (3) diverging central commands. This phenomenon, known as *enslaving*, has traditionally been studied in isometric pressing tasks. The purpose of this project was to build a device, an Inverse Piano (IP), to study finger interaction in non-isometric pressing tasks. The IP allows for fingers to be unexpectedly raised or lowered during pressing tasks. Fingers are perturbed by linear motors located directly under uni-dimensional force sensors, which serve as the "piano keys".
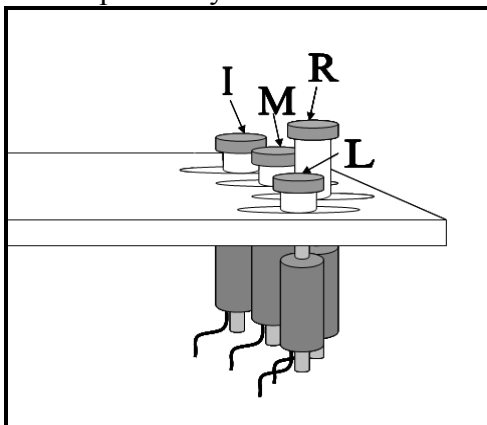
Figure 1: Schematic of Inverse Piano.

Motors are triggered using National Instruments LabVIEW. This allows key position and finger force data to be recorded simultaneously. The IP makes possible the studying of several factors on the finger force outcome and coordination. In particular, the following factors can be explored: (a) Finger combination. There are 15 combinations of the key manipulation: four 1-finger tasks (I, M, R, L, where the letters designate the index, middle, ring, and little finger respectively); six 2-finger tasks (IM, IR, IL, MR, ML, RL); four 3-finger tasks (IMR, IML, IRL, MRL) and one 4-finger task (IMRL). (b) Predictability of the key raising. The options are innumerable but can be roughly classified into three groups: (1) both the sequence and time intervals are unknown to the subjects; (2) the sequence is known but the time intervals are unknown; and (3) both the sequence and time intervals are known in advance. (c) Amplitude of key movement. The IP is capable of displacing fingers up to 2 cm, in increments less than 1 mm. (d) The speed of key movement. The IP can vary key movement rates of between 2 mm/s to 4,687 mm/s. (e) Resistance of the keys to the external force. The resistance can mimic different mechanical properties, e.g. elastic resistance which is proportional to the key displacement, damping resistance proportional to the speed, dry friction, etc. The magnitude of the resistance, e.g. 'stiffness', can also be varied. (f) Feedback with various options: (1) visual feedback on the computer screen, the subject can also see his/her hand; (2) no visual feedback on the

screen, however the subject can see his/her hand; and (3) no feedback on the screen, the subject cannot see his/her hand. Thus far experimentation using IP has only investigated effects of varying magnitude of displacement.

Methods

During testing, subjects sat comfortably facing IP and computer monitor. Forearm and hand position were constrained. Initial 4-finger pressing force level was varied from 0, 10, 20, 30, 40 and 50% of maximum voluntary contraction (MVC) for a four-finger pressing task. Subjects were given the instructions "Do not pay attention to what happens after fingers are perturbed." After subjects demonstrated constant force production at this level motor movement was randomly triggered. Only 1-finger key raising tasks (I, M, R, L) were performed. Fingers were displaced either 10 mm or 20 mm, randomly. Speed of key movement was kept constant. Subjects were not given feedback of finger force and could not see their hand. Three trials of each condition were performed for a total of 144 trials (4 fingers x 6 initial force levels x 2 displacements x 3 trials of each condition = 144 trials).

Data analysis focused on change in magnitude of finger forces after perturbation and timing of force changes after perturbation. A two-way ANOVA was used to determine the effect of initial force level and displacement on force changes displayed by non-master fingers.

Results and Discussion

An exemplary recording is presented in Figure 2. It is seen that in response to the perturbation of the ring finger, the finger force increases while the force exerted by the middle finger decreases. Forces of other fingers change in a more complex way. The preliminary data do not agree with an opinion that the finger interaction is determined mainly by the tendon connections between the fingers.
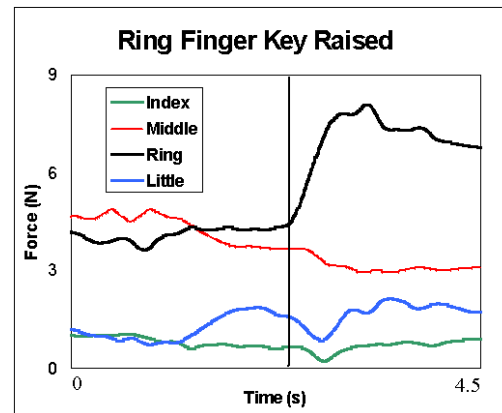
Figure 2: Graph of finger force changes from single trial with ring finger perturbation.

Summary

The results show that the IP can be a valuable tool for investigating the coordination of finger forces. Numerous experiments may be performed on the IP due to the large number of variables that can be manipulated.

References

Kilbreath SL and Gandevia SC (1994). *Journal of Physiology,* 479:487-497.
Li ZM et al. (2004). *Motor Control*, 8: 1-15.
Zatsiorsky VM (2000). *Experimental Brain Research*, 131: 187-195.

THE EFFECTIVENESS OF WRIST GUARDS FOR REDUCING WRIST AND ELBOW ACCELERATIONS FOLLOWING SIMULATED FORWARD FALLS.

Timothy A. Burkhart[2] and David M. Andrews[1]

[1]Department of Kinesiology, University of Windsor, Windsor ON, Canada
dandrews@uwindsor.ca
[2]Department of Industrial and Manufacturing Systems Engineering, University of Windsor, Windsor ON, Canada, burkha3@uwindsor.ca

INTRODUCTION

Fractures to the wrist and forearm account for approximately 25% of reported in-line skating injuries (Scheiber et al., 1996). In-line skaters have been encouraged to utilize wrist guards with force absorbing rigid volar splints. Joint changes at the elbow have also been suggested as a method of damping the effects of impact forces (DeGoede and Ashton-Miller, 2002). While there is little agreement on the efficacy of wrist guards for preventing impact related injuries, there appears to be a clear consensus that changing elbow angles decreases ground reaction forces. However, the capacity of these interventions for reducing impact induced accelerations at the wrist and elbow has not been documented in living people. Therefore, the purpose of the current study was to determine the effectiveness of a wrist guard in attenuating the impact force effects on the upper extremity in different elbow orientations. The acceleration response at the wrist and elbow were analyzed following impacts from simulated forward falls.

METHODS AND PROCEDURES

A seated human pendulum apparatus was used to simulate the flight phase of a forward fall in a controlled fashion. Healthy university aged subjects (15 males and 13 females) were asked to arrest their forward motion with the palmar soft tissues of both hands while upper extremities were extended. Impacts of approximately 0.4-0.5 times body weight, at a velocity of approximately 1.0 m/s were targeted (Chiu and Robinovitch, 1998), and were executed with, and without an off-the-shelf wrist guard in place (Firefly Sport Line, model number: 065627). Straight arm (180°) and natural arm (168°) elbow angles were also studied and were measured by an electro-goniometer (Biometrics SG110 Biometrics Ltd., Gwent, UK). A skin-mounted accelerometer (MMA1213D and MMA3201D, Freescale Semiconductor, Inc, Ottawa ON, Canada) was firmly attached at the wrist and the elbow, to measure the impact response characteristics (peak acceleration (PA), acceleration slope (AS), and the time to peak acceleration (TPA)), in the axial (aligned with the long axis of the forearm) and off-axis (normal to the long axis of the forearm in the sagittal plane) directions.

RESULTS

The peak axial acceleration response at the wrist was unaffected by the wrist guard (Figure 1), however, the AS_{axial} increased by almost 60%, when the wrist guard was in place. Conversely, the off-axis acceleration responses (e.g. PA) decreased significantly by more than 50% on average, from the unguarded to the guarded condition (Figure 1). Contrary to the findings at the wrist, the magnitude of all acceleration responses in the axial and off-axis directions at the elbow decreased significantly from the unguarded to

the guarded conditions. PA_{axial} and PA_{off} were decreased by 1.9g and 2g, respectively, while the AS_{axial} and AS_{off} were decreased by 537g/s and 592g/s, respectively.

At the wrist, PA_{axial} was found to increase significantly, although by only 1g, from the straight arm to natural arm conditions. PA_{off} was unaffected by any change in elbow angle. At the elbow, there were no changes in the axial parameters, however, the peak off-axis accelerations increased significantly in magnitude and experienced a change in direction on average (-1.7g to 3.7g) during natural arm impacts. AS_{off} was affected in a similar manner increasing from -421g/s to 1083g/s between straight arm and natural arm conditions, respectively.

Figure 1. Mean peak axial and off-axis accelerations at the wrist in the un-guarded and guarded conditions ($*p<0.05$)

DISCUSSION

The off-axis responses at the wrist, and the full set of responses at the elbow, suggest that the volar splint tested in this study, was capable of significantly absorbing the energy produced by the impact forces. However, the axial response at the wrist supports the findings of Kim et al. (2006) that suggest that splints simply transmit the force across the wrist joint, increasing the risk of injury to susceptible structures that are more proximal.

Small changes in peak acceleration were noted in the axial direction at the wrist in the

different elbow conditions. This may have been due to the fact that the difference in elbow angle between the two conditions was not large (only 12°). The change in loading direction at the elbow may be a result of the localized impact of the distal humerus within the trochlear notch. When a straight arm impact occurs, the distal humerus is inline with the long axis of the radius and ulna. However, when the arm is flexed, the trochlea would have rotated in the sagittal plane within the trochlear notch, becoming more aligned with the off-axis at the elbow.

SUMMARY

The results of this study show that the wrist guard tested is beneficial in decreasing the potentially damaging off-axis forces discussed by Troy & Grabiner (2007).. Eliminating or reducing the transmission of the axial accelerations through the wrist, as a result of improved wrist guard design, and studying the effects of elbow angle when the elbow is allowed to move through a full, dynamic range of motion, is a basis for future research.

REFERENCES

Chiu, J., & Robinovitch, S. N. (1998). *J. Biomech.*, 31:1169-1176.

DeGoede, K.M., & Ashton-Miller, J. A. (2002). *J. Biomech.*, 35**:**843-838

Kim, K. J. et al. (2006). *Am. J. Sport. Med.,* 34**:**637-643.

Scheiber et al. (1996). *New Eng. J. Med.,* 335**:** 1630-1636

Troy, K. L., & Grabiner, M. D. (2007). *J. Biomech.,* 40:1670-1675.

ACKNOWLEDGEMENTS

THE EFFECTIVENESS OF WRIST GUARDS FOR REDUCING WRIST AND ELBOW ACCELERATIONS FOLLOWING SIMULATED FORWARD FALLS.

Timothy A. Burkhart[2] and David M. Andrews[1]

[1]Department of Kinesiology, University of Windsor, Windsor ON, Canada
dandrews@uwindsor.ca
[2]Department of Industrial and Manufacturing Systems Engineering, University of Windsor, Windsor ON, Canada, burkha3@uwindsor.ca

INTRODUCTION

Fractures to the wrist and forearm account for approximately 25% of reported in-line skating injuries (Scheiber et al., 1996). In-line skaters have been encouraged to utilize wrist guards with force absorbing rigid volar splints. Joint changes at the elbow have also been suggested as a method of damping the effects of impact forces (DeGoede and Ashton-Miller, 2002). While there is little agreement on the efficacy of wrist guards for preventing impact related injuries, there appears to be a clear consensus that changing elbow angles decreases ground reaction forces. However, the capacity of these interventions for reducing impact induced accelerations at the wrist and elbow has not been documented in living people. Therefore, the purpose of the current study was to determine the effectiveness of a wrist guard in attenuating the impact force effects on the upper extremity in different elbow orientations. The acceleration response at the wrist and elbow were analyzed following impacts from simulated forward falls.

METHODS AND PROCEDURES

A seated human pendulum apparatus was used to simulate the flight phase of a forward fall in a controlled fashion. Healthy university aged subjects (15 males and 13 females) were asked to arrest their forward motion with the palmar soft tissues of both hands while upper extremities were extended.

Impacts of approximately 0.4-0.5 times body weight, at a velocity of approximately 1.0 m/s were targeted (Chiu and Robinovitch, 1998), and were executed with, and without an off-the-shelf wrist guard in place (Firefly Sport Line, model number: 065627). Straight arm (180°) and natural arm (168°) elbow angles were also studied and were measured by an electro-goniometer (Biometrics SG110 Biometrics Ltd., Gwent, UK). A skin-mounted accelerometer (MMA1213D and MMA3201D, Freescale Semiconductor, Inc, Ottawa ON, Canada) was firmly attached at the wrist and the elbow, to measure the impact response characteristics (peak acceleration (PA), acceleration slope (AS), and the time to peak acceleration (TPA)), in the axial (aligned with the long axis of the forearm) and off-axis (normal to the long axis of the forearm in the sagittal plane) directions.

RESULTS

The peak axial acceleration response at the wrist was unaffected by the wrist guard (Figure 1), however, the AS_{axial} increased by almost 60%, when the wrist guard was in place. Conversely, the off-axis acceleration responses (e.g. PA) decreased significantly by more than 50% on average, from the unguarded to the guarded condition (Figure 1). Contrary to the findings at the wrist, the magnitude of all acceleration responses in the axial and off-axis directions at the elbow decreased significantly from the unguarded to

the guarded conditions. PA_{axial} and PA_{off} were decreased by 1.9g and 2g, respectively, while the AS_{axial} and AS_{off} were decreased by 537g/s and 592g/s, respectively.

At the wrist, PA_{axial} was found to increase significantly, although by only 1g, from the straight arm to natural arm conditions. PA_{off} was unaffected by any change in elbow angle. At the elbow, there were no changes in the axial parameters, however, the peak off-axis accelerations increased significantly in magnitude and experienced a change in direction on average (-1.7g to 3.7g) during natural arm impacts. AS_{off} was affected in a similar manner increasing from -421g/s to 1083g/s between straight arm and natural arm conditions, respectively.

Figure 1. Mean peak axial and off-axis accelerations at the wrist in the un-guarded and guarded conditions (*p<0.05)

DISCUSSION

The off-axis responses at the wrist, and the full set of responses at the elbow, suggest that the volar splint tested in this study, was capable of significantly absorbing the energy produced by the impact forces. However, the axial response at the wrist supports the findings of Kim et al. (2006) that suggest that splints simply transmit the force across the wrist joint, increasing the risk of injury to susceptible structures that are more proximal.

Small changes in peak acceleration were noted in the axial direction at the wrist in the

different elbow conditions. This may have been due to the fact that the difference in elbow angle between the two conditions was not large (only 12°). The change in loading direction at the elbow may be a result of the localized impact of the distal humerus within the trochlear notch. When a straight arm impact occurs, the distal humerus is inline with the long axis of the radius and ulna. However, when the arm is flexed, the trochlea would have rotated in the sagittal plane within the trochlear notch, becoming more aligned with the off-axis at the elbow.

SUMMARY

The results of this study show that the wrist guard tested is beneficial in decreasing the potentially damaging off-axis forces discussed by Troy & Grabiner (2007).. Eliminating or reducing the transmission of the axial accelerations through the wrist, as a result of improved wrist guard design, and studying the effects of elbow angle when the elbow is allowed to move through a full, dynamic range of motion, is a basis for future research.

REFERENCES

Chiu, J., & Robinovitch, S. N. (1998). *J. Biomech.*, 31:1169-1176.
DeGoede, K.M., & Ashton-Miller, J. A. (2002). *J. Biomech.*, 35**:**843-838
Kim, K. J. et al. (2006). *Am. J. Sport. Med.*, 34**:**637-643.
Scheiber et al. (1996). *New Eng. J. Med.,* 335**:** 1630-1636
Troy, K. L., & Grabiner, M. D. (2007). *J. Biomech.,* 40:1670-1675.

ACKNOWLEDGEMENTS

UPPER EXTREMITY SOFT AND RIGID TISSUE MASS PREDICTION USING SEGMENT ANTHROPOMETRIC MEASURES AND DXA

Katherine L. Arthurs[1], Timothy A. Burkhart[1,2] and David M. Andrews[1]

[1]Department of Kinesiology, University of Windsor, Windsor, ON, Canada,
dandrews@uwindsor.ca
[2]Department of Industrial & Manufacturing Systems Engineering, University of Windsor,
Windsor, ON, Canada, burkha3@webmail1.uwindsor.ca

INTRODUCTION

Wobbling mass (WM) models (e.g. Gruber et al., 1998) require knowledge of the magnitude of segment soft tissue masses, but little in-vivo data are available. Dual Energy X-ray Absorptiometry (DXA) can accurately quantify bone mineral content (BMC), fat mass (FM) and lean mass (LM) for the entire body. However, DXA can be expensive and may not be readily available for use in a non-clinical research setting. Holmes et al. (2005) addressed these limitations by developing tissue mass prediction equations for the lower extremity segments of living subjects from simple anthropometric measures and subject characteristics. The equations were validated against masses from DXA. The purpose of this study was to expand on this work by developing BMC, FM, LM and WM (WM=FM+LM) prediction equations for the arm, forearm, and forearm with hand segments, and validate them using DXA.

METHODS AND PROCEDURES

One hundred healthy adults (50 M, 50 F: mean age, mass, and height of 21.8±6.2 years, 70.4±94.96 kg, and 170.8±19.4 cm), gave consent prior to participation. The study was approved by the Research Ethics boards of the University of Windsor and Windsor Regional Hospital. Participants were randomly assigned to two subgroups: a generation sample (38 M, 38 F) used to develop the prediction equations; and an independent validation sample (12 M, 12 F) to assess predicted mass accuracy (Holmes et al., 2005). Actual tissue masses were determined from DXA whole body scans (GE Lunar Prodigy Advance). Using enCORE software (2006, GE Healthcare, v. 10.51.006), custom regions of interest (ROI) were utilized to segment the upper limbs as per Clarys & Marfell-Jones (1986) and Dempster (1955).

After scanning, 6 lengths, 6 circumferences, 8 breadths, and 4 skinfolds were recorded bilaterally from the upper extremities (shoulder to wrist) by two trained measurers, while in anatomical position. The reliability of these measures has been shown to be excellent, between and within measurers (Burkhart et al., 2008). Multiple linear stepwise regression was used to generate prediction equations for BMC, FM, LM, and WM of the arm, forearm, and forearm with hand segments. Predicted and actual tissue masses were compared (%error, RMS$_{error}$).

RESULTS

Anthropometric measures for the generation and validation samples were statistically similar (p>0.05), suggesting that the groups were homogeneous. Twelve prediction equations were generated using these anthropometric measures and subject variables such as height, body mass and sex. Adjusted R^2 values for these equations were high (range ~ 0.85 to 0.97). SEEs ranged from 7.7 g (BMC forearm) to 154 g (LM arm).

Actual and predicted tissue masses compared very well in general, with mean errors across all segments and tissue types ranging from 0.25 g for arm WM to 31.6 g for the arm and forearm with hand LM. Mean %errors ranged from - 2.2% to 15.5%, with 10 of the 12 equations resulting in mean tissue errors of < ± 4.3%. RMS_{errors} ranged from 7.9 g to 180.3 g, with 9 of 12 equations having RMS_{errors} <86.0 g. The actual and predicted tissue masses were highly correlated, with R^2 values for lines of best fit ranging from 0.68 (forearm LM) to 0.97 (arm WM) (Figure 1). Generally, the R^2 values for the WM tissues were the highest of all the tissue types.
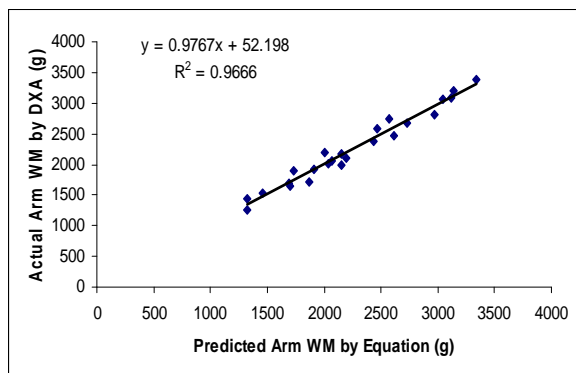
Figure 1. Scatter plot of actual (DXA) and predicted (equation) arm WM.

DISCUSSION

The generated tissue mass prediction equations resulted in a mean R^2 of 0.91 across all tissue types and segments. The errors in predicted tissue masses were small in general, and compared favourably to previous work for the lower extremities (Holmes et al., 2005).

The ability to accurately estimate segment soft tissue masses in-vivo is very important for biomechanical applications such as wobbling mass modeling (Gruber et al., 1998). These equations will enable the development of wobbling mass models that have segment mass compositions that are subject-specific. Improvements such as these will hopefully increase the predictive ability of such models for evaluating the segment response of individuals to impacts.

Small errors in predicted tissue masses may have resulted from measurement errors made between the two measurers. However, Burkhart et al. (2008) showed very high measurement reliability between and within measurers, with mean intra-class correlation coefficients (ICCs) of 0.860 and 0.895, respectively, for the same measurements used in the current study.

SUMMARY

The results of this study indicate that surface anthropometric measurements can be used to accurately predict the magnitudes of the hard and soft tissue masses of the upper extremity segments of young, healthy adults. These equations will allow subject-specific tissue masses to be determined for the upper extremities without the use of expensive imaging technologies, such as DXA.

REFERENCES

Burkhart, T.A. et al. (2008). *J. Biomech.* (in press).
Clarys, J.P. & Marfell-Jones, M.J. (1986) *Human Biology,* 58(5):771-782.
Dempster, W.T. (1955). WADC TR, 55-159.
Gruber, K. et al. (1998). *J. Biomech.,* 31(5):439-444.
Holmes, J. et al. (2005). *J. Appl. Biomech.,* 21(4):371-382.

ACKNOWLEDGEMENTS

EFFECTS OF FOOTWEAR ON PLANTAR FOOT SENSITIVITY ARE FREQUENCY DEPENDENT: A STUDY WITH FORMULA 1 FOOTWEAR

Günther Schlee, Thorsten Sterzing, Thomas L. Milani

Department of Human Locomotion, Chemnitz University of Technology, Chemnitz, Germany,
guenter.schlee@phil.tu-chemnitz.de

INTRODUCTION

The sensory function of the human foot allows the perception of different mechanical stimuli. These stimuli provide important sensory information, which are used for the fine regulation of movements. Through mechanoreceptors located in the skin, the foot is able to recognize different stimuli such as touch and vibration. Studies have shown that foot vibration sensitivity of healthy subjects is influenced by age (Inglis et al., 2002), foot region (Sterzing et al., 2006), and vibration frequency (Nurse & Nigg, 1999).
Furthermore, clinical studies have shown that diseases of the Central Nervous System, e. g. Diabetes and Morbus Parkinson, have negative effects on vibration sensitivity of the plantar foot (Dyck et al., 1987; Prätorius & Milani, 2004).
Foot sensitivity is also important for sports performance. Schlee et al. (2007) showed that gymnasts have better mean foot vibration sensitivity than volleyball players. They concluded that technical demands of the sport as well as footwear usage during practice and competition may influence the vibration sensitivity of athletes. Effects of footwear on plantar foot vibration sensitivity need to be investigated, since most of the studies involving foot sensitivity are performed barefoot. Additionally, according to Formula 1 drivers, their footwear must provide "pedal feeling", which is very important for driving performance. Therefore, the objective of this research is to investigate the effects of Formula 1 footwear on plantar foot vibration sensitivity.

METHODS AND PROCEDURES

The Sample was composed of 25 male subjects (age: 24.8 ± 2.6years, height: 173.7 ± 3.3cm, weight: 69.5 ± 7.1kg). Five foot/shoe conditions were analyzed: Barefoot (BF), Shoe 1 (S1) and Shoe 2 with three insoles differing in hardness (S2a: soft, S2b: middle, S2c: hard). Shoe 1 presented a common Formula-1 outsole, while Shoe 2 had a decoupled outsole. Vibration thresholds were measured with a vibration exciter at 30 and 200Hz under three anatomical locations of the right foot: Rearfoot, Metatarsal Head I and Hallux. The order of the measured structures and foot/shoe conditions was randomized. Subjects were seated during the measurements. Vibration amplitude was raised from zero until the amplitude where the subjects could perceive it (vibration perception threshold).
Five repetitive trials were performed for each location and foot/shoe condition. For data analysis the lowest CoV of at least three trials was used to select the most homogeneous measurements. Means and standard deviations were calculated from this data. Student's paired T-test ($p<0.05$) was used to compare vibration thresholds measured at both frequencies. Vibration thresholds among the 5 foot/shoe conditions measured at the same frequency were compared with a repeated measures ANOVA ($p<0.05$).

RESULTS
Figure 1 below compares thresholds measured barefoot to overall mean threshold values from all shoe conditions.

Fig. 1 - Vibration thresholds: BF vs. Shoe
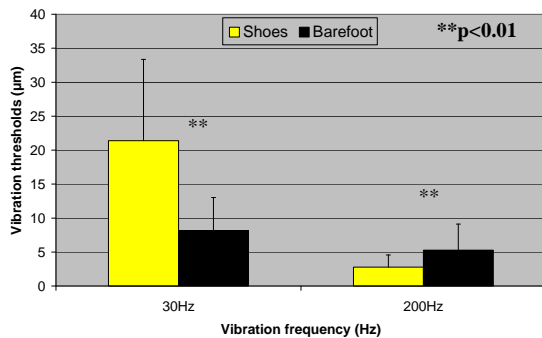
Results show significantly lower threshold values in the BF condition compared with all shoe conditions at 30Hz (p<0.01). Opposite to these results, measurements at 200Hz show significantly lower threshold values in all shoe conditions compared with the BF condition (p<0.01).

Figure 2 shows overall mean threshold values calculated from the three measured anatomical locations at 30Hz and 200Hz.

Fig. 2 - Vibration thresholds: Frequency comparison
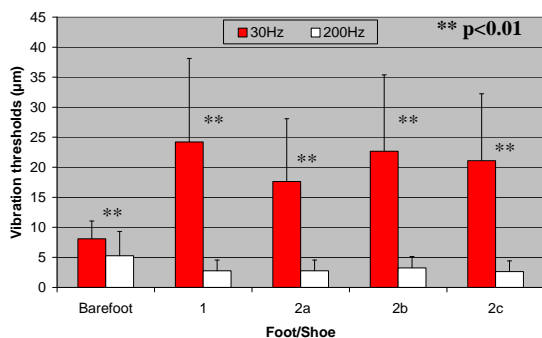
Results show that thresholds measured at 200Hz are significantly lower than thresholds measured at 30Hz in all measured foot/shoe conditions (p<0.01). There were no systematic differences among the four shoe conditions

DISCUSSION

Vibration sensitivity of the plantar foot at 200Hz was increased by the use of footwear compared to barefoot, indicating a frequency-related influence of footwear on vibration sensitivity. It seems that shoe outsole

materials in this study allow the high frequent stimuli to pass more easily through the material than the low frequent stimuli. Additionally, lower thresholds measured in the BF condition at 200Hz compared with barefoot results at 30Hz indicate better foot sensitivity at higher frequencies and confirm previous literature results (Nurse & Nigg, 1999; Inglis et al., 2002). Similar results were found in the shoe comparisons, indicating that the footwear used in this study did not affect this physiological pattern.

SUMMARY

Footwear influence on plantar foot vibration sensitivity is frequency-dependent. Further studies are needed to understand the interaction of foot and footwear with regard to foot sensitivity as well as the importance of foot sensitivity for sports performance in general.

REFERENCES

Dyck PJ et al. (1987). *Diabetes Care*, 10: 432-40.

Inglis TJ (2002). *Adv Exp Med Bio,* 508: 111-17.

Nurse MA, Nigg BM (1999). *Clinical Biomechanics*, 14: 667-72.

Prätorius B, Milani TL (2004). *13. Conference of the Canadian Society of Biomechanics*: Halifax, Canada 176.

Schlee G, Sterzing T, Milani TL (2007). *ISBS*: Ouro Preto, Brazil, 285.

Sterzing T et al. (2006): *Symp. dvs Biomechanik, Sportmotorik & Trainings-wissenschaft"*. Bad Sassendorf, Deutschland.

ACKNOWLEDGEMENTS

A NEW METHODOLOGY FOR THE ASSESSMENT OF MOVEMENT REPEATABILITY IN FUNCTIONAL UPPER LIMB TASKS

Sibylle Thies[1], Phil Tresadern[1], Laurence Kenney[1], Dave Howard[1], Yannis Goulermas[1]

[1]Centre for Rehabilitation & Human Performance Research, University of Salford, Manchester, UK, s.thies@salford.ac.uk

INTRODUCTION

There is a real need for robust metrics for the description of upper limb motions in functional tasks. Previous work focused on the forward reach and arm retraction in pointing tasks (e.g. Cirstea and Levin, 2000). However, grasping an object and its manipulation and release are crucial to many everyday tasks and central to rehabilitation of the upper limb. Previous approaches have relied on standard camera-based motion analysis systems, not applicable to the clinical domain (Buckley et al 1995,van Andel et al. 2008). More importantly, these studies did not go beyond a description of the kinematics. We present a new, inexpensive and user-friendly assessment method for unilateral and bilateral functional tasks that goes beyond a simple description of upper limb kinematics and has potential to provide information about changes in motion due to pathology or recovery. This paper introduces the method and reports on test-retest reliability.

Upper limb movement variability may well be a useful outcome parameter when studying pathologies (Reinkensmeyer et al. 2003). Our assessment method therefore uses software algorithms to determine movement repeatability for 3D accelerometer signals of two constrained functional tasks: a) drinking, b) moving a plate to the side.

METHODS AND PROCEDURES

Eight healthy young adults performed the "drinking task" with their dominant hand; both hands were used to move the plate from the center to their 'dominant' side. Hand position at begin and end were fixed and the object was picked up from and returned to a target position. Each subject performed eight trials per task on two days, two months apart. A triaxial accelerometer placed on the wrist provided 3D accelerations, sampled at 100 Hz. Movement begin and end were defined with an acceleration threshold algorithm.

The repeatability of any given inertial signal consists of two parts: 1) repeatability of the timing of the signal, e.g. the timing of a characteristic spike present in each trial 2) repeatability of the signal's quantity, e.g. peak value of a characteristic spike present in each trial. Timing errors between trials are addressed using established curve registration techniques (Sadeghi et al. 2000). For each trial-to-trial comparison a reference trial (trial 1) is defined onto which the other trial (trial 2) is "time-warped" (Figure 1). For each data point in trial 1, we define the 'cost' of matching it to a given data point in trial 2 as the distance between the two points in 3D space. Computing this cost for every possible pairing of data points gives a cost surface (Figure 2) in which the axes represent time in trials 1 and 2 respectively; red areas indicate a high cost between points while blue areas indicate low cost between points. The least cost path (Figure 2) is calculated under the constraint that the temporal order of the data points in trial 2 is unchanged; this path defines the optimal warping of trial 2 onto trial 1. The difference between this path of least error and an ideal 45° line ('no

warping') reflects the amount of time-warping done and therefore how well the subject reproduced the motion with regard to timing of the acceleration signal. Finally, the ability to reproduce motion signals that are similar in quantity is reflected by the RMS error and correlation coefficient, R, between the reference trial and the warped trial. For each trial-to-trial comparison, RMS errors and R values were obtained for curve-fitted x, y, and z accelerations and the average across all three axes was calculated. This was done for both tasks and both days of every subject. Paired t-tests were used to compare day 1 and day 2 repeatability measures of each subject to check parameters for their reliability.
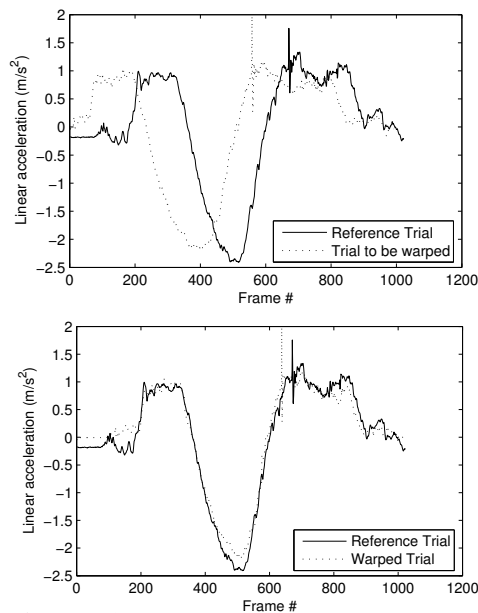
Figure 1. Accelerations of two trials before (top) and after (bottom) time-warping.
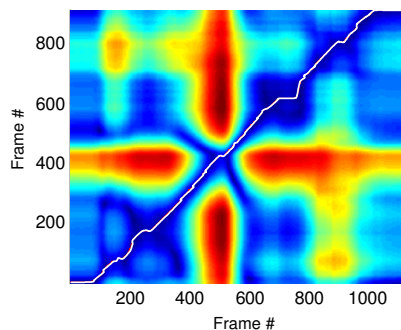
Figure 2. Cost surface. Least cost path: white.

RESULTS

Day-to-day differences in parameters were insignificant (Table 1).

	Variable	Day 1	Day 2	P
Glass	Warp Cost	14.62(3.32)	12.80(5.70)	0.3
	R	0.97(0.02)	0.98(0.01)	0.2
	RMS(m/s^2)	0.57(0.09)	0.56(0.12)	0.9
Plate	Warp Cost	19.62(4.80)	16.51(7.78)	0.3
	R	0.89(0.07)	0.89(0.05)	0.7
	RMS(m/s^2)	0.67(0.10)	0.66(0.12)	0.7

Table 1. Group mean(group std) for glass task and plate task.

DISCUSSION

Test-retest reliability of the protocol and outcome measures is confirmed: day-to-day differences did not reach significance in this group of healthy young adults. We conclude that the methodology can be used to gain insights in group differences when comparing patients to healthy controls, with the advantage of providing information on repeatability of signal timing and signal quantity, separately.

REFERENCES

Buckley MA, et al. (1996) Proc Inst Mech Eng [H].;210(4):241-7.
Cirstea MC and Levin MF (2000). *Brain,* 123: 940-53.
Reinkensmeyer DJ et al. (2003). *Neural Comput,* 15, 2619-42.
Sadeghi H et al. (2000). *Gait Posture,* 12, 257-64.
van Andel CJ et al. (2008). *Gait Posture,* 27:120-7.

ACKNOWLEDGEMENTS

PREDICTING FEMALE ARM STRENGTH FROM HAND LOCATION

Christopher C. Freeman[1] and Jim R. Potvin[2]

[1]Department of Kinesiology, University of Windsor, Windsor, ON, Canada,
[2]Department of Kinesiology, McMaster University, Hamilton, ON, Canada
potvinj@mcmaster.ca

INTRODUCTION

Upper limb strength limits plays an important role in determining acceptable loads for many workplace tasks. To date, most efforts to estimate limits for these tasks have relied on biomechanical models to estimate the static strength at the shoulder (about three axes) and about the elbow flexion/extension axis. However, errors in these strength calculations at each joint can summate to affect the validity of the final estimates. The purpose of the current study was to directly measure maximum arm efforts at the hand, for a wide variety of hand locations relative to the ribcage. In addition, predictive regression equations were developed to predict the average population strength for a variety of hand positions.

METHODS AND PROCEDURES

A total of 29 female subjects were studied and they were divided into three groups: 1) 10 between 20-29 years, 2) 10 between 30-39 yrs and, 3) 9 between 40-55 yrs. Subjects stood upright and an extending padded rod was used to control the location of their manubrium (ie. ribcage). Data were collected with the hand in 18 locations, which were at a combination of three heights (shoulder, head/stature and waist height), three rotations over the transverse plane (hand directly in front of the shoulder, hand rotated 45 degrees, and hand directly lateral to the shoulder) and two reaches (approximately 40% and 80% of the maximum reach). The head/stature and waist heights were an average of 18 cm above and 33.5 cm below the shoulder, respectively. The 40 and 80% reaches were an average horizontal distance of 22 and 44 cm from the shoulder, respectively. In each of the 18 hand positions, subjects performed two trials of maximum voluntary efforts (MVEs) in each of the following six directions: anterior push, posterior pull, up, down, medial (left) and lateral (right). All subjects were right-hand dominant and performed the efforts with the right hand, which grasped a vertically oriented, 2 cm diameter padded bar that was attached to a triaxial force plate and rigidly affixed to the testing apparatus. Subjects could stabilize themselves by grasping the apparatus with their left hand. Each effort was 3-5 seconds in duration and maximum forces were determined from a 2 second sliding average window. The higher of the two trials was recorded for each of the six directions in each hand position.

Stepwise regression analyses were performed to predict the average maximum force for a given hand location and effort direction combination. Separate equations were developed for each direction and it was determined that separate equations were needed for efforts at, or above, shoulder height and those at, or below, shoulder height. This resulted in a total of 12 equations and each had some combination of the horizontal (H), vertical (V) and lateral (L) displacement of the hand, relative to the shoulder location. Specifically, H, V, L, H^2, V^2, L^2, HxL, HxV and LxV were used as input variables.

RESULTS

There were substantial interactions between height, reach and angle for the MVEs in most directions, but there were some general trends observed. Height: the Down average MVE was highest at head height; Push, Pull, Medial and Lateral were highest at shoulder height; and Up was highest at waist height. Reach: while differences existed within reach/angle combinations, the pooled averages were similar between reaches for all six directions. Angle: average MVEs were highest when the hand was positioned in front of the shoulder for Push, Pull and Down directions and when rotated 90° (hand lateral) for the Medial and Lateral efforts. The highest average force was 160.7 N (36 lbs) for one of the eighteen Down efforts. Generally, the regression equations were very effective in estimating the group means for each of the 18 hand positions for each of the 6 directions (Table 1, Figure 1).

DISCUSSION

Overall, more than 97% of the variance was explained and the RMS errors were only 4 N (>1 lb) and 5%. Across all 108 combinations, the largest error was only 14.3 N (~3lbs) and even this was less than 10% of the criterion value. All directions maintained errors < 6% and r^2 values >94% (Table 1). Within each combination, the CVs were observed to range from 18%-43%, but were generally close to 30% for each direction, such that 25th percentile values can be approximated by multiplying the predicted equation values (50th %ile) by 0.80.

Future studies will determine if MVEs from 2 or 3 axes can be combined to predict strengths in any direction. This will allow for maximum forces to be estimated for efforts that are directed outside the 6 main axes tested. In addition, data will be collected for efforts performed with the hands above head height.

	Min (N)	Mean (N)	Max (N)	RMS Error (N)	RMS Error (%)	r^2
Push	51.6	85.5	130.2	3.9	4.5%	96.7%
Pull	50.4	87.2	142.4	4.5	5.2%	96.6%
Up	55.9	86.0	114.3	2.7	3.1%	97.6%
Down	76.3	111.2	160.7	6.1	5.5%	94.5%
Medial	63.8	89.2	135.0	2.2	2.4%	98.6%
Lateral	53.2	67.3	96.4	3.5	5.2%	92.0%
Overall	**50.4**	**87.7**	**160.7**	**4.0**	**4.6%**	**97.2%**

Table 1. Scatter plot of empirically measured, average maximum forces versus predicted, regression model outputs.
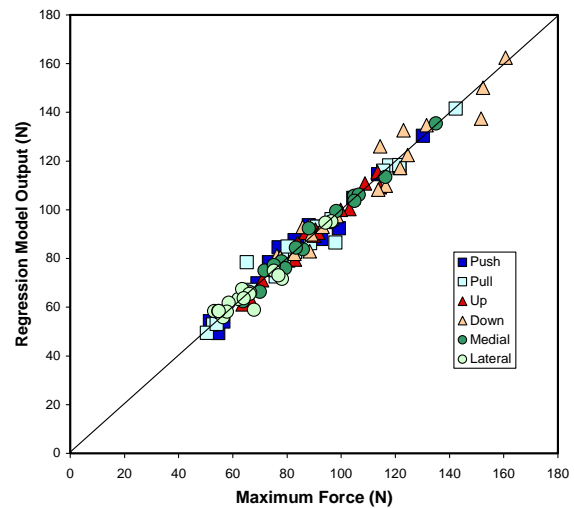

Figure 1: MVE statistics for each of the six directions. Regression statistics are provided for RMS error and correlation between the equation outputs and empirical data. Each number is calculated across the 18 positions.

SUMMARY

This study has successfully produced predictive equations to estimate arm strength in the six primary directions and determine acceptable loads in the workplace.

ACKNOWLEDGEMENTS

PROACTIVE ERGONOMIC ANALYSES WITH DIGITAL HUMAN MODELING: A VALIDATION STUDY OF PERCENT CAPABLE VALUES

Jim R. Potvin[1], James Chiang[2], Monica Jones[2], Brian McInnes[3], Allison Stephens[2]

[1]Dept. of Kinesiology, McMaster, University, Hamilton, ON, Canada, potvinj@mcmaster.ca
[2]Ford Motor Company, Dearborn, MI, USA
[3]Dept. of Kinesiology, University of Windsor, Windsor, ON, Canada

INTRODUCTION

Ergonomics was a reactive discipline for many decades. Tasks were designed, some resulted in worker injuries and some of those were redesigned to reduce their associated risk. More recently, a number of industries have started to use proactive methods to improve the human factors and ergonomics of their products and manufacturing designs and reduce costs. One such method is performed at a computer terminal and involves the manipulation of a digital human model within a virtual environment. However, assumptions must be made regarding how the workers would posture themselves. Alternatively, motion capture (MoCap) technology also uses a computer-generated environment while observing real human motion in a virtual reality lab. However, much more research is needed to assess the assumptions made with both these methods. Thus, the purpose of this study was to determine the validity and reliability of various proactive methods employing either static digital human model manipulation or MoCap methods to predict joint postures and injury risk for a wide variety of automotive assembly tasks.

METHODS

Twelve automotive assembly line Tasks were studied (6 each from a car and truck plant). An ergonomic assessment was performed on each task using 5 different proactive methods. The first used a manual manipulation of the Classic Jack mannequin (Siemens PLM Software Inc, Plano, TX) (termed "Static") and the remaining four all used MoCap technology (Motion Analysis Corp, Santa Rose, CA). These were collected with each combination of: 1) Non-operators or "NO" (no assembly line experience) or untrained operators or "UT" (assembly line workers unfamiliar with the specific task), and 2) using either minimal physical props ("Crude") or with as many props as was possible ("Buck"). A sixth condition had the actual ("Real") workers perform the task in the MoCap environment, but they simulated the actual plant performance using video feedback. For each Task, there were 6 Static, 10 UT, 10 NO and 3 Real subjects. Hand loads ranged from 4 N (Task 3) to 89 N (T5). Three repeat trials were performed with each condition. For the Static subjects, these were spaced at least a week apart.

The Jack Static Strength Prediction (JSSP) model and JackScript API were used for each trial to calculate a large number of kinematic and kinetic variables. However the current paper will focus on the total percent of population strength capability (%Cap) values, which were the lowest value from the 3 trunk, 6 shoulder and 2 elbow bilateral axes. This number is used most often to determine if a task is "acceptable". An ANOVA was used to determine the effects of Task (n = 12) and Method (n = 6). For this paper, an emphasis was placed on comparing between Methods for each Task.

RESULTS

There were few cases were the proactive Methods differed substantially from the Real for a given Task (Figure 1). When compared with the Real criterion, the %Cap RMS errors ranged from 8-11%. When comparing the four combinations of MoCap methods to each other, the RMS differences were generally less than 10 %Cap and there was no trend for any Method to consistently result in higher or lower values than the others, except for Static which was often somewhat higher than the other Methods and Real values.

In rare cases (Task 12, 1, 8) different decisions would have been made each Method regarding the acceptability of a Task. However, this was also observed to occur when comparing between the results of the 3 Real subjects within a Task.
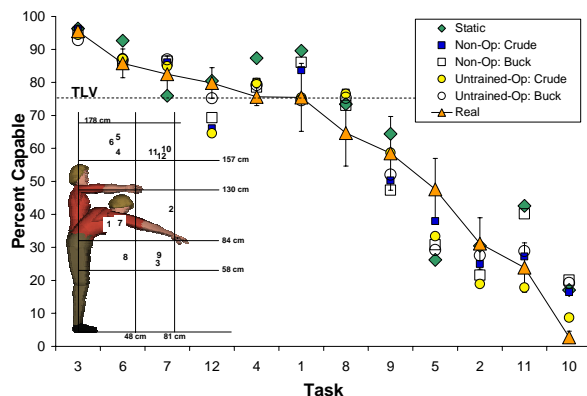
Figure 1: The total %Cap value for each Method /Task combination (sorted by the Real value, least to highest risk). The inset shows the hand locations for each Task. TLV limit shown at 75 %Cap.

DISCUSSION

When using a Static method (eg. Classic Jack), it is recommended that an attempt be made to keep trunk and shoulder postures as close to neutral as is possible and/or feasible. This appears to be the strategy employed by the Real subjects in this study. Postures should be adopted that allow for vision of the part (unless if it is obvious that vision will not be necessary) and two hands should be used whenever it is feasible. For tasks that are not performed overhead, users should be encouraged to move the mannequin as close as possible to the location of exertion.

When using MoCap, there appeared to be no functional benefit to using actual assembly line worker s (UT) as subjects in the motion capture testing. Overhead tasks should be assessed with MoCap so the subject can subjectively account for risk to the neck and wrist (not assessed with Jack). One-handed overhead Tasks appear to benefit from Buck props, especially where the other hand would likely be needed for support. However, there appeared to be no benefit of Buck over Crude for overhead tasks that use two hands (and don't require a support hand). For one-handed tasks being done below shoulder height, there is a need for a physical support for the other hand, although more complex props are not necessary. Finally, every effort should be made to recreate the actual forces required for part installation during MoCap studies. This will ensure that the postures adopted are appropriate for the task demands.

SUMMARY

This study has evaluated the validity of various proactive ergonomic methods. The resulting recommendations will improve the accuracy of these ergonomic assessments but much more research is needed to evaluate the current proactive processes being used.

ACKNOWLEDGEMENTS

BIOMECHANICAL MECHANISMS OF KNEE OSTEOARTHRITIS

Janie L. Astephen[1,2], Kevin J. Deluzio[1,3], Graham E. Caldwell[4], Michael J. Dunbar[1,5],
Cheryl L. Hubley-Kozey[1,6]
[1]School of Biomedical Engineering, Dalhousie University, Halifax, NS, Canada
[2]Department of Human Biology, University of Cape Town, Cape Town, South Africa
[3]Department of Mechanical & Materials Engineering, Queen's University, Kingston,ON, Canada
[4]Department of Kinesiology, University of Massachusetts Amherst, Amherst, MA, USA
[5]Department of Surgery, Dalhousie University, Halifax, NS, Canada
[6]School of Physiotherapy, Dalhousie University, Halifax, NS, Canada

INTRODUCTION

Knee Osteoarthritis (OA) is a metabolically active disease of the musculoskeletal system that has no definitive cure and produces substantial societal cost. The pathomechanics of knee OA are poorly understood, largely due to the progressive and multifactoral nature of the disease process. Treatment options for persons with moderate levels of knee OA have therefore been limited to pharmacological and therapeutic interventions of unknown effectiveness. Numerous risk factors for the disease have been identified, and mechanical factors have been linked to the progression of the disease. However, little attention has been paid to how these risk factors interact to progress the disease.

METHODS AND PROCEDURES

The anterior-posterior and lateral radiographs of the affected knee of 40 subjects diagnosed with moderate, medial-compartment knee OA were assessed by an experienced orthopaedic surgeon with a visual analog severity score (VAS), representative of the radiographic severity of the joint. Gait analysis was performed for all subjects, and three-dimensional joint angles and net external moments at the hip, knee and ankle joints were calculated. Surface electromyography (EMG) was simultaneously recorded from two hamstrings, two gastrocnemius and three quadriceps muscles. Principal component analysis (PCA) was applied to each joint angle and moment and the EMG waveforms for each muscle separately to extract major patterns of variation of the waveforms. A stepwise regression analysis was used to obtain the subset of biomechanical variables that best explained radiographic knee OA disease severity, defined by the visual analog severity (VAS) score.

RESULTS

Five variables were selected as optimal for the prediction of the VAS, including (in order) the knee adduction moment PC1, the medial gastrocnemius PC2, BMI, the ankle adduction angle (i.e. the toe out angle of the foot) PC2, and the ankle rotation moment PC3. The total variation explained (R^2) by this five variable model was 67.4%. Separately, only the knee adduction moment PC1 had a significant but mild univariate correlation with VAS ($r^2=0.214$).

High severity was associated with high overall magnitudes of the knee adduction moment during stance (Figure 1a), a phase shift in peak activation of the medial gastrocnemius muscle towards later stance and an increase in activation of the muscle in late stance (Figure 2), high BMI, a greater and more sustained toe out angle of the foot relative to the tibia during mid to late stance (Figure 1b), and a greater net resultant eversion moment of the foot mid-stance.
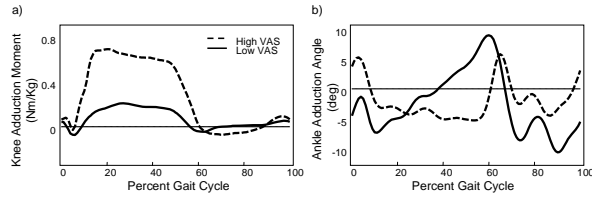
Figure 1: Representative waveforms of subjects with high and low severity (95th percentiles) indicated that a higher overall level of the knee adduction moment (a) and a more prolonged toe out (i.e. adduction) angle of the foot (b) was associated with greater severity.
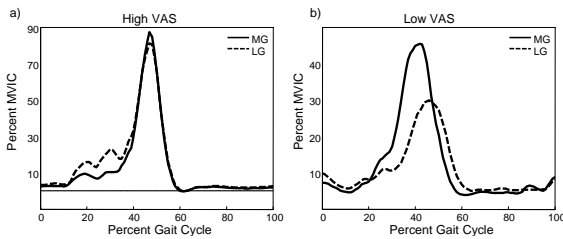

Figure 2: Representative EMG waveforms of subjects with high (a) and low (b) severity indicated that a more delayed and greater peak activation of the medial gastrocs were associated with greater severity.

DISCUSSION

The results of this study suggest that the role of biomechanical factors in the radiographic progression of knee OA is multivariate in nature. Radiographic disease severity within a moderate knee OA subject group was well explained by a multifactoral combination of biomechanical changes ($R^2 = 67.4\%$). The knee adduction moment, which is the gait variable most associated with knee OA disease progression (Miyazaki et al., 2002), was important only *in combination* with other biomechanical changes (Figure 1a). Obesity also consistently emerges as a risk factor in the onset and progression of musculoskeletal conditions (Felson, 1992), but the mechanism of its role in the pathomechanics of knee OA has remained unclear. These results support previous findings that its role is multivariate in nature (Astephen and Deluzio, 2004). Also included in the severity model were changes in ankle joint biomechanics during gait (Figure 1b), which are suggestive of a mechanism to move the line of action of the

ground reaction force more laterally during mid-stance. The fifth factor in the prediction model represented an abnormal neuromuscular control strategy of the gastrocnemius muscles (Figure 2) which may represent a mechanism to provide frontal plane stability to the diseased joint.

SUMMARY

The radiographic severity of a moderate knee OA population was well explained by a combination of obesity, gait and neuromuscular changes. The mechanism defined by the model should be studied further with longitudinal and simulation studies to understand its potential role in the initiation and progression of disease and to develop more appropriate early diagnostic and treatment strategies for patients with moderate knee OA. These results highlighted the importance of considering multiple factors simultaneously in the study of knee OA, and the need for more multivariate biomechanical analyses that include information from multiple joints and neuromuscular information from electromyography.

REFERENCES

Astephen, JL and Deluzio, KJ (2005). *Clin. Biomechanics*, 20(2):209-17

Felson,DT et al. (1992). *Ann Intern Med*, 1;116(7):535-9.

Miyazaki, T et al. (2002) *Ann.Rheum.Dis*. 61(7):617-22.

ACKNOWLEDGEMENTS

VIBRATION TRANSMISSIBILITY OF MULTI-BODY SEGMENTS IN REACH MOVEMENTS UNDER WHOLE-BODY VIBRATION EXPOSURE

Heon-Jeong Kim[1] and Bernard J. Martin [2]

[1]Department of Mechanical Engineering, University of Michigan, Ann Arbor, Michigan, USA,
heonjeon@umich.edu
[2]Departments of Industrial and Operations Engineering, University of Michigan, Ann Arbor, Michigan, USA, martinbj@umich.edu

INTRODUCTION

Vehicle vibration is transmitted to the whole body of the seated driver and operators, thus causing discomfort and interfering with their movements in this dynamic environment. More specifically, vibration can affect the speed and accuracy of reaching and manipulating tasks associated with vehicle operations (Rider et al, 2003). Several studies have examined the effects of vibration on seated human to improve comfort, safety or performance. The apparent mass of the upper torso in static seated postures was analyzed as a function of vibration variables (Griffin, 1990), (Paddan and Griffin, 2002). Reach performance in ride motion was quantified by finger-tip trajectory and aiming error (Rider et al, 2003 and 2004). The present study investigates vibration transmissibility of multi-body segments along the transmission path, with the goal to develop an active biomechanical model for the proper evaluation of whole-body vibration (WBV) effects on reach performance.

METHODS AND PROCEDURES

A biodynamic reach experiment was conducted on the ride motion simulator (RMS) of the US Army to generate vehicle vibration. Six sinusoidal vibration inputs were produced by combining three vibration frequencies (2, 4, or 6Hz) and two vibration directions (vertical or fore-and-aft). Six participants performed self-paced reaches in a random order with one repetition to five targets representing the right reach hemisphere. Reach movements were recorded by an optical motion capture system (VICON) using twenty-six retro-reflective markers attached to selected body landmarks. Transfer functions of the torso, right upper arm, and right lower-arm-hand were estimated by Fast Fourier Transform (FFT) applied to motion capture data. Vibration transmissibility along the right arm was investigated by comparing peak perturbations of the right shoulder, elbow, and index finger.

RESULTS

As expected, the transfer functions along the right upper body segment vary as a function of vibration frequency (Figure 1 and 2). Vibration transmissibility along the right arm shows the same characteristics regardless of vibration direction such as vertical and fore-and-aft axis. Peak transmissibility increases from the right shoulder to the right index fingertip for the 2 Hz frequency, while it decreases along the right arm path for the 6 Hz frequency. For the 4 Hz frequency, the peak transmissibility decreases from the shoulder to the elbow and does change form the elbow to the finger.

The peak transmissibility for individual upper body segments varies as a function of vibration direction as well as vibration

frequency. For the vertical WBV, the frequency at which the peak transmissibility is observed varies as a function of body segment or joint (Figure 1). The peak frequencies for the shoulder, elbow, and finger occur at 4 Hz, 2 and 4 Hz, and 2 Hz respectively. For the fore-and-aft WBV, the peak frequencies for all segments occur at 2 Hz, as all peaks decrease monotonously when the input frequency increases (Figure 2).
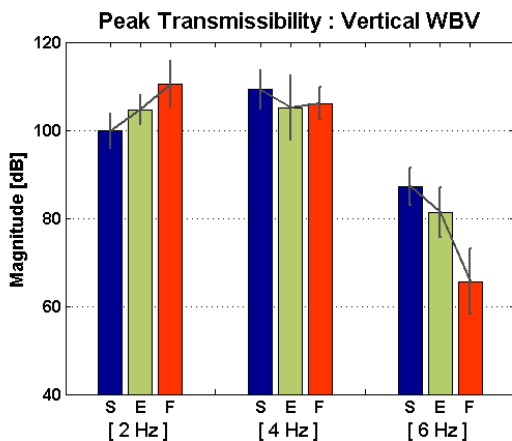

Figure 1. Peak transmissibility of upper body segments as a function of vertical WBV frequency: S (right shoulder), E (right elbow), and F (right index finger).
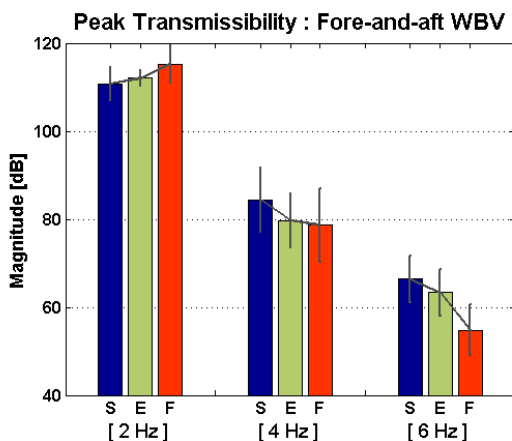
Figure 2. Peak transmissibility of upper body segments as a function of fore-and-aft WBV frequency: S (right shoulder), E (right elbow), and F (right index finger).

DISCUSSION

Vibration transmissibility of body segments may be affected by target location as well as vibration input. Indeed, different target location requires changes in reach direction and movement coordination which affect posture and thus stiffness of the upper body. The effect of target location will be analyzed in detail to develop an active biodynamic model. This model will be used to test vehicle designs and improve vehicle controls or interfaces.

SUMMARY

Vibration transmitted to the seated operator can affect the transmissibility along body segment path as it can be amplified or attenuated along the transmission path depending on WBV frequency. The frequency of peak transmissibility also varies as a function of vibration direction and body segment. The effect of reach posture and movement on transmissibility will be investigated.

REFERENCES

Griffin, MJ (1990). *Handbook of Human Vibration.* San Diego: Academic Press.

Paddan, GS and Griffin, MJ (2002). *J Sound and Vibration* 253(1): 215-241.

Rider, K et al. (2004). Technical Paper 2004-01-2180. SAE International, Warrendale, PA

Rider, K et al. (2003). Technical Paper 2003-01-0589. SAE International, Warrendale, PA.

Mansfield, NJ (2005). *Human Response to Vibration.* CRC Press.

Can Between-Day Kinematic Reliability Be Improved?

Brian Noehren[1] and Irene Davis [1,2]

[1] University of Delaware, Newark, DE, USA
[2] Drayer Physical Therapy institute, Hummelstown, PA, USA E-mail: bwn51@yahoo.com

INTRODUCTION

Instrumented gait analyses are often used to assess the effect of interventions on mechanics over time. Therefore, the reliability of these gait measures is extremely important. This reliability is heavily dependent on the repeatability of marker placement between sessions. In a study of sagittal plane motion during walking, Maynard et al. (2002) reported low to moderate reliability at the ankle (ICC = 0.45) and hip (ICC =0.62), with higher values for the knee (ICC=0.87).
In a 3D study of running, Ferber et al. (2002) reported good reliability of sagittal plane motions (ICC=0.85 to 0.93). However, they found values were lower (ICC=0.54 to 0.83) for secondary planes of motions. These results are similar to those found in a walking study by Kadaba et al. (1989). These authors reported the best results in the sagittal plane, with the lowest reliability in the secondary planes. These authors also noted an overall offset in these motions. They attributed this problem to the reapplication of the markers, as the waveforms were very similar after removing the offset (Kadaba et al. 1989). These results suggest that we may be limited in our ability to measure changes in secondary plane mechanics over time as a result of an intervention.

Therefore, the purpose of this study is to examine the effect of a marker placement device designed to improve the day-to-day reliability of kinematic data. We hypothesized that differences in peak angles between days would be reduced with the use of a Marker Placement Device (MPD).

METHODS

This is an ongoing study to be included subjects must be healthy and between the ages of 18-50. To date, 4 subjects have been tested. The study consists of three visits. During the first visit, anatomical markers were manually placed. Following a three-minute warm-up, subjects ran at 3.58 m\s (8 mph) for two minutes.   The 3D trajectories were captured at 200 Hz using an 8 camera, Vicon motion analysis system (Vicon, Oxford, UK). Force data were collected at 1000 Hz using an instrumented treadmill (AMTI, Watertown, MA) for the purposes of identifying stance.

During the second visit, the anatomical markers were placed on the lower extremities as in the first visit. The subject then stepped into the MPD (Figure 1). This device consists of horizontal and vertical pieces that are adjusted to align with a marker. There are laser pointers located at the end of each arm. The base can be adjusted for stance width, and levers can be rotated to align with the lateral border of the foot. A back support is provided to maintain trunk position.

Figure 1: Marker placement device

First, the subject selected a comfortable stance width and foot angle, which was recorded using

the device. The horizontal and vertical pieces of the device were adjusted so that the laser lined up with the center of the marker. Next, the positions of all anatomical landmarks were recorded. The running trials were then collected as described in session one.

On the third visit, the subject stepped into the MPD again, with the foot width and angle position adjusted from the previous session. Once standing in the device, the arms were adjusted to the previously recorded locations. A marker was then placed such that the laser was pointed directly at its center. The running trials were again collected. Five running trials were collected in each session. Peak joint angles during the stance phase were calculated using visual3D software (C motion, MD, USA). Angles resulting from manual marker placement were compared to those derived from MPD positioning, using the absolute average difference between days and typical error (TE).

RESULTS

Results are summarized in Table 1. The absolute average difference and typical error were consistently lower with the MPD. A representative curve between all three sessions for knee internal rotation is presented in figure 2. This figure shows less of a difference when using the device (days 2 and 3) than manual placement (days 1 and 2).

Table 1: Absolute average difference and typical error (TE), in degrees, for angles derived with manual and MPD placement

		Manual Abs Dif	TE	MPD Abs Dif	TE
Rearft	DF	3.6	3.2	0.7	0.7
	Ever	3.7	3.4	1.8	1.6
	Abd	5.4	5.3	0.9	1.0
Knee	Flex	3.5	2.9	2.9	2.5
	Abd	2.1	1.8	1.5	1.3
	IR	2.5	2.2	1.2	1.1
Hip	Flex	3.7	4.1	2.8	2.0
	Add	2.8	2.9	1.5	1.3
	IR	6.9	5.7	2.1	1.8
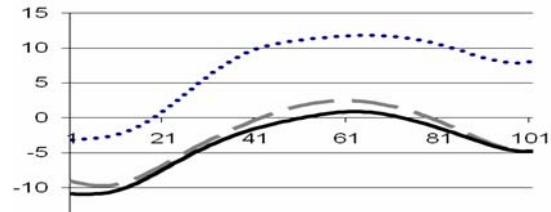
Figure 2: A representative knee IR curve, session 1 is the dotted line, session 2 is the dashed line and session 3 is the solid line.

DISCUSSION

Many factors may influence the reproducibility of gait mechanics. This device has attempted to alter one factor that has a large influence on repeatability. The lower absolute average difference suggests that there is less of an offset in day-to-day peak values when using the device. Additionally, the lower TE values suggest that there is less variance in the differences between days. The TE values using the MPD (0.7-2.5 degrees) were also about half of those reported by Ford et al. (2007) (1.3 -5.5 degrees). Lower errors allows for greater confidence in interpreting differences as being a result of an intervention, rather than the result of marker placement. Interestingly, using this device resulted in lowering the absolute average difference and TE in the secondary planes so they were similar to the results in the sagittal plane. Therefore, this type of device might have its biggest impact in interventions concerned with repeated measures in secondary planes of motion, as these motions have previously had the worst reproducibility. These results may be strengthened as additional subjects are added.

SUMMARY

These early results suggest that it is possible to improve the day-to-day repeatability of peak angles by using the marker placement device.

REFERENCES

Ferber, R., et al. 2002. *J Orthop Res* 20: 1139-1145.
Ford et al. 2007 *MSSE* 39: 2021-2028.
Kadaba, M., et al. 1989 *J. Orthop. Res*. 7:849–860
Maynard, V., et al. 2002 *Gait and Posture*. 59-67

The effect of gender on abdominal muscle activation in response to an asymmetrical leg loading task in healthy adults

Melissa McKeon[1], Sarah Gordon[1] and Cheryl Hubley-Kozey[1,2],

[1]School of Physiotherapy, Dalhousie University, Halifax, NS, Canada, mmckeon@dal.ca
[2]School of Biomedical Engineering, Dalhousie University, Halifax, NS, Canada

INTRODUCTION

The ability of the trunk muscles to respond to external moments of force is important to maintain a healthy spine. Differences in muscle strength and structure have been suggested as possible reasons why muscle activation patterns of men and women differ. Perez & Nussbaum (2002) found no significant effect of gender when looking at trunk muscle response to isometric contractions against uni-planar and multi-planar forces. In contrast, Anders et al. (2007) found women had higher abdominal amplitude response than men during a whole body tilt perturbation, and that women exhibited greater co-contraction among trunk muscles than men. Both studies focussed on amplitude measures only and on responses to static loading. Hubley-Kozey and colleagues (2002a, 2002b, 2005) have examined trunk muscle amplitude and temporal patterns including both healthy adults and those with low back pain during a dynamic task. Gender was not examined as a potential influence on patterning. Thus, the *purpose* of this study was to determine whether gender had a significant effect on abdominal amplitude and temporal patterns in response to an asymmetrical leg-loading task.

METHODS AND PROCEDURES

Eighteen healthy men and 19 women aged 20 to 50 years participated. After standard skin preparation, twelve (12) pairs of Ag/AgCl Meditrace[TM] (10 mm diameter) surface electrodes were placed bilaterally over lower (LRA) and upper rectus abdominis (URA), external oblique (E01-anterior, EO2-lateral, EO3-posterior), and internal oblique (IO). Electromyographic (EMG) signals were amplified (Bortec[TM,] Canada) and digitized at 1000 Hz while participants performed 3 trials of an asymmetrical leg loading task (ASLLT) and a series of maximum voluntary isometric contractions (MVIC). A Flock of Birds[TM] magnetic sensor was fixed on the left iliac crest and was digitized at 50 Hz to monitor 3D pelvic motion. The root mean squared (RMS) amplitudes was calculated for the leg extension phase of the ASLLT and normalized to percent MVIC. The raw signals were also full wave rectified and low pass filtered at 6 Hz to yield a linear envelop waveform for the total exercise. Principal component analysis (PCA) was applied to the waveforms to quantify shape and amplitude characteristics. Effects of gender, muscle, and side on amplitude and temporal patterns were analyzed using a General Linear ANOVA Model and post-hoc Tukey tests in Minitab software.

RESULTS

Subject demographics are presented as Means ± Standard Deviations in Table below.

	Age (yrs)	Mass (kg)	Height (cm)	BMI (kg/m^2)
Males (N = 18)	30.1 ±7.4	78.8 ±11.3	179.1 ±6.5	24.5 ±2.8
Females (N = 19)	31.2 ±8.6	61.6 ±12.0	164.5 ±4.3	22.7 ±4.0

There was no significant difference (p>0.05) in pelvic motion between genders (X: 3.9°, Y: 2.5°, Z: 2.9°). There were significant gender, side and muscle effects (p<0.05) on RMS amplitude (Figure 1).
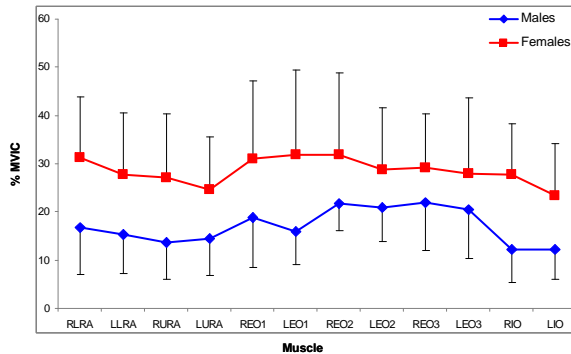

Figure 1: RMS amplitudes: Means (SD)

PCA found that 4 patterns explained 89% of the variance in the waveforms. PC1 (79%) captured the overall shape and magnitude and was highly correlated with the RMS amplitude (r=0.98). Therefore the ANOVA showed a similar significant main effects (p<0.05). PC2 captured the difference in activation between the initial and middle of the leg extension phase. There was a muscle effect (p<0.05) only with EO1 and IO higher than the other muscles (Figure 2). PC3 and PC4 captured the difference in peaks between the burst during the second leg lift off and the peak during the initial leg lowering. There was a significant muscle by side interaction for PC3 and a gender by muscle interaction for PC4. The only gender difference for the PC4 was for the EO1 muscle (Figure 2).
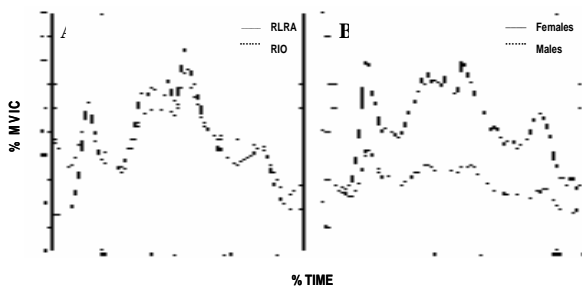
Figure 2: A) mean waveforms for RLRA and RIO of the women; B) mean waveforms of LIO for both men and women.

DISCUSSION

The results showed that women recruited all of their abdominal muscles to higher percent MVIC to perform this task. This could be explained by the typical strength differences expected between men and women. PCs (2-4) showed minor variations in muscle patterning in response to the ASLLT. There were shape differences between muscles as seen for IO and LRA above. This higher initial EO1 and IO activity was preparatory for the ASLLT. PC3 explained the response of the left EO2, EO3, and IO to the left leg lift off the bed. The only shape difference between the groups was the EO1 (PC4) activity in response to the left leg lift off the bed and left leg lowering (women had more distinct responses as seen in Figure 2). Thus men and women had similar responses to this dynamic challenge.

SUMMARY

Gender affects RMS amplitude and only EO1 temporal patterning in healthy adults. Therefore when amplitude differences are examined gender should be considered, but this is not necessary for temporal patterns.

REFERENCES

Anders,C et al. (2007). *Eur J Appl Physiol*, 101:195-205.
Perez, MA and Nussbaum, MA (2002). Spine, 27:1326-1335.
Clarke-Davidson, K and Hubley-Kozey, CL (2005). *Arch Phys Med*, 86:216-223.
Hubley-Kozey, CL and Vezina, J (2002a). *Arch Phys Med*, 83:1100-1108.
Hubley-Kozey, CL and Vezina, J (2002b). *Clin Biomech*, 17:621-629.

ACKNOWLEDGEMENTS

MINIMISING TRUNK ANGLE PREDICTION ERRORS ASSOCIATED WITH FIELD GONIOMETRY BY UTILIZING A SUBJECT SPECIFIC CALIBRATION OF PLANAR LEG MOVEMENTS IN SEATED DRIVERS

Robert J. Jack[1,2], Michele Oliver[1,2]

[1] Department of Biophysics, University of Guelph, Guelph ON, rjack@uoguelph.ca
[2] School of Engineering, University of Guelph, Guelph ON

INTRODUCTION

The quantitative assessment of trunk postures while driving is desired since trunk postures can be related to low-back pain (Harstella, 1990). This assessment can be performed by aligning a goniometer over the hip to measure trunk flexion/extension angles. Note that this approach assumes the goniometer is aligned properly and that the lower limb is stationary. For convenience, goniometers are often mounted on vehicle operators while they are standing outside the vehicle. This can lead to goniometer misalignment with tissue displacements as operators move to a seated posture within the vehicle cab. Misalignments can result in inaccuracies in goniometer determined angles, but much of this error can be reduced with an "on-subject zeroing" described by Jack and Oliver (2006). Furthermore, occasional voluntary and involuntary leg movements by drivers can lead to erroneous results. It is possible to control for these movements by monitoring the operator's knee angle and predicting associated trunk angle changes while the leg is constrained by the seat and the floor (r^2-values of 0.97 and standard prediction errors of 2.67˚ have been found (Jack and Oliver, 2006)). Controlling for operator movements becomes more difficult when the foot leaves the floor. Preliminary attempts to control for these elevated leg movements proved promising, but demonstrated the need for improvement. It was found that differences in movement patterns between subjects were limiting the prediction of trunk angles while the foot was elevated (standard prediction errors >7.36˚ and >4.90˚ while the leg was raised and lowered respectively (Jack and Oliver, 2006b)). The purpose of this study was to determine if the trunk angle prediction errors while raising and lowering the foot could be reduced by determining the subject specific relationship between knee and trunk angles with a series of planar calibration motions.

METHODS AND PROCEDURES

Nine male subjects had reflective markers placed over the ankle (lateral malleolus), knee (axis of rotation), hip (axis of rotation), and shoulder (glenohumeral joint). Each subject sat with their back against a backrest in an upright posture with their arms crossed to minimise extraneous shoulder movements. While adopting this posture, subjects preformed a series of sagittal plane lower limb movements summarized in Table 1. Dot product calculations using marker positional data recorded with six M^2mcam cameras and a VICON™ 460 motion capture system (sampled at 120Hz) were then conducted to obtain planar knee and trunk angles (a virtual marker was created to make trunk angles relative to vertical). Step-wise multiple linear regression analyses were then conducted to produce least-square fit polynomial equations for the prediction of trunk angle changes from patterns of knee angle change specific to the individual for a series of leg movement conditions (refer to Table 2). R^2-values and standard errors of the estimate were calculated to determine how well the regression models preformed for each movement condition.

Table 1: A summary of the subject specific calibration procedure

General Step	Description
1) Define knee angle ranges	Used to establish ranges of foot distances from the seat base. The subject's knee angle is recorded while the foot is placed at the start and end of each range so that the knee angle can be used to determine the position of the foot relative to the seat base
2) On floor calibration	To determine the trunk/knee angle relationship when the foot is moved while in contact with the floor
3) Single range calibrations	To determine the trunk/knee angle relationship when the foot leaves and contacts the ground in the same distance range from the seat base. The foot is raised to three different heights (0-15cm, 15-30cm and >30cm).
4) Multiple range calibrations	To determine the trunk/knee angle relationship when the foot leaves and contacts the ground in different distance ranges from the seat base. The foot is also raised from one distance range and lowered into another while being moved through the same height levels mentioned above.

RESULTS

The results demonstrate that a subject specific calibration of planar motion can be used to accurately predict changes in trunk angle with changes in knee angle while the lower limb undergoes short duration movements to relocate the foot (Table 2). On average, the prediction equations specific to each subject showed a good fit to the data (r^2-values >0.76)

Table 2. Mean r^2-values and standard errors for the subject specific prediction equations.

Selection Condition	r^2 -value	Standard Error
Foot on floor	0.99±0.01	0.08±0.05
Foot raised from range 1	0.93±0.09	1.82±1.06
Foot raised from range 2	0.80±0.15	3.64±1.06
Foot raised from range 3	0.76±0.17	3.81±1.27
Foot lowered to range 1	0.90±0.11	2.09±1.42
Foot lowered to range 2	0.88±0.17	2.39±1.15
Foot lowered to range 3	0.79±0.14	3.54±0.98

for all movement conditions. More importantly, mean standard prediction errors were below 4° for all movement conditions.

DISCUSSION

This study was able to determine that a subject specific calibration of lower limb movements can help reduce the standard prediction errors of least-square fit equations for the prediction trunk angle changes from knee angle changes. By measuring knee angle changes and accurately predicting the associated trunk angle changes, researches and ergonomists can remove erroneous trunk angle data by removing the predicted trunk angles them from measured trunk angles. The removal of the predicted trunk angles will leave only the trunk angles that would have been captured if the leg was stationary.

REFERENCES

Harstella, P (1990). *Int J Ind Ergon* 5:219-226.

Jack, R.J. and Oliver, M (2006). *2006 Canadian Society of Biomechanics Biannual Conference*. Waterloo, Ontario.

Jack, R and Oliver, M (2006b). *2006 Ontario Biomechanics Conference*. Barrie, Ontario.

LOWER EXTREMITY KINEMATIC EFFECTS OF MEDIAL ARCH SUPPORT AMONG FUNCTIONALLY FLATFOOTED INDIVIDUALS

E. Anne Cunningham and Stephen D. Perry

Department of Kinesiology and Physical Education, Wilfrid Laurier University, Waterloo, ON, Canada
Email: cunn4290@wlu.ca URL: http://www.biomechanics.wlu.ca

INTRODUCTION

Running is a physically demanding activity as the body is placed under increased stress in order to perform. Previous research has demonstrated an increase in lower extremity kinematic variables with running as opposed to walking (Perry et al., 1995). Further physical demands are seen during running among individuals with functional flatfoot (FFF) which contributes to a higher incidence of running related injuries among this population (McClay et al., 1998). Orthotics are commonly used to restore the medial arch in FFF however the effectiveness and the mechanism by which orthotics function remains unclear in the literature (Stacoff et al., 2000).

The objective of this research study is to determine the effects of medial arch supports on maximum rearfoot motion and maximum internal transverse tibial rotation among individuals with FFF.

METHODS AND PROCEDURES

A total of 19 healthy subjects (mean ± standard deviation: age, 23.8 ± 3.7 years; height, 173.8 ± 9.3 cm; weight, 71 ± 14.4 kg) with FFF performed a total of 24 running trials at 2 different speeds. Participants were deemed eligible if they fit our predetermined FFF criteria and they had no functional limitations of their lower extremity. Eligible participants were casted in a subtalar neutral position by a Certified Pedorthist. Medial arch supports were then constructed for each participant at 33%, 66% and 100% of their maximum arch height. Randomized running trials were completed in four conditions: barefoot, and the orthotic interventions of 33%, 66% and 100%. All conditions were conducted on a treadmill at speeds of 2.0m/s and 3.0m/s with three trials carried out during each condition. Kinematic data was collected using infrared light-emitting diodes (IRED's) by two OptoTrak 3020 (Northern Digital Inc., ON, Canada) camera banks. A total of 20 IRED's were placed on the rearfoot and tibia which allowed for measurement of the rearfoot motion and transverse tibial rotation that resulted from the running trials performed during each running condition. Statistical analysis was completed using a repeated measures ANOVA with apriori alpha value set at 0.05.

RESULTS

Preliminary findings (n=9) suggest a significant decrease in maximum rearfoot motion during orthotic intervention (p=0.001) at both speeds (p=0.004). Specifically, maximum rearfoot motion decreased as the orthotic arch height increased while running at 2.0m/s and 3.0m/s (Figure 1; Table 1). Significance was observed while comparing each orthotic condition except for the barefoot and 33% comparison (Table 2).
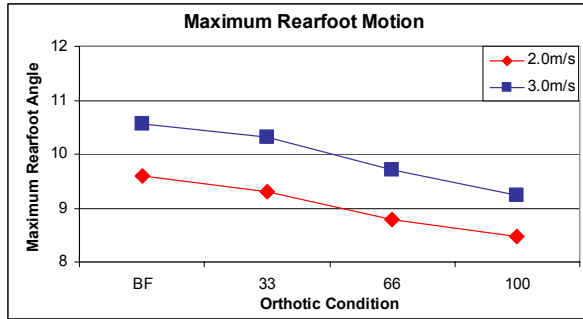
Figure 1: Maximum rearfoot angles obtained during running speeds of 2.0m/s and 3.0m/s.

Table 1: Maximum rearfoot angles obtained at each orthotic condition at both velocities (mean (standard deviation)).

Running speed (m/s)	Orthotic Intervention			
	BF	33%	66%	100%
2.0	9.6° (4.4)	9.3° (3.9)	8.8° (4.3)	8.5° (3.8)
3.0	10.6° (4.7)	10.3° (4.4)	9.7° (3.9)	9.2° (4.0)

Table 2: The symbol (*) denotes significance of p<0.05 when comparing the orthotic conditions.

	BF	33%	66%	100%
BF			*	*
33%			*	*
66%	*	*		*
100%	*	*	*	

The preliminary results further suggest that maximum internal transverse tibial rotation was not affected by the orthotic intervention (p=0.19). However, an increase in maximum internal transverse tibial rotation was observed while running at 3.0m/s when compared to 2.0m/s (Table 3).

Table 3: Maximum transverse internal tibial rotation obtained during running trials at both speeds (mean (standard deviation)).

Running Speed	Max. Internal Tibial Rotation
2.0 m/s	9.9° (10.3)
3.0 m/s	10.8° (10.0)

An investigation into the rate at which the foot and the tibia reached their maximum angles was conducted. The preliminary results suggest that the orthotic intervention had no significant effect on the rearfoot (p=0.78) or tibial (p=0.68) rates.

DISCUSSION

Although the results presented in this abstract are preliminary, they suggest that there is a significant difference in maximum rearfoot motion while wearing medial arch supports. More specifically, as the medial height of the orthotic increased a significant decrease in maximum rearfoot motion was observed. Maximum internal transverse tibial rotation was not significantly affected by the orthotic intervention.

SUMMARY

Orthotic intervention significantly reduces rearfoot motion while running at speeds of 2.0m/s and 3.0m/s.

REFERENCES

McClay, I et al. (1998). *Clin Biomch,* 13(3): 195-203.
Perry, SD et al. (1995). *Clin Biomch,* 10(5): 253-257.
Stacoff, A et al. (2000). *Clin Biomch,* 15: 54-64.

ACKNOWLEDGEMENTS

DIFFERENCES BETWEEN JOINT WORK AND MUSCLE FIBER WORK DURING STEADY-STATE WALKING

Kotaro Sasaki[1], Richard R. Neptune[1] and Steven A. Kautz[2]

[1]Department of Mechanical Engineering, University of Texas at Austin, Austin, Texas, USA,
justkoit@mail.utexas.edu
[2]Department of Physical Therapy, University of Florida, Gainesville, Florida, USA

INTRODUCTION

Joint work derived from inverse dynamics techniques has been used to estimate muscle mechanical energy expenditure in various human movement analyses (e.g., Winter, 1983). However, the accuracy of such estimates is not established. Differences between joint work and muscle fiber work can occur due to co-contraction of agonist and antagonist muscles, muscle tendon elastic energy storage and return, and intercompensation of joint power by biarticular muscles. The overall objective of this study was to use a muscle-actuated forward dynamics simulation to assess the difference between estimates of joint and muscle fiber work during walking.

METHODS AND PROCEDURES

A sagittal-plane musculoskeletal model was developed using SIMM (MusculoGraphics, Inc.) and consisted of a trunk, two legs and 25 Hill-type musculotendon actuators per leg. There were 13 degrees-of-freedom in the model including trunk anterior-posterior tilt, trunk horizontal and vertical translation, hip, knee, ankle, mid-foot and toe flexion-extension for both legs. Visco-elastic elements were attached to each foot to model foot-ground contact (Neptune et al., 2000). Passive joint torques representing the forces applied by ligaments, passive tissue and joint structures (Davy and Audu, 1987) were applied at each joint. The equations of motion were generated using SD/FAST (PTC, Needham, MA).

Muscle excitation patterns were fine-tuned using a simulated annealing optimization algorithm such that the simulation emulated group averaged experimental kinematic and ground reaction force data over a complete gait cycle. The experimental data were collected from ten young healthy subjects during walking at 1.6 m/s on a split-belt instrumented treadmill with embedded force plates. Several measures of joint and muscle mechanical work were computed from the simulation data as the time-integral of: 1) net joint power, 2) passive joint power, 3) muscle joint power (i.e., the joint power excluding passive joint power), 4) musculotendon power, 5) muscle fiber power and 6) muscle tendon power. Positive, negative, total and net mechanical work were quantified separately. The contributions of biarticular muscles to joint work were quantified as the difference between the muscle joint work by biarticular muscles and biarticular musculotendon work.

RESULTS

The net joint, musculotendon and muscle fiber work over the gait cycle was positive (Table 1). The majority of the positive net work was offset by the negative work done by the visco-elastic foot contact elements (not shown in Table 1), which yielded a total net work over the gait cycle close to zero. The difference in net work between the joint and muscle fiber work was relatively small (11.0 J), which was primarily due to the net passive joint work. Total joint work did not provide a reasonable estimate of muscle fiber work

(Table 1: Total - Joint: 361.0 J, Muscle fiber: 424.8 J). Further, the total muscle joint work was less than the total musculotendon work by 184.8 J, which represents the influence of co-contraction on the total joint work. Total muscle joint work by biarticular muscles was ~66 J higher than the biarticular musculotendon work, which provided a positive net contribution to the total joint work.

DISCUSSION

The net positive joint work over the gait cycle was consistent with previous inverse dynamics-based analyses (e.g., DeVita et al., 2007). Muscle co-contraction and tendon elastic energy storage and return caused the joint work to underestimate muscle fiber work. In contrast, biarticular muscle contributions to the total joint work caused an overestimation of muscle fiber work, which was consistent with previous studies (e.g., Prilutsky et al., 1996). The magnitude of the over- or underestimation caused by muscle co-contraction, elastic energy storage and return and biarticular muscle work would most likely be different across motor tasks. For example, previous studies have shown that elastic energy storage and return varies across different walking speeds (e.g., Sasaki and Neptune, 2006). If the net passive work done during walking is small, *net* joint work may be used to estimate *net* musculotendon or fiber work since the net elastic energy storage and return over the gait cycle is zero.

SUMMARY

Total joint work over a complete gait cycle does not accurately estimate total muscle fiber work. Co-contraction and tendon elastic energy storage and release cause joint work to underestimate muscle fiber work, while biarticular muscle contributions cause an overestimation of muscle fiber work.

REFERENCES

Davy DT and Audu ML (1987). *J Biomech,* 20: 187-201.
DeVita P et al. (2007). *J Exp Biol,* 210: 3361-73.
Neptune RR et al. (2000). *Comp Methods Biomech Biomed Eng,* 3: 321-34.
Prilutsky BI et al. (1996). *J Biomech,* 29: 405-15.
Sasaki K and Neptune RR (2006). *Gait Posture,* 23: 383-90.
Winter DA (1983). *Clin Orthop Rel Res,* 175: 147-54.

ACKNOWLEDGEMENTS

Table 1. Mechanical work over the full gait cycle

	Positive (J)	Negative (J)	Total (J)	Net (J)
Joint	204.6	-156.4	**361.0**	48.2
Passive joint	59.8	-71.8	**131.6**	-12.0
Muscle joint	163.6	-103.4	**267.0**	60.2
Musculotendon	256.0	-195.8	**451.8**	60.2
Muscle fiber	242.0	-182.8	**424.8**	59.2
Tendon	75.7	-74.7	**150.4**	1.0

A SIMPLE, ANATOMICALLY BASED CORRECTION TO THE CONVENTIONAL ANKLE JOINT CENTER

Dustin A. Bruening [1, 2], Ashlie N. Crewe [3], and Frank L. Buczek [2, 4]

[1] Health, Nutrition, & Exercise Science Department, University of Delaware, Newark DE, USA
[2] Shriners Hospitals for Children, Erie PA, USA, dbruening@gmail.com
[3] Physical Therapy Department, Gannon University, Erie PA, USA
[4] National Institute for Occupational Safety & Health (NIOSH), Morgantown WV, USA

INTRODUCTION

The conventional gait model defines the ankle joint center as the midpoint of the most medial and lateral aspects of the malleoli (Kadaba et al., 1990; Davis et al., 1991), yet *in vivo* studies suggest a more distal location would be more accurate. Lundberg et al. (1989) placed tantalum beads in bones of the foot and shank, and obtained radiographs as sagittal, coronal, and transverse plane rotations occurred about the ankle complex (i.e., the aggregate of joints between the foot and shank). Helical axes for these rotations all passed near a point at the center of the talus, approximated by the midpoint of the tips of the malleoli. In a study of six degree-of-freedom (6DoF) joint powers, Buczek et al. (1994) reported translational joint velocities when the conventional ankle center was used, and hypothesized that these were due to an incorrect center of rotation. When an ankle center consistent with Lundberg et al. (1989) was used, these velocities were nearly eliminated for much of stance phase.

The purpose of this study was to develop and evaluate an anatomically based offset that would move the conventional ankle joint center to a more accurate location, without requiring medical imaging or markers at the tips of the malleoli. We hypothesized that common anthropometric measurements could be used to define the offset, and that its use would reduce calculated joint translations at the ankle complex during gait.

METHODS AND PROCEDURES

Existing coronal plane lower extremity radiographs from 30 pediatric subjects (ages 7-16 yr.) were chosen at random in this Human Subjects Exempt study; patients with pathologies likely to adversely affect normal bony geometry were excluded. Locations for conventional motion capture markers were estimated at the skin surface, and from these, virtual points were derived (Figure 1). A line was drawn between KC and AC, and extended inferiorly to intersect a line drawn between LT and MT. This intersection point did not always fall on the midpoint between LT and MT, but the difference was considered negligible (< 0.5 mm), and the intersection point was considered the true ankle center (AC'). Distance measurements were then made to the nearest half millimeter,

Figure 1. Radiograph. Physical marker locations were estimated at the skin surface, permitting derivation of virtual points at the knee and ankle joint centers.

ME: medial epicondyle
LE: lateral epicondyle
MM: medial malleolus
LM: lateral malleolus
MT: medial malleolus tip
LT: lateral malleolus tip
KC: knee center
AC: ankle center (conv)
AC': ankle center (true)
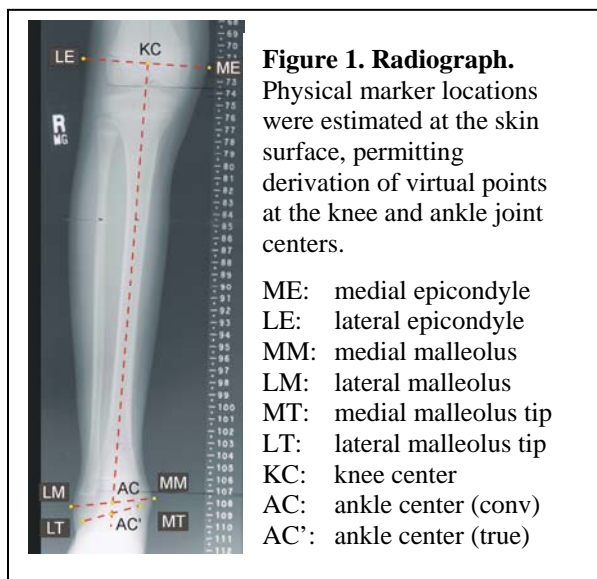
and linear regression analyses were used to relate these to the desired Offset:

KW: distance between ME and LE
AW: distance between MM and LM
SL: distance between KC and AC
Offset: distance between AC and AC'

To evaluate the performance of the regression equation providing the best correlation, a 6DoF foot model (Walker et al., 2008) was applied to gait data from eight normal subjects, using both AC and AC'. Joint translations were calculated in Visual3D (C-Motion, Inc., Rockville MD, USA) and averaged over one gait cycle for each subject. A two-tailed, paired t-test was used to detect differences in joint translations obtained using AC and AC'.

RESULTS

Offsets measured on the 30 radiographs ranged from 6.0 to 13.0 mm (mean 9.7 mm, SD 1.7). Of the three radiographic measurements, SL showed the best bivariate linear correlation with Offset, with a Pearson coefficient, r, of 0.89 (0.76 for KW and 0.71 for AW). The line of best fit passed very close to the origin (y-intercept = 0.2 mm), suggesting that a simple percentage of SL would provide sufficient accuracy:

Offset (predicted) = 0.027 SL

Using this equation, the mean error in predicting Offset for these 30 radiographs was 0.6 mm (6% mean Offset), and the maximum error was 1.7 mm (18% mean Offset). Mean joint translations during a gait cycle obtained using AC' (1.8 mm, SD 0.5) were significantly smaller (p = 0.0001) than those obtained using AC (2.4 mm, SD 0.6). These joint translations were reduced for each of the eight subjects (Figure 2).
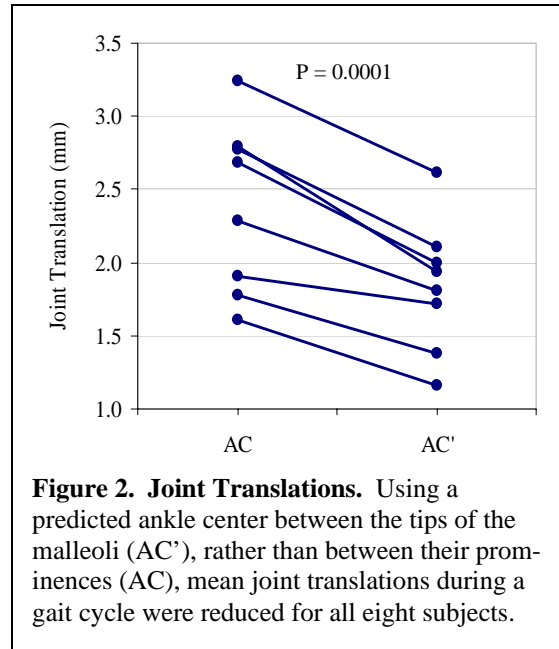
Figure 2. Joint Translations. Using a predicted ankle center between the tips of the malleoli (AC'), rather than between their prominences (AC), mean joint translations during a gait cycle were reduced for all eight subjects.

DISCUSSION

Using measurements easily derived from markers associated with the conventional gait model, we developed a simple correction for AC that results in AC', an ankle joint center consistent with *in vivo* studies free from skin movement artifact. Reductions in joint translations associated with AC' suggest that a greater level of accuracy was achieved for normal gait. Effects on gait kinetics were not studied, but are likely to be small due to the magnitude of the required Offset (< 13 mm).

REFERENCES

Buczek FL et al. (1994). *J Biomechanics*, 27:1447-1457
Davis RB et al. (1991). *Hum Mov Sci*, 10:575-587.
Kadaba MP et al. (1990). *J Orthop Research*, 8:383-392.
Lundberg A et al. (1989). *J Bone Joint Surg Br,* 71:94-9.
Walker M et al. (2008). in: Harris GF (Ed), *Foot and Ankle Motion analysis*, Boca Raton, CRC Press.

QUANTIFICATION USING FLUOROSCOPIC RSA OF SYNDESMOTIC MOTION IN THE INTACT STATE AND FOLLOWING SIMULATION OF HIGH ANKLE SPRAIN

Angela E. Kedgley and Thomas R. Jenkyn

Wolf Orthopaedic Quantitative Imaging Laboratory and Department of Mechanical and Materials Engineering, University of Western Ontario, London, ON, Canada
tjenkyn@eng.uwo.ca

INTRODUCTION

The distal tibiofibular syndesmosis lies between the tibia and fibula at the ankle. Four ligaments maintain the stability of this articulation. Sprains of the syndesmosis are fairly rare, but are frequently misdiagnosed (Lin et al, 2006) with the range of disability and time to recovery being highly variable (Amendola et al, 2006). This may be because these injuries are not being diagnosed correctly and consequently are not receiving optimal treatment. A better understanding of syndesmosis sprain kinematics should assist clinicians in proper differential diagnosis.

Non-invasive *in-vivo* studies are commonly confounded by skin motion artefact (Benoit et al, 2006). In this study, two techniques were utilized to quantify syndesmosis kinematics– optical skin-mounted markers and beaded fluoroscopic radiostereometic analysis (RSA). The aims of this study were 1) to quantify the range of motion present in the syndesmosis and 2) to determine whether skin-mounted markers accurately measure syndesmosis kinematics in intact and injured states.

METHODS AND PROCEDURES

Motion at the syndesmosis was manually simulated in a fresh-frozen cadaveric foot and ankle. Four 0.8mm tantalum beads were implanted into both the tibia and fibula. Two fluoroscopic units (SIREMOBIL Compact-L, Siemens, Malvern, PA) were positioned nearly orthogonally with the specimen in both fields of view. RSA reconstruction of bead locations was performed with custom-coded software (MatLab, MathWorks, Natick, MA). From these, bone-fixed reference frames were created on the tibia and fibula and relative rotations and translations were calculated with an Euler angle analysis.

Auto-reflective markers were affixed to the skin on the medial and lateral malleoli, heel, distal second ray and anterior tibial ridge to approximate the shank and foot portions of the Helen Hayes marker set (Kadaba et al, 1990). Rigid marker triads were affixed to the tools used for manual manipulation of the specimen to capture the applied bone displacements. The markers were tracked optically with a 4-camera motion capture system (Hawk cameras, EvaRT system, Motion Analysis Corp, Santa Rosa, CA).

Passive full-range ankle dorsi- and plantar-flexion and medial-lateral separation of the tibia and fibula via inferiorly applied forces were performed. Motions were first carried out with all ligaments intact, then repeated after complete sectioning of the anterior tibiofibular ligament. The kinematics recorded by the skin-mounted markers were compared to the kinematics obtained from the bone-fixed coordinate systems using RSA.

RESULTS

The kinematics measured with RSA were different from those obtained from optical motion analysis of skin-mounted markers,

particularly the change in distance between the two malleoli during plantar- and dorsi-flexion (Figure 1A). RSA was considered the gold standard with which to compare the skin-mounted marker measurements. During plantar-flexion the tibia and fibula incorrectly appeared to move approximately 1.3mm closer together with the optical system. During dorsi-flexion the tibia and fibula incorrectly appeared to move about 1.3mm further apart with the optical system.

Differences were also noted between the intact and injured states, especially upon the application of the inferiorly-directed forces on the tibia and fibula. Using the RSA measurements, in the intact state these forces had almost no effect on the distance between the malleoli (Figure 1B). However, once the anterior tibiofibular ligament was sectioned, the application of the forces increased the separation of the tibia and fibula.
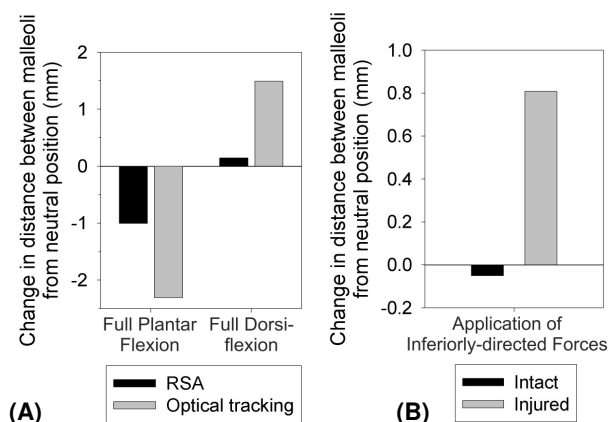
Figure 1. Change in the distance between the medial and lateral malleoli as measured (A) by RSA and by optical surface markers during full plantar flexion and full dorsiflexion and (B) by RSA during medial-lateral separation via inferiorly applied pressure

DISCUSSION

The 'extra' motion observed when using skin-mounted markers and an optical motion capture system during plantar- and dorsi-flexion is most likely the result of skin motion relative to the underlying bone. If this is the case, this artefact in the observed motion would represent an error of similar magnitude to the bone kinematics under investigation. In standard gait analysis the foot and lower leg are treated as rigid bodies that articulate at the ankle joint. This variation in relative optical marker positions would usually be treated as error in the rigid body assumption and corrected by smoothing. Therefore, optical motion analysis with skin-mounted markers is inadequate for quantifying syndesmosis motion *in-vivo*.

The results of this work suggest there is a poor correlation between motion observed by skin markers and the actual kinematics of the underlying bones. They do however suggest that RSA is an appropriate modality for investigating these kinematics, as it is able to accurately track the motions of the bones. Ultimately, the goal is to determine whether distinct modes of syndesmotic injury exist which result in differing abnormal kinematics. The next step is to apply this approach *in-vivo* to more accurately characterize the kinematics of the distal tibiofibular syndesmosis in the normal state and following a high ankle sprain.

REFERENCES

Amendola, A et al. (2006). *Sports Med Arthrosc,* 14:232-236.
Benoit, DL et al. (2006). *Gait Posture,* 24:152-164.
Kadaba, MP et al. (1990). *J Orthop Res,* 8:383–392.
Lin, C-F et al. (2006). *JOSPT,* 36:372-384.
Takao, M et al. (2001). *Arthroscopy,* 17:836-843.
Teramoto, A et al. (2008). *Am J Sports Med,* 36:348-352.

TOTAL KINETIC ENERGY PRODUCTION OF BODY SEGMENTS IS DIFFERENT BETWEEN RACING AND TRAINING PACE IN ELITE OLYMPIC ROWERS.

Daniel J Bechard, MSc[1]; Angela Kedgley, MESc[2]; Volker Nolte, PhD[3]; Thomas Jenkyn, PhD[2,3]

[1]Faculty of Health Sciences, Department of Health and Rehabilitation Science, University of Western Ontario, London, ON, Canada dbechard@uwo.ca
[2] Faculty of Engineering, Department of Mechanical and Materials Engineering, UWO
[3]Faculty of Health Sciences, School of Kinesiology, UWO

INTRODUCTION

The goal of competitive rowing is to cover a set distance as fast as possible (Baudouin and Hawkins, 2004). The role of the coach is to optimize each athlete's technique and physiology through training to maximize their motive force and endurance. Training should therefore replicate the conditions of competition, at least in part, so that each athlete is prepared for the technical and physiological tasks demanded during the race. Different stroke rates are used in training sessions to achieve different goals. The majority of training is performed at 'low' stroke rate (18-22 strokes per minute) to improve endurance and technique. A much smaller portion of training sessions are performed at 'high' stroke rate (32-40 strokes per minute). This stroke rate is analogous to race conditions and is used for race familiarization and evaluation of athletic performance (Harrison et al., 2000).

The purpose of this study was to calculate total kinetic energy (TKE) for each body segment of Olympic rowers during on-water training and to compare TKE, as a proxy for metabolic cost (Turvey et al., 1999), between low and high stroke rates.

METHODS AND PROCEDURES

28 Canadian National Team members who qualified for the 2004 Olympic Games were recruited. A series of 5 sequential strokes (high and low) were recorded via digital camera (Sony DCR-TRV33) from a motorboat traveling parallel at approximately 25m separation. The joint centres and two stationary points on each boat were digitized. Digitization repeatability and error were calculated to be 7.5±1.4mm and 4.2±.7mm respectively. The stroke was normalized to 100%, beginning and ending at the 'catches', with the drive phase occurring first and recovery second. Anthropometric measures were used to calculate linear and angular kinetic energies from which TKE was determined. The ratio between TKE magnitudes at 80% (recovery) and 15% (drive) of the stroke cycle was calculated for each segment of each athlete. High to low stroke rates were then compared.

RESULTS
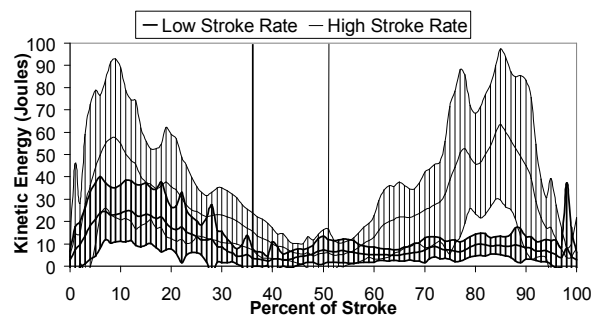
Figure 1. Total kinetic energy (TKE) production: TKE of the entire body (all segments summed) at low stroke rate (thick line) and high stroke rate (thin line) averaged for all athletes throughout one stroke. Also shown for each condition is plus and minus one standard deviation. The horizontal axis is normalized to 100% stroke. The average

drive-recovery transition ('finish' position) is indicated with a vertical line (thick line for low stroke rate and thin line for high rate).
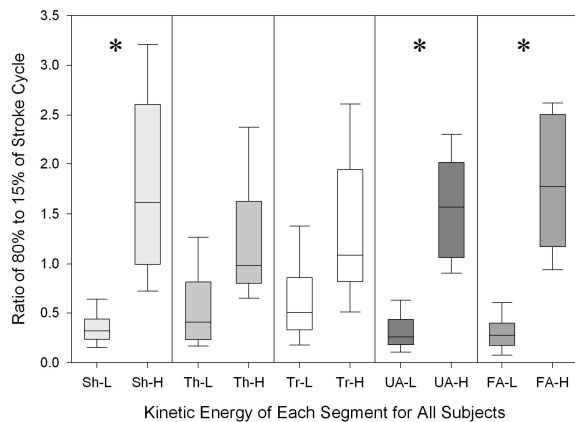
Figure 2. Recovery-to-drive TKE ratios by body segment: Box plots showing the recovery-to-drive TKE ratio (80%-to-15% of stroke) for low (L) and high (H) stroke rates averaged for all athletes comparing each body segment. Segments included are the lower leg (Sh), thigh (Th), trunk (Tr), upper arm (UA) and forearm (FA). Significance at $p<0.05$ is indicated (*).

Variable	Male (N=16)	Female (N=12)
Age (years)	27.8 (3.6)	28.0 (4.1)
Height (m)	190.2 (4.8)	176.3 (4.5)
Mass (kg)	86.5 (9.0)	71.4 (6.8)

Table 1. Athlete demographics: Average age, height and mass with (SD). Number of participants indicated in (N).

DISCUSSION

In all cases examined, the ratio of recovery-to-drive TKE showed that at high rates a quicker recovery phase resulted in an increased ratio relative to the low stroke rate, with the shank, upper arm, and forearm, showing significance ($p<.05$). The same trend is also observed when comparing by sex and boat size with women showing significance ($p<.05$). At high stroke rate the recovery increasingly becomes an energy

costing phase. This is a key result because a vast majority of training time in elite rowing teams is dedicated to low stroke rate training for the purposes of technique and fitness development. This raises the question of whether athletes are training appropriately for race conditions which are performed at high stroke rates. Possible implications of a failure to train for the relatively high values of TKE needed during high rate recovery phase are technical errors that are not likely to occur at low stroke rate training such as "rushing the slide". In this case the recovery phase is uncontrolled and the proper sequencing of body segments is disrupted as the athlete rushes towards the next catch.

SUMMARY

The greatest impact in identifying the increased TKE required for recovery during high stroke rates is to properly train for the accompanying increased metabolic cost. During gait, Usherwood (2005) eludes to the increased cost in achieving higher than natural frequencies in segment rotation. Athletes in race conditions are required to expend an increased amount of energy moving their body forward during the recovery phase at high stroke rates. This contradicts the common belief among many coaches that the recovery is 'passive' and therefore unimportant. This study suggests otherwise. Training for this is essential to athletic success.

REFERENCES

Baudouin, A., and Hawkins, D(2004). *Journal of Biomechanics*, 37: 969 – 976.

Harrison, D et al. (2000). *Level Two Coaching Manual*. Rowing Canada Aviron.

Turvey, M et al. (1999). *Journal of Motor Behavior*, 31, 3: 265.

Usherwood, JR. (2005). *Biology Letters,* 1: 338 – 341.

THE ACUTE EFFECTS OF CHRONIC TREKKING POLE USE
ON STATIC AND DYNAMIC BALANCE

Julianne Abendroth-Smith[1], Victoria Swigart[1], and Michael Bohne[2]
[1]Willamette University, Salem OR, jabendro@willamette.edu
[2]Utah Valley University, Orem UT USA

INTRODUCTION

Hiking is a fast growing recreational activity, but there are inherent risks involved with hiking outdoors. Boulware et al. (2003) determined musculo-skeletal injuries to be the most common type of injury suffered while hiking. A typical way to suffer such an injury would be through a loss of balance. Hence, many hikers have adopted the use of trekking poles due to the unpredictable terrain that is encountered on many trails. Pole use allows for an increase in the base of support, and thus an increase in overall stability (Jacobson, et al., 1997).

The International Mountaineering and Climbing Federation (UIAA) suggests continuous pole use has an adverse effect on acute balance.

> "Continuous use of hiking sticks can decrease the hiker's coordination ability and through this his steadiness, although, in his own mind, he may feel safer. This disadvantage is becoming more and more evident and can lead to certain balancing problems, especially in difficult mountain areas, where stick users cannot use his hiking sticks (i.e. narrow ridges or climbing terrain). In fact, the most common type of hiking accident, the fall by tripping or stumbling, can actually be made a greater risk as a result. For these reasons such accidents occur even during the use of sticks."
> (UIAA, 1994).

In other words, if a person is out on a hike and are using trekking poles, when they come to a situation where they must put the poles away, their balance may be worse than if they had not used poles at all. The purpose of this study was to examine the effects of continuous hiking pole use on acute static and dynamic balance in experienced hikers.

METHODS AND PROCEDURES

Ten active, female participants with experience using trekking poles while hiking were recruited (ages 21-62). Boulware (2004) noted that women backpackers did not experience significantly more musculo-skeletal injuries than men; therefore the use of women only should still allow for generalization. Approval was obtained from the University IRB and participants signed informed consents. An Aeromat foam pad was used for the Balance Error Scoring System (BESS) static balancing task. The 4-camera Falcon Motion Analysis System was used to collect kinematic data during the dynamic balancing task, using a simulated 3.3m log that participants walked across (60 Hz; filtered at 6 Hz). Knee angles of both legs, stride length and time, right and left arm elevation, and medial/lateral and vertical trunk motion were analyzed. EMG was used to record the erector spinae (ES), bicep femoris (BF), vastus lateralis (VL), tibialis anterior (TA), and the gastrocnemius (GA) (Bortec Inc.; 1000 Hz; rectified, and filtered at 4 Hz).

Walkers participated in both the poles and no poles condition. Participants first performed baseline static and dynamic balance tasks. Then each participant walked for 15 minutes with or without trekking poles (counter-balanced) to achieve a steady state pace, hiking both up and down a 20 degree ramp, before repeating the balancing tasks. Immediately before each balancing task, they were required to set down the poles, if in use, and perform the task as

though they had come to a log or narrow ridge on a hike and had to put away the poles to maximize they safety while crossing. Five trials of each balancing task were completed, while continuing to walk with or without poles between each trial. Repeated measures ANOVAs were used to examine statistical sig. (alpha = 0.05).

RESULTS AND DISCUSSION

Results showed fewer errors on average in the pole condition for the static balance task, though not statistically significant (p=0.7). Significantly greater knee flexion was noted in the pole condition (p=0.03) (Figure 1).
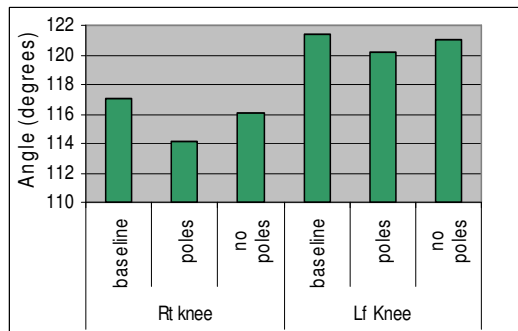
Figure 1. Knee joint flexion angles for the dynamic balance task.

A greater stride length was noted in the pole condition, though not significant (p=0.2). Significantly faster stride times were found in the pole condition compared to the baseline condition (p<.01). No significant differences were seen in arm elevation or trunk sway between pole conditions. The greatest overall muscle activity was elicited in the baseline condition, and the least activity was seen in the pole condition, although no statistically significant differences were noted (p=.4) (Figure 2).

A decrease in stride time and knee flexion angles suggest that the participants had an increased sense of stability because they were more comfortable spending less time in the double support phase of the gait cycle.

The lower amount of muscle activity in the pole condition may also indicate an increased sense of stability after pole use, and less need for the individual to use muscular force and co-contraction in order to maintain stability.
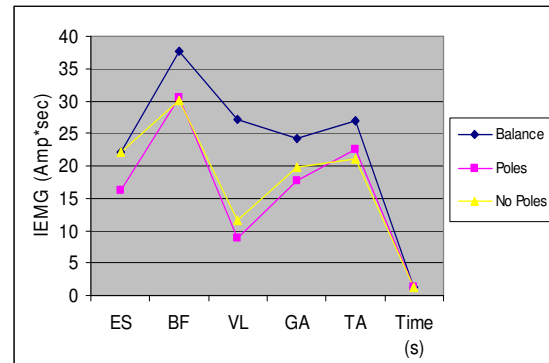
Figure 2. IEMG activity during the dynamic balance task.

SUMMARY

The primary implication of this study was for hiker safety. UIAA suggested that trekking pole use could lead to injury while hiking. The two primary reasons hikers use trekking poles are to increase stability while hiking by increasing their base of support and to lessen the forces placed on the lower extremity joints (Bohne & Abendroth-Smith, 2007). Because no statistical significance was found in this study to show that trekking pole use has a negative effect on subsequent balance tasks, it is suggested that hikers should continue to use trekking poles while hiking to increase stability and lessen the forces placed on the lower extremity.

REFERENCES

Bohne, M. & Abendroth-Smith, J. (2007) *Med Sci Sport & Exer.* **39**(1), 177-183.

Boulware, D.R. (2004). *Wild and Env Med*, 15, 175-180.

Boulware, D., Forgey, W., & Martin, W. (2003) *The Amer J of Medicine.* **114**(4). pp. 288-293.

International Hiking and Mountaineering Federation. (1994). *Official Standards of the UIAA Medical Commission*, (vol. 3).

Jacobson, B.H., Caldwell, B., & Kulling, F.A. (1997). *Perceptual and Motor Skills*, 85, 347- 350.

THE IMPACT OF MEDIAL PLANTAR FLEXOR DYSFUNCTION ON MID FOOT JOINT PRESSURES

Dong-gil Lee[1,2], Robb W. Colbrunn[1], Antonie J. van den Bogert[1,2], Peter R. Cavanagh[1,2] and Brian L. Davis[1,2]

[1]Department of Biomedical Engineering, Cleveland Clinic Foundation, Cleveland, Ohio, USA
[2]Department of Chemical and Biomedical Engineering, Cleveland State University, Cleveland, Ohio, USA

INTRODUCTION

Medial plantar flexors serve as (i) an inverter acting from mid stance phase of gait in order to push-off and (ii) a support of the medial longitudinal arch. Dysfunction of the tibialis posterior is known as a cause of adult flat foot deformity. This can result in altered mechanical stress in foot and ankle joints, potentially leading to arthritis. The purpose of this study is to evaluate joint pressures changes for two groups (normal/diabetic), where medial plantar flexor dysfunction can be introduced during simulated gait with a robotic system.

METHODS AND PROCEDURES

The robotic system consists of 6 a degree-of-freedom robot, 5 tendon actuators, a force plate, and control software (LabVIEW). The force plate was vertically mounted on the robot platform. The tibia was fixed to the robotic system frame and the force plate position and orientation was controlled by the robot. In addition, five muscle forces were generated by tendon actuators (the Triceps Surae, tibialis posterior, tibialis anterior, flexor hallucis longus, and peroneus longus). A subject's normal gait pattern was measured in a gait laboratory to provide kinetic and kinematic data for the robotic simulation. The control software was programmed to generate ground-tibia motions and tendon forces which replicated in vivo gait kinematics and kinetics during stance, after

scaling to ¼ speed and 66.7% body weight was simulated. In order to match desired ground reaction forces and center of pressure from the subject, the robot motion and each tendon force was iteratively adjusted by an optimization process until the collected data was comparable to the target profiles. After collecting baseline data on the fully actuated foot, the robotic system ran combinations of the same optimized gait profiles without medial plantar flexor's tendon actuators to simulate dysfunction of medial plantar flexor. The tibialis posterior and flexor hallucis longus were chosen for medial plantar flexors.
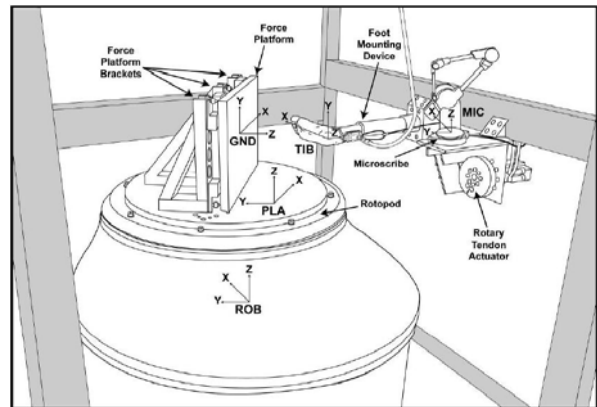
Figure 1. Illustration of the robotic system with mounted cadaver specimen

Three healthy control specimens and four diabetic experimental specimens were used in order to compare joint pressure at 4 mid foot joints (joint between the first metatarsal and first cuneiform, between the first cuneiform and navicular, between the second cuneiform and navicular, and between the first

cuneiform and second cuneiform).
FlexiForce sensors were used to measure joint pressure.

Variables	Control	DM
Average Age (years)	82.33	78.25
Average Body weight (lbs)	143	122.5
Gender	1F/2M	3F/1M

Table 1. Variables in two specimen groups

RESULTS

For each group, joint pressure between the 2nd cuneiform and navicular bone showed the highest value (Figure 2 and 3). This study shows that there is a significant difference in peak mid foot joints pressure during simulated medial plantar flexor dysfunction. In particular, the diabetic group shows a more significant difference at mid foot joints during simulated medial plantar flexor dysfunction and 278% higher mid foot joint pressures than the control group, across all conditions.
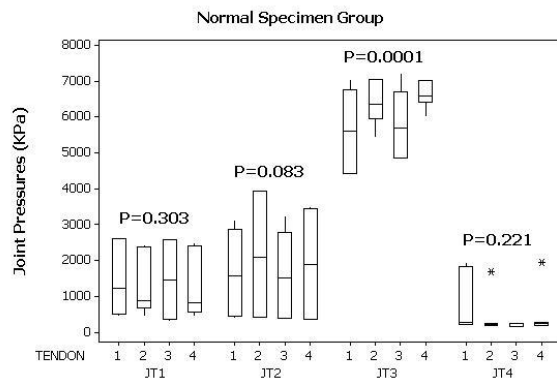
Figure 2. Statistical results for each joint pressure in control group (JT1: 1st Metatarsal & 1st Cuneiform, JT: 1st Cuneiform & Navicular, JT3: 2nd Cuneiform & Navicular, JT4: 1st Cuneiform & 2nd Cuneiform, TENDON 1: all tendons, 2: W/O tibialis posterior, 3:W/O flexor hallucis longus, 4: W/O tibialis posterior & flexor hallucis longus)
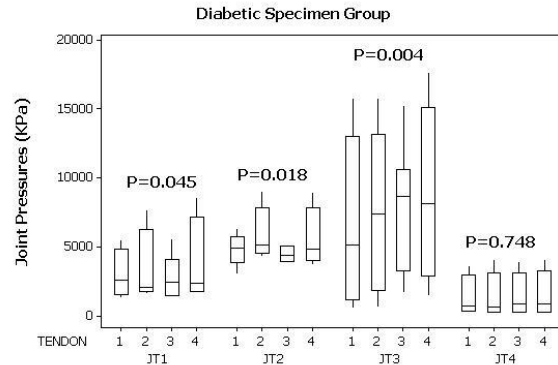
Figure 3. Statistical results for each joint pressure in diabetic group

DISCUSSION

The acquired data show that dysfunction of medial plantar flexors results in an increase in mid foot joint pressures during walking. We consider that abnormal foot function in a diabetic foot could cause this increased joint pressure.

SUMMARY

Four mid foot joint pressures were measured during simulated medial plantar flexor dysfunction. In this preliminary study, we found statistical significance in mid foot joint pressure for the two groups. This result implies that patients with diabetes could have a higher likelihood of developing foot joint problems such as Charcot joint disease.

REFERENCES

Wright V. (1993). Mechanics of human joints. New York. Marcel Dekker, INC. p83-108

ACKNOWLEDGEMENTS

UPPER BODY POSTURE DURING TREE PLANTING WORK

Tegan Upjohn[1] Peter Keir[2] and Genevieve Dumas[3]

[1]School of Kinesiology and Health Studies, Queen's University, Kingston, ON, Canada
5tru@queensu.ca
[2]Department of Kinesiology, McMaster University, Hamilton, ON, Canada
[3]Department of Mechanical and Materials Engineering, Queen's University, Kingston, ON, Canada

INTRODUCTION

Although injury rates in most industrial sectors have decreased in Canada over the past decade, injury rates in the forestry sector have not seen such a favourable decline; total days lost due to injury increased by nearly 40% from 2001 to 2004 (WSIB 2005, OFSWA, 2004). Forty-eight percent of injuries are work-related musculoskeletal disorders, and can be attributed to the repetitive nature of the work (Lyons, 2001). The aim of this study is to define upper body and trunk postures during the tree planting task that contribute to musculoskeletal symptoms among tree planters, and to determine whether posture remains constant throughout the work shift.

METHODS AND PROCEDURES

Fourteen tree planters (8 male, 6 female) from a reforestation camp in Northern Ontario (age 21.83(0.75) yrs, height 1.75(0.09)m, mass 75.7(8.8)kg) volunteered to participate in the study. Workers were filmed with a standard digital video camera for 15 minutes at both the start and the end of the work shift, for three consecutive work days. Trunk flexion and lateral bend were also recorded for 6 of the 14 subjects during a full work shift using a Virtual Corset (MicroStrain, VT, USA) worn at the sternum.

Five events of interest were identified during the tree planting task: 1. shovel at highest vertical position before entry into ground, 2. shovel entry into ground, 3. shovel at furthest horizontal position from the trunk, 4. shovel at closest horizontal position to the trunk, and 5. tree insertion into ground.

Video data were digitized using DartFish video analysis software (ProSuite 4.0, Lausanne, Switzerland). Trunk flexion, shoulder flexion, shoulder abduction and elbow flexion were determined for each of the above events for 10 planting cycles at both the start and end of the work shift.

Virtual Corset data were filtered using a low pass Butterworth filter with a cutoff frequency of 2 Hz. An amplitude probability distribution function (APDF) analysis was performed to determine 10th, 50th and 90th percentiles of trunk flexion during the first 15 minutes of the shift, for 15 minutes 6 hours into the shift (end of shift), and during the entire shift.

A repeated measures ANOVA with 2 factors (day and time) was performed on the video data to determine differences in posture between days, and from start to end of a work shift. T-tests were used to determine postural differences in trunk flexion (Virtual Corset data) from beginning to end of the shift. Statistical significance was set to 0.05.

RESULTS

Upper body postural data are presented in Table 1 for each event in the tree planting

cycle. No significant differences were found from start to end of the work shift (p>0.05).

Table 1. Mean (SD) upper body posture data (combined for start and end of work shift) for events 1-5 in the tree planting cycle. (n = 14)

	Upper Body Angle (degrees)			
	Trunk Flexion	Shoulder Flexion	Shoulder Abduction	Elbow Flexion
1	39.4(11.6)	50.0(24.9)	60.9(10.0)	60.9(16.0)
2	64.6(12.9)	66.7(11.0)	15.3(5.4)	133.3(17.5)
3	84.5(12.0)	96.3(14.3)	17.9(2.3)	147.2(20.0)
4	102.2(10.7)	44.4(13.2)	36.0(10.4)	95.3(20.0)
5	105.3(8.2)	4.8(24.5)	64.7(23.5)	48.9(17.5)

Mean trunk angles for the 10th, 50th and 90th percentiles for the start, end, and full work shift are presented in Figure 1. Trunk angles were not significantly different from start to end of shift. Fifty percent of the work day (4.3 hours) was spent in trunk flexion greater than 45 degrees.
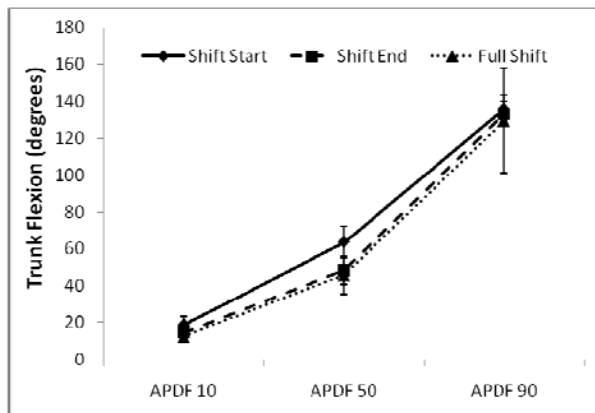
Figure 1. Mean APDF values for trunk flexion for the start of the shift, the end of the work shift, and the full work shift. Error bars are standard error of the mean. (n = 6)

DISCUSSION

The aim of this study was to define upper body and trunk postures during tree planting that contribute to musculoskeletal symptoms, and to determine whether posture remains constant throughout the work shift. Although studies have shown that worker *physiology* changes throughout the work shift (Roberts

2002, Trites et al, 1993), the present study suggests that upper body *posture* does not change. Therefore over the course of the work shift, workers must exert progressively higher physiological effort to maintain the biomechanical motions constrained by the work task itself.

APDF analyses show that workers spend 50% of the work shift at greater than 45 degrees of trunk flexion. Working in such a flexed posture may lead to a decrease in compressive strength of the spine, and may eventually lead to increased risk of disc failure (Gunning et al, 2001).

SUMMARY

Upper body posture in tree-planting does not change from start to end of the work shift. Fifty percent of the work shift is spent working in trunk flexion greater than 45 degrees. Large amounts of time spent in trunk flexion, coupled with the repetitive nature of the task may lead to an increased risk for developing low back disorders.

REFERENCES

Gunning, JL et al. (2001). *Clin Biomech,* 16:471-480.
Lyons, A (2001) *UBC Undergrad Thesis*
OFSWA (2004) Forestry health and safety in 2004 www.ofswa.on.ca
Roberts, D (2002). *J OEM,* 44:559-567.
Trites, DG et al. (1993). *Ergonomics*, 36:935-949.
WSIB (2005) Statistical Supplement to the 2005 annual report. 5-19. www.wsib.on.ca

ACKNOWLEDGEMENTS

AGE-RELATED CHANGES IN THE NEUROMUSCULAR COORDINATION OF HUMAN WALKING

[1]Anne Schmitz, [1]Amy Silder, [1,2]Bryan Heiderscheit, [3]Jane Mahoney and [1,2,4]Darryl Thelen

Departments of [1]Biomedical Engineering, [2]Orthopedics and Rehabilitation, [3]Medicine and [4]Mechanical Engineering, University of Wisconsin-Madison, Madison, WI
Contact: Anne Schmitz ambaus@wisc.edu

INTRODUCTION

Age-related changes in joint kinetics (DeVita and Hortobagyi, 2000) and metabolic energy expenditure (Malatesta et al., 2003) are observed in the gait of healthy older adults. However, the underlying factors that drive these changes are less well understood. In particular, it is unclear whether biomechanical changes in muscle or adaptations in neuromuscular coordination play a more prominent role. For example, it is feasible that neuromuscular coordination patterns are unchanged with age, and that the changes in joint kinetics are simply a result of muscle weakness and/or a loss of flexibility (Kerrigan et al., 1998). Alternatively, the changes in gait mechanics may reflect a diminished ability to sense and actuate movement (Dean et al., 2007). To gain insights in this issue, we measured the modulation of lower extremity electromyography (EMG) signals with walking speed in young and older adults. We hypothesized that older adults would exhibit decreased plantar flexor activity but increased hip extensor activity. We also hypothesized that older adults would exhibit increased co-contraction about the ankle during single support, similar to that seen during challenging postural tasks (Benjuya et al., 2004).

METHODS

Nineteen healthy older (age, 73±5 years) and eighteen healthy young (age, 26±3 years) adults participated in the study. Each subject performed five walking trials at 80 (slow), 100 (preferred), and 120% (fast) of preferred speed.

Surface EMG signals were recorded from the soleus (SOL), gastrocnemius (GAS), biceps femoris (BF), medial hamstrings (MH), tibialis anterior (TA), vastus lateralis (VL), and rectus femoris (RF). Each signal was rectified, low-pass filtered, and then normalized to the mean signal of that muscle over a gait cycle at the subject's preferred speed. Mean activities were then determined over the loading, mid-stance, terminal stance, pre-swing, initial swing and terminal swing phases of gait. A two-way repeated measures analysis of variance was used to assess the effects of age (young, old) and speed (slow, preferred, and fast) on the activities, with a univariate post-hoc test to assess significance ($p < 0.05$) between groups at each speed.

RESULTS

There were no significant differences between the older and young adults with respect to preferred walking speed, cadence, or the percent of the gait cycle spent in swing. However, the older adults exhibited significantly greater TA, SOL and VL activity during mid-stance at all walking speeds (Table 1). In addition, at the fastest speed, older adults exhibited lower SOL activity during terminal stance and pre-swing, and greater MH activity from loading through mid-stance (Figure 1). VL activity in loading was also slightly greater at the fast speed.

DISCUSSION

We observed two fundamental changes in the neuromuscular coordination of walking with age. First, at all speeds, the older adults exhibited greater co-contraction of the uni-articular dorsi- and plantar-flexors during mid-stance. This likely increases ankle stiffness, but could also contribute to the increased metabolic expenditure observed in older adult gait (Malatesta et al., 2003). Secondly at the fast speed, the older adults exhibited less soleus activity during push-off and more hamstring activity through mid-stance. This could represent a compensation for plantar-flexor weakness, whereby hip extensor activity is preferably used to power walking at faster speeds.

In summary, age-related changes in the neuromuscular coordination of walking are clearly present among healthy older adults. The differences observed may represent an increased concern with balance during single support, and a greater reliance on hip power generation at faster walking speeds.

REFERENCES

Benjuya N et al. (2004). *J Gerontol A Biol Sci Med Sci* 59A: 166-171.
Dean JC et al. (2007). *Trans on Biomed Engr* 54: 1919 – 1926.
DeVita P, and Hortobagyi T (2000). *Journal of Applied Physiology,* 88: 1804-1811.
Kerrigan DC et al. (1998). *Arch Phys Med Rehabil* 79: 317-322.
Malatesta D et al. (2003). *J Appl Physiol* 95: 2248-2256.

ACKNOWLEDGEMENTS

Table 1. Significance of age on mean EMG activities during phases of the gait cycle at slow, preferred and fast walking speeds.

Phase	Muscle	Walking Speed		
		Slow	Pref	Fast
Loading Response (0-10% of the gait cycle)	TA			
	BF			
	VL			p<0.05+
	MH			P<0.05*
Mid-stance (10-30%)	TA	p<0.05*	p<0.05*	p<0.05*
	SOL	p<0.05*	p<0.05*	p<0.05*
	GAS			
	BF			
	VL	p<0.05*	p<0.05*	p<0.05*
	MH			p<0.05*
Terminal stance and pre-swing (30 – 60%)	SOL			p<0.05+
	GAS			
Pre and Initial Swing (50 – 73%)	RF			
Terminal Swing (87 – 100%)	BF			
	MH			

* older adults show greater activity
+ younger adults show greater activity
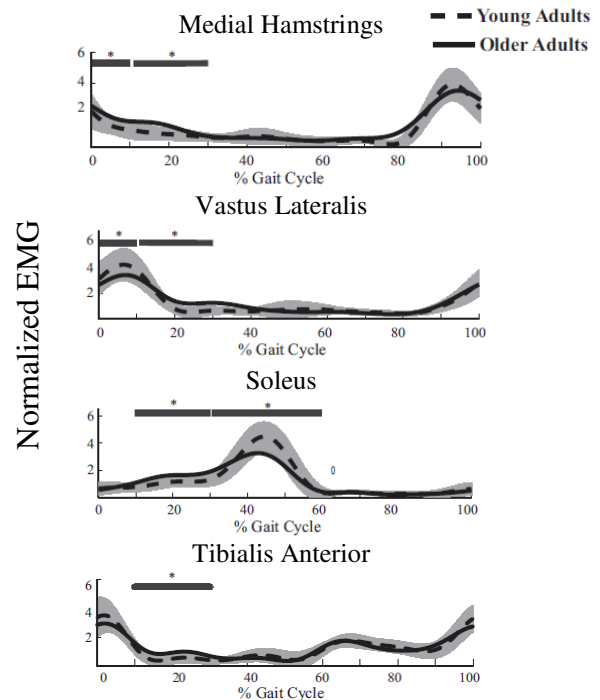
Figure 1. Ensemble EMG over a gait cycle for the young and older adults at fast walking speed. Shaded curves represent ±1 sd of the young adult data. The horizontal bars represent where age is significant.

A TECHNIQUE FOR OPTIMIZING THE CENTER OF PRESSURE AND KINETIC DATA OBTAINED FROM A SPLIT-BELT INSTRUMENTED TREADMILL

Saryn R. Goldberg[1], Thomas M. Kepple[2], and Steven J. Stanhope[2, 3]

[1] Department of Engineering, Hofstra University, Hempstead, NY, USA, eggszg@hofstra.edu
[2] Department of Health, Nutrition, and Exercise Sciences, University of Delaware, Newark, DE
[3] Department of Mechanical Engineering, University of Delaware, Newark, DE, USA

INTRODUCTION

As split-belt instrumented treadmills become more common in biomechanical research (Lee and Hidler, 2007; Riley et al., 2007), it is important to assess the accuracy of these measurement tools and determine how to optimally integrate them with motion capture technology. We have developed a technique for optimizing the center of pressure (COP) data and subsequent calculation of kinetic data obtained from a split-belt instrumented treadmill by correcting for crosstalk between the treadmill's output channels, as well as minimizing error associated with calculating the transformation between the motion capture (MC) and treadmill force plate (TFP) coordinate systems.

METHODS

We worked with a split-belt instrumented treadmill that output 6 channels of digital data, consisting of 3-dimensional forces and moments (Bertec Corp., Columbus, OH). Our calibration techniques were based on the Caltester tool (C-Motion Inc., Germantown, MD) assessment of COP measurement error. Caltester is a pointed rod fitted with tracking targets that is used to measure the error between the rod tip location and orientation as determined via the MC system and the TFP (Holden et al., 2002). Assuming the MC data is accurate, error is attributed to the TFP.

Our calibration approach addresses two possible sources of error in determining the COP. The first is our ability to accurately determine the transformation between the MC and TFP coordinate systems. The second is crosstalk between the channels of data measured by the treadmill which would affect the COP calculation.

The transformation between the MC and TFP coordinate systems is traditionally determined using a technique that employs a jig fitted with targets that are at "known" locations relative to the TFP corners. Small errors in these known locations can lead to error in the subsequent COP calculation. To compensate for this, a correction technique was used, in which three trials of Caltester data were collected in each of the four corners of the TFP. An optimization scheme was then used to find the set of translations and rotations between the MC and TFP coordinate systems that would minimize the error in the COP from these Caltester trials.

To minimize error due to crosstalk, known vertical and shear loads were applied at known locations, as determined by a digitizing arm (FARO Technologies Inc., Lake Mary, FL), across the surface of the treadmill. A 6x6 correction matrix was calculated which, when applied to the output data, minimized the error between the applied and measured forces and moments. A 3x3 correction matrix, which only included F_z, M_x, and M_y, was also calculated to determine whether it was necessary to correct for crosstalk between the F_x, F_y, and M_z channels, since known shear loads are difficult to apply.

To evaluate our techniques, we collected trials of Caltester data across the surface of the stationary treadmill and collected gait data from a normal subject walking on the treadmill at 1.3 m/s. We compared the data processed with the traditional and corrected transformation techniques and corrected with the 3x3 and 6x6 calibration matrices.

RESULTS AND DISCUSSION

We measured a significant 10 mm error in the traditionally transformed, uncorrected COP data. Using the corrected transformation technique resulted in a substantial decrease in this error (Table 1). Applying the 3x3 and 6x6 correction matrices to the corrected transformation data resulted in further improvement in the COP measurement.

(mm)	Traditional Transform	Corrected Transform	3x3 Matrix & Corrected Transform	6x6 Matrix & Corrected Transform
Front	**10.9** (0.7)	**5.7** (1.2)	**2.6** (0.8)	**2.0** (0.3)
Middle	**9.9** (0.3)	**3.5** (0.8)	**3.0** (0.7)	**2.4** (0.2)
Rear	**10.9** (0.2)	**3.5** (0.3)	**3.6** (0.6)	**3.0** (0.4)

Table 1. Average error (SD) in measured position of COP from Caltester (in mm) after successive correction steps at 3 positions along the length of the treadmill.

More meaningfully, there was a significant change in the calculation of the sagittal hip joint moment when a 3x3 versus a 6x6 correction matrix was applied to the treadmill gait data (Figure 1). With the 3x3 correction, there is a significant difference between right and left hip moments for a subject who walked symmetrically overground. After the 6x6 correction was applied, data from both the right and left treadmills shifted to be more bilaterally symmetrical.

The 6x6 correction matrix minimized crosstalk between the F_y and F_z data channels which, upon inspection of the data, affected the calculation of the anterior GRF. Applying just the 3x3 matrix resulted in errors large enough to result in data misinterpretation, suggesting that it is necessary to correct for crosstalk across all 6 data channels.

a)

b)
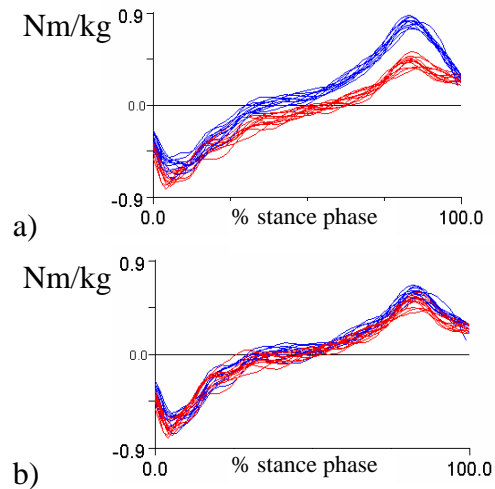
Figure 1. Stance phase sagittal hip moments for right (red) and left (blue) legs calculated using corrected transformation technique and a (a) 3x3 or (b) 6x6 correction matrix.

Using the corrected transformation technique and correcting for crosstalk between all 6 data channels reduced errors in the COP measurement to levels close to those measured for fixed force plates (Holden et al., 2002). Thus, Caltester offers a valuable means for measuring and, in conjunction with optimization algorithms, correcting error in treadmill COP measurements. These correction concepts should be applicable to other treadmill models.

REFERENCES

Holden JP et al. (2002). *Gait Posture,* 11: 131-139.
Lee SJ and Hidler J (2007). *J Appl Physiol,* in press.
Riley PO et al. (2007). *Gait Posture,* 26: 17-24.

ACKNOWLEDGEMENTS

GENDER DIFFERENCES DURING A RUN TO CUT TASK ON SURFACES WITH DIFFERENT FRICTION INTERACTIONS: IMPLICATIONS FOR ACL INJURY RISK

Ariel Dowling[1], Stefano Corazza[1], Todd Alamin[1], Ajit Chaudhari[3], Thomas Andriacchi[1,2]

[1] Stanford University, Stanford, CA, USA
[2] Veteran's Administration Palo Alto Health Care System, Palo Alto, CA, USA
[3] The Ohio State University Medical Center, Columbus, OH, USA
E-mail: adowling@stanford.edu   Web: biomotion.stanford.edu

INTRODUCTION

Anterior cruciate ligament (ACL) injury occurs at a 4 to 6 times greater rate in female athletes compared with male athletes (Arendt, 1995). Most ACL injuries occur during landing or deceleration before a change in direction (Olsen, 2004), suggesting the importance of the alignment of the support limb for stability. In addition, a decreased knee flexion angle, specifically at foot contact, has been suggested as an ACL injury risk factor (Hewett, 2006; McLean, 2005). Changing the coefficient of friction of the shoe-surface interface can influence the body posture of the subject (Heiden, 2006). Additionally, increasing the coefficient of friction of the surface leads to increased incidence of ACL injury during sporting events involving run to cut maneuvers (Steffen, 2007; Orchard, 1999).

This study examined the hypotheses that the alignment of the center of mass relative to the support limb and kinematic (knee flexion angle) risk factors for ACL injury in sideways cutting are altered more in female athletes than male athletes by the changing the coefficient of friction of the surface.

METHODS

Twelve healthy subjects (5 male and 7 female, age 22.2 yrs ± 2.4 yrs, BMI 22.8 ± 1.8) with no prior knee, hip, or ankle injuries were evaluated. Subjects performed a 60° cut on two different surfaces in random order at a constant speed: a rubber pad (high friction = 0.99), and surgical booties placed over the subject's shoes (low friction = 0.38). The speed was self-selected for safety in the reduced-friction condition. The subjects were allowed to train on the surfaces before their trials were recorded, so this was an anticipated cut.

An innovative MMC system (Corazza, 2006; Mündermann, 2006) was used to measure full-body kinematics from video captured from 8 VGA cameras. The center of the subject's volume was measured and the center of mass (COM) approximated assuming homogeneous density of the body. A full body laserscan was used to create a subject-specific model for tracking the video data. The alignment of the COM relative to the ankle of the support limb and the knee flexion angle were examined during landing. Data was analyzed using two-tailed paired t tests ($\alpha = 0.05$) to determine if the variables of interest were significantly different between the low friction and high friction trials for the male and female subjects.

RESULTS AND DISCUSSION

The trials performed on the higher coefficient of friction surface had a lower ($p < 0.001$) knee flexion angle and more medial alignment of the COM (relative to the support limb ankle) at landing compared to the low friction trials (Table 1).

Variable	Low Friction	High Friction
Knee Flexion Angle: degrees	24.51 (6.83)	20.93 (5.84)
Ankle COM Medial: cm	18.1 (3.7)	22.4 (4.3)

Table 1. Statistically significant (p < 0.001) differences between low and high friction surfaces for all subjects

When the results were split by gender, at foot contact females had statistically significant decreased knee flexion angle and a smaller shift of the COM in the medial direction when compared to males on both surfaces (Figure 1).
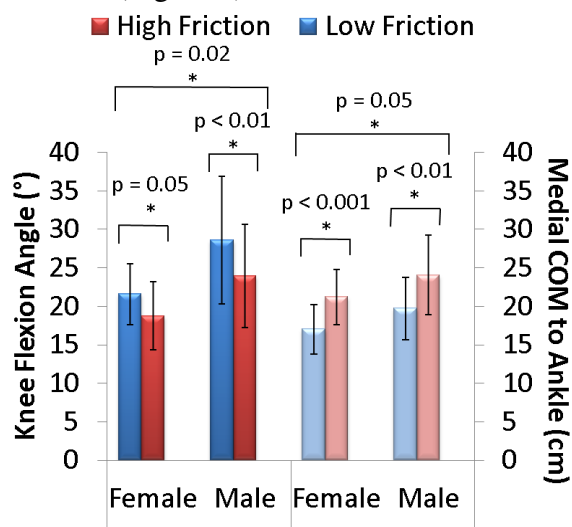
Figure 1. Differences between males and females for both surfaces at foot contact

These results suggest that the greater incidence of ACL injury observed on high friction surfaces may be caused by a decrease in knee flexion angle and a COM further in the medial direction (compared to the ankle position). The subjects anticipated the surface friction and modified their movements based on perceived stability, altering their risk for an ACL injury.

Additionally, at foot contact females on the low friction surface do not have as much knee flexion as males on the high friction surface, and the alignment of the COM relative to the support limb has a smaller medial offset. This smaller medial offset for females could be related to changes in the position of the upper body. These results suggest that females do not alter their movements enough to compensate for each surface condition, and that the combination of gender and high friction further increases the risk for ACL injury.

SUMMARY/CONCLUSIONS

The results suggest that surfaces with high COF influence patterns of movement in a manner that can increase risk of ACL injury. In addition, female subjects are likely more at risk for ACL injury on high COF surfaces than male subjects.

REFERENCES

Arendt E, Dick R (1995). *Am J Sports Med*, 23(6): 694-701.
Corazza S et al. (2006). *Annals Biomech Eng,* 34(6), 1019-1029.
Heiden TL et al. (2006) *Gait Pos*, 24(2): 237-46.
Hewett TE et al. (2006). *Am J Sports Med*, 34: 229-311.
McLean SG et al. (2005). *J Sci Med Sport*, 8(4): 411-22.
Mündermann L et al. (2006). *J Neuroeng Rehab*, 3(6).
Olsen OE et al. (2004). *Scand. J. Med. Sci. Sports.* 13(5), 299-304.
Orchard J et al. (1999). *Med. J. Aust.* 170(7), 304-6.
Steffen K et al. (2007). *Br. J. Sports Med.* Epub Jun 5, 33-7.

ACKNOWLEDGEMENTS

The Relationship between Hip and Knee Kinematics to the Knee Adduction Moment in Asymptomatic Individuals with Genu Varum

Joaquin A. Barrios[1] and Irene S. Davis[1,2]

[1] University of Delaware, Newark, DE, USA
[2] Drayer Physical Therapy Institute, Hummelstown, PA, USA
E-mail: joaquin@udel.edu

INTRODUCTION

Medial knee osteoarthritis (OA) is a common and disabling condition, affecting millions of Americans. It has been shown to be associated with genu varus (GV) alignment, as well as an increased knee adduction and a high knee adduction moment (KEAM) during gait (Sharma et al, 2001; Baliunas et al, 2002). It was recently reported that adults with genu varus (GV), but with otherwise healthy knees, are at a two-fold increased risk for later developing medial knee OA (Brouwer et al., 2007). It is possible that these individuals, like those with medial knee OA, also exhibit mechanics associated with a high KEAM. GV alignment is likely to be associated with hip abduction (or reduced hip ADD) and external rotation (ER) and knee adduction (ADD) and ER. These motions, in turn, may be associated with the KEAM. Understanding these mechanics may lend insight into the increased risk of developing knee OA. However, the gait mechanics of these individuals have not been studied.

Therefore, the purpose of this study was to assess the relationship between the frontal and transverse plane motions of the hip and knee with KEAM. The focus of this study is on individuals with GV, but no evidence of knee OA. We hypothesized that since the KEAM is a frontal plane moment, frontal plane kinematics would be more closely related to it than the transverse plane kinematics.

METHODS

To ensure that the individuals with GV were asymptomatic, they completed the Sports and Recreational Activities subscale of the Knee Injury and Osteoarthritis Outcome Score Knee Survey (KOOS) (Roos et al., 1998). A score of $\leq 2/20$, where 0/20 means no symptoms and 20/20 means extreme symptoms, was needed to qualify for the study. To be classified with GV, the frontal plane mechanical axis of the tibia was measured using a caliper-inclinometer device (Hinman et al., 2006). A value of $\geq 11°$ from vertical was needed to qualify for the study.

To assess gait mechanics, retro-reflective markers were placed on the lower extremity with greater GV. Three-dimensional motion analysis was performed as the subject walked at a controlled speed at 1.46 m/s ($\pm 5\%$) along a 25 m walkway. Kinematic data were captured using an 8-camera VICON motion analysis system (120 Hz). Kinetic data were captured using a Bertec force platform (1080 Hz). Five usable trials were collected for each subject. Data was processed and analyzed using Visual 3D and custom Labview software. The frontal and transverse plane hip and knee kinematics at the time of the first peak of the KEAM (Figure 1) were extracted for each trial, and then averaged for each subject. These four variables were then correlated to the KEAM.
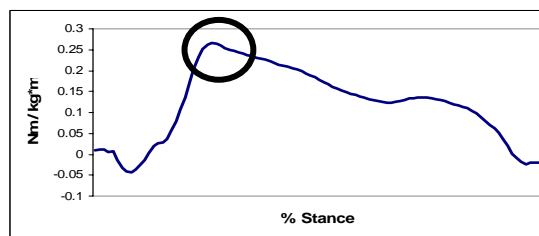
Figure 1 The KEAM peak during the 1st half of stance

RESULTS

This is an ongoing study, of which seven (two female, 5 male) asymptomatic subjects have been recruited, to date (Table 1).

Table 1 Demographic data for seven subjects

Variable	Mean (SD)
Age (years)	23.9 (3.7)
Height (m)	1.73 (0.1)
Mass (kg)	70.2 (10.3)
KOOS-S (0-20)	0.4 (0.8)
Tibial Mech. Axis (°)	101.4 (0.5)

The mean peak KEAM value for the group was 0.363 (0.06) Nm/ht*wt. Knee ADD was most strongly correlated with peak KEAM (Figure 2). A moderately strong correlation was seen for hip IR, and a moderate correlation for knee ER. A poor relationship was seen for hip ADD angle.
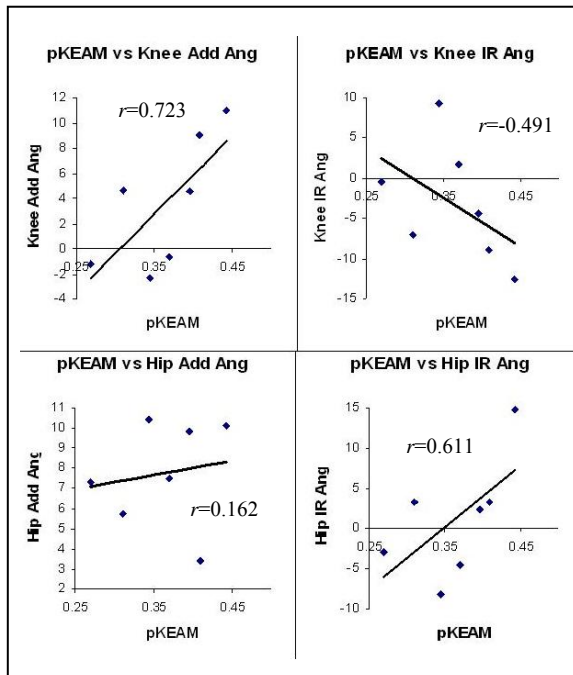
Figure 2 Scatterplots depicting the relationships between the kinematic variables (in degrees) and peak KEAM (in Nm/ht*wt).

DISCUSSION

Young, asymptomatic individuals with GV appear to ambulate with elevated KEAM values (0.363 Nm/ht*wt) that are similar to those with medial knee OA (0.379 Nm/ht*wt) (Butler et al., 2007). This may explain their increased risk of later development of medial knee OA. Understanding the kinematic patterns that produce this high KEAM may be particularly valuable to researchers and clinicians aiming to reduce medial joint loading in this population. These preliminary data suggest that the knee ADD angle was most closely related to the peak KEAM. This is not surprising as they are both frontal plane knee mechanics. In addition, as expected, knee ER was moderately correlated with the KEAM. Surprisingly, hip IR, and not ER, was correlated with the KEAM.

These findings, if supported at the conclusion of this study may indicate that altering the knee adduction angle may be helpful in reducing medial compartment loading. This may help to delay or prevent the onset of medial knee OA in these individuals with GV.

SUMMARY

The frontal plane knee angle at the time of peak KEAM is strongly related to the magnitude of the peak KEAM during the first half of stance in asymptomatic individuals with GV.

REFERENCES

Sharma et al. (2001). *JAMA,* 286:188-195.
Baliunas et al. (2002). *Osteoarth Cart,* 10:573-579.
Brouwer et al. (2007). *Arth & Rheum,* 56:1204-1211.
Zhao et al. (2007). *J Orthop Res* 25:789-97.
Roos et al. (1998). *JOSPT* 78(2): 88-96.
Hinman et al. (2006). *Arthr & Rheum,* 55:306-313.
Butler et al (2007). *J Orthop Res* 25:1121-1127.

ACKNOWLEDGEMENTS

THE EFFECT OF STRIDE-LENGTH CHANGES ON TRICEPS SUREA EXCITATION DURING WALKING

David J. Sanderson, Ryan Cawsey, Scott Apperley, Julia Wilkes

School of Human Kinetics, University of British Columbia, Vancouver B.C. Canada
david.sanderson@ubc.ca

INTRODUCTION

Sanderson et al (2006) examined the effect of cadence and power output manipulation on the operating length, velocity of shortening, and triceps surae excitation during cycling. They showed that there was a cadence-sensitivity in gastrocnemius but not soleus, the soleus and gastrocnemius muscles were at times acting in opposite direction, and that there was evidence of the stretch-shorten cycle. This study was designed to investigate whether these observations were similar in a weight-bearing activity, walking. Our hypothesis was that with increased cadence, there would be an increase in both lateral and medial gastrocnemius activity while soleus will be insensitive to cadence changes.

METHODS AND PROCEDURES

After determining the preferred walking speed and stride length, subjects walked for 2 mins at 8 randomly presented cadences (85, 90, 95, 100, 105, 110, 115, 120% of preferred cadence) on a treadmill. Lower-limb sagittal plane 2D kinematics collected were determined from video recordings of reflective markers placed over the greater trochanter, lateral midline of the knee, lateral malleolus, the posterior aspect of the calcaneous, and the head of the 5th metatarsal. EMG was recorded from the lateral gastrocnemius, medial gastrocnemius, and soleus muscles, amplified at the electrodes (gain = 35) before being sampled at 1200Hz. Muscle lengths were calculated from marker kinematics using equations developed from

Hawkins and Hull (1990). These data were differentiated using the central differences method to generate muscle velocities. The first ten strides were selected for data analysis. EMG data were demeaned, rectified, and filtered using a 4th order dual-pass Butterworth filter at 6Hz. EMG was normalized to the highest 100ms window of the linear envelope of the EMG data at the preferred cadence. Both EMG and kinematic data were separated into strides and interpolated to the number of points of the shortest stride within each condition. For each condition, the ten strides were averaged to create one representative data set per subject.

RESULTS

Figure 1. Mean iEMG for each muscle
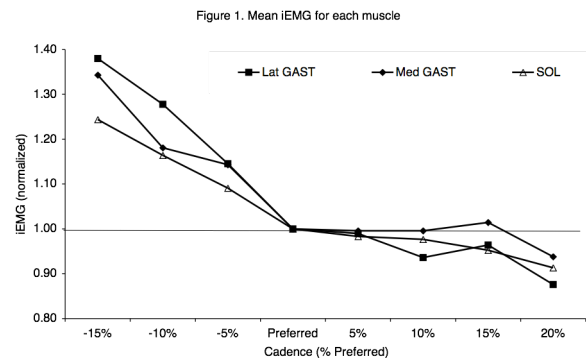
Figure 1, above, presents the mean integrated EMG for the medial and lateral gastrocnemius and soleus muscles collapsed across subjects for each cadence condition.

Figure 2: Medial and Lateral Gastroc Length Min, Max and Range
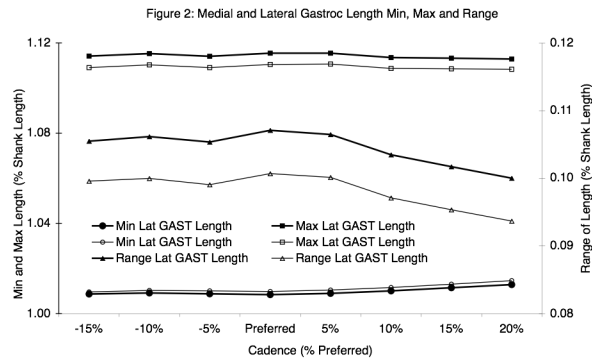
Figure 2, above, presents the length changes for the medial and lateral components of gastrocnemius collapsed across subjects for each cadence condition.

Figure 3: Soleus Length Min, Max and Range
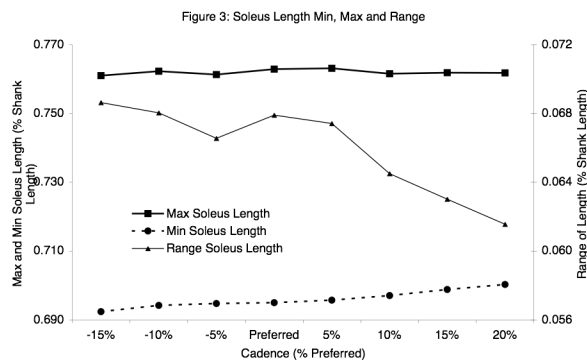
Figure 3, above, presents the length change data for the soleus muscle collapsed across subjects for each cadence condition.

DISCUSSION

Both walking and cycling require rhythmical leg movements with periods of loading and unloading, sequences of muscle contraction, during periods of lengthening and shortening. A major difference however is that walking is a weight-bearing task whereas cycling is not. Data presented here suggest major differences in muscle recruitment and the mechanical response of muscles in walking compared to cycling. Unlike during cycling, there was cadence sensitivity for both parts of gastrocnemius and for soleus. There was a significant decrease in the IEMG for medial

gastrocnemius ($F_{7,56}$=13.6, p<0.0001), lateral gastrocnemius ($F_{7,56}$=21.8, p<0.0001), and soleus ($F_{7,56}$=25.9, p<0.0001). Post-hoc Scheffé revealed the primary contributor to the significant difference for each of the muscles was due to the large increase in excitation at the very short cadence. There were only minor effects of cadence on the lengths of these muscles. There was a small but non-significant increase in the minimum length of both groups of muscles, which resulted in a similar non-significant decrease in the range of length change. Similarly, shorten/lengthening velocity of these two muscles was essentially unaffected by the changes in cadence. During cycling there was a consistent effect of cadence manipulation on triceps surea excitation and muscle kinematics.The data presented here for walking show that in spite of the 35% change in the stride length (from -15% to +20%) the triceps surea kinematic features remain unaffected. Both soleus and gastrocnemius showed similar sensitivity to cadence manipulation. One of the explanations could lie in the fact that the foot remained on the floor during walking whereas during cycling the pedal is free to rotate. As Sanderson et al (2006) suggested part of the ankle muscle activity could be focussed on maintaining a level pedal whereas during walking Winter (19xx) argued that the ankle musculature provide 80% of the mechanical power during propulsion. These results suggest that during walking the triceps surae acts with a common purpose not seen in the cycling activity.

REFERENCES

Sanderson, DJ et al. (2006). EMG Kines, 16:642-649.
Hawkins, D and Hull, M. (1990). JOB 23: 487-494.
Sale, D. et al. (1982). *J Appl Physiol* 52, 1636-1642.

STABILITY MARGIN DURING GAIT:
IDENTIFYING BALANCE IMPAIRMENT IN THE ELDERLY

Vipul Lugade, Sue Ewers, Chu Jui Chen,
Sujitra Boonyong, Patima Silsupadol and Li-Shan Chou

Motion Analysis Laboratory, Department of Human Physiology, University of Oregon, Eugene, Oregon, USA, chou@uoregon.edu
URL: http://biomechanics.uoregon.edu/MAL/

INTRODUCTION

The purpose of this study was to present a dynamic description of a person's balance control during gait. Balance has been defined as maintenance of the center of mass within the base of support; however a clear definition of the base of support during the entire gait cycle has not been defined. Therefore, a proposal for quantifying the dynamic base of support during gait is presented here, with the stability margin calculated for healthy adults and elderly fallers. We hypothesized that elderly fallers would show a deficit to maintain their extrapolated center of mass within the base of support during gait, and would maintain a smaller, more conservative stability margin when compared to healthy young and older adults.

METHODS AND PROCEDURES

This study included 10 healthy young adults (HY) (21.6 ± 2.2 years; 1.7 ± 0.1 m; 70.6 ± 15.2 kg), 10 healthy elderly adults (HE) (74.7 ± 6.3 years; 1.7 ± 0.1 m; 66.9 ± 10.2 kg), and 10 elderly fallers (EF) (80.3 ± 4.3 years; 1.7 ± 0.1 m; 67.0 ± 10.2 kg). Subjects recruited from the community were asked to walk at a self-selected pace along a 10-meter walkway.

Three dimensional marker trajectories were collected at 60Hz with an eight-camera motion tracking system (Motion Analysis, Santa Rosa, CA). Twenty-nine reflective markers were placed on bony landmarks of the body (Hahn & Chou, 2004). Markers and estimated joint centers were used to calculate the three-dimensional locations of segmental center of mass (CoM). Whole body CoM position data was calculated as the weighted sum of 13 body segments. The extrapolated center of mass (XcoM) was calculated using a combination of the CoM postion and CoM velocity: $XcoM = \sqrt{p + v/\omega_o}$, where $\omega_o = \sqrt{gravity/vertical\ CoM\ position}$, $v =$ CoM velocity and $p =$ CoM position (Hof et al. 2005).

The base of support (BoS) was defined under two conditions, single limb support and double limb support as shown in Figure 1A and B, respectively. The shortest distance from the CoM or XcoM to the BoS was calculated for each time frame, with the maximum distance outside the base of support throughout the gait cycle defined as the stability margin. When the CoM and XcoM were within the base of support, the person was in a stable configuration, and such results were indicated as a negative stability margin in our analysis.

A custom program was written in MATLAB (Mathworks, Lowell, MA) to calculate the BoS and stability margin. All statistical analyses were performed with SPSS 14.0 using a one way ANOVA to determine group differences between HY, HE and EF, with significance level set at 0.05.
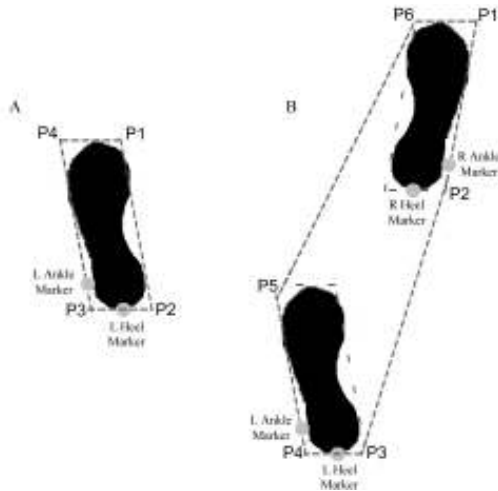
Figure 1: Dashed lines indicate the boundary of support for gait during single limb support (A) and double limb support (B).
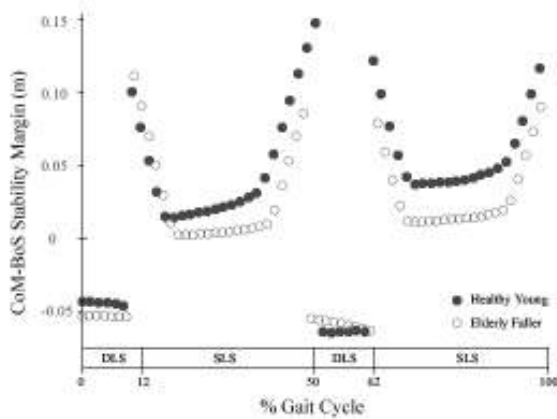
Figure 2: The CoM stability margin for healthy young and elderly fallers.

RESULTS

During single limb support, all subjects maintained the CoM and XcoM on the medial side of the support foot. Both the CoM and XcoM remain within the base of support for the EF during double limb support, while the XcoM did travel outside the BoS for healthy individuals. The CoM stability margin for HY and EF is shown in Figure 2 during one complete gait cycle. The stability margin showed that HY and HE were able to extend their CoM and XcoM a significantly further distance away from the base of support than EF (Table 1; p < .001).

DISCUSSION

Elderly fallers had a significantly smaller stability margin than both healthy groups indicating a conservative strategy during gait. It has been shown in that past that older adults at risk for falling adopt a compensatory gait pattern due to their reduced physical capabilities, and such a pattern was seen among our elderly fallers (Woolacott and Tang 1997).

By characterizing the base of support and stability margin throughout the gait cycle, it might be possible to understand and improve an elderly fallers walking pattern to reduce the risk of falling.

REFERENCES

Hof A.L., et al. (2005). *J. Biomech,* **38**, 1-8.
Hahn M.E., Chou L-S. (2004). *J. Biomech,* **37**, 837-844.
Woollacott M.H., Tang P.F. (1997). *Phys Therapy,* **77**, 646-660.

Table 1: Margin of stability for CoM and XcoM when compared to the BoS (mean ± SD).

	Healthy young	Healthy elderly	Elderly fallers	*p*-values
CoM – BoS Stability Margin (cm)	15.1 ± 3.6 [a]	14.6 ± 6.5 [a]	10.9 ± 3.0 [b]	*p* < .001
XcoM – BoS Stability Margin (cm)	57.9 ± 8.1 [a]	55.2 ± 9.2 [a]	42.6 ± 6.4 [b]	*p* < .001

Note: Differing superscripts (a, b) refer to groups with significant differences ($p < 0.01$).

COMPARISON OF VARIABILITY BETWEEN OVERGROUND AND TREADMILL RUNNING

Rebecca E Fellin [1] and Irene S Davis [1,2]

[1] University of Delaware, Newark, DE, USA
[2] Drayer Physical Therapy Institute, Hummelstown, PA, USA
Email: fellin@udel.edu

INTRODUCTION

Treadmill analyses have multiple advantages to overground analyses including ease of collecting multiple sequential footfalls and less required space. During overground running, individuals are free to vary their speed from stride to stride. But, with treadmill running, the runner is constrained to the same speed during each stride.

Because speed is constant with treadmill running, it is possible there is less variation between strides. In a study comparing overground and treadmill running, Wank and colleagues (1998) found less variation during treadmill running than overground running. Specifically, they found lower standard deviations in knee and ankle joint angles. However, they did not report standard deviations at the hip, and their analyses were limited to the sagittal plane.

Therefore, the purpose of this study was to compare the variability of treadmill and overground running through a 3D lower limb kinematic analysis. We hypothesized that lower limb hip, knee and rearfoot angles would exhibit decreased variability during treadmill running compared to overground running.

METHODS

This study included 20 male and female individuals (25.2 ± 6.2 yrs), who run at least 10 mpw. All subjects were rearfoot strikers and comfortable with treadmill running. Retroreflective markers were applied to the right lower extremity of each subject. Subjects then completed both the overground (OG) and treadmill (TM) running in the same laboratory, within the same calibrated volume. The order of OG and TM running was counterbalanced. For the OG trials, subjects ran along a 25m runway. Speed was monitored via photocells, and trials within 3.35 m/s $\pm5\%$ were accepted. A VICON (Oxford, UK) motion analysis system captured kinematic data at 120Hz. Kinematic data were filtered at 12Hz.

Although a forceplate was available for OG trials, stance was determined using kinematic methods for both conditions to ensure consistency. Footstrike was identified at the change in vertical velocity from negative to positive of the distal heel marker. Toe-off was identified at peak knee extension. These methods were previously validated for OG running (Fellin and Davis, 2007). Using an instrumented treadmill in another location, an analysis of 10 recreational runners confirmed that these methods are similarly accurate in estimating footstrike and toe-off during treadmill running. Errors of less than one video frame at 120Hz for toe-off and less than 3 video frames for footstrike were obtained.

For each trial, hip, knee and rearfoot angles were calculated at both initial contact (IC), and at peak (PK) (first 75% of stance). Five trials were averaged for each subject. The standard deviations of the 3D hip, knee and rearfoot angles (IC and PK) were computed for each condition. Next, the difference between the conditions was calculated for each subject, and then averaged across subjects.

RESULTS

At initial contact, subjects exhibited smaller standard deviations during TM running for seven of nine joint angles (Table 1). For peak angles, there were smaller standard deviations during TM running for eight of the nine angles. All of these standard deviation differences were less than half a degree. Overall, 15 out of 18 measures supported our hypothesis of TM running being less variable than OG running. The largest difference between the two modes (0.45 degrees), occurred at the rearfoot in the frontal plane for initial contact.

DISCUSSION

Overall, variability of TM running was lower than OG running. These results agreed with Wank and associates (1998). However, their differences were greater than those found in this study. They reported decreases in standard deviations of 0.6 degrees in PK knee angle and 1.7 degrees in ankle angle at IC during TM running. Their subjects ran 4 m/s compared to 3.35 m/s in this study. Additionally, their subjects exhibited 10 times the SD for IC ankle angle and 1.5 times the SD for PK knee angle compared to the results of this study. Both of these differences may have contributed to the smaller differences in standard deviations found in this study.

The relatively large reduction in rearfoot variability for the frontal plane at IC on the TM was surprising. Individuals often drift side-to-side while running on a TM, which could potentially increase frontal plane variability. However, the narrow width of the TM belt (45 cm) may have constrained footstrike position resulting in lower variability.

Previous research suggested that variability in movement patterns may reduce the risk of running-related injuries. (Hamill et al., 1999). These authors promoted the theory that reduced variability of movement causes very consistent loading patterns in the lower extremity, leading to overuse. However, TM surfaces are typically more compliant than those surfaces that individuals run OG. In fact, compared to OG running, TM running external loads were reduced (Willy and Davis, 2008). Thus it is unclear as to which mode of running results in lowered injury risk.

CONCLUSIONS

Subjects exhibited decreased variation during TM running compared to OG running for 15 out of 18 lower limb 3D kinematic variables. The largest difference was frontal plane rearfoot position at initial contact.

REFERENCES

Fellin, R.E. and Davis I.S. (2007). *American Society of Biomechanics Annual Meeting*.
Hamill, J. et al. (1999). Clin Biomech 14(5), 297-308.
Wank, V. et al. (1998). *Int J Sports Med*. 19: 455-461.
Willy, R. and Davis, I.S. (2008) *American College of Sports Medicine Annual Meeting*.

Table 1: Group mean standard deviations for TM and OG running. Differences are the average of the individual differences between conditions. Negative differences indicate TM SD < OG SD. (All units degrees)

Condition	Joint	Sagittal			Frontal			Transverse		
		TM SD	OG SD	Diff	TM SD	OG SD	Diff	TM SD	OG SD	Diff
Initial Contact	Hip	1.15	1.40	**-0.26**	1.22	1.30	**-0.08**	1.17	1.19	**-0.02**
	Knee	1.58	1.77	**0.19**	0.54	0.46	**0.08**	1.18	1.40	**-0.22**
	Rearfoot	1.80	1.95	**-0.15**	1.37	1.82	**-0.45**	1.57	1.52	**-0.04**
Peak	Hip	1.25	1.51	**-0.27**	1.05	1.34	**-0.30**	0.99	0.99	**0.00**
	Knee	1.13	1.36	**-0.24**	0.54	0.57	**-0.03**	0.83	1.06	**-0.23**
	Rearfoot	1.18	1.41	**-0.23**	0.78	0.95	**-0.17**	1.08	1.27	**-0.20**

AN INNOVATIVE METHOD TO ANALYZE THE CHONDROCYTE RESPONSE TO MECHANICAL INJURY BOTH TEMPORALLY AND SPATIALLY

McCabe, D J; Stroud, N J; Pedersen, D R; Martin, J A

Department of Orthopaedics and Rehabilitation, University of Iowa, Iowa City, IA
nstroud@engineering.uiowa.edu

INTRODUCTION

The initiation of post-traumatic osteoarthritis (PTOA) is attributable in part to acute necrosis and apoptosis of chondrocytes that occurs subsequent to high-energy impact loading of articular cartilage. Ongoing work in our lab has revealed that cell death following an injury begins quickly and continues for at least 8 hours after injury. Essential to this work is the ability to determine the viability of an impact site non-invasively. By creating a device that allows precise movements across a cartilage surface and accurate placement of an objective at specific points throughout this surface we can spatially describe the biological response to mechanical injury. This non-destructive analysis allows the use of the same impact site across time which offers increased statistical power in the detection of the cartilage response to injury.

METHODS AND PROCEDURES

Osteochondral explants (2.5cm x 2.5cm) were harvested from the lateral load-bearing areas of adult bovine tibial plateaus and incubated overnight under standard culture conditions. A drop tower was used to impart a blunt impact insult (~7J/cm^2, 2kg, 7cm high) to the cartilage surface via a 5mm diameter platen. Post impact, the explants were incubated for 2 hours and subsequently stained with biological fluorophores for an additional hour. The biological fluorophores consisted of ethidium homodimer and calcein AM;

staining dead or live cells respectively. After staining, the explants were transported in a custom-built tissue chamber/holder complex and mated to a purpose-built x-y tissue stage that attaches to a 1024 *BioRad* confocal microscope. Predetermined sites (Figure 1) were then imaged using 568nm (ethidium homodimer) and 488nm (calcein AM) wavelengths and scanned through the superficial layer to a depth of approximately 200 microns. This was done by separately imaging focal planes which were 20 microns apart in the z-axis. The resulting z-slices were assembled and analyzed in *ImageJ* providing the tissue viability for each imaged site.
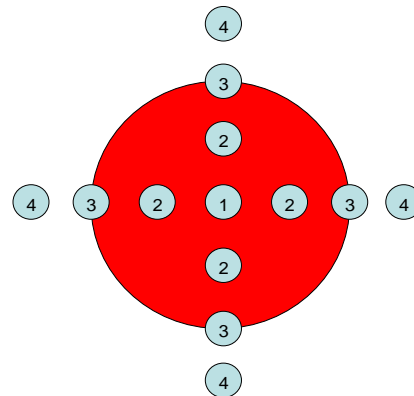
Figure 1. Distribution of analysis sites within an impact area. Impact area is indicated by red circle (diameter = 5mm). Blue circles indicate microscopically imaged areas (diameter = 1mm); there is 0.25mm from the outside of 1 to 2 and from 2 to 3, 1.5mm from 3 to 4.

RESULTS

Referring to the areas indicated in Figure 1 three hours post-impact, the center of area 1 showed a viability of ~40% and area 2 had a viability of approximately 60%. Sites in area 3 were determined to be ~80% viable which was expected considering that these sites were precisely on the impact border and cell death was almost entirely inside the border. The control regions have a center that was 5.0mm away from the center of the impact site; these regions boasted over 97% viability. Figure 2 illustrates the images that were collected via confocal microscopy.
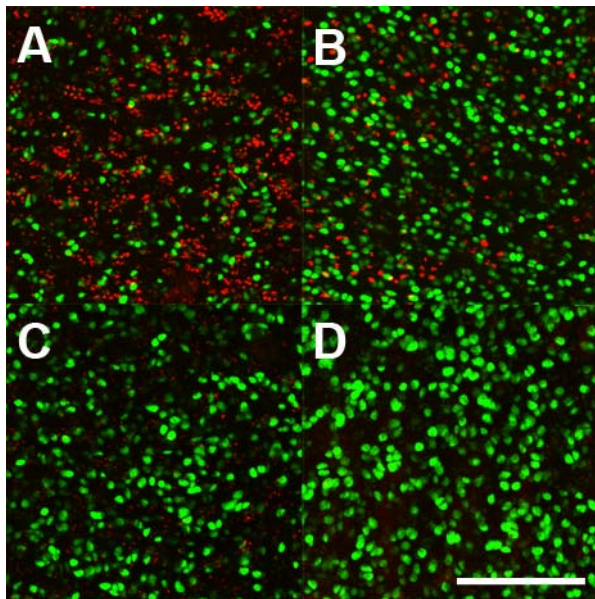
Figure 2. Representative images from the four different regions analyzed: A is from area 1, B is from area 2, C is from area 3, and D is from area 4 (scale bar = 200 microns).

DISCUSSION

Previous work has provided data from randomly chosen spots inside an injured site, but without the x-y tissue stage we were only able to determine the representative cell viabilities for the two broad groups, within or outside of the impacted area. The 60% viability in area 2 was consistent with our previous studies. In this earlier work, the sites were sampled entirely inside the impact region, but not in the absolute center of the impact site. Examination of area 3 supports the idea that immediate chondrocyte death is limited to the impact area; this is apparent because there was a distinct boundary enclosing the cell necrosis.

SUMMARY

The ability to map the cellular response to injury will improve our understanding of the response to injury as data points can be precisely defined temporally and spatially. This will allow for clear observation of the initiation and progression of all death inside and outside the impact site. Additionally, with the available echelon of control, observed biological responses of impacted cartilage can be used to validate finite element models of the tissue and subsequently describing the relationship between stress and strain tensors and cell necrosis. Clinically, the information concerning cell death and its relationship to the progression of PTOA could be used for non-invasive arthroscopic tests to determine the condition of a patient's cartilage post injury. This in turn can be used for deciding the level and variety of medical care.

Future revisions of the x-y tissue stage will include an environmental chamber with submerged specimens. This innovative technique would allow events to be followed through time at the same image site allowing for a more accurate representation of *in vivo* experimental conditions.

ACKNOWLEDGEMENTS

NATIVE ULNAR COLLATERAL LIGAMENT STRAIN UNDER A REHABILITATION PROTOCOL

Ramon A. Ruberte Thiele[1], Geoffrey A. Bernas[2], Karen Kinnaman[3], Bruce S. Miller[1], and James E. Carpenter[1]

[1]Department of Orthopaedic Surgery, University of Michigan, Ann Arbor, MI.
[2]Department of Orthopaedic Surgery, State University of New York at Buffalo, Buffalo, NY.
[3]University of Michigan Medical School, Ann Arbor, MI.
rruberte@med.umich.edu

INTRODUCTION

Overhead throwing athletes of sports like baseball and football subject their elbows to high valgus and extension loads, which often lead to injury (Cain et al., 2003). The anterior bundle of the medial ulnar collateral ligament (UCL) absorbs much of these loads, and is repetitively subjected to near-failure moments during the throwing motion (Wilk et al., 2004). After UCL injury, typical nonoperative treatment starts with a period of rest and immobilization, followed by restricted motion and then a progressive strengthening program that includes isometric exercises (Cain et al., 2003; Wilk et al., 2004). However, little is known about the strains generated in the UCL as a result of these exercises. Our goal was to determine the strains obtained in the native UCL under a rehabilitation protocol.

METHODS AND PROCEDURES

Specimens: Eight fresh-frozen cadaveric arms (7 male, 1 female; mean age: 74.6 years; range: 51-87 years) were used (# based on power analysis). There were no macroscopic or radiographic signs of osseous or soft-tissue abnormalities. Arm preparation: Arms were amputated at mid-humerus, leaving rest intact. Solid-braided nylon rope was sutured to the tendon insertions of biceps brachii, brachialis and triceps muscles with Number 2 Ethibond (Ethicon, Inc.). Experimental setup: The proximal humerus was cleared of soft tissue and secured to a fixture allowing full, unconstrained range of motion (ROM). The ropes were run along the muscles' lines of action and attached to weights of 1, 1, and 2 kg respectively via a system of pulleys. This ratio represents 5% of their maximal potential force to simulate joint compressive loads (Morrey et al., 1991). The Optotrak Certus® Motion Capture System (Northern Digital, Inc.) and MotionMonitor™ software (Innovative Sports Training, Inc.) were used to collect and analyze the joint kinematics. Strain measurement: Differential variable reluctance transducers (DVRTs, MicroStrain, Inc.) were secured to the anterior and posterior bands of the anterior bundle to measure strain. All strains were reported as a percentage from the reference angle of 30°. Testing sequence: Strain was measured in: 1. passive ROM in neutral, supination, and pronation; 2. isometric resisted exercises with 5 lbs in flexion and extension, and varus and valgus loading with 2.5 lbs hand weight (3.34 N*m torque) at 90° of flexion. Statistical analysis: Two-way ANOVA was used to determine if forearm rotation and flexion angle significantly affected UCL strain. The change in strain between the unloaded and loaded conditions for the varus and valgus testing was analyzed with a paired t-test.

RESULTS

There was a significant increase in strain with increasing elbow flexion for both the anterior

and posterior bands of the UCL (p < 0.001). The anterior band had less strain than the posterior band for all flexion angles studied (Figure 1). Strain was not significantly different between forearm rotations (anterior band: p = 0.312; posterior band: p = 0.290).

Isometric testing showed no measurable change in strain between the unloaded and loaded conditions at 90° of flexion. However, there was an increase in strain simply by flexing the elbow to 90°. A varus and valgus torque of 3.34 N*m produced a significant strain between the unloaded and loaded states (p < 0.01). Strain decreased 0.85 +/- 0.59% on the anterior band and 1.07 +/- 0.61% (mean +/- SD) on the posterior band during varus loading. The valgus load increased strain 2.01 +/- 1.31% on the anterior band and 2.59 +/- 1.06% (mean +/- SD) on the posterior band.
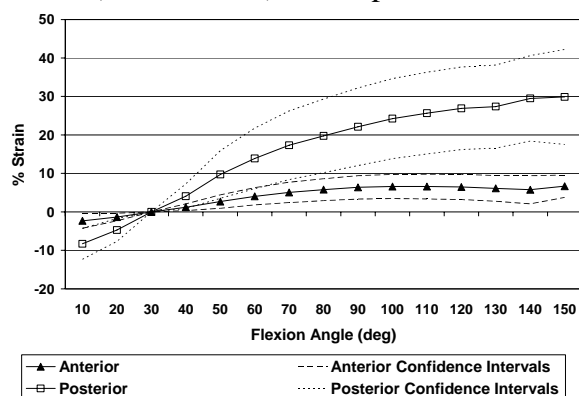
Figure 1. Anterior and posterior band mean strain with 95% confidence intervals per flexion angle in neutral forearm position.

DISCUSSION

We have shown that both bands of the UCL anterior bundle increase in strain as the elbow is flexed without a forearm rotation effect. However, the anterior band tends to relax as the flexion angle increases, while the posterior band gradually increases in tension over the entire flexion/extension arc. Overall, peak strains for the anterior band occurred in the range of 90°-110°, and 130°-150° for the posterior band. Our data is supported by

Pribyl et al. (1999) who demonstrated that strain values approached 50% in full flexion for the anterior bundle of the UCL, and forearm position had no effect on strain.

Elbow flexion at 90° is a common position for splinting, performing isometric contractions and valgus loading. In our study, isometric exercises and varus and valgus torques as performed did not create strains greater than 3%, but we noted an increase in strain in both bands just by flexing to 90°. This is consistent with studies that report strain values between 3-6% for the anterior bundle of the UCL under comparable torques at 90° of flexion (Andrews et al., 2001; Levin et al., 2004).

SUMMARY

Our work demonstrates increasing ligament tension as one approaches full flexion of the elbow. Varus and valgus testing confirmed that the UCL becomes lax when subjected to varus loading and taut when subjected to valgus loading. Isometric exercises and varus and valgus torques as performed generated a low amount of strain, but just flexing the elbow to 90° produced strains > 5% in both bands. This information should be taken into consideration when selecting an appropriate rehabilitation program after UCL injury.

REFERENCES

Andrews JR et al. (2001). *Am J Sports Med*, 29(6):716-721.
Cain EL et al. (2003). *Am J Sports Med*, 31(4):621-635.
Levin JS et al. (2004). *J Shoulder Elbow Surg*, 13(1):66-71.
Morrey BF et al. (1991). *Clin Orthop Relat Res*, 265:187-195.
Pribyl CR et al. (1999). *Orthopedics*, 22(6):607-612.
Wilk KE et al. (2004). *Clin Sports Med*, 23(4):765-801, xii.

MECHANISMS UNDERLYING INCREASED WALKING SPEED AFTER REHABILITATION IN PERSONS WITH POST-STROKE HEMIPARESIS

Jessica L. Allen[1], Mark G. Bowden[2], Steven A. Kautz[2,3,4] and Richard R. Neptune[1]

[1]Department of Mechanical Engineering, University of Texas, Austin, TX,
jessica.allen@mail.utexas.edu
[2]Brain Rehabilitation Research Center, Malcolm Randall VA Medical Center, Gainesville, FL
[3]Dept of Physical Therapy and [4]Brooks Center for Rehabilitation Studies, University of Florida

INTRODUCTION

Slower walking speeds and asymmetry typically characterize patients with post stroke hemiparesis and are often the result of neuromuscular deficiencies related to impaired muscle strength and recruitment that changes their motor control pattern. These impairments vary among patients, and therefore different mechanisms are used to generate their walking pattern.

A recent study has identified step length ratio (SLR = paretic step length / non-paretic step length, symmetric = 1.0) as a clinical measure that offers a window into the underlying motor impairments and compensatory strategies used by patients with post-stroke hemiparesis (Balasubramanian et al 2007). Due to the high variability between subjects, SLR may distinguish between subjects who attain similar speeds with different compensatory strategies. SLR was found to negatively correlate with another measure of asymmetry, (PP = paretic propulsion / paretic + nonparetic propulsion, symmetric = 50%), which quantifies the percent of the propulsive ground reaction forces provided by the paretic leg (Bowden et al 2006, Balasubramanian et al 2007). These propulsive impulses are important to the mechanics of walking and attaining higher walking speeds. Recent studies have found multiple contributions to PP and speed increases in hemiparetic subjects. Ankle plantar flexor moment impulse and leg orientation positively correlated while hip flexor moment impulse negatively correlated with propulsion

(Peterson 2007). Additionally, peak ankle power in late stance was found to correlate with increased speed (Parvataneni 2007). The goal of the present work was to analyze two case studies and identify the mechanisms that contributed to similar individual speed increases following rehabilitation.

METHODS AND PROCEDURES

Two subjects greater than six months post-stroke completed a 12-week body weight supported treadmill rehabilitation training program. Bilateral kinematics, GRFs and EMG were collected at their fastest comfortable speed pre- and post-rehabilitation. Intersegmental joint moments and powers were calculated using standard inverse dynamics techniques. All data were normalized to one complete gait cycle and joint moment impulses were calculated during the propulsive phase. PP, SLR, peak late stance ankle power, peak leg orientation (angle between the pelvis COM and foot COM), and hip flexor and ankle plantar flexor propulsive moment impulses (i.e., time-integral of the positive and negative moment curves, respectively) were calculated pre- and post- rehabilitation.

RESULTS

Subject A increased their plantar flexor moment impulse (increases of 10.5 paretic and 6.9 nonparetic, Nm•s-%BW), ankle peak power (0.08 paretic and 0.17 nonparetic, W-%BW) and leg orientation (11.0 paretic and 5.4 nonparetic, degrees) on both legs. Paretic
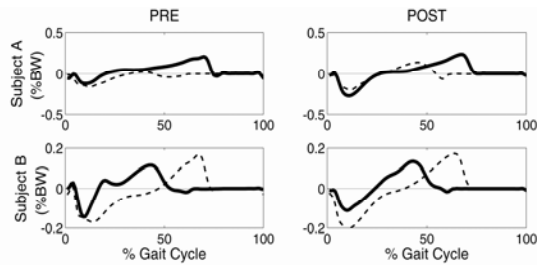
Figure 1: Anterior-posterior ground reaction forces show asymmetry in propulsion between legs (paretic, - - - ; nonparetic, —)

leg hip flexor moment impulse decreased while the nonparetic leg impulse increased (-2.9 and 1.4, Nm•s-%BW, respectively). Subject B increased their hip flexor moment impulse (8.2 paretic and 4.5 nonparetic, Nm•s-%BW), peak ankle power (0.04 paretic and 0.06 nonparetic, W-%BW) and leg orientation (6.2 paretic and 6.3 nonparetic, degrees) on both legs while their ankle plantar flexor moment impulse increased on the paretic leg but decreased on the nonparetic leg (1.6 and -3.1, Nm•s-%BW, respectively).

Table 1: Pre- and post-training speed, SLR and PP

		Speed (m/s)	PP (%)	SLR
Subject A	Pre	0.70	5.8	1.46
	Post	1.00	33	0.99
Subject B	Pre	0.80	48	1.00
	Post	1.10	44	0.99

DISCUSSION

Both subjects had similar pre-intervention speeds and speed increases following rehabilitation. However, different values for pre-rehabilitation PP and SLR suggest the subjects had different neuromotor deficits. Subject A initially had very little contribution from the paretic leg to forward propulsion, as shown by the low PP. A large increase in the paretic leg contribution to propulsion (PP increase) resulted in increased walking speed. Increased paretic leg ankle plantar flexor output, seen in the moment impulse and peak power, contributed to the PP increase. Also, a decrease in paretic leg hip flexor moment

impulse facilitated an increase in peak leg orientation (i.e., foot more posterior of pelvis) and the improved mechanics helped increase propulsion.

In contrast, Subject B initially had a symmetric gait pattern. Increases in both ankle plantar flexor and hip flexor output from both legs contributed to the speed increase. The paretic leg ankle plantar flexor output increased in both the moment impulse and peak power. However, the values of these variables post-rehabilitation were much lower than those of the nonparetic leg and did little to change PP. Additionally, the hip flexor moment impulse increased from both legs, but more so on the paretic leg (PP decrease). These increases at the hip, despite acting to decrease propulsion generation, contributed to increased step lengths, and thus increased walking speed.

CONCLUSION

Assessment of SLR and PP can reveal whether increased speed following gait rehabilitation of persons with post-stroke hemiparesis was achieved by different mechanisms that depended on different individual deficits.

REFERENCES

Balasubramanian, CK et al (2007). *Arch Phys Med Rehabil,* 88:43-49.
Bowden, MG et al (2006). *Stroke.* 37:872-876.
Parvataneni, K et al (2007). *Clin Biomech,* 22:813-820
Peterson, CP (2007). *MS Thesis, UT-Austin.*

ACKNOWLEDGEMENTS

PERCEPTION OF WEIGHT-BEARING DISTRIBUTION DURING SIT-TO-STAND TASKS IN HEMIPARETIC AND HEALTHY INDIVIDUALS

Anabèle Brière, Séléna Lauzière, Denis Gravel and Sylvie Nadeau

Centre de recherche interdisciplinaire en réadaptation, Institut de réadaptation de Montréal
Ecole de réadaptation, Université de Montréal, (Québec), H3C 3J7, Canada.
Sylvie.nadeau@umontreal.ca

INTRODUCTION

Transferring from sitting to the standing position is important to maintain independence in everyday life. Following a stroke, the ability to rise from a chair is characterised by an asymmetry in the weight-bearing (WB).The hemiparetic individuals prefer to place more weight on their non-paretic foot, even though they have the capacity to perform more symmetrically on demand, with visual feedback (Engardt, 1994) or by altering the foot position (Roy et al., 2006). This asymmetrical performance has been associated with paresis and loss of postural control. It is not well known whether the hemiparetic subjects are aware about this asymmetry of WB and if they perceive it adequately. In sit-to-stand (STS), one study reported that the correlation between the strokes individuals' own estimation of WB distribution on a visual analogue scale and the actual WB distribution while rising was low (Engardt and Olsson (1992). The main purpose of this study was to compare the error between the perception of WB and the actual WB distribution of hemiparetic and healthy individuals during the STS task.

METHODS AND PROCEDURES

Eleven individuals with a chronic left hemiparesis (57.0 ± 14.1 yrs), as well as 15 healthy elderly individuals (65.1 ± 3.8 yrs) participated in this study. The hemiparetic group presented a moderate level of motor impairment and, except for one that had a hypoesthesia at the foot; others had good tactile and proprioceptive sensation. Their mean time to complete the Five repetition Sit-to-Stand Test was 16.6 s (±6.6 s) whereas for the healthy participants it was 10.9 s (±1.9 s).

The participants were required to rise at natural speed from an instrumented chair equipped with platforms. Forces under each foot were measured by two force plates. Two foot conditions were assessed: spontaneous (SP) and symmetric (S). For the latter, verbal instructions to put equal WB on each foot was given prior to executing the task. After each trial, the participants rated their perceived WB distribution on a visual analogue scale. Two trials were performed for each condition. The WB distribution on the right side (mean of two trials), expressed in percent, was computed using the vertical ground reaction forces (seat and foot), averaged from -0.5 s before the seat-off event to 0.5 s after. For each condition, four errors were computed: 1) raw error (difference between the actual WB distribution and the perception); 2) normalized raw error (raw error/% of actual WB distribution); 3) absolute error (absolute difference between the actual WB distribution and the perception and 4) normalized absolute error (absolute error/% of actual WB distribution). The results of the two groups were compared using descriptive statistics and independent Student t-tests ($p < 0.05$).

RESULTS

The mean (SD) values of WB distribution and errors of perception for each condition are presented in **Table 1**. Results revealed a more asymmetrical WB distribution in the hemiparetic group in comparison to the healthy subjects ($p < 0.001$). The patients

presented significantly greater errors of perception than healthy individuals and overestimated systematically the weight under their left (affected) foot.

DISCUSSION

Since no other study evaluated the errors of perception of WB during the STS task, comparisons with other results are not possible. For upright stance, a study of Bohannon et al. (1989), in which healthy subjects had to attempt to bear 50% of their weight on one of their lower limb, the mean absolute error of WB perception was of 3.3 % (± 3.7 %). This is very close to the mean absolute error of 2.8% we obtained for the healthy individuals. In a second study (Bohannon and Tinti-Wald, 1991), they assessed stroke individuals with the same protocol. They found that, although making significantly greater errors (5.2 ± 4.0 %) in WB than healthy subjects, the stroke individuals did not systematically bore less weight on their paretic limb. In our study, the hemiparetic individuals, as a group, also made greater errors of perception than the healthy individuals but all, except for two, bore less weight on the paretic foot. The different mechanical demands required between standing and performing a STS might explain these results. Actually, we do not have results to explain the greatest errors found in the stroke group. However, it could be hypothesized that they rated their perceived effort distribution rather than their weight distribution (force) as predicted by the principle of bilateral matching effort proposed by Bertrand et al. (2004) in bilateral matching tasks performed at the upper limbs. Other clinical characteristics, such as the type and localisation of the lesion might also have an influence.

SUMMARY

The results of this study revealed greater WB asymmetry and errors of WB perception in hemiparetic compared to healthy individuals during the STS task. However, before assuming that stroke patients can not perform symmetrically, other factors, such as the sense of effort, have to be studied.

REFERENCES

Bertrand AM et al. (2004). *J Neurophysiol, 91*: 1579-85.
Bohannon RW et al. (1989). *Percept Mot Skills, Dec; 69 (3 Pt 1)*: 875-80.
Bohannon, RW and Tinti-Wald, D (1991). *Percept Mot Skills, Jun; 72(3 Pt 1)*:935-41.
Engardt, M. (1994). *Scand J Rehabil Med, 26*: 65-69.
Engardt, M and Olsson, E (1992). *Scand J Rehabil Med, 24*(2), 67-74.
Roy G et al. (2006). *Clin Biomech, 21*(6), 585-593.

ACKNOWLEDGEMENTS

Table 1: WB (right side) and errors of perception (%) for the healthy and hemiparetic groups.

Groups	Conditions	Mean (SD) WB (%)	Types of errors			
			Raw	Normalized raw	Absolute	Normalized absolute
Healthy	SP	50.0 (2.7)	-1.1 (3.3)	-2.5 (6.7)	2.7 (2.2)	5.5 (4.4)
	S	49.7 (3.5)	-0.5 (3.7)	-1.5 (7.6)	2.8 (2.4)	5.7 (5.0)
Hemiparetic	SP	60.1 (7.8)	6.0 (6.4)	9.3 (10.5)	7.5 (4.3)	12.2 (6.6)
	S	58.2 (7.3)	7.3 (5.0)	12.2 (8.4)	7.9 (4.0)	13.3 (6.0)

MANUAL PATIENT TRANSFER TRAINING: STUDENT NURSE PERCEPTIONS

Paula M. van Wyk[1], David M. Andrews[1] and Patricia L. Weir[1]

[1]Department of Kinesiology, University of Windsor, Windsor, ON, Canada,
vanwyk@uwindsor.ca, dandrews@uwindsor.ca, weir1@uwindsor.ca

INTRODUCTION

Performing physically demanding tasks in non-neutral postures with heavy loads can hinder nurses from remaining injury free at work. Several studies have cited manual patient transfers (PT) as the primary reason for musculoskeletal injuries among nurses (Owen and Garg, 1993; Yassi et al., 1995). Although biomechanical study supports nurses' perceptions that PT are the most physically stressful tasks they perform, their risk of injury may be increased due to improper or inadequate training (Evanoff et al., 2003; Nelson et al., 2003). This study is part of a larger project on the training and use of PT by student nurses, and the confidence they have in their PT ability. This study sought to determine if there are differences in PT training received in both academic and clinical settings. If there are differences in training, this might lead to changes in nursing curricula regarding PT training, which might in turn better prepare nurses for clinical practice.

METHODS AND PROCEDURES

The study sample was 163 nursing students (age: 24.36 +/-4.64 years) from the University of Windsor who volunteered to complete a survey. The participants were asked to respond (yes/no/unsure) if they were trained at school and while on clinical placement for 19 PT (10 PT from the side of a bed, and 9 PT from a chair). For both the bed and chair PT, there were non-assistive PT (hook and hug) and assistive PT (gait and transfer belts). All

PT were illustrated in the survey using pictures of a nurse and patient. The participants were also asked how often (never, rarely, sometimes, occasionally, very often) they performed each of the 19 illustrated PT, over the last month, 6 months and 12 months. Additionally, they were asked to provide a percentage of confidence (0-100%) for their ability to perform each of the 19 PT accurately, without harm to the patient, and without harm to themselves. The analyses for this paper will be limited to the academic and clinical training portion of the survey. Chi-square analyses were performed to compare yes/no/unsure responses to determine if, for each of the 19 PT, there was a significant difference between the locations (academic vs. clinical settings) of training ($p \leq .05$). Expected frequencies were balanced across responses (i.e. 33.3%).

RESULTS

Participants indicated "yes" they were trained how to use 32% (6/19) of the PT. The identified PT were all non-assistive hook lifts. For all 6 of these PT, more participants indicated that they received training in the clinical setting. Interestingly, these non-assistive hook lifts are not taught as part of the nursing curriculum at the University. In comparison, for the PT traditionally taught as part of the curriculum (non-assistive hug lift and assistive transfer belt lift, both from the side of a bed and a chair), 50% fewer students perceived that they had been trained on these PT in either setting (Figure 1).
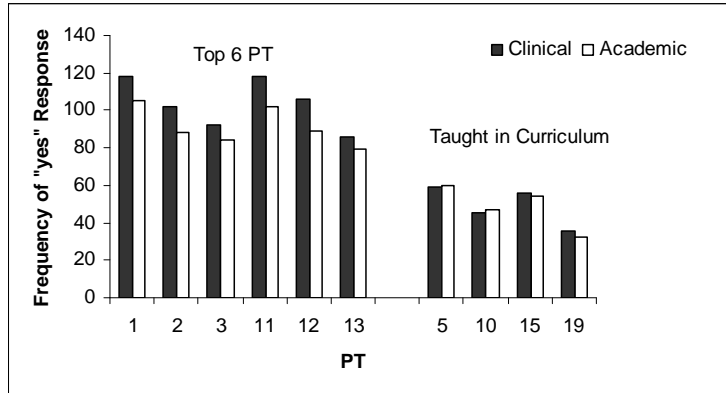
Figure 1. Frequency of "yes" responses for the top 6 patient transfers, and the patient transfers taught in the University curriculum.

DISCUSSION

It is important to study manual PT as they are one of the leading risk factors for work-related injuries. Garg and Owen (1992) reported that 98% of nurses choose to perform transfers manually even when a mechanical lift is available. Thus, it is critical to understand how nurses are trained to perform these demanding tasks. Our findings suggest that there is a potential disconnect between what they learn in the classroom and in clinical practice. Not one of the top 6 PT identified by our sample of student nurses was even taught in the standard nursing program. While the data show that the perception of training on these PT was higher in the clinical setting, it is a concern that the academic frequencies were as high as they were. Many students perceived they were trained on certain PT when they were not, or didn't perceive they were trained on the PT that they were trained on; scenarios which could both put nurses at an increased risk of injury.

Two critical questions arise from this. First, do clinical placements skew nursing students' perceptions for which PT they were actually provided training for in courses and labs? A lack of exposure to education regarding the biomechanics of lifting and PT may also play a major role in students' misperceptions. Secondly, is the current curriculum an accurate representation of what nurses are experiencing on the job? Future analyses on the use and confidence data will provide a deeper understanding of these issues, because although nurses do receive training for PT, it may not be for the ones they use most often, or have the most confidence in performing without injuring themselves or their patients.

SUMMARY

Practice not only allows a person to enhance their skills but also to develop their confidence to perform a task well. The multi-factorial approach of this research project will continue to address the interplay between PT curriculum development, clinical practice, and the prevalence of work-related injuries.

REFERENCES

Garg, A and Owen, B (1992). *Ergonomics,* 35:1353-1375

Evanoff, B. et al. (2003). *American Journal of Industrial Medicine,* 44:451-457.

Nelson, A. et al. (2006). *International Journal of Nursing Studies,* 43:717-733.

Owen, B.D. and Garg, A. (1993). *American Journal of Nursing,* 93:48-51.

Yassi, A. et al. (1995). *Occupational Medicine,* 45:215-220.

Effects of ice hockey facial protectors on response time

Patrick M Dowler and David J Pearsall

Dep. of Kinesiology & Physical Education, McGill University, Montreal, QC, Canada
URL: http://icehockeyscience.mcgill.ca

Introduction

While the added protection given to ice hockey players through the use of visors and cages has been well documented (Benson et al., 2002; Stevens et al., 2006; Lemair & Pearsall, 2007), a perception in the hockey community remains that cages and visors impair the field of vision, and in turn delay response time and subsequent movements. In ice hockey, a fast paced sport that heavily relies on vision and reaction time, any impairment in the field of vision has the potential to lower one's level of play. Furthermore, a slight latency in one's response time could have effects on both performance and safety on the ice. Some prior studies examining the effects of visors and sports goggles on visual function do report a reduction in peripheral vision (Ing et al., 2002). However, no studies have addressed the subsequent effects on movement response time. This forms the basis for the current study.

Methods and Procedures

Healthy subjects from the McGill University male and female varsity ice hockey teams (n=28) were recruited to participate in this study. Each subject stood in front of 13 light targets, arranged at equal intervals along a 180° horizontal arc array positioned at shoulder height and a distance of 1.3 arm lengths away. Three test conditions were examined wearing a helmet and: (1) no facial guard (control), (2) a cage, and (3) a visor. During each trial, upon random illumination of lights in the array, the subject was instructed to respond as quickly a possible to reach out and touch the activated light with their index finger. With button switches in the lights, as well as on the subject's chest (i.e. start hand position on mid-sternum), reaction time (RT), movement time (MT) and response time (RsT= RT + MT) were measured for each light target. Several trials per target were collected in random sequence among the 13 lights, controlled by an I/O DAQ board and software (National Instruments™, Labview™ 8). In addition, six Vicon® infrared cameras captured subject kinematics through each trial (figure 1). Passive reflective markers were placed at body landmarks on the subject in accordance with Vicon's® full body model. Records of body movement for each trial were synchronized with the above response time data.
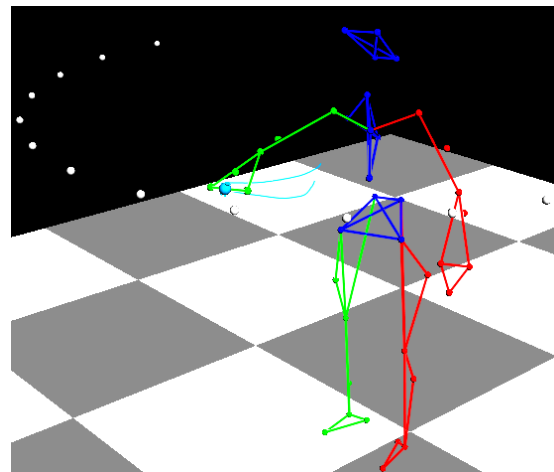
Figure 1: Example trial of the reach and point task.

For the purposes of this abstract, only the former variables will be discussed. Following subject testing, RT, MT and RsT data were statistically evaluated in Matlab® and SPSS®, incorporating a two-way repeated measures ANOVA.

Results

Significant differences were present between subjects' RsT. Pairwise comparisons indicated that these differences existed between the cage and control conditions (p=0.039). A rank order was observed between these cage, visor, and helmet conditions, with RsT means of 866, 855, and 843 ms, respectively, with an upper bound of 47 ms existing between the cage and helmet conditions (table 1).

Condition	Mean (ms)	Std. Error
Control	843	18.2
Cage	866	18.1
Visor	855	19.4

Table 1: Mean RsT times (ms) and standard error values.

Though similar ranking was observed for RT and MT measures, repeated measures analysis showed no significant differences.

Discussion

Though RT and MT values were not affected significantly by the test conditions, the cumulative RsT scores were delayed, in particular with the cages (~23 ms). This was a consistent observation for most of the light targets. In addition, the largest differences were detected within 45° of subjects' central focal point. This was unexpected, given the results of the aforementioned study by Ing et al (2002), in large part due to the

unique qualities of cages versus goggles/visors.

Summary

The effect of three ice hockey facial protection conditions on reaction, movement and cumulative response times in a goal directed task was investigated. Results indicated that RsT is significantly different when comparing a subject wearing a helmet with no facial protection versus wearing a cage. Given the above results, further study is warranted to validate these findings during on-ice conditions and with respect to game specific skills. As well, re-evaluation of cage design and construction to optimize safety and functionality should be pursued.

References

Benson et al. (2002). *Br J Sports Med*, 36, 27-32.
Ing et al. (2002). *Can J Opthalmol*, 31, 161-167.
Lemair M. & Pearsall D.J. (2007). *Sports Eng*, 10, 65-74.
Stevens et al. (2006). *J Sci Med Sport*, 9, 238-242.

Acknowledgements

Reproducing Human Arm Motion Using a Kinematically Coupled Humanoid Shoulder-Elbow Complex

Craig M. Goehler[1] and Michael M. Stanišić[2]

[1]Applied Research in Musculoskeletal Simulation Lab, Sensory Motor Performance Program, Rehabilitation Institute of Chicago, Chicago, Illinois, USA, cgoehler@alumni.nd.edu
[2]Mechanisms and Mechatronics Lab, Department of Aerospace and Mechanical Engineering, University of Notre Dame, Notre Dame, Indiana, USA, stanisic@nd.edu

INTRODUCTION

This work presents a mechanism capable of reproducing voluntary human reaching motions, along with a method of implementing the coupled motions that exist within the human shoulder complex and shoulder-elbow complex.

INVERSE KINEMATICS PROCEDURE

The humanoid shoulder-elbow complex considered here is an extension of the parallel mechanism shoulder complex of (Lenarćić and Stanišić, 2003) into a whole arm mechanism which includes an elbow. The kinematic descriptions and equations were formulated using Denavit and Hartenberg parameters and frame assignments outlined in (Craig, 1989). This results in a six degree of freedom system: θ_1 and θ_2 describe the shoulder girdle configuration, θ_3 and θ_4 control the direction of the humerus, θ_5 represents humeral roll and θ_6 accounts for flexion/extension at the elbow joint.

The inverse kinematics problem of the humanoid shoulder-elbow complex is defined as: given the coordinates of the wrist in the base frame, determine the values of the joint variables θ_1-θ_6, a problem with three equations in six unknowns, i.e. three redundant degrees of freedom. Three constraints need to be imposed to resolve the redundancy and importantly, these constraints must conform to human shoulder-elbow complex motions.

Two constraints which couple the first four degrees of freedom come from (Lenarćić and Stanišić, 2003) and account for the approximate 2:1 ratio between human humerus and scapula rotation. Another two constraints come from (Stanišić et al., 2007), which couple the direction of the elbow axis to the reaching direction for voluntary human reaching motions. This leads to an over-constrained system.

The two pairs of couplings can be separated from each other during the solution, since the effect of one pair on the other is weak. This allows the problem to be solved using the method of successive iterations, an example of which is presented in (Dobrowolski, 1965). This method allows the inverse kinematics problem to be solved as follows:

Given: Wrist coordinates in base frame
1) Set θ_1=0° and θ_2=180° (corresponds to solution that neglects scapula motion).
2) Solve inverse kinematics problem for θ_3-θ_6, implementing the coupling between reaching direction and elbow axis direction found in voluntary reaching (Stanišić et al., 2007).
3) Knowing θ_1-θ_4, determine the direction of the humerus.
4) Calculate new values for θ_1 and θ_2, implementing the coupling between human humerus and scapula rotation (Lenarćić and Stanišić, 2003).

5) Iterate Steps 2-4 until the change in the values of the joint angles satisfies a convergence criterion. (Iterations are required because the solution in Step 4 affects the location and orientation of the glenohumeral joint, which alters the solution in Step 2.)

EVALUATION OF HUMANOID SHOULDER-ELBOW COMPLEX MOTION

With the kinematics of the humanoid shoulder-elbow complex mechanism established, it is possible to evaluate the resulting motion both quantitatively and qualitatively by comparing the configuration of the mechanism to that of the arm.

The humanoid shoulder-elbow complex was animated and the animation was qualitatively compared to voluntary human reaching motions. **Figure 1** displays an example of one of the trajectory snapshots.

Figure 1. Qualitative comparison of humanoid mechanism to human.

The data from the human motion studies in (Stanišić et al., 2007) was utilized to attain the quantitative comparison. The mean difference between the reaching direction of the mechanism and the reaching direction from the data was 12.08^{o} with a standard deviation of 8.64^{o}. The mean difference between the elbow axis direction of the mechanism and the elbow axis direction from the data was 20.96^{o} with a standard deviation of 11.56^{o}. When the mechanism was able to reproduce a similar shoulder center position for a desired wrist position (the best case scenario), there existed a difference between reaching directions of 0.58^{o} with a difference between elbow axis directions of 3.39^{o}.

CONCLUSION

This work presented an algorithm for the kinematic control of a humanoid shoulder-elbow complex mechanism that reproduces the range of motion of the human shoulder-elbow complex. The kinematic solution replicates the motion of the human shoulder complex and closely approximates the coupling between the reaching direction and elbow axis direction for voluntary reaching motions. The algorithm used the method of successive iterations to solve the kinematically complex and coupled system. Replication of human shoulder-elbow complex motion was verified quantitatively and qualitatively.

REFERENCES

Craig, J.J. (1989), *Introduction to Robotics: Mechanics and Control, Second Edition*, New York, Addison-Wesley.

Dobrowolski, J.A. (1965), *Applied Optics*, 4:937-946.

Lenarćić, J. and Stanišić, M. (2003), *IEEE Transactions on Robotics and Automation*, 19:499-506.

Stanišić, M.M., Goehler, C.M., and Tomsić, M. (2007), *Applied Bionics and Biomechanics*, 4:47-55.

BIOMECHANICAL MODELING TO PREDICT THE RISK OF DEVELOPING PAINFUL KNEE OA

Krishna S. Iyer, Donald D. Anderson, Jennifer Baker, James C. Torner,
Thomas D. Brown, Neil A. Segal

– for the Multicenter Osteoarthritis Study Group –
Department of Orthopaedics and Rehabilitation, University of Iowa, Iowa City, IA, USA
e-mail: don-anderson@uiowa.edu   URL: http://poppy.obrl.uiowa.edu

INTRODUCTION

The Multicenter Osteoarthritis (MOST) study is an investigation of the incidence and progression of knee osteoarthritis (OA) in a cohort of 3026 men and women, 50–79 years old. It aims to link physical activity, weight, diet and other factors to the onset of knee pain and OA, using primarily associative epidemiological methods.

Subjects did not have knee OA symptoms upon entry to the study, but were selected as being at risk for its development. In addition to physical check-ups, MRI scans were obtained of subjects' knees at baseline and at regular intervals over a 30-month period, providing a unique opportunity to identify biomechanical risk factors for knee OA.

Discrete element analysis (DEA – Li et al. 1997) is a means of estimating articular joint contact stress, using bone surface geometries derived from CT or MRI. The utility of DEA for studying MOST subjects was previously established (Anderson et. al 2007). In the current study, the correlation of DEA-based estimates of contact stress with the onset of knee OA was investigated, in a nested matched case-control study of MOST subjects.

METHODS

Thirty MOST subjects who developed symptomatic knee OA after a 15-month follow-up (OA cases) and 30 subjects who did not (controls) were selected at random. Standardized MRI scans of subjects' knees were obtained at the baseline visit, as were weight-bearing bilateral 30º flexed knee radiographs. MRI images were segmented using OsiriX software (www.osirix-viewer.com), yielding a 3D cloud of points defining subchondral bone surfaces of both the femurs and the tibias.

Smoothed surfaces were fit to the points using Geomagic Studio software (Geomagic; Research Triangle Park, NC). Surfaces were registered using bilateral radiographs (Li et al. 2004) to obtain loaded knee alignment. Next the smoothed bone surfaces were imported into MATLAB (The Mathworks, Inc.; Natick, MA), where DEA solutions were computed (Figure 1). The cartilage was assumed to be 6 mm thick (combined femoral and tibial), with an elastic modulus of 12 MPa, and a Poisson's ratio of 0.42.
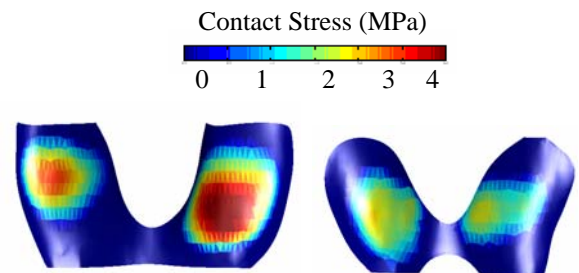
Contact Stress (MPa)

Figure 1: DEA-computed contact stress distributions for OA case (left) and control (right), with geometry derived from MRI

RESULTS AND DISCUSSION

The DEA contact stress distributions took less than a minute to compute, yielding mean and maximum contact stress values for each of the 60 subjects. The series-wide average peak contact stress for OA cases was 3.66 ± 0.13 MPa, a value that differed significantly from controls (2.99 ± 0.14 MPa). Series-wide average area engagement histograms showed that subjects' knees from the OA cases had a larger percentage of joint surface bearing higher stresses compared to the controls (Figure 2).
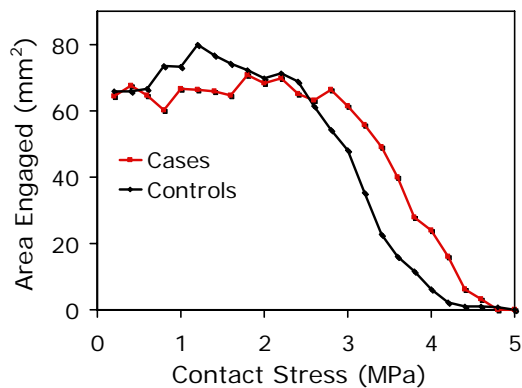
Figure 2: Area engagement histogram for OA cases and controls (n = 30 each). A significant difference was observed between the two groups (p < 0.001)

SUMMARY/CONCLUSIONS

This study incorporates biomechanical modeling of knee joint contact stress (using DEA), working from baseline radiographic images. It bridges the gap between associative and physical models of knee OA, enabling an epidemiological model to test whether identified risk factors may act through increased articular surface loading.

The speed and simplicity of this method for estimating knee joint contact stresses makes its application to subject-specific modeling highly attractive. This type of study has not previously been possible with more complex computational stress analysis techniques (i.e., finite element analysis).

By identifying thresholds of contact stress that predict development of painful knee OA, this type of study has the potential to improve patient care, and to guide the utilization of expensive interventions as they become available.

REFERENCES

Kawai T and Takeuchi N. *ASCE Int. Conf. Comput. Civ. Engng*, New York, 1981.
Li G, Sakamoto M, Chao EY. *J Biomech* 30:635-8, 1997.
Anderson, D, Segal N, Torner J, Brown T. *Am. Soc Biomech Conf,* California, 2007.
Li G, Wuerz TH, DeFrate LE. *J. Biomech Eng*. 126: 314-318, 2004.

ACKNOWLEDGEMENTS

HEAD ANGULAR ACCELERATION PULSE CHARACTERISTICS AFFECT BEHAVIORAL OUTCOMES FOLLOWING MILD DIFFUSE BRAIN INJURY

Brian D. Stemper, Ronald J. Fijalkowski, Thomas A. Gennarelli,
Narayan Yoganandan, and Frank A. Pintar

Department of Neurosurgery, Medical College of Wisconsin,
Department of Veterans Affairs Medical Center
Milwaukee, WI, stemps@mcw.edu

INTRODUCTION

Diffuse brain injury results from high rate head rotation. Characteristics of the head angular acceleration versus time pulse were theorized to influence injury severity (Gennarelli and Thibault, 1982; Ommaya et al., 1973). However, independent effects of acceleration magnitude and duration have not been clearly defined. This study was conducted to determine effects of increasing angular acceleration magnitude and duration on behavioral outcomes following mild DBI.

METHODS AND PROCEDURES

The experimental protocol was approved by our Institutional Review Board. Thirty adult male Sprague-Dawley rats were subjected to the experimental protocol, resulting in diffuse brain injury (DBI) through coronal plane head angular acceleration (Fijalkowski et al., 2007). Five control rats were subjected to the entire protocol minus induction of loading. Experimental and control rats were given anesthesia prior to the protocol and were given a reversal agent immediately following. Unconscious time was measured as the time from reversal agent administration to reappearance of the corneal response.

Experimental rats were divided into five test groups based on head angular acceleration pulse characteristics. Angular acceleration magnitude and duration were independently varied across three levels (Table 1).

Test Group	Magnitude (krad/s2)	Duration (msec)
Controls	--	--
M1D2	300	2.0
M2D2	425	2.0
M3D2	530	2.0
M2D1	425	1.0
M2D3	425	3.0

Table 1. Head angular acceleration pulse characteristics for experimental groups.

Rodent activity when placed in a Y-maze has been used to quantify spatial memory impairment (Fernandez-Gonzalez et al., 2008). All rats were placed in a Y-maze for 15 minutes approximately one hour after reversal agent administration. The entire maze was imaged from above using a digital video camera. The number of arm changes was quantified for each five-minute period. ANOVA determined statistically significant differences ($p < 0.05$) between test groups in unconscious time and number of arm changes during each time period.

RESULTS

All experimental rats survived head angular acceleration without skull fracture. Unconscious times were significantly longer for each experimental group compared to controls, and increased with increasing angular acceleration magnitude (M1D2 = 207±44 sec, M2D2 = 364±26 sec, M3D2 = 446±28 sec) and duration (M2D1 = 200±12

sec, M2D2 = 364±26 sec, M2D3 = 630±105 sec).

Post-injury behavioral activity was assessed using Y-maze activity (Figure 1). In general, activity was greatest during the initial time period, with a decreased number of arm changes during the second and third time periods. Number of arm changes was not significantly different between groups during the initial time period. Activity levels significantly varied between groups for the second and third time periods.
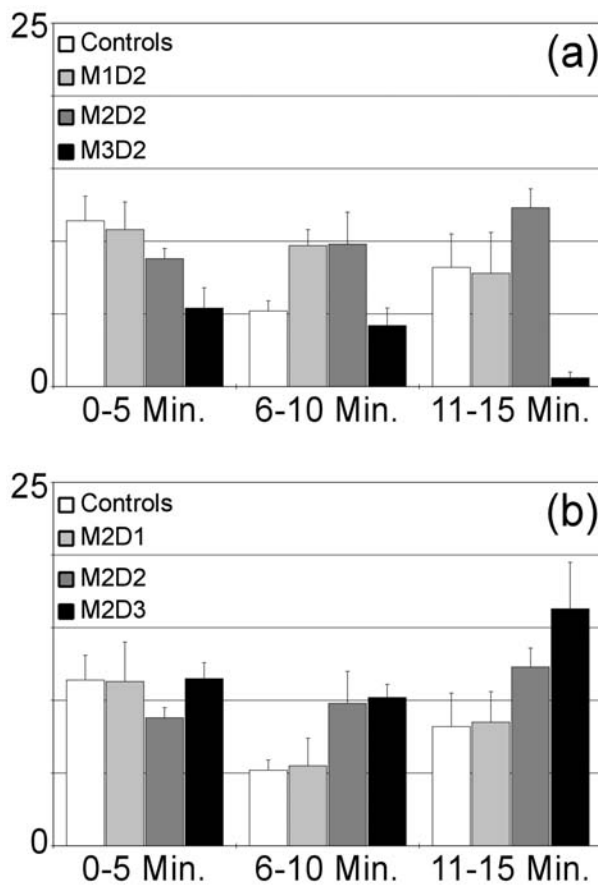
Figure 1. Number of Y-maze arm changes for increasing (a) magnitude and (b) duration.

Post-hoc analysis revealed that rats subjected to the highest magnitude pulse (M3D2) demonstrated significantly decreased Y-maze activity during the second and third time periods. Additionally, the longest duration group demonstrated significantly increased Y-maze activity during the third time period.

DISCUSSION

All experimental rats sustained DBI, as demonstrated by significantly longer unconscious times than controls, with longest unconscious times in the highest magnitude and longest duration groups. Although unconscious times were longer in all DBI groups, behavioral outcomes varied based on acceleration pulse characteristics. Decreased Y-maze activity in the high magnitude group (M3D2) may indicate neuronal damage in the superficial motor regions of the brain (parietal cortex). However, significantly increased Y-maze activity during the second and third time periods in the long duration group (M2D3) may indicate some level of spatial memory impairment, due to lack of habituation. This deficit can result from damage to the hippocampus, which is located deep to motor regions in the rat brain. Therefore, longer duration impacts may manifest as longer sustained strains within the subcortical fiber tracts of the hippocampus.

REFERENCES

Fernandez-Gonzalez R, et al. Long-Term Effects of Mouse Intracytoplasmic Sperm Injection with DNA-Fragmented Sperm on Health and Behavior of Adult Offspring. Biol Reprod, 2008.

Fijalkowski RJ, et al. New rat model for diffuse brain injury using coronal plane angular acceleration. Journal of neurotrauma, 2007; 24: 1387-98.

Gennarelli TA, Thibault LE. Biomechanics of acute subdural hematoma. The Journal of trauma, 1982; 22: 680-6.

Ommaya AK, et al. Head injury in the chimpanzee. 1. Biodynamics of traumatic unconsciousness. Journal of neurosurgery, 1973; 39: 152-66.

COMPARISON OF COMPUTATIONAL AND EXPERIMENTAL RESULTS FOR FEMUR FRACTURE RISK FOLLOWING DOUBLE-BUNDLE ACL RECONSTRUCTION

*O'Farrell M E, Lopes Jr. O V, Yoo Y, Fu F H, Smolinski P J
University of Pittsburgh, Pittsburgh, PA
*mae7@pitt.edu

INTRODUCTION

The traditional method of ACL reconstruction is to replace the ligament with a single graft (single bundle). However, studies have shown that the ACL is made up of the anterior medial (AM) and posterior lateral (PL) functional bundles (Zelle 2006). For this reason, double-bundle (DB) ACL reconstructions are now being performed in order to more closely restore normal, intact knee anatomy and kinematics (Yagi 2002).

Previous studies used finite element models of the femur, from both a sawbone model and CT scan data, to assess femur fracture risk after the addition of the PL tunnel (Bell 2006), and according to tunnel location (Egan 2007). These studies determined that the double-bundle technique did not increase the risk of femur fracture when compared to a single-bundle (SB) reconstruction, and that slight variations in tunnel placements do not significantly increase the risk of femur fracture. In the current study, cadaver femurs were used to validate the results of the computational finite element studies. The result of the experimental testing of the cadavers will be compared to the computational results.

METHODS

Eleven fresh-frozen cadaver femurs were used in this study. Both the AM and PL tunnels were drilled in the bone. A strain gage rosette was then attached to the bone just outside the AM tunnel (Figure 1), which has been shown by the computational studies to be an area of high stress (Bell 2006, Egan 2007). The strain gage rosette (Vishay-Micro Measurements) is made up of three gages stacked on top of each other (Figure 1), and allows for detection of the principle strains in an area.
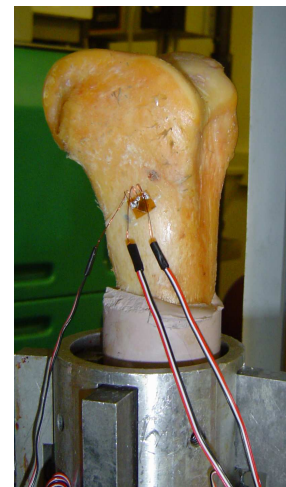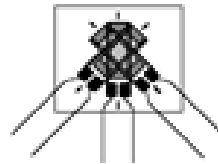
Figure 1 Strain gage rosette with leads (left), potted cadaver with strain gage attached (right)

After gage attachment, the proximal end of the femur (mid-shaft) was potted using a fast drying cement and inserted into an axial testing machine. A force sensor was used to determine the amount of force applied to the condyles in compression. Loads were applied by pressing a flat metal plate against the femoral condyles. Using load control software, loads were applied in 100 N intervals from 0 to 1300 N, and strain readings were recorded at each load. The principle strains were computed and the maximum principle strain was used in comparison to the computational strains from both the sawbone and CT scan finite element models.

RESULTS

The results of the experimental testing were plotted as micro-strain versus load applied (N). A least squared analysis was used to determine the linearity of the experimental lines. Table 1 shows the resulting r-squared value used to measure linearity (1 being linear), and the slope of each line.

Table 1 r^2 values and slope of cadaver results and computational models when plotted as micro-strain vs. load (N)

	Cadaver Average	Cadaver Std. Dev.	Sawbone Model	CT Model
r^2	0.991436	0.010449	1	1
slope	0.239245	0.088764	0.299	0.318

Using the student's t-test for small sample sizes, there was shown to be no significant difference between the slope values of the cadaver tests and the models. Also, the relationship between strain and load was shown to be close to linear (i.e. r^2=1), for cadavers 1-11. The strain was also analyzed at each load for both models and cadavers. Figure 2 shows the resulting strains at 1000 N in compression. Using the same statistical analysis, there was shown to be no significant difference among the values of strain at each load. (Note: all statistics reported at 98% confidence level)
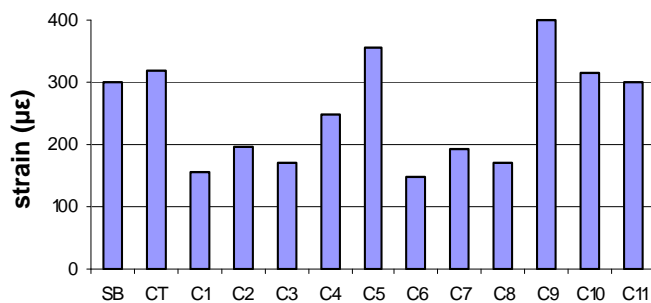
Figure 2 Chart showing strain ($\mu\varepsilon$) at 1000 N for sawbone model (SB), CT scan model (CT) and cadaver tests 1-11 (C1-C11)

DISCUSSION

The results of this study support the validity of the computational results obtained from the sawbone and CT scan models. As shown above, there was no significant difference between computational and experimental results for strain. The slight differences in slope can be attributed to the heterogeneous material properties of bone, which differ from specimen to specimen, and the homogenous material properties of the sawbone model. The steeper slope of both the sawbone and CT scan models suggests a stiffer material than that of the cadavers. This may be due to the loading techniques used in the experimental (distributed load) and computational (point loads) testing.

In the future, more physiological loading should be modeled by using the tibia-femoral joint. Eventually, an entire knee joint could be modeled to most accurately mimic physiological movement and loading.

REFERENCES

Zelle BA et al. *Sports Medicine*. 2006; 36(2): 99-108.
Yagi M et al. *Am. J. of Sports Medicine*. 2002; 30(5):660-666.
Bell KM et al. ORS#1142 2006
Egan M et al. ORS#825 2007

ACKNOWLEDGEMENTS

JOINT COUPLING OF THE REARFOOT AND KNEE IN RUNNERS WITH PATELLOFEMORAL PAIN SYNDROME DURING A PROLONGED RUN

Tracy A. Dierks[1] and Irene Davis[2]

[1]Department of Physical Therapy, Indiana University, Indianapolis, IN, USA, tdierks@iupui.edu
[2]Department of Physical Therapy, University of Delaware, Newark, DE, USA
URL: http://www.shrs.iupui.edu/pt/bios/dierks.php

INTRODUCTION

Patellofemoral pain syndrome (PFPS) is one of the most prevalent running overuse injuries. Excessive eversion has often been proposed as a mechanism associated with PFPS (Powers, 2003). However, recent literature suggests that joint coupling between the foot and knee may be related to running injuries (Heiderscheit et al, 2002; Dierks et al, 2007). Vector coding is a method that yields a coupling angle that is essentially a continuous excursion ratio. Coupling angles of 45° indicate equal amounts of joint motion. As values increase towards 90°, the amount of relative distal motion increases, whereas values that decrease towards 0° indicate increases in the amount of relative proximal motion.

As PFPS symptoms typically increase throughout a running session, we were interested in examining coupling over the course of a prolonged run. Therefore, the purpose of this study was to investigate coupling between the foot and knee in runners with PFPS over the course of a prolonged run. It was hypothesized that the PFPS group would display larger coupling angles due to relatively greater eversion at baseline. We also expected that these angles would increase to a greater degree in the PFPS group at the end of the run.

METHODS

Twenty runners with PFPS and 20 uninjured runners participated in the study. All were between the ages of 18 and 45 and ran at least 10 miles per week. Each subject performed a prolonged run on a treadmill at a self-selected pace. 3D kinematic data (120 Hz) of the leg with the most painful knee (random for uninjured) were collected for 20 consecutive footfalls at the beginning and end of the run. The prolonged run ended when 1 of 3 events occurred: 1) 85% heart rate maximum was reached, 2) 17 was reached on the rating of perceived exertion scale, and 3) for the PFPS group, 7 out of 10 was reached on a visual analog pain scale. Total run time varied from 20-45 minutes.

A modified vector coding method was used to evaluate joint coupling (Dierks et al, 2007). Coupling relationships of interest included rearfoot eversion (EV) with knee flexion (KF), knee adduction (KADD), and knee internal rotation (KIR). Angle-angle diagrams were constructed for each coupling relationship and coupling angles were then calculated (Sparrow et al, 1987). Coupling angles were assessed within 2 periods during the first half of stance. Period 1 occurred from heel-strike to the first impact peak of the vertical ground reaction force, while period 2 occurred from this peak to the maximum peak at approximately midstance. Within each period, coupling angles were averaged for each subject and group means were calculated. A 2-factor ANOVA for each period (group by time) was used to assess each coupling angle relationship ($p \leq 0.05$).

RESULTS AND DISCUSSION

No significant interaction effects were observed, as both the PFPS and uninjured groups responded similarly to the prolonged run. However, significant group and time effects were observed. Unexpectedly, in the

EV-KADD and EV-KIR couplings, the PFPS group exhibited significantly lower coupling angles during period 1 compared to controls (Figure 1). While not significant, the EV-KF coupling was also lower. This indicates that the runners with PFPS displayed less EV relative to knee motion during the initial loading period. However, no group differences were detected for the remainder of stance (period 2). Runners with excessive eversion have been reported to exhibit increased knee flexion, knee internal rotation, and less knee adduction (McClay et al, 1998). These knee motions may adversely effect the patellofemoral joint alignment and lead to PFPS. Therefore, this relatively reduced eversion may have been a compensatory control strategy to minimize abnormal knee mechanics. This period of early loading is important as the patella is not yet well seated into the femoral trochlea and is vulnerable to malalignment.

Interestingly, by period 2, coupling angles were similar between the 2 groups for all relationships. As this is the period of maximal loading, the PFPS group may not have been able to maintain the relatively reduced EV seen in early loading.

Finally, both groups increased their coupling angles in period 1 at the end of the prolonged run compared to the beginning. This may be an indication of fatigue, as EV has been shown to increase over the course of prolonged running (Derrick et al, 2002).

SUMMARY

It appears that coupling angles are lower at initial loading in the PFPS group. This may be an attempt to control EV during early loading in the PFPS group. During maximal loading in period 2, coupling angles are generally similar between groups. Finally, both groups increased their coupling angles over the course of the prolonged run.

REFERENCES

Derrick T, et al (2002). *Med Sci Sports Exerc*, 34:998-1002.
Dierks T, et al (2007). *Clin Biomech*, 22:581-591.
Heiderscheit B, et al. (2002). *JAB*, 18:110-121.
McClay IS, et al (1998) *Clin Biomech*, 13:195-203.
Powers (2003). *J Orthop Sports PT*, 33:639-646.
Sparrow A, et al. (1987). *J Mot Behav*, 19:115-129.
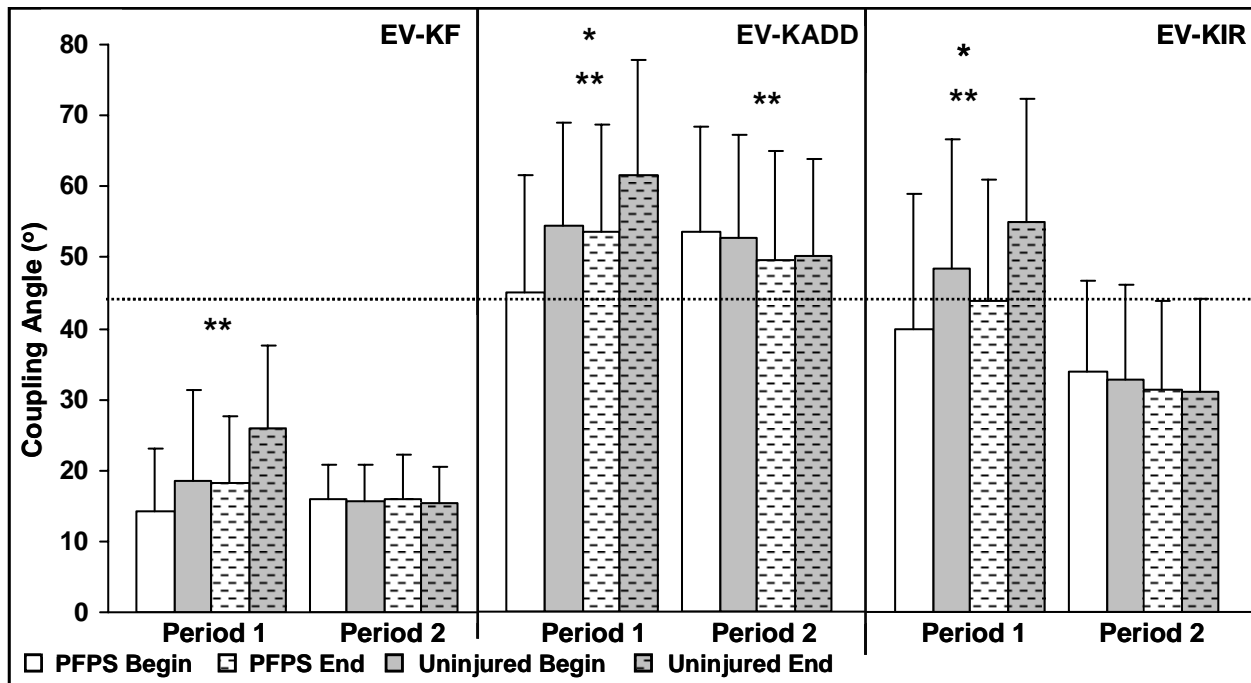
Figure 1. Coupling angle group means during the 2 loading periods of stance at the beginning and end of the run. * = Significant main effect for group in a period. ** = Significant main effect for time in a period. Horizontal dashed line at 45° indicates point of equal amounts of EV and knee excursion.

Elucidating the Relationship Between Residual Incongruities, Elevated Contact Stresses, and Cartilage Degeneration in Fractures of the Tibial Plafond

Thaddeus P. Thomas, Chris Van Hofwegen, Donald D. Anderson, JL Marsh, Thomas D. Brown
[1]Orthopaedics & Rehabilitation, The University of Iowa, Iowa City, Iowa, USA
thaddeus-thomas@uiowa.edu

INTRODUCTION

Residual incongruities following intra-articular fractures have been associated with aberrant articular contact stress distributions, linked indirectly to the onset of post-traumatic osteoarthritis (OA) (Wagner et al. 1996). The purpose of this study was to improve current understanding of the relationship between patterns of abnormal contact stress exposure and of cartilage degeneration, using advanced image analysis techniques and patient-specific finite element (FE) modeling.

METHODS

Articular joint contact stresses following surgical fracture reduction were quantified using a validated patient-specific contact finite element (FE) analysis (Anderson et al, 2007). FE models were created from post-reduction CT studies in a series of 11 tibial plafond fracture patients. The chronic contact stress exposure over a simulated gait cycle (contact stress times the resident time in gait, summed over all time steps) was calculated as a metric of degeneration propensity.

Cartilage outcome was evaluated from dual contrast multi-detector CTs obtained six months and two years post injury, for six patients. The contrast agent injected into the joints enabled segmentation of the subchondral bone and cartilage surfaces by a senior orthopaedic resident. Cartilage thickness was then calculated across the articulating surface using purpose-written MATLAB code.
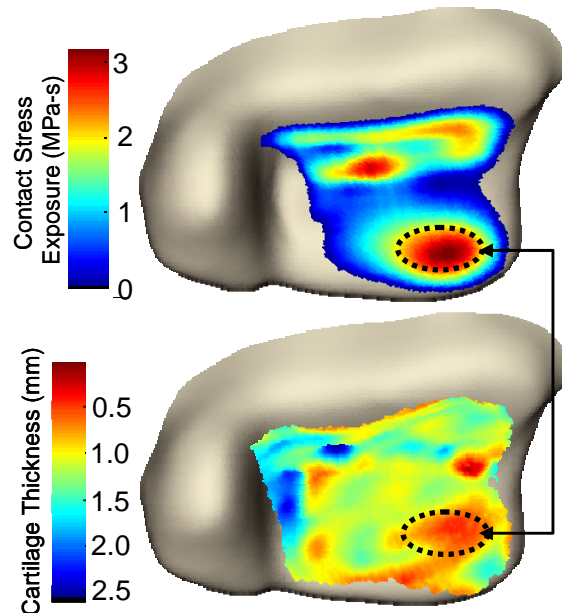
Figure 1. These antero-inferior views of a fractured tibia's articular surface illustrate the FE results (top) and cartilage thickness analysis (bottom). Spatial registration enabled pixel-by-pixel correlation between contact stress exposure and cartilage thickness.

Registration of the post-op FE simulations to the two year cartilage thickness maps was necessary for spatial comparison. Geomagic Studio software was used to obtain the necessary transformation to place post-op and two-year data into the same space. This was accomplished by aligning iso-surfaces created from metallic screws placed during fracture reduction. Registration was completed by transforming the surfaces and linearly interpolating cartilage thickness data to coincide with the FE nodal locations. The resulting cartilage thickness maps were quantitatively compared to the FE-computed contact stress exposures.

RESULTS

Localized areas of cartilage thinning generally corresponded to areas exposed to elevated contact stresses. Contact stress exposures of 2 MPa-s or greater were associated with a focal loss of cartilage [Fig 2]. For these six patients, the percent reduction in cartilage volumes from a pre-fractured state ranged from 11 to 81%. The most severely comminuted fractures experienced the greatest loss of cartilage, in addition to having the greatest contact stress exposures as assessed by FE. The area of cartilage loss ranged from 0 to 241 mm^2.

DISCUSSION

Clinical experience has shown that residual articular incongruity is poorly tolerated and is a likely factor in the progression of joint degeneration. FE modeling coupled with advanced imaging analysis techniques is improving our understanding of the mechanopathology of PTOA. No conclusive statements relating aberrant contact stresses to cartilage thinning can be made from the limited number of patients included. However, there is a clear spatial connection between elevated contact stress exposures over small and large regions, and focal areas with cartilage degeneration for this series of patients.

SUMMARY

The results from this study support an association between elevated contact stress exposure and focal cartilage degeneration. Restoration of normal subchondral anatomy may decrease cartilage loss and slow the development of post-traumatic osteoarthritis.
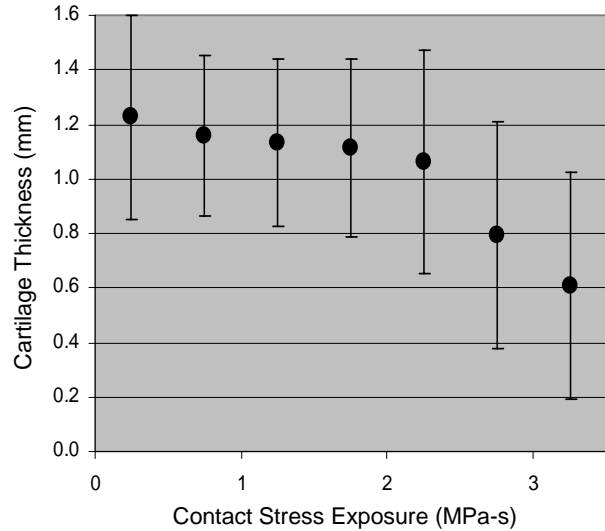
Figure 2. Point-by-point comparisons between computed contact stress exposure and cartilage thickness measures were made over the loaded articular surface. Cartilage thickness decreases as the exposure exceeds roughly 2 MPa-s.

REFERENCES

Anderson DD, et al. *J Biomech.* 2007;40(8):1662-9. Epub 2007 Apr 12.
Wagner Jr., W.F. et al. 1996. *Journal of Hand Surgery [American]* 21 (4), 554–560.

ACKNOWLEDGEMENTS

TYRAMINE-BASED HYALURONAN HYDROGELS FOR NUCLEUS PULPOSUS REPLACEMENT: CHARACTERIZATION BY MAGNETIC RESONANCE IMAGING

Ediuska Laurens[1,2], Aniq Darr [1,3], William Montgomery [4], Lars Gilbertson [4], Peter Zahos [5], Carl Winalski [1,6], Erika Schneider[6], Amit Vasanji[1], Anthony Calabro [1]

[1] Department of Biomedical Engineering, Cleveland Clinic Foundation, Cleveland, OH, USA, laurene@ccf.org.
[2] Department of Biomedical Engineering, Cleveland State University, Cleveland, OH, USA.
[3] Department of Biomedical Engineering, CASE Western University, Cleveland, OH, USA.
[4] The Center for Spine, Cleveland Clinic Foundation, Cleveland, OH, USA.
[5] Department of Neurosurgery, Cleveland Clinic Foundation, Weston, FL, USA.
[6] Imaging Institute, Cleveland Clinic Foundation, Cleveland, OH, USA.

INTRODUCTION

Degeneration of the intervertebral disc is a major etiological component of lower back pain (John, 1998). This disc degeneration is characterized by a decrease in water content due to decreased synthesis of glycosaminoglycans in the form of proteoglycans and their resulting loss from the extracellular matrix of the nucleus pulposus (Keun, 2004). Hyaluronan (HA), a hydrophilic glycos-aminoglycan, is a normal component of the extracellular matrix in the nucleus pulposus and the major un-sulfated glycosaminoglycan in this tissue (Shu-Hua, 2005). This study examines the feasibility of injection of tyramine-based HA (TB-HA) hydrogel into the nucleus pulposus to rehydrate degenerate discs in a rabbit needle puncture model of disc degeneration. In this study, the average signal intensity within the nucleus pulposus as measured and defined by magnetic resonance imaging (MRI) was used as measure of disc hydration and thus glycosaminoglycan content.

METHODS AND PROCEDURES

In this study, conventional carbodiimide chemistry was used to chemically generate tyramine-substituted HA (TS-HA).

Horseradish peroxidase was subsequently added to the purified TS-HA, and then the TS-HA was enzymatic cross-linked in vitro through the addition of dilute hydrogen peroxide to form TB-HA hydrogel. A rabbit model (three female New Zealand white rabbits, 4-5 kg BW) of early disc degeneration was utilized (Satoshi, 2004). Disc degeneration was induced by a 5 mm deep puncture with a 16-gauge needle into the nucleus pulposus of intervertebral discs at the L2-L3, L3-L4, and L4-L5 levels. After 6 weeks, the punctured discs were injected with 20-50 µl of TB-HA hydrogel at 25 mg/ml and examined after 1 week of injection. MR images of the discs were obtained at three time points: 1) prior to surgery (Pre-surgery); 2) after induction of disc degeneration (Post-puncture); and 3) after injection of TB-HA hydrogel (Post TB-HA). A 4 Tesla Seimans Bruker MRI scanner was utilized to obtain Sagittal T1 images with a gradient echo sequence (TR = 15 ms, TE = 3.4 ms), FOV 144 x 256 mm, and slice thickness 3.0 mm. Axial T2 images were also obtained at three echo times to create a T2 map with a turbo-spin echo sequence (TR = 5050 ms, TE = 19 ms, 38 ms, 76 ms, 133 ms), FOV 112 x 160 mm, and slice thickness 2.0 mm. A region-of-interest represented by the nucleus pulposus was defined, and its average signal intensity,

which is correlated to the water and glycosaminoglycan content, was measured using Image J software. Statistical analysis was performed using One Way ANOVA Student-Newman-Keuls Method (SNKM).

RESULTS

Table 1 provides the mean, and standard deviation of the average signal intensity of the discs of one rabbit at the different time points of the study.

Discs	n	ASI Mean ± SD
Pre-Surgery	3	48.8 ± 0.3
Post-Surgery	3	31.9 ± 4.7
Post TB-HA	3	44.2 ± 5.4

Table 1. Comparison of the average signal intensity (ASI) of the nucleus pulposus on T2 MRI maps.

DISCUSSION

Compared to the pre-surgical discs, the above data shows a loss of average signal intensity in the nucleus pulposus following induction of disc degeneration by needle puncture validating the needle puncture model. A recovery of average signal intensity in the nucleus pulposus of the degenerate discs to near normal levels was observed following injection of TB-HA hydrogel. Utilizing SNKM, a significant difference ($P < 0.05$, with power of 0.931) is observed between the normal discs (Pre-surgery) and the degenerate discs (Post-puncture) and between degenerate discs (Post-puncture) the TB-HA injected discs (Post TB-HA). However, no significant differences were found between normal discs (Pre-surgery) and the TB-HA injected discs (Post TB-HA).

SUMMARY

These results suggest that the TB-HA hydrogel has the ability to replace the glycosaminoglycan content lost due to disc degeneration, and potentially aid in the recovery of degenerate discs. Further research consists of using magnetization transfer imaging to quantify the glycosaminoglycan content in intervertebral discs and TB-HA hydrogel.

REFERENCES

John Antoniou et al, (1998), *MR in Medicine*, 40:900-907.

Keun Su Kim et al, (2004). *Spine,* 30:33-37.

Sobajima et al. (2004). *Spine,* 30:15-24.

Shu-HuaYang et al, (2005), *Artificial Organs*, 29**:**806-814.

ON THE PREDICTED BUCKLING BEHAVIOR OF THE HUMAN UPPER EXTREMITY UNDER IMPULSIVE END-LOADING: AGE AND GENDER EFFECTS

Yunju Lee[1] and James A. Ashton-Miller[2]

[1,2]Biomechanics Research Laboratory, Department of Mechanical Engineering,
University of Michigan, Ann Arbor, Michigan, U.S.A. yunjulee@umich.edu
URL: http://me.engin.umich.edu/brl/

INTRODUCTION

Falls are a leading cause of injury in the population (CDC, 2006). When an arm is used to 'break' a fall, the impulsive end-load at the wrist can easily reach one body-weight (1*BW) or more (DeGoede, 2002 & 3). Should the extremity collapse under that load, the head can strike the ground. In fact, fall-related head injuries are a problem in the elderly (Kannus, 2007) and they increase dramatically with age (Jacobsson, 2007).

We are not aware of any estimates of how age or gender affects the buckling load of a human extremity. This is likely due to the risk of injuring a subject's limb extensor muscles by a sudden stretch. To avoid this risk, we used computer simulation to calculate the load-displacement behavior of an upper extremity axially end-loaded by an impulsive load up to 1* BW, as in arresting a forward or lateral fall. We tested the hypothesis that the yield load depends on (1) the lumped rotational stiffness and viscosity of the elbow extensor and shoulder flexor muscles, which will in turn depend on age and gender, (2) the initial elbow angle at impact, and (3) the magnitude of the end load.

METHODS AND PROCEDURES

A planar, two-link, lumped parameter, musculoskeletal model of the adult upper extremity was developed with frictionless revolute joints at the wrist, elbow and shoulder. Anthropometric properties and ground surface stiffness were taken from DeGoede (2003). The resistance of the precontracted elbow extensor muscles to forced flexion was modeled with a rotational spring and damper at the elbow whose linear coefficients we identified from impulsive measurements in 5 females and 3 males (Mathias, 2006). These coefficients varied linearly with muscle preactivation levels, as they do with muscle force (Blanpied, 1993). The maximum volitional isometric shoulder flexor muscle strength, rotational stiffness and viscous coefficients were assumed to be 2.0-times and 1.5-times those for the elbow extensor muscles in healthy males and females, respectively (Stobbe, 1982). The model limb was flexed 10 degrees and end loaded by an axial impulsive force of known magnitude and time course (DeGoede, 2002). Simulations were run in ADAMS 2005 r2 using 10 ms increments. To simplify comparisons, we normalized the results to those involving the usual (70% MVC) muscle pre-contraction levels measured in forward falls (DeGoede, 2002). Compared to young males, size-matched young females (~25 years) and older males (~70 years) were assumed to exhibit a 0.2 decrement, and older females (~70 years) a 0.4 decrement in their arm strength-to-weight ratios and stiffness and viscosity coefficients.

RESULTS

The yield load of the healthy young male upper extremity was found to be 715 N (or just under 1*BW [73 Kgf]) (Figure 1) [with a

greatest allowable elbow deflection permitted by young males (103 degrees, DeGoede, 2002) of 880 N ('YM' in Figure 1)]. The corresponding yield [and allowable] loads for young female, older male and older female were 565 N [595 N], 565 N [700 N] and 420 N [440 N], respectively (Figure 1). The limb deflection behavior is divided into 'pre-yield', 'pseudo-yield' and the 'deflection hardening' regions (Figure 1).
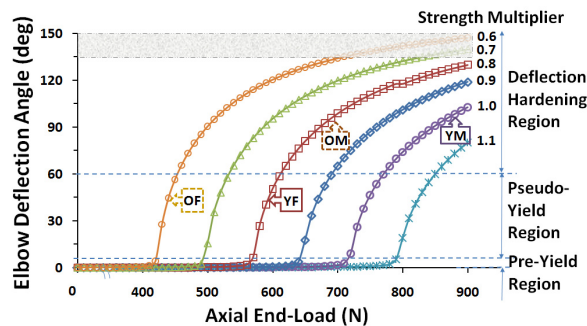
Figure 1. Predicted elbow deflection behavior as a function of upper extremity axial end-load and 'strength multiplier' (age, gender or muscle preactivity). The shaded region (at top) denotes limb collapse whereby the head would be predicted to strike the ground.

Initial elbow angle was found to significantly affect the yield load of the extremity (Figure 2), but not the load at which the head would strike the ground (i.e., 665 N in 'OF').
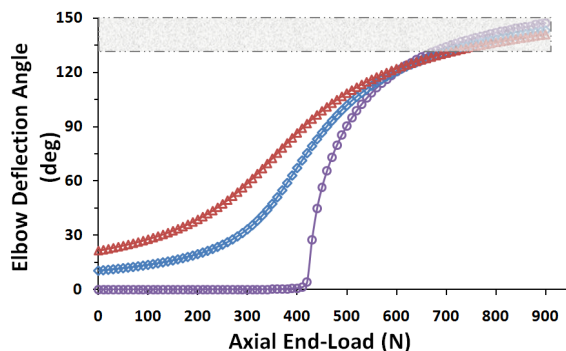
Figure 2. Effect of initial elbow angle (0, 10 and 20 deg.) on the limb deflection behavior of the older female limb.

DISCUSSION

These are the first estimates of the yield load of a slightly flexed extremity in a fall arrest scenario. The deflection hardening behavior may be overestimated in that post-impact muscle inhibition was not considered. The 'strength multiplier' results (Figure 1) show that yield loads decrease roughly linearly with a reduction in muscle pre-activity, and vice versa. Despite a number of simplifying assumptions, we believe the model makes reasonable predictions because the behavior of the young adult model extremity matches that we have measured in actual forward falls. In summary, the results underline the importance of older individuals maintaining as much arm protraction strength as possible.

CONCLUSIONS

Age and gender adversely affect upper extremity yield loads. This helps explain why fall-related head injuries increase with age.

REFERENCES

Centers for Disease Control and Prevention (2006). www.cdc.gov/ncipc/wisqars.
DeGoede, KM and Ashton-Miller, JA (2002). *J Biomech,* 35:843-848.
DeGoede, KM and Ashton-Miller, JA (2003). *J Biomech,* 36:413-420.
Kannus P et al. (2007). *Injury,* 38:81-83
Jacobsson LJ et al. (2007). *Acta Neurol Scand,* 116:300-6.
Mathias A et al. (2006). *WCB* Abstract.
Blanpied, P and Smidt, GL (1993). *J Gerontol,* 48:M58-63.
Stobbe TJ (1982). Ph.D. thesis, University of Michigan.

ACKNOWLEDGEMENTS

The effect of starting location on posture during a fine assembly part insertion task

Sean Y. Abdulla and Anne E. Moore

School of Kinesiology and Health Science, York University, Toronto ON, Canada,
amoore@yorku.ca

INTRODUCTION

Ergonomic workspace design can affect postures used by workers and associated muscle and joint loading (Grandjean 1969, Bao et al., 1997). Fine assembly work typically entails tasks involving high repetition and low loads (Mathiassen and Winkle, 1995) and poorly designed workspaces for such work may lead to the development of musculoskeletal injuries. Ideally, a workspace is designed appropriately in the first place rather then modified after injuries occur. However, it is not known whether the posture and associated muscle loading is predictable in the design process and if so what factors must be accounted for. The purpose of this study was to examine the role the location a worker obtains a part plays on posture at the location of part insertion. We hypothesized that starting location will have no affect on a subject's final posture during a fine assembly task.

METHODS AND PROCEDURE

Seven healthy university students (2 males, 5 females, mean age= 21.3 (+/- 2.2)) participated in the study. Subjects provided informed consent, as approved by the human participants review sub-committee (HRPC) of York University, Ontario Canada. Participants picked up an 18 mm x 13mm 6 pin relay from 1 of 4 bins (4 cm high) mounted at each corner of the workspace, oriented and fit the relay into 90 marked and labeled areas on a printed circuit board grid (77.5 cm x 57.3 cm) mounted on a tabletop. Table height was normalized to the participants elbow height at $90°$ flexion when standing in an erect posture. Kinematic data was collected at 60 Hz using a 7-camera (3 MX-F40, 4 MX40+) Vicon motion capture system and associated full body plug-in gait model. A 4 x 9 x 10 repeated measures ANOVA was performed. Independent measures included: starting location (4) (front right corner, front left corner, back right corner and back left corner), row (10) (saggital plane reach) and column (9) (frontal plane reach). Dependent measures included the 3 joint or segment axis angles at point of insertion (X: medial-lateral tilt, Y: anterior-posterior tilt: Z: rotation) for the head and trunk segments and the neck and shoulder joints. All angles calculated in rotation order Y, X', Z''. Means for each angle across each independent variable were calculated and the range (maximum mean – minimum mean) determined.

RESULTS

Significant main effects were found for row and column on each angle. Starting location had significant main effects for 8 of 12 angles: head X; neck X, Z; trunk Y, Z; and shoulder X, Y, Z. The mean ranges associated with each independent variable were: Starting location, 4.5º (1.3-10.2), Column, 19.9º (4.8-42.6) and Row 18.7º (3.0-37.3). Only 2 joints experienced starting location ranges greater than 5 degrees (table 1).

		SL	Column	Row
Neck	X	3.8*	11.5*	4.6*
	Y	2.2	6.7*	32.2*
	Z	10.2*	27.3*	12.8*
Shoulder	X	3.5*	25.1*	28.4*
	Y	5.9*	23.2*	51.5*
	Z	10.1*	39.7*	37.3*

Table 1. Angular Range (degrees) over starting location (SL), column and row at the neck and shoulder. (*sig. $p < .05$)

Shoulder posture was the most affected by starting location particularly in rotation. The trunk was the least affected (figure 1).
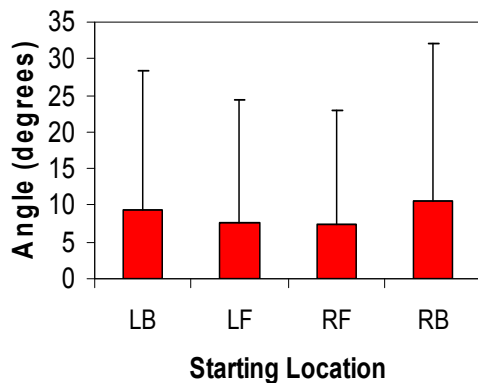
Figure 1. Mean trunk Y angles at each starting location.

DISCUSSION

Our results suggest that the starting location does influence the final posture prior to insertion. To date previous results in the prehension control literature are mixed. Desmurget et al (1998) did find initial location influenced final posture, where as Grea et al (2000) did not. This may reflect a difference in task – Grea et al (2000) had their participants grasp a sphere while Desmurget et al (1998) grasp an oriented cylinder. Perhaps the ability or need to "pre-orient" the hand or part is what makes the difference.

Compared to final location the effect of SL is small. For example, the 3.2º shift in trunk flexion between the four starting locations, while significant, may have minimal effect on the static muscle loading experienced in the low back during part insertion. Further collection of EMG and kinetic data will further clarify this question. Minimal utilization of the trunk throughout the task suggests that participants relied heavily on shoulder and head postures.

SUMMARY

The ability to predict posture in the design process would be beneficial. The results here suggest that for fine parts insertion tasks, there is a small effect of starting location on posture at insertion. Further work will examine the implications of this difference on kinetic variables.

ACKNOWLEDGEMENTS

REFERENCES

Bao, S. et al. (1997). *Int J Ind Ergon*, 20: 75-85.

Desmurget, M. et al. (1998). *Exp Brain Res*, 119:511-516.

Grandjean, E (1969). *Fitting the Task to the Man, an Ergonomic Approach. 1st ed.* Great Britain: Talor & Francis.

Grea, H. et al. (2000). *Exp Brain Res,* 134:155-162.

Mathiasson, S.E. and Winkel, J. (1996). *Int Arch Occup Environ Health*, 68: 94-108.

DETECTION OF GAIT IMBALANCE USING THE EXTRAPOLATED CENTER OF MASS

Vipul Lugade , Sue Ewers , Chu-Jui Chen ,

Sujitra Boonyong , Patima Silsupadol , Li-Shan Chou

Department of Human Physiology, University of Oregon, Eugene, Oregon USA
E-mail: chou@uoregon.edu, Web: biomechanics.uoregon.edu/MAL/index.html

INTRODUCTION

Falls are the leading cause of accidental death among older adults. An accurate quantification of balance control is needed to provide early detection before falls occur. Instantaneous inclination angles between the whole body center of mass (CoM) and center of pressure (CoP) during gait were reported to detect gait imbalance in the elderly (Lee and Chou 2006). However, one limitation of this parameter is that it is a quasi-static measure and does not account for the instantaneous CoM velocity.

Hof et.al. (2005; 2007) proposed the extrapolated centre of mass position (XcoM) which utilized the CoM position and velocity to determine an appropriate stability region during stance. Thus, the purpose of this study was to calculate the inclination angle formed by the line connecting XcoM and CoP during gait and test its feasibility to identify elderly people who are prone to fall. We hypothesized that adults with balance impairment would demonstrate a greater deviation of their XcoM with respect to their CoP as compared to healthy young and healthy older adults.

METHODS AND PROCEDURES

Ten elderly fallers (EF) (mean age = 80.3 ± 4.3), 10 healthy elderly controls (HE) (mean age =74.7 ± 6.3), and 10 healthy young adults (HY) (mean age = 21.6 ± 2.2) were recruited

for this study. Subjects were asked to walk along an 8-meter level surface at a self-selected pace while barefoot. Whole body motion was captured using an 8-camera motion analysis system at 60 Hz (Motion Analysis Corp., Santa Rosa, CA). A total of 29 markers defined a 13-segment model (Chou et al. 2003). Two force plates (AMTI, Watertown, MA) were used to collect ground reaction forces for the calculation of CoP. Inclination angles of the lines formed by the CoM and CoP as well as by the XcoM and CoP were computed for each frame through a gait cycle (Fig.1). Also, the ratio of the maximum anterior-posterior CoM-CoP to medial CoM-CoP (A-P/M-L CoM-CoP) inclination angle was calculated.

The effects of subject groups on the three variables were assessed using a one way analysis of variance. The significance levels for all tests were set at 0.05.
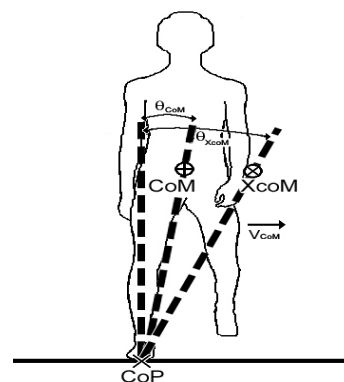
Figure 1. CoM-CoP and XcoM-CoP medial inclination angles are shown by θ_{CoM} and θ_{XcoM}.

RESULTS

The maximum medial CoM-CoP inclination angle indicated a possible group effect ($p = .054$), while the maximum medial XcoM-CoP angles were found to be significantly different between groups ($p = .007$). The tukey post hoc test showed the maximum medial XcoM-CoP inclination angle of elderly fallers was significantly greater than the healthy young adults ($p = .043$). The ratio of the maximum anterior-posterior CoM-CoP to medial CoM-CoP (A-P/M-L CoM-CoP) inclination angle in elderly faller was significantly smaller than both healthy young and healthy elderly groups. (Table 1.)

DISCUSSION

The CoM-CoP inclination angle identified fallers from non-fallers (Lee and Chou 2006), but only demonstrated a trend to discriminate between subject groups included in this study. When incorporating the CoM velocity, statistically significant group differences were detected in our subjects. This result confirms our hypothesis that a greater deviation may be measured among elderly fallers than healthy adults and further strengthens the use of the medial XcoM-CoP inclination angle.

It has been shown that an increased frontal plane angle usually accompanies a reduced sagittal plane angle in the elderly. Therefore, the ratio of the maximum anterior-posterior CoM-CoP to medial CoM-CoP inclination angle was examined to confirm this pattern. As was expected, the elderly fallers had the significantly smaller CoM-CoP ratios, when compared to both healthy groups.

SUMMARY

Findings of this study indicate that the XcoM-CoP frontal plane inclination angles and the ratio between A-P and M-L inclination angles might provide a more sensitive detection of elderly fallers.

REFERENCES

Chou, L. S., K. R. Kaufman, et al. (2003). *Gait & Posture,* 18: 125-33.

Lee, H. J. and L. S. Chou (2006). *J Biomech,* 87: 569-575.

Hof, A. L., M. G. Gazendam, et al. (2005). *J Biomech*, 38: 1-8.

Hof, A. L., R. M. van Bockel, et al. (2007). *Gait Posture*, 25: 250-8.

Table 1
Maximum medial CoM-CoP and XcoM-CoP inclination angles and ratio of sagittal-frontal plane inclination angles (mean ± SD).

Subjects	Healthy young	Healthy elderly	Elderly fallers	$p*$
Med. CoM-CoP	3.99 ± 0.79	4.29 ± 1.15	4.69 ± 1.68	.054
Med. XcoM-CoP	5.55 ± 1.25 [a]	6.31 ± 1.86 [a b]	7.20 ± 3.17 [b]	.007
A-P/M-L CoM-CoP ratio	3.79 ± 1.15 [a]	3.20 ± 0.95 [b]	2.63 ± 0.97 [c]	< .001

Note: Group means sharing a common superscript are not significantly different ($p > 0.05$). Differing superscripts (a,b,c) refer to groups with significant differences ($p < 0.05$).

Validation of Walkway Slip Resistance Measurements: A Gait Based Approach

Christopher M. Powers, Ph.D.[1], Mark G. Blanchette, M.S. (mgblanch@usc.edu)[1], John R. Brault, M.S.[2], Jim Flynn, P.E.[3], Gunter P. Siegmund, Ph.D., P.Eng.[4]

[1]Musculoskeletal Biomechanics Research Lab, Division of Biokinesiology & Physical Therapy, University of Southern California, 1540 E. Alcazar St., CHP-155, Los Angeles, CA 90089
[2]MEA Forensic Engineers & Scientists, 23281 Vista Grande Dr., Laguna Hills, CA 92653
[3]J2 Engineering Inc., 7636 N. Ingram Ave, Suite 108, Fresno, CA 93711
[4]MEA Forensic Engineers & Scientists, 11-11151 Horseshoe Way, Richmond, BC, Canada V7A 4S5

INTRODUCTION

Tribometers are devices that measure the slip resistance of walkway surfaces. There are over thirty tribometers that are commercially available, and each varies in its mechanical design and friction calculation method (Chang, Gronqvist et al. 2001). As a result, different tribometers yield varied measurements of friction for the same surface (Chang 1999; Gronqvist, Hirvonen et al. 1999; Chang 2002; Powers, Brault et al. 2007). The variability in tribometer-based friction measurements suggests that a value obtained from a given tribometer may or may not represent a measure of a pedestrian's risk of slip; a fact that undermines the validity of all tribometers. The purpose of the current study was to use slip risk (as quantified during human subject walking trials) to create a reference standard against which tribometer readings could be validated.

METHODS AND PROCEDURES

Eighty subjects (23 males, 57 females) between the ages of 20 and 39 were randomly assigned to walk across one of four walkway surfaces conditions (polished black granite, porcelain, ceramic tile and vinyl composition tile). Each floor condition was tested under wet conditions. To control for the influence of footwear, subjects were provided with a pair of Oxford-style shoes in their size. During testing, subjects wore a fall-arresting body harness attached to an overhead trolley. The ranking of surface slipperiness was based on the number of slip events (either heel or toe slips) observed for each condition. To confirm whether a slip occurred, an eight camera Vicon motion analysis system (Oxford Metric Ltd., Oxford, UK) was used to record the position of reflective markers placed on the heel and second metatarsal.

Following the human subject testing, eleven tribometers were used to measure the coefficient of friction (COF) of the four surfaces. For each surface condition, the COF was measured four times. The results of the tribometer measurements were then compared to the gait-based ranking of surface slipperiness using two criteria: 1) Did the tribometer measurements correctly rank the slipperiness of the different surfaces? 2) Did the tribometer measurements differentiate between surfaces with significantly different levels of slipperiness? To test for differences in the number of slips that occurred for each surface, a chi-squared test was used. A one-way analysis of variance (ANOVA) was used to compare tribometer readings across the four floor conditions. This analysis was repeated for each tribometer. *Post hoc* tests were run using a Fischer least significant difference (LSD) test to identify surfaces that were significantly different from one another.

RESULTS

The results of the human subject walking trials are presented in Table 1. All four surface conditions were significantly different from each other with respect to levels of slipperiness.

Surfaces	No Slips	Toe Slips	Heel Slips	Ranking
Granite	1	6	13	Most slippery
Porcelain	5	11	4	Moderately
Vinyl	13	7	0	Less
Ceramic	20	0	0	Least
Total	39	24	17	N = 80

Table 1. Results of human subject testing

The eleven tribometers produced widely varying friction measurements for the four surfaces (Table 2). Our results revealed that only four of eleven tribometers (Wessex pendulum, Sigler pendulum, Mark II and Mark III) met our compliance criteria by correctly ranking the four floor conditions and differentiating between surfaces of differing degrees of slipperiness. Of the seven tribometers that failed, two did not pass criteria #1 (Tortus III, HPS), two did not pass criteria #2 (Mark I, Bot 3000 static & dynamic) and three did not meet either criterion (English XL, C1028, Tortus II).

DISCUSSION

The results of our tribometer measurements were consistent with the conclusions of previous studies in that different tribometers give varied COF values for the same surface. In the current study, only four of the eleven tribometers tested met our compliance criteria by both correctly ranking all four conditions and differentiating between surfaces of differing degrees of slipperiness as established by the walking trials. These findings reinforce the need for objective criteria to ascertain which tribometers

effectively evaluate floor slipperiness and a pedestrian's risk of slipping. Moreover, this experimental protocol demonstrates that human gait-based measures of slipperiness can be used to create reference standards against which the output of tribometers can be validated.

Tribometer	Granite	Porcelain	Vinyl	Ceramic
English XL	0.18	0.23	0.21	0.49
Bot 3000 S	0.30	0.62	0.85	0.94
Bot 3000 D	0.20	0.23	0.38	0.74
C1028	0.22	0.44	0.65	0.58
Tortus II	0.35	0.47	0.64	0.60
Tortus III	0.14	0.21	0.34	0.24
HPS	0.32	0.61	0.85	0.73
Wessex	0.05	0.19	0.24	0.49
Sigler	0.13	0.16	0.20	0.42
Mark I	0.21	0.42	0.48	0.67
Mark II	0.18	0.22	0.31	0.69
Mark III	0.20	0.32	0.37	0.63

Table 2. Tribometer COF measurements. For the Bot 3000, S denotes static mode and D denotes dynamic mode.

REFERENCES

Chang, W. R. (1999). Int J Ind Ergon 24(299-313).

Chang, W. R. (2002). Saf Sci 40: 593-611.

Chang, W. R., R. Gronqvist, et al. (2001). Ergonomics 44(13): 1233-61.

Gronqvist, R., M. Hirvonen, et al. (2001). Appl Ergon 32(2): 163-71.

Powers, C. M., J. R. Brault, et al. (2007). J Forensic Sci 52(2): 400-5.

ACKNOWLEDGEMENTS

EFFECT OF ABILITY ON FREESTYLE SWIMBENCH STROKE CHARATERISTICS

Tracy H Spigelman, Tim L Uhl, David R Mullineaux, Thomas J Cunningham, Scott Mair, Robert Shapiro

University of Kentucky, Lexington, KY, USA
tray.spig@uky.edu

INTRODUCTION

Elite level swimmers are distinguished from non-elite swimmers by longer stroke lengths (SL) and faster stroke rates (SR), and decreased lag time between propulsive phases during freestyle defined by the Index of Coordination (IdC) (Seifert *et al*., 2004). Motor control research suggests elite performers have an enhanced ability to reorganize the sensory-motor system as greater constraints are placed on the system (Kelso *et al*., 1984). In swimmers this means making subtle adjustments in SL, SR, and IdC as necessary (Potdevin *et al*., 2006, Seifert *et al*., 2007).

Coaching swimmers poses a challenge in that the majority of technique is obscured by occurring under the water. A swimbench, designed to reproduce the biomechanical and physiological demands of swimming, may assist coaches in observing technique.

This study investigated the spatial-temporal, coordinative structures and kinematics of different ability levels swimmers on a dryland swimbench. Information gained from this research would provide evidence to support the use of a dryland device to coach swimming.

METHODS AND PROCEDURES

A sample of 11 elite (>85% of 100 m freestyle World Record time; age 22.9±4.1 yrs; height 180±8 cm; 6 Male; 5 Female), 10 intermediate (60-85% WR; 34.8±10.5 yrs; 172±8 cm; 5 M; 5 F) and 9 novice (<60% WR; 40.3±9.8 yrs; 174±11 cm; 3 M; 6 F) healthy collegiate and masters' swimmers volunteered for this study. All participants signed approved consent forms. Freestyle stroke was performed on a swimbench (Swimworks, Inc, Santa Rosa, CA) allowing kicking and rotation of the trunk about the cranial-caudal axis.
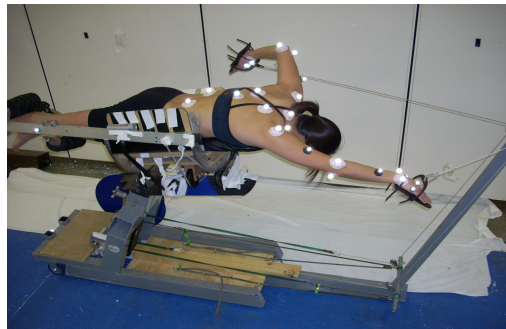
Figure 1. Freestyle swimming on swimbench

Following a 30-minute familiarization session, 30 reflective markers were attached on the upper extremity and torso of the swimmer. Each swimmer performed four ten second trials of freestyle swimming on the swimbench at a 100 m race pace.

Kinematic data were collected at 200 Hz using EVART 5.0 (Motion Analysis Corporation, Santa Rosa, CA). Raw data were exported into Visual 3-D (C-motion, Gaithersburg, MD) for calculation of joint trajectories and division in to stroke phases during each trial. Data were smoothed using a low pass Butterworth filter with cutoff frequencies determined via residual analysis

of 4 Hz for the shoulder, elbow, and hand, and 2 Hz for the trunk.

Dependent measures were SL calculated as maximum hand displacement in the cranial-caudal plane and SR calculated as number of stroke cycles per second (c/s). IdC was calculated as previously described (Seifert *et al.,* 2007) as the mean times 'between the first right arm pull and the first left arm exit' and 'second left arm pull and the second right arm exit' presented as a percentage of the stroke cycle (%ofS). These dependent measures were analyzed between groups and within trials using two-way mixed ANOVAs.

RESULTS

No significant differences were found between groups or within trials for SL, SR or IdC ($p > 0.05$; see Table 1).

	Novice	Intermed	Elite
SL (m)	1.13±3.2	0.91±.21	0.88±.19
SR (c/s)	0.53±.12	0.65±.13	0.61±.15
IdC (%ofS)	-20±18	-11±20	-8±12

Table 1. Novice, intermediate and elite level swimmers stroke characteristics.

DISCUSSION

Large variability between swimmers has been reported previously (Schnitzler *et al*., 2007, Seifert *et al*., 2007) as swimmers often use a different techniques to achieve the same goal.

As well as large variability, the mechanical construct of the bench likely contributes to the lack of difference between ability levels. As swimmers placed their hand in a fixed length pulley system this could have prevented a full range of motion. SL values on the swimbench were much less than values reported in water (elite male 2.54±0.27, recreational male 2.14± 0.26, elite female 2.15±0.13 recreational female 2.07±0.15 m; Schnitzler *et al*., 2007).

This would be expected since there is no glide on the swimbench as there is in the water.

Values for the IdC are similar to those noted by Siefert *et al*. (2004) for elite male swimmers during a 100m freestyle (IdC = -1.1±4.5%) as the trend for IdC was closer to zero for elite swimmers. This indicates a longer period of propulsion and suggests a better ability to organize the sensory motor system when the environment is altered. The tendency for better swimmers to have an IdC closer to zero and higher SR is logical as an increased arm speed is needed to achieve a longer duration in the propulsive phase.

SUMMARY

Freestyle SL, SR, and IdC can not be distinguished between skill levels on a swimbench. IdCs closer to zero and increased SR support that elite swimmers may have advanced levels of sensory-motor organization as environmental constraints are modified. The use of the swimbench may not help coaches discriminate between swimmers skill levels, but may have other training benefits not yet identified.

REFERENCES
Kelso, J.A.S. *et al*. (1984). *Am J Physio,* 246:R1000-4.
Potdevin, F. *et al*. (2006). *IJSM,* 3:193-8.
Schnitzler, C. *et al*. (2007). *IJSM,* 28(2): 164-71.
Seifert, L. *et al*. (2004). *J Sport Sci*, 22:651-660.
Seifert, L. *et al*. (2007). *Human Mov Sci*, 26: 68-86.

THE COMPARISON OF KINETICS AND KINEMATICS AMONG DIFFERENT TYPES OF RESISTANCE TRAINING

Hsiang-Hsin Wang[1], Tzyy-Yuan Shiang [2] and Chuan-Show Chen[3]

[1]Doctoral candidate, Institute of Coaching Science, Taiwan Sport University, Taoyuan, Taiwan,
mystarmailbox@yahoo.com.tw
[2] Professor, Institute of Exercise and Sport Science, National Taiwan Normal University, Taipei,
Taiwan, tyshiang@yahoo.com.tw
[3] Professor, Graduate Institute of P.E.,Taiwan Sport University, Taichung, Taiwan,
chenyy@ntcpt.edu.tw

INTRODUCTION

Most athletes have been using resistance training technique to enhance their jumping, striking or throwing performance. These rapid acceleration movements require a high power output of the involved muscles rather than high force production. Therefore, recent resistance training emphasized velocity specificity of resistance training, which has demonstrated that the greatest strength gains occur at or near the training velocity (Behm and Sale 1993). The evidence indicated that performed resistance training with maximal velocity and no deceleration phase may represent a method for overloading the neuromuscular system effectively throughout the range of motion and result in greater training effect in rapid and explosive performance than traditional resistance training (Newton et al. 1996). The purpose of this study was to compare the mechanism (Kinematics, Kinetics, and Muscle activation) among slow ramp movement, ballistic movement and functional isometric movement. The result of this study may reveal which is the superior form of resistance training for the development of power.

METHODS AND PROCEDURES

Subjects: Sixteen male taekwondo athletes, who were currently training for national intercollegiate athletic game in Taiwan, volunteered to be the subjects in this study. The subjects' mean ($\pm$SD) age, height, and weight were 20.6 ± 2.0 years, 175.4 ± 2.9 cm, and 70.2 ± 8.2 kg, respectively. **Procedure:** There were two testing phases in this study. The first testing phase involved the design of a brake system, which was combined with knee extension training machine for performing function isometric movement. During this phase, maximal knee extension strength (1RM) was also assessed by having the subjects perform a concentric-only knee extension for comparison of EMG recorded during later trial and arrangement of testing load. The load lifted in the best successful attempt was recorded in kilograms. After 20minutes warm-up exercise, the second phase began. Each subject was instructed to complete knee extension action 5 times with 30% 1RM resistance. The mode of three types of resistance training was demonstrated in figure 1. **Equipment:** A goniometer was attached on the joint of levers to measure the range of concentric phase during testing movement. From staring position to full extension position, the range was set as 0~100° which could be divided into every 10% of total concentric movement. The displacement of weigh stack was measured by UD-300 displacement sensor that was installed above the weigh stack. Load cell was connected with cable of machine to measure the pulling force. The surface electrode module was attached over the belly of rectus

femoris to measure muscle activity during concentric phase.
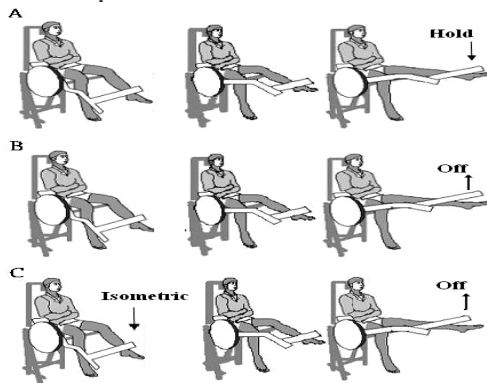
Figure 1. Diagram of SRM slow ramp movement (A), BAM ballistic movement (B) and FIM functional isometric movement (C).

RESULTS

Peak velocity was no difference among three types of resistance movement, but the average velocity was significant higher for BAM and FIM compared to SRM (figure 2). Further analysis revealed that velocity was higher during BAM and FIM after beginning and remained better acceleration till the end of the movement. The average force and peak force were significantly higher for the BAM and FIM compared to the SRM. The average force was also significantly higher for BAM compared to FIM (Figure3). The peak EMG was not different among three types of resistance movement, but the average EMG was significantly higher for BAM compared to SRM (Figure 4).
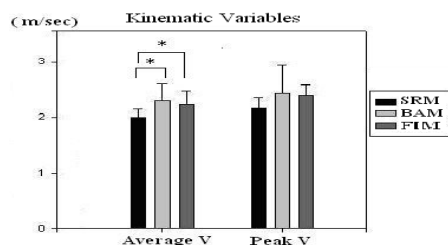
Figure 2. Weight stack velocities of concentric phase among three types of resistance movements.
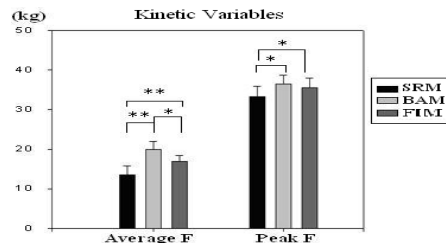
Figure 3. Pulling forces of concentric phase among three types of resistance movements.
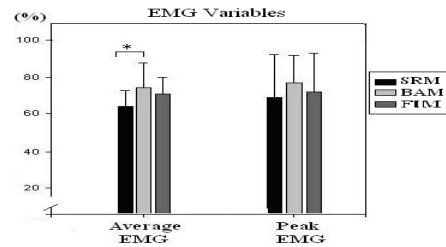
Figure 4. EMG activity of concentric phase among three types of resistance movements.

DISCUSSION

The primary result of this study demonstrated that attempting to perform BAM and FIM as fast as possible with 30% of 1RM load could result better velocity, force and EMG activity than SRM. The rectus femoris of these two types of movement was active throughout the concentric phase and maintained better acceleration and force output over the entire range of motion. It has been proposed that this type of movement could provide superior loading condition for neuromuscular system and increase muscle power effectively.

SUMMARY

BAM and FIM could perform higher velocity and maintain better acceleration than SRM. These types of movement are ideal training method for improving explosive strength.

REFERENCES

Behm, DG and Sale, DG (1993). *Sports Medicine,* 15(6):374-388.
Newton RU et al. (1996). *Journal of Applied Biomechanics,* 12: 31-43.

PHYSICAL ACTIVITY FOR MAINTAINING HEALTHY BONE DENISTY WITH AGING

Katherine Boyer, Jonathan Rylander, B. Jenny Kiratli, Tom Andriacchi, Gary Beaupre

[1]Mechanical Engineering, Stanford University, CA, USA
[2]VA Bone and Joint Rehabilitation R & D Center, Palo Alto, CA USA
E-mail: kboyer@stanford.edu

INTRODUCTION

Complications associated with falling, specifically fractures, are a large problem in the aging population. Exponential increases in hip fracture rates occur with age (Samelson et al.,2002) and age-related loss in bone mineral density (BMD) is a major factor for osteoporotic fractures (Rivadeneira et al.,2007). Decreases in BMD of 6.6 to 8.8 % per decade have been reported in the literature (May et al.,1994). Bone density is strongly influenced by the magnitude and frequency of the applied loading (Carter et al.,1987) and the importance of physical activity on bone healthy is well established. However, while levels of physical activity (duration and intensity) typically decrease with age (Bohannon,2007), it is not clear to what degree the decline in BMD and increase in fracture risk are inevitable parts of aging. That is, to what degree does age-associated reduction in physical activity contribute as opposed to aging alone. Therefore the purpose of this study was to investigate the relationship of BMD with physical activity in older men and women.

METHODS

Walking speed and ground reaction force (GRF) data were collected for 87 healthy active older volunteers (27 men, 68.0 yrs ± 1.5; BMI 25.9 ± 0.6 & 60 women 62.9 yrs ± 1.1; BMI 23.8 ± 0.4) as they walked at self-selected slow, normal, and fast speeds on an 11m long walkway. BMD was quantified for the total femur region using dual energy X-ray absorptiometry (GE/Lunar iDXA). The habitual daily activity history for each subject was assessed using an activity monitor worn on an ankle sleeve (AMP 231/ 331 Dynastream Innovations Inc. Canada). The mean of five days of activity was used to quantify average number of steps per day and average walking velocity for each subject.

A mathematical model of bone density regulation as a function of the daily tissue "effective" stress has been derived and modified for application in vivo (Whalen et al.,2001). In this model, "bone density index" (BDI), considers both the influence of the magnitude of loading at the joint, as estimated by GRF (% BW), and the number of loading cycles, n_{steps}, on bone mineral density (BMD).

$$BDI = \left(n_{steps} \times (\beta \times GRF_{ave})^m\right)^{1/2m}$$

where $m=3$ is an empirically determined constant and β=BW/pooled mean BW. The linear regression equation for the walking velocity and vertical GRF (in % BW) relationship was determined using measured GRF and speed for this population. This was used to estimate GRF_{ave} based on the individuals' average walking speed from the activity monitoring. This GRF_{ave} was then used along with the average number of steps

per day to calculate BDI for each subject.

Multiple regression models were used to look at the effects of BDI and age on BMD. To assess the effect of age on BMD, the subjects were grouped by decade (50, 60 and 70's) into three age categories. Age effects were assessed by entering age group as a variable into the model.

RESULTS

The association between BDI and BMD was statistically significant. BDI accounted for 14.8% of the variance in BMD. Adding age into the regression model did not significantly improve the model prediction (r^2=0.155). The slope of the regression for BDI-age and BMD-age was not different from zero. (Figure 1). No differences in walking velocity or body weight were found between the three age groups.
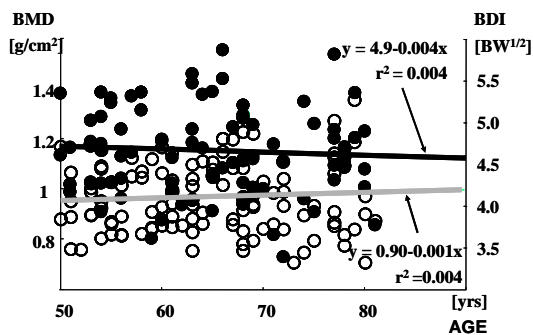
Figure 1: Relationships between BMD and age (unfilled pts and gray line); BDI and age (black pts and line). Based on the iDXA (GE/Lunar) normative database, we would expect a 12% decrease in total femur BMD for males and a 21 % decrease in females between the ages of 50 and 80 yrs.

DISCUSSION

The results of this study suggest loss of BMD is not an inevitable part of aging.

Daily physical activity, as quantified by the BDI value, can provide the required mechanical stimulus to maintain homeostasis in bone remodelling rates. The magnitude of the dynamic loading is strongly correlated with BW and movement speed. Physical activity also helps maintain lean muscle mass and is thus an important factor in creating a significant mechanical stimulus for bone (Gjesdal et al.,). BMD decreases with disuse are well documented. The results of this study suggest that if activity levels are maintained and thus the habitual stress stimulus for lower extremity bones does not change that the previously documented bone loss with aging can to some degree be mitigated. Future work should focus on quantifying whether an activity quantity or intensity threshold level exists.

Reference List

Bohannon,R.W.,(2007), *PHYS THER*, **87**, 1642-1650.

Carter,D.R. et al.,(1987), *J Biomech*, **20**, 785-794.

Gjesdal,C.G. et al.,*Maturitas*, **In Press, Corrected Proof**,

May,H. et al.,(1994), *Age and Aging*, **23**, 235-240.

Rivadeneira,F. et al.,(2007), *J Bone Miner Res*, **22**, 1781-1790.

Samelson,E.J. et al.,(2002), *American Journal of Public Health*, **92**, 858-862.

Whalen,R.T. and Breit,G.A.,(2001), Patent **US 6,183,425 B1**,

EFFECTS OF AN UNSTABLE SHOE CONSTRUCTION IN LOW SPEED RUNNING

[1,2]Katherine A. Boyer, Katerina Blazek, [1,2]Thomas Andriacchi

[1]Mechanical Engineering, Stanford University, CA, USA
[2]VA Bone and Joint Rehabilitation R & D Center, Palo Alto, CA USA
E-mail: kboyer@stanford.edu

INTRODUCTION

Prevention of running injuries by inducing changes in the lower extremity kinetics with shoe interventions is a research area with high interest. While a traditional shoe constructions aim to provide stability new shoe developments have focused on creating an unstable environment with the goal of improving strength of the static and dynamic stability muscles. Such a device has been developed by the Masai Barefoot Technologies (MBT) group. The MBT shoe has a rounded sole in the anterior-posterior direction. Recent studies with the MBT shoe have shown changes in the lower extremity muscle activation patterns, joint kinematics and kinetics compared with traditional shoes in walking (Nigg et al.,2006). Joint moment magnitudes have been suggested to be important factor in the development in running injuries (Stefanyshyn et al.,2006; Ward et al.,2004).Similar changes in the joint moments for running as walking might suggest the MBT shoe could be a training device to maximize gains in fitness while minimizing overuse injury development as It is thus of interest to determine if the accommodations to the unstable sole design results in beneficial reductions in the joint moments during running. **Therefore the purpose of this study was to investigate the effects of low speed running in the MBT shoe compared with a conventional athletic shoe on lower extremity gait characteristics.**

METHODS AND PROCEDURES

19 healthy volunteers were tested, all with no history of lower-limb injury or pain: 11 women (age: 28.9 +/- 7.3 years; BMI: 22.7 +/- 2.9) and 9 men (age: 32.6 +/- 7.5 years; BMI: 23.5 +/- 1.8). Informed consent was obtained from all subjects per Stanford University IRB guidelines. The subjects were asked to wear the shoe for a two week period prior to testing. Kinematic marker data and ground reaction forces (GRF) were collected as subjects perform low speed running at a self-selected comfortable pace in a traditional athletic shoe and an MBT shoe. The intersegmental joint forces and external joint moments were calculated using inverse dynamics and a previously published link model (Andriacchi et al.,1997). Paired Student's t-tests were used to compare the shoe conditions.

RESULTS

The self-selected jogging speed in the MBT (2.53 m/s) shoe was significantly slower (0.11m/s or 4.4 %) than for the athletic shoe ($p < 0.05$). The differences in sagittal plane joint kinematics at both heel-strike and toe-off were greatest at the ankle. No significant kinematic differences were found at the knee at either heel-strike or toe-off or at hip joints at heelstike. A smaller hip extension angle at toe-off was found ($p < 0.05$).

There was significant decrease in the hip flexion and abduction moments, the knee adduction and internal rotation moments and the ankle dorsi-flexion, plantar-flexion and inversion moments ($p < 0.05$). An increase in the knee flexion moment and ankle eversion moments was found ($p < 0.05$). (Figure 1). There were no differences in the magnitude of the impact or active peaks in the vertical GRF, or the loading rate of the impact peak between the MBT and athletic shoe.

DISCUSSION

Similar to walking in the MBT (Nigg et al., 2006) the most dramatic kinematic differences occurred at the ankle joint during running while very little change in the knee and hip angles were found despite the dramatic change in the sole structural properties. Changes in the joint moments responsible for the movement task (sagittal plane) suggest changes in the muscle activation patterns. Specifically, the decrease in ankle dorsi and plantar flexion moments suggest less tibialis anterior and triceps surae muscle activations. In the absence of increased antagonistic muscle activity this suggests the joint loading at the ankle is reduced. The increased flexion moment in the MBT shoe suggests an increase in quadriceps muscle activity and thus an increase in contact force and stress in the tibio-femoral and patello-femoral joint. (Ward et al., 2004).

The effect of subtle changes in the shoe midsole or insert geometry on the joint kinematics and kinetics is often small and not among test subjects in running (Nigg,2001). However, the results of this study indicate that if a dramatic change in the sole construction is made that predictable changes in the joint kinematics and kinetics can be invoked.

REFERENCES

Andriacchi,T.P. et al.,(1997), Basic Orthopedic Biomechanics, 37-68.
Nigg,B.M.,(2001), *Clin.J.Sport Med.*, **11**, 2-9.
Nigg,B.M. et al.,(2006), *Clin.Biomech.(Bristol., Avon.)*, **21**, 82-88.
Stefanyshyn,D.J. et al.,(2006), *American Journal of Sports Medicine*, **34**, 1844-1851.
Ward,S.R. and Powers,C.M.,(2004), *Clinical Biomechanics*, **19**, 1040-1047.
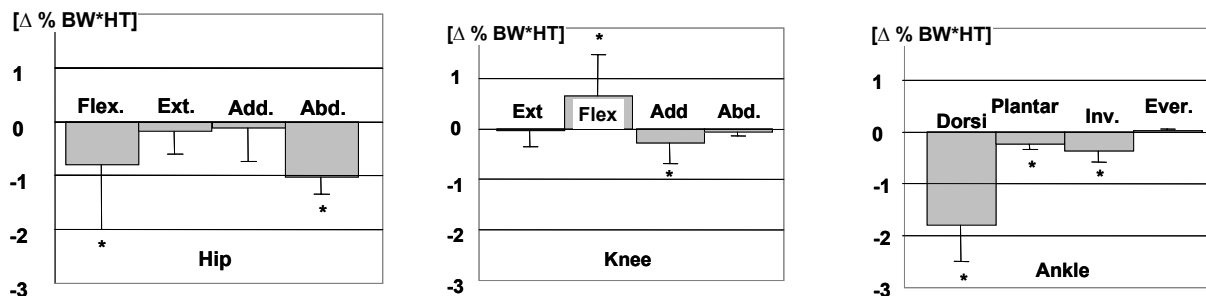
Figure 1: Mean ± SE change in the peak external joint moments during stance phase of jogging. A positive value indicates there was an increase in the MBT shoe.* indicates a significant difference between the MBT and the athletic shoe ($p<0.05$).

DEVELOPMENT OF AN APPARATUS TO PRODUCE HIGH IMPACT EXTREMITY LOADING WITH AN APPLICATION IN THE LOWER LEG

Cheryl E. Quenneville[1], Gillian S. Fraser[2], Cynthia E. Dunning[1]

[1]The Jack McBain Biomechanical Testing Laboratory, Department of Mechanical & Materials Engineering, The University of Western Ontario, London, ON, Canada, cdunning@uwo.ca
[2]General Dynamics Land Systems Canada, Engineering Design & Development, London, ON, Canada

INTRODUCTION

High impact loading of the lower leg occurs during various events, including ejection seat and parachute landings, and direct or indirect (*i.e.* in-vehicle) contact with landmines. Different from car crashes, these events have higher peak forces over shorter time spans. To protect the legs, injury tolerance levels for the shank must be defined. The current standard for military vehicles exposed to mine blasts is to maintain axial shank loading below 5.4 kN (AEP-55, 2006). However, it is of interest to know whether this load level alone is a suitable tolerance level, or if the energy and/or momentum imparted must also be limited. This paper outlines the design and validation of an impacting apparatus capable of applying controlled axial loads to cadaveric or Anthropometric Test Device (ATD) tibias. This will be used in future investigations of lower leg injury criteria.

METHODS AND PROCEDURES

The test area of the impacting apparatus (Figure 1) includes a stainless steel sheet with a linear rail, which supports two brackets on bearings. These brackets support both ends of a test specimen. The proximal bracket has attachment points for either a potted cadaveric tibia or an ATD tibia.

A projectile (Figure 1, inset), accelerated through a tube by pressurized air, supplies the required impact load to the distal end of the specimen. It consists of a threaded rod with multiple discs that can be added to alter its mass. A flange ring at the exit of the acceleration tube allows the projectile to strike the bracket, but not fully exit the tube.
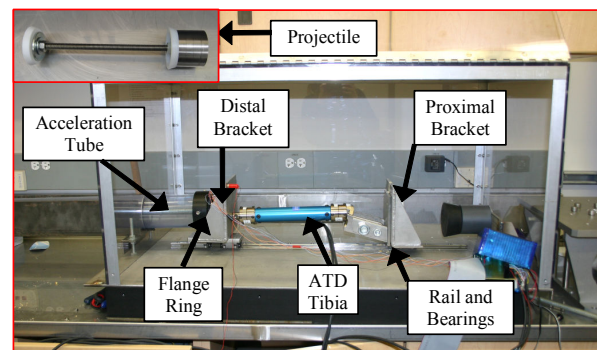
Figure 1. Impacting Apparatus. A projectile (inset) supplies an impulse to a specimen.

The required compressed air is stored in a tank, whose pressure is controlled by an electronic regulator (500-AG, ControlAir Inc., Amherst, NH, USA). Air is released from the tank to the acceleration tube by a fast-acting solenoid valve (VXR2380, SMC Corporation, Tokyo, Japan). Varying the pressure allows control over the projectile's exit velocity, which is quantified using two reflective optical sensors attached to the flange ring.

Design criteria for this device included the ability to achieve impact velocities in the vicinity of 5 m/s (characteristic of indirect mine blast; Manseau and Keown, 2005) and axial forces in the range of 4.3 to 11.4 kN (reported to produce leg injuries; Yogonandan *et al.*, 1996), over a range of input energy and

momentum levels. To verify the apparatus' ability to meet these criteria, the roles of the independent variables (pressure, projectile mass, and projectile travel distance) on the dependent variables of interest (projectile exit velocity and force imparted to the distal leg) were examined. Three masses (m_1=2.6 kg, m_2=3.6 kg, and m_3=4.6 kg) were each projected from three firing distances (d_1=8 cm, d_2=16 cm, and d_3=24 cm). Pressures were then adjusted to achieve velocities and forces in the desired ranges. All tests were performed against an ATD leg, and the imparted axial force measured from its distal internal load cell (Model 3644, Robert A Denton, Inc, Rochester Hills, MI, USA). Force and velocity data were collected at a sampling rate of 6500 Hz. Repeatability was quantified by the standard deviation in both force and velocity over 5 trials for each mass at a single pressure and distance.

RESULTS

Figures 2 and 3 graph exit velocity and imparted force, respectively, versus pressure. For all mass-distance combinations, velocity varied linearly with pressure ($R^2 > 0.98$), as did force ($R^2 > 0.96$). Increasing projectile mass decreased both velocity and force. The standard deviation among repeated trials ranged from 2-3% for velocity and 6-9% for force.
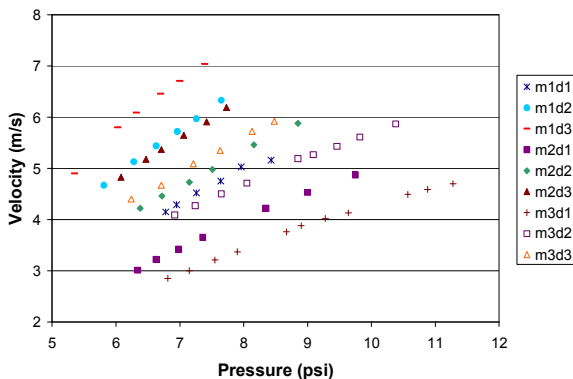
Figure 2. Velocity vs. Pressure for each mass over the three travel distances.
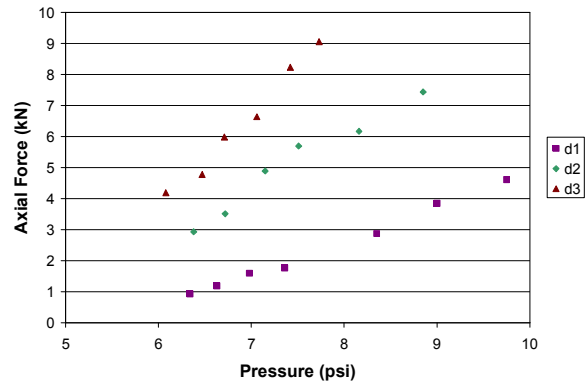
Figure 3. Axial Force vs. Pressure for 3.6 kg mass only, over three travel distances.

The energy and momentum associated with the target force value of 5.4 kN ranged between 46-54 J and 15-22 Ns, respectively.

DISCUSSION

Lower leg damage resulting from high impact loads can be lifestyle-altering. By properly identifying injury thresholds, such injuries may be avoided. This device is an important tool for this assessment, allowing experimental tests over a span of impact levels to be conducted in a controlled environment.

This device is capable of producing impact events within the range of critical velocity and force parameters described by others in a controlled, repeatable manner. Furthermore, targeted load levels can be achieved while varying the energy and momentum input to the system. This apparatus may now be used to develop a shank injury criterion specific to high-impact events.

REFERENCES

AEP-55 Vol. 2 (2006). *NATO/PIP*, pp. 43-46.
Manseau, J and Keown, M (2005). *IRCOBI Conference*, pp. 299-310.
Yogonandan, N. *et al.* (1996). 962426 *SAE*, pp. 207-218.

ROLE OF PELVIC FLOOR MUSCLE IN URINARY CONTINENCE DURING A STRESS TO THE BLADDER: AN ELECTROPHYSIOLOGICAL AND BIOMECHANICAL EVALUATION ON FEMALE RATS

HH Jiang[1,3], L Salcedo[1], AM Gustilo-Ashby[1], B Song[3], MS Damaser[1,2]

[1] Cleveland Clinic, Cleveland, OH, USA, Damasem@ccf.org
[2] Louis Stokes VA Medical Center, Cleveland, OH, USA
[3] Southwest Hospital, Third Military Medical University, Chongqing, CHINA

INTRODUCTION

Pelvic floor muscle (PFM) exercise has been regarded as a primary choice for treatment of stress urinary incontinence (Wells, 1990). To determine if PFM activity contributes to urinary continence, we tested PFM electromyogram (EMG) response to an externally applied bladder pressure on female animals.

METHODS

Thirty-one female adult Sprague-Dawley rats were studied under urethane-anesthetization with simultaneous electrophysiological and mechanical recordings of filling cystometry (CMG; 5 ml/h) via transurethral catheter, PFM (pubo- or iliococcygeus muscle) EMG and external urethral sphincter (EUS) EMG. These muscles were accessed directly by the opening of pubic symphysis in a supine position. An external increase in bladder pressure until urinary leakage (ΔP) was made by slowly pressing a cotton swab on the bladder and removing it quickly at the first sign of leakage at the urethral meatus. Six of the rats underwent repeat ΔP testing after bilateral transection of the levator ani nerve, which innervates the PFM (pubococcygeus muscle and iliococcygeus muscle). Another six of the rats underwent repeat ΔP testing after bilateral transection of the pudendal nerve, which innervates the EUS.

RESULTS

During filling CMG, EUS EMG showed steady tonic activity during continence and bursting activity during voiding. Some rats (n=13) showed steady tonic activity in the PFM EMG during bladder filling and decreased activity (*arrow c*) during voiding (Fig. 1).
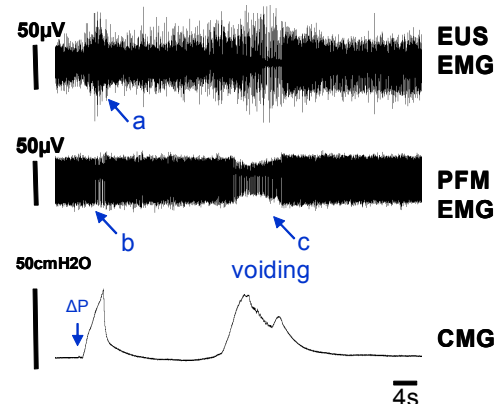
Fig.1. the simultaneous recordings of EUS EMG and PFM EMG during ΔP testing & during filling CMG (PFM EMG showed tonic activity during continence). arrow a and arrow b, EUS and PFM response to ΔP testing; arrow c; PFM response to voiding.

PFM EMG in other rats (n=18) showed no tonic activity during filling, but could be activated by pinching the perineal skin around the urethra meatus. This activity could be maintained unless voiding occurred (Fig. 2).

The ΔP to leakage caused increased EUS EMG activity, or a bladder-to-urethra guarding reflex to prevent urinary leakage (*arrow a*). However, there was no such

positive response in PFM EMG to contribute urinary continence. In contrast, 36% of the ΔPs caused a decrease in PFM EMG activity (*arrow b*). This may reflect a mechanism of PFM response intended to protect the bladder and upper urinary tract from high pressure by allowing urinary leakage.
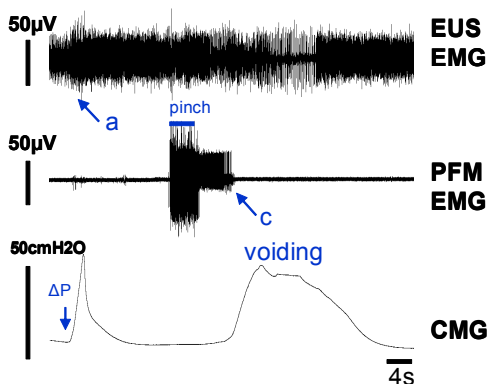
Fig.2. the simultaneous recordings of EUS EMG and PFM EMG during ΔP testing & during filling CMG (PFM EMG showed no tonic activity, but activated by pinching perineal skin). arrow a, EUS response to ΔP testing; arrow b, PFM response to voiding.

ΔP was not significantly different after bilateral levator ani nerve transection (41 ± 6 cmH$_2$O) compared to the same animals when intact (47 ± 4 cmH$_2$O; Fig. 3). In contrast, ΔP was significantly decreased after bilateral pudendal nerve transection (23 ± 5 cmH$_2$O) compared to the same animals when intact (44 ± 6 cmH$_2$O).
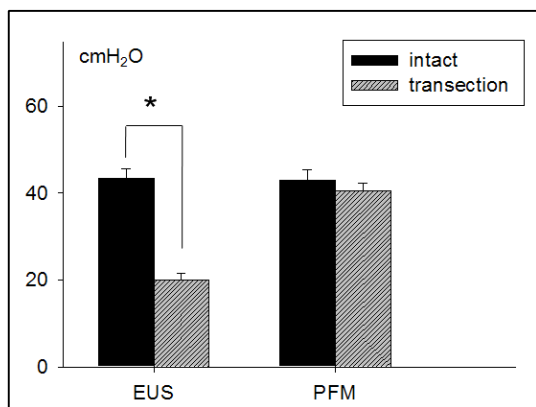
Fig. 3. ΔP to urinary leakage before & after transection of the nerves which innervate the EUS or PFM. PFM, pelvic floor muscles; EUS, external urinary sphincter (* $P < 0.01$; paired-t-test).

DISCUSSION

In the classical anatomical view, the levator ani muscles are dually innervated by the pudendal nerve on the perineal surface and by branches of the sacral nerves on the pelvic surface (De Lancey JOL, 1997). However, recent studies in human cadavers indicate that the levator ani muscles are innervated solely by a nerve traveling on the intrapelvic surface of the muscles without innervation of the pudendal nerve in the ischiorectal fossa (Wallner et al., 2006). This anatomical assessment was also confirmed in rats (Bremer et al., 2003).

From our electrophysiological and biomechanical investigations, we suggest that the PFM, unlike the EUS, has no contribution to prevention of incontinence during an applied increase in bladder pressure (bladder-to-urethra guarding reflex). Probably, PFM exercise facilitates continence by reinforcing the PFM to decrease bladder neck mobility or prolapse since the PFM supports the pelvic organs. The PFM is involved in multiple aspects of urogenital and anorectal function, but is not involved in the above mechanism to maintain continence during an external increase in bladder pressure.

REFERENCES

Bremer, RE. *et al.* (2003). Anat.Rec.A Discov.Mol.Cell Evol.Biol. 275, 1031-1041.

De Lancey JOL, (1997). Surgical anatomy of the female pelvis. In: Te Linde's operative gynecology. Philadelphia, Lippincott-Raven.

Wallner, C. *et al.* (2006). Obstet.Gynecol. 108, 529-534.

Wells, TJ. (1990). J Am.Geriatr.Soc. 38, 333-337

NEUROMUSCULAR CONTIRBUTION OF THE LEG FLEXOR MUSCLES TO KNEE JOINT STIFFNESS FOLLOWING A SUDDEN LEG PERTURBATION

Joel A. Cort and Jim R. Potvin

Department of Kinesiology, McMaster University, Hamilton, ON, Canada, cort@mcmaster.ca

INTRODUCTION

In previous work, sEMG has been used as an analog to determine joint stability or joint rotational stiffness (JRS) (Chiang et al., 2001). Although this approach may lack the fidelity needed for full JRS analysis, this sEMG amplitude (AMP) approach provides investigators with an understanding of activation levels when muscles attempt to contribute to JRS. Also, the sEMG approach has been used to understand the neuromuscular responses to perturbations (Granta et al., 2004). The purpose was to utilize sEMG AMP to examine the response of muscles crossing the knee joint before, and immediately after, the initiation of a sudden perturbation (PERT).

METHODS AND PROCEDURES

Nineteen subjects participated in the study, (10 males: 26.4±2.8 years, 74.3±9.8 kg, 1.8±0.06 m; 9 females: 25.2±2.8 years, 62.9±7.8 kg, 1.7±0.06 m). sEMG from the leg flexors: biceps femoris (BF), semimembranosus (SM), medial gastrocnemius (MG), lateral gastrocnemius (LG), and the leg extensors: rectus femoris (RF), vastus lateralis (VL), vastus medialis (VM) of the right leg were recorded. For the purpose of this paper, only the knee flexor muscles will be presented. Subjects were fitted with an ankle brace to resist ankle motion and positioned prone on a table where they maintained a right knee angle of 90° before the PERT. A pneumatic PERT device forced each subject's right knee into sudden extension via a rapid push force (78±2.2N) to the posterior of the ankle brace, such that the forces acted directly through the ankle joint (minimal ankle moment). Two PERT timing knowledge (TK) conditions were tested: 1) known timing (KT) was self-elected via control button, 2) unknown timing (UT) delivered after a random duration between 1-15 sec). Three masses were fastened to the top of the ankle brace to manipulate the Potential Energy (PE) of the lower leg/foot (0, 7.5 & 15% of leg mass). sEMG data (1000 Hz) were band-passed filtered (2nd order Butterworth, 100-498 Hz), full wave rectified, normalized to an MVE contraction AMP and dual-pass low pass filtered (2.5 Hz). A uni-axial goniometer measured the extensor rotation of the knee. The sEMG data were windowed into 3 time periods (TP) and the average AMP was calculated for each: 1) baseline (BLTP) from 150-100 ms prior to the PERT, 2) Pre-PERT (PPTP) from 15-0 ms prior to the PERT, 3) Reflex (RFTP) from 25-150 ms post PERT.

RESULTS

A repeated measures ANOVA (p<0.05) was completed for each muscle and Tukey's Post hocs were completed between PE conditions at each TP. Results can be viewed in Figure 1. An interaction between TP and PE was found for the BF. During the RFTP, the BF showed an sEMG AMP decrease of 12% MVE in the PE15 condition when compared to both the PE0 & PE 7.5. The SM had a main effect of TK as well as an interaction between TP and PE. For the main effect of TK, the SM was 26 %MVE greater during the KT condition compared to UT. The TP/PE interaction

revealed that the sEMG AMP were lower by 9 & 14 %MVE during the RFTP when PE was 15, compared to 0 & 7.5, respectively. The MG muscle had a main effect of TP where the RFTP had higher sEMG AMP than both the BLTP and PPTP. During the RFTP, the MG had sEMG AMP 64 & 44 %MVE greater than the BLTP and PPTP, respectively. The LG muscle also had a main effect of TP. This muscle had sEMG AMP 53 & 38 %MVE higher during the RFTP, compared to BLTP & PPRT, respectively.

DISCUSSION

The results suggest that, when following a PERT, the neuromuscular system responds by increasing the activation of muscles that have roles in aiding in JRS. Specifically, the reflex time period for all muscles, in all cases, had greater sEMG amplitudes than the two time periods preceding the perturbation. This exhibits the importance of this system, as it is the first to respond to a system disturbance. In addition, it is evident that the neuromuscular system chooses specifically, based on mechanical and physiological characteristics, muscles that will aid in the safety of the joint. This is evident in this study as BF and SM had EMG amplitudes that were that were, on

average, 65 and 55% greater than both the MG and LG.

The results also show that the neuromuscular system may be affected by an increase in PE. During the RFTP, when PE was increased there was a statistically significant decrease in the activation of the muscles that would contribute most to JRS (ie. BF & SM). Whether this decrease is biomechanically relevant is debateable, as the most dramatic changes were only 21.4-19.1%MVE for the BF and 16.7-14.7%MVE in the SM. Further biomechanical modeling, including calculated muscle force and restorative muscle moments, may provide insight into why this decrease occurred in both the BF and SM muscles.

REFERENCES

Chiang, J., Potvin, J. R., (2001). *Spine* **26**, 1457-1464.
Granata, K. P. et al. (2004). *J. of Biomechanics* **37**, 241-247.

ACKNOWLEDGEMENTS
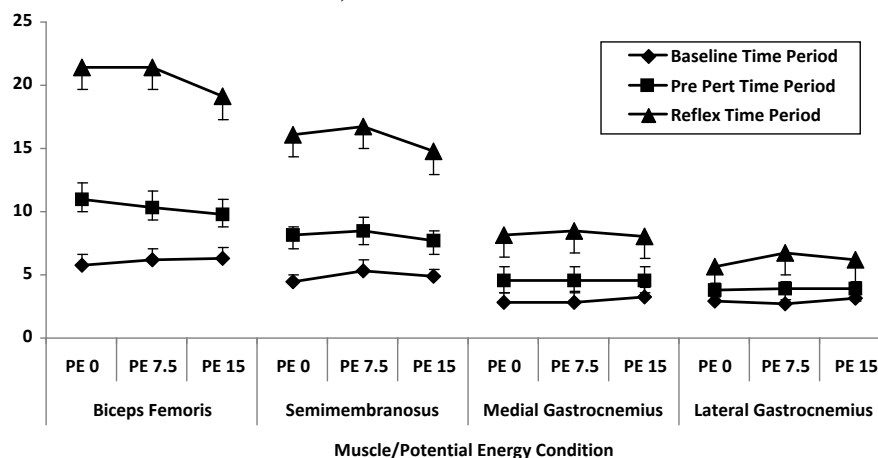
Figure 1. Averages of sEMG amplitudes of each leg flexor muscles exhibiting, the interaction effect, between PE conditions and TP when the amplitudes are calculated. Standard error bars are shown (n=19).

Three-Dimensional Analysis of the Trajectory of the Ankle While Running

Thomas J. Cunningham[1], Tim L. Uhl[2], Robert Shapiro[1], Carl G. Mattacola[2]

[1]Department of Kinesiology and Health Promotion, College of Education, [2]Division of Athletic Training, College of Health Sciences, University of Kentucky, Lexington, KY, USA,
tommyc@uky.edu

INTRODUCTION

The ankle is a possible attachment point between the lower extremity and a device which can guide the lower extremity through motions similar to running. There is a lack of published data to statistically support descriptions of the trajectories of the lower limb during running. The following research was conducted to provide additional detail and understanding to previous works studying ankle trajectories over several running speeds.

METHODS AND PROCEDURES

Twenty-six running athletes of varying experience and training frequency volunteered for this study (age=23±4 yrs, weight=78±10 kg, height=1.80±.06 m). Retro-reflective markers were placed on the subject's right lower extremity at the following locations; the ASIS, lateral femoral epicondyle and the lateral malleolus. Subjects then ran on a treadmill for 10-15 seconds at four speeds, 2.0, 3.8, 4.52 and 5.36 m/s, respectively.

Coordinate data of each marker were collected at 200 Hz using 4 Hawk cameras (Motion Analysis, Santa Rosa CA). Data were filtered using a low-pass 4th order Butterworth filter with a cutoff frequency of 5 Hz with exception of the ASIS marker in the horizontal and depth direction which was cutoff at 1 Hz to account for treadmill translation. Cutoff frequencies were chosen using methods described by Winter (1990). Maximum anterior femoral position was used to differentiate between gait cycles. Twelve gait cycles were normalized to 201 points and ensemble averaged for each speed. All trajectory data were offset relative to the ASIS and maximum displacement range in each direction was calculated for statistical comparison across 4 speeds.

RESULTS

A repeated measures ANOVA with a Bonferonni correction revealed that the displacement range of the ankle significantly increased both horizontally and vertically across all speeds ($p<.0083$). Results were mixed in the depth direction with a significant difference in displacement range occurring between the top speed of 5.36 m/s and the speeds of 3.8 and 4.52 m/s, respectively. There was, however, no significant difference in the depth displacement range when running at 3.8 m/s compared to 4.52 and 2.0 m/s. Displacement range values are shown in Table 1.

Speed (m/s)	Direction (cm)		
	Horizontal	Vertical	Depth
2.0	63.8 (6.8)	27.0 (5.3)	6.0 (2.3)
3.8	88.6 (6.6)	49.2 (9.4)	5.9 (1.9)
4.52	95.9 (8.2)	55.5 (9.4)	6.4 (1.8)
5.36	101.5 (8.4)	60.0 (8.8)	7.1 (2.0)

Table 1. Mean displacement ranges (±SD) of the ankle in each direction for every speed. The Horizontal displacement is along the length of the treadmill.

Greater detail concerning the actual path of the ankle can be seen in Figure 1 where the

average trajectory paths for each speed are plotted.
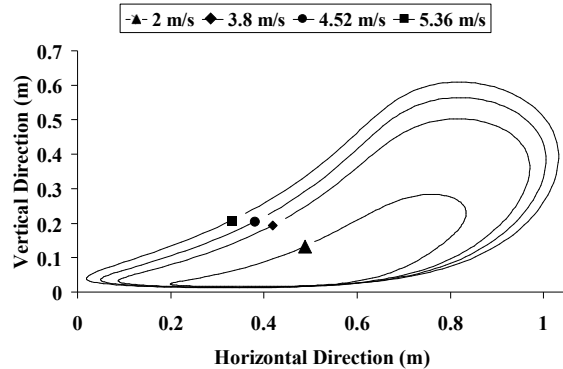
Figure 1. Sagittal plane trajectory displacement for the ankle at each speed tested. Subjects are facing left and the ankle traverses the path counterclockwise. Marker location indicates ankle position at maximum anterior femoral position.

Trajectory data in the frontal plane projected from a rear view is illustrated in Figure 2. There is a large difference in scaling of the horizontal axis when compared to Figure 1 due to the small amount of depth motion.
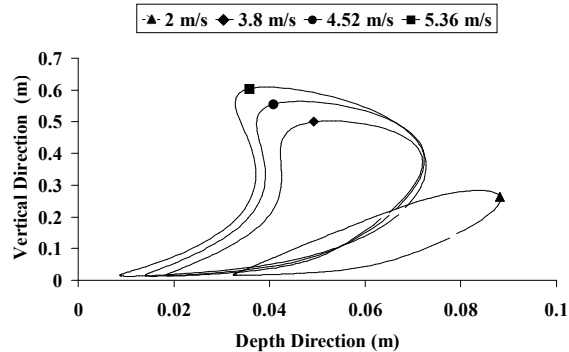
Figure 2. Frontal plane trajectory displacement for the ankle at each speed tested. Subjects are viewed from the rear and the foot traverses the path in a clockwise fashion. Marker only indicates different speeds.

DISCUSSION

The goal of this research was to have a better quantitative understanding of the path of the ankle during running. Our findings agree

with that of Cavanagh (1990) who found similar path tracings and ranges in the sagittal plane at similar speeds. The lack of difference found in the depth direction at the slowest speed might be due to the proximity of the transition speed of walk to jog for some runners. A differing transition speed between runners would inherently lead to a larger amount of variance. Movement in the depth direction was substantially less than that in the sagittal plane but should not be disregarded. If attempting to replicate motion at these speeds, these seemingly small movements might have significant clinical consequences and should not be disregarded.

SUMMARY

Speeds used in this study can be classified as a slow jog to a fast run. As speeds increased we found that range displacements also increased. A limitation of this study was the maximum speed of our treadmill, 5.36 m/s. Qualitative findings at elite running speeds (Hoshikawa and Miyashita 1973, and Mah et al., 1994) suggest that ranges will continue to increase for higher speeds. Future research should test this hypothesis and elaborate on these findings. With higher speeds documented, ankle trajectory for the entire spectrum of gait speeds should be well understood and the design of exercise devices focusing on specificity training of the running gait can be more accurate.

REFERENCES

Cavanagh, P. (1990). *Biomechanics of Distance Running,* Illinois, Human Kinetics

Hoshikawa, T and Miyashita, M (1973). *Medicine and Sport,* 8:342-48.

Mah, C. et al. (1994). *Journal of Motor Behavior,* 26(2):83-102.

Winter, DA. (1990). *Biomechanics of Human Movement.* New York, Wiley

RECOVERY OF POSTURAL SWAY AFTER STATIC STRETCH OF THE ANKLE JOINT

Tomoaki Iwata[1] , Akinori Nagano[1] , Zhi-wei Luo[1,2]

[1]Department of Computer Science and Systems Engineering, Kobe University, Japan
freddy_toro@cs11.cs.kobe-u.ac.jp
URL: http://www.research.kobe-u.ac.jp/eng-ro-man/mainpage.htm
[2]Environment Adaptive Robotic Systems Laboratory
Bio-Mimetic Control Research Center, RIKEN, Japan

INTRODUCTION

It has been well assumed that stretching is an effective exercise for the purpose of warming up, improving flexibility and preventing injury (Ferber et al., 2002; Wilson et al., 1991). However, recently it has also been reported that stretching decreases muscular force development and delay the onset of muscle power (Cornwell et al., 2002; Fowles et al., 2000; Young & Elliott, 2001). It was also reported that balance maintenance ability decreases with stretch (Behm et al., 2004). An additional experiment was conducted to evaluate the effects of stretching, vision and their interaction on postural sway (Nagano et al., 2006). Although the preceding study investigated the change in postural sway, it did not consider the trend after stretching. Therefore the purpose of this paper was to investigate the effects of vision and stretching on postural sway during quiet standing and to evaluate the recovery phase after stretching.

METHODS AND PROCEDURES

Healthy male subjects participated in this study. Participants quietly stood as upright as possible on a force plate (9286A, Kistler Instrumente AG, Winterthur, Switzerland) while ground reaction force data were collected. Both feet were arranged on the center of the force plate. Arms were crossed in front of the chest. In the eyes-open condition, participants stared at a marker placed in front of the face 2m apart at the eye level. In the eyes-closed condition, participants voluntarily closed their eyes and stood upright. Recordings were initiated after the posture became stable on the force plate. Data were recorded at 100 Hz (PowerLab, ADInstruments, Colorado Springs, CO, USA). Thirty seconds were recorded and utilized for analysis. The sway of ground reaction force center of pressure (COP) was calculated from the force plate data. In order to apply stretch, participants were asked to quietly stand as upright as possible on a device that caused a static dorsiflexion (STR-158, COMBI Wellness, Tokyo, Japan). The device was set to 20° for the first one minute. Then it was set to 25° for ten minutes (Figure 1).

Figure 1. The standing posture on the stretching device.

Measurements were conducted in two parts, with a total of four experimental conditions. Two conditions were first measured without stretch, i.e., eyes-open and eyes-closed. These conditions will be called "pre-stretch eyes-open" and "pre-stretch eyes-closed". Six trials of each were performed in random order, resulting in 12 total trials. A ten minutes of static stretch was applied after these measurements. Following the stretch, two conditions were measured as described previously. These conditions will be called "post-stretch eyes-open" and "post-stretch eyes-closed". Each condition was performed for seven times. The subjects took a rest of one minute on a chair after every two trials.

RESULTS

There was a clear change in the sway speed associated with stretch: (1) the sway speed of the COP increased after stretching, (2) the sway speed increased when vision was removed, (3) the sway speed recovered to the original level in about 20 minutes (Figure 2). Similar trends were found for the standard deviation (RMS) and maximal sway range of the COP trajectory.
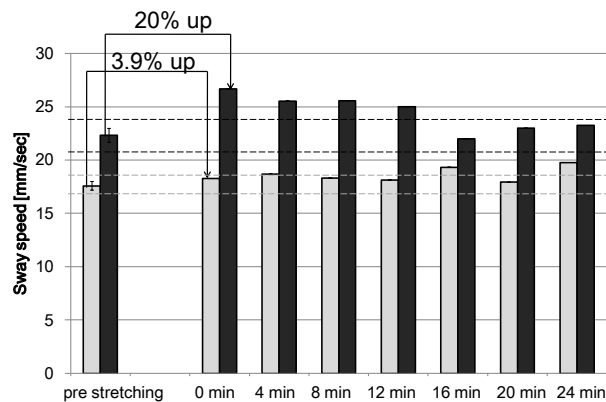
Figure 2. Trend of the sway speed. Light color shows "eyes-open" and dark color shows "eyes-closed". The magnitude of sway recovered to the original level in 20 minutes.

DISCUSSION

Through this experiment, it was confirmed that there are clear effects of vision and stretching on postural sway. Moreover, it was found that the sway speed of the COP recovered to the original level while repeating the measurements. This result may suggest that the force deficit caused by stretching disappears after approximately 20 minutes, although this point was not tested in this study. We will work on the development and evaluation of a training apparatus that contributes to the improvement of balance ability (decrease in postural sway) in the future.

REFERENCES

Behm et al. (2004) *Medicine and Science in Sports and Exercise*, 36: 1397-1402.
Cornwell et al. (2002) *J Applied Physiology*, 86: 428-434.
Ferber et al. (2002) *J Electromyography and Kinesiology*, 12: 391-397.
Fowles et al. (2000) *J Applied Physiology*, 89: 1179-1188.
Nagano et al. (2006) *Human Movement Science*, 25: 422-434.
Wilson et al. (1991) *J Sports Medicine*, 12: 403-407.
Young and Elliott (2001) *Research Quarterly for Exercise and Sport*, 72: 273-279.

ACKNOWLEDGEMENTS

EFFECT OF THE BOSTON BRACE ON STANDING BALANCE IN ADOLESCENT IDIOPATHIC SCOLIOSIS

Heydar Sadeghi[1] and Paul Allard[2]

[1]Department of Kinesiology, Tarbiat Moallem University, Tehran, IRAN, sadeghih@yahoo.com

[2]Laboratoire d'Étude du Mouvement, Research Center, Sainte-Justine Hospital, Montreal, QC, Canada

INTRODUCTION

There is evidence that traditional time-domain measures are not sensitive to the changing dynamic properties of the postural control system [1]. Frequency domain measures such as the spectral characteristics associated with sway may be more effective in detecting important but not easily identifiable changes in the physiological control systems underlying balance [1]. Frequency domain analysis has not yet been performed to study standing balance in AIS but has been applied on the ground reaction forces developed during gait by Giakas et al. [2] in scoliotic and healthy individuals. The objective of this study was to use time and frequency domain analyses to test if the Boston brace affect balance in AIS.

METHODS AND PROCEDURE

Fifteen AIS girls were fitted with a Boston brace. At the four month follow-up, standing balance was assessed using the center of pressure (COP) displacements measured from a force plate. Subjects were tested with and without the brace.Quiet standing balance was tested at the four month follow-up using an AMTI force platform (AMTI, Newton, MA, USA). Values for each set of time and frequency parameters were averaged for each condition. Paired t-tests were performed to compare out-of-brace and in-brace conditions at the four month follow-up. Differences of $p<0.05$ were considered statistically significant. A Bonferroni correction procedure was applied to control Type I error by adjusting the p values when analyzing the above-mentioned parameters [3].

RESULTS

The mean position of the COP and the sway area were similar with or without a body brace. Figures 1 and 2 illustrate the average power spectra distribution of the center of pressure displacements as it was measured in the antero-posterior and medio-lateral directions, respectively. Though the first peak in the power spectra was not statistically significant while the-second peak was statistically smaller with the Boston brace in the antero-posterior direction ($p = 0.012$) and larger along the medio-lateral axis ($p = 0.022$).
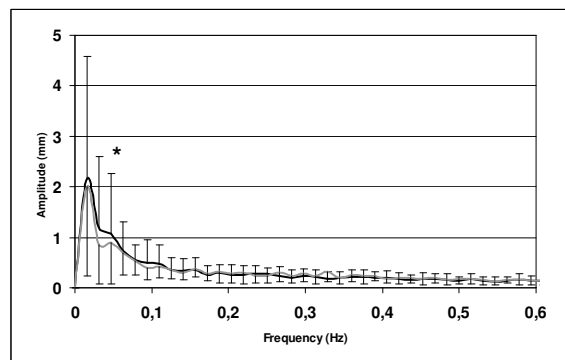
Fig 1. Average spectrum of the center of pressure measured in the antero-posterior direction of scoliotic girls without (dark) and with (grey) a Boston brace.

In the antero-posterior direction, there was a statistically significant shift towards higher mean ($p = 0.012$) and median ($p = 0.003$) frequencies with the brace on, whereas no difference was noted in the medio-lateral direction. Time domain parameters did not prove useful for differentiating between the in- and out-of-brace conditions in AIS individuals. The second peak in the power spectra could be associated with an inverse double pendulum motion.
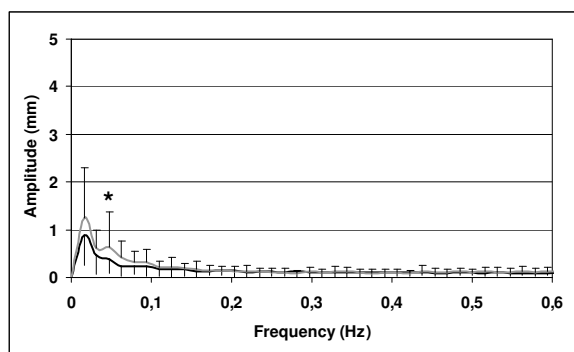
Fig 2. Average spectrum of the center of pressure measured in the medio-lateral direction of scoliotic girls without (dark) and with (grey) a Boston brace.

DISCUSSION

A body brace is usually prescribed to control spinal deformities that are less than 40° and progressive. Few studies have addressed its effect on balance and, of those that have, all of them have used time-related parameters such as displacements of the center of pressure. The objective of our study was to use time and frequency domain approaches to test the hypothesis that a Boston brace could result in less balance control in adolescent idiopathic scoliosis. Giakas et al. [2] consider harmonic analysis more appropriate and more sensitive than time domain analysis for showing differences between scoliotic and non-scoliotic girls. Using only time domain data, one could assume that the Boston brace restrains the lateral deviation of the spine without disturbing the standing balance of scoliotic subjects. Our time-dependent results were fairly similar to those previously reported [4,5,6]. The absence of statistical significance in the time domain parameters could be due in part to larger variations in individuals fitted with a Boston brace, although the mean values were usually higher.

To our knowledge, no one has reported the effect of bracing on the mean positions of the COP. In our study, the use of a Boston brace did not substantially displace the mean COP in either the antero-posterior or the medio-lateral direction. However, it was khown by Aubin et al. [7] that the Boston brace shifts the spine and rib cage anteriorly, and that forward displacement of the top vertebra is likely to increase the hypokyphosis and decrease the normal physiological curvatures. Korovessis et al. [8] corroborated these observations. In our study, the mean antero-posterior COP was not statistically affected by use of the Boston brace. It can therefore be assumed that any forward shift of the trunk and spine caused by the brace was offset by a backward shift in other body segments. According to a study by Karlsson et al. [9], frequency analysis can be used to detect fundamental differences in postural sway that cannot be observed visually. In our study, only the frequency-dependent parameters have shown that standing balance was affected in adolescent idiopathic scoliosis subjects fitted with a Boston brace.

SUMMARY

Time-dependent parameters used in this study did not prove useful for differentiating between the in-brace and out-of-brace conditions. Spectral analysis highlighted increased stiffness in the antero-posterior direction and less control in the medio-lateral axis in standing balance between in-brace and out-of-brace conditions in AIS.

REFERENCE

[1] Williams et al. Arch Phys Med & Rehabil 1997; 78: 737-44.
[2] Giakas et al. Spine 1996; 19: 2235-42.
[3] Holland BS, Copenhaver M. Psychological Bulletin, 1988; 104: 145-9.
[4] Gauchard et al. Spine 2001; 26: 1052-8.
[5] Bernard J-C, Valero J-P. Kénésithér 1999; 26: 145-53.
[6] Alder et al. J Orthop Res 1986; 4: 102-07.
[7] Aubin et al. Spine 1996; 22: 629-35.
[8] Korovessis et al. Spine 2000; 25: 2064-71.
[9] Karlsson et al. Clin Biomech 2000; 15: 541-5.

CHANGE OF POSTURAL FEEDBACK GAIN SCALING BY AGING

Seyoung Kim[1] , Fay B. Horak[2] and Sukyung Park[1]

[1]Department of Mechanical Engineering, KAIST, Daejon, KOREA
[2]Neurological Sciences Institute, Oregon Health & Science University, USA

INTRODUCTION

We examined how age affects how postural strategies change as perturbation magnitude changes. Previous studies showed that young adults continuously scale postural response gains from ankle strategy to more and more hip strategy with increasing biomechanical constraints but it is now known whether elderly subjects show the same scaling (Park et al.,2004). Postural responses were analyzed with full-state feedback control whose gain parameters characterize the response of each group. The gain scaling indicates that the elderly relies more on hip strategy, while the young continuously changes from ankle to hip with perturbation magnitude.

METHODS AND PROCEDURES

Subjects
Young (7 females, 23-28 yrs) and elderly (6 males and 1 females, 53-81 yrs) subjects with no history of balance problem participated after signing the consent form.

Experiment data collection
Backward perturbations of magnitude ranged from 3-15cm were applied to the subjects with duration of 275msec. The maximum magnitude was designed to induce frequent heel-lifts or steps. Subjects stood upright on a movable force plate, and were instructed to keep the balance, not to lift their heels off the ground if possible. All subjects experienced total five sets of seven randomly ordered perturbations. For each trial, ground reaction force and kinematic data were recorded for 10 seconds including the early 2 seconds prior to perturbation onset (Park et al., 2004).

Biomechanical model with feedback gain
Human body was modeled as two segment inverted pendulum in sagittal plane. Full-state feedback control model was used to describe the human postural response to external perturbations. Control gain parameters of full-state feedback model were obtained by optimization method using MATLAB.
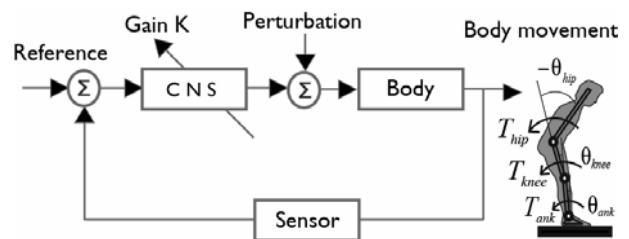
Figure 1. Human postural feedback loop

RESULTS

Full-state feedback simulation reproduced the experimental data with the goodness of fit ($R^2=0.84\pm0.35$ in the young and 0.86 ± 0.30 in the elderly).
Joint kinematic data showed that the elderly relies more on hip strategy. Joint angle trajectories of the elderly are composed of smaller ankle and larger hip motion in compared to those of the young (Figure 2 top).
Joint torque trajectories were more uniformly scaled with perturbation magnitude for the elderly (Figure 2 bottom left). However, joint trajectories of the young continuously change its characteristic shape when perturbation magnitude increases (Figure 2 bottom right).
Maximum allowable ankle joint torque significantly reduced for the elderly (Figure 2 bottom right). Though it is not shown in the figures, the elderly experienced frequent heel-lifts or steps at large perturbation magnitudes.

Gain parameters corresponding to 15cm perturbation were not included to fit the scaling trend with linear regression (Figure 3) because most of the elderly subjects violated flat foot constraint.
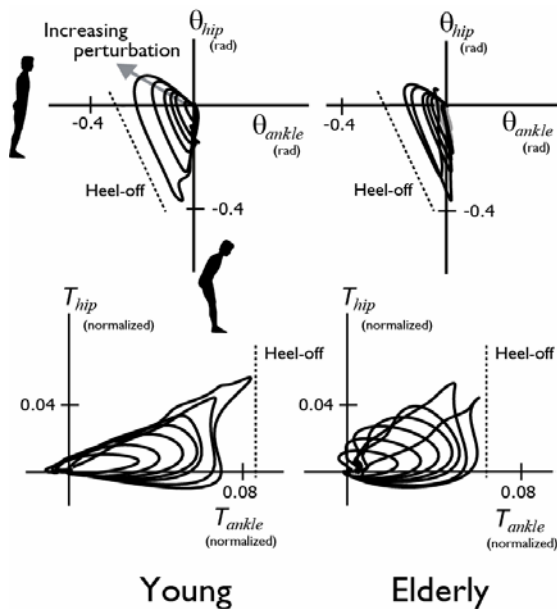
Figure 2. Averaged postural responses of all subjects for increasing perturbations(3-15cm) in terms of joint angles(top), and joint torques (bottom). Joint toques were normalized by subject's weight × height
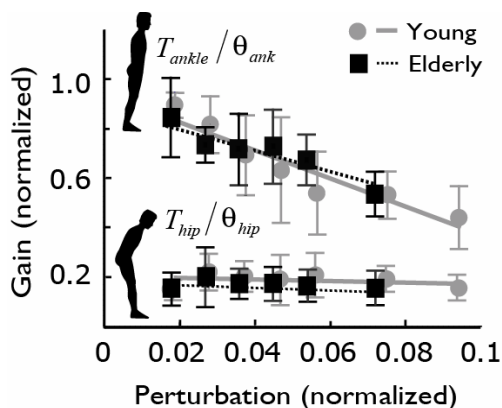
Figure 3. Comparison of averaged postural feedback gain scaling: Young vs. Elderly. Gains and perturbations were normalized by subject's body parameters. Linear regression was used to describe the scaling trend in the perturbation ranges.

Feedback gain scaled with perturbation magnitude for young subjects, but not significantly for the elderly. The young gradually scaled T_{ank}/θ_{ank} as a function of perturbation magnitudes, while the elderly barely changed the gain at the intermediate perturbations (Figure 3 top). They also showed smaller and almost invariant gain T_{hip}/θ_{hip} with perturbation magnitudes, while the young showed slightly increasing trend.

DISCUSSION

Smaller ankle motion in combination with large hip motion indicates that the elderly rely more on hip strategy in response to broad range of perturbation. Less flexible strategy change from ankle to hip was also observed from the gentle gain scaling slope. Reduced maximum ankle joint torque of the elderly might be attributed by their fear of fall, which was reflected in discontinuous postural strategy change as well as frequent heel-off or steps at large perturbations

SUMMARY

The elderly relies more on hip strategy, while the young continuously changes from ankle to hip with perturbation magnitudes. These strategy changes could be quantified by gain scaling slope.

REFERENCES

Park S, Horak FB and Kuo AD (2004). *Postural feedback responses scale with biomechanical constraints in human standing, Exp Brain Res,* 154:417-427.

ACKNOWLEDGEMENTS

RELATIONSHIP BETWEEN MECHANICAL, BIOMECHANICAL AND PERCEPTUAL PARAMETERS OF CUSHIONING PROPERTIES IN RUNNING SHOES

Julia Augustijn, Thorsten Sterzing, Thomas L. Milani

Department of Human Locomotion, Chemnitz University of Technology, Chemnitz, Germany
julia.augustijn@phil.tu-chemnitz.de

INTRODUCTION

Cushioning is one aspect of running shoe research and development. Inadequate running shoe cushioning may lead to overuse injuries. There are several innovative cushioning designs in running shoes available, e.g. Nike Shox [TM], Asics Gel, Adiprene. Damping elements made of different materials and geometries are placed in or completely replace the midsole of running shoes. These concepts should be tested by a comprehensive approach including mechanical, biomechanical and perceptual testing (Milani and Hennig, 2002). The purpose of this study was to analyze the relationship between these testing approaches for rearfoot cushioning of an innovative running shoe design.

METHODS AND PROCEDURES

The innovative running shoe design used in this study allowed modifying rearfoot hardness by interchangeable TPU units. These units had a shore hardness of 75A, 80A, 85A and 90A. A commercially available traditional cushioning running shoe served as a reference shoe (TRS). Mechanical testing was performed by vertical application of a loading profile according to force-time characteristics of a heel-to-toe specific running speed of $3.5 \ ms^{-1}$ (Cavanagh and Lafortune, 1980). Maximum deformation [mm] and stiffness [N/mm] were measured. For biomechanical and perceptual testing 20 male subjects (25.6yrs +/- 4.6; 177.0cm +/- 5.1; 71.0kg +/- 6.1) were recruited. During biomechanical testing running speed was set to $3.5 \ ms^{-1}$ (+/- 0.1). Five repetitive heel strike running trials across a Kistler force platform (9287BA) were recorded. Simultaneously, tibial acceleration was measured by a lightweight accelerometer (EGAX-F-100). Shoes were tested in randomized order. For perceptual testing, subjects ran at individual self-selected running speed on an indoor track. Perceptual ratings were obtained while running in each shoe condition for 200m. The intensity of heel impact was rated using a 9-point category estimation scale (1: much lower to 5: equal to 9: much higher) compared to a reference. The shoe condition with medium hardness according to mechanical testing results was used as the reference shoe and was set to be 5 on the rating scale. Subjects performed one 200m lap wearing the reference shoe prior to testing each of the remaining shoe conditions. For data evaluation mean values of left and right shoes for mechanical testing and mean values of the five repetitive trials for biomechanical testing were calculated. For statistical analysis a repeated measures ANOVA and Post-Hoc comparisons according to Fisher's LSD were used. Additionally, correlation analyses between parameters of the three testing areas were performed.

RESULTS

Mechanical testing shows less deformation (75A=9.5mm to 90A=7.4mm) and higher stiffness (Figure 1) for harder shoes. The TRS

shows higher deformation (12.8mm) and lower stiffness than the innovative shoe design.
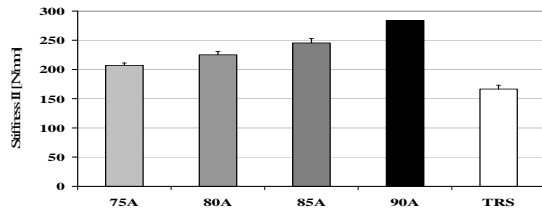
Figure 1: Mechanical stiffness

Results for biomechanical testing show no differences between shoe 75A, 80A, 85A and 90A in force rising rate (69.4 - 71.3N/(bw*s)) and tibial acceleration (Figure 2). The TRS shows significant lower tibial acceleration (p < 0.01) and force rising rate.
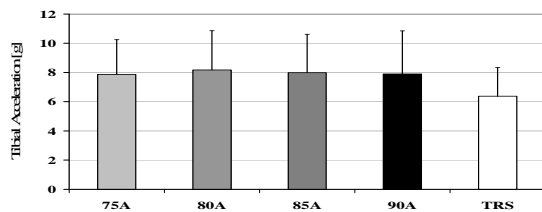
Figure 2: Tibial acceleration

In perceptual testing subjects rated the softest and the hardest shoe condition of the innovative shoe design according to mechanical stiffness values (Figure 3).
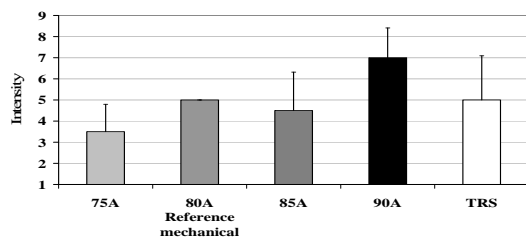
Figure 3: Rearfoot hardness – intensity rating

For the two different shoe concepts, statistical analyses result in high correlation between mechanical and biomechanical parameters (e.g. deformation and tibial acceleration: $r = 0.91$; $p < 0.05$), but within the innovative shoes no correlation is present ($r = 0.13$; $p = 0.87$). No relationship was found between mechanical and perceptual parameters or perceptual and biomechanical parameters.

DISCUSSION

In mechanical testing differences between all shoe conditions are present. The results in the biomechanical test show significant differences between both running shoe concepts, but - surprisingly - no differences within the shoes of the innovative running shoe concept. This may indicate that differences are too small to influence running biomechanics. Otherwise, in perceptual testing subjects identified the softest and the hardest shoe condition according to mechanical testing results. Adaption behaviour may be the reason for this result (Hennig et al., 1996). Subjects may have perceived differences between shoe conditions and adapted the running style to avoid high heel impacts.

SUMMARY

It was shown that differences in midsole hardness between and within two running shoe concepts can be measured mechanically. These differences do not necessarily need to be detected during biomechanical testing. This is most likely due to movement adaptation of runners. During perceptual testing subjects perceived differences of rearfoot hardness within the innovative shoe conditions. Further investigations would be desirable to evaluate the movement adaptation. Foot strike angle in the saggital plane may be a parameter of interest.

REFERENCES

Cavanagh PR and Lafortune MA (1980). J. Biom., 13 : 398-406.
Hennig EM et al. (1996). J Applied Biomechanics, 12: 143-150.
Milani TL and Hennig EM (2002). *J Med. Orth. Tech.,* 122: 68-75.

ACKNOWLEDGEMENTS

A PRELIMINARY STUDY ON MUSCULOSKELETAL FINITE ELEMENT MODEL WITH ACCURATE MUSCLE MOMENT ARMS IN HUMAN ELBOW

Hideyuki Kimpara[1], Takahiko Sugiyama[1], Chikara Nagai[1], Kyuengbo Min[1], Yuko Nakahira[1], and Masami Iwamoto[1]

[1]Toyota Central R&D Labs., Inc., Safety Crashworthiness Laboratory, Nagakute, Aichi, Japan, h-kimpara@mosk.tytlabs.co.jp

INTRODUCTION

Muscle activation must be considered in the crashworthiness as an essential effect in biomechanical responses and occupant injuries (e.g. Sugiyama et al., 2007). Further investigation on the detailed mechanism for muscle effects on the body is needed. A musculoskeletal model would be a key technique to estimate biomechanical body responses. However, there were limitations in previous researches, especially on application for the impact biomechanical simulations. Consequently, we postulated three technical targets in the simulation: accurate muscle moment arms, forward dynamic analysis, availability on commercially available software, which is widely used in real design and engineering. In this study, we developed a new musculoskeletal model on an explicit finite element (FE) code. This report presents preliminary works of motion generation.

METHODS

The anthropometry of a model (Figure 1) was an American Male 50th percentile (AM50). The joint centers and inertia of body segments were obtained from Schneider et al., (1983). Right upper and lower arm bones were modeled as rigid, and an elbow joint was represented as a revolute joint. A Hill-type muscle model (*MAT_MUSCLE in LS-DYNA material library) was engaged. Muscle properties of cross-sectional area, maximum force, passive element, and the functions of the tension-length and tension-

velocity for active skeletal muscles were determined from the literature (Winters and Woo, 1990; Gans, 1982; Thelen, 2003). Nine muscles of the elbow joint were represented as series of discrete truss elements. The muscle paths were connected between origin and insertion points, and assumed as fixed via points and edge-to-surface contact interfaces to prevent muscle paths from crossing over the joint centers. Activation levels of nine muscles were controlled by four nerves, so that the elbow motion was determined by four nerve inputs.
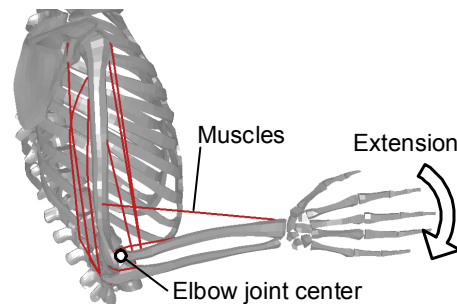
Figure 1. Musculoskeletal FE model

Objective motions of elbow flexion-extension for the model were obtained from a volunteer test. A well informed male volunteer subject who had similar height and weight of AM50 agreed to participate in the test. A 3D motion analysis system (Eagle/Hawk digital system, Motion Analysis, USA) and an EMG measurement system (MP150, Biopac systems, USA) were used.

Simulations of forward dynamics were conducted on a commercially available explicit finite element (FE) solver code, LS-

DYNA 971 (LSTC, Livermore, CA). A commercially available optimization tool, iSIGHT-FD ver 2.5 (Engineous Software Inc., Cary, NC) was used to minimize the following objective function O to fit the elbow angle of the model to the test data.

$$O = \left(\theta_{model} - \theta_{test}\right)^2 + E_{muscle}$$

where θ_{model} and θ_{test} are elbow angles of the model and test data, respectively. E_{muscle} is whole energy of muscle.

RESULTS

Computational time for elbow motion of 1.0 sec termination time was 165 seconds on a 64-bit Linux, one core of Intel Xeon 5160 3.0 GHz machine. Calculated muscle moment arms (Figure 2) of the model were well validated against several experimental data (Murray et al., 1995; Amis et al., 1979). The results of motion generation in elbow extension were reasonably matched with the experimental data; the error of angle was 1.4 ± 0.7 degree in a 15 degree of elbow extension.
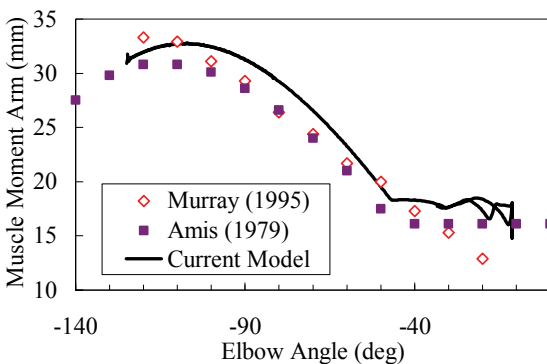
Figure 2. Brachialis muscle moment arms between literature data and the model

DISCUSSION

This study presented the method of muscle path determination by combination of fixed via points and edge to surface contact interfaces, and made accurate muscle moment arms. Since the geometry of contact surface can be freely modified, the muscle moment arms were designed as requested. In case of brachialis muscle (Figure 2), muscle path was discontiguous from −140 to −45 degrees of elbow angle, however, muscle moment arm of 20 mm was kept after −45 degree of elbow angle by the contacts. This prevented brachialis muscle path from crossing over the elbow joint.

The error of predicted elbow angle was less than 10%. When the number of numerical parameters for optimization was increased, the accuracy can be improved more.

In previous studies, most proposed musculoskeletal models were developed on the original software (e.g. Delp et al., 1990). However it is difficult to apply it on impact simulations, due to limitation of boundary condition and absence of vehicular models. In contrary, other musculoskeletal models developed on the commercially available solvers (e.g. Chancey, et al., 2003) appeared not to be validated for muscle moment arms. The musculoskeletal FE model developed in this study could be useful to apply musculoskeletal dynamics to the impact analysis.

REFERENCES

Amis AA et al. (1979). *Eng Med*, 8-1: 41-48
Chancey VC et al. (2003). *Stapp*, 47:135-153
Delp SL et al. (1990). *IEEE Computing in Science and Engineering*, 2:46-55
Gans C (1982). *Exerc Sport Sci Rev*, 10: 160-207
Murray WM et al. (1995). *J of Biomechanics*, 28-5: 513-525
Schneider LW et al. (1983). *UMTRI-83-53-1*
Sugiyama T et al. (2007). *IRCOBI*: 127-140
Thelen DG (2003). *J Biomech Eng*, 125(1): 70-77
Winters, JM and Woo, SL (1990). *Multiple Muscle Systems.* New York, Springer.

A QUANTITATIVE ANALYSIS OF JOINT PHASING AND EFFICIENCY IN THE OLYMPIC CLEAN

Justin Byers, Tom Wu and Pierre Gervais

Sports Biomechanics Laboratory, Faculty of Physical Education and Recreation, University of Alberta, Edmonton, AB, Canada, jbyers@ualberta.ca

INTRODUCTION

For an athlete to be successful in the classical lifts, the clean and jerk and the snatch, he or she must display excellent coordination between body segments in a powerful fashion (Jones, 1991). These characteristics make Olympic style weightlifting highly beneficial and transferable to other sports (Caravan et al, 1996). It is widely accepted that to produce the maximum force, all three of the hip, knee and ankle joints must be fully extended (Martyanov, 1988). It is theorized that the premature extension of the trunk, in relation to the knees, will lead to excessive horizontal bar movement and subsequent loss of force, or failure to lift. The purpose of this study was to examine joint phasing for efficiency during the Olympic power clean. The results would be important for the development of future coaching protocol to aid in the continuing improvement of the technical mastery of the Olympic style lifts across all applications.

METHODS AND PROCEDURES

Six elite male subjects who have been involved in the sport competitively for at least 3 years volunteered in the study. Subjects were fitted with reflective markers placed on left side of body joints at the 5th toe, heel, ankle, knee, hip, shoulder, ear and the collar of the weightlifting bar. Each subject performed 5 clean repetitions at the designated 75% of subject's current training one repetition maximum with one-minute break between all trials. Each trial was performed on a standard Olympic weightlifting platform; the weights and bar were also certified and standardized. Video trials were obtained using a JVC high-speed digital camera operated at 60 Hz. The camera was placed to capture left sagittal view of the subjects. A total of 25 video trials were filmed and analysed with the APAS™ motion analysis system. Data were smoothed with a digital filter (X and Y cut-off = 5 Hz). Smoothed spatial data were used to determine joint angle changes over time and the horizontal movement of the bar, Figure 1. A bivariate correlation was conducted between each variable and horizontal deviation of the bar at $\alpha = 0.05$. SPSS statistical analysis system was used for all statistical tests.
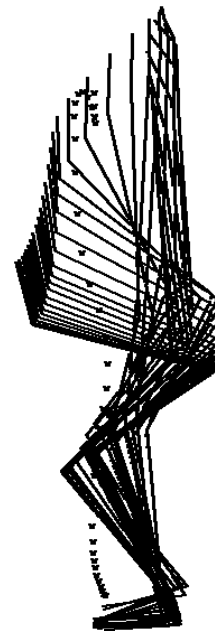
Figure 1. Horizontal bar movement.

RESULTS

To determine joint phasing, the time of peak extension for the hip and knee were recorded and the difference (time of peak hip extension angle – time of peak extension knee angle) was calculated, Table 1. A bivariate correlation analysis was performed between the peak knee extension and the horizontal deviation of the bar, the peak hip extension and the horizontal deviation of the bar and finally the joint phasing and the horizontal deviation of the bar, and the results of the correlations calculated were -0.3, -0.7 and 0.7, respectively.

S	H.E. (°)	K.E. (°)	J.P. (s)	H.D. (m)
1	166.4	157.0	0.07	0.13
2	167.5	152.3	0.06	0.27
3	179.2	166.5	0.03	0.16
4	177.3	160.7	-0.07	0.08
5	177.8	161.4	0.01	0.14
6	178.7	151.3	0.00	0.23
Mean	174.5	158.2	0.02	0.17
(SD)	(5.9)	(5.8)	(0.05)	(0.07)

Table 1. Peak joint angles of hip extension (H.E) and knee extension (K.E.), joint phasing (J.P.) and horizontal deviation of the bar (H.D.).

DISCUSSION

None of the correlations were shown to be statistically significant. Regardless, some potentially interesting findings were shown. In the study a moderate correlation was noted, indicating that premature extension of the knees in relation to the hips results in increased horizontal movement of the bar. This moderate correlation observed is sufficient to warrant future research utilizing a larger sample size.

The bar path kinetics observed throughout the study are concurrent with the findings of Garhammer (1985, 1993). The bar moved positively (toward the body) during the initial pull phase and then negatively during the second pull or explosion phase. During the catch phase the bar moved positively again. The amount to which the bar deviated in either direction (horizontal deviation) was highly variable as it is affected by both technical proficiency (Takano, 1987) and body segment length (Garhammer, 1985).

SUMMARY

Despite the lack of significant findings, the present study does warrant future research in the area. Given a larger sample size more generalizable results should be available. The close proximity of the camera to the subject can introduce error into the proximal data (Garhammer, 1993). To nullify this problem the camera placement can be placed further away or 3D filming can be utilized. This study has shown promising connections between both knee extension and joint phasing to horizontal deviation of the bar. Continued research in this area will provide a valuable coaching tool in evaluating and improving power clean technique.

REFERENCES

Caravan P et al. (1996). *J. Strength and Cond Research*, 10(2):127-130.

Garhammer J (1985). *ISBS*, 1:122-130.

Garhammer J (1993). *J. Strength and Cond Research*, 7(2):76-89.

Jones A (1991). *Natl Strength Cond Assoc J*, 13(6):50-51.

Martyanov S et al. (1988). *Teoriya i Praklika Fizicheskoi Kultury*, 2:38-40.

Takano B (1987). *Natl Strength Cond Assoc J,* 9(5):50-59.

GENDER DIFFERENCES OF 2-POINT TOUCH SENSITIVITY THRESHOLDS OF THE HUMAN FOOT

Sabrina Kunde, Thorsten Sterzing, Thomas L. Milani

Department of Human Locomotion, Chemnitz University of Technology, Chemnitz, Germany
sabrina.kunde@phil.tu-chemnitz.de

INTRODUCTION
With regard to 2-point touch sensitivity thresholds (2PT) of the human body Weber et al. (1835) showed that fingertip, tongue and lips are the most sensitive regions, whereas the back is the most insensitive area. The 2PT is the minimal distance at which two simultaneously given stimuli at a specific anatomical location can be discriminated. Clinically, 2PT of the hand or foot are used to assess sensory nerve functions of patients (Barber et al. 2001). Stevens et al. (1996) reported declining discrimination capability with age at different body regions. Only little information could be found in the literature about the 2PT of healthy feet; hallux (2PT = 4-22 mm) and plantar midfoot (2PT = 10-35 mm) according to age were studied (Stevens et al. 1996). There are two main approaches to test 2PT: Conventionally, subjects judge whether one or two stimuli are applied (Stevens et al. 1992). Another method is the two-point gap threshold test, in which subjects decide between a configuration with gap and one without (Stevens et al. 2003). 2PT of different foot regions are important factors with regard to the fit perception of footwear. The purpose of this study was to determine 2PT at different foot regions and to compare those of healthy women and men.

METHODS AND PROCEDURES
20 women (age: 23.1±2.4 years; height: 169.0±6.4 cm; weight: 62.5±9.7 kg) and 20 men (age: 22.5 ±2.7; height: 184.8±7.3; weight: 79.8±8.6 kg) took part in the study. The 2PT of the dominant foot were tested at 8 different anatomical locations:

Plantar: Calcaneus (PC), Caput Os Met I (PCMI), Hallux (PH)
Dorsal: Basis Os Met III (DBMIII), Caput Os Met I (DCMI) and V (DCMV)
Medial: Caput Os Met I (MCMI),
Lateral: Basis Os Met V (LBMV)
Testing was performed in randomized order. Subjects were lying in supine position. Room temperature was maintained constant at 23.6 (±0.95) °C. Skin temperature of the tested foot was kept constant at 27.6 (±1.6) °C by use of an infra-red lamp. The measurement device was a modified digital vernier calliper (Technologiezentrum W-tec, Wuppertal, Germany) equipped with a customized force transducer. The absolute accuracy of the system is 0.02mm. Stimuli were given at a controlled force of 15-25 grams. The conventional 2PT testing method was used by applying a modified version of Dyck`s 4-2-1 algorithm for measurements with Semmes Weinstein Monofilaments. The initial 2PT distance was set to be 11 mm. Step size was 0.5 mm and stimuli were applied for 1 sec. Each distance was tested five times, twice as one point stimulus and three times as two point stimulus. Four of five correct recognitions were necessary to proceed to the next distance level.
Mean values for each anatomical location and mean values of both gender groups were calculated. Anatomical locations were compared using a repeated measure ANOVA, gender differences were examined using unpaired T-Tests.

RESULTS
The repeated measures ANOVA reveals

statistically significant differences between anatomical locations (p<0.01). PH shows the lowest 2PT whereas DCMI and DBMIII show the highest 2PT (Figure 1).
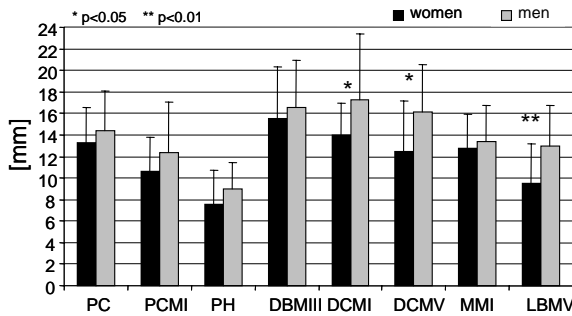
Figure 1: 2PT of anatomical locations

2PT of women compared to men show lower values for all anatomical locations; statistically significant differences are present at dorsal Met I and V and lateral Met V.
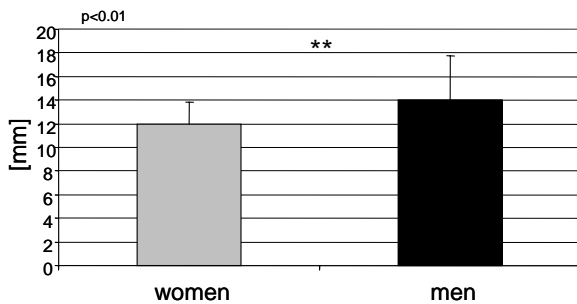
Figure2: 2PT across all anatomical locations

Across all anatomical locations women have significantly lower mean 2PT at the foot compared to men (p<0.01) (Figure 2).
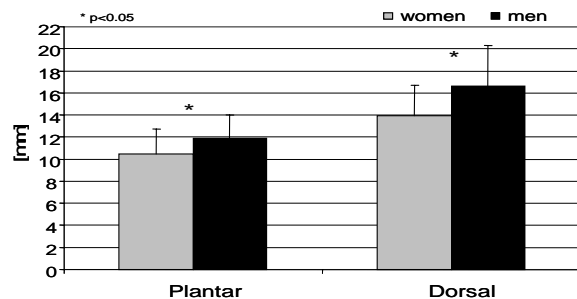
Figure 3: 2PT of foot regions

The dorsal foot region is less sensitive compared to the plantar foot region (p<0.01).

DISCUSSION
2PT at the human foot differ due to foot region and specific anatomical locations. Women are more sensitive compared to men with regard to 2PT. These gender differences are also present with regard to single touch sensitivity (Hennig et al. 2004). In contrast to this, Stevens et al. (1996) found no significant differences for 13 body regions between genders by using the two-point gap threshold test. This indicates the necessity to investigate the influence of different testing methods on the findings of 2PT tests.

SUMMARY
The human foot shows different 2PT due to different anatomical locations. Women have lower 2PT at the foot compared to men. Considerable differences were found for the anatomical locations dorsal Met I and V and lateral Met V. These findings may have consequences for the perception of footwear fit.

REFERENCES

Barber M. A. et al. (2001). *Journal of the American Podiatric Medical Association.*

Dyck PJ (1993). *Neurology*, 43. 1508-1512.

Hennig E et al. (2004). *Proceedings, 13. Biennial Conference, Canadian Society for Biomechanics,* Halifax.

Stevens JC et al. (1996). *Somatosensory and Motor Research,* Vol. 13, 2, 153-166.

Stevens JC et al. 1992. *Journal of gerontology*, 47, 35-40.

Stevens JC et al. (2003). *Somatosensory and Motor Research*, Vol. 20, 3-4, 271-279.

Weber EH (1835). *Archiv für Anatomie, Physiologie und wissenschaft. Medizin.* 152-160.

ACKNOWLEDGEMENTS

Validation of agonist and antagonist muscle force estimation during jumping at three different effort levels

Kevin R. Ford[1,2] , Antonie J. van den Bogert[3], Gregory D. Myer[1],
Robert Shapiro[2] and Timothy E. Hewett[1,4]
[1]Cincinnati Children's Hospital, Sports Medicine Biodynamics Center, Cincinnati, OH
[2]University of Kentucky, Department of Kinesiology and Health Promotion,
Lexington, KY
[3]Department of Biomedical Engineering, Cleveland Clinic Foundation, Cleveland, OH
[4]Departments of Pediatrics, Orthopaedic Surgery, Biomedical Engineering, and Rehabilitation
Sciences, University of Cincinnati, College of Medicine Cincinnati, OH
kevin.ford@cchmc.org

INTRODUCTION

Non-invasive analyses of neuromuscular control and joint loading are critical to the delineation of the potential mechanisms that underlie increased risk of musculoskeletal injury. Static optimization techniques may be used in an attempt to resolve the indeterminacy of muscle forces. While debate remains concerning the ability to correctly estimate forces in antagonistic muscles, methods are technically feasible and should be validated to determine if they provide physiologically accurate data (Herzog and Binding 1992). The purpose of this project was to validate a static optimization musculoskeletal model used to estimate lower extremity muscle forces. Specifically, EMG patterns of agonist/antagonist muscles were compared to estimated muscle forces during counter-movement jumps at varied efforts.

METHODS AND PROCEDURES

Fourteen female volleyball players were enrolled in the current study. Surface Ag/AgCL dual electrodes were applied to the vastus medialis (QUAD) and semimembranosus (HAM) on the right lower extremity. 37 retroreflective markers were placed on each subject. Counter-movement jumps were performed at three effort levels (50%, 75% and 100% of maximum). Three trials of each type of jump were collected with a ten camera motion analysis system (Motion Analysis Corp. 240Hz). Two force platforms (AMTI)
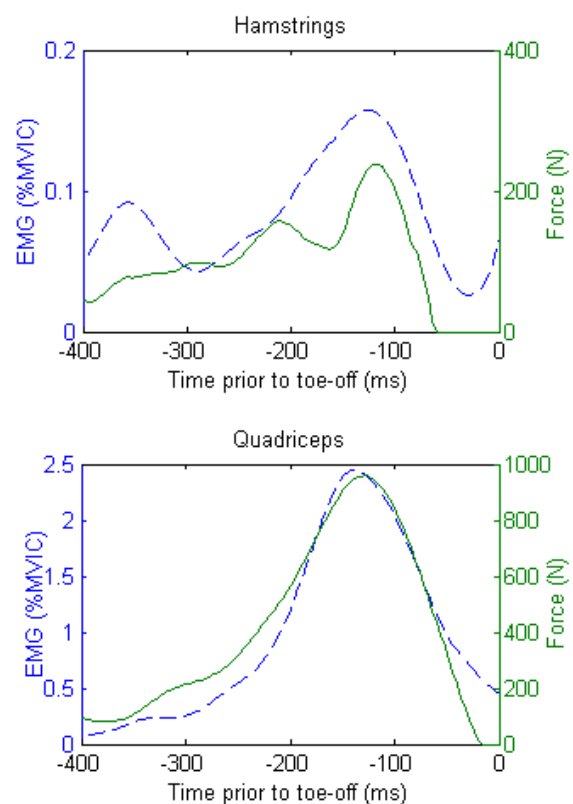
Figure 1. Example countermovement trial of hamstrings and quadriceps muscle force (green, solid line) and EMG (blue, dash line).

and telemetry EMG system (Noraxon) were sampled at 1200 Hz. Lower extremity joint angles and moments were calculated. Moment arms for 43 lower extremity muscles were calculated as a function of joint angles (Delp et al., 1990) and muscle forces were solved from joint moments by minimization of the sum of cubed muscle stresses, using the

Matlab optimization toolbox. EMG was high pass (30Hz Butterworth) filtered to remove movement artifact and then full-wave rectified and low pass (6Hz) filtered (Besier et al., 2003). Maximum muscle force and EMG were used for comparison. Cross correlation analysis was used to correlate the estimated muscle force to normalized EMG during each trial (400ms phase prior to toe off, Figure 1). This procedure measured the maximum correlation, taking into account phase shifts, between signals. A 3 factor (50, 75, and 100%) ANOVA was used to determine the effect of jump effort on measured EMG and estimated force variables ($p<0.05$).

RESULTS
The static optimization estimated significant co-contraction of HAM and QUAD at all three effort levels. The average cross-correlation between EMG and maximum force were fair ($r >0.4$) for HAM (50% r=0.52 [CI: 0.46-0.57], 75% r=0.57 [CI: 0.51-0.64] and 100% r=0.53 [CI: 0.47-0.59]) and QUAD (50% r = 0.65 [CI: 0.59-0.72], 75% r = 0.53 [CI: 0.47-0.59] and 100% r = 0.47 [CI: 0.39-0.54]). There were significant increases in maximum EMG and muscle force in both the quadriceps and hamstrings as the effort level increased ($p<0.005$) (Figure 2). Post-hoc analyses showed significant increases in estimated muscle forces for the QUAD and HAM ($p<0.05$) between each effort level.

EMG data showed similar increases from the 75% to 100% effort level, but did not demonstrate a significant increase between 50% and 75% of QUAD and HAM EMG.

DISCUSSION
The results demonstrated that static optimization methods can predict co-contraction of antagonistic muscles. This model incorporated muscles acting across multiple joints and simultaneous estimation of muscle forces in the entire lower extremity (Herzog and Binding 1992). Maximum estimated force and EMG in HAM and QUAD showed similar increases from the 75% to 100% jump height. Conversely, the decreased relationships between EMG and estimated maximal force at the 50% effort level indicate decreased validity of the static optimization techniques used in the current study during sub-maximal tasks.

REFERENCES
Besier TF et al. (2003). *Med Sci Sports Exerc*, 35: 119-27.
Delp SL et al. (1990). *IEEE Trans Biomed Eng*, 37: 757-67.
Herzog W and Binding P (1992). *Math Biosci*, 111: 217-29.

ACKNOWLEDGEMENTS

Figure 2. Mean hamstrings and quadriceps maximum force (green, ♦) and EMG (blue, ●).

EFFECTS OF OPTIC FLOW WHEN SPONTANEOULY ACCELERATING TOWARDS THE WALK-TO-RUN TRANSITION

Kristof De Smet, Philippe Malcolm, Veerle Segers, Matthieu Lenoir and Dirk De Clercq
Ghent University (Belgium), Department of Movement and Sport Sciences
e-mail: kristof.desmet@ugent.be

INTRODUCTION

Understanding the interplay between the use of exproprioceptive information, such as optic flow, and the body dynamics could help us to gain insights into the control mechanisms of gait, and more specific, of gait transitions. Therefore, the purpose of this study is to investigate the influence of optic flow on spontaneous overground walk-to-run transitions (WRT), during which subjects were asked to accelerate in their own preferred manner (De Smet et al., 2008). As subjects did not accelerate in a pre-determined way (like on treadmill), it was not only possible to investigate the influence of the optic flow on the WRT-speed, but also on the entire walking acceleration prior to reaching transition.

METHODS AND PROCEDURES

13 female subjects participated in the study. The experiment took place in a hallway (1.8 m wide, 28 m long and 2.25 high). Black and white stripes (20 cm) were rear-projected on the sidewalls of the hallway. Three visual conditions were tested. In the control condition, static stripes were presented. In the forward condition, the stripes moved in the same direction as the subject at $+2$ m.s^{-1} (= slower optic flow). In the backward condition, the stripes moved in the opposite direction as the subjects at -2 m.s^{-1} (= faster optic flow). Each subject performed 12 trials divided into four blocks of three trials.

Subjects were asked to start walking from a stand still position in a spontaneously accelerating way, until the moment it would be more comfortable for them to run. Subjects' speed was measured at 1000 Hz by Noptel® Distance Laser (CMP2-30). Footscan® insoles (500 Hz) were used to detect foot contacts.

Subjects' speed profile of accelerated walking contains the speed of all walking steps, from the first walking step until the last walking step before transition, plotted against normalized time. Through each speed profile, a best curve was fitted by 4th degree polynomials. To gain insight into the underlying factors that determine the speed profile, a best fit through subjects' SF- and SL-profile was also calculated. A repeated-measures ANOVA compared the profiles at every 10% of the time to transition (TT), in order to reveal whether significant differences between the visual conditions existed.
The transition step (= step 0) was defined as the first step with a flight phase. The last walking step before transition was defined as step -1, while the first running step was defined as step +1.

RESULTS

No significant main effect for visual condition was obtained for the time to transition (TT) ($F = .861$, $p = .435$), nor for the steps to transition (ST) ($F = .820$, $p = .452$) (Table 1).

Table 1 Mean time to transition (TT) and steps to transition (ST)

	TT (s) mean ± sd	ST (n) mean ± sd
Backward	3.094 ± 0.913	6.8 ± 1.9
Control	3.226 ± 0.873	7.1 ± 1.9
Forward	3.113 ± 0.958	6.9 ± 2.0

Subjects' speed, SF- and SL- profiles prior to reaching WRT are shown in Fig. 1. No differences between the visual conditions were observed, nor for speed, nor for SF and SL.
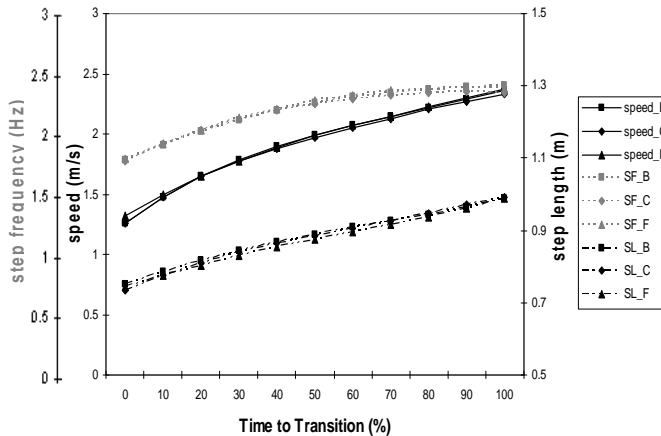
Fig. 1 Speed-, step frequency (SF)- and step length (SL)- profiles during the entire walking acceleration prior to reaching the WRT. Backward condition = B, control condition = C, Forward condition = F. No differences between visual conditions were observed.

For step 0, post-hoc pairwise comparison showed that speed and SL were lower in the backward condition than in the control condition. The same inter-conditional differences were observed for the speed and SL of step +1.

DISCUSSION

It is remarkable that the walking acceleration prior to reaching WRT was not influenced by a modified optic flow, whereas the average speed of step 0 was lower in the backward condition, caused by a smaller SL. This difference was also observed for step +1.

Three major discussion topics can be put forward:

1) the walking acceleration appears to be controlled by a control mechanism which is not online influenced by visual feedback.
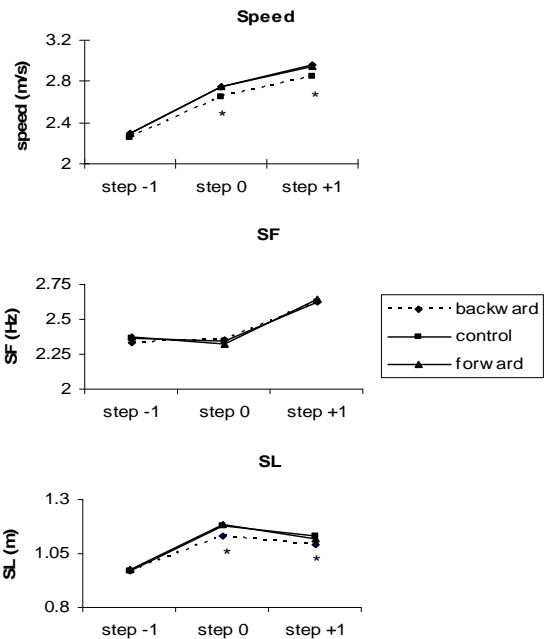
Fig. 2 Speed, step frequency (SF) and step length (SL) of step -1, step 0 and step +1. * significant difference between the backward and the control condition ($p < .05$).

2) backward flow induced a decrease in the WRT-speed. As such, subjects 'jumped' to a lower running speed after the WRT-step when experiencing a faster optic flow (= feed-forward). This was not observed when experiencing a slower optic flow.

3) starting from the WRT-step, the optic flow induced changes in the SL, which is in accordance with Prokop et al (1997).

SUMMARY

The modified optic flow influenced the WRT-step, but not the walking acceleration prior to reaching the WRT.

REFERENCES

De Smet et al. (2008). *Gait Post*, resubmitted
Prokop et al. (1997). *Exp Brain Res,* 28: 225-236.

ACKNOWLEDGEMENTS

FINITE ELEMENT MODELING OF INTRANEURAL GANGLION CYSTS OF THE COMMON PERONEAL NERVE

Shreehari Elangovan[1], Gregory Odegard[1], Duane Morrow[2] and Robert Spinner[3]

[1]Dept. of Mechanical Engineering - Engineering Mechanics, Michigan Technological University,
[2]Biomechanics and Motion Analysis Lab, Mayo Clinic
[3]Departments of Neurosurgery and Orthopaedic Surgery, Mayo Clinic
E-mail: gmodegar@mtu.edu

INTRODUCTION

Intraneural Ganglion Cysts (IGC) are mucinous cysts which form within the epineurium of peripheral nerves, most commonly the Common Peroneal Nerve (CPN). They produce neurologic deficit (i.e., a foot drop). It pathogenesis and treatment are subjects of intense debate for clinicians. Previous studies (Spinner, Atkinson et al., 2003) support the theory that synovial fluid from the superior tibiofibular joint enters the articular branch of the CPN subsequent to joint capsule disruption through injury. The increased pressure caused by continuous influx of fluid compresses nerve fascicles, expands the nerve radially (Fig. 1 - stage I) and causes further propagation proximally into the CPN (Fig. 1 - stages II, III and IV). To effectively treat IGC and eliminate the common situation of postoperative recurrence, surgeons would benefit from an understanding of the underlying mechanics that influence cyst growth. The objective of this study is to introduce computational modeling as a tool for analysis of cyst development. In particular, this study will explore the phenomenon of proximal cyst propagation.
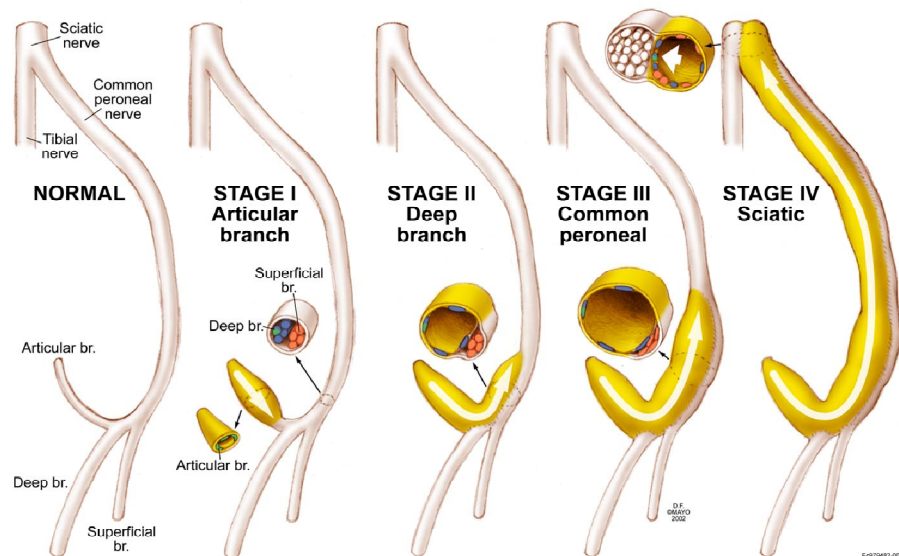
Figure 1. Growth stages of a peroneal intraneural ganglion cyst

METHODS AND PROCEDURES

A two-dimensional planar finite element model of the junction between the articular and the deep branches of the CPN has been constructed (Fig. 2). The articular branch, labelled AB in the figure, meets the deep branch (DB) at an acute angle of 45˚. The positive X-axis represents the proximal direction and the negative X-axis represents the distal. The model contains two regions: a blue region, representing the fascicular region, modeled as a Mooney-Rivlin hyperelastic isotropic material with properties of collagen (α_1 = 168700 Pa, α_2 = 10600 Pa) (Hirokawa and Tsuruno, 1997), surrounded by a red region, representing the softer epineurium, modeled as a Mooney-Rivlin material with properties that are an order of magnitude less than that of the fascicle. Dimensions are taken from intra-operative images and MRI images. The model is meshed with plane-183 elements of ANSYS. The boundary conditions include translational restraints at the two ends along the X-axis and the application of a pressure load of 7932.31 Pa (corresponding to a 15 N load) in the U-shaped cyst face region in the articular branch.
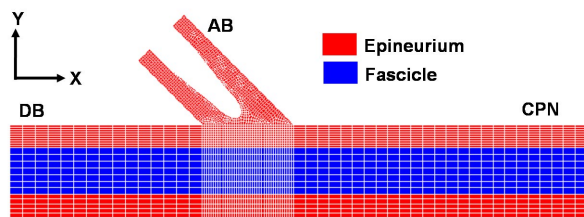
Figure 2. Finite element mesh showing different regions of the nerve

RESULTS

Figure 3 is a vector plot of the first principal stresses around the cyst face where the direction of the arrows represents the principal direction and the length represents the magnitude. It shows that the greatest tensile stresses occur below and to the right of the cyst face and their directions support the clinical observation of the tendency of the cyst to propagate proximally.

DISCUSSION

The location of the peak tensile stresses' occurring on the right side of the cyst face is believed to be a primary reason for the chosen direction of cyst propagation in the proximal direction. It is also believed that the fascicular portion of the articular branch acts as a "road block" that impedes cyst from propagating distally. A three-dimensional finite element model needs to be constructed and analyzed to further investigate the latter point.
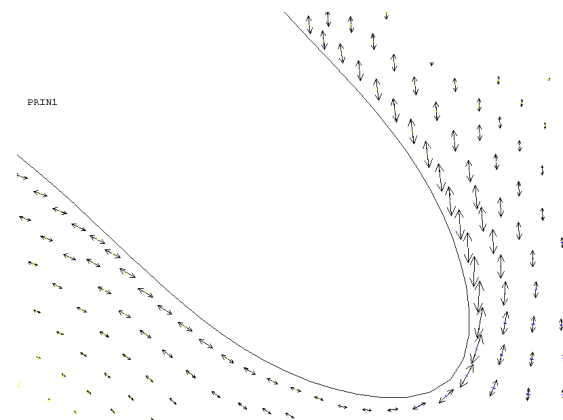
Figure 3. Principal stress directions below the cyst face

REFERENCES

Hirokawa, S. and Tsuruno, R., (1997). *Medical Engineering & Physics* 19 (7) 637-651.

Spinner, R. J., et al., (2003). *Journal of Neurosurgery* 99 (2) 319-329.

ACKNOWLEDGEMENTS

EXAMINATION OF JOINT WORK DURING WALKING IN OLDER ADULTS

Cory Christiansen[1] and Gary Heise[2]

[1]Assistant Professor, Department of Physical Medicine & Rehabilitation, University of Colorado Denver, Aurora, CO, USA, cory.christiansen@uchsc.edu

[2]Professor, School of Sport & Exercise Science, University of Northern Colorado, Greeley, CO, USA, gary.heise@unco.edu

INTRODUCTION

It has been shown that humans walking on level surfaces require net positive work to overcome energy losses by other tissues (DeVita et al., 2007). During stance, hip and ankle work is predominantly positive, while negative work is greater than positive at the knee. The purpose of the present study was to test these relationships in older adults walking on a level surface.

METHODS AND PROCEDURES

A volunteer sample of 15 healthy people participated (age: 71.9 years ± 6.0 years; mass: 74.5 kg ± 16.7 kg; height: 1.64 m ± 0.07 m; sex: 13 women and 2 men). Subjects walked on a 6-m walkway with an imbedded force platform (AMTI, Inc., Watertown, MA) while a video camera (JVC, TK-C1480) captured sagittal plane motion. The video signal (60 Hz sampling frequency) was fed directly to an event and video control unit and synchronized with analog data from the force platform (1020 Hz sampling frequency). Motion data were reduced via digitization of reflective markers and low-pass filter (Vicon, Englewood, CO).

Gait speed was set at 1.5 m/s; established as the normative "fast" mean walking speed for similar aged individuals (Waters et al., 1988). Examination at this speed also allowed comparison to previous data obtained from younger adults (DeVita et al., 2007). Speed was monitored with two photocells set apart 2.44 m along the walkway. Any trial outside ±0.1 m/s of the set speed was re-performed.

Analysis of hip linear velocity and hip height was used to ensure stability of kinetic and potential energy, respectively. All trials demonstrating more than 5% change in hip velocity or vertical position from start to end of stance were removed from analysis.

Sagittal plane joint moments and powers at the hip, knee, and ankle were calculated using inverse dynamics. Joint work was derived as area under the joint power vs. time curve; separated into positive and negative phases during stance. Paired t-tests were used to compare absolute positive and negative work values at each joint as well as for total (summed) joint values during stance.

RESULTS

Figure 1 presents joint work data.
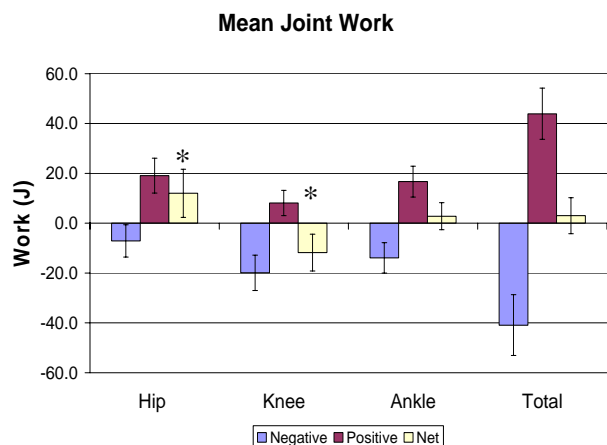
Figure 1. Joint work during stance phase.
*significant difference between positive and negative work absolute values at $\alpha = 0.05$.

Positive work was 169% larger than negative at the hip ($P < 0.001$) and negative 146% larger than positive at the knee ($P < 0.001$). At the ankle, there was no difference between positive and negative work. Total positive and negative work was 43.9 J and –40.9 J, respectively with no significant difference. Of all participants, 10 had total positive and 5 total negative work during stance.

DISCUSSION

The finding of no difference between total positive and negative work during level walking indicates a difference in older adults compared to previous findings with younger adults (DeVita et al., 2007). In their study, DeVita and colleagues found total positive work to be 16.2 J greater than negative. Based on their findings, the authors formulated the hypothesis that overall muscle function in human walking is biased toward mechanical energy production over dissipation.

The current data reveals a bias of net positive work performed at the hip and negative work at the knee; similar to data presented for younger adults (Devita et al., 2007). However, no difference between positive and negative work at the ankle was seen in older adults. In contrast, Devita and colleagues found positive ankle work to be 180% greater than negative work.

Previous studies have established differences between age groups in joint torque and power distribution during walking (DeVita & Hortobagyi, 2000; Judge et al., 1996; Savelberg et al., 2007). Specifically, older adults demonstrate less torque and power at the ankle and knee with greater values at the hip compared to young adults at similar gait speeds. It has been theorized that the hip may compensate for decreased neuromuscular function distally (DeVita & Hortobagyi).

Results of the current study are consistent with this theory.

Current data reveal a higher positive to negative work ratio at the hip than the previous examination of young adults (DeVita et al. 2007). Young adults demonstrated 62% greater positive than negative work at the hip, while positive work is 169% greater than negative in the current sample of older adults. However, the increased percentage of hip work is insufficient to attain net positive lower extremity work. As a result, older adults walk with total net values near zero.

This study is limited to sagittal plane work at the hip, knee, and ankle during stance. It is possible that total joint work, when including all joints and planes of motion throughout the gait cycle, would be different. Additionally, the gait speed examined is faster than customary for the sample of older adults. Older adults walking at customary speed may demonstrate a different joint work profile.

SUMMARY

In conclusion, no net lower extremity work was produced during stance in older adults. Our findings support the idea that net neuromuscular function at the hip may compensate for declines distally (at the knee and ankle) with aging. Further study is warranted.

REFERENCES
DeVita, P & Hortobagyi, T. (2000). *J Appl Physiol*, 88:1804-1811.
DeVita, P et al. (2007). *J Exp Biol*, 210:3361-3373.
Judge, JO et al. (1996). *J Gerontol A Biol Sci Med Sci*, 51:M303-312.
Savelberg, HH et al. (2007). *Gait Posture*, 25:259-266.
Waters, RL et al. (1988). *J Orthop Res,* 6:215-222.

BLOOD FLOW AND OXYGEN LEVEL CHARACTERIZATION OF THE FOREARM WITH CHANGES IN NORMAL AND SHEAR LOAD

Abinand Anbazhagan Manorama, Seungik Baek, Tamara Reid Bush

Department of Mechanical Engineering
Michigan State University, East Lansing, MI, USA
E-mail: anbazhag@msu.edu, sbaek@egr.msu.edu, reidtama@msu.edu
Web: www.egr.msu.edu/~reidtama

INTRODUCTION

Decubitus ulcers are localized areas of tissue-breakdown in the skin and the underlying tissues. Ulcers are more prevalent in subjects who are wheelchair-bound or bed-ridden. The external factors leading to pressure ulcers include pressure, friction, shear force and moisture.

It is well known that mechanical loading is a major factor affecting tissue breakdown. However, it is not clear how the external loading conditions, including normal and shear forces, affect regional blood flow and trans-cutaneous oxygen levels.

Thus, our goal was to study the oxygen levels and blood perfusion in the skin when normal and shear loads were applied to the forearm. Results of this study will provide information that can be related to ulcer development and help inform seating design.

For this study, our hypothesis was that with the addition of shear loading (normal load already present), the blood perfusion and the oxygen levels would decrease as compared to when only a normal force was applied.

METHODS AND PROCEDURES

A total of 15 human subjects were tested for changes in blood perfusion and trans-cutaneous oxygen during the application of normal and shear forces. Each subject participated in two test sessions, with a gap of one week between each session. Each session consisted of 7 test conditions (Table 1). Each condition lasted for a minute, and any two conditions were separated by a resting time of 2 minutes.

A continuous measurement of blood perfusion and trans-cutaneous oxygen was performed on the forearm using a laser Doppler system. The forearm was resting on a fixture connected to an AMTI multi-axis load cell. Along with the two physiological measures, the normal and shear forces were measured by fixing two probes on the lower side of the forearm. A wooden fixture was carved out in such a way that the probes fit into the fixture. The temperature of the blood perfusion probe was maintained constant at 37°C.

For each test condition a time interval of 20 seconds was selected in which the fluctuations of the force values were minimal. Then, the mean values of the blood perfusion and oxygen levels were calculated for the pre-selected 20 second time interval. A statistical analysis was performed to determine the effect of loading on the blood flow and the trans-cutaneous oxygen.

RESULTS AND DISCUSSION

Results of our data show that that the shear and normal loads were highly

individualized. For a relaxed resting arm, ranges from 9.7 N to 33.1 N were obtained. The condition where the subjects applied what they felt to be their maximum amount of shear loading to the base of their forearm showed ranges of shear values from 0.4 N to 35.6 N. Finally, for the condition when the subjects were asked to lean on their forearm using the weight of their upper body and to apply as much load as they felt comfortable, the following ranges of normal 24.9 N to 117 N, and shear 3.1 N to 57.6 N were obtained.

Because of the highly individualized loads, the results of the blood flow and trans-cutaneous oxygen levels were evaluated for with-in subject comparisons. We compared the blood perfusion and oxygen levels between conditions 2 and 3 (Table 1). A Paired t-test (α =0.05) was used to assess blood perfusion. However, the data for the trans-cutaneous oxygen levels did not demonstrate normality. Hence, a Wilcoxon Signed Rank Text (α =0.05) was performed for these measures.

The results of these tests indicated that significant differences were exhibited between the condition of normal loading, and the combination of normal and shear loading. Specifically, blood perfusion and oxygen levels were reduced with the addition of shear loading ($p=0.006$ and $p < 0.001$ respectively).

SUMMARY/CONCLUSIONS

From the statistical analysis, we obtained positive results that support our hypotheses; the blood perfusion and the trans-cutaneous oxygen levels decreased when there was combined loading (shear and normal).

One limitation to this work is the variability of the forces across subjects. This will be addressed in future studies.

REFERENCES

Bansal et al. (2005). *Intl. J. of Dermatology,* 44:805-810.
Kanj et al. (1998). *J. American Academy of Dermatology,* 38:898-104.
Bouten et al. (2003). *Arch Phys Med Rehabil,* 84:616-9.

Table 1: Description of test conditions

Test condition	Description of loading while blood perfusion and trans-cutaneous oxygen levels are measured.
1.	No load is applied on the forearm and no contact with load cell.
2.	The forearm rests on the load cell arrangement, without the application of any additional loads.
3.	A shear force is applied to the base of the forearm in addition to the weight of the arm (normal force)
4.	An additional 2 lbs is applied on the forearm without applying shear force.
5.	A shear force is applied to the forearm in addition to the force mentioned in 4.
6.	An additional 4 lbs is applied on the forearm without applying shear force.
7.	Normal and a shear forces are applied by resting all the body weight on the forearm.

LUMBAR SPINE MOVEMENT AND PAIN DURING PROLONGED SEATED WORK

Nadine M. Dunk, Jack P. Callaghan
Department of Kinesiology, Faculty of Applied Health Sciences
University of Waterloo, Waterloo, ON
Corresponding author email: nmdunk@ahsmail.uwaterloo.ca

INTRODUCTION

With the high prevalence of computer users in the workplace, the issue of postural fixity in seated postures has emerged. Little is known about how movement in the lumbar spine influences the mechanical changes and potential injurious effects of the prolonged flexion associated with seated postures. Specially designed chairs or devices that induce movement in sitting have been used as a method for alleviating LBP provoked by prolonged sitting (van Deursen et al., 1999). The purpose of this study was to examine the postural responses and pain scores of low back pain (LBP) sufferers compared with healthy individuals in order to understand the biomechanical factors that may be associated with LBP during sitting.

METHODS

Sixteen participants with sitting-aggravated LBP were age- and gender-matched with 16 healthy participants. Participants performed 90 minutes of standardized seated computer work in six 15-minute blocks. Ratings of perceived discomfort were obtained at the beginning of each time block as well as at the end of the protocol. Lumbo-sacral (LS) spine and pelvic postures were continuously measured using tri-axial accelerometers (S2-10G-MF, NexGen Ergonomics, Montreal, QC) placed at L1 and on the sacrum. Outputs were proportional to the angle between the sensitive axis and the gravitational vector. Accelerometers were calibrated by aligning their sensitive axes at known orientations in the gravitational field and custom software

was written to convert the output into angles. Full standing LS flexion range of motion (RoM) was measured before and after prolonged sitting. Lumbar spine posture was examined over the 90-minute sitting period using various analysis techniques including calculating the range of movement and a shift analysis similar to Duarte & Zatsiorsky (1999). The number of lumbar spine shifts were calculated by comparing average values of two moving windows ($\bar{x}_{w1}$ and $\bar{x}_{w2}$, duration = 15 s) separated by a period of 3 s. Any two consecutive windows satisfying Equation 1 were classified as a shift:

$$|\bar{x}_{w1} - \bar{x}_{w2}| \geq 5° \qquad (1)$$

RESULTS

Healthy participants had greater LS RoM than those with LBP. In general, all participants had less RoM after sitting for 90 minutes. Individuals with LBP reported large increases in pain (described as achy, sore or tired) in their low back region, while healthy individuals generally reported little pain anywhere in their body. Over time, postures were quite variable, due to the amplitude of lumbar spine movement increasing as time passed (Figure 1). Individuals with LBP had larger amplitudes of lumbar spine movement than healthy individuals throughout the 90-minute sitting period, and had an increasing number of shifts over each 15-minute time block. Over the entire sitting period, LBP sufferers shifted once every 7.2±4.7 minutes, whereas healthy participants shifted every 12.6±4.6 minutes.
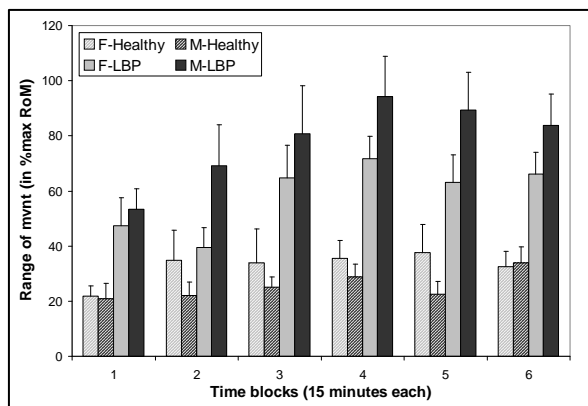
Figure 1: The range of movement of the lumbar spine (in percent of maximum lumbar flexion) calculated as (max flexion angle – min flexion angle) during each 15-minute time block of the 90-minute

DISCUSSION

The results of the current study demonstrate that individuals with sitting-induced LBP exhibit large shifts in lumbar spine postures in conjunction with increased pain in that region. In general, LBP sufferers exhibited a dynamic sitting pattern (i.e. using up to 100% of their lumbar RoM) while healthy individuals tended to adopt a small number of single 'static' positions within 40% of their RoM. It has been observed that increased whole body movement is associated with increased discomfort over time (Fenety et al., 2000; Vergara & Page, 2002) and that small, frequent postural shifts may be more effective at relieving discomfort (Vergara & Page, 2002). Low frequency, small amplitude continuous passive lumbar motion has also been shown to reduce pain in LBP patients over a period of prolonged sitting (Reinecke et al., 1994; van Deursen et al., 1999). However, given that the individuals in the current study suffered from LBP prior to their participation, a causal relationship between spine movement and pain remains difficult to discern. There is little information in the literature regarding how total lumbar spine movement affects the mechanics of the intervertebral joint, in particular height

changes and pressure distribution within the intervertebral disc. Further work examining the time-varying effect of movement on the mechanical properties of the intervertebral joint *in vitro* will give insight into the potential pain generating mechanisms that can exist from exposure to prolonged sitting.

SUMMARY

Lumbo-sacral spine posture and movement was examined during 90 minutes of seated computer work in 16 LBP sufferers who were age- and gender-matched with 16 healthy control participants. Individuals with sitting-induced LBP exhibit large shifts in lumbar spine posture in response to increased pain in the lumbar region. It has been suggested that frequent large spine movements are an effect of discomfort while small, quick movements tend to alleviate it.

REFERENCES

Duarte M & Zatsiorsky VM (1999). *Motor Control*, 3; 12-27

Fenety PA et al. (2000). *Appl Ergon,* 31; 383-393.

Reinecke SM et al. (1994). *J Spinal Disord*, 7; 29-35.

van Deursen LL et al. (1999) *Eur Spine J*, 8; 187-193.

Vergara M, Page A (2002). *Appl Ergon,* 33; 1-8.

ACKNOWLEDGEMENTS

NEUROMUSCULAR BIOMECHANICS SIMULATION ONTOLOGY

Anders Sandholm[1], Daniel Thalmann[1]

[1] Virtual Reality Laboratory, Department of Information Technology and Computer Science, Swiss Federal Institute of Technology (EPFL), Lausanne, Switzerland, anders.sandholm@epfl.ch

INTRODUCTION

Today several fields are developing, or have developed, ontology's for there sub-domains. One of the more public known is the Gene Ontology (Ashburner et al. 2000) which is used in the field of biology. In this paper the author present a new ontology aimed towards the neuromuscular simulation field. Today this field utilizing knowledge from several subdomains, such as orthopaedics, electronics, mechanics, mathematics, computers science, computer graphics and statistics. When developing new models or simulation tools people collaborate over these subdomains, for example, the implementation of new simulations methods where knowledge from orthopaedics, tissues mechanics is used by the software developer. Commonly this knowledge are stored in text books, journals or in project documentation with no linkage between the subdomains. In an ontology all information is ordered and classified according to a vocabulary which is a set of rules for combining and linking words and expressions (Gruber 1993). Each of these instances can been seen as a class with properties and relationships to other classes. When the ontology grows it create a web between the subdomains that link the different knowledge domains together and makes them interactive.

In the 3D Visual Anatomical Human Project (3DAH 2008) we are developing an simulation ontology to increase the collaboration and knowledge sharing between partners in different subdomains. The aim is to create a reusable knowledge infrastructure that allow both subdomain knowledge to be shared and to be reused.

METHODS AND PROCEDURES

The implementation of the extended biomedical ontology is based on the idea of reusable knowledge libraries (Benjamin et al. 1996) with the extension that information from models and simulation is combined with information from the common knowledgebase. Our aim is to extend the ontology concept so it will be able to handle model specific data, simulation setup, results and discussions/conclusions. The ontology also support exchange of knowledge without sending the complete ontology implementation. To fulfill these goals an overlaying architecture and dataflow design where constructed (figure 1). The implementation uses a main database to store all common knowledge who is extended with information from the experiment database, result files and software tool documentation.
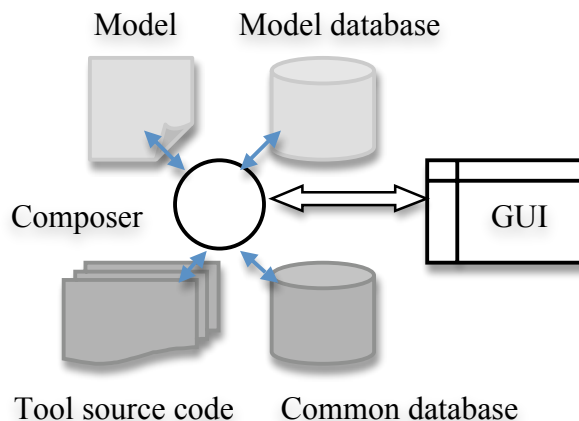
Figure 1. Ontology component interaction.

RESULTS

The first implementation part of the neuromuscular biomechanics simulation ontology has been completed and is currently been populated with subdomain knowledge. Today several model/result formats is used depending on the simulation tool. Currently the ontology presented in this paper only support OpenSim (Delp et al. 2007) XML based model and result files. When the user loads a model or result file, information is extracted from the xml file and combined with the knowledge from the other domains. Information can also be extended into the XML file along with references to other recourses. To access knowledge from the simulation tool, information is extracted from the source code documentation using the doxygen markup language. In figure 2 the current graphical user interface are shown displaying information and data from a muscle in a model, general information about the muscle comes from the common database, model parameters are loaded from the associated model file.
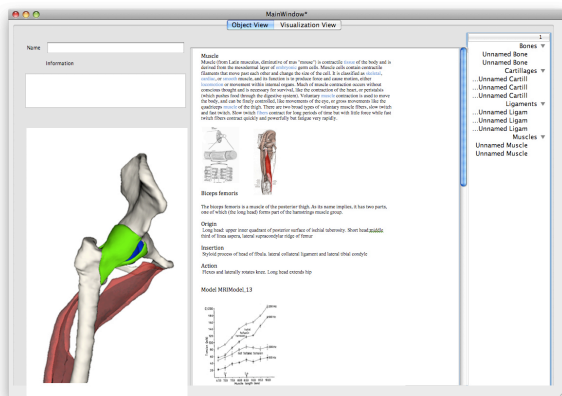
Figure 2. Graphical user interface of the ontology

DISCUSSION

By extending the traditional ontology idea to contain model and simulation result more information can be viewed and exchanged.

Knowledge that is derives from an experiment can be integrated into the knowledgebase and reused in other experiments. Further work will include development of functionality to propagate edited and added information to the right information source.

SUMMARY

The field of neuromuscular biomechanics consist of several subdomains, such as orthopaedics, mathematics and computer science. This paper outline an extended ontology implementation where knowledge is represented in a reusable way, along with model and experiment information.

REFERENCES

Ashburner, M et al. (2000). *Gene Ontology: tool for the unification of biology Nature Genetics 25, 25 – 29*

Benjamin, J et al. (1996). Ontology Construction for Technical Domains, *Proceedings of the 9th European Knowledge Acquisition Workshop on Advances in Knowledge Acquisition*, 98-114.

Delp SL, et al. (2007). OpenSim: Open-source Software to Create and Analyze Dynamic Simulations of Movement. IEEE Transactions on Biomedical Engineering.

Gruber, T.R. (1993). *A Translational Approach to Portable Ontology Specifications. Knowledge Acquisition, Vol. 5, Number 2.*

3DAH (2008), 3D anatomical functional models for the human musculoskeletal, *Sixth Framework Programme, EU, http://3dah.miralab.unige.ch/*

ACKNOWLEDGEMENTS

REPEATED EXPOSURE TO SMALL POSTURAL PERTURBATIONS LEADS TO IMPROVEMENTS IN BALANCE RECOVERY

Kathleen A. Bieryla[1], Bradley S. Davidson[2], and Michael L. Madigan[1]

[1]Virginia Tech, Blacksburg, VA, USA
[2]University of Colorado Health Science Center, Denver, CO, USA
E-mail: kbieryla@vt.edu, Web: www.biomechanics.esm.vt.edu

INTRODUCTION

In 2005, falls caused 14.2% of occupational fatalities in the United States (BLS, 2005). Additionally, 39% of all fatal falls were from workers 55 years and older (BLS, 2005). One potential approach to help prevent these falls is balance training.

The main purpose of this study was to determine if repeatedly exposing participants to a small postural perturbation would result in performance adaptations. It was hypothesized that participants would demonstrate performance adaptations that were consistent with an improvement in balance recovery performance (BRP).

METHODS

Sixteen younger (mean $19.4 \pm$ SD 1.4 years) and 13 older (62.8 ± 5.5 years) adults were recruited to participate in the study from the university population and surrounding community, and informed consent was obtained prior to participation. The experiment consisted of three testing sessions with approximately one week between consecutive sessions. During each session participants were exposed to 20 forward and backward postural perturbations delivered via ballistic pendulums in a random order (Fig 1). Only forward perturbations are reported here. The magnitude of the forward perturbations was defined as the linear momentum just prior to impact and was approximately 10 N·s.

Figure 1: Participants stood relaxed with their eyes closed. Perturbations were administered with two padded and weighted ballistic pendulums placed both in front of and behind the participant

Whole-body kinematics were recorded during all trials. Body segment data was sampled at 100 Hz (Vicon, CA).

BRP was quantified using several center of mass (COM) based measures. Whole body COM was estimated using anthropometric measurements. BRP measures were peak COM displacement, time-to-peak COM displacement, and time-to-boundary of the COM (Van Emmerick, 2002) . To allow comparisons between groups, COM displacement measurements were normalized by ankle to toe distance. A two-way ANOVA was conducted on BRP measures with session (1, 2, or 3) and age (young or old) as independent variables. Multiple comparisons were performed using a Bonferroni correction ($\alpha=0.017$).

RESULTS AND DISCUSSION

Peak COM displacement decreased 2.2% from Session 1 to Session 3 ($p<0.001$) (Fig 2). Time-to-peak COM displacement decreased 4.7% from Session 1 to Session 3 ($p<0.001$). Time-to-boundary of the COM increased 3.6% from Session 1 to Session 3 ($p<0.001$). Significant Session x Age interaction effects were seen in all three dependent measures ($p<0.01$).
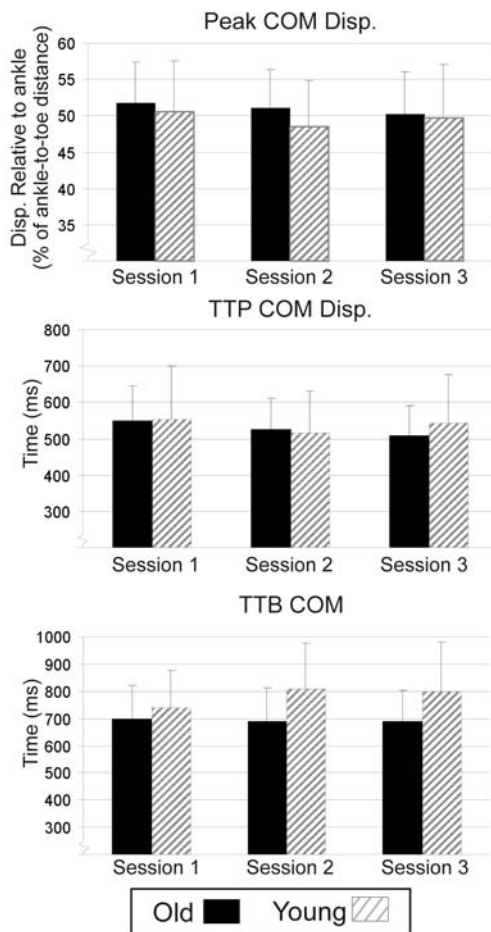
Figure 2: Peak COM displacement, time-to-peak COM displacement, and time-to-boundary of the COM for all three sessions, old and young. Error bars represent standard deviation.

In general, BRP measures improved with repeated exposure to a balance perturbation. Maintaining a low COM displacement can be associated with greater postural stability (Shumway-Cook and Woollacott, 2000).

Older adults were not able to increase their time-to-boundary of the COM between the sessions while the young adults were able to do so. A lower time-to-boundary measure indicates greater postural instability (Van Emmerick, 2002) suggesting that the young adults were able to improve their stability more than older adults.

Although the effects of training were significant, it is unclear if they were large enough to provide meaningful benefits.

SUMMARY/CONCLUSIONS

In conclusion, both young and older adults were able to improve measures of balance recovery and demonstrate short term performance adaptations when exposed to low level perturbations. These results suggest it may be beneficial to expose workers to balance perturbations to allow them to adapt to the situation in a safe controlled environment which may translate to the occupational setting, but further work on the effect size of training is necessary.

REFERENCES

Bureau of Labor Statistics. (2005). National Census of Fatal Occupational Injuries in 2004. US Department of Labor.
Shumway-Cook A and Woollacott MH (2000). *Motor Control: Theory and Practical Applications*. Baltimore, Lippincott Williams & Wilkins.
Van Emmerick, REA and van Wegen, EEH (2002). *Exerc Sport Sci Rev*, 30:177-183.

ACKNOWLEDGEMENTS

ANTHROPOMETRIC PARAMETERS IN THE ELDERLY: A DXA-BASED STUDY

April J. Chambers[1], Jean L. McCrory[2], Alison L. Sukits[1] and Rakié Cham[1]

[1]Human Movement and Balance Laboratory, Department of Bioengineering
[2]Department of Health and Physical Activity, University of Pittsburgh, Pittsburgh, PA, USA
email: chambers@engr.pitt.edu, web: www.hmbl.bioe.pitt.edu

INTRODUCTION

Anthropometric data are required in biomechanical studies of gait and balance. Regression equations are typically based on two types of source measurements: (1) cadaveric (Dempster, 1955), or (2) imaging (de Leva, 1996). The use of these non-age specific regression equations has yielded inaccurate estimates in both children (Ganley & Powers, 2004b) and older adults (Durkin & Dowling, 2003). For example, Durkin noted errors of over 50% in the center of mass position estimation using traditional regression equations in older adults.

Tissue density varies within and between segments, and that distribution varies with age, gender and body type (Stoudt, 1981; Jensen 1978; Jensen & Fletcher, 1994). Dual energy x-ray absorptiometry (DXA) can be used to take into account these effects and has been proven a reliable in-vivo method to derive body segment parameters (Durkin & Dowling, 2003; Ganley & Powers, 2004a). The goal of this preliminary study, part of a larger research project, is to compute the magnitude of potential errors in the estimates of anthropometric variables derived based on traditional regression models in the elderly. These errors will be estimated relative to the "true" DXA-based values.

METHODS AND PROCEDURES

Eight healthy older adults (4 F, 4 M), screened for metal implants and equally divided into two obesity groups (BMI≤30 / BMI>30), underwent a whole body DXA scan (Hologic QDR 1000/W). Participants represented a range of body types (Table 1).

Table 1. Participant characteristics. Means (SD) and [Range] are tabulated

Age (years)	Body Mass (kg)	Height (m)
71 (4)	80.9 (22.6)	1.67 (.06)
[66-75]	[54.4-122.5]	[1.61-1.79]

For each DXA scan, segment boundaries were identified (Table 2) (Dempster, 1955; de Leva 1996). Additionally, detailed body measurements were collected.

Table 2. Boundaries used to identify body segments from DXA scans

Segment	Proximal end	Distal end
Shank	Lateral epicondyle	Inferior lateral malleolus
Thigh	Superior greater trochanter [1]	Lateral epicondyle
Trunk	Superior greater trochanter	Superior acromion

[1] Mass of pelvis not included

Segment mass as a percent of body mass (SM), segment length as a percent of body height (SL), distance from the center of mass to the proximal end of the segment as a percent of segment length (COM), and frontal plane radius of gyration as a percent of segment length (r) were determined (Ganley & Powers, 2004b; Durkin & Dowling, 2003). These dependent variables, derived using de Leva (1996), were each entered individually as dependent variables in a within-subject

ANOVA. The independent factors were derivation method (de Leva / DXA), gender (M/F), obesity group (BMI≤30 / BMI>30), and their interactions. Statistical significance was set at 0.05. Percent root mean square errors (%RMSE) were calculated for each dependent variable using the following:

$$\%RMSE = 100 \times \sqrt{\frac{1}{N(=8)} \sum_{i=1}^{i=N(=8)} \frac{(deLeva_i - DXA_i)^2}{DXA_i^2}}$$

RESULTS

No significant differences were found across males/females or BMI group. These groups were combined for the remaining results. Statistically significant differences in all anthropometric variables for all segments were noted between the de Leva estimates and DXA-based parameters except for the shank SM. These errors were typically large in magnitude (Figure 1). The greatest errors were seen in the thigh segment.
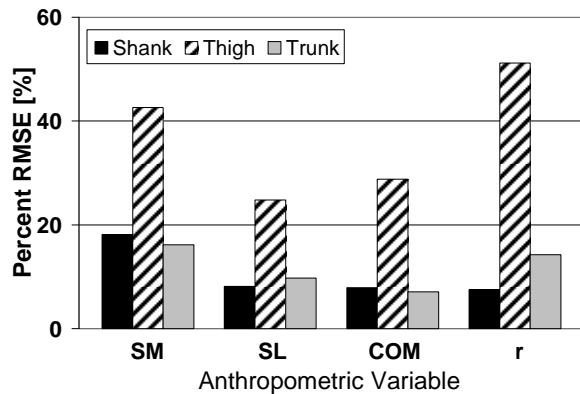
Figure 1. %RMSE comparing DXA and de Leva methods.

DISCUSSION

Significant differences were found across all segments and variables of interest except shank SM. These large errors associated with the traditional regression-based methods have been noted previously in various populations (Ganley & Powers, 2004b; Durkin & Dowling, 2003). The errors reported here

may be attributed to regression models assuming a constant density. This assumption can be a source of error as age-related mass redistribution between and within segments is ignored. Also, the elderly are known to have different body shapes compared to the populations on which the traditional equations are based. One limitation of this study is the small sample size. We suspect that with a larger N, gender and obesity effects may be significant.

SUMMARY

This preliminary study underlines the need to develop accurate methods to predict age-specific anthropometric data needed to study the biomechanics of postural control and gait in the elderly.

REFERENCES

de Leva, P (1996). *J Biomech,* 29:1223-30.
Dempster, WT (1955). *Space Requirements of the Seated Operator*. 55.
Durkin, JL and Dowling, JJ (2003). *J Biomech Eng,* 515-22.
Ganley, KJ and Powers, CM (2004a). *Clin Biomech*. 19:50-6.
Ganley, KJ and Powers, CM (2004b). *Gait & Posture*, 19:133-40.
Jensen, RK (1978). *J Biomech*, 11:349-58.
Jensen, RK and Fletcher, P (1994). *J Biomech,* 27:89-96.
Stoudt, HW (1981). *Hum Factors,* 23:29-37.

ACKNOWLEDGEMENTS

DOES MIDSOLE DEFORMATION REFLECT REARFOOT MOTION DURING RUNNING? – A MULTIPLE REGRESSION APPROACH TO EVALUATE PRONATION BY HALL SENSORS

Thomas L. Milani, Torsten Brauner, Thorsten Sterzing, Doris Oriwol

Department of Human Locomotion, Chemnitz University of Technology, Chemnitz, Germany
thomas.milani@phil.tu-chemnitz.de

INTRODUCTION

Although many studies have been performed in the research area of rearfoot motion the relationship to running injuries and their etiology are still unclear (Grau et al., 2003). Nevertheless, pronation and pronation velocities during running are accepted to be linked to overuse injuries like PFPS and achilles peritendinitis. The majority of studies to analyze rearfoot motion are performed by using motion analysis systems. A convenient and fast measurement method was introduced by using an electrogoniometer (Milani & Hennig, 1995) that is fastened at the heel cup of the running shoe.

The rotation of the hind foot from the supinated position at touchdown to pronation during early stance phase induces a load shift from lateral to medial (Hennig & Milani, 2000). Hagman et al. (2001) used a mathematical model to build a relationship between pressure plate data and 3D rearfoot motion, but no biomechanical validation was reported. Brauner et al. (2008) used single plantar piezoceramic sensors to calculate an algorithm for the determination of pronation and pronation velocities.

The goal of this study was to determine the range of rearfoot motion (TPR) and maximum pronation velocity (MPV) by analyzing the midsole deformation using Hall sensors that are placed in the midsole of an EVA prototype running shoe.

METHODS AND PROCEDURES

30 runners (26.1 yrs ($\pm$5.3), 71.5 kg ($\pm$7.8)) were in the subject pool: 17 served for the algorithm calculation, whereas 13 different runners were used for its validation. All subjects were familiar with the laboratory testing conditions and categorized as heel-toe runners. Running velocity (3.5m/s $\pm$0.1) was controlled by photoelectric barriers. Subjects performed five repetitive trials on a runway across an integrated KISTLER force plate (9287BA). All subjects used an EVA test shoe with 10 Hall sensors placed into the EVA midsole around the heel cup (Figure 1).

Figure 1: EVA Test shoe with Hall Sensors

As a reference for rearfoot motion an electrogoniometer was used (Milani & Hennig, 1995). Maximum (max) deformation and time of this maximum (tmax) deformation of each Hall sensor signal was used as independent variable in Multiple Regression Analyses, whereas goniometer data served as dependent variables. With the determined regression coefficients, TPR$_{Hall}$ and MPV$_{Hall}$ were calculated for each trial and compared to the

goniometer data (Fig. 2). Over all subjects mean rearfoot motion parameters were calculated. Furthermore, the mean error and regression coefficients as well as the mean error of the validation procedure ($\varnothing_{\text{error-V}}$) and its correlation coefficients were evaluated.
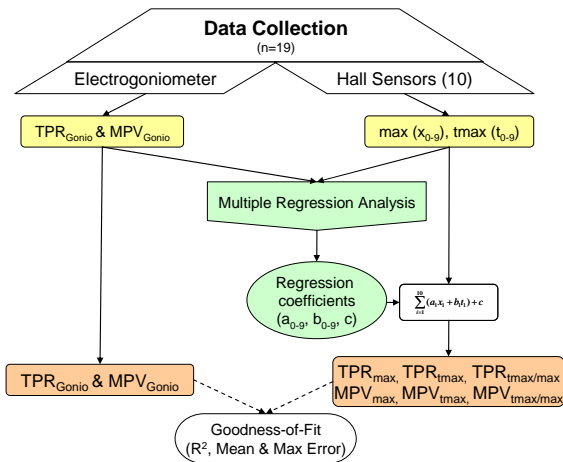
Figure 2: Data Processing Procedure

RESULTS

Hall sensor signals were successfully applied to determine TPR_{Hall} and MPV_{Hall}. In Table 1 the determined Hall mean values, regression coefficients and mean errors are listed.

Parameter	$\varnothing$Mean	$\varnothing_{\text{error}}$	R^2	$\varnothing_{\text{error-V}}$
$TPR_{\text{Hall}}°$	13,1(3,7)	1,1	.86	3,5
$MPV_{\text{Hall}}°/s$	365(91)	32	.78	150

Table 1: Mean parameters of rearfoot motion determined by Hall and by goniometer

The regression analyses showed good regression coefficients for the determination of rearfoot motion parameters. The combination of the variables max/tmax resulted in higher regression coefficients. The validation study with different runners showed higher mean errors (TPR $\varnothing_{\text{error-V}}$ & MPV$\varnothing_{\text{error-V}}$) and lower correlation coefficients (R_{TPR}=.73; R_{MPV}=.41).

DISCUSSION

Hall sensors that are placed in the midsole of the heel area of an EVA running shoe were used to analyze local midsole deformation and to calculate rearfoot motion parameters. The algorithms resulted in sufficient regression coefficients when determining TPR and MPV. The validation procedure of the algorithms showed relatively high mean errors resulting in relatively low correlation coefficients. Data evaluation showed that highly different individual rearfoot motion patterns are resulting in insufficient correlation values.

SUMMARY

Heel midsole deformation can be used to calculate rearfoot motion parameters such as pronation and maximum pronation velocity in a modified EVA shoe. Modification of the location of the Hall sensors and increasing subject numbers might improve the algorithm and therefore result in higher validation values.

REFERENCES

Brauner, T. et al. (2008). Submitted to *ESM 2008,* Dundee, Scotland.

Grau, S. et al. (2003). D. Z. Spo Med 54 (1), 17-24.

Hagman, F. et al. (2001), Proc. of the 5th Symp. on Footwear Biomech. Zuerich /Switzerland. 42-43.

Hennig E. M. & Milani, T. L. (2000), Sportverletz Sportschaden. 14: 90-97.

Milani, T. L. & Hennig, E. M. (1995). J. Appl. Biom. 177-187.

ACKNOWLEDGEMENTS

ACTIVELY GENERATED FORCE AND STIFFNESS TRANSMISSION THROUGH LAYERS OF THE RAT ABDOMINAL WALL

Stephen H.M. Brown and Stuart M. McGill

Department of Kinesiology, University of Waterloo, Waterloo, ON, Canada,
shmbrown@uwaterloo.ca

INTRODUCTION

The anatomical architecture of the abdominal wall is highly unique. Three broad sheet-like muscles (internal oblique, external oblique, transverse abdominis), each with fibres obliquely oriented relative to one another, are adhered in a layered architecture through a network of loose connective tissues. This composite laminate arrangement appears well suited to facilitate transmission of muscularly generated force and stiffness between adjacent layers (Hwang et al., 2005). The purpose of this study was to test this hypothesis by disrupting the normal route of force/stiffness transmission in the rat abdominal wall.

METHODS AND PROCEDURES

Fifteen male rats were anaesthetized (5% isofluorane), and the abdominal wall was cut away from the rib cage and pelvis and sutured to a force/displacement transducer. The transverse abdominis (TrA) muscle was stimulated (100Hz (0.1 ms/pulse) 800ms trains) directly with surface electrodes. Rapid muscle length changes were administered during contraction, enabling the recording of both muscle force and stiffness (1000Hz).

In ten rats the aponeurosis of the transverse abdominis was then surgically cut (Figure 1), negating force and transmission via this route, and the muscle wall was re-stimulated and force and stiffness were again recorded.
In the remaining five rats an amount of time approximately equal to the amount of time required to perform the cutting of the aponeurosis (average of three minutes) was allowed to elapse and the force and stiffness tests were repeated. In these rats the aponeurosis remained intact. This control group served to test the hypothesis that an elapse of time, in the compromised surgical state, caused a decrease in the force and stiffness generating capabilities of the abdominal wall muscle group.

RESULTS

Force and stiffness generated by the abdominal wall were reduced 10.6% and 10.7%, respectively, after cutting of the aponeurosis. Based on measurements made of the thickness and fibre orientation of each muscle, however, it was estimated that an approximate 39% reduction in these parameters should have occurred had the contribution of the transverse abdominis been completed eliminated. Thus, the majority of actively generated force and stiffness was still transferred through to our recording system.

Further, in the control group in which the aponeurosis was not mechanically cut but time was allowed to elapse between tests, drops of 7.9% and 8.2% were found in active force and stiffness, respectively. This indicates that at least a portion of the drop in these parameters was a result of the passage of time in a compromised muscular state.

intact aponeurosis   linea alba   cut aponeurosis

wire to force/displacement transducer

transverse abdominis   stimulating electrodes
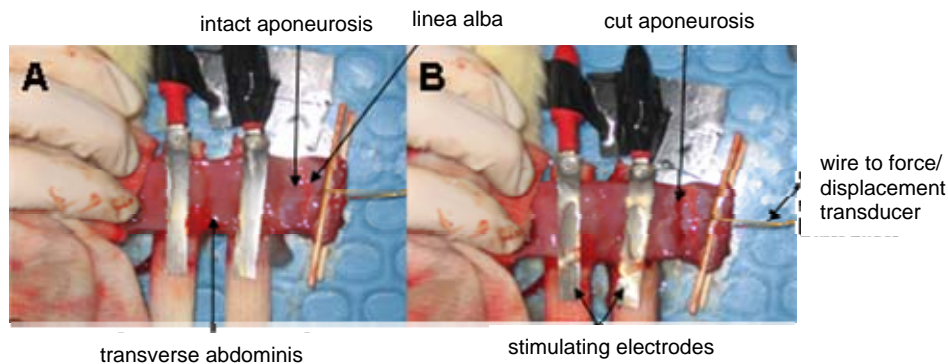
Figure 1. Picture of the abdominal wall in the intact state (A) and with the TrA aponeurosis cut (B).

DISCUSSION

The vast majority (72%) of the force and stiffness generated by the transverse abdominis was transferred to our recording device, despite the elimination of its normal route of transmission. Force and stiffness were most likely transferred through the connective tissue network intervening the muscle layers. It is not possible from the current study to determine the degree to which, if at all, this inter-muscle connective tissue transmission route is utilized in the healthy or undamaged state; however, it can be stated that the force produced by the muscles will be transferred in the majority through the stiffest path. A suspected high shear modulus suggests that force would be readily transferred between the muscle layers during in vivo situations. This indicates a functionality of the abdominal wall as a composite laminate structure, enabling a substantial generation and transmission of multi-directional stiffness around the torso. This has important consequences for the effective stabilization of the lumbar spine.

SUMMARY

The abdominal wall musculature has a unique anatomical arrangement that would appear designed to facilitate myo-fascial force transmission between the muscular layers. This study confirmed that, in the absence of its normal route of transmission (the anterior aponeurosis), the majority of actively generated transverse abdominis force and stiffness can still be transferred around the abdomen. The most likely alternative path of transmission is through the connective tissue network that intervenes the three muscular layers. This may enlighten the ability of these muscles to work in a mechanically synergistic fashion, essentially forming a composite material thought to be necessary to stabilize the spinal column, through the effective linking of force and stiffness during contraction.

REFERENCES

Hwang, W et al. (2005). *J Appl Physiol,* 98: 1829-1835.

ULTRASOUND ANALYSIS OF IN-VIVO CONNECTIVE TISSUE DEFORMATIONS OF THE HUMAN ABDOMINAL WALL

Stephen H.M. Brown and Stuart M. McGill

Department of Kinesiology, University of Waterloo, Waterloo, ON, Canada,
shmbrown@uwaterloo.ca

INTRODUCTION

The abdominal wall components, specifically muscle and connective tissue, must meet and accommodate a wide range of force demands for torso movement, spine stabilization, and respiration. The wall is comprised of three muscle groups (internal oblique (IO), external oblique (EO), transverse abdominis (TrA)) and has a composite laminate arrangement that assists torque generation about the three axes and forms stiffening hoop stresses facilitating function. The purpose of this exploratory study was to examine the deformations of the abdominal wall, with a special focus on both the internal oblique aponeurosis and the tendinous intersections of the rectus abdominis (RA), using ultrasound imaging, during relatively simple contractions of the abdominal musculature.

METHODS AND PROCEDURES

Eight healthy males volunteered from the University population. Participants performed a series of static abdominal brace contractions in a modified sit-kneel position, designed to keep the spine in a neutral posture. Target contraction levels were set to 25%, 50% and 100% of the maximum activation capability of the right EO in the testing position. To view the aponeurosis of the IO muscle, ultrasound images were taken with the probe at the level of the umbilicus on the left side of the body, with the lateral position adjusted to ensure a view of the IO aponeurosis between the medial edge of the IO muscle and the lateral edge of the RA muscle. For a sub-set of four participants another series of the identical contractions were performed with the probe at two additional orientations: 1) angled 35 degrees inferior-laterally (along the approximate line of the IO fibres); 2) angled 60 degrees superior-laterally (along the approximate line of the EO fibres). For the RA tendon, the ultrasound probe was positioned over the intersection lying most closely superior to the umbilicus, oriented in the inferior-superior direction along the anterior of the RA muscle, and positioned approximately mid-way between the linea alba and linea semilunaris. Two still ultrasound images were captured on a video cassette and digitized for each trial, the first when the muscles were relaxed and the second when the target activation level had been reached at a steady state. For the IO aponeurosis images trials, the length and thickness of the aponeurosis were measured in both the relaxed (Figure 1) and contracted image (Figure 2). The same measures (length and thickness) were taken for the RA tendon.

Surface EMG was recorded from the RA, EO, and IO muscles, and used to estimate (based on cross-sectional area, maximum stress, and length) the force generated in each of these muscles (along with the TrA) during contraction.

RESULTS

The most unique finding was that both the IO aponeurosis and RA tendon displayed deformations in nearly 50 percent of
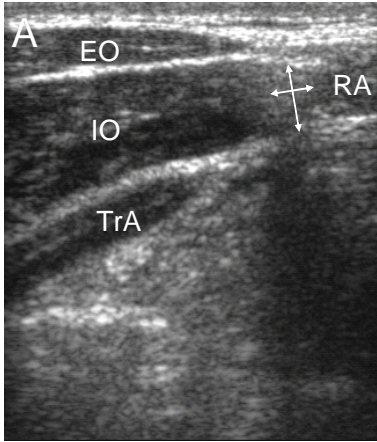
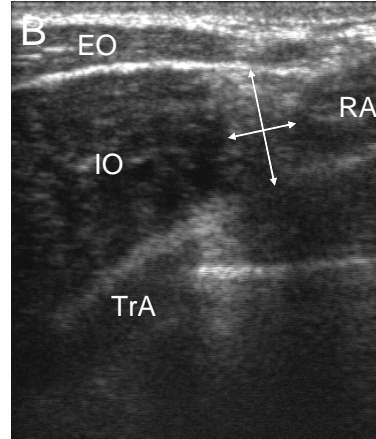**Figure 1.** Ultrasound image, taken transverse through the abdomen, of the IO aponeurosis (indicated by arrows) at relaxation.

Figure 2. Ultrasound image, taken transverse through the abdomen, of the IO aponeurosis (indicated by arrows) at 100% contraction.

contractions that would be characterized by a simultaneous expansion in multiple planes. Also, the lateral border of the RA muscle was pulled more laterally upon contraction in 68% of trials. The ratio of summed oblique muscle (EO, IO, TrA) force to RA muscle force was used to assess a relationship with the lateral displacement of the RA muscle, with an exponential R-squared fit of 0.54. This indicates that the lateral forces produced by the oblique and transverse muscles dominate over the longitudinal force of the RA muscle, causing the RA to be pulled laterally.

DISCUSSION

The primary finding of this study is that the connective tissues supporting the various attachments to the muscles of the anterior abdominal wall take on a complex arrangement that allow them to deform in complex manners to conform to the different forces acting throughout the system. In particular, the apparent simultaneous tissue expansion in multiple planes is hypothesized to occur as the layered nature of the abdominal wall and aponeurotic or fascial structures allows for such expanding deformations by accommodating separation

between the layers in response to the diverse forces acting on the various tissues. Further, the laterally produced forces of the oblique and transverse muscles appear to dominate the longitudinally produced force of the RA muscle, such that the connective tissues intervening these muscles (specifically the transverse RA tendons and linea alba) must function to accommodate such force distribution.

SUMMARY

This exploratory work has documented unique in-vivo deformations of the human abdominal wall connective tissues that cannot be explained by simple mechanical and tissue properties; a complex network of fibres and matrix interact to accommodate the deformations necessary for varying demands. In particular, the composite laminate nature of the connective tissues appears to allow for expansion and/or retraction in multiple planes simultaneously. In addition, the high laterally produced forces of the oblique and transverse muscles appear to dominate over the longitudinal force of the RA, suggesting a role of the transverse tendons within the RA to transmit hoop stresses around the torso.

FORCES IN ANTERIOR CRUCIATE LIGAMENT DURING SIMULATED WEIGHT-BEARING FLEXION WITH ANTERIOR AND INTERNAL ROTATIONAL TIBIAL LOAD

JiaHsuan Lo; Otto Müller; Markus Wünschel; Steffen Bauer; Nikolaus Wülker

Department of Orthopaedics, University of Tübingen, Tübingen, Germany

INTRODUCTION

Although ACL forces during unloaded knee flexion have been investigated extensively (Xerogeanes, et al., 1995), experimental data on the ACL force during muscle-loaded flexion is scarce. Therefore, the objective of the current study was to experimentally determine the ACL force profile in a weight-bearing knee flexion and investigate the effect of external tibial loads on the ACL force during a weight-bearing flexion. We hypothesized that in a simulated knee flexion movement with muscle loads at a physiological level, (a) there is no significant difference in the ACL force at different flexion angles; (b) the external tibial load (anterior tibial force and internal rotation tibial torque) does not affect the ACL force.

METHODS AND PROCEDURES

An upright knee simulator was developed to simulate dynamic weight-bearing knee motion. The hip and ankle joints in the knee simulator were designed to allow unconstrained tibiofemoral movement in all six degrees of freedom. Linear electrical servo motors (Parker Hannifin, Offenburg, Germany) were incorporated to provide the vertical movement of the hip and to generate the forces in three quadriceps and two hamstrings tendons.

Nine fresh-frozen human cadaveric knee specimens with an age at the time of death of 71 ± 16 years (mean ± standard deviation) were mounted on the dynamic knee simulator.

Knee flexions with a prescribed 100N of body weight were simulated, while a robotic/universal force sensor (UFS) system was used to provide external tibial loads during the movement. Three external tibial loading conditions were simulated, including no external tibial load (termed BW only), a 50 N anterior tibial force(termed ATF), and 5 Nm internal rotational torque (termed ITT). The tibial and femoral kinematics was measured with an ultrasonic motion capture system (ZEBRIS® CMS100, Isny, Germany). These movement paths were then accurately reproduced on a robotic testing system before and after transecting the ACL, and the in-situ force in the anterior cruciate ligament was determined via the principle of superposition (Fujie, et al., 1993).

A two-way repeated-measure analysis of variance was conducted (SAS®, SAS Institute Inc., Cary, NC) to investigate the effect of flexion angle and external loading on the ACL force. A post hoc test using Tukey-Krammer method was also performed.

RESULTS

The first null hypothesis that there is no significant difference in the ACL force at different flexion angles was rejected, because our results of ACL in-situ force show the flexion angle affected the magnitude of the ACL in-situ force (p < 0.001). Meanwhile, the second null hypothesis was also refuted, since the tibial loading significantly changed ACL in-situ force (p < 0.003).

Comparing to the "BW only" condition, the addition of 50N anterior tibial force (ATF) significantly increased ACL force at flexion angles from 15 to 55 degree ($p<0.04$, Figure 1), while no difference was found in the ACL force between the "ITT" and "BW only" trials for all flexion angles ($p>0.05$, Figure 2). In each loading conditions, the ACL force remained nearly constant before it gradually decreased beyond 40 degree of knee flexion. The peak ACL forces of the "BW only", "ATF", and "ITT" trials was 33 ± 11 N (mean $\pm$ standard error), 54 ± 10 N, and 35 ± 5 N, respectively.
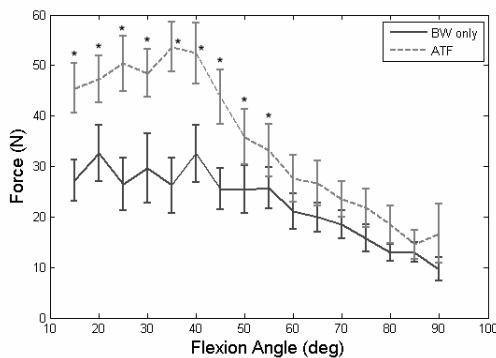
Figure 1. ACL force profiles in the "BW only" and "ATF" trials. Error bars represent one standard error. * denotes significant difference in the ACL force between the two loading conditions ($p<0.04$).
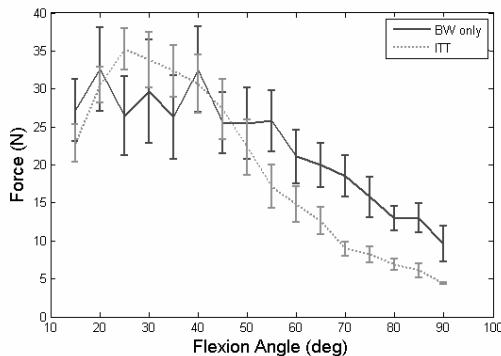
Figure 2. ACL force profiles in the BW only and "ITT" trials. Error bars represent one standard error.

DISCUSSION

This study shows that, during a simulated weight-bearing flexion ("BW only" trials), the ACL is slightly loaded, and its magnitude decreases with knee flexion. This experimentally corroborates the widely-perceived belief that ACL forces are relatively low during squatting exercise (Shelbourne and Nitz, 1990).

Our results suggest that, in the presence of the muscle loading, ACL provides resistance primarily to an anterior tibial draw but not to a 5 Nm internal rotation torque. It therefore implies that the quadriceps tendons, joint capsule, and collateral ligaments are more likely the structures that restrict the rotational tibial torque.

SUMMARY

We experimentally verified that, in weight-bearing knee flexion, the magnitude of the ACL force is relatively low and decreases with increasing flexion angle. The anterior cruciate ligament plays a limited role in restricting axial rotation in a weight-bearing knee flexion exercise.

REFERENCES

Fujie, H et al. (1993), J Biomech Eng 115(3), 211-7

Shelbourne, KD and Nitz, P (1990), Am J Sports Med 18(3), 292-9

Xerogeanes, JW et al. (1995), Knee Surg Sports Traumatol Arthrosc 3(1), 9-13

DIFFERENT APPROACH TECHNIQUES IN VOLLEYBALL SPIKE

Claas H. Kuhlmann, Karen Roemer, Thomas L. Milani

Department of Human Locomotion, Chemnitz University of Technology, Germany
claas.kuhlman@phil.tu-chemnitz.de

INTRODUCTION

In volleyball spikes the impact height of hand and ball is a relevant parameter for success (Tillman et al., 2004). A higher ball impact location allows more possibilities for technical and tactical variation. Therefore, the optimisation of jump height (JH) is in the focus of research.

In the literature coherencies between different parameters of lower limb to the JH were analysed (e.g. Coutts, 1982). However, most of the published studies have been performed under laboratory conditions.

The purpose of this study was to analyse if a coherency to JH could be found in selected parameters of the lower limb (e.g. foot angle at take off) in top-level athletes under contest conditions.
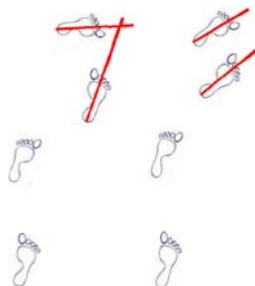
Figure 1. Different foot angles at take off. Angle (left) and Parallel (right).

METHODS AND PROCEDURES

Four digital high speed cameras (3x Basler, 1x Vosskühler), sited around the court, were used for the motion analysis with a frame rate of 100 Hz. Those cameras were controlled and triggered by "SIMI Motion-Capture" software.

Spike movements performed by players of the national teams of Croatia, Estonia, Germany and the Netherlands were recorded during European league tournament. Since the favourite spike-position used by international top level teams is position four (Kuhlmann et al., 2008) only diagonal spikes from this position have been considered. All subjects performed a step-close technique, identified by Coutts (1982). Another criterion was the flight angle of the ball after impact from 110° to 145° to the net. From the sum of all recorded spikes achieving those criteria, 10 spikes from 10 different attackers were chosen in a randomised order. No difference was made with respect to the national team. The average weight of the selected subjects was 92.0 ±5.35 kg, the average height was 198.8 ±4.4 cm.

Analysed parameters were foot angle at take off, closing time, ground contact time and running speed at the approach. Also the arm movement has to be considered when examining dependence of the approach to the JH of a volleyball spike. Statistical analysis was made with SPSS 14.0.

RESULTS

In the arm swing, the lower reversal point has to pass along with the lower reversal point of the centre of mass (COM). Otherwise, there would be a negative effect between these two impulses. The mean time difference was calculated with 10 ± 10.5 ms. The mean time difference from the arm block to the last frame with ground contact was calculated

with 5.4 ± 5.1 ms (left arm) and 5.7 ± 3.5 ms (right arm). The time difference of the maximum angular velocity to the last frame with ground contact was calculated with 13.8 ± 2.7 ms (left arm) and 13.2 ± 4.1 ms (right arm).

The JH of the sample was 63.2 ± 6.2 cm. The closing time was 18.7 ± 3.9 ms. Over all ground contact time (both feet) was 34.4 ± 7.2 ms. The average foot angle at take off was 16.03 ± 16.62°. When calculating Pearson's correlation test, no relationship between the parameters foot angle, ground contact time and closing time to JH was detected.

DISCUSSION

The arm movements of the examined subjects were nearly similar. Therefore, an inhomogeneous influence can be neglected for this sample.

Concerning the parameters ground contact time, closing time and foot angle at take off, no apparent effect on JH could be detected. From a biomechanical point of view, no specific benefit of one technique can be postulated for maximum jump height in volleyball spikes. These results lead to the assumption that the technique of spike jumps seems to be highly individual in top level athletes. This is in line with Tokuyama et al. (2005), who showed in a laboratory-study, that intra-individual variation was significantly smaller than inter-individual variation for female attackers.
These results raise the question, if educating young players by traditional techniques lead to an optimal individual performance for the spike. The approach of differential learning showed that better and more continuous results in performance were reached when motion was taught with a big range of variability in contrast to a conventional

method. An overview on some experimental studies concerning differential learning with similar results in different disciplines was given by Frank et al. (2008). According to these authors this method could support athletes to find their specific motion pattern for maximum performance, which could differ from the conventional one.

SUMMARY

In this study 10 top level athletes were analysed during international competition. No apparent effect on JH was detected in the analysed parameters of the lower limb although the sample was considered to be homogeneous with regard to the performance ability. This could be an indication for highly individual technique in top level sports. It prompts the question if methods like e.g. the approach of differential learning could be useful to gain higher individual performance. It may be easier for athletes to find their specific technique, when using methods with different variation of motion.

REFERENCES

Coutts, KD. (1982). *Med. Sci. Sports Exerc.*, 14, 1, 57-59.
Frank, TD., Michelbrink, M., Beckmann, H., Schöllhorn, WI. (2008). *Biol Cybern*, 98, 19-31.
Kuhlmann, CH., Roemer, K., Zimmermann, B., Milani, TL., Froehner, B. (2008). *Leistungssport*. In Press.
Tillman, MD., Haas, CJ., Brunt, D., Bennett, GR. (2004). *J. Spo. Sci. Med.*, 3, 1, 30-36.
Tokuyama, M., Ohashi, H., Iwamoto, H., Takaoka, K., Okubo, M. (2005). *J of Biomechanics*, 38, 2050-2057.

ACKNOWLEDGEMENTS

HAND LOAD CONTRIBUTIONS TO CERVICAL SPINE COMPRESSIVE FORCES

Adam Pickens[1] and Jeff Woldstad[2]

[1]Texas Tech University, Department of Industrial Engineering, Lubbock, Texas, U.S.,
adampickens@suddenlink.net
[2]Texas Tech University, Department of Industrial Engineering, Lubbock, Texas, U.S.,
jeff.woldstad@ttu.edu

INTRODUCTION

Musculoskeletal injuries to the cervical region of the spine have historically been linked to many different injury mechanisms. These injury mechanisms range from acceleration injuries (whiplash) to injuries associated with lifting heavy loads (Hagberg, 1987; Herberts et al., 1981). Aaras and Ro (1997) found that frequently repeated lifts, as low as 1% of the MVC, are correlated to musculoskeletal injuries of the neck and shoulder. In epidemiologic studies by NIOSH (1997), it has been found that repetition, forceful exertion, and extreme postures contribute to musculoskeletal disorders of the cervical spine and shoulder. These musculoskeletal disorders have led to an increase in the number of permanent disability cases due to degeneration of cervical spine discs (Nygren et al., 1995).

METHODS AND PROCEDURES

It has been demonstrated (Woldstad & Nicolalde, 2001) that EMG levels increase in the musculature of the neck as hand loads are increased. From their findings, Woldstad and Nicolalde (2001) theorized that this increase in muscle activity corresponds to an increase in the compressive forces acting on the cervical spine. Currently, while there

are predictive shoulder models and predictive neck models, the need for a combined neck and shoulder model exists. That is the aim of this study, to test the validity of using outputs from existing an existing shoulder model as inputs for a current neck model in an attempt to quantify the compressive forces exerted on the spine due to hand loads. For the purposes of this study, the shoulder model that will be the focus is the Chalmers Computerized Shoulder Model. This model is based on the shoulder modeling work done by Hogfors et al. (1987) and a series of papers by various authors following that original publication by Hogfors et al. The Chalmers shoulder model uses anthropometric, static posture, and muscle parameter inputs to estimate muscle forces in shoulder muscles and the resultant forces on the shoulder.

Output for this model is given in the form of force as a percentage of estimated maximum force for each muscle. The muscles in question are muscles shared by the cervical spine and the shoulder girdle: sternocleidomastoid, splenius, trapezius, and levator scapulae.

To test the model outputs, ten (5 male, 5 female) subjects were used for data collection. Surface EMG electrodes were attached to the specified muscles and each subject performed a series of

maximum voluntary isometric tasks (MVC) designed to isolate the muscles. Upon completion of the MVC tasks, subjects performed a series of lifting tasks modeled after the luggage-lifting task performed by Transportation Security Administration baggage screeners at airports, a task historically associated with high shoulder and neck injury rates. Subjects performed four (4) randomized trials each of nine (9) different luggage size/weight combinations.

Three-dimensional motion capture data was recorded for each trial for position input into the model.

Peak EMG values during the lifting task for each muscle for each trial were compared to the values of the MVC peak EMG values. In an attempt to replicate the data output of the Chalmers model, the peak trial values were calculated as percentages of the maximum values collected during the MVC collection period.

RESULTS

While data collection and analysis for all ten subjects has been performed, statistical analysis still remains to be completed for this study. The statistical analysis will center on testing the hypothesis that the Chalmers model accurately predicts muscle activity for given hand loads. The hypothesis test will compare the Chalmers model predictions of the percentage of maximum activity for each muscle during each combination to the observed results collected during the lifting task.

REFERENCES

Aaras, A., & Ro, O. (1997). (EMG) – Methodology and application in occupational health. *Ind. Ergonomics*, 20, 207-214.

Hagberg, M. (1987). Shoulder pain – pathogenesis. In *Clin. Concepts in Regional Musculoskeletal Illness*, pp. 191-200. Grune & Stratton Inc., New York, NY.

Hogfors, C., Sigholm, G., & Herberts, P. (1987). Biomechanical model of the human shoulder – I: Elements. *J. Biomechanics*, 20(2), 157-166.

Herberts, P., Kadefors, R., Hogfors, C., & Sigholm, G. (1984). Shoulder pain in heavy manual labor. *Clin. Orthopedics and Related Research*, 191, 166-178.

Nygren, A., Berglund, A., & Von Koch, M. (1995). Neck and shoulder pain, an increasing problem. Strategies for insurance material to follow trends. *Scand. J. Rehab. Med*., 32, 107-112.

Musculoskeletal disorders and workplace factors. Retrieved from the NIOSH website: September 21, 2007. http://www.cdc.gov/niosh/docs/97-141/

Woldstad, JC. & Nicholalde, J. (2001). The contribution of hand loads to cervical disc compression. Procedings, 45th annual meeting of the Human Factors and Ergonomic Society, Minneapolis, MN.

CADAVERIC MEASUREMENT OF IMPACT FORCE
ON TOTAL HIP ARTHROPLASTY SURGICAL INSTRUMENTATION

Cristina West and J. Craig Fryman
E-mail: cristina.west@zimmer.com
Zimmer, Inc., Warsaw, IN, USA

INTRODUCTION

Total hip arthroplasty implant components are commonly implanted by impact loads applied by a surgical mallet through an intermediary insertion instrument. The quantity (per surgical procedure) and magnitude of these impact forces are of engineering interest in regards to development and testing of both implant components and surgical instruments. Maximum and average impact force magnitudes and average impacts per surgical procedure were recorded during this investigation for insertion of acetabular cups and liners (ceramic, metal and polyethylene), and femoral rasping.

METHODS AND PROCEDURES

Impact forces for several surgical procedures performed by eight Orthopaedic surgeons were measured during a cadaveric study (Zimmer, Inc.). Surgical procedures included acetabular cup insertion, femoral rasping and insertion of liners of various materials. Measurements were taken on size 48 mm, 50 mm, 52 mm and 60 mm hemispherical acetabular cups and corresponding sized liners from several Zimmer acetabular implant systems. The acetabulum in all cases was reamed undersized by 1mm or 2mm increments relative to the cup size for a perfect hemispherical press fit. Impact forces applied to Zimmer M/L Taper rasps size 6mm, 7.5mm, 8mm, 9mm, 11mm and 12.5mm during femur preparation were also recorded.

The impact forces were measured with two instrumented mallets (standard 907 gram surgical mallets with piezoelectric load cell transducers rigidly fastened to the strike zone). The conditioned output signal was recorded with two National Instruments modular data acquisition systems.

The output voltage file was post-processed by a software routine in LabVIEW 8.5 (National Instruments, Austin, TX). The "Peak Detector.vi" Virtual Instrument (supplied with LabVIEW) was used to detect the impacts in the file and the data point address. The data point address combined with the sampling frequency was used to determine the time between impacts.

RESULTS

The influence of particular surgeons was not analyzed due to the lack of repetitive data per surgeon per technique. Figure 1 shows the average peak impact force per surgical procedure. The total number of each procedure in which measurements were recorded, the max peak impact force, and average number of impacts per procedure are listed in Table 1.
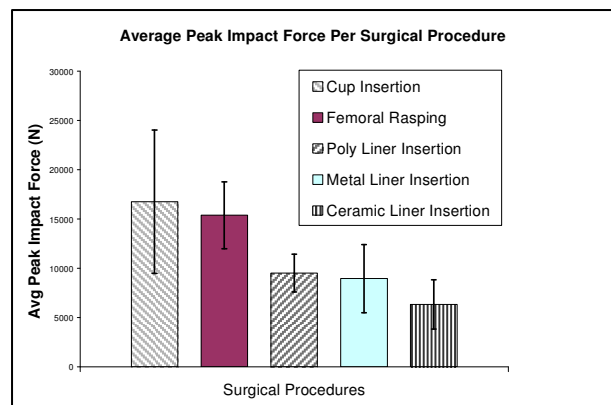
Figure 1: Average peak impact force magnitudes recorded per surgical procedure

Surgical Procedure	No. of Procedures	Max Peak Force (N)	Average Peak Force (N)	Avg No. of Impacts Per Procedure
Cup Insertion	10	27490	16750 (7270)	5 (2)
Femoral Rasping	10	22090	15380 (3400)	12 (9)
Poly Liner Insertion	7	11710	9515 (1910)	4 (2)
Metal Liner Insertion	10	15660	8940 (3450)	4 (1)
Ceramic Liner Insertion	20	12950	6335 (2500)	5 (3)

Table 1: Impact force data measured per procedure and total number of each procedure recorded

On average, the time between impacts was 0.429 (0.165) seconds or approximately 2.3 Hz excluding procedures where significant surgical delay occurred. No significant differences in the average number of impacts per procedure with consideration of standard deviation and number of procedures performed were observed.

DISCUSSION

The measured mean peak impact forces for cup insertion and femoral rasping were greater in magnitude compared to those measured for liner insertion (regardless of liner type). The number of impacts per procedure was greatest for the rasping procedure. However no significant difference in impact force magnitude can be drawn between surgical procedures due to the large standard deviations for both the force and number of impacts per procedure.

The maximum and average peak rasping impact forces measured are comparable to values obtained during a prior cadaveric study on rasp and tamp instruments (Kold S et al.). In addition, an intra-operative study recorded mean peak impact broaching forces during total hip arthroplasty ranging from 20,551 to 29,919 N which correspond to the rasping measurements of this investigation (Markel D et al.).

SUMMARY

Mean peak impact forces recorded for acetabular cup insertion and femoral rasping were approximately 17,750 (7270) N and 15,380 (3400) N respectively. These values were greater in magnitude than those recorded for liner insertion. Liner insertion mean peak forces ranged from 9,515 (1910) N to 6,335 (2500) N depending on liner type.

Overall, the average number of impacts measured for cup insertion, femoral rasping and liner insertion (all types) were 5, 12 and 4 respectively.

REFERENCES

Kold S et al. (2003). Clin Orthop, 408: 180-188.
Markel D et al. (2006). AAOS Poster Exhibit P071.

RESISTANCE TRAINING ALTERS JOINT POWERS IN MULTIPLE SCLEROSIS PATIENTS

Jessie M. Huisinga[1], Mary Filipi[2], and Nicholas Stergiou[1,3]
[1]Nebraska Biomechanics Core Facility, University of Nebraska at Omaha, Omaha, NE
[2]University of Nebraska Medical Center, College of Nursing, Omaha, NE
[3]University of Nebraska Medical Center, College of Public Health, Omaha, NE
Email: jhuisinga@mail.unomaha.edu   URL: http://biomech.unomaha.edu

INTRODUCTION

Multiple Sclerosis (MS) is a progressive, debilitating, neurological disease which currently affects over 400,000 Americans. Symptoms vary widely among patients and may include sensory disturbances, optic neuropathy, trunk and limb parasthesias, limb weakness, gait ataxia, and severe fatigue (White and Dressendorfer, 2004). Treatment options depend greatly upon the range and severity of symptoms and may include medication, physical therapy treatments, and steroids. Physical activity had previously been discouraged in order to protect the current physical functioning of the patient. Recently, exercise interventions have been shown to positively affect MS patients with respect to aerobic fitness and quality of life measures. (Mostert and Kesselring, 2002). The current study employed a progressive resistance training program to determine the effects of resistance training on the lower extremity joint powers during walking in MS patients. It was hypothesized that the training would result in joint powers measures that were closer to those of healthy controls.

METHODS AND PROCEDURES

Eleven MS patients (age 42.3 ± 10.8 yrs) and 5 healthy controls (age 34.2 ± 10.9 yrs) participated in the study. Patients and controls walked through a 10 meter walkway at their self-selected walking pace, while kinetics and kinematics were collected for 10 trials with a Kistler force plate (600Hz) and an 8-camera Motion Analysis system (60 Hz). Data collection was performed before and after the MS patients participated in three months of a twice weekly supervised, progressive resistance training program that included lower extremity, upper extremity, and core exercises. Hip, knee, and ankle joint powers were calculated from the ground reaction forces and the kinematics. The maximum power absorption and generation were identified for the hip, knee, and ankle joints. Student t-tests were used to compare between the MS patients and the controls, before and after training.

RESULTS

Before training, MS patients as compared to controls exhibited significantly decreased ankle plantarflexor power generation during late stance (A2), decreased power generation at the knee during late stance (K2), increased power absorption at the knee during pre swing (K3), decreased power absorption of the hip flexors during late stance (H2), and decreased hip extensor power generation during pre-swing (H3) (Figure 1). Following training, MS patients as compared to controls showed significant differences only for power generation of the ankle plantarflexors during pre-swing (A2) and power absorption at the knee during pre-swing (K3). Resultant power values were comparable to results presented in the literature (Graf et al., 2005)
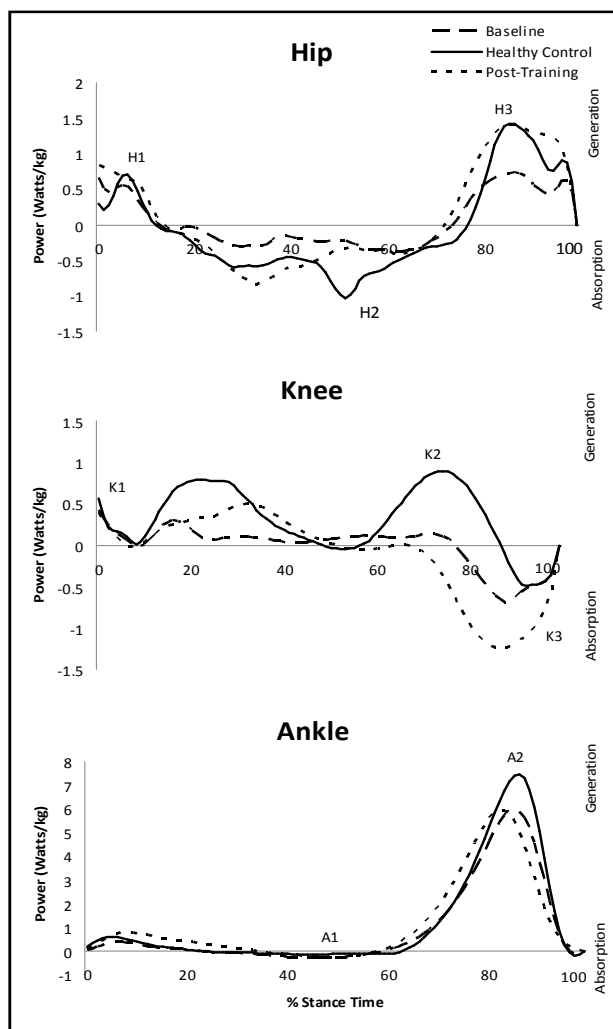
Figure 1: Representative Joint Powers for Baseline, Post-Training, and Healthy Controls with specific discrete points indicated

DISCUSSION

Baseline differences between healthy control and MS patient joint powers were present prior to the intervention. These differences indicate that MS patients had significantly decreased power generation and decreased power absorption at all three joints. Inability to generate and absorb power during gait would result in a significantly stiffer walking pattern due to lack of joint movement as well as shorter step length since the hip flexors and ankle plantarflexors are not able to efficiently propel the limb off of the ground and into swing. Changes in the joint powers were revealed following the resistance training intervention which reduced the number of differences between the controls and MS patients. The differences that remained between the two groups were present during the pre-swing phase of the gait cycle indicating a remaining deficiency in MS patients' ability to propel the leg into swing after the stance phase due to decreased power generation at the ankle. The inability to bring the leg fully into swing could result in dragging of the foot and significantly increase the probability of falls. The addition of gait initiation training could supplement the improvements to gait parameters gained as a result of resistance training. The changes identified in this study indicated that inexpensive, non-invasive treatments could greatly improve ambulatory capabilities in MS patients. Further study is necessary to conclude what specific exercise programs are the most effective in improving MS patient symptoms.

REFERENCES

Graf, A et al. (2005) *Arch Phys Med Rehabil*. 86:2177-2183.

Mostert, S and Kesselring, J (2002) *Mult Scler*. 8(2):161-8.

White LJ, Dressendorfer RH. (2004) *Sports Med*. 34(15):1077-100.

ACKNOWLEDGEMENTS

A TEST METHOD FOR THE FATIGUE TESTING OF TIBIAL INTRAMEDULLARY NAILS USING SEGMENT CONSTRUCTS

J. Craig Fryman[1], Balz Mueri[2], Barbara Kralovic[1] and Roger Kenyon[1]
E-mail: craig.fryman@zimmer.com
[1]Zimmer, Corporate Research, Warsaw, IN, USA
[2]Zimmer, Corporate Research, Winterthur, Switzerland

INTRODUCTION

Fractures of the tibia are the most common fractures for adults. The tibial intramedullary (IM) nail is the preferred treatment of these fractures since the tibia has very little soft tissue coverage and is very susceptible to skin irritation when plated. The tibia is also a major load bearing bone during normal walking. With the desire to have a patient ambulatory as soon as possible after surgery, the strength of these implants is critical. However, the failure rate of IM tibial nails is relatively low (Hahn; Hutson; Ruiz).

A new test method is needed to improve on the tests in ASTM F1264, which test "away from screw holes or other interlocking features" in four-point bending, and those designed by Brumback et al. for antegrade femoral nails, which may cause excessive nail deflection.

The objective of this study was to develop a method to fatigue test tibial nails using physiologically based loads and fixation.

METHODS

The fixturing was designed to replicate the physiological load location present on the tibia during walking.   All load locations were chosen in a worst case manner (i.e. largest offsets). For the distal load location, the AP coordinate was coincident with the intramedullary canal and the ML coordinate was taken to be 10mm medial of the centerline of the IM canal (Duda; Gaebler; Hutson). The inferior location of the distal load was determined to be 40mm distal to the tip of the nail. In the AP plane, the proximal load location was determined by finding the center of contact during gait. This location has been found to be between 0 and 7mm posterior of

the midline of the tibial plateau (Dennis '01; '03). Hicks et al also found that the intramedullary canal is 7 to 10mm anterior and 1.5 to 3mm medial of the center of the tibial plateau. This indicates that, in a worst case scenario, the load location could be 17mm posterior of the IM canal. The ML coordinate of the proximal load location was approximated to be 23mm medial of the centerline of the tibial plateau during the peak loading during gait (Gaebler). The superior location for the proximal load location is based on the assumption that the tibial nail should be inserted until the most superior surface of the nail is flush with the bone. Surgeons have the option of inserting the nail up to 15mm farther down into the canal while using a nail cap. Thus, the proximal load location was chosen to be 15mm superior of the most proximal part of the nail. As desired, these load locations produce an inversion moment at the ankle and a flexion and adduction moment at the knee.
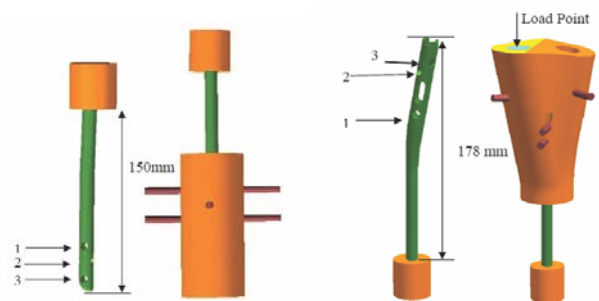
Figure 1: Setup of Distal and Proximal Constructs

The fixturing was made of a material and design that replicates the average stiffness of the tibia. Cristofolini et al measured cadaveric tibias and found an average outer diameter of 27.6mm and an average inner diameter of 18.6mm. The calculated moment of inertia (I)

for the average tibia is 22,800mm^4. The average elastic modulus (E) of tibial cortical bone reported in the literature is 17.5GPa (Duda). The equivalent stiffness of the tibia, EI, was estimated to be 399N-m^2.

Using this equivalent stiffness, an inner diameter of 18mm was chosen so that various nail sizes could be tested with the same fixturing. Spacers are used to establish the proper clearance as specified by the surgical technique. The outer diameter was adjusted in order to recreate the stiffness of the tibia.

Ten, 8mm x 140cm M/DN Tibial nails were tested (Zimmer, Inc.). The nail was sectioned 150mm from the distal end and 178mm from the proximal end. Each segment was potted in 50.8mm of PMMA from the section end. Each segment was oriented vertically (0°) in both the ML and AP planes as measured from the midshaft of the nail. This section of the nail was collinear with the IM canal of the long bones.

Fixturing was secured to the nail using the screws specified in the surgical technique. Three screws were used with each construct. (Figure 1) The location of the screws had been pre-determined via FEA in order to place the largest relevant stress on the nail (Hahn; Ruiz). Samples were tested on a uniaxial fatigue frame (MTS, Minneapolis, MN) at a rate of 10 Hz in 0.9% Saline solution. The tests were run to 1 million cycles or fracture whichever occurred first.

RESULTS

Figure 2 shows the fatigue results for the proximal and distal segments of the 8mm diameter nail.

DISCUSSION

The failures from the fatigue test were able to replicate the failure modes reported in the literature (Hahn). Figure 3 shows a fracture in the distal segment of the nail through the most

proximal screw hole as observed by Hahn et al. Similar fractures were found in the proximal segment at the most distal hole. These failures were at the highest stress location as predicted in FEA.
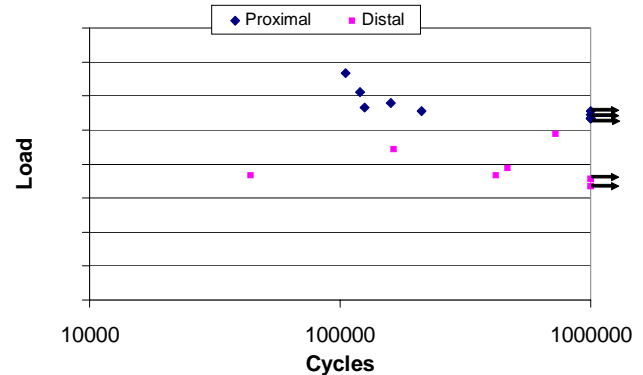
Figure 2: Fatigue results for proximal and distal constructs for an 8mm diameter nail

SUMMARY

This method was able to replicate fractures of tibial nails that have been observed clinically. This method uses physiologic load points that better replicate the stresses that a tibial intramedullary nail will experience in vivo than the existing ASTM test methods.

Figure 3: Representative failure of tibial nail: distal segment

REFERENCES

Brumback RJ et al (1999). *JBJS*. 81:1538-44.
Cristofolini L and Viceconti M; (2000) *J. Biomech.* 33:279-288
Dennis D et al (2001) *JBJS*. 83-A Sup. 2, Pt 2: 104-115
Dennis DA et al (2003) *CORR*. 410:114-130
Duda GN et al (2001), *JBiomech*. 34:639-650
Gaebler C et al (2001), *Injury*. 32:108-712
Hahn D et al (1996), *Injury*. 27(5):323-7
Hicks CA et al (1995), *CORR*. 321:111-116
Hutson JJ et al (1995), *CORR*. 315:129-137
Ruiz AL et al (2000), *Injury*. 31(5):359-62

THE RELATIONSHIP BETWEEN STATIC ARCH HEIGHT AND ARCH STIFFNESS

Andrew Barnes[1], Jonathan Wheat[1], Clare E. Milner[2]
[1]The Centre for Sport and Exercise Science, Sheffield Hallam University, UK.
Web: www.shu.ac.uk/cses. email: a.barnes@shu.ac.uk
[2] Dept of Exercise, Sport, and Leisure Studies, University of Tennessee, TN, USA

INTRODUCTION

Foot type, and particularly arch height is an intrinsic injury risk factor which has received much attention within the literature (Cowan et al. 1993). However, the relationship between foot type and injury is somewhat unclear. In addition to arch height, arch stiffness may be important in trying to relate foot type to injury. It is commonly thought that high arches tend to be more rigid, and lower arches more flexible. Furthermore, it is suggested that more flexible feet with lower arches may serve as more effective natural shock absorbers than more rigid foot types. A higher incidence of shock related bony injuries has been reported in high arched runners (Williams et al. 2001). Zifchock et al. (2006) measured the foot structure of 145 individuals in both 10% and 50% of weight bearing, with relative arch deformation between conditions used as a means of assessing arch stiffness. Although a relationship between variables was observed, only 9% of the variance in arch stiffness could be explained by arch height (Zifchock et al. 2006). During shod running, vertical ground reaction forces can reach 2-3 times body weight. Assessing arch characteristics in loaded conditions closer to those seen during running may provide insight into dynamic arch stiffness and its potential relationship to injury. The aim of the present study was to assess the relationship between arch height and arch stiffness in 10% and 90% of weight bearing. It is suggested that calculating arch stiffness between these conditions may give a better indication of foot function in loaded conditions, such as gait.

METHOD

After ethics approval, 101 male participants (age 20.0±2.8, height 176±19 cm, mass 76.9±10.5 kg) gave informed consent to take part in the investigation. Measurements were taken on the right foot of participants in 10% and 90% of weight bearing, using a previously validated measurement system (Williams and McClay, 2000). A portable force plate was used to determine percentage weight bearing, with the 10% condition measured in a sitting and the 90% in a standing position. Dorsum height at 50% of foot length divided by truncated foot length was used as a measure of arch height index (AHI). Relative arch deformation between 10% and 90% of weight bearing was calculated using the equation described by Williams and McClay (2000). Relative arch deformation was normalised to body weight (BW) to give a measure of arch stiffness, with a lower arch stiffness score indicating a flexible arch structure, and a higher score indicating a more rigid arch. A one-tailed Pearson's correlation was used to examine the relationship between each AHI measure and arch stiffness. Significance was accepted at ($p<0.05$).

RESULTS

Based on normality analysis, arch stiffness data were found to be positively skewed. A log transform ($\log_{10}$) was applied to all data, resulting in normal distribution of all variables. The relationship between arch stiffness and AHI in 10% and 90% weight bearing can be seen in Figures 1 and 2 respectively. No significant relationship was seen between AHI in 10% of weight bearing and arch stiffness ($R^2= 0.024$, $p = 0.063$). A relationship was observed between AHI in 90% of weight bearing and arch stiffness, although it was a relatively weak one ($R^2=0.14$, $p= 0.0001$). The observed trend suggests that a higher arch equates to a more rigid foot, and a lower arch a more flexible foot.
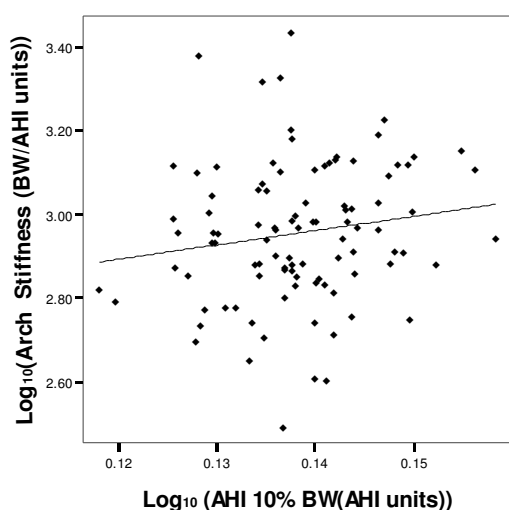
Figure 1. Relationship between AHI 10% and arch stiffness ($R^2= 0.024$, $p = 0.063$)
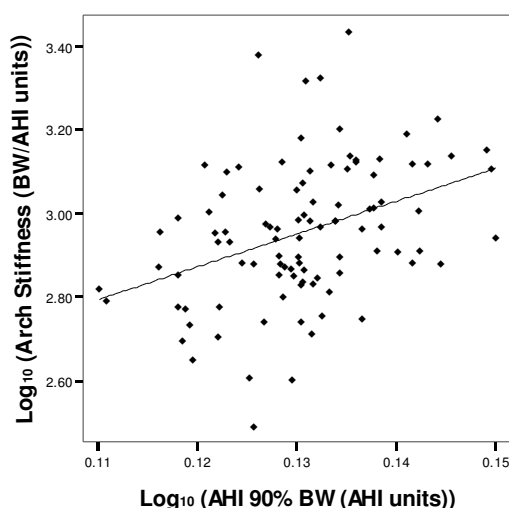
Figure 2. Relationship between AHI 90% and arch stiffness ($R^2=0.14$, $p= 0.0001$).

DISCUSSION

The findings of the present study suggest no relationship between AHI 10% and arch stiffness, and only a weak relationship between AHI 90% and arch stiffness. In support of the hypothesis regarding height and stiffness, a higher arch was suggestive of a more rigid foot, and a lower arch a more flexible foot. However, only 14% of the variance seen in arch stiffness can be explained by arch height. These findings do suggest a marginally higher association than the 9% variance previously reported

(Zifchock et al. 2006). Such differences may be due to the population measured, or the use of AHI at 90% rather than 50% weight bearing. Although 90% AHI represented an increased degree of loading, it was still below the level that would be expected during running. Evidence from this study and the study by Zifchcock and colleagues (2006) suggests static measures of arch height offer a limited indication of arch stiffness characteristics. Given the small amount of variance explained by arch height, other factors must be of importance in determining foot stiffness. Such factors might include foot mobility and the range of motion within the joints of the foot, particularly the midfoot. Significant rotations about the joints of the midfoot have been reported during walking (Lundgren et al. 2007). The degree to which bone and soft tissue structures permit motion between relative joints as they are loaded, is likely a crucial factor in determining arch stiffness. Future research should consider the three dimensional motions at the joints of the foot as it is loaded. Analysis of dynamic situations such as running should be a priority, in an attempt to establish links between foot stiffness and injury.

SUMMARY

A relationship between arch height and arch stiffness was only observed using AHI at 90% of weight bearing. Although this measure does provide some indication of arch stiffness, it is limited. The use of static measures may not reflect the dynamic function of the foot.

REFERENCES

Cowan DN et al. (1993). *Arch Fam Med* , 2: 773-777.

Lundgren P et al. (2007). *Gait Posture*, Online first.

Zifchock RA et al. (2006). *Foot Ankle Int*, 27: 367-372.

Williams, DS and McClay, IS (2000) *Phys Ther*, 80: 864-871.

Williams DS et al. (2001). *Clin Biomech*, 16: 341-347.

DYNAMIC FOOT MOBILITY IN HIGH AND LOW ARCHED INDIVIDUALS

Andrew Barnes[1], Jonathan Wheat[1], Clare E. Milner[2]
[1]The Centre for Sport and Exercise Science, Sheffield Hallam University, UK.
Web: www.shu.ac.uk/cses. email: a.barnes@shu.ac.uk
[2] Dept of Exercise, Sport, and Leisure Studies, University of Tennessee, TN, USA

INTRODUCTION

Evidence relating injury to any one foot type is limited (Kaufman et al. 1999). However, a higher incidence of shock-related bony injuries have been reported in high arched (HA) runners (Williams et al. 2001a). This incidence may be linked to the higher observed loading rates in this population (Williams et al. 2001b). During early stance the foot pronates, a tri-planar motion consisting of dorsiflexion, eversion and abduction. Pronation has been suggested to serve as a shock attenuation mechanism. Perry and Lafortune (1995) reported increased impact loading when normal pronation was restricted. Given this, one may expect the range of motion within the joints of the foot to be crucial in determining its shock attenuation ability. The purpose of this study was to compare the relative foot mobility and tibial shock in those with HA and those with low arches (LA). More specifically, it sought to test the hypothesis that those with LA have more mobile feet and are better able to absorb shock dynamically than more rigid HA feet. It is suggested that those with greater range of motion at the joints of the foot (LA) will have lower tibial shock compared to those with more rigid feet (HA).

METHODS

After ethics approval, 101 male participants (age 20.0±2.8, height 176±19 cm, mass 76.9±10.5 kg) gave informed consent to take part in the investigation. Measurements were taken on the right foot of participants at 90% of weight bearing, using dorsum height at 50% of foot length divided by truncated foot length to give a measure of arch height index (AHI) (Williams and McClay, 2000). This population was used as a normative database from which participants in the upper (HA)

and lower (LA) most quartiles were selected for further analysis and comparison. The study included seven LA (age 20.2±2.2 yrs, height 179±5 cm, mass 75.4±4.5 kg, AHI 0.316±0.014) and eight HA (age 19±0.9 yrs, height 177±5 cm, mass 82±11 kg, AHI 0.383±0.014) participants. A measure of arch stiffness taken between 10% and 90% of weight bearing (Williams and McClay, 2000) was calculated and normalised to body weight (STFF). A lower STFF score indicated a more flexible arch structure, and a higher score indicated a more rigid arch. Participants completed 10 good trials of running (3.5m/s ±5%) wearing gait sandals (Bite, Orca). A three segment model (adapted from Carson et al. 2001) comprising the shank, rearfoot and forefoot was used, where markers were fixed directly to the skin. All three dimensional kinematic data were collected using an eight camera motion capture system (Motion Analysis Corporation), sampling at 500Hz. A force platform (Kistler, 9281CA) and uniaxial accelerometer (PCB, piezotronics) mounted on the anterior medial aspect of the distal tibia were sampled simultaneously at 1000Hz. Tibial acceleration data were filtered (50Hz) and corrected for angular motion and gravity (Lafortune and Hennig, 1991), before peak positive acceleration (PPA) was calculated. The raw coordinate data were filtered (8 Hz), and cropped to the stance phase of gait using the force data (15N threshold). Rearfoot motion was calculated relative to shank, and forefoot relative to rearfoot, using a joint coordinate system adapted from Cole et al. (1993). Rearfoot (RFDF) and forefoot (FFDF) dorsiflexion excursion were defined from initial maximum plantarflexion to maximum dorsiflexion during stance. Rearfoot eversion (RFEV), rearfoot abduction (RFABD), forefoot eversion (FFEV) and forefoot abduction (FFABD) excursion were all

defined from footstrike to peak values during stance. Cohen's *d* values were calculated as a measure of effect size. The following classifications were used to interpret effect values: *d*=.20 small, *d*=.50 medium, *d*=.80 large.

RESULTS

Results of all variables for both LA and HA groups can be seen in Table 1. PPA was found to be greater in the HA group, with a *d* value approaching a medium effect (*d*=0.49). A higher STFF score was also seen in the HA group with a large effect (*d*=1.80). Greater range of motion was seen in the HA group for RFABD (*d*=0.52), FFEV (*d*=0.69) and in particular FFABD in which a large effect was observed (*d*=1.18).

Variable	LA	HA	*d*
PPA(*g*)	6.1(1.8)	6.9(1.5)	0.49
STFF	780(256)	1261(270)	1.80
RFDF(°)	13.0(2.6)	11.8(3.2)	0.41
RFEV(°)	14.4(4.2)	13.7(3.2)	0.19
RFABD(°)	5.5(1.8)	6.7(2.5)	0.52
FFDF(°)	7.9(2.2)	8.1(1.8)	0.01
FFEV(°)	2.6(1.5)	3.9(2.2)	0.69
FFABD(°)	3.7(0.8)	5.3(1.7)	1.18

Table 1. Means (SD) of variables for LA and HA groups, as well as effect sizes (*d*).

DISCUSSION

The purpose of this study was to compare foot mobility and tibial shock during running in those with HA and LA. Results show the HA group exhibited a higher mean tibial shock than the LA group. This finding is supported by the higher loading rates previously reported in HA individuals (Williams et al. 2001b), and may offer some explanation for the higher incidence of shock-related bony injuries (Williams et al. 2001a). A stiffer arch structure was observed in the HA group, evidenced by the higher STFF score. This supports the theory that HA feet are stiffer, and LA feet are more flexible. Although this may offer some explanation for the higher tibial shock in the HA group, the STFF score is based solely on static measures and does not reflect dynamic foot function. However, the assessment of dynamic foot mobility in the present study does not provide a clear explanation for the higher tibial shock measured in HA individuals. Sagittal (RFDF, FFDF) and frontal (RFEV) plane excursions were similar between groups. This does not support the findings of Williams et al. (2001b), who reported greater RFEV in LA (13.9°) compared to HA (11.9°) individuals. This difference may be due to the sampling of more extreme foot types (very LA and very HA) than in the present study. Contrary to expectation, greater excursions were seen for RFABD, FFEV and FFABD in the HA group. This may be due to a limited available range of motion for these rotations in LA individuals. LA feet exhibit a more pronated foot position than HA feet during running. Therefore, as the foot is loaded and pronation occurs, the joints in LA feet have less range of motion through which to pass, thereby limiting excursion for these rotations. These findings suggest the relationship between arch height and foot mobility to be complex, and one which certainly warrants further investigation.

SUMMARY

Tibial shock was greater in HA compared to LA individuals. While LA feet were more flexible (lower STFF), increased excursions within the feet of LA individuals were not found.

REFERENCES

Carson MC et al. (2001). *J Biomech,* 34: 1299-1307.

Cole GK et al. (1993). *J Biomech Eng*, 115: 344-349.

Kaufman KR et al. (1999). *Am J Sports Med*, 27: 585-593.

Lafortune, MA and Hennig, EM (1991). *Med Sci Sports Exerc*, 23: 360-363.

Perry, SD and Lafortune, MA (1995). *Clin Biomech*, 10: 253-257.

Williams, DS and McClay, IS (2000) *Phys Ther*, 80: 864-871.

Williams DS et al. (2001a). *Clin Biomech*, 16: 341-347.

Williams DS et al. (2001b). *J Appl Biomech,* 17: 153-163.

EVALUATION OF FOOTSWITCHES TO DETECT HEEL CONTACT

Jennica L. Roche, Daniel P. Steed, and Mark S. Redfern

Human Movement and Balance Laboratory, Department of Bioengineering, University of Pittsburgh, Pittsburgh, PA, USA
Email: JLR59@pitt.edu URL: http://hmbl.bioe.pitt.edu/home.htm

INTRODUCTION

Force plates, gait kinematics, and footswitches have been used to detect heel contact (HC). The ground reaction forces (GRFs) from force plates are used to detect HC by identifying a sharp peak in the vertical force as the heel strikes the ground (Findlow, 2004). However, since force plates are expensive and require imbedding into the floor, uses are limited to the lab setting (Findlow, 2004). Additionally, kinematic data allows HC detection, but a practical and robust algorithm for this approach has not yet been developed, and the large amount of required data processing renders this method unusable for real-time collection (Findlow, 2004). Footswitches remove location constraints and allow real-time feedback. However, commercially available switches are costly and research developed switches are unreliable and often have limited or unknown accuracy (Hausdorff, et al., 1995).

The purpose of this study was to examine the accuracy and reliability of numerous commercially available switches. From these results, we will propose optimal criteria of a footswitch that could reliably identify heel contact in real-time.

METHODS AND PROCEDURES

Mechanical and membrane switches of varying area, thickness, actuation force, and tactical response, were tested on six healthy subjects of age 21±1 years (Table 1).
We placed each switch inside the shoe, under the right heel. Force plate GRFs, (Bertec, Inc., model 4060A) as well as motion capture data, (Vicon 612 / M2 camera system) were collected during walking. The motion capture system allowed us to visualize reflective markers placed on the heel, ankle, and toe.

Switches were tested under "normal," "light," and "shuffle" walking styles. The "light" and "shuffle" walking styles were employed to mimic the cautious gait of older adults. "Shuffle" walking is a strategy where the subject walks flat-footed with truncated step length. "Light" walking is a strategy of decreased gait speed and step length, as well as decreased pressure on the heel. To determine reliability, the activations were visually compared to heel vertical trajectory. Reliability was qualitatively categorized into "good," "fair," and "poor" based on an accurate count of HCs. The step count accuracy was determined by identifying the HCs, troughs in the heel trajectory, and ensuring that only one footswitch rising edge, square pulse, was present. Switch activations, heel marker trajectory, and GRF plots also allowed footswitch delay to be calculated by comparison against a 5N threshold on the GRFs measured from the force plates.

RESULTS

Qualitative analysis of the data showed the membrane switches performed better than their mechanical counterparts. As displayed in Table 1, the majority of the membrane switches performed "good" for all trials. Figure 1 shows an example of what could be considered "good" reliability. Activation delay followed the same trend. The mechanical switches had long delay times, as well as higher variability (Table 1). Most of

the membrane switches performed well with delays under 40ms and variance under 3ms.
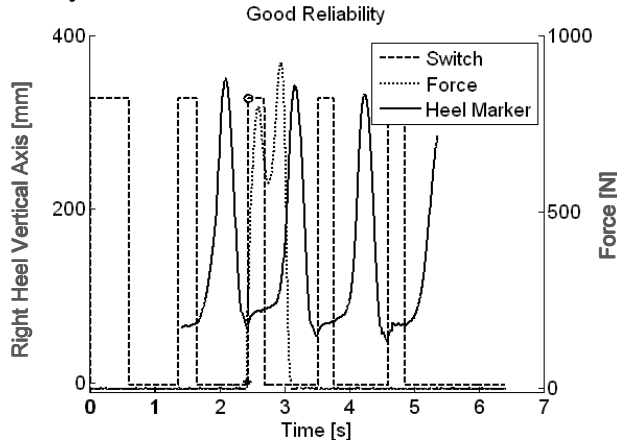
Figure 1. An example trial of a footswitch with good reliability. The footswitch signal (dashed) is high when activated. The vertical heel trajectory (solid) denotes HCs at the troughs and the GRF is dotted.

DISCUSSION

Initial testing indicated that the switches with less variance, but slightly longer delays performed more robustly to abnormal gait, assuming actuation occurs. Moreover, thin, tactile, membrane switches were the most reliable performers in terms of heel contact detection and precision. The membrane switches featuring a lag-time below 40ms allowed for precise detection of heel contact while still recording in real-time, since heel contact occurs about every 600ms.

The major limitations of our study are the limited subjects tested to-date, and the homogeneity of the subject population. All subjects tested were young and healthy. Ongoing testing will include older adults and adults with mobility impairments.

SUMMARY

There is great variability in footswitch performance and cost. Objective criteria for switch performance were evaluated, identifying desirable switch characteristics. A new footswitch will be developed utilizing optimal characteristics that can identify heel contact with accuracy and precision.

REFERENCES

Findlow, AH et al. (2004) *9th Annual Conference of the International FES Society*. 1-3.
Hausdorff, JM et al. (1995). *J Biomech*. 3:347-51.

ACKNOWLEDGEMENTS

Table 1. Switch specifications and quantitative and qualitative results

	Switch	Actuation Force [N]	Thickness [mm]	Area [mm²]	Activation Pressure [N/mm²]	Type		Accuracy	Precision	Heel Contact Reliability		
								Delay [ms]	Stdev [ms]	Normal	Light	Shuffle
Digi-key	A	4.4	2.5	2.8	1.6	Tactile	Mech.	95	74	Fair	Poor	Poor
	B	3.4	3.5	6.6	0.52	Tactile	Mech.	59	3.7	Good	Fair	Fair
	C	3.1	5.2	5.3	0.59	Tactile	Mech.	52	45	Good	Poor	Poor
	D	1.6	3.1	16.6	0.094	Tactile	Mech.	8.3	N/A	Good	Fair	Fair
Motion	EMG	0.5	1	176.1	0.0028	Non-Tactile	Mem.	N/A§	N/A§	Poor	Poor	Poor
Pannam	Blue	5.0	1.5	314.2	0.016	Tactile	Mem.	17	2.6	Good	Good	Good
	Help	4.4	1	113.1	0.039	Tactile	Mem.	37	2.6	Good	Good	Good
Nelson	A	-	1	113.1	-	Non-Tactile	Mem.	13	0.92	Good	Good	Good
	B	1.9	1	113.1	0.016	Tactile	Mem.	34	2.3	Good	Good	Good
	C	2.6	1	113.1	0.023	Tactile	Mem.	69	4.2	Good	Fair	Poor
	D	3.3	1	113.1	0.029	Tactile	Mem.	N/A†	N/A†	Poor	Poor	Poor
	E	3.4	1	113.1	0.0303	Tactile	Mem.	N/A†	N/A†	Poor	Poor	Poor

** Actuation force, thickness, and type are taken from manufacturer specifications. Button area and activation pressure were measured. § Activated by lacing of shoe † Never activated

EFFECTS OF SEATED WHOLE-BODY VIBRATION ON SEATED POSTURAL SWAY

Gregory P. Slota, Kevin P. Granata, Michael L. Madigan

Virginia Polytechnic Institute & State University
School of Biomedical Engineering & Sciences
The Kevin P. Granata Musculoskeletal Biomechanics Laboratory
Corresponding Author Email: gslota@vt.edu

INTRODUCTION

Low back disorders (LBDs) and their prevention are of great importance for companies and their employees. Whole-body vibration (WBV) is thought to be a risk factor for LBDs, but the neuromuscular, biomechanical, and/or physiological mechanisms responsible for this increased risk are unclear. The purpose of this study was to measure the acute effect of seated WBV on the postural control of the trunk during unstable seated balance.

Measures of seated postural sway during unstable seated balance have been used as surrogate measures of trunk postural control (Cholewicki et al, 2000) and have been related to spinal stability (Reeves et al, 2006). Seated WBV was investigated because machine operators are typically exposed to vibration while in a seated posture. It was hypothesized that WBV would impair postural control of the trunk, suggesting a loss of spinal stability and perhaps an increased risk for low back injury.

METHODS AND PROCEDURES

Twenty-one healthy subjects aged 23 ±4 years were tested on a wobble chair (Figure 1) designed to measure trunk postural control. Measurements of kinematic variance and non-linear stability control were based on seat angle before and after 30 minutes of seated whole-body vibration (bandwidth = 2 – 20 Hz, root-mean-squared amplitude =1.15 m/s^2). Fourteen of the 21 subjects completed a second experiment during which WBV was replaced with quiet sitting. The goal of this second experiment session was to identify any effects of prolonged sitting on postural control of the trunk.

The wobble chair is designed to provide an unstable seating condition for the subjects to balance upon. A single central pivot point with 4 radially located springs allows for adjustability of the balancing task. Kinematic variance of the seat tilt angle was determined using common measures of postural sway including the 95% ellipse area, root-mean-squared (RMS), and path length. Non-linear stability control measures of the seat tilt angle consisted of Lyapunov exponent, stability diffusion analysis (SDA), and Hurst rescaled range analysis (HRRA).
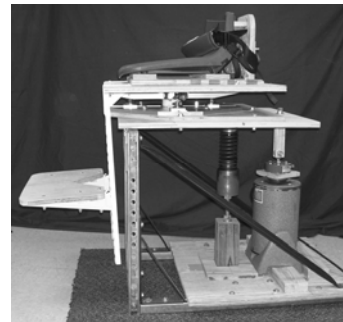
Figure 1: Wobble chair on top of vibration platform

The vibration platform (Figure 1) consisted of an electro-mechanical shaker on the back of the platform, a spring in the middle to offset the subject's weight, and a hinge in the front

to allow vertical movement of the chair (approx. ±1"). The shaker was computer controlled using feedback from an accelerometer to maintain the desired RMS amplitude of vibration.

RESULTS

WBV increased all measures of kinematic variance (Table 1). For example, ellipse area increased 35.5% ±50.5%, RMS increased 17.9% ±21.0%, and path length increased 12.2% ±15.1%. WBV also increased all non-linear stability control measures (Table 1). Lyapunov exponent increased 8.78% ±10.9%, SDA increased 1.95% ±2.8%, and HRRA increased 5.2% ±4.0%. Thirty minutes of sitting without WBV (control group) did not affect most measures of kinematic variance or non-linear stability control measures, but the medial/lateral components of RMS and SDA decreased (P =0.027, and P =0.019 respectively) after prolonged sitting.

Variable	Before	After
Ellipse Area*	58.6 ±40.5	79.4 ±40.9
RMS*	2.45 ±.778	2.89 ±.767
Path Length*	173.2 ±60.3	194.3 ±60.1
Lyapunov Exp*	0.613 ±.082	0.667 ±.074
SDA*	0.608 ±.022	0.620 ±.025
HRRA*	0.853 ±.024	0.897 ±.026

(* indicates p<0.05)

Table 1: Kinematic variance & stability assessment measures of unstable seated balance both before and after WBV exposure

DISCUSSION

The goal of this study was to investigate the effects of seated WBV on the postural control of the trunk. All measures of kinematic variance and non-linear stability control during unstable seated balance increased following WBV, suggesting that the postural control of the trunk was impaired. It is commonly believed that greater variability indicates greater instability (Dingwell & Marlin, 2006). Therefore, the results of this study imply an impairment of spinal stability with WBV. The results of the control group analysis suggest that the changes in postural control were not due to sitting alone.

Spinal stability is maintained through contributions from passive tissue stiffness, active muscular stiffness, and neuromuscular reflexes. The effect of WBV on any of these subsystems could conceivably alter postural control of the trunk, and explain the changes found in the present study.

SUMMARY

In conclusion, WBV impaired postural control of the trunk, which may indicate impaired spinal stability. Future studies are required to further explore the affects of WBV on the subsystems of the neuromusculoskeletal system that control spinal stability, as well as to understand the effects of different vibration characteristics, exposure durations, and recovery time-line.

REFERENCES

Cholewicki J et al. (2000). *J Biomech,* 33: 1733-7.
Dingwell JB & Marlin LC (2006). *J Biomech*, 39: 444-52
Reeves NP et al. (2006). *Exp Brain Res*, 174: 694-700.

ACKNOWLEDGEMENTS

CHANGES IN NATURAL FREQUENCY OF THE TRUNK WITH EXPOSURE TO SEATED WHOLE-BODY VIBRATION

Gregory P. Slota, Michael L. Madigan

Virginia Polytechnic Institute & State University
School of Biomedical Engineering & Sciences
The Kevin P. Granata Musculoskeletal Biomechanics Laboratory
Web: www.biomechanics.esm.vt.edu
Corresponding Author Email: gslota@vt.edu

INTRODUCTION

The prevention of low back disorders is the goal of ongoing research which studies various risk factors, such as whole-body vibration (WBV). The purpose of this study was to measure the changes in the natural frequency characteristics of the trunk during seated whole-body vibration as measured by transmissibility. The natural frequency and amplitude of the frequency response function of the trunk is related to the biomechanical properties of stiffness and damping, which contribute to spinal stability.

METHODS AND PROCEDURES

Twenty-one subjects (mean age 23 ±SD 4 years) without history of low back pain were exposed to 30 minutes of seated WBV at 2 – 20 Hz bandwidth and 1.15 m/s^2 RMS amplitude. Vibration was administered using a vibration platform that was designed with an electro-mechanical shaker, spring to offset the subject's weight, and hinge joint (Figure 1). Maximum vertical displacement during vibration was ±1 inch. Computer control with acceleration feedback maintained the desired RMS amplitude of vibration.
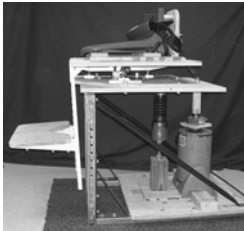
Figure 1: Vibration platform

Data were sampled from two accelerometers at the person/seat interface and on a bite-bar for 1 minute at the beginning and end of the 30 minutes. The transmissibility frequency response function (equation 1) was calculated from the ratio of acceleration at the mouth with a bite-bar, $Acc_{body}(f)$, and the acceleration at the person/seat interface, $Acc_{seat}(f)$, in the frequency domain.

$$TR(f) = \frac{Acc_{body}(f)}{Acc_{seat}(f)} \qquad (1)$$

The natural frequency of the trunk was identified as the highest amplitude of this function (Figure 2).
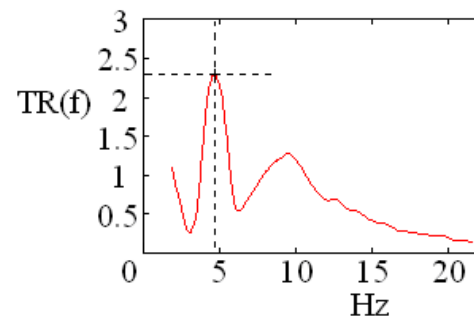
Figure 2: Transmissibility frequency response function with the natural frequency of the system indicated. A second characteristic frequency can be seen with the peak value near 10 Hz.

RESULTS

WBV caused the natural frequency to decrease 3.0% (p=0.030) and the peak amplitude of the transmissibility frequency response function to increase 41.7% (p<0.001) (Figure 2A, 2C).

The transmissibility frequency response function also showed a second characteristic frequency in the area of 10 Hz, as seen in other studies (Fairley & Griffin, 1989). WBV caused the second characteristic frequency to decrease 4.2% (p=0.005) while the amplitude increased 41.7% (p<0.001) (Figure 2B, 2D).

DISCUSSION

The goal of this study was to investigate changes in the natural frequency of the human trunk during exposure to seated WBV. Changes in the natural frequency are related to trunk stiffness (equation 2, assuming mass (m) as a constant) and the decrease in the natural frequency (F_n) found here implies a decrease in stiffness (k).

$$F_n = \sqrt{(k/m)} \qquad (2)$$

Based on the percent changes for the characteristic frequencies (natural, secondary) of the system and equation 2, the respective stiffness could have decreased by 5.83% and 14.2% due to 30 minutes of WBV exposure. Similar results were reported in studies describing a "softening" of the body where the natural frequency decreased from 6-4 Hz

as vibration magnitude increased from 0.25-2.0 m/s^2 RMS (Fairley & Griffin, 1989).

Similarly, changes in the peak value recorded at the natural frequency are related to the system damping of the trunk and the increase in the peak value found here implies a decrease in the system damping.

SUMMARY

In conclusion, WBV caused changes to the characteristics of natural frequency of the trunk and implied changes to the biomechanics, which may result in impaired spinal stability control that can lead to low back pain. Future studies are required to further explore how the progressive changes affect the human body with WBV exposure.

REFERENCES

Fairley TE & Griffin MJ, (1989) *J Biomech* 22:81-94.

ACKNOWLEDGEMENTS
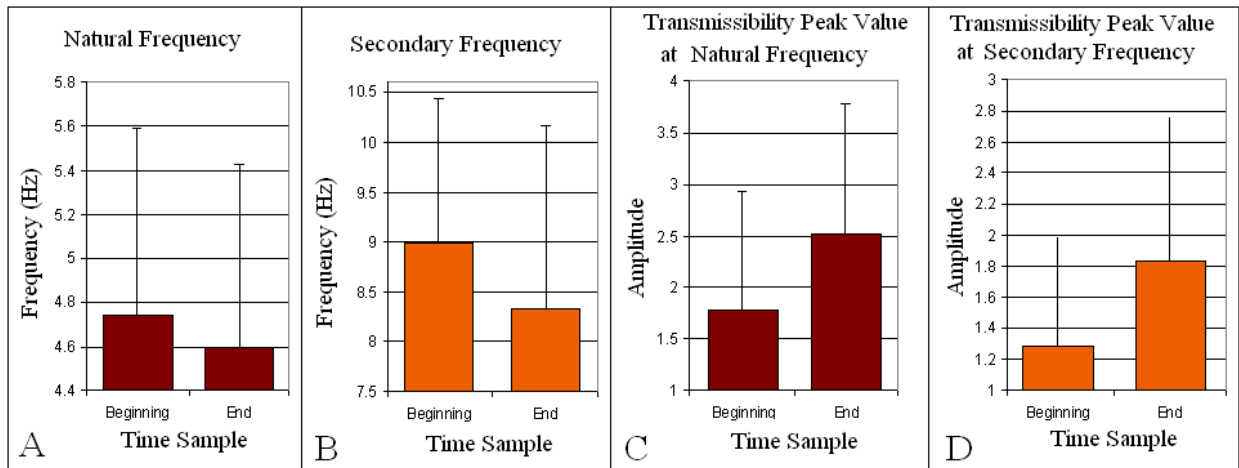
Figure 2: Results for natural frequency characteristics at the beginning and end of 30 of WBV exposure. A) Natural Frequency, B) Secondary Frequency, C) Transmissibility Peak Value at Natural Frequency), D) Transmissibility peak value at secondary frequency. Error bars represent inter-subject standard deviation.

EFFECTS OF ASYMMETRIC ANKLE PLANTARFLEXOR RECRUITMENT ON POST-STROKE WALKING: A 3D SIMULATION STUDY

Ming Xiao and Jill Higginson

Department of Mechanical Engineering, University of Delaware, Newark, DE, USA
Email: mx@udel.edu, Lab URL: http://www.me.udel.edu/higginson

INTRODUCTION

Studies based on experimental data have identified the relationship between ankle plantarflexor weakness and gait deviations in individuals with stroke (Kim and Eng 2003). Mulroy et al. (2003) suggested that other muscle groups may be used to provide body support for ankle plantarflexors. Higginson et al. (2006) used forward simulation to examine the reorganized muscle coordination in post-stroke walking but the model was 2D thus the study of hip muscle function was limited.

In this study, we generated the first 3D forward simulation of a complete gait cycle of post-stroke hemiparetic gait in OpenSim (Delp et al. 2007). The aims of this study were to examine bilateral ankle muscle moments in post-stroke walking and to identify compensatory strategies by other muscles for impaired ankle plantarflexor function.

METHODS AND PROCEDURES

Three-dimensional kinematic and kinetic data were collected from one subject (183cm, 109.5kg) with hemiparesis secondary to stroke. After signing an informed consent approved by the human subjects review board, the subject walked on an instrumented split-belt treadmill at the comfortable speed (0.67 m/s) without any handrails while motion analysis data was collected.

A 3D musculoskeletal model was built in OpenSim with 13 segments and 12 joints. It had 23 degrees-of-freedom and was actuated by 54 muscle-tendon units to enable movements in the sagittal plane, frontal plane and transverse plane. The equations of motion for the model were derived from SD/Fast (PTC).

Predicted muscle excitation patterns from OpenSim were compared between paretic and non-paretic sides. Individual muscle forces and moments were also compared.

RESULTS

A complete cycle of hemiparetic gait was simulated by OpenSim within 5 hours on a personal computer. Simulated body movements and joint angles were very close to experimental measurements (within ±5º). Asymmetric kinematics and kinetics (Fig. 1), including insufficient hip and knee flexion, and excessive hip abduction and internal rotation on the paretic side were observed.

Predicted muscle excitations were generally consistent with recorded EMG signals. We noticed that peak plantarflexion moment generated by soleus (SOL) on the paretic side was only 20% of that on the non-paretic side during late stance phase (Fig 2), indicating the subject had weak ankle plantarflexors on the impaired leg. Knee extensors vastii (VAS) and rectus femoris (RF) on the paretic side were activated during mid-stance to late-stance. Gluteus medius (GMED) had asymmetrical excitation patterns with delayed activity on the non-paretic side (Fig. 3).
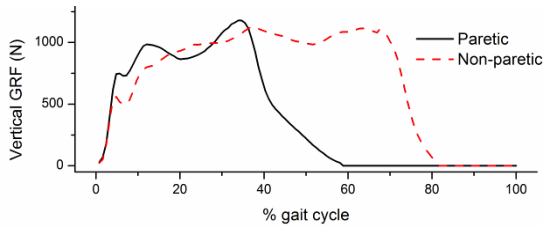
Figure 1. Vertical ground reaction forces on the paretic side (solid) and non-paretic side (dashed). Data were normalized to one gait cycle starting from heel strike. Non paretic stance duration (80% gait cycle) was much longer than the paretic side (60% gait cycle).
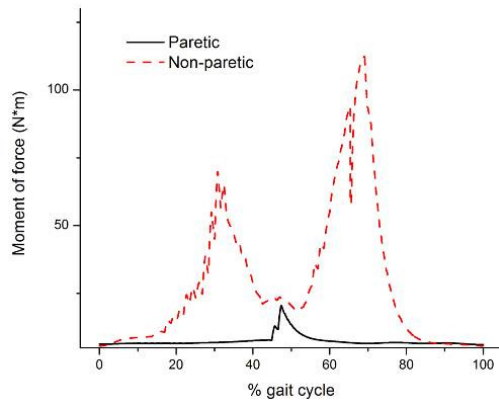
Figure 2. Ankle plantarflexion moment generated by paretic SOL (solid) was much smaller than that on the non-paretic side (dashed).

DISCUSSION

We built a 3D musculoskeletal model in OpenSim to simulate a full cycle of post-stroke hemiparetic walking.

SOL was shown to be much less active on the paretic side of the subject and consistent with reports of ankle plantarflexor weakness. Impaired force and torque generation by the ankle plantarflexors would necessitate a change in the coordination patterns of other muscle groups. Instead of SOL, VAS and RF were activated from mid to late-stance phase to extend the knee joint and contribute to body weight support. GMED on the paretic side was activated during the entire stance phase in contrast with that on the non-paretic

side, which was silent during the first half of single-leg stance where SOL was not weak. We believe this is because the subject maintained his COM over the non-paretic side most of the time, so GMED should not be needed in early to mid-stance for lateral COM stability.
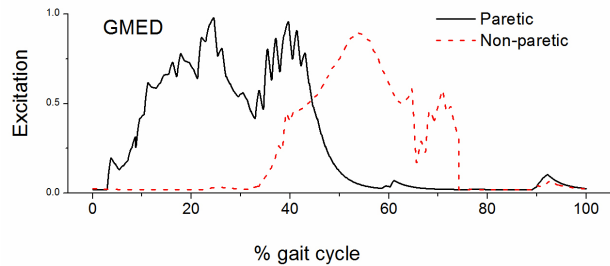
Figure 3. Predicted muscle excitation of GMED on both legs. Data were normalized to one gait cycle starting from heel strike.

Ankle plantarflexors are believed to be responsible for stabilizing the ankle and knee joint and supporting the COM. Our results from forward simulation showed that several other muscles can be utilized to compensate for the weakness of ankle plantarflexors. Future work will use simulations to investigate individual muscle contributions to abnormal movement patterns common in post-stroke hemiparesis.

REFERENCES
Delp SL et al. (2007). *IEEE Trans Biomed Eng.* 54, 1940-1950.
Higginson JS et al. (2006). *J Biomech*, 39, 1769-1777
Kim CM and Eng JJ. (2003). *Phys Ther,* 83, 49-57
Mulroy S et al. (2003). *Gait Posture*.18, 114-125.

INFLUENCE OF CADENCE, POWER OUTPUT AND HYPOXIA ON THE JOINT POWERS AND MUSCLE EXCITATION DURING CYCLING

David J. Sanderson[1], Guillaume Mornieux[2], Jordan A. Guenette[1], A. William Sheel[1]

[2]Institut für Sport und Sportwissenschaft, Universität Freiburg, Germany
[1]School of Human Kinetics, University of British Columbia, Vancouver, BC, Canada
david.sanderson@ubc.ca

INTRODUCTION

Analysis of the relative joint distribution to the global lower-limb activity was initially presented by Ericson et al. (1986). They described the percentage contribution of each joint to the total positive and negative work and reported that the main relative energy producers were the knee extensors (39%) and the hip extensors (27%), whereas the plantar flexors (57%) and the hip extensors (32%) were the main relative energy absorbers at 120 W and 60 rpm. Ericson (1988) described the influence of pedalling cadence and power output on the relative proportions of the total positive work at the hip, knee, and ankle joints. Pedalling cadence was found to have no influence, while power output showed only a significant effect on the hip flexors and ankle extensors, both decreasing their proportions with increased power output from 0 to 240 W. Recently, Mornieux et al (2007) provided data showing the relative insensitivity of the ankle, knee, and hip joint moment to variations in cadence and power output. Even in the presence of hypoxia this relative insensitivity remained. The data presented here came from the same project and expand on the notion of insensitivity.

METHODS AND PROCEDURES

The anthropometrical data of the 7 subjects were 27 (3) years, 84.1 (9.5) kg and 190 (5) cm. Subjects came twice to the laboratory on two separate days where normoxic (fraction of inspired oxygen $FIO_2 = 20.9\%$) and hypoxic ($FIO_2 = 15\%$) cycling conditions were tested. These 2 sessions were conducted in a single-blind randomised fashion. Trials were performed comprising the combination of 3 pedalling cadences (60, 80, and 100 rpm) at 250 W and that of the 3 power outputs (150, 250, and 350 watts) at 80 rpm. Riders rode a standard bicycle, mounted on a Schwinn Velodyne ergometer, instrumented with 2 piezo-electric tri-axial transducers (Kistler 9251A) in the right pedal (Sanderson et al., 2000). Force data were recorded at 240 Hz while lower-limb kinematics were recorded at 60 Hz using a video camera oriented perpendicular to the sagittal plane of the rider. Using these data, calculations of the absolute relative joint powers at the hip, knee and ankle were done using conventional inverse dynamics (Hull and Jorge 1985). Muscle activity was recorded at 1200 Hz using surface electrodes affixed over the gluteus maximus, biceps femoris, rectus femoris, vastus lateralis, gastrocnemius lateralis, tibialis anterior, and soleus. The data were rectified, low-pass filtered and the mean within-cycle average was computed for each subject and condition. EMG data were normalized to the 250 watts/ 80 rpm condition recorded at the beginning of each testing session. A term, global EMG, was computed as the sum of the integrated across cycle EMG for all muscles.

RESULTS

Table 1, below, presents the average absolute relative joint power as a function of cadence

manipulation. There were no significant effects of cadence nor oxygen on the relative joint power at the ankle but there was a significant effect at the hip and knee joints.

Cadence Effect		60 rpm	80 rpm	100 rpm
Ankle	Normoxic	12%	12%	11%
Knee		37%	38%	44%
Hip		51%	51%	46%
Ankle	Hypoxic	12%	11%	10%
Knee		38%	40%	48%
Hip		50%	49%	42%

Table 2, below, presents the average absolute relative joint power as a function of the power output manipulation. There was no significant effect of power output nor oxygen at the ankle joint but there was at the knee and hip joints.

Power Effect		150 watts	250 watts	350 watts
Ankle	Normoxic	11%	12%	12%
Knee		42%	38%	35%
Hip		48%	51%	52%
Ankle	Hypoxic	10%	11%	13%
Knee		48%	40%	35%
Hip		42%	49%	53%

Figure 1 presents the global EMG response to the power output manipulation while Figure 2 shows the global EMG response to the cadence manipulation. While there was a significant increase in global EMG with increased power output there was no significant difference in response to cadence manipulation. These effects were similar for each of the 7 muscles assessed.

DISCUSSION

These data were consistent with Mornieux et al (2007) and serve to support their conclusion that the cycling task is a robust complex movement. The ankle joint remained insensitive to all manipulations but the hip

and knee joints appeared to interact in such a way that they compensated for changes in

Figure 1
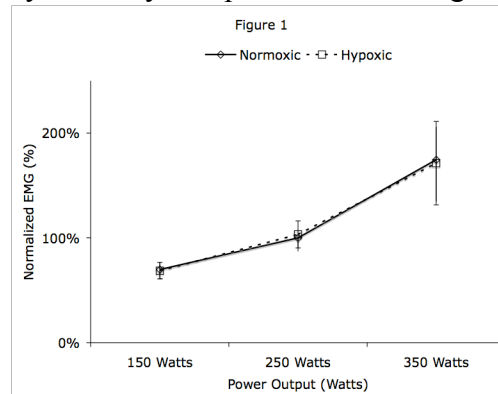
each other as a means to maintain the each

Figure 2
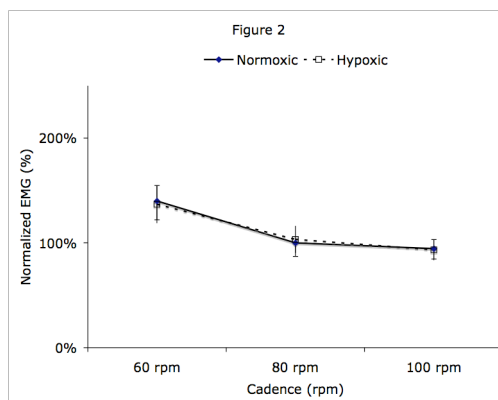
other as a means of providing the needed pedal force. Even in the presence of a strong perturbation by reducing the available oxygen concentration, the riding mechanics remain unchanged. These data suggest that when a rider is working at maximum, as in a competitive event, the underlying movement biomechanics are relatively fixed. Training in environments of reduced oxygen is unlikely to produce changes in this movement pattern nor in the underlying muscular events.

REFERENCES

Ericson et al. (1986). SJRM 18:165-172.
Ericson et al. (1988). JAPOP 24:382-387.
Hull and Jorge 1985). JOB 18:631-644.
Mornieux et al. (2007). EJAP 102:11-18.
Sanderson, DJ et al. (2000). JSS 18:173-181.

A MULTI-SUBJECT EVALUATION OF UNCERTAINTY IN ANATOMICAL LANDMARK LOCATION ON SHOULDER KINEMATIC DESCRIPTION

Joseph E. Langenderfer[1*], Paul J. Rullkoetter[2], Peter J. Laz[2]

[1]Department of Engineering and Technology, Central Michigan University, Mount Pleasant, MI
[2]Computational Biomechanics Laboratory, University of Denver, Denver, CO
*e-mail: j.langend@cmich.edu

INTRODUCTION

Uncertainty in identifying and locating anatomical landmarks (ALs) via digitization has potential to affect reported joint kinematics. Many studies have characterized sources of AL variability and their effects on kinematic descriptions using repeated measures experimentation (e.g. DeGroot, 1997, Meskers et al., 1998). Alternatively, probabilistic analysis techniques including the Monte Carlo (MC) simulation and the more efficient Advanced Mean Value (AMV) method have been used to evaluate the variability in knee kinematic descriptions resulting from AL location uncertainty (Morton et al., 2007). Probabilistic analyses predict bounds of kinematics and the input parameters that most affect performance, but have typically been applied to single subjects (Morton et al., 2007; Langenderfer et al., 2006). The purpose of this study was to apply probabilistic methods to quantify the effect of AL location uncertainty on scapular and humeral kinematic descriptions for multiple subjects, and to evaluate the consistency of results. The hypothesis was that the probabilistic analysis would yield similar bounds and sensitivity factors across multiple subjects.

METHODS

Eleven healthy volunteers participated in this study; informed consent was obtained from all participants, and University Institutional Review Board approval was attained. The experimental procedure has been described previously (Mell et al., 2005). Data consisted of digitized ALs and position and orientation of electromagnetic sensors attached to the sternum, forearm, humerus and scapula while the subjects performed humeral elevation from 30° to horizontal within the scapular plane. Data were processed to calculate Euler angles describing humero-thoracic motion (elevation, plane of elevation, and humeral rotation angle), and for scapulo-thoracic motion (medial-lateral (M-L) rotation, anterior-posterior (A-P) tilt, and protraction).

The probabilistic model, linking NESSUS (Southwest Research Institute, San Antonio, TX) and custom code, predicted the 1 and 99 percentile bounds for each Euler angle. Uncertainty in ALs was simulated by assigning Normal distributions to each coordinate of the AL digitization data. For each landmark, the mean was the digitized location, while standard deviations of 4 mm were assumed. This standard deviation is at the upper bound of intra-observer variability measured *in vivo* (Meskers et al., 1998). After confirming excellent agreement between the MC and AMV methods for one subject, the AMV method was used for subsequent evaluations. The absolute sensitivity of each Euler angle to each anatomical landmark was averaged over the elevation motion for each subject. Sensitivities were analyzed with 2-way ANOVAs to detect differences attributable to ALs and subjects.

RESULTS

The AMV analysis yielded excellent agreement with the MC results; average difference of the 1 to 99 percentile ranges between the two methods was 0.18 degrees. Uncertainty in AL location resulted in 1 to 99 percentile ranges of 7.3 ± 0.6^{o} (mean ± standard deviation) for humeral elevation angle (Figure 1), 15.8 ± 1.7^{o} for humeral plane of elevation, and 11.3 ± 1.5^{o} for humeral rotation angle. For the scapular angles, 1 to 99 percentile ranges were: 12.3 ± 1.0^{o}, 11.7 ± 1.1^{o}, and 16.6 ± 1.4^{o} for M-L rotation, A-P tilt and protraction, respectively.
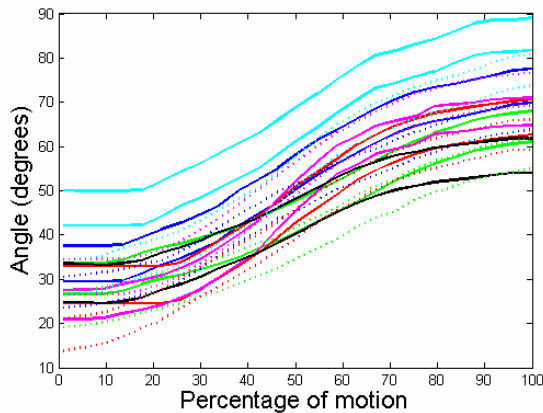
Figure 1: 1-99 percentile for humeral elevation angle for the eleven subjects.

There were statistically significant differences in sensitivities of Euler angles to ALs ($p<<0.05$), but no statistically significant differences in sensitivities across subjects ($p>0.5$) (Figure 2). For example, humeral elevation angle was most sensitive to thorax landmarks: seventh cervical vertebrae (C7), eighth thoracic vertebra (T8), incisura jugularis (IJ), and processus xiphoideus (PX) (all 0.41 ± 0.02), as well as processus coracoideus (PC) (0.26 ± 0.07), medial and lateral epicondyles (EM & EL) (both 0.24 ± 0.02), and the AC joint (0.23 ± 0.04). Likewise, humeral rotation angle was most sensitive to thorax landmarks (all 0.39, S.D. 0.03), EM and EL (both 0.28, ±0.05), and PC

(0.24 ± 0.05). Scapular M-L rotation was most sensitive to trigonum spinae (TS) and angulus acromialis (AA) (both 0.61 ± 0.03), and then thoracic ALs (all 0.25 ± 0.04).
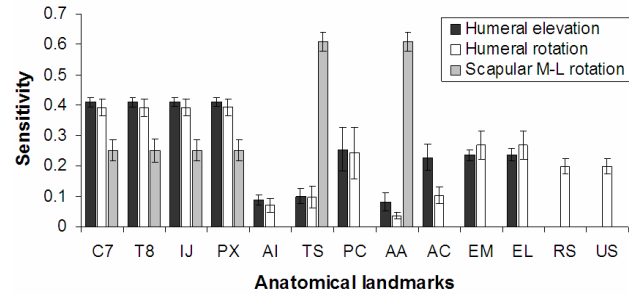
Figure 2: Mean (S.D.) sensitivities of Euler angles to anatomical landmarks.

DISCUSSION AND CONCLUSIONS

Probabilistic analysis using the AMV method provides an efficient approach to evaluate variability in reported kinematic descriptions for multiple subjects. The probabilistic platform yielded consistent results in calculated kinematic ranges and sensitivities to ALs across multiple healthy subjects. A similar analysis could be used to understand how ALs may contribute to kinematic descriptions differently for patients with joint pathologies, which is a relevant issue in understanding pathologic kinematics. The consistent sensitivity findings provide insight into the important AL affecting kinematics with the potential to impact computer-assisted surgical techniques used to align joint implants.

REFERENCES

DeGroot (1997) *Clin Biomech* 12, 461-472.
Langenderfer et al. (2006) *ASME Sum Bio Conf*, 157639.
Mell et al. (2005) *J Shoulder Elbow Surg*, 14, 58S-64S.
Meskers et al. (1998) *J Biomech*, 31, 93-96.
Morton et al. (2007) *J Orthop Res*, 25 1221-1230.

A THREE-DIMENSIONAL MODEL TO EXAMINE THE EFFECTS OF POSTURE ON CARPAL TUNNEL SIZE AND SHAPE

Jeremy P.M. Mogk[1] and Peter J. Keir[2]

[1]Sensory Motor Performance Program, Rehabilitation Institute of Chicago, Chicago, IL, USA, j-mogk@northwestern.edu
[2]Department of Kinesiology, McMaster University, Hamilton, ON, Canada, pjkeir@mcmaster.ca

INTRODUCTION

Carpal tunnel syndrome is the most common peripheral compression neuropathy. Deviated wrist posture has been linked to its development, with reduced carpal tunnel (CT) area and dimensions representing mechanisms for median nerve compression (Keir and Rempel, 2005). Wrist posture is reported to alter CT size and shape (*c.f.* Bower et al., 2006); however, changes are consistent with non-orthogonal alignment of scans relative to the tunnel (Mogk and Keir, 2007). As a result, it remains unclear how posture alters CT size and shape, as well as how these factors contribute to median nerve compression. The purpose of this study was to evaluate the effect of wrist posture on CT dimensions using several indices of size and shape.

METHODS AND PROCEDURES

Three-dimensional static models were created using a hybrid of reconstructed MRI data and modelled bone surfaces. Digitized data of six individuals were imported into Maya™ (v7.0, Alias®, Toronto, Canada) to reconstruct the CT surfaces, and bone positions in three wrist postures (30° flexion, neutral and 30° extension). Bone positions were recreated in each posture using an anatomical set of bone surfaces (radius, ulna, 8 carpals and 5 metacarpals) placed according to the digitized bone contours. Bone surfaces were used to identify the tunnel boundaries and ensure that measurements in each posture lay within the anatomically "landmarked" volume, defined by specific vertices located on the pisiform and scaphoid tubercle (proximally), and the most distal aspects of the hook of the hamate and ridge of the trapezium (distally).

Tunnel dimensions were measured at 1.5 mm increments from the reconstructed CT surfaces using a simulated imaging plane, aligned perpendicular to the tunnel on a slice-by-slice basis to obtain "physiological" cross-sections. Dimensions included CT cross-sectional area (CTA), circumference, width (CTW) and depth (CTD). The broadest distance was used to represent width, with depth measured perpendicular to the width dimension. Shape was evaluated using two ratios. Carpal tunnel ratio (CTR) was calculated as the width to depth ratio, with values less than 1.0 when tunnel width exceeds its depth. A non-circularity ratio (NCR) was calculated as the ratio between tunnel area and the area of a circle with the same circumference. A perfect circle carries a value of 1.0, with smaller values indicating less circular or elongated shapes. Dimensions were evaluated at the proximal (scaphoid tubercle) and distal ends (distal extent of ridge of trapezium), and using an "average" measurement which included all slices throughout the CT length.

RESULTS

Carpal tunnel area and depth were smaller at the proximal end in extension than neutral ($p<0.01$) or flexion ($p<0.05$) (Table 1). The proximal end was wider than the distal in both

extension (p=0.01) and neutral (p<0.01), and narrowed from neutral to flexion (p=0.01) (Table 1). Significant differences between proximal and distal end dimensions were only noted for CT width, both within and between postures. No significant differences were noted at the distal end between postures for any dimensions. Average measurements showed similar patterns of significance.

Table 1. Summary of mean (s.d.) dimensions at proximal (P) and distal (D) tunnel ends.

		30° Ext	Neutral	30° Flex
CTA	P	163.6 (23.3)	180.5 (19.7)	172.4 (20.7)
(mm^2)	D	160.9 (26.6)	170.8 (21.6)	172.2 (25.6)
CTD	P	9.3 (1.0)	10.5 (0.7)	10.8 (1.0)
(mm)	D	9.5 (0.7)	10.1 (0.7)	10.5 (1.5)
CTW	P	23.1 (1.4)	22.5 (1.6)	20.9 (1.5)
(mm)	D	21.4 (2.1)	21.4 (1.6)	21.0 (1.5)
CTR	P	0.401 (0.035)	0.467 (0.029)	0.516 (0.063)
	D	0.447(0.036)	0.474 (0.032)	0.498 (0.057)
NCR	P	0.686 (0.037)	0.752 (0.026)	0.792 (0.058)
	D	0.746 (0.022)	0.781 (0.025)	0.804 (0.035)

Using the CTR, the proximal end appeared flatter in extension than neutral (p<0.05) and flexion (p<0.01). The distal end was flatter than the proximal in flexion (p<0.01), but no differences were noted distally between wrist postures. Using the NCR, the tunnel in extension was less round proximally than flexion (p=0.01), and distally relative to neutral (p<0.05) and flexion (p=0.01).

DISCUSSION

Building upon previous findings (Mogk and Keir, 2007), three-dimensional hybrid models were constructed to examine posture-related changes in carpal tunnel size and shape. Results suggest that our prior understanding of posture-related changes in CT dimensions reflects slices aligned relative to the forearm, rather than the tunnel itself. Where others have reported sizeable posture-related changes at the distal end (*c.f.* Bower et al.,

2006), current results indicate less variable changes between postures distally than proximally. The generally smaller dimensions found in the extended posture support measured CT pressure increases with extension (Keir and Rempel, 2005). Concern has been raised over the effectiveness of width-depth ratios to evaluate the "shape" of non-elliptical cross-sections (Bower et al., 2006) (Figure 1). Non-circularity does not vary with the directionality of width and depth measurements, and thus accounts for shape irregularities resulting from bony projections which may prove valuable in locating sites of impingement. Slice alignment with the tunnel may improve the consistency of findings within and between patient and control populations, and enhance the diagnostic utility of clinical imaging.

CTA = 171.0 mm^2 CTA = 172.3 mm^2
Circumference = 53.4 mm Circumference = 51.3 mm
NCR = 0.753 NCR = 0.824

Width = 21.4 mm   Depth = 10.3 mm
CTR = 0.480
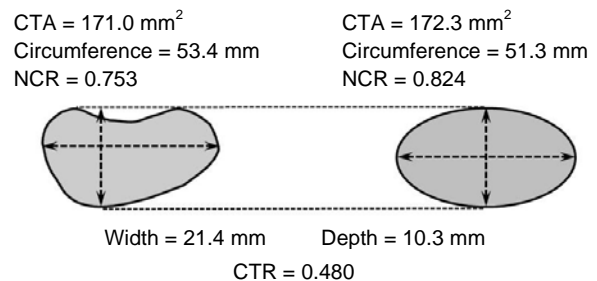
Figure 1. Comparison of size and shape indices for a digitized cross-section (left) versus the equivalent ellipse (right) based on the measured width and depth parameters.

REFERENCES

Bower, JA et al. (2006). *Clin Biomech*, 21: 816-825.
Mogk, JPM and Keir, PJ (2007). *J Biomech*, 40: 2222-2229.
Keir, PJ and Rempel, DM (2005). *J Hand Ther*, 18: 259-269.

ACKNOWLEDGEMENTS

DEVELOPMENT OF A SEMI-AUTOMATED METHOD FOR GENERATION OF HEXAHEDRAL FEMORAL CARTILAGE MESHES FROM MRI

Mark A. Baldwin[1], Joseph E. Langenderfer[2], Peter J. Laz[1], Paul J. Rullkoetter[1*]

[1]Computational Biomechanics Laboratory, University of Denver, Denver, CO
[2]Department of Engineering and Technology, Central Michigan University, Mount Pleasant, MI
*e-mail: prullkoe@du.edu

INTRODUCTION

Patient-specific finite element (FE) models which incorporate anatomic articular surface and soft tissue geometric representations can provide important insight into knee mechanics (Li et al., 1999; Shirazi-Adl et al., 2004). However, the generation of patient-specific meshes with hexahedral elements required for an accurate contact formulation is a manual, time-consuming process (Muccini et al., 2000). Extraction of three-dimensional (3D) anatomic surfaces is accomplished with manual segmentation of medical images, but the resulting meshes are not useable for contact in FE analysis. For this reason, more efficient methods for generating patient-specific hexahedral meshes are required. Thus, this study's objectives were: to assess the feasibility of using a semi-automated morphing method to create specimen-specific hexahedral meshes of femoral surfaces from MR images and to compare the accuracy and efficiency of meshes generated with the semi-automated method and with a traditional preprocessor-segmentation based method.

METHODS

This study adapted a previously described method of generating tibial and patellar cartilage surface meshes to generate femoral cartilage meshes (Baldwin et al. 2008). Similar to the previous study, a generic 3D hexahedral mesh for the femoral cartilage was generated in Hypermesh 7.0 (Altair, Inc., Troy MI). The mesh was aligned to the sagittal plane with three elements (≈2.5 mm edge length) between the bone and articular surface and a medial-lateral width of 3 mm. Within each mesh, groups of adjacent elements were created with moveable control handles located on the group corners. Using the Hypermesh morph tool, control handle movement linearly influenced all elements' nodes within the groups, and allowed the mesh to be stretched (morphed) while element quality (i.e. shape and skewness) was maintained. Sagittal plane MR images were displayed with a graphical user interface (GUI) developed in Matlab (Mathworks, Natick, MA). The morphing process is initiated by specifying image details (e.g. field-of-view dimensions, image resolution, etc.) to scale the generic mesh in the medial-lateral (M-L) direction. Then, the most anterior, posterior, inferior and superior points are found on the femoral cartilage (not shown) to scale the generic mesh in the respective directions. Next, three points are dragged on each image to denote the anterior-posterior (A-P) and inferior-superior (I-S) femoral surface locations (Figure 1, red) and then additional points corresponding to mesh control handles (cyan) are dragged to identify the entire surface. Finally, the meshes are smoothed by fitting piecewise polynomials to handle locations in the sagittal, coronal and frontal planes. Differences between the initial generic and final control handle 3D coordinates are calculated and exported as a script to morph the meshes in Hypermesh. The morphing method was used to generate hexahedral meshes for the femoral cartilage

from MR images (CISS sequence, 512x512 pixels, 0.35 mm in-plane resolution, 1 mm slice thickness) of two healthy adult cadaver specimens. Hexahedral meshes for each femur were also generated by a combination of traditional segmentation using ScanIP (Simpleware, Exeter, UK) and manual solid mesh generation techniques in Hypermesh. Mesh differences were quantified by calculating the root mean square (RMS) difference between the 3D mesh nodal coordinates generated with each method.
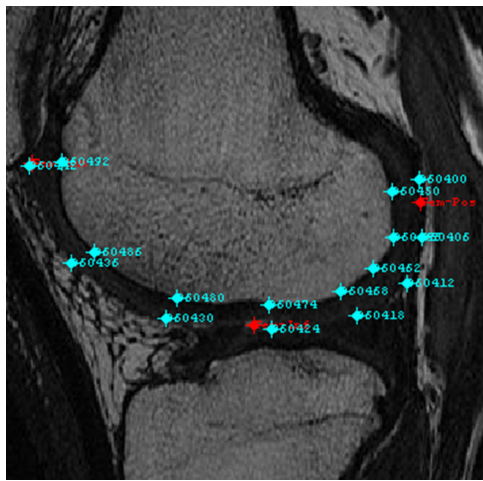
Figure 1: GUI with points designating femoral A-P and I-S locations (red) and contour (cyan).
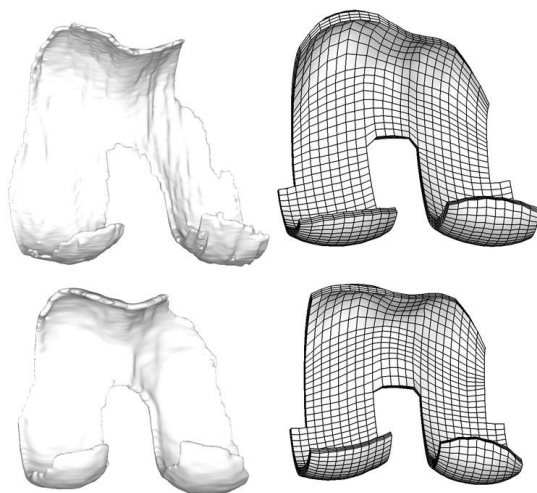
Figure 2: Segmented femoral (left) and GUI-generated (right) hexahedral solid meshes for two specimens.

RESULTS

The RMS differences between the GUI-morphed and manually segmented femoral surfaces for the two specimens were 0.63 and 1.24 mm, respectively (Figure 2). Meshes generated with the semi-automated method were appropriate for contact analysis and required approximately 30 minutes per femur, while generation of meshes with traditional segmentation and meshing procedures averaged 3 hours per femur.

DISCUSSION AND CONCLUSIONS

This study utilized a novel semi-automated GUI-based method to generate specimen-specific hexahedral meshes of femoral cartilage. Additionally, meshes generated with the semi-automated technique were compared to meshes generated with traditional segmentation, with an average RMS difference of 0.94 mm. This difference is comparable to RMS differences (0.34-0.62 mm) found for patellar and tibial cartilage mesh generation with a similar technique (Baldwin et al., 2008), and is within the reported range (0.5-4 mm) for semi-automated mesh generation of bones (Shim et al., 2007). These results imply that semi-automated mesh generation for other joints, such as the shoulder and hip, may be possible with appropriate MR scans.

REFERENCES

Baldwin et al. (2008) *Trans ORS* 635.
Li et al. (1999) *J Biomech Eng* 121, 657-662.
Muccini et al. (2000) *J Med Eng Tech* 24, 145-8.
Shim et al. (2007) *J Biomech* 40, 26-35.
Shirazi-Adl et al. (2004) *CMBBE* 8, 17-24.

ACKNOWLEDGEMENTS

THE STEPS OF MUSCLE MYOSIN II

A. Mehta[1], W. Herzog[2]

[1]Faculty of Kinesiology, University of Calgary, Calgary, Canada, mehtaa@ucalgary.ca
[2]Faculty of Kinesiology, University of Calgary, Calgary, Canada, walter@kin.ucalgary.ca

INTRODUCTION

According to the cross-bridge theory, the chemo-mechanical cycle by which a muscle contracts is governed by a deterministic process that stipulates the myosin molecules are only able to pull the actin filaments, or perform the power stroke, in a specific direction (Huxley, 1957). Each myosin has a mid axis symmetry such that half myosins pull the actin filaments toward the middle of the sarcomere, thereby causing sarcomeres to shorten. However, in experiments of single actin-cross-bridge interactions, it has been shown that cross-bridges pull actin filaments in both directions: a preferred direction towards the positive charged end of actin (forward steps), and a less frequently observed stepping towards the negative end of actin (backward steps). However, it is not clear if the direction of cross-bridge stepping is determined by the polarity of actin or the orientation of the cross-bridge. The purposes of this study were (i) to determine if the preferred direction of pulling is governed by the orientation of the myosin cross-bridge or the polarity of the actin filament, and (ii) to quantify if there are mechanical differences between forward and backward steps.

METHODS AND PROCEDURES

A three-bead laser trap setup, as first developed by Finer et al. (1994), was used for testing single cross-bridge interactions with actin (Figure 1). Briefly, two micron-sized beads were attached to the ends of the actin filament and were held by two independently controlled lasers for manipulation, force and step size measurement. A cross-bridge (a heavy meromyosin, double headed construct) was placed on top of a surface fixed bead for interaction with the actin filament. Upon attachment of the cross-bridge, the direction of actin movement, force, step size, and the time of attachment (dwell time) were recorded at low ATP concentrations, so that attachment events could be clearly identified.

Once a set of cross-bridge attachment events had been recorded for a given construct, the actin filament orientation was changed by 180° so that the plus and minus end of the filament were reversed and a second set of attachment events were recorded in this new configuration.

Non-parametric tests were used to determine if there was a significant difference between dwell times, step sizes and forces of the forward and backward steps

RESULTS

Step size and associated force were greater for forward (15 ± 1nm) than backward steps (12 ± 1nm), while dwell times were the same. Backward steps (32%) occurred in random order.

Following the change in actin orientation by 180°, the primary stepping direction was reversed (Figure 2).
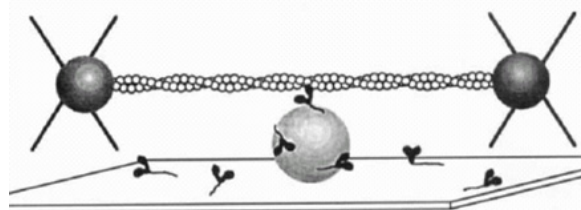
Figure 1. "Dumbbell" setup first proposed by Finer et al. (1994). Two micron sized beads hold an actin filament in place as it interacts with a single cross-bridge.
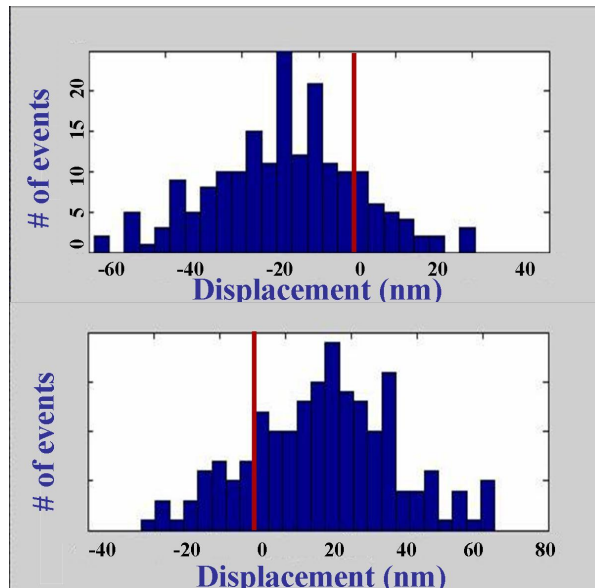
Figure 2. Displacement histogram showing the number of forward and backward steps before and after a 180° change in direction of an actin filament. Note the change in preferred step direction following actin reorientation.

DISCUSSION

Single cross-bridge interactions with actin show a preferred direction that depends on the orientation of the actin filament. Thus, we conclude that it is likely actin orientation, and not cross-bridge orientation, that determines the direction of force production in sarcomeres. However, there were a significant number of "backward" steps, indicating that cross-bridge interactions with actin are not deterministic as described in traditional cross-bridge models (Huxley, 1957; Huxley and Simmons, 1971).

Step size and force were significantly greater for "forward" compared to "backward" steps, suggesting that whatever the detailed molecular mechanisms of actin-myosin interaction, they are more effective in the more frequently occurring forward direction. Backward steps have been observed previously in laser trap setups (Kitamura et al, 2005, Guilford et al., 1997, Veigel et al., 1998), but to a smaller degree. Possibly, the relatively soft laser trap setup used here, which allows for large Brownian motion of the actin filament, might partly be responsible for the high percentage of backward stepping and it would be interesting to determine if trap stiffness, and by implication the amount of Brownian motion, affects the percentage of observed backward steps.

Dwell times were the same for the forward and backward steps, indicating that the basic ATP hydrolysis kinetics of the cross-bridge cycle was the same for both step directions.

SUMMARY

The results of this study indicate that the polarity of the actin filament determines the direction of force application and that actin-myosin interactions, at least in a three bead laser trap setup, are not deterministic as described in traditional cross-bridge models.

REFERENCES

Finer, J.T., Simmons, R.M., Spudich, J.A. (1994). *Nature.* 368:113-119

Guilford et al. (1997). *Biophysical Journal.* 72:1006-1021

Huxley, A.F., (1957). *Prog Biophys Biophys Chem.* 7: 255-318

Kitamura, K. et al. (2005). *Biophysics.* 1:1-19

Veigel et al., (1998). *Biophysical Journal.* 75:1424-1438

ACKNOWLEDGEMENTS

THE EFFECTIVENESS AND USER-ACCEPTABILITY OF A PERSONAL LIFT ASSIST DEVICE (PLAD) IN REDUCING ERECTOR SPINAE DEMAND ASSOCIATED WITH AN AUTOMOTIVE ASSEMBLY TASK

Ryan B. Graham[1], Joan M. Stevenson[1], Michael J. Agnew[2], Mohammad Abdoli-E[3]

[1]School of Kinesiology and Health Studies, Queen's University, Kingston, ON, Canada,
0rbg@qlink.queensu.ca
[2] Department of Industrial and Systems Engineering, Virginia Tech, Blacksburg, VA, USA
[3]School of Occupational and Public Health, Ryerson University, Toronto, Ontario, Canada

INTRODUCTION

Forward bending and static holding are prominent ergonomic risk factors (RFs) that often occur concurrently in automotive occupational settings (Punnett et al., 1991). As a result, many workers experience a low back disorder (LBD) at some point in their careers. Ergonomic aids such as hoists, lifts, and body slings are some of the strategies used to reduce worker's mechanical exposure to these acute and cumulative RFs (Hermans et al., 1999). The Personal Lift Assist Device (PLAD) is an on-body ergonomic aid that has been proven effective at reducing low back muscular demand and localized muscle fatigue in laboratory simulated lifting tasks (Abdoli-E et al., 2006, 2007; Lotz et al., 2007). The purpose of this study was to investigate the effectiveness and user-acceptability of the PLAD at an automotive manufacturing facility, with operators who perform an assembly process requiring forward bending and static holds.

METHODS AND PROCEDURES

The assembly task analyzed required ten volunteer workers (M=8, F=2) to spend half of their time in a static flexed forward posture and half in a standing posture. Data collection occurred on operators who were building cars on-line over two consecutive and randomized days (Condition 1= No PLAD, Condition 2= PLAD). The task duty cycle was 55 seconds in length, and this was repeated for an entire 2 hour job rotation. PLAD spring stiffness was chosen to provide the right tension for supporting 20% of each individual's upper body during the task. This was done using "sizing" equations that we developed to keep the assistance of the device relatively constant across subjects, based on body posture and anthropometry.

Surface EMG data were collected at six sites on the low back and abdomen using a Bluetooth® telemetry system. A tri-axial accelerometer was mounted on each subjects' sternum to measure trunk flexion. User-acceptability was assessed via verbal and/ or written surveys administered prior, during and after each testing period.

EMG signals were normalized to a reference contraction (trunk flexed to 45° while holding a 16kg box) and quantified based on the 10th, 50th, and 90th percentile activation amplitudes obtained from an amplitude probability distribution function analysis (APDF). Repeated-measures ANOVAs were applied to the data to determine significant differences between the two conditions.

RESULTS

Use of the PLAD significantly reduced the thoracic erector spinae (TES) and lumbar erector spinae (LES) muscle activity at the 10th, 50th, and 90th percentile levels, without any significant increases in rectus abdominus (RA) activity (Figure 1). Similarly, rating of perceived exertion (RPE) was significantly lower when wearing the PLAD (p=0.006). Finally, trunk flexion was not significantly different between days (p=.298).
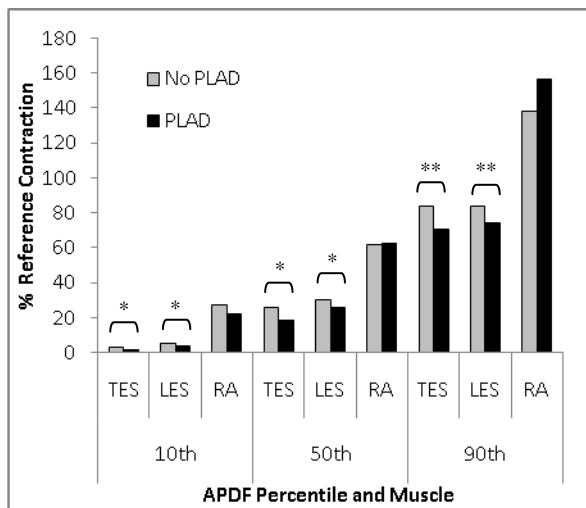
* and ** represent significant differences at p=0.05 and p=0.01

Figure1. EMG activation as a percentage of reference contraction for thoracic and lumbar erector spinae, and rectus abdominus at three APDF percentiles.

Subjective opinions were positive, with workers providing an overall score of 4.2 out of 5 (84%) on a questionnaire aimed at determining user-acceptability. All subjects reported feeling positive assistance from the device, and 8/10 (80%) said that it did not interfere with any aspect of their job and they would wear the device every day. However, areas of concern were noted by operators in terms of shoulder comfort and heat stress. With slight modifications, workers believed that PLAD could be very beneficial in reducing LBDs for similar automotive assembly tasks.

DISCUSSION

Use of the PLAD as an engineering control was effective at reducing low back muscular demand during a static forward bending task. These results were hypothesized and are similar to previous in-lab results, but were achieved in field on workers doing real tasks. One setback related to an assistive device such as the PLAD may be that workers will tend not to wear them if they are restricting, uncomfortable, unsightly, or a hazard. However, the operators in this study were pleased with, and would wear the current PLAD to prevent low back discomfort. With slight alterations, PLAD may be beneficial at reducing low back forces and discomfort in a variety of industrial tasks placing excessive biomechanical loading on the low back.

REFERENCES

Abdoli-Eramaki, M et al. (2006). *Clin Biomech*, 21: 456-465.
Abdoli-Eramaki, M et al. (2007). *J Biomech*, 40: 1694-1700.
Hermans, V et al. (1999). *Int J Ind Ergon*, 24: 657-664.
Lotz, C et al. (2007). *ISEK*, In Press.
Punnett, L et al. (1991). *Scand J Work Environ Health*, 17: 337-346.

ACKNOWLEDGEMENTS

Interjoint compensation stabilizes leg length and orientation during human locomotion

Arick Auyang[1], Jasper Yen[1,2], Young-Hui Chang[1,2]

[1]Comparative Neuromechanics Lab, GeorgiaTech, Atlanta, GA, USA

[2]Biomedical Engineering Program, Emory Univ/GeorgiaTech, Atlanta, GA, USA

Email: arick.auyang@gmail.com

http://www.ap.gatech.edu/chang/CNLmission.htm

INTRODUCTION

Evidence for the simplification of motor control of the limbs through dimensional collapse exists in areas of research such as neuroscience, robotics, and biomechanics (Bosco et al., 2000; Raibert et al, 1984; Farley and Morgenroth, 1999). Human hopping in place is the simplest form of a bouncing gait that can be modeled as a spring-mass system (McMahon and Cheng, 1990; Blickhan 1989). It also provides a well studied locomotion model by which to study how the locomotor system achieves stability of performance variables, leg length and orientation, through structuring inter-joint coordination. Leg length and orient-tation have been implicated as important performance variables in both biomechanics and neurophysiology research. This study seeks to provide the first evidence for how the redundancy of human leg joints may be simply controlled to stabilize these low degree of freedom kinematic templates that represent whole body movement during locomotion.

The Uncontrolled Manifold (UCM) analysis allows us to analyze whether segment angle variance is purposefully structured to exploit this redundancy and stabilize a kinematic performance variable (Scholz, 1999). We investigated 2.2 Hz one-legged human hopping in place within the framework of the UCM hypothesis to study stabilization of leg length and leg orientation. We hypo-thesized that leg length and orientation would each be stabilized throughout the entire hopping cycle. We further tested the effect of constraining the segment angle state space by having our subjects hop at faster frequencies, which increased the difficulty of the locomotor task. We hypo-thesized that at higher frequencies, subjects would more tightly control the structure of segment angle variance to remain within a task stabilizing subspace (i.e., the UCM).

METHODS

We collected 3-D kinematics data on 11 healthy subjects who gave informed consent before participating in this study. Subjects hopped on their dominant leg at 2.2, 2.8, and 3.2Hz. Segment angles were calculated using Matlab. We ran the UCM analysis for each performance variable (leg length and leg orientation) at 1% bins over the entire hopping cycle. We calculated an Index of Motor Abundance (IMA, Tseng et al, 2005) at each time point to test whether subjects actively utilized motor redundancy in the joints to stabilize each performance variable, indicated by an IMA greater than 0.

RESULTS

Qualitatively, segment angle trajectories showed no obvious strategy for stabilizing leg length or orientation (Fig 1). UCM analysis, however, revealed a quantitative structure to the joint variance at 2.2Hz hopping that acted to stabilize leg length throughout most of the hop cycle with a peak occurring at mid-stance (Fig. 2a). Leg orientation was stabilized primarily in the aerial phase with IMA peaking in the latter half (Fig. 2d). Average IMA for leg length stabilization significantly increased with increasing hopping frequency (Fig. 2b-c, daggers). Average IMA for leg orientation stabilization did not change with frequency (Fig. 2e & f).
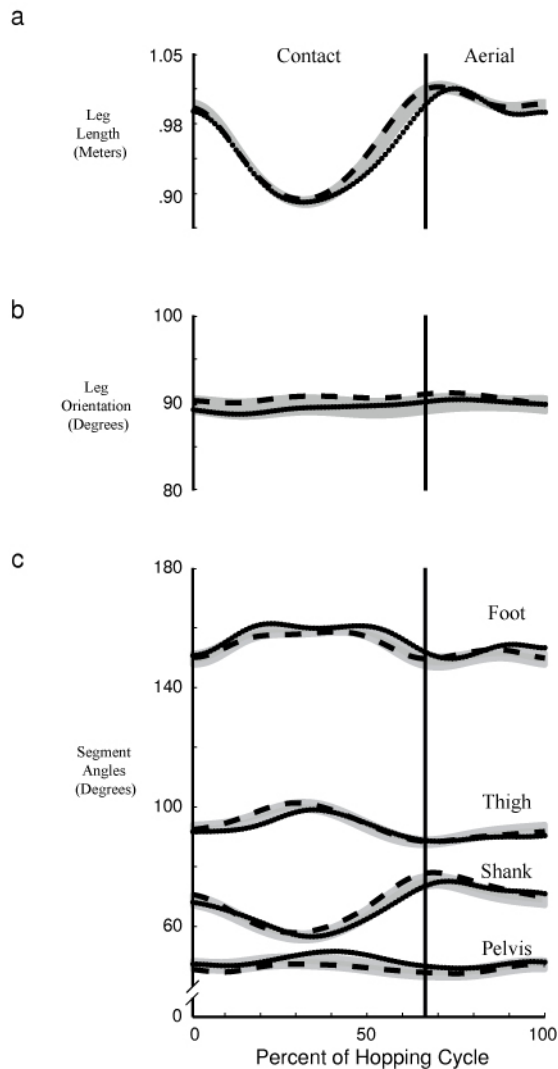
Fig 1. (a-b) Leg length and orientation trajectories and (c) segment angle trajectories. Data from representative subject. Black lines are two random cycles. Gray area is mean± 1 SD.

DISCUSSION

The period during mid-stance where we observed peak IMA for leg length stabilization is when leg length is most susceptible to control errors due to small changes in joint angles. The increased mechanical difficulty associated with hopping at higher frequencies resulted in increased average IMA stabilization of leg length. Leg orientation at foot contact is important for center of mass stability and controlling forward
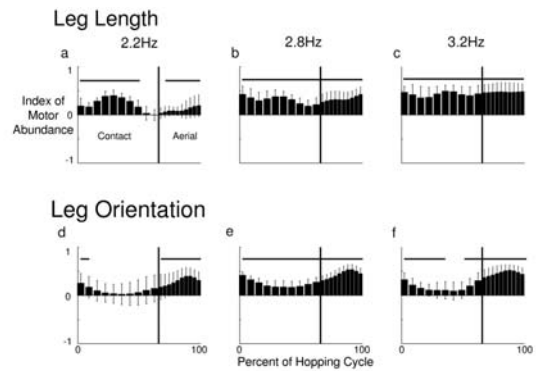
Fig. 2. (a-c) IMA for leg length and (d-f) IMA for leg orientation. Vertical bar separates contact and aerial phase. Horizontal bar denotes IMA >0 ($\alpha<0.05$).

velocity throughout stance phase (Raibert et al,1984). Stabilization of leg orientation during the aerial phase, particular the latter half, would allow for more precise foot placement at contact and forward velocity control during the stance phase. Future work will investigate leg control during forward running. Preliminary results suggest IMA for leg orientation stabilization increases with forward running speed and with targeted foot placement. In summary, we have found that humans exploit musculoskeletal redundancy in the legs to stabilize leg length and leg orientation, each at respectively critical periods of the hopping cycle.

REFERENCES

Blickhan, R. (1989). *J Biomech*. 22, 1217-27.

Bosco G, Poppele RE and Eian J (2000). *J Neurophysiol*. 83: 2931-2945.

Farley CT and Morgenroth DC (1999). *J Biomech*. 32: 267-273.

McMahon, T.A. and G.C. Cheng. (1990). *J Biomech*. 23, 65-78.

Raibert MH, Brown HB and Murthy SS (1984). *International Journal of Robotics Research* 3: 75-92.

Scholz, J.P. and G. Schoner. (1999). *Exp Brain Res*. 126, 289-306.

Tseng YW and Scholz JP. (2005). *Motor control* 9: 75-100.

THE ROLE OF KNEE EXTENSOR STRENGTH IN LANDING PHASE CHARACTERISTICS OF A BALANCE-RESTORING STEP RESPONSE

Gregory W. King[1] and Carl W. Luchies[2]

[1]Department of Civil and Mechanical Engineering, University of Missouri – Kansas City, Kansas City, MO, USA, kinggr@umkc.edu
[2]Department of Mechanical Engineering, University of Kansas, Lawrence, KS, USA

INTRODUCTION

A stepping response is often used to restore balance after a fall-provoking disturbance. Various researchers have reported age-related changes in balance recovery step characteristics, some of which may be associated with declines in lower extremity strength. Most of this work has focused on the initiation and execution phases of the step response; few studies have investigated the landing phase of the step response, which is likely associated with larger biomechanical strength requirements (Won, 2001).

The goal of this study was to investigate the role of lower extremity strength on the landing phase of a step response in an environment not influenced by other age effects. We hypothesized that young adults, after undergoing a strength-reducing lower extremity activity, would use a step response characterized by altered landing phase center of pressure (COP) and center of mass (COM) characteristics.

METHODS AND PROCEDURES

Participants. Twelve young (mean age 25 ± 3.0 years) adult males were recruited and screened for major musculoskeletal, cardiovascular, and neurological disorders. Participants provided informed consent as approved by the institution's human subjects committee.

Tasks. Each participant received balance perturbations facilitated by release from a forward leaning configuration pre and post an exercise task. The participant was instructed to recover his balance by taking a single step. The exercise consisted of strength-reducing contractions of stepping leg knee extensors: isokinetic knee extensions were performed on a dynamometer at a rate of 60 degrees per second until peak knee extension torque fell below 50% of the isokinetic maximum voluntary contraction torque. The knee extensor musculature was chosen due to its role in energy absorption during the landing phase and whose strength likely has the greatest impact on balance recovery ability (Decker et al., 2003).

Measurements. Kinetic data, consisting of foot-floor reaction forces and moments, were sampled at 1 kHz from force plates (AMTI, Watertown, MA, USA) placed under initial left and right foot stance positions and under the step foot landing position.

Data Analysis. Outcome variables included horizontal plane COP and COM speeds averaged over the landing phase. COP locations were calculated using an equilibrium analysis of forces and moments about the origin of the landing force plate. COM locations were calculated using double-integration of the shear force scaled to body mass. Average COP and COM speeds were calculated by dividing landing phase duration time into summed COP and COM sway paths, respectively.

Statistical Analysis. Statistical analysis was performed with SPSS (SPSS, Inc., Chicago, IL, USA). Exercise effects were assessed with paired t-tests (pre versus post exercise) performed on the outcome variables. Comparisons with p-values <0.05 were considered statistically significant.

RESULTS

Post-exercise trials, compared to pre-exercise, were characterized by increased COP and COM average landing phase speed (p<0.05). Results are shown graphically in Figure 1.
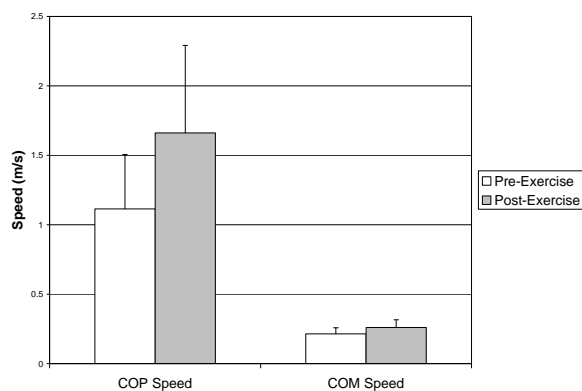
Figure 1: Average landing phase COP and COM speeds.

DISCUSSION

The observed exercise-related increases in average COP and COM speed indicate more movement of the body's center of mass, suggesting a decline in the knee joint's ability to absorb the energy associated with a forward fall. While few studies have investigated such sway characteristics during the landing phase of a step response, our results appear to be similar to those observed by Schulz (Schulz et al., 2005), who demonstrated age-related decreases in landing phase momentum attenuation. The apparent similarity between these studies may suggest that age-related declines in the ability to absorb the energy and attenuate the body's

center of mass momentum during a step response are related to declines in lower extremity strength. If such a deficit progressed to a point at which the lower extremity joints were unable to absorb fall-related energy using a single step, a multiple step response might be necessary, which may be associated with higher fall risk (Mansfield et al., 2007; McIlroy & Maki, 1996).

SUMMARY

The results of this study suggest that strength-reducing activity of young adults' knee extensor musculature is associated with reduced energy absorption performance during the landing phase of a step response used to arrest a forward fall. This may suggest that strength deficits contribute to age effects observed in the step response landing phase during balance recovery.

REFERENCES

Decker, MJ et al. (2003). *Clin Biomech (Bristol, Avon)*, 18:662-669.
Mansfield, A et al. (2007). *BMC Geriatr*, 7:12.
McIlroy, WE and Maki, BE (1996). *J Gerontol A Biol Sci Med Sci*, 51:M289-296.
Schulz, BW et al. (2005). *Gait Posture*, 22:198-209.
Won, YS (2001). Doctoral Dissertation, University of Kansas.

ACKNOWLEDGEMENTS

ELASTIC ENERGY AND OPTIMAL STRIDE FREQUENCY IN RUNNING: THE EFFECTS OF UPHILL AND DOWNHILL

Kristine L. Snyder[1, 2] and Claire T. Farley[1]

University of Colorado, Boulder, CO
[1]Department of Integrative Physiology
[2]Department of Applied Mathematics, Kristine.Snyder@colorado.edu

INTRODUCTION

Each runner strongly prefers a stride frequency that is close to the 'optimal' stride frequency that minimizes metabolic cost (Cavanagh and Williams, 1982). We investigated the role of elastic energy recovery in determining the optimal stride frequency during level and hill running.

Because we expected less useful elastic energy storage and recovery in hill running, we hypothesized that altering stride frequency would change metabolic cost less during hill than level running. Further, we hypothesized that increased metabolic cost would cause runners to prefer stride frequencies closer to optimal on an uphill vs. on the level. Finally, we hypothesized that increased impact forces would lead runners to choose stride frequencies faster than optimal on a downhill.

METHODS

We measured metabolic rate and normal and parallel ground reaction forces as ten male subjects ran at 2.8 m/s on a force treadmill on the level, at 3˚ uphill, and 3˚ downhill. Each subject performed seven 7-minute trials on each slope: a standing trial, a trial to determine preferred stride frequency (PSF), and five trials using a metronome to set stride frequency. Net cost of transport (J/kg/m) was determined for minutes 4-6 by subtracting resting metabolic rate, and dividing by speed. From thirty seconds of force data, a Matlab program calculated kinetic and potential energy of the center of mass (CoM) from the force data over the course of a step. These data were used to analyze the maximum CoM energy that can be stored elastically and then returned on each slope. An ANOVA tested for significant changes across slope and stride frequency ($p \leq .05$).

RESULTS

As expected, stride frequency and slope affected metabolic cost, but for all slopes, metabolic cost depended on stride frequency similarly ($p=0.38$). Additionally, runners tended to prefer approximately the optimal stride frequency regardless of slope. PSF mean (SEM) values were 1.44 (0.02), 1.47 (0.03), and 1.43 Hz (0.02) for the level, uphill and downhill, respectively.
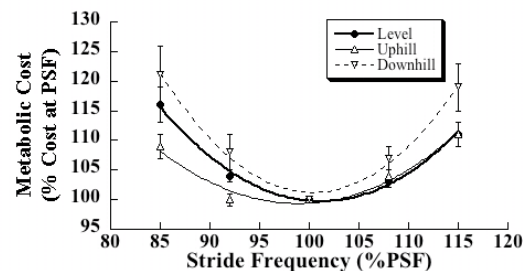
Figure 1. Normalized metabolic cost versus and normalized stride frequency for level, 3˚uphill and 3˚ downhill. Error bars = SEM.

CoM fluctuation patterns changed distinctly with slope and stride frequency (Figures 2 and 3). From these data, we can infer possibilities for elastic energy storage. Based on the energy fluctuations of the CoM, the maximum CoM energy that can be stored elastically and

then used to lift and accelerate the CoM later in stance is reduced during hill running. The CoM energy fluctuates asymmetrically during hill running (Figure 2). This asymmetry indicates that in uphill running, less energy can be stored elastically than is needed to increase the CoM energy during the second half of stance. Correspondingly, during downhill running, more CoM energy can be stored than is needed later in stance. This indicates that some dissipation of elastic energy must occur. Varied stride frequencies show symmetrical patterns with more CoM energy per stride available for elastic storage and return at slower stride frequencies than faster ones.
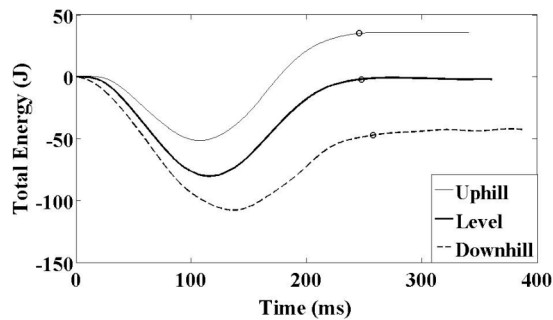
Figure 2. Fluctuations of total CoM energy over a step for a representative subject for 3° downhill, level, and 3° uphill at PSF. Circle indicates end of contact time.
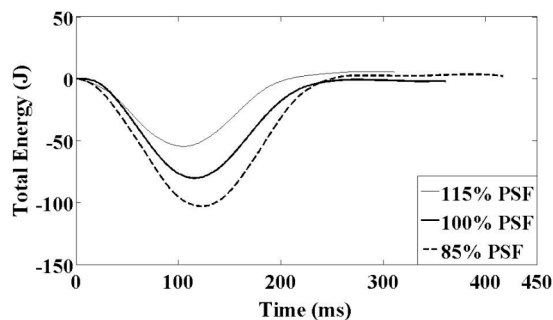
Figure 3. Fluctuations of total CoM energy over a step for the same subject for 85, 100, and 115% PSF during level running.

DISCUSSION

We reject our hypothesis that reduced elastic energy storage leads to shallower stride frequency vs. cost curves in hill running.

It is possible that elastic energy storage/return was not sufficiently impaired on the slopes used to lead to a shallower stride frequency vs. cost curve. However, calculations from the CoM data showed that the maximum possible amount of useful elastic return was reduced by an average of 19%. This suggests that other factors also influence the optimal stride frequency. Possibilities include change in internal work and the increased cost of producing force as a function of contact time (Kram and Taylor, 1990).

We reject our hypotheses that runners choose stride frequencies closer to optimal uphill and faster than optimal downhill. Runners were as likely to use the optimal stride frequency on hills as on the level. The fact that runners used the optimal stride frequency downhill indicates that minimizing metabolic cost outweighs avoidance of high impact forces.

SUMMARY

The relationship between stride frequency and metabolic cost does not change from level to hill running, suggesting that factors other than elastic energy storage are also influencing the stride frequency vs. metabolic cost curve.

REFERENCES

Cavanagh, PR and Williams, KR (1982). *Med. Sci. Sports Exerc.* 14:30-35.
Kram, R and Taylor, CR (1990). *Nature* 346:265-267.

GRASPING A HANDLE WITH CONSTANT EXTERNAL TORQUE AND VARIABLE LOAD

Jason Friedman, Mark L. Latash, and Vladimir M. Zatsiorsky

Dept. Kinesiology, Penn State University, University Park, PA. Email: jason.friedman@psu.edu

INTRODUCTION

The grip force applied by the fingers to an object has been observed to increase linearly with increases in the load force (Johansson and Westling, 1984). In five-finger grasping of an object with non-zero external torque, linear scaling of the grip force of all the fingers with the increase in the load in general will not maintain rotational equilibrium. Rather, the grip and load forces applied by the fingers must be coordinated in order to maintain this equilibrium. In a redundant system such as this, there are many possible solutions to this problem. We aim to quantify the strategies used by the central nervous system (CNS) to maintain rotational equilibrium while increasing appropriately the load force.

METHODS

A novel apparatus, shown in Figure 1, was constructed for this study. Five 6-DOF force sensors (4 ATI Nano-17, and one Nano-25 sensor for the thumb) were attached to a handle in a comfortable grasping position. A bar was attached to the bottom of the handle, allowing the application of different external torques by sliding a 0.514 kg weight, giving external torques of 0, $\pm 0.45 Nm$, $\pm 0.91 Nm$, $\pm 1.36 Nm$. The apparatus was designed such that it allowed movement in only two directions. Firstly, the entire handle could move up and down, in a nearly frictionless manner as the handle was attached to the base through a linear bearing. Additionally, the handle could rotate about an axis going through the center of the handle (see Figure 1).

The handle was attached to a motor through an extension spring. By extending the spring a known distance, a particular force could be applied to the handle. A counter-weight was connected to the handle in order that there was no net vertical force on the handle initially.

In each 10s trial, after 1s, the force increased linearly over 3s to a peak of 12N, remained there for 2s, then decreased linearly over 3s to 0N. Each external torque condition was repeated 5 times. Additionally, the subjects held the handle when it was not connected to the motor or the counter-weight for 5s, repeated 3 times for each torque condition. Each trial began only after the subject had maintained the handle orientation vertical, as determined by a bubble level. Eight healthy young male subjects participated in this study. Subjects sat comfortably in front of the apparatus, with their forearm and wrist strapped to a stand.
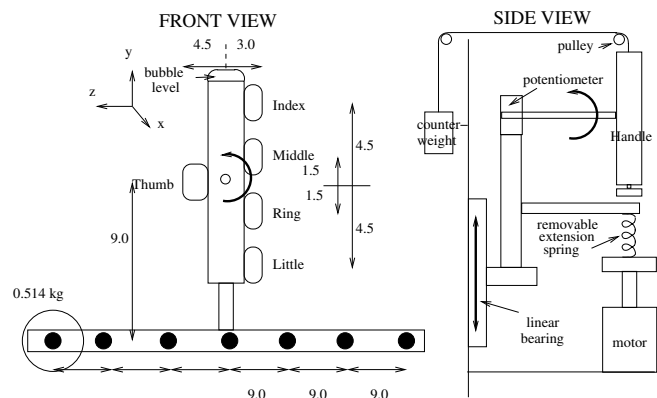
Figure 1. The experimental apparatus. The bold lines show the two directions in which movement is possible.

RESULTS AND DISCUSSION

Based on a preliminary analysis of the data, several initial observations can be made. Subjects were able to very quickly learn the task, and applied sufficient force such that the handle did not move or rotate during the force application.

The force patterns were analyzed in terms of the force produced by the thumb, and the combined forces of the other four fingers, known as the virtual finger (VF), as well as at the individual finger level. The moment of force applied by the fingers on the handle, about the axis of rotation of the handle, can be divided into two components, those due to the normal forces, M^n, and those due to the tangential forces, M^t, which can be further divided into the components due to the thumb and the virtual finger, i.e., $M^n_{th}, M^n_{VF}, M^t_{th}, M^t_{VF}$.

Despite large changes in both the normal and tangential forces, the values of M^n and M^t changed very little in all conditions with the application of the force. F^t increased to counter the load, although M^t changed very little. This was achieved by sharing the increase of the load between the thumb and the virtual finger such that

$$d^t_{VF} \Delta F^t_{th} = -d^t_{th} \Delta F^t_{VF}$$

where d^t_{VF} and d^t_{th} are the moment arms of the virtual finger and the thumb (in this case fixed by the sensor positions).

The moment of the normal forces also remained nearly constant. For M^n_{th}, as the moment arm is zero, this is trivial, however for M^n_{VF} as the normal force increased, the effective moment arm of the virtual finger must decrease appropriately. This is achieved by altering the force sharing relationship between the fingers.

This implies that for each finger in the VF, in general the relationship between F^n and F^t is different, apart from the case where there is no external torque. This can be observed for a typical subject in Figure 2.
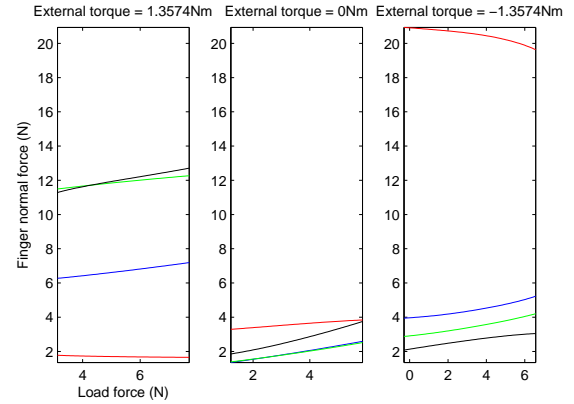
Figure 2. The normal forces of the fingers as the load force increases for three different external torque conditions.

The preliminary results suggest that the principle of superposition (Arimoto et al., 2001; Zatsiorsky et al., 2004) at the level of the thumb and virtual finger may be used by the neural controller, because the load force and the grip force can be increased independently without either of the changes altering the moment of force and hence the rotational equilibrium.

REFERENCES

Arimoto, S, et al. (2001), *Robotica*, 19, 21–28.
Johansson, R and Westling, G (1984), *Exp Brain Res*, 56, 550–564.
Zatsiorsky, V, et al. (2004), *Robotica*, 22, 231–234.

ACKNOWLEDGEMENTS

BIOMECHANICAL CHANGES DURING PROLONGED RUNNING

Lisa Stirling, Vincent Von Tscharner, Seong Hoon Kim and Benno Nigg

Human Performance Laboratory, Faculty of Kinesiology,
University of Calgary, Calgary, AB, Canada,
e-mail: lstirling@kin.ucalgary.ca, URL: http://www.kin.ucalgary.ca/hpl/

INTRODUCTION

The purpose of this study was to investigate changes that occur in gait mechanics during endurance running as a function of exercise time and perceived exertion. Previous studies have often used either short, intense bouts of running (Candau, et al., 1998, Derrick, et al., 2002) or long duration running followed by a recording session (Kyröläinen, et al., 2000, Nicol, et al., 1996) to examine the effects of exhaustion or fatigue on gait mechanics. The protocol used in our study allowed us to measure kinematic and psychological variables throughout the duration of a constant speed prolonged treadmill run.

METHODS AND PROCEDURES

Fifteen female volunteers (age 30.8 ± 7.6 years, mean $\pm$ std) were used in this study. All experimental protocols were approved by the University of Calgary Conjoint Health Research Ethics Board. Maximum aerobic treadmill speed was determined for each subject during a preliminary running session (7.2 ± 0.9 mph). Subjects were asked to return for a 1-hr treadmill running session during which kinematic data were collected. During these running sessions, the treadmill belt speed remained constant at approximately 95% (93.7 ± 2.9%) of their maximum aerobic speed. This speed was reduced for 3 subjects in which the required speed exceeded their perceived 1-hr sustainable leg speed. Subjects were not permitted to listen to music during the running sessions.

Kinematics of the right leg and arm were obtained using an 8 camera capture system (Motion Analysis Corporation. Santa Rosa, California). Kinematic data were collected for 30 second periods at 2 minute intervals throughout the 60 minute run. Ankle, knee, and trunk angles were extracted and analysed for data recorded near the beginning of the run (after 8-10minutes of running) and near the end of the run (with 4-6 minutes remaining). Stride period was determined using a heel-strike detection algorithm. Runners were also asked to rate their perceived exertion at 6 minute intervals throughout the run using the 15 point Borg scale. Runners were classified into low exertion and high exertion groups based on the maximum Borg number reported during their run (between 9-14 and 15-20 for low and high effort runners, respectively).

The kinematic and psychological data were used to: (1) track the changes in gait mechanics as a function of running time and (2) compare the gait mechanics of subjects running at low versus high perceived exertion levels.

RESULTS

Ankle and knee angles measured in all three axes of rotation showed very little variability within steps taken during each 30 sec period. Some change was observed between the patterns of single individuals obtained early and late in the run but these changes were not consistent across subjects or effort groups. The mean trunk angle of individual subjects

was found to decrease from start to finish of the run, indicating a more forward leaning posture (figure 1). Stride period (figure 2) increased for most (but not all) individuals with a trend towards larger absolute changes in subjects within the high effort group (P = 0.07).
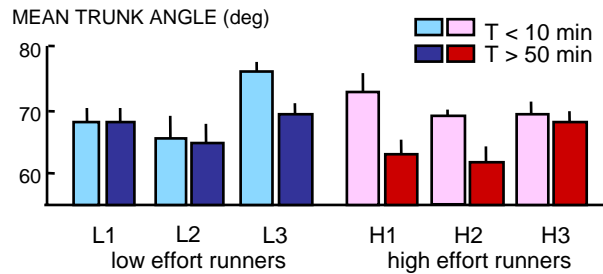
Figure 1. Mean trunk angle for 3 low effort runners (L1, L2, L3) and 3 high effort runners (H1, H2, H3) measured at T < 10 minutes T > 50 minutes.
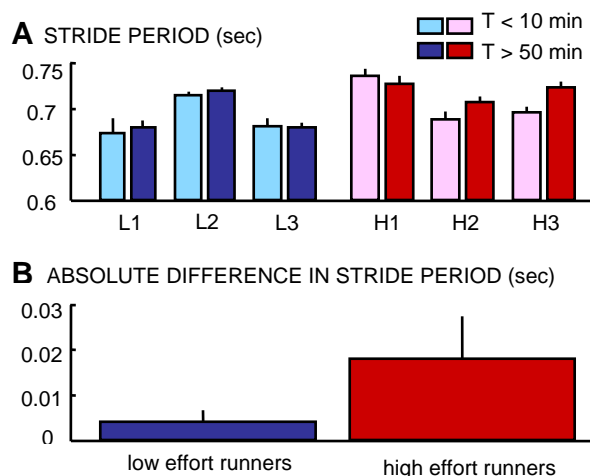
Figure 2. Stride period for 3 low effort runners and 3 high effort runners (A) measured at T < 10 minutes and T > 50 minutes and (B) the absolute change in stride period grouped perceived exertion.

DISCUSSION

The relationship between running mechanics and time and distance travelled has not been clearly established in the literature. However, it has been proposed that during running the body tries to minimize oxygen consumption by optimizing running mechanics. The forward leaning posture adopted by our subjects is a characteristic seen in runners having a lower oxygen consumption than those who maintain a more upright posture (Williams and Cavanagh, 1987). Our subjects may use this modification of their posture to compensate for increased demands for oxygen later in their run. Changes in stride period may be due to an effort to match the resonant frequency of the mass spring model of the limb (Avogadro, et al., 2003). High effort runners may experience larger differences in limb properties (such as stiffness) than low effort runners resulting in greater tuning of the optimal stride period.

.

SUMMARY

The optimization of running mechanics throughout an endurance run is a highly individual process. Changes in joint angles are not consistent across subjects, however, consistent trends in trunk angle and stride period can be explained by an effort to maximize running efficiency.

REFERENCES

Avogadro, P et al. (2003). *Eur J Appl Physiol*, 90:165-70

Candau, R et al. (1998). *Eur J Appl Physiol Occup Physiol*, 77:479-85

Derrick, TR et al. (2002). *Med Sci Sports Exerc*, 34:998-1002

Kyröläinen, H et al. (2000). *European Journal of Applied Physiology*, 82:297-304

Nicol, C et al. (1996). *Eur J Appl Physiol Occup Physiol*, 72:401-9

Williams, KR and Cavanagh, PR (1987). *J Appl Physiol*, 63:1236-1245

ACKNOWLEDGEMENTS

RADIOSTEREOMETRIC ANALYSIS (RSA) CALIBRATION ACCURACY IS UNAFFECTED BY NON-ORTHOGONAL IMAGES

Angela E. Kedgley and Thomas R. Jenkyn

Wolf Orthopaedic Quantitative Imaging Laboratory
Department of Mechanical and Materials Engineering, University of Western Ontario
London, ON, Canada
tjenkyn@eng.uwo.ca

INTRODUCTION

Traditionally, when radiostereometric analysis (RSA) is performed, the two imaging devices – whether x-ray films or fluoroscopy image intensifiers – are placed perpendicular to one another (Selvik, 1989). However, to obtain the best view of a structure of interest, sometimes the imaging devices must be positioned in a non-orthogonal orientation. Calibration frames for RSA are generally designed based on the assumption that the imaging devices will be perpendicular, and are built so that their fiducial and control planes lie at 90° angles (Valstar et al, 2005). An alternate approach is to use a uniplanar calibration cage (Valstar et al, 2005). This type of calibration is more common in instances that require the imaging devices to be oriented at a small angle relative to each other.

The aims of this study were to determine whether RSA can be performed when the imaging devices are not at 90° using (1) a calibration frame whose fiducial and control planes lie at 90° to one another and (2) a calibration frame whose fiducial and control planes lie parallel to one another but not at 90°.

METHODS AND PROCEDURES

A custom-designed calibration frame was constructed from acrylic sheet. Each fiducial and control plane was embedded with 45 beads. The fiducial points were 1mm in diameter and had a grid spacing of 20mm by 25mm and the control points were 2mm in diameter and had a grid spacing of 15mm by 20mm. Fiducial and control planes could be adjusted into one of three patterns, in which the opposing planes were always parallel to one another (Figure 1). An accuracy phantom was also constructed. This consisted of four 2mm stainless steel beads with relative locations determined by a coordinate measuring machine (Swift, Hexagon Metrology S.p.A., Italy).
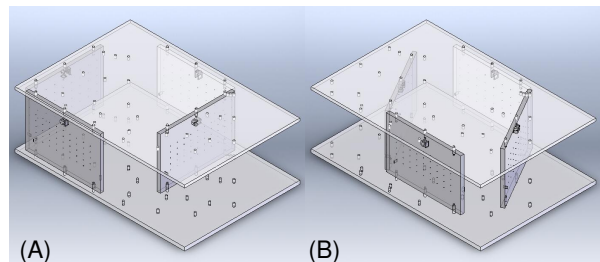
Figure 1. The calibration frame in (A) the 90° configuration and (B) one of the two parallelogram configurations (this one for 120°).

Two fluoroscopy units (SIREMOBIL Compact-L, Siemens, Malvern, PA) were positioned orthogonally with the accuracy phantom in both fields of view. Calibration was performed with the calibration frame in the 90° configuration. 40 sets of images of the phantom were obtained without moving the phantom. The fluoroscopy units were

then reoriented to a 105° angle relative to one another and the system was calibrated with the fiducial and control planes of the calibration frame parallel to the image intensifiers. 40 sets of images of the phantom were then obtained. Next, 40 additional sets of images were taken with the RSA units still at 105°, but the calibration frame set to 90°. The fluoroscopy units were once again reoriented, this time to a 120° relative angle. Again, 80 sets of images were taken, the first 40 calibrating with the custom parallelogram frame oriented to match the angles of the image intensifiers, and the second 40 calibrating with the 90° frame.

RSA reconstruction of bead locations was performed with custom-coded software (MatLab, MathWorks, Natick, MA). The average location of each bead was calculated from the 40 trials and the three-dimensional distance from the average location to each individual trial was then determined. In this case, the precision and best-case accuracy of the system are the same, since each set of 40 images were taken without any movement of the phantom in between trials (Ranstam et al, 2000). Statistical analysis was performed using a Two-way Analysis of Variance followed by post-hoc Tukey multiple comparisons ($p < 0.05$).

RESULTS

A significant difference in precision was found when the fluoroscopy units were placed at 105° relative to one another, with better results when the parallelogram frame was configured to 105° ($p = 0.012$). No differences were noted between the two configurations of the calibration frame when the fluoroscopy units were placed at a 120° relative angle. Furthermore, no differences were found when the calibration frame was set to a 90° angle and the fluoroscopy units were reoriented (Figure 2).
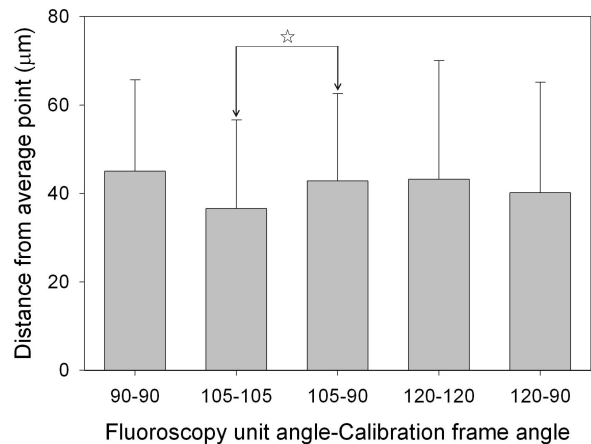
Figure 2. Average distance (mean + SD) in 3-dimensions over 40 trials from the average location of a 2mm bead determined by RSA for fluoroscopy units placed at relative angles of 90°, 105° and 120° (first value) and calibrated with a frame whose planes had relative orientations of 90°, 105° and 120° (second value; ☆ significant).

DISCUSSION

While one significant difference was noted between the parallelogram calibration frame and the 90° calibration frame, this was not consistent at both 105° and 120°. Therefore, it cannot be concluded that a superior calibration is obtained by orienting the fiducial and control planes such that they are parallel to the imaging planes. However, this study does show that as long as a sufficient number of beads in the calibration frame can be viewed in the image, RSA may be performed with the imaging devices at relative angles other than 90° while still maintaining accuracy.

REFERENCES

Ranstam, J et al. (2000). *Acta Orthop Scand*, 71:106-108.
Selvik, G (1989). *Acta Orthop Scand*, Suppl 232:1-51.
Valstar, ER et al. (2005). *Acta Orthop Scand*, 76:563-572.

INDUCED LOWER EXTREMITY VASCULAR OCCLUSION AFFECTS GAIT VARIABILITY

Sara A. Myers[1], Iraklis Pipinos[2,3], Jason M. Johanning[2,3], Nick Stergiou[1,2]

[1] University of Nebraska at Omaha
[2] University of Nebraska Medical Center
[3] Veterans Affairs Medical Center, Omaha, NE
E-mail: sfagan@mail.unomaha.edu   Web: biomech.unomaha.edu

INTRODUCTION

Peripheral arterial disease (PAD) is a manifestation of atherosclerosis that leads to a decrease of lower extremity blood flow. The most common symptom is intermittent claudication, a cramping pain occurring in the calves, thighs and/or buttocks brought on by physical activity and relieved with rest. PAD leads to reduced mobility and physical functioning and poor health outcomes (Nehler et al., 2003). Our previous studies (Myers et al., 2007) indicate that PAD patients have altered gait variability patterns prior to the onset of claudication pain. However, it is unclear if the contributing factor to gait dysfunction is a result of the underlying cellular abnormalities in the lower extremity muscle and nerves (Pipinos et al., 2006) or the restriction of the blood flow to the extremities with ambulation. Therefore our study investigated the potential effect of vascular occlusion on ambulatory function by examining gait variability. We hypothesized that there would be significant differences in gait variability before and after induced lower extremity vascular occlusion in normal subjects without underlying muscle or nerve dysfunction.

METHODS

Ten healthy young subjects walked on a treadmill while kinematics (60 Hz) were recorded using a Motion Analysis system. Walking trials of three minutes were captured during natural walking at subjects' self selected pace. Next, pneumatic blood pressure cuffs were placed on the upper thighs and inflated to 220 mmHg for three minutes to induce lower extremity vascular occlusion while subjects were standing. Following the 3 minutes of vascular occlusion, the cuffs were removed and subjects immediately walked at the same speed for another three minutes. This condition simulated the ischemic walking condition. Relative lower extremity joint angles were calculated for thirty strides from both before and after induced occlusion. The time series from the unfiltered joint angles were analyzed using the Chaos Data Analyzer (professional version; Sprott & Rowlands, 1995) to calculate the largest Lyapunov Exponent (LyE) for each subject-condition. The LyE describes variability by quantifying the exponential separation in the trajectories of the joint angles with time in state space. More divergence means more variability and higher values. The calculation of the LyE was performed according to the procedures previously described by Buzzi et al. (2003). Baseline and ischemic conditions were compared using paired t-tests.

RESULTS

The ischemic walking condition had significantly larger LyE values compared with the baseline condition at the ankle ($p = .009$) and the knee ($p = .021$). No differences between conditions were found at the hip.

DISCUSSION

Our results demonstrated that gait variability is altered following induced lower extremity ischemia through vascular occlusion. This is consistent with our previous work that found increased gait variability in patients with PAD (Myers et al., 2007), and also agrees with findings for the elderly population (Kurz and Stergiou, 2003). Increased variability in the ischemia condition may reflect a diminished capacity of the neuromuscular system to find a stable gait. Impaired lower extremity function in PAD patients is commonly attributed to intermittent claudication however, the current study showed that decreased blood flow is also contributing to altered nonlinear dynamics in these patients. Gait variability is an indicator of motor control and has been related with several physiological factors such as neural control, muscle function and posture (Stergiou et al., 2006). Increased variability in elderly individuals has been linked to increased risk of falling (Maki, 1997) and patients with PAD have impaired balance and increased risks of falls (Gardner and Montgomery, 2001). Therefore, restoring normal blood flow may reduce the risk of falling and improve mobility in patients with PAD.

Our results also imply that level of occlusion in the ischemic process is important. The differences in LyE between conditions decreased from the ankle to the hip, with the hip demonstrating no significant differences between conditions. This suggests that muscles and nerves distal to the occlusion will be more affected and thus, the joints distal to the vascular occlusion will be the ones demonstrating abnormalities.

SUMMARY

Induced lower extremity ischemia led to increased gait variability in young healthy subjects. The larger LyE values in the ischemic condition indicate that reduced blood flow, in the absence of neuromuscular

abnormalities results in increased variability in gait patterns. This study suggests reduced blood flow is a mechanism contributing to altered gait variability patterns. The current work sheds light into the mechanisms of altered gait function in patients with PAD and has direct implications for future evaluation of treatment methodologies, and the development of rehabilitation and diagnostic protocols aiming to prevent disease progression, improve physical function, and decrease fall risk in patients with PAD.

REFERENCES

Buzzi U et al. (2003). *Clin Biomech,* 18:435-443.

Gardner, A and Montgomery, P (2001). *J Gerontol,* 56A:M454-458.

Kurz, M and Stergiou, N (2003). *Neurosci Lett,* 34:155-158.

Maki B (1997). *J Am Geriatr Soc,* 45:313-320.

Myers S et al. (2007). *Proceedings of the ASB 2007.* Stanford, CA.

Nehler N et al. (2003). *Vasc Med*, 8**:**115-126.

Pipinos I et al. (2006). *Free Radic Biol Med,* 41: 262-269.

Sprott, J and Rowlands, G (1995). *Chaos Data Analyzer: Professional Version,* Human Kinetics Publishers.

Stergiou N et al. (2006). *J Neurol Phys Ther,* 30:120-129.

ACKNOWLEDGEMENTS

Table 1. Group means for the largest Lyapunov Exponent (mean ±SD) in the pre and post induced occlusion conditions. Significant differences (P < .05) are marked with an asterisk (*).

Joint	Pre	Post
Ankle*	.076 ±.02	.098 ± .01
Knee*	.063 ± .02.	.093 ± .02
Hip	.071 ± .01	.084 ± .02

REAL-TIME ESTIMATION OF MUSCLE FORCES FROM INVERSE DYNAMICS

Antonie J. van den Bogert[1], Thomas Geijtenbeek[2], Oshri Even-Zohar[2]

[1]Department of Biomedical Engineering, Cleveland Clinic Foundation, Cleveland, OH, USA
[2]Motek Medical B.V. Amsterdam, The Netherlands
bogerta@ccf.org, tgeijten@e-motek.com, oshri@e-motek.com

INTRODUCTION

Model-based estimation of muscle forces through inverse dynamic analysis is a well established research technique with potential applications in orthopaedic and neurological rehabilitation (Erdemir et al., 2007). With the advent of real-time 3D motion analysis technology and increased computer power, we can consider doing such analyses in real-time. This can provide information to the therapist which can be utilized within the same therapeutic session. Information can also be presented to the patient, in a game-like virtual reality environment for biofeedback assisted rehabilitation. Here we present a system with these capabilities, and an initial validation with EMG measurements.

METHODS AND PROCEDURES

The analysis uses a human body model (HBM), consisting of 18 body segments and 46 kinematic degrees of freedom. Subject-specific model parameters are defined during model initialization based on 3D marker coordinates. Mass properties are computed from total body mass, gender, and bone lengths (de Leva, 1996). The current version of the model contains 43 muscle elements in each leg, using data from Delp et al. (1990).

During real-time processing, the 46 generalized coordinates are solved from 3D coordinates of 47 markers. Skeleton kinematics and ground reaction forces are filtered by a real-time low pass filter which also outputs first and second derivatives (generalized velocities and accelerations). Joint moments are then solved from equations of motion. Muscle forces $\mathbf{F} = (F_1 \ldots F_{86})$ are estimated from the joint moments by minimizing a static cost function

$$\sum_{i=1}^{86} \left(\frac{F_i}{F_{\max,i}} \right)^n ,$$

with linear equality constraints to satisfy the known joint moments. The optimization problem was solved in real-time by a recurrent neural network (Xia and Feng, 2005). The real-time analysis was implemented within the CAREN system for virtual reality assisted rehabilitation (Motek Medical, Netherlands).

Test data were collected at 120 fps with a 12-camera motion capture system (Vicon Motion Systems, Oxford, UK) and two force platforms (AMTI .Watertown, MA). One male subject was instrumented bilaterally with pre-amplified EMG electrodes on Vastus Lateralis, Vastus Medials and Rectus Femoris (Twente Medical Systems, The Netherlands).

The subject performed six trials of typical postural control tasks, including single leg balancing and knee bending exercises, for a total of 150 seconds. EMG envelope was obtained by rectification followed by a 4 Hz low pass filter. Low pass filters in the inverse dynamics processing were set to 4 Hz also. Muscle forces were solved with cost function exponents (n) of 2, 3, 4, and 5. The EMG-force relationship was quantified by the maximum of the cross-correlation function. Cross correlation values for each muscle were averaged across trials and left and right limbs.

RESULTS

On a 2 GHz Pentium processor, the analysis required about 1 ms for kinematics, 1 ms for inverse dynamics, and 6 ms for muscle force estimation (with n=2), which is well within real time performance at 120 fps data rate. Figure 1 shows typical normalized muscle forces and EMG of the six muscles. Cross-correlations (Table 1) were lowest for the Rectus Femoris and tended to be increase with higher cost function exponents, but this was not statistically significant.
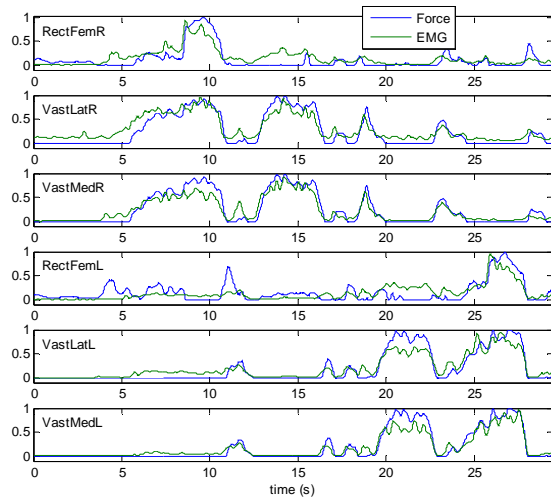
Figure 1. Normalized muscle force estimates (using n=2) and EMG signals during single leg balance (right leg, followed by left).

n	RectFem	VastLat	VastMed
2	0.611	0.829	0.907
3	0.639	0.828	0.914
4	0.662	0.824	0.915
5	0.665	0.820	0.912

Table 1. Cross-correlation between muscle force and EMG for different cost functions.

DISCUSSION

Having a full biomechanical analysis available in real time allows the design of innovative biofeedback protocols in which patients can learn to control specific kinematic variables, joint moments, or muscle

forces. Muscle forces can be presented to the patient and therapist on a real-time animation (Fig. 3). Results can be streamed to disk for conventional offline processing and reporting.

The comparisons with EMG suggest that the analysis provides information of similar quality as EMG, with the advantage of not requiring electrodes and providing information for all muscles, including those not accesible by EMG. Our results suggest that correlations may be worse for two-joint muscles or weaker muscles, Additional studies are required to examine validity for other muscle groups and other movements.

REFERENCES

de Leva P (1996*) J Biomech* **29**: 1223-1230.
Delp SL, et al. (1990) *IEEE Trans Biomed Eng* **37**: 757-767.
Erdemir A, et al. (2007) *Clin Biomech* **22**: 131-154.
Xia Y, Feng G (2005) *Neurocomputing* **64**: 359-374.

ACKNOWLEDGEMENTS
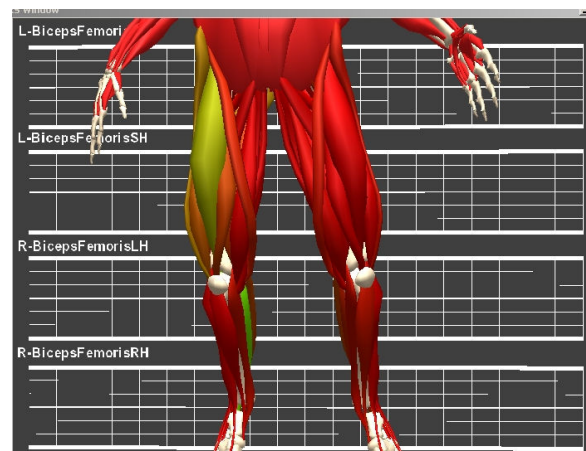
Figure 3. Real-time visualization with color animation to visualize muscle forces.

A PROPORTIONAL DERIVATIVE CONTROLLER FOR PLANAR HUMAN ARM MOVEMENT USING FUNCTIONAL ELECTRICAL STIMULATION

Kathleen Jagodnik[1,2], Robert Kirsch[1] and Antonie van den Bogert[2]

[1]Department of Biomedical Engineering, Case Western Reserve University, Cleveland, OH USA
(http://bme.case.edu/faculty_staff/kirsch/ ; rfk3@case.edu)
[2]Department of Biomedical Engineering, Lerner Research Institute, Cleveland, OH, USA
(http://www.lerner.ccf.org/bme/bogert/ ; bogerta@ccf.org)

INTRODUCTION

Functional Electrical Stimulation (FES) involves the electrical activation of peripheral nerves and muscles for the restoration of motor function. To date, FES technology has been applied to simple motions in both lower extremity (LE) and upper extremity (UE) systems. However, there remains a need for controllers capable of accomplishing more complex and goal-directed motions, such as reaching. The development of a control algorithm for UE FES systems that facilitates complex dynamic movements will expand the types of motion available to those with neurological impairments.

In this project, we applied a feedback controller to both a simulated UE FES system and to a human subject with a spinal cord injury (SCI). We selected Proportional Derivative (PD) control as our feedback controller due to its similarity to Equilibrium Point control, which has been shown to approximate human movement well (Feldman et al., 1998). The purposes of this study were (i) to design a PD controller stimulating six arm muscles to perform goal-directed reaching movements in the horizontal plane for a 2-segment arm model with realistic muscle properties, (ii) to evaluate its performance in a computational model of musculoskeletal dynamics, and (iii) to test this controller in a human subject.

METHODS AND PROCEDURES

Controller performance was evaluated using a biomechanical model for arm movement. The model had 2 segments (upper arm, forearm), 2 hinge joints (shoulder, elbow) and was driven by 6 muscles, which were modeled using a Hill-based approach.

A PD controller was applied to the arm model. This controller generates a response whose magnitude is proportional to the errors in joint angles and their time-derivatives. The controller has 24 gain parameters (6 muscles x 4 sensors). Optimal gains were found by minimizing a weighted sum of reaching error and muscle force, over a given set of 12 reaching movements.

The effect of controller architecture was tested by varying the number of free parameters (24, 16 and 2) in the PD controller.

Controller generality and robustness were tested by applying the optimized controllers to a set of 1,000 random reaching tasks; muscles were randomly weakened for the robustness test.

The 2-parameter PD controller was tested in a SCI human subject. Multiple trials of an elbow-extension task were performed with shoulder immobilized.

RESULTS & DISCUSSION

PD controller architecture was found to have a small effect on performance: it improved as the number of parameters specifying the controller increased.

The performance of the optimized 24-parameter controller on a typical simulated reaching movement is shown in Figure 1:

(a)

(b)
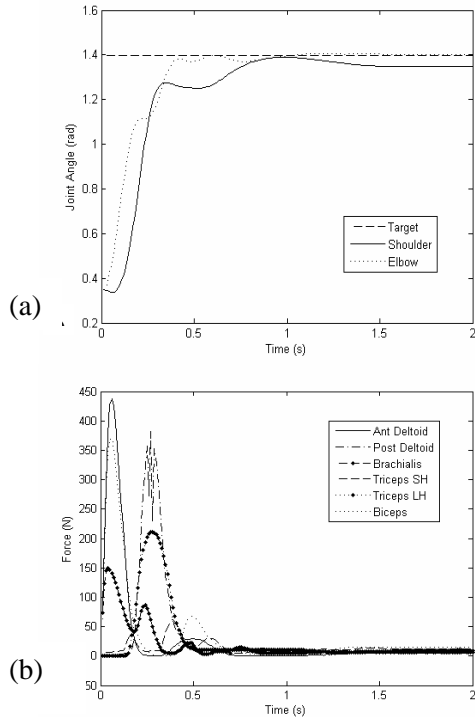
Figure 1. Optimized 24-parameter controller outputs for a (20° shoulder, 20° elbow) to (80°, 80°) reaching task. (a) Shoulder and elbow joint angles. (b) Muscle forces.

Performance on the generality test improved as the number of parameters specifying the controller increased (Table 1). All 3 controllers performed well, characterized by good accuracy and low muscular effort. In the robustness test, performance was less accurate for all 3 controllers than in the generality test, but was still acceptably good (Table 1).

Human subject trials showed generally good performance of the tuned PD controller. Performance variations from day to day, and within day, were observed and were attributed to spasticity.

SUMMARY

PD controller performance for our UE FES system was found to be good in simulation, with performance slightly improving as controller complexity increased. In our human system, PD controller performance could be good, provided that the human system was not subject to excessive anomalous behaviour.

REFERENCES

Feldman AG et al. *Motor Control*, 2(3): 189 – 205, 1998.

ACKNOWLEDGEMENTS

PD Controller (# of parameters)	Test	Avg. Error (deg)	Avg. Effort (N)	# Failed Trials
24	Generality	5.29	22.18	0
	Robustness	7.28	15.69	107
16	Generality	5.32	23.26	0
	Robustness	7.41	16.00	117
2	Generality	5.50	25.10	0
	Robustness	7.51	17.31	122

Table 1. Generality and robustness test results. Number of Failed Trials is out of 1,000, defined as failure to terminate within 5 deg of both target joint angles.

Kinematic Comparison of Circles in Cross Support and Circles in Side Support

Toshiyuki Fujihara and Pierre Gervais

Sports Biomechanics Laboratory, Faculty of Physical Education and Recreation,
University of Alberta, Edmonton, AB, Canada, toshiyuk@ualberta.ca

INTRODUCTION

"Circles" is one of the most basic skills on pommel horse. Circles can be divided into two types in terms of their supporting orientation with respect to the horse: Circles in side support—when gymnasts face perpendicular to the long axis of the horse (Side-Circles, see Fig.1) and Circles in cross support—when gymnasts face parallel to the long axis of the horse (Cross-Circles, see Fig.2). Although both types of Circles are equally essential for pommel horse performance, most attention has been devoted exclusively to Side-Circles. Clarifying the difference between these two types of Circles will be important for better comprehension of the skill. The purpose of this study is to investigate the kinematic difference between Side-Circles and Cross-Circles on pommel horse.

Figure 1. Circles in side support

Figure 2. Circles in cross support

METHODS AND PROCEDURES

Four national level male gymnasts performed three sets of ten Cross-Circles and Side-Circles on a pommel horse. The gymnasts were fitted with 37 retro reflective markers attached at anatomical landmarks to facilitate analysis using de Leva's (1996) suggested body segment parameters. Either Side-Circles or Cross-Circles were randomly assigned as

their first set of ten. Gymnasts alternated between the two types of Circles in subsequent sets. All the experimental protocols were approved by our local institutional ethics committee. Details of the experiment were explained to all the gymnasts and each gave written informed consent prior to participating in the study. Kinematic data was acquired using twelve Qualysis Proreflex motion tracking cameras operating at 120 Hz. Temporal information related to duration of the Circles was derived from the 3-D time-histories of the data collected. The velocity for the body's center of mass and for the ankle centers were found using central differences Angles between body segments were calculated based on the three-dimensional coordinate of the segments. For each set of Circles, seven were used for analysis (from the third to ninth Circle). Therefore, mean data for each variable was computed from the data of twenty one Circles (three sets of seven Circles). The data are compared between Cross-Circles and Side-Circles. The repeated measures t-test was used to compare the mean data of the four subjects' Cross-Circles to their Side-Circles. Within each subject, an independent t-test was used to compare the mean data of his twenty-one Cross-Circles to his Side-Circles. The statistical significance was set at $p < 0.05$.

RESULTS

The data for the Side-Circles in this study agreed with results from previous research (Fujihara and Fuchimoto, 2006). In the horizontal plane, the center of mass rotates elliptically, with the major axis parallel to the way in which the gymnasts faced. In general,

Cross-Circles involved similar horizontal movement of the center of mass. Regarding the vertical movement of the center of mass, however, they were different from each other. The center of mass reached the lowest position in the double-hand rear support during Side-Circles, although it dropped in the double-hand front support during Cross-Circles (Fig. 3). While average velocity of the center of mass in the front support was significantly greater than that in the rear support during Cross-Circles (0.48 ± 0.08 m/s vs. 0.38 ± 0.06 $t = 4.6, p < 0.05$), it was significantly less in the front support than in the rear support during Side-Circles (0.28 ± 0.07 m/s vs. 0.39 ± 0.03 $t = 3.9, p < 0.05$). The duration of a single Side-Circle (0.95 ± 0.02 s) was significantly longer than that of a single Cross-Circle (0.92 ± 0.03 s, $t = 3.2, p < 0.05$). Also, Cross-Circles had the shorter duration for the double-hand rear support phase than Side-Circles (0.15 ± 0.02 s, 0.18 ± 0.03 s, $t = 4.2, p < 0.05$). When gymnasts performed Cross-Circles, they placed their hands closer to each other (0.32 m in the front support, 0.34 m in the rear support) than when they did Side-Circles (0.52 ± 0.00 m in the front support, 0.53 ± 0.01 m in the rear support). All gymnasts tended to bend their hip (omphalion - center of hips - center of knees) more in the double-hand rear support of Cross-Circles (150 ± 8°) than in Side-Circles (159 ± 6°, $t = 4.4, p < 0.05$). Their lower trunk (xiphion - omphalion - center of hips) had greater angles in the same phase as well (166 ± 5°, 170 ± 4° $t = 4.4, p < 0.05$).

DISCUSSION

To avoid collision with a pommel horse during Cross-Circles, gymnasts must raise their body high in the rear support (Fig. 3). High rear support position with narrow hands-distance requires excellent shoulder flexibility.
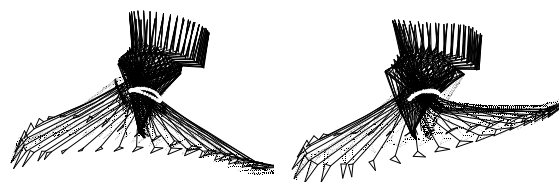
Figure 3. Layered stick figures of a gymnast performing Side-Circles (left) and Cross-Circles (right) viewed from right hand side. White circles indicate the center of mass.

In fact, the results of this study showed that a gymnast tended to bend their body more in the rear support during Cross-Circles than during Side-Circles, in which there was no obstacle in the rear support position. This difficulty in maintaining shoulder hyper-extension along with hip extension in the rear support may also result in the shorter rear support durations. The fact that the center of mass moved faster in the lower side—the front support during Cross-Circles and the rear support during Side-Circles—implied that gymnasts took advantage of gravity to accelerate their Circles. According to Fujihara and Fuchimoto (2006), the vertical movement of the center of mass corresponded to the vertical component of the reaction force. Therefore, it was suggested that gymnasts exert their force on a pommel horse differently according to the orientation of the pommel horse on which they are so that they can avoid collision with the pommel horse and utilize gravity to preserve the rotation of the center of mass.

REFERENCES

de Leva, P. (1996). *J. Biomech,* 29(9), 1223-1230

Fujihara, T., & Fuchimoto, T. (2006). *Jap. J of Biomech. in Sports & Exercise*, 10(1), 27-41. (in Japanese)

TIMING AND VELOCITY OF SHOULDER AND HIP HORIZONTAL ROTATION IN NOVICE AND SKILLED GOLFERS

Isao Okuda [1], Junji Shinohara [2], and Charles Armstrong [2]

[1] College of Art and Science, Department of Exercise and Sport Performance, University of New England, Biddeford, ME, USA Iokuda@une.edu
[2] Applied Biomechanics Laboratory, University of Toledo, Toledo, OH, USA

INTRODUCTION

Previous golf studies have identified several key factors that distinguish between expert and novice golfers when executing a full swing shot. One particularly important factor is that involving differences in the position of various body segments during the swing. Although the number of studies that have examined is limited, and there remains some conflicts of opinion, it appears that these two groups consistently differ in the patterns of rotation of the hip and shoulder that are seen during the swing (Burden AM et al., 1998). However, these differences have only been examined at selected events in the swing, including the top of the back swing and ball impact. While this is significant, the degree to which these groups differ throughout the entire swing has not been examined. Therefore, the purpose of this study was to examine the motion patterns of the hip and shoulder across the entire downswing motion with the intent of distinguishing between skilled golfers and novice golfers.

METHODS AND PROCEDURES

Thirteen skilled golfers (SG – handicap less than five) and seventeen novice golfers (NG – handicap from 20 to 36), ranging in age from 19 to 35 years volunteered to participate in this study. Eight high-speed video cameras, operating at 240 Hz, and the associated hardware (Motion Analysis Corporation, Santa Rosa, CA) were used for data collection. EVa (Version 6.1.5) and Kintrak (version 6.2.2) software were used for calibration, data collection, tracking, data processing, and data analysis (Motion Analysis Corporation, Santa Rosa, CA). Thirty-two reflective markers were placed over specific anatomical landmarks, as well as on the golf club (a driver), to create the model used in examining segmental motions. Specifically, to define the shoulder, the markers were placed bilaterally on the acromion processes at the C7 level. At the hip, the markers were placed bilaterally on the ASIS. All data collection was done in a single laboratory testing session using an indoor driving range. The data from five swings for each participant were averaged to obtain single values for each of the dependent variables. These variables included maximum velocity of horizontal rotation in the shoulder and hip segments, timing of the appearance of these maximums, and the maximum club head velocity. Since the duration of the downswing time was different for each participant, the timing of the maximum velocity was expressed as a percentage of the downswing time in each participant. Independent t-tests (significance level of .05) were used for each dependent variable to identify those variables for which a significant

difference existed between the two groups.

RESULTS

Figure 1 illustrates that the SG demonstrated a slightly greater maximum velocity in both of the segments, although the differences were not significant for either the shoulder ($p < .307$) or the hip ($p < .345$). Table 1 illustrates that, relative to the time of ball impact for both segments, the point in the swing when the SG reached peak velocity was significantly earlier than that of the NG. Additionally, for both groups, the hip velocities peaked earlier than those of the shoulder. The maximum club head velocity of the SG (43.7 m/s) was significantly greater ($p < .01$) than that of the NG (33.6 m/s), and in both cases was achieved slightly before ball impact.
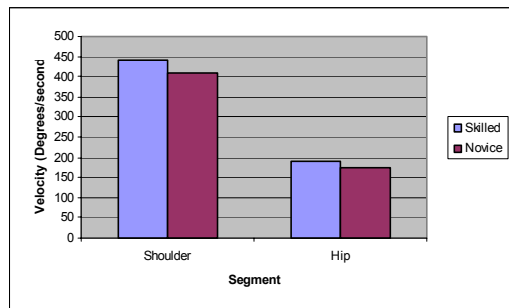
Figure 1: Maximum velocity of the shoulder and hip segments.

	Novice	Skilled	P value
Shoulder	85.2 ± 6.6	72.9 ± 7.6	.001
Hip	77.5 ± 7.9	69.1 ± 8.1	.01

Table1: Timing of the maximum hip and shoulder velocity, expressed as a percentage of the downswing motion.

DISCUSSION

The current study determined that the timing of the maximum hip and shoulder velocities achieved in the downswing is of greater importance in differentiating the skill levels than the maximum absolute velocities of these segments. This suggests that proper timing contributes to maximizing club head velocity. The result of the current study confirms a previous study reporting a positive correlation between club head velocity and golf skill level (Fradkin AJ et al. 2004). Putnam (Putnam, CA, 1991) theorized a need to decelerate a proximal segment to accelerate a distal segment. To maximize this segmental interaction, timing of the deceleration is critical, especially in a multiply linked system. The results of our study are consistent with this, in that the trunk rotation velocities peaked earlier in the downswing than that of the shoulder. Thus the associated hip (proximal segment) deceleration contributed to optimizing shoulder (distal segment) acceleration.

SUMMARY

The current study demonstrated that the timing of the maximum velocity of horizontal rotation in the shoulder and hip segments occurs significantly earlier in the downswing motion for skilled golfers than for novice golfers. However, the maximum velocity of the two segments was not significantly different between the two groups.

REFERENCES

Burden AM et al. (1998). *J Sport Science*, 16:165-176

Fradkin AJ et al. (2004). *J Sci Med Sport*, 7(4): 465-472

Putnam CA (1991). *Med Sci Sports Exerc*, 23:130-141

THE FORCE-LENGTH RELATIONSHIP OF THE CAT SOLEUS MUSCLE

Marco Aurélio Vaz[1], Cíntia de la Rocha Freitas[2], Tim Leonard[3], Walter Herzog[3]

[1]School of Physical Education, Federal University of Rio Grande do Sul, Porto Alegre, RS, Brazil, marcovaz@esef.ufrgs.br
[2]Faculty of Physical Education, Lutheran University of Brazil, Canoas, RS, Brazil,
[3]Faculty of Kinesiology, University of Calgary, Calgary, AB, Canada, walter@kin.ucalgary.ca

INTRODUCTION

Rack and Westbury (1969) measured the force-length properties for the cat soleus and found the plateau region of this relationship at sarcomere lengths of approximately 3.0μm, while the optimal length would be expected to occur between 2.3-2.5μm. However, they did not account for possible sarcomere shortening associated with force production and the corresponding stretching of series elastic components. This neglecting of series elasticity might be justified in cat soleus, as it is a virtually parallel fibred muscle with a rigid tendon (Barratta and Solomonow, 1990). The purpose of this study was to repeat Rack and Westbury's (1969) study, while measuring fibre and average sarcomere lengths. We hypothesized that the plateau of the force-length relationship occurs at sarcomere lengths between 2.3-2.5μm, rather than 3.0μm, and that fibre length changes would be smaller than the corresponding muscle length changes.

METHODS AND PROCEDURES

Testing was performed on six soleus muscles of adult male cats. After anaesthesia and intubation, a nerve cuff stimulation electrode was fixed on the tibial nerve (Herzog & Leonard, 1997). Supramaximal electrical stimulation was applied with monopolar rectangular pulses (0.1 ms duration) at frequencies of 1, 2, 10, 30 and 100 Hz. The soleus muscle, its tendon and the calcaneus were carefully dissected and isolated from surrounding tissues. The tendon was cut with a remnant part of bone and fixed to a muscle puller. Force and excursion were measured continuously. Sonomicrometry crystals were implanted at the ends of a proximal and a distal fascicle and sutured fixed underneath the fascia. Optimal soleus length was defined as the length of maximal active isometric force at 100Hz stimulation and was designated as 0mm length. Isometric forces were measured for lengths ranging from approximately -20 to +20mm relative to the optimal length for all stimulation frequencies. Following testing soleus muscles were fixed in a 10% formalin solution and five fascicles were extracted from the medial, central and lateral part of the muscle. Fascicle lengths were measured using video analysis. Mean sarcomere lengths were obtained from six measurements along each fascicle by laser diffraction (Butterfield & Herzog, 2006). Sarcomere number was determined by dividing the fascicle length by the average sarcomere length. In situ sarcomere lengths were calculated from the fascicle lengths measured during the experiments and the known serial number of sarcomeres. For each stimulation frequency, the active peak force was obtained by subtracting the passive from the total force. In situ fascicle lengths were obtained from the sonomicrometry system and were synchronized with the corresponding force values.

RESULTS AND DISCUSSION

The sarcomere force-length relationship showed an ascending and descending part with a plateau between 2.0-2.3µm (Figure 1). Therefore, peak forces were obtained at smaller average sarcomere lengths than reported by Rack and Westbury (1969), and closer to the optimal sarcomere length based on sliding filament considerations. There was a decrease in the optimal sarcomere length with increasing stimulation frequencies. Optimal length was about 2.2 µm for 1-2 Hz and 2.1 µm for 30-100 Hz, respectively (Figure 2).
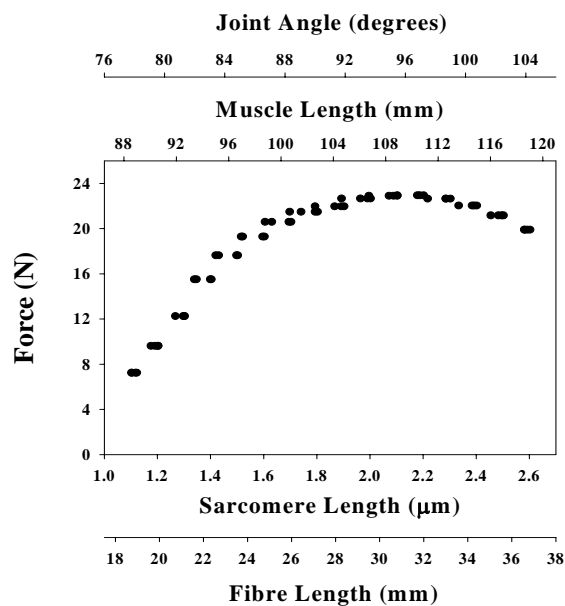
Figure 1. Force (100 Hz) as a function of sarcomere length, fiber length, muscle length and joint angle.

Fibre lengths increased with increasing muscle lengths and decreased with increasing forces at a given muscle length. For muscle length changes of 40mm, fibre lengths changed by 14mm or about 35% of the muscle length changes in the passive muscle and by about 24mm or 60% in the active muscle. Therefore, fibre length changes were

substantially smaller than muscle length changes despite the small angle of pennation (6.4°; Spector et al., 1980) and virtually rigid tendon (Baratta and Solomonow, 1990) associated with the cat soleus. These substantial differences in fibre and muscle length changes are partly responsible for what we think was a vast overestimation of the optimal sarcomere length in the Rack and Westbury (1969) study. We conclude that optimal cat soleus length is associated with near optimal sarcomere lengths.
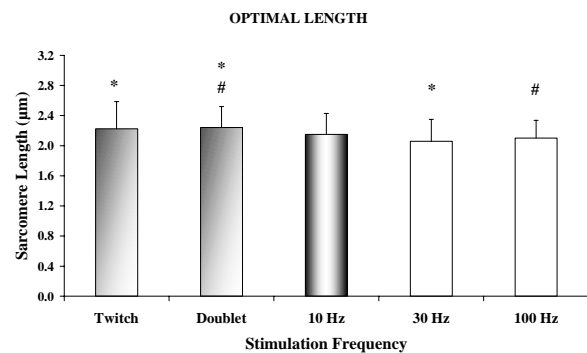
Figure 2. Optimal length as a function of stimulation frequency. Symbols indicate $p < 0.05$ after a Friedman's repeated measures analysis on ranks.

REFERENCES

Baratta, RV and Solomonow, M (1990). *IEEE Trans Biomed Eng*, 37(3):243-251.
Butterfield, T and Herzog, W (2006). *Pflugers Arch- Eur J Physiol*, 451:688-700.
Herzog, W and Leonard, TR (1997). *J Biomech*, 30 (9): 865-872.
Rack, MH and Westbury, DR (1969). *J Physiol*, 204:443-460.
Spector, SA et al. (1980). *J Neurophysiol*, 44(5):951-960.

DIETARY EFFECTS ON BONE
MECHANICAL PROPERTIES AND MOLECULAR MARKERS

Caeley R. Lorincz[1], Raylene A. Reimer[1] and Ronald F. Zernicke[2, 3]

[1]Faculty of Kinesiology, Human Performance Laboratory, Roger Jackson Centre for Health and Wellness Research, University of Calgary, 2500 University Drive NW, Calgary, Alberta, Canada, crlorinc@ucalgary.ca, reimer@ucalgary.ca
[2]Faculties of Kinesiology, Medicine and Engineering, McCaig Centre for Joint Injury and Arthritis Research, University of Calgary, 3300 Hospital Drive NW, Calgary, Alberta, Canada
[3]Director, Musculoskeletal Injury Prevention and Rehabilitation Center, Dept of Orthopaedic Surgery, University of Michigan, Ann Arbor, Michigan, USA, zernicke@umich.edu

INTRODUCTION

The changeover of disease etiology in the past century has brought to the forefront the need to examine environmental factors that have influenced the epidemic of chronic disease affecting our society. For bone, fracture associated with osteoporosis can lead to severe morbidity and/or mortality and is increasing faster than demographic changes in the population (Salem et al., 1992). Concurrently, an increase in the consumption of saturated fats and refined carbohydrates has been documented (Wohl et al., 1998). Emerging data suggest diets high in saturated fat and sucrose (HFS) have a negative effect on skeletal structural integrity and should be investigated to substantiate this risk factor to bone health (Zernicke et al., 1995). The purpose of this study was to investigate the effects of consuming a HFS diet on mechanical, molecular, and blood markers of bone turnover.

METHODS AND PROCEDURES

Female C57BL/6 mice (aged 9 wk) were randomly assigned to one of two custom prepared dietary cohorts: high-fat-sucrose (HFS, n=36) or adjusted starch (n=36) diet. Mice were fed their respective diets for 10 weeks. Prior to sacrifice, blood was extracted by way of cardiac puncture and used to test serum levels of vitamin D, intact parathyroid hormone (iPTH), osteocalcin (biomarker of bone formation, OC), and tartrate resistant acid phosphatase (biomarker of bone resorption, TRAP). Upon sacrifice, tibiae were dissected and randomly assigned to group A or group B. Group A tibiae underwent mechanical testing and morphological analysis, while group B tibiae were used to measure the expression of two genes, osteoprotegerin (OPG) and receptor activator for nuclear factor κ B ligand (RANKL).

RESULTS

For blood markers of bone homeostasis, no significant differences were observed between dietary cohorts for vitamin D, PTH, or OC. In contrast, TRAP levels were significantly increased (30%) in the HFS cohort when compared to the starch cohort ($p < 0.05$). HFS mice were significantly heavier than the starch mice ($p < 0.05$). After normalizing for body mass, the mice fed a HFS diet had 23% reduced load at max, 25% smaller cross-sectional area, and 28% thinner cortex when compared to their starch-fed counterparts ($p < 0.05$). Real-time PCR analysis found that both OPG and RANKL were slightly depressed in the HFS cohort relative to their starch counterparts.

DISCUSSION

Mice fed an HFS diet had significantly compromised skeletal integrity. Cross-sectional area, cortical thickness, and maximal load were significantly decreased in HFS mice relative to starch fed controls. Structural—but not material—properties of the skeleton were affected, consistent with previous reports (Li et al., 1990, Salem et al., 1992, Zernicke et al., 1995). Elevated serum TRAP data suggested a negative balance in bone remodeling independent of calcium metabolism, which is consistent with the structurally compromised skeletal tissue observed within the mice fed a high-fat-sucrose diet. Both OPG and RANKL were slightly down-regulated in the HFS cohort relative to their starch counterparts. However, since they were down-regulated to the same extent, the OPG/RANKL ratio remained constant, suggesting that an alternate gene pathway was responsible for the observed outcome measures.

SUMMARY

Diets high in saturated fat and sucrose (HFS) appear to be detrimental to skeletal structural integrity, likely by way of increasing osteoclastic and bone resorbing activities. These results offer insights into the potent effect of diet on bone integrity and suggest potential non-pharmacological (dietary) methods to improve or sustain bone health across the life span.

REFERENCES

Li KC et al. (1990). *Calcif Tissue Int,* 47: 308-313.
Salem GJ et al. (1992). *Am J of Physiol,* 262: R318-R321.
Wohl GR et al. (1998). *Calcif Tissue Int,* 63: 74-79.
Zernicke RF et al. (1995). *Bone*, 16: 25-31.

ACKNOWLEDGEMENTS

NEUROMECHANICS OF MUSCLE SYNERGIES DURING CYCLING

James Wakeling[1] and Tamara Horn[2]

[1]School of Kinesiology, Simon Fraser University, Burnaby, BC, Canada, wakeling@sfu.ca

[2]ETH Zurich, Switzerland

INTRODUCTION

Movements and locomotion require the co-ordinated contraction of many different muscles within the body, and this poses a complex challenge to the motor control system. One solution is to contract different muscles in a few set patterns, called synergies. Typically, many complex movements can be co-ordinated using relatively few synergies. Muscle synergies have been demonstrated for a range on movements such as walking, jumping, cycling and corrections to postural perturbations, and the same sets of synergies can even be used for different types of movement (Ivanenko et al. 2004; Raasch and Zajac, 1999; Ting et al. 1999).

One remarkable property of our locomotor systems is the ability to generate co-ordinated movements across a wide range of speeds and loads. We know that the relative levels of individual muscle contractions can vary with changing speed and load (Wakeling et al. 2006), but it has not been established whether these can be incorporated by the same muscle synergies. The purpose of this study was to identify whether the muscle synergies adapt to the load and velocity of a movement task by altering the relative contributions of the synergistic muscles.

METHODS AND PROCEDURES

The electrical activity (EMG) was measured for three synergistic groups of muscle in the leg for 9 trained cyclists: ankle extensors (soleus, SOL, medial gastrocnemius, MG and lateral gastrocnemius, LG), knee extensors (vastus medialis, VM, rectus femoris, RF and vastus lateralis, VL), and knee flexors (biceps femoris, BF and semitendinosus, ST). Subjects cycled on a stationary dynamometer for 9 conditions at a range of cadences (60 to 140 revolutions per minute), torques (6 to 41 N m) and power outputs (35 to 260 W) with the different conditions presented in a randomised-block format. The EMG intensity was determined for 20 intervals in each pedal cycle using wavelet analysis (von Tscharner, 2000). The effects of the mechanical conditions on the patterns of EMG intensity across the different muscles were classified using principal component analysis and statistically quantified using multivariate ANOVA.

RESULTS

Within the triceps surae both the MG and LG were used much more for increasing cadence tasks than the SOL. The maximum intensity of the MG had a 45.4 % greater dynamic range than for the LG (Fig. 1). Within the quadriceps there was a slightly (3.4 %) higher dynamic range for the maximum intensity of the VM than for the VL. The timing of the EMG for the RF became progressively delayed for higher crank torque tasks. Within the hamstrings the BF was used more (41.8 % greater dynamic range) for increasing cadence tasks than the ST. The timing of the EMG in both the BF and ST was delayed for higher crank torques.
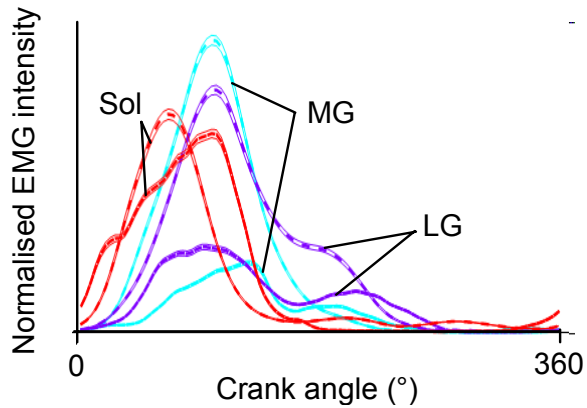
Figure 1. EMG intensity for the triceps surae muscles during cycling. Lines show mean ± s.e.m. for 756 pedal cycles from the 9 subjects: MG blue, LG purple and SOL red. Wide dashes show trials at a cadence of 140 r.p.m. and a crank torque of 9.5 N m. Solid lines show trials at a cadence of 60 r.p.m. and a crank torque of 41.4 N m.

DISCUSSION

Within each synergistic muscle group there were agonist muscles that responded differently to altered mechanical demands, even when they shared similar anatomical origins and insertions. The fundamental synergistic patterns of activation therefore adapted to the altered mechanical demands on the leg. These variations in recruitment may reflect differences in composition or architecture of the different muscles within each group.

REFERENCES

Ivanenko YP et al. (2004). *J. Physiol.* 556, 267-282.

Raasch CC and Zajac FE (1999). *J. Neurophysiol.* 82, 515-525.

Ting LH et al. (1999). *J. Neurophysiol.* 81, 544-551.

Wakeling, JM et al. (2006). *J. Roy. Soc. Interface* 3, 471-587.

von Tscharner, V. 2000 *J Electromyogr Kinesiol* 10, 433-445.

SIMPLE MODELS OF DROP JUMPS: EVALUATING A MODEL AGAINST THE SUBJECT SPECIFIC GROUP OF MODELS FROM WHICH IT WAS DEVELOPED

Matthew T.G. Pain and Steph Forrester

School of Sport and Exercise Sciences, Loughborough University, Loughborough, UK
Email: M.T.G.Pain@lboro.ac.uk, URL: www.lboro.ac.uk

INTRODUCTION

Simulation modelling is an important research tool in the study of human movement and evaluation of a model is a key step in its development. In multi-muscle models direct evaluation of the muscle model cannot be carried out as the *in vivo* comparison measures cannot be made. Evaluation is commonly effected by taking the model performance and showing that it lies within a range of subject performances and then inferring that the muscle performance is correct. In this process the model is usually constructed from generic parameters and thus the model does not represent any of the subjects it is compared against and may not even represent an average of the subjects.

An alternative is to use subject specific models where model parameters are equal to the same parameters measured on the subject, and compare the model to the single subject performance. In this case the complexity of the model is limited as muscle performance can only be expressed at the joint level and the evaluation is still not perfect as the subject is not measured under all possible conditions.

Simple models have regularly been used to assess general principles. Replacing the subject group with a group of subject specific simple models allows the average simple model to be constructed from precisely know parameters and the model performance can then be compared back to the model 'subjects' performances.

The aims of this study are: 1) to use 7 subject specific, simple Alexander (1990) type jumping models to produce a population of 'subject' performances for a drop jump; 2) to produce an average model from this 'subject' group and compare the performance of the average model with respect to the group mean and standard deviation (sd).

METHODS AND PROCEDURES

The 2-segment simulation model of Alexander (1990) was used to produce 7 models with subject specific knee extensor muscle function and anthropometry. Isovelocity data were collected for each model from 7 male subjects who had given consent (age 27.5 ± 5.0 yrs, mass 81 ± 11 kg, height 1.77 ± 0.05 m) and a seven parameter torque – angular velocity strength curve was fitted to them, as described by Yeadon *et al.* (2006). An average model was created from the mean anthropometrics and an average strength curve fitted to the normalised isovelocity data of the 7 models. Two average models using anthropometrics from, and strength curve fits to, the data of Alexander (1990) and Challis (1998) were also created.

Each subject specific model and average model was applied to a two-legged drop jump from a height of 0.6 m, in which the activation dynamics of the knee extensor were optimised to maximise the reactivity coefficient (R = jump height / ground contact time). The activation was a simple sigmoid function. Penalties were incurred if the knee

flexed below 60°, or if activation was <25% or > 75% at touchdown. The mean and standard deviation of the results of the subject specific performances were calculated. Strength curves and anthropometrics from all models were transposed to look at variations in performance that could arise.

RESULTS

The subject specific model, the average model and literature model results are presented in Table 1. The most notable result is that the performance of the average model is more than 1 sd larger than the mean performance of the subject specific models. However, it has produced a jump similar to Subject 7. Overall the performance of the average model lies between the literature models but, unsurprisingly given the female population in Challis (1998), tends towards the Alexander model. By applying the average model strength curve to individual subjects or the average anthropometry to individual subjects and re-optimising, different subjects gave: a maximum R = 2.65, ground contact = 105 ms and jump height = 29.1 cm, all outside the range of values for individual subjects.

DISCUSSION

Given that the average model results are more than 1 sd from the mean performance of the 'subjects' it would be normal to consider this a poor model. However, this is hard to justify as the structural components are identical for the 'subjects' and the average model, all 'subject' parameters are explicitly known and the same data processing was carried out.

Given the non-linearity of the strength curves and the non-linear interactions of even this simple system it is not surprising that the average model did not perform like the mean of the 'subjects'. It is somewhat surprising that it performed outside the 'subject' range though. One reason for the improved performance is that the strength curve fitting looks to determine the maximal voluntary performance. As such the average model may be biased to have a shallower hyperbolic concentric phase when the 'subject' data are grouped, even though the same algorithms are used for all strength curve fits.

A good example of the non-linear response to parameter changes was found when parameters were transposed. With high eccentric torques R was rapidly maximised by reducing tgc even at the expense of jump height. The variability in results seen when 'subject' parameters were switched and different average parameters used indicate quite high sensitivity.

SUMMARY

An average model developed from 7 subject specific models failed to reproduce performance characteristics within 1 sd of the mean of the subject specific models.

REFERENCES
Alexander, RMN (1990). *Philos Trans R Soc B,* 329: 3-10.
Challis, JH (1998). *Hum Mov Sci,* 17: 307-325.
Yeadon et al. (2006). *J Biomech,* 39: 476–482.

		S1	S2	S3	S4	S5	S6	S7	Mean (sd)	Average	Challis	Alexander
JH	(cm)	23.4	23.1	26.5	22.1	21.7	25.7	28.4	24.4 (2.5)	27.1	17.9	29.4
R	(m/s)	1.80	1.60	1.69	1.32	1.56	1.92	2.22	1.73 (0.29)	2.19	2.34	2.33
tgc	(ms)	130	144	157	168	139	133	128	143 (14.9)	124	76	126

Table 1. Jump Height (JH), Reactivity Coefficient (R) and time of ground contact (tgc) for the subject specific models, along with the mean results, and the group average models.

HOW DOES ISOLATED GASTRONEMIUS CONTRACTURE AFFECT PLANTAR PRESSURE IN NEUORLOGICALLY HEALTHY SUBJECTS?

Nicole Chimera[1] Michael Castro[2], and Kurt Manal[1]

[1]University of Delaware, Department of Mechanical Engineering, Center for Biomedical Engineering Research, Newark, DE, USA,
[2]Pennsylvania Orthopaedic Foot & Ankle Surgeons, Philadelphia PA.

E-mail: chimera@udel.edu, Web: www.cber.udel.edu

INTRODUCTION

Isolated gastrocnemius contracture (IGC), a type of equinus, is characterized by limited ankle dorsiflexion with full knee extension. Patients with IGC are at a mechanical disadvantage during walking because they can not attain sufficient gastrocnemius length for knee extension and ankle dorsiflexion to occur at the same time. It is commonly accepted that the ankle must reach at least 10° of dorsiflexion during the stance phase of gait just prior to heel lift when the knee is at or near full extension to achieve normal walking (Root, 1977).

A proposed compensatory strategy for people with IGC is early heel rise during stance (Hill 1995). While this strategy may reduce strain in the gastrocnemius muscle, it may also increase plantar pressure (Figure 1); this has been noted in diabetic patients with ankle equinus deformity (Lavery, Armstrong et al. 2002). Early heel rise distributes the ground contact force over a smaller area and for a larger proportion of stance. Early heel rise

Increased Peak Fore-Foot Pressure

Early Heel Rise

Figure 1. Demonstration of early heel rise resulting in increased peak fore-foot pressure.

and thus increased fore-foot plantar pressure may provide insight into the link between IGC and associated foot injuries. Retrospectively, 65% of healthy patients with foot pathologies had IGC (DiGiovanni et al., 2002). We hypothesized that neurologically healthy patients with foot pathologies associated with IGC would demonstrate early heel rise and increased peak fore-foot plantar pressure during stance.

METHODS AND PROCEDURES

Plantar pressures were measured on 5 IGC subjects and 5 healthy control subjects using an ultra-thin, high-resolution pressure mat (HR Mat, Tekscan, South Boston, MA). Plantar pressures were recorded during the stance phase of gait. Subjects performed three walking trials at a self-selected speed. A trial was not accepted if the subject altered their stride or visually targeted the pressure mat. Plantar pressure data was sampled at 50 Hz and passed through a PC Interface Board (Super-Receiver) to a desktop computer. Data was made available for storage and analysis through the HR Mat System Software. Peak fore-foot plantar pressure and heel rise were directly measured using the system software. For each subject individual trials were averaged. Independent t-tests were used to compare peak pressures and heel rise between patients with foot pathologies associated with IGC and healthy control subjects.

Heel Rise During The Stance Phase of Gait
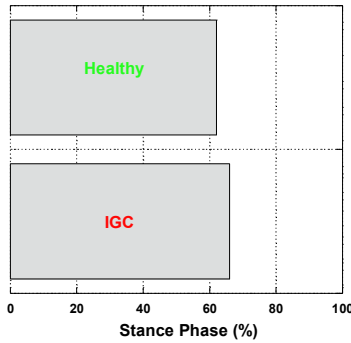
Figure 2. Time to heel rise recorded during the stance phase of normal gait from patients with IGC and healthy control subject without history of foot

RESULTS

Our preliminary results suggest that there is no difference in time of heel rise between IGC and healthy control subjects (Figure 2). Additionally patients with IGC do not have increased peak fore-foot plantar pressures compared to healthy control subjects (Figure 3).

DISCUSSION

Neurologically healthy patients with foot pathologies associated with IGC do not exhibit early heel rise or increased peak fore-foot plantar pressures. While this seems to contradict previous reports that diabetic patients with ankle equinus were nearly three times more likely to have increased plantar pressure compared to those without equinus (Lavery et al., 2002), our subjects were sensate and thus could feel pain. Perhaps early heel rise increases foot pain, and therefore patients with IGC may not exhibit this compensatory strategy. Because the gastrocnemius muscle functions at both the ankle and the knee, patients with foot pathologies associated with IGC may attempt to reduce gastrocnemius strain by increasing knee flexion.

SUMMARY

Patients with IGC do not have early heel rise or increased peak pressure during stance. We propose that these patients' exhibit alternate compensatory strategies, which may be reflected knee joint kinematics. Further assessment is necessary to explore relevant changes that may occur in this population.
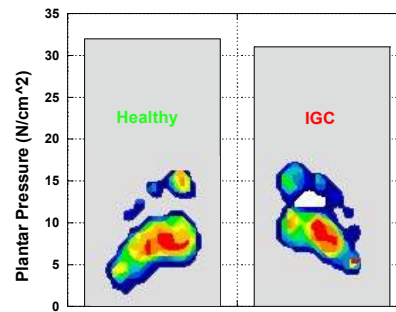
Figure 3. Peak fore-foot plantar pressures recorded during normal gait from patients with IGC and healthy control subjects without history of foot pathology.

REFERENCES

DiGiovanni CW et al. (2002*). J Bone Joint Surg Am,* 84-A(6): 962-970.
Hill RS (1995). *J Am Podiatr Med Assoc,* 85(6): 295-300.
Lavery LA et al. (2002). *J Am Podiatr Med Assoc,* 92(9): 479-482.
Root ML et al. (1977). *Normal and abnormal function of the foot: Clinical Biomechanics*. Los Angeles, Clinical Biomechanics Corp.

ACKNOWLEDGEMENTS

DYNAMIC PRESSURE MAPPING OF THE HEAD-HELMET INTERFACE

Ryan Ouckama and David J Pearsall

Department of Kinesiology and Physical Education
McGill University, Montréal, Québec, Canada
URL: http://icehockeyscience.mcgill.ca

INTRODUCTION

Despite the widespread use of helmets in construction, automotive and sporting industries, an alarmingly high rate of minor traumatic brain injuries (mTBI), or cerebral concussions exist (e.g. 503/10000 individuals, Bazarian *et al.* 2005). mTBI can result from a direct blow to the head causing a series of contact and inertial stresses to propagate throughout the cranium (Biasca *et al.* 2005). In principle, protective helmets are designed to attenuate these stresses below magnitudes leading to neuronal disruption.

Helmet testing standards (CSA, ASTM, ANSI, NOCSAE, DOT, SNELL) typically measure peak linear acceleration at the center of mass (CoM) of a surrogate head form during a guided monorail drop (Bishop, 2000). Arguably, evaluating helmet effectiveness based solely on this single acceleration measure is too general and not the appropriate metric to explain all head injury mechanisms. For example, finite element modeling studies have demonstrated substantial non-uniform stress distributions in cranial and cerebral tissues during simulated impacts. Standard physical tests using acceleration based safety criterions (e.g. GADD, HIC) are not sensitive to focal impact stresses. This situation was demonstrated by Bishop (2000), wherein maximal surface cranial pressures were directly recorded during impacts to the side of a helmet. Local pressures (3.1MPa) capable of causing skull fracture were observed while acceleration measures were within the acceptable safety criterions. Thus, in addition to acceleration measures, it is necessary that pressure be mapped discretely.

Recent advances in technology enable assessment of local pressures at the helmet-head interface at high magnitudes and sample rates through the use of an array of capacitive pressure sensors. The primary purpose of this research will be to evaluate these pressure sensors in conjunction with acceleration measures at multiple impact velocities.

METHODS AND PROCEDURES

A 4.8 kg magnesium ISO head form was fitted with a 5.5 gram triaxial accelerometer (Dytran 3053B1, Chatsworth, CA) mounted at the CoM. A single 25x25mm capacitive pressure sensor (ConTacts C500, PPS) was adhered to the crown of the head form and encased in a plastic sheath to reduce possible shear force damage. Using a guided rail system, the head form was repeatedly dropped onto a 16mm thick vinyl nitrile foam pad at impact speeds of 1 m/s, 2 m/s and 3m/s. Drop velocity was measured just prior to impact using a fixed light trap and 50 mm tab mounted to the drop rig. Impact data were collected using a USB acquisition board (NI USB-6210) sampling 5 channels at 10000 Hz. Acceleration signals were low-pass filtered at 1680Hz using a 4th order Butterworth digital filter. Pressure signals were low-pass filtered at 2000 Hz as this was the published response bandwidth of the sensor.

RESULTS

A statistical summary for each drop condition is presented in Table 1. Average acceleration and pressure profiles were plotted against time for three different drop speeds and are presented below (Figure 1).

Table 1. Velocity, acceleration and pressure values for three drop speeds. Data are mean(s.d.). n=9 for each measure.

	Target Velocity		
	1 m/s	2 m/s	3m/s
Impact Velocity (m/s)	1.00 (0.00)	1.97 (0.03)	3.06 (0.01)
Z-Acceleration Maximum (G)	18.69 (0.18)	42.15 (1.17)	97.63 (1.32)
Max Pressure (KPa)	239.06 (9.37)	434.87 (19.35)	1060.11 (29.28)
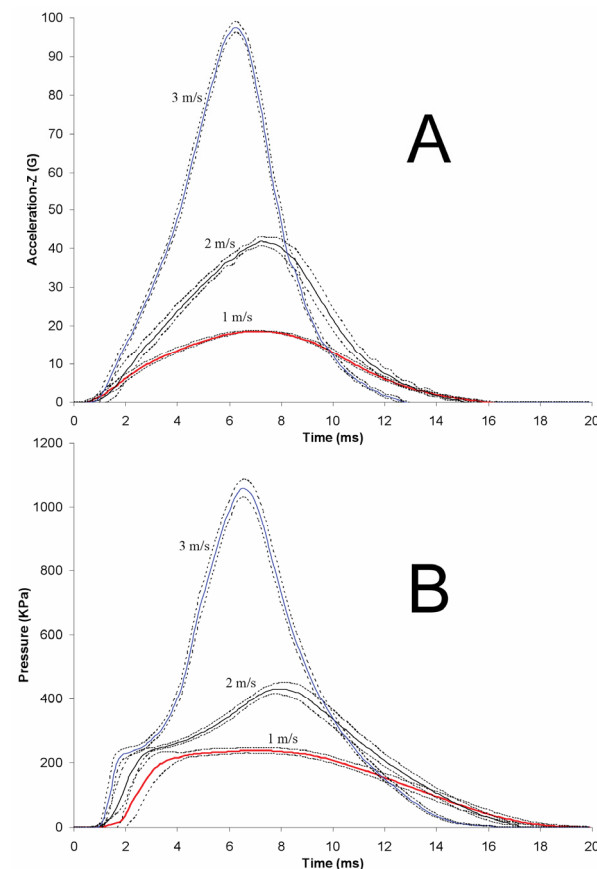
Figure 1. Average acceleration (A) and pressure (B) profiles of impacts at drop velocities of 1, 2, and 3 m/s. Dashed lines represent mean ± 1 standard deviation.

DISCUSSION

The capacitive sensors were effective in measuring dynamic pressure profiles. The low deviations of the averaged signals (Fig.1B) demonstrated measurement repeatability. Average maximal pressures of 1.06 MPa were recorded from the relatively flat area of the crown. Although this was below the approximate 3 MPa threshold for bone fracture, higher focal pressures can be expected at areas on the head form with more complex skeletal geometry, in particular structures with relatively smaller radii of curvature. Nonetheless, given the relatively modest impact velocities, surface pressures were in the order of magnitude close to the bone fracture threshold. Acceleration and pressure measures corresponded closely under the current test configuration but they may also be expected to diverge as the complexity of focal geometry increases.

SUMMARY

Repeatable measurement of cranial surface pressure during impact was possible at high temporal resolution. Construction of a multiple sensor matrix is feasible to map pressure distribution and would be a relevant tool to address helmet design, material and construction parameters.

REFERENCES

Bazarian, J.J. *et al.* 2005. *Brain Injury*, 19:85-91.
Biasca, N. *et al.* 2005. *European Journal of Trauma*, 2:105-116.
Bishop, P.J. 2000. *Safety in Ice Hockey: 3* ASTM STP 1341: 113.

ACKNOWLEDGEMENTS

DES MOINES UNIVERSITY FOOT MODEL: RELIABILITY AND CASE REPORT

Vassilios Vardaxis[1,2,3], Greg Iwaasa[2], Phillip Hasler[2], James Mahoney[2]

[1]Doctor of Physical Therapy Program, [2]College of Podiatric Medicine and Surgery
[3]Human Performance Laboratory, Des Moines University, Des Moines, IA, USA
E-mail: vassilios.vardaxis@dmu.edu

INTRODUCTION

Currently, foot and ankle surgeons assess deformity, plan surgical procedures and determine outcomes solely on radiographic images and clinical evaluations. While these procedures have been proven useful over the years they provide limited data in terms of functional/quantitative characteristics of the foot during dynamic tasks such as gait. Considering that pes cavus, planus, and hallux valgus and limitus are some of the more prevalent pathologies, considerable interest has been developed in a multi-segment foot model.[1-5] The objective of this study was to develop and test the reliability of a lower leg/foot model for mid/fore-foot functional assessment during clinical gait analysis. The efficacy of the model in foot deformity and surgery outcome evaluation was assessed .

METHODS AND PROCEDURES

A six segment model of the leg below the knee (tibia, hindfoot, midfoot, lateral forefoot, medial forefoot, and hallux) was developed in MATLAB and was used to assess foot function in bilateral stance and gait. 26 skin mounted markers were placed on each lower leg, of 5 healthy volunteers (10 feet) and a single hallux valgus patient (pre-operative on the right and 6 months post bunionectomy on the left). The 3D positions of the markers were captured by an 8-camera system motion capture system (EVaRT, Motion Analysis Ltd.) @ 120 Hz on 2 separate days, 2 sessions per day. A total of 10 trials (5R & 5L) were recorded at each session: 3 out of 5 trials per foot were analyzed for a total of 120 trials. The reliability between trials, sessions, days, and examiners in terms of consistency (RMSE, Root Mean Square Error) and waveform reproducibility error (VR, Variability Ratio) of the medial longitudinal (MLA) and the 1st metatarsophalangeal (MTP) projection angles on the foot midsagittal plane was assessed.

RESULTS / DISCUSSION

Both of the clinical measures assessed here were consistent and reproducible across 10 feet (Figure 1). The average error for both

Table 1: The means and standard deviations of the RMSE (°) and the VR (%) for Medial Longitudinal Angle (MLA), and 1st MetaTarso-Phalangeal joint angle (1st MTP)

	Between Trials (B_Tr)	Between Sessions B_S	Between Days B_D	Between Examiners B_E
RMSE values				
MLA	1.34	1.36	1.09	1.47
	(± 0.23)	*(± 0.78)*	*(± 0.32)*	*(± 0.23)*
1st MTP	1.45	1.46	1.12	1.62
	(± 0.31)	*(± 0.70)*	*(± 0.25)*	*(± 0.36)*
VR values				
MLA	15.0 %	16.4 %	10.6 %	21.9 %
	(± 6.2)	*(± 9.8)*	*(± 4.4)*	*(± 12.1)*
1st MTP	5.7 %	7.2 %	2.2 %	4.1 %
	(± 2.3)	*(± 8.9)*	*(± 1.1)*	*(± 2.0)*

clinical measures was small ranging between 1.09° to 1.47° for the MLA and between 1.12° and 1.62° for the 1st MTP (Table 1). Considering the 23.4° average deformation angle range of the MLA (for all 10 feet) the MLA RMSE value of 1.47° reflects 6.3% error. The waveform reproducibility of the MLA ranged between 10.6% and 21.9%. The percent error for the 1st MTP joint angle was 3.5% based on the average dorsiflexion angle range of 48.4°. The 1st MTP waveform reproducibility was excellent ranging between 2.2% and 7.2%. The worst reproducibility values were found between examiners for the MLA which is potentially due to small variation in marker placement.[4]
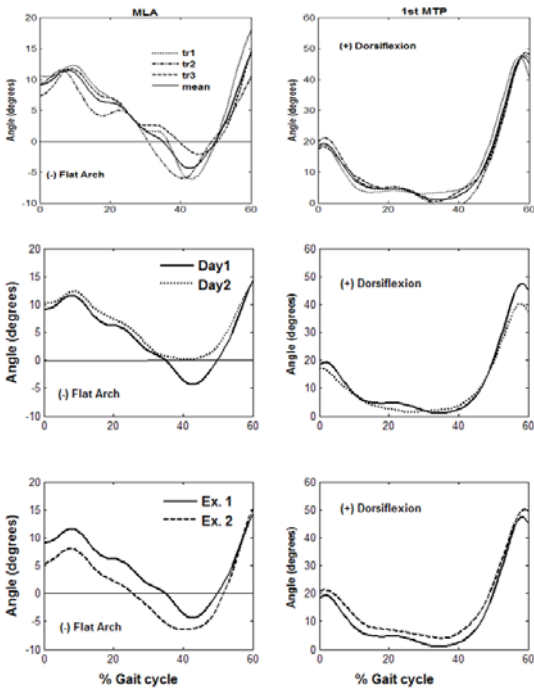
Figure 1. MLA change and 1st MTP angle during stance in gait. **Top** – Single session 3 trials and the mean. **Middle** – Between days comparison (3 trial) average waveforms. **Bottom** – Between examiners comparison.

CASE STUDY

The pre surgical data for the MLA indicate limited mobility for the 0-50% of the gait cycle in the pes planus direction. The MLA remains in a relative pes cavus position during the entire stance phase of the gait cycle. The

post surgical MLA data indicate marked changes and while there is some residual rigidity (observed clinically); the MLA waveform presents remarkable similarity to control. The 1st MTP function during gait shows marked improvements as well especially over the initial 40% gait cycle. The surgery has restored much of the dorsiflexion range of motion at the 1st MTP and it improved its overall mobility for the entire stance phase of the gait cycle.
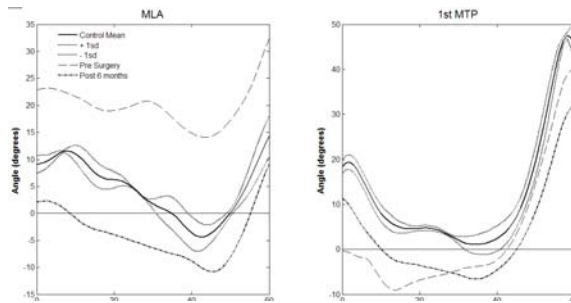
Figure 2. Time normalized waveforms of the MLA change and the 1st MTP angle. Normative data and hallux abducto-valgus (pre surgery – dash), and post-surgical bunion (post 6 months – dash/dot).

SUMMARY

The results support the use of the Des Moines University Foot Model to assess foot function during gait. The medial longitudinal angle change (reflecting deformation of the arch) and the 1st metatarsal joint angle (reflecting dorsiflexion of the 1st MTP joint) are both robust and consistent. The shape of the entire waveform of these parameters is highly reproducible and maybe useful for diagnostic purposes of foot function during gait. The model shows potential in planning and assessment of surgery outcome as shown by the single hallux abducto-valgus case.

REFERENCES

1. Carson et al (2001) *J Biomech*, 34:1299-7
2. Leardini et al (2007) *G&P*, 25:453-62
3. MacWilliams et al (2003) *G&P*, 17:214–4
4. Simon et al. (2006) *G&P*, 23:411-24
5. Stebbins et al. (2006) *G&P*, 23:401-14

ACHILLES TENDON MOMENT ARMS VIA A HYBRID METHOD USING MOTION ANALYSIS AND ULTRASOUND: *IN VIVO* ESTIMATIONS IN MALE SUBJECTS

Justin D. Cowder, Thomas S. Buchanan, Kurt T. Manal

University of Delaware, Department of Mechanical Engineering, Center for Biomedical Engineering Research, Newark, DE, USA
E-mail: manal@udel.edu, Web: www.cber.udel.edu

INTRODUCTION

Developing accurate estimates of muscle-tendon parameters are important for use in biomechanical studies. The muscle moment arm (MA) is one such parameter; transforming the linear force developed by a muscle into a moment about a joint. The plantar flexion (PF) moment during stance is generated primarily by the gastroc-soleus acting through the Achilles tendon MA. Recently, we developed a novel hybrid method for computing Achilles tendon MA using ultrasound (US) and motion analysis (Cowder *et al*., 2007). The method has been validated using an animal model and found to have good accuracy (3.3% error). In this paper, we use this new technique to determine the average Achilles tendon MAs of 10 subjects.

PROCEDURE AND METHODS

The hybrid method was used to determine the Achilles tendon MAs of ten healthy male subjects with average age: 24.1±2.3 years, height: 1.77±0.05m, and mass: 76.07±9.07 kg. All subjects submitted written informed consent prior to testing and the testing protocol was approved by the Human Subjects Review Board at the University of Delaware. Subjects were positioned in an isokinetic dynamometer (Biodex System 3, Shirley, NY) (Figure 1). The Biodex was used to monitor ankle joint angle and to provide resistance for isometric PF maximum voluntary contraction (MVC).

Figure 1. Subject placement in Biodex with markers and gel standoff pad attached. Ankle is in neutral angle with knee at 90º.

Reflective markers were placed on the subject's lateral and medial malleoli to define the ankle joint axis. The ankle joint center was assumed to lie at the midpoint between the markers. In addition, markers were placed on the US probe to establish a correspondence between the ankle joint center and the US image. A seven camera motion capture system (Qualisys ProReflex, Gothenburg, Sweden) was used to capture marker locations during testing. B-mode US images at 10 MHz of the Achilles tendon were recorded using a 60mm linear probe and gel pad (Aloka SSD-5000, Tokyo, Japan) (Figure 2).
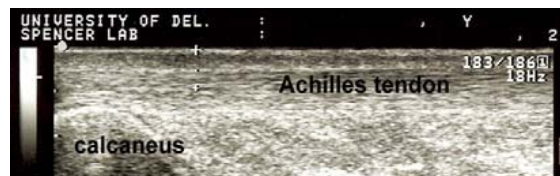
Figure 2. Sonogram with Achilles tendon.

A gel pad was used for acoustic coupling. US recording was synchronized with motion data using a contact switch

attached to the freeze image button on the US console. Two trials at rest and two trials at MVC were collected at each of 5 ankle angles ranging from 20º dorsiflexion (DF) to 20º PF in increments of 10º.

RESULTS

Hybrid method estimates for Achilles tendon MAs with SD error bars are shown in Figure 3. MAs at rest increased in length from 34.5±1.9 mm at 20º DF to a peak 36.9±1.9 mm at 10º PF. During MVC, MAs increased from 35.5±1.8 mm at 20º DF to 38.1±2.6 mm at 20º PF. Small increases in MA length between rest and MVC were observed with an average increase of 3.4±0.9%.
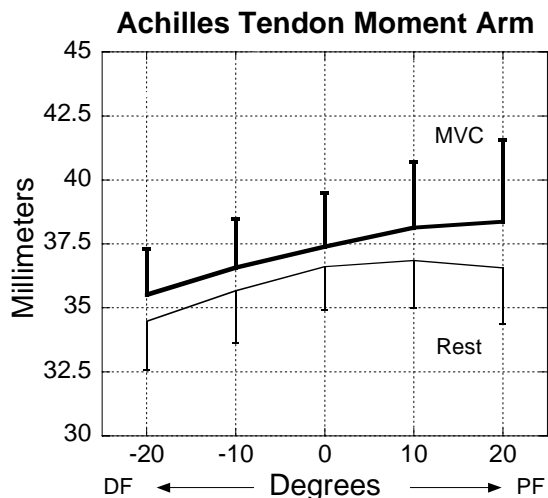
Figure 3. Achilles tendon MAs at rest (thin curves) and at MVC (bold curves).

DISCUSSION

We observed an increase in the MA as the ankle angle progressed from DF into PF. We also noted that MAs were slightly greater (3.4%±0.9%) during MVC than at rest. These observations are similar to findings reported by Maganaris *et al.* (2000). They too observed a similar trend of increasing MA from DF to PF and also increased MAs during MVC compared to

rest. In contrast, the magnitude of the MAs between studies were significantly different. The hybrid MAs were 15% to 35% smaller than those reported by Maganaris. Subjects in both studies were similar in size and therefore not likely the reason for such large differences. MAs computed by Maganaris were based on the concept of virtual work (An *et al.*, 1984) and requires a change in joint angular position to approximate the MA. They used a change of 15º (i.e., ± 7.5º) when computing the MA for a specific angle and therefore each MA may be thought of as an average value over the range. This may be a potential source of error contributing to differences between studies. Our hybrid method uses measurements made directly at the angle of interest and thus requires fewer potentially error prone measurements.

SUMMARY

MAs computed using the hybrid method showed the same trend as values reported in the literature, although, the magnitudes were less. Based on the results of our validation experiments we are confident the MAs for subjects in our study are physiologically representative of their true Achilles tendon MA.

REFERENCES

An, K.N. *et al.* (1984). *J Biomech Eng*, 3: 280-282.
Cowder, J.D. *et al.* (2007). In Proceedings of 2007 ASB Annual Conf. Stanford University, Palo Alto, CA.
Maganaris, C.N. *et al.* (2000). *Eur J Appl Physiol*, 83: 363-369.

ACKNOWLEDGEMENTS

COMPRESSION APPAREL EFFECTS ON SOFT TISSUE VIBRATIONS

Aurel Coza and Benno M. Nigg

Human Performance Laboratory, Faculty of Kinesiology, University of Calgary, Calgary, AB, Canada, acoza@kin.ucalgary.ca

INTRODUCTION

Compression apparel has been reported to have positive effects on performance (Kraemer et al., 1998). Mechanisms to explain the improved performance included change in kinematics, change in blood flow and the damping of soft tissue vibrations. Soft tissue vibrations are important for the energetics of running (Nigg and Wakeling, 2001) since muscle activity is required to damp these vibrations (Boyer and Nigg, 2006). Consequently, damping the soft tissue vibrations through apparel should decrease the muscle activity and, therefore, decrease the needed energy. However, the effect of compression apparel on vibration damping and muscle activity has never been quantified.

The goal of this study was to quantify the effects of compression apparel on (a) the damping of soft tissue vibration and (b) muscle activity during treadmill running.

METHODS

Four young, active subjects (2 females, 2 males) participated in this study. All subjects were free of any injuries at the time of the experiments. Subjects were wearing the test or the control apparel.

Three 3-D accelerometers were taped to the skin overlying the soft-tissue compartments of the triceps surae, quadriceps, and hamstrings soft tissue compartments . EMG signals were recorded for the vastus medialis, gastrocnemius lateralis and biceps femoris muscles with a sampling frequency of 2400 Hz.

The damping coefficient was computed for each step by fitting the acceleration data in the interval 0 to 200ms after heel strike to an exponential decay function.

Muscle activity was computed as the Root Mean Square (RMS) of the EMG activity in the interval 100ms before heel contact to heel contact (*pre-activation*) and heel contact to 100ms after heel contact (*post-activation).*

Two apparel conditions were tested: compression and control apparel.

The average damping coefficient was computed for the time interval 0 to 200 ms after heel strike for all steps in each trial. The pre/post-EMG-activity was computed as the RMS-EMG mean of all the steps in each trial.

Each subject was asked to run on a treadmill at five different speeds wearing 3 different shoes. Acceleration and EMG data were recorded and used to determine the speed/shoe combination that produced the highest vibration of the soft tissue

compartments, which may be related to resonance.

Each subject performed two series of 4 running trials at the speed with the highest acceleration and EMG (resonance) at two different days, wearing the test and the control apparel in different order. Acceleration and EMG data were collected for 1 minute for each trial. In total each subject had to perform 8 trials (4 test, 4 control), corresponding to approximately 90 steps for each trial.

The relative change between test and control condition was calculated as the mean relative change over all three soft tissues for each muscle. This averaging was done since the relative changes for the three soft tissue compartments were similar.

A series of t-tests were used to examine whether the change in damping coefficient and the change in muscle activity due to the compression apparel was significantly different from the control condition.

RESULTS AND DISCUSSION

The compression apparel condition showed an 8% (±2.1%) average increase (p=.05) in the damping coefficient when compared to the control apparel.

There was an 8.2% (±1.8%) average decrease (p=.05) in the muscle pre-activation and a 6.5% (±1.6%) decrease in post-activation values for the compression apparel condition compared to the control apparel (Fig.1)

CONCLUSION

The results showed that the compression apparel increased the damping and decreased the muscle activity. Since the addition of the compression apparel was the only change implemented it is concluded that the compression apparel was responsible for the observed changes in damping and muscle activity.
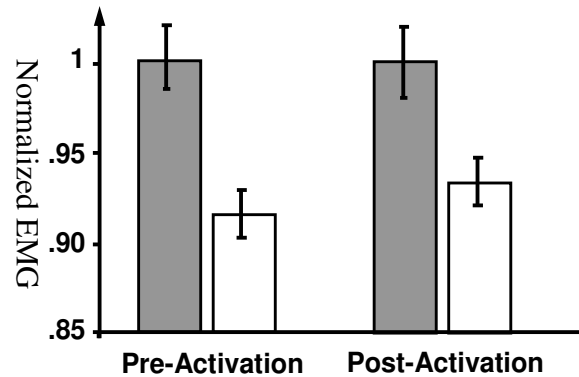
Figure 1. Normalized pre- and post-EMG-activation (mean and standard deviation) for the compression (white bars) and control apparel (grey bars).

Compression apparel has a positive effect on soft tissue vibration damping and muscle activity in running. It is speculated that these changes may have an effect on performance. However, this speculation requires further investigation.

REFERENCES

Boyer, KA and Nigg, BM (2006). *J. Biomech Eng, 128(6): 815-822.*
Kraemer, WJ et al. (1998). *J. Strength and Cond. Res., 10: 180-183.*
Nigg, BM and Wakeling, JM (2001). *Ex. and Sport Sci. Rev., 29(1): 37-41.*

AKNOWLEDGMENTS

TIBIOFEMORAL CONTACT PRESSURES AND OSTEOCHONDRAL MICROTRAUMA DURING ACL RUPTURE DUE TO EXCESSIVE COMPRESSIVE LOADING AND INTERNAL TIBIA TORSION

Eric G. Meyer, Timothy G. Baumer and Roger C. Haut
Michigan State University, East Lansing, MI, USA
E-mail: haut@msu.edu, Web: www.obl.msu.edu

INTRODUCTION

Participation in sports increases the risk of acute and chronic injuries, such as ligament sprains or OA. The knee is one of the most frequently injured joints with approximately 80,000 ACL tears in the US each year with a total cost of nearly one billion dollars (Griffen, 2000). The most common kinematic scenarios for ACL injuries are internal twisting or combined loading during a hard landing (Ettlinger, 1995). Rupture of the ACL is associated with degenerative changes in the joint, and 50-70% of patients have radiological changes consistent with chronic disease after 15-20 yrs (Gilquist, 1999). In 80% of these cases, a characteristic osteochondral lesion occurs, which is often associated with an overt loss of articular cartilage (AC) overlying the "bone bruise" within 6 months of injury (Vellet, 1991). The objective of the current study was to document the levels of contact pressure developed in the cadaveric human knee joint during rupture of the ACL via excessive axially compressive loading or internal rotation of the tibia. Additionally, this study was designed to investigate acute injury to AC and underlying subchondral bone (SB). A hypothesis of the study was that the types and extent of these injuries would depend on the mechanism producing ligamentous injury to the knee.

METHODS

Paired compression and torsion experiments were conducted on 7 cadaver tibiofemoral (TF) joints (55.8 ± 5.7 yrs). The bone ends were potted in cylindrical aluminum sleeves. The tibia was attached to a low friction rotating shaft or rotary actuator. The femur was attached to an XY translation table with the knee flexion angle set to 30 deg. Compression was applied to one joint from each pair by a haversine (10 Hz) load-controlled waveform in 1 kN increments until catastrophic injury of the joint. Internal torsion was applied in 10 Nm increments to the tibia of the opposite joint with a similar load-time waveform. The varus/valgus angle was constrained in neutral for compression experiments and unconstrained in torsion experiments. Pressure film was inserted into the TF joint to record contact area and pressure on each facet. Following testing, samples of each tibia were prepared for standard histology. Four types of damage were recorded: vertical cracks, horizontal cracks, AC damage, and compression lines in the AC. Statistical differences reported for $p < 0.05$.

RESULTS AND DISCUSSION

All compression and torsion failures involved the ACL, although there were frequently other ligamentous or meniscal injuries. The compressively loaded specimens had a peak load of 5.5±2.0 kN, while the torsionally loaded specimens failed at 37.4±16.8 Nm. For compression, the contact area and pressure were slightly higher in the medial compartment than the lateral compartment (Table 1). For torsion experiments, the medial facet also had slightly higher contact areas than the lateral facet, although the distributions were dissimilar (Figure 1).

Indirect joint compression produced significantly lower contact areas in the torsion experiments. The compression experiments also had more contact area that was above a pressure threshold likely to cause AC damage (>25 MPa) and significantly higher maximum pressure values than torsion experiments. Analysis of the histological samples revealed significantly more damage to the tibial plateau in compression experiments than in torsion experiments in both lateral and medial facets. There was also more vertical micro-cracking in compression than in torsion experiments, with a significant difference in both the lateral and medial facets. There was significantly more damage to the AC in compression than in torsion. Finally, there were more AC compression lines in compression than in the torsion experiments.

Table 1. Pressure film data from failure experiments. *Significant difference relative to compression specimens. # Significant difference between medial and lateral compartments.

	Average Contact Area (mm²)		Average Contact Pressure (MPa)	
	Medial	**Lateral**	**Medial**	**Lateral**
Compression	187 (116)	142 (104)	15 (4)	15 (4)
Torsion	56 (52)*	37 (42)*	12 (5)#	10 (4)*
	Area > 25 MPa (mm²)		Maximum Pressure	
Compression	25 (35)	18 (29)	34 (13)	33 (11)
Torsion	3 (2)	0 (0)	25 (11)#	16 (7)*
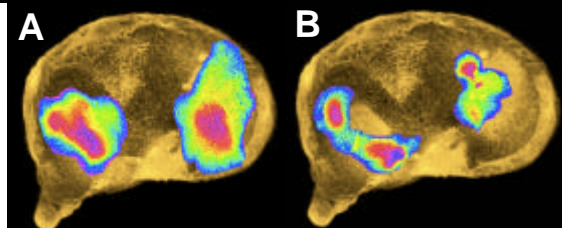
Figure 1. Representative contact pressure distributions for A) compression and B) torsion experiments.

SUMMARY/CONCLUSIONS

High levels of tension were developed in the ACL for all experiments. Compression experiments resulted in regions of high contact pressure on the posterior tibial plateaus. Torsion experiments resulted in contact regions, posteriorly on the lateral plateau and anteriorly on the medial plateau.

These regions of high contact pressure in compression specimens may be associated with bone bruises seen in the posterior-lateral and medial aspects of the tibia (Sanders, 2000; Speer, 1992). In addition to generating ACL injuries, the number of microcracks at the interface between AC and SB and the extent of AC damage was higher for compression specimens than torsion specimens. Interestingly, a higher percentage of the damage in torsion specimens, especially in the lateral facet, were horizontal microcracks, which may be related to high shear stresses versus compressive stress producing vertical microcracks. These associated damages may form the basis for the development of post-traumatic OA in both ACL-reconstructed and non-reconstructed patients (Mykleburst, 2005). The location of the high contact pressure and bone bruises clinically may also be an indicator of anterior tibial drawer. Indeed, compressive loading of the TF joint, as seen in the current and previous studies (Meyer, 2005), resulted in anterior drawer of the tibia. Compressive loads between 5-7 kN could easily be generated during an uncontrolled jump landing or other noncontact injury situation, and might lead to clinical symptoms of OA 5-10 years post-injury.

REFERENCES

Ettlinger C. (1995) *Am J Sports Med.* 23, 531-7.
Gilquist J. (1999) *Sports Med.* 27, 143-56.
Griffen L. (2000) *J Am Acad Orthop Surg.* 8, 141-50.
Meyer E. (2005) *J Biomech.* 38 2311-16.
Mykleburst G. (2005) *Brit J Sport Med.* 39, 127-31.
Sanders T. (2000) RadioGraphics. 20, S135-51.
Speer K. (1992) *Am J Sports Med.* 20, 382-9.
Vellet A. (1991) *Radiology.* 178, 271-6.

ACKNOWLEDGEMENTS

SEGMENTATION OF COMPUTED TOMOGRAPHY DATA AND CREATION OF A THREE-DIMENSIONAL REPRESENTATION OF THE WRIST

Vincent T W Lo[1], Michele L Oliver[1], Robert D Dony[1], Anne Agur[2], and David Salonen[2]

[1]School of Engineering, University of Guelph, Guelph, ON, Canada, vlo@uoguelph.ca, moliver@uoguelph.ca
[2]University of Toronto, Toronto, ON, Canada

INTRODUCTION

As a result of load transmission from the hand to the forearm, the wrist and associated structures are prone to injuries and diseases such as osteoarthritis, carpal tunnel syndrome, and carpal bone fractures. Studies of the effects of loads on the wrist are important because they could lead ultimately to less patient discomfort in therapies and more accurate prediction of fracture risk (Carrigan et al., 2003; Ulrich et al., 1999).

While previous studies have utilized Computed Tomography (CT) scans of the wrist to develop Finite Element Analysis (FEA) models (Carrigan et al., 2003; Ulrich et al., 1999), little research exists on scans of the wrist under variable loading conditions.

The objectives of this study were: a) to develop a method of applying variable loading conditions to the wrist of a cadaveric forearm specimen; b) to acquire CT scans under variable loading conditions; and c) to segment the CT data in order to demonstrate the potential to create a 3-D model for FEA.

METHODS AND PROCEDURES

To apply variable loads during imaging, a jig and force applicator were designed to fit through the opening of a CT scanner. When designing them, the use of metals was avoided because they might cause beam hardening artifacts. The specimen was held in place by the jig in order to avoid motion artifacts in the CT scans. The jig held the specimen in place by sandwiching it between two panels which were joined together using nylon rod-ends and nuts (Figure 1).
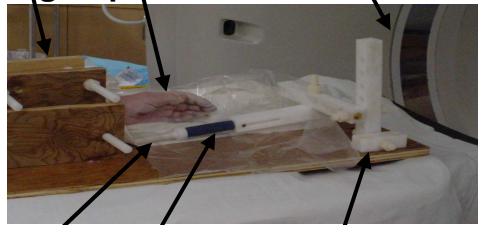
Figure 1: A detailed view of the experimental setup used to obtain the CT images.

The force applicator was designed with the ability to apply loads in six degrees of freedom. The force applicator had three linkages with holes along each linkage. The linkages were joined together using nylon nuts and bolts which allowed the force applicator to be adjusted to apply a range of force magnitudes and directions. The direction of the loads applied by the force applicator was determined by measuring the angles between the linkages using a protractor. When a force was applied to the specimen, the magnitude and direction of the force was varied by manipulating the position and alignment of the force applicator tip. The tip had a circular cross-section with a 0.5 inch diameter. The magnitude of the force was determined by measuring compression (displacement in mm) of the spring in the force applicator. Spring displacement was

monitored using digital calipers. Three different polyurethane springs were designed and constructed for this experiment. Spring constants were determined by compression testing using an Instron Model No. 8872 (Instron: Norwood, MA) testing machine. The Instron monitored both force as well as the corresponding displacement. A best fit line (f=kx) was fit to each set of compression testing data using linear regression ($R^2 \geq 0.96$) with the slope (k) of each line considered to be the spring constant.

An Introfiant-embalmed cadaveric specimen of the left forearm was scanned. Introfiant is a mixture containing the following ingredients: formaldehyde, methanol and propylene glycol. A Toshiba Aquilion 64 Multislice CT (Toshiba America Medical Systems Inc.: Tustin CA) scanner was used to acquire images in this study. Eight sequences of images were acquired. In four of the eight sequences, no force was applied. In the remaining four sequences, four different magnitudes of compressive forces (10 N, 21 N, 48 N, and 54 N) were applied to the base of the palm of the specimen using the force applicator while the specimen was held in place in the jig (Figure 1). Compressive loads were chosen based upon a previous wrist FEA study (Carrigan et al., 2003).

After the CT images were acquired, 421 images from one of the sequences with no load were processed to generate a three-dimensional representation of the wrist. Maximum entropy thresholding (Kapur et al., 1985) and the Canny (Canny, 1986) edge detection method were used to automatically segment the radius and ulna. Carpal bones were manually segmented. Maximum entropy thresholding was implemented using ImageJ (NIH: Bethesda, MD) while the Canny method was performed in Matlab™ (The Mathworks, Inc.: Natick, MA). Manual segmentation was done in ImageJ using a

custom plug-in application (Bonnet et al., 2007).

Segmented data were imported into MicroView (GE Healthcare: Buckinghamshire, UK) as point clouds and the resulting surface model was input into NX (Siemens PLM Software: Plano, TX). The resulting 3-D representation of the radius, ulna and carpal bones is shown in (Figure 2).
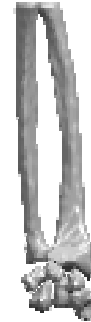
Figure 2: Palmar view of the three-dimensional representation of the radius, ulna and carpal bones of the left hand.

SUMMARY

This paper describes the design and testing of a variable load application device for image acquisition to be used in the development and validation of FEA models. The acquired data were segmented and a 3-D representation of the wrist was generated.

REFERENCES

Bonnet, N et al. (2007). Plug-ins ImageJ: Manual segmentation. http://helios.univ-reims.fr/Labos/INSERM 514/ImageJ/

Canny, J (1986). *IEEE Trans Pattern Anal Mach Intell*, **8**(6), 679-698.

Carrigan, SD et al. (2003). *Ann Biomed Eng,* **31**(6), 718-725.

Kapur, JN et al. (1985). *CVGIP*, **29**(3), 273-285.

Ulrich, D et al. (1999). *J Biomech,* **32**(8), 525-526.

A NOVEL TECHNIQUE TO DETERMINE GRAVITATIONAL AND PASSIVE JOINT TORQUES FROM DYNOMOMETER-MEASURED PASSIVE TORQUE DATA

Dennis E. Anderson, Michael L. Madigan and Maury A. Nussbaum

Virginia Polytechnic Institute and State University, Blacksburg, VA, USA
Email: dennisa@vt.edu, Web: www.biomechanics.esm.vt.edu

INTRODUCTION

Isokinetic dynamometers are widely used in testing of muscular strength, as they allow simultaneous measurement of joint torque, angle and angular velocity. However, the torque measured by a dynamometer does not equal the torque applied about a joint by active muscle loading due to contributions from gravitational torque and passive joint torques. Gravitational torque is due to the weight of the limb and dynamometer arm (Herzog, 1988). Passive joint torque is caused primarily by elastic deformation of tissues crossing the joint, including muscles, tendons and ligaments (Yoon and Mansour, 1982).

Passive torque may be modeled as the sum of gravitational torque and passive joint torques. The gravitational torque has frequently been modeled as a simple sine or cosine function (Herzog, 1988, Nelson & Duncan, 1983) based on measurements at specific joint angle(s). For these models, the angle of maximum gravitational torque is 90° or 0°, respectively. However, this assumes that the center of mass of the limb distal to the joint plus the dynamometer attachment is aligned with the centerline of the segment defining the joint angle. This assumption is not valid in all cases. Passive joint torques have typically been modeled as exponential functions (Hoang et al., 2005, Yoon and Mansour, 1982). Previously, we have used optimization to fit a model of passive torque to measured passive torque data (Anderson et al., 2007). The purpose of this work was to create a simple algorithm for directly calculating the model parameters.

METHODS AND PROCEDURES

Passive torque profiles were collected for the ankle, knee and hip using a Biodex System 3 dynamometer as part of a larger study. Thirty-four healthy adults, ages 18-73, half male and half female, participated. Informed consent was obtained prior to participation. The dynamometer moved through two full cycles of joint motion at 5°/s while the subject was relaxed. Torque, angle and angular velocity were sampled at 200 Hz.

The passive torque model was fit to measured passive torque data (Figure 1). The passive torque model was defined as:

$$T_{PASSIVE} = A_1 \sin(\theta) + A_2 \cos(\theta) + B_1 e^{k_1 \theta} + B_2 e^{k_2 \theta}$$

where θ is the dynamometer angle. The constants A define the gravitational torque as a general sinusoid. The constants B and k define passive joint torques with two exponential functions, one for each end of the range of motion (ROM).

The gravity torque parameters A were determined by performing a least squares fit in the gravity-only region of the data where passive joint torques are negligible (Figure 1). Note that in the gravity-only region:

$$T_{PASSIVE} + \frac{d^2 T_{PASSIVE}}{d\theta^2} = 0$$

To determine the location of the gravity-only region, a cubic polynomial regression was performed on the entire passive torque profile, added to its second derivative and equated to zero. The real root(s) of this equation should represent the center of the gravity-only region. Based on the previously calculated passive torque functions, it was assumed that

the gravity-only region spans at least 40% of the ROM. Thus, the gravity-only region was defined as encompassing these root(s) plus 20% of the ROM on either side.

The exponential passive joint torque functions are determined to match quadratic best fits of the data. The data were gravity-corrected and split in two at the center of the gravity-only region. A quadratic least squares fit of each end was performed. The parameters B and k were determined as:

$$k = \frac{T'_{FIT}}{T_{FIT}}$$

$$B = T_{FIT}\,e^{-k\theta_{FIT}}$$

where T_{FIT} and T'_{FIT} are the quadratic best fit and its first derivative evaluated at θ_{FIT}, defined as the angle where the torque was half of the peak torque at the end of the ROM.

RESULTS

The models determined using this technique fit measured passive torque profiles well. The average coefficient of determination (r^2) was 0.977 (range 0.714 – 0.999) across all subjects and joints. This is comparable to the average r^2 of 0.982 (range 0.722-0.999) for fits found using optimization (Anderson et al. 2007).

DISCUSSION

The approach presented here offers several advantages in determining gravitational torque corrections. It may be more accurate than methods based on specific joint angle(s), as it uses data from the entire range of motion. The model makes no assumptions about the dynamometer angle at which gravitational torque will be maximum or minimum. It also explicitly accounts for and models passive joint torques. However, the accuracy of the technique in separating gravitational torques from joint torques has not been evaluated.
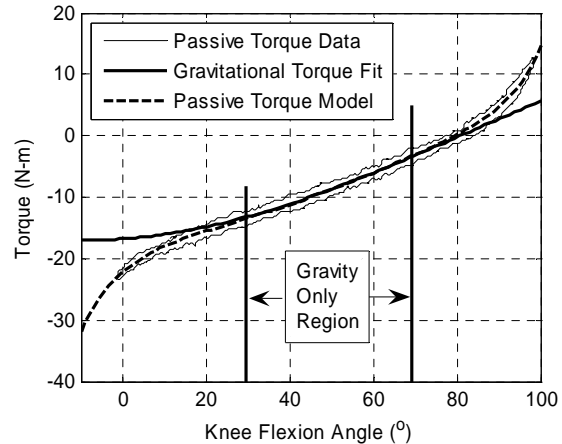
Figure 1. An example of a passive torque profile for the knee with the corresponding passive torque model. The gravitational torque was fit within the gravity-only region.

SUMMARY

The technique presented here can accurately fit dynamometer-measured passive torque data encompassing the entire joint ROM. The model accounts for gravitational torque and passive joint torque as separate components of the measured passive torque.

REFERENCES

Anderson DE et al. (2007). *J Biomech,* 40: 3105-3113.
Herzog W (1988). *J Biomech,* 21: 5-12.
Hoang PD et al. (2005) *J Biomech,* 38: 1333-1341.
Nelson, SG and Duncan, PW (1983). *Phys Ther*, 63: 674-676.
Yoon, YS and Mansour, JM (1982). *J Biomech,* 15: 905-910.

ACKNOWLEDGEMENTS

NEUROMUSCULAR ACTIVATION IN THE WRIST DURING ISOMETRIC CONTRACTIONS

Sarah Eby and Michael Hahn

Movement Science Laboratory, Department of Health and Human Development,
Montana State University, Bozeman, MT USA
E-mail: mhahn@montana.edu

INTRODUCTION

Distal radius fractures are among the most frequently treated fractures, though the nature of the injury often leads to poor clinical results (Fölhdazy, et al., 2007). Improving post-injury outcomes must begin with investigation of the non-injured neuromotor control system. Neuromuscular activation patterns at the wrist indicate a certain level of muscle specificity, and distinct neural systems have been identified in flexion/extension stability (Buchanan, et al., 1993, Suminski, et al., 2007). The force envelope for the thumb has been identified (Li and Goitz, 2003), and similar research to determine the range of normal function and activation should benefit wrist rehabilitation. The purpose of this study was to develop a baseline neuromuscular map of wrist function for use in future research that will compare the activation patterns associated with distal radius fracture to help retain hand/wrist function. It was hypothesized that the anatomical position of wrist musculature should dictate each muscle's primary function, with some tendency for coactivation.

METHODS AND PROCEDURES

Ten right-handed, healthy young adults (5 male, 5 female, 24.6 yrs) with no reported history of right-arm musculoskeletal injury were recruited for this study. Muscle activity was monitored for the extensor carpi radialis longus/brevis (ECR), extensor carpi ulnaris (ECU), flexor carpi ulnaris (FCU), and flexor carpi radialis (FCR) of the right arm using passive bipolar surface electromyography (EMG). Using fibreglass-casting tape, a rigid apparatus was molded for the subject's right hand, attaching a bolt to the medial surface of the hand, perpendicular to the longitudinal axis. Subjects were seated with shoulder and wrist in neutral, and elbow flexed to 90°. Clamps immobilized the subject's elbow and fixed the wrist in a neutral position. The hand was firmly fastened to a 6 degrees-of-freedom load cell (MC3A, AMTI, Watertown, MA) using the casted bolt attachment (Figure 1).
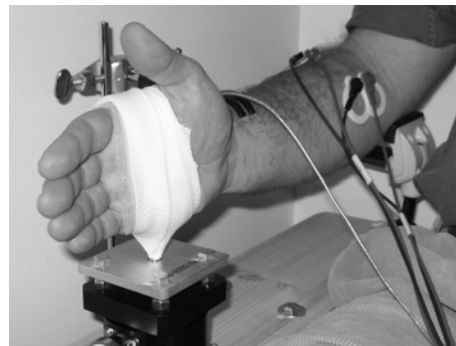
Figure 1. Testing apparatus.

Baseline force production and EMG data were collected at 1000 Hz for the maximum voluntary contraction (MVC) at eight experimental torque angles using the Myopac Jr. (Run Technologies, Inc., Mission Viejo, CA). A custom written LabVIEW program (National Instruments, Austin, TX) provided real-time visual feedback of force production to monitor the torque magnitude and direction. Two submaximal trials were conducted at each of three load magnitudes (20%, 30%, 40% MVC) at the eight torque angles. Surface EMG activity was collected for the final 1.5 seconds of each 5 second

trial. The order of target-matching trials was randomized.

Raw EMG data were filtered using a digital band-pass filter (10-1,000Hz), full wave rectified and passed through a linear envelope. The filtered EMG signals were normalized to each subject's MVC activation level for the respective muscle. The average level of neural activation was determined for each muscle in each testing direction.

RESULTS

Neuromuscular activation levels increased with greater force production. The mean submaximal activation levels plotted on polar coordinate graphs illustrate the range of normal activation levels (Figure 2). Different regions of neuromuscular activity were evident for each muscle, though overlap by the FCR was especially pronounced.
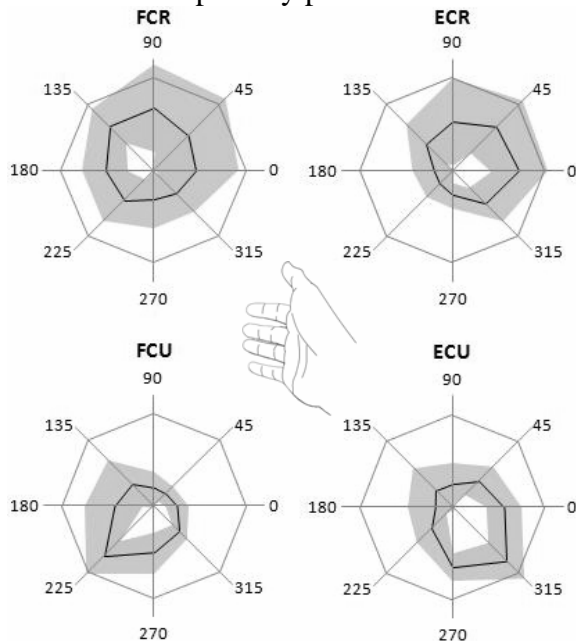
Figure 2. Neuromuscular activation plots of baseline data for 30% MVC. Black line indicates Mean, +/- SD (shaded region).

DISCUSSION

The purpose of this study was to determine the neural activation patterns for the four major wrist muscles during isometric contractions in the neutral position. The results indicate a moderate level of muscular specialization, as shown by high agonist levels of activation and lower antagonistic levels of activation. However, some muscles showed higher levels of coactivation, namely the FCR and the ECR. These patterns of coactivation may indicate a strategy for gaining additional stability at the wrist during the fine motor contractions required in the testing protocol. High variability of muscle function and coactivation patterns between subjects depicts a range of possible strategies for wrist stability and function.

SUMMARY

High levels of activation were found in agonist muscles, and low levels in antagonist muscles for most directions of contraction. Some levels of muscular coactivation were found during certain directions of contraction, indicating the need for additional stabilization in those directions. Additional research will examine the activation patterns to identify adaptation or coping strategies associated with recovery from distal radius fracture.

REFERENCES

Buchanan, TS, et al. (1993). *J. Biomech,* 26: 547-60.
Földhazy, Z, et al. (2007). *J. Hand Surg,* 32A: 1374-84.
Li Z-M, and Goitz, RJ (2003). *Technol Health Care,* 11: 233-43.
Suminski AJ, et al. (2007). *J Neurophysiol,* 97: 1527-45.

ACKNOWLEDGEMENTS

COMPARISON OF STRENGTH BETWEEN PREGNANT AND NON-PREGNANT WOMEN

Geneviève Dumas[1] , Karine Charpentier[1] , Mei Wang [2] , Andrew Leger[3]

[1]Department of Mechanical and Materials Engineering, Queen's University, Kingston, ON, Canada, dumas@me.queensu.ca
[2]Department of School of Kinesiology, University of Western Ontario, London, ON, Canada,
[3] Centre for Teaching and Learning, Queen's University, Kingston, ON, Canada.

INTRODUCTION

Pregnant women have been found to have lower upper extremity strength than non-pregnant women (Masten and Smith, 1988). Similarly, decreases in strength have been demonstrated in women after compared to before pregnancy (Treuth et al., 2005). These findings have important implications for the safety of pregnant women as well as for job assignment. The objective of this study was to compare strength in handgrip, back extension and quadriceps muscles in pregnant women and paired controls.

METHODS AND PROCEDURES

Twenty women were recruited and tested at the beginning of the second trimester of pregnancy, at 14.8(1.7) weeks. They were paired with 20 non-pregnant women of childbearing age according to height and weight (Table 1).

All measurements were performed using the same equipment and protocol as in Wang et al. (2005). Maximal power grip was determined with a hand held dynamometer (Preston). For back strength, the participants sat in the Isometric Trunk Ergonomic Chair in a semi-kneeling posture and pulled back against two load cells connected to two straps attached to a harness (Figure 1). The straps were attached at the level of T9. For quadriceps strength, the participant sat on a plinth with both knees bent to 90° and with a

1338N load cell connected above the ankle of the dominant leg. The participant was asked to contract her quadriceps muscles gradually and maximally in an attempt to extend her lower leg and pull against the load cell.

For all strength measurements, the participants performed three trials after some practice, and the highest value among the three trials was recorded. Correlations and Student t-tests were calculated for each variable of interest to compare the two groups.
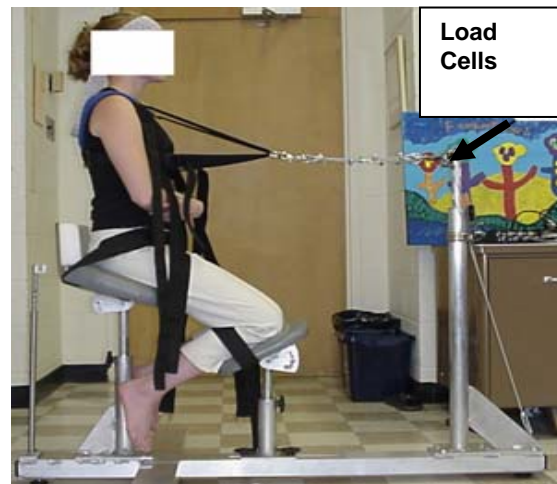
Figure 1: The Isometric Trunk Ergonomic Chair Used for Testing Back Extensor Strength.

RESULTS

The groups were almost perfectly matched for height and mass (r>0.98, *p*<0.005), Table 1. The pregnant group was slightly older than

the non-pregnant group, but the difference did not reach significance.

Strength was lower for the pregnant group on all measures (Table 1). The difference between the two groups reached significance for the two measures of back strength (over 30%) and for quadriceps strength (over 24%), but not for handgrip (~10%), Table 1.

DISCUSSION

The results of this study are consistent with previous data from the literature (Treuth et al. 2005) showing a decrease of strength associated with pregnancy, except for handgrip where no significant difference between the groups was found in this study contrary to Masten and Smith (1988). Small changes in grip strength were also mentioned by Morrissey (1998). This could be caused by a lack of statistical power due to a smaller sample for this parameter (14 subjects instead of 20), or reflect a true lack of difference.

SUMMARY

In this study, 20 women in the early second trimester of pregnancy were paired with 20 non-pregnant women by height and weight. Grip strength, back extensor strength (sitting) and quadriceps strength were measured for the two groups. Strength was significantly lower for the pregnant group for back strength (by over 30%) and quadriceps strength (~25%).

REFERENCES

Masten WY and Smith JL, (1988). *J Occup Med*, 30(5):451-456.
Morrissey SJ, (1998). *Int J Ind Ergon* 21:383-395.
Treuth, MS et al., (2005). *Med Sci Sports Exercise,* 37(5):832-837.
Wang M, et al., (2005). *Clin Biomech,* 20; 685-692.

	Pregnant N = 20	Non-pregnant, N = 20	Correlation R (*p*)	*p* for t-test difference
Age (years)	28.6 (4.56)	26.1 (4.67)	-.08*(.74)*	.12
Height (m)	1.65 (.06)	1.65 (.06)	.99*(.00)*	.74
Mass (kg)*	61.57 (6.64)	61.38 (6.48)	.98*(.00)*	.53
BMI (kg/m^2)	22.78 (2.72)	22.72 (2.66)	.98*(.00)*	.63
Grip strength (N)**	246.65 (47.26)	273.49 (72.91)	.54*(.04)*	.13
Max Back Moment (Nm)	98.41 (33.51)	141 (24.08)	.11*(.64)*	.00
Back strength (N)	477.02 (132.94)	716.82 (106.18)	.28*(.22)*	.00
Quadriceps strength(N)	404.26 (118.19)	534.19 (138.11)	.41*(.07)*	.00

*For pregnant women, this is the pre-pregnancy mass,
** N = 14 for grip strength due to missing data for the pregnant group.

Table 1. Demographic and strength data for the two groups. Means (SD) in the first two columns.

EFFECT OF TREADMILL EXERCISE IN TIBIAE OF OVARIECTOMIZED RATS: A BIOMECHANICAL ANALYSIS

Patrícia Blóes, Ariane Zamarioli, Antônio C. Shimano, Priscila A. Simões, José B. Volpon, Luís H. A. Pereira and Francisco C. Mazzocato
Department of Biomechanics, Medicine and Rehabilitation of the Locomotor Apparatus of
Faculty of Medicine of Ribeirão Preto of University of São Paulo
http://www.fmrp.usp/bioengenharia

INTRODUCTION

Bone is a dynamic tissue in a continuous process of formation and resorption that are performed by osteoblasts and osteoclasts, respectively (Canalis, 1996). After menopause, the reduction of estrogens increases the osteoclastic resorption that exceeds the rate of osteoblastic formation, resulting in a bone mass loss (osteopenia or osteoporosis). In modern ages these conditions have been object of interest in research as they represent a serious health problem; mostly for women and elderly people. The mechanical stress produced by the physical exercise increases bone mass (Smith and Raab, 1986). In this way, exercises are widely used as a preventable method to minimize the loss of bone mass (Bonnet et al., 2007; Chen et al. 1994; Gala et al., 2001 and Notomi et al., 2003), as it has been shown to improve the bone quality in rats and in women after estrogen depression (Nelson and Fiatarone, 1994). Furthermore, the therapeutic effects of physical training in osteopenic rats have been reported by Barengolts et al. (1993), Iwamoto et al. (1998), Notomi et al. (2003), Ocarino et al. (2007), Yeh et al. (1993) and Yeh et al. (1994).
This study aimed at investigating the influence of the treadmill running on mechanical properties of the tibiae of ovariectomized rats using biomechanical analysis with three-point ventral bending tests.

METHODS AND PROCEDURES

Thirty three-month-old female Wistar rats were divided into 3 groups: control group (A, n=10); non-exercised ovariectomized group (B, n=10) and exercised ovariectomized group (C, n=10).
The ovariectomy procedure was based on Zarrow et al. (1964) and it was used to cause osteopenia.
The rats from group C began the training 60 days after the ovariectomy.
The physical exercise program consisted of running on a flat-bed treadmill 4 days a week, 1 hour per day at 15 m/min from the beginning of the training until the sixth week. Then the speed was increased to 19 m/min during the remaining six weeks.
At the end of the experiment, the animals were killed under anaesthesia and the tibiae were harvested, cleaned of soft tissues and tested in three-point ventral bending in a universal testing machine with speed of 10 milimeters per minute and the maximal strength was obtained. After sacrifice a laparotomy was made and the uterus gross conditions were observed. Data were analyzed using analysis of covariance - ANOVA Two Way Analysis of Variance to test the differences among the groups. The level of significance was set at 5%.

RESULTS

The results were based on 29 rats (A=C=10, B=9). There was one exclusion along the course of the study because of one death after the ovariectomy in group B.

The mean of maximal strength was: A (54.52 ± 18.47) N; B (31.05 ± 20.62) N and C (37.17 ± 13.14) N. There was a statistical difference between groups A and B and also between A and C (p<0.01), but not between B and C (Figure 1).
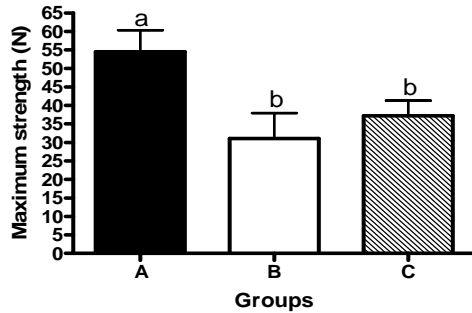
Figure 1. Maximum strength of the groups A, B and C. Different letters show significant statistical difference.

DISCUSSION

Previous studies have shown that ovariectomy in rats is a suitable experimental model for postmenopausal osteopenia that reasonably reproduces the changes observed in women (Bonnet et al., 2007; Notomi et al., 2003 and Ocarino et al., 2007). At the sacrifice we observed the uterus was atrophied, suggesting a successful ovariectomy procedure. Many authors reported that exercising produces a positive effect on bone tissue in osteopenic rats (Notomi et al., 2003; Ocarino et al., 2007; Barengolts et al., 1993; Iwamoto et al., 1998; Yeah et al., 1993 and Yeh et al., 1994). Physical training may be achieved by tower climbing exercise (Notomi et al., 2003) but in the majority, the running exercise in a treadmill is used based on different protocols (Notomi et al., 2003; Ocarino et al., 2007; Barengolts et al., 1993; Iwamoto et al., 1998; Yeah et al., 1993 and Yeh et al., 1994). Based on our findings we concluded that the ovariectomy in rats induced a decrease of the maximal strength in both non-exercised and exercised groups. The exercise did not recover the initial state of the tibiae strength. However, it was demonstrated a tendency of recuperation. One possible explanation is that we mainly tested the cortical bone of the tibiae (diaphysis) that is more compact than the cancellous bone and would require a longer time of training to depict some structural change caused by physical exercing.

REFERENCES

Barengolts, EI et al. (1993). *Calc Tissue International,* 52: 239-243.

Bonnet, N et al. (2007). *J Bone Miner Res*, 22: 578-588.

Canalis, E (1996). *Primer on the Metabolic Bone Disease and Disorders of Mineral Metabolism.* New York, Lippincott-Raven.

Chen, MM et al. (1994). *Bone*, 15: 313-319.

Gala, J et al. (2001). *British J Nutrition,* 86: 521-527.

Iwamoto, J et al. (1998). *J Bone Miner Res*, 13: 1308-1317.

Nelson, ME and Fiatarone, M (1994). *JAMA*, 272: 1909-1914.

Notomi, T et al. (2003). *J Bone Miner Res*, 18: 140-149.

Ocarino, NM et al. (2007). *J Musculoskelet Neuronal Interact*, 7: 84-93.

Yeh, JK (1993). *J Bone Miner Res*, 8: 677-683.

Yeh, JK et al. (1994). *Bone Miner*, 24: 223-234.

Zarrow, MX et al. (1964). *Academic press*, 1: 39-40.

ACKNOWLEDGEMENTS

VIRTUAL FORCEPLATE: PREDICTING GROUND REACTION FORCES DURING SINGLE LEG HOPPING USING ONLY KINEMATIC MEASUREMENTS

Alison L. Sheets[1], Stefano Corazza[1] and Thomas P. Andriacchi[1,2,3]

[1]Biomotion Laboratory, Department of Mechanical Engineering, Stanford University, Stanford, CA, USA, alsheets@stanford.edu
[2]Department of Orthopaedics, Stanford University, Stanford, CA, USA
[2]Bone and Joint Center, Palo Alto Veterans Affairs, Palo Alto, CA, USA

INTRODUCTION

Kinetic analyses of human motion have typically been confined to controlled environments in which subjects strike a force plate to measure ground reaction forces (GRF) and use bottom-up inverse dynamic methods. Thus opportunities to analyze activities where environment (e.g. sports fields) can influence movement patterns have been limited.

Combining developments in markerless motion capture methods and a top-down kinetics approach offers the opportunity to accurately capture motion in an unconfined environment and analyze it without force plate data. Markerless capture methods could potentially reduce top-down approach error because: exact limb geometry is used to estimate subject specific limb masses, 3D center of mass (CM) locations and moments of inertia, and motion is tracked using the whole limb rather than specified points.

This study predicts vertical, medio-lateral and anterior-posterior GRF during a single-leg hop using a markerless motion capture method.

METHODS AND PROCEDURES

A single-leg hop performed by a female subject (mass=59.19 kg, ht=1.59 m) was recorded at 120 Hz using eight synchronized VGA cameras. Joint positions and body segment orientations were measured using a markerless motion capture method (Corazza, 2006, Mündermann et al., 2006). The body was automatically divided into 15, 6 degree-of-freedom, rigid segments: head, upper torso, pelvis and two upper arms, forearms, hands, thighs, shanks, and feet (Corazza et al., 2007). Segment masses, and the 3D CM locations and moments of inertia were estimated from the body surface topography measured with a laser scanner (Sheets et al., 2008) and assuming constant densities (Dempster, 1955). Motion data was filtered with an 18 Hz (Farley and Morgenroth, 1999) low pass Butterworth filter. Flight and stance phases were automatically identified by tracking toe-ground contact (Figure 1).

Individual segment CM positions and masses were used to calculate a whole body CM location for each instant in the recorded hop. The three GRF components were estimated using only the whole body CM acceleration (a_{CM}). Accelerations were filtered using a kalman filter with a relatively small measurement noise to state noise ratio (5:1) during stance, and a very large ratio (75:1) during flight. Flight a_{CM} should be constant, and the large filtering ratio attributes variations to noise. After separately filtering the phases, all data was combined and filtered (kalman, 1:1) to eliminate discontinuities. Predicted GRF were verified with filtered (kalman, 5:1) and unfiltered force plate measurements collected at 120 Hz.

RESULTS

Peak vertical GRF predicted using the a_{CM} of the rigid 15 segment model were within 1% of measured unfiltered GRF. The rms GRF errors with respect to the filtered data in the vertical, medio-lateral and anterior-posterior directions were 81.2N (4.9% of maximum resultant force), 36.8N (2.2%) and 44.3N (2.7%), respectively (Figure 2).
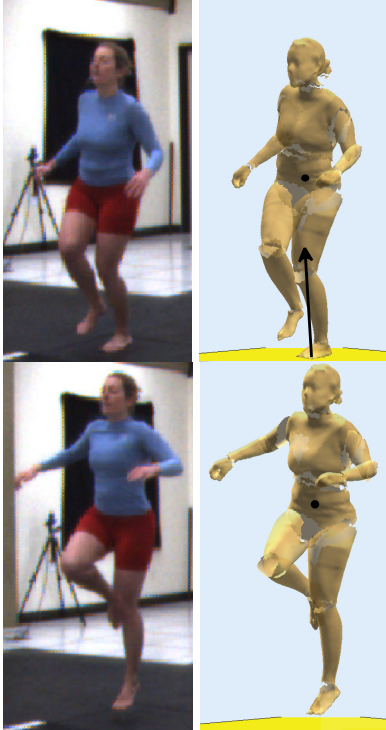
Figure 1. Video and model stance (top) and flight (bottom) phases during single-leg hop

DISCUSSION

Predicted vertical GRF most closely match the measured values because they had the largest signal to noise ratio. Errors in phase transitions can be attributed to discontinuities between filtered flight and stance data. Also, the rigid segment assumption and filtering removed predicted oscillations during stance.

The method presented here can be applied to other activities with single-leg stance. The filtering frequencies for flight a_{CM} would be the same for all motions and stance phase

filtering could be tuned for each activity if a sample GRF is measured. If not, the defined filter values could be used, although a_{CM} peaks may be slightly attenuated during high frequency motions.
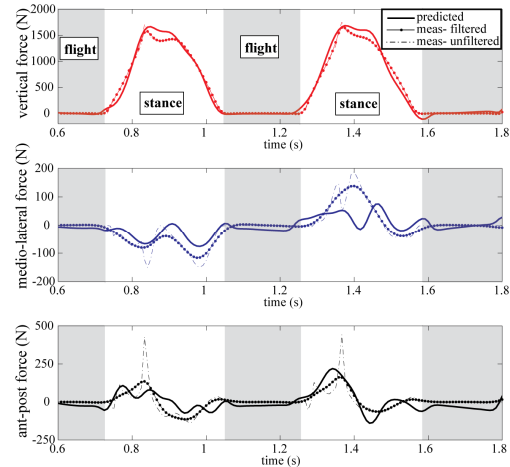
Figure 2. Predicted (solid), measured-filtered (dotted) and measured-unfiltered (dashed) GRF during single-leg hop

SUMMARY

Results of this study confirm the possibility of conducting kinetic analyses of motion studies without force plates. This work is particularly relevant to analyzing sport since studies could be conducted on various surfaces and could provide new insights into the biomechanics of natural movement.

REFERENCES

Corazza, S et al. (2006). *Annals Biomed. Eng.*, 34 (6):1019-1029.
Corazza, S and Andriacchi, TP (2007). *ASB 2007 Conf Proceedings.*
Dempster, WE (1955). WADC-Technical Report, Wright Air Development, Ohio.
Farley, CT and Morgenroth, DC (1999). *J Biomech*, 32:267-273.
Mündermann, L et al. (2006). *J NeuroEng Rehab*, 3(1): 6.
Sheets, AL (2008). *ASME 2008 Summer Bioeng Conf Proceedings*.

EFFECTS OF OBESITY ON SINGLE STEP BALANCE RECOVERY FROM A FORWARD FALL

Michael J Whitley, Michael L Madigan, and Kevin P Davy

Virginia Tech, Blacksburg, VA, USA
E-mail: mwhitley@vt.edu, Web: www.biomechanics.esm.vt.edu

INTRODUCTION

Falls are a major medical problem in older adults due to high fall rates and a greater likelihood of injury and death from a fall. Obesity has the potential to exacerbate this problem, but little is known about its effect on the ability to prevent falls (Wearing 2006). To address this gap in the research, this study investigated the effects of obesity on single step balance recovery from a forward fall. In addition, the effect of obesity on the relative strength required during single step balance recovery was investigated.

METHODS

Sixteen subjects participated including eight obese adults (age = 64.9 ± 5.4 years, BMI = 33.2 ± 2.4) and eight age- and gender-matched non-obese adults (age = 64.0 ± 6.4 years, BMI = 24.8 ± 1.8). Subjects were initially released from a static forward lean of 10 degrees, and attempted to recover their balance with a single step. Upon successful balance recovery, the task was repeated with progressively larger lean angles until the largest lean angle that could be recovered from upon release was determined. After a brief rest, subjects performed a battery of muscle strength tests on a Biodex System 3 dynamometer to determine the maximum isometric joint torque that could be produced at each joint of the lower extremity.

Sagittal plane joint torques in the lower extremity were estimated for all trials using a 2D rigid-link model and inverse dynamics analysis. Joint torques were then normalized to peak joint torques measured during strength tests to express joint torques as a percentage of their maximum values (i.e. relative joint torques).

RESULTS AND DISCUSSION

The maximum lean angle achieved by the obese subjects (13.75 ± 3.54 degrees) was smaller (p=0.024) than that achieved by the non-obese subjects (18.13 ± 2.59 degrees) (Figure 1).
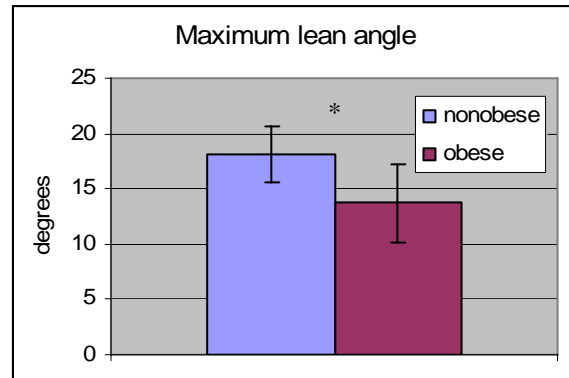
Figure 1. Maximum lean angle for both non-obese (left bar) and obese (right) subjects. Error bars represent standard deviation. * indicates p<0.05.

This suggests that obese subjects have a poorer ability to recover from a forward fall with a single step.

No differences in peak knee or hip extension torques during recovery from a 15 degree lean angle were found between the groups (p>0.05). However, peak ankle plantar

flexion torque was higher in obese subjects as compared to non-obese subjects (p=0.035) (Figure 2).
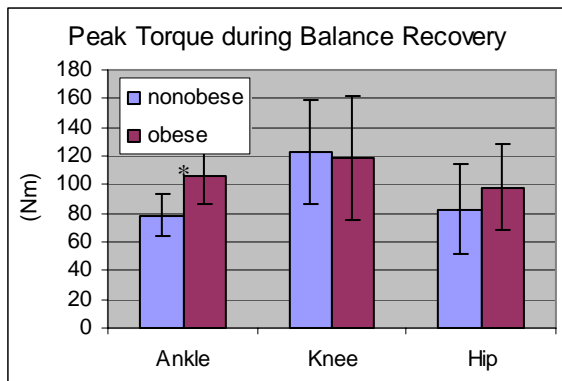
Figure 2. Peak joint torque during balance recovery for both non-obese (left bars) and obese (right) subjects during recovery from a 15° lean angle. * indicates p<0.05.

Similarly, no differences in peak knee or hip extension relative torques during recovery from a 15 degree lean angle were found between groups (p>0.05). However, peak ankle plantar flexion relative torque was higher in the obese subjects compared to the non-obese subjects (p=0.35) (Figure 3). This suggests that the obese used a larger percentage of their maximum ankle plantar flexion joint torque during recovery from a forward fall compared to non-obese subjects.

It should be noted that some of the peak relative torques were above the theoretical maximum of 100% strength estimated by the MVC. This was likely attributed to sub-maximal effort during strength tests.
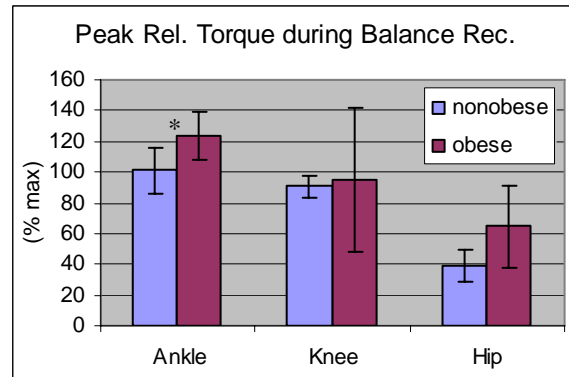
Figure 3. Peak relative joint torque during balance recovery for both non-obese (left bars) and obese (right) subjects during recovery from a 15° lean angle. * indicates p<0.05.

SUMMARY

In conclusion, obese subjects exhibited a poorer ability to recover from a forward fall with a single step, and used a higher percentage of their total ankle strength compared to non-obese subjects. Obese subjects also tended to use a higher percentage of their total hip strength, but this did not reach statistical significance. Considering these results together, they suggest that the poorer ability of recovering from a forward fall in the obese may be related to increased exertions levels during balance recovery.

REFERENCES

Wearing, SC et al. (2006). *Obesity Reviews,* 7:13-24.

ACKNOWLEDGEMENTS

MUSCULAR DEMANDS DURING PROSTHETIC LEG SWING INCREASE DUE TO INCREASED INTERACTIONS AMONG SEGMENTS

Jeremy D Smith[1] and Philip E. Martin[2]

[1]School of Sport & Exercise Science, University of Northern Colorado, Greeley, CO, USA,
Jeremy.Smith@unco.edu
[2]Department of Kinesiology, The Pennsylvania State University, University Park, PA, USA,
pmartin@psu.edu

INTRODUCTION

Early modeling research (e.g., Mena et al., 1981) suggested that walking asymmetries would be minimized if inertia properties of the prosthesis matched those of the intact leg. Empirical data, however, suggest that matching prosthesis inertia to that of the intact leg exacerbates existing asymmetries and results in higher metabolic costs during walking (e.g., Smith & Martin, 2007). Walking asymmetries and metabolic costs in general appear to be exacerbated to a lesser extent when the additional masses are positioned more proximally within the prosthetic leg (Smith & Martin, 2007). The higher cost associated with greater prosthesis inertia suggests increased muscular control during swing of the prosthetic leg. According to Bernstein (1967) muscle forces are often utilized to counteract the effects of forces and moments generated from interactions among segments and gravity (Zernicke et al., 1991). Thus, the purpose of this study was to test the hypothesis that muscle, gravitational, and interaction moment magnitudes increase with increasing prosthesis inertia.

METHODS AND PROCEDURES

Subjects were six unilateral, transtibial amputees (age: 47±16 yrs, mass: 105±10 kg, height: 175±8 cm) who were fully ambulatory, used energy storing prostheses, and were physically active in their vocational and/or daily activities.

Prosthesis inertia properties were measured using oscillation and reaction board techniques. Seven load conditions were studied (2 loads x 3 positions) plus an unloaded baseline condition (NL). 100% and 50% of the estimated mass difference between the intact and prosthetic legs were added at each of the following load positions: a) near the prosthetic ankle, b) near the prosthesis center of mass, and c) near the prosthetic leg's thigh center of mass. Participants walked at their preferred velocity for all load conditions as motion and ground reaction force data were measured. An intersegmental dynamics analysis was used to partition net joint moments at the hip, knee, and ankle into interaction, gravitational, and muscle moment components (Zernicke et al., 1991). Absolute angular impulses of each moment component served as dependent variables. A single-factor MANOVA with nine planned contrasts was used to statistically identify significant load magnitude and position effects during the swing phase of walking.

RESULTS

More distally positioned masses and larger mass magnitudes resulted in greater absolute angular impulses for each of the moment components (Figure 1). These systematic effects were exhibited by all three moment components at the hip and knee. Although statistically significant differences were also

found for the prosthetic ankle during swing, these differences were quite small (< 0.01 Nm·s) and suggest they were of questionable importance, particularly in light of the much larger loading influences at the hip and knee.
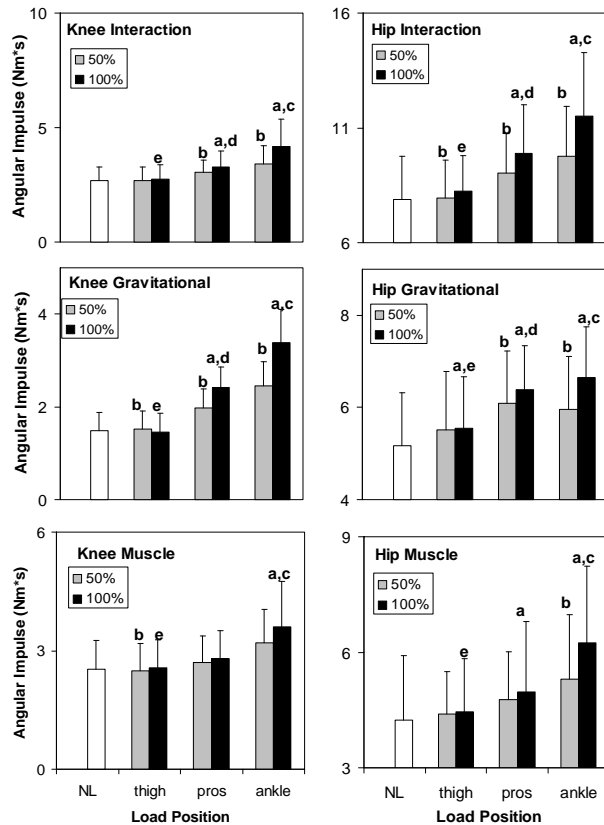
Figure 1. Load effects on knee (left panels) and hip (right panels) intersegmental dynamics of the prosthetic leg during swing (means ± SD). $p<0.05$ considered significant.
a – NL vs 100% mass for load position
b – 50% vs 100% mass for load position
c – 100% ankle vs 100% pros
d – 100% pros vs 100% thigh
e – 100% thigh vs 100% ankle

DISCUSSION

During swing, muscle and gravitational moments were mostly in phase with one another (e.g., both flexor or both extensor for similar periods of swing), but out of phase with the interaction moment (e.g., when interaction moment was flexor, gravitational and muscle moments were usually extensor). Increased muscular demands associated with loading of the prosthetic leg were attributable to increases in interaction moments that were not offset by increases in the gravitational moment at each joint. These findings were consistent with Bernstein's notion that muscle often counteracts the effects of interactions arising from linked segment motion. The increased muscular control was also consistent with our findings of higher metabolic costs for higher inertia conditions reported previously (Smith & Martin, 2007).

SUMMARY

Consistent with our hypothesis, muscle, gravitational, and interaction moment magnitudes increased as prosthesis inertia increased. Thus, greater muscular control was needed to provide corrective action during swing with increasing prosthesis inertia. Consequently, increasing the inertia of the prosthesis would not be beneficial to the amputee due to the higher aerobic and muscular demands.

REFERENCES

Bernstein, NA (1967). *Biodynamics of Locomotion*. New York, Pergamon Press.
Mena, D, et al. (1981). *J Biomech*, 14: 823-32.
Smith, JD and Martin, PE (2007). American Society of Biomechanics 31st Annual Meeting, Palo Alto, CA.
Zernicke, RF, et al. (1991). *Intersegmental dynamics during gait: Implications for control*. North-Holland, Netherlands, Elsevier Science Publishers B.V.

ACKNOWLEDGEMENTS

DIFFERENCES IN CORRELATIONS OF ANTERIOR-POSTERIOR GROUND REACTION FORCES WITH PARETIC AND CONTROL LEG GAIT VARIABLES

Carrie L. Peterson[1], Richard R. Neptune[1] and Steven A. Kautz[2,3,4]

[1] Department of Mechanical Engineering, University of Texas, Austin, TX, USA
[2] Brain Rehabilitation Research Center, Malcom Randall VA Medical Center, Gainesville FL
[3] Department of Physical Therapy and [4] Brooks Center for Rehabilitation Studies, University of Florida, Gainesville, FL. clpeters@mail.utexas.edu

INTRODUCTION

Stroke is the leading cause of long-term disability with less than 50% of surviving stroke patients walking in the community. Forward propulsion of the body center of mass (COM) is a central task of walking that depends on the generation of appropriate anterior-posterior ground reaction forces (A-P GRFs). In a recent study, propulsive impulses (i.e. the time integral of the positive A-P GRF) generated by 47 hemiparetic subjects were computed. The average percentage of total propulsion generated by the paretic leg was 16%, 36% and 49% for those with high, moderate and low hemiparetic severity, with paretic propulsion being strongly correlated with walking speed (Bowden et al., 2006). Because most of propulsion is generated during the second half of stance, we believe that the decreased paretic leg propulsion is related to the person's inability to produce appropriate muscle forces then.

The ankle plantar flexors are the primary contributors to the propulsive impulse in healthy walking (e.g., Neptune et al., 2001). Hemiparetic individuals demonstrate deficits in kinetic and EMG measures of the plantar flexors (Chen et al., 2005). Thus, impairments affecting plantar flexor output may be partly responsible for decreased paretic propulsion. In addition, exaggerated flexor muscle activity acting to offload the leg (Turns et al., 2007) and indirect mechanics (e.g., leg angle relative to the pelvis) may also contribute to decrease paretic propulsion. The purpose of this study was to gain insight into the underlying causes of decreased paretic propulsion generated by hemiparetic subjects. We hypothesized that the plantar flexor moment and leg angle would positively correlate with the A-P impulse in both the paretic and control legs, but a stronger correlation would exist among control subjects. We also hypothesized a stronger negative correlation between the paretic hip flexor moment and paretic A-P impulse would be found compared to controls.

METHODS AND PROCEDURES

3D kinematic, GRF and bilateral EMG data were recorded during treadmill walking from 39 persons with post-stroke hemiparesis and 19 age-matched control subjects. Subjects walked at their self-selected speed on a split-belt instrumented treadmill while EMG were recorded from eight muscles including the rectus femoris (RF), soleus (SO), and medial gastrocnemius (MG). Control subjects completed additional trials at 0.6 m/s. All data were time normalized to the paretic and right leg gait cycle for hemiparetic and control subjects, respectively. The second half of stance was divided into two phases: single leg support and pre-swing (i.e., double support phase proceeding toe-off). Joint moment impulses, average leg angle (angle between the pelvis COM and foot COM, positive when foot is posterior to the pelvis), and average EMG activity in each phase were computed for each gait cycle. Pearson correlation coefficients were computed between the A-P

impulse and the hip flexor and plantar flexor moment impulses, and average leg angle and EMG activity for each phase and subject. Two-sample t-tests with unequal variances (Satterthwaite's method) were used to determine whether differences in paretic and control leg correlations exist.

RESULTS

Significant differences in correlation coefficients between paretic and control leg variables with their respective A-P impulses were found during the second half of ipsilateral stance (Table 1).

Variable	Paretic leg	Control (right) leg	P-value
Single support			
Hip Imp	-.268	-.222	.599
Ankle Imp	.231	.073	.099
Leg Angle	.592	.375	.014[*]
Pre-swing			
Hip Imp	-.423	-.175	.008[*]
Ankle Imp	.115	.511	.048[*]
Leg Angle	.315	.500	.079
RF EMG	-.171	.095	.005[*]
SO EMG	-.083	.306	.0001[*]
MG EMG	-.066	.148	.004[*]

[*]Significant at $p < 0.05$

Table 1. Mean correlation coefficients for each variable with the A-P impulse in single support and pre-swing. P-values represent the probability that there is no difference in paretic and control leg correlations.

In single support, a stronger positive correlation was found between the paretic leg angle with the paretic A-P impulse compared to the control leg. In pre-swing, a stronger negative correlation was found between the paretic hip flexor moment impulse (Hip Imp) and RF activity with the paretic A-P impulse. Also in pre-swing, stronger positive correlations were found between the control plantar flexor moment impulse (Ankle Imp)

and SO and MG activity with the A-P impulse compared to the paretic leg.

DISCUSSION

The hypothesis that a stronger positive correlation between the plantar flexor moment and A-P impulse would exist in the control subjects was supported in pre-swing. A positive, but weaker ankle moment correlation in the paretic leg suggests other factors also contribute to the paretic A-P impulse in pre-swing. Indeed, the strong negative correlation between the paretic hip flexor moment impulse and paretic A-P impulse in pre-swing supports a previous study suggesting increased paretic leg flexor activity acts to prematurely offload the paretic leg, which interferes with plantar flexor contributions to propulsion (Turns et al., 2007). In single support, strong positive paretic ankle moment and leg angle correlations with the A-P impulse suggest increasing paretic ankle output and leg angle (extension) has the potential to increase paretic leg propulsion.

In conclusion, paretic and control hip and ankle moments, EMG activity and leg angles correlated differently with the A-P impulse during the second half of stance. The paretic leg hip and ankle output and leg angle each contribute to the decrease in propulsion generated by the paretic leg.

REFERENCES

Bowden MG et al. (2006). *Stroke,* 37: 872-6.
Chen G et al. (2005). *Gait Posture*, 22: 51-6.
Neptune RR et al. (2001). *J Biomech,* 34: 1387-98.
Turns LJ et al. (2007). *Arch Phys Med Rehabil*, 88: 1127-35.

ACKNOWLEDGEMENTS

EVALUATION OF A HUMAN FOOT PLACEMENT MODEL

Matthew Millard*, Derek Wight, John McPhee, Eric Kubica, and David Wang
Systems Design Engineering, University of Waterloo, Waterloo ON, Canada N2L 3G1
*mjhmilla@engmail.uwaterloo.ca

INTRODUCTION

Falls account for 30% of all hospital admissions in Canada, and are the second leading cause of injury, after motor vehicle collisions (Health Canada 2006). Foot placement has been identified as the primary means used to restore balance to the body, preventing falling (A.E.Patla et al 1999). Work in the field of bipedal robotics echoed this finding [D.Wight et al (2008), Pratt and Tedrake (2006)]. An experimentally-validated mathematical model for foot placement would be extremely useful for understanding and treating dynamic-balance ailments and reducing preventable falls. A promising new foot placement model (D.Wight et al 2008) has been proven to be a useful method for dynamically balancing bipedal robots. Here the model is tested to see if it is able to predict human foot placement during walking, including gait initiation and termination.

MODEL

Wight et al's foot placement estimator (FPE) will *restore* balance to an unbalanced biped — in contrast to previous control strategies for *maintaining* balance (M.Vukobratovic and B.Barovac 2004). Wight et al considered a simplified biped consisting of a single body with 3 degrees of freedom (planar translation and rotation), and two contact points attached to the body through rigid, massless links as shown in Figure 1. The solution to Equation 1 gives ϕ, the angle the lead limb should be held to cause the model to transition to the metastable pose after impact, as pictured in Figure 1.C. This ϕ can be found iteratively using Newton's method, Equation 1 and the biped's iner-
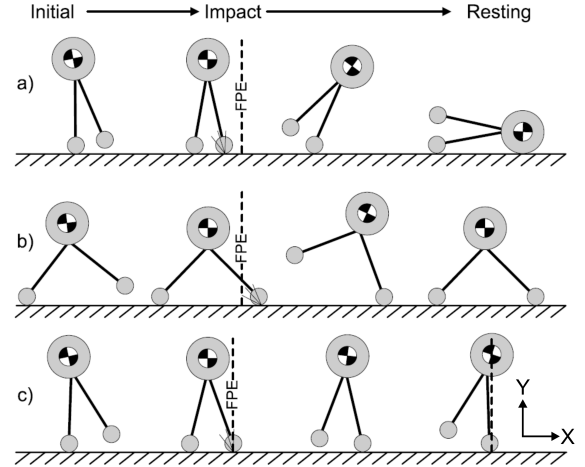
Figure 1: A simplified biped stepping relative to the FPE (D.Wight et al 2008). a) Stepping closer than the FPE results in falling forward. b) Stepping further than the FPE causes the biped to fall back onto the swing leg. c) Stepping precisely on the FPE will balance the center of mass above the standing foot.

tia (m, I_{com}), height at impact (h), linear and angular velocities (v_x, v_y, $\dot{\theta}$). The FPE can be applied to more complicated systems by calculating the FPE for a momentum and inertia equivalent single body biped. For brevity $sin\phi$ and $cos\phi$ have been shortened in Equation 1 to $s\phi$ and $c\phi$.

$$0 = \frac{[mh(v_x\, c\phi + v_y\, s\phi)c\phi + I_{com}\dot{\theta}_1\, c^2\phi]^2}{mh^2 + I_{com}\, c^2\phi} + 2mgh\, c\phi(c\phi - 1) \qquad (1)$$

METHODS

Ten healthy subjects (5 males and 5 females) with a wide range of heights (1.42 - 1.92m)

and masses (69.5 - 114.5 kg) were instrumented with OptoTrack IRED markers to track their movements in the sagittal plane while they walked. IREDs were placed on the distal head of the 5th metatarsal, fibular trochlea of the calcaneus, the lateral malleolus, the proximal fibular head, and the greater trochanter of both legs as well as at the acromion process of both shoulders. Subjects walked with their arms crossed (eliminating the need to track arm movements) at their natural pace, and then at $\pm 20\%$ of their natural cadence using a metronome to cue timing. The three different paces of walking were repeated 10 times through the collection volume. Trials were recorded of constant cadence walking (Thru), and of walking that included gait initiation and termination (I.T.).

The FPE was calculated as in Equation 1 using the equivalent single body velocity and inertia for each subject. The human choice for foot placement was defined as being the horizontal location of the lateral malleolus marker just as the foot contacted the ground; this location was compared to the location the FPE predicted. Foot contact onset was defined as being when the calcaneus marker was 10 mm away from its minimum vertical value between steps. The calculated FPE locations were compared to the measured ones to see how well they correlated (using a Spearman correlation). Probability plots were used to see if the differences followed a normal distribution, after which means and standard deviations were calculated.

RESULTS

In all cases the FPE is highly correlated with human foot placement choices as shown in Table 1. At the same time, the probabilities returned by the Student's t-test clearly illustrate that it is extremely unlikely that the FPE aligns exactly with the location of the lateral malle-

I.T.	Slow	Nat.	Fast
μ	-0.068	-0.029	-0.020
σ	0.019	0.015	0.014
ρ	0.999	0.999	0.9995
t	0.0004	0.0159	0.0975
Thru	Slow	Nat.	Fast
μ	-0.042	-0.006	-0.002
σ	0.036	0.0333	0.0297
ρ	0.997	0.997	0.998
t	0.0008	0.4410	0.8162

Table 1: FPE error means μ and standard deviations σ (in units of meters), Spearman correlation values ρ and t-test probabilities. Trials that included gait initiation and termination are labeled 'I.T.', trials of just constant cadence walking are labeled 'Thru'.

olus at foot contact — with the exception of the natural and fast 'Thru' trials. Probability plots indicate that the errors follow a fat-tailed Normal distribution very closely, proving that the model is accounting for all of the systematic behaviour of human foot placement selection. Thus the resulting error is random, and the FPE is modeling human foot placement with low variability during gait initiation, termination and regular walking across a range of velocities, but with a cadence-dependent offset.

REFERENCES

Canadian Inst. for Health Info. 2006.

A.E.Patla N.Wijneberg and S.W.D.Hill. *Gait and Posture*, 9, 1999.

J. Pratt and R. Tedrake. In *Ruperto Carola Symp. on Fast Motions in Biomech. & Robots*, September 2006.

M.Vukobratovic and B.Barovac. *J. Humanoid Robotics*, 1(1):157–173, 2004.

D.Wight E.Kubica and D.Wang. *J. of Comp. and Nonlinear Dyn*, 2008

HIERARCHICAL SYNERGIES IN BIMANUAL PREHENSION

Stacey L. Gorniak, Vladimir M. Zatsiorsky, Mark L. Latash
Department of Kinesiology; The Pennsylvania State University, University Park
Email: mll11@psu.edu

INTRODUCTION

Recent studies have reported multi-finger force and moment of force stabilizing synergies (FSSs; MSSs) among fingers of the hand during one-hand prehension tasks (Shim et al 2003, 2005). In such studies, synergies have been defined as co-variation among finger forces (or moments of force) across trials, which reduces the variation of total force (or moment of force) production. Studies of one-dimensional force production tasks have shown FSSs are not always present among fingers within-a-hand during bimanual tasks (Gorniak et al 2007a,b). In this study, we investigated within-a-hand and between-hand FSSs & MSSs in bimanual tasks involving one or two persons.

METHODS

Five six-component force-moment sensors were mounted on a handle of adjustable width, narrow (10 cm) and wide (32 cm). A level on the top of the handle provided visual feedback to subjects. Subjects were instructed to grasp the handle using different finger combinations (six for the narrow configuration and five for the wide configuration) and hold it statically in an upright position for 10 s. Finger combinations were: T_R + VF_R, T_L + VF_R, T_E + VF_R, I_L + VF_R, I_E + VF_R, Object + VF_R (where VF_R = 'virtual finger', i.e. the four fingers of the right hand; T = thumb, I = index finger, subscripts R, L, and E denote right, left, and experimenter hands, respectively; Object refers to an inanimate object). Fifteen trials for each condition were collected. Normal and tangential forces of VF_R (F_{VF}^z and F_{VF}^y), their moments of force (M_{VF}^n and M_{VF}^t), and safety margin (SM) were calculated in the grasp plane. Both M_{VF}^n and M_{VF}^t were computed with respect to the axis passing through the center of the handle orthogonal to the grasp plane (see Shim et al 2003). Total moment in the grasp plane was also calculated for VF_R (M_{VF} = M_{VF}^n + M_{VF}^t).

For each point in time, the following variables and their respective variances were calculated for F_{VF}^z, F_{VF}^y, M_{VF}^n, M_{VF}^t, and M_{VF} : output of VF_R, output of individual fingers of VF_R (D_i), output of thumb (or other opposing effector: I_L & I_E), and output of all digits involved (including the opposing effector). An index of co-variation, ΔV, was calculated at two levels: the individual finger (IF) and virtual finger-thumb (VF-T) level ($\Delta V_{IF} = \Sigma$ Var(D_i) -Var(total output)/ ΣVar(D_i) and $\Delta V_{VF-T} = ((Var(VF_R) + Var(T)) - Var(\text{total output})) /(Var(VF_R) +Var(T))$.

RESULTS

Overall, it was found that the SM, F_{VF}^z, and M_{VF}^n outputs were all highest in the single-hand task (T_R + VF_R) and lowest in tasks involving two people (T_E + VF_R & I_E + VF_R) [$p < 0.001$], see Figure 1. In contrast, F_{VF}^y (and M_{VF}^t) were lowest in the case where the handle was partially supported by an inanimate object or by fingers of a single hand [$p < 0.001$]; M_{VF} was lowest if the handle was supported by an inanimate object. For all mechanical variables (F_{VF}^z, F_{VF}^y, M_{VF}^n, M_{VF}^t, and M_{VF}), the finger I_R within VF_R had significantly higher contributions to each variable compared to the other fingers within

VF$_R$ [p < 0.001] (with the exception of M_{VF}^t in the single-hand task).
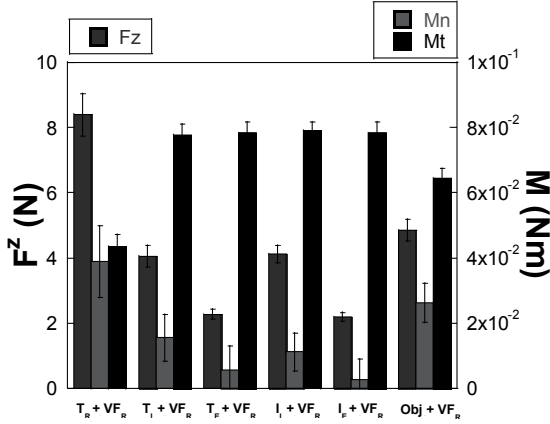
Figure 1: Mean (±SE) F_{VF}^z, M_{VF}^n, and M_{VF}^t data across all finger configurations and subjects; only narrow width data shown

Co-variation indices (ΔV) showed co-variation at one or more levels for each of the mechanical variables, see Table 1.

Variable	VF-T	IF
F_{VF}^y	**ΔV > 0**	**ΔV > 0**
F_{VF}^z	**ΔV > 0**	ΔV ~ 0
M_{VF}^t	ΔV < 0	**ΔV > 0**
M_{VF}^n	**ΔV > 0**	ΔV < 0
M_{VF}	ΔV ~ 0	**ΔV > 0**

Table 1. Co-variation indices for each variable. ΔV > 0 (in bold) indicate the existence of synergies at a given hierarchical level.

DISCUSSION

Regarding mechanical variables, we find that safety margin (SM), grip force (F_{VF}^z), and its moment of force (M_{VF}^n) were highest in the single-hand task and lowest in tasks involving two people. It is likely that subjects used less grip force in trials involving two persons in order to reduce perturbations to the handle. However, load force (F_{VF}^y) and its moment of force (M_{VF}^t) showed an opposite trend. This

is likely since a decrease in M_{VF}^n output by one person necessitates an increase in M_{VF}^t to balance the total rotational moment produced by the same person in a two-person task.

Since the index finger produces higher values of each mechanical variable (with the exception of F_{VF}^y in the single-hand task), it is likely that the thumb (or other opposing effector) exhibits chain effects to compensate for the imbalance of forces and moments caused by the index finger. Thus, coord-ination of moments is not exhibited at both hierarchical levels (see Table 1) due to the existence of these chain effects.

Regarding synergies, our finding of ΔV > 0 at one or more levels of the individual finger-virtual finger system provides evidence for hierarchical control of forces and moments of force produced by the hand. With ΔV > 0 at the IF and VF-T levels for F_{VF}^y, it appears that the CNS actively stabilizes tangential force output of the individual- and virtual-finger system at the same time, while it stabilizes F_{VF}^z (and M_{VF}^n) only at the VF-T level. In contrast, it appears that the CNS stabilizes M_{VF}^t and M_{VF} at the IF level only, particularly since M_{VF}^t and M_T^t are affected by chain effects caused by the index finger. Thus, it we argue that FSSs and MSSs do exist, but are not necessary, at multiple levels of a hierarchy in order to successfully complete a novel prehensile task.

REFERENCES

Gorniak SL et al (2007a). *Exp Brain Res,* 179(2): 167-180.
Gorniak SL et al (2007b). *Exp Brain Res,* 183(2) : 259-270.
Shim JK et al (2003). *Exp Brain Res,* 152: 173-184.
Shim JK et al (2005). *J Neurophysiol,* 93 : 766-776.

BIOMECHANICAL ANALYSIS OF OPENING GLASS JARS: USING KINEMATICS TO INFORM DESIGN

Joseph R. Fair[1], Tamara Reid Bush[2], and Laura Bix[1]
[1]School of Packaging, Michigan State University, East Lansing, MI, bixlaura@msu.edu
[2]Department of Mechanical Engineering, Michigan State University, East Lansing, MI,
reidtama@msu.edu URL: http://www.egr.msu.edu/~reidtama/

INTRODUCTION

Most of the published research regarding the usability of jars focuses on opening forces (Langley et al., Yoxall et al., Crawford et al., Voorbij and Steenbekkers) while few studies address the kinematics. Other factors that may play a role in how people open jars include dexterity, hand size, handedness, or laterality. The goals of research presented here include:

- Development of a methodology for capturing kinematic data when opening a jar in restrained and unrestrained conditions.
- Determination of whether or not requiring the jar to remain on a support surface during opening impacts kinematics.

METHODS AND PROCEDURES

It is theorized that there are three motions that exist when opening jars with lug style closures. These motions are: (1) only the hand on the closure moves, (2) the hand placed on the base of the jar rotates while the hand on the closure remains nearly stationary, (3) and a combined movements of both hands.

Twelve subjects, 7 men and 5 women with an average age of 25 and without a history of injury to the hands, wrists, arms or shoulders were selected for testing. Prior to testing subjects, demographic information was collected. Subject anthropometrics, laterality and preferred dexterity were also recorded. Grip strength and pinch strength (lateral, tip and key) were tested in accordance with tests standards specified by the American Society of Hand Therapists.

Pilot work suggested that subjects employed two styles of opening. In method one, the subject placed their hand on the closure and the other hand around the center of the jar. Subjects that employed the second opening style put one hand on the closure, and used the other hand to grasp the base of the jar, i.e. the palm spanning the jar's bottom thus making the two palms parallel. Two fixtures were created to accommodate each of the two opening styles for testing. This preliminary test of opening style served to inform researchers which of two test fixtures subjects would require during testing.

Two jars with diameters of 87mm and 109mm were used for testing, each with a closure diameter of 70mm and a height of 150mm. Prior to each trial, test jars were fitted with a new closure and torqued to 35 in-lb. Two conditions were tested, one where the subjects were asked to keep the jar on a table and open it (restrained), and a second condition where subjects were asked to pick up the jar and open it (unrestrained). Each subject opened a

total of twelve jars; three trials were recorded for each of the two jars in the restrained and unrestrained conditions. Trials were randomized to mitigate any effect of fatigue on test results. Data were recorded using a five camera Qualisys motion capture system and software.

RESULTS

Preliminary findings indicate that right handed individuals open the jar by placing the right hand on the closure and their left hand on the jar. This is true for both the restrained and unrestrained conditions. Eleven of the 12 subjects opened the restrained jars by rotating their closure hand. Therefore, the dominate hand moved when opening in the restrained condition. Table 1 shows a sampling of the motion data

Gender	Preferred Dexterity	Top Hand	R Hand	L Hand
M	R	R	77	3
M	R	R	89	0
F	R	R	40	0
F	L	L	37	31

Table 1. Sample of the opening motion when restricted to opening the jar on a table at a fixed height of 36" (values in degrees).

In order to open the jars, a total of 30 degrees of rotation is needed. Instances where the total rotation was greater than 30 degrees resulted from the continuation of the movement past the initial point of opening; this is likely due the force necessary to overcome the torque applied prior to opening.

DISCUSSION

Current data suggests that when restricted, subjects tend to use one of two motions to open jars, the closure hand alone, or a combination of both hands. However, further testing is needed to generalize this finding.

SUMMARY

Preliminary findings indicate that only two of the opening motions are used when subjects are required to keep the jar on the table. Further analysis will compare differences in the kinematics for each subject between unrestrained and restrained protocols. This research provides a methodology for use in future research evaluating the affects of ageing on accessibility of packaging.

REFERENCES

Crawford JO, Wanibe E, Nayak L (2002) Ergonomics 45: 922-933

Langley J, Janson R, Wearn J, Yoxall A (2005) Packaging Technology and Science 18: 285-293

Voorbij AIM, Steenbekkers LPA (2002) Applied Ergonomics 33: 105-109

Yoxall A, Janson R, Bradbury SR, Langley J, Wearn J, Hayes S (2006) Packaging Technology and Science 19: 219-225

ACKNOWLEDGEMENTS

IN VIVO COMPRESSIVE STRESSES IN THE INTERVERTEBRAL DISC

Donita Bylski-Austrow, David Glos, Frank Sauser, Alvin Crawford, Eric Wall
Department of Orthopaedics, Cincinnati Children's Hospital Medical Center, Cincinnati
Ohio, USA, donita.bylski-austrow@cchmc.org

INTRODUCTION

While preclinical tests of spine instrumentation often use quadrupedal animal models, differences in *in vivo* biomechanical conditions compared to bipeds are not well defined. The purpose of this study was to determine whether **1)** normal physiological activity of a quadruped correlated with variations in disc compressive stress, and **2)** implant insertion increased the baseline disc stress under surgical conditions. Supporting *in vitro* experiments were performed to determine whether staple implantation immediately **3)** increased the baseline static compressive stress, **4)** created a side-to-side stress differential, and **5)** attenuated dynamic stresses asymmetrically.

METHODS AND PROCEDURES

Using microelectromechanical (MEMS) techniques, custom compressive stress sensor packages were fabricated using piezoresistive dies in a full Wheatstone bridge configuration (Silicon Microstructures Inc., Milpitas, CA). Dies were incorporated into a metallic package to withstand dynamic stresses and attach firmly to vertebrae. Sensors were electrically connected to carriers using ultrasonic wire-bonding. Four package designs were tested for longer-term durability. Each sensor was dynamically calibrated in fluid (hydrostatic pressure), solid contact stress, and *in situ* before implantation and after spine harvest.

In 6 live skeletally immature domestic pigs (approved by an IACUC), a right thoracotomy approach was used to implant 4 sensors and a custom titanium implant. The sensors were placed in pairs at T7-8 and T5-6, with the implant across the right side of one disc space. Wires were routed subcutaneously and out the posterior cervical region. Placement was documented using fluoroscopy. Stresses were measured for durations of 100 seconds at 670 Hz, during surgery, postoperatively 3 times per week, and at 2, 4, 6 and 8 weeks with the animal prone and anesthetized. Video was used to document activities. Stress–time histories were categorized into segments using video: during implant insertion, during walking, manual bending and flexion. After 8 weeks, spines were harvested; instrument placement was documented with CT, and the sensors were retrieved for recalibration. Fourier analysis was used to quantify frequency content.

In 5 isolated porcine motion segments, custom stress sensors were inserted into left and right sides of the annulus. Specimens were tested before and after insertion of a custom staple. Axial compression of 400 N was applied along the longitudinal axis (y) of the spine. Displacement range and rate were controlled. Load-displacement curves were used to define baseline and peak compressive stresses. The MEMS sensors were used to measure compressive stress component σ_{yy} before and after staple insertion, as in surgical conditions.

RESULTS

In vivo, dynamic stresses were recorded at both levels, including on the stapled side. Mean stresses during breathing were 0.05-0.10 MPa; and during walking, 0.2 MPa. Manual bending and flexion resulted in peak stresses of 1.9 MPa. Compressive stresses ranged from 15% to 50% of reported values in humans, depending on activity. Staple implantation resulted in an increase in baseline stress of 0.1 to 0.2 MPa immediately post-operatively. Calibration factors proved stable (< 1% change) after 8 weeks *in vivo* for 2 sensors of the final design.

In *in vitro* biomechanical tests, staple insertion resulted in an increase in baseline stress of 0.10 MPa (± 0.03). Staple insertion resulted in a decrease in mean peak dynamic compressive stresses *in vitro*. After stapling, mean peak dynamic compressive stresses were 77% of control values.

DISCUSSION

Compressive stresses measured *in vivo* in the intervertebral discs of a quadruped ranged from 15% to 50% of reported values in humans, depending on activity. Staple implantation increased mean compressive stresses in the intervertebral disc in both *in vivo* and *in vitro* tests. Stresses were dynamic at both control and stapled levels.

In vitro, hemiepiphyseal stapling produced an immediate increase in the magnitude of the baseline static compressive stress. It also decreased peak dynamic compressive stresses, but not dramatically. The baseline magnitude increase corresponded to the *in vivo* study. The baseline stress increase was likely due to at least in part to the angle between the blades which drew vertebrae together during insertion. The cantilevered blades transmitted most peak stresses, and indicated that the disc was subjected to both static and dynamic stress gradients.

Stresses may be compared to prior human *in vivo* stress measurements (Nachemson and Morris, 1964, Wilke et al., 1999). This study indicates that mean stresses were approximately 30% of those reported in the nucleus of human lumbar discs.

SUMMARY

Dynamic compressive stresses of up to 2 MPa were measured *in vivo* in quadruped spines during activities. A method of hemiepiphysiodesis reported to slow vertebral growth asymmetrically was shown to increase the static baseline stress at time of implantation. The disc was not isolated from physiological compressive stresses. This study indicates the extent to which constraining joint displacement on one side of the spine reduces the motion of the intervertebral joint, and shields disc and bone from compressive stresses.

REFERENCES

Nachemson, Morris. *J Bone Joint Surg*., 46A: 1077-1964, 1964.
Wall et al, *Spine* 30:1148-1153, 2005.
Wilke et al, *Spine* 24:755-762,1999.

ACKNOWLEDGMENTS

AN OBJECTIVE EVALUATION OF SEGMENTED FOOT MODELS USING A ROBOTIC DYNAMIC ACTIVITY SIMULATOR

Nori Okita[1,3], Steven A. Meyers[3], John H. Challis[1], and Neil A. Sharkey[1,2]

Departments of [1]Kinesiology, [2]Orthopaedics and Rehabilitation, and [3]Mechanical and Nuclear Engineering, The Pennsylvania State University, University Park, PA 16802, USA
Email: nas9@psu.edu; URL: http://www.biomechanics.psu.edu

INTRODUCTION

Over the last several years investigators have proposed methods for measuring the motions of different regions of the foot to quantitatively assess foot function in health and disease. These methods consider the foot as a system of segments, whereby the tibia (TIB), hindfoot (HF), and forefoot (FF) are treated as separate rigid bodies that move relative to each other. The goal of the current study was to objectively verify the utility of this approach by comparing the multi-segment kinematic data calculated from skin- and bone-mounted markers. By using a high fidelity cadaveric Robotic Dynamic Activity Simulator:RDAS (Hoskins, 2006), comparisons were conducted under five simulated neuromuscular conditions.

METHODS AND PROCEDURES

A total of ten normal fresh frozen cadaver extremities (5M/5F, 59.2 ± 14.2 years) were evaluated. The RDAS was employed to conduct dynamic simulations of the stance of gait at 1/20th the velocity of typical walking. For each specimen, the baseline *Normal* simulation was achieved by adjusting sagittal plane tibia kinematics and six muscle actuations (Tibialis Anterior:TA, Tibialis Posterior:TP, Peroneus longus, Flexor hallucis longus, Flexor digitorum longus, Triceps Surae) until target ground reaction forces were attained. Four additional conditions simulating common neuromuscular pathologies were examined by altering specified muscle activation patterns while holding other simulation parameters at normal values: *NoTP* (no TP activation during stance phase), and three hyperactive conditions set at 75% of the normal peak output through out stance phase: *ExtTA* (hyperactive TA), *ExtTP* (hyperactive TP), and *ExtTATP* (hyperactive TA and TP).

A seven-camera passive marker 3D photogrametry system (Motion Analysis Corporation, Santa Rosa, CA) was employed to capture marker motion at 100 Hz with a typical 3D reconstruction residual of 0.3 mm. A three-segment foot and ankle model (TIB, HF, FF) was developed based on Buczek et al. (2003). The joint angles were obtained by taking ZYX Cardan decomposition of the distal segment with respect to the proximal segment.

The first marker configuration (referred to as "REAL markers") utilized external skin markers (3/8" diameter) adhered with cyanoacrylate on the following 9 landmarks: medial and lateral malleoli; medial, posterior, and lateral calcaneus; bases and heads of Metatarsals 1 and 5, respectively.

Following successful collection of 15 trials (5 conditions × 3 repetitions each) with REAL markers, every bone of the foot except for the phalanges was instrumented with marker clusters (four 1/8"-dia. markers on carbonfiber rods), and another 15 trials were collected. The second marker configuration (referred to as "VIRTUAL markers") was then calculated as the virtual skin markers from the collected motion of bone-mounted

markers and fixed local vectors in respective bones. The local vectors were determined by merging the static data with skin and bone markers. The static trials were extracted from normal walking trials when the tibia was aligned with vertical axis to reflect muscle action.

A General Linear Model ANOVA (Minitab, State College, PA) was used to examine the significance of interaction term "Condition × Marker type" with $\alpha=0.05$, and followed by post-hoc comparisons with Bonferroni correction ($\alpha=0.05$).

RESULTS

As listed in Table 1, significant Condition × Marker type interaction term was found in the Int/Ext rotation profiles of all joints. Only the hyperactive conditions resulted in significantly different means. Representative results for *ExtTA* are shown in Figure 1. The maximum difference between the REAL and VIRTUAL data in significantly different joint angles was approximately 2.5 degrees.

INT/EXT Axis	ANOVA	Bonferroni Group Comparison for REAL v.s. VIRTUAL				
		Normal	NoTP	ExtTA	ExtTP	ExtTATP
HF_TIB	0.000	0.280	1.000	**0.000**	0.100	**0.000**
FF_TIB	0.000	0.090	1.000	**0.000**	1.000	**0.000**
FF_HF	0.004	1.000	1.000	1.000	**0.020**	1.000

Table 1: Results of ANOVA and Bonferroni Comparisons. Significance level was set at p<0.05.

DISCUSSION

Based upon the current results, all joint angles calculated from REAL or VIRTUAL markers under *Normal* and *NoTP* resulted in statistically similar measured angles. Hyperactive conditions resulted in significantly different measurements but only in Int/Ext rotation angles. One possible explanation is that the foot was mostly constrained by the floor during 0~90% of stance, allowing transverse rotation of bones due to the imbalance caused by hyperactive muscle force, but constraining abnormal motions in the sagittal and frontal planes.
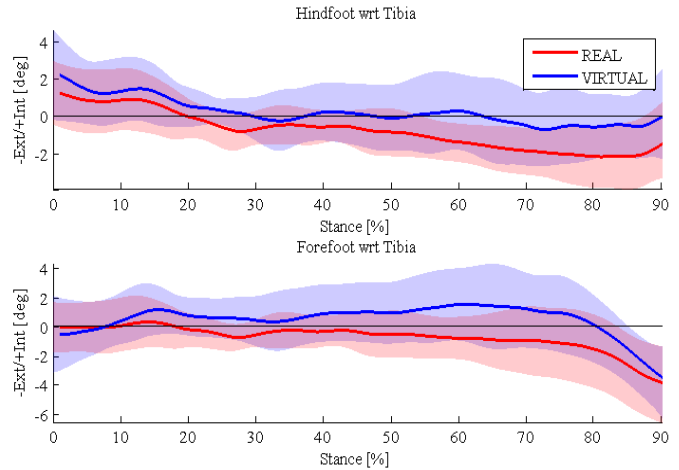
Figure 1: Int/Ext rotation of left HF_TIB and FF_TIB joints under ExtTA condition. Each shade represents ±sd.

Overall, the REAL and VIRTUAL marker data agreed well (within 2.5° mean difference even in Int/Ext rotation). This good agreement between the REAL and VIRTUAL marker data may be due to the scaled speed (1/20) of the simulation. Reduced velocity would tend to minimize extraneous marker jiggle and skin motion artefact. On the other hand the reduced velocity of the simulations would tend to amplify viscoelastic effects, allowing the soft tissues to creep and bones to move more than at normal velocity.

SUMMARY

The current study suggests that a three segment foot model based on external skin markers provides a reliable means of assessing overall internal skeletal motion in the sagittal and frontal planes, although detectable inaccuracies exist in the transverse plane (Int/Ext rotation).

REFERENCES

Buczek, FL et al. (2003). *Proc. Pediatric and Adult Foot and Ankle,* NIH.
Hoskins, AH (2006). *PhD Dissertation,* The Pennsylvania State University.

ACKNOWLEDGEMENTS

CONSTRAINED HANDGRIPPING REDUCES MAXIMAL ARM STRENGTH AND MUSCLE ACTIVATION OF THE UPPER EXTREMITIES

Martin P. Smets[1], Jim R. Potvin[1], and Peter J. Keir[1]

[1]McMaster Occupational Biomechanics Laboratory, Department of Kinesiology, McMaster University, Hamilton, ON, Canada, smetsmp@mcmaster.ca

INTRODUCTION

Many industrial tasks require that hand gripping and cognitive effort occur in conjunction with repetitive shoulder exertions. Predictive algorithms are often used to estimate static strength in various postures. These predictions are used in job design to optimize efficiency while minimizing the risk of worker injury. However, task complexity, in the form of concurrent hand gripping or increased mental effort, has been found to reduce deltoid muscle activity and, thus, total arm strength (Sporrong, 1995; MacDonell & Keir, 2005). Currently, these factors are not considered in standard strength prediction methods. The purpose of this study was to evaluate the effect of constrained and unconstrained hand gripping on maximal arm strength.

METHODS AND PROCEDURES

Ten female subjects performed seated maximal arm exertions in five directions (up, down, left, right, push), at two heights (elbow and shoulder), and two grip conditions (Constrained: 30% maximum voluntary grip (MVG) and Freestyle: where subjects were free to grip as they chose). The hand, positioned anterior to the shoulder with a reach equal to 70% of subject arm length, grasped a vertically oriented handgrip dynamometer. Grip force feedback was displayed on a monitor. During the Constrained 30% MVG condition, subjects were given a visual target to guide their grip force. Arm strength was measured with a triaxial force transducer mounted to the base of the handgrip dynamometer. EMG was collected on the following eight muscles of the right upper extremity; trapezius, anterior deltoid, middle deltoid, posterior deltoid, biceps brachii, triceps brachii, flexor carpi ulnaris, and extensor carpi ulanaris.

RESULTS

Subjects were found to target the 30% MVG trials accurately (mean = 31.7 ±0.4%). In the Freestyle condition, a significant interaction was found between grip, direction and height. At shoulder height, the Freestyle grip for the down and push forward directions were 22% higher and 41% lower, respectively, when compared to the Constrained 30% MVG (Figure 1). However, regardless of these grip force differences, the Constrained gripping always resulted in decreased arm strength across all directions (mean % decrease = 21.5 ±5.8%) (Figure 2).
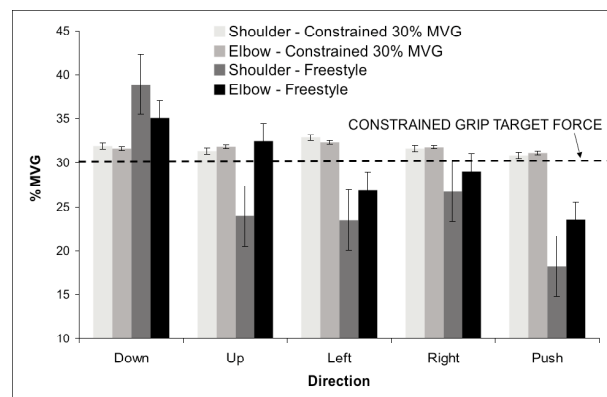
Figure 1. Mean grip forces (%MVG with SEM) forces, pooled by direction of force application at different heights. In the Freestyle grip trials, subjects adopted

grips that were sometimes higher and at other times lower than what was used in the Constrained grip trials.
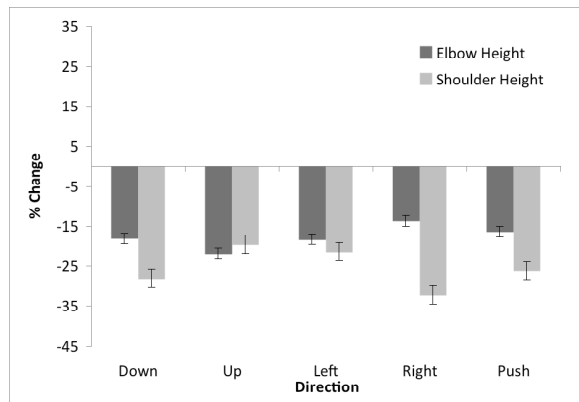
Figure 2. Mean percent decrease (with SEM) in maximal arm strength in the Constrained grip condition, relative to Freestyle grip. Significant decreases were seen in all directions (F=2.741, P<0.05). This effect was greater at shoulder height versus elbow height for arm exertions to the left, right, down, and pushing forward.

Muscle activation decreased in all muscles when the grip was constrained (all $F_{1,9} > 6.013$, all P<0.05). Overall, activation levels decreased by 30.6% at shoulder height and 14.8% at elbow height.

DISCUSSION

These findings indicate that increased grip forces alone may not be responsible for decreases in maximal arm strength. Unconstrained gripping resulted in greater maximal arm strengths, compared to the 30% MVG conditions, regardless of whether or not individuals chose a grip force that was higher or lower than the constrained value. Additionally, there was a consistent decrease in muscle activation with constrained gripping. This decrease occurred across all muscles even if their function did not contribute to the direction of movement. It would seem that there is an overall muscular inhibition (or a redistribution to muscles not monitored here) when cognitive demands are present during maximal force production. These findings are consistent with other studies looking at force and muscle activation changes during concurrent hand gripping and mental tasks (Au & Keir, 2007; MacDonell & Keir, 2005). MacDonell and Keir (2005) observed decreases in shoulder strength and muscle activity with sub-maximal hand gripping and further decreases when sub-maximal hand gripping was combined with mental effort. Others have seen increases in rotator cuff activity during intermittent and static hand gripping tasks (Sporrong, 1995 MacDonell & Keir, 2005). It is possible that the decreases in deltoid activity, and subsequent strength reductions, are part of a preventative mechanism to protect the sensitive stabilizing muscles of the rotator cuff.

SUMMARY

The results of this study indicate that maximal arm force is consistently reduced when hand gripping is constrained. These decreases seem to have less to do with the chosen grip force, and more to do with the mental effort required to maintain a sub maximal grip through visual target matching. Significant decreases in maximal arm strength in all directions were coupled with similar reductions in muscle activation. This information is valuable considering the wide use of force prediction software in job design.

REFERENCES

Au, A & Keir, PJ (2006) *J of Electromyog Kinesiol* Vol 17(5):578-586
Sporrong, H. (1995) *Eur J Appl Physiol Vol* 71:485-492.
MacDonell, C & Keir PJ (2005) *Ergonomics* 41(15):1749-1769

ACKNOWLEDGEMENTS

TIBIOFEMORAL CONTACT PRESSURES AND OSTEOCHONDRAL MICROTRAUMA FROM ACL RUPTURE VIA HYPEREXTENSION AND JOINT COMPRESSION

Eric G. Meyer, Timothy G. Baumer and Roger C. Haut
Michigan State University, East Lansing, MI, USA
E-mail: haut@msu.edu, Web: www.obl.msu.edu

INTRODUCTION

Participation in sports increases the risk of acute and chronic injuries, such as ligament sprains or OA, respectively. The knee is one of the most frequently injured joints with approximately 80,000 ACL tears in the US each year with a total cost of nearly one billion dollars (Griffen, 2000). Interestingly, 50-70% of patients with ACL rupture have radiological changes consistent with chronic disease after 15-20 yrs (Gilquist, 1999). In 80% of these cases, a characteristic osteochondral lesion occurs, which is often associated with an overt loss of articular cartilage (AC) overlying the "bone bruise" within 6 months of injury (Vellet, 1991). These associated damages in patients may form the basis for the development of post-traumatic OA in both ACL-reconstructed and non-reconstructed patients (Mykleburst, 2005). The objective of the current study was to document the levels of contact pressure developed in the cadaveric human knee joint during rupture of the ACL via isolated axial compressive loading and isolated hyper-extension. Additionally, this study was designed to investigate acute injury to the underlying subchondral bone (SB). A hypothesis of the study was that the types and extent of these injuries would depend on the relative joint motion producing ligamentous injury to the knee.

METHODS

Experiments were conducted on 6 pairs of cadaver tibiofemoral (TF) joints (49.4 ± 9.6 yrs). The bone ends were potted in cylindrical aluminum sleeves and in both experiments, axial tibia rotation was fixed, but varus/valgus angular rotation was unconstrained. Hyperextension was applied via four-point bending, with the moment applied to the potting cups. The femoral cup was mounted on an XY translational table to allow medial/lateral and proximal/distal motion. Angular displacements were applied via repeated, increasing magnitudes until catastrophic injury of the joint. Compression was applied axially in the tibia on a 30° flexed knee using a similar method. Pressure film was inserted into the TF joint to record contact area and pressure in the medial and lateral compartments. After testing, the film was scanned and converted to pressures using a calibrated density-to-pressure scale. The area over 25 MPa and maximum pressure during failure were also documented to compare the location of potentially microdamaged AC and SB. Finally, samples of each tibia were prepared for standard histology. Microcracks, including both horizontal and vertical cracks, occurring at the cartilage-bone interface were recorded. Statistical differences for $p < 0.05$.

RESULTS AND DISCUSSION

All failures involved the ACL, although there were frequently other ligamentous or meniscal injuries, including five of the six hyperextension specimens which included a partial tear of the PCL and posterior capsule. The hyperextension moment was 292±118 Nm at failure with an extension angle of 26±8.7°. The compression specimens had a peak load of 6.7±1.6 kN and posterior displacement of the femur of 24±9.7 mm relative to the tibia. Both types of experiments

generated slightly higher contact area in the medial compartment than in the lateral compartment (Figure 1). Compression experiments resulted in similar values between the medial and lateral compartments for both the average contact pressure and maximum pressure, while the hyperextension pressures were higher in the medial compartment (Table 1). There were not differences in peak or average pressure between the two experiments, although the distribution and locations were different due to the femur's posterior drawer in compression and anterior rotation in hyperextension. Analysis of the histological samples for micro-damage revealed significantly more micro-cracks in the lateral compartment of compression specimens than in hyperextension specimens. In addition, the hyperextension specimens revealed significantly more microcracks on the medial facet than on the lateral facet. Finally, the micro-cracks were located central to anterior in both compartments of hyperextension specimens, and central to posterior in both compartments of compression specimens.

Table 1. Pressure film data from failure experiments. *Significant difference between medial and lateral compartments.

	Average Contact Area (mm^2)		Average Contact Pressure (MPa)	
	Medial	**Lateral**	**Medial**	**Lateral**
Compression	151 (90)	113 (101)	16 (3)	14 (3)
Hyperextension	90 (44)	71 (42)	19 (3)*	14 (2)
	Area > 25 MPa		**Maximum Pressure**	
Compression	19 (29)	2 (3)	31 (10)	25 (5)
Hyperextension	15 (19)	1 (1)	34 (8)*	24 (7)
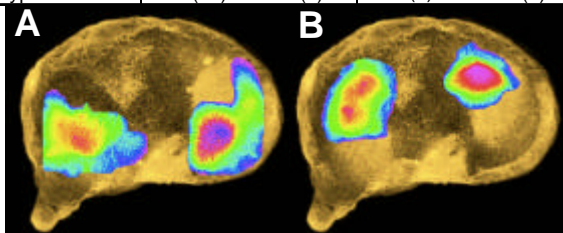
Figure 1. Representative contact pressure distributions for A) compression and B) hyperextension experiments.

SUMMARY/CONCLUSIONS

Compression experiments resulted in regions of high contact pressure on the posterior tibia plateau, while hyperextension experiments resulted in regions of high contact pressure on the anterior tibial plateau. Bone bruises seen in the posterolateral and medial aspects of the tibia in failure mechanisms with a large compressive force (Kaplan, 1999) and in the anterior aspect of the tibia with hyperextension (Sanders, 2000) may be associated with high contact pressures shown in the current study. Although in different locations, the number of microcracks at the cartilage-bone interface were similar between compression and hyperextension specimens. A comparison of this data with similar previous compression experiments involving constrained varus/valgus bending and unconstrained axial tibia rotation (Meyer, in press) revealed no differences in either histological or pressure film results. This may be due to coupling between valgus moments and internal tibia rotation. Finally, 5/6 specimens tested in pure hyperextension also suffered PCL and capsular damages, suggesting that isolated ACL injuries do not occur for the clinical hyperextension case where the loading is due to a pure bending moment on the knee. In contrast, three point bending tests can induce shear force in the knee joint that can generate isolated ACL rupture (Fornalski, 2008).

REFERENCES

Fornalski S. (2008) *Am J Sports Med*. 36, 80-4
Gilquist J. (1999) *Sports Med*. 27, 143-56.
Griffen L. (2000) *J Am Acad Orthop Surg*. 8, 141-50.
Kaplan P. (1999) *Radiology*. 211, 747-53.
Meyer E. (in press) *Am J Sports Med.*
Mykleburst (2005) *Brit J Sports Med*. 39, 127-31.
Sanders T. (2000) RadioGraphics. 20, S135-51.
Vellet A. (1991) *Radiology*. 178, 271-6.

ACKNOWLEDGEMENTS

KNEE JOINT RELATIVE MOTION DURING ACL RUPTURE BY INTERNAL TIBIAL TORSION OR TIBIOFEMORAL COMPRESSION

Eric G. Meyer, Timothy G. Baumer and Roger C. Haut
Michigan State University, East Lansing, MI, USA
E-mail: haut@msu.edu, Web: www.obl.msu.edu

INTRODUCTION

The knee is one of the most frequently injured joints in the human body. Approximately 91% of ACL injuries occur during sporting activities, usually from a non-contact event (Paul, 2003). The most common kinematic scenarios for ACL injuries are internal twisting or combined loading during a hard landing (Ettlinger, 1995). Biomechanical studies confirm that the ACL is a primary stabilizer of the knee for internal tibial rotation (Markolf, 1995) and TF joint compression (Torzilli, 1994), especially between full extension and 30° of flexion. ACL strain measurements *in vivo* show similar magnitudes between weightbearing loads of 40% and 10 Nm of internal tibia torque (Flemming, 2001). Few studies however, have documented relative knee joint displacements at failure levels of force. The goal of the study was to induce ACL rupture in the knee joint by isolated internal tibial torsion or TF compression and measure the relative joint motions that occur prior to, and following, the injury. These relative motions of the knee joint may be important for the interpretation of injury mechanisms from video-based studies of clinical ACL tears.

METHODS

Experiments were conducted on 20 cadaver tibiofemoral (TF) joints (53.5 ± 7.9 yrs). The bone ends were potted in cylindrical aluminum sleeves. For both compression and torsion experiments the flexion angle was fixed at 30° and the femur was attached to an X/Y translational table that had linear encoders attached to record anterior/posterior as well as medial/lateral motions relative to the tibia. Compression was applied axially through the tibia via repeated, increasing load tests until catastrophic injury of the joint. In one series of experiments (C1, n=7) axial rotation of the tibia was unconstrained and internal/external rotation was recorded with a rotary encoder, but varus/valgus rotation was prevented. The opposite, paired joints from this series of experiments were loaded with an internal torque (T) that was applied through the tibia with a similar repeated loading protocol. Femur varus/valgus rotation was unconstrained and recorded with a rotary encoder. In a second series of experiments (C2, n=6), TF joints were also loaded in compression, similar to C1, with the exception that femur varus/valgus rotation was unconstrained and recorded, but tibia internal/external rotation was prevented. The peak forces and relative joint motions were documented from the tests immediatedly prior to failure (SF) and during failure (F). Statistical t-tests were used to test for significant differences ($p < 0.05$).

RESULTS AND DISCUSSION

Internal tibia rotation produced a coupled posterior and lateral displacement and valgus rotation of the femur (Table 1). The results for the two series of compression experiments were similar and also showed posterior femur displacements. However, when axial rotation of the tibia was allowed there was a slight medial motion, but when varus/valgus rotation was allowed there was lateral motion of the femur. Most of the displacements produced significantly higher magnitudes in F tests than SF tests with one notable exception. There was internal tibia rotation in C1 experiments before ACL failure, but after

failure the rotation switched to external. The largest increase in displacement after failure for compression was posterior displacement of the femur.

All failures involved the ACL, although there were frequently other ligamentous or meniscal injuries. The compressively loaded specimens had a peak load of 6.0±1.9 kN, while the torsionally loaded specimens failed at 37.4±16.8 Nm. Avulsion fractures occurred in 7 specimens and there were significant differences between the failure loads in these versus midsubstance failures for compression experiments (6.8 versus 4.3 kN), but not for torsion experiments. The displacement values were similar between injury types (p values between 0.18-0.37).

Table 1. Average (SD) for compression and torsion experiments. # Difference between SF and F, * difference between C1 and C2.

		Compressive Load (kN)/ Torque (Nm)	Posterior Femur Displacement (mm)	Lateral Femur Displacement (mm)	Internal Tibia Rotation (Deg)	Valgus Femur Rotation (deg)
C1	SF	5.0 (1.9)#	12 (5.2)#	-2.1 (4.8)	3.9 (4.0)#	
	F	5.4 (2.0)	27 (15)	-1.5 (8.1)*	-6.1 (4.3)	
C2	SF	5.8 (1.6)#	12 (4.3)#	0.1 (2.1)#		1.3 (3.2)#
	F	6.7 (1.6)	24 (9.7)	5.6 (3.9)		8.0 (3.6)
T	SF	36 (14)#	8.4 (3.3)	6.3 (5.1)#	46 (16)#	11 (6)#
	F	37 (17)	10 (4.1)	11 (4.0)	58 (18)	20 (5.7)

SUMMARY/CONCLUSIONS

Our laboratory has previously documented ACL rupture from TF compressive loading for knee flexion angles of 60, 90 and 120° (Meyer, 2005). The current study provides new information for important joint motions, such as the maximum anterior drawer and internal rotation of the tibia, that occur prior to injury. During compression, the femur displaced posteriorly relative to the tibia in SF tests and with a significantly higher magnitude in F tests (Figure 1). Others have

also documented a similar "anterior neutral shift" of the tibia during weightbearing (Torzilli, 1994) that could predispose the ACL to rupture. In C2 and T experiments there was a significant increase in valgus angular displacement after ACL failure. The study confirmed that joint motions can vary before and after failure of the ACL. There was also approximately 4° of internal tibia rotation before failure, but 6° of external rotation after. External tibial rotation and valgus joint motions are frequently documented in video analyses of sports related ACL injuries. However, the exact time when the ACL ruptures is unknown (Olsen, 2004). The current study may suggest these video documented motions actually occur after rupture of the ACL.
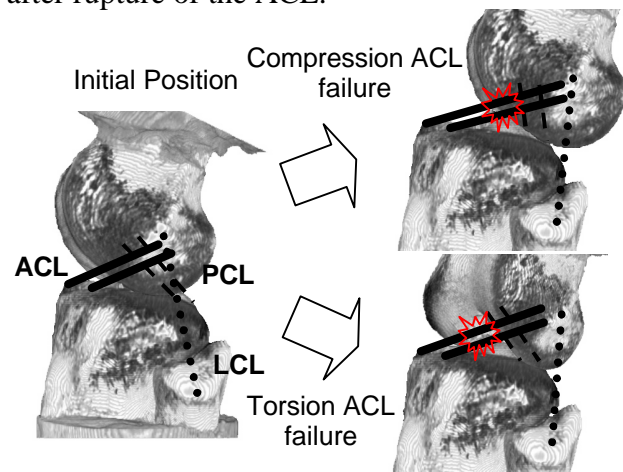
Figure 1. Sagittal view, for a fixed tibia, of the relative TF joint motion.

REFERENCES

Ettlinger C. (1995) *Am J Sports Med*. 23, 531-7.
Flemming B. (2001) *J Biomech*. 34, 163-70.
Markolf K. (1995) *J Orthop Res*. 13, 930-5.
Meyer E. (2005) *J Biomech*. 38, 2311-16.
Olsen O. (2004) *Am J Sports Med*. 32, 1002-12.
Paul J. (2003) *Clin J Sports Med*. 13, 1-5.
Torzilli P. (1994) *Am J Sports Med*. 22 105-12.

SEPARABILITY OF INDIVIDUALS WITH NON-SPECIFIC ARM PAIN FROM ASYMPTOMATIC SUBJECTS USING EMG SPIKE SHAPE ANALYSIS

Kristina M. Calder[1], David A. Gabriel[2], and Linda McLean[1]

[1]School of Rehabilitation Therapy, Queen's University, Kingston, ON, Canada,
4kmc2@queensu.ca
[2]Faculty of Applied Health Sciences, Brock University, St. Catharine's, ON, Canada

INTRODUCTION

The wrist extensor muscles have been implicated in a work-related upper limb disorder referred to as non-specific arm pain, which, as the names suggest, has an unknown pathophysiology. Patients with NSAP complain of diffuse forearm pain during and after repetitive tasks, and have muscle pain and tenderness on palpation. A recent study used quantitative motor unit potential analysis techniques to investigate differences in the eletrophysiological characteristics of motor units (MUs) among healthy subjects, subjects at-risk for NSAP, subjects with lateral epicondylitis (LE) and subjects with NSAP and found evidence that individuals with NSAP may have myopathic changes in their wrist extensor muscles (Calder et al., 2007). Although concentric needle electromyography can provide such important information, it is an invasive approach to studying MU properties.

An alternative method of studying MU properties is to use surface electromyography (SEMG) as presented by Gabriel (2000) to determine differences in MU firing patterns detected from the SEMG interference pattern (IP). This non-invasive technique, called 'spike shape analysis' uses the shape of individual spikes within the SEMG IP to make inferences about changes in MU firing patterns (Table 1).

Table 1. Predicted changes in the SEMG spike parameters for alterations in MU recruitment.

	MSA	MSF	MSS	MSD	MNPPS
firing frequency	−	↑	−	↓	−
recruitment	↑	↑	↑	↓	↑
synchro-nization	↑	↓	↑	↑	↓

In this study we compared changes in SEMG spike shape analysis parameters across different levels of isometric wrist extension contractions among individuals with NSAP, individuals deemed at-risk for NSAP, and asymptomatic control subjects. The purpose of the study was to determine (i) if SEMG recorded from the extensor carpi radialis brevis (ECRB) muscle show spike shape changes with increasing isometric force within the three groups; and (ii) if measurable differences in spike shape analysis parameters exist among the groups.

METHODS AND PROCEDURES

Twenty-two asymptomatic control subjects, eight subjects deemed at-risk for NSAP, and sixteen subjects with NSAP participated. Subjects were seated with the elbow of their most affected limb (NSAP subjects) or dominant arm (control subjects and at-risk subjects) flexed to 90º and with their forearm pronated and resting on a custom-built table. Maximum isometric wrist extension force was measured in Newtons by a strain gauge secured to the bottom of the testing table with adjustable straps secured around the dorsum of

the hand. SEMG data were recorded from the ECRB muscle during 5-s randomized isometric wrist extension contractions at 10, 20, 30, 40, 50, 60, and 70% of maximum voluntary force.

Five criterion measures: mean spike amplitude (MSA), mean spike duration (MSD), mean spike slope (MSS), mean spike frequency (MSF), and mean number of peaks per spike (MNPPS), were calculated using spike shape analysis, as described in detail by Gabriel et al.(2007). The measures were compared across contraction levels within groups using one way repeated measures analyses of variance. Analyses of covariance were used to determine the effects of group and contraction level across the measures. The α-level was set at 0.05.

RESULTS

All groups behaved in a predictable manner, whereby firing frequency and recruitment appeared to be the primary mechanisms for increases in force production. Four parameters significantly changed across the contractions levels for the control and NSAP and at-risk subjects ($p>0.05$) (Table 2). Significant interactions between group and contraction level were observed for MSA and MSS, where the NSAP group exhibited significantly lower positive slopes than the control subjects ($p<0.05$)

DISCUSSION

In myopathic conditions, compensatory mechanisms may occur whereby increased recruitment of MUs and greater MU firing rates occur at lower levels of contraction because the low number of muscle fibers in a given MU cannot produce adequate force. This may explain the absence of change in MNPPS with increasing force output in the NSAP group. Degeneration of muscle fibers with subsequent regeneration is reflected by short-duration, low-amplitude and polyphasic individual MU potentials might explain the lower MSS and MSA slopes found in the NSAP group.

SUMMARY

This work provides evidence that a non-invasive approach to MU morphological analysis may be possible using SEMG. The results of the spike shape analysis support our previous findings using decomposition-based MU potential morphological analysis on these same experimental samples, which also suggested that individuals with NSAP demonstrate myopathic changes in their ECRB muscle.

REFERENCES

Calder, KM et al., (2007). *PREMUS*, Boston, USA
Gabriel, DA (2000). *Clin Neurophysiology*, 40: 423-30.
Gabriel, DA et al., (2007). *J Neurosci Methods*, 159: 146-52.

ACKNOWLEDGEMENTS

Table 2. Slope values of the spike shape parameters with increasing force production.

Group	MSA(mV)	MSF(Hz)	MSS (mV/ms)	MSD(ms)	MNPPS
Asymptomatic control subjects	+0.19*	+4.07*	+0.03*	-0.09	-0.01*
At-risk subjects	+0.07*	+4.10*	+0.01*	-2.12	-0.01*
NSAP subjects	+0.06*	+5.96*	+0.01*	-0.32*	-0.00

*Significant at the 0.05 level

MUSCLE ACTIVATION CORRELATES WITH VIBRATION INTENSITY MEASURED DURING ALPINE SKIING

Peter Federolf[1], Benno Nigg[1], Vinzenz von Tscharner[1], Martin Gimpl[2], Erich Mueller[2]

[1] Human Performance Laboratory, University of Calgary, Alberta, Canada
peter.federolf@kin.ucalgary.ca URL: www.kin.ucalgary.ca/hpl
[2] Christian Doppler Laboratory Biomechanics in Skiing, University of Salzburg, Austria, Europe.

INTRODUCTION

Vibration exposure is known to affect muscle physiology and neuromuscular activity. Research of the effect of whole body vibration on muscle activation has focused on passenger safety in vehicles and on work place safety, for which guidelines and international standards have been developed (ISO 2631). However, in many sports the athlete is also exposed to substantial continuous vibrations (e.g. inline skating, mountain biking, alpine skiing) or recurring impact shocks (e.g. running, soccer, tennis). The later have received some scientific attention, however, there are very few studies investigating the impact of continuous vibration exposure on neuromuscular activity during the execution of a specific movement in sports.

The purpose of this study was to quantify simultaneously vibration exposure and muscle activation on four muscles of the lower extremities during alpine skiing.

METHODS AND PROCEDURES

Ten experienced skiers completed 24 runs performing 5-7 short turns, 6 carving turns, and gliding in a tuck position. The 24 trials of each subject were conducted between 9am, and 12.30pm. For eight of the ten subjects, snow conditions changed from hard frozen to soft snow during this time. The skiers were equipped with 1-D acceleration sensors (Analog Devices[TM] (ADXL series), range: 35 to 120g) placed in axial direction on the shaft of the ski boot (parallel to the tibia), on the muscle compartments of the triceps surae, quadriceps and hamstrings, and on skin covering bones close to the ankle, knee hip and neck joints. Muscle activation was measured using bipolar surface EMG sensors on vastus medialis, vastus lateralis, m. semitendinosus, and gastrocnemius. All sensor signals were recorded with a mobile EMG measurement device (Biovision[TM]) carried in a backpack. Measurement frequency was 2000 Hz.

For each run three specific movements were selected for further analysis: four consecutive short turns (2.8 ± 0.3 sec.), four consecutive carving turns (6.4 ± 0.6 sec.) and two seconds of gliding in a tuck position. Short turns are highly dynamic movements in which the muscles act mainly concentric. Carving turns are executed at high speeds with little body motion. Due to centripetal forces the skiers' muscles are loaded eccentrically. Gliding was executed in the tuck position which is characterized by small hip and knee angles. In this position the muscles are mainly isometrically contracted.

The recorded acceleration signal was resolved with a wavelet transformation into intensities calculated for a set of 22 center frequencies between 0.6 and 80 Hz. EMG data was resolved using 13 wavelets with center frequencies between 6.9 and 542 Hz. In both cases, wavelet transformations (von Tscharner, 2000) were used, because in this wavelet definition the intensity calculated

for each wavelet is normalized with respect to the energy content of the original signal. To compare muscle activation levels or vibration exposure between trials, total signal intensities were averaged over the duration of the analyzed movement. Correlation between muscle activation and vibration exposure was analyzed by calculating Pearson's correlation coefficient.

RESULTS

The vibrations the skiers' body is exposed to, determined from the acceleration senor at the subjects' ankles, had amplitudes around 10g, 6g, and 2g for short turns, carving, and gliding, respectively. High vibration intensities were found in the frequency range 5-35 Hz.
Average vibration intensities decreased by a factor 2 to 3 as the snow turned from hard frozen to soft. In many cases, a substantial decrease in the average EMG intensity was observed as the vibration intensities decreased (Figure 1). Table 1 lists the number of subjects for which statistically significant correlations between average EMG intensity and average vibration intensity were found.

DISCUSSION

The movement task executed by the muscles determines muscular activation levels. If the body is additionally exposed to whole body vibrations, then muscular activation levels of selected muscles increase in many cases. Reasons for increased muscle contraction
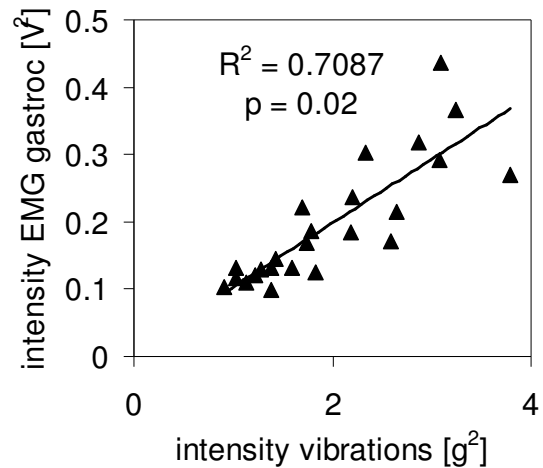
Figure 1: Average EMG intensity of the gastrocnemius muscle vs. average vibration intensity for the 24 trials of subject 6 performing short turns.

could be (a) active damping by the muscles, (b) increased co-contraction to change damping or transmissibility properties of the lower extremities, (c) necessity for additional adjustments in movement execution or body posture and/or (d) damping of resonances of muscle compartments by muscle tuning.
The magnitude of the observed increases in muscle activation levels suggests that movement execution and, thus, performance might be affected in sports with high vibration exposure. Furthermore, vibration exposure might accelerate fatigue and, consequently, the risk of falls and injuries.

REFERENCES

Von Tscharner (2000). Journal of Electromyography and Kinesiology 10, 433-445.

movement	biceps femoris	gastrocnemius	vastus lateralis	vastus medialis
Short Turns:	6	7	6	5
Carving Turns:	7	8	6	5
Straight Gliding:	1	2	2	3

Table 1: Number of subjects for whom statistically significant correlations were found between EMG activity and vibration intensity (out of 10 subjects in this study).

VIRTUAL REALITY IN STROKE REHABILITATION

Martha Walker PT, PhD[1], Stacie Ringleb, PhD[2], George Maihafer PT, PhD[1], Jessica Crouch PhD[3], Nigel Tierney BS[3], Bonnie Van Lunen, ATC, PhD[4], Gianluca De Leo PhD[2], Jean Shelton, MD, FAAP[5], Robert Walker MD[5], Hector Garcia MS[2]

[1] School of Physical Therapy, Old Dominion University, [2]Virginia Modeling Analysis and Simulation Center, Old Dominion Unviersity [3] Department of Computer Science, Old Dominion University,[4]Department of Exercise Science, Old Dominion University, [5] Department of Physical Medicine and Rehabilitation, Eastern Virginia Medical School
SRingleb@odu.edu

INTRODUCTION

Approximately 700,000 people each year are diagnosed with a stroke (American Heart Association, 2007), and up to 90% of the survivors report one or more disabilities (Duncan, 1991). Previous research in motor learning and motor recovery has shown that if the involved extremities are used in a repetitive and purposeful manner following a stroke, neuroplasticity can occur in brain, resulting in new synaptic connections and a re-learning of motor function (Levin, 2006). For this practice to be effective, it must be a meaningful, goal-directed activity rather than a mindless movement (Levin, 2006). Virtual reality has the potential to give purpose to the repetitive activity of treadmill walking. The purpose of this study was to demonstrate the feasibility of using a virtual reality (VR) environment in conjunction with partial body weight support treadmill walking for gait rehabilitation in patients following stroke.

METHODS AND PROCEDURES

Five patients with hemiparesis, who had a stroke within the previous year, were recruited for this study. Each patient was more than 6 months post-stroke, had completed inpatient and outpatient physical therapy, and had reached a plateau of physical progress. The patients were able to ambulate at least 20 feet with or without a cane, understand 3-step commands, see and hear well enough to watch a television program.

The VR system consisted of a large flat-screen TV placed in front of a treadmill with an overhead suspension system for partial body weight support. While the subject walked, he or she viewed a city environment from the perspective of a person walking down the street. Included in the scene were pedestrians, car traffic, and a random configuration of buildings that was newly generated with each session. During walking, an avatar companion stayed in view and gave the patient encouragement and feedback.

The effect of the VR training on walking ability was assessed by examining changes in various gait related measures, including a) functional gait assessment (FGA) scores, b) walking speed, c) walking duration and d) percent of body weight supported during gait.

RESULTS

Overall, all subjects improved across all measures, and 2 subjects discontinued the use of a cane. As highlighted in Figure 1, subjects exhibited notable increases in walking speed (34%) and walking time (97%) as a result of training. Similarly, the percent body weight supported decreased for each subject by 10% on average while their FGA scores increased by approximately 30% (Figure 2).
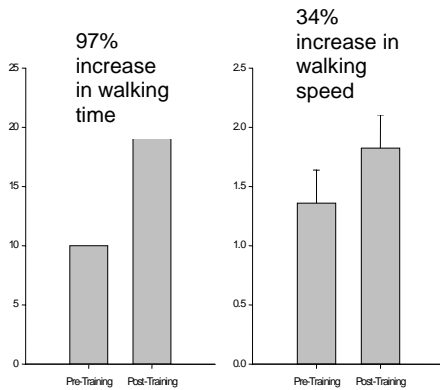
Figure 1. Improvements seen in walking time and walking speed observed across the five stroke patients following 4 weeks of VR training.
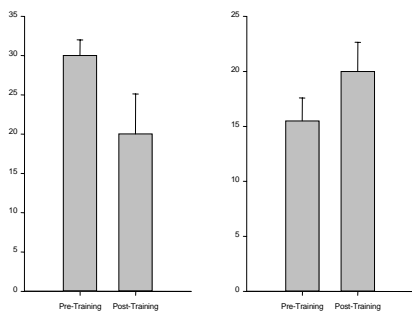
Figure 2. Average changes in Functional Gait Assessment (FGA) scores and percent body weight supported during walking trials for the group of stroke patients following 4 weeks of VR training.

DISCUSSION

This study demonstrated that patients who had reached a plateau in their physical progress could improve their gait with additional gait training using a treadmill with body weight support and virtual reality. Fung et al. also used a treadmill system with VR for gait training and demonstrated that two patients with hemiparesis as a result of stroke increased their speed and learned to walk on a slight slope. This suggests that VR has beneficial effects for rehabilitation and motor relearning. Future studies will include comparing rehabilitation with the treadmill alone and using a treadmill with VR.

SUMMARY

For the five subjects, training using a VR-enhanced treadmill system with partial body weight suspension resulted in improvement in duration of walking and in FGA scores.

REFERENCES
American Stroke Association, http://www.strokeassociation.org/presenter.jhtml?identifier=1033, accessed September 17, 2007.
Duncan, PW. (1991) Physical Therapy, 74: 30-39.
Fung et al. (2004) CyberPsychology&Behavior, 9: 157-162
Levin. (2006) Arch Phys Med Rehabil 87: S1.

COMPENSATORY GAIT MOVEMENTS POST STROKE: THE INFLUENCE OF SYNERGIES

Theresa Hayes Cruz, MS [1,2], Yasin Dhaher, PhD [1,2]
[1]Northwestern University, [2]Rehabilitation Institute of Chicago, Chicago, IL, USA
E-mail: theresacruz2008@u.northwestern.edu Web: www.ric.org/smpp

INTRODUCTION

Although most patients regain the ability to walk after stroke, several sagittal plane impairments (i.e. reduced paretic knee flexion, hip flexion, and ankle dorsiflexion) compromise toe clearance during swing. Compensatory frontal plane movements, including circumduction and hip hiking, may be employed to facilitate toe clearance (Perry 1992; Kerrigan, Frates et al. 2000). Despite the recovery of walking, persistent gait disorders are linked to increased energy expenditure (Olney and Richards 1996; Chen, Patten et al. 2005), which can negatively impact endurance and rehabilitation. Given this clinical significance, the goal of this study is to quantify the differential effects of sagittal and frontal plane joint strength measures on compensatory kinematics. Additionally, the frontal and sagittal plane deviations in gait kinematics suggest that abnormal multi-joint synergistic torque coupling previously observed in the lower limbs of stroke subjects may contribute to overground gait behaviors (Cruz and Dhaher 2008). We hypothesize that paretic hip sagittal plane weakness and abnormal across-joint coupling will relate to gait deviations. Delineating the effects of these impairments may improve future rehabilitation therapies.

METHODS

Eighteen stroke subjects (>12 months post monohemispheric CVA) and eight age-matched controls were tested. Data collection consisted of two parts: gait analysis and isometric strength measures. Overground gait analysis was performed using standard procedures and equipment (Cleveland Clinic marker set and an eight camera Motion Analysis Corp, data sampled at 120 Hz). Subjects walked with comfortable shoes on a 10m walkway at a self-selected walking speed for a minimum of five trials. Stroke subjects were tested without ankle-foot-orthoses (AFOs) and canes when possible. Given that walking is a dynamic task influenced by many factors, the rates of change of compensatory movements at the initiation of the swing phase were selected as outcome measures. Specifically, the deviations from the normal rate of change of hip abduction/adduction angle and hip pelvic obliquity angle at toeoff were used.

For the isometric data collection, stroke subjects' lower limbs were secured in an instrumented exoskeleton locked in the standing toeoff posture (Cruz and Dhaher 2008). Subjects were instructed to produce maximum hip frontal and sagittal plane torque and hold for 200ms, while receiving real-time visual feedback. Subjects were unaware that knee flexion/ extension torque measurements were recorded simultaneously, providing a measure of across joint coupling. Paretic knee and ankle sagittal plane strength was measured using a Biodex® chair.

To determine which strength measures were related to compensatory kinematics, multiple linear regression models were used as follows:

$$\Delta = \beta_i \alpha_i + \varepsilon,$$

where Δ is the deviation in the rate of change of the kinematic variable, β_i are the coefficients for the α_i variables and ε is the error.

RESULTS AND DISCUSSION

The groups significantly differed in pelvic joint angle at toeoff (p = 0.005, see Figure 1), but not in frontal plane angle (p = 0.44). The stepwise regression procedure found four of the ten variables to be related to the deviation from normal in the rate of change of pelvic obliquity angle at toeoff in the stroke group, including hip flexion and extension strength, knee flexion strength, and abnormal hip adduction\knee extension hip\knee coupling. As expected, the regression model revealed that abnormal coupling resulted in increased deviations from normal, while increases in paretic hip extension and flexion, and paretic knee flexion strength reduced the deviations from normal, see Table 1. The regression algorithms were unable to find a relationship between the strength variables and the deviation from normal in the rate of change of hip frontal plane angle at toeoff. These findings reveal that proximal joint sagittal plane strength measures are the most important factors when determining abnormal pelvic frontal plane compensatory kinematics.
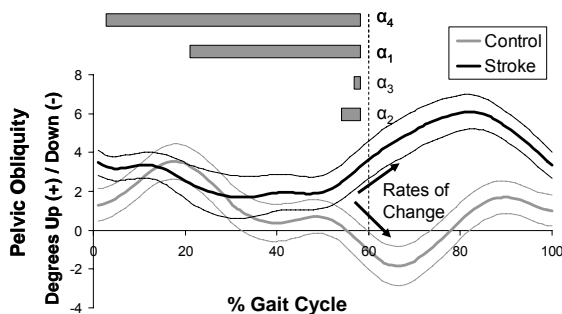
Figure 1: Mean (SE) pelvic frontal plane angle for one gait cycle (heelstrike= 0% and toeoff = 60%) and mean strength measures from Table 1.

SUMMARY/CONCLUSIONS

This study suggests that given the relationships among abnormal across joint coupling, single joint strength, and gait kinematics, task specific training may improve the quality of gait following stroke. The subsequent reduction of compensatory movements is anticipated to lessen energetic costs and improve rehabilitation potential. These findings also support the hypothesis that pelvic movement is a major compensatory strategy post stroke.

REFERENCES

Chen, G., C. Patten, et al. (2005). Gait Posture **22**(1): 51-6.

Cruz, T. and Y. Dhaher (2008). Stroke **39**(1): 139-47.

Kerrigan, D. C., E. P. Frates, et al. (2000). Am J Phys Med Rehabil **79**(3): 247-52.

Olney, S. and C. Richards (1996). Gait Posture **4**: 136-48.

Perry, J. (1992). Gait Analysis: Normal and Pathological Function. Thorofare, NJ, SLACK

ACKNOWLEDGEMENTS

Table 1 – ANOVA for Multiple Regression Model for Pelvic Obliquity

Source (α_i)	Coefficient (β_i)	R^2	Probability Level	Power 5%
Hip Flexion (α_1)	-0.01		**0.002**	.966
Hip Adduction/Knee Extension Ratio (α_2)	-0.08		**0.000**	1.00
Knee Flexion (α_3)	-0.31		**0.000**	.993
Hip Extension (α_4)	-0.02		**0.000**	1.00
Model (Intercept)	1.38	.957	**0.000**	1.00

GAIT CHARACTERISTICS OF THE CENTRE OF PRESSURE IN SUB-ACUTE STROKE PATIENTS.

Amanda E Chisholm[1,2], Stephen D Perry[1,2,3], William E McIlroy[1,2,4]

[1]Graduate Department of Rehabilitation Science, University of Toronto, Toronto, ON, Canada,
amanda.chisholm@utoronto.ca
[2] Toronto Rehabilitation Institute, Toronto, ON, Canada
[3] Kinesiology & Physical Education, Wilfrid Laurier University, Waterloo, ON, Canada
[4]Department of Kinesiology, University of Waterloo, Waterloo, ON, Canada

INTRODUCTION

Following a stroke, impaired walking function leads to long-term disability and reduced participation in daily activities. Improved walking function is the goal most often stated by individuals with stroke and recovery usually occurs within 3-6 months (Jorgensen 1995). Common features of walking after stroke include slow velocity, poor efficiency, reduced muscle co-ordination and asymmetrical pattern (Olney and Richards, 1996). However, relatively few studies have looked at centre of pressure (COP) patterns during gait. Since the COP controls the forward progression of the centre of mass, altered patterns may reveal difficulties in controlling dynamic stability. The purpose of this study was to describe temporal and spatial parameters of the COP pattern during the single support phase of the gait cycle in patients early after stroke.

METHODS AND PROTOCOL

Twelve sub-acute stroke patients (61 ± 15 years old, 46 ± 20 days post stroke) were asked to walk a distance of 10m over a pressure sensitive mat (GaitRite, CIR Systems, Clifton, NJ) with their regular footwear under two conditions; 1) at their preferred pace and 2) at the fastest pace at which they felt safe. Three trials were recorded per condition. Participants were allowed to use their walking aids during the trials, which included rollators, canes and ankle-foot orthoses. The Chedoke-McMaster Stroke Assessment (CMSA) Impairment Inventory is a clinical tool used to evaluate the level of impairment in motor control at the leg and foot. This measure was completed by each participant with a physiotherapist or trained research assistant. The analysis of the walking trials included four consecutive foot contacts (two paretic and two non-paretic) recorded in the middle of the mat from each trial to give a total of twelve foot contacts per condition.

RESULTS

Preliminary analysis (n=11) shows no significant difference for the average velocity of the COP between the non-paretic (15.02 cm/s and 26.09 cm/s) and paretic foot (17.1 cm/s and 24.2 cm/s) for both preferred and fast conditions, respectively. However, there is a significant difference between paretic (14.8 cm/s) and non-paretic (16.0 cm/s) foot for the average velocity in the heel region (p <0.05; figure 1). Although, no difference between limbs was found for the amount of time COP spent in each foot region, the majority of the single support phase occurred on the lateral and middle aspects of the heel and mid-foot regions. The distance to the initial COP point (relative to foot length) showed a trend towards a greater length under the paretic foot (30.7% and 27.1%) as compared to the non-paretic foot (28.1% and 25.7%) for both preferred and fast conditions, respectively.

COP Velocity

Legend:
- Paretic - Preferred
- Non-Paretic - Preferred
- Paretic - Fast
- Non-Paretic - Fast
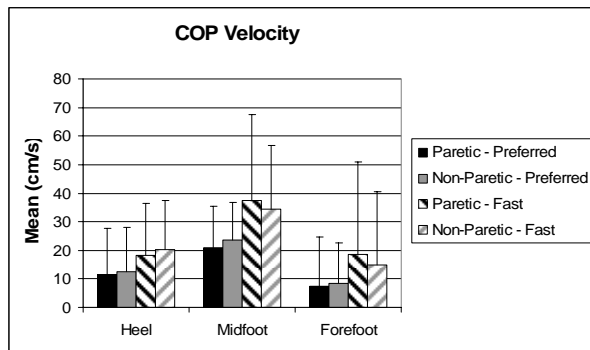
Figure 1. The average velocity of the COP in each foot region; heel, mid-foot and forefoot.

DISCUSSION

Gait dysfunction has been characterized well in the stroke population with respect to temporal, spatial and force parameters. This study examined components of the COP pattern to reveal how impairments in sensorimotor control impact the progression of the centre of mass (COM) during gait. The average velocity of the COP was similar between the paretic and non-paretic limb, which suggests the temporal control of the COM is consistent during gait. The velocity of the COP displays a normal peak in the mid-foot region representing the transition onto the forefoot (Cornwall and McPoil, 2000). The single support phase occurred more under the heel and mid-foot regions. The distance to the initial COP point was longer under the paretic foot, which indicates that the single support phase begins closer towards the mid-foot

region. This may be a compensatory strategy of increasing the duration of double limb support. Since, the analysis combined individuals with low and high sensorimotor control together, some inter-limb differences may have been masked, which will be considered in a future analysis.

SUMMARY

The initial findings suggest that alterations in temporal and spatial components of the COP pattern may reflect dynamic instability as well as sensorimotor dyscontrol. Ongoing work will examine the relationship between COP parameters and the level of severity in sensorimotor control. This work highlights the importance of evaluating dynamic stability as an indicator of walking ability and to identify those at a higher risk of falling.

REFERENCES

Jorgensen, HS et al. (1995) *Arch Phys Med Rehabil*. 76; 27-32.
Cornwall MW and McPoil TG. (2000) *J Am Podiatr Med Assoc*. 90;(7) 334-338.
Olney, SJ and Richards, C. (1996) *Gait & Posture*. 4; 136-148.

ACKNOWLEDGEMENTS

QUANTIFYING AND PREDICTING ELEVATION ANGLE ERROR USING TRI-AXIAL ACCELEROMETER DURING DYNAMIC MOTION

Tal Amasay[1] and Andrew Karduna[1]

[1]Orthopaedic Biomechanics Laboratory, Department of Human Physiology, University of Oregon, Eugene, OR, USA, tamasay@uoregon.edu, karduna@uoregon.edu.
URL: http://biomechanics.uoregon.edu/obl/

INTRODUCTION

Linear accelerometers are commercially available and are commonly used in evaluation of segments' posture by means of uni-axial (Paquet et al. 2001) , bi-axial (Boonstra et al. 2006) and tri-axial (Hansson et al. 2001) accelerometers. However, the main problem with linear accelerometers is that any non-gravity linear acceleration will bias the calculated elevation angles. Therefore the purpose of this study is to test and evaluate triaxial accelerometer accuracy under dynamic conditions and the ability to predict the elevation angle error.

METHODS AND PROCEDURES

The Virtual Corset, (Microstrain Inc,VT, USA) is a pager sized, battery powered tri-axial accelerometer with an integrated 2 Mb data logger and a sampling rate of approximately 7.6 Hz. A SW22B Wirewound precision single turn potentiometer (ETI Systems Inc, CA, USA), with a linearity tolerance of $\pm$ 0.5%, was connected to an aluminum arm to create a pendulum. It was felt that a pendulum would result in a controlled environment that introduced high and variable levels of angular velocities and accelerations. To predict the angle error (θ) in elevation angle, the angle between the actual resultant and gravity acceleration vectors was calculated. This equation can be represented by angular velocity (ω) and acceleration (α), radius (r), and elevation angle (β).

$$\sin\theta = \frac{(\alpha r + g\sin\beta)\cos\beta - (\omega^2 r + g\cos\beta)\sin\beta}{\sqrt{(\alpha r + g\sin\beta)^2 + (\omega^2 r + g\cos\beta)^2}}$$

To check the accuracy of this prediction equation the VC was mounted on the pendulum's arm at nine different radii: 0-10cm in 2cm increments and 0–25cm in 5 cm increments. For each trial, the pendulum's arm was released from an angle of 105° of elevation and data were collected from the VC and potentiometer for 15 seconds and saved. The potentiometer data were sampled at 1000Hz. These settings were repeated for each of the VC at three different positions which represent, the frontal, scapular and sagittal planes. The actual angle error and the predicted angle error were compared.

To validate the use of the VC beyond the pendulum setting for in vivo measurement, data from a previous reaching study were used. The subjects performed a controlled continuous seven arm elevations and depression (Constrained) and also two unconstrained reaching movements of reaching overhead (Overhead) and reaching to a seat belt (Belt). These data were used to calculate the averaged RMS and absolute maximum predicted angle errors for each task.

RESULTS

Under in-vitro dynamic conditions the calculated elevation angle error was increased as the radius increased and as the angular acceleration increased (Figure 1). The calculated predicted elevation angle errors

from the pendulum's data were found to be similar to the VC calculated elevation angle errors (Figure 2). Using a radius of 10cm on the in-vivo previously collected data, constrained arm elevation had the lowest averaged RMS and maximum predicted angle errors (Table 1).
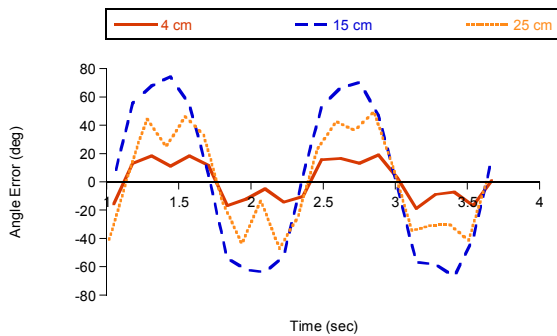
Figure 1. Difference error between the potentiometer calculated angle and the VC calculated angle at three different radii
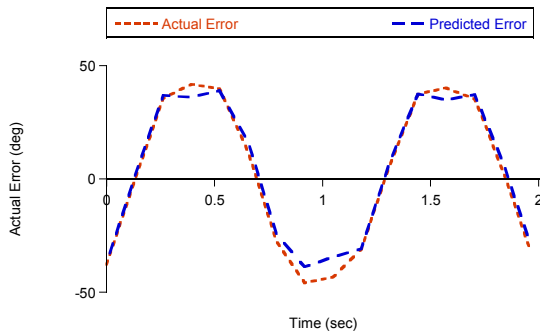
Figure 2. Difference between the actual angle error and the predicted angle error at a radius of 20cm

DISCUSSION

The farther the VC is located from the axis of rotation the higher the errors. The same was true for larger angular accelerations. The angular velocity did not have a large impact under these settings because the radial acceleration was parallel to the gravitational acceleration vector. It was also found that plane of elevation did not affect the error. Our proposed prediction equation has the ability to predict the error, which may help the

investigator to make a decision on how appropriate the VC is for measuring exposure in a specific job environment.

	Constrained		Belt		Overhead		Pendulum	
	Max	RMS	Max	RMS	Max	RMS	Max	RMS
Angle error (deg)	9.1	1.0	12.2	2.8	21.5	5.1	38.4	23.2

Table 1. Averaged maximum and RMS angle error at a radius of 10 cm during constrained arm elevation, Belt and Overhead tasks and pendulum.

SUMMARY

The VC can be used to reconstruct elevation angles. In order to improve data collection qualities we offer the following recommendations:
1. Locate the VC as close as possible to the joint center of rotation.
2. Estimate the maximum and average angular velocity and acceleration of the task.
3. Determine the typical and maximal range of humeral elevation angle.
4. Use the prediction equation to determine whether the expected errors are within acceptable tolerances for the given experiment.

REFERENCES

Boonstra, M. C., et al. (2006). J Biomech 39(2): 354-8.
Hansson, G. A., et al. (2001). Med Biol Eng Comput 39(4): 405-13.
Paquet, V. L., et al. (2001). Appl Ergon 32(3): 215-24.

ACKNOWLEDGEMENTS

TEMPORAL CHANGES IN MOTOR IMPAIRMENTS
AND GAIT FUNCTION POST STROKE

Theresa Hayes Cruz, MS [1,2], Yasin Dhaher, PhD [1,2]
[1]Northwestern University, [2]Rehabilitation Institute of Chicago, Chicago, IL, USA
E-mail: theresacruz2008@u.northwestern.edu Web: www.ric.org/smpp

INTRODUCTION

The ability to safely ambulate is the prime factor that determines whether a stroke patient will be discharged to a skilled nursing facility or return home, and whether he or she will return to pre-morbid levels of social and occupational activities (Wall and Turnbull 1986). Therefore understanding the factors that contribute to gait recovery, as well as how they change with time are important research topics. Specifically, it remains to be seen how the evolution of multiple impairments contributes to improvements in functional activities throughout the recovery process. In order to determine these relationships, the time course of these variables must first be determined. Therefore, the goal of this investigation is to acquire a set of quantitative and clinical measures of impairments and activity at monthly intervals between the onset of the disease and twelve months post stroke. We hypothesize that onset of walking ability will vary with subject. We further hypothesize that increased strength may not mirror functional improvements. The outcomes of this study may provide insight into factors that influence clinical discussions regarding the return to pre-morbid activities of daily living and allocation of resources.

METHODS

Subjects with first ever, monohemispheric CVAs were recruited within two months of the onset of CVA and tested every two months up to one year post-stroke. Several types of impairment measures and functional outcomes were collected as able by the subjects, including overground gait, isometric strength, across joint synergies, balance, endurance, and spasticity. Overground gait analysis was performed using standard procedures and equipment (Cleveland Clinic marker set and an eight camera Motion Analysis Corp). Subjects walked with comfortable shoes on a 10m walkway at a self-selected walking speed for a minimum of five trials. Stroke subjects were tested with and without assistive devices (ankle-foot-orthoses and canes), as able. Kinematic, kinetic, and spatial-temporal variables were measured.

For the isometric data collection, a previously published experimental paradigm was used (Cruz and Dhaher 2008). Briefly, the subjects' lower limbs were secured in an instrumented exoskeleton locked in the standing toeoff posture. Subjects were instructed to produce maximum hip frontal and sagittal plane torque and hold for 200ms, while receiving real-time visual feedback. Subjects were unaware that knee flexion/ extension torque measurements were recorded simultaneously, providing a measure of across-joint coupling. The paretic knee and ankle sagittal plane strengths were measured in the seated posture using a Biodex® chair. Finally, balance, endurance, and spasticity were measured using the Berg Balance Scale (Berg, Wood-Dauphinee et al. 1995), six minute walk test, and Modified Ashworth (Bohannon and Smith 1987), respectively. These values were recorded every two months from the acute, sub-acute and chronic phases of stroke recovery (2 to 12 months post stroke).

RESULTS AND DISCUSSION

Seven subjects have been recruited; four have completed the twelve month study, and three will complete the program within the next four months. Preliminary findings reveal different non-linear changes over time with regards to all variables collected; see Figures 1 A, B, and C for exemplar data.

A

B

C
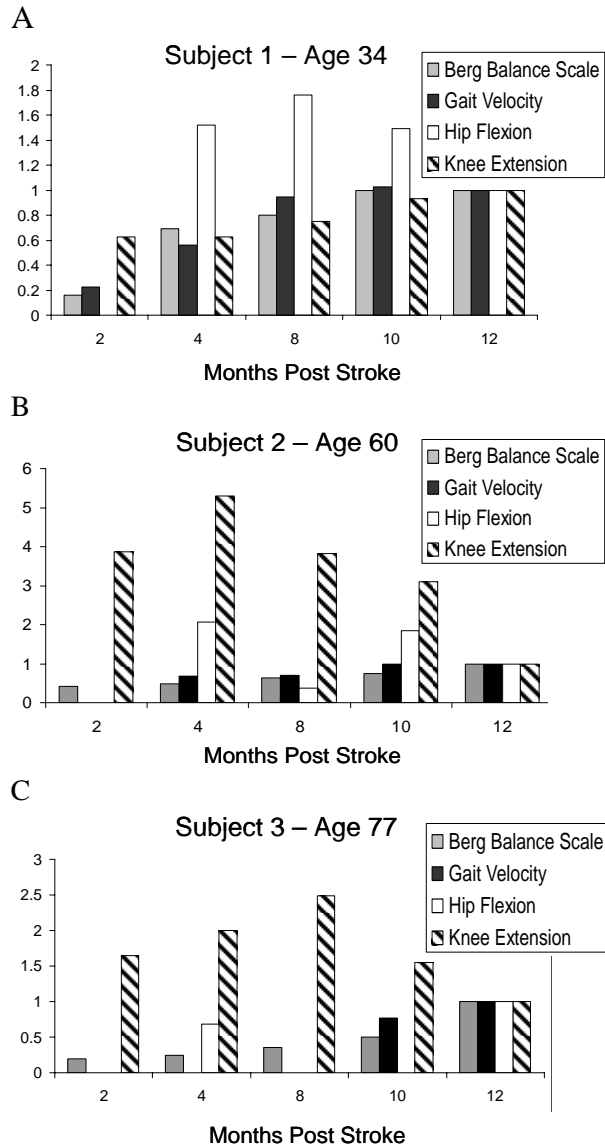
Figures 1 A, B & C: The recovery of function and strength by high (A), middle (B), and low functioning (B) stroke survivors. Data normalized to chronic values within a subject.

For example, the onset of walking varied with subject and appears to be related to age, as younger subjects walked earlier than older subjects. While the evolution of functional measures (walking speed and balance) were similar within a subject, the rate of change of all strength measures did not mirror these improvements. Moreover, the patterns of return differed between the functional and strength measures. Specifically, the functional measures logarithmically approached asymptotic chronic values, while the strength measures appeared parabolic. More data is required to define these trends.

SUMMARY/CONCLUSIONS

Consistent with clinical observations, recovery was found to be subject specific. Larger datasets may provide distinct clusters of subjects, and this data may reveal insights into the modes of walking recovery. For example, it may be determined how changes to lower limb motor impairments influence gait recovery. This information may be used to design therapeutic interventions and better allocate resources.

REFERENCES

Berg, K., S. Wood-Dauphinee, et al. (1995). Scand J Rehabil Med **27**(1): 27-36.

Bohannon, R. W. and M. B. Smith (1987). Phys Ther **67**(2): 206-7.

Cruz, T. and Y. Dhaher (2008). Stroke **39**(1): 139-47.

Wall, J. C. and G. I. Turnbull (1986). Arch Phys Med Rehabil **67**(8): 550-3.

ACKNOWLEDGEMENTS

THE EFFECTS OF MUSCLE TENSION ON HUMAN BIOMECHANICAL RESPONSE AND PERCEIVED IMPACT INTENSITY

F. Tsui and M.T.G. Pain

Loughborough University, Loughborough, UK
Email: F.Tsui@lboro.ac.uk, Web: www.lboro.ac.uk

INTRODUCTION

Despite anecdotal evidence of muscle tensing during impacts, its role in preventing or reducing injury is still unclear. Tensing has been found to significantly increase thoracic stiffness in human volunteers during low-intensity simulated car crashes (Stalnaker, 1976; Patrick, 1981), but not influence the occurrence of catastrophic injury such as rib fractures or organ injuries (Kent et al., 2006). Subsequent impact injury research and design of Anthropometric Test Dummies (ATDs) has since ignored the effects of muscle tension.

Omitting the role of muscle tension during impact eliminates a real set of possible injuries and ignores its influence in low-intensity impacts prevalent in contact sports. These impacts can affect performance by tearing and contusing muscle, but are not considered to be 'serious'. As such, muscle tension may play an important role in reducing non-catastrophic impact injury by altering the biomechanical response of the muscle and thus, the body as a whole.

The aim of this study was to determine the influence of muscle tension on the human biomechanical response and perceived impact intensity, measured in terms of the discomfort caused to each subject.

METHODS AND PROCEDURES

Five Mixed Martial Artists (age 22.8 ± 2.6 yrs, body mass 80.7 ± 7.3 kg, height 176.6 ± 6.6 cm) provided informed voluntary consent for this study. Measurements of the right leg were taken to calculate inertial parameters using the model of Yeadon (1990).

Participants were seated on a bench with their right foot resting on the ground and their knee at 90°. Each participant performed a single Maximum Voluntary Isometric (MVI) knee extension and the force generated was measured with a force plate. In subsequent trials requiring muscle tension, subjects were asked to produce ~ 60% of this MVI force.

In each trial, a medicine ball (m = 3.9 kg) was dropped from 1.0 m – 1.6 m onto the thigh under relaxed and tensed muscle conditions. Perceived discomfort was assessed using a Borg CR10 scale. At impact, force was measured at 500 Hz using Tekscan sensors (Boston, MA) and filmed with a Phantom camera (Vision Research Inc.) at 2000 Hz. Video footage was digitised with Simi Motion (SIMI Reality Motion Systems) to provide impact and rebound velocities. The energy absorbed by the thigh was calculated using these velocities and the energy expended to deform the medicine ball. This deformation energy was estimated using the thigh impact force and results obtained from separate medicine ball impacts against a rigid surface.

RESULTS

Across all drop heights, tensed muscle had higher impact forces and less energy absorbed when compared to relaxed muscle (Fig. 1). Discomfort was also higher when the muscles were relaxed (4.4 ± 1.1) versus trials in which

they were tensed (1.6 ± 0.7).
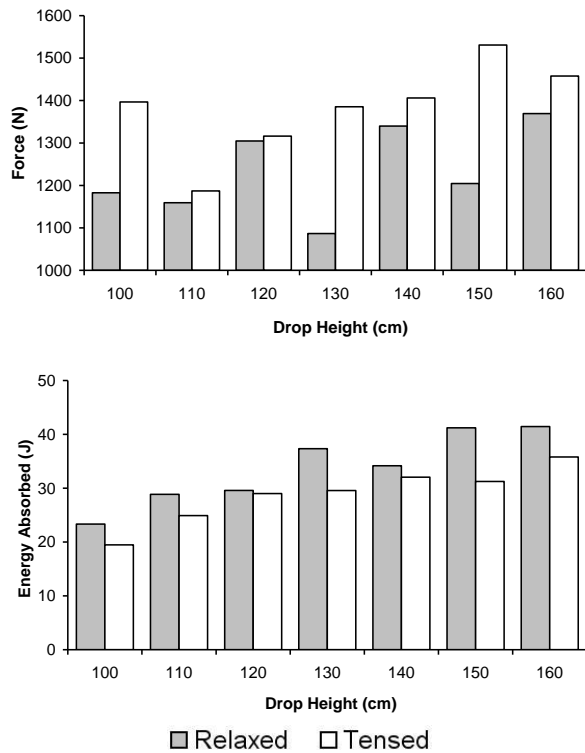
Figure 1. Average impact force and average energy absorbed (by the thigh) at each drop height.

DISCUSSION

Although these impacts did not cause injury, this study assumed that the stimulus from the nociceptors, which senses discomfort, is directly related to the risk of tissue injury (i.e. higher discomfort indicates a higher risk of tissue damage). While muscle tension can influence the actual transmission of stimuli from the nociceptors, this research only examines mechanical predictors of injury.

The higher impact forces and lower energy absorption at each height for tensed muscle supports early research that stiffness increases with muscle contraction. This suggests that muscles are compressed much less when tensed and this likely contributes to lower perceived impact intensities. The high-force, low-intensity relationship also implies that force is not the most accurate predictor of

muscle injury. This is critical since Personal Protective Equipment (PPE) performance is often assessed by its ability to reduce force. Therefore, future PPE designs should shift focus to decreasing the energy absorbed by the body and localised deformation.

These results also suggest that sports-related impact intensities obtained from current ATDs suffer from low biofidelity. Not only does it ignore all muscle injuries, it also fails to account for the viscoelastic and deformable nature of both colliding bodies. Thus, impact intensities are likely to be understated as athletes risk injury from maximally striking a non-deformable surface.

The variability in the average impact force was likely caused by the differences in body types and composition. While subject inertial parameters were calculated, more subjects are required to produce a reliable normalisation. Further testing will be conducted to establish a more distinct trend in the data for both impact force and energy absorption.

SUMMARY

Omitting muscle tension in impacts reduces the biofidelity of the biomechanical response. Tensed muscle decreases the deformation and energy absorbed by the body lowering the perception of discomfort and subsequent risk of soft tissue injury.

REFERENCES

Kent RW et al. (2006). *ProcIMechE, 220: 853 – 868.*
Patrick JW (1981). *Stapp Car Crash Conf., SAE Paper 811014.*
Stalnaker RL et al. (1973). *Human Impact Response.* New York, Plenum Press.
Yeadon MR (1990). *J Biomechanics, 23: 67 - 74.*

A FORWARD BIO-DYNAMIC MODEL FOR A THREE-SEGMENT OPEN-CHAIN SYSTEM: AN APPLICATION TO MUTLI-FINGERED HAND MOVEMENT

Kang Li[1, 2] and Xudong Zhang[2, 3]

[1]Department of Mechanical Science and Engineering, University of Illinois at Urbana-Champaign, IL, USA, kangli2@uiuc.edu
[2]Department of Orthopaedic Surgery, [3]Department of Mechanical Engineering & Materials Science, University of Pittsburgh, PA, USA, xuz9@pitt.edu

INTRODUCTION

Biodynamic models are powerful means for describing the production or consequences of a human movement. Most existing forward dynamic models cannot replicate the observed kinematics and kinetics simultaneously. Sophisticated models such as the ones driven by muscle activation patterns also suffer from impractical computational time. In this work, we propose a novel forward dynamic model for three-segment open-chain biomechanical systems. It is capable of reproducing realistic multi-joint movements in both kinematics and kinetics at a low computational cost. We use the modeling of multi-fingered hand movement to illustrate the application of the proposed model.

METHODS AND PROCEDURES

The dynamics of a general 3-segment, 3-DOF linkage system without considering the gravity at time t can be represented by the following equations of motion:

$$M(\theta(t))\ddot{\theta}(t) = V(\theta(t), \dot{\theta}(t)) + \tau(t),$$

where $\theta(t) \in \Re^{3\times 1}$ is the angle vector; $\tau(t) \in \Re^{3\times 1}$ is the torque vector at the joints; $M(\theta(t)) \in \Re^{3\times 3}$ is a positive definite mass matrix, $V(\theta(t), \dot{\theta}(t)) \in \Re^{3\times 1}$ is the centrifugal and Coriolis force. We hypothesize that the torque actuator of each joint has two components: one component $\tau_{\text{flexor}}(t)$ represents the flexor action and the other

$\tau_{\text{extensor}}(t)$ represents the extensor action. Both torques are controlled by proportional-derivative (PD) controllers and modulated by distribution functions that emulate muscle contractile mechanics as:

$$\tau(t) = \tau_{\text{flexor}}(t) + \tau_{\text{extensor}}(t),$$
$$\tau_{\text{flexor}}(t) = -q(t)[K^{p}_{\text{flexor}}\Delta\theta(t) + K^{d}_{\text{flexor}}\Delta\dot{\theta}(t)]$$
$$\tau_{\text{extensor}}(t) = -s(t)[K^{p}_{\text{extensor}}\Delta\theta(t) + K^{d}_{\text{extensor}}\Delta\dot{\theta}(t)]$$

where K^{p}_{flexor}, K^{p}_{extensor}, and K^{d}_{flexor}, K^{d}_{extensor} are the associated proportional and derivate gains; $\Delta\theta$, $\Delta\dot{\theta}$ are the angle and angular velocity changes; $q(t)$ is gamma distribution function; $s(t)$ is a beta distribution.

An optimization routine that minimizes the discrepancy between the model-predicted and the measured angle profiles can be formulated to estimate the control parameters:

$$\text{Min} \int_{0}^{t_{max}} (\theta(t) - \tilde{\theta}(t))^2 \, dt$$
$$\text{s.t. } M(\theta(t))\ddot{\theta}(t) = V(\theta(t), \dot{\theta}(t)) + \tau(t)$$
$$\tau(t) = \tau_{\text{flexor}}(t) + \tau_{\text{extensor}}(t)$$
$$\frac{1}{t_{max}}\int_{0}^{t_{max}} (\tau(t) - \tilde{\tau}(t))^2 \, dt < tol$$

where $\tilde{\theta}(t)$ is the measured kinemics, and $\tilde{\tau}(t)$ the torque derived using inverse dynamics at time t; tol is the tolerance in root-mean-square difference between measured and model-predicted torque profiles. The kinemics data were acquired in a previous study (Lee and Zhang, 2007).

RESULTS & DISCUSSION

The proposed model successfully replicated the experimental kinetics (Figure 1) and kinematics (Figure 2 and 3). The flexor and extensor torque components have consistent spatial-temporal patterns across joints, digits (Figure 4) and subjects (not shown here). This model can also predict the experimental kinematics and kinetics by directly applying the control parameters of one subject to another and produce close matches (not shown here).
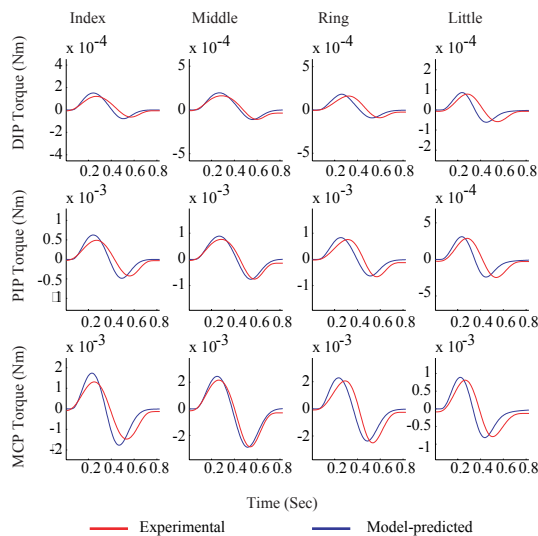
Figure 1. Model-predicted kinetics vs. experimental kinetics.
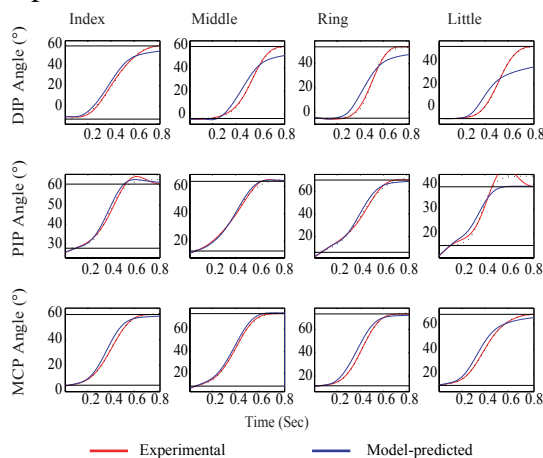
Figure 2. Model-predicted angular kinematics vs. observed kinematics.
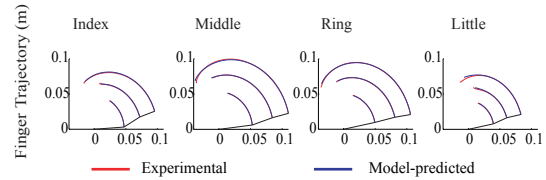
Figure 3. Model-predicted finger trajectory vs. observed trajectory.
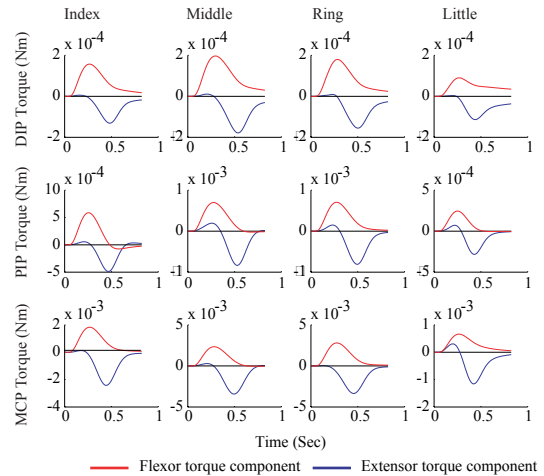
Figure 4. Torque components across joints and digits.

SUMMARY

We demonstrated that the proposed model was able to produce multi-fingered movements that are realistic in both kinetics and kinematics. This is the first forward dynamic model we are aware of that can achieve such biomechanical realism at a low computational cost. The model also provides a solution to alleviate the inverse dynamics failure problem (Risher et al., 1997). Some aspects of the model are yet to be explored such as motor control interpretation of the model and correlation between the torque component profiles and EMG patterns.

REFERENCES

Lee, SW and Zhang, X (2007). *J Biomech,* 40(14):3215-3222.

Risher DW et al. (1997). *J Biomech Eng-T ASME,* 119(4):417-422.

TECHNIQUE DIFFERENCES AMONG MALE AND FEMALE INTERMEDIATE HURDLERS AND STEEPLECHASERS

Laurence Bollschweiler, Iain Hunter, J. Brent Feland, and J. Ty Hopkins
Department of Exercise Sciences, Brigham Young University, Provo, UT, USA
iain_hunter@byu.edu URL: http://biomech.byu.edu

INTRODUCTION

In the sport of track and field, proper hurdling technique is a complicated combination of various running and jumping kinematics. With most research having been done on sprint hurdling, there is a need for further research on hurdling events of different distances. The intermediate hurdles (IH) and the steeplechase (SC) are two events where there are a number of differences in hurdling technique. This study compared the differences in hurdling technique between events (IH and SC) as well as the differences in technique between genders.

METHODS AND PROCEDURES

Subjects for this study consisted of 20 elite intermediate hurdlers (10 male, 10 female) and 20 elite steeplechasers (10 male, 10 female). Subjects were filmed performing their respective events at the 2006 USA Outdoor Track and Field National Championships. A 2-D analysis was performed on each subject to determine differences between events and genders for the following variables: loss of horizontal velocity, peak center of mass height above hurdle, horizontal position (relative to the hurdle) at peak height of center of mass, deviation angle at takeoff (center of mass to takeoff toe relative to vertical), hurdle step length, penultimate, and recovery step lengths, takeoff and landing distance, minimum lead leg hip angle (saggital plane), trail leg knee height relative to the hip at peak height, trunk angle at peak height, landing angle (center of mass to landing toe relative to

vertical), and hurdle velocity (Figure 1). Variables (other than hurdle velocity) were all divided by horizontal velocity of the center of mass through the measured area to account for any differences between groups that were due to speed rather than event or gender. A 2x2 ANOVA determined differences between gender and event.
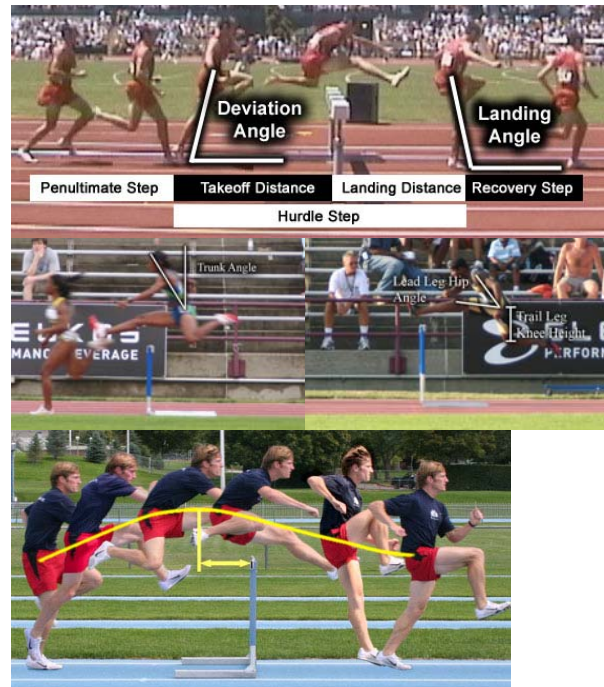
Figures 1: Visual definitions of dependent variables. a) Step distances, takeoff, and landing angles, b) trunk angle, c) lead leg hip angle and trail leg knee height, d) horizontal position at peak height of center of mass.

RESULTS

Significant differences ($p < .05$) were observed in 13 of the 14 variables analyzed (Table 1).

DISCUSSION

As athletes and coaches go about evaluating and training hurdling technique, it is important to remember the differences that exist between events and between genders. For instance, SC tend to take off with a greater deviation angle in order to obtain the appropriate peak height – a height which we have shown to be significantly higher than IH. As well, hurdlers appear to perform the tasks that help promote a low center of mass clearance over the hurdle. These include a high kick of the lead leg, raising the trail leg high and away from the body, and a pronounced forward lean. Due to the high energy demands of these tasks and the economy required for steeplechasers, they tend to perform them on a smaller scale.

Although less understood, some gender differences are worth noting. Males maintain smaller deviation angles, greater leg kick of the lead leg and higher knee height of the trail leg. All of these variables help to maintain a low center of mass through the hurdle, allowing the runner to have a quick return to running. Males demonstrated smaller landing angles than females. Smaller landing angles help to minimizing horizontal braking and loss of horizontal velocity. Although males have a lower barrier clearance than females, they have a taller barrier which forces them to jump higher than the females. These gender differences are likely a result of this higher barrier requirement.

SUMMARY

Even after accounting for horizontal velocity through the obstacle, many differences exist between SC and IH and between gender. Coaches and athletes should realize these differences and train according to the needs of their respective events.

REFERENCES

Brown, G (1988). *Modern Athlete and Coach*, 26:39-41.
McDonald, C and Dapena, J (1991). *Med and Sci in Sports and Exer*, 23:1382-1391.

	MIH	WIH	MSC	WSC
Deviation Angle (degrees)*#	64	64	74	71
Landing Angle (degrees)*#	107	109	101	102
Minimum Lead Leg Hip Angle (degrees)*#	66	78	70	67
Peak Height over Barrier (m)*#	0.42	0.45	0.57	0.56
Horizontal Position of Peak Height (m)	-0.18	-0.08	-0.07	-0.19
Trail Leg Knee Height Relative to Hip (m)*#	0.24	0.28	0.23	0.28
Trunk Angle at Peak Height (degrees)	37	26	29	33
Takeoff Distance (m)#	2.43	2.09	1.73	1.61
Landing Distance (m)*#	1.86	1.67	1.60	1.21
Hurdle Step Length (m)*#	4.29	3.76	3.33	2.82
Penultimate Step Length (m)#	2.18	1.93	1.65	1.66
Recovery Step Length (m)#	1.73	1.59	1.35	1.23
Loss of Horizontal Velocity (%)#	11.3	8.10	12.3	16.0
Hurdle Velocity (m/s)#	9.15	8.29	5.88	5.26

Table 1: Group means by hurdle velocity. *Represents significant differences between gender after accounting for horizontal velocity. #Represents significant differences between events.

THE RELATIONSHIP BETWEEN INTERJOINT COORDINATION DURING GAIT AND STRENGTH, SPASTICITY AND SELECTIVE VOLUNTARY MOTOR CONTROL IN CHILDREN WITH SPASTIC DIPLEGIC CEREBRAL PALSY

Evan Goldberg[1], Loretta Staudt[1], Marcia Greenberg[1], William Oppenheim[1], and Eileen Fowler[1]

[1]Center for Cerebral Palsy, Department of Orthopaedic Surgery, University of California, Los Angeles, Los Angeles, California, USA
egoldberg@mednet.ucla.edu

INTRODUCTION

Inadequate terminal knee extension during the swing phase of gait is common in spastic diplegic cerebral palsy (CP), frequently manifesting as a shorter stride length and decreased walking speed. Hamstring spasticity or contractures may contribute to inadequate knee extension (Tuzson et al., 2003); however, not all patients who undergo hamstring lengthenings walk with improved knee extension post-operatively (Thometz et al., 1989). Muscle weakness has also been proposed as a contributing factor (Arnold et al., 2007). The influence of selective voluntary motor control (SVMC) on terminal knee extension has not been examined. Patients with impaired or absent SVMC are often unable to move the hip, knee and ankle joints independently of one another and may rely on gross flexion and extension synergy patterns to varying degrees (Perry, 1975). Patients with good SVMC may be more capable of using non-synergistic patterns to simultaneously flex the hip and extend the knee during the swing phase of gait. The purpose of this study was to examine the relationship between the coordination of the hip and knee during the swing phase of gait and spasticity, strength and SVMC in children with spastic diplegic CP.

METHODS AND PROCEDURES

Fifteen subjects were recruited for this study. Subjects met the follow inclusion criteria: (1) diagnosis of spastic diplegic CP, (2) minimum of twelve months post orthopedic or neurological surgery, (3) minimum of 6 months post baclofen pump implantation and (4) ability to walk independently indoors for short distances, with or without assistive devices (Levels I-IV of the Gross Motor Function Classification System (GMFCS)). Subjects with "stiff-knee" gait were excluded due to limited knee motion. The mean age of the subjects was 11.5 years (SD = 4.7, range = 5-20). Each subject was evaluated for his or her lower extremity SVMC ability using the UCLA Selective Voluntary Motor Control Assessment of the Lower Extremity tool (SCALE). A total score between 0 and 10 (0 = poor SVMC, 10 = normal SVMC) was given for each limb. Clinical assessments of spasticity and strength were performed using the Modified Ashworth Scale and the Manual Muscle Test, respectively. Spasticity and strength indexes were calculated for each limb by summing the individual scores throughout the lower extremity. Gait data were collected using an eight-camera system (Motion Analysis Corp.), and kinematics were computed using Orthotrak.

Dynamic Systems Theory methods (Stergiou, 2004) were used to quantify interjoint coordination of the hip and knee during gait. Joint velocity versus joint angle was plotted for the hip and knee. Phase angles were then computed (phase angle = arctan (velocity/angle)). The relative phase (i.e., the difference between the hip and knee

phase angles) was calculated throughout the gait cycle. A relative phase angle close to zero indicated that the two joints were moving in phase (synergy); a relative phase angle approaching $\pm$ 180 degrees indicates that the joints were moving out of phase (non-synergistic). A positive value indicated that the hip was leading the knee in the phase space. A negative value meant the knee was leading the hip. The minimum relative phase during swing (MRP) was correlated with the SCALE score, spasticity index and strength index using Pearson correlations (r) for the right limb of each subject. We evaluated the impact of SVMC, spasticity and strength on MRP using stepdown regression methods with a liberal $p < 0.15$ retention criterion.

RESULTS

Significant correlations ($p<0.05$) were found between the MRP and SCALE score, spasticity index and strength index (Table 1). The strongest correlation was that of the SCALE score ($r = -0.81$) (Figure 1), as subjects with high SCALE scores tended to demonstrate more out-of-phase movement during swing (i.e., flexing the hip while extending the knee). In the stepdown regression model, SVMC remained the most important predictor, but spasticity was a factor and modified this relation ($R^2 = 0.75$).

	Pearson r	p
SCALE Score	-0.81	0.0001
Spasticity Index	0.67	0.0045
Strength Index	-0.57	0.0203

Table 1. Pearson correlations (r) between MRP and SCALE score, spasticity index and strength index.

DISCUSSION

The results of this study indicate that SVMC is a stronger predictor of hip and knee coordination during the swing phase of gait

than spasticity or strength. While CP is a multifaceted disorder, the ability to perform purposeful voluntary movement appears to be a key determinant in achieving non-synergistic movements during gait. Patients with poor SVMC ability may be constrained by their neurological capability and unable to dissociate hip and knee movement during swing regardless of hamstring length. Patients with good SVMC ability, initially constrained by biomechanical factors, may be able to utilize their increased range of motion following hamstring lengthenings. An understanding of influence of SVMC on swing phase mechanics during gait may help establish appropriate goals for interventions, in particular hamstring lengthenings.
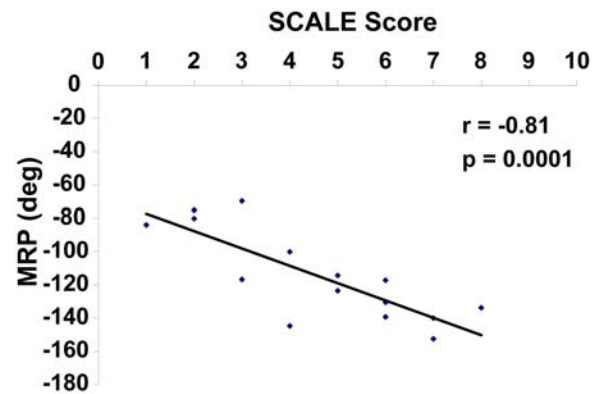
Figure 1. SCALE scores versus MRP for the right limb.

REFERENCES

Arnold, AS et al. (2007). *J Biomech,* 40:3314-3324.

Perry, J (1975). Cerebral Palsy Gait. In: Samilson, RL (Ed.) *Orthopaedic Aspects of Cerebral Palsy CDM Nos. 52/53.* Philadelphia, JB Lippincott.

Stergiou, N (2004). *Innovative Analyses of Human Movement.* Champaign, Human Kinetics.

Thometz, J et al. (1989). *J Bone Joint Surg,* 71-A:345-353.

Tuzson, AE et al. (2003). *Arch Phys Med Rehabil,* 84:1363-1368.

ANGULAR MOMENTUM PRIMITIVES AS GAIT INVARIANTS

Bradford C. Bennett[1,2], Shawn D. Russell[2], and Mark F. Abel[1]

[1] Department of Orthopaedic Surgery, University of Virginia, Charlottesville, VA USA,
bcb3a@virginia.edu
[2] Department of Mechanical and Aerospace Engineering, University of Virginia, Charlottesville, VA USA

INTRODUCTION

The mechanics and control of walking are complex processes that have received extensive study. However, the angular momentum of a person during locomotion has received little attention. Recent work (Popovic, et al, 2004) has suggested that angular momentum is "conserved to a large extent" and that the primitives of this momentum are independent of walking velocity. Yet, there has been little data presented to validate this claim.

This research examines the variance of the angular momentum and its primitives as a function of walking speed. The normalized angular momentum about an individual's CoM and its primitives are determined for adults walking at 0.7, 1.0, and 1.3 times their comfortable walking speed (CWS).

METHODS AND PROCEDURES

Data were collected on retrospective sample of 11 adults without gait problems. Subjects had a mean age of 28.3±12.4 years, a mean a mean height of 181±6.3 cm, and a mean mass of of 76.5±9.0 kg. All tests were conducted in the Motion Analysis and Motor Performance Laboratory at the University of Virginia. Subject consent was approved by the University of Virginia's Human Investigation Committee and was obtained for all subjects. A full body marker set of 38 markers was attached to the subjects. Three-dimensional kinematic data were collected using an 8 camera Vicon Motion Analysis System at 120 Hz. Subjects performed multiple trials and 3 trials at each speed were analyzed. A 12 segment model of each walker was created and the center of mass (CoM) and

angular momentum of each segment and the entire body was computed. The momenta were normalized by the walking speed and subject height and mass. Principal Component Analysis (PCA) was performed on each segment's angular momentum to generate the angular momentum primitives. The eigenvalue problem of the 12 by 12 (there were 12 body segments) data covariance was solved. In this way a new 12-dimensional basis was obtained where the basis vectors were linearly independent.

RESULTS

The normalized angular momenta were highly regulated in all trials. The patterns shown in the average curves of Figure 1 are stereotypical of what has been reported in the literature. The results in the frontal plane reveal the small side to side motion of walking. The total momentum in the
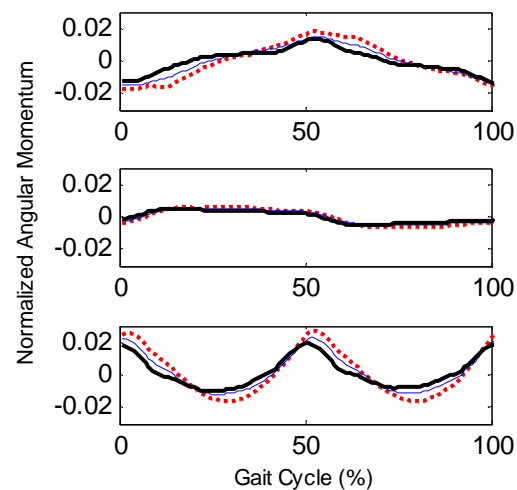
Figure 1. The total body normalized angular momentum during a gait cycle. Starting at the top the momentum in the frontal, transverse, and sagittal planes. Thin lines are at CWS, dotted lines are slow, and thick lines are fast walking.

transverse plane is smallest as the upper and lower body contributions are in opposite directions and cancel each other. The largest values are in the sagittal plane and are the result of the swinging legs and arms in this plane. The extrema of each curve at each speed were different from each other ($p<0.001$) with the largest values at the slowest walking speed.

For all speeds and about all axes the first three primitives accounted for more than 95% of the variability of the data. Fig. 2 shows the first 3 PCs of angular momentum (primitives) in the sagittal plane. To compare the PCs at two speeds their dot product was computed. The average value for all subjects for all speeds about each axis was greater than 0.969 for the first PC, 0.930 for the second PC, and 0.979 for the third PC, revealing that the basis vectors for each individual were nearly co-linear with those of all other subjects.
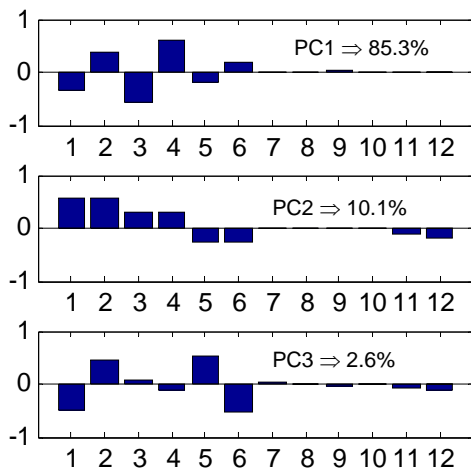
Figure 2 The first three angular momentum primitives in the sagittal plane and their percent data explained. The abscissa numbers correspond to the following human segments: Left (L) foot (1), Right (R) foot (2), L shank (3), R shank (4), L thigh (5), R thigh (6), L upper arm (7), R upper arm (8), L forearm/hand (9), R forearm/hand (10), head (11), torso (12)

DISCUSSION
The angular momenta contribution from all body segments was computed from measured gait parameters. We found that the angular momenta about a subject's CoM scaled with respect to each individual's CWS,

their most economical walking speed. The strength of this organization is emphasized by the fact that the angular momenta at CWS reported here are almost identical to values computed for children walking at their CWS (Bennett, et al. In press)

The collective behaviour of the primitives of the angular momenta was independent of gait speed that ranged from 0.7 to 1.3 times each individual's CWS. We also observed that using the angular momentum primitives reduced the dimensionality of the problem and that three primitives effectively explain all of the walking data.

From a dynamical systems perspective the primitives of angular momentum represent low dimensional collective variables of walking. This makes them candidates for organizational parameters of motor control (synergies) and controls parameters for walking simulations. Popovic et al. (2004) used the sagittal plane primitives to control a walking model with movements constrained to the sagittal plane. We have used a slightly different approach and implemented a full 3-D model using the angular momenta themselves (Ledoux, et al, 2007). Future work will entail modifying our 3-D model to use the primitives themselves.

SUMMARY
Angular momentum and its primitives are excellent candidates for both the control of walking simulations and motor control synergies for walking.

REFERENCES
Bennett, et al., *In Press*

Ledoux, et al. (2007), *ASB Conf, Stanford*.

Popovic, et al., Proc. (2004) *IEEE/RSJ Int. Conf. of Int. Robots & Sys.*

ACKNOWLEDGEMENTS

KNEE-JOINT LOADING VARIABILITY DURING GAIT DOES NOT DIFFER BETWEEN INDIVIDUALS WITH AND WITHOUT KNEE OSTEOARTHRITIS

Todd Royer[1], Jeremy Crenshaw[1], Joaquin Barrios[2], and Irene Davis[2]

[1]Dept of Health, Nutrition, and Exercise Sciences and
[2]Dept of Physical Therapy, University of Delaware, Newark, Delaware, USA
royer@udel.edu

INTRODUCTION

Research has shown that the magnitude of joint loading is elevated in persons with knee osteoarthritis (OA) and increases with disease severity (Sharma et al, 1998). From a mechanical perspective, kinematic and kinetic variability may be beneficial in reducing risk of overuse injury. Force variability would indicate the joint is exposed to a variety of force magnitudes. Kinematic variability suggests joint forces are dealt to different regions of the joint structure. Therefore, low variability may indicate a joint is exposed to repetitive joint force magnitudes or perhaps the same region of the joint is repeatedly exposed to load. While it is logical that force magnitude contributes to joint degradation, it is also plausible that invariable joint loading may contribute to knee osteoarthritis.

The purpose of this study was to examine within subject variability measures related to knee joint loading among subjects with contrasting knee OA severities. It was hypothesized that variability would be least in subjects with advanced knee OA and greatest in subjects with no OA symptoms.

METHODS AND PROCEDURES

Seventeen persons with no self reported knee OA, 17 individuals with K-L (Kellgren & Lawrence, 1957) grade II knee OA, and 14 individuals with K-L grade IV knee OA served as subjects (Table 1). There were no differences in age, BMI or walking speed between groups. Five walking trials at self selected speeds were recorded using a three-dimensional motion analysis system and force plate. A traditional inverse dynamics approach was used to calculate the internal knee abduction moment (normalized to body weight and height), which reflects the magnitude of knee joint loading.

Stance phase was time normalized to 100 points. The standard deviations of 5 walking trials were calculated at each time point; these standard deviations were then averaged to determine stance phase variability for the internal knee abduction moment ($AbMom_{stance}$) and vertical (GRF_{vert}) and medial/lateral (GRF_{ML}) ground reaction forces. Variability of discrete variables was also calculated for the peak internal knee abduction moment ($AbMom_{peak}$) and knee flexion angle at the instant of peak abduction moment ($Ang@AbMom_{peak}$, reflecting the region along the anterior-posterior axis is maximally stressed). A series of one-way ANOVAs were used to test for significant differences ($p < 0.05$) between groups.

RESULTS

There were no between-group differences in knee abduction moment stance phase variability or peak variability (Table 2). Likewise, there were no differences in knee flexion angle variability at the instant of peak knee abduction moment or in vertical and medial/lateral ground reaction force variability over stance phase (Table 2).

DISCUSSION

Invariable knee position and velocity during the swing phase of running has been associated with chronic patellofemoral pain (Hamill et al., 1999). There was a trend for our grade IV OA subjects to have approximately a 37% smaller $Ang@AbMom_{peak}$ variability than both non-OA and grade II OA subjects. This trend suggests subjects with more advanced knee OA may consistently load a specific region of cartilage from stride to stride.

Lewek and colleagues (2006) did not find differences in joint coordination variability between groups with and without knee OA. While increased joint laxity is observed in knee OA patients, it was suggested that medial knee joint co-contraction in OA subjects may influence motion variability.

SUMMARY

In theory, invariable joint motion and forces have the potential to contribute to joint injury. Repeatedly and invariably stressing a joint may accelerate cartilage degradation and lead to osteoarthritis. However, this relationship was not supported in our study.

REFERENCES

Hamill, J et al (1999). *Clin Biom*, 14:297-308.
Kellgren, JH and Lawrence, JS (1957). *Ann Rheum Dis*, 16: 494-502.
Lewek, M et al (2004) *Osteo Cart*, 23:505-11.
Sharma, L et al. (1998). *Arth and Rheum*, 41:1233-40.

ACKNOWLEDGEMENTS

Table 1: Subject characteristics. Data are mean and one standard deviation. There were no significant differences between groups.

Group	No OA (n=17)	Grade II OA (n=17)	Grade IV OA (n=14)
male:female	9:8	10:7	5:9
age (yrs)	56.2 (10.8)	61.1 (8.8)	63.6 (8.8)
BMI (kg/m^2)	28.2 (5.3)	32.6 (6.2)	34.0 (8.7)
walking speed (m/s)	1.45 (0.10)	1.44 (0.17)	1.46 (0.22)

Table 2: There were no between group differences in variability measures. Data are mean and one standard deviation.

Variable (units)	No OA	Grade II OA	Grade IV OA
$AbMom_{stance}$ (Nm/BW/ht)	0.0204 (0.0062)	0.0219 (0.0079)	0.0233 (0.0055)
$AbMom_{peak}$ (Nm/BW/ht)	0.0210 (0.0063)	0.0273 (0.0119)	0.0215 (0.0104)
$Ang@AbMom_{peak}$ (degrees)	1.87 (1.82)	1.87 (1.74)	1.36 (1.21)
GRF_{vert} (%BW)	0.0303 (0.0059)	0.0318 (0.0136)	0.0300 (0.0068)
GRF_{ML} (%BW)	0.00875 (0.00224)	0.00851 (0.00263)	0.00977 (0.00309)

WALKING EXERCISE DIFFERENTLY ALTERS THE METABOLIC ACTIVITY OF BONE IN THE KNEE MEASURED WITH 18F-fluoride PET/CT BETWEEN HEALTHY AND OSTEOARTHRITIC KNEES

Seungbum Koo[1], Andrew Quon[1], David Clark[2], Garry Gold[1], Thomas Andriacchi[3]

[1]Department of Radiology, Stanford University, Stanford, CA, USA
[2]Department of Anesthesiology, Stanford University, Stanford, CA, USA
[3]Department of Mechanical Engineering, Stanford University, CA, USA
Email of the first author: skoo@stanford.edu

INTRODUCTION

Walking biomechanics play an important role in the progression of knee osteoarthritis (OA) (Andriacchi, 2004). There remains a lack of understanding of the influence of walking mechanics on the interaction between subchondral bone and cartilage changes in osteoarthritic joints. However, this information is important since OA affects not only articular cartilage but also subchondral and trabecular bone (Lavigne, 2005). Positron Emission Tomography (PET) offers a unique opportunity to examine the metabolic activity of subchondral bone in patients with OA. Recently, ^{18}F-fluoride PET was used to measure the skeletal response to damaging fatigue in rat ulna (Silva, 2006) and an association between the level of loading and ^{18}F-fluoride accumulation in the damaged ulna was found.

The objective of this study was to measure the metabolic activity in bone from OA knees using ^{18}F-fluoride and to test the hypothesis that the joint loading by walking can alter the bone metabolic activity differently between healthy and OA knees.

METHODS

Three healthy subjects (age 57±5, BMI 25.3 ±4.0, 1 female and 2 males) without history of knee injury and two bilateral medial knee OA subjects (age 60±6, BMI 29.5±0.0, 2 males) were recruited for the study. Each knee (n=10) was treated as an independent sample. The study was approved by the IRB and an informed consent was obtained from each subject prior to testing. Each subject underwent PET/CT tests on 2 consecutive days. Subjects were advised to avoid any exercise and walking before the PET/CT scans and maintain the same activity levels between the two days. On day 1, each subject rested on a chair to unload the knee for at least 30 minutes, and then received about 15 mCi of ^{18}F-fluoride intravenously. The subject rested for an additional 60 minutes and then underwent PET/CT scan. On day 2, each subject rested for 10 minutes and then walked for 20 minutes at a normal walking speed prior to the ^{18}F-fluoride injection. The rest of the procedure was the same as day 1.
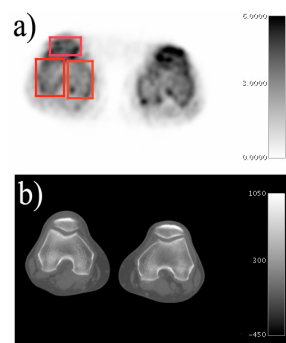
Figure 1. (a) PET and (b) CT images in the transverse plane of the knee at femoral epicondyle level

The PET and CT data were loaded into OsiriX software (Rosset, 2004) and mean and peak values of PET standardized uptake value (SUV) were measured from five regions (three-dimensional box shape region of interest), medial and lateral femur (MF &

LF), medial and lateral tibia (MT & LT) and patella (Pat), for each knee. For each region, the mean and peak values were compared between healthy (n=6) and OA (n=4) knees with Student's t-test at a significance level of alpha=0.05.

RESULTS

The day 1 (baseline) results showed higher metabolic activity in OA knees compared to healthy knees with the peak values significantly different in the medial femur (p<0.01) and medial tibia (p=0.02) (Fig. 2a).
.
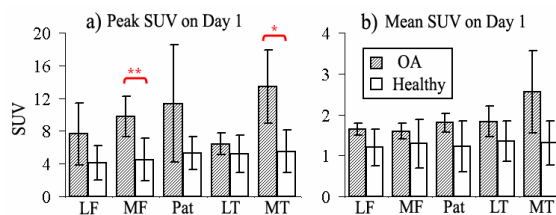
Figure 2. Peak and mean SUVs for five regions in the knee on day 1

Following the 20 minutes walking exercise the bone metabolic activity at the knee increased for both the healthy and OA knees. However the increase of mean SUVs in the medial tibia (p=0.02) and lateral tibia (p<0.01) was greater for healthy knees (Fig. 3).
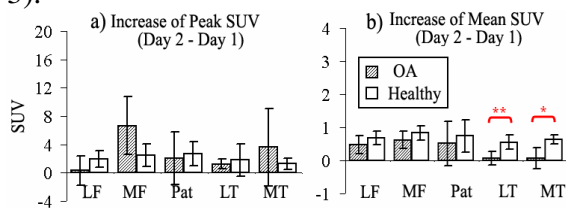
Figure 3. Change of peak and mean SUVs between day 1 and day 2

DISCUSSION

The finding that metabolic activity in bone of the OA knees responded with a lower increase than healthy knees following twenty minutes of walking suggest the potential for reduced sensitivity of subchondral bone to functional loading during walking in patients with knee OA.

This different response to loading in OA knees could be due to the fact that the metabolic activity is already high in these knees. The higher metabolic activity in OA knees on day 1 (resting) is consistent with clinical observations of hot spots in OA knees with bone scan (Schauwecker, 2003). While the altered bone cell metabolism with OA has been investigated (Westacott, 1997), the response of the bone cells in OA joints to loading has not been understood.

A previous study using ^{18}F-FDG could not find significant uptake in cartilage (Nakamura, 2007) which could be due to the low metabolic activity of cartilage. Bone has much higher metabolic activity than cartilage, which could be visualized in this study.

CONCLUSIONS

The differential bone metabolic response to loading in knee OA relative to healthy knees suggests the possibility for using this technique for evaluating the role of bone changes in the progression of OA.

REFERENCES

Andriacchi TP, Mündermann A et al. (2004). *Ann Biomed Eng*, 32:447-57.
Lavigne P, Benderdour M et al. (2005). *Osteoarthritis Cartilage*, 13:310-7.
Nakamura H, Masuko K et al. (2007). *Osteoarthritis Cartilage*, 15:673-81.
Rosset A, Spadola L et al. (2004). *J Digit Imaging*, 17:205-216.
Schauwecker DS (2003), in *Osteoarthritis*. Oxford University Press.
Silva MJ, Uthgenannt BA et al. (2006). *Bone*, 39:229-36.
Westacott CI, Webb GR et al. (1997). Arthritis Rheum, 40:1282-91.

AUTOMATIC EXTRACTION OF DISTAL FEMUR ARTICULAR GEOMETRIC MEASURES FROM 3D SURFACE DATA

Kang Li[1, 3], Scott Tashman[1], Christopher Harner[1], and Xudong Zhang[1, 2]

[1]Department of Orthopaedic Surgery, [2]Department of Mechanical Engineering and Materials Science, University of Pittsburgh, Pittsburgh, PA, USA, xuz9@pitt.edu
[3]Department of Mechanical Science and Engineering, University of Illinois, Urbana, IL, USA

INTRODUCTION

Quantitative knowledge of the distal femur articular surface geometry is critical to understanding the relation between the anatomy and function of the knee joint. It is also the foundation for clinical applications such as total knee arthroplasty (TKA) and surgical navigation. The interest in such knowledge has recently intensified with the advances in imaging and visualization techniques allowing more effective and accurate studies of joint surface geometry (Eckhoff et al., 2001, 2003, 2005; Martelli and Pinskerova, 2002; Martelli et al., 2006a, 2006b). What plagued these previous studies, however, was the fact that subjective trial-and-error visual inspections and judgments were required in extracting geometric information from the image data.

We propose a new computational framework consisting of three algorithms to enable automated analysis of the distal femur articular geometry based on 3D surface data. We demonstrate the proposed framework by an analysis of 3D distal femur surface data of 12 knees acquired using CT.

METHODS AND PROCEDURES

The proposed computational framework consists of three algorithms. The first is a pattern recognition algorithm that identifies and separates the articulating portion from the entire sagittal-view profiles. It is based on the observation that the articulating portion of a profile exhibits detectable curvature changes around the posterior and anterior extremities. Thus, the extremities of the cartilage can be located by determining the curvature extrema. An enhanced curvature-scale-space (CSS) based corner detection method (He and Yung, 2004) is adapted and incorporated into our algorithm to identify the curvature extrema (i.e., local maxima) with noise present in the data. The second algorithm fits the articulating portion of a sagittal-view condyle profile with a parametric-form ellipse, extracting geometric measures that describe the size, shape, position, and orientation of the ellipse. The more generic parametric ellipses are used instead of circles, as the algorithm is intended to be applicable to profiles from cross-sections of varied orientation. The third algorithm seeks to correct the original sagittal planes either embedded in the data acquisition (e.g., inherited from the CT-based coordinate system) or subjectively determined in pre-processing of the data. It provides a consistent objective means to establish a unified sagittal plane. The premise is best illustrated using a model of a series of parallel cross-sectional "cuts" of a cylindrical object (Figure 1). The algorithm systematically varies the plane for a series of "cuts" near the central aspects of both femoral condyles, and searches for a cutting plane that minimizes the dispersion of the centers or focuses of ellipses fitted to the surface profiles. This cutting plane is deemed as the unified sagittal plane.
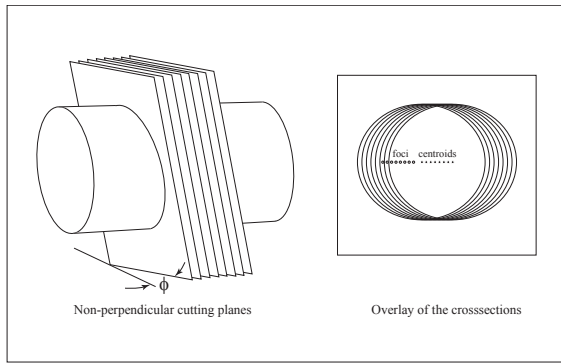
Figure 1. A conceptual model for algorithm 2 that identifies a unified true saggital plane.

We tested the algorithms using data from an ongoing study of ACL reconstruction. As part of this study, bilateral computed tomography (CT) scans were collected with slice spacing of 1.25 mm, 28 cm field of view and 512x512 pixels per image (0.547 mm/pixel in-plane resolution). The femur was segmented using a combination of thresholding and manual segmentation. The resulting slices were reconstructed into 3D solid figures using a regularized marching tetrahedra algorithm (Treece et al., 1999).

RESULTS & DISCUSSION

The proposed computational framework, implemented as a Matlab program, is able to process the CT-acquired 3D distal femur surface data and generate desired geometric measures automatically. The least-squares ellipses identified by algorithm 2 fit the articulating portion of distal femur profiles with small residual errors (Table 1). Correcting and unifying the sagittal planes reduces the dispersion of focus locations by more than 50% on average while having minimal effects on the fitting residuals, or the shape and size of the fitted ellipses (Table 1).

The framework is intended to be general and applicable for 3D surface data acquired using a variety of modalities (CT, MRI, surface digitization, etc.), while the specific working and outcomes may depend on the data quality.

The noise present in the data and resolution in data acquisition could affect the effectiveness and efficiency of the algorithms. Some fine tuning may be necessary, for example, to adjust the criterion for selecting the extreme points in algorithm 1, or the cutting intervals or search steps in algorithm 3.

		Original	Unified
dispersion (mm)		1.6 (0.5)	0.7 (0.2)
residual error (mm)		0.2 (0.04)	0.2 (0.04)
a (mm)	medial	30.0 (3.2)	29.4 (4.2)
	lateral	33.4 (2.6)	33.6 (2.6)
b (mm)	medial	22.3 (2.0)	22.0 (2.2)
	lateral	23.0 (2.1)	24.0 (2.0)

Table 1. The focus dispersion, fitting residual error, and the major (*a*) and minor (*b*) axis lengths before and after unifying the sagittal plane.

SUMMARY

We have proposed and demonstrated a computational framework integrating three algorithms to facilitate automated analysis of the distal femur articular geometry. It can empower and accelerate the studies of knee joint morphology and kinematics, and minimize the subjectivity and methodological inconsistency in such studies.

REFERENCES

Eckhoff DG et al. (2001). *J Bone Joint Surg Am,* 83A: 43-50.
Eckhoff DG et al. (2003). *J Bone Joint Surg Am,* 85A: 97-104.
Eckhoff DG et al. (2005). *J Bone Joint Surg Am,* 87A: 71-80.
He, XC and Yung, NHC (2004). *ICPR'04,* 2: 791-794.
Martelli S et al. (2006a). *Comput Meth Prog Bio,* 83(1): 50-56.
Martelli S et al. (2006b). *J Mech Med Biol,* 6(1): 55-73.
Martelli, S and Pinskerova, V (2002). *J Bone Joint Surg Br,* 84B(4): 607-613.
Treece GM et al. (1999). *Comput Graph,* 23: 583-598.

AUTOMATIC EXTRACTION OF DISTAL FEMUR ARTICULAR GEOMETRIC MEASURES FROM 3D SURFACE DATA

Kang Li[1, 3], Scott Tashman[1], Christopher Harner[1], and Xudong Zhang[1, 2]

[1]Department of Orthopaedic Surgery, [2]Department of Mechanical Engineering and Materials Science, University of Pittsburgh, Pittsburgh, PA, USA, xuz9@pitt.edu
[3]Department of Mechanical Science and Engineering, University of Illinois, Urbana, IL, USA

INTRODUCTION

Quantitative knowledge of the distal femur articular surface geometry is critical to understanding the relation between the anatomy and function of the knee joint. It is also the foundation for clinical applications such as total knee arthroplasty (TKA) and surgical navigation. The interest in such knowledge has recently intensified with the advances in imaging and visualization techniques allowing more effective and accurate studies of joint surface geometry (Eckhoff et al., 2001, 2003, 2005; Martelli and Pinskerova, 2002; Martelli et al., 2006a, 2006b). What plagued these previous studies, however, was the fact that subjective trial-and-error visual inspections and judgments were required in extracting geometric information from the image data.

We propose a new computational framework consisting of three algorithms to enable automated analysis of the distal femur articular geometry based on 3D surface data. We demonstrate the proposed framework by an analysis of 3D distal femur surface data of 12 knees acquired using CT.

METHODS AND PROCEDURES

The proposed computational framework consists of three algorithms. The first is a pattern recognition algorithm that identifies and separates the articulating portion from the entire sagittal-view profiles. It is based on the observation that the articulating portion of a profile exhibits detectable curvature changes around the posterior and anterior extremities. Thus, the extremities of the cartilage can be located by determining the curvature extrema. An enhanced curvature-scale-space (CSS) based corner detection method (He and Yung, 2004) is adapted and incorporated into our algorithm to identify the curvature extrema (i.e., local maxima) with noise present in the data. The second algorithm fits the articulating portion of a sagittal-view condyle profile with a parametric-form ellipse, extracting geometric measures that describe the size, shape, position, and orientation of the ellipse. The more generic parametric ellipses are used instead of circles, as the algorithm is intended to be applicable to profiles from cross-sections of varied orientation. The third algorithm seeks to correct the original sagittal planes either embedded in the data acquisition (e.g., inherited from the CT-based coordinate system) or subjectively determined in pre-processing of the data. It provides a consistent objective means to establish a unified sagittal plane. The premise is best illustrated using a model of a series of parallel cross-sectional "cuts" of a cylindrical object (Figure 1). The algorithm systematically varies the plane for a series of "cuts" near the central aspects of both femoral condyles, and searches for a cutting plane that minimizes the dispersion of the centers or focuses of ellipses fitted to the surface profiles. This cutting plane is deemed as the unified sagittal plane.

Figure 1. A conceptual model for algorithm 2 that identifies a unified true saggital plane.

We tested the algorithms using data from an ongoing study of ACL reconstruction. As part of this study, bilateral computed tomography (CT) scans were collected with slice spacing of 1.25 mm, 28 cm field of view and 512x512 pixels per image (0.547 mm/pixel in-plane resolution). The femur was segmented using a combination of thresholding and manual segmentation. The resulting slices were reconstructed into 3D solid figures using a regularized marching tetrahedra algorithm (Treece et al., 1999).

RESULTS & DISCUSSION

The proposed computational framework, implemented as a Matlab program, is able to process the CT-acquired 3D distal femur surface data and generate desired geometric measures automatically. The least-squares ellipses identified by algorithm 2 fit the articulating portion of distal femur profiles with small residual errors (Table 1). Correcting and unifying the sagittal planes reduces the dispersion of focus locations by more than 50% on average while having minimal effects on the fitting residuals, or the shape and size of the fitted ellipses (Table 1).

The framework is intended to be general and applicable for 3D surface data acquired using a variety of modalities (CT, MRI, surface digitization, etc.), while the specific working and outcomes may depend on the data quality.

The noise present in the data and resolution in data acquisition could affect the effectiveness and efficiency of the algorithms. Some fine tuning may be necessary, for example, to adjust the criterion for selecting the extreme points in algorithm 1, or the cutting intervals or search steps in algorithm 3.

		Original	Unified
dispersion (mm)		1.6 (0.5)	0.7 (0.2)
residual error (mm)		0.2 (0.04)	0.2 (0.04)
a (mm)	medial	30.0 (3.2)	29.4 (4.2)
	lateral	33.4 (2.6)	33.6 (2.6)
b (mm)	medial	22.3 (2.0)	22.0 (2.2)
	lateral	23.0 (2.1)	24.0 (2.0)

Table 1. The focus dispersion, fitting residual error, and the major (a) and minor (b) axis lengths before and after unifying the sagittal plane.

SUMMARY

We have proposed and demonstrated a computational framework integrating three algorithms to facilitate automated analysis of the distal femur articular geometry. It can empower and accelerate the studies of knee joint morphology and kinematics, and minimize the subjectivity and methodological inconsistency in such studies.

REFERENCES
Eckhoff DG et al. (2001). *J Bone Joint Surg Am,* 83A: 43-50.
Eckhoff DG et al. (2003). *J Bone Joint Surg Am,* 85A: 97-104.
Eckhoff DG et al. (2005). *J Bone Joint Surg Am,* 87A: 71-80.
He, XC and Yung, NHC (2004). *ICPR'04,* 2: 791-794.
Martelli S et al. (2006a). *Comput Meth Prog Bio,* 83(1): 50-56.
Martelli S et al. (2006b). *J Mech Med Biol,* 6(1): 55-73.
Martelli, S and Pinskerova, V (2002). *J Bone Joint Surg Br,* 84B(4): 607-613.
Treece GM et al. (1999). *Comput Graph,* 23: 583-598.

LOWER EXTREMITY MECHANICAL WORK EXPLAINS INTERINDIVIDUAL VARIABILITY OF RUNNING ECONOMY

Gary D. Heise[1], Jeremy Smith[1], and Philip E. Martin[2]

[1]School of Sport and Exercise Science, University of Northern Colorado, Greeley, CO, USA,
gary.heise@unco.edu, jeremy.smith@unco.edu
[2]Department of Kinesiology, Penn State University, University Park, PA, USA

INTRODUCTION

The metabolic cost of running has been linked to the cost of supporting one's mass and the time course of generating force during stance (Kram, 2000). Data from various animal species and speeds of locomotion support this claim (Kram & Taylor, 1990). Several researchers suggest that the mechanical work done by muscles is strongly tied to the metabolic cost of walking (e.g., Umberger & Martin, 2007). The work of DeVita et al. (2006) suggested that level walking and running result in a bias or "overproduction" of positive mechanical work by the musculature of the lower extremity in order to overcome dissipation by other tissues. For runners, they reported 8% more total positive work than negative work. Taken collectively, the aforementioned research points to the importance of the stance phase of locomotion and the mechanical power generated and dissipated in the lower extremity as potential determinants of metabolic energy cost. In the present study, correlations between running economy (RE; the metabolic cost at a given speed) and the positive and negative mechanical work at lower extremity joints were examined. It was hypothesized that the dominance of positive work during stance, especially at the hip and ankle, would be positively correlated to RE. Correlations between RE and mechanical energy dissipation (i.e., negative work) at each lower extremity joint were also investigated, but no specific hypotheses were formulated.

METHODS AND PROCEDURES

Sixteen well-trained men (mean VO_{2max} = 62.2 ml·kg^{-1}·min^{-1}) performed treadmill running for determination of RE and overground running for which biomechanical measures were determined (running speed = 3.35 m·s^{-1}). A single video camera (60 Hz) recorded a sagittal-plane view of runners as they contacted an AMTI force platform (480 Hz) with their right leg. Using coordinate data from a motion analysis system (Vicon Motus), ground reaction force data, and an inverse dynamics analysis, net joint moments were calculated for the ankle, knee, and hip during ground contact. Mechanical power was calculated as the product of net joint moment and angular velocity at each joint. Mechanical work was then quantified by integrating the power-time curves. Resulting positive and negative work values at the ankle, knee, and hip were correlated with RE.

RESULTS

Scatterplots of RE and positive and negative work values, along with correlation coefficients, are shown in Figure 1. As hypothesized, higher RE was associated with greater positive work at the hip and ankle. In addition to expectations, more economical runners (lower RE) exhibited greater negative work at the hip, greater positive work at the knee and less negative work at the ankle.
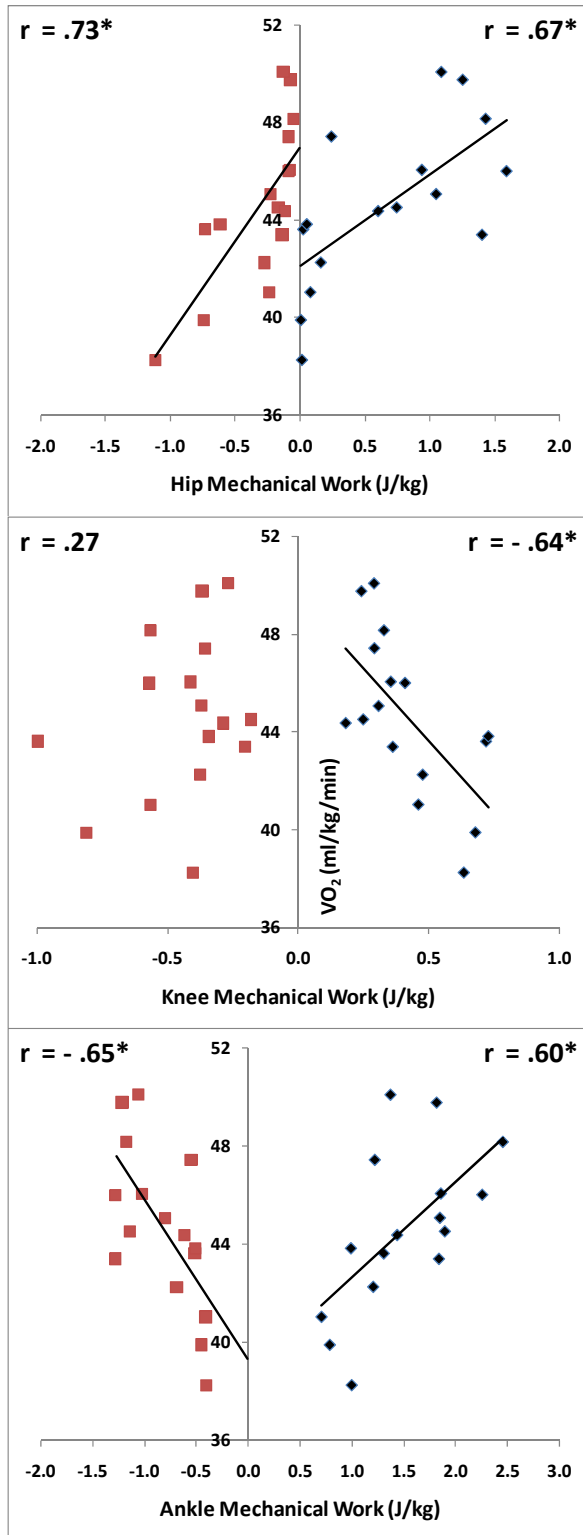
Figure 1. Scatterplots of metabolic cost (ml·kg^{-1}·min^{-1}) and positive/negative mechanical work at the hip (top), knee (middle), and ankle (bottom). *p<.05

HIP	0.67 $\pm$ 0.59	-0.30 $\pm$ 0.32
KNEE	0.42 $\pm$ 0.18	-0.44 $\pm$ 0.22
ANKLE	1.50 $\pm$ 0.52	-0.82 $\pm$ 0.33

Table 1. Mean ($\pm$ SD) Positive and Negative Mechanical Work (J·kg^{-1}).

DISCUSSION

As shown in Table 1, the hip and ankle displayed more positive work than negative work, similar to the findings of DeVita et al. (2007). During stance, the total positive work (2.59 J·kg^{-1}) produced by all joints of the lower extremity was greater than the total negative work (-1.56 J·kg^{-1}). The work at the knee, however, did not agree with DeVita et al. and showed no difference between positive and negative work. Positive work at the hip and ankle are both nearly double the corresponding negative work (see Table 1) and both share positive correlations with RE.

Minimizing energy generation at the hip and ankle, while maximizing energy generation at the knee appear to be important considerations for economical running. The independence of the mechanical work terms will need further consideration in order to make more precise recommendations. In addition, the action of biarticular muscles, which have a prominent role during stance phase (Kram, 2000), may be involved in energy transfer. This mechanism was not addressed by the analytical approach used in the present study.

REFERENCES

DeVita, P et al. (2007). ASB *Proceedings*, Palo Alto, CA.

Kram, R (2000). *Exerc Sport Sci Rev,* 28: 138-143.

Kram, R & Taylor, CR (1990). *Nature*, 346: 265-267.

Umberger, BR & Martin, PE (2007). *J ExperBiol,* 210: 3255-3265.

SKELETAL MUSCLE MYOFIBRILS FAIL AT DIFFERENT FORCES BUT SIMILAR SARCOMERE LENGTHS FOR ACTIVE AND PASSIVE STRETCHING.

Tim Leonard and Walter Herzog
Faculty of Kinesiology, University of Calgary,
Calgary, AB, Canada, leonard@ucalgary.ca

INTRODUCTION

Lengthening contractions can cause significant injury to muscle fibres (McCully and Faulkner, 1985) and severe mechanical injury or failure is associated with forced lengthening of activated muscle (Faulkner et al., 1993). Previous work has shown that the force required to fail activated muscle fibres was 30% greater than that required to fail fibres stretched passively. Furthermore, the extra force measured at failure was attributed to both the displacement of cross bridges during stretch and to sarcomere length non-uniformities at the beginning of stretch resulting from connective tissue compliance (Tidball et al.,1993). Patel and Lieber (1997) suggested that three parallel force transmission systems exist in skeletal muscle fibres; the cross bridge pathway, the titin pathway and the costamere pathway (Z disc-costamere-basement membrane system). Recent work by Claflin and Brooks (2008) used this model in their work on sarcomere failure with incomplete activation in the *mdx* mouse, where the costamere pathway is impaired, and they concluded that in inactive sarcomeres, the cross bridge (inactive) and costamere (absent) pathways are not able to support stretch forces and hence the titin system must support all the force and sometimes it fails. We decided to determine failure forces in single myofibrils since myofibrils have no costamere pathway and inactive myofibrils would support stretch forces solely through the titin pathway. Activated myofibrils would support stretch forces via the titin pathway and also the cross bridge pathway. However, at sarcomere lengths beyond actin-myosin filament overlap, the force supporting system would revert back to the titin pathway alone. Therefore, we hypothesized that forces in active myofibrils would be greater than those for inactive myofibrils if failure occurred at sarcomere lengths less than the "no overlap" length, but would be the same if failure was observed at sarcomere lengths beyond myofilament overlap.

METHODS AND PROCEDURES

Rabbit psoas muscle myofibrils were obtained and tested on an inverted microscope system described elsewhere (Joumaa et al., 2007). Myofibrils with 3 to 8 sarcomeres in series were used. Myofibrils were stretched actively (n=7), passively (n=12) or passively with titin deleted (n=6) at 0.1 µm/sarcomere/s from the plateau region of the force length relationship to a length where failure occurred. Failure was defined at the point when the force-time curve changed from a positive to a negative slope (Tidball et al., 1993). All forces were normalized by the cross sectional area of the myofibrils and results are reported as stress ($nN/\mu m^2$). Mean sarcomere length for the myofibril was determined by measuring the length of the specimen and dividing it by the number of sarcomeres. Individual sarcomere lengths were determined during stretch using the striation pattern of the myofibrils which was projected onto a high resolution linear photo-diode array. The plateau region of rabbit psoas occurs between sarcomere lengths of 2.26µm and 2.43µm and loss of actin-myosin overlap occurs at 3.91µm (Herzog et al., 1992).

RESULTS & DISCUSSION

Stress (nN/µm^2)
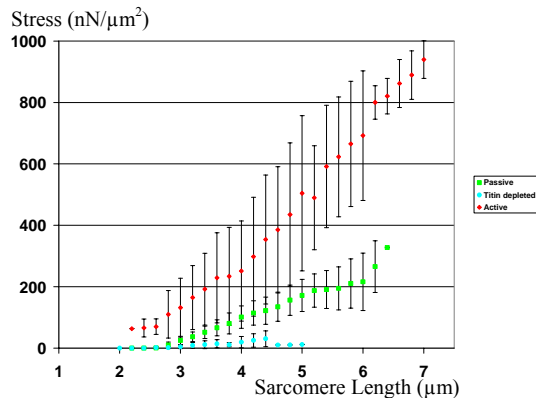
Figure 1. Stress and sarcomere length during continuous stretching for active, passive and titin depleted myofibrils (means ± 1 S.D.)

Figure 1 shows stress values versus sarcomere length during stretch. At sarcomere lengths above 4µm active force traces should have mirrored those observed for purely passive lengthening because the active cross bridge pathway of force production is no longer able to support force (Gordon et al., 1966).

Stress (nN/µm^2)
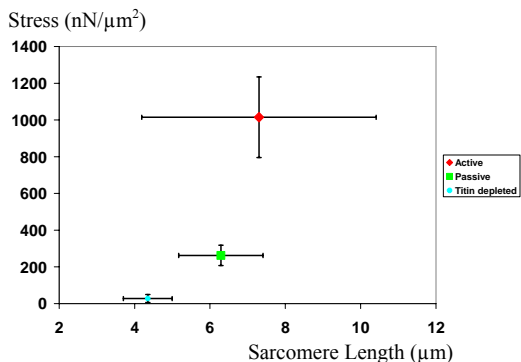
Figure 2. Stress and sarcomere lengths of myofibrils at failure (means and ± 1 S.D.)

Figure 2 shows failure stress and sarcomere lengths for active stretching, passive stretching, and the titin depleted passive myofibrils. The average sarcomere lengths at failure were the same for all three experimental conditions (p=0.42, α=0.05), while the failure stresses were significantly different (p<0.0005, α=0.05). The titin depleted myofibrils show drastically reduced failure stresses compared to the normal passive myofibrils, suggesting that titin is the primary passive force constraint in myofibrils. The activated myofibrils show the greatest failure stresses. Since actin-myosin overlap, and therefore active cross-bridge force, is lost at sarcomere lengths greater than 4.0µm, this result suggests that titin stiffness is increased in an activation (calcium) dependent manner. It has been suggested previously that titin is be a calcium-dependent molecular spring (Labeit et al., 2003). Our results support this idea, but demonstrate that this is true not only for physiological sarcomere lengths but also for sarcomere lengths beyond actin-myosin overlap. Furthermore, increases in titin stiffness have been found to be modest within the physiological range of sarcomere lengths, while the present results suggest a dramatic increase in titin stiffness in the presence of calcium, a result that will need explanation in the future.

REFERENCES

Claflin, D. and Brooks, S. (2008) *Am. J. Physiol-Cell Physiol* 294:C651-658.

Faulkner, J. et al., (1993) *Physical Therapy* 73:911-921.

Gordon, A.M. et al. (1966) *J Physiol* 184(1):170-192.

Herzog et al., (1992) *J. Biomech* 25:945-948.

Joumaa, V. et al., (2007) *Pflugers Arch* 455(2) :367-371.

Labeit, D. et al., (2003) *PNAS* 100:13716-21.

McCully, K and Faulkner J.A. (1985). *J Appl Physiol* 59: 119-126.

Patel, T. and Lieber, R. (1997) *Exerc Sport Sci Rev* 25:321-363.

Tidball, J. et al., (1993) *J Appl Physiol* 74:1280-1286.

ACKNOWLEDGEMENTS

PATELLAR TENDINOPATHY ALTERS THE DISTRIBUTION OF LOWER EXTERMITY JOINT EFFORT DURING HOPPING

Richard Souza[1], Shruti Arya[2], Christine Pollard[3], George Salem[4], and Kornelia Kulig[5]

[1,2] PhD Candidate, Department of Biokinesiology and Physical Therapy, University of Southern California, Los Angeles, CA, USA, rsouza@usc.edu

[3] Assistant Professor of Research, Division of Biokinesiology and Physical Therapy, University of Southern California, Los Angeles, CA, cpollard@usc.edu

[4] Associate Professor and Co-Director, Musculoskeletal Biomechanics Research Laboratory, Division of Biokinesiology and Physical Therapy, University of Southern California, Los Angeles, CA, gsalem@usc.edu

[5] Associate Professor of Clinical and Co-Director, Musculoskeletal Biomechanics Research Laboratory, Division of Biokinesiology and Physical Therapy, University of Southern California, Los Angeles, CA, kulig@usc.edu

INTRODUCTION

A hop is an extensively studied task with a potential to reveal the impact of pathology on intersegmental dynamics. A composite measure of intersegmental dynamics is the support moment. It is the *relative contribution* of each lower extremity joints, to the total support moment, that has the potential to provide unique information regarding the movement strategies utilized to accomplish complex, coordinated, multi-joint tasks. The purpose of the current investigation was to quantify the relative contributions of the hip, knee and ankle to the total support moment, in athletes with and without patellar tendinopathy. We hypothesized that subjects with patellar tendinopathy would demonstrate altered sagittal plane moments during hopping when compared to healthy controls, shifting the relative effort away from the knee and to the hip and/or ankle.

METHODS AND PROCEDURES

Two groups of subjects were recruited for this study. Seven males with a history of patellar tendinopathy served as the experimental group and seven males without a history of knee pain or injury constituted the control group. All subjects were elite volleyball players either playing at the collegiate (local Los Angeles area universities) or professional levels. Kinematic data (VICON Oxford Metrics; 250 Hz) and ground reaction forces (AMTI; 1200 Hz) were collected while subjects performed 20 repetitions of self-selected hopping and an externally-imposed frequency (1.66 Hz) hopping. Sagittal net joint moments (inverse dynamics), total support moment, and joint contribution to the total support moment were analyzed. Group differences were explored using 2 x 2 (group x hopping frequency) multivariate ANOVAs with repeated measures.

RESULTS

For net joint moments, a significant group effect (no interaction) was observed across hopping frequencies (p=0.018). However, although the average moments varied, univariate analysis revealed that no single variable was statistically different between groups. When averaged across frequencies, the patellar tendinopathy group generated a 72% greater average hip extensor moment

(p=0.078), 23% less knee moment (p=0.082) and 5% greater ankle moment (p=0.429).

No group effect or interaction was found for the average total support moment generated across hopping tasks. Contrastingly, the individual contributions of the hip, knee, and ankle to the total support moment, demonstrated a significant group effect (no interaction) across hopping frequencies (p=0.022). When averaged across hopping frequencies, subjects with patellar tendinopathy demonstrated greater hip contribution (p=0.030), less knee contribution (p=0.006), and similar ankle contribution (p=0.773) compared to the control participants (Figure 1).
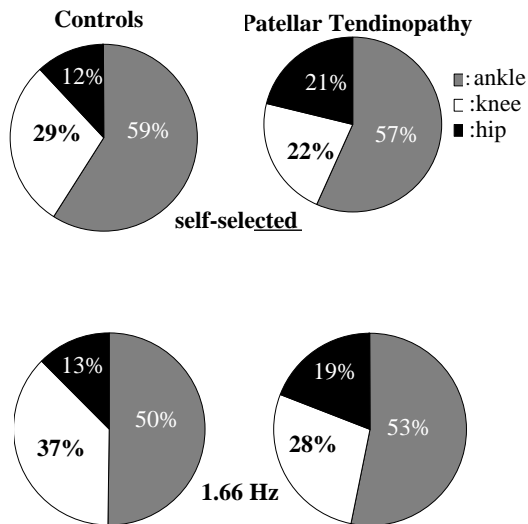
Figure 1. Contribution to total support moment during hopping

DISCUSSION

These results are in support of previous findings of observed decreased knee contribution to total support moment where subjects are apparently "off-loading" their knee either not willing or able to involve the pathologically affected joint. It should be noted that the task investigated in the current study was relatively low-effort-level compared with the cohort's typical exercise

intensities. Patellar tendinopathy subjects had no reports of pain during either of the hopping task. Despite this, subjects chose to use a strategy that decreased the demand on the knee.

These results illustrate the importance of examining both the *absolute* kinetic parameters of an activity (e.g. average net joint moments), but also the *relative contribution* of the individual joints to an overall objective—support of body mass against gravity during hopping.

SUMMARY

Subjects with patellar tendinopathy were observed to generate greater average hip extensor contribution and decreased knee extensor contribution to the total support moment. These findings were consistent across hopping frequencies. It is important to note that the distribution of joint effort to the total support moment analysis revealed important information regarding painful subject's knee contribution that would have gone undiscovered using standard net joint moment analyses. Future studies investigating joint effort in the presence of pathology may want to consider a similar analysis.

REFERENCES

Flanagan SP and Salem GJ. (2005). *J Appl Biomech,* 21:181-8.
Hurd WJ and Snyder Mackler L. (2007), *J Orthop Res.* 25:1369-1377.
Webster et al. (2004). *Knee Surg Sports Traumatol Arthrosc,* 12: 15-21.
Winter DA. (1980) *J Biomech.* 6:183-201.

DETERIORATION OF KINEMATIC AND MUSCLE PERFORMANCE AND ASSOCIATED CORTICAL ACTIVITY RELATED TO INCREASED SHOULDER ABDUCTION DRIVE IN CHRONIC HEMIPARETIC STROKE

Albert Chen, Jun Yao, Ana Maria Acosta and Julius Dewald

Northwestern University, Chicago, IL, USA
E-mail: alchen@northwestern.edu, Web: http://www.dewaldlab.com

INTRODUCTION

A very important cause of upper-extremity motor disability following chronic hemiparetic stroke is abnormal joint coordination between the shoulder and elbow. Abnormal movement patterns caused by this discoordination, described by Brunnstrom (Brunnstrom 1970) as flexion and extension synergies, involve the coupling of elbow and shoulder movements, thus severely limiting the ability to make functional movements such as reaching. Previous static (Dewald and Beer 2001) and dynamic (Beer et al. 1999; Sukal et al. 2007) studies have shown that independent torque generation, arm workspace and reaching ability can all be seriously affected when stroke survivors increase the amount of shoulder abduction drive needed to lift the arm against gravity.

To investigate the neural mechanisms behind the appearance of abnormal coordination patterns during post-stroke recovery, we used an experimental setup consisting of a high-density electroencephalogram system (EEG), an electromyographic (EMG) system and a robotic device. This study experimentally and quantitatively investigates peripheral performance measures such as muscle and kinematic activity simultaneously with cortical activity. Our results provide evidence for a deterioration of elbow/shoulder kinematic and muscle coactivation variables combined with changes in cortical activity during realistic upper-extremity reaching movements when increasing shoulder abduction torques.

METHODS AND PROCEDURES

Eight able-bodied subjects (51-62 years old, all with right hand dominance) and 10 chronic hemiparetic stroke subjects (52-69 years old, all with subcortical white matter lesions) participated in our study. The experimental setup included EMG, EEG, and a robotic system known as the Arm Coordination Training 3D (ACT^{3D}) system.

Surface EMG signals were recorded from 12 muscles of the arm and trunk on the dominant limb side of control subjects or the paretic limb of stroke subjects. Scalp recordings were made with a 160-channel Biosemi EEG system.

Three different reaching tasks were performed in the horizontal plane with different required levels of shoulder abduction drive, in order to deal with different gravitational loads while reaching. The three reaching tasks consisted of making a ballistic reaching movement to a visual display target while supported by a haptic planar surface (abbreviated as TbRe), while supported in free space by a constant force equal to the weight of the arm (0Re), or while having to lift 25% of their maximum abduction force (25Re). 120 trials were performed for each task.

Quantitative indices were developed using a biomechanics-based method that represents muscle activations as 3D vectors in joint

torque space (Yao et al. 2006). Indices included a Muscle Selectivity (MS) Index, which quantifies muscle coactivation (a higher MS indicates higher coactivation), and an Effective Torque Contribution (ETC) Index, which quantifies muscle contributions to torque generation in the expected directions (a higher ETC indicates expected behavior).

RESULTS AND DISCUSSION

Stroke subjects demonstrated muscle activity consistent with movement synergy patterns during the motor tasks, as well as significant decreases in kinematic performance, as shoulder abduction drive was increased. As deltoid activity increased to abduct the paretic arm, elbow extensor activity decreased and elbow flexor activity increased as part of the flexion synergy. Both shoulder and elbow joint excursions and velocities decreased significantly between the TbRe and 25Re tasks by about 40-60% ($p<0.005$).

The MS and ETC indices also clearly indicated differences between stroke and control subjects in performance of the tasks. The TbRe task did not produce significant differences between control and stroke subjects. However, the 0Re task showed significantly lower ETC values (30%, $p<0.05$) for stroke subjects during the movement, suggesting that paretic limb muscles were contributing to torques in unexpected directions. For the 25Re task, MS values for stroke subjects were significantly higher after 20 ms after movement onset (75%, $p<0.05$). Overall, control subjects showed a decreasing trend in MS as the gravitational load was increased, while stroke subjects showed an increasing trend. This increasing trend suggested that control subjects were able to coactivate more muscles to deal with lifting and reaching (low MS), while stroke subjects were unable to reach while lifting (high MS).

Accompanying these peripheral changes, it was found that stroke subjects began to use more of the ipsilateral, or contralesional, hemisphere when they increased the amount of shoulder abduction drive. Furthermore, more heavily impaired stroke subjects (as determined by Fugl-Meyer Assessment scores) exhibited more ipsilateral cortical activity than lesser impaired subjects.

SUMMARY

Our results show differences between control and stroke subjects in quantitative peripheral performance of motor tasks and for corresponding differences in brain activity. This provides insight into the underlying mechanisms behind abnormal joint coordination following stroke. More specifically, results suggest that increases in abnormal discoordination are linked with the increased use of contralesional areas and their projections, which may include bilateral ventromedial bulbospinal pathways.

REFERENCES

Beer, R., et al. (1999). Prog Brain Res **123**: 455-60.

Brunnstrom, S. (1970). Movement therapy in hemiplegia : a neurophysiological approach. New York, Harper & Row.

Dewald, J. P. and R. F. Beer (2001). Muscle Nerve **24**(2): 273-83.

Sukal, T. M., et al. (2007). Exp Brain Res **183**(2): 215-23.

Ward, N. S. (2004). Curr Opin Neurol **17**(6): 725-30.

Yao, J., et al. (2006). J Biomech **39**(8): 1527-30.

ACKNOWLEDGEMENTS

KNEE MECHANICS WHILE WALKING ON DIFFERENT SURFACES AFTER TOTAL KNEE REPLACEMENT

Clare E. Milner & Michael W. Smith
University of Tennessee, Knoxville, TN, USA. Email: milner@utk.edu

INTRODUCTION
Total knee arthroplasty (TKA) is a very successful surgery in terms of reducing pain and improving function of the affected joint. Despite the decrease in pain and improvement in mobility after TKR, evidence indicates that patients had not lost weight one year after surgery (Donovan et al., 2006). However, Sisto and Malanga (2006) cautioned against an activity program that includes fast walking without paying attention to lower-limb biomechanics. Recent evidence indicates that knee kinematics do not return to normal following TKA (Milner, in press). This population may be suitable candidates for gait retraining to improve lower extremity kinematics. This is typically done on a treadmill to provide a controlled environment. However, the effect of treadmill walking on gait mechanics in this population is unknown.

Therefore, the aim of this study was to determine whether sagittal plane knee mechanics during overground and treadmill walking are similar after unilateral total knee arthroplasty. In particular, peak knee flexion (KFLEX) and knee excursion during weight acceptance (KEXC) in the involved knee were compared among laboratory (LAB), treadmill (TM), indoor hallway (HALL), outdoor sidewalk (SW) and outdoor running track (TK) conditions.

METHODS
These data are preliminary findings of an ongoing study of walking mechanics on different surfaces following TKA. Adults who were fully recovered from a previous unilateral TKA were recruited into the study. Exclusion criteria included rheumatoid arthritis, conditions likely to affect gait, current lower extremity or low back pain and body mass index greater than 40 (extreme obesity). All subjects provided informed consent to participate. Knee kinematics were recorded via an electrogoniometer as participants walked on each of the five surfaces (stratified to indoor and outdoor and randomized within strata) at their freely chosen speed. Practice trials were used to familiarize the participants with each condition. Five good trials were recorded. These were consecutive steps collected at the end of the walk in all conditions, except LAB. Separate trials were collected in the LAB condition, replicating a typical gait analysis. Knee flexion angles were calculated for the involved limb. One way repeated measures ANOVA was used to compare peak knee flexion and knee flexion excursion (footstrike to peak) amongst the conditions. Tukey post-hoc tests were used to identify where any differences lie. Data are presented for 9 subjects with TKA (age: 61 ± 6 y; height: 1.69 ± 0.09 m; mass: 84.4 ± 14.8 kg).

RESULTS AND DISCUSSION
Both peak knee flexion and excursion were significantly different between conditions. Peak knee flexion values during treadmill walking and walking trials in the laboratory were similar to each other and lower than the three other conditions. Furthermore, peak knee flexion values during walking in the hallway, on the sidewalk and on the track were not significantly different from each other. This is a very interesting finding and suggests that the laboratory environment may be affecting the gait pattern of

individuals with TKA. The laboratory condition replicated a typical gait analysis with discrete walking trials that require the subject to walk over a force plate and make a clean footstrike on the plate. Consequently, this overground condition is more constrained than the others, in which the participant simply walks continuously as data are collected.

Table 1: Peak knee flexion and knee flexion excursion in different walking conditions, mean (sd)

	Peak knee flexion (°)	Knee flexion excursion (°)
LAB	13.6 (4.9)	14.6 (5.7)
TM	12.3 (4.9)	6.2 (4.4)
HALL	17.7 (6.6)	15.4 (5.8)
SW	17.7 (6.8)	16.1 (5.3)
TRK	17.6 (5.7)	16.9 (6.6)

Even more startling was the difference in knee flexion excursion between treadmill walking and all four other conditions. Knee flexion excursion on the treadmill was less than half that in the overground conditions. Knee excursion in the overground conditions was generally similar, although excursion in the lab was significantly less than on the track. The small knee flexion excursion in the treadmill condition was partly due to both lower peak knee flexion and increased knee flexion at footstrike.

Several factors may have contributed to these changes in gait during treadmill walking. Subjects walked at their freely chosen speed in all conditions. There is some evidence in the literature that this leads to significantly lower walking velocities on the treadmill compared to overground (Marsh et al., 2005). Slower velocities during treadmill walking were also observed in the present study (0.79 ± 0.20 m/s TM vs 1.26 ± 0.09 m/s LAB). Furthermore, older adults may require an extended period of habituation to the treadmill. Wass et al. (2005) reported that the knee mechanics of older adults changed during the first four minutes of treadmill walking. They suggested that the overall gait pattern was not the same as during overground walking even after 14 minutes of habituation. However, it should be noted that two-thirds of the participants in their study walked while holding the treadmill handrail for the entire period. None of the participants in the present study held the handrail during data collection. Finally, several participants reported that the safety harness used during treadmill walking was cumbersome. This additional factor may have affected their gait pattern and is a limitation of the study. Future work involving treadmill walking after total knee replacement should incorporate an extended habituation period, ideally spanning several sessions. This may result in a treadmill gait that is more similar to overground walking.

SUMMARY
Knee mechanics after unilateral TKA are different during treadmill walking compared to overground walking in the laboratory, in a hallway, on a sidewalk and on a track. Specifically, peak knee flexion and knee flexion excursion are lower on the treadmill compared to the overground conditions (excluding peak knee flexion in the laboratory).

REFERENCES
Donovan, J. et al. (2006). *ANZ J. Surg.* **76**, 222-225.
Sisto, S.A. & Malanga, G. (2006). *Am. J. Phys. Med. Rehabil.* **85**, S69-78.
Milner, C.E. (2008). *Gait Posture*, in press.
Marsh, A.P. et al. (2006). *Med. Sci. Sports Exerc.* **38**, 1157-1164.
Wass, E. et al. (2005). *Gait Posture* **21**, 72-79.

CONTRIBUTION OF ACTIVE DORSIFLEXION TO TOE CLEARANCE IN TRANSTIBIAL AMPUTEES: A CASE STUDY

Noah Rosenblatt[1], Jeremy Crenshaw[1], Jason Wenning[2], Mark Grabiner[1],

[1] Department of Kinesiology and Nutrition, University of Illinois, Chicago, IL, USA
nrosenbl@uic.edu, URL: http://www.uic.edu/ahs/biomechanics
[2] Scheck & Siress Orthotics & Prosthetics, Oak Park, IL, USA

INTRODUCTION

Successful negotiation of varying terrains and obstacles is critically dependent upon minimum toe clearance, the distance between the walking surface and the toe of the swing limb, at midswing (MTC). For transtibial amputees (TTA), the absence of active ankle dorsiflexion during swing initiation lowers MTC. The associated increased probability of hitting an unseen obstacle (Best et al, 2007) may contribute to the 42.9% of TTA that reported falling over a 1 month period (Gauthier-Gagnon et al, 1999).

A recently designed prosthesis, with active control of swing phase dorsiflexion, was developed to provide adaptation to variable terrains, while increasing MTC (Ragnarsdóttir 2005). However, MTC depends not only on ankle kinematics, but also those at the hip and knee (Moosabhoy et al. 2005) all of which are walking speed-dependent (Borghese et al 1996). For this reason, active dorsiflexion alone may be insufficient to improve MTC. Therefore the purpose of this study was 1) to compare MTC for TTA on level and inclined surfaces, at varying speeds, with and without actively controlled dorsiflexion and 2) to develop a model to quantify the contribution of ankle kinematics to MTC. In all cases, we expected MTC and ankle contributions to increase with actively controlled dorsiflexion.

METHODS AND PROCEDURES

One subject (male, age 40, 81.6 kg, 1.8m) who suffered a traumatic transtibial amputation 12 years prior, and uses a prosthesis with active ankle dorsiflexion control (Proprio Foot ®, Ossur, Aliso Viejo, CA) participated. The subject walked on a treadmill for 30 sec at a slow, preferred and fast speed on 2 different inclines: level and 5° uphill, with and without the control feature of the prosthetic engaged ("on" and "off" respectively). The motion of 22 passive reflective markers was recorded at 60 Hz and used to calculate MTC and hip, knee and ankle kinematics from toe off (TO) to midswing (MS).
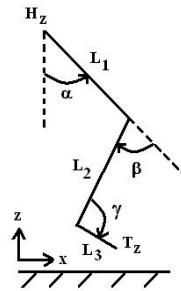
Figure 1. Three segment model of the swing limb in the sagittal plane. Positive joint angles are shown with arrow. Vertical toe and hip position (T_z and H_z respectively) and segment lengths (L_1, L_2, L_3) are noted.

A three segment model of the lower limb (Figure 1) lead to the following relationships:

$$T_z(t) = H_z(t) - L_1 \cos(\alpha(t)) - L_2 \cos(\beta(t) - \alpha(t))$$
$$- L_3 \cos(\pi + \alpha(t) - \beta(t) - \gamma(t))$$

$$MTC = Tz(MS) - Tz(TO) = dT_z =$$

$$\int_{TO}^{MS} \left(\frac{\partial T_z}{\partial H_z} \frac{dH_z}{dt} + \frac{\partial T_z}{\partial \alpha} \frac{d\alpha}{dt} + \frac{\partial T_z}{\partial \beta} \frac{d\beta}{dt} + \frac{\partial T_z}{\partial \gamma} \frac{d\gamma}{dt} \right) dt$$

The partial derivatives (i.e. $\partial T_z / \partial \gamma$) represent the sensitivity, or rate of change of T_z with

respect to each angle (Moosabhoy et al, 2005) or to hip position. Multiplying this rate of change by the observed changes (i.e. $d\alpha/dt$) and integrating over time, the "total contribution" of each joint to MTC, expressed in mm, is obtained. A positive value suggests the cumulative motion of the joint from TO to MS acts to increase MTC. Contributions for each joint are calculated on a step-to-step basis, averaged across steps (N=15 steps), and theoretically sum to MTC. Contributions can not be determined by direct comparison of single joint kinematics.

RESULTS

MTC for the "on" condition was larger than that of the "off" condition for the preferred and fast walking speeds. At slow speeds the two conditions were similar (Figure 2). For the "on" condition, MTC increased from slow to preferred speed, and the ankle contribution became positive. For the "off" condition, ankle contribution was always negative.
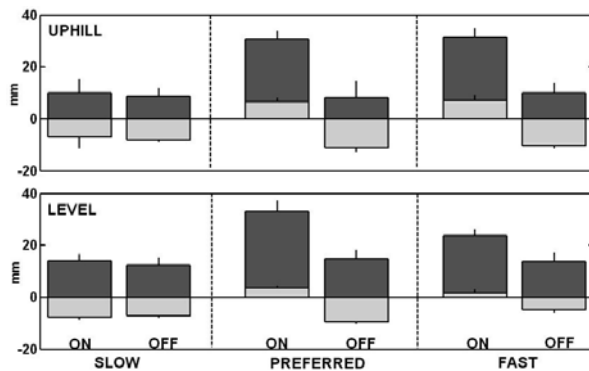
Figure 2. MTC (dark grey bar) and contribution of the ankle to MTC (light grey) for level and uphill walking, at three speeds, during on and off conditions (mean ± SD).

DISCUSSION

Active control of ankle dorsiflexion had the greatest influence on MTC at faster speeds during uphill walking. This is evidenced by the fact that MTC and ankle contributions were the largest for "on" trials at preferred

and fast speeds. In addition to a positive ankle contribution, the increased MTC at higher speeds also reflects a more positive contribution from hip and knee joints. We found that ankle dorsiflexion, from TO to MS, always increased MTC ($\partial T_z/\partial\gamma<0$). A negative ankle contribution may be explained by one of two scenarios. One, the ankle does not dorsiflex ($d\gamma/dt>0$), as observed in all of the "off" trials. Two, ankle dorsiflexion begins too close to MS to counter the negative contribution due to plantarflexion in early swing. Thus, negative contributions during the "on" condition may reflect an inability of the prosthesis to properly adapt to slow speeds. Since ankle contributions were greatest during uphill walking, which requires greater dorsiflexion to clear the surface, we believe that the foot can successfully adapt to changing terrain.

Although our results constitute strategies adopted by an individual, the strength of this study lies in the variety of conditions tested and the novelty of the quantitative methods used.

SUMMARY

Active control of swing phase dorsiflexion by a prosthetic foot was directly linked to an increased MTC at preferred and fast speeds on level ground and inclines. It is unclear why ankle control at slow speeds was not associated with a positive effect on MTC.

REFERENCES

Gauthier-Gagnon et al. (1999). *Arch Phys Med Rehabil,* 80:706-13.
Best, R et al. (2008). *J Biomech,* doi:10.1016/j.jbiomech.2007.11.023.
Moosabhoy, MA et al. (2005). *Gait Posture* 24: 493-501.
Ragnarsdóttir HG (2005). *J of Proc AAOP.*
Borghese et al. (1996). *J Physiol* 494: 863-79.

CAN CHILDREN CONTROL THEIR JOINT VARIABILITY IN STANDING WHILE CONFRONTING A PERTURBATION OF TENDON VIBRATION?

Jianhua Wu[1], Sandra McKay[2] and Rosa Angulo-Barroso[3]

[1]Biomechanical Laboratory, Department of Kinesiology and Health, College of Education, Georgia State University, Atlanta, GA, USA, jwu11@gsu.edu
[2]Center for Studies in Aging, Sunnybrook Health Sciences Center and Health Care Technology and Place, University of Toronto, Canada, sandra.mckay@sri.utoronto.ca
[3]Division of Kinesiology, University of Michigan, Ann Arbor, MI, USA, rangulo@umich.edu

INTRODUCTION

Stable control of center-of-mass (COM) is a prerequisite to performing human movements. Children acquire this ability starting in their infancy and make progress throughout their childhood. One important component in balance control is the ability to adapt to external perturbations. This study examined how children control their COM while confronting a perturbation of tendon vibration in standing. A framework of uncontrolled manifold (UCM) was used to examine the use of variability in the joint configuration space.

METHODS AND PROCEDURES

Three groups of healthy people participated in this study: (1) young children (YC) n=8, age 6.3 (SD 0.6) yrs; (2) older children (OC) n=9, age 10.3 (SD 0.9) yrs; (3) young adults (YA) n=10, age 20.5 (SD 1.4) yrs. Reflective markers were placed bilaterally on toe, ankle, knee, hip, shoulder, elbow, wrist, and temple, and one on C7 spine. A six-camera Vicon Peak® motion capture system was used to collect data. A small motor was attached above the right ankle to alter proprioceptive information in muscle spindles, which produced false impression of body movement.

Participants stood on a Bertec® force platform. Two visual conditions were examined: eyes-open (EO) and eyes-closed (EC). Three 40-second trials were collected in each condition. The first 10 seconds of each trial was standing without vibration. Then, vibration (8 seconds) was triggered when the ground reaction force and moment on the sagittal plane were both pointing to forward sway. Posterior COM sway was elicited during vibration, and maximal posterior COM sway was chosen to study joint variability using the UCM analysis. All the analyses were conducted in the sagittal plane.

Geometric model relating the COM to the joint configuration space is:

$COM_{AP} = m_{foot} \cdot l_{foot} \cdot d_{foot} \cdot \cos(\theta_{foot}) + m_{shank} \cdot [l_{shank} \cdot d_{shank} \cdot \cos(\theta_{shank}) + l_{foot} \cdot \cos(\theta_{foot})] + m_{thigh} \cdot [l_{thigh} \cdot d_{thigh} \cdot \cos(\theta_{thigh}) + l_{foot} \cdot \cos(\theta_{foot}) + l_{shank} \cdot \cos(\theta_{shank})] + m_{trunk} \cdot [l_{trunk} \cdot d_{trunk} \cdot \cos(\theta_{trunk}) + l_{foot} \cdot \cos(\theta_{foot}) + l_{shank} \cdot \cos(\theta_{shank}) + l_{thigh} \cdot \cos(\theta_{thigh})] + m_{head} \cdot [l_{head} \cdot d_{head} \cdot \cos(\theta_{head}) + l_{foot} \cdot \cos(\theta_{foot}) + l_{shank} \cdot \cos(\theta_{shank}) + l_{thigh} \cdot \cos(\theta_{thigh}) + l_{trunk} \cdot \cos(\theta_{trunk})]$

in which m and d are proportional mass and location of segment COM, respectively, l is segment length, θ is the elevation angle to the horizontal. Values of m, l and d were adopted from Winter (2005) for YA group and from Jensen (1986) for YC and OC groups.

The UCM analysis calculates the Jacobian of the geometric model to linearize the joint configuration space, and then partitions the variance from all the θs to two orthogonal

subspaces: task-relevant (V_{UCM}) and task-irrelevant (V_{ORT}). The details on calculating V_{UCM} and V_{ORT} can be referred to Scholz and Schoner (1999). The UCM ratio was defined as V_{UCM}/V_{TOTAL}, where V_{TOTAL} is the sum of V_{UCM} and V_{ORT}. A higher ratio suggests more joint variability is partitioned to the task-relevant subspace to help stabilize the COM.

Dependent variables include: (1) SD of pre-vibration COM (8 seconds before vibration), (2) Max posterior COM sway (from the mean of pre-vibration COM), (3) total joint variance (V_{TOTAL}), and (4) UCM ratio. The first two variables were normalized to the foot length. ANOVAs (3 Group x 2 Visual) with repeated measures were conducted on each variable.

RESULTS

Before the vibration, both YC and OC groups produced significantly greater COM sway than YA group ($p<.0001$; SD of pre-vibration COM in Table 1). Participants produced greater COM sway in the EC than in the EO ($p=.005$). During the vibration, YC group produced significantly greater maximum posterior COM sway than YA group ($p=.009$; Max posterior COM sway in Table 1). Participants produced greater max COM sway in the EC than in the EO ($p=.005$).

At the maximal posterior COM sway, both YC and OC groups produced significantly

greater values of total joint variance than YA group ($p=.005$; V_{TOTAL} in Table 1). No visual effect was significant for this variable. As for the UCM ratios, all the three groups produced similar group means (ranged from 0.73 to 0.84; Table 1). Neither group difference nor visual effect was significant.

DISCUSSION

It is not surprising to find that YC group produced significantly greater COM sway before and during the vibration compared to YA group. However, at the maximal posterior COM sway due to the vibration, YC group partitioned the joint variability similarly as YA group such that the majority of joint variance was directed to the task-relevant space to help stabilize the COM. This finding suggests that YC group, though their balance control is not mature, start to show the adult-like variability-partitioning strategy when confronting external perturbations.

REFERENCES

Jensen RK (1986) *J Biomech,* 19: 359-368.
Scholz JP and Schoner G (1999). *Exp Brain Res,* 126:289-306.
Winter DA (2005). *Biomechanics and Motor Control of Human Movement.* New Jersey, Wiley.

Table 1: Mean (SD) of the dependent variables

	EO			EC		
	YC	OC	YA	YC	OC	YA
SD of pre-vibration COM	0.025 (0.009)	0.013 (0.005)	0.009 (0.004)	0.031 (0.009)	0.016 (0.005)	0.010 (0.004)
Max posterior COM sway	-0.076 (0.037)	-0.072 (0.031)	-0.041 (0.013)	-0.119 (0.071)	-0.087 (0.029)	-0.055 (0.026)
V_{TOTAL} (rad^2)	0.0033 (0.0026)	0.0032 (0.0041)	0.0005 (0.0006)	0.0022 (0.0031)	0.0016 (0.0016)	0.0001 (0.0003)
UCM ratio	0.84 (0.20)	0.77 (0.24)	0.84 (0.09)	0.74 (0.30)	0.77 (0.16)	0.78 (0.22)

DOES RESTRAINING ARM MOTION ALTER GROUND REACTION FORCES DURING RUNNING?

Ross H. Miller, Graham E. Caldwell, Richard E.A. Van Emmerik,
Joseph Hamill, and Brian R. Umberger
Department of Kinesiology, University of Massachusetts, Amherst, MA, USA
Email: rhmiller@kin.umass.edu   Web: http://www.umass.edu/sphhs/kinesiology

INTRODUCTION

Running mechanics can be studied with computer simulations that attempt to replicate, or "track" experimental data, such as ground reaction forces (GRF), to generate realistic movement patterns (Wright *et al*., 1998). To simplify the simulation problem, the upper body is often modeled as a single segment representing the head, arms, and trunk. This simplifying assumption is questionable, since the upper body moment of inertia changes due to arm motion, and the arms contribute to total-body momentum (Hinrichs, 1990). Further, upper body muscles can influence lower extremity mechanics through dynamic coupling (Zajac & Gordon, 1989).

Knowledge of the influence of the arms on experimental tracking variables such as the GRF could provide strategies for defining musculoskeletal models. A model with no arms that tracks experimental data will attempt to reproduce these data using lower extremity muscles only. The GRF is robust to some (Wright *et al*., 1998) but not all (Derrick *et al*., 2000) perturbations, and the effects of perturbing arm motion are currently unknown. If arm motion contributes substantially to GRF patterns, a potential mismatch will exist between modeled and actual lower extremity muscle actions. Therefore, the purpose of the study was to determine the effects of restrained arm

motion on GRF during running. We hypothesized that restrained arm motion would increase the peak medial-lateral GRF due to a loss in transverse angular momentum regulation, while the peak vertical GRF would decrease due to a loss of 'lift' (*i.e.* vertical linear momentum regulation; Hinrichs, 1990).

METHODS

Six subjects (28±2 years) ran overground and landed on a force platform with the right foot. Subjects completed five trials each of normal running (NO), running with the arms restrained across the chest (RC), and running with the arms restrained behind the back (RB). All trials were performed at the subject's preferred speed from the NO condition. Subjects were allowed numerous practice trials to become comfortable with the RC and RB conditions. GRF data were sampled at 5000 Hz.

Peak GRF magnitudes and times of occurrence were compared across conditions by ANOVA ($\alpha = 0.05$). To compare GRF time series between conditions, Pearson's *r* correlations (Derrick *et al*., 1994) and cross-correlations were calculated.

RESULTS

There were no significant differences across conditions in GRF timing as evidenced by

cross-correlation or peak timing. The medial-lateral GRF was the least similar time series across conditions, although r was large (> 0.96) for all components. The vertical and medial-lateral GRF peaks were disrupted by conditions RC and RB (Fig. 1). When arms were restrained, the vertical GRF peak fell by 11-14% body weight (BW) and the lateral GRF peak rose by 4-7% BW. Table 1 summarizes GRF peaks between conditions. Regardless of condition, variability between subjects (8% BW) was on average twice as large as variability within subjects (4% BW).
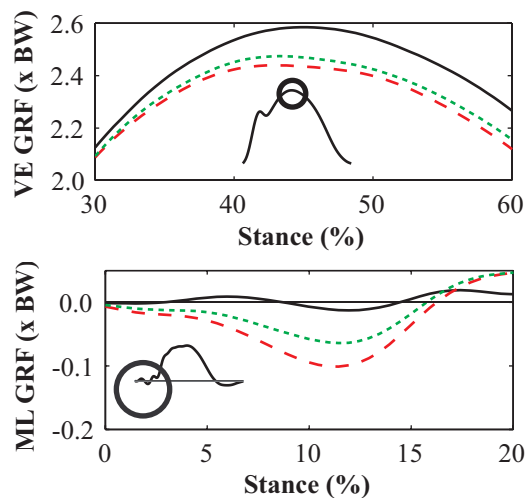
Figure 1. Vertical (VE, top) and medial-lateral (ML, bottom) GRF for the **NO**, **RC (dashed)**, and **RB (dotted)** conditions.

DISCUSSION

The hypotheses were supported, as restrained arm motion decreased the vertical GRF peak and increased the lateral GRF peak. Changes are likely due to losses in momentum control provided by the arms (Hinrichs, 1990). Similarities between RC and RB suggest that the GRF disruptions were due primarily to the loss of arm motion rather than adjustments in the center-of-mass location. The restrained arm conditions approximate the capabilities

Table 1. Changes in GRF peak magnitudes (in % BW) between conditions. $* = p < 0.05$.

Parameter	RC - NO	RB - NO	RC - RB
VE impact	7.1	2.0	5.1
VE second	-13.7*	-10.8*	-1.9
AP brake	4.2	2.4	1.8
AP propel	-0.8	-1.4	0.6
ML medial	-0.2	-0.1	-0.1
ML lateral	6.8*	3.7*	3.1

of a computer model with no arm articulation. Because differences in GRF peaks between RC/RB and NO were inside two between-subjects standard deviations, we conclude that tracking experimental GRF from normal running with an armless computer model is likely a valid general simulation method. However, because peak differences were large relative to within-subjects variability, for subject-specific simulations researchers may consider tracking experimental data from human runners with restrained arm motion, or including muscle-actuated arms in the model. It remains to be seen how arm motion affects other commonly tracked variables, such as lower extremity joint kinematics (Wright *et al.*, 1998).

REFERENCES

Derrick TR *et al.* (1994). *Med Sci Sports Exerc*, 26:919-928.

Derrick TR *et al.* (2000). *J Appl Biomech*, 16:36-51.

Hinrichs RN (1990). In: *Biomechanics of Distance Running*. Human Kinetics.

Wright IC *et al.* (1998). *Clin Biomech*, 13:521-531.

Zajac FE & Gordon ME (1989). *Exerc Sport Sci Rev*, 17:187-230.

TRIP-RECOVERY STRATEGIES OF A TRANSFEMORAL AMPUTEE

Jeremy Crenshaw[1], Kenton Kaufman[2], and Mark Grabiner[1]

[1]Department of Kinesiology and Nutrition, University of Illinois at Chicago, Chicago IL,
jcrens2@uic.edu, URL: http://www.uic.edu/ahs/biomechanics
[2]Department of Orthopaedic Surgery, Mayo Clinic, Rochester, Minnesota USA

INTRODUCTION

During a one month period, 63.9% of adults with a unilateral, transfemoral amputation (TFA) reported falling (Gauthier-Gagnon et al., 1999). The high incidence of falls necessitates an understanding of fall mechanisms and the identification of appropriate recovery strategies that are amenable to intervention.

Adults with no amputation have demonstrated two distinct trip-recovery strategies (Eng et al., 1994, Pavol et al., 2001). An elevating strategy occurs when a limb is obstructed during the swing phase and then elevates over the obstacle. A lowering strategy occurs when a swing limb is obstructed, lowers to the ground, and the contralateral limb is used as the leading limb to cross the obstacle. These strategies have been associated with active control of the stance and swing limbs' knees and ankles. It is unknown if similar strategies are appropriate and feasible for individuals with a TFA.

Strategy-specific mechanisms leading to a trip-induced fall have been identified in older adults (Pavol et al., 2001). Walking quickly, excessive trunk flexion, and deficient stepping responses distinguished fallers from non-fallers. Similar variables have yet to be measured during a trip recovery in lower limb amputees.

The purpose of the present study was to identify and describe trip recovery strategies of a person with a unilateral TFA.

METHODS AND PROCEDURES

The subject (female, age 27 years, height 165 cm, mass 62.5 kg) suffered a traumatic, TFA of the left limb 3 years and 6 months prior to participation. Her prosthesis consisted of a microprocessor knee (C-Leg[®,] Otto Bock, Minneapolis, MN) and a dynamic response foot.

The subject walked through a motion capture volume at a self-selected speed. When triggered, a concealed, pneumatically-controlled obstacle rose 5 cm above the floor. The obstacle was situated in between two force plates (AMTI, Watertown, MA). The subject was first tripped by obstructing the prosthetic limb (PL). During a subsequent walking trial, the subject's non-prosthetic limb (NPL) was obstructed. Marker position and ground reaction forces were recorded at 120 Hz and 1200 Hz respectively.

The following kinematic variables were calculated:

- Forward velocity of the pelvic centroid at the time of obstacle contact (v_{pelvis}).
- Recovery step length (d_{rec}). Recovery step is defined as the step crossing the obstacle.
- Trunk flexion at the time of recovery step contact (TrunkAng).
- Trunk flexion velocity at the time of recovery step contact (TrunkVel).

RESULTS

The subject successfully recovered from both trips. She reported both trips to be unexpected.
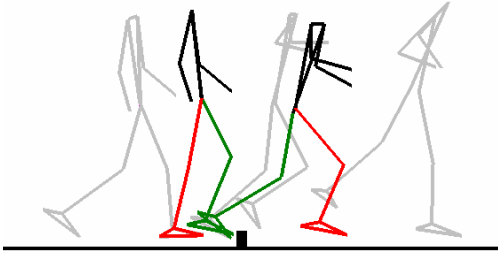
Figure 1. Obstruction of the PL (green). The subject demonstrated a lowering strategy (see video on website). Based on peak ground reaction forces, the PL supported up to 57.6% of the subject's body weight as the NPL crossed the obstacle. After landing on her NPL, the subject hopped on the limb twice before bearing weight on the PL.
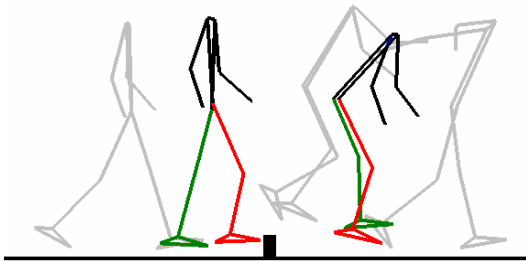
Figure 2. Obstruction of the NPL (red). The subject lowered the NPL to the ground and hopped over the obstacle, landing on the NPL (see video). During subsequent strides, the subject hopped on the NPL.

DISCUSSION

This is the first study to report a trip response by a subject with a TFA. These observations demonstrated that, despite a high level of ambulatory function, this individual relied on trip-recovery strategies that favored the NPL. A previously undocumented "hopping strategy" was observed when the NPL was obstructed. Compared to the lowering strategy used when the PL was obstructed, the hopping strategy was accompanied by a shorter recovery step, as well as a larger and increasing trunk flexion at recovery step. The hopping strategy was associated with a step length and trunk flexion velocity similar to that resulting in a fall in older adults (Table 1). Although the subject did not fall, a hopping strategy may be impracticable for older amputees with plantarflexion or trunk extension weakness.

REFERENCES

Eng, JJ et al. (1994). *Exp Brain Res,* 102:339-349.

Gauthier-Gagnon, C et al. (1999). *Arch Phys Med Rehabil,* 80:706-713.

Pavol, MJ et al. (2001). *J Gerontol,* 56A, M428-M437.

Variable	Obstructed Limb		Older Adults		
	PL	NPL	Non-fallers	DS Fall	AS Fall
v_{pelvis} (m/s)	1.13	1.15	1.13 ± 0.19	1.45 ± 0.12	1.29 ± 0.09
d_{rec} (%bh)	33.1	27.6	49.4 ± 5.7	36.9 ± 8.3	49.1 ± 8.0
TrunkAng (deg)	12.93	37.22	36.0 ± 12.6	48.3 ± 4.7	55.2 ± 11.4
TrunkVel (deg/s)	-20.82	23.52	-43.0 ± 52.8[#]	81.6 ± 41.4[#]	36.1 ± 40.9[#]

Table 1. Kinematic variables when the PL and NPL were obstructed, as well as comparable variables from older adults employing a lowering strategy (Pavol et al., 2001). Body height = bh; During-step fall = DS Fall; After-step fall = AS Fall. [#]Reported as Hip-HAT COM velocity.

CONFLICT RESOLUTION TASK EFFECTS ON GAIT BALANCE AFTER A CONCUSSION

Robert D. Catena, Paul van Donkelaar, and Li-Shan Chou

University of Oregon, Eugene, OR, USA, chou@uoregon.edu,
URL: http://biomechanics.uoregon.edu/MAL/

INTRODUCTION

Conflict resolution (a function of the executive controller) deficits exist long after a concussed individual returns to normal activity (Halterman et al., 2006). It was also shown that divided attention results in gait imbalance long after a return to normal activity (Parker et al., 2006). The purpose of this experiment was to analyze the effects of conflict resolution on balance control during gait following a concussion, and the effects of gait on conflict resolution to see if perhaps tasks requiring executive functioning may result in physical deficits. We expected an executive function task to result in minor gait stability changes; however, an analysis of conflict resolution was expected to indicate even poorer performance when conflicting stimuli were presented to concussed subjects. This study will indicate if executive dysfunction in concussed patients interferes with gait balance control and aid clinicians making a decision in timing of a return to certain activities following a concussion.

METHODS AND PROCEDURES

Ten grade II mTBI subjects were tested at 2, 6, 14 and 28 days post-injury. Gender, age, stature and athletic participation matched controls were tested at four equivalent intervals. Each test included single task walking, walking with a concurrent congruent auditory Stroop task, and with an incongruent Stroop task. Whole body motion data were collected with an 8-camera motion analysis system. Twenty-nine reflective markers were used to create a thirteen-link model. The whole-body CoM was calculated using the weighted sum of each of the 13 segments. Center of pressure (CoP) data were found with two force plates.

CoM motion in relation to the CoP was examined via inclination angles in sagittal and coronal directions (Lee and Chou, 2006). Stroop performance was examined via reaction times. A three-way mixed model analysis was used to assess significant differences. A linear regression was used to measure the conflict resolution/balance correlation

RESULTS AND DISCUSSION

Contrary to our hypothesis, balance control deficits were the only deficits evident in our analysis. A three-way interaction ($p = .008$) was observed in medial CoM-CoP angular range of motion (figure 1). Concussed individuals consistently had balance control deficits denoted by larger medial ranges of motion than controls. Concussed individuals had particular large medial motion at the 14 day testing in walking with a congruent Stroop presentation. Their medial CoM motion at this point was significantly larger than control individuals ($p = .006$), larger than testing sessions before ($p = .002$) and after ($p < .001$), and larger than single task walking ($p = .003$). This follows similar findings of ours in a separate concussed

group where individuals showed increased balance deficits a couple weeks after testing began because they had a premature return to normal activity (Parker et al. 2006).

There were no differences in Stroop reaction times between the two groups. Since conflict resolution deficits have been well documented following concussions, and the Stroop tasks has been determined an effective way to test conflict resolution, we believe either the auditory version of the Stroop task is too variable given the number of trials we used or is not as sensitive as other conflict resolution tasks. But because this auditory version of Stroop doesn't require a visual stimulus we thought that it could be a possibly effective method to test the relationship between balance and conflict resolution. Interestingly, we only found a weak correlation between sagittal plane motion and reaction time during the Stroop task, and no correlation between medial motion and the Stroop reaction time.

SUMMARY

Our results indicate that conflict resolution deficits do not interact importantly with balance deficits following a concussion. However, concussed individuals displayed balance deficits; particularly after a couple weeks during the congruent presentation of the Stroop task. This may be due to a premature return to normal activity and/or an inappropriate belief in their improved health following their concussion.

REFERENCES

Halterman et al. (2006) *Brain* **129**, 747-753.
Parker et al. (2006) *MSSE* **38**(6), 1032-1040.
Lee and Chou (2006) APMR **87**(4), 569-75.

ACKNOWLEDGEMENTS
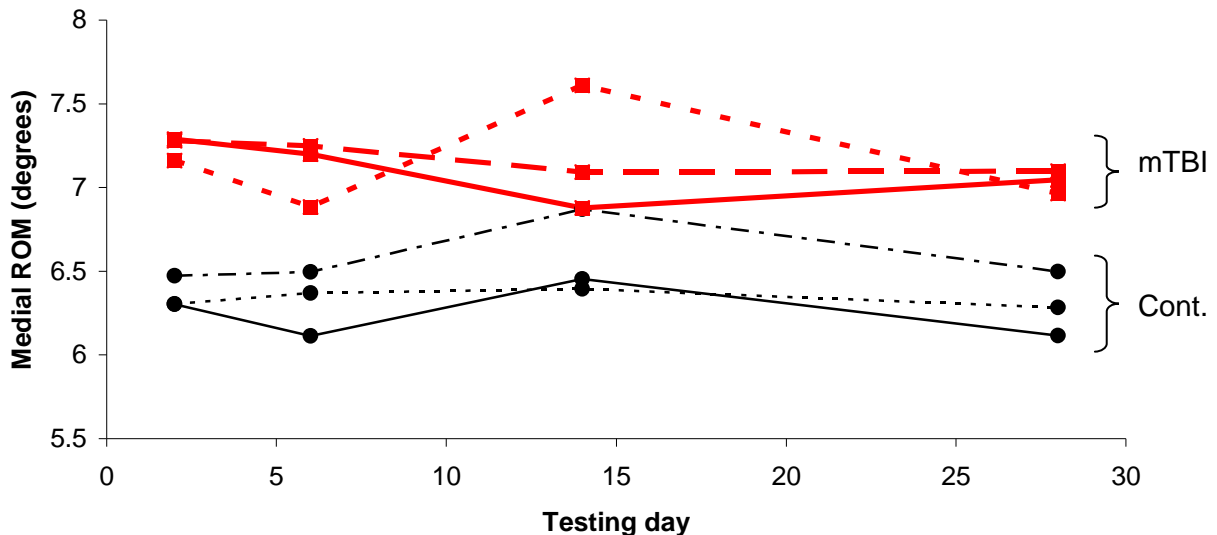
Figure 1: Medial angular range of motion of center of mass with respect to center of pressure over 28 days of testing. Concussed subjects are represented by "mTBI" to the right of the graph and control subjects are represented by "Cont." Solid lines represent single task walking, highly perforated lines represent Stroop walking during congruent task presentation, and slightly perforated lines represent Stroop walking during incongruent task presentation.

Step to step variation in step width suggests a link to variations in trunk kinematics

Christopher Hurt[1], Karrie Hamstra-Wright[1], Noah Rosenblatt[1], Karen Troy[1], Mark D. Grabiner[1]

[1]Department of Kinesiology and Nutrition, University of Illinois at Chicago, Chicago, IL, USA
churt2@uic.edu, URL:http://www.uic.edu/ahs/biomechanics

INTRODUCTION

During human walking, maintenance of frontal plane balance requires that the body center of mass (COM) remain within the laterally-directed boundaries of the base of support (BOS) (MacKinnon & Winter 1993). Proper placement of the foot can be guided by active feedback processes (Kuo 1999). Therefore, given the mass of the trunk and its capacity to act as a inverted pendulum having its axis at the hip, control of balance may rely upon the ability to temporally and spatially coordinate lateral placement of the foot on the ground with trunk states during gait. For this reason, we would expect to observe an association between trunk kinematics and foot placement, as measured by step width (SW).

Sensing of trunk states relies on information from the visual, vestibular and/or somatosensory systems. As humans age, the fidelity of sensory information from these systems decreases (Kuo 2007). Age related differences may also be compounded by a decreased ability of older adults to execute motor commands (Barry et al. 2005). Reliance on degraded signals and/or execution of motor commands would be expected to result in a loss of control accuracy and/or precision.

In this study we tested the hypothesis that step-to-step variations in step width are associated with step-to-step variations in preceding trunk states. We also tested the hypothesis that the association between step-to-step variations in step width and preceding trunk states would differ between young and older adults.

METHODS AND PROCEDURES

Twelve healthy young adults (6 males 6 females, age 25 ± 3.3 years) and eleven healthy older adults (4 males 7 females, age 61 ± 5.6 years) participated. Each subject walked on a motorized treadmill at a self-selected speed for 10 min. Kinematics were captured using an eight camera motion capture system.

SW and the frontal plane position (y) and acceleration ($\ddot{y}$) of the trunk COM were identified using custom software. SW was calculated as the difference between successive left to right foot centroids. The COM of the trunk segment was estimated from the positions of the shoulder and pelvis markers. Values for y and $\ddot{y}$ were taken at the when frontal plane lateral velocity was zero. This instant represents the point when the COM begins to "fall towards" from the stance foot, and may set the initial conditions that influence step width adjustment.

Statistics:
The relationship between trunk kinematics and SW for the aggregate datasets of each group was quantified using stepwise linear regression. The regression coefficients β_1 and β_2 were statistically examined for between-group differences.

RESULT

Step to step variations in y and $\ddot{y}$ explained over half of the shared variance with SW. SW appeared to be more sensitive to changes in trunk position, evidenced by a larger standardized coefficient for position than acceleration of the trunk COM (Table 1). In addition, position of the trunk COM accounted for 43% (of 55%) and 60% (of 63%) of the shared variance for young and older adults respectively. The regression equations were not parallel. The beta coefficients for position and acceleration of the trunk COM of the young and older adults were significantly different ($p<0.05$).

	Young	Old
Position	1.03± 0.018 (.568)	1.29 ± 0.040 (.690)
Accleration	0.082±0.02 (.359)	0.040±0.02 (.201)

Table 1.Unstandardized Beta coefficients for position and acceleration of trunk COM ± standard error. Beta coefficients are given in the parentheses**.**

DISCUSSION

Insofar as step to step variations in step width were strongly and significantly associated with step to step variations in position and acceleration of the trunk COM we accepted the first hypothesis. Frontal plane balance during walking is primarily maintained through step to step adjustment in SW. The present results suggest that SW is a function of the sensing of and responses to trunk states during the swing phase.

Given that the between-group differences for the trunk state beta coefficients were significant we accepted the second hypothesis of an age-related effect. In the regression model more of the explained variance in step width was accounted for in older adults than younger adults. Because balance control in

older adults is subject to increased sensor and processor noise (Kuo 2007) we reject the possibility that older adults may have a more robust control system than younger adults.

The degradation of sensory input may play a weaker role in the relationship between trunk states and step widths than other age-related physiological changes. For example older adults exhibit increased joint stiffness due to less compliant soft tissue. Older adults also demonstrate increased trunk roll stiffness (Allum 2002), which reduces the motion of the trunk relative to the pelvis and considerably decreases frontal plane postural stability.

Coupled translations of the trunk, pelvis and lower extremity in the frontal plane due to reduced lumbosacral and hip joint stiffness could account for the larger observed R^2 of the older adults. It would be of value, therefore, to develop a method to parse out the effects of active control and passive motion that may be reflected in the overall relationship.

SUMMARY

To our knowledge, this is the first study to link step to step variations in SW to step-to-step variation in trunk position and acceleration. This relationship was different in the young and old.

REFERENCES

Allum et al. (2002) *JPhysiology* 542: 463-663.
Barry BK et al. (2005). *J GerontolA Biol Series,* 60: 232-240.
Kuo AD (1999). *Int J. Robot Res.* 18:917-930.
Kuo AD(2007). *IEEE.* 54:1919-1926
MacKinnon and Winter (1993). 26:633-644.

EFFECT OF ANKLE INSTABILITY ON THE LOAD BEARING CHARACTERISTICS OF THE ANKLE-FOOT STRUCTURE DURING TOUCHDOWN

Jason Tak-Man Cheung[1], Victor Valderrabano[2], Scott Landry[1] and Benno M. Nigg[1]

[1]Human Performance Laboratory, Faculty of Kinesiology, University of Calgary, Calgary, Alberta, Canada, jcheung@kin.ucalgary.ca, slandry@kin.ucalgary.ca, nigg@kin.ucalgary.ca
[2]Orthopaedic Traumatology Department, University Hospital of Basel, University of Basel, Basel, Switzerland, v.valderrabano@bluewin.ch

INTRODUCTION

Ankle sprains are the most common injuries in sports and recreational activities. Lateral ankle sprain is the main cause of ligamentous posttraumatic ankle osteoarthritis. (Valderrabano, 2006). In lateral ankle sprain, the ligaments which lesion and rupture most are the anterior talofibular ligament (ATFL) and calcaneofibular ligament (CFL), which often result in ankle instability. Despite the close correlation with chronic ankle instability and ankle osteoarthritis, its pathomechanics is not clear. In this study, the biomechanical consequence of ankle instability was quantified using a three-dimensional finite element (FE) ankle-foot model with an aim to provide the biomechanical rationale behind ankle instability associated osteoarthritis.

METHODS AND PROCEDURES

The current FE analysis (ABAQUSv6.7) was done based on a previously developed 3D FE ankle-foot and shoe model (Cheung et al., 2005, Cheung and Nigg, 2007), consisting of 28 bones, 72 ligaments and the plantar fascia embedded in a volume of bulk soft tissue and an assembled shoe structure. The soft tissue and shoe soles were defined as hyperelastic while the foot bones, ligaments, ground support and uppershoe shell were assumed as linearly elastic. Surface contact among the major joints, foot-insole and shoe-ground interfaces were defined. Nine extrinsic muscle forces for simulating touchdown instances from initial contact to impact peak (Figure 1) were defined as contraction forces via axial connector elements. The muscle forces were first estimated from normalized EMG data (Perry, 1992) and physiological cross-sectional area (Klein Horsman et al., 2007) assuming a linear EMG-force relationship with varied force gains across muscles. The muscle forces were further adjusted to fit the measured kinematics (Motion Analysis Corp.) and plantar pressure (Novel GmbH.) of the same subject, whose MR images were obtained for the FE model. The measured ground reaction forces (Kistler Corp.) were applied at the inferior ground support of which its inclination relative to the shank was prescribed. The superior surfaces of the soft tissue, distal tibia and fibula were constrained throughout the simulation.

The biomechanical consequence of two different unstable ankle structures, which was simulated by deleting the ATFL (Cut1) followed by an additional deletion of the CFL (Cut2), was compared to the normal condition. The loading and boundary conditions were kept the same in all cases.

RESULTS

Figure 1 depicts the predicted deformations of the ankle-foot structure and shoe soles during touchdown.
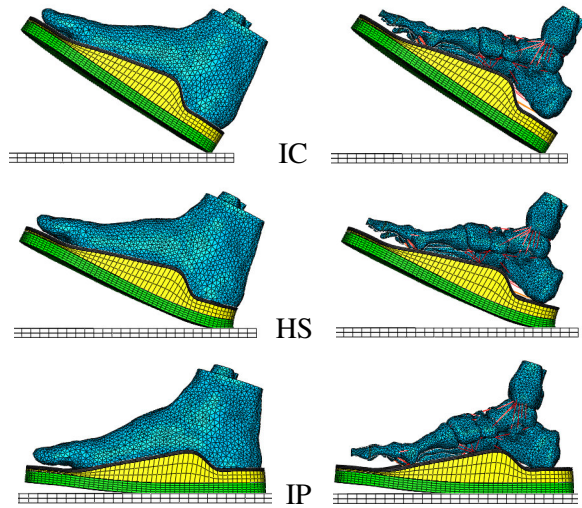
Figure 1. The deformed plots of the foot soft tissue and bony structures from initial contact (IC), heelstrike (HS) and impact peak (IP).

The maximum tensions of ankle ligaments and contact stress of talus during touchdown are tabulated in Table 1 and Table 2. Simulation of immediate ATFL rupture (Cut1) reduced the tensions of the anterior Deltoild ligaments of up to about 12% during touchdown while negligible effect was predicted in the rest of the ankle ligaments. Minimal change in contact stress of the talus of up about 0.02 MPa was found. Further CFL rupture produced minimal effects.

Ligaments	Normal	Cut1	Cut2
ATFL	79.5N	-	-
CFL	4.8N	4.8N	-
ATiFL	116.1N	116.1N	115.6N
Deltoid-AT	226.6N	205.2N	205.4N
Deltoid-TN	122.3N	120.8N	120.9N
Deltoid-TC	13.1N	13.1N	13.7N
Deltoid-PT	0.1N	0.1N	0N

Table 1. Maximum tensions predicted in the ankle ligaments. ATiFL refers to the anterior tibiofibular ligament. Deltoid ligaments are divided into the anterior tibiotalar (AT), tibionavicular (TN), tibiocalcaneal (TC) and the posterior tibiotalar (PT) parts.

Talus	Normal	Cut 1	Cut 2
CP	5.76 MPa	5.78 MPa	5.79 MPa
APS	0.05 MPa	0.04 MPa	0.04 MPa
MLS	0.05 MPa	0.06 MPa	0.06 MPa

Table 2. Maximum contact pressure (CP), antero-posterior shear (APS) and medio-lateral shear (MLS) of talus.

DISCUSSION

Rupture of the ATFL and CFL was not found to increase the forces in the surrounding ankle ligaments during touchdown. A minimal increase in contact pressure and medial-lateral shear was found. ATFL and CFL rupture caused only minimal changes in contact stress of the ankle joint during touchdown.

SUMMARY

A biomechanical link between ankle instability and osteoarthritis could not be found during touchdown. Further simulations are to be conducted to investigate the loading response during later stance instances.

REFERENCES

Cheung JT et al. (2005). *J Biomech*, 38, 1045-54.

Cheung JT and Nigg BM. (2007). *Sports Orthop Trauma*, 23: 264 – 271.

Klein Horsman MD et al. (2007). *Clin Biomech*, 22: 239-47.

Perry J (1992) *Gait analysis: normal and pathological function*. Thorofare, SLACK.

Valderrabano V et al. (2006). *Am J Sports Med*, 34: 612-620.

ACKNOWLEDGEMENTS

THE EFFECTS OF REFLEX DELAYS ON POSTURAL CONTROL
DURING UNSTABLE SEATED BALANCE

N. Peter Reeves[1], Jacek Cholewicki[1], and Kumpati Narendra[2]

[1]Osteopathic Surgical Specialties, College of Osteopathic Medicine, Michigan State University, East Lansing, MI, USA, reevesn@msu.edu

[2]Deptartment of Electrical Engineering, Yale University, New Haven, CT, USA

INTRODUCTION

Patients with low back pain (LBP) exhibit longer trunk muscle reflex latencies (Radebold et al., 2000) and poorer postural control (Radebold et al., 2001) than healthy subjects. We hypothesized that balance during a simulated postural control task would become impaired when the delays exhibited by LBP patients were incorporated into neuromuscular control. The task chosen for this investigation was seated balancing, which emphasizes trunk muscles' contribution to postural control.

METHODS AND PROCEDURES

The seated balancing task was modeled (Figure 1) in Simulink as a fourth order linearized system with feedback delays. Optimization (minimizing error between experimental and model data) of state variables was used to determine neuromuscular control. Experimental data was obtained for 7 subjects during 5 perturbation trials while balancing on a 40 cm diameter half-cylinder with eyes closed. Feedback delays in modeled neuromuscular control were increased by 5 msec increments to determine their effect on task stability, seat displacement, and trunk moment.

The linearized model was able to capture the movement dynamics of all subjects except two who had difficulty maintaining equilibrium after perturbation (Figure 2 & 3).

The two "bad balancers" data were not used for further analysis.
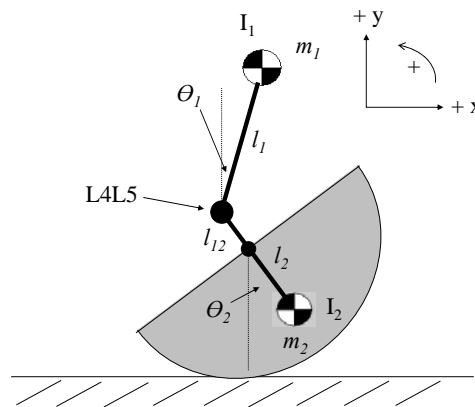
Figure 1. Simple inverted pendulum model of balancing on a half-cylinder.
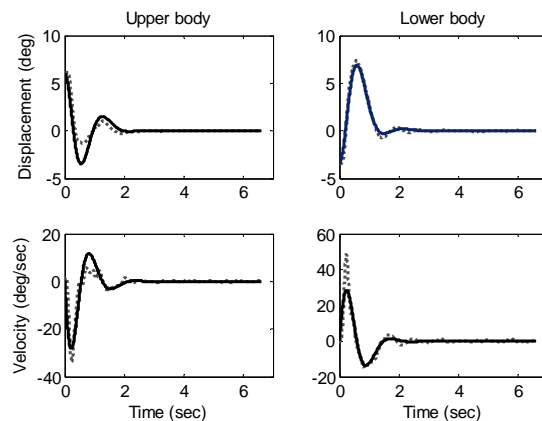
Figure 2. Experimental (broken line) and modeling (solid line) state variables for a single trial of a "Good Balancer".

Upper body · Lower body
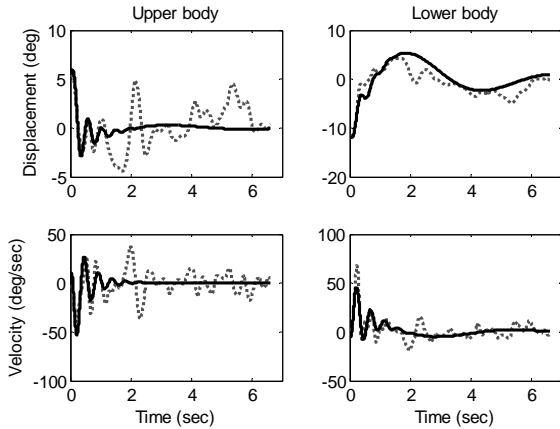
Figure 3. Experimental (broken line) and modeling (solid line) state variables for a single trial of a "Bad Balancer".

RESULTS

Simulations showed that longer delays found in LBP patients (20 msec.), in general, did not produce unstable balancing. Only 4 out of 25 trials became unstable.
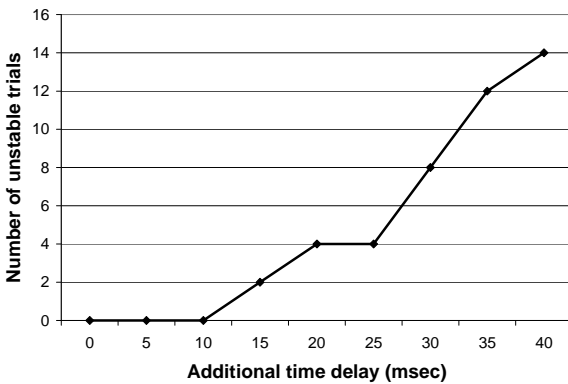
Figure 4. The number of unstable trials (seat displacement greater than 20 degrees representing seat "touch down").

However, delays of 20 msec and longer, did result in increased displacement ($p=.02$) and trunk moment required to stabilize the system ($p=.04$) (Figure 5).
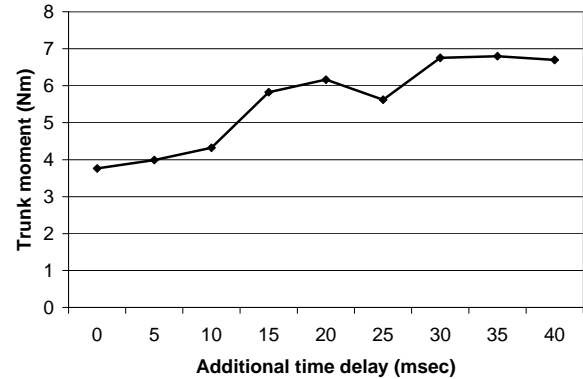
Figure 5. The average trunk moment produced during perturbation response.

DISCUSSION

Longer trunk muscle reflex delays found in LBP patients did not affect postural stability, but did affect postural performance in our simulated balancing task. Longer delays caused larger trunk displacement and higher trunk moments to maintain stability. Increase in spine displacement and loading could be problematic in LBP patients who may have diminished tissue tolerances.

SUMMARY

Longer trunk muscle reflex latencies found in LBP patients can affect their postural control and may increase their risk for re-injury.

REFERENCES

Radebold A, et al. (2000). *Spine,* 25(8):947-954.

Radebold A, et al. (2001). *Spine* 26(7):724-730.

ACKNOWLEDGEMENTS

DEFORMABILITY OF THE CARPAL TUNNEL WITH AND WITHOUT THE TRANSVERSE CARPAL LIGAMENT

Kai-Hua Xiu, Joo-Han Kim, Zong-Ming Li

Hand Research Laboratory, Department of Orthopaedic Surgery, University of Pittsburgh, Pittsburgh, PA, USA, zmli@pitt.edu, URL: http://www.pitt.edu/~zmli/handlab/

INTRODUCTION

The carpal tunnel at the wrist is formed by the interconnected carpal bones at its medial, lateral and dorsal borders, and the transverse carpal ligament (TCL) at its volar border. Carpal tunnel syndrome (CTS) results from compression on the median nerve in the tunnel. Previous research indicated that the carpal tunnel can be mechanically expanded (e.g. myofascial manipulation) to reduce the carpal tunnel pressure (Sucher BM,1993). The effectiveness of such a procedure is predominantly determined by the deformable characteristics of the carpal tunnel. In addition, the role played by the TCL in stabilizing the tunnel structure is limited (Garcia-Elias, 1989). The goal of this study was to examine the deformability of the carpal tunnel in response to the application of inward and outward forces to the TCL insertion sites. In particular, the effect of TCL transection on the deformability of the carpal tunnel was studied.

METHODS

Six fresh-frozen cadaver arms (one male and five females) with no prior history of injury or disease involved in the hands were used in the study. The mean age was 58 ± 17 years. For dissection preparation, a large skin flap was made by two longitudinal and two horizontal cuts at volar surface to expose the subcutaneous tissue. Then dissection was carried out to the TCL, exposing its proximal and distal edges and four insertion sites. The carpal tunnel was evacuated all of its contents. A piece of custom designed plywood with a 20 degree inclination was fixed onto a metal plate. Inclination of the plywood was to provide a functional neutral position for the wrist. The specimen was then mounted onto the plywood with a pin through the middle of the third metacarpal, and with a

Velcro strip around the forearm. After the fixation, the four insertion sites of TCL to the carpus were marked and individual holes were drilled. Cortex screws (Synthes Inc, West Chester, PA) with a 2.0 mm diameter and 10~12 mm in length were inserted into these drilled holes. Individual wires were attached to the screws. Four pulleys were constructed for force application by weight suspension. Each pulleys can be adjusted in horizontal and vertical directions for force alignment. Two pairs of forces were applied, one aligned with the connection line between the hamate and trapezium distally, and the other aligned with the connection line between the pisiform and scaphoid proximally (Figure 1).
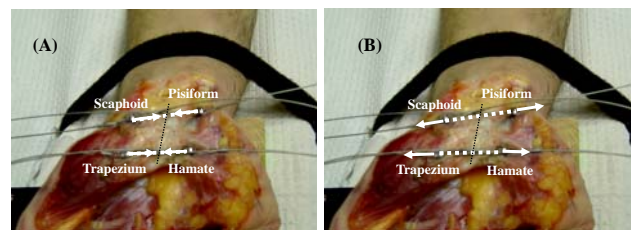
Figure 1. Two pairs of forces applied to the carpal tunnel in the inward (A) and the outward (B) directions

The forces applied to each carpus were 2, 4, 6, 8 and 10 N. These forces were applied in both inward and outward directions. The testing was repeated on the same specimen with the TCL transected. While a force was applied, the coordinates of the four insertion points of the TCL were collected by a 3D digitizer (Microscribe GX2, Immersion Corp., San Jose, CA). The distal distance between the hamate and trapezium (HT) and proximal distance between the pisiform and scaphoid (PS) were calculated for each trial. Statistical differences between conditions with TCL and with TCL transection and differences between inward and outward

force application were evaluated with One-way repeated measures ANOVA ($\alpha = 0.05$).

RESULTS

For inward force at 10 N, the HT distances decreased by 2.6 ± 1.1 mm and 2.5 ± 1.1 mm for the TCL-intact and TCL-transected conditions, respectively. The decreases for the PS distance were 10.5 ± 1.6 mm and 10.5 ± 2.2 mm for the TCL-intact and TCL-transected conditions, respectively. TCL transection didn't significantly affect the changes of the HT ($p = 0.212$) or PS ($p = 0.887$) distances. For outward force at 10 N, the HT distance increased by 0.9 ± 0.4 mm and 2.2 ± 0.9 mm for the TCL-intact and TCL-transected conditions, respectively. The increases for the PS distance were 5.6 ± 1.6 mm and 9.4 ± 2.7 mm for the TCL-intact and TCL-transected conditions, respectively. TCL transection had a significant effect on the changes of the HT ($p = 0.003$) and PS ($p < 0.001$) distances.
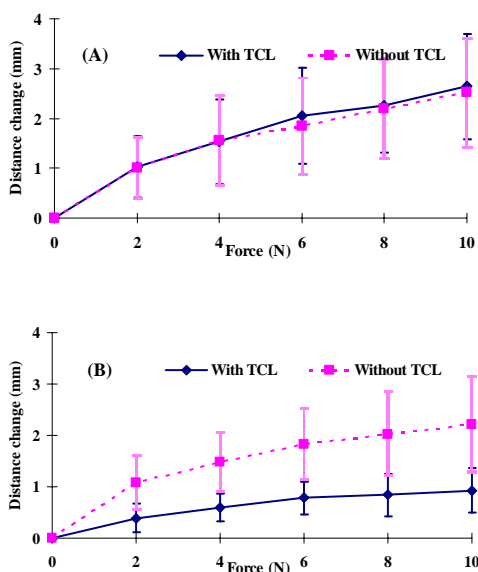
Figure 2. Force-distance change curves for the HT with TCL and without TCL during inward (A) and outward (B) force

Compliance was defined as the slope of the linear regression of the force-distance data at HT level (Figure 2). For the inward direction, the HT compliance was 0.21 ± 0.06 mm/N and $0.18 \pm$ 0.07 mm/N for the TCL-intact and TCL-transected conditions, respectively. For the outward direction, the HT compliance was 0.06 ± 0.03 mm/N and 0.14 ± 0.06 mm/N for the TCL-intact and TCL-transected conditions, respectively. The transection of the TCL significantly affected the outward compliance at the HT level ($p = 0.008$). However, TCL transection did not significantly affected the inward compliance at the HT level ($p = 0.055$). However, the compliance at the PS level was not considered due to the nonlinearity of the force-distance data.

DISCUSSION

In this study, we found that the proximal level of the carpal tunnel was more flexible than the distal level. This flexibility was evidenced by the larger amount of changes in PS distance in the inward or outward force direction, whether the TCL was intact or transected. Mobility of the carpal tunnel at the proximal level may help explain the post-operative "pillar pain" possibly associated with the pisiform-triquetral joint. Our results also showed that the TCL played an important role in stabilizing the carpal tunnel as indicated by the increases of the distance changes or compliance in the outward direction after TCL transection. As such, carpal tunnel release may cause biomechanical instability of the tunnel. However, TCL transection did not influence the inward deformability of the carpal tunnel, which is expected because the ligament does not resist compression forces.

REFERENCES

Sucher BM (1993). *J Am Osteopath Assoc*, 12: 1273-1278.
Garcia-Elias et al. (1989). *J Hand Surg [AM]*, 14A:277-282.

ACKNOWLEDGEMENTS

EFFECTS OF OBESITY ON BALANCE IN RESPONSE TO SMALL POSTURAL PERTURBATIONS

Emily M. Miller, Michael L. Madigan, Sara L. Matrangola

Virginia Polytechnic Institute and State University, Blacksburg, VA, USA
E-mail: millerem@vt.edu, Web: http://www.biomechanics.esm.vt.edu/

INTRODUCTION

Balance may be degraded by obesity (Teasdale et al., 2007). In particular, balance in response to forward postural perturbations would seem to be challenged by increased body mass and the center of mass being displaced anteriorly with respect to the spine. This displacement is due to an increased anterior abdominal mass associated with obesity. However, obese individuals typically exhibit increased muscle strength (Maffiuletti et al., 2007) and have a larger mass moment of inertia about the ankle. These may offset the presumed increase in difficulty during recovery from a forward perturbation.

The goal of this study was to investigate the effects of obesity on balance in response to small postural perturbations. We hypothesized that obese individuals would exhibit poorer balance as a result of their increased body mass.

METHODS

Twenty male subjects including 10 lean (mean ± standard deviation BMI = 21.9 ± 1.4) and 10 obese (BMI = 33.2 ± 2.3) participated in the study and provided informed consent prior to participation. Each subject performed perturbation trials while standing on a force platform. They were instructed to stand relaxed with their eyes closed and hands clasped behind their back. A ballistic pendulum was used to apply forward perturbations of 1, 2, 3, 4, 5, 6 and 8 N·s just inferior to the scapula. These perturbations were small enough so that no step was required to maintain balance. Backward perturbations were also applied intermittently to the sternum to prevent subject anticipation, but they were not included in this study. Four trials were performed at each perturbation magnitude.

Force platform data was sampled at 1000 Hz during all trials (Bertec Corporation, Columbus, OH) and filtered with a low-pass 4th order Butterworth filter (7 Hz cut-off, zero-lag). The anterior-posterior position of the center of pressure (COP) was determined for all trials. Balance was quantified using peak COP displacement from the heel and peak COP velocity.

A 2-way ANOVA was used to investigate the effects of obesity, perturbation magnitude, and their interaction on balance in response to perturbations. Pairwise comparisons were performed using Tukey's HSD. Weight was also used as a covariate during a secondary analysis to account for the fact that perturbation amplitudes were not relative to body weight.

RESULTS

Peak COP displacement (Figure 1) showed main effects of group (p<0.001), perturbation magnitude (p<0.001), and a group × perturbation magnitude interaction (p<0.001). Similarly, peak COP velocity showed main effects of group (p=0.003), perturbation magnitude (p<0.001), and a group × perturbation magnitude interaction (p=0.009).

Pairwise comparisons revealed differences between groups for both peak COP displacement and velocity at levels of 3, 5, 6, and 8 N·s in that lean measures were always greater than obese.
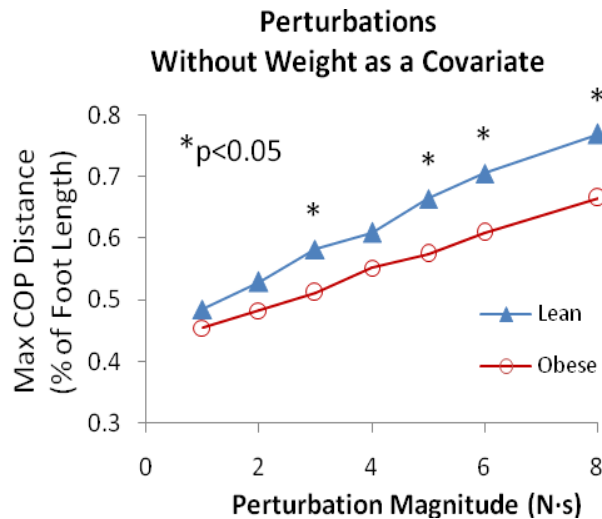
Figure 1. Least squares means of peak COP displacement without weight as a covariate.

When the analysis was repeated with weight as a covariate, there were *no* main effects of obesity or interactions found for either peak COP displacement (Figure 2) or velocity.
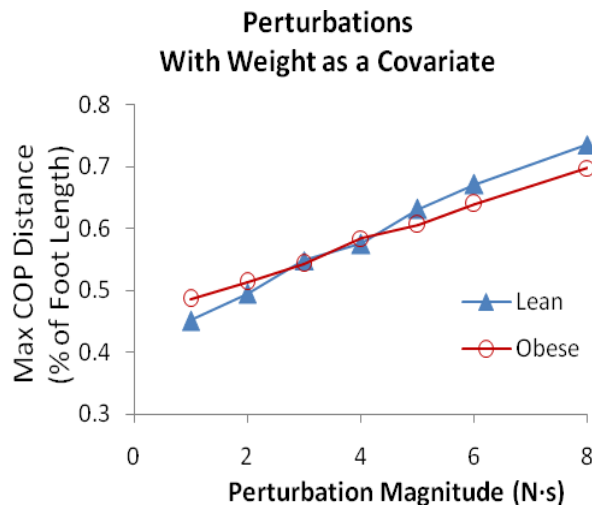
Figure 2. Least squares means of peak COP displacement with weight as a covariate.

DISCUSSION

Results indicate obese subjects exhibited better balance, as quantified by peak COP displacement and velocity, for perturbations, in general, larger than 3 N·s. This was contrary to our expectations. However, this may be the result of our experimental protocol. Obese subjects have larger mass than lean subjects, and thus will experience a smaller increase in velocity in response to increasing applied impulses (see impulse-momentum relation). This smaller velocity may be more easily controlled than the larger increase in velocity experienced by the lean subjects. When weight was used as a covariate to account for dependence of our balance measures on weight, all differences between lean and obese were lost. In other words, there were no differences in balance between lean and obese when equal perturbations relative to body weight were applied.

SUMMARY

Obese subjects exhibited better ability at recovering from small magnitude perturbations compared to lean subjects. However, no differences were found with the secondary analysis accounting for the fact that perturbation magnitudes were not relative to body weight. These findings may help to understand the factors and conditions involved in the increased risk of falls in the obese.

REFERENCES

Teasdale N et al. (2007). *Int J Obes (London)*, 31:153-60.
Maffliuletti NA et al. (2007). *Eur J Appl Physiol,* 101:51-59.

STRATEGIES FOR WALKING ON A LATERALLY OSCILLATING TREADMILL

Brian T. Peters[1], Rachel A. Brady[1], Jacob J. Bloomberg[2]

[1]Wyle's Life Sciences Group, Houston, TX, USA, brian.peters-1@nasa.gov
[2]Neuroscience Laboratory, NASA Johnson Space Center, Houston, TX, USA

INTRODUCTION

Most people use a variety of gait patterns each day. These changes can come about by voluntary actions, such as a decision to walk faster when running late. They can also be a result of both conscious and subconscious changes made to account for variation in the environmental conditions. Many factors can play a role in determining the optimal gait patterns, but the relative importance of each could vary between subjects. A goal of this study was to investigate whether subjects used consistent gait strategies when walking on an unstable support surface.

METHODS AND PROCEDURES

We used a treadmill mounted on a six degree-of-freedom motion base (Moog, East Aurora, New York) to provide support surface motion to walking subjects. After two minutes of normal treadmill walking at 1.1 m/s, subjects continued to walk for another twenty minutes while the treadmill oscillated laterally. Data from nineteen subjects is reported here. The amplitude of the sinusoidal motions was 25.4 cm for all subjects, but eleven were exposed to oscillations at 0.2 Hz and the remaining were tested using 0.3 Hz. Data from both groups are combined here because no differences were found in the variables of interest. Video-based motion analysis was used to record movement of the trunk, feet and treadmill. These were analyzed using custom software (Matlab, The Mathworks, Inc., Natick, MA). A frequency domain data analysis was conducted on the lateral trunk position and subjects' step width was also determined. Data reported here represent the final ten minutes of the data trial when all subjects had achieved a stable walking pattern.

RESULTS

After subtracting the treadmill position from a body midline marker positioned near T12, the resulting waveforms varied between subjects. For some, the predominant feature of the signal was the oscillatory pattern associated with the natural lateral motion that occurs with each stride. For others, this stride-related signal was superimposed on a sinusoid that had the same frequency as the lateral treadmill motions. This was an indication that some subjects were remaining more fixed in space (FIS) while others were more fixed to the base (FTB). A ratio was calculated for each subject comparing the amplitude of the torso signal to the amplitude of the support surface motion at the base motion frequency. These data are shown in Figure 1. We classified those subjects with ratios on a continuum between 0.05 and 0.3 as FTB and the four subjects with ratios above 0.4 as FIS.
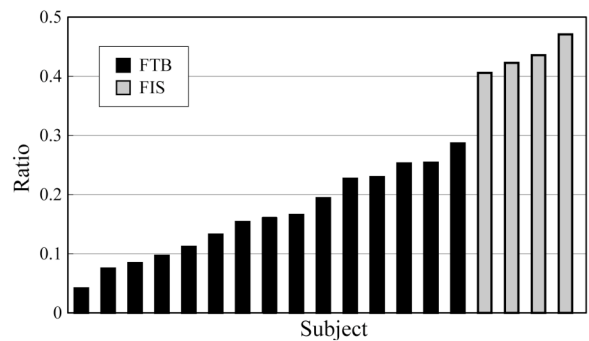
Figure 1. Ratio of lateral torso amplitude to lateral base amplitude at the base frequency.

Step width was originally calculated to confirm an assumption that it would be wider while the support surface was being manipulated. A more striking result was the increase in variability of the step width throughout the trial. The data were further analyzed to account for the movement of the support surface. In Figure 2, the step width data for one subject is shown on a polar plot. The angular coordinate for each point is determined by the lateral position and velocity of the support surface during its oscillation. The distance from the center of the plot to each point is the normalized right-foot-to-left-foot step width.
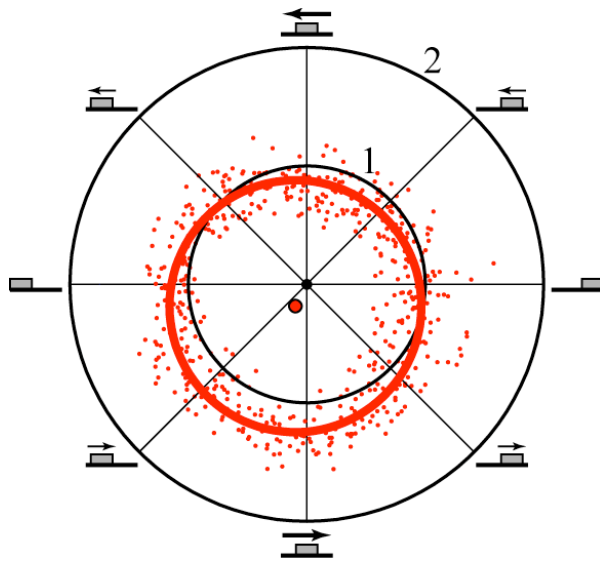
Figure 2. Polar plot showing right-foot-to-left-foot step width data for one FIS subject. Graph "labels" depict treadmill position and velocity. The unity circle defines mean step width during normal walking period of test.

A shift in the center of a best-geometric-fit circle is an indication that the subject is adjusting their step width according to the treadmill movements. Interestingly, this shift is predominantly downward for FIS subjects and upward for FTB subjects. The downward shift indicates that as the support surface is moving to the right, the FIS subjects take a wider step when transferring support from the right leg to the left. They take a narrower right-to-left step when the treadmill is moving to the left. The opposite is true for the other FTB subjects. In either case, modulation of the step width, according to the movement of the base, accounts for some of the increased step width variability that was observed.

DISCUSSION

Two strategies can be observed when subjects' are exposed to lateral oscillations of the support surface during treadmill walking. Some subjects maintain their position with respect to the support surface and move with it. Others are more fixed relative to space and allow the treadmill to travel beneath them. Warren et al. (1996) found similar differences between subjects during an investigation in which it was the visual scene that was manipulated instead of the support surface. Further investigation is required, but it is assumed that these strategies emerge based on individual differences in the relative weighting that is place on the sensorimotor inputs used during the gait optimization process. An ability to rapidly re-weight these inputs could be beneficial for maintaining stable gait.

A goal of our laboratory is to develop a training program that facilitates the rapid adaptation of gait when astronauts are exposed to novel environmental conditions. A better understanding of subjects' natural tendencies will allow us to tailor our training paradigms to each individual.

REFERENCES

Warren et al. (1996). *J Exp Psychol Hum Percept Perform* 22:818-838

ACKNOWLEDGEMENTS

PREFERRED POSITION AND ASSOCIATED FORCES FOR LOWER BACK SUPPORT IN VEHICLE AND OFFICE SEATING ENVIRONMENTS

Zahid Rampurawala and Tamara Reid Bush

Department of Mechanical Engineering, Michigan State University, East Lansing, Michigan, USA,
rampuraw@msu.edu reidtama@msu.edu, www.egr.msu.edu/~reidtama

INTRODUCTION

The contour of a seat can influence the posture achieved by an individual. For example, an excessive forward contour at the shoulder region could prevent some individuals from achieving an erect posture, influencing the amount of support needed in the lower back or lumbar regions. Thus, the goal of our work was to measure the preferred locations and forces on lower back supports independent of a seat contour in vehicle and office seating environments.

METHODS AND PROCEDURES

For this study, an experimental laboratory seat was designed and built. Using two small motors activated by a subject-controlled switch, the seatback allowed the lower back support pads to move in vertical as well as fore-aft directions.

Two multi-channel force transducers were used along with the experimental seat, one was behind the fixed thoracic support while the other was behind the lower back support pad and moved with the pad. These force transducers measured support forces in the three axial directions F_x, F_y and F_z. The two force transducers together helped record forces exerted by the subject in the upper as well as lower back regions. Each of the two force transducers had a capacity of 250lb (1112 N).

Three dimensional positions of retro-reflective targets secured to both the experimental seat and bony landmarks of the subject were captured using a five camera 60 hertz Qualisys motion measurement system. Using these three-dimensional coordinates, the location of each force transducer could be computed relative to subjects' anthropometry. Eight subjects were placed in four different seating configurations marked by variation in seatback recline angle – 10º and 15º for office, 20º and 24º for vehicle seating environments. The footrest was allowed vertical as well as fore-aft adjustment in the office environment, but only fore-aft movement in the vehicle seating tests. The seat pan for vehicle testing was inclined at 14˚ with respect to the horizontal unlike the zero inclination for the office test seat pan.

RESULTS

Table 1 shows the preferred location of the support pads (average distance along the seat back). This distance was also converted to a percentage of each subject's seated height. Table 2 shows the average forces exerted by each subject on the thoracic and lower back supports as measured by the force transducers.

DISCUSSION AND CONCLUSIONS

The average vertical locations of all the support pads in the office and vehicle seating environments were measured and calculated to be 167.2mm, 173.5mm, 166.9mm and 161.8mm above the seat pan at each of the four recline angles respectively. All these values fall between the averages of the third lumbar vertebra (L3 = 195.1mm) and the posterior superior iliac spine (PSIS = 93.7mm). Hence, it appears that

Subject ID	Pad apex location along seat back at each recline angle (mm)				Seated Height (erect) (mm)	Pad apex height as percentage of Seated Height (%)			
	10°	15°	20°	24°		10°	15°	20°	24°
P2A	199.0	207.5	195.2	197.7	863.6	23	24	23	23
P2B	116.0	99.5	105.3	91.2	952.5	12	10	11	10
P2C	126.8	161.0	153.5	116.0	895.3	14	18	17	13
P2D	164.2	170.5	155.7	168.2	876.3	19	19	18	19
P2E	188.2	189.0	199.7	205.7	889.0	21	21	22	23
P2F	202.3	229.7	174.5	178.7	901.7	22	25	19	20
P2G	184.5	179.8	189.0	187.7	914.4	20	20	21	21
P2H	156.2	150.7	162.0	149.3	914.4	17	16	18	16
Averages	167.2	173.5	166.9	161.8	900.9	19	19	19	18
Std. Dev.	32.4	39.2	30.6	40.4	27.2	3.9	4.7	3.7	4.7

Table 1. Distance from seat pan to support pad apex (averages of all three pads) along the seat back. This distance is also reflected as a percent of seated height. All distances are in millimeters.

Recline Angle	Normal forces (N)		Vertical Shear forces (N)		Lateral Shear forces (N)	
	Thoracic	Lower Back	Thoracic	Lower Back	Thoracic	Lower Back
10°	-58.2	-54.2	-9.2	-12.8	-2.1	-2.5
15°	-71.3	-53.7	-7.2	-12.3	-2.1	-2.5
20°	-121.5	-89.9	-15.3	-14.7	-2.2	-1.3
24°	-132.7	-91.2	-13.6	-12.5	-2.2	-1.7

Table 2. Average forces exerted by subjects on lower back and thoracic supports at different recline angles. All forces are in Newtons. Negative sign indicates direction of force – into the pads for normal forces, downward for vertical shear forces and leftward for lateral shear forces.

subjects prefer to position the lower back support pads between L3 and the PSIS when a seat contour is not present.

Greater normal forces were exerted on both the lower back and thoracic supports in the vehicle seating as compared to the office seating indicating the correlation between recline angles and support forces. This is expected because with an increase in recline angle, the distribution of body forces on the seat shifts relatively more towards the subject's back (Bush and Hubbard, 2007). Also, the inclination of the vehicle seat pan with respect to the horizontal causes an increase in normal forces on the seat back.

SUMMARY

Since all lower back support movements were subject controlled, the data recorded were the preferred positions of the supports with the associated forces. These data have the potential to be used as an input for seat future design.

REFERENCES

Bush TR and Hubbard RP (2007), *ASME Journal of Biomechanical Engineering.*

Measuring In-vivo Humeral Head Translation using Fluoroscopy: A Comparison of Static and Dynamic Positioning

San Juan J.G.[1], Karduna A.R.[1]

[1]University of Oregon, Eugene, OR, USA, bsanjuan@uoregon.edu

INTRODUCTION

Subacromial impingement syndrome (SAIS) of the shoulder is the most common disorder of the shoulder, accounting for 44 – 65% of all complaints of shoulder pain during a physician office visit (Michener et al., 2003). Abnormal superior translation of the humeral head is believed to be one of the major causes of this pathology (Deutsch et al., 1996). There are numerous techniques used to assess humeral head translation. The most common techniques utilize include roentgenogram (X-ray), fluoroscopy, and magnetic resonance imaging (MRI). During data collection, images of the shoulder complex are either taken statically or dynamically. Numerous authors have argued that dynamic shoulder motion occurs frequently in everyday living, although, to our knowledge, there have been no studies comparing humeral head motion between static and dynamic motions. Therefore, the purpose of this study is to compare humeral head translations between static and dynamic trials in healthy individuals.

METHODS AND PROCEDURES

Three healthy subjects (age 22 ± 2.2, weight 68.9 ± 5.4 kg, height 166.8 ± 10.4 cm) participated in the study. Subjects were asked to perform two different conditions of shoulder elevation. The first condition involved dynamic shoulder elevation and the second condition involved holding the arm statically at different angles of shoulder elevation (i.e. 30°, 60°, 90°, and 120°). Each condition consisted of one trial. There was a 5 minute rest interval between conditions. Subjects started with their arm at the side.

During condition 1 (dynamic), the subject elevated their dominant arm in the scapular plane up to 120° of shoulder elevation for three repetitions. They were instructed to elevate their arm within 4 seconds and lower their arm also in 4 seconds. For the second condition (static), the subject was passively positioned by the investigator in five different elevation angles (0°, 30°, 60°, 90°, and 120°) in the scapular plane and was directed to hold their arm actively in the set position. In each of the trials, fluoroscopic images were taken.

During practice trials, the investigator positioned the subject so that the anterior side of the scapula was perpendicular to the field of view of the fluoroscope (Figure 1). By doing this, projection errors were minimized. During the dynamic trials, continuous imaging was utilized to capture shoulder elevation (8 pps).

Kinematic data were collected using a GE (OEC) 9800 Fluoroscopy unit. In addition, points were digitized on the glenoid face, the humeral head and the humeral shaft using Space (University of Oregon), which is an edge detection software. Humeral head translation was measured using a 2-D registration technique developed by Crisco et al (1995). In order to compare the static and dynamic trials, humeral elevation angles for both conditions were matched by calculating the humeral angle of each static position with respect to gravity. The measured superior humeral head translation was calculated in

each humeral elevation angle with respect to the resting position, which is defined as the 0° position during the static trial. This method of measuring humeral head translation was previously validated by the investigator with a measured error of less than 0.5 mm.

Fig. 1. Subject set-up during testing protocol.

RESULTS

During the static trials, the greatest measured superior humeral head translation occurred when the humerus was at 60° of elevation (4.4 ± 1.7). During the dynamic trials, both the 60° (4.2 ± 1.5) and 120° (4.2 ± 0.9) of humeral elevation angle showed the largest measured superior translation. There was a large difference in measured superior humeral head translation when the humerus was at a 120° of elevation (3.0 ± 1.1).

DISCUSSION

Dynamic motions performed during shoulder experiments better represent the actions Performed in activities of daily living. This study has shown that there is a difference in the measurement of humeral head translation between static and dynamic trials. The greatest difference occurred at 120° with a measured difference of 3.0 ± 1.1 mm. In this study, the dynamic trial had a greater amount of measured humeral head translation

(1.4mm) above 90°. This result is important because studies have shown that overhead activities occur above 90° of humeral elevation, and repetitive overhead activities could lead to SAIS. However, care should be taken when interpreting the results of this study due to the limited number of subjects. This is an ongoing research study and the investigators are planning on testing more subjects.

SUMMARY

The dynamic motion of the shoulder should be taken into consideration during experimental protocol design especially when measuring glenohumeral kinematics. Static trials might elicit different muscle activation patterns to stabilize the humeral head compared to dynamic motions during shoulder elevation.
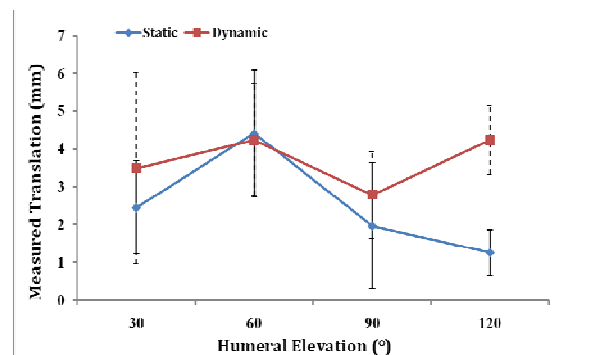
Fig. 2. Measured superior humeral head translation of static and dynamic trial.

REFERENCES

Crisco et al., *J Biomech*. (1995) 28, 119-124.
Deutsch et al., *J Shldr Elb Surg*. (1996) 5, 186-193.
Michener et al., (2003), *Clin Biomech*., 18, 369-379.

ACKNOWLEDGEMENTS

TOWARD A MINIMAL INPUT MODEL FOR JOINT MOMENT ESTIMATION DURING GAIT

Michael Hahn

Movement Science Laboratory, Department of Health and Human Development,
Montana State University, Bozeman, Montana, USA
mhahn@montana.edu

INTRODUCTION

There is a perceived disconnect between laboratory-based locomotion research and broad spectrum clinical application. Use of neural networks and other machine learning (ML) techniques may provide a viable solution to bridge that gap. These techniques have become more common in niche areas of biomechanics and have shown effectiveness in mapping surface measures onto internal mechanical outcomes (Hahn, 2007; Liu et al., 1999; Luh et al., 1999; Wang and Buchanan, 2002). Two previous ML models estimated lower extremity kinematics and kinetics during gait (Goulermas et al., 2005; Sepulveda et al., 1993). However, their findings have been limited in clinical application. The long-term goal of this research is to provide a joint dynamics estimation model which may be accessed and implemented with minimal equipment. With this objective in mind, the purpose of the current study was to develop a model to estimate joint moments for the lower extremity during gait using a minimized list of input data.

METHODS AND PROCEDURES

Nineteen healthy young subjects were recruited for this study (12 female, 7 male; 22.3 ± 1.6 years; 1.73 ± 0.08 m; 72.0 ± 13.3 kg) within the guidelines of the Institutional Review Board. Informed consent was obtained from each subject before participation. All participants were self-reported to be free of neuromuscular and musculoskeletal pathologies.

Standard gait analysis procedures were used to collect all data types: demographics (D), anthropometrics (A), electromyography (E), kinematics (K), and ground reaction forces. Inverse dynamics was used to calculate net internal joint moments for the hip, knee and ankle. All subjects walked at a self-selected pace, wearing comfortable walking/running shoes.

The ML modeling technique used in this study was a three layer feed-forward neural network structure, with 11-fold cross-validation. A unique network was trained and tested for each joint. The input layer contained a variable list of data types, based on category. The hidden layer contained 30 processing units. The output layer contained the experimental net internal moment, serving as the target against which the network was trained. The hidden layer used a sigmoidal transfer function and the output layer contained a linear transfer function. A Levenberg-Marquardt algorithm was used for error correction, with an error goal of 0.01.

The input data set was varied by category (see Table 1) to determine which combination of inputs is best suited to provide a balance between accurate estimation and ease of measurement in the clinical setting. Accuracy was assessed for general model performance using the coefficient of determination (r^2). Case-specific validation was tested with root

mean squared error (RMSE) magnitude between experimental and estimated joint moments in a single representative case.

RESULTS

Joint moment estimation accuracy was acceptably high with all data types entered as input (r^2 from 0.94 - 0.99). Next best accuracy was seen in models with all data but electromyography, followed by an input list of just kinematics and demographics (K, D; see Table 1). Case-specific validation revealed similar effects, with the most accurate joint moment estimation coming from models without electromyography (RMSE from 0.02 – 0.07 Nm/kg). The best fit joint moment curve came from an input list of kinematics and demographics (see Figure 1).

DISCUSSION

Model accuracy was comparable to that reported by Goulermas et al. (2005) and Sepulveda et al. (1993). Results indicate that estimation accuracy was not enhanced by the inclusion of electromyography; requiring only kinematic and demographic data to achieve accurate joint moment patterns.

SUMMARY

These findings provide progress towards the goal of a minimal input joint moment estimation model. Use of electrogoniometers and a record of demographics would be sufficient to utilize these models in the non-research setting. Future efforts will include clinical cases and test the field application validity of these models.
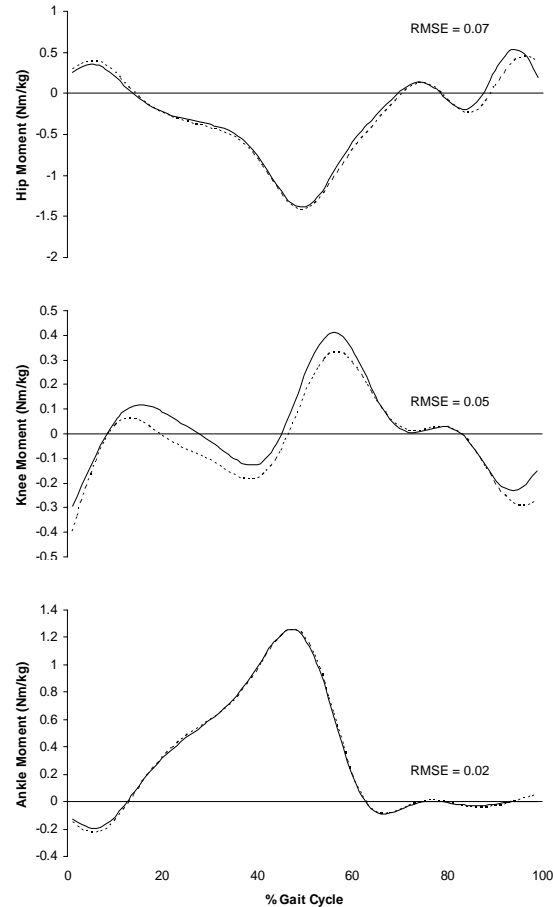
Figure 1. Joint moment estimation, with input list of K, D; solid = experimental, dashed = estimated.

REFERENCES

Goulermas et al. (2005) *J Biomech Eng*, 127, 1020-1024.
Hahn, ME (2007). *J Biomech,* 40, 1107-1114.
Liu et al. (1999). *J Electromyogr Kinesiol*, 9, 391-400.
Luh et al. (1999). *J Electromyogr Kinesiol*, 9, 173-183.
Sepulveda et al. (1993). *J Biomech*, 26, 101-109.
Wang and Buchanan (2002). *IEEE Trans Neural Syst Rehabil Eng*, 10, 30-37.

Table 1. Coefficient of determination (r^2) values for each joint model based on input categories.

	All Input	**K, A, D**	**E, A, D**	**K, D**	**E, D**	**K**	**E**
Hip	0.95	0.96	0.77	0.95	0.75	0.93	0.58
Knee	0.94	0.94	0.81	0.94	0.78	0.70	0.54
Ankle	0.99	0.98	0.92	0.98	0.91	0.96	0.84

GAIT VARIABILITY IS REDUCED BY SUB-THRESHOLD VIBRATIONS TO THE FEET

Hyun Gu Kang[1,2], Andrew M. Galica[1], Attila A. Priplata[3,], Olga V. Starobinets[1], Susan E. D'Andrea[4], James J. Collins[5], Lewis A. Lipsitz[1,2,6]

[1]Institute for Aging Research, Hebrew SeniorLife, Boston, Massachusetts, USA
[2]Harvard Medical School, Boston, Massachusetts, USA
[3]Stryker Corporation, Cambridge, Massachusetts, USA
[4]Afferent Corporation, Providence, Rhode Island, USA
[5]Department of Biomedical Engineering, Boston University, Boston, Massachusetts, USA
[6]Gerontology Division, Beth Israel Deaconess Medical Center, Boston, Massachusetts, USA

URL: http://www.hebrewseniorlife.org   hyungukang@hrca.harvard.edu

INTRODUCTION

Decreases in somatosensory function result in diminished motor performance and falls (DeMott et al., 2007). Increased stride-to-stride variability in stride length, speed, and double-support time is predictive of fall risk (Maki 1997). Subsensory mechanical noise applied to the soles of the feet can enhance sensory function and reduce postural sway in quiet standing via a mechanism called stochastic resonance (Priplata et al., 2003). The goal of this study was to determine whether the application of subsensory noise vibrations to the soles of the feet could reduce gait timing variability, an indicator of fall risk in older adults.

METHODS AND PROCEDURES

41 older adults (ages 76.5 ± 4.7 years) without neurological conditions were recruited from the Mobilize Boston Study, an ongoing population-based study of 800 community-dwelling older adults (Leveille et al, 2007). 22 were recurrent fallers who fell 2 or more times in the last year. 19 were non-fallers who fell 0-1 times (non-fallers) in one-year period, matched by age and sex. 12 healthy young adults (ages 26 ± 5 years) also participated. Participants walked at a self-selected comfortable pace around a 22m elliptical track for 3 trials of 6 minutes each, while wearing custom vibrating sandals. The sandals delivered a white-noise vibration signal that was adjusted to be up to 90% of each individual's sensory threshold in the feet during each gait phase. During walking, noise was applied during first or second half of each trial, and the application order was randomized. Heel-strike and toe-off events were captured using force-sensing resistors in the sandals. Variability of the stride, stance, and swing time intervals for each half of each trial were quantified as the standard deviation (SD). The effects of the vibrations and the group (faller, non-faller, young) were compared using a mixed-model ANOVA (SAS 9.1).

RESULTS

Sub-threshold vibrations reduced stride time SD ($p < 0.04$), stance time SD ($p< 0.02$), and swing time SD ($p = 0.06$) in all subjects, but did not affect gait speed ($p = 0.76$). Without the vibratory stimulus, recurrent fallers exhibited greater baseline stride time SD than non-fallers or young adults ($p < 0.002$; Figure 1). During vibration, stride time SD was significantly reduced only in the faller group ($p = 0.025$; Tukey LSD). Group by vibration interactions were not present ($p > 0.4$), Reduction of SD due to the vibration

correlated with baseline SD. This correlation was strongest in stride time variability in fallers (r = 0.65, p < 0.002) and weaker in non-fallers (r = 0.45, p = 0.051; Figure 2).

Stance time SD was reduced in both fallers (p < 0.04) and non-fallers (p < 0.03) during the vibration. Reduction of stance time SD was correlated with baseline SD, but this relationship was stronger in the non-fallers (r = 0.66, p < 0.002) than in fallers (r = 0.25, p = 0.26).   The correlations in swing time were similar between the two groups.
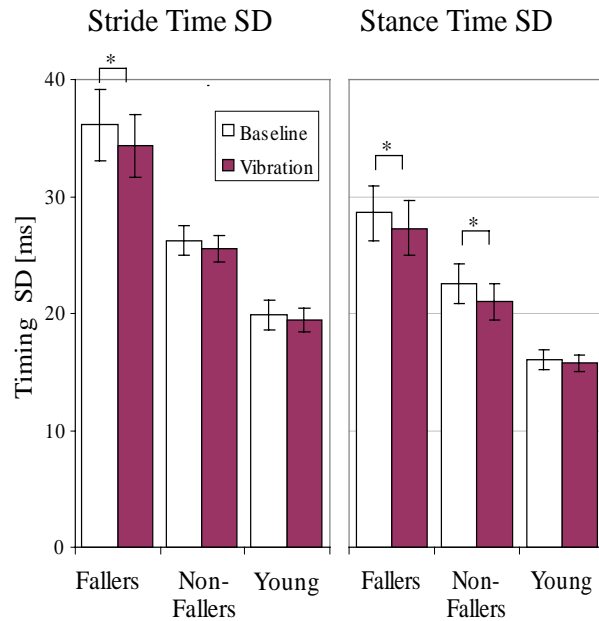
Figure 1. Stride Time and Stance Time Variability. Reduction in SD was most noticeable in Fallers.

DISCUSSION

Sub-threshold vibratory noise applied to the soles of the feet reduced gait variability. This effect was most prominent in older adults with recurrent falls and with large variability in stride time. Application of noise may increase somatosensation via a mechanism known as stochastic resonance. Older adults

with recurrent falls and large gait variability may benefit the most from this novel intervention.

REFERENCES

DeMott TK, *et al*. *Am J Phys Med Rehabil*. 2007
Leveille SG et al. (2007). *Gerontologist,* 47(S1):352.
Maki BE. *J Am Geriatr Soc* (1997) 45:313-320.
Priplata AA, *et al*. *Lancet* (2003) 362:1123-4.

ACKNOWLEDGEMENTS
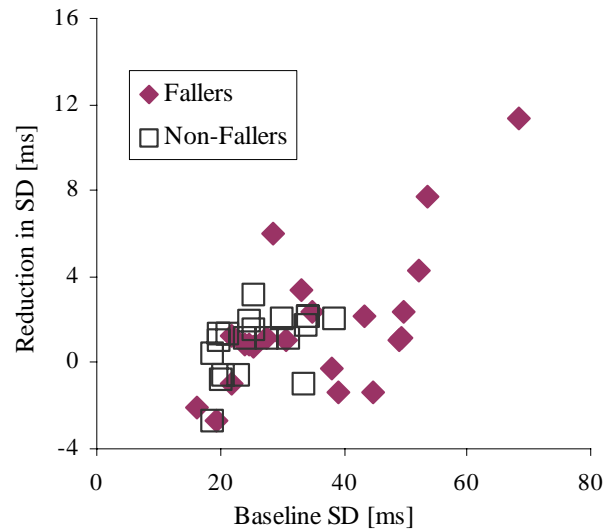
Figure 2. Reduction in Stride Time SD with Vibration vs. Baseline SD. Vibration reduced SD in fallers with large baseline SD. The effect on fallers seems to be present only on those with high baseline SD.

GAIT DYNAMICS ON A CROSS-SLOPE WALKING SURFACE

Phil Dixon, David Pearsall

Department of Kinesiology and Physical Education
McGill University, Montreal, QC, Canada, david.pearsall@mcgill.ca

INTRODUCTION

The biomechanics of level walking have been studied extensively in the past, but few studies have explored the body's adaptation to transversely inclined (cross-sloped) surfaces (DeGarie et al., 2000; Nicolaou et al., 2002; Pearsall et al., 2007)

Cross-slopes are a regular feature of our physical environment. Sidewalks and roadways are tilted between 5-7° mainly to permit water drainage (National Guide to Sustainable Municipal Infrastructure, 2004).

For young adults, cross-slopes do not represent a significant challenge, however for special populations (elderly, blind, amputees, wheelchair users, *etc*), the asymmetrical demands of cross-slope walking may introduce functional muscular-skeletal and balance barriers. Cross-slopes may too be a causative factor in falls, a major concern for elderly populations (Lockhart et al., 2007; Donald and Bulpitt, 1999). Hence, a better understanding of the dynamics of cross-slope walking may aid in the design prostheses and walking aids to accommodate for this terrain obstacle.

METHODS AND PROCEDURES

A sample of ten young healthy adult males performed flat (0º) and cross-slope (6º) walking trials at a self-selected pace (Figure 1).

Excluded were subjects with a leg length discrepancy (LLD) greater than 2.0 cm.
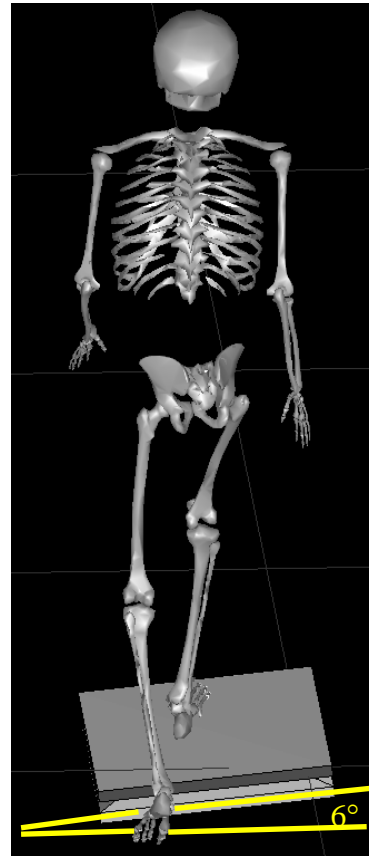
Figure 1 Cross-slope walking.

An inclinable walkway was used containing two AMTI^{TM} (AMTI, model 0R6-7-1000, Watertown, MA, USA) force plates within its surface. Force plates recorded ground reaction forces (GRF) and ground reaction moments (GRM) in all three-dimensions (960 Hz) while a six camera Vicon^{TM} (Vicon, Los Angeles, USA) system collected kinematic data

from passive optical markers (240 Hz). Data were synchronized and used to compute the joint reaction forces (JRF) and joint reaction moments (JRM) using a standard Inverse Dynamics Analysis (IDA) approach (Vaughan et al., 1999).

RESULTS

The ankle, knee and hips responded asymmetrically to the cross-slope condition by substantially changing (1) the medio-lateral GRF pattern, (2) the sagittal and frontal plane kinematics, and (3) the medio-lateral JRF and frontal plane JRM. For brevity, only the hip medio-lateral JRF (Figure 2) and hip frontal plane JRM (Figure 3) data are shown.
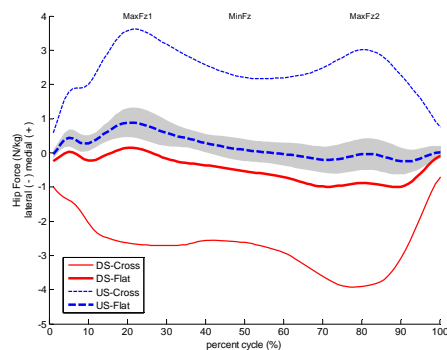
Figure 2 – Hip medio-lateral JRF (N/kg). Grey region is the SD of the US-flat condition.
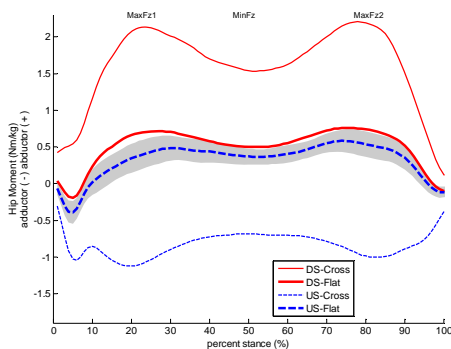
Figure 3 – Hip moment (Nm/kg). Grey region is the SD of the US-flat condition.

DISCUSSION

The body adopts a functional LLD, presumably to maintain an upright trunk position, causing main kinematic and kinetic changes in the lower-limb sagittal plane profiles. In addition, the medio-lateral GRF are modified due to the cross-slope, producing a cascading effect of asymmetrical and substantially greater JRF and JRM in the lower-limb joints particularly in the frontal plane.

SUMMARY

The modest cross-slope condition induced substantial asymmetrical changes in the lower-limb locomotor patterns and may well represent a substantial physical obstacle to populations with restricted mobility.

REFERENCES

DeGarie, L and Pearsall, DJ (2000). *Proceedings of the XIth Congress of the Canadian Society for Biomechanics. Montreal, 111*.

Nicolaou et al. (2002). *Proceedings CD of the IVth World Congress for Biomechanics. Calgary, Canada.*

Pearsall, DJ et al. (2007). *International Society for Posture & Gait Research, Burlington, Vermont.*

National Guide to Sustainable Municipal *On-line. Retrieved Sept 24, 2007, from http://infraguide.ca.*

Lockhart, TE et al (2007). *Gait & Posture*, 26:142-149.

Donald, IP et al. (1999). *Age and Ageing*, 28:121-5.

FLEXOR TENDON AND MEDIAN NERVE EXCURSION IN HEALTHY AND SELF-IDENTIFIED SYMPTOMATIC WRISTS

Melanie M. Lopes[1] & Peter J. Keir[2]

[1]School of Kinesiology & Health Science, York University, Toronto, ON
[2]Department of Kinesiology, McMaster University, Hamilton, ON, pjkeir@mcmaster.ca

INTRODUCTION

Due to the arrangement of the finger flexor tendons within the carpal tunnel, the tendons impose loads on each other and the median nerve, especially when the wrist is deviated (Keir et al., 1997). Histologically, evidence of friction and mechanical loads has been found in the synovium of carpal tunnel syndrome (CTS) wrists (Schuind et al., 1990). Increased adherence of the subsynovial connective tissue (SSCT) to the flexor tendons may decrease movement of the two structures, or increase dissociation from the tendon, predisposing the SSCT, tendon, and median nerve to further friction (Ettema et al. 2007).

Studies have examined the motion of the median nerve using cadavers, and surgical methods (Erel et al., 2003; Nakamichi and Tachibana, 1995). Investigating median nerve and flexor digitorum superficialis (FDS) tendon excursion will improve understanding of movement, which may help diagnose distal upper extremity disorders. In addition, it will help with nerve and tendon gliding protocols utilized in CTS recovery, and flexor tendon repair. A new technique, "Spectral Doppler ultrasound", can be used to track velocities of nerves and tendons.

The purpose of this study was to use Spectral Doppler ultrasound to determine excursions of FDS tendons and the median nerve under various hand and wrist motions.

METHODS AND PROCEDURES

Twenty-two volunteers participated in the study, 16 in the healthy (H) group (9♀, 7♂), and 6 in the self-identified symptomatic (S_x) group (4♀, 2♂).

Grey-scale sonography examinations were performed with a 12-5 MHz linear array transducer (HDI Philips 5000 ultrasound machine, Philips Canada). Both wrists were scanned from the volar aspect, using static and dynamic measurements.

Motion of the (FDS 2,3) tendon bundle, and median nerve were examined using spectral Doppler scanning. Each participant completed 5 motions for each hand (Table 1), recording FDS and median nerve movement on a separate scan for each structure.

Table 1. The 5 wrist/finger motions

#	MOTION and DESCRIPTION
1	Move fingers from extension to 90º MCP flexion
2	Move fingers from extension to full flexion (loose fist)
3	Move from neutral wrist to 60º wrist extension (fingers extended)
4	Flex fingers and wrist from 60º wrist extension to neutral
5	Move 60º wrist extension wto neutral with pinch grip

For each of the five dynamic motions, the output screen indicated the location of the measurement (Fig. 1 top) and the velocity plotted against time (Fig. 1 bottom). The excursion velocities were traced, resulting in an area for each curve traced [Image J

software, USA]. The velocity-time integral (VTI) was also determined for both the FDS and median nerve using the collection software of the ultrasound machine.
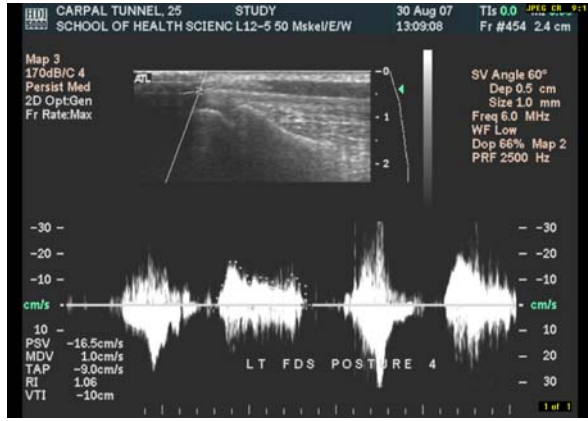
Fig. 1: Sample ultrasound output screen for the left FDS using motion #4.

RESULTS

The smallest FDS and median nerve excursions occurred with motion #1, and the largest with motion #4. There was a high positive correlation between VTI and excursions measured via post-hoc tracings of the velocity curves, however, there was no relationship between VTI and excursions estimated with existing equations.

Table 2. Mean ratio (SD) of median nerve excursion as a % of FDS displacement for healthy (H) and symptomatic (S_x) groups.

MOTION # & GROUP		MN % of FDS	
		Left	Right
1	H	53.4 (17.4)	52.3 (18.0)
	S_x	36.8 (20.2)	31.2 (8.8)
2	H	47.7 (18.8)	40.1 (11.5)
	S_x	40.5 (23.2)	39.3 (21.8)
3	H	65.6 (26.5)	61.0 (16.1)
	S_x	122.0 (26.1)	78.4 (38.1)
4	H	58.4 (19.5)	61.6 (14.8)
	S_x	48.2 (12.4)	38.4 (10.5)
5	H	78.9 (30.7)	70.7 (31.1)
	S_x	101.0 (30.9)	95.6 (53.6)

DISCUSSION

In this preliminary study, there appeared to be more motion of both the FDS and nerve with motions that incorporated both wrist and finger motions, compared to isolated joint motions.

The ratio of median nerve to FDS excursion was higher (Table 2) than the 43% found in cadaveric specimens (Szabo et al., 1994). It is possible that the underlying connective tissue that is in close contact with the FDS tendons might have been adhered to the tendons via fibrosis (Ettema et al., 2007).

Ultrasound imaging was able to reliably measure static components of the carpal tunnel. However, the resolution of the velocity curves was limited for measuring tendon and nerve excursions. The implications of this research immense as it can impact rehabilitation protocols used to treat CTS and post-surgical tendon repair.

REFERENCES

Erel et al. (2006) *J Hand Surg*, 28B: 439-43.
Ettema, AM et al. (2007) *Hand*, 20: 292-9.
Keir et al. (1997) *J Hand Surg*, 22A: 628-34.
Nakamichi, K and Tachibana, S (1995) *J Hand Surg*, 20B: 460-4.
Schuind et al. (1990) *J Hand Surg*, 15A: 497-503.
Szabo et al. (1994) *J Hand Surg*, 14A: 624-7.

ACKNOWLEDGEMENTS

LOSS OF COMPLEXITY IN BALANCE DYNAMICS DURING QUIET STANDING AND DUAL-TASK: A MARKER OF FRAILTY IN ELDERLY PEOPLE

Hyun Gu Kang[1,2], Madalena Costa[2,3], Olga V. Starobinets[1], Ary L. Goldberger[2,3], Chung-Kang Peng[2,3], Dan K. Kiely[1], L. Adrienne Cupples[5], Lewis A. Lipsitz[1,2,4]

[1]Institute for Aging Research, Hebrew SeniorLife, Boston, Massachusetts, USA
[2]Harvard Medical School, Boston Massachusetts, USA
[3]Division of Interdisciplinary Medicine and Biotechnology and [4]Gerontoloy Division, Beth Israel Deaconess Medical Center, Boston Massachusetts, USA
[5]Department of Biostatistics, Boston University, Boston Massachusetts, USA

URL: http://www.hebrewseniorlife.org   and   http://reylab.bidmc.harvard.edu
hyungukang@hrca.harvard.edu

INTRODUCTION

The ability to maintain balance during standing is attributable to the complex, nonlinear interactions of multiple postural control systems, which is manifest as the highly irregular displacements in center of pressure (COP) during standing. The complexity of COP displacements can be quantified by metrics such as multiscale entropy (MSE), which measures system dynamics over multiple time scales (Costa et al., 2007) and is a more sensitive measure of physiologic health than simple variability (Costa et al, 2002). Traditional methods of measuring balance do not quantify the dynamic interactions of these systems.

The process of aging, and age-associated syndromes such as frailty may result in the degradation of complex interactions among postural control systems and manifest as a loss of complexity in COP dynamics. Furthermore, frail individuals may not be able to adapt to a superimposed stress or distraction that challenges balance, leading to falls and other adverse outcomes. Therefore, we hypothesized that frail elderly people would show a loss of complexity in COP displacements during quiet standing compared to healthy elderly controls, and that a divided task would further reduce the complexity of balance dynamics in frail individuals.

METHODS AND PROCEDURES

Data were analyzed from the Mobilize Boston Study, an ongoing population-based study of 800 community-dwelling older adults (Leveille et al., 2007). Each participant's frailty status (not frail, pre-frail, frail) was determined using the five symptoms of unintentional weight loss, slow gait, weakness, low activity, and exhaustion as defined in (Fried et al., 2001). Frailty is predictive of future falls, disability, and death. Participants exhibiting 1-2 symptoms were denoted "pre-frail," and those with 3 or more were denoted "frail."

Participants (n = 571, age 77.9 ± 5.5) stood on a 6-DOF force plate for 30 seconds for 10 trials. Of the ten, five trials were performed concurrently with a serial subtraction mental arithmetic dual-task. Center of pressure (COP) excursions in anterioposterior (AP) and mediolaterial (ML) directions were sampled at 240Hz. The recorded COP data was detrended using empirical mode decomposition to remove low-frequency artefacts (Wu et al., 2007). Sample entropy

was calculated after each successive coarse-graining (averaging then down-sampling) of the COP signal. Entropy values were integrated over the time scales to calculate MSE. MSE was calculated for each trial, and averaged over the 5 trials of the same condition. The effect of the dual-task and frailty on MSE was assessed using mixed-model ANOVA (SAS 9.1).

RESULTS

Of the participants 37% were pre-frail and 7% were frail. Baseline MSE of AP sway was lower in the pre-frail group, compared to the non-frail group, and it was even lower in the frail group compared to the other groups ($p<0.002$). MSE of COP was lowered with the dual-task for both AP and ML sway ($p<0.001$; Figure 1). The decrease of MSE during the dual-task was similar for all groups. RMS sway increased with dual-task as previously reported (Shumway-Cook et al, 1997) but it was not correlated with MSE ($r^2 < 1\%$).
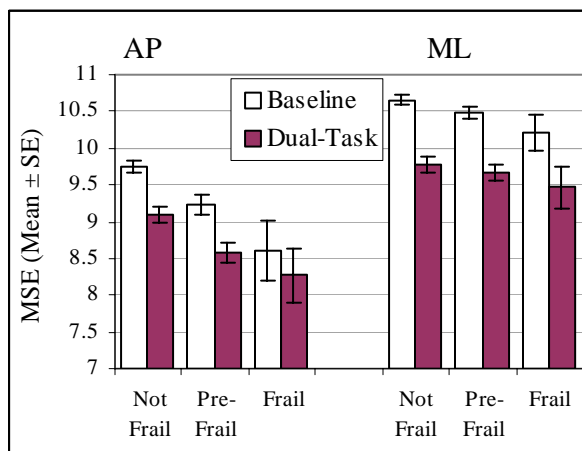
Figure 1. Multiscale Entropy of Postural Sway in AP and ML directions. Frailty was associated with lower MSE. Dual-task lowered MSE.

DISCUSSION

Frailty was associated with a loss of complexity in the dynamics of postural sway. This may be because frailty is associated with the degradation of integrated postural control networks that enable the body to maintain upright stance. Performance of a dual-task further reduced this complexity. This may be because the dual-task utilizes frontal lobe resources necessary for attention, sensory integration, and motor control, thus diminishing the reserves necessary to maintain balance (Yogev-Seligmann et al., 2007).

Being frail did not predict a larger reduction in MSE with dual-task, but postural control may be further compromised by the dual-task. Thus, frail elderly people may be at increased risk of falls when distracted by cognitive activities during standing.

REFERENCES

Costa M, et al. (2002). *Phys Rev Lett*, 89:068102.
Costa M et al. (2007). *Europhys Lett*, 77:68008.
Fried LP et al. (2001). *J Geron A,* 56:M146-156.
Leveille SG et al. (2007). *Gerontologist,* 47(S1):352.
Shumway-Cook A et al. (1997). *J Geron A,* 52:M232-40
Wu Z, et al. (2007). *PNAS*, 104:14889-14894
Yogev-Seligmann G et al. (2007). *Mov Disord*, in press.

ACKNOWLEDGEMENTS

TRUNK BEND AND TWIST COORDINATION IN RUNNERS WITH LOW BACK PAIN

Joseph Seay[1], Richard van Emmerik[2], and Joseph Hamill[1]

[1]Biomechanics and [2]Motor Control Laboratories, Department of Kinesiology, University of Massachusetts, Amherst, Massachusetts, USA
joseph.seay@us.army.mil

INTRODUCTION

Low back pain (LBP) affects at least 75% of US and Canadian citizens. Injury literature indicates that injuries to the pelvis and low back can be very debilitating [1] and that performance issues linger even after LBP has resolved [2]. Additionally, the ergonomics literature has implicated occupational tasks that combine trunk flexion and axial rotation ("bend and twist") as contributing to LBP in the workplace [3], but these claims seem as yet unsubstantiated by empirical data.

Research utilizing dynamical systems methods, such as Continuous Relative Phase (CRP) and CRP variability (CRPvar), has demonstrated differences in transverse plane (axial rotation) coordinative patterns during locomotion for individuals with chronic LBP. Specifically, individuals with chronic LBP demonstrated diminished capacity to transition axial pelvis-trunk coordination from in-phase to anti-phase as walking speed increased on a treadmill [4]. However, from this research it is not clear whether individuals with LBP also demonstrate changes in trunk axial rotation and lateral flexion coordination during locomotion.

The purpose of this study was to examine three-dimensional trunk range of motion (ROM) and trunk sagittal motion – axial rotation ("bend and twist") coordination during treadmill locomotion in three groups of runners classified by LBP status. We hypothesized that a group of runners currently experiencing LBP and a group of runners for whom LBP had resolved would demonstrate decreased ROM, coordination (CRP) and coordination variability (CRPvar) as compared to a control group.

METHODS AND PROCEDURES

Data were collected on three groups of runners with varying degrees of LBP. One group was currently experiencing mild to moderate LBP (LBP group, n=14), another group had recovered from a single bout of LBP and had been running pain-free for at least six months (RES group, n=14), and the third group had never experienced LBP (CTR group, n=14). All participants were recreational runners from the community, ran at least 20 km per week, and were free of lower extremity orthopaedic injuries.

After an appropriate acclimatization period, subjects ran (2.3, 2.8, 3.3, 3.8 m/s) on a treadmill for 30 sec per speed. Trunk segment 3-D kinematic data were collected using an 8-camera high speed motion capture system (240 Hz) for the last 20 sec at each speed.

Two-way repeated measures ANOVA (Group by Speed) ($p < 0.05$) were performed for (1) three-dimensional trunk ROM and (2) trunk sagittal-axial plane CRP and CRPvar. Effect size (ES) was also calculated to express differences relative to a pooled standard deviation.

RESULTS

T-tests revealed no significant differences among groups for age, height, body mass, or

preferred running speed (Table 1). The LBP group demonstrated significantly lower CRP (122.1 ± 28 degrees) as compared to the CTRL group (112.4 ± 21 degrees) (Figure 1), regardless of speed, with a correspondingly large ES (ES=2.84). A large ES was also noted between the RES v. LBP (ES=1.72) and CTR v. RES groups (ES=1.13). There were no differences between groups in CRPvar or three-dimensional trunk ROM during running.

Table 1. Group means (±SD) characteristics for age, height, body mass, and preferred running speed (PRS) for three experimental groups used in this study.

	CTRL	**RES**	**LBP**
Age (yr)	35.7 ± 11	32.6 ± 9	29.9 ± 8.5
Height (m)	1.7 ± 0.1	1.72±0.1	1.69 ± 0.1
Mass (kg)	73.9 ±13	71.4 ±9.8	63.9 ±10.1
PRS (m/s)	3.07 ± 0.3	2.91 ±0.5	2.84 ± 0.4
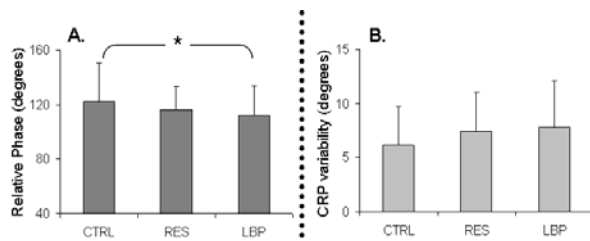
Figure 1. Mean CRP (A.) and CRPvar (B.) of trunk sagittal (lean) and axial rotation for CTRL, RES, and LBP groups, averaged across all running speeds. Error bars represent SD, * denotes significant differences.

DISCUSSION
Differences were observed between groups for sagittal-transverse coordination (CRP) during running, indicating that runners with LBP had experienced difficulty moving toward anti-phase coordination. While no significant differences were reported for the RES group, large effect sizes were noted compared to LBP and CTR groups, which suggest that clinical differences may exist between all three groups [5]. Contrary to our hypothesis, no differences were observed between our groups for three-dimensional trunk ROM or sagittal-transverse coordination variability (CRPvar). These results were present despite low disability levels of our LBP group, and despite the fact that running involves relatively little "bend and twist" motion as compared to even the most common work-related tasks.

While these results are interesting in the context of the current study, the measures used in this study can be applied to job-specific tasks to examine the effect of LBP on coordination between planes. We suggest that the multi-planar coordination analysis similar to that used in this study will aid in elucidating the relationship between LBP and "bend-and-twist" motion specific to occupational tasks.

SUMMARY
We examined sagittal-transverse (bend and twist) coordination coupling within the trunk segment, an action that has been associated with low back injury in the ergonomic literature. We found coordination differences between individuals with and without LBP, and suggest that this measurement may prove useful for analyzing a myriad of workplace activities. These data add to a growing body of literature that is attempting to quantify kinematic and coordinative differences between individuals with and without LBP.

REFERENCES
1. Geraci, M. Aspen, MD, 1998.
2. Nadler et al., *Clin J Sport Med* **12**, 73-78, 2002.
3. Riihimaki et al. *Scand J Work Environ Health*. **15**, 415-23, 1989.
4. Selles, et al., Clin Biomech **16**, 175-181, 2001.
5. Cohen, J. Earlbaum, New Jersey, 1988.

ACKNOWLEDGEMENTS

FLUCTUATION OF EMG PATTERNS AT MULTIPLE WALKING SPEEDS

Hyun Gu Kang[1,2], Jonathan B. Dingwell[3]

[1] Institute for Aging Research, Hebrew SeniorLife, Boston, Massachusetts, USA
[2] Harvard Medical School, Boston, Massachusetts, USA
[3] Nonlinear Biodynamics Lab, Dept. of Kinesiology, University of Texas, Austin, Texas, USA

E-mail: hyungukang@hrca.harvard.edu   Web: http://www.hebrewseniorlife.org

INTRODUCTION

Falls pose a tremendous risk to those over 65 and most falls occur during walking. To prevent falling, a person must generate both the correct motor patterns to facilitate stable walking, and the proper corrective responses to perturbations. Fluctuations in kinematics may reflect the health of the motor system (Hausdorff et al. 1997), but little is known about how these fluctuations occur and are controlled. Kinematic patterns during gait were less variable than EMG over multiple speeds (Ivanenko et al, 2002) and slower walking is associated with both increased variability in timing of EMG Patterns (Chung and Giuliani, 1997). However, existing studies have used subjective self-selected speeds or imposed fixed speeds, without accounting for an individual's preferred walking speed, and did not systematically relate kinematic variability with EMG variability across age and walking speed. Therefore we quantified the variability of EMG linear envelopes in the leg muscles at multiple speeds in young and older adults.

METHODS AND PROCEDURES

Eighteen healthy older adults (age 72±6) and 17 sex, height and weight-matched young adults (23±3), with no orthopedic or neurological impairments, participated with informed consent. Each subject walked for 5 minutes on a Woodway treadmill at each of 5 speeds: 80%, 90%, 100%, 110%, and 120% of their preferred speed (PWS) (Kang and Dingwell, 2008). EMG from *v. lateralis* (VL), hamstrings (HA), *gastrocnemius* (GA), *t. anterior* (TA) were recorded at 1080Hz. Linear envelopes were calculated after bandpass filtering (20-300 Hz), normalizing, rectifying and smoothing using a convolution filter. Average stride-to-stride variability (MeanSD) (Kang and Dingwell, 2008) and average peak amplitudes of these EMG linear envelopes were calculated for each subject and each speed. The groups and speeds were compared using ANOVA (SPSS 14).

RESULTS

The healthy older subjects tested here walked with the same preferred walking speeds as the younger subjects ($p = 0.86$). The kinematic variability results are reported elsewhere (Kang and Dingwell, 2008). Variability of EMG increased with walking speed in VL, HA and TA muscles ($p < 0.0001$). Variability was also larger in older adults in HA ($p <0.004$) and TA ($p < 0.001$) muscles. Age × Speed interaction effects were not significant. Older adults displayed higher peak amplitudes of linear envelopes in VL ($p <0.003$), HA ($p < 0.001$), and GS ($p < 0.03$). When MeanSD's were normalized by Peak EMG amplitudes, age- and speed- related differences were no longer significant ($p > 0.05$).

DISCUSSION

Variability of EMG patterns during gait increased with speed and EMG amplitude, except in the GS. This demonstrated the

signal-dependent noise phenomenon, also observed in isometric contractions (Harris and Wolpert, 1998). Age-differences were seen only in HA and TA. That variability of GS pattern is consistent across speeds and age groups may be because GS is important during the push-off phase of gait, a propulsive event that introduced mechanical energy to the locomotor system. Keeping its behavior consistent maybe especially important in maintaining stability during gait.

The response of EMG variability to walking speed and age is unlike that of kinematic variability of the leg joint angles (Kang and Dingwell, 2008). Although these muscles are primarily involved in sagittal motion, the variability of sagittal joint angles did not vary with age or speed. This suggests that variability of EMG patterns does not predict kinematic variability in response to walking speed.

REFERENCES

Chung, S.H. and Giuliani, C.A. (1997). *Gait & Posture*, 6: 110-118.

Dingwell, J.B. and Marin, L.C. (2006). *J Biomech,* 39: 444-452.

Harris, C.M. and Wolpert, D.M. (1998) *Nature*, 394: 780-4.

Hausdorff, J.M. et al. (1997). *J App Physiol*, 82:262-9.

Kang, H.G. and Dingwell, J.B. (2008). *Gait & Posture*,doi:10.1016/j.gaitpost.2007.07.009

Shiavi, R. et al. (1987). *J Rehabil Res Dev*, 24:13-23.

Ivanenko et al. (2002). *J Neurophysiol*, 87:3070-89
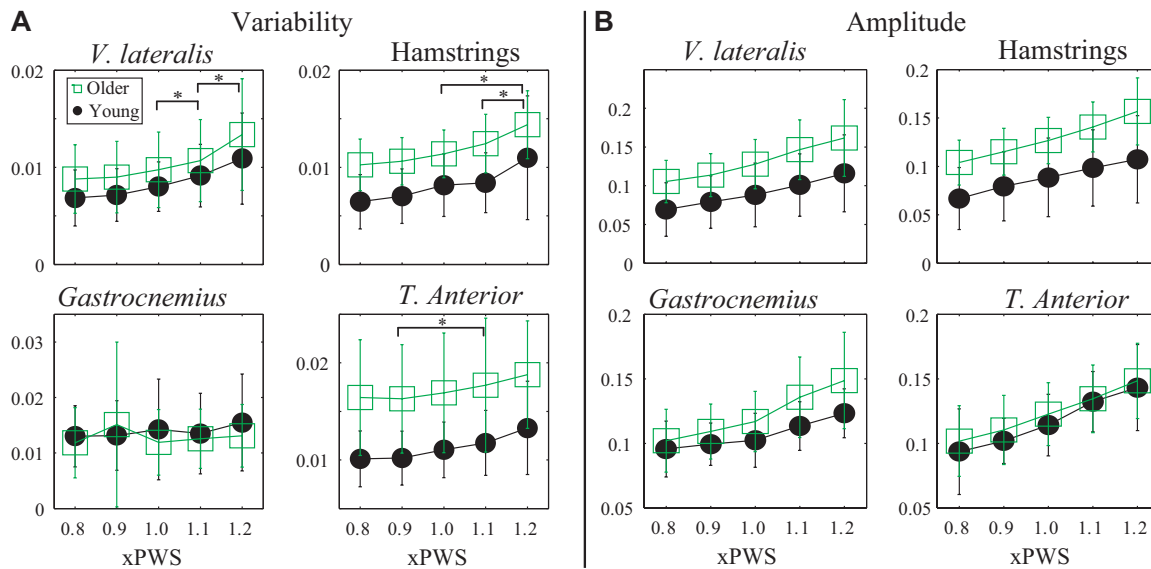
Figure 1. **A:** MeanSD of EMG linear envelopes vs. walking speed. Speed effects were significant in all muscles but the GA. Age effects were significant in HA and TA. **B:** Between-strides average of EMG linear envelope peak amplitudes. Amplitudes increased with speed (p < 0.001). Horizontal brackets denote significant Tukey's LSD post-hoc comparisons at p < 0.005.

EFFECTS OF WALKING SPEED ON STEP WIDTH AND STEP LENGTH VARIABILITY

Daniel S. Peterson[1*] and Philip E. Martin[1]

[1]Pennsylvania State University, Department of Kinesiology, University Park, PA, USA
*dsp167@psu.edu

INTRODUCTION

Step to step variability is an inherent feature of gait. Not only has variability been shown to be associated with stability and falls in older adults (e.g., Maki, 1997), recent work has suggested that it also may be important to metabolic cost during walking (e.g., Donelan et al., 2002). Several studies (Helbostad and Moe-Nilssen, 2003; Sekiya et al., 1997; Yamasaki et al., 1991) have reported mediolateral (M/L) and anteroposterior (A/P) movement variability as a function of walking speed. Results, however, have been equivocal. We examined the effect of walking speed on step width (SW), SW variability (SWV), stride length (SL), and SL variability (SLV) in young, healthy adults.

METHODS AND PROCEDURES

Five males and one female (mean age = 24.3 yrs) walked on a motorized treadmill for 3-5 minutes at each of five speeds (0.90, 1.11, 1.35, 1.56, and 1.77 m/s). Variable sampling times were used to obtain between 350 and 400 steps for each speed. Reflective markers on the heel and over the third metatarsal of each foot were sampled at 100 Hz using a Motion Analysis system. Marker position data were low pass filtered at 2 Hz. Heel strike and toe off events for each foot were determined using an algorithm described by Herljac and Marshall (2000). M/L foot position for each step was defined as the average location of the midpoint of heel and 3rd metatarsal markers during single leg support. SW was computed as the M/L distance between right and left feet during consecutive stance periods. SL was determined by multiplying the time between consecutive same foot heel strikes by walking velocity (figure 1).
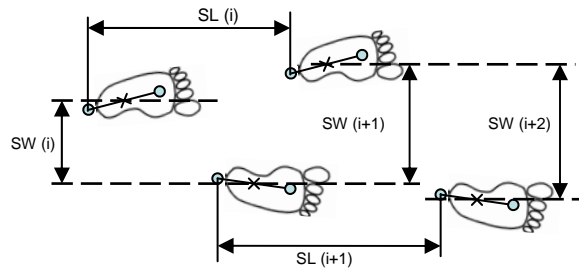
Figure 1. Stride length (SL) and step width (SW) determination.

Three hundred sixty-eight steps, the minimum number of steps recorded in any trial, were analyzed for all conditions. Step width variability (SWV) and stride length variability (SLV) were defined as the standard deviation of SW and SL, respectively, at each speed. SW, SL, SWV, and SLV were normalized to each subject's leg length (LL). The effect of speed on SW, SWV, SL, and SLV were analyzed using single factor ANOVA's with speed as the repeated measure. Preferred walking speed (PWS) was averaged over 10 trials of overground walking along a 10m gaitway.

RESULTS

Neither SW nor SWV (figure 2a) were affected by walking speed (SW: F=0.07, p=0.99; SWV: F=0.26, p=0.90). As expected, SL increased systematically with walking speed (F=58.78, p<0.001). SLV was also significantly affected by walking speed

(F=4.64, p=0.006) and reflected a curvilinear association with speed (figure 2b). PWS (1.47±0.06 m/s) was intermediate to the speeds that resulted in the two lowest SLV's (1.35 and 1.56 m/s).
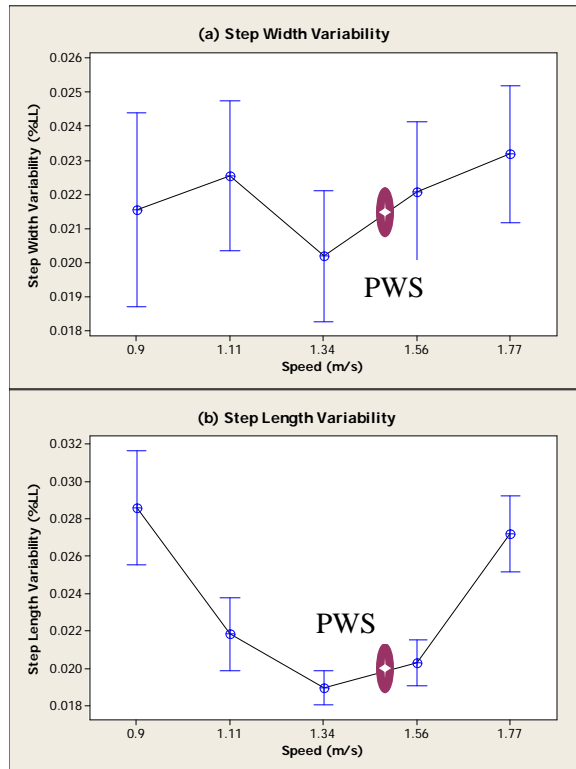
Figure 2. SWV (a) and SLV (b) as a function of walking speed.

DISCUSSION

Gabel and Nayak (1984) suggested kinematic measures primarily in the A/P plane, such as SL and step time, are determined predominantly by a gait-patterning mechanism, whereas measures in the M/L direction are determined by a balance control mechanism. Our results are consistent with this suggestion. The U-shaped relationship between SLV and speed has been reported previously (Sekiya et al., 1997; Yamasaki et al., 1991) and implies PWS elicits the most consistent pattern of movement in the A/P direction. This U-shaped relationship matches changes in gait economy as a function of speed (Martin et al., 1992; Ortega

and Farley, 2007). Donelan et al. (2002) found SL above or below preferred SL at a given walking speed substantially increased metabolic cost. The lower cost at PWS may be due in part to the minimized SLV which also occurs near PWS.

Consistent with previous studies (Kang and Dingwell, 2007; Helbostad and Moe-Nilssen, 2003), SWV was not affected by walking speed. In contrast to our results, Sekiya et al. (1997) found SWV increased linearly with walking speed and suggested this was related to "a speed dependent balance function but not to rhythmicity control of walking" (p.271). If M/L variability is linked to a balance mechanism, walking between 0.90 and 1.77 m/s apparently did not cause a substantial perturbation to M/L balance in our sample of young healthy subjects.

SUMMARY

In conclusion, SLV but not SWV, was affected significantly by walking speed. SLV was minimized near PWS, suggesting SLV may be associated with minimization of walking energy cost.

REFERENCES

Donelan, JM et al. (2002). *J Exp Biol,* 205:3717-27.
Gabel, A and Nayak, USL (1984). *J Gerontol,* 39:662-666.
Herljac, A and Marshall, RN (2000). *J Biomech,* 33:783-786.
Maki, B (1997). *J Gerontol,* 45:313-20.
Martin, PE et al. (1992). *J Appl Physiol*, 73:200-206.
Ortega, JD and Farley, CT (2007). *J Appl Physiol*, 102:2266-73.
Sekiya, M et al. (1997). *J Orthop Sports Phys Ther,* 26:266-72.
Yamasaki, M et al. (1991). *Eur J Appl Physiol*, 62:99-103.

IMPLICATIONS OF ALTERNATE STAIR DESCENT STRATEGIES ON KNEE BIOMECHANICS: BACKWARDS DESCENT IS LESS DEMANDING

[1]T.B.R. Cluff and [2]D.G.E. Robertson
School of Human Kinetics, University of Ottawa, Ottawa, ON, Canada, K1N 6N5
Email: [1]tcluf077@uottawa.ca, [2]dger@uottawa.ca

INTRODUCTION

Considerable research has been dedicated to understanding the demands imposed by stair ambulation (McFadyen and Winter, 1988; Reiner *et al.*, 2001). Peak knee moments and powers are larger in descent than ascent and level-walking, rendering descent a difficult mechanical task. In descent, lower limb muscles are required to generate force while lengthening, thereby dissipating gravitational energy and performing negative work. As such, elderly and clinical populations commonly develop compensatory gait strategies to modulate the imposed demand. However, we know little about the mechanics of these strategies. The purpose of this research was to delineate differences between traditional forwards stair descent and two alternate patterns; forwards step-by-step and backwards descent. Only the peak knee extensor moments and dissipative powers will be considered here, which represent the knee dissipating energy and contributing to controlled lowering during single-support, when the contralateral limb is in terminal swing.

METHODS AND PROCEDURES

Healthy males (*n*=9) and females (*n*=9) participated in the study. All subjects were free of neurological and musculoskeletal conditions. Subjects performed 10 trials in forwards (FD) and backwards descent (BD). Trials were initiated with the subject's preferred limb and performed at a self-selected pace. Twenty step-by-step (SBS) trials were performed, 10 to analyze lead limb kinetics (STSL), 10 for trail limb kinetics (SBST). Condition presentation was counterbalanced across subjects.

The staircase was instrumented with four force plates embedded in steps 2 through 5 (step 2 & 5: Kistler 9286A; step 3 & 4: AMTI OR6-7-1000 & OR6-7-2000). The stairs dimensions were 30 cm run and 20 cm rise (Ontario Building Code, Section *9.8.3*, 2006). Force platform data were sampled at 200 Hz. Seven Vicon MX-13 cameras sampled displacement data at 200 Hz. Analog data were low-pass filtered with a 4th-order Butterworth digital filter (f_c =10 Hz force; 6 Hz for displacement data). Data were ensemble averaged and subjected to 4 × 4 repeated-measures ANOVA with stair step and condition as factors for peak knee extensor moments and powers.

RESULTS

Peak knee extensor moment depended on stair ($F_{(3, 15)} = 6.45$, $p<0.001$) and condition ($F_{(3, 15)}$) $= 59.59$, $p<0.001$) main effects and a stair × condition interaction ($F_{(9, 9)} = 10.93$, $p<0.001$). Figure 1 shows that both main effects were annulled by the interaction.

Peak knee extensor power was influenced by stair ($F_{(3, 15)} = 8.81$, $p<0.001$) and condition ($F_{(3, 15)} = 110.6$, $p<0.001$) main effects and a stair × condition interaction (($F_{(9, 9)} = 14.62$, $p<0.001$). Figure 1 shows the stair step main effect was washed out by the stair step × condition interaction.
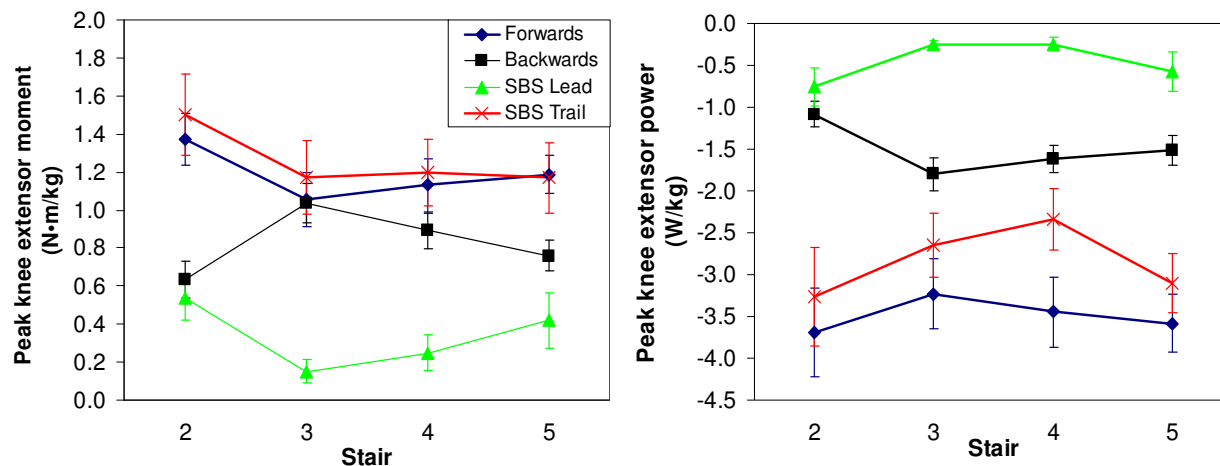
Figure 1. Body-mass normalized peak knee extensor moments and powers over four consecutive gait cycles in forwards, backwards and step-by-step stair descent (lead and trail limbs). Error bars show 95% confidence intervals.

DISCUSSION

In all conditions, the peak knee moment decreased into the mid-stair region and stabilized. Conversely, in BD the trend was opposite. While the lowest peak knee moments were associated with SBSL, there were no apparent differences between those associated with SBST and FD. The condition main effect was preserved for peak knee extensor power. Peak knee extensor powers were larger in FD and smaller in SBSL than other conditions. In BD, peak powers were smaller than those observed at the SBST knee. In terms of the interaction, peak knee power was largest during transition and decreased in absolute magnitude thereafter, except in BD, where the trend was reversed.

SUMMARY

Peak knee extensor moments and powers stabilized following one complete gait cycle. Further, peak knee moments and powers were larger in FD than the alternate gait patterns. As such, compensatory strategies reduced the demand at the knee during stair descent. However, the overall pattern of net moments and powers was idiosyncratic; it depended on both strategy and stair. This was illustrated with BD, where peak knee moments and powers increased at the step 1 transition but decreased thereafter. As such, BD is recommended as an alternative to FD for individuals with pronounced weakness of knee extensor musculature. Furthermore, reduced powers with BD imply forces were applied at lower levels. While similar results were observed in SBS descent, the reduction only occurred for the lead limb. Therefore, BD might represent a more feasible strategy in individuals with bilateral knee extensor weakness.

REFERENCES

Ministry of Municipal Affairs & Housing (2006). *Ontario Building Code.* Toronto: Housing Development & Buildings.
McFadyen, BJ and Winter, DA (1988). *J Biomech,* 21: 733-744.
Reiner, R *et al.*(2002).*Gait Posture* 15:32-44

ACKNOWLEDGEMENTS

STABILITY OF SUPERIOR SEGMENTS DURING GAIT IN OLDER ADULTS

Hyun Gu Kang[1,2], Jonathan B. Dingwell[3]

[1] Institute for Aging Research, Hebrew SeniorLife, Boston, Massachusetts, USA
[2] Harvard Medical School, Boston, Massachusetts, USA
[3] Nonlinear Biodynamics Lab, Dept. of Kinesiology, University of Texas, Austin, Texas, USA

E-mail: hyungukang@hrca.harvard.edu   Web: http://www.hebrewseniorlife.org

INTRODUCTION

The ability to maintain steady motion diminishes with age (Cromwell et al., 2002; Kang and Dingwell, 2008). Active control of trunk motion is believed to enable stable walking (Winter et al., 1993). Head movement is always tightly controlled during various tasks, and this control may not function as well in older adults (Cromwell et al., 2002). Acceleration amplitudes from shocks from walking are absorbed as they move up from the feet to the head (Ratcliffe and Holt, 1997). The nervous system may therefore prioritize the stability of the superior segments during walking. We tested whether superior segments exhibited less dynamic instability than inferior segments, and whether these stability relationships between segments are altered with age. We hypothesized that increased control of superior segments would be reflected in decreased local instability and that the deterioration of this control with normal aging would lead to increased local instability.

METHODS AND PROCEDURES

Eighteen healthy older adults (age 72±6) and 17 height- and weight-matched young adults (23±3), with no orthopedic or neurological conditions, participated with informed consent. Each walked for 5 minutes on a Woodway treadmill at their preferred speed (PWS) (Kang and Dingwell, 2008). VICON was used to measure the motion of trunk, pelvis, thigh, shank, and foot segments using a custom market set. Custom MATLAB routines were used to determine dynamic stability for the trunk, pelvis, thigh, shank, and foot segments separately. Local dynamic stability was quantified as local divergence exponents that estimate the sensitivity of gait pattern to small intrinsic perturbations, using established algorithms (Dingwell et al, 2007). The effects of the small perturbations over 0-1 strides (λ^*_S), and 4-10 strides (λ^*_L) were quantified. Differences between the two age groups and the five body segments were compared using ANOVA (SPSS 14).

RESULTS

The preferred walking speeds of our healthy older adults were no different than our young adults (1.29 ± 0.13 m/s, $p = 0.86$). Superior segments were less sensitive to small local perturbations ($p < 0.0001$; Fig. 1). Older adults exhibited higher local divergence exponents ($p < 0.001$; Fig. 1) than the young adults, and thus were less stable across all segments. Segment × age interaction effect was also present ($p < 0.02$), where the age-differences were stronger at superior segments for (λ^*_S).

DISCUSSION

The trunk segment was less sensitive to local perturbations. The larger mass of the trunk may make it less sensitive to perturbations. The trunk segment is often involved in other

motor tasks during gait, and therefore may require additional stability during gait to allow other activities.

Older adults exhibited greater instability in all segments, despite walking at the same preferred speeds as young adults. This may indicate diminished control of body segment motion even in healthy older adults, although this difference may not be obvious from their gait speed. This age-related difference was larger in the stability of superior segments. Measuring dynamic stability of trunk motion during gait may be more indicative of future gait disorder and falls in older adults than measures based on lower extremity movements.

REFERENCES

Cromwell R.L. et al. (2002). *J Geron A,* 57: M442-8.
Dingwell, J.B. et al (2007). *J Biomech,* 40: 1723-1730.
Kang, H.G. et al. (2008). *Gait Posture* doi:10.1016/j.gaitpost.2007.07.009
Ratcliffe, R.J. and Holt, K.G. (1997). *Gait Posture,* 5:93-100.
Winter, D.A. et al. (1993). *Prog Brain Res,* 97: 359-67.

ACKNOWLEDGEMENTS
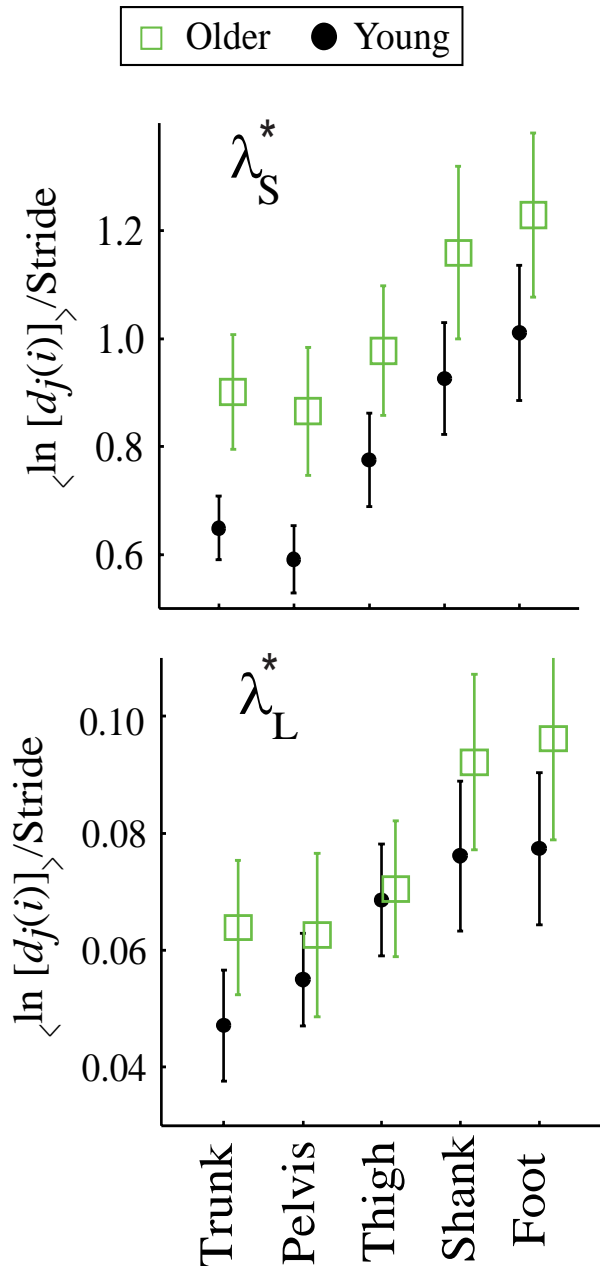
Figure 1. Local Divergence Exponents vs. Age and Body Segment.

MINIMAL FOOT CLEARANCE IN STAIR DESCENT: APPLICATION OF A SIMPLE, ROBUST EMPIRICAL METHODOLOGY

[1]T.B.R. Cluff and [2]D.G.E. Robertson
School of Human Kinetics, University of Ottawa, Ottawa, ON, Canada, K1N 6N5
Email: [1]tcluf077@uottawa.ca, [2]dger@uottawa.ca

INTRODUCTION

Debilitating stair falls motivate researchers to understand the factors that predispose both young and elderly populations to falling. Foot clearance has received considerable attention as such a factor (Hamel *et al*., 2005). Foot clearance quantifies the distance between the stair edge and the foot during swing phase. To date, the majority of research focused on clearance in descent since falls in descent are three times more numerous than those incurred in ascent (Cohen, 2000). In short, it appears clearance might be refined to progressively smaller values as the individual descends stairs and accomplishes a steady-state descent pattern.

METHODS AND PROCEDURES

Healthy males (*n*=9) and females (*n*=9) participated in the study. All subjects were free of neurological and musculoskeletal conditions. Subjects performed 10 trials in forwards (FD) and backwards descent (BD). Trials were initiated with the subject's preferred limb and performed at a self-selected pace. Condition presentation was counterbalanced across subjects. Stair dimensions were 30 cm tread and 20 cm riser according to local building codes. Seven Vicon MX-13 cameras sampled displacement data of four foot marker--hallux, calcaneus, 1st and 5th metatarsal-phalangeal joints --at 200 Hz. Analog data were low-pass filtered with a 4th-order Butterworth digital filter with 6 Hz cutoffs. Filtered marker trajectories were imported to

MATLAB and analyzed with a custom script. Marker clearance was computed according to the formula:

$$d = \frac{\left|(\underline{x}_2 - \underline{x}_1) \times (\underline{x}_1 - \underline{x}_0)\right|}{\left|(\underline{x}_2 - \underline{x}_1)\right|}$$

where d is the minimal distance between a marker and the line that defines the stair edge; $\underline{x}_1$ and $\underline{x}_2$ are points at the corners of the stair edge; and $\underline{x}_0$ represents the coordinates of a foot marker. Data were ensemble averaged and subjected to 2×5 repeated-measures ANOVA with descent condition and stair (number) as factors.

RESULTS

There were significant stair ($F_{(4, 13)} = 51.43$, $p<0.001$) and condition ($F_{(1, 16)} = 109.57$, $p<0.001$) main effects and a stair $\times$ condition interaction ($F_{(4, 13)} = 37.22$, $p<0.001$) for the dependent variable, minimal clearance. Figure 1 shows ensemble averaged minimal clearances over five consecutive stairs during the swing phases of FD and BD. In addition, Figure 1 demonstrates that clearance was dependent upon levels of both stair and condition so that neither main effect was relevant. In other words, clearance increased and stabilized in the mid-stair region in BD and was subsequently larger than that demonstrated in FD. However, there was no discernible difference in transition (first stair). In both conditions, subjects demonstrated a tendency to increase clearance at stair 5, the transition to level walking.
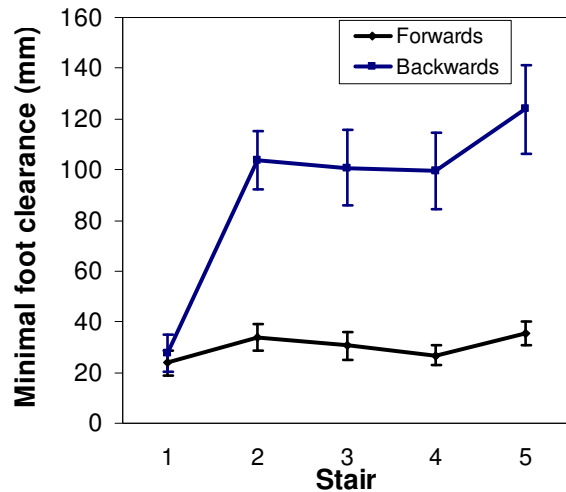
Figure 1. Ensemble averaged minimal foot clearance over five consecutive stairs in forwards and backwards descent. Error bars represent ±1 SD.

DISCUSSION

As demonstrated in Figure 1, clearance was substantially larger in BD than FD, except for the transition at stair 1. Transition represents the initiation of descent where the foot need only clear one step. Therefore, it seems the constraints imposed during transition to stair descent reduced foot clearance as compared to subsequent stair step-downs; making it the most dangerous. This phenomenon was especially pronounced in backwards descent, where clearance over stair 2 saw a fivefold increase in contrast to that of stair 1. Aside from the apparent transition effect and despite greater intra- and inter-subject variability, clearance in BD was markedly larger than that of FD. As a result, there is significantly less likelihood of contacting a stair in the swing phase of BD than FD. In conjunction with kinetic analyses conducted in our laboratory, BD might be suggested as an alternative to FD since the peak knee extensor moment and dissipative power are substantially reduced, while subjects are less likely to

sustain contact with the stair edge during the swing phase of the descent gait cycle.

Moreover, the minimal clearance results shown in Figure 1 agree well with the literature (Hamel *et al.*, 2005), in that clearance became progressively smaller as the individual descended the stairs and achieved a steady-state pattern. Therefore, the methodology presented here appears to be robust and suitable for application in clinical and research settings.

SUMMARY

Minimal foot clearance revealed that the first gait cycle represented a transition in stair descent. In transition, clearance was markedly smaller than during steady-state progression. However, as an individual descends, clearance progressively decreased. In steady-state progression, clearance was substantially greater in backwards as compared to forwards descent. Future research should consider the feasibility of backwards descent in elderly and clinical populations.

REFERENCES

Hamel, K.A. *et al.* (2005). *Gait Posture* 21: 135-140.

ACKNOWLEDGEMENTS

WALKING SPEED, LEG STRENGTH, RANGE OF MOTION, AND DYNAMIC STABILITY IN THE GAIT OF HEALTHY OLDER ADULTS

Hyun Gu Kang[1,2], Jonathan B. Dingwell[3]

[1] Institute for Aging Research, Hebrew SeniorLife, Boston, Massachusetts, USA
[2] Harvard Medical School, Boston, Massachusetts, USA
[3] Nonlinear Biodynamics Lab, Dept. of Kinesiology, University of Texas, Austin, Texas, USA

E-mail: jdingwell@mail.utexas.edu   Web: http://www.edb.utexas.edu/faculty/dingwell/

INTRODUCTION

Falls pose a tremendous risk to those over 65 and most falls occur during walking. Slow gait speed is common in the elderly and may predict fall risk (Alexander, 1996). Slower speeds are related to fear of falls (Maki, 1997) and so may be a strategy to improve stability. In young adults, walking slower leads to improved local dynamic stability, despite also leading to greater variability (Dingwell and Marin, 2006). However, older adults who walk slower may still be at higher risk of falls. Very healthy active elderly who walk at the same preferred speeds as younger adults still exhibit greater variability, which also increases at slower speeds (Kang and Dingwell 2008). To resolve this seeming paradox, we determined if healthy older adults also improved their dynamic stability by walking slower, and if leg strength and flexibility modulate this relationship.

METHODS AND PROCEDURES

Eighteen healthy older adults (age 72±6) and 17 height- and weight-matched young adults (23±3), with no orthopedic or neurological impairments, participated with informed consent. Each subject walked for 5 minutes on a Woodway treadmill at each of 5 speeds: 80%, 90%, 100%, 110%, and 120% of their preferred speed (PWS) (Kang and Dingwell, 2008). VICON was used to measure motions of the trunk segment. Custom MATLAB routines were used to quantify dynamic

stability using local divergence exponents and maximum Floquet multipliers (FM) (Dingwell et al., 2007). Local divergence exponents estimate the sensitivity of gait patterns to small perturbations. Maximum FM quantify the amount of a perturbation to the gait pattern that remains after one complete stride. Maximum FM magnitudes < 1 indicate stable movement (i.e., perturbations get smaller) and smaller FM indicate better stability. Maximum FM were quantified at 0%, 25%, 50%, and 75% of the gait cycle (Dingwell 2007). Isometric leg strengths and passive range of motion (ROM) were also measured to account for age-related differences. The two groups and 5 walking speeds were compared using ANOVA (SPSS 14). Effects of strength and ROM were then included as covariates in ANCOVA.

RESULTS

The healthy older subjects tested here walked with the same preferred walking speeds as the younger subjects (p = 0.860). However, these older adults still exhibited greater local divergence exponents (p<0.0001; Fig. 1) and higher maximum FM (p<0.007; Fig. 2) than young adults at each walking speed. These older adults remained more unstable (p<0.04) even after adjusting for their lower strength and ROM. In both age groups, local divergence exponents decreased at slower speeds and increased at faster speeds (p<0.0001). Maximum FM showed similar changes with speed (p<0.02).
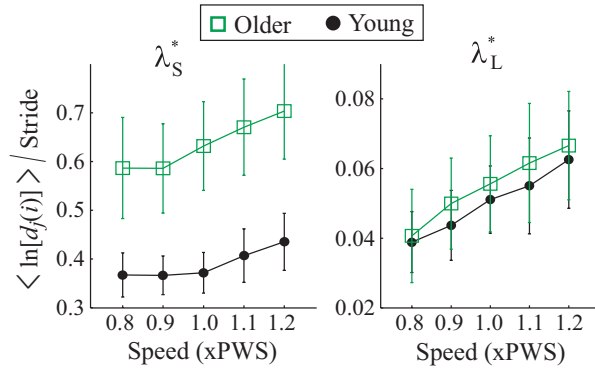
Figure 1. Local divergence exponents (λ^*) vs. walking Speed and Age. Older adults exhibited greater short-term (0-1 strides) (λ^*_S; $p < 10^{-13}$), but not long-term (4-10 strides) (λ^*_L; $p = 0.192$) local instability. Both groups exhibited decreased local dynamic instability at slower speeds and increased instability at faster speeds ($p < 0.001$) for both λ^*_S and λ^*_L.

DISCUSSION

Slower speeds and increased gait variability are commonly reported in older adults and those at risk of falls. Surprisingly, however, no study to date has directly examined how changes in walking speed affect variability and/or dynamic stability in older adults.

The older adults in this study were healthy enough to walk at normal speeds. However, they were still more unstable than the young adults, *independent* of walking speed. This greater instability was *not* explained by loss of leg strength and ROM. Thus, other age-related physiological changes, like increased neuromotor noise, may be equally important determinants of walking stability.

Slower speeds led to greater dynamic stability in both groups. Thus, older adults can *also* improve dynamic stability by walking slower, despite *in*creased gait variability). These results suggest that changes in dynamic instability might possibly be more sensitive indicators of future fall risk and gait disability than changes in gait speed or variability.

REFERENCES

Alexander, N.B. et al. (1992). *J Gerontol A,* 47: M79-M87.

Dingwell, J.B. and Marin, L.C. (2006). *J Biomech,* 39: 444-452.

Dingwell, J.B., Kang, H.G., and Marin, L.C. (2007). *J Biomech,* 40: 1723-1730.

Kang, H.G. and Dingwell, J.B. (2008). *Gait & Posture,*doi:10.1016/j.gaitpost.2007.07.009

Maki, B.E. (1997) *J Am Geriatr Soc,* 45: 313-320.
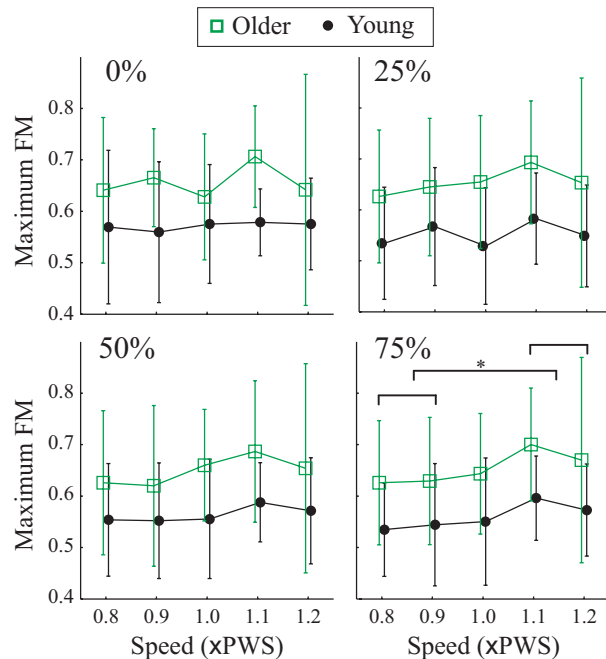
Figure 2. Floquet Multipliers vs. Speed at 0%, 25%, 50% and 75 of the gait cycle. Older adults exhibited larger FM values. The horizontal bracket denotes significant post-hoc tests (Tukey LSD). At 75% of the gait cycle, maximum FM at faster speeds were larger than that at slower speeds.

SPINAL STIFFNESS MEASURES DO NOT CHANGE WITH CHIROPRACTIC MANIPULATION EVEN WITH CLINICAL IMPROVEMENT

E Owens[+], D Wilder*, MR Gudavalli[+], J DeVocht[+], W Meeker[#]

[+]Palmer Center for Chiropractic Research, Davenport, Iowa, USA
*The University of Iowa, Iowa City, Iowa, USA
[#]Palmer College of Chiropractic-West, San Jose, California, USA

INTRODUCTION

Chiropractors and other practitioners of spinal manipulation use manual techniques to assess their patient's spinal function. In one test, therapists displace the spinal tissues in a posterior-to-anterior (PA) direction while subjectively sensing the force required to produce that displacement. The test results are used as an indication of what spinal segments are relatively less compliant and likely to benefit from spinal manipulation, which is thought to increase compliance. Therapists will often re-evaluate the spine after manipulation to evaluate the treatment's effectiveness.

We developed a testing system to perform an objective PA spinal stiffness measurement for use in clinical trials of spinal manipulation for patients with low back pain (LBP). The system uses a hand-held plastic rod to apply loads normal to the skin surface over the spinous processes of patients lying prone on a hard flat bench. An electro-magnetic tracking system monitors displacement of the rod tip while an inline force transducer measures the applied load. The force-displacement plot typically shows a linear region in the force range of 50-80N. We use the slope of this region of the force-displacement plot as a measure of spinal stiffness. The development and reliability of the system was described in Owens, 2007 and Owens, 2007b.

METHODS AND PROCEDURES

The system was used to measure PA stiffness in a group of patients with sub-acute or chronic LBP before and after a 2-week course of spinal manipulation following procedures described in Owens, 2007. After screening, participants were randomly assigned to one of 3 treatment groups: high-velocity low-amplitude (HVLA) manipulation, low-velocity variable-amplitude (LVVA) manipulation or wait list control. All treatments were delivered manually by chiropractors and were directed only to the L4-L5, L5-S1 segments, or either sacroiliac joint. The clinical results were generally positive in nature as seen by improved scores on the Roland Morris Questionnaire (RMQ). A comparison between groups showed that patients undergoing either HVLA or LVVA had greater improvement in RMQ scores than did wait list controls. The clinical results of that trial will be reported elsewhere (Meeker, 2008). This report focuses on the changes seen in PA Stiffness.

RESULTS

We collected complete PA Stiffness data on 136 patients in the study. In an earlier study, we determined that our method of PA stiffness measurement is subject to artifact in participants with thick skin or fat overlying the lumbar spinous processes. This was especially true in the lowest lumbar segments. We calculated a corrected PA Stiffness value using a factor based on regression with Body Mass Index (BMI) and Lumbar segment. The BMI correction tended to increase the PA Stiffness, especially at L4 & L5. The corrected PA Stiffness values range between

10-18.4 N/mm, with the stiffness increasing, on the average, from L1 to L5.

A one-way analysis of variance (ANOVA) shows no treatment effect for any treatment group. We also did a more detailed exploration of the dataset using a graphical approach (Figure 1). In the chart we plotted the change in PA stiffness at L5 (Baseline minus 2-week PAS) versus each participant's initial stiffness. Many participants showed less than 2 N/mm change in PAS, which we consider the limits of accuracy of our system. Participants with large (>20 N/mm) initial PAS tended to show a decrease in stiffness after care. And participants with initial PAS < 15 N/mm tended to show increased stiffness at 2-weeks. The effect is most notable in the group that received HVLA treatments.
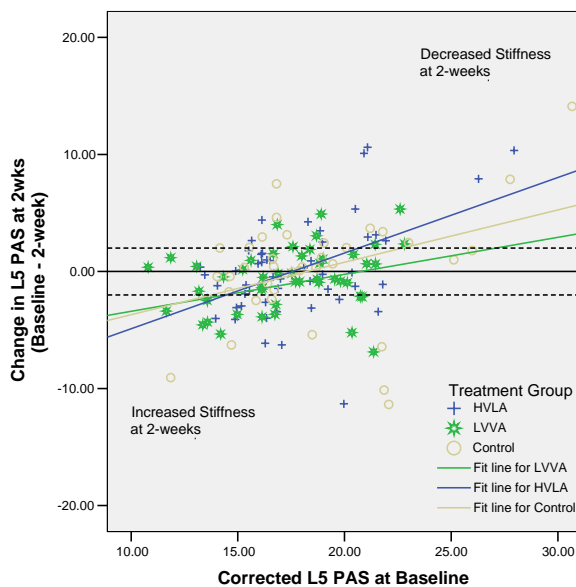
Figure 1. Change in PA Stiffness at 2-weeks versus baseline PA stiffness at L5
.

DISCUSSION

Based on these results, it is not possible to conclude that a 2-week course of spinal manipulation has a consistent effect on spinal stiffness. This is most interesting because participants in the study did experience relief of their symptoms as shown by changes in RMQ scores. The HVLA and LVVA groups experienced a 40%

improvement in RMQ overall, while the wait list control experienced less that 15% improvement on average (Meeker, 2008). The changes are indicative of clinically significant decreases in pain and disability with a short course of spinal manipulation.

Our analysis of change in PA Stiffness correlated to initial stiffness has the look of regression to the mean: participants with initially low scores showed increases in stiffness while participants with initially high scores showed relative decreases in stiffness at 2-weeks. Hence, on the average, the ANOVA showed no change with treatment. It is very interesting, however, that improvements based on RMQ can be associated with increases or decreases in PA stiffness. This implies a more complex definition of what is "normal" or "improved" spinal stiffness.

REFERENCES

Owens EF, DeVocht JW, Wilder DG, Gudavalli RM,. Meeker WC (2007) *J Manipulative Physiol Ther* 30:116-123.
Owens EF, DeVocht JW, Wilder DG, Gudavalli RM,. Meeker WC (2007b) *J Manipulative Physiol Ther* 30:493-500.
Meeker WC et al (2008) manuscript in preparation.

ACKNOWLEDGEMENTS

HyperSpectral Imaging to Assess and Predict Diabetic Foot Ulcers

Samantha Keevey[1], Brian L. Davis, PhD[1], Byron Hoogwerf, MD[1], Emile Mohler, MD[2],
Elizabeth Medinilla, MD[2], Marie Neverov[3], Aksone Nouvong, DPM[4], Kevin Schomacker, PhD[3]

[1]Lerner Research Institute, Cleveland Clinic, keeveys@ccf.org
[2]University of Pennsylvania Health Systems.
[3]HyperMed Inc.
[4]UCLA/David Geffen School of Medicine.

INTRODUCTION

Diabetic foot ulcers seriously impact the lives of people with diabetes. A lower extremity ulcer develops in about 15% of patients with diabetes during their lifetime. Up to 24% of diabetics with a foot ulcer will require amputation (R.G. Frykberg et als, 2000). The current procedure for diagnosing a diabetic foot is a clinical examination. The evaluation includes a thorough medical history, vascular history, physical examination, neurologic evaluation for neuropathy and a thorough vascular examination (Frykberg, RG, 2002). The next step for a patient with significant peripheral vascular or diabetic foot disease is non-invasive testing, which can include ankle brachial index (ABI), transcutaneous oxygen measurements (TcPO2), and pulse volume recordings (using duplex ultrasound). All these measurements are highly subjective and there is currently no method to accurately assess serious foot complications.

METHODS AND PROCEDURES

A method to accurately assist clinical evaluations; to define tissue at risk and prevent initial ulcer formation would be extremely favorable. This study is part of a multicenter study by HyperMed Inc., using Medical HyperSpectral Imaging (MHSI) to identify tissue at risk for ulceration, evaluate the healing capability of an ulcer and monitor treatment efficacy. MHSI uses a digital camera which is modified with special filters to take images of the subjects' skin. A spectrum of reflected light is acquired for each pixel in a region, containing the chemical signature of the outer layer of skin at that location. The images are then analyzed in order to quantifying the type, location and relative concentration of chromophores in the skin including oxyhemoglobin and deoxyhemoglobin. The multicenter study is divided into two groups, an ulcer healing group and an ulcer prediction group. The ulcer group consists of 66 type 1 and 2 diabetic subjects with at least one foot ulcer. The ulcer and tissue surrounding the existing ulcers is measured using the MHSI camera at 11 visits over 6 months. The ulcer prediction group consists of 210 type 1 and 2 high risk diabetic subjects. Their feet are surveyed and measurements taken using the MHSI camera over 24 months. The data is then used to assess the healing of an ulcer if one already exists or to predict the occurrence and location of future ulcers.
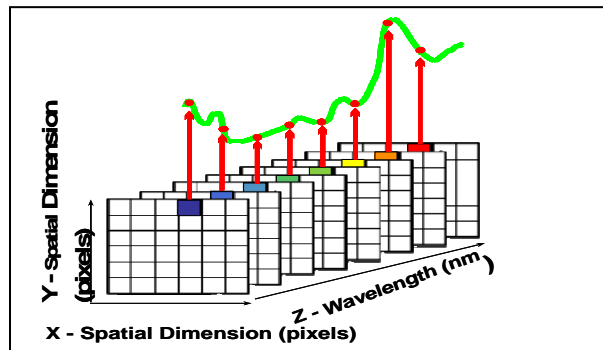
Figure 1. When the data is processed every pixel in the image has a spectrum embedded that reflects the tissue oxygenation status.

RESULTS

Through factor analysis we found that there is a relationship between (i) MHSI oxygenation and deoxygenation values and (ii) the two groups (Prediction and Ulcer). All of the "deoxy" values (i.e., for each of six foot regions) were associated with the same factor that was associated with patients who had an ulcer. While "oxy" values were not associated with active-ulcer patients, the thought is that they relate more to those patients whose ulcers will heal more rapidly.
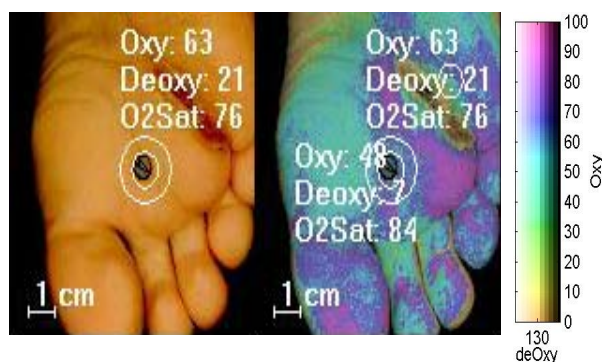
Figure 2. Two images from the ulcer group: On the left a visible image of the foot and on the right a spectral image of the foot and region of interest. With the spectral image the "oxy" and "deoxy" values throughout the foot can be obtained by outlining the region of interest. Mean values are calculated from a 1 cm wide region outside the outline.

SUMMARY/CONCLUSION

These initial findings relate to our hypothesis that MHSI-Oxy/MHSI-Deoxy values can be used to signify ulcers likely to heal along with predicting areas at risk for ulceration. MHSI offers an assessment of tissue oxygenation and deoxygenation, providing for the first time (i) a relevant analysis of the potential of an existing ulcer to heal and (ii) a method for defining tissue at risk for ulceration from a single patient visit. MHSI information can be collected in the clinic or physician office and has the potential to assist in the management of foot problems.
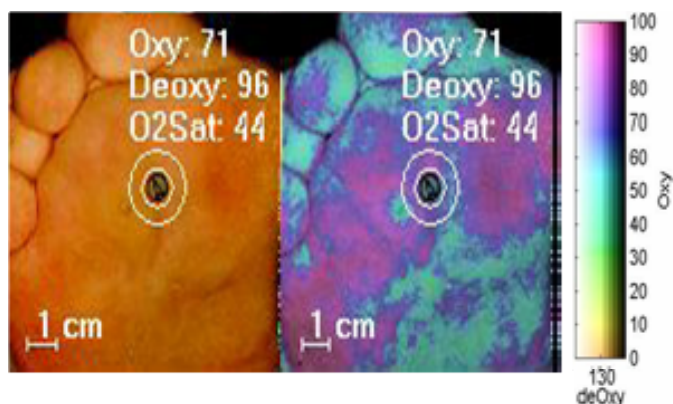
Figure 3. Two images from the prediction group: On the left a visible image of the foot and on the right a spectral image of the foot and region of interest. With the spectral image the "oxy" and "deoxy" values throughout the foot can be obtained by outlining the region of interest with a computer tool. Mean values are calculated from a 1 cm wide region outside the outline.

REFERENCES

R.G. Frykberg et als, *J. Foot Ankle Surg*. 39:5, Suppl. 2000.
Frykberg RG. Diabetic foot ulcers: pathogenesis and management. Am Fam Physician. 2002 Nov 1;66(9):1655-62.

ACKNOWLEDGEMENTS

EVALUATION OF A DYNAMIC LOAD SHARING APPROACH FOR THE LOWER EXTREMITY

M.D. Klein Horsman[1,2], H.F.J.M. Koopman[1], H.E.J. Veeger[3] and F.C.T. van der Helm[1]
[1]Laboratory of Biomedical Engineering, University of Twente, Enschede, the Netherlands
[2]Human Performance Laboratory, University of Calgary, Calgary, Canada
kleinhorsman@kin.ucalgary.ca
[3]Faculty of Human Movement Sciences, Vrije Universiteit, Amsterdam, the Netherlands
URL: http://www.ctw.utwente.nl/staff/BW/M.D.KleinHorsman/

INTRODUCTION

Muscle force can be used to describe the interaction between muscles and the skeleton. It provides insight in tissue loading and muscle control. The use of musculoskeletal models in the estimation of muscle force has been widely reported in the literature and showed to have clinical potential. However, many technical challenges still have to be overcome before application in clinical practice is achievable (Erdemir et al., 2007). Specifically, current models (a) use different anatomical data sets and fitting procedures for the anatomical information, (b) have often unrealistic force changes because the effect of excitation and activation dynamics are excluded and (c) use cost functions that typically activate only large muscles.

We have developed a musculoskeletal model of the lower extremity with the following added value in relation to previous models: (a) The model is based on a complete anatomical dataset (Klein Horsman et al., 2007); (b) it uses an inverse-forward dynamic optimization (IFDO) approach that includes activation dynamics (van der Kooij et al., 2003) and (c) it uses a cost function that has a good correspondence with muscle energy consumption (Praagman et al., 2006).

The goal of this project is to evaluate the validity of the dynamics of the model by comparison of (1) calculated joint reaction forces with in vivo measurements of joint reaction force and (2) simulated muscle activation with EMG patterns during gait.

METHODS

In this two-legged model, 10 joints are crossed with 264 Hill-type muscle elements, defined by muscle parameters such as optimal fiber length. 'Via' points and wrapping geometries were defined in case of a curvature in muscle line of action (Klein Horsman et al., 2007). Muscle dynamics are described by a third-order muscle model with excitation, active state and length of the contractile element as state variables. To evaluate the dynamic model properties, gait kinetics and EMG of the main flexors and extensors of the lower extremity were collected for a healthy male subject (age 21, mass 85 kg, length 1.85m). The size of the model and the muscle parameters (e.g. optimal fiber length) were scaled to the length of the segments of the subject. PCSA was scaled to subject mass. The load sharing problem was solved by using the IFDO approach. The muscle activation dynamics that were taken into account prevent unrealistic fast force transitions (van der Kooij et al., 2003). A recently proposed energy related cost function was used, representing the two-major energy processes in the muscle: re-uptake of calcium and detachment of cross bridges (Praagman et al., 2007).

RESULTS

Joint moments determined with the model fall well within the wide range of moments found in the literature. The calculated hip

compression force is in agreement with measured hip forces (Bergmann et al., 2001) (figure 1). The difference in the second peak (figure 1) is due a higher hip moments in the current study when compared to the study of Bergmann et al., 2001.

Calculated muscle activation and measured EMG agreed well (figure 2).
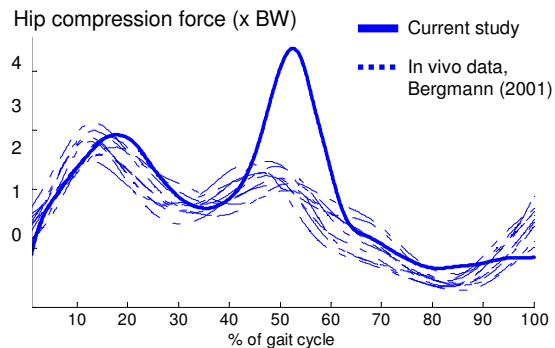
Figure 1. Hip compression force calculated with the model (solid) and measured with instrumented prosthesis (dashed) (Bergmann et al., 2001).
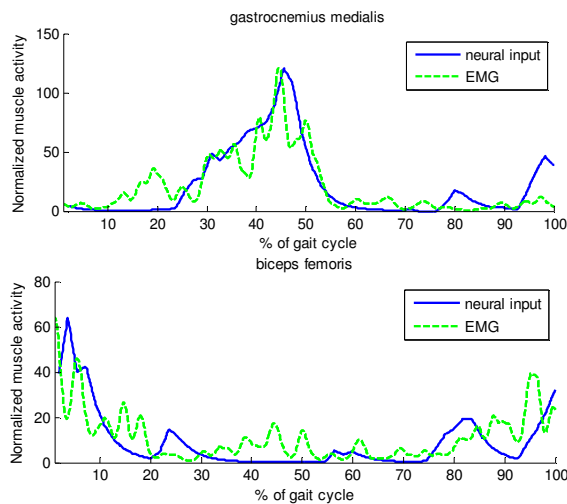
Figure 2. Muscle activation predicted by the model in comparison to measured EMG.

DISCUSSION

The effect of model assumptions is eminent. Load-sharing is highly dependent on geometry (e.g. muscle tendon paths) and force

generating properties (e.g. optimal fiber length). The presented model is unique for different reasons: First, it is based on one consistent anatomical dataset (Klein Horsman et al., 2006 and 2007). This is a major advantage with respect to other models based on different anatomical datasets, since it avoids possible inaccuracies caused by inter-individual anatomical differences and co-variance between parameters. Second, the IFDO approach prevented unrealistic fast transitions in muscle force, which were present in most previous model results because they did exclude the effect of excitation and activation dynamics. Third, the energy related cost function induced synergistic muscle activity resulting in solution where large and small muscles participate. This is an improvement when compared to traditional cost functions based on muscle force and cross sectional area only, which typically activate only large muscles.

The proposed model seems to be an improvement in muscle modeling. Yet, improvements can be made in muscle dynamics to obtain a better fit of activation and EMG.

REFERENCES

Bergmann et al. (2001). Journal of Biomechanics 34:859-71

Erdemir A, et al. (2007). Clin Biomech, 22: 131-54.

Klein Horsman MD, et al. (2007). Clin. Biomech, 22:239-47.

Klein Horsman MD, et al. (2006). Proceedings World Congress of Biomech., Munich, Germany, abstract 7233, 2006

Praagman M, et al. (2006). Journal of Biomechanics, 39:758-65.

Van der Kooij H, et al. (2003). Proceedings of ISCSB, Sydney, Australia.

Biomechanical Testing of the Shear Modulating Diabetic Insoles: An Engineering Perspective

Dan Lanctot[2] BS, David G Armstrong[1] DPM, PhD, Manish Bharara[1] PhD, Ryan T Crews[1] MS
[1]Center for Lower Extremity Ambulatory Research, Rosalind Franklin University of Medicine & Science, North Chicago, IL 60064, manish.bharara@rosalindfranklin.edu
[2]Diabetica Solutions Inc., San Antonio, TX 78249

INTRODUCTION

Peripheral neuropathy causes sensory loss, which leads to patient's inability to know when the foot is injured. This unnoticed trauma or any potential triggering factor leads to pressure or shearing injury, subsequently causing ulcerations and hospitalisation. Conventional diabetic foot care only address the foot problem from one perspective - "Cushioning or Pressure Offloading". This is only partially helpful. The new prescription diabetic insoles from Vasyli Medical addresses both pressure and shear, which in combination cause the traumatic impact to the foot. This novel product improvement uses two thin intervening layers of low friction materials sandwiched around a thn layer of Kevlar as part of a viscoelastic insole. Initial clinical studies have observed a 90% reduction in ulceration rate in individuals using this technology. The purpose of this investigation was to objectively assess the shear modulating capability of this device.
.

METHODS AND PROCEDURES

As part of the scientific validation, biomechanical assessment of the orthotic was carried out with the intent of evaluating the shear modulating capability. The assessment protocol is consistent with the regulatory guidelines, which suggest Medicare reimbursed, diabetic, heat moldable insoles must be heated to 230-240ºC to soften the EVA base material to allow better conformability for patient feet. Insoles were heated at 230ºC for three minutes in an oven. The mechanical test rig shown below was used to measure the shearing force for three diabetic insoles:

1) Prescription Diabetic Insoles (Vasyli Armstrong, Vasyli, USA) -These are heat moldable shear modulation insoles, designed with patented Glidesoft shear technology. Insoles consist of memory foam and offer temperature control using Outlast Adaptive comfort technology by NASA.

2) Non-Prescription Diabetic Insoles (Orthaheel, Vasyli, USA) - These are non-heat moldable shear modulation insoles, designed with Plastazote.

3) Standard Insoles - These are laminar construction, non-heat moldable, non-prescription insoles with no shear modulation. This simply offers vertical pressure offloading.

The test procedures and its reliability have been published in an earlier study (Lavery et al. 2005). A typical testing procedure involved, application of load using cylindrical indenter and translating the slide assembly in a reciprocating pattern with 2.3mm maximum displacement. The reactive force and displacement were measured with electronic transducers. The main objectives of our assessment were to quantify the changes in shear upon heating and to compare the prescription insoles with the non-prescription insoles.

RESULTS

Figure 1 illustrates the comparative results from the assessment of all three types of insoles, represented as error bars. Error bars represent shearing force as, mean±SD for

prescription (3687.2±13.42), non-prescription (4309.4±65.87) and standard (6846.4±41.2) insoles. The mean shearing force (mean One sample of each type was tested five times to determine peak shearing force. Figure 2 illustrates summary of the complete dataset in the form of 'box plots' emphasizing the median and extreme values in datasets. Four samples of each type were tested five times using the mechanical test rig described above. to determine the shearing force in grams. Figure 3 illustrates the effect of heating the prescription insole on the shearing force. Data from 20 tests runs on four samples is presented in the form of 'box plots' with median and extreme values.

Figure 1: Comparative results for three diabetic insoles.
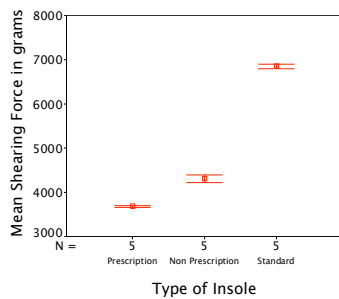
Figure 2: Summary of biomechanical assessment for prescription and non prescription insoles.
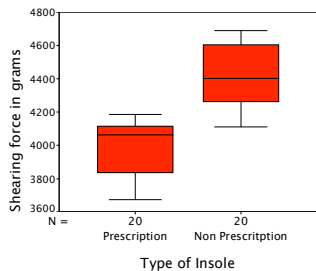
Figure 3: Summary of effect of heating on prescription insoles.
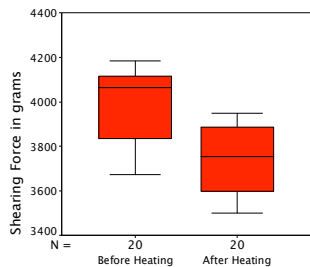
DISCUSSION

Both prescription and non-prescription diabetic insoles have shear modulation capability. However, prescription insoles offer superior shear modulation and enhanced offloading technology based on NASA's Memory Foam. Therefore, it would stand to reason that the patients with high-risk for foot ulceration will benefit more. Heating induced changes in the orthotic material can potentially alter the shear modulation capability. Our current assessment procedure confirmed that the elastic threads are able to withstand the heat required for shaping the insole.

SUMMARY

In our earlier study (Lavery et al. 2005), we have demonstrated that the Glidesoft shear technology can reduce the shear force up to half when compared to a standard pressure relieving insole. Using the identical assessment protocol, we found that the heating the novel prescription insoles (by Vasyli Medical) for patient conformability does not significantly alter shear modulation capability. Our assessment also justifies that prescription insole has superior shear modulation capability when compared to the to the non-prescription and laminar construct insoles. It must be emphasized that Orthaheel still provides a high degree of shear modulation using Glidesoft shear technology, which is novel. The authors recommend the specific use of prescription insoles for Foot Ulcer risk category 2 and 3 (Lavery et al.2008 and Peters et al. 2007).

REFERENCES

1.Lavery LA, et al. *Diabetes Technol Ther*. 2005 Aug;7(4):638-46.
2.Lavery LA, Peters EJ, Armstrong DG. *International Wound Journal*. 2008:In Press
3. Peters EJ, Armstrong DG, Lavery LA. *Diabetes Care*. 2007.

EFFECTS OF LOAD AND FREQUENCY ON MUSCLE ACTIVITY IN A REPETITIVE UPPER EXTREMITY TASK

Melissa M. Brown and Peter J. Keir

McMaster Occupational Biomechanics Laboratory, Department of Kinesiology, McMaster University, Hamilton, Ontario, Canada. brownmm@mcmaster.ca

INTRODUCTION

Work-related musculoskeletal disorders (WMSD) of the upper extremity currently rank second to lumbar spine disorders as the most common workplace injury claims in Ontario. Several factors that place workers at an increased risk for the development of WMSDs include high repetition (Silverstein et al. 1986) high force (Silverstein et al. 1986) non- neutral postures (Malchaire et al. 1996) and high angular velocities (Marras et al. 1993). There is also strong evidence that the combination of high force and high repetition places individuals at a higher risk (Moore 2002; Silverstein et al. 1986).

The purpose of this study was to examine the effects of force and repetition on muscle activity during a pushing, task with and without grip.

METHODS AND PROCEDURES

Ten male and ten female participants participated after given informed consent. Participants performed a series of bimanual push-grip tasks on a custom made apparatus, which includes two tracks with a grip dynamometer on the right side and a matching post on the left each attached to linear potentiometer (Figure 1). A combination of three force levels (2 kg, 4 kg, and 8 kg), three frequencies (4/min, 8/min, and 16/min) and two grip conditions (30% maximum grip and unconstrained grip) were performed. Ratings of perceived exertion (RPE) were taking after each trial. The muscle activities of eight upper extremity muscles were collected via bipolar surface electromyography (EMG) (Bortec Biomedical Ltd., AB, Canada). Muscles recorded were: posterior deltoid, anterior deltoid, biceps brachii, triceps brachii, extensor digitorum (ED), extensor carpi radialis (ECR), flexor digitorum superficialis (FDS) and flexor carpi radialis (FCR). Grip force, potentiometer data and EMG was sampled at 2048 Hz using a custom made Labview program. All EMG was normalized to maximum voluntary exertion (MVE).
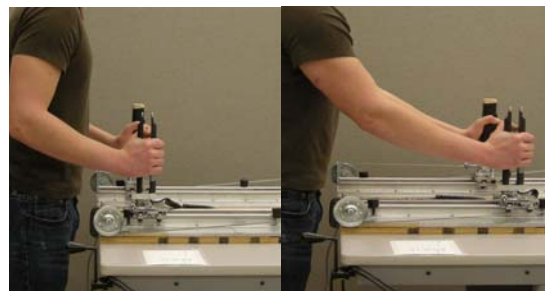
Figure 1. Custom made track. Grip dynamometer on right and matching post on left.

RESULTS

Preliminary results indicate an increase in muscle activity when, during the 30% grip condition, the frequency of the task is increased (Figures 2&3). During all tasks, regardless of gripping condition, it appears that the anterior deltoid muscle activity increases when both the load and frequency are increased. Forearm muscle (ED, ECR, FDS, FCR) activity appears to rise with increases in frequencies yet seems to be unaffected by increases in load, during the gripping tasks. In addition, the RPE for the high load, high frequency condition with no

grip had a mean of 3.25 ± 0.5 and for the 30% grip task the mean RPE was 5.25 ± 0.5.
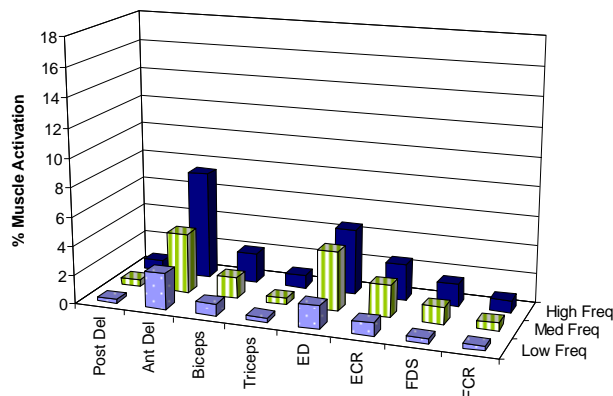
Figure 2. Mean muscle activity (%MVE). No grip and high load condition with all frequencies shown.
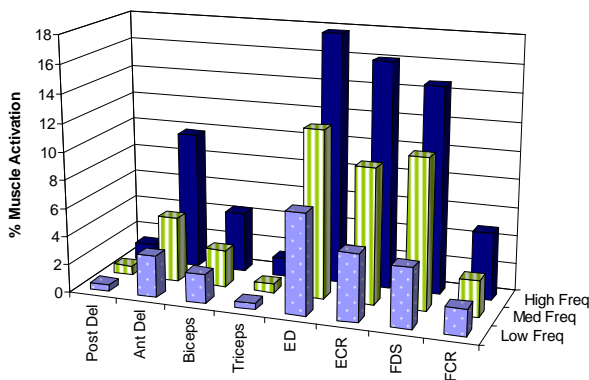
Figure 3. Mean muscle activity (%MVE). Grip and high load condition with all frequencies shown.

DISCUSSION

We found increases in EMG with force and frequency supporting the contention that high force, high repetition, and the combination of high force and high repetition appear to be central in the development of MSDs (Malchaire et al. 1996, Marras et al. 1993, Moore 2002). Preliminary results of this study indicate an increase in forearm muscle activity as the frequency of the task increases during the 30% of maximum grip condition yet these muscles appear to be unaffected by changes in load. Previous work found altered forearm muscle activity during static push and grip tasks (Di Domizio 2006). Simultaneous gripping and pushing are common in the workplace and detailed examination of the muscular response to loading and frequency parameters will provide further insights to potential injury mechanisms. The relative effects of force and frequency on muscle activity should be incorporated into upper extremity assessment tools.

REFERENCES

Di Domizio J. (2006) MSc. Thesis, York University. Toronto

Malchaire, J. B et al. (1996). Scand J Work Environ Health, 22(3), 176-181.

Marras, W. S. et al. (1993). Ergonomics, 36(4), 341-351.

Moore, J. S. (2002). Am J Indust Med, 41(5), 353-369.

Silverstein, B. A. et al. (1986). Br J Indust Med, 43(11), 779-784.

ACKNOWLEDGEMENTS

DETERMINATION OF CALCANEAL BONE STRAIN DURING SIMULATED WALKING WITH CADAVER LEGS

Lawrence D. Noble[1,2], Dong-gil Lee[1,2], Robb W. Colbrunn[1], Ton van den Bogert[1,2], Peter R. Cavanagh[1,2] and Brian L. Davis[1,2]

[1]Dept. of Biomedical Eng., Cleveland Clinic Foundation, Clev., Ohio, USA, noblel2@ccf.org
[2]Dept. of Chemical and Biomedical Eng., Cleveland State University, Cleveland., Ohio, USA

INTRODUCTION

A musculoskeletal simulator (MS) has been developed to enable fundamental research of cadaver joint loading. The MS can accurately simulate the biomechanics of human motion by including (i) a set of actuators that, when connected to selected tendons traversing a joint, can imitate muscular contractions, and (ii) a rotopod (a six degree of freedom robot similar to a hexapod, but additionally capable of 720 degrees of rotation) that can simulate contact between the specimen being tested and the environment. The benefit of these coupled systems is that they, for the first time, permit musculoskeletal simulations with joint loading approaching physiological levels at real-time or near real-time.

The purpose of this paper is to present calcaneal strain results from a NASA study that utilized the MS to measure tibial and calcaneal bone strain during simulated walking with cadaver feet. The objective of the study was to quantify the amount of strain that occurs under loading conditions designed to simulate walking. The results are expected to provide insight to whether current exercise countermeasure devices used by astronauts are capable of providing sufficient mechanical stimuli to bones.

METHODS AND PROCEDURES

The major mechanical components required to load the cadaver foot to simulate walking are shown in Figure 1.
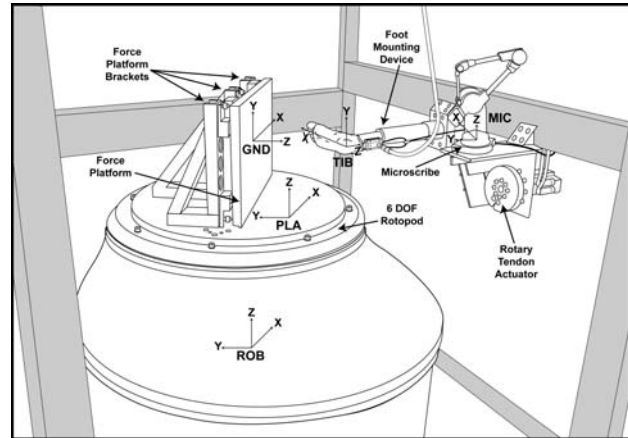
Figure 1. Simplified illustration of the Musculoskeletal Simulator configured for the foot study.

The rotopod was programmed to move the force platform through a trajectory that simulated the relative 3-dimensional motion measured in a gait lab by a live subject. Five (5) servomotor actuators were programmed to simulate the forces of five key muscles used during walking (triceps surae, tibialis posterior, tibialis anterior, flexor hallucis longus, and peroneus longus). The starting point for muscle force profiles were approximated from electromyogram (EMG) data (Perry, 1992) and linearly scaled based on muscle cross-sectional area. Software optimization was employed to adjust the muscle force profiles to achieve normal ground reaction forces before recording bone strain data. The stance phase was simulated to achieve full physiological loading of the cadaver foot over a timeframe of four (4) seconds to minimize inertial effects. One (1) stacked rectangular rosette (Vishay Part No.

C2A-06-031WW-120) was bonded to the lateral surface of the calcaneus following manufacturer's recommendation for bonding to bone.

RESULTS

Fifteen experiments were performed on six (6) cadaver specimens at full physiological loading of the Achilles tendon. The average maximum normal strain (Ep-tension) and average minimum normal strain (Eq-compression) were determined to be 535 and -1,914 microstrain, respectively, during the toe-off phase of stance. Figure 2 shows the typical calcaneal bone strain measured during simulated walking of a cadaver foot when plotted against Achilles tendon force (triceps surae muscle group).
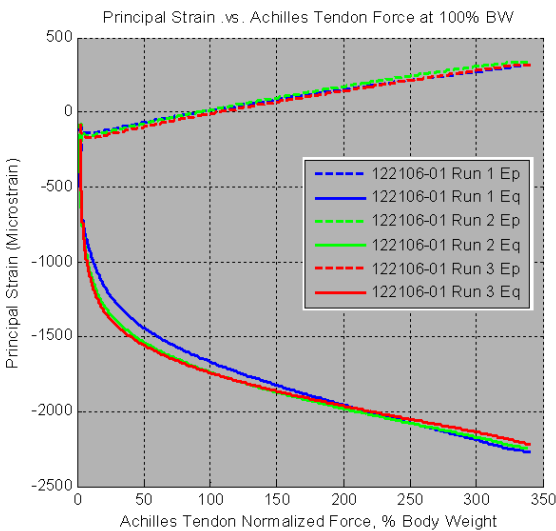
Figure 2. Calcaneal bone strain measured during three runs of the same specimen at 100% body weight (BW).

DISCUSSION

It has been shown that bone loss is associated with peak bone strain magnitudes less than 1,000 microstrain for cortical bone (Rubin and Lanyon, 1985). As seen in Figure 2, the Ep for this specimen was determined to be

approximately 300 microstrains and Eq was 2,300 microstrains under the maximum Achilles loading condition expected for walking (approximately 340 %BW). From these results we can state the following:

- The minimum Achilles tendon force required to achieve healthy bone strain (> 1000 microstrain) is 20 %BW
- Exercise regimens should be specified at Achilles tendon forces above 50 %BW to ensure predictable response, since the strain drops rapidly under this levels
- Good repeatability in results were observed between experiments of the same specimen using the MS
- Full-physiological loading of the Achilles tendon was achieved with the MS

SUMMARY

The cadaver test results from simulated walking show that a minimum Achilles tendon force of 20 %BW is necessary to stimulate the calcaneus to maintain healthy bone homeostasis.

REFERENCES

Perry J (1992). *Gait Analysis – Normal and Pathological Function.* New Jersey, Slack Incorporated.

Rubin, CT and Lanyon, LE (1985), *Regulation of Bone Mass by Mechanical Strain Magnitude*, Calcif. Tissue Int., 37:411-417

ACKNOWLEDGEMENTS

REFINEMENTS OF MOMENT-BASED COST FUNCTIONS IMPROVE PREDICTION OF EXPERIMENTAL MOMENT PROFILES IN CYCLING

Herman van Werkhoven[1*], H. Joseph Sommer III[2], and Philip E. Martin[1]

[1]Department of Kinesiology and [2]Department of Mechanical and Nuclear Engineering,
Penn State University, University Park, PA, USA, [*]hxv114@psu.edu

INTRODUCTION

Many cycling simulations (e.g., Gonzalez & Hull, 1989; Kautz & Hull, 1995) have employed joint moment-based computer models. A common cost function in simulations is based on the sum of squares of ankle, knee, and hip moments (e.g., Kautz & Hull, 1995; Redfield & Hull, 1986). In its simplest form absolute joint moments are used with equal weighting of concentric and eccentric contributions and equal contributions of the three joints. Potential refinements include using net joint moments expressed relative to maximum flexion and extension moment capacities, representing eccentric effort as some fraction of concentric effort, and weighting contributions from the ankle, knee, and hip differently (e.g., Kautz (1992) doubled the relative cost of the knee in cycling simulations). Our purpose was to evaluate the effect of these three refinements on the accuracy of predicting experimentally-derived lower extremity moments for 250 W cycling at 90 rpm. We predicted each of these refinements would result in more accurate lower extremity moment profiles.

METHODS

The leg-bicycle system was modeled as a planar five bar-linkage for each leg. The three degree of freedom (DOF) model was reduced to a one DOF system by constraining the ankle motion to follow experimentally collected data. The problem was formulated using a dynamic forward optimization framework that minimized a given cost function for the system task and constraints. Joint moments were parameterized using 12 discrete nodes; values between nodes were calculated through interpolation. The optimization problem was solved using a standard non-linear optimization routine. Four cost functions were used:

CF1: $\int_0^{t_f} \left(M_h^2 + M_k^2 + M_a^2 \right) dt$

CF1 used absolute moment amplitudes, provided no distinction between concentric and eccentric contributions, and equally weighted effort at the hip, knee, and ankle. It served as the nominal condition to which other cost functions were compared.

CF2: $\int_0^{t_f} \left(\% M_h^2 + \% M_k^2 + \% M_a^2 \right) dt$

CF2 expressed moments as a percentage of maximum isometric moment capacity.

CF3: $\int_0^{t_f} \left(M_h^{*2} + M_k^{*2} + M_a^{*2} \right) dt$

CF3 weighted eccentric contributions at 1/3 those of concentric contributions.

CF4: $\int_0^{t_f} \left(M_h^2 + 2M_k^2 + M_a^2 \right) dt$

CF4 doubled the importance of knee contributions as suggested by Kautz (1992). A final model (ALL) incorporated all three modifications to examine their collective effect. Optimized joint moment histories for all cost functions were compared to experimental cycling joint moments from Kautz and Hull (1995). Root mean square error (RMSE) between experimental and simulated results were calculated for each

cost function at each joint and averaged across joints.

RESULTS

ALL matched experimental hip joint moment most accurately, although each of the cost functions underestimated maximum hip extension moments (Figure 1a). CF2 predicted experimental knee joint moment most accurately (Figure 1b). Each of the other cost functions underestimated the knee extensor moment. The ankle moment was simulated effectively by all cost functions (Figure 1c), but was matched most closely by ALL. The mean RMSE between experimental results and simulation outputs using individual cost functions was the lowest for CF2, followed by CF4, CF3 and CF1 (Table 1). The difference between CF3 and CF1, however, was negligible. ALL showed the biggest reduction in RMSE.

DISCUSSION

A moment-based cost function expressing moments relative to maximum capabilities (CF2); which recognizes that moment generating capacity is not equal across the ankle, knee, and hip; improved prediction of experimental moment profiles substantially relative to the nominal case (CF1). Increasing the importance of the knee moment (CF4) made the second largest improvement in prediction of experimental profiles. This result suggests the relative importance of the knee musculature during the cycling task. Reducing the importance of eccentric contributions (CF3) had little effect on model predictive ability. This is presumably linked to the limited eccentric effort reflected in the cycling task. Overall, results indicate more physiologically sound cost functions improve the accuracy of prediction of experimental results.
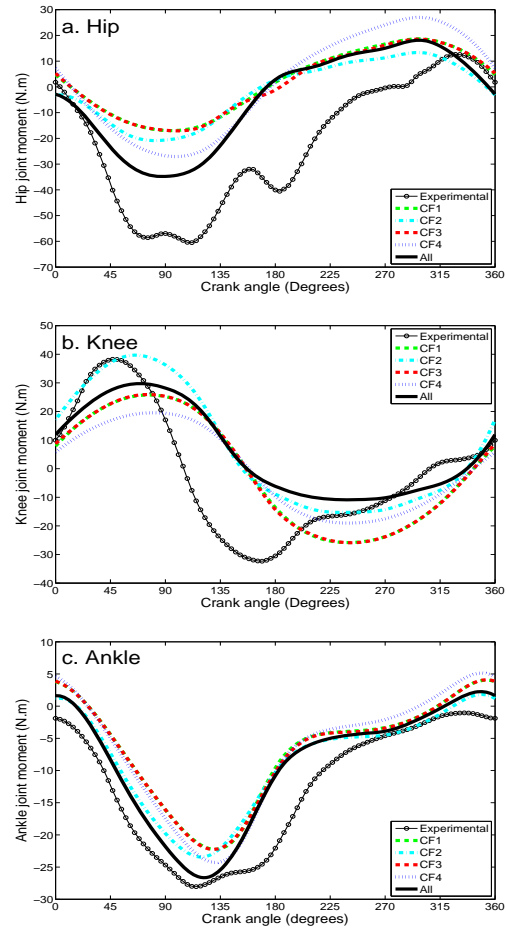
Figure 1. Experimental and simulated joint moments at the hip (a), knee (b), and ankle (c).

	CF1	CF2	CF3	CF4	ALL
RMSE	**17.3**	**16.1**	**17.1**	**16.5**	**14.3**
% change	-	6.7%	1.1%	4.6%	17.3%

Table 1. Mean RMSE across all joints for different cost functions and percent change relative to original cost function (CF1).

REFERENCES

Gonzalez, H and Hull, ML (1989). *J of Biomechanics,* 22:1151-1161.

Kautz, SA (1992). *Ph.D. thesis, Biomedical Engineering Group, UC Davis.*

Kautz, SA and Hull, ML (1995). *J of Biomechanics,* 28:1391-1401.

Redfield, R and Hull, ML (1986). *J Biomechanics*, 19:523-540.

MEASUREMENT OF DYNAMIC MUSCLE FUNCTION VIA ELECTRICAL STIMULATION SYNCHRONIZED TO THE GAIT CYCLE

Antonio Hernández and Darryl G. Thelen

Departments of Mechanical and Biomedical Engineering, University of Wisconsin-Madison
ahernandez2@wisc.edu, URL: http://www.engr.wisc.edu/groups/nmbl/

INTRODUCTION

An understanding of dynamic muscle function is highly relevant to the diagnosis and treatment of gait disorders. However, using standard gait analysis techniques to discern muscle function is challenging due to muscle redundancy and inter-segmental dynamics (Zajac et al., 2002). Dynamic simulation models account for these complexities, but require a number of assumptions that are not fully validated (Piazza, 2006). A couple of recent studies have introduced the use of electrical stimulation to directly measure dynamic muscle function (Hernández et al., 2007; Stewart et al., 2007). The objective of this study was to empirically characterize rectus femoris (RF) function before and after toe-off by synchronizing stimulation pulses to the gait cycle. We tested the hypothesis that RF would act to induce increases in both hip flexion and knee extension.

METHODS AND PROCEDURES

Subjects performed 60-second walking trials on a treadmill at self-selected speeds. Real-time monitoring of heel contact and toe-off (with foot switches) was used to control when a 90 ms pulse train (33 Hz) was delivered to the RF via surface electrodes. The following procedure was used to ensure that subjects could not predict when stimulation would occur: five non-stimulated strides were first allowed for the subject to reach a steady-state pattern; stimulation was then randomly introduced to the RF at either 50 or 60% of the gait cycle during one of the following five strides. Whole body kinematics (100 Hz) and lower extremity EMG activities (2000 Hz) were synchronously recorded throughout. Inverse kinematics was used to compute hip and knee angles, and EMG was used to identify the onset of stimulation.
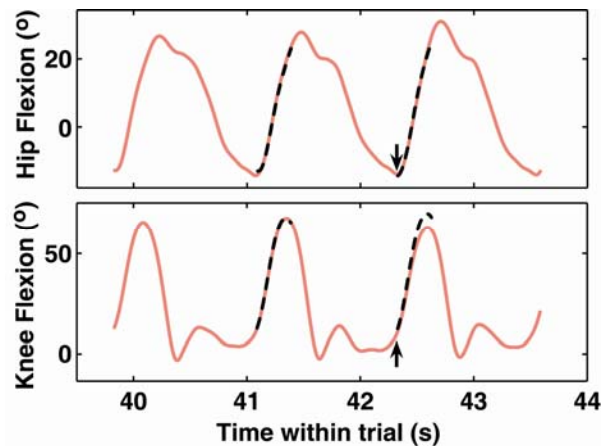
Figure 1. Measured (solid) and predicted (dotted) flexion angle curves for RF stimulation delivered at 50% of the gait cycle. Arrows indicate the stimulation time.

A linear periodic prediction model of the form $\theta(t+\tau) = \alpha + \beta\,\theta(t)$ was used to predict hip and knee flexion based on measured angles from the previous stride. In this model, τ represents the stride period, while α and β account for slight offset and drift from stride to stride. Model parameters were first identified using data from the two strides preceding the stimulus. We then used the model to predict the hip and knee flexion angles expected during a 300 ms window after the stimulus was delivered (Fig. 1). The maximum deviations of measured angles relative to predicted values were used to identify the stimulation-induced movement.

RESULTS

The knee flexed significantly less in both subjects when RF stimulation was delivered at 50% of the gait cycle (start of double support) than when it was delivered at 60% of the gait cycle (approximately toe-off, Fig. 2). The effects of RF stimulation on hip flexion were substantially smaller in both cases.
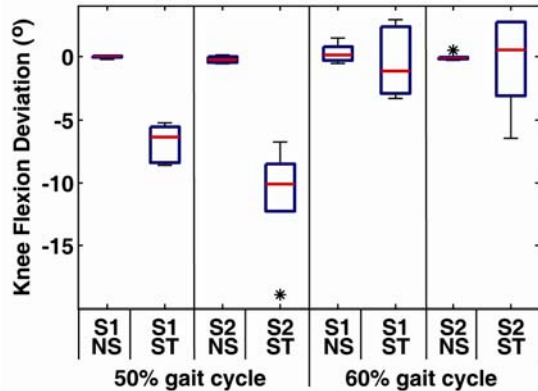
Figure 2. Knee flexion deviations by subject. S1=subject 1, S2=subject 2, ST= stimulation trials, NS = non-stimulated trials. Boxes summarize 6 observations per subject and represent upper and lower quartiles, with the medians indicated by central lines. Whiskers show data limits and asterisks denote outliers.

DISCUSSION

We have introduced a well controlled experimental protocol for measuring dynamic muscle function during walking. We used foot switches to time the stimulation to specific phases of the gait cycle. Similar timing could be achieved via real time monitoring of ground reactions on an instrumented treadmill. Such an approach would provide the additional advantage that perturbations to ground reactions could also be used to characterize the effects of stimulation on center of mass movement.

A key component of our approach is the linear periodic prediction model which is used to delineate the perturbation to movement induced by stimulation. During unperturbed walking, we found that the model was capable of accurately predicting joint angles one stride ahead, with rms errors typically less than 1 deg. Predicting joint angles two strides ahead resulted in slightly larger errors, which is reflected in the larger variability of our angle deviations (Fig. 2). Nevertheless, by delivering the stimulus to multiple strides, key patterns emerge by which to empirically characterize dynamic muscle function.

Our data clearly show the effects of RF activity on knee motion. In particular, an average reduction of 5 to 10 deg of knee flexion during swing was obtained by stimulating RF for 90 ms at the start of double support (50% of the gait cycle). Similar effects were not observed if the same stimulus was introduced at the start of swing. This result is consistent with the idea that muscle actions during double support affect the toe-off conditions, and thus ultimately determine the amount of knee flexion present (Piazza and Delp, 1996; Goldberg et al., 2003). Such empirical validation is important for validating model predictions, and ultimately for establishing a scientific basis for treating gait disorders.

REFERENCES

Goldberg SR et al. (2003). *J Biomech,* 36:1111-6.
Hernández et al. (2007) *JBiomech,* 41:137-144.
Piazza SJ (2006). *J Neuroeng Rehabil,* 3:5.
Piazza SJ and Delp SL (1996). *J Biomech,* 29:723-733.
Stewart C et al. (2007) *Gait Posture* 26:482-8.
Zajac et al. (2002) *Gait Posture* 16:215-232.

LATERAL REACHING FROM FIXED LADDERS

Justin Young[1], Hogene Kim[2], Chuck Woolley[1], Tom Armstrong[1], James Ashton-Miller[2]

[1] Department of Industrial & Operations Engineering, [2] Department of Mechanical Engineering,
University of Michigan, Ann Arbor, Michigan, USA, jgy@umich.edu
URL: http://www.engin.umich.edu/dept/ioe/C4E/index.html

INTRODUCTION

The incidence rate of injuries among ladder users is very high, and though reaching laterally from a ladder is a common activity, it hasn't been studied thoroughly. Some studies have explored lateral reaching on stepladders (Clift and Navarro, 2002; Juptner, 1976) where the ladder may become unstable, however they do not address fixed ladders or the forces applied to the hands. This aim of this study is to quantify the forces exerted by workers on fixed ladders as they perform a lateral reaching task.

METHODS AND PROCEDURES

Twelve healthy subjects (6 males, 6 females) were recruited for this study. Their mean (± SD) age, height, weight, and arm span was 21±2 years, 172±11 cm, 625.2±139.2 N and 150±14 cm respectively. While standing with both feet on the ladder, subjects were instructed to reach to their left and touch a target that was one full arm span away from the centerline of the ladder. Subjects then returned back to the ladder after a short pause. Two lateral reaching exercises (holding the left rail or holding the rung) were performed on two fixed ladder orientations (oriented vertically or pitched 10 degrees forward from vertical). There were three repetitions of each treatment. Orthogonal forces on the rungs or rail were recorded over the duration of the reach/return exercises. For data analysis purposes, the duration of a reach exercise was defined as the point when a left-lateral force was positive. Forces were normalized by each subject's bodyweight, and sampled evenly over the duration of the reach exercise.

RESULTS

Peak resultant forces during reach exercises were between 27 and 34 percent of body-weight, with rail forces being higher than rungs and the vertical ladder force higher than on the tilted (repeated measures ANOVA, $p<0.05$).
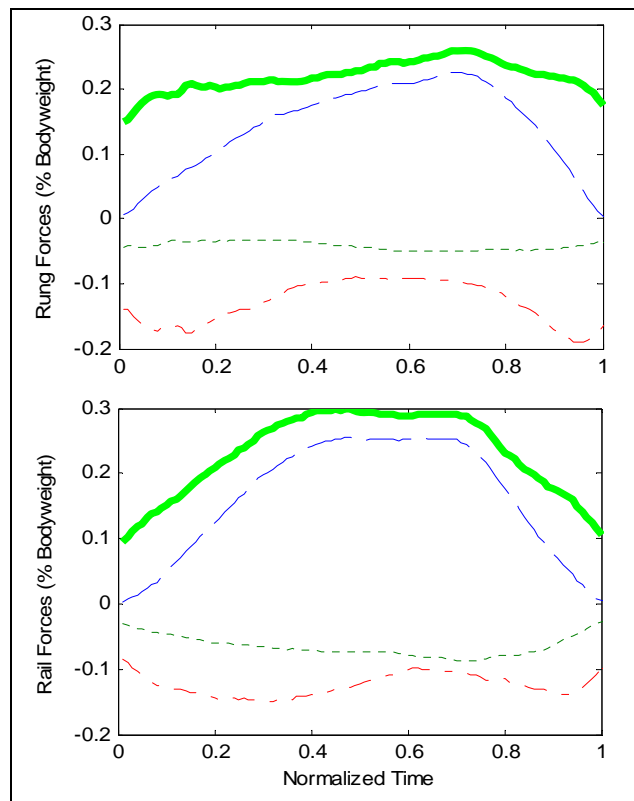
Figure 1. Vertical ladder: Mean hand force (% bodyweight) applied to the ladder rung (above) and ladder rail (below) during a reach/return exercise. See legend (Figure 3).

Component forces were dominated by lateral forces (x), but on the vertical rail, in/out (z) forces were larger during the initial reach and the return phase of the exercise. This was not the case for the tilted ladder.
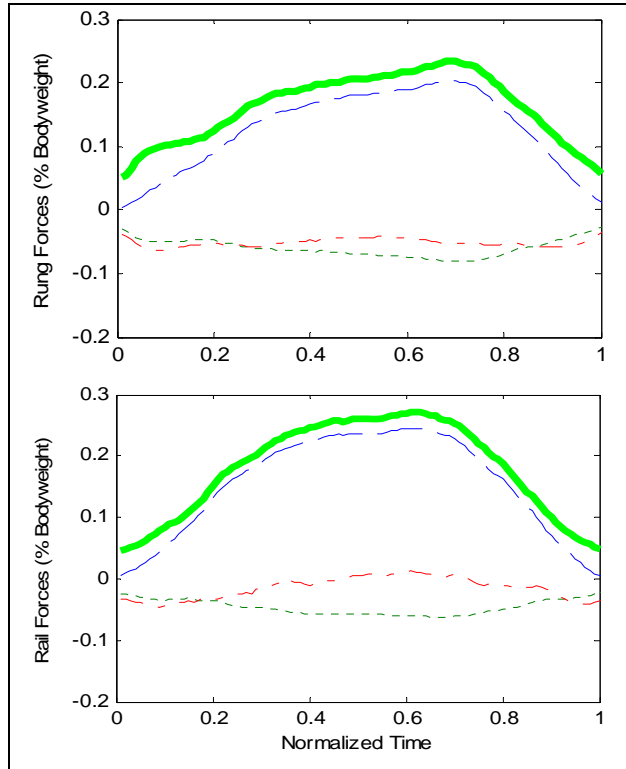
Figure 2. Ladder tilted 10º: Mean hand force (% bodyweight) applied to the ladder rung (above) and ladder rail (below) during a reach/return exercise. See legend (Figure 3).
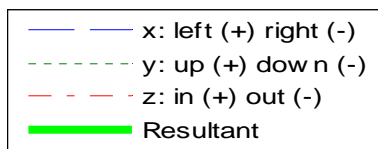
Figure 3. Legend: Resultant force is the thick line and component forces are dashed lines.

DISCUSSION

These results show a significant amount of force is required to perform a reach one arm span from the center of the ladder. Holding the rails may have resulted in greater force by allowing the body's center of mass to move more laterally. These reach exercises were slow, mostly quasistatic, and if the subject were to increase speed, we would see larger forces on the hand. If the ladder is slippery, the required reaching force may exceed the grasp capability of the hand, or the required friction for the feet to resist lateral load.

On vertical ladders we see a difference in the component forces as compared to the tilted ladder. On a vertical ladder, the body's center of mass is outside the vertical plane. When reaching we see the subject exert a large inward force pulling themselves toward the ladder at the beginning and ends of the reach task. On tilted ladders, the subject can balance their center of mass over their feet and use minimal inward force when reaching.

This study may be useful in predicting the effort a worker will have to exert while performing a lateral reach task such as painting. Fixed ladders are also a good analogue for climbing on fixed equipment such as trucks or racks. In future studies we will increase sample sizes, and explore the effects of reaching with tools, difficulty of the task requiring the reach, and the effects of aging. We may also examine friction on the rungs and torques at the base of the ladder.

REFERENCES

Clift L & Navarro T (2002). *Ergonomics evaluation into the safety of stepladders: User profile and dynamic testing - Phase 2*. London, Health and Safety Executive.
Juptner H. (1976). *Applied Ergonomics*. 7(4): 221-223.

ACKNOWLEDGEMENTS

IMPACT ATTENUATION THROUGH HUMAN BODY DURING HEEL-TOE RUNNING WITH DIFFERENT CUSHIONING SHOES

Yongkoo Lee, Martijn Klein Horsman and Benno M. Nigg

Human Performance Laboratory, Department of Kinesiology, University of Calgary, Calgary, AB, Canada, ylee@kin.ucalgary.ca, URL:http://www.kin.ucalgary.ca/hpl/

INTRODUCTION

During running, the human body experiences repeated impact forces between the foot and the ground (Cavanagh and Lafortune, 1980). The impact forces have been associated with injury, comfort and performance (Voloshin and Wosk, 1982, Nigg, 1997). Shoemakers have developed shoes with various cushioning properties. The impact is attenuated not only in the shoe but also throughout the body (Mercer et al., 2002). However, to the best of the authors' knowledge, the attenuation of the impact throughout the human body with different shoe cushioning has not been studied. Therefore, the purpose of this study was to determine the impact attenuation throughout the body for different shoe properties.

METHODS AND PROCEDURES

Three male expert heel-toe runners with a mean mass of 70 kg (SD 10kg) and a mean age of 27 years (SD $\pm$ 6 years) consented to participate in the study. All of the subjects were injury-free at the time of testing. Three (soft, medium and hard midsole) pairs of shoes were used in the study. The subjects ran heel-toe at a constant speed of 12 km/h $\pm$ 5% in the lab.

The impact from heel to neck was measured at a frequency of 2,400 Hz using 5 uniaxial accelerometers (ADXL 278, Analog Devices, mass < 3 g) , mounted on the outsole of the shoe (heel), tibia tuberosity (knee), greater trochanter (GT), lumbar (low back) and cervical vertebral column (neck).

To analyze the impact attenuation, a spectral analysis method suggested by Shorten and Winslow (1992) was adopted. With acceleration data, the transfer function from the spectral analysis was calculated for four sections through the body (heel-knee, knee-GT, GT-low back and low back-neck).

RESULTS

The impact attenuation through the body is presented in figure 1. Each graph shows the transfer function for each body section with respect to the frequency along with the impact propagation direction. Positive transfer function means impact gain during the propagation while negative means impact attenuation.

From heel to knee the impact was attenuated for input frequencies that were less than 8 Hz or greater than 20 Hz. In that region the solid line is lowest, while the dotted line is the lowest in the region of 8 to 20 Hz. For the section from knee to GT, most transfer functions are negative for frequencies greater than 5 Hz. For the section from GT to the low back, the transfer functions were negative when the frequency was greater than 7 Hz and the solid line remained the lowest until 27 Hz. From the low back to the neck impact enhanced since most transfer functions were positive for frequencies greater than 7 Hz.
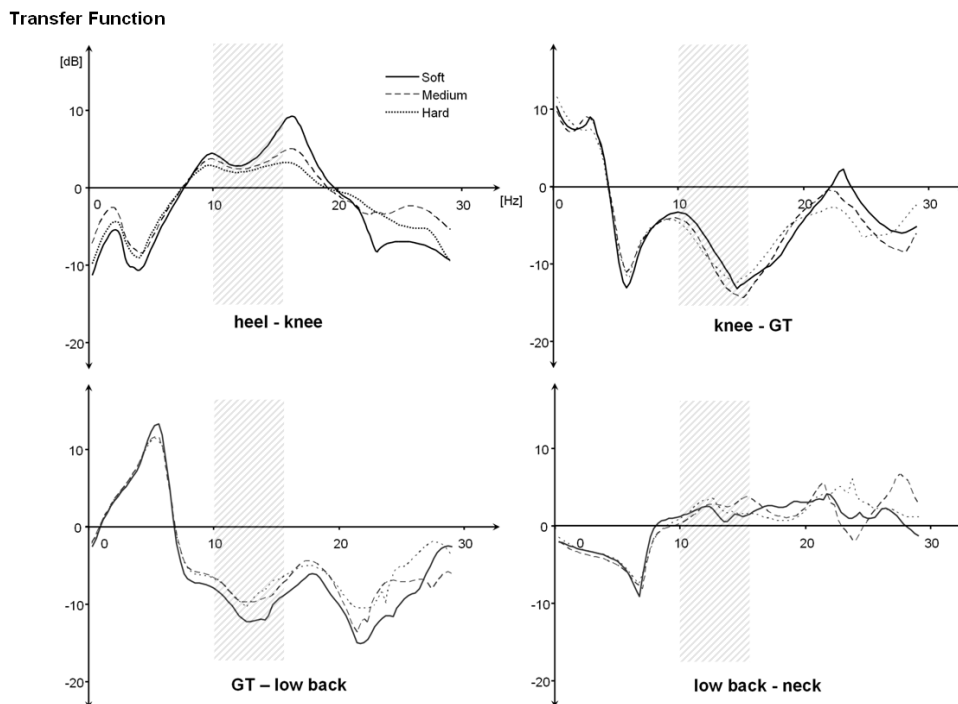
Figure 1. Transfer function of impact attenuation through the human body during running.

DISCUSSION

The ground reaction force during the heel-toe running has two peaks, the impact and the active peak. The impact peak reaches its peak about 20 to 50 ms after heel strike. This corresponds to a signal frequency of about 10-15 Hz (crosshatched regions in figure 1). In this frequency range, the impact increased from heel to knee and from low back to neck, while impact attenuations occurred from knee to GT and from GT to the low back. The increased impact from heel to knee and from low back to neck might be because the muscles within those sections could not reduce impact properly and/or because of resonance phenomena in these regions. Further investigations are needed to understand these speculations.

SUMMARY

In this study spectral analysis was carried out in order to observe impact attenuation through the human body during heel-toe running. The result that impact is not attenuated in certain frequency regions is surprising and needs further studies. It may be possible that such increases are related to the quality of cushioning provided through the shoe and/or running style.

REFERENCES

Cavanagh, PR and Lafortune, MA (1980). *J Biomech,* 13:397-406.
Mercer, JA et al. (2002). *Eur J Appl Physiol,* 87:403-408.
Nigg, BM (1997). *Curr Opin Ortho,* 8:43-47
Shorten, MR and Winslow, DS (1992). *Int J Sport Biomech,* 8:288-304.
Voloshin, AS and Wosk, J (1982). *J Biomech*, 15:21-27.

ACKNOWLEDGEMENTS

MOTOR UNIT DISCHARGE DURING STEADY ISOMETRIC CONTRACTIONS WITH THE DORSIFLEXOR MUSCLES

Mark Jesunathadas[1], Malgorzata Klass[2], Jacques Duchateau[2], and Roger M. Enoka[1]

[1]Department of Integrative Physiology, University of Colorado, Boulder, USA
[2]Laboratory of Applied Biology, Universite Libre de Bruxelles, Brussels, Belgium

Email: Mark.Jesunathadas@colorado.edu

INTRODUCTION

Recent studies have had success in simulating the discharge characteristics of the 180 motor units of the first dorsal interosseous muscle (FDI) during steady isometric contractions (Barry et al. 2007, Moritz et al. 2005). To assess the extent to which these relations generalize to other muscles, the purpose of this study was to compare the variation in activity of motor units in the tibialis anterior (TA) muscle with that observed in FDI during steady isometric contractions.

METHODS

The study involved two experimental protocols: measurement of motor unit discharge activity, and measurement of isometric force steadiness across a wide range of forces. The activity of 13 single motor units was quantified from 5 healthy adults (5 men; 31.4 ± 7.50 yrs) during brief contractions that spanned the range between the recruitment threshold of the motor unit to an average of 30.6 ± 17.4% of the maximal voluntary contraction (MVC) force above recruitment threshold.

The fluctuations in force during steady isometric contractions of the ankle dorsiflexor muscles were measured in 8 healthy adults (6 men; 30.4 ± 5.89 yrs). Subjects performed steady isometric contractions at target forces of 2, 5, 15, 30, 50, 70, 85, and 95% MVC. Visual feedback was given for the first half of the contraction and then removed. The steadiest 1 s portion of the force trace without visual feedback was used to quantify the coefficient of variation (CV) for force.

A model of motor unit recruitment and rate coding originally developed by Fuglevand et al. (1993) was modified to simulate the motor units of the TA. The model was modified to match the mechanical properties of motor units previously reported by Van Cutsem et al. (1997) and the discharge characteristics of motor units observed in the present study. The model included 250 motor units with an exponential distribution of motor unit peak twitch forces and contraction times. The upper limit of motor unit recruitment was at 80% MVC. The minimum discharge rate of motor units varied linearly as a function of recruitment threshold (range: 7.71 – 13.75 pps), whereas peak discharge rates were constant at 25 pps. The variability in motor unit discharge was 30% at recruitment and decreased rapidly to 10% as force increased above recruitment.

RESULTS AND DISCUSSION

The average recruitment threshold of the motor units was 36.5 ± 17.9% MVC (range: 18.7 – 67.6% MVC). Similar to the results for FDI, the minimal discharge rate of the units increased from 8.80 to 13.1 pps as a function

of recruitment threshold ($r^2 = 0.69$, $P < 0.01$). In contrast to the FDI, however, the peak discharge rates of motor units did not vary with recruitment threshold and were on average 24.4 ± 6.58 pps ($r^2 = 0.08$, $P = 0.73$). Furthermore, the average CV of interspike interval at recruitment was $20.2 \pm 12.1\%$ and rapidly decreased to $13.4 \pm 4.76\%$ as force increased above recruitment threshold.

Although the CV for force of the ankle dorsiflexors was less than that of the FDI at 2, 30, 50, 70, and 85% MVC ($P < 0.05$), the CV for force did decline with an increase in target force, as observed with the FDI. The CV for force was the greatest in the dorsiflexors at a target force of 2% MVC force ($2.73 \pm 1.73\%$) and decreased rapidly to $0.82 \pm 0.52\%$ at a target force of 15% MVC where it remained relatively constant at the higher target forces.

The computer model was only able to match the fluctuations in force observed experimentally at target forces of 2 and 5% MVC. At target forces of 15% MVC and above, the simulated CV for force was significantly greater than the values measured experimentally ($P < 0.01$).

SUMMARY AND CONCLUSIONS

The discharge characteristics of single motor units in TA and the fluctuations in force exerted by the dorsiflexor muscles were measured at a range of target forces and compared with those observed with the FDI. The results indicate that the fluctuations in force of the dorsiflexor muscles are lower than that of the FDI muscle. Furthermore, the computer simulation was not able to match the experimental fluctuations in force at higher target forces. Thus, it appears that the current model of motor unit recruitment and rate coding fails to characterize the discharge of motor units in the leg muscle during steady isometric contractions.

REFERENCES

Barrry, B.K. et al. (2007). *J Neurophysiol*, 97: 3206-3218.
Fuglevand, A.J. et al. (1993). *J Neurophysiol*, 70:2470-2488.
Moritz, C.T. et al. (2005). *J Neurophysiol*, 93: 2449-59.
Van Cutsem, M. et al. (1997). *Can J Appl Physiol*, 22:585-597.

ACKNOWLEDGMENTS
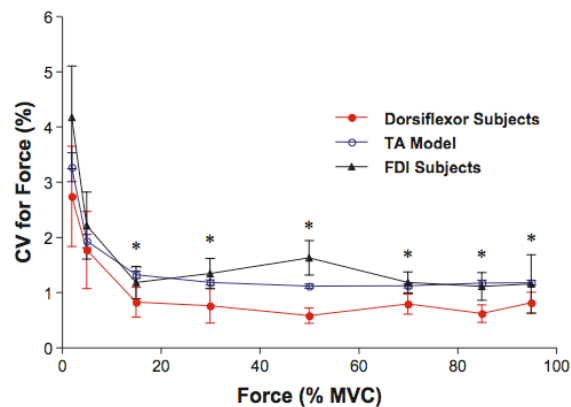
Figure 1. Relation between the experimental and simulated CVs for force across the operating range of the ankle dorsiflexor muscles and the FDI. *Significant differences between the experimental and simulated CVs for force of the ankle dorsiflexors ($P < 0.05$).

OVERHEAD GRASP CAPABILITY FOR TYPICAL LADDER HANDHOLDS

Justin Young[1], Michael Sackllah[1], Chuck Woolley[1], Tom Armstrong[1], James Ashton-Miller[2]

[1] Department of Industrial & Operations Engineering, [2] Department of Mechanical Engineering,
University of Michigan, Ann Arbor, Michigan, USA, jgy@umich.edu
URL: http://www.engin.umich.edu/dept/ioe/C4E/index.html

INTRODUCTION

Performance of the hand is central to safety during ladder climbing. According to the Bureau of Labor Statistics, more than 20,000 American workers are injured every year by falls from ladders (BLS 2005). Barnett and Poczynk (2000) defined three distinct phases after a ladder fall event has started: (I) A freefall phase that is a function of reaction time and the grasping movement; (II) The time it takes for the victim's muscle forces to increase to a maximum, (III) The interval when the victim decelerates to a stop. If the maximum coupling force that the victim's hand can exert on the ladder in the third phase is less than the force of the body's weight and inertia, then victim will fail to arrest the fall.

In trying to stop a fall from a ladder, an individual may try to hold onto either the vertical side rails or the horizontal rungs of the ladder. If the hands are on the side rails when the feet slip, friction will be produced between the hand and the rail which will act against the force of the falling body. If the rung is grasped, a power or hook grip will provide the friction plus mechanical interference to arrest the fall.   The aim of this study examined how much vertical force subjects could exert on overhead rails and rungs.

METHODS AND PROCEDURES

To achieve the aim of this study, twelve (6 male, 6 females) subjects stood on a weighted, height-adjustable platform which lowered at a constant 14.5 cm/sec. A weightlifter's dipping belt was used to secure the subject to the platform so that they could not flex their ankles or lift themselves off the platform. Three instrumented handles could be fixed overhead. Two vertically-oriented handles simulated typical ladder rails (a 1" diameter cylinder and a 2½"× 3/8" plate). The third handle was a 1" diameter horizontally-oriented cylinder that simulated a typical ladder rung.

The experiment consisted of a total of fifteen maximum strength trials: three grip strength tests and twelve overhead grasp strength tests. Grip strength was measured for both hands. Subjects were tested grasping each of the three handles using the dominant hand, and the also the horizontal rung in the non-dominant hand. There were three repetitions for each treatment. The order of the trials was randomized. Between each trial the subjects were given breaks of at least two minutes.

For each of the overhead grasp strength tests, the subject was instructed to exert their maximum strength capability and hold onto the handle as long as possible. Subjects were asked if they were ready and were then lowered at a steady rate until their hand decoupled from the overhead handle. The forces exerted on the handle were recorded. Data were analyzed using repeated measures ANOVA with $p < 0.05$ being significant.

Subjects were recruited to participate in this study. Their mean ($\pm$ SD) age, height, weight, and dominant hand grip strength was 21±2

years, 172±11 cm, 625.2±139.2 N and 426.3±123.5 N respectively. On average, males were 196 N heavier, 15 cm taller and had mean grip strengths 245 N greater than females.

RESULTS

Handle Type	Grasp Strength (N)	Grasp Strength / Body-weight	Grasp Strength / Grip Strength
Horizontal Rung	667.9 (237.0)	1.05 (0.20)	1.52 (0.23)
Vertical Rail	434.7 (121.3)	0.70 (0.11)	1.02 (0.17)
Vertical Plate	336.9 (146.3)	0.53 (0.13)	0.78 (0.22)

Table 1. Mean (SD) grasp strength results by handhold type (all subjects, dominant hand).
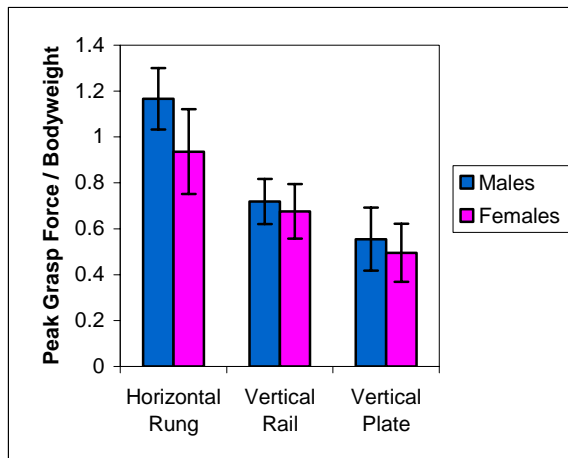
Figure 1. Mean (SD) grasp strength divided by the subject's bodyweight for each type of handhold, by gender.

The peak forces exerted on the three overhead handles (grasp strength) were significantly different (p<0.05): largest for the horizontal handle and smallest for the vertical plate (Table 1). Similar results were found when normalized by bodyweight and grip strength and when stratified by gender (Figure 1).

DISCUSSION

The aim of this research was to examine the total strength capability of the hand as it grasps an overhead handle of varying shape and orientation, similar to that found on industrial fixed ladders. It was shown that, on average, only males would be able to support their own bodyweight with one hand, and only when grasping a horizontal rung. For any other handle type, bodyweight exceeds the maximum grasp force. Females, on average, were not able to support their bodyweight with one hand for any of the handles. The grasp strength developed with the non-dominant hand was not significantly less than the dominant hand.

These results imply that only relatively strong persons, or relatively light persons would be able to arrest themselves with one hand if they fell while climbing a ladder, and only if they were holding a ladder rung. In the future we plan to increase group sizes and address the effect of heavy tool belts, advancing age and certain disease conditions. Other factors such as wearing gloves and different rail/rung materials and surfaces will be examined.

REFERENCES

Barnett, R and Poczynck, P (2000). *Safety Brief (Triodyne Inc.)* 16(4): 1-15.
BLS (2005). *Census of fatal occupational injuries summary 2004.* Washington, DC, US Bureau of Labor Statistics: 1-3.

ACKNOWLEDGEMENTS

EFFECTS OF LONG-DURATION SPACE FLIGHT ON TOE CLEARANCE DURING TREADMILL WALKING

Chris Miller [1], Brian Peters [1], Rachel Brady [1], Ajitkumar Mulavara [2],
Jason Richards [1], Matthew Hayat [2] and Jacob Bloomberg [3]

[1] Neurosciences Laboratory, Wyle Laboratories, Houston, TX; [2] Universities Space Research
Association, Houston, TX; [3] NASA Lyndon B. Johnson Space Center, Houston, TX, USA
E-mail: chris.miller-1@nasa.gov

INTRODUCTION

Upon returning from long-duration space flight, astronauts and cosmonauts must overcome physiologic and sensorimotor changes induced by prolonged exposure to microgravity as they readapt to a gravitational environment. Their compromised balance and coordination lead to an altered and more variable walking pattern (Bloomberg & Mulavara, 2003; McDonald, et al., 1996). Toe trajectory during the swing phase of locomotion has been identified as a precise motor control task (Karst, et al., 1999), thus providing an indication of the coordination of the lower limbs (Winter, 1992). Failure to achieve sufficient toe clearance may put the crew member at a greater risk of tripping and falling, especially if an emergency egress from the vehicle should be necessary upon landing. The purpose of this study was to determine the pre- to post-flight changes in toe clearance in crew members returning from long-duration missions and the recovery thereafter.

METHODS

Ten crew members (mean ± SD: 46.0 ± 5.6 yrs) from five missions (duration = 188 ± 6 days) aboard the International Space Station gave informed, written consent and participated in this study (part of a larger investigation examining the effects of long-duration space flight on the sensorimotor system). Data collection sessions were performed pre-flight (60-80 days before launch), and six times post-flight (R+, in days after landing): R+1, R+2, R+(3-4), R+(6-7), R+(11-30), and R+(168+).

Subjects wore lab-supplied shoes with footswitches (Motion Lab Systems, Baton Rouge, LA) affixed to soles beneath the heels and toes. The footswitch data (sampled at 1000 Hz) were used to determine heel strike and toe-off events. Retroreflective markers were affixed to landmarks on the subject to define the head, torso, pelvis and right leg segments. Specifically on the right shoe, markers were placed on the lateral aspect of the calcaneus, the lateral aspect of the 5th metatarsal head, and over the superior aspect of the navicular bone. A six-camera motion capture system (Motion Analysis, Santa Rosa, CA) recorded the three-dimensional positions of the markers at a sampling rate of 60 Hz. Toe position was tracked via a virtual marker, computed at a point near the distal tip of the 2nd toe, at the level of the 5th metatarsal marker (Miller, et al., 2007). The virtual marker indicated the shoe location that would most likely contact the walking surface during a stumble or trip.

For each session, subjects performed four 30-sec trials where they walked on a motorized treadmill (Gaitway, Kistler Instrument Corp., Amherst, NY) at 1.8 m/sec (4.0 mph) while performing a dynamic visual acuity task set at

a "far" target distance of 4.0 m (Peters & Bloomberg, 2005). Toe clearance (TCl) was computed for each stride (~30 strides per trial), relative to the virtual toe marker's height during a static trial recorded before the walking trials. Instead of mean and SD, the median and interquartile range (IQR) of TCl were computed for each trial due to skewness of the data (Begg, et al., 2007). A three-way ANOVA with random effects (subjects) was used to determine significant effects of session and trial on TCl median and IQR ($p < 0.05$). Twelve contrasts of the six post-flight sessions vs. pre-flight and six paired trial combinations were tested for significance with a Bonferroni-corrected p-value of 0.004.

RESULTS AND DISCUSSION

Median TCl showed a nearly significant session effect ($p = 0.052$), however the contrast analysis (Figure 1) indicates a trend of increased median TCl two to four days post-flight, followed by a recovery back to pre-flight values. Surprisingly, median TCl on R+1 was not different than pre-flight.
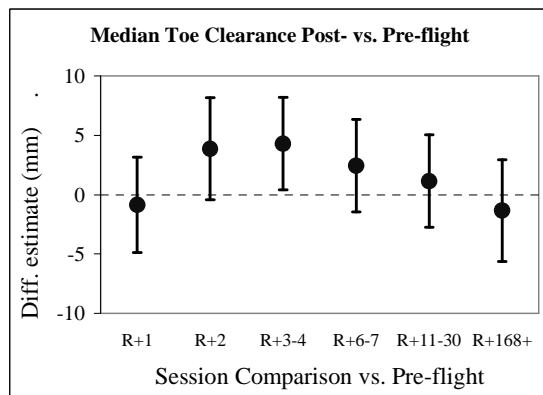
Figure 1. Median TCl difference contrast estimates (Mean ± 2SE) between post-flight sessions and pre-flight.

Median TCl was significantly affected by trial ($p < 0.001$). All paired comparisons were significant ($p < 0.001$), except for trial 3 vs. 4 ($p = 0.01$). Median TCl was greatest for trial 1, then decreased with successive trials.

TCl IQR was also affected by trial ($p < 0.01$), with trial 1 vs. 4 being the only significant paired comparison ($p = 0.002$). While the ANOVA showed that session was not a significant factor on IQR overall ($p = 0.14$), the contrast analysis revealed a significant increase of IQR one day post-flight compared to pre-flight ($p = 0.0039$).

SUMMARY

Crew members returning from long-duration spaceflight walk with an increased variability in toe clearance one day after landing, but return to pre-flight values by post-flight day two, thus reflecting a change in motor control. However from post-flight days two through four, crew members exhibit a slightly increased median toe clearance, possibly indicating that they are giving themselves a "margin for error" during readaptation to the gravity environment.

REFERENCES

Begg R., et al. (2007). *Gait Posture,* 25(2), 191-8.
Bloomberg J.J., Mulavara A.P. (2003). *IEEE Eng Med Biol Mag,* 22(2), 58-62.
Karst G.M., et al. (1999). *J Gerontol A Biol Sci Med Sci,* 54(7), M343-7.
McDonald P.V., et al. (1996). *Exp Brain Res,* 112(2), 325-34.
Miller C., et al. (2007). *Proceedings of ASB 2007*, #7.
Peters B.T., Bloomberg J.J. (2005). *Acta Otolaryngol,* 125(4), 353-7.
Winter D.A. (1992). *Phys Ther,* 72(1), 45-53.

ACKNOWLEDGEMENTS

THE EFFECT OF PARKINSON'S DISEASE ON THE RESPONSE TO A BACKWARDS PULL: CENTER OF PRESSURE

Molly A. McVey[1], Antonis P. Stylianou[1,2], Carl W. Luchies[1,2], Michael Haines[1,2], Kelly E. Lyons[3], Rajesh Pahwa[3]

[1]Department of Mechanical Engineering, The University of Kansas, Lawrence, KS, USA
luchies@ku.edu
[2]Landon Center on Aging, The University of Kansas Medical Center, Kansas City, KS, USA
[3]Parkinson's Disease and Movement Disorder Center, The University of Kansas Medical Center, Kansas City, KS, USA

INTRODUCTION

Postural instability is one of the most disabling symptoms of Parkinson's disease (PD) and often leads to falls. Falls can have severe physical, psychological, and economic impacts including fractures, fear of falling, and loss of independence (Bloem, Grimbergen et al. 2001). The response to a large balance perturbation often involves a step response to reconfigure the base of support, which must be done quickly and appropriately in order to prevent a fall. PD impairs the step response and subjects typically use shorter than normal steps, multiple anticipatory postural adjustments, have a longer step foot liftoff time, and are less consistent in the choice of stepping limb (Jacobs, Horak et al. 2005; Jacobs and Horak 2006). The goal of this study was to investigate the effect of low severity PD on the center of pressure movement during the step response to a backwards pull. The response was characterized in a group of PD participants at Hoehn & Yahr stage 2, with no signs of postural instability, and a group of age-range matched healthy controls.

METHODS AND PROCEDURES

Participants: Ten subjects with idiopathic Parkinson's disease and 10 healthy controls (PD: age range 48-77, mean age 63.2 ± 8.9 years; HC: age range 48-79, mean age 67.2 ± 10.9 years) were tested. All participants gave informed consent for the study as approved by the Institutional Review Board at the University of Kansas Medical Center.

Task: Each participant stood in an upright and relaxed position, with arms crossed at the chest. A rigid waist harness was attached to a cable and weight-drop mechanism, which when released, delivered a posterior waist pull to the participant. The participant was asked to respond naturally to the disturbance. The weight-drop mechanism was loaded with a weight equal to 20% of body weight and pulled the participant backwards a distance equal to 8.7% of waist height, corresponding to a 5° equivalent disturbance angle (Luchies, Alexander et al. 1994).

Data Collection: Foot-floor reaction forces were measured by three force plates (Advanced Medical Technology, Inc.; Watertown, MA) sampled at 1080 Hz.

Data Analysis: The whole body center of pressure (COP) was calculated for the time period of disturbance onset to liftoff of the first step, and divided into two stages. Stage one was defined as disturbance onset to weight shift onset. Stage two was defined as weight shift onset to step foot liftoff. Weight shift onset was defined as the last change in the location of the COP in the medial-lateral

(ML) direction prior to liftoff. The anterior-posterior (AP) and ML distance traveled and the duration of each stage were calculated. Statistical analysis was performed with SPSS (SPSS, Inc., Chicago, IL, USA).T-tests were used to assess group differences with p-values <0.05 considered statistically significant.

RESULTS AND DISCUSSION

Group differences were evident in the COP patterns in response to the backwards pull. In the first stage, the PD group, compared to controls, took longer to shift their weight and the COP traveled further backwards. In the second stage, the duration of the stage and the COP distance traveled were similar between groups. The results suggest that the increase in liftoff time observed in PD may be due to a delay in weight shift to the stance foot in preparation for a step in response to an external perturbation.

	HC	PD	t-test
AP distance S1 (mm)	-3.81 (36.10)	-54.97 (44.12)	.024*
ML distance S1 (mm)	12.45 (11.79)	19.40 (38.72)	.635
Duration of S1 (ms)	198.75 (73.39)	468.53 (275.54)	.018*
AP distance S1 (mm)	-25.47 (17.86)	-9.95 (22.50)	.149
ML distance S1 (mm)	-140.91 (18.43)	-142.26 (56.53)	.950
Duration of S2 (ms)	146.86 (40.16)	154.19 (38.58)	.715

Table 1. COP parameters; S1= disturbance onset to weight shift onset, S2= weight shift onset to liftoff; *indicates p < .05

SUMMARY

These results suggest that PD impairs the ability to respond quickly and effectively to a backwards pull. PD increased the time required for weight shift and the posterior distance traveled by the COP prior to weight shift onset. This altered response may represent an impairment that reduces the effectiveness of the step response to a postural disturbance for PD patients.

ACKNOWLEDGEMENTS

Figure 1. Whole body COP in HC and PD.

REFERENCES

Bloem, B. R., Y. A. Grimbergen, et al. (2001). *J Neurol* **248**(11): 950-8.
Jacobs, J. V. and F. B. Horak (2006). *Neuroscience* **141**(2): 999-1009.
Jacobs, J. V., F. B. Horak, et al. (2005). *Gait and Posture* **21**(S1): S94-S95.
Luchies, C. W., N. B. Alexander, et al. (1994). *J Am Geriatr Soc* **42**(5): 506-12.

LEARNING EFFECTS OF SIMULTANEOUS GRIP AND SHOULDER EXERTION ON MUSCLE ACTIVITY

Joanne N. Hodder and Peter J. Keir

McMaster Occupational Biomechanics Laboratory, Department of Kinesiology, McMaster University, Hamilton, ON, Canada, hodderjn@mcmaster.ca , pjkeir@mcmaster.ca.

INTRODUCTION

Research has suggested that the performance of a combination of physical and cognitive tasks have an effect of muscle activation patterns. In a study by MacDonell and Keir (2005), an interference effect was found during the combination of simultaneous grip, shoulder exertion and cognitive tasks. Changes in deltoid muscle activity were observed with the combination of tasks, indicating complex co-activation patterns. Au & Keir (2007) also demonstrated interference in muscle activation patterns with combined submaximal tasks.

Recent observations from the McMaster Occupational Biomechanics laboratory questioned whether maintenance of grip force via visual feedback represents a cognitive task in itself. If so, repetition of the task should reduce this effect.

The purpose of this study was to further examine the interference effect of gripping during shoulder exertions. Repeated trials were used to examine whether there was a learning effect and thus indicate a cognitive component to grip maintenance.

METHODS AND PROCEDURES

Twelve healthy, right hand dominant males (182.5±10.5 cm, 72.2±6.7 kg) participated in this study. Participant arm length was collected to calculate shoulder moment. The muscle activities of eight right shoulder muscles were collected via bipolar surface electromyography (EMG) (Bortec Biomedical Ltd., AB, Canada). The muscles collected were the anterior (AD), medial (MD) and posterior (PD) deltoids, trapezius (TR), infraspinatus (INF), teres major (TM), latissimus dorsi (LD) and biceps brachii (BB). EMG was normalized to maximum voluntary excitations after removing bias collected during a quiet trial. Both EMG and grip force were sampled at 2048 Hz in a custom made LabView program (National Instruments, TX, USA).

The protocol consisted of 21 trials in total. During the first three trials, participants were required to maintain 90° shoulder abduction in the scapular plane for 10s while holding a grip dynamometer, without any constraint on grip. Participants than performed 15 trials in the same posture, however with a simultaneous 30% maximum grip for 10s. During these trials, visual feedback was provided with a ± 3% window. Finally, three trials without constraint on grip were conducted again.

RESULTS

Preliminary results suggest that there is a redistribution of muscle activity within the shoulder girdle musculature with gripping. With gripping in this task, the anterior deltoid activity decreased while the posterior deltoid increased with a simultaneous grip (Figure 1).

A learning effect due to repetition was not apparent after 15 trials in grip force or muscle activity, thus only the 15th trial is shown in

Figure 2. Interestingly, it appears that training did not occur in 15 trials but some of the subjects who had prior experience in maintaining grip force had lower variation trial-to-trial and in the standard deviation of each trial.
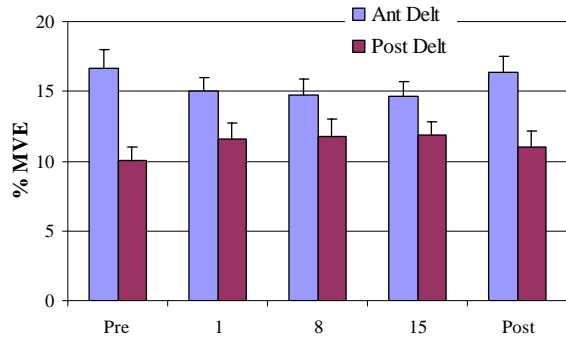
Figure 1. Mean (SD) anterior and posterior deltoid activation for pre and post trials, trial 1, 8, 15.
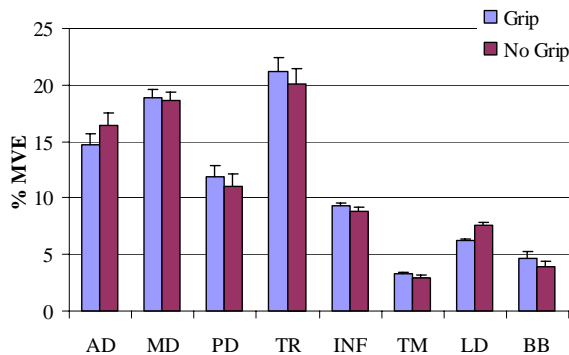
Figure 2. Mean muscle activity (%MVE with SD) for grip and no grip conditions.

The mean grip force during the no grip trials was $2.1 \pm 0.4\%$ and $2.2 \pm 0.9\%$, for the pre- and post training trials, respectively. For the 30% target grip force trials, the mean value was $27.9 \pm 1.9\%$, which was within the allowable target range.

Participants who had no previous experience maintaining a 30% grip force had larger variance in grip (standard deviation of 2.3% versus 1.4 %).

DISCUSSION

Preliminary results of this study do not readily suggest a learning effect during repeated simultaneous grip and shoulder exertions. There were no apparent changes in mean muscle activation, mean grip and standard deviations from 1st to 15th gripping trials when all participants were considered.

Differences were observed between participants with previous experience in maintaining 30% grip and novice participants. Greater variance in grip maintenance was demonstrated for novice participants, suggesting more difficulty with the task. As well, further investigation of muscle activation patterns based on subject experience seem to indicate that novice participants have greater overall amplitude during gripping conditions. Thus there may be a learning effect that requires more than the 15 repetitions used in the current study, however, some participants may likely experience fatigue if the session was lengthened.

There was some evidence of a learning effect from the alterations in both grip and muscle activation patterns seen with the experience of the participants but not in the protocol per se.

REFERENCES

Au and Keir (2007). *J Electromyogr Kinesiol,* 17(5): 578-586.
MacDonell and Keir (2005). *Ergonomics,* 48(15): 1749-1769.

ACKNOWLEDGEMENTS

EFFECTS OF GENDER ON KINEMATICS OF THE HIP, KNEE, AND ANKLE IN UNANTICIPATED DROPLANDINGS OF ADOLESCENT SOCCER PLAYERS

Michelle B. Sabick, Seth M. Kuhlman, Ronald P. Pfeiffer, Benjamin Cooper, David Clark, and Kevin G. Shea

Center for Orthopaedic & Biomechanics Research, Boise State University, Boise, Idaho, USA
URL: http://coen.boisestate.edu/cobr

INTRODUCTION

Female athletes participating in sports requiring highly dynamic movements are at four to six times greater risk of knee injury than their male counterparts (Ford, 2005). Several theories based on differences between genders in joint kinematics, hormones, and other variables have been offered to explain the disparity. For example, Ford *et al* (2003) found that high school aged female athletes displayed greater knee valgus angles than males during landing. However, few studies have tested adolescent subjects to establish whether kinematic differences also exist at a younger age, especially in unanticipated paradigms that replicate real game situations.

This purpose of this study was to identify kinematic differences between male and female adolescent soccer players that might be precursors of knee injuries. Our hypothesis was that male and female adolescent soccer players would display comparable lower extremity kinematics due to their similar skeletal structures.

METHODS

A cohort of 6 male (age = 10.7 years, height = 1.46 m, weight = 343 N) and 8 female (age = 10.3 years, height = 1.47 m, weight = 351 N) youth soccer players were recruited to participate. Each subject dropped 30.5 cm from an overhead bar landing on his or her dominant leg. Prior to landing, a set of lights directed the subject to complete one of three tasks in random order: a forward run to the center (C), a side-step cut of 30° (SS), or a cross-over cut of 30° (XO, Figure 1). Subjects were instructed to give maximum effort on all tasks. Kinematic data for the landing leg was collected during the trials at 250 Hz using a six-camera motion capture system. Ground reaction forces acting on the landing leg were collected at 1250 Hz.
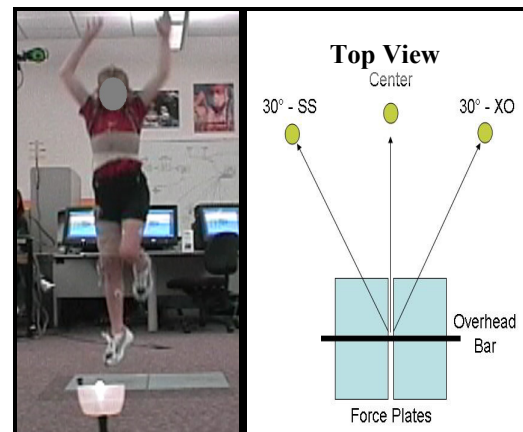
Figure 1. Subject preparing for landing (left), and diagram of landing tasks (right).

Hip, knee, and ankle kinematics were analyzed from 300 ms before initial ground contact to 300 ms after contact. Kinematic data from the instant that peak ground reaction force (pGRF) occurred were compared between genders. A 2x3 (sex x joint) Factorial Analysis of Variance was conducted within each task and each plane of motion: sagittal, frontal, and transverse. The α-level was set at 0.05 for all tests.

RESULTS

Significant differences were found between male and female subjects in frontal plane kinematics at pGRF in the center run (p = 0.037) and SS cut (p = 0.014) tasks (Table 2). In both cases, the male subjects tended to display greater hip abduction, knee varus, and ankle inversion angles. The most striking difference between groups was that male subjects landed with hips abducted approximately 7-11° more than the females across all three tasks (Table 1). Differences at the knee and ankle were much more subtle.

No significant differences between groups were detected in the sagittal plane or transverse plane kinematic variables.

Table 1: Joint angles at pGRF

		Sagittal Plane		Frontal Plane		Transverse Plane	
		Male	Female	Male	Female	Male	Female
Center	Hip	-17 (13)	-16 (8)	10 (7)	3 (5)	3 (11)	8 (14)
	Knee	31 (12)	28 (11)	-1 (4)	2 (5)	-5 (2)	-5 (20)
	Ankle	-21 (6)	-22 (10)	2 (5)	0 (6)	3 (4)	5 (10)
XO	Hip	-18 (13)	-17 (10)	10 (6)	2 (6)	4 (9)	7 (14)
	Knee	33 (11)	28 (6)	2 (4)	1 (8)	-6 (17)	-5 (17)
	Ankle	-21 (9)	-20 (7)	1 (5)	2 (7)	1 (5)	4 (10)
SS	Hip	-17 (13)	-13 (19)	12 (7)	1 (8)	4 (10)	5 (15)
	Knee	33 (11)	28 (21)	0 (3)	1 (6)	-5 (5)	-7 (12)
	Ankle	-21 (9)	-10 (14)	1 (4)	-3 (3)	0 (4)	3 (10)

Table 2: Results of the factorial analysis of variance

Sagittal Plane		Frontal Plane		Transverse Plane	
P-value	Power	P-value	Power	P-value	Power
Center Task					
0.903	0.064	0.037 *	0.630	0.076	0.512
Crossover Task					
0.651	0.115	0.169	0.363	0.961	0.056
Sidestep Task					
0.412	0.195	0.014 *	0.762	0.909	0.063

* P < 0.05

DISCUSSION

This is the first study to look at an unanticipated task in middle school aged subjects. For the majority of the kinematic variables analyzed, no significant differences were observed. This was not unexpected as there should be few skeletal or hormonal differences between the groups. Ford et al (2005) also found no differences in knee flexion angles in their cohort of 12-18 year old athletes. However, they did observe a difference in hip flexion angle between sexes that was not observed in the present study. This discrepancy may be due to differences in the study paradigm or subject population.

Unlike the current study, Landry et al (2005) observed no frontal plane differences between sexes in 14-18 year old adolescent soccer players. However, the significant differences between sexes occurred in the center and SS tasks, with none being found in the XO task. We had similar findings in the current study. Therefore it appears that there are sex and task related interactions.

Given that the frontal plane knee and ankle angles were similar, the differences in hip abduction angles between sexes suggest a difference in pelvic tilt at pGRF. This could indicate a difference in balance control strategy between sexes.

One of the most interesting qualitative findings of this study was that the unanticipated paradigm posed a significant challenge to our young subject group. Many subjects had a difficult time reacting immediately upon landing. This seems to validate our assumption that the unanticipated task more closely replicates game situations than many other paradigms.

REFERENCES

Ford KR et al. (2003). MSSE, 35(10): 1745-50.
Ford KR et al. (2005). MSSE, 37(1): 124-29.
Landry SC et al. (2007). AJSM, 35(11): 1888-1900.

VIDEO EVALUATION OF DISTAL UPPER EXTREMITY POSTURE

Aaron M. Kociolek and Peter J. Keir

McMaster Occupational Biomechanics Laboratory, Department of Kinesiology, McMaster University, Hamilton, ON, Canada, kociolam@mcmaster.ca, pjkeir@mcmaster.ca

INTRODUCTION

Limited tools are available to assess injury risk of the distal upper extremity. Observational posture-based tools are most commonly used in the workplace to quantify risk of injury because they are practical and provide reliable measures (Bao et al., 1999). Most of these assessment methods require onsite observation or video capture and posturing-sampling strategies to approximate a still-frame image representative of the task. However, several sampling techniques, including extreme, average and most frequently occurring postures, are reported in the literature and often predict different results (Bao et al., 1999). Also, posture-based observation methods for the wrist and forearm continue to be applied in the workplace without validation of their posture classification schemes (Lowe, 2004).

To eliminate posture sampling dependency from injury risk predictions researchers have employed real-time posture-based observation methods with low-to-moderate reliability (Burt & Punnett, 1999). It has been suggested that accurate and reliable observations were limited since too many body joints and posture categories were required to adequately code posture (Bao et al., 1999). However, slow motion video playback while focusing on individual joint movements might allow observers to reliably code posture. The purpose of this study was to test the effects of video playback speed (real-time, half-time and quarter-time) and number of representative bins on observational outcomes.

METHODS AND PROCEDURES

Eight graduate students with previous experience in human movement observation participated in this study. Occupational videos were cut to include 3 to 5 cycles (approximately 20 seconds) of automotive seat assembly tasks. An adaptable observation software suite (Observer 6.0, Noldus Information Technology, VA, USA) was used to code forearm pronation/supination, wrist flexion/extension, wrist radial/ulnar deviation and hand postures from video at three playback speeds (real-time, half-time, quarter-time) and two different categorical scales (6 bins, 3 bins) for flexion/extension (Figure 1).
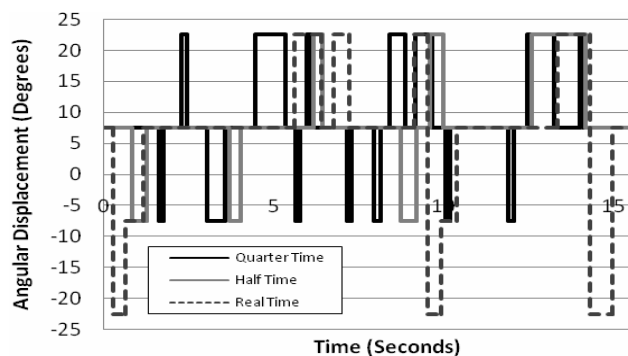
Figure 1. Example time series data of angular wrist flexion/extension displacement across three playback speeds with 6 bins.

RESULTS

Preliminary results demonstrated an effect of video playback speed on observed posture categorical ratings (Figure 2). Using a 6-bin scheme to catalogue wrist flexion/extension, real-time analysis appears to result in fewer postural observations and increased

disagreement when compared to quarter-time analysis (Figure 2a). However, the effect of speed is diminished when percent duration is considered (Figure 2b). Using a 3-bin scheme, both count and percent duration agreeability are improved across quarter-, half- and real-time video analysis (Figure 2c, 2d).

DISCUSSION

These results suggest that slower playback speeds might not significantly improve rater ability to classify postures during continuous time video analysis. The application of this finding to ergonomic tool development could drastically reduce analysis time associated with current video-based frame-by-frame procedures.

Also, fewer bins appear to improve posture coding agreement for flexion/extension trials.

This finding is consistent with research conducted by Lowe et al. (2004). However, future research is required to further investigate the tradeoff between precession and misclassification with categorical posture coding.

REFERENCES

Bao S et al. (1999). *Ergonomics* 50 (12); 2118–2136.
Burt S & Punnett L (1999). *Applied Ergonomics* 30; 121–135.
Lowe B (2004). *Ergonomics* 47 (5); 527–554.
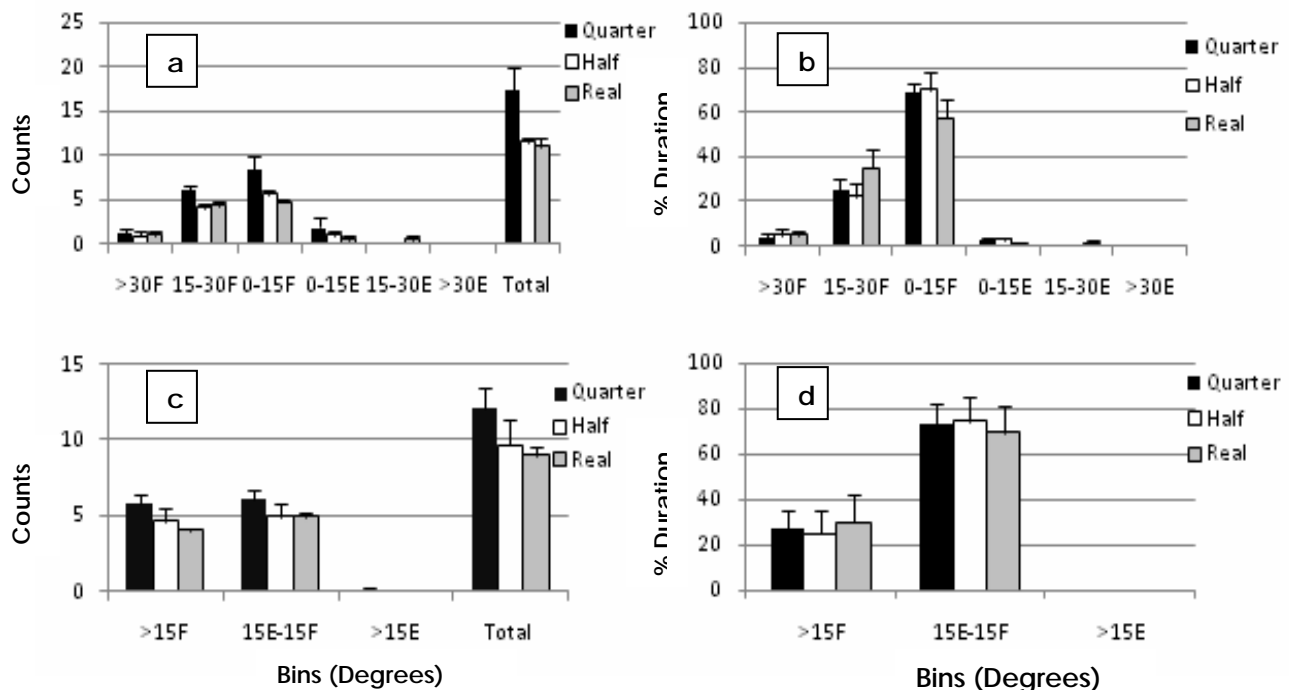
Figure 2. Recorded mean counts and percentage durations with standard error of the mean across wrist flexion/extension trials with three playback speeds and two posture classification schemes: a.) counts over a six bin classification scheme; b.) % duration over a six bin classification scheme; c.) counts over a three bin classification scheme; d.) % duration over a three bin classification scheme. Bin abbreviations are as follows: F – flexion; E – extension.

THE EFFECTS OF LEG DOMINANCE ON KNEE JOINT KINETICS DURING CUTTING

Szu-Ping Lee [1,2] , John W. Chow [1,3] , Mark D. Tillman [1]

[1] Department Applied Physiology and Kinesiology, University of Florida, Gainesville, Florida, USA

[2] Division of Biokinesiology and Physical Therapy, University of Southern California, Los Angeles, USA

[3] Center for Neuroscience and Neurological Recovery, Methodist Rehabilitation Center, Jackson, Mississippi, USA

email: szupingl@usc.edu, website: http://www.hhp.ufl.edu/apk/ces/labs/biomech/

INTRODUCTION

A quick change of direction initiated by pushing off with single lower limb or cutting is a maneuver often cited as one of the primary causes for non-contact anterior cruciate ligament (ACL) rupture [1, 3]. Studies have suggested lower-limb dominance as a possible etiologic factor in predicting ACL injury because joint of the non-dominant limb were thought to be more unstable during such maneuver. Excessive translational shear forces, internal rotation and valgus moments at the knee during cutting have been identified as possible kinetic stresses that place increased strain on the ligament of the pushing leg [2]. Thus, how the forces and torques acting on the joints differ between limbs during high risk movements deserve a closer examination.

The purpose of this study was to compare the peak ground reaction force (GRF) and hip and knee joint resultants during the push off of a side-step cutting exhibited by the dominant and non-dominant limbs. We hypothesized that cutting with non-dominant leg would exhibit higher risk characteristics and therefore indicating increased susceptibility to ACL injury.

METHODS

Thirty-four subjects (15 male, 19 female, age 18-30 yrs) with no previous history of lower limb injuries were recruited to participate the study. The dominant pushing leg was determined by the single-leg hop test [6]. Subjects were then instructed to perform the preplanned side-step cutting action 45° toward both sides while running at self-selected speed. If the cut was intended to the right, the pushing leg would be the left and vice versa. Participants were told to try to push off as hard as they can. Kinematic and kinetic data were collected using a 7-camera Hawk® digital motion capturing system (Motion Analysis Corporation) and two 40 x 60 cm Bertec® forceplates. The data captured were then imported into Orthotrak® software package (Motion Analysis Corporation) to calculate the kinematics, forces and torques at the knee and the hip joints. Resultant forces were normalized with bodyweight and moments were normalized with bodyweight × height. Paired-sample t-test was used to compare dominant and non-dominant limb with peak joint resultant forces and moments as dependent variables (α=.05, two-tailed).

RESULTS AND DISCUSSION

The results were mixed relative to our original hypothesis. We found that pushing with non-dominant leg exhibits comparable peak resultant ground reaction force to pushing with the dominant leg (1.89 to 1.84 BW. p=0.551). A significantly higher lateral force was found

at the non-dominant hip joint and a significantly larger posterior force at the knee joint. However, the posterior force at the non-dominant hip joint was significantly smaller.

Limb asymmetry has long been identified in strength, stability and functional performances. Bilateral differences in neuromuscular control have been hypothesized to cause postural instability and predispose one side to higher risks of injury. Traditional assessment of limb dominance such as the kick-ball method overemphasized the mobilizing function of the leg more while overlooking leg's stabilizing role. We believed this was not an appropriate assessment especially when the motion in question demands more stability than mobility. Our findings supported the notion that there existed significant bilateral differences in lower extremity joint kinetics during cutting even the pushing force exerted (resultant GRF) was comparable. However, the non-dominant leg didn't exhibit the high risk characteristics we expected to see. Our results, suggested that dominant and non-dominant legs had different neuromuscular control strategy to achieve

a similar level of movement performance.

REFERENCES

1. Boden, B.P., et al. *Orthopedics* 23, 573-578, 2000.
2. Kevin R.F., et al. *Med Sci Sports Exerc* 37, 124-129, 2005.
3. Gerwyn Hughes and James Watkins. *Sports Med* 36(5),   411-428, 2006.
4. Rodney J.N., et al. *J. Strength Cond. Res.* 21(1), 270-273, 2007.
5. Matava, M.J., et al. *J. Knee Surg.* 15, 11-16, 2002.
6. Carl G. and Susan H. *J. Gen Psych.* 123(4), 289-296, 1996.

	Dominant	Non-dominant	Mean standard error	Significance
Peak resultant GRF	1.84BW	1.89BW	0.08BW	0.55
Hip:				
Posterior force	0.76	0.56	0.07	0.009
Lateral force	0.25	0.32	0.02	0.003
Internal rotation moment	0.51	0.59	0.19	0.746
Abduction moment	1.98	2.27	0.20	0.154
Knee:				
Posterior force	0.09	0.13	0.01	<0.001
Lateral force	0.60	0.61	0.04	0.797
Internal rotation moment	1.23	1.33	0.19	0.569
Valgus moment	1.42	1.49	0.26	0.787

Table 1: Peak Joint kinetic measures of dominant and non-dominant limbs during cutting (α=.05, two-tailed).

MANUAL SEGMENTATION OF DXA SCAN IMAGES RESULTS IN RELIABLE UPPER AND LOWER EXTREMITY TISSUE MASS ESTIMATES

Timothy A. Burkhart[1,2], Katherine Arthurs[1] and David. M. Andrews[1]

[1]Department of Kinesiology University of Windsor, Windsor ON, Canada,
dandrews@uwindsor.ca
[2]Department of Industrial and Manufacturing Systems Engineering, University of Windsor, Windsor, ON, Canada, burkha3@uwindsor.ca

INTRODUCTION

Wobbling mass models more accurately represent the impact response of the human body (e.g. Gruber et al., 1998). However, quantifying the masses of both soft and rigid tissues in living people continues to limit the use of such models. Holmes et al. (2005) validated tissue mass prediction equations for the lower extremity against tissue masses from DXA scans. Tissue masses can be parceled out for specific segments via DXA software. Users can create custom regions of interest (ROI) by manually tracing polygons around individual segments. While DXA is generally accepted as a valid method for quantifying body composition, the reliability of segment tissue masses that result from the manual segmentation of DXA scan images using ROIs, has yet to be well documented, between and within-measurers.

METHODS AND PROCEDURES

One hundred healthy adults (50 M, 50 F: mean age, mass, and height of 21.8±6.2 years, 70.4±94.96 kg, and 170.8±19.4 cm), gave consent prior to participation. The study was approved by the Research Ethics boards of the University of Windsor and Windsor Regional Hospital. Each subject underwent a full body DXA scan (GE Lunar Prodigy Advance) in a supine position. Using enCORE software (2006, GE Healthcare, v. 10.51.006), custom ROIs (e.g. Figure 1) were drawn manually to segment the upper and lower limbs, as per

Clarys & Marfell-Jones (1986) and Dempster (1955). Actual tissue masses were quantified from the ROIs, including fat mass (FM), lean mass (LM), bone mineral content (BMC) and wobbling mass (WM=LM+FM), for the arm, forearm, forearm and hand, thigh, leg, and leg and foot segments bilaterally. Three measurers independently segmented each scan twice, after all scans were completed the first time. Mean measurement differences were evaluated with a two-way (3 measurers x 2 attempts) repeated measures ANOVA. Intraclass correlation coefficients (ICCs) were used to determine between and within-measurer reliability. Good to excellent reliability was accepted at an ICC of 0.75 (Portney &Watkins, 2000).
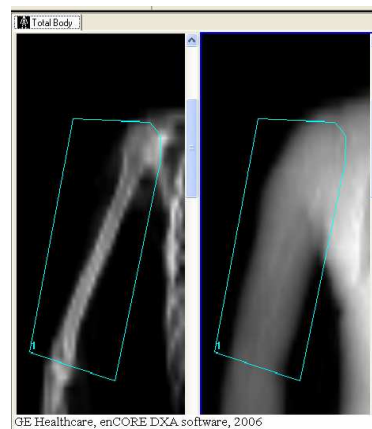
Figure 1. Sample ROI on a DXA scan for an arm segment.

RESULTS

In the upper extremities there were significant differences in all mean tissue mass types between-measurers (p<0.05). However, these differences were fairly small in general,

ranging from 4.4g (5.9%) to 211.6g (13.6%) for the BMC and WM, respectively. For all tissue types and segments, differences between-measurers were greater overall than those between attempts by the same measurer. Differences in arm tissue masses were greater than for the forearm and forearm and hand segments, by approximately 46% and 56%, between and within-measurer. On average, within-measurer reliability (ICC, 0.978) was greater than between-measurer reliability (ICC, 0.956) for all upper extremity tissue masses.

In the lower extremities, there were significant differences in 75% of the mean tissue masses between-measurers (p<0.05). However, these differences were small in general, ranging from 19.5g (7.5%) to 153.3g (3.4%) for the BMC and WM, respectively. For all tissue types and segments, differences between-measures were greater overall than those between attempts by the same measurer. Differences in thigh tissue masses were greater than the leg, and leg and foot segments by approximately 70% and 9%, between and within-measurer. On average, within-measurer reliability (ICC, 0.870) was greater than between-measurer reliability (ICC, 0.781) for all lower extremity tissue masses.

DISCUSSION

The small measurement differences, combined with the overall high ICCs, confirm that manual segmentation of DXA scan images is a fairly reliable method for obtaining tissue masses of individual segments. Overall, within-measurer tissue mass differences were smaller, and the segmentations more reliable than between-measurers. The larger differences associated with the soft tissues, such as LM and FM, are likely a result of not having a complete separation between the upper extremities and the trunk, and between the two lower extremities, in some cases. This was due to the limited scan space on the DXA bed. Smaller differences in BMC resulted because the bones remained visually separate on the scans. The larger differences for the bigger segments, such as the thighs, may be attributed to scale effects (Burkhart et al., 2008).

SUMMARY

The current study indicates that manual segmentation of DXA scan images using ROI is a fairly reliable method for determining segment tissue masses of living people, with reliability within a measurer being better than between. Using the manual ROI option allows researchers to fine-tune their segmentations from scan images, to more closely represent anatomically relevant sections used in cadaver-based studies.

REFERENCES

Burkhart, TA et al. (2008) *J. Biomech*. (In press).
Clarys, J.P. & Marfell-Jones, M.J. (1986) *Human Biology,* 58(5):771-782.
Dempster, W.T. (1955). WADC TR, 55-159.
Gruber, KR et al. (1998). *J. Biomech*., 31:439-444
Holmes, JD et al. (2005). *J. Appl. Biomech*., 21:371-382.
Portney, LG & Watkins, MP. (2000). *Foundation of Clinical Research Applications to Practice (2nd Ed)*. New Jersey: Prentice Hall.

ACKNOWLEDGEMENTS

SUBJECT SPECIFIC ANATOMIC PARAMETERS IMPROVE MOMENT PREDICTIONS OF AN EMG-DRIVEN KNEE JOINT MODEL

Liang-Ching Tsai, John Popovich, Mark Lyle, and Christopher Powers

University of Southern California; email: liangcht@usc.edu; URL: pt.usc.edu/labs/mbrl

INTRODUCTION

A valid EMG driven model requires appropriate anatomical and muscle parameters (Pandy, 2001). Although most EMG driven models are based on mathematical optimization procedures to estimate muscle parameters (Lloyd and Besier, 2003), it is not known how subject-specific anatomic parameters influence joint moment predictions. The purpose of this pilot study was to examine whether an EMG-driven model that uses subject-specific physiological cross-sectional areas (PCSA) and lever arms of the lower extremity musculature would improve knee moment predictions when compared to an EMG-driven model using generic anatomical parameters.

METHODS AND PROCEDURES

One male subject (28 yrs, 1.72 m, and 72 kg) performed three trials of drop-landing task and isokinetic knee extension on a Kin-Com dynamometer (60°/sec; 90°-0° of knee flexion). Lower extremity kinematics and ground reaction forces during drop-landing were recorded using VICON motion analysis system (250 Hz) and AMTI force platforms (1500 Hz). The net sagittal-plane moment at the knee joint was calculated using inverse dynamics equations. The Kin-Com dynamometer was used to directly measure the knee extensor moment during the isokinetic knee extension exercise.

Muscle activation levels during the two tasks were recorded from the vastus lateralis (VL), vastum medialis (VM), rectus femoris (RF), semitendinosis (ST), biceps femoris long head (BFL), medial gastrocnemius (MG), and lateral gastrocnemius (LG) using surface electrodes. Raw EMG signals were band-pass filtered (35-500 Hz), smoothed (10-Hz low-pass filter), and normalized to a maximum voluntary isometric contraction. Muscle activation of the vastus intermedius (VI) was estimated as the average of the VM and VL EMG. Semimembranosis (SM) was assumed to have the same activation as ST; and the biceps femoris short head (BFS) was assumed to have the same activation as BFL (Lloyd and Besier, 2003). An 80 ms electro-mechanical delay was used to adjust for the difference between EMG and force output.

Sagittal and axial magnetic resonance (MR) images of the lower extremity were obtained using a 3T MRI system. For each muscle used in the model, the cross sectional area was measured on each axial image to calculate the total muscle volume. The total volume was combined with the muscle pennation angle and fiber length (Friederich and Brand, 1990) to yield the PCSA for each muscle. Lever arms of the quadriceps, medial and lateral hamstrings, and MG and LG were measured from the sagittal MR images at 10, 20, 40, and 60° of knee flexion. The lever arm was defined as the perpendicular distance from the knee joint center to the line of action of the muscle. A second order polynomial curve fitting procedure was used to estimate lever arm from 0 to 120° of knee flexion.

SIMM software (Delp et al., 1990) was used to create an anatomical knee joint model. The model included 10 musculotendon actuators: VL, VI, VM, RF, ST, SM, BFL, BFS, MG, and LG. Muscle EMG and joint kinematics

were used as input variables to estimate muscle forces and the net knee moment. Knee sagittal-plane moments were calculated using the generic SIMM model and the model with subject-specific PCSA and lever arm data.

Moments calculated by the two models were compared to gold-standard knee moment measurements consisting of inverse dynamics (drop-landing) and Kin-Com dynamometer (isokinetic knee extension). Coefficient of multiple correlation (CMC) and mean absolute differences were calculated for each trial to examine the accuracy of the models in predicting the knee sagittal-plane moment.

RESULTS

The knee sagittal-plane moments during drop-landing and isokinetic knee extension are shown in Figure 1. For both tasks, the subject-specific SIMM model had a higher CMC value and a smaller mean absolute difference than the generic SIMM model, indicating better agreement with gold-standard moment measurements (Table 1).
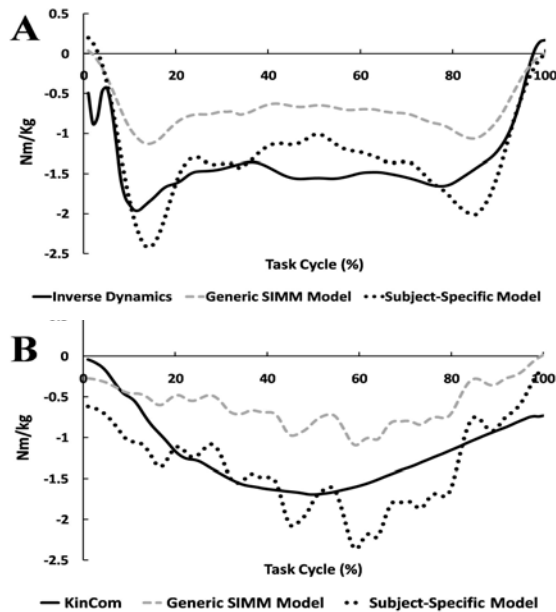
Figure 1. Knee extensor moment (negative values) during drop-landing (A) and isokinetic (60°/sec) knee extension (B).

		Generic Model	Subject-Specific Model
Landing	CMC	0.57	0.84
	Abs. Diff.	0.67	0.31
Isokinetic	CMC	0.62	0.84
Extension	Abs. Diff.	0.61	0.36

Table 1. CMC and mean absolute differences (Nm/kg) for the two knee joint models.

DISCUSSION

The results of this study demonstrate that moment predictions can be improved when subject specific anatomic parameters are used. Given that the net joint moment is the sum of the individual muscle moments, it stands to reason that anatomic parameters that would lead to more accurate muscle force predictions (e.g., individual muscle PCSA) and muscle moment estimations (e.g., lever arms), would compare more favorably to gold standard measures of joint kinetics (e.g., inverse dynamics and dynamometry).

SUMMARY

An EMG-driven model that uses subject-specific anatomic parameters may provide a more valid assessment of knee joint kinetics.

REFERENCES

Delp, SL et al. (1990). *IEEE Trans Biomed Eng*, 37: 757-767.
Friederich, JA and Brand, RA (1990). *J Biomech*, 23: 91-95.
Lloyd, DG and Besier, TF (2003). *J Biomech*, 36: 765-776.
Pandy, MG (2001). *Annu Rev Biomed Eng*, 3: 245-273.

ARM SWING OF VOLLEYBALL SPIKE JUMP PERFORMANCE BETWEEN ADVANCED AND RECREATIONAL FEMALE PLAYERS

ChengTu Hsieh[1] and Gary D. Heise[2]

[1]University of Texas, Pan American, Edinburg, TX, USA, hsiehc@utpa.edu
[2]University of Northern Colorado, Greeley, CO, USA, gary.heise@unco.edu

INTRODUCTION

Numerous studies have shown that arm swing has a significant influence on jump height (e.g., Lees et al., 2004). These studies indicated that an arm swing increases the angular velocity and torque at lower extremity joints, COM height, and velocity at takeoff for a countermovement jump. Additionally, Hsieh and Heise (2006) found that arm swing was one of the most important factors which contributed to volleyball spike jump height.

Studies found that the takeoff velocity can be enhanced by 6-12% when comparing countermovement jumps with arm swing to no arm swing. Arm swing raised the COM height at takeoff by 2-3% when compared to no arm swing (Feltner et al., 1999; Harman et al., 1990; Lees et al., 2004; Ravn et al., 1999). Although these studies examined the effect of arm swing on jump height, few of them have examined the performance of the arm swing in different skill level players. Additionally, few of the volleyball coaching texts adequately explain the importance of arm swing for the volleyball spike jump.

Therefore, the main purpose of present study was to investigate the difference of arm swing performance patterns between advanced and recreational female volleyball players.

METHODS

Twenty female volleyball players were recruited from college-level teams. Ten players (mean body height = 1.75 ± 0.09 m; mean body mass = 66.0 ± 8.5 kg) were playing on a highly competitive team (NCAA Division I) and the other ten players (mean body height = 1.71 ± 0.11 m; mean body mass = 62.3 ± 7.4 kg) were actively playing volleyball at a local recreation center. All policies and procedures for the use of human subjects were followed and approved by the local Institutional Review Board.

Each subject was required to warm-up for at least 5 min by stretching all major muscle groups for jump performance and practicing several normal spike jumps in front of a net and camera (see Figure 1). All subjects performed 10 volleyball spike jumps.
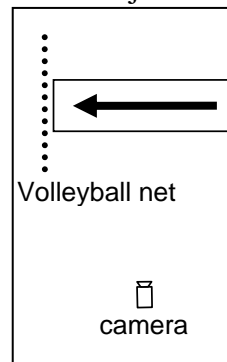
Figure 1. Experimental set-up showing one camera and volleyball net.

Two-dimensional coordinate data from one side of the body were obtained with a 60-Hz video camera in conjunction with a motion analysis system (Vicon Motus). Data were collected from movement onset until after the peak of the jump. Coordinate data were filtered and then kinematic variables of arm swing were examined: the range of motion (*X1*), angular velocity (*X2*), the coordination of arm swing (*X3*), hyperextension joint angle at shoulder joint (*X4*), and the jump

height (*X5*) (see Figure 2 for *X3*, *X4*, & *X5*). The coordination of arm swing was defined as the time when maximum hyperextension of shoulder joint was occurred prior to the feet impact. The data were analyzed and compared (t-test, p < .05) between advanced and recreational female volleyball players.
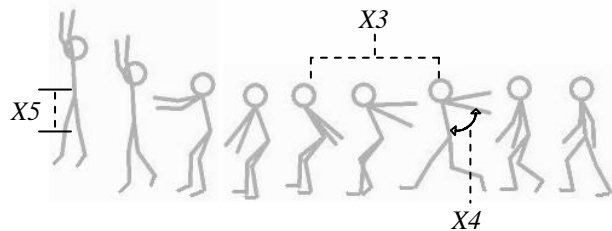
Figure 2. Three kinematic variables of arm swing (*X3*, *X4*, & *X5*) of a volleyball spike jump.

RESULTS AND DISCUSSION

Results showed that the kinematic variables of arm swing were significantly greater in the advanced volleyball players group. Additionally, the jump height of advanced female volleyball players was significantly higher than recreational female players. Table 1 shows the kinematic variables of arm swing and jump height for both advanced and recreational female volleyball groups. The skilled female volleyball players demonstrated the ability to use the arm swing to facilitate the spike jump by swinging arms faster with a greater range of motion. Advanced volleyball player illustrated earlier onset of arm swing with greater shoulder hyperextension joint angle when compared to the recreational female volleyball players.

A successful volleyball spike jump consists of several different factors and a balanced combination of these variables. Arm swing was recognized as one of these variables. During the approach phase, skilled players brought the arm back farther and earlier prior to the impact of both feet when compared to recreational players. This process assists the arm to store and release the energy from the muscle and tendon at lower extremities meanwhile help the trunk to move upward (Lees et al., 2004). That is, the increased range of motion for the arm swing in addition to the earlier time of initiation allowed the arm to generate more energy, which is transferred to various body points to improve vertical jump performance.

Pedagogically, instructors, coaches, and trainers may want to focus on the coordination of arm swing during the performance of a volleyball spike jump. Arm swing forward should have begun before the feet planted at the last step.

REFERENCES

Feltner, ME et al. J. *J Sports Sci*, 17, 449-466, 1999.

Harman, EA et al. *Med Sci Sports Exerc*, 22, 825-833, 1990.

Hsieh, C. & Heise, G. D. *Proc Annu Meet*, Virginia Tech, Blacksburg, VA, 2006

Lees, A. et al. *J of Biomech*, 37, 1929-1940, 2004.

Ravn, S. et al. *Scand J Med Sci Sports*, 9, 201-208, 1999.

Table 1: Kinematic variables of arm swing performance for advanced and recreational female players. * (p < 0.05)

Variables	Advanced (mean ± SD)	Recreational (mean ± SD)
Jump Height* (*X5*)	0.45 ± 0.05 m	0.30 ± 0.03 m
Range of Motion* (*X1*)	225.43 ± 37.63˚	165.07 ± 40.91˚
Angular Velocity* (*X2*)	-456.96 ± 59.49˚	-375.82 ± 70.93˚
Hyperextension Joint Angle* (*X4*)	95.01 ± 34.74˚	68.87 ± 34.74
Coordination* (*X3*)	0.24 ± 0.06 s	0.20 ± 0.03 s

FUNDAMENTAL BIOPOTENTIAL ANALYSIS FOR QUANTIFICATION OF PUDENDAL NERVE INJURY RECOVERY

Bradley C. Gill (gillb@ccf.org)[1-3] Hai-Hong Jiang[1,4] Jonathan B. Glaab[1]
Paul J. Zaszczuryski[1,3] Margot S. Damaser[1-4]

[1]Department of Biomedical Engineering, Cleveland Clinic, Cleveland, OH, USA
[2]Department of Biomedical Engineering, Case Western Reserve University, Cleveland, OH
[3]Research Service, Louis Stokes Veterans Administration Medical Center, Cleveland, OH
[4]Glickman Urological and Kidney Institute, Cleveland Clinic, Cleveland, OH
URL: http://lerner.ccf.org/bme/damaser

INTRODUCTION

The current presentation of electromyography (EMG) and electroneurography (ENG) in the clinically-oriented literature is largely qualitative. On the opposite end of the spectrum, engineering literature related to biopotential analysis often appears overly complex to clinicians. Finding a middle ground between these two extremes can help increase the clinical and physiological impact of data produced from these measurements. The objective of this project was to develop a simple, yet fundamentally-based quantitative analysis method for biopotentials recorded in assessing external urethral sphincter and pudendal nerve function.
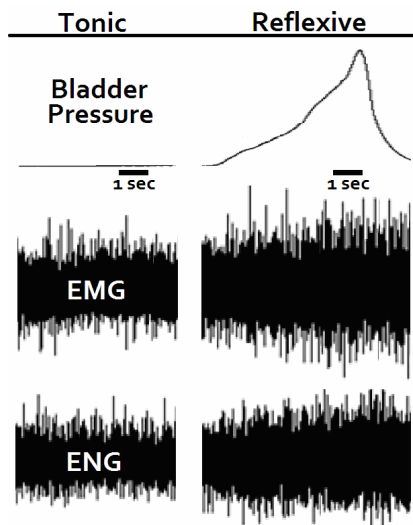
Figure 1. A typical data set analyzed using the method described. The reflexive state 1 second sample was defined by peak bladder pressure.

METHODS

In response to increased bladder pressure, the guarding reflex of the external urethral sphincter was studied using EMG and ENG. Sprague-Dawley rats were anesthetized and the pudendal nerve motor branch and urethra were isolated within the pelvic cavity. Platinum needle electrodes (30 gauge, 2 mm separation) were placed on the surface of the external urethral sphincter. A similar electrode having right-angled needle ends was used to suspend and isolate the pudendal nerve. Data was recorded prior to and during the gradual application of pressure to the exposed bladder.

All EMG and ENG recordings were amplified and band pass filtered (3 Hz - 3 KHz) prior to recording. Data was sampled at 10,000 Hz to ensure high temporal resolution (Gut, Moschytz, 2000). Following acquisition, recordings were visually analyzed and 1 second segments were isolated for processing. Segments included baseline, or tonic states and guarding, or reflexive states (Figure 1). The determination of these states was based upon bladder pressure recordings from a fluid-filled catheter system (Damaser MS, et al., 2003).

Line noise (60 Hz) and its first harmonic (120 Hz) were first removed from all data with two digital, 8th order, Bessel band stop filters (59-61 Hz and 119-121 Hz) having 60 dB attenuation (Clancy, et al., 2001). Signal amplitude was analyzed by first rectifying all

samples recorded from an animal in the non-reflexive state, calculating the mean amplitude of each 1 second segment, and subsequently the mean of means. Next, filtered EMG and ENG signals were divided by this value to account for variability in amplitude across animals. Finally, mean amplitudes were determined for each sample and experimental group. Frequency analysis was carried out using a zero-crossing threshold method. Through observing multiple data sets the average noise amplitude in the tonic state (0.2 mV for this setup) was determined and used as a threshold to eliminate noise. Signals were shifted by this magnitude and frequency was calculated as the detected number of zero crossings divided by two.

RESULTS

Amplitude and frequency analysis in 13 animals demonstrated significant increases when bladder pressure was applied (Figure 2).
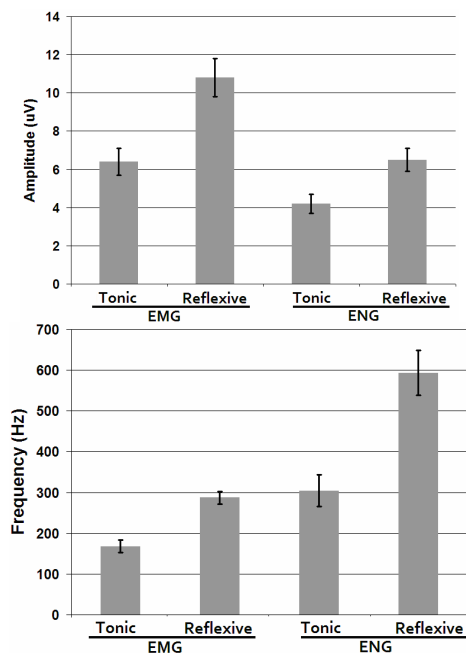
Figure 2. EMG and ENG amplitude (top) and frequency (bottom) in tonic and reflexive states. Data are means with standard error bars. Differences are significant across states (Wilcoxon Signed Rank Test, p<0.01).

DISCUSSION

Electromyography has demonstrated pudendal nerve injury induced reduction in function of external urethral sphincter striated muscle (Peng CW, et al., 2006). The methods in clinically-targeted studies of this nature have been largely qualitative, focusing upon visual inspection and description of waveforms or duration measurements of binary variables. Electroneurography has also been used to analyze PN function, correlating nerve activity and EUS contractions (Boggs JW, et al., 2006). While still notably qualitative, the ENG analysis in this manuscript produced clear quantitative results with simple and straight forward methods, similar to those presented.

Amplitude and frequency increase as additional motor units are recruited, such as in a reflexive state. Therefore, the ability to draw substantial functional conclusions from the amplitude and frequency content of EMG and ENG exists. This capability is underutilized currently by their dichotomous presentation in clinical and engineering research. The use of a straight forward, quantitative EMG and ENG analysis scheme will likely help appreciate the full scientific potential these recordings offer.

REFERENCES

Boggs JW, et al. (2006). *J Physiol*. 577: 115.
Clancy EA, et al. (2001). *IEEE Eng Med Biol Mag*. 20(6): 47.
Damaser MS, et al. (2003). *J Urol*. 170: 1027.
Gut R, Moschytz GS (2000). *IEEE Trans Sig Proc*. 48(9): 2487.
Peng CW, et al. (2006). *Neurourol Urodyn*, 25: 388.

ACKNOWLEDGEMENTS

MECHANICAL CHARACTERISTICS OF NATIVE TENDON SLICES FOR TISSUE ENGINEERING SCAFFOLD

Ting-Wu Qin[1,2], Chun-Feng Zhao[1],Yu-Long Sun[1], Scott P. Steinmann[1], Peter C. Amadio[1], Kai-Nan An[1]

[1]Orthopedic Biomechanics Laboratory, Mayo Clinic, Rochester，MN, USA，

Qin.tingwu@mayo.edu; an.kainan@mayo.edu

[2]Institute of Stem Cell and Tissue Engineering, West China Hospital, Sichuan University, Chengdu, P.R.China, Tingwuqin@hotmail.com

INTRODUCTION

Engineered tendon scaffolds require enough mechanical strength, appropriate pore size and porosity for temporary mechanical support, cell infiltration and survival (Butler el al, 2000; Whitlocka et al, 2007). Meanwhile, tendon extracellular matrix (ECM) components play the important roles in modulating the biological activities of tenocytes or tendon stem cells (Bi et al, 2007). Few artificial and native scaffolds have been developed to satisfy the above criteria. In order to develop a novel scaffold to possess the sufficient mechanical strength, efficient cell seeding area and natural ECM micro-architecture of native tendons, we plan to investigate the scaffold made from acellular tendon slices. In present study, we determined the mechanical characteristics of native tendon slices to identify the minimum thickness of tendon slice which has the elemental mechanical characteristics of native tendon. We hypothesized that there would be mechanical alterations with varying thicknesses of native tendon slices.

METHODS AND PROCEDURES

Eight hind limbs were obtained from 4 dogs, which were euthanized for Institutional Animal Care and Use Committee approved studies. Three bundles of each Achilles tendon (AT) were dissected from one hind limb. Each bundle was fixed on a cryostat (Leica CM1850, Germany) with Tissue-Tek® optimal cutting temperature compound (Sakura Finetek USA, Inc., USA), and sliced with varying thickness of 100, 200, 300, 400, and 500 μm in succession. AT bundles (n=12) and AT slices (n=60) were used in present study. The ends of the AT bundles and slices were wrapped with saline-soaked sandpaper, and mounted into custom made grips on an uniaxial load frame (MTS 312, MTS Co., MA) for failure testing. Cross-sectional area and the distance between the grips were measured prior to testing with digital calipers. Bundles and slices were pre-loaded to 0.2 N, and then stretched to failure at a rate of 12 mm/min. Samples were kept moist during testing with PBS. Ultimate tensile stress (UTS), failure strain, and elastic modulus were calculated from the load and displacement data obtained from the test.

RESULTS

Typical stress-strain curves for one AT bundle and representative slices are shown in Figure1.For the thicknesses of more than 300μm, the toe regions were apparent, followed by linear regions, which continued until ultimate failure. However, there seemed to be no toe region for 100μm thick slice.
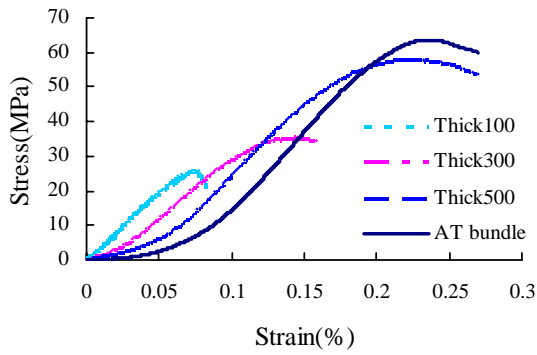
Figiure 1. Typical stress-strain curves for AT slices and one AT bundle.

The mean UTS and modulus values exhibited a gradual rise with increasing thickness (Table1). For 300µm thick slice, the UTS and modulus reached mean values of 70 and 77 per cent of AT bundles, respectively. Also, the failure strain of 300µm thick slice was remarkably higher than that of 100 or 200µm thick slice, reaching a mean value of 87 per cent of native AT bundles.

Thickness	UTS	Failure strain	Modulus
(µm)	(MPa)	(%)	(MPa)
100	17.5(10.1)	9.3(2.9)	230.3(99.2)
200	27.3(10.5)	9.3(2.4)	351.9(87.6)
300	40.9(11.6)	16.0(2.2)	375.2(113.1)
400	42.1(14.4)	16.4(2.0)	378.8(85.0)
500	55.1(11.8)	16.5(5.8)	468.8(76.6)
AT bundle	58.3(11.2)	18.3(4.5)	484.7(88.6)

Table1. Mechanical properties of AT slices and AT bundles (n=12 for each group).

DISCUSSION

The tendon is a fibrous connective tissue, consisted predominantly of type I collagen fibres. The collagen fibrils follow a natural periodic crimp, which is planar with respect to the alignment of the tendon structure. The dimension of fibres with crimp waveform is approximately 10-50µm. When the slice was cut with thickness of 100-200µm, there would be more or less damage to the crimp structure and some fibrils were likely to be broken off. Macroscopically, the slice with 100 or 200µm exhibited weak mechanical strength. This is mainly caused by adjacent fibre sliding and without the initial crimp straightening. In contrast, the slices with more than 300µm, equivalent to the fascicle level (50-400µm), retained most of the crimp structure and collagen fibrils. The mechanical properties of these slices are determined by the straightening of crimped collagen fibres and subsequent fibre slipping with increasing load. These slices showed a standard stress-strain curve similar with native AT bundles.

SUMMARY

This study demonstrated that mechanical characteristics of slices from AT bundles depended largely on the thickness of the slice. The slice with the thickness of 300 µm seemed to be the thinnest slice to keep the essential mechanical characteristics of the AT bundle. These findings are fundamental to the selection of tendon slices as engineered tendon scaffolds.

REFERENCES

Bi YM et al. (2007). *Nat Med*, 13(10): 1219-1227.

Butler DL et al.(2000). *J Biomech Eng*, 122: 570-575.

Derwin KA et al.(2006). *J Bone Joint Surg Am*, 88:2665-2672.

Whitlocka PW et al.(2007).*Biomaterials*, 28 : 4321–4329

SUBJECT-SPECIFIC FORCE-LENGTH PARAMETERS OF THE ANKLE PLANTARFLEXORS IN YOUNG ADULTS

Ross H. Miller, Christopher J. Hasson, and Graham E. Caldwell
Department of Kinesiology, University of Massachusetts, Amherst, MA, USA
Email: rhmiller@kin.umass.edu   Web: http://www.umass.edu/sphhs/kinesiology

INTRODUCTION

Neuromuscular aspects of human athletic activities are often investigated by computer simulations that actuate a musculoskeletal model with Hill-based muscle models. Many simulations solve tracking problems, where design variables within the simulation are optimized to minimize the error between the model's performance and the performances of human subjects (*e.g.* Neptune *et al.*, 2000).

If simulations are performed on a subject-specific basis (tracking kinematics and kinetics from specific individuals; Neptune *et al.*, 2000; McLean *et al.*, 2003), it is important to tune the parameters of the muscle models to the force production capabilities of each individual to faithfully simulate the muscle mechanics of the movement. However, muscle model parameters are often taken from the literature and are not derived on an individual basis.

Previous research has suggested the need for subject-specific muscle model parameters by demonstrating the sensitivity of simulation output to input parameter values, in particular the maximum isometric muscle force (Fo), the optimal contractile component length (Lo), and the unloaded series elastic component length (Lu) (Pandy, 1990; Scovil & Ronsky, 2006; Redl *et al.*, 2007). It would seem important, therefore, to know how these parameters vary among individuals. If muscle model parameters vary considerably between individuals, they should be derived on an individual basis in order for simulations to be truly subject-specific.

The purpose was to determine subject-specific muscle model parameters for the plantarflexors in healthy young subjects, and to compare their values to values used for subject-specific simulations in the literature.

METHODS

Twelve young, active subjects (six males, six females) performed maximum isometric plantarflexion on a dynamometer. Trials were performed at five different ankle angles, and at two different knee angles to account for the biarticularity of gastrocnemius. Moment and angle data were sampled at 1000 Hz. Peak ankle joint moments developed at each angle were extracted to construct experimental ankle joint moment-angle (M-θ) relationships.

Simulations were performed at each joint configuration with a musculoskeletal model of the leg actuated by Hill models of soleus (SO) and gastrocnemius (GA). Simulations assumed full plantarflexor activation and no dorsiflexor co-activation. Muscle lengths and moment arms were estimated using OpenSim software and scaled to the segment lengths of each subject. Fo, Lo, Lu, and force-length parabola widths (W) for SO and GA were then optimized by genetic evolution to minimize the error between modeled and experimental M-θ curves.

RESULTS

Subject-specific results are presented for four subjects (two males, two females). The average error between experimental and modeled moments was < 5 Nm (*e.g.* Fig. 1). Moments and muscle forces dropped as the plantarflexion angle increased. Muscles operated on the ascending limb of the force-length relationship.
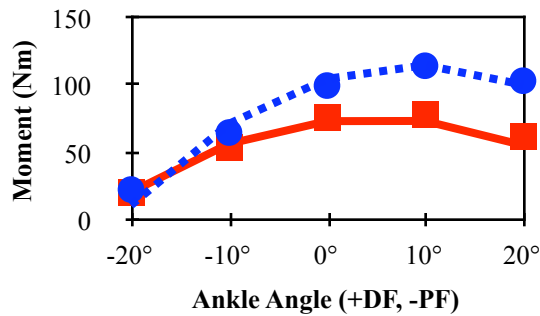
Figure 1. Modeled (symb.) and experimental (line) M-θ profiles with the knee **flexed** (—) and **extended** (· · ·) for Subject #1.

Fo, Lo, and *W* varied substantially between subjects, with coefficient of variation (CV) values between 20-40%, while *Lu* was more consistent (CV: 2% for SO, 10% for GA). Table 1 shows results for these four subjects.

Table 1. Muscle model parameters for SO and GA in four subjects. N00: Neptune *et al.*, 2000. M03: McLean *et al.*, 2003.

	Fo (kN)		*Lo* (cm)		*Lu* (cm)		*W* (% *Lo*)	
Subj	**SO**	**GA**	**SO**	**GA**	**SO**	**GA**	**SO**	**GA**
#1 m	2.0	1.7	5.4	4.4	23.1	41.5	35	67
#2 f	2.2	2.8	3.4	7.7	22.1	35.5	52	60
#3 m	2.9	1.3	7.6	8.9	23.3	36.0	43	98
#4 f	1.8	0.9	6.1	6.9	23.2	32.8	82	100
Mean	2.2	1.6	5.6	7.0	22.9	36.7	53	81
SD	0.5	0.8	1.8	1.9	0.5	3.6	20	20
CV	21	49	31	28	2	10	38	25
N00	5.6	3.2	2.7	4.3	26.8	40.8	--	--
M03	2.8	1.6	3.0	5.1	26.8	40.1	1.0	0.9

DISCUSSION

Plantarflexor force-length parameters varied substantially between subjects. These findings were evident even though the subjects were similar in age and fitness level. Values for *Fo* were comparable to McLean *et al.* (2003), but were much smaller than Neptune *et al.* (2000). *Lo* tended to be longer than both referenced studies. *Lu* was relatively homogenous between subjects, and slightly shorter than the references. Further work is needed on other muscle groups.

The ranges of values exhibited for *Fo*, *Lo*, and *W* were similar to the ranges tested by Scovil and Ronsky (2006), who found that joint kinematics and ground reaction forces during locomotor simulations were highly sensitive to input values for *Fo* and *Lo*. Subject-specific simulations should therefore derive these parameters on a subject-specific basis in order to faithfully represent the muscle mechanics of the modeled individual. Applicable methods include modeling, optimization, and imaging (MRI, ultrasound).

ACKNOWLEDGEMENTS

REFERENCES

McLean SG *et al*. (2003). *J Biomech Engr*, 125:864-874.

Neptune RR *et al*. (2000). *Clin Biomech*, 15:611-618.

Pandy MG (1990). In: *Multiple Muscle Systems*, Springer-Verlag.

Redl C *et al*. (2007). *Hum Mov Sci*, 26:306-319.

Scovil CY and Ronsky JL (2006). *J Biomech*, 39:2055-2063.

SUBJECT-SPECIFIC CHANGES IN KNEE LOADING IN RESPONSE TO AN UNSTABLE SHOE INTERVENTION

Katerina Blazek[1], Katherine A. Boyer[1,2], Thomas Andriacchi[1,2]

[1]Mechanical Engineering, Stanford University, CA, USA
[2]VA Bone and Joint Rehabilitation R&D Center, Palo Alto, CA USA
E-mail: kblazek@stanford.edu

INTRODUCTION

Interventions aimed at reducing lower extremity joint loads and pain associated with osteoarthritis (OA), specifically medial knee OA, have become a focus of recent research (Fisher, 2007; Nigg, 2006; Romkes, 2006). One such intervention, developed by Masai Barefoot Technologies (MBT), is the unstable sole shoe, which is designed with a rocker sole and compliant heel to activate and strengthen the stabilizing muscles of the lower limb. Previous investigations with the MBT shoe have shown significant changes compared to a general athletic shoe in gastrocnemius and tibialis anterior muscle activation patterns and increased ankle dorsiflexion angle and plantarflexion moment during stance (Nigg, 2006; Romkes, 2006). These findings indicate there is a locomotor adaptation to the MBT shoe, particularly at the ankle joint. However, the effects on the knee and hip joints are not clear. The severity and progression of medial knee OA has been correlated to the magnitude of the knee adduction moment and the total force in the joint (Muendermann, 2004). Therefore in order to evaluate the usefulness of the unstable sole shoe as an intervention to reduce pain and slow the progression of knee osteoarthritis, the effect of the shoe on the forces and moments at the knee should be determined. **The purpose of this study was thus to identify the kinematic and kinetic adaptations to an unstable shoe intervention and the effect on the total and medial compartment knee joint force in healthy subjects.**

METHODS AND PROCEDURES

19 healthy volunteers were tested, all with no history of lower-limb injury or pain and who had never worn the MBT shoe before: 11 women (age: 28.9 +/- 7.3 years; BMI: 22.7 +/- 2.9) and 8 men (age: 32.6 +/- 7.5 years; BMI: 23.5 +/- 1.8). Informed consent was obtained from all subjects per Stanford University IRB guidelines. Each subject wore the shoe for a two week period prior to testing. Kinematic marker data and ground reaction forces were collected at 120 Hz while each subject walked at a self-selected normal pace in the MBT and the subject's own casual shoe. Intersegmental joint forces and moments were calculated using inverse dynamics and a previously published link model (Andriacchi, 1997). Paired Student's t-tests were carried out to determine differences in the group response between the two shoe conditions.

RESULTS

There was no significant difference in speed between the casual (1.38 m/s) and MBT shoe (1.4 m/s) (p=.43). However, the response to the MBT shoe showed substantial variations, with individual subjects showing 6 differing adaptation patterns of lower-body kinetics. Three of the patterns (12 subjects) showed a decrease in the knee flexion and knee adduction moments, two patterns (5 subjects) showed an increase in both knee flexion and adduction moments, and the last (2 subjects) showed an increased knee flexion moment but a reduced adduction moment. In the 3 groups with a reduction in the knee flexion moment, patterns differed in whether subjects increased or decreased hip flexion and adduction; in the

increased knee flexion groups, strategies differed in whether the ankle dorsiflexion moment increased or decreased (Figure 1).
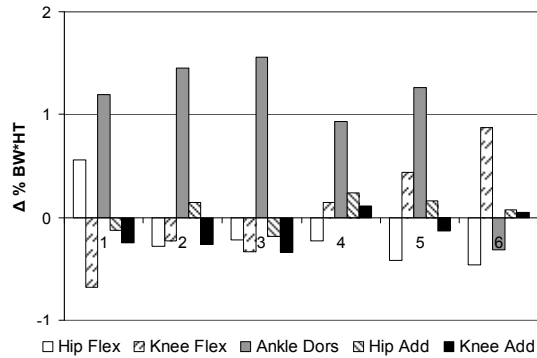
Figure 1: Different strategies used to adapt to the MBT shoe; plotted are average changes in moments between the MBT and the casual shoe.

Regardless of strategy, in the MBT shoe, all subjects walked with a more flexed knee and more dorsiflexed ankle at heelstrike and a more flexed knee at toe-off (p < 0.05). On average, subjects showed significant increases in the knee extension and the ankle plantarflexion moments and decreases in the hip extension moment and knee adduction moment (p < 0.05) (Figure 2).

DISCUSSION

This study suggests that in contrast to other shoe interventions (Fisher, 2007), the adaptations and therefore changes in knee joint loading with an unstable shoe intervention are subject-specific. This could be due to the unstable construction of the shoe, which presents a different stimulus to each wearer and thus encourages different locomotor adaptations. These differing responses indicate that the shoe may be beneficial for some but harmful to other OA patients. A pattern of decreased knee flexion and adduction moments will tend to reduce the total knee loads and redistribute them to the lateral compartment, and would thus be a positive response for a medial knee OA

patient. However, an increase in both moments will tend to increase the total force in the medial compartment, and so this pattern could potentially harm the OA patient. A decreased adduction and increased flexion moment pattern may redistribute the force laterally, but will tend to increase the overall force and thus no change in the medial compartment loading is expected. The results of this study thus highlight the individual nature of gait adaptations to this shoe intervention and the importance of patient monitoring during the clinical use of an unstable-soled shoe.
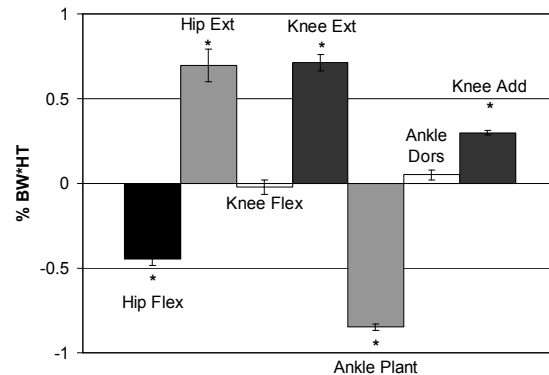
Figure 2: Differences (mean ± SE) between the MBT and casual shoe sagittal and frontal plane moments.

REFERENCES

Andriacchi, et al. (1997) *Basic Orthopaedic Biomechanics,* 37-68.
Fisher, et al. (2007) *J Orthop Res*, **25**, 540-546.
Muendermann, et al. (2004) *Arthritis Rheum*, **50**, 1172-1178.
Nigg, et al. (2006) *Clin Biomech,* **21,** 82-88.
Romkes, et al. (2006) *Clin Biomech,* **21,** 75-81.

ACKNOWLEDGEMENTS

ARE ASYMMETRIES IN JOINT KINETICS RELATED TO LIMB DOMINANCE?

Matthew K. Seeley [1], Brian R. Umberger [2], and Robert Shapiro [3]

[1] Brigham Young University, Provo, UT, USA, matt_seeley@byu.edu
[2] University of Massachusetts, Amherst, MA, USA
[3] University of Kentucky, Lexington, KY, USA

INTRODUCTION

Bilateral asymmetries have been documented for kinematic, kinetic, and electromyographic data during normal gait, yet their causes remain unclear (Sadeghi et al., 2000). One explanation for these asymmetries has been termed functional asymmetry. According to this explanation, the non-dominant (ND) leg contributes more to supporting the center of mass, while the dominant (D) leg contributes more to propulsion of the center of mass (Sadeghi et al., 2000). Impulses due to vertical and propulsive ground reaction forces are symmetrical during normal gait (Seeley et al., In Press), indicating that, at a global level, the ND and D legs contribute similarly to support and propulsion. However, these symmetrical impulses do not necessarily imply symmetry for "local" measures, such as joint kinetics. Asymmetries in joint kinetics may be related to different functional roles of the ND and D legs, in a manner that is consistent with the functional asymmetry perspective.

The purpose of this study was to determine if joint kinetic asymmetries during normal gait are related to these hypothesized functional differences between the ND and D legs (support and propulsion, respectively). We formulated three hypotheses that were based upon this idea of functional asymmetry: 1) joint mechanical work associated with support during gait would be greater for the ND leg than for the D leg, 2) joint work associated with propulsion would be greater for the D leg, relative to the ND leg; and 3) with increases in walking speed, propulsion-related joint work would increase disproportionately for the D leg, when compared to the ND. This limb × speed interaction was not predicted for support-related work because, although propulsive requirements increase as walking speed increases, support requirements remain relatively steady due to the constancy of gravity.

METHODS AND PROCEDURES

The gaits of 20 healthy subjects (age = 25 ± 3 yr; ht = 1.7 ± 0.1 m; mass = 70 ± 14 kg) were evaluated at three walking speeds: preferred (1.49 ± 0.20 m/s), -20% (1.24 ± 0.15 m/s), and +20% (1.78 ± 0.20 m/s). We quantified joint mechanical work associated with support and propulsion by integrating joint mechanical power, with respect to time, during specific power bursts that are associated with support or propulsion (Eng & Winter, 1995; Allard et al., 1995). Power bursts associated with support included the first ankle sagittal (A1S), combined first and second knee sagittal (K1S/K2S), first hip sagittal (H1S), and second hip frontal (H2F). Propulsion-related bursts included the second ankle sagittal (A2S) and third knee sagittal (K3S). Power was the product of joint angular velocity and net joint moment. Work was normalized to body weight × limb length. A repeated measures ANOVA ($\alpha = 0.05$) was performed (SPSS) to detect the effects of limb and speed on joint work. Variables exhibiting a limb × walking speed interaction were bilaterally compared at each speed via *post hoc* analyses. All other data were pooled from each speed and compared bilaterally.

RESULTS

For mechanical work associated with support: 1) significantly more work was performed by the ND leg during the A1S (data were pooled from each speed) and K1S/K2S (preferred and fast speeds) power bursts; and 2) significantly more work was performed by the D leg during the H2F power burst (data pooled from each speed; Table 1). Regarding propulsion-related work, significantly more work was performed by the ND leg during the A2S (data were pooled from each speed) and K3S (fast speed) power bursts (Table 1).

DISCUSSION

The data did not consistently support our hypotheses, indicating that asymmetries in joint work during walking are probably not related to different functional roles of the ND and D legs, as conceptualized within the functional asymmetry framework. Mechanical work performed during the A1S, K1S/K2S, H1S, and H2F joint power bursts is associated with center of mass support. As expected, the work performed during two (A1S and K1S/K2S) of these bursts was greater for the ND. However, there was no difference for work performed during the H1S burst, and work performed during the H2F burst was significantly greater for the D, which was in opposition to our first hypothesis. Propulsion-related work (A2S and K3S) consistently contradicted our second hypothesis, as both were greater for the ND. Finally, the walking speed manipulation described in the third hypothesis was not supported, as the only limb × speed interaction observed for propulsion-related work, was in a direction that was opposite to the third hypothesis.

SUMMARY

Bilateral asymmetries for joint mechanical work are probably not related to limb dominance in a manner that is consistent with the functional asymmetry idea, which states that the ND and D legs contribute more to support and propulsion, respectively. Other causes of asymmetries in joint kinetics should be explored, as clarification of this issue will advance our understanding of normal gait.

REFERENCES

Eng J & Winter D (1995). *J Biomech,* 28**:** 753-758.
Allard P et al. (2004). *Hum Mov Sci,* 15**:** 327-346.
Sadeghi H et al. (2000). *Gait Post,* 12: 34-45.
Seeley M et al. (In Press). *Gait Post.*

Mean Work × 10⁻³					
Support	**ND**	**D**	**Propulsion**	**ND**	**D**
A1S * (*p* < 0.001)	17 ± 5	10 ± 4	A2S * (*p* < 0.001)	26 ± 6	15 ± 5
K1S/K2S (slow)	13 ± 7	12 ± 5	K3S (slow)	11 ± 6	12 ± 5
K1S/K2S (preferred) * (*p* = 0.008)	19 ± 6	15 ± 5	K3S (preferred)	14 ± 8	14 ± 5
K1S/K2S (fast) * (*p* < 0.001)	28 ± 8	22 ± 6	K3S (fast) * (*p* < 0.001)	22 ± 6	17 ± 5
H1S	21 ± 12	21 ± 13			
H2F * (*p* < 0.001)	3 ± 4	10 ± 6			

Table 1. Work, normalized to body weight × limb length, performed at the ankle, knee, and hip joints of the non-dominant (ND) and dominant (D) legs during specific joint power bursts (see text for details) during normal gait. * Asterisks indicate statistical significance.

EFFECTS OF CYCLIC STRETCH ON BEHAVIOR OF TENOCYTES SEEDED IN ACELLULAR TENDON SCAFFOLDS

Ting-Wu Qin[1,2], Cheng-Jun Liu[1], Zhi-Ming Yang[1], Chun-Feng Zhao[2],Yu-Long Sun[2], Kai-Nan An[2]

[1] Institute of Stem Cell and Tissue Engineering, West China Hospital, Sichuan University, Chengdu, P.R.China, Tingwuqin@hotmail.com

[2]Orthopedic Biomechanics Laboratory, Mayo Clinic, Rochester，MN, USA，

Qin.tingwu@mayo.edu; an.kainan@mayo.edu

INTRODUCTION

The bio-scaffold and mechanical stimulation have been stressed in development of functional engineered tendons (Butler et al, 2008). We have developed a method for preparing an acellular tendon scaffold using chemical reagents to minimize host immune response. This study is designed to understand whether such bio-scaffold would provide an optimal micro-architecture to promote efficient tenocyte seeding, infiltration, and function under cyclic stretch. We investigated the effects of cyclic stretch on behavior of tenocytes seeded in the acellular tendon scaffold. We hypothesized that with cyclic mechanical stimulation, the tenocytes seeded in the acellular tendon scaffold would be accelerated in cell growth, infiltration, and function compared to those without cyclic stretch.

METHODS AND PROCEDURES

The flexor digitorum profundus (FDP) tendons were obtained from fresh cadavers. The acellular FDP tendon scaffold was prepared according to the following procedures. Briefly, dynamic treatment in a thermostatic water bath (37°C), defatting/decellularizing, and partly deproteining with chemical reagents were performed using a custom designed instrument. The scaffold was then freeze-dried and sterilized with ethylene oxide. Tenocytes were obtained from explant culture of rat tail tendons and cultivated in fresh F12 medium containing 10% FCS, 6mg/L penicillin, 0.1g/L streptomycin. Before seeded on the scaffolds at a density of 1×10^6 cell/scaffold, the 2-4 passages of tenocytes were digested from the culture flask with 0.25% trypsin (Gibico Co.). After 24h static culture, tenocyte-scaffold composites experienced a cyclic stretch culture (0.2Hz, 10% elongation, 15min/h) for 48h with a custom designed culture device. Then the composites were taken out for morphological observation, histological examination, and collagen assay. Sections were cut and stained with H&E. Collagen synthesis was quantified by measuring the hydroxyproline that was present in the composites using high performance liquid chromatography. Student's T-test was used for the statistical analysis. $P<0.05$ was considered significant.

RESULTS

The growth of tenocytes on the scaffolds under the static and stretched culture conditions was observed with SEM (Figure 1a and b). The acellular tendon scaffold was suitable for adhesion and growth of tenocytes. The cells well attached on the scaffold and

grew to a high density.
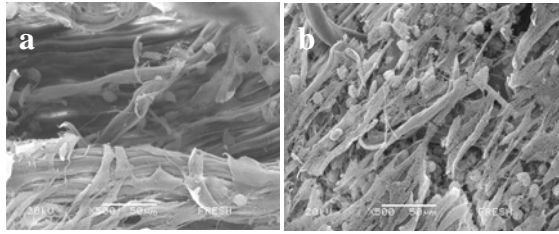
Figure 1. Tenocyte morphology cultured on acellular scaffolds (72h). Non-stretch(a); stretch(b) (SEM,×500).

Histological results showed there were a large number of tenocytes on the upper layer of scaffold for the static culture (Figure 2a). However, the tenocyte infiltrated thoroughly into the scaffold with cyclic stretch and the fibers of the scaffold became loose (Fig.2b).
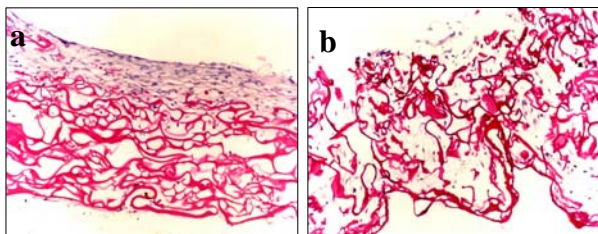
Figure 2. Histology of the tenocyte-scaffold composites (72h). Non-stretch (a); stretch (b) (H&E stain, ×100).

The collagen content from production of hydroxyproline demonstrated a statistically significant difference between static and stretched culture ($P<0.05$) (Figure 3).
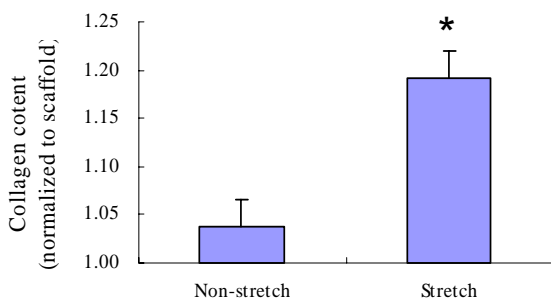
Figure 3.The collagen content ratio to the original collagen in scaffold (72h).* $P<0.05$ to non-stretch.

DISCUSSION

The results demonstrated that the acellular FDP tendon scaffold was cytocompatible when assessed via morphological observation. Furthermore, increased tendon pore size and porosity were produced using chemical reagents to produce the scaffold that is more likely to allow cell infiltration and repopulation. For the static culture, the cell infiltration was only present at the periphery. However, the tenocytes were observed within the inner matrix as well as at the periphery of the scaffold under stretch. This homogenous tenocyte infiltration under stretch suggested the importance of cyclic stretch for the maintenance of tenocyte distribution within scaffold. Additionally, the stretch culture significantly improved the collagen synthesis. This is in agreement with the results of previous studies (Garvin et al, 2003; Screen et al, 2005).

SUMMARY

The study showed that the acellular FDP tendon scaffold is of optimal micro-architecture to promote efficient tenocyte adhesion, infiltration, and function of the seeded tenocytes under cyclic stretch culture.

REFERENCES

Butler DL et al.(2008). *J Orthop Research,* 26:1-9.
Garvin J et al.(2003).*Tissue Eng*, 9:967-979.
Screen HRC et al.(2005). *Biochem Bioph Res Co*, 336: 424–429.

ACKNOWLEDGEMENTS

THE EFFECTS OF TASK ROTATION ON MUSCLE ACTIVITY AND FATIGUE

Michael W.R. Holmes, Kia Sanei and Peter J. Keir

McMaster Occupational Biomechanics Laboratory, Department of Kinesiology, McMaster University, Hamilton, ON, Canada, holmesmw@mcmaster.ca

INTRODUCTION

Job rotation has become a common approach to reducing the incidence of work related musculoskeletal injury risk. However, the literature has provided mixed results with respect to tangible evidence towards the benefits of job rotation (Frazer et al., 2003). Task variation is one method whereby changing posture and muscular loading will provide rest to muscles that would otherwise be continually used (Mathiassen, 2006).

A widespread task rotation design may alternate between tasks primarily focused on the upper extremity muscles with a second task that would focus on the lower extremity or back muscles. However, upper extremity muscles, especially those used during gripping activities may be used substantially during lifting activities. This may prove vital in the design of job rotation protocols. Thus, the purpose of this study was to evaluate the effect of task order when alternating between lifting and gripping activities.

METHODS AND PROCEDURES

Ten male participants volunteered for this study. After signing informed consent each participant performed a combination of lifting and gripping tasks. Task A required lifting and lowering a box at a frequency of 6 lift/lowers per minute. Task B was a 20% maximal gripping task of the same frequency. All combinations of the two tasks were performed for 30 minutes. In total 4 randomized task variations were completed by each subject (Table 1). Between trials 30 minutes rest was given, with no more than 2 trials (task combinations) being performed on one day. The load lifted was 15kg, participants hands started at 55 cm above the ground and the handles of the box were 50 cm apart. Participants were free to lift as they desired, while keeping their feet fixed with a shoulder width stance. The grip task was a 20% maximal grip using a hand held grip dynamometer. An intermittent grip task of 5 seconds grip followed by 5 seconds of no grip was performed. Participants were instructed to maintain a 90° flexed elbow posture (arm and dynamometer unsupported) during contraction and return to the holding position during rest cycles.

Table 1. Each task represents 15 minutes of activity. Trial 1 and 4 represent 30 minutes of the same task.

Trial	Task Combination	
	Task 1 - 15 min	Task 2 - 15 min
1	Lift	Lift
2	Lift	Grip
3	Grip	Lift
4	Grip	Grip

Eight muscles on the right side of the body were monitored using surface EMG (Bortec Biomedical Ltd., AB, Canada). Muscles included: flexor carpi radialis (FCR), flexor digitorum superficialis (FDS), extensor carpi radialis (ECR), extensor digitorum (ED) and upper/lower erector spinae (UE/LE). EMG was normalized to muscle specific maximal voluntary exertions (MVE). EMG and grip force data was collected at 2048 Hz and stored for further analysis.

RESULTS

Average EMG (AEMG) was evaluated during the 1st, 7th, and 14th minute of each 15 minute task. Average muscle activity was evaluated for all cycles during each time period. Muscle activity in the forearm flexors and extensors during gripping resulted in activation levels only slightly larger than those found during the lifting task (Figure 1). It appears that continuous low level muscle activity is evident in the forearm muscles for the duration of the lifting tasks. With respect to the upper and lower erector spinae muscles they demonstrated large variability during lifting trials. Prior to testing, maximum isometric lifts were performed by each participant and when the test load was expressed as a percent maximum, a large range between individuals was observed (19.5 – 45.2 %MVC). Finally, rated perceived exertion levels for each trial were collected and results suggest very similar scores with an average rating of 4.2 ± 0.75 on a 10 point scale.

DISCUSSION

Forearm muscle activities appear similar during the lifting and gripping tasks. These results suggest that further evaluation is needed of continuous low level efforts that are apparent in the upper extremity during lifting. While job rotation may provide rest to muscles primarily not being used (Frazer et al., 2003) these muscles may still be activated at lower levels and contribute to cumulative effects.

Mathiassen (2006) suggested that task variation is a commonly used intervention to share muscular loading. Our initial results indicate that overall average forearm muscle activity is slightly higher for the grip – lift task when compared to the lift – grip task (Trial 3 vs. Trial 2). This could suggest fatigue during the gripping task, which may influence the lifting task to follow. It is believed that further evaluation of these findings along with rated perceived exertion scores may provide insight towards the importance of proper task variation during job rotation design.

REFERENCES

Frazer, MB et al. (2003). *Ergonomics*, 46: 904 - 919.
Mathiassen S. (2006). *Appl Ergon*, 37: 419 - 427.

ACKNOWLEDGEMENTS
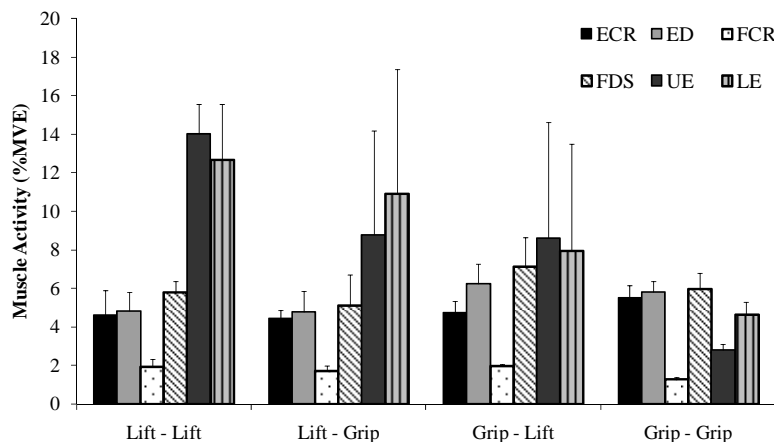
Figure 1. AEMG (% MVE and Standard Deviation) for selected muscles during each trial

A MATHEMATICAL MODEL OF FORCE TRANSMISSION BY DESMIN IN SKELETAL MUSCLE

Gretchen A. Meyer[1], Miklos Kellermeyer[2], Samuel R. Ward[1], Richard L. Lieber[1]

[1]Departments of Bioengineering, Orthopaedic Surgery, and Radiology, University of California-San Diego and Veterans Affairs Medical Center, La Jolla, CA 92093 USA
[2]Department of Biophysics, University of Pécs, Szigeti ut 12. Pécs H-7624, Hungary
Email: rlieber@ucsd.edu, Web: http://muscle.ucsd.edu

INTRODUCTION

Desmin is the intermediate filament protein in skeletal muscle fibers that forms a mesh-like network around Z-disks, binding them laterally and anchoring them to costameres at the sarcolemma. This localization ideally suits desmin to function as a mechanical integrator of the cell, maintaining lattice connectivity and enabling efficient force transmission. Studies performed on desmin knockout (DKO) muscle fibers revealed a reduction in sarcomere alignment and a reduction in isometric force production compared with wild-type (WT) fibers. (Sam et al. 2000)

There have been no known attempts to model the quantitative effect of individual desmin filaments on muscle fiber mechanics. Thus, the objective of this research was to develop a viscoelastic finite element model of a muscle fiber incorporating experimentally-measured desmin filament properties and then to compare model predictions with experimental data from real fibers.

METHODS

A muscle fiber model was developed in which sarcomeres were represented by a viscoelastic four-element model. Sarcomeres are rigidly connected longitudinally at Z-disk nodes and each node is connected to the node above and below it by a desmin elastic element creating a finite element mesh. The parameters of the model are based on twenty experimentally-measured properties of mouse muscle taken from the literature. A Matlab routine evaluates the equations-of-motion at quasi-equilibrium, progressing through time to determine the transient fiber deformation for the specified parameters.

Ten simulations of passive stretch and isometric contraction were performed on DKO and WT muscle fibers that include random variation in passive tension. The sarcomere misalignment, or Z-disk variability, was then expressed as the mean variance of the nodal displacement across the fiber. Additionally, isometric force generation was determined as a function of desmin concentration.

RESULTS

For the cases of simulated passive stretch, mean Z-disk variability increased in DKO fibers relative to WT (Fig 1).
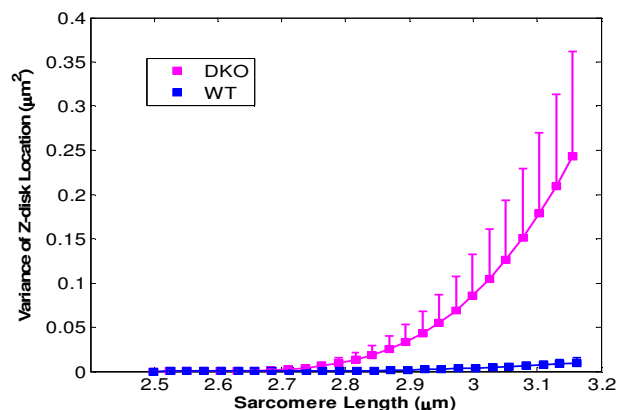
Figure 1: Z-disk variance in simulated fibers.

When compared to passive stretch applied to real WT and DKO fibers (Fig 2), it can be seen that in both cases Z-disk variability increases non-linearly with increasing strain. A similar non-linear relationship is seen for Z-disk variability as a function of time during simulated isometric contraction.
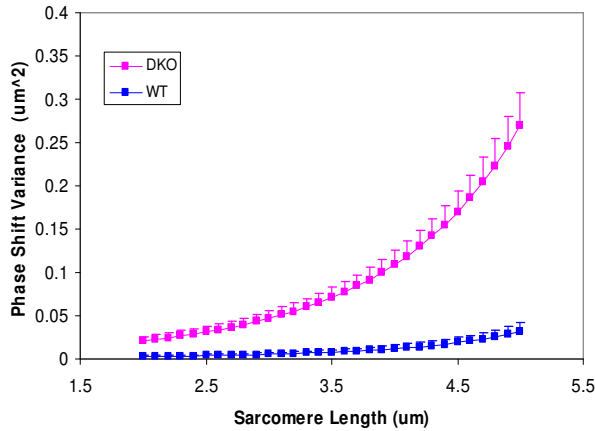
Figure 1: Experimental fibers (B) subjected to passive stretch as a function of sarcomere length (Shah et al., 2004).

Experimental fibers transfected with varying percentages of desmin show both a decrease in isometric stress production and a non-linear relationship between desmin concentration and percent isometric stress decrease following eccentric contraction (Fig 3).]
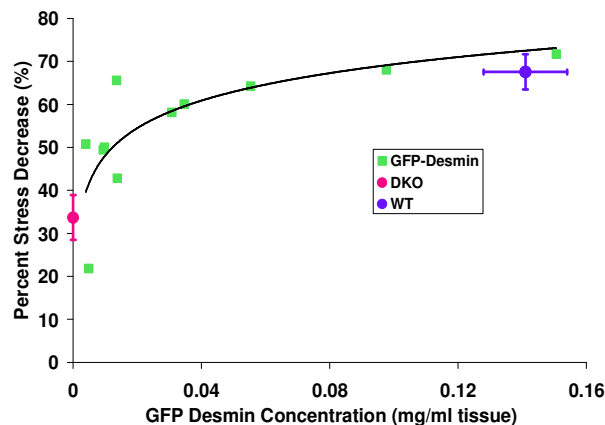
Figure 3: Percent stress decrease following eccentric contraction as a function of percent desmin concentration (unpublished).

Varying the concentration of desmin in the simulated fiber with and without preferential localization shows a similar non-linear relationship between percent desmin and isometric force production (Fig 4).
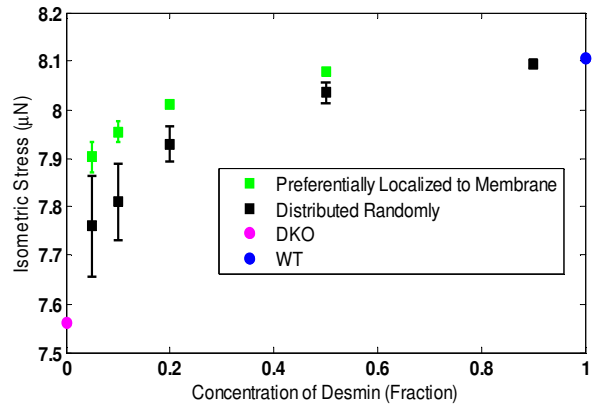
Figure 4: Active force production as a function of desmin concentration in simulated fibers. Force decreases with desmin fraction.

DISCUSSION

A finite element model of a skeletal muscle fiber was developed which faithfully simulates the WT and DKO fiber mechanical behavior, including predictions of decreased sarcomere alignment, decreased isometric force production and a non-linear relationship between desmin content and force production. Future studies will focus on further experimental work to investigate model predictions of desmin localization.

REFERENCES

Morgan et al. (1982). *Biophys. J.,* 39:189-96
Shah et al. (2004). *Biophys. J.,* 86:2993-3008.
Kiss et al. (2006). *J. Struct. Biol.,* 155:327-39.
Sam et al. (2000). *Am. J. Physiol Cell Physiol* 279: C1116-C1122

ACKNOWLEDGEMENTS

KINEMATIC AND KINETIC CHANGES DURING GAIT BEFORE AND AFTER BOTULINUM TOXIN A TREATMENT IN CHRONIC STROKE

Alison C. Novak[1], Stephen Bagg[2], Brenda Brouwer[3]

[1]School of Rehabilitation Science, Motor Performance Laboratory, Queen's University, Kingston, ON, Canada, 5acn@queensu.ca
[2]Providence Care, St. Mary's of the Lake Hospital, Kingston, ON, Canada,
[3]School of Rehabilitation Science, Queen's University, Kingston, ON, Canada,

INTRODUCTION

Following stroke, decreased mobility and reduced function can be attributed in many cases to excessive muscle tone of the plantarflexors (Lamontagne et al., 2002). Botulinum toxin A (BTX-A) is becoming a more common treatment in clinical practice to reduce muscle stiffness. However, the biomechanical effectiveness of BTX-A treatment in the ankle plantarflexors on gait has not been established. This study describes the kinematic and kinetic profiles of the lower limbs during walking to determine the impact of BTX-A injections of the ankle plantarflexors on gait performance.

METHODS AND PROCEDURES

Nine hemiparetic stroke subjects with plantarflexor hypertonicity were recruited for the study. The subjects were instructed to walk at a self-selected pace numerous times over an 8 metre long walkway instrumented with two AMTI force platforms. Full lower limb, three dimensional, bilateral gait analysis (Optotrak 3020 motion analysis system) provided joint angle and power profiles of the ankle, knee and hip throughout stance. Data were collected at baseline, two weeks post BTX-A treatment of the ankle plantarflexors (T1), and 10 weeks post treatment (T2). Repeated measures ANOVA was used to determine if joint kinematics or kinetics changed over time.

RESULTS

Following BTX-A injection, subjects demonstrated reduced plantarflexion (p=0.05) and increased ankle range of motion (p<0.05) on the affected side throughout stance (Figure 1a). At the knee, a significant reduction in the maximum knee extension angle (p=0.034) of the affected leg was seen at T2. The percentage of stance in which the knee was in hyperextension demonstrated a trend towards reduction (p=0.097) (average of 59.3% (S.D. 35.3%) to 45.2% (S.D. 34.7%)). (Figure 1b). There were no significant kinematic changes seen at the hip.
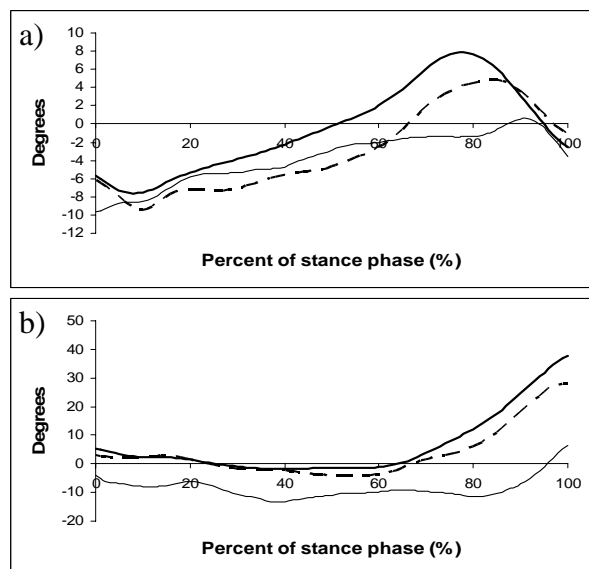
Figure 1. Representative kinematic profiles for one subject of the affected ankle (a) and knee (b) at baseline (thin line), two weeks post treatment (dashed line) and ten weeks post treatment (solid thick line)

Of the kinetic variables, no significant changes were detected post injection relative to baseline. However, examination of the individual data revealed four of the nine subjects were able to increase power generation at the ankle post injection and six subjects demonstrated increased positive work at the hip post treatment (Table 1), with only three subjects demonstrating improvements in both ankle and hip positive power profiles by 10 weeks post-injection.

	Max ankle power (W/kg)	Positive hip work (J/kg)
Baseline	0.44 (0.38)	9.61 (9.12)
T1	0.61 (0.45)	11.36 (10.91)
T2	0.59 (0.40)	12.18 (10.11)

Table 1. Joint power and work variables of the affected ankle and hip. Data are means (SD), from subjects who demonstrated improvements compared to baseline only. T1=Two weeks post-injection; T3=ten weeks post-injection.

DISCUSSION

Hypertonicity of the ankle plantarflexors restricts passive movement and therefore limits rotation of the ankle during stance (Perry et al., 1978). Following BTX-A treatment, subjects were able to achieve increased range at the ankle and reduced hyperextension at the knee. It is likely that increased compliance of the plantarflexor muscles allowed rotation of the leg over the foot, resulting in improved functional kinematics (Sutherland et al., 1999). Kinematic changes were seen at two weeks post-injection, but significance at ten weeks post-injection suggested that gains in muscle distensibility were sustained.

Only four of the nine subjects achieved increased ankle power post treatment. However, six subjects demonstrated increased positive work at the hip. It is possible that decreasing plantarflexor tone would allow the full extent of the plantarflexor muscle

weakness to manifest, and an increase in hip work was required to generate sufficient power as a compensation (Nadeau et al., 1999) in subjects who were not able to take advantage of the normalized ankle and knee kinematics (improved rotation of the leg over the foot in stance). In these subjects, perhaps adjunct therapy (such as strength training of the ankle musculature) should be used in conjunction with BTX-A treatment to maximize the benefits of tone reduction.

SUMMARY

Botulinum Toxin A injection of the ankle plantarflexors results in improved ankle and knee kinematics throughout the stance phase of gait. Although there were no significant changes in terms of kinetics, some subjects were able to increase ankle power generation. In the cases where increased work at the hip was seen with no increases in ankle power, the reduction of tone may have exposed the impact of the underlying weakness of the ankle musculature. BTX-A may be best used as a tool in conjunction with other therapy to maximize the benefits of tone reduction.

REFERENCES

Lamontagne A et al. (2002). *Gait Posture,* 15:244-255.
Nadeau S et al. (1999). *Clin Biomech,* 14: 125-135.
Perry J et al. (1978). *Clin Orthop Relat Res,* 131:47-53.
Sutherland DH et al. (1999). *Gait Posture,* 10:1-9.

ACKNOWLEDGEMENTS

FEEDBACK DRIVEN LOCOMOTOR ADAPTATION IN A HUMAN SPINAL CORD INJURY POPULATION

Keith Gordon[1], Ming Wu[1, 2], Jennifer Kahn[1] and Brian Schmit[1, 2, 3]

[1] Rehabilitation Institute of Chicago, Chicago, IL, USA
[2] Northwestern University, Chicago, IL, USA
[3] Marquette University, Milwaukee, WI, USA
e-mail: keith-gordon@northwestern.edu

INTRODUCTION

Spinally transected rats are capable of rapidly adapting locomotor patterns in response to external perturbation (Heng and de Leon, 2007). This finding has important clinical implications for gait rehabilitation following spinal cord injury. We have demonstrated that during stepping, humans with spinal cord injury increase hip extension torque when a dorsiflexor torque is applied about the ankle during stance phase (Gordon et al., 2007). We hypothesized that humans with spinal cord injury would adapt their locomotor patterns (demonstrated by aftereffects) following a short training period of stepping with an externally applied ankle-foot load. Specifically, we expected to see a lasting increase in hip extension torque following training. We also performed catch trials to investigate changes in the control strategy underlying locomotor adaptation.

METHODS AND PROCEDURES

We recorded EMG, kinematics and joint torque from the lower limbs of eight subjects with incomplete spinal cord injury, ASIA C and D, actively performing airstepping (stepping movements performed with 100% body weight support). A Lokomat provided kinematic assistance at the knee and hip joints. Bilateral, powered ankle-foot orthoses were used to mechanically load the ankle and foot. When powered, the orthoses created a

dorsiflexor torque (~0.5 Nm/kg) during the stance phase of the step cycle. In the disengaged state, the orthoses allowed free sagittal plane rotation about the ankle.

Subjects performed airstepping for 12 minutes (~300 steps). No load was applied to the subjects' ankle and foot during the first and last 100 steps. During the intermediate 100 steps, subjects received bilateral, ankle-foot stance load. Twelve catch trials, distributed across the three testing conditions, were included to investigate the feed forward / feedback components of the subjects' locomotor strategy. Catch trials during the two no load conditions consisted of loading a single limb during the stance phase of one step cycle. Conversely, catch trials during the stance load condition consisted of removing load unilaterally during a single step cycle.

RESULTS

During the initial no load condition subjects increased hip extension work by ~ 59% when given stance load catch trials (0.35 J/kg) compared to the immediately preceding no load step (0.22 J/kg), ($p < 0.05$) (Fig. 1, 2). Hip extension work also increased significantly ($p < 0.05$), ~160%, during the stance load condition (0.57 J/kg) compared to the initial no load condition (Fig. 1). Hip extension work during the first no load catch trial (0.46 J/kg) was not significantly different from preceding stance load step ($p > 0.05$).
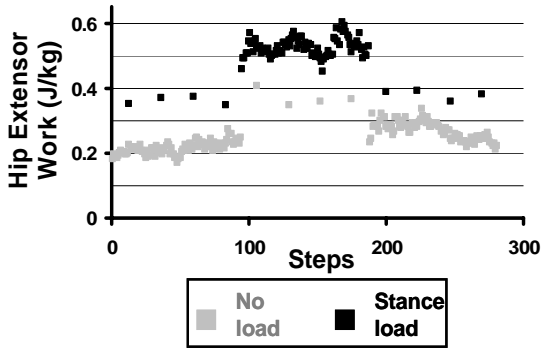
Figure 1. Mean hip extension work increased significantly when load was applied. Changes in the difference between catch trials and baseline may indicate changes in locomotor control strategy.

This additional increase can be attributed to several factors including load afferents from the contralateral limb and a progressive increase in reflex response to the repetitive stimulation. These factors may also explain why hip extension work did not return to the no load baseline levels during the catch trials of the stance load condition. Following the stance load condition, subjects' hip extension torque remained elevated for an extended period after ankle-foot load was removed. The change in hip extension work observed during the catch trials vs. no load stepping during the final condition suggests that the elevation in hip extension torque may have been a result of subjects initially adjusting their neural strategy to rely more on feed forward / non-ankle-load related feedback control. These findings may be valuable for improving gait rehabilitation methods.

However, work performed during the stance load step immediately preceding the final no load catch trial was ~58% greater than work performed during the catch trial (0.36 J/kg) ($p < 0.05$) (Fig. 1, 2). Following the transition from the stance load condition to the no load condition subjects decreased hip extension work significantly ($p < 0.05$) (Fig. 1). However, hip extension work initially remained elevated during the final no load condition compared to the initial no load condition (Fig. 1). During the final no load condition, hip extension work performed during the first stance load catch trial (0.38 J/kg) was not significantly different than work performed during the preceding no load step (0.30 J/kg) ($p > 0.05$). In contrast, hip work during the final stance load catch trial (0.38 J/kg) was significantly greater than the preceding no load step (0.24 J/kg) ($p < 0.05$).

DISCUSSION

Results from catch trials performed during the initial no load condition suggest that in spinal cord injury subjects potentially 60% of hip extension work performed during stepping is regulated by feedback from ipsilateral ankle-foot load. In addition, we observed further increases in hip extension work when subjects received multi-step bilateral ankle-foot load.

REFERENCES

Gordon KE, Wu M, Schmit BD (2007) Annual Meeting of the ASB, Palo Alto, CA.
Heng C and de Leon RD (2007). J. Neurosci. 27, 8558-8562.

ACKNOWLEDGEMENTS
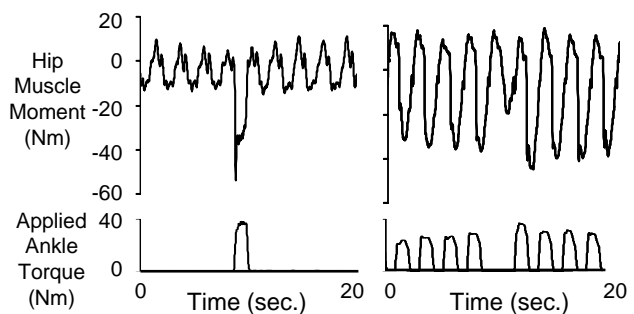
Figure 2. Individual data from the initial no load and stance load stepping conditions.

PREDICTING QUADRICEPS FATIGUE DURING ELECTRICALLY STIMULATED NON-ISOMETRIC CONTRACTIONS

Susan Marion[1], Maury Hull[2] and Anthony Wexler[3]

[1]Biomedical Engineering, University of California, Davis, CA 95616, msmarion@ucdavis.edu
[2]Mechanical and Aeronautical Engineering and Biomedical Engineering Programs, University of California, Davis, CA 95616, mlhull@ucdavis.edu
[3]Mechanical and Aeronautical Engineering, Civil and Environmental Engineering, and Biomedical Programs, University of California, Davis, CA 95616, aswexler@ucdavis.edu

INTRODUCTION

Functional electrical stimulation (FES) is increasingly used by individuals with paralysis to regain functional movement, but muscle fatigue can limit the applicability of this technology. The ability to predict FES-induced muscle fatigue would enable design of control strategies for producing functional limb movements repetitively. An existing force model together with a fatigue model can predict isometric fatigue in the quadriceps (Ding et al., 2000) The force model has been expanded to predict force in non-isometric contractions (Perumal et al., 2006), but a fatigue model for these contractions has not been developed. This study's objectives were to 1) determine whether modifications to the fatigue model are necessary to predict fatigue in non-isometric contractions, 2) if so, then incorporate necessary modifications into the fatigue model, and 3) test the predictive accuracy of the modified model on human subjects.

METHODS AND PROCEDURES

The force model (Perumal et al., 2006) incorporates muscle activation and contraction dynamics. The input is stimulation timing. The output is torque, angle, and angular velocity as functions of time. The isometric fatigue model (Ding et al., 2000) predicts changes in force model parameter during fatigue. The input is force predicted by the force model and the outputs are three of the force model parameters, A_θ, K_m and τ_1, as functions of time. Experiments were conducted using a computer-controlled stimulator that sent trains of pulses to surface electrodes on the thighs of seven able-bodied subjects; force was measured at the ankle. The pulse duration was 600 μs and the amplitude was set to produce maximal excursion of the leg with 9.1 kg applied to the distal leg. Three non-isometric and one isometric fatiguing leg extension sessions per subject were required to identify the fatigue model parameters and to assess the model accuracy. Each session was separated by >48 hours. All sessions included both isometric and non-isometric non-fatiguing leg extension tests to identify the force model parameters (Perumal et al., 2006). During the non-isometric leg extensions, either 0, 4.5, or 9.1 kg was applied to the freely swinging distal leg.

Model parameters were identified by minimizing the sum of squares error between the model and observations. Predictive accuracy was determined from linear regression analyses and RMSE of the maximum angular displacement and angular velocity.

RESULTS

The fatigue model required modification. Angular velocity and three parameters were

added. The new parameters are functions of the other parameters within the existing force-fatigue model.

The predictive accuracy of the force-fatigue model was relatively high. Increasing the applied load increased both the measured and predicted fatigue, as determined by the reduction in angular velocity and angular displacement (Figure 1).
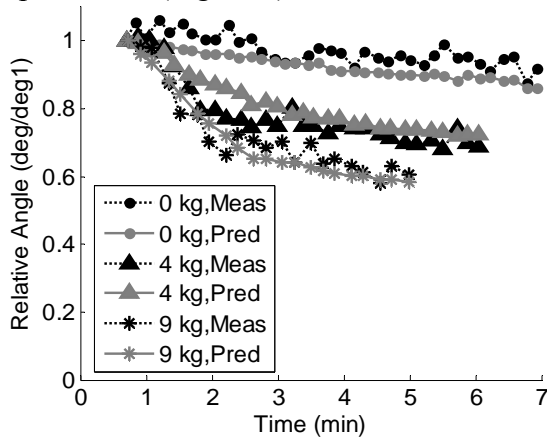
Figure 1. Average relative angular displacements in response to 33 Hz pulse trains. Every 6th contraction is shown and is normalized to first contraction (deg1).
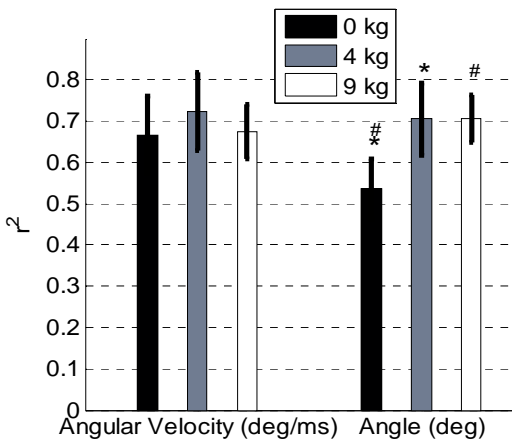
Figure 2. Average linear regression coefficients of determination (r^2; ± 95% confidence limit). Matching symbols significantly different at p = 0.0005.

Average r-squared values for the maximum angular velocity for all applied loads were > 0.65 (Figure 2). The average r-squared values

for the maximum angular displacement for the 4.5 kg and 9.1 kg loads were 0.7 (Figure 2), however the average r-squared value for 0 kg was 0.54. In general, at least 65% of the variability in the measurements was explained by the model.

The RMSE values were low compared to the initial and final angular velocities and displacements. For angular displacement, the maximum initial values ranged from 68 to 58 deg, and minimum final values ranged from 59 to 31 deg, for 0 and 9 kg, respectively. Average RMSE values were 7.5, 5.5, and 7.0 deg for 0, 4.5, and 9 kg, respectively.

DISCUSSION

Others have shown that a decrease in force and a decrease in maximum velocity are consequences of non-isometric fatigue (De Ruiter et al, 1999). When our force-fatigue model was modified to account for angular velocity, fatigue was reasonably well predicted. Day-to-day differences in the number and types of muscle fibers recruited, in the initial conditions, and in the resting position of the freely swinging leg before each contraction may have contributed to the random error.

REFERENCES

Ding J et al. (2000). *J Appl Physiol,* 89:1322-32.

Perumal R et al. (2006). *J Biomech*, 39: 2826-36.

ACKNOWLEDGEMENTS

GENDER DIFFERENCES IN POSTURAL CONTROL STRATEGIES DURING PROLONGED STANDING

Erika Nelson-Wong, Diane E. Gregory, David A. Winter and Jack P. Callaghan

Department of Kinesiology, Faculty of Applied Health Sciences, University of Waterloo, Waterloo, ON, Canada, enelsonw@ahsmail.uwaterloo.ca

INTRODUCTION

Gender differences in hip muscle function have been found in athletic populations during high-demand tasks. Females were found to use a significantly lower percentage of their available gluteal muscle strength compared to males to control a single leg drop landing (Zazulak, et al., 2005). These findings appear to be due to differences in control strategy rather than in strength.

It has been demonstrated that medio-lateral control of the centre of pressure (COP) is primarily due to activation of the hip abductors and adductors through a load-unload mechanism. This has been found to be independent of the ankle musculature which controls the antero-posterior COP (COP_{A-P}) (Winter, 2003). Therefore it is the purpose of this work to determine if females demonstrate a pattern of decreased utilization of hip abductors for control of medio-lateral centre of pressure (COP_{M-L}) during a low-demand activity of prolonged standing compared to males.

METHODS AND PROCEDURES

Twenty-three participants (twelve male, eleven female) stood for two hours in a constrained area for this study. Ten channels of continuous electromyography (EMG) were collected from four bilateral trunk and left and right gluteus medius muscles (LGM, RGM). Force plate measurements were used to calculate COP_{M-L} and COP_{A-P}.

Cross-correlation analyses were used to quantify the common signal (R_{xy}) between each linear enveloped EMG signal and COP excursion in the antero-posterior and medio-lateral directions to provide information about postural control. Root mean square values of the COP excursion (COP_{rms}) and normalized, linear enveloped EMG (EMG_{rms}) for fifteen minute windows were also calculated to compare average COP movement and muscle activation between groups. Dependent measures of R_{xy}, EMG_{rms}, and COP_{rms} were entered into a general linear model with a between factor of gender, and within factor of time with eight repeated measures over the 2-hour standing period. Significance was set at $P < .05$.

RESULTS

There was no main effect of time, and no interactions between time and gender for any of the dependent measures.

No significant differences were seen between genders in COP_{rms} for antero-posterior or medio-lateral directions.

There were significant differences in EMG_{rms} of the LGM between genders ($F_{1,21}$=4.972, P = .037), but not in RGM (Figure 1). There was no main effect of gender in R_{xy} values for EMG signals cross-correlated with COP_{A-P}.

Only the LGM and RGM EMG signals cross-correlated with COP_{M-L} were found to have a significant main effect of gender ($F_{1,21}$=

13.836, $P = .001$, $F_{1,21} = 20.672$, $P < .001$ respectively).
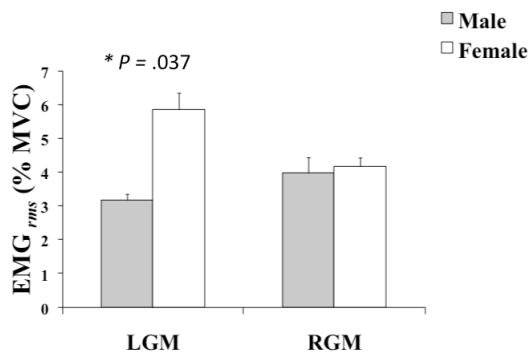
Figure 1. Females demonstrated greater average LGM activation over the 2-hour standing period than males.

Figure 2 shows the average R_{xy} values over the two-hour standing period for LGM and RGM cross-correlated with COP$_{M-L}$. Note that R_{xy} values for LGM-COP$_{M-L}$ are negative due to the polarity of the COP signal. As the LGM is activated, the COP moves towards the left, which is in the negative direction, resulting in a negative R_{xy} value.
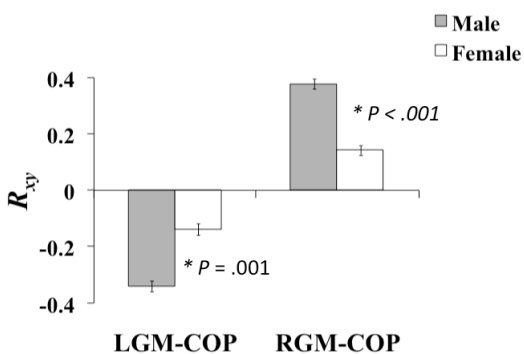
Figure 2. Males demonstrated higher correlation of LGM and RGM activation with COP$_{M-L}$ movement than females.

DISCUSSION

Both males and females demonstrated a load-unload mechanism through the hip abductors for control of medio-lateral COP in standing. Males however appear to be more hip-dominant in their medio-lateral postural control than females. It is interesting that although females do not appear to control the COP movement from the hip as much as males do, they actually demonstrated higher average activation at the left hip abductors than males did during this 2-hour standing activity. This is in contrast to findings from studies involving higher demand activities, where females were found to have lower activation of the hip musculature than males.

An obvious limitation of this study is that EMG was not collected from the hip adductors or from other lower extremity musculature. Therefore it is difficult to isolate more clearly the particular control strategy used by females during prolonged standing.

SUMMARY

Males and females clearly demonstrate different strategies for medio-lateral postural control during standing. More work is required in this area to further investigate these differences and isolate specific mechanisms.

REFERENCES

Winter DA, et al., (2003). *J Electromyogr Kinesiol,* 13: 49-56.

Zazulak, BT, et al., (2005). *JOSPT,* 35(5): 292-299.

ACKNOWLEDGEMENTS

GROUND REACTION FORCES IN SKATEBOARDING: THE OLLIE

Matthew Nevitt[1], Jeremy Determan[1], Joseph Cox[1] and E. C. Frederick[2]
[1]Sole Technology Institute, Lake Forest, CA, USA, Matthew.Nevitt@soletechnology.com
[2]Exeter Research, Inc., Brentwood, NH, USA

INTRODUCTION

Skateboarding is a popular activity that had over 11 million participants in 2006 in the US alone; a 5.2% growth over 2005 (SGMA, 2007). Skateboarding's continued growth in participation now exceeds total participation rates for tackle football and regular participation rates for baseball by more than one million participants (SGMA, 2007). Despite its popularity, little is known about even the most basic of skateboard maneuvers.

The Ollie is one of the most common movements in skateboarding. This maneuver allows the rider to hop onto, off of, and over obstacles encountered while skateboarding all without ever touching the skateboard with his hands. This basic movement is a key component of many other skateboard maneuvers.

Despite its importance to skateboarding, little is known about the biomechanics of this movement. In 2006 a study was published on the kinetics of the Ollie using professional skateboarders for test subjects (Frederick et al., 2006). They studied the movement using a single platform height of 45.7CM, a height considered relatively tall by many amateurs. Therefore, the purpose of this study was to examine the Ollie at various heights and compare how the kinetics might vary between professional and amateur skateboarders.

METHODS AND PROCEDURES

Ten male, amateur skateboarders visited the laboratory at the Sole Technology Institute to participate in this study (mean body mass = 68.8KG, SD = 8.3KG). Although amateur, all subjects far surpass the "frequent participant definition" (SGMA, 2007). Each subject performed six movements: Ollie Up Conditions 1-3 (OU1, OU2, OU3) and Ollie Down Conditions 1-3 (OD1, OD2, OD3).

The OU2 and OU3 movements required the subject to ride his board onto the force plate, mounted at floor level, and Ollie up onto a level wooden platform either 22.9CM (OU2) or 45.7CM (OU3) above floor level and either 26.7CM (OU2) or 45.7CM (OU3) beyond the end of the force plate. For the OU1 condition the wooden platform was removed and the subject was instructed to Ollie up as high as necessary to land with all four wheels completely off the force plate (landing at floor level).

The OD2 and OD3 movements required the subject to roll toward the edge of the wooden platform (located 22.86CM [OD2] or 45.72CM [OD3] above floor level) and Ollie off the platform down onto the force plate mounted at floor level. For the OD1 condition the wooden platform was removed and the subject was instructed to Ollie before the force plate, from floor level, and land on the center of the plate.

A large AMTI model BP12001200 force plate was used to measure ground reaction forces (GRFs). GRF data were collected for ten trials of each condition for each subject. The GRF data were collected at 1000Hz and low-pass filtered using a fourth-order Butterworth filter with a 50Hz cut-off frequency. All

subjects were required to wear the same model of skate shoe (Model: éS EK-01). Subjects were allowed to use their own skateboards.

RESULTS

For each OU condition the resulting Vertical Ground Reaction Force (VGRF) had a consistent two humped shape as observed in the previous study (Frederick et al., 2006). For all subjects and all OU trials the Nose/Tail Ground Reaction Force (N/T GRF) had a consistent two peak shape. The second of these N/T GRF peaks corresponds to what skateboarders refer to as the "tail-smack" phase of an Ollie. The direction of this force is toward the tail of the skateboard and thus in the lateral direction of the subject's rear foot while skating forward. This movement causes the board to rapidly rotate around the rear axel, "smack" into the ground, and then rebound into the air. Mean peak VGRFs for all subjects and trials as well as mean peak N/T GRFs for all subjects and OU trials are shown in Table 1.

Platform Height(CM)	Peak OU VGRF(BW)	Peak OD VGRF(BW)	Peak N/T GRF(BW)
0	2.13 (.20)	3.77 (.70)	.074 (.02)
22.86	2.18 (.21)	4.61 (.80)	.072 (.02)
45.72	2.14 (.22)	5.44 (.88)	.079 (.02)

Table 1. Mean Peak VGRFs and N/T Tail-Smack Forces for All Subjects and Trials Normalized to Body Weights (SD).

DISCUSSION AND CONCLUSION

Average peak VGRFs for all subjects for all OU conditions were found to be quite similar regardless of the wooden platform height. Further analysis of the GRF, motion capture, and video data collected for this study may be necessary to understand the reason(s) for this unexpected similarity.
Average peak VGRFs for all subjects for all OD conditions were higher than expected given the previous study of Ollie kinetics (Frederick et. al., 2006). In that study average peak VGRFs for professional skateboarders Ollieing down from a 45.7CM platform were found to be $4.519 \pm .582$BW. The authors noted that these forces were higher than expected given relatively lower VGRFs from other jump landing studies. They concluded that this was caused by the subjects intentionally "spiking" their landings in order to stabilize themselves on top of the skateboard. In our study average peak VGRFs for subjects Ollieing down from a similar height were found to be .92BW greater. Perhaps amateur skateboarders need to spike their landings even harder to stabilize themselves. It is also possible that this difference in force was due to a difference in the height the subjects Ollied off the 45.7CM platform before landing down on the force plate.

Average peak N/T tail-smack forces were unexpectedly similar in magnitude among all OU conditions and trials for all subjects. Interestingly this peak N/T GRF corresponded with a peak vertical tail-smack force. The magnitude of this force is not reported in this abstract.

REFERENCES

Frederick, E.C. et al. (2006). *J Appl Biomech*, 22:33-40.

SGMA (2007). *SGMA 2007 Sports & Fitness Participation Report from the USA Sports Participation Study*, 1-5.

DETERMINING BIOMECHANICAL PROPERTIES OF FALLS USING AN ADULT ANTHROPOMETRIC DUMMY

Daniel P. Steed, Jennica L. Roche, Mark S. Redfern

Human Movement and Balance Laboratory, Department of Bioengineering,
University of Pittsburgh, Pittsburgh, PA, USA
Email: dps3@pitt.edu URL: http://hmbl.bioe.pitt.edu/home.htm

INTRODUCTION

The future of fall detection may be a wearable device that automatically notifies emergency services. To create such a device, it is essential to characterize the biomechanics of falls. Previous studies have investigated falls while protecting subjects from injury using a padded floor or harness (Smeesters, 2001 & Pijnappels, 2004). These methods render the collection of body kinematics at ground impact impossible, thus a literature gap exists that characterizes full-body fall impact biomechanics. The purpose of this study was to characterize head, thorax, and pelvis accelerations in anterior, posterior, and lateral falls using a Hybrid III anthropometric test dummy (ATD).

METHODS AND PROCEDURES

A "50th percentile male" adult Hybrid III ATD (First Technology Safety Systems, MI) was used to investigate anterior, lateral, and posterior falls. Motion capture data (Vicon 612 / M2 camera system) was collected to orient accelerations based on anatomical segments. The head, thorax, and pelvis were each instrumented with a triaxial accelerometer (head & pelvis: Analog Devices ADXL330; thorax: Freescale Semiconductor MMA7261QT; 110Hz per axis) to record angular accelerations relative to their anatomical position.

The ATD was suspended by a single head bolt with only its feet touching the floor in a near-vertical position. With the joint stiffness adjusted to minimally support the weight, anterior, posterior, and lateral falls were tested. Anterior falls were performed with the knee and hip joints loose and rigidly locked in a straight-leg position. In all cases, the ATD was allowed to fall freely on the vinyl tile floor below.

RESULTS

The head, thorax, and pelvis all experienced accelerations under 19gs. Averaged over all fall types, the average peak acceleration for the head, pelvis, and thorax was 15.56g (±3.24), 2.04g (±1.08), and 0.64g (±0.05), respectively.

Two types of posterior falls were experienced. In the first type ("posterior sit"), the ATD fell backward into a seated posture. In this situation, only the pelvis contacted the floor. The head and thorax experienced vibrations due to shock through the body, not from physical contact with the floor. In the other type ("posterior lay"), the backward fall continued from a seated posture to a laying position that caused the pelvis, thorax, and head to all contact the floor.

Figure 1 shows the average peak acceleration values averaged over all anterior, posterior and lateral fall iterations. Overall, the head experienced the greatest average acceleration magnitude of in lateral falls. Minimum head accelerations were experienced in "posterior sit" falls.
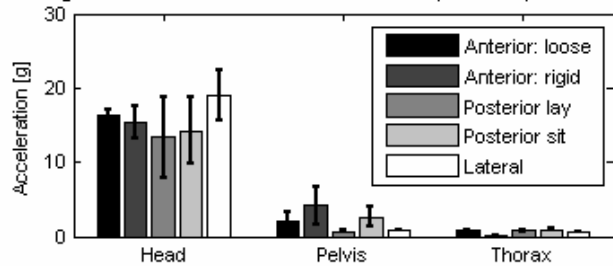
Figure 1. Average peak acceleration values of the head, thorax, and pelvis in anterior, posterior, and lateral falls with standard deviations.

DISCUSSION

Anterior falls with "loose" joints may occur from syncope or from other pathologies. Anterior falls were also performed with rigid leg joints to mimic the responses of patients with Parkinson's disease who lack the ability to make quick, controlled movements. Thus, of all falls tested, these may be the most realistic. Lateral falls are often experienced by the elderly due to loss of balance and may lead to hip fracture.

Of the three segments tested, the head experienced the greatest overall average acceleration. The head falls from the greatest height allowing more momentum and inertia before contact with the floor.

The thorax experienced the lowest overall average acceleration. This may be due to the fact that the thorax is protected by the surrounding areas of the body. When striking the ground with the head or the pelvis, the shock is absorbed by other body parts, consequently diminishing the acceleration in the thorax.

The accelerations experienced by the pelvis were much smaller than those in the head for every fall condition. The greatest overall average accelerations in the pelvis occur in fall conditions where it hit the ground before the head or thorax. The posterior falls had the greatest variability in average peak acceleration due to the unpredictable nature of the segments that actually contact the ground as well as the fall itself.

The ATD model suffered from a few limitations. First, it is a passive system. The ATD does respond in the same physiological manor as a conscious human would. Thus, the data is useful only for specific types of falls. Second, the ATD was not made for fall testing, thus ill-equipped for fall replication. Lastly, the power of this study is diminished due to the low repetitions.

SUMMARY

The need exists for a device that automatically detects falls and contacts the emergency services. This study examined head, thorax, and pelvis accelerations during anterior, poster, and lateral falls using an adult Hybrid III ATD. In these three types of falls, the head experiences the greatest overall acceleration and the thorax experiences the least.

REFERENCES

National Safety Council (Feb 19, 2008). <http://www.nsc.org/index.htm>
Pijnappels et al. (2004). *J Biomech,* 38:627-634.
Smeesters et al. (2001). *J Biomech,* 34:309-317.

ACKNOWLEDGEMENTS

COMPARISON OF THREE DIMENSIONAL PATELLOFEMORAL JOINT REACTION FORCES IN PERSONS WITH AND WITHOUT PATELLOFEMORAL PAIN

Yu-Jen Chen and Christopher M. Powers

Musculoskeletal Biomechanics Research Laboratory, Division of Biokinesiology and Physical Therapy, University of Southern California, Los Angeles, CA
URL: http://pt2.usc.edu/labs/mbrl/   e-mail: yujensch@usc.edu

INTRODUCTION

Patellofemoral pain (PFP) is one of the most common disorders affecting the lower extremity. [1,2] Although it is commonly assumed that PFP is the result of abnormal patellofemoral joint loading, [3] there is little evidence to support this premise. Using a subject specific three dimensional model, the purpose of this study was to determine if persons with PFP demonstrate differences in patellofemoral joint reaction forces (PFJRF) compared to pain-free controls.

METHODS AND PROCEDURES

Twenty individuals with PFP and twenty pain-free controls were recruited for this study. All subjects underwent two phases of data collection: 1) MRI assessment of the knee, patellofemoral joint, and thigh, and 2) kinematic, kinetic and EMG analysis during walking (80 meters/min), running (200 meters/min) and ascending/descending stairs (50 steps/min).

An overview of the model is illustrated in Figure 1. Using data obtained from magnetic resonance imaging (MRI) and clinical measurements, a subject specific representation of the extensor mechanism was created using SIMM modeling software (MusculoGraphics, Santa Rosa, CA). Individual gait data were used to drive the model (via an optimization routine) and three dimensional vasti muscle forces and subsequent three dimensional PFJRF's were computed. The following subject specific input variables were used in the model: 1) three dimensional kinematics of the lower extremity, 2) net knee joint moment in the sagittal plane, 3) hamstring and gastrocnemius EMG, 4) extensor mechanism lever arm, 5) vasti muscle orientation, 6) vasti muscle physiological cross-sectional area proportions, 7) patella flexion angle, and 8) patella ligament orientation. Model outputs consisted of the resultant PFJRF as well as the posterior, superior and lateral components of the PFJRF. Comparisons of peak forces were made between groups across conditions using a 2-factor ANOVA. This analysis was repeated for the resultant PFJRF and each component of the PFJRF
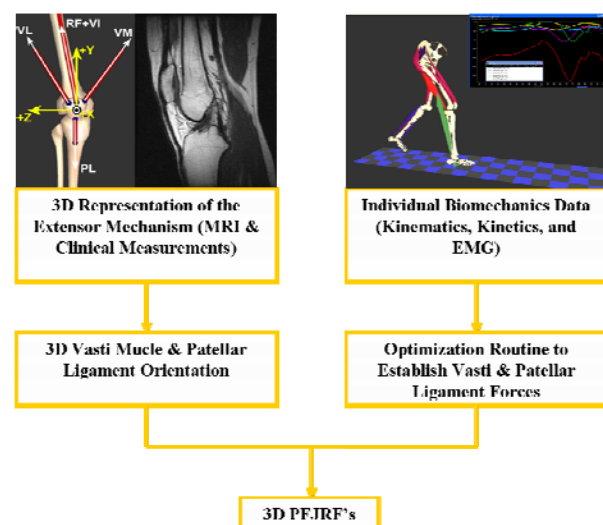
Figure 1. Patellofemoral joint model used to estimate 3D patellofemoral joint reaction forces

RESULTS

When averaged across all conditions, the PFP group demonstrated lower peak resultant PFJRF's compared to the control group (25.9 vs. 32.2 N/kg-bwt; Fig.2). Although similar decreases were observed in the PFP group for the peak posterior (24.2 vs. 30.5 N/kg-bwt) and superior (7.9 vs. 10.4 N/kg-bwt) components of the PFJRF, the PFP group had higher peak lateral forces compared to the control group across all conditions (5.0 vs. 2.2 N/kg-bwt).
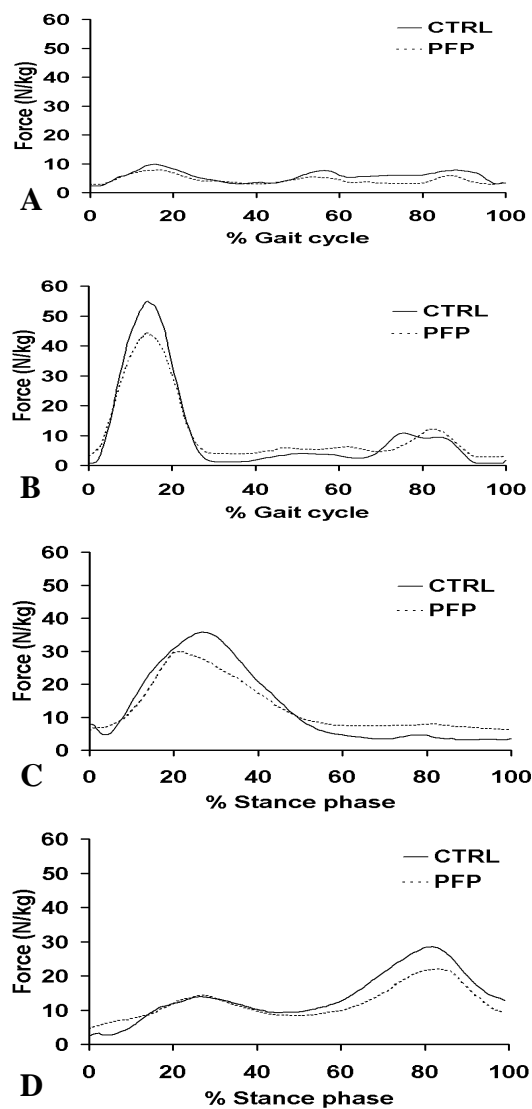
Figure 2. Resultant PFJRF's during walking (A), running (B), ascend stairs (C), and descend stairs (D).

DISCUSSION

When average across all conditions, the peak resultant PFJRF's were 20% lower in the PFP group. This finding is consistent with Heino et al. who reported a 22% and 33% decrease in peak PFJRF's in persons with PFP during walking and stair ascent respectively.[4,5] When the resultant PFJRF was broken down into its orthogonal components, the forces were always in the posterior, superior, and lateral directions. Despite the lower posterior and superior forces, the PFP individuals demonstrated higher peak lateral forces when compared to the control group. This finding was observed in three of the four tasks.

SUMMARY

The lower resultant, posterior and superior forces observed in the PFP group support the premise that these individuals may be employing strategies to minimize patellofemoral joint forces (i.e. quadriceps avoidance). However, the higher lateral forces in the PFP group are consistent with clinical observations of lateral patella subluxation in this population.

REFERENCES

1. Fulkerson JP. (2002). *Am J Phys Anthrop,* 30:447-456.
2. Malek M, and Mangine R. (1981). *J Orthop Sports Phys Ther,* 2:108-116.
3. Goodfellow J et al. (1976). *J Bone Joint Surg Br*, 58:291-9.
4. Heino Brechter J, and Powers CM. (2002). *Med Sci Sports Exerc*, 34:1582-93.
5. Brechter JH, and Powers CM. (2002). *Gait Posture*, 16:115-23.

ACKNOWLEDGEMENTS

THE DYNAMIC QUADRICEPS ANGLE:
A COMPARISON OF PERSONS WITH AND WITHOUT PATELLOFEMORAL PAIN

Yu-Jen Chen and Christopher M. Powers

Musculoskeletal Biomechanics Research Laboratory, Division of Biokinesiology and Physical Therapy, University of Southern California, Los Angeles, CA
URL: http://pt2.usc.edu/labs/mbrl/   e-mail: yujensch@usc.edu

INTRODUCTION

Lateral subluxation of the patella is commonly thought to be contributory to the development of patellofemoral pain (PFP).[1,2] The tendency for the patella to track laterally is largely dictated by the angle between the resultant quadriceps force vector and patellar ligament force vector (ie. Q-angle). Typically, the Q-angle is quantified statically using a goniometer. However, it has been recently proposed that segmental motions of the lower extremity during dynamic tasks may increase Q-angle and the lateral force acting on the patella (i.e. dynamic Q-angle).[3] Using a subject specific 3D model of the patellofemoral joint,[4] it is possible quantify the Q-angle during dynamic tasks. The purpose of this study was to determine if persons with PFP demonstrate higher dynamic Q-angles compared to pain-free controls during functional activities.
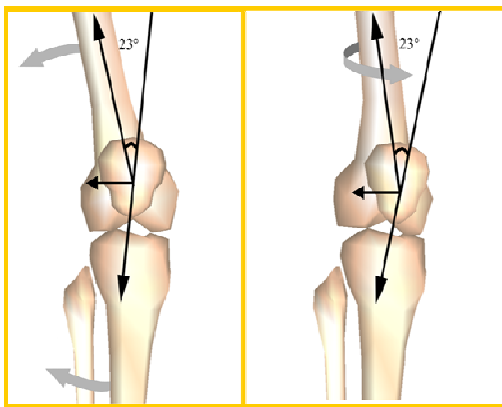
Figure 1. Segment motions that increase Q-angle during dynamic tasks

METHODS AND PROCEDURES

Twenty individuals with PFP and twenty pain-free controls were recruited for this study. All subjects underwent two phases of data collection: 1) MRI assessment of the knee, patellofemoral joint, and thigh, and 2) kinematic, kinetic and EMG analysis during walking (80 meters/min), running (200 meters/min) and ascending/descending stairs (50 steps/min).

Using data obtained from magnetic resonance imaging (MRI) and clinical measurements, a subject specific representation of the extensor mechanism was created using SIMM modeling software (MusculoGraphics, Santa Rosa, CA). Individual gait data were used to drive the model (via an optimization routine) and three dimensional vasti muscle forces and subsequent three dimensional PFJRF's were computed (Figure 1). The following subject specific input variables were used in the model: 1) three dimensional kinematics of the lower extremity, 2) net knee joint moment in the sagittal plane, 3) hamstring and gastrocnemius EMG, 4) extensor mechanism lever arm, 5) vasti muscle orientation, 6) vasti muscle physiological cross-sectional area proportions, 7) patella flexion angle, and 8) patella ligament orientation.

The dynamic Q-angle was calculated as the frontal plane projection of the angle between the 3-D quadriceps force vector and the 3D patellar ligament force vector. Group differences in the average dynamic Q-angle across conditions were assessed using a 2-factor ANOVA (group x condition).
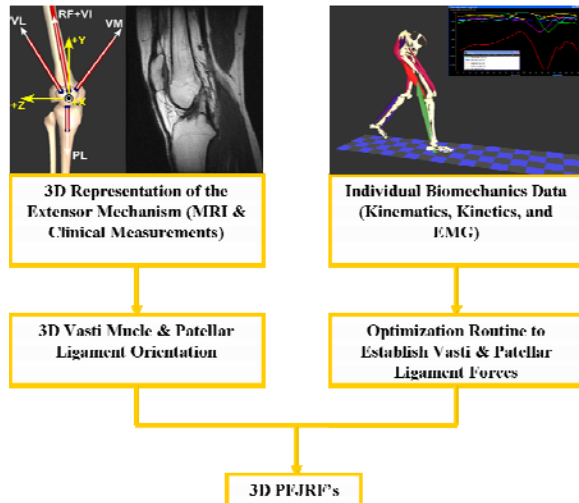
Figure 1. Patellofemoral joint model used to estimate the dynamic Q-angle.

RESULTS

ANOVA results revealed a significant group effect (no interaction). When averaged across all conditions, the average dynamic Q-angle was significantly higher in the PFP group compared to the control group (34.9 vs. 22.3 degree). The average dynamic Q-angle difference was greatest during stair descent (39.1 vs. 24.2 degrees).
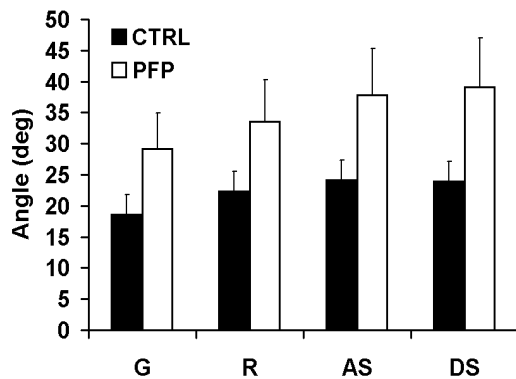
Figure 2. Average dynamic Q-angle during functional tasks between groups (G=gait, R=running, AS=ascend stairs, DS=descend stairs).

DISCUSSION

The higher dynamic Q-angles observed in the PFP group indicate that these individuals are more susceptible to lateral patella forces during dynamic tasks. The greatest group difference was observed during stair descent which happens to be the task most commonly associated with clinical symptoms. The average dynamic Q-angle values for both groups exceed previously reported values for "normal" static measurements (ie. 15-20 degrees).[5] This finding reinforces previous assumptions that the pathomechanics associated with patellofemoral joint dysfunction may be related to dynamic function.

SUMMARY

Persons with PFP demonstrated greater average dynamic Q-angles compared to pain-free controls. This finding suggests that these individuals are more susceptible to laterally directed forces acting on the patella and is consistent with the clinical observations of lateral patellar subluxation in this population.

REFERENCES

1. Goodfellow J et al. (2002). *J Bone Joint Surg Br,* 58:291-299.
2. Moller BN et al. (1989). *Acta Orthop Scand,* 60:188-191.
3. Powers CM. (2003). *J Orthop Sports Phys Ther,* 33:677-685.
4. Chen YJ et al. (2007). *ISB 2007 proceeding abstract.*
5. France L, and Nester C. (2001). *Clin Biomech,* 16:710–713.

ACKNOWLEDGEMENTS

Tibiofemoral Moments of Force and Co-Stabilization:
Revisiting the Non-Contact Mechanism of Anterior Cruciate Ligament Injury

Jeffery T. Podraza P.T., M.S.[1,2] and Scott C. White Ph.D.[1]

[1] Dept. of Exercise & Nutrition Sciences, School of Public Health & Health Professions
University at Buffalo, Buffalo, NY
Email: swhite@buffalo.edu
[2] Department of Physical Therapy, Adjunct Associate Faculty, Daemen College, Amherst, NY

INTRODUCTION

The majority of ACL injuries are caused by the non-contact deceleration (Boden et al., 2000). Large knee extensor moments and quadriceps overload with the knee near full extension are considered the primary components of these ACL injuries (DeMorat et al., 2004). The hamstrings are viewed as capable antagonists to quadriceps overload (MacWilliams et al., 1999) but their ability to counterbalance this load dynamically has been questioned (Colby et al., 2000). Knee moments and the stabilizing influence of lower limb muscles during deceleration impact landings at different knee flexion angles have not been described. The present study reports changes to knee moments and co-contraction indices using a controlled, impact landing model. It was hypothesized that knee extensor moments would increase with greater knee flexion at landing and that there would be an associated increase in knee muscle co-contraction.

METHODS AND PROCEDURES

Ten males performed a lunge deceleration movement from a height of 10.5 cm. Ground reaction forces (GRFs) and video data were collected for 3 trials with subjects landing with knee flexion angle ranges of $0 – 25^0$, $25 – 50^0$ and $50 – 75^0$. Knee joint moments were calculated via inverse dynamics using a similar data filtering strategy advocated by Bisseling & Hof (2006). Filter cut-offs were determined individually for each landing, for each subject based on frequency analyses of GRFs. Surface EMG was collected using bipolar Ag/AgCl electrodes placed over the vastus medialis and lateralis, medial and lateral hamstrings, medial gastrocnemius and the lateral soleus. EMG signals were analog to digitally sampled (16 bit) at 2400 Hz after being amplified and bandpassed from 10 to 500 Hz. EMG RMS values were determined for a 0.6 sec window starting 0.3 s prior to the peak vertical GRF at landing. Muscle moments from the EMG RMS values were calculated for each muscle based on linear EMG-to-torque regression equations. The equations were determined from EMG-to-torque modeling calibration trials performed on a Cybex II isokinetic dynamometer. The equations were based on variable effort contractions and considered EMG-to-torque as a function of joint angle.

Peak knee extensor moments and muscle torque values were averaged for each condition across all subjects. Co-contraction (CCI) and co-stabilization (CSI) indices were calculated (Winter, 1990) using:

$$\%cocon = 2M_{antag} / (M_{agon} + M_{antag}) \cdot 100$$

The quadriceps and gastrocnemius were considered agonists and hamstrings antagonists for the CCI. The CSI calculation included soleus as an antagonist based on its closed chain posterior translation effect on the tibia (Elias et al., 2004).

RESULTS AND DISCUSSION

The peak knee extensor moment significantly increased (p < .05) as knee flexion at landing increased (Fig. 1). The CCI (Fig. 2) and CSI (Fig. 3) significantly decreased (p < .05) for the two deepest flexion angles. Greater extensor moments were expected due to an increased external flexor moment arm with increasing knee flexion. A decrease in CCI and CSI was unanticipated as more co-contraction for stabilization was expected with greater knee extensor moments. Higher hamstring moments to counterbalance anterior tibial draw was anticipated but our results show the opposite trend. Deceleration ACL injuries occur with the knee near full extension; therefore, high knee extensor moments and low co-contraction indices were expected for the $0-25^0$ condition, which was not the case. Interestingly, the inclusion of soleus as an antagonist for the CSI calculation resulted in complete counteraction of the anterior tibial draw muscles with the knee near full extension $0-25^0$ (Fig. 3). This outcome suggests protection of the ACL might be enhanced if soleus was more active during deceleration activities. The results of the present study are limited to our controlled experimental protocol but suggest the accepted view of the non-contact mechanism of ACL injury requires further consideration.

REFERENCES

Bisseling & Hof, (2006) *J Biomechanics* 39:2438-2444
Boden et al. (2000) *Orthopedics*. 23:573-578
Colby et al. (2000) AJSM, 28:234-240
DeMorat et al. (2004) *AJSM,* 32:477-483
Elias et al. (2004) *AJSM*, 31:241-246
MacWilliams et al. (1999) *J Orthop Res*. 17:817-822
Winter, DA. (1990) *Biomechanics and Motor Control of Human Movement* 2nd ed. John Wiley & Sons, Inc.
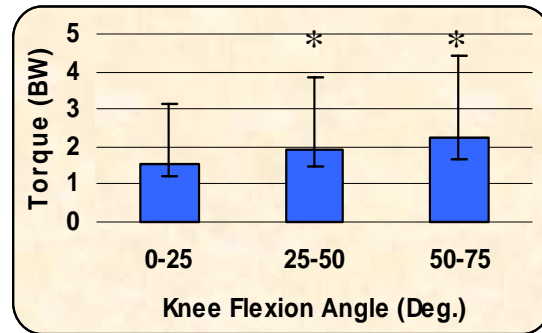
Figure 1. Peak knee extensor moments normalized to bodyweight (BW).
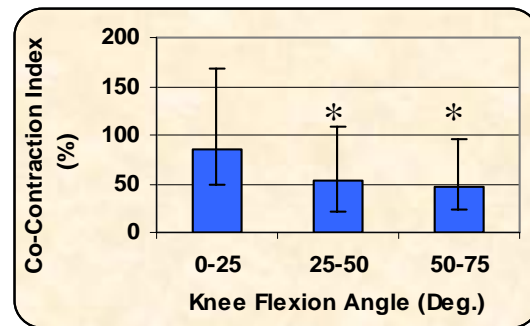
Figure 2. Co-contraction index between the quadriceps-gastrocnemius and hamstrings. 100% equals full co-contraction, < 100% implies extensor moment dominance.
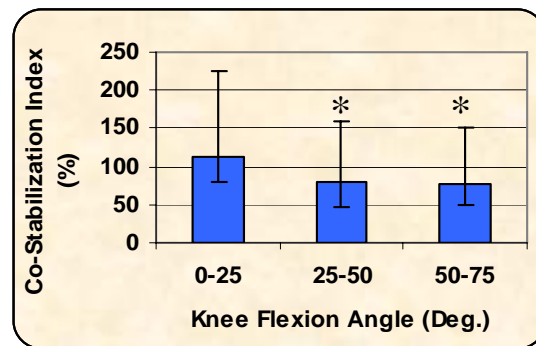
Figure 3. Co-stabilization index between the quadriceps-gastrocnemius and hamstrings-soleus. 100% equals full co-contraction, < 100% implies extensor moment dominance.

Pulling a Fast One: Mechanical Response of Articular Cartilage to High Frequency Loading

Matt Szarko[1] and John Bertram[2]

[1]PhD Student, Department of Medical Science, University of Calgary, Calgary, AB, Canada,
mjszarko@ucalgary.ca
[2]Professor, Department of Cell Biology and Anatomy, University of Calgary, Calgary, AB,
Canada

INTRODUCTION

An important, yet neglected area of articular cartilage research is understanding biomechanical responses to the full range of physiological loading rates. Investigations have shown that during heel strike, skeletal transients greater than 60 Hz (Simon *et al* 1981; Gillespie and Dickey 2003) are experienced by the lower limb and transfer up the boney skeleton, largely unattenuated, to the skull (Light *et al* 1980). The current study investigates the biomechanical behaviours of articular cartilage dynamically loaded between 0-100 Hz. Additionally, fast rates of loading were used to identify the mechanical properties of the principle solid matrix components of articular cartilage (type II collagen and proteoglycans).

METHODS AND PROCEDURES

Osteochondral dowels (8mm diameter) from mature bovine tibiae (obtained from a local abattoir) were harvested and split into three groups (N=20 per group) to more closely study the functional role of specific cartilage components in dynamic loading. Collagenolytic digestion (*C. histolyticum* - Worthington Biochemical Corp.) cleaved the collagen matrix, attempting to isolate proteoglycan behaviour. Chemical extraction with 4M GUHCl (Sigma-Aldrich) removed proteoglycans to isolate collagen behaviour. Controls were kept in PBS solution, while sham samples were exposed to either 0.05M Tris HCl or DMEM F12 media.

Samples were exposed to a spectrum of compressive loading rates (0-100 Hz). Loading was applied sinusoidally with an electrodynamic vibrator (Ling Dynamic Systems), driven by a function generator (SE Labs SR780). Waveform frequencies utilized a 'chirp' function, comprising equal amplitude sine waves perfectly periodic in the time record over the frequency spectrum. Loading was non-destructive and very low amplitude (0.01 MPa) in order to focus primarily on loading rate. Comparisons of input (displacement transducer) and output (force beam) signals were gathered and analyzed in the function generator. Phase angles and complex stiffness values were determined from storage and loss moduli and were used as measures mechanical behaviour. Testing occurred at 0hr, 4hr, and 8hr time points to identify changing biomechanics with increased matrix component isolation.

Two-way, repeated measures ANOVA with Tukey HSD post-hoc statistical tests were utilized in isolating differences between sample groups.

RESULTS

Biomechanical properties relating to viscous behaviours (phase angle measurements) significantly depended on the rate of loading. Under lower frequency loadings (0-15 Hz) no

significant differences were found between any of the treatments. At faster rates of loading (> 15 Hz), however, disparities were seen. Collagenase treated specimens witnessed a significant increase in fluid-like behaviours (seen as an increased phase angle) while GUHCl treated specimens showed a significant decrease in viscous properties (seen as a decreased phase angle).

Intriguingly elastic properties (shown by complex stiffness measurements) appear only to have been affected by the GUHCl treatment under all loading rates. These specimens experienced a significant decrease in complex stiffness.

DISCUSSION

Interestingly the results of this study reveal that alteration of specific matrix components oppositely affect the viscous properties of articular cartilage, but that these mechanical changes only occur under faster rates of loading. Elastic properties remain unaffected by loading rate, and only appear to be affected by proteoglycan leaching.

A compromised collagen matrix appears to significantly heighten the viscous behaviour of articular cartilage, while proteoglycan removal causes more linearly elastic, less viscous behaviour.

Additionally, the fact that proteoglycan removal causes decreased cartilage stiffness suggests that they play an important role in the maintenance of normal biomechanics both in terms of viscous and elastic material properties.

In osteoarthritis, contention whether initiation begins with collagen degeneration or proteoglycan leaching remains undecided (Buckwalter and Lane 1997). Insights gained from this investigation suggest that high frequency loading plays an important role in differentiating how articular cartilage behaves with a compromised matrix. Further, this study places an importance on identifying which matrix component is initially affected, since mechanical behaviours change depending on the matrix component compromised.

SUMMARY

This study reveals a previously unexplored area of articular cartilage biomechanics; high loading rate, low magnitude compressive loading. Results show specific biomechanical importance on each of the principle matrix components within articular cartilage with increasing loading rate.

REFERENCES

Buckwalter, JA and Lane, NE (1997). *AM J Sports Med,* 25: 873-881.

Gillespie, KA and Dickey, JP (2003). *Clinical Biomechanics,* 18: 50-59.

Light, LH et al. (1980). *J Biomech,* 13: 477-480.

Simon SR et al. (1981). *J Biomech,* 14: 817-822.

ACKNOWLEDGEMENTS

Stability of Multi-Finger Prehension Synergy: Exploration with Transcranial Magnetic Stimulation

Xun Niu, Vladimir M. Zatsiorsky and Mark L. Latash

Department of Kinesiology, The Pennsylvania State University, University Park, PA, USA, xun100@psu.edu

INTRODUCTION

The control of hand action is commonly viewed as based on a two-level hierarchy (Arbib et al. 1985): (1) The task is shared between the thumb and a virtual finger (VF, an imagined digit with the mechanical effect equal to that of the four fingers); and (2) VF action is shared among the actual fingers. Synergies at both levels can be studied as patterns of co-variation of its elements that stabilize the overall output (Zatsiorsky and Latash, 2004). We used single-pulse transcranial magnetic stimulation (TMS) as a perturbation to explore the stability of the three components of the prehension synergies: (a) internal forces, (b) resultant force, (c) moment of force exerted on the hand-held object.

METHODS AND PROCEDURES

Six male right-hand dominant subjects participated in the experiment. Five six-component force/moment transducers were mounted on an aluminum handle at the bottom of which a horizontal aluminum bar was attached. Three loads attached along the bar generated seven external torques clockwise and counterclockwise, as well as a zero torque. Focal TMS was delivered with a Magstim-200 stimulator with a 70-mm figure-of-eight coil, and was applied over the subject's hand projection in the left primary motor cortex.

The subjects were instructed to keep the handle vertically in the air exerting minimal grasping force. They looked at an air bubble level at the top of the handle. In each trial, a TMS stimulus was applied unexpectedly; the subjects had sufficient time to re-stabilize the handle. Three trials were performed in a block for each load/torque combination.

Force and moment of force signals were collected and changes in three components of the prehension synergy (corresponding to three equations of statics in two dimensions) were analyzed at the thumb–VF level for each task. Two stages of synergy restoration were identified.

RESULTS

The TMS-induced quick changes of digit forces showed increments in proportion to their background values. This led to predominantly positive co-variation among finger forces that violated two out of three components of the prehension synergy.

The normal forces showed a quick TMS-induced increase that was proportional to the background force. This was also true for the tangential forces produced by the thumb, middle and ring fingers but not by the index and little fingers. The total moment of force changed proportionally to its background value with predominance of supination responses. During the quick force response to TMS, patterns of digit force co-variation stabilizing the total tangential force and total moment were violated. Two stages of synergy restoration were identified taking about 0.3 s and 1.5 s. These times differed among the three synergy components (Table 1).

DISCUSSION
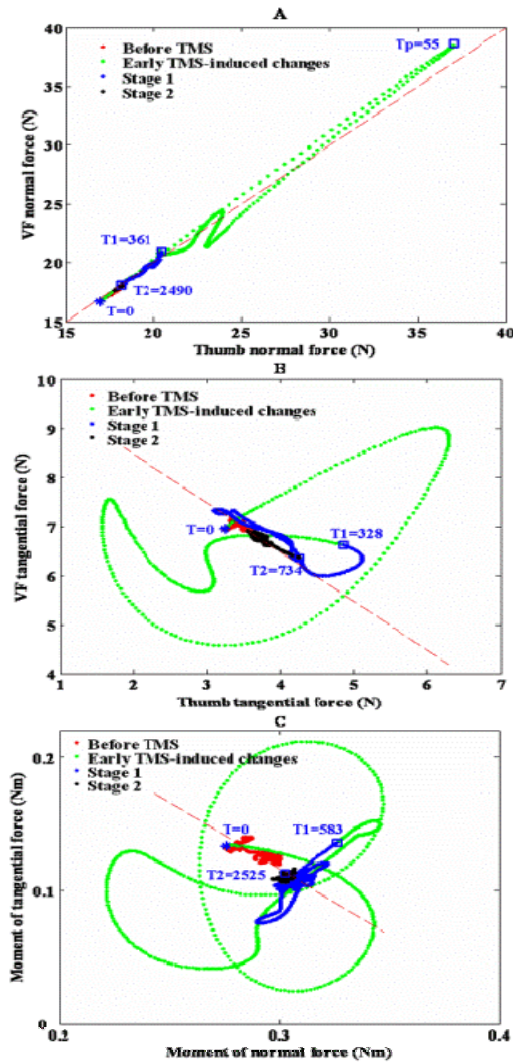
Figure 1. The relations between the VF and thumb normal forces (A), tangential forces (B), and moments produced by the normal and tangential forces (C) before and after a TMS stimulus. T=0 is the time when TMS occurred.

The results corroborate earlier observations on a close to proportional increase in finger force response to TMS with an increase in the background finger force (Danion et al., 2003). Our data show that this rule is valid for the normal finger forces and tangential forces produced by some of the digits, and for the total moment of force.

After a TMS pulse, patterns of co-variation between pairs of elemental variables corresponding to the equations of statics restored first, followed by a change in the magnitude of the performance. These observations support the idea of synergies as conjoint changes in elemental variables (Zatsiorsky and Latash, 2004) by showing that synergies stabilizing a certain mechanical variable exerted on the hand-held object may be present while there are still ongoing changes in the magnitude of that variable. This conclusion is also supported by the fact that the timing of synergy restoration was not affected by manipulations of the external load and torque, while the magnitudes of the mechanical variables produced by the hand were all affected by these factors as required by the equilibrium constraints. The results support an idea on independent control of the total force and moment of force as required by the principle of superposition (Zatsiorsky et al., 2004).

	Total normal force	Total tangential force	Total moment
Stage-1, T1	301±47	296±30	357±68
Stage-2, T2	1517±201	1181±168	1496±160

Table 1. Timing of synergy restoration. Data are mean ± SE.

REFERENCES

Arbib, MA et al. (1985). *Hand Function and the Neocortex.* Berlin, Springer Verlag.

Danion, F et al. (2003). *Clin Neurophysiol* 114: 1445-1455.

Zatsiorsky, VM and Latash, ML (2004). *Exerc Sport Sci Rev*, 32: 75-80.

Zatsiorsky, VM et al. (2004). *Robotica* 22: 231-234.

ACKNOWLEDGEMENTS

Grasping force magnitude affects the force sharing pattern in multi-finger prehension

Xun Niu, Mark L. Latash and Vladimir M. Zatsiorsky

Department of Kinesiology, The Pennsylvania State University, University Park, PA, USA, xun100@psu.edu

INTRODUCTION

To keep an object at rest in the air, the performers distribute the digit normal and tangential forces to satisfy the task requirements. A mechanically redundant task can be performed by various combinations of the digit forces and moments. It has been reported that human performers alter the magnitude of the total force by scaling the forces generated by the contributing elements (Valero-Cuevas, 2000). For example, at any combination of friction values at the individual fingertip-object contacts the performers select a certain 'template' of digit forces and then scale it linearly with the weight of the hand-held object (Niu et al. 2007). In this study, we are interested in (a) the effect of grasping force magnitude on the prehension synergies, i.e. conjoint changes of finger forces and moments, and (b) whether the scaling of a certain template is a universal mechanism of force control.

METHODS AND PROCEDURES

Subjects (n=7) were required to stabilize in the air vertically an instrumented handle with prismatic grasping. The forces and moments exerted by individual digits were recorded with 6-component sensors (ATI Industrial Automation, Garner, N.C.). Nine external torques that the subjects should resist varied among the trials from zero to 0.46 Nm both in clockwise and counterclockwise directions. The experiment had two phases. First, the subjects were instructed to hold the handle vertically with minimal normal (grip) force for 3 s. The computer recorded the force and then set a target force level at double the thumb normal force value. Visual feedback on the grip force and on target force was provided on the computer screen. Subjects were instructed to squeeze the handle until the force matched the target. The second phase lasted 17 s.

RESULTS

The ratio 'moment arm after force doubling/moment arm prior to the doubling' deviated from the 'gold standard' value of 0.5 necessary to maintain the moment of the normal force constant: it was larger than 0.6 at all pronation effort tasks and below 0.4 at all supination effort tasks (p<0.05). Moment arm is formed by the force couple of thumb and virtual finger (VF, an imagined digit with the mechanical effect equal to that of the four fingers). The moments of the normal forces M^n changed after the force doubling: the moment magnitudes decreased in the supination tasks and increased in the pronation tasks (Figure 1). The changes in the moments of the tangential forces (M^t) were opposite to the M^n changes; M^t increased in the supination tasks and decreased in the pronation tasks.

In the non-zero torque tasks the normal finger forces did not scale proportionally with the grasping force; the sharing percentage of the individual finger forces in the VF normal force changed with the grasping force increase. These changes depended on finger function (Figure 2), whether the finger acted against (moment agonist) or with the external torque (moment antagonist). In particular, in the tasks where the index and little fingers acted as moment antagonists, their forces

increased much more than in the tasks where these fingers served as torque agonists. The effects of the finger function on the middle and ring finger forces were less striking.
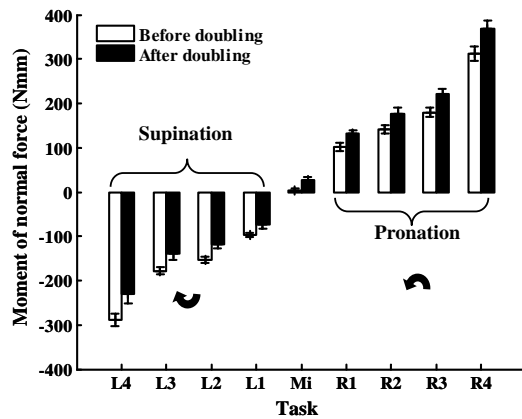
Figure 1. Changes of the moments of the normal forces after the virtual finger normal force doubling Group averages and standard errors.
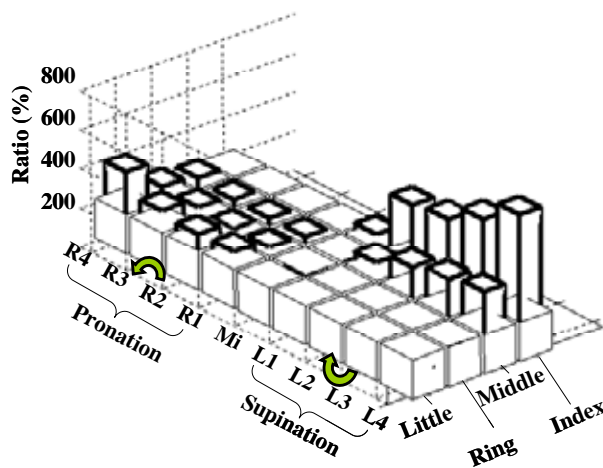
Figure 2. The normal finger forces after the doubling in % of their values before the doubling. The values above 200% are shown. A 200% value signifies the doubling of the individual finger force.

The grasping force doubling was accompanied by an increase in the thumb tangential force and a decrease of the VF tangential force such that the total force acting on the object in the vertical direction stayed constant. The decrease of the VF tangential force was achieved mainly by a decrease in the tangential force exerted by the index finger.

DISCUSSION

The M^ns after the doubling differed systematically from the values prior to the doubling. Hence, the central controller did not solve the problem of rotational equilibrium by adjusting only the normal finger forces; rather it preferred to prevent object tilting by simultaneous adjustments of both the normal and tangential forces.

The data indicate that the finger tangential forces are generated actively: the substantial changes of the index finger tangential force observed after the grasping force doubling cannot be explained by the passive mechanical properties of the fingers.

The total force doubling induced changes both in the percentage sharing of the total VF force among individual fingers and in the tangential forces exerted by individual fingers. Hence, in the present study the pattern of finger forces in grasping, i.e. their relative values, depended on the grasping force magnitude. Thus, the present study confirms that the scale invariance is not a general law of motor control; it is valid only for some tasks.

REFERENCES

Valero-Cuevas, FJ. (2000). *J Neurophysiol* 83:1469–1479
Niu, X et al. (2007). *J Neurophysiol*, 98: 16-28.

ACKNOWLEDGEMENTS

PRE AND POST ASSESSMENT OF NORMAL PRESSURE HYDROCEPHALUS PATIENTS USING A HEAD MOUNTED ACCELEROMETER

Brandy Wozniak[1], Stephen Dombrowski[2], Brian L. Davis[3], and Mark Luciano[2]

[1] Cleveland Clinic, Biomedical Engineering, Cleveland, OH, wozniab@ccf.org
[2] Cleveland Clinic, Pediatric and Congenital Neurosurgery, Cleveland, OH
[3] Cleveland Clinic, Biomedical Engineering, Cleveland, OH

INTRODUCTION

Normal pressure hydrocephalus (NPH) is a neurologic condition. It is diagnosed with imaging to confirm enlarged ventricles of the brain and little to no increase in intracranial pressure. NPH is generally seen in elderly patients (age≥55y.o.), and is attributed to cerebrospinal fluid (CSF) accumulation and abnormal brain compliance. The standard treatment is a surgical procedure, where a shunt is implanted to divert the CSF away from the brain. Neuropsychological and stability testing are helpful in the diagnosis and treatment of patients on an individual basis and in assessing the effects of shunting.

METHODS AND PROCEDURES

We assessed 59 patients (31 males and 28 females), ranging from 47 to 94 years old who underwent 36-hour CSF trial drainage as part of the diagnostic protocol for NPH. Patients who were diagnosed with NPH that went onto CSF shunt treatment (N= 27) were also assessed after 3 and 12 months.

Patients were asked to stand and perform a Romberg-type assessment with an accelerometer placed upon their head (Figure 1). A total of six tests were completed; three with the eyes open and three with the eyes closed. Random walk theory (Collins and DeLuca, 1993) was used to assess the path of antero-posterior versus medio-lateral head accelerations. Short term correlations (H1 values) were selected as the primary outcome variable.

Figure 1. Placement of head accelerometer on a subject.

RESULTS

Our statistical analysis shows that there is a significant difference (p = .001) between each visit (Figure 2) visit As the value H1 decreases, this indicates more coordination of movement, as a patient strives to maintain a steady upright posture. The time when H1 decreased corresponds to the 3rd visit, i.e., 3 months post-shunt.
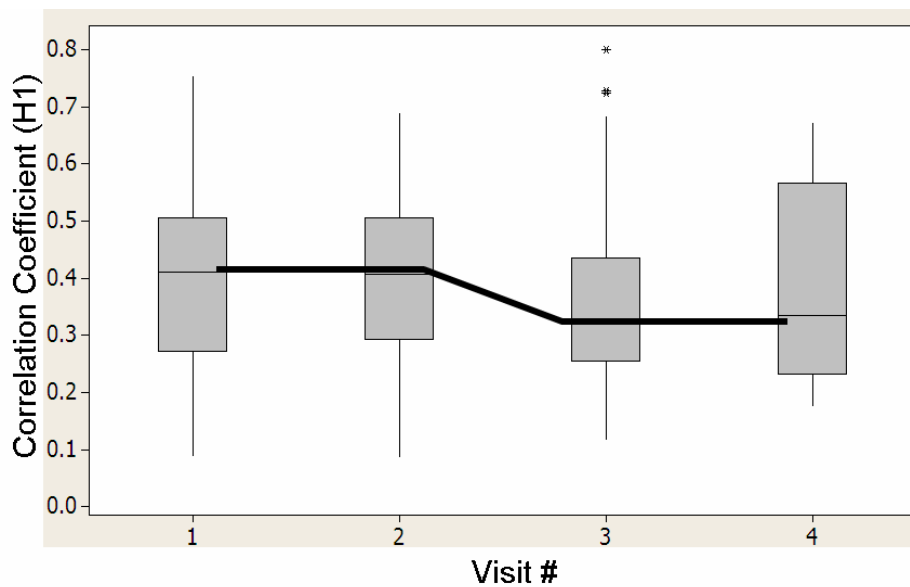
Figure 2. Average coefficients plotted at each visit. Visit 1 corresponds to the baseline condition, visit 2 is "post drainage", visits 3 and 4 are 3 months and 12 months post-op, respectively.

DISCUSSION

The maintenance of balance has always been a concern to various neurological patient populations, especially those with NPH. Gait disturbance and postural instability are prominent symptoms in patients with NPH, thus making these patients at risk for injuries relating to falling. Blomsterwall et al. found larger displacements and sway areas in NPH patients when compared to controls during quiet standing (Blomsterwall et al., 2000).

While the Romberg test itself is simple to administer, the head mounted accelerometer is a very small and convenient piece of equipment to use along with the test. The device is the size of a pager and simply requires placement upon the head and can be used in any preferred location.

At this time, biomechanical postural analysis has not been done on NPH patients. Having used the cranial accelerometer and analysed the data, we can see a significant difference in patients stability three months post shunt.

SUMMARY

Decisions for shunt placement are based on gait evaluation, cognitive testing, and patient/family self-report. Our head mounted accelerometer testing protocol, and the novel manner of assessing multiple trials easily, allows clinical decisions to be made as to whether patients' gait and dynamic balance have improved.

REFERENCES

Collins JJ, De Luca CJ. Open-loop and closed-loop control of posture. *Exp Brain Res* 1993; 95:308-18

Blomsterwall, E. et al. *Acta Neurologica Scandinavica* **102**, 284-291

ACKNOWLEDGEMENTS

ELECTROMYOGRAPHY EVALUATION OF MANUAL MUSCLES TESTS

Rebecca Brookham[1], Clark Dickerson[1] and Linda McLean[2]

[1]Kinesiology Department, Univ. of Waterloo, Waterloo, ON, Canada, rlbrookh@uwaterloo.ca
[2] School of Rehabilitation Therapy, Queen's Univ., Kingston, ON, Canada.

INTRODUCTION

The rotator cuff (RC) helps to stabilize the glenohumeral joint by depressing the humeral head and centering it in the glenoid fossa (Ferro et al., 2003). RC weakness could jeopardize this stability, ultimately resulting in compression and injury of the subacromial tissues (Burke et al., 2002). Manual muscle tests (MMTs) of the RC are maximal exertions used to evaluate muscle function and strength. These tests are intended to isolate specific RC muscles by minimizing contributions from surrounding musculature. However, few electromyography (EMG) evaluations have rigorously assessed the ability of MMTs to isolate RC muscles and confirm the diagnostic utility of these tests. Additionally, there is little information available on the effectiveness of alternative MMT posture/force configurations in achieving muscle isolation. The purpose of this study was to evaluate the ability of 29 MMTs to isolate the four RC muscles.

METHODS AND PROCEDURES

12 right-handed male subjects participated. EMG was recorded using a 16 channel Noraxon Telemyo[TM] 2400T G2 (Noraxon, Arizona, US). One bipolar intramuscular electrode was inserted into each of the four RC muscles. Ten bipolar surface electrodes were placed over surrounding muscles: deltoid (3), trapezius (2), p. major (2), lat. dorsi, biceps and triceps. Subjects performed maximal contractions against a stationary 3-axial force transducer during 29 MMTs. These MMTs represented 7 groups in two categories. 3 groups were MMTs often used by clinicians to target specific muscles: subscapularis, external rotators (infraspinatus and t. minor), and supraspinatus. 4 groups were resistance direction-defined groups of flexion and abduction exertions at 0° (at side), 45°, and 90° (horizontal) arm elevation. The force was directed four ways with respect to the hand: palmar, dorsal, radial, and ulnar.

Isolation ratios (IRs) were calculated for each RC muscle for all MMTs (Eq. 1). The resultant force produced at the hand was calculated in quadrature for each MMT from the 3-D hand force data. Maximal IR values indicate highest isolation of specific muscles.

$$IR = \frac{\dfrac{\% \text{ MVC for muscle i}}{100}}{\dfrac{\sum \% \text{ MVC for all other muscles}}{1300}} \qquad (1)$$

RESULTS

Currently, data for 6 of the 12 subjects have been fully analyzed. Tested MMTs generally isolated the RC muscles, but performance across subjects varied (Table 1), and the MMT for which maximum IRs existed was not identical across the subject pool.

Table 1. Range and mean of maximal IRs.

Muscle	Infra	Supra	T. Minor	Subscap
Range	1.6 - 5.8	1.4 - 5.3	1.0 - 6.6	0.7 - 8.2
Mean	3.3	3.3	3.2	3.2

Maximum specific muscle IRs often occured in the clinical MMTs groups (Figure 1), supporting their continued clinical utility. However, MMTs from these groups did not universally identify maximum IRs.

DISCUSSION

Our results show that some of the MMTs studied effectively isolate RC muscles, with activity up to eight times the average of other recorded muscles in cases. MMTs that yield maximal RC IRs aid muscle-specific strength evaluation, as other muscle contributions are minimal. This limits bias in clinical interpretation of forces produced at the hand.

   This study fills gaps in the rigor of clinical muscle strength assessment, which is critical in evaluating injury treatment programs. Few prior studies have investigated positions that most isolate RC muscles. Kelly et al (1996) defined optimal MMTs for the rotator cuff (excluding teres minor) during 29 isometric contractions based on a combination of maximal muscle activation, minimal synergist contributions, minimal pain provocation, and good test-retest reliability. However, unlike in our study, RC synergists were assumed to be consistent regardless of posture and hand force, neglecting data establishing that RC muscle function changes with posture (i.e. Liu et al., 1993), which may have biased results.

SUMMARY

Our results showed that specific MMTs can isolate RC muscles, and that current clinical assessment techniques are often effective in accomplishing these isolations. Multiple MMTs may be required for population analysis, as variation in MMTs producing maximal IRs existed across subjects.

REFERENCES

Burke, WS et al. (2002). *Clin Orth Rel Res,* 402:292-298.
Ferro, RT et al. (2003). *Adv Stud Med,* 3:518-26.
Kelly, BT et al. (1996). *Amer Jour Sports Med, 24*: 581-588.
Liu J et al. (1997). *Clin Biomech,* 12:32-38.
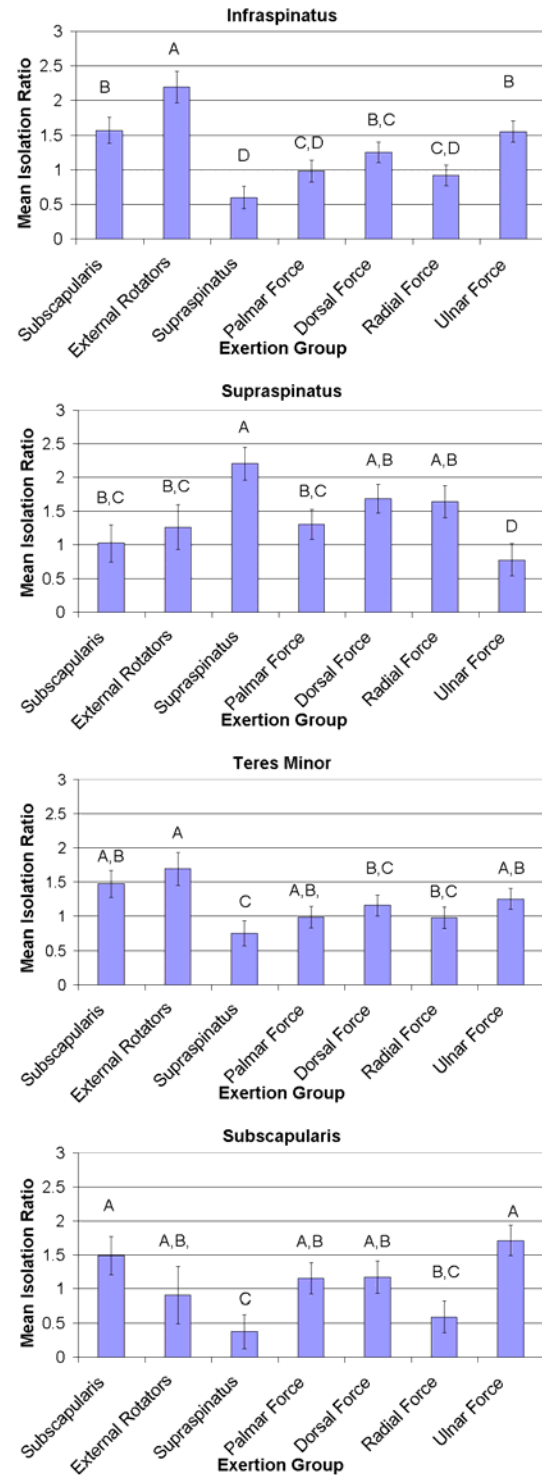
Figure 1. Mean (6 subjects) RC IRs organized by exertion group. Different letters denote significantly different groups. From top: results for infraspinatus, supraspinatus, teres minor, and subscapularis.

Kinematics of a Walking Spinal Cord:
Insights from a Novel Isolated Spinal Cord-Hindlimb Preparation

Heather Hayes[1], Shawn Hochman[1,2], Young-Hui Chang[1,3]

[1] Biomedical Engineering, Georgia Tech/Emory Univ, Atlanta, GA, USA
[2] Physiology, Emory Univ, Atlanta, GA, USA
[3] Applied Physiology, Georgia Tech, Atlanta, GA, USA
Email: heather.brant.hayes@gmail.com , http://www.ap.gatech.edu/chang/CNLmission.htm

INTRODUCTION

While the spinal cord contains all the circuitry required for producing the basic rhythmic motor patterns that underlie locomotion (central pattern generator, CPG), sensory information is known to play a vital role in refining the spatiotemporal features (Pearson 1995; Pearson et al. 1998). Many of the mechanistic details of the CPG have been elucidated using the isolated rodent spinal cord *in vitro*, in which the CPG can be reliably recruited via neurochemicals. While such preparations offer exquisite neural accessibility and control, the isolated cord ignores vital sensory and mechanical influences and lacks the ability to biomechanically characterize locomotor behavior (Atsuta et al. 1990; Cowley and Schmidt 1994a)

Here we describe a novel rodent spinal cord-hindlimb preparation (SCHP) that combines the neural accessibility and manipulability of *in vitro* preparations with the appropriate mechanical and sensory influences of *in vivo* locomotion. We present a biomechanical characterization of neuromochemically-induced hindlimb locomotion *in vitro*. We also compare hindlimb kinematics across mechanical conditions and between *in vitro* and *in vivo* conditions to show the importance of sensory and mechanical context in refining centrally generated motor output.

METHODS

Following spinal cord-hindlimb isolation from a neonatal rat (D1-D4), the SCHP was transferred to a locomotor chamber and perfused with oxygenated artificial cerebrospinal fluid. The cord was pinned dorsal-up onto a Sylgard step, with the hindlimbs hanging over the edge and allowed to locomote on a custom treadmill (Figure 1). Locomotion was then induced by 40-60µM serotonin (5HT) and 2-4µM N-methyl D-aspartate (NMDA) and sagittal plane kinematics collected using a video camera. Kinematics of the SCHP in the biomechanically-appropriate dorsal-up posture were compared to kinematics in a ventral-up posture. Dorsal-up SCHP kinematics were also compared to intact rat treadmill kinematic to determine whether the SCHP could produce typical movement patterns when provided with appropriate sensory and mechanical feedback.

RESULTS

In the dorsal-up posture, the SCHP exhibited kinematics similar to normal rat locomotion (Gillis and Biewener 2001). Both the ankle and hip extended during stance and flexed during swing, while the knee yielded at the beginning of stance under the weight of the hindquarters as expected (Figure 2). The joint trajectories produced in the ventral-up posture differed considerably from those in the dorsal-up posture. All joints were much more extended throughout the cycle, with large end-of-stance plateaus, and the knee failed to exhibit stance-phase yielding characteristic of normal stepping (Figure 2). Finally, the kinematics produced by the SCHP in the dorsal-up posture were strikingly similar to those observed in intact rat treadmill locomotion (Figure 2),

while the ventral-up kinematics compared well with intact rat airstepping kinematics (Stehouwer et al. 1994).

DISCUSSION AND SUMMARY

Together these results show the importance of mechanical context and sensory feedback in determining motor outcomes. The SCHP produced kinematic patterns that strongly resembled the patterns from the corresponding mechanical condition *in vivo*, suggesting that the SCHP preparation can exhibit task-appropriate kinematics despite being a reduced *in vitro* model. The similarities between the dorsal-up SCHP and intact rat joint trajectories show that the SCHP model is capable of producing locomotor patterns kinematically similar to normal rat behavior when given the appropriate environment, verifying that the dorsal-up SCHP can be used to study the CPG under behaviorally-relevant sensory and biomechanical influences.

REFERENCES
Atsuta Y, Garcia-Rill E, and Skinner RD (1990). *J Neurophysiol* 64: 727-735.
Cowley KC, and Schmidt BJ (1994). *Neurosci Lett* 171: 142-146.
Gillis GB, and Biewener AA (2001). *J Exp Biol* 204: 2717-2731.
Pearson KG (1995). *Curr Opin Neurobiol* 5: 786-791.
Pearson KG, Misiaszek JE, and Fouad K (1998). *Ann N Y Acad Sci* 860: 203-215.
Stehouwer DJ, McCrea AE, and Hartesveldt CV (1994). *Dev Brain Res* 82: 143-151.

Figure 1. Experimental Setup.
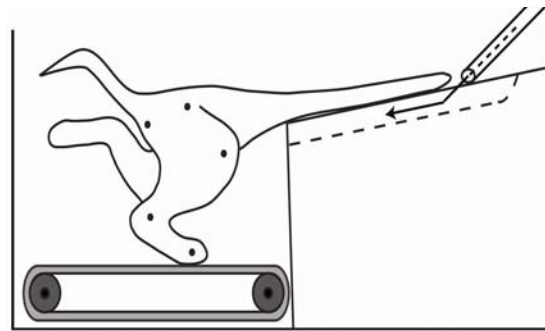
Figure 2. A) *In vitro* hindlimb joint angle trajectories in the ventral-up posture (gray) compared to dorsal-up posture (black) from representative rats. **B)** *In vivo* hindlimb joint angle trajectories from normal adult treadmill locomotion from a representative rat. In all cases, trajectories have been time normalized and averaged across cycles (n=20 cycles for ventral-up *in vitro*, n=17 for dorsal-up *in vitro*, n=13 for *in vivo*). All data are represented as mean (solid) ± standard deviation (dashed).
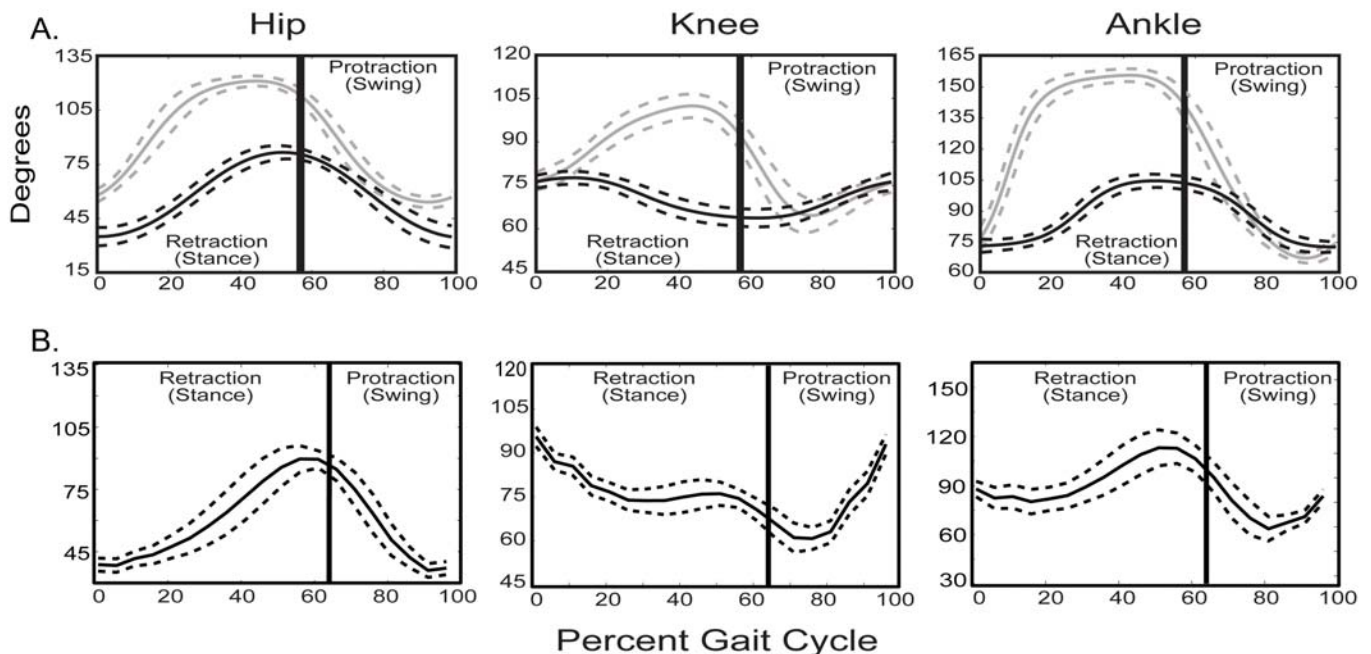
THE USE OF ARTIFICIAL NEURAL NETWORKS AS A DATA REDUCTION APPROACH IN DETERMINING CUMULATIVE EXPOSURES

Robert J. Parkinson and Jack P. Callaghan
University of Waterloo, Waterloo, ON, Canada, rjparkin@uwaterloo.ca

INTRODUCTION

Research indicates that the cumulative amount of loading (compression, shear, moments) to which a worker is exposed will affect the likelihood of their reporting low back pain or the occurrence of injury (Norman et al., 1998, Seidler et al., 2001). However, these conclusions are based upon external loads alone or simplified joint models which are not sensitive to individual differences in task performance. Simplified approaches have been used as obtaining the data required to implement models sensitive to individual performance is not currently possible in industry. For this reason, it is necessary to search for alternative approaches that will allow for predictions of loading in industry that are equivalent to those obtained with more sophisticated laboratory based methods. The ability of artificial neural networks (ANNs) to learn complex non-linear relationships may allow them to predict cumulative loading variables equivalent to those obtained with more intensive laboratory based models while requiring less input data than the laboratory based approaches.

DATA COLLECTION PROCEDURES

Data was obtained from 10 male and 10 female subjects (table 1) who performed lifts and lowers in several direction combinations (left, right and sagittal) and at two separate weights (7.56 and 9.73 kg). For each direction and load level participants were asked to perform 6 lifts and lowers in a continuous manner, resulting in 216 total manual material handling cycles.

Figure 1: Data collection set-up.

Electromyographic (EMG) signals were recorded bilaterally from 5 trunk muscle sites (Mirka and Marras, 1993) to be normalized and used in a gender specific EMG driven model that includes passive tissue contributions about all three L5S1 axes. Model anatomy was obtained from the work of Jorgensen et al. (2005) and Marras et al. (2001). Spine posture was tracked using the Lumbar Motion Monitor while 3D kinematic data was measured with an Optotrak Certus system. To allow for determination of joint moments and reaction forces at the L5S1 joint, participants performed all lifts while standing on a force platform (figure 1).

	Male	Female
Age (years)	25(3)	22 (2)
Height (m)	1.82 (0.09)	1.66 (0.07)
Mass (kg)	86.8 (7.9)	69.7 (8.0)

Table 1. Anthropometrics (means (SD)).

NEURAL NETWORK PROCEDURES

Two networks were created based upon preliminary data analysis. In order to determine which variables were most associated with the computed L5S1 muscle moments and bone on bone forces, correlation

coefficients were determined for each input-output combination. Using the most strongly correlated variables, three layer feed-forward neural networks were developed and trained to minimize the mean square error between the simulated and original L5S1 muscle moments and bone on bone forces. The following results are based upon networks created using data from two females (joint moments) and two males (forces), further tested with independent data from one additional gender matched subject.

RESULTS

Joint Moment: A neural network was developed to predict the L5S1 muscle moments about each of three axes with a mean error of 17.4 Nm using spine angles and vertical hand forces alone. Testing the network with a novel data set resulted in an overall underestimation of cumulative moment exposure of 28%, while testing of trials used to train the network indicated cumulative differences below 1%. The flexion moment from one lift/lower (novel data) is illustrated in figure 2.
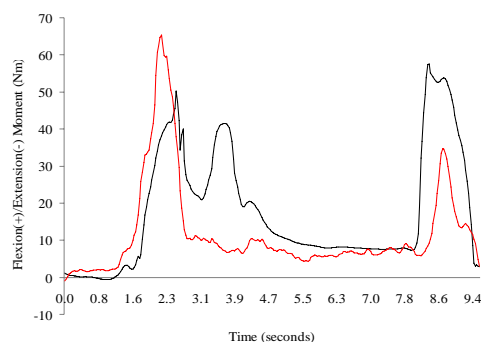
Figure 2. Original (black) and simulated (red) flexion moments.

Forces: It was found that spine forces can be estimated based on the input of bilateral latissimus dorsi and erector spinae (L3) activation as well as spine flexion angle. The network was trained to predict spine force with a mean error of 212.5 N. Exposure to a

novel data set resulted in errors in cumulative compression prediction of 11.5% (figure 3).
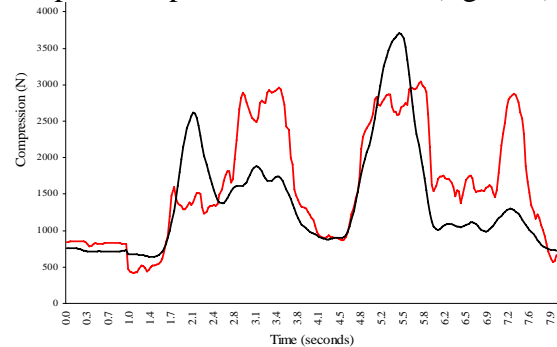
Figure 3. Original (black) and simulated (red) spine compression.

DISCUSSION

While ANNs have been used previously to bypass the limitations of industrial data collection by predicting EMG and spine loading based upon kinematic inputs (Hou et al., 2004), this study represents a novel attempt to reduce the amount of input data necessary to obtain strong estimates of cumulative exposure. Although errors can exceed 20% when the networks are presented with novel data, the low error levels for the data used in training indicates that future work expanding the number of subjects and trials in training may lead to improved network generalization.

REFERENCES

Hou, Y et al. (2004). *Proc 2004 Int Con Mac Learn and App.* 360-365.
Jorgensen, MJ et al. (2005). *Clin Biomech.* 20: 242-246.
Marras, WS et al. (2001). *Clin Biomech.* 16: 38-46.
Mirka, GA and Marras, WS. (1993). *Spine.* 18: 1396-1409.
Norman, RW et al. (1998). *Clin Biomech.* 13: 561-573.
Seidler, A et al. (2001). *Occup Environ Med.* 58: 735-746.

AUTOMATED METHOD FOR TRACKING CHANGE IN MUSCLE FASCICLE LENGTH FOR ULTRASOUND IMAGES

Manku Rana[1] and James Wakeling[1]
School of Kinesiology, SFU Canada, mrana@sfu.ca

INTRODUCTION

Amongst the main factors that determine the functional properties of a muscle are muscle architecture, muscle strain and strain rate. During concentric contraction fascicle length shortens and pennation angle increases. Ultrasonogrophy can be used to directly visualize in vivo skeletal muscle. Real time images of muscles can be obtained using B-mode ultrasound during any dynamic activity. To date there are no reliable methods to automatically track the fascicle orientations or strain from ultrasound images. The purpose of this study was to find an automated method to track change in length of muscle fascicles.

METHODS AND PROCEDURES

Ultrasound images (Echoblaster, Telemed; LT) were obtained from distal part of vastus lateralis close to knee from left leg of a subject during cycling. Images were extracted per frame from the video sequence (fig.1).Each image was segmented to obtain muscle fascicles. Methods used to find length change of fascicles are described below.
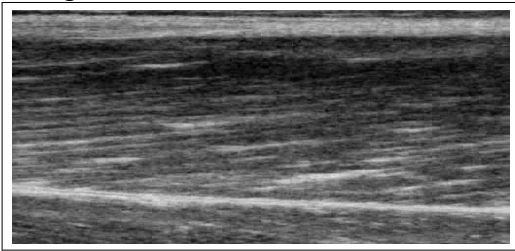
Figure 1 Image obtained from ultrasound

Multiscale vessel enhancement filtering was used to enhance tube like structure of muscle fascicles [Frangi et al].The image was first convolved with Gaussian of a particular scale (which is same as standard deviation of Gauss Function) and then a Hessian matrix was obtained at each pixel. Eigen values of the Hessian matrix were used to define vesselness function ($Vo(s)$) as follows:

$$V_o(s) = \begin{cases} 0 & if \lambda_2 > o \\ \exp\left(-\dfrac{R_\beta^2}{2\beta^2}\right)\left(1 - \exp\left(\dfrac{-S}{2c^2}\right)\right) \end{cases}$$

where λ_1 and λ_2 are Eigen values of Hessian such that $|\lambda_1| > |\lambda_2|$, $R_\beta = |\lambda_1|/|\lambda_2|$ is measure of line like structure and S= Frobenius norm of Hessian is low in background. β and c are arbitrary contants depending on image and in this case both are 0.5.

The whole process was repeated at each pixel for different scales and then the one giving maximum vesselness value was used. The image after vessel enhancement is shown in fig.2.
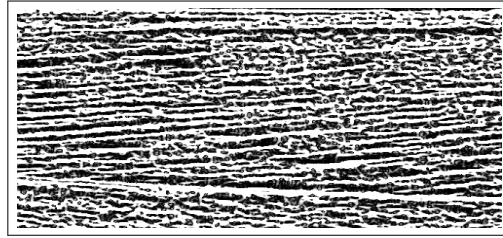
Figure 2 Image after vessel enhancement filtering

Mean orientation of fascicles was obtained by two methods.
1. Radon Transform (Khouzani, Zadeh) was used to obtain to obtain mean orientation of fascicles.
2. Muscle fascicle orientation at each pixel was by using anisotropic wavelet analysis. The image was convolved with anisotropic wavelets at different orientations to obtain local orientations at each pixel. Eq. Of wavelet used

$$\omega = \frac{\exp(-\dfrac{x_s^2}{2} + \dfrac{1}{90}(-x^2 - y^2))Cos(2\Pi v x_s)}{2\Pi}$$

$$x_s = \frac{\Pi(xCos\theta - ySin\theta)}{2f}$$
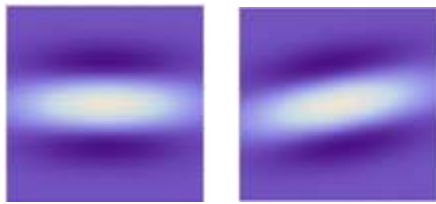
Figure 2 for $\theta=0^o$ **Figure 3** for $\theta=10^o$

Fascicle directions were found by tracking through the vector field found from method 2...

RESULTS

Fig. 2 was convolved with anisotropic wavelets to obtain local orientation at each pixel. The computed fascicle trajectories (shown in red dots) matched those visible by eye, and followed local curvature that occurred naturally within each fascicle (fig. 5 and fig. 6).
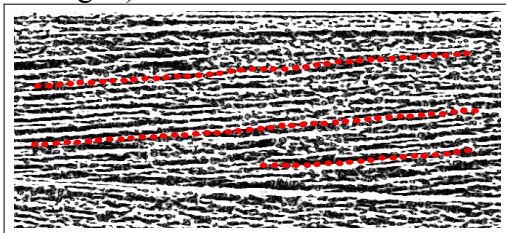
Figure 5 Orientations obtained after convolving fig4 with wavelets
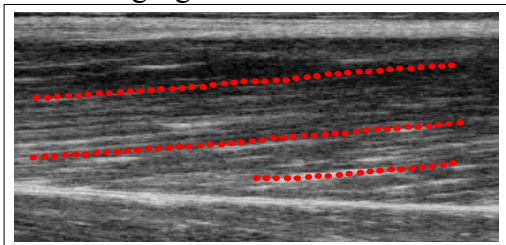
Figure 6 Orientations shown on original ultrasound image

DISCUSSION

The results obtained depend on the factors f and v in the wavelet expression. Results are best at some optimal value (f = 6.5 and v =0.3) in a sequence so seems to be determined by muscle structure and resolution of

image).This is very effective method for automatic tracking of muscle fascicle length change. The methods will be validated by extracting orientation of parallel lines at some known angle or comparing to physical phantoms.

SUMMARY

Images of muscle obtained using ultrasonography were filtered using multiscale vessel enhancement filtering to enhance muscle fascicle structure. Orientation of the fascicles was obtained using both Radon Transform and anisotropic wavelet. Muscle fascicle strains can be quantified by this information tracked through the vector field of their orientations.

REFERENCES

A.F. Frangi, W.J. Niessen, K.L. Vincken, M.A. Viergever (1998). Multiscale vessel enhancement filtering. In Medical Image Computing and Computer-Assisted Intervention - MICCAI'98, W.M. Wells, A. Colchester and S.L. Delp (Eds.), Lec.notes in Comp Sc1496,30-137.

 K.J Khouzani and H.S Zadeh, (2005) Radon Transform Orientation estimation for rotation invariant texture analysis.

EXPERIMENTAL STUDY OF THE DEFORMATION AND FLEXIBILITY OF INSECT WINGS

Xiaolin Wang, Afzal Khan, Lingxiao Zheng and Rajat Mittal

Department of Mechanical & Aerospace Engineering, George Washington University, Washington D.C. mittal@gwu.edu
URL: http://www.gwu.edu/~cobre/

INTRODUCTION

An insect wing is a key determinant of flight performance. In the past few decades, insect flight mechanisms have been extensively studied theoretically, computationally and experimentally. The seminal work of Weis-Fogh (Weis-Fogh, 1956 and 1973) uncovered the "clap-and-fling" mechanism that is known to be used by a number of insects and birds. Ellington (Ellington et al., 1996) drew attention to the importance of the leading-edge stall vortex as a key factor in lift generation by insects. More recently, Dickinson and coworkers (Dickinson and Gotz, 1996; Dickinson et al., 1999) identified delayed stall, rotational circulation and wake-capture as three distinct mechanisms that appear in experiments conducted with a dynamically scaled fruitfly wing. Wing-wing interaction in functionally four-winged insects such as dragonflies has also been studied by Mittal et al. (Mittal et al., 2006 and 2008) and Wang et al. (Wang et al., 2005). All of the studies mentioned above have assumed insect wings perfectly rigid. This however, is far from reality since wing flexibility and the associated deformation is widely accepted to play a significant role in insect flight (especially large insects such as moths, butterflies and dragonflies as shown in Figure 1) (Wootton, 1981 and 1993). The potential that wing deformation leads to the generation of aerodynamic mechanism of lift/thrust production that are not possible with rigid wings has been hinted by a number of researchers (Combes et al., 2001; Lehmann, 2008; Sane, 2003; Wootton, 1993) but experiments or computational studies to date have found it hard to investigate this issue. Insects are difficult to visualize and model with a high level of detail as they are small, fast moving and flap their wings at high frequencies. Despite some recent quantitative visualization of insect in free flight (Sunada et al., 2002), the current literature lacks the necessary 3-D detail of body and wing kinematics needed for input into CFD analyses. As a result, no computational models of flapping flight have been validated with experimental data from freely flying insects. The effect of insect wing deformation and flexibility on the aerodynamics and flight performance has been even more difficult to quantify (Dudley, 2000). Not a single study to date has managed to extract the kinematics of an insect wing that is undergoing significant deformation.

In recent years, direct linear transformation (DLT) (Abdel-Aziz et al., 1971; Chen et al., 1994) has been employed quite extensively in high-speed videogrammetry systems by Lauder et al. (Lauder et al., 2006; Standen et al., 2005) and

Hedrick et al. (Hedrick et al., 2004 and 2007) for reconstructing fish swimming and avian flight kinematics respectively. However, it has not been applied to the study of the insect flight kinematics. In this work, we will experimentally measure 3-D kinematics (position, velocity and acceleration) for a grid of points on the surface of both the wings and body of free flying butterflies and different maneuvers (climbs, turns and hovers) with high-speed videogrammetry and DLT algorithm. This data is to be used in the CFD-FSI tool which is based on an existing Navier-Stokes immersed-boundary solver (Mittal et al., 2005 and 2006) developed to simulate the hydrodynamics of flexible fish pectoral fins (Lauder et al., 2006; Mittal et al., 2006). In future, the solver will be modified to simulate the aerodynamics of insect flight and quantify the role of wing deformation and flexibility on the flight performance.

(a)   (b)   (c)
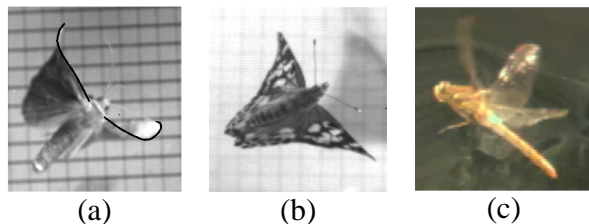
Figure 1. Various insect in flight showing wing flexibility. (a) Moth in climbing flight (b) Butterfly in flight hover (c) Dragonfly in flight (Thomas et al., 2004).

METHODS AND PROCEDURES

The insects studied in this work are Painted Lady butterflies (*Vanessa Cardui*) and Monarch butterflies (*Danaus plexippus*) and are shown in Figure 2. The insect flight videogrammetry setup is shown in Figure 3. Butterflies are kept in a holding facility and transferred into glass chambers (chamber size varies according to the butterfly size) before the experiments. These butterflies fly inside the chambers which are illuminated by halogen photo optic lamps (OSRAM, 54428) with heat shields. Note that past studies have

found that butterflies flying in enclosure maintain the allometry of their natural (unconstrained) flight (Dudley et al., 1994). Three synchronized Photron FASTCAM 1024 PCI high-speed cameras with 1024×1024 pixel resolution, operated at 1000 Hz with at least 1/3000 sec. shutter speed are applied to capture the butterfly free flight videos. Given that the butterflies flap at about 20Hz, this provides us excellent temporal and spatial resolution of the butterflies in flight. The cameras are calibrated in three-dimensions using a portable calibration rig (shown in Figure 3) which is recorded at the end of each set of videogrammetry trial. The calibration rig was rapid prototyped with a precision of 0.25mm that allows accurate reconstruction of the positions of the body and wings during flight.
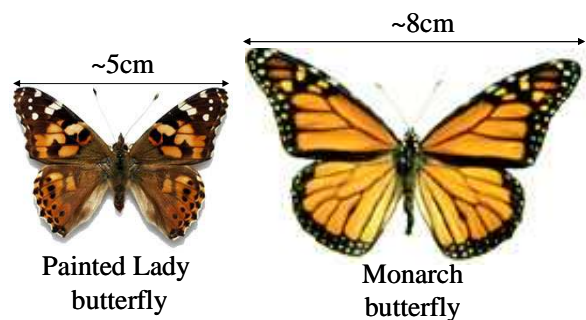
Figure 2. Painted Lady butterfly and Monarch butterfly.

Various flight modes are elicited using fresh flowers, sugar water and other stimuli. The recorded sequences from the three cameras are downloaded continuously to a desktop computer for subsequent analysis. The video sequences are then examined and useable segments (segments where we get good quality visualization of 4-5 wing beats in level, climbing, hover or turning flight modes) identified for detailed DLT analysis. The objective of the DLT videogrammetry analysis is to determine with accuracy in time and space, the geometric conformation of the wings and body during flight. The individual

body parts (wings, head, thorax, and abdomen) of the butterflies are weighed with a 0.01 mg accuracy balance (Ohaus, Analytica Plus). The wings are cut into about 25 pieces and each piece weighed individually to determine the center-of-mass and moment of inertia of the wings (note that total weight of a butterfly is about 150 mg).
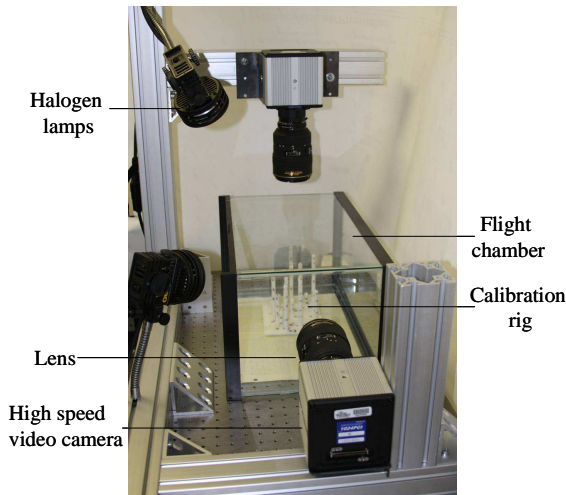
Figure 3. High-speed insect flight videogrammetry setup.

Natural markers on the butterfly wings and body are identified in image pairs and DLT is used to extract the 3D coordinates of these points at roughly 15 time-instants during each wing beat. An accurate representation of this butterfly in flight is constructed from the DLT analysis at each time instant.

RESULTS

Preliminary tests have been performed reconstructing the 3-D geometry and measuring the 3-D trajectory, velocity and acceleration of Painted Lady butterflies performing level and climbing flights.
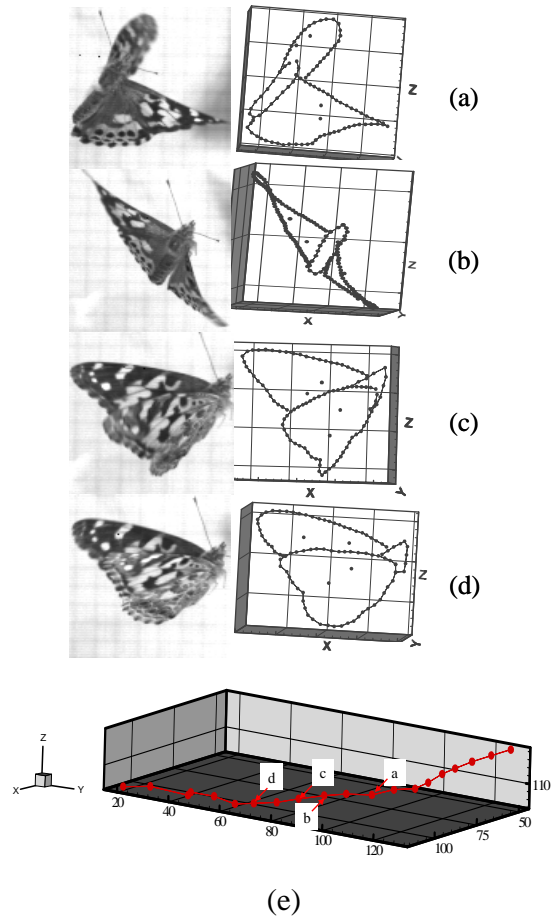
Figure 4. Preliminary reconstruction of wing kinematics and flight trajectory using high-speed videogrammetry. (a-d) Frames from high-speed videos and reconstructed wing and body coordinates using DLT. (e) Flight trajectory of the butterfly tracked using location of head.

Figure 4 shows reconstruction of wing kinematics and flight trajectory of a butterfly performing level flight using high-speed videogrammetry. The four images (a-d) on the left are extracted from the same flapping cycle showing apparent wing deformation. The 3-D reconstructed body and wing coordinates are shown on the right. The trajectory of the butterfly is also obtained by tracking the position of the head via DLT and is shown in Figure 4e. A critical component of these 3-D kinematic studies is the analysis of body acceleration. Determination of the

mass distribution of insect body and wings and total body mass allows direct determination of net flight forces if whole body accelerations is measured accurately and inertial components of motion are accounted for. Determination of body acceleration together with a knowledge of the mass distribution of the butterfly body allows a quantitative comparison of different maneuvers and provides data for the validation of forces calculated from the CFD models. Figure 5 shows experimental estimates of the acceleration of this butterfly by tracking the position of the head. The high values of the instantaneous acceleration (up to 3*g*) are experienced by the butterfly, and similar high values have been reported in other studies (Sunada et al, 1993). Furthermore, the acceleration clearly allows us to determine the flapping frequency of the butterfly and is about 16Hz. The same procedure is used to obtain the 3-D kinematics of different points in the body and wings.
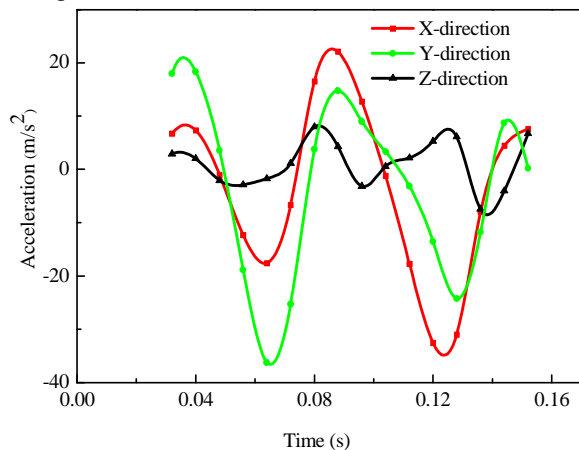
Figure 5. Body acceleration of Painted Lady butterfly in level flight extracted via videogrammetry.
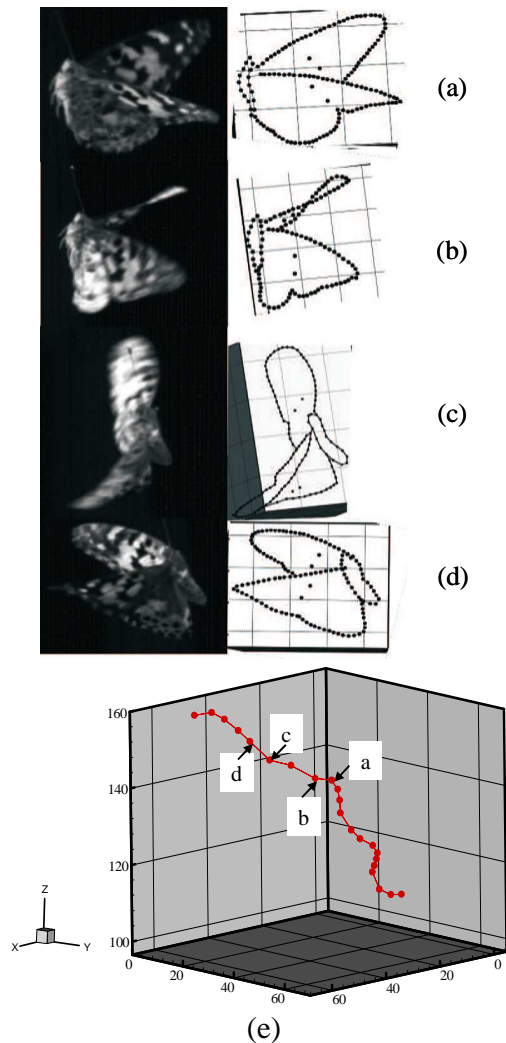
Figure 6. Preliminary reconstruction of wing kinematics and flight trajectory using high-speed videogrammetry. (a-d) Frames from high-speed videos and reconstructed wing and body coordinates using DLT. (e) Flight trajectory of the butterfly tracked using location of head.

Similarly, Figure 6 shows reconstruction of wing kinematics and flight trajectory of a Painted Lady butterfly performing climbing flight. The four images (a-d) on the left are extracted from the same flapping cycle showing apparent wing deformation. The reconstructed body and wing coordinates are shown on the right. The trajectory of the butterfly is also obtained by tracking the head

location via DLT study and shown in e. The acceleration of the butterfly is shown in Figure 7 which indicates the flapping frequency of the butterfly to be about 20Hz.
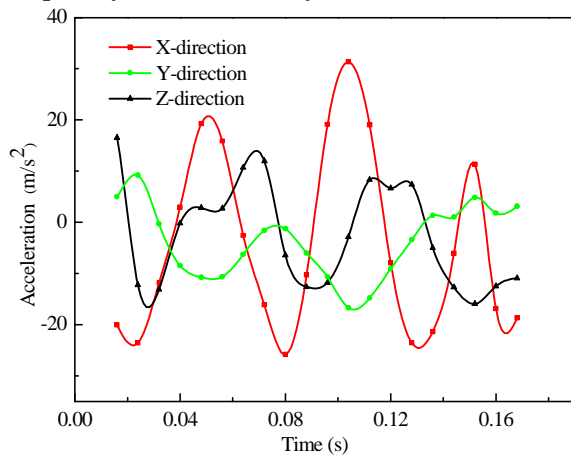
Figure 7. Body acceleration of Painted Lady butterfly in climbing flight extracted via videogrammetry.

DISCUSSION AND SUMMARY

In this work, the high-speed videogrammetry setup and the DLT algorithm are employed for reconstructing butterflies flight kinematics. It turns out that various flight modes of the butterflies are elicited using fresh flowers, sugar water and other stimuli. To date, the level and climbing flight of Painted Lady butterflies have been reconstructed, and the 3-D geometry, trajectory, velocity and acceleration have been measured. The acceleration profiles are quite periodic, and the maximum acceleration value is comparable with the value reported in literature. In addition, the flapping frequency obtained from the acceleration profiles is 16~20Hz, which agrees with the frequency observed from the flapping videos.

Our particular interest is to study the role of wing deformation and flexibility on aerodynamics and force production for the free flight of insects with our high-speed insect flight videogrammetry setup, DLT algorithm, and CFD-FSI tool. Study of different maneuvers (turns and hovers) of butterflies are anticipated prior to the conference. These measurements will aid in quantifying the kinetics of a grid of points in the butterfly body and wings and serve as input for our CFD-FSI tool modeling to simulate insect free flight for better understanding the fundamental role of wing deformation and flexibility on the flight performance of the insects.

REFERENCES

Abdel-Aziz, YI and Karara, HM (1971). *Proceedings of the Symposium on Close-Range Photogrammetry*, Falls Church, VA.

Chen, L et al. (1994). *J. Biomech.* 27: 493-500.

Combes, SA and Daniel, TL (2001). *J. Exp. Biol.* 204: 2073-2085.

Dickinson, MH and Gotz, KG (1996). *J. Exp. Biol.* 199: 2085-2104.

Dickinson, MH et al. (1999). *Science* 284: 1954 -1960.

Dudley, R (2000). *The Biomechanics of Insect Flight: Form, Function, Evolution. Princeton*. NJ: Princeton University Press.

Dudley, R and Srygley, R (1994). *Journal of Computational Physics* 191: 125-139.

Ellington, C et al. (1996). *Nature* 384: 626-630.

Hedrick, TL et al. (2004). *J. Exp. Biol.* 207: 1689-1702.

Hedrick, TL and Biewener, AA (2007). *J. Exp. Biol.* 210: 1897-1911.

Johansson, LC and Lauder, GV (2004). *J. Exp. Biol.* 207: 3945-3958.

Lauder, GV et al. (2006). *Bioinspiration & Biomimetics*, 1: s25-s34.

Lehmann, F (2008) *J. Exp. Biol.* 211: 224-233.

Mittal, R et al. (2002). AIAA-2002-0865.

Mittal, R et al. (2008). To appear in *Journal of Computational Physics*.

Mittal, R. and Iaccarino, G. (2005). Immersed boundary methods. *Annual Review of Fluid Mechanics*, 37: 239-261.

Mittal, R, et al. (2006). AIAA-2006-2867.

Sane, SP (2003) *J. Exp. Biol.* 206, 4191-4208.

Standen, EM and Lauder, GV (2005). *J. Exp. Biol.* 208, 2753-2763.

Sunada, S et al (1993). *J. Exp. Biol.* 183, 249-277.

Sunada, S et al. (2002). *JSEM International Journal B* 45: 836-842.

Thomas, ALR et al. (2004) *Journal of Experimental Biology* 207: 4299-4323

Wang, H et al. (2003). *J. Exp. Biol.* 207: 745-757.

Wang, J. K. and Sun, M. (2005). *J. Exp. Biol.* 208: 3785-3804.

Weis-Fogh, T (1956). *Phil. Trans. R. Soc. London. Ser B.* 239: 459-510.

Weis-Fogh, T (1973). *J. Exp. Biol.* 59: 169-230.

Wootton, RJ (1981). *J. Zool., Lond.* 193: 447-468.

Wootton, RJ (1993). *J. Exp. Biol.* 180: 105-117.

THE INFLUENCE OF MUSCLE ACTIVATION-DEACTIVATION DYNAMICS ON THE CHAINRING SHAPE THAT MAXIMIZES AVERAGE CRANK POWER

Jeffery W. Rankin and Richard R. Neptune

Department of Mechanical Engineering, The University of Texas at Austin, Austin, TX, USA
jwrankin@gmail.com

INTRODUCTION

Previous studies have sought to improve cycling performance by altering various aspects of the pedaling motion using novel crank-pedal mechanisms and non-circular chainrings (e.g. Belen et al., 2007; Kautz and Hull, 1995). Non-circular chainrings can potentially increase crank power relative to a conventional circular chainring by acting to slow down the crank angular velocity during the power phase, which allows muscles to generate power longer and produce more external work. However, non-circular chainrings can also cause muscles to quickly change from shortening to lengthening during deactivation, which can result in increased negative work relative to a circular chainring. Thus, to maximize crank power, the shape and orientation of the optimal chainring may be sensitive to muscle activation-deactivation dynamics. The purpose of this study was to determine the influence of muscle activation-deactivation dynamics on the optimal chainring shape that maximizes crank power during pedaling at 90 rpm.

METHODS AND PROCEDURES

A detailed musculoskeletal model (Neptune and Hull, 1998) with 15 individual muscle actuators per leg and forward dynamic simulations were used with dynamic optimization to determine the optimal chainring shape that maximizes average crank power during isokinetic pedaling at 90 rpm. Two optimizations were performed: one using fast activation and deactivation time constants (10 and 20 ms, respectively) for all muscles and one using slower, muscle-specific time

constants based on Winters and Stark (1988) with average values of 15 and 55 ms. The muscle actuators were governed by Hill-type muscle properties including force-length-velocity relationships. Activation-deactivation dynamics were modeled with a first order differential equation (Raasch et al., 1997).

Following each optimization, the eccentricity and orientation (measured counter clockwise from the crank arm) for each chainring was determined. In addition, the average single-leg crank power over the crank cycle was determined and total mechanical work produced by each muscle was determined by time integrating the musculotendon power within the power (45° to 135°) and subsequent transition (135° to 225°) phases of the crank cycle. Of particular interest was the influence of chainring shape on the power produced by the hip (GMAX) and knee (VAS) extensors, which are the primary power producing muscles in cycling.

RESULTS

The eccentricity of the optimal chainring, average crank power and mechanical work of the VAS and GMAX muscle groups within the power and transition phases all decreased with the slower activation-deactivation dynamics (Table 1, Fig. 1, SLOW). The average crank power decreased by 16.5% relative to the faster deactivation-activation dynamics. The decrease in muscle work was more pronounced in VAS than in GMAX, with the amount of VAS positive and negative work decreasing 9.9 J and increasing 10.0 J, respectively (Fig. 1). Little difference in

orientation between the two chainring shapes was observed (Table 1).

Time Constants	Eccentricity	Orientation	Crank Power
Fast	1.29	91.84^o	1028W
Slow	1.22	93.78^o	858W

Table 1. Eccentricity and orientation of the chainring and single revolution average crank power output for the two optimizations.
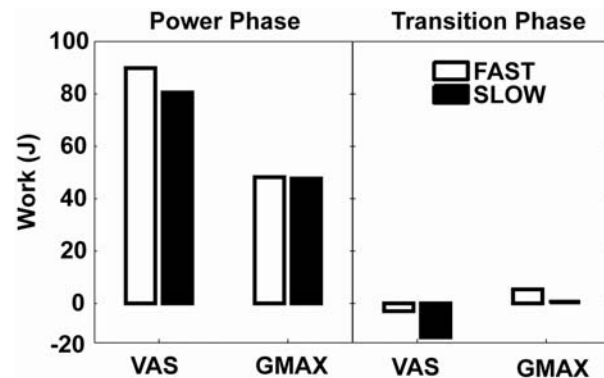
Figure 1. Single-leg mechanical work for the VAS and GMAX muscle groups produced during the power and subsequent transition phases for each optimization.

DISCUSSION

The faster time constants resulted in a more eccentric chainring shape as well as increased average crank power relative to the slower time constants. The increase in crank power was due primarily to increased muscle work during the power phase and reduced negative crank work in the transition phase. The decrease in eccentricity was consistent with Neptune and Kautz (2001), who showed there is a trade-off between maximizing the time spent generating power during the downstroke and minimizing negative work that occurs during deactivation in the subsequent transition phase and upstroke. Similarly, the reduction in crank power with the slower time constants was consistent with Soest and Casius (2000) who showed that the net crank

power in their model increased dramatically when activation-deactivation dynamics were removed from their model. Therefore, the optimal chainring shape that maximized average crank power balanced the competing demands of increasing the eccentricity to increase external work generated by muscles during the power phase and reducing the eccentricity to minimize negative work during the subsequent transition phase as muscles deactivate.

CONCLUSIONS

These results suggest that an individual's muscle fiber composition is an important consideration when customizing chainring shape to improve performance. For example, an endurance cyclist with predominately slow twitch muscle fibers and consequently slower deactivation dynamics may find greater improvements in power output with less eccentric shapes. Thus, the results of the present study suggest that developing subject-specific models that include activation-deactivation dynamics based on individual fiber types (e.g. Umberger et al., 2006) can better match chainring shapes to individual cyclists.

REFERENCES

Belen, L, et al. (2007). *Eur J Appl Physiol*, 101: 721-6.

Kautz, SA and Hull, ML (1995). *J Biomech*, 28: 1391-1401.

Neptune, RR and Hull, ML (1998). *J Biomech Eng*, 120: 334-341.

Neptune, RR and Kautz, SA (2001). *Exerc Sport Sci Rev*, 29: 76-80.

Raasch, CC, et al. (1997). *J Biomech*, 30: 595-602.

Soest, AJ and Casius, LJR (2000). *Med Sci Sports Exerc*, 32: 1927-1934.

Umberger, BR, et al. (2006). *J Biomech*, 39: 1472-1479.

Winters, JM and Stark, L (1988). *J Biomech*, 21: 1027-41.

A TECHNIQUE FOR CALCULATING AND MAPPING FOCAL CARTILAGE THICKNESS

William Anderst, Eric Thorhauer and Scott Tashman
University of Pittsburgh, Department of Orthopaedic Surgery, anderst@pitt.edu

INTRODUCTION

Cartilage thickness is typically measured from single plane magnetic resonance image (MRI) slices. Due to the curvature of underlying bone tissue, thickness measurements from single plane slices may not provide accurate thickness values (Akhtar, Poh, and Kitney, 2007). Additionally, the correlation between cartilage thickness and anatomical location is difficult to visualize and quantify on two-dimensional MRI slices.

The objective of this project was to determine cartilage thickness within specific focal regions on load-bearing femur and tibia surfaces. The new technique measures 3D distances between inner and outer cartilage surfaces, rather than determining thickness from 2D slice data.

METHODS

Five subjects (4M, 1F; 34±5 yrs.; 83±17kg) received bilateral, sagittal, 3T knee MRIs using a 3D SPGR sequence. All knees were asymptomatic for OA. MRI field of view was 160 x 160 mm with 2 mm slice spacing. Cartilage was segmented using both Mimics software (Materialise) and manual segmentation. Sagittal slices were interpolated to produce (0.312 x 0.312 x 0.333) mm voxels.

Segmented MRI slices were reconstructed into 3D volumetric models by applying a regularized marching tetrahedra algorithm to the 2D slice data (Treece, Prager and Gee, 1999) (Figure 1).
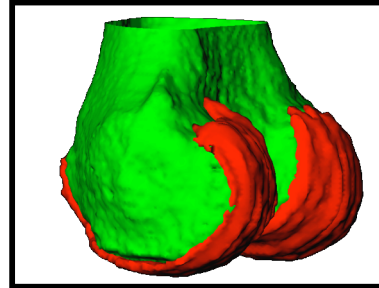

Figure 1: Distal femur (green) and cartilage (red). Femoral cartilage within the region of interest included all cartilage below a horizontal plane passing through the center of the femur condyles.

Cartilage volumes were grouped into focal regions within the medial and lateral compartment (Figure 2) to include surfaces likely to be loaded during walking and running.
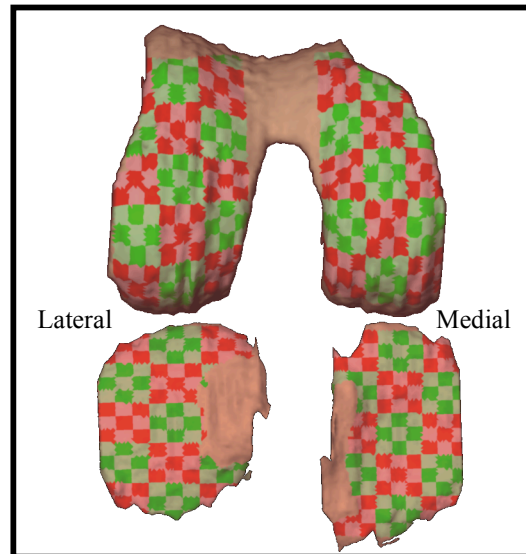

Figure 2: Regions on femur cartilage (above) were defined by the intersection of a cylinder centered on the condyle and the cartilage surface. The intersection cylinder contained regions every 10° around the cylinder (for 180° total) and nine medial-to-lateral regions on each condyle. Regions on tibia cartilage (below) were defined by the intersection of the cartilage surface with a 9 x15 region box aligned to the tibia anatomical axes.

Inner (touching bone) and outer (touching opposing cartilage) cartilage surfaces were identified using information contained within the 3D reconstruction of each cartilage volume. The minimum 3D distance from the outer cartilage surface to the inner cartilage surface was calculated, and average thickness values for each focal region was calculated.

RESULTS

Although medial and lateral compartment average cartilage thickness on the femur was nearly identical (2.38 mm and 2.38 mm, respectively), there was not a high correlation between corresponding regions within the medial and lateral femur ($R^2 = 0.37$). Likewise, medial and lateral compartment average thickness on the tibia was similar (2.33 mm and 2.30 mm, respectively). The correlation between corresponding regions within the medial and lateral tibia was higher than in the femur ($R^2 = 0.49$).
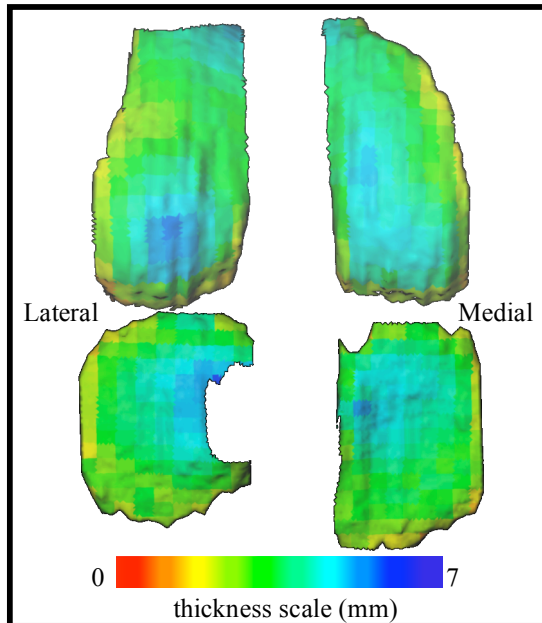

Figure 3: Group average cartilage thickness for the medial and lateral compartments of femur (above) and tibia (below) cartilage. Regions (as defined in Figure 2) are color-coded according to average thickness for 5 subjects.

Lateral femur cartilage thickness was greatest in a the posterior-central region, while medial femur cartilage was thickest over a relatively large range, from the posterior-central to the anterior-medial region of the cartilage (Figure 3).

Lateral tibia cartilage was thickest near the tibial spine, while medial tibia cartilage was thickest in the center of the posterior medial plateau (Figure 3).

DISCUSSION

There were two primary advantages to the current technique. First, cartilage thickness was determined using 3D distances between inner and outer cartilage surfaces, rather than by 2D single plane slices. Second, cartilage thickness was measured and visualized in defined focal regions, enabling comparisons within and among subjects.

This technique may be useful for tracking changes in cartilage thickness over time in a single individual (such as an OA patient or ACL-reconstructed patient) and for comparing cartilage thickness between subjects at specified anatomical regions.

We intend to combine this technique with high-speed biplane x-ray data to test for a relationship between cartilage thickness and areas of cartilage overlap during dynamic loading during walking and running.

REFERENCES

Akhtar, S, Poh, CL, and Kitney, RI (2007). *Osteo. and Cartilage*, 15:1070-1085.
Treece, GM, Prager, RW and Gee, AH (1999). *Comp. and Graph.*, 23:583-598.

ACKNOWLEDGEMENTS

A TECHNIQUE FOR CALCULATING AND MAPPING FOCAL CARTILAGE THICKNESS

William Anderst, Eric Thorhauer and Scott Tashman
University of Pittsburgh, Department of Orthopaedic Surgery, anderst@pitt.edu

INTRODUCTION

Cartilage thickness is typically measured from single plane magnetic resonance image (MRI) slices. Due to the curvature of underlying bone tissue, thickness measurements from single plane slices may not provide accurate thickness values (Akhtar, Poh, and Kitney, 2007). Additionally, the correlation between cartilage thickness and anatomical location is difficult to visualize and quantify on two-dimensional MRI slices.

The objective of this project was to determine cartilage thickness within specific focal regions on load-bearing femur and tibia surfaces. The new technique measures 3D distances between inner and outer cartilage surfaces, rather than determining thickness from 2D slice data.

METHODS

Five subjects (4M, 1F; 34±5 yrs.; 83±17kg) received bilateral, sagittal, 3T knee MRIs using a 3D SPGR sequence. All knees were asymptomatic for OA. MRI field of view was 160 x 160 mm with 2 mm slice spacing. Cartilage was segmented using both Mimics software (Materialise) and manual segmentation. Sagittal slices were interpolated to produce (0.312 x 0.312 x 0.333) mm voxels.

Segmented MRI slices were reconstructed into 3D volumetric models by applying a regularized marching tetrahedra algorithm to the 2D slice data (Treece, Prager and Gee, 1999) (Figure 1).

Figure 1: Distal femur (green) and cartilage (red). Femoral cartilage within the region of interest included all cartilage below a horizontal plane passing through the center of the femur condyles.

Cartilage volumes were grouped into focal regions within the medial and lateral compartment (Figure 2) to include surfaces likely to be loaded during walking and running.

Figure 2: Regions on femur cartilage (above) were defined by the intersection of a cylinder centered on the condyle and the cartilage surface. The intersection cylinder contained regions every 10° around the cylinder (for 180° total) and nine medial-to-lateral regions on each condyle. Regions on tibia cartilage (below) were defined by the intersection of the cartilage surface with a 9 x15 region box aligned to the tibia anatomical axes.

Inner (touching bone) and outer (touching opposing cartilage) cartilage surfaces were identified using information contained within the 3D reconstruction of each cartilage volume. The minimum 3D distance from the outer cartilage surface to the inner cartilage surface was calculated, and average thickness values for each focal region was calculated.

RESULTS

Although medial and lateral compartment average cartilage thickness on the femur was nearly identical (2.38 mm and 2.38 mm, respectively), there was not a high correlation between corresponding regions within the medial and lateral femur ($R^2 = 0.37$). Likewise, medial and lateral compartment average thickness on the tibia was similar (2.33 mm and 2.30 mm, respectively). The correlation between corresponding regions within the medial and lateral tibia was higher than in the femur ($R^2 = 0.49$).

Figure 3: *Group average cartilage thickness for the medial and lateral compartments of femur (above) and tibia (below) cartilage. Regions (as defined in Figure 2) are color-coded according to average thickness for 5 subjects.*

Lateral femur cartilage thickness was greatest in a the posterior-central region, while medial femur cartilage was thickest over a relatively large range, from the posterior-central to the anterior-medial region of the cartilage (Figure 3).

Lateral tibia cartilage was thickest near the tibial spine, while medial tibia cartilage was thickest in the center of the posterior medial plateau (Figure 3).

DISCUSSION

There were two primary advantages to the current technique. First, cartilage thickness was determined using 3D distances between inner and outer cartilage surfaces, rather than by 2D single plane slices. Second, cartilage thickness was measured and visualized in defined focal regions, enabling comparisons within and among subjects.

This technique may be useful for tracking changes in cartilage thickness over time in a single individual (such as an OA patient or ACL-reconstructed patient) and for comparing cartilage thickness between subjects at specified anatomical regions.

We intend to combine this technique with high-speed biplane x-ray data to test for a relationship between cartilage thickness and areas of cartilage overlap during dynamic loading during walking and running.

REFERENCES

Akhtar, S, Poh, CL, and Kitney, RI (2007). *Osteo. and Cartilage*, 15:1070-1085.
Treece, GM, Prager, RW and Gee, AH (1999). *Comp. and Graph.*, 23:583-598.

ACKNOWLEDGEMENTS

MUSCLE EXCURSION SCALES WITH NORMALIZED FIBER LENGTH IN A RABBIT MODEL

Taylor M. Winters[1], Mitsuhiko Takahashi[1], Richard L. Lieber[1], Samuel R. Ward[1]

[1]Departments of Bioengineering, Orthopaedic Surgery, and Radiology, University of California-San Diego and Veterans Affairs Medical Center, La Jolla, CA 92093 USA
Email: twinters@ucsd.edu, Web: http://muscle.ucsd.edu

INTRODUCTION

Muscle architecture is defined as the macroscopic arrangement of muscle fibers relative to the axis of force generation (Gans et al., 1965). Architectural features are important in current musculoskeletal modeling techniques because they form the basis for predictions of muscle force, excursion, and velocity.

There are excellent data demonstrating the robust relationship between muscle architecture and maximum force-generating capacity (Powell et al., 1984) and shortening velocity (Bodine et al., 1982). However, similar data do not exist for muscle excursion. Therefore, the purpose of this project was to examine the relationship between muscle fiber length (the architectural parameter predicting excursion) and the range over which a muscle can shorten and lengthen (excursion).

METHODS

The basic experimental assumption was that a unit change in muscle length was uniformly distributed over all sarcomeres arranged serially within a fiber. This provided the *a priori* framework, or model, to which experimental data were compared.

Tibialis anterior (TA, n = 3), extensor digitorum longus (EDL, n = 2), and extensor digitorum II (EDII, n = 14) from New Zealand white rabbits were chosen due to their varied architectural properties—primarily, their normalized fiber length (38.08 mm for TA, 15.34 mm for EDL (Lieber & Blevins, 1989), and 10.71 mm for EDII (Takahashi et al., 2007)). The distal tendon of the muscle of interest was transected and clamped to a servomotor at the muscle-tendon junction. Maximum isometric tension was measured at various lengths via direct nerve stimulation.

Post-operatively, the muscle was excised and fixed. Muscle fiber bundles were dissected and length was measured. Using laser diffraction, sarcomere length was measured and used to compute normalized fiber length.

Isometric forces were normalized to peak isometric force. A parabolic regression was applied to the length tension curve (LTC) and then shifted to ensure that maximum tension (P_o) aligned with optimal normalized fiber length (L_o). The width of the LTC was quantified using full width at half max (FWHM).

Linear regression was applied to the FWHM plotted against L_o. The intraclass correlation coefficient (ICC) was used to validate the measured FWHM with the theoretical FWHM. Data are shown as mean $\pm$ SD, and significance level was set to $p < 0.05$.

RESULTS

The theoretical P_o occurs at the literature value of L_o (Figure 1).

The experimental P_o occurs at the measured L_o of 39.27 ± 3.96 mm for TA, $16.10 \pm .02$ mm for EDL, and $8.90 \pm .41$ mm for EDII (Figure 2).
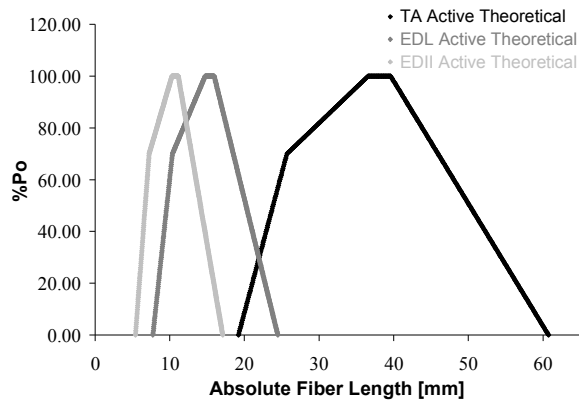
Figure 1. Theoretical active LTC for the TA, EDL, and EDII are derived from a sarcomere LTC for rabbit.
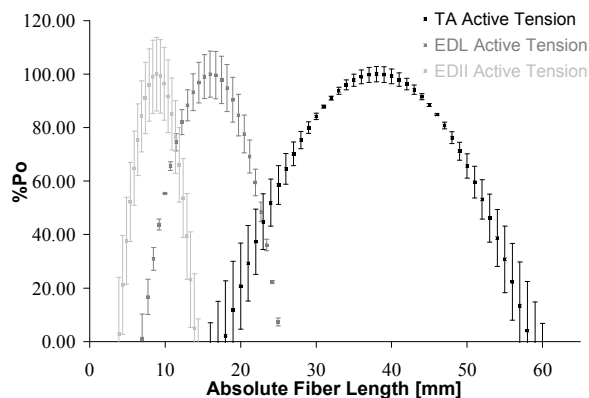
Figure 2. Experimental active LTC for the TA, EDL, and EDII.

Linear regression of FWHM versus L_o demonstrated a highly significant relationship between these variables ($r^2 = 0.982$, $p < 0.001$) and the slope of this line was $0.76 \pm .018$ mm/mm (Figure 3).
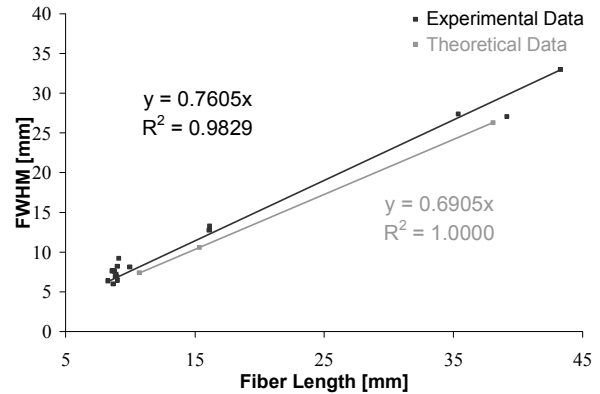
Figure 3. Linear regression of FWHM vs. L_o for experimental ($p < 0.001$) and theoretical ($p < 0.001$) data.

The ICC for FWHM predicted vs. FWHM measured was 0.993 ($p < 0.001$).

DISCUSSION

These data suggest that the width of the LTC scales proportionally with the normalized fiber length of the muscle. Specifically, a muscle is capable of producing greater than or equal to 50% of P_o through a range of lengths equal to 76% of fiber length. Furthermore, the basic assumption that a unit change in muscle length is distributed uniformly over all sarcomeres arranged serially within a fiber is validated by the statistical significance of the ICC. Therefore, the LTC of a muscle can be safely derived from the literature value of normalized fiber length and a sarcomere LTC with an error of only ~2%.

REFERENCES

Bodine SC et al. (1982). *J Neurophysiol*, 48(1): 192-201

Gans C & Bock WJ. (1965). *Adv Anat Embryol Cell Biol*, 38: 115-142

Powell PL et al. (1984). *J Appl. Physiol*, 57(6): 1715-1722

Lieber RL & Blevins FT. (1989). *J Morphol*, 199: 93-101

Takahashi M et al. (2007). *J Hand Surg*, 32A: 612-617

CAN WE ASSUME THAT THE INDIVIDUALS WITH INCOMPLETE SPINAL CORD INJURY HAVE A SYMMETRICAL GAIT PATTERN?

Sylvie Nadeau[1,2,3], Hugues Barbeau[4], Christiane Garneau[1] and Cyril Duclos[1,2,3]

[1]Laboratoire de pathokinésiologie, Centre de recherche interdisciplinaire en réadaptation, site Institut de réadaptation de Montréal, [2]École de réadaptation, Université de Montréal, Qc, Canada, [3]Équipe multidisciplinaire en réadaptation locomotrice, sylvie.nadeau@umontreal.ca
[4]School of Physical and Occupational Therapy, McGill University, Canada

INTRODUCTION

One of the most important goals for individuals after a spinal cord injury (SCI) is the recovery of safe, symmetrical and effective reciprocal gait pattern. Results of animal studies and randomized control trials have led to intensive locomotor training being implemented in rehabilitation units to enhance gait recovery in this population (Dobkin et al., 2007). Astonishingly, available biomecha-nical gait data about the gait pattern of these subjects is limited: more often data is reported for only one side of the body (Leroux et al., 1999). The main purpose of this study was to determine whether the natural gait pattern of individuals with incomplete SCI (ISCI) is less symmetrical than that of healthy subjects walking at a matched cadence.

METHODS AND PROCEDURES

Fourteen men with chronic traumatic ISCI (ASIA D; mean age: 46.9± 13.5 yr) able to walk 50 m independently and 14 healthy subjects (7 women, 7 men; mean age: 46.0 ± 13.3 yr) participated in the study. Kinematic gait parameters were measured bilaterally with an infrared movement analysis system (Optotrak) using 3D coordinates obtained from markers placed on the body segments. Ground reaction forces were recorded using force plates. The net moments and powers at the hip, knee and ankle joints were calculated using an inversed dynamic approach. The stride characteristics of each gait cycle were computed with foot-switches. For the ISCI group, the less (healthy: dominant) and more (healthy: non-dominant) involved lower limbs were identified using the clinical data (lower extremity motor score [LEMS; sum of the ASIA motor score of 5 key muscles (L2, L3, L4, L5, and S1) per extremity, and neurological sensory score of the ASIA]. The mean asymmetry (absolute difference) in the angular displacements, moments and power parameters were obtained by computing the absolute difference between sides (less affected or dominant – more affected or non dominant) at each 5% of the gait cycle and then averaging the results over the number of intervals (n=21). The differences between sides were also examined for the time-distance parameters and for the peak values of moment and power during the energy generation phases of gait (A2, H1 and H3) in ISCI to characterize the pattern of asymmetry. The results of the ISCI and healthy subjects were compared at matched cadence using descriptive statistics and independent Student t-test ($p<0.05$).

RESULTS

The mean natural gait speed of the ISCI was 0.78m/s (SD: 0.34) and the cadence 84 steps/min (SD: 14). The mean LEMS was different between sides (less affected vs. more affected: 22.7 vs. 21.7/25; $p<0.05$). Three participants did not present a difference between sides in the LEMS; in those cases, the more affected side was identified by referring to the ASIA sensory score. Except for the time-distance parameters and the gait parameters at the ankle, the differences

between sides were greater for the ISCI group and they tended to increase from distal to proximal joints (hip > ankle; Table 1).

Table 1: Mean absolute differences

Gait Parameters	ISCI	Healthy	P-value
Time-distance	Mean(SD)	Mean(SD)	
Stride length*	2.3 (2.0)	2.5 (2.5)	NS
SSupport (%)	2.2 (1.2)	2.8 (2.6)	NS
Support(%)	2.2 (1.2)	2.8 (2.7)	NS
Angular displacements (º)			
Ankle	2.9 (1.4)	2.5 (0.9)	NS
Knee	6.3 (3.6)	4.2 (1.7)	0.03
Hip	8.3 (4.5)	4.3 (1.7)	0.00
Joint moments (Nm/kg)			
Ankle	0.10 (0.05)	0.09 (0.05)	NS
Knee	0.11 (0.05)	0.08 (0.03)	0.02
Hip	0.13 (0.05)	0.09 (0.06)	0.01
Joint powers (W/kg)			
Ankle	0.14 (0.08)	0.13 (0.07)	NS
Knee	0.14 (0.06)	0.09 (0.03)	0.02
Hip	0.22 (0.10)	0.16 (0.05)	0.06

* Stride length normalised to height.

Respectively, six (42%) and seven (50%) participants with ICSI had a longer stride length and a longer single support (SSupport or support) duration on the more affected side than on the less affected one. The peak moments and powers at the ankle did not differ between sides. For the hip extensors and flexors, the moment and power values were generally greater on the less affected side during the H1 and H3 phases of gait. As example, over 70% of the subjects presented power values near or higher than zero on the less affected side.

DISCUSSION

As expected, the gait speed of the ISCI was reduced and corresponds grossly to 70% of the natural speed of healthy controls. It was important to compare the two groups at a similar cadence to control for effects of the magnitude of the moments and power values on the difference between sides. Overall, the biomechanical parameters of gait are less symmetrical in ISCI individuals than in healthy subjects walking at a similar cadence. Interestingly, we found that the ankle gait parameters are similar between sides whereas significant differences were noted at the hips. This finding might reflect different levels of impairments or recovery patterns for distal and proximal muscles groups in this population. The results also revealed that the gait asymmetry did not follow the clinical pattern of asymmetry closely for the time-distance parameters or the ankle power (A2 peak values). Thus, no specific locomotor characteristics can be identified for the less and more affected sides, except at the hips where the less affected side can be said to generate more energy.

SUMMARY

This study assessed the level of asymmetry of gait parameters in 14 individuals with ISCI walking at preferred speed. Results revealed that these participants could not be considered as having a symmetrical gait pattern, with greater differences between sides at the hip than at the ankle. Moreover, the results revealed that, in general, clinical asymmetry of motor and sensory scores can not be used to infer on the asymmetry of the gait parameters, except at the hip.

REFERENCES

Dobkin B. et al. (2007). *Neurorehabil Neural Repair.* 21:25-35.
Leroux A. et al. (1999). *Exp Brain Res.* 126: 359-68.

ACKNOWLEDGMENTS

DEVELOPMENT OF A LASER REFLECTANCE SYSTEM TO MEASURE THE CROSS-SECTIONAL AREA OF SOFT TISSUE

Gabriel Pokhai[1,2], Karen Gordon[1], Michele Oliver[1]

[1]School of Engineering, University of Guelph, Guelph, ON, Canada
[2]Email: gpokhai@uoguelph.ca

INTRODUCTION

Accurate cross-sectional area (CSA) measurements are required to determine biomechanical properties of soft tissue. Measuring the CSA of tendons and ligaments is difficult because they are irregularly shaped and easily deformed. Of the many methods of measuring CSA that have been reported, there are concerns with contact methods that can deform the specimen, and non-contact methods that require geometric assumptions (Moon et al., 2006).   The objective of this work was to design and verify a non-contact laser reflectance system (LRS) for accurate CSA measurement of soft tissue.

METHODS AND PROCEDURES

The system includes a Keyence LB-10 laser micrometer (Keyence Corp., Woodcliff Lake, NJ), which is mounted on a turntable bearing (Kaydon Corp., Muskegon, MI) and rotated with a stepper motor (Automation Direct, Cumming, GA). The entire assembly is mounted on an Instron 8872 servo-hydraulic testing machine (Instron Corp., Canton, MA) (Figure 1). Laser readings are collected by a personal computer, and along with the angle of rotation are used to calculate the CSA via Reimann sums with Microsoft Excel spreadsheets (Microsoft Corp., Redmond, WA).

Machined metallic specimens of various sizes were placed in the centre of the assembly and the laser was orbited at 5° angle increments around the specimen. The system was validated by repeating the measurements with a previously reported casting method (Goodship and Birch, 2005).

As a "gold standard" measurement, photographs of the specimen cross-sections were taken with 10 megapixel digital camera and CSA values were calculated using ImageJ image analysis software (National Institutes of Health, Bethesda, MD). The CSA values from the LRS and the casting method were compared with these values.

As a preliminary study, the CSA of five bovine deep digital flexor tendons (DDFT) were measured with the LRS. The tendons were first stained with ink to prevent
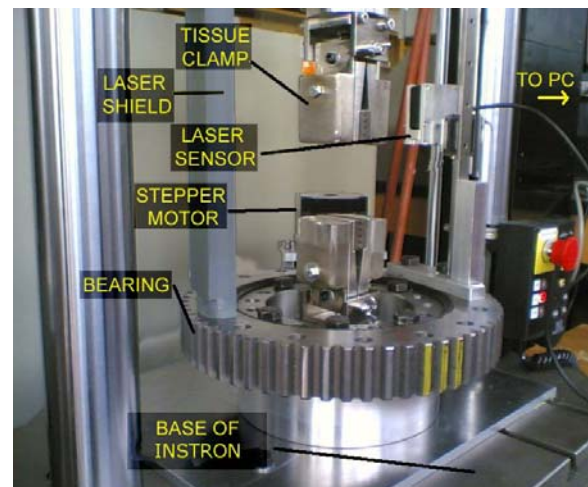

Figure 1. Laser reflectance system, as installed on Instron testing machine.

Shape	Photograph CSA	Laser CSA	Laser Error (%)	Casting CSA	Casting Error (%)
Small Circle	29.95	29.55	1.32	29.35	2.00
Large Circle	506.75	508.08	0.26	501.91	-0.95
Kidney Bean	307.18	316.15	2.92	324.79	5.73

Table 1. CSA measurements of various metallic shapes. CSA is given in mm^2.

penetration of the laser beam into the specimen (Moon et al., 2006). Transverse sections of the mould and tendon were cut at the same level measured with the LRS and digital images of both were taken. The CSA values of these sections were calculated in image analysis software as above.

A 2-way analysis of variance (ANOVA) was performed to determine if there were significant differences between the CSA values obtained from the LRS and the casting method (p≤ 0.05), for both machined and soft tissue specimens.

RESULTS

The LRS was able to measure circular areas of the metallic specimens to within 2% and a complex "kidney bean" shape to within 3% (Table 1). No significant differences were found between the LRS and casting methods (p = 0.448).

The LRS measured the CSA of the tendon specimens with an average error of 1.11 ± 8.25% relative to the gold standard (Table 2). The CSA as determined by the casting method had an average error of 11.22 ± 3.83% (data not shown). Statistical analyses again showed no significant difference between measurement methods (p = 0.052).

DISCUSSION

The LRS produced CSA values with minimal errors equivalent or less than the established casting method for both metallic

Tendon	Photograph CSA	Laser CSA	Laser Error (%)
1	187.88	200.30	6.61
2	155.54	160.04	2.89
3	167.96	149.61	-10.93
4	158.41	153.75	2.94
5	159.61	175.44	9.92
Mean	165.88	167.83	1.11
(SD)	(13.14)	(20.64)	(8.25)

Table 2. Tendon CSA measurements. CSA is given in mm^2.

and soft tissue specimens. The accuracy of both methods decreased when measuring the tendon specimens.

SUMMARY

A soft tissue laser measurement system was designed and successfully validated against an existing casting measurement method, producing accurate CSA measurements for several machined specimens of various shapes and radii. The system's installation on an Instron testing machine will permit future studies where CSA of tendon specimens is measured simultaneous with tensile testing to facilitate calculation of true stress values.

REFERENCES

Goodship, AE and Birch, HL. (2005). *J Biomech*, 38:605-8.
Moon, DK et al. (2006). *J Biomech*, 39:3071-5.

DEVELOPMENT OF A LASER REFLECTANCE SYSTEM TO MEASURE THE CROSS-SECTIONAL AREA OF SOFT TISSUE

Gabriel Pokhai[1,2], Karen Gordon[1], Michele Oliver[1]

[1]School of Engineering, University of Guelph, Guelph, ON, Canada
[2]Email: gpokhai@uoguelph.ca

INTRODUCTION

Accurate cross-sectional area (CSA) measurements are required to determine biomechanical properties of soft tissue. Measuring the CSA of tendons and ligaments is difficult because they are irregularly shaped and easily deformed. Of the many methods of measuring CSA that have been reported, there are concerns with contact methods that can deform the specimen, and non-contact methods that require geometric assumptions (Moon et al., 2006). The objective of this work was to design and verify a non-contact laser reflectance system (LRS) for accurate CSA measurement of soft tissue.

METHODS AND PROCEDURES

The system includes a Keyence LB-10 laser micrometer (Keyence Corp., Woodcliff Lake, NJ), which is mounted on a turntable bearing (Kaydon Corp., Muskegon, MI) and rotated with a stepper motor (Automation Direct, Cumming, GA). The entire assembly is mounted on an Instron 8872 servo-hydraulic testing machine (Instron Corp., Canton, MA) (Figure 1). Laser readings are collected by a personal computer, and along with the angle of rotation are used to calculate the CSA via Reimann sums with Microsoft Excel spreadsheets (Microsoft Corp., Redmond, WA).

Machined metallic specimens of various sizes were placed in the centre of the assembly and the laser was orbited at 5° angle increments around the specimen. The system was validated by repeating the measurements with a previously reported casting method (Goodship and Birch, 2005).

As a "gold standard" measurement, photographs of the specimen cross-sections were taken with 10 megapixel digital camera and CSA values were calculated using ImageJ image analysis software (National Institutes of Health, Bethesda, MD). The CSA values from the LRS and the casting method were compared with these values.

As a preliminary study, the CSA of five bovine deep digital flexor tendons (DDFT) were measured with the LRS. The tendons were first stained with ink to prevent

Figure 1. Laser reflectance system, as installed on Instron testing machine.

Shape	Photograph CSA	Laser CSA	Laser Error (%)	Casting CSA	Casting Error (%)
Small Circle	29.95	29.55	1.32	29.35	2.00
Large Circle	506.75	508.08	0.26	501.91	-0.95
Kidney Bean	307.18	316.15	2.92	324.79	5.73

Table 1. CSA measurements of various metallic shapes. CSA is given in mm^2.

penetration of the laser beam into the specimen (Moon et al., 2006). Transverse sections of the mould and tendon were cut at the same level measured with the LRS and digital images of both were taken. The CSA values of these sections were calculated in image analysis software as above.

A 2-way analysis of variance (ANOVA) was performed to determine if there were significant differences between the CSA values obtained from the LRS and the casting method (p≤ 0.05), for both machined and soft tissue specimens.

RESULTS

The LRS was able to measure circular areas of the metallic specimens to within 2% and a complex "kidney bean" shape to within 3% (Table 1). No significant differences were found between the LRS and casting methods (p = 0.448).

The LRS measured the CSA of the tendon specimens with an average error of 1.11 ± 8.25% relative to the gold standard (Table 2). The CSA as determined by the casting method had an average error of 11.22 ± 3.83% (data not shown). Statistical analyses again showed no significant difference between measurement methods (p = 0.052).

DISCUSSION

The LRS produced CSA values with minimal errors equivalent or less than the established casting method for both metallic

Tendon	Photograph CSA	Laser CSA	Laser Error (%)
1	187.88	200.30	6.61
2	155.54	160.04	2.89
3	167.96	149.61	-10.93
4	158.41	153.75	2.94
5	159.61	175.44	9.92
Mean	165.88	167.83	1.11
(SD)	(13.14)	(20.64)	(8.25)

Table 2. Tendon CSA measurements. CSA is given in mm^2.

and soft tissue specimens. The accuracy of both methods decreased when measuring the tendon specimens.

SUMMARY

A soft tissue laser measurement system was designed and successfully validated against an existing casting measurement method, producing accurate CSA measurements for several machined specimens of various shapes and radii. The system's installation on an Instron testing machine will permit future studies where CSA of tendon specimens is measured simultaneous with tensile testing to facilitate calculation of true stress values.

REFERENCES

Goodship, AE and Birch, HL. (2005). *J Biomech*, 38:605-8.
Moon, DK et al. (2006). *J Biomech*, 39:3071-5.

ADAPTATIONS AND AFTEREFFECTS OF MUSCLE ACTIVATION PATTERNS AND FOOT KINEMATICS FOLLOWING PASSIVE SWING PHASE ASSISTANCE

M. Thajchayapong[1], B.D. Schmit[2,4], T.G. Hornby[3,4]

[1]Dept of Mechanical Engineering, Northwestern University, Evanston, IL, [2]Dept of Biomedical Engineering, Marquette University, Milwaukee, WI, [3]Dept of Physical Therapy, University of Illinois at Chicago, Chicago, IL, [4]Dept of Physical Medicine and Rehabilitation, Northwestern University, Chicago, IL

INTRODUCTION

The purpose of the present study was to investigate alterations in lower extremity kinematics and muscle activity during and following application of anteriorly directed swing assistance during treadmill walking. A previous investigation showed that during applied swing phase assistance, muscle activity is altered (Gottschall and Kram, *J Appl Physiol*. 2005 99:23-30). Changing other types of environmental demands and task constraints produces adaptation in human locomotion (Reisman et al., *Brain*. 2007 Jul;130(Pt 7):1861-72). Similarly, preliminary data indicated that aftereffects and adaptations were also observed following removal of swing phase assistance.

METHODS AND PROCEDURES

Using a device similar to that described previously (Gottschall and Kram, *J Appl Physiol*. 2005 99:23-30), we applied a pulling force of 3-10% body weight (BW) at the foot during mid-stance to mid-swing phases of the gait cycle during treadmill walking in 10 able-bodied subjects. Electromyographic activity of six lower extremity muscles and hip and knee kinematics were collected from both legs during constant velocity treadmill walking using an accelerometer secured to the foot. Data were sampled at 1000 Hz and collected prior to, during, and following application of passive swing phase assistance.

RESULTS
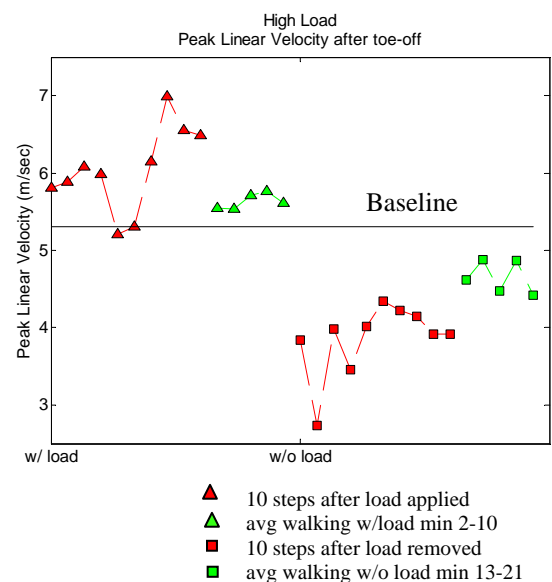
Figure 1: Peak linear velocity after toe-off for 10 minutes of treadmill walking with a high load (6-10% BW) swing phase assistance and 10 minutes following load removal. Data collected for the first 10 steps following load application (red triangles) revealed elevated foot linear velocity, which gradually decreased towards baseline during minutes 2-10 (green triangles, data averaged over 1 min every 2nd min). Upon removal of the assistance, data demonstrate a rapid decline in peak linear velocity for the first 10 steps (red square), which gradually increased back to baseline over 10 min (green square). Similar results were observed for low load (3-5%BW) conditions.
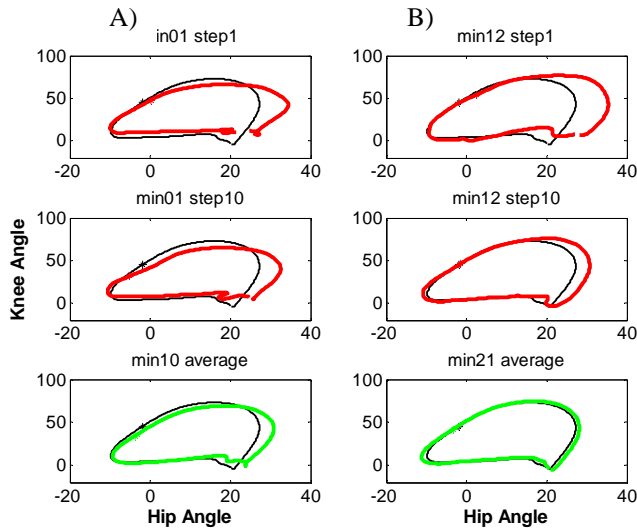
Figure 2. Hip and knee angle profiles during a) the 1st and 10th step following high load application (red traces), at 10 min following loading (green trace), and B) following assistance removal (1st, 10th steps, 10th min). Baseline walking is shown in gray. After load application, there is an increase in hip flexion and slight decrease of knee flexion. After 10 min of walking, the subject adapted their walking closer to baseline. Subjects flexed the hip to greater extent following removal of assistance. Walking profile returned to baseline by the 10th min.
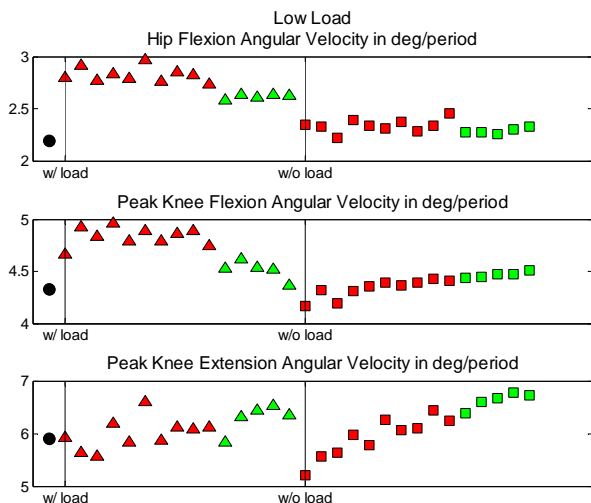
Figure 3. Angular velocity of hip flexion, knee flexion and knee extension with a low assistive load (3-5% BW). The black circle

indicates average baseline data. Similar legends as in Figure 1. A large increase in hip and knee peak flexion velocity was observed following load application, with slight adaptation towards baseline following a 10 min stepping bout and little aftereffect following removal. In contrast, peak knee extension velocity demonstrated a substantial reduction following load removal. Elevation of medial hamstring activity during swing partially accounted for the reduced knee extension velocity.

DISCUSSION
The data presented demonstrated adaptation and after-effects in lower extremity kinematics in response to applied assistance loads. Subjects adapted to the perturbation (load applied) after a brief period of training, and demonstrated reduced end-point velocity, and altered joint kinematics and muscle activity following load removal. With the increasing use of therapist or robotic-assistance to facilitate treadmill stepping in individuals with neurological impairments, understanding the alterations in kinematics and muscle activity patterns following applied forces becomes paramount to optimizing perturbations to augment recovery.

REFERENCES
Gottschall and Kram, *J Appl Physiol*. 2005 99:23-30
Reisman et al., *Brain*. 2007 Jul;130(Pt 7):1861-72

ACKNOWLEDGEMENTS

A Preliminary Study: Tracking 3D Kinematics of the Goat Knee Joint In-Vivo

D.L. Miranda, M.J. Rainbow, E.L. Brainerd, B.C. Fleming
Dept. of Orthopaedics, Warren Alpert Medical School of Brown University, Providence, RI

INTRODUCTION

ACL injury has reached epidemic levels. In the United States, it is estimated that 100,000-200,000 people sustain an ACL injury annually. ACL injury is thought to alter knee mechanics, disrupting cartilage metabolism. These changes in knee joint mechanics have been linked to increased incidence of osteoarthritis (OA); however, the precise mechanism is poorly understood (Tapper 2005). Developing an *in vivo* method for accurately tracking 3D bone kinematics during relative movements of articular surfaces during load-bearing movements in both healthy and injured knees may be useful for exploring the relationship between joint motion and OA. The goal of this study was to introduce a novel method for tracking 3D kinematics of the healthy and ACL-transected goat knee joint.

METHODS AND PROCEDURES

Surgical Technique: One Nubian goat (64.2kg) received surgical ACL-transection, while another goat (53.1kg) received a sham surgical procedure. A total of 12 spherical radiopaque tantalum markers were embedded in the distal femur and proximal tibia (6 markers per bone) of each goat during surgery.

Fluoroscope Motion Capture: Each goat knee joint was imaged using a high-speed, biplanar video fluoroscopy system comprised of two C-arm (OEC 9400) fluoroscope assemblies. Each C-arm assembly was retrofitted with an X-ray source opposite a 12-inch image intensifier optically coupled to a digital high-speed video camera (Photron Fastcam-X 1024pci, 250 frames/s). Each goat walked on a standard treadmill while video sequences were synchronously recorded with both video cameras at shutter speeds of 0.001 seconds. X-ray source voltage and current

were independently set (camera one: 100 kVp 3.2 mA, camera two: 110 kVp 3.0 mA) to best visualize the bone markers during gait cycles. Markers were identified for each frame using marker digitization software (XrayProject; CTX Technology Development Project, Brown University, Providence, RI).
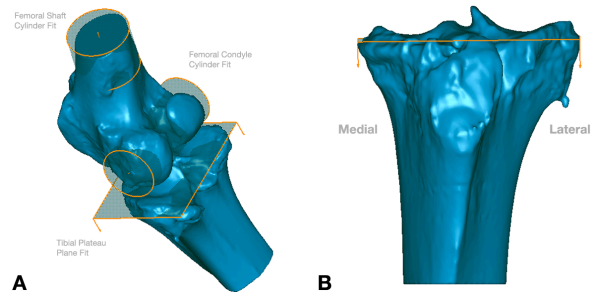
Figure 1. (A) Cylinder fits of femoral shaft and condyles, and plane fit of tibial plateau. (B) Plane fit of tibial plateau (coronal view).

Anatomical Coordinate System Determination: 3D bone models were created from CT scans (LightSpeed; GE, Piscataway, NJ) for the tibia and femur of each goat knee. Manual segmentation software (Mimics 9.11; Materialise Ann Arbor, MI) was used to produce 3D models of bone. 3D bone features, including the surface of the tibial plateau, the volume between the most medial and most lateral points on the femoral condyles, and the femoral shaft were found using geometry analysis software (Geomagic Studio 9; Geomagic, Durham, NC). The FE axis of the femoral coordinate system was designated as the first axis, based on the best cylindrical fit of the volume between the femoral condyles. The AB/ADD axis was designated as the second axis, defined by taking the cross product of the cylindrical fit through the femoral shaft with the FE axis. Finally, the third axis of the femoral coordinate system was defined by crossing the FE axis with the AB/ADD axis (Figure 1). The tibial coordinate system was defined

using the plane that was the best-fit to the surface of the tibial plateau. The plane was finite, with its corners approximating the length and width of the tibial plateau. Its normal vector approximated the tibial shaft, and the other two axes were defined by bisecting the plane perpendicular to its edges. **_3D Joint Kinematic Data Processing:_** 3D modeling and animation software (Maya 8.5; Autodesk, San Rafael, CA) was used to link, rotoscope, and animate the digitized bone markers to the 3D bone models and the anatomical axes. The animated anatomical axes generated in Maya were loaded into motion analysis software (Visual3D; C-Motion, Germantown, MD) to perform kinematic analysis on local reference frames. A joint coordinate system was defined from the tibial and femoral anatomical axes using the method of Grood and Suntay (Grood, 1983). The ordered sequence of rotations was FE (x-axis), AB/ADD, (y-axis), and IE rotation (z-axis). AP translation of the femur relative to the tibia was also determined. The average ROM in each goat knee joint was defined as the difference between the maximum and minimum peaks of each rotation.
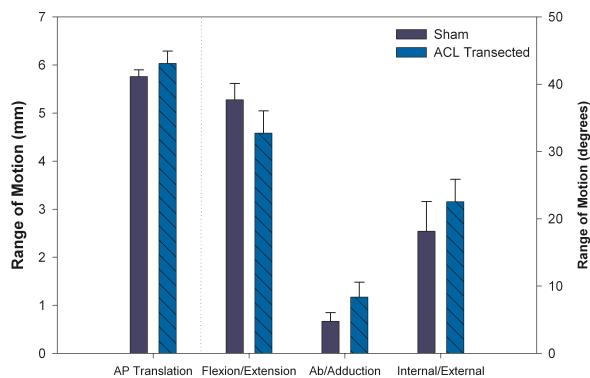
Figure 2. Bar chart depicting mean range of motion (left y-axis in mm, right y-axis in degrees) between goat gait strides with standard deviation bars.

RESULTS
The kinematic rotational and translational patterns were similar for the sham and ACL-transected joints (Figure 2). The largest ROM was FE (sham 37.7°±2.43°, ACL-transected 32.7°±3.30°), followed by IE rotation (sham 18.1°±4.41°, ACL-transected 22.5°±3.33°), and then AB/ADD (sham 4.76°±1.29°, ACL-transected 8.37°±2.21°). The AP translations of the femur relative to the tibia were 5.76±0.138mm and 6.03±0.256mm for the sham and ACL-transected knees, respectively.

DISCUSSION
This study has introduced a novel method for tracking 3D kinematics of healthy and ACL-transected goat knee joints. The relative rotational and translational motion of the goat knee joint were quantified by determining ROM in a sham and ACL-transected goat knee. Any differences observed in kinematics between the two subjects tested may have been due to ACL-transection altering joint mechanics or to differences in the defined knee coordinate systems. Further studies are needed to validate the robustness this method. ROM measurements (Figure 2) are consistent with other more invasive marker tracking quadruped kinematic studies by Frank et al. (Tapper, 2008). The results of this preliminary study indicate the feasibility and repeatability of tracking 3D kinematics *in vivo*.

REFERENCES
Grood ES et al. 1983. A joint coordinate system for the clinical description of three-dimensional motions: application to the knee. J. Biomech. Eng., 105:136-44.

Tapper JE et al. 2005. Dynamic in vivo kinematics of the intact ovine stifle joint. J. Orthop. Res., 24:782-92.

Tapper JE et al. 2008. Dynamic in vivo three-dimensional (3D) kinematics of the anterior cruciate ligament/medial collateral ligament transacted ovine stifle joint. J. Orthop. Res.

A Comparison between Two Systems for the Quantification of Lower Extremity Kinematic Gait Data

Andrew Kraszewski MS, Sherry Backus PT DPT MA, Rebecca Zifchock PhD, Mark W. Lenhoff, Howard J. Hillstrom, PhD
Hospital for Special Surgery, Rehabilitation Services, Leon Root, MD, Motion Analysis Laboratory, New York, NY
KraszewskiA@hss.edu   URL: http://hss.edu/rehab-motion-analysis-lab.asp

INTRODUCTION

The collection of three-dimensional (3D) gait analysis, while more common, continues to lack standardization for motion capture systems, marker sets, and analysis algorithms. Given multiple alternatives, the comparisons between and even within gait laboratories across data capture and analysis systems is important particularly as technology and data processing capabilities improve and more complex marker sets can be routinely implemented.

The goal of this study is to examine the differences between two gait analysis systems that examine lower extremity (pelvis, hip, knee, and ankle) kinematics and kinetics. A "system" is the combination of a digital representation of the limbs (marker set) and the specific analysis algorithm used to calculate gait parameters. This pilot study focused on two systems: a Cleveland Clinic marker set implemented in Orthotrak (CC-OT) and a six degree-of-freedom (6DOF) marker set implemented in Visual3D (6DOF-V3D). It was hypothesized that sagittal plane kinematics and kinetics would not differ between CC-OT and 6DOF-V3D systems, whereas transverse and frontal plane results would differ.

METHODS AND PROCEDURES

As part of an ongoing prospective IRB approved study, the gait of 12 subjects during level walking (6 healthy individuals, 6 individuals with altered gait patterns who were referred for clinical gait analysis) were analyzed. The inclusion of a variety of gait patterns in this study permitted a more robust estimation of the differences between the three systems. Sixty-four retro-reflective passive markers were placed on each subject to located anatomical and tracking frames for the simultaneous data collection of 3D trajectories of both marker sets (100 Hz). Where possible, identical markers were shared by both systems. For example, in the 6DOF-V3D system, the thigh tracking frame consists of four markers; three of those markers were selected to match the tracking frame triad used in the CC-OT system. The 6DOF set used ISB recommended anatomical locations for the pelvis, thigh, and shank segments. Hip joint centers were calculated using a functional method (Schwartz and Rozumalski, 2005)(Orthotrak 6.5 (2007). Data analysis were performed on a randomly chosen side for a single gait cycle (0-100%). Identical marker data were analyzed and used to represent both markersets. Marker trajectories were then analyzed separately in Visual3D 3.99.2 (C-Motion, Bethesda, MA) and Orthotrak 6.5.1 (Motion Analysis Corporation, Santa Rosa, CA) to produce kinematic waveforms for the pelvis, hip, knee, ankle, and foot in all three planes of rotation. The waveforms were compared using four measures: Trend Symmetry, Range Offset, Range Amplitude Ratio, and Phase Offset (Crenshaw and Richards, 2006). Subjects averaged 25 ± 10 years of age. There were nine males and three females.

RESULTS

	Trend Symmetry where 1 = perfect agreement		Range Offset (deg)		Range Amplitude Ratio (% total excursion)		Phase Offset (%Gait Cycle)	
	Mean	SD	Mean	SD	Mean	SD	Mean	SD
Pelvic Tilt	0.905	0.272	0.202	1.790	0.946	0.299	0.923	1.115
Pelvic Obliquity	0.891	0.272	0.089	0.484	0.895	0.314	-0.462	1.506
Pelvic Rotation	0.912	0.274	0.337	1.635	0.979	0.352	0.846	0.899
Hip Flexion	0.919	0.276	0.893	2.814	0.848	0.259	1.000	1.472
Hip Ad/Abduction	0.901	0.271	-0.106	2.594	0.843	0.293	-0.308	1.797
Hip Rotation	0.899	0.272	0.060	3.265	0.877	0.277	0.231	1.641
Knee Flexion	0.909	0.273	0.412	1.960	0.894	0.272	1.308	2.057
Knee Varus/Valgus	0.865	0.266	1.017	3.666	0.819	0.293	0.769	2.127
Knee Torsion	0.903	0.273	9.446	12.560	0.886	0.285	1.000	1.683
Ankle Flexion	0.891	0.271	0.762	3.614	0.924	0.319	1.077	1.935
Ankle In/Eversion	0.713	0.428	5.478	11.944	1.025	1.479	0.769	8.824
Ankle Rotation	0.894	0.270	-9.682	12.856	0.860	0.309	0.846	1.463
Foot Orientation	0.894	0.272	-0.312	1.328	0.988	0.333	1.385	2.434

Table 1. All difference were calculated as (6DOF-V3D)-(CC-OT).

DISCUSSION

Trend symmetry values in all planes and at all joints, with the exception of ankle inversion/eversion, expectedly show a high level of agreement (average 0.88) between systems. This indicates both marker sets are moving in parallel paths because their tracking markers were either in close proximity or were shared between systems. Comparisons made for ankle inversion/ eversion show disagreement due to the fact the tracking frame of the 6DOF set is located entirely on the foot where the CC set uses a shared point on the tibia. In general we do not consider it a fair comparison at the foot, yet it is reported for inclusiveness. Range offset magnitude was typically small except for knee rotation and ankle rotation and inversion/eversion. Knee and ankle rotation offsets are nearly equally opposed because of differences in coordinate system construction between systems. The 6DOF set uses four points to define the shank where the CC set

uses three, and thus they point in average in slightly different directions. This was common among patients where it was difficult to locate the tibial condyles for maker placement due mainly to excess tissue or structural deformity. Range amplitude ratios overall conclude that the excursion reported by Orthotrak was smaller than that of Visual3D. Because both sets shared the same tracking frames on the thigh and shank, it is possible these differences are due to the separate software processing algorithms

SUMMARY

There is high agreement between systems where markers are commonly shared, especially for sagittal plane kinematics.

REFERENCES

Crenshaw, SJ, and Richards, JG (2006). *Gait Posture*, 24(4):515-21.
Schwartz, MH, and Rozumalski, DM (2005). *JBiomech,* 38(1):107-116.
Orthotrak 6.5 Gait Analysis Software Reference Manual (2007), *Motion Analysis Corporation*

BIOMECHANICAL ANALYSIS OF THE LUMBAR SPINE ON THE FACET JOINT FORCE AND INTRADISCAL PRESSURE— A REALISTIC FINITE ELEMENT STUDY

Hsuan-Teh Hu[1], Ruey-Mo Lin[2], Ching-Sung Kuo[1,3], Po-Chun Lin[1], Zheng-Cheng Zhong[4], Mu-Lin Hsieh[1], and Kuo-Yuan Huang[2]

[1] Department of Civil Engineering, National Cheng Kung University, Tainan, Taiwan

[2] Department of Orthopaedics, National Cheng Kung University Hospital, Tainan, Taiwan

[3] Center for General Education, Nan Jeon Institute of Technology, Yenshui, Taiwan, n6890104@mail.ncku.edu.tw or dgkcs@mail.njtc.edu.tw

[4] Department of Mechanical Engineering, National Chiao Tung University, Hsinchu, Taiwan

INTRODUCTION

The lumbar spine often leads to a high incidence of disc diseases, such as herniated disc, sciatica and low back pain. Biomechanical analyses of lumbar spine have been used to explore the related problems using in vitro studies or finite element simulations. Most of the previous FE studies have used simplified models such as a quarter of the vertebrae and discs, a half of the vertebrae, or a simple whole spine model. This study developed and validated an FE model of the lumbosacral spine with a realistic geometric shape to simulate the lumbar spine subjected to several loading conditions. The effects of symmetric postures such as left and right axial rotations on the facet joint forces at various levels of the lumbar spine were compared. In addition, we investigated the effect of postures on the intradiscal pressures in the nuclei pulposi.

METHODS AND PROCEDURES

CT images were acquired from scanning a specimen of a lumbosacral spine model. Bony boundary outlines were depicted from each DICOM image filtered using a gray value threshold, and then a smooth surface model was created by smoothing the sawtooth shapes of the boundary outlines and stacking. The surface model was further preprocessed with PATRAN to retain the accurate geometry of the lumbosacral spine (Fig. 1). Properties of the materials used in this study are listed in Table 1. The contact behavior of facet joints was simulated by setting the coefficient of friction to 0.1. The model used solid tetrahedral linear elements instead of hexahedral ones to simulate the posterior bone, cancellous bone, and annulus ground substance, near incompressible tetrahedral elements for the nucleus pulposus, triangular shell elements for the cortical shell, endplate, and annulus fiber layers, and narrow strip-shaped bilinear membrane elements for the ligaments under the control of no resistance in compression. Several loading conditions included an evenly distributed load of 300, 460, or 600 N, and combinations of a preload of 300, 460, or 600 N with bending or rotation moment of 5, 10, 15, or 20 Nm on the superior surface of the L1 vertebral body. The boundary condition imposed in the model involved setting the sacroiliac joint to fully constrained in all directions.
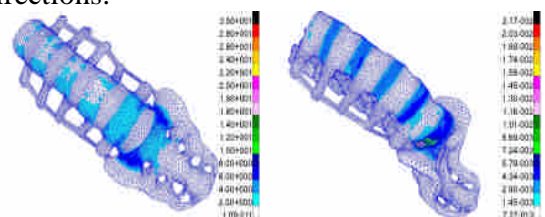
Figure 1. A realistic finite element model of the lumbosacral spine. (under a preload of 460 N; left/right for stress/strain distribution.).

Material	Young's (MPa) modulus, E	Poisson ratio, ν
Cortical shell	12000	0.3
Cancellous bone	100	0.2
Endplate	12000	0.3
Posterior bone	3500	0.25
Nucleus pulposus	1	0.4999
Ground substance	4.2	0.45
Fiber (inner/outer)	(360/550)	0.3

Table 1. Material properties of this model.

RESULTS

Figure 2 indicates that the facet joint forces were affected slightly by the preloads in the range of 300 to 600 N, particularly in right rotation. Left rotation resulted in a larger facet joint force in the contralateral (right) facet joint than that in the homolateral (left) joint at the same level, and vice versa. Figure 3 shows that intradiscal pressures in the nuclei pulposi increased with preloads and became more noticeably with flexion than with extension or left/right rotation.
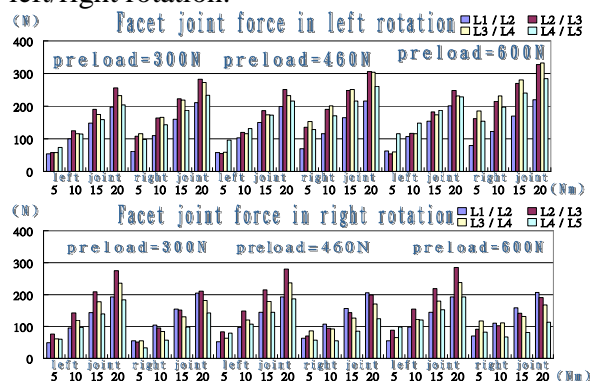
Figure 2. Facet joint forces at various levels under different combinations of preloads and loadings in left/right (top/bottom) rotation.
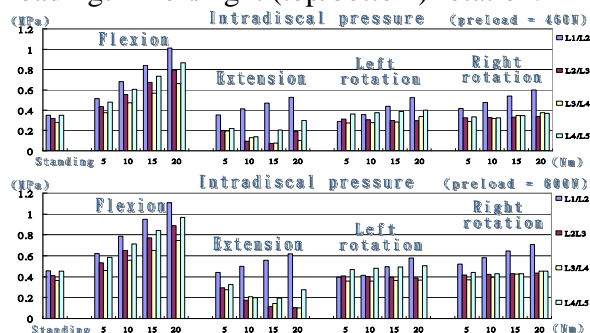
Figure 3. Intradiscal pressures at various levels of the lumbar spine. (under preloads of 460 and 600 N and different loadings.).

DISCUSSION AND CONCLUSIONS

With regard to the facet joint forces, forward/backward bending and axial rotation produced asymmetric responses in the facet joints. It appeared that the influence of the magnitude of preloads on the facet joint force was less important than that due to the various postures. The intradiscal pressures, in extension postures, decreased temporarily at levels L2/L3, L3/L4, and L4/L5 under different preloads, and considering all levels of the lumbar spine, it showed that the pressure at level L1/L2 was greatest for the various postures － flexion, extension, and axial rotation.

REFERENCES

Baroud G et al. (2003). *Eur Spine J*, 12:421-426.

Cao KD et al. (2001). *Spine*, 26:E253-E260.

Chosa E et al. (2004). *J Spinal Disord*, 17:134-139.

Kim YE et al. (1991). *Spine*, 16:331-335.

Lee CK et al. (2000). *Spine*, 25:2431-2439.

Natarajan, RN and Andersson, GBJ (1997). *Comp Structures*, 64:1291-1297.

Pitzen T et al. (2001). *Eur Spine J*, 10:23-29.

Polikeit A et al. (2003). *Eur Spine J*, 12:413-420.

Ramos, A and Simoes, JA (2006). *Med Engng Phys*, 28:916-924.

Rohlmann A et al. (2005). *Eur Spine J*, 14:445-453.

Rohlmann A et al. (2007). *Eur Spine J*, 16:1223-1231.

Shirazi-Adl A et al. (1984). *Spine*, 9:120-134.

Totoribe K et al. (2004). *J Spinal Disord*, 17:147-153.

White, AA and Panjabi, MM (1990). *Clinical biomechanics of the spine*. Philadelphia: J.B. Lippincott.

INFLUENCE OF WHEELCHAIR SUSPENSION ON SEAT FORCES AND HEAD ACCELERATIONS DURING CURB DESCENT LANDINGS

Philip S. Requejo[1], Jill McNitt-Gray[2], Henryk Flashner[3]

[1]Rehabilitation Engineering Program, Rancho Los Amigos National Rehabilitation Center, Downey, California, USA, prequejo@larei.org
[2]Biomechanics Research Laboratory, Departments of Kinesiology and Biomedical Engineering, University of Southern California, Los Angeles, California, USA, mcnitt@usc.edu
[3]Department of Aerospace and Mechanical Engineering, University of Southern California, Los Angeles, California, USA, hflashne@usc.edu

URL: http://www.ranchorep.org

INTRODUCTION

For many persons with a spinal cord injury (SCI), a common method of mobility is a wheelchair. Shocks experienced during manual wheelchair use can decrease an individual's comfort, increase the rate of fatigue, result in injury, and consequently limit mobility and community participation[1]. The objective of this study was to determine the forces transmitted from the seat and accelerations experienced by wheelchair riders during independent curb descents on a rigid and 3 rear suspension type wheelchair frames. We hypothesized that rear suspension wheelchairs will significantly reduce the seat forces and head accelerations compared to non-suspension wheelchairs.

METHODS AND PROCEDURES

Eight men with paraplegia (T12; ASIA-A) performed an independently-controlled curb descent manoeuvres in four different wheelchairs: a rigid frame wheelchair (Quickie GPV) and three rear-wheel suspension wheelchairs (Invacare A4, Colours Boing, Quickie XTR). Subjects performed the curb descents from a 4 inch height, 5 times in each wheelchair. Load cells mounted on each seat frame measured the 3D seat reaction forces and accelerometers attached to a helmet measured the subjects head accelerations[2]. Resultant seat forces at initial contact normalized to body weight (BW), change in resultant seat force from initial contact to peak force, rise time (initial contact to peak force); and peak vertical, forward (positive) and backward (negative) head accelerations were compared between wheelchairs.

RESULTS

Change in seat resultant force was lower in the suspension frames (XTR=1.51 ± 0.64 BW, A4=1.69 ± 0.48 BW, Boing= 1.87 ± 0.52 BW) compared to the rigid frame wheelchair (GPV=2.03 ± 0.35 BW). Rise time was shorter in the rigid frame (GPV = 59 ± 14 ms) compared to suspension frame wheelchairs (A4=68 ± 14ms, Boing = 90 ± 7 ms, XTR=103 ± 11 ms). Peak vertical head acceleration was lower in the suspension frames (XTR=1.33 ± 0.29 g, A4=1.51 ± 0.41g, Boing = 1.57 ± 0.37g) compared to the rigid frame wheelchair (GPV=1.69 ± 0.44g). Peak forward head acceleration was lower in the suspension frames (XTR=1.08 ± 0.51 g, Boing=1.46 ± 0.82g, A4= 1.47 ± 0.60g) compared to the rigid frame wheelchair (GPV=1.95 ± 0.80 g). Peak backward head

acceleration was reduced in the suspension frames (XTR=-0.23 ± 0.43g, Boing = -0.65 ± 0.51g, A4 = -0.96 ± 0.53g) compared to the rigid frame wheelchair (GPV=-1.10 ± 0.41g). Resultant seat force at initial contact was inversely related to change in seat force (Figure 1), peak vertical head acceleration, and peak backward head acceleration (Figure 2); indicating that wheelchair riders can reduce the reaction forces and head accelerations by increasing the seat reaction force prior to initial ground contact.
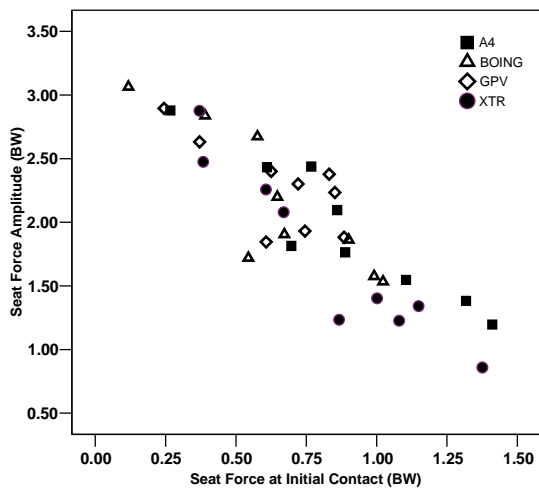
Figure 1. Change in seat force amplitude as a function of seat force at initial contact.
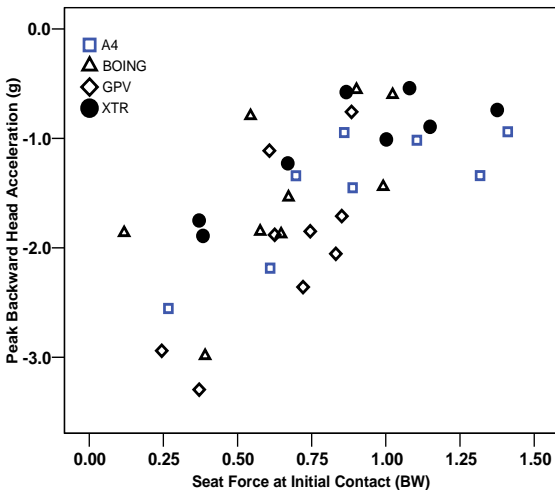
Figure 2. Peak backward head acceleration as a function of seat force at initial contact.

DISCUSSION
Rear wheel suspension systems can reduce the forces transmitted from the wheelchair to the user by extending the peak force rise time. This resulted in decreased head acceleration for the wheelchair riders. Among the suspension frame wheelchairs, the Quickie XTR demonstrated the greatest attenuation of forces and reduction in head accelerations. However, wheelchair riders can also control the magnitude of the seat reaction forces and head accelerations during curb descent landings by controlling the velocity at contact as indicated by the magnitude of seat force.

SUMMARY
Rear suspension is effective in absorbing shocks and vibration during wheelchair use. However, the suppression performance varies as a function of rear suspension configuration and landing strategies at contact.

REFERENCES
1. Cooper RA, Boninger ML, Spaeth DM, et al. *IEEE Trans Neural Syst Rehabil Eng.* Dec 2006;14(4):438-455.
2. Kerdanyan G, Minkel J, et al. Measurement of Force and Acceleration Experienced in a Manual Wheelchair. Paper presented at: RESNA 28th Annual Conference, 2005; Atlanta, GA.

ACKNOWLEDGEMENTS

IMPROVED LOCOMOTION IN HUMAN SCI TRHOUGH MOTOR ADAPTATION

Ming Wu[1,2] T. George Hornby[1,2,3] W. Zev Rymer[1,2], Brian D. Schmit[1,2,4]

[1]Sensor Motor Performance Program, Rehabilitation Institute of Chicago, Chicago, IL, USA
[2]Depertment of Physical Medicine & Rehabilitation, Northwestern University, Chicago, IL, USA
[3]Department of Physical Therapy, University of Illinois at Chicago, Chicago, IL, USA
[4]Department of Biomedical Engineering, Marquette University, Milwaukee, WI, USA
E_mail: w-ming@northwestern.edu

INTRODUCTION

While body weight supported treadmill training (BWSTT) has been shown to provide greater improvements in locomotor ability, motion function, and balance than conventional rehabilitation techniques (Behrman and Harkema 2000; Dietz et al. 1995), the efficacy of the technique is likely to be improved by minimizing the amount of assistance provided and allowing independent walking practice. Evidence from spinalized mice indicates that motor learning is more effective with assistance as needed compared with a fixed trajectory paradigm (Cai et al. 2006). In addition, results from human subjects show that motor learning is accelerated by amplifying, rather than reducing, movement errors (Emken and Reinkensmeyer 2005). We propose that providing targeted resistance load as tolerated, instead of persistent assistance, may increase patient effort and further improve the efficacy of BWSTT by engaging adaptive sensorimotor process.

METHODS AND PROCEDURES

Two subjects with incomplete (ASIA D) C5 and T10 SCI, and 4 control healthy subjects were recruited to participate into this study. The average ages for patient and healthy subjects were 41 ± 6 and 36 ± 6 years old. The average time post injury was 32 ± 8 months. Their scores on the Walking Index for Spinal Cord Injury II (WISCI II) were 16/20 and 13/20 respectively. Their 10-Meter walking speed were 0.51 and 0.16m/s.

The subject was fitted into an overhead body weight support system through a harness (for safety only; no body weight was supported) and walked on a treadmill with the speed was set at their maximum comfortable speed. A custom-designed cable-driven actuator was used to apply load at the ankle of the subject. A cable was attached to the right leg at the ankle using a strap, which was then connected to a cable spool to provide a constant resistance (backward) or assistance (forward) load to the lower leg. The loads applied to the legs were controlled through a PC using custom LabVIEW software.

Two types of loads, resistance and assistance, were applied to the right leg through the cable, with a 10 minute interval between the application of the loads to allow washout of any lingering aftereffects. A constant load, 5 N for the first 20 steps, 15 N afterwards, was applied to the ankle through the cable robot for the purpose of this pilot test. For each test run, the subject walked on the treadmill without load for 2 minutes, defined as the baseline period, and then a resistance or assistance load was applied to the leg for 5 minutes, defined as the adaptation period, and after that, the load was removed and the subject continued to walk on the treadmill for another 1 minute, defined as the post-adaptation period.

Surface EMG data from 6 muscles of right leg were recorded using active Delsys electrodes (model De 2.1, Delsys Inc., Boston, MA). Kinematic data from the hip, knee and ankle were recorded using three electrogoniometers (Biometrics, Inc, UK) attached at the hip, knee and ankle. The length of the lower leg, measured between the ankle and knee axes of rotation, the length of the femur were measured for subsequent calculations of the step height and stride length. All data were sampled at 1000 Hz using a data acquisition card (National Instruments, Austin, TX). The step height and stride length were calculated using recorded hip and knee joints positions signals and the length of lower limb.

RESULTS

1. Enhanced muscle activity during resistance training.
As shown in Figure 1, enhanced muscle activity was observed during resistance training. The RF EMG was increased substantially by the resistance load, especially during late stance and early swing (Figure 1).
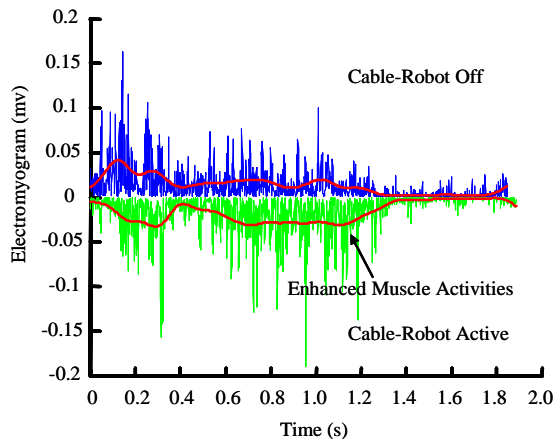
Figure 1. The effects of Cable-Robot (with/without) resistance load on the rectus femoris EMG are shown for a SCI patient.

2. Motor adaptation to resistance load and its aftereffect following load release.
An aftereffect consisting of increased step height and stride length following the load release was observed. Following 5 minutes of resistance training, both the step height and stride length increased, although a more significant increase was observed for step height, as shown in Figure 2. In contrast, the assistance load applied to the ankle appeared to reduce the subject effort during treadmill stepping and had a detrimental effect on gait parameters post-adaptation.
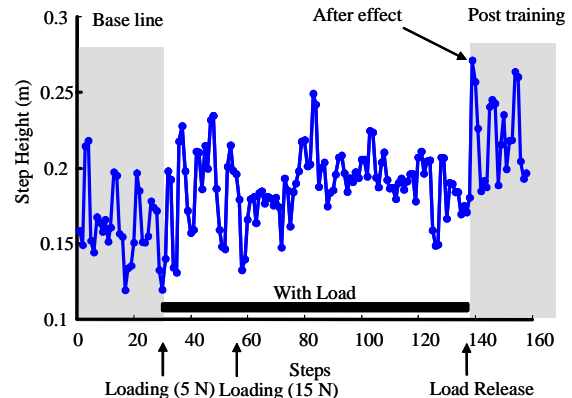
Figure 2. Stride by stride plot of step height for one subject with incomplete SCI.

SUMMARY

In summary, results from this pilot study suggest that a swing phase resistance load could enhance the training effects of BWSTT through increased patient effort and by engaging adaptive sensorimotor processes

REFERENCES

Behrman AL, Harkema SJ (2000). *Phys Ther*, 80: 688-700.
Cai LL et al (2006). *J Neurosci*, 26: 10564-8.
Dietz V et al (1995). *Ann Neurol*. 37: 574-82.
Emken JL, Reinkensmeyer DJ (2005). *IEEE Trans Neural Syst Rehabil Eng*. 13: 33-9.

ACKNOWLEDGEMENTS

GENDER AND PASSIVE TISSUE RESPONSES TO PROLONGED SITTING IN AN AUTOMOBILE SEAT

Diana E. De Carvalho and Jack P. Callaghan
Department of Kinesiology, University of Waterloo, Waterloo, ON, Canada,
ddecarva@ahsmail.uwaterloo.ca

INTRODUCTION

A substantial amount of research has linked low back pain development with prolonged sitting both in office chairs and automobile seats.   Recent work has found that men and women sit differently and demonstrate different passive lumbar spine stiffness characteristics after prolonged seated exposure in an office chair (Beach et al., 2005). An investigation of the gender based postural responses to an automobile seat showed that while gender differences exist, they are opposite to the responses found in office chairs (Coke et al, Submitted 2007). Men exhibited more flexed postures in office chairs, whereas in automotive seats women exhibited greater lumbar flexion. The impact of these postural changes on passive tissues of the spine from prolonged driving are critical to support the design of automobile seats.

METHODS AND PROCEDURES

Nineteen subjects (10 males and 9 females), recruited from a student population, were exposed to a 2 hour simulated driving task. Passive lumbar range of motion was measured at three points during the prolonged driving trial. To generate a measure of stiffness, passive moment-angle relationships were calculated from normalized lumbar angle data captured by video and the cable tension needed to pull subjects into flexion while side lying on a low friction table. EMG was collected bilaterally over the thoracic and lumbar erector muscles and normalized to ensure activation levels were less than 5% MVC during passive range of motion trials.

Two tri-axial accelerometers (S2-10G-MF, NexGen Ergonomics Inc., Montreal, Canada) were fixed over the spinous processes of L1 and S1 to provide a time-varying external measure of lumbar lordosis angle and pelvic tilt during driving. Time varying seat pan and backrest pressure distributions were collected with a pressure mapping system fitted to the car seat (Xsensor Technology Corporation, Calgary, AB, Canada). Ratings of Perceived Discomfort using a 10 cm VAS were taken at three points throughout the prolonged simulated driving trial.

RESULTS

During the prolonged simulated driving trial females were found to have significantly greater lumbar flexion on average than men: 53.4 degrees (SD 6.9) and 48.9 degrees (SD 1.7) respectively ($p < 0.0458$). Trends indicate that women changed their lumbar flexion angle at approximately twenty minute intervals during prolonged sitting in an automobile seat.
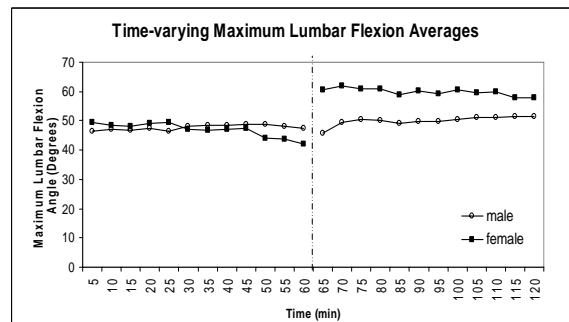
Figure 1: Time varying maximum lumbar flexion angles measured by tri-axial accelerometers.

Women demonstrated a significant increase (59.9 degrees SD 1.3 from 45.2 degrees SD 2.2) in maximum lumber flexion angle as they returned to the automobile seat for the second hour of simulated driving ($p<0.003$). Time varying lumbar flexion angles showed an increasing trend in both women and men over the two hour simulated driving trial. Pelvic angles, both with respect to the vertical and with respect to standing, were not statistically different between men and women: 29.77 (SD 0.45) and 28.97 (SD 0.32) respectively.

Trends indicated that total area, total pressure and peak pressure increased over time in both males and females. Center of pressure was found to move anteriorly on the seat pan for men only and superiorly on the backrest over time for both men and women.

On average, passive lumbar spine stiffness in both males and females initially increased after one hour of sitting and then decreased by the end of the second hour. At the end of the driving trial males were marginally stiffer than their initial measurements while female subjects exhibited decreased stiffness and exceeded their initial range of motion measurements.
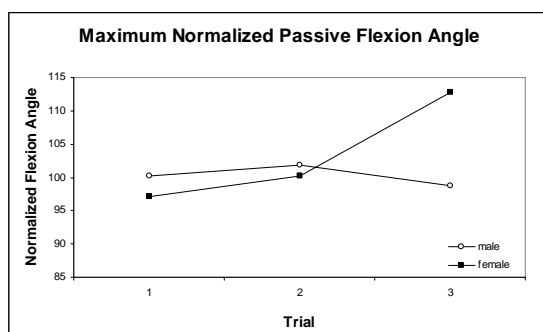
Figure 3: Normalized maximum passive flexion angle across trials between men and women.

DISCUSSION

The spine posture and seat pressure results from this study agree well with those noted previously (Coke et al., Ergonomics Submitted 2007). The remarkably static pelvic angles that were measured for both genders are reflective of the posture constraint the automobile seat imparts. If the pelvis is fixed and lumbar flexion is increased it is logical that this posture will result in some degree of viscoelastic creep in pelvic and lower lumbar ligaments resulting in decreased stiffness. Since females were shown to sit with greater lumbar flexion compared to men, it is not surprising that they also demonstrated decreased passive flexion stiffness in the passive moment-angle trials. The increased stiffness in males, however, prompts the suggestion that there may be a gender specific response to passive tissue strain at the cellular level.

SUMMARY

This study examined the effect a two hour simulated driving trial had on passive lumbar spine stiffness. Postural differences between genders were clearly demonstrated in this study. Passive stiffness appeared to increase in males over time and decrease in females over time. In order to prevent injury to the passive elements of the spine during prolonged driving, gender specific ergonomic interventions for the automobile seat are indicated.

REFERENCES

Beach T.A.C. et al. (2005). *The Spine Journal* 5; p. 145-154.
Coke S. et al. (Submitted 2007). *Ergonomics*

ACKNOWLEDGEMENTS

MOMENT ARMS OF THE MUSCLES CROSSING THE ANATOMICAL SHOULDER

David C. Ackland and Marcus G. Pandy,
ackland@pgrad.unimelb.edu.au
Department of Mechanical Engineering, University of Melbourne, Australia

INTRODUCTION

The moment arm (MA) of a muscle force represents the mechanical advantage of a muscle and largely determines its role, for example, as a stabilizer or a prime mover. Many biomechanical models rely on accurate muscle-path and MA data to represent the anatomical shoulder during movement. To our knowledge, no study has investigated the instantaneous MAs of functionally distinct muscle sub-regions within the rotator cuff, pectoralis major or latissimus dorsi through scapula plane abduction (scaption), coronal-plane abduction and forward flexion. Furthermore, muscle MAs have not been reported over a continuous range of humeral elevation exceeding 100°, as most studies ignore scapulothoracic motion.

METHODS AND PROCEDURES

MAs of the musculature spanning the glenohumeral joint were measured in 8 fresh-frozen, entire upper extremities using the tendon excursion method (An et al., 1984). Specimens were mounted on a custom designed dynamic shoulder cadaver testing apparatus (DSCTA) designed to produce and quantify 6 degree-of-freedom glenohumeral joint motion by means of simulated muscle force and scapula rotation. Tendons of the following muscles and muscle sub-regions were exposed by resection: deltoid (anterior, middle, posterior), subscapularis (inferior, middle, superior), supraspinatus (anterior, posterior), infraspinatus (superior, inferior), latissimus dorsi (superior, middle, inferior), and pectoralis major (superior, middle, inferior).

Nylon-lines were sutured to all tendons and passed through a pulley system to hanging weights of 10 N; the pulleys were positioned to reproduce each muscle's line-of-pull, as determined by visual inspection and using a computational model (Garner and Pandy, 2001). Retro-reflective markers were placed on each hanging weight, and marker triads placed on the humerus and scapula. The humerus was passively elevated in the scapula plane, coronal plane and sagittal plane to 120°. During elevation, the scapula was rotated on the DSCTA to simulate scapulohumeral rhythm as reported by Inman et al., (1944).

Tendon excursion (vertical trajectory of hanging weight) and joint angle were measured from the retro-reflective marker trajectories using a 6-camera Vicon motion capture system, and instantaneous muscle MAs were then computed from the gradient of the plot of tendon excursion vs. joint angle. Scapula and humeral coordinate systems were defined by digitizing bony prominences, as described in Garner and Pandy (2001).

RESULTS

Significant differences in MAs were reported across sub-regions of all muscles ($p < 0.01$) (Table 1). The most effective elevators in abduction were the anterior and middle deltoid, while the most effective depressors were the posterior deltoid and inferior and middle latissimus dorsi (Figure 1A). In flexion, the superior pectoralis major was the most effective elevator (Figure 1B), while teres major and superior latissimus dorsi had the largest depressor MAs. Division of multi-pennate shoulder muscles of broad-origins into sub-regions highlighted distinct functional differences across those sub-regions. Most significantly, we found that the clavicular fibres of the pectoralis major were

able to exert substantial elevator torque in flexion, whereas the sternal and lower costal fibres behaved as stabilizers and flexion antagonists.

Muscle/muscle subregion	Scaption		CP abduction		Flexion	
	Ackland et al (2008)		Ackland et al (2008)		Ackland et al (2008)	
	AG	AN	AG	AN	AG	AN
Superior Subscapularis	9.8	2.2	7.2	-9.5	35.3	-5.4
Middle Subscapularis	1.8	-2.4	1.3	-12.7	24.2	-0.6
Inferior Subscapularis	-1.5	-9.5	-2.2	-16.6	10.4	-3.4
Anterior Supraspinatus	32.4	9.2	23.2	5.6	41.8	0.6
Posterior Supraspinatus	31.9	13.8	26.8	10.4	13.4	2.7
Superior Infraspinatus	22.2	7.1	13.4	5.6	7.1	1.7
Inferior Infraspinatus	12.2	1.9	10.9	3.8	4.2	-6.8
Teres minor	2	-0.8	5.1	-3.3	2.2	-18.7
Teres major	-18.6	-47.3	-12.1	-46.1	-19.7	-54.4
Anterior Deltoid	39.3	2.1	30.2	2	40	11.6
Middle Deltoid	33.1	6.7	29.1	8.3	12.2	0
Posterior Deltoid	3	-14.9	2	-15.9	-16.3	-33
Superior Pectoralis major	30.2	3.1	11.2	-1.8	53.7	-32.9
Middle Pectoralis major	-2.9	-12.7	-17.7	-32.9	15.9	4.4
Inferior Pectoralis major	-12.4	-22.2	-16.2	-33.6	1.9	-9.3
Superior Latissimus dorsi	-7.8	-31.5	-2.1	-29.9	-0.1	-22.1
Middle Latissimus dorsi	-6.4	-21	-10.1	-38.6	-0.6	-15.3
Inferior Latissimus dorsi	-9.9	-28.9	2.6	-38.1	-2.9	-10.8

Table 1. Peak muscle MAs. Positive values signify agonistic muscle action; negative values signify antagonistic muscle action. (AG), maximum elevation agonistic MA; (AN), maximum elevation antagonist MA.
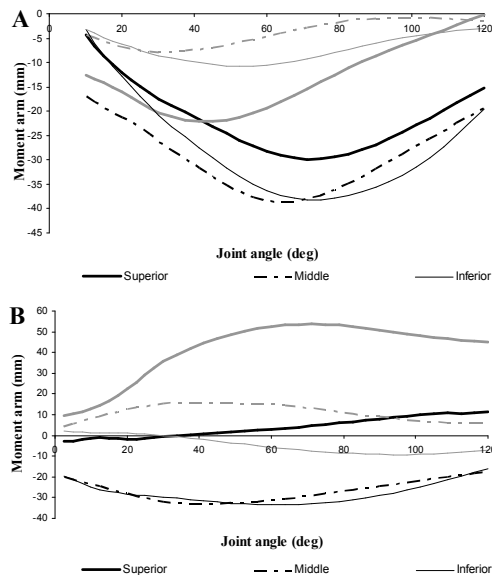
Figure 1. MAs arms of (A) latissimus dorsi, and (B) pectoralis major. Black lines show scaption data and grey lines flexion data.

DISCUSSION

The MA data presented in this study may facilitate the design and validation of biomechanical models of the shoulder complex. The data presented are valid for an intact shoulder free of pathology and joint dysfunction; any condition that is likely to effect joint congruency may change muscle moment arm quantities due to eccentric joint centre of rotation. Demonstrating the torque-producing potential of the glenohumeral joint musculature helps to establish a better understanding of the normal function of the shoulder joint and its surrounding structures, and therefore may provide knowledge for the design and implantation of joint prostheses and ligament replacements in diseased or injured shoulders.

SUMMARY

Quantifying the MAs of sub-regions of multi-pennate shoulder muscles provided biomechanical evidence for the torque-producing potential of such muscles across the glenohumeral joint, as well as the moment inducing potential of the muscle fibers across their extensive origins. Such evidence cannot readily be obtained by approximating broad-origin muscles as single lines-of-force. Knowledge of MA differences between muscle sub-regions may assist in identifying the functional effects of muscle sub-region tears, assist surgeons in planning tendon reconstructive surgery, and aid in the development and validation of computational models.

REFERENCES

An et al. (1984) *J Biomech Eng* 106, 280-2

Garner and Pandy (2001) *Comp Meth Biomech Biomed Engin* 4, 93-126

Inman et al (1944) *JBJS* 58, 1-30

MUSCLE CONTRIBUTIONS TO JOINT STABILITY IN THE ANATOMICAL SHOULDER

David C. Ackland and Marcus G. Pandy

ackland@pgrad.unimelb.edu.au Department of Mechanical Engineering, University of Melbourne, Australia

INTRODUCTION

During the course of normal shoulder movement, muscles and tendons translate and rotate with their bone-embedded origins and insertions. Because the spatial relationship between the origins and insertions of these structures varies according to joint motion, muscle lines-of-action (LOA) and moment arms must also change through the range of movement. As a result, articulating forces, bone-stress distributions, and joint stability may vary significantly. The present study investigated the contribution of shoulder musculature LOA to the superior stability of the glenohumeral joint. At present, no study has measured the LOA of all the major muscles spanning the shoulder in flexion and abduction, nor quantified the contribution of these muscles to joint stability.

METHODS

Eight fresh-frozen, entire upper extremities were mounted on a custom designed dynamic shoulder cadaver testing apparatus. Tendons of the following muscles and muscle sub-regions were identified and separated: deltoid (anterior, middle, inferior), subscapularis (inferior, middle, superior), supraspinatus (anterior, posterior), teres minor, latissimus dorsi (superior, middle, inferior), and pectoralis major (superior, middle, inferior).

To remove muscle-slack, nylon-lines were sutured to all tendons and passed through a pulley system to hanging weights of 10 N; the pulleys were positioned to reproduce each muscle's line-of-pull, as determined by visual inspection and using a computational model (Garner and Pandy,

2001). Retro-reflective marker triads were inserted into the humerus and scapula, and joint angles computed from the marker trajectories using a 6-camera Vicon motion capture system. Scapula and humeral coordinate systems were defined by digitizing bony prominences, as described in Garner and Pandy (2001). The humerus was passively held at 30°, 60°, 90° and 120° of elevation in scapula-plane abduction (scaption) and flexion. At each joint angle, LOA were calculated by digitising bony and soft tissue landmarks using a marker wand. Muscle LOA for each scapulohumeral muscle bundle were defined by the force-vector projection from the last tendon wrapping via-point (the point where the muscle-tendon loses contact with the head of the humerus), to the centroid of origin of the muscle sub-region, and expressed in the scapula reference-frame.

Stability ratios were computed to assess muscle potential contributions to glenohumeral joint stability; superior stability ratios (SSR) were computed by dividing superior shear components of the muscle's LOA by the compressive component.

RESULTS

The inferior latissimus dorsi was a potential inferior destabiliser, but may stabilise the glenohumeral joint with the combined superior shear of the superior pectoralis major and the anterior deltoid, particularly in flexion (Figure 1). The superior subscapularis and anterior supraspinatus had the greatest stabilising capacity of the rotator cuff muscles during scaption and flexion, while the inferior subscapularis and teres minor had the greatest destabilising potential.
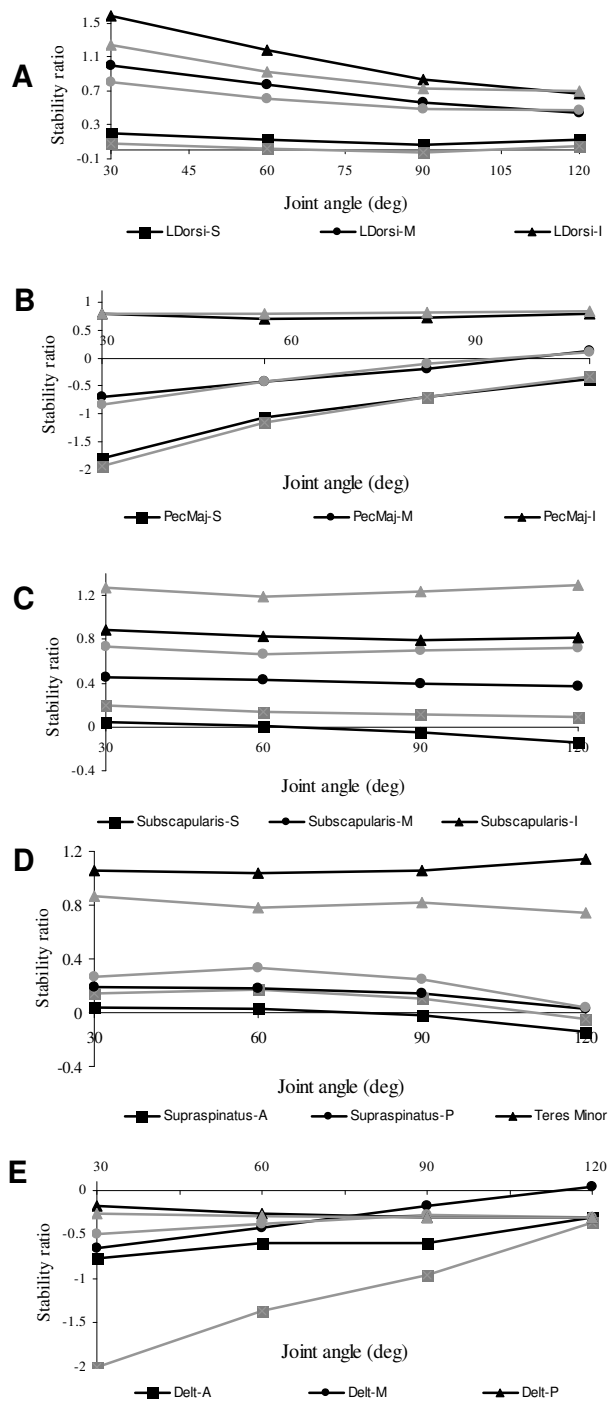
Figure 1. Superior stability ratios for (A) latissimus dorsi, (B) pectoralis major, (C) subscapularis, (D) supraspinatus and teres minor, and (E) deltoid Black lines show scaption data and grey lines flexion data

DISCUSSION

The results of this study provided anatomical evidence of the superior stabilising potential of specific rotator cuff muscles, and how the potentially destabilising prime movers of the shoulder may interact to produce stable leverage during elevation. At present, contributions of latissimus dorsi and pectoralis major to joint stability have received very little attention in the literature and are not well understood; for the first time in a study of glenohumeral joint stability, multi-pennate muscles of broad origin were divided into functionally distinct sub-regions and investigated individually.

Quantifying the LOA and stabilising potential of the shoulder musculature helps to establish a better understanding of the normal function of the glenohumeral joint, and may assist surgeons in planning shoulder joint surgery including arthroplasty or reconstructive procedures such as tendon-transfer.

SUMMARY

Measuring the lines-of-action and stability ratios of sub-regions of the shoulder muscles during scaption and flexion demonstrated the potential contribution of the shoulder musculature to glenohumeral joint stability during arm elevation. The results presented provided evidence for specific muscle sub-region function, which may assist in the planning of surgery for the diseased or injured shoulder. The data presented may also assist in development and validation of computational models of the shoulder complex.

REFERENCES

Garner and Pandy (2001) *Comp Meth Biomech Biomed Engin* 4, 93-126

IMAGE-BASED MESH GENERATION AND ITS ROLE WITHIN COMPUTATIONAL BIOMECHANICS

Philippe Young[1], Terry Beresford-West[2] and Frank Murphy[3]

[1]Associate Professor, School of Engineering, Computing and Mathematics, University of Exeter, Exeter, UK, Philippe.G.Young@exeter.ac.uk
[2]Senior Software Developer, Simpleware Ltd., Exeter, UK, t.west@simpleware.com
[2]Computational Modeling Engineer, Kx Simulation Technologies Inc., Cincinnati, OH, frank.murphy@kxinc.com

INTRODUCTION

Although a wide range of mesh generation techniques are currently available these, on the whole, have not been developed with meshing from segmented 3D imaging data in mind. Generating high quality computational models from 3D segmented imaging data presents a number of challenges but also unique opportunities for presenting more realistic and accurate geometrical descriptions of the computational domain. It is simply the 'only option' for a wide range of applications within and beyond the computational biomechanics field.

MESH GENERATION FROM PATIENT-SPECIFIC DATA

The majority of approaches adopted have involved generating a surface model (either in a discretized or continuous format) from the scan data, which is then exported to a commercial mesher – a process which is time consuming, not very robust and virtually intractable for the complex topologies typical of image data. A more 'direct approach' presented in this paper is to combine the geometric detection and mesh creation stages in one process. This approach involves identifying volumes of interest (segmentation of 3D image) and then directly generating the volumetric mesh based on a unique in-house developed multi-part marching cubes algorithm. The resulting meshes can then be directly exported to a number of major commercial CAE solvers which provides more flexibility and efficiency for researchers in the computational biomechanics community.

Image-based mesh generation raises a number of issues which are different from CAD-based model generation some of which are discussed below:

CAD-based versus Image-based Meshing
CAD-based approaches use the scan data to define the surface of the domain and then create elements within this defined boundary (Cebral and Loehner, 2001). The element creation process was initially quite simplistic, but automatic meshing has been an area of great interest in the FEA/CFD community, with applications well beyond the biomedical field, and so reasonably robust algorithms are now available (Antiga et al., 2002). These techniques do not easily allow for more than one domain to be meshed as multiple surfaces generated are often non-conforming with gaps or overlaps at interfaces where one or more structures meet.

A more direct approach would be to combine the geometric detection and mesh creation stages in one process. In this paper a methodology is used that generates 3D hexahedral or tetrahedral elements throughout the volume of the domain, thus creating the mesh directly. This technique was originally developed for FE analysis of bones, for both stress and vi-

bration analysis (Weber and Young, 2003), and has been implemented as a set of computer codes (ScanIP, ⁺ScanFE and ⁺ScanCAD).

Robustness and Accuracy
In the case of modeling complex topologies with possibly hundreds of disconnected domains (e.g. inclusions in a matrix), approaching the problem via a CAD-based approach is virtually intractable. By contrast treating the problem using an image-based meshing approach is remarkably straightforward, robust, accurate and efficient. Indeed meshes can be generated automatically which is of image-based accuracy with domain boundaries of the finite element model lying exactly on the iso-surfaces thereby taking into account partial volume effects and providing sub-voxel accuracy (Figure1).

a)

b)
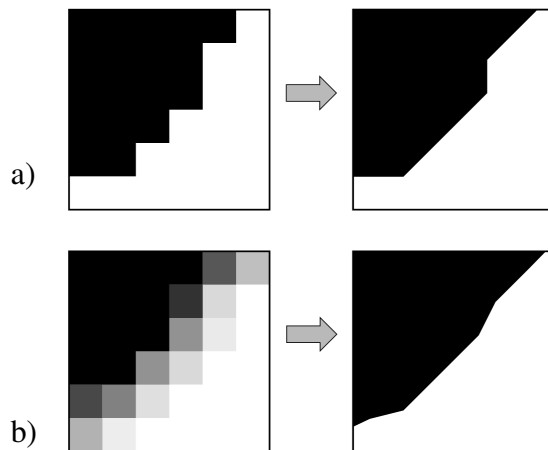
Figure 1. 2D surface reconstruction a) from binary image, and b) using partial volumes information present in the scan.

Anti-aliasing and Smoothing
Where anti-aliasing and smoothing is applied to the segmented volumes, the presented technique is both topology and volume preserving. If appropriate algorithms are not used, the process of smoothing and anti-aliasing the data can introduce significant errors in the reconstructed geometry and topology. Most implemented smoothing algorithms are not volume preserving and lead to shrinkage of convex hulls and in many cases topological changes (Figure 2). Whilst this is not particularly problematic when the purpose is merely enhanced visualization, the influence can be dramatic when the resultant models are used for metrology or simulation purposes.
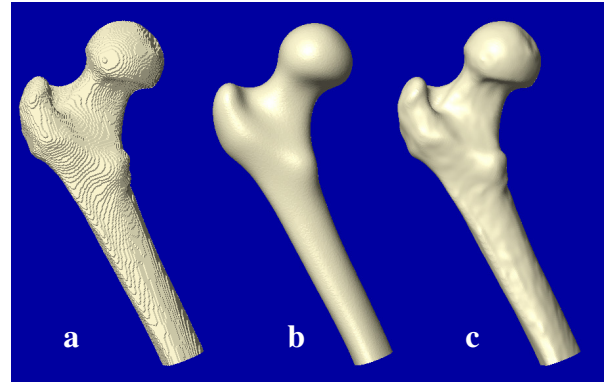
Figure 2. a) Original image, unsmoothed ($203,238$ mm^3); b) Traditional smoothed ($180,605$ mm^3, Δvolume = -11.14%); c) Exeter developed proprietary ($202,534$ mm^3, Δvolume = -0.35%).

DISCUSSION

The ability to automatically convert any 3D image dataset into high quality meshes, is becoming the new *modus operandi* for anatomical analysis. The techniques presented guarantee the generation of robust, low distortion meshes from 3D data sets for use in finite element analysis (FEA), computer aided design (CAD) and rapid prototyping (RP).

REFERENCES

Antiga, L et al. (2002), *Computerized Medical Imaging and Graphics*, 26:227-235.
Cebral, JR and Loehner, R (2001) *Int.J.Num.Methods Eng.*, 51:985-1008.
Weber, I and Young, P (2003), *3D Modelling Paris, France*, 23-24.

POSTURAL BALANCE DURING ONE LEG STANDING IN PATIENTS WITH TOTAL HIP ARTHROPLASTY AND SURFACE REPLACEMENT ARTHROPLASTY

Marc Therrien[1], Julie Nantel[1-4], Martin Lavigne[2-3], Pascal-André Vendittoli[2-3] and François Prince[1,2,4]

[1]Gait and Posture Laboratory, Marie Enfant Rehabilitation Center, Montreal, QC, Canada
[2]Department of Surgery, Faculty of Medicine, University of Montreal, Montreal, QC, Canada
[3]Orthopaedic Department, Maisonneuve-Rosemont Hospital, Montreal, QC, Canada
[4]Department of Kinesiology, University of Montreal, Montreal, QC, Canada
francois.prince@umontreal.ca

INTRODUCTION

Osteoarthritis (OA) is the world most common joint condition, affecting over 20 millions people in USA (Garstang and Stitik, 2006). Of these, the hip is the second most common site of OA after the knee, causing the patient to experiment pain in their activities of daily living. One way to relieve this pain is to make a hip arthroplasty. Traditionally performed, the total hip arthroplasty (THA) with a large head using metal on metal bearing surface is a frequent and successful procedure that requires the resection of the whole femoral head and part of the neck. Consequently, THA does not always allow a precise reconstitution of the normal hip biomechanics, particularly for the abd/adductor muscles. In opposition, the surface replacement arthroplasty (SRA) does not present these draw-backs. Considering that balance control in medio-lateral (ML) is mostly regulated by the abd/adductor muscles (Winter, 1995), the objective of this study was to examine if the SRA would be more advantageous than THA to maintain postural control in a challenging task like one leg stance. In addition, we wanted to determine whether a difference persists between the affected and the sound side.

METHODS AND PROCEDURES

Two groups of patients with unilateral hip OA who underwent THA or SRA were evaluated at six and twelve months post-surgery while a control group was evaluated once. Characteristics of the groups are presented in Table 1. Each surgery was performed using a posterior surgical approach. All subjects performed two 10-sec.-one leg standing trials for each side on a force platform (AMTI, Advanced Mechanical Technology Inc, MA, USA) recording at 120 Hz the position of their center of pressure (COP). The data were then filtered and analysed to extract the range (maximum-minimum), root-mean-square amplitude (RMS) and the velocity of the COP (V_{COP}), in both the ML and antero-posterior (AP) directions . In addition, the total path length (TPL) of the COP was measured. The results were then averaged for each side and analysed by means of a repeated measures ANOVA (3 groups X 2 sides X 2 evaluations). If necessary, the results were analyse with Tukey post-hoc tests and paired-t tests. Statistical threshold was set at 0.05.

RESULTS

Table 1 shows the characteristics of the groups. No significant differences were observed between the groups ($p<0.05$).

Subjects	THA	SRA	Control
Age (y)	50.3 (6.6)	49.1 (6.8)	44.4 (8.5)
Gender	6 F/11 M	9 F/11 M	6 F/8 M
Weight (kg)	76.3 (11.9)	78.9 (15.0)	75.2 (13.4)
Height (m)	1.68 (0.05)	1.68 (0.07)	1.70 (0.07)
BMI(kg/m^2)	27.0 (3.5)	27.7 (3.6)	25.8 (3.3)

Table 1. Means (SD) of the group's characteristics.

The statistical analysis revealed only a main group effect for the V_{COP} in both ML (p=0.045) and AP (p=0.010) directions and for the TPL variable (p=0.040). No main effect of evaluation time or side was found. In addition, no interaction was found between the three factors for all variables. Table 2 presents the Tukey post-hoc tests used for the significant main group effect. The results show no difference between THA and SRA for these biomechanical variables but they present significant difference with the control group.

Subjects	THA	SRA	Control
Range ML	3.4 (1.0)	3.4 (1.0)	3.3 (1.0)
Range AP	4.0 (1.2)	4.1 (2.0)	3.9 (0.8)
RMS ML	0.8 (0.2)	0.8 (0.3)	0.7 (0.2)
RMS AP	0.8 (0.3)	0.8 (0.3)	0.8 (0.2)
V_{COP} ML	4.1 (1.4)*	3.9 (1.3)	3.4 (0.9)*
V_{COP} AP	3.8 (1.4)*	3.9 (2.3)λ	2.8 (1.0)* λ
TPL	60.8(18.4)*	60.7 (27.6)λ	49.0 (15.1)*λ

Table 2. Means (SD) of COP range, RMS, TPL (cm) and velocity (cm/s) for the main group effect, independently of evaluation time and side. *: Significant difference between THA and Control, λ: Significant difference between SRA and Control.

DISCUSSION

The absence of significant effect of side or evaluation time indicate that both legs performed the task similarly as soon as 6 months, which is consistent with an improvement of the hip function three to six months post-surgery (Laupacis et al., 2002). However, this improvement is not sufficient to reach the performance of the control group even at 12 months post-surgery. In fact, even if the amplitude of displacement of the COP is similar between our 3 groups (range, RMS); the velocity of the displacement made by the two patient groups is higher than for the control group (V_{COP}, TPL). This reflects an increased neuromuscular activity needed for maintaining their postural stability not only in ML, but also in AP for the same displacement of the COP. Finally, even if no significant group difference where found between SRA and THA for the V_{COP} in ML, the former seems to better performs between 6 and 12 months. These results could be linked to a better recovery of the abd/adductors muscles which, combined with a more natural hip biomechanics (femoral head and neck), may improve their postural control by means of a better proprioceptive function and stronger muscles strength (Nantel et al., 2007).

SUMMARY

One leg standing is a challenging task for control participants. It is even more for patients undergoing arthroplasty because of the muscles affected during the surgery. Even at 12 months post-surgery, these patients did not reach the performance showed by control participants. However, as soon as 6 months post-surgery, no difference subsists between the two supporting legs. Finally, even if no significant group difference between THA and SRA was found, the latter seems to better performs between 6 and 12 months.

REFERENCES

Garstang, SV and Stitik, TP (2006). *Am J Phys Med Rehab,* 85:S2-11.
Laupacis, A et al. (2002). *J Bone Joint Surg Am*, 84A:1823-1828.
Nantel, J et al. (2007). *J Clin Biomech*, in press.
Winter DA (1995). *A.B.C of Balance during Standing and Walking*. Waterloo, Ontario.

ACKNOWLEDGEMENTS

IMPLEMENTATION OF FACET JOINTS IN A DETAILED MUSCULOSKELETAL LUMBAR SPINE MODEL BASED ON INVERSE DYNAMICS

Mark de Zee[1], Peter Mikkelsen[2], Christian Wong[3], and Erik B. Simonsen[4]

[1]Dept. of Health Science and Technology, Aalborg University, Denmark, mdz@hst.aau.dk
[2]Orthopaedic Department, Glostrup Hospital, Denmark
[3]Orthopaedic Department, Næstved Hospital, Denmark
[4]Institute of Medical Anatomy, University of Copenhagen, Denmark
URL: http://www.anybody.aau.dk

INTRODUCTION

Recently, De Zee *et al.* (2007) presented a detailed musculoskeletal model of the lumbar spine using data from the literature (Hansen *et al.*, 2006). The model is based on inverse dynamics, where the redundancy problem is solved using optimization in order to compute the individual muscle forces and joint reactions. This model is, however, not equipped with facet joints. This limits the use of the model, because it has been proven experimentally that facet joints can carry a significant amount of load in some situations (Schendel *et al.*, 1993). Facet loading will therefore have an effect on the muscle recruitment in an inverse dynamics model and on the estimated reaction forces in the disc. Implementation of facet joints in an inverse dynamics model is not straightforward. One cannot just use a contact algorithm as one would in FEM. This work presents a new methodology for implementation of facet joints in the lumbar spine model developed by De Zee *et al.* (2007).

METHODS AND PROCEDURES

The already existing lumbar spine model (De Zee *et al.*, 2007) formed the basis for the implementation of the facet joints. In short this model consists of seven rigid segments with 18 degrees-of-freedom and 154 muscles and was built in the AnyBody Modeling System. The mathematical and mechanical methods of this software are described in detail by Damsgaard *et al.* (2006).

The location of each facet joint was defined as a node in the center of the facet contact site on each vertebra. This resulted in four nodes on each vertebra representing the location of the two superior and two inferior facet joints. The orientation of each node in the local coordination system was changed in such a way that the x-axis was perpendicular to the facet joint surface. For doing this the data generated by Masharawi *et al.* (2004) was used.

The contact points between the superior and inferior facet joints can transfer compression forces perpendicular to the facet joint surfaces. The strength of the contacts depends on the distances between the contact points. If the distance is zero, the contact is capable of providing a compression force; otherwise, no compression force is present. The unknown facet forces then become part of a redundant system of equilibrium equations for the entire system including the muscles. This redundant system is subsequently solved uniquely via the system's advanced muscle recruitment algorithms.

In order to test the implemented facet joints, the following situation was simulated. The spine model was driven from 20 degrees flexion to 5 degrees extension, for which we estimated the muscle forces, facet joint forces

and the compression forces between the vertebrae.

RESULTS

Figure 1 shows the model in 5 degrees extended position. The blue lines indicate the orientation and amplitude of the facet forces in this position.
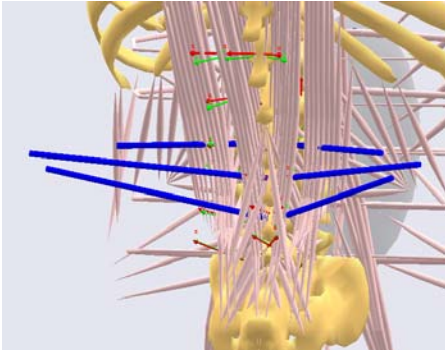
Figure 1. The model in extended position with estimated facet joint forces.
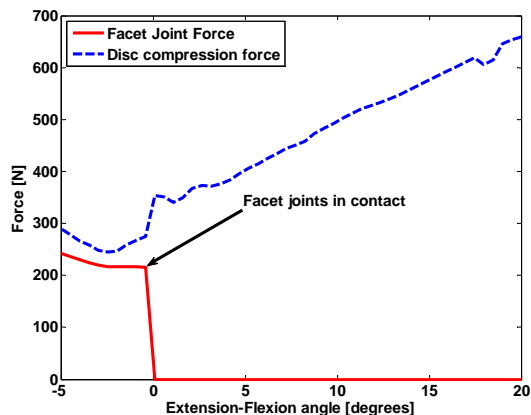
Figure 2. The estimated facet joint force and axial force between L2 and L3 as a function of spine angle.

Figure 2 shows the compression forces between L2 and L3 and one of the facet forces as a function of spine angle. It can be seen that during flexion the disc compression forces are high, due to the necessary muscle activity. At the point where the facet joints come into contact with each other, there is a significant loading of the facet joints and a

drop can be seen in the disc compression force.

DISCUSSION

Traditionally, computational studies of facet loads have used the finite element method (FEM) (e.g. Shirazi-Adl, 1991). This method is, however, computationally heavy, and it is difficult to analyze dynamic movements together with the force generating muscles. The present approach of rigid-body musculoskeletal models based on inverse dynamics takes the whole lumbar spine into account together with its muscles making it possible to analyze the effect of whole body movements and loads on facet joint loading. The ratio of load transfer for the presented case is within the range found in the literature.

REFERENCES

Damsgaard,M., Rasmussen,J., Christensen,S.T., Surma,E., and de Zee,M. (2006) *Simulation Modelling Practice and Theory* **14,** 1059-1070.

de Zee,M., Hansen,L., Wong,C., Rasmussen,J., and Simonsen,E.B. (2007) *J Biomech.* **40,** 1219-1227.

Hansen,L., de Zee,M., Rasmussen,J., Andersen,T.B., Wong,C., and Simonsen,E.B. (2006) *Spine.* **31,** 1888-1899.

Masharawi,Y., Rothschild,B., Dar,G., Peleg,S., Robinson,D., Been,E., and Hershkovitz,I. (2004) *Spine.* **29,** 1755-1763.

Schendel,M.J., Wood,K.B., Buttermann,G.R., Lewis,J.L., and Ogilvie,J.W. (1993). *J Biomech.* **26,** 427-438.

Shirazi-Adl,A. (1991). *Spine.* **16,** 533-541.

ACKNOWLEDGEMENTS

LOCOMOTION STABILITY IN SIMULATED MARTIAN GRAVITY: INSIGHTS ON THE INFLUENCE OF LOAD LOCATION

Melissa Scott-Pandorf[1], Dan O'Connor[1], Charles S. Layne[1], Krešimir Josić[2], and Max J. Kurz[1]

[1] Laboratory of Integrated Physiology, Department of Health and Human Performance, University of Houston, Houston, TX, USA, mmscott-pandorf@uh.edu or mkurz@uh.edu
[2] Department of Mathematics, University of Houston, Houston, TX, USA

INTRODUCTION

Due to recent aspirations to extend space exploration to Mars, NASA has a revitalized interest in reduced gravity locomotion for designing the next generation of space suits. A new suit, to be worn during extravehicular (EVA) tasks, must provide life-sustaining supplies without inhibiting the astronauts' ability to efficiently perform tasks on the surface of Mars. Review of the video archives from the Apollo missions on the Moon revealed an issue of repeated instances of astronauts falling. It appeared that the portable life support system (PLSS) the astronauts wore during the Apollo missions influenced the dynamic balance of the gait pattern. It has been speculated that this may have been due to the distribution of the PLSS load. The influence of load location on the dynamic stability of the gait pattern in a Martian environment is largely unknown. This information is essential to prevent the occurrence of falls during the future Mars EVA missions.

The purpose of this investigation was to explore the stability of the gait pattern in simulated Martian gravity while wearing a rig that simulates the possible load placement configurations for the PLSS being considered by NASA.

METHODS

Five participants (62.2±7.8 kg, 167.6±2.5 cm, 26.6±8.8 yrs) walked on a treadmill for
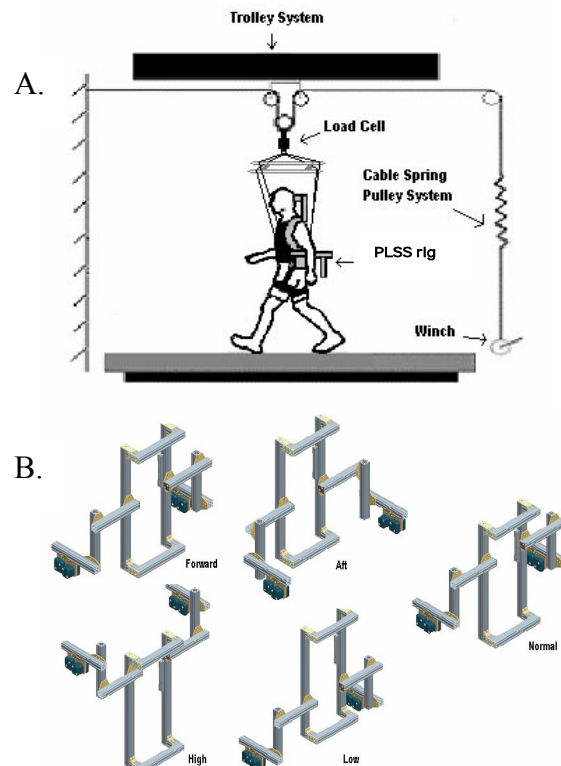
Figure 1. (A) Schematic of the body-weight suspension system that was used to simulate the Martian gravity, (B) the five configurations (Forward, Aft, Normal, High and Low) for the different PLSS rig load placement conditions.

four minutes while suspended by a custom-built body weight suspension system which off-loaded the participants to a simulated 3/8 gravity (Figure 1A). While suspended, participants wore a 20 kg PLSS rig that could be rearranged into five different load placement conditions (Figure 1B). Due to the novelty of the experiment, all participants practiced walking in the suspension system while wearing the rig in its respective configurations at least one day before data was collected.

A six-camera motion capture system (100 Hz) was used to collect the right leg's ankle, knee and hip joint sagittal plane kinematics. The kinematics were filtered with a ninth order digital filter with a six Hz cut-off. A first central difference method was used to differentiate the filtered angular kinematics.

The state vector (**x**) was used to evaluate the stability of the locomotive system. **x** was defined by the joint positions and velocities of the hip, knee, and ankle at mid-stance. Floquet analysis was used to quantify the dynamic stability of the gait pattern (Hurmuzlu et al., 2001). This involved linearizing the first-return map about **x*** to satisfy the following relationship

$$\delta x^{n+1} = \mathbf{J} \delta x^{n}$$

where δ denotes the deviation about **x*** at each nth step, and **J** is the Jacobian. δx^{n} and δx^{n+1} were defined as

$$\delta x^{n} = [x_n - x^*, x_{n+1} - x^*, x_{n+2} - x^*, \ldots]$$
$$\delta x^{n+1} = [x_{n+1} - x^*, x_{n+2} - x^*, x_{n+3} - x^*, \ldots]$$

A least squares algorithm was used to solve for **J** (Tedrake, 2004). The largest eigenvalue (β) was computed from **J** and was used to quantify the stability of the gait pattern. A β value further away from zero signified a less stable gait.

A one-way repeated measures ANOVA was used to determined difference in load location with Bonferonni t-tests for post-hoc analysis ($p<0.05$).

RESULTS AND DISCUSSION

The PLSS load placement did have a significant influence on the stability of the gait pattern during stance ($p=0.014$; Figure 2). The Normal and Aft load placement conditions were significantly more stable than the Forward load placement ($p = 0.022$ and $p = 0.026$, respectively). These results indicate that the gait pattern is more stable with the load at the sides of the torso (*i.e.,* Normal condition) and behind an individual (*i.e.,* Aft condition).

SUMMARY

PLSS loads at the side of the torso or behind improves locomotive stability in simulated Martian gravity and should therefore be considered as the next generation space suit is designed. Our current work is directed toward determining how the weight of the space suit and PLSS influences the stability of gait in a Martian environment.

REFERENCES

Hurmuzlu, YB, et al. (2001). *ASME J. Biomech. Eng.,* 118: 405-411
Tedrake R et al. (2004). *Proc. IEEE ICRA,* 5:4656-4661.

ACKNOWLEDGEMENTS
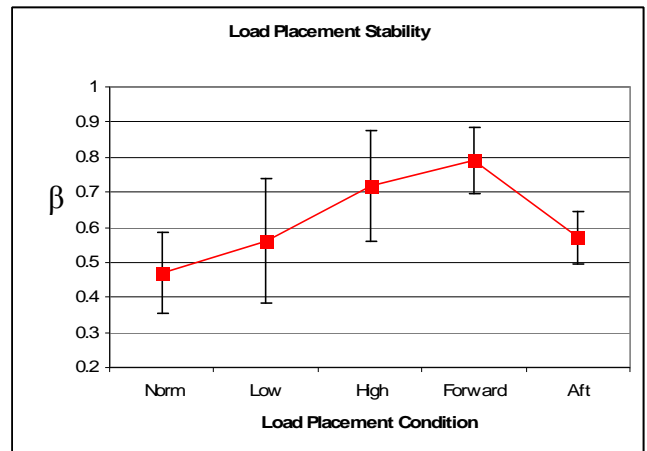
Figure 2. β values for each load placement condition.

BIOMECHANICAL SIMULATION OF A GREATER TROCHANTER FIXATION SYSTEM

Kajsa Duke[1,2], G.Yves Laflamme[2] and Yvan Petit[1,2]

[1]École de technologie supérieure, Department of Mechanical Engineering, Montreal, Quebec, Canada. Yvan.Petit@etsmtl.ca
[2]Hôpital du Sacré-Cœur, Research Center, Montreal, Quebec, Canada.

INTRODUCTION

Reattachment of the greater trochanter fragment is frequently treated with cable grip type systems. Fracture of the greater trochanter is a relatively common complication (4.3%) of hip replacement surgery (Claus et al. 2002). In addition, to improve exposure during hip revision surgeries an osteotomy of the greater trochanter is often performed. During reattachment, one concern is the effect the cables tightness has on the integrity of the system. The objective is to create a femur implant model and vary the cable tension, common muscle forces and the placement of the femoral neck cut in order to analyse trochanter fragment displacement in terms of both shear and gap.

METHODS AND PROCEDURES

A finite element model (FEM) of a femur with simulated greater trochanter osteotomy (30º) was combined with the femoral component of a hip prosthesis and a greater trochanter reattachment system with 4 cables (Cable-Ready®, Zimmer). The surface geometry for the femur was developed by Papini (2003) and was obtained from the Bel repository. Cable geometry is specific to the femur as the shape was projected onto the bone surface. The femur, implants and cables were meshed with total of 64971 tetrahedral elements (Figure 1). Femur geometry and mechanical properties represent the Sawbones third-generation composite femur model, with

cancelous (137 MPa) and cortical bone (7600 MPa) (Pacific Research laboratories Inc. Vashon, WA). In total there are 6262 contact elements. For example, the cortical and cancelous bone was assembled with *fastened connections* to insure that they behave as a single body. The contact between the trochanter fragment and the femur is a *contact connection* which allows the fragment to slide and separate. No friction was assumed at the fragment interface in order to represent a worst case scenario.
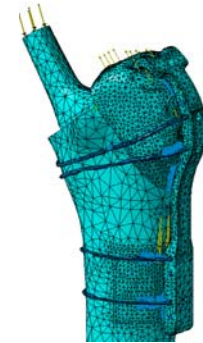
Figure 1. Finite element model of a greater trochanter fixation system.

A total of 18 simulations were modeled in a full factorial design using three independent variables; cable tightening, muscle forces and femoral neck cut (Table 1). Cable tightening was 355.9 N (80 lbf) based on the manufacturer's recommendation; in addition 177.9 N (40 lbf) and 533.8 N (120 lbf) were tested. Muscle forces were held at zero or applied to simulate walking and stair climbing as described by Heller et al. 2005. Finally, the placement of the femoral neck cut was simulated in two positions: 10 mm and 15 mm above the lesser trochanter. The relative gap and shear displacement magnitudes were determined at three points around the perimeter of the fracture surface: two at the top corners and one at the bottom.

A local coordinate system was defined with the x,y plane (shear) on the fracture surface of the femur and z perpendicular (gap). Interfragmentary displacements were resolved at each point into gap and shear components and the maximum was determined. During statistical analyses, differences were considered significant if they were greater then 0.1mm and $p \leq 0.05$.

Cable tension (N)	Muscle forces	Femoral neck cut (mm)
177.9	0	10
355.9	Walking	
533.8	Stair Climbing	15

Table 1. Independent variables

RESULTS

The placement of the femoral neck cut closer to the lesser trochanter (10mm) reduced the osteotomy contact surface area by over 20% and significantly increased the fragment displacement. Maximum gap (0.38 mm) and maximum total displacement (0.41 mm) was observed during stair climbing, while the cables were tightened to 177.9 N and with the femoral neck cut at 10 mm. Excessive cable tightening provided no reduction in fragment displacement. In fact, maximum shear (0.20 mm) occurred while the cables were tightened 533.8 N and the 10 mm femoral neck cut. The gap displacement at the upper points was zero. Actually, these points were subject to shear but primarily served as a pivot and the maximum gap (0.38 mm) was present at the bottom of the fracture (Figure 2).
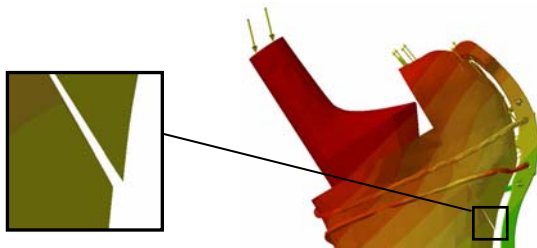
Figure 2. Location of the maximum gap

DISCUSSION

The results obtained with the proposed FEM are generally in accordance with the literature. In particular, Plausanis et al. 2003 observed trochanter displacement generally less then 0.5 mm. One limitation was that friction was not simulated in our model but was neglected providing a worst case scenario. Because pivoting was observed at the proximal line of the osteotomy surface, friction is potentially inconsequential. Complete validation of this FEM against an experimental model is currently underway. However, it allows us to highlight key findings regarding the relative importance of cable tightening, muscles forces and contact area.

SUMMARY

Lowering the femoral neck cut reduced contact surface area and significantly increased fragment displacement. Preservation of the contact surface area is recommended. Excessive cable tightening provided no reduction in fragment movement. Caution must be used to not over tighten the cables. This model can be used to test and compare the performance of new implant designs.

REFERENCES

Claus, A.M. et al. (2002). J Arthroplasty, 17:706-712
Heller et al. (2005) J of Biomechanics. 38:1155-1163
Papini, M. (2003) BEL repository
Plausinis, D et al. (2003) Clinical Biomechanics, 18:856-863

ACKNOWLEDGEMENTS

SENSORY INTEGRATION FOR VISUALLY INDUCED ROLL TILT PERCEPTION

Heewon Park and Sukyung Park

Department of Mechanical Engineering, KAIST, Daejeon, Korea
Heewon_Park@kaist.edu, sukyungp@kaist.edu, URL: http://biomt.kaist.ac.kr

INTRODUCTION

States of human body movement and its motion perception are estimated from multi-sensory integration of vision, vestibular input and proprioception. However it is under investigation which sensory information contributes more to the body posture and its motion perception, and whether there are dynamic characteristics in resolution of sensory conflict. In this study, we examined the visually induced postural response and corresponding tilt perception under sensory conflict condition.

METHODS AND PROCEDURES

Six healthy young subjects (Six male, 23.5 yrs ± 3.74) with no history of sensory illness volunteered for this study. Written informed consent was obtained according to KAIST IRB protocols. Subjects stood on a force plate and were instructed to maintain upright posture in response to randomly ordered roll rotational visual cues. Visual cues were applied through three LCD monitors with peak velocity of 13.2 deg/sec over the stimulus frequency ranged from 0.01 to 0.7Hz (Park H, 2006). Subjects participated in two test sessions of different body constraint conditions: 1) free sway and 2) body strapped condition, in which subject's body movement was restrained by a shoulder immobilizer. Center of pressure (COP) and subjective tilt perception were measured using portable force plate and somatosensory bar, respectively. The somatosensory bar, located at about waist level, was aligned with subject's medial-lateral sway. Subjects were instructed to align the bar to their perceived horizontal. Experimental data were band-pass filtered with cut off requencies at 0.5 and 3.5Hz. Cycle by cycle sinusoidal fit was used to quantify the magnitude of tilt perception.
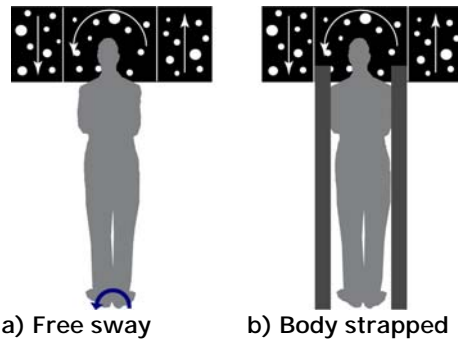
a) Free sway   b) Body strapped
Figure 1. Roll rotational visual stimulus.

RESULTS

Strong vection was induced by visual stimulus in both free sway and body strapped condition. In free sway, body sway measured in terms of COP and tilt perception were compensative to visual stimulus (Figure 2).
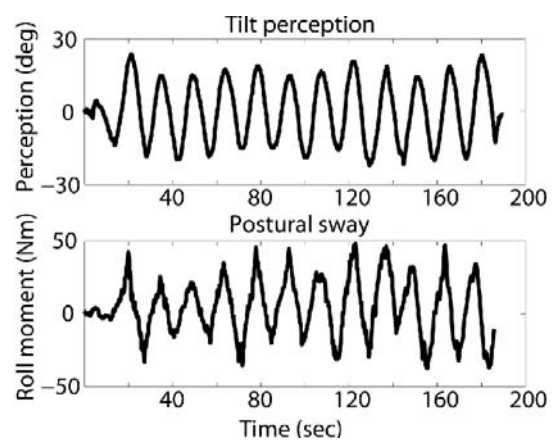
Figure 2. Tilt perception and body sway in free sway condition.

With body immobilized, significant roll tilt perception was observed (Figure 3). The vection started about a half minute after onset of visual stimulus, and was irregularly ceased and resumed. Magnitude of tilt perception of body strapped trials was smaller than that of free sway trials (Figure 4). Both COP and tilt perception decreased with stimulus frequency.
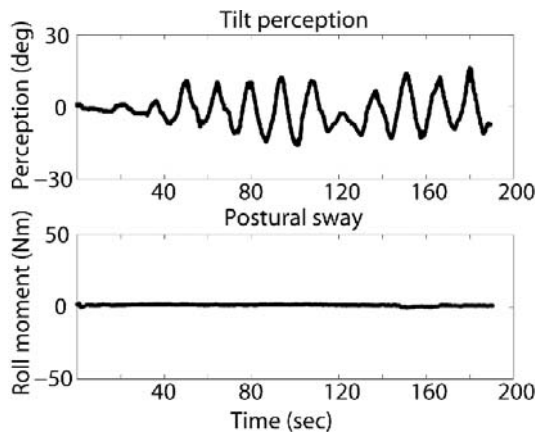
Figure 3. Tilt perception and body sway in body strapped condition.
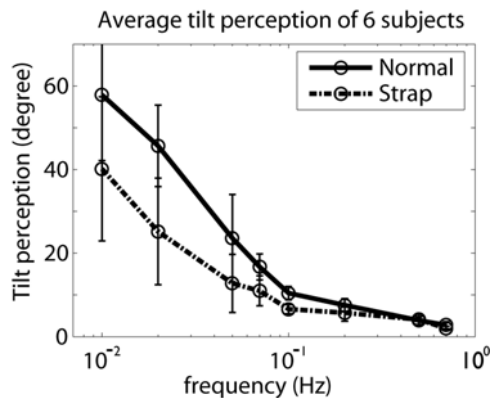
Figure 4. Magnitude of frequency response of tilt perception.

DISCUSSION

Significant roll tilt perception without body sway implies that vision has relatively dominant effect on tilt perception over vestibular and proprioceptive input. Delayed onset of vection observed under sensory conflict condition can be explained by continuous sensory reweighting among vision, vestibular input and proprioception by the CNS. Increased sensory weight on vision may also attribute to the fact that the vision is the only source of motion cues, which would be processed with more significance by the nervous system. As oppose to the delayed onset of vection at the beginning of the trials, instant cease and resumption of vection in the middle of trial was observed. This may imply that the perception mechanism has dynamic characteristics so that the previous vection experience would promote prompt resolution of sensory conflict. Frequency responses of body sway and tilt perception showed low-pass filter characteristics having decrease in magnitude as a function of stimulus frequency, and this result is consistent to previous visually induced postural sway study (Peterka and Benolken 1995).

SUMMARY

We examined the visually induced postural response and corresponding tilt perception under sensory conflict condition. Significant roll tilt perception was observed without body sway, but with delayed onset and temporal irregularity. This implies the CNS performs continuous sensory reweighting in resolving sensory conflict.

REFERENCES

Park, H (2006). *Master's thesis*, KAIST
Peterka, RJ and Benolken, MS (1995). *Experimental Brain Research*, 105:101-10.

ACKNOWLEDGEMENTS

THE INFLUENCE OF NOISE AND TIME SERIES LENGTH ON TWO COMMON MEASURES OF ENTROPY

Tobin Silver, Chris K. Rhea, Breanna E. Studenka, Joong Hyun Ryu, Charmayne Mary Lee Hughes, and Jeffrey M. Haddad

Department of Health and Kinesiology, Purdue University, West Lafayette, IN.
tasilver@purdue.edu

INTRODUCTION

Measures of entropy assess the overall regularity of a time series and are often used to quantify the degree of chaos in a system. Recently, there has been a lot of interest in extending these measures to human movement data. It is believed that measures of entropy can detect information in movement patterns that is not detectable using more traditional techniques. For example, Lipsitz and Goldberger (1992) suggested that a decrease in movement complexity (smaller entropy) is a signature of aging and disease.

Direct measures of entropy, such as Kolmogrov-Sinai entropy, can only be used on time series that contain many noise free data points (Richman and Moorman, 2000). Since direct measures of entropy are not practical in the analysis of human movement, a variety of indirect measures that approximate entropy have been developed. Sample Entropy (SampEn) and RQA entropy (RQAEn) are two indirect measures of entropy that are widely used.

In human movement, the various indirect entropy techniques have been employed in a variety of data sets. However, due to differences in calculations, it is difficult to make interpretations regarding entropy between studies. Specifically, differences in the length and amount of noise in the time series may affect the final entropy calculation. The purpose of this study was to examine the effects of noise and time series length on SampEn and RQAEn measures.

METHODS AND PROCEDURES

5Hz sine waves (one second in duration) were generated with either 500, 1000, 1500 or 2000 samples. White noise that was 0% (no noise), 5%, 10% or 20% the amplitude of the original wave was added to each sine wave, resulting in a total of 16 sine waves (4 frequencies X 4 levels of noise).

RQAEn and SampEn were calculated for each of the 16 sine waves using the algorithms published by Weber and Zibult (2005) and Richman and Moorman (2000) respectively. In each of these techniques the original time series must be embedded in a multidimensional state space using a time lag. The appropriate embedding dimension was determined using the false nearest neighbors technique. The appropriate time lag was determined using the average displacement technique (Hasson et al. 2008).

When calculating both RQAEn and SampEn, a radius value (a value that determines a threshold of similarity) must also be determined. A detailed description regarding how to choose the appropriate radius to perform the SampEn and RQA calculations can be found in Richman and Moorman (2000) and Weber and Zibult (2005) respectively. The radius parameters were chosen using the recommendations from these publications.

RESULTS

Four main results emerged from this data. 1) The number of data points in the time series affected both the SampEn and RQAEn calculations. 2) RQAEn tended to increase as the number of data points increased while SampEn tended to decrease as the number of data points increased. 3) In RQAEn, the number of data points had the greatest influence at low noise levels. In SampEn, the total number of data points equally affected the final entropy value at all noise levels. 4) As noise was added to the sine wave, RQAEn and SampEn exhibited different trends.
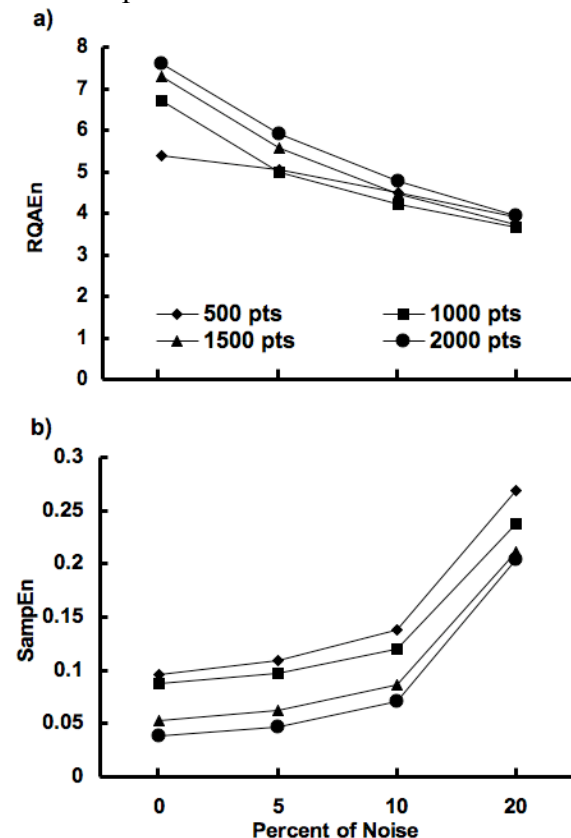
Figure 1. a) RQAEn and b) SampEn of the various sine waves.

DISCUSSION

SampEn and RQAEn were both affected by the amount of noise and length of the data set. Interestingly at the lower levels of noise the effects of time series length were largest. It is important to note that the signal to noise ratio in movement data would be in the region where the greatest differences were observed.

Care should be taken when comparing entropy results both between and within studies. Within study comparisons may be problematic because some studies (e.g. reaching studies) often have data series of varying length. In this case, entropy may differ between conditions simply because of differences in time series length.

When comparing results between studies, it is important to recognize that not all entropy calculations are equal. Two studies that use similar methodologies may obtain completely different values of entropy. Varying values may emerge because of 1) differences in calculations between different entropy measures; 2) the use of different input parameters; 3) differences in the signal to noise ratio (e.g. different filter cut-offs); 4) differences in the number of data points.

SUMMARY

Non-linear measures such as entropy can provide rich information regarding the dynamics of human movement. Given the power of these techniques, more researchers are beginning to use entropy measures when analyzing their data. However, it is important to recognize the assumptions and limitations when interpreting measures of entropy.

REFERENCES

Hasson et al. (2008). *Gait Post,* 27:416-422.
Lipsitz, LA and Goldberger, AL (1992). *JAMA*, 267:1806-1809.
Richman, JS and Moorman, JR (2000). *Am J Physiol*, 278:H2039-H2049.
Weber, C and Zibult, J (2005). *Tutorials in contemporary nonlinear methods for the behavioral sciences,* pp. 26-94.

RELIABILITY OF JOINT ANGLE MOVEMENTS DURING ROCK CLIMBING

Paris L. Malin, Shinya Abe, Randall L. Jensen, Phillip B. Watts

Department of Health Physical Education Recreation,
Northern Michigan University, Marquette, MI USA, rajensen@nmu.edu

INTRODUCTION

The nature of rock climbing requires the individual to transport body mass vertically, with varying degrees of support, through a series of complex movements and body positions. Although more researchers have begun to study physiological responses (Watts, 2004); only Sibella et al. (2006) have reported kinematic data of actual climbing. Their study examined center of mass movement, but did not address joint angle changes, or whether these changes are consistent. Thus the purpose of the current study was to assess the reliability of joint angle movements during repeated trials of rock climbing.

METHODS AND PROCEDURES

Ten subjects (mean ± SD: age = 31.6±13.9 years; height = 177.5±8.6 cm; body mass = 73.8±10.7 kg) wore their own rock climbing shoes during testing. Each subject completed four trials of a climbing movement sequence on a vertical indoor wall (Figure 1). The specific movement sequence is known to climbers as a *high-step* Climbers performed two trials (T1, T2) randomized by conditions of foot placement (1) Inside edge = where the area on the inside of the shoe near the base of the great toe is used for contact and support; and (2) Toe-in = where the front part of the shoe at the toe is used for contact and support. Subjects self-selected the rate of movement and specific body positioning, other than the right foot, during each climbing trial. Subjects gave informed consent prior to participating in the study which had IRB approval.

Reflective markers placed on the subject's right ulnar head, lateral humeral epicondyle, acromion, greater trochanter, fibular head, lateral malleolus and atop the great toe were used to determine joint angles using Peak Motus 8.5. Data were acquired at 60 Hz and a 2nd order Butterworth filter with a cut off of 3-6 Hz was used to smooth the data (Winter, 2005).

Intraclass correlation (two way mixed analysis) and repeated measures ANOVA were used to estimate reliability and test differences among trials via SPSS 15.0. The parameters of interest were maximum (MAX), minimum (MIN), and average (AVE) joint angles for the elbow, shoulder, hip, knee, and ankle.

Figure 1. A subject performing the climbing movement.

RESULTS

Intraclass correlation coefficients (ICC) for the MAX, MIN, and AVE joint angles are displayed in Table 1. Significant differences (p <0.05) were found between trials for MAX Ankle (108.3±5.7° vs. 110.1±6.3°), and MIN Ankle (90.9±5.9° vs. 92.7±5°.9). None of the other joint angles differed between trials (p > 0.05).

	MAX	MIN	AVE
Elbow	0.913	0.891	0.947
Shoulder	0.893	0.824	0.890
Hip	0.920	0.937	0.918
Knee	0.887	0.913	0.928
Ankle	0.957	0.850	0.951

Table 1. Intraclass correlation coefficients for maximum, minimum, and average joint angles (n=20).

DISCUSSION

The results of the Intraclass correlation indicate, that for the joints examined, the consistency of movements in repeated trials while rock climbing are high (R > 0.820). This is similar to the findings of Ford et al. (2007) who examined joint angles during jump landings. Also for most joints the lack of difference between trials suggests that subjects perform the movement the same in repeated trials.

The variation across trials for the ankle joint may be due to this joint being closest to main support of the body. Watts (2004) has noted that climbers typically use the feet to help provide support during climbing. Quaine et al. (1995) found that when one handhold was removed the load maintained by the hands only increased from 5-6 to 9-10 kg with both feet contributing support. Furthermore, unpublished data from our lab indicates that there is a greater amount of force supported by the feet than the hands. In the current study support was provided by one foot; thus variations in technique and supporting force of the foot could result in changes of the ankle joint movement and explain the differences in MAX ankle and AVE ankle across trials.

SUMMARY

The current study found that minimum, maximum, and average joint angles display a high degree of consistency for most joints during a repeated rock climbing movement based on ICC and lack of difference across trials. This information should provide additional knowledge for researchers investigating rock climbing movements.

REFERENCES

Ford, KR et al. (2007) *Med Sci Sports Excerc* 39: 2021-2028.

Quaine F, et al. (1995) *J of Appl Biomech* 13: 14-23.

Sibella, F, et al. (2006) *Proc of XXIV Int Symposium on Biomech in Sports* 821-824.

Watts, PB. (2004) *Eur. J. Applied Physiol.* 91: 361-372.

Winter DA (2005). *Biomechanics of Motor Control and Human Movement 3rd Ed.* New York, Wiley.

ACKNOWLEDGEMENTS

THE INFLUENCE OF TRANS-TIBIAL PROSTHESES' MECHANICAL PROPERTIES ON THE PERFORMANCE OF THE AMPUTEE

Matthew J. Major, Martin Twiste, Laurence Kenney, and David Howard

Centre for Rehabilitation and Human Performance Research, University of Salford, Salford, United Kingdom, M.J.Major@pgr.salford.ac.uk
URL: http://www.ihscr.salford.ac.uk/CRHPR

INTRODUCTION

There is a wide range of commercially available modular components that prosthetists can select in order to assemble a trans-tibial prosthesis. Each component's mechanical properties will have a direct influence on the performance of both the prosthesis and, consequently, the user. The effects of various trans-tibial components on user performance have been thoroughly investigated (Hafner, 2002). Additionally, the stiffness and damping properties of prosthetic feet have been described previously (Van Jaarsveld, 1990). However, there appears to be very little quantitative evidence supporting manufacturers' claims that particular foot designs provide the wearer with a biomechanical or physiological advantage compared to alternative designs. The objective of this study was to design a controlled method of investigating the influence of trans-tibial prosthesis stiffness properties on the biomechanical and physiological performance of the amputee. Preliminary results will also be presented.

METHODS AND PROCEDURES

The primary objective of this study was to investigate, in a controlled manner, the influence of mechanical properties on user performance. In order to do so, a purpose-built prosthesis was designed with adjustable ankle-joint stiffness characteristics. This allowed for a comprehensive investigation of the effects of a wide range of prosthetic stiffness properties on gait. The mechanical model known as "roll-over shape" was adopted in order to quantify the mechanical behaviour of the prosthesis (Hansen, 2000). Roll-over shape is a quasi-static representation of how the prosthesis deflects during the single-limb stance phase of gait. This information on compliance during weight-bearing reflects the dorsiflexion and plantar flexion stiffness of an assembled prosthesis. The roll-over shape of the prosthesis is measured by a custom-designed test-rig, utilizing a 6-component load cell that is installed between the prosthesis socket and the pylon (Major, 2007).

RESULTS

The purpose-built prosthesis used during gait experimentation is comprised of four components, described from most proximal to most distal: i) socket, ii) load cell, iii) pylon, and iv) foot-ankle mechanism (Figure 1). A custom-designed foot-ankle mechanism allows for adjustment of the mechanical properties of the prosthesis. The ankle stiffness, and hence roll-over shape, is determined by two linear compression springs which can be moved along a track to vary their distance from the central pivot. The ankle dorsiflexion stiffness ($K_{rot,1}$) and plantar flexion stiffness ($K_{rot,2}$) is then described by the following equation:

$$K_{rot,i} = K_{lin,i} \times r_i^2 \qquad \text{for i=1,2}$$

where $K_{lin,i}$ is the linear stiffness of the respective spring in dorsiflexion or plantar flexion, and r_i is the fixed distance of that spring from the pivot. An important feature of this device is that the dorsiflexion and plantar flexion stiffness can be modified independently of each other. The custom test-rig is used to quantify the mechanical properties of the assembled prosthesis (i.e., all components distal to the socket) for various arrangements of the springs independent of the amputee.
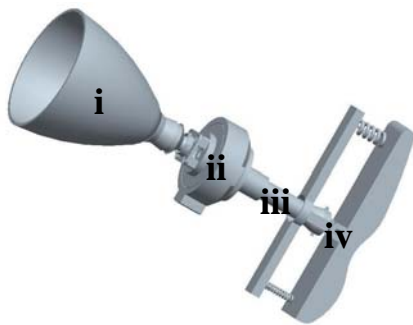
Figure 1. Purpose-built prosthesis used during gait experimentation.

DISCUSSION

The purpose-built prosthesis displayed in Figure 1 is being used for controlled investigations of the effects of different mechanical properties on amputee gait kinematics, gait kinetics and physiological performance. These parameters will be observed during self-selected and fast walking (133% of self-selected speed) on a level surface, a +5% grade and a -5% grade. During gait experimentation, the foot-ankle mechanism will be setup such that each walking condition is tested against all combinations (four in total) of high and low dorsiflexion stiffness, and high and low plantar flexion stiffness. The levels of high and low stiffness are defined by a previous study of the mechanical properties of commercial products which reflect the prosthetic foot function of a standard, non-dynamic foot and an "energy-storage and return" foot (Lehmann, 1993).

SUMMARY

This paper discusses a new approach to investigating the influence of the mechanical function of a trans-tibial prosthesis on the performance of the user. The novelty of this approach is that the methodology provides for a systematic exploration which is decoupled from the use of commercial products. The results from this study will provide insight into appropriate prosthetic prescription of modular components and assist in establishing improved design guidelines for future prostheses.

REFERENCES

Hafner, BJ et al. (2002). *Clin Biomech*, 17: 325-344.
Hansen, AH et al. (2000). *Prosthet Orthot Int*, 24: 205-215.
Lehmann, JF et al. (1993). *Arch Phys Med Rehab*, 74: 1225-1231.
Major, MJ et al. (2007). *J Biomech*, 40(S2): S595.
Van Jaarsveld, HW et al. (1990). *Prosthet Orthot Int*, 14: 117-124.

ACKNOWLEDGEMENTS

EFFECT OF PROPRIOCEPTIVE AND VISUAL PERTURBATIONS ON POSTURAL CONTROL ABOUT THE VERTICAL AXIS IN QUIET STANDING

Marlène Beaulieu[1,2], Martin Simoneau[3], Georges Dalleau[4], Charles-Hilaire Rivard[2] and Paul Allard[1,2]

[1]Département de Kinésiologie, Université de Montréal, Montréal, QC, Canada,
[2]Laboratoire d'Étude du Mouvement, Research Center, Sainte-Justine Hospital, Montreal, QC, Canada, marlene.beaulieu@umontreal.ca
[3]Faculté de médecine, Division de Kinésiologie, Groupe de Recherche en Analyse du Mouvement et Ergonomie, Université Laval, Québec, Canada
[4] Centre Universitaire de Recherche en Activités Physiques et Sportives, Faculté des Sciences et Technologies, Université de la Réunion, Le Tampon, France

INTRODUCTION

Tough many studies investigated balance strategies about the antero-posterior (AP) and medio-lateral (ML) axes, little is known about the contribution of the free moment (T_Z) about the vertical axis on postural control. Beaulieu et al. (submited) found that T_Z can be dissociated in part from the center of pressure (COP) displacements in both AP and ML directions during quiet standing. However, when stability was challenged in single leg stance and/or reduced vision conditions, the relationship between T_Z and COP increased. This is suggestive of a strategy about the vertical axis contributing to reduce body oscillations in horizontal plane in perturbed testing conditions. The aim of this study is to investigate the mechanism underlying this strategy on postural control during and after uni- and bilateral proprioceptive disturbance. The visual contribution on postural control about the vertical axis will also be studied.

METHOD

Eleven young adults stood on two force plates (one under each foot) and maintained their balance during eight conditions namely vision [eyes opened (EO), eyes closed (EC)] and/or proprioception [left leg muscle vibration (LVib), right leg muscle vibration (RVib),

left and right leg muscle vibration (L+RVib)]. Three trials of 30 s were performed for each condition. All trials were separated into three periods: baseline (10 s with no vibration), vibration (10 s) and recovery when vibration stops and where the subject returns to the baseline condition (10 s). From the force-plate's data, four parameters were computed. COP Range in AP was calculated to estimate subject stability. ML axis was not considered because vibrations were only applied to muscles responsible for AP body displacements. RMS COP AP and T_Z reflected their oscillations about the sagittal and the vertical axis respectively. Lastly, T_Z integral was calculated to quantify its total absolute value over the period. Multifactor ANOVAs of 2 (Vision) x 3 (Vibration) x 3 (Periods) were performed on COP and T_Z parameters to test the differences among conditions. When these tests were statistically significant ($P < 0.05$), Tukey post-hoc analysis were performed.

RESULTS

During EO and L+RVib condition, COP AP range increased significantly by 62% from baseline to the vibration periods. During the recovery COP AP range maintained greater or equal values than the vibration period. The same general findings were obtained for the EC and

L+RVib conditions (Figure 1). In EO condition, LVib provided similar results as L+RVib, but RVib did not show any effect of periods. However, in EC condition LVib and RVib did not bring out any difference between the three periods. RMS COP AP displayed similar results as COP AP range.
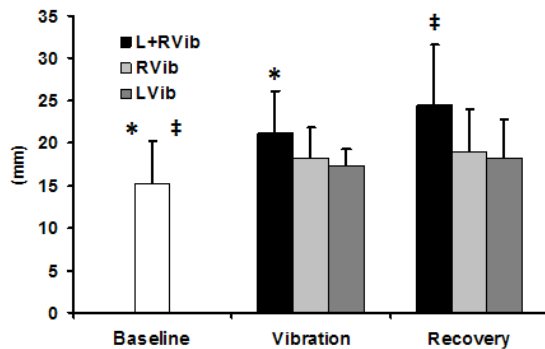
Figure 1. COP AP range values (mm) during the trial periods as function of the vibration type in the EC condition.

EO and L+RVib condition showed an increase of 200 % for T_Z integral between the baseline and the vibration periods. No significance difference was found for the recovery periods. T_Z integral behaved similarly in both LVib and L+RVib conditions. No difference was found between RVib in the recovery and the vibration periods and between the EO and EC visual conditions (Figure 2).
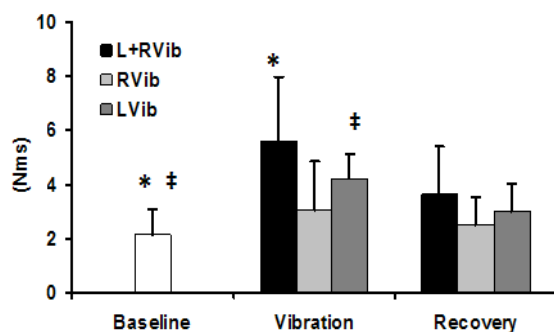
Figure 2. T_Z integral values (Nms) during the trial periods as function of the vibration type in the EC condition.

RMS T_Z showed different results than T_Z integral in few conditions. During L+RVib trials in the EC condition, RMS T_Z was greater in vibration and recovery periods compared to the baseline period and to EO condition.

DISCUSSION

Kavounoudias et al., (1999) reported that muscles vibration had an impact on body oscillations in the sagittal axis during and after the presentation of the leg muscle vibration. However, when only one leg muscle was vibrated, postural response depended on the laterality of the vibration. This difference between the left and the right sides suggest an asymmetry in the body-weight repartition on both stances. Rotational component of postural control also responded to the laterality. In contrast to COP AP displacement did not necessitate a period of recovery to return to normal values. Moreover, visual information did not have an effect on the quantity of moment deployed about the vertical axis but did enhance its variability when eyes were closed.

SUMMARY

Rotational component about the vertical axis was affected by bilateral proprioceptive disturbance. The impact of unilateral vibration on free moment depended on which leg received the vibratory stimulus. Once the perturbation was over, the body rotational component returned to its normal behavior. Availability of visual cues had an impact on variability of free moment, but not on the quantity of torque.

REFERENCES

Beaulieu M et al. (Submitted) *Am J Phys Med Rehab*

Kavounoudias et al. (1999) *Exp Brain Res* 124:80-88.

ACL RUPTURE IS AN *IN VIVO* IMPACT MODEL

Pedersen, DR[1]; Thedens, DR[2]; Martin, JA[1]; Tadimalla, S[1]; Ramakrishnan,PS[1]; Amendola, A[1]

[1]Department of Orthopaedics and Rehabilitation, University of Iowa, Iowa City, IA, USA,
doug-pedersen@uiowa.edu
[2]Department of Radiology, University of Iowa, Iowa City, IA, USA
URL: http://mnypt.obrl.uiowa.edu/

INTRODUCTION

Anterior cruciate ligament tears are among the most frequent major musculoskeletal injuries affecting physically active men and women. Disruptions of the ACL display a range of characteristics also representative of many other types of joint injury. In 85-90% of acute ACL ruptures, lateral femoral condyle bone bruising is detected by standard anatomic magnetic resonance imaging (MRI). Bruising is caused by a sudden subluxation and blow to the femoral condyle, which also results in focal injury to the overlying cartilage (Figure 1). ACL rupture provides an
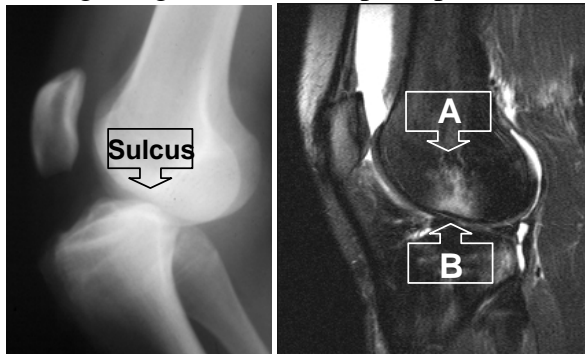
Figure 1: Pre-reduction radiograph of ruptured ACL blunt trauma (Left) and, (Right) an anatomic knee MRI showing (A) bone bruise and (B) apparent cartilage damage.

in vivo vehicle to study the ability of MRI to quantify impacted cartilage compositional changes in human knees. Immediate physical damage in the form of surface disruption and chondrocyte death into the ECM, are thought to instigate a degenerative cascade (Figure 2). This model connects *in vivo* whole joint MRI to cellular level assessment of articular cartilage condition following blunt impact injury.

METHODS AND PROCEDURES

Patients who sustained an ACL rupture and chose to receive an ACL reconstruction received a pre-surgery battery of hydration (T2) and proteoglycan (PG) specific T1ρ and delayed gadolinium-enhanced MRI (dGEMRIC) imaging. During arthroscopic ACLR a 3.5mm osteochondral biopsy is harvested from the damaged sulcus, anterior to the weight-bearing region of the lateral femoral condyle.
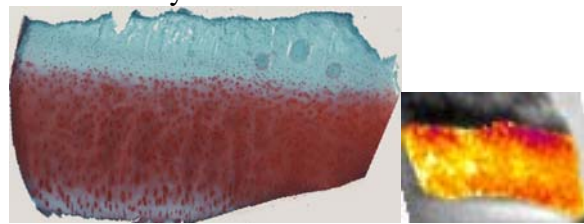
Figure 2: Safranin-O/fast green stains for PG distribution, and surface roughness indicates superficial damage. Linear recession of PG is accented by isolated chondrocytes generating pericellular PG but unable to replenish ECM. Corresponding 4.7T T1ρ map shown at right.

A second biopsy from the uninjured trochlear notch is a measure of normal cartilage. The trochlear region serves as the patient-specific *in vivo* control for MRI follow-up evaluations. Immediately post-surgery, explants are imaged at high resolution in a small bore 4.7T Varian MR imager. Then mechanical properties of the cylindrical chondral explants are assessed in a specimen-tailored device for Young's modulus and creep-strain (Park et al,

2004), before each explant is cut along the midline. One half is used for DMMB PG assay (μg/mg wet weight) and the other half is cryo-embedded for histological microscopy.

RESULTS

MRI imaging reveals differences in articular cartilage relaxation time constants both within a single scan and between images of the same tissue across time (Figure 3). Mechanical testing measures differences in load-bearing responses of normal cartilage and post-impact (Figure 4). DMMB measures of PG content in normal and post-impact cartilage exhibit a direct relationship to $T1\rho$ variation (Figure 5).
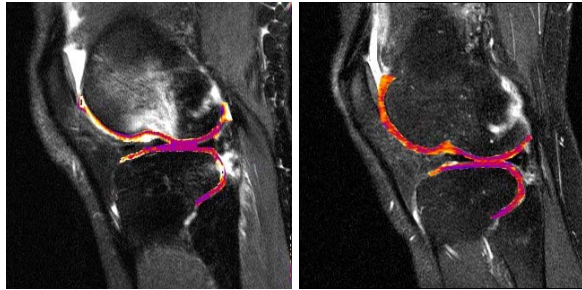
Figure 3: Presurgery and 5 month follow-up $T1\rho$ MRI showing blunt impact severity and temporal resolution of the bone bruise. However, the overlying cartilage still exhibits PG depletions.
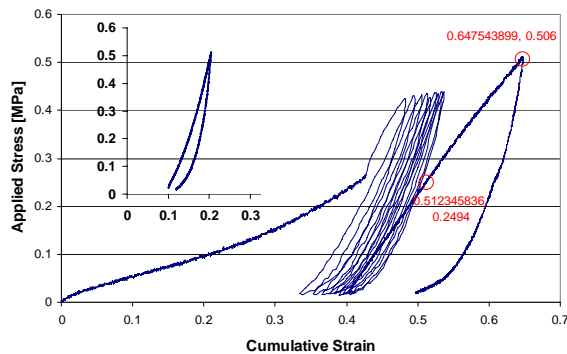
Figure 4: Impacted cartilage height 1.93mm, Young's Modulus 1.90MPa; Inset, normal cartilage height 2.82mm, E=5.98 MPa. Impact injury has diminished the cartilage stiffness.
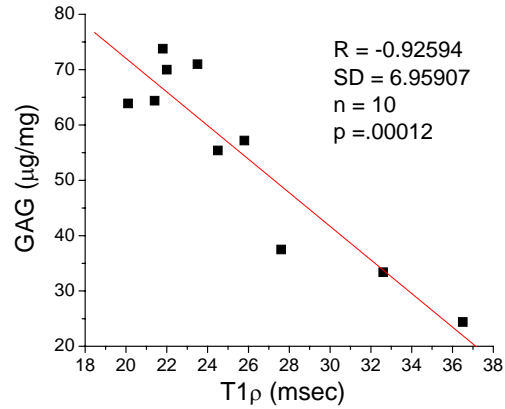
Figure 5: Glycosaminoglycan loss correlates with increasing $T1\rho$ relaxation evaluation.

SUMMARY

The effects of blunt impact injury on articular cartilage have been studied extensively *in vitro* and in animal models, but there is a paucity of information on the pathogenic effects of such injuries in humans. However, ACL rupture serves as a naturally occurring model in humans. Furthermore, we here show that non-invasive MR imaging potentially could be used to study cartilage damage and degeneration subsequent to impact injury *in vivo*.

REFERENCES

Park, S; Hung, CT; Ateshian, GA (2004), *OA and Cartilage*, 12: 65-73.

ACKNOWLEDGEMENTS

STABILITY AND ADAPTABILITY OF PASSIVITY-BASED BIPEDAL LOCOMOTION WITH FLAT FEET AND ANKLE COMPLIANCE

Qining Wang[1], Yan Huang[1], Long Wang[1] and Dongjiao Lv[2]

[1]Intelligent Control Laboratory, College of Engineering,
Peking University, Beijing 100871, China
[2]Department of Biomedical Engineering, Peking University, Beijing 100871, China

INTRODUCTION

Over the past years, several studies have investigated how much of the human walking motion can be modeled with passive dynamics (e.g. Garcia et al., 1998; Kuo, 2002; Wisse et al., 2004). However, only a few studies have been done on a flat foot shape in passive dynamic models (e.g. Kwan Hubbard, 2007). These studies proposed that the flat foot with a geometric parameter (foot length) can introduce a toe-strike collision in addition to the heel-strike impulse and influence the passive dynamics of walking. It has been investigated that flat feet can distribute the energy loss per step over these two collisions. Additionally, experiments on human subjects and robot prototypes revealed that the tendon in ankle joint is one mechanism that favors locomotor economy (Fukunaga et al., 2001; Collins et al., 2005). However, no effort has been made to analyze the adaptability and stability of adding compliant ankles to passive dynamic models that have flat feet.

The general goal of this study was to provide insight on the role of ankle compliance in human walking, by using a passivity-based bipedal locomotion model that is more close to the human motion in view of walking stability and adaptability.

MODEL

We proposed a 2D passivity-based bipedal locomotion model that consists of two three-segmented rigid legs interconnected through a passive hinge with a rigid upper body connected at the hip, as shown in Fig.1. The foot is mounted on the ankle with a torsional spring. A kinematic coupling is used to keep the body midway between the two legs.
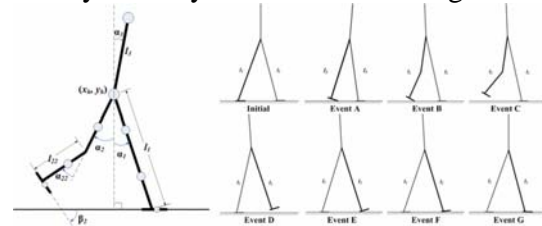
Figure 1. Model and walking sequence of the passive dynamic walker with flat feet and compliant ankle joints.

We divided one step into seven events (see Fig. 1). A hip torque was added between the swing leg and the stance leg to compensate the energy consumption. The configuration of the walker is defined by the coordinates of the point mass on hip joint and six angles, which can be arranged in a generalized vector $q = (x_h, y_h, \alpha_1, \alpha_2, \alpha_{11}, \alpha_{22}, \beta_1, \beta_2)^T$. Then we can obtain the Equation of Motion (EoM) :

$$\begin{bmatrix} M_r & \Sigma^T \\ \Sigma & 0 \end{bmatrix} \begin{bmatrix} \ddot{q} \\ F_c \end{bmatrix} = \begin{bmatrix} F_r \\ -\Psi \end{bmatrix} \qquad (1)$$

where M_r is a reduced mass matrix. F_r is the external force in generalized coordinates, while F_c is the contact force. Matrix $\Sigma = \dfrac{d\xi}{dq}$ transfers independent generalized coordinates $\dot{q}$ into constraint equation $\dot{\xi}$. Consequently, matrix $\Psi = \dfrac{\partial(\Sigma \dot{q})}{\partial q} \dot{q}$. In Event *A*, *B*, *F*, we consider that the ankle joint of the swing leg is constrained to move in a circular orbit with toe as the center and distance between toe and ankle joint as the radius. The force generated

by the spring on the swing leg should be considered as external force.

RESULTS AND DISCUSSION
By introducing flat feet and ankle compliance, the bipedal walking has a specific resistance of 0.06 at a scaled speed of 0.45 (walking speed/leg length). It is more efficient than not only the passive dynamic model with upper body (Wisse et al., 2004), but also human beings walking at the similar speed (Ralston, 1958). We found that the model is stable for small disturbance, with parameter values from Table 1 and a certain combination of initial conditions ($\alpha_1(0)$ =0.20203, $\dot{\alpha}_1(0)$ =-0.89034, $\dot{\alpha}_2(0)$ =-0.17253). In addition, by applying the cell mapping method, we found that the model performs well in the concept of global stability. This can be inspected by the evaluation of the basin of attraction as shown in Fig.2(a). One can find that such cyclic walking emerges even if the initial step is nearly fourfold as large. Fig.2(b) indicates that a relatively small ankle compliance (k) will lead to more stable points and an inappropriate k may be worse than a stiff ankle in the view of walking stability.
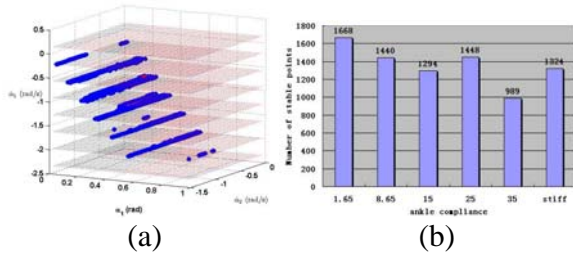
(a)   (b)
Figure 2. Results of walking stability.

By adding compliance to ankle joints, the adaptability of bipedal walking is no surprise: the passive dynamic walker can achieve adaptive bipedal locomotion with larger ground disturbance on uneven terrain. Having the hip torque *0.38Nm* and ankle spring *8.65Nm/rad*, the passive walker performs a stable walking on the ground with *-10mm* disturbance with no active control. It indicates that by adding ankle compliance, bipedal

walking can keep stable on uneven terrain with no active control. Fig.3(a) presents the results of terrain adaptability of walking with different ankle compliance. The relation between maximum allowable disturbance and ankle compliance is nearly linear. Big ground disturbance needs a small k. Fig3(b) reveals that more ankle compliance results in more visible sensitivity to the hip torque.

Parameter	mass	length
Body	*0.81kg*	0.62m
Pelvis	*15.03kg*	-
Thigh	*0.56kg*	0.45m
Shank	*0.56kg*	0.35m
Foot	*2.05kg*	0.15m

Table 1. Parameters in simulations.
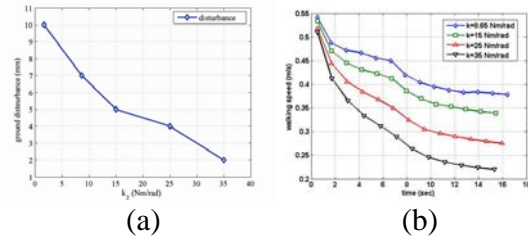
(a)   (b)
Figure 3. Results of terrain adaptability.

SUMMARY
In this paper, we presented a passivity-based bipedal locomotion model with flat feet and compliant joints. Both the theoretic analysis and the simulation results show that ankle compliance can improve the stability and efficiency of bipedal walking, which may reveal the role of ankles in human walking.

REFERENCES

Collins S et al. (2005). *Science*, 307:1082-1085.
Fukunaga T et al. (2001). *Proc. Biol. Sci.*, 268:229-233.
Garcia M et al. (1998). *ASME J. Biomech. Eng.*, 120: 281-288.
Kuo AD (2002) *ASME J. Biomech. Eng.*, 124:113-120.
Kwan M and Hubbard M (2007). *J. Theor. Biol.*, 248331-339.
McGeer, T (1990). *Int. J. Robot. Res.*, 9: 68-82.
Ralston HJ (1958) *Int. Z. Angew. Physiol.*, 17: 277-283.
Ruina A (2006). J. Biomech, 39(Sl): S359.
Wisse M et al. (2004) *Robotica*, 22: 681-688.

AUTOMATED MANKIN SCORING OF OSTEOARTHRITIS SEVERITY IN RABBITS

Amendola, RL; Martin, JA; Kurriger, GL; Moussavi-Harami, SF; Brown, TD; Pedersen, DR

Department of Orthopaedics and Rehabilitation, University of Iowa, Iowa City, IA, USA,
Richard-Amendola@uiowa.edu
URL: http://mnypt.obrl.uiowa.edu/

INTRODUCTION

The severity of osteoarthritis is often assessed by histologic appearance, the most commonly utilized index being the 14-point histological-histochemical grading scale (Mankin et al. 1971). On this scale (normal = 0), cartilage is graded on structural compromise (0-6 points), loss of matrix staining (0-4), cellularity anomalies (0-3), and violation of tidemark integrity (0-1). Mankin scorings have been dependent on human observer subjectivity, and thus have drawn criticism on the basis of the associated inter- and intra-observer variability (Ostergaard et al. 1997). Histologic assessments typically utilize only spot samplings, rather than continuous spatial mappings of abnormality grading, which is a substantial limitation in applications for which heterogeneity of cartilage pathology (and/or of therapeutic response) is an important consideration. Recently a fully automated and objective assessment of Mankin score by image-analysis tools was introduced for human articular cartilage (Moussavi-Harami et al. 2007). Since the rabbit knee is a common laboratory model for OA, these imaging techniques were adapted to build a species-dependent Mankin Scorer.

METHODS AND PROCEDURES

For the structural abnormality component, cleft/defect depths must be categorized. Since normal (non-OA) cartilage possesses a smooth surface, piecewise quadratic curve fits are used to represent the surface reference datum. A comparable datum line is fitted near the tidemark between calcified cartilage and subchondral bone. Cleft depths are calculated as the distance between the actual cartilage surface and its datum. These cleft depths are in turn normalized to cartilage thickness, and stratified into ranges corresponding to Mankin structural damage categories (Figure 1).
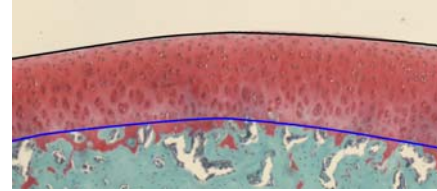
Figure 1. Safranin-O / Fast Green stained cartilage with surface (black) and tidemark curve fits (blue) for a non-OA specimen, having a surface defect score of 0.

The characteristic decrease in proteoglycan (PG) content in OA is manifest histologically by reduced safranin-O staining. In order to computationally assign Mankin sub-scores for PG loss, the algorithm digitizes the stained cartilage's color content, using the Hue-Saturation-Intensity color scale. This allows quantifying the saturation level of specific hues, of which red most closely corresponds to PG staining.

For cellularity sub-scoring, hematoxylin-stained cells are detected by area-based neighborhood thresholding, with the segmented objects' sizes being used as a basis for filtering to remove staining artefacts (Figure 2). Cell density scorings are then computed based on variations in local cell density from corresponding location-normalized values for normal cartilage. Twenty rabbit medial femoral condyles were decalcified, paraffin-embedded and sectioned into 5 μm-thick sections for histology assessment. Safranin-O specifically binds to PG; Fast Green provides a contrast stain; and

hematoxylin darkens chondrocyte nuclei. Cartilage zones were determined by cell size and orientation
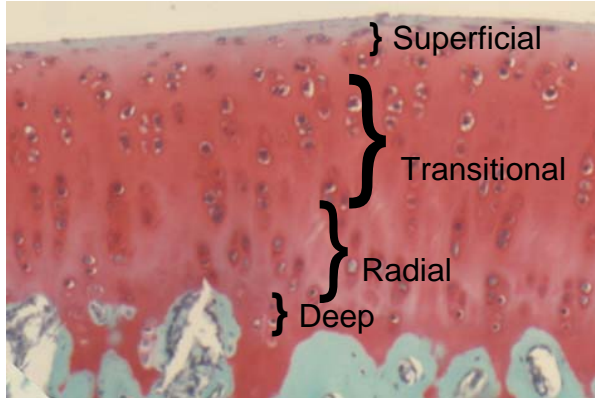
Figure 2. Four zones were measured. 1) Superficial contains small cells with flattened nuclei running parallel to the surface 2) Transitional shows scattered chondrocytes with round nuclei and intense Safranin O staining in the matrix 3) Radial consists of columns of cells oriented perpendicular to the articular surface with intense Safranin O staining immediately surrounding the lacunae, but less intense in the matrix   4) Deep shows intense Safranin O staining at the border of calcification.

Finally, for tidemark violation sub-scoring, the presence versus absence of penetrating blood vessels is determined by auto-segmenting the tidemark-facing base of the red-stained PG region, combined with size-filtering and shape-detection operations, to identify blood-vessel-sized disruptions of the calcified/non-calcified interface.

RESULTS
Zones that were measured for 20 medial condyles are recorded as percent of cartilage thickness. Cell counts were made within each of the four cartilage zones in 20 rabbit femoral condyles. Cell counts and cell density per square mm are also reported (Table 1).

Zone Depth [% thickness (SD)]			
Superficial	Transitional	Radial	Deep
9(2)	48 (9)	29(10)	14(5)
Cellularity [count (SD)]			
Superficial	Transitional	Radial	Deep
65(17)	270(40)	132(24)	123(24)
Cell Density [count/mm^2 (SD)]			
694(144)	546(90)	438(62)	855(187)

Table 1. Cartilage Measurements

DISCUSSION
Mankin scaling by automated image analysis, developed originally for assessment of human cartilage, was adapted for rabbit cartilage. The cellularity data from normal specimens shown in Table 1 serves as a reference for comparison to specimens with varying degrees of degeneration. Thus, the computer program makes it possible to consistently evaluate cellularity, a parameter that human observers often score discordantly. Furthermore, the automated system enables spatial mapping of degenerative changes, facilitating evaluation of cartilage lesion severity and progression in rabbit models.

SUMMARY
Automated image analysis tools were developed for objective Mankin scaling of cartilage degeneration in rabbits, eliminating inter-observer variation. This capability greatly improves our ability to detect and measure degenerative changes and treatment effects in this common model system.

REFERENCES
Mankin et al. (1971). *JBJS*, 53A: 523-37.
Ostergaard et al. (1997). *Arth & Rheum*, 40: 1766-1771.

ACKNOWLEDGEMENTS

EFFECT OF INLCINE ON MULTI-SEGMENT FOOT KINEMATICS

Kirsten Tulchin, MS, Michael S. Orendurff, MS

Texas Scottish Rite Hospital for Children, Dallas, TX USA, ktulchin@tsrh.org

INTRODUCTION

Lower extremity changes during incline walking have been previously reported by McIntosh et al in 2006. In 2002, Urry described foot pressure changes during side slope walking. However, the specific effects of incline on multi-segment foot kinematics remain unclear. Understanding the mechanism of adaptation to incline in the healthy foot may provide a means to better identify and describe pathological foot motion in the future

METHODS AND PROCEDURES

Ten adults (average age 23.9 ± 3.7yrs) underwent gait analysis with IRB informed consent. Each subject was instrumented with a modified Helen Hayes marker set, and an eight marker multi-segment foot marker set (Tulchin, 2003). Marker trajectories were collected using a VICON motion capture system at 120Hz and filtered with a Woltring spline with MSE of 10.Subjects walked on a treadmill at 3.0mph at inclines of 0% to 12% grade in 3% increments. Decline trials were conducted with the treadmill at 3.0mph by placing wooden blocks under the rear of the treadmill, at approximately 7.5% grade.
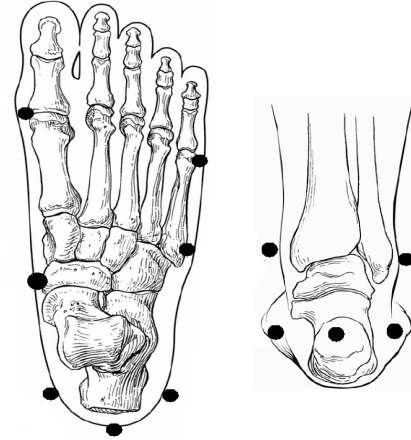
Figure 1: Skin marker placement for the foot kinematic model.

ANOVA's with Scheffe's test post hoc were used to detect differences between grades. It was hypothesized that there would be significant differences in hindfoot and forefoot sagittal motion with changes in treadmill grade.

RESULTS

Significant differences were seen in sagittal plane hindfoot motion between inclines. Maximum hindfoot plantarflexion during first rocker was significantly less for the 9%

	Decline		Incline			
	~ -7.5%	Level (0%)	3%	6%	9%	12%
Max HF PF 1st rocker (degs)	5.8 (4.0) [9, 12%]	4.3 (4.0) [9, 12%]	4.0 (3.9) [9, 12%]	4.0 (5.8) [9, 12%]	0.9 (4.3)	-0.4 (3.4)
Max HF DF Stance (degs)	7.6 (3.0) [12%]	8.1 (3.2)	8.7 (3.2)	8.7 (3.0)	9.4 (3.6)	10.2 (3.5)
Time Max HF DF Stance (%gc)	42 (6) [6, 9, 12%]	39 (3) [9, 12%]	40(3) [9, 12%]	38 (4) [9, 12%]	34 (6)	32 (6)

Table 1: Significant differences were seen in hindfoot sagittal plane motion between incline conditions. Mean (Stdev). ** Significant difference from the condition shown by superscript

and 12% grades as compared to decline walking, level walking and lower incline conditions. (p<0.0001) The timing of peak hindfoot dorsiflexion occurred significantly earlier in the gait cycle during the higher incline conditions. (p<0.0001)

There were no significant differences in sagittal plane forefoot motion or timing of peak motion.

SUMMARY

As expected incline does appear to affect foot kinematics, particularly at the hindfoot. Specifically, the hindfoot has been shown to achieve less dorsiflexion during decline walking, and more dorsiflexion during incline walking during the first half of stance phase. The timing of peak sagittal hindfoot motion occurs earlier in the gait cycle as treadmill incline increases. Incline related changes in foot segment kinematics have not been previously reported.

Interestingly, the sagittal plane forefoot motion did not change with varying grades of treadmill walking. This implies that the ankle is able to accommodate the changes in grade and no changes in forefoot motion is needed. Additional changes were seen in the coronal plane in both segments.

The ability to alter ankle motion to accommodate incline walking may not be possible in the pathological foot, which may lead to associated changes, particularly in forefoot motion, not seen in the healthy population.
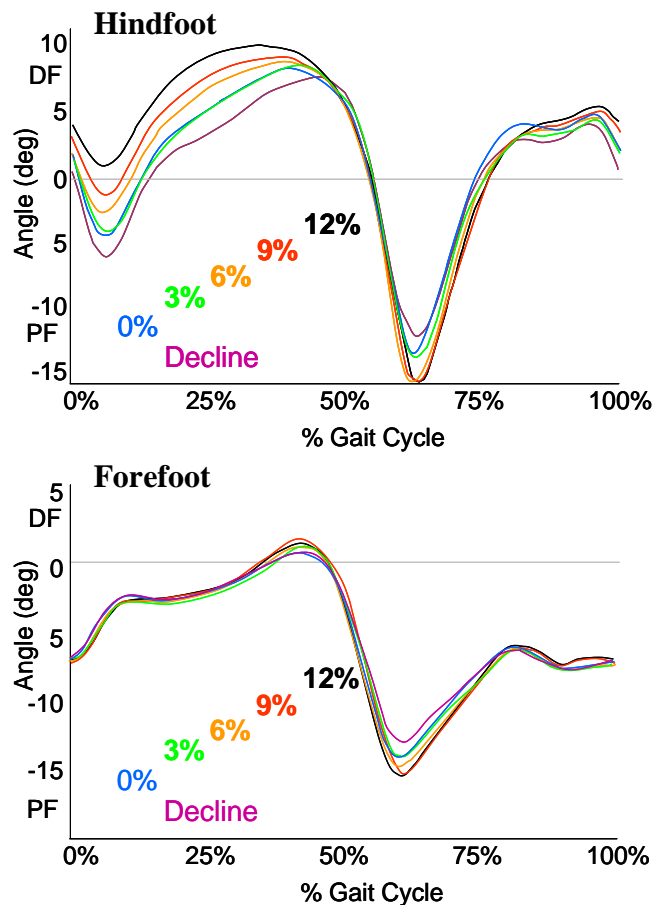
Figure 2 *Significant changes in sagittal plane hindfoot motion were seen with incline treadmill walking, however there were no changes in sagittal plane forefoot motion.*

REFERENCES:

McIntosh AS, et al (2006). *J Biomech,* 39(13):2491-502.
Urry (2002), *Foot & Ankle,* 23(12):1112-1118.
Tulchin, K and Haideri, N, (2004) *Proceed 8th annual ISB-3D*, p:25-28.

QUADRICEPS EMG DURING WEIGHTED KNEE EXTENSION FOLLOWING TOTAL KNEE ARTHROPLASTY

Jeannette M. Byrne[1] and Stephen D. Prentice[2]

[1]Assistant Professor, School of Human Kinetics and Recreation, Memorial University of Newfoundland, St. John's, Newfoundland, jmbyrne@mun.ca
[2]Associate Professor, Department of Kinesiology, University of Waterloo, Waterloo, ON

INTRODUCTION

Total knee arthroplasty (TKA) results in decreased pain and improved function. Despite these improvements, deficits in knee function persist after surgery. Research has shown persistent decreases in knee extensor moments during gait (Benedetti et al 2003) and stepping tasks (Byrne et al 2002). Altered knee kinematics has also been reported (Byrne et al 2002; Wilson et al 1996). More recent research has examined muscle activation following TKA, finding deficits in both EMG timing (Benedetti et al 2003) and amplitude (Mizner and Snyder-Mackler 2005).

A question that remains unanswered is whether the changes in joint kinematics and kinetics observed in this population are secondary to some underlying alterations in muscle function or whether the changes observed in EMG are simply indicative of the altered movement patterns exhibited by this patient group. In an effort isolate the effect of TKA on muscle function, EMG was recorded from knee muscles while individuals (with and without TKA) performed a seated knee extension. This task was chosen as it enabled the kinematic and kinetic demands to be controlled, ensuring that both groups were exposed to similar conditions.

METHODS

Two groups of individuals were examined in this study. The first group consisted of 6 individuals (mean age=71 years, SD=10) who had undergone unilateral knee joint replacement at least one year previous to testing (actual times post-op: 31, 25, 26, 19, 19 and 72 months). The second group consisted of age matched controls (mean age =70 years, SD=4) with no history of knee injury. EMG was recorded from vastus medialis (VM), vastus lateralis (VL), rectus femoris (RF), medial and lateral hamstrings, and medial and lateral gastrocnemius using a Bortec EMG system. Data were sampled at a rate of 1200Hz and bandpass filtered (10Hz – 500Hz) prior to being digitally sampled. All subjects were seated in a chair that allowed them to fully flex and extend their knee without restriction. During all trials the hip was positioned at 90º. Subjects completed a total of 18 knee extension trials during which they were instructed to fully extend their knee from a flexed position. Trials consisted of six weight conditions: extension with no weight, and knee extension with weights of 1.1 kg, 2kg, 2.9kg, 3.8kg or 4.7kg attached to the ankle. Temporal feedback was provided to ensure that all participants

completed the task in the same amount of time.

EMG data were first full-wave rectified, linear enveloped and normalized to a maximum contraction. EMG signals were then integrated (trapezoidal rule) for the time period from the start of knee extension until full extension was reached. Average integrated EMG (AiEMG) was determined by dividing iEMG by the total time it took to complete the knee extension trial. A two-way repeated measures ANOVA (1 repeated factor (weight) and 1 between subject factor (control or patient)) was then performed on the AiEMG measures.

RESULTS

Patients had significantly greater AiEMG than controls for both VM (p=0.048) and VL (p=0.0197). Rectus femoris exhibited a similar trend, although it did not reach significance (Figure 1). No statistically significant differences existed between the groups for the other muscles. All interaction effects were non-significant. The time to complete the task was 2.3s. Time did not differ significantly either between the groups or across weight
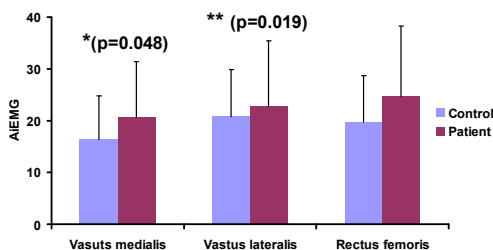
conditions.

Figure 1: AiEMG for VM, VL and RF during seated knee extension for patient and control groups. (* and ** significant difference between patient and control for muscle indicated.)

DISCUSSION

Preliminary analysis of this data found that following TKA, individuals activate VM and VL to a greater extent then do age matched controls. Activation levels of the hamstrings and gastrocnemius, the other primary muscles crossing the knee joint, showed no differences between the groups. Because the seated knee extension task requires the same gross knee kinematics and places similar kinetic demands on the knee, the observed changes in muscle activation may be attributed to alterations in muscle function. While muscle weakness is one factor that must certainly be considered, alteration in muscle moment arms may also contribute. Further research is underway to examine these issues.

SUMMARY

The current study examined AiEMG during a seated knee extension task in individuals following TKA. Findings indicate increased AiEMG in VL and VM in the patient group.

REFERENCES

Benedetti MG et al. (2003). *Clin Biomech,* 18: 871-876.
Byrne et al. (2002): *Clin Biomech,* 18:580-585.
Mizner RL, Snyder-Mackler L (2005): J *Orthop Research,* 23:1083-1090.
Wilson SA et al. (1996): *J Arthop*, 11:359-367.

EVALUATION OF PHYSICAL STRESS DURING HAND GESTURES FOR HUMAN MACHINE INTERACTION

Raziel Riemer, Adi Ronen, Helman Stern, Yael Edan

Department of Industrial and Management Engineering, Ben Gurion University of the Negev, Beer-Sheva, Israel. rriemer@bgu.ac.il

INTRODUCTION

Human machine interfaces based on hand gestures offer an alternative to traditional direct manipulation devices (e.g. joystick) (Stern, et al. 2008). Hand gesture communication involves several muscles that control finger, hand and wrist positions. When developing hand gesture vocabulary it is important to encourage natural postures and to avoid postures that cause strain (for ease of use and to prevent cumulative trauma disorders). There are two common approaches for determining the level of physical effort, subjective (Borg, 1982) and objective measurement i.e. electromyography (EMG)

In the past EMG has been used to investigate the level of effort in the muscle involved in physical activities (Skotte et al., 2002, Agarabi et al., 2004). While there are several studies that investigated the relation between perceived effort and muscle activity, No studies were found that investigated the level of effort during hand gestures. Previous studies investigated individual muscles only (Agarabi et al., 2004; Thuresson et al., 2005). However, performing a hand gesture is a complex task involving the activity of several muscles. The effect of the combined activity of the muscles on the perceived effort is unknown.

The objectives of this research are: to examine the differences between the perceived efforts from the different hand gestures, and to determine the relationship between EMG signals and perceived effort during different gestures.

METHODS AND PROCEDURES

Nine right-handed male subjects (age 31.4 ±6.8 years, weight 72.0 ±8.8kg, and height 1.76 ±0.06m), with no musculoskeletal problems in the forearm and hand, participated in the study. During the first part of the experiment the subject's placed their right arm and hand on a table in a neutral posture (Snell et al, 2000) and relaxed their muscles. Then each subject performed eight hand gestures (Figure 1). All gestures were performed with the forearm resting on the table. Hand gestures 1-6 were hand gestures that were identified by users as good candidates for hand gestures vocabulary (Stern, et al. 2008), while 7 and 8 hand gestures were added to increase the range of difficulty. Each gesture was initiated from a rest posture (hand open with palm facing down), after which the subject executed the gesture for 15 seconds. After which the gesture was released to the starting posture for 15 seconds of rest. This cycle was repeated three times for each gesture. The sequence of presentation of the gestures to each of the subjects was varied. For each gesture pose EMG signals were measured (Bagnoli-8, Delsys, Boston, MA) using a sampling rate of 2048Hz from the following muscles: Pronator teres, Flexor carpi radialis, Flexor carpi ulnaris, Extensor carpi radialis brevis+Extensor carpi radialis longus, Extensor carpi ulnaris, and Extensor digitorum. In addition, each subject reported a self perceived evaluation of effort required to perform each gesture execution using a 0-10 Borg scale (Borg, 1982).
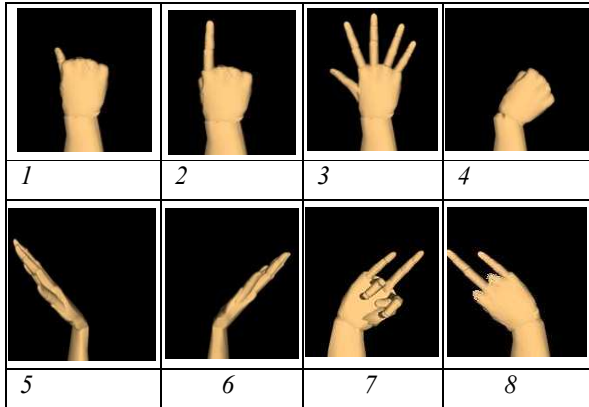
Figure 1: Hand gestures used in the study

Data analysis

Non-parametric Friedman and least significant difference (LSD) tests were used to determine if the perceived effort of the gestures varied, and if any pair of gestures were statically different. Moving RMS of the EMG signal was calculated using a time window of 0.125sec with an over-lapping of 0.0625sec. An average RMS for each of the muscles was calculated after the gesture was completed. This value was normalized by the average RMS of the same muscle obtained during the neutral posture

The relation between perceived (average Borg rating) effort and the level of muscle activity (average RMS) were investigated using Spearman correlation. Also, the relation between a single EMG parameter representing all muscle readings (maximum value and average value) and the Borg rating were investigated.

RESULTS

Non parametric Friedman test of Borg scores for the eight gestures, indicated a difference between the perceived effort in performing the eight gestures ($p= 2.3e-05$). The average score of each gesture yielded the following order of difficulty, from easy to difficult: 3, 1, 5, 2, 6, 4, 7, 8. An LSD test showed that gestures 3 and 1 were different from 4, 7 and 8, and that gesture 5 was different from 7 & 8.

Correlations between perceived levels of effort (Borg) to an average EMG (RMS) for each gesture (during static hand gesture) were executed. These correlations across all subjects revealed that, the muscle EMG and the Borg ratings for all gestures had three significant correlations. The Flexor carpi ulnaris signle ($r=0.39$), average EMG($r=0.33$), and maximum EMG ($r=0.31$). Correlations between individual subject's perceived effort and the muscle EMG showed that all the subjects except one had at least one correlation (r) higher than 0.73. However, there was no consistency among subjects regarding which muscle or parameters best predicted the relationship between the EMG and the perceived effort.

DISCUSSION

The statistical analysis indicated that even among hand gestures identified as good candidates for vocabulary, there was a perceived difference in the level of effort required for each gesture. These results emphasize the need to choose hand gestures that are easy to perform. The correlations across all subjects are relatively low ($R=0.39$, 0.33, 0.31) and suggest that an EMG measurement may not be sensitive enough to determine the perceived level of effort in the muscles.

REFERENCES

Agarabi, M. et al. (2004). *Conf Proc IEEE Eng Med Biol Soc*, 4: 2450-3.

Borg, G.A.,(1982). *Med Sci Sports Exerc* 14(5):377-81.

Skotte, J.H., et al. (2002). *J Biomech* 35(10): 1357-66.

Snell, R.S., (2000). *Clinical Anatomy for Medical Students*. Washington D.C., Williams & Wilkins.

Stern, H. et al. (2008), *Int. J. Semantic Computing,* (to appear April).

Thuresson, M., et al. (2005*). J Elect and Kines* 15(3): 323-331.

ASSESSMENT OF MOTION OF LONG-STEMMED TIBIAL IMPLANT

Jill Schmidt[1] and Heidi-Lynn Ploeg[2]

[1]PhD Student, Department of Mechanical Engineering, University of Wisconsin, Madison, Wisconsin, USA, jschmidt1@wisc.edu
[2]Assistant Professor, Departments of Mechanical Engineering, University of Wisconsin, Madison, Wisconsin, USA, ploeg@engr.wisc.edu
URL: http://www.engr.wisc.edu/groups/BM/

INTRODUCTION

Aseptic loosening is one of the most prevalent reasons for primary (Sharkey et al., 2002) and revision (Gofton et al., 2002) knee arthroplasty failures. Previous studies have shown correlations between aseptic loosening and initial implant motion (Freeman and Plante-Bordeneuve, 1994; Krismer et al, 1999). Therefore, several studies have used initial motion of an implant relative to the bone as a method to predict its clinical performance. In recent years, there has been a trend towards using three-dimensional (3D) optical marker systems to measure small motion in-vitro instead of the traditional means of one degree of freedom linear variable transducers. Previous studies using optical markers involving the tibial tray have investigated the effect of boney defects (Conditt et al., 2004) or the presence of a stem (Rawlinson et al., 2005), but none have explored the source of specimen-specific differences. The goal of this study was to perform an in-vitro study to investigate inter-specimen variability. Future work will be performed to develop specimen-specific finite element (FE) models to investigate possible sources of variability.

METHODS AND PROCEDURES

Six matched pair cadaveric tibias (n=12) were implanted with an appropriately sized Precoat A/P Wedge tibial tray with a 100 mm Offset Stem Extension (Nex Gen, Zimmer Inc., Warsaw, IN). The intramedullary canal was reamed until the reamer was felt to "chatter", and a stem with the same diameter as the final reamer was used. The implant had cement applied to the proximal cut surface and the underside of the tray, but not along the stem. Marker carriers with four optical markers were rigidly attached to the tibial tray, stem tip, and bone collar (Figure 1). A 60-to-40 medial-to-lateral sinusoidal load from 150 - 1500 N was applied at a frequency of 1 Hz for 5000 cycles. Displacements of the three bodies were measured with an optical marker system (Optotrak 3020, Northern Digital Inc., Ontario, Canada), which has a reported 3D resolution of 10 microns. Motion was captured during seven 30 second intervals and results are reported as a mean and standard deviation over all trials. The relative motion between the tray and the bone along the axis of the stem is reported.
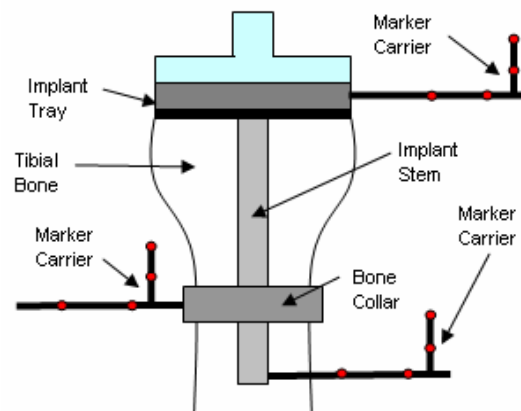
Figure 1. In-vitro test set-up of tibial bone with stemmed tibial tray and marker carriers.

RESULTS

The overall relative displacement for all bones was 51 ± 27 microns. The relative motion between the tray and the bone had high inter-specimen variability, but low intra-specimen variability (Figure 1). The intra-cadaver variability was large for most specimens.
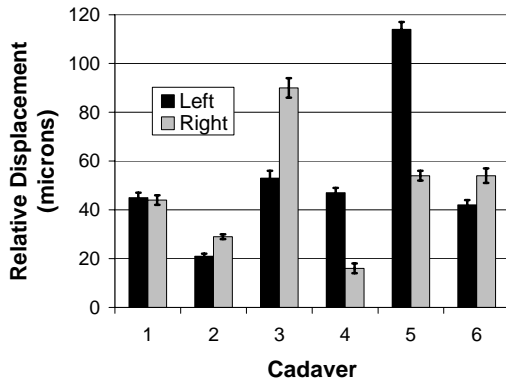
Figure 1. Relative displacement between the tray and bone along the axis of the stem.

DISCUSSION

The reported relative displacements between the bone and the implant were small (<120 microns). Similar magnitudes have previously been reported by Rawlinson et al., who performed a similar study measuring relative tray motion using an optical marker system (Proflex, Qualisys, Glastonbury, CT).

The relative displacement results between the tray and the bone for all specimens was highly variable (SD = 29 microns, coefficient of variation = 53%). Due to intra-cadaver variability it is predicted that variability is not only due to patient specific parameters (i.e. age, sex, etc.), but also implant specific parameters (i.e. tray size, stem diameter, etc.). This result is of particular interest since the implant specific parameters may be modified with implant design or surgical technique.

Finite element analysis (FEA) provides the opportunity for 3D analysis of implant motion, along with investigations of parameter effects. Therefore, future work is proposed using the bones of the current study to create specimen-specific FE models from computed tomography data. The relative displacement reported in the current study can provide validation for the FE models, which can be used to perform correlation studies on modifiable parameters.

SUMMARY

The relative motion between the tibial tray and bone of six matched-pairs of tibial bones demonstrated high inter-specimen and intra-cadaver variability. The results presented are a portion of a rich set of experimental data which will serve to validate subsequent numerical analyses. Future work will be performed to develop specimen-specific FE models to investigate the source of inter-specimen variability.

REFERENCES

Conditt et al. (2004). *J Arthrolasty, 19(7 Suppl 2): 113-8.*

Freeman and Plante-Bordeneuve (1994). *J Bone Joint Surg Br, 76(3):432-8.*

Gofton et al. (2002). *Clin Orthop Relat Res, 404: 158-68.*

Krismer et al. (1999). *J Bone Joint Surg Br, 81(2): 273-80.*

Rawlinson et al. (2005). *Clin Orthop Relat Res, 440: 107-16.*

Sharkey et al. (2002). *Clin Orthop Relat Res, 404: 7-13.*

ACKNOWLEDGEMENTS

FINITE ELEMENT MODELLING AND ANALYSIS OF CUSTOM FOOT ORTHOTICS

Lieselle Trinidad[1], Sundar Krishnamurty[1], Ryan Chang[2], Joseph Hamill[2]

[1]Department of Mechanical and Industrial Engineering, [2]Department of Kinesiology,
University of Massachusetts Amherst, Amherst, MA
e-mail: skrishna@ecs.umass.edu

INTRODUCTION

This paper presents an engineering approach to the modeling and analysis of Custom Foot Orthotics (CFOs). Although orthotics have become widely used and accepted as devices for the prevention of and recovery from injuries, the design process continues to be based on empirical means. A deeper understanding of the therapeutic effects of a CFO and its design for optimal performance can be achieved through systematic simulation-based engineering modeling and analysis studies. Towards this goal, this paper presents the development of a methodical simulation-based approach using Finite Element Analysis (FEA). Salient steps for the development of accurate CFO models include the creation of FEA models through approximation of complicated nonlinear material properties, as well as a methodical process for the replication of the complex three-dimensional geometry.

Despite the common practice of modeling and analysis through FEA in product design, tools related to these systems have not been utilized when designing custom prescription foot orthotics. This is primarily due to the fact that the engineering analysis is complex and the dynamics of human gait characteristics are difficult to model. Recently the use of FEA has been used to gain insight into the effectiveness of ankle-foot orthotics (Lam, et al 1985) and accommodative orthotics (Lemmon, et al. 1995). This work further extends the use of FEA to model and analyze prescription CFOs.

METHODS AND PROCEDURES

1) Nonlinear Material Property Estimation
An initial challenge when creating a FEA of CFOs results from the limited availability of material properties. This challenge is compounded by the highly complex and nonlinear traits of these materials. For this study, we considered the most popular material used in typical semi-rigid style CFOs: polypropylene. Ten sample sheets of polypropylene with varying thicknesses (2mm, 3mm, and 4mm) provided by Kintec Footlabs were examined using ASTM standard D575-91, and D412. Material properties were approximated through rigorous uniaxial tensile testing and resulting stress-strain behaviours were constructed.

To capture the nonlinear material properties, the Mooney-Rivlin strain energy function was adopted and the constants were calculated. (Finney and Kumar, 1988) and can be expressed as:

$$S = 2(a-a^{-2})\ (C_1+C_2*a^{-1});\ G = 2*(C_1+C_2) \quad (1)$$

Where S is stress; a is the principal stretch ratio $(1+dL/L)$, and material constants C_1 and C_2 relate to the shear modulus.

2) Geometry Construction
The replication of CFO geometry using CAD tools is extremely time consuming and almost impossible to accurately represent. An alternative approach involves using laser scanning technology to generate the geometry. Laser scanning captures an object's geometry in a point cloud surface image, simplifying the process while creating

the most accurate result. In this project, a semi-rigid CFO was scanned using a laser digitizer and the point cloud image was converted into a solid image using 3-Matic a commercial imaging tool from Materialise Inc.

3) Modeling of Constraints and Loads

Engineering analyses rely on the identification of kinematic constraints and applied forces. The mid-stance phase of gait was modeled. The boundary conditions applied were: 1) zero degrees of freedom (DOF) in the underside of the heel region; 2) zero horizontal movement on the back, lateral and front edges; and 3) zero movement in the vertical direction on the bottom area. The arch area was left unconstrained. Finally, a uniform surface pressure load was applied using a static large deflection model to the entire top surface.

RESULTS

The ANSYS finite element package was used to run the analyses on three separate weight classifications and the maximum von Mises stress and deflection results were acquired (Figures 2 and 3).

Figure 2 is a plot of the applied load versus the deflection of the arch area using three weight classifications. Each line represents a different model which only varies by thickness. The larger the load applied, the more deflection is seen in the arch as well as the thicker the model the less deflection there is.
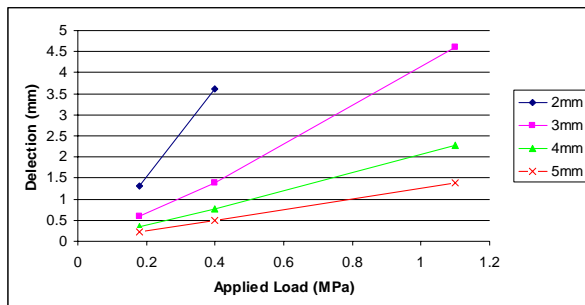
Figure 2. Maximum deflection versus the applied load by orthotic thickness.

Figure 3 shows a representative plot of the von Mises stress distribution which shows that the maximum stress areas are around the edge of the arch.
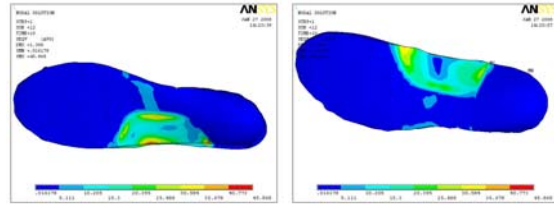
Figure 3. Stress distribution view (a) top and (b) bottom.

DISCUSSION AND SUMMARY

The engineering-model based results for the different thicknesses are consistent with the clinical study findings. As expected, the deflection differences between the 3mm and 4mm models are minimal for low values of applied loads, but the differences become significant at the higher applied loads. Figure 3 also shows positive performance since the distribution of stress is displayed as expected.

This paper details a simulation-based design procedure for the systematic design of custom foot orthotics. Properly employed, these models have the potential to replace the empirical tables currently used for designing custom foot orthotics. This model may enable optimal CFO designs based on a patient's body weight, activities, loading conditions, foot deformities, etc. Finally, these models and the corresponding results promise to form the basis of a new generation of custom foot orthotics.

REFERENCES

Finney, R.H., and Kumar, A. *Rubber Chemistry and Technology* (1988)

Lam, P. C., et al. (1985) *AB ASME*

Lemmon, David R., et al. (1995) *ASME IMECE*

MacLean, C., et al. (2006) *Clinical Biomechanics.*

INCREASED EXPOSURE TO AN OBSTACLE CROSSING TASK DECREASED TOE ELEVATION AT OBSTACLE CROSSING, BUT NOT ESTIMATION OF OBSTACLE HEIGHT

Chris K. Rhea, Julia E. Drifmeyer, and Shirley Rietdyk
Purdue University, West Lafayette, IN, USA
E-mail: crhea@purdue.edu

INTRODUCTION

Humans commonly encounter obstacles that require them to deviate from steady state gait, such as stairs, curbs, or objects in their pathway (Shumway-Cook, Patla, Steward, Ferrucci, Ciol, & Guralnik, 2002). Locomotion behavior can change as a function of experience with a locomotor task (Rhea & Rietdyk, 2005; Rietdyk, McGlothlin, & Knezovich, 2005). While some research has examined how the action of locomotion is coupled with perception of the environment (Cornus, Montange, and Laurent, 1999; Warren, 1984), these studies did not assess how perception changes with increased locomotor experience.

Previous research has shown that subjects' estimation of obstacle height is correlated to their toe elevation when crossing the obstacle (Rhea & Rietdyk, 2007). It has also been shown that toe clearance decreases with increased exposure to a consistent obstacle height (Rhea & Rietdyk, 2005). The purpose of this project was to examine if an obstacle height estimation task changed as a function of proprioceptive information gained from crossing an obstacle multiple times. Three hypotheses were tested: 1) toe clearance would decrease with increased exposure, 2) estimation of obstacle height would be more accurate with increased exposure, and 3) with increased exposure to the obstacle, subjects' height estimation would more closely reflect their toe elevation while crossing the obstacle.

METHODS

Ten subjects (age: 21.7 ± 1.6 yrs; mass: 76.4 ± 18.5 kg; height: 1.7 ± 0.1 m) participated in the study and gave informed consent. Four infrared emitting diodes (IREDs) were placed on the subjects' toe and heel on the lateral aspect of their right foot and medial aspect of their left foot. Displacement data was collected at 120 Hz with one Optotrak 3020 sensor (Northern Digital, Inc.).

A 10 cm obstacle was placed in the middle of an 8 m walkway. Prior to walking over the obstacle, subjects were told to stand approximately three steps from the obstacle and raise and lower their toe 10 times to their perceived height of the obstacle (Figure 1). Subjects then crossed the obstacle for 50 consecutive trials. Following the obstacle crossing trials, subjects performed the height estimation task again. The estimation trials prior to and following obstacle crossing were termed pre-estimation and post-estimation, respectively.

The dependent variable was toe elevation in the pre- and post-estimation trials and when the foot was directly over the obstacle during crossing. Toe elevation was measured as the vertical displacement of the toe from the ground. Toe elevation at obstacle crossing was examined for trials 1-5 and trials 46-50 to explore behavioral changes with increased exposure to the obstacle crossing task.
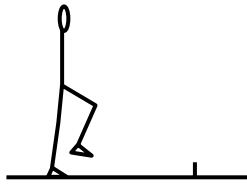
Figure 1. Estimation of obstacle height.

RESULTS AND DISCUSSION

Toe clearance values significantly decreased from the first five obstacle crossings to the last five obstacle crossings ($p < .05$, mean = 20.2 cm and 18.3 cm, respectively), supporting the first hypothesis. The range of height estimation values decreased from the pre- to post-estimation (5.9-21.8 cm, 7.7-20.4 cm, respectively), however subjects did not get more accurate in the estimation task ($p > .05$). This finding did not support the second hypothesis. Figure 2 shows the relationship between height estimation and obstacle crossing for the pre-estimation and first five obstacle crossings (Figure 2a) and the post-estimation and last five obstacle crossings (Figure 2b).
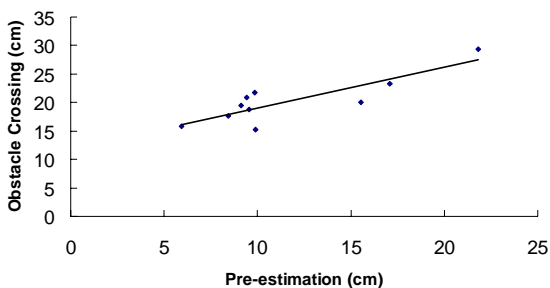
Figure 2a. Toe elevation during the pre-estimation and first five obstacle crossings.
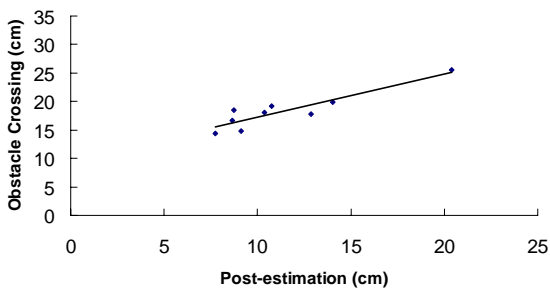
Figure 2b. Toe elevation during the post-estimation and last five obstacle crossings.

The correlation between subjects' pre-estimation and their first five obstacle crossings was .72. A strong correlation between the post-estimation and the last five obstacle crossings was also observed (r = .83), but the correlations were not significantly different ($p > .05$), which did not support the third hypothesis.

SUMMARY/CONCLUSIONS

Increased exposure to an adaptive locomotor task had an effect on toe elevation when subjects crossed the obstacle, but not on subjects' estimation of obstacle height. In general, the difference between toe elevation for the estimation task and obstacle crossing task was smaller for subjects who perceived the obstacle to be larger than its actual size. Previous research has examined perception at the beginning of an adaptive locomotor task and our results indicate that subjects' perception in an obstacle crossing task is robust and may not change as a result of task experience.

REFERENCES

Cornus S. et al. (1999) *Ecological Psychology*, 11(4), 249-267.

Rhea, C.K. & Rietdyk, S. (2005) *Proceedings of the XX Congress of the International Society of Biomechanics*.

Rhea C.K. & Rietdyk, S. (2007) *Preceedings of the American Society of Biomechanics Meeting.*

Rietdyk, S. et al. (2005) *Clinical Biomechanics*, 20(10), 1085-1093.

Shumway-Cook, A. et al. (2002) *Physical Therapy*, 82(7), 670-681

Warren, W.H. (1984) *JEP: HPP*, 10(5), 683-703.

ACKNOWLEDGEMENTS

AGE-ASSOCIATED DOPAMINERGIC INFLUENCES ON FOOT-TAPPING AND TEMPORAL GAIT PARAMETERS IN HEALTHY OLDER ADULTS

Chris W Bogan[1], NI Bohnen[2, 3, 4], RA Koeppe[2], KA Frey[2], RL Albin[3, 4], & MLTM Müller[2]

Departments of Mechanical Engineering[1], Radiology[2], Neurology[3], &
GRECC/Neurology[4] (VA)
Functional Neuroimaging, Cognitive and Mobility Laboratory
http://sitemaker.umich.edu/pdresearch/home, crbogan@umich.edu
University of Michigan & VA Healthcare System, Ann Arbor, MI, USA

INTRODUCTION

Gait is a complex motor task that requires both low level rhythmic pattern generation as well as higher order cerebral control. With aging neurophysiological changes occur that may affect the ability to maintain stable gait. The purpose of this study was to examine the interrelationships between striatal dopaminergic denervation, oscillatory rhythmic foot movements, and gait in healthy older adults.

METHODS AND PROCEDURES

Presented here is preliminary data of a larger research effort into underlying mechanisms of falling. The data of 17 normal healthy older adults (5/12 f/m, age = 66.7 ± 11.7 yrs., range 50-84 yrs.) has been analyzed thus far. Subjects were normal upon neurological and physical examination. Mobility and motor functioning were assessed, of which the gait and foot-tapping data are presented here. All subjects provided IRB-approved written informed consent prior to testing.

Dopamine Imaging: Standard [11C]-DTBZ Positron Emission Tomography (PET) imaging of the vesicular monoamine transporter type 2 (VMAT2) ligand was performed. Standard VMAT2 PET analyses methods were used to determine the striatal

(i.e. bilateral caudate nucleus and putamen) binding potential (BP) for dopamine. This is a unitless estimate of the amount of dopamine in the striatum (Figure 1).
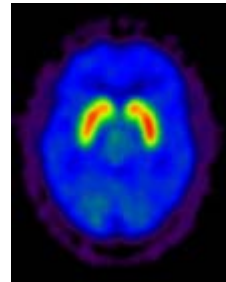
Figure 1. Binding of [11C]-DTBZ to VMAT2 in the striatum of a healthy older adult.

Gait Testing: A telemetry system (BIOPAC Systems, Inc) was used to record heel and toe strike through pressure-sensitive transducers (Figure 2). Subjects were asked to walk in their own shoes at a self-selected normal pace for 8 meters. This was repeated four times. All subjects wore a safety harness and were trailed closely to prevent from falling. Standard temporal gait parameters were calculated.

Rhythmic Pattern Generation Assessment: Foot tapping was taken as a measure for the ability to generate rhythmic oscillatory movements. A new device was designed and built in our lab that was able to measure

oscillatory rotations of the foot, the so-called foot-tapper (Figure 3).
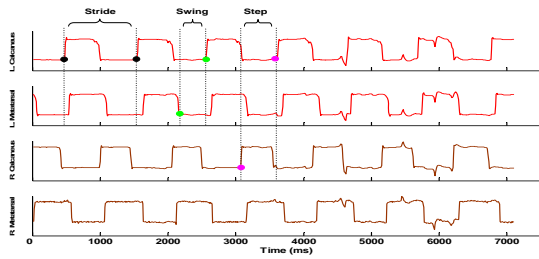
Figure 2. Typical gait data from the heel (row 1) and toe (row 2) transducers of the left foot (top 2 rows) and the right foot (bottom 2 rows).
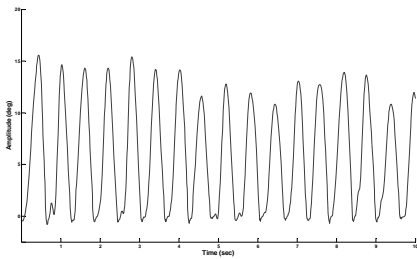
Figure 3. Typical oscillations recorded electronically with ADAMView (Advantech) from the foot-tapper device.

The foot-tapper consists of a rotary encoder (Encoder Products Co.) attached to a foam-covered wooden pedal that could rotate freely. Testing was done with shoes off, and the subject was asked to generate as many foot taps as possible in ten seconds with one foot. This was repeated five times and the task was repeated with the other foot. Total number of taps, frequency and amplitude were calculated.

RESULTS

Corrected for age and walking speed, there were significant negative correlations between striatal VMAT2 BP and measures of temporal gait variability, i.e. with Stride Time variability (r=-0.730, p=0.011), Stance Time variability (r=-0.735, p=0.010), and Step Time variability (r=-0.769, p=0.006). Corrected for age, none of the foot-tapper measures correlated with striatal VMAT2 BP, nor did any of the foot-tapper measures correlate with any of the gait measures.

DISCUSSION

These preliminary results showed negative correlations between striatal dopaminergic BP and temporal measures of gait variability, independent of age and walking speed. With a decrease in striatal dopamine, temporal aspects of gait became more unstable. There were no robust associations between dopaminergic BP and foot-tapper measures.

Also, foot-tapper data did not correlate with gait data. This finding is in line with findings by Hausdorff et al. (2005), who showed that a complex catching task was associated with gait control, whereas rhythmic finger tapping showed no relationship.

SUMMARY

Striatal dopaminergic control plays an important role in the regulation of gait, but not in the regulation of oscillatory foot movements. Oscillatory foot movements are not robustly correlated with gait parameters. More data is needed to strengthen or disprove these statements.

REFERENCES

Hausdorff JM et al. (2005). *Exp Brain Res, 164(4)*: 541-548.

ACKNOWLEDGEMENTS

AN ASSOCIATION BETWEEN PREOPERATIVE GAIT PATTERNS AND POSTOPERATIVE TOTAL KNEE IMPLANT MIGRATION

D. Wilson[1,2], J.L. Astephen[1,2], M. Dunbar[1,3], K.J. Deluzio[1,4]

[1]School of Biomedical Engineering, Dalhousie University, Halifax, Canada
[2]Department of Human Biology, University of Cape Town, Cape Town, South Africa
[3]Department of Surgery, Dalhousie University, Halifax, Canada
[4]Department of Mechanical and Materials Engineering, Queen's University, Kingston, Canada

INTRODUCTION

Total knee arthroplasty (TKA) is the current gold standard treatment for severe osteoarthritis of the knee. However, early aseptic loosening of the implant commonly leads to costly, invasive revision surgery (CJRR). Associations between preoperative biomechanical patterns and postoperative TKA surgery success have been identified (Hilding et al., 1995), but the relationship between preoperative kinematic and kinetic patterns and the amount and direction of postoperative implant migration have not been explored. The purpose of this study was to investigate the association between preoperative biomechanical patterns and the postoperative migration of both cemented and uncemented total knee arthroplasty measured with Radiostereometric analysis (RSA).

METHODS AND PROCEDURES

Forty-three patients with primary osteoarthritis of the knee underwent gait analysis trials in the week prior to total knee joint replacement surgery. Three-dimensional net external knee joint moments and angles were calculated. Principal component analysis (PCA) was applied to each of the joint angles and joint moments separately to extract major patterns of variation within the waveforms. A set of principal component scores for each subject were calculated by projecting original waveforms onto the principal components.

The subjects were randomized to receive the uncemented Nexgen TM monoblock (n = 22; mean age = 66 years; mean BMI = 32) or the cemented cobalt chrome, modular posterior-stabilized knees (n=21; mean age=65 years; mean BMI=33). Four experienced surgeons followed a standardized surgical technique (PCL resection, patella resurfacing, RSA bead placement in polyethylene and tibia) and post-operative protocol (CPM as tolerated, no drains, WBAT). Within four days of surgery and at six months post-operatively, patients had bi-planar knee RSA x-rays taken. RSA analysis was performed with MB-RSA (MEDIS, Leiden). RSA results at six months were reported as maximum total point motion, and six degrees of freedom translations and rotations. Due to the non-parametric distribution of the data, Spearman's rank correlations were used to examine the relationship between the first three principle component (PC) scores for each gait variable and the RSA metrics (P<0.05).

RESULTS

There was a moderate, significant correlation between maximum total point motion (MTPM) and the first principal component (PC) of the knee adduction moment, which represented the overall magnitude of moment during the stance phase of the gait cycle (r = 0.459, P = 0.005). Higher preoperative knee adduction moment magnitudes were associated with greater MTPM postoperatively (Figure 1).

Internal rotation of the tibial implant with respect to the tibia was correlated with the second PC of the net resultant rotation moment at the knee, which represented the magnitude of the moment at load acceptance (r = 0.341, P = 0.042) (Figure 2).
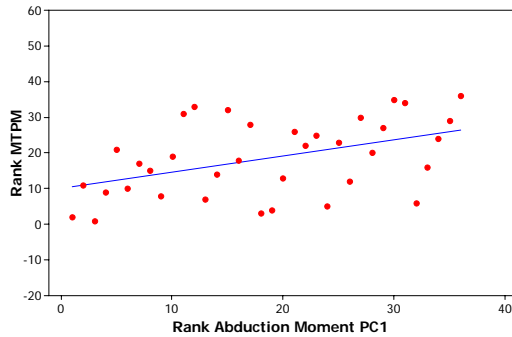
Figure 1: Scatter plot of the rank of maximum total point motion (MTPM) vs. the rank of the first principle component (PC) of the knee adduction moment.
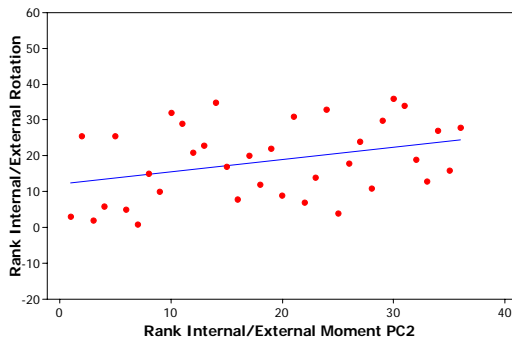

Figure 2: Scatter plot of the rank of the internal/external rotation of the tibial component vs. the rank of the second principle component of the internal rotation of the knee.

DISCUSSION

The knee adduction moment is the biomechanical variable most associated with knee osteoarthritis both pre and postoperatively, and has been identified as predictive of high tibial osteotomy surgery outcome (Prodromos et al., 1985). In the current study, the overall magnitude of the knee adduction moment during stance was shown to relate to postoperative TKR migration, and therefore may be an important factor in patient-specific implant selection. Greater resultant internal rotation moments of the tibia relative to the femur at load acceptance, preoperatively, were associated with higher tibial component internal rotations postoperatively (Figure 2). This has important clinical implications because in the longitudinal RSA study on the same subject group, internal rotation of the tibial component was associated with continuous migration.

SUMMARY

The amount of postoperative migration of the tibial component of total knee arthroplasty was found to be associated with preoperative gait patterns, particularly to the magnitude of the knee adduction moment and the knee internal rotation moment. These results suggest that surgical success may be dependent on the preoperative mechanical environment of the knee joint.

REFERENCES

Hilding MB et al. (1995) *Acta Orthop Scand*, 66(4):317-20.
Prodromos, CC et al. (1985) *J Bone Joint Surg Am.* 67(8): 1188-1194.

ACKNOWLEDGEMENTS

3-D Strength Surfaces for Shoulder Internal and External Rotation

Gary Pierce[1] and Laura Frey Law[1,2]

[1]Virtual Soldier Research program, College of Engineering, gmpierce@engineering.uiowa.edu
[2]Physical Therapy and Rehabilitation Science, College of Medicine, laura-freylaw@uiowa.edu
The University of Iowa, Iowa City, IA, USA

INTRODUCTION

Normative static strength databases are repeatedly used in biomechanics related fields. However, increasingly dynamic strength information is needed due to advances in predicting dynamic joint torque. 3-D strength surfaces can be used to better delineate the relationships between angle and velocity on joint torque. Theoretical 3-D strength surfaces have been proposed as well as 3-D strength surfaces for lower limb joints (Anderson, 2007). However there is currently no literature available providing data for a 3-D surface of the shoulder joint. The only shoulder strength data available includes 2D torque-velocity or torque-position relationships (Mayer, 1994; Alderink & Kuck, 1985). The shoulder relies predominantly on the rotator cuff, i.e. internal and external rotators, to provide joint stability. However, it is not clear whether dynamic shoulder strength follows predicted lower extremity surfaces, or varies differentially with angle and velocity. Thus, the purpose of this research project was to evaluate how dynamic shoulder internal and external rotation (IR/ER) strength is influenced by velocity and joint position variables. This information may be useful for both clinical rehabilitation applications as well as with biomechanical and digital human models.

METHODS AND PROCEDURES

Four subjects were recruited: 2 males 2 females (23 ± 1yrs). Written informed-consent, approved by the Institutional Review Board at the University of Iowa was obtained from each subject before testing was performed. This study tested static and dynamic strength in the IR/ER plane of motion with the arm abducted 45 degrees at the shoulder joint, using an isokinetic dynamometer (Biodex System 3, New York, USA). Subjects were positioned according to the Biodex System standard procedures.

Isometric torque was tested at 5 positions across the full ROM. The zero angle of the ROM was defined as the most extreme point of external rotation, achievable by the subject. At each of the 5 positions the subject completed 6 maximal voluntary contractions (MVCs) alternating directions between each MVC (e.g. 3 IR and 3 ER). Between contractions a 45 second rest was provided. The order of testing positions was randomized. Isokinetic testing involved 5 angular velocities (60, 120, 180, 240, and 300 deg/sec) performed in a randomized order. Prior to maximal testing at each velocity, a minimum of 3 submaximal repetitions were performed to familiarize the subject with the speed and ROM. A set of 4 to 7 maximum repetitions were performed at each velocity with a 3 minute rest between each speed.

The raw, analog data was sampled at 1000 Hz and analyzed using MATLAB (MathWorks USA). Necessary corrections for gravity and passive tension were performed based on passive torque measured at each isometric test position. Peak torque was extracted for both IR and ER at each position – velocity combination (5 positions x 6 velocities including isometric). 3-D strength surfaces were plotted for IR and ER directions.

RESULTS

Representative 3-D strength surfaces for a single subject are shown in figures 1 and 2. The torque-velocity relationship varied across position for each subject. For example, IR at 10, 60 and 125 deg, IR torque decayed a total of 13.9%, 44.3%, and 74.6%, respectively for sub 3 (fig 1). Similarly, ER strength at 10, 60, and 125 deg, decayed a total of 54.2%, 53.5%, and 17.1% respectively (fig 2). Peak torque values for the four subjects are provided in Table 1.
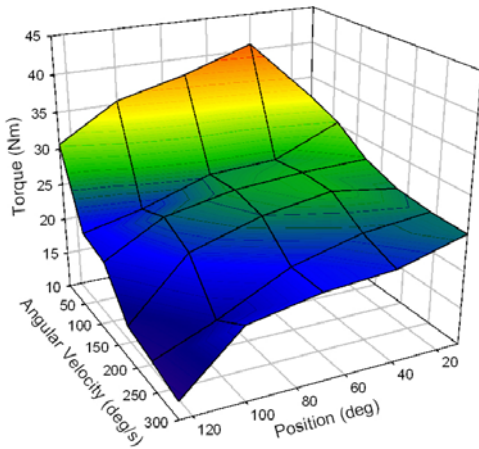

.
Figure 1. Internal rotation 3-D strength surface for subject 3.
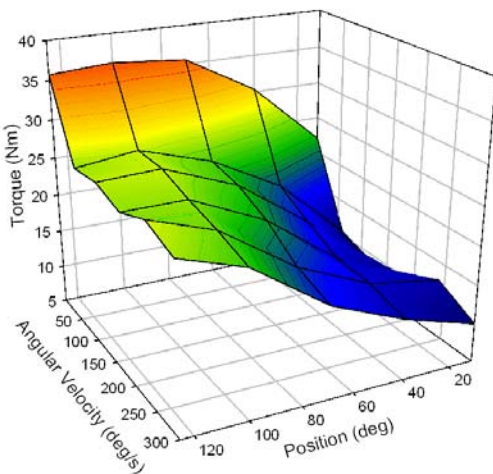
Figure 2. External Rotation 3-D strength surface for subject 3.

Sub #	Sex	IR (Nm)	ER (Nm)
1	F	27.4	25.8
2	F	23.9	26.0
3	M	40.8	36.3
4	M	60.5	37.7

Table 1. Peak Torque for individual subjects.

DISCUSSION

IR strength was generally greater than ER strength, and torques were greater for males than females, consistent with previous 2-D shoulder strength data. However, the torque-velocity relationship did not follow a constant Hill's force-velocity decay across the ROM. Interestingly, the region of peak torque decayed the least for both IR and ER. Further, these 3-D surfaces demonstrate strength nonlinearities that are not represented by simple 2-D or static strength estimates.

SUMMARY

IR/ER shoulder peak torque varies with velocity and position. This information may be useful for biomechanical and digital human modeling.

REFERENCES

Alderink GJ, Kuck DJ (1986) *Journal of Orthopaedic and Sports Physical Therapy.*, 7(4):163-172.
Anderson DE et al. (2007) *Journal of Biomechanics.*, 40:3105-3113.
Mayer F et al. (1994). *Int. J. Sports Med.*, 15:S19-S25.

ACKNOWLEDGEMENTS

CARTILAGE CELL VIABILITY AFTER SUBMAXIMAL AND MAXIMAL MUSCLE LOADING WITH AND WITHOUT IMPACT LOADING

Doug Bourne[1], John Matyas[2], Ken Muldrew[2] and Walter Herzog[1]
[1]Human Performance Laboratory, Faculty of Kinesiology, University of Calgary, Canada,
[2]Faculty of Medicine, University of Calgary, Canada
dbourne@kin.ucalgary.ca

INTRODUCTION

Injury to articular cartilage is thought to be an initiator of osteoarthritis. One possible mechanism of cartilage degeneration is that cells are killed due to impact. The resulting metabolic load on the remaining cells prevents them from properly maintaining the extracellular matrix, leading to matrix degeneration. In vivo impact models have been used as models of osteoarthritis (Haut et al., 1995). Cartilage is a viscoelastic material whose response to loading is dependent on loading history. Pre-straining cartilage explants has been shown to decrease cell death after injurious loading (Morel et al., 2005). The purpose of our study was to determine the susceptibility of cartilage to impact loading after one of two loading conditions. The first loading condition was fifty minutes of repetitive submaximal loading. This was chosen to represent a repetitive activity such as running. The second loading condition was a maximal muscle contraction that one might do when trying to avoid an injury.

METHODS AND PROCEDURES

Testing was performed on patellofemoral joints of New Zealand white rabbits. Animals were anaesthetized and a nerve cuff electrode was surgically implanted over the femoral nerve of each leg. Rabbits were then fixed in a custom stereotaxic frame where their hips were pinned and the experimental knee supported at an angle of 90 degrees. Six knees underwent muscle stimulation for 50 minutes with one 20% of maximal effort, 0.5s contraction every 2 seconds. Three of these

six joints were then impact loaded while the others were not. Impact loading was applied by dropping a 1.5kg mass from a distance of 33cm (Figure 1).
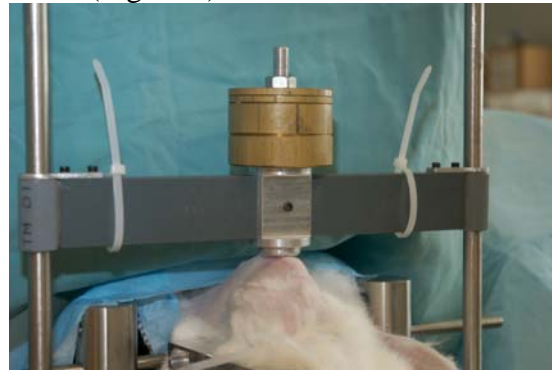
Figure 1 Impact device shown in contact with rabbit patella.

Two further knees were received maximal muscle loading; one of them received an impact load during the muscle loading. Seven knees were just impact loaded and seven knees were not loaded and served as controls. Following loading, rabbits were sacrificed and the knees dissected. The cartilage was stained with SYTO 13 and SYTOX orange overnight. The patellae and distal femurs were then mounted in a Petri dish with PBS and imaged with a confocal microscope. First, the surface of the patella was scanned to identify areas of cell death. Then image stacks were taken from different areas of the patella including the loaded areas of interest. Live (green) and dead (orange) cells were counted with a custom cell counting program. The two scans with the highest percentage of dead cells were averaged to determine a cell death value for each specimen.

RESULTS

All results are summarized in Figure 2. The 50 minute muscle stimulation group showed greater cell death than the unloaded controls (Figure 3). The 50 minute muscle stimulation plus impact groups showed higher cell death than the impact only group. The one patella from the maximum muscle stimulation group showed similar cell death to the controls, while the patella for the maximal muscle contraction plus impact showed less cell death than the impact only group.
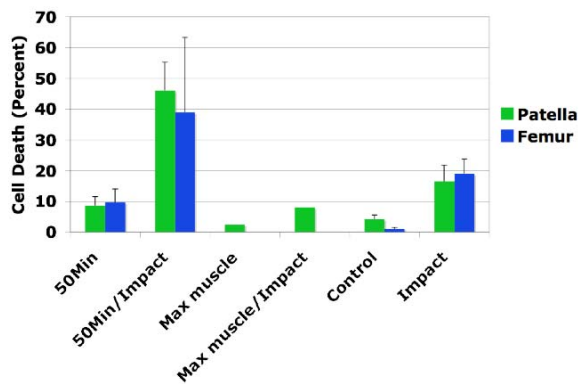

Figure 2 Cell Death for the different loading conditions.

DISCUSSION

It appears that not only does 50 minutes of submaximal muscle contraction make cartilage more susceptible to impact loading but it also kills chondrocytes. This contradicts work done in explant studies where it was found that prestraining cartilage had a protective effect (Morel et al. 2005). However, in the explant study, low strain rates were used to apply the prestrain while we used a cyclical muscle contraction, thus we cannot discern if the differences are caused by the different pre-load application or the different test specimens (intact vs. explant).

While only one patella had been tested at abstract submission, the results for the maximum muscle contraction and impact test are intriguing and will be further studied. The expected patellofemoral joint contact

pressures for this condition would be high since previous work has shown that impact loading and maximal muscle loading produce peak pressures of 45MPa and 25MPa, respectively. Cell death is lower for the maximal muscle contraction plus impact group compared to just the impact group suggesting that muscle contraction potentially produces a protective effect. The nature of such an effect needs investigation.
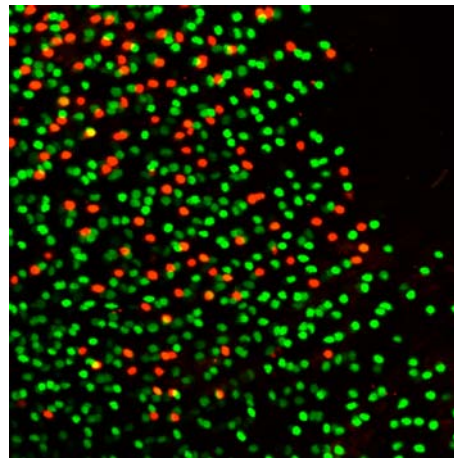
Figure 3 Sample depth-projection from the 50 minute muscle stimulation group.

SUMMARY

The results of this study suggest that repetitive muscle stimulation kills chondrocytes and makes chondrocytes more susceptible to impact loading while a single maximum contraction concurrent with impact loading may have a protective effect. We will add further animals to the various testing groups and measure the patellofemoral pressure distributions directly in the experimental animals

REFERENCES

Haut, R.C., Ide, T.M. and De Camp, C.E. (1995) *J Biomech Eng* 117, 402-8.

Morel, V., Mercay, A., and Quinn, T.M. (2005) *Osteoarthritis and Cartilage* 13(11), 964-70

THE EFFECT OF DRYWALL STILTS ON THE CONTROL OF QUIET STANDING

Jeremy W. Noble, Jonathan C. Singer, Kaitlin M. Gallagher and Stephen D. Prentice
University of Waterloo, Waterloo, ON, Canada
E-mail: jwnoble@uwaterloo.ca

INTRODUCTION

Currently in Ontario, drywall tapers and insulation installers must use a bench to reach elevated heights, as the use of stilts is prohibited. The goal of the present study is to investigate the effect of stilt use on total body sway during quiet standing in a group of experienced stilt users and a group of novice stilt users. It is hypothesized that the stilts will change the sway measures similar to those observed standing at an increased height.

METHODS

A group of 6 experienced stilt users and a group of 6 novice stilt users participated in this experiment. The participants were outfitted with 21 infra-red emitting diodes (iREDS) on anatomical landmarks described by Winter (2005).

The participants performed 5 trials of quiet standing on the ground, while standing on a platform (60cm x 120cm) raised 60 cm off the ground, and while using a pair of drywall stilts, raised to 60 cm. All standing trials were 30 seconds long. In order to replicate some of the postures that would be used during drywalling, the participants performed an additional 5 standing trials with their head extended to look at the ceiling, and 5 trials with their head extended and their dominant hand reaching towards the ceiling. These postures were completed for each standing condition (Ground, Platform, Stilts). The locations of the markers were measured during the standing trials with the use of an OPTOTRAK system (Northern Digital Inc., Waterloo ON).

The location of the total body centre of mass (COM) was determined from the locations of specific iREDS in the Anterior/Posterior (A/P) and Medial-Lateral (M/L) directions over the entire 30s standing trial. In order to determine the magnitude of sway in each direction the mean value was subtracted from the COM, and the root-mean-square (RMS) value was determined in the A/P and M/L directions. The frequency of the sway was determined assessed by determined the mean power frequency (MPF) from the power spectral density function of sway measures.

A three-way repeated measures ANOVA was used to determine the effect of experience (expert or novice), standing condition (ground, bench, stilts) or posture (normal, head extended, head and arm extended).

RESULTS

The RMS sway values and MPF values for the quiet standing posture, for all standing conditions are shown in Figures 1 and 2. Standing on the stilts resulted in decreased sway magnitude in the A/P direction, without any change in the MPF for both the expert and novice groups. No change in A/P sway magnitude was observed in the bench condition, although a significant increase in the sway frequency was observed for both the expert and novice stilt users.

No differences were observed in the magnitude of the M/L sway across standing conditions; however the expert group had a lower sway frequency when standing on the bench and the stilts, despite having similar

MPF in the M/L direction while standing on the ground. The various postures tested resulted in no significant differences in either the sway magnitude or the frequency.
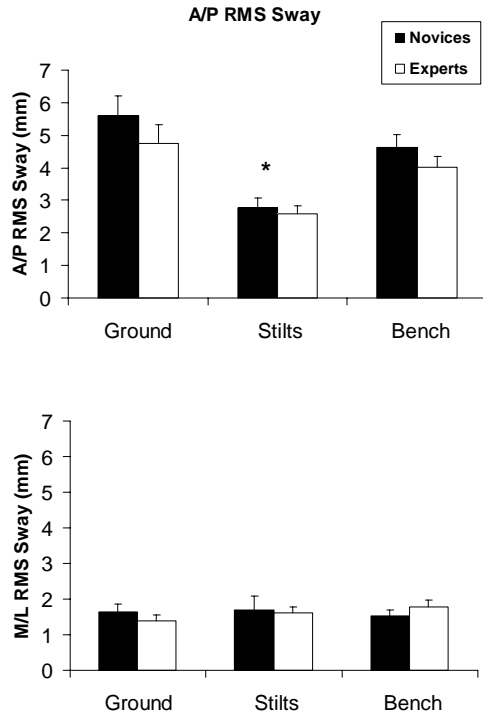
A/P RMS Sway

Figure 1: RMS sway values of the COM. An asterisk (*) indicates a significant difference across standing conditions.

DISCUSSION

It has previously been shown that standing at a height results in a decreased sway magnitude, and increased sway frequency (Carpenter et al, 2001). Although the participants in this study did not show a decrease in the magnitude of A/P sway when standing on the bench, they did show a significant increase in the MPF, indicating tighter control in this condition (Winter et al, 1998). Standing on the stilts resulted in a significant decrease in sway for both groups. This is likely due to the fact that the springs that are a part of the ankle of the stilt allowed for less sway then the human ankle. An interesting finding was that the expert group showed lower sway frequencies

in the M/L direction when standing on the bench, and while standing on the stilts. This finding could indicate that the novice group was controlling their balance more tightly in these conditions due to lack of experience.

A/P Sway MPF

M/L Sway MPF
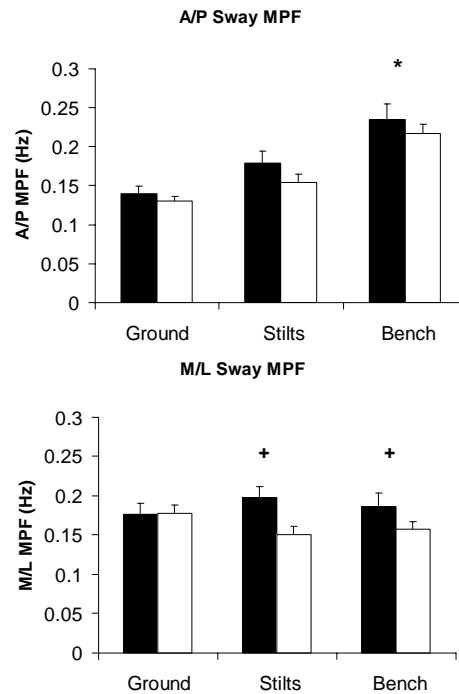
Figure 2: Sway **frequency (**MPF). An asterisk (*) indicates a significant difference across standing conditions while a plus sign (+) indicates a significant difference between groups.

REFERENCES

Carpenter MG et al. (2001). *Exp Brain Res*. 138:210-8.
Winter DA (2005). Biomechanics and Motor Control of Human Movement. New York. Wiley.
Winter DA. et al. (1998). *J Neurophysiol.* 85: 2630-3.

CONTINUOUS MOTION MONITORING OF THE CERVICAL SPINE

[1]Andrew C. Sterling, BS; [2]Daniel G. Cobian, BS; [2,3]Paul A. Anderson, MD; [2,3]Bryan C. Heiderscheit, PhD, PT

Departments of [1]Mechanical Engineering, [2]Orthopedics and Rehabilitation and [3]Biomedical Engineering, University of Wisconsin-Madison, Madison, WI 53706; asterling@wisc.edu

INTRODUCTION

Information pertaining to the daily and activity-specific frequency and magnitude of cervical motion is currently unavailable. Such information would quantitatively assess normal movement behavior in healthy young adults for comparison with individuals suffering from a cervical pathology and could potentially influence treatment methods. Likewise, the design and evaluation of cervical disc prostheses requires this information for annual wear estimations (ASTM, 2006). Therefore, the objective of this study was to quantify the daily frequency and magnitude of cervical motion in healthy human subjects.

METHODS

Ten healthy young adults (ages 18-24) were recruited to participate in this study. Subjects were fitted with a portable motion measurement device comprised of a data logger and two inclinometer arrays that measure angular displacements during flexion-extension (FE) and lateral bending (LB), and angular velocities during axial rotation (AR). Participants were instructed to wear the unit continuously over a 5-day period except during activities that may damage the unit (e.g. showering or contact sports). Subjects were required to document their day-to-day activities in a journal. Following the collection period, motion peaks about each axis were identified, and motion magnitude between two consecutive peaks was calculated with the frequency of motions within 5° increments determined. The average motion frequency was extrapolated to yield daily and yearly values of total neck motion, as well as that attributed to the C5-C6 level (18%, FE; 17%, LB; 10% AR) (White AA 1990). These results were then compared to the excursions recommended within ASTM standard F 2423-05, the current wear analysis protocol for intervertebral disc prostheses. Finally, subject journal logs were used to characterize the neck motion during specific tasks (e.g. athletics, travel, work, miscellaneous and sleeping).

RESULTS

The estimated annual motion distribution is shown in Figure 1. Estimates of the average daily/annual excursions are listed in Table 1 as are the estimates of the C5-C6 level contributions. The average motion peaks per hour are shown in Table 2.

DISCUSSION

Overall, FE movements were twice as frequent as movements along the other two axes with a median motion magnitude of 13°. The total number of movements per hour for all axes, regardless of amplitude, was highest during athletic activity and lowest during sleeping. The wear analysis protocol described in ASTM standard F2423-05 currently prescribes 10 million cycles at 24° excursions for both LB and axial-rotation and 10 million cycles at 30° excursions in flexion extension. Our data suggests that the current protocol is inadequate for FE and may need to be amended.

This study is unique because it is the first to attempt to quantify cervical motion using a continuous motion monitoring instrument. This allows for data collection during routine activities of daily living outside of a laboratory setting. The application of a continuous motion device would allow clinicians to survey and address factors such as movement avoidance in their assessment of patient disability and would also aid in their assessment of patient recovery following a surgical procedure.

SUMMARY

The results of this study provide a baseline of the frequency and magnitude of neck motion during normal activities of daily living for healthy young adults. These findings can assist physicians and physical therapists in identifying activities that will likely be problematic for patients with limited cervical motion.

REFERENCES

(2006). "Standard Guide for Functional, Kinematic, and Wear Assessment of Total Disc Prostheses." ASTM International.

White AA, P. M. (1990). Clinical Biomechanics of the Spine. Philadelphia.

Table 1: Mean (SD) daily and annual estimates of neck excursions (°) (x 10^6).

	Daily Excursion	Annual Excursion	ASTM F2423-05
FE			
total	0.92 (0.29)	335.6 (107.4)	-
C5-C6	0.17 (0.05)	60.4 (19.3)	30
LB			
total	0.30 (0.10)	108.8 (35.1)	-
C5-C6	0.05 (0.02)	18.5 (5.9)	24
AR			
total	0.46 (0.15)	167.0 (55.4)	-
C5-C6	0.05 (0.02)	17.0(5.5)	24

Table 2: Mean (SD) motion peaks per hour for each of the 5 primary activities of daily living (x 10^2)

	FE	LB	AR
Athletics	84.9 (75.4)	46.2 (47.4)	34.2 (26.1)
Travel	61.1 (51.2)	23.4 (18.5)	21.8 (15.2)
Work	33.1 (16.5)	15.2 (5.9)	16.4 (5.0)
Misc.	30.2 (21.0)	13.3 (8.8)	14.2 (7.9)
Sleeping	2.4 (2.1)	0.9 (0.8)	1.3 (0.8)
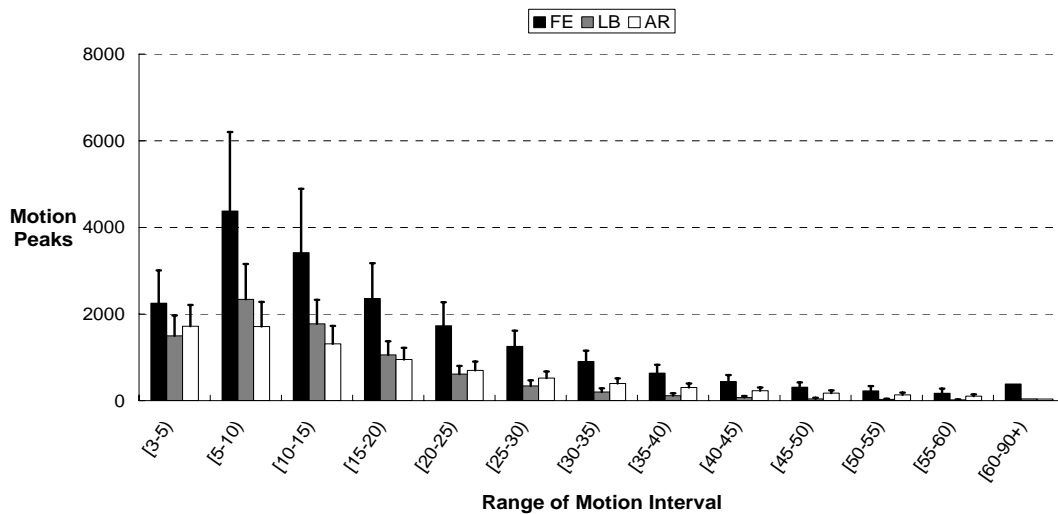
Figure1: Annual frequency estimates for each axis of motion. Values are distributed within the range of motion interval reflective of the corresponding motion magnitude. (x 10^3)

A NEURO-MUSCOLOSKELETAL MODEL FOR TESTING BIPEDAL LOCOMOTOR CONTROL HYPOTHESES

Jeremy W. Noble and Stephen D. Prentice
University of Waterloo, Waterloo, ON, Canada
E-mail: jwnoble@uwaterloo.ca

INTRODUCTION

Recently, neuro-mechanical simulations of animal and human locomotion have been used to gain insight into various aspects of locomotor control that cannot be assessed with traditional experimental techniques (Pearson et al, 2006). These simulations consist of models representing known neural control mechanisms interacting with a model of the musculoskeletal system, and all observation of the resulting movements. The majority of these simulations have used very basic musculoskeletal models, or non-human musculoskeletal models.

The goal of the present study is to define the characteristics of a human neuro-musculoskeletal model for testing hypotheses on the control of adaptive hypothesis locomotion. This model will improve on previous models, through the inclusion of a reasonable set of musculature including bi-articular muscles. The model will be tested by applying a reciprocal muscle activation pattern to flexor and extensor muscles present in the model, and the kinematic outputs of the model will be evaluated. A further goal of the present experiment was to determine whether this simple periodic neural input would result in a complex periodic kinematic pattern over several cycles.

METHODS

A two-dimensional mechanical model consists of 7 segments (2 Feet, 2 Legs, 2 Thighs and a Lumped Head, Arms and Trunk Segment (HAT)), resulting in 6 articulations (2 Hips, 2 Knees and 2 Ankles). Anthropometric data (length, mass and moment of inertia) were estimated from a 50th percentile male. Range of motion of the joints was limited by non-linear rotational springs at the joints, with data taken from human subjects (Silder et al, 2007). A ground contact model was implemented by placing a non-linear spring-damper under the heel and toe of each foot, a coulomb friction model was used to determine the ground reaction force in the horizontal direction. The model was implemented in Simulink, a component of MATAB (Mathworks Inc., Natwick MA). Equations of motion wither integrated forward in time with a variable step integrator with a tolerance of 10^{-5} rads or rads/s.

The joints in the model were actuated by nine musculo-tendonous units, there are six uniarticular muscles (Soleus, Tibalis Anterior, Vastus Group, Short Head of Biceps, Gluteus Maximus, Psoas Major), and three biarticular muscles (Gastrocnemius, Rectus Femoris and Hamstrings Group). Muscle forces were determined by a neural input, and subject to force-length (active and passive) and force-velocity effects. Joint moments were determined by multiplying these muscle forces by a constant moment arm. Neural input signals were subject to a first order delay to emulate excitation-contraction coupling.

For the purpose of testing the model, a simple neural input was used. The neural input consisted of a pulse input, alternating between the flexors and extensors, and applied only to the uniarticular muscles. The position of the HAT segment was held constant for testing purposes, as no balance controller is present in the model at this time.

RESULTS

A sample of the neural input provided to the model is shown in Figure 1. All of the neural inputs had a period of 1s, with a pulse width of 50% of the period. The amplitude of the pulse was 0.15 for the extensors, and 0.4 for the hip flexor, 0.01 for the knee flexor, and 0.5 for the ankle flexor.
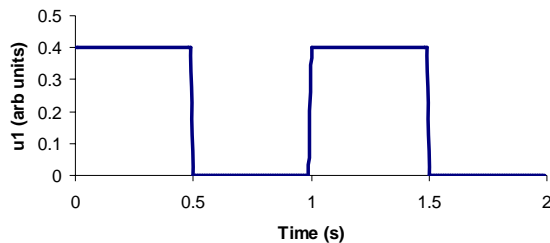
Figure 1: Sample neural input.

With the previously described neural input, the model was able to successfully simulate a periodic movement, with cyclical limb movements. A sample of the kinematic outputs is shown in Figure 2.

DISCUSSION

Although the model was able produce a complex periodic movement, there was some variability in the kinematics, from cycle to cycle. This is most likely due to the fact that no feedback mechanisms have been implemented in the model at this point. The model also had difficulty transitioning between stance and swing phases, which may be aided by the addition of feedback
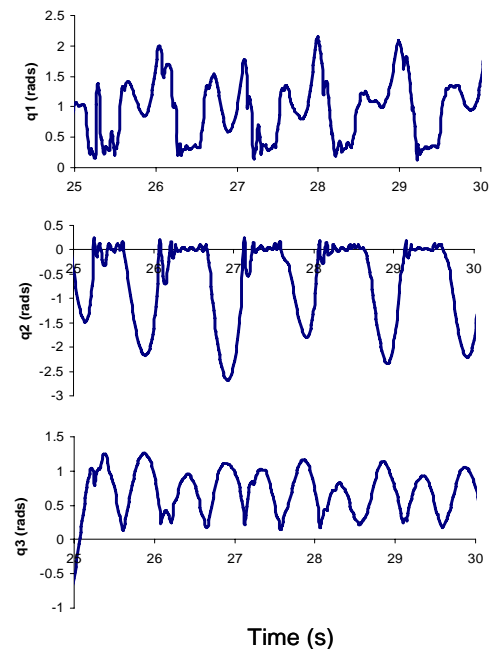
Figure 2: Kinematic variables vs. time, q1 is the right hip angle, q2 is the right knee angle, and q3 is the ankle angle.

mechanisms (Ekeberg & Pearson, 2005). A more realistic walking pattern may also be achieved by actively using the bi-articular muscles in the model. These muscles likely have an important role to re-distribute the segmental energy within the limb (Zajac, 2002).

This model appears to contain the necessary neural, muscular, and mechanical components to move forward with the creation of more complex neural models of locomotor control.

REFERENCES

Pearson, K.G. et al. (2006). *Trends Neurosci.* **29**, 625-631.
Ekeberg, O., Pearson, K.G. (2005). *J Neurophys.* **94,** 4256-4268.
Silder, A. et al. (2007). *J Biomech.* **40**, 2628-2635.
Zajac, F.E. (2002). *J Biomech.* **35**,1011-101.

GAIT AND BALANCE COMPARISIONS BETWEEN LEATHER AND RUBBER BOOTS IN PROFESSIONAL FIREFIGHTERS

Chip Wade[1], Ryan Garten[2], Scott Breloff [3], and Ed Acevedo[4]

[1]Department of Industrial and Systems Engineering, Auburn University, Auburn, AL, USA,
cwade1@auburn.edu
[2]Departments of Exercise and Sports Science, University of North Carolina Greensboro, Greensboro, NC, USA.
[3]Departments of Health and Exercise Science, University of Mississippi, Oxford, MS, USA.

[4]Departments of Health and Human Performance, Virginia Commonwealth University, Richmond, VA, USA.

INTRODUCTION

Firefighters are presented with numerous occupational challenges that elevate the risk of death and injury. The challenge of fighting fire is exacerbated by environmental hazards (i.e., working on roofs, in smoky places, and on slippery surfaces) and the use of protective equipment, including fire-protective clothing and a self-contained breathing apparatus (SCBA). The National Fire Protection Association estimates that 80,800 firefighter injuries occurred in the line of duty in 2002. Results by type of duty indicate that 37,860 or 46.9% of all firefighter injuries in 2002 occurred during fire-ground operations. Overexertion and strain (32%), and falls, slips, and jumps (25.9 %) were the leading causes of fire-ground injuries (Karter AND Molis, 2003). Unpredictable and rapidly changing work conditions, in association with high physical strain, require an alert postural control system for firefighters. In addition, lifting and carrying victims in rescue work demands continuous control of balance. Those tasks also necessitate the use of fire-protective clothing and equipment that increase challenge to the postural control system and might predispose the firefighter to postural instability (Kincl et. al. 2002).

A firefighter's boots play a critical role in working effectiveness and personal safety. The OSHA regulations and standards for appropriate foot and leg protection for fire brigades state that this must include either fully extended boots which provides protection for the legs or protective shoes or boots worn in combination with protective trousers. Firefighters use two types of boots that meet these requirements, a rubber boot and a leather boot. An argument can be made that although the rubber boot may provide greater protection from chemical hazards, the leather boot provides greater tactile sensitivity. This sensitivity may be important in maintaining balance and limiting falls.

The purpose of this study is to examine differences in balance and gait in professional firefighters wearing rubber and leather boots participating in a fire simulation activity.

METHODS AND PROCEDURES

Twelve professional firefighters (33 ± 6.8 years; height of 179 ± 6.47 cm; weight of 95.08 ± 21.47 kg), whom received, within the past 8 months a medical evaluation, including resting 12-lead EKG analysis, and clearance by a physician to participate in firefighting participated in this study. Each firefighter participated in two identical testing sessions [leather (5.37 ± 0.45 lbs) and rubber boots (6.45 ± 0.53 lbs)] on two separate days.

During each session, firefighters performed 2 sets of a three minute simulated firefighter stair climb wearing a 50 lb weighted vest to simulate their typical personal protective equipment, two 12.5 lb weights on the shoulders to simulate the weight of a high-rise pack (hose bundle), and a Helen Hayes marker set (motion capture retro-reflective markers). The 12.5 lb weights were only worn during the stair climbs.

On each condition day (leather, rubber) the firefighter conducted 10 gait trials (6-M2-camera VICON system 460 at 120 Hz), followed by a balance assessment (Sensory Organization Test: Equitest, NeuroCom) consisting of 6 sensory conditions: eyes open/closed, fix/sway referenced visual scene, fix/sway referenced surface. Dependent measures for gait included stride length (SL), stride width (SW), step period (SP), and walking velocity (V); dependent measures for balance was sway velocity. Following the initial gait and balance protocol, the firefighter conducted a Simulated Firefighter Stair Climb (The Fire Service Joint Labor Management Wellness/Fitness Initiative - Candidate Physical Ability Test, 1999) for 3 minutes at a rate of 60 steps per/min. At the completion of the stair climb, the firefighter repeated the gait and balance procedure. Following a 3 minute rest period, the complete procedure (gait, balance, stair climb) was repeated. A total of 3 gait and balance procedures and 2 stair climbs were completed.

RESULTS

A series of repeated measures ANOVA analyses revealed a statistically significant between boots difference(s) for all balance (Figure 1.) and gait measures (Table 1.).
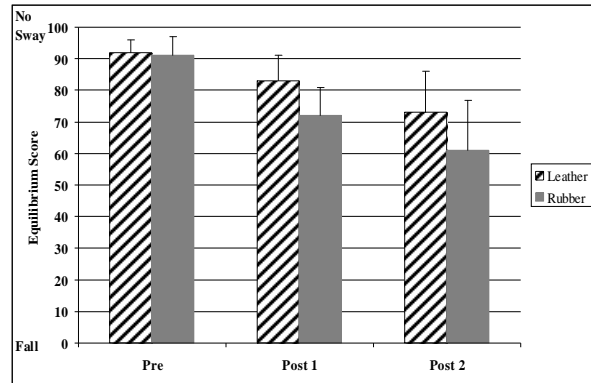
Figure 1. Ensemble average (100 = least sway velocity, 0 = Fall) of each of the 6 sensory conditions

DISCUSSION

In general, while postural stability degrades over both dynamic balance conditions, the results suggested that the leather boots contributed less to the degradation than that of the rubber. These findings have practical implications in the firefighting occupation when developing a safety and personal protective strategy. The implications lead to an assumption that given the varying degrees of advantages and disadvantages of each type of boot, the leather boot provides a stability advantage.

REFERENCES

Karter MJ. and Molis JL. (2003). NFPA Journal, Nov/Dec, 66-67.

Kincl et al. (2002). *Applied Occupational & Environmental Hygiene*, 17, 4, 256-266.

Table 1. Stride length, stride width, step period, and walking velocity, normalized by height, for each boot type.

	Leather			Rubber		
	Pre	Post 1	Post 2	Pre	Post 1	Post 2
SL(m/ht)	.54±.01	.48±.01	0.45±.01	.52±.01	.43±.01	.36±.02
SW(cm)	90±.44	10.2±.18	11±.32	10.3±.18	11.2±.31	12.1±.32
SP(s)	.68±.01	.63±.01	.56±.02	.66±.01	.46±.01	.38±.01
V(m/s)	.78±.02	.75±.02	.61±.02	.76±.01	.63±.02	.58±.01

ASSOCIATION BETWEEN 30SEC MAXIMAL TETHERED SWIMMING AND SWIMMING PERFORMANCE IN FRONT CRAWL

Pedro Morouço[1,2,3], Susana Soares[1], J. Paulo Vilas-Boas[1,3] and Ricardo Fernandes[1,3]

[1]Faculty of Sports, University of Porto, Portugal
[2]School of Education, Polytechnic Institute of Leiria, Portugal, pmorouco@esel.ipleiria.pt
[3]Portuguese Swimming Federation
URL: http://www.spormor.com

INTRODUCTION

Tethered swimming has been in use for long in order to measure and evaluate swimmers propulsive force (Magel, 1970; Yeater et al., 1981). Besides being a valid and reliable test (Dopsaj et al., 2003 and Kjendlie & Thorsvald, 2006) its relationship with performance in swimming is questioned (Smith et al., 2002), mainly because changes of arm and hand action seem to occur (Maglischo & Maglischo, 1984). Gathering these factors, studies developed with elite swimmers are required. The aim of the present study was to analyze the relationship among forces and velocity produced by elite swimmers in tethered and free swimming.

METHODS AND PROCEDURES

Sample included elements of the Portuguese national swimming team: (i) Group 1 – 6 swimmers with an age range of 18 to 21 years and (ii) Group 2 – 13 swimmers with 14 to 17 years. Basic descriptive characteristics were: (i) Group 1 – high = 179.3±12.1cm; body mass = 73.6±6.2kg; (ii) Group 2 – high = 171.3±9.1cm; body mass = 60.6±10.9kg. After a 1200m warm-up each subject performed a 30sec maximum intensity crawl tethered swimming. Individual force to time - F(t) - curves were obtained with swimmers attached by a non-elastic cable to a strain-gauge system (Globus, Italy). The load cell had a data cable connected to a PC computer that uses a data acquisition system – Ergometer Globus. SPSS v15.0 was used in order to obtain average pulling force in 30sec (AvgF), average maximum peak force (MaxF), average minimum force (MinF) and average of MaxF minus MinF ($Ran_{max-min}$). 24 hours later, the same swimmers performed a normal swimming test. Group 1 did a 50m maximum freestyle and Group 2 a 200m one. Both distances were covered in a long course pool. Time was registered in order to calculate average velocity of the 50meters (V50m) and of the 200meters (V200m).

RESULTS

Table 1 includes basic descriptive and inferential statistic results showing the differences obtained between groups. As expected, older swimmers (Group 1) got higher values for all variables calculated. However no statistical difference was obtained in $Ran_{max-min}$.

Variable	Group 1 (n=6)	Group 2 (n=13)
AvgF (N)**	121.7 (13.7)	61.4 (22.8)
MaxF (N)*	257.4 (33.9)	194.8 (66.2)
MinF (N)*	159.2 (26.8)	110.6 (38.1)
$Ran_{max-min}$ (N)	98.2 (22.1)	84.1 (32,1)
V50m (ms^{-1})	1.86 (.07)	-
V200m (ms^{-1})	-	1.47 (.10)

Table 1. Mean and standard deviation of each variable studied. **represents $p<.01$ and *$p<.05$

In Table 2 the correlation values obtained within studied variables according to Pearson product moment can be observed. Only positive correlations were found meaning that increasing variables correspond to improved performances.

	AvgF	MaxF	MinF	Ran$_{max-min}$
MaxF	.87**			
MinF	.87**	.94**		
Ran$_{max-min}$	.68**	.87**	.64**	
V50m	.93**	.81*	.47	.69
V200m	.94**	.93**	.82**	.94**

Table 2. Correlations obtained among parameters. **represents p<.01 and *p<.05

DISCUSSION

In the present study, differences between groups were obtained for AvgF (p<.01), MaxF and MinF (p<.05), meaning that older swimmers present higher strength producing capacity in tethered swimming. As expected, mean velocity of the 50meters freestyle was superior to the 200meters one. Statistical significant differences weren't found in the Ran$_{max-min}$, indicating that the decrease shown in strength curves is similar within groups. As referred earlier, AvF is highly correlated with all variables, getting higher values on V200m and V50m respectively (r=.94, r=.93). These results point out that mean force calculated in 30sec maximal tethered swimming can induce performance results for crawl stroke in short and middle distance events. D'Acquisto & Costill (1998) have shown high correlations for power and performance in 100 and 400yard events. However those data refers to breaststroke and evaluation were performed using partially tethered swimming. Another result to point out is the high correlation of Ran$_{max-min}$ with MaxF meaning that swimmers who reach higher peak forces aren't able to keep their pulling force values for so long. For each distance, there was a higher correlation for MaxF than for MinF, suggesting that the first half of the tethered swimming event is a stronger predictor than the second half. Obtained data seems to indicate the possibility of the mean force obtained through a 30 s fully tethered swimming test predict the mean velocity correspondent to a 50m front crawl (v = 0.004*tethered force + 1.331), and 200m front crawl (v = 0.004*tethered force + 1.208). In the near future we will focus on analyzing the slope obtained from MaxF point to MinF point.

SUMMARY

Association between AvF and mean velocity in 50m and 200m events was found. Tethered swimming seems to be a tool for results prediction in front crawl swimming.

REFERENCES

D'Acquisto, LJ and Costill, DL (1998). *J. Swim Res*, 13: 8-14.

Dopsaj M et al. (2003). *Physical education and Sport*, 1 (10): 11-12.

Kjendlie, PL and Thorsvald, K (2006). *Proceedings BMS X*, 231-233.

Magel JR (1970). *Res Q*, 41 (1): 68-74.

Maglischo, CW and Maglischo, EW (1984). *Proceedings ISBS: Sports Biomechanics*, 163-176.

Smith DJ at al. (2002). *Sports Med*, 32 (9): 539-554.

Yeater RA et al. (1981). *J Biomech*, 14 (8): 527-537.

A COMPARISON OF THE REPEATABILITY OF SUBMAXIMAL AND MAXIMAL METHODS COMMONLY EMPLOYED FOR NORMALIZATION OF THE ERECTOR SPINAE MUSCLES IN THE THORACIC AND LUMBAR REGION

Jennie A. Jackson[1], Niall V. O'Brien[2], Patrick G. Dempsey[2], Jack P. Callaghan[1]

[1]Department of Kinesiology, University of Waterloo, Waterloo, ON, Canada
ja2jacks@uwaterloo.ca
[2]Liberty Mutual Research Institute for Safety, Hopkinton, MA, USA

INTRODUCTION

In ergonomics research, work task EMG recordings are typically normalized to maximal voluntary exertions (MVE) or sub-maximal reference voluntary exertions (RVE). Currently, a wide range of normalization postures and efforts are utilized to normalize erector spinae (ES) EMG, however, little research has been done to quantify the repeatability of these different techniques. Further, the process of normalization introduces error to work task EMG data and there is little information on the magnitude of this error or the impact different normalization tasks may have on the interpretation of the dataset. The overall goal of this study was to examine the use of RVE and MVE tasks to normalize work task EMG data and to determine, quantitatively, how different normalization tasks may impact the interpretation of work tasks. The specific purpose for this portion of the study was to determine the repeatability of seven RVE and three MVE normalization tasks.

METHODS AND PROCEDURES

Fifteen male subjects aged 20 – 50 completed the three day study. Subjects had a mean age, height, weight and BMI of 32 (SD 11) years, 180 (SD 10) cm, 76.6 (SD 13.2) Kg and 25.1 (SD 3.5) Kg/m^2, respectively. On each day, subjects performed four repeats of ten normalization posture and effort combinations (Table 1). Postures were selected based on: repeated appearances in the literature; potential applicability to clinical populations; and postures corresponding to physiologically relevant events. Seated and prone tasks were conducted with subjects secured in a Biodex™ machine to standardize postures. Standing trial trunk flexion angles were set using a digital inclinometer. RVE trials were 10s long and MVEs were a 3s ramp and 2s maximal effort hold. EMG was collected bilaterally from the ES musculature at the level of thoracic vertebrae 9 (T9) and lumbar vertebrae 1 and 5 (L1, L5). EMG data was collected at 1024 Hz using a Noraxon TeleMyo2400T system. EMG data were then high passed filtered at 30Hz to remove heart rate (Drake et al., 2005) and linear enveloped (single low pass Butterworth filter at 2.5 Hz). For RVE trials, average EMG amplitude was calculated from seconds 3 – 8; for MVE trials the peak single value was recorded, as was a 1 second average around the peak single value. The coefficient of variation (CV) was calculated for all normalization tasks at each of the EMG sites and for both MVE processing methods to investigate repeatability.

Standing Trials		Seated Trials		Lying Trials
▪ 20˚ flexion	▪ 50˚ flexion	▪ Upright - 0˚ flexion	▪ 20˚ flexion	▪ Prone
- body wt only	- body wt only	- MVE	- MVE	- MVE
- 10 Kg wt	- 10 Kg wt – msd.	- 30% MVF	- 30% MVF	- Body weight only

Table 1: Summary of normalization trial postures and efforts. Msd = measured using a digital inclinometer; Est. = estimated using an angle marked on the wall behind the subject.

RESULTS

Results from the first seven subjects show CV values at all muscle sites for prone tasks at both submaximal and maximal levels were significantly lower than those for similar exertions in seated or standing postures (Table 2). EMG amplitudes at L1 and 5 were higher during prone MVE efforts than during any of the other tasks; T9 EMG was not consistently higher during any single task. EMG from levels L1 and 5 proved more repeatable (lower CV) than EMG at level T9 across all tasks. RVE tasks requiring higher muscle activation were more repeatable at trunk angles up to 20° flexion (ex. standing flexed at 20° holding 10 Kg had lower CV than 20° flexion with body weight); at 50° of trunk flexion, the opposite was true. RVE and MVE reliability values were similar for prone tasks. Interestingly, the repeatability of MVEs calculated using a single peak value was not significantly different from the repeatability of the corresponding MVEs calculated using the 1s average technique.

Trunk flexion angles calculated from digitized images during seated and prone trials showed similar variability of trunk angle deviation between trials for both postures: 1.7 – 2.0° for RVE trials and 2.3 – 3.3° for MVE trials.

DISCUSSION

The large range of CV values indicates normalization tasks are not all equally repeatable; task selection should be made accordingly. Arguments have been made that RVE or MVEs at multiple trunk angles should be used for normalizing dynamic work; preliminary findings from this study indicate this practice may induce varying error to the normalized dataset since the repeatability of normalization tasks varied by trunk angle. The difference in repeatability between sites along the ES muscles may be indicative of functional divisions along the length of the ES muscles, with preferential activation of lower level ES musculature during the extension efforts examined. Further study is required to determine a more repeatable normalization method for higher ES EMG recording sites.

SUMMARY

The repeatability of ten normalization methods was examined. Prone posture tasks proved the most repeatable at both sub-max and maximal efforts.

REFERENCES

Drake and Callaghan (2005). *J Electromyogr Kinesiol.* 16:175-87.

ACKNOWLEDGEMENTS

	RVEs								MVEs - 1 s avg			MVEs - max val		
	prone	sit_0	sit_20	st_20.10	st_20.bw	st_50.10	st_50.bw	st_50.eb	prone	sit_0	sit_20	prone	sit_0	sit_20
RT9	0.12	0.42	0.39	0.27	0.54	0.17	0.23	0.12	0.22	0.27	0.28	0.21	0.26	0.25
	(0.08)	(0.33)	(0.22)	(0.32)	(0.41)	(0.09)	(0.26)	(0.06)	(0.14)	(0.20)	(0.12)	(0.13)	(0.18)	(0.09)
RL1	0.07	0.31	0.16	0.14	0.26	0.15	0.10	0.18	0.09	0.18	0.17	0.09	0.18	0.17
	(0.04)	(0.29)	(0.11)	(0.11)	(0.27)	(0.13)	(0.07)	(0.30)	(0.05)	(0.09)	(0.10)	(0.05)	(0.09)	(0.07)
RL5	0.07	0.26	0.10	0.09	0.11	0.12	0.07	0.15	0.10	0.17	0.18	0.10	0.17	0.18
	(0.03)	(0.29)	(0.10)	(0.05)	(0.07)	(0.14)	(0.03)	(0.38)	(0.06)	(0.10)	(0.08)	(0.05)	(0.11)	(0.08)
LT9	0.14	0.56	0.43	0.28	0.62	0.16	0.28	0.15	0.21	0.30	0.28	0.21	0.29	0.25
	(0.09)	(0.44)	(0.24)	(0.27)	(0.61)	(0.11)	(0.28)	(0.11)	(0.09)	(0.16)	(0.13)	(0.08)	(0.15)	(0.11)
LL1	0.07	0.25	0.15	0.12	0.18	0.12	0.17	0.15	0.10	0.21	0.23	0.10	0.17	0.19
	(0.04)	(0.25)	(0.12)	(0.07)	(0.15)	(0.12)	(0.42)	(0.31)	(0.05)	(0.12)	(0.15)	(0.06)	(0.08)	(0.11)
LL5	0.07	0.23	0.08	0.08	0.11	0.16	0.14	0.14	0.11	0.18	0.16	0.12	0.19	0.14
	(0.04)	(0.33)	(0.04)	(0.05)	(0.07)	(0.32)	(0.42)	(0.37)	(0.05)	(0.13)	(0.06)	(0.06)	(0.11)	(0.07)

Table 2: Summary of CV values (± SD) for RVE and MVE normalization tasks. MVEs were calculated (i) as a 1 second average around the peak trial value (MVE – 1s avg) and (ii) as the peak trial value (MVEs – max val).

MEASUREMENT OF ELBOW MEDIAL ULNAR COLLATERAL LIGAMENT STRAIN: CHOICE OF REFERENCE LENGTH REDUCES INTERSPECIMEN VARIABILITY

Laurel Kuxhaus[1,2], Florian Thomines[4], Angela M. Flamm[1], Patrick J. Schimoler[1,3], Mandy L. Brogdon[1,3], Jeffrey S. Vipperman[1,2,3], Patrick J. DeMeo[1], and Mark Carl Miller[1,2,3]

[1]Orthopaedic Biomechanics Laboratory, Allegheny General Hospital, Pittsburgh, PA, USA
Departments of [2]Bioengineering and [3]Mechanical Engineering and Materials Science,
University of Pittsburgh, Pittsburgh, PA, USA
[4]Ecole Normale Superieure de Cachan, France
mcmiller@wpahs.org

INTRODUCTION

The medial ulnar collateral ligament (mUCL) of the elbow is an important stabilizer. It is of particular importance to fast motions such as baseball pitching. The anterior bundle of this ligament is composed of two bands, one anterior and one posterior. It has been suggested that the anterior and posterior bands of the anterior bundle behave in an opposing fashion, with the anterior band becoming taut in extension and the posterior band in flexion. (Callaway *et al.*, 1997) The strain in this ligament during elbow motions has not been quantified. The goal of this study was to measure the deformation in the anterior band of the anterior bundle of the mUCL and determine the best *in situ* reference length to be used in computation to permit meaningful comparisons of strain across different specimens.

METHODS AND PROCEDURES

Five cadaver specimens (4 left, 3 male, mean age 63.25 years) were used. The mUCL was carefully exposed and four circular markers were sutured to both the anterior and posterior bands of the anterior bundle. On each band, one marker was placed over the bony insertion sites on each end, and the remaining two markers were equispaced in the midsubstance. The elbow specimens were

actuated with an existing elbow simulator. (Kuxhaus *et al.*, 2005) Flexion movements were performed. A Peak5 camera system (ViconPeak, Oxford, UK) recorded the markers' movements and an inclinometer (X3Q, US Digital, Vancouver, WA) recorded the elbow's flexion angle.

Each movement with data collection was performed three times. After digitizing the optical data, custom MATLAB (The MathWorks, Natick, MA) software was used to calculate the strain between all pairs of markers for each band. Tensile strain was defined in its simplest form as the ratio of the length change to a reference length, or $\Delta L/L_0$, where L_0 is the reference length.

The choice of reference length was determined after each test. Initial computations used the length at set flexion angles across all specimens. These computations were performed from 50° to 130° of flexion. (One specimen was excluded from the 130° computation since it could not reach that position.) Additionally, a specimen-specific reference length (SSRL) was used for a final computation of strain. The length between two markers, when expressed as a function of flexion angle, displayed a cusp or inflection point demarcating a region with little change in length and a region with a greater slope. This

boundary point between these regions indicated a change in the load carried by the anterior band. The SSRL was chosen to be the length at this inflection point in the length-time plot, i.e., where a sharper change in slope was observed.

To compare the effects of the different reference lengths on the computation of strain, the variability across specimens was assessed using the standard deviation of the maximum computed strain for each reference length. The hypothesis is that use of the SSRL will yield the lowest variability.

RESULTS

The variability across all specimens is shown in Table 1. Note that the variability when using fixed-angle reference lengths is lowest at 80° of flexion. However, the variability when using the SSRL is markedly lower.

The strain results using the SSRL in computation are shown in Figure 1. Note the consistent trends across specimens: the strain decreases as flexion angle increases. Negative strain values indicate buckling of the ligament, and are an artifact of the optical methods used to track the ligament.

Table 1. Variability in maximum strain using different reference lengths.

Reference length:	Variability in Max. Strain
Length at 50°	0.097
Length at 60°	0.096
Length at 70°	0.092
Length at 80°	0.083
Length at 90°	0.094
Length at 100°	0.115
Length at 110°	0.158
Length at 120°	0.133
Length at 130°	0.086
SSRL	*0.034*
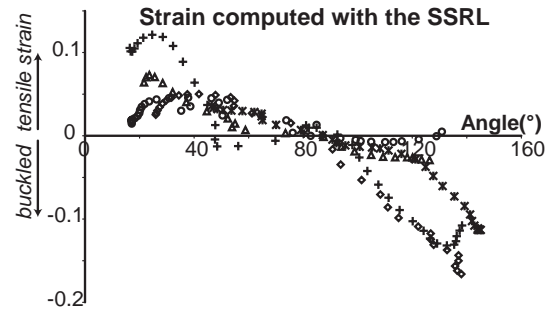
Figure 1. Anterior band strain as a function of flexion angle. Different symbols indicate different specimens.

DISCUSSION

The reduced variability across specimens shows the superiority of choosing the SSRL as the reference length as opposed to using the length at fixed angles across different specimens. This makes clinically-meaningful comparisons across specimens possible. The results presented here are only those from one pair of the four markers placed on the anterior band. Future work will analyze the results for the other marker pairs as well as for the posterior band.

SUMMARY

In summary, the movement of the anterior band of the mUCL was measured during flexion-extension motion. The variability in maximum strain was lowest using the SSRL, which makes physiologically-meaningful comparisons across specimens possible.

REFERENCES

Callaway *et al.* (1997). *J Bone Joint Surg.* 79A: 1223-1231.
Kuxhaus *et al.* (2005). *Amer Soc Biomech.*

MECAHNICAL LOADING OF IN SITU CHONDROCYTES IN THEIR NATIVE ENVIRONMENT

Sang-Kuy Han[1,2] and Walter Herzog[2,1]

[1]Department of Mechanical Engineering, University of Calgary, Calgary, AB, Canada,
shan@ucalgary.ca
[2]Human Performance Laboratory, Faculty of Kinesiology, University of Calgary, Calgary, AB, Canada. URL: http://www.kin.ucalgary.ca/hpl/

INTRODUCTION

Fifty percent of all people 60 years and older suffer from functional deficits related to joint problems. The proper functioning of joints is critically dependent on the health of the joint surface lining provided by articular cartilage. Chondrocytes, the living cells in articular cartilage, play a major role in maintaining cartilage healthy, as they synthesize the extracellular matrix. Furthermore, the mechanical environment is known to influence the biosynthetic activity of chondrocytes, and the relationship between cartilage loading and biosynthetic responses of the cells has been studied extensively (Choi et al., 2007; Clark et al., 2003; Guilak et al., 1995). However, because of technical limitations of conventional experimental approaches, it has not been possible to measure the mechanical responses of cells for dynamic loading conditions while fully embedded in cartilage that is attached to its native bone.

The purpose of this study was to measure the deformations behaviour of in situ chondrocytes within articular cartilage that was fully attached to its native bone.

METHODS AND PROCEDURES

In order to observe chondrocyte deformations in intact articular cartilage, we designed an indentation system that allows for microscopic imaging of chondrocytes through an indentor made of glass (diameter 1.64mm thickness 1.7mm: Mindrum Precision Inc., USA, : Figure.1). The indentation system was designed for mounting on the XY stage of a confocal microscope (Zeiss LSM 510, Carl Zeiss, Germany: Figure 1.a).

Experiments were performed with three fully intact patellae from mature New Zealand white rabbits. Dextran Alexa (3 kMW, 0.8 mg/ml, Dulbecco's Modified Eagle's Medium, Invitrogen, U.S.A.) was used to identify cells.

After 4 hours of staining at 4°C, cartilage samples were fixed in a specimen holder using dental cement and were immersed in a phosphate-buffered saline solution throughout testing (Figure 1b). A series of planar optical sections were recorded at a spacing of 0.5 μm per section. 1 and 2 MPa indentation loads were applied to the patella using a constant ramp speed (250 mV/s) and then kept constant until steady state (1200 s). The magnitude of the applied load was in the physiological range of rabbit patellofemoral joint loading (Clark, et al., 2004). A 60×0.7 N.A air objective (Olympus, Japan) was used to capture cell images corresponding to an image pixel size of $0.26 \times 0.26 \times 0.5$ μm. After testing, cartilage thickness was measured by needle indentation. Average local tissue strain was calculated by measuring the distance between identified cells in the loading direction. Six cells from

each sample were selected for cell morphology analysis.

RESULTS

1 and 2 MPa compressive loading of the cartilage surface resulted in an average compressive tissue strain of 15.3±1.3% and 32.1±10.3% respectively, and an average compressive local tissue strain in the superficial layer of 27.7±12.0% and 42.2±1.3%, respectively. At steady state, cell height decreased by 12.8±2.4% and 27.3±2.3%, and cell volume deceased by 13.9±6.8% and 19.5±4.9% for the 1 MPa and 2 MPa loading, respectively (Figure 2.).
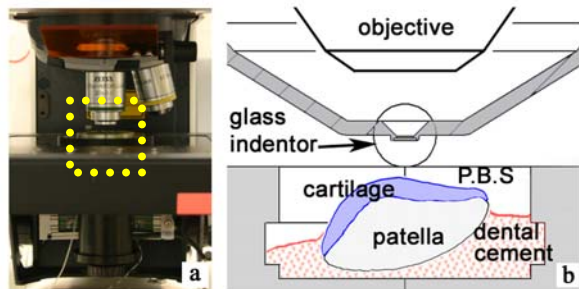
Figure 1: Custom-designed indentation system; a: indentation system on confocal microscope, b: schematic illustration for the area marked with the dashed line in a.
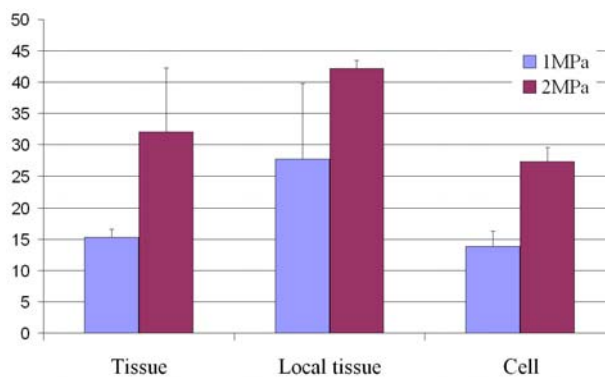
Figure 2: Tissue and cell morphology changes at steady state following loading.

DISCUSSION

The results of this study provide evidence that the superficial zone cartilage is softer than the average tissue, as the local tissue strains exceeded the global tissue strains for the applied indentation loads. However, cell deformations in the superficial zone were smaller than expected based on the superficial zone strains, suggesting that cells do not just deform in the same manner as the surrounding matrix. Rather it appears that cells are somehow protected from the rather large superficial zone tissue strains. Although it is not clear what might provide this protective effect, it has been speculated that the chondron, an organized structural tissue component surrounding chondrocytes might provide protection for cells in their native environment (Poole et al., 1987)

REFERENCES

Choi, J.B., et al., (2005) *Journal of Biomechanics*, 40:2596-603

Clark, A.L., et al., (2003). *Journal of Biomechanics*, 36: 553-568.

Clark, A.L., et al., (2004). *J. Musculoskel. Res.,* 8(1): 1-12.

Guilak, F. et al., (1995). *J. Orthop. Research,* 13: 410-421.

Poole, C.A., et al., (1987). *J. Orthop. Research,* 6: 509-522.

ACKNOWLEDGEMENTS

POSTURAL STABILITY IN INDIVIDUALS WITH NORMAL AND LOW BONE MINERAL DENSITY

Chip Wade[1], Andrea Johnson[2], Scott Breloff [2], and M. Allison Ford[2]

[1]Department of Industrial and Systems Engineering, Auburn University, Auburn, AL, USA,
cwade1@auburn.edu
[2]Departments of Health and Exercise Science, University of Mississippi, Oxford, MS, USA.

INTRODUCTION

Fractures resulting from a fall incident have been documented as a leading cause of traumatic injury in older adults in the United States. Nearly 90% of hip fractures result from the impact of a fall with an expected 6.25 million by 2050. However, little is known about the aging relationship between biomechanical variables associated with postural stability and low bone mineral density (BMD). The average annual risk of falling for an older adult over 65 years ranges from 30% to over 50%; meaning roughly one in three older adults fall each year (Tinetti et al., 1995). Furthermore, older adults over 75 years of age have almost three times the incidence of falls compared to older adults aged 60-75 years (Scuffham et al., 2003). The consequences of falls include injury, fear of falling, decreased activity, functional deterioration, social isolation, depression, reduced quality of life, institutionalization, and death. Nearly 90% of hip fractures result from the impact of a fall. In 1990, there were an estimated 1.66 million hip fractures worldwide, and the numbers are expected to escalate to 6.25 million by 2050 (Cooper et al., 1992). Even with the fracture of weak bone, some type of traumatic event is usually present. A fall of just a few feet may cause a fracture in a person with low bone density. Falling is as common as osteoporosis in the elderly. At least one fall per year occurs in 30 percent of persons 70 years of age or older. Thus, the incidence of falls in the elderly and associated outcomes and costs are evidence of

the imperative need to develop clinical/rehabilitation intervention programs that reduce the rate of fall accidents. The increasing incidence rate of falls among older adults compared to the rest of the population has motivated the extensive investigation of natural aging effects on the ability of maintaining balance. While, little is known about aging effects on biomechanical variables affected by low BMD, balance impairments have been identified in people with osteoporosis; specifically, a relationship between osteoporosis-associated postural changes. The purpose of this study was to investigate the balance performance characteristics of individuals without postural alignment issues, which may be unique to this population.

METHODS AND PROCEDURES

Two groups of participants were tested: 20 individuals with low BMD (osteopenia/osteoporosis) and 20 healthy, adults with normal BMD. Non-dominant femoral BMD was measured by a dual energy x-ray absorptiometer (DEXA). Following DEXA examination, participants completed a balance protocol consisting of the Sensory Organization Test (SOT) (Equitest, NeuroCom) experimental conditions utilized the sway-referencing capabilities of the platform to produce six conditions: standing w/ (1) eyes open and (2) eyes closed with the platform and visual surroundings stable, (3) with the platform stable, eyes open with the visual surroundings sway referenced, (4)

standing on the platform sway referenced w/ eyes open, (5) standing on the platform sway referenced w/ eyes closed, and (6) standing on the platform, eyes open, with the platform and visual surrounding sway referenced. Each trial last 60 seconds, with CoP being recorded at a sampling rate of 50 Hz. One minute of seated rest was provided between trials to minimize fatigue effects. A total of 3 trials per condition were performed in random order, resulting in 18 total trials. Data were analyzed using a within participants ANOVA with repeated measures ($p \leq .05$), with follow up univariate comparisons when warranted by significant main effects.

RESULTS

Compared to participants with normal BMD, participants with low BMD had significantly greater sway measures in all of the six sensory organization test conditions ($p = .031$, .027, .04, .037, .022, .038, respectively) (Figure 1). Participants in both groups demonstrated improvement on the second test relative to the first, a result indicating a learning or practice effect. In addition, the results suggested the Low BMD group relied more on a hip strategy for stability, while the Normal BMD group elicited a more consistent ankle strategy for stabilization.
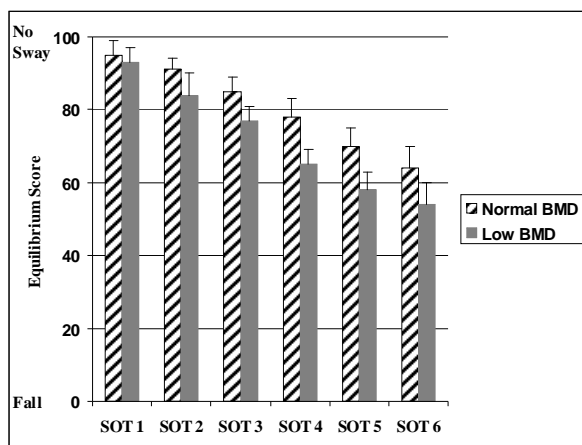
Figure 1. SOT between group comparisons.

DISCUSSION

These differences indicate a corollary relationship between balance characteristics and bone mineral density. Furthermore, the results may be important for both clinical and research studies in examining the correlation between a biomechanical mechanism and BMD. Previous research has described balance characteristics of patients with osteoporosis, particularly those with alignment issues (kyphosis), as having unique balance features that may destabilize them during activities of daily living. Previous research has suggested that the increased reliance, of individuals with Low BMD, on hip strategies may have resulted from the flexed posture, shifting the body's center of gravity closer to the limits of stability. The current findings suggest that the postural alignment issues are not the only contributing factor in instability in this population. Consequently, the current results have implications for additional rehabilitation techniques when addressing the populations fall risk. The results warrant additional research into the neuromuscular and biomechanical mechanisms of postural control in individuals with low BMD.

REFERENCES

Tinetti et al. (1995). *J Amer Ger Soc*, 43, 1214-21.

Scuffham et al. (2003). *J Epi and Com Health*, 57, 740-4.

Cooper et al. (1992). *Osteo Int*, 2, 285-9.

A 3-D KINEMATIC COMPARISON BETWEEN SINGLE-BELT AND SPLIT-BELT TREADMILL WALKING

Allison Altman BS,[1] Michael Pohl PhD,[1] Joaquin Barrios DPT, and Irene Davis PT PhD[1,2]

[1] Department of Physical Therapy, University of Delaware, aaltman@udel.edu
[2] Drayer Physical Therapy, Hummelstown, PA.

INTRODUCTION

Walking mechanics are often studied using a treadmill as one can collect multiple, consecutive steps in a small volume. Instrumented treadmills designed for walking studies have two belts, each associated with an independent force plate. These belts can either be arranged front to back or side-by-side (split-belt configuration). Altman et al, (2008) reported that base of gait widens by 4 cm when walking on a split-belt treadmill. This may lead to alterations of joint kinematics, particularly in the frontal plane.

Therefore, the purpose of this study was: a) to compare gait kinematics between single-belt and split-belt treadmill walking; and b) to determine whether split-belt kinematics are altered following an accommodation period. We hypothesized that there will be an interaction between belt configuration and time. Specifically, the rearfoot will be less everted (EV), the knee will be less adducted (ADD), and the hip will be less ADD in the split-belt condition. However, we anticipated that the split-belt mechanics would become more similar to the single-belt mechanics over the accommodation period.

METHODS AND PROCEDURES

Sixteen healthy subjects, experienced with treadmill walking, were recruited for the study (28 ± 9.3 yrs). A split-belt instrumented treadmill (AMTI, Watertown, MA) with one wide belt (0.66 m) and one narrow belt (0.33 m) was used in this study. Subjects warmed up on the single-belt for 3 minutes at a self-selected speed. Kinematic data were collected at 200 Hz using an 8-camera motion analysis system (VICON, Oxford, England).

Five stance phases were collected while subjects walked at 1.3 m/s. Baseline mechanics for the single-belt were then collected at 0 minutes (T0). Data were collected again following 10 minutes (T10) of walking. Subjects then rested for 5 minutes. Following the rest, the subjects repeated the walking protocol with one foot landing on each belt (split-belt) for 10 minutes. Data were again collected at T0 and T10.

3D angles at the hip, knee, and rearfoot were calculated using Visual 3D (C-Motion, Rockville, MD) and customized software (LabVIEW, National Instruments, Austin, TX). Peak angles during the first 75% of stance were calculated for each belt condition and at T0 and T10. The frontal plane angles of the hip, knee and rearfoot were compared statistically using a two-way, repeated measures ANOVA (belt x time) ($p < 0.05$). Results for the sagittal and transverse planes were analyzed descriptively.

RESULTS

Surprisingly, no belt x time interactions were noted. However, main effects were found for both belt and time (Figure 1). Rearfoot EV ($p = 0.03$) and knee ADD ($p = 0.05$) were lower by 1.5 and 1.2 degrees respectively, in the split-belt condition. In general, these differences were noted throughout stance (Figure 2). No differences were noted at the hip between belt conditions. Overall, frontal plane angles at the rearfoot and knee did not

change with time. However, hip ADD did increase (1.2 º) over time across conditions (*p* = 0.03).
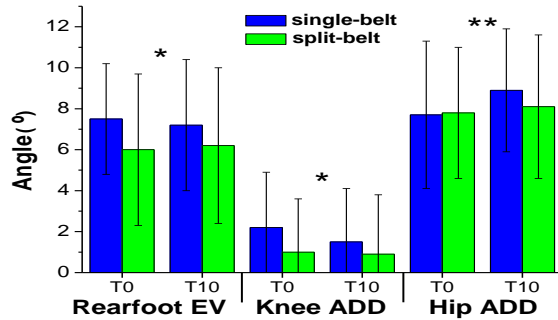
Figure 1. Mean (SD) peak angles in frontal plane in first 75% of stance. * significant belt effects, ** significant time effects.
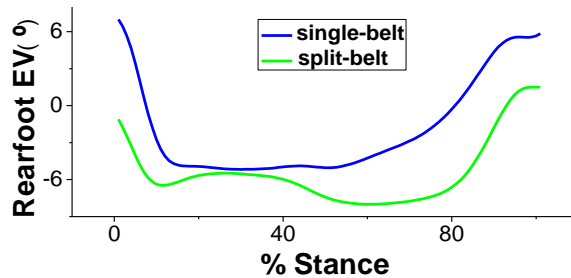
Figure 2. Mean rearfoot EV from one subject over stance. Note the offset between the belt conditions.

For the other planes of motion, the differences in peak angle were small across belts and time (Table 1).

Table 1. Mean (SD) peak angles in sagittal and transverse plane during the first 75% stance.

	T0		T10	
	single	*split*	*single*	*split*
Rearft DF (+)	11.6 (3.9)	11.8 (2.8)	11.7 (2.8)	12.2 (3.3)
Rearft ABD (-)	-10.4 (4.4)	-10.2 (4.4)	-10.0 (4.6)	-11.2 (7.8)
Knee FL (-)	-15.6 (5.8)	-15.2 (5.8)	-16.2 (6.5)	-16.0 (6.3)
Knee IR (+)	8.2 (11.8)	8.6 (12.0)	8.9 (12.8)	10.7 (15.7)
Hip FL (+)	22.0 (6.1)	21.8 (6.1)	21.7 (6.0)	22.1 (6.0)
Hip IR (+)	-2.1 (11.6)	-2.4 (11.2)	-2.6 (11.1)	-2.8 (11.7)

DISCUSSION

As split-belt treadmills become more common, it is important to understand the effects they may have on mechanics, and

whether these effects are lessened with accommodation time. The results show that there were no interactions between time and belt configuration. This is mostly due to the lack of change over time in the split-belt configuration. These results are consistent with Zeni et al. (2008) who found no significant kinematic changes over 10 minutes on a split-belt treadmill. These findings indicate that either, subjects do not accommodate to the split-belt, or that more time is required.

The time effect for hip ADD resulted from the increased peak observed on the single-belt. We did not expect changes in single belt mechanics over time. However, it must be noted that this difference was only 1.2 degrees.

The same was true for the other frontal plane angles. The differences between peak angles in the split and single-belt configurations were less than two degrees. However, the total rearfoot eversion excursion is only eight degrees, indicating that a 1.2 degree difference can account for about 15% of the total excursion at the joint. In knee adduction, the total excursion is only five degrees, so a one degree change in peak angle is 20% of the joint excursion in the frontal plane. However, the clinical relevance of these differences is still questionable.

SUMMARY

Differences in the rearfoot and knee frontal plane movement were found in split-belt, compared to single-belt treadmill walking. These differences remained following a 10-minute accommodation period.

REFERENCES

Altman et al., (2008) ACSM National Conference (accepted abstract).
Zeni et al., (2008) *Gait Posture*, in review.

DO VESTIBULAR INPUTS TRIGGER UPPER BODY RESPONSES DURING A SLIP?

Kurt Beschorner[1], Mark S. Redfern[1], Peter N. Sandrian[1], and Rakie Cham[1]

[1] Human Movement and Balance Laboratory, Department of Bioengineering, University of Pittsburgh, keb52@pitt.edu
URL: http://hmbl.bioe.pitt.edu/

INTRODUCTION

After a slip is initiated, the body attempts to regain balance by generating postural responses at the knee, hip and shoulder (Cham and Redfern, 2002; Sandrian and Cham, 2007). Shoulder responses are of particular interest because previous research has indicated that the arm is used to brace the body for a fall during a severe slip, but moves the arm in the opposite direction in an effort to recover from a non-severe slip (Sandrian and Cham, 2007). However, it is not known what triggers these complex and rapid arm responses. We hypothesize that vestibular inputs sense the fall and trigger these responses.

The purpose of this study is to explore the association between changes in vertical head acceleration, which would be sensed by the vestibular system, and shoulder reaction moment onset time.

METHODS AND PROCEDURES

A total of 31 healthy subjects (13 older and 18 young) were recruited to take part in the study. Written informed consent was obtained prior to enrolment. Four subjects were not included in the analysis due to technical or testing problems. Subjects performed 2-5 baseline walking trials and then were unexpectedly slipped with a liquid glycerol contaminant. Subjects were harnessed to prevent injury. An eight-camera motion analysis system recorded whole body motion via a 79 marker set.

Shoulder moments and head acceleration were calculated from marker data. Shoulder moments were calculated by performing a distal to proximal inverse dynamics method from the hands up to the shoulders. Segment masses and moments of inertia were determined as per (de Leva, 1996). Head motion was tracked by generating a virtual head center of mass trajectory based on 4 markers placed on the head. Head marker data was filtered using a 2nd order butterworth filter with cutoff frequency of 10 Hz and then was twice differentiated via a 3-point method.

The two primary variables were the time of negative vertical head acceleration and the time of shoulder flexion moment deviation from baseline non-slip trials. Head acceleration time was determined to potentially result in a vestibular queue when vertical head acceleration switched from positive (up) to negative head acceleration (down). This time point, time of head acceleration direction change (THADC) was chosen as a measure of deviation from normal walking during the slip. In addition, the THADC was required to deviate from baseline dry walking trials. If THADC did not deviate from baseline walking, the trial was excluded. This measure therefore resulted in a time at which the fall could be sensed by the vestibular system. To determine shoulder moment reaction times, the flexion moment ipsilateral to the slip was analyzed. The ipsilateral flexion moment was chosen because its magnitude correlated best with slip severity (Sandrian and Cham, 2007).

Shoulder reaction time was identified as the time when the moment during the slip trial differed from the dry trials by 3 standard deviations. Standard deviations were calculated from the difference of the slip and dry trial for 0.5 sec before heel contact. When no shoulder reaction or very late reaction moments were found, the trials were not analyzed. A mixed model ANOVA was run with subject as a random effect; THADC, slip severity and THADC-slip severity interaction as the fixed effects on shoulder reaction time.

RESULTS

The timing of head acceleration direction change (THADC) was significantly correlated with shoulder reaction time ($p<0.05$). (Figure 1) The slope of the regression line is 0.84. The intercept of the line is 0.104 s, which is significantly different from 0 ($p<0.05$) On average, the THADC occurred 116 ms after heel contact, and the moment generation reaction time was 204 ms after heel contact. Slip severity did not significantly influence the relationship.
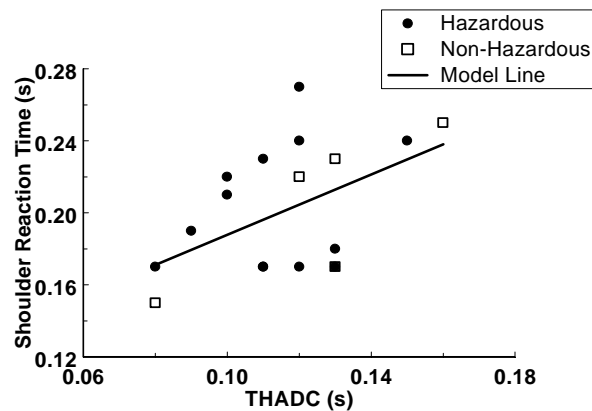
Figure 1. Shoulder reaction time plotted against THADC shows a positive correlation.

DISCUSSION AND SUMMARY

This study suggests that the vestibular system may play a role in sensing the fall and initiating the upper body postural response to a slip. The ANOVA further supports the claim. For example, if an upper body postural response only occurred after receiving vestibular input, the slope of the line between vestibular input time and reaction time would be 1. Our analyses revealed the slope of the line was near to that value. Furthermore, the intercept of the line, which would represent the time for signal processing, decision making, signal transition time and muscle activation, is 104 ms. Because of the proximity of the vestibular system, neural processing center and shoulder, a reaction in 104 ms is reasonable.

One limitation of this study was the measure of head acceleration and shoulder reactions. Future studies will include accelerometers to get more accurate acceleration profiles and shoulder EMG's for improved quantification of shoulder reaction onset.

REFERENCES

Cham, R. and Redfern, M.S., 2001, *J Biomech* 34, 1439-45.
deLeva, P., 1996, *J Biomech* 29, 1223-30.
Sandrian, P.N. and Cham, R., 2007, *Human Factors Ergo Society.*

ACKNOWLEDGEMENTS

CO-ACTIVATION DIFFERENCES IN LOWER LIMB MUSCLES BETWEEN ASYMPTOMATIC CONTROLS AND THOSE WITH VARYING DEGREES OF KNEE OSTEOARTHRITIS DURING WALKING

Cheryl Hubley-Kozey[1,2] , Nicholas Hill[2], Derek Rutherford[2] and William Stanish[3]

[1]School of Physiotherapy, Dalhousie University, Halifax, NS, Canada, clk@dal.ca
[2]School of Biomedical Engineering, Dalhousie University, Halifax, NS, Canada
[3]Department of Surgery, Dalhousie University, Halifax, NS, Canada.

INTRODUCTION

Increased muscle co-activation during gait has been identified as a neuromuscular alteration associated with knee osteoarthritis (OA). Lewek *et al.* 2004 reported higher co-activation indices during initial stance in those with medial compartment OA. A high degree of co-activity among muscle sites, based on principal component analysis (PCA), has also been found in those with severe knee OA (Hubley-Kozey *et al.*, 2008). While differences have been noted between controls and individuals with OA, levels of co-activation among varying degrees of OA has not been established. Muscle activation characteristics could be a valuable adjunct in the diagnostic classification of those with knee OA given the poor association between radiographic scores and symptoms (Creamer *et al.* 2000).

The purpose of this study was to determine if differences in co-activation could be detected among asymptomatic (ASYM) controls, those with moderate OA (MOA) and those with severe OA (SOA) using i) a co-activation index (CCI) during the initial phase of the gait cycle and ii) PCA.

METHODS AND PROCEDURES

Sixty three ASYM, 59 MOA and 48 SOA participated. The study was approved by the Institutional Ethics Board. Assignment to MOA and SOA was based on both radiographic and functional assessments. After standard skin preparation, surface electrodes (Meditrace[TM] Graphics Control) were placed in a bipolar configuration over the vastus lateralis (VL) and medialis (VM),), lateral (LH) and medial hamstring (MH) and lateral (LG) and medial (MG) gastrocnemius muscles of the affected leg for OA groups and a randomly selected leg for ASYM. Subjects walked at their self-selected walking velocity along a 6 meter walkway while electromyographic (EMG) signals were amplified (Bortec[TM]) and digitally converted at 1000Hz. The raw signals were bias adjusted, full-wave rectified then low-pass filtered (Butterworth 6Hz recursive). The EMG waveforms were amplitude normalized to MVIC and time normalized to the gait cycle. First CCIs were calculated for the initial stance phase using the method of Lewek *et al.* 2004. Then waveforms from all participants for all muscles formed a matrix (101 by 1190) that was entered into a principal component analysis model (Hubley-Kozey *et al.*, 2008). Differences between the co-activation indices were tested among groups using a Kruskal-Wallis test. A mixed model ANOVA (group, muscle) tested for differences in the principal component score. Post hoc analyses were performed on significant results ($\alpha=0.05$).

RESULTS

Demographic data are in Table 1. There was a significant group effect ($p<0.05$) for all four CCIs. ASYM was less than SOA for all CCIs, but only different from MOA for VLLH. MOA was significantly lower than

SOA for all CCIs except VMMH. The waveforms for the VL and LH muscle sites and the CCIs are in Figure 1.

Variable	ASYM	MOA	SOA
Age (years)	49(10)	58(9)	64(8)
BMI	25 (4)	31 (5)	32(5)
Velocity (m/s)	1.37 (.1)	1.27 (0.2)	0.97(0.2)
KL score	--	2.47 (0.8)	3.2 (0.4)

Table 1. Subject Demographics. Means (SD).
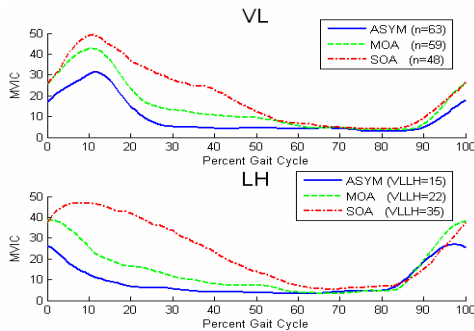
Figure 1: Waveforms with median CCI in brackets on lower graph.

Four principal patterns explained over 90% of the variance in the waveforms. PC1 (46% variance) captured the magnitude of the waveforms indicative of the relative level of activity over the stance phase (Figure 2a). ANOVA revealed a significant ($p < 0.05$) group by muscle interaction for PC1 scores (Figure 2b). Post hoc analyses showed that the MG was higher than all other muscle sites for the ASYM whereas no significant muscle differences were found for MOA. Two vasti and LH were higher for the SOA. Significant differences were found between the ASYM and OA groups as well as between the two OA groups (Figure 2b).

DISCUSSION

CCIs for the ASYM group are similar to those reported in the literature (Lewek *et al.* 2004). There are no CCIs reported for MOA and SOA groups separately and the values in the present study are different from Lewek's findings. The only CCI difference among all three groups was VLLH (Figure 1), resulting from increased VL and LH activity with increased disease severity. PC1 shape is similar to that reported for severe OA (Hubley-Kozey *et al.*, 2008). The group by muscle interaction captured variation in strategies unique to each group. Key features include the VM working at higher %MVIC for the SOA perhaps to stabilize the medial compartment. The higher LH and VL activity in both OA groups aimed to unload the medial compartment and differential recruitment of MG in ASYM.
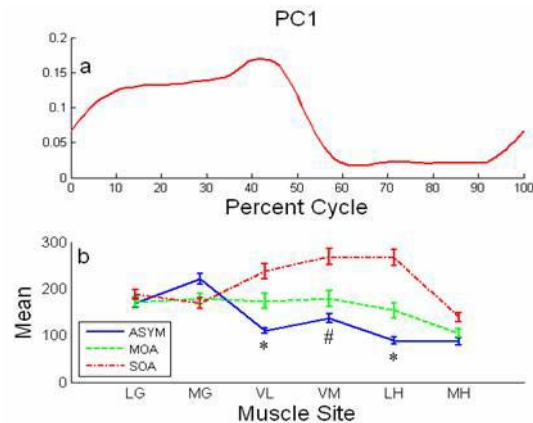
Figure 2: a) PC1 and b) interaction plot of Mean (SEM) PC1 scores. (* all groups different, # ASYM=MOA< SOA α=0.05)

SUMMARY

Both CCI and PCA captured differences in co-activity patterns among the three groups and most importantly, between the two OA groups. These findings suggest that measures of muscle co-activity provide valuable information related to severity of knee OA.

REFERENCES

Creamer *et al.* (2000)
   Rheumatology 39, 490-496.
Lewek M.D *et al.* (2004)
   Osteoarthritis Cartilage **12**, 745-751.
Hubley-Kozey *et al.* (2008)
   Clin Biomech 23, 71-80.

ACKNOWLEDGEMENTS

CAN THINKING BE HAZARDOUS TO YOUR BALANCE? THE EFFECTS OF COGNITION ON POSTURAL STABILITY IN OLDER ADULTS.

Jeffrey M. Haddad[1], Winona Snapp-Childs[2], Richard E. A. Van Emmerik[3] and Matthew Davidson[4]

[1]Department of Health and Kinesiology, Purdue University, West Lafayette, IN, USA,
jmhaddad@purdue.edu
[2]Department of Psychology, Indiana University, Bloomington, IN, USA.
[3]Department of Kinesiology, University of Massachusetts, Amherst, MA, USA.
[4]Department of Psychology, University of Massachusetts, Amherst, MA, USA.

INTRODUCTION

Older individuals are often prone to falls as they perform routine activities of daily life (i.e. reaching for an item or walking around clutter in the home). To address this issue, there has recently been an increase in research examining how older individuals control posture as they are engaged in some other activity. Since most activities of daily life require some degree of cognition, many of these studies have examined how individuals control posture as they are concurrently performing some other cognitive task.

In both older and younger adults, research has shown that the magnitude of postural sway does change when people perform a concurrent cognitive task (Woollacott & Shumway-Cook, 2002). However, exactly how posture changes appears to be a matter of debate. For example, Swan et al. (2004) found that in older adults, as the cognitive difficulty of a concurrent task increased, postural sway decreased. Consequently, Woollacott & Shumway-Cook (2002) reported that older individuals tend to increase postural sway when performing a concurrent cognitive task.

Additionally, changes in the magnitude of sway while performing a cognitive task are often believed to reflect changes in overall postural stability (Woollacott & Shumway-Cook, 2002). However, recent research on postural control has demonstrated the importance of spatiotemporal measures in relation to the stability boundary at the base of support for assessing postural stability (Haddad et al. 2006).

The purpose of this study was to examine changes in posture using spatial and stability boundary (time-to-contact) measures of postural sway as younger and older individuals performed a cognitive task that systematically increased in difficulty.

METHODS AND PROCEDURES

A group of older adults (N=6; 65-80 yrs) and younger adults (N=12; 18-30 yrs) stood on a force plate facing a computer monitor while holding a button under each thumb. Subjects performed five blocks of trials: SIMPLE (Ss pressed the right button whenever a letter appeared in the center of the screen); CHOICE (Ss pressed the left button when an 'A' appeared and the right button when a 'B' appeared in the center of the screen); WHAT and WHERE (letters were presented laterally on the screen, and the auditory cues 'what' or 'where' sounded before the display of each letter. In the what trials, Ss pressed the left or right button when the letter 'A' or 'B' appeared respectively. In the where trials, Ss pressed the button corresponding to the location of the displayed letter); TASK-SWITCHING (the

'what' and 'where' games were mixed together and letter presentation was either congruent or incongruent). Center of pressure (the anterior-posterior range) and virtual time-to-contact (VtC) data were analyzed according to the procedures in Haddad et al. (2006).

RESULTS
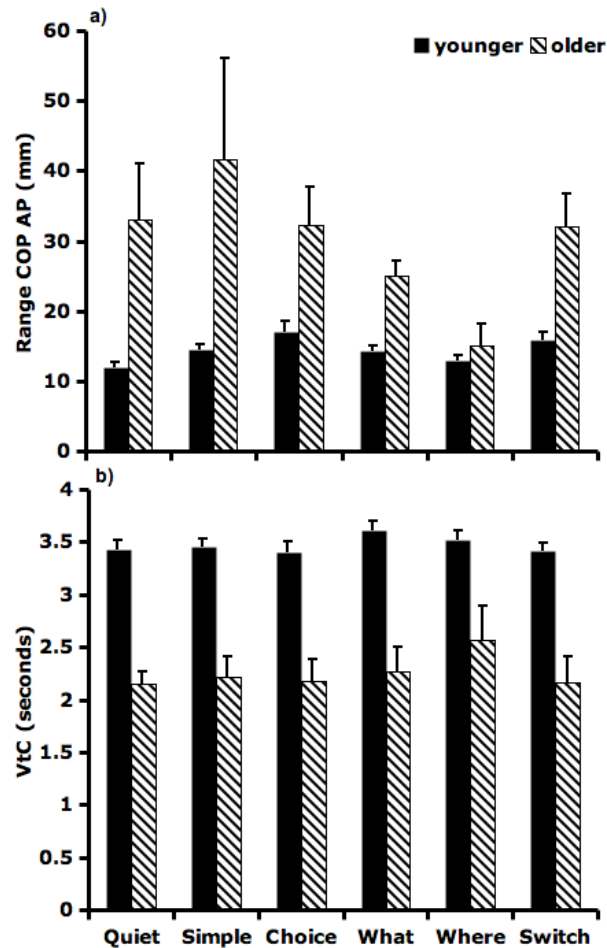
Figure 1. a) The anterior-posterior (AP) range and b) the virtual time to contact (VtC) of the center of pressure (COP).

In the young subjects, the range of the COP in the AP direction did not change across conditions.   However, the older subjects tended to exhibit a U-shaped function, where, sway decreased from low (SIMPLE) to moderate cognitive loads and then increased at high cognitive loads (TASK SWITCH condition). The young subjects maintained a longer time to the stability boundary compared to the older subjects. However, VtC remained constant in both groups between conditions.

DISCUSSION

Two main conclusions can be drawn from this research. 1) In older individuals, the U-shaped function in postural sway with increases in cognitive load can explain some of the differences in past studies. Specifically, based on these findings, studies that used easy cognitive tasks would have obtained different results compared to studies that used difficult cognitive tasks. This U-shaped function also agrees with recent data from Huxhold et al. (2006). 2) Although individuals change the magnitude (AP range) of sway during a cognitive task, a constant temporal margin to the stability boundary is maintained. This may suggest that in both older and younger subjects overall postural stability is maintained despite increases in cognitive load.

SUMMARY

Based on traditional postural measures we observed differential responses to task difficulty. The VtC results however indicate that changes in postural sway (at least in this postural task) have no consequences for postural stability. Therefore, performing a concurrent cognitive task does not appear to influence overall postural stability.

REFERENCES

Haddad JM et al. (2006). *J App Biomech,* 22:155-161.
Huxhold O et al. (2006). *Brain Res Bull,* 69:294-305.
Woollacott M and Shumway-Cook A (2002). *Gait Posture,* 16:1-14.
Swan L et al. (2004). *Brit J Psych,* 95:31-40.

GENDER COMPARISONS BETWEEN UNILATERAL AND BILATERAL LANDINGS

Joshua Weinhandl, Mukta Joshi, and Kristian O'Connor

University of Wisconsin-Milwaukee, Milwaukee, WI, USA
E-mail: weinhan2@uwm.edu   Web: www.chs.uwm.edu/neuromechanics

INTRODUCTION

Approximately 70% of all ACL injuries are caused by non-contact mechanisms and the ACL injury rates in females have been reported to be 4-6 times greater than males competing in the same sports (Hewett et al., 2005). Boden et al. (2000) suggested that ACL injuries occur more commonly during unilateral landings rather than bilateral landings, typically during deceleration, lateral pivoting, or landing tasks that are often associated with high external knee joint loads.

Although ACL injuries can occur during unilateral and bilateral landings, Pappas et al. (2007) suggested that the observed kinematic difference in unilateral landings increased injury risk. They attributed this to a decreased base of support and increased demand on the lower extremity musculature to absorb the impact. However, they did not report any kinetic measures, and all subjects performed landings from a 40 cm height. Conversely, landings from a height equal to individuals' maximum jumping ability may more closely simulate reality. Therefore, the purpose of this study was to determine whether females and males utilize different landing strategies (kinematic and kinetic) during unilateral and bilateral landings from a height equal to their individual jumping abilities.

METHODS AND PROCEDURES

Nine males and eleven females participated in this study. All were recreationally active and free from musculoskeletal injury. Each subject was asked to perform unilateral and bilateral drop landings from a box height equal to their maximum jump height. Five trials of each task were recorded.

Three-dimensional kinematic data were collected using a seven-camera Motion Analysis Eagle system (200 Hz), and force data were collected with an AMTI force platform (1000 Hz). Three-dimensional joint kinematics and kinetics were calculated, touchdown angles, range of motion (ROM), peak moments, and joint work were extracted for each plane. The peak moment and joint work parameters were normalized by body mass*body height*√landing height. A repeated measures ANOVA was performed for each dependent variable ($p < 0.05$).

RESULTS AND DISCUSSION

There was a significant interaction between task and gender for hip adduction angle at touchdown. Subjects exhibited increased abduction during unilateral landings in order to shift their center of mass over the stance leg and prevent pelvic drop to the contralateral side. However, it was unclear why males exhibited a greater increase in hip abduction than females during unilateral landings. At the knee, subjects performed unilateral landings with significantly less knee flexion at touchdown and subsequent ROM (Figure 1). These findings were consistent with Pappas et al. (2007) who suggested that a more extended knee during unilateral landings may be a compensatory mechanism to more effectively utilize the quadriceps in absorbing the impact of landing. Unilateral landings were also characterized by decreased knee

abduction at touchdown, and subsequent ROM. Thus, there is an apparent attempt to increase stability by limiting motion at the knee, which may increase injury risk during an unbalance landing (Decker et al., 2003).
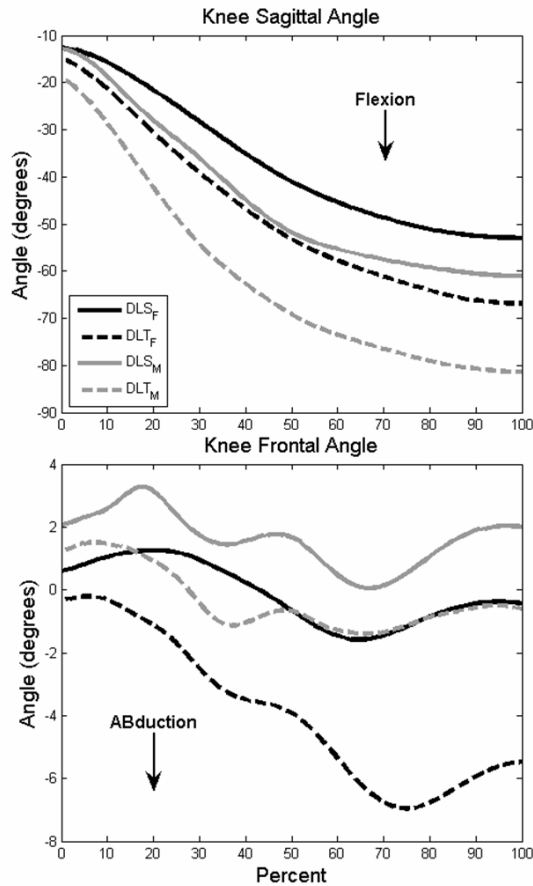
Figure 1. Mean knee flexion and adduction angles for males (grey) and females (black) single (solid) and two leg (dashed) landings.

Analysis of the sagittal plane joint work (Figure 2) revealed a significant task by gender interaction for sagittal ankle work. During bilateral landings females performed more work (36%) than males (28%). However, during unilateral landings males and females performed similar amounts of work at the ankle (males 44%, females 45%). This increase in ankle work during unilateral landings was accompanied by a significant decrease in knee work by both males (-10%) and females (-13%). At the hip, males

exhibited a 6% decrease while females exhibited a 4% increase in sagittal plane work. However, this difference was not statistically significant.
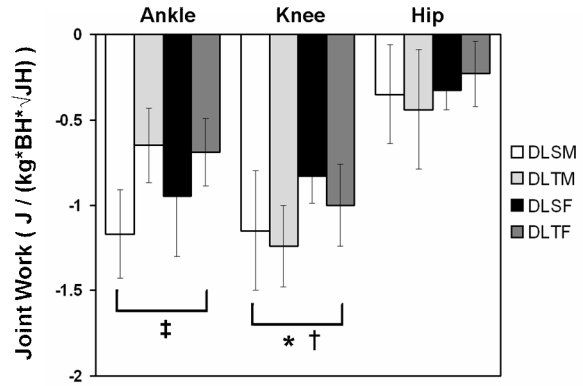
Figure 2. Mean sagittal plane joint work. [†]indicates significant gender difference. *indicates landing type difference. [‡]indicates significant interaction.

SUMMARY

Unilateral landings were characterized by significant differences in hip and knee kinematics that have been linked to increased injury risk (Boden et al., 2000; Hewett et al., 2005). The ankle musculature was utilized more for impact absorption during unilateral landing, which required increased joint extension at touchdown and may increase injury risk during an unbalanced landing.

REFERENCES

Boden et al. (2000). *Orthopedics,* 23:573-8.
Decker et al. (2003. *Clin Biomech,* 18:662-9
Hewett et al. (2005). *Am J Sport Med,* 33(4):492-501.
Pappas et al. (2007). *Clin J Sport Med,* 17(4):263-8.

ACKNOWLEDGEMENTS

MODELING TIME VARYING MOMENT PROFILES DETERMINED FROM AUTOMOTIVE ASSEMBLEY WORKERS USING A FIRST ORDER SYSTEM RESPONSE

Steven Fischer[1], Wayne Albert[2] and Jack P. Callaghan[1]

[1]Department of Kinesiology, University of Waterloo, Waterloo, ON, Canada,
sfischer@uwaterloo.ca
[2]Faculty of Kinesiology, University of New Brunswick, Fredericton, NB, Canada,

INTRODUCTION

The assessment of mechanical exposure has traditionally focused on either its amplitude or its duration. However, the important time varying pattern information is often disregarded (Wells et al. 2004) or lost due to difficulties in documenting these exposures. One of the difficulties with interpreting time varying load patterns is the lack of definitive relationships with injury mechanisms. Wells et al. (2004) argued that the best way to interpret external load with respect to internal tissue load, is to model exposure indices at the tissue level. Cumulative load, the area under the load time curve, is used as an index of exposure; however it lacks information about the tissue's response to a load. Krajcarski and Wells (2008) recently used a first order system response 'filtering' technique to predict the tissue time varying load profile from time varying mechanical exposure data. Their indices of tissue exposure lead to enhanced identification of low back pain (LBP) cases.

The purpose of this research was to determine if the peak or cumulative moment modeled using a first order system response to time varying flexion/extension net joint moment profiles were correlated with LBP as measured on a 10 point VAS score, when a net joint peak (NJPM) or cumulative moment (NJCM) measure examined previously were not correlated.

METHODS AND PROCEDURES

A sub-sample of 30 workers was selected from a database of automotive assembly jobs developed over the past 3 years. The jobs consisted of a wide range of postural requirements and loading demands. All original video and force data were input into 3DMatch (Callaghan 2003) a posture matching approach, to determine the L4/L5 lumbar spine flexion /extension moment profile for each video clip. All post processing from that point was done with custom designed software written in MATLAB© (Mathworks, MA, USA).
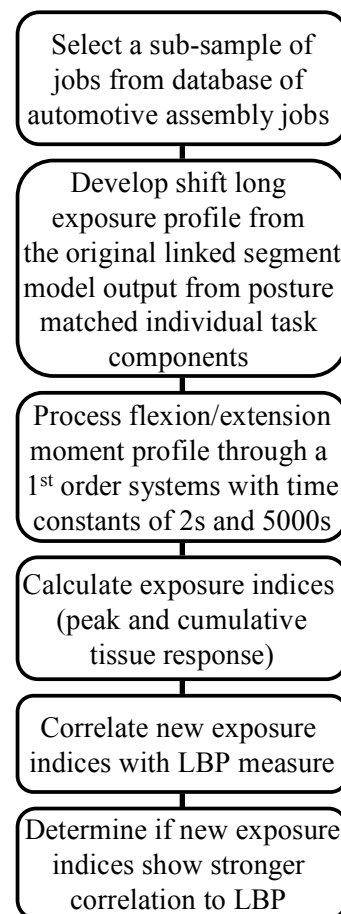
Figure 1 - Flow of Data Processing adopted from Krajcarski and Wells (2008).

The daily shift profile was created by concatenating moment profiles from individual tasks in the order in which they were completed by the worker. A modest flexion /extension moment of 5 Nm was assumed during all breaks, as there was no documentation of the workers postures and loads during their break time. Four exposure indices were calculated from the modeled response: a peak (PTR2) and cumulative (CTR2) tissue response using a time constant of 2s, and a peak (PTR5000) and cumulative (CTR5000) tissue response using a time constant of 5000s. Peak responses were determined as the maximum value occurring during the modeled shift profile, and cumulative tissue responses were calculated as the area under the modeled tissue response curve for the work shift. Pearson correlations were calculated between the two peak tissue responses and the two cumulative response with the LBP-VAS scores, using SPSS (SPSS, Illinois,USA).

RESULTS

The use of a modeled peak or cumulative tissue response exposure measure calculated using time constants of 2 or 5000 seconds did not result in a higher correlation with the LBP-VAS measure than the original NJPM or NJCM. Subjects were then categorized into two groups, LBP (VAS>0, n=18) or no LBP (VAS=0, n=12), and T-tests showed that neither peak or cumulative tissue responses, modeled at either time constant could distinguish between those with and those without LBP.

A subsequent analysis was run using only those 12 participants that reported some level of LBP. Correlations were again run between all of the modeled tissue response variables, net joint variables and LBP-VAS score within the subset of those with LBP. The CTR2 and CTR5000 were significantly correlated with LBP-VAS, where NJCM and all peak measures were not (Table 1).

Table 1- Correlations between LBP-VAS score and each of the exposure measures for a subset of 12 workers reporting LBP

Correlations with LBP-VAS	All	LBP Only
NJPM	-0.234	-0.322
PTR2	-0.240	0.022
PTR5000	-0.152	-0.080
NJCM	-0.121	0.225
CTR2	0.089	**0.710**
CTR5000	0.086	**0.669**

DISCUSSION

Although this modeling approach did not create exposure measures that could distinguish between those with and those without LBP in this population, the CTR did correlate with LBP-VAS. Those with LBP were more likely to report higher LBP-VAS scores if they sustained higher cumulative tissue response values. These findings suggest that the modeled tissue response does share some relationship with the level discomfort in those with LBP. More work is needed using a larger sample of data to determine if this relationship holds true, and to begin to parse out how the modeled response may be related to injury mechanics and the reporting of LBP.

SUMMARY

The use of a 1st order system to model the tissue response to a shift moment profile revealed a relationship with the magnitude of LBP in those reporting pain amongst a sample of automotive assembly workers yet failed to separate this group from pain free individuals.

REFERENCES

Callaghan JP et al. (2003). *Proceedings of the 2003 meeting of ACE*.
Krajkarski S & Wells R (2008). *TIES,* 9(1): 45-71.
Wells R, Van Eerd D & Hägg G (2004). *Scan J Work Environ Health*, 30:179-190.

REGULATION OF MECHANICAL ENERGY GENERATED DURING WALKING IN HEALTHY CHILDREN

Brian Umberger[1], Sam Augsburger[2], JoAnne Resig[2],
Donna Oeffinger[2], Robert Shapiro[3], & Chester Tylkowski[2]

[1]Dept. of Kinesiology, Univ. of Massachusetts, Amherst, MA, USA, umberger@kin.umass.edu
[2]Motion Analysis Laboratory, Shriners Hospital for Children, Lexington, KY, USA
[3]Dept. of Kinesiology & Health Promotion, Univ. of Kentucky, Lexington, KY, USA

INTRODUCTION

The generation and regulation of mechanical energy is a requirement for successful locomotion. Disruptions in the flow of energy throughout the body are believed to be a major factor contributing to the elevated metabolic cost of walking in children with gait disorders (Olney et al., 1987). Commonly used methods for investigating the energetics of gait, based on segment kinematics or joint kinetics, can be used to identify abnormal mechanical energy patterns. However, these techniques provide limited insight as the causes of the abnormal patterns. Newer segmental power techniques allow the energetic effects of each force or moment on every segment in the body to be determined (Fregly & Zajac, 1996). This should allow the causes of gait disorders to be better identified.

Our broader goal is to use segmental power analysis as a complement to traditional gait analysis procedures in the evaluation of children with gait pathology. As a first step in that direction, this project focused on developing a model for computing segmental powers during gait, and characterizing the powers in a group of healthy children.

MODEL DESCRIPTION

A three dimensional model of the whole body was developed that consisted of seven rigid segments representing the right and left foot, shank, and thigh, as well as a lumped head-arms-trunk (HAT) segment. The inertial properties of the HAT were determined using a second, static model that included separate segments representing the trunk, head, upper arms and lower arms (including the hands). During periods of ground contact, the feet were constrained to the ground at the center of pressure. The model was actuated by hip, knee, and ankle joint moments. During model development, we found that the minimum set of actuators necessary for the model to reproduce experimental kinematics was: hip flexion/extension, hip abduction/adduction, knee flexion/extension, and ankle dorsi/plantarflexion. The equations of motion for the model were generated using Autolev 4.1 and coded in Matlab[TM], along with routines for performing the segmental power analyses.

METHODS

Subjects included 33 normal healthy children aged 5-17 years, who were subdivided into young (5-7 yr, n=10), middle (8-11 yr, n=12), and older (12-17 yr, n=11) groups. Kinematic (60 Hz) and kinetic (960 Hz) data were collected as subjects walked along a 10 m walkway at their self-selected speed. Experimental data were processed using EvaRT 5.0 and OrthoTrak 6.3.4. The kinematic data were used to scale the model to each subject, and to configure the model at the start of the gait cycle. The experimental moments were then applied to the model one at a time, and the mechanical power of each segment was computed. This process was repeated for each sample ($\Delta t = 0.0167$ s) over the entire gait cycle.

RESULTS & DISCUSSION

The contribution of the right hip, knee, and ankle moments to the power of the HAT, thigh, shank, and foot are shown for a representative subject (male, 16 yr) in Fig. 1. The joint moments primarily served to transfer energy between the leg and HAT, with the ankle moment having an opposite energetic effect from the hip and knee moments over much of the gait cycle. These patterns were in general agreement with data from Siegel et al. (2004) for adults.

The results tended to be similar across age groups; however, there were some consistent age effects. For example, the thigh power due to the knee moment tended to be negative around 10% of the gait cycle for older children, while it was usually positive for
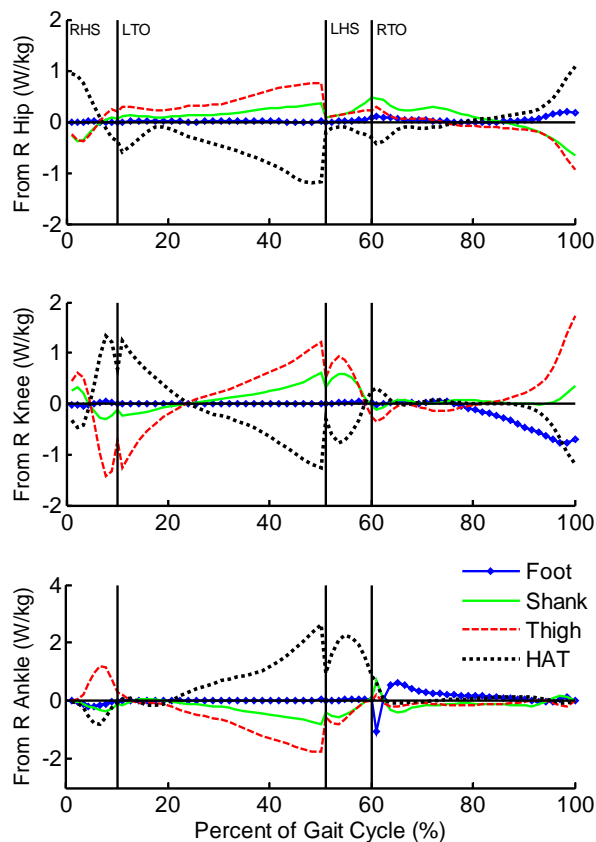
Figure 1. Segmental powers due to the right hip, knee, and ankle joint moments.
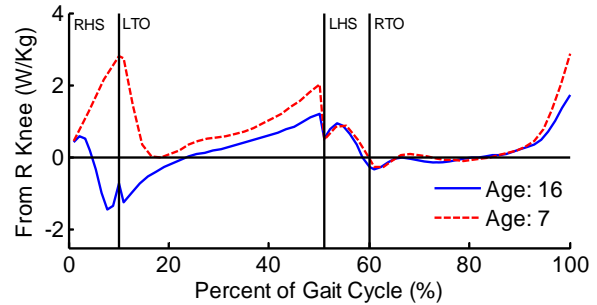
Figure 2. Thigh power due to the knee joint moment for two different aged subjects.

younger children (Fig. 2). This difference is due partly to the lack of a pronounced knee extensor moment in young children at this point in the gait cycle (Cupp et al., 1999).

SUMMARY

Regulation of mechanical energy during walking in healthy children was found to arise from the concerted actions of moments with opposite energetic effects, similar to what has been reported in adults. However, some differences were noted, which may reflect maturation of the gait pattern during development. Our future efforts will be focused on comparing results obtained in children with cerebral palsy to healthy children, as well as comparing data from pre- and post-surgical intervention.

REFERENCES

Cupp, T, et al. (1999). *J Ped Ortho,* 19:475-478.
Fregly, BJ & Zajac, FE (1996). *J Biomech,* 29:81-90.
Olney, SJ, et al. (1987). *Phys Ther,* 67:1348-1354.
Siegel, KL, et al. (2004). *Gait Post,* 19:69-75.

ACKNOWLEDGEMENTS

MUSCLE ACTIVITY IN VARIOUS OVERHEAD WORK POSTURES

Steven Fischer[1], Jaclyn Chopp[1] and Clark Dickerson[1]

[1]Department of Kinesiology, University of Waterloo, Waterloo, ON, Canada,
sfischer@uwaterloo.ca

INTRODUCTION

Overhead work, defined as working above shoulder height, has been linked to the development of upper extremity discomfort and disorders (Bernard et al., 1997). Further, in a study of autoworkers reporting shoulder pain, Punnett et al. (2000) found a strong association between shoulder abduction or flexion of greater than 90° and shoulder disorders. These and other studies suggest that working in an overhead posture contributes to the likelihood of work-related shoulder fatigue or pathology.

It is often difficult to eliminate these postures in industrial practice, however, and it remains uncertain as to which tasks require specific muscle contributions. This study examined overhead tasks to determine the relative importance of three factors:

- Work location angle from vertical
- Direction of applied hand force
- Subject-specific or generic work placement

METHODS AND PROCEDURES

Fourteen right-handed male volunteers with no history of shoulder pain participated in this study (age: 22.0 ± 2.0 years). Bipolar surface electrodes were placed over eleven muscle sites on the right side of the body (anterior, middle and posterior deltoid, upper and lower trapezius, biceps, triceps, pec major clavicular insertion and sternal insertions, infraspinatus and latissimus dorsi). Muscle activity was recorded using the Noraxon T2000 EMG system (Noraxon, Arizona, USA). The four overhead work angles tested were: -15°, 0°, 15° and 30° measured from the center of the

hips, with 0° being a hand position vertically above this center of the hips. At each location, participants applied and maintained a 5-second, 30N force in each of five randomly ordered directions: forward, back, up, down and medially. Force was measured using a multi axis transducer (MC3A, AMTI MA, USA) and visual force feedback was provided with custom LabVIEW software. (National Instruments, Texas, USA). The protocol was repeated twice: once with the force cube fixed at 120 cm above the floor along the work angles, and once where the force cube was placed along the defined angles at a distance equal to 75% of the combined magnitudes of torso length and arm length. Recorded muscle activity was linear enveloped and normalized to activation produced during maximal voluntary contractions (MVC). Three-second windows were used to calculate mean %MVC EMG levels for each muscle for each trial.

RESULTS

The direction of force application had the largest effect on muscle activation of the three factors studied. Pulling backward resulted in the highest activity, while pushing forward or downward resulted in the lowest level of muscle activity for several muscles (Table 1).

Work angle also influenced muscle activity for the anterior (Figure 1) and middle deltoid, and the upper and lower trapezius, but this effect depended on force application direction due to a significant interaction between these factors. The stature-based protocol resulted in slightly lower %MVC for all muscles compared to the fixed placement protocol, with decreases ranging from 0-3% MVC.

Table 1- Range of muscle activity measured during back, forward and downward force application directions in muscles significantly affected by direction of force application.

Muscle	Direction of Force Application	
	Back	Front/Down
Anterior Deltoid	17-31%	< 5%
Upper Trapezius	13-19%	< 5%
Lower Trapezius	5-15%	< 5%
Biceps	6-9%	< 5%
Infraspinatus	12-14%	< 5%
Middle Deltoid	8-12%	< 5%
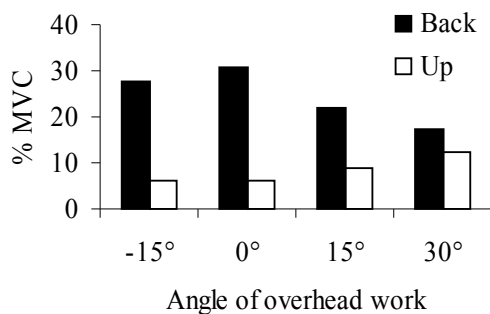
Figure 1 - Anterior deltoid muscle activity while pushing back or up at each work angle.

DISCUSSION

The direction of force application dominated the studied factors in determining the level of muscle activity associated with applying overhead force. This issue has received little attention in the past. The results of our study suggest that preferred force application directions exist and are dependant on the angle at which the overhead work occurs.

Anton et al. (2001) examined the influence of overhead work angle during upward drilling and found that working directly overhead rather in front of the body resulted in the lowest muscle activity. Our findings agree with these results, in that the lowest activation was measured at 0° for an upward force application. Wiker (1987), in contrast, demonstrated increased fatigue trends for more elevated postures in repeated simulated fastening tasks. In this study, the angle effect was not consistent for the various force application directions tested, indicating their central importance to overhead work. For example, as shown in Figure 1, when a backward force was applied, activity decreased as the work moved forward from directly overhead. Configuring overhead work to account for stature variability typically lowered muscle requirements, although this reduction was modest compared to the other studied factors. This argues for population scalability in work design, which has long been advocated by ergonomists.

SUMMARY

The level of muscle activity associated with overhead work tasks was affected by three factors, in descending order of influence:
- Direction of force application
- Angle of overhead work position
- Subject-based versus generic work design

The interaction between direction and angle has practical importance, as it suggests that these factors should be considered collectively in guiding workplace design decisions. Further, configuring overhead work designs to respect individual anthropometry may slightly reduce overall muscle load.

REFERENCES

Anton D et al. (2001). *Ergonomics* 44:489-501.

Bernard B et al. (1997).*NIOSH Pub No 97-141*. Cincinnati, OH.

Punnett L et al. (2000). *Scan J Work Environ Health* 26(4):283-291.

Wiker S et al. (1989). *Ergonomics* 32:211–237.

ACKNOWLEDGEMENTS

Prediction of Fracture Load and Initiation Location of Acetabular Fractures by means of Nonlinear FEM – a Feasibility Study

Peter Vaitl[1], Vickie Shim[2], Joerg Boehme[1], Roland Huelse[1], Ian Anderson[2] and Christoph Josten[1]

[1] Clinic for Trauma-, Plastic- and Reconstructive Surgery of the University of Leipzig, Germany
petervaitl@web.de, med02kmy@studserv.uni-leipzig.de
[2]Institute of Biomedical Engineering, University of Auckland, New Zealand

INTRODUCTION

Minimally invasive, computer navigated operation methods and fracture stabilising hip implants are a great challenge in today's acetabular surgery. The use of biomechanical tools like FE models therefore gains more and more valuability in order to provide methods for treatment and management options. Aim of the project was to create a FE model that can predict acetabular fracture location and fracture load and validate its performance by a mechanical experiment. Additionally two types of osteosynthesis were tested on stability against each other. On the one side conventional plate osteosynthesis, on the other side percutaneous acetabular screws.

METHODS AND PROCEDURES

Three sets of synthetic pelvis and femur models (Pacific Research Laboratory, WA, USA) were used to develop an experimental set-up for acetabular fracture testing. The loading condition was similar to the one described in Dalstra et al. (1995), which simulated a standing position. Each pelvis was positioned with the iliac crests fixed in acrylic cement. The matching femoral head was cut from the femoral neck and then attached to the crosshead of the Instron Machine (the 5800 series, Instron Ltd., Norwood, USA) (Fig. 1). To achieve more stable and better fit between the synthetic femoral head and the acetabulum, the femoral head was covered with liquid latex, a compliant material to obtain an effect similar to having a layer of cartilage. A vertically directed force was applied to the acetabulum until failure at a rate of 40N/s. Resulting fracture load and location were recorded.

The synthetic pelvis model was CT scanned and a FE model was generated using a previously validated FE mesh generation method (Shim et al. 2007). For mechanical simulations, we used finite deformation elasticity rather than linear elasticity. This required the use of full Green's strain tensors and a strain energy function in the governing equation. Although computationally more expensive, this setup allowed us to use any constitutive relations as well as nonlinear material behaviours, required in fracture analysis. Two materials – solid rigid polyurethane foam and cellular foam – were incorporated and their properties were obtained from the manufacturer. The latex layer was also modelled with properties obtained from the literature. The contact between the femoral head and the acetabulum was modeled using a contact mechanics penalty method involving Coulomb friction (μ=0.3). The same loading and boundary condition as the experiment were used and the FE model of the pelvis was also loaded with a vertical force in steps of 500N until failure is detected. To predict the fracture load of a femur, a factor of safety (FOS) for each gauss point was computed using the distortion energy theory of failure (Keyak et al. 1998). The fracture load and location were compared with experimental results.
The fractured pelvises were stabilized either

with 12 hole reconstruction plates or with single percutaneous screws. The pelvises were then loaded cyclic from 300N to 900N whereas the crack opening was detected optically.

RESULTS

The same experiment was repeated three times to check whether the result is consistent. All three pelves showed a very similar fracture patterns, that is posterior column fracture (Figure 1). The average fracture load was 3600N (3200-4000N). The FE models failed at a similar load (4000N) and the location where the fracture started was superior dome of the acetabulum, which closely matched the pattern of posterior column fracture (Figure 2).
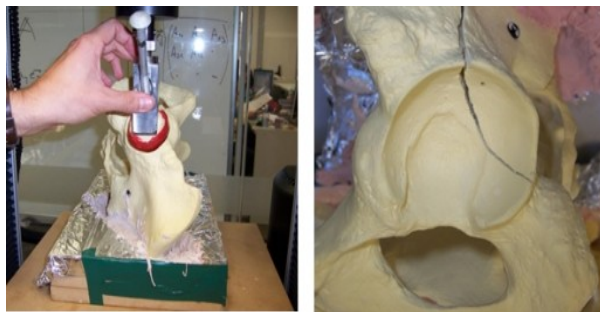
Figure 1. Left shows our experimental set-up. The red layer on the femoral head is the latex layer. Right shows the resulting posterior column fracture on one of the left hemipelvis.
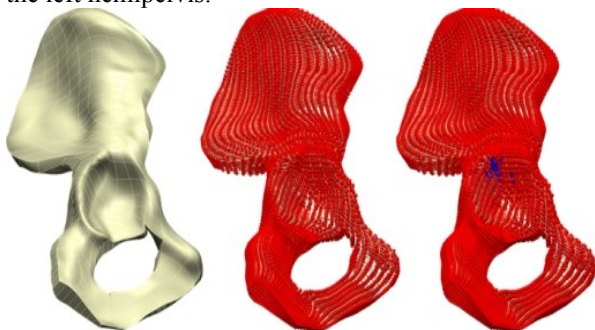
Figure 2: FE simulation results. The left is the initial mesh. The center shows the result at 2000N where no sign of fracture is present. The right shows the result at 4000N. Fracture is initiated at the superior dome of the acetabulum close to the area of posterior column fracture. The blue dots indicate the Gauss points that

have failed according to the FOS criterion.

Displacement in the plate fixation group was 0.11mm – 0.91mm, in the single screw group 0.21mm – 1.10mm respectively.
The plate osteosyntheses gave higher stability to the fractured pelves whereas the single screws gave also a high stability related to the low material use.

DISCUSSION

The current study demonstrated that non linear finite element models with finite deformation assumption can predict fracture load and fracture initiation location accurately. Although validated with synthetic bones, the agreement achieved between the experiment and FE simulation can be a good indicator for the usefulness of our model. Future works will involve biomechanical assessments of various treatment options for the acetabular fractures using the current model.
Moreover it could be shown, that single screw fixation in acetabular fracture can not only reduce collateral damage in surgery, but can also provide sufficient initial stability.

REFERENCES

Dalstra, M et al. *J Biomech Eng* 1995;117:272-278
Keyak, J. H. et al. *J Biomech, 1998* 31:125-133.
Shim, V.B., et al., *J Biomech*, 2007. 40(1): p. 26-35

LEVODOPA INFLUENCES THE REGULARITY OF THE ANKLE JOINT KINEMATICS IN INDIVIDUALS WITH PARKINSON'S DISEASE

Max J. Kurz[1], Ashley Hickerson[1], Chris Arellano[1], J. G. Gabriel Hou[2], and Eugene C. Lai[2]

[1] Laboratory of Integrated Physiology, Department of Health and Human Performance, University of Houston, Houston, TX, USA, mkurz@uh.edu
[2] Parkinson's Disease Research, Education & Clinical Center, Michael E. DeBakey VA Medical Center, Baylor College of Medicine, Houston, TX, USA

INTRODUCTION

Parkinson's disease (PD) is a progressive, degenerative neurological disease that results mainly from a loss of dopaminergic neurons in the substantia nigra. These nuclei, together with other related brain structures, compose the basal ganglia, which are largely attributed to controlling the amplitude and timing of movement patterns. The impairment of the basal ganglion functions appears to be the cause for the larger amount of stride-to-stride variability seen in PD patients (Schaafsma et al., 2003).

Levodopa is a metabolic precursor for dopamine, which is largely effective in improving motor symptoms in PD, including gait. It was demonstrated that levodopa therapy reduced the magnitude of the variations present in the stride time interval dynamics (Schaafsma et al., 2003). Most likely these changes resided in an improved regulation of the lower extremity joint kinematics. However, the influence of levodopa on the regularity of the structural variations found in the joint kinematics is largely unknown.

The purpose of this investigation was to explore the effect of levodopa on the regularity of the structural variations present in the lower extremity joint kinematics. We hypothesized that levodopa will reduce the variations of the lower extremity kinematics in PD patients.

METHODS

Eight participants with idiopathic PD walked on a treadmill for three minutes while "off" and then "on" their levodopa therapy. Characteristics of the participants are detailed in Table 1. All participants were initially assessed in the morning without taking their PD medications, including levodopa, for at least eight hours. Immediately after the walking on the treadmill while "off" levodopa, the participants took their morning dose of levodopa. We waited 45 minutes for the levodopa to be turned "on" before having the participant repeat the walking bout.

A six-camera motion capture system (200 Hz) was used to collect the right leg's ankle, knee and hip joint sagittal plane kinematics. Approximate entropy (ApEn) was used to assess the regularity of the structural variations present in the respective joint's angle kinematics (Pincus, 1981; Equation 1).

$$ApEn(m, r) = \ln\left(\frac{C_m(r)}{C_{m+1}(r)} \right) \quad \text{Equation 1.}$$

Table 1. Participants' characteristics.

Age (years)	76±6
Height (meters)	1.74±0.1
Weight (kg)	71.9±12
Walking Speed (m/s)	0.62+0.4
UPDRS III	28.6±4.6
Hoehen & Yahr Score	2.8±0.7

where $C_m(r)$ is the number of data points of length m that are similar, $C_{m+1}(r)$ is the number of data points of length m+1 that are similar, and r is the similarity criterion. For this investigation, m was 2 and r was 20% of the standard deviation of the time series (Pincus, 1991). A lower ApEn value indicates a greater regularity in the structural variations present in the joint kinematics.

We used a two factor repeated measures ANOVA (drug x joint) with a Tukey HSD post-hoc to evaluate the effect of levodopa on the regularity of the structural variations present in the joint kinematics. All statistical tests were performed at a 0.05 alpha level.

RESULTS AND DISCUSSION

Our analysis revealed that there was a significant joint-medication interactive effect ($F(2,14) = 6.74$; $p = 0.009$; Figure 1). Our post-hoc analysis indicated that the structural variations present in the ankle joint kinematics were more regular while being "on" levodopa ($p < 0.0001$). No significant differences in the regularity of the structural variations were found in the knee ($p > 0.05$) and hip ($p > 0.05$) joints' kinematics.

According to the above results, levodopa improves the Parkinsonian motor symptoms by regulating the performance of the ankle joint. We suggest that the changes previously noted in the magnitude of the stride-to-stride variations by levodopa may be related to the ankle joint's ability to regulate a consistent muscular performance (Schaafsma et al., 2003). This notion is supported by a previous investigation that demonstrated that individuals with PD have a decreased amount of ankle power at push-off if not taking levodopa (Morris et al., 1999). The perceived resistance of the knee and hip joints to levodopa may be related to
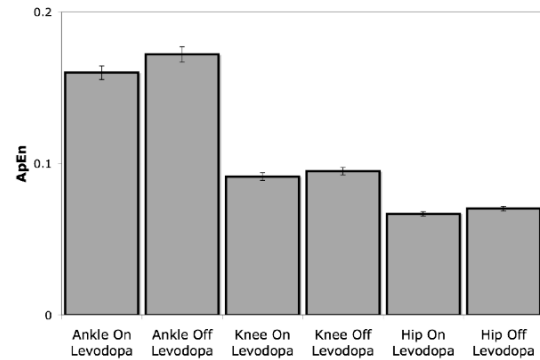
Figure 1. ApEn values for the respective joints while "on" and "off" levodopa.

the fact that our investigation was conducted on a treadmill. Potentially, the treadmill may have acted as an external cueing device that reduced the structural variations present in the knee and hip joint kinematics. This notion is partially supported by an investigation that found that the magnitude of the stride-to-stride variations is reduced when PD patients walk on a treadmill (Frenkel-Toledo et al., 2005).

SUMMARY

Levodopa influences the regularity of the structural variations present in the ankle joint kinematics of individuals with PD. We suggest that an impaired ability to regulate the ankle joint may be related to gait abnormalities in PD. Future investigations the variations present in the Parkinsonian gait pattern should account for the medicated state of the patient.

REFERENCES

Frenkel-Toledo et al. (2005). Mov Disord, 20:1109-1114.
Morris ME et al. (1999). J Hum Mov Sci, 18:461-83.
Pincus SM (1991). Proc Nat Acad Sci, 88:2297-2301.
Schaafsma JD et al. (2003). J Neuro Sci, 212:47-53.

A MR-COMPATIBLE LOADING DEVICE FOR DYNAMICALLY IMAGING SHORTENING AND LENGTHENING MUSCLE CONTRACTIONS

Christopher Westphal[1], Amy Silder[2], and Darryl Thelen[1,2]
Departments of [1]Mechanical and [2]Biomedical Engineering, University of Wisconsin-Madison
Madison, Wisconsin, USA. Email: thelen@engr.wisc.edu

INTRODUCTION

Dynamic magnetic resonance (MR) imaging is a powerful approach for characterizing in vivo muscle mechanics. For example, recent studies have used MR imaging to investigate the effects of surgery on muscle function (Asakawa et al. 2003), and to measure spatial strain distributions within contracting muscle (Zhou et al. 2007, Zhong et al. 2008). While providing valuable insights, the requirements of dynamic MR impose unique constraints on the motion and loading conditions that can be studied within the scanner. In particular, cine phase contrast (cine PC) imaging requires many motion cycles to characterize all pixel velocities within an image plane (Asakawa et al. 2003). Prior studies have addressed this challenge by using a device to guide repeatable flexion-extension motion against elastic loads (e.g. Pappas 2002). We have designed and built a MR compatible device that can impose either elastic or inertial loads on the hamstrings, which is important for distinguishing muscle mechanics during shortening and lengthening contractions. Our objective in this study was to use motion analysis to assess repeatability of movement performed with the device, and to characterize the muscle activities and joint moments induced.

METHODS AND PROCEDURES

The device is constructed of non-ferrous materials and designed to fit within the 60 cm diameter bore of a MR scanner. Subjects are positioned prone on a rigid platform with the knee aligned with the shaft of a leg support assembly. A large sprocket mounted on the knee shaft is chained to a loading assembly

mounted on the platform just distal to the foot (Figure 1). Inertia disks and/or stainless steel torsion springs can be mounted on the loading shaft. An overall gear ratio of 10:1 is achieved, such that the reflected inertia or stiffness felt at the knee is 100 times larger than that on the loading shaft.
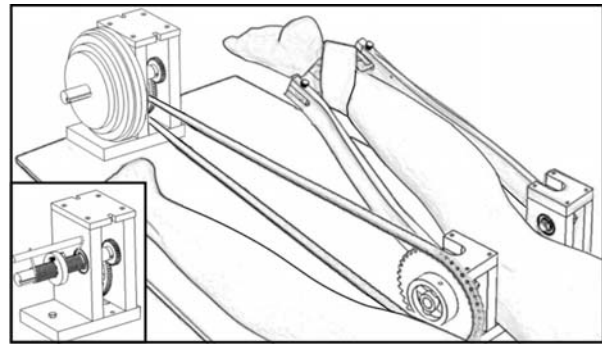
Figure 1. MR compatible loading device can be configured to impose either inertial or elastic loads (inset) on the knee.

Five limbs of three healthy young adults (age 26±3y) were tested. Each subject performed cyclic flexion-extension at 28 cycles per minute against both inertial and elastic loads (peak loads of ~15% maximum) for 90 sec. A semi-circular covering was used to emulate the physical constraints of an MR bore. Knee angle was measured using motion capture and chain tension was measured via load cells embedded in the chain. The net internal knee moment was computed using inverse dynamic analysis. Both medial and lateral hamstring EMG activity were simultaneously acquired to assess when the hamstrings were active within the flexion-extension cycle.

RESULTS

Peak knee flexion moments and hamstring activity occurred when the knee was flexed

under the elastic loading, and when the knee was extended under the inertial loading condition (Figure 2). The range of knee motion achieved varied from 24 to 29 deg, depending on the height of the subject. The standard deviation of peak knee angles and moments were ~1 deg and ~0.5 Nm, respectively, over 50 repeat cycles of motion under each loading condition (Table 1).
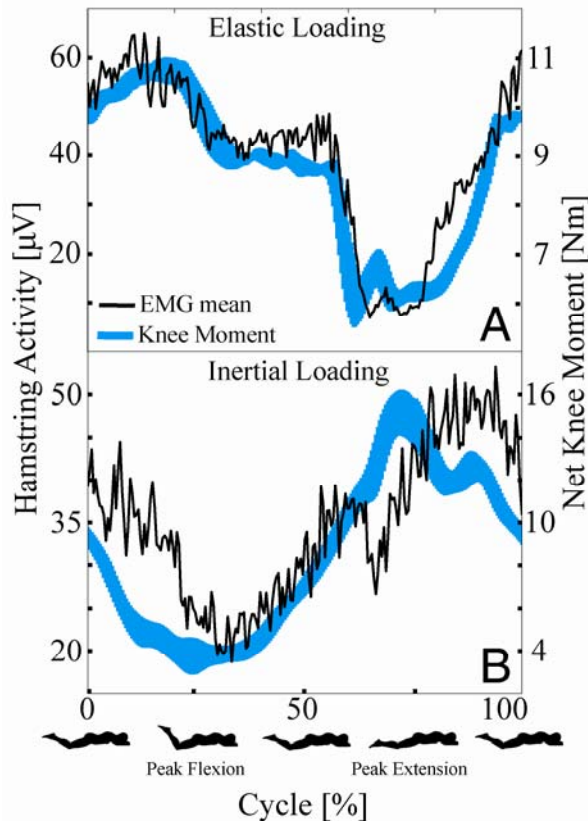
Figure 2. Mean (s.d.) joint moments and hamstring activity under (a) elastic and (b) inertial loading conditions.

DISCUSSION

We have successfully constructed a MR compatible device that guides repeatable knee flexion-extension motion while imposing either elastic or inertial loads on the hamstrings. This device can be used together with a dynamic MR imaging sequence to investigate how muscle strain distributions vary between shortening and lengthening contractions. Given the strong link between lengthening contractions and muscle injury, this information is important for investigating potential injury mechanisms. Furthermore, the empirical data is extremely valuable for the further development and validation of three-dimensional muscle models (Blemker and Delp 2005).

REFERENCES

Asakawa, DS et al. (2003). *Semin Musculoskelet Radiol*, 7(4):287-95.
Blemker, SS and Delp, SL (2005). *Ann Biomed Eng*, 33(5):661-73.
Pappas, GP et al. (2002). *J Appl Physiol*, 92(6):2381-9.
Zhong, X et al. (2008). *J Biomech*, in press.
Zhou, H and Novotny, JE (2007). *J Magn Reson Imaging*, 25(1):175-84.

ACKNOWLEDGEMENTS

Table 1. Mean (s.d.) peak knee flexion (θ_{max}), moment (*M*) and cyclic period (*T*).

Limb	Elastic Loading Condition			Inertial Loading condition		
	θ_{max} (deg)	M (Nm)	T (s)	θ_{max} (deg)	M (Nm)	T (s)
1	42.6 (0.6)	13.6 (0.2)	2.13 (0.09)	42.4 (0.8)	14.5 (0.6)	2.14 (0.07)
2	42.5 (0.7)	13.2 (0.2)	2.13 (0.07)	42.6 (0.8)	14.4 (0.5)	2.14 (0.07)
3	40.3 (0.9)	12.1 (0.5)	2.14 (0.06)	40.2 (0.8)	14.7 (0.7)	2.14 (0.05)
4	46.5 (0.9)	14.0 (0.2)	2.14 (0.05)	48.2 (1.0)	14.7 (0.8)	2.14 (0.05)
5	45.5 (1.1)	13.5 (1.3)	2.13 (0.09)	45.5 (1.4)	14.6 (0.6)	2.14 (0.06)

THE EFFECTS OF LOCAL VIBRATION ON A JOYSTICK PURSUIT-TASK

Joseph Soltys[1], John Keighley[2], and Sara Wilson[1]

[1]Human Motion Control Laboratory, Department of Mechanical Engineering,
University of Kansas, Lawrence, KS, Jsoltys@ku.edu and Sewilson@ku.edu
[2]Department of Biostastistics, KU Medical Center, KC, KS, Jkeighle@kumc.edu

INTRODUCTION

Sensory elements (*muscle spindle organs*) throughout the body contribute to perception of position and movement. It has been demonstrated that sensory afferents are altered by vibration (Roll and Vedel, 1982). This has been seen as increased position targeting errors for up to 30 minutes post vibration, suggesting neuromotor habituation or adaptation to vibratory stimulus (Li and Wilson, 2005).

The purpose of this study is to examine how such adaptation may alter the ability to do dynamic hand motions and develop a metric that can be used in an advanced imaging environment. Previous vibration imaging investigations have used static limbs (Romaiguere et al., 2003) A task-based fMRI protocol may provide more insight into the role of the motor and sensory regions of the brain during this adaptation.

METHODS AND PROCEDURES

In this study, six young, healthy subjects (2F, 4M, age 24.5 ± 2.3) consented to this protocol, which was approved by the University of Kansas Human Subjects Committee. Participants were limited to right-handed individuals.

Subjects were instructed to sit upright in a cubicle on a stationary chair facing a computer monitor at eye level. A standard USB computer joystick, with the zeroing spring removed, was located on a platform

Figure 1. Experimental Protocol
Solid line/triangle represents the target, dashed line/open-triangle represents subject trace. Relative timing for trials with during-vibration (start: 5-mins. post vibration onset) omitted.
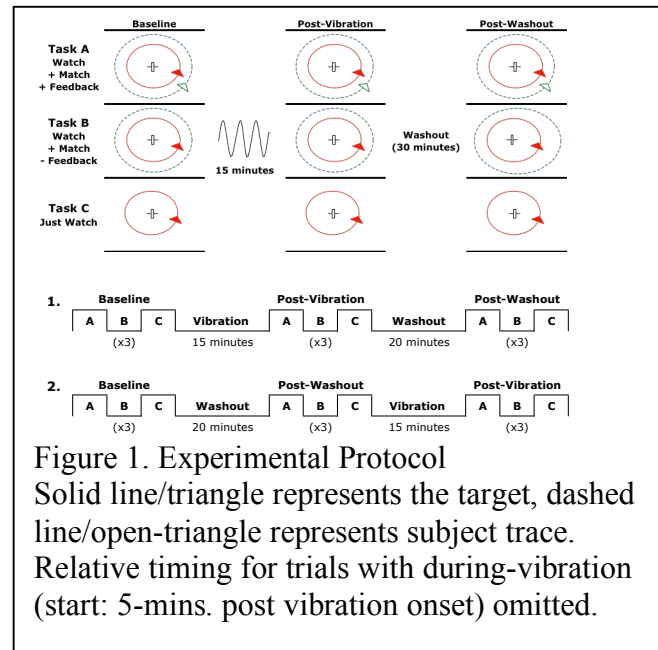
just to the right of the subject and hidden from view. The height of the chair was adjusted so that the angle between the forearm and upper-arm was approximately 90° when the joystick was held in the neutral position. To ensure wrist flexion, subjects were instructed to adopt a firm grip and to rest the edge of their hand against the hilt of the joystick.

For each trial, subjects were presented with three tasks provided in an ABC block paradigm (Figure 1). The three task levels were: A.) Watching a red target cursor move about a circular path at a given speed (3 sec/rev) while trying to match the target position with a *visible,* green, joystick controlled cursor, B.) Watching the target and trying to match the target with an *invisible* joystick controlled cursor, and C.) Watching the target cursor while remaining motionless.

Three blocks were presented sequentially with the duration of each task condition presented for 30 seconds and no delay between conditions. The interface was created using Labview and data were collected at 50 Hz. After an initial training session, trial data were collected at each of four time-points (baseline, during-vibration, immediately post-vibration, and post-washout). A washout period of 20 minutes was used in this study. The 70 Hz vibration was applied to the right wrist flexor group for 15 minutes. Subjects were randomly assigned to a group indicating the order of vibration and washout.

RESULTS

A typical trace of the joystick cursor location can be seen in Figure 2. From this data, the average per-revolution errors in subject angle and radius were calculated (Table 1). The angle error and radius were found to increase after exposure to vibration relative to washout.
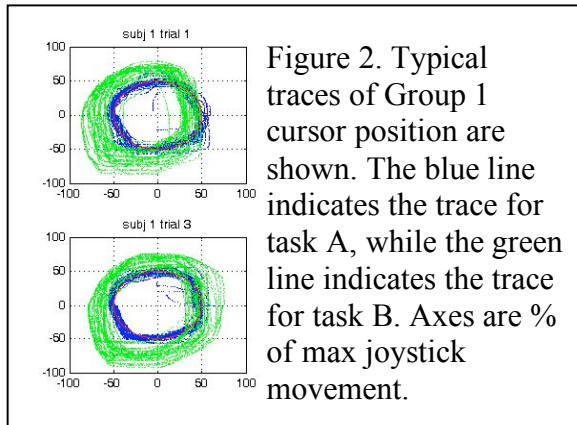
Figure 2. Typical traces of Group 1 cursor position are shown. The blue line indicates the trace for task A, while the green line indicates the trace for task B. Axes are % of max joystick movement.

DISCUSSION

Variability was observed to increase during task B for all conditions in both groups, indicating the greater difficulty of the task. The results presented here are sensitive to extreme per-revolution values as they are mean-based and each group consists of only 3 subjects. Additionally, the measures presented here are only representative of the average

revolution; dividing each revolution into sections corresponding to wrist: flexion, extension, and ab/adduction will produce a stronger physiological link to what is occurring.

SUMMARY

The measures and methodology developed here are useful in understanding how post-vibration effects may alter dynamic neuromotor control. Future investigations will examine these effects utilizing fMRI technology. Vibration is considered to be a risk factor for occupational injury so the results here will serve to further elucidate the role of vibration in injury etiology.

Group 1	Angle Error (*Deg.*)				Radius			
	A		B		A		B	
T1 - B	-0.63	(8.48)	27.90	(34.18)	48.89	(2.87)	62.40	(12.90)
T2 - DV	-3.77	(7.42)	6.72	(15.35)	49.59	(3.71)	65.14	(12.85)
T3 - PV0	-7.17	(7.09)	13.30	(30.90)	51.50	(2.75)	77.44	(14.92)
T4 - PW	-2.41	(7.74)	10.98	(17.85)	50.49	(2.64)	70.38	(12.38)

Group 2	Angle Error (*Deg.*)				Radius			
	A		B		A		B	
T1 - B	-3.70	(6.88)	2.34	(14.13)	52.98	(2.24)	72.68	(10.23)
T2 - PW	-1.84	(6.21)	-4.01	(15.16)	52.51	(2.03)	65.95	(7.05)
T3 - DV	-6.51	(13.80)	-11.11	(19.79)	51.81	(4.92)	62.69	(11.25)
T4 - PV0	-3.57	(5.18)	-8.64	(10.64)	53.14	(2.16)	70.53	(11.19)

Table 1. Preliminary Results
Preliminary results and (SD) for groups 1 & 2 are reported for the average per-revolution user radius (% $_{max}$ joystick movement) and Angle Error (deg.). Sign of angle error indicates whether the subject cursor was following the target (-), or ahead of the target (+).

REFERENCES

Li, L and Wilson, SE (2005). *ASME SBC,* Vail, CO.
Roll, JP and Vedel, JP (1982). *Ex Brain Res,* 47: 177-90.
Romaiguere, P et al. (2003). *Brain Res Cogn Brain Res,* 16: 74-82.

ACKNOWLEDGEMENTS

COORDINATION PATTERNS IN CHILDREN WITH SPASTIC DIPLEGIA: PRE-, 1- AND 5-YEARS POST-OPERATIVE

Elizabeth M. Russell, M.S.[1], George E. Gorton, III, Ph.D.[2], Peter D. Masso, M.D.[2], Richard E.A. van Emmerik, Ph.D.[1], Joseph Hamill, Ph.D.[1]

[1]University of Massachusetts, Department of Kinesiology, Amherst, MA, U.S.A.,
[2]The Shriner's Hospital for Children, Clinical Outcomes Laboratory, Springfield, MA, U.S.A.
erussell@kin.umass.edu

INTRODUCTION

Spastic diplegic cerebral palsy (CP) is often characterized by excessive hip and knee flexion and ankle plantar flexion. This leads to impaired coordination and coupled lower extremity motion patterns known as the "extension synergy", which can negatively influence gait and stability (Thelen, *et al.*, 2003). Surgical lengthening of the affected biarticular muscles can produce joint angle profiles similar to those in healthy children. However, over time post-surgery, CP children tend to revert back to a crouched gait with increased knee flexion due to spasticity in the hamstrings and the constant pull from gravity. The majority of literature on CP gait focuses on the kinematics of the hip, knee and ankle and not the interactions between the joints. The purpose of this study was to examine intra-limb coordination patterns pre-operatively and approximately one- and five-years post-operatively.

METHODS AND PROCEDURES

Five (4 males, 1 female; age 7.33 (1.86) years at first surgery) children with spastic diplegia all underwent surgical procedures bilaterally to transfer the rectus to the sartorius and lengthen the hamstrings and heel cords. Surgeries were not limited to these three procedures; however, no orthopaedic surgeries were performed. Three-dimensional kinematic gait analyses were collected pre-operatively and approximately one- (1.17 (0.79) years) and five-years (6.19 (1.75) years) post-operatively as subjects walked through the collection area without assistive devices and at their preferred speed. Sagittal plane hip, knee and ankle joint angles for the right and left legs were calculated during the stance phase of gait, normalized to 100 data points and averaged within a subject. The angular position of the hip relative to the knee, and the knee relative to the ankle were graphed and a vector coding approach (Heiderscheit, *et al.*, 2002) was applied to assess frame-by-frame changes in coordination. Vector angles (γ) were grouped in bins in Table 1 to classify coordination.

Proximal	$0°$ $\leq$	γ	$\leq 22.5°$;
	$157.5° <$		$\leq 180°$
Distal	$67.5° <$	γ	$\leq 112.5°$
In-phase	$22.5° <$	γ	$\leq 67.5°$
Anti-phase	$112.5° <$	γ	$\leq 157.5°$

Table 1. In-phase is flexion/extension of both joints; anti-phase is flexion of one joint and concurrent extension of the other; proximal signifies change in the proximal joint angle relative to a stationary distal joint angle; distal signifies the distal joint changing angle relative to a stationary proximal joint angle.

RESULTS

Surgical lengthening of biarticular muscles crossing the hip, knee and ankle did not show a major change in the coordination between the hip and knee during stance but a clear shift in the coordination pattern is seen between the knee and ankle (see Figures 1 &

2). The angle between two points can be grouped into the bins in Table 1 to quantify coordination.
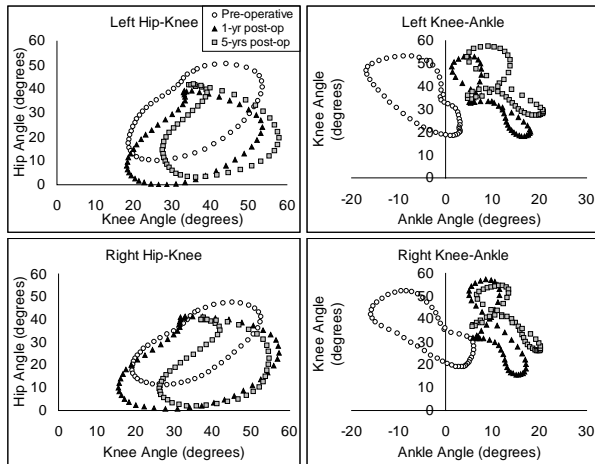
Figure 1. Mean intra-limb coordination patterns pre-operatively, 1- and 5-years post-operatively in children with spastic diplegia.

Subjects did not show a major shift post-surgery in percent stance spent in each coordination pattern. Figure 2 displays that no single pattern predominated between the hip and knee but the knee spent almost half of stance either flexing or extending while the ankle joint did not change.
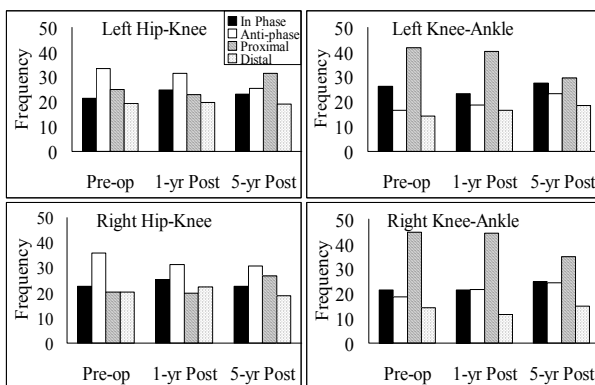
Figure 2. Frequency of occurrence of the different coordination patterns during stance.

DISCUSSION

Previous studies have found changes in coordination patterns post-operatively in children with spastic diplegia using correlations between joint actions as the coupling parameter (Baddar, *et al.*, 2002). Analysis using vector coding showed a clear change in the shape of the coordination patterns, particularly between the knee and ankle, post-operatively. We expected that the improvements post-surgery towards a more "normal" gait pattern would decrease the amount of concurrent hip and knee flexion and ankle plantar flexion; however, the percentage of in-phase coupling across the stance phase remained stable after surgery. The "in-phase" coordination characteristic of CP gait is actually a combination of all four different types of coordination. The type of coordination did not change with surgery or over time and no single pattern was preferred post-surgery.

SUMMARY

A vector coding approach quantified coordination changes in children with spastic diplegia, one- and five-years post-surgery. Surgical lengthening of the hamstrings, rectus femoris and gastrocnemius improved range of motion and altered the shape of the coupling pattern between the knee and angle, in particular. Future clinical treatments for CP may establish procedures to remedy the synergistic activity of the lower extremity musculature while maintaining healthy joint motion.

REFERENCES

Baddar A, Granata K, Damiano DL, et al. (2002). *J Bone Joint Surg*, 84A(5):736-34.

Heiderscheit BC, Hamill J, van Emmerik REA (2002) *J Appl Biomech* 18:110-21.

Thelen DD, Riewald SA, Asakawa DS, et al. (2003) *Muscle Nerve*, 27(4):486-93.

AN EMG-DRIVEN FORWARD SIMULATION OF SINGLE SUPPORT PHASE DURING GAIT

Qi Shao and Thomas S. Buchanan

Center for Biomedical Engineering Research
University of Delaware, Newark, DE, USA
E-mail: shao@udel.edu
URL: www.cber.udel.edu

INTRODUCTION

Simulations based on forward dynamics have been used to study the relationship between joint torques (Kepple et al., 1997), muscle forces (Anderson and Pandy, 2001; Neptune et al., 2001; Thelen and Anderson, 2006) and the resulting movement. In these models, dynamic optimization and a computed muscle control algorithm were used to determine a set of muscle excitations that generate a simulation to best reproduce experimental data. However, these models cannot account for different neural control strategies that may be used by different people, and may have difficulty predicting different muscle recruitment patterns during various tasks. This may be resolved by using electromyography (EMG) as input.

In this report we describe for the first time a forward dynamics model that incorporates an EMG-driven model, and we apply this approach in a pilot study to estimate joint moments, muscle forces and measured kinematics during single support phase of gait.

METHODS

Two healthy young subjects who gave informed consent were included in this study. EMGs, joint positions and force plate data were collected from 4 walking trials. EMGs were collected from the major muscle groups of the right leg (MG, LG, Sol, TA, RF, VM/VL/VI, BFL/BFS, SM/ST) using surface electrodes. Kinematics of the lower extremity, pelvis and trunk were determined using a Qualysis System. Maximum voluntary contraction trials were collected for normalization of EMG. The subjects were required to strike the force plate using their right feet. In this study we simulated the single support phase of the walking trials.

An inverse dynamics model was developed using SD/FAST (Symbolic Dynamics, Inc., Mountain View, CA). The musculoskeletal model was constructed using SIMM (Motion Lab Systems, Inc., Baton Rouge, LA). It includes 12 segments: femur, tibia/fibula, talus, calcn and toes of both limbs, pelvis, back. Here the back segment includes the mass and inertial properties of the torso, head and arms. This model has 10 DOF in sagittal plane: lumbar rotation, horizontal and vertical position of pelvis, pelvis rotation, hip, knee and ankle extension/flexion of both limbs. Our model solved the equations of motion of the whole body, and was different from the traditional bottom-to-up approach. The measurement of the upper body's movement is relatively inaccurate and may influence the results of our full-body model, so we implemented an optimization algorithm to calibrate the kinematics of the pelvis and back, reducing the residual forces and torques there.

An EMG-driven model (Buchanan et al., 2004) was used to estimate the muscle forces of the right leg to match the calculated inverse dynamic joint moments.
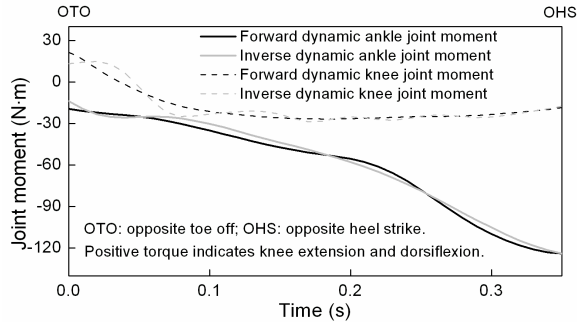
Figure 1. Forward and inverse dynamic right knee and ankle joint moment profile.

The forward dynamics model was developed using the same musculoskeletal model described above. Muscle forces, F_M, calculated from our EMG-driven model were used to drive the model spanning the right ankle and knee joint. For the other joints, the model was driven by the joint torques calculated using inverse dynamics, T_{inv}. The dynamical equations of motion were derived and solved using SD/FAST. We only included hip flexor, RF, and hip extensors, BFL, SM and ST, and did not include the other flexor/extensors and ligaments across the hip, so the right hip joint moment applied to the model was calculated as the term T_{others}^{hip}.

$$T_{others}^{hip} = T_{inv}^{hip} - T_{RF}^{hip} - T_{BFL}^{hip} - T_{SM}^{hip} - T_{ST}^{hip} \qquad (1)$$

Ground reaction forces during the simulation were prescribed to the experimental values and a couple of translational and rotational spring-dampers were applied under each foot to account for the variance between calculated kinematics and experimental kinematics (Thelen and Anderson, 2006). The stiffness and damping of the spring-dampers were tuned using dynamic optimization to accurately track the measured kinematics.

RESULTS

The forward dynamic knee and ankle joint moments calculated from the EMG-driven model matched the inverse dynamic joint moments (Figure 1). The calculated right hip,
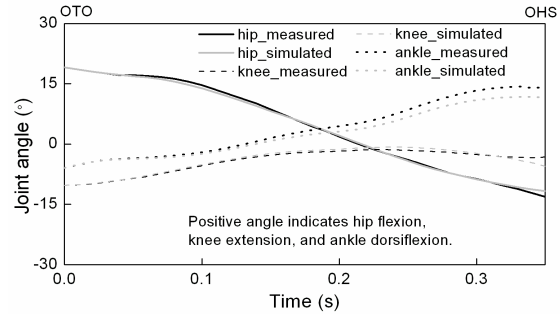
Figure 2. Simulated joint kinematics and measured kinematics.

knee and ankle joint kinematics matched the measured kinematics (Figure 2).

DISCUSSIONS AND SUMMARY

We have developed a forward dynamics model that uses EMGs as input. It successfully tracked measured kinematics during single support phase of gait. It demonstrated for the first time that muscle forces calculated from an EMG-driven model can be used to drive forward modeling of kinematics. This technique has great potential in study of the inter relationships between muscles and the resulting movements in healthy and impaired subjects.

REFERENCES

Anderson, FC and Pandy, MG (2001). *J Biomech Eng*, 123: 381-90.
Buchanan, TS et al. (2004). *J Applied Biomech*, 20: 367-95.
Kepple, TM et al. (1997). *Gait & Posture,* 6:1-8.
Neptune, RR et al. (2001). *J Biomech,* 34:1387-98.
Thelen, DG and Anderson, FC (2006). *J Biomech,* 39:1107-15.

ACKNOWLEDGEMENTS

QUANTIFYING THE PLANARITY OF THE FIELD HOCKEY HIT

Alexander Willmott and Jesús Dapena
Department of Kinesiology, Indiana University, Bloomington, IN, USA,
swillmott@lincoln.ac.uk

INTRODUCTION

The concept of a 'swing plane' in golf was popularized by Cochran and Stobbs (1968) based upon their qualitative observation that the clubhead moves in a single inclined plane for much of the downswing. The assumption of planar arm and club motions has been central to most modeling of the swing, though its validity has been questioned (see, for example, Coleman and Anderson, 2007).

The planarity of the field hockey hit has not been investigated. The purpose of this study was to initiate such an analysis by developing a quantitative version of Cochran and Stobbs' approach and applying it to the path followed by the stickface during the downswing.

METHODS AND PROCEDURES

Thirteen experienced female field hockey players were asked to hit a stationary ball after a single approach step. They were filmed with two cameras at 200 fps, and the DLT method was used to calculate the positions of three stick markers at 0.005 s intervals between the start of the downswing and impact. These data were used to reconstruct the 3D motion of the center of the stickface during the downswing.

The positional data for the center of the stickface were then resampled to give equal weight to all parts of its curved path. For this, quintic spline interpolation was used to calculate points at even 0.1 m intervals from the position at impact back along the path followed by the stickface.

The planarity of the stickface motion was investigated by determining planes of best fit for the points defining progressively longer sections of the downswing path, each of which ended at the impact position. The first section included the final 0.2 m of the stickface path, to provide the minimum of three points required for plane fitting. Each subsequent section included a further 0.1 m along the path until the start of the downswing was reached. The planes were calculated using Total Least Squares (Orthogonal) Regression, since this allows for error in each of the three coordinate directions (Nievergelt, 1994). The closeness of fit of each plane to the data points was measured using the mean absolute residual, expressed as a percentage of the distance traveled by the stickface in that section.

RESULTS

A mean absolute residual of 1% of the distance traveled by the stickface was selected as the cutoff defining planar motion. Using this criterion, the entire downswing was planar in 10 of the 13 subjects. Figure 1 shows a typical subject within that group. For the remaining three subjects the stickface motion was planar during the final 83, 91 and 92% of the downswing path.

Figure 2 illustrates the close fit of the stickface path to a plane for mean absolute residuals of 1% or less.
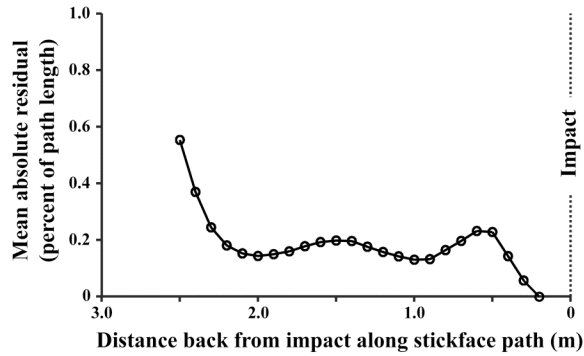
Figure 1. Mean absolute residuals for Subject 13 over sections of increasing path length back from impact.
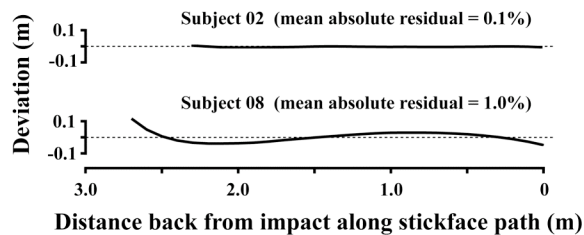
Figure 2. Deviations of the stickface path from the plane fitted to the downswing in two subjects chosen to illustrate the quality of fit at large and small values of the mean absolute residual.

Direction of hit
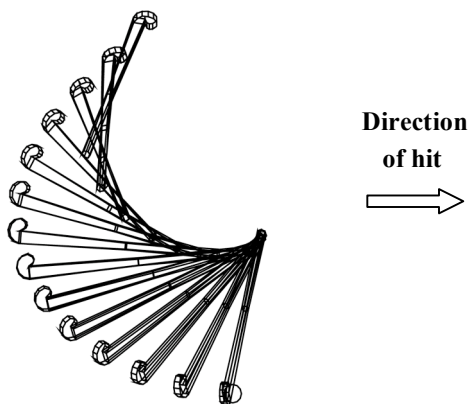
Figure 3. Motion of the stick, viewed perpendicular to the plane, for Subject 12.

In the 10 subjects whose entire downswing was planar, the stickface traveled between 2.1 and 2.8 m during this phase. In the three remaining subjects, the range of the downswing was longer, between 3.0 and 3.4 m, and the length of the planar portion was between 2.7 and 2.9 m.

Figure 3 shows the stick motion, viewed perpendicular to the stickface plane, for the subject with the median downswing path length (2.6 m).

DISCUSSION

The results indicate that the curved path followed by the center of the stickface is remarkably planar for all, or almost all, of the downswing of a field hockey hit.

Future work should investigate the motions of the stick shaft and of the arms, and how they relate to the plane fitted to the path followed by the center of the stickface.

SUMMARY

A method has been developed for quantifying the planarity of the motion of a selected landmark. The application of this approach to the field hockey hit indicates that the curved path followed by the center of the stickface is very close to planar for all, or almost all, of the downswing.

REFERENCES

Cochran, A and Stobbs, J (1968). *The Search for the Perfect Swing*. Philadelphia, Lippincott.

Coleman, S and Anderson, D (2007). *J Sports Sci* 25: 739-748.

Nievergelt, Y (1994). *SIAM Review* 36: 258-264.

COMPARISON OF MOMENT-ANGLE PROFILE OF ELBOW FLEXORS – EXTENSORS IN ELITE YOUNG OVERHEAD ATHLETES

Maria Elissavet Nikolaidou and Konstantinos Boudolos

Department of Sport Medicine and Biology of Exercise, Faculty of Physical Education and Sport Science, National and Kapodistrian University of Athens, Greece, mnikola@phed.uoa.gr

INTRODUCTION

In in-vivo conditions, the moment vs. joint angle curve (M-A profile) is typically used to examine the force-length characteristics of muscles. During attack in volleyball (VB) and water-polo (WP), the elbow moves through an arc of $\approx 60°$-$70°$ joint flexion suggesting that the flexor and extensor muscles operate in similar joint configurations, therefore muscle lengths. Previous studies (Herzog et al., 1991) have shown different extensor moment-knee angle relations between different athletes that were attributed to adaptation of muscle function to different functional requirements. The purpose of this study was to compare the moment-elbow angle profile between elite young overhead athletes.

METHODS AND PROCEDURES

The sample consisted of 10 elite young VB and 10 WP athletes with body mass, height and age values (mean±SD) being 80.0±8.0 kg, 185.7±5.1 cm and 17.2±1.0 years, and 76.1±15.0 kg, 174.8±8.0 cm and 15.2±0.9 years, respectively. Subjects executed 3.0 sec maximum dominant elbow flexion–extension contractions on a Cybex II+ dynamometer at angles of 45-60-75-90-105-120° of joint flexion (0°=full extension) in a random order, being in a supine position with the shoulder joint at 45° of horizontal abduction and the forearm in neutral position. Maximal isometric flexor–extensor moment (Nm) was calculated. Data collection (Fs=1000 Hz) and data analysis used the AcqKnowledge software. A 2nd-order polynomial curve fitting approach was used to predict the M-A profile

and the optimal elbow joint angle (A_{opt}) for moment production. Possible differences in A_{opt} of the M-A profile and in the flexors-extensors moment magnitude across tested elbow joint angles between groups were examined with t-test for independent samples and univariate anovas, respectively ($p<.05$).

RESULTS

In both groups, results showed that the flexor moment was stronger on positions of greater elbow joint extension and was reduced as the joint became more flexed (Figure 1), while the extensors showed a relatively constant moment-generating capacity over the range of the tested elbow angles (Figure 2). The predicted A_{opt} of the flexors M-A profile was at 72° and 70° and the corresponding one for the extensors M-A profile at 74° and 70° of elbow flexion in VB and WP athletes, respectively, however no significant differences were observed between groups. VB athletes generated higher elbow extensor moment than WP athletes at 45° of elbow joint flexion (Figure 2), whereas no significant differences between groups were found for the flexor moment (Figure 1).
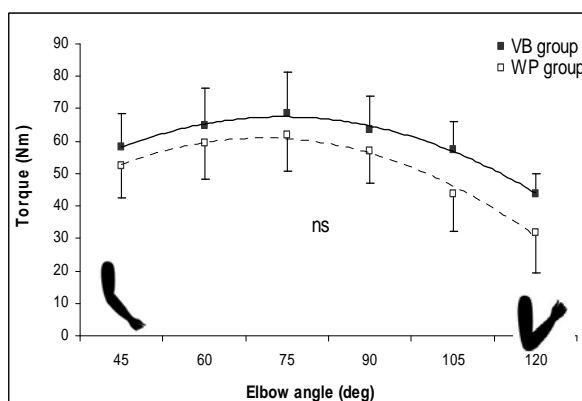
Figure 1. Maximal isometric moment (Nm) of elbow flexors as a function of changes in joint angle from 45° to 120° of elbow flexion (M-A profile) in VB and WP groups. No significant (p>.05) differences in the magnitude of the elbow flexors moment across tested joint angles were found between groups. Data are means (SD).
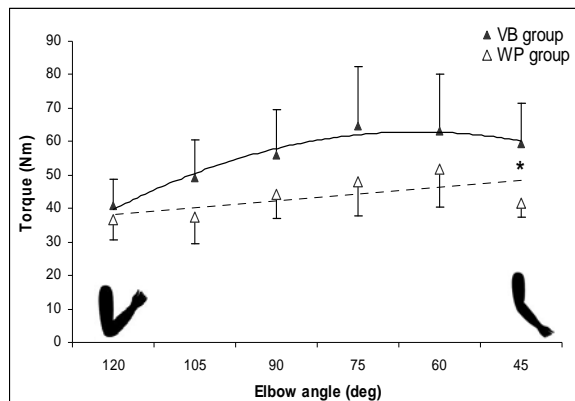
Figure 2. Maximal isometric moment (Nm) of elbow extensors as a function of changes in joint angle from 120° to 45° of elbow flexion (M-A profile) in VB and WP groups. *Significant (p<.05) differences in the magnitude of the elbow extensors moment across tested joint angles were found between groups. Data are means (SD).

DISCUSSION

Present results agree well with previous studies on the isometric functional capacity of the muscles crossing the elbow (Murray et al., 2000). The identical shape of the elbow flexor – extensor M-A profile in VB and WP athletes suggests similar adaptations of the elbow muscles to similar functional requirements. However, the observed difference in the extensor moment magnitude between groups at the joint configuration of greater elbow extension, which is more frequently seen in volleyball, provides evidence for adaptations of muscle function that may either relate with different competition conditions (Herzog et al., 1991) or may result from existing differences in muscle volume between groups, which become more pronounced in critical elbow joint angles for these sports. Further research where other factors that could affect the shape and magnitude of the M-A profile of athletes with specific long-term physical activity at the elbow joint can be examined is necessary.

SUMMARY

This study compared the profile of possible changes in the elbow flexor – extensor maximal moment as a function of changes in the elbow joint angle (M-A profile) between two groups of elite young overhead athletes. The shape of the M-A profile of the elbow flexors – extensors was similar between groups, however a difference found in the extensor moment magnitude may be associated with different elbow joint configuration during training and/or competition, thus providing evidence for adaptations of muscle function to specific functional requirements.

REFERENCES

Herzog W et al. (1991). *Med Sci Sports Exerc*, 23:1289-96.
Murray WM et al. (2000). *J Biomech*, 33:943-952.

ACKNOWLEDGEMENTS

THE EFFECT OF UNLOADER BRACES ON KNEE LOADS DURING GAIT

Kristin Whitney, Ian Jones, Trevor Birmingham and Thomas Jenkyn

Wolf Orthopaedic Biomechanics Laboratory, Fowler Kennedy Sport Medicine Clinic, The University of Western Ontario, London, ON, Canada, kwhitne2@uwo.ca

INTRODUCTION

Unloader or valgus bracing is a common method of decreasing pain and increasing knee function in patients suffering from medial compartment knee osteoarthritis (OA). Although there have been many studies conducted on unloader braces, there is only one study, which used a computer model of internal knee joint loading (Pollo et al., 2002), that investigated the internal biomechanics of an osteoarthritic knee joint while wearing an unloader brace. However the generalizability of this study's assumptions and therefore the influence of the brace on internal knee joint loading remain unclear.

This study follows a protocol similar to past studies (Draganich et al., 2006; Lindenfeld et al., 1997; Pollo et al., 2002) and evaluates the effect of the unloader brace on medial and lateral knee joint loads during gait.

METHODS AND PROCEDURES

3D kinematics and kinetics were measured using an eight-camera motion capture system (Eagle cameras, EvaRT system, Motion Analysis Corp., Santa Rosa, CA) and an integrated floor-mounted force platform (AMTI, Watertown, MA). Three male patients with knee OA and lower limb varus alignment were recruited from a tertiary care centre. Each subject's own custom-fit unloader brace (Unloader XT, Ossur) was used during testing. Subjects were tested on two separate occasions: 1) the day of initial brace fitting, and 2) after a two-week period of normal use to allow for familiarization.

Each individual test session involved level walking at preferred gait both with and without the brace. The order of brace conditions was randomized (Draganich et al., 2006).

Inverse dynamic analysis was performed to determine the external knee kinetics. Data was further processed to find the peak knee adduction moment, including individual components: ground reaction force (GRF) and the lever arm of the GRF in the frontal plane.

An optimization model of mechanical equilibrium of the internal structures of the knee joint, previously developed and validated (Bhatnagar and Jenkyn, 2007), is then used to calculate internal joint loading on the tibial plateau. The model includes 6 muscles, 4 ligaments and the medial and lateral tibial plateau articulating surfaces. The peak values of the external kinetic measures and the ratio of medial-to-lateral compartment compression are compared between brace and no-brace conditions.

RESULTS

Peak external knee adduction moment for the braced limb appeared to be similar when tested immediately after brace application versus after two weeks of brace wear (Table 1, Figure 1-A). The peak external adduction moment for the affected limb was less at both visits for the braced condition (Table 1, Figure 1-B).

Frontal plane lever arm decreased immediately after brace application with

similar results at Visit 2 (Table 1). No differences were found between visits and conditions for frontal plane GRF (Table 1).

1-A

1-B
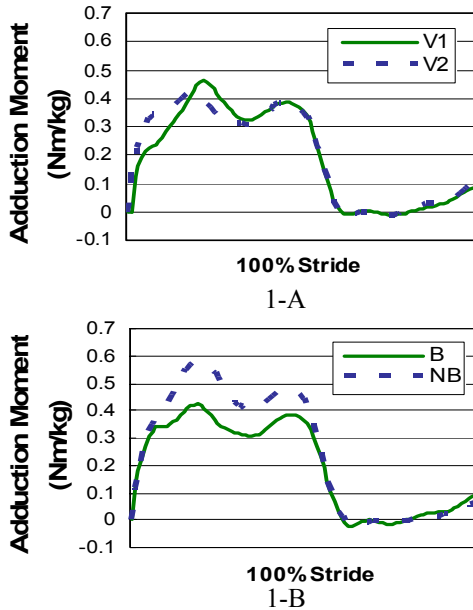
Figure 1. External knee adduction moments comparing conditions for one representative subject. Fig 1-A: Brace at Visit 1 and Visit 2. Fig.1-B: Brace and No Brace at Visit 2.

	Kinematic Results (Affected Limb)			
	Visit 1		Visit 2	
	B	NB	B	NB
M_{add}	1.97 (0.39)	2.67 (0.62)	1.91 (0.69)	2.49 (0.93)
LA	0.04 (0.01)	0.06 (0.01)	0.04 (0.01)	0.06 (0.02)
GRF	1.04 (0.01)	1.05 (0.02)	1.05 (0.01)	1.06 (0.04)

Table 1. Kinematic results for brace (B) and no brace (NB). M_{add} – normalized average peak external adduction moment (% body weight(BW) x height); LA – lever arm (m); GRF – (BW).

DISCUSSION

The consistency in peak adduction moment for both braced and unbraced conditions from Visit 1 to Visit 2 of the affected limb support

previous studies which indicate that the mechanical effects of an unloader brace occur immediately upon brace application (Draganich et al., 2006). As well, the decrease in peak external adduction moment about the knee between the brace and unbraced conditions for the affected limb is consistent with previous studies (Draganich et al., 2006; Lindenfeld et al., 1997; Pollo et al., 2002). The decreases in lever arm with no change in GRF may indicate that the reduction in adduction moment is a result of the brace.

This study is currently on-going and it is expected there will be 12 subjects at the time of press. Further analysis will include mathematical modeling of the medial and lateral compartment loads.

SUMMARY

The preliminary findings of this study are consistent with previous studies and suggest that unloader braces cause a reduction in external adduction moment about the knee and may also reduce the loading in the medial compartment (Draganich et al., 2006; Pollo et al., 2002). Unloader braces appear to be an effective method of treatment for knee osteoarthritis, however further investigation of the internal structures is recommended to understand the complexity and individual role of structures on the decrease in external adduction moment.

REFERENCES

Bhatnagar, T and Jenkyn, TR (2007). *ASB Conference*, Abstract.
Draganich L et al. (2006). *J Bone Joint Surg Am*, 88:2645-2652.
Lindenfeld TN et al. (1997). *Clin Orthop Relat Res*, 344:290-297.
Pollo FE et al. (2002). *Am J Sports Med*, 30:414-421.

DYNAMIC STABILTIY OF THE PARKINSONIAN GAIT

Christopher J. Arellano, Ashley Hickerson, Melissa Scott-Pandorf, Vladimir Ivkovic
and Max J. Kurz

Laboratory of Integrated Physiology, Department of Health and Human Performance,
University of Houston, Houston, TX, USA
E-mail: carellano@uh.edu or mkurz@uh.edu, URL: www.hhp.uh.edu

INTRODUCTION

One of the hallmark features of Parkinson's disease (PD) is its affect on gait. Individuals with PD often walk at a slower pace, have a shorter stride length and an increased amount of stride-to-stride variability (Morris et al, 1999). Many of these gait changes have been speculated to be strategies that attempt to prevent falls. However, 70% of PD patients experience an annual fall (Bloem et al., 2003). Despite the considerable amount of experimental work on the gait and postural balance of individuals with PD, clinical metrics that adequately measure fall susceptibility remains elusive.

Recently, floquet analysis has emerged as a potential measure for quantifying fall susceptibility in the aging (Granata and Lockhart, 2008). Floquet analysis quantifies how disturbances or errors in the gait cycle are attenuated over many steps. A fall is more likely if it takes a longer time to correct the errors or disturbances that occur during the gait cycle. Historically, floquet analysis has been used extensively to determine the stability of walking robots (McGeer, 1990; Tedrake, 2004); however, its utility as a clinical measure of gait stability in humans remains for the most part unknown.

The purpose of this investigation was to determine if floquet analysis discriminates between individuals with PD, who are susceptible to falls, and the young individuals, who have limited fall susceptibility.

METHODS AND PROCEDURES

Seven healthy young adults (height = 1.76 ± 0.07 m, weight = 77.61 ± 13.79 kg, age = 23.29 ± 2.21 yrs.) and seven individuals with PD participated in this investigation. Characteristics of the PD participants are detailed in Table 1. A six-camera motion capture system (200 Hz) was used to collect the right leg's ankle, knee and hip joint sagittal plane kinematics as the subjects walked on the treadmill at a self-selected pace. All participants held onto the handrails while walking. The PD participants performed the walking trial while off their levodopa medication.

A state vector ($\mathbf{x}$) was created to evaluate the stability of the locomotive system. This vector was defined by the joint position and velocity of the hip, knee, and ankle at heel-contact. Floquet analysis was used to quantify the dynamic stability of the gait pattern (Granata and Lockhart, 2008).

Table 1. PD participants' characteristics.

Age (years)	76.0±6.0
Height (meters)	1.74±0.1
Weight (kg)	71.9±12
UPDRS III	28.6±4.6
Hoehen & Yahr Score	2.8±0.7
Range of annual falls	0-30

This involved linearizing the first-return map about **x*** to satisfy the following relationship

$$\delta \chi^{n+1} = \mathbf{J} \delta \chi^{n}$$

where δ denotes the deviation about **x*** at each nth step, and **J** is a 6 x 6 constant coefficient matrix that represented the Jacobian. $\delta \chi^{n}$ and $\delta \chi^{n+1}$ were defined as

$$\delta x^{n} = [x_n - x^*, x_{n+1} - x^*, x_{n+2} - x^*, \ldots]$$

$$\delta x^{n+1} = [x_{n+1} - x^*, x_{n+2} - x^*, x_{n+3} - x^*, \ldots]$$

A least squares algorithm was used to solve for **J** (Tedrake et al., 2004). The largest eigenvalue (β) was computed from **J** and was used to quantify the stability of the gait pattern at the instance of heel- contact. A β value further away from zero signified a less stable gait.

RESULTS

The young (1.21±0.3 m/s) walked significantly (p<0.001) faster than the participants with PD (0.62±0.4 m/s). β was significantly greater (p = 0.011) for the individuals with PD compared to the young (Figure 1). The PD participants had a less stable gait than the healthy young adults.

DISCUSSION

Our results indicate that individuals with PD have a less stable gait that may be more susceptible to future falls. The larger β seen in the PD participants indicates that it takes them longer to correct for disturbances that were present in the gait cycle. The inability to quickly respond to disturbances that arise during gait may be the reason why some of the PD participants in this investigation had a high incidence of falls last year (Table 1). The β values for the PD participants were similar to what was previously reported
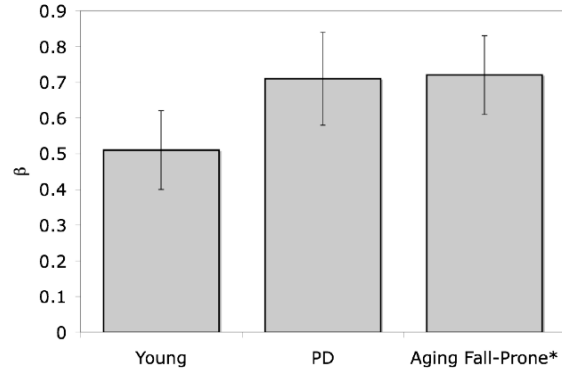
Figure 1. β values for each group (mean ± SD), * indicates that the β values for the aging are from Granata and Lockhart (2008).

for the aging that had a history of falls (Figure 1). Taken together, these results provide further support for the use of floquet analysis as a metric for fall susceptibility. We are currently collecting data from a larger number of PD patients to determine if floquet analysis can be used to predict future falls.

SUMMARY

Individuals with PD have a less stable gait than young individuals. Since our results are similar to what has been previously reported for the fall prone aging, floquet analysis may augment clinical measures that are directed at identifying potential fallers.

REFERENCES

Bloem BR et al. (2003). *Curr Opin Neurol* 16:15-26.

Granta KP and Lockhart TE (2008). *J Electr Kines*, in press.

McGeer T (1990). *Int J Robotic Res*, 9:62-82.

Morris et al. (2001). *Clin Biomech* 16:459-470.

Tedrake R et al. (2004). *Proc IEEE ICRA*, 5: 4656-4661.

COMPARING UNIAXIAL AND BIAXIAL STRAIN RESPONSES OF THE PORCINE ANNULUS FIBROSUS

Diane E. Gregory and Jack P. Callaghan

Department of Kinesiology, University of Waterloo, Waterloo, ON, Canada,
dgregory@uwateloo.ca

INTRODUCTION

The annulus fibrosus is primarily a collagenous tissue that is required to withstand tensile forces during various loading and postural scenarios. This is especially true for the outer annulus, which is comprised of type I collagen fibres, similar to those found in tendons and ligaments (Lo et al., 2002, Pritchard et al., 2002). However, to date, the tensile loading properties of the annulus fibrosus have only been examined uniaxially, while the annulus is likely loaded in all directions *in vivo*. Due to the structural organization of the annulus, each layer is subject to vertically orientated strains as well as circumferentially orientated strains. Therefore, it is important to determine the response of the annulus fibrosus under multiple axis loading. The purpose of the current study was to compare the force-displacement profile of porcine annulus layers under uniaxial and biaxial tension.

METHODS AND PROCEDURES

Ten 5mm by 5mm annulus samples (average thickness 0.52mm, S.D. 0.16mm) were dissected from the outer anterior portion of the intervertebral discs from four C3/4 and six C5/6 porcine functional spinal units. These functional units have been shown to be morphologically and functionally similar to human lumbar functional units (Yingling et al., 1999, Oxland et al., 1991). Each tested sample consisted of two adjacent annular layers and

were dissected such that the orientation of the fibres of the superficial layer were running in a vertical orientation and therefore the fibre orientation of the adjacent layer was approximately 30 degrees deviated from vertical. Each sample was subjected to 20% uniaxial strain (applied transversely to the orientation of the vertical fibres) at a strain rate of 2%/s, and subjected to biaxial strain (20% in both the transverse (perpendicular to fibre orientation) and vertical (parallel to fibre orientation)) at a rate of 2%/s. The order in which these strains were presented were randomized. Samples were strained using a custom biaxial testing system (BioTester 5000, CellScale, Waterloo Instruments Inc, Waterloo, ON). Variables of interest (all in the transverse direction) were peak force, peak displacement, and stiffness. A two-way ANOVA (uniaxial versus biaxial, and functional unit type, i.e. C3/4 versus C5/6) was conducted in order to determine any main effects on the previously mentioned variables. An alpha level of 0.05 was used in order to determine significance.

RESULTS

As expected, the biaxial strained tests resulted in significantly higher stiffness values (uniaxial average (S.D.) stiffness: 1.79 N/mm (0.86); biaxial stiffness: 3.44 N/mm (1.36); $p<0.0001$) as well as peak force values (uniaxial average (S.D.) peak force: 0.71N (0.36); biaxial peak force: 1.39N (0.59); $p=0.001$). Figures 1a and 1b depict the stiffness and peak forces values,

respectively. It is also important to note that the peak displacement for the uniaxial versus biaxial tests were not significantly different (p=0.831). In addition, the stiffness, peak force, and peak displacement were not significantly different between the C3/4 and C5/6 functional unit specimens (p=0.326, 0.273, 0.297, respectively).
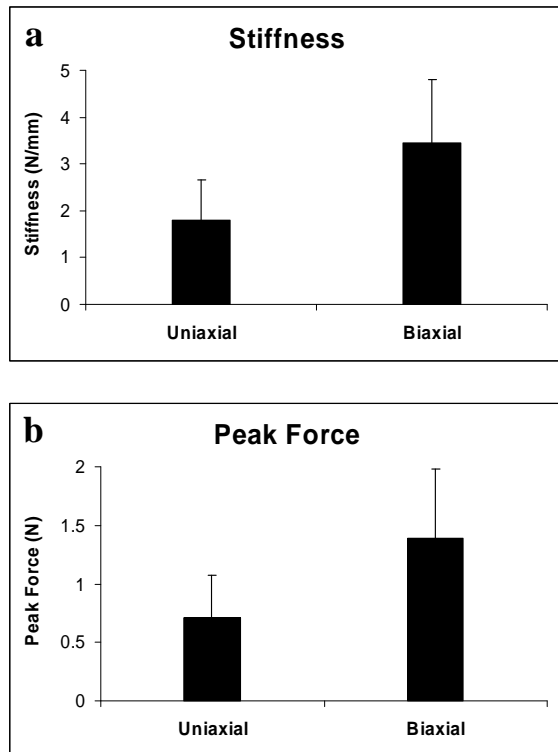
Figure 1. a) Average stiffness (p<0.0001) and b) average peak force (p=0.001) for the uniaxial and biaxial tensile tests to 20% strain. Error bars represent standard deviation.

DISCUSSION

Prior to the current study, the annulus fibrosus had only been studied under applied uniaxial tensile loads *in vitro*. However, it is generally accepted that the annulus, and most biological tissues, undergo multi- directional tensile loads. Therefore, it is important to determine how these tissues respond to multi-directional

strains. The current study showed that the annulus fibrosus requires almost double the force to strain to the same magnitude when under biaxial tensile load as compared to uniaxial tensile load. Further, the tissues are approximately twice as stiff under biaxial tension as compared to uniaxial tension. Therefore, the annulus fibrosus experiences a higher stress for a given strain during multi-directional tension, which is a more physiological scenario, then what has been previously documented uniaxially. This is important for determining tissue tolerance levels as well as the injury potential of various tensile loading situations, as currently these tissue tolerances are based solely on uniaxially applied strains.

SUMMARY

This study was the first to document biaxial tensile loading for the annulus fibrosus. The most important finding is that the annulus fibrosus experiences much higher stress levels (approximately 95% higher peak forces) at a given strain magnitude when under biaxial tension as compared to uniaxial tension, which is a far more biologically relevant scenario.

REFERENCES

Lo, IK et al. (2002). *Histol Histopathol,* 17:523-537.
Pritchard, S et al. (2002). *Biophys J,* 83:2502-2510.
Oxland, TR et al. (1991). *J Orthop Res,* 9:452-462.
Yingling, VR et al. (1999). *J Spinal Disord,* 12: 415-423.

LONG-TERM MORPHOLOGICAL AND FUNCTIONAL CHANGES FOLLOWING AN ACUTE HAMSTRING STRAIN INJURY

Amy Silder, Darryl G. Thelen, Michael J. Tuite, and Bryan Heiderscheit
University of Wisconsin-Madison, Madison, WI, USA, silder@wisc.edu

INTRODUCTION

Approximately 30% of all athletes that experience a hamstring strain injury will re-injure within the first year after returning to sport (Woods et al., 2004), with subsequent injuries often more severe and requiring more time away from sport than the initial injury (Koulouris et al., 2007). Long-term follow-up of acute strain injuries have shown scar tissue to enclose the previously injured tendon (Rask and Lattig, 1972). Such morphological changes may alter both the passive and active force-length properties of musculotendons. This may pre-dispose previously injured muscle to re-injury when a movement is performed that requires lengthening contractions, such as sprinting. The objective of this study was to investigate long-term changes in hamstring morphology, passive stiffness, and joint kinematics following an acute hamstring strain injury.

METHODS AND PROCEDURES

Eleven athletes were recruited who had experienced a hamstring strain injury between 5-13 months prior. Bilateral comparisons were made between the previously injured and non-injured limbs. We first measured 3D full body kinematics (200Hz) and EMG signals (2000Hz) while subjects ran on a treadmill at speeds ranging between 60 to 100% of maximum. Scaled musculoskeletal models were then created of each subject, and used to estimate joint angles and hamstring lengths from measured kinematics. Bilateral EMG signals from the biceps femoris, medial hamstrings, rectus femoris, and vastus lateralis were compared during loading, propulsion, initial swing, and the terminal swing phases of running. All sprinting measures were averaged across strides and compared between limbs and speeds. Secondly, we measured and modeled the passive force-length relationship of the hamstrings on each limb (Silder et al., 2007). The hip and knee angles during sprinting corresponding to peak biceps femoris musculotendon stretch were used as inputs into the passive stiffness model, resulting in the peak passive hip extension moment during terminal swing. Third, isokinetic knee flexion strength was measured at 60deg/sec. Finally, high resolution bilateral MR images were obtained to evaluate the presence of residual scar tissue and muscle volume changes. Hamstring muscle and tendon volumes were manually outlined on each slice (Figure 1). Volumes were calculated as the product of the inter-slice distance and the summed cross-sectional areas from each axial slice.
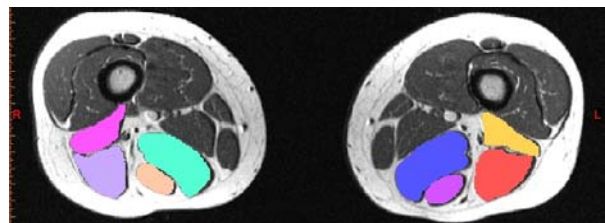
Figure 1. Hamstring muscles and tendons were outlined on each axial slice and used to quantitatively compare differences in musculotendon morphology between limbs.

RESULTS

Eleven subjects experienced biceps femoris injuries (seven proximal, four distal). Nine of 11 subjects presented with enlarged regions of low intensity signal along the proximal biceps femoris long head (BFLH) musculotendon junction adjacent to the site of prior injury, suggesting the presence of residual scar tissue

(Figure 2). Atrophy of the previously injured BFLH and/or hypertrophy of the biceps femoris short head (BFSH) was present in 8 of 11 subjects and showed a moderate inverse relationship (r=-0.50), though not significant. Significant differences were observed between the previously injured and non-injured proximal biceps femoris tendon (BFT), BFLH, and BFSH volumes (Table 1).

Asymmetries in hamstring strength (peak torque and angle of peak torque), passive hamstring musculotendon stiffness, muscle activity during sprinting, and peak hamstring lengths during sprinting were present, but consistent differences were not observed across subjects.
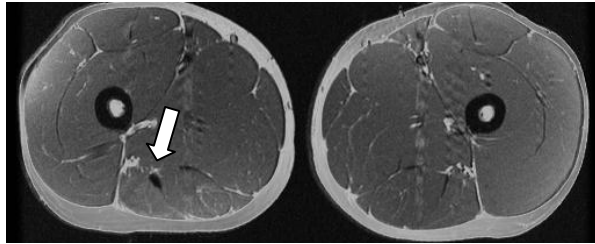
Figure 2: Increased area of low-signal intensity was clearly present near the proximal biceps femoris musculotendon junction near the site of prior injury.

Table 1. Average percent difference in muscle or tendon volume between the previously injured and non-injured limbs. Positive indicates an increase in volume of the previously injured limb, when compared to the un-injured limb.

BFLH	BFSH	BFT
-10% p<0.01	+12% p<0.01	+57% p<0.05

DISCUSSION

The goal of this study was to use a combination of biomechanical analyses and MRI to investigate long term changes muscle morphology and hamstring mechanics following an acute hamstring strain injury. The most consistent observation was the presence of scar tissue along the musculotendon junction, which could alter internal muscle mechanics and increase risk for re-injury. However, we could not identify any consistent asymmetries between the limbs of previously injured individuals using passive stiffness, strength, or joint kinematic measures. While differences in rehabilitation following the initial injury may have contributed to this inconsistency, it is possible that the local morphological changes may not be observable at the joint level. For example, the consistent reduction in BFLH volume and increases in BFSH volume could represent a compensatory process to maintain knee flexion strength following injury. Further study is needed to determine the extent to which initial injury and rehabilitation program influences hamstring musculotendon remodeling and function, and whether these factors influence re-injury risk.

SUMMARY

We conclude that long term morphological changes persist following an acute hamstring strain injury. However, these changes do not translate to asymmetries that are consistently detectable at the functional performance level.

REFERENCES

Koulouris, G et al., (2007). *Am J Sports Med,* 35(9): 1500-6.
Rask, MR and Lattig, GJ (1972). *JAMA,* 221(3):268-9.
Silder, A et al., (2007). *J Biomech* 40(12):2628-35.
Woods, C et al., (2004). *Br J Sports Med,* 38(1):36-41.

ACKNOWLEDGEMENTS

DIFFERENCES IN HAMSTRING MECHANICS BETWEEN SHORTENING AND LENGTHENING CONTRACTIONS REVEALED BY DYNAMIC MRI

Amy Silder, Christopher Westphal, Scott B. Reeder, and Darryl G. Thelen
University of Wisconsin – Madison, Madison, WI, USA, silder@wisc.edu

INTRODUCTION

Muscle injuries are thought to occur as a result of excessive strain during active lengthening contractions (Lieber and Friden 1993). Given that acute injuries most often occur along the musculotendon junction (DeSmet and Best, 2000), it is possible that regional variations in muscle strain influence injury potential. Dynamic MR imaging is a useful tool for characterizing spatial variations in muscle contraction mechanics (Pappas et al., 2002), and thus could provide insights into injury mechanisms. However, dynamic imaging studies to date have focused primarily on shortening muscle contractions performed against either constant or elastic loads. Our objective was to assess differences in hamstring mechanics between shortening and lengthening contractions using cine phase contrast (CINE PC) MRI.

METHODS AND PROCEDURES

Three healthy limbs (ages 26-29y) were tested. A MR-compatible device was used to guide the knee through ~30 deg of flexion/extension while simultaneously while imposing either an elastic or inertial load on the limb (Figure 1). Each loading condition required a knee moment of ~15% of the subject's isokinetic (30°/s) knee flexion strength. Peak loading occurred when the knee was extended in the inertial loading case (lengthening contraction), and when the knee was flexed during the elastic loading (shortening contraction). CINE PC was used to measure pixel velocities within a sagittal-oblique imaging plane through the biceps femoris long head (Figure 2). Subjects performed cyclic flexion/extension at a rate of 28 cycles/min to the beat of a metronome. Each scan lasted 1min 39s. Scanning

parameters were: spatial resolution = 1.4x1.4x6mm, VENC=5cm/s, 256×256 matrix, TR/TE=21.6/7.1ms, 2 lines of k-space/cycle, and 40 reconstructed frames/cycle.
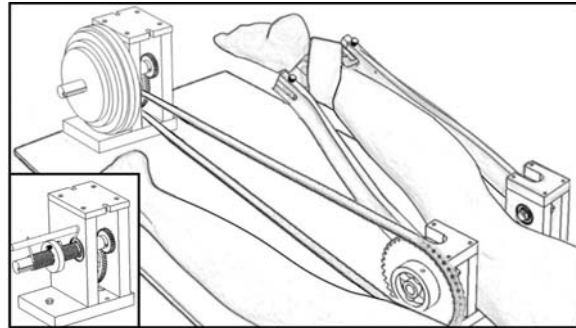
Figure 1. The subject lay prone within the scanner. Lengthening contractions were induced using inertial loading (shown), while shortening contractions were induced using an elastic load (see inset).

From the magnitude image at the first frame (~5° short of full extension), a set of 11x11mm regions of interest (ROIs) were drawn along the midline of the muscle (Figure 2). The trajectory of each ROI was then computed by integrating vertical and horizontal velocities (Pelc et al., 1995). Through plane velocities were checked to ensure out of plane motion was minimal.

RESULTS

There were marked differences in velocities and overall muscle motion between the two loading conditions. Comparing the same knee flexion angle, ROI velocities were more vertically oriented in the proximal region under the inertial load, compared to the elastic load (Figure 2). As a result, the inertial load resulted in ~30% less overall change in muscle length. Both loads induced non-uniform shortening along the muscle, with the

greatest shortening occurring in the mid-proximal region (Figure 3).

(a)   (b)
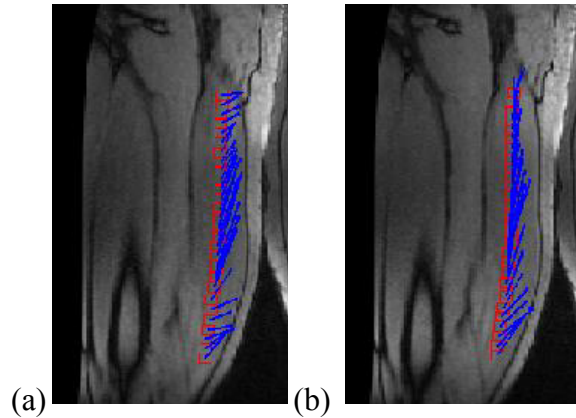
Figure 2. ROIs were drawn along the midline of the muscle and tracked throughout the knee motion. Arrows represent the velocity of each pixel at the current frame and demonstrate more vertically oriented motion in the proximal region for the (a) elastic load than the (b) inertial load.

DISCUSSION

Observable differences in muscle mechanics were revealed when loading required a lengthening contraction. In this condition, a more vertically oriented velocity profile during knee flexion resulted in a smaller overall muscle excursion. This difference likely resulted from greater tendon stretch (greater force) when the knee was extended in the inertial loading case.

Substantial variations in muscle stretch were observed along the length of the muscle for both contraction types. These variations may arise due to the biceps femoris musculotendon architecture. The large shortening in the mid-proximal region may reflect a portion of the muscle with the smallest aponeurosis, being distal to the proximal tendon, yet proximal to sheath-like distal aponeurosis of the biceps long head (Woodley et al., 2005). Given the large variations in strain, it is possible that strain gradients within the muscle play a role in the propensity for injury to occur at specific regions within the muscle. More

refined spatial strain mapping using dynamic MR imaging techniques (Zhong et al. 2007) could provide further insights into this issue.
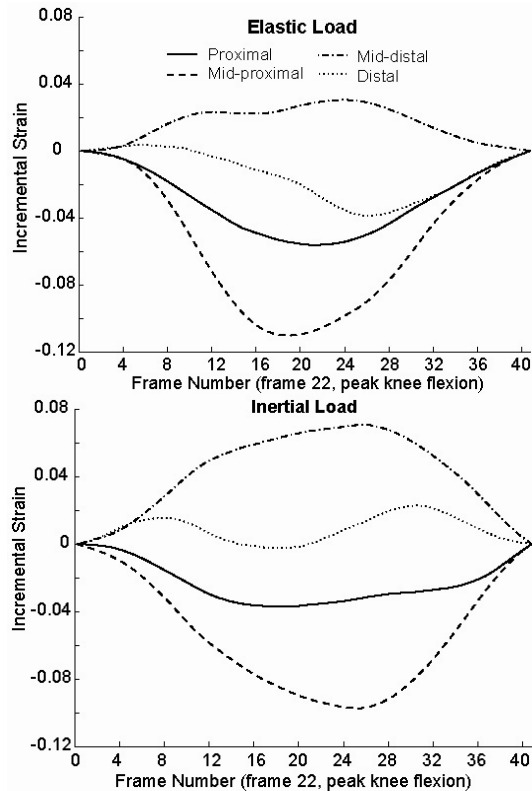
Figure 3. Average muscle strain measured from four sections of the muscle highlight the variations in local muscle mechanics along the length of the muscle.

REFERENCES

Desmet, AA and Best, TM (2000). *AJR Am J Roentgenol*, 174(2):393-9.
Lieber, RL and Friden, J (1993). *J Appl Physiol,* 74:520-6.
Pappas, GP, et al., (2002). *J Appl Physiol,* 92:2381-9.
Pelc JN, et al., (1995). *J Magn Reson Imaging,* 5(3):339-45.
Woodley SJ, et al. (2005). *Cells Tissues Organs,* 179: 125-141.
Zhong, X et al. (2008). *J Biomech,* in press.

ACKNOWLEDGEMENTS

A COMPARISON OF MUSCULOSKELETAL MODEL PREDICTIONS OF MUSCLE STRAIN WITH DYNAMIC MRI MEASURES

Amy Silder, Scott B. Reeder, and Darryl G. Thelen
University of Wisconsin-Madison, Madison, WI, USA, silder@wisc.edu

INTRODUCTION

Musculoskeletal models provide a foundation for characterizing muscle mechanics and describing how muscles induce movement. With recent advances in computational techniques (Delp et al., 2007), such models are being used increasingly in both research and education. Unfortunately, the validity of many model predictions, such as muscle strain, cannot be easily verified during normal movement. Therefore, the purpose of this study was to compare model predictions of muscle strain with measures obtained from dynamic MRI during two well controlled loading conditions.

METHODS AND PROCEDURES

Three healthy limbs were tested (2 females, 1 male; age 26±3y). A MR compatible device was used to load the hamstrings during cyclic knee flexion-extension performed at 28 cycles/min (Figure 1a). Two loads were considered: a) shortening contractions induced via a torsional spring, and b) lengthening contractions induced via inertia disks. A 10:1 gear ratio built into the device amplified the loads at the knee, such that knee moments of ~15% of each subject's maximum were experienced for each condition.

The experimental protocol was first performed in a motion analysis lab. A calibration trial was used to create a scaled musculoskeletal model of the lower extremity (Figure 1b) for each subject. Knee angle and chain tension were measured over ~50 cycles of knee flexion-extension for both conditions (~30 deg range of motion). These data were ensemble averaged across repeated cycles. We subsequently used computed muscle control (Thelen et al. 2003) to generate muscle-actuated simulations of each subject's movement. The model utilized a Hill-type representation of musculotendon mechanics, resulting in predictions of muscle strain across a flexion-extension cycle for each subject and loading condition.
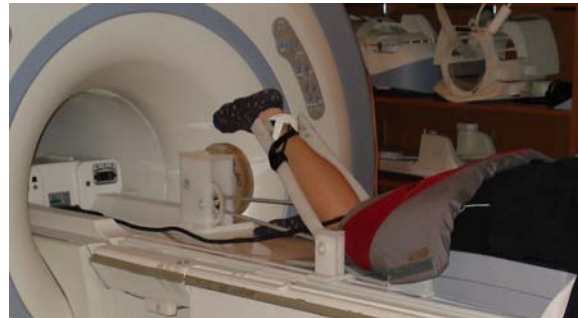
(a)
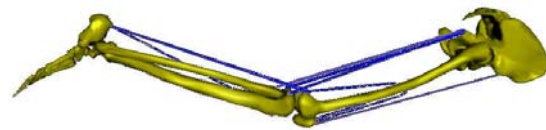
(b)

Figure 1. (a) Knee flexion-extension was performed while a device imposed elastic or inertial loads on the hamstrings. (b) Hill-type models were used to simulate musculotendon mechanics during the movement.

CINE PC images of the biceps femoris long head (BFLH) were also obtained for each subject and from each loading condition. Each scan lasted 1min 39sec. Scanning parameters were: spatial resolution=1.4 x 1.4 x 6mm, VENC=5cm/s, 256×256 matrix, TR/TE =21.6/7.1ms, 2 lines of k-space/cycle, and 40 reconstructed frames/cycle. From the magnitude image at the first frame (~5° short of full extension), a set of 11x11mm ROIs were drawn along the midline of the muscle. The motion of each ROI was computed by integrating vertical and horizontal velocities

(Pelc et al. 1995). Strain was defined as the normalized change in distance between ROIs, relative to the first frame.

RESULTS

The model predicted a larger change in muscle fiber length for the elastic load (9.7±2.0mm) compared to the inertial load (8.3±1.7 mm). This translated into an estimated 13% greater fiber strain for the elastic load. MR measures revealed qualitatively similar results. Quantitatively, strain estimates agreed most closely with model predictions in the mid-proximal region of the muscle (Figure 2), which represents the muscle portion spanning from 25 to 50% of the length from the proximal origin. Strain measures in other regions of the muscle were substantially less than model-based estimates.

DISCUSSION

The goal of this study was to compare model predictions of muscle strain with *in vivo* measurements obtained from dynamic MRI. Both model and image-based measures of strain were larger across a flexion-extension cycle for the elastic loading, compared to the inertial loading. Since overall musculotendon lengths were similar for both contraction types and muscle strain was larger for the elastic load, we conclude that the differences in strain are a result of increased tendon stretch when the knee is extended (lengthening contraction) during inertial loading.

Discrepancies between model and *in vivo* estimates are likely a result of fundamental model assumptions. In particular, we observed non-uniform strains along the entire length of the muscles' midline in both contraction types, which is consistent with the observations of Pappas et al. (2002). Our strain measures were largest in the mid-proximal portion of the muscle, but substantially smaller on either side. This may

reflect the BFLH architecture, characterized by a long rope-like tendon extending into the muscle on the proximal end and a sheath-like aponeurosis that inserts onto a shared distal tendon (Woodley et al., 2005). In contrast to our observations, the muscle model assumes uniform fiber shortening across the length of the muscle. We conclude that the use of three-dimensional muscle models (Blemker et al. 2005) seems appropriate when applications require strain data more refined than average estimates provided by Hill-type models.
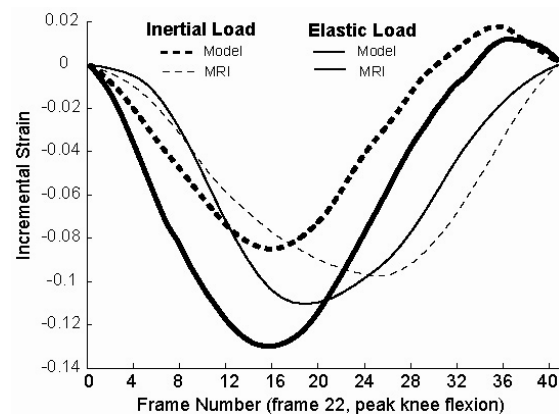
Figure 2. Model-based estimates of strain variations across a flexion-extension cycle agreed most closely with MR measures in the mid-proximal region of the muscle.

REFERENCES

Blemker SS, et al. (2005). *Ann Biomed Eng*, 33: 661-73
Delp SL, et al. (2007). *IEEE Trans Biomed Eng*, 54: 1940-1950.
Pappas GP, et al. (2002). *J Appl Physiol*, 92: 2381-2389
Thelen DG, et al., (2003). *J Biomech*, 36: 321-328.
Woodley SJ, et al. (2005). *Cells Tissues Organs,* 179: 125-141.

ACKNOWLEDGEMENTS

THE EFFECTS OF MID-AIR ADJUSTMENTS ON KNEE JOINT LOADING WHEN LANDING FROM A JUMP

Guan Q. Tan[1] and Timothy R. Derrick [1]

[1]Department of Kinesiology, Iowa State University, Ames, IA, USA
gqtan@iastate.edu URL: http://www.hhp.hs.iastate.edu

INTRODUCTION

One of the most common injuries involving the knee joint is an anterior cruciate ligament (ACL) tear. Female basketball and soccer players have about 3 time's higher risk of ACL injury versus male athlete counterparts (Prodromos et al., 2007).

Mid-air adjustments to the upper extremities will cause equivalent reactions in the lower extremities. This may cause jumpers to land asymmetrically and possibly increase the potential for ACL injuries. Variables of interest in ACL injury potential include knee shear forces, knee adduction moments and knee internal rotation moments (McLean et al., 2007). The purpose of this study was to determine if these variables are affected by landing from a jump with mid-air adjustments.

METHODS AND PROCEDURES

Eleven healthy college female students (age 21.8 ± 1.62 yrs, height 1.7 ± 0.5 m, mass 64.1 ± 11.7 kg) participated in the study. Three tennis balls were suspended from the ceiling according to Figure 1. After maximum jump height was established, subjects were instructed to jump from and land on two force platforms (AMTI, 1000 Hz). Approximately 100 ms after leaving the force platform an LED positioned near one of the balls was illuminated. Subjects were asked to tap this ball using both hands. They were told to jump as high as possible for each of 21 randomly selected trials. A total

of 23 retroreflective markers on the right and left lower extremities were used to determine the 3D orientation of the segments (Peak Motus, 120Hz).

Inverse dynamics were used to calculate joint moments and reaction forces at the knee joint. Kinematics were imported to a scaled SIMM (MusculoGraphics, Inc.) model to obtain the maximal muscles forces, muscle moment arms and muscle orientations for 88 lower extremity muscles. Static optimization using a cost function that minimizes the sum of the muscle stress squared was used to estimate the individual muscle forces. The knee joint contact forces were then calculated as the sum of the muscle forces and the joint reaction forces. The peak adduction knee joint moment, peak internal knee joint moment and peak anterior shear force were used to assess the potential for ACL injury. A 3 x 2 x 2 (reaching direction by right vs left leg by ipsilateral vs contralateral leg) repeated measures ANOVA was used to determine statistical significance.
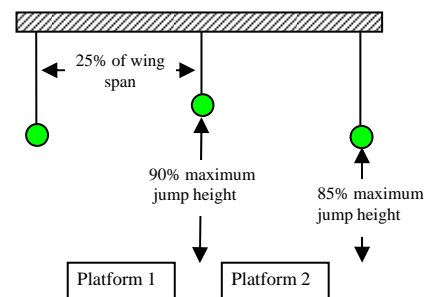
Figure 1. The jumping-landing tasks setup.

RESULTS

The average peak values for anterior shear force, rotation moment and adduction moment are given in Table 1.

	Reaching Direction	Ant. Shear Force	Rot. Mom.	Add. Mom.
Left Leg	Right	0.64 (0.56)	0.17 (0.10)	0.16 (0.08)
	Left	0.60 (0.55)	0.17 (0.09)	0.16 (0.08)
	Middle	0.59 (0.55)	0.14 (0.08)	0.14 (0.08)
Right Leg	Left	0.66 (0.51)	0.14 (0.09)	0.16 (0.10)
	Right	0.81 (0.57)	0.14 (0.07)	0.17 (0.10)
	Middle	0.68 (0.54)	0.11 (0.07)	0.15 (0.10)

Table 1. Mean (SD) of selected ACL injury potential variables during landing from a jump with possible mid-air adjustments. Forces are in body weights (BW) and moments are in BWm.

The anterior shear force was significantly greater on the right knee compared to the left and the rotation moment was significantly greater on the left knee compared to the right. However, data were also analyzed without reference to which leg had the highest peak values. The average peak difference between the middle ball condition and the greater value of the ipsilateral and contralateral legs from the side reaching conditions is given in Table 2. This shows that anterior shear forces, rotational moments and adduction moments all increased in one of the legs when reaching to the side.

Variables	average peak difference	p value
Ant. Shear Force	0.14 BW	0.05
Rot. Mom.	0.05 BWm	<0.01
Add. Mom.	0.03 BWm	0.02

Table 2. Loading increases during the side reaching conditions when compared to the middle reaching condition.

DISCUSSION

The results suggests that reaching to the side balls had a higher risk of ACL injury than reaching to the middle ball. This result was not apparent when looking at right/left leg effects or ipsilateral/contralateral leg effects because subjects adopted different strategies to deal with the mid-air adjustments that are necessary when reaching to a side ball. Some subjects always landed on their dominant leg, some subjects always landed on the ipsilateral leg etc.

SUMMARY

Understanding how the movement of the body in the air can affect the potential for ACL injury can be of benefit to athletes, coaches, athletic trainers and researchers. We found an increased potential for ACL injury when jumpers land from a jump in which they are required to reach to the right or left during the flight phase.

REFERENCES

Prodromos CC et al. (2007). *Arthroscopy, 23:1320-1325.*
Chappell JD et al. (2002). *Am J Sports Med, 30:261-267.*
Boden BP et al. (2000). *Orthopedics, 23:573-578.*
McLean SG et al. (2007). *Med Sci Sports Exerc, 39:502-514.*

DYNAMICAL MODELS OF REPEATED GOAL-DIRECTED MOVEMENTS

Joby John and Joseph P. Cusumano
Nonlinear Dynamics Laboratory, Department of Engineering Science and Mechanics,
Pennsylvania State University, University Park, PA, USA, jzj109@psu.edu

INTRODUCTION

A class of discrete dynamical systems for modeling repeated goal-directed kinematically redundant human movements is presented. The approach is based on the definition of movement tasks using goal functions and Goal Equivalent Manifolds (GEMs) (Cusumano and Cesari, 2006), which helps us to address "Bernstein's degrees of freedom problem". The example of a ball-throwing task is used to illustrate the central ideas. The resulting perception-action models have a hierarchical structure involving in-trial action templates and an inter-trial stochastic optimal error correction. The models identify the important factors on which variability in repetitive skilled performance depends.

THROWING TASK EXAMPLE

Consider a ball-throwing task as is schematically shown in Fig. 1. The manipulandum starts from rest ($\theta = 0, \omega = 0$) and throws a ball at the target on the wall. Knowing (θ, ω) at release completely determines if the ball hits the target. The scalar goal function for this task in the kth trial can be written as,

$$f(\theta_k, \omega_k; H) = \frac{L + R\cos\theta_k}{\tan\theta_k} - \frac{g}{2}\left(\frac{L + R\cos\theta_k}{\omega_k R\sin\theta_k}\right)^2$$
$$+ R\sin\theta_k - H = 0, \qquad (1)$$

The set of all $\mathbf{x} = (\theta, \omega)$ that satisfies Eq.(1) constitutes the goal equivalent manifold (GEM). In order to attain the release values (θ, ω) the manipulandum has to be actuated from rest. Experimental observations suggest that optimization principles govern discrete movements (Engelbrecht, 2001). Here, for the sake of simplicity, we assume that the manipulandum follows an *in-trial action template*
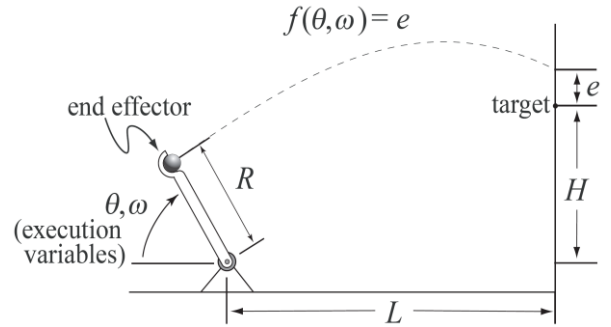
Figure.1 A Ball-throwing task. The goal is to hit the target at height H.

given by a minimum mean squared torque path such that, $\delta\int_0^{\tau_k}\left(\ddot{\theta}\right)^2 d\tau = 0$. This transforms the execution variables to the action variables as: $\theta_k = \frac{1}{6}\beta_k\tau_k^3$; $\omega_k = \frac{1}{2}\beta_k\tau_k^2$, where β is a jerk parameter and τ is the rescaled dimensionless actuation time to release. We can now equivalently express the GEM for the throwing task in terms of the actuation variables as:

$$f(\theta_k, \omega_k) = f\left(\tfrac{1}{6}\beta_k\tau_k^3 \; \tfrac{1}{2}\beta_k\tau_k^2\right) \triangleq \tilde{f}(\beta_k, \tau_k).$$

Figure 2 shows the GEM in action space with two constant error contours depicting $\pm 10\%$ error at the target. We notice that the "thickness" imparted to the GEM by these constant error contours is not constant and varies along the GEM. For small perturbations off of the GEM, the singular values s of the matrix of partial derivatives of the goal function with respect to the body variables (A), quantify the effective thickness property of the GEM and determine how body errors are magnified to goal level errors. This property of the goal function is referred to as *passive sensitivity* and is central to our analysis of variability arising in repeated trials of skilled tasks.
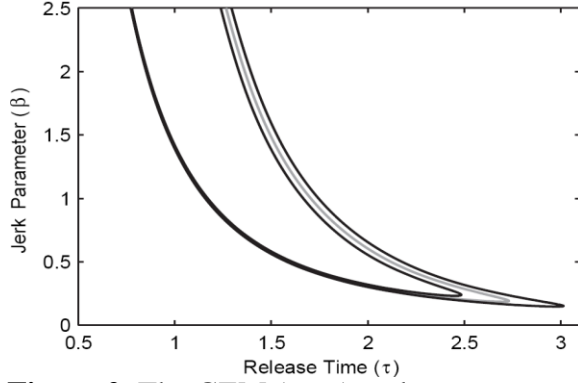
Figure 2. The GEM (grey) and constant error $(\pm 10\% \, \text{error})$ contours (black) in the actuation space for the throwing task.

PERCEPTION-ACTION LOOP

The schematic representation in Fig. 3 is used to illustrate the repeated performance of a goal oriented task. This template is fairly general and can be used to model a variety of repetitive skilled tasks. The inter-trial dynamics can be modeled as a simple update equation :

$$\mathbf{x}_{k+1} = \mathbf{x}_k + (G + M)\,\mathbf{v}(\mathbf{x}_k) + \mathbf{n}, \qquad (2)$$
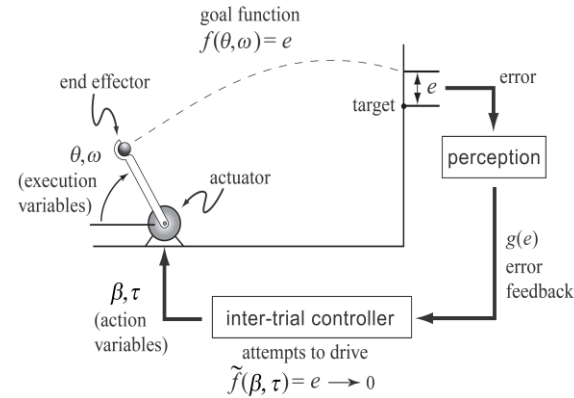
Figure 3. The perception-action loop. Each component in this template can be modified according to the task being modeled.

where $\mathbf{x}_k = (\beta_k, \tau_k)$ are the body state variables in the action space, in the kth trial, $\mathbf{v}(\mathbf{x}_k)$ is the control input, $\mathbf{n}$ is the additive noise and G and M are diagonal matrices of controller gain and multiplicative noise respectively. An error-correcting stochastic optimal feedback controller (Todorov & Jordan,

2005) is employed to compute the input $\mathbf{v}(\mathbf{x}_k)$. For small deviations $\mathbf{u}$ from the GEM, Eq.(4) is linearized as $\mathbf{u}_{k+1} = (I + GJ)\,\mathbf{u}_k + \mathbf{n}$, where J is the Jacobian matrix of the control input $\mathbf{v}$ evaluated at $\mathbf{x}^*$. The eigenvalues of the matrix $(I + GJ)$ determine the stability of the system. Transforming the linearized dynamics to the eigen coordinates, it can be shown that the performance at the target scales linearly with the passive sensitivity of the GEM, i.e.,

$$\frac{\sigma_e}{\sigma} = \frac{s}{\sqrt{1 - \lambda^2}}, \qquad (4)$$

where σ_e^2 is the variance of error at the target, σ^2 is the variance of the isotropic additive noise, s passive sensitivity, and λ is the eigenvalue of the linearized controller corresponding to a direction orthogonal to the GEM. Repetitive performance based on Eq.(2) at 20 different locations along the GEM, for two different controllers (optimal: $\lambda = 0$, suboptimal: $\lambda = 0.6$) and two different additive noise levels ($\sigma = 10^{-4}$ and $\sigma = 10^{-2}$), was numerically simulated. The variance at the target (σ_e) was found to agree very well with the prediction of Eq.(4).

SUMMARY

We showed how the concepts of goal equivalence and goal equivalent manifolds can be used to developed a class of models for the trial-to-trial dynamics of skilled movements. Applying the approach to a throwing example, we found that the performance at the target depends on passive sensitivity (s), noise level (σ), and the stability of the inter-trial controller (λ). Experiments to test these predictions are currently being constructed.

REFERENCES

Cusumano J. P. & Cesari P. (2006), *J. Biol Cybernetics*, **94** (5), 367-379.

Engelbrecht, S. E., (2001), *J. Math. Psych,* **45**, 497-542.

Todorov, E. & Jordan, M. I., (2002), *Nature: Neuroscience*, **15** (11), 1226-1235.

IN-VITRO INVESTIGATION OF MENISCAL MOVEMENT USING MEDICAL IMAGING

Maeghan Innes[1,2,3,4], Mark Hurtig[2,3,4,5], David Holdsworth[2,6] and Karen Gordon[1,3,4]

[1]School of Engineering, University of Guelph, Guelph, ON, Canada, innesm@uoguelph.ca
[2]Canadian Arthritis Network, Canada
[3]Comparitive Orthopaedic Research Group, University of Guelph, Guelph, ON, Canada
[4]Proknee Group, Toronto, ON, Canada
[5]Clinical Studies, Ontario Veterinary College, University of Guelph, Guelph, ON, Canada
[6]Robarts Research Institute, London, ON, Canada

INTRODUCTION

Medical imaging used in conjunction with joint loading devices can yield valuable information with regards to the response of the knee joint to load. However, it is difficult to replicate physiologic loading in an in-vitro environment. In addition, some previous studies have removed a portion of the joint, making the loading scenario less relevant (Song et al., 2006). The objective of this work was to study the in-vitro response of the medial meniscus to physiologic loading.

METHODS AND PROCEDURES

A device was designed to apply physiologic loads of 1.5 to 2 times body weight (BW) (Taylor et al., 2006) while maintaining an intact ovine (sheep) stifle (knee) from the mid femur to mid tibia at flexion angles (40-60 degrees) representing the stance phase of gait (Tapper et al., 2004). The fresh frozen left knee of a 31.5kg sheep, approximately 1 year old, was dissected to remove as much muscle and soft tissue as possible without damaging the joint capsule. Beekley™ markers were placed above bony landmarks on the proximal end of the tibia and distal end of the femur (Beekley Inc., CT, USA). The knee was potted in polymethylmethacrymate (PMMA), and mounted within the device. A 50/50 saline and ioxaglate (meglumine 39.3% and sodium 32%) solution was used as a contrast agent and was injected into the joint space. The device and joint were placed into the μCT bore and connected to an air compressor. A custom built μCT compatible piston was used to apply the desired joint load.

Figure 1. Device used to apply physiologic loads to a secured ovine stifle joint at various flexion angles

A General Electric Health Care (GEHC) eXplore Locus Ultra μCT scanner was used to collect this data. The anatomical scan protocol was set with an acquisition time of 8 seconds and x-ray exposure energies of 120kVp, 20mA. The reconstruction matrix size was 330 x 420 x 340 with voxel dimensions of 0.307mm x 0.307mm x 0.307mm.

The μCT images were acquired simultaneously with load application. Images were taken first in the unloaded state, followed by an applied load of 60% BW (imaged at 1 & 3 minutes following load application). The load was increased to 100% BW, and images were acquired at 8, 11, 18, 28 & 49 minutes after the initial load. The distance between the centroid of the medial

meniscus and the tibia origin, established as midway between the medial and lateral Beekley™ markers, were calculated for the unloaded and loaded images. The response of the medial meniscus was quantified as the difference between these distances.

RESULTS

There were displacements of the meniscus in both the anterior-posterior and medial-lateral directions with load application. It initially moved 0.55mm posteriorly but 49 minutes after initial load returned to a position 0.98mm anterior to the unloaded meniscus centroid. The medial meniscus initially moved 0.63mm medially when the 60% BW load was applied but stabilized to a position 0.26mm medially compared to the unloaded state. With the load increased to 100% BW the meniscus moved medially to 0.37mm but after 20 minutes returned to 0.23mm displacement. The resolution of the images, 0.307mm, is sufficient to show displacements of less than a millimetre in the medial meniscus of the sheep.

DISCUSSION

There are several factors that may affect the accuracy of the results. Segmentation of the meniscus was performed manually since the contrast between soft tissue is limited, which decreases the accuracy of these displacement measurements. It is also difficult to align the knee to ensure a neutral (minimal stress) initial orientation. The initial position of the joint may apply small loads to the soft tissues, and affect the resulting movement of the meniscus.

There was a medial shift of the meniscus upon loading, which is expected in the medial meniscus of the left knee (Shefelbine et al., 2006; Thompson et al., 1991; Vedi et al., 1999). The medial movement occurred during the first minute following load application. There was an inconsistent anterior-posterior movement of the medical meniscus under load. The meniscus will move posteriorly when the knee experiences cyclic loading (Kenny et al., 1997; Shefelbine et al., 2006). The current study found an initial posterior followed by an anterior displacement. This discrepancy may arise due to the different loading conditions. Quantification of meniscal movement in normal, healthy tissue will aid in determining variations that occur with injury, disease and healing; and provide insight into the trajectory of tissue degeneration that leads to osteoarthritis.

SUMMARY

From this initial data, it is clear that this device will allow for the investigation of the movement of the meniscus during axial loading. Continuing work with a greater number of specimens will enable a quantification of the response of the healthy meniscus to physiologic load. Further investigations into the response of the meniscus following degeneration, injury and repair will help elucidate disease mechanisms and optimize repair methods for the knee joint.

REFERENCES

Kenny, C. (1997). *Clin Orthop & Related R*, 339: 163-173.
Shefelbine et al. (2006). *J Orthop R*, 24(6): 1208-1217.
Song et al. (2006). *J OA & Cartilage*, 14: 728-737.
Tapper et al. (2004). *J Biomech Eng*, 126: 301-306.
Taylor et al. (2006). *J Biomech*, 39(5):791-8.
Thompson et al. (1991). *AJSM,* 19(3): 210-6.
Vedi et al. (1999). *J Bone and Joint Surgery,* 81: 37-41.

MODELING MUSCLE FATIGUE FOR MULTIPLE JOINTS

Ting Xia[1] and Laura Frey Law[1,2]

[1]Virtual Soldier Research program, Center for Computer-Aided Design, College of Engineering, University of Iowa, Iowa City, IA, USA, txia@engineering.uiowa.edu
[2]Graduate Program in Physical Therapy and Rehabilitation Science, College of Medicine, The University of Iowa, Iowa City, IA, laura-freylaw@uiowa.edu

INTRODUCTION

Muscle fatigue prediction is an important area in ergonomics to prevent workers from occupation-related musculoskeletal disorders. Studies have shown that muscle fatigue is affected not only by work intensity but also intrinsic properties such as muscle composition (i.e. fatigability) and joint torque-velocity-angle relationship. We propose a theoretical muscle fatigue model addressing these factors. The purpose of this work is to examine if the model can represent realistic fatigue behavior, particularly the endurance time (ET)-work intensity relationship, of major body joints.

The fatigue model is a compartment-based muscle fatigue model (Liu et al., 2002) with a bounded proportional controller. The muscle tissue is considered to be in one of three states at any time: resting (M_R), activated (M_A), or fatigued (M_F). Muscle activation-deactivation is regulated by the controller to achieve a given task intensity. The fatigue and recovery processes are regulated by two factors, F and R, representing the fatigue and recovery properties of a particular joint, respectively. The system is able to maintain a steady torque output by increasing muscle activation until failure, i.e. ET.

METHODS AND PROCEDURES

To examine the model's ability to represent different joint ET - intensity profiles from the literature, F and R were varied for each joint (Table 1). Isometric work intensities ranging from 10% to 90% of maximum voluntary contraction (%MVC) were modeled for the elbow, shoulder, back and the whole-body, and compared to published regression models (El ahrache et al., 2006).

RESULTS

The simulated ET-Intensity curves for the elbow, shoulder, and back joints, as well as the whole-body are presented in Figures 1-4, respectively, along with the statistical regression models from the review by El ahrache et al. (2006). Our theoretical model reproduces the average (i.e. <10% error for < 50%MVC and ~ 20% error for > 50% MVC) of the previous statistical models. Note, however, there is significant variability between the other models (see figures).
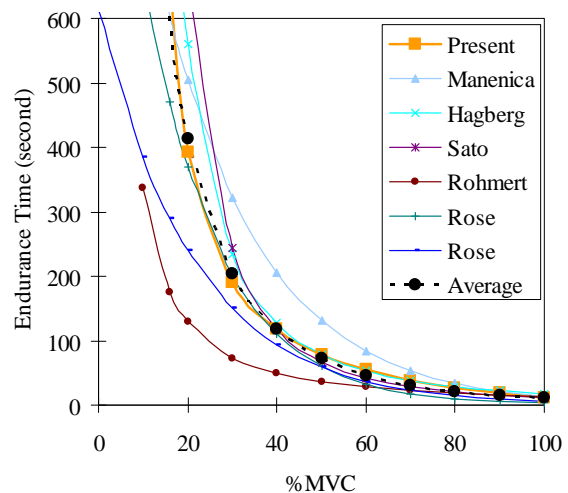
Figure 1. Elbow joint ET-Intensity curves.
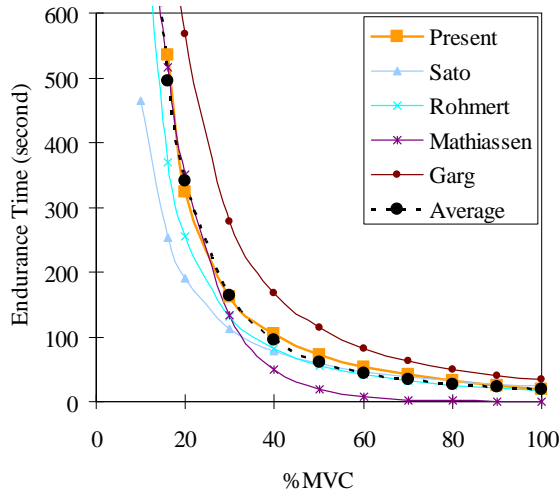
Figure 2. Shoulder joint ET-Intensity curves.
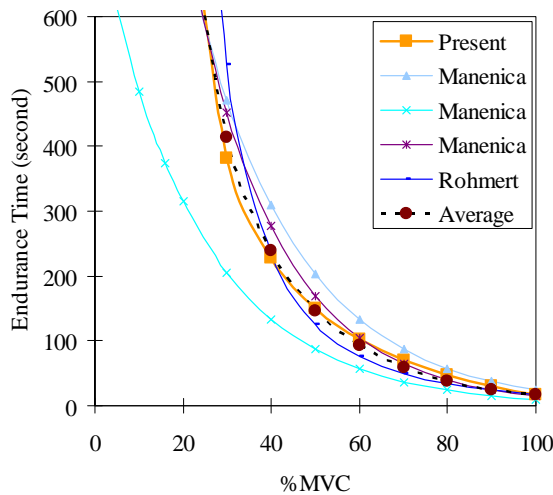
Figure 3. Back joint ET-Intensity curves.
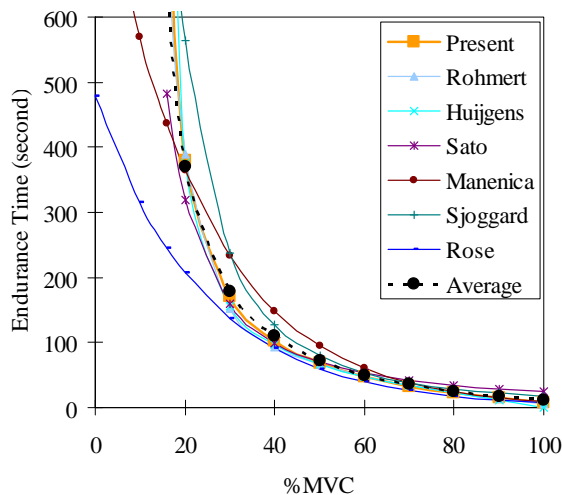
Figure 4. Whole-body ET-Intensity curves.

Joint	F	R
Elbow	0.016	0.0024
Shoulder	0.02	0.003
Back	0.0083	0.0015
Whole-Body	0.0187	0.0033

Table 1. Fatigue and recovery factors.

DISCUSSION

Modeling muscle fatigue is very challenging due to the complexity of the phenomenon. Previous ET-work intensity curves have been modeled statistically based on experimental data. Our model uses a theoretical approach to represent muscle fatigue that is able to reproduce a variety of joint ET-work intensity profiles. Additionally, the smaller magnitude of the back F value suggests that back muscles are, as expected, less susceptible to fatigue than muscles surrounding the elbow or shoulder joints. These simulations demonstrate the model's ability to adjust to varying joint fatigability. The potential advantage of this approach is that it may be applied to more complex tasks that simple static ET curves cannot.

SUMMARY

Reasonable ET predictions for different body joints suggest that this theoretical muscle fatigue model provides a reasonable approach and acceptable accuracy for ergonomic applications.

REFERENCES

El ahrache K et al. (2006). *Int J Ind Ergon*, 36: 99-108.
Liu JZ et al. (2002), *Biophys J*, 82: 2344-59.

ACKNOWLEDGEMENTS

INCREASED INERTIAL FORCES REDUCES LOCOMOTIVE STABILITY

Christopher J. Arellano, Daniel P. O'Connor, Melissa Scott-Pandorf, Charles S. Layne
and Max J. Kurz

Laboratory of Integrated Physiology, University of Houston, Houston, TX, USA
E-mail: carellano@uh.edu or mkurz@uh.edu, URL: www.hhp.uh.edu

INTRODUCTION

Adding a load around the center of mass (COM) increases both the gravitational and inertial forces acting on the body. However, when adding a load, the independent effect of inertia on the stability of the locomotive system is not readily evident. It is possible that the inertial forces play an important role in the stability of the locomotive system since they govern how the COM is accelerated and decelerated throughout the gait cycle. In this study, we investigated the influence of increased inertial forces on the stability of the locomotive system. It was hypothesized that stability would decrease as inertia increased.

METHODS AND PROCEDURES

Right lower extremity joint kinematics (120 Hz) were recorded in the sagittal plane for twenty-three subjects (height = 1.7 ± 0.1 m, weight = 63.9 ± 8.7 kg, age = 23.8 ± 4.5 yrs.) walking on an treadmill for three minutes at a self-selected speed while inertia was increased from 0%, 10%, 20%, and 30% of normal body weight. To increase inertia only, thin lead strips (0.45 kg each) were firmly attached in symmetry around the waist via a modified belt, while an upward vertical force was applied by a body weight support system. The upward force was equal to the amount of weight added to the participant. Therefore, the subject weighed the same but was carrying additional mass. The addition of mass, with

no increase in weight, effectively increased the inertia acting at the COM of the body. The state vector (**x**) of the locomotive system was used to evaluate the stability at the instance of heel-contact and mid-swing. **x** was defined by the joint positions and velocities of the hip, knee, and ankle. Figure 1 depicts an example first-return map for the hip joint component of **x** over successive gait cycles.
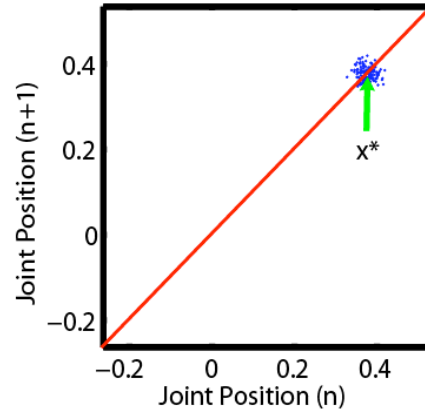
Figure 1. First -return map for the hip joint. x* represents the hip joint's equilibrium point.

Floquet analysis was used to quantify the dynamic stability of the gait pattern (Hurmuzlu et al., 2001). This involved linearizing the first-return map about **x*** to satisfy the following relationship

$$\delta x^{n+1} = \mathbf{J} \delta x^{n}$$

where δ denotes the deviation about **x*** at each nth step, and **J** is a 6 x 6 constant coefficient matrix that represented the Jacobian. δx^{n} and δx^{n+1} were defined as

$$\delta x^{n} = [x_{n} - x^*, x_{n+1} - x^*, x_{n+2} - x^*, \dots]$$

$$\delta x^{n+1} = [x_{n+1} - x^*, x_{n+2} - x^*, x_{n+3} - x^*, \dots]$$

A least squares algorithm was used to solve for **J** (Tedrake, 2004). The largest eigenvalue (β) was computed from **J** and used to quantify the stability of the gait pattern at the instance of heel- contact and mid-swing. A β value further away from zero signified a less stable gait.

RESULTS

Repeated measures ANOVA showed that the main effects of inertia (p = 0.040) and instance of the gait cycle (p = 0.0001) were significantly different. However, no significant interaction was found (p = 0.751). Post hoc analysis revealed that the locomotive system was significantly less stable while walking with 30% inertia when compared to walking without added inertia (p = 0.031; Figure 2) and significantly less stable at heel-contact than at mid-swing (p = 0.0001), indicating greater instability at heel-contact. Additionally, our trend analysis indicated a significant increasing linear trend for β as inertia increased (p = 0.007).
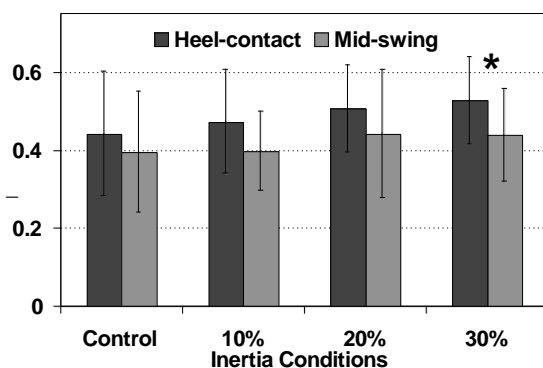
Figure 2. β values across conditions (mean ± SD).

DISCUSSION

Our results support the hypothesis that stability decreases as inertial forces are increased. Potentially, the loss of stability may be related to how the locomotive system controls the forces that influence the acceleration and deceleration of the COM throughout the gait cycle. On the other hand, previous experiments show that the redirection of the COM during the step-to-step transition points is a critical determinant of gait (Kuo, 2007). Possibly the control of the inertial forces at these transition points may have an impact on the stability of the gait pattern. Our results also indicate that the value of β at heel-contact was greater than at mid-swing. Interpretation of the data suggests that these differences may be due to the initial collision that occurs at heel-contact. It is also possible that these differences may be due to the fact that our experimental design directly manipulated the stance dynamics.

SUMMARY

Overall, gait stability decreased as inertia increased. Our future investigations will test whether these results hold when walking at slower and faster speeds. It seems reasonable that the control of the deceleration and acceleration of the COM will become increasingly important at faster speeds and may affect gait stability.

REFERENCES

Hurmuzlu, YB, et al. (2001). *ASME J. Biomech. Eng.,* 118: 405-411.
Kuo, AD (2007). *Hum Mov Sc,* 26: 617-656.
Tedrake, R, et al. (2004). *Proc. IEEE ICRA.,* 5: 4656-4661.

ACKNOWLEDGEMENTS

A SURFACE EMG STUDY OF HEALTHY JAW FUNCTION

Steph Forrester[1], Matthew T.G. Pain[1], Andy Toy[2] and Ron Presswood[3]

[1]School of Sport & Exercise Sciences, Loughborough University, Loughborough, LE11 3TU, UK, s.forrester@lboro.ac.uk, URL: http://www.lboro.ac.uk
[2] Gorse Covert Dental Practice, Loughborough, LE11 4RZ, UK
[3] 8801 Gaylord, Houston, Texas 77024, USA

INTRODUCTION

A number of studies have linked temporomandibular disorders (TMD) to altered activation patterns of the masticatory muscles during occlusion (Ciancaglini et al., 2002). Treatment of TMD aimed at restoring neuromuscular function requires knowledge of how occlusal contact is achieved in the healthy population. The purpose of this study was to identify common masticatory muscle function patterns in the healthy population for maximum clenching on a range of symmetric and asymmetric occlusal interferences.

METHODS

Fifteen volunteers (12 males and 3 females, age 26.1 ± 4.5 years) with healthy jaw function gave informed consent to participate. Subjects were seated in the alert feeding position and, following a short familiarisation of sub-maximal clenches, completed maximal clenches for the following six conditions: natural dentition (ND); lucia jig (LJ); left molars on a tongue blade (TBL); right molars on a tongue blade (TBR); front teeth on a tongue blade angled at ~45° below the horizontal (TBF); both sets of molars on cotton rolls (CR). In each trial the subject was instructed to start relaxed, clench maximally for 4 seconds, and relax again. Surface EMG were collected bilaterally for the temporalis anterior (TA), masseter superficial (MS), digastric anterior (DA) and sternocleidomastoid (SCM) muscles using active bipolar surface electrodes. The signals were recorded at 2000 Hz and bandpass filtered at 10-600 Hz. EMG amplitude was evaluated as an RMS average over a 50 ms window and normalised based on the global maximum value recorded in all trials. Onset times were determined using the algorithm recommended by Hodges and Bui (1996). Selected EMG amplitude and onset timing parameters for the six maximal clench conditions were compared using one-way repeated measures ANOVAs and Tukey's HSD post-hoc test ($p \leq 0.05$).

RESULTS

Figure 1 presents the mean ± 1 standard deviation in each condition for: maximum normalised amplitude (AMPNmax) of the TA and MS; bilateral symmetry coefficient (POC) for the TA and MS; torque coefficient (TC); and anterior-posterior coefficient (APC). POC TC and APC from Ferrario et al. (2006).

DISCUSSION

Occlusal interferences that prevented molar contact (LJ, TBD) significantly reduced maximum AMPN of both the TA and MS by at least 50% as reported previously for the LJ (Becker et al., 1999). This has been suggested to result from the loss of periodontal ligament proprioreceptive feedback. However, these interferences also produce geometrical changes in the position of the mandible relative to the maxilla, which could equally generate the feedback mechanisms that result in reduced muscle

activity. Indeed, the significantly different APC values for these interferences compared to ND condition, indicate differing amplitude reductions in the TA and MS which supports a geometry based feedback mechanism.

Asymmetric interferences (TBL and TBR) had minimal effect on MS but significantly affected the contralateral TA amplitude. For TBL, maximum AMPN of the RTA was significantly lower than that of the LTA, and vice versa for TBR. Similarly, the bilateral symmetry (POC) and torque coefficient (TC) values for the TA were significantly different between the TBL and TBR with both conditions generating significant asymmetry. There was also evidence for asymmetric onset timing in TA muscle activity with the contralateral TA activating first. However, a larger sample size is required to confirm the statistical power of this observation.

SUMMARY

This preliminary study has indicated some well defined activation patterns in the jaw musculature for maximum clenching under different symmetric and asymmetric conditions in the healthy population. Neuromuscular performance of the TA appears to be more affected by the presence of occlusal interferences compared to the MS.

REFERENCES

Becker, I et al. (1999). *J Prosthet Dent*, 82:22-26.
Ciancaglini, R et al. (2002). *J Oral Rehab*, 29:1082-1090.
Ferrario, VF et al. (2006). *J Oral Rehab,* 33:341-348.
Hodges, PW and Bui, BH (1996). *Electroencephalogr Clin Neurophysiol,* 101:511-519.

ACKNOWLEDGEMENTS
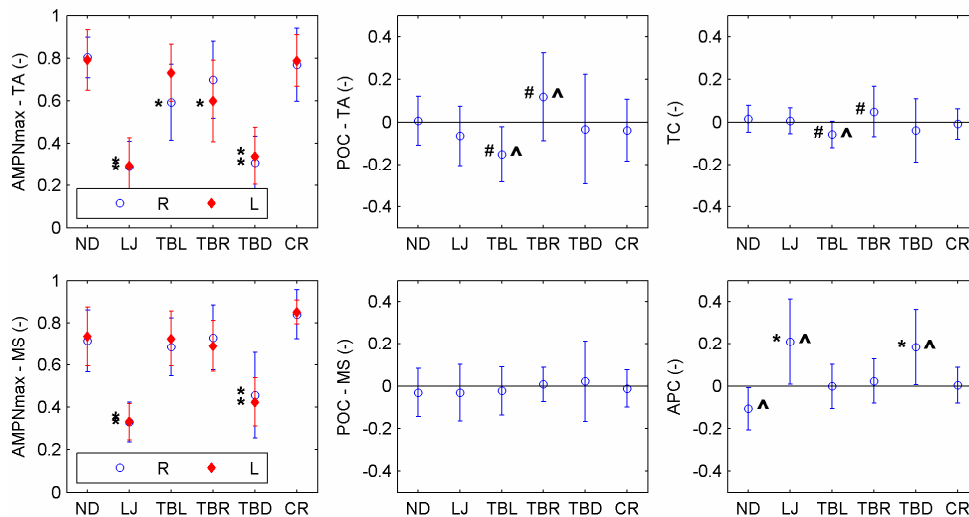
Figure 1. Amplitude parameters for the MS and TA in the six maximum clenches conditions (mean ± sd). Significant differences: compared to ND (*); between TBL & TBR (#); non-zero POC, TC & APC (^).
POC = bilateral symmetry [0 = symmetric → ± 1 = left dominant (-1) or right dominant (+1)]
TC = latero-deviating torque [0 = no torque → ± 1 = left dominant (-1) or right dominant (+1)]
APC = anterior-posterior displacing force [0 = no force; posterior dominant -1; anterior dominant +1]

ACL RECONSTRUCTION AFFECTS LOWER EXTREMITY ENERGY ABSORPTION MORE THAN TASK DIVERSION DURING ONE LEG LANDINGS

Marissa A. Link & Steven T. McCaw
Illinois State University, Normal
email: smccaw@ilstu.edu   web: www.cast.ilstu.edu/mccaw

INTRODUCTION

Drop landings are used to investigate energy absorption by the lower extremity, allowing for control and/or manipulation of factors such as height, distance, surface, and footwear that affect energy absorption. The effect of perturbing a subject's information processing while landing remains equivocal. Previous research has reported both more (Buckley et al, 2005) and less (Santello et al, 2001) lower extremity joint ROM with restricted vision, using healthy old and young subjects, respectively, while the act of catching a ball altered leg muscle activity patterns among those with previous ACL injury (Cowling & Steele, 2001). Our purpose was to determine the effect of task distraction and rehabilitated ACL reconstruction on individual joint energetics during one leg drop landings. We hypothesized greater bilateral differences in the absolute and relative energy absorptions by the ankle, knee and hip among those with ACL reconstruction, and that the differences would be accentuated when the information processing demands were increased by diverting the subject from the landing task.

METHODS

Physically active females participated in the study. The ACLr group (n=10) had been surgically reconstructed at least 1y prior, and had medical clearance to return to pre-injury activity. The Healthy group (n=10) were recreationally competitive athletes. All were injury free for 6 months prior to testing, and each provided informed consent.

Landings were performed from a .3 m box set .1 m from the force plate. A six-camera optotrak system recorded (200Hz) 5 trials of one leg landing onto a force platform (1000 Hz) in each of four conditions created by crossing the Leg (injured/uninjured for the ACLr group, right/left for the healthy group) and the Diversion (Non-diverted/diverted) factors. Diversion was attained by requiring subjects to identify the colour of randomly flashing lights. The conditions were performed in random order by each subject. Instructions were to "land comfortably".

GRF data were smoothed (20 Hz) to reduce artifacts in the calculated joint torques (Bisseling & Hof, 2006). Sagittal plane joint torques (JT) were calculated using standard inverse dynamic techniques, and mechanical power was calculated as $JT \cdot \omega$. Power curve integrals at each joint from initial contact to the end of knee joint flexion were calculated to quantify energy absorption. The five trial condition means of each subject were entered into a 3 way mixed factor ANOVA (Between: group; Within: Leg & Diversion) for statistical comparisons ($\alpha = .05$).

RESULTS AND DISCUSSION

Joint power curves were similarly shaped for both groups in all conditions (Fig.1). Diversion interaction and main effects were not statistically significant (Table 1). Less total energy was absorbed by the ACLr group, most evident when landing on the reconstructed leg. A significant group by leg interaction revealed a bilateral difference in
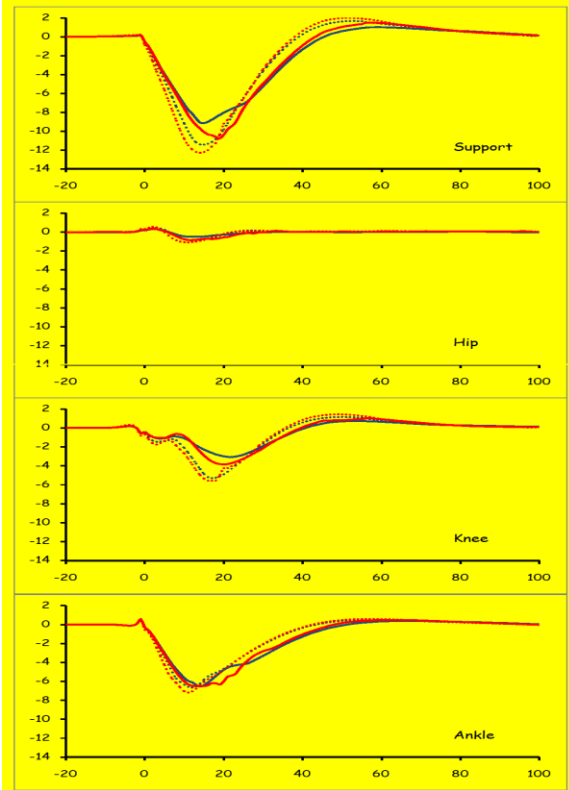
Figure 1. Grande ensemble power curves (mean data only) by conditions: Legend: Blue Dashed: ACLr non-diverted; Blue Solid: ACLr Diverted; Red Dashed: Healthy Non-diverted; Red Solid: Healthy Diverted. Vertical axes: J/kg. Ground contact at 0. Haxis: % time from contact to end knee extension.

SUMMARY/CONCLUSIONS

Although reduced energy absorption by the reconstructed knee was evident in the power curves of the ACLr, results did not support the hypothesis that bilateral differences in lower extremity energetics would be accentuated when an additional task is imposed on a one leg drop landing.

REFERENCES
Bisseling, R & Hof, A (2006) *J Biomech* 39, 2438-2444.
Buckley, JG et al. (2005) *Gait Posture* 21, 65-71
Cowling, EJ & Steele, JR (2001) *J Bone Joint Surg.,* 83A, 35-41.
Santello, M et al. (2001). *JAP*, **537.1**, 313-327.

knee energy absorption only for ACLr; the injured knee absorbed ~30% less energy than the uninjured knee. With no significant compensating increase at the hip or ankle there are significant bilateral differences in the relative contribution of the ankle and knee to total energy absorption.

Table 1. Descriptive statistics of joint work and % joint contribution to total energy absorption.

		Negative Work (J/kg)									
		ACLr Group					Healthy Group				
		ACLr Leg		Healthy Leg			Right Leg		Left Leg		
		Non-Div	Div	Non-Div	Div		Non-Div	Div	Non-Div	Div
Total	Mean	-1.06	-1.03	-1.23	-1.19	Mean	-1.42	-1.41	-1.28	-1.38
	SD	0.27	0.30	0.20	0.24	SD	0.32	0.36	0.33	0.42
Hip	Mean	-0.06	-0.04	-0.06	-0.05	Mean	-0.07	-0.06	-0.06	-0.09
	SD	0.06	0.04	0.04	0.02	SD	0.06	0.05	0.07	0.12
Knee	Mean	-0.35	-0.33	-0.50	-0.49	Mean	-0.61	-0.61	-0.47	-0.54
	SD	0.19	0.20	0.16	0.17	SD	0.17	0.23	0.17	0.23
Ankle	Mean	-0.65	-0.66	-0.67	-0.65	Mean	-0.74	-0.74	-0.75	-0.75
	SD	0.17	0.18	0.13	0.17	SD	0.19	0.16	0.14	0.13
		Relative Work (%)									
		ACLr Group					Healthy Group				
		ACLr Leg		Healthy Leg			Right Leg		Left Leg		
		Non-Div	Div	Non-Div	Div		Non-Div	Div	Non-Div	Div
Hip	Mean	5.6	4.1	5.2	4.2	Mean	5.0	4.1	4.4	5.5
	SD	4.7	3.3	3.6	2.2	SD	3.1	2.8	3.6	4.9
Knee	Mean	31.0	30.1	40.3	40.7	Mean	42.9	42.8	35.9	37.9
	SD	12.7	12.0	7.4	9.9	SD	7.2	6.9	6.1	8.2
Ankle	Mean	63.3	65.7	55.2	54.6	Mean	52.1	53.1	59.7	56.6
	SD	14.2	12.6	9.1	7.1	SD	8.4	8.4	7.1	9.2

POSTURAL CONTROL DURING QUIET STANDING IN PATIENTS WITH A TOTAL HIP ARTHROPLASTY OR A HIP RESURFACING

Vicky Bouffard[1-4], Marc Therrien[1], Martin Lavigne[3], Pascal-André Venditolli[3]
François Prince[1-2-4]

[1]Gait and Posture Laboratory, Marie Enfant Rehabilitation Center, Montreal, Qc, Canada
[2]Department of Surgery, Faculty of Medicine, University of Montreal, Montreal, Qc, Canada
[3]Ortopaedic Department, Maisonneuve – Rosemont Hospital, Montreal, Qc, Canada
[4]Department of Kinesiology, University of Montreal, Montreal Qc, Canada
francois.prince@umontreal.ca

INTRODUCTION

Osteoarthritis (OA) is a disease affecting 15% of the American population (Issa and Sharma, 2006) with a higher prevalence for people older than 65 years (Buckwalter, 2006). In most cases, it generates an overwhelming pain. In order to relieve this pain, several prostheses are used in a surgical procedure called hip arthroplasty. The first main type of hip replacement is the total hip arthroplasty using a large femoral head (THA). Over the years, this prosthesis has proved its worthiness and is now recognized as an effective, reproducible and frequently used therapeutic option (Vendittoli, et al., 2006). The second main type is the surface replacement arthroplasty (SRA). The major advantage of this prosthesis is to keep the femoral head and neck assuring a better restoration of the patient's anatomy (Nantel et al., 2007). A lot of studies have shown results about THA or SRA but so far, only a few compared the two prostheses together. The objective of this study is to compare the postural stability of the patients after THA or SRA at six and twelve months post-surgery, during a quiet standing task with open eyes (OE) and closed eyes (CE).

METHODS AND PROCEDURES

All patients (THA: n= 18 SRA: n=20) from the two groups were diagnosed with hip OA and had a surgical intervention using a posterior approach. A control group (n=12) was used for comparison. The characteristics of the groups are shown in Table 1. All subjects were performing a quiet standing task in two different conditions (OE and CE) while standing on a force platform (AMTI, Advanced Mechanical Technology Inc, MA, USA). They were first asked to stand still during 2 minutes with their eyes open and secondly, with their eyes closed at 6 and 12 months post-surgery. The data relative to the center of pressure (COP) were extracted, analysed and filtered using a second-order low pass Butterworth with a cut-off frequency fixed at 10 Hz. From those data, the range (max-min), root-mean-square (RMS) amplitude and the velocity of the COP were calculated in the medio-lateral (VML) and anterio-posterior (VAP) directions respectively. Moreover, the area covering 85% of the data and the total path length (TPL) of the COP, were calculated. The results were then averaged for each task and analysed with an ANOVA with repeated measures with 2 fixed factors (3 groups X 2 tasks X 2 evaluations). The results were then further analysed if necessary, with Tukey post-hoc test and paired-t-tests. All analyses were done with a level of signification set at 0.05.

RESULTS

Table 1 demonstrates no significant differences between our groups.

Subjects	THA	SRA	Control
Age (y)	50.2 (6.4)	49.1 (6.8)	44.4 (9.2)
Gender	6 F/12 M	9 F/11 M	4 F/8 M
Mass (kg)	78.1 (13.8)	78.9 (15.0)	77.0 (13.8)
Height (m)	1.68 (0.06)	1.68 (0.07)	1.72 (0.07)
BMI(kg/m^2)	27.4 (3.7)	27.7 (3.6)	26.0 (3.4)

Table1. Means (SD) of the group's characteristics. No significant differences were observed between the three groups.

During the quiet standing, the statistical analyses (see Tables 2, 3 and 4) revealed a main effect on the period for the range in the ML direction ($F (1,100) = 6.238$, $p= 0.014$) and for the type of prostheses ($F (1,100) = 3.578$, $p=0.024$). It also revealed a main effect for the experimental conditions for the COP velocity in both directions and for TPL (VML: $F (1,100) = 4.946$, $p= 0.029$; VAP: $F (1,100) = 22.265$, $p= 0.000$; TPL: $F (1,100) = 19.493$, $p= 0.000$). No interaction between the factors was found for all variables.

Period	6 months*	12 months*
Range_ML (cm)	1.47 (0.67)	1.31 (0.46)

Table2. Mean (SD) of the range in ML.
 *Significant difference between 6 and 12 months.

Subjects	THA	SRA*	CTRL*
Range_ML (cm)	1.40 (0.68)	1.26 (0.46)	1.59 (0.56)

Table3. Mean (SD) of the range in ML.
* Significant difference between SRA and Control.

	Open Eyes*	Closed Eyes*
VML (cm/s)	0.43 (0.10)	0.45 (0.15)
VAP (cm/s)	0.69 (0.16)	0.93 (0.31)
TPL (cm)	110.5 (21.4)	139.7 (41.1)

Table4. Mean (SD) of COP velocity and TPL.* Significant difference between open and closed eyes

DISCUSSION

The presence of a significant difference between the two periods demonstrates that the patients need six additional months to complete their rehabilitation. During those six months, the muscles needed to maintain a good postural stability in the ML direction, mainly with the abductors/adductors muscle groups (Winter et al., 1996). Patients have also more time to restore their muscular force and endurance, so they may be more efficient and show a more normal postural control. In addition, a significantly improvement has been observe in the SRA group compared to the control group. For the SRA, the femoral head and neck are kept preserving better proprioception functions than the THA (Nantel et al., 2007). Moreover, the surgery used could cause less muscular damage, facilitating than a return to

a more normal activity of the affected muscles. Surprisingly, this difference is not shown when we compare the two experimental conditions. The postural control is a more complex task in lack of vision because the body needs to compensate this loss by a higher use of the other sensorial information source. In the present study, there is no difference between the period and the type of prostheses. The significantly increase of the COP velocity and TPL suggest that the patients, without visual inferences, used their proprioception functions in a similar way. In fact, they need to do more corrections of their COP to be able to keep it in the same zone.

SUMMARY

Quiet standing is often involves in daily living activities. The range in the ML direction of the patients with hip arthroplasty needs more than 6 months to return to a more normal postural control condition. Patients with SRA prosthesis showed more improvement in their rangeML, indicating a better preservation of their proprioception. However all patients are using their proprioception functions in a similar way when they closed their eyes.

REFERENCES

Buckwalter, Martin (2006). *Adv Drug Deliv Rev,* 58: 150-167.

Issa, SN, Sharma, L (2006). *Curr Opin Rheumatol*, 18: 147-156.

Nantel, J, Termoz, N, Centomo, H et al. (2007). *J Clin Biomech*, in press.

Vendittoli, Pa,Lavigne, M, Roy, AG et al. (2006). *Hip Int*, 16 :S73-81.

Winter, D.A, Prince, F, Frank, J.S et al. (1996). J. Neurophysiol. 75, 2334-2343.

ACKNOWLEDGEMENTS

INFLUENCE OF INCREMENTAL INCREASES IN ORTHOTIC HEIGHT ON DYNAMIC STABILITY IN FUNCTIONAL FLATFOOTED INDIVIDUALS

Stephen D. Perry and Kelly M. Goodwin

Dept of Kinesiology and Physical Education, Wilfrid Laurier University, Waterloo, ON, CAN
Email: sperry@wlu.ca URL: http://www.biomechanics.wlu.ca

INTRODUCTION

Flatfoot deformity or pes planus is the most common foot pathology in patients of all ages (Lee et al., 2005). The deformity may be associated with discomfort and pain, instability, serious foot, ankle, knee, and lower back joint problems, misalignments, and postural strain (Lee et al., 2005). Within pes planus, flexible flatfoot (FFF) is defined as a hypermobile foot with excessive hindfoot valgus and minimal medial-longitudinal arch height (Lee et al., 2005). Most often, FFF is treated with custom orthotics to aid in arch realignment and to provide stability. Imhauser and colleagues (2002) quantified and compared the efficacy of orthoses in the treatment of flatfoot deformity of cadaveric models in the static phase and determined orthoses to stabilize and restore the medial longitudinal arch. Furthermore, Kitaoka et al. (2002) demonstrated a significant improvement in arch alignment and structural alignment of the lower limbs with the use of orthoses in cadavers. Within the limited literature the transferability of the findings has little value to everyday life as all studies have focused primarily on static movement. In hopes to resolve the variable findings, this study will determine the influence of arch height on dynamic balance control in FFF subjects and identify the optimal arch height associated with dynamic balance in FFF subjects.

METHODS AND PROCEDURES

Participants (n=10) had both feet casted in the subtalar neutral position by a pedorthist. From their casts, identically styled laboratory walking shoes and custom-fit flat insoles were assigned. Arch inserts of 0%, 33%, 66%, and 100% of their subtalar neutral arch height were created for each participant. During the participant's visit to the laboratory, manual muscle tests, cutaneous sensation, and hindfoot valgus were measured. Static balance was also tested. Forty-eight dynamic balance trials were conducted using an uneven terrain set-up; three trials within each combination of four differently arranged series of platforms and four arch height conditions. The arch height condition was randomly varied by inserting the arch inserts of 33%, 66%, and 100% into the participant's shoes and fixing them by means of a soft adhering Velcro. Measurements of dynamic stability were 1) the relative position of the body's center of mass (COM) to base of support (BOS) and 2) the relative position of the center of pressure (COP) to COM.
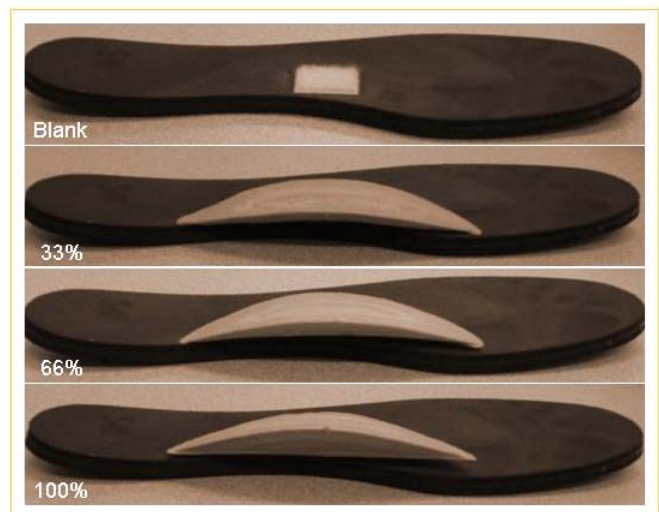
Figure 1: Arch insert conditions (0, 33, 66 & 100 %) adhered to shoe insole.

RESULTS

Increases in insert height demonstrated an improvement (p=0.035) in dynamic stability predominantly at the 66% arch height. During the left single support phase, the medial-lateral COM-BOS difference presented the lowest maximum (0.12m) and highest minimum values (0.07m) at 66% insert height.
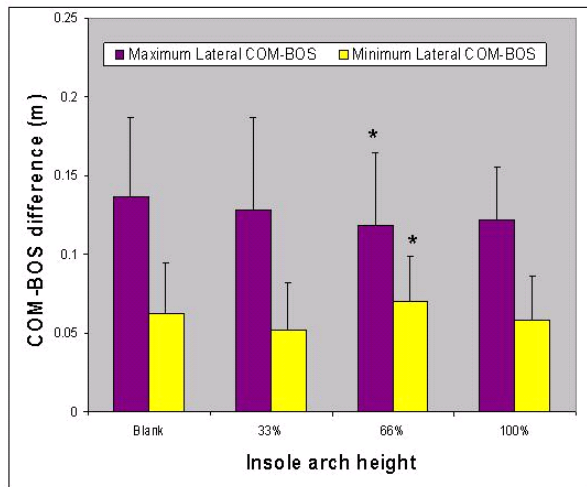
Figure 2: Medial Lateral COM-BOS results for the left single support phase
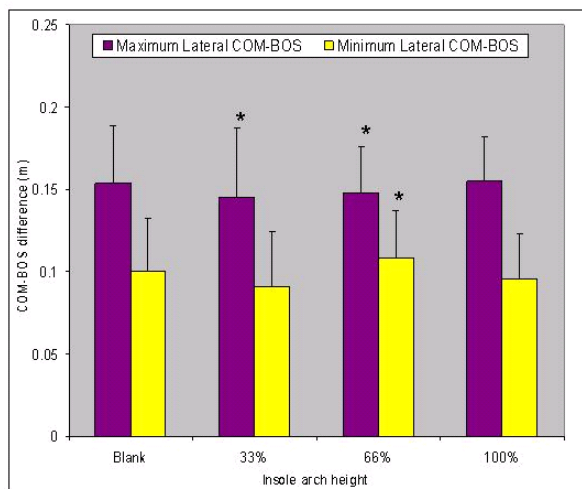
Figure 3: Medial Lateral COM-BOS results for the right single support phase

In addition, the medial-lateral COM-BOS difference during the right single support phase presented the lowest maximum (0.14m)

at 33% and 66% and highest minimum values (0.11m) at 66% insert height. No significant differences were found for COM-COP measurements due to insert height.

DISCUSSION

These results indicate a greater control of dynamic stability is observed primarily at the 66% arch insert height. Thus, individuals with pes planus, FFF, experience increased dynamic stability when wearing arch inserts that are 66% of their subtalar neutral arch height. These findings will aid in fall prevention research, contribute to production of orthoses and insoles, and could be generalized across multiple age groups.

REFERENCES

Lee, M. et al. Diagnosis and Treatment of Adult Flatfoot. J Foot Ankle Surg. 44 (2):78-113, 2005.
Imhauser, M. et al. Foot Ankle Int. Aug; 22(8): 727-37, 2002.
Kitaoka, H. et al. Arch Phys Med Rehabil. June; 83: 876-79, 2002.

ACKNOWLEDGEMENTS

PORTABLE STRAIN MEASUREMENT SYSTEM FOR ICE HOCKEY STICKS

PM Magee[1], P Dixon[1], TJ Stidwill[1], DJ Pearsall[1], RA Turcotte[1], and K Covo[2]

[1]Department of Kinesiology and Physical Education, McGill University, Montreal, QC, Canada,
[2]Nike-Bauer Hockey Inc, Research, Design and Development, St. Jerome, QC, Canada,
URL: http://icehockeyscience.mcgill.ca/

INTRODUCTION

Bending of an ice hockey stick is commonly observed during slap and wrist shots, wherein the shaft deformation stores elastic energy that may be transferred (in part or in whole) to the puck for higher projection velocity (Villasenor-Herrara *et al*, 2006). Hence, understanding the optimal bend stiffness characteristics is important to both athletes and manufactures of these specialty products. Previous studies have used high speed video recording (Wu *et al*, 2003), or infrared motion tracking (Worobets *et al,* 2006) for successful estimates of gross deflection. Alternatively, pioneering studies by Roy *et al* (1979) used strain gauges adhered to hockey sticks to obtain greater resolution of material deformation properties. Given advances in miniaturization and data storage, it may now be feasible and practical to use this latter approach. The purpose of this study was 1) to develop a portable strain gauge measurement system for evaluation of stick dynamic deformation characteristics during puck shooting tasks and 2) to demonstrate its utility for both in lab and on ice testing conditions.

METHODS AND PROCEDURES

Four paired strain gauges measured shaft bend (B1 to B4) and two obliquely oriented gauges measured shaft torsion (T2 to T3) at 15 cm intervals. These were positioned on the lower end of the stick shaft (Fig 1). The strain gauge system consists of: 1) a half-active Wheatstone bridge composed of 350 Ω, 0.125" long strain gauges with a 5 V DC battery excitation; 2) a signal conditioning unit capable of acquiring signals in ±100 mV and amplify to a 0 to 5 V range; 3) an 8 channel DAQ (using LabVIEW 8) at 2.5 kS/s

for 2 seconds. Acquired data were stored on a laptop computer. The above components could be contained within a backpack. Fine wires connecting the strain gauges to DAQ were tethered along the stick shaft and upper limb of a subject with minimal encumbrance to the swinging motion.
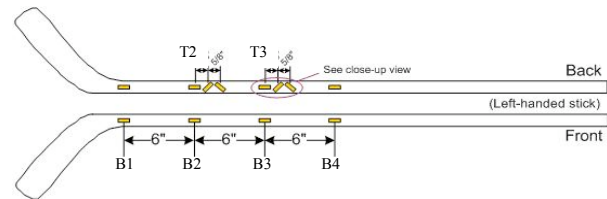
Figure 1. Strain gauge placement along hockey stick.

Calibration of the system was conducted at the ambient air temperature of the test environment (lab = 20°C, arena = 2°C) prior to testing. As a subject, a high calibre hockey player executed a several wrist and slap shots. For in lab conditions, shots were performed on top of a synthetic gliding surface (0.6 cm thick polyethylene sheets with silicon lubricant). Subsequently, the same subject repeated the skill on the ice in the hockey arena.

RESULTS

Initial inspection of the acquired strain data demonstrated both high temporal response and discrimination between strain by shaft location. Also, quantitative differences between skills were displayed. With regards to the wrist shot (Fig 2) the 6 strain-pair records corresponding to "pre-shot gathering", shot loading, and recoil strain coincided in time (600, 100, and 200 ms in length respectively) but with different magnitudes (800 to 200 µE). Greatest deflection occurred at B4 (near lower hand position) and least at B2. Concurrent torsion measures occurred

from 50 to 200 μE. For the slap shot (Fig 3), similar temporal synchronization and rank order was shown though the loading phase was shorter (~100 ms) and the magnitudes of maximal strains were greater (1000 to 3500 μE). In-lab versus on-ice strain records showed almost identical patterns (Fig 4).
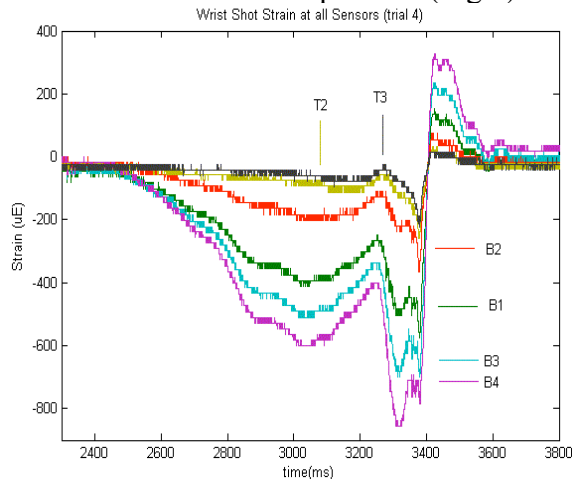
Fig 2. Wrist shot: example data for all strain gauges.
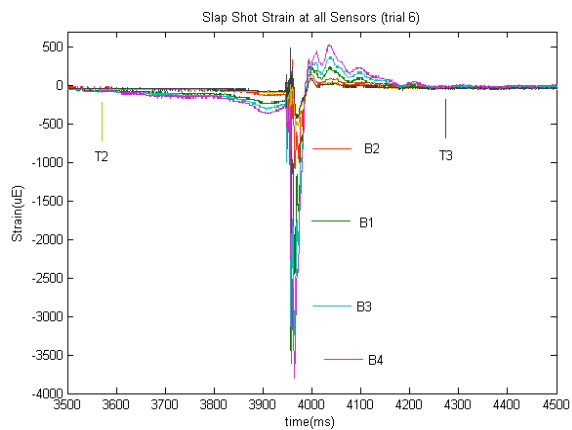
Fig 3. Slap shot: example data for all strain gauges.

DISCUSSION
The objective to create a portable system was successful. The use of several strain gauges revealed heterogeneous bending and torsional strain magnitudes along the shaft during the shooting task, similar to dynamic cantilever loading. Equally important, the testing system was sensitive enough to demonstrate different strain rate behaviours between skills. Finally, the high similarity in strain profiles between in-lab and on-ice testing gives confidence in the measurement consistency.
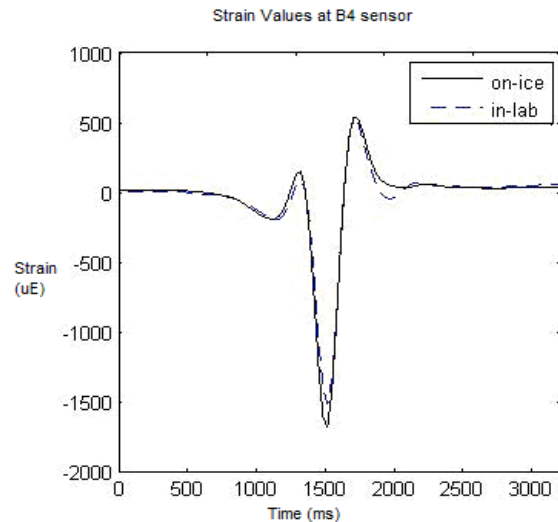
Fig 4. Wrist shot: B4 strain in lab versus on-ice

SUMMARY
The above results indicate that strain gauge technology is robust enough and portable for testing in both lab and real game cold environments. It also possesses the necessary spatial and temporal resolution to identify material behaviour responses during dynamic activities that other conventional video based technologies detect. After more extensive verification of the system's accuracy, future studies addressing material properties and construction properties will be pursued.

REFERENCES
Roy B et al. (1979) *Can J Appl Sport Sci* 4:1-7
Villasenor-Herrara A *et al* (2006)
    J Appl Biomech 22(3): 202-211
Worobets *et al* (2006) *Sports Eng* 9(4):
    191-200
Wu T-C *et al* (2003) *Sports Eng* 6(1):31-39

ACKNOWLEDGEMENTS

NEURAL COUPLING BETWEEN THE UPPER AND LOWER LIMBS IN INDIVIDUALS WITH INCOMPLETE SPINAL CORD INJURY

Helen J. Huang[1] and Daniel P. Ferris[1,2,3]

Departments of [1]Biomedical Engineering, [2]Movement Science, and [3]Physical Medicine and Rehabilitation, University of Michigan, Ann Arbor, Michigan, USA
hjhuang@umich.edu

INTRODUCTION

Growing evidence suggests that there are spinal connections between upper limb motor neurons and lower limb motor neurons in humans that facilitate coordinated interlimb movements (Zehr and Duysens, 2004). Upper limb muscle activation has been shown to facilitate lower limb muscle activation during passive locomotor-like movements of the lower limbs in neurologically intact individuals (Ferris et al 2006; Huang & Ferris, 2004; Kao & Ferris, 2005).

The purpose of this study was to examine neural coupling between the upper and lower limbs in individuals with incomplete spinal cord injury. We wanted to determine if a) upper (or lower) limb muscle activation facilitates lower (or upper) limb muscle activation during passive locomotor-like movement of the lower (or upper) limbs, and b) maximal effort simultaneous upper and lower limb muscle activation results in greater muscle activation compared to maximal effort upper limb only or lower limb only muscle activation.

METHODS AND PROCEDURES

Ten individuals with incomplete spinal cord injury (ASIA C & D) performed recumbent stepping (Fig.1) using four different combinations of upper and lower limb effort (active-A, passive-P). For active effort, we instructed subjects to use maximal effort. For passive effort, we instructed subjects to relax
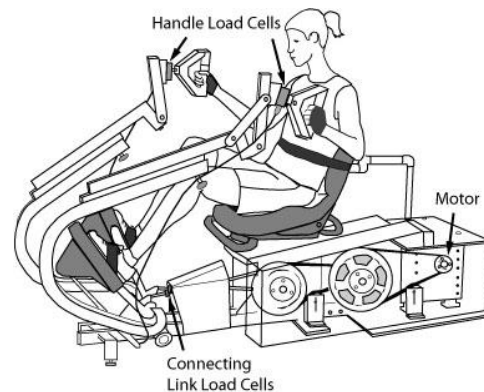
Figure 1: Recumbent stepping machine with real-time computer-controlled resistance and force and position sensors (modified TRS 4000, NuStep Inc, Ann Arbor, MI).

and exert minimal effort. The four conditions were: passive upper & passive lower (PU-PL), passive upper & active lower (PU-AL), active upper & passive lower (AU-PL), and active upper & active lower (AU-AL). Velcro gloves, pedal straps, and a torso strap secured subject's hands, feet, and torso to the handles, pedals, and seat, respectively. The stepping frequency was 1.25 Hz.

We collected electromyography (EMG) and joint kinematic data from upper and lower limbs. We calculated limb forces from load cells on the handles and pedals. For each condition and muscle, we calculated the root-mean-square (RMS) EMG. We normalized RMS amplitudes to the AU-PL data for the upper limb muscles and to the PU-AL data for the lower limbs. We used an ANOVA with Tukey-Kramer post-hoc tests to determine differences between pairs of conditions.
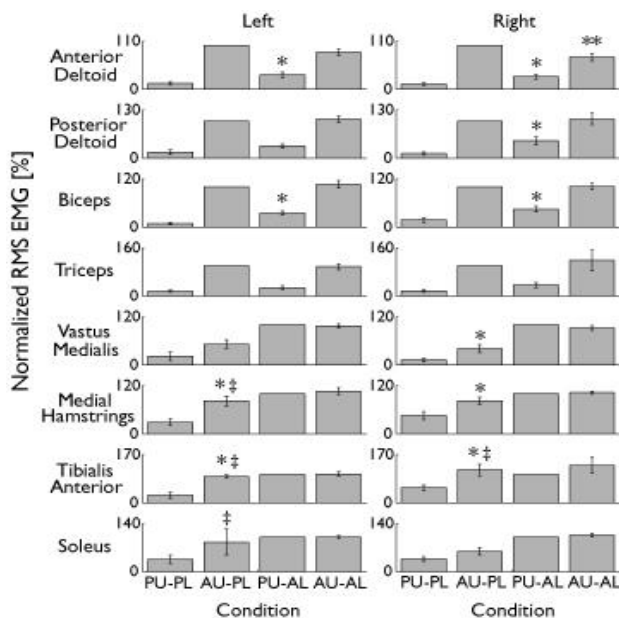
Figure 2: Group averaged normalized RMS EMG with standard error bars. *Significantly different from PU-PL condition. **Significantly different from AU-PL condition. ‡Not significantly different from AU-AL condition.

RESULTS

Upper limb exertion resulted in greater muscle activation of passive lower limb muscles (Fig. 2 *). AU-PL RMS amplitudes were significantly greater than PU-PL amplitudes for the right vastus medialis, the left and right medial hamstrings, and the left and right tibialis anterior. The effect was large enough that AU-PL amplitudes were not significantly different from AU-AL for the left medial hamstrings, both tibialis anterior, and left soleus (Fig. 2 ‡). Similarly, lower limb exertion resulted in greater muscle activation of passive upper limb muscles (Fig. 2 *). PU-AL amplitudes were significantly higher than PU-PL amplitudes for the left and right anterior deltoid, the right posterior deltoid, and the left and right biceps.

During simultaneous upper and lower limb exertion, EMG amplitudes were not significantly different compared to just upper limb exertion or just lower limb exertion. The right anterior deltoid was the only exception (Fig. 2, **AU-AL < AU-PL).

DISCUSSION

Upper limb exertion does not facilitate lower limb muscle activation during maximal effort tasks in individuals with incomplete spinal cord injury. There was no additive interlimb effect on recruitment. However, therapeutic exercise and activities of daily living are often performed at submaximal levels. Our results do not rule out the possibility that upper limb exertion provides an excitatory effect on lower limb muscles during submaximal exercise. Transcranial magnetic stimulation (TMS) could be used to determine if there is an excitatory interlimb coupling during submaximal muscle activation that results in less supraspinal descending neural drive to the lower limbs with upper limb exertion.

SUMMARY

These results suggest that neural coupling between upper limbs and lower limbs is bidirectional during locomotor-like movements in individuals with incomplete spinal cord injury. At maximal levels, there is no facilitation of muscle activation.

REFERENCES

Ferris, DP et al. (2006) *Ex. Sp. Sci. Rev.*, 34(3):113-120.
Huang, HJ and Ferris, DP (2004). *J Appl Physiol,* 97(4): 1299-308.
Kao, PC and Ferris, DP (2004). *Motor Control,* 97(4): 1299-308.
Zehr, EP and Duysens, J (2004). *Neuroscientist,* 10(4):347-61.

ACKNOWLEDGEMENTS

THREE DIMENSIONAL KINEMATICS AND KINETICS OF THE CENTER OF MASS OF THE CAT DURING WALKING ON A NARROW WALKWAY

Brad Farrell[1], Irina Beloozerova[2], and Boris Prilutsky[1]

[1]School of Applied Physiology, Georgia Institute of Technology, Atlanta, GA,
Farrell@gatech.edu
[2]Barrow Neurological Institute, St. Joseph's Hospital and Medical Center, Phoenix, AZ

INTRODUCTION

Many quadrupedal animals manage to maintain balance in the frontal plane while walking along very narrow paths, like cats walking on top of narrow fences. In order not to fall, the cat must control the medial and lateral displacement of the general center of mass (GCM) such that its projection on the support surface does not move too far outside the base of support. We hypothesized that to walk along a narrow path, the cat constrains the medial-lateral movement of the GCM either by decreasing the medial-lateral accelerations of the GCM (by reducing the medial-lateral ground reaction forces) or by applying additional medial and lateral forces to counteract excessive GCM displacements in the medial and lateral directions. The goal of this study was to compare kinematics and kinetics of the cat GCM during walking on a narrowed walkway to those during normal (or simple) walking.

METHODS

Two cats were trained to walk across a level walkway under two conditions: simple level walkway (12 cm) and a narrow walkway (5 cm). During the experiment, 22 body segments (5 segments per limb, trunk, and neck-head segment) were marked by light reflective markers 6 and 9 mm in diameter. 3D marker positions and ground reaction forces were recorded during walking using a motion capture system (Vicon, UK; sampling rate 120 Hz) and a force platform embedded

in the walkway floor (Bertec, USA; sampling rate 360 Hz), respectively (for details, see Gregor et al., 2006; Prilutsky et al., 2005). Linear displacements, velocities and accelerations of each body segment and the GCM in three dimensions were calculated using the marker positions and inertial segment parameters (Hoy and Zernickie, 1985). All kinematic variables and the ground reaction forces were time normalized and then averaged across trials of each cat and between cats.

RESULTS

During walking on a narrow walkway, the cat appears to minimize medial-lateral acceleration of the general center of mass in order to maintain balance over its narrowed base of support (Fig. 1).
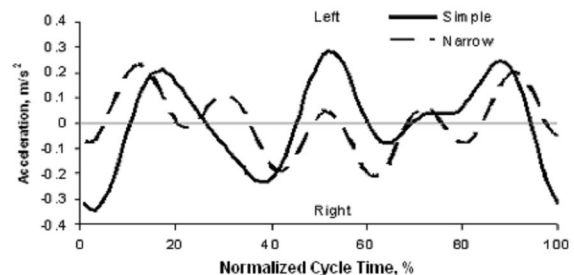
Figure 1 Average medial-lateral acceleration of the general center of mass during one cycle of "narrow" and simple walking (n=30, 15 cycles for each cat). Positive and negative values indicate accelerations in the left and right directions, respectively.

The way in which the cat accomplishes the decreased acceleration is through reducing the magnitude of the lateral forces exerted on the ground during locomotion (Fig. 2). The lateral

forces (positive) are decreased while the cat walks on the narrow walkway compared to the forces exerted during simple walking.
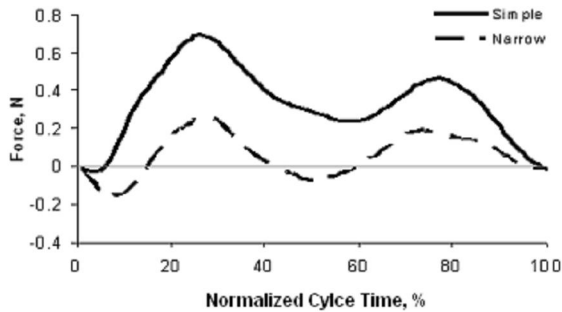
Figure 2. Medial and lateral ground reaction forces exerted by forelimbs during one cycle of "narrow" and simple walking (n=30, 15 cycles for each cat averaged across left and right limbs).. Positive values indicate laterally directed force.

Another indicator of this is seen when examining the peak GCM accelerations and the peak medial forces. For example, absolute peaks of medial-lateral accelerations in simple walking ($0.63 +/- 0.21$ m/s^2) were significantly ($p < 0.05$) higher than during simple walking ($0.44 +/- 0.15$ m/s^2) (Fig. 3). Also peak lateral forces in the forelimbs were significantly ($p < 0.05$) higher in simple walking ($0.72 +/- 0.17$ N) compared to narrow walking ($0.42 +/- 0.14$ N; Fig. 3)
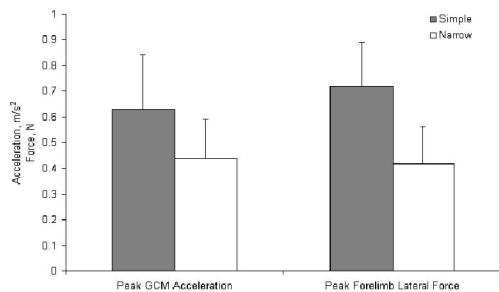
Figure 3. Peak medial-lateral accelerations of GCM and peak lateral ground reaction forces under forelimbs in "narrow " and simple walking. Peak GCM acceleration was calculated as the absolute value of the peak acceleration in either left or right direction.

No statistical difference was found in vertical and anterior-posterior ground reaction forces, joint angles, and stride length between the two walking conditions.

DISCUSSION

To maintain balance in frontal plane during quiet standing, the GCM must remain within the base of support. During locomotion this task becomes more complicated because the cat must maintain forward momentum and also control medial-lateral displacement of the GCM. The results of this study suggest that the cat controls the medial and lateral displacement of the GCM by reducing medial and lateral forces exerted on the ground by the legs. The hip and shoulder abductors and adductors are likely the major contributors in regulating ground reaction forces in the medial-lateral directions. Given that most hindlimb and probably many fore-limb muscles create moments outside the plane of progression when active (e.g., Lawrence et al. 1993), the reduction of the medial and lateral ground reaction forces without changing anterior-posterior forces may involve coordination of all major limb muscles operating in all three planes.

SUMMARY

The cat maintains balance while walking along a narrow base of support by reducing the magnitude of acceleration and exerted ground reaction forces in the medial and lateral directions.

REFERENCES

Gregor et al. (2006) *J Neurophysiology*, **95**, 1397-1409.
Hoy et al. (1995) *J Biomech*. **18**, 49-60.
Lawrence et al. (1993) *J Neurophysiology*. **69,** 282-285.
Prilutsky et al. (2005) *J Neurophysiology*. **94**, 2959-2969.

ACKNOWLEDGEMENTS

IN VIVO SKELETAL MUSCLE FIBRE FUNCTION DURING CYCLING

Neal Austin, Tim Keren, Chris Wieland, and Walter Herzog

INTRODUCTION

There has been a vast amount of research on skeletal muscle function, either in whole muscle preparation or in single fibres isolated from muscle. Comparatively, there has been little research on the functional characteristics of muscle in vivo during dynamic voluntary movements. With the technological advances in medical imaging, ultrasound has allowed for the in vivo representation of muscle fascicles during movement (Henriksson-Larsen et al., 1992), which allows for a better understanding of muscle contractile characteristics during voluntary human movement. The purpose of this project was to investigate the architectural changes, specifically fascicle length, and the associated force-length relationships in the vastus lateralis (VL) muscle during stationary cycling with variations in pedaling frequencies and power outputs.

METHODS AND PROCEDURES

Six male subjects underwent testing that involved the determination of the torque-angle and torque-fascicle length relationships for the vastus lateralis. Subjects performed maximal isometric voluntary contractions at knee angles ranging from 10° and 100° at 10° increments, with full extension defined as 0°. At each angle, torque, activation of the muscle, knee angle, and fascicle length were collected using the Biodex System 3, EMG, an electric goniometer, and ultrasound imaging, respectively. Torque, muscle activation, and kinematic data were synchronized with a function generator. All data were collected at 1kHz, except the ultrasound images which were collected at 49Hz. Subjects were then seated on a cycle ergometer (SRM Training System) and asked to cycle at 4 different pedaling conditions; 50rpm at 100 and 250 watts and maximal effort, and 80rpm at 100 and 250 watts.

Power output, pedaling frequency, muscle activation, knee angle and VL fascicle lengths were collected.

Muscle Fascicle lengths were calculated using Image J software and assuming that aponeuroses and fascicles could be approximated with straight lines if they were not fully visible in the filed of view (Narici et al., 1996; Fig. 1).
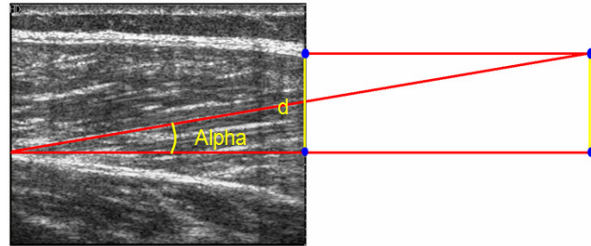
Figure 1. Fascicle length determination assuming that aponeuroses and fascicles can be approximated with straight lines.

RESULTS

The torque-angle relationships had an ascending and descending limb with peak torque production at around 70° for all subjects and approximated knee extensor strength curves observed in many previous studies (Kulig et al. 1984; Figure 2). However, the torque-fibre length curves showed a steep ascending limb, and fibre lengths remained virtually constant for knee angles of 40° and lower (Figure 2). Although not perfectly consistent, fibre lengths decreased during cycling for increased power output (at constant pedalling rates; Figure 2) or for decreasing pedalling rates (at constant power output), indicating that higher pedal force requirements were associated with shorter fascicle lengths. Typically, fibre lengths during cycling were on the ascending limb of the torque-angle and torque-fibre lengths relationships (Figure 1).
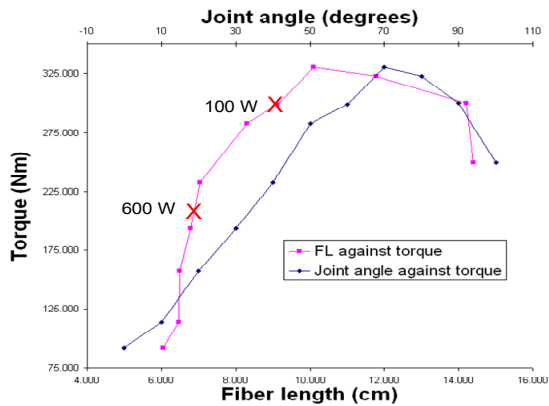
Figure 2. Torque-angle and torque-fascicle length relationships for an exemplar subject. Note the steep ascending limb of the torque-fascicle length relationship and the fascicle length at maximal force production for pedalling at 50rpms and 100 and 600W (maximal effort) on the ascending limb.

DISCUSSION

This study revealed two rather surprising results. First, despite vastly differing knee torques from 40 to 0º of knee extension, fascicle lengths remained virtually the same, and second, increased pedal force requirements during cycling are associated with shifts of the fascicle length to shorter values on the ascending part of the torque-angle relationship. Thus, as more force is required, the knee extensors are shortening to less favourable force conditions on the force-length relationship.

The first result, the virtually constant fibre length for vastly different torque (and thus presumably force) production can be explained from a mechanical point of view by the decrease in knee extensor lengths with decreasing knee angles. Since fibre lengths depend on muscle length and force, it appears that the shortening of the fascicles associated with muscle shortening while going from a knee flexion angle of 40º to full knee extension, is offset by the decrease in torque (force) production for the same knee extensor range. However, in the classical literature, fascicle length is uniquely associated with

force, and shortening on the ascending limb should be associated with less force, while here, less force is associated with the same fascicle length. Obviously, the behaviour of fascicles in muscles does not represent the behaviour of isolated fascicles or fibres tested in vitro. This result might have far reaching implications and needs careful investigation in the future.

Higher pedal force requirements during cycling are associated with shorter fibre lengths, which makes perfect sense from a mechanical point of view. However, since cycling is associated with fibre lengths on the ascending limb of the torque-angle curve, this implies that increased force requirements during cycling are associated with a decreased force potential of the fascicles. This seems counter intuitive and might reflect that human knee extensor muscles were not optimized for cycling. Since our subjects were not cyclists, it would be interesting to investigate if long term cycling, such as in elite athletes, might change the force-length properties of the knee extensors such that decreased fascicle lengths would be associated with an increase in force potential, as one would obtain on the descending part of the torque-angle relationship.

SUMMARY

The torque-fascicle length relationship of VL has a very steep ascending limb that produces vastly different torques for virtually identical fibre lengths, and fascicle lengths during cycling are typically on the ascending limb of the force-length relationship.

REFERENCES

Henriksson-Larsen K. et al. (1992). *Eur J Appl Physiol,* 64: 68-72.

Kulig K, Andrews JG, Hay JG. (1984). Exerc Sport Sci Rev, 12:417-66.

Narici et al. (1996). J. Physiol, 496: 287-297.

CHANGES IN WHEELING KINEMATICS AFTER 8 WEEKS OF PUSHRIM-ACTIVATED POWER-ASSISTED WHEELCHAIR USE

Mark D. Tillman[1], John W. Chow[2], Kim A. Fournier[1], Srikant Vallabhajosula[1], Peter Giacobbi, Jr.[1], Frederick D. Dietrich[1], Sandra Hubbard[3,4] and Charles E. Levy[3,4]

[1]Department of Applied Physiology & Kinesiology, University of Florida, Gainesville, FL, USA, mtillman@hhp.ufl.edu
[2]Center for Neuroscience and Neurological Recovery, Methodist Rehabilitation Center, Jackson, MS, USA
[3]Department of Occupational Therapy, University of Florida, Gainesville, FL, USA
[4]North Florida/South Georgia Veterans Health System, Gainesville, FL, USA

INTRODUCTION

Two types of wheelchairs have traditionally been available to the public: manual (wheeler pushes himself or herself.) and power (wheeler drives a chair powered by electricity). More recently, pushrim-activated power-assisted wheelchairs (PAWs) have become available as an intermediate alternative. PAWs require the user to apply a force to the pushrims which propels the chair and activates small, lightweight motors which continues to drive the wheels for a brief period of time (Levy et al., 2004). Although the wheeler is given assistance, he or she must continue pushing in order to keep moving. In our earlier work, we analyzed the acute changes in wheelchair propulsion while using PAWs. However, the long-term changes in wheeling mechanics remained unstudied. Thus, the purpose of this study was to evaluate basic PAW wheeling mechanics before and after 8 weeks of use.

METHODS

Thirteen male and six female full-time manual wheelchair users (age 43.1±15.0 yrs) who had no musculoskeletal disorders in their upper extremities served as the participants. Each participant was asked to wheel over three different surfaces at their own self-selected pace: a flat vinyl floor (approximately 28m including three turns), a thick carpet (approximately 21m including two turns), and a 4m long ramp inclined to 6° (three repetitions). Data were collected during three separate visits. During the first session (S1) the participant used his/her own wheelchair. During the second session (S2) the participant used his/her own wheelchair fitted with e.motion power-assisted wheels (www.ulrich-alber.de) after a few minutes of practice. For the final session (S3), each participant was tested using the power-assisted wheels after 8 weeks of full time PAW activity.

Each trial was recorded using seven digital Hawk cameras collecting at 60 Hz (Motion Analysis Corp, Santa Rosa, CA) and a Sony digital camcorder (60 Hz). The time to complete each trial, the number of pushes required to complete each trial, and the average velocity while performing each task were calculated. Only the ascending part of ramp trials was analyzed.

The average values of each dependent variable from a pair of analysts were used in subsequent statistical analyses. More specifically, separate one-way ANOVA with repeated measures were computed to determine if any differences occurred across sessions. A traditional level of statistical

significance was utilized (α=0.05). When appropriate, Bonferroni posthoc analyses were performed.

RESULTS

Across sessions, completion time decreased 5% for the flat surface, 19% for carpet, and 37% for the ramp. The number of pushes decreased 15% on the flat surface, 20 % on the carpet, and 14% on the ramp. In addition, velocity increased 6% on the flat surface, 13% on the carpet, and 12% on the ramp. However, no significant differences were detected for the time elapsed to complete the tasks across sessions, the number of pushes required to complete each task, or the average velocity during each task (p>0.05). See Figures 1, 2, and 3.

DISCUSSION

Despite the apparent decrease in time to complete each task, decrease in number of pushes to complete each task, and increase in velocity across the different surfaces, no significant differences were detected. One of the possible explanations is that participants were asked to push at their own self-selected speeds.

Even with power-assisted wheels, they elected to push at speeds they felt comfortable with. The other possible explanation is that the variability inherent in this population of test participants might have masked any significant differences between testing sessions.

SUMMARY

Our data suggest that there is no significant performance advantage to using a PAW compared to a manual wheelchair for the tasks used in the present study. Additional research is warranted on a larger population of wheelers and the use of more challenging tasks in order to more definitively parse out the potential benefits of PAW use.

REFERENCES

Levy, C.E. et al. (2004). *Am J Phys Med Rehabil*. 83, 166-167.

ACKNOWLEDGEMENT
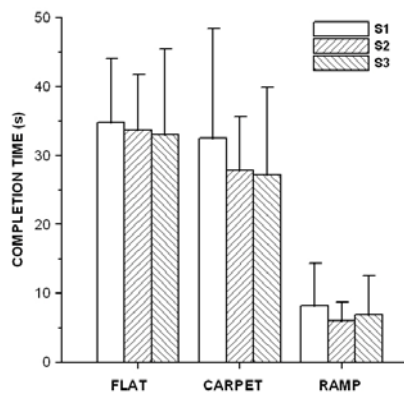
Figure 1. Time to complete each task.
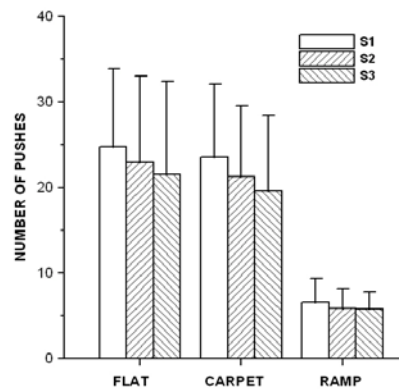
Figure 2. Number of pushes to complete each task.
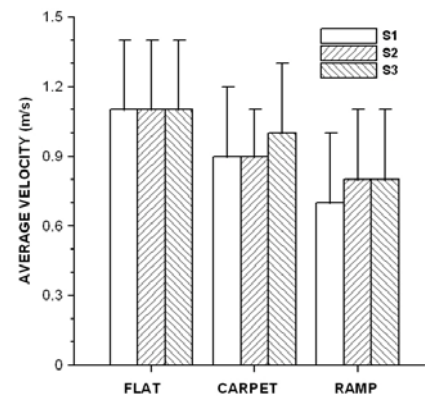
Figure 3. Average velocity during each task.

SELF-SELECTED TRANSITION BETWEEN MOVEMENT PATTERNS ON A MOVING PLATFORM

Venkata Gade, Nitin Moholkar, Jerome Allen, and W. Thomas Edwards

Kessler Medical Rehabilitation Research and Education Center, West Orange, NJ, USA
E-mail: tedwards@kmrrec.org   Web: www.kmrrec.org

INTRODUCTION

Movement response to a platform translating sinusoidally in the anterior-posterior direction can be used to understand balance. Prior studies have demonstrated that maintaining balance on a translating platform involves choosing a balance strategy that depends on the frequency of platform translation. Two primary strategies were proposed by Buchanan and Horak (2003): head-fixed-to-platform (HF-platform) and head-fixed-in space (HF-space). At lower frequencies either strategy could be evoked on command. However, at higher frequencies (>0.6 Hz) only the HF-space strategy was seen. Our objective was to determine the subject's preference for employing these strategies and to relate this choice to the dynamic conditions.

METHODS

Fifteen healthy adult individuals participated in the study. The subjects were free of neurological, audiological, opthalmological and internal pathologies, and medications affecting balance. All the participants gave their informed consent for participation.

A NeuroCom Research Balance Platform consisting of two independent AMTI force plates provided the anterior-posterior translations and gathered the ground reaction forces. Subjects stood on the platform with their feet shoulder width apart with one foot on each forceplate. Motion data along with the forceplate information was collected using a six camera Vicon system. The platform translated sinusoidally with fixed frequencies (0.1, 0.25, 0.5, 0.75, 1.0, and 1.25 Hz) with a peak to peak amplitude of 6 cm. Each translation frequency was repeated three times with both eyes open and closed conditions. Subjects were protected from falling by using a safety harness system.

Individual trails in which subjects made a transition from one motion pattern to another were selected from the complete set. The motion patterns were defined by the relative magnitude and phase of the head and ankle motions, Fig. 1.
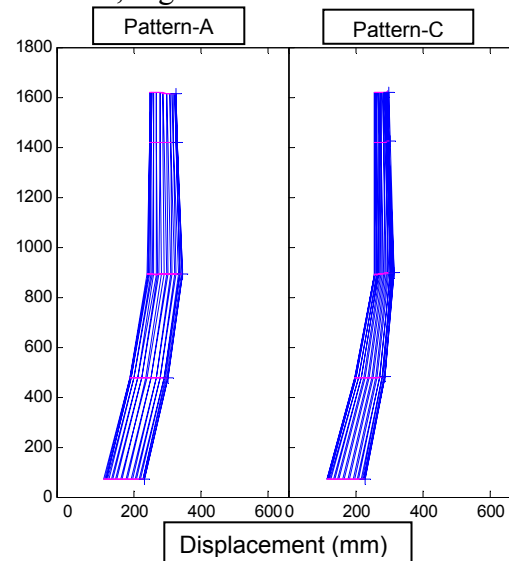
Figure 1. Motion patterns: Pattern-A reflects HF-Platform and Pattern-C reflects HF-Space motion.

The effort required to maintain balance during a trial was calculated from the average power of the power spectrum of the movement of the Center of Pressure (COP) (Roy 2002). The power spectrum was calculated from the FFT of the zero-mean COP trajectory.

RESULTS

Transitions occurred in 35 trials, 13 trials at lower frequencies and 22 trials at higher frequencies. Thirty-two of the trials were eyes-open and three were eyes closed. At the lower frequencies, the motion of the knee, hip and head increased to more closely match the motion of the platform, Fig 2a. At the higher frequencies the motions decreased showing a transition towards HF-space strategy, Fig 2b. Each transition between patterns resulted in a reduction in the power required to stand, shown by the power of the COP, Fig 3.

Average RMS_error before and after transition for low frequency (0.1, 0.25, & 0.5 Hz) trials

Average RMS_error before and after transition for high frequency 0.75, 1.0, & 1.25 Hz trials
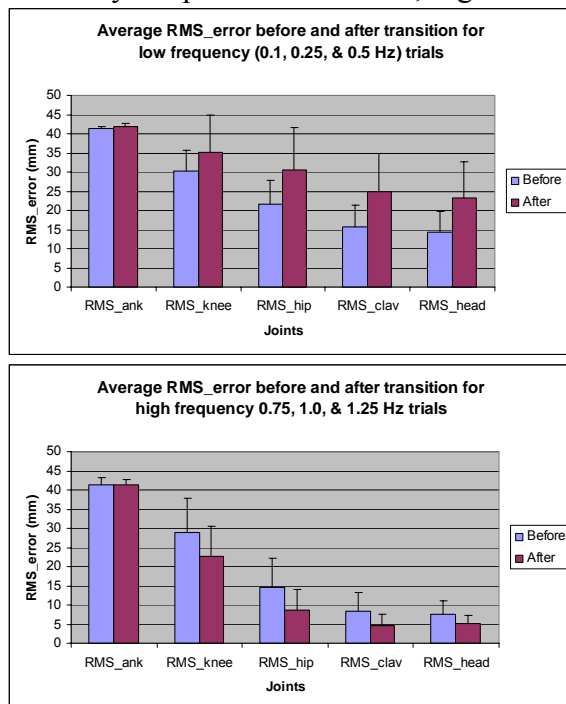
Figure 2. The RMS motion of five levels from the ankle to head at lower platform frequency. 2a, and at higher frequencies, 2b.

DISCUSSION

This study examines processes involved when subjects spontaneously transition between balance patterns in response to a sinusoidally moving platform. In similar studies by Buchanan and Horak at frequencies up to 1.0 Hz, they found HF-platform patterns at frequencies ≤0.4Hz. At higher frequencies they observed the HF-space pattern and concluded that an independent or separate control of the upper and lower body was acting. Based on the present results and prior models (Edwards 2007) subjects are able to dynamically tune their bodies to obtain a response pattern matched to platform frequency. The results show a synergetic response across the ankle knee and hip for such tuning and that tends to reduce effort (power) required for balance.

Center of Pressure Power
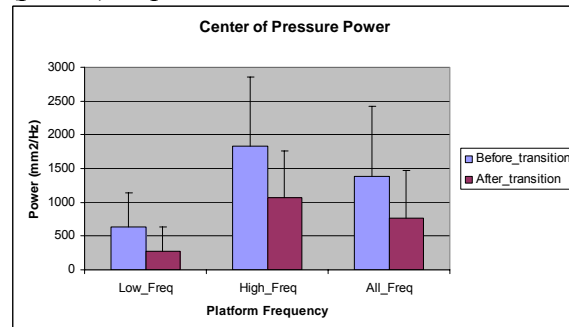
Figure 3: Average power across the subjects for the COP movement before and after pattern transition. (Low freq ≤0.5Hz; high freq ≥0.75Hz).

This study, quantifies the dynamics of transitions between self-selected movement patterns to maintain balance on an oscillating platform. These results indicate that subjects can select more efficient balance patterns during a single trial by tuning the response of the ankle and hip. These experimental protocols have potential for new diagnostic and treatment techniques for balance rehabilitation using whole body oscillations and other therapies.

REFERENCES

Buchanan, J.J., Horak, F.B. (2003). *Behavioural Brain Research*, **143**, 121-40.
Edwards, W.T. (2007). *Gait&Posture*. **25**, 432-39.
Roy, M., H., (2002). *Principles of Random signal analysis and low noise design*.

ACKNOWLEDGEMENTS

EFFECTS OF A SUBTALAR STRAPPED WEDGE ON KNEE DYNAMICS DURING GAIT IN YOUNGER AND OLDER ADULTS

Kristian O'Connor, Nandina Hill, Barbara Hart, and Jennifer Earl

Department of Human Movement Sciences
University of Wisconsin-Milwaukee, Milwaukee, WI, USA
E-mail: krisocon@uwm.edu   Web: www.chs.uwm.edu/neuromechanics

INTRODUCTION

A majority of older adults have been diagnosed with or have medial tibiofemoral osteoarthritis (Bolen et al., 2005). Costly and invasive surgical procedures have not always been effective treatments in the reduction of loading at the affected compartment of the knee. Therefore, the use of laterally wedged insoles is becoming more commonplace. Previous literature has shown this type of intervention to be generally effective in pain reduction but to have somewhat mixed results on an individual basis for the reduction of the abduction moment (Crenshaw et al., 2000; Maly et al., 2002). Some authors have proposed that movement at the subtalar joint may cause these differences in efficacy (Toda et al., 2001). Thus, a lateral wedge was developed that included subtalar strapping to restrict this motion (Taketora USA, Inc.). Clinical studies have shown greater reductions in pain and in the tibiofemoral angle with this strapped wedge as compared to the more traditional inserted lateral wedge (Toda et al., 2001). However, a dynamic assessment of joint moments had yet to be conducted in order to elucidate the mechanism and the effect at the knee joint. Additionally, studies examining the general effect of wedging have yielded mixed results (Crenshaw et al., 2000; Kakihana et al., 2004), and one possible factor could be the use of younger or older subjects. The purpose of this study was to examine the effects of subtalar strapping of a lateral wedge on knee dynamics during gait in healthy younger and older adult women.

METHODS

Fifteen younger (21 ± 2 years) and ten older (66 ± 5 years) women with no lower extremity musculoskeletal disorders or gait restrictions were recruited for participation. Each participant completed a functional knee scale to assess joint health (WOMAC). All participants performed ten walking trials at a controlled gait velocity (1.3 m/s) under four wedge conditions; no orthotic (CONTROL), traditional 6° lateral heel wedge (TRAD), 11° softer lateral heel wedge strapped to the foot (STRAP), and the 11° wedge without the strap (NO STRAP).

Three-dimensional kinematic data were collected using a seven-camera Motion Analysis Eagle system (200 Hz), and force data were collected with an AMTI force platform (1000 Hz). The following variables were extracted at the instant of the first peak (F1) of the vertical ground reaction force (GRF); frontal plane internal knee moment and GRF moment arm about the knee, knee adduction angle, medial-lateral center of pressure location in the foot (COP FOOT) and global (COP-GCS) coordinate systems, and the angle of progression of the foot. Each dependent variable was analyzed with a repeated measures 2×4 ANOVA (age × condition) with a significance level of 0.05.

RESULTS AND DISCUSSION

There were no significant differences in the WOMAC scores between age groups. There were also no significant interactions between age and condition for any of the gait variables, nor were there any significant age effects. The moment profiles were similar between conditions (Figure 1), but there was a significant increase in the knee abduction moment at F1 with the strapped wedge (Figure 2). There were no differences in the ground reaction forces, but there was a significant difference in the GRF moment arm about the knee (Figure 2). The moment arm change appears to be due to an interaction between a COP-FOOT location and the orientation of the foot relative to the line of progression (Table 1).
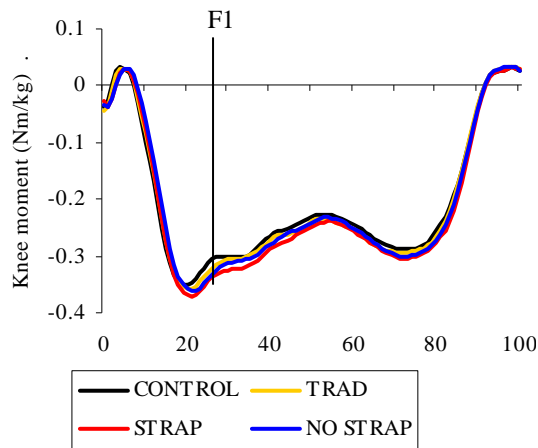
Figure 1. Group mean frontal plane knee moment during stance. Vertical line represents F1.
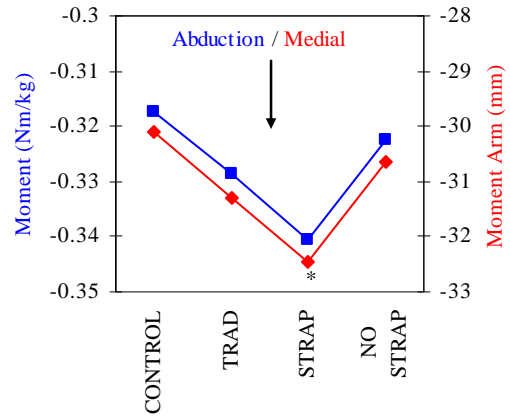
Figure 2. Mean frontal plane knee moment and the medial-lateral center of pressure position at F1. * indicates significant difference from other conditions.

SUMMARY

Similar to the findings of Maly et al. (2002), the overall orthotic results of this study appear to contradict the clinical outcomes previously reported. In addition, the strapping accentuated the negative effects.

REFERENCES

Bolen et al. (2005). *Morbility & Mortality Weekly Report*, 54(5), 119-123.
Crenshaw et al. (2000). *Clin Orth & Rel Res*, 375, 185-192.
Kakihana et al. (2004). *Am J Phys Med Rehab*, 83(4), 273-278.
Maly et al. (2002).*Clin Biomech*, 17, 603-610.
Toda et al. (2001). *J Rheumatology,* 29, 541-545.

Table 1. Medial-lateral center of pressure location in the foot and laboratory coordinate systems, and the foot angle relative to the line of progression. Negative displacements are medial, and negative angles are toed out.

	CONTROL	TRAD	STRAP	NO STRAP	p
M/L COP-FOOT (mm)	-8.2 ± 7.2	-7.3 ± 7.6	**-5.2 ± 9.9***	-8.9 ± 9.4	0.032
M/L COP-GCS (mm)	-1.1 ± 6.8	-2.0 ± 7.6	-1.2 ± 9.2	**-5.5 ± 6.6***	<0.001
FOOT ANGLE (°)	**-5.3 ± 5.5***	-3.8 ± 4.8	-3.6 ± 5.9	-2.9 ± 5.8	0.007

USING VICON TO DETERMINE THE AREA AND VOLUME OF BODY SEGMENTS

Idafe Pérez Jiménez

Sports Biomechanics and Motor Control Research Group. School of Sport & Exercise Sciences, Loughborough University, Loughborough, UK. I.Perez-Jimenez@lboro.ac.uk

INTRODUCTION

The accurate determination of areas and volumes of body segments is important for several areas of biomechanics research. The shape of a segment can change due to its movement or to its interaction with other segments and external objects. In an impact, a mechanical wave propagates through the segment producing surface area changes that can be detected. Those changes can provide information on energetic interactions and the properties of underlying tissues underlying. Also, when the volume of a segment changes during an action, so do inertia parameters. An experimental technique was designed to use the Vicon system to allow obtaining data on areas and volumes of

METHODS AND PROCEDURES

Markers: The election of the type of marker to be used is conditioned by the size of the marker and its detectability by the system. Ideally, the marker should be as small as possible to better reproduce the movement of the skin it is attached to. Three different types of markers (flat, 3 mm and 5 mm hemispherical) were placed on a cylinder and on different segments to evaluate how well they could be detected.

Camera setup: Eight to ten cameras were used at frequencies from 250 Hz to 2000 Hz, covering a volume of sufficient dimension to detect the movement of a single segment.

Preliminary determination of accuracy: 130 markers (3 and 5 mm hemispherical)

were used to cover an area of $(52\pm1.8)\text{x}10^3$ mm^2 on a cylinder. Five static and five dynamic trials were performed and the area covered by the markers calculated.

Area changes: Seventy-eight 5 mm hemispherical markers were placed on the anterior and lateral sides of a subject's thigh, and around the waist (see Figure 1). Surface areas were measured when performing different leg movements (abduction, flexion and rotation around the hip joint centre), to test the ability of the system to measure changes related with these actions.

RESULTS

Optimal setup: A setup with eight cameras close up successfully detected 3mm and 5 mm hemispherical markers up to 1000 Hz. Flat markers were only detectable under ideal circumstances. If cameras were taken further back or the frequency was raised, even hemispherical markers were eventually lost.

Preliminary determination of accuracy: The system provided an area of $(53.5\pm0.2)\text{x}10^3$ mm^2. This represents an overestimation of 2.9%, but within the error margin. All trials were within the error margin as well. Other experiments have provided a similarly small overestimation.

Area changes: The setup was able to successfully measure changes in areas of very different magnitudes. Figure 2 shows the different behaviour of two areas situated near the hip and near the knee respectively, when

Figure 1. Marker placement for local area changes in leg movements.
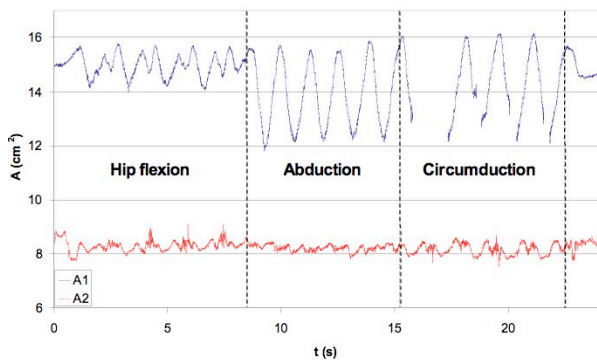
Figure 2. Area for a region near the hip (A1, top) and one near the knee (A2, bottom).

the subject performed hip flexion, abduction and circumduction.

DISCUSSION

The setup proved able to measure areas and volumes in static and dynamic situations. The accuracy shown in an object of regular shape is promising, but further assessment need to be made for actual segments.

3mm and 5 mm markers appear to be small enough to adequately reproduce the movement of the skin they are attached to. The ability of recording changes in areas with a frequency up to 1000 Hz will allow studying the behaviour of soft tissues under impacts, through examining how the mechanical wave propagates. It can also provide a quick way for determining volumes of segments and allow the calculation of inertia parameters.

The need for a setup in which cameras are very near each other limits the volume that can be covered and therefore the actions that can be captured. The estimation of areas and volumes for small segments, like hands or feet, will be less accurate than for the bigger ones, due to the higher gradient in their surfaces.

SUMMARY

An experimental method has been developed to use Vicon to measure areas and volumes on body segments, and their change during actions. The preliminary assessment of accuracy is promising but further trials need to be made. The technique has shown to be useful in several applications, like determining the shape of a segment for later recreation, assessing the skin artifact associated with certain movements or studying the propagation of a mechanical wave through a segment after an impact.

A FINITE ELEMENT MICROMECHANICAL MODEL OF MUSCLE TO EXPLORE THE ROLE OF INTRAMUSCULAR CONNECTIVE TISSUE

Bahar Sharafi, Silvia S. Blemker
Department of Mechanical and Aerospace Engineering, University of Virginia
bahar@virginia.edu, URL: http://www.mae.virginia.edu/muscle/

INTRODUCTION

Intramuscular connective tissue (IMCT) is thought to play an important role in the transfer of force between neighboring muscle fibers (Huijing, 1999, Purslow, 2002). The role of the IMCT in lateral force transmission can be investigated by assessing its contribution to the effective along-fiber shear modulus of the muscle tissue (a higher shear modulus would indicate a greater ability to transmit force laterally, and vice-versa). It is generally assumed that the shear modulus of the IMCT is much smaller than that of muscle fibers and that the effective shear modulus of muscle tissue is determined by the shear modulus of the IMCT (Purslow, 2002, Huijing 1999, Blemker 2005). The purpose of this study was to create a finite element micromechanical model of muscle to test this assumption. We built models of varying geometric complexity and explored the dependence of muscle tissue's along-fiber shear properties on the properties and geometry of the microstructure.

METHODS AND PROCEDURES

Finite-element models that represent four different microstructure geometries (Fig. 1A-D) were created. Both the muscle fibers and the IMCT were assumed to be passive, hyper-elastic, almost incompressible and transversely isotropic. The following functional form was used to represent the contribution of along-fiber shear to the strain energy (Blemker, 2005): $W_1 = G_1 B_1^2$, where B_1 is the along-fiber shear strain and G_1 is the along-fiber shear modulus.
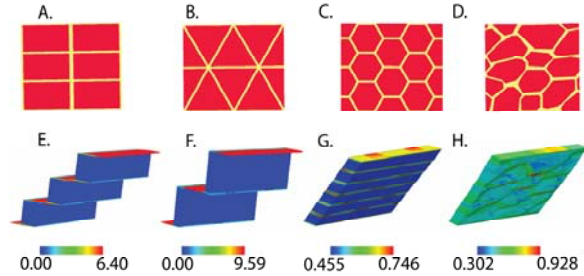
Figure 1: Regular geometrical shapes (A, B, and C), intra-fascicular muscle fiber geometry defined from a muscle histological cross-section (D), where red areas represent fibers and yellow areas represent the IMCT. The fiber volume ratio is 85% for all geometries. Along-fiber shear strain distributions for rectangular (E), triangular (F), and hexagonal (G) fibers, and real muscle tissue (H). The fiber to IMCT modulus ratio is 1×10^4 for these simulations.

Three-dimensional finite element simulations were performed using NIKE3D, a nonlinear implicit code (Puso, 2006). The concept of a repeating unit cell (RUC) and periodic boundary conditions (Drago and Pindera, 2007) were employed to derive the effective along-fiber tissue properties from the simulations.

Simulations were performed for a range of fiber and IMCT moduli. These simulations showed that the distribution of strains and the ratio of the effective tissue modulus to the IMCT shear modulus depends on the ratio of fiber shear modulus to IMCT shear modulus (Fig. 1E-H), independent of the absolute magnitudes of the shear moduli. Therefore, we present our results in terms of these ratios so that our conclusions are not sensitive to the assumed values of the shear moduli.

RESULTS

The microstructure geometry was an important factor in determining the tissue's effective along-fiber shear modulus (Fig. 2). For rectangular and triangular fiber arrays (Fig. 1A-B), most of the shear strain was concentrated in the IMCT (Fig. 1E-F). The effective tissue shear modulus approached a constant value and was not dependent on the fiber shear modulus except for low fiber to IMCT modulus ratios (Fig. 2A). This was not true of the hexagonal and the muscle microstructures (Fig. 1C-D). In these models, the strain distributions were relatively uniform between the fiber and IMCT (Fig. 1G-H) and effective tissue shear modulus was highly dependent on fiber shear modulus for the whole range of fiber modulus to IMCT modulus ratios (Fig. 2B).
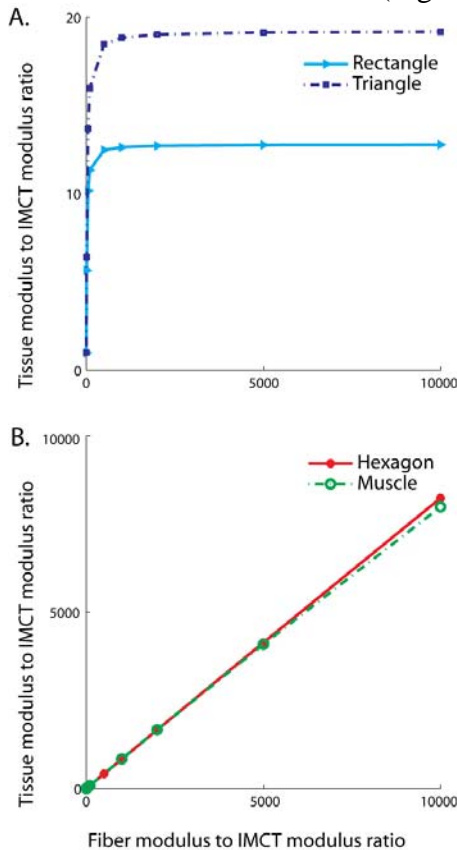
Figure 2: Relationship between the effective tissue along-fiber shear modulus and fiber shear modulus, normalized by IMCT modulus.

DISCUSSION

Our results challenge the common assumption that the effective shear modulus of muscle tissue is predominantly determined by the shear modulus of the IMCT. For the actual fiber microstructure, the effective tissue shear modulus was highly dependent on both the IMCT shear modulus and the fiber shear modulus. For a given fiber modulus and a given IMCT modulus, the intra-fascicular microstructure led to a higher effective shear modulus as compared to triangular and rectangular fiber geometries. This suggests that the intra-fascicular fiber arrangement provides a microstructure for effective lateral force transmission through the endomysium.

SUMMARY

Finite element simulations were performed for four different microstructures over a range of fiber and IMCT moduli. Our results indicate that the microstructure of muscle makes the IMCT an effective lateral force transmitter. Here we focused on the intra-fascicular structure, and therefore assessed the role of the endomysium in lateral force transmission. Our next step will be to analyze the inter-fascicular structure and assess the role of perimysium in lateral force transmission. The models presented here provide a new paradigm for assessing muscle structure and function at the microstructure level.

REFERENCES

Blemker et al. (2005). *J Biomech*, 38:57-665
Drago and Pindera (2007). *Compos Sci Technol*, 67:1243–1263.
Huijing (1999). *J Biomech*, 32:329-345.
Purslow (2002). *Comp Biochem Physiol*, Part A, 133:947-966.
Puso et al. (2006). *Lawrence Livermore National Labs Technical Report*, UCRL-MA-10526.

THE EFFECTS OF WALKING SPEED AND SURFACE ON DYNAMIC STABILITY IN YOUNG ADULTS WITH UNILATERAL TRANS-TIBIAL AMPUTATIONS

Shawn J. Scott[1], Jonathan B. Dingwell[1], and Jason M. Wilken[2]

[1]Nonlinear Biodynamics Lab, Department of Kinesiology and Health Education, University of Texas, Austin, TX, USA, shawn.scott1@us.army.mil
[2]The Center for the Intrepid, Brooke Army Medical Center, Ft. Sam Houston, TX, USA.

INTRODUCTION

Dynamic stability is commonly defined as the ability to maintain balance during locomotion. Hof (2005) introduced a dynamic stability margin (DSM) based on how the center of mass (COM) moves relative to the base of support. Unilateral trans-femoral amputees exhibited larger DSMs on their involved sides. These also increased at faster walking speeds (Hof 2007). This finding seems counterintuitive and suggests that amputees adopt larger DSMs to *compensate* for an increased sensitivity to perturbations (either real or perceived). DSMs have not been assessed when walking stability has been overtly challenged.

Patients with locomotor impairments are especially challenged when walking over uneven or unstable surfaces (Richardson 2004). To date, however, these studies have not yet controlled for walking speed. This study determined how both walking speed and an uneven surface affected DSMs in adults with unilateral trans-tibial amputation (TTA). We hypothesized that DSMs would increase on the involved side at faster walking speeds and would also increase more on the involved limb when walking over loose gravel.

METHODS AND PROCEDURES

Five male military service members (27.6 ± 5.4 yrs) volunteered to participate with written informed consent (Table 1). All patients had unilateral TTA. These were due to blast related injuries in 3 patients, gunshot wounds

in 1 patient, and a motorcycle accident in 1 patient. Prosthetic devices varied for subjects based on individual needs.

Patients walked at 3 height-adjusted speeds over both a level walkway and a loose gravel surface. All subjects completed 6-10 trials over each surface at each speed. Full body kinematics were recorded during each trial using 55 markers and a 19 camera Motion Analysis system. A 15-segment model was used to estimate whole body COM motions.

Frontal plane DSMs were defined as the minimum perpendicular distance between the velocity adjusted COM vertical projection and the lateral borders (5th metatarsal head) of the forward supporting foot (Hof 2005). In theory, larger DSMs should reflect a safer (i.e., more stable) gait pattern (Hof 2005). Minimum DSM values during the stride were extracted for statistical analyses. A three factor ANOVA was used to determine differences between limbs, speeds, and surfaces.

RESULTS

DSMs exhibited minima shortly after heel strike (Fig. 1), as in Hof (2005, 2007). Minimum DSMs (Fig. 2) were significantly larger when patients walked on the gravel surface compared to level ground ($p = 0.037$). There was a trend for DSMs to increase slightly at faster walking speeds ($p = 0.097$). There were no significant differences between involved and uninvolved limbs ($p = 0.321$). There were no significant interaction effects.

There were occasional individual subject trials over the loose gravel where the DSMs were only a few millimeters. During these trials, some subjects exhibited stumbling responses, including occasional cross-over stepping. However, the DSMs never became negative and no subject experienced a fall.

Subject - Limb*	Age (yr)	Ht (m)	Wt (kg)	Time in Prosthesis (wk)
1 - L	26	1.80	67.50	8
2 - R	19	1.72	63.18	17
3 - L	32	1.86	83.86	120
4 - L	29	1.75	75.50	8
5 - R	32	1.76	77.27	21

Table 1. Demographic data for patients with trans-tibial amputation. *The prosthesis limb.

DISCUSSION

Patients adapted to the unstable loose gravel surface by increasing their DSMs. This provides additional evidence that these DSMs reflect how patients *compensate* to maintain balance when their stability is challenged. This directly extends recent results presented in trans-femoral amputees (Hof 2007). However, it is not yet known if these changes in DSM directly predict changes in fall risk.

The lack of differences between intact and prosthetic limbs in these TTA patients contrasts with previous results obtained in trans-femoral patients (Hof 2007). This was likely due either to differences in level of amputation, activity/fitness level, or both. That the TTA patients in this study achieved relatively symmetric gait patterns and DSMs supports the idea that amputees do not have to sacrifice symmetry to achieve sufficient stability.

Further research needs to determine how these DSMs are related to actual fall risk and how gait symmetry, stability, and fall risk are inter-related in both trans-tibial and trans-

femoral amputees. The present findings nevertheless provide important insights into how TTA patients adapt their gait patterns to challenging walking environments.
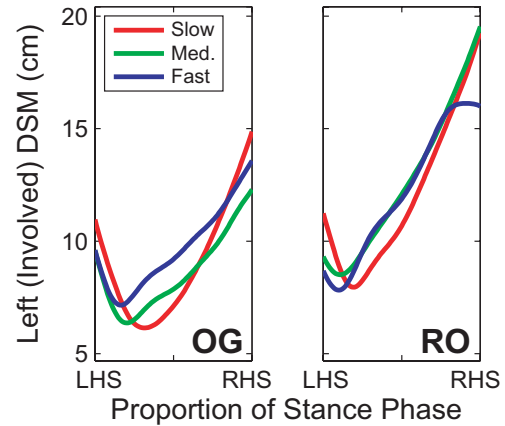
Figure 1. DSMs for the involved limb of a typical subject while walking over level ground (OG) and loose gravel (RO).
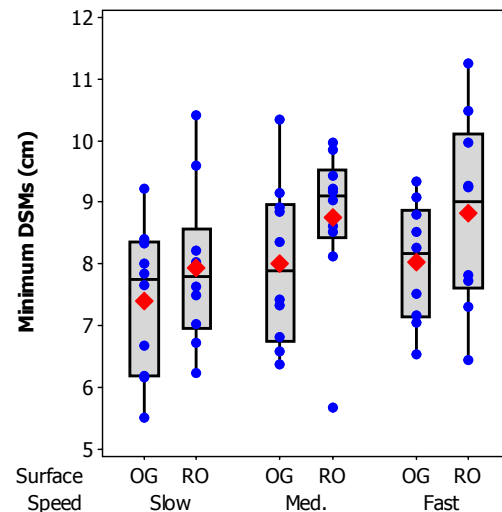
Figure 2. Box plots of DSMs. Dots are individual means, diamonds are group means. OG=overground (level), RO=rocks (gravel).

REFERENCES

Hof, A. L., M. G. Gazendam, et al. (2005). J *Biomech* 38(1): 1-8.

Hof, A. L., R. M. van Bockel, et al. (2007). *Gait Posture* 25(2): 250-8.

Richardson, J. K., S. B. Thies, et al. (2004). J *Am Geriatr Soc* 52(9): 1532-7.

DYNAMIC STABILITY OF WALKING DURING ANTERIOR-POSTERIOR AND MEDIO-LATERAL SUPPORT SURFACE AND VISUAL FIELD TRANSLATIONS

Patricia M. McAndrew[1, 2], Jonathan B. Dingwell[1], Jason M. Wilken[2]

[1]Nonlinear Biodynamics Lab, Dept. of Kinesiology, University of Texas, Austin, TX, USA
[2]Center for the Intrepid, Brooke Army Medical Center, Ft. Sam Houston, TX, USA

E-mail: mcandrew@mail.utexas.edu   Web: http://www.edb.utexas.edu/faculty/dingwell/

INTRODUCTION

Improving the ability to react to perturbations during daily activities like walking is a key to effective fall prevention training. Quantifying how walking stability changes in response to de-stabilizing events is critical for assessing how effective gait training interventions are. In robotics, walking stability is commonly quantified using Floquet multipliers (FM) (Hurmuzlu 2004). Healthy elderly exhibited larger maximum FM (i.e., more unstable) than young subjects during *un*perturbed walking (Kang 2008). However, FM did *not* increase when perturbations of increasing amplitude were applied to a dynamic model of walking (Su 2007). Changes in FM have not been assessed in humans during *perturbed* walking.

Virtual reality (VR) environments such as the Computer Assisted Rehabilitation ENvironment (CAREN) system at the Center for the Intrepid (CFI; Fig. 1) provide a unique opportunity to understand how humans control gait stability. These systems can apply well-controlled and repeatable visual and mechanical perturbations during gait. This study determined how continuous pseudo-random horizontal oscillations of the walking surface and visual field affected gait stability.

METHODS AND PROCEDURES

Four young healthy subjects participated with informed consent. Each subject completed five 3-min walking trials in the CAREN under each of 5 conditions: no perturbations (NORM), anterior-posterior platform (APP) or visual (APV) translations or mediolateral platform (MLP) or visual (MLV) translations. All translations were applied as a pseudo-random sum of sines with incommensurate frequencies of 0.16, 0.21, 0.24 and 0.49 Hz. Kinematic data for the head, trunk, pelvis and feet were collected using Vicon at 60 Hz.

Fig. 1. The CAREN at CFI is an immersive VR system contained in a 7m diameter dome with a six degree of freedom platform with a built-in instrumented treadmill.

Motions of a single marker placed on the seventh cervical (C7) vertebra were analyzed. Power spectral analyses were performed to quantify the strength of the coupling or entrainment between the perturbation input and the movement output.

To quantify orbital stability, maximum Floquet multipliers (FM) were computed for each time series using standard techniques

(Su 2007; Kang 2008). State-spaces were generated using 3-dimensional velocities and accelerations of the C7 marker. The maximum FM defines the amount by which a perturbation away from the mean reference trajectory grows or decays after one complete cycle. If the maximum FM has magnitude < 1, perturbations decay after successive strides, and the system is orbitally stable. Smaller FM indicate greater stability. The results were analyzed using 2-factor ANOVA.

RESULTS AND DISCUSSION

C7 marker movements exhibited significantly increased spectral power ($p \leq 0.004$) at all 4 input frequencies for all perturbation conditions (Fig. 2, Left). This demonstrates that the applied perturbations significantly altered each subjects' kinematics. Subjects perceived that the MLV and APV conditions affected them the most and least, respectively.

Conversely, subjects remained orbitally stable throughout the gait cycle for all experimental conditions (Fig. 2, Right). Maximum FM magnitudes did not increase significantly ($p \geq 0.104$) for any of the perturbation conditions. These results confirm modeling predictions, where orbital stability did not change as perturbation amplitudes increased (Su 2007).

Interestingly, there was a trend for subjects to exhibit slightly greater responses to *platform* translations in the AP direction, whereas they exhibited slightly greater responses to *visual field* translations in the ML direction.

Even with substantial perturbations, subjects still maintained stable gait for all conditions. It is important to note that no subjects fell during this study. Also, FMs theoretically reflect the inherent stability of the *system*, which should not depend strongly on the specifics of the perturbations applied. This was reflected in these stable FM values.

These results indicate that inducing greater movement, and thus greater movement *variability* (Fig. 2, Left) does not necessarily induce greater *instability*. What these FMs do not reflect, however, is how people *achieved* stability. While these FM appear to represent overall gait "stability", they may not in fact be sensitive enough to predict *risk* of falling.
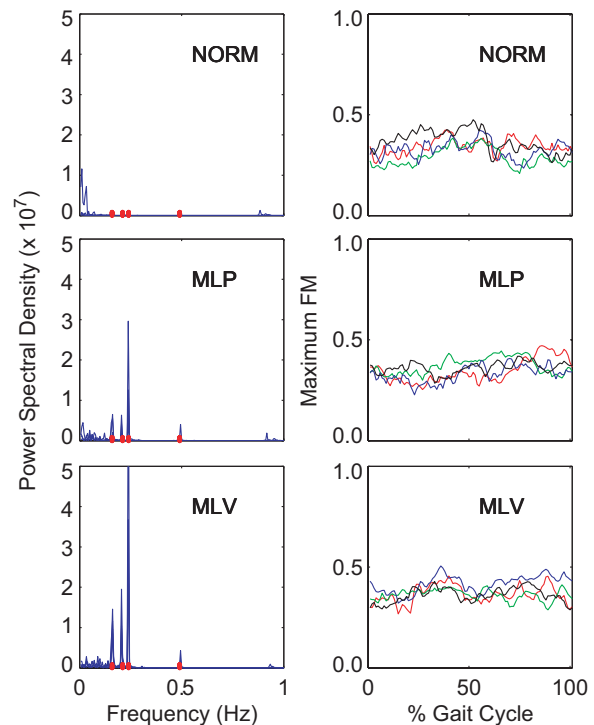
Fig. 2. Left: Representative power spectra of the mediolateral C7 marker motions for the NORM, MLP and MLV conditions. Red lines indicate the frequencies of the applied perturbation. Right: Corresponding maximum FM for all subjects. Each line represents the mean result for one subject.

REFERENCES

DeMott, T.K. et al. (2007). *Am. J. Phys. Med. Rehabil.,* 86(2): 125-132.
Hurmuzlu, Y. et al. (2004). *Automatica,* 40(10): 1647-1664.
Kang, H.G. and Dingwell, J.B., (2008). *J Biomech.*, In Review.
Su, J.L. and Dingwell, J.B., (2007). *J Biomech Eng.,* 129:802-810.

VERTICAL GROUND REACTION FORCES AND CENTER OF PRESSURE EXCURSION DURING TWO-HAND PUSH EXERTIONS

Suzanne Hoffman[1], Matthew Reed[2], and Don Chaffin[2]

[1]Manufacturing Systems Research Lab, General Motors Research and Development, Warren, MI, suzanne.hoffman@gm.com
[2]Center for Ergonomics, Industrial and Operations Engineering, University of Michigan, Ann Arbor, MI

INTRODUCTION

For certain tasks, balance has been shown to be more limiting than floor traction or joint muscle strength with respect to force exertion capability (Holbein & Chaffin, 1997). Functional stability limits are dependent on load and foot position conditions as shown by Holbein and Chaffin (1997), Holbein and Redfern (1997), and Lee T-H and Lee Y-H (2003). Holbein and Chaffin (1997) also showed that, in general, increased separation of the feet in a given direction allows for greater displacement of the center of gravity in that direction without loss of balance. In high-force pushing and pulling tasks, a fore-aft split-stance may allow for greater body weight utilization.

This paper examines load distribution between the rear and lead foot during two-hand push exertions to determine the extent to which foot placements can be predicted from balance considerations.

METHODS AND PROCEDURES

Nine men and ten women were recruited from a student population and paid for their participation. All were required to be right-hand dominant and none had a history of musculoskeletal disorders. All participants were young (median age 21 years) and relatively thin (median body mass index 23 kg/m2).

Posture data were obtained using a passive optical motion tracking system (Figure 1). Participants exerted force on a fixed cylindrical handle covered with foam rubber that provided a high-friction grip. Forces and moments at the hands were measured via a 6-DOF load cell (JR3, Woodland, CA). Hand force feedback was presented visually to the subject allowing subjects to achieve and maintain requested hand forces.
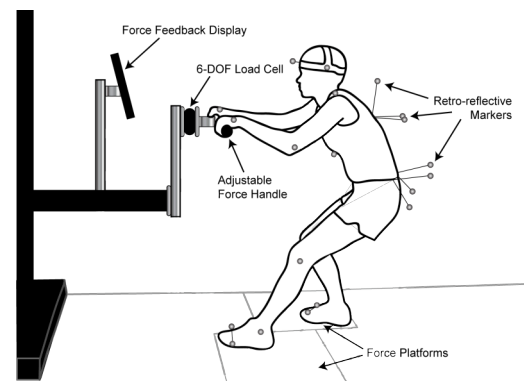
Figure 1: Laboratory configuration with optical motion tracking system, visual force feedback display, 6-DOF load cell, and moveable force platforms.

For the current analysis, data from two-handed push exertions performed on a horizontal handle at elbow height (63% of stature) were used. Subjects exerted forces spanning from 25% to 100% of their maximum capability. For each trial, data were analyzed with respect to the *hand force plane*, defined as the vertical plane containing the measured hand force vector. Center-of-pressure (COP) excursion is defined as the Euclidean distance from the center of the

base-of-support (BOS) to the COP location computed from force plate data (Figure 2).
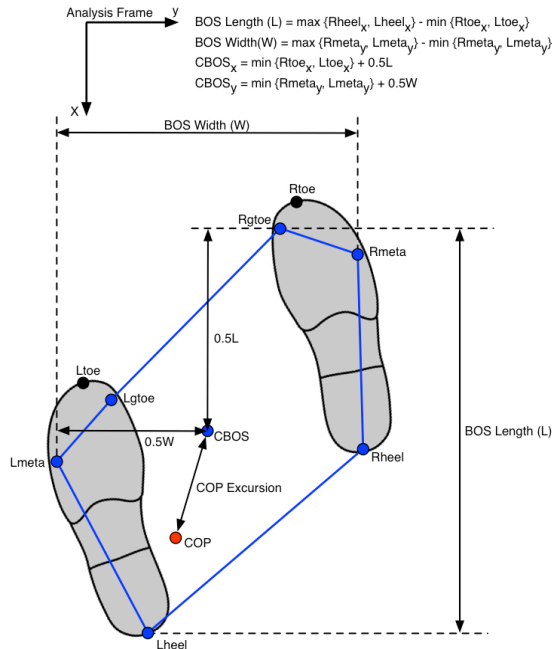
Figure 2: Base-of-support is defined by heel, 5th metatarsal, and toe locations.

RESULTS

An increase in horizontal push force is associated with a loading of the rear foot (Figure 3) and unloading of the lead foot (Figure 4). This change in load distribution corresponds to a shift in COP location towards the rear edge of the BOS (Figure 5).
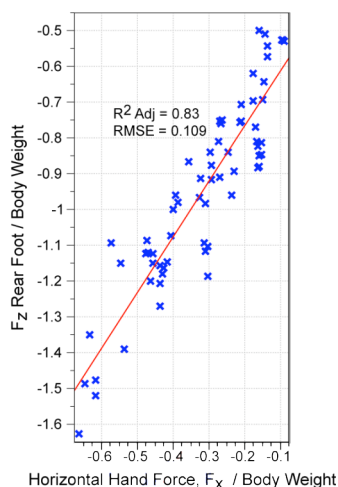
Figure 3: Vertical ground reaction force measured at the rear foot as a function of the horizontal push force.
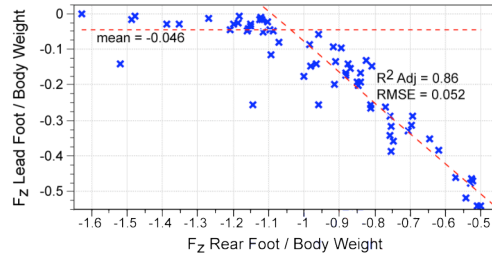
Figure 4: Load distribution between lead and rear foot.
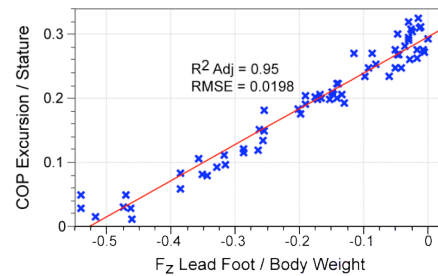
Figure 5: Shift in COP from center of BOS to rear edge of BOS with unloading of lead foot.

DISCUSSION

Horizontal push force magnitude is a strong predictor of vertical reaction force distribution between the rear and lead foot and COP excursion is well predicted by vertical force at the lead foot. These findings suggest that static balance requirements can be used to predict foot placements with respect to the pelvis.

REFERENCES

Holbein, M. and Chaffin, D. (1997). *Human Factors*, 39(3):456–68.
Holbein, M. and Redfern, M. (1997). *Int J Ind Ergonom*, 19(5):387–395.
Lee, T. and Lee, Y. (2003). *Ergonomics*, 46(5):446–54.

ACKNOWLEDGEMENTS

LOCOMOTOR INITIATION: INFLUENCE OF CHRONIC ANKLE INSTABILITY

Chris J Hass, [1] Erik Wikstrom, [1] Kimberly Fournier, [1] Amruta Inamdar[1], Mark Bishop[2]

[1] Department of Applied Physiology and Kinesiology , University of Florida,
Gainesville, FL, USA cjhass@hhp.ufl.edu
[2]Department of Physical Therapy, University of Florida, Gainesville, FL, USA

INTRODUCTION

The injury occurs within 100ms but the sequela of instability can last a lifetime for almost 75% of people that sprain their ankle (Gerber et al, 1998). Currently, the underlying neurophysiologic mechanism of chronic ankle instability (AI) is unknown but preliminary evidence suggests that both feed forward and feedback mechanisms may play a role. Recently, we have shown that both feed forward and feedback control are altered in this population using planned and unplanned gait termination as a perturbation model (Wikstrom et al., 2008).

Postural control during dynamic activities such as gait termination and initiation requires the integration of multiple sensory and motor pathways so that the central nervous system can coordinate the anticipatory/postural and intentional/movement components of the task. Recent studies indicate that people with unilateral AI have altered gait patterns and bilateral increases in postural sway when compared to healthy controls (Ross et al., 2004). This finding suggests that reorganization in the feed-forward neuromuscular control may occur in this population. The purpose of this study was to determine if AI leads to alterations in neuromuscular control during gait initiation.

METHODS AND PROCEDURES

Forty subjects, 20 healthy (20.85±1.6yr, 164.3±7.9cm, 64.2±10.62kg) and 20 with AI (20.5±1.0yrs, 169.8±9.8cm, 74.2±20.2kg) participated in this investigation. AI was defined as a history of at least one grade-two ankle sprain that required immobilization and at least one recurrent sprain within the past 6 months.

Gait initiation trials began with the participant standing quietly with each foot on separate force platforms (Bertec, Columbus Ohio) mounted flush with the laboratory floor. Initial positioning of the feet was self selected. In response to an auditory signal, the participants initiated walking self selected pace and continued to walk for several steps. For each participant, five data collection trials were collected from each stepping leg.

Kinematic data were collected using an 8 camera 3D Optical Capture system (Vicon Peak, Oxford, UK) collecting at 120Hz. Thirty-nine passive reflective markers were attached to the body in accordance with the Vicon Plug-in-Gait marker system.

Electomyographic recordings were also collected bilaterally at 1200Hz, from the tibialis anterior, soleus, and gluteus medius. Ground reaction forces were collected using the two multi-component force platforms (Bertec Corp). Force platform data were subsequently used to calculate the instantaneous COP.

The center of pressure (COP) during gait initiation (GI) was divided into three periods (S1, S2, S3) by identifying two landmark events (Figure 1).The first section (S1) began

with the initiation command and ended with the COP located in its most posterior and lateral position toward the initial swing limb (Landmark 1). The second section (S2) was characterized by a translation of the COP towards the stance limb ending at Landmark 2. The third section (S3) extended from Landmark 2 until toe off of the initial stance
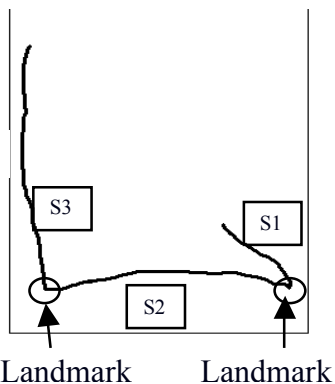
Landmark   Landmark

Figure 1: Landmark identification and the subsequent defined periods S1, S2, and S3 of the COP trace during GI.

Dependent COP variables were computed to include peak COP excursions and average velocities. Magnitudes were normalized based on self-selected stance width. Separate 2 x 2 (Group x Limb) ANOVA's were used to test for overall group differences during each GI period.

RESULTS

During the initial GI period, a significant Goup × Limb interaction was observed for the resultant displacement of the COP which was strongly influenced by the mediolateral component of the shift. During the S2 period, a statistical trend for a Group × Limb (p= 0.06) interaction was observed in mediolateral component of the COP shift. In both cases, the magnitudes of the displacements decreased when stepping with the dominant limb in the healthy controls and increased when stepping with the injured side in those with AI. During S3, the time period where the COP moves forward under the stance foot, a

significant Leg main effect was observed for mediolateral COP oscillations. Greater movement and velocities were observed during trials where stepping occurred with the non-dominant or non affected limb when compared to trials where stepping occurred with the involved or non-dominant limb.

DISCUSSION

During GI, movement of the COP towards the initial stepping limb drives the center of mass forward and towards the stance limb. The present findings suggest that subjects may alter COP excursions based on perceived stability of the initial stance limb. For example, individuals with AI reduced the COP excursions towards the unaffected stepping limb. Thus, the magnitude of stance side COM momentum would be less as it travels towards the affected leg. Similarly, the healthy controls produced less swing side COP excursions when stepping with the dominant limb, possibly in an effort to reduce the postural requirements of the non-dominant stance limb.

SUMMARY

Ankle instability appears to alter feed-forward control of gait initiation particularly in the postural shift mechanisms.

REFERENCES

Gerber J et al. (1998) *Foot Ankle Int*: 19; 653-60

Ross, S and Guskiewicz,K (2004) *Clin J Sports Med* 14: 332-338

Wikstrom E et al. (2008) *SEATA Conference Proceedings, Franklin, TN*

ACKNOWLEDGEMENTS

Calculation of Vertical Load Rates in the Absence of Vertical Impact Peaks

Richard Willy, MPT[1] Michael B. Pohl, PhD[1] and Irene S. Davis, PhD, PT[12]

[1]University of Delaware, Department of Physical Therapy, Newark, DE, USA.
[2]Drayer Physical Therapy Institute, Hummelstown, PA, USA
Email: rwilly@udel.edu

INTRODUCTION

High vertical ground reaction force load rates during gait have been associated with injuries such as anterior knee pain in walking (Radin at al. 1991) and tibial stress fractures in running (Milner et al., 2006). Rearfoot strikers typically demonstrate a clear vertical impact peak (**VIP**) during running. Vertical load rate is calculated as the slope of the force-time curve between foot strike and VIP. However, midfoot and forefoot strikers often exhibit an attenuated, or missing VIP. Without a well-defined impact peak, it is difficult to discern the period over which the loading rate is calculated. However, there may be other force or impact related variables that correlate well, in time, with the vertical impact peak. If so, the time to these events might serve as a surrogate for the timing of an attenuated or missing VIP. This would then provide a time period over which to calculate a vertical load rate.

The purpose of this study was to examine the timing of a number of impact-related variables with the timing of the VIP in a group of rearfoot strike runners. A subset of those variables was then used to determine VIP in a separate group of rearfoot strikers. Based on its association with impact, it was hypothesized that the timing of peak tibial acceleration would be the best surrogate for the timing of VIP

METHODS

Twenty male and female recreational rearfoot strike runners (age 25.2, ±8.32),

currently running at least six miles per week were tested. Subjects were healthy and had no injury, illness, or any condition, which might affect their ability to run.

A triaxial accelerometer (PCB Piezotronics, Depew, NY) was firmly attached to the anteromedial aspect of the distal tibia on the dominant limb. Five trials were collected as each subject ran approximately at 3.35 m/s (8 min/mile pace) across a forceplate (Bertec, Worthington, OH). Force and accelerometer data were collected at 1000hz. All signals were filtered at 50 Hz with a fourth order, zero lag, low pass digital Butterworth filter.

Data were analyzed using custom LabVIEW software (National Instruments, Austin, TX). We first calculated the time (in %stance) of the VIP. This was used as a reference for later comparison. We then calculated the mean and standard deviation (sd) of the times (in %stance) to peak: positive acceleration (**PPA**), braking force (**BF**), vertical force (**VF**) and lateral force (**LF**). Next, we correlated these times with the time to VIP. Variables with nonsignificant correlations were then removed from the analysis, resulting in a reduced set.

We then used these variables to estimate the time to VIP in a separate set of 30 recreational runners whose force and accelerometry data had been collected in a similar manner previously. Finally, we calculated the rms error between the estimated time and actual time to the VIP in this new group of runners.

RESULTS

The mean and sd, and correlation between the variables of interest are presented in Table 1.

Table 1. Initial variables of interest (mean and sd (in % stance) and correlation to VIP

	mean	sd	r	p
VIP	0.13	0.02		
PPA	0.11	0.02	0.49	**0.03**
BF	0.24	0.03	0.43	**0.06**
VF	0.45	0.03	-0.05	0.84
LF	0.23	0.16	0.35	0.13

Based on the non-significant correlations of VF and LF, these variables were removed from the data set, leaving times to PPA and BF along with VIP to be validated on the separate set of runners (Figure 1)
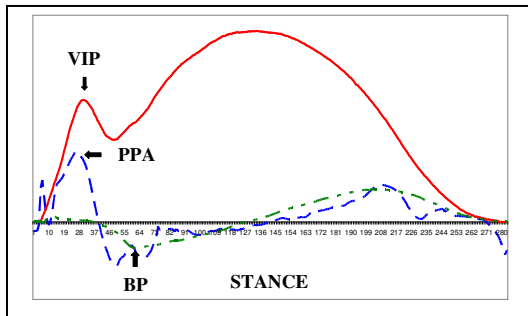
Figure 1. Relative timing of variables used to predict time to VIP

While the time to BF was consistent across subjects and was moderately correlated with the time to BF, it occurred later in stance. Therefore, we calculated the time of VIP relative to the time of BF to create a correction factor for BF, which was 0.55 BF, or 13% stance. The rms values of VIP, PPA and the corrected BF (CBF) between the estimated and actual time of VIP in a new data set were 0.03, 0.03, and 0.04 respectively.

DISCUSSION

Calculation of vertical load rates is problematic when vertical impact peaks are attenuated or missing. We sought to determine whether other force or impact related variables could be used as a surrogate measure.

It was apparent from the first part of the study that time to VF (even with a correction factor applied) would not be a good measure to use. This is because there was essentially no relationship between the time to VIP and VF. Along with a weak and insignificant correlation between time to VIP and LF, time to LF was more variable than the rest of the values. During running, there is a typical peak in the lateral GRF at initial contact. However, this was missing in a few subjects whose peak lateral force then occurred much later in stance.

When applied to the new data set, the rms values for all three variables were small. This suggests that any one of these could be used as surrogates for time to VIP. However, in individuals with low PPA values, the peak values are much less distinct. Additionally, accelerometry may not be part of the gait data. These may provide rationales for using one of the other force measures when impact peaks are missing.

SUMMARY

Based on the results of these data, it appears that either time to PPA, time to CBF or a set value of 13% stance could be used as a surrogate for time to VIP when vertical impact peaks are missing.

REFERENCES

Milner, CE et al. (2006) *MSSE* 38-323-328.
Novacheck, TF (1998) *Gait and Posture,* 7:77-95
Radin EL et al. (1991). *J Orthop Res,* 9:398-405.

Neuromechanical representations of leg orientation and length control are preferentially conserved after peripheral nerve injury during cat locomotion

Young-Hui Chang[1], Arick Auyang[1], John P. Scholz[2], T. Richard Nichols[1]

[1]School of Applied Physiology, GeorgiaTech, Atlanta, GA, USA

[2]Department of Physical Therapy, University of Delaware, Newark, DE, USA

Website: http://www.ap.gatech.edu/chang/CNLhome.html   E-mail: yh.chang@ap.gatech.edu

INTRODUCTION

There is a paucity of data on common gait compensation principles that span different pathologies. Such understanding would yield important insights into how legged locomotion is controlled in able-bodied and impaired persons. As a first step to study what may guide intralimb compensation in impaired gait, we studied cat locomotion after peripheral nerve injury. Surgical cut and repair of nerves in cats results in muscle paralysis (~1 month) followed by gradual self-reinnervation and complete return of motor function within 9-12 months (Cope et al., 1994; Cope and Clark, 1993). We hypothesized that a neuromechanical representation of whole leg function (orientation and length) guides intralimb compensation after injury and would be preferentially conserved over individual joint function.

METHODS

After training five cats to walk on a treadmill at 0.8 m/s, we surgically transected and repaired nerves supplying each of the triceps surae muscles (3 cats) or only soleus muscle (2 cats). We collected hindlimb kinematics before injury (P0), during the paralytic stage (P1), and after muscle reinnervation (P14). On average, we analyzed 38±25 (SD) step cycles for each cat and condition (range: 17-100). We quantified kinematics trajectories from individual joints (MTP, ankle, knee, and hip) and toe-to-hip leg vector (orientation and length). We compared post-injury kinematics to P0 trajectories by calculating average coefficient of determination across cats, R^2. An $R^2=0$ represents the control strategy of an immobilized joint or leg, while an $R^2=1$ denotes perfect return to the pre-injury trajectory shape for that variable. We tested across cats for consistent maintenance of pre-injury trajectories during the initial weight acceptance period and over the entire stance phase. An $R^2>0.5$ denotes that the majority of post-injury kinematics variance is accounted for by a pre-injury control strategy (1-tailed t-test, $\alpha=0.05$).

RESULTS
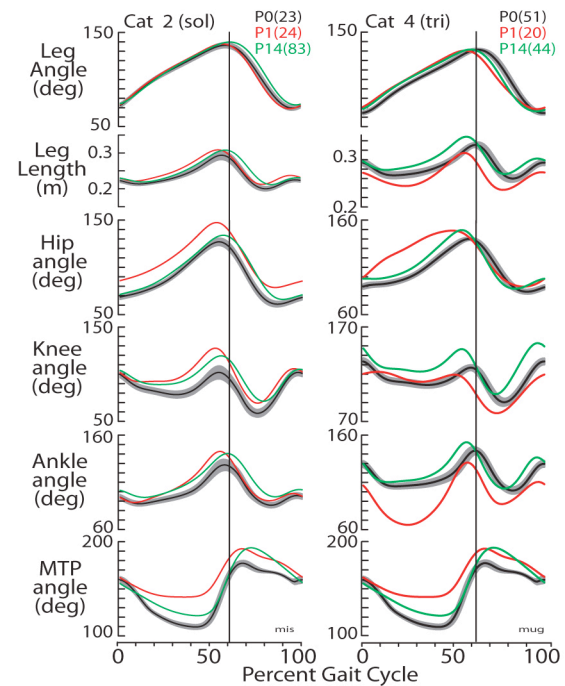
Fig 1. Mean trajectories for 2 cats at P0 (black; gray shading is ±1SD), P1 (red) and P14 (green). Vertical lines indicate end of stance. Number of step cycles in parentheses.

In general, animals with entire triceps surae injuries showed greater deficits (Fig 1). We did not, however, see any consistent trend in trajectory shapes correlating with injury type.

During initial weight acceptance, only leg orientation and leg length control strategies were conserved in both paralytic ($R^2 \geq 0.82$,

p≤0.003) and reinnervated (R^2≥0.83, p≤0.009) stages. Knee joint control at P14 was the only joint level variable that returned to a pre-injury strategy at weight acceptance (R^2=0.69±0.20, p=0.238).

Only leg orientation control was conserved over the entire stance phase during paralytic stage (R^2=0.99±0.002, p<0.001). Leg orientation (R^2=0.97±0.04, p<0.001) and leg length (R^2=0.83±0.24, p=0.0352) control strategies were both conserved after reinnervation. Ankle joint (R^2=0.81±0.24, p=0.039) and hip joint (R^2=0.95±0.06, p<0.001) control also returned to pre-injury trajectories after muscle reinnervation. R^2 data are summarized in Figure 2.
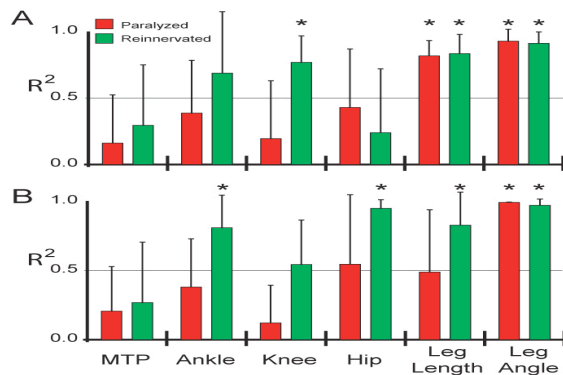
Fig 2. Avg. R^2 values for P1 (red) and P14 (green) trajectories at A) weight acceptance and B) stance phase compared to P0. Data are means ± SD. * indicates >0.5 (α=0.05).

DISCUSSION

We have shown joint level responses to muscle paralysis likely act to conserve whole leg function during walking. These compensation strategies appear to persist after muscle reinnervation, at 14 months post-injury. Our findings imply adaptive processes within the central nervous system preferentially stabilize leg control over joint control and that joint deficits observed after injury may reveal a coordinated strategy for stabilizing the leg. We also have preliminary data from a rat model indicating limb function is conserved over joint function after peripheral nerve injury, which suggests this

may be a fundamental principle for mammalian locomotor compensation.

Our findings are consistent with the idea that whole limb control is dictated and referenced at higher levels of the central nervous system while compensatory joint level adjustments are coordinated at lower levels. Both leg orientation and length have been observed to be encoded in the cat spinal cord by dorsal spinocerebellar tract neurons that deliver sensory information to higher brain centers (Bosco et al., 1996). We are also pursuing direct testing of this hypothesis with a novel *in vitro* preparation involving spinally generated locomotion in an isolated rat spinal cord with hindlimbs attached.

SUMMARY

Locomotor compensation subsumes that one or more elements of the system change in response to an injury with a higher purpose of conserving function in another element. Such joint level changes are described as deficits, but little attention is usually given to how these deficits are coordinated to preserve higher locomotor function after the injury. We have shown that leg function is preferentially conserved after injury despite large deficits in joint function. Further study of how compensatory responses of joints can stabilize leg function is needed to construct a theoretical framework to better understand intralimb locomotor compensation.

REFERENCES

Bosco G, Rankin A, and Poppele R (1996). *J Neurophysiol.* 76:715–726.

Cope TC, Bonasera SJ, Nichols TR (1994). *J Neurophysiol* 71:817-820.

Cope TC, Clark BD. 1993. *J Neurophysiol* 70:1787-1796.

ACKNOWLEDGEMENTS

CHANGES IN PASSIVE MUSCLE PROPERTIES OF CEREBRAL PALSY PATIENTS

Megan Yaraskavitch and Walter Herzog

Faculty of Kinesiology, University of Calgary, Calgary, Alberta, Canada
walter@kin.ucalgary.ca

INTRODUCTION

Cerebral palsy (CP) is a condition characterized by a static lesion in the immature brain caused by a congenital development defect, a neonatal etiology or a traumatic event at birth leaving individuals with a permanent motor impairment (Miller, 2005). It has been found that spastic muscle cells from cerebral palsy patients are stiffer than normal muscle cells (Fridén and Lieber, 2003). However the mechanism for this difference remains unclear. Past research suggests that the molecular spring titin is a main contributor to the development of passive force upon stretch in normal muscle (Wang, 1991) and that changes in the passive stiffness of myocytes are accompanied by changes in titin isoforms (Granzier, 2004). The purpose of this study is to examine the passive force length properties of spastic muscle myofibrils from cerebral palsy patients to investigate whether the increased stiffness can be attributed to changes in the mechanical properties of titin.

METHODS AND PROCEDURES

Spastic muscle samples (1 cm x 0.5 cm) were collected from various lower limb muscles of children with CP undergoing routine tendon lengthening/release surgeries at the Alberta Children's Hospital. One sample from each muscle was prepared for single myofibril force-length testing using a specifically designed apparatus (accuracy < 1nN) while another sample was frozen for gel electrophoresis to determine titin isoforms. Single muscle myofibrils (n=4) were isolated as described earlier (Rassier et al. 2003). Once isolated, one end of the myofibril was attached to a glass needle and the other end to a nanolever, which upon stretch to various physiological sarcomere lengths deflected relative to a control lever allowing the passive force to be calculated. After the passive force-length relationship was determined for an individual myofibril, the protease trypsin was added to degrade titin and the passive force-length relationship was remeasured (without the added contribution of titin). Passive stress-sarcomere length (SL) traces were plotted to account for varying diameters of myofibrils.
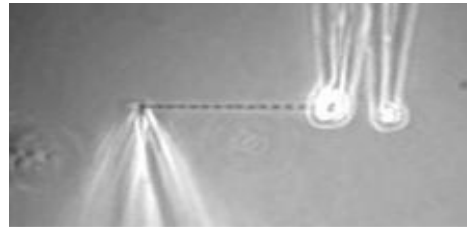
Figure 1. Isolated human spastic psoas myofibril in force-length testing apparatus.

RESULTS

Preliminary results of the spastic psoas (n=2) and spastic tibialis anterior (n=2) suggest that, for a given sarcomere length, passive forces of spastic muscle are considerably higher than we have seen using normal skeletal muscles from the rabbit. Previous work with rabbit psoas indicates a peak passive stress of approximately 50 nN/μm^2 at a SL of 3.4 μm (Joumaa, 2007). Results at the same SL with human spastic psoas suggest stresses 2 to 8 times higher. Following the addition of

trypsin, passive forces were reduced with the degradation of titin. This confirms that titin is a main contributor to passive force development in spastic muscle.
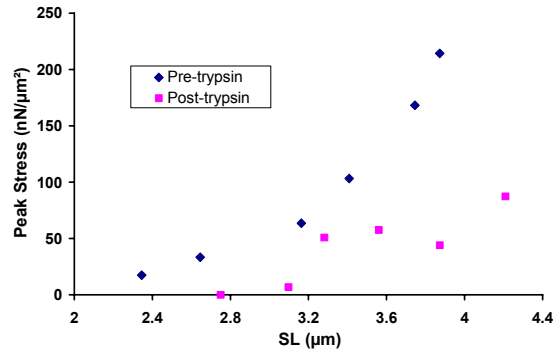
Figure 2. Stress-SL trace of a human spastic psoas myofibril.

DISCUSSION

The results of our preliminary study describe a potential mechanical difference in spastic muscle from CP children which may be explained by a possible structural difference in titin. As it is known that the mechanical properties and titin isoforms can differ between skeletal muscles of the same and different species (Freiburg, 2000), our next step is to conduct comparisons between the same muscle of a spastic and normal individual. Normal muscle samples will be collected from the gastrocnemius of adult subjects and from other lower limb muscles of healthy adults receiving orthopaedic surgery for traumatic injury. Force-length testing and gel electrophoresis will then be performed with the same normal and spastic human muscle so that a relative comparison of the mechanical properties and related titin isoforms can be determined.

SIGNIFICANCE

Understanding the passive properties of spastic muscle from CP patients is the first step towards understanding the condition and the possible effects of routine treatment surgery. If our further investigation continues to support the findings of our preliminary work, this study may provide evidence for a structural remodelling of spastic muscle as a result of CP.

REFERENCES

Freiburg, A et al. (2000). *Circ. Res*. 86, 1114-1121.

Fridén, J and Lieber, RL (2003). *Muscle nerve*, *27*(2), 157-64.

Granzier, HL and Labeit, S (2004). *Circ Res*, 94(3), 284-295.

Joumaa, V (2007). *Pflugers Arch – Eur J Physiol.* 455, 367-371.

Miller, F (2005). *Cerebral Palsy*. Anonymous New York: Springer Science+Business Media, Inc.

Rassier, DE et al. (2003). *Proc. R. Soc. Lond. B 270*(1525), 1735-40.

Wang, K et al. (1991). *PNAS*, *88*(16), 7101-7105.

ACKNOWLEDGEMENTS

ESTIMATING THE APPROPRIATE SAMPLE SIZE FOR THE DETERMINATION OF OPTIMAL FIBER LENGTH

Benjamin W. Infantolino and John H. Challis

Biomechanics Laboratory, Department of Kinesiology, The Pennsylvania State University,
University Park, PA, USA
E-mail: bwi100@psu.edu

INTRODUCTION

The force-length properties of muscle dictate the force a muscle can produce isometrically at a given length (Gordon et al,. 1966). A key parameter required to describe the force-length properties of a muscle is the fiber's optimum length. The optimum length will determine where on the force-length curve a muscle operates *in vivo* (Lieber and Friden, 2004). Fiber optimum lengths have been estimated by counting the number of sarcomeres for a given length of the whole fiber and from these data extrapolating the optimum length of the whole fiber (Wickiewicz et al., 1983). The purpose of this study was to determine the appropriate fraction of the total number of sarcomeres which must be counted to permit estimation of optimum fiber length.

METHODS

Muscle fascicles from the first dorsal interosseous muscle were removed and placed in a solution of 20% nitric acid to digest the connective tissue surrounding the muscle fibers. Whole muscle fibers were removed using a dissecting stereomicroscope and fine forceps. Each fiber was placed on a microscope slide and checked to ensure that it was indeed an entire fiber.

Once it was determined that the fiber was single, complete, and intact, the microscope was focused at 200x magnification. The whole fiber was imaged in sections.

Beginning at one end of the fiber, a stage driver was used to advance the fiber a repeatable distance to ensure that no portion of the muscle fiber would be missed or double counted. Digital images of the fiber were obtained along the entire length of the fiber (Figure1).
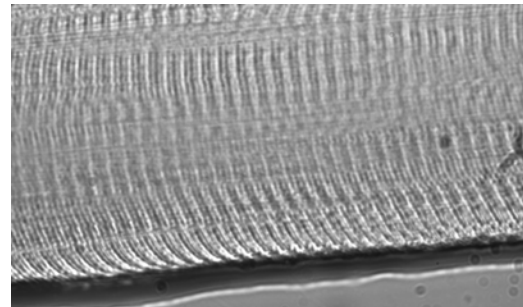
Figure 1: Muscle fiber at 1000x magnification.

Custom MATLAB code was used to count the sarcomeres in the muscle fiber per unit length. The program has been previously validated for accuracy and repeatability. The program output was individual sarcomere lengths along the entire muscle fiber and total fiber length.

The procedure selected for estimating optimum fiber length was based on the method used in a laboratory environment (e.g. Meijer et al., 1998). Samples of the whole fiber were selected to estimate whole fiber optimum length. The sample sizes were 10, 20, 40, 60, 80, 100, 200, 300, 400, 500, 600, 700, 800, 900, and 1000 sarcomeres. Each sample began at a randomly selected location along the muscle

fiber. Five hundred random locations were used.

The optimum fiber length was calculated for each individual sample size, at each location. The mean and standard deviation of the optimal fiber length from the 500 random samples for each sample size were calculated.

Three fibers were analyzed, each comprising more than 2000 sarcomeres per fiber.

RESULTS AND DISCUSSION

As the number of sarcomeres sampled increased, two trends in the data were observed (Figure 2). First, as sarcomere sample number increased, the estimated optimal fiber length became closer to the actual optimal fiber length. Secondly, as the sample size increased, the standard deviation of the estimated optimal fiber length decreased.
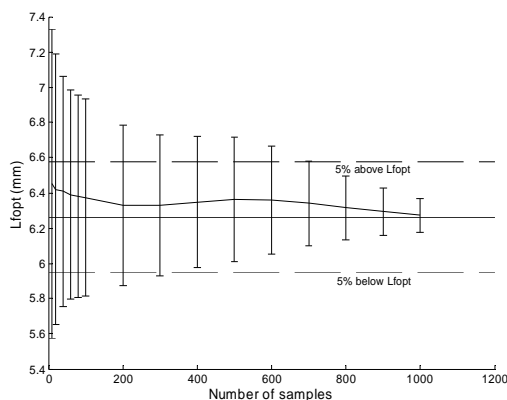
Figure 2: Representative graph of the mean estimated optimal fiber length (bars represent the standard deviations). The solid horizontal line is the actual optimal fiber length.

The minimum sample size for the estimation of optimal fiber length is important as optimal fiber length is a parameter in many musculoskeletal models. Without an accurate estimation of optimal fiber length musculoskeletal models are not realistic representations of the system they seek to simulate. Therefore, to estimate optimal fiber length in the first dorsal interosseous muscle, a sample size of over 600 sarcomeres is suggested.

An alternative method of estimating fiber optimum length is laser diffraction (e.g., Cleworth and Edman, 1969; Delp et al., 2001). Langenderfer et al. (2004) estimated the minimum number of samples needed to achieve an appropriate sample size that would allow for the calculation of mean sarcomere length in upper extremity human muscles. However, the entire muscle fiber was not inspected, therefore it is difficult to definitively state if the minimum number estimated is indeed appropriate.

Langenderfer et al. (2004) estimated that 60 sarcomeres would be a minimal sample size for estimating optimum fiber length. Based on the current study, over 600 sarcomeres must be measured to estimate the optimal fiber length within 5% of the true value. Six hundred sarcomeres translates to 30% of total fiber sarcomere number.

REFERENCES

Cleworth, D et al. (1969). *Science,* 163**:**296-298.
Delp, SL et al. (2001). *J Biomech,* 34:371-375.
Gordon, AM et al. (1966). *J Physiol,* 184:170-192.
Langenderfer, J et al. (2004). *Clin Biomech,* 19:664-670.
Lieber, RL et al. (2004). *Clin Orthop Relat Res*, 419:267-279.
Meijer, K et al. (1998). *J Appl Biomech,* 14:62-79.
Wickiewicz, TL et al. (1983). *Clin Orthop Relat Res*, 179**:**275-283.

DYNAMICS ANALYSIS OF ANKLE, KNEE AND HIP JOINT IN SAGITTAL PLANE USING A WEARABLE SENSOR SYSTEM

Rencheng Zheng*; Tao Liu; Yoshio Inoue; Kyoko Shibata; Kun Liu

Department of Intelligent Mechanical Systems Engineering, Kochi University of Technology, Kami City, Kochi County, 782-8502, Japan, 106404x@gs.kochi-tech.ac.jp

URL: http://www.lab.kochi-tech.ac.jp/robodyna/

INTRODUCTION

The joint kinetics analysis of ankle, knee and hip joint during gait in daily activities is fundamental for clinical decisions processing but they are commonly obtained by means of expensive laboratory-restricted equipments like a force plate and an optical camera analysis systems, which need sophisticated computing programs and professional operating procession. For using human kinematics and kinetics to biomedical applications conveniently indoors and outdoors, a wearable sensor system was improved for this study.

METHODS AND PROCEDURES
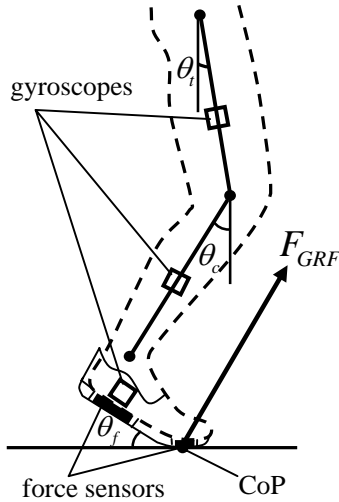
Fig. 1 Leg model wore the sensor systems

A leg model wore the sensor system in the pre swing phase was shown in fig. 1. The wearable sensor system was developed by integrating of a motion sensor system for detecting kinematical information of lower limb, an instrumented shoe for measuring ground reaction force (GRF) and center of pressure (CoP), and a logger for collecting data.

3 gyroscopes units were worn on the part of the foot, calf and thigh respectively as was shown in fig. 1. Two force sensors were inserted into a modified common shoe as a prototype of the instrumented shoe. One was under the heel part of the shoe, and another under the forefoot part of the shoe. The data logger was strapped around the waist part.

The identification of detailed phases in stance phase is based on the signals of the foot angular displacements θ_f. When $\theta_f > 0$, gait phase is being in weight acceptance, and $\theta_f = 0$ in single limb support, and $\theta_f < 0$ in pre swing.

Position and orientation of ankle, knee and hip joint, in a global coordinates system, can be sequentially estimated based on the identification of gait phase by equation (1), (2) and (3) respectively.

$$^g\{P\}_{ank} = \{^g\{P\}_{ank-wa}, {}^g\{P\}_{ank-sls}, {}^g\{P\}_{ank-pw}, {}^g\{P\}_{ank-sw}\} \quad (1)$$

$$^g\{P\}_{kne} = \{^g\{P\}_{kne-st}, {}^g\{P\}_{ank-sw}\} \quad (2)$$

$$^g\{P\}_{hip} = \{^g\{P\}_{hip-st}, {}^g\{P\}_{ank-sw}\} \quad (3)$$

In whole gait cycle, the joint moments at the ankle, knee and hip joint in global coordinates systems are calculated using the inverse dynamic equation by

$$^gM_{k,k+1} = -(^g r_{CoP} - {}^g r_{k,k+1}) \times F_{GRF} - \sum_{i=1}^{k}\left[(^g r_i - {}^g r_{k,k+1}) \times m_i \cdot g\right]$$

$$+ \sum_{i=1}^{k}\left[(^g r_i - {}^g r_{k,k+1}) \times m_i \cdot a_i\right] + \sum_{i=1}^{k}\frac{d}{dt}(I_i \cdot \theta_i)$$

$$k = 1, 2, 3 \quad (4)$$

The joint powers were computed as the scalar product of the joint moment and joint angular velocity in the global coordinates frame.

RESULTS

By gait experiments of 12 subjects, the joint kinetics is calculated using data measured synchronously by the wearable sensor system and a traditional analysis system of a force plate and an optical camera system. The root mean square (RMS) difference of the ankle moments using the two systems was (2 ± 0.34) (mean ± standard deviation) Nm, being $(5.4 \pm 0.7)\%$ of the maximal magnitude. The RMS difference of the knee moments was (7.2 ± 1.34) Nm, being $(6 \pm 0.32)\%$ of the maximal magnitude. The RMS difference of the hip moments was (11.2 ± 1.3) Nm, being $(6.1 \pm 0.25)\%$ of the maximal magnitude. The RMS difference of the ankle power calculated by using the two systems was (4.2 ± 0.4) W, being $(8.4 \pm 0.4)\%$ of the maximal magnitude. The RMS difference of the knee powers calculated by using the two systems was (5.7 ± 2.1) W, being $(4.1 \pm 0.5)\%$ of the maximal magnitude. The RMS difference of the hip joint powers calculated by using the two systems was (5.7 ± 0.3) W, being $(6.4 \pm 0.4)\%$ of the maximal magnitude.

(a) (b) (c) (d) (e) (f)
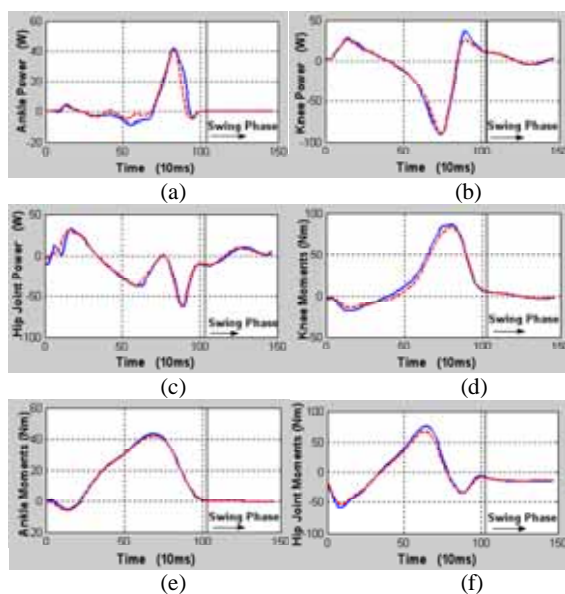
Fig. 1 Joint moments and joint powers estimated using wearable sensor systems (solid line), and force plate & Hi-DCam camera systems (dashed line). (a) Ankle moments. (b) Knee moments. (c) Hip joint moments. (d) Ankle powers. (e) Knee powers. (f) Hip joint powers.

DISCUSSION

In our study, the joint kinetics analysis during whole gait phases on level walking using the wearable sensor systems is presented. An inverse kinetics method integrating of the sensing signals and gait characteristics is developed as a first attempt to estimate the joint kinetics.

SUMMARY

The experimental results testified the joint kinetics assessment of ankle, knee and hip joint based on wearable sensor systems is feasible as well as effective for a daily application of gait analysis.

REFERENCES

At L. Hof (1992). J. Biomechanics, 25(10): 1209-1211.

Jessica Rose and James G. Gamble (2006). Human Walking. New York, Lippincott Williams & Wilkins.

Tao Liu, et al. (2006). Pro. of IEEE CIRA, 1655-1660.

Contribution of Joint Torque Coordination to Vertical Force Stabilization during Human Locomotion is Speed Dependent

Jasper Yen[1,2], Arick Auyang[1] and Young-Hui Chang[1,2]

[1]Comparative Neuromechanics Lab, School of Applied Physiology, GeorgiaTech, Atlanta, GA, USA
[2]Biomedical Engineering Program, Emory Univ/GeorgiaTech, Atlanta, GA, USA
Website: http://www.ap.gatech.edu/chang/CNLhome.html   E-mail: yh.chang@ap.gatech.edu

INTRODUCTION

High level performance task variables can be stabilized by structuring low level elements redundant for the task to vary within a goal equivalent solution space, or Uncontrolled Manifold (UCM) (Scholz & Schöner 1999). We previously found that humans hopping in place vary joint torques within the UCM to stabilize vertical force at the beginning middle and end of stance (Yen & Chang 2007). This stabilization can be due to a coordination of joint torques when the UCM lies obliquely to joint torque axes (Fig. 1A). Alternatively, when the UCM aligns with one or more joint torque axes, minimization of independent variance along the remaining joint axis is the sole contributor to performance stability (Fig.1B). Actual behavior likely reflects some combination of these two extremes (Fig.1C).
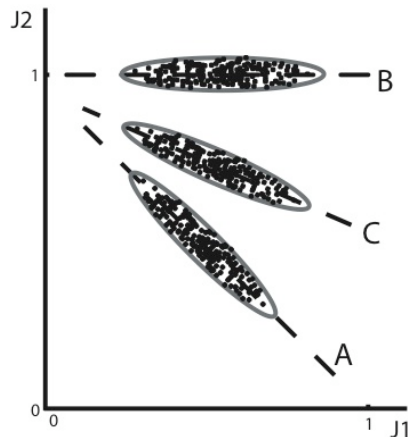
Fig.1. Hypothetical 2-D system with 1-D UCM (dashed line). A) Coordination of J1 & J2 results in max. variance along UCM. B) Task stability due to minimizing J2 variance when UCM aligns with J1. C) Contribution of both strategies.

We hypothesized that the contribution of coordinated joint torque variance would decrease with increased hopping frequency due to the adoption of extended leg postures.

METHODS

We collected sagittal plane kinematics (120 Hz) and ground reaction forces (1080 Hz) from 11 subjects hopping in place on their right leg at 2.2, 2.8, and 3.2 Hz. Three trials were collected at each frequency and pooled for analysis (~100 hops). We created a three-link biomechanical model that related ankle, knee, and hip torques to vertical end-point force (vGRF). The null space of the model represented the UCM. For every 1% of stance phase, we calculated relative amount of joint torque variance residing in the UCM as the Index of Motor Abundance for vGRF stabilization (IMA, Tseng & Scholz 2005). IMA>0 indicates vGRF stabilization by structuring joint torque variance along the UCM.

We then permutated the data set into one containing every possible ankle, knee, and hip torque combination to nullify stabilization through interjoint coordination (Müller & Sternad 2003). E.g., a data set of 100 hops would result in 100^3 total hop cycles. We re-ran the IMA analysis on the permutated data set to distinguish the fraction of IMA due only to independent joint variance (IV-IMA). Subtracting this from IMA left only the contribution of coordinated joint torque variance (CoV-IMA).

RESULTS

At 2.2 Hz, the vGRF stabilizing joint torque variance (||UCM) was unimodal in shape with a peak at mid-stance, while the destabilizing variance was bimodal (Fig.2A). The resulting IMA was 'W'-shaped (Fig.2B).

IV-IMA revealed the source of vGRF stability at foot contact (Fig.2C). CoV-IMA retained its peak at mid-stance (Fig.2D).
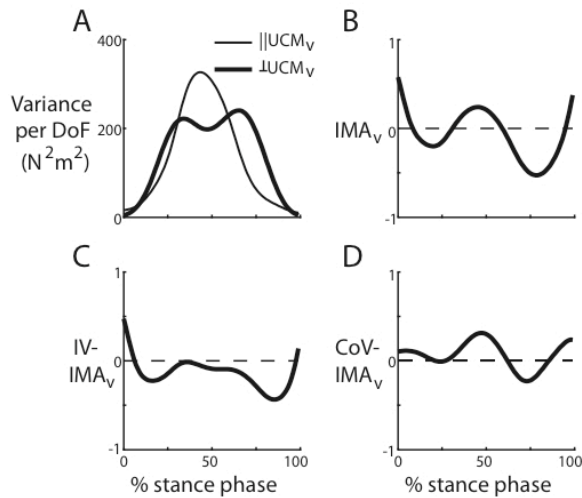

Fig.2. Representative subject at 2.2 Hz. A) ||UCM and ⊥UCM variance components. B) IMA. C) IV-IMA. D) CoV-IMA.

IMA retained the 'W' shape and exhibited little change across frequencies (Fig.3A). IV-IMA also did not change substantially with frequency. CoV-IMA decreased dramatically with frequency (Fig.3B). The extended leg posture at foot contact resulted in alignment of the UCM plane within 4° of the hip torque axis, 20° of the knee torque axis and 70° of the ankle torque axis.

DISCUSSION

The contribution of joint coordination to vertical force stability decreased as hopping rate increased. Yet, overall task stability was maintained at all frequencies. At high frequencies, greater alignment of the UCM plane with the hip and knee joint torque axes effectively decreased the influence of joint coordination on vGRF stability. This greater alignment was due to the increasingly extended limb postures adopted by our subjects at high frequencies. At these extended limb postures, the ankle joint was nearly orthogonal to the UCM plane and stability of vGRF was achieved by minimizing independent joint variance at the ankle joint.
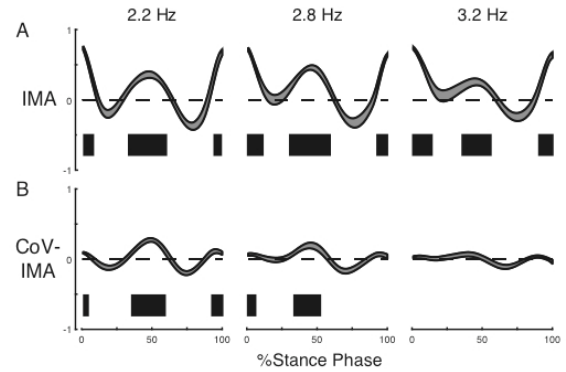
Fig 3. Ensemble means±1SEM A) IMA and B) CoV-IMA across hopping frequencies. Bars show when IMA or CoV-IMA >0 (1-tailed t-test, α=0.01).

SUMMARY

Two different strategies exist for structuring joint torque variance to stabilize vGRF during human hopping. Both strategies simplify control of vertical force generation during hopping through either coordinated action from multiple joints or through localized control of a single joint. Coordinating variance across the joints is the predominant contributor to vertical force stability at slow frequencies. At faster rates, an extended leg posture mechanically constrains the hip and knee torque axes within the UCM such that the controller need only minimize ankle torque variance independently. The degree to which each strategy contributes to task stability is rate dependent. Translational studies in walking and running may elucidate the ubiquity of these intralimb compensation principles for able-bodied and pathological locomotion.

REFERENCES

Müller H and Sternad D (2003). *Biol Cyb*. 89:22-33.

Scholz JP and Schöner G (1999). *Exp Brain Res*. 126, 289-306.

Tseng YW and Scholz JP (2005). *Motor Control*. 9:75-100.

Yen J and Chang Y-H (2007) *ASB abstract*.

RECTUS FEMORIS MOMENT ARMS ESTIMATED OVER A LARGE RANGE OF MOTION FROM REAL-TIME MRI

Niccolo Fiorentino[1], Jonathan Lin[2], Michael Guttman[2], Elliot McVeigh[2,3], and Silvia Blemker[1]

[1] Department of Mechanical & Aerospace Engineering, University of Virginia
[2] Laboratory of Cardiac Energetics, NHLBI, National Institutes of Health
[3] Department of Biomedical Engineering, Johns Hopkins University
Email: niccolo@virginia.edu

INTRODUCTION

In vivo estimates of muscle moment arms are needed to characterize muscle function and test musculoskeletal models. However, muscle moment arms are challenging to measure *in vivo*, as they may vary substantially with body position and loading condition, especially for a muscle with a complex path geometry like the rectus femoris.

Previous studies of rectus femoris muscle moment arms have used cadaveric specimens, static conditions, passive motion, and/or a limited range of motion (Buford et al., 1997; Sheehan, 2007; Wretenberg et al., 1996). The goal of this study was to quantify rectus femoris muscle moment arms *in vivo* over a large range of motion using real-time dynamic MR images of the knee.

METHODS

Six healthy volunteers were scanned in the left lateral position inside a wide-bore (~70 cm) Siemens Espree MRI scanner during right knee joint flexion (Figure 1). Scanning was performed in a sagittal slice through the rectus femoris muscle, patella, and patellar tendon insertion on the tibia. Images were acquired with a real-time spoiled gradient-recalled echo sequence at a temporal resolution of 3 frames per second during flexion at 15 – 20 cycles/min (Figure 2).

Moment arm calculations were performed based on the tendon excursion method (An et al., 1984). Knee angle and rectus femoris muscle-tendon lengths were measured directly on sagittal MR images, and muscle-tendon length was plotted versus knee angle for each flexion cycle (Figure 3). The muscle-tendon length data were fit with a 4th order polynomial, and the rectus femoris moment arm was calculated by taking the analytical derivative of the muscle-tendon length polynomial fit with respect to joint angle (Murray et al., 1995).
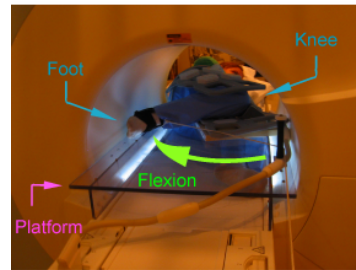
Figure 1. Volunteer in the MRI scanner. As viewed from the back, the volunteer moves his or her knee in flexion on top of a platform to ensure a repeatable motion.
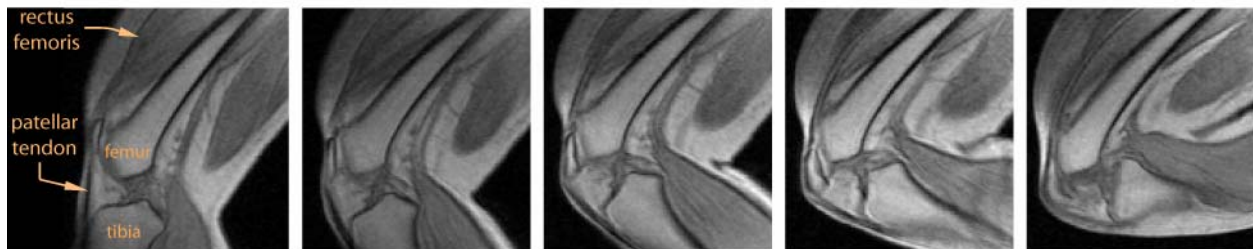
Figure 2. Example real-time MR images of the knee and distal thigh (flexion ⟶)
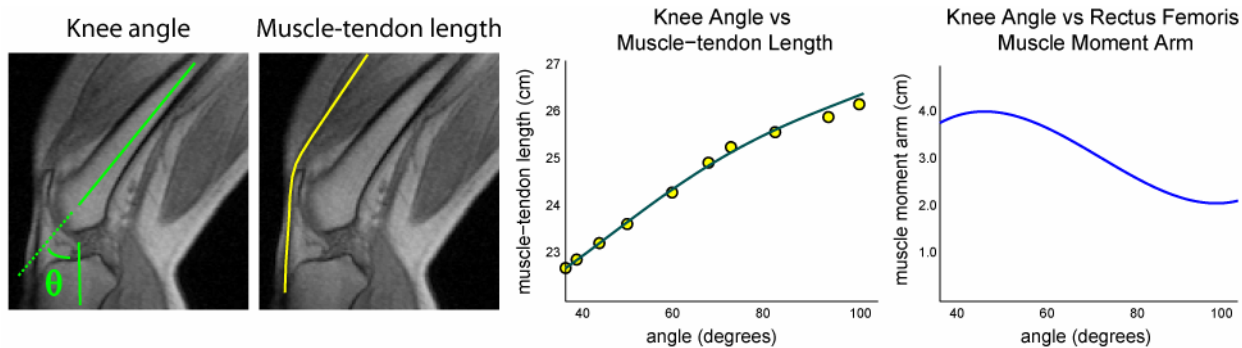
Figure 3. Moment arm estimation technique with example angle and muscle-tendon length measurements. Plotted are one cycle's muscle-tendon measurements with 4th order fit and corresponding moment arm result.

RESULTS AND DISCUSSION

The real-time images conveyed the complex path of the rectus femoris muscle as it wraps around the anterior portion of the distal femur throughout the knee joint range of motion (Figure 2).

The moment arm results compare well with those from previous cadaveric studies, with the data from Buford et al. (1997) falling within one standard deviation from the mean of this study's results (Figure 4). In this study, the peak moment arm was 3.5 +/- 0.8 cm across all the subjects. The minimum moment arm occurred at the large flexion angles, and was 2.5 +/- 1.0 cm across all the subjects.

These results demonstrate the potential of large-bore real-time MR imaging as an effective tool for measuring muscle moment arms *in vivo* over a large range of motion. Further optimization in the method will include synchronizing multiple slices to acquire three-dimensional muscle and bone motion.

There are several potential applications for the technique described here, including characterizing moment arms under various loading conditions, studying other muscles that have complex muscle paths, and investigating the effects of bone deformities on muscle moment arms.
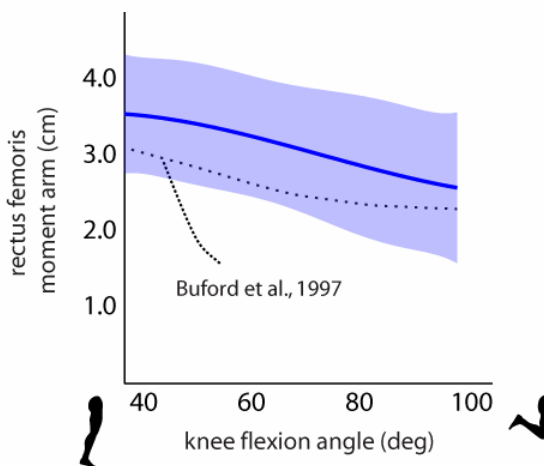
Figure 4. Moment arm results. Mean rectus femoris moment arm for all six volunteers plotted with one standard deviation above and below the mean shaded. Buford et al. results plotted on same axes for direct comparison with moment arm data from cadavers.

REFERENCES

An, KN et al. (1984). *J Biomech Eng*, 106:280-282.

Buford, WL et al. (1997). *IEEE Trans Rehabil Eng*, 5:367-379.

Murray, WM et al. (1995). *J Biomech*, 5:513-525.

Sheehan, FT (2007). *J Biomech*, 40:1968-1974.

Wretenberg, P et al. (1996). *Clin Biom*, 11:439-446.

ACKNOWLEDGEMENTS

EFFECTS OF DOWN SYNDROME ON MEDIOLATERAL MOTION DURING WALKING AT DIFFERENT SPEEDS

Stamatis Agiovlasitis[1], Michael J. Pavol[2], Jeffrey A. McCubbin[2], and Joonkoo Yun[2]

[1]Department of Kinesiology and Community Health, University of Illinois at Urbana-Champaign, Champaign, IL, USA, agiovlas@uiuc.edu
[2]Department of Nutrition and Exercise Sciences, Oregon State University, Corvallis, OR, USA

INTRODUCTION

The inherent joint laxity and muscle hypotonia of adults with Down syndrome (DS) may result in reduced gait stability (Kubo and Ulrich, 2006). This could have negative impacts on both general mobility and energy expenditure. Balance in the mediolateral (ML) direction may be of particular challenge to adults with DS. ML stability appears to depend on the active control of step width (Kuo, 2007), together with passive knee stiffness and active control of the hip abductors in the stance limb (MacKinnon and Winter, 1993), each of which may be diminished in DS. The challenge of ML balance control in adults with DS may be intensified at slow walking speeds, where the time between steps is the greatest. This study thus examined how ML body motion and step width were affected in adults DS as a function of walking speed.

METHODS AND PROCEDURES

15 adults with DS (27 ± 8 yrs) and 15 adults without DS (28 ± 6 yrs) underwent a series of randomly presented treadmill walking trials. Walking speeds were determined as Froude numbers, based on leg length, to account for the shorter legs of persons with DS. Participants walked at Froude numbers of 0.1, 0.2, 0.3, 0.4, 0.5, 0.6, and, for adults without DS, 0.7. A motion capture system was used to collect kinematic data for 30-35 steps after 4 minutes of walking at each speed. All participants were experienced

with treadmill walking at the tested speeds. Informed consent was obtained.

The ML position of the body center of mass (COM) was determined from the filtered kinematic data using a 15-segment model (Plug-in Gait, Vicon, Lake Forest, CA). Instants of heel strike were identified and the range of COM ML position determined for each stride. The variability of COM ML motion was quantified by the root-mean-square value of the between-stride standard deviation (SD) of COM position at each 2% of stride. Dependent variables for each trial were the mean range of COM ML position, the root-mean-square SD of COM ML position, and the mean and SD of step width.

Effects of group and walking speed were analyzed with 2 x 6 repeated-measures ANOVA ($\alpha = 0.05$). When warranted, a between-group ANOVA with a Bonferroni-adjusted α was performed at each speed.

RESULTS

Adults with DS showed greater and more variable COM ML motion ($p < 0.05$), independent of walking speed (Figure 1). Step width did not differ between the groups (DS: 12.3 ± 4.1 cm; Non-DS: 10.2 ± 2.5 cm; $p > 0.05$). However, step width was more variable ($p < 0.05$) in adults with DS across all speeds except Froude 0.1.

Walking speed influenced the range and variability of COM ML motion ($p < 0.05$),

independent of group. Qualitatively, the range of COM ML position decreased as speed increased, whereas variability in COM ML position increased. Step width did not differ between speeds, but its variability appeared to increase at greater speeds.
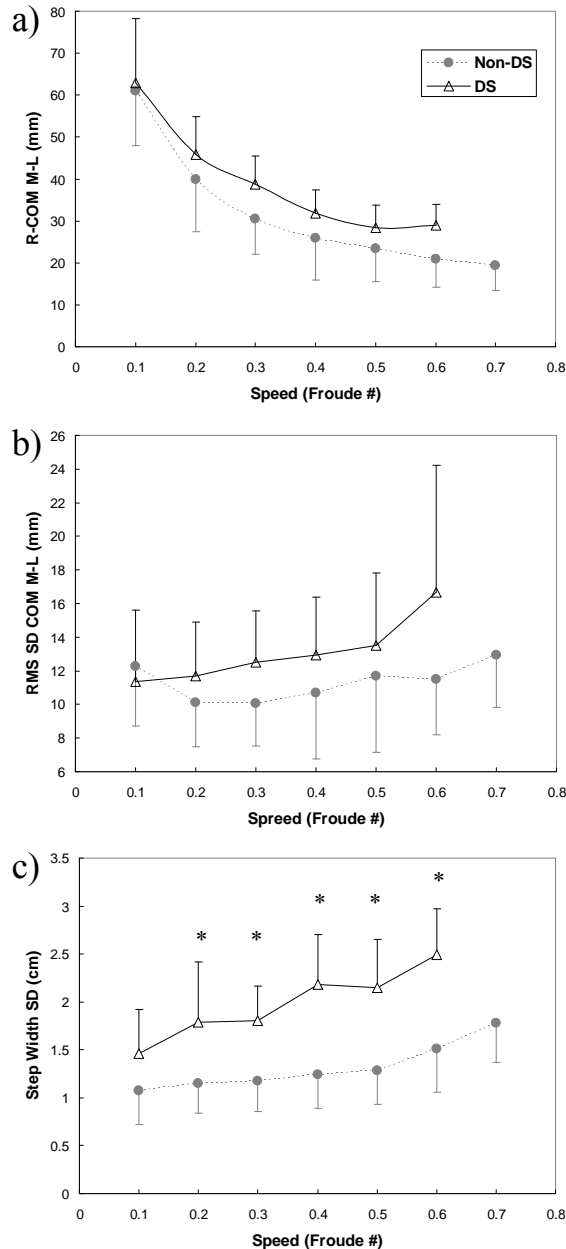

Figure 1. Mean ± SD (a) Range of COM ML motion, (b) Root-mean-square SD of COM ML position, (c) SD of step width, as a function of walking speed in adults with and without DS. *= p<0.008 between groups

DISCUSSION

Greater and more variable COM ML motion is characteristic of imbalance (Chou et al., 2003). Thus, consistent with observations in children with DS (Kubo and Ulrich, 2006), the greater and more variable COM ML motion in adults with DS may reflect lesser ML stability during gait. This relative deficit appears to exist across walking speeds.

Notably, adults with DS did not widen their steps to compensate for their greater COM ML motion. However, they appeared to actively adjust their step widths to greater extent in response to their more variable COM motion. This difference in step width control appears to widen as speed increases. Because active stabilization has a metabolic cost (Kuo, 2007), energy expenditure during walking may be greater among adults with DS, especially at faster speeds.

SUMMARY

Adults with DS exhibit greater and more variable ML motion of the COM during gait. They appear to compensate through actively adjusting step widths to a greater extent.

REFERENCES

Chou, L-S et al. (2003). *Gait Posture,* 18: 125-133.
Kubo, M and Ulrich, B (2006). *Gait Posture,* 23: 512-518.
Kuo, AD (2007). *Hum Mov Sci,* 26: 617-656.
MacKinnon, CD and Winter DA (1993). *J Biomech,* 26: 633-644.

ACKNOWLEDGEMENTS

TRACKING GAIT ASYMMETRIES DURING REHABILITATION USING REGIONS OF DEVIATION MEASURES: A CASE STUDY

K. Alex Shorter, John D. Polk, Karl S Rosengren, and Elizabeth T. Hsiao-Wecksler

University of Illinois at Urbana-Champaign, IL, USA
E-mail: ethw@uiuc.edu, Web: mechse.uiuc.edu/research/ethw

INTRODUCTION

Quantitative gait analysis, in combination with qualitative observational analysis, is a versatile clinical tool used to identify pathology or acute injury and assess recovery from injury (Perry, 1992). Quantitative tools typically consist of univariate gait parameters that measure events at discrete and easily defined points in time (e.g., heel-strike, mid-stance, toe-off) (Vaughan, 1999). Such measures fail to capture the motion that occurs between these discrete temporal events, and fail to assess how problems at one joint affect other joints. We address these shortcomings with new regions of deviation measures (ROD) that are used to identify: (i) joint angles affected by an injury, (ii) the timing during the gait cycle when these effects are prominent, and (iii) how an injury at one joint affects ipsilateral and contralateral joints (Shorter et. al., 2007). In that work, bracing was used to create artificial asymmetries in the gait of healthy walkers. The goal of the current work is to apply the analysis techniques to an individual subject with an acute lower limb injury and track recovery.

METHODS AND PROCEDURES

The subject had surgery to repair a torn right meniscus. Data were collected on a treadmill at three walking speeds (Self-selected (SS), SS + 25% (FS), and SS - %25 (SL)) and at four time points: before surgery (TB), one week (T0), three months (T3), and six months (T6) post-surgery. Kinematic data were collected using a six camera motion analysis system at 120 Hz (Vicon Model 460, Oxford,

UK) and were used to calculate the ROD measures. The first metric, symmetry regions of deviation (SROD), identifies regions of deviation in bilateral joint angle symmetry ($\Delta\theta_j = \theta_{j,Affected} - \theta_{j,Unaffected}$).

$$SROD = \begin{cases} \langle\Delta\theta_j\rangle - \left(\langle\Delta\theta_j^{Norm}\rangle + SD_j^{Norm}\right), & \langle\Delta\theta_j\rangle > SNorm^+ \\ \langle\Delta\theta_j\rangle - \left(\langle\Delta\theta_j^{UB,Norm}\rangle - SD_j^{UB,Norm}\right), & \langle\Delta\theta_j\rangle < SNorm^- \\ 0, & SNorm^- \leq \langle\Delta\theta_j^i\rangle \leq SNorm^+ \end{cases}$$

where: $SNorm^+ = \langle\Delta\theta_j^{UB,Norm}\rangle + SD_j^{UB,Norm}$, $SNorm^- = \langle\Delta\theta_j^{UB,Norm}\rangle - SD_j^{UB,Norm}$
$j \in$ [Ankle, Knee, Hip] SD = Standard Deviation $Norm$ = Control Data

The second metric, individual regions of deviation (IROD), identifies regions of deviation in an individual joint angle.

$$IROD = \begin{cases} \langle\theta_j\rangle - \left(\langle\theta_j^{Norm}\rangle + SD_j^{Norm}\right), & \langle\theta_j\rangle > INorm^+ \\ \langle\theta_j\rangle - \left(\langle\theta_j^{Norm}\rangle - SD_j^{Norm}\right), & \langle\theta_j\rangle < INorm^- \\ 0, & INorm^- \leq \langle\theta_j\rangle \leq INorm^+ \end{cases}$$

where: $INorm^+ = \langle\theta_j^{Norm}\rangle + SD_j^{Norm}$, $INorm^- = \langle\theta_j^{Norm}\rangle - SD_j^{Norm}$
$j \in$ [RAnkle, RKnee, RHip, LAnkle, LKnee, LHip]

RESULTS AND DISCUSSION

SROD values plotted in Figure 1 show the effect of walking speed on the level of asymmetry present in the joint behaviors post surgery (T0). Asymmetries tended to be larger during swing when the subject was walking at the FS pace, and larger during stance at the SL pace. By T6, the asymmetries were reduced substantially (Fig 2) and did not vary greatly with walking speed. After identifying regions of the gait cycle with asymmetry in T0 data, IROD measures were used to interpret how the repaired knee was affecting the subject's other joints. IROD values showed that the behaviors of ipsilateral and contralateral joints were modified to maintain functional gait. Specifically, the affected-side hip was utilized to compensate for the knee's

restricted range of motion to maintain toe clearance during swing and to modify load bearing of the affected leg during stance. The ankle joint on the affected side was also used to maintain toe clearance.

SROD values of the subject's fast walking trials in Figure 2 illustrate recovery from the surgery. Fast walking trials are shown in the figure because the subject demonstrated the most asymmetric behavior at this condition (Fig 1). At the ankle joint, asymmetric behavior seen at T0 was no longer visible by T6. The knee and hip joints both showed reduced asymmetry: an 88% reduction in peak knee asymmetry during swing, an 80% reduction in peak hip asymmetry during swing and a 33% reduction in asymmetry during stance. These reductions in asymmetric behavior are an indication of subject recovery.

SUMMARY/CONCLUSIONS

Common gait analysis measures consisting of univariate measurements do not capture the spatio-temporal complexity of the gait cycle, and provide little information on interactions between joints during recovery from injury. ROD analysis addresses these deficiencies by providing information about the magnitude of the asymmetry resulting from injury, the locations in the gait cycle where gait is perturbed, and information about how a joint specific injury affects the coordinated motion of associated joints. ROD data provides a useful supplement to qualitative observational gait analysis and an improvement over current univatiate measures.

REFERENCES

Perry, J. (1992). *Gait Analysis: Normal and Pathological Function*. SLACK Inc.
Vaughan, C. L. et al. (1999). *Dynamics of Human Gait.* Human Kinetics Publishers.
Shorter, K. A. et. al. (In Press). *Clinical Biomechanics*
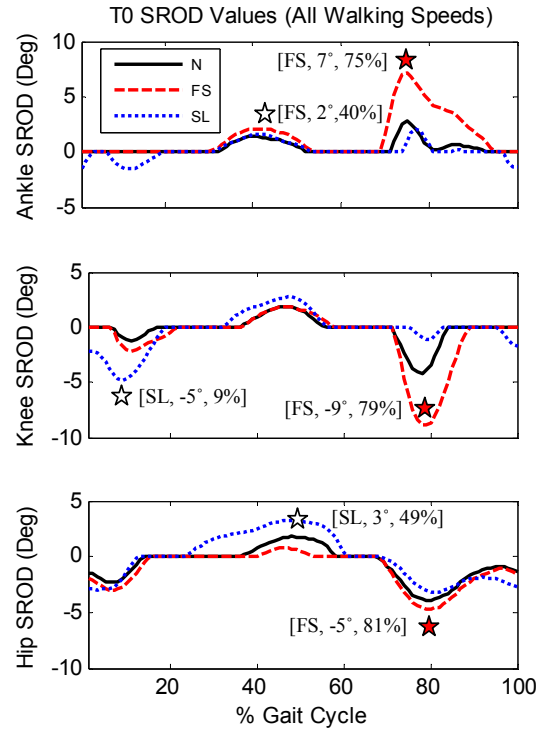
Figure 1. Effect of walking speed on asymmetry. Peak values are marked with the stars and labeled with the value and position during the gait cycle.
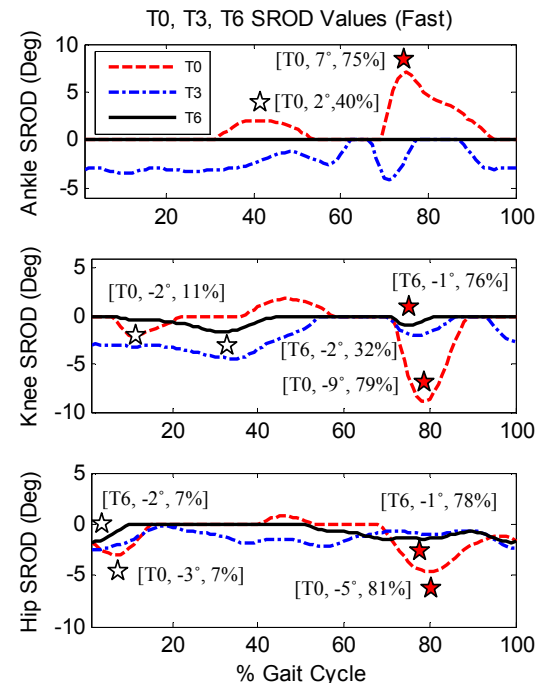
Figure 2. SROD values showing decreasing asymmetry during recovery.

STEPPING TASKS THAT REQUIRE GREATER EXECUTIVE CONTROL INDUCE MULTIPLE POSTURAL ADJUSTMENTS

Joseph J Lacko[1], Mark S Redfern[3,1,2], Joseph M Furman[2,1,3], Patrick J Sparto[1,2,3]

Departments of Physical Therapy[1], Otolaryngology[2], and Bioengineering[3], Univ. of Pittsburgh
Corresponding Author: PJ Sparto, psparto@pitt.edu

INTRODUCTION

Compared with young adults, older adults have delays in step initiation, and these delays increase as the number of potential choices of step direction increase. Jacobs and Horak (2007) recently observed that uncertainty about step direction induced multiple postural adjustments. We have developed a step initiation task that increases the level of executive control by varying the choice of step direction based on the congruity or incongruity of visual cues. The purpose of this study was to examine if this paradigm caused older subjects to generate multiple postural adjustments which could measure the impact of executive functioning on mobility.

METHODS AND PROCEDURES

Eight subjects (4 female, ages 72-84 years) performed a visually-cued step task that included simple step reaction time (SSRT) and choice step reaction time (CSRT) blocks (Table 1). Subjects always stepped laterally in the direction that an arrow was pointing.

Table 1. Experimental conditions.

Blocks	Description
1-4	**SSRT**: In each block, all arrows pointed left or pointed right. (Fig. 1)
5-6	**CSRT(control)**: In each block, an equal number of left or right arrows were shown in random order. (Fig. 1)
7-8	**CSRT(exec)**: Left or right arrows were shown on either the right or left side of the screen in random order. Subjects stepped to the side that the arrow was pointing. (Fig. 2)

In 50% of the CSRT(exec) trials, the arrow direction and location indicated the same step response (<u>congruent</u> trials). In the other half, the cues were incongruent (arrow direction and location <u>incongruent</u>). The CSRT(exec) task requires executive control because during the incongruent cue trials, the subject must suppress a potent step response toward the side of the monitor in which the arrow was located. To potentiate the incorrect response, 2 blocks were interleaved in which subjects were instructed to step toward the same side where the arrow was located. Similar paradigms are known to involve areas of the brain important for executive function.
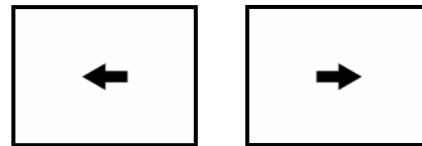

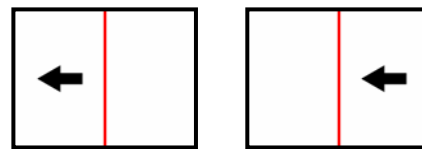**Fig. 1.** SSRT and CSRT(control) trials.

Fig. 2. Congruent (left) and incongruent (right) CSRT(exec) trials.

The lateral step responses induced vertical ground reaction force (VGRF) curves that included either one or multiple postural adjustments (Fig. 3). The onset of the first postural adjustment (**1st PA**), identified by the initial positive or negative deflection in the VGRF, was recorded, as was the time of liftoff (**LO**), when all weight has been shifted to the stance leg and the vertical ground reaction force of the step leg goes to 0.
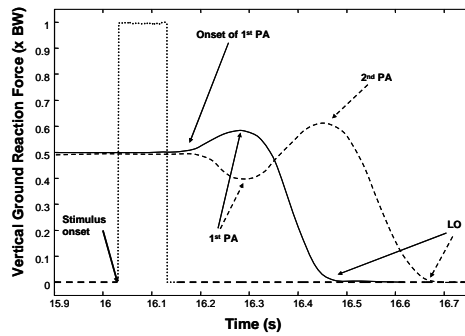
Fig. 3. Components of VGRF during step responses with single postural adjustment (solid) and multiple postural adjustments (dashed). Vertical scale is proportion of body weight (xBW).

Following the removal of outliers, we collapsed data across identical block conditions and determined the mean value of the number of multiple Pas, onset of 1st PA, and time of LO. There were no differences between left and right steps. The non-parametric Friedman test was used to compare the number of multiple adjustments made during each condition. Because the behaviors were different for steps that elicited a single postural adjustment versus multiple postural adjustments, the onset of the 1st PA and time of LO were compared, with the Friedman test, using the data from steps which generated a single PA.

RESULTS
Increasing the challenge of the step task resulted in a great number of multiple postural adjustments and delays in the onset of the **1st PA** and time of **LO** (Tab 2). The number of multiple postural adjustments made was significantly affected by the step task condition (Friedman $\chi^2(3) = 20.3$, $p < 0.001$).

There were virtually no multiple PAs during the SSRT condition. As the uncertainty about step direction increased in the CSRT conditions, the number of multiple PAs increased, up to 37% when the directional cue was incongruent with the location cue. When the step cues were congruent, there appeared to be a facilitation effect because the number of multiple PAs was only 4%.

The onset of the **1st PA** (Friedman $\chi^2(3) = 13.8$, $p = 0.003$) and time of **LO** (Friedman $\chi^2(3) = 23.0$, $p < 0.001$) both showed a significant increase with increasing cognitive control of stepping.

DISCUSSION
The results suggest that the impact of executive function on stepping can be measured using the CSRT. The method augments previous work by incorporating the executive function task directly into the postural task. The occurrence of multiple postural adjustments and delayed step initiation time during conditions that restrict a person's ability to preplan step direction may have important implications if a rapid step is required to avoid a fall.

REFERENCES
Jacobs JV and Horak FB (2007) *Experimental Brain Research*, 179:29-42.

ACKNOWLEDGEMENTS

Table 2. Effect of step task condition on percentage of trials with multiple postural adjustments, onset of first postural adjustment (1st PA), and time of liftoff (LO). Values are mean (SD).

Variable	SSRT	CSRT (control)	CSRT(exec) congruent	CSRT(exec) incongruent
% Multiple PA	0.3 (0.7)	18 (17)	4 (4)	37 (26)
Onset of 1st PA (ms)	245 (23)	275 (34)	289 (59)	374 (101)
LO (ms)	553 (75)	651 (115)	730 (180)	868 (209)

FREQUENCY INFLUENCES THE REGULARITY OF THE STRUCTURAL VARIATIONS PRESENT IN THE LEG SWING KINEMATICS

Vladimir Ivkovic and Max J. Kurz

Laboratory of Integrated Physiology, Department of Health and Human Performance, University of Houston, Houston, Texas, USA, vivkovic@mail.uh.edu or mkurz@uh.edu
URL: www.hhp.coe.uh.edu

INTRODUCTION

Human locomotion is variable. However, the magnitudes of the variations present in the stride and swing time intervals are disproportionate and respond differently to changes in the walking speed (Gabel and Nayak, 1980; Frenkel-Toledo et al., 2005). The magnitudes of the variations present in the stride time intervals are smaller and more sensitive to changes in walking speed. Alternatively, the magnitude of the variations present in the swing phase is larger and less sensitive to changes in walking speed. It has been suggested that these different responses are related to the neural mechanism that are controlling the respective phases. It has been postulated that the stride dynamics are governed by an automatic rhythmic stepping mechanism, while the swing phase dynamics are governed by active balance control mechanisms (Gabel & Nayak, 1980; Frenkel-Toledo et al., 2005). Although these hypotheses seem plausible, the actual biomechanical factors that govern the kinematic variations seen in the respective phases of the gait cycle are largely unknown.

The purpose of this investigation was to use a simple leg swing task to initially explore how frequency influences the structural variations present in the leg swing kinematics.

METHODS AND PROCEDURES

Twenty-one healthy young subjects (*age*=20.05±1.2 yrs., *height*= 1.70±0.08

Figure 1. Frame and apparatus set up for the investigated leg-swinging task

meters, *mass*= 73.88±15.74 kg) swung their leg at three different frequencies. A goniometer was placed over the hip joint and measured the position of the leg in the sagittal plane at 100Hz. A custom built frame was used to hold the participants upright and isolated the movement to only the leg evaluated (Figure 1). A lightweight knee brace was worn to prevent any flexion of knee during the conditions. Participants swung their leg at the preferred pendular frequency, and frequencies that were 20% faster and slower. A metronome was set to twice the period of prescribed frequency and provided audible target cues. Equation 1 was used to calculate the period of the prescribed leg-swinging task.

$$T = 2\pi\sqrt{\frac{I}{mg\ell}}$$ Equation 1.

where T is the period, I is the inertia of the leg, m is mass, g is gravity and ℓ is the length of the leg (ℓ=0.86$\pm$0.06). Inertia was defined based on the anthropometric values listed in Winter 2006. For each condition the subject swung their leg for two-minutes.

Approximate entropy (ApEn) was used to quantify the regularity of the structural variations present leg swinging performance (Equation 2; Pincus 1991).

$$ApEn(m,r) = \ln\left(\frac{C_m(r)}{C_{m+1}(r)}\right) \quad \text{Equation 2.}$$

where $C_m(r)$ is the number of data points of length m that are similar, $C_{m+1}(r)$ is the number of data points of length m+1 that are similar, and r is the similarity criterion. For this investigation, m was 2 and r was 20% of the standard deviation of the time series (Pincus, 1991). A lower ApEn value indicates a greater regularity in the structural variations present in the leg kinematics.

RESULTS

A significant main effect was found for the regularity of the structural variations (F (2,40)=80.182, p<0.0001). Post-hoc analysis revealed that the regularity of the structural variations was significantly different for all the respective frequencies (p<0.0001 for all comparisons). Additionally, a significant (p<0.001) increasing linear trend was found for the structural variations (Figure 2). Hence, the structural variations were more regular for the slow frequency and less regular for the fast frequency.

DISCUSSION

Regularity of the structural variations was influenced by the frequency that the leg was swung. Our experiment was far simpler
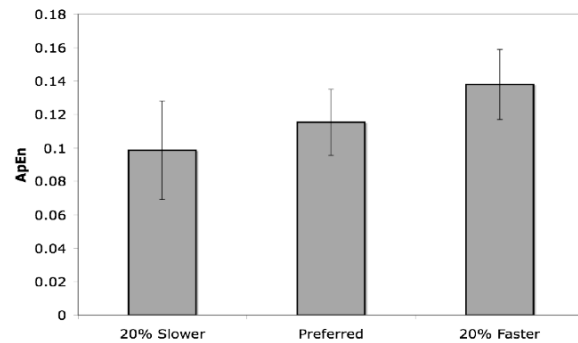
Figure 2. ApEn values for the respective leg swing tasks.

than the complexities seen in human walking. However, outcomes presented here may have relevance for explaining what biomechanical factors influence the variability of the swing phase kinematics. For example, if the swing phase kinematics is more variable then the limb is possibly being rapidly actuated to ensure the gait pattern remains stable. Moreover, if the swing phase kinematics is less variable then the limb dynamics may possibly be damped to ensure stability.

SUMMARY

We have shown that the frequency that the leg is swung influences the structural variations. The experimental data presented in this investigation is representative of healthy young individuals. We are currently exploring if the outcomes from our experiments can be extended to individuals with motor control deficits (*e.g.*, Parkinson's Disease).

REFERENCES

Gabell A & Nayak US (1980). *J Gerontol*, 39:662-666.
Frenkel-Toledo S et al. (2005). *J NeuroEng Rehab*, 2:30.
Pincus, SM (1991). *Proc Nat Acad Sci*, 88: 2297-2301.
Winter DA (2006). *Biomechanics and Motor Control of Human Movement*, John Wiley & Sons Inc.

LINE OF SIGHT AND DRIVING POSTURE EVALUATION: WHAT AN OPERATOR CANNOT SEE INFLUENCES DRIVING POSTURE

Tammy Eger[1], Alison Godwin[2], Sylvain Grenier[2], and Jack Callaghan[3]

[1]Assistant Professor, School of Human Kinetics, Laurentian University, Sudbury, ON, CND.
teger@laurentian.ca
[2]Assistant Professor, School of Human Kinetics, Laurentian University, Sudbury, ON, CND.
[3]Associate Professor, Department of Kinesiology, University of Waterloo, Waterloo, ON, CND.

INTRODUCTION

Operators of industrial vehicles are at risk of developing musculoskeletal injuries due to continued daily exposure to awkward driving postures (combination of rotation, flexion and lateral neck & trunk bend) they adopt in an attempt to compensate for restricted sightlines. Therefore, the interplay between line-of-sight and posture must be explored in order to identify solutions aimed at preventing future accidents and musculoskeletal injuries associated with the operation of industrial vehicles. In this regard the ability to accurately measure line-of-sight and posture during the operation of industrial vehicles is essential. Furthermore, the ability to use the collected information to subsequently model and estimate postural loading is critical. This study will report driving postures adopted during the operation of a load-haul-dump vehicle (underground mining vehicle) and lift-truck. Line-of-sight from the operator's compartment and operator point-of-regard data will also be reported.

METHODS AND PROCEDURES

Driving posture, line-of-sight, and point-of regard data were collected during the operation of a LHD vehicle and a lift-truck. An ASL eye-tracking system was used to measure point-of-regard during vehicle operation, two-four portable digital video cameras were used to record the overall driving posture of the vehicle operator, and a computer simulation program (Classic JACK) was used to model line-of-sight from the operator's position of the vehicle. The digital video cameras and the eye-tracking system were synchronized. The LHD vehicle operator and lift-truck operator were monitored when driving their respective vehicles forward, backward, turning right and turning left while unloaded and while carrying a load.

Point-of-regard data and driving posture data are presented for each task. The point-of-regard data showed what the driver looked at in the environment and a subsequent interview with the operator was used to determine why the operator looked at specific "targets" in the environment. Driving posture was evaluated via a 3D-Match analysis in order to predict the percentage of time the operator spent in mild, moderate and severe postures and associated peak and cumulative loading at the low back (Eger et al., 2008). Available line-of-sight to the operator is presented as a line-of-sight boxplot, where areas that are theoretically visible from the operator's compartment are shown in green and areas that are not visible are shown in red.

RESULTS AND DISCUSSION

Preliminary findings are presented for a lift-truck operator (Figure 1) and a LHD operator (Figure 2).

The lift-truck operator was able to maintain a relatively neutral neck and trunk posture when driving forward without a load; however, driving with a load created restricted sightlines leading to awkward driving postures (Figure 1). Postural analysis in 3D-Match revealed the lift-truck operator spent 27% of the time with the trunk flexed forward between 20-45 degrees and 9% of the time the trunk flexed forward more than 45 degrees while neck rotation was minimal (less than 15 degrees of neck rotation 97% of the time). The peak compressive force associated with driving posture at the L4/L5 level of the spine was 2282 N.
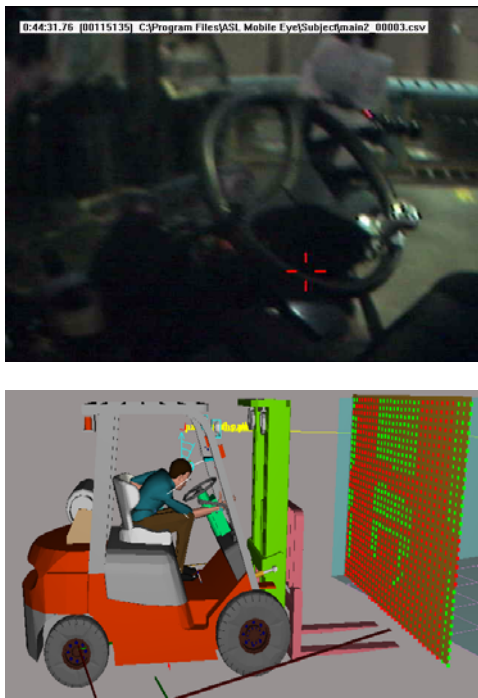
Figure 1. Point-of regard (at an instant in time) for a lift-truck operator driving forward with a load (top) and modeled line-of-sight (bottom) are shown.

LHD operators sit sideways to the direction of travel which requires them to rotate their neck and trunk to operate the vehicle (Figure 2). Line-of-sight is restricted; therefore, the LHD operator adopts an awkward neck position when driving. Postural analysis in 3D-Match revealed the LHD operator spent over 94 % of the time with their neck rotated more than 40 degrees when operating the vehicle. The peak compressive force associated with driving posture at the L4/L5 level of the spine was 2059 N.
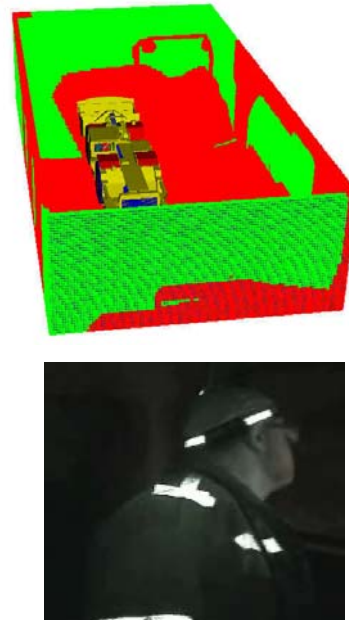
Figure 2. Line-of-sight from the operator's position of an LHD vehicle (top) and typical posture adopted by an LHD operator when driving forward (bottom).

SUMMARY

Available line-of-sight and the importance of visual cues required to safely operate mobile equipment have an influence on the posture adopted by vehicle operators.

REFERENCES

Eger, TR et al. (2008). IJIE (In Press).

ACKNOWLEDGEMENTS

STATIC OPTIMIZATION OF MUSCLE FORCES DURING DROP LANDINGS: A COMPARISON OF COST FUNCTIONS

W. Brent Edwards [1], Brett J. Sealine [1], Ross H. Miller [2], Jason C. Gillette [1], and Timothy R. Derrick [1]

[1] Department of Kinesiology, Iowa State University, Ames, IA, USA
[2] Department of Kinesiology, University of Massachusetts, Amherst, MA, USA
E-mail: edwards9@iastate.edu Web: www.kin.hs.iastate.edu

INTRODUCTION

A fundamental problem in movement science is the determination of force patterns in individual muscles. Muscle forces can provide insights into the internal loading of the body, and reflect the coordination of movements at the neuromuscular level. The redundancy of the musculoskeletal system allows for an infinite number of muscle force combinations capable of producing the resultant joint moments observed during a movement. This "force sharing" problem is often solved through static optimization by determining the set of muscle forces that minimizes a specified cost function.

Previous research has yet to determine an appropriate static optimization cost function to solve the force sharing problem during drop landings. The purpose of this study was to compare six different cost functions, and determine which one produces muscle forces that best agree with electromyography (EMG) patterns during drop landings.

METHODS

Nine young adult subjects (four males, five females) participated in this study. Motion-capture (160 Hz), force platform (1600 Hz), and EMG data (1600 Hz) were collected synchronously while subjects landed from three separate heights (26, 39, 52 cm). Ten trials were performed at each height.

Kinematics of the trunk, pelvis and right lower-extremities were calculated in a flex/ext, abd/add, int/ext sequence. Resultant reaction forces and joint moments at the hip, knee, and ankle were calculated using inverse dynamics. Kinematic data were imported into a scaled SIMM 4.0 model to obtain maximal dynamic muscle forces and muscle moment arms for 43 lower extremity muscles. Muscle forces during the first 200 ms of landing were calculated using the *fmincon* optimization routine in Matlab 7.0.4 (sequential quadratic programming). Muscle forces were constrained to reproduce the experimental joint moments (three orthogonal hip moments, sagittal knee and ankle moment), and were bounded above zero and below the maximal dynamic forces.

For each trial, the optimization routine was performed with six different cost functions:

a) $\sum F_m$

b) $\sum \left(F_m\right)^2$

c) $Max\left(F_m / PCSA_m\right)$

d) $\sum \left(F_m / PCSA_m\right)$

e) $\sum \left(F_m / PCSA_m\right)^2$

f) $\sum \left(F_m / PCSA_m\right)^3$

where F_m is the mth muscle force and $PCSA_m$ is the physiological cross sectional area of the mth muscle.

EMG data for gluteus maximus, vastus lateralis, medial hamstrings, medial gastocnemius, and tibialis anterior were full-wave rectified and low-pass filtered at 6 Hz to produce a linear envelope. Time series

comparisons of the linear envelopes and corresponding optimized muscle forces were performed using root mean squared error (RMSE) and cross-correlations at zero-lag. Prior to time series analysis, linear envelopes were scaled to peak muscle force magnitudes. The RMSEs and z-scores from the correlations were average across muscles and conditions. Repeated measures ANOVAs were used to test differences in RMSEs and z-scores between each cost function (α=0.05) with Bonferroni adjustments for pairwise comparisons.

RESULTS

No difference in RMSE was observed between cost functions. A small but significantly lower correlation was observed for $\sum (F_m)^2$ when compared to all other cost functions (Table 1). Figure 1 displays representative time series comparisons.

Table 1. Mean time series comparisons. * denotes significantly different z-score from other cost functions (p<0.003).

Cost Function	RMSE (N)	r
a	130.06	0.90
b	142.28	0.86 *
c	131.88	0.90
d	131.87	0.90
e	132.27	0.90
f	131.66	0.90

DISCUSSION

Little difference in muscle force to EMG comparisons was observed between cost functions. However, the choice of cost function should be theoretically supported by physiologically based criteria (Crowninshield & Brand, 1981). During fatigued drop landings, the researcher may want to choose a cost function that maximizes muscular endurance. In this circumstance $\sum (F_m / PCSA_m)$, or some power of, may be most appropriate.

SUMMARY

In general, each cost function showed close agreement to EMG profiles. These findings suggest that static optimization during drop landings is fairly robust and insensitive to cost function choice, and is a reasonable method for estimating muscle forces during drop landings based on EMG comparisons.

REFERENCES

Crowninshield, RD and Brand, RA (1981). *J. Biomech*, 14: 793-801.

ACKNOWLEDGEMENTS

Figure 1. Representative muscle forces and EMG linear envelopes for vastus lateralis (VL), medial hamstring (MHAM), and medial gastrocnemius (MGAS) (solid green line = $\sum F_m$; dashed blue line = $\sum (F_m)^2$; dotted red line = EMG).

AGE RELATED CHANGES IN POSTURAL MUSCLE RESPONSES WITH INCREASING PERTURBATIONS TO THE UPPER BACK

Luis Rosado, Christopher J. Hasson, Richard E.A. Van Emmerik, and Graham E. Caldwell
University of Massachusetts Amherst, MA, USA, lrosado@kin.umass.edu

INTRODUCTION

Older adults display reduced postural stability associated with age-related neuromuscular deficits (Woollacott et al., 1986). If their base of support is suddenly moved backwards, older adults take longer to activate muscles needed to stop their forward rotation (Peterka & Black, 1990). Magnifying the support platform perturbation velocity alters muscular onset latencies and activity magnitudes in older subjects (Lin & Woollacott, 2002).

An external force perturbation applied to the upper back will also induce sudden forward rotation. In these and other perturbations, rapid balance recovery relies on various sensory inputs including muscle stretch receptors and the vestibular system. However, the force perturbations to the upper back likely cause greater head accelerations and neural responses from sensory mechanisms in the cranium. Because balance recovery responses are sensitive to the dynamics of the perturbation (Brown et al., 2001), external force perturbations might produce different age-related responses than platform motions.

Therefore, our purpose was to examine the relation between perturbation magnitude and plantarflexor muscle responses in young and old adults subjected to a series of increasing force perturbations to the upper body.

METHODS AND PROCEDURES

Healthy young [Y, n=9; 27±3 yrs, 1.73±0.11 m, 71±15 kg] and older [O, n=9; 71±5 yrs, 1.71±0.10 m, 82±16 kg] subjects stood on a force plate while wearing a safety harness anchored to the ceiling. Subjects were strapped to a backboard designed to constrain motion to the sagittal plane about the ankle joints. During quiet stance, a weighted pendulum was released to impact the subject on the upper back. Subjects were instructed to resist the subsequent forward sway and re-establish upright stance quickly without stepping. The perturbation magnitude was controlled by the pendulum release angle, which was increased sequentially until the subject could not recover without stepping. The perturbation level was quantified as the instantaneous pendulum angular velocity upon impact, computed from pendulum motion tracked at 200 Hz with a Qualisys camera system.

A force transducer in the pendulum striker was sampled at 1000 Hz to measure the perturbation impact. Activity levels for the gastrocnemius (GA) and soleus (SO) muscles were measured with electromyography (EMG) sampled at 1000 Hz. The EMG data were full wave rectified and low pass filtered at 50 Hz. EMG onsets were defined manually with the aid of a nominal threshold three standard deviations above baseline activity. Muscle onset latencies were calculated as the time from perturbation impact to EMG onset. Muscle activity magnitude was represented by the peak EMG value in the time period after onset, scaled relative to the largest value in the perturbation trials for that subject.

Correlations between pendulum impact velocity and muscle response variables were computed for each subject. Differences between age groups were assessed for maximum impact velocity before stepping, onset latencies, and correlations with t-tests, using $p < .05$ to determine significance.

RESULTS

Younger subjects were able to withstand greater pendulum velocities before stepping than the older adults (Mean±SD; Y: 496±137 deg/s; O: 380±107 deg/s; p =.032). Onset latencies for both muscles were longer in the older group than in the young (GA: p = .024; SO: p < .001; Fig. 1).
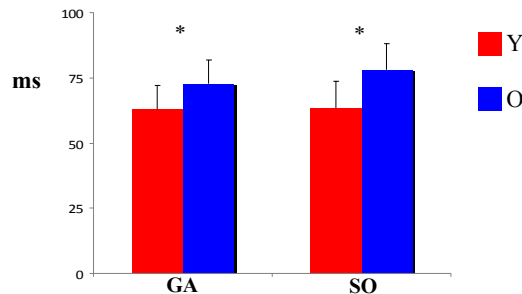

Figure 1. *Mean + 1 SD onset latencies for GA and SO muscles in young (red) and older (blue) groups (*p < .05 Y vs O).*

Correlation coefficients for onset latencies and impact velocity were negative for both muscles and age groups (Table 1), indicating shorter latencies with larger perturbations. In contrast, correlations between peak EMG and perturbation size were positive; as pendulum velocity increased so did the muscle activities for both age groups (Fig. 2). There were no age group differences in correlations for either onset latencies or EMG magnitudes.

Table 1. *Correlations (r) of muscle response variables with pendulum velocity (Mean±SD).*

	GA	SO
Onset Latency		
Young	-.43 ± .43	-.31 ± .53
Older	-.39 ± .38	-.07 ± .33
p	.844	.263
EMG Magnitude		
Young	.71 ± .24	.84 ± .09
Older	.46 ± .45	.68 ± .28
p	.160	.114

DISCUSSION

Our finding of longer onset latencies in older adults agrees with Peterka & Black (1990).
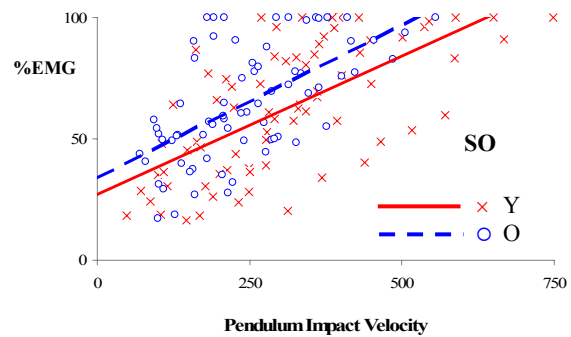
Figure 2. *SO Peak EMG activity plotted as a function of perturbation magnitude (Y: red × ; O: blue ○).*

Likewise, the correlations with perturbation magnitude for both EMG onset latency and activity agree with Lin & Woollacott (2002).

These similar findings occurred despite the use of a very different perturbation method than in these moving platform studies, and the findings of Brown et al. (2001) who showed how responses are modulated by the details of platform accelerations. The pendulum used here delivered a brief forward acceleration, with subsequent movement dictated solely by the subject response. Platform motion causes backward acceleration of the feet followed by subsequent deceleration that may occur within the response period. Onset latency and peak EMG measures may reflect only the first acceleration phase shared by both protocols.

REFERENCES

Brown, L.A., et al. (2001). *Gait and Posture*, 14, 256-263.

Peterka, R.J., and Black, F.O. (1990). *J Vest Res: Equil and Orient*, 1, 87-96.

Lin, S., and Woollacott, M.H. (2002). *J Mot Behav*, 34, 37-44.

Woollacott, M.H., et al. (1986). *Int J Aging and Hum Devel*, 23, 97-114.

ACKNOWLEDGEMENTS

CREATION OF THE GEOMETRY FOR A FINITE ELEMENT MODEL OF THE WRIST UNDER LOADED AND UNLOADED CONDITIONS

Charlotte Curtis[1], Robert Dony[1], Michele Oliver[1], Anne Agur[2], David Salonen[2], and Vincent Lo[1]
[1]School of Engineering, University of Guelph, Guelph, ON, Canada,
{curtisc,rdony,moliver}@uoguelph.ca
[2]University of Toronto, Toronto, ON, Canada

INTRODUCTION

Repetitive strain injuries to the wrist are common in occupations ranging from office work to mobile machine operation (Grieco et al. 1998). In order to avoid such injuries, ergonomic considerations should be made when designing work stations and equipment. However, the biomechanics of the wrist joint are not well understood (Oliver et al. 2007).

The development and validation of a finite element (FE) model of the wrist will provide insight into the loading conditions that may result in wrist injuries. Specific challenges presented by the wrist joint such as the complex interactions between bone and soft tissue make creation of the basic geometry a difficult task (Carrigan et al. 2003). In this work, geometry of the wrist in loaded and unloaded positions were created through manual segmentation and image registration.

METHODS AND PROCEDURES

Computed tomography (CT) scans with a resolution of 0.337 mm in the coronal and saggital directions and 0.5 mm in the axial direction were acquired of a cadaveric hand and forearm in an unloaded position and under a 54.3 N axially compressive load. Each bone of the loaded image was segmented using the medical visualization software MeVisLab (MeVis Research, Bremen, Germany). The radius, ulna, and phalanges could be automatically outlined with a threshold of 250 HU. However, due to close spacing and poor definition between
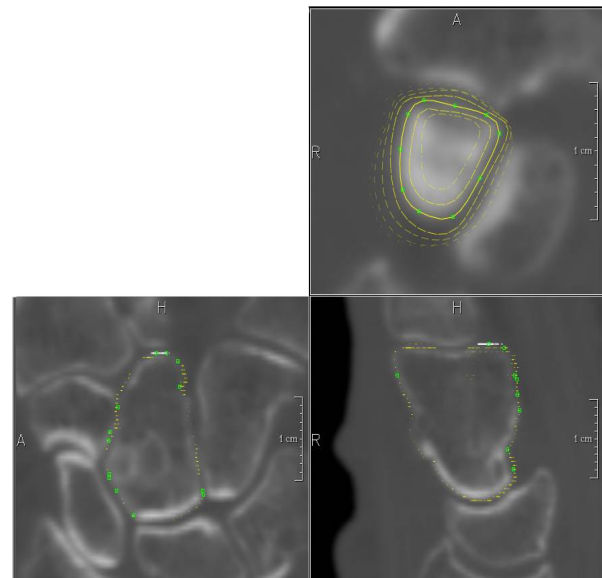
Figure 1: Manually segmenting the carpal bones of the wrist

individual bones, segmentation of the carpal bones could not be automated. For these bones, contour splines were drawn by hand on each slice. The splines of the previous slices were displayed as increasingly faded lines to ensure continuity, and each of the three orthogonal views was examined to ensure accuracy (Figure 1).

The manually and automatically drawn contour splines were rasterized and filled to create binary segmentation objects which were then smoothed and triangulated to created individual surface mesh objects. A custom program to rigidly register the unloaded scan to the loaded scan was written in C++ using the open-source Insight Toolkit. The registration was confined to the bounding box containing each bone, and a least squares

metric was used to find the optimal fit. The resulting 3D rigid transformation matrices were applied to the manual segmentations to create the geometry of the unloaded wrist.

RESULTS

Two sets of surface meshes were created to represent the geometry of the wrist under loaded and unloaded conditions (Figure 2).
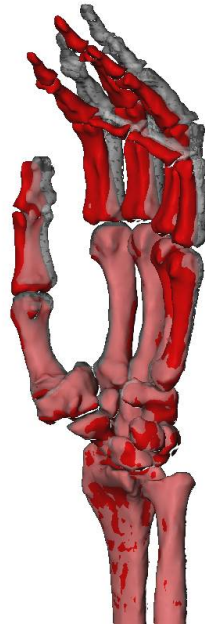

Figure 2: The final geometry (loaded in red, unloaded in grey)

DISCUSSION

The method of registering the unloaded and loaded images to create the second segmentation has several advantages over the more conventional approach of creating two separate models. The rigid transformation matrix provides a quantitative measure of the deformation between the two positions that can be used to fine-tune finite element model parameters such as material properties and interactions between bones. In addition, this method has the advantage of maintaining the same geometry for each bone, reducing the

impact of errors introduced during the segmentation process. Finally, the registration process is significantly faster than the manual segmentation process, allowing for more loading scenario models of the same sample to be generated quickly and easily.

For a validated finite element model, future work is required to ensure that the segmentations are accurate. Due to the discrete nature of the CT images and the reliance on manual segmentation, it is likely that the geometry created differs slightly from the cadaveric sample. Also, a single reference point is insufficient for fine-tuning of model parameters; therefore, future work will be required to create the geometry of additional loading scenarios.

SUMMARY

Computed tomography images of a cadaveric wrist in two different loading scenarios were acquired. Each bone of the loaded wrist was manually segmented and meshed to generate surface mesh objects. The unloaded scan was rigidly registered to the loaded scan and the segmentations were transformed accordingly to create the geometry of the unloaded scan.

REFERENCES

Grieco, A. et al. (1998). *Ergonomics*. Vol. 41 (9); pp. 1253–1260.

Oliver, M. L. et al. (2007). *Ergonomics*. Vol. 49 (3); pp. 249–268.

Carrigan, S. et al. (2003). *Annals of Biomedical Engineering*. Vol. 31 (6); pp. 718-725.

THE INFLUENCE OF INCREASING STEADY-STATE WALKING SPEED ON MUSCLE COORDINATION IN BELOW-KNEE AMPUTEES

N. P. Fey[1], A. K. Silverman[1], A. A. Portillo[2], J. G. Walden[2], G. Bosker[3], and R. R. Neptune[1]

[1] Dept of Mechanical Engineering, The University of Texas at Austin, Austin, TX
[2] Physical Medicine & Rehabilitation Service, Audie L. Murphy VA Hospital, San Antonio, TX
[3] Dept of Rehabilitation Medicine, University of Texas Health Science Center, San Antonio, TX

INTRODUCTION

Previous studies have shown that below-knee amputees exhibit greater energy expenditure and bilateral asymmetry relative to non-amputees at their self-selected walking speed (e.g., Hafner et al., 2002). These differences are attributed to the functional loss of the ankle plantar flexors, which are critical to providing body support, forward propulsion, and swing initiation in non-amputee walking (Neptune et al., 2004). Identifying how amputee muscle coordination changes in response to changes in task demands, such as increased walking speed, will provide insight into the compensatory mechanisms used by amputees. Previous studies have examined muscle activity during amputee walking, but have either analyzed a small set of muscles (typically < 3) or not compared their results with control subjects under the same conditions. Furthermore, no study has examined amputee muscle activity over a wide range of walking speeds. The purpose of this study was to examine bilateral muscle activity across a wide range of walking speeds to identify changes in muscle coordination in below-knee amputees.

METHODS AND PROCEDURES

Fourteen below-knee amputees and 10 control subjects walked at 0.6, 0.9, 1.2 and 1.5 m/s. Kinematic, ground reaction force (GRF), and electromyographic (EMG) data were collected using a Vicon motion capture system (Oxford Metrics, Inc.). EMG data were collected using surface electrodes from eight intact leg muscles including the tibialis anterior (TA), medial gastrocnemius (GAS), soleus (SOL), vastus lateralis (VAS), rectus femoris (RF), biceps femoris long head (BF), gluteus medius (GMED), and gluteus maximus (GMAX), and from five residual leg muscles including VAS, RF, BF, GMED, and GMAX. Integrated EMG (iEMG) magnitude was calculated over the gait cycle and within three subphases including braking (~0-50% stance), propulsion (~50-100% stance) and swing. Gait cycle and subphase iEMG magnitudes were normalized by the gait cycle iEMG value at 1.5 m/s. This method of normalization was performed at the individual subject level, and individual values were averaged for each group.

Statistical analyses compared iEMG values and included five, three-factor (group, leg, speed) repeated measures ANOVAs for the upper-leg muscles and three, two-factor (group, speed) repeated measures ANOVAs for the intact and control leg ankle muscles. The same analysis was repeated for the gait cycle and each subphase. When significant differences were found, Bonferroni pairwise comparisons were used to determine which values were significantly different ($p \leq 0.05$).

RESULTS

The most notable differences occurred within the residual leg muscles. During braking, significantly higher activity was found in the residual leg VAS (all speeds compared to the intact leg) and BF (all speeds compared to the

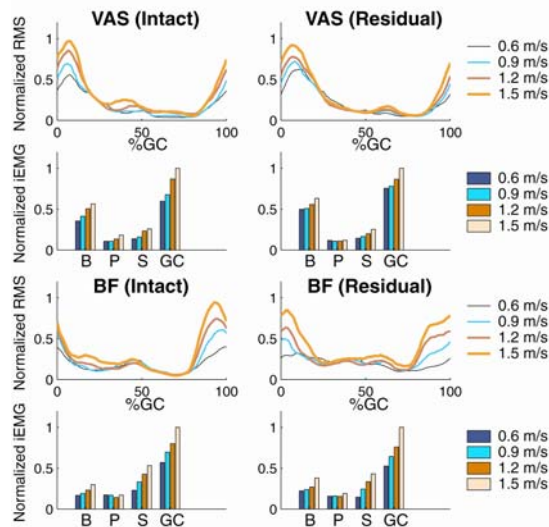intact leg, and at 1.5 m/s compared to the control leg) (Fig. 1).

Figure 1. Intact and residual leg EMG profiles and iEMG magnitudes for VASL and BF muscles within Braking (B), Propulsion (P), Swing (S), and the gait cycle (GC).

Other significant findings included increased residual leg RF activity during braking (0.9, 1.2, and 1.5 m/s compared to the intact leg, and at 0.9 and 1.2 m/s compared to the control leg) which resulted in a more systematic response to walking speed compared to the intact and control legs. Similar to the residual leg VAS, the residual leg GMAX exhibited significantly higher activity during braking compared to the intact leg GMAX at 0.6 and 0.9 m/s. Also, GMED activity in all legs was largely insensitive to changes in walking speed.

DISCUSSION

The heightened and prolonged residual leg VAS and BF activity (Fig. 1), especially at the slower speeds, suggest a need for increased stability in the absence of the plantar flexors (e.g., Rietman et al., 2002). In addition, the heightened and prolonged residual leg BF activity may help to reduce residual leg braking. Previous modeling and simulation studies of non-amputee walking

have shown BF to contribute positively to the anterior/posterior GRF throughout stance (e.g., Neptune et al., 2004). Thus, increased activity of this muscle in early stance could provide propulsion, and therefore reduce the net braking impulse.

The higher activity of the residual leg RF during braking at 0.9 and 1.2 m/s, compared to control legs, suggests that it may be transferring more energy from the leg to the trunk to provide additional body support (e.g., Neptune et al., 2004). In addition, the residual leg GMAX, along with the residual leg VAS muscles, may provide increased body support in the absence of the ankle plantar flexors (e.g., Neptune et al., 2004). The insensitivity of GMED to walking speed is consistent with its primary role to provide body support (Anderson and Pandy, 2003).

In summary, most amputee EMG patterns across legs were similar to the control subjects and systematically increased with speed. The most notable differences were observed in the residual leg BF, VAS, RF and GMAX muscles, which exhibited increased output, especially at slower speeds, and appear to provide needed body support and propulsion in the absence of the plantar flexors.

REFERENCES

Anderson, FC and Pandy MG (2003). *Gait Posture,* 17:159-169.
Hafner, BJ et al. (2002). *Clin Biomech,* 17:325-44.
Neptune, RR et al. (2004). *Gait Posture,* 19:194-205.
Rietman, JS et al. (2002). *Prosthet Orthot Int,* 26:50-7.

ACKNOWLEDGEMENTS

SYNERGIES HIERARCHIES DURING ACCURATE ROTATIONS TASKS

Wei Zhang[1], Vladimir M. Zatsiorsky[2], and Mark L. Latash[1]

[1]Motor Control Laboratory, [2]Biomechanics Laboratory,
Department of Kinesiology, The Pennsylvania State University, PA 16802, USA,
wuz107@psu.edu, mll11@psu.edu

INTRODUCTION

Synergies stabilizing forces and moment of forces (Latash 2008) have been mostly observed in multi-finger pressing tasks and static prehension tasks. Recently, rotational actions have been studied in the framework of the uncontrolled manifold (UCM) hypothesis (Scholz and Schöner, 1999) to detect and quantify synergies (Zhang et al, 2008). However, there have been no studies of multi-digit synergies during accurate voluntary rotational actions in 3D space. In current study, we explored the two levels of a hypothetical hierarchy involved in the control of the hand during rotation of a hand-held object. We expected an interaction between the synergies at the two control levels.

METHODS AND PROCEDURES

Ten (5 males, 5 females) young healthy right-handed subjects participated in this study. During the experiment, subjects sat comfortably facing a vertically oriented handle (Figure 1). Five six-component force/torque transducers (NANO17/25; ATI inc.) were mounted on the two sides of the handle to record the individual digit forces and local moments of forces. Two inertial loads (100 g each) were attached along the middle vertical line, 9.5 cm from the center on a PVC disc (25cm in diameter), which was connected to the handle by a 19-cm aluminum rod. The weight and orientation of the handle-rod-disc system was balanced by a counter-load, such that the subjects only had to

produce rotational efforts, not to support the weight of the system.
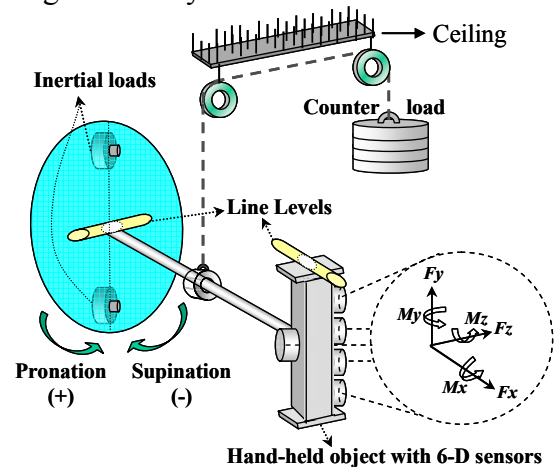
Figure 1. Experiment set up.

A torsiometer (Biometrics inc.) was used to record the pronation-supination angle. With the forearm fixed, subjects were instructed to voluntarily rotate the handle 60 degrees at two speeds (naturally slow/fast, SL/FA) in two directions (pronation/supination, PR/SU). Holding the initial position before and final position after the rotations were also parts of the task. Twenty-four trials were performed for each condition.

The data were aligned by the onset of rotation for each trial, and the rotation duration was normalized to 100%. The UCM hypothesis was used to compute an index (ΔV) reflecting multi-digit synergies stabilizing mechanical outputs of the digits at each time sample over sets of trials for each condition and each subject separately. The UCM analysis was performed at two hierarchical levels, the

virtual finger-thumb level (VF-TH), and the individual finger level (IMRL).

RESULTS

Over all conditions, the rotational action was produced by changes in both forces and lever arms of individual fingers. In particular, the index finger was the main finger to initiate rotation in PR tasks and to brake rotation in SU tasks by changes in its normal force, while the middle and ring fingers showed relatively constant shares of the total normal force.

Indices ΔV computed at the VF-TH level for both normal forces and tangential forces showed high positive values, corresponding to stabilization of their combined output, in all four conditions. These indices were consistently negative at the IMRL level before, during and after the rotational action (Figure 2).
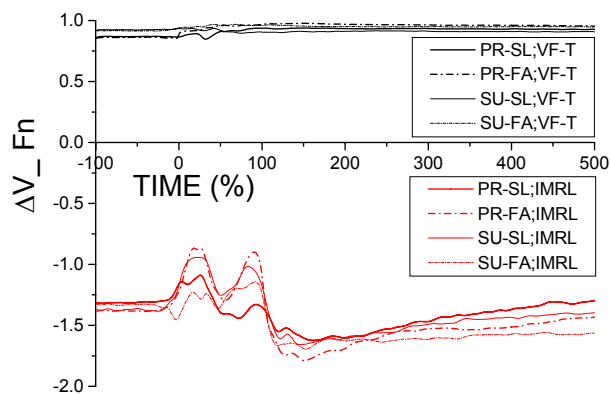
Figure 2. ΔV index for normal forces at the VF-TH (black four lines) and IMRL levels (red four lines) for the four conditions. Note highly positive ΔV at the VF-TH level, but negative values at the IMRL level.

DISCUSSION

Sharing patterns of individual fingers revealed their task-related functional behaviors, which is that the forces of the 'peripheral' (index and little) fingers mainly defined the total

moment of force time profile while the forces exerted by the 'central' (middle and ring) fingers reflect both load and torque requirements (Zatsiorsky et al, 2002).

The fact that force-stabilizing synergies were present at the higher level of the control hierarchy but absent at its lower level might suggest a potential limitation in the ability of the CNS to organize synergies at both levels of the control hierarchy simultaneously (Gorniak et al, 2007).

REFERENCES

Gorniak, SL et al. (2007). *Exp Brain Res,* 179: 167-180.
Latash, ML et al. (2002). *Exerc. Sport Sci. Rev.*, **30**, 26-31
Latash, ML (2008) Synergies. Oxford
Scholz JP, and Schöner G (1999). *Exp Brain Res,* 126:289-306.
Zatsiorsky VM et al (2002). *Biol Cybern*, 87:50-57
Zhang W et al. (2008). *J Neurophysiol,* 99:500-513

ACKNOWLEDGEMENTS

THE RELATIONSHIP BETWEEN CENTER OF PRESSURE DISPLACEMENT AND ESTIMATED INSTABILITY OF DANCERS AND NON-DANCERS WHILE IN A MOVING ROOM

Leigh Schanfein and Shirley Rietdyk
Department of Health and Kinesiology, Purdue University, West Lafayette, IN, USA.
lschanfe@purdue.edu

INTRODUCTION

Balance is an innate aspect of dance, which leads one to believe that dancers receive "balance training" (Schmit et al., 2005) in the process of developing their technical and artistic abilities. Dancers are significantly less stable than controls when proprioceptive information is unreliable (Simmons, 2005), and they are only more stable than controls when standing with eyes closed (Perrin et al., 2002) suggesting that dancers are less dependent on vision than non-dancers. It may be that, through dance training, dancers are able to maintain postural control when reliance on the visual system is jeopardized by more effectively distributing sensory weightedness away from the visual system to the proprioceptive and/or vestibular sensory systems. If such adaptation occurs, the dancer would be less susceptible to illusions of self-motion induced by a moving visual surround (called vection) than controls but potentially unable to utilize stationary references within an advantageous distance to further aid postural stabilization. The current project proposes to examine if balance control is altered and vection reduced by the addition of stable visual references, in central and/or peripheral vision, within a moving visual surround. Additionally, it will examine if vection, measured as estimated instability, is correlated to center of pressure (COP) displacement.

METHODS AND PROCEDURES

Ten advanced-level university modern dancers (22 ± 1.7 yrs) and ten athletic controls (20.3 ± 2.2 yrs) stood on a forceplate inside a moving room. Visual references were stationary black vertical poles (2 m height, 6.25 cm diameter). Eight visual conditions were examined: (1) static visual field, the room not moving and no references present; the room was moving for the remaining seven conditions: (2) without references, (3) peripheral references within the room, (4) peripheral references outside the room, (5) central references within the room, (6) central references outside the room, (7) both central and peripheral references within the room, (8) both central and peripheral references outside the room. Two trials were observed for the first condition, and five trials for the latter seven conditions, for a total of 37 trials. Each trial lasted 70 seconds. Perception of instability was assessed after each trial; subjects were instructed to provide a number between 1 and 10, 1 indicating "I felt solid as a rock" and 10 indicating "I felt I was about to fall over." COP displacement was quantified as root mean square (RMS) in the anterior-posterior direction (AP).
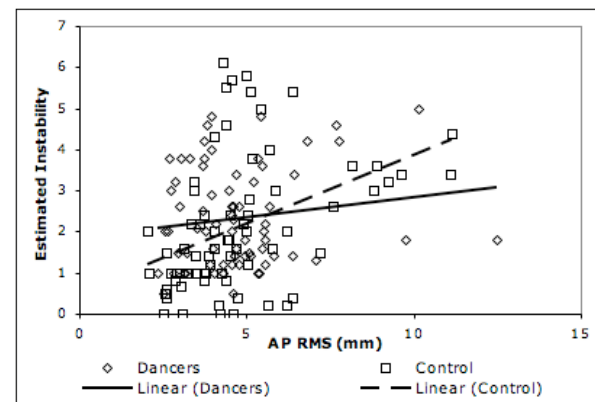
RESULTS AND DISCUSSION

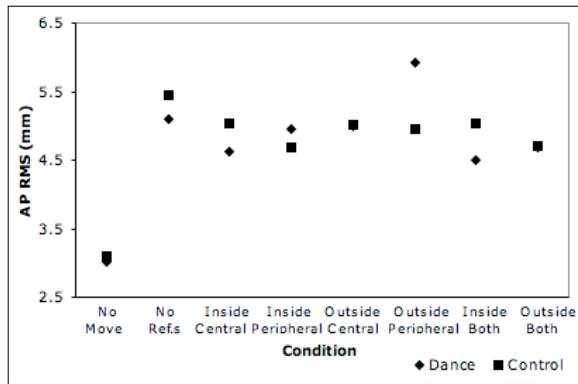**Figure 1**. Estimated instability plotted against AP COP RMS.

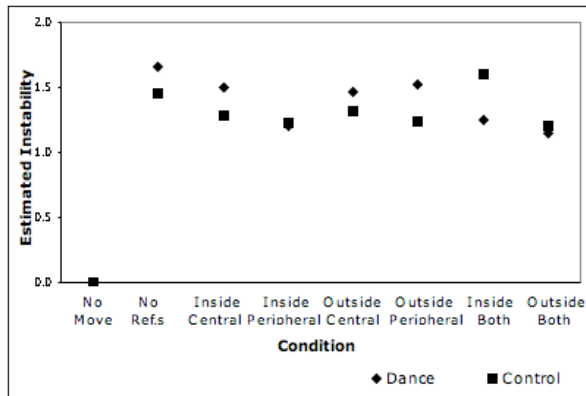**Figure 2**. AP COP RMS for each group by visual condition.

Figure 3. Estimated instability for each group by visual condition. Values are normalized to baseline measure obtained through subjective estimate of instability during the no room movement condition.

Estimated instability and AP COP RMS were linearly correlated for controls ($R^2 = 0.168$, $p < .001$), but not for dancers ($R^2 = 0.021$, $p = .258$) (Figure 1). Therefore, COP displacement appears to affect estimated instability for the control group but not for the dancers, the group with "balance training." This is consistent with the interpretation that increased COP displacement does not necessarily reflect decreased stability, and may indicate increased behavioral flexibility (Schmit et al, 2005).

An interaction effect was observed for AP COP RMS ($p = .008$); post hoc analysis revealed that dancers demonstrated significantly greater AP COP RMS with references in the outer periphery than with any other reference positioning, including having no references (Figure 2, third condition from right). This observation does not support the concept that dancers are less visually dependent (as suggested by Perrin et al. 2002; Simmons, 2005). Increased AP COP RMS with outside peripheral cues may reflect that the dancers are "dancing with the room," providing further evidence of increased behavioral flexibility.

Estimated instability was affected by condition ($p < .001$); the greatest instability was perceived with no references. Estimated instability was reduced when inside peripheral references were available or outside central and peripheral references were in place (Figure 3). Estimated instability was also affected by group ($p < .001$); dancers had higher estimated instability than controls, which does not support the concept that dancers are less visually dependent, although one must take into account that this measure is subjective.

SUMMARY

This study did not support the concept that dancers are less visually dependent, either with subjective or objective measures. However, dancers do respond differently to visual cues within a dynamic visual environment than non-dancers, consistent with the idea that dance training modifies how dancers use visual cues. This may reflect increased behavioral flexibility.

REFERENCES

Perrin P, Deviterne D, Hugel F, Perrot C. Gait and Posture 15 (2002): 187 – 194.

Schmit JM, Regis DI, Riley MA. Experimental Brain Research 163 (2005): 370 – 378.

Simmons RW. International Journal of Neuroscience 115.1 (2005): 87 – 97.

MUSCLE FORCE ESTIMATES FOR WALKING USING AN EMG-DRIVEN MUSCULOSKELETAL MODEL OF THE KNEE ARE RELIABLE WITHIN AND BETWEEN DAYS

Kurt Manal[1], Lynn Snyder-Mackler[1,2], Michael Axe[1,2] and Thomas S. Buchanan[1]
[1]Center for Biomedical Engineering Research, University of Delaware, Newark, DE, USA
[2]Department of Physical Therapy, University of Delaware, Newark, DE, USA
E-mail: manal@udel.edu

INTRODUCTION

Muscle forces during dynamic movements are generally estimated using some form of a computer model. The validity of these estimates is difficult to ascertain given the lack of experimental data for direct comparison. Reliability is an integral component of validity, and therefore a well-constructed model should yield reliable data when repeatable results are expected. Joint kinematics, kinetics and muscle activity during normal gait have been shown to exhibit good within and between day repeatability (Winter, 1991; Kadaba et al., 1989). This paradigm was used to evaluate the within and between-day reliability of our EMG-driven muscle force estimates. Our a priori expectation was that model forces would demonstrate good repeatability for subjects with normal gait.

PROCEDURE AND METHODS

Six subjects performed 5 natural cadence walking trials on 2 separate occasions. Testing sessions were separated by approximately 4 weeks. Muscle forces were computed using an EMG-driven musculoskeletal model. Details of this model have been presented elsewhere (Buchanan et al., 2004) and are summarized here. Muscle activations for 10 muscles crossing the knee: semimembranosus (SM), semitendinosus (ST), biceps femoris longus (BFL), biceps femoris short head (BFS), medial and lateral gastrocnemii (MG & LG), rectus femoris (RF) and the vasti (VM, VL & VI) were computed from recorded EMGs . Standard motion analysis was used to compute joint kinematics and kinetics for the stance phase of normal walking. The EMGs and joint kinematics served as inputs to a Hill-type muscle model to compute individual muscle forces. Within day repeatability was assessed using the coefficient of variation (CV) and between-day repeatability evaluated using the coefficient of multiple determination (R^2). For each subject, the CV and R^2 values were computed for each muscle and then averaged across subjects to create an average CV and R^2 for each muscle.

RESULTS

In general the results indicate good repeatability of muscle force estimates both within and between-days. This is characterized by the CV and values reported in Table 1. Visual inspection of the between-day muscle forces revealed an overall similarity in magnitude and shape of the force profiles.

DISCUSSION

The CV and R^2 reported in Table 1 are consistent with values reported for joint kinematics and kinetics, and smaller than the variability associated with EMG for the major leg muscles (Winter, 1991;

Kadaba et al., 1989). Based on the CV and R^2 values, and through visual inspection of muscle force curves we believe our EMG-driven model yields reliable force estimates under conditions in which repeatable forces are to be expected (i.e., normal gait). Although this approach does not speak directly to the question of construct validity, it is nonetheless an important test of the model output and a key finding since demonstrating model reliability is a necessary component of model validity.

SUMMARY

Muscle force estimates were repeatable both within and between days. This finding suggests it is appropriate to make pre & post muscle force comparisons using our EMG-driven model.
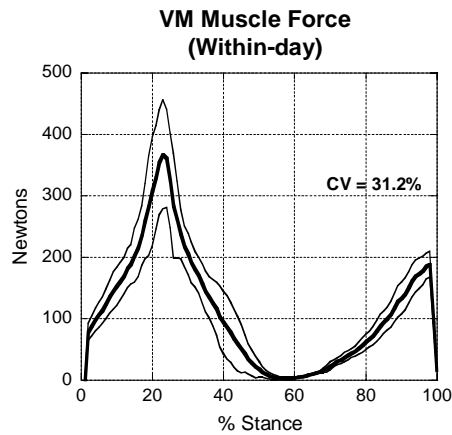
Figure 1. Representative within-day variability for the VM force.

Figure 2. Representative between-day variability for the VM force.

REFERENCES

Buchanan TS et al.(2004). *J Appl Biomech* 20, 367-395.
Kadaba MP et al. (1989). *J Orth Res* 7,849-860.
Winter DA (1991). *Biomechanics and Motor Control of Human Gait.* University of Waterloo Press.

ACKNOWLEDGEMENTS

Table 1. Average coefficient of variation (CV) for individual muscle forces during stance. CV was used as an estimate of within-day reliability. The similarity of the muscle force estimates between days was evaluated using R^2. Standard deviations reported in parentheses

Muscle Force Reliability Measures

	SM	ST	BFL	BFS	MG	LG	RF	VM	VL	VI
CV%	29.6	41.9	39.5	37.9	30.7	34.3	35.5	32.5	40.5	33.1
(SD)	(12.3)	(19.5)	(13.4)	(14.6)	(13.1)	(23.9)	(15.4)	(10.0)	(12.6)	(11.5)
R^2	0.83	0.83	0.88	0.62	0.88	0.56	0.75	0.94	0.93	0.94
(SD)	(0.13)	(0.15)	(0.05)	(0.31)	(0.05)	(0.22)	(0.25)	(0.04)	(0.05)	(0.03)

USE OF ULTRASOUND TO DYNAMICALLY EVALUATE ACHILLES TENDON MECHANICAL PROPERTIES IN STROKE

Heng Zhao[1] and Li-Qun Zhang[1, 2]

[1]Department of Physical Medicine and Rehabilitation, Feinberg School of Medicine, Northwestern University, Chicago, Illinois, USA, hengzhao@northwestern.edu
[2]Rehabilitation Institute of Chicago, Chicago, Illinois, USA, l-zhang@northwestern.edu

INTRODUCTION

Recent findings show that the metabolic activity in human tendon is remarkably high which affords the tendon the ability to adapt to changing demands (Magnusson et al. 2008). Studying the tendon mechanical properties of the stroke survivors may help to understand the physiological mechanism of spasticity/contracture and provide guidance for rehabilitation.

B-mode ultrasound imaging has been widely used to investigate human tendon displacement, *in vivo*, during muscle maximum voluntary isometric contraction (MVC). However, due to muscle weakness, stroke survivors can only generate about 20%~40% of an average healthy subject MVC. Therefore smaller muscle-tendon junction (MTJ) displacement becomes more susceptible to error, indicating the need for more objective and accurate measurement. Moreover, decorrelation is inevitable between ultrasound frames due to out-of-plane motion and noise. Frame-by-frame analysis is a way to avoid severe decorrelation and allow the MTJ displacement to be studied dynamically with changes in load, but it is too labour intensive. Some automatic tracking methods have been developed (Magnusson et al. 2003; Loram et al. 2006). However the methods are limited to tracking the regions with high intensity gradient or consistently clear features. In this paper, a block-matching method based on minimum sum of absolute differences (MSAD) algorithm is introduced to measure the displacement of Achilles-soleus MTJ under voluntary contraction. The viscoelasticity, as well as the Young's modulus of a stroke survivor's Achilles tendon was evaluated and compared to a healthy subject.

METHODS AND PROCEDURES

Figure 1. The experiment setup.

MSAD Block-Matching Algorithm:
A method was proposed recently to quantify regional myocardial dysfunction in mice (Li et al. 2007). Compared to previous methods, MSAD does not require clear features and is more robust to the false noisy speckles which are common in ultrasound images. Moreover, the MSAD implementation is highly computationally-efficient and compatible with different types of CPUs (Li et al. 2007).

Experiment Setup:
The setup consists of a custom knee-ankle device (Figure 1) and a LOGIQ-9 (GE, Waukesha, WI) ultrasound machine.

Experiment Protocol:

The subject was seated upright with the knee and ankle attached to the knee-ankle device (Figure 1). The Achilles tendon length at rest was measured using an extended field-of-view technique with a 14 MHz probe. The moment arm and the cross-sectional area of the Achilles tendon was measured using the method in (Maganaris and Paul 2002). A camcorder was used to monitor the calcaneus motion and the EMG of dorsiflexors was recorded. The subject performed a voluntary isometric contraction and relaxed following a ramping up and down pattern displayed on the screen. The ultrasound images, the synchronization signal, and the joint moment were recorded.

Data Processing:
The soleus MTJ displacement was calculated as an average of multiple tracked blocks. Sub-pixel displacement was estimated using parabolic interpolation. The recorded joint moment data were filtered and aligned with displacement data using the synchronization signal. The stress and the strain of the Achilles tendon were calculated.

RESULTS

The stress-strain relation curves of a representative stroke survivor and a healthy subject during dynamical loading are shown in Figure 2.
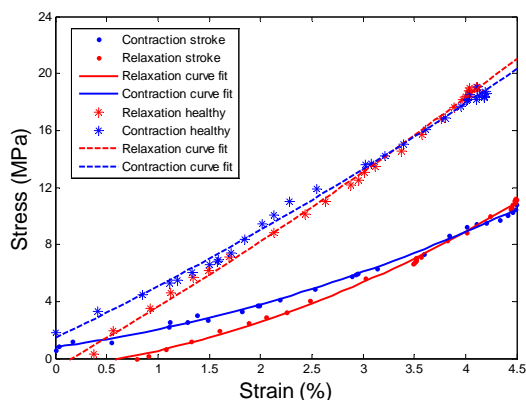
Figure 2. Stress-strain relation curves of a stroke survivor and a healthy subject.
The dots and the stars represent the stress-strain relation of the stroke survivor and the

healthy subject, respectively. The blue and red colors represent the contraction and relaxation process, respectively. The stress-strain loops were fitted using quadratic polynomial curves. The maximum Young's moduli of the stroke survivor and the healthy subject were 469.5 MPa and 269.6 MPa, respectively. The hysteresis area (between the loading and unloading curves) of the stroke survivor and the healthy subject are 19% and 6.5% of the area between each loading curve and the abscissa, respectively.

DISCUSSION

Although the task was relatively easy, the stroke survivor still needed to go through considerable training, and the compensations for antagonist co-contraction and calcaneus motion need to be dealt with properly. Since the test was carried out within the toe region of the tendon elasticity curve, the Young's moduli of both subjects are lower than some previous results (Magnusson et al. 2003).

SUMMARY

A robust, computationally-efficient block matching method is introduced to study the Achilles tendon mechanical properties using ultrasound. Results show that the Achilles tendon of the stroke survivor is more compliant than the healthy subject. The larger hysteresis area of the stroke survivor indicates larger energy loss during locomotion.

REFERENCES

Li Y et al. (2007). *Ultrasound Med Biol,* 33:894-904.
Loram ID et al. (2006). *J Appl Physiol,* 100:1311-23.
Maganaris CN and JP Paul (2002). *J Biomech,* 35:1639-46.
Magnusson SP et al. (2003). *Acta Physiol Scand,* 177:185-95.
Magnusson SP et al. (2008). *J Physiol,* 586:71-81.

STRUCTURAL PROPERTIES OF TRABECULAR CORES FROM FEMORAL HEADS

Sylvana García-Rodríguez[1], Meghan C.M. Crookshank[2], Norma J. MacIntyre[2,3] Mark Harrison[2], Everett L. Smith[4], Rick Sellens[2] and Heidi-Lynn Ploeg[1]

[1]Department of Mechanical Engineering and [4]Department of Population Health Sciences, University of Wisconsin, Madison, WI, USA, http://www.engr.wisc.edu/groups/BM/
[2]Human Mobility Research Centre, Kingston General Hospital, Queen's University, Kingston, ON, Canada, http://me.queensu.ca/hmrc/
[3]School of Rehabilitation Science, McMaster University, Hamilton, ON, Canada

INTRODUCTION

Bone density and fracture risk are clinically assessed by dual-energy x-ray absorptiometry (DXA). The advantages of DXA are its accessibility, low radiation dose and established ability to predict population-based fracture risk in postmenopausal women; however, it provides two-dimensional data, limiting its ability to accurately predict bone's structural properties. Computed tomography (CT) has grown as a tool to evaluate the three-dimensional (3D) mechanical properties of bone, which may serve to improve the ability to predict bone fracture risk for individual men and women.

The purpose of this study was to establish a comprehensive dataset of structural properties (e.g. CT x-ray attenuation in Hounsfield units HU, bulk density ρ_{blk}, apparent density ρ_{app}, mineral content MC, and apparent elastic modulus E_{app}) of trabecular bone from human femoral heads. This dataset will provide valuable insights into the probability density functions of, and correlations between, these measured properties.

METHODS AND PROCEDURES

Seven femoral heads were donated by hip replacement recipients with Research Ethics Board approval (age 66 – 87 y; two male, five female). The hip heads were CT scanned (GE Lite Speed Plus) pre- and post-operatively.

Two to three, 7 mm thick slices were cut (Exact diamond-coated band saw) from each head. The slices were oriented approximately perpendicular to the hip joint load. From each slice, 10 mm diameter trabecular bone cores were extracted and milled to a 5 mm height. Bulk dimensions and wet weights were recorded.

The femoral head with cores removed were "reassembled" and CT scanned with the same pre-machined scan parameters. A custom-made registration algorithm aligned the pre- and post-machined segmented CT data before the data were subtracted from each other. The resulting data set corresponded to the prepared bone cores, therefore providing their x-ray attenuation data (HU).

Compression testing was performed on each core using *ZETOS* (Jones et al., 2003; García-Rodríguez et al., 2008). With 10 N preload, displacement of 30 µm was applied quasi-statically (0.7 µm/s) while measuring force (Kistler, type 9011A). Force and displacement were normalized to stress and strain, respectively, using bulk dimensions. E_{app} was determined from the slopes of the stress-strain curves. Cores with E_{app} outside the *ZETOS* operating range (58.3-1860 MPa) were excluded.

The cores were dried in a 70°C oven (24 hrs) and defatted in a soxhlet extractor (24 hrs). Ashing was performed in a 700°C oven

(24 hrs). Dimensions and weights were recorded before and after the drying and defatting procedures. Dry, defatted weight (W_{dd}) over dry, defatted bulk volume ($V_{dd,blk}$) gave ρ_{app}. Material mineral content (MMC) was determined by dividing ash weight by W_{dd}. The ratio of ash weight to $V_{dd,blk}$ was defined as structural mineral content (SMC) (Cowin, 2001). Histograms of HU, ρ_{app}, MMC, SMC and E_{app} were analyzed for normality using the Anderson-Darling test.

RESULTS

From seven femoral heads, 85 cores were prepared and 20 were excluded due to low compression stiffness (E_{app}<58.3 MPa). Figure 1 shows the probability density functions of the measured properties. Only MMC and E_{app} were not normal, but were normalized by Johnson transformations.
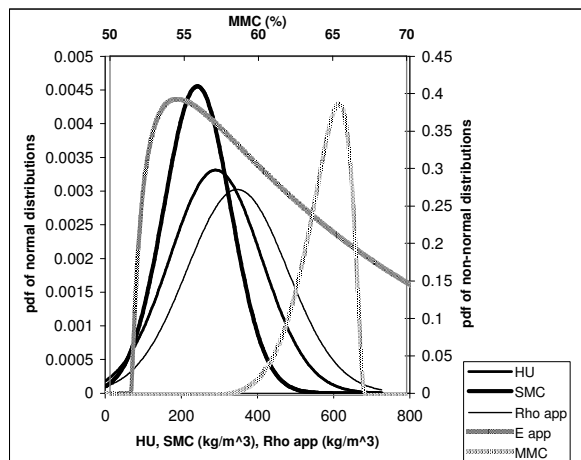
Figure 1. Probability density functions of measured structural properties of trabecular bone cores from human femoral heads.

DISCUSSION

CT scan data and mechanical properties were found for 85 trabecular bone cores. These measures provided probability density functions and correlations of importance to CT-based structural analyses of bone. The HU, SMC and ρ_{app} were normally distributed; however the E_{app} distribution was skewed to the left and MMC distribution was skewed right. Although it seems contradictory that E_{app} is skewed left, this result supports the hypothesis that MMC alone does not define structural properties. High MMC may indicate thicker trabecular struts; however the stiffness of the structure may be compromised by micro damage or reduced connectivity, as in osteoporotic bone.

SUMMARY

Eighty five human femoral trabecular cores (10 mm diameter, 5 mm height) were obtained from seven femoral heads. CT data registration and Boolean operations provided HU data for each core. Compression testing was performed using *ZETOS* to determine E_{app}. Dry, defatted bulk dimensions and weight were used to calculate ρ_{app}. Ashing provided data for determining MMC and SMC. All histograms except E_{app} and MMC passed Anderson-Darling normality tests. The skewed distributions for E_{app} and MMC may be an indication of osteoporotic bone. A valuable dataset of trabecular bone properties was obtained, relevant for future studies on bone fracture prediction.

REFERENCES

Cowin, SC (2001). *Bone Mechanics Handbook*. USA, CRC Press.
Jones, DB et al. (2003). *Eur Cell Mater*, 5: 48-60.
García-Rodríguez, S et al. (2008). *J Biomech Eng* (in press).

ACKNOWLEDGEMENTS

PROPRIOCEPTIVE SENSITIVITY IN CONSTRAINED AND UNCONSTRAINED DEGREES OF FREEDOM

Martha Cammarata[1,2] and Yasin Dhaher[1,2]
[1] Department of Biomedical Engineering, Northwestern University, Chicago, IL, USA
[2] Sensory Motor Performance Program, Rehabilitation Institute of Chicago, Chicago, IL, USA
E-mail: m-cammarata@northwestern.edu

INTRODUCTION

Biomechanical demands during general joint movements necessitate the use of a number of motor templates to generate movement in the targeted degree of freedom (DOF) while maintaining posture or stability in secondary DOFs. This task is more complicated when secondary DOFs are highly constrained and poorly actuated. Key examples include the metacarpophalangeal, elbow, and knee joints. It has been suggested that proprioception plays a substantial role in the selection of the appropriate motor template for a given task (Dietz et al.1987). While the perception of movement in primary DOFs has been studied (Lephart et al. 2002, Pai et al. 1997), little is known regarding proprioceptive sensitivity to movements in the constrained DOF. We hypothesize that sensitivity to joint movement and position is increased in these directions. We argue that the increased sensitivity is part of a motor control strategy designed to maintain the integrity of joint passive tissues. Using the knee as an experimental model, the aim of this study is to examine proprioceptive sensitivity in the frontal and sagittal planes. Given the potential detrimental role of loading in the frontal plane to joint injury and disease (Weidow et al. 2006), understanding the differential proprioceptive sensitivity between these two DOFs has both clinical and scientific importance.

METHODS AND PROCEDURES

Five healthy subjects (4 females, ages 21-33 years) participated in the study. For testing in the frontal plane, subjects were seated in an experimental chair with the right knee fully extended. The right ankle was placed in a cast and secured to a servomotor, which rotated into varus and valgus. Brackets were fastened around the knee to prevent translation. In the sagittal plane, subjects were seated in the chair with the knee at 30° of flexion and the servomotor center of rotation was aligned with the femoral epicondyles. Subjects wore headphones and an eyemask to reduce auditory and visual cues.

Proprioception was assessed under both passive and dynamic conditions. In the first test, subjects' threshold to detection of passive movement (TDPM) was tested by rotating the knee into varus or valgus (flexion or extension) at 1°/s. Subjects were instructed to press a handheld button as soon as movement of the limb was detected. TDPM was defined as the position difference between the actual onset of the movement and subjects' detection of movement. Two sample t-tests were used to assess differences in TDPM between the two planes.
A second test was created to assess joint position sense (JPS) under dynamic conditions. A series of rapid ramp and hold valgus (or extension) perturbations of varying amplitude were applied to the knee at a loading rate of 60°/s (Figure 1). Subjects were instructed to compare the magnitude of consecutive perturbations, using the handheld button to indicate if the current stretch felt larger, smaller, or the same as the previous stretch. The relative angular difference between consecutive perturbations ranged from 0° to ±5° in the frontal plane, and 0° to ± 11° in the sagittal plane. For each amplitude of these angular comparisons, accuracy was

determined as the ratio of correct responses to total observances. In this way, the sensitivity
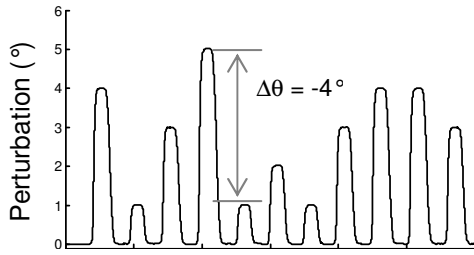

Figure 1. Movement profile used in the dynamic test. Shown is a difference of -4° between consecutive perturbations.

for detecting relative differences in joint position was examined.

RESULTS

TDPM results are presented in Table 1. The threshold for detecting movements in varus was not significantly different than in valgus (P >0.05). Likewise, no significant differences were found between TDPM in flexion and extension. When comparing between the two degrees of freedom, TDPM was significantly greater (P = 0.02) in the sagittal plane ($1.06° \pm 0.37°$) than the frontal plane ($0.84° \pm 0.27°$).

Table 1. Mean (SD) TDPM results reported in degrees.

Varus	0.84(0.36)	Extension	1.15(0.49)
Valgus	0.84(0.17)	Flexion	0.97(0.18)

During the dynamic tests, subjects had an overall accuracy rate of 83 ±6.4% in the frontal plane and 81 ± 3.8% in the sagittal plane. In both planes, a clear threshold for detecting relative differences in the amplitude of rapid perturbations was noted. In the frontal plane, all subjects were able to accurately detect when the second perturbation was at least 2° larger or 3° smaller than the previous one (Figure 2). In comparison, the threshold for detecting differences in knee extension was larger, ranging from -4° and 4°.
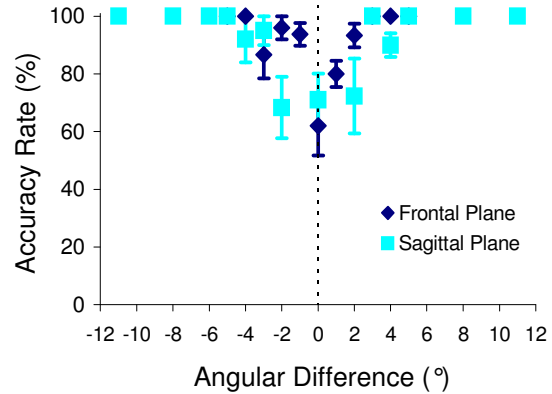
Figure 2. Accuracy rate across all subjects for detecting differences in rapid ramp and hold perturbations. Error bars are SE.

DISCUSSION AND SUMMARY

In this study we have presented preliminary psychophysical data on joint proprioception in constrained and unconstrained degrees of freedom at the knee. While further testing on a larger sample size is necessary, our results indicate that the neuromuscular system is more sensitive to movements in the frontal plane than the sagittal plane, for both passive and dynamic tests. This heightened proprioceptive acuity may enable more precise neuromuscular control in constrained DOFs to maintain stability and prevent joint injury.

REFERENCES

Dietz V et al. (1987). *J Physiol.* 386:149-63.
Lephart SM et al. (2002). *Arthroscopy.* 18:770-8.
Pai YC et al. (1997). *Arthritis Rheum.* 40:2260-5.
Weidow JR et al. (2006). *J Orthop Res.* 24:1890-9.

ACKNOWLEDGEMENTS

DETERMINING THE BIOMECHANICAL PROPERTIES OF NULLIPAROUS AND PAROUS VAGINAL TISSUE

Andrew Feola[1], Keisha Jones[2],
Pam Moalli[2], Steven Abramowitch[1,2]

[1]Musculoskeletal Research Center, Department of Bioengineering, ajf12@pitt.edu
[2] Magee Womens Research Institute, Department of Obstetrics and Gynecology and Reproductive Sciences at Magee Womens Hospital, University of Pittsburgh

INTRODUCTION

Roughly three million women in the United States give birth vaginally each year (National Vital Statistics, 2001). Clinically, the vagina undergoes pronounced adaptations up to the time of delivery, presumably to afford passage of the fetus (Lowder et al, 2007). Nevertheless, vaginal injury at the time of delivery occurs quite frequently and is considered one of the greatest risk factors for developing a pelvic floor disorder (i.e. urinary dysfunction and pelvic organ prolapse) later in life (Delancey et al. 2003). Thus, questions remain regarding the impact of vaginal delivery on the vagina and its supportive tissues and the degree to which these tissues are able to recover following an insult.

The nonhuman primate (NHP) is arguably the best animal model to study the impact of vaginal delivery because, like the human, it has a much larger fetal size relative to the vaginal diameter and commonly does develop pelvic floor disorders. Thus, the objective of this study was to determine the impact of vaginal delivery by comparing the uniaxial mechanical properties of the vaginal wall in the longitudinal direction between nulliparous and parous nonhuman Rhesus macauqes. We hypothesize that the tissues of vaginally parous animals will display evidence of vaginal injury which will be characterized by inferior mechanical properties (tangent modulus, tensile strength) compared to the nulliparous animals.

METHODS

Experimental: The vaginas of three nulliparous and six parous primates, at least one year from the most recent delivery, were harvested for uniaxial tensile testing. At sacrifice, NHP were in the follicular phase of the menstrual cycle. Vaginal tissue was placed in saline soaked gauze in a plastic bag and stored at $-20^{o}C$ (Abramowitch et al., 2004). On the day of testing, the tissue was thawed and a longitudinal section of tissue was isolated avoiding areas near the urethra. Each sample was then gripped using custom designed clamps and further dissected to a dog-bone shape with an aspect ratio of 5. Subsequently, cross-sectional area and geometry was measured using a laser micrometer system (Abramowitch et al., 2004). Throughout this protocol the sample was kept moist with 0.9% saline.

Contrast markers were placed on the tissue near the mid-line of the sample at a distance of 1 cm apart for strain measurements using a camera system (Keyence CV-2600) and motion analysis software (Spicatek, Inc. Maui, HI). Biomechanical testing of the tissue sample was conducted in a $37^{o}C$ saline bath fixed to the base of an Instron[TM] testing machine (Instron 5565) (Abramowitch et al., 2004). Each specimen was allowed to equilibrate in the bath for 30 minutes prior to testing. Next, a small 0.5 N preload was applied to the tissue sample and ten cycles of preconditioning were performed to 7% clamp-to-clamp strain. The tissue was then allowed to recover for ten minutes prior to a load to failure test at an elongation rate of 10 mm/min (Abramowitch et al., 2004). The linear region of the resulting stress-strain curve was defined as the tangent

modulus, while the tensile strength and ultimate strain were recorded at failure. The strain energy density was calculated by taking the area underneath the stress-strain curve until failure. An unpaired t-test was utilized to make comparisons between parous and nulliparous samples with significance set at $p < 0.05$.

RESULTS

Typical stress-strain curves are shown in Figure 1 for each group. Both curves demonstrated nonlinear behavior with a distinct toe, linear, and failure region. However, the nulliparous group was more nonlinear beyond 3% strain. This is demonstrated by the higher slope of the stress-strain curve even though differences were not detected for the tangent modulus with this sample size ($p>0.05$). The nulliparous group also displayed a significantly higher tensile strength, which measured almost 3 times that of the parous group (Table 1; $p<0.05$). Correspondingly, it was found that strain energy density was also more than 3 time greater than the parous group (Table 1; $p<0.05$). No differences were detected for ultimate strain ($p>0.05$).

DISCUSSION

This study utilized a uniaxial tensile testing protocol to measure and compare the mechanical properties of nulliparous and parous NHP vaginal tissue in the longitudinal direction. In spite of our relatively small sample size, the results demonstrate a very different mechanical response between the two groups, with nulliparous animals demonstrating a significantly higher tensile strength and strain energy density. These results support our hypothesis, that the vaginal tissue of parous animals would have inferior mechanical properties, which may result from incomplete recovery of maternal adaptations during pregnancy or injury during vaginal delivery. These findings confirm clinical observations that the vagina of parous women is palpably different from nulliparous women.

To confirm whether it is injury or incomplete recovery at this time point, longer studies which include abdominal delivery will have to be performed. Nevertheless, this study suggests that the primate is a suitable animal model to investigate the mechanisms of birth injury and the factors which mediate recovery.
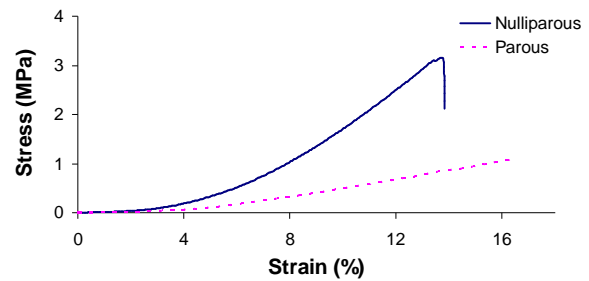

Figure 1. Representative stress-strain graph for nulliparous and parous primates

	Nulliparous	Parous	p-value
Tensile Strength (MPa)	2.77 ± 0.34	0.96 ± 0.26	0.02*
Ultimate Strain (%)	20 ± 6	16 ± 5	0.38
Tangent Modulus(MPa)	27.15 ± 13.9	12.79 ± 6.6	0.09
Strain Energy Density (MPa)	0.21 ± 0.08	0.07 ± 0.02	0.02*

Table 1. Mechanical properties of nulliparous and parous NHP. Data are means (SD)

REFERENCES

Abramowitch S.D. et al. (2004). *Annals of Biomedical Engineering,* 32(3):329-335

Births: Final Data for 1999, in *National Vital Statistics Reports*, National Center for Health Statistics: Atlanta: Centers for Disease Control and Prevention 2001

Delancey J.O.L. et al. (2003). *The American College of Obstetricians and Gynecologists,* 101:46-53

Lowder, J.L. et al. (2007). *Obstetrics and Gynecology,* 109(1):136-143

ACKNOWLEDGMENTS

EFFECTS OF THE SEAT ARMREST AND ASSISTIVE DEVICES ON LUMBAR KINETICS DURING DEPENDENT TRANSFERS ON AN AIRCRAFT

Kristof Kipp and Michael Pavol

Department of Nutrition and Exercise Sciences, Oregon State University, Corvallis, OR, USA,
mike.pavol@oregonstate.edu

INTRODUCTION

A concern related to air travel by people with mobility disabilities is the risk of low-back injuries to the persons transferring a traveler to or from the aircraft seat. Such transfers result in large lumbar loads in the rear transferor (Higginson et al., 2007). One potential means of reducing the risks of low-back injury is to remove spatial obstructions, such as a fixed seat armrest, that may hinder the ability to use safe lifting technique. Another possible means of reducing the risk of low-back injury is through the use of assistive devices. The purpose of this study was to determine the effects of a fixed armrest and of using either a transfer board and slide or a transfer sling on the lumbar forces and moments in the rear transferor during a two-person dependent transfer between a wheelchair and an airplane seat.

METHODS

Twenty-five pairs of healthy men ($n = 35$) and women ($n = 15$) transferred an anthropometric dummy (mass: 78 kg; height: 178 cm) between an aircraft aisle wheelchair and an airplane seat. Mean ± SD age, mass, and height of the rear transferors (22 men, 3 women) were 24 ± 5 yr, 81 ± 11 kg, and 180 ± 7 cm. IRB approval and written informed consent were obtained.

Two-person, dependent transfers were performed in the presence of the spatial constraints imposed by the surrounding seats in a laboratory simulation of an aircraft interior (Higginson et al., 2007). The basic transfer technique used consisted of the two-person "front-and-rear" technique (Pelosi and Gleeson, 1988) with the seat armrest raised. This represented the Control condition. After instruction, warm-up, and practice, participants completed transfers for four conditions: Control, with the Armrest lowered, using a Board+Slide (Accessible Designs, San Antonio, TX; ScanMedical, Medford, MA), and using a Sling (Broadened Horizons, Maple Grove, MN). Participants completed each transfer in two directions: wheelchair-to-seat = outboard; seat-to-wheelchair = inboard. Transfer condition and direction were randomized.

The movements of the rear transferor were recorded at 60 Hz by a motion capture system. Reaction forces acting on each foot and the outboard thigh of the rear transferor were recorded by two floor-mounted force plates and a seatback force plate. From the kinematic and force data, resultant forces and moments acting at a lumbar joint located at the estimated position of L3-L4 were calculated with a three-dimensional inverse dynamics approach.

Dependent variables included peak shear and compressive forces, as well as peak extension, bending, and twisting moments. Absolute values were used in determining peak values for lateral shear forces and bending and twisting moments. Two-way repeated measures ANOVA were used to test the effects of transfer condition and direction on the dependent variables.

Effects were considered significant at $\alpha = 0.05$. Post-hoc analysis employed paired t-tests with Bonferroni adjusted α-levels.

RESULTS

Transfer condition had significant main effects on the peak lumbar kinetics of the rear transferor (Table 1). Peak posterior shear and compressive forces were larger for the Armrest condition than for the Control. In contrast, the Board+Slide and Sling each resulted in smaller peak anterior shear forces, compressive forces, and extension moments than for the Control condition. The Sling also resulted in smaller peak twisting but larger peak bending moments.

Significant effects of transfer direction were observed only for the Armrest and Board+ Slide conditions. Most notably, peak posterior and lateral shear forces and peak bending moments were 46, 24, and 28% greater for inboard than outboard transfers in the Armrest condition, respectively.

DISCUSSION

Transfers over a fixed armrest and the use of assistive devices both affected the lumbar loading of the rear transferor. The greater peak loads for transfers over the armrest were likely due to the extra height that the dummy had to be lifted. The added constraints of lifting over or around the seatback further increased the loading during inboard transfers over the armrest. In contrast, the smaller peak loads in using the transfer board and slide were likely because the dummy did not need to be lifted. The smaller loads for the transfer sling were likely because the sling's handles allowed the transferor to maintain a more erect torso, thereby decreasing the load moment arm.

SUMMARY

The transfer of a traveler with disabilities over a fixed seat armrest on board an aircraft results in greater lumbar loading, and likely greater risk of injury, in the rear transferor. The use of a transfer board and slide or a transfer sling appears to reduce lumbar loading. The results suggest that travelers with disabilities be seated in a seat with a moveable armrest and that one of the tested assistive devices be used during transfers.

REFERENCES

Higginson, B et al. (2007). *American Society of Biomechanics, 31st Annual Meeting,* Stanford, CA.

Pelosi, T and Gleeson, M (1988). *Illustrated transfer techniques for disabled people.* Melbourne, Churchill Livingstone.

ACKNOWLEDGMENTS

Table 1: Mean $\pm$ SD peak lumbar loading of the rear transferor as a function of condition

		Transfer Condition			
		Control	Armrest	Board+Slide	Sling
Anterior Shear Force	(N)	$162.4 \pm 94.5^{\ddagger\S}$	$157.3 \pm 90.4^{\ddagger\S}$	$86.7 \pm 64.1^{*\dagger}$	$74.7 \pm 75.2^{*\dagger}$
Posterior Shear Force	(N)	$59.8 \pm 76.6^{\dagger}$	$130.3 \pm 73.0^{*\ddagger\S}$	$49.2 \pm 63.0^{\dagger}$	$60.7 \pm 70.3^{\dagger}$
Lateral Shear Force	(N)	144.6 ± 39.4	$158.6 \pm 38.9^{\S}$	143.0 ± 42.5	$120.2 \pm 28.0^{\dagger}$
Compressive Force	(N)	$946.7 \pm 112.7^{\dagger\ddagger\S}$	$1012.6 \pm 119.8^{*\ddagger\S}$	$754.1 \pm 94.0^{*\dagger\S}$	$884.2 \pm 97.4^{*\dagger\ddagger}$
Extension Moment	(Nm)	$275.2 \pm 52.1^{\ddagger\S}$	$287.8 \pm 48.7^{\ddagger\S}$	$217.5 \pm 36.4^{*\dagger}$	$225.2 \pm 40.6^{*\dagger}$
Bending Moment	(Nm)	$67.1 \pm 22.8^{\S}$	$79.3 \pm 22.0^{\ddagger}$	$59.0 \pm 12.4^{\dagger\S}$	$86.7 \pm 24.8^{*\ddagger}$
Twisting Moment	(Nm)	$54.8 \pm 18.9^{\S}$	$63.7 \pm 19.1^{\S}$	$58.1 \pm 22.9^{\S}$	$43.6 \pm 14.6^{*\dagger\ddagger}$

* $p < 0.0083$ vs. Control, † $p < 0.0083$ vs. Armrest, ‡ $p < 0.0083$ vs. Board+Slide, § $p < 0.0083$ vs. Sling

AN INSTURMENTED HANDRAIL STAIRWAY VALIDATION

Matija Radovic[1], Nicholas Hanson[1], Palav Deka[1], Shing-Jye Chen[1]

[1]School of Health Physical Education and Recreation (HPER)
Biomechanics Laboratory
University of Nebraska at Omaha, USA

INTRODUCTION

Stairs negotiation is one of the most common activities of daily life. For those who are aged developing with neuromuscular disease, climbing stairs is a great challenging task that leads to falls (Williamson and Fried, 1996). To prevent falling during stair negotiation, assistive handrail has been designed to provide safety maintaining body stability on stairs. However, to directly quantify handrail forces necessary to provide body support during stairs negotiation is very limited. The purpose of this study was to validate an instrumented handrail of a 4-step stairway system by determining any cross talks among steps where force plates were embedded and detecting any vibration created by the current design of the handrail.

METHODS AND PROCEDURES

A 4-step stairway was built with light weighted rigid aluminum frames to rigidly support the stairs. Each step of the stairs was embedded with one AMTI force plate (OR6-7-1000) which was independently supported (see Figure 1a). Two individual right and left handrails are lightweight tubular metal rails. Each handrail has a continuous tubular loop and is directly secured to one end of a rectangular long support beam (L (1.2m) x W (0.2m) x H (0.3m); mass: 44 kg). The base of the support beam was securely anchored to another AMTI (handrail) force plate beneath the stairway. Thus, three dimensional (3D) handrail forces were measured. To validate static 3D handrail forces, a 90N torus plate was vertically suspended and redirected its

downward force to the anterior/posterior (AP) and medial/ lateral (M/L) directions via a pulley system. Three testing sites (P1, P2, P3) of each handrail were tested (Figure 1). The 90N object was then compared to the forces measured directly from the handrail force plate.
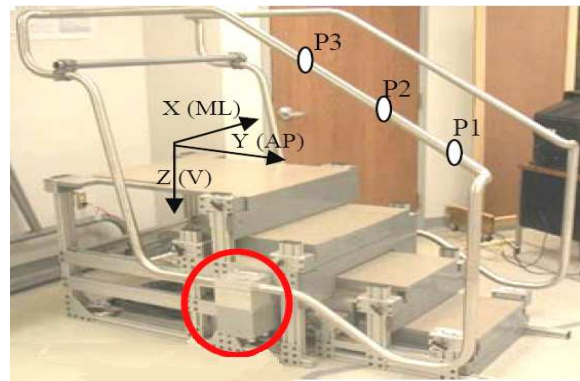
Figure 1: Instrumented 4-step staircase and two handrails which directly measure 3Dforces.

To determining any cross talks among the force plates and vibration from the handrails, the suspended 90N object was swung into ML and AP directions to simulate a dynamic handrail grasping condition when a subject climbing the stairs. The three handrail locations (P1, P2, P3) were tested again during the dynamic swinging. The natural frequency of the swinging object was predetermined to differentiate noise created by the handrail. The calculated frequency was between 0.6-0.7 Hz based on the moment of inertia (I) and mass (m) of the torus plate, and the distance (L) from the center of the plate to the suspended site of the handrail (see Equation 1) .

$$f = \frac{1}{2\pi}\sqrt{\frac{mgL}{I}}$$

The known frequency of the swung plate was compared to that of the 3D handrail forces measured during the dynamic swing test. In addition to the dynamic swing test, one subject was asked to fast ascend and descend the stairs (2 steps/sec) while grasping one side of the handrails. Maximum errors were computed for the 3D handrail forces during the static, and cross talks among the plates were also computed during the dynamic. Power Spectrum Density of the forces measured from the handrail and each step plate was analyzed using a "Hann" window by a custom made Matlab program (MathWorks, Inc). All forces of the stairway and handrail were amplified using the AMTI MSA-6 amplifier (with built-in 1000 Hz low pass filter) and acquired by a data acquisition system (EvaRT 5.0, Motion Analysis Co, Santa Rosa, CA). All forces were sampled at 1200 Hz for 5 seconds.

RESULTS

Results showed that maximal errors during the static was smallest in the vertical direction at three locations (P1: 0.08%, P2: 0.13% and P3: 0.13%) and in the M/L direction (P1: 0.83% and P2: 11.7% and P3: 0.69%), but the greatest errors in the AP direction (P1: 9.68 %, P2: 8.72 % and P3: 9.88 %). The greatest cross talks were found among the 3D handrail forces at the P1 (5.36%) during the dynamic swinging in both AP and ML directions, and the least found at the P2 (0.28%) and P3 (0.34 %). No force crosstalk among the step and handrail force plates were detected during the subject's fast stair walking. The natural frequency of the 3D handrail forces was found to be reliable in all force directions during the dynamic swing test (see Table 1.). The highest frequency of 3D handrail forces during ascending and descending was detected at 50 Hz and 35 Hz, respectively.

	P 1 (Hz)	P 2 (Hz)	P 3 (Hz)
Handrail	Right / Left	Right / Left	Right / Left
A-P	0.6 / 0.7	0.7 / 0.7	0.6 / 0.6
M-L	0.6 / 0.74	0.6 / 0.74	0.6/ 0.6
Vertical	1.3 / 1.3	1.3 / 1.2	1.3 / 1.3

Table 1. Natural frequency responses when a 90N torus plate was dynamically swung at three handrail locations.

DISCUSSION

The crosstalk and maximum errors of the handrail forces were found to be within the reported ranges (Chapdelaine, 2005). The frequencies of the handrail forces were higher during a fast climbing than during a dynamic pendulum motion. This high noise frequency of the touched handrail could be filtered. No crosstalk was found among the force plate signals while the handrail force was measured.

SUMMARY

Both static and dynamic tests of the current instrumented handrail stairway system validate the instrumented handrail stairway system with least cross-talk at midway of the handrail and no cross talks among the steps and the handrails.

REFERENCES

Williamson JD, Fried LP (1996). *J Am Geriatr Soc* 44:1429-1434.
S. Chapdelaine, et al. (2005). *Medical and Biological Engineering and Computing,* 43: 552-556.

ACKNOWLEDGEMENTS

EXPERIMENTAL AND FINITE ELEMENT INVESTIGATIONS OF THE PRESS-FIT FIXATION OF A BONE IMPLANT INTERFACE IN THE DISTAL FEMUR

Travis Burgers[1] and Heidi Ploeg[2]
[1]University of Wisconsin-Madison, Department of Mechanical Engineering, tburgers@wisc.edu
[2] University of Wisconsin-Madison, Department of Mechanical Engineering, Department of Biomedical Engineering

INTRODUCTION

In 2005 the number of total knee arthroplasties (TKAs) in the US was over 500,000, an increase from previous years (USCDC, 2007). Aseptic loosening is the most common cause for TKA failure with cementless femoral loosening occurring at a rate of approximately 1% (King and Scott, 1985). While this is a small percentage of the TKA population it amounts to a large number of patients due to the volume of TKAs annually and is thus worth studying (King and Scott, 1985; Sharkey et al., 2002). This study assessed the press-fit fixation of a femoral knee component by comparing implant strains after *in vitro* implantation and in a finite element (FE) model.

METHODS AND PROCEDURES

A NexGen® (Zimmer, Inc.) femoral knee component was surgically implanted *in vitro* on three cadaveric femurs. The three bones were chosen because of their range of bone density (assessed radiographically). Principal strains were determined from strain gauge rosette measurements at two anterior and two posterior locations on the femoral knee component before and after implantation. The strains were measured for at least 10 minutes following implantation.

Specimen-specific FE models were created from computed tomography (CT) scan data of each of the cadaveric bones. Virtual implantation was performed on each to model the press-fit bone-implant interface. Quadratic tetrahedrons were used to mesh the bone and the implant. The modulus of elasticity was assigned using a modulus-density relationship from Rho et al. (1995). Viscoelasticity was defined using relaxation data (Lakes et al., 1979). The bone was modeled as perfectly elastic-plastic (Taylor et al., 1995) using a 1.3% yield strain (Burgers et al., 2008).

The initial overclosure from the press-fit was resolved and friction was defined on the bone-implant surfaces. Principal strains were calculated on each implant in the same four locations as the strain gauges in the experimental study. The average strain energy density (SED) was calculated for each bone within the implant.

RESULTS

The magnitude of the strains measured immediately after implantation decreased with time (Figure 1). The strains measured in the *in vitro* testing (Figure 1) and calculated in the FE models increased with increasing bone density. SED calculated for low and medium density bones immediately after implantation (shown in Figure 2) also demonstrated increased SED for higher density bone.

DISCUSSION

The increased component strains and bone SED with increasing bone density demonstrates that the degree of press-fit fixation increased for higher density bone.
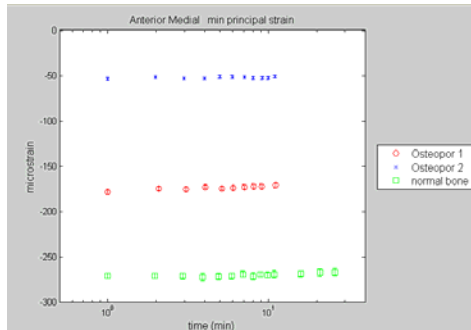
Figure 1. Anterior Medial minimum principal strains measured *in vitro* in the three bones.
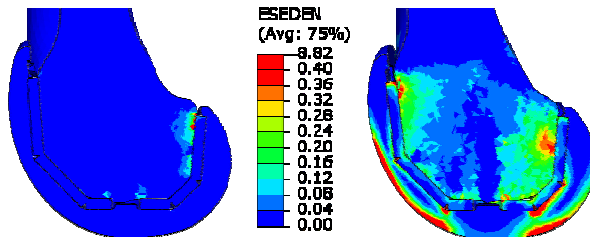

Figure 2. SED distribution in low density bone (left) and medium density bone (right).

The magnitude of strain on the external face of the implant is a measure of the primary fixation strength of the implant. The bone-implant interface pressure causes the anterior shield and posterior condyles to bend out. The larger the magnitude of the minimum principal strain, the larger the compressive bending strain at the strain gauge locations. The decrease in the magnitude of the minimum principal strains at these locations over time demonstrated that the fixation strength decreased over time. While the magnitude of the fixation strength differed in each bone, the trend of decreasing strength over time was approximately the same in each bone.

SED also increased as the bone density increased. Strain energy has been used as a stimulation signal in bone modelling/remodelling laws (Fyhrie and Carter, 1986). As SED increases, bone modelling is stimulated and therefore osseointegration and secondary fixation strength will increase. The SED results predict improved long-term fixation outcomes for press-fit components on higher density bones.

SUMMARY

The *in vitro* testing found that the absolute value of the minimum principal strain decreased over time and was larger for higher density bones. Minimum principal strains in the femoral knee component predicted by FE analysis also increased with higher density bone. These findings suggest bone density improves the primary fixation strength of the press-fit femoral knee component.

FE-predicted SED in the post-operative bone was greater in the higher density bone, suggesting increased bone modeling and improved longterm fixation rates for press-fit femoral knee components on higher density bones.

REFERENCES

Burgers, T. et al. (2008). *J Biomech*, in press.
Fyhrie, DP and Carter DR (1986), *J Orthop Res, 4(3):304-317.*
King, TV and Scott, RD (1985). *CORR*, (194): 285-90.
Lakes, RS et al. (1979). *J Biomech*, 12(9):679-87.
Rho, JY et al. (1995). *Med Eng Phys*, 17(5):347-55.
Sharkey, PF et al. (2002). *CORR*, 404:7-13.
Taylor, M. et al. (1995), *J Mater Sci - Mater Med*, 6(12):808-12.
US Centers for Disease Control and Prevention (2007) www.cdc.gov/nchs/data/ad/ad385.pdf

ACKNOWLEDGEMENTS

Two-Dimensional Sequential Analysis of the Underhand Softball Pitch

John C. Garner, Ph.D., CSCS[1], Wendi H. Weimar, Ph.D.[2], Nels H. Madsen, Ph.D.[2]

[1] University of Mississippi, University, MS, USA
[2]Auburn University, Auburn, AL, USA
E-mail: jcgarner@olemiss.edu

INTRODUCTION

Proximal to distal sequencing is a process most readily associated with extension motions such as kicking and overhand throwing. Unfortunately, motions dominated by flexion movements have gone largely ignored in the literature. Therefore, the purpose of this research was to determine if the upper extremity exhibits the quantitative criteria of proximal to distal sequencing during the underhand windmill pitch via kinematic, kinetic, and electromyographic analysis.

METHODS AND PROCEDURES

5 Collegiate Varsity Softball Pitchers (ht: $1.83 \pm .065$ m, mass: 87.27 ± 5.44 kg) were asked to throw 5 pitches at game speed. The pitch with the highest velocity was used for analysis. The motions of the upper extremity and the muscle activity of the triceps and biceps brachii were captured using an integrated Motion Reality Inc. (Marietta, GA) motion capture and Noraxon Electromyography (EMG) (Scottsdale, AZ) system. Further mathematical analyses allowed for a description of moments at the joints of interest.

RESULTS AND DISCUSSION

The results from velocity and moment calculations revealed that the underarm throwing pattern does indeed follow the proximal to distal sequencing as expected. The velocity (figure 1 and figure 2) followed the expected pattern where the distal segment's (lower arm) peak velocity is

achieved at a point near the proximal segment's (upper arm) minimum velocity with the appropriate corresponding changes in acceleration.
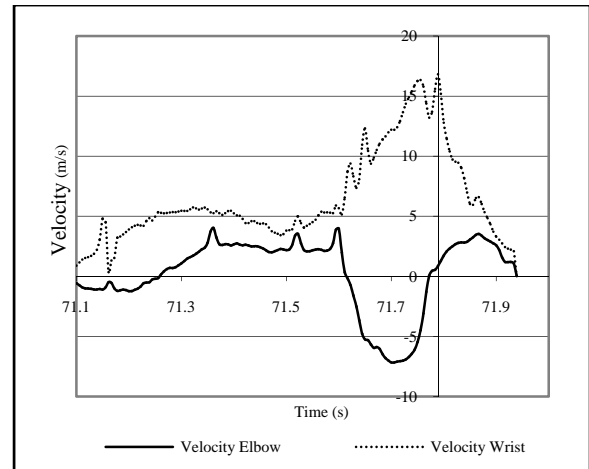
Figure 1. Linear velocity of elbow and wrist
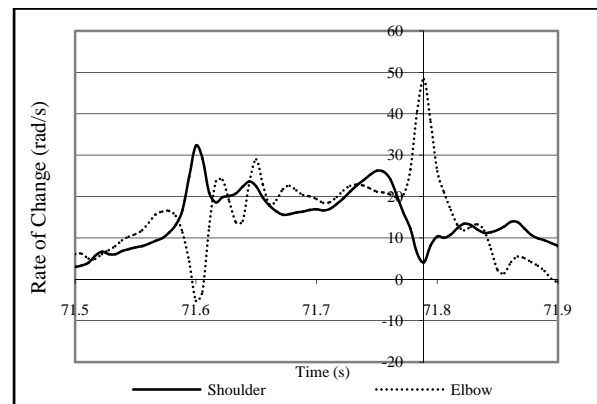
Figure 2. Sagittal plane angular rate of change of elbow and wrist.

The EMG results (figure 3) revealed an attenuated bicep and increased tricep activation at the time of peak distal segment

velocity, suggesting little elbow flexion muscle contribution.
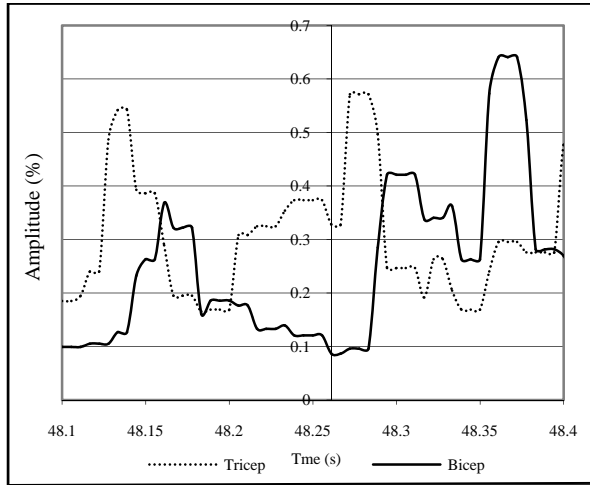
Figure 3. Electromyographic Analysis of Biceps and Triceps

The reversal of accelerations and velocities seen in the results of this study confirmed the existence of a proximal to distal sequential motion in the windmill pitch. It also provides evidence that this summation of speed at the elbow occurs through a reversal of accelerations caused by an inertial acceleration of the lower arm with a negative acceleration of the upper arm rather than an activation of the elbow flexion musculature. Furthermore, the moment graphs indicating the direction of the moment at the shoulder, in conjunction with the moment at the elbow further allowed the researcher to classify the action of the underhand pitch as classic proximal to distal sequencing. Figure 4 is a graphical representation of the moment about the shoulder during the underhand pitch. Figure 5 is a graphical representation of the moment about the elbow during the underhand pitch.

The instant of release is marked by the location of the y-axis on the graph. The negative moment at the shoulder with the small negative moment at the elbow, during the time of separation of velocity lines between the upper arm and lower arm,

suggest that there is a negative acceleration of the proximal segment with a corresponding positive acceleration of the distal segment, conserving angular momentum. Furthermore, the negative moment seen at the elbow may be indicative of the reactive moments produced by the hard end point of the bone on bone contact at the joint during the transfer of momentum from the proximal to distal segments.
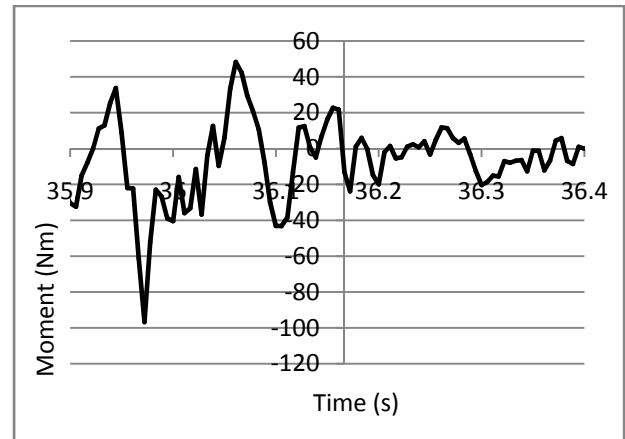
Figure 4. Sagittal plane moment about the shoulder
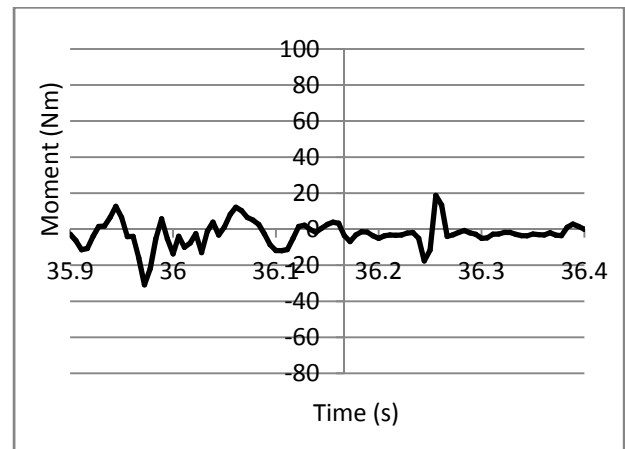
Figure 5. Moment about the elbow

These findings in conjunction with velocities and accelerations that rival those seen in overhand pitching, are a vital step in understanding the injury mechanisms and performance enhancements that may be associated with windmill pitching.

EFFECT OF NEUTRAL TRIAL ON DYNAMIC FOOT KINEMATICS

Rebecca Shultz[1], B.Eng and Thomas R. Jenkyn[2], PhD

[1]PhD Candidate, Department of Kinesiology, University of Western Ontario, London, ON, Canada, rshultz2@uwo.ca
[2]Associate Professor, Departments of Mechanical and Materials Engineering, University of Western Ontario, London, ON, Canada

INTRODUCTION

A static trial is commonly used to establish the zero point for joint coordinate systems. But should a separate static trial be used for each footwear or orthotic condition? Nester et al. (2007) suggest that error may arise by assuming a constant foot alignment is valid throughout conditions. This study examines the influence of the static trial conditions on reported foot kinematics.

METHODS AND PROCEDURES

The study used an 8-camera motion capture system (Eagle Camera, EvaRT system, Motion Analysis Corporation, Santa Rosa, CA). Digitization of bony landmarks were collected with the subject in quiet standing (Jenkyn et al., 2007). A quiet standing static trial was collected while subjects stood in the center of the capture volume at a standard width. Each subject stood barefoot, in Nike Frees (CO), a forefoot plate condition (FF), and a full-length plate condition (FL).

The foot was functionally divided into five segments (hallux, lateral and medial forefoot, midfoot and hindfoot) with a rigid marker triad attached to each segment at the skin (Jenkyn et al., 2007). Three average inter-segment static positions were reported: forefoot and hindfoot motion with respect to the midfoot segment in the frontal plane, and the height-to-length ratio of the medial longitudinal arch (MLA). The barefoot position was subtracted from each condition.

RESULTS

Figures 1 through 3 show the neutral position for the 10 subjects measured with static trials for each specific condition. Most subjects show clinically significant differences between the conditions ($>5°$) (Nester et al.,2007).
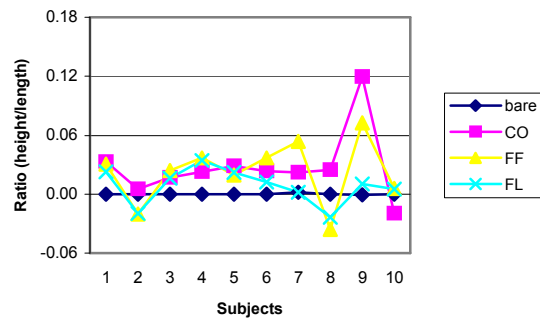

Figure 1. Neutral values of the medial longitudinal arch height-to-length ratio for 4 conditions over the 10 subjects.
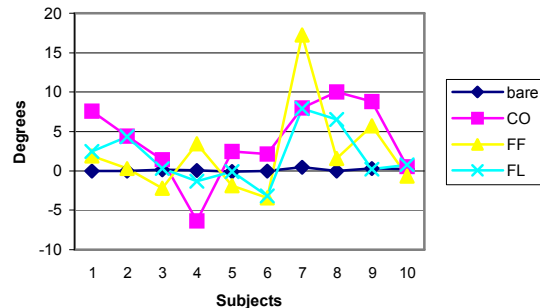

Figure 2. Neutral positions of the forefoot with respect to midfoot in the frontal plane for 4 conditions over the 10 subjects.
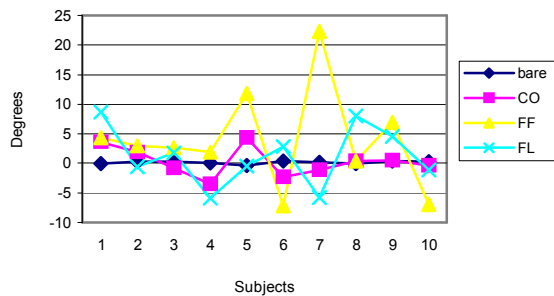
Figure 3. Neutral positions of the hindfoot with respect to midfoot in the frontal plane for 4 conditions over the 10 subjects.

DISCUSSION

These results demonstrate a clinically significant difference between neutral positions in all three kinematic measurements reported. Therefore care should be taken in setting up a research protocol that compares footwear conditions. The condition-dependent differences in neutral position can be important methodologically whether one is interested in absolute joint angles or relative changes.

If the objective is to examine absolute joint motions across conditions then a single static trial (i.e. quiet barefoot standing) should be used to account for the static change in neutral due to footwear or orthotic change. If the objective is to compare the relative motion (i.e. ranges of motion about neutral) then a condition-specific static trial should be used. This would ensure that differences in the static trials do not affect the pattern of the motion or the range of motion reported for each condition.

Additionally, the range of motion of a joint may remain constant with a change of footwear condition and yet show a clinically significant shift in its neutral position. Accurately reporting the absolute joint position would be necessary to indicate whether the joint was moving toward the edge

of its neutral zone during the dynamic tasks, and therefore at increased risk of soft tissue injury. This would be missed if a condition-specific static trial were used.

SUMMARY

Researchers need to be aware of the influences of the static trials on the dynamic trials outcome. The collection method of the neutral trial needs to be considered in the planning of research studies and clearly stated in the study's methodology.

REFERENCES

Nester et al. *J Biomech*, 40:3412:3423 (2007).

Jenkyn, TR and Nicol, AC *J Biomech*, 40(14): 3271-8 (2007).

ACKNOWLEDGEMENTS

VALIDATION OF WINDOWS FOR EXAMINING KINEMATICS OF THE FOOT WITH RESPECT TO THE SHOE USING A MULTI-SEGMETNED FOOT MODEL

Rebecca Shultz, B.Eng, Trevor Birmingham, PhD and Thomas R. Jenkyn, PhD

Wolf Orthopaedic Biomechanics Laboratory, Fowler Kennedy Sport Medicine Clinic, The University of Western Ontario, London, ON, Canada, rshultz2@uwo.ca

INTRODUCTION

Shoes designed for specific foot types are speculated to decrease running injuries by encouraging different foot kinematics. One method to test this hypothesis is to track reflective markers affixed to the foot via windows cut in the shoe. The window size should be small enough to maintain the shoe's structural integrity but large enough to allow easy visualization the markers.

Only one study has a detailed description of the method used to validate window sizes in the hindfoot [1]. The objective of this study was to validate window sizes for five different locations in the shoe: calcaneus, navicular, first metatarsal, fifth metatarsal and hallux using an optical tracking system.

METHODS AND PROCEDURES

One subject was tested under 3 different shoe conditions (motion control, stability and cushioning) with standard gait analysis using an 8-cameras system motion capture system (Eagle camera, EvaRT system, Motion Analysis Corporation, Santa Rosa, CA) synchronized with a floor-mounted force plate (AMTI, Watertown, MA).

For the first 10 trials, the shoe was intact with a heel and toe markers affixed to the shoe. For the next four conditions, windows of increasing size were cut into the shoe above the calcaneus, navicular, first metatarsal, fifth metatarsal and hallux bone.

Triad marker clusters were affixed to the skin of the foot via the windows.

A neutral trial and digitization of bony landmarks were collected in quiet standing for each condition (Jenkyn et al, 2007). The subject then walked at a self-selected pace over an 8m runway and struck the force plate with her right foot.

The deformation of the shoe was assessed using the toe and heel markers on the shoe, and lateral malleolus marker. The foot was tracked as five individual segments (Jenkyn et al, 2007). The forefoot and hindfoot with respect to the midfoot in the frontal plane and the height-to-length ratio of the medial longitudinal arch were measured and compared for each window size (Jenkyn et al, 2007).

Shoe deformation was assessed by comparing mean differences between each window sizes and the intact shoe at the instant of heel raise. Foot kinematic differences were compared as mean differences between the first hole size and the following three hole sizes at heel raise. Sensitivity of the system was considered to be less than 3°. Any mean differences below 3° were considered insignificant.

RESULTS

Both the shoe and the foot calculations demonstrated that a window size of less than 2.5 cm diameter was appropriate for all three shoes. Window sizes above this deviated

from the original motion of the foot. Shoe motion generally remained constant. The forefoot graph for the foot motion (Figure 1) and the heel-ankle-toe angle graph (Figure 2) for the shoe deformation are shown here as examples.
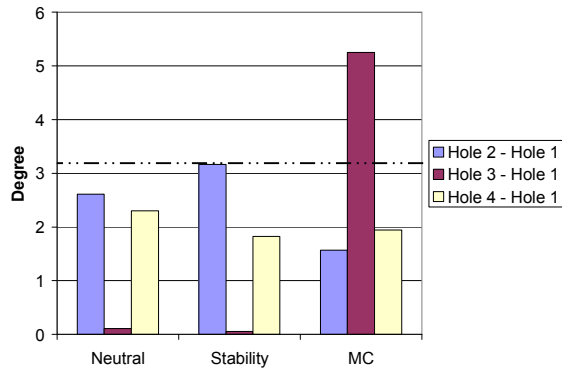

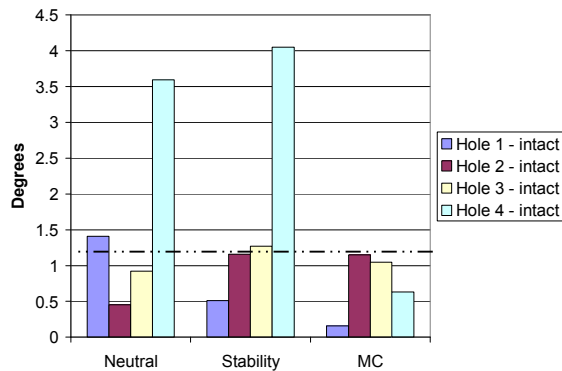**Figure 1.** All mean differences for the second hole (2.5 cm) are insignificant.

Figure 2. The heel-ankle-toe angle mean difference of the second hole (2.5 cm) and the intact shoe at approximately 1 degree for each shoe type.

DISCUSSION

Results show that the 2.5 cm holes were a valid window sizes in the three shoes. The first marker size was not chosen since larger windows increased camera visibility of the markers on the foot and the decreased the possibility of marker-shoe contact.

Comparing the heel validated hole size to that found in Stacoff et al. (1991) (1.7 x 2.1 cm), the window size in this study is slightly larger. There is a difference in methodology; however it is assumed that the difference in heel window size is most likely due to the varying functional properties of the shoes. Walking pace may also have influenced the window size since it has been shown that pace can influence joint range of motion. Large foot motion with respect to the shoe would require larger windows to avoid shoe-marker contact.

The study was limited by the fact that only one subject was tested, using one shoe per condition. Future investigation of different shoes during different movements should be conducted since window size is speculated to depend on shoe type, shoe brand and activity.

SUMMARY

A validation method was developed and was successfully used to validate window sizes for three different shoes in five different locations within the shoe.

REFERENCES

Stacoff, et al. (1991). *Med Sci Sports Exerc*. 23(4): 482-90.

Jenkyn, TR and Nicol, AC (2007). *J Biomech*, 40(14): 3271-8.

ACKNOWLEDGEMENTS

CHANGES IN THORACOLUMBAR KINEMATICS AND CENTRE OF PRESSURES WHILE PERFORMING A LIFTING AND LOWERING TASK IN A MARINE ENVIRONMENT

Carolyn A. Duncan[1], Scott N. MacKinnon[2], Wayne J. Albert[3]

[1] Faculty of Engineering and Applied Science, Memorial University of Newfoundland, St. John's, NL, Canada, carolyn.duncan@mun.ca
[2] SafetyNet, Memorial University of Newfoundland, St. John's, NL, Canada
[3] Human Performance Lab, Faculty of Kinesiology, University of New Brunswick, Fredericton, NB, Canada

INTRODUCTION

Research has established that tasks including lifting and maneuvering of loads significantly increases musculoskeletal injury risk, particularly to the lower back (Marras, 1995). These effects may be exacerbated when the body is forced to execute these tasks in motion-rich environments where compromises in postural stability can occur. Understanding how an operator compensates for poor stability control is paramount to understanding the mechanisms for injury. While using simulated motion environments provides an element of experimental control, it does not fully replicate the high wave amplitudes and accelerations that are typical of marine environments. While there are few empirical studies examining the kinetics during manual materials handling (MMH) in marine environments (Faber et al., 2007, Kingma et al. 2003, Torner et al. 1994) none to date have examined issues of the effects of motion-induced postural perturbations on lower back function and stability. The purpose of this study was to examine the effects of wave induced ship motions on trunk kinematics and foot centre of pressures (CoP) while performing a sagittal lifting task.

METHODS

Twelve subjects, (nine male, three female), who were free of any known musculoskeletal diseases or injuries, performed a continuous lifting and lowering task during three sessions performed on separate days. The three testing sessions differed by the magnitude of platform motions (baseline while tied along side the wharf, low and high sea states) . The motion sessions took place on a 76 metre research vessel (CFAV Quest) while at sea approximately 160 kilometres from Canada's Eastern coast. Thoracolumbar kinematics were collected using a Lumbar Motion Monitor and CoP velocities for each foot during the tasks were monitored using the F- Scan mobile, a resistive-based insole foot pressure system. A custom built motion pack capable of measuring changes in all six degrees of freedom was used to monitor the motion of the platform in a location nearby the subject. Statistical analyses were performed to identify significant differences in thoracolumbar and CoP velocities between motion conditions for both successful lifts and lowers.

RESULTS

During high sea state condition, both thoracolumbar flexion/extension velocities during lifting and lowering were

significantly lower than the baseline motion. These were associated with significant increases in peak CoP velocities. There were also cases of significant decreases in thoracolumbar velocities with accompanied significant increases in peak CoP velocities in the anterior-posterior direction were seen between high and low motion conditions.
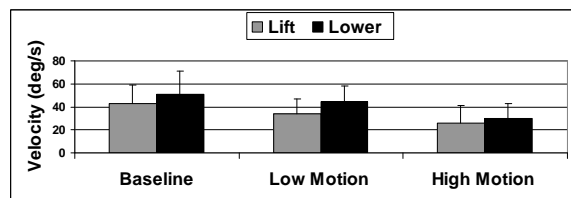

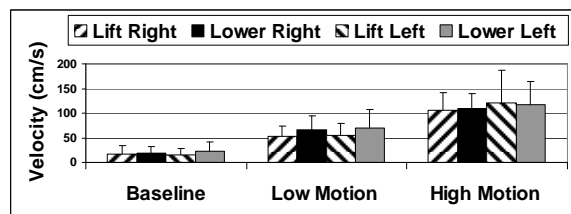**Figure 1: Lifting and lowering sagittal velocities for all motion conditions**

Figure 2: Left and right foot anterior-posterior CoP for all motion conditions

DISCUSSION

Until recently, few attempts have been made to examine how motion-rich environments influence strategies for postural stability when performing MMH tasks. Results of this study are similar to those done in previous simulated motion environment studies (Holmes et al, Duncan et al,Submitted). Significant decreases in sagittal thoracolumbar velocities during the high sea state motion condition suggests that as the severity of the deck motion increases, the speed in which the MMH task is performed must decrease so that postural stability can be maintained. Yet, postural stability, by definition, continues to be challenged as evidenced by the increases in CoP values observed during increased motion states. Although not examined in this

study, this severity of motion may cause a change in lifting technique to a slower technique that protects against loss of balance such as a squat or semi-squat technique opposed to a stoop technique similar to those seen in studies that examined lifting without knowledge of the load being lifted (Heiss et al. 2002).

SUMMARY

When handling manual materials in motion-rich environments it is critical that stability is maintained. The CoP data suggests that in provocative motion states, an operator will choose to slow the speed of the lifting and lowering task. While this strategy may allow for opportunities to correct posture in order to maintain balance, it is certainly adding to the energetic cost to complete the activity. Kinematic and neuromuscular analysis of the changes in the lifting technique while performing MMH in moving environment is required to gain a greater understanding the effects of moving environments on MMH activities.

REFERENCES

Duncan, CA et al. (Submitted). *Occ. Ergo.* Heiss, DG et al. (2002). *Arch. Phys. Med. Rehab.,* 83: 48-59.

Holmes, M et al. (Accepted). *J. Applied. Biomech.*

Faber, GS et al. (2007). *J Biomech*, 40: S29.

Kingma, I et al. (2003). *Int. J. Ind. Ergonomics*, 32: 51-63.

Marras, WS. et al. (1995). *Ergonomics*, 32: 377-410.

Torner, M et al. (1994). *Ergonomics,* 37: 345-362.

FOOT KINEMATICS DURING BAREFOOT RUNNING AND CUTTING

Rebecca Shultz[1], B.Eng and Thomas R. Jenkyn[2], PhD

[1]PhD Candidate, Department of Kinesiology, University of Western Ontario, London, ON, Canada, rshultz2@uwo.ca
[2]Associate Professor, Departments of Mechanical and Materials Engineering, University of Western Ontario, London, ON, Canada

INTRODUCTION

Despite the vast amount of walking research, there is limited knowledge of foot joint kinematics during barefoot running and lateral cutting movements. Kinematic cutting studies tend to examine the parameters of a running shoe or orthortic compared to barefoot walking or running. The objective of this research is to examine the three-dimensional kinematics of the foot complex during barefoot lateral cutting compared to barefoot running.

METHODS AND PROCEDURES

The study used an 8-camera motion capture system (Eagle Camera, EvaRT system, Motion Analysis Corporation, Santa Rosa, CA) synchronized with a floor-mounted force plate (Kistler Instruments, Inc., Amherst, NY). A relaxed neutral trial at a standard foot width and digitization of bony landmarks were collected with the subject in quiet standing (Jenkyn et al, 2007).

Three male subjects (27± 7 years, 69 ± 5 kg) performed two tasks: barefoot running (7 min/mile ± 5%) and barefoot lateral cutting (70% maximum effort). For each task, 7 right foot trials were collected. For the lateral cutting trials, subjects approached the force plate at 60° and left at the same angle. Shear forces of each cutting trial were calculated from the force plate and compared to ensure consistency across trials.

The foot was functionally divided into five segments (hallux, lateral and medial forefoot, midfoot and hindfoot) with a rigid marker triad attached to each segment at the skin (Jenkyn et al, 2007). Three inter-segment motions are reported: forefoot and hindfoot motion with respect to the midfoot segment in the frontal plane, and the height-to-length ratio of the medial longitudinal arch (MLA).

All results were normalized to 100% stance cycle. Average maximum differences between the running and cutting trials were calculated. Clinical significance was assumed to be 5° (Nester et al, 2007). Mean differences between movements for individuals were also calculated.

RESULTS

During the first half of the stance phase the forefoot direction of motion was opposite to that of running (Figure 1). The MLA dropping peak was delayed for the lateral cutting movement compared to running (Figure 2). For the hindfoot, clinically significant differences (MD = 11.4^o) were seen in the first 25% and the last 20% of the stance phase (Figure 3). Within subject analysis also resulted in clinically significant maximum differences for the hindfoot across all subjects (S1=23.5^o, S2=10.2^o, S3=18.1^o).
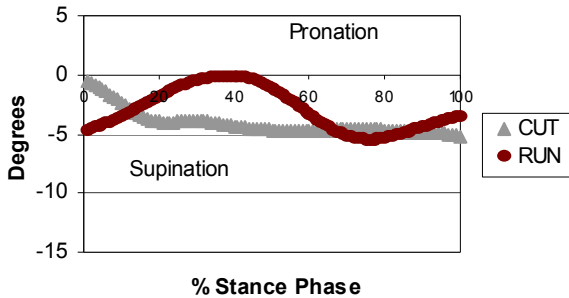
Figure 1. Forefoot motion with respect to midfoot during cutting and running during stance phase of 1-100%.
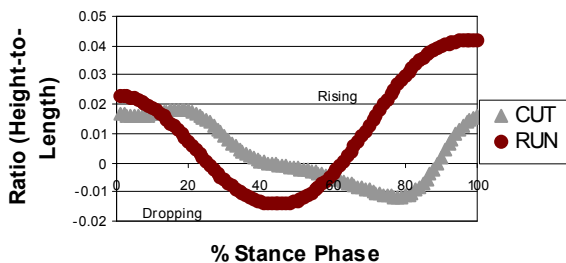

Figure 2. Height-to-length ratio during cutting and running during stance phase of 1-100%.
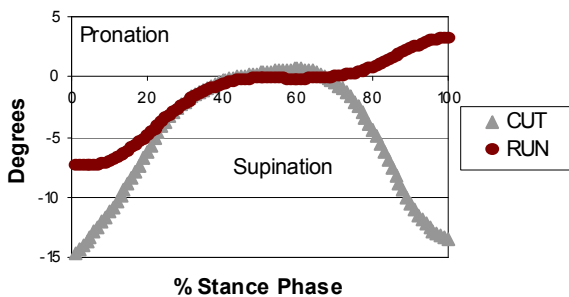

Figure 3. Hindfoot motion during running and cutting during stance phase of 1-100%.

DISCUSSION

Comparing the barefoot lateral cutting to barefoot running, all three joint movements showed different trends during stance phase with clinical significance occurring for the hindfoot. The differences were likely due to the medial lean of the lower leg relative to the foot during cutting compared to running.

It should be noted that absolute measurements were not the objective of this study. There is always error with skin markers, particularly in smaller distal segments of the foot and in dynamic activities, such as running (Reinschmidt et al. 1997). The objective of this study was to compare kinematics of the foot using relative measurements.

This study includes an important addition to the numerous walking studies by exploring barefoot lateral cutting and barefoot running. It provides a basis for more research to be conducted that examines the foot kinematics during running and cutting using a clinical multi-segmented model.

SUMMARY

A pilot study using a non-invasive model was used to explore the joint kinematics of the foot during running and lateral cutting.

REFERENCES

Jenkyn, TR et al. (2007). *J Biomech*, 40(14): 3271-8.

Nester et al. (2007). *J Biomech*, 40: 412:3423.

Reinschmidt et al. (1997). *Clin. Biomech,* 12(1):8-16.

ACKNOWLEDGEMENTS

COMPARISON OF STOPPING TASKS USED TO ASSESS ACL INJURY RISK

Mukta Joshi, Joshua Weinhandl, and Kristian O'Connor

University of Wisconsin-Milwaukee, Milwaukee, WI, USA
E-mail: krisocon@uwm.edu   Web: www.chs.uwm.edu/neuromechanics

INTRODUCTION

A majority of ACL injuries in sports are caused by non-contact injury mechanisms, and many of these occur during a rapid deceleration (Boden et al., 2000). Some have suggested that sagittal loading may play a major role in causing these injuries, although it is unclear whether a direct sagittal plane mechanism is at play, or whether it combines with out of plane motion to place stress on the ACL. Less knee flexion may place the knee at greater risk. While some studies have reported less knee flexion for women, others have reported no differences. Studies that have focused on stopping horizontal motion have used protocols that require athletes to stop on one leg from a single stride (Hass et al., 2003) or on two legs from a multi-step approach (Chappell et al., 2002). However, rapid stopping during play usually occurs in response to a stimulus. When running at high speed, the athlete will likely require multiple steps to come to a complete stop. This raises the question about whether the previous stopping protocols have been able to capture the mechanics that occur during a more stressful stopping task. In addition, there may be another constrained task that can better replicate the lower extremity dynamics of high-speed stopping, such as a box landing from a distance. Therefore, the purpose of this study was to compare the sagittal plane mechanics of several single- and two-legged stopping tasks across genders.

METHODS

Nine males and eleven females participated in this study. All were recreationally active and free from musculoskeletal injury. Each subject was asked to perform running, stopping and cutting maneuvers where they were randomly cued to either run straight, stop rapidly (RUN task), or cut 45°. Subject approached at 4.0-5.0 m/s, and the timing of the stimulus forced subject to apply a large braking impulse on their next stride. The dynamics of the task made it impossible for subject to come to a complete stop on the forceplate. Subjects also performed landing tasks from; a) a box height equal to their maximum two-leg jump height at a distance from the force plate (3× box height) with a single leg (BOX-SL) b) with two legs (BOX-TL), c) a two-leg jump stop after a multiple step approach (JS), and d) a single-leg stride landing (STRIDE) from level ground. Both two-leg stopping tasks required the subject to land with only their dominant leg on the forceplate. Five trials of each task were recorded.

Three-dimensional kinematic data were collected using a seven-camera Motion Analysis Eagle system (200 Hz), and force data were collected with an AMTI force platform (1000 Hz). Sagittal plane touchdown angles, range of motion, peak moments, and net joint work were extracted for each joint. A repeated measures 5×2 ANOVA (task × gender) was performed for each dependent variable ($p < 0.05$).
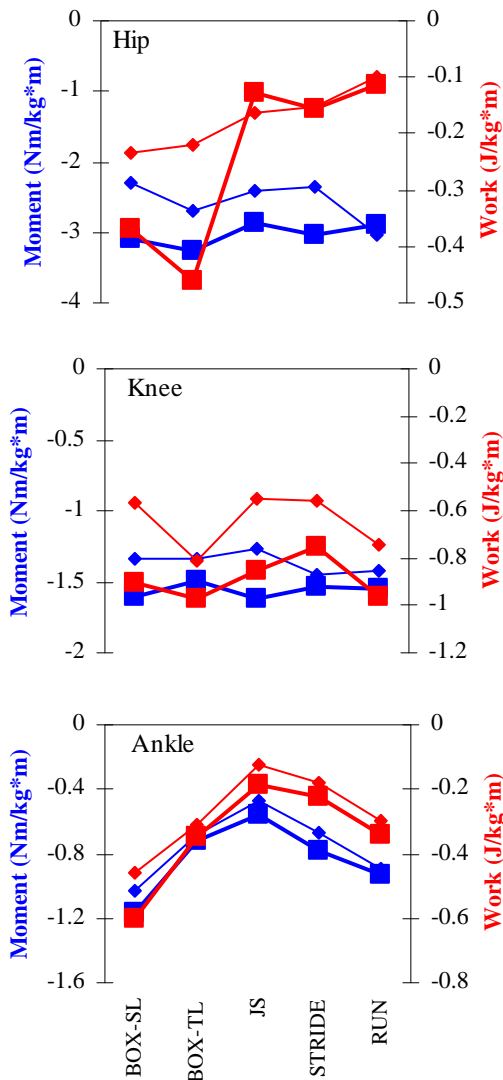
Figure1. Mean peak moment and net joint work for all joints. Extension and plantarflexion moments are negative.

RESULTS AND DISCUSSION

Tasks differences were observed across all joints in touchdown angles and range of motion. Maximum knee flexion was greater in the male subjects as compared to the female subjects across all tasks, and the RUN and BOX-TL tasks exhibited the greatest knee ROM. There was a significant interaction between task and gender at the hip for both the peak moment and net joint work (Table 1). At the knee, there were no significant differences for the peak moment, but the work was greatest for the RUN and BOX-TL tasks. At the ankle, there was a systematic task difference for both the moments and work. The JS task was the smallest, while the BOX-SL task had the greatest plantarflexion moment and energy absorption.

SUMMARY

Overall, the two-leg box landing (BOX-TL) kinematics and kinetics were most similar to those of the RUN. The JS and STRIDE tasks substantially differed from the RUN task, and may not adequately capture the task demands occurring during a game .

REFERENCES

Boden, B.P. et al. (2000). *Orthopedics,* **23**, 573-578.
Chappell, J.D. et al. (2002), *Am. J. Sports Med.,* **30,** 261-267.
Hass, C.J. et al. (2003). *J.Appl. Biomech.,***19***,* 139-152.

ACKNOWLEDGEMENTS

Table 1. *p* values for sagittal plane moments and work. Significant differences are highlighted.

	Hip		Knee		Ankle	
	Moment	**Work**	**Moment**	**Work**	**Moment**	**Work**
Task × Gender	*0.003*	0.006	0.072	0.398	0.857	0.348
Task	0.004	<0.001	0.535	<0.001	<0.001	<0.001
Gender	0.034	0.243	0.101	0.009	0.208	0.109

A COMPARISON BETWEEN THREE DOWNSWINGS FOR THE MOY TO SUPPORT AND GIANTS ON PARALLEL BARS IN MEN'S GYMNASTICS

Pierre Gervais, Pierre Baudin, Toshiyuki Fujihara and Tom Wu

Sports Biomechanics Laboratory, Faculty of Physical Education and Recreation, University of Alberta, Edmonton, AB, Canada, pgervais@ualberta.ca

INTRODUCTION

The cast to support on parallel bars has long been used as a transition skill from under-bar swings to backward swings in support. More recently the Moy has replaced the cast as the primary transition skill taught in Canadian Gymnastics. The Moy is either a required element or a development skill required in competitive boys level 3 (age 10-12) to level 6 (aged 16 up) in both provincial and national streams. Most often the Moy is first taught from a support swing but eventually from a straight body downswing from handstand when the goal is to catch the skill in support (Figure 1). This downswing resembles that of the downswing in back giants on horizontal bar and is therefore used as a precursor to giants on parallel bars (Figure 2).
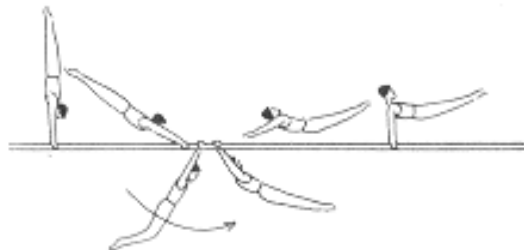

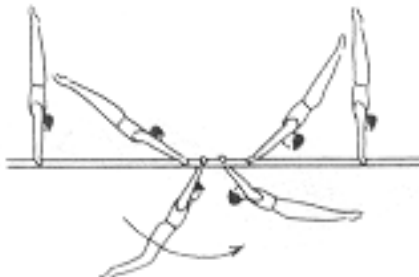**Figure 1**. Moy from handstand to support

Figure 2. Giant swing backwards

As the gymnast grows both in skill and stature he must contend with the height constraint imposed by the parallel bars and their height restriction. This is generally manifested in a bent knee swing through the bottom of the swing. Prassas (2005) and Tsuchiya *et. al.* (2004), using college level gymnasts, both suggested close technique similarity between giants on horizontal bar and parallel bars except for the knee excursion. This is also seen in the Moy using the 'giant downswing'. However a further progression of the Moy is a Tippelt or piked Moy in which the gymnasts initiates the down swing with shoulder hyperflexion and a large back arch followed by rapid hip flexion (Figure 3)
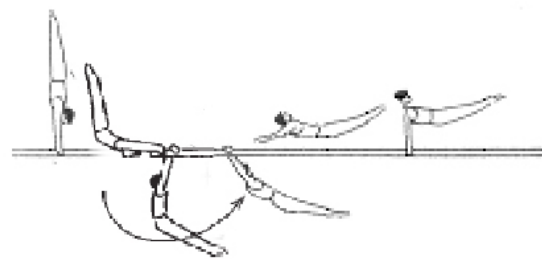

Figure 3. Moy piked (figures taken from FIG Code of Points, 2006)

The purpose of this study was to look at the angular Momentum characteristics of these 3 potential Moy downswings, *no height constraint, back-giant* and *Moy piked* and to compare these individual Moys to their giant technique used on parallel bars.

METHODS AND PROCEDURES

Three National level Junior male gymnasts volunteered and gave informed consent to participate in this study. Subjects were fitted with retro-reflective markers on the joints for the right side of the body closest to the cameras. 3D data was collected using 4 Qualisys ProReflex cameras operating at

120Hz. Since the parallel bar rail obscures the wrist during some of the downswing, the wrist was also manually digitized using the APAS system and a synchronized video record (60Hz) of the performances. Sampling rates were matched using linear interpolation. Angular Momentum was normalized by dividing the subject's mass times the square of their height (Hinricks *et. al*. 1983).

RESULTS

Each subject performed 3 successful Moys and giants. Only their best performances of each skill are described here. The purpose of the downswing is to create the necessary conditions for release and catch either in support or in handstand with sufficient momentum for a smooth transition into the next element. Table 1 lists the Angular Momentum maximums, where they occur in the downswing and the body configuration at those points. The angle of incidence is defined as the angle formed between a positive right horizontal, the wrists and the body's Centre of Mass. Angular Momentum was taken about a horizontal axis through the wrist. Both subject 1 and 3 maintained straight legs during their Moys due to no height constraint and a piked hip respectively. All subjects had similar

shoulder and hip angles in their giants with subject 1 showing straight legs throughout.

DISCUSSION

Tsuchiya *et. al.* (2004) discussed the importance of shoulder flexion during the up swing following shoulder extension during the tap in the bottom of the swing. Subjects 1 & 2 had greater similarity between their positions at maximum Angular Momentum with noted differences in the hips in the giants. The shoulders are more flexed in the Moys in preparation for release where the hips are fully extended in all cases. However, the piked Moy had the least shoulder flexion than any of the observed skills. In summary, this case study provided evidence of good similarity between the giants and the developmental skill (Moy) but not for the more advanced Moy piked.

REFERENCES

Hinricks, R.N. *et. al*. (1983) Biomech VIII-B, 641-647.
Prassas, S. (2005, August). *XXIII ISBS*, Beijing, China, 156.

Tsuchiya, J., *et. al. (2004) Int J Sport & Health Sci*, 2, 211-221.

Table 1 Angular Momentum

Subject	Shoulder-ankle (m)	Skill	Ang Mom (/s)	Ang Incidence [o]	Shoulder [o]	Hip [o]	Knee [o]
1	1.162	Moy	2.73	226.3	161.2	218.9	160.4
		Giant	3.40	284.6	149.6	185.7	162.6
2	1.343	Moy	3.59	264.8	170.9	165.6	80.7
		Giant	2.65	265.2	156.6	181.9	88.1
3	1.318	Moy	2.34	284.0	143.7	126.9	174.1
		Giant	2.92	278.4	153.9	190.8	86.2

INDIPENDENT EFFECTS OF WEIGHT AND MASS ON PLANTAR FLEXOR MUSCLE FUNCTION: A COMPARATIVE MODELING AND SIMULATION STUDY

Craig P. McGowan[1], Rodger Kram[2] and Richard R. Neptune[1]

[1]Department of Mechanical Engineering, University of Texas at Austin, Austin, TX, USA, cpmcgowan@mail.utexas.edu
[2]Department of Integrative Physiology, University of Colorado at Boulder, Boulder, CO, USA

INTRODUCTION
In a recent study, we used independent manipulations of body weight and body mass to examine the relative contributions of the individual ankle plantar flexors, soleus (SOL) and gastrocnemius (GAS), to body support and forward propulsion. Based on relative changes in muscle activity, we concluded that both SOL and GAS contribute to body support, while SOL is the primary contributor to forward propulsion. Our analysis assumed that the function a muscle performs during normal walking (e.g. body support) will be enhanced (depressed) when the demands for that function are increased (decreased) using experimental manipulations (e.g. added weight and/or weight support). While this was deemed a reasonable assumption, this type of analysis provided little insight into changes in mechanical output from the plantar flexor muscles or how these manipulations influenced walking dynamics.

In the present study, we expand on our previous analysis by using a detailed musculoskeletal model and forward dynamical simulations to gain a better understanding of how plantar flexor muscle function is modulated in response to changing mechanical demands. Based on our previous work, we predict that both GAS and SOL will increase (decrease) power delivered to the trunk segment in the vertical direction in response to added weight (weight support). However, only SOL will increase horizontal power delivered to the trunk during added weight and added mass only conditions.

METHODS
Experiential data were collected from ten healthy subjects walking at 1.3 m/s on a dual belt instrumented treadmill. In addition to a control trial, subjects walked with trunk loads (increasing both weight and mass), with weight support (decreasing weight only), and with a combination of equal added trunk weight and weight support (increasing mass only). Each perturbation was preformed at 25% and 50% of the subject's body weight for a total of seven conditions.

Simulations of the experimental conditions were developed using a previously described 2-D bipedal musculoskeletal model [1] using SIMM (MusculoGraphics, Inc.). Briefly, the model consisted of rigid segments representing the trunk and two legs, with 25 Hill-type musculotendon actuators per leg. The trunk was allowed to translate and rotate in the sagittal plane, and the hip, knee, ankle, mid-foot and toe joints were allowed to flex and extend (13 degrees of freedom total). Ground contact was modeled using viscoelastic elements attached to the bottom of each foot. The equations of motion for the model were generated using SD/FAST (PTC).

Muscle excitations were defined using multiple block patterns. A simulated annealing optimization algorithm identified the excitation patterns that best reproduced the group averaged experimental data (ground reaction forces, kinematics) for each condition.

Added loads were modeled in the simulation by increasing the mass and inertial properties of the trunk segment, while weight

support was modeled by applying a constant upward force to the trunk segment center of mass.

RESULTS AND DISCUSSION

The simulation results generally agreed with our predictions. The amount of power delivered to the trunk from both GAS and SOL increased with added load (Fig. 1A) and decreased with weight support (Fig. 1B). Further, during the added mass trials, the horizontal power delivered to the trunk by SOL increased substantially, while the horizontal power from GAS actually decreased slightly (Fig. 2).
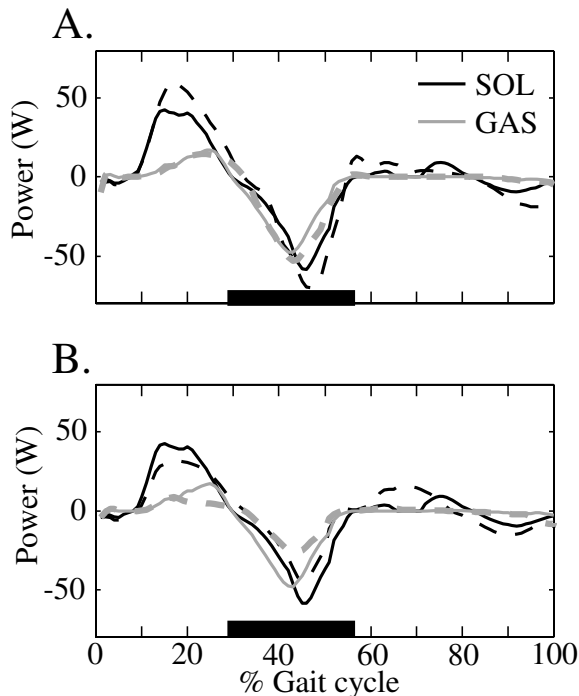
Fig.1 Vertical power delivered to the trunk during the A.) 25% added weight and B.) 25% weight support conditions. Control trials are the solid lines and experimental conditions are the dashed lines. The black bar indicates when the trunk is moving down.

Interestingly, the relative increase in vertical power due to added load was greater in SOL than GAS, whereas the decrease in vertical power delivered to the trunk during weight support was greater in GAS than SOL. This
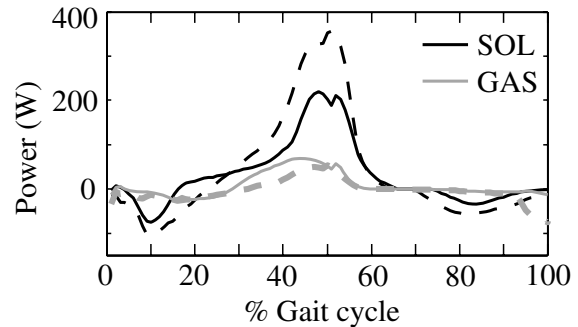
Fig 2. Horizontal power delivered to the trunk by GAS and SOL during control (thin lines) and 25% added mass conditions (dashed lined).

suggests that SOL cannot be modulated to increase vertical or horizontal power independently. Because SOL delivers vertical and horizontal power to the trunk simultaneously in late stance, an increase in SOL power output to accelerate the load forward will also deliver power vertically. Similarly, because SOL must maintain horizontal power output for forward propulsion during weight support trials, it cannot substantially decrease its vertical power. These results are consistent with previous simulation analyses [2].

SUMMARY

Our results support our previous conclusions about individual function of the ankle plantar flexors. Our simulations suggest that the roles that each muscle plays during normal walking are enhanced or depressed during experimental conditions; however, muscles are likely not able to modulate contributions to vertical and horizontal power independently.

REFERENCES

[1] Sasaki et al (2008) *Gait & Posture*, 27: 440-446.
[2] Neptune et al. (2001). *J Biomech*, 34: 1387-1398.

ACKNOWLEDGEMENTS

MOVING ENVIRONMENTS AND THEIR EFFECTS ON THORACOLUMBAR KINEMATICS AND CENTRE OF PRESSURE WHEN PERFORMING STATIONARY TASKS

Carolyn A. Duncan[1], Scott N. MacKinnon[2], Wayne J. Albert[3]

[1] Faculty of Engineering and Applied Science, Memorial University of Newfoundland, St. John's, NL, Canada, carolyn.duncan@mun.ca
[2] SafetyNet, Memorial University of Newfoundland, St. John's, NL, Canada
[3] Human Performance Lab, Faculty of Kinesiology, University of New Brunswick, Fredericton, NB, Canada

INTRODUCTION

Ship motions are often unpredictable and pose a threat to postural stability during the execution of manual materials handling (MMH) tasks. Past research examining the biomechanical responses to work in moving environments has focused primarily on lifting tasks (Torner 1994, Matthews et al., 2007, Faber et al., 2007). Although lifting is one of the most common MMH activities, other tasks including, holding, pushing and pulling activities are also typical (Cirello, 1999). The purpose of this study was to examine the effects of ship motions on thoracolumbar kinematics and centre of pressure (CoP) when performing standing and load holding activities.

METHODS

Twelve (9 male and 3 female) healthy participants performed two tasks during three motion sessions (baseline while tied along side the wharf, low and high sea states) performed on separate days aboard a research vessel located off the coast of Nova Scotia, Canada. The sessions differed in the magnitude of the motion of the platform on which the tasks were performed. Thoracolumbar kinematics were collected using a Lumbar Motion Monitor and foot CoP velocities during the tasks were determined using the F-Scan mobile. Angular and linear ship kinematics were monitored using a custom built motion pack placed near the participants. Statistical analyses identified significant differences in thoracolumbar and CoP velocities between motion conditions.

RESULTS

When performing standing and holding tasks both thoracolumbar kinematics in all directions and centre of pressures in the anterior-posterior direction were significantly greater during these tasks when wave motions were the greatest.
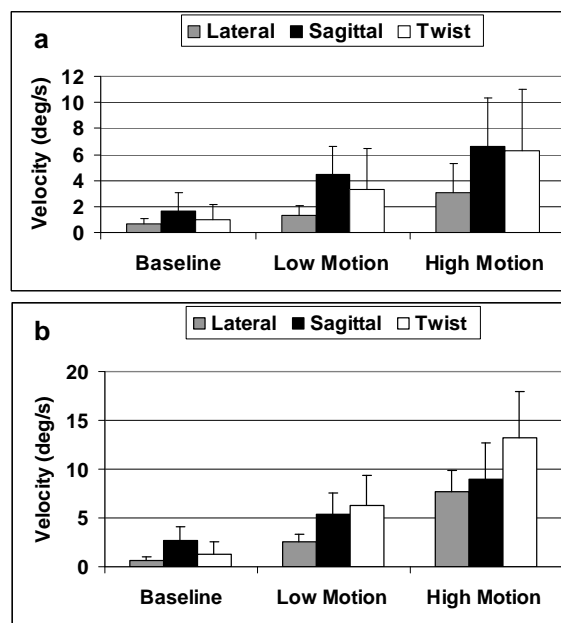

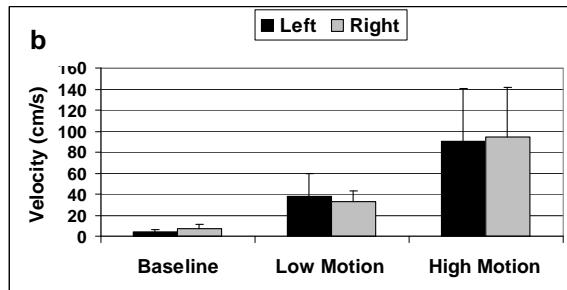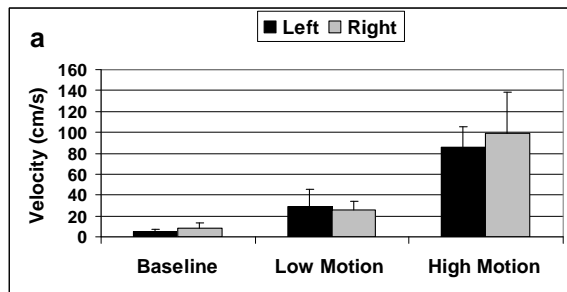**Figure 1: Thoracolumbar velocites while holding a) a 10kg load and b) no load**

Figure 2: Left and right foot CoP velocities when a) standing and b) holding a 10kg load

DISCUSSION

Platforms under motion pose a major threat to those working in offshore industries. Performing MMH tasks and maintaining postural stability in moving environments requires both the complex coordination of skeletal and neuromuscular systems. When working in moving environments the operator must cope with two simultaneous perturbations to their dynamic stability: destabilization as a result of the execution of a MMH task and the unstable environment in which the work is being performed. This theoretically complicates the manner in which postural adaptations are executed. The purpose of this current exploratory field study was to assess human responses to large and unpredictable platform motions. This work follows-on research done employing motion simulation technologies. While the current study does

provide some important insights into the biomechanical adaptations required while working in moving environments, continued work examining the postural adaptations associated with maintaining postural stability in moving environments is necessary.

SUMMARY

Results of this study confirm that type of wave motion has a significant effect on the thoracolumbar velocities and CoP profiles while performing stationary MMH tasks. Large trunk velocities suggest that attempts to maintain balance in moving environments will likely increase mechanical joint loading and concomitant risk of musculoskeletal injury.

REFERENCES

Cirello VM et al. (1999). *Int J Ind Ergon*, 24: 379-388.

Faber GS et al. (2007). *J Biomech*, 40: S29.

Matthews JD et al. (2007). *Int J Ind Ergon*, 37: 43-50.

Torner M et al. (1994). *Ergonomics,* 37: 345-362.

DEVELOPMENT OF SARCOMERE LENGTH NON-UNIFORMITY DURING LENGTHENING CONTRACTIONS OF PERMEABILIZED SINGLE MUSCLE FIBERS FROM RAT

Appaji Panchangam[1], Dennis R. Claflin[2], Mark L. Palmer[1,3], and John A. Faulkner[1,4]

Departments of [1]Biomedical Engineering, [2]Surgery (Plastic Surgery Section), [3]Kinesiology, [4]Molecular & Integrative Physiology, University of Michigan, Ann Arbor, MI 48109

INTRODUCTION

Structural damage is evident by electron microscopy (Macpherson et al. 1997) immediately following stretches of maximally activated skeletal muscle fibers ('lengthening contractions'). The damage is localized within single sarcomeres or small groups of sarcomeres that appear to be distributed randomly among the intact sarcomeres. Steady-state models of muscle contraction predict that, when maximally activated fibers are lengthened, longer sarcomeres stretch more than shorter sarcomeres (Morgan, 1990), increasing the likelihood that the longer sarcomeres will become damaged by over-stretch. We tested the hypotheses that: (1) regions of activated fibers that contain sarcomeres at longer lengths prior to a lengthening contraction undergo greater increases in the lengths of sarcomeres (L_s) during the lengthening contraction, and (2) the non-uniform lengthening behavior takes place during the slow phase of the tension rise that accompanies the stretch.

MATERIALS AND METHODS

To test the hypotheses, we used a laser diffraction technique (Panchangam et al. 2006, 2008) to make rapid measurements ($500\ s^{-1}$) of the L_s in 20 contiguous regions of permeabilized single fiber segments ('fibers') undergoing lengthening contractions with a strain of 27 % and a strain rate of $54\ \%\ s^{-1}$ (Figure 1). Stretches were initiated at mean L_s of $2.54 \pm 0.12\ \mu m$. Sixteen (16) fibers, obtained from the *soleus* muscles of adult male rats, were used in the study. Measurements of L_s were obtained 50 ms

before (pre-stretch), 50 ms after and at the peak of the stretch (Figure 1). Relative pre-stretch L_s was computed as the ratio of pre-stretch L_s to the fiber mean for each region of the fiber. Similarly, the increase in L_s and the relative increase in L_s, defined as the ratio of increase in L_s to the mean L_s increase, were computed at both 50 ms after onset and at the peak of the stretch.
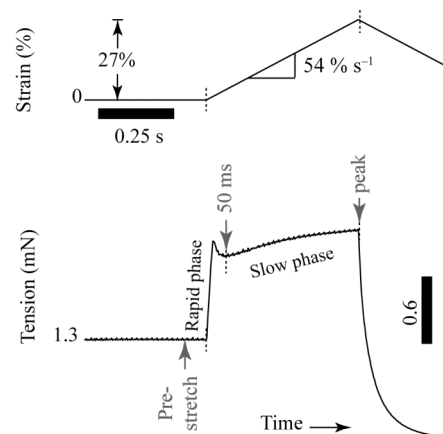

Figure 1. Tension response (bottom) of a fiber to a lengthening contraction with a strain of 27% (top).

RESULTS

The data from a representative fiber are shown in Figure 2*A* and suggest a correlation between the pre-stretch L_s and increase in L_s during the stretch, but the relationship did not develop until after the first 50 ms of the stretch. Data pooled from all 16 fibers are presented in Figure 2*B&C*. The relationship between relative increase in L_s at 50 ms and relative pre-stretch L_s showed no correlation (Figure 2*B*), indicating no systematic growth in L_s non-uniformity during this phase. In

contrast, the relative increase in L_s at the peak of the stretch correlated with relative pre-stretch L_s (Figure 2*C*).
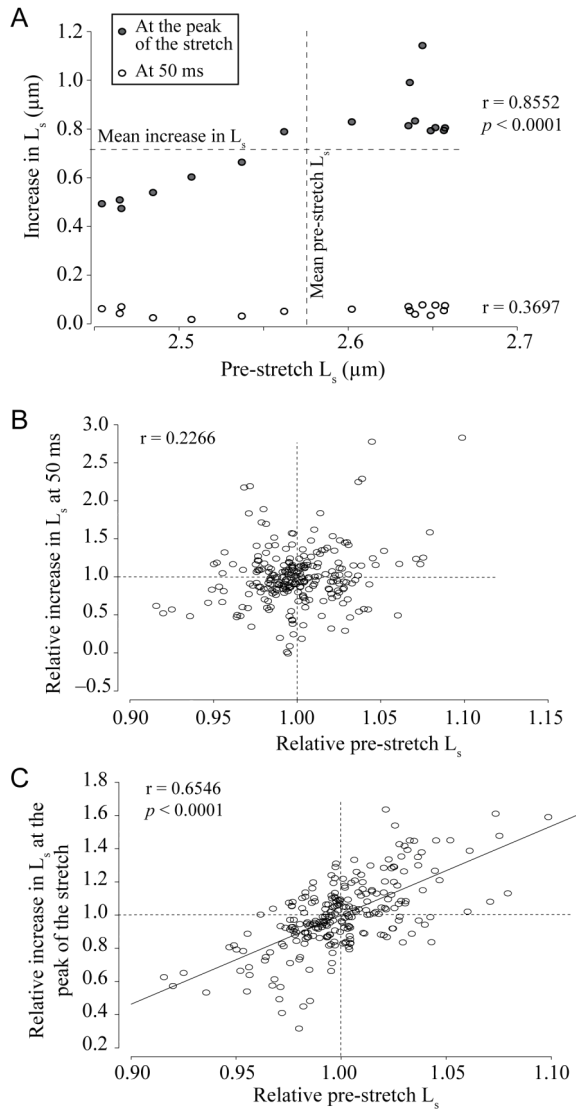

Figure 2. *A*. Data from a representative fiber. *B & C*. Relationship between relative increase in L_s and relative pre-stretch L_s.

DISCUSSION

The results show that non-uniformity in L_s increases during a lengthening contraction as regions of single permeabilized fibers containing longer sarcomeres undergo a greater increase in L_s during the stretch. The correlation between relative pre-stretch L_s and relative increase in L_s developed during the slow phase of tension increase with stretch, not during the rapid phase.

For a sarcomere operating at lengths longer than the optimum, continued increase of tension with stretch cannot be explained by static properties of activated muscle. Morgan (1990) explained the increase by incorporating L_s non-uniformities into his computer models and proposed that, during activated stretches, some weak sarcomeres undergo a rapid transition to long lengths where filament overlap is lost and the sarcomere becomes permanently damaged. The results of the present study support the contention that the slow increase in force during stretch is accompanied by a growth of L_s non-uniformity. However, because laser diffraction measurements reflect the average behavior of a large number of sarcomeres within the illuminated volume, the hypothesis that a small number of individual sarcomeres are undergoing rapid elongation cannot be tested using this technique.

SUMMARY

The findings support the hypothesis that sarcomeres operating at longer lengths stretch more during a lengthening contraction, and that development of non-uniformity in L_s during a lengthening contraction coincides with the slow phase of the force increase.

REFERENCES

Macpherson PC et al. (1997). *J Physiol*, 500:523-533.
Morgan DL (1990). *Biophys J*, 57:209-221.
Panchangam et al. (2006). *Proc SPIE*, 6088(1):08-11.
Panchangam et al. (2008). *Biophys J,(in press)*.

ACKNOWLEDGMENTS

GRAVITAIONAL EFFECTS UPON LOCOMOTION POSTURE

John K. DeWitt[1], Jason R. Bentley[1], W. Brent Edwards[2], Gail P. Perusek[3] and Sergey Samorezov[4]

[1]Wyle's Life Sciences Group, Houston, TX, USA; [2]The Iowa State University, Ames, IA, USA; [3]NASA Glenn Research Center, Cleveland, OH, USA; [4]ZIN Technologies, Cleveland, OH, USA. email: john.k.dewitt@nasa.gov

INTRODUCTION

Researchers use actual microgravity (AM) during parabolic flight and simulated microgravity (SM) obtained with horizontal suspension analogs to better understand the effect of gravity upon gait. In both environments, the gravitational force is replaced by an external load (EL) that returns the subject to the treadmill. However, when compared to normal gravity (N), researchers consistently find reduced ground reaction forces (GRF) and subtle kinematic differences (Schaffner et al., 2005).

On the International Space Station, the EL is applied by elastic bungees attached to a waist and shoulder harness. While bungees can provide EL approaching body weight (BW), their force-length characteristics coupled with vertical oscillations of the body during gait result in a variable load. However, during locomotion in N, the EL is consistently equal to 100% body weight.

Comparisons between AM and N have shown that during running, GRF are decreased in AM (Schaffner et al, 2005). Kinematic evaluations in the past have focussed on joint range of motion rather than joint posture at specific instances of the gait cycle. The reduced GRF in microgravity may be a result of differing hip, knee, and ankle positions during contact. The purpose of this investigation was to compare joint angles of the lower extremities during walking and running in AM, SM, and N. We hypothesized that in AM and SM, joints would be more flexed at heel strike (HS), mid-stance (MS) and toe-off (TO) than in N.

METHODS AND PROCEDURES

Five subjects (2M/3F) completed treadmill walking at 1.34 m·s^{-1} (3 mph) and running at 3.13 m·s^{-1} (7 mph) in SM, N, and AM. SM trials were collected on the enhanced Zero Gravity Locomotion Simulator (eZLS) at NASA Glenn Research Center. N trials were collected on a laboratory treadmill immediately following the SM trials. AM trials were collected during parabolic flight onboard a DC9 aircraft at NASA Johnson Space Center. The EL during AM and SM with EL were approximately 88% BW (SM = 89.0 ± 4.2 % BW; AM = 87.3 ± 6.6 %BW).

Kinematic data were collected with a video motion capture system (SMART Elite, BTS Bioengineering SPA, Milanese, IT) at 60 Hz. The 3-D positions of lower extremity and trunk markers were recorded, rotated into a treadmill reference frame, and projected on to the sagittal plane. All subsequent kinematic calculations were completed in 2-D.

Hip, knee, and ankle joint angles were computed as the angles between markers defining the long axes of adjacent segments. The HS and TO events were found using toe and heel markers. MS was defined as the event 20% between HS and TO. Contact time (CT) was the time between TO and HS, and stride time (ST) was the time between successive HS. Multiple strides were analyzed for each condition. Joint angle means were tested for differences using repeated measure

ANOVAs with location as the main effect. Tukey-Kramer multiple comparison post hoc tests were used to determine pairwise differences ($p < 0.05$).

RESULTS (Figure 1)

During walking, the hip flexion angle at HS was greater in AM than in SM or N. Knee flexion angle at HS was greater in AM than N. At MS, the ankle dorsiflexion angle was greater in N than AM, and at TO, SM ankle dorsiflexion angle was greater than AM.

During running, ST was less in AM than SM. The hip flexion angle at HS and MS was greater in AM than SM and N. The ankle dorsiflexion angle at TO in AM was less than in SM or N.

Walking Joint Angles with Significant Differences

Running Joint Angles with Significant Differences
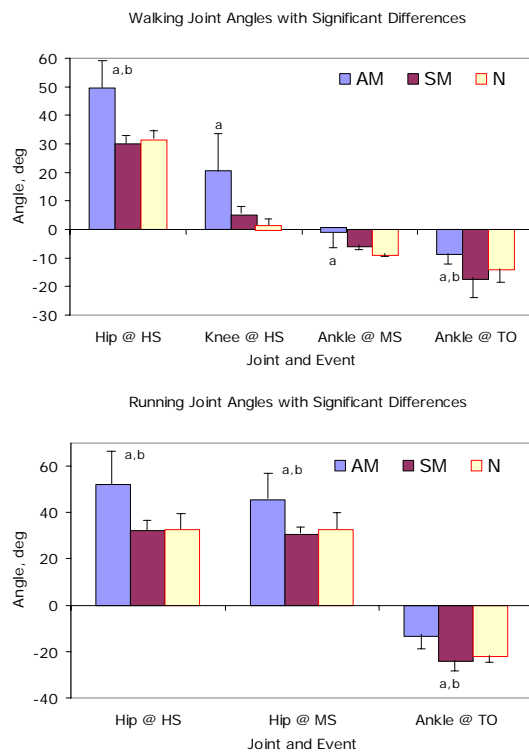
Figure 1. Walking (upper) and running (lower) joint angular displacements. [a]different than N, [b]different than SM

DISCUSSION

While temporal kinematics were similar between conditions during walking, and there were no differences in temporal kinematics between AM and N during running, differences were detected in joint angular displacements during specific instances of the gait cycle. Therefore, reporting only the range of motion of the lower extremity joints may not completely describe the effects of reduced gravity upon locomotion. Surprisingly, there were differences in joint angles between SM and AM, but no differences between SM and N, suggesting that locomotion in SM and N are more similar to one another than locomotion in AM.

McMahon et al. (1987) showed that when running with increased flexion at the knees, GRF were attenuated. The dampened GRF reported during locomotion in AM may result from the increased hip and knee flexion that occurs as a response to the EL being applied to the waist and shoulders via the harness.

SUMMARY

Locomotion in AM results in postural differences when compared to SM and N. The postural differences may explain attenuations in GRF. Increasing the EL to obtain greater GRF in AM may not be the best solution due to kinematic adaptations in response to the increased loads.

REFERENCES

McMahon et al. (1987). *J Appl Physiol,* 62: 2326-2337.
Schaffner, G. et al. (2005). *NASA/TP-2005-213169.*

ACKNOWLEDGEMENTS

CONSTRAINTS TO OVERGROUND WALKING VELOCITY ELICITE DECREASED WITHIN SUBJECTS GAIT VARIABILITY

Adam M. Fullenkamp[1] and James G. Richards[2]

[1]Dissertation Fellow, Department of Health, Nutrition, and Exercise Sciences, University of Delaware, Newark, Delaware, USA, Adam.Fullenkamp.ctr@WPAB.AF.MIL
[2]Associate Dean, Department of Health, Nutrition, and Exercise Sciences, University of Delaware, Newark, Delaware, USA, jimr@udel.edu

INTRODUCTION

In the interest of developing robust gait recognition solutions, it is critical to scrutinize the perturbations that might adversely affect gait matching performance. These perturbations may be as complicated as altered terrain or as simple as normal changes in gait velocity. Obviously, the transient fluctuation of gait velocity is a common attribute that allows us to adapt our locomotion to changing environments. However, when we alter gait velocity in the laboratory setting it is difficult to be sure that kinematic measures of gait are sufficiently consistent to make our findings generalizable. This concept is valid for a wide spectrum of gait-related research areas. There is existing evidence that gait variability is artificially reduced when subjects are asked to walk on treadmills (Dingwell et al., 2001). The assumption is often made that controlling gait velocity during overground walking promotes less variable measures of gait, however, this has not been substantiated. The purpose of our experiment was to investigate changes in overground gait variability as a function of artificially constrained gait velocity.

METHODS AND PROCEDURES

Gait data were collected from 94 healthy adult subjects. All subjects provided informed consent prior to testing. The variables identified for use in this study were obtained from a gait recognition system being developed in-house (Table 1). The gait recognition platform is a hybrid system that incorporates a commercial off-the-shelf 2D video camera and an instrumented walkway. The video camera observes a sagittal plane image of subjects walking as the instrumented walkway gathers temporal/spatial information. During data collection, each subject performed five walking trials at each of three different walking velocities: self-selected (SS) velocity, SS + 20%, and SS – 20%. Gait velocity was estimated using the instrumented walkway and subjects achieved the faster and slower velocities by consciously altering their gait velocity to fall within a +/-5% window of the +20% and -20% targets. In order to facilitate a more rapid adoption of the alternate gait velocities, verbal feedback was provided following each trial to inform subjects of their trial velocity relative to the target velocity.

The data were analyzed by first calculating the within subjects standard deviations for each measure. Subsequently, a One-Way ANOVA with repeated measures was performed to determine the velocity effects on within subjects gait variability. A Tukey HSD post-hoc test was performed for measures the displayed significant group effects.

Table 1. Mean and SD of within subjects variability are reported for each speed condition. The p-values from the ANOVA and the corresponding Tukey HSD post-hoc results are also presented.

	+20%	self-selected	-20%	p-value	Tukey HSD post-hoc
Step Length (cm)	1.2 (0.5)	1.4 (0.7)	1.1 (0.6)	0.022*	-20% vs SS
Toe In/Out Angle (deg)	0.8 (0.3)	0.9 (0.4)	0.9 (0.4)	0.053	-
Step Width (cm)	0.9 (0.4)	0.9 (0.4)	0.9 (0.4)	0.439	-
Trailing Shank Angle (deg)	1.1 (0.6)	1.1 (0.6)	0.8 (0.4)	0.000*	-20% vs +20%, -20% vs SS
Leading Shank Angle (deg)	1.0 (0.5)	1.0 (0.4)	0.8 (0.4)	0.005*	-20% vs +20%, -20% vs SS
Face Angle (deg)	2.9 (4.8)	2.9 (5.4)	1.6 (3.0)	0.004*	-20% vs +20%, -20% vs SS
Trunk Angle (deg)	2.2 (2.0)	2.0 (1.7)	1.3 (0.8)	0.000*	-20% vs +20%, -20% vs SS

* indicates a significant effect at the $\alpha = 0.05$ level
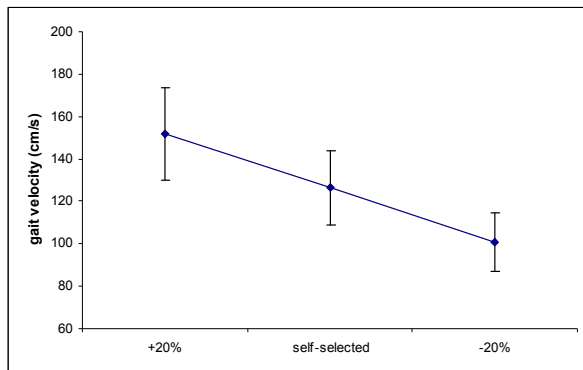
Figure 1. Mean and SD of the observed gait velocities are plotted for each of the three speed conditions.

RESULTS

Figure 1 depicts the mean gait velocities observed for all 94 subjects in each of the three velocity conditions. The variability of gait velocities in the -20% condition was found to be significantly smaller than the other two conditions. This finding corresponds with the variability results reported in Table 1. Specifically, step length showed less variability in the -20% condition compared to the SS condition. Further, all four of the kinematic measures showed significantly less variability in the -20% condition than the other two speed conditions.

DISCUSSION

There is often specific cause for controlling gait velocity in locomotion research. Whether interrogating the limits of a gait recognition system, investigating the nuances of dynamic stability, or merely measuring velocity-dependent gait energetics, it is important to know that the method used to control gait velocity does not confound the analysis of observed measures. A number of studies have shown that treadmill walking may cause decreased kinematic variability compared to overground walking (Dingwell et al., 2001; Nelson et al., 1972; Wank et al., 1998). The results of the current study demonstrate that a similar decrease in variability may be observed in overground walking when gait velocity is constrained. It is possible that subjects reduced their kinematic variability to ensure that their gait velocity consistently fell within the target windows. Although these data represent a small subset of relevant gait features, they highlight the potential limitations of controlling gait velocity in studies of overground walking. Ultimately, there is the danger of finding significant differences between speed conditions due to artificially reduced variability.

REFERENCES

Dingwell et al. (2001). *Journal of Biomechanical Engineering,* 123, 27-32.
Nelson et al. (1972). *Medicine and Science in Sports,* 4(4), 233-240.
Wank et al. (1998). *International Journal of Sports Medicine,* 19(7), 455-461.

ULTRASTRUCTURAL DISORDER IN D₂O-EQUILIBRATED BONE TISSUE STUDIED BY POLARIZED RAMAN SPECTROSCOPY - IMPLICATIONS FOR BIOMECHANICS

Mekhala Raghavan[1], Michael D. Morris[2], Nadder D. Sahar[1], David H. Kohn[1,3]

[1] Department of Biomedical Engineering, University of Michigan, Ann Arbor, MI, USA 48109, mekhala@umich.edu
[2] Department of Chemistry, University of Michigan, Ann Arbor, MI, USA 48109
[3] Department of Biologic and Materials Sciences, School of Dentistry, University of Michigan, Ann Arbor, MI USA 48109
URL: www.umich.edu/~morgroup/index.html

INTRODUCTION

Water is an abundant component of bone, and its roles in determining bone's mechanical properties are less studied than those of the apatite mineral and organic matrix. It is known that the aqueous environment of the bone influences the structure and mechanical properties of the mineral and collagenous matrix (Nalla, 2005). A simple and direct way to disrupt the aqueous environment of bone tissue is to replace water with deuterium oxide (D₂O) as deuterium ions form weaker hydrogen bonds than protons (Steiner, 2002). In the present study, the effect of D₂O-equilibration on orientation and organization of the ultrastructural components of murine cortical bone tissue is investigated using polarized Raman microspectroscopy.

METHODS AND PROCEDURES

Twelve murine femora (strain: F2 generation produced from the C57BL/6J Female x 129S1/SvImJ Male) were obtained. Six femora each were assigned to the control and the D₂O-equilibrated groups randomly. The control specimens were immersed in phosphate buffered solution (PBS) prepared with water and frozen for 3 weeks until use. The D₂O-equilibrated specimens were soaked in PBS prepared with deuterium oxide (99.9% from Sigma Aldrich, USA) and frozen for 3 weeks until use. Before spectral acquisition, the specimens were thawed. Polarized Raman spectra were collected from the mid-diaphysis region of the murine femora using a locally-constructed Raman microprobe (Crane, 2005). In all experiments, the polarization of the incident laser beam was maintained either parallel to or perpendicular to the long axis of the diaphysis, i.e. along the proximal distal (pd) or medial-lateral (ml) direction. The polarization analyzer was adjusted to pass either the component of Raman scatter polarized parallel (pd) to or perpendicular(ml) to the polarization direction of the incident laser.

RESULTS

Collagen amide I bands are strongly polarized perpendicular to the direction of the collagen fibril axis in normal bone tissue. This observation agrees with the orientation effects reported by Kazanci and co-workers (Kazanci 2006, 2007). Equilibration with deuterium oxide results in depolarization caused by disordering of the collagen chains. Because there is specific water binding to the peptide backbone and water hydrogen bond bridges between peptide chains (Brodsky 2005) deuteration changes collagen secondary structure. The weaker hydrogen bonds cause reduced order in the triple helix, resulting in the observed depolarization.

Similarly, because the crystallographic c-axes of the mineral crystallites align along the long axis of the collagen fibres and the crystallites are bound to collagen (Weiner 1986), equilibration with D_2O causes depolarization of the phosphate v_1 band indicating loss of mineral orientation. There are no detectable changes in the position or shape of the mineral phosphate and carbonate bands, strongly suggesting that there is little or no change in mineral crystallite composition or crystallinity. The orientation data for phosphate $_1$ are summarized in Figure 1 as depolarization ratios for the D_2O-equilibrated and control specimens. The depolarization ratio of the D_2O-equilibrated group increases significantly, implying that the mineral crystals are less well-aligned.
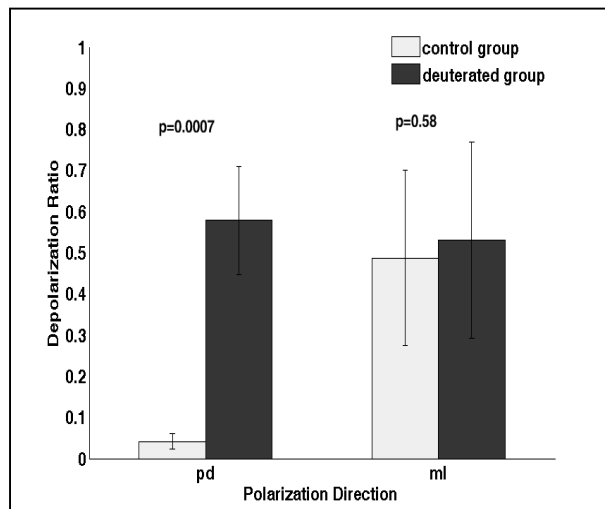
Figure 1. Depolarization ratios of the phosphate v_1 band for control and deuterium-equilibrated groups.

DISCUSSION

Deuterium-equilibration results in depolarization caused by disordering of both mineral and collagen chains. There is no spectroscopically observable change in the composition of the mineral itself, although crystallite surface water is probably displaced by D_2O. More tightly bound water in the crystallites themselves is probably not displaced, because this water can not be removed even at elevated temperature (Wilson 2006). Further studies on the deformation of orientation and structure simultaneously in the bone tissue will help assess the effects of mechanical loading and age on bone tissue.

SUMMARY

This study demonstrates that disruptions to the normal aqueous environment of bone tissue change the collagen structure and orientation by weakening hydrogen bonds and also affect mineral orientation. It is proposed that controlled substitution of deuterium for labile protons can be used to model ultrastructural defects that result in disordered bone matrix.

REFERENCES

Brodsky B et al., (2005) *Adv. Prot. Chem.* Vol. 70. Academic Press, pp 301-339.
Crane NJ et al., (2005) *J. Biomed. Opt.* **10**(3)**:**031119.
Nalla RK, et al. (2005) *Acta Biomat.* **1**(1)**:**31-43.
Kazanci M, et al., (2006) *J. Struct. Biol.* **156**(3)**:**489-496.
Kazanci M, et al., (2007) *Bone* **41**(3)**:**456-461.
Steiner TT (2002) *Ange. Chem. (Int. Ed.)* **41**(1)**:**49-76.
Weiner SS et al., (1986) *FEBS Lett.* **206**(2)**:**262-6.
Wilson EE, et al., (2006) *Biophys. J.* **90:**3722–3731.

ACKNOWLEDGEMENTS

MATCHING PERFORMANCE OF A HYBRID GAIT RECOGNITION SOLUTION

Adam M. Fullenkamp[1] and James G. Richards[2]

[1]Dissertation Fellow, Department of Health, Nutrition, and Exercise Sciences, University of Delaware, Newark, Delaware, USA, Adam.Fullenkamp.ctr@WPAB.AF.MIL
[2]Associate Dean, Department of Health, Nutrition, and Exercise Sciences, University of Delaware, Newark, Delaware, USA, jimr@udel.edu

INTRODUCTION

The state of the art in gait recognition approaches typically involves the use of a commercial off-the-shelf (COTS) video camera (Johnson & Bobick, 2001; Wang et al., 2004). Accordingly, these systems rely on the analysis of human silhouette images that have been extracted from surveillance video footage. The advantage of video-based systems is the ability to observe human motion at a distance. However, there are a number of factors that may limit the utility of video-based systems. To begin with, these systems rely heavily on the post-processing techniques that extract the human silhouette from the background image. Furthermore, model-based recognition systems hinge on the ability to determine high-fidelity models from which gait features may be estimated. At present, it is still unclear whether human gait provides sufficient information to uniquely identify individuals.

The purpose of this project was to develop a hybrid gait recognition system that incorporates both a COTS video camera and an instrumented walkway. The addition of foot contact data offers indices of temporal/spatial parameters and basic foot anthropometrics. Although the inclusion of an instrumented walkway obviates true standoff recognition, a walkway made to look like regular carpeting could still accomplish a more surreptitious observation of gait features.

METHODS AND PROCEDURES

The hybrid gait recognition system developed for this project included a GAITRite[TM] instrumented walkway and a Sony DCR-SR80 Handycam digital video camera collecting at 30 frames per second. The camera was oriented in a position 28ft. from the walkway with a sagittal plane view of the walking direction. Gait and anthropometric measures were calculated and analyzed in custom software. To evaluate the system's recognition performance, data were collected from 94 healthy adult subjects. One trial from each subject was identified as a template trial and another was identified as an unknown trial. This allowed for the evaluation of matching performance across the test sample.

The gait and anthropometric variables measured by the system were used to develop match scores describing the similarity between two given trials. Because it was hypothesized that a match score derived from a combination of variables could provide matching performance greater than any one measure, we compared all combinations of uncorrelated measures. We then computed the area under the Receiver Operating Characteristic (ROC) curves (AUC) using the match scores from each variable combination and combination of template and unknown trials. It should be noted than an AUC of 1.0 indicates perfect recognition and an AUC of 0.5 indicates random selection.

Table 1. Multivariate matching performance based on the template and unknown databases. The AUC of each measure is compared to the largest AUC (0.981).

Combined Variables	AUC	SE	p-value
Toe In/Out Angle, Silhouette Height, Trunk Angle	0.981	0.010	1.000
Toe In/Out Angle, Silhouette Height	0.979	0.010	0.739
Toe In/Out Angle, Foot Length, Leading Shank Angle	0.975	0.011	0.346
Silhouette Height, Step Width, Trunk Angle	0.974	0.011	0.272
Silhouette Height, Step Width	0.970	0.012	0.109
Toe In/Out Angle, Leading Limb Length, Leading Shank Angle	0.967	0.013	0.061
Toe In/Out Angle, Silhouette Height, Trunk Angle, Face Angle	0.967	0.013	0.061
Toe In/Out Angle, Foot Length, Trunk Angle	0.965	0.013	0.063
Toe In/Out Angle, Silhouette Height, Face Angle	0.964	0.014	0.037*
Toe In/Out Angle, Trailing Limb Length, Trunk Angle	0.964	0.013	0.023*

* indicates a significant difference from the largest AUC (0.981) at the $\alpha = 0.05$ level

Finally, the multivariate solution that produced the largest AUC was compared to the top ten solutions (Hanley & McNeil, 1983).

RESULTS

The multivariate solution that produced the largest AUC (0.981) included toe in/out angle, silhouette height, and trunk angle (Table 1).
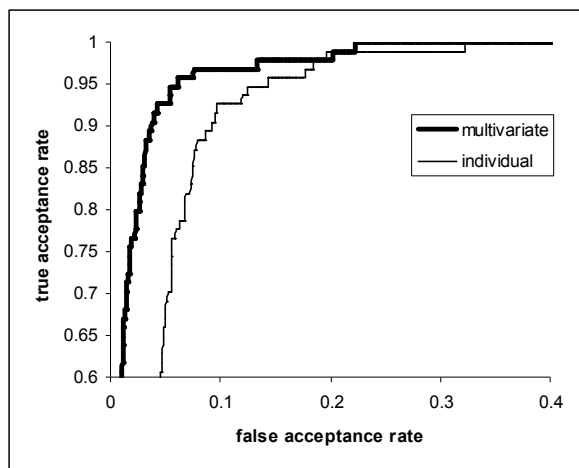
Figure 1. ROC curves for the multivariate and individual matching solutions with the largest AUC's.

Also, the best multivariate solution provided significantly greater matching performance than the best individual solution (AUC = 0.981 vs. AUC = 0.953 from silhouette height alone) (Figure 1).

DISCUSSION

The purpose of this project was to report the preliminary performance of a hybrid gait recognition system. The results of our testing confirmed our original hypothesis that a match score combining multiple variables could outperform the best individual measure. Although an AUC of 0.981 is excellent for purposes of medical diagnostics, it is insufficient for applications that require the identification of one person out of thousands. Specifically, for the best matching solution presented, the False Acceptance Rate (FAR) is 22% when the True Acceptance Rate (TAR) is 100%. This means that we have a 22% percent chance of obtaining a false positive. However, we can reduce the FAR to 5% and still obtain a TAR of 93%. While the current system is still in its infancy, the results of this preliminary testing show promise for the ultimate development of a viable gait recognition system.

REFERENCES

Hanley, J.A. & McNeil, B.J. (1983). *Radiology,* 148, 839-843.

Johnson, A.Y. & Bobick, A.F. (2001). *LNCS,* 2091, 301-311.

Wang et al. (2004). *IEEE TC&SVT,* 14(2), 149-158.

THE INFLUENCE OF TIME INTERVAL BETWEEN LOADINGS ON HEEL PAD PROPERTIES

Daniel J. Gales [1,2] and John H. Challis [1]

[1] Biomechanics Laboratory, Department of Kinesiology, The Pennsylvania State University, University Park, PA, USA
[2] Lock Haven University of Pennsylvania, Lock Haven, PA, USA
E-mail: djg153@psu.edu

INTRODUCTION

The mechanical properties of the human heel pad have been measured in cadaver specimens using pendulum tests (Aerts et al., 1995) and servo-hydraulic testing (Bennett and Ker, 1990). Typical reported mechanical properties include force deformation characteristics, hysteresis, and stiffness properties of the heel pad. Under servo-hydraulic loading the specified loading pattern and interval between loadings are applied to the heel pad.

Each foot has a period during gait when it is not in contact with the ground, presumably during which the heel pad has the potential to recover from the previous loading. Research examining the temporal characteristics of gait have reported that the stride time intervals during walking (Hausdorff et al., 1995) and running (Jordan et al., 2007) demonstrate long term correlations. Therefore, the stride interval times are not normally distributed but have fractal like properties. No study to date has examined the influence of physiologically realistic intervals between loadings on heel pad mechanical properties. Therefore the purpose of this study was to compare the mechanical properties of heel pads in cadaver specimens using a servo-hydraulic compression device with rest times which reflect the rest times experienced in vivo.

METHODS

Eleven injury free runners were recruited for this study, each ran on an instrumented treadmill at their preferred running speed for eight minutes. The treadmill had two force plates under the belt, these plates permitted determination of the vertical ground reaction forces. From the force profiles the intervals between footfalls was computed. The preferred running speed was 3.52 ± 0.97 m.s^{-1}, and the subjects experienced 1663 ± 79 footfalls. Examination of the time interval between footfalls using the Detrended Fluctuation Analysis (Peng et al., 1994) showed the presence of long-term correlations. The time intervals between strides for one representative subject were used as the time intervals between loadings when the cadaver heel pads were tested.

Four fresh-frozen cadaver feet were thawed to room temperature before completing all procedures. All tissues superior to a 45 mm horizontal line marked on the foot above the uncompressed heel were removed using blunt dissection. Heel pads remained fixed to the calcaneus and the foot and toes and overlying skin remained intact throughout the testing procedures.

Dynamic mechanical testing of the heel pads was completed using a servo-hydraulic material test system (MTS model 858). It was operated in force control and

programmed to compress these specimens 808 times to a maximum impact peak based on subject data scaled to body weight. Each heel pad was subjected to three stride time interval conditions: minimum in the experimental time series, the maximum, and actual. For all conditions applied force and pad displacement were collected at 500 Hz, from which the heel pad deformation, hysteresis, and stiffness were computed.

RESULTS AND DISCUSSION

Given the small sample size trends in the data will be reported. It was anticipated that there would be differences between the heel pad properties under the minimum and maximum time conditions, and this was the case. For all the loadings for each heel pad the deformation was greater for the maximum time interval compared with the minimum time interval (maximum: 6.22 mm ± 0.05; minimum: 6.09 mm ± 0.05). The hysteresis was greater for each heel pad under the maximum time interval compared with the minimum time interval (maximum: 70.4% ± 6.38; minimum: 68.0% ± 4.7). These data suggest that the increased time between footfalls provides the heel pad time to recover. This recovery probably corresponds with the return of the fat filled septa, comprising the heel pad, to their original state. For each heel pad the stiffness was greater for the maximum time interval compared with the minimum time interval (maximum: $101.0 ± 7.31$ N.mm^{-1}; minimum: $99.4 ± 7.4$ N.mm^{-1}). Under the fractal loading conditions deformation was similar to the maximum time condition; hysteresis was intermediate between the minimum and maximum time interval conditions; and stiffness was smallest for the fractal condition. These data suggest the fractal time intervals provide a softer impact (less stiffness and more heel pad deformation).

The comparisons to date have been for all the footfalls, and suggest that the time interval between footfalls does influence heel pad behavior during loading. To investigate this further one loading was also examined. The footfall with the smallest time interval preceding it for the fractal condition was examined, and compared with the same footfall under the minimum time interval loading condition. These data would indicate the influence of not just the time interval for the preceding footfall but for all prior footfalls. Deformation was greatest for the fractal loading, hysteresis was greater, and stiffness was less compared with the minimum time interval condition. In a similar fashion the footfall with the largest time interval preceding it for the fractal condition was examined, and compared with the same footfall under the maximum time interval loading condition. Deformation was greatest for the fractal loading, hysteresis was greater, and stiffness was similar when compared with the minimum time interval condition.

These results indicate that physiologically realistic time intervals between loadings do influence the properties of the human heel pad, potentially conferring some advantage in its ability to attenuate the forces associated with loadings.

REFERENCES

Aerts, P et al. (1995). *J Biomech*, 28:1299-1308.
Bennett, MB and Ker, RF (1990). *J Anat*, 171:131-138.
Hausdorff, JM et al. (1995). J Appl Physiol, 78:349-358.
Jordan, K et al. (2007) *Hum Mov Sci*, 26:87-102.
Peng, CK et al. (1994) *Phys Rev E*, 49:1685-1689

HOW IS SARCOMERE LENGTH AFFECTED BY THE PROCEDURES FOR INTRAOPERATIVE MEASUREMENTS USING LASER DIFFRACTION?

Huub Maas[1], Jeremy Eagles[1], Thomas G. Sandercock[1], Wendy Murray[2,3]

[1] Department of Physiology, Northwestern University, Chicago, IL, USA
[2] Departments of Biomedical Engineering and Physical Medicine and Rehabilitation, Northwestern University, Chicago, IL, USA
[3] Research Service, Edward Hines Jr., VA Hospital
h.maas@fbw.vu.nl -- w-murray@northwestern.edu

INTRODUCTION

Measurement of sarcomere lengths in human muscles during reconstructive surgery provide valuable information for the evaluation and optimization of surgical outcome (2). Intraoperative measurement of sarcomere lengths via laser diffraction involves dissecting a small bundle of muscle fibers on the surface of the muscle belly so that a laser myometer can be inserted underneath the fibers (Fig. 1). A 5 mW He-Ne laser beam is projected through a prism, which reflects the beam through the fiber bundle, resulting in a diffraction pattern that characterizes sarcomere spacing (1). If placement of the myometer elevates the fiber bundle relative to the muscle surface, sarcomere lengths in the bundle can be artificially increased. Previous work indicates that the intraoperative technique implemented by experienced users of the laser myometer introduces errors in sarcomere lengths of less than 0.2 µm (1).
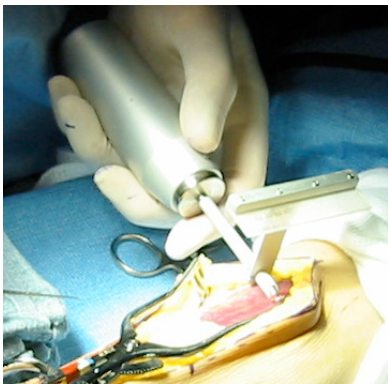
Figure 1. Intraoperative measurement of muscle sarcomere lengths via laser diffraction.

The goal of this study is to quantify how different elevations of the fiber bundle relative to the muscle surface influence sarcomere length in the elevated bundle. Our ultimate aim is to provide guidelines to instruct novice users of the laser myometer and to identify surgical approaches that will minimize the potential for error during intraoperative data collection.

METHODS AND PROCEDURES

In the deeply anesthetized cat, the soleus muscle was dissected free from surrounding tissues while its origin and insertion were left intact. At maximal dorsi-flexion of the ankle (~30°), two fiber bundle segments of 20 mm length were exposed. Each fiber bundle was elevated and either 1 or 2 rubber pieces (1.5 mm thick, 5 mm wide) were inserted underneath them. The muscle (still attached to the skeleton at maximum dorsi-flexion) was fixed in 10% formalin for 48 hours. Connective tissue was mildly digested in 30% nitric acid for 24 hours. The elevated fiber bundles were excised and 4 smaller samples from each bundle were mounted on a microscope slide. The average sarcomere length of each sample was measured using light microscopy (×630). The average sarcomere lengths from two control fiber bundles were also measured from the same muscle, again using 4 samples per bundle. The control bundles were neither dissected nor elevated before fixation.

RESULTS

The average sarcomere length of each of the elevated fiber bundles was significantly ($p < 0.05$) longer than average sarcomere length of the two control bundles (Fig. 2). We observed sarcomere length increases that ranged from ~0.2 µm to ~0.4 µm. The average sarcomere length of the fiber bundle that was elevated by 1.5 mm was 6.9% longer than the average sarcomere length of the two control bundles. The average sarcomere length of the fiber bundle that was elevated by 3.0 mm was 11.3% longer than the control bundle.
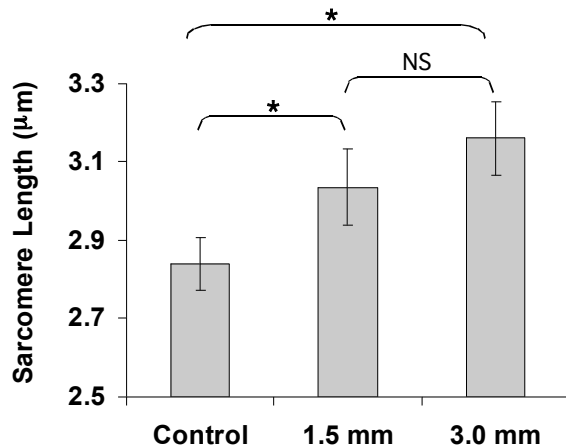
Figure 2. Mean (±SD) sarcomere length for the elevated and control bundle segments. Asterisk denotes a significant difference ($p < 0.05$).

Simple geometric calculations suggest that the length of the dissected fiber bundle may influence the increase in sarcomere length that is imposed by a given elevation of the fiber bundle (Fig. 3). For example, our calculations suggest that dissecting a fiber bundle of 40 mm length (rather than 20 mm length) would substantially reduce the increase in sarcomere length that is associated with 3 mm of fiber bundle elevation. We calculate the length of the entire fiber bundle would increase by only 1.5% (from 40 mm to 40.6 mm) with a 40 mm bundle. This is four times less than our calculation of the length increase (6%, from 20 mm to 21.2 mm)

associated with a 3mm elevation of a 20 mm fiber bundle.
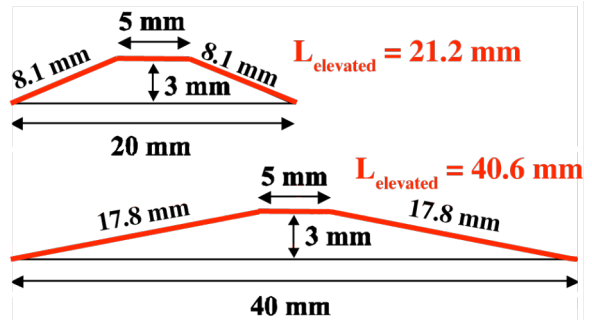
Figure 3. Increasing the fiber bundle dissection length has the potential to minimize the increase in sarcomere length caused by fiber elevation.

DISCUSSION AND SUMMARY

Our work indicates that elevation of fiber bundles by 1.5 mm to 3.0 mm can result in significant increases in sarcomere length. However, the sarcomere length increase associated with fiber bundle elevation could be highly sensitive to the length of the fiber bundle that is dissected. Ongoing work in our laboratory is now aimed at evaluating the potential for minimizing the error imposed by fiber elevation by dissecting longer fiber bundles. This work will ultimately provide information that will help us to instruct novice users of the laser myometer device how to collect the most accurate data possible. In addition, it will help us to evaluate the potential error associated with intraoperative measurements of sarcomere lengths.

REFERENCES
1. Lieber et al. (1994). *J Neurophysiol* **71**: 874-81.
2. Lieber et al. (2005) *J Hand Surg* **30A**: 273-82, 2005.

WALKING STABILITY ANALYSIS OF BRACE AND FES-BASED INTERVENTIONS FOR MULTIPLE SCLEROSIS

Vanessa Q. Everding, Anirban Dutta, and Elizabeth C. Hardin

Department of Biomedical Engineering, Case Western Reserve University and
Cleveland FES Center, Louis Stokes Cleveland VA Medical Center,
Cleveland OH, USA, vqe@case.edu

INTRODUCTION

Walking stability is a key parameter in the diagnosis of gait disorders and the development of medical devices for gait assistance. Traditionally, walking stability measures have been derived from logical assumptions about what causes an ambulating subject to fall. Recently, investigators have studied the feasibility of using nontraditional measures, including Lyapunov exponents (England and Granata 2007, Dingwell and Marin 2006, Rosenstein et al 1993).

Walking stability degrades with motor impairment, a consistent feature of chronic multiple sclerosis (MS). Within 15 years of diagnosis, 50% of persons with MS will need walking assistance. A characteristic problem of their walking gait is foot drop, for which the commonly prescribed interventions are an ankle-foot orthoses (AFO) or a functional electrical stimulation (FES) based device. The aim of this study is to measure walking stability with and without these interventions in persons with MS. We hypothesize that: 1) walking stability will improve with the AFO and FES; and 2) the traditional and nontraditional stability measures will not agree.

METHODS

Two subjects with multiple sclerosis (MS) performed a set of walking trials on a motorized treadmill (ADAL3D-F-COP-Mz , HEF Medical Development, France). Their motion was captured at 60 Hz (Vicon, Oxford, UK). Each subject walked under the following experimental conditions: 1) while wearing an AFO, 2) while using an Odstock Dropped Foot Stimulator (ODFS, Odstock Medical, Salisbury, UK), and 3) without an assistive device.

For a traditional measure of stability, the mean standard deviation (meanSD) of trunk motion was calculated (Dingwell and Marin, 2006). For a nontraditional measure, the largest Lyapunov exponent (LLE) was calculated (Rosenstein et al 1993).
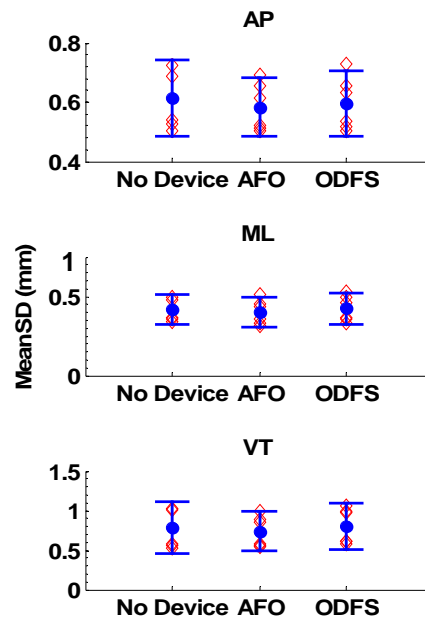

Figure 1. MeanSD of trunk motion during the three walking conditions for each movement direction.

RESULTS

Figure 1 displays the meanSD for the three walking conditions. The three plots are for each movement direction: anterior/posterior (AP), mediolateral (ML), and vertical (VT). The center filled circle is the average meanSD value between subjects, and the horizontal lines above and below indicate ± one standard deviation. The extent and concentration of the data is shown by the open diamonds, which display the meanSD values for all trials for both subjects. The average meanSD values were very similar between the three conditions: **without any device** (AP = 0.6142; ML = 0.4203; VT = 0.7862), **with an AFO** (AP = 0.5838; ML = 0.4022; VT = 0.737), and **with an ODFS** (AP = 0.5947; ML = 0.4249; VT = 0.8017).

Figure 2 displays the LLE for the three walking conditions. The axes and plots are represented in the same manner as in Figure 1. The average value for the LLE was greatest in all three directions when the subjects walked **without any device** (AP =

0.2426; ML = 0.3944; VT = 0.2017). The average values decreased and were very similar **with an AFO** (AP = 0.2086; ML = 0.3503; VT = 0.1865) and **with an ODFS** (AP = 0.2168; ML = 0.3760; VT = 0.1805).

DISCUSSION AND CONCLUSIONS

The meanSD measure showed little sensitivity to the three conditions. This could be explained by the fact that this traditional measure is a measure of variability between strides and not system stability. This is because the computation requires division of the data into strides and compares the characteristics of all strides separately.

The nontraditional measure, LLE, seemed to be more sensitive during the interventions. This measure uses the time series data from the walking trials to represent the whole system. It measures how the trajectories change over time, acquiring information that could potentially describe the function of the controller. Although the number of subjects was small, they were more stable (smaller LLE) when they walked with an assistive device (both AFO and ODFS), so these results suggest that system stability, and possibly neuromuscular control, improve when an assistive device is used.

Future experiments will attempt to further highlight the differences between these assistive devices using stability measures. Additional subjects will be examined and the use of nontraditional stability measures will be expanded.

REFERENCES

Dingwell, JB and Marin, LC (2006). *JBiomech, 40:1723-1730.*
England, SA and Granata, KP (2007). *Gait & Pos, 25:172-178.*
Rosenstein, MT et al (1993). *Phys D, 65:117-134.*

Figure 2. LLE of during the three walking conditions for each movement direction.

LONGITUDINAL STRAIN ESTIMATION IN MUSCLES, TENDONS, AND OTHER INCOMPRESSIBLE GENERALIZED CYLINDERS

Qi Wei [1, 2] and Dinesh K. Pai [1]

[1] Department of Computer Science, University of British Columbia, Vancouver, BC, Canada
[2] Department of Computer Science, Rutgers University, New Brunswick, NJ, USA
E-mail: pai@cs.ubc.ca, URL: www.cs.ubc.ca/~pai

INTRODUCTION

Estimation of the mechanical properties of soft tissues is critical for better understanding their functions and conducting realistic simulation. However, measuring mechanical parameters *in vivo* is challenging. Advanced imaging techniques (Akasawa et al., 2003; Osman et al., 1999) and physical markers (Miller et al., 2006) have been investigated to track the tissue deformation. However, applications of these techniques are limited by their availability.

We propose a simple algorithm for measuring longitudinal strain of generalized cylindrical objects. It is particularly useful when images are inadequate in providing information for the object interior deformation due to image resolution or homogeneity. Usually the boundaries are relatively easy to segment because of the contrast between different tissues. Our goal is to compute the 1D axial strain fields along the major deformation axis, given only the 3D boundaries of the tissue. It can be applied to study generalized cylindrical tissues, including skeletal muscles and tendons. We validate our method by performing experiments with MR images of rubber phantoms and sensitivity analysis. We show that the approach is accurate and practical even in the presence of noise.

METHODS

The key point of our approach is that it is a good approximation to model soft tissues as incompressible. In other words, tissue volume is well preserved in different deformed states. By using this physical property together with the assumption of uniform stress and stain over cross sections, we manage to find segment-to-segment correspondences from which strains are computed.

Given the geometries of the object in two deformation states, we first compute the cumulative volume function along the longitudinal axis. Then the total volume is uniformly partitioned into segments. Under the assumption of uniform stress and strain, each material segment before deformation can be associated with one afterwards, following the sequential order along the longitudinal axis. Instead of tracking point-to-point correspondences, 1D segment-to-segment correspondences are established using incompressibility. The longitudinal strain of each segment is computed as $s_i = (w'_i - w_i) / w_i$, where w_i and w'_i are the weighted average widths of the ith segment in two states. Figure 1 illustrates the method on a 2D example.
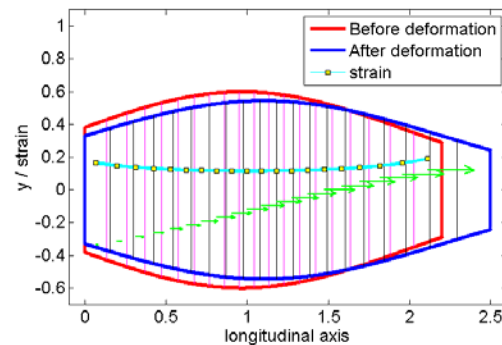

Figure 1. Segment correspondences are set from uniform volume partitions.

RESULTS

In order to validate this approach in real applications, evaluation was first performed on real MR images of a rubber phantom made from silicone rubber (Smooth-On, Easton, PA) embedded with glass beads (BioSpec, Bartlesville, OK). T1 weighted gradient echo 3D MR images (voxel resolution: 0.5mm) were acquired from a Philips Achieva 3.0 Tesla MRI scanner while the phantom was stretched to different elongation states.
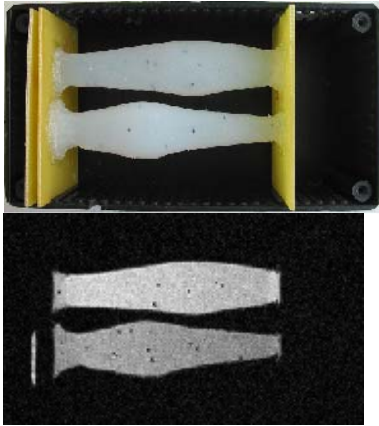

Figure 2. Photo and one representative MR image of the phantom elongated by 125.6%.

Our approach was validated by computing the error between the axial marker displacement predicted from our approach and the actual marker displacement obtained by tracking the glass beads. Figure 3 shows the absolute errors of the markers in three elongation states. Notice that the absolute errors were bounded by the scan resolution 0.5mm. The relative errors were bounded by ±0.05 except for four markers with small displacements.

We also conducted sensitivity analysis by perturbing the input using simulated examples. We first added shearing to the deformation. Linear relationship between the shear angles and marker errors were observed. In other experiments, object boundaries were corrupted with additive noise of different frequency and magnitude. We conclude that our approach is robust even with noise.
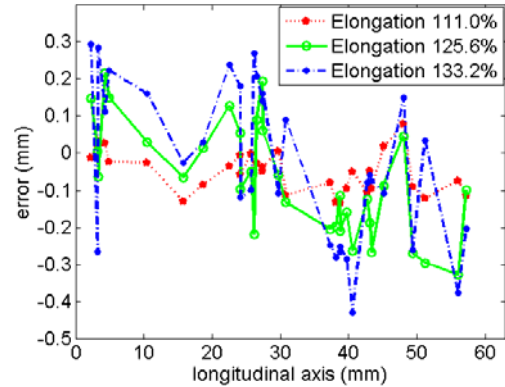

Figure 3. Marker axial displacement errors.

SUMMARY

We present a simple and effective method for estimating longitudinal strains in musculotendons and other generalized cylinders, in cases where local correspondences are hard to find. Validation on real MR images of a rubber phantom and sensitivity analysis on simulated experiments shows the accuracy of this approach. This approach is limited to 1D strain estimation and is not suitable for complex deformation such as cardiac strains.

In future work, we plan to estimate extraocular muscle deformations using MR scans of the human orbit. We are also interested in estimating strains from more general deformation with shearing.

REFERENCES

Asakawa, DS et al. (2003). *Seminars in Musculoskeletal Radiology.* 7:287-295.
Osman, NF et al. (1999). *Magn Reson Med.*42:1048-60.
Miller JM et al. (2006). *J Vision.* 6:5:616-624.

ACKNOWLEDGEMENTS

ASYMMETRIC TONIC NECK REFLEXES INDUCED CHANGES IN JOINT TORQUE GENERATION IN THE HEMIPARETIC UPPER EXTREMITY: PRELIMINARY RESULTS

Julius Dewald, Michael Ellis and Thierry Keller

Northwestern University, Chicago, IL, USA
E-mail: j-dewald@northwestern.edu, Web: http://www.dewaldlab.com

INTRODUCTION

A central abnormality following hemiparetic stroke is the loss of independent joint control in the paretic limb expressed as stereotypic multi-joint movement patterns as described by Brunnstrom (Brunnstrom 1970). Specifically in the paretic upper limb, shoulder abduction/elbow flexion (flexor-synergy) and shoulder adduction/elbow extension (extensor-synergy) are coupled in moderately to severely impaired individuals with stroke. The underlying neurological mechanism responsible for its manifestation remains largely unknown. We designed a protocol to measure single-joint maximum torque generation abilities for the shoulder and elbow while the head was rotated toward and away from the paretic arm. We hypothesized that the asymmetric tonic neck reflex (ATNR) would affect isometric torque generation abilities in the paretic arm. This would provide indirect evidence for an enhanced bulbospinal drive as a mechanism underlying the expression of abnormal muscle/torque synergies.

METHODS AND PROCEDURES

Eight individuals including 5 men and 3 women, ages 44-73, with chronic unilateral cortical and/or subcortical stroke and nine individuals without stroke including 1 man and 8 women, ages 23-43, participated in the study. Stroke subjects scored 21-36 out of 66 on the Fugl-Meyer Motor Assessment. Study participants were strapped to a Biodex chair in a fixed posture of 75° shoulder abduction, 40° shoulder flexion and 90° elbow flexion with the lower arm placed in a rigid cast and attached to a 6 degrees-of-freedom load cell. The head was then rotated 5º less than full active range of motion toward or away from the paretic (stroke) or non-dominant arm (control) and a LCD monitor was placed in front of the subject displaying a dial that provided real time visual feedback of the elbow or shoulder torques generated by the subject. Head rotation angles were measured with a compass and with a mounted laser pointer mounted to the top of the helmet. Good reproducibility of the vertical and horizontal head rotation angles was obtained by asking subjects to maintain the laser dot in the center region of the dial on the LCD monitor. Subjects were instructed to generate isometric maximum voluntary torques (MVTs) in the directions of elbow flexion, elbow extension, shoulder abduction, shoulder adduction, shoulder flexion and shoulder extension while maintaining the laser dot in the center region of the feedback dial. MVTs were recorded for all subjects and for both head rotation directions. The torque generated in the instructed direction was labeled as the primary torque while the spontaneous torques generated in other directions at the same or other joint were labeled as secondary torques. For each torque direction, participants rotated the head to acquire and maintain the laser dot at the center of the displayed dial and then

performed the strongest possible contraction for 2-4 seconds. Following each repetition, the participant rotated the head back to a resting position.

RESULTS AND DISCUSSION

In individuals with stroke there was a significant effect of head rotation on the primary torque directions of EF ($p=0.0027$) and EE ($p=0.0109$). With the head rotated away from the impaired side, average normalized elbow flexion (0.95 ± 0.04) was $31\pm8\%$ greater than when the head was rotated toward the impaired side (0.74 ± 0.06). Incongruent with the individuals with stroke, there was no effect of head rotation on MVTs in the control group. The effects of head rotation also carried over into secondary joint torques but only for torques about the elbow joint. There were significant primary (head rotation, $p=0.0065$); torque direction, $p=0.0001$) and interaction (head rotation x torque direction, $p=0.0281$) effects on secondary elbow flexion/extension torque. Post hoc analysis showed that during shoulder abduction MVTs, average normalized secondary elbow flexion torque was significantly greater ($p=0.0281$) when rotated away from the impaired arm (0.85 ± 0.04) than when rotated toward the impaired arm (0.61 ± 0.11). Additionally, during shoulder flexion MVTs, secondary elbow extension torque was significantly less ($p=0.0001$) when rotated away from the impaired arm (0.00 ± 0.11) than when rotated toward the impaired arm (0.44 ± 0.08) . Unlike individuals with stroke, there was no interaction effect (head rotation x torque direction) for secondary elbow flexion/extension during MVTs in shoulder flexion/extension or shoulder abduction/adduction in the control group.

Research in animal models has demonstrated that the ATNR is initiated when neck muscle spindle afferents are excited by the muscle stretch resulting from head rotation. These neck receptors project onto and result in the activation of reticular and vestibular brainstem motor nuclei. The finding that during maximum voluntary torque generation the expression of joint torque couples is uniquely affected by the ATNR in the paretic upper limb therefore provides indirect evidence for a greater excitability of brainstem motor nuclei in chronic stroke survivors.

SUMMARY

The aim of this study was to investigate whether an enhanced bulbospinal drive contributes to abnormal torque patterns in stroke. If an augmented response to asymmetric tonic neck reflex (ATNR) would be present in stroke survivors, as opposed to control subjects, this would constitute support for this hypothesis. Our results provide evidence for changes elbow/shoulder joint torque patterns as a function of head rotation in the paretic arm of stroke subjects only.

REFERENCES

Brunnstrom, S. (1970). Movement therapy in hemiplegia : a neurophysiological approach. New York, Harper & Row.
Dewald, J. P. and R. F. Beer (2001). Muscle Nerve 24(2): 273-83.

ACKNOWLEDGEMENTS

TENDINOPATHY ALTERS MECHANICAL PROPERTIES OF THE ACHILLES TENDON

Shruti Arya[1] and Kornelia Kulig[2]
[1]PhD Candidate, Division of Biokinesiology and Physical Therapy, University of Southern California, Los Angeles, California, USA; arya@usc.edu
[2]Associate Professor and Co-director, Musculoskeletal Biomechanics Rehabilitation Laboratory, Division of Biokinesiology and Physical Therapy, University of Southern California, Los Angeles, California, USA; kulig@usc.edu
URL: http://pt.usc.edu/labs/mbrl/index.html

INTRODUCTION

Achilles tendinopathy causes considerable morbidity and functional impairment among the athletic and general populations. It remains a clinically challenging condition, recalcitrant to most current treatment protocols. Tendinopathy is accompanied by tendon thickening and altered tendon composition. However, alterations in mechanical properties of tendons in the presence of tendinopathy remain largely unknown. Considering the crucial role of the tendon in transfer of muscle forces and production of coordinated movement, alterations in tendon mechanical properties will likely have a discernable effect on locomotion. Therefore, an understanding of the mechanical characteristics of tendons in the presence of pathology has important implications for prevention of injuries and optimization of performance. Hence, this study was conducted to test the hypothesis that individuals with Achilles tendinopathy will exhibit lower tendon stiffness and higher strain compared to healthy controls.

METHODS AND PROCEDURES

Male subjects with Achilles tendinosis were identified through grayscale ultrasound (US) imaging (**Figure 1**). Subjects in the Achilles tendinopathy group (n = 12) and the healthy control group (n = 12) were matched for age, gender and activity level. Tendon cross-sectional area (CSA) and length measurements were obtained through US imaging. All subjects performed maximal isometric plantar flexion contractions on a hydraulic dynamometer (Kin-Com 500H, Chattanooga, TN, USA). The excursion of the Achilles tendon during the contraction
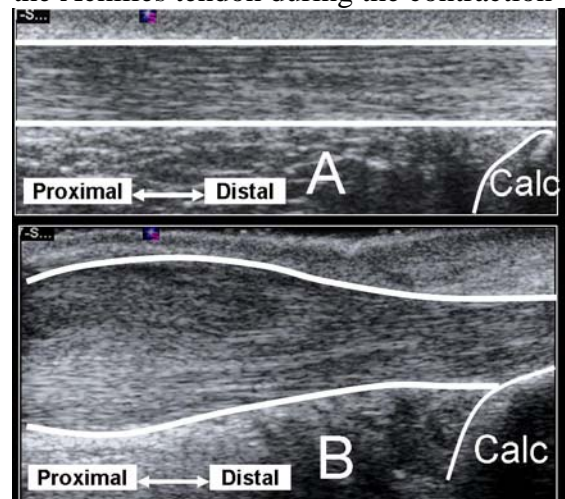

Figure 1: Grayscale US images of normal (A) and tendinosed (B) Achilles tendon. The tendon and calcaneal borders (calc) are outlined. B demonstrates significant focal thickening of the tendon.

was recorded simultaneously through dynamic ultrasound imaging (VFX 5-13, Siemens Sonoline Antares, PA, USA). Tendon elongation was measured by manually tracking the displacement of the medial gastrocnemius muscle myotendinous junction (NIH Image Software). Net plantar flexion torque was corrected for co-activity of the tibialis anterior and divided by the internal moment arm of the Achilles tendon

(obtained through the tendon excursion method), to estimate the force acting on the tendon (Maganaris CN and Paul JP, 1999). Heel contact foot switches were used to ensure no movement of the foot during the isometric contraction. Tendon stiffness was calculated as the ratio of tendon force and elongation. Tendon stress was obtained through the ratio of tendon force and CSA. The ratio of tendon elongation and original tendon length provided a measure of tendon strain. Independent sample t-tests were used to determine differences in tendon stiffness, stress and strain between the two groups.

RESULTS

These data indicate significant differences in the Achilles tendon's morphology and mechanical properties between the two groups **(Table 1)**. Individuals in the tendinopathy group demonstrated significantly higher CSA measures compared to controls (p = .003). Tendon

Group	CSA (mm^2)	Force (N)	Elongation (mm)	Stiffness (N/mm)	Stress (N/mm^2)	Strain (%)
Control	55.7 (12.8)	2089 (433)	12.2 (3.3)	180 (32.2)	35.5 (10.2)	4.7 (1.7)
Tendinopathy	96.6 (14.3)	1875 (64)	15.7 (4.1)	115.4 (41.1)	20.4 (7.7)	5.5 (1.2)

Table 1: Mean (SD) values for Achilles tendon cross-sectional area, force, elongation, stiffness, stress and strain measures in control and tendinopathy group.

force was significantly lower (p = .001), and tendon elongation was significantly higher (p = .028), in the tendinopathy group. Tendinopathy group demonstrated significantly lower stiffness and stress (p = .033 and .008) and significantly higher strain measures (p = .006) compared to controls.

DISCUSSION

The results of this study indicate that Achilles tendons in individuals with chronic tendinopathy are mechanically weaker compared to their healthy counterparts. Lower tendon stiffness may affect the force transmission capabilities of the tendon and thus, negatively impact rate of force development at the limb segments. Sustained alterations in tendon mechanical properties may have deleterious effects on functional performance, predisposing the tendon to further injury, perpetuating the disabling condition. The effect of the observed increase in tendon compliance on functional performance and its implications for injury potential warrants further investigation.

SUMMARY

The present investigation demonstrated significant differences in mechanical properties of Achilles tendons in individuals with chronic tendinopathy compared to controls. These findings are imperative for construction of effective preventive and rehabilitative strategies that can specifically address mechanical deficits, promote faster healing and enhance functional recovery.

REFERENCES

Maganaris CN, Paul JP (1999). *Journal of Physiology*, 15: 307-313.

ACKNOWLEDGEMENTS

THE INFLUENCE OF RATE OF MUSCLE ACTIVATION ON THE NEURAL ADAPTATIONS TO RESISTANCE EXERCISE

Clayton Peterson, Michel Ladouceur, and Warren Darling

Department of Integrative Physiology, University of Iowa, Iowa City, IA, USA.
Correspondence directed to: clayton-peterson@uiowa.edu

INTRODUCTION

Skill training and strength training both involve optimization of spatiotemporal muscle activation patterns, yet reported adaptations in motor cortex (M1) generally differ between the two (Adkins, Boychuk et al. 2006). Skill training commonly results in modification of movement representations within M1. However, several studies have failed to find changes in M1 following strength training (Carroll, Riek et al. 2002; Jensen, Marstrand et al. 2005). Though much evidence indicates that skill and strength training result in different neural adaptations, not all results support this notion. A force production task resulted in M1 reorganization when performed ballistically but not when performed slowly (Muellbacher, Ziemann et al. 2001). Furthermore, one strength training study has indicated that adaptations within M1 may occur (Griffin and Cafarelli 2006), contrasting with earlier findings (Carroll, Riek et al. 2002; Jensen, Marstrand et al. 2005). This study did not specify the nature of the training contractions, though testing was ballistic in nature. The other studies used slow, controlled contractions. This suggests a potential role of rate of activation (ROA) in determining the nature of the neural adaptation to strength training.

This study explores the influence of ROA on the acute (within a single session) neural changes subsequent to isometric knee extensor training through use of transcranial magnetic stimulation (TMS) and femoral nerve stimulation (FNS).

METHODS AND PROCEDURES

Subjects underwent strength testing, electrophysiological testing, and training. Training consisted of maximum, isometric knee extensions performed on a Cybex II dynamometer. Sessions consisted of three sets of eight isometric knee extensions (~1 per 5 seconds, 5 minutes between sets). Subjects were instructed to maximize ROA, and verbal encouragement was given.

Strength testing (2 maximum efforts separated by 60s) was done prior to training. Subjects received the same instructions as for training. Max torque, max rate of torque development (RTD), and EMG were measured during testing and training contractions.

Electrophysiological testing targeted rectus femoris (RF) and vastus lateralis (VL). FNS was used to elicit a maximal muscle compound action potential (M_{max}) and to elicit H-reflexes. TMS was applied over RF hotspot and elicited motor evoked potentials (MEPs) during resting conditions in both RF and VL. The response to submaximal FNS (ascending slope of H-reflex recruitment curve) and TMS (120% resting motor threshold) was monitored prior to and following training.

RESULTS

Peak-to-peak (p-p) MEP amplitude increased following training in both RF (Figure 1) and VL (not shown) in all subjects. H-reflex could only be elicited in one subject. In this

subject, H-reflex amplitude did not change from pre- to post-training.
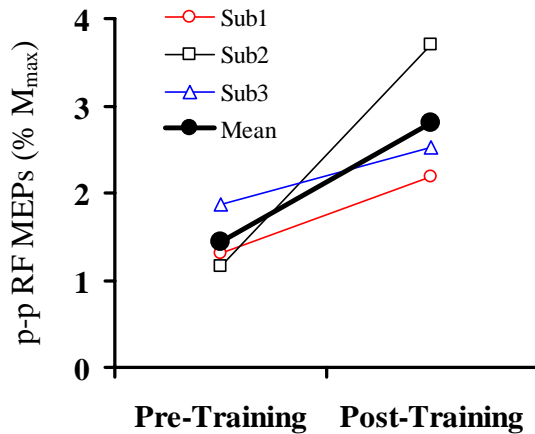

Figure 1. RF MEPs elicited at rest (120% threshold stimulus) prior to and after isometric knee extensor training emphasizing maximum ROA.

Max torque did not increase during training. However, max RTD increased in all subjects (Figure 3).
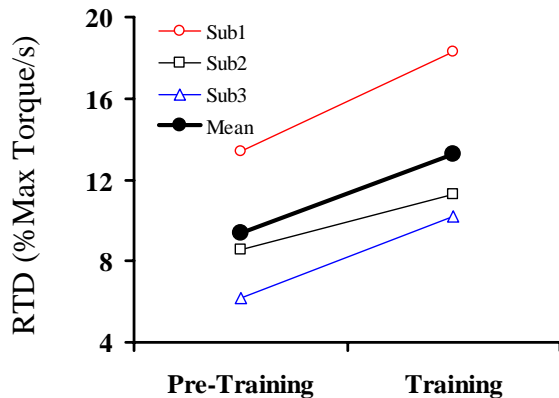

Figure 3. Max RTD, expressed as a % of maximum torque/second, prior to and during training

DISCUSSION

The excitability of the M1 area corresponding to RF and VL seems to increase during isometric knee extension training emphasizing a high ROA. This increase is associated with an increase in RTD during maximum contractions.

Future studies will investigate the location of the adaptation and compare the effects of different ROA on the M1 adaptation.

SUMMARY

Strength training with an emphasis on ROA led to an increase in M1 excitability. This result is similar to results seen with skill training, but runs counter to those often seen with strength training. Further studies are required to verify this result. If verified, it would highlight the importance of ROA training in order to maximize neural adaptation potential.

REFERENCES

Adkins, D. L., J. Boychuk, et al. (2006). "Motor training induces experience-specific patterns of plasticity across motor cortex and spinal cord." J Appl Physiol **101**: 1776-82.

Carroll, T. J., S. Riek, et al. (2002). "The sites of neural adaptation induced by resistance training in humans." J Physiol **544**: 641-52.

Griffin, L. and E. Cafarelli (2006). "Transcranial magnetic stimulation during resistance training of the tibialis anterior muscle." J Electromyogr Kinesiol. **4**: 446-52.

Jensen, J. L., P. C. Marstrand, et al. (2005). "Motor skill training and strength training are associated with different plastic changes in the central nervous system." J Appl Physiol **99**: 1558-68.

Muellbacher, W., U. Ziemann, et al. (2001). "Role of the human motor cortex in rapid motor learning." Exp Brain Res **136**: 431-8.

ACKNOWLEDGEMENTS

DECREASED STABILITY OF MULTISEGMENTAL POSTURAL COORDINATION IN ACL-INJURED FEMALE ATHLETES

Adam W. Kiefer[1], Kevin R. Ford[2,3], Mark V. Paterno[2], Gregory D. Myer[2],
Michael A. Riley[1], Kevin Shockley[1], & Timothy E. Hewett[2,4],

[1] Department of Psychology, University of Cincinnati, Cincinnati, OH, USA,
kieferac@email.uc.edu
[2] Sports Medicine Biodynamics Center, Cincinnati Children's Hospital, Cincinnati, OH
[3] University of Kentucky, Department of Kinesiology and Health Promotion, Lexington, KY
[4] Departments of Pediatrics, Orthopaedic Surgery, Biomedical Engineering, and Rehabilitation
Sciences, University of Cincinnati, Cincinnati, OH

INTRODUCTION

Bilateral proprioceptive deficits result from anterior cruciate ligament (ACL) injury and may persist up to two years after ACL reconstruction (e.g., Corrigan et al. 1992). Proprioception plays a key role in neuromuscular control, as indicated by performance impairments resulting from perturbations of proprioception (e.g., Serrien et al. 2001). High levels of neuromuscular control are important for athletic actions such as landing and cutting, which are associated with ACL injury (Boden et al. 2000). Because deficient neuromuscular control has been implicated as contributors to ACL injury risk (Hewett et al. 2002, 2005), proprioceptive deficits following ACL reconstruction may place athletes at risk for a second ACL injury.

Standard tests of proprioception may not capture the functional deficits that contribute to ACL injury (Co et al. 1993). In this study we determined whether a dynamic postural coordination task was sensitive to the proprioceptive and neuromuscular deficits that characterize ACL-injured subjects. The task (Bardy et al. 2002) required subjects to track the position of an oscillating visual target by keeping the head at a fixed position relative to the target. This is achieved by coordinating sagittal-plane rotations of the body about the ankle with sagittal-plane oscillation of the trunk and upper body about the hips. This coordination is mediated by proprioceptive feedback, so proprioceptive deficits were expected to manifest as decreased stability of the coordination pattern.

METHODS AND PROCEDURES

Twenty-two females participated in the current study (11 ACL injured; 11 controls). The ACL-injured subjects were medically cleared to return to sport. Four trials (two low-frequency, two high-frequency) of anterior/posterior target oscillation were examined. Front-to-back ankle and hip angular displacement was recorded using a 10-camera motion analysis system (Motion Analysis Corp., 60 Hz sampling rate). All trials lasted for 10 front-to-back-to-front oscillations that took approximately 15 s and 1 min to complete for the high and low frequency conditions, respectively.

Subjects stood on either the left or right leg with their arms crossed in front of them. The computer-generated, oscillating target was displayed on a monitor placed 1 m from the participant. Participants were instructed to use body movements to track the front-to-back oscillations of the target, doing their best to move in phase with the target, which oscillated at either 0.2 or 0.7 Hz. Motion data

were filtered using a low-pass Butterworth filter (4th order, 5 Hz cut-off frequency).

Postural coordination was indexed on each trial by continuous relative phase (ϕ), the difference between the ankle and hip phase angles θ (i.e., $\phi = \theta_{ankle} - \theta_{hip}$). Relative phase variability (SDϕ, the within-trial standard deviation of ϕ) quantifies the stability of ankle-hip coordination—higher SDϕ indicates more variability in the phase relation, hence lower coordination stability—and was the dependent variable of interest.

RESULTS

A group (ACL injured vs. control) × leg (injured vs. non-injured) × frequency (low vs. high) mixed-model ANOVA revealed a significant group × frequency interaction (see Figure 1), $F(1,25) = 10.03$, $p < .01$. Follow-up tests revealed significantly higher SDϕ for the control group in the high frequency than the low-frequency condition ($p < .05$; $M = 43.70°$ vs. 29.49°, respectively), and significantly higher SDϕ for the ACL injured than the control group in the low frequency condition ($p < .05$; $M = 37.03$ vs. 29.49, respectively).
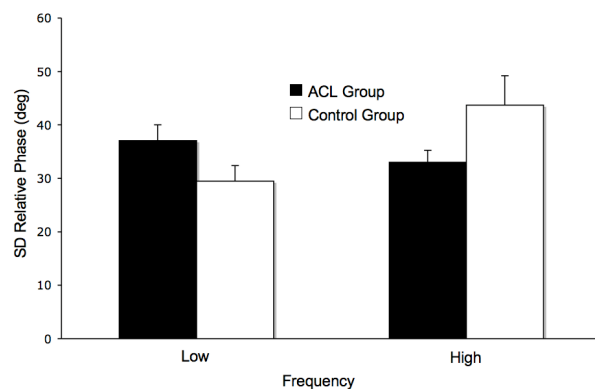
Figure 1. Group × frequency interaction for standard deviation of relative phase (SDϕ).

DISCUSSION

Postural coordination was affected differently for the ACL-injured and control groups by the frequency manipulation. ACL-injured subjects exhibited significantly greater variability than controls in the low-frequency condition. The stability of the postural coordination decreased significantly in the high-frequency condition for controls, but not for the ACL-injured subjects. The low-frequency condition required slow, controlled muscular contractions to oscillate the body in the sagittal plane so as to track the looming target—arguably this presented a greater challenge in terms of neuromuscular control. The multi-segmental, dynamic postural coordination task, which depends heavily on proprioceptive feedback, may have utility in predicting risk for ACL re-injury.

SUMMARY

ACL-injured subjects exhibited less stable hip-ankle coordination when performing a postural coordination task that required slow oscillations about the ankle and hip.

REFERENCES

Bardy BG et al. (2002). *J Exper Psychol: Hum Percept Perform*, 28:499-514.
Boden GP et al. (2000). *Orthop*, 23:573-578.
Co FH et al. (1993). *J Orthop Res*, 11:696-704.
Corrigan JP et al. (1992). *Bone Joint Surg Br*, 74:247-250.
Hewett TE et al. (2002). *Clin Orthop*, 402:76-94.
Hewett TE et al. (2005). *Am J Sports Med*, 33:492-501.
Serrien DJ et al. (2001). *Exp Brain Res*, 140:411-419.

ACKNOWLEDGEMENTS

ALTERED REFLEX MODULATION TO CHANGES IN MECHANICAL ENVIRONMENT FOLLOWING STROKE

Randy D. Trumbower [1], James Finley [2], Jonathan Shemmell [1], Eric J. Perreault [1, 2, 3]

[1] Rehabilitation Institute of Chicago, Chicago, IL, USA
[2] Biomedical Engineering, Northwestern University, Chicago, IL, USA
[3] Physical Medicine and Rehabilitation, Northwestern University, Chicago, IL, USA

INTRODUCTION

The human central nervous system regulates limb mechanics during interactions with the physical world. This regulation is due, in part, to involuntary mechanisms including the stretch reflex. Single joint studies in unimpaired subjects have shown that longer latency (M2) components of this reflex become more sensitive during interactions with compliant objects, suggesting that these responses contribute to limb stability (Perreault et al., 2008) when that stability is not provided by the environment. A substantial amount of evidence also indicates that these reflex components are influenced by neural elements within the cortex (Matthews, 1991), which may provide the flexibility needed for task appropriate reflex modulation.

Stretch reflexes are known to be altered following stroke. To date, however, most studies have focused on the spinal components of the reflex, thought to be mediated through short latency (M1), monosyaptic pathways. These pathways contribute impairments such as spasticity and tremor, but the relationship between spasticity and stroke-related disabilities is not clear (Sommerfeld et al., 2004).

A few studies also have examined M2 responses following stroke. This longer latency response is known to be attenuated relative to unimpaired subjects (Dietz et al., 1991; Lee and Tatton, 1978), decreasing its potential efficacy in tasks that require enhanced limb stability. These previous studies have been conducted only during interactions with a stiff environment and it is unclear if stroke subjects retain the capacity to modulate M2 responses during interactions with compliant loads. Addressing that question was the purpose of this study.

METHODS AND PROCEDURES

Five chronic stroke (Fugl-Meyer scores 16-31) and 8 healthy control subjects were seated with the paretic (stroke) or dominant (control) arm positioned in 70° of shoulder abduction and 90° of elbow flexion with the forearm in the neutral position. The forearm was supported in neutral and the hand was rigidly attached to a linear motor (Fig 1). Perturbations displaced the hand 25mm at 200mm/s to induce elbow extension while subjects applied a voluntary flexion torque equivalent to 5% of their maximum voluntary contraction. Subjects were instructed not to resist the perturbation while they interacted with either a stiff (50kN/m) or compliant (10N/m) environment. Surface electromyography (EMG) was used to measure muscle activity from brachioradialis (BRD) and triceps lateralis.

Averaged rectified EMG within pre-perturbation (background), short-latency (M1), and M2 stretch reflex time periods were calculated from 20 trials collected in each environment. 20msec windows were used for each average. M1 and M2 onsets were identified by visual inspection.
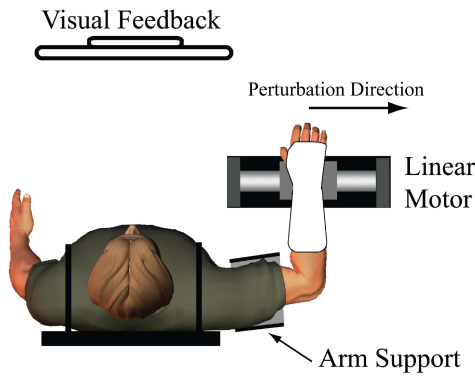
Fig 1. Experimental Setup.

RESULTS

Reflex responses in the stroke subjects were characterized by a large M1 and a smaller M2 response. In addition, the M2 response was substantially delayed following stroke with a mean onset of 86.9±9.0ms (Fig. 2).

In strong contrast to the control subjects, the stroke subjects exhibited decreased sensitivity of the M2 during interactions with the compliant environment (Fig 3; *p<0.05, Sign-Rank Test). This reduction in M2 relative to the stiff environment was not due to differences in background or M1 activity, which were controlled in all experiments.
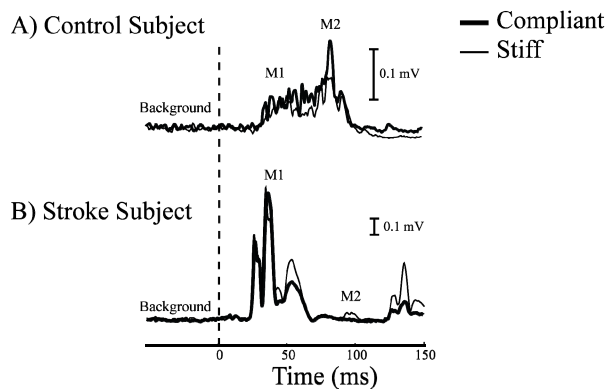
Fig 2. Typical stretch reflexes. Dashed line indicates perturbation onset.

SUMMARY/DISCUSSION

Our stroke subjects were unable to modulate their M2 reflex responses during interactions with a compliant environment. This inability

to regulate reflex sensitivity in a task appropriate manner may lead to impairments during object manipulation or other tasks that require precise control of limb mechanics and stability. Future studies are necessary to determine if this abnormal reflex modulation is associated with lesion location and physical disability.
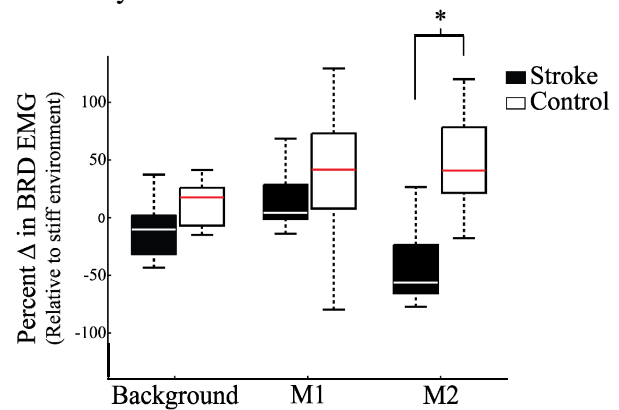

Fig 3. Boxplots representing the median and inter-quartile ranges for the change in BRD activity during interactions with the compliant environment relative to the EMG recorded in the stiff environment.

REFERENCES

Dietz V, Trippel M, Berger W. *Ann Neurol* 1991; 30: 767-79.

Lee RG, Tatton WG. In: Desmedt J, editor. *Cerebral motor control in man.* Vol 4. Basel, NY, 1978: 320-333.

Matthews PBC. *Trends in Neurosciences* 1991; 14: 87-91.

Perreault EJ, Chen K, Trumbower RD, Lewis GN. *J Neurophysiol* 2008.

Sommerfeld DK, Eek EU, Svensson AK, Holmqvist LW, von Arbin MH. *Stroke* 2004; 35: 134-9.

ACKNOWLEDGEMENTS

DETERMINATION OF THE OPTIMAL SEAT POSITION THAT MAXIMIZES AVERAGE CRANK POWER: A THEORETICAL STUDY

Jeffery W. Rankin and Richard R. Neptune

Department of Mechanical Engineering, The University of Texas at Austin, Austin, TX, USA

jwrankin@gmail.com

INTRODUCTION

As competitive cycling becomes more popular, there is increased demand to develop new methods to improve performance. One method is to alter the bicycle-rider geometry to change the lower extremity kinematics and take advantage of muscle force-length-velocity relationships to increase power output. A common way to change the geometry is to modify the seat position relative to the crank center. Indeed, there are differences in preferred seat position even among racing disciplines (e.g., road racers vs triathletes). Although altering different aspects of seat position (e.g. Nordeen-Snyder, 1977) on cycling performance have been investigated, there has been no study that has systematically assessed the sensitivity of crank power to a wide range of seat positions. The purpose of this study was to use modeling and simulation techniques to determine the optimal seat position that maximizes average crank power while pedaling at 90 rpm.

METHODS AND PROCEDURES

A detailed musculoskeletal model (Neptune and Hull, 1998) with 15 individual muscle actuators per leg and forward dynamic simulations were used with dynamic optimization to determine the optimal seat position that maximizes average crank power during isokinetic pedaling at 90 rpm. Two sets of optimizations were performed. First, the muscle excitation patterns and seat position (i.e. location and seat orientation) that maximized crank power over a single revolution were determined. The seat was allowed to vary ± 35 cm in the fore/aft and ± 40 cm in the vertical directions relative to the crank center. These variations in seat position essentially altered the seat tube angle and seat height. Second, optimal excitation patterns and crank power were optimized over a wide range of seat tube angles relative to the solution obtained in the first optimization to assess the sensitivity of crank power to seat tube angle. In the model, the muscle actuators were governed by Hill-type muscle properties including the force-length-velocity relationships. Activation-deactivation dynamics were modeled with a first-order differential equation (Raasch et al., 1997) using activation and deactivation time constants of 20 and 30ms, respectively.

Following each optimization, the location of the seat relative to the crank center and the seat height (i.e. distance along the seat tube angle) were determined. Seat orientation was calculated as the angle between the seat's vertical axis and the seat tube angle (0° angle corresponds to a seat perpendicular to the seat tube) and provides an indication of pelvis tilt since the pelvis is fixed to the seat in the model. In addition, average crank power and the range of motion (ROM) and mean values for the hip, knee, ankle, and pedal angles were determined to assess how the different seat positions influenced joint kinematics.

RESULTS

Interestingly, the maximum crank power varied little (within 6.4 watts) over a wide range of seat positions with a maximal value of 976.8 W (Fig. 1). The optimal solutions had a consistent seat height and orientation, with average (SD) values of 0.8041 (0.0014) m and -13.65(-0.45) degrees, respectively. Joint ROM and means for the hip, knee and ankle were consistent among all the optimal solutions with the largest variation occurring in the hip angle ROM (Table 1). Mean pedal

angle varied greatly among the solutions (Table 1), but rotated clockwise in a systematic fashion as the seat moved forward.
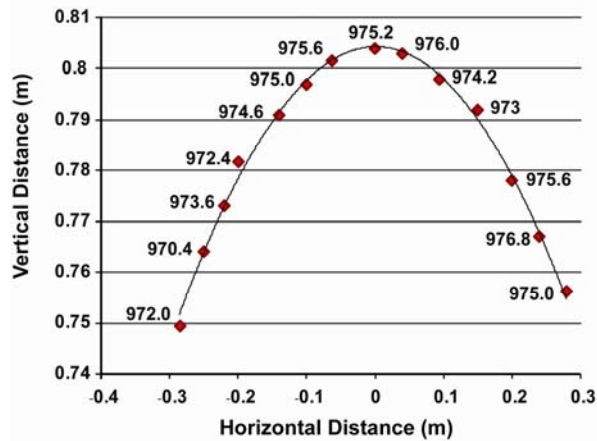

Figure 1. Location of optimal solutions (relative to crank center) and corresponding crank power output (W).

Angle	Mean° (SD)	ROM° (SD)
Hip	54.35 (0.56)	54.74 (0.36)
Knee	-78.27 (0.26)	94.06 (0.51)
Ankle	11.85 (0.37)	32.64 (0.42)
Pedal	-25.7 (13.63)	44.59 (0.52)

Table 1. Mean angle and ROM values for the pedal and lower extremity joint angles across optimal solutions. SD = standard deviation.

DISCUSSION

Maximum power was consistent across the optimal solutions, with differences within 1% of the highest power output. Maximal power was obtained within a small range of seat heights and orientations. However, the seat tube angle did not affect power output.

Previous studies have shown that seat height alters joint kinematics during cycling (e.g. Nordeen-Snyder, 1977). Therefore, the narrow range for optimal seat height suggests that specific knee and ankle angles are optimal for producing power. Additionally, the small variation in these angles, regardless of seat tube angle, were consistent with the findings of Heil et al. (1997) who showed there is little variation in these angles over a range of seat tube angles at a given seat height. The consistent seat height and orientation across the optimal solutions also produced a constant hip angle (Table 1). Previous studies have shown that extreme hip angle values increase $\dot{V}O_2$ output during sub-maximal cycling (e.g. Heil et al., 1997). A possible explanation for these findings and for the consistent optimal seat orientation in the present study is that altered hip kinematics cause muscles crossing the hip joint to operate on non-optimal regions of the force-length curve, and therefore increase metabolic cost.

While pedal ROM was nearly constant among solutions, the average pedal angle systematically changed (rotated clockwise) as the seat moved forward, which allowed the joint kinematics to remain constant and near optimal for producing power (Table 1). This was consistent with Browning et al (1992) who showed pedal rotation was directly related to seat position in competitive cyclists.

CONCLUSIONS

There is an optimal seat height and orientation that maximizes crank power, but the maximum power is relatively independent of seat tube angle. Instead, the pedal angle is used to adjust the joint kinematics such that the joint angles remain within their optimal range that allows muscles to operate in a more favorable region of the force-length relationship and produce maximum power.

REFERENCES

Browning, RC, et al. (1992). *Med Sci Sports Exerc*, 24: S186.

Heil, DP, et al. (1997). *Eur J Appl Physiol Occup Physiol*, 75: 160-5.

Neptune, RR and Hull, ML (1998). *J Biomech Eng*, 120: 334-341.

Nordeen-Snyder, KS (1977). *Med Sci Sports*, 9: 113-7.

Raasch, CC, et al. (1997). *J Biomech*, 30: 595-602.

A COMPARISION BETWEEN SLOPED AND LEVEL SURFACE GAIT INITATION

Scott P Breloff [1], Dwight E. Waddell [1], Chip Wade [2]

[1]Department of Health, Exercise Science & Recreation Management, The University of Mississippi, Oxford, MS, USA
[2]Department of Industrial & Systems Engineering, Auburn University, Auburn, AL, USA
Email: sbreloff@olemiss.edu

INTRODUCTION

Gait initiation is a functional task representing one of the first voluntary, destabilizing behaviors observed in the development of locomotor patterns as the whole body center of mass transitions from a large to a small base of support (Hass et al., 2008). Gait initiation has been used to provide insight into dynamic postural control and the changes that occur in the control system with advancing age and disability (Halliday et al., 1998). Specifically, the trajectory of the body's center of pressure (COP) has been used to detect instability during both forward and lateral gait initiation in various populations. It has also been shown that individuals are more likely to fall when walking on a sloped rather than a level surface (Hsiao & Simeonov, 2001). Since gait initiation is a destabilizing activity and COP represents the response of the central nervous system during postural adjustments, the purpose of this study was to investigate the differences in COP trajectories during gait initiation along a sloped versus a flat surface in a young, healthy male population.

METHODS AND PROCEDURES

Twelve male subjects (18-30 years) participated in the study. Subjects wore Stanley Model 211 6" STWB steel toe construction boots which laced up past the ankle. A mock roof which was 8.53m long and 2.44m wide was constructed with a 6\12 pitch (26.50° slope). Two horizontal force plates (AMTI, MA) were placed beneath the roof and a rigid extender, which matched the pitch of the roof, was constructed and fixed to the force plates. Force plate data were collected at 1080 Hz. Subjects stood quietly on the force plates until given a command to "begin walking" forward either along the pitch of the roof or the flat surface depending on the trial. For flat conditions, all subjects started walking with their right leg as bilateral symmetry for COP trajectories have been shown for young healthy populations in previous data. For sloped walking, subjects initiated gait with both their uphill and down hill foot as referenced by the pitch of the roof.

Total displacement, average velocities, and smoothness scores (a jerk cost function) in the X & Y direction were calculated for three defined segments of the COP trajectory (Figure 1). Segments (S1, S2 and S3) were defined using visual inspection and estimated time indices of heel and toe off for both the swing and stance leg. Multivariate analysis of variance (MANOVA) with repeated measures was used to test for over all group differences between COP variables for flat, "uphill swing foot" and "downhill swing foot" conditions. Follow up tests on separate univariate comparisons were conducted if needed. An alpha level of $p <= 0.05$ was set for all statistical tests.

RESULTS

Statistical analysis indicated a significant difference between the level and sloped surface conditions for all dependent variables: displacement, average velocity, and smoothness in the X and Y directions. These
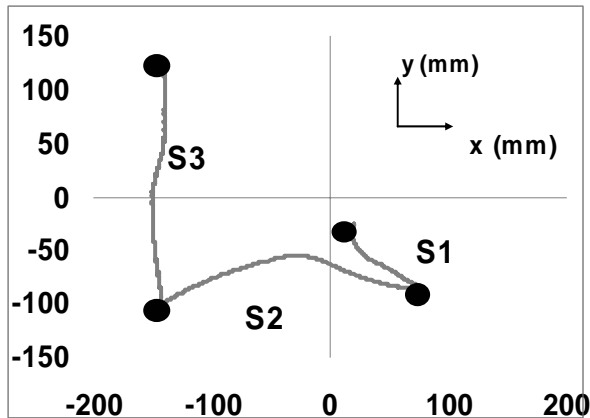
differences were found to be significant at p >.000.

Figure 1: Center of Pressure Trace with Segments Defined

DISCUSSION

While initiating gait on a sloped surface, changes in the displacement, average velocity, and smoothness in the X and Y directions suggest an increased challenge to the postural control system due to the volitional transition from a condition of relatively static stable support to one of the continuously unstable posture during locomotion (Halliday et al., 1998). These challenges seem to be increased when initiating gait along a sloped surface. It also appears that increased instability while initiating gait on a sloped surface depends on the choice of the swing leg (uphill versus downhill).

SUMMARY

There is a serious need for research to prevent falls from roofs, both by improving the existing work practices, and by developing new approaches, methods and systems for fall preventions and protection. Studying the role and the effect of the main factors that may lead to disruption in the control of balance on

inclined surfaces may provide a scientific basis for new fall-prevention strategies.

REFERENCES

Halliday, S. E. et al., (1998). The initiation of gait in young, elderly, and Parkinson's disease subjects. *Gait & Posture.* 8,8-14

Hass et al. (2008). Gait initiation in older adults with postural instability. *Clinical Biomechanics*. In press.

Hsiao, H., & Simeonov, P. I. (2001). Preventing falls from roofs: A critical review. *Ergonomics,* 44, 537-561

ACKNOWLEDGEMENTS

INITIAL ELECTROMECHANICAL REACTION TO REARWARD PERTURBATION

Nitin Moholkar, Venkata Gade, Jerome Allen, and W. Thomas Edwards

Kessler Medical Rehabilitation Research & Education Center, West Orange, NJ, USA
E-mail: nmoholkar@kmrrec.org, Web: www.kmrrec.org

INTRODUCTION

Falls are a major health concern due to the increased morbidity, mortality, and healthcare costs, as well as the decreased quality of life. A sudden rearward perturbation to balance will lead to a fall without a proper response. The nervous system needs to send the proper signal to the muscles, and the musculo-tendon units (MTU) need to respond in an appropriate and timely manner. This mechanical response can be broken down into three components: preset properties of the MTU due to current activation, reflex changes to the MTU, and active changes to the MTU.

Prior studies examining the EMG response of muscles crossing the ankle joint in similar situations have observed short, medium, and long latency responses (Schieppati and Nardone 95), usually linked to reflexes of agonists (short and medium) and reflexes of antagonists (long). But the mechanical effect of the EMG responses has not been adequately investigated.

In our study, we examined the combined EMG and mechanical response to a rearward perturbation and categorized the responses into the three categories (preset, reflex, & active) described earlier. We hypothesized that it is the active response that provides the bulk of balance recovery.

METHODS AND PROCEDURES

Seven healthy adult subjects gave informed consent and were screened to exclude internal pathologies or medications affecting balance.

Subjects stood on a NeuroCom Research Platform. The platform oscillated 12 cm in the anterior-posterior direction at three different frequencies (0.75, 1.0, and 1.25 Hz), with the initial movement in the rearward direction. Each condition was repeated three times with eyes open, for a total of 9 trials per subject. Motion data was collected at 100 Hz using a Vicon motion capture system and reflective markers placed on anatomical landmarks. Subjects wore a safety harness attached to a metal frame to prevent a fall. Ground Reaction Force (GRF) data was collected through the NeuroCom Research Platform at 200Hz. Motion and GRF data were combined through inverse dynamics to calculate ankle joint moments in the sagittal plane. EMG data from ankle extensor muscles was collected at 1000 Hz. All data was synchronized through the Vicon motion capture system.

To determine initial reaction to the platform movement, the initial movement cycles were compared to later cycles, by which point subjects had fully adjusted to the platform motion. Both timing and magnitude of EMG and force and moment data were examined to separate observed changes into preset mechanical properties of the joint, reflex response, and active response to the perturbation. All results presented are group averages plus/minus standard error of the mean.

RESULTS

EMG response: There was a burst starting at 75 ± 4 ms, 60 ± 4 ms, and 60 ± 4 ms after the

onset of movement, lasting for 216±16 ms, 210±10 ms, and 203±7 ms for the 0.75, 1.0, and 1.25 Hz trials (figure 1, first peak in EMG curve). In all trials, there was a second burst starting approximately 70±10 ms later. After two to three cycles, the EMG activity became more consistent and coincided with the movement of the platform.
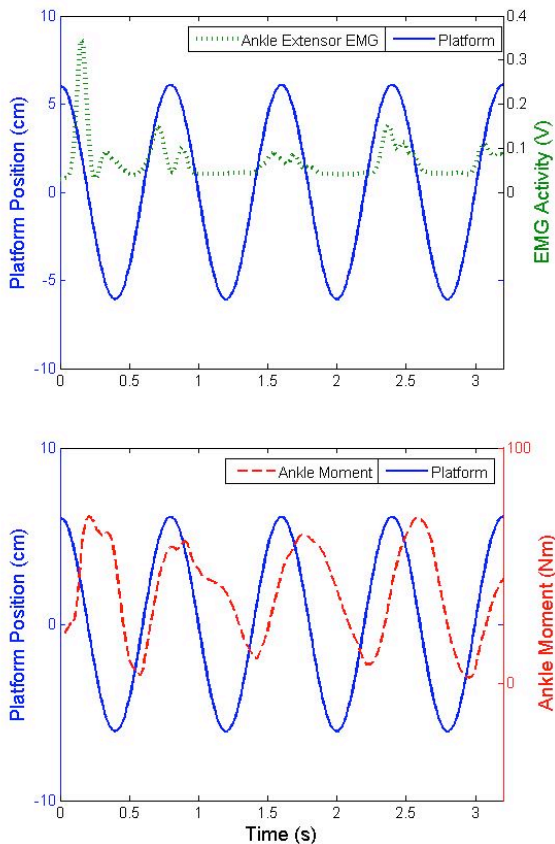

Figure 1 : Ankle EMG (top, dotted green), ankle moment (bottom, dashed red) and platform position (both, solid blue) vs time.

Ankle Moment Response: The ankle moment increased immediately as the movement started (figure 2). This was followed by a cycle where the timing of the moment is synchronizing with the platform movement. After two to three cycles, the ankle moment becomes more consistent and timed with the platform movement.

DISCUSSION

The timing of the first two ankle extensor EMG bursts in response to the initial movement of the platform matched well with values in the literature for reflex activity. Furthermore, they matched well with the timing of small deviations in the ankle moment response, with small time delays, explained by electromechanical delay. By the third cycle of movement, the EMG and extensor moment had settled into their patterns.

If preset conditions and reflex activity were sufficient to respond to perturbations, there would not have been a two cycle settling time before reaching a consistent pattern. An active response was necessary to prevent a fall. This study further demonstrates that reflexes alone are insufficient to balance recovery after a perturbation.

SUMMARY

Initial preset condition of the ankle extensor muscles combined with reflex activity is not sufficient to maintain balance on a moving platform. Following an initial reflex reaction, further active control is required to match the timing (phase) of the ankle moment and the platform motion and avoid a loss of balance. This study provides new insight for the diagnosis of postural deficits.

REFERENCES

Schieppati M & Nardone A (1995) *J Physiol* 487 (Pt 3) : 787-96.

ACKNOWLEDGEMENTS

WALKING STEP WIDTH DURING THE TRANSITION BETWEEN LEVEL AND SLOPED SURFACES

Nori Okita and Jinger S. Gottschall

Department of Kinesiology, The Pennsylvania State University
University Park, PA 16802 USA
nxo118@psu.edu and jsg20@psu.edu

INTRODUCTION

Falls are the leading cause of injury death for older adults and the second leading cause of death for all ages. The National Safety Council states that during walking, the main reason for the a) high incidence rate of falling and b) low mobility percentage after falling, is instability due to steep slopes and uneven terrain (Klein and Ritzel, 2000). Therefore, our goal is to quantify walking stability, estimated with step width, during the transition between level and sloped surfaces.

Prentice et al (2004) conducted a thorough investigation on the transition from a level surface to an incline slope that provided an ideal preface for the current project. They collected walking kinematic data during the approach to the slope and during the initial step on the slope for 3, 6, 9, and 12-degree conditions. Both limb and trunk motion was modified in a scaled fashion in order to navigate surface slope transitions. They observed that participants anticipate the transition by modifying their trunk orientation and leg swing trajectory prior to the first step on the sloped surface. Subsequent to the transition, the first step ensured foot clearance onto the final surface while the second step tailored the trajectory for the new surface. In short, these data indicate that there is a transition phase that may compromise stability.

Step width is an exemplary gait variable utilized to assess stability (Branch et al, 2005). For example, walking adults may increase their step width as a compensation strategy during steep slopes and uneven terrain. We propose to study when and how step width changes during surface slope transitions in an effort to initially evaluate stability. Specifically, we hypothesize that compared to steady-state level walking, step width will be greater during the last step on the initial surface and the first step on the final surface. Additionally, we hypothesize that step width will be the greatest when the gradient difference between the initial and final surfaces is largest.

METHODS

Two men and three women volunteered. All of these healthy, adults provided written informed consent that followed the guidelines of the Pennsylvania State University Biomedical Review Board. For the kinematic recordings, we placed markers on the base of the sacrum, greater trochanter, lateral femoral condyle, lateral malleolus, posterior calcaneous, fifth metatarsal, and first metatarsal. These pilot experiments were completed in our gait laboratory, which was oriented with a 50 foot level pathway leading to the 6 foot surface inclined at 6 degrees. We instructed the participants to approach the inclined slope and continue walking up to the top of the ramp. The participants also completed an additional condition of walking uphill at

6 degrees on a treadmill to compare step width of steady-state steps to transition steps.

RESULTS

Step width was two times greater than level walking during the transition between the initial level surface and the final uphill surface. Additionally, step width during steady-state uphill walking was also greater than level walking. In summary, the participants overcompensated for the surface slope transition by increasing their base of support.
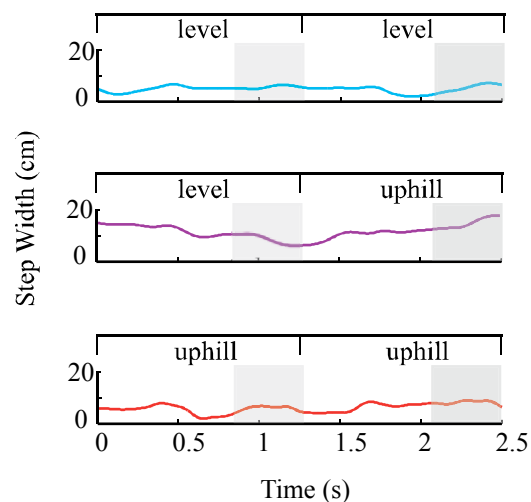

Figure 1. Step width data of two steps for the left leg during steady-state level walking (TOP), transition steps, level walkway to uphill ramp (MIDDLE), and steady-state uphill walking (BOTTOM). Representative data was taken from a single participant with a mean velocity of 1.25 m/s. The shaded areas correspond to the swing phase.

Overall, our kinematic data resembled Prentice et al (2004). The most significant modifications to level walking kinematics were during the swing phase of the first step onto the incline slope. However, we also documented significant increases in both hip and knee flexion in anticipation of the slope

at least two steps prior to the transition. As for the ankle, during the last step on the level prior to the transition, the ankle trajectory actually mimicked the trajectory of uphill walking. It is remarkable that the transition between the two surfaces (level-uphill) is seamless and it will be interesting to analyze if other surface combinations produce similar strategies.

DISCUSSION

Our preliminary methodology suggests that stability is compromised during surface slope transitions. This conclusion is based upon the significant increase in step width during transition walking compared to steady-state level or steady-state uphill walking.

Due to these intriguing pilot results, we plan to expand upon our methods in two aspects. First, we will incorporate electromyography measurements in six lower leg muscles (rectus femoris, biceps femoris, tensor fascia latte, adductor longus, medial gastrocnemius, anterior tibialis). Second, we will increase the number of conditions by adding three protocols with varying slope gradients (downhill-level, uphill-downhill, downhill-uphill).

In the future we will combine these supplementary methods with calculations of dynamic stability (Hof et al, 2005). Ultimately, our objective is to quantify walking stability during surface slope transitions in an effort to decrease falls.

REFERENCES

Brach et al (2005) *J Neuro Rehab* 26:2-21
Hof et al (2005) *J Biomech* 38:1-8
Klein and Ritzel (2000) *National Security Council Resources and Research*
Prentice et al (2004) *Gait Post* 20:255-265

CORRELATION BETWEEN FOCAL CARTILAGE THICKNESS AND FEMUR CARTLIAGE CONTACT REGIONS DURING RUNNING

William Anderst, Eric Thorhauer and Scott Tashman

University of Pittsburgh, Department of Orthopaedic Surgery, anderst@pitt.edu

INTRODUCTION

The relationship between tibio-femoral cartilage thickness and cartilage contact during dynamic knee loading is unknown. It was hypothesized that cartilage is thicker in regions that are habitually loaded during walking and running.

The purpose of this study was to determine the correlation between focal cartilage thickness on the femur and cartilage contact location during the impact phase of running.

METHODS

Four subjects (3M, 1F) received bilateral, sagittal, 3T knee MRIs using a 3D SPGR sequence. All knees were asymptomatic for OA. MRI field of view was 160 x 160 mm with 2 mm slice spacing. Cartilage was segmented using both Mimics software (Materialise) and manual segmentation. Sagittal slices were interpolated to produce (0.312 x 0.312 x 0.333) mm voxels.

Segmented MRI slices were reconstructed into 3D volumetric models by applying a marching tetrahedra algorithm to the 2D slice data (Treece, Prager and Gee, 1999).

Cartilage volumes were grouped into focal regions within the medial and lateral compartment (Figure 1) to include surfaces likely to be loaded during running. Average thickness of each focal region was determined by 3D distances from the outer to inner cartilage surface.
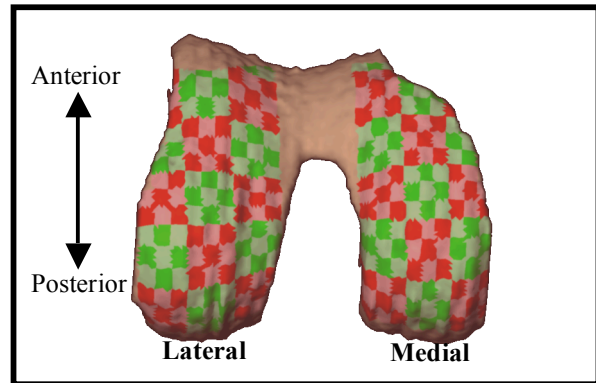

Figure 1: *Femur (above) cartilage regions of interest (red-green checkerboard). Regions of interest were divided into focal regions of approx. 6 mm².*

Cartilage surfaces were co-registered with bone surfaces, and animated according to bone motion recorded with a high-speed biplane x-ray system (Tashman and Anderst, 2003). Precise in-vivo knee kinematics were acquired at 250 frames/s during downhill treadmill running for 3 trials per subject.

Contact areas were estimated from femur-to-tibia cartilage distances, which were calculated for each frame of the loading phase of each running trial (approx. 200 ms after foot strike). The average distance between cartilage surfaces over this time period was determined for each focal region, with average distances below 7 mm included in the analysis to exclude non-contacting regions.

Cartilage thickness within each focal region was correlated to average distance between cartilage surfaces within each focal region during the running trials, and the average correlation for each subject was determined.

RESULTS

Correlation between focal cartilage thickness and distance between cartilage surfaces was low within both the medial (average $R^2 = .10$; R^2 range .03 to .30) and lateral (average $R^2 = .12$, R^2 range .02 to .36) compartment on the femur.

Cartilage thickness in relation to minimum distance was similar, but not close enough to result in a high focal region correlation (Figures 2 and 3).
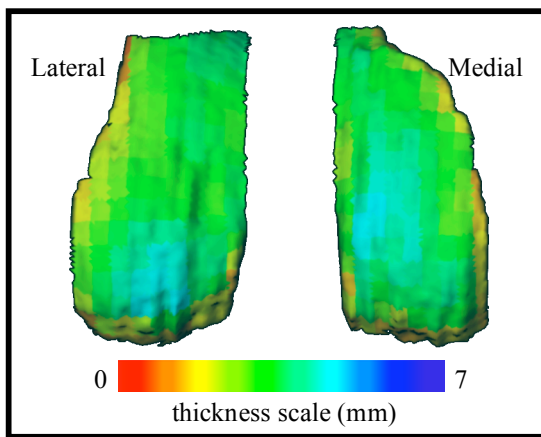

Figure 2: Cartilage thickness for the medial and lateral compartments of the femur of one subject. Focal regions (as defined in Figure 1) are color-coded according to average thickness within each region.
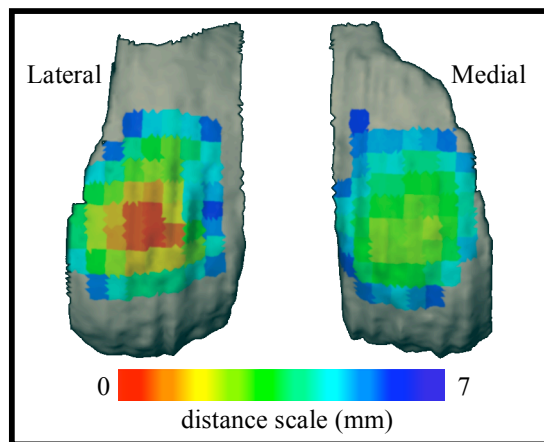
Figure 3: Average distance from femur to tibia cartilage surfaces during the loading phase of running for the same subject shown in Figure 2. Focal regions are color-coded according to average distance between cartilage surfaces for 200 ms after footstrike.

DISCUSSION

These findings do not support the hypothesis that cartilage thickness in the femur is related to cartilage contact regions during dynamic loading.

These results contradict previous reports that cartilage contact location during static loading was related to cartilage thickness (Li, Park, DeFrate, et al., 2005). It should be noted that sample size was small for both studies, and Li, et al. correlated cartilage thickness on one group of subjects with static contact locations from another group of subjects. Also, the focal region size used by previous authors (Li, Park, DeFrate, et al., 2005) was large compared to the present study. As Figures 2 and 3 show, the regions of close cartilage contact on the lateral condyle are only slightly anterior to the thickest cartilage regions, while medial close cartilage contact was located slightly lateral to the thickest focal regions. Increased focal region size may improve the correlation between contact regions and cartilage thickness.

REFERENCES

Li, G, Park, SE, DeFrate, LE, et al. (2005). *Clin. Biomech.*, 20:736-744.
Tashman, S and Anderst, W (2003). *J. Biomech. Eng.*, 125:238-245.
Treece, GM, Prager, RW and Gee, AH (1999). *Comput. and Graph.*, 23:583-598.

ACKNOWLEDGEMENTS

MAXIMUM ALLOWABLE FORCE ON A SAFETY HARNESS CABLE TO DISCRIMINATE A SUCCESSFUL FROM A FAILED BALANCE RECOVERY

Marc-André Cyr and Cécile Smeesters

Research Center on Aging, Sherbrooke QC, Canada
Human Performance and Safety Laboratory (PERSEUS), Sherbrooke QC, Canada
Department of Mechanical Engineering, Université de Sherbrooke, Sherbrooke QC, Canada
E-mail: Cecile.Smeesters@USherbrooke.ca   Web: http://www.usherbrooke.ca/gmecanique

INTRODUCTION

A safety harness system is essential in experiments at the threshold of balance recovery where avoiding a fall is not always possible. An unsuccessful balance recovery then occurs when the maximum allowable force on the safety harness cable is exceeded. This maximum allowable force cannot be too small, as a minimum load is always generated just by the displacement of the safety harness system when the participant takes one or more steps (Wojcik *et al.*, 1999). Similarly, it cannot be too large, as the safety harness system then assists the participant in balance recovery and may be the only reason a fall is avoided. Unfortunately, the maximum force used varies a great deal. Moreover, to our knowledge, no one has explained how this maximum force is determined. The purpose of this study was thus to propose a method to determine the maximum allowable force on a safety harness cable to discriminate a successful from a failed balance recovery.

METHODS AND PROCEDURES

Data from 12 healthy younger adults, who participated in experiments to determine the maximum forward lean angles that participants could be suddenly released from and still recover balance using three different limits on the number of steps, were used (Cyr and Smeesters, 2007; submitted 2008).

Starting at 15 deg, the initial lean angle was increased in 2.5 deg increments at each trial, until the participant failed to recover balance twice at a given initial lean angle and was thus no longer able to avoid a fall. For this study, balance recovery was considered definitely unsuccessful if the vertical force on the safety harness cable was more than 50 % of the participant's body weight (%BW).

For each participant, the coefficients of the following asymptotic regression, between the maximum vertical force on the safety harness cable and the initial lean angle at each trial below 50 %BW, were evaluated by a least squares method:

$$\theta_i = a\left(1 - e^{-F_{\max}/b}\right) + c$$

F_{max} = max vertical force (%BW)
θ_i = initial lean angle (deg)
$a = \theta_i\left(F_{\max} = \infty\right)$ with respect to c (deg)
b = force constant (%BW)
$c = \theta_i\left(F_{\max} = 0\right)$ (deg)

RESULTS

The proposed asymptotic regression represented well the behaviour of the initial lean angle as a function of the maximum vertical force on the safety harness cable with a = 15.7 ± 7.8 deg, b = 4.6 ± 4.9 %BW, c = 17.0 ± 7.8 deg and $0.5742 \leq r^2 \leq 0.8807$ (Figure 1).
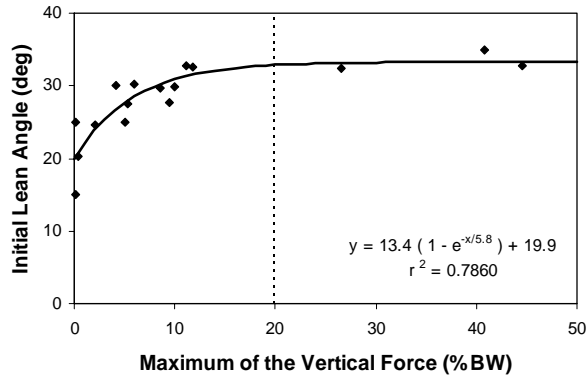
Figure 1. Asymptotic regression for a typical participant (full line) and the proposed 20 %BW threshold (dotted line).

It established that the initial lean angle reached 99 % of its steady state value a with respect to its initial value c when the maximum vertical force was five times the force constant b or 23.0 %BW. Rounding towards zero to avoid false positives, we thus proposed a 20 %BW threshold for the maximum allowable vertical force to discriminate a successful from a failed balance recovery for our experiments.

As the participants stepped forward, the anterior-posterior forces on the safety harness cable did increase (Figure 2). However, for trials at the maximum forward lean angle, the contributions of the medial-lateral (0 %) and anterior-posterior (2 %) forces were negligible relative to the vertical forces (98 %) at the maximum vertical forces.

DISCUSSION AND SUMMARY

The proposed asymptotic regression and threshold for the maximum allowable vertical force on a safety harness cable of five force constants discriminates well a successful (below the threshold) from a failed (above the threshold) balance recovery for experiments at the threshold of balance recovery.

Furthermore, although the amplitude of the horizontal forces should not be neglected in safety harness system designs, their contribution can be neglected in experiments at the threshold of balance recovery.

Finally, although our five force constants method could be used on other safety harness systems, the actual value obtained for the maximum allowable vertical force probably varies between systems.
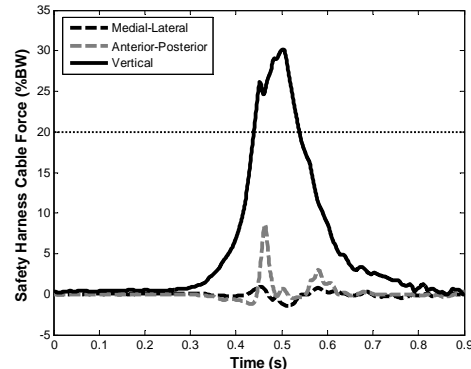

Figure 2. Horizontal (dashed lines) and vertical (full line) forces on the safety harness cable for a typical participant during the first trial to exceed the proposed 20 %BW threshold (dotted line).

REFERENCES

Cyr MA and Smeesters C (2007). *J Biomech*, 40(13): 2857-2864.
Cyr MA and Smeesters C (submitted 2008). *Gait Posture*.
Wojcik LA et al. (1999). *J Gerontol*, 54A(1): M44-50.

ACKNOWLEDGEMENTS

COMPUTER SIMULATION OF INTERNAL STRUCTURAL LOADING: APPLICATION TO OVERUSE RUNNING INJURIES

Ross H. Miller and Joseph Hamill
Department of Kinesiology, University of Massachusetts, Amherst, MA, USA
Email: rhmiller@kin.umass.edu   Web: http://www.umass.edu/sphhs/kinesiology

INTRODUCTION

Despite a large volume of research on injuries in distance runners, incidence rates of overuse injuries remain high, and most injury mechanisms are not well-understood. Injury research tends to focus on external measures of loading, such as ground reaction forces (GRF) and joint kinematics (*e.g.* Messier & Pittala, 1988). Overuse injuries generally arise from trauma accumulation through the internal loading of susceptible tissues (Hreljac, 2004). However, changes in internal loading are not necessarily reflected by changes in external loading (Nigg *et al.*, 1987; Wright *et al.*, 1998). External loading is thus limited in its ability to quantify the effects of training interventions on reducing the internal loading of at-risk tissues.

Running injury research, and ultimately injury prevention, may benefit from a shift in focus from external to internal loading. Methods that directly estimate internal loading, such as computer simulations, may be useful in elucidating injury mechanisms and prescribing training interventions to attenuate harmful internal loads.

The purposes of the study were to demonstrate the utility of computer simulations of running for (1) quantifying internal structural loading of injury-prone tissues, and (2) investigating the effects of potential training interventions on loading modulation at these sites.

METHODS

The impact phase of running was simulated with a two-dimensional musculoskeletal model of the body (Fig. 1). The model was actuated by nine Hill-based muscle models per leg. Wobbling masses modeled soft tissue oscillations during impacts. In the 'Normal' simulation, muscle model excitation signals were optimized by genetic evolution to minimize errors between modeled and experimental joint angles and GRF. Experimental data were collected from a healthy 27-year old male running at 4.5 m/s.
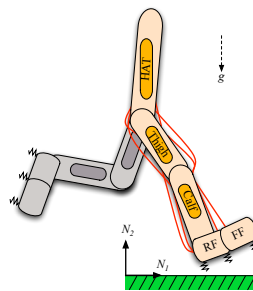

Figure 1. The musculoskeletal model used to simulate running. Swing leg muscles are not shown. HAT = head, arms, and trunk.

To demonstrate the utility of the model in predicting internal loading, a popular training intervention (adjustments in footwear) was simulated by adjusting the stiffness and damping parameters of the model's ground contact elements to approximate harder or softer midsoles (Aerts & De Clercq, 1993) and re-running the simulations. The Normal simulation's muscle excitation signals were used in all simulations (Wright *et al.*, 1998). Outcome variables were peak bone contact forces at the distal tibia, and peak muscle forces.

RESULTS

As shoe stiffness increased from soft to hard, peak compressive tibial contact force increased by 8% of the Normal level, and peak shear tibial contact force increased by 11% (Figs. 2 and 3). Shoe stiffness did not have a consistent effect on changes in peak muscle forces; some forces increased (tibialis anterior, vasti), while some forces decreased (hamstrings) or were unaffected (glutei).
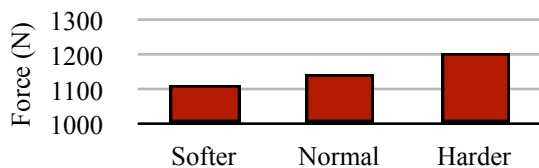

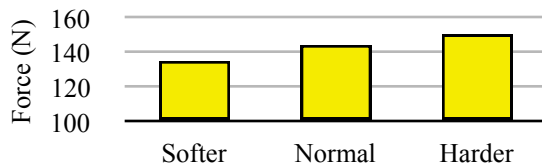**Figure 2.** Peak compressive tibial contact force versus shoe stiffness.

Figure 3. Peak shear tibial contact force versus shoe stiffness.

DISCUSSION

Biomechanical research of overuse injuries has focused for many years on measures of external loading that do not directly quantify trauma-inducing internal loads. New directions in the analysis of running injuries are needed if our understanding of injury mechanisms is to improve. The present results, along with previous research (Neptune *et al.*, 2000), indicate that computer simulations are a powerful tool for achieving this goal through the quantification of internal loading, which cannot necessarily be extrapolated from external loading measures such as the GRF (Wright *et al.*, 1998).

Forward dynamics and optimal control are attractive for their ability to predict responses to novel conditions, as demonstrated by the present simulations. This predictive nature allows researchers to identify causal relationships between input parameters, such as shoe stiffness, and output responses, such as bone loading (Neptune, 2000).

As computers become more powerful, simulations will become increasingly more sophisticated. Subject-specific simulations with model parameters tuned to a particular individual may be useful in clinical settings for investigating internal sources of pain and injury. Modeling and simulation can be used to predict outcomes of potential interventions, such as equipment selection, technique adjustments, and strength and flexibility training, on health and performance.

ACKNOWLEDGEMENTS

REFERENCES

Aerts P and De Clercq D (1993). *J Sports Sci*, 11:449-461.

Hreljac A (2004). *Med Sci Sports Exerc*, 36:845-849.

Messier SP & Pittala KA (1988). *Med Sci Sports Exerc*, 20:501-505.

Neptune RR *et al*. (2000). *Clin Biomech*, 15:611-618.

Neptune RR (2000). *Phys Med Rehab Clin N Amer*, 11:417-434.

Nigg BM *et al*. (1987). *J Biomech*, 20:951-959.

Wright IC *et al*. (1998). *Clin Biomech*, 13:521-531.

PERCEPTUO-SENSORY, COGNITIVE AND SENSORY-MOTOR CHARACTERISTICS THAT INFLUENCE THE ABILITY TO RECOVER BALANCE TO AVOID A FALL

Alessandro Telonio[1,2,3], Hélène Corriveau[1] and Cécile Smeesters[1,2,3]

[1] Research Center on Aging, Sherbrooke QC, Canada
[2] Human Performance and Safety Laboratory (PERSEUS), Sherbrooke QC, Canada
[3] Department of Mechanical Engineering, Université de Sherbrooke, Sherbrooke QC, Canada
E-mail: Cecile.Smeesters@USherbrooke.ca   Web: http://www.usherbrooke.ca/gmecanique

INTRODUCTION

There are still only a small number of studies that have attempted to take tasks related to falls to the threshold of balance recovery. Moreover, there are controversies among these studies as to the effect of perceptuo-sensory, cognitive and sensory-motor deficits on the ability to recover balance to avoid a fall. The purpose of this study was thus to determine the characteristics of younger and older healthy adults that influence the most the ability to recover balance to avoid a fall.

METHODS AND PROCEDURES

Data from 32 adults, who participated in experiments to determine the maximum forward, sideways and backward lean angles that they could be suddenly released from and still recover balance using a single step, were used (Telonio and Smeesters, 2007).

The perceptuo-sensory (vision, vestibular system, distal sensibility, reaction time), cognitive (attention, executive functions) and sensory-motor (movement speed, range of motion, muscular strength, balance and coordination) characteristics of each participants were evaluated by a physical therapist, producing a total of 246 variables.

Eliminating variables with pearson correlation coefficients smaller than 0.200 and using a collinearity diagnostics analysis, we reduced the set to 26 independent variables (Table 1).

Table 1. Pearson Correlation Coefficients with the maximum lean angles

Variable (x_i)	For-ward	Side-ways	Back-ward
1. Knee extension power	0.811	0.810	0.852
2. Age group	-0.774	-0.755	-0.631
3. Grip strength	0.678	0.704	0.700
4. Choice upper limb reaction time	-0.669	-0.690	-0.700
5. Hip flexion power	0.645	0.722	0.688
6. Ankle dorsiflexion power	0.611	0.662	0.666
7. Hip extension power	0.535	0.615	0.692
8. Hip adduction power	0.532	0.578	0.679
9. Knee flexion power	0.520	0.641	0.625
10. Stroop test ink	-0.570	-0.642	-0.561
11. F distance for F SSL	0.678	0.538	0.524
12. FB sway for B SSL	-0.631	-0.648	-0.455
13. Trail making test B	-0.596	-0.589	-0.508
14. Hip abduction power	0.539	0.548	0.588
15. Contrast sensitivity D	0.551	0.517	0.594
16. DN sway speed for F SSL	-0.603	-0.574	-0.451
17. DN sway speed for B SSL	-0.633	-0.603	-0.376
18. FB sway speed for D SSL	-0.587	-0.562	-0.434
19. D+N distance for D+N SSL	-0.510	-0.428	-0.474
20. Simple lower limb reaction time	-0.454	-0.454	-0.483
21. Comfortable walking speed	-0.528	-0.437	-0.417
22. N distance for N SSL	-0.448	-0.395	-0.533
23. D one legged balance	0.465	0.486	0.412
24. Ankle plantarflexion power	0.344	0.408	0.441
25. D malleolus vibration sensibility	-0.324	-0.383	-0.382
26. D palm light touch sensibility	-0.440	-0.328	-0.259

SSL: Static Stability Limit, F: Forward, D: Dominant, N: Non dominant, B: Backward.

For each lean direction, we then determined the characteristics of the participants that influenced the most the maximum lean angle using a stepwise multiple linear regression analysis. Alternative best fit regression models were also computed for comparison.

RESULTS

The stepwise multiple linear regression analyses resulted in model R^2 explaining 75-82 % of the variability in the maximum lean angles (Table 2). Knee extension power was the strongest predictor (64-72 %) in all three lean directions. Static stability limit (11-17 %), simple reaction time (4 %) and other power (4 %) variables contributed to a lesser extent.

Alternative best fit regression models showed nearly identical model R^2 (73-81 %). These showed that hip flexion power (50 %), age group (2-23 %), grip strength (5-7 %), choice reaction time (2 %), and Stroop test (1 %) variables could equally well contribute to the variability in maximum lean angles.

DISCUSSION AND SUMMARY

Therefore, in healthy adults, sensory-motor characteristics were the best predictors of the ability to recover balance to avoid a fall. In particular, muscular strength (57-72 %) and balance (4-17 %) characteristics were the most influential.

However, perceptuo-sensory and cognitive characteristics also contributed to the ability to recover balance to avoid a fall. In particular, reaction time (2-4 %) and executive functions (1 %) characteristics were important. Note that age group could also contribute 2-23 %.

Finally, slightly different characteristics influenced balance recovery in each lean direction. These may thus explain the greater age-related reduction in sideways (36 %) maximum lean angle compared to forward (29 %) and backward (24 %) maximum lean angles (Telonio and Smeesters, 2007).

REFERENCES

Telonio A and Smeesters C (2007). *31st Annual Meeting of the American Society of Biomechanics*, Stanford CA, Aug 22-25.

ACKNOWLEDGEMENTS

Table 2. Stepwise multiple linear regression models and alternative best fit regression models

Lean direction	Type of regression	Regression Model $\theta_{max}=\beta_a x_a+\beta_b x_b+\beta_c x_c+\beta_d$	Partial R^2			Model R^2
			x_a	x_b	x_c	
Forward	**Stepwise**	$\theta_{max}=2.877x_1-0.471x_{17}+0.072x_{11}+13.406$	0.6457	0.1392	0.0320	0.8169
	Alternatives	$\theta_{max}=2.294x_1-4.260x_2+0.077x_{11}+12.850$	0.6457	0.1238	0.0371	0.8066
		$\theta_{max}=2.848x_1-0.377x_{17}-2.877x_2+21.211$	0.6457	0.1392	0.0191	0.8040
Sideways	**Stepwise**	$\theta_{max}=2.370x_1-0.505x_{17}+1.501x_5+13.274$	0.6448	0.1147	0.0350	0.7945
	Alternatives	$\theta_{max}=1.571x_1-5.037x_2+0.143x_3+11.811$	0.6448	0.1059	0.0504	0.8011
		$\theta_{max}=1.364x_5-5.758x_2+0.155x_3+13.525$	0.5049	0.2260	0.0661	0.7970
Backward	**Stepwise**	$\theta_{max}=2.497x_1-0.017x_{20}+14.987$	0.7168	0.0371		0.7539
	Alternatives	$\theta_{max}=2.229x_1-0.027x_4+17.046$	0.7168	0.0234		0.7402
		$\theta_{max}=2.451x_1-0.253x_{10}+12.711$	0.7168	0.0148		0.7316

EFFECTS OF ANKLE STRETCHING ON PASSIVE AND ACTIVE MUSCLE-TENDON PROPERTIES OF PLANTAR FLEXORS IN STROKE

Fan Gao[1-2] and Li-Qun Zhang[1-4]

[1]Rehabilitation Institute of Chicago, Chicago, IL, USA
Departments of [2]Physical Medicine and Rehabilitation, [3]Orthopaedic Surgery, and [4]Biomedical Engineering, Northwestern University, Chicago, IL, USA
E-mail: l-zhang@northwestern.edu

INTRODUCTION

Passive ankle stretching has been used in stroke rehabilitation and the efficacy has been demonstrated. Specifically, motor driven devices have allowed both controllable treatment and quantitative outcome evaluations. Intelligent stretching is effective in treating ankle contracture/spasticity in stroke survivors, with reduced ankle joint resistance torque, stiffness, and increased range of motion (Zhang et al. 2002). However, there is a lack of evaluation of changes in muscle-tendon properties.

The objective of the study was to investigate *in vivo* the passive and active changes of muscle-tendon units of plantar flexors induced by passive ankle stretching in stroke survivors. We expected that stretching would alter muscle-tendon properties, including decreased stiffness, shortening of the Achilles tendon (AT) associated with relaxation of muscle fibers, and improved muscle force-generating capacity.

METHODS

Ten stroke survivors (2 female and 8 male; age: 55±10 year; body mass: 81.9±11.2 kg; height: 174±11.2 cm) and ten gender age-matched healthy subjects (age: 53±18 year; body mass: 70±14.5 kg; height: 170±9 cm) without any neurological disorder participated in the study.

Experimentally, an intelligent stretching device was used for both treatment and evaluations (Zhang et al. 2002). The same evaluations were conducted before and after treatment.

For treatment, the stretching typically reached the peak resistance torque at 15-20 Nm in dorsiflexion and 3 Nm in plantar flexion. In total, there were twelve intermittent stretching sessions of 5 min each (one hour in total).

For evaluation of joint properties, initially, the subjects were asked to relax and the resting position and torque were recorded as baseline values. The resistance torque at the neutral position (90° flexion) was also recorded. The torque-angle relationship during stretching was plotted to establish the hysteresis loops (Figure 1). Index of hysteresis was calculated as the ratio of area within the loop to the area below the ascending limb and presented in percentage.

For evaluation of muscle contraction properties, the triceps surae muscle was activated through electrical stimulation at a constant level across various ankle positions, covering the ankle range of motion. The stimulation-induced torque across the ROM was curve-fitted based on a published model (Otten 1987).

For evaluation of tendon properties, the AT length was measured from the calcaneus notch to the soleus muscle tendon junction using a GE ultrasound machine operating in LOGIQView[TM] mode. The AT cross sectional area (CSA) was measured at a position of 3 cm away from the insertion. Mechanical

properties of the AT, including strain, stress and Young's modulus were derived at the neutral ankle position.
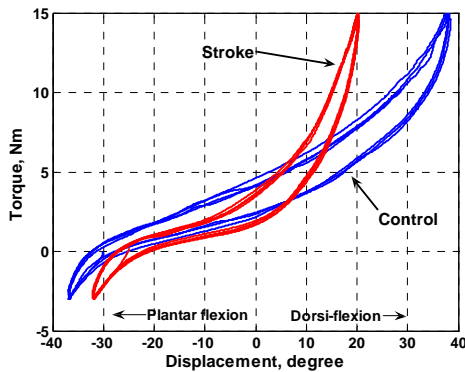

Figure 1. Typical torque-angle relationship of stroke and control subjects during passive stretching.

Student T-test (SPSS, Inc.) was conducted and statistical significance was set at $P<0.05$.

RESULTS AND DISCUSSION

Compared to healthy controls, stroke survivors had a significantly shorter and thinner AT ($P\leq0.042$). The AT lengths were 54.4±8.2 mm and 72.5±17.2 mm and the CSAs were 56.16±7.40 mm^2 and 67.4±8.53 mm^2 for stroke and control, respectively.

The active torque-angle relationship of the stroke survivors shifted towards plantar flexion compared to that of healthy control. Before treatment, the optimum ankle position corresponding to the peak torque was 13.41±5.23^o and 1.25±1.41^o dorsiflexion for control and stroke groups, respectively ($P<0.001$).

After stretching treatment, the ankle joint of stroke survivors was loosened with joint stiffness reduction, especially in dorsiflexion. For instance, the averaged resistance torques of the ascending limb of the passive torque-angle curve at 20° dorsiflexion were 11.9±3.2 Nm and 10.4±3.3 Nm pre- and post-treatment respectively ($P=0.009$). Similarly, a

significantly drop in stiffness was observed (pre: 0.60±.13 Nm/^{o}; post: 0.49±.14 Nm/^{o}). In addition, the index of hysteresis was reduced post-treatment (.37±0.06 and 0.33±0.05 pre- and post-treatment respectively, $P = 0.002$).

Post treatment, the active force-generating capacity of stroke survivors, represented by active torque-angle relationship established through constant electrical stimulation, was significantly improved especially around the neutral ankle position ($P<0.05$). At the tendon level, the AT length of stroke survivors decreased from 54.4±8.2 to 46.5±12.2 mm after treatment ($P = 0.009$), while the AT length of control changed little (from 72.5±17.2 to 71.2±21.8 mm). In addition, in a typical stroke survivor, the tendon become more compliant with the AT stiffness decreased from 96.3 N/mm to 67.9 N/mm at a tension level of 150 N.

SUMMARY

Compared to healthy control, stroke survivors had shorter and thinner Achilles tendons and shifted torque-angle relationships. Repeated ankle stretching could loosen the ankle joint, decrease ankle joint stiffness, and increase passive ROM and could also alter the mechanical properties of the muscle-tendon, such as increased compliance, shortening of the Achilles tendon indicating relaxation of muscle fibers, and improved muscle force-generating capacity.

REFERENCES

Zhang, L.Q. et al. *IEEE Trans Neural Syst Rehabil Eng*, 2002. 10: p.149-157
Otten, E.J. *Neurosci Methods*, 1987. 21: p.287-302

ACKNOWLEDGEMENTS

RELATIONSHIP BETWEEN STATIC ARCH STIFFNESS AND MEDIAL-LONGITUDINAL ARCH BEHAVIOR DURING WALKING

Pedro Rodrigues, Trampas TenBroek, Alan Tomasko and Joseph Hamill

Department of Kinesiology, Biomechanics Laboratory, University of Massachusetts-Amherst, Amherst, MA, USA; email: prodrigues@kin.umass.edu

INTRODUCTION

Static foot measurements are used by researchers and clinicians to predict dynamic foot function. Arch stiffness (AS) is one such measure which attempts to quantify arch flexibility using a vertical force and the corresponding deformation of the arch. There are a number of variations, as some authors scale stiffness calculations to foot length (Zifchock et al., 2006) or a relatively unweighted arch height (Williams et al., 2000) whereas the classical definition does not.

Both active and passive structures contribute to AS. However, stiffness measures are generally taken in static postures, where extrinsic and intrinsic foot musculature is relatively inactive (Mann and Inman, 1964). As a consequence these measures may be representative of the "passive" stiffness of the arch. In dynamic situations, e.g. walking or stair climbing, the contribution of active structures to arch stiffness would presumably increase (Mann and Inman, 1964), possibly rendering the passive measure less relevant. Therefore, the purpose of this experiment was to 1) examine the correlation between different AS measures and 2) determine if static AS measures are good predictors of medial longitudinal arch behavior during a dynamic activity.

METHODS AND PROCEDURES

Twenty male and 19 female subjects were recruited for this study (age 24.2 ± 5.3, height 1.7 ± 0.1 m, mass 71.2 ± 12.6 kg). A certified physical therapist measured right foot length (FL), truncated foot length (TFL), and dorsum height (DH at 50% FL), in sitting and standing. These measurements were made using a Arch Height Index Measurement System and used to calculate arch height index (AHI) and AS using the following equations (Williams et al., 2000, Zifchock et al., 2006)

- $AHI = DH / TFL$

- $AS\text{-}C = (0.4 \times BW)/(DH_{sit} - DH_{stand})$

- $AS\text{-}W = ((DH_{sit} - DH_{stand}) / DH_{sit}) \times (10^4/BW)$

- $AS\text{-}Z = (0.4 \times BW)/(AHI_{sit} - AHI_{stand})$

The foot was modeled as two rigid segments composed of the rearfoot and the medial side of the forefoot allowing for information on the medial longitudinal arch to be calculated. Subjects wore sandals, allowing retro-reflective markers to be directly attached to skin (Figure 1).
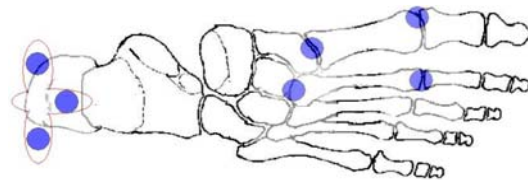

Figure 1. Marker configuration.

A standing calibration was taken then subjects walked at 1.35 ± 0.5 m/s while kinematic and kinetic data was captured at 240 and 1200 Hz. Vertical GRF profiles were used to determine the stance phase. Forefoot motion relative to the

rearfoot was calculated using an Xyz Cardan rotation sequence and then scaled to the standing calibration trial.

The correlation between each stiffness measure was assessed using a Pearson's product-moment. Linear regression analyses were utilized to assess the relationship between AS and the following stance phase kinematic variables: 1) total sagittal plane motion 2) peak dorsiflexion 3) peak plantarflexion.

RESULTS

All AS calculations were highly correlated, with r values between 0.83 and 0.99. Stiffness measurements demonstrated a weak relationship with the kinematic variables during stance (Table 1). The classical definition appeared to have the best fit with the total sagittal plane range of motion (Figure 2). The definition used by Williams et al (2000) appeared to have the best fit with peak dorsiflexion (Figure 3) and plantarflexion.

	C	W	Z
Total Sagittal	0.02	< 0.01	0.01
Dorsiflexion	<0.01	0.07	0.01
Plantarflexion	0.03	0.07	0.02

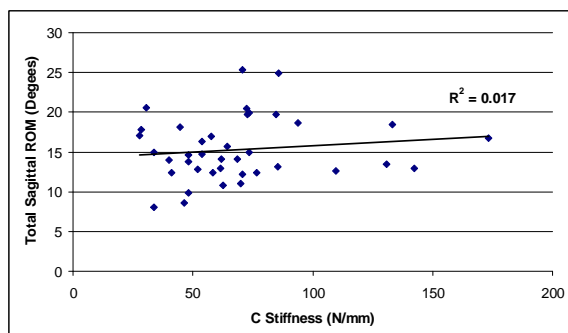**Table1**. R-squared values for linear regression

Figure 2. Classical definition of AS vs. total sagittal plane range of motion during stance
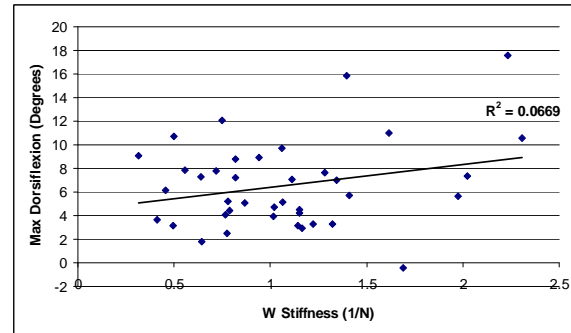

Figure 3. Williams et al. equation of AS vs. maximum dorsiflexion during stance

DISCUSSION

All AS definitions were highly correlated regardless of whether the calculations were scaled to foot length or the relatively unweighted arch height. However, static AS measures do not appear to be predictive of the arch ROM during walking. This implies that although muscle may not be actively contributing to the static stiffness measures they may be appreciably contributing to the arch during some dynamic movements.

Combining static AS measures with dynamic arch kinematics may offer a more complete understanding of the contributions of active and passive tissues to medial longitudinal arch function.

SUMMARY

Current measures of AS are largely inter-correlated. However, none of these measures are good predictors of medial longitudinal arch motion during the stance phase of walking.

REFERENCES

Mann R and Inman VT (1964). *J Bone Joint Surg*, 46-A: 469-481.
Williams, DS and McClay, IS (2000). *Phys Ther*, 80: 864-871.
Zifchock RA et al. (2006). *Foot Ankle Int*, 27: 367-372.

PERFORMANCE MEASURES THAT INFLUENCE THE MOST
THE ABILITY TO RECOVER BALANCE TO AVOID A FALL

Alessandro Telonio and Cécile Smeesters

Research Center on Aging, Sherbrooke QC, Canada
Human Performance and Safety Laboratory (PERSEUS), Sherbrooke QC, Canada
Department of Mechanical Engineering, Université de Sherbrooke, Sherbrooke QC, Canada
E-mail: Cecile.Smeesters@USherbrooke.ca   Web: http://www.usherbrooke.ca/gmecanique

INTRODUCTION

There are still only a small number of studies that have attempted to take tasks related to falls to the threshold of balance recovery, i.e., far enough so that falls can occur. Indeed, to our knowledge, only Madigan and Lloyd (2005) and Wojcik et al. (1999) have shown an age-related reduction in the maximum forward lean angles that healthy adults could be released from and still recover balance using a single step. They both attributed this to an age-related reduction in stepping speed. We wondered if the same held true for other lean directions. The purpose of this study was thus to determine the performance measures of younger and older healthy adults that influence the most the ability to recover forward, sideways and backward balance.

METHODS AND PROCEDURES

Data from 16 younger and 16 older healthy adults, who participated in experiments to determine the maximum forward, sideways and backward lean angles that participants could be suddenly released from and still recover balance using a single step, were used (Telonio and Smeesters, 2007).

For each lean direction, 12 performance measures were evaluated for each participant (Table 1). One variable measured how long after lean release the participants initiated a response: reaction time. Eight variables measured how fast participants executed a

response: step leg push time, support leg push time, weight transfer time, step time, absorption time, maximum step velocity, mean step velocity and maximum step acceleration. Finally, three variables measured the geometry of the step: step length, step height and step width.

Table 1. Pearson Correlation Coefficients with the maximum lean angles

Variable (x_i)	For-ward	Side-ways	Back-ward
1. Max step velocity	0.914	0.888	0.813
2. Max step acceleration	0.849	0.827	0.672
3. Step length	0.789	0.798	0.674
4. Mean step velocity	0.641	0.904	0.665
5. Step height	0.651	0.790	0.554
6. Weight transfer time	-0.602	-0.619	-0.455
7. Step time	-0.489	-0.442	-0.281
8. Step leg push time	-0.298	-0.378	-0.437
9. Reaction time	-0.461	-0.080	-0.541
10. Absorption time	-0.086	-0.459	-0.132
11. Step width	-0.016	-0.133	-0.178
12. Support leg push time	-0.030	-0.009	-0.174

For each lean direction, we then determined the performance measures of the participants that influenced the most the maximum lean angle using a stepwise multiple linear regression analysis. Alternative best fit regression models were also computed for comparison.

RESULTS

The stepwise multiple linear regression analyses resulted in model R^2 explaining 70-89 % of the variability in the maximum lean angles (Table 2). Maximum and mean step

velocities were the strongest predictors (65-83 %) in all three lean directions. Weight transfer time (5 %), step time (3 %), maximum step acceleration (3 %) and absorption time (2 %) variables contributed to a lesser extent.

Alternative best fit regression models showed nearly identical model R^2 (66-88 %). These also showed lesser contributions to the variability in maximum lean angles form absorption time (5 %), maximum step acceleration (4 %), step time (1 %), step length (1 %) and weight transfer time (0.4 %).

DISCUSSION

Therefore, in healthy adults, performance measures describing how fast participants executed a response were the best predictors of the ability to recover balance to avoid a fall. In particular, maximum (65-83 %) and mean (81 %) step velocities were the most influential in all three lean directions.

Other response execution variables (0.4-5 %) and to a lesser extent step geometry variables (1 %) also had a small contribution to the ability to recover balance to avoid a fall. However, how long after lean release the participants initiated a response did not contribute to the ability to recover balance to avoid a fall.

SUMMARY

The age-related reduction in stepping speed was the best predictor of balance recovery in all three lean directions. However, there were slight differences in the other performance measures that also influenced balance recovery in each direction. These may thus explain the greater age-related reduction in sideways (36 %) maximum lean angle compared to forward (29 %) and backward (24 %) maximum lean angles (Telonio and Smeesters, 2007).

REFERENCES

Madigan ML and Lloyd EM (2005). *J Gerontol*, 60A(4): M481-485.
Telonio A and Smeesters C (2007). *31st Annual Meeting of the American Society of Biomechanics*, Stanford CA, Aug 22-25.
Wojcik LA et al. (1999). *J Gerontol*, 54A(1): M44-50.

ACKNOWLEDGEMENTS

Table 2. Stepwise multiple linear regression models and alternative best fit regression models

Lean direction	Type of regression	Regression Model $\theta_{max}=\beta_a x_a+\beta_b x_b+\beta_c x_c+\beta_d x_d+\beta_e$	Partial R^2				Model R^2
			x_a	x_b	x_c	x_d	
Forward	Stepwise	$\theta_{max}=4.154x_1+0.114$	0.830				0.830
	Alternative	$\theta_{max}=3.839x_1-28.386x_6+6.442$	0.830	0.004			0.834
Sideways	Stepwise	$\theta_{max}=5.066x_4+28.529x_7-9.170x_{10}$ $+0.189x_2-6.683$	0.811	0.034	0.020	0.028	0.893
	Alternative	$\theta_{max}=1.861x_1-10.702x_{10}+0.230x_2$ $+8.142x_3+1.328$	0.782	0.046	0.042	0.009	0.879
Backward	Stepwise	$\theta_{max}=2.987x_1-26.369x_6+6.425$	0.650	0.045			0.695
	Alternative	$\theta_{max}=3.091x_1-7.728x_7+5.182$	0.650	0.011			0.661

COMPUTATIONAL VERIFICATION OF WRIST FLEXION-EXTENSION AND RADIAL-ULNAR DEVIATION MUSCLE MOMENT ARMS

John W. Ramsay, Jessica R. Maglott, and Roger V. Gonzalez

LeTourneau University Biomedical Engineering
Longview, TX, USA; E-mail: rogergonzalez@letu.edu

INTRODUCTION

Experimental verification of muscle moment arms from a musculoskeletal model is vital for accurate calculations of joint moment. Currently, many literature values for muscle moment arms during elbow flexion-extension, forearm pronation-supination, and wrist flexion-extension exist to validate these models. However, few sources exist for radial-ulnar deviation moment arms, and none exist that describe wrist moment arms as a function of both wrist flexion-extension and radial-ulnar deviation. Murray et al (1995) noticed that forearm muscle moment arms changed as a function of both elbow flexion-extension and forearm rotation. Since wrist muscle moment arms appear to be dependant on multiple joint angle configurations, then an accurate model should reproduce the same results.

Using the tendon excursion technique to obtain muscle moment arms has been used in past studies. (Horii et al 1993) Utilizing this method, experimental values of both wrist flexion-extension and radial-ulnar deviation moment arms were calculated individually and as a function of the other, and compared to an existing forearm-wrist model developed by Hunt and Gonzalez. (2004)

METHODS AND PROCEDURES

An experimental fixture was designed to restrict an embalmed human cadaver arm in two degrees-of-freedom (*df*s): wrist flexion-extension and radial-ulnar deviation. The dissected specimen was positioned with the elbow flexed at 90° with the wrist in neutral pronation-supination. Ten wrist mover tendons were sutured to cables connected to potentiometers to measure tendon excursion, representing the change in muscle-tendon length (∂l^{mt}). An electrogoniometer was used to measure the wrist joint angle (θ) in both *df*s. One motor fixed a specified joint angle at a constant value while a second motor using position feedback from the electrogoniometer maintained a constant velocity as it travelled through the secondary *df*.

For each fixed joint angle (e.g. r/u deviation), the wrist was moved throughout the secondary *df* (e.g. wrist f/e) and the rotation of each potentiometer recorded the tendon excursion. Once tendon excursion was measured throughout the range of motion, each muscle's moment arm was calculated from the tendon excursion-joint angle relationship given by the equation (An et al. 1997):

$$MA = \frac{\partial l^{mt}}{\partial \theta}$$

Experimental cadaver moment arms were then compared to those of the computational model.

RESULTS

Preliminary results of wrist flexion-extension tendon excursion are shown in Figure 1 for a single trial performed at 0° radial-ulnar deviation through a full range of wrist

flexion-extension of the specimen. Results are similar in shape as found by Horii et al. (1993) (Figure 2). Extensors have positive excursions, where as flexors have negative excursions.
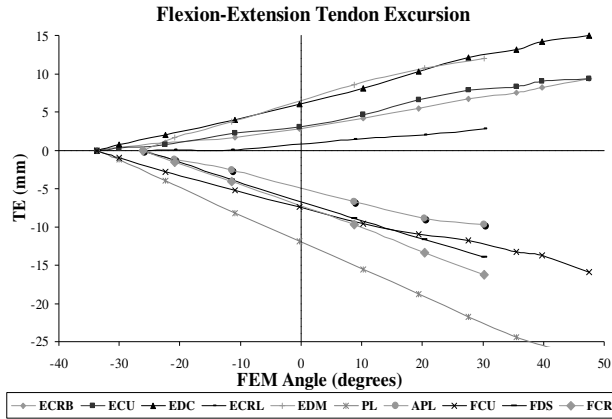

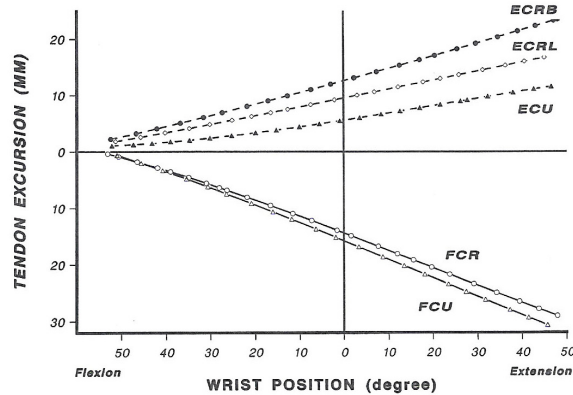**Figure 1: Experimental wrist flexion-extension tendon excursion.**

Figure 2: Literature wrist flexion-extension tendon excursion (Horii et al. 1993)

Three additional specimens are currently being prepared for further testing, and will be compared to our musculoskeletal model as well as relevant literature.

DISCUSSION

Although our tendon excursion data is similar in its trend to that of Horii et al (1993), our data differs in that its magnitude is smaller, likely due to the preservation and limited mobility of our specimen.

Our forearm-wrist model uses only one literature source for radial-ulnar deviation, and this study will provides additional data-sets. However, most studies in the literature use fresh frozen cadavers for the tendon excursion technique, where our cadavers are preserved. Therefore, prior to comparing our preserved muscle moment arms to the model, our moment arms must first be similar to fresh cadaver studies at known joint angles.

Our current musculoskeletal model has shown minimal changes in muscle moment arm as both wrist flexion-extension and wrist deviation occurs. Yet, if noticeable changes in our cadaver specimens are observed, the model will be modified to represent these changes.

CONCLUSION

While our study is still in its early stages, the additional data for radial-ulnar deviation moment arms as well as an original data-set of wrist moment arms as a function of two *df*s will be useful for not just our wrist model, but others as well. We anticipate a full set of results will be available by the time of the presentation.

REFERENCES

An, KN et al. (1984). *J Biomech Engng*, 106: 280-282

Horii, E et al. (1993). *J of Hand Surgery*, 18: 83-90.

Hunt, BV and Gonzalez, RV (2004). *ASME National Congres*s, Anaheim, CA.

Murray, WM et al. (1995). *J Biomech,* 28: 513-525

ACKNOWLEDGEMENTS

A 3-D FINITE ELEMENT MODEL OF ANTERIOR VAGINAL WALL SUPPORT FOR EVALUATING MECHANISMS UNDERLYING CYSTOCELE FORMATION

Luyun Chen[1], James A. Ashton-Miller[1], Yvonne Hsu[2], John O.L. DeLancey[2]

[1] Department of Biomedical Engineering, [2] Department of Obstetrics and Gynecology,
University of Michigan, Ann Arbor, Michigan, U.S.A. luyunc@umich.edu
URL: http://me.engin.umich.edu/brl/

INTRODUCTION

Anterior vaginal wall prolapse (hernia), clinically known as 'cystocele', is the most common form of pelvic organ prolapsed in women (Hendrix 2002). It is also the site with the highest rate of persistent and recurrent support defects (Shull 2000). However the mechanism of cystocele still remains unknown. The goal of this study was to develop a 3-D finite element model based on living woman's anatomy to investigate how intraabdominal pressure affects prolapse size in the presence of increasing defects in the two systems of anterior vaginal wall support: muscular support and connective tissue support, including apical support and paravaginal support.

METHODS

A 3-D volumetric model was created from magnetic resonance images (MRI) of a 34 year-old healthy nulliparous woman to establish the geometry of anterior vaginal wall and surrounding support tissues using 3D Slicer 2.1b1 (*ad modam* Chen 2006) is shown in Figure 1A & B. The volumetric model was then simplified using the I-DEAS Surfacer (Figure 1C) and then imported into ABAQUS (Version 6.6-1 ABAQUS, Inc) for meshing and finite element analysis (Figure 1D). The anterior vaginal wall and levator ani muscles were modeled as deformable shell elements. The posterior compartment including posterior vaginal wall and rectum were modeled as a deformable 3-D solid. 3-D truss elements were used to represent the ligamentous connections to vaginal wall.

There are total 11553 nodes and 11968 elements. All the model elements were assigned hyperelastic material properties based on literature values (Yamada 1970, Bartscht 1988) and our own tissue testing. Simulations were run by modeling defects as % loss in tissue stiffness and incrementing intra- abdominal pressure.
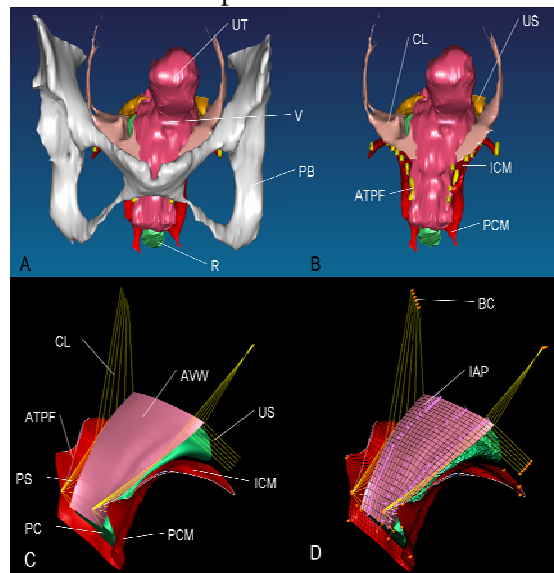

Figure 1, Model development. A: 3-D volume rendering model of anterior support system including pubic bone；B: 3-D volume rendering model without pubic bone; C: Geometry simplified surface model; D: 3-D finite element model with mesh, boundary condition (orange pin representing ligaments and muscle origin is pinned to pubic bone and pelvic sidewall), and abdominal pressure loading. PB: pubic bone; UT: uterus; V: vagina；R: rectum; CL: cardinal ligament; US: uterosacral ligament; ATFP: arcus tendineus fascia pelvis; ICM: iliococcygeus

muscle; PCM: pubococcygeus muscle; AVW: anterior vaginal wall; PC: posterior compartment; PS: paravaginal support; IAP: abdominal pressure

The model was validated by comparing the mid-sagittal anterior vaginal wall deformation under increasing abdominal pressure with that measured in a dynamic mid-sagittal MRI of a patient with stage III cystocele performing the same maneuver. The simulated prolapse size was measured as vertical distance between the most dependent point of deformed vaginal wall to ATFP origins from pubic bone on mid-sagittal plane.

RESULTS

A typical 3-D displacement-time simulation sequence is shown in Figure 2 with increasing intraabdominal pressure, which is run on a IBM T42 with Intel Pentium 1.8GHz processor and 1.25GB RAM for 456mins. The main finding is that prolapse size was sensitive to impairments in apical connective tissue, paravaginal connective tissue, as well as to abdominal pressure (Table 1).
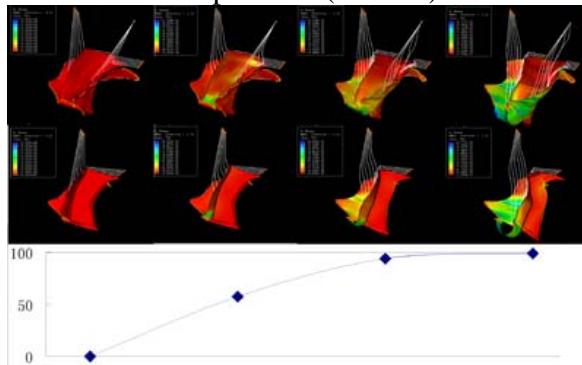

Figure 2. The sequential development of a simulated cystocele at 4 time steps (left-to-right). In this simulation, levator ani muscle had a 60% defect, apical and paravaginal support were set be to 50% defects and abdominal pressure rose from 0 to 99 cmH$_2$O. The first row shows three-quarter views, the second row sagittal cut views, while the plot gives the pressure (y-axis, in cm H$_2$O) at each time point (x-axis).

Defect Severity		Abdominal Pressure (cmH$_2$O)		
Apical Defect	Para-Vaginal Defect	50	99	168
Prolapse Size (cm)				
90%	0%	*0.7*	*1.8*	*4.1*
0%	90%	*0.6*	*1.5*	*2.9*
50%	50%	*0.8*	*1.9*	*4.9*

Table 1: Prolapse size (in cm) of the simulated cystocele with different defect combinations under different maximum intraabdominal pressure (in cmH$_2$O).

DISCUSSION

This is the one of the first attempts to simulate cystocele formation using 3-D finite element analysis. The model correctly reproduces the development of a cystocele under increasing intraabdominal pressure, as seen clinically. The model lends itself to be used to systematically examine the interactions of different combinations of anatomic defects in causing cystocele formation in a way that would not be ethical in living humans.

CONCLUSIONS

A cystocele can form due to impairments in muscle and/or connective tissue supports of the anterior vaginal wall.

REFERENCES

Bartscht, KD and Delancey, JO (1988). *Obstet Gynecol,* 72:940–3
Chen, L et al (2006). *Obstetrics & Gynecology,* 108(2):324-32
Hendrix, SL et al (2002). *Am J Obstet Gynecol, 186:1160–6.*
Shull, BL et al (2000). *Am J Obstet Gynecol*, 183(6):1365-73
Yamada, H. (1970) *Strength of Biological Materials*, Williams & Wilkins 205–70.

ACKNOWLEDGEMENTS

ANALYSIS OF AMPUTEE GAIT USING CENTER-OF-MASS VELOCITY

Peter Gabriel Adamczyk[1,†], Michael Orendurff[3], Joseph Czerniecki[2], Ava Segal[2],
Hannah Sutton[2], Glenn Klute[2], Arthur D. Kuo[1]

[1]Department of Mechanical Engineering, University of Michigan, Ann Arbor, MI USA
[2]U.S. Department of Veterans Affairs Center for Limb Loss Prevention and Prosthetic
Engineering, V.A. Puget Sound Health Care System, Seattle, WA USA
[3]Movement Science Laboratory, Texas Scottish Rite Hospital for Children, Dallas, TX USA
[†]email: padamczy@umich.edu

INTRODUCTION

Clinical gait evaluation in a laboratory produces abundant data regarding kinematics, moments, and powers at the joints. Although joint motion is critical to walking, there are few measurements that evaluate motion of the body center of mass (COM). Such measures could potentially augment joint data and contribute to understanding of gait abnormalities. Here we show that a cyclic plot of the COM's trajectory in velocity space, called a COM *hodograph*, exhibits distinct features that differ between normal and pathological gait. The features arise from abnormalities such as asymmetric work output and impaired push-off. They can be linked to unilateral leg function for highlighting gait asymmetry, and can be quantified for objective comparison.

METHODS

We measured ground reaction forces (GRF) while unilateral transtibial amputees (n = 4) and non-amputees (n = 10) walked over two in-floor force plates. From the measured GRF and walking speed, we computed COM velocity over a complete stride cycle (Cavagna, 1975). We plotted the COM hodograph as the vertical component of COM velocity versus its fore-aft component (Fig 1; Greenwood,1988). We noted prominent features differentiating the hodographs of amputees (Fig 2) and non-amputees (Fig 1). We compared these features to the underlying GRF in

order to determine the functional abnormalities that caused them.

A typical COM hodograph for a non-amputee is shaped like a rounded letter D, with one counter-clockwise loop for each leg's stance phase (Fig 1). Double support spans the right (highest-speed) portion of each loop and single support spans the left portion. Just before heel strike, the trailing leg commences push-off, reducing the downward COM velocity and giving the bottom of the D an upward slope. During double-support both legs redirect the COM velocity upward, forming the rounded portion of the D. The maximum up-
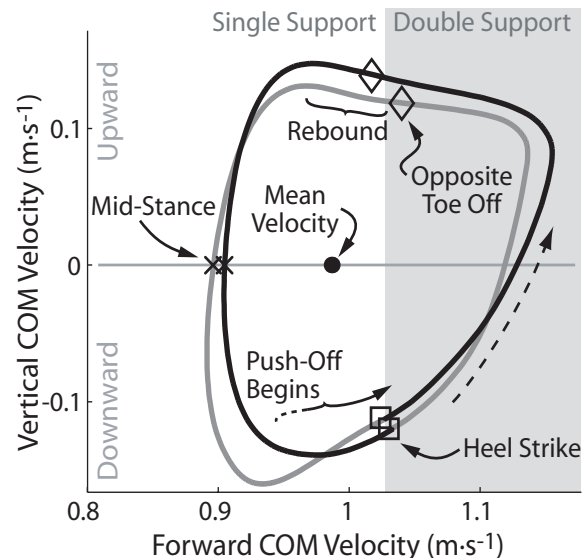

Figure 1: Sample COM hodograph for a complete stride cycle of a non-amputee walking at 1.0 m·s⁻¹. Labels indicate mean velocity and the timing of heel strike, opposite toe off, rebound, mid-stance (defined as zero vertical velocity), and early push-off. Light: Left Stance; Dark: Right Stance
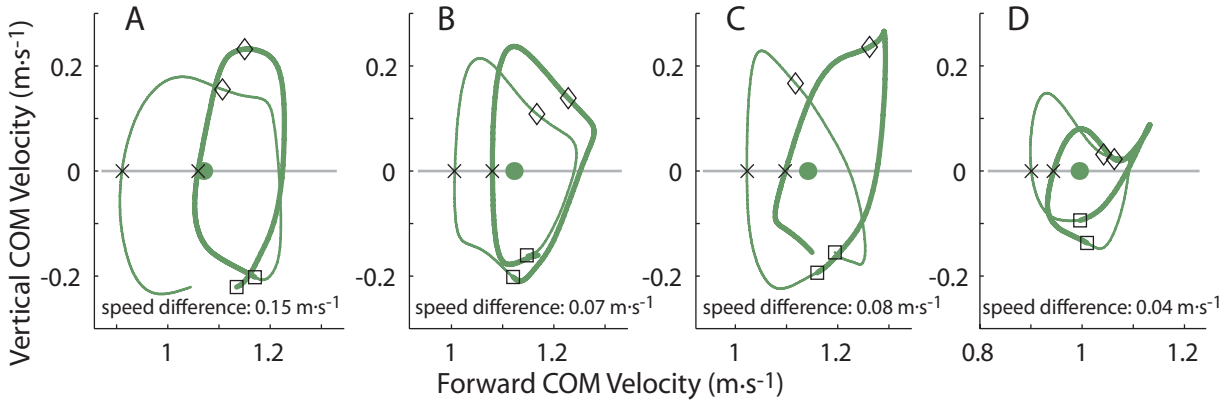
Figure 2: COM hodographs from four unilateral transtibial amputees. One abnormality is that mid-stance forward speed is higher during prosthetic stance than during intact stance, indicating asymmetric acceleration and deceleration of the COM (A-D; speed difference is given for each subject). Other features such as asymmetric forward speed range (A), downward acceleration at intact heel strike (A,C,D), and negative vertical acceleration during late double-support (C-D) may yield additional subject-specific insight. Thin lines: Intact Leg Stance; Thick lines: Prosthetic Leg Stance. Gait events denoted by symbols as in Fig 1.

ward COM velocity occurs after toe-off as a "rebound" from leg compression. Finally, the middle portion of single-support is characterized by a smooth downward acceleration.

RESULTS AND DISCUSSION

One feature of the amputee COM hodographs is substantial asymmetry in walking speed. We quantified this by comparing the forward COM velocity at mid-stance for the two legs. Intact subjects had only slight speed asymmetry (Fig 1; absolute value of speed difference 0.0123 ± 0.0125 m·s^{-1}, mean $\pm$ S.D.), while amputees exhibited speed asymmetry of 0.04 to 0.15 m·s^{-1} (intact-affected speed difference, Fig 2A-D). This may be due to a reduced ability to push off with the prosthetic leg and compensations such as increased push-off with the intact leg.

Additional features of the amputee COM hodographs may provide additional insight into the specific gait of each individual. For example, three amputees exhibited downward (rather than normal upward) acceleration at the time of intact heel strike (Fig 2 A,C,D). For these amputees, prosthetic side vertical push-off GRF does not exceed body weight before heel strike as it does in most intact

limbs. Other features include asymmetries in speed fluctuation (Fig 2A) and unusual downward acceleration during late double-support (Fig 2 C-D). These features may be helpful for understanding how a wide variety of gait impairments influence COM motion, and could potentially be quantified as with speed asymmetry.

The hodograph provides a simple summary of COM motion that can complement traditional gait rehabilitation techniques. It highlights abnormal gait patterns in ways that cannot be observed visually. It does not require extensive equipment, and can be constructed with as little as a single force plate.

REFERENCES

Cavagna, GA (1975) *J. Appl. Phys.* 39:174-9.
Greenwood, DT (1988) *Principles of Dynamics.* Prentice-Hall, New Jersey.

ACKNOWLEDGEMENTS

Liquid Plug Dynamics in Microfluidic Flexible Channels – a Small Airway Model

Ying Zheng[1], Hideki Fujoka[1], Yusuke Torisawa[1], Shuichi Takayama[1,2], James B. Grotberg[1]

[1]Department of Biomedical Engineering, [2]Department of Macromolecular Science and Engineering, University of Michigan, Ann Arbor, MI

INTRODUCTION

Chronic obstructive pulmonary disease is the fourth leading cause of death in America with characteristics of airflow obstruction, airway closure and airway wall remodeling. Liquid plugs can form due to interfacial instability, airway wall collapse or a combination of both. The propagation of a formed plug can produce high pressure, high shear stress, and large gradients of each, which may damage the cells lining the wall (Fujioka and Grotberg, 2004; Zheng, 2007).

This study is motivated by an interest in the effect of wall flexibility on the plug propagation and its resulting wall stresses in small airways. Cell injuries have been investigated experimentally during airway reopening in Gaver's group (Bilek, 2003; Kay, 2004) by propagating the semi-infinite air bubbles through a rigid chamber lined with airway epithelial cell and in Huh et al. (Huh, 2007) of liquid plug propagation and rupture on human airway epithelial cells lined microengineered airway system. Fluid stress and stress gradients on the rigid walls during the two phase flow has been demonstrated to be responsible for the cell injuries in these experiments. Understanding is needed on the plug dynamics and wall stresses in flexible channels to mimic the real physiologic situations.

METHODS AND PROCEDURES

Experiments: The flexible microchannel is made by two layers: main channel layer, which is fabricated with soft lithography method using materials of PDMS at a curing ratio of 10:1; and a thin membrane layer with thickness of 5-7 μm, which is spin-coated on a silanized clean glass cover slide. The channel dimensions are around 100μm in height and 100μm in width. The two layers were sealed against each other using a plasma oxidizer (11005-plasma Prep II, SPI, West Chester, PA). The microchannels were filled with the liquid. The inlet and outlet are connected to reservoirs which were open to the atmosphere. A pair of air bubbles was injected in the liquid to form a plug, which propagated with a specified pressure from the gravity pump. A CCD camera (Hamamatsu Orca-100), connected to an inverted fluorescent microscope (TE-300, Nikon, Tokyo, Japan), and SIMPLE PCI software (Compix Inc.) were used to record the plug motion and wall deformation.
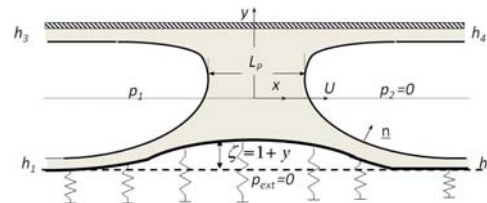
Mathematic Model:

Figure 1. Schematic of propagation of liquid plug with length L_p in flexible channel with speed U and driven by the pressure drop p_1-p_2.

The steady plug propagation is numerically simulated in a 2-D channel with top wall rigid and bottom wall flexible, shown in Figure 1. The flow governing equations are $\nabla p = \nabla^2 \underline{u}$, $\nabla \cdot \underline{u} = 0$. On the flexible wall, the fluid stress balances with the wall tension: $T_L \kappa_{LW} - f(\zeta) = -Ca \underline{n}_w \cdot \underline{\underline{T}} \cdot \underline{n}_w$ in which, T_L is the longitudinal tension scaled with the surface tension; $\zeta(x)=1+y$ is the lower wall deformation with undeformed wall $\zeta(x)=0$; $f(\zeta)$ is the nonlinear spring tension with respect to the wall deformation, obtained by fitting the pressure-deformation curve

measured in the experiments with the formula $f(\zeta)=A\zeta^3 + B\zeta$ where A=76.8 and B=0.13. The wall damping and inertia are neglected in the wall equation due to the fact of thin flexible membrane and Stokes flow regime. The curvilinear computational grid was generated from two dimensional Poisson's equation. SIMPLER algorithm is used to solve momentum and pressure equations. The wall equation is solved using Newton's method.

RESULTS
The wall deformation is observed during plug propagation for different plug length and propagation speed. Figure 2 shows the plug dynamics and wall deformation for 3 different situations of plug length and speed.

(a) LP ~ 2.5 H, U ~ 1.0cm/s

(b) LP ~ 0.56 H, U ~ 0.63cm/s   (c) LP ~ 0.08 H, U ~ 0.3cm/s
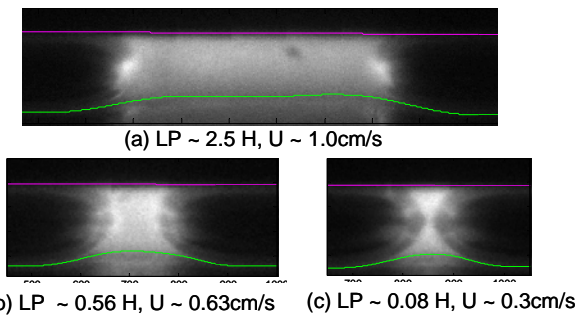
Figure 2. Instantaneous flexible wall deformation during plug propagation. H is the channel height, which is about 100μm.

Image analysis was performed to extract the wall shape and quantify the wall deformation. The maximum wall deformation for the three cases shown in Figure 2 is measured to be (a) 15.5 ±1μm, (b) 12.5±1μm, and (c) 11±1μm. It shows to increase with increasing plug length and speed. The average strain along the wall, defined as the arc length difference normalized by the original wall length, is measured to be (a) 0.7% (b) 1.0% and (c) 1.2%, which increases with decreasing plug length and speed.

The plug flow pattern is calculated as shown in Figure 3 with the fluid stress and stress gradients comparing the flexible wall and rigid channel walls.
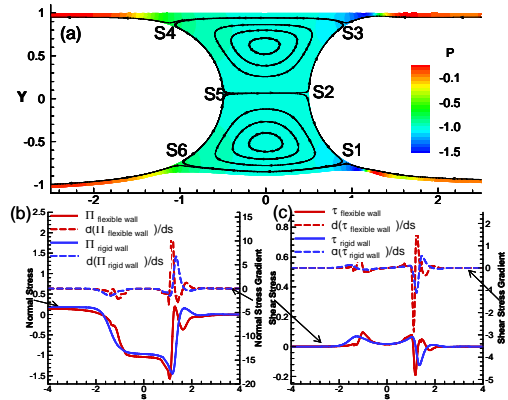

Figure 3. (a) The plug flow patter with pressure contour and flow streamlines at Ca=0.01, LP=1, Re=0 and T_L =1.(b) Normal fluid stress and stress gradients along x direction (c) Shear stress and stress gradients from the fluid along x direction.

The maximum flexible wall deformation is measured to be around 10% of the channel width at this parameter set, which is in the same order as what we measured in the experiment (11-15%). The normal stress shows little changes with wall flexibility but the normal stress gradient has a larger peak for the flexible wall. Shear stress and its gradient increases largely on flexible wall, which increases the risk on the cell damages during diseases like emphysema.

SUMMARY
We experimentally observed the flexible wall deformation during plug propagation and numerically predicted high stress and stress gradients due to the increase of wall flexibility. Diseases like emphysema may cause more cell/tissue damages during airway reopening process.

REFERENCES

Fujioka H and Grotberg JB (2003). *J Biomch. Eng.,* 126: 567-577.
Zheng Y et al (2007). *Phys. Fluids,* 8,082107.
Bilek AM et al (2003). *J App Physio.*, 94: 770-783.
Kay SS et al (2004). *J App Physio.*, 97: 269-276.
Huh D et al (2007). PNAS, 104: 18886-18891.

ACKNOWLEDGEMENTS

ELASTIC ROD MODEL FOR PROTEIN MEDIATED DNA LOOPING

Todd D. Lillian[1], Sachin Goyal[2], Edgar Meyhöfer[3], and Noel C. Perkins[4]

[1]Doctoral Candidate, Mechanical Engineering Department, University of Michigan, Ann Arbor, MI, USA, tlillian@umich.edu
[2]Visiting Assistant Professor, Theoretical & Applied Mechanics Department, Cornell University, Ithaca, NY, USA
[3]Professor, Mechanical Engineering Department, University of Michigan, Ann Arbor, MI, USA
[4]Professor, Mechanical Engineering Department, University of Michigan, Ann Arbor, MI, USA

INTRODUCTION

DNA looping is a common gene regulatory mechanism whereby two distant DNA operator sites are bound by a regulatory protein that deforms the intervening DNA into a loop. The Lactose repressor (LacI), of the bacterium E. coli, is a classical example, and is responsible for regulating the production of proteins necessary to digest lactose. LacI functions by blocking access to genes when the loop is formed.

Although LacI has been the subject of much research (see, for example, Becker et al., 2005, Müller et al., 1996) several issues remain unresolved. For instance, the crystal structure of LacI has been resolved (Lewis et al., 1996); refer to Figure 1. However, the energetics and topology of the DNA loop remain unknown. The energy of loop formation is important because it influences the probability of gene repression. Here we exercise a computational elastic rod model (Goyal et al., 2005) to predict the energetics of loops of various lengths. The continuum model describes the long-length scale and three-dimensional deformation of the DNA helical axis as illustrated in Figure 1.
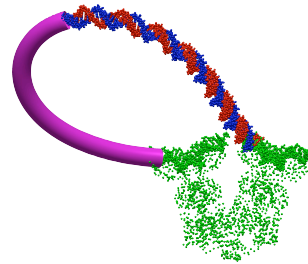

Figure 1. LacI DNA loop complex. The LacI protein structure (Lewis et al., 1996) is represented with all-atom detail (green). The DNA loop is shown in two representations, an atomistic approximation and an elastic rod.

METHODS AND PROCEDURES

The application of our elastic rod model to DNA looping is recently reported in (Goyal et al. 2007). Our rod model accounts for large DNA bending and twisting deformations that arise in order to satisfy the boundary conditions imposed by looping. The molecule binds to LacI at two specific sites in the sequence (operator sites). DNA bending and torsional stiffnesses are approximated by published experimental measurements (Schlick, 1995). Figure 1 illustrates the rod model approximation to the all-atom structure of DNA. The model treats the length of the DNA as an important parameter that can be experimentally altered and thus controlled. As

the length of the intervening DNA increases, the the torsional alignment of the operator sites adjusts as dictated by the helical structure of DNA which possess about 10.5 basepairs per helical turn.

RESULTS AND DISCUSSION

In Figure 2 we present the elastic energy (kT), including the torsional and bending components, of loop formation as a function of DNA length. Two major observations are apparent. First, the total elastic energy reduces at a rate of about 1/L, where L is the length of the DNA loop. (This becomes even more apparent as the length is increase beyond the 15 helical turns shown.) Basic rod theory predicts that the strain energy of an elastic rod deformed into a circle is inversely proportional to its length. This suggests that long loops are more efficient at repressing gene activity because of their low energy. By contrast, experiments suggest an optimal DNA length for maximum repression (Müller et al., 1996). We attribute this discrepancy to the high entropic contribution to the free energy of looping for long lengths of DNA (longer than about 10-20 helical turns). The calculations reported here neglect this entropic contribution and their utility is restricted to shorter lengths of DNA, where the entropic contribution to the free energy remains on the order of 10% or less (Wilson et al., 2007).

Second, the total elastic energy oscillates with a one helical turn period. This is a direct result of the helical construction of DNA, as observed experimentally (Becker et al., 2005, Müller et al., 1996). As the torsional alignment of the DNA operators changes with increasing length, their alignment with the protein binding sites changes. One might
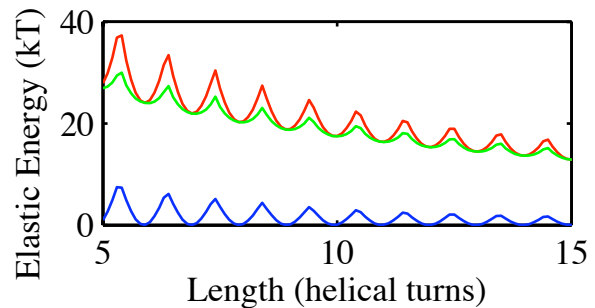

Figure 2. Loop elastic energy (kT) dependence on DNA length: torsional (blue), bending (green), and total (red).

expect the torsional component of the energy to be primary source of of these oscillations (Becker et al., 2005). However, Figure 2 shows that both bending and torsional components of the elastic energy oscillate with similar amplitude. Therefor the loop adjusts to changes in the alignment of the operator sites by both bending and twisting the DNA helical axis in three dimensions.

REFERENCES

Becker, NA et al. (2005). *J Mol Biol,* 349:716-730.

Goyal, S et al. (2005). *J Comput Phys,* 209:371-389.

Goyal, S et al. (2007). *Biophys J,* 92:4342-4359.

Lewis, M et al. (1996). *Science,* 271:1247-1254.

Müller, J et al. (1996). *J Mol Biol,* 257:21-29.

Schlick, T (1995). *Curr Opin Struct Biol,* 5:245-262.

Wilson, DP et al. (2007). *Proc SPIE,* 6602:660208.

ACKNOWLEDGEMENTS

LOWER-BACK COMPRESSIVE FORCES DURING DROP LANDINGS

Christopher J. Sorensen, W. Brent Edwards, Brett J. Sealine, Jason C. Gillette,
and Timothy R. Derrick

Department of Kinesiology, Iowa State University, Ames, IA, USA
E-mail: chriss40@iastate.edu   Web: www.kin.hs.iastate.edu

INTRODUCTION

Lower back injuries account for 10 to 15% of all injuries in athletes (Tall and Devault, 1993). A study of 31 Olympic athletes with lower back pain suggested that the most frequently affected area was the joint between the 5th lumbar and 1st sacral vertebrae (L5S1) (Ong et al., 2003).

Athletes suffering from L5S1 pain are often involved in sports that require repetitive landing from various heights. This type of repetitive loading may lead to L5S1 joint degeneration, and subsequent joint pain, if compensatory strategies are not undertaken to reduce the loading environment.

Research focusing on L5S1 joint loading during landing activities is sparse. The purpose of this study was to determine L5S1 compressive forces during landings from three heights. We hypothesized that L5S1 compressive forces would increase with landing height.

METHODS

Five females (age 21.2 ± 0.5 yrs, height 1.6 ± 0.1 m, mass 59.1 ± 8.5 kg) and four males were recruited for this study (age 27.5 ± 3.9 yrs, height 1.8 ± 0.1 m, mass 82.4 ± 2.1 kg). Motion-capture (160 Hz) and force platform data (1600 Hz) were collected while subjects landed from three separate heights (26, 39, 52 cm) in a balanced order. Ten trials were collected at each height.

Kinematics of the trunk, pelvis and right lower-extremities were calculated in a flex/ext, abd/add, int/ext sequence. Assuming symmetry of both legs, a bottom-up inverse dynamics approach was used to obtain reaction forces and the flex/ext moment at the L5S1 joint. Anthropometrics of the lower extremity and pelvis were obtained from Vaughn et al. (1992) and Zatsiorky (2002), respectively. The reaction forces and moment were calculated in the global reference frame and then rotated into a local L5S1 reference frame. The local L5S1 reference frame was estimated from a -45° rotation of the pelvic reference frame about the medial-lateral axis.

Kinematic data were imported into a scaled SIMM 4.0 model to obtain lower back flex/ext moment arms. Using these moment arms, compressive L5S1 contact forces were calculated as follows:

$$F_c = RF_{axial} + \frac{M}{r}$$

where F_c is the L5S1 compressive contact force, RF_{axial} is the axially oriented reaction force, M is the flex/ext moment, and r is the corresponding flex/ext moment arm (depending on the direction of the moment).

Peak compressive forces during the first 200 ms of landing were determined for each trial. Mean peak compressive forces were calculated at each height. Differences in peak compressive forces were examined using a repeated measures ANOVA ($\alpha = 0.05$) with Bonferroni adjustment for pairwise comparisons ($\alpha = 0.017$).

RESULTS

Group ensemble curves for L5S1 compressive forces are displayed in Figure 1. The assumption of sphericity was not met (Huynh-Feldt $\varepsilon = 0.68$) for the univariate repeated measures ANOVA. Therefore, multivariate tests were used and a significant Pillai's Trace statistic was observed ($F = 5.65$, $p = 0.035$). Pairwise comparisons revealed that the 39 and 52 cm drop heights had larger L5S1 compressive forces than the 26 cm drop height. No differences in L5S1 compressive forces were found between the 39 and 52 cm drop heights (Figure 2).
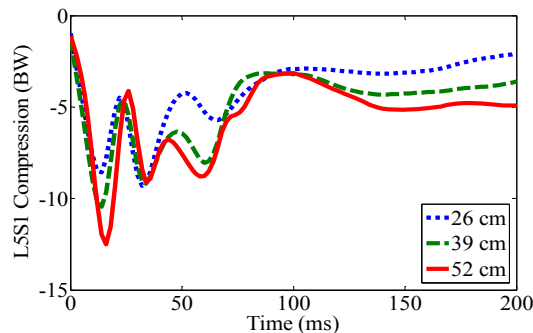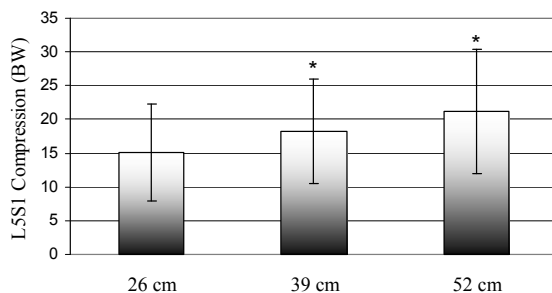

Figure 1. Group ensemble L5S1 compressive forces.

Figure 2. Mean peak L5S1 compressive forces (* significantly different from 26 cm).

DISCUSSION

Our hypothesis was only partially supported by the results of this study. L5S1 compressive forces increased from 26 to 39 cm, and no change was observed from 39 to 52 cm. Caster and Bates (1995) suggested that subjects may choose from one of two strategies during landings: 1) a mechanical strategy in which forces increase in accordance with Newton's 2nd law, and 2) a neuromuscular strategy in which compensatory strategies are undertaken to reduce loads. Further review of within subject differences, suggested that only 1 subject adopted a neuromuscular strategy from 26 to 39 cm, but 4 subjects adopted a neuromuscular strategy from 39 to 52 cm. This discrepancy in landing strategies may have led to the larger variance in L5S1 compressive loads during the highest drop, preventing significant differences between the 39 and 52 cm conditions.

SUMMARY

L5S1 compressive forces increase from a 26 to 39 cm drop height, but not from a 39 to 52 cm drop height as some subjects may adopt a landing strategy that prevents further increases in loads. Athletes able to adopt compensatory landing strategies at higher drop heights may be at a lower risk for L5S1 joint pain.

REFERENCES

Caster B & Bates B (1995). *Med Sci Sports Exerc*, 27:736-744.
Ong A et al. (2003). *Br J Sports Med*, 37:263-266.
Tall R & Devault W (1993). *Clin Sports Med*, 12:441-448.
Vaughan C et al. (1992). *Dynamics of Human Gait*. Champaign, IL, Human Kinetics.
Zatsiorsky V (2002). *Kinetics of Human Motion*. Champaign, IL, Human Kinetics.

ACKNOWLEDGEMENTS

Changes in Patellofemoral Contact Pressure Caused by Imbalance of the Knee Extensor Muscles

Andrew Sawatsky, Doug Bourne, Azim Jinha, Walter Herzog
University of Calgary, Calgary, AB Canada
E-mail: aj_sawatsky@hotmail.com

INTRODUCTION

Strength imbalance of the knee extensor muscles has been associated with problems in patellofemoral tracking (Powers, 2000), joint pain, and osteoarthritis. Changes in patellar tracking and pressure distribution are suspected to cause patellofemoral pain (PFP). The main region of pain is the lateral aspect of the patellofemoral joint. Weakness of the vastus medialis (VM) relative to the vastus lateralis (VL) is the usual imbalance associated with PFP (Cowan et al., 2002; Lefebvre et al., 2006). The fibers of VM are aligned about 50° medially, and this structural arrangement has been thought to pull the patella medially while the vastus lateralis has been assumed to provide the corresponding lateral balance.

A commonly used treatment for PFP is exercises directed at increasing the strength of the VM in the hope of balancing the lateral pull of VL. Although the idea that muscle imbalance causes maltracking of the patella and so causes pain makes intuitive sense and has clinical and anecdotal support, it has not been tested scientifically.

The purpose of this study was to create an animal model of quadriceps imbalance and to test the effect of extreme imbalance on patellofemoral contact pressures. Muscle imbalance was produced by eliminating the action of VM by cutting it in mid-belly. We hypothesized that the elimination of VM causes a lateral shift of the patellofemoral contact pressures, and might cause lateral patellar subluxation.

METHODS

All experiments were performed on knees (n=12) of six months old New Zealand white rabbits (mass 4.5-7.7kg). Measurements of patellofemoral contact pressures were performed before and after VM transection at 5-8 of force levels and three knee angles. Experiments were approved by the Animal Ethics Review Committee of The University of Calgary.

In order to assess changes in patellofemoral contact pressures, low grade and medium grade pressure sensitive film (Fuji) was used. Prior to measurement, rabbits were placed in a stereotaxic frame with only the tibia and foot of the test limb being mobile. The film was inserted into the joint through bilateral, retinacular, 20-25mm incisions while the joint was fully extended. The tibia was then placed behind a restraining bar at knee angles of 30°, 60° and 90 °. The restraining bar measured knee extensor forces. Patellofemoral contact pressures were measured while stimulating the knee extensor muscles through the femoral nerve at supra-maximal currents and frequencies ranging from 25 to 200Hz. Contact pressures were always measured with the low grade film (range = 1-16Mpa). If the low grade film became saturated, measurements were repeated using a medium grade film (range = 18 - 52MPa). Contact area measurements were all determined from the low grade film, while peak and average pressures were determined from the low and medium grade films.

Peak joint contact pressure was defined as the maximal pressure obtained in an area of at least 0.25mm^2. Average pressure was calculated as the total contact force divided by the total contact area.

RESULTS AND DISCUSSION

Average pressure increased with increasing knee extensor forces but remained the same for a given knee extensor force before and after VM transection. There was a change in shape with a slight lateral shift (figure 1), while contact area showed no consistent change with VM transection. There was a distinct lateral shift in pressure distribution at knee angles of 60° (Figure 2) and 30° but not for knee angles of 90°
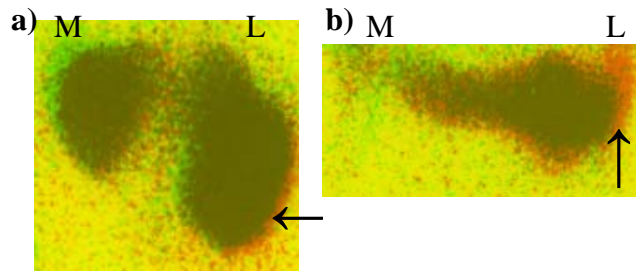

Figure 1 Overlay of contact area before transection (green) and after transection (red) for an exemplar joint and knee angle of a) 60 ° and b) 30 °
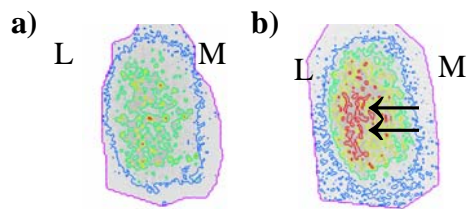

Figure 2 Pressure distribution for an exemplar joint and a knee angle of 60 °. Red dots indicate regions of high pressure a) normal b) post VM transection

Clinical and anecdotal evidence has led to the common notion that knee extensor imbalance causes PFP through changes in the patellofemoral contact pressure distribution. Here, we found that elimination of the VM caused a lateral shift in the patellofemoral joint pressures at knee angles of 30 and 60° but not at 90° . One common treatment for PFP is the strengthening of the VM because it has been assumed implicitly that weakness of VM relative to VL is the primary cause of the joint pain. Our results suggest that VM strengthening might be the correct intervention for extended knee angles in the rabbit but not at angles of around 90°. Interestingly, pressure distribution changes in our model only occurred at non-physiological joint angles (30 and 60°), while in the physiologically relevant joint position (90° in the rabbit), ablation of the VM did not cause changes in the patellofemoral contact pressures for the same knee extensor forces. This result suggests that VM weakness in the rabbit does not cause changes in patellofemoral contact pressures for physiological angles but causes the "expected later shift" in contact pressure at non-physiological angles. If this was true for other species including humans, the idea of VM strengthening to alleviate patellofemoral joint pain might not hold as the joint stabilizes itself in the presence of vast knee extensor imbalances

References

Cowan, S.M., et al., 2002. *Med SciSport Exerc* **34**:1879-1885

Goh, J.C., et al., 1995. *Brit edit soc bone jt surg*. **77**-B:2:225-231

Lefebvre, R.,et al., 2006. *J manip physiol therap*. **2**:139-144

Powers, C.M., 2000. *Physic Therap* **80**:10:956-964

FLEXOR AND EXTENSOR CONTRIBUTIONS TO THE JOINT MOMENT DURING STAIR ASCENT FOR HEALTHY SUBJECTS AND THOSE WITH KNEE OA

Joseph Gardinier[1] and Kurt Manal[1,2]
[1]Biomechanics and Movement Science, University of Delaware, Newark, DE, USA
[2]Center for Biomedical Engineering Research, University of Delaware, Newark, DE, USA

E-mail: manal@udel.edu

INTRODUCTION

Stair climbing can be difficult for people with knee osteoarthritis (OA). Understanding joint mechanics in this group of patients is important for developing better treatment strategies. The net extensor moment during stair ascent reaches a peak during the 1st half of the upward motion. In contrast, the ankle plantarflexion moment is small during the 1st half and peaks during late stance. The soleus and gastrocnemii are the main plantarflexors, and the gastrocnemii have the potential to flex the knee as they plantarflex the ankle. The knee extends during stance and therefore any flexor moment developed by gastrocnemii must be offset by an extensor moment for normal knee kinematics to occur. We suspect the quadriceps develop a significant moment during late stance, much larger than one might expect based on the net joint moment alone. Moreover, people with knee OA exhibit increased co-contraction of the hamstrings (Hortobagyi et al., 2005) and thus we hypothesize they develop a greater extensor moment during late stance than healthy subjects. This can not be evaluated using inverse dynamics because the resultant moment is the sum total of the flexor and extensor contributions. In this study we used an EMG-driven model to compute individual muscle forces to determine how the flexors and extensors contribute to the net joint moment during stair ascent.

PROCEDURE AND METHODS

The EMG-driven musculoskeletal model and data processing methods have been described elsewhere (Buchanan et al., 2004). Joint kinematics, kinetics and EMG signals were collected during stair ascent for 6 healthy controls and 6 subjects with knee OA. Each subject performed 5 trials at a self-selected speed. Knee joint moments were computed using Visual3D and normalized to BW*Height. The muscle-tendon lengths and moment arms of 10 muscles crossing the knee were determined using SIMM and the lower extremity anatomical model developed by Delp (1990). The knee extensor moment was computed from individual force estimates for the rectus femoris, the vastus lateralis, medialis and intermedius. The flexor moment was computed using forces from the 4 hamstrings and medial and lateral gastrocnemius. Data were evaluated qualitatively due to small subject numbers.

Table 1. Subject characteristics

	Healthy	OA
Age	58.2 (9.9)	59.2 (6.2)
Height (m)	1.67 (0.09)	1.65 (0.09)
Weight (kg)	70.8 (12.1)	72.0 (16.7)
BMI	25.1 (2.5)	26.2 (4.4)

RESULTS

Control subjects had a greater net joint moment than subjects with OA, and the net moment for both groups was small during late stance (Figure 1).
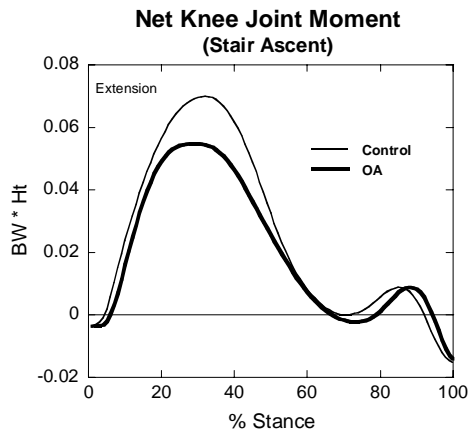
Net Knee Joint Moment
(Stair Ascent)

Figure 1. Net joint moment from inverse dynamics.

Flexor & Extensor Contribution
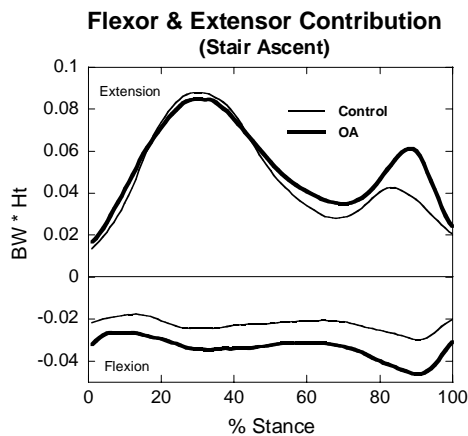**(Stair Ascent)**

Figure 2. Flexor and extensor contributions to net joint moment.

Figure 2 shows the EMG-driven model flexor and extensor contributions to the net joint moment. Note the extensor peak during the 1st half was similar for both groups but subjects with OA had a greater

flexor component. As expected, both groups developed significant extensor moments during late stance when the net joint moment was small.

DISCUSSION

Individuals with knee OA have altered kinematics, kinetics and muscle activity during walking and stair climbing (Hortobagyi et al., 2005). It has been suggested the reduced moment for those with OA may be an effort to minimize pain associated with activity (Hurwitz et al., 2002). Results of our study suggest that subjects with OA did not unload the joint and may actually experience greater loading than healthy control subjects. This has implications for disease progression and highlights a key limitation of inverse dynamics.

SUMMARY

Our findings illustrate how using an EMG-driven model to estimate individual muscle forces and resulting moments can offer added insight into joint mechanics associated with normal and pathological gait.

REFERENCES

Buchanan TS et al.(2004). *J Appl Biomech,* 20, 367-395.
Delp S et al. (1990). *IEEE Trans Biomed Eng*, 37, 757-767.
Hortobagyi T et al. (2005). *Clin Biomech*, 20, 97-104.
Hurwitz D et al. (2002). *J Orthop Res,* 20, 101-107.

ACKNOWLEDGEMENTS

VALIDATION OF THE COMPUTATIONAL KNEE JOINT MODEL UNDER HIGH COMPRESSIVE LOADING CONDITIONS

Bhushan S. Borotikar and Antonie J. van den Bogert

Department of Biomedical Engineering, Lerner Research Institute, Cleveland Clinic, Cleveland, OH, USA bogerta@ccf.org
URL: http://www.lerner.ccf.org/bme/bogert/

INTRODUCTION

The study of knee joint mechanics has important clinical applications, including surgery, rehabilitation and injury diagnostics and prevention.

Cadaveric studies (Blankevoort et al., 1988; Kanamori et al., 2000) give insight in the kinematic response and tissue stresses but are difficult to extrapolate beyond the loading conditions that were tested. Computational modeling (Pandy et al., 1998; Li et al., 1999; Blankevoort et al., 1996) can overcome these limitations but always require experimental validation.

Because of technical limitations, experimental studies and model validations have not yet explored high compressive loading conditions. Such conditions occur in vivo and, because of complex articular contact geometry, may significantly affect joint kinematics and soft tissue. In this study we present a validation of a computational knee model, in complex loading conditions which include compressive loading.

METHODS

A medial parapatellar arthrotomy was conducted on a 41 year old female cadaveric knee to check the meniscal and ligamentous integrity. The tibia was mounted on a 6-component load cell (SI-2500-400, ATI Industrial Automation, Apex, NC) and femur was attached to a six degree of freedom (DOF) motion platform (R2000, Parallel Robotic Systems Corp., Hampton, NH). In-house software was developed using Labview (National Instruments Corp., Austin, TX) for mixed motion-load control in a standard joint coordinate system (JCS). Flexion angle was motion controlled, and load control was applied to the 3D force, internal-external rotation moment, and varus-valgus moment.

We applied combinations of valgus torque (0 Nm and 10 Nm) and compressive load (0 N, 100 N, 700 N) on the tibia, while changing the internal rotation moment from 0 Nm to 5 Nm in steps of 1 Nm and keeping the flexion fixed at 0^0. We also performed a Lachman test by changing the anterior drawer force on the tibia from 0 N to 100 N in steps of 10 N. Kinematic data were recorded at each loading combination.

A computational model of the same specimen was generated from sagittal plane MRI scans. Articular surfaces were digitized and four ligaments (ACL, PCL, MCL and LCL) were represented by 3 line elements each. Ligament and articular cartilage parameters were taken from earlier work (Blankevoort et al., 1996). The experimental protocol described above was simulated on the model, using software for 3D-quasi static joint modeling (Kwak et al., 1999). Model simulations were compared to experimental data, and ligament pre-strains were modified to evaluate model sensitivity.

RESULTS

Figure 1 shows the tibial internal rotation during internal rotation and valgus loading at three levels of compression. Model simulations agreed qualitatively with experimental data but were sensitive to ligament pre-strains (Fig. 1), suggesting that pre-strains can be robustly estimated by fitting the model to the experimental data.
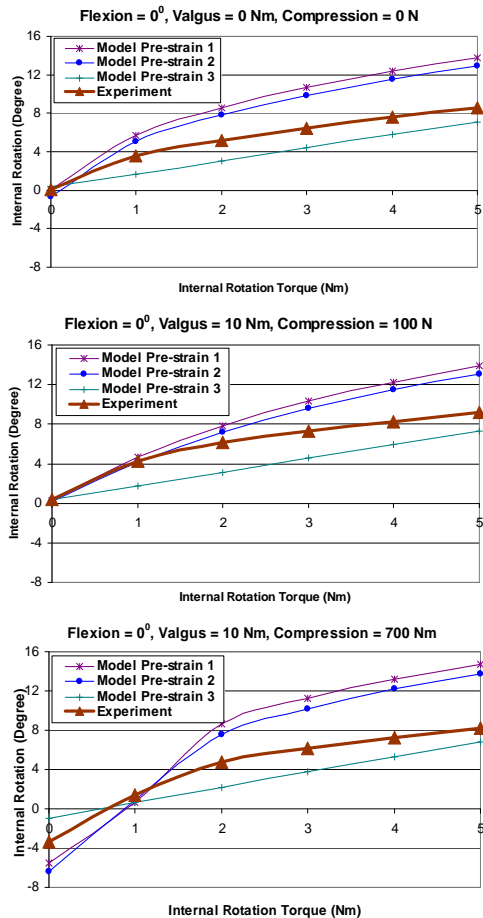

Figure 1. Kinematic response of the knee during combined internal rotation, valgus, and compression loading. Pre-strain of the MCL was varied from 1 to 6%.

In the experiment as well as in the model, there was a slight reduction in absolute internal rotation at higher internal rotation torques, as the compression increased from 100N to 700N. For the Lachman test, it was observed that the model tibia was getting externally rotated during anterior drawer load while the experimental data suggested internal rotation of the tibia.

DISCUSSION

High compressive loads may put the joint ligaments in higher stress and make the joint vulnerable to injury. We demonstrated with a model that joint kinematics under rotational load is affected by compressive load, and this was confirmed by experimental data.

Incorrect prediction of tibia rotation in the Lachman test can be attributed to differences in the JCS axes between experiment and model co-ordinates, which we will eliminate by attaching MRI-compatible registration objects to the bones. Currently the model pre-strains are changed manually. Further work will be directed towards optimizing these parameters to fit kinematic data from all experimental loading conditions. Such a model can be further used to study different knee or ligament injury mechanisms.

REFERENCES

Blankevoort, L. et al. (1988). *J of Biomech*. 21: 705-720.

Blankevoort L. et al., (1996). *J of Biomech*. 29: 955-961

Kanamori et al. (2000). *J of Arthroscopic & Related Surgery*. 16: 633-639.

Kwak et al., (2000). *Comp Meth Biomech Biomed Engg*. 3: 41-64

Li et al. (1999). *J of Biomech. Engg*. 121: 657-662

Pandy et al. (1998). *Comp Meth Biomech Biomed Engg* 1: 265-283

ACKNOWLEDGEMENTS

POOR GLUCOSE CONTROL IS RELATED TO REDUCED BALANCE CONTROL IN ADULTS WITH TYPE II DIABETES

Brandi Row, Kathy Knutzen, Lorrie Brilla, Jeanne Freeman, Ying Li, & Billie Lindsey

[1]Department of Physical Education, Health and Recreation, Western Washington University, Bellingham, WA, USA, Brandi.Row@wwu.edu, URL: http://www.wwu.edu/pehr

INTRODUCTION

Patients with Type II Diabetes Mellitus (T2DM) exhibit compromised performance on postural balance measures, particularly when affected by peripheral neuropathy (Boucher et al., 1995; Cavanagh et al., 1993; Ducic et al., 2004; Nardone et al., 2006; Oppenheim et al., 1999; Yamamoto et al., 2001). The purpose of this study was to determine if postural balance measures in adults with T2DM are associated with an indicator of long-term glucose control, the glycosylated hemoglobin (HbA1c) blood test. This cross-sectional analysis includes the pre-intervention results of a study to determine the effects of high intensity resistance training on numerous health and performance outcomes in adults with T2DM.

METHODS AND PROCEDURES

Forty subjects (age range 37-84 years, mean 60.8 (SD 10.8) years) participating in a resistance training intervention study were tested prior to the onset of exercise. Glucose control (HbA1c) was measured by the subjects' physicians prior to entry into the study.

Standing balance measures were evaluated for 30 seconds using a force platform (Advanced Mechanical Technology, Inc.) under the conditions of comfortable stance and feet together stance widths (during eyes open and eyes closed conditions). Center of pressure (COP) excursions, mean & maximum COP velocity, and variability of excursions and velocities (standard deviation, SD) were calculated during these trials. Only the results of the feet together, eyes closed (FTEC) condition is reported here, as it had the greatest variance in performance of the static balance trials.

Dynamic balance was assessed using an anterior-posterior 'limits of stability' (LOS) test, where subjects maintained their bodies as straight as possible, while leaning as far forward and backward as possible for a period of 30 seconds. LOS performance was calculated as the total anterior-posterior excursion of the COP relative to shoe length.

A dynamic challenge to medial-lateral balance was conducted with a rapid step up (RSU) test, where the subject placed the foot on a 15 cm high step as rapidly as possible when cued, after which the foot remained lightly placed on the step for at least five seconds, and the subject balanced mostly on one leg. Performance on the RSU test was calculated as maximum COP velocity during the weight shift period, the medial-lateral excursion of the COP as percentage of foot width following the foot placement on the step. Only the performance during a left leg trial is reported, where the subject remained standing on the right leg.

Partial correlation analyses, which controlled for the effect of age, were conducted to determine the relationships between glucose control and balance parameters.

RESULTS AND DISCUSSION

For the FTEC condition, several measures of COP displacement, velocity, and variability of COP velocity were mildly correlated with HbA1c, after controlling for age (Table 1), and this was particularly so with ML COP measures. These results reveal that reduced long-term glucose control was related to larger COP excursions, velocities, and the respective variability for each.

For the LOS condition, higher HbA1c scores were associated with reduced AP COP velocity, reduced variability of AP COP velocity, and *increased* variability of ML COP excursion amplitude (Table 1). These results indicate that reduced glucose control is related to more conservative, yet more variable AP COP velocity. Further, the results demonstrate that reduced glucose control is related to more variable ML COP excursion even during this test that challenges AP COP excursion.

For the RSU condition, higher HbA1c scores were associated with increased ML COP excursion, velocity, and variability of the velocity (Table 1). Therefore, reduced glucose control is associated with greater and faster COP excursions, and greater variability of excursions and velocities during this challenge to ML balance control. Further, following the placement of the foot on the step, increased HbA1c scores were related to higher ML COP amplitudes, expressed as a percentage of the shoe width ($r = .432$, $p = .005$) and variability of ML COP excursions ($r = .420$, $p = .006$).

COP measures on the three tests, as well as HbA1c, were also related to body composition measures (not presented) when controlling for age.

SUMMARY

Reduced long-term glucose control in adults with T2DM is associated with reduceds balance control. While the association between peripheral neuropathy and balance has been repeatedly established, this study demonstrates a direct relationship with a common measure of long-term glucose control, confirming the importance of the basic management of diabetes for optimal balance function.

REFERENCES

Boucher P, et al. (1995). *Diabetes Care*, 18(5):638-45.
Cavanagh PR, et al. (1993). *J Biomech*, 26 Suppl 1:23-40.
Ducic I, et al. (2004). *Ann Plast Surg*, 52(6):535-40.
Nardone A, et al. (2006). *Gait Posture*, 23(3):364-73.
Oppenheim U, et al. (1999). *Diabetes Care*, 22(2):328-32.
Yamamoto R, et al. (2001). *Diabetes Res Clin Pract*. 52(3):213-21.

Table 1: Partial correlation coefficients (controlling for age) of HbA1c and COP measures:

	COP Amplitude		SD, COP amplitude		Max. COP Velocity		Mean COP Velocity		SD, COP velocity	
	ML	AP	ML	AP	ML	AP	ML	AP	ML	AP
FTEC	.345	.313	.289	*ns*	.388	ns	.355	.297	.355	ns
LOS	ns	ns	.338	ns	ns	ns	ns	-.303	ns	-.294
RSU	.304	ns	ns	ns	.337	ns	.286	ns	.324	ns

All correlations presented are statistically significant partial correlations ($p < .05$).
ns = non-significant. SD = standard deviation. ML = medial-lateral, AP = anterior-posterior.

THE EFFECT OF THE OBJECT DISTANCE ON HAND MOVEMENT DURING REACH-TO-GRASP TASKS

Sungchan Bae and Thomas J. Armstrong

University of Michigan, Ann Arbor, Michigan, USA
Email: scbae@umich.edu

INTRODUCTION

Biomechanical models of the hand movement are needed to predict hand posture and force in biomedical and ergonomic fields (Sancho-Bru, 2001). To improve the models, previous studies examined quantitative aspects of the hand movement. Mathematical approach was employed (Braido, 2004) and the effect of object properties was considered (Choi, 2007; Paulignan, 1997). This study investigates the effect of object distances on temporal aspects of hand movement during reach-to-grasp task.

METHODS AND PROCEDURES

Six healthy right-handed subjects (3 males, 3 females), distributed from 16 percentile female to 70 percentile male by the hand length, participated in the experiment. The subjects were asked to reach for and grasp the cylindrical object of 3.8 cm in diameter with pulp pinch at their voluntary speed. The object was located at three distances (20, 30, and 40 cm from the subject's wrist). To measure the 3D position of hand movement, thirty markers were attached on the object as well as on all the finger joints/tips and wrists, which were then recorded by OptoTrak® Certus™ motion tracking system.

The data obtained were processed with MATLAB® software; the raw data were low-pass filtered with a cut-off frequency of 3Hz, after which the inter-digit joint angles were calculated. Figure 1 illustrates mean DIP (Distal Interphalangeal) joint angle and distance from the object to the wrist over time during 400 mm reach-to-grasp tasks. The starting point was detected when the movement velocity first exceeds 25 mm/sec on the distance curve whereas the ending time was the point where the joint angular velocity becomes less than 5 °/sec. On the joint angle profile, delay time is a period where the joint angle stays within 5 °/sec right after the starting point. Then open time continued until the finger reaches a maximum opening, followed by close time during which the finger flexes to the final posture. Total time is summation of delay, open, and close times. Reach time, defined on the distance profile, indicates duration where the hand is in reach motion. ANOVA tests were performed to examine the effect of the distance on these temporal parameters of the index finger.

RESULTS AND DISCUSSION

Mean values of temporal parameters of the index finger joints – DIP, PIP (Proximal Interphalangeal), and MCP (Metacarpo-
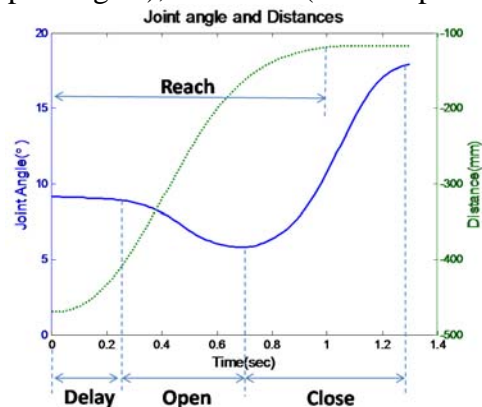

Figure 1. Mean DIP joint angle (solid) and distance (dotted) for 400mm reach-to-grasp task over time with key temporal parameters.

phalangeal) – are shown in Table 1. Total, delay, and reach times during reach-to-grasp task were significantly affected by object distances at all joints (p<0.05) except that delay time at MCP was slightly insignificant (p=0.053). Total time and delay time, ranged from 0.82 to 1.31 and from 0.05 to 0.2 seconds, respectively, increased as well as normalized reach time from 0.7 to 0.91 for farther distances throughout joints. On the other hand, the effects of distances on open and close times depend on the joint; open time at DIP was affected, close time at PIP, and none of them at MCP. However, open time for PIP becomes significant when normalized by total time (p<0.05). Total and open time results were comparable to the previous studies (Choi, 2007; Paulignan, 1997).

Final postures of DIP and PIP at grasping remained statistically the same for different levels of object distances (p>0.05), but MCP
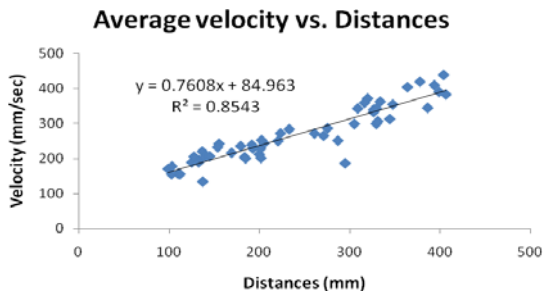

Figure 2. Average velocities of the hand for traveling distances with regression equation

was more extended as the object was located farther. In addition, actual moving distances of the wrist during reach were calculated from the distance curve and its effect on average velocity of the hand was considered. Figure 2 illustrates that average velocity during reach is linearly related to the distance travelled by the wrist with a high R^2 value of 0.85.

CONCLUSIONS

Distance from the object is a significant factor in hand movement pattern. Total, delay, and reach times are changed while behavior of opening and closing the finger is affected by distance as well. Also, reach velocity of the hand is notably related to object distances. The results can provide biomechanical models with standards of temporal variables so that they can identify abnormal performance.

REFERENCES

Braido and Zhang (2004). *Human Mov Sci,* 22
Choi and Armstrong (2007). *ASB conference*
Paulignan et al. (1997). *Exp Brain Res*, 114
Sancho-Bru et al. (2001). *J Biomech*, 34

ACKNOWLEDGEMENTS

Table 1. Pooled movement times of the index finger joints for six subjects reaching 20, 30 and 40 cm and grasping a 3.8 cm diameter cylinder with pulp pinch. Means (SD)

Joints	DIP (sec)			PIP (sec)			MCP (sec)		
Distances(cm)	20	30	40	20	30	40	20	30	40
Total	1.00 (0.26)	1.19 (0.20)	1.30 (0.21)	0.82 (0.14)	1.01 (0.14)	1.09 (0.13)	0.98 (0.21)	1.17 (0.18)	1.31 (0.22)
Delay	0.11 (0.07)	0.13 (0.07)	0.20 (0.05)	0.07 (0.04)	0.11 (0.06)	0.12 (0.08)	0.05 (0.07)	0.07 (0.08)	0.10 (0.07)
Open	0.40 (0.09)	0.53 (0.12)	0.53 (0.12)	0.44 (0.10)	0.51 (0.09)	0.58 (0.06)	0.28 (0.20)	0.41 (0.24)	0.43 (0.30)
Close	0.49 (0.16)	0.53 (0.15)	0.58 (0.15)	0.31 (0.10)	0.40 (0.10)	0.39 (0.11)	0.65 (0.15)	0.69 (0.23)	0.78 (0.30)
Reach	0.70 (0.11)	0.90 (0.11)	0.99 (0.08)	0.71 (0.11)	0.92 (0.10)	0.99 (0.09)	0.70 (0.10)	0.92 (0.11)	0.97 (0.08)

A Biomechanical Investigation of the Forces Applied to Lift Truck Steering Wheels: Effects of Posture, Gender and Steering Forces on Cumulative Low Back Loading

Sylvain G. Grenier*, Aaron M. Kociolek and Tammy Eger*
Department of Kinesiology, McMaster University, Hamilton, Ontario, Canada
*School of Human Kinetics, Laurentian University, Sudbury, Ontario, Canada.
sgrenier@laurentian.ca

INTRODUCTION

LBP is the leading cause of disability to employees working physically demanding jobs (Davis and Jorgensen, 2005). Although 90% of workers return to work in less than 6 months time, 20% to 44% of this population experience reoccurring LBP, which results in future time off work (Rossignol et al., 1988).

Mobile equipment operators, including lift truck (LT) drivers, frequently suffer from the detrimental effects of LBP. Lift truck vehicles are designed for forward direction operation. Nevertheless, large cargo loads frequently block operator line-of-sight (LOS), which forces operators to drive in reverse (Tyson, 1995). Reverse driving consequences include prolonged neck rotation greater than 45º, trunk rotation greater than 25º, and lateral trunk flexion greater than 15º. Musculoskeletal pain and discomfort associated with sustaining awkward postures during LT operation is well documented (Bovenzi et al. 2002).

Although the steering wheel is the most frequently used control system in lift trucks, its biomechanical effects on cumulative low back loading and its interaction with awkward postures are unknown. The goal of this research project is to quantify the hand forces applied to the typical lift truck steering wheel and the resulting lumber cumulative low back loading exposure variables. We hypothesized that hand forces would significantly reduce compression values at the L4/L5 level of the spine.

METHODS

Steering forces applied to the typical lift truck steering wheel were quantified in a laboratory setting to determine their effects to cumulative low back loading. Participants underwent three repetitions of a randomized series of postures common during LT operation. Cumulative loading exposure variables were estimated with a quasi-dynamic link segment model for four representative lift truck operating postures (neutral sitting, forward flexion, lateral flexion, backward rotation) in three male and three female university students. Movement speed was was controlled by restricting subjects to narrow trunk posture ranges during recorded trials.

Forces collected at the platform were assumed equal to steering forces. AVI video clips of the postures were loaded into 3D-Match. The program was first used to posture code all trials, neglecting hand forces, to estimate cumulative forces in the back. Then, the hand forces collected with the force platform were added to the 3DMatch analysis to the same trials. The original prediction of cumulative loads were compare with these revised estimates.

RESULTS

The addition of hand forces to the loading model utilized in 3D-Match significantly reduced predicted mean L4/L5 cumulative compression in forward bending posture conditions (Table 1). Mean cumulative L4/L5 compression was significantly decreased in forward bending postures for both male and female participants. Males achieved

significantly reduced cumulative compression for forward bending and lateral bending postures when hand forces were considered but increased for lateral bending postures.

SUMMARY

The steering wheel control system was effectively used as an assistive device whereby operators used the wheel to decrease spinal loading.

Table 1. Average (mean+/-standard deviation), minimum and maximum forces (N) applied to the steering wheel apparatus in each translational axis over 30-second trials reported over male (M) and female (F) participants in neutral sitting (NS), forward bending (FB), lateral bending (LB) and backward rotation (BR) posture conditions

subject	gender	posture	Average			Minimum			Maximum		
			X	Y	Z	X	Y	Z	X	Y	Z
1,2,4	M	NS	5.31 +/- 7.43	31.35 +/- 8.72	0.013 +/- 1.37	-25.19	0.00	-6.52	54.73	63.37	8.18
		FB	-11.0 +/- -9.50	101.7 +/- 26.06	0.042 +/- 2.78	-54.42	0.00	-11.78	86.65	191.16	11.95
		LB	3.99 +/- 8.03	31.99 +/- 5.74	-6.52 +/- -2.91	-29.43	0.00	-51.54	68.86	62.53	17.24
		BR	6.74+/- 6.03	13.60 +/- 4.32	2.59 +/- 3.51	-13.79	-0.44	-9.59	48.05	51.17	14.59
3,5,6	F	NS	2.88 +/- 6.55	23.47 +/- 7.37	-0.398 +/- 1.67	-20.38	-9.13	-9.65	42.24	41.14	7.86
		FB	-0.97+/- 8.04	44.46 +/- 16.47	-0.237 +/- 3,39	-42.17	-7.49	-13.25	37.74	124.75	27.27
		LB	4.50 +/- 7.00	14.72 +/- 7.07	-6.70 +/- 4.81	-25.54	-12.62	-36.52	50.28	48.58	6.1
		BR	6.91 +/- 7.52	10.88 +/- 5.14	2.07 +/- 3.39	-14.65	-7.37	-6.65	76.61	33.55	27.78

Mean scores reflect the average of all three trials for male and female participants within each posture condition.
Minimum and maximum scores reflect absolute peaks over all trials for both male and female participants respectively.

– Forces in the x-axis (anterior-posterior axis) are negative if the resultant force is a push away and positive a pull towards the body.
– Forces in the y-axis (vertical axis) are negative if the resultant force is a lift and positive for a push down to the ground.
– Forces in the z-axis (medial/lateral axis) are positive if the resultant force is a push/pull towards the left and negative to the right.

The results confirm the need to account for gender-based differences in occupational environments (Dunk and Callaghan, 2005) and during design and development of mobile equipment. While the steering wheel placement may not have been optimal for females to relieve compressive force, perhaps an optimally placed handle would relieve compression on the same scale as the steering does for males.

REFERENCES

Bovenzi, M., Pinto, I. and Stacchini, N. 2002. *Journal of Sound and Vibration,* 253 (1), 3–20.

Davis, K. and Jorgensen, M. 2005. *Occupational Ergonomics,* 5, 57-76.

Dunk, M. and Callaghan, J.P. 2005. *Clinical Biomechanics,* 20, 1101-1110.

Rossignol, M., Suissa, S. and Abenhaim, L. 1998. *Quebec Journal of Occupational Medicine,* 30, 502-505.

Tyson, J. 1995.Pulp and Paper Health and Safety Association, North Bay Canada.

Zimmerman, C.L., Cook, T.M. and Rosecranse, J.C. 1997. *Applied Occupational Environmental Hygiene,* 12 (7), 480-484.

ACKNOWLEDGEMENTS

GROUND REACTION FORCES RECORDED UNDERNEATH HANDS DURING SITTING PIVOT TRANSFERS IN INDIVIDUALS WITH SPINAL CORD INJURY

Dany Gagnon[1], Sylvie Nadeau[1], France Piotte[1], Luc Noreau[2] & Denis Gravel[1]

[1] Université de Montréal/Centre de recherche interdisciplinaire en réadaptation du Montréal métropolitain, Montreal, PQ, Canada, E-mail : dany.gagnon.2@umontreal.ca
[2] Université Laval/Centre interdisciplinaire de recherche en réadaptation et intégration social, Quebec City, PQ, Canada

INTRODUCTION

The performance of sitting pivot transfers (SPTs) ranks among the most strenuous wheelchair-related activities for the upper extremities (U/Es) among individuals with spinal cord injury (SCI) (Allison, 1997; Nyland et al, 2000; Gagnon, 2008). Given the paucity of biomechanical studies focusing on these functional activities, limited knowledge is available on SPT kinematics. Only Forslund et al (2006) have investigated vertical reaction forces (VRFs) under hands during SPTs among individuals with SCI. They documented substantial peak VRF approaching 50% of the body weight (BW) for men with SCI at one time under each hand during SPTs (Forslund et al, 2006). A tendency for the trailing U/E to be exposed to a greater mean VRF than the leading arm was also observed (Forslund et al, 2006). The horizontal reaction force (HRF) underneath hands has never been studied. The main objective of this study was to quantify the VRFs and HRFs exerted under hands when individuals with SCI perform SPTs from an initial seat to a target seat of same or high heights.

METHODS

Twelve males (age= 41.5 ± 8.4 years; mass = 81.8 ± 18.5 kg; height = 1.76 ± 0.09 m; time post-injury = 9.7 ± 11.1 years) with complete motor thoracic SCI (T4 to T11) participated in this study. Participants had the ability to independently transfer between seats of even or uneven heights and routinely used SPTs in daily life (number of SPTs performed daily= 20±7).

Participants performed SPTs from an initial force-sensing seat toward a height-adjustable target force-sensing seat, while the leading (right) and trailing (left) hands were each placed on distinct hand force-sensing surfaces attached to the side of the initial and target seats (Figure 1) (Gagnon et al, 2008). With both seats initially set at a height of 50 cm, three SPT trials were first recorded with the right and left U/Es always playing a leading and trailing role, respectively. After, only the target seat and leading hand surface heights were raised to 60 cm, and three additional SPTs were recorded
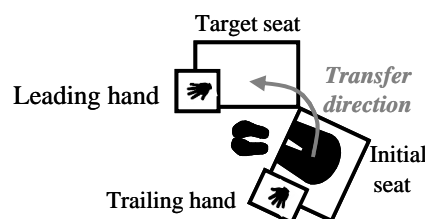

Figure 1: Top view of the experimental set-up used to assess sitting pivot transfers.

Each SPT trial was divided into pre-lift, lift and post-lift phases (Gagnon et al, 2008). The lift phase started when the VRF equalled zero at the initial seat and ended when the VRF reached its peak value (impact force) on the target seat for the SPTs. The start of the pre-lift and end of the post-lift phases coincided with the start of the acceleration and end of the deceleration phase of the head and trunk segments, respectively. Reaction forces were time-normalized to 100 data point per phase for a total of 300 data points for each trial, and then expressed as a percentage of body weight.

For each hand, outcome measures were the overall peak VRF and HRF values reached during SPTs as well as their mean values computed during the lift phase of the SPTs.

RESULTS

Peak VRFs were greater underneath the trailing hand compared to the leading one ($p<0.02$), and reached its highest value when transferring to the high target seat ($p=0.003$).
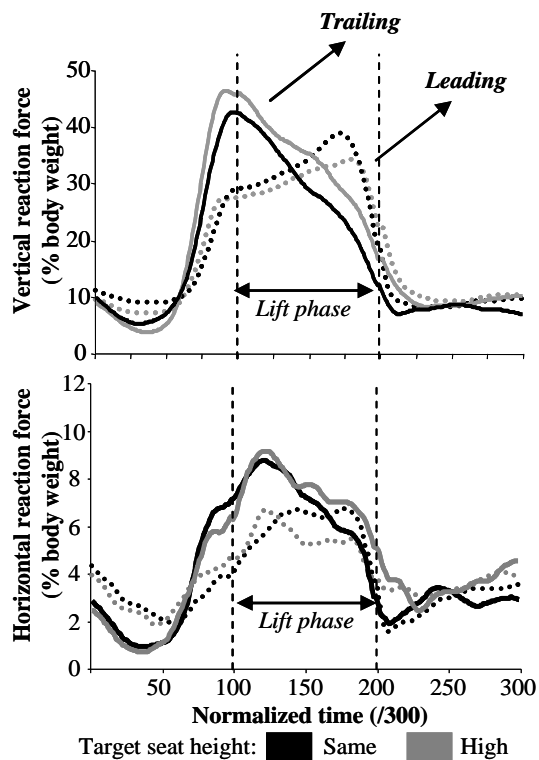

Figure 2: Overall mean vertical and horizontal reaction forces recorded under the leading (dotted lines) and trailing (solid lines) hands during transfers.

Similar mean VRFs were found between hands for each transfer studied ($p>0.088$). Unexpectedly, the mean VRF underneath the leading hand was greater when transferring to a target seat of same height compared than doing so to a high target seat ($p=0.021$), and vice-versa for the trailing hand ($p=0.0001$). Peak and mean HRFs were always higher underneath the trailing hand than the leading hand, independently of target seat height ($p<0.001$).

DISCUSSION

In conformity with the results previously reported by Forslund *et al* (2006), the peak VRFs were found to be higher underneath the trailing hand (same=45%; high=49%) than the leading hand (same=40%; high=36%) during SPTs. However, similar mean VRFs were found between the leading and trailing hands (same=32% versus 29%) when transferring between seats of same height which contradicts previous finding (Forslund et al, 2006).

The HRFs were quantified for the first time during SPTs. The peak (9-10%) and mean HRFs (5-8%) reached their highest values at the trailing U/E, and were not affected by target seat height. These HRFs may have their greatest effects at the shoulder joint where the rotator cuff muscles might be challenged.

The VRFs and HRFs found may exacerbate the development of secondary U/E impairments among this population. To reduce this risk, promoting the use of the strongest U/E, or of the pain-free one, as the trailing one during SPTs to a target seat of same or high height may be indicated in light of the current results. However, further research is required to assess relative muscular and mechanical demands during SPTs in individuals with SCI.

SUMMARY

This study assessed the VRF s and HRFs underneath hands during SPTs in individuals with spinal cord injury. The main results revealed that the peak VRF and HRF were always higher at the trailing hand when compared to the leading hand during SPTs, independent of the target seat height. Moreover, transferring to the high target seat shifted additional VRF at the trailing U/E accompanied by a decline of VRF at the leading U/E.

REFERENCES

Allison, G. (1997) Crit Rev Phys Rehab Med, 9:131-150.

Gagnon, D (2008) PhD Thesis, Faculty of Medicine, University of Montreal.

Gagnon D *et al.* (2008) J Biomech [In Press]

Nyland J *et al.* (2000) Spinal Cord, 38:649-657.

ACKNOWLEDGEMENTS

DIFFERENCES IN LOWER EXTREMTIY COODINATION IN HIGH- COMPARED TO LOW-ARCHED FEMALE ATHLETES DURING RUNNING

Douglas Powell[1], Songning Zhang[3], Clare Milner[3], Benjamin Long[2], Matt Bice[1]
[1]Biomechanics Laboratory, University of Texas of the Permian Basin, Odessa, TX
[2]Biomechanics Laboratory, East Carolina University, Greenville, NC
[3]Biomechanics/Sports Medicine Lab, The University of Tennessee, Knoxville, TN
e-mail: powell_d@utpb.edu

INTRODUCTION

Aberrant foot function is associated with an increased propensity for injury within the foot, shank, thigh and pelvis (Williams et al. 2001). It has been suggested that high-arched (HA) compared to low-arched (LA) athletes exhibit unique injury patterns at these sites. Several studies have examined the lower extremity kinematic and kinetic patterns of HA and LA individuals (Williams 2001; Hunt and Smith 2004; Williams et al. 2004). However, the variability of movement within the lower extremity of HA and LA athletes has not been studied. Differences in coordination patterns and variability may explain some differences in the injury patterns of these two groups. Continuous relative phase (CRP) is an effective method of determining coordination between two segments (Stergiou 2004). In addition, it has also been suggested that the standard deviation of the continuous relative phase, the deviation phase (DP) curve provides a measure of stability concerning the organization of the neuromuscular system (Stergiou 2004). The purpose of the current study was to investigate the multi-planar coordination patterns and variability within the lower extremity of HA and LA athletes. Specifically, femoral adduction-tibial internal rotation (FAdd-TIR) and tibial internal rotation-calcaneal eversion (TIR-CEv) were examined.

METHODS

Ten HA (AI>0.375) and ten LA (AI<0.290) female recreational athletes performed five barefoot running trials at a self-selected speed while three-dimensional kinematics (240 Hz; VICON*PEAK*) and ground reaction force (1200 Hz; AMTI) were collected simultaneously. Visual 3D was used to calculate kinematic and kinetic data as well as phase plots and CRP. Relationships examined include femoral adduction-tibial internal rotation (FAdd-TIR) and tibial internal rotation-calcaneal eversion (TIR-CEv).

SPSS 14.0 was used to conducted curve correlation between high- and low-arched groups to examine point differences within CRP and DP curves. Alpha level was set at p<0.05.

RESULTS

HA compared to LA runners were more out of phase after mid-stance during running (Fig. 1). Specifically, HA compared to LA are more out of phase in TIR-CEv coordination from 67%-87% of the stance phase. These differences in coordination may result in altered loading patterns during the propulsive phase of running gait.
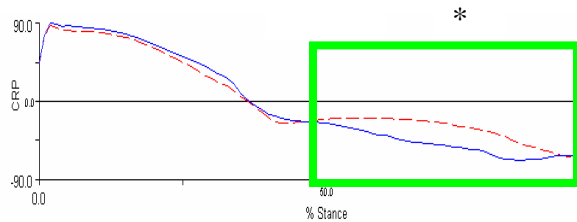
Figure 1. Tibial internal rotation – calcaneal eversion continuous relative phase curve during stance in HA (solid) compared to LA (dashed) runners.

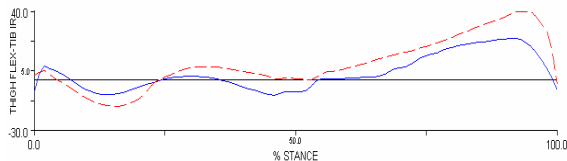No statistical differences were found in FAdd-TIR coordination patterns between HA and LA athletes (Fig. 2).

Figure 2. Femoral adduction – tibial internal rotation continuous relative phase curve during stance in HA (solid) compared to LA (dashed) runners.

No differences were observed in deviation phase (DP) between HA and LA athletes during the stance phase of running gait.

DISCUSSION

These data suggest the tested coordination patterns at the knee may not be related to injury patterns within these two groups. These data also suggest that both coordination patterns exhibit similar stability. The neuromuscular system of HA and LA athletes produced stable coordination patterns as evidenced by DP.

Different coordination patterns within HA and LA athletes occurs at the ankle after mid-stance. These data give rise to the possibility that unique injury patterns may occur not due to shock attenuation and unique loading patterns during load response, but due to muscular force associated with propulsion.

The TIR-CEv Angle-Angle data show that HA compared to LA athletes had a greater amount of eversion at a given TIR angle after mid-stance.

These data show differences in coordination patterns at the ankle only during active propulsion as opposed to shock attenuation. It is possible this relationship contributes to lower extremity injury. Alternatively, unique injury patterns in HA and LA athletes may not be dominated by foot dysfunction alone, but by an interaction of foot, ankle, knee and hip dysfunction.

REFERENCES

Hamill, J., et al. (1999). Clin Biomech **14**(5): 297-308.

Hunt, A. E. and R. M. Smith (2004). Clin Biomech **19**(4): 391-7.

Stergiou, N. (2004). *Innovative Analyses of Human Movement: Analytic Tools for Human Movement Research.* Champaign, IL, Human Kinetics.

Williams, D. S., 3rd, et al. (2004). Gait Posture **19**(3): 263-9.

Williams, D. S., 3rd, et al. (2001). Clin Biomech **16**(4): 341-7.

Williams, D. S., et al (2001). J Appl. Biomech. **17**: 153-163.

IS UPPER EXTREMITY LOADING SYMMETRIC DURING WEIGHT-RELIEF LIFTS PERFORMED BY INDIVIDUALS WITH SPINAL CORD INJURY?

Dany Gagnon, Sylvie Nadeau, France Piotte & Luc Noreau

Université de Montréal/Centre de recherche interdisciplinaire en réadaptation du Montréal métropolitain, Montréal, PQ, Canada, E-mail : dany.gagnon.2@umontreal.ca

INTRODUCTION

Individuals with spinal cord injury (SCI) routinely perform weight-relief lifts (WRLs) in daily life to preserve skin and soft tissue integrity and to reposition themselves, for examples. This functional task is highly demanding for the upper extremities (U/Es), especially for the shoulder (flexors, adductors) and elbow (flexors, extensors) muscles (Reyes et al, 1995; Newsam et al, 2003; van Drogolen et al; Gagnon et al, 2008a). The mechanical demand imposed at the U/Es has generally been assumed to be symmetrical.

No study has thoroughly documented the vertical reaction force (VRF) during WRLs among individuals with SCI. The first objective of this study was to quantify the VRF underneath hands during WRLs. The second objective was to determine the level of U/E symmetry while performing this task.

METHODS

Thirteen right-handed males (age: 43.6 ± 8.8 years; mass: 79.9 ± 18.2 kg; height: 1.75 ± 0.08 m; time post-injury: 9.70 ± 10.6 years) with SCI (C6 to T11) participated in the study. Participants presented no signs or symptoms of musculoskeletal impairments affecting the trunk or U/Es or any other conditions that may have altered U/E symmetry.

Each participant completed three WRLs while sitting on an instrumented seat (Figure 1), set at a height of 50 cm, while their hands were symmetrically placed in a hand-flat position on two additional instrumented surfaces set 10 cm higher than the seat (Gagnon et al, 2008b). Participants were instructed to lift body weight off the seat as high as possible, hold the lift for three seconds, and come down on the seat using their habitual movement strategy. For each instrumented surface, VRFs were collected at a sampling frequency of 600 Hz during the entire duration of the WRL.
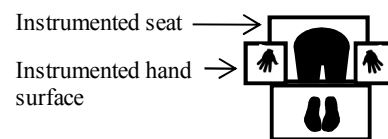

Figure 1: Top view of the experimental set-up used to assess weight-relief lifts.

Each WRL trial was divided into ascent, hold and descent phases (Gagnon et al, 2008b). The hold phase started when the VRF equalled zero at the seat and ended when the impact force (VRF) reached its peak value on the seat. The start of the ascent phase and the end of the descent phase coincided with the start of the acceleration and end of the deceleration phase of the head and upper trunk segments, respectively. VRFs were time-normalized to 100 data point per phase for a total of 300 data points for each trial. Each VRF data point was expressed as a percentage of body weight (% BW).

For the dominant and non-dominant hands, the overall peak VRF value reached during the WRL and the mean VRF measured during the hold phase were calculated. A symmetry index (SI) was also computed at each data point using a ratio between the dominant (dom) and non-dominant (ndom) U/Es (Gilleard et al, 2008):

$$\text{SI (\%)} = [VRF_{dom}/(VRF_{dom}+VRF_{ndom})]*100$$

Values ranging between 0.45 and 0.55 express symmetry whereas values ≥ 0.55 and ≤ 0.45 confirm an asymmetry.

RESULTS

For the dominant and non-dominant hands (Figure 2), near-identical mean VRF patterns were found with greater intensity observed during the hold phase of the

WRLs. At this time, similar (p=0.87) mean VRFs were calculated underneath the dominant (37.19%) and non-dominant (37.3%) hands. Comparable (p=0.96) peak VRFs were also measured underneath the dominant (39.18%) and non-dominant (39.22%) hand during the WRLs.
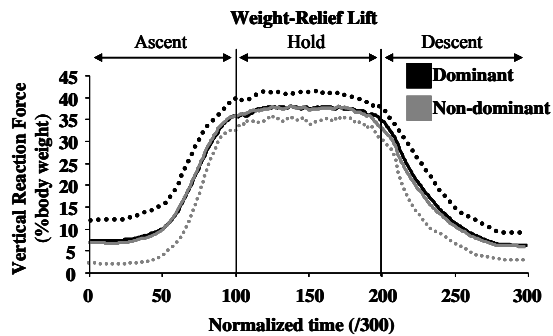

Figure 2: Mean+SD (dominant) and mean-SD (non-dominant) of the VRF measured underneath hands during WRLs (solid line=mean; dotted line=SD).

On average, the magnitude of the VRFs were symmetrical between the dominant and non-dominant U/Es during the performance of WRLs, with near-perfect symmetry reached during the hold phase (mean±SD symmetry index=49.88±1.61) (Figure 3).
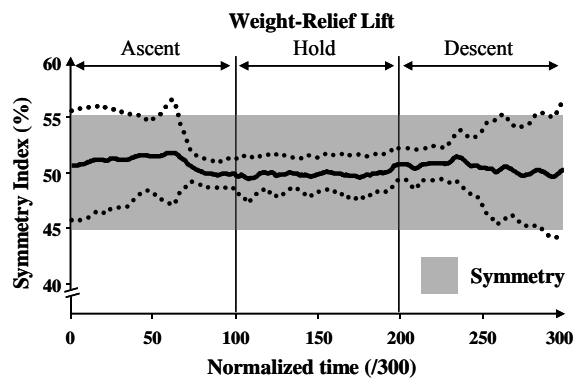
Figure 3: Mean±SD of the symmetry index measured during WRLs.

DISCUSSION

The substantial weight bearing role played by U/Es among individuals with SCI, especially during the hold phase of WRLs, is confirmed in this study. The elevated VRFs recorded under the hands may explain the high demands documented at the shoulder (flexors and adductors) and elbow (flexors and extensors) most likely required to move body weight and assure dynamic postural stability during WRLs. Such elevated

demands may increase the likelihood of developing secondary U/E impairments among this population.

Symmetric load distribution between the dominant and non-dominant U/E during the performance of WRLs is also demonstrated in this study. This symmetry may be crucial to maintain proper body alignment and secure balance during WRL. Despite the VRFs symmetry, relative EMG and mechanical demands sustained may differ between U/Es during WRLs, particularly if U/E muscle imbalance (dominance) is substantial, for example.

Further investigation of the antero-posterior and medio-lateral components of the reaction forces recorded underneath hands is required as it may provide insights on dynamic balance requirements during WRLs. Whether U/E dominance or sensory-motor deficit altering postural control affects symmetry during WRLs among individuals with SCI remains to be investigated.

SUMMARY

This study assessed U/E loading during WRLs among 13 individuals with SCI. The results support the assumption that the performance of WRLs is a symmetrical motor task that highly solicits U/Es.

REFERENCES

Gagnon D *et al.* (2008a) J Rehabil Res Dev [In Press]
Gagnon D *et al.* (2008b) J Biomech [In Press]
Gilleard W *et al.* (2008) Gait Posture, 27:8-15.
Newsam CJ *et al.* (2003) J Spinal Cord Med, 26:59-64.
Reyes ML *et al.* (1995) Arch Phys Med Rehail, 76:433-439.
van Drogolen S *et al.* (2005) Arch Phys Med Rehabil, 86:1214-1220.

ACKNOWLEDGEMENTS

FEMUR BONE MASS AND BONE GEOMETRY AFTER SPINAL CORD INJURY

Gail F Forrest[1], Thomas J Beck[2], Chris Cirnigliaro[3], Arvind Ramanujam[1], Steven Kirshblum[4], William A. Bauman[3], John Mores[1], Susan Harkema[5]

[1]Kessler Medical Rehabilitation Research and Education Center (KMRREC), West OrangeNJ.
[2]Johns Hopkins University, School of Medicine, Baltimore, MD.
[3]VA RR&D Center of Excellence for the Medical Consequences of Spinal Cord Injury, Bronx, NY., NY
[4]Kessler Institute for Rehabilitation, NJ
[5]Department of Neurological Surgery, University of Louisville,KY
email:gforrest@kmrrec.org

INTRODUCTION

Over 200,000 persons in the United States have spinal cord injuries (SCI) with varying degrees of immobilization, associated with disuse atrophy of bone and muscle. Skeletal fragility with potential fracture risk is a well recognized secondary complication of SCI (Garland et al., 2004). The lack of strength of the musculoskeletal system may limit walking or loading ability. Densitometry has been used to study the effect SCI on changes in bone and lean body mass. Bone mineral density (BMD) does not account for bone structure and size (Kiratli et al. 2000). The distal femur and proximal tibia are sites most prone to fracture and are, thus, regions of heightened interest. The purpose of this preliminary study was: a) to use geometric properties (with BMD) to describe the femoral shaft, b) to examine the relationship between the geometric properties and bone strength to unloading and leg lean mass in individuals with chronic SCI.

METHODS AND PRODEDURES

Five participants with chronic SCI (Table 1) were consented in accordance with KMRREC's Institutional Review Board.

Table 1: Physical Characteristics				
Post Injury (years)	Age (years)	Height (cm)	Weight (kg)	Loading 1=Yes; 2=No
4.52	45.08	176.60	79.20	1.60
±2.40	±15.20	±7.40	±11.00	±0.55

Femur Measurements: Dual energy x-ray absorptiometry (GE Lunar Prodigy iDexa, Lunar Inc., Madison, WI) was used to determine BMD (g/cm^2). Distal femur was measured by one scan image. Measures of femur length (FL) were made from the total body scan to calculate FL/3. The distance FL/3 proximal from the knee joint (apex of patella) was marked on the participant while supine. Scan length included at least 2 cm above this mark.

Analyses: On the scan image:
a) The point measured FL/3 proximal from the knee joint is marked (A)
b) A rectangular region across the long bone axis, centered at this distance A is marked.
c) The fixed region length (L) along the femur axis was between 1 and 2 cm (Table 2). L was measured from the scanner software.
d) BMD was measured in the region of interest using the AP spine software. The region bone area (BA) was also recorded.
e) The average outer diameter of the bone (W) within the region = BA/L.

The bone CSA is computed as:
$$CSA = \frac{BMD * W}{\rho_m}$$

Where ρ_m is the effective density of bone mineral in fully mineralized bone tissue (~1.05 g/cm^3).

Table 2.

The section modulus (Z) is computed as:

$$Z = \frac{CSMI}{W/2}$$

Measure of Strength: Strength of long bone varies with:

$$Z/FL$$

The cross-sectional moment of inertia (CSMI) is computed as:

$$CSMI = \frac{\pi}{4}\left(\left(\frac{W}{2}\right)^4 - \left(\frac{ED}{2}\right)^4\right)$$

Where ED is the estimated endosteal diameter.

$$ED = 2\sqrt{\left(\frac{W}{2}\right)^2 - \frac{CSA}{\pi}}$$

An estimate of mean cortical thickness is given by:

$$t = (W - ED)/2$$

Buckling ratio can then be estimated as:

$$BR = \frac{W/2}{t}$$

(Developed by Beck, T.J., 2008)

Non parametric Spearman's Rank Order Correlation determined relationship between geometry variables and loading and lean mass.

RESULTS

Summary values for bone mineral density and geometry parameters are presented in Table 2. There was a high negative correlation (-0.608) between with z/FL and loading. A high positive correlation (0.66) also was noted between leg lean mass and strength (Z/FL). Both sets of correlations increased slightly when controlling for age (unloading: -0.66; lean mass 0.67).

DISCUSSION

This study presents preliminary data to explore bone geometry and strength response after chronic SCI. The use of BMD only assumes that size, shape and material distribution is relatively less important. The section modulus normalized to femur length allows for a more accurate representation of strength. The limitations of the study relate to the small sample size and the lack of comparison to able-bodied controls.

SUMMARY

The potential significance of this study is: a) to examine the changes in bone geometry (CSMI, t, Z, Z/FL) in response to interventions, b) to improve clinical evaluation of bone and the estimation of fracture threshold using bone geometry (with BMD) rather than BMD alone for individuals with SCI.

ACKNOWLEDGEMENTS

REFERENCES

Beck. T., J. et al., *ftp.cdc.gov/pub/Health_*
Garland, D., E, et al., *J Spinal Cord Med.*2004; 27:207-11.
Kiratli, B., J. et al., *Journal of Rehabiliation Research and Development*, 2000, 37(2) 225-233.
Visintin, M., Barbeau, H. *Can. J. of Neurol. Science.* 1989; 16(3) 315-325.

Table 2: Bone Mineral Density and Geometry Parameters

	t (cm)	CSMI (cm^4)	Z (cm^3)	BR	BMD (g/cm^2)	L (cm)	Z/FL	Lean mass legs (gm)	Fat mass legs (gm)
Mean	0.94	3.58	2.41	1.59	2.08	1.99	0.06	16688.60	8382.60
Std	±0.18	±1.41	±0.73	±0.27	±0.30	±0.01	±0.02	±2794.76	±4760.69
Range	.65-1.08	2.17-4.64	1.68-2.96	1.33-2.05	1.62-2.24	1.98-.99	.04-.08		

INTERVERTEBRAL NEURAL FORAMINA DEFORMATION DUE TO TWO TYPES OF REPETITIVE COMBINED LOADING

Janessa D.M. Drake[1] and Jack P. Callaghan[2]

[1]Department of Kinesiology, Faculty of Human Kinetics, University of Windsor, Windsor, Ontario, Canada, jdrake@uwindsor.ca
[2]Department of Kinesiology, Faculty of Applied Health Sciences, University of Waterloo, Waterloo, Ontario, Canada, callagha@healthy.uwaterloo.ca

INTRODUCTION

The effects of posture and load combinations on the nerve roots have only been addressed for the cervical spine region, but it has been shown that the size of the neural spaces are dependent on posture (Harrison et al., 1999). In addition, pressure on neural tissue has been shown to elicit pain responses in rats (Hubbard et al., 2007). Altered mechanics of the spine have been observed in in-vitro experiments that exposed functional spinal units to a repetitive combined loading paradigm (Callaghan & McGill, 2001; Drake et al., 2005). This loading paradigm may also modify neural space size. Recently, it has been demonstrated that larger twist angles can be achieved when coupled with forward flexion in-vivo (Drake & Callaghan, 2008). These findings suggest a postural mechanism may be responsible for modulating the load distribution between the facets and the disc. The contribution of intervertebral disc (IVD) damage to the development of constricted neural spaces has not been explored. The objectives of this study were two-fold, to measure the occlusion of the intervertebral foramina (IVF) due to two types of repetitive loading, and to investigate whether repetitive combined axial twist loading can generate IVD injury. The outcome measures were compared to known levels of mechanical neural compression, which have been shown to cause pain, to assess viable pain generating mechanisms associated with IVD injury.

METHODS AND PROCEDURES

Sixteen porcine cervical spine motion segments (C5/6) were subjected to 1500N of compression combined with either passive range repetitive flexion/extension motions (15.5±1.4° flexion,-4.75±1.6° extension) or static flexion (16.4±2.1°) combined with repetitive left axial twist motion (5.2°). A custom 3-axis servo-hydraulic system was used to apply the loads. Pressure was measured in the IVF of both the left and right side of the specimens using 5mm diameter flexible plastic tubing and a custom pressure monitoring system. The tubes, which were the same size as the nerve roots, were inserted anterior-laterally through the IVF and terminated in the spinal canal (Figure 1) after the nerve roots and spinal cord had been removed.
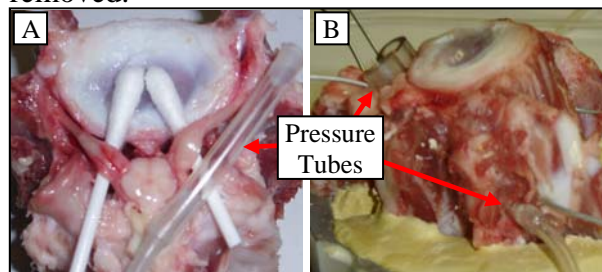

Figure 1. The nerve roots in the IVF were removed and were replaced with plastic tubing bilaterally (A). The tubes ran through the IVF to the spinal canal (B).

Prior to loading and following blocks of 1000 loading cycles the specimens were subjected

to flexion-extension range of motion testing and planar radiography to document the IVD condition. The range of motion tests flexed and extended the specimens to the limits of the neutral zone five times at a rate of 0.5°/s. Resultant structural failure of the disc and vertebrae were compared to the measured pressure changes, flexion-extension stiffness, and specimen height. Testing was terminated when herniation was determined radiographically or after 10,000 loading cycles had been applied.

RESULTS

There was significantly different bilateral pressure (pre-post difference) in the IVF of specimens that were repetitively flexed-extended (P=0.028) compared to those that were repetitively twisted (Figure 2).
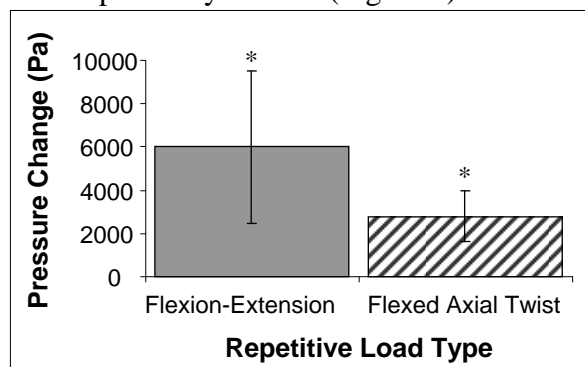
Figure 2. Pre-post pressure changes measured in the intervertebral foramina under two types of repetitive loading: flexion-extension motions, and left axial twist motion combined with static flexion were different(*).

The failure of the specimens was different between the repetitively loaded groups. All of the flexed-extended specimens herniated after an average of 5750 ±1065 cycles of loading. The repetitively axial twisted group sustained 9750 ±463 cycles of loading, with two specimens having no observable damage, one having a facet fracture with no IVD damage, and five having incomplete herniations. There was no significant difference of the vertical

height loss or percent difference flexion-extension stiffness between the groups (P>0.199). The height loss was 3.50±0.88mm, and the pre-post percent difference stiffness (normalized to endplate area) was 54.9±23.4%.

DISCUSSION

The average pressure for the repetitive flexion-extension and axial twist loading respectively were approximately 46% and 21% of the pressure threshold reported to elicit pain behaviours in rats (Hubbard et al., 2007). These values ranged as high as 97% and 34% respectively. Based on the injury data, if the duration of exposure to repetitive axial twist was increased, greater injury to the IVD may be sustained causing further increases in IVF pressure. This information may be useful to consider when determining treatment and rehabilitation to address nerve root compression.

SUMMARY

Repetitive loading of dynamic flexion-extension motions is a viable pain generating pathway.

REFERENCES

Callaghan JP, and McGill SM, (2001) *Clin Biomech* 16:28-37.
Drake JDM, and Callaghan JP, (2008) *Clin Biomech* Epub Ahead of Print.
Drake JDM, et al., (2005) *Clin Biomech* 20:1038-45.
Harrison DE, et al., (1999) *J Manipulative Physiol Ther* 22:227-234.
Hubbard RD, et al., (2007) *J Biomech* Epub Ahead of Print.

ACKNOWLEDGEMENTS

A ROBOTIC CADAVERIC FLATFOOT SIMULATION OF STANCE PHASE

Lyle T. Jackson,[1,2] Patrick M. Aubin,[1,4] Matthew S. Cowley,[1] Bruce J. Sangeorzan[1,5] and William R. Ledoux[1,3,5]

[1] RR&D Center of Excellence, VA Puget Sound, Seattle, WA
[2] School of Medicine, Departments of [3] Mechanical Engineering, [4] Electrical Engineering, and [5] Orthopaedics & Sports Medicine, University of Washington, Seattle, WA
email: wrledoux@u.washington.edu, web: www.seattlerehabresearch.org

INTRODUCTION

The pes planus or flatfoot deformity is the most common foot pathology (Gould, *et al.* 1980). It is often associated with posterior tibialis tendon insufficiency (PTTI) (Mann 1999; Niki, *et al.* 2001). A number of studies have generated cadaveric flatfoot models, but most consider only midstance. We are unaware of a study that has characterized all of the stance phase of the gait cycle, used inputs from flatfoot subjects and simulated both translational and rotational motion. Our purpose was to create a six-degree of freedom (DOF) cadaveric flatfoot model with PTTI that quantified bony motion and ground reaction forces (GRF) during the entire stance phase of gait.

METHODS

Previously, gait kinematics and GRFs were recorded from ten flatfoot subjects using a Vicon® twelve-camera motion analysis system. A single fresh frozen cadaver lower limb was acquired for study. Proximal to the ankle, soft tissue was dissected away leaving intact the extrinsic tendons, tibia and fibula. Retro-reflective markers were placed on the tibia, calcaneus, talus, navicular, medial cuneiform and first metatarsal. The foot was mounted in the Robotic Gait Simulator (RGS), a dynamic gait simulator consisting of a parallel axis robot (R-2000), force plate, dedicated motion analysis system and tendon actuators (Figure 1, Aubin *et al.* 2008). The RGS moves the "ground" relative to a cadaveric foot. Physiologic extrinsic tendon forces were applied, the gait kinematics (rotations) were prescribed and translations were adjusted to match the vertical GRF. Cadaveric bony motion and GRFs were recorded at 10 discrete (static) instances between 0 and 90% of stance phase. The foot was then conditioned flat using surgical ligament attenuation and cyclic loading (Blackman *et al.* in review). Each foot was tested again in the RGS without loading the posterior tibialis to simulate PTTI. The normal and flatfoot conditions were compared.
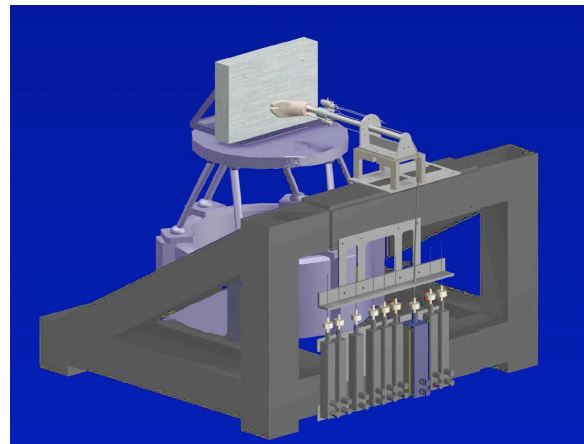

Figure 1: The RGS with a cadaver foot.

RESULTS

The RGS was able to recreate the kinematics and kinetics of the *in vivo* flatfoot subjects by prescribing the correct angular rotation of the "ground" with respect to the foot and generating the correct vertical GRF (data not shown). The cadaveric foot demonstrated collapse of the medial arch as indicated by plantar flexion of the talus relative to the tibia and dorsiflexion of the following: the first metatarsal with respect to the talus (Figure 2), the medial cuneiform with

respect to the navicular and the navicular with respect to the talus. Forefoot abduction was seen by the first metatarsal with respect to the talus (Figure 3). Unexpectedly, the calcaneus inverted slightly rather than everted relative to the tibia (Figure 4).
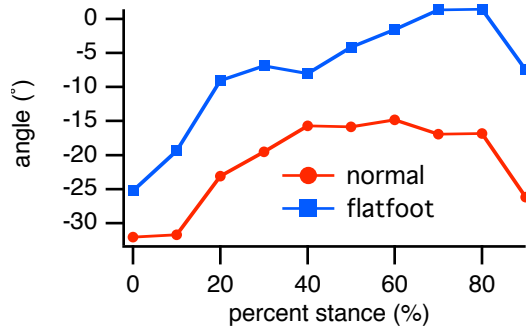

Figure 2: First metatarsal with respect to the talus, sagittal plane, - = plantar flexion
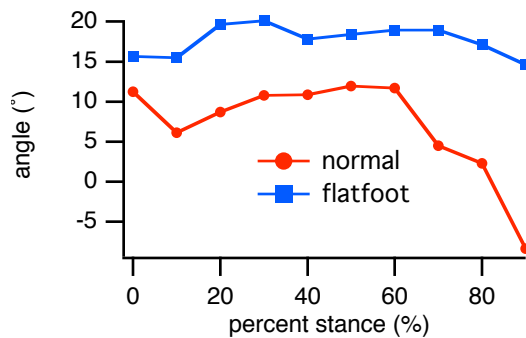

Figure 3: First metatarsal with respect to the talus, transverse plane, + = abduction
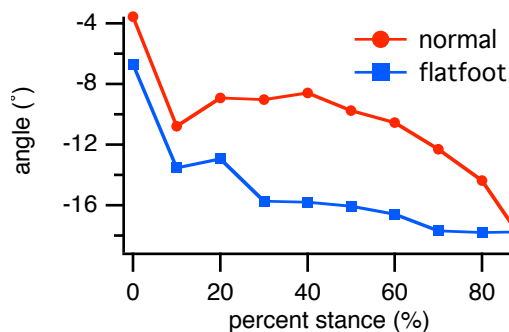

Figure 4: Calcaneus with respect to the tibia, coronal plane, - = inversion

DISCUSSION

With the exception of the calcaneus, the cadaveric flatfoot model demonstrated changes consistent with a flatfoot deformity resulting from PTTI. The common bony motion changes expected with a flatfoot are collapse of the medial arch, plantar flexion of the talus, abduction of forefoot and eversion of the calcaneus (Johnson and Strom 1989; Mann 1999). The RGS was able to generate the correct kinematics and kinetics in six DOF based on *in vivo* pes planus subjects and estimated extrinsic muscle forces for 10 discrete (static) points during the stance phase of gait. The cadaveric flatfoot model with PTTI showed changes consistent with the acquired flexible flatfoot pathology including collapse of the medial arch and abduction of the forefoot. Whereas other cadaveric models only considered midstance or a few positions within the stance phase, this simulation has the potential to evaluate both non-invasive treatments and surgical treatments throughout the entire stance phase of gait perhaps eliciting unknown advantages or disadvantages of these treatments at other points in the gait cycle. Future work will include dynamic simulation of gait.

REFERENCES

Aubin, P. M., et al. (2008) IEEE Trans Biomed Eng **55**(3): in press
Blackman, A. J., et al. Submitted to J of Orthopaedic Research.
Gould, N., et al. (1980). Foot Ankle **1**(1): 8-10.
Johnson, K. A. and D. E. Strom (1989). Clin Orthop Relat Res (239): 196-206.
Mann, R. A. (1999). M. J. Caughlin and R. A. Mann. St. Louis, Mosby. **1:** 733-767.
Niki, H., et al. (2001). Foot Ankle Int **22**(4): 292-300.

ACKNOWLEDGEMENTS

SHAPE MEMORY ALLOYS, AN ALTERNATIVE ACTUATION METHOD FOR ORTHOSIS DEVICES

Ehsan Tarkesh Esfahani[1], Mohammad H Elahinia[1], Mohamed S Hefzy[1], Charles W Armstrong[2]

[1]Mechanical Industrial and Manufacturing Engineering Department, University of Toledo
[2]Kinesiology Department, University of Toledo, Toledo, OH

INTRODUCTION

There are millions of individuals who cannot experience the pleasures of walking. Only in the US, approximately 866,000 people use an orthosis on a lower extremity and 8 million people are in immediate need for new technologies in orthosis and/or prosthesis that will help them walk. The main objective in developing active orthoses for the lower extremity is to enable patients to walk closer to normal. The first efforts in building a powered assistive device goes back to mid-1970s with hydraulic actuators [Hughes, 72]. More recently, Mckibben mussels [Ferris, 05] and DC motors have been used to provide actuation for orthosis [Blaya, 04]. The need of light weight and flexible actuation with a high power to mass ratio brings the idea of using novel actuation such as Shape Memory Alloys (SMA).

The key feature of this material is its ability to undergo large seemingly plastic strains and to subsequently recover these strains when a load is removed or the material is heated. A secondary useful feature of many SMAs is their biocompatibility characteristic. Nitinol (Ni-Tn) is known for their capabilities in applying both large forces (stress of 600 MPa) and large displacements (strain of 10%) which make it suitable in our application. Using SMA wires have also some disadvantages namely slow response, low energy efficiency due to conversion of heat to mechanical energy, and motion control difficulties due to hysteresis, nonlinearities and parameter uncertainties. Using nonlinear control method, however, it is possible to overcome most of these difficulties.

The aim of this paper is to introduce shape memory alloys as an alternative solution for actuating an ankle foot orthosis. In this paper, simplicity of the actuation, high actuation force, and large actuation displacement of SMA wires is combined with proper control algorithms to develop an effective active foot orthosis.

SMA FOOT ORTHOSIS

Figure1 shows that ankle function during controlled plantar flexion closely resembles a linear torsional spring as ankle moment is proportional to ankle position. Thus by using a rotation spring at orthosis joint, it is possible to produce the unloading part of the curve which occurs between mid-stance and toe off. At the same time SMA actuator provides one-way actuation and therefore, must be deformed by a bias force in martensite in order to achieve repetitive motions. The torsional spring therefore can be used here to deform the SMA wire to the initial position at a same time that it is producing the unloading torque.
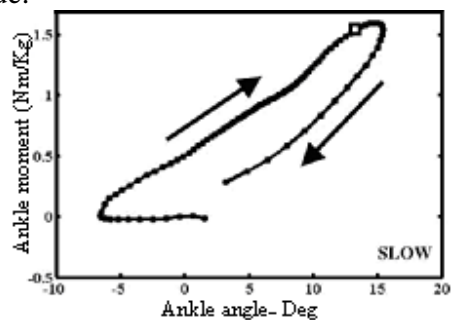

Figure 1 Ankle's behaviour during slow walking [Hansen, 04]

_____
*Send correspondence to mohamamd.elahinia@utoledo.edu

MODELING AND CONTROL

SMA actuation is the result of increased stress in the wire as a consequence of martensite to austenite phase transformation. It can be achieved by passing an electrical current through the SMA wire and simply increasing the temperature of the wire.

Model of SMA actuation system consists of the SMA element, dynamics of the system and heating and cooling method. Behaviour of the The input of the actuation model is the applied voltage and the output is the angular displacement of the orthosis. The modeling block of SMA actuation is shown in Figure 2. Since the actuation of SMA is combined with nonlinearity and uncertainties, it is important to use an adaptive robust controller. In this work, an adaptive PID is used which update the gains based on the sliding criteria.
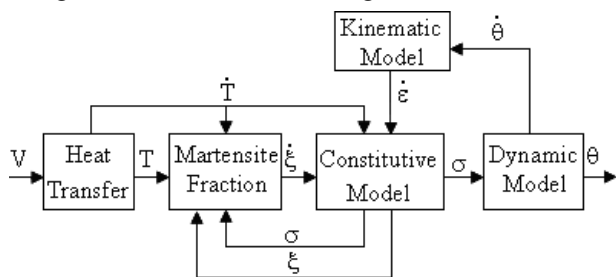

Figure 2 Block diagram of SMA actuation

RESULTS

Using the SMA model and the adaptive PID controller it is possible to simulate the walking cycle at different time cycles. The simulation results show that the tracking error of almost all controllers will increase dramatically for frequencies more than 0.3 Hz. This in turn results in an error up to 20° at the hill strike while the landing angle is about $20^o - 30^o$, hence this amount of error can not be acceptable. Therefore time cycle of 5sec (freq = 0.2 Hz) is selected for running the experiments. The performance of the controller in tracking the real ankle angle is shown in Figure 3. More details about the experimental setup, controller and modeling can be found in author's previous works.
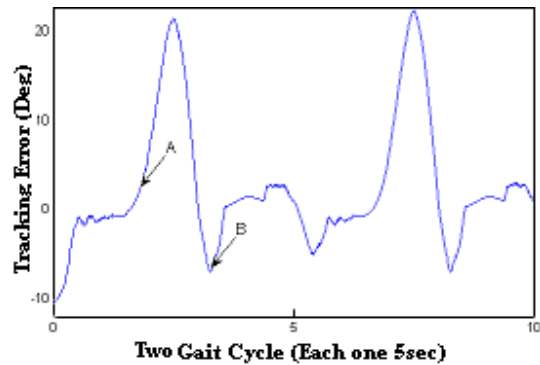

Figure 3 Tracking error for 5 sec gait cycle

DISCUSSION

As it is shown in Figure.3 the system has a largest error between point 'A' and 'B' where no voltage is applied and the wire is cooling down. The passivity of cooling process causes the tracking error and therefore the performance of the system in this part is not related to the controller and can be improved by adjusting the spring stiffness. Although this actuation method shows promising results both in simulation and experiments, yet there is a need to develop the actuation method during cooling process.

REFERENCES

Blaya, JA., Herr H., (04) *Adaptive control of a variable-impedance ankle-foot orthosis to assist drop-foot gait.* IEEE Trans Neural Sys Rehab Eng, 12(1):24–31.

Ferris, D.P., Czerniecki, J.M. and Hannaford, B., (05) *An ankle-foot orthosis powered by artificial pneumatic muscles.* J. App Biomec, 21:189-197.

Hughes,J.,(72) *Powered lower limb orthotics in paraplegia.* Paraplegia.1972;9:191–193.

Hansen, A.H., Childress, D.S., Miff, S.C., Gard, S.A. and Mesplay, K.P., (04) *The human ankle during walking: implications for design of biomimetic ankle prostheses.* J. Biomech, 37; 1467-1474.

FRICTIONAL PROPERTIES OF INTACT MUTANT PRG4 MOUSE KNEE ARTICULAR CARTILAGE

Elizabeth Drewniak[1], Michael Rainbow[1], Gregory Jay[2], Braden Fleming[1], and Joseph Crisco[1]

[1]Bioengineering Laboratory, Department of Orthopaedics, Brown Medical School/RIH, Providence, RI, USA 02903, Joseph_Crisco@brown.edu
[2]Department of Emergency Medicine, Brown Medical School/RIH, Providence, RI, USA 02903

INTRODUCTION

Osteoarthritis (OA) can be characterized by the degeneration of articular cartilage (AC) in synovial joints. In order to better understand this disease, many have focused their research efforts on joint lubrication and coefficient of friction (μ). Various methods have been utilized to measure the μ of AC including the use of pendulums with intact joints serving as the fulcrum of the system, the rubbing of cartilage plugs against a variety of surfaces, and atomic force microscopy. Pendulums have been used with of a variety of intact joints including human ankles and hips, porcine and bovine shoulders, and guinea pig knees; μ values ranged from 0.001 to 0.13 (Forster and Fisher, 1996l; Teeple et al, 2007). There is a need for a better understanding of joint lubrication and μ. Lubricin, a glycoprotein encoded by the PRG4 gene, provides chondro-protection (Jay, 2004). The objective of this study is to measure μ of PRG4 mouse hind limbs and compare the results using two models, a linear decay model and an exponential decay model that accounts for viscous damping.

METHODS AND PROCEDURES

Ten hind limbs from 10-week old PRG4 (+/+) mice were excised post-euthanasia. Skin and musculature were removed. Each intact knee was mounted in a pendulum with the arm (weighing ~50 g) fitted to the proximal end of the femur and the tibia fixed to the base, creating a resting angle of ~70°. Reflective markers were fixed to the pendulum arm and the base of the system for motion tracking. The joint was placed at an initial angle of 10±2°. The pendulum arm was released and allowed to oscillate freely until it came to a stop. Five trials of oscillations were collected for each joint with VICON (Centennial, CO) cameras and software. Oscillation data was processed with Visual3D (C-Motion, Inc., Germantown, MD) and custom MATLAB (MathWorks, Inc, Natick, MA) code to calculate the μ for each joint using the Stanton linear decay model (Lin μ) and an exponential decay model (Exp μ) that accounts for viscous damping (Crisco et al, 2007). The fit of each model to the experimental data was determined using root mean square error (rmse). Repeatability was quantified using means (SD) and coefficient of variance analysis.

RESULTS

The Lin μ ranged from 0.031 to 0.080 with a mean of 0.042 (0.016) and a coefficient of variance of 5.0%. The Exp μ ranged from 0.016 to 0.037 with a mean of 0.022 (0.007) and a variance of 17.98%. The damping coefficient ranged from 1.364×10^5 to 1.245×10^4 with a mean of 2.969×10^5 (3.409×10^5) and a variance of 16.83%. The rmse for the Exp model was less than half that of the Lin model, indicating that it better fits the experimental data, however there was greater variability in the Exp μ given the higher coefficient of variance (Figure 1; Table 1).
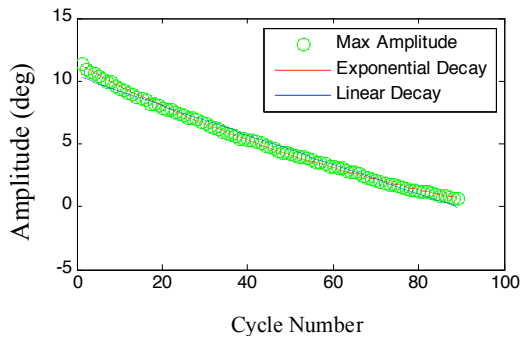
Figure 1. A representative plot demonstrating the decay of the oscillations (green circles) and the linear (blue) and exponential (red) decay models.

ID	Lin μ	Lin rmse	Exp μ	Exp rmse	Damping
874R	0.058	0.360	0.031	0.132	3.738E-05
874L	0.049	0.273	0.037	0.154	1.503E-05
875R	0.034	0.651	0.016	0.308	2.474E-05
875L	0.036	0.393	0.019	0.096	2.064E-05
876R	0.080	0.644	0.016	0.210	1.245E-04
876L	0.031	0.263	0.019	0.152	1.577E-05
928R	0.033	0.375	0.018	0.191	1.570E-05
928L	0.032	0.352	0.018	0.173	1.505E-05
929R	0.034	0.330	0.021	0.120	1.448E-05
929L	0.034	0.266	0.023	0.112	1.364E-05
Overall	0.042	0.391	0.022	0.165	2.969E-05

Table 1. Mean coefficient of friction (Lin μ and Exp μ), rmse (Lin and Exp), and damping values for each specimen and overall.

DISCUSSION

The objective of this study was to examine the frictional properties of the AC of PRG4 mouse knee joints with two mathematical models, a linear decay model and an exponential decay model that accounts for viscous damping. While the use of a small animal model for biomechanical testing poses design challenges, there are several advantages to using mutant PRG4 mice. This *ex vivo* pendulum testing takes the joint geometry into consideration. Also, the use of genetically modified mice reduces variability and allows for the further examination of

lubricin. Numerous studies have investigated the frictional properties of a variety of intact joints. The values obtained in this study fall within the accepted published results. Also, two other studies have investigated the μ of PRG4 mouse AC. Methods varied from this study, including the use of a different pendulum apparatus and μ calculations derived from the deceleration of the pendulum as well as the use of atomic force microscopy. These studies also examined different PRG4 genotypes. Results from these three studies of PRG4 mouse AC μ varied by as much as an order of magnitude, proving that more research is needed in this area (Coles et al, 2007; Elsaid et al, 2007). This study marks the first phase in our investigation of the effects of lubricin on μ of AC. Future work will examine μ values of PRG4 (+/-) and (-/-) AC, as well as the effects of wear on μ. More research focusing on μ, joint lubrication, and AC wear is needed to better understand OA.

REFERENCES

Coles, JM et al (2007). *JBiomech*, Epub.

Crisco, JJ et al (2007). *Proc IMechE*, 221: 325-33.

Elsaid, KA et al (2007). *Trans Orthop Res Soc*.

Forster, H and Fisher, J (1996). *Proc IMechE*, 210(2): 109-19.

Jay, GD (2004). *Curr Opin Orthop*, 15: 355-59.

Teeple, E et al (2007). *Osteo Cart*, 15: 309-15.

ACKNOWLEDGEMENTS

VIBROTACTILE TILT FEEDBACK REDUCES MEDIOLATERAL TILT IN VESTIBULOPATHIC SUBJECTS DURING LOCOMOTOR TASKS

Kathleen H. Sienko[1,2,3], Kennyn D. Statler[2], Lars I.E. Oddsson[4], Conrad Wall III[2,3]

[1]Dept. of Mechanical Engineering, Univ. of Michigan, Ann Arbor, MI, USA, sienko@umich.edu
[2]Jenks Vestibular Diagnostic Lab., Massachusetts Eye & Ear Infirmary, Boston, MA, USA
[3]Harvard-MIT Division of Health Sciences & Technology, Cambridge, MA, USA
[4]NeuroMuscular Research Center, Boston University, Boston, MA, USA

INTRODUCTION

We have developed a novel wearable device that augments or replaces compromised vestibular information by providing vibrotactile cues of body motion. Estimates of body tilt derived from accelerometers and gyroscopes are presented to a subject's torso in the form of small vibrations by vibrotactile elements similar to pager motors. Single- and multi- axis vibrotactile feedback has been shown to significantly reduce the root-mean-square (RMS) tilt in vestibulopathic subjects during quiet standing and single- and multi-axis perturbations (Kentala et. al, 2003, Kentala and Wall, 2005, Sienko et. al, 2008).

METHODS AND PROCEDURES

Eight vestibular-deficient subjects participated in a proof-of-concept study involving real-time M/L vibrotactile tilt feedback during various locomotor tasks including slow- and self-paced walking, walking on a foam surface, and walking along a narrow walkway. Locomotor tasks ranging from easy to challenging were selected for this exploratory study since the utility of vibrotactile feedback for improving gait stability was previously unproven. Prior to testing, subjects trained for approximately 45 minutes with the device. Two feedback configurations in addition to the device off configuration were tested: continuously displayed M/L tilt (continuous) and M/L tilt displayed for 200 ms beginning at the heel-strike event (intermittent). The intermittent display design was motivated by the findings of Bent et al. (2004) demonstrating that vestibular information is used during double support phase to affect the M/L position of subsequent foot placement. The RMS tilt was calculated for all locomotor tasks by taking the square root of the squared sum of the estimated tilt as derived from the processed inertial sensing assembly data. Step width was calculated by taking the difference between the M/L shank positions derived from kinematic data. Step width variability was characterized by averaging the standard deviation step width values for all single support phases within a trial. Step length was calculated by taking the difference between the A/P shank positions. A modified five point Likert scale was used to assess the subject's impression regarding the usefulness of the device in improving stability. A one-way, repeated-measure analysis of variance was performed on each dependent variable, with a level of significance set at $p < 0.05$.

RESULTS

Use of M/L vibrotactile tilt feedback resulted in decreased M/L tilt for slow-, self-paced, narrow stance, and foam walking tasks. This decrease was statistically significant for the narrow stance walking task (Figure 1). Step width and step length were significantly reduced during slow-paced walking when M/L tilt feedback was provided. Step width variability was significantly reduced by M/L

tilt feedback for both slow- and self-paced walking trials. Although not significant, subjects decreased their pace during trials in which feedback was provided. The subjects perceived the usefulness of the device as 4.05 and 3.73 out of 5 (where 1 = very unhelpful, 3 = neutral, and 5 = very helpful) for the continuous and intermittent feedback displays, respectively.
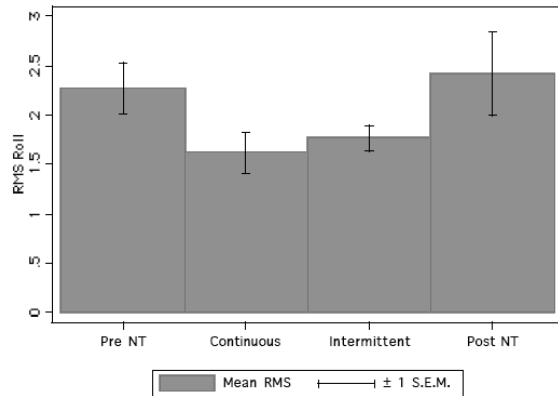

Figure 1. Average RMS M/L tilt (RMS roll) for narrow stance walking trials. Pre NT = device off (no feedback) trials preceding device on (feedback) trials. Post NT = device off trials following device on trials.

DISCUSSION

This study is the first to show that M/L vibrotactile tilt feedback improves M/L stability in vestibular deficient subjects during locomotor tasks. M/L tilt feedback resulted in decreased M/L tilt for all locomotor tasks; however, the difference was only significant for the narrow stance trials (the most challenging locomotor task). Additional subjects should be evaluated to determine if this trend is significant for slow-, self-paced, and foam walking tasks. In general, subjects walked at a slower, although not significantly slower pace when feedback was provided. Subjects were likely decreasing their gait velocity in an attempt to cognitively process and use the feedback information. This finding may suggest that the subjects were not sufficiently practiced at using the device and

that long training sessions potentially spanning days may be required for effective use of a biofeedback device during locomotor activities. No significant difference was identified between the two device configurations evaluated. Subjects as a whole found the continuous display configuration to be more useful and verbally indicated an increased level of confidence when their tilt information was displayed continuously vs. intermittently.

SUMMARY

This proof-of-concept study demonstrates that vestibular-deficient subjects can decrease their RMS M/L tilt during narrow stance walking by using M/L vibrotactile tilt feedback.

REFERENCES

Bent, L. et. al, *J Neurophysiol, 2004. **92(3):** p. 1269-75.*

Sienko, K. et. al, *XXV Bárány Society Meeting, March 31-April 3, 2008, Kyoto Japan.*

Kentala, E. et. al, *Ann Otol Rhinol Laryngol, 2003. **112(5):** p. 404-9.*

Wall, C., 3rd and E. Kentala, *J Vestib Res, 2005. **15(5-6):** p. 313-25.*

ACKNOWLEDGEMENTS

THE PULSED FLOW EQUATIONS FOR MODELING PHYSIOLOGICAL SYSTEMS IN BIOLOGICAL ORGANISMS AS QUASI-1D FLUID FLOWS

Anne Staples[1], Jay Boris, and Elaine Oran

Laboratory for Computational Physics and Fluid Dynamics, Naval Research Laboratory, Washington, DC, USA, [1]astaples@lcp.nrl.navy.mil

INTRODUCTION

Extensive research has been done on modeling human physiology. Most of the work has been aimed at developing detailed models of specific components of physiological systems such as a cell, a vein, a molecule, or a heart valve. One example of such an effort is the three-dimensional computational model of the heart developed at NYU (Peskin and McQueen, 1993). While efforts such as these are invaluable to our understanding of human biology, if we were to construct a global model of human physiology with this level of detail, computing even a nanosecond in this computational being's life would certainly be prohibitively expensive.

With this in mind, we derive the Pulsed Flow Equations (PFE), a set of coupled one-dimensional (*1D*) partial differential equations, specifically designed to capture two-dimensional (*2D*) viscous, transport, and other effects, and aimed at providing accurate and fast-to-compute global models for physiological systems modeled as networks of quasi one-dimensional (quasi-*1D*) fluid flows. Our goal is to be able to perform faster-than-real time simulations of global processes in the human body on desktop computers.

METHODS AND PROCEDURES

We seek to derive a system of equations that govern the velocity, u, the pressure, p, and the area, A, in internal biological fluid flows, while capturing what we feel are essential effects occurring in biological fluid flows that are not captured by the standard equations for incompressible fluid flows in *1D*. We begin with the constant-property Navier-Stokes equations in two dimensions with s as the variable in the radial direction, and x as the variable in the axial direction. To capture *2D* effects vital in modeling biological fluid flows, we consider the *2D* velocity profile found in fully developed channel flow:

$$u_p(x,s) = \frac{1}{4\mu}\frac{\partial p}{\partial s}\left(R^2 - x^2\right), \qquad (1)$$

where μ is the dynamic viscosity and R is the channel (a blood vessel or the trachea) radius, substitute this expression into the Navier-Stokes equations, and integrate over the radial direction:

$$\int \left[\frac{\partial u_p(x,s,t)}{\partial t} + (u_p(x,s,t)\cdot\nabla)u_p(x,s,t)\right.$$
$$\left. + \frac{1}{\rho}\nabla p(x,s,t) - \upsilon\nabla^2 u_p(x,s,t) - g(x,s,t)\right]dx = 0$$
$$(2)$$

resulting in a modified, quasi-*1D* momentum equation:

$$\frac{\partial u(s,t)}{\partial t} + (u(s,t)\cdot\nabla)u(s,t) =$$
$$-\frac{1}{\rho}\nabla p(s,t) + \upsilon\nabla^2 u(s,t) + \frac{8\pi\upsilon}{A}u + g(s,t),$$
$$(3)$$

where $A = \pi R^2$.

We then introduce the standard mass conservation equation:

$$\frac{\partial A}{\partial t} = -\frac{\partial}{\partial s}(Au),\qquad(4)$$

and a constitutive relation that models that relationship between the pressure at a point in the channel and the area at that point:

$$p = p^{eq} + \frac{1}{\varepsilon}\left(A - A^{eq}\right),\qquad(5)$$

where p^{eq} and A^{eq} are equilibrium values for the pressure and area, respectively, to close the system.

RESULTS

The resulting quasi-*1D* momentum equation is similar to the Navier-Stokes equation in *1D*, but with an extra term on the right hand side. This term, the contribution from the assumed parabolic velocity profile, captures some of the *2D* transport and viscous effects associated with that profile. Using the analytical approach here, the same term that others have added empirically to the standard *1D* momentum equation for biological fluid flows (see, for example, Quateroni, 2001) is recovered. In addition, branching effects can be captured by employing a branching scheme of the form $A = \pi R^2 = nS$, where *n* is the number of concurrent channel (branches) and *S* is a reduced area. Finally, the resulting system of equations, once discretized, can be put into tridiagonal form, leading to solutions in *O(N)* operations for each time step, where *N* is the size of the computation. Thus the goal of deriving a set of equations for performing faster-than-real time computations of global processes in physiological systems has been achieved.

DISCUSSION

The model derived here can be considered as a macroscopic model for a multiscale model of a physiological system in the human body. For example, the PFE equations could be used to compute blood flow through a computational model of the circulatory system, with computational visits to microscopic levels of description (molecular dynamics simulations to determine the shear stresses, for example) as needed on the fly.

The choice of the velocity profile (1) was somewhat arbitrary. Another velocity profile, such as that for fully developed turbulent pipe flow, or laminar or turbulent channel flow, could be used.

SUMMARY

The PFE equations, a set of coupled partial differential equations, were derived as an accurate low-dimensional model for physiological systems in the body. The approach to deriving the equations recovers previous empirical results, and it is found that the equations can be put in tridiagonal form, leading to faster-than-real-time computations of global processes in the human body.

REFERENCES

Peskin, CS and McQueen, DM (1989) *J. Comp. Phys.,* 81:372-405

Quarteroni, A (2001) *SIAM News,* 34(6):1-3

ACKNOWLEDGEMENTS

CHILDREN'S POSTURAL HABITS WHILE WORKING AT COMPUTER WORKSTATIONS

Carol Murphy[1], Joan Stevenson and Mohammad Abdoli[2]

[1]Department of Kinesiology and Health Studies, Queens University, Kingston, ON, Canada,
2cam9@queensu.ca
[2]School of Occupational and Public Health, Ryerson University, Toronto, ON, Canada

INTRODUCTION

The increasing incidence and disability associated with repetitive stress disorders and musculoskeletal disorders and their frequency among computer users has led to concern. This concern has been extended to young children who are potentially also at risk for these injuries (Jacobs et al., 2002; Gerr et al., 2004). Jacobs (2002) has shown that children are reporting moderate amounts of musculoskeletal discomfort and this discomfort can be related to computer use. This risk is increased by the fact that children are often required to play and work on computer workstations which are designed for adult anthropometrics. The purpose of this study was to examine the quality and quantity of postural movements exhibited by children when using an adult workstation and an ideal children's computer workstation to play a computer game.

METHODS AND PROCEDURES

Nine, 8 and 9 year old children were recruited with consent. Children were outfitted with eight Liberty® sensors on their head, hand, forearm, arm, acromion process, C7, T12 and iliac crest to allow quantification of 3D motions of the wrist, elbow, shoulder, head tilt and poke, upper and lower trunk angles and motions of the pelvic girdle and shoulder girdle. The children were tested in two conditions: one at an adult workstation with adult computer equipment and one at an ergonomically-adjusted child's workstation with children's computer equipment. Data were collected for 20 minutes while the children played an educational computer game. Segment and joint angles and displacements relative to the neutral starting posture were determined and compared to recommended postures by Occupational Safety and Health Associations (OSHA). Both descriptive and statistical comparisons were made to determine the 3D postures and durations in each posture over the time course of data collection. Adult vs. Ideal Child's workstations were compared in the primary area of concern, namely: spinal curves, upper extremity postures and head-on-neck postures. Children were also asked to complete a Visual Analog Scale (VAS) and a Perceived Children's Rate of Exertion. (PCERT) to assess their pre- and post-musculoskeletal aches and pains.

Children's Workstation

Adult Workstation

RESULTS

Spinal curve changes were significant showing adaptive postural strategies to the two conditions for the different spinal curves. Arm positions were also adaptive to the adult workstation. The wrist was more dorsi-flexed at the adult's workstation. (Figure 1) The elbow angles were not significantly different; however there was greater shoulder flexion (Figure 1) as well as abduction. (Figure 2)
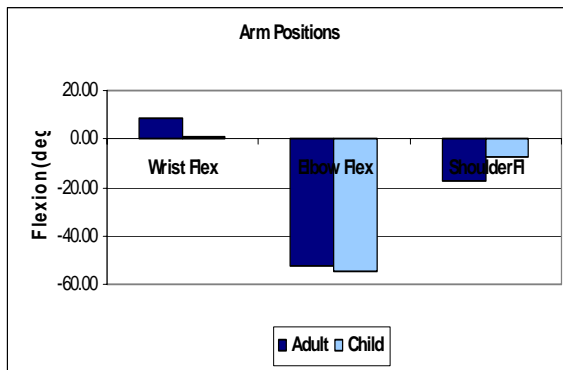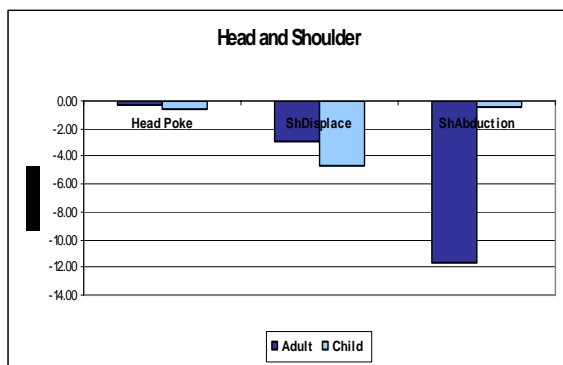

Figure 1

Figure 2

DISCUSSION

Analysis of children's postures at adult workstations show that children are not following OSHA guidelines and spend little of their time in the recommended neutral resting posture.
The main areas of concern identified from the adult workstation were:

- Spinal curves were compromised from their neutral positions.
- Wrist postures show increased wrist dorsi-flexion and deviation.
- Shoulder abduction occurs throughout.
- Children self-report more perceived exertion at an adult workstation.
- Children self-report more discomfort on a VAS using an adult workstation.

SUMMARY

Based on these results it would be advisable to devise recommendations and guidelines for children's workstation design. This need is deemed to be imperative based on the increasing use of computers both in school and at play and the increasing amount of time spent at the computer on a daily basis. (Jacobs, 2002)

REFERENCES

Gerr, F. et al (2004) *J. Electromyographical Kinesiology*. Feb;14(1):25-31.
Gerr, F. et al. (2002) *Am J Ind Med*. Apr; 41(4):221-35
Jacobs, K and Baker, N.A. (2002) *Work.* 2002:18(3):221-6

ACKNOWLEDGEMENTS

INFLUENCE OF POSTERIOR CRUCIATE LIGAMENT TREATMENT ON QUADRICEPS DEMAND IN TKR: A COMPUTER SIMULATION STUDY

Michael W. Hast[2], Ryan L. Landon[2], Stephen J. Piazza[1,2,3]

Depts. of [1]Kinesiology, [2]Mechanical and Nuclear Engineering and [3]Orthopaedics & Rehab., The Pennsylvania State University, University Park, PA, USA, *piazza@psu.edu*

INTRODUCTION

Treatment of the posterior cruciate ligament (PCL) is an important consideration for surgeons who perform total knee arthroplasty. Cruciate-retaining (CR) knee replacement designs rely upon the natural PCL to control anteroposterior movement of the femur upon the tibia, while posterior-stabilized (PS) designs sacrifice the PCL and employ a cam-post mechanism to accomplish the same task. These different approaches have the potential to affect the efficiency of the extensor mechanism, which is critical to regaining function postoperatively. Yoshiya et al. (2005) measured tibiofemoral contact points *in vivo* and found PS knees to have more 'posterior rollback' than did CR designs, but it was not clear if these kinematic differences corresponded to changes in extensor mechanism efficiency. The purpose of this study was to use a computational model to investigate the influence of PCL treatment (CR versus PS) on the demands of the quadriceps and location of the axis of rotation following knee arthroplasty.

METHODS AND PROCEDURES

The lower extremity model described by Delp et al. (1990) was reconfigured into a 12-degree-of-freedom forward-dynamic model to replicate an 'Oxford Rig' cadaver test arrangement in which a controlled knee flexion from 20° - 120° was performed under quadriceps control. A 30 kg mass was placed at the pelvis to simulate body weight, and the attachments of the vastus intermedius were used to represent a lumped quadriceps muscle group. The quadriceps force necessary to lower the pelvis at a constant rate (3.9 cm/s) was determined using a modified version of the Computed Muscle Control algorithm described by Thelen et al. (2003).

The PCL was modeled by ten ligament fibers with slack lengths chosen such that the PCL engaged at 80° of knee flexion when normal knee motions were applied (Makino et al., 2006). Passive muscle forces and collateral ligaments were modeled with force-length and force-velocity relationships. PS and CR versions of the same knee replacement design (Scorpio; Stryker Orthopaedics, Inc.) were compared using the simulation. Patellofemoral and tibiofemoral contact was modeled using a rigid body spring model (Li et al., 1997).

Knee joint angles were computed following the convention of Grood and Suntay (1983). Axes of rotation between the femur and tibia were located throughout the flexion movement by computing finite helical axis.

RESULTS AND DISCUSSION

The quadriceps forces required to perform the knee flexion task were found to be similar for PS and CR designs at low knee flexion angles. At angles higher than 70°, however, the quadriceps in the CR model were required to exert forces that were 5% - 10% higher than those demanded of the quadriceps when effecting the same motion for the PS-implanted model (Figure 1).

The axes of rotation between the tibia and femur were nearly immobile in the femoral frame of reference for both PS and CR knees from 20° - 70° of flexion (Figure 2). At

higher flexion angles, however, there was substantial motion of the axis of rotation for the PS design, while the axis for the CR design remained in place. The greater motion of the axis of rotation in the PS design is likely caused by the action of the cam-post mechanism, which was found to engage at 70°.
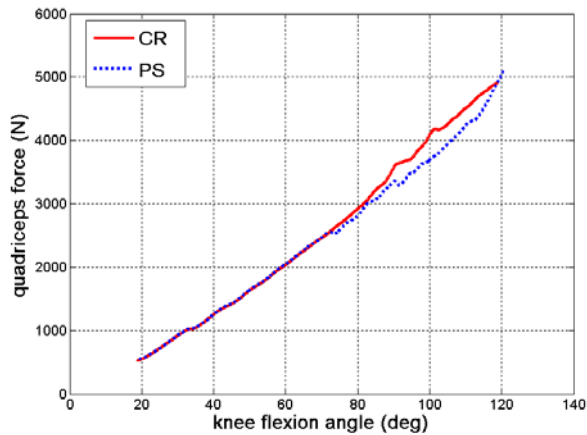

Figure 1: Vastus intermedius forces plotted against knee flexion angle for CR and PS knees.

SUMMARY/CONCLUSIONS

Investigations of the determinants of knee extensor efficiency afforded by different implant designs are important for improving functional outcomes following knee replacement. In this study, the movement of the axis of rotation at high flexion angles mediated by the cam-post mechanism of the PS design appears to lessen the demands on the quadriceps at high flexion angles.

REFERENCES

Delp SL et al. (1990) *IEEE Trans. Biomed Eng.*, 37, 757-767.
Grood ES, Suntay WJ. (1993). *J. Biomech Eng,* **105,** 136-44.
Li G, et al. (1997). *J. Biomech*, **30**, 635-38.
Makino A et al. (2006) Arthroscopy, 22:684.e1-5.
Thelen DG, et al. (2003). *J. Biomech, **36,** 321-28.
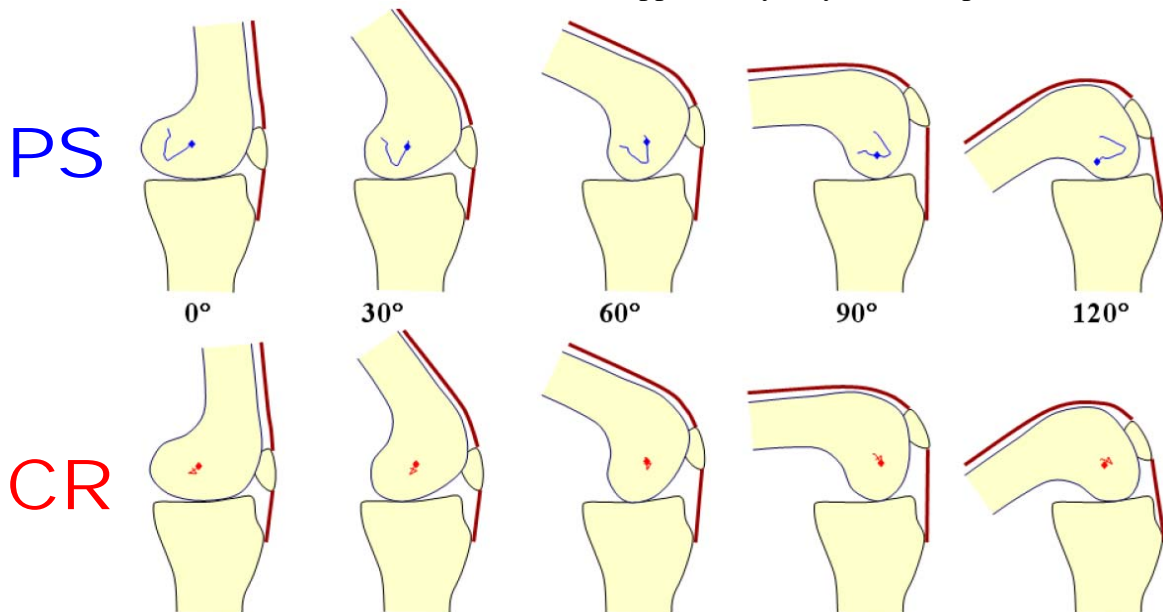Yoshiya S, et al. (2005). *J. Arthroplasty,* **20,** 777-83.

ACKNOWLEDGMENTS

Figure 2: A cartoon representing the paths of the axes of rotation. Translations are noted by the blue lines (PS) and red lines (CR) on the femur. The colored dot represents the current location of the axis of rotation for the knee flexion angle shown.

FORCE ENHANCEMENT REACHES A PLATEAU AT CRITICAL STRETCH MAGNITUDES

Brandon Hisey, Tim Leonard, and Walter Herzog[†]

Human Performance Laboratory, Faculty of Kinesiology, University of Calgary, Calgary, AB. Canada.
[†]Corresponding author: email walter@kin.ucalgary.ca

INTRODUCTION

It has been widely observed that the steady-state isometric force following active stretch is greater than the force obtained during purely isometric contractions at the corresponding length (Abbott and Aubert, 1952). This phenomenon has been termed force enhancement (FE). FE cannot be explained within the framework of the reigning paradigm of muscle contraction, the cross-bridge theory. However several mechanisms for FE have been advanced in the literature (Rassier and Herzog, 2004). Edman et al. (1978) found that FE increases with increasing stretch magnitude, however this finding was recently found to be only partially correct, as FE was found to increase with increasing stretch magnitudes, but reached a plateau at critical stretch magnitudes (Bullimore et al., 2007). However, for lack of direct fibre length measurements, and because experiments were only performed for one final muscle length, the reason for this plateau effect could not be speculated upon. Therefore, the purpose of this study was to investigate the stretch magnitude dependence of FE at different final lengths and with simultaneous fibre and sarcomere length (SL) measurements. We hypothesized that FE increased only for stretches covering the plateau and descending limb of the force-length relationship, while additional stretching on the ascending limb would not contribute to FE.

METHODS AND PROCEDURES

Experiments were performed on cat soleus (n=6). All procedures were approved by the Animal Ethics Committee of the University of Calgary. Soleus was isolated from surrounding tissues, and its tendon was rigidly attached to a muscle puller (MTS) with a remnant piece of bone. The muscle puller applied computer controlled length changes and had a sensor for force measurements. A cuff-type, stimulating electrode was placed on the tibial nerve to deliver controlled stimulation to the soleus. Sonomicrometry crystals were implanted at the ends of a fascicle for online fibre length recordings.

The experimental protocol consisted of isometric reference contractions and stretch test contractions. The isometric reference contractions were performed at three lengths corresponding respectively to lengths of 9mm longer (test 1), 3mm longer (test 2) and 3mm shorter (test 3) than optimal soleus length. The stretch test contractions consisted of active soleus stretches ranging from 3-24mm that finished at the three reference lengths identified above. Stretch speed was 12mm/s for all tests.

Following testing, animals were sacrificed and the soleus was removed and fixed at optimal length in 10% formalin. Following fixation, fascicles were isolated, fascicle length was measured using a video analysis system, and SL was determined using a laser diffraction system. The number of

sarcomeres in a fascicle was calculated by dividing fascicle length by the average SL. Knowing the number of sarcomeres within a fascicle and the instantaneous fascicle length at any given time, the instantaneous average SL could be calculated.

RESULTS

Steady-state force following stretch was equal or greater than the corresponding isometric reference force (Figure 1). The amount of FE depended on the end length (p<0.001), with the greatest values observed at 9mm longer than optimal (+9mm) and the lowest values observed at 3mm shorter than optimal length (-3mm, Figure 1). FE reached a plateau in tests 1 and 2 at stretch magnitudes of 12mm and 6mm, respectively, and remained virtually constant in test 3 (Figure 1). Maximal isometric force was observed at a SL of approximately 2.5µm while a length of 3mm shorter than optimal length (-3mm) corresponded to a SL of about 2.4µm (theoretical plateau = 2.3-2.5 µm). Thus, FE increased for stretches in the range of the descending limb and plateau, but not the ascending limb of the force-length relationship (Figure 2).
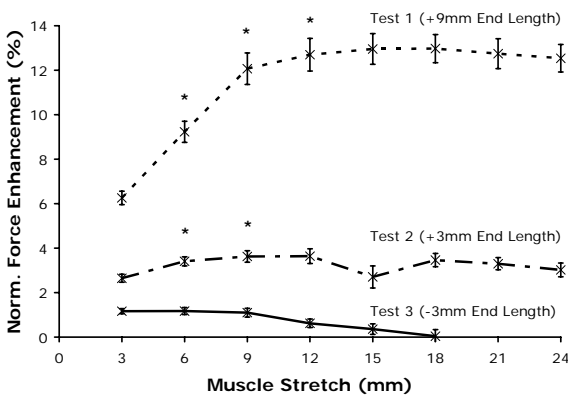

Figure 1. Mean normalized FE as a function of muscle stretch (error bars = ±1SEM). Asterisks indicate cases when FE was greater than FE for the preceding stretch magnitude.
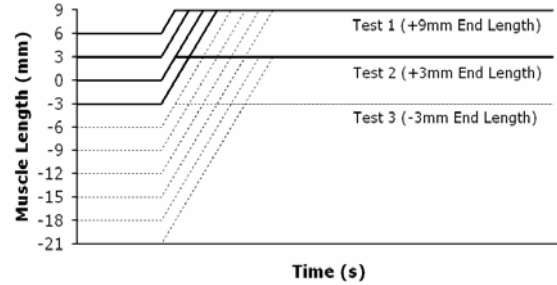

Figure 2. Muscle length histories during stretch contractions. The darker lines indicate the stretches for which FE increased.

DISCUSSION

For the past fifty years (Abbott and Aubert, 1952), FE had been thought to increase with increasing stretch magnitudes. Here we demonstrate that this result only holds for stretches covering the plateau and descending limb of the force-length relationship, but not the ascending limb. Since passive forces occur at around optimal length in cat soleus, and since passive FE was found to increase in parallel with the active FE (results not shown), we propose that the increase in FE depends critically on the existence of a passive force. The detailed nature of this dependence needs further investigation.

SUMMARY

Contrary to the literature, FE does not continue to increase with increasing stretch magnitudes but reaches a plateau at critical stretch lengths that depend crucially on the final muscle length.

REFERENCES

Abbott, BC and Aubert, XM (1952). *J. Physiol* 117: 77-86.

Bullimore, SR et al. (2007). *J. Biomech* 40: 1518-1524.

Edman, KAP et al. (1978). *J. Physiol (Lond)* 281: 139-155.

Rassier, DE and Herzog, W (2004). *J. Appl Physiol* 96: 419-427.

POSTURAL CONTROL DURING A STANDING TURNING TASK IN YOUNG AND OLDER ADULTS

Jennifer Baird and Richard Van Emmerik

Department of Kinesiology, University of Massachusetts Amherst, Amherst, MA,
bupt95@kin.umass.eduT

INTRODUCTION

More than one-third of adults fall each year, with 3-5% of those falls resulting in a fracture. About 30% of these falls occur while turning (Patla et al., 1992), which can result in a debilitating hip fracture (Cumming and Klineberg, 1994). Older adults demonstrate adaptations in spinal rotation during turning (Baird and VanEmmerik, 2007) that may indicate difficulty in control of turning. Turning movements would seem to challenge mediolateral control of posture, which has been reported to decrease with aging based on analysis of both the center of pressure and the center of mass (Lord et al., 1999). The purpose of this study was to investigate age-related differences during a visually-guided standing turning task, with analysis of both center of pressure and center of mass (Panzer et al, 1995).

METHODS

Ten young (25 ± 1.3 years) and 10 older adults (74.8 ± 5.3 years) participated. Subjects stood with one foot on each of two force platforms with feet hip-width apart. Targets (47.5 cm^2) were placed at eye level 130° to the right and left from the front of the collection space. A light was placed at eye level two meters from the subject. A headpiece was fitted with a laser pointer that had to contact the target for the trial to count. Prior to each trial, subjects were instructed to turn at a self-selected pace to the right or left. When the light was illuminated, they turned, hit the target with the laser pointer, and returned to face the front of the room. There were two conditions. In condition one (constrained), subjects were not allowed to move their feet. In condition two (unconstrained), subjects were allowed to move their feet if they chose. There were twelve trials in each condition, with direction of turn randomized in advance. Net center of pressure (COP) and center of mass (COM) range in the anterioposterior (AP) and mediolateral (ML) directions were calculated for both conditions; foot rotation was calculated for the unconstrained condition. Foot rotation and COM were calculated from retroreflective markers placed on the subject. A one-way repeated measures ANOVA, with subject as the repeated measure, was used for between group comparisons of all dependent variables for the constrained and unconstrained conditions independently.

RESULTS

Feet Constrained:
COP - Older adults demonstrated greater AP COP range than younger adults (5.39 cm vs. 3.40 cm, p<0.0001). No differences were observed between groups in ML COP range (p=0.82). Additionally, the young adults demonstrated greater COP ML range than COP AP range (6.45 cm vs. 3.40 cm, p=0.0002) (See Figure 1)
COM - Older adults had a greater AP (3.63 cm vs. 2.17 cm, p<0.0001) and ML (3.89 cm vs. 2.69 cm, p=0.014) COM range than young adults. (See Figure 2)
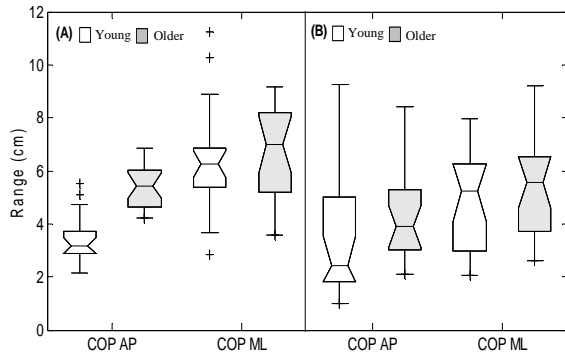
Figure 1. Box and whisker plot of the center of pressure range in the AP and ML directions for (A) constrained and (B) unconstrained conditions. The box has lines at the lower quartile, median, and upper quartile values. The whiskers are lines extending from each end of the box to show the extent of the rest of the data.
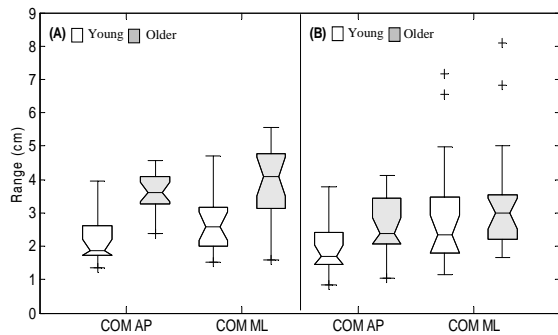

Figure 2. Center of mass range in the AP and ML directions for (A) constrained and (B) unconstrained conditions.

Feet Unconstrained:

COP - There were no differences between the young and older adults in the AP or ML COP range. (See Figure 1)

COM - There were no differences between the young and older adults in the AP or ML COM range. (See Figure 2)

Foot movement - 30% of young adults and 60% of older adults moved their feet greater than five degrees. The range of foot rotation varied greatly; young adults ranged from 0.50°-42° of rotation (mean=4.5°), while foot rotation in older adults ranged from 0.80°-77° (mean=10°).

DISCUSSION

With feet constrained, the COP results alone indicate that the older adults were more challenged than the young adults in the AP direction, but they performed as well as the young adults in controlling the task in the ML direction. The COM ranges, however, seem to indicate that the older adults are not as stable as the young adults in either direction. Taking both together provides a more complete picture. In both the AP and the ML direction, the greater COP range seen in the older adults compared to the young leads to greater movement of the COM. However, in the AP direction, there is greater COM movement within a smaller COP range.

With the feet unconstrained, the COP and COM results indicate that young and older adults control the task equally well. The older adults used foot movement in this condition to increase the ease of controlling the turning movement, while the young adults did not need this additional foot movement.

SUMMARY

A standing turning task requires more control in the AP than in the ML direction. Older adults use foot movement to make control of this task easier when given the option of doing so. Additionally, inclusion of the COM as a dependent measure provides a more complete picture of this task.

REFERENCES

Baird, J.L. and Van Emmerik, R.E.A. (2007) Podium presentation, ISPGR.
Cumming, R.G. and Klineberg, R.J. (1994) *J Amer Geriatr Soc*, 42(7): 774-8.
Lord, S. R., et al. (1999) *J Amer Geriatr Soc,* 47, 1077-1081.
Panzer VP et al 1995. *Arch Phys Med Rehabil* 76:151-157.
Patla, A. E., et al. (1992) *Canadian J Public Health,* 83, S29-33.

DIFFERENCES IN GASTROCNEMIUS ARCHITECTURE BETWEEN SPRINTERS AND NON-SPRINTERS: IMPLICATIONS FOR MUSCLE FUNCTION

Sabrina S.M. Lee[1] and Stephen J. Piazza[1,2,3]

Depts. of [1]Kinesiology, [2]Mechanical & Nuclear Engineering, and [2]Orthopaedics & Rehabilitation, The Pennsylvania State University, University Park, PA, USA, *piazza@psu.edu*

INTRODUCTION

The role of a muscle in producing a specific movement is determined in part by the muscle's force-generating capacity. This capacity depends on muscle architecture parameters and the muscle's fiber length and shortening velocity. The relationships between these parameters and muscle function have been explored in animal models (Lieber and Boakes, 1988; Lutz and Rome, 1994), but the influence of muscle and joint structure on *in vivo* function in humans has received less consideration. The results of previous investigations have suggested that sprinting is an activity that is especially well suited to elucidating these relationships. The fascicle lengths of gastrocnemius in sprinters have been found to be greater than those of non-sprinters (Abe et al., 2000; Abe et al., 2001) and gastrocnemius fascicle length has been found to positively correlate with sprint performance while its pennation angle has been shown to negatively correlate with performance (Kumagai et al., 2000). No studies, however, have reported these parameters in sprinters along with Achilles tendon moment arm, which should critically influence F-L and F-V characteristics.

The purposes of this study were (1) to compare lateral gastrocnemius fascicle length, pennation angle, and Achilles moment arm measured in sprinters and non-sprinters; and (2) to use a simple model to investigate the mechanisms by which these factors influence sprint performance.

METHODS AND PROCEDURES

Fascicle length, pennation angle, and plantarflexion moment arm of the lateral gastrocnemius were measured in 12 male collegiate sprinters (age 19.4± 1.2 y, height 1.81 ± 0.08 m, body mass 77.5 ± 6.5 kg) and 12 young adult males (27.3± 5.7 y, 1.80 ± 0.07 m, 76.9 ± 9.2 kg) who were not engaged in competitive sports. All subjects gave informed consent prior to testing and all procedures were approved by our university's Institutional Review Board. Fascicle length and pennation angle were determined from images captured using B-mode ultrasonography (Aloka 1100; transducer: SSD-625, 7.5 MHz). These images were made of the central region of the muscle while subjects were standing in anatomical position. To measure moment arm, the foot was rotated from 10º dorsiflexion to 20º plantarflexion using a potentiometer-instrumented rotating foot platform while ultrasound images of the musculotendinous junction were captured. The experimenter manually controlled plantarflexion during each trial while each subject plantarflexed maximally against the foot plate with the knee in full extension. Tendon excursion versus angle data were well approximated by linear fits; plantarflexion moment arms were taken to be the slopes of these lines. Two-tailed t-tests were used to test for differences between sprinters and non-sprinters for each parameter. Pearson correlation coefficient was calculated to test for correlation between moment arm and fascicle length.

A one-muscle, 2-DOF, planar model was used to simulate a sprint push-off subject to co-variation in muscle fiber length and plantarflexion moment arm. This simulation was developed using SIMM/Dynamics Pipeline and SD/FAST.
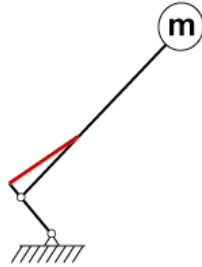

Figure 1. Sprint push-off model.

RESULTS

Fascicle lengths were significantly larger and moment arms were significantly smaller in sprinters compared to non-sprinters (Table 1). The pennation angles of sprinters were smaller on average than those of non-sprinters, but this difference was not found to be significant. The work done by the plantarflexor muscle during simulated sprint push-off increased with fiber length but maximal work was produced when the muscle moment arm was between 2 –3 cm (Figure 2).

parameter	SPR	Non-SPR	p
moment arm (cm)	31.0 (3.7)	41.6 (5.5)	< 0.001
fascicle length (cm)	7.0 (0.6)	6.1 (0.6)	0.001
pennation angle (°)	12.8 (1.1)	14.1 (1.8)	0.055

Table 1. Mean architecture parameters of lateral gastrocnemius of sprinters (SPR) and non-sprinters. (SD values in parentheses)

DISCUSSION

The architecture parameters measured for the lateral gastrocnemius in sprinters enhance the force generating capacity of this muscle, enabling sprinters to produce higher ground reaction forces for longer periods of time during push-off. Longer fascicle lengths, which may correspond to longer optimal fiber lengths will correspond to a wider plateau of the active force-length curve and a increase in

v_{max}, the intercept of the force-velocity curve, when each of these is expressed in un-normalized, absolute terms (Abe et al., 2001). Smaller moment arms result in smaller length changes for a given ankle rotation, resulting in more favorable operating ranges on the force-length and force-velocity curves.
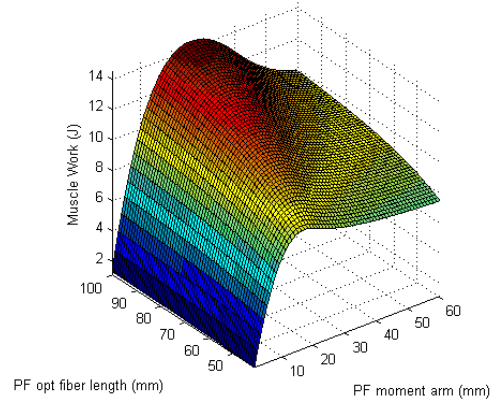

Figure 2. Simulated push-off work.

SUMMARY

Differences between sprinters and non-sprinters in gastrocnemius-Achilles architecture seem to permit sprinters to operate over more favorable ranges on the force-length and force-velocity curves for this muscle. The present study offers insights into the determinants of muscle function during sprinting that may also be relevant during push-off during walking and stair-climbing.

REFERENCES

Abe, T et al. (2000). *Med Sci Sports Exerc,* 32:1125-1129.
Abe, T et al. (2001). *J Physiol Anthropol,* 20(2):141-147
Kumagai, K et al. (2000). *J Appl Physiol,* 88:811-816.
Lieber, RL and Boakes, JL (1988). *Am J Physiol Cell Physiol,* 254:C769-C722.,
Lutz, GJ and Rome, LC (1994). *Science,* 263:370-372.

ACKNOWLEDGMENT

The Influence of Height and Edge Proximity on Balance and Reaction Time

Wendi Weimar, John Garner, Brian Campbell & Paul St. Onge
Auburn University, Auburn, AL.
weimawh@auburn.edu

INTRODUCTION

Previous research has indicated that standing on incline surfaces at heights can attenuate flat surface balance (Wade, Weimar and Davis, 2004). However, research indicating changes in static balance as a result of being on a platform above the ground has received little attention. It is the documentation of the prevalence of falls and the lack of understanding regarding the influence of height on balance that has led to the current study. The purpose of this study is to assess the static balance and information processing demands of standing on an elevated platform. The results of this study will aid in the understanding of the mechanisms that bring about these decrements in balance.

METHODS

This study utilized the Modified Clinical Test of Sensory Interaction on Balance (mCTSIB) of the NeuroCom® Basic Balance Master System™. The mCTSIB protocol quantifies dual support sway velocity. This study employed the eyes open condition only, for thirty seconds, at each of the three height conditions. The three height testing conditions consisted of (1) flat, level ground, (2) the middle of the 5 meter diving platform and (3) the edge of the 5 meter diving platform. Two spotters were present during all balance testing sessions. In addition, a Dekon Human Performance Analyzer was used to collect reaction time data following an auditory stimulus. The auditory stimulus, was a 1000 Hz tone, presented at 60 dB through an external speaker on the front of the data collection unit, located at eye level one meter behind the subject. The participants were asked to report to the Aquatics Center on three separate testing days. Each person was randomly assigned to a height condition order. Once at the Aquatics Center the participant's balance was measured at the predetermined height condition for thirty seconds. Next balance and reaction time measures were taken over the same interval. This balance and reaction time trial took approximately 4 minutes and included sixty reaction time trials. Sway velocity in degrees/seconds were averaged over the thirty seconds to provide a single balance score for balance alone and balance during reaction time trials for each height condition. In addition, the sixty reaction time trials were averaged and provided a single reaction time score for each height condition.

RESULTS

Balance conditions were measured alone and in conjunction with the reaction time task. A significant main effect was noted across all height conditions for the balance alone scores ($F(2,24) = 8.977$, $p = 0.000$, $\eta^2 = 0.418$). Follow up tests indicate that significant differences exists between the ground and the 5 meter edge conditions ($F(1,25) = 17.495$, $p = 0.000$, $\eta^2 = 0.412$) as well as between the 5 meter mid and the 5 meter edge conditions ($F(1,25) = 15.949$, $p = 0.001$, $\eta^2 = 0.389$). A significant main effect was also noted across all height conditions measured during the reaction

time trials ($F(2,24) = 7.05$, $p = 0.002$, $\eta^2=0.185$). Follow up tests indicate that significant differences exists between the ground and the 5 meter mid conditions ($F(1,25) = 7.017$, $p = 0.013$, $\eta^2=0.185$) and a significant difference exists between the 5 meter mid and the 5 meter edge conditions ($F(1,25) = 7.836$, $p = 0.009$, $\eta^2=0.202$). A significant main effect was also noted for balance measured across all height conditions measured alone and during the reaction time task ($F(5,125) = 16.843$, $p = 0.000$, $\eta^2=0.403$). Follow up tests indicate that significant differences exists between the ground and the ground with reaction time balance measures ($F(1,25) = 29.409$, $p = 0.000$, $\eta^2=0.541$) and a significant difference between the 5 meter mid and the 5 meter mid with reaction time balance measures ($F(1,25) = 21.661$, $p = 0.000$, $\eta^2=0.464$) and a significant difference between the 5 meter edge and the 5 meter edge with reaction time balance measures ($F(1,25) = 20.261$, $p = 0.000$, $\eta^2=0.448$). No significant difference was noted across any of the height conditions for reaction time.

Balance Condition	Ground	5M Mid	5M Edge
Balance Alone (deg/sec)	0.313 (0.12)	0.402 (0.33)	0.563 (0.32)
Balance w/RT (deg/sec)	0.258 (0.11)	0.311 (0.16)	0.486 (0.28)

Table 1: Mean and standard deviations of the balance scores alone and taken during the reaction time measures.

DISCUSSION

These results indicate that height and proximity to the edge contributes to the decrement in one's balance, or at least the increase sway velocity. Interestingly, balance under these height conditions improved when the participant was asked to perform the reaction time task. It was originally thought that a decrement would be noted in the task, while balance would remain relatively constant. However, it appears that the height condition is great enough to cause the participant to devote attention to losing one's balance, but that a task is distracting enough to this concern regarding losing balance to actually decrease the sway velocity. To explain this more simply, being at height caused the participants to focus only on remaining balanced and it appears that this focus caused them to sway more (perhaps in an attempt to elicit more information from their proprioceptors). However, the introduction of a task, allowed the performer to not focus so much on remaining balanced, to devote attention away from balance to the reaction time task. This is supported by the results that balance improved during the reaction time task vs the balance alone scores and that reaction time did not degrade at the various height conditions.

These results suggest that care be taken to ensure that safety precautions are in place when people are going to be close to the edge of a platform at some height above the ground. Particularly in situations when the uninitiated are going to have cause to be near the edge as is the case in amusement parks, zoos and other sightseeing or recreational settings. Perhaps attention diverting devices could be implemented to distract the individuals at height from focusing only on the fact that they are high above the ground.

REFERENCES

Wade, LR, et. al., 2004, *Ergonmics*, 15: 1614-1623.

DEVELOPMENT OF A FIBER-OPTIC FORCE SENSING GLOVE TO PROVIDE CLINICAL BIOMECHANICS MEASUREMENTS

David J. Nuckley[1], David R. Linders[2], and Wei-chih Wang[3]

[1]Musculoskeletal Biomechanics Research Laboratory, Department of Physical Medicine and Rehabilitation, University of Minnesota, Minneapolis, MN, USA, dnuckley@umn.edu.
[2]Department of Bioengineering and [3]Department of Mechanical Engineering, University of Washington, Seattle, WA, USA.   URL: http://www.mbrl.umn.edu

INTRODUCTION

Most Americans will receive physical treatment from musculoskeletal ailments such as muscle strains, ligament sprains, joint replacements, and arthritis at some point in their lives. Greater than 70% of the U.S. population will seek clinical care that is physical / biomechanical in nature (physical therapy, orthopaedic surgery, or chiropractic care) (Andersson, 1999). For these clinicians, their effectiveness is dependent on the forces they apply to their patients. Current hospitals and clinics lack a way to measure these forces, affecting diagnosis and treatment.

Clinical biomechanical assessments and treatments contain variability between clinicians and visits which has influenced the outcome of care (Hintermeister, RA, *et al.*, 1998; McQuade, KJ and Murthi, AM, 2004). While a few clinicians have attempted to use devices to assist in identifying the loads they are applying to their patients, no off-the-shelf system can be universally applied in spite of the need for clinicians to apply forces to their patients that are sensitive and accurate. Thus, we have developed a force sensing glove aimed at assisting in clinical biomechanics diagnosis and treatment.

METHODS AND PROCEDURES

To minimally affect a clinician's function, obtain maximal signal to noise in a medical environment, and maintain patient safety, a fiber-optic sensor is being developed for this application. This fiber-optic sensor, embedded within a latex glove is low profile (1.1 mm) enabling a clinician to feel a patient quantitatively. Furthermore, the use of light as a transduction media makes the sensor inert to hospital or clinical 'noise' and more importantly enables this tool to operate without affecting or interfering with other critical medical instrumentation.

The sensor's design is based on microbend loss properties of optical fiber whereby the attenuation of light through a fiber is related to the bending of that fiber through a series of corrugated teeth (Fig 1). These evenly spaced teeth create multimode bending in the fiber when loaded which optimizes the light loss. In this way, the force applied can be related to the light lost.
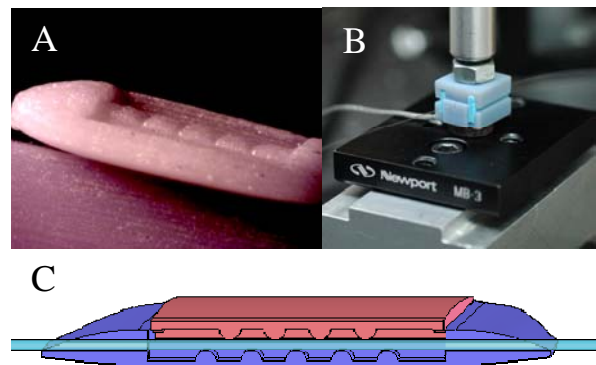

Figure 1. Fiber-Optic Force Sensor. The 1.1mm thick sensor (A) was tested on a stage with integrated load cell (B). The fiber-optic cable passes between the sensor teeth creating light loss proportional to applied force (C).

The fiber-optic sensor was cast into polymer and embedded into a latex glove along with the fiber. Once produced, we characterized the output of the sensor and its applicability for use in a clinical setting. First, a linear ramp was applied at 1mm/sec to the sensor using rigid boundary conditions measuring the force beneath the sensor (Sensotec button load cell) and the sensor light intensity output. Next, the sensor was worn by a user who physically applied a force to the load cell with the force sensing glove (Fig 2).

Figure 2. Force Sensing Glove Prototype.

RESULTS

The finished single sensor thickness was 1.1mm within a latex glove. Upon mechanical testing, the sensor exhibited a monotonically increasing load-light intensity curve. The response was sensitive (0.4N) and repeatable (max 3% error full scale) for this sensor in a controlled test. The single finger sensor when exercised by a human user produced a response with a 2N threshold, 95N range, and resolution of 0.4N. The sensitivity of the sensor (Fig 3) followed the theoretical Gaussian relationship and was reproducible upon loading. There was hysteresis in the glove sensor (less then 9%) which was due to its elastic nature. The calibration of the sensor was reproducible and accurate on separate days and sensor response was robust to temperature and moisture.
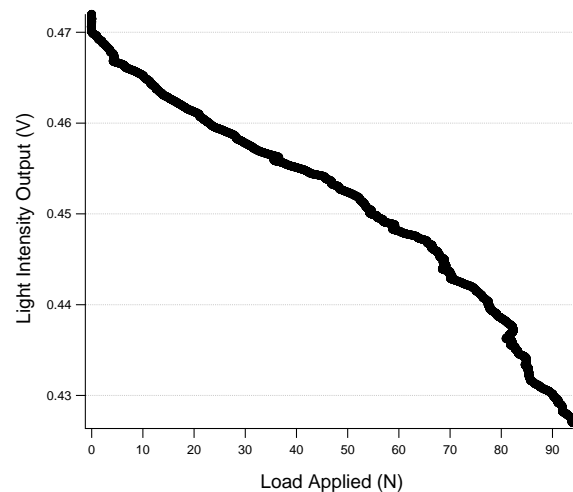

Figure 3. Sensitivity Curve for the Force Sensing Glove. The response of the prototype meets the biomechanical design criteria.

DISCUSSION

This optical biomechanics sensor provides force feedback which has the potential to improve clinical effectiveness for patient diagnosis and treatment. Further characterization of a multiple sensor glove will elucidate its full potential, but initial outcomes indicate a force measurement sensor which meets design criteria and may have significant clinical utility.

SUMMARY

A clinical force sensing glove has been designed, fabricated, and characterized for use in improving clinical diagnosis and treatment of biomechanical pathologies and injuries.

REFERENCES

Andersson, GB. 1999. *Lancet* 354(9178): 581-5.
Hintermeister, RA, *et al.* 1998. *J. Orthop Sports Phys Ther* 28(1): 40-50.
McQuade, KJ and Murthi, AM 2004. *Clinical Biomechanics* 19: 10-15.

THREE-DIMENSIONAL ENDPOINT FORCE PRODUCTION OF MUSCLES IN THE EXTENDED THUMB: POSSIBLE EVIDENCE FOR A TRANSLATIONAL DEGREE OF FREEDOM AT THE BASE JOINT THAT DRAMATICALLY AFFECTS FORCE PRODUCTION

Joseph D. Towles[1], Vincent R. Hentz[2]

[1]Sensory Motor Performance Program, Rehabilitation Institute of Chicago; Chicago, IL, USA

towles@northwestern.edu

[2]Department of Surgery, Stanford University

[3]Hand Surgery Service, VA Palo Alto Health Care System; Palo Alto, CA, USA

INTRODUCTION

An accurate understanding of thumb mechanics is critical to the development of models that can be used to study the effects of disease on grasp. Until recently, the thumb was thought to have only rotational joints that mattered for movement and force production e.g., (Hollister, Buford et al. 1992) despite the fact that the first metacarpal sits adjacent to carpal bones which translate in the wrist (Berger 2001). A recent study of muscle endpoint force production in the flexed thumb (Pearlman, Roach et al. 2004) suggested that the transformation between tendon force and endpoint force was possibly influenced by carpal bone movement. It is unclear whether muscle endpoint force production in the extended thumb is also affected by potential carpal bone motion. The purpose of this study was to examine the map between tendon force and endpoint force in the extended thumb.

METHODS

Endpoint forces produced by the muscles of the thumb were measured in 6 upper extremity cadaveric specimens by adapting an experimental approach previously applied to the study of fingertip force production (Valero-Cuevas, Towles et al. 2000). Briefly, a force of 10 N was applied to the tendons of nine thumb muscles (flexor pollicis longus, FPL; flexor pollicis brevis (radial and ulnar heads); FPBr, FPBu; adductor pollicis, ADP; abductor pollicis

longus/brevis, APL, APB; extensor pollicis longus/brevis, EPL, EPB; opponens pollicis, OPP) and the resulting three-dimensional (3D) thumb-tip force was quantified using a force sensor. The wrist was positioned in neutral and the thumb was fixed in an extended posture characterized by neutral adduction of all joints, and 35° to 50° of trapeziometacarpal (TMC) joint extension and near neutral extension of the metacarpophalangeal (MP) and interphalangeal (IP) joints. For each muscle, median endpoint force components across the specimens tested and associated interquartile ranges (IQRs) were computed. Using these data, endpoint force magnitude and the ratio of the proximal force component to the magnitude of the remaining force components (i.e., the proximal force component ratio) were determined for each muscle. These values were compared (Wilcoxon 2-sample Test, $\alpha = 0.05$, 1-tail) to the those calculated using data from a previous study (Towles, Hentz et al. 2008) in which the same tendon force was applied to the muscles of the thumb in a flexed posture.

RESULTS

In the extended posture, most muscles (7 of 9) produced larger endpoint forces than those produced in the flexed posture. As a group they produced 41% larger forces ($p = 0.038$) (Table 1). Moreover in the extended posture, muscle endpoint forces were in general proximally directed (Fig. 1A). The proximal

force component ratio was larger in the extended posture for all muscles than that calculated in the flexed posture. As a group, the proximal component was 4.16 more times larger in the extended thumb ($p = 0.001$) (Table 1).
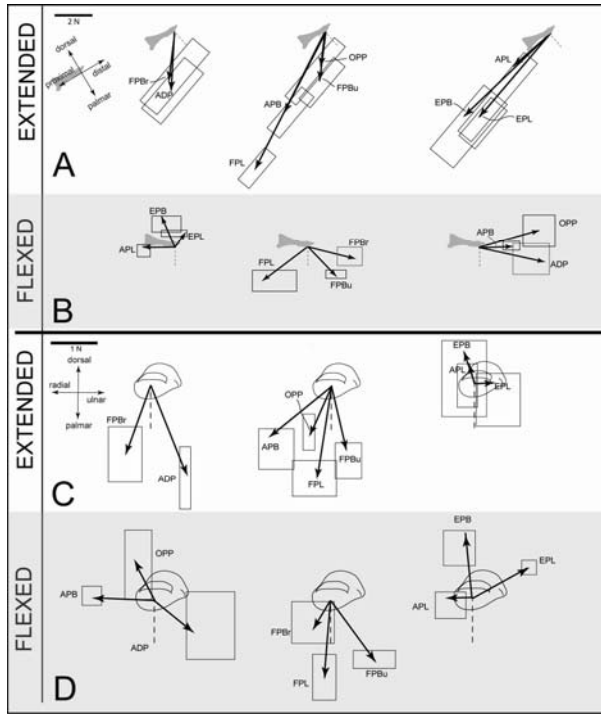

Figure 1: Thumb muscle endpoint force data in extended (white) and flexed (gray) postures

Table 1: Endpoint force magnitudes and ratio

Muscle	% MAG DIFF	RATIO DIFF
FPL	193	2.89
FPBr	12	5.24
EPB	252	8.63
EPL	248	17.19
FPBu	4	2.30
APL	41	3.24
OPP	-39	4.53
ADP	-3	4.16
APB	126	3.95
median (IQR)	**41 (3, 193)***	**4.2 (3.2, 5.2)***

*$p < 0.05$. Negative values indicate negative proximal force component (i.e., distal).

DISCUSSION

The goal of this study was to evaluate the map between tendon force and endpoint force in the extended thumb. In the flexion-extension (FE) plane (Fig. 1A, B), endpoint force direction seemed to be less influenced by the muscle's primary action when the thumb was extended than when it was flexed (cf. EPL and FPL, Fig. 1A). In the ab/adduction (AA) plane (Fig. 1C, D) however, endpoint force directions were diverse in both postures.

The fact that most muscle endpoint force vectors were largest in the extended posture suggests that the gain of the map between tendon force and endpoint force increases with extension. The fact that muscle endpoint force vectors were more proximally directed in the FE plane irrespective of the muscle and simultaneously oriented along various directions in the AA plane (Fig. 1C) suggests that the map consists of both translational and rotational joint properties. It is likely that the interface between the thumb and wrist provides an additional DOF in the extended thumb. Of note, the presence of a translational joint could also account for the increase in the gain of the map between tendon force and endpoint force (Yoshikawa 1990). Importantly this work provides insight into a potentially relevant aspect of thumb mechanics which is not currently modeled.

REFERENCES

Berger, RA (2001). *Hand Clinics,* 17(4):525-32.

Hollister, A et al. (1992). *Orthop Research,* 10: 454-60.

Pearlman et al. (2004). *J. Orthop Research,* 22: 306-12.

Towles et al. (2008). *Clin Biomech,* in press.

Valero-Cuevas et al. *J Biomech,* 33:1601-09.

Yoshikawa, T. *Found of Robotics,* 13-80.

MOMENT-GENERATING CAPACITY OF TENDONS IN FINGER MOVEMENTS: EVALUATION OF THE TENDON MOMENT ARMS OBTAINED FROM THE EXCURSION METHOD

Sang Wook Lee[1] and Derek G. Kamper[2]

[1] Rehabilitation Institute of Chicago, Chicago, IL, USA. E-mail: sanglee2@northwestern.edu
[2] Rehabilitation Institute of Chicago and Illinois Institute of Technology, Chicago, IL, USA

INTRODUCTION

A tendon moment arm, defined as the distance between the joint center and the tendon line of action, is generally used to assess the moment-generating capacity of the muscle-tendon unit around the joint. Excursion method that utilizes the relationship between the tendon excursion and the joint rotation (An et al., 1983) has been commonly employed to estimate the \moment arm values. In the human finger, however, some tendons generate the rotation of the segments into which they do not have insertions; for example, the flexor digitorum profundus (FDP) tendon is involved in generating flexion or extension of the proximal phalanx (PP), into which they do not have apparent insertions. Instead, the rotation of the PP is generated via the joint reaction forces, transmitted from the distal segments into which the tendon inserts, or pulley forces that constrain the tendon paths. It is thus unclear if the tendon moment arm values obtained from the excursion method can be employed to estimate the joint moment produced via such mechanisms.

In this study, we examined if the moment arms of the finger tendons estimated by the excursion method can represent their moment-generating capacity in hand movements. We utilized two different models of the finger, one employing the moment arm values from the excursion method, and the other considering more realistic joint moment generation mechanisms (via joint reaction forces and pulley forces). The spatial and temporal coordination of the multi-joint flexions obtained from the two models were examined and compared for this purpose.

METHODS

Two types of the dynamic models of the index finger were developed. The first model (model 1) employed the moment arm values of the tendons obtained from the excursion method (An et al., 1983) in order to estimate the joint moments generated by the tendon forces, whereas the second model (model 2) estimated the joint moment magnitudes directly from the force and moment balance equations considering the pulling forces at insertions, subsequent joint reaction forces, and the forces acting on the pulley structures.

In both models, the index finger was represented as an open chain of three rigid segments connected through three one degree-of-freedom (DOF) joints. The abduction (or adduction) of the MCP joint was not considered in the model, since the flexion or extension of the three joints were mainly examined and little abduction/adduction is generated by FDP or FDS tendons. The finger segments are represented as conical cylinders with density of $1.1 (g/cm^3)$, and the dimensions of finger segments were acquired from the literature (An et al., 1979; An et al., 1983). Passive stiffness and damping values at each joint obtained from Kamper et al. (2002) were also incorporated in the models. In the model 1, the joint moment magnitude generated at each joint in response to the tendon force application was estimated by directly

multiplying its moment arm value to the tendon force. In contrast, the second model (model 2) calculated the joint moments by incorporating the force and moment equilibrium equations at all three joints. Here, three types of moment generating mechanisms were considered: 1) the direct tendon pulling forces from the insertions ($\mathbf{b}_T$), 2) the joint reaction forces that transmit the tendon forces from the adjacent segments ($\mathbf{b}_R$), 3) the forces acting on the tendon pulleys constraining tendon path ($\mathbf{b}_P$) (Roloff et al., 2006), 4) passive stiffness and damping ($\mathbf{b}_S$), and 5) Coriolis force ($\mathbf{b}_C$) term (Eq. 1).

$$\mathbf{I}\ddot{\boldsymbol{\theta}} = \mathbf{b}_C(\boldsymbol{\theta},\dot{\boldsymbol{\theta}}) + \mathbf{b}_T(\boldsymbol{\theta},\mathbf{f}_t)f + \mathbf{b}_R(\boldsymbol{\theta},\mathbf{f}_t) + \mathbf{b}_P(\boldsymbol{\theta},\mathbf{f}_t) + \mathbf{b}_S(\boldsymbol{\theta},\dot{\boldsymbol{\theta}}) \quad (1)$$

($\mathbf{I}$: inertia matrix, $\boldsymbol{\theta}$: joint angle vector)

Tendon forces of FDP = 4 (N) and FDS = 3.2 (N) were applied. Forward dynamic simulations for both models were performed using the 4th-order Runge-Kutta method in MATLAB (MathWorks, Inc. Natick, MA).

RESULTS AND DISCUSSION

Noticeably different joint flexion patterns were produced by two models (Fig. 1). The model 1, adopting the moment arm values from the excursion method, resulted in larger flexion angle in the MCP joint (>90°) than PIP joint, whereas the PIP joint flexion angle was greater than the MCP flexion in the movement generated by the model 2. Similar movement patterns were observed in the different FDP/FDS force combinations. Both models were capable of producing realistic sigmoidal angular profiles and inter-joint temporal coordination pattern (Holguin et al., 1999).

Note that the joint flexion patterns generated by the electrical stimulation of the FDP/FDS muscles (Kamper et al., 2002) were more comparable to the movement obtained from the model 2 (PIP>MCP). Similar joint flexion patterns were also reported in Long and Brown (1964), in which the electromyography confirmed that the FDP and FDS were the main muscles for generating such movements.
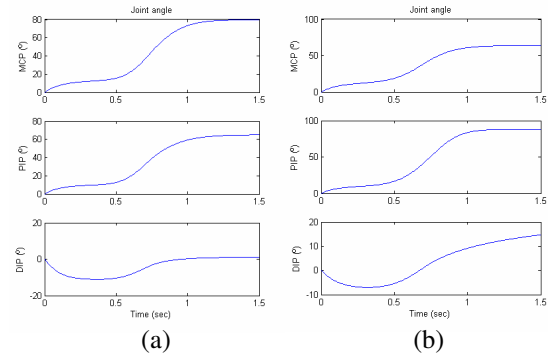

Figure 1. Joint angles simulated by two models (a) model 1: MCP>PIP>DIP (b) model 2: PIP>MCP>DIP

We also examined the contribution of different elements to the angular acceleration of each joint, i.e. from the tendon pulling forces ($\mathbf{I}^{-1}\mathbf{b}_T$), joint reaction forces and tendon pulley forces ($\mathbf{I}^{-1}(\mathbf{b}_R + \mathbf{b}_P)$), passive stiffness/damping ($\mathbf{I}^{-1}\mathbf{b}_S$), and the Coriolis force $\mathbf{I}^{-1}\mathbf{b}_C$, in the model 2 (Fig. 2). Here, $\mathbf{b}_P$ and $\mathbf{b}_R$ are specifically found to be functionally important in most joints.
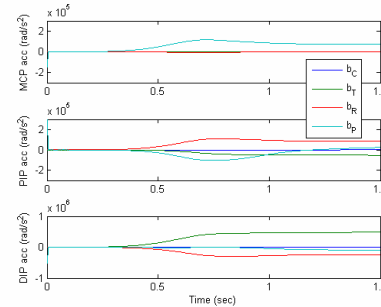

Figure 2. Contribution of different elements to the joint angular acceleration

The results of this study indicate that the excursion method can overestimate the moment generating capability of some tendons, specifically when the tendon is not directly inserted into the segment. Also, the analysis of different elements (Fig. 2) suggests that factors other than direct tendon pulling force should be carefully considered in analyzing the dynamics of the finger movement generation.

REFERENCES

An KN et al. (1983). *J Biomech*, **16**, 419-25.
Holguin PH et al. (1999). *Clin Orthop*, **362**, 117-24.
Kamper DG et al. (2002). *J Biomech*, **35**, 1581-89.
Roloff I et al. (2006). *J Biomech*, **39**, 915-23.

SUBTALAR JOINT KINETICS DURING STANDING AND WALKING

Tara L. Sulewski[2] , Tamara L. Cohen[2], Gregory S. Lewis[2], Stephen J. Piazza[1,2,3]

Depts. of [1]Kinesiology, [2]Mechanical & Nuclear Engineering, and [2]Orthopaedics & Rehabilitation, The Pennsylvania State University, University Park, PA, USA, *piazza@psu.edu*

INTRODUCTION

Hip, knee, and ankle joint moments are regularly assessed in clinical gait analysis and in biomechanics research. Internal joint moments about the subtalar joint axis, however, are not readily computed because there is no established means for locating this axis *in vivo* on a subject-specific basis. Normative values for subtalar joint moments would be useful for treating frontal-plane gait abnormalities such as hindfoot varus and pes planus.

Scott and Winter (1993) estimated subtalar joint moment arms during walking in three subjects after locating the joint axis by visualizing skin movement during applied inversion-eversion moments. The authors found inversion moment arms throughout stance phase that peaked at approximately 30 Nm at 75% of stance phase. Procter and Paul (1982) used a model-based assessment of subtalar joint moment with an assumed subtalar joint axis and predicted peak inversion moment of approximately 35 Nm at 85% of stance. A new method for subject-specific location of the subtalar joint axis from measured ankle motion (Lewis et al., 2007) may permit true subject-specific measurement of subtalar joint moments.

The purpose of this study was to make subject-specific measurements of normative internal subtalar joint moments during the standing and walking of healthy young subjects.

METHODS AND PROCEDURES

Subtalar joint moments during standing and walking were measured in 13 healthy subjects (8M, 5F; ages 19-29 y; height 1.73 ± 0.13 m; body mass 72.3 ± 14.5 kg), who provided informed consent prior to testing. All procedures were approved by our university's Institutional Review Board.

Subtalar joint axes were found by placing four reflective markers on the skin over the right tibial crest and four over the lateral aspect of the calcaneus and then applying inversion eversion motions in concert with a dorsiflexion load (Lewis et al., 2007). This loading is intended to limit talocrural motion, permitting the subtalar joint axis to be located by computing finite helical axes between the tibia and calcaneus. Marker locations during these motions and subsequent standing and walking trials were measured using an 8-camera Eagle motion analysis system (Motion Analysis Corp.; Santa Rosa, CA).

During standing trials, the subject stood with the right foot on a force plate and the left foot on the floor next to the force plate for 3 s. During walking trials, subjects walked at self-selected speeds, striking the force plate with the right foot. Subtalar joint moments were approximated for standing and walking trials by taking the moment of the ground reaction force about the calcaneus-fixed subtalar joint axis. The foot weight and inertia were assumed to be negligible in this analysis.

RESULTS

Subtalar joint axis orientations were found to vary across subjects in a manner and degree similar to that previously reported for subtalar joint axes measured in cadaver specimens (Inman, 1976).

All subjects exhibited inversion moments during standing. The mean internal subtalar joint moment across subjects was 0.085 ± 0.041 N m / kg.

Subtalar joint moment patterns during walking were generally similar in shape across subjects, with peak inversion moments greater than peak eversion moments (Figure 1). The average peak inversion moment was 0.378 ± 0.182 N m / kg and this peak occurred at 58 ± 16% of stance on average.
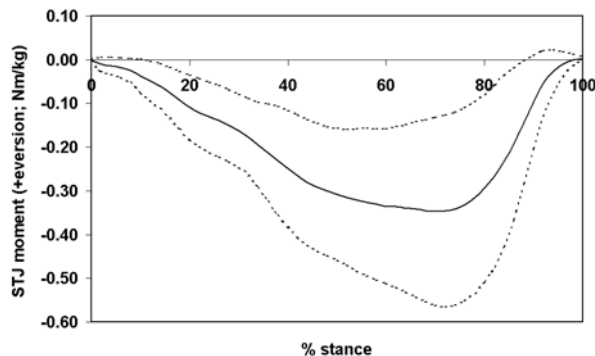
Figure 1. Normalized subtalar joint moments during walking, averaged across subjects. Moments are normalized by body mass, and negative moments correspond to an internal inversion moment. The solid line represents the mean; dashed lined represent plus and minus one standard deviation.

DISCUSSION

The results presented in the present study represent the first normative subtalar joint moments computed using subject-specific subtalar joint axes computed from measured ankle complex motions. The subtalar joint patterns during the walking of 13 subjects (Figure 1) are similar in shape and magnitude to those reported previously by Scott and Winter (1993) in three subjects. Normalized moments were found to vary substantially across subjects; future work is necessary to determine if this variation is attributable to variability in the orientation of the subtalar joint axis, which has been demonstrated to be substantial in cadaver studies (Inman, 1976).

SUMMARY

Subtalar joint moments were measured in healthy young adult subjects during standing and walking. Moments were computed about axes that were determined using a new motion-based method for subtalar joint axis location. The magnitudes of the measured moments were variable across subjects, even when normalized by body mass, perhaps due to inter-subject variability in the axis orientation.

REFERENCES

Inman VT (1976) *The Joints of the Ankle*. Williams and Wilkins.
Lewis GS et al. (2007) *Gait & Posture*, **25**, 63-69.
Scott SH and Winter DA (1993) *J Biomechanics*, **26**, 1091-1104.
Proctor P and Paul JP (1982) *J Biomechanics,* **15**, 627-634.

ACKNOWLEDGMENT

THE RELATIONSHIP BETWEEN KNEE VALGUS WHEN SQUATING AND DURING VERTICAL JUMP TAKEOFF AND LANDING

Mostafa Afifi, Kristinn Heinrichs, & Richard Hinrichs
Arizona State University, Tempe, AZ, USA
e-mail: mostafa.afifi@asu.edu

INTRODUCTION

Anterior cruciate ligament (ACL) injuries are a major problem for today's athletes as an estimated 1 in 3000 of the population experiences an ACL injury.

The knee valgus is viewed as a non favorable position as it has been linked to ACL injuries (Russell et al., 2006). This hazardous position can be observed not only during landing from a jump but also during the countermovement (squat) prior to the takeoff. Knee valgus is caused by a combination of hip adduction internal rotation and abduction external rotation of the lower leg as it is clear that in many jumpers the two knees come closer to each other. If the quantity of valgus experiences during a countermovement or a squat is related to that experienced during landing from a jump, a double legged squat test could be used as a screening tool prior to sports participation.

Thus, the purpose of the study was to investigate if a relationship exists between knee valgus observed during the countermovement prior to a vertical jump, knee valgus seen during landing, and knee valgus experienced during the downward phase of a squat.

METHODS

Sixteen active college students (8 males, 8 females) volunteered to participate in the study. Participants were excluded if they had any orthopedic condition that would prevent them from jumping.

Subjects were asked to do three squats and three maximal vertical countermovement jumps standing with the feet shoulder's width apart. The order of the trials was balanced. Electromagnetic motion sensors (240 Hz, Polhemus Liberty) were used to calculate the distance between the knees during the jumps and squats.

Pearson product correlations were used to identify the relationship between the change in distance between the two knees during the downward phase of the takeoff phase and the downward phase during landing, the downward phase of the squat. Linear regression analyses were conducted to identify the predictability of the distance between the knees during landing from the distance between the knees during the squat and countermovement.

RESULTS AND DISCUSSION

Results showed significant correlations between the three variables (Table 1).

Table 1. Pearson production correlations between the three conditions

	Take off	Landing	Squat
Take off	1	0.656*	0.959*
Landing		1	0.637*
Squat			1

* Significant at the 0.01 level (2-tailed)

Each variable had a strong positive correlation with the other two variables. This suggests valgus motion during the

countermovement meant valgus motion during landing as well as during a squat.

Linear regression analysis identified the average change in distance between the two knees during the countermovement jump as a significant predictor of the average change during landing from a jump (Figure 1). However, the R^2 value is relatively low (0.43) which suggests this variable by itself cannot predict the change in knee position during landing.
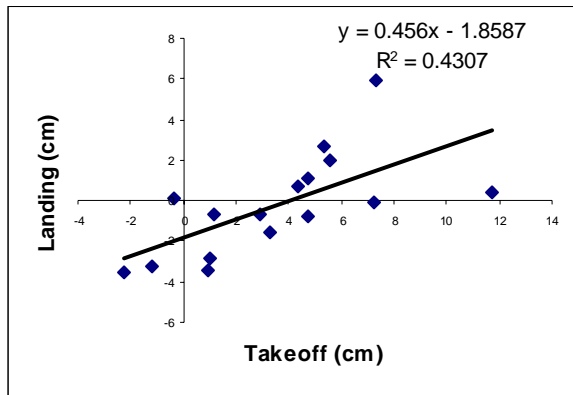

Figure 1. The relationship between change position during countermovement and during landing.

Similar results were seen when attempting to predict the change in distance between the knees from the change in position during squatting ($R^2 = 0.41$, Figure 2).
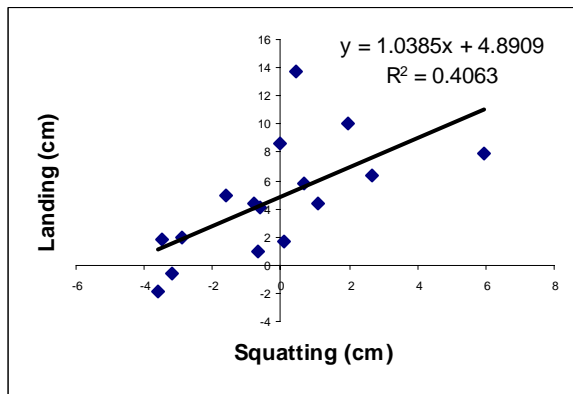
Figure 2. The relationship between change position during squatting and during landing.

Linear regression analysis showed the change in knee position during the squat was a strong predictor of the change in position during the countermovement ($R^2 = 0.92$, Figure 3).
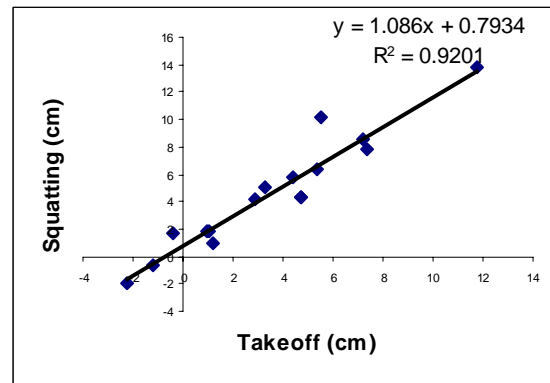

Figure 3. The relationship between change position during squatting and during the countermovement.

The predictability of the change in distance during the countermovement from squatting suggests that when designing a field test squatting may replace the need to have the subjects do an actual countermovement jump to be tested.

SUMMARY/CONCLUSIONS

This study examined the ability to predict the change in distance between the knees during landing from a jump from the change during the countermovement and the change during the squat. This distance rather than actual knee valgus was used as it would be a measure that can be taken on the field. Both were significant predictors, however, neither factor by itself can predict the change during landing. Future studies should focus on multiple regression using factors as the height, weight, leg length, muscle strength, and other factors that can be measured in the field.

REFERENCES
Russell, K. A., et al. (2006). *Journal of Athletic Training, 41,* 166-171.
Swartz, E.E. et al. (2005). *Journal of Athletic Training, 40,* 9-14.

DISC HEIGHT REDUCTION IS A BETTER PREDICTOR OF CERVICAL DISC DEGENERATION PROGRESSION THAN REDUCTION IN THE AREA OF NUCLEUS PULPOSUS – A FINITE ELEMENT ANALYSIS

Mozammil Hussain[1] and Rodger Tepe[1]
[1]Division of Research, Logan University, Chesterfield, Missouri, USA
E-mail: mozammil.hussain@logan.edu

INTRODUCTION

Disc degeneration (DD) is multi-factorial cascading process which is still not clearly understood. Several changes occur in the disc due to DD. Some of the most common are – changes in the disc tissue matrix from solid-fluid to more like a solid and changes in the disc morphology. Increase in the disc area, decrease in the disc height and decrease in the nucleus pulposus (NP) area are some of the changes in the disc morphology that occur due to DD. Literature studies has shown that the effect of DD on disc area is very negligible, whereas disc height and NP area are drastically affected. Several biomechanical finite element (FE) studies exist in the literature that incorporates degenerative changes in the material properties and/or degenerative changes in the disc height and NP area. To the best of our knowledge, none of the studies has addressed that which one could be a better predictor of DD (increased stiffness) – decrease in the disc height or decrease in the NP area?

Therefore, the aim of the present study was to investigate the changes in the segmental stiffness due to three types of degenerative changes in the disc morphology – reduction in the disc height alone, reduction in the NP area alone and combined reduction in the disc height and NP area. Two stages of DD were included – moderate and severe.

METHODS

A previously validated three-dimensional finite element (FE) model of a cervical motion segment was used (Hussain and Tepe, In Review). The model components included cortical bone, cancellous bone, endplates, annulus fibrosus (AF) and NP. The model represented the morphology and material properties of the normal disc that were adopted from the literature. Two grades of degeneration were induced into the normal disc – moderate and severe. DD was simulated by modifying both material properties and geometry of the normal disc. The material properties (elastic modulus and poisson's ratio) of only NP were changed (equivalent to the AF properties) in the moderate stage of DD, whereas both AF and NP properties (elastic modulus was doubled as compared to the moderate degeneration) were varied in severely degenerated disc. To understand the segmental biomechanics from the viewpoint of degenerative morphological changes in the disc, three different types of geometry changes were included into the normal disc at both moderate and severe stages of DD – change in the disc height alone, change in the NP area alone and combined changes in the disc height and NP area. The disc height and NP area was decreased by 4% each in the moderate DD and by 40% each in the severe DD as compared to the normal disc height and NP area. An axial compressive load of 50 N (equivalent to upper body weight) was simulated on the superior surface of the top vertebra, and the inferior surface of the bottom vertebra was constrained in three planes. The finite element software

(ABAQUS) was used to perform the analysis.
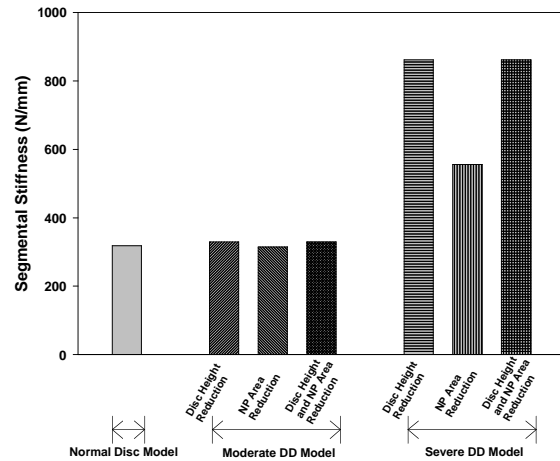
RESULTS

Figure 1. Segmental stiffness due to three different degenerative geometry changes in the disc – disc height reduction, NP area reduction and combined disc height and NP area reduction

The results of the present study showed that the segment was stiffer when the disc height alone was decreased than when the NP area alone was decreased (Figure 1). At each stage of degeneration, the segmental stiffness due to disc height reduction was same as that of the stiffness due to combined disc height and NP area reduction. No significant difference in the stiffness was observed between the moderate stage of DD and normal disc state, and the stiffness of the severe DD model was higher than the other two models.

DISCUSSION

This study was successful in addressing the changes in the segmental stiffness due to degenerative change(s) in the disc morphology – disc height and/or NP area. Increased stiffness is an indication of degenerative progression, particularly in the stabilization phase of degeneration. We think that the reduction in the disc height is a better predictor of DD than reduction in the NP area. This is because the disc height reduction alone and combined disc height and NP area reduction resulted into same stiffness. Based our results, it is very likely that the biomechanical effect of DD is more dependent on the sagittal plane geometry (disc height) than on the transverse plane geometry (NP area).

SUMMARY

In summary, we investigated the stiffness behavior of the cervical motion segment at moderate and severe stages of DD by simulating three different degenerative changes in the disc morphology – reduction in the disc height alone, reduction in the NP area alone and combined reduction in the disc height and NP area. We found that the reduction in the disc height affects degenerative stiffness more than reduction in the NP area.

REFERENCES

Hussain, M and Tepe, R (In Review). *Summer Bioengineering Conference (ASME)*, Marco Island, Florida.

Hand Approach Velocity and Impact Force during Manual Wheelchair Propulsion

Shashank Raina[1], Jill L. McNitt-Gray[1, 2, 3], Philip S. Requejo[2, 4]
[1]Depts. of Biomedical Engineering, [2]Kinesiology, [3]Biological Sciences, USC, Los Angeles, CA
[4]Pathokinesiology Laboratory, Rancho Los Amigos National Rehabilitation Center, Downey, CA
E-mail: sraina@usc.edu

INTRODUCTION

Wheelchair users frequently develop shoulder pain or suffer from an overuse injury (Sie et al., 1992). Shoulder injury is often associated with the mechanical loading of the upper extremity during wheel chair propulsion. Raina et al. (2007) have found that large rim forces experienced immediately after hand contact with the rim contribute to relatively large shoulder net joint moments. The purpose of this study was to determine if the magnitude of the peak rim forces immediately after contact were associated with specific recovery phase techniques used when propelling a wheel chair. Four distinct recovery patterns have been previously observed: semicircular, single looping over propulsion (SLOP), double looping over propulsion (DLOP), and arcing (Boninger et al., 2002; Shimada et al., 1998). We hypothesized that the peak rim forces immediately after hand contact are related to the recovery patterns used and the magnitude of the rim forces are directly related to the approach velocity of the hand at rim contact. We expected users with limitations in muscle control (e.g. cervical level injury) to exhibit different recovery patterns, initiate contact at higher hand velocities and experience higher rim forces than users with more muscle control (e.g. thoracic level injury).

METHODS

Individuals with SCI were recruited from outpatient clinics through Rancho Los Amigos Rehabilitation Institute. Eight users with 3 with thoracic level and 5 with cervical level spinal injury participated in this study.

The average age of the participants was 45(8) years, average mass was 75(13) kg and average height was1.7 (0.06) m. Reflective markers were used to monitor the 3D motion (Vicon®). The data was processed in Visual 3D® and Matlab®. The force applied to the wheelchair during propulsion was measured using force transducers mounted along the spokes of the wheel. The peak rim force immediately after contact was identified as the impact rim force. A four-segment 3D upper extremity model was generated using segment kinematics. All users propelled the wheelchairs at two velocities normal and self selected fast. The wrist marker was used to track the propulsion pattern. The velocity of the hand/wrist prior to rim contact was used to characterize approach velocity of the hand.

RESULTS

Recovery patterns were not specific to level of muscle control or hand/wrist approach velocities (Figure 1).Three of the five cervical level users used a modified SLOP recovery pattern with an average hand/wrist approach velocity of 0.77(0.35) m/s. Two cervical level users an arcing recovery pattern with an average hand/wrist approach velocity of 0.57(0.59) m/s. The three thoracic level users used SLOP, semi circular and DLOP patterns with hand/wrist velocities of 0.64(0.34) m/s, 1.66 m/s and 0.73(0.42) m/s respectively.

Larger resultant hand/wrist approach velocities were found to be associated (0.78) with larger impact rim forces immediately after contact (Figure 2).
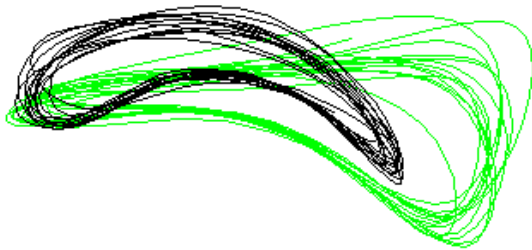
Figure 1: A modified SLOP recovery pattern of a user with a cervical level injury (black) and a traditional SLOP pattern (green) of a user with a thoracic level injury.
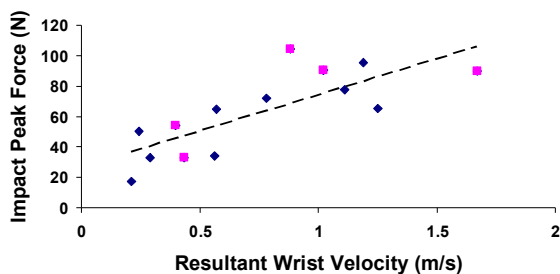

Figure 2: The correlation (0.78) between the impact force and the resultant hand/wrist velocity prior to rim contact. Users with thoracic (square) and cervical (diamond) level injury.

DISCUSSION

In this study, the magnitude of the peak rim forces immediately after contact were found to be associated with resultant hand/wrist velocity prior to rim contact. As the resultant hand/wrist velocity increased, the magnitude of the impact peak force increased. Recovery phase technique was not specific to user injury level or resultant hand/wrist approach velocity. Establishing a relationship between recovery technique and hand/wrist velocities was limited by a small sample size.

Users with cervical level injuries used a modified version of the SLOP recovery pattern as often reported for users with thoracic level injuries (Boninger et al., 2002) The modified SLOP recover pattern (Figure 1) tended to have larger resultant hand velocities than users using the arcing pattern. The larger resultant hand velocities may

provide a mechanism for users to generate a relatively larger friction forces and compensate for limited gripping ability. Future studies will explore the relationship between gripping abilities and hand/wrist approach velocities in different user populations and identify ways of modifying wheel chair design to lower impact forces without compromising the grip on the pushrim.

SUMMARY

Shoulder injury is often associated with the mechanical loading of the upper extremity during wheel chair propulsion and large rim forces experienced immediately after hand contact with the rim contribute to relatively large shoulder net joint moments. In this study, the magnitude of the impact peak forces were found to be associated with resultant hand/wrist velocity prior to rim contact even with a limited sample size. These preliminary results indicate that recovery patterns are not specific to injury level or hand/wrist approach velocities. Future studies, benefiting from a larger sample size, will investigate whether larger hand/wrist approach velocities prior to contact are inherently specific to recovery patterns and/or related to gripping ability.

REFERENCES
Sie et al., (1992). Arch Phys Med Rehabil; 73(1):44-8.
Raina et al., (2007). ASB, Palo Alto, CA.
Boninger et al., (2002). Arch Phys Med Rehabil; 83(5):718-23.
Shimada et al., (1998) J Rehabil Res Dev; 35(2):210-8.

REDUCING RESIDUAL FORCES AND MOMENTS IN A THREE-DIMENSIONAL SIMULATION OF RUNNING

Samuel R. Hamner[1], Chand T. John[3], Frank C. Anderson[2], Jill S. Higginson[4], Scott L. Delp[1,2]

Departments of [1]Mechanical Engineering, [2]Bioengineering, [3]Computer Science, Stanford University, Stanford, CA
Department of [4]Mechanical Engineering, University of Delaware, Newark, DE
E-mail: samner@stanford.edu, Web: http://nmbl.stanford.edu

INTRODUCTION

Understanding the actions of muscles during running is a challenging problem because important variables, such as muscle forces, are generally not measurable. To gain insight into muscle actions we are creating three-dimensional simulations of running that track experimentally measured running dynamics and allow estimation of muscle forces and the motions they produce. Unfortunately, due to experimental errors and modeling assumptions, such as lumping arms into a rigid trunk segment, dynamic inconsistencies between experimental kinematics and ground reaction force arise (Kuo, 1998). To resolve dynamic inconsistencies an additional force and moment (called residuals) must be applied to a model such that the sum of the residuals and the ground reactions equal the mass-acceleration products of the body segments. To improve the dynamic consistency of forward dynamic simulations, Delp et al. (2007) developed a residual reduction algorithm (RRA). By slightly adjusting body segment mass distributions and experimental kinematics, residuals applied to the model can be significantly reduced. The purpose of this study is to investigate the performance of RRA in reducing the residuals in a three-dimensional simulation of running.

METHODS AND PROCEDURES

Data were collected on an adult male subject (height 1.83 m, mass 65.9 kg) running at 3.9 m/s on a Bertec split-belt instrumented treadmill (Fig. 1). A 6-camera Motion Analysis system recorded the positions of markers placed according to a modified Cleveland Clinic marker set. A three-dimensional 10-segment, 23 degree-of-freedom musculoskeletal model (Thelen and Anderson, 2006) with 92 muscles was scaled to match the anthropometry of the subject. An inverse kinematics problem was solved using weighted least squares optimization to determine experimental kinematics (e.g., joint angles) that minimized the error between experimental markers and markers on the model. A forward simulation of a running gait cycle that reduced residuals and tracked the experimental kinematics was then created using OpenSim (Delp et al., 2007).
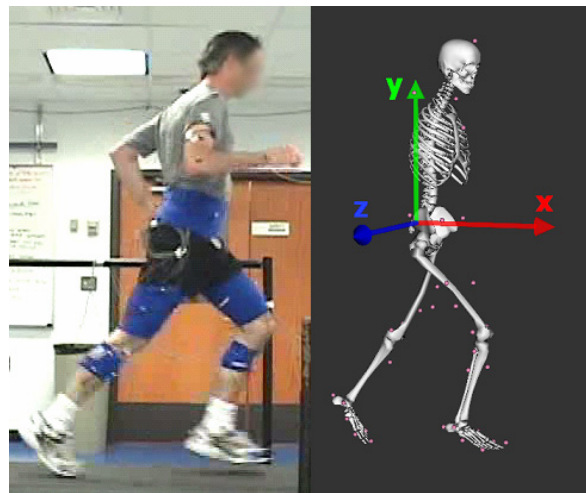

Figure 1. A three-dimensional simulation of running generated from motion capture data. Coordinate axes are shown for reference.

To investigate the performance of RRA, joint moments and residuals were calculated before and after use of RRA. In both cases, residuals were applied to the mass center of the pelvis segment. To reduce the residuals, RRA adjusted the torso mass center, the total mass, and the experimental kinematics.
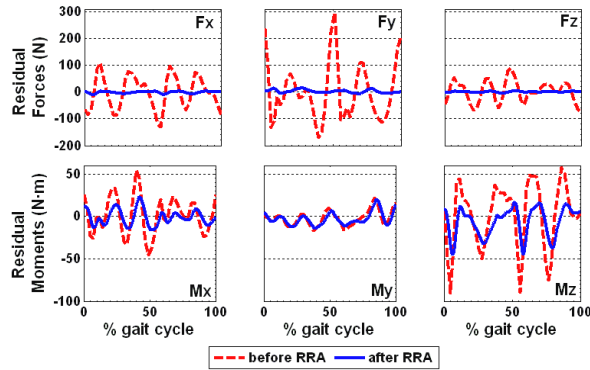
Figure 2. Residual forces and moments calculated before (dashed line) and after (solid line) RRA.

Figure 3. Maximum and RMS differences in kinematics (i.e., joint angles) before and after RRA.

RESULTS & DISCUSSION

Applying RRA substantially reduced the residuals. Prior to RRA, the residual forces were large. For example, F_y, the vertical force applied to the pelvis, was as large as 300 N. After application of RRA, the amplitudes of the forces applied to the pelvis were less than 15 N (Fig. 2, top row). RRA reduced M_x and M_z, the residual moments in the frontal and sagittal planes, by about 50%. In contrast, RRA did not appreciably reduce M_y, the moment in the transverse plane, perhaps reflecting that arm swing was not accounted for in the model. The maximum value of M_y (19.8 N·m) is similar to measured peak transverse moments due to arm swing (14.5 N·m; Cavanagh, 1990).

Our experimentally measured hip, knee, and ankle joint kinematics and moments were consistent with literature data (Winter, 1983; Swanson and Caldwell, 2000). The simulation tracked the experimentally measured joint angles to within 2.5º (Fig. 3). Maximum changes in pelvis translation were 9 mm in the anterior-posterior and superior-inferior directions, and 12 mm in the medial-lateral direction. The torso mass was adjusted 0.14 kg and its mass center was moved less than 1 mm.
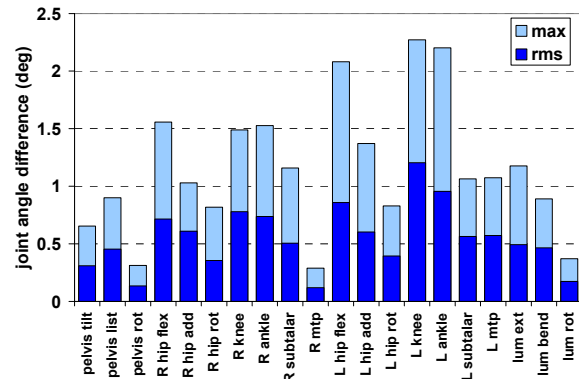
Moments at the knee and ankle were not appreciably altered by RRA, but changes in back joint moments were as large as 20%. This suggests that residual reduction may not be important when estimating forces generated by ankle and knee muscles. However, reducing residuals may be important for estimating forces generated by hip and torso muscles. Future work will use the altered kinematics and mass properties from RRA to create three-dimensional muscle-actuated forward simulations of running to investigate the action of muscles.

REFERENCES

Cavanagh (1990) *Biomechanics of Distance Running*. Champaign, IL, Human Kinetics.
Delp et al. (2007) *IEEE Trans Biomed Eng* 55:1940-50.
Kuo (1998) *J Biomech Eng* 120:148-59.
Swanson and Caldwell (2000) *Med Sci Sports Exerc* 32:1146-55.
Thelen and Anderson (2006) *J Biomech* 39:1107-15.
Winter (1983) *J Biomech* 16:91-97.

ACKNOWLEDGEMENTS

EFFICIENCY OF STEP-TO-STEP TRANSITION WORK IN HEMIPARETIC GAIT.

Daniel Hewson[1], Arrlann Christie[1], Janice Eng[2], and Max Donelan[1]

[1]School of Kinesiology, Simon Fraser University, Burnaby, BC, Canada, dhewson@sfu.ca
[2]Department of Rehabilitation Science, University of British Columbia, Vancouver, BC, Canada

INTRODUCTION

The mechanical work required to redirect the center of mass velocity during step-to-step transitions is a major determinant of the metabolic cost of healthy walking (Donelan et al., 2002). Physics-based models of this transition predict the requisite work is minimized when leading leg negative work and trailing leg positive work are equal and simultaneous. This optimal transition hypothesis, supported by experiments on healthy subjects, has consequences for hemiparetic gait: if a paretic leg cannot perform the required positive work, mechanical work and metabolic cost would be predicted to increase. To calculate the contribution of transition work to metabolic cost, experimental designs that isolate it from other metabolic cost contributors are necessary. Donelan et al., (2002) demonstrated that subjects walking faster by increasing only step length had proportional increases in transition work while controlling for limb swing cost. In this set of experiments, we use a length-modulated walking protocol to determine if sub-optimal transitions explain the metabolic cost of hemiparetic gait. Our hypothesis is that transition work efficiency during hemiparetic gait is equal to that measured during healthy walking; any increase in metabolic cost is due to an increase in mechanical work.

METHODS AND PROCEDURES

We determined each hemiparetic subjects' preferred step frequency and length during overground walking at 0.7m/s, then enforced this frequency by having subjects match the beat of a metronome forcing length to be directly proportional to speed. Step length was enforced with tape placed on the ground. To determine mechanical work using the individual limb method, subjects walked across ground-mounted force plates while wearing active joint markers. Subjects were asked to walk with as many of the step lengths corresponding to speeds between .5 and 1.1m/s they were capable of. To calculate metabolic cost, subjects performed 6 min walk tests under the above conditions. We measured rates of O_2 consumption and CO_2 production using a portable metabolic analysis system.

RESULTS

Subjects accurately maintained equal step lengths at the enforced frequency using their paretic limb to complete a wide range of speed trials using the length-modulated protocol (Hewson et al, 2007). Preliminary analysis of a single subject shows a substantial difference between the power profiles of the paretic and non-paretic limbs. The paretic limb is unable to generate enough push-off power during double support, which must then be produced during single support (Fig 1. In support of our hypothesis, the associated work rate is noted to increase with walking speed (Fig 2). Figure 2 also shows that net metabolic power associated with step-to-step transitions increased with step length. The slope of line comparing metabolic power and mechanical work is equal to the efficiency of step-to-step transition work (Fig 3). The measured efficiency for this subject is

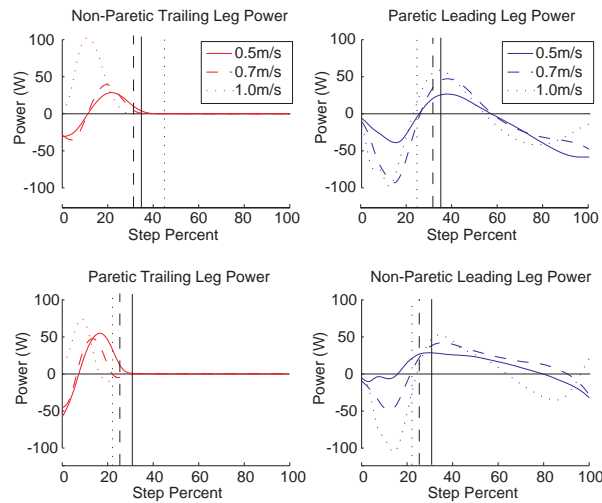22% which is comparable to healthy walkers (Donelan et al., 2002).

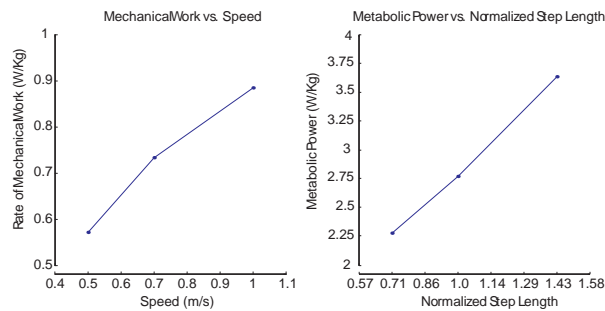**Figure 1.** Average external mechanical power. Vertical lines denote double support.

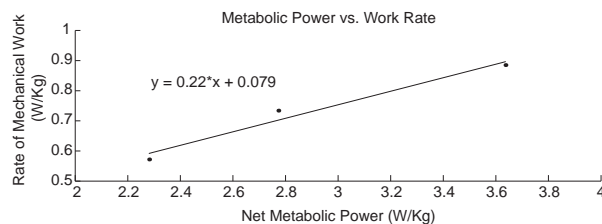**Figure 2.** Work rate and metabolic power vs. step length.

Figure 3. Work rate and metabolic power vs. step length.

DISCUSSION

The optimal transition hypothesis suggests that walkers may perform up to four times the amount of mechanical work during the step-to-step transition if they are unable to perform positive mechanical work appropriately. This

work exacts a metabolic cost. Using our length modulated protocol, we are able to compare the increased mechanical work of step-to-step transitions with the associated increase in metabolic cost; this corresponds to the efficiency of performing step-to-step transition work. The efficiency can then be used to determine the contribution of step-to-step transition work to the overall metabolic cost of hemiparetic walking during non-length modulated trials. The results will provide insight into the design of rehabilitation strategies and devices aimed at lowering metabolic cost and increasing patient mobility by improving the step-to-step transition. The potential significance of this research goes beyond its specific application to stroke rehabilitation. In principle, predictions regarding the effect of asymmetrical transitions on metabolic cost apply to all forms of gait diseases and disorders that result in biomechanical asymmetry including amputation and spinal cord injury.

SUMMARY

A preliminary analysis of one hemiparetic subject performing a length modulated walking protocol to control for the cost of leg swing reveals a 22% efficiency for producing work during the step-to-step transition which is equivalent to the efficiency of step-to-step transition work in healthy walkers.

REFERENCES

Donelan JM et al. (2002). *J Exp Bio,* 205:3717-3727.
Hewson DN et al. (2007). *ISPGR,* 166.

ACKNOWLEDGEMENTS

CROSSOVER AND FREE MOMENT DURING RUNNING

Stacey A. Meardon and Timothy R. Derrick

Iowa State University, Ames, IA, USA
E-mail: smeardon@iastate.edu

INTRODUCTION

As the merits of exercise for health and wellness have gained public acceptance, running has become an exercise of choice for many. Unfortunately, the risk for injury is well documented in the literature. While the exact cause of overuse injury in runners is multifactorial, altered lower extremity kinematics and loads have been associated with overuse injury.

The free moment is the torsional force about a vertical axis due to friction between the foot and the ground. This moment has been used as an estimate of torsion in the lower extremity. Peak absolute free moment is positively associated with overuse injury in runners, specifically stress fracture (Milner *et al.*, 2005 and 2006). Furthermore, altered dynamic hip and knee kinematics have also been reported in persons with a history of stress fracture (Milner *et al.*, 2005). Specifically, hip adduction is increased in runners with a history of tibial stress fracture compared to a control group (Milner *et al.*, 2005).

Increased crossover of the lower extremity relative to the pelvis during the stance phase of gait would logically result in greater hip adduction angles and potentially increase one's risk for injury. Moreover, a crossover gait pattern could result in greater pelvic rotation that needs to be countered at the foot, via the free moment. The relationship between lower extremity crossover and the free moment has not been established. The purpose of this study was to identify the relationship between the magnitude of crossover and the free moment.

METHODS

Eight male and six female (26.1 ± 6.51 years) recreational runners participated in this study. None of the subjects had lower extremity abnormalities at the time of data collection that would affect their ability to participate in this study.

Three dimensional kinematic data were collected using a 120 Hz eight-camera motion capture system (Vicon Peak, Centennial, CO). Twenty-three retro-reflective markers were secured on both legs. Ground reaction forces and moments were collected at 1200 Hz.

Ten successful trials were collected for each limb. All subjects ran at a self-selected 5k race pace and were required to maintain this self-selected pace during each trial (average speed: 3.90 ± 0.33 m/s). Data were exported to Matlab 7.0.4. and smoothed using a low-pass Butterworth filter with a cutoff frequency of 8 Hz for kinematics and 50Hz for kinetics.

Peak positive and peak negative free moment peaks were identified as the free moment tends to display a sinusoidal pattern. The magnitude of crossover was calculated as the difference between a sacral marker and the center of pressure in the medial/lateral direction.

All free moment peaks and crossover values were averaged across trials to obtain subject means. Linear regression determined the relationship between the magnitude of crossover occurring at the peak positive and peak negative free moment peaks.

RESULTS

Significant correlations existed between the magnitude of crossover and the both the peak positive and peak negative free moments (p=.009 for both) (Figures 1 & 2). In both cases, an increase in the magnitude of the free moment was associated with a greater magnitude of crossover.
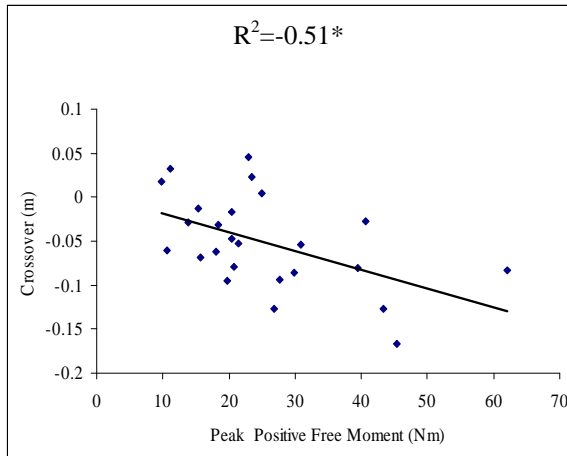

Figure 1. The relationship between crossover and peak positive free moment. A more negative crossover value indicates a greater magnitude of crossover.

DISCUSSION

The purpose of this study was to identify the relationship between the magnitude of crossover and the free moment. A 1 cm increase in crossover resulted in a 4.76 Nm increase in the peak positive free moment. Similarly, a 1 cm increase in crossover resulted in a 3.70 Nm increase in the peak negative free moment.

The free moment, associated with crossover gait patterns in this study, has been related to overuse injury in runners. Thus, methods of controlling crossover may lead to new strategies preventing or managing injury.
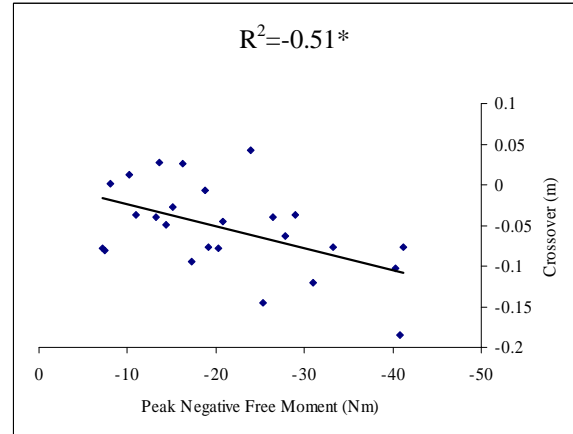

Figure 2. The relationship between crossover and peak negative free moment. A more negative crossover value indicates a greater magnitude of crossover.

SUMMARY

The free moment, a measure of torsion in the lower extremity, has been associated with running injury. In this study, crossover of the lower extremity was significantly related to the free moment during running. Cues and/or training designed to decrease crossover may be beneficial in minimizing detrimental loads.

REFERENCES

Milner, C.E. et al. (2006) *Med. Sci. Sports Exer.*, **38**(2), 323-328.
Milner, C.E. *et al.* (2005). *J. Biomech.*, **39**(15), 2819-25.
Milner, C.E. et al. (2005). *Med. Sci. Sports and Exer.*, **37**(5), S346.

DEVELOPMENT AND VALIDATION OF A VERSITILE INTRA-ARTICULAR PRESSURE SENSING ARRAY

J.W. Welcher[1,3,4], J. M. Popovich, Jr.[2,3], T.P. Hedman[1,2,5] and W. Tawackoli[3]

[1]Department of Biomedical Engineering, USC, Los Angeles, CA
[2]Division of Biokinesiology and Physical Therapy, USC, Los Angeles, CA
[3]Department of Surgery, Cedars-Sinai Medical Center, Los Angeles CA
[4]Biomechanical Research & Testing, LLC, Long Beach, CA
[5]Orthopeutics, L.P., Georgetown, TX
E-mail: Welcher@usc.edu

INTRODUCTION

Many studies attest to the high frequency of back complaints in society with 60–85% of all people having back pain at some time in life (Andersson, 1997). The etiology of low back pain remains controversial; however, the relationship between anatomical structures, including the lumbar facet joints, and pain clearly exists (Manchikanti, et al., 2004). The facet joints are the major load bearing elements in the lumbar spine posterior column. They also share the vertebral column loads and help control the amount and type of motion available in the lumbar spine.

Of the research that has been conducted on examining intra-articular facet joint loading, technology such as externally mounted strain gauges (Suezawa, et al., 1980), pressure sensitive films, or force sensitive resistors (Hedman, 1992) have been utilized, These measurement methods are either indirect, lack temporal or spatial specificity, or are quantified with sensors that produce large errors (Wilson 2006). Therefore, the purpose of this investigation was to develop and validate sensor technology that would measure accurate spatial and temporal parameters of facet loading in-vitro.

METHODS

Numerous existing technologies were investigated to determine their potential feasibility. Each system was independently evaluated depending on their progressive meeting of the criteria for utilization including: sensor thickness less than 0.8 mm, steady state response, linear response, minimal or correctable errors associated with curvature, and durability. Inability of the commercially available technology to meet our design criteria necessitated the construction of a custom made system. This new system consisted of an array of miniature pressure sensors (0-500psi range) embedded in electrically resistant durable Kapton tape (Figure 1).
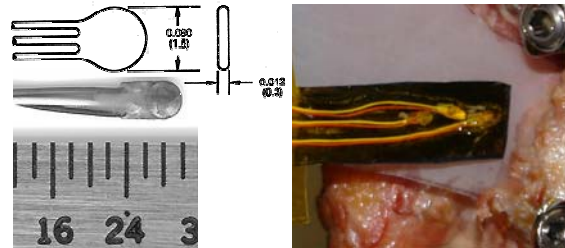

Figure 1: Pressure sensor geometry (left) and sample 1x3 array configuration being placed in the lumbar L4-5 facet joint (right).

Validation was conducted in a pressure vessel with a hermetically sealed 30-wire pass through on one end and an Omega Engineering PX35 High Accuracy pressure transducer and pressure regulator on the other. Initial sensor validation data was

collected on a 16-bit resolution TDAS-Pro data acquisition system certified to NHTSA, FAA, ISO 6487 and SAE J211.

A frozen human lumbosacral (L1-Sacrum) specimen was thawed, dissected and potted in a two-part polyurethane potting solution such that the superior endplate of the fourth lumbar vertebra was aligned horizontally. Hydration of the specimen was maintained by spraying with isotonic saline solution.

The specimen was secured in an eight-axis Bose Kinematic Spine Tester (Bose Corporation). A 1x3 array of the pressure sensors was utilized for preliminary testing. The array was placed in the approximate vertical midline of the right L4-5 facet. The testing protocol consisted of five loading cycles ($\pm$ 10Nm) of continuous sagittal plane (flexion/extension) pure bending moment at a rate of 1.0 degrees/sec. Kinematic and kinetic data were recorded at a sampling rate of 50Hz. To allow for preconditioning, the fourth bending cycle was used for analysis.

RESULTS

The new sensors were able to capture the signal power over a range of physiologically relevant frequencies up to at least 6 Hz Sensor hysteresis was found to be 0.631% (+/-0.358%) and total combined system and sensor signal-to-noise ratio was nominally 50 dB. Analysis of other sensor characteristics such as thermal drift ($\leq$1% of load at 16 minutes), sensitivity to curvature (no artifactual load with curvature), and cross talk ($\leq$2% of load with sensors adjacent to one another) were evaluated and found to comply with our utilization criteria. The combined tape-sensor-tape construct was approximately 0.6 mm thick. Figure 2 illustrates the intra-facet pressure sensor results of the third through fifth loading cycles during in-vitro testing.
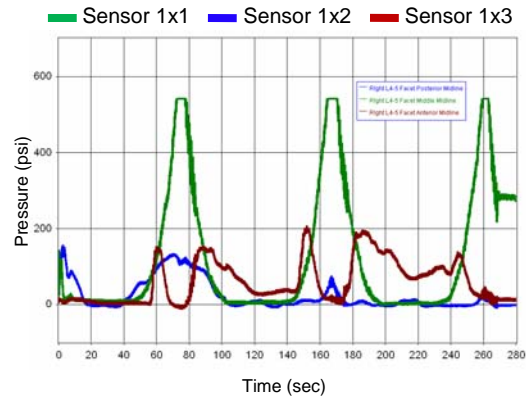

Figure 2: Example of intra-facet pressure recording of the 1x3 sensor array during flexion and extension. Increased loading is noted during lumbar extension.

DISCUSSION

Our new sensor system satisfied all the design requirements; with sensor thickness well below 0.8 mm, a linear and steady state response, and are configurable to eliminate curvature effects without added cross talk. Preliminary measured in-vitro facet pressure data is consistent with the limited prior research for similar loading conditions.

SUMMARY

A new sensor for spatial and temporal intra-facet pressure measurement was developed and tested. Additional work is in progress developing more robust and spatially relevant sensor arrays.

REFERENCES

Andersson, GBJ. (1999). *Lancet*, 581-585. .
Hedman TP. (1992). *Journal of Biomechanics*, 25, 69-80.
Manchikanti, L, et. al. (2004). *BMC Musculoskeletal Dis*, 5, 15.
Suezawa, Y., et. al. (1980). *International Orthopaedics*, 4, 205-209.
Wilson DC, et al. (2006) *Journal of Biomechanics.* 39(2):348-53.

TRANSITION WORK IN SIMULATED PATHOLOGICAL WALKING

Caroline Soo and J. Maxwell Donelan

School of Kinesiology, Simon Fraser University, Burnaby, BC, Canada, chsoo@sfu.ca
URL: http://www.sfu.ca/locomotionlab

INTRODUCTION

The energy expenditure of pathological walking is significantly elevated relative to healthy walking (Waters and Mulroy, 1999). Our research aims to understand the determinants of this increase in metabolic cost.

Mechanical work is needed to redirect the centre-of-mass velocity during step-to-step transitions (Donelan et al., 2002). Physics-based mathematical models show that, during transitions, the front leg performs negative work while the back leg performs positive work to redirect the centre of mass velocity into the next step. This model also predicts that there is an optimal way to perform this work (Ruina, et al., 2005; Kuo et al., 2005). *Optimal transitions* occur when equal magnitudes of positive and negative work are performed in a coordinated fashion. If one or both legs are not able to perform this, the walking models predict that *sub-optimal transitions* will require a greater magnitude of total mechanical work than optimal transitions.

Healthy humans perform near-optimal transitions at all walking velocities (Donelan et al., 2002). However, no studies to date have looked at the mechanical consequence of sub-optimal transitions in humans. Our general hypothesis is that the major cause of increased metabolic demands underlying all pathological walking, regardless of aetiology, is the inability to perform transition work with the correct magnitude and timing. We test whether sub-optimal transitions increase the total amount of mechanical work.

METHODS AND PROCEDURES

The major determinant of the metabolic cost of walking is transition work, contributing to 65 – 70% of the total metabolic cost (Kuo et al., 2005). To isolate transitions from other contributors of the metabolic cost of walking such as leg swing (Doke et al., 2005), we use an established sagittal plane rocking paradigm (Soo et. al., 2007).
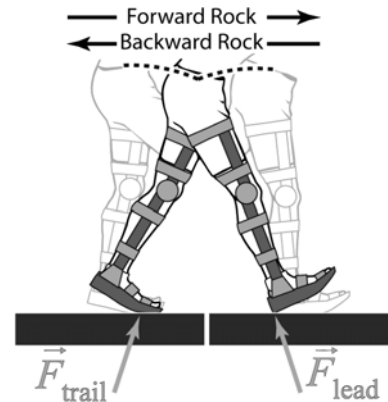

Figure 1. Sagittal plane rocking paradigm.

To simulate the biomechanical effects of gait pathology while controlling for other contributors of the metabolic cost associated with pathology such as spasticity (Waters and Mulroy, 1999), we immobilise the knee and ankle joints using braces in healthy subjects (Figure 1). We compare three conditions: (a) both legs unlocked, (b) locked back leg and (c) locked front leg. Subjects rock at 0.04 Hz and at 80% of their leg length to ensure that subjects perform a substantial amount of work. We use ground reaction forces to calculate individual limb work (Donelan et al., 2002) of each leg.
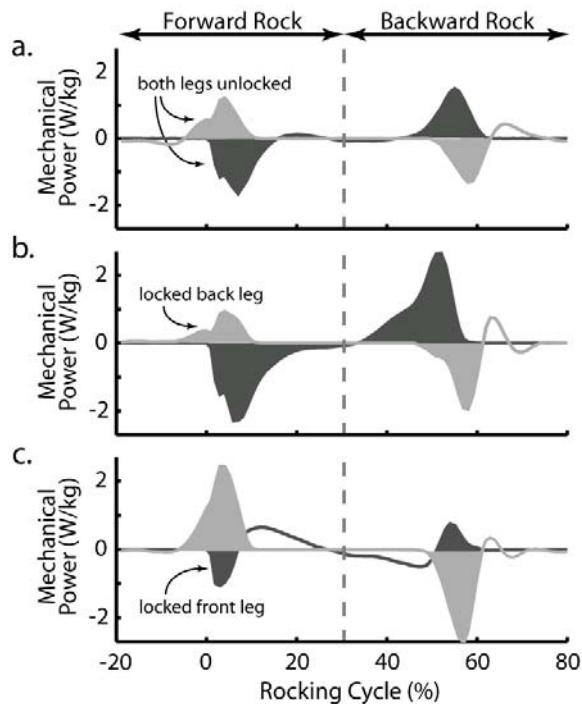
RESULTS

Figure 2. Leg mechanical power for one subject showing (a) both legs unlocked, (b) back leg locked and (c) front leg locked conditions. Shaded areas represent leg work. Dark grey areas are front leg work; light grey areas are back leg work.

Preliminary analyses have shown that the braces can simulate sub-optimal transitions. When both legs were unlocked (Figure 2a), the subject was able to perform near optimal transitions as evidenced by relatively equal positive and negative work magnitudes. When the back leg was braced (Figure 2b), the subject was unable to perform positive work resulting in net negative total mechanical work during forward rock. When the front leg was braced (Figure 2c), the subject was unable to perform negative work resulting in net positive mechanical work during forward rock. For this subject, immobilising the leg to produce sub-optimal transitions has increased the total positive mechanical work by 146% and 122% for the back leg locked condition and the front leg locked condition,

respectively, compared to the unlocked condition.

DISCUSSION

Further analyses will assess the relationship between sub-optimal transitions and the total mechanical work. Irrespective of the hypothesized outcomes, these experiments will be the first to determine the effect of sub-optimal transitions on mechanical work. The outcome of this study may provide a novel biomechanical approach to explain why pathological gait is so expensive.

SUMMARY

We hypothesize that the inability of one or more legs to perform transition work with correct magnitude and timing increases the total mechanical work. Preliminary results show that biomechanically simulating sub-optimal transitions does increase the total mechanical work.

REFERENCES

Brockway, JM (1987). *Hum Nutr Clin Nutr*, 41(6): 463-471.
Donelan, JM et al. (2002). *J Exp Biol*, 205: 3717-3727.
Doke J et al. (2005). *J Exp Biol*, 208:439-445.
Kuo, AD et al. (2005). *Exerc Sport Sci Rev*, 33(2):88-97.
Ruina, A et al. (2005). *J Theo Biol*, 235:170-192.
Soo, CH et al. (2007). *Proceedings from ISPGR Conference 2007*. University of Vermont, Vermont.
Waters, R and Mulroy S (1999). *Gait & Posture*, 9(3):207-231.

ACKNOWLEDGEMENTS

KINEMATIC ANALYSIS ON INFLUENCE OF AN EXTRA WEIGHT IN HORIZONTAL ARM SWING

Young-Kwan Kim and Richard Hinrichs

Department of Kinesiology, Arizona State University, Tempe, Arizona, USA,
E-mail: Young-Kwan.Kim@asu.edu

INTRODUCTION

Forceful human limb motions such as throwing, kicking, and striking are governed by open kinetic chain principle. It is characterized by a sequential order of proximal-to-distal segmental rotation, a tapered mass distribution (i.e., more massive at proximal segment and less massive at distal segment), and the highest linear velocity at the most distal segment (Kreighbaum & Barthels, 1990).

In order to improve the distal end performance, some warm-up or training devices in sports (e.g., a donut on a baseball bat and ankle weights of runners) are designed to put extra weight(s) on the distal segment. Intuitionally the extra weight on the distal segment is believed to reduce the performance. However, the effect of an extra weight on the proximal segment was a little investigated (Southard, 1998).

The purpose of this study was to investigate change in arm swing speed and inter-segmental coordination in an open kinetic chain motion (i.e., horizontal arm swing) according to different location and amount of an extra weight.

METHODS AND PROCEDURES

20 participants (10 male and 10 female) who had no neuromuscular diseases in the upper extremities participated in this study. They came to lab at two different days for two different extra weight conditions (upper arm vs. forearm extra weight).

For each extra weight condition, six different masses (i.e., 0, 25, 50, 75, and 100% segmental mass) were applied (see Table 1).

Extra weight	Upper arm (kg)	Forearm (kg)
0%	0	0
25%	0.50±0.10	0.30±0.06
50%	1.00±0.20	0.60±0.12
75%	1.51±0.30	0.90±0.18
100%	2.01±0.40	1.20±0.24

Table 1. Different location and amount of extra weight (mean±SD).

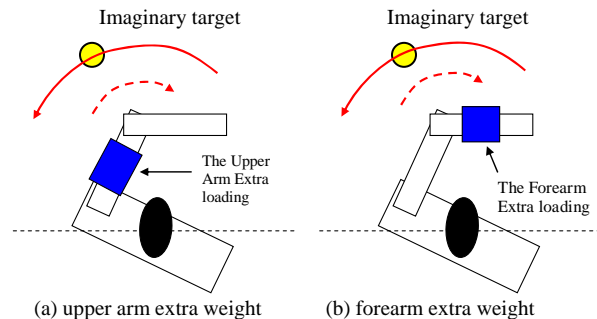(a) upper arm extra weight   (b) forearm extra weight

Figure 1. Three segment upper arm model and different location of an extra weight in forceful horizontal arm swing: a) upper arm, and b) forearm

The task was to execute a fast horizontal arm swing toward an imaginary target after countermovement action (see Figure 1). The electro-optical motion measurement system (Optotrack®, NDI, Canada) was used to record three-dimensional position data of Infrared-emitting diode (IRED) markers on the upper body. Its sampling rate was 300 Hz.

The locations of five markers were the trailing shoulder, the leading shoulder, the elbow, the wrist, and the imaginary target. Since this task mimicked the baseball bat swing motion, the leading arm was the non-dominant arm.

RESEULTS

The arm swing speed was defined as the peak linear velocity at the wrist when the arm passed the imaginary target. A two-way (Location × Amount) repeated measures ANOVA on the arm swing speed showed a significant interaction ($F(76, 4) = 40.9$, $p < .01$). For the upper arm extra weight, there was no main effect by the amount of an extra weight. However, there was a significant main effect by the forearm extra weight ($F(76, 4) = 79.5$, $p < .01$). The swing speed was significantly reduced with increase in the forearm extra weight (except 50% and 75% conditions) (see Figure 2).
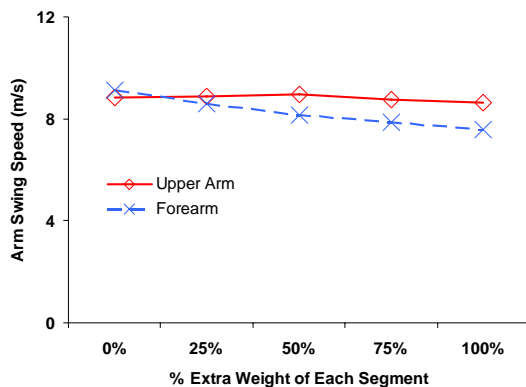

Figure 2. Changes in arm swing speeds according to the amount of an extra weight and its location.

Inter-segmental coordination, represented by the temporal lags of peak angular velocities between adjacent segments, showed that the only significant interaction was detected at the fore arm extra weight (see Figure 3). The temporal lag between upper arm (UA) and trunk (TR) was significantly lengthened according to the increased forearm extra

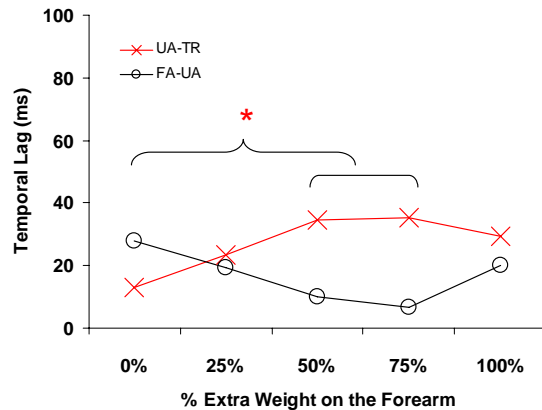weight, while that between forearm (FA) and UA was shortened by the compensation.

Figure 3. Change in temporal lag according to the forearm extra weight. * significant different mean values ($p < 0.05$).

DISCUSSION

The extra weight on the upper arm did not affect the performance and inter-segmental coordination, while the extra weights on the forearm reduced the arm swing speed significantly and changed inter-segmental coordination when it was increased. This might be attributed to the increased moment of inertia (MOI). Since the MOI is the function of the squared distance from the segment to the axis rotation, the farther location of an extra weight (i.e., forearm) might increase the rotational resistance than the upper arm extra weight did.

SUMMARY
The extra loading on the proximal segment did not affect the swing speed and inter-segmental coordination until 100% extra weight was added during horizontal arm swing.

REFERENCES
Kreighbaum, E and Barthels KM (1990). *Biomechanics.* New York, NY: Macmillan.
Southard, D. (1998). *Res Q Exerc Sport*, 69, 355-367.

TREATMENT INSIGHT FROM SUBJECT-BASED SIMULATION OF CROUCH GAIT

Ajay Seth[1], May Q. Liu[2], Michael H. Schwartz[3], Frank C. Anderson[1], and Scott L. Delp[1,2]

[1]Department of Bioengineering, Stanford University, Stanford, CA, USA
[2]Department of Mechanical Engineering, Stanford University, Stanford, CA, USA
[3]Center for Gait & Motion Analysis, Gillette Children's Specialty Healthcare, St. Paul, MN, USA
E-mail: aseth@stanford.edu   URL://www.stanford.edu/group/nmbl/

INTRODUCTION

Crouch gait, characterized by excessive knee flexion in stance, is common in individuals with cerebral palsy (CP). If uncorrected, crouch gait can lead to chronic knee pain, skeletal deformities, and loss of independent ambulation. Muscle lengthening and tendon transfer surgeries are employed to correct excessive knee flexion by reducing tightness in muscles that flex the knee. Strengthening exercises and surgeries to correct skeletal deformities are also performed to increase the capabilities of muscles to extend the knee. It is difficult, however, to determine how these treatments affect the actions of muscles because of the complex dynamic coupling between body segments. Dynamical models describe cause-and-effect relationships that enable quantitative analysis of muscle actions. The purpose of this study is to determine the role (if any) of tightness in iliopsoas, hamstrings and/or gastrocnemius to flex the knee, and possible weakness of gluteus maximus, vasti, and/or soleus to insufficiently extend the knee, as factors of a patient's crouch gait. This information can provide insight into treatment planning.

METHODS AND PROCEDURES

 A child with CP (7yrs, 136cm, 34kg, spastic diplegia) with crouch gait (mean stance-phase knee flexion > 27°) was selected for analysis. Physical exam indicated hip flexor tightness with no spasticity, knee flexor tightness with slight spasticity, and ankle plantar flexor tightness and spasticity. Gait data included: surface-marker positions, functional joint-centers locations and joint kinematics; EMG of 5 muscles in each limb (medial and lateral hamstrings, quadriceps, gastrocnemius, and tibialis anterior), and ground reaction forces and moments from two consecutive force-plate strikes.

A generic musculoskeletal model was scaled to match the joint centers, surface markers, and total body mass measured from the subject. The SimTrack workflow in OpenSim (Delp et al. 2007) was used to generate a muscle-actuated forward dynamics simulation. Model joint angles were within 2° root-mean-square error of the experimentally determined joint angles and muscle activities for the model were in temporal agreement with EMG for measured muscles. Perturbation analysis (Liu et al. 2006) was used to compute the muscle-induced accelerations of the stance knee as well as the body mass center to elucidate the function of individual muscles during the subject's gait.

RESULTS

Simulation results showed gastrocnemius to be the most significant contributor to stance-phase knee flexion acceleration (Fig. 1A) and body support (Fig. 1B) for the subject with crouch gait. In contrast, a typically developing (unimpaired with an upright gait) child of similar stature (137cm, 32.4 kg) had little knee extension acceleration from gastrocnemius walking at a self-selected speed. Iliopsoas in crouch gait also accelerated the knee into flexion, but it represented a much smaller

deviation from the muscle's action in the unimpaired subject (Fig. 1A). In the crouch simulation, hamstrings had a net extensor acceleration at the knee but took away from the support of the body (Fig. 1B). Gluteus maximus, vasti, and soleus acted with greater knee extension acceleration and body support in the subject with crouch gait compared to the unimpaired subject (Fig. 1).
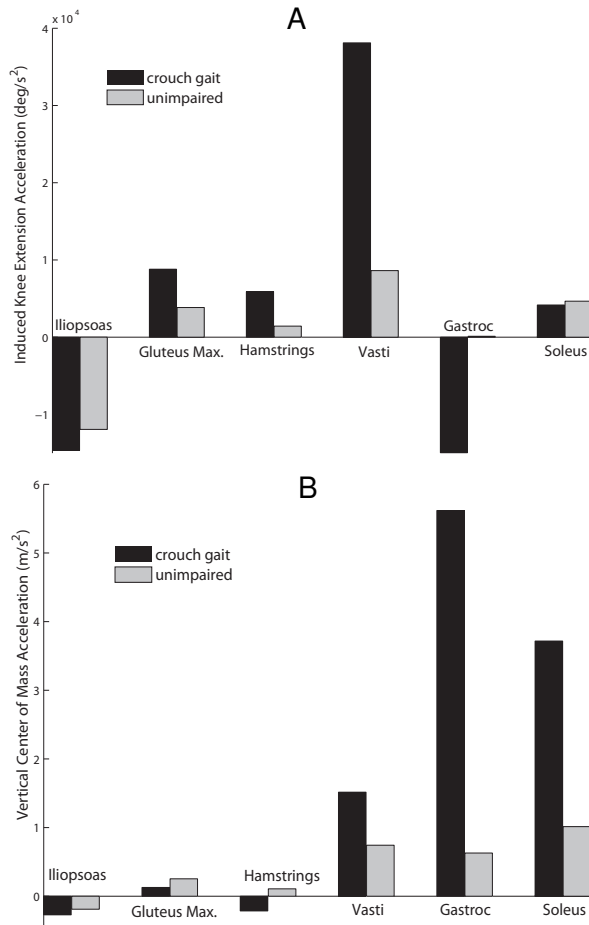

Figure 1. Average stance-phase muscle-induced accelerations of the knee (A) from a simulation of a child with crouch gait compared to an unimpaired child. Muscle-induced accelerations of the mass center in the vertical (support) direction (B).

DISCUSSION

The results highlight several unexpected findings. First, gastrocnemius can strongly accelerate the knee towards flexion (Fig. 1)

while significantly contributing to support (Fig. 2B). This can be understood in context of our toe-walking subject with a crouch gait. In crouch, plantar flexors have diminished capacity to extend the knee (Hicks et al. 2008) and thus gastrocnemius' knee flexion moment dominates at the knee while its plantar flexion moment contributes to support. Second, the two powerful plantar flexors, gastrocnemius and soleus, can have differential roles at the knee. In the unimpaired case, soleus acted to extend the knee while gastrocnemius had no action at the knee. In the subject with crouch, soleus also extended the knee but gastrocnemius accelerated the knee into flexion (Fig. 1A). Finally, hamstrings do not necessarily increase knee flexion acceleration during stance. Our simulation of a child with crouch gait indicated that hamstrings can increase its contribution to knee extension (Fig. 1A) compared to an unimpaired subject.

Based on our analysis, gluteus maximus, vasti, and soleus strength were sufficient for support (Fig. 1B) in the subject, and crouch gait was not a consequence of weakness. Rather, gastrocnemius tightness/spasticity had a dominant and detrimental effect at the knee (Fig. 1A). Interestingly, the subject had a fractional lengthening of gastrocnemius and botulinum toxin injected into the medial hamstrings (without surgical lengthening) with an excellent outcome– near normal knee flexion during gait after treatment.

REFERENCES

Delp SL et al. (2007). *IEEE Trans. Biomed. Eng,* 54:1940-50.
Hicks JL et al. (2008). *J Biomech*, in press.
Liu MQ et al. (2006). *J Biomech,* 39:2623-30.

ACKNOWLEDGEMENTS

IN VIVO SARCOMERE LEGNTH AND FIBER TENSION MEASUREMENTS

Yi-Ning Wu[1], Yupeng Ren[1] and Li-Qun Zhang[1,2]

[1]Sensory Motor Performance Program, Rehabilitation Institute of Chicago, Chicago, IL, USA,
[2]Departments of Physical Medicine and Rehabilitation, Biomedical Engineering, and
Orthopaedic Surgery, Northwestern University, Chicago, IL, USA
l-zhang@northwestern.edu

INTRODUCTION

Spasticity, contracture, and muscle weakness are commonly occur in neurological disorders. The symptoms are closely related to each other and are major factors contributing to disabilities in patients with neurological impairments. Biomechanical properties of spastic muscle fibers have been investigated in *in vitro* experiments. It was reported that single fibers from spastic muscle of children with cerebral palsy developed passive tension at significantly shorter lengths of about 1.84 μm (Friden and Lieber, 2003). On the other hand, only sarcomere length was measured *in vivo* and the sarcomere length of spastic muscles was found significantly longer in vivo, averaging 3.48 μm (Lieber and Friden 2002).

It is not clear whether spastic fibers are under higher tension and thus elongated and stiffer under in vivo condition. There is a need for simultaneous *in vivo* evaluation of the fiber tension and the sarcomere length changes for better understanding of spasticity, contracture and muscle weakness. The purpose of this study was to simultaneously evaluate the fiber tension and sarcomere length *in vivo*.

METHODS AND PROCEDURES

The tibialis anterior (TA) muscle of Sprague-Dawley rats was investigated in this study. A small bundle of fibers was isolated with the two ends still attached to the remaining muscle bulk. A custom device was used to measure the force of the small bundle of fibers and sarcomere length in vivo by lifting the bundle of fibers moderately (Fig. 1).

Sarcomere/fiber images were recorded *in vivo* through an objective and CCD camera. The tension of the fiber bundle and the lifting distance of the fibers were recorded by a force sensor and a linear position sensor, respectively (Fig. 1). Z stage 1 was used to focus the objective and Z stage 2 was for lifting the fiber bundle. The evaluation was done at the 45º dorsiflexed, neutral, 45º plantar flexed positions.
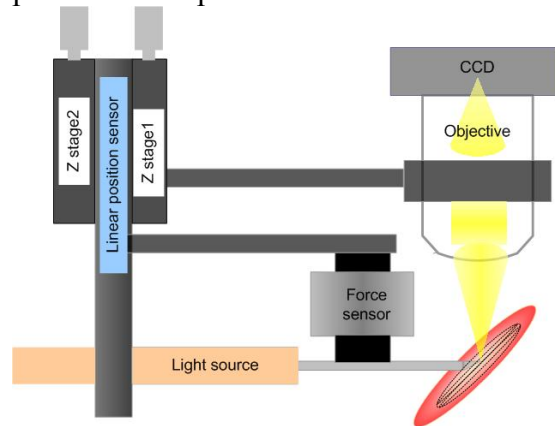

Figure 1. A novel device for evaluating fiber tension and sarcomere length *in vivo*.

Assuming the fiber bundle was lifted at the middle, the axial tension (F_x) along the fiber bundle was estimated from the lifting force (F_y) and the lifting distance (y), based on the equations below.

$$F_x = \frac{F_y}{2\sin(\theta)}$$

$$\theta = \tan^{-1}\left(\frac{y}{x}\right)$$

Figure 2. The relationship between the axial tension and the lifting force. *x* is half of the fiber bundle length, y the lifting

distance, θ the lifting angle of the fiber bundle.

An in vitro corroboration setup was used to corroborate the in vivo measurement (Fig. 3). After the in vivo measurement, the small bundle of fibers was dissected out with the two ends mounted to the tips of a linear motor and a force sensor, respectively. The width and thickness of the bundle was measured.
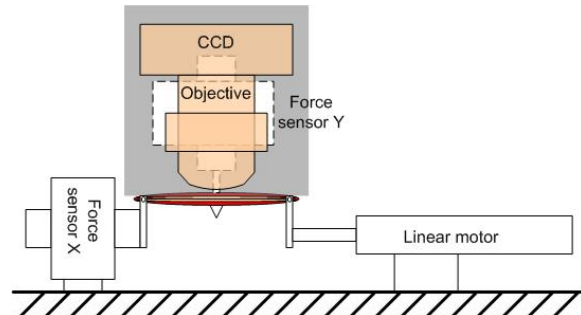

Figure 3. In vitro validation setup. The horizontal force sensor was used to directly record the axial force of the small bundle of fibers with the linear motor controlling the fiber tensions. The custom *in vivo* device in Fig. 1 was shown in the shaded area.

RESULTS

Images recorded from the fiber bundle showed clearly the sarcomere length increase with lifting (Fig. 4).
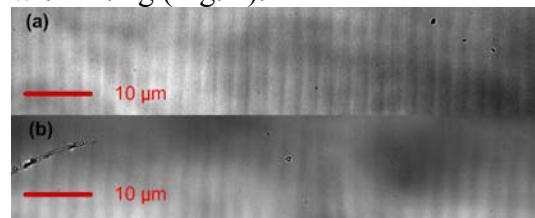

Figure 4. Images of the sarcomeres from the fibers being lifted. (a) is the image of the fiber bundle before lifting (sarcomere length = 2.61 μm). (b) gives the sarcomere length after the fiber bundle was lifted to a lifting angle of 28°(sarcomere length = 2.82 μm).

A steeper slope of the lifting force versus lifting angle indicated higher axial tension. The axial tension became higher as the ankle was moved to plantar flexion. The fiber bundle generated higher tension during the lifting when the ankle was at a plantar flexed position with the TA stretched. The axial tension of the TA bundle was higher at plantar flexion, as compared to the neutral and dorsiflexion position with the TA more relaxed.

The *in vitro* experiment corroborated the in vivo measurements on the axial tension along the fiber bundle (Fig. 5). The estimated axial force derived from the lifting force matched closely with the measured axial force.
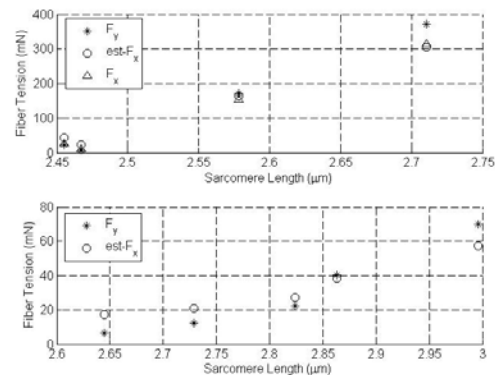

Figure 5. Results of in vitro validation. The upper plot shows the goodness of the estimation. The lifting force (F_y ,denoted by the star) and axial tension (F_x ,denoted by the triangle) were measured by the vertical and horizontal force sensors, respectively. The estimated axial force (est-F_x) was derived from the equation. The bottom plot shows the increases of the axial tension and sarcomere length during the lifting *in vivo*.

DISCUSSION & SUMMARY

We have demonstrated the feasibility of measuring sarcomere length and fiber tension *in vivo*. The combination of force and sarcomere length measurement allows us to investigate the tension in spastic muscle for better understanding of the mechanisms underlying spasticity and motor impairment.

REFERENCES

Friden J, Lieber RL (2003). *Muscle Nerve*. 27:157-64.
Lieber RL, Friden J (2002). *Muscle Nerve*. 25:265-270.

DOES DECOMPRESSIVE SPINAL SURGERY FOR OLDER PATIENTS WITH CERVICAL MYELOPATHY IMPROVE GAIT ON FLAT AND IRREGULAR SURFACES?

Fatima Makhzoum[1], James A. Ashton-Miller[1], Frank La Marca[2]

[1] Biomechanics Research Laboratory, Biomedical Engineering, University of Michigan, Ann Arbor, MI, USA, fmakhzou@umich.edu
[2] Department of Neurosurgery, University of Michigan, Ann Arbor, MI, USA

INTRODUCTION

Cervical Myelopathy (CM), which is prevalent in elderly populations, causes chronic spinal cord compression and problems with balance and gait. Although decompression surgery is a treatment option, we are unaware of a clinical trial that evaluates whether its efficacy is superior to conservative treatment in terms of gait variability. If treatment of CM is successful, then it should show improved gait both on a flat surface, as well as an irregular surface. In this paper, we test the (null) hypothesis that operative treatment of CM is not superior to conservative treatment in terms of gait variability on a flat and irregular surface at one year follow-up. The expectation was that that cervical decompression surgery will improve mean speed, as well as the following secondary parameters: step length (SL), step time (ST) and step width (SW).

METHODS AND PROCEDURES

A prospective, case-control, trial was conducted with 1-year follow-up. At baseline, patients, 11 males (mean [SD]: 52.0 [9.8] years) and 5 females (54.6 [10.1] years), were placed into two groups: those who underwent surgical decompressive cervical procedure (n=8) and a conservatively-treated control group (n=8). Both groups were evaluated at baseline and at 3-, 6- and 12-months post-operatively.

All subjects walked at a comfortable speed along a 10 m walkway under normal lighting. Fifteen trials were completed under the following two conditions, presented in randomized order: (1) flat surface (vinyl-tiled floor); and (2) irregular surface (wooden prisms distributed randomly under carpet, Thies et al. 2005). Two force-sensing resistors ("foot switches") taped underneath the insole of each shoe were used to indicate single and double support intervals. Two infrared-emitting diode markers were located at each ankle, and a fifth marker was located in the mid-sagittal plane ventral to the umbilicus. The 3-D kinematic and foot switch data were recorded at 100 Hz using an Optotrak 3020 motion analysis system. Forward progression of the waist marker over time was assumed to be representative of the subject's walking speed. The kinematic and force data were processed using a custom algorithm written in MATLAB® to quantify step width, step length, and walking speed (Thies et al. 2005). The hypotheses were tested using a repeated measures analysis of variance with $p < 0.05$ being considered statistically significant.

RESULTS

The null hypothesis was rejected in that decompressive surgical treatment significantly increased mean speed on both the flat and irregular surfaces by 11% (MS, p=0.034, Table 1), and there was a trend

towards increased SL (p=0.073) at one year follow-up. Surface type had a significant effect on mean speed (p=0.001) and ST (p=0.002). Both time post-baseline (p<0.001) and surface type (p=0.001) significantly affected mean speed, with cases increasing their mean speed by 5.1 % over the course of one year. There was also a significant interaction of time * group (p=0.034). The gait of the control group remained fairly stable over the one year study.
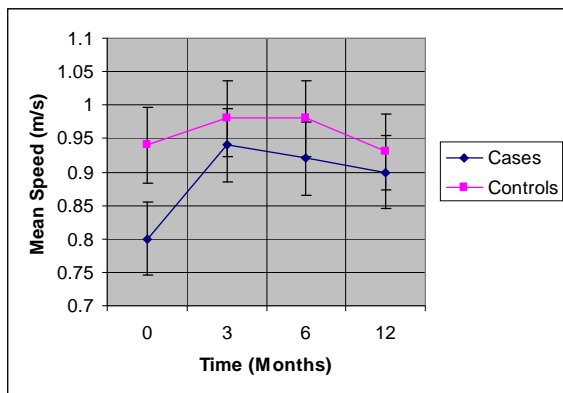

Figure 1 - Mean [SD] speed plotted by group. Cases exhibited a significantly greater improvement over time.

DISCUSSION

It has not been known whether surgical decompression for cervical myelopathy improves gait function. This is the first study to show that the procedure is helpful for modestly improving gait both on flat as well as on a (more challenging) irregular surface after the first 3 months (Figure 1). The results held at one year follow-up, but longer follow-up is desirable. Limitations of the study include the fact that a reduced marker set was used (compared with that used in traditional clinical gait analysis), but this reduced set has been shown to yield reproducible results when measuring the stepping variability on flat and irregular surfaces (as demonstrated by Thies et al. in a series of papers).

SUMMARY

Surgical decompression for cervical myelopathy results in modest, but significant, improvements in gait at 1-year follow-up.

REFERENCES

Thies, SB, Richardson, JK, and Ashton-Miller, JA (2005). *Gait and Posture,* 22:26-31.

ACKNOWLEDGEMENTS

Group	Surface	Test	Step Width (mm)	Step Length (mm)	Step Time (s)	Mean Speed (m/s)
Cases	Even	Baseline	167.2 [31.8]	495.1 [41.8]	0.73 [0.17]	0.87 [0.14]
		1-Year	157.5 [28.6]	519.9 [83.0]	0.78 [0.27]	0.97 [0.13]
	Irregular	Baseline	172.8 [28.9]	485.7 [47.1]	0.86 [0.25]	0.79 [0.09]
		1-Year	170.9 [31.3]	514.7 [80.3]	0.88 [0.24]	0.89 [0.15]
Controls	Even	Baseline	161.8 [45.5]	561.3 [94.4]	0.68 [0.13]	1.01 [0.24]
		1-Year	165.9 [47.1]	552.5 [76.8]	0.68 [0.14]	0.99 [0.23]
	Irregular	Baseline	170.2 [42.7]	556.3 [106.1]	0.71 [0.13]	0.97 [0.27]
		1-Year	176.5 [42.8]	541.5 [94.1]	0.73 [0.17]	0.97 [0.25]

Table 1 - Overall effect of treatment and surface on mean [SD] gait parameters

JOINT POWERS BUT NOT JOINT TORQUES DISCRIMNATE HIGHLY MOBILE AND FUNCTIONAL OLD FROM YOUNG ADULTS

P. DeVita, P. Rider, B. Long, K. Steinweg, A. Gruber, S. Solnik & T. Hortobagyi
Dept. Of Exercise and Sport Science, East Carolina University, Greenville, North Carolina, USA, devitp@ecu.edu, http://www.ecu.edu/cs-hhp/exss/biomechlab.cfm

INTRODUCTION

It is well established that old vs. young adults demonstrate mechanical plasticity in gait by increasing and decreasing proximal hip and distal knee and ankle muscle function, respectively (DeVita et al, 2000, Kerrigan et al, 1998). These adaptations are further increased in old adults who exhibit low physical performance (Graf et al, 2005). We now ask, do old adults who exhibit high levels of physical performance show reduced adaptations? The purpose of this study was to compare lower extremity joint torques and powers in fully healthy and highly mobile young and old adults during level walking at three walking speeds.

METHODS AND PROCEDURES

All potential subjects were screened with a health and behavior questionnaire and all old adults were examined by a geriatric physician using extensive exclusion criteria. These methods enabled us to test only healthy, highly functional and mobile participants. Ground forces and 3D kinematics were obtained from 20 young (21 yr) and 20 old (77 yr) volunteers during 1.2, 1.5, and 1.8 m/s level walking after obtaining written informed consent. Sample size was based on previous data and provided over 80% statistical power. All subjects performed the tasks without difficulty. Self-selected walking velocity was also measured in each subject. Inverse dynamics were used to derive 3D joint torques and powers throughout the stride. Extensor angular impulse and positive work were derived from the torque and power data.

2-by-3 ANOVAs (age by speed, $p<0.05$) were used to identify age by speed interactions and age effects followed by post hoc t-tests in the case of significant interactions ($p<0.05$).

RESULTS

Self selected walking speed was statistically identical for young (1.53 ± 0.19 ms^{-1}) and old (1.46 ± 0.13 ms^{-1}) adults (t-test, $p>0.15$). Significant interaction ($p<0.05$) was seen in stride length. Old stride length was 2% shorter at slow but 7% shorter at fast speed. No interactions or age effects were observed for extensor angular impulses at any joint (figure 1). Significant interactions were seen in positive work at all joints (all $p<0.05$). Old had 18% and 24% greater hip work at slow and fast speeds; 27% and 32% less knee work at slow and fast speeds; and 2% and 22% less ankle work at slow and fast speeds. In short, as speed increased Old vs Young had greater increases in hip work and lower increases in knee and ankle work. Old also had on average 22% greater hip work and 29% less knee work at each speed (both $p<0.05$).

DISCUSSION

The identical self-selected walking speeds between age groups supports the premise that we tested highly mobile and functional Old adults. These novel joint torque data are the first demonstration of the retention of Young adult joint torque characteristics in Old adults during walking and we can conclude that Old adults who maintain a high level of gait performance walk with joint torques identical to those of Young adults. A distal to proximal

shift in muscle function was observed in joint powers and this effect increased with walking speed. The surprising result of statistically identical torques but different powers was produced through the subtle alterations in stride length. Old adults increased hip joint angular velocity (data not shown) to increase stride rate and maintain the test speeds with shorter strides. Thus Old adults shifted power and work production to the hip joint during all conditions and also to increase walking speed. The retention of torque but the reduction of power at knee and hip may be related to the reduced loss of muscle torque production but the larger loss of muscle power production observed isokinetically (McNeil et al, 2007).

SUMMARY

Highly mobile and functional Old adults retain the lower extremity joint torque patterns used by Young adults but show a distal to proximal shift in joint power production during walking. This mechanical plasticity increases with walking speed.
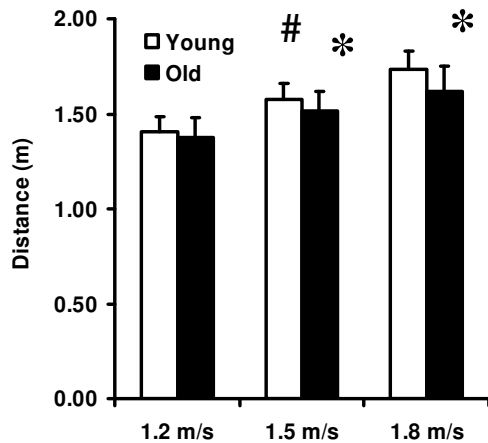

Fig 1. Mean (sd) stride lengths. #: significant age by speed interaction and *: significant age effect within a speed, both p<0.05.
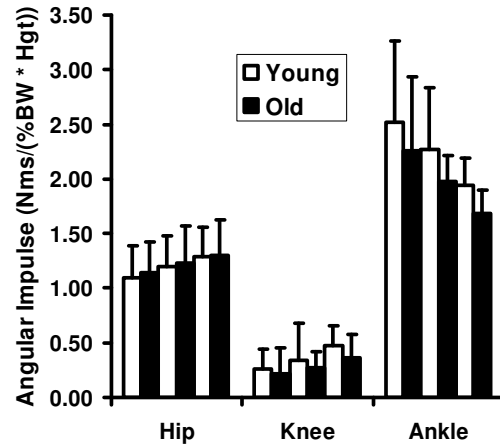
ACKNOWLEDGEMENTS

Fig 2. Mean (sd) extensor angular impulse across speeds (left to right: 1.2, 1.5, 1.8 m/s within each joint). No statistically significant age or interaction effects were observed.
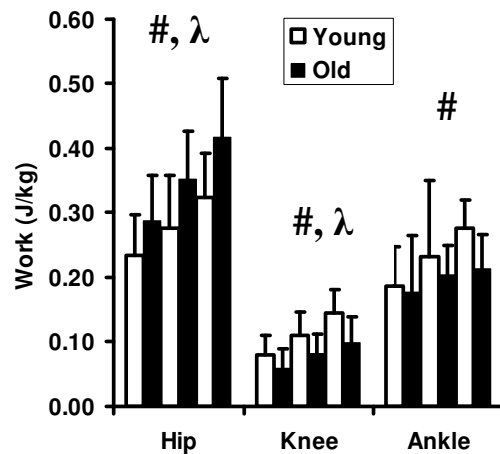
Fig 3. Mean (sd) positive joint work across speeds (left to right: 1.2, 1.5, 1.8 m/s within each joint). #: significant age by speed interaction and λ: significant age main effect, both p<0.05.

REFERENCES

DeVita, P et al. (2000). *J Appl Physiol*, 88: 1804-1811.

Graf, A et al. (2005). *Arch Phys Med Rehab*, 86: 2177-2183.

Kerrigan D et al. (1998). *Arch Phys Med Rehab*, 79: 317-322.

McNeil C el al. (2007). *J Appl Physiol,* 102:1962-1968.

EFFECT OF SPEED ON EMOTION-RELATED KINEMATICS DURING WALKING

Rebecca Edgeworth, Brendan Keen, Elizabeth Crane, and Melissa Gross
Department of Movement Science, University of Michigan, Ann Arbor, MI, USA
mgross@umich.edu URL: http://sitemaker.umich.edu/mgrosslab

INTRODUCTION

Emotion can be expressed through multiple physiological channels including face, voice, autonomic responses, and through the body. A recent study on the effect of emotion on gait kinematics suggests that high arousal emotions (e.g., anger) are associated with an increased speed and stride length compared to low arousal emotions (e.g., sadness), and that joint kinematics change in characteristic ways when specific emotions are expressed (Gross et al., 2007). Because others have demonstrated that knee, hip, and lumbo-pelvic angles change with walking speed (Saunders et al., 2005; Kirtley et al., 1985; Crowninshield et al., 1978), it is important to separate the effects of gait speed and emotion expression on gait kinematics. The purpose of this study was to systematically test the effects of speed and felt emotion on joint kinematics during gait.

METHODS

Twenty university students (50% females; 19.7 ± 1.6 yrs) participated after giving informed consent form. Participants were asked to recall an experience in which they felt one of three target emotions (anger, sadness, neutral), and then to walk across the lab (5 m). Participants performed three trials for each emotion in a block. Next, participants were asked to walk at speeds that matched the target emotion trials but without any particular feeling. Participants were asked to adjust their walking speed until they matched the speed criterion (<6% of their average target emotion speed). Pre and post-baseline trials were also recorded. After each emotion or speed trial, walkers rated the intensity of 9 emotions (3 target; 6 non-target) using a 5-item Likert scale. Only trials in which participants felt the target emotion with at least moderate intensity were included in the kinematic analysis.

Whole body motion data were acquired using a video-based, 6-camera system. Side view video was recorded simultaneously with the motion data. Walking speed was calculated using a photocell system and Lab View software. Marker coordinate data were filtered at 6 Hz. Gait parameters and postural and limb angular data were calculated using Visual 3D software. Stride length and velocity were normalized by body height. A linear mixed model with random effects of walker and fixed effects of emotion, speed and gender was used to model means on the response variables ($p<0.05$). Post hoc pair-wise comparisons with Bonferroni correction were used to detect differences in emotions and speeds.

RESULTS

Walkers felt the angry and sad emotions at levels of at least "moderate" intensity in all of the emotion trials. In the speed-matched trials, walkers reported feelings similar to their neutral emotion trials.

On average, gait speed increased 24% (range=6-59%) in angry trials compared to neutral trials. Gait speed in angry trials ranged from 1.2-1.9 m/s. The difference in gait speed between angry and speed-matched trials was 2.0% (range = 0.3-5.2%).

On average, gait speed decreased 8% (range=10-26%) in sad trials compared to

neutral trials. Gait speeds in sad trials ranged from 0.8-1.1 m/s. The difference in gait speeds between sad and speed-matched trials was 2.2% (range = 0.2-5.4%).

Gait velocity, cadence, and stride length were affected by emotion but were not different between target emotion and corresponding speed-matched trials (Table 1). Velocity and stride length were greater for the high activation emotion (anger) than for neutral or sad. Emotion-based velocity changes were due primarily to changes in cadence rather than stride length.

Preliminary analysis of joint angular data showed the differences expected for changes in speed. That is, with increasing speed, range of motion increased in hip flexion, shoulder flexion, elbow flexion, trunk rotation, and trunk tilt.

Emotion did not affect limb variables such as elbow flexion, shoulder flexion and hip flexion. However, postural variables were significantly different between emotions and between target emotion and corresponding speed-matched trials. In sad trials, the neck was 7.4, 8.7, 11.1, 8.2 deg more flexed than in angry, angry speed-matched, neutral, and sad speed-matched trials, respectively. Similarly, range of motion for trunk lateral tilt was 1.9, 2.5, 3.0, and 3.5 deg greater in angry than in angry speed-matched, neutral, sad, and sad speed-matched trials, respectively.

DISCUSSION

Bodily expression of angry and sad emotions was associated with changes in both gait parameters and joint kinematics. Changes in gait parameters were consistent with changes in gait speed associated with emotion expression and thus were not explained by some other, emotion-specific effects. Similarly, joint kinematics for upper and lower extremity motions during walking changed with gait speed and were similar in the target emotion and corresponding speed-matched trials.

Differences in some postural variables emerged that were dependent on emotion expression alone. It may be that changes in limb motions with emotion expression are constrained by task requirements of gait, especially as speed changes, but that postural variables were less biomechanically constrained by gait requirements and thus were more available for emotional expression during walking.

REFERENCES

Crowninshield RD et al. (1978). *Clin. Orthop. Rel. Res.*, 132: 140-144.
Gross, MM et al. (2007). *Proc. Ann. Mtg. Am. Soc. Biomech.*, Palo Alto, CA.
Kirtley C et al. (1985*). J. Biomed. Eng.* 7: 282-288.
Saunders SW et al. (2005). *Clin. Biomech.*, 20: 784-793.

Table 1. Effect of each emotion and speed matched trial on gait parameters (mean ± SD).

Gait Parameter	Anger		Sadness		Neutral
	Emotion	**Speed-Matched**	**Emotion**	**Speed-Matched**	
Velocity (m/s)	1.52±0.23[1]	1.48±0.22[1]	1.12±0.21[2]	1.14±0.20[2]	1.22±0.17[2]
Cadence (steps/min)	121.7±9.6[1]	119.2±11.1[1]	106.4±11.5[2]	106.2±11.2[2]	111.3±10.3[1,2]
Stride Length (m)	1.49±0.14[1]	1.48±0.11[1]	1.27±0.24[2]	1.28±0.11[2]	1.31±0.09[2]

[1] Significantly different from sad trials
[2] Significantly different from anger trials

DETERMINATION OF SUBJECT-SPECIFIC MECHANICAL PROPERTIES OF INDIVIDUAL ANKLE JOINT MUSCLES

Christopher J. Hasson, Ross H. Miller, and Graham E. Caldwell
University of Massachusetts Amherst, MA, USA, *cjhasson@kin.umass.edu*

INTRODUCTION

The mechanical properties of human muscles govern their force response to neural commands, and thus have a profound effect on human movement. Due to redundancy in the human muscular system, the mechanical properties of individual muscles are difficult to measure *in vivo,* with direct measurement possible only with highly invasive techniques (Komi *et al.* 1987). While such methods produce accurate data, they can only be applied to animal models or in rare human cases. A less invasive method is to collect data on the properties of whole joints and use modeling and optimization techniques to estimate individual muscle properties (Caldwell & Chapman 1991; Garner & Pandy 2003). With this approach, subject-specific measures are combined with data from the literature to compute muscular properties. Of importance is the need to use as many subject-specific measures as possible, because muscle mechanical properties change with training, disuse, aging, and disease.

Therefore, the purpose of this study was to develop a method that integrates joint and muscle measurements with modeling and optimization techniques to estimate the subject-specific mechanical properties of individual muscles controlling the ankle joint.

METHODS AND PROCEDURES

Dynamometer Experiments
Three male subjects (27-29 yrs) produced maximal effort dorsi- and plantarflexor torque sequences across a range of isometric ankle angles and isovelocity angular velocities. EMG was recorded from the tibialias anterior (TA), gastrocnemius (GA), and soleus (SO) muscles. From these trials subject-specific isometric torque-angle (Tθ) and dynamic torque-angular velocity (Tω) relations were determined (Caldwell & Chapman, 1991).

Muscle Imaging
For each subject, TA, GA, and SO muscle volumes were computed from cross-sectional areas measured from serial axial magnetic resonance images (MRI) of the entire leg. Physiological cross-sectional areas (PCSAs) were estimated by dividing the volumes by fiber lengths reported in the literature. Ultrasound imaging was used to assess internal muscle elasticity during 30 s ramped isometric dorsi- and plantarflexion trials. Displacements of points on the deep muscle aponeuroses were plotted against measured ankle torque to create torque-extension (TΔL) relations for ankle dorsi- and plantarflexion.

Modeling, Simulation, and Optimization
A musculoskeletal model of the ankle joint was used to simulate the dynamometer experiments. Muscle dynamics were represented by two-component models (Hill 1938), consisting of contractile (CC) and series elastic (SEC) components. CC behaviour was characterized by force-length (FL) and force-velocity (FV) relations, while the SEC compliance was represented by a nonlinear force-extension (FΔL) relationship.

First, model FL and FΔL parameters were optimized through isometric simulations that tried to match the experimental Tθ and TΔL relations, with GA and SO relative force capabilities constrained by their PCSA sizes. CC FV parameters were then optimized in isovelocity simulations that tried to replicate the experimental Tω relations, with model kinematics and excitation onset times based on dynamometer and EMG data, respectively.

RESULTS AND DISCUSSION

The root-mean-squared error between the optimized model and experimental Tθ and Tω data averaged 0.63 ± 0.47 Nm (Mean ± SD). For all subjects, the only area where the model and experimental data did *not* closely match was for eccentric dorsiflexion (*Fig. 1*). This may be because there were more concentric data points available, biasing the optimization. Plantarflexor Tω data matched better because there were twice as many free muscle parameters to optimize.

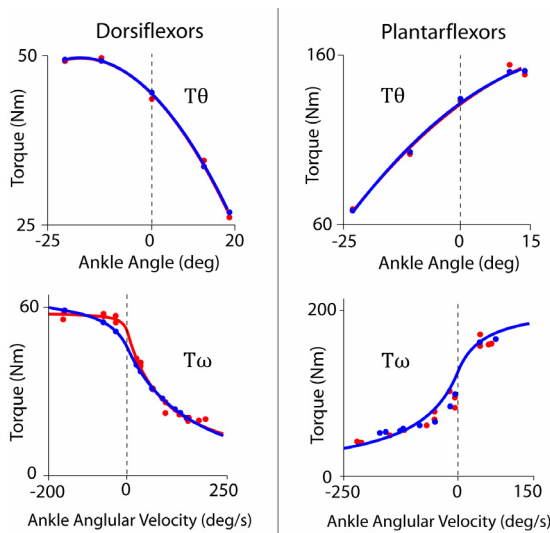**Figure 1.** *Experimental (red) and model (blue) Tθ and Tω curves for Subject 3 (S3). (+θ DF)*

Optimized muscle properties are shown for one subject in *Fig. 2*. On average, the extension of the TA FΔL at P_0 (7.5%) was larger than the GA (6.7%) and SO (6.9%). The FL parabola was narrowest for TA (0.77-1.23 L_0), and wider for the GA (0.75-1.25 L_0) and SO (0.72-1.28 L_0). Coefficients [a/P_0, b/L_0] defining the FV relation averaged [0.1, 0.58] for TA, [0.5, 2.0] for GA, and [0.55, 0.3] for SO. Optimized P_0 values (*Table 1*) were lower than Gerritsen et al. (1998), who reported values of 1528 N for TA, 1639 N for medial GA only, and 3883 N for SO.

This methodology has improved upon that described in Garner & Pandy (2003) by including subject-specific data from MRI and ultrasound imaging, and concentric and eccentric isovelocity dynamometer data. We are currently refining the methods in studies examining changes in muscle mechanical properties that occur with age.

Table 1. *Optimized model P_0 values and estimated PCSAs from MRI volume data.*

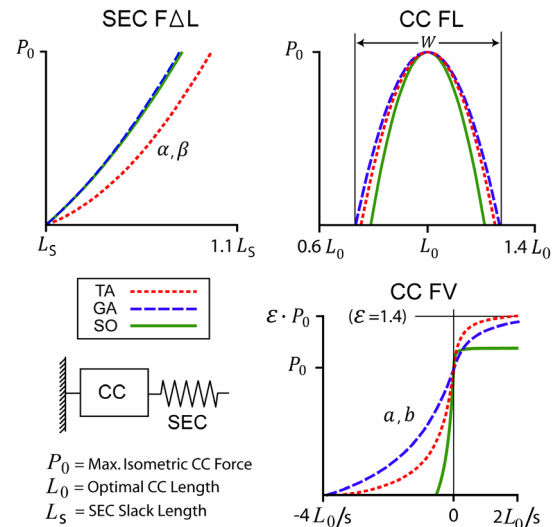| Muscle	Property	S1	S2	S3
TA	P_0 (N)	1182	790	1247
	PCSA (cm^2)	38	32	36
GA	P_0 (N)	1753	1300	1767
	PCSA (cm^2)	113	98	104
SO	P_0 (N)	2814	2154	2334
	PCSA (cm^2)	170	148	137

Figure 2. *Optimized model properties of the ankle joint muscles for Subject 3 (S3)*

REFERENCES

Caldwell GE & Chapman AE (1991) *Hum Mov Sci,* 10:355-92.

Garner BA & Pandy MG (2003) *Ann Biomed Eng*, 31:207-20.

Gerritsen KGM *et al*. (1998) *Motor Control*, 2:206-20.

Hill AV (1938) *Proc Royal Soc Lond*, 126B:136-95.

Komi PV *et al*. (1987) *Int J Sports Med*, 8:3-8.

ACKNOWLEDGEMENTS

Achilles Tendon Injury: Predisposing Factors in Men between 30 and 50 Years of Age

Kathryn Antle [1,3], David Hawkins [1,2, 3]

[1] Biomedical Engineering Graduate Group
[2] Section of Neurobiology, Physiology and Behavior, dahawkins@ucdavis.edu,
[3] Human Performance Laboratory
University of California, Davis CA 95616

INTRODUCTION

The Achilles tendon plays an important role in human locomotion and if injured can severely affect a person's movement capability and quality of life (Mazzone and McCue, 2002). Based on previous research findings and basic biomechanical principles, we hypothesized that people susceptible to Achilles tendon injury would have (1) a larger active muscle to tendon stiffness ratio than other individuals, (2) a larger maximum tendon stress and strain experienced during a maximum isometric ankle plantar flexion than other individuals, and (3) a muscle tendon unit (MTU) stiffness that deviates by more than 1 standard deviation relative to normative MTU stiffness values.

METHODS

The hypotheses were tested by quantifying and comparing the triceps surae muscle group and Achilles tendon mechanical properties between two groups of physically active male subjects, 30-50 years of age: one group experiencing pain in the midsubstance of the Achilles tendon, in one leg, during and after physical activity within the past year (n=5) and another group that had no prior history of Achilles tendon injuries (n=9). It was assumed that the asymptomatic leg of the injured group would have MTU properties reflective of the injured MTU prior to injury and could be compared to uninjured controls.

Subjects performed controlled isometric and eccentric ankle plantar flexion efforts in a custom testing chamber while force and muscle-tendon image data were collected simultaneously using a force transducer and a Hitachi EUB 6500 Ultrasound System (Hitachi Corporation) with dual EUP L53 linear probes. Force data were used to determine forces in the gastrocnemius-soleus-Achilles complex (GSATC). For the analysis, the posterior aspect of the lower leg was categorized into four regions: M_P - muscles proximal to the gastrocnemius muscle-tendon junction (MTJ), M_T - total muscle comprised of muscles proximal to the soleus MTJ, T_T - total tendon located between the osteotendinous junction (OTJ) and gastrocnemius MTJ, and T_F - free tendon located between the OTJ and soleus MTJ. Ultrasound images were digitized to determine muscle and Achilles tendon deformation during loading and Achilles tendon cross-sectional area. The average active muscle to tendon stiffness ratio, the Achilles tendon stress and strain during a maximum isometric ankle plantar flexion effort, and the MTU stiffness were calculated and compared between the uninjured control group and the asymptomatic leg of the Achilles tendon injured group.

An unpaired t-test was used to test the first and second hypotheses. The third hypothesis was tested by comparing individual MTU stiffness values to the range of MTU stiffness

values obtained from the uninjured group. A p-value of 0.05 was considered statistically significant while a p-value between 0.05 and 0.2 was considered marginally significant.

RESULTS

Hypothesis 1 (Injured individuals have a larger stiffness ratio of active muscle and tendon than uninjured individuals) was rejected. There were no significant differences (p>0.38) in the uninjured group $M_P:T_T$ (n=7, 0.88 ± 0.76) and $M_T:T_F$ (n=5, 0.49 ± 0.25) stiffness ratios compared to the injured asymptomatic group $M_P:T_T$ (n=5, 0.95 ± 0.58) and $M_T:T_F$ (n=3, 0.69 ± 0.25) stiffness ratios.

Hypothesis 2 (Injured individuals have a larger maximum tendon stress and strain experienced during a maximum isometric ankle plantar flexion than uninjured individuals) was partially supported. There was a statistical trend (p=0.170) between the mean T_T strain for the uninjured group (n=9, 1.80 ± 0.81 %) compared to the injured asymptomatic group (n=5, 2.69 ± 1.51 %). There was no statistical difference (p=0.215) in T_F strain of the uninjured group (n=9, 1.67 ± 1.45 %) compared to the injured asymptomatic group (n=4, 4.21 ± 3.71 %). There were no significant differences (p>0.75) in the uninjured group mean T_T (n=9, 14.9 ± 5.5 MPa) and T_F (n=9, 18.0 ± 6.8 MPa) stress values compared to the injured asymptomatic group mean T_T (n=5, 16.5 ± 13.8 MPa) and T_F (n=4, 22.2 ± 11.4 MPa) stresses.

Hypothesis 3 (Injured individuals have a muscle tendon unit (MTU) stiffness that deviates by more than 1 standard deviation relative to normative MTU stiffness values) was not supported. The MTU stiffness for the uninjured group (n=7) ranged from 66.6-131.3 N/mm. Two injured subjects had MTU stiffness values that fell outside of the ± 1 standard deviation range of the normal uninjured data, with values of 57.1 N/mm and 299.6 N/mm. Three subjects had values that fell within the normal range: MTU stiffness values of 67.0, 113.2, and 83.3 N/mm respectively.

DISCUSSION

The Achilles tendon plays a vital role in human locomotion and is commonly injured in physically active people 30-50 years of age. Identifying injury risk factors is an important first step for developing injury prevention interventions. Based on the results of this study, physically active people having a total tendon strain exceeding 2.4% during MVC may be at risk for an Achilles tendon injury. However, there was considerable variation in the data suggesting that identifying a person at risk for injury based on one or two MTU mechanical properties may not be realistic. We believe that quantifying Achilles tendon loading during daily activities and combining the loading history with the MTU mechanical properties may prove more useful in predicting injury risk than only quantifying MTU mechanical properties; the combination of data would provide a more complete biomechanical profile.

ACKNOWLEDGEMENTS

REFERENCES

Mazzone, M. F. and T. McCue (2002). *American Family Physician* 65: 1805-1810.

EVIDENCE FOR GOAL EQUIVALENT CONTROL IN TREADMILL WALKING

Joseph P. Cusumano[1*], Joby John[1], and Jonathan B. Dingwell[2]

[1]Department of Engineering Science & Mechanics, Penn State University, University Park, PA
[2]Department of Kinesiology, University of Texas, Austin, TX
*Email: jpc3@psu.edu

INTRODUCTION

Fluctuations in the repeated performance of human movements provide important information about the function and health of the neuromotor system (Osborne et al., 2005; Stein et al., 2005). In walking, reflexes are important for regulating gait cycle timing (Zehr & Stein, 1999). Thus, changes in appropriately defined measures of gait fluctuations should reflect changes in neuromotor control. This work uses the concepts of goal functions and goal equivalent manifolds (GEMs) (Cusumano & Cesari, 2006, Gates & Dingwell, 2008) to gain new insights into the nature and structure of neuromotor control humans use during treadmill walking.

GEM THEORY

The goal function for steady walking is
$$L_n - vT_n = 0 , \qquad (1)$$
Where v is treadmill speed, L_n is the length of stride n, and T_n stride time. The GEM is the set of all vectors (L_n, T_n) satisfying Eq. (1). We then decompose the perturbations $\boldsymbol{\delta}_n = (T_n, L_n) - (T^*, L^*)$ about the mean values (T^*, L^*) into components tangential and perpendicular to the GEM (Fig. 1) by
$$\boldsymbol{\delta}_n = \delta_T \hat{e}_T + \delta_P \hat{e}_P . \qquad (2)$$
The speed of stride n is $v_n = L_n/T_n$. Linearizing about the mean values and transforming into perpendicular and tangential coordinates, one can show that
$$e_n = \left(\sqrt{1 + v^2}/T^* \right) \delta_P , \qquad (3)$$
where $e_n = v_n - v$ is the goal-level error, i.e., the deviation in stride speed from treadmill speed. Thus, perturbations along the GEM, δ_T, to lowest order have *no effect on walking speed*, whereas perturbations perpendicular to
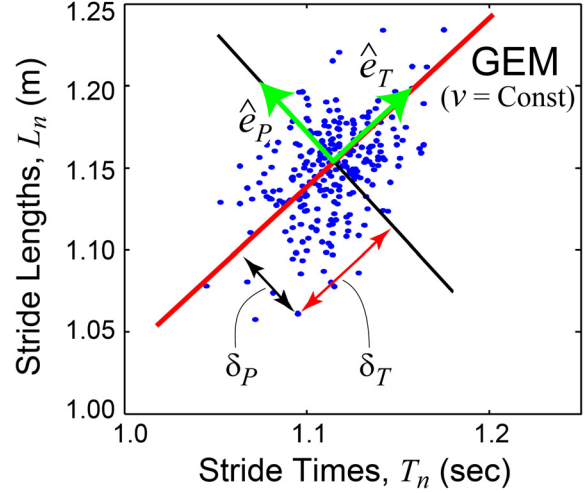

Figure 1 Stride times T_n and lengths L_n for each stride for a typical subject, showing the GEM and scalar deviations δ_P and δ_T.

the GEM, δ_P, do. This means fluctuations in walking speed scale with those of δ_P as:
$$\sigma_e/\sigma_P = \sqrt{1 + v^2}/T^* , \qquad (4)$$
where σ_e and σ_P are the standard deviations in stride speed and deviation δ_P, respectively.

We posit that the neuromotor control acts to drive the stride states onto the GEM, and are thus led to the following three hypotheses:

H1. The variability in δ_P will be significantly less than the variability in δ_T.

H2. The fluctuations in δ_P will show evidence of strong control, those in δ_T will show only weak control.

H3. The variability of walking speed will scale according to Eq. (4).

EXPERIMENTAL METHODS

17 healthy older (65-85 yr) subjects participated. Each subject walked on a level motorized treadmill (Woodway USA) at 5 speeds: preferred, ±10%, and ±20%. There were two
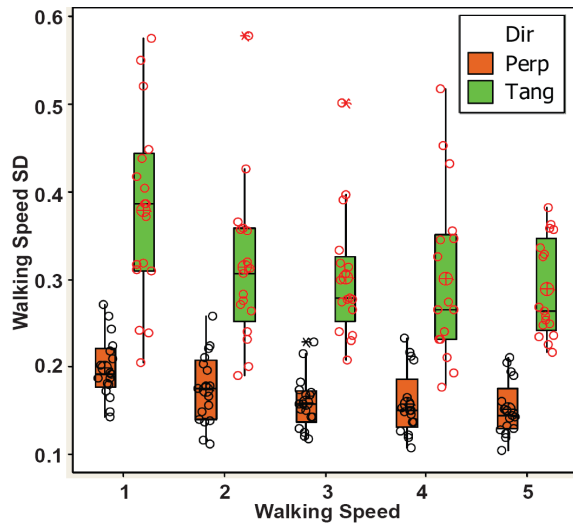
Figure 2 Walking speed variability perpendicular and tangent to the GEM.

Figure 3 Detrended fluctuation results perpendicular and normal to the GEM

5 min trials at each speed. Stride lengths and times were computed from movements of 5 reflective markers attached to each foot (Vicon, Oxford Metrics, Oxford, UK). The GEM for each subject was constructed using their average speed across all strides. The time series of perturbations δ_P and δ_T were computed for each subject via Eq. (2), as in Fig. 1.

Detrended fluctuation analysis (DFA; Peng et al., 1992) was used to quantify the statistical structure of stride-to-stride variations in the perturbation time series. DFA yields a scaling exponent, α: $\alpha = 0.5$ indicates a white noise time series; $\alpha > 0.5$ implies *persistent* correlations (i.e., deviations in one direction are more likely to be followed by deviations in the same direction); $\alpha < 0.5$ implies *antipersistent* correlations (i.e., positive and negative deviations are more likely to alternate).

RESULTS AND DISCUSSION

All subjects showed highly significantly ($p < 0.0005$) smaller variability perpendicular to the GEM than tangent to it (Fig. 2). Also, across all subjects, the DFA analysis yielded α values highly significantly different ($p < 0.0005$) in both directions: α tended to be under 0.5 for perturbations perpendicular to the GEM, indicating antipersistence consistent with error correcting control, whereas α was
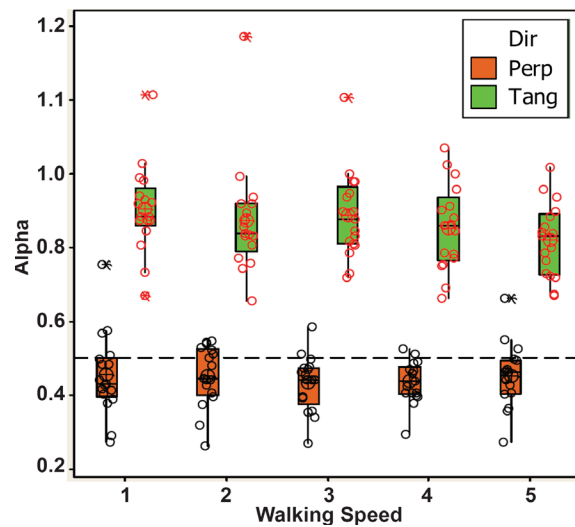
almost always over 0.5 for tangential perturbations, indicating long-range persistent correlations that are consistent with weak or indifferent control. Finally, the scaling behavior of Eq. (4) was satisfied by all subjects with an R^2 value in excess of 99%.

CONLUSIONS

All three hypotheses H1-H3 were satisfied, consistent with the theoretical task dynamical model developed using the concepts of goal-equivalence. The GEM was not found to be strictly "uncontrolled", however there is strong evidence that the GEM structure is used in maintaining a steady walking speed, at least for treadmill walking.

REFERENCES

Cusumano J.P. & Cesari P. (2006) *Biol. Cybern.*, 94:367-379.

Gates D.H. & Dingwell J. B. (2008) *Exp. Brain Research*, In Press.

Osborne L.C. et al. (2005) *Nature*, 437:412-416.

Peng C.K. et al. (1992) *Nature*, 356: 168-70.

Stein R.B. et al. (2005) *Nature Rev. Neurosci.*, 6:389-397.

Zehr E.P. & Stein R.B. (1999) *Prog. Neurobiol*. 58: 185-205.

Muscle activation timing influences muscle-tendon mechanical performance during cyclic contractions

Gregory S. Sawicki[1] Emanuel Azizi[1] and Thomas J. Roberts[1]

[1]Dept. of Ecology and Evolutionary Biology, Brown University, Providence, RI, USA
E-mail: gsawicki@brown.edu

INTRODUCTION

During cyclic movements (e.g. running, walking) muscle fibers at distal joints can produce force nearly isometrically, performing little mechanical work, while series elastic tendons store and return elastic energy in the interaction with the external environment (Roberts, Ishikawa). The 'tuned' elastic behavior of muscle-tendon likely requires a specific pattern (timing and amplitude) of muscle force output (Ettema). The goal of this study was to determine how the <u>timing</u> of muscle activation onset influences the mechanical performance of the contractile element (CE) in a compliant muscle-tendon (MT) undergoing a fixed sinusoidal length change. We hypothesized that as activation phase advanced from initial MT lengthening (i.e. 0% phase) the CE would shorten more and perform more positive mechanical work.

METHODS

We tested six bullfrog (*Rana catesbeiana*) plantaris-Achilles tendons *in vitro*. For each preparation, we used a muscle ergometer to drive the MT through a fixed sinusoidal length change ($\pm$ 4mm, 4 Hz) (**Fig 1.**) We set the rest length of the MT to correspond with the onset of passive MT force from an experimentally determined force-length curve. We attached a nerve-cuff to the sciatic nerve and stimulated the muscle using a 4V, 100 ms pulse train (0.2 ms pulses, 100 pps) with activation phases of -12.5%, 0% (onset of MT lengthening),12.5%, 25%, 37.5% and 50% of the cycle period (**Fig. 1**). We also collected a control condition with no muscle stimulation (NS).
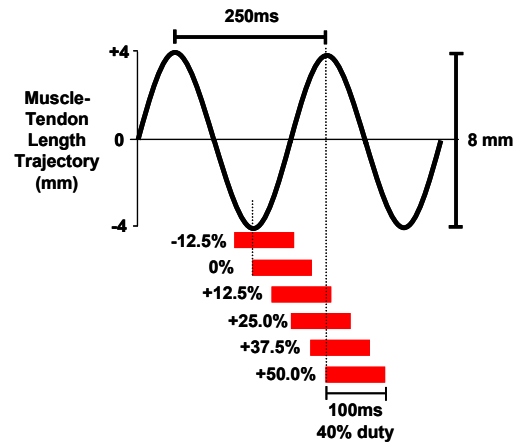

Figure 1. Schematic of experimental conditions. An ergometer maintained a sinusoidal (4Hz; $\pm$ 4mm) muscle-tendon length trajectory. We stimulated the muscle for 100 ms with activation phases ranging from -12.5% to 50% of the cycle period (red bars).

We recorded (1) MT force and length from the ergometer and (2) muscle fiber length from surgically implanted sonomicrometry crystals. To calculate CE length change we multiplied muscle fiber length by a gearing factor (~1.6) to account for the effects of muscle pennation. Series elastic element (SEE) length changes were computed as the difference between MT length (from the ergometer) and CE length (from sonomicrometry). Power was calculated as the product of force and velocity for each element. We integrated the positive regions of the power curves and divided by MT mass to obtain mass-specific MT and CE positive work over a cycle. We used a repeated measures ANOVA to determine if there were differences in CE length change over the MT shortening phase, CE positive work, MT peak force and MT peak power between activation phase conditions.

RESULTS

Activation phase had a significant effect on CE length change (ANOVA, p<0.0001). During MT shortening (50%-100% of the contraction cycle), the CE lengthened only slightly in the 0% phase condition (+0.3 ± 0.1 mm (mean ± s.e.)) but shortened considerably (-7.0 ± 0.4 mm) in the 50% phase condition (**Fig. 2C, 2D**). MT peak force was markedly higher (+324%) in the 0% phase condition when compared to the 50% phase condition (ANOVA, p<0.0001) (**Figs. 2A-C**). As a result, CE positive mechanical work increased then decreased as activation timing advanced from 0% to 50% phase (**Fig. 2E**). MT peak power was maximum (497.3 ± 18.6 W/kg) in the 0% phase condition and decreased significantly as phase advanced (ANOVA, p<0.0001) (**Fig. 2F**).

CONCLUSIONS

These results indicate that muscle activation timing is critical for exploiting the mechanical and energetic benefits of tendon elasticity. In a 'tuned' MT (i.e. 0% activation phase) effective tendon recoil allows maximum MT peak mechanical power to be achieved with very little CE mechanical work. These findings could be applied to improve the neuromechanical design of artificial muscle-tendon actuators for lower-limb powered orthoses and prostheses.

REFERENCES

Roberts, T.J. et al. (1997). *Science,* 275(5303):1113-1115.

Ishikawa, M. et al. (2005). *J Appl Physiol,* 99(2):603-608.

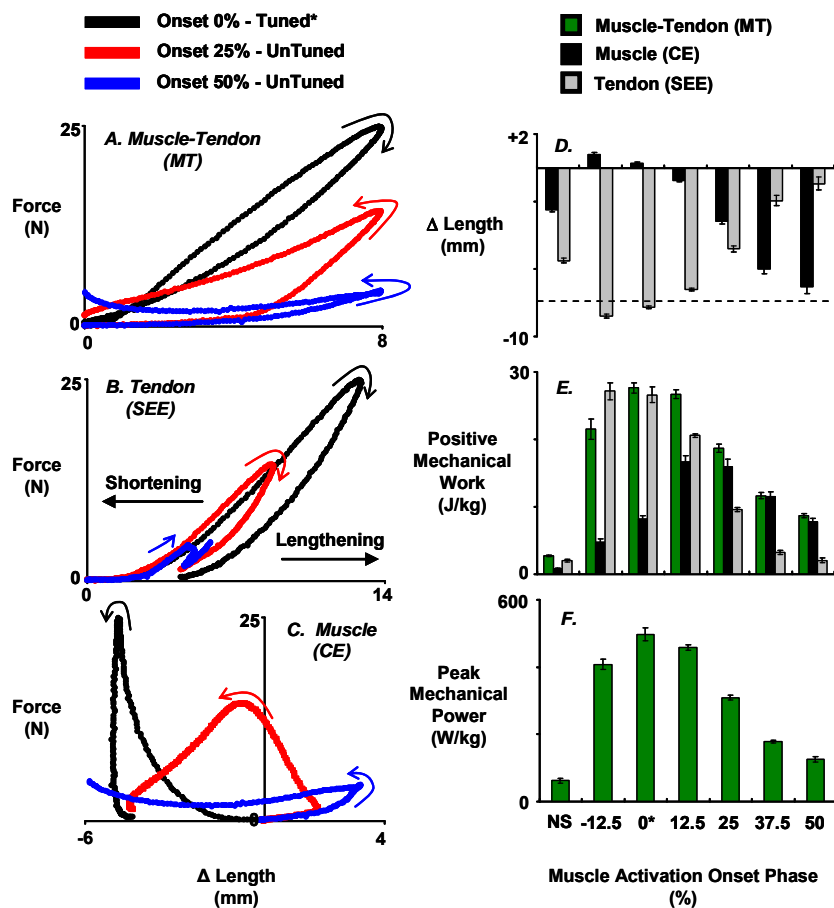**Ettema, G.J.C. (1996).** *J Exp Biol,* 199(Pt. 9):1983-1997.

Figure 2. (**Left Panel**) Force (N) versus length (mm) plots for the (**A**) muscle-tendon (MT) (**B**) tendon (SEE) and (**C**) muscle (CE) during one sinusoidal contractile cycle (0%-100%). Three activation phases (black=0%; red=25%, blue=50%) are plotted for a single *in vitro* muscle-tendon preparation. Negative length changes indicate shortening. Colored arrows indicate the time evolution of force-length state. Counter-clockwise loops indicate net positive work. (**Right Panel**) (**D**) Length change over 50%-100% of the MT length change cycle for the CE (black) and SEE (gray). Negative values indicate net shortening. Dashed horizontal line indicates MT length change (-8mm). (**E**) Mass specific positive mechanical work (J/kg) over 0%-100% of the MT length change cycle for the MT (green), CE (black) and SEE (gray). (**F**) Mass-specific (W/kg) peak mechanical power over 0%-100% of the MT length change cycle. In all subplots bars are mean ± standard error for six preparations for each muscle activation onset condition (-12.5%-50% phase) and the control (NS) condition. In the 0% phase condition the muscle stimulation onset coincides with initial MT lengthening (see Fig. 1).

A COMPARISON OF THE KINEMATICS OF LADDER CLIMBING USING RUNGS VS SIDE RAILS

Hogene Kim[1], Justin Young[2], Chuck Woolley[2], Tom Armstrong[1,2] and James A. Ashton-Miller[1,3]

[1]Department of Biomedical Engineering, [2]Department of Industrial & Operations Engineering, [3]Department of Mechanical Engineering, University of Michigan, Ann Arbor, Michigan, USA.
hogenek@umich.edu, URL: http://me.engin.umich.edu/brl/

INTRODUCTION

More than 20,000 American workers are injured, and over 100 die, every year as a result of falls from ladders (BLS 2005). Studies of the gait pattern of climbing on vertically tilted ladders have shown a large variation of the chosen method (McIntyre, 1983). 'Lateral gait' (i.e., synchronous ipsilateral hands and feet movement) and 'diagonal gait' (i.e., synchronus contralateral hand and foot movement) were reported as the most common climbing styles. However, an individual can change his/her climbing style even within the same ladder climb (Hammer 1992) . Both Dewar (1977) and Hakkinen (1988) reported the use of both ladder rungs and rails as handholds. Bloswick (1992) studied vertical fixed ladder climbing, but only with the use of rungs.

The goal of this study was to contrast and compare the kinematics of climbing a fixed vertical ladder using two different climbing strategies: grasping rungs or grasping rails.

METHODS AND PROCEDURES

A custom-made, instrumented, fixed vertical ladder 10' in length was constructed. Nine 16" wide rungs were spaced 12" apart (OSHA, 1910.27 Fixed Ladder standards). Ladder rungs and rails were 1-inch diameter cylindrical steel rods and were cleaned with steel wool before testing. The ladder rungs were attached to the ladder frame at the center post so the rungs could be mounted on 3-axis force and 3-axis moment transducers (AMTI® MC3 and ATI® Theta). Four of the rungs were instrumented – two for the feet and two for the hands. Twelve healthy subjects (6 males, 6 females, age: 21±2 years, height: 172±11cm, weight: 625.2±139.2 N and arm span: 150±4 cm) volunteered for this study. Subjects were instructed to climb a vertical fixed ladder at a comfortable speed using one of two climbing styles: grasping the rungs or the side rails. From a bipedal stance on the ground, subjects climbed 5 rungs, paused, and then return to the ground. Three repetitions of each treatment were conducted.

Bilateral optoelectric cameras (Optotrak 3020) recorded body kinematics at 100 Hz using 22 infrared markers placed on body landmarks including the head, acromion, lateral epicondyle, wrist, hand, greater trochanter, knee, malleolus, and feet. For the sake of brevity, we only report the descriptive statistics for the major joint motions. Paired, two-sided, t tests were used to compare joint motions in the two climbing styles, with $p < 0.05$ being considered significant.

RESULTS

Figure 1 shows data from one climbing movement cycle from a representative trial of a subject beginning a climb while grasping the side rails. The cycle starts with the onset of right knee and hip flexion and ends in full knee and hip extension after climbing one step. In general, hip and knee flexion are out of phase with elbow and shoulder extension.
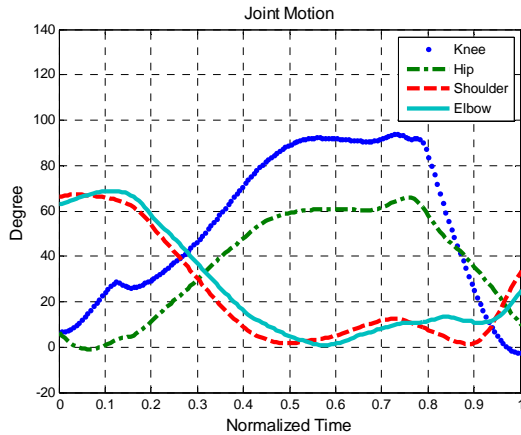
Figure 1. Sample data from a male showing contralateral style of vertical climbing using side rails. Positive (+) direction denotes flexion, negative (-) direction is extension.

This movement pattern was universally observed whether climbing with rungs or side rails in this study.

Mean (SD) range of joint motion data for one climbing cycle [mean (SD) time: 2.27 (0.35 s)] for the 12 subjects climbing with each climbing style (rung vs rail hand-holds) are shown in Table 1. There were no significant difference in the ranges of motion used, although less variability was observed in climbing with rungs than with the rails. Greater kinematic variability in hip joint motion is noticeable when climbing with side rails. Variability in lower limb use was generally smaller than that with the upper limb.

Joint	Climbing with center rungs N=10	Climbing with side rails N=10
Elbow	**24.1 (11.5)**	**29.8 (16.1)***
Shoulder	**38.8 (13.4)**	**36.8 (15.3)**
Hip	**55.0 (6.7)**	**54.7 (11.4)**
Knee	**56.7 (5.9)**	**53.9 (8.1)**

Table 1. Mean (SD) joint range of motion (in deg.) used for the two climbing styles.
* p = 0.139

DISCUSSION

Although Table 1 gives a summary of the kinemetic data by climbing style, systematic differences in anthropometry (height and arm span) between the males and females will have increased the data scatter in that table. Joint ranges of motion may well be determined by stature and rung spacing. In the future we hope to expand group sizes and investigate the effect of anthropometry, age, ladder inclination and rail design on the kinematic and kinetic variables.

SUMMARY

No significant differences were found in joint ranges of motion used to climb by grasping the rungs or the rails. Perhaps the kinematics were largely determined by rung spacing.

REFERENCES

BLS (2005). *Census of fatal occupational injuries summary.* Washington, DC, US Bureau of Labor Statistics: 1-3.
Bloswick, DS (1990). *Int J Ind Ergon.*, 6, 17-27.
Dewar, ME (1977). *Ergon*, 20 (1), 67-86.
Hakkinen, KK (1988). *J. Occup. Accid.* 10, 1-19.
Hammer, W (1992). *Safety Sci*, 15, 21-38.
McIntyre, DR (1983). *Hum. Mov. Sci.* 2, 187-195.
Vaughan CL (1992), *Dynamics of Human Gait*. Human Kinetics Publishers

ACKNOWLEDGEMENTS

DETERMINANTS FOR DIRECTION OF OBSTACLE AVOIDANCE DURING GOAL-DIRECTED LOCOMOTION

Michael E. Cinelli[1] and William H. Warren[1]

Department of Cognitive and Linguistic Sciences, Brown University, Providence, RI, USA
Michael_Cinelli@brown.edu

INTRODUCTION

What causes an individual to avoid a stationary obstacle or another person walking towards him/her to the left or right? Previous work has shown that environmental layout (Cinelli and Patla, 2007), goal location relative to an obstacle (Fajen and Warren, 2003), or direction of movement of the obstacle determine the direction that an individual will circumvent an obstacle. The purpose of this study was to determine what causes and individual to change his/her travel path to the right or left when approaching and avoiding an obstacle placed in-line with (or close to) a goal. The three hypotheses tested were: 1) when the obstacle's location is off-center with the goal, the individual will avoid to the opposite side; 2) as soon as individuals get within a certain distance of the obstacle, they will avoid towards the side opposite that of their stance leg; and 3) individuals will avoid the obstacle towards the side of their dominant hand, foot, or eye.

METHODS AND PROCEDURES

Participants walked along a 9m path towards a goal (i.e. a pole 2.5m tall) straight ahead and had to avoid an obstacle (i.e. a pole 2m tall) placed 5m from the start. The obstacle was placed in one of 7 positions in the horizontal plane (i.e. inline with the goal, ± 2.5cm, ± 5cm, or ± 7.5cm from middle). Each participant performed 56 completely random trials (i.e. 8 trials x 7 obstacle locations). In order to eliminate learning and to keep each trial novel, four start locations were used, each separated by 20cm in the A/P direction and randomly selected at the start of each trial, and the participants were not told which foot to start with.
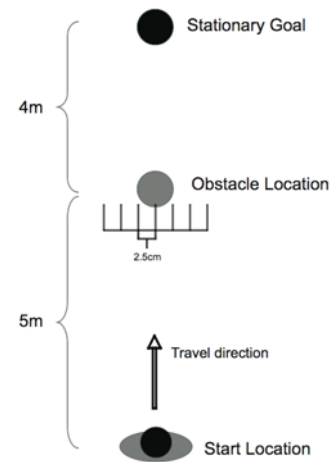

Figure 1- Experimental set-up. The study took place in a large space with no environmental constraints

The participants were instrumented with LCD goggles, which were opaque at the start of each trial but became transparent after the participant walked for 2s (i.e. 1.5m). The LCD goggles were used to prevent the participants from having prior knowledge of the obstacle's location and to elicit a natural reactive response. Kinematic data was collected and sampled at 60Hz using an Optotrak Certus Motion Capture System (NDI, Waterloo, ON). Markers were placed on the left and right shoulders, C7, and T10 (to calculate torso COM displacement) as well as markers on the right and left foot (to determine their locations). M/L torso COM location for the first 1s of each trial was averaged and the point when the COM fell outside 2SD of the average was considered to be the point at which a change in travel path had taken place and the direction of the new travel path. At the end of the study, participants filled out *Waterloo Handedness and Footedness Questionnaires* and tested for eye dominance.

RESULTS

The data presented is only preliminary results from four participants.

Hypothesis 1: The results did not show that obstacle location relative to the goal's position determined direction of avoidance (Fig. 2)
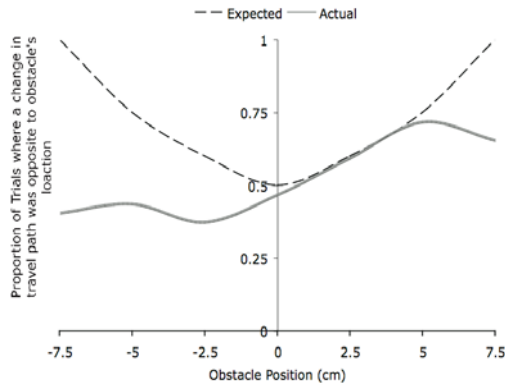

Figure 2- Expected versus actual results if the location of the obstacle with respect to the middle affected the change in direction of travel path.

Hypothesis 2: On average the participants avoided the obstacle when they were 3.56m from it, however, their stance leg did not determine the side of avoidance (Table 1).

Table 1- Average distance (SD) from obstacle when a change in travel path was initiated and the proportion of trials that the side of deviation was opposite to the stance foot for all participants.

Participant	Distance from Obstacle (cm)	Proportion of trials
BS	355.56 (35.2)	0.47
EC	391.45 (98.1)	0.5
GR	352.11 (129.6)	0.55
JV	327.59 (96.1)	0.36

Hypothesis 3- All participants were right-hand dominant, two were right-foot dominant, and another two were right-eye dominant. The results showed that eye dominance has the largest impact on the side of avoidance. Regardless of the obstacle's location, over 70% of avoidances were towards the side of the dominant eye, whereas the other two body segments were at chance (i.e. 50%) (Fig.3).
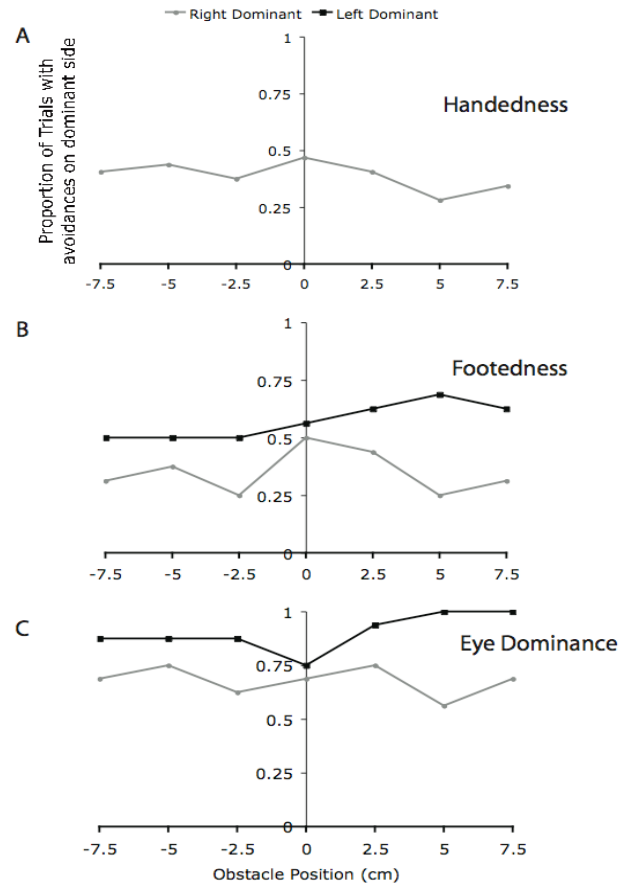

Figure 3- Determining which body segment lateralization (hand, foot, eye) best predicts which direction an individual will change his/her path.

DISCUSSION

Although the study is in its infancy, it appears as though eye dominance plays a crucial role in determining the direction of avoidance. Even though, (perceptual view) a change in the lateral position of the obstacle or (biomechanical view) stance leg at time of avoidance should have a large influence. Therefore, individuals may always choose to avoid obstacles or other individuals on the side of their dominant eye, sometimes this works out well and other times it does not.

REFERENCES

Cinelli ME and Patla AE. (2007). *Gait & Posture,* 26:186-93
Fajen, BR and Warren, WH. (2003). *J Exp Psychol Hum Percept Perform,* 29:343-62
Gerin-Lajoie, M et al. (2005). *Motor Control,* 9: 242-69

ACKNOWLEDGEMENTS

DESIGN OF LOW STIFFNESS FLOORS FOR PREVENTING HIP FRACTURES IN HIGH RISK ENVIRONMENTS: COMPARISON OF FORCE ATTENUATION AND INFLUENCE ON BALANCE

Andrew C. Laing[1] and Stephen N. Robinovitch[2]
[1] Ph.D. Candidate, School of Kinesiology, Simon Fraser University, Burnaby, BC, Canada, alaing@sfu.ca
[2] Associate Professor, Schools of Kinesiology and Engineering Science, Simon Fraser University, Burnaby, BC, Canada, stever@sfu.ca

INTRODUCTION

The prevention of hip fractures in the elderly is a public health priority. 90% of fractures are due to falls, and low stiffness flooring may be an effective means for preventing fractures in high-risk environments. However, this would only be true if such floors can attenuate impact force sufficiently, without impairing balance so much that falls would be more likely. Previous studies have shown that padded carpeting can attenuate peak impact forces by 15%, without causing a measurable impairment in balance (Gardner et al., 1998, Maki and Fernie 1990, Dickinson et al. 2002). In the current study, we extended this line of enquiry to examine the effect of a wider range of floor stiffness on (a) peak impact force during a simulated sideways fall on the hip, and (b) measures in healthy elderly women of postural stability during daily activities.

METHODS AND PROCEDURES

We investigated five floors. The 'Rigid' floor was a 2 mm thick layer of dense natural rubber used in institutional settings. The SmartCell anti-fatigue mat (2.54 cm thick) and SofTile playground surface (10 cm thick) are composite rubber floors comprised of a continuous surface layer bonded on elastic columns. The Firm Foam (density = 32.0 kg/m^3) and Soft Foam (density = 22.2 kg/m^3) floors consisted of 10 cm thick open-cell polyurethane foams of the type commonly used in gymnasium mats.

We used a hip impact simulator, consisting of an impact pendulum and surrogate pelvis (Laing et al., 2006), to measure the attenuation in peak force applied to the femoral neck provided by each floor, for impact velocities of 2, 3, and 4 m/s (simulating falls of low, medium, and high severity, respectively).

We also acquired measures of balance from fifteen healthy elderly women (mean age = 75.0 (8.1) yrs) on each floor. These included Get Up and Go (GUG) test time (Podsiadlo and Richardson, 1990), postural sway during quiet stance (quantified by range and velocity of the centre-of-pressure in the anterior-posterior direction), and success in recovering balance in five repeated backwards floor translations. We also used a questionnaire to acquire participant ratings of balance confidence and practicality for each floor.

RESULTS

The mean attenuation in peak femoral neck force ranged from 24.5% by SmartCell to 76.6% by Firm Foam (Table 1). When compared to the Rigid floor, the SmartCell and SofTile caused no impairments in ability to recover balance and GUG time, and were ranked as high for balance confidence and practicality. While all floors affected postural sway during quiet stance, the effect was most dramatic for Firm Foam, which caused more than a doubling in sway range and velocity.

	Rigid	SmartCell	SofTile	Firm Foam	Soft Foam
force attenuation (%)[a]	0	24.5 (8.4)	47.2 (3.5)	76.6 (11.3)	52.4 (14.1)
GUG time (s)	11.7 (1.9)	11.4 (1.9)	12.0 (2.4)	14.0 (3.2)[b]	14.0 (3.1)[b]
recovery success	0.79 (0.36)	0.85 (0.32)	0.79 (0.33)	0.45 (0.42)[b]	0.67 (0.38)
sway range (mm)	15.1 (4.0)	18.7 (5.5)[b]	20.3 (4.4)[b]	33.3 (6.2)[b]	23.4 (5.5)[b]
sway velocity (mm/s)	8.0 (2.4)	9.1 (3.2)	9.3 (2.3)[b]	20.3 (6.5)[b]	12.8 (2.4)[b]
balance confidence	9.5 (1.1)	9.6 (0.6)	9.3 (1.5)	5.4 (2.8)[b]	5.5 (3.1)[b]
practicality	9.1 (2.1)	8.5 (1.8)	8.2 (2.4)	2.6 (2.6)[b]	1.9 (2.4)[b]

Table 1: Mean values (with standard deviations in parentheses) of outcome parameters for each of the five floors. [a] all floors significantly different from each other. [b] significantly different from the Rigid floor.

DISCUSSION

Our results suggest that currently available flooring systems (e.g. the SofTile playground system) can attenuate peak femoral impact force by up to 47%, while causing only minimal effects on postural stability in elderly women. Further reductions in floor stiffness, while leading to greater force attenuation, caused substantial negative effects on postural sway, balance recovery ability, and balance confidence.

The force attenuation provided by the floors we studied was significantly larger than the 4–15% observed for carpet (Gardner et al., 1998, Maki and Fernie, 1990), and the 12-24% observed for wearable hip protectors tested on our hip impact simulator (Laing et al., 2006). In addition to attenuating force more effectively than hip protectors, low stiffness floors are not dependent on user compliance, and likely reduce the risk of fall-related upper extremity fractures and head injuries, in addition to hip fracture.

SUMMARY

Two of the four floors we examined substantially reduce the force applied to the hip during simulated sideways falls, and are unlikely to increase fall risk compared to typical rigid floors. Furthermore, these floors were rated as practical by a sample of elderly women. A simple cost-benefit analysis projects a pay-off period of 1.5 years for installing such floors in high-risk areas of nursing homes, assuming a direct cost of $26,500 CAD per hip fracture (Wiktorowicz et al., 2001), differential material costs of $134 CAD/m^2 and a 50% reduction in hip fracture incidence. Overall, this comprehensive biomechanical study supports the value of low stiffness floors for preventing hip fractures in high risk environments.

REFERENCES

Dickinson, JI et al. (2002). *Gerontologist* 42:552-559.
Gardner, TN et al. (1998). *Med Eng Phys*, 20:57-65.
Laing, AC et al. (2006). *Osteoporos Int*, 17:S231.
Maki, BE and Fernie, GR (1990). *App Ergon*, 21:107-114.
Podsiadlo, D and Richardson, S (1991). *J Am Geriatr Soc*, 39:142-148.
Wiktorowicz, ME et al. (2001). *Osteoporos Int*, 12:271-278.

ACKNOWLEDGEMENTS

Direction-Dependent Weighting of Vision for Balance During Walking

Shawn M. O'Connor and Arthur D. Kuo

University of Michigan, Ann Arbor, MI, USA
E-mail: smoconno@umich.edu

INTRODUCTION

Humans rely on information from vision, vestibular sensors, and proprioceptors to stabilize balance during walking. Not only is information from multiple modalities weighted differentially, but even a single modality such as vision can contain multiple attributes that may themselves be weighted differentially. Vision is sensitive to multiple directions of visual field motion, and the importance of these directions may depend on the degree of feedback stabilization that must be provided by the central nervous system. Identification of those attributes of vision most critical for walking balance could contribute to assessment and rehabilitation of individuals with poor sensorimotor function. We investigated whether visual motion cues are differentially weighted in the anterior-posterior and medio-lateral directions, using a virtual reality environment to apply unexpected perturbations to the visual field, and using foot placement variability as an indicator of active feedback..

METHODS

Three-dimensional walking models indicate that gait may be passively stable in the anterio-posterior (A-P) direction but unstable in the medio-lateral (M-L) direction (Kuo 1999). Visual and other sensory information pertaining to side-to-side movement may therefore be more important for actively controlling balance than that for fore-aft movement. This active control is largely achieved by corrective placement of the leading foot at heel-strike.

Six healthy subjects (aged 25 ± 2.6 yrs., mean ± s.d.) provided consent and participated in this study. Subjects walked on a split-belt instrumented force treadmill. A virtual reality display (Figure 1) presented a visual field resembling a virtual dark hallway tiled with randomly placed white rectangles (Warren 1996). Head tracking was not used. During all conditions, subjects walked at a constant speed of 1.25 m/s while viewing a speed-matched hallway. The visual field was perturbed with unexpected oscillations of the visual flow in the horizontal plane, at six uniformly distributed angles relative to M-L direction. There was also a control condition with no oscillations.
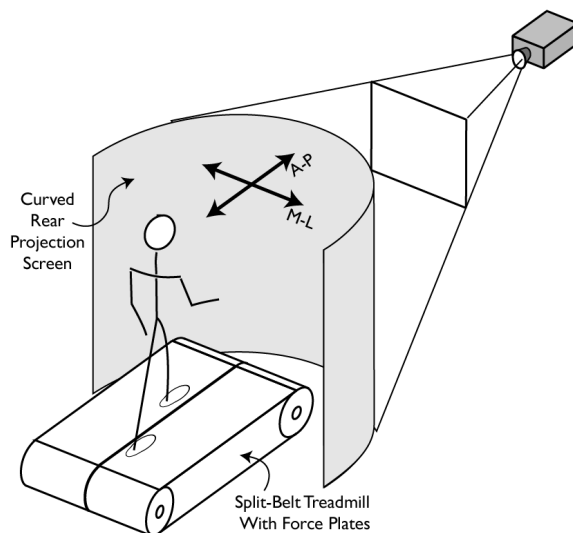

Figure 1: Depiction of experimental setup with instrumented force treadmill and curved rear projection screen.

The oscillations were composed of a sum of sine waves at frequencies of 0.058 0.135, 0.250, 0.442, and 0.827 Hz with a total peak to peak amplitude of 40 cm. The effect of the oscillations was assessed by measuring root-mean-square (RMS) variability in step length and step width recorded from individual limb COP estimated at mid-step over at least 300 steps.
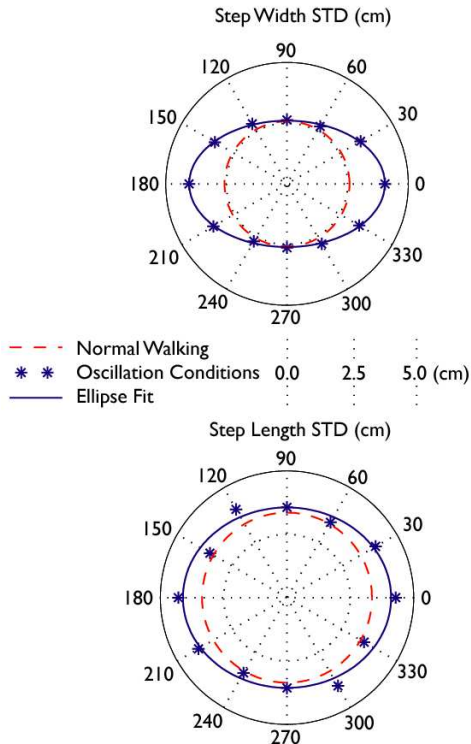

Figure 2: Effect of visual oscillation direction on step width and step length variability averaged across subjects.

RESULTS AND DISCUSSION

To test for differential directional sensitivity to vision, we calculated subject specific ellipses summarizing foot placement variability as a function of oscillation direction (see polar plot, Fig. 2). Each ellipse was determined through linear regression and characterized by an eccentricity, defined as the ratio of the distance between the foci to the length of the major axis (a circle has zero eccentricity).

Eccentricity was significantly greater than zero in the M-L direction for both step length ($P<0.001$) and width ($P < 0.001$) variability.

A significant increase in step width variability for M-L visual perturbations, with no corresponding change in step length variability for A-P perturbations, indicates that visual information pertaining to side-to-side movement may be more useful for controlling balance during walking than information about fore-aft movement.

We also noted that M-L perturbations had a larger effect on step length variability than A-P perturbations, suggesting that visual information in the M-L direction may contribute to walking balance in all directions. This may be explained by mechanical coupling between step width and step length, found in three-dimensional passive dynamic walking models (Bauby & Kuo 2000).

SUMMARY/CONCLUSIONS

Visual sensory information is differentially weighted to actively control medio-lateral balance during walking, which appears to be unstable. Anterio-posterior information is de-emphasized, perhaps due to passive stability of walking in that direction.

REFERENCES

Kuo, A. D. (1999). *Int. J Robotics Research*, **18**, 917-930.
Warren, W.H. et al. (1996). *J Exp. Psych.,* **22**, 818-838.
Bauby, C.E., Kuo, A.D. (2000). *J. Biomechanics.* **33**, 1433-1440.

ACKNOWLEDGEMENTS

VERTICAL STIFFNESS DURING THE DOUBLE SUPPORT PERIOD OF WALKING

John R. Rebula, Shawn M. O'Connor, and Arthur D. Kuo

University of Michigan, Ann Arbor, MI, USA
[jrebula\smoconno\artkuo]@umich.edu

INTRODUCTION

Bipedal walking is often modeled with an inverted pendulum, but running is usually described as a mass spring system that may be characterized with a vertical stiffness (McMahon and Cheng, 1990). This stiffness models the redirection of the body center of mass (COM) velocity during ground contact of running. The double support phase of walking also redirects the COM velocity, and might also resemble a mass-spring system. In this study, we examined the double support phase of human walking in this context, calculating a vertical stiffness analogous to that of running. We calculated the vertical stiffness of humans during the redirection phase of walking and running, over a range of speeds. We found that double support during walking redirects the COM velocity vertically in a spring-like manner not unlike ground contact during running.

METHODS AND PROCEDURES

We measured individual limbs ground reaction forces of five ($N = 5$) healthy humans walking and running on a split-belt force instrumented treadmill. Subjects each walked at a range of speeds from 0.75, 1.0, 1.25, 1.5, 1.7, and 2.0 m/s. Running trials were performed at 2.0, 2.3, and 2.6 m/s.

For each subject, ground reaction forces were measured over 5 steps and integrated twice to yield velocity and position. Periodicity constraints were used to reduce drift, and data were also low-pass filtered at 25Hz. For walking, the double support period was demar-cated by the times when both legs had substantial vertical ground reaction force. For each double support period, a vertical stiffness was found by fitting a line to the vertical force plotted against the vertical displacement (see Fig. 1). The same method was used to calculate stiffness of the stance phase of running, where the stance phase was defined by the period of ground contact. All data were non-dimensionalized using body mass, gravity acceleration, and leg length.

We considered an additional parameter to describe a running gait, Q, the fraction of a vertical oscillation period spent in the redirection phase. Previous work (McMahon and Cheng, 1990) includes predictions of Q for a spring mass running model,

$$k_{vert} = \frac{4\pi^2 Q^2}{t_c^{\,2}} \quad \textbf{(1)}$$

where t_c is the non-dimensionalized time of contact. We used the vertical stiffness and duration of double support to calculate Q for walking using the same equation, for comparison with running.

RESULTS

We found that double support yielded a fairly linear force vs. displacement (Fig. 1) which could be characterized reasonably well with a linear fit (average R^2 of .695). Vertical stiffness of the double support phase in walking increased with walking speed (see Fig. 2). This can be explained by the need to redirect similar vertical velocities during increasingly shorter redirection periods. Also, at comparable speeds, the vertical stiffness of
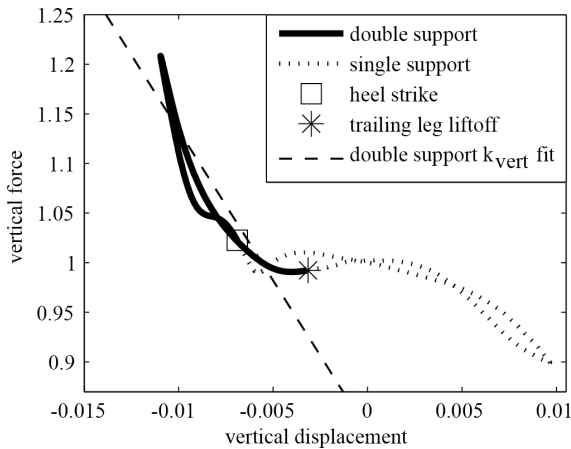
Figure 1. Sample trial of vertical ground reaction force vs. vertical COM displacement for one walking stride, with stiffness quantified as slope during double support stiffness. Data shown are in dimensionless units.

the redirection phase in walker is higher than the vertical stiffness of running. This is associated with the shorter time of contact in walking as compared to running, due to ground contact of two legs, both of which are kept fairly straight.
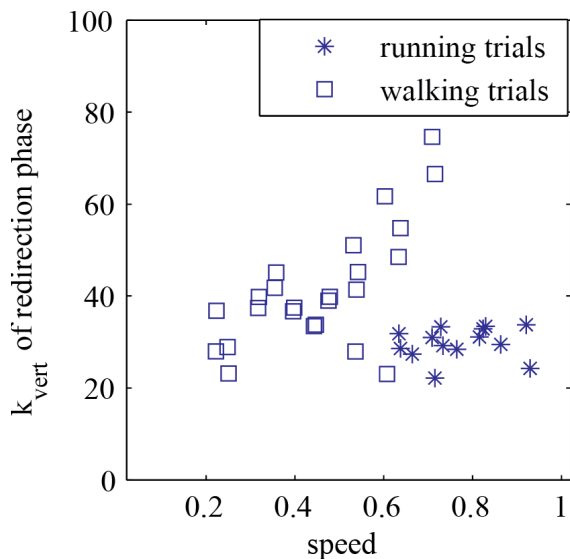

Figure 2. Vertical stiffness of the velocity redirection phase as a function of speed for walking and running. All quantities are non-dimensionalized.

We also found that the duration of the redirection phase (Fig. 3) was inversely related to vertical stiffness, as predicted by the mass-spring model. A single equation (Eq. 1 with an additional stiffness offset term) is fit to both the running and walking data. The offset term is 26.9 (95% confidence interval 23.7 to 30.0), Q is 0.21 (95% confidence interval 0.18 to 0.23), and the R^2 of the fit is 0.701.
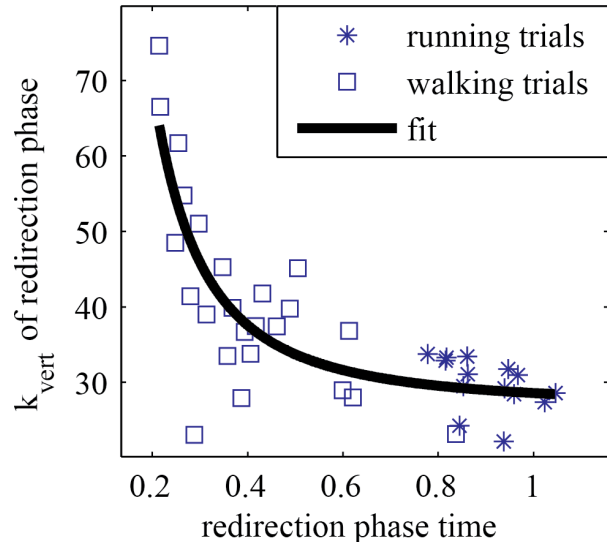

Figure 3. Vertical stiffness as a function of the duration of the redirection phase. The R^2 of the fit is 0.701.

DISCUSSION

A single measure of vertical stiffness of the redirection (double support) phase can be used to compare walking to running. While the single support phase of walking is commonly modeled using an inverted pendulum, human data show that the double support phase is analogous to the ground contact phase of running using a simple relationship based on a mass spring system.

REFERENCES

McMahon, T.A. and Cheng, G. C. (1990). *J Biomechanics,* 23:65-78

PHYSICAL ASSISTANCE CAN BE DETRIMENTAL TO LEARNING WALKING BALANCE

Antoinette Domingo[1] and Daniel P. Ferris[1]

[1]Human Neuromechanics Laboratory, University of Michigan, Ann Arbor, MI, USA,
adomingo@umich.edu

INTRODUCTION

Balance impairments are common in patients with neurologic injury and in the elderly. Designing therapeutic interventions for improving walking balance could greatly improve functional mobility in millions of individuals. Although physical assistance is often provided during rehabilitation therapies to improve balance, it is not clear how assistance affects motor learning of complex skills. The purpose of our study was to determine how physical assistance affects motor learning of walking balance. Physical guidance may be detrimental to learning because it removes opportunities for error detection and correction.

In this study, two groups of subjects were evaluated before and after 30 minutes practice walking on a narrow treadmill mounted balance beam (beam-mill). The first group practiced the task without assistance (Unassisted), while the second group practiced with assistance (Assisted) provided by a lateral assist device (Donelan et al., 2004) (Figure 1). The device used springs to provide a restoring force whenever the pelvis moved away from the beam-mill center. We hypothesized that the group that practiced the task without assistance would improve their ability to walk on the beam more than the group using assistance.

METHODS AND PROCEDURES

Seven subjects walked on a treadmill mounted balance beam for 5-minute pre- and post- practice evaluations. The beam was 2.5 cm wide and 2.5 cm tall. Treadmill speed was set at 0.22 m/s. Subjects were given instructions to walk heel-to-toe with arms crossed and not to lean forward, twist, angle their feet away from the longitudinal direction of the beam, or look down at their feet. View of the walking surface was obscured by using dribble goggles. All subjects wore standardized shoes. If the subject stepped off the beam, she had to wait five seconds before attempting to walk on it again.

Figure 1. A subject walking on the beam-mill with a lateral assist device used to provide a restoring force towards the center of the beam.

Four subjects were in the Assisted group and three subjects were in the Unassisted group. During practice, the Assisted group walked on the beam-mill with the lateral assist device, and the Unassisted group did not. The practice duration was 30 minutes with rest breaks every 10 minutes.

Subjects were evaluated over a 3-minute period during unassisted walking on the beam-mill before and after training. We assessed beam walking performance by calculating the percentage of time the subject was on the beam (not touching the treadmill surface with either foot) and by calculating

the root-mean-square (RMS) and the standard deviation (SD) of the medio-lateral movement of markers placed at the sacrum and the left shoulder, respectively (Motion Analysis Corporation, Santa Rosa, CA; 120 Hz).
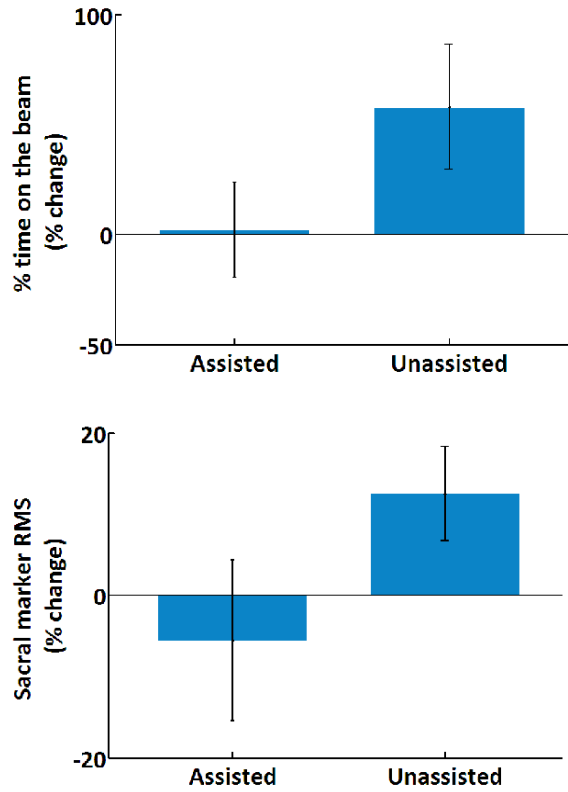
RESULTS AND DISCUSSION

Figure 2. Percent change after training in time on the beam and sacral marker RMS. Vertical lines indicate standard error of the mean.

The Unassisted group made greater improvements in time spent on the beam (~58%) than the Assisted group (~2%) (Figure 2). This suggests that practicing without the assistance was more beneficial for learning beam walking balance because it was task specific and allowed the subjects to explore the dynamics of the task. The Unassisted group spent less than half the practice time on the beam (~44%). When subjects used the assistance, error was minimized during practice (on the beam ~86% of practice time), decreasing opportunities to learn error detection and correction.

In the Unassisted group, subjects had larger movements in the sacral marker after training. This suggests that either these subjects preferred to use movement at the pelvis to maintain balance or they were more comfortable allowing greater movement at the pelvis because they were aware of their limits of stability.

SUMMARY/CONCLUSIONS

Unassisted practice was more beneficial to learning walking balance than assisted practice in neurologically intact subjects. This was demonstrated by the greater improvements in time walking on the beam-mill for the Unassisted group compared to the Assisted group. Future studies need to separate the effects of assistance and the amount of error experienced during practice as confounding factors affecting learning.

REFERENCES

Donelan, JM et al. (2004). *J Biomech*, 37, 827-835.

ACKNOWLEDGMENTS

INVARIANT ANKLE MOMENT PATTERNS WITH PLANTAR FLEXOR ASSISTANCE FROM A POWERED ANKLE ORTHOSIS

Cara L. Lewis[1], Pei-Chun Kao[1], and Daniel P. Ferris[1]

[1]Division of Kinesiology, University of Michigan, Ann Arbor, MI, USA
E-mail: caralew@umich.edu

INTRODUCTION

Robotic lower limb orthoses hold considerable potential to improve human mobility. It is critical, however, to identify principles of motor adaptation to powered assistance in order to guide orthosis development. Healthy humans rapidly learn to walk with mechanical plantar flexor assistance from a powered ankle-foot orthosis under proportional myoelectric control of the soleus (Gordon and Ferris, 2007). With treadmill training, subjects reduced soleus electromyography (EMG) to reach steady-state kinematic and EMG patterns within two 30-minute sessions. The purpose of this study was to compare ankle joint kinetics with and without powered assistance after adaptation to determine if subjects walking with the powered orthosis use kinetic patterns similar to walking with the orthosis unpowered.

METHODS AND PROCEDURES

Two healthy subjects adapted to walking with the powered orthosis using an established protocol (Gordon and Ferris, 2007). Briefly, subjects walked with a custom powered ankle-foot orthosis for two 30-minute training sessions. A pneumatic muscle under proportional myoelectric control of the soleus provided plantar flexion assistance. During a subsequent testing session, subjects walked on a force measuring treadmill at 1.25 m/s with the orthosis powered and unpowered. We collected kinematic, kinetic, and EMG data. Joint kinematics and kinetics were calculated using Visual 3D software. EMG data were high-pass filtered, rectified, and low pass filtered (f_c= 6 Hz).

To compare unpowered and powered data, we calculated the root mean square difference (RMSD) between the average gait cycle curves of the two conditions. The variables evaluated were the ankle angle, velocity, moment, and power, as well as the ground reaction force and soleus EMG. The RMSD for each variable was normalized from 0 to 1 for the range of that variable in order to allow comparison across variables with different magnitudes. For each variable within each condition, we also calculated the RMSD comparing each individual trial with the mean of the trials within that condition. Comparing the within condition RMSD to the between condition RMSD tested whether the difference between the two conditions was greater than the difference expected due to the within condition variability alone.

RESULTS

While there were substantial differences in soleus EMG and ankle angle patterns between conditions, there was virtually no difference in the total ankle moment pattern between powered and unpowered conditions (Fig. 1). The difference between the soleus EMG powered and unpowered curves was much greater than the variability within the curves (Table 1). Ankle angle and ankle power RMSDs between conditions were also much higher than their respective RMSDs within conditions. Ankle moment, ankle velocity, and the three ground reaction forces, however, had RMSDs between conditions that were much more similar to RMSDs within conditions (Table 1).

DISCUSSION

After training with the powered orthosis, subjects adopted a walking pattern with substantially lower soleus recruitment and substantially less dorsiflexion during stance. These results were consistent with our previous study using 10 subjects but that study did not measure ankle moments during unpowered and powered walking after adaptation (Gordon & Ferris, 2007). In spite of these differences in muscle activity and ankle kinematics, the total ankle moment and ground reaction forces showed very little differences between powered and unpowered walking. This is particularly remarkable given that the orthosis was providing ~40% of the total net muscle moment at the ankle during push-off during the powered condition.

SUMMARY

When walking with a powered orthosis providing plantar flexion assistance, subjects adopted a walking pattern with substantial kinematic differences from normal but an almost identical ankle moment pattern as normal walking. This supports the concept that joint moments may be intrinsically represented in the neural control of human walking (Shemmell et al., 2007).

REFERENCES

Gordon, KE and Ferris, DP (2007). *J Biomech,* 40: 2636-2644.

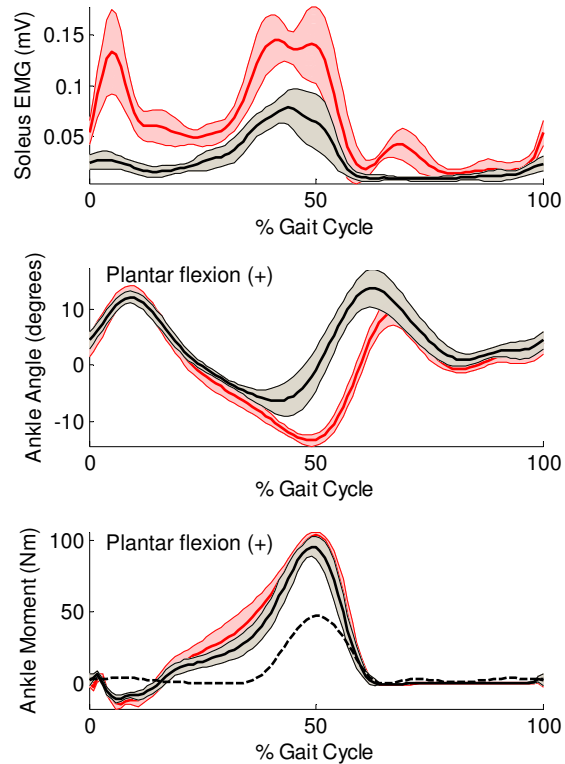Shemmell, J et al. (2007) *J Neuroeng Rehab*, 4:10.

Figure 1: Soleus EMG, ankle angle and total ankle moment curves (mean±s.d.) during the unpowered (red) and powered (black) conditions. Dashed line in the moment graph is the orthosis portion of the ankle moment for the powered condition.

ACKNOWLEDGMENTS

	Between Conditions	Within Powered	Within Passive
Soleus EMG	0.546 (0.086)	0.159 (0.013)	0.108 (0.007)
Ankle Angle	0.220 (0.066)	0.159 (0.008)	0.041 (0.003)
Ankle Velocity	0.053 (0.005)	0.036 (0.003)	0.027 (0.002)
Ankle Moment	0.058 (0.002)	0.048 (0.004)	0.034 (0.003)
Ankle Power	0.150 (0.057)	0.088 (0.007)	0.041 (0.005)
GRF (lateral)	0.067 (0.011)	0.071 (0.005)	0.060 (0.003)
GRF (posterior)	0.040 (0.001)	0.039 (0.002)	0.031 (0.002)
GRF (superior)	0.039 (0.007)	0.039 (0.003)	0.029 (0.003)

Table 1. Normalized root mean square differences (RMSD) as mean (s.e.m.)

FLEXIBLE REPRESENTATIONS OF DYNAMICS ARE USED IN OBJECT MANIPULATION

Alaa A. Ahmed[1], Daniel M. Wolpert[1], and J. Randall Flanagan[2]

[1]Computational and Biological Learning Lab, Department of Engineering, University of Cambridge CB2 1PZ, United Kingdom; aaa52@cam.ac.uk
[2]Department of Psychology and Centre for Neuroscience Studies, Queen's University, Kingston, Ontario, K7L 3N6, Canada; flanagan@queensu.ca

INTRODUCTION

To manipulate an object skilfully, the brain must learn its dynamics, specifying the mapping between applied force and motion. A fundamental issue in sensorimotor control is whether such dynamics are represented in an extrinsic frame of reference tied to the object or an intrinsic frame of reference linked to the arm. Although previous studies have suggested that objects are represented in arm-centered coordinates (Shadmehr and Mussa-Ivaldi, 1994; Bays and Wolpert, 2006), all of these studies have used objects with unusual and complex dynamics. Thus it is not known how objects with natural dynamics are represented. Here we test the hypothesis that when manipulating a novel object, dynamics are learned in an object-centered reference frame.

METHODS AND PROCEDURES

We used a bimanual object manipulation task in which participants grasped the handles of two robotic manipulanda (vBOTs) attached by a virtual elastic band (Fig. 1) and moved the right hand to stretch the band while holding the left hand still. In this task, subjects learn to compensate for the effects of
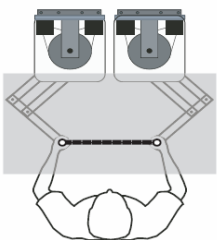

Figure 1 Setup. Seated participants grasped two robotic handles and looked down onto a horizontal semi-silvered mirror, located above the hands that displayed circles representing their hand positions in the plane of movement.

right hand movement by generating appropriate forces with the left hand. To assess learning in the training position (Fig. 2), we included catch trials, in which we measured the force applied by left hand while locking the left handle in place. To determine whether participants represent the learned dynamics in object or arm-centered coordinates, we used transfer trials, which were catch trials where the object was moved (1 in 10 trials) to a new location involving a 30° clockwise rotation about the left shoulder (transfer position). After 380 trials, the object was moved to the transfer position, where participants performed a further 110 trials, including catch trials to assess steady-state learning in the transfer position.

Thirty-six subjects were randomly allocated to one of 6 groups (Fig 3). Each group was exposed to 1 of 3 object conditions (straight-visible, straight-invisible, or pulley), in 1 of 2 arm configurations (transverse or sagittal). In the straight conditions, the object was a visible or invisible elastic band. In the pulley condition, the band was visible and wrapped 90° around a pulley which rotated as the band was stretched.

Steady-state performance in the training and transfer locations was quantified as the median angle of the force vector measured on catch trials during learning in that position. To quantify transfer of learning we compared steady-state performance in the transfer position to performance on transfer trials. That is, for each subject we subtracted the median force vector measured on catch trials

in the transfer position after learning from the median force vector measured on transfer trials. A transfer angle of 0° or 30° would indicate perfect transfer in object- or arm-centered coordinates, respectively. Effects of condition and configuration on transfer angle, were determined using a 2-way (3x2) between-subjects ANOVA.

RESULTS

All subjects learned the dynamics of the task and generated appropriate compensatory forces on catch trials in the training and transfer positions after learning. However, performance on transfer trials revealed that when vision was available the dynamics of the straight band generalized mainly in object-centered coordinates whereas the dynamics of the band and pulley were represented primarily in arm-centered coordinates (Figs 2,3). And when vision of the straight band was removed, an intermediate representation was observed (Fig. 3). Significant effects of both object condition ($F_{2,30}$=22.5; p<0.01) and arm configuration ($F_{1,30}$=6.7; p<0.015) were observed, without interaction ($F_{2,30}$=0.55; p<0.58) . Moreover, the transfer angle was greater in the pulley condition than in the two straight band conditions combined (p <0.001). Vision of the object also played a significant role; the transfer angle was greater when the object was not visible (p = 0.043).

DISCUSSION

These results indicate that the way in which we represent object dynamics is flexible and depends on the complexity of the dynamics. When experiencing the relatively complex dynamics of the elastic band wrapped around the pulley, participants represent learning in arm-centered coordinates. In contrast with previous studies, our results show that objects with simpler dynamics can be represented in
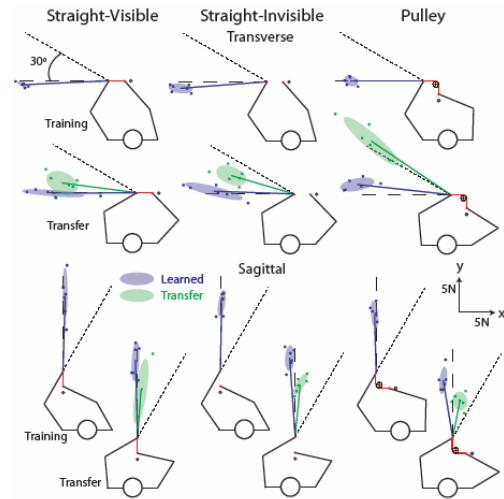

Figure 2 Force vectors Arm configurations in the training and transfer conditions are shown for object conditions (columns) and arm configurations (top and bottom panels). Subjects stretched an elastic band to a target (black circles). Each blue cross represents a subject's median force vector angle after learning in that position. The green crosses show the subject's median force vector angle on transfer trials. Thick lines show mean force vectors, with the corresponding 50% confidence ellipses. Object- and arm centered predictions are shown by the dashed and dotted lines, respectively.

object-centered coordinates. And when visual cues are removed, learning generalizes in an intermediate reference frame between object- and arm-centered coordinates. We suggest that with experience the representation of the dynamics of a manipulated object may shift from a coordinate frame tied to the arm to one linked to the object.
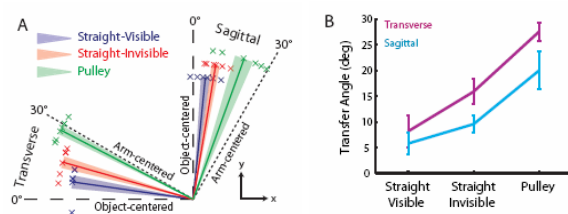

Figure 3 Transfer Angles. A. The transfer angles are presented as normalized unit vectors (± 1SE) in polar coordinates. B. The magnitude of the average transfer angle (± 1SE) for each object condition is presented.

REFERENCES

Bays, PM and Wolpert, DM (2006). J Neurosci, 26:7121-7126.

Shadmehr, R and Mussa-Ivaldi, F (1994). J Neurosci, 14:3208-3224.

VISCO-HYPERELASTIC PROPERTIES OF THE PELVIC FLOOR MUSCLES IN HEALTY WOMEN

Dejun Jing[1], Kuo-Cheng Lien[1], James Ashton-Miller[1] and John O. DeLancey[2]

[1]Biomechanics Research Laboratory, Department of Mechanical Engineering, and
[2]Department of Obstetrics & Gynecology, University of Michigan, Ann Arbor, Michigan, USA
djing@umich.edu URL: http://me.engin.umich.edu/brl/

INTRODUCTION

Vaginal birth increases the chance that a woman will develop pelvic organ prolapse 4- to 11-fold (Mant 1997). The underlying mechanisms are poorly understood. Finite element analysis offers a powerful tool to investigate these mechanisms. However, such models require reliable constitutive equations for each tissue type involved. We are unaware of any such data having been published on the female pelvic floor muscles. So, existing finite element models of the pelvic floor have had to 'borrow' material properties from other soft tissues, such as cardiac tissue (d'Aulignac 2005) and tongue muscle (Lee 2005).

The purpose of this study was to make the requisite measurements and derive the constitutive laws for healthy female human pelvic floor (levator) muscles. Since pelvic floor muscle deformation during vaginal birth is time-dependent, finite and nonlinear, the derivation of the constitutive equations was based on the theory of hyper-viscoelasticity. A servo-controlled bi-axial tensile test system was developed to measure the visco-hyperelastic properties of these muscles.

METHODS

Up to six fresh specimens of puboviseral muscle (PVM), illiococcygeal muscle (ICM) and perineal body (PB) were collected from six fresh cadavers for uniaxial tension tests. Each specimen was preconditioned first with 5 cyclic stretches up to 30% strain under a stretching rate of 0.1mm/second. After a 15-minute rest for recovery, the specimen was stretched in the "ramp-and-hold" mode (first stretched up to double the initial length at a stretch rate of 0.5mm/second, then held at that fixed length for at least one hour), while the values of stress and strain were synchronously recorded by a video-based strain measurement system and computer.

The Quasi-Linear Viscoelasticity (QLV) theory (Fung 1972) was used to form the constitutive equations for the pelvic floor muscles. The nonlinear stress response was characterized using a 2nd-order polynomial hyperelastic strain energy function

$$W = C_{10}(I_1 - 3) + C_{01}(I_2 - 3) + C_{11}(I_1 - 3)(I_2 - 3)$$

where I_1 and I_2 are invariants of right Cauchy-Green tensor. The reduced relaxation function takes the form of Prony series

$$G(t) = 1 - \sum_{i=1}^{3} g_i \left(1 - e^{-t/\tau_i}\right)$$

with constraints of g_i, $\tau_i > 0$ and $G(0) = 1$.

A nonlinear optimization code using Matlab was developed to curve-fit the experimental data to extract material parameters C_{10}, C_{01}, C_{11}, g_i and τ_i.

RESULTS

Figure 1 and 2 show curves fit to the experimental tissue stiffness and relaxation data respectively, while Table 1 lists the

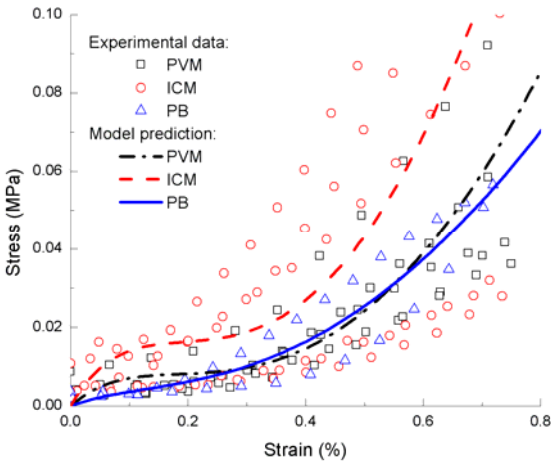material constants obtained from data regression by region of levator muscle.

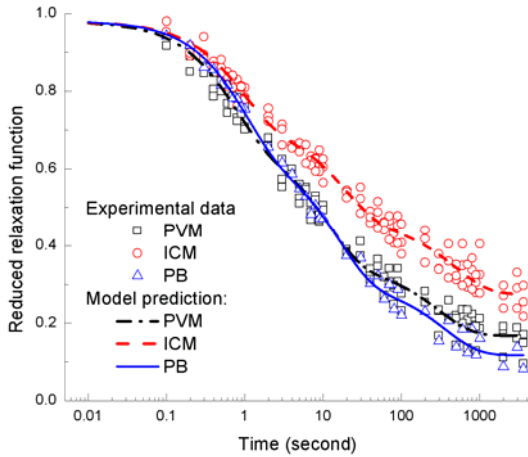**Figure 1:** Instantaneous elastic responses of PVM, ICM and PB.

Figure 2: Reduced relaxation function of PVM, ICM and PB muscles.

DISCUSSION

The regression analysis shows that introducing a 2nd-order term to the strain energy function can better characterize muscle stress responses in both small and large strain regions, obviating the difficulty of commonly used Mooney-Rivlin model (1st-order polynomial). It can be seen that the short- and long-term relaxation behavior can be well modeled with 3-term Prony series.

Even though the results presented here are preliminary data based on uniaxial tests, they are the first publication of viscoelastic data of human pelvic floor muscles to our knowledge. Currently a series of biaxial tests are being performed on these muscles in our lab.

SUMMARY

The human levator muscle exhibits visco-hyperelastic behaviour and this appears to vary systematically by region.

REFERENCES

D' Aulignac, D et al. (2005). *Compt. Meth. Biomech Biomed Eng,* 8(5), 339-47.

Lee, SL et al. (2005) *Int Conf Med Image Comput Comput Assist Interv,* 8, 360-7

Fung Y.C. (1972) *Biomechanics- Its Foundations and Objectives*. Prentice Hall, 181-207.

Mant, J et al. (1997) *Brit J Obstet Gynaecol* 104:579-85

ACKNOWLEDGEMENTS

	C_{10}	C_{01}	C_{11}	g_1	g_2	g_3	τ_1	τ_2	τ_3
PVM	-0.106	0.129	0.038	0.325	0.308	0.179	11.39	0.708	297.99
ICM	-0.20	0.244	0.069	0.25	0.265	0.19	18.40	0.907	483.47
PB	-0.03	0.04	0.019	0.346	0.335	0.183	15.397	0.968	357.05

Table 1: Material constants obtained from curve-fitting test data. (Number of specimens: PVM=5, ICM=6, PB=2)

SHEAR THICKENING FLUID BASED PROTECTIVE FOAM PADDING

Sarah Trager,[1] Norman J. Wagner[2] and C. Buz Swanik[1]

[1] Department of Health, Nutrition and Exercise Sciences, University of Delaware, Newark, Delaware, USA, strager@udel.edu
[2] Department of Chemical Engineering, University of Delaware, Newark, Delaware, USA

INTRODUCTION

Unintentional falls are the leading cause of non-fatal injury in almost all age groups (CDC, 2002). These episodes may result in bone fracture, bruising, and/or swelling of the impacted region. In older adults, hip fractures resulting from falls are common and present a significant public health problem due to the difficult recovery and increased risk for secondary health issues.

Previous research has shown that protective padding is effective at reducing the peak force on the hip at impact (Kannus, et al., 1999; van Schoor, et al., 2006). Two types of pads exist currently – those with a hard shell (energy shunting) and those that are soft (energy absorbing). The hard pads have been shown to be more effective in decreasing impact forces, but these pads are often bulky and uncomfortable which reduced patient compliance. An ideal solution is one that combines the comfort of a soft pad with the protective properties of the hard shelled pad.

Shear thickening fluid (STF) is a material that is fluid in its resting state, but hardens once force is applied to it. The purpose of this project was to determine the effectiveness of combining the properties of the shear thickening fluid with soft padding (closed cell foam) in attenuating impact forces.

METHODS AND PROCEDURES

A drop weight impact tester was used to measure the impact force of a 2.5cm round, flat cylinder as it was dropped from 15.9 cm above the sample. The impact tester was fitted with weights totalling 13.4 kg. The load cell in the impact head transmitted information to the computer during the impact tests.

A steel plate served as the base upon which the samples were placed and impacted. Four layers of rubber matting (total 14mm thickness) were placed between the plate and sample (Figure 1). The rubber matting was placed under the sample to represent force attenuation that would occur due to the presence of soft tissue in a typical biological system.
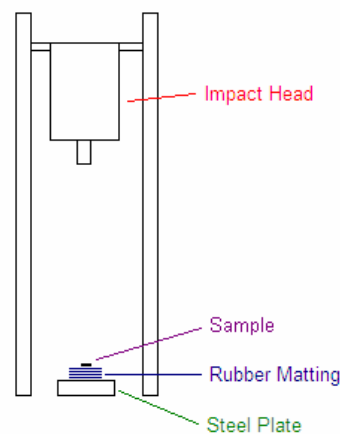

Figure 1. Instrumentation set-up for impact tests.

A calibration run was performed by dropping the impact head directly onto the rubber matting. Following the calibration run, neat foam, a packet filled with STF, a foam/STF combination, and a HipSaver pad were tested.

The foam/STF combination samples were 0.95cm thick foam pads with STF inserted into vertical holes that had been punched into the foam. Holes were placed in a hexagonal pattern using a standard 1/4" diameter punch, approximately 1/4" apart.

The packet filled with STF was constructed to be the same thickness as the neat foam and foam/STF combination samples.

Peak impact force and loading rate data was analyzed using custom LabView software. Due to small sample sizes, only descriptive statistics were run. Averages of 2 trials of each type of sample are reported.

RESULTS AND DISCUSSION

Peak impact forces and loading rates from tests run with no sample, neat foam, STF packet, foam/STF combination, and the HipSaver are shown in Table 1.

The lowest peak impact forces were recorded during the STF packet trials. While this is promising, the weight and form of the STF packet is prohibitive to consideration as a protective product on its own.

The foam/STF combination performed similarly to the HipSaver, a commercially available soft hip protection device. The key advantage to the foam/STF combination is the thickness, or lack thereof. The force attenuation properties of the HipSaver were achieved by a much thinner pad. As previously stated, people are more likely to make use of protective padding if it is comfortable and unobtrusive.

Typical soft hips pads attenuate impact force by absorbing energy. By filling holes in soft foam with STF, impact forces can be absorbed by the foam, while energy is also used by the fluid to harden, thereby transmitting less energy (and force) to the biological tissue underneath the pad.

Although the foam/STF combination did not result in drastically lower forces than the HipSaver product that is currently available, the results were promising. Future projects will focus on developing the current technology to be even more effective at decreasing impact forces in a variety of settings.

REFERENCES

Control, N.C.f.I.P.a. (2002). CDC Injury Research Agenda. A.G. Centers for Disease Control and Prevention.

Kannus, P, Parkkari, J, and Poutala, J. (1999). *Bone,* 25:229-235.

Van Schoor, NM, van der Veen, AJ, Schaap, LA, Smit, TH, Lips, P (2006). *Bone,* 39:401-407.

ACKNOWLEDGEMENTS

Table 1. Results from all samples tested. *Weight of HipSaver is approximate as the actual sample is much larger in area than the other samples. This weight is proportionate according to the area of our other samples.

Sample	Thickness (cm)	Weight (g)	Peak Force (kN)	Loading Rate (kN/sec)
Rubber Matting only	N/A	N/A	6.56	.88
Neat Foam	.95	6.6	4.93	.52
STF packet	.95	69.9	3.29	.31
Foam with STF	.95	19.9	3.85	.37
HipSaver	1.5	20.69*	3.89	.37

NON INVASIVE DETERMINATION OF BODY SEGMENT PARAMETERS IN LABRADOR RETRIEVERS

Chantal A. Ragetly[1], Dominique J. Griffon[1], Jason E. Thomas[2], Ayman A. Mostafa[1], David J. Schaeffer[3], Gerald J. Pijanowski[3], Elizabeth T. Hsiao-Wecksler[2]

[1]Department of Small Animal Surgery, Small Animal Clinic (cimbs2@uiuc.edu), [2]Department of Mechanical Science and Engineering (ethw@uiuc.edu) and [3]Department of Veterinary Biosciences, University of Illinois, Urbana, IL, USA

INTRODUCTION

Inverse dynamics gait analyses have greatly contributed to the understanding of normal and pathological movement in humans; however, nearly all canine gait analyses have involved only kinematic or ground reaction forces (GRF) gait parameters. Application of inverse dynamics to dogs has been limited by the lack of data regarding inertial body segment parameters (BSP), i.e., mass, location of the center of mass (COM) and mass moment of inertia. Colborne et al. (2005) determined hind limb segment masses and COM locations, but these were from a small cadaveric sampling of three Labrador Retrievers and four Greyhounds.

Computerized tomography (CT) allows for non invasive determination of BSP, but this approach requires general anesthesia and is both time-consuming and expensive. Estimating BSP based on simple morphometric parameters (such as body mass and/or segment length, width or girth) provides a basis for wide spread studies using inverse dynamics to investigate hind limb biomechanics in dogs. Therefore, the objectives of the current study were to (1) determine BSP of hind limb segments using a non invasive method based CT in a large sampling of living Labrador Retrievers, and (2) develop regression equations for the estimation of hind limb BSP in Labradors using simple morphometric measurements.

METHODS AND PROCEDURES

Test subjects were part of a larger study examining differences in hind limb morphology and gait behavior due to cranial cruciate ligament (CCL) deficiency. Hind limb morphometric measurements and CT scans were collected on 24 dogs (14 normal and 10 with unilateral CCL deficiency). Bone, muscle and fat areas were identified according to CT pixel intensity (Figure 1). BSP were determined based on individual tissue densities in the thigh, crus and foot (Zatsiorsky, 2002). Stepwise regression models were used to develop predictive equations to estimate BSP for each leg type.
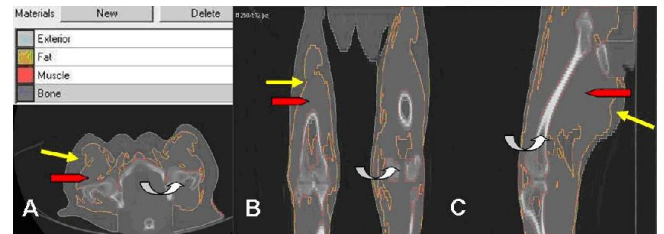

Figure 1: 3-D CT scan pixel values attributed to fat (yellow), muscle (red) and bone (dark grey outline, curved white arrow) in transverse view at the hip (A), frontal (B) and para-sagittal (C) views at mid femoral level.

RESULTS/DISCUSSION

Average BSP values from the test limbs and regression equations to predict these BSP were documented in normal healthy, CCL-deficient, and contralateral hind limbs of Labradors. The thigh and crus of CCL-deficient limbs were found to be lighter than

their matched contralateral segments (Table 1). The thigh also weighed less in CCL-deficient than normal limbs. The moment of inertia of the thigh was decreased in CCL-deficient limbs compared to contralateral values. The COM of the crus was found to be located more distally in normal limbs compared to other limbs.

Lighter thigh and crus and decreased mass moment of inertia are consistent with muscle atrophy observed in limbs with CCL disease. This is likely secondary to pain and decreased use of the CCL-deficient limb, and advanced activity of the compensating contralateral limb (Rumph et al, 1995). The more proximal position of the COM in CCL-deficient and contralateral crus compared to normal limbs is unlikely to be solely due to CCL disease since contralateral limbs displayed the same distribution. These contralateral limbs can be considered as predisposed to CCL deficiency based on the incidence of bilateral CCL disease in dogs (Doverspike et al, 1993). A relatively greater proportion of bone and/or muscle in the proximal portion of the crus may be a factor predisposing dogs to CCL disease.

Regression equations based on morphometric measurements were identified to estimate segment mass, location of the COM relative to the proximal joint, and mass moment of inertia for all three limb types. For example, in a normal healthy limb, mass (in g) for the thigh could be predicted for a given dog's body mass (BM), thigh circumference ($Girth_{thigh}$), and latero-medial stifle joint width ($Width_{stifle}$) using the following expression ($R^2 = 0.95$, 5.0%

error, standard error of 127):

$$Mass_{thigh} = -2723 + 31BM + 51Girth_{thigh} + 296Width_{stifle}$$

We constructed regression equations based on parameters that are fast, non invasive, technically simple and cost effective to generate. This novel approach will facilitate clinical studies of canine gait mechanics, offering for the first time new strategies to investigate the pathogenesis of non-traumatic joint diseases in living animals. Analysis of muscular pattern and internal force at each joint of interest using an inverse dynamics method will provide valuable insights for orthopaedists or neurologists.

SUMMARY

For the first time, the mass, COM and mass moment of inertia of hind limb segments in Labradors were calculated non-invasively from CT imaging. In this study, we also establish with a series of predictive equations for estimating BSP based on simple morphometric parameters. These equations provide a basis for inverse dynamics studies, which will facilitate clinical studies of canine gait biomechanics.

REFERENCES
Colborne et al. (2005) *Am J Vet Res*, 66: 1563-1571
Doverspike, et al. (1993) *J Am Anim Hosp Assoc*, 29:167-170
Rumph, et al. (1995) *Vet Surg*, 24:384-389
Zatsiorsky (2002) *Kinetics of human motion*. Champaign, IL, Human Kinetics

Table 1: Mean (±SD) of mass, mass moment of inertia, and COM location relative to the proximal joint for thigh, crus and foot for normal, CCL-deficient and contralateral limbs. **A**, **B**: groups with different letters differ statistically.

Segment	Group	n	Mass (g)	Mass (% BM)	Mass moment of inertia (g.cm²)	Mass moment of inertia (I/BM)	COM (cm)	COM (% L)
Thigh	Normal	28	2231 (±581)	6.05 (±0.51)A	92,875 (±44,294)	2,423(±561)AB	9.0 (±1.0)	42 (±5)
	CCL-deficient	10	1939 (±398)	5.48 (±0.34)B	79,074 (±24,596)	2,199(±276)A	9.1 (±0.4)	45 (±4)
	Contralateral	10	2192 (±374)	6.22 (±0.30)A	87,981 (±23,795)	2,459(±210)B	9.1 (±0.4)	44 (±3)
Crus	Normal	28	516 (±113)	1.41 (±0.16)AB	16,242 (±6,778)	433 (±35)	6.3 (±0.7)	31 (±2)B
	CCL-deficient	10	484 (±112)	1.36 (±0.09)A	15,174 (±5,699)	421 (±80)	6.3 (±0.5)	28 (±1)A
	Contralateral	10	512 (±116)	1.44 (±0.11)B	15,941 (±6,210)	441 (±35)	6.4 (±0.4)	28 (±1)A
Foot		20	249 (±25)	0.70 (±0.09)	7,228 (±1,223)	203 (±24)	8.7 (±0.4)	47 (±3)

THE EFFECT OF A LINEAR IN-FLIGHT PERTURBATION ON LANDING BIOMECHANICS

Scott W. Arnett[1], Yang-Chieh Fu[2], Ryan Thompson[3], Petur Sigurdsson[2], & Kathy J. Simpson[2]

[1]Western Kentucky University, Bowling Green, KY, USA, scott.arnett@wku.edu;
[2]University of Georgia, Athens, GA, USA;
[3]University of Tennessee at Chattanooga, Chattanooga, TN, USA
URL: http://www.wku.edu/chhs/cms/index.php/departments/pe-recreation/pe-rec

INTRODUCTION

The exact mechanisms occurring at the time of an ACL injury are still elusive at this time. Although this type of injury is not gender specific, it occurs more prevalently in females (AAOS, 2003), which has led to research on risk factors within the individual. Personal factors, such as anatomical, hormonal, and biomechanical, have been implicated in increasing the risk of incurring an ACL injury during sports participation (Boden et al., 2000; Childs, 2002; Griffin et al., 2000; Markolf et al., 1995). More recently, the focus of ACL injury research has been extended to include the interaction of biomechanical and environmental factors. One such interaction is an in-flight perturbation. Although these events have been implicated in ACL injuries (Hewett et al., 2006; Krosshaug et al., 2007), the effects of these events on drop landing biomechanics are not known at this time. Therefore, the purpose of this study was to determine the effect of a linear in-flight perturbation on landing biomechanics.

METHODS AND PROCEDURES

Thirteen college-aged female soccer and basketball athletes (Table 1) performed double-leg drop landings 0.6 m from the ground with (PERT) and without (CON) in-flight perturbations being applied. Three-dimensional ground reaction forces (1200 Hz) and lower extremity joint kinematics (240 Hz) and kinetics were analyzed for the right limb using paired t-tests ($\alpha = 0.05$).

RESULTS

Compared to the non-perturbed condition (CON), peak vertical ground reaction force (VGRF) was decreased during the perturbed condition (PERT). No significant differences were demonstrated for peak posterior ground reaction force (GRF) or lower extremity joint kinematics between conditions. Peak hip and knee extensor net muscle moments and peak plantarflexor net muscle moments were significantly greater during the PERT compared to the CON condition (Figure 1).

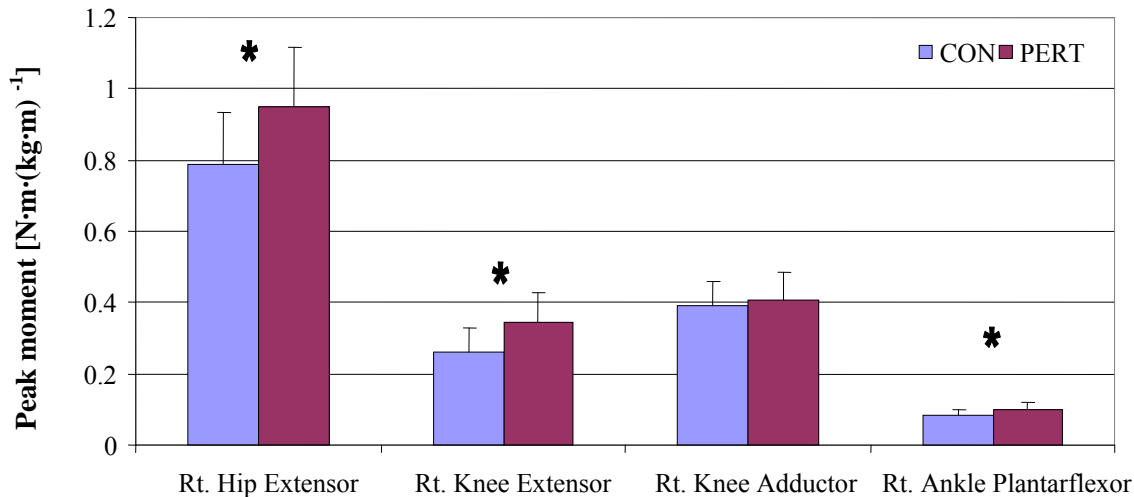|	Mean ± SD	Range
Age	20.3 ± 1.9	18-24
Body Mass (kg)	62.8 ± 8.2	52.5-79.4
Body Height (cm)	167.9 ± 7.3	159.6-187.7
No. yr participation Soccer	8.2 ± 6.0	<1-18
Basketball	7.2 ± 3.6	4-12

Table 1. Participant characteristics.

Figure 1. Peak joint moments during the CON and PERT conditions. Data are means with SD error bars. * denotes statistical significance (p<0.01)

DISCUSSION

The significant differences found between conditions for peak vertical ground reaction force and moments are insightful and at the same time raise questions. The difference in peak VGRF could be interpreted as anticipation by the performer leading to an altered landing strategy. During the PERT compared to the CON condition, increased force could be placed on the ACL due to the shear force created by the peak knee extensor moment (DeMorat et al., 2004; Simpson & Kanter, 1997). Inter-individual variation occurring at the knee joint between conditions supports that individuals utilized different strategies when landing and this variation could possibly be linked to increased risk for an ACL injury.

SUMMARY

While the in-flight perturbation used in this study was light in magnitude, it remains that an in-flight perturbation does influence landing biomechanics.

REFERENCES

AAOS. (2003). http://www.aaos.org/about/papers/advistmt/1024.asp.

Boden, BP et al. (2000). *Orthopedics 23*, 573-8.

Childs, SG (2002). *Orthop Nurs 21*, 35-40.

DeMorat, G et al. (2004). *Am J Sports Med 32*, 477-83.

Griffin, LY et al. (2000). *J Am Acad Orthop Surg 8*, 141-50.

Hewett, TE et al. (2006). *Am J Sports Med 34*, 299-311.

Krosshaug, T et al. (2007). *Am J Sports Med 35*, 359-67.

Markolf, KL et al. (1995). *J Orthop Res 13*, 930-5.

Simpson, KJ & Kanter, L (1997). *Med Sci Sports Exerc 23,* 522-7.

INVERSE DYNAMIC ANALYSIS OF THE STIFLE JOINT IN LABRADOR RETRIEVERS WITH CRANIAL CRUCIATE LIGAMENT DEFICIENCY

Chantal A. Ragetly[1], Dominique J. Griffon[1], Jason E. Thomas[2],
Ayman A. Mostafa[1], and Elizabeth T. Hsiao-Wecksler[2].

[1]Department of Small Animal Surgery, Small Animal Clinic (cimbs2@uiuc.edu), [2]Department of Mechanical Science and Engineering (ethw@uiuc.edu) University of Illinois, Urbana, IL, USA

INTRODUCTION

Inverse dynamic analyses combine kinematics, morphometric and ground reaction force (GRF) data in a segmental model of the limb, and have greatly contributed to the understanding of normal and pathological movement in humans (Winter, 2005). Cranial cruciate ligament (CCL) disease is the leading cause of degenerative joint disease in the stifle (knee) of dogs. No published information describes the net joint moment, power or reaction forces associated with lameness due to CCL disease, therefore limiting our knowledge about CCL-deficient gait mechanism. The objectives of this study were to (1) quantify for net joint moments, powers and joint reaction forces (JRF) during the stance and the swing phases of the gait cycle across the stifle joints in Labrador Retrievers with and without CCL disease, and (2) investigate differences in joint mechanics between normal, CCL-deficient and contralateral hind limbs.

METHODS AND PROCEDURES

The inertial properties were determined using 3-dimension computerized tomography images in 14 normal dogs and 10 dogs with unilateral CCL-deficiency. Thirteen spherical reflective skin markers identified bilateral thigh, crus and foot segments. Kinematic data of trotting dogs were collected using a 6-camera optical motion capture system (Vicon 460, Lake Forest, CA) synchronized with a force plate (AMTI, model BP600900, Watertown, MA). A minimum of 3 valid trials were collected for each hind limb. X-, y- and z-directions were defined as forward-backward, medio-lateral and vertical, respectively (Figure 1). An inverse dynamic approach was used to compute, in the sagittal plane, stifle net moment (in Nm/kg), power (in W/kg) and joint reaction force (peak in N/kg, and impulse in N.s/kg) during the stance and swing phases of the gait cycle. Mann-Whitney and Wilcoxon tests were used to compare data between groups.
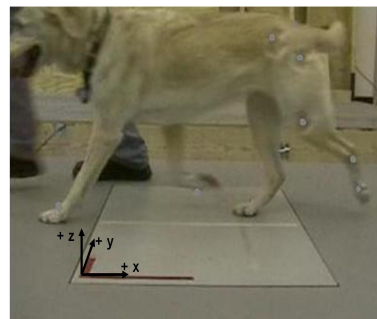

Figure 1: Dog trotting over the force plate with reflective markers on specific bony prominences.

RESULTS

This study documents for the first time gross differences in stifle joint mechanics between normal, CCL-deficient and contralateral limbs in dogs (Table 1). Curves of mean ± SE for net moment and power values are plotted to reflect between-limb variation within each group (Figure 2). Moment, power and JRF patterns were similar in shape, but amplitudes were larger for contralateral limbs compared to normal limbs, and for normal compared to affected limbs. The amplitude of peak power

generation in late stance in contralateral limbs was about 3 times that measured in normal limbs and 15 times greater than that of CCL-deficient limbs.
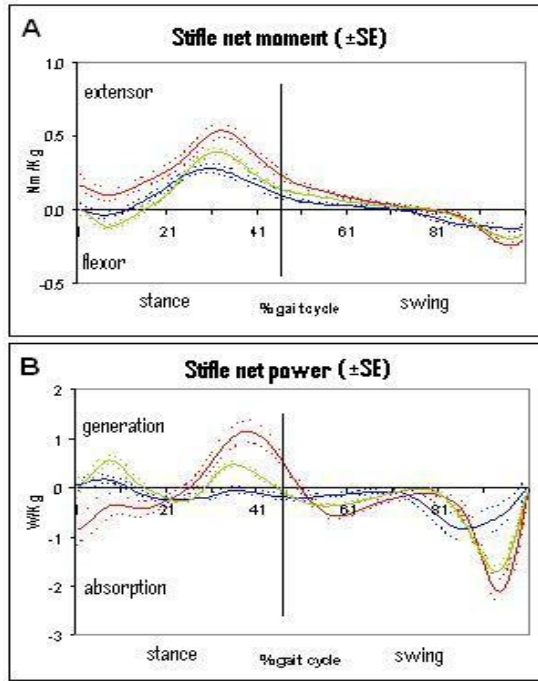

Figure 2: Mean (±SE) of stifle joint net moment (A) and power (B) for normal (green), CCL-deficient (blue) and contralateral (red) limbs.

DISCUSSION

The only previous publication of stifle kinetics in dogs was based on a small sampling of healthy, musculoskeletal disease-free Labradors (n=3) and Greyhounds (n=4) (Colborne et al, 2005). Our study reports, for the first time, net moment, power and JRF around the stifle joint in Labrador Retrievers with or without CCL disease. Reductions in stifle joint net moment and power peaks and in stifle JRF peaks and impulses were interpreted as modifications adopted to reduce or avoid painful mobilization of the injured stifle joint (Andriacchi, 1990). Kinetics data identified an advanced activity of the contralateral side (increased loading and power generation), which may correlate with the predisposition of contralateral limbs to CCL deficiency in dogs (Doverspike et al, 1993).

SUMMARY

This study describes for the first time gross differences in stifle joint mechanics between normal, CCL-deficient and contralateral limbs indicating a reduced activity of the injured side compensated by an advanced activity of the contralateral limb.

REFERENCES
Andriacchi (1990) *J. Biomech,* 23:99-105
Colborne, Innes, Comerford et al (2005) *Am J Vet Res*, 66:1563-1571
Doverspike, Vasseur, Harb et al (1993) *J Am Anim Hosp Assoc*, 29:167-170
Winter (2005) *Biomechanics and Motor Control of Human Movement.* New York, Wiley

Measurement		CCL-deficient	Contralateral	Normal
Moment (N.m/kg)	flexor peak stance	-0.08 (±0.05) A	0.03 (±0.09) B	-0.17 (±0.07) C
	extensor peak stance	0.31 (±0.12) A	0.57 (±0.15) B	0.42 (±0.14) A
	flexor peak swing	-0.15 (±0.03) A	-0.26 (±0.06) B	-0.21 (±0.04) C
Power (W/kg)	peak generation	0.10 (±0.27) A	1.56 (±0.83) B	0.64 (±0.40) C
	peak absorption	-1.06 (±0.58) A	-2.33 (±0.46) A	-1.95 (±0.33) A
JRF (N/kg, N.s/kg)	vertical peak	-3.02 (±1.70) A	-6.51 (±0.85) B	-5.98 (±0.99) B
	vertical impulse	0.41 (±0.23) A	1.02 (±0.17) B	0.87 (±0.13) C
	propulsion peak	0.71 (±0.24) B	1.09 (±0.23) A	0.85 (±0.22) B
	propulsion impulse	0.11 (±0.03) B	0.15 (±0.37) A	0.12 (±0.02) B
	braking peak stance	-0.27 (±0.25) A	-0.57 (±0.39) B	-0.80 (±0.20) B
	braking impulse stance	0.01 (±0.01) A	0.03 (±0.02) B	0.05 (±0.01) B
	braking peak swing	-0.51 (±0.14) A	-0.89 (±0.23) B	-0.71 (±0.16) C
	braking impulse swing	0.04 (±0.01)	0.04 (±0.01)	0.04 (±0.01)

Table 1: Mean (±SD) of net moment, power and JRF for the stifle joint of normal, CCL-deficient and contralateral limbs. **A**, **B, C**: groups with different letters differ statistically.

HIGH ENERGETIC COST OF SUDDEN CENTER-OF-PRESSURE ADVANCEMENT DURING HUMAN WALKING

Peter Gabriel Adamczyk[†] and Arthur D. Kuo
Department of Mechanical Engineering, The University of Michigan, Ann Arbor, MI USA
[†]email: padamczy@umich.edu

INTRODUCTION

In normal human walking, the stance foot and ankle interact in such a way that the entire lower leg behaves much like a single curved body rolling on the ground (Hansen et al., 2000). When foot or ankle function is impaired, interventions include walking boots that immobilize the ankle and shoes that redistribute plantar pressure. Both typically employ a rocker bottom shape that facilitates forward progression of the center of pressure (COP) similar to normal. Previous results show that rocker curvature can significantly reduce energy expenditure (Adamczyk et al., 2006). Here we show that, when the foot bottom has little curvature, very subtle differences in shape can greatly increase energy expenditure. Nearly flat rockers with slightly convex or concave profile yield large differences in COP progression and walking energetics, demonstrating the importance of smooth rolling of the foot.
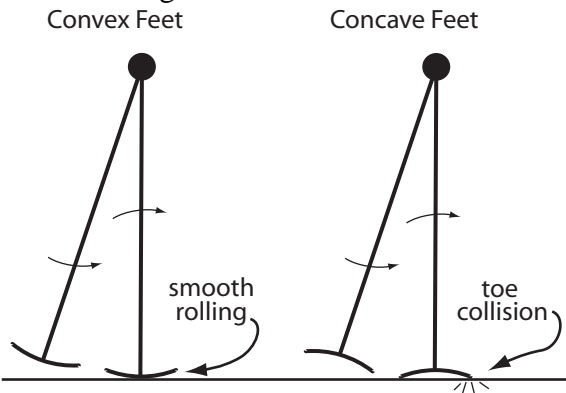

Figure 1: Walking models with convex and concave feet. Convex feet facilitate smooth rolling through the stance phase, a behavior that human feet emulate during normal gait. The only energy loss occurs in a collision at heel strike. Concave feet have an additional "toe-strike" collision as the contact point advances suddenly to the toe.

METHODS

A simple model of a rolling rigid body (Ruina et al., 2005) suggests that convex *versus* concave profiles should dramatically change the amount of work required to roll at given speed. This concept can be applied to a simple model of walking comprising a point mass pelvis and two rigid massless legs with infinitesimal mass at the bottoms of shaped feet (Fig 1). With convex feet, this model dissipates energy through ground collisions at heel-strike but rolls smoothly through each stance phase. With concave feet, heel strike is similar but there is also a second collision loss at the toe in mid-stance. The second collision increases the total work for concave feet. Because work by muscle exacts a metabolic cost, we hypothesized that humans would expend more energy to walk with a concave foot bottom shape than with a convex shape.

We immobilized subjects' ankles using a rigid plastic boot on each foot, modified to allow wooden blocks to be interchanged on the bottom surface (Fig 2). We designed two nearly flat wooden blocks to be superficially indistinguishable, but with one slightly convex and the other slightly concave (radius of curvature approximately ± 5.0 m).

We measured metabolic cost while normal young subjects (n = 8) walked at 1.25 m·s-1 on a treadmill. Subjects first walked in normal shoes as a control condition. They next walked on the two blocks in random order. We estimated average metabolic energy expenditure rate using indirect calorimetry. Metabolic rates were non-dimensionalized
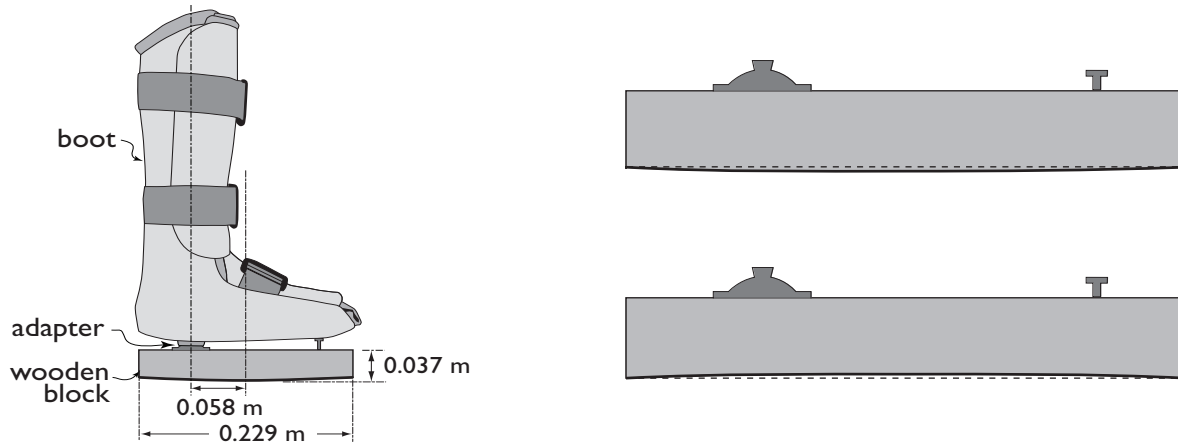
Figure 2: Rigid boot with interchangeable wooden blocks, used to immobilize the ankle and enforce a foot bottom shape. Right: Superficially similar, nearly flat blocks: one slightly convex, the other slightly concave.

using base units gravitational acceleration *g,* body mass *M,* and leg length *L*. We separately asked subjects to visually inspect the two wooden blocks and identify any perceived differences.

RESULTS AND DISCUSSION

Both wooden blocks caused subjects to expend substantially more energy than during normal walking (Fig 3). The cost for walking on the slightly convex block was 45.6% higher than for normal walking (P = 2×10^{-5}, ANOVA), due to both block shape and the
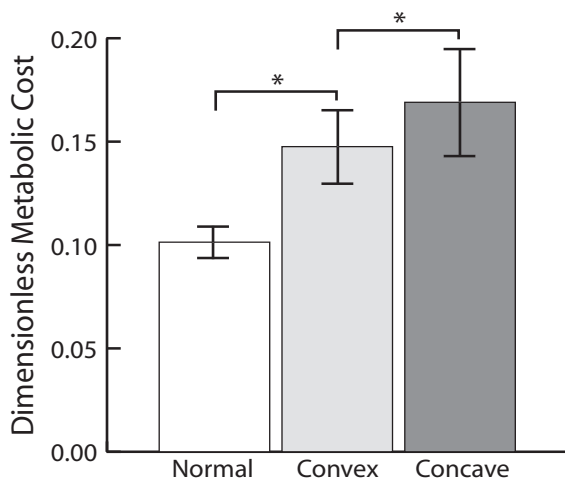

Figure 3: Energy expenditure rate (mean ± S.D.) for normal walking and walking with convex and concave foot bottom shapes. Dimensionless cost in excess of quiet standing is shown. Asterisks denote significant differences, P < 0.05.

extra apparatus mass attached to the feet (Adamczyk, 2006). The cost for the slightly concave block was 66.7% higher than normal (P = 2×10^{-7}), and 14.5% higher than for the convex block (P = 0.012). As an indicator that the foot bottoms were superficially similar, 5 of 8 subjects were unable to identify bottom curvature as the main difference between them. But all subjects could correctly identify which was better while walking on them, demonstrating the mechanical significance of the very subtle difference in curvature.

The toe-strike collision of humans is less pronounced than in a model, possibly because of body and apparatus compliance and/or motor adaptation. The cost increase may arise in part from altered joint moments in response to an abnormally sudden advancement of the center of pressure underfoot. But whether or not the toe collision is avoided, foot bottom shape can greatly affect energy expenditure.

REFERENCES

Adamczyk, PG et al. (2006). *JEB* 39:3953-63
Hansen, AD et al. (2000). *POI* 24(3):205-215
Ruina A et al. (2005) *JTB* 237:170-92

ACKNOWLEDGEMENTS

UNCONSTRAINED SHOULDER JOINT POSITION SENSE DOES NOT CHANGE WITH BODY ORIENTATION

Jason Chapman[1], David N Suprak [2], Andrew R Karduna[1]
[1]Department of Human Physiology, University of Oregon, Eugene, Oregon 97403
[2] Department of Health Sciences, University of Colorado, Colorado Springs, Colorado 80918
email: karduna@uoregon.edu; website: biomechanics.uoregon.edu/obl

INTRODUCTION

Muscle forces at the shoulder play a predominant role in maintaining joint stability. There is evidence in the literature that an increase in muscle activation results in an improvement in joint proprioception, which may help enhance joint stability. To our knowledge, a previous study from our laboratory was to first to demonstrate a graded response in joint position sense (JPS) at different levels of muscle activation (Suprak et al., 2006). However, one of the limitations of that study was that changes in muscle activation were also accompanied by changes in joint angle. Therefore, the changes in JPS could have been due to either of these factors. The present study was designed to overcome previous limitations. By manipulating trunk angle, we propose a model in which we can directly compare JPS at different joint angles (at the same resistive torque) and at different resistive torques (at the same joint angles).

METHODS AND PROCEDURES

Twenty-four healthy volunteers (22.1 ± 3.5 years) participated in this study. Kinematic data of the humerus and thorax were collected with a Polhemus Fastrak 3Space magnetic tracking system (Colchester, VT, USA). Bony landmarks were digitized in order to establish anatomical coordinate systems (Wu et al., 2005). A head mounted display (I-O Display Systems, Sacramento, CA) allowed for the presentation of kinematic data to the subject while suppressing any extraneous visual cues. A chair was designed to allow the torso of each subject to be tilted backward by 45 degrees (figure 1). A total of six target positions (45, 60, 75, 90, 105, and 120 degrees of humerothoracic elevation) were presented to the subjects in a randomized order. Testing at each target was performed both with the subject upright and tilted.

Figure 1 – Experimental Setup

In the head-mounted display, the subject was presented with the output from the sensors which served to guide the subject to the target position. The screen then went blank and the subject was required to maintain the position for five seconds and then returned the arm to the starting position. The subject then attempted to replicate the presented arm orientation. The angle between the presented position and reproduced position in 3D was calculated as the vector error (Suprak et al., 2006). A two-way, repeated measures ANOVA was conducted with two within subject factors (tilt and target angles). Three target positions for each tilt were matched so as to require the same torque. An additional two-way repeated measures ANOVA was

performed with two within subject factors (tilt and joint torque).

RESULTS

The two-way ANOVA with matching joint angles revealed no main effect of tilt (p = 0.494) and a significant interaction between condition and joint angle (p<0.05) (figure 2A). Follow-up paired t-tests demonstrated that for all joint angles, there was no significant difference between conditions (p>0.05). The two-way ANOVA with matching joint torques revealed a main effect of tilt (p = 0.002) and no significant interaction between condition and joint angle (p=0.970) (figure 2B).
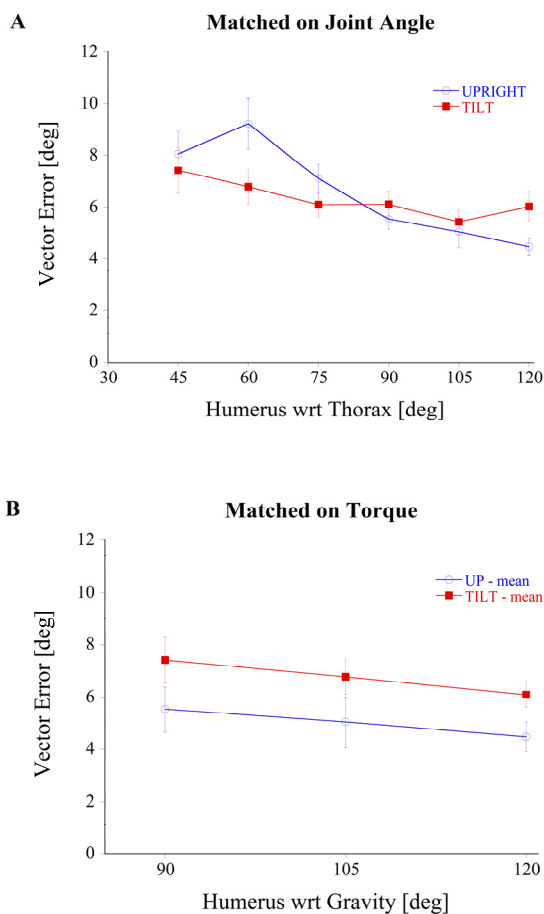

Figure 2 – Analysis of data matched on (A) Joint angle and (B) Torque

DISCUSSION

The results from the present study demonstrated no significant difference when the two conditions were compared on the basis of joint angle, but there was a significant effect when they were matched on joint torque. In a parallel study in our lab, we found that by increasing joint torque with the addition of weights, there was an increase in JPS accuracy (Suprak et al., 2007). However, the magnitude of that effect was much lower than what we observed in our elevation study. One theory that would fit the data from all three experiments is that there is an effect of both joint angle (present study) and joint torque, but the effect of joint angle is much stronger. It is likely that humans incorporate both muscle activation and some intrinsic coordinate system based on muscle length, joint receptor activation and skin deformation when positioning a joint. It seems intuitive that the body may preferentially use one input more than another or in combination with another as opposed to selecting which afferent system to utilize at a given time.

SUMMARY

In summary, when comparing upright and tilted conditions, we found matching based on elevation angle demonstrated no significant difference, while there were differences when matching was based on resistive torque. This would appear to implicate elevation angle at the shoulder as playing a more important role in joint position sense than joint torque. However, we cannot rule out an effect of torque that was overshadowed in the present study.

REFERENCES

Suprak et al. (2006) JOR, 24: 559-568
Suprak et al. (2007) J Mot Beh, 39: 517-25

Wu et al., (2005), J Biomech, 38, 981-992

COMPARISON OF MUSCLE ACTIVITY DURING COMMON LOWER EXTREMITY REHABILITATION EXERCISES

Sabrina Silver[1], Cara L. Lewis[1] and Riann Palmieri-Smith[1]

[1]Division of Kinesiology, University of Michigan, Ann Arbor, Michigan, USA,
caralew@umich.edu

INTRODUCTION

Similar to the muscle redundancy problem in musculoskeletal modeling, rehabilitation specialists face a challenge when designing exercises to preferentially strengthen one muscle within a group of muscles that perform similar functions. For example, targeting the iliopsoas muscle separate from the rectus femoris muscle or the vastus medialis separate from the other knee extensor muscles is difficult. The purpose of this study was to evaluate muscle activity during the performance of commonly utilized rehabilitation exercises proposed to preferentially target specific muscles within a synergistic group.

METHODS AND PROCEDURES

Eight subjects participated voluntarily in this study. Subjects with current or recent history of significant hip or knee pain or neurological disorders were excluded. Each subject gave informed consent prior to participation.

Reflective markers were placed on the subject's trunk, pelvis and legs. Surface electromyography (EMG) electrodes were placed over the muscle bellies of the vastus lateralis, vastus medialis, rectus femoris, medial hamstrings, lateral hamstring and iliopsoas muscles. Iliopsoas was placed lateral to the femoral pulse, medial to rectus femoris, and inferior to the inguinal ligament (Gottschall and Kram, 2005). To ensure correct placement of iliopsoas electrode, each subject performed a pair of movements in quadruped as recommended by Cram and Kasman (1998). For the first movement, with the knee raised slightly off of the ground the subject brought the knee to the chest. For the second movement, the subject extended both the hip and knee out behind. If electrode placement was correct, an iliopsoas burst is seen only during the first movement of hip flexion. If questionable muscle activity was noted, the electrodes were repositioned and retested.

Kinematic and electromyographic data were collected while subjects performed supine hip flexion with knee flexion (heel slide) and supine hip flexion with knee extended (straight leg raising) under different conditions. Subjects performed heel slides naturally, and with the instruction to "dig" into the surface while sliding the heel. It is a clinical belief that performing a heel slide while digging into a surface will elicit iliopsoas activity without eliciting rectus femoris activity, despite both muscles' role as hip flexors. Subjects performed straight leg raises under three conditions: with the leg in neutral rotation, lateral rotation and medial rotation. Performing straight leg raises in different positions of femoral rotation is thought to target the knee extensor muscles differently. A metronome was used to regulate the speed of each movement which was performed through the same range of motion for each condition. We randomized the order of the conditions and collected five trials of each condition.

For each muscle, the average root mean square (RMS) of the EMG data was

calculated from the start of movement to the end of movement as determined by the kinematic data. For each subject, we averaged the values from the five trials. We used repeated measures analysis of variance followed by paired t-tests if appropriate to determine differences in muscle activity between exercises.

RESULTS

Variations in the exercises had an effect on the activity of certain muscles. The rectus femoris muscle activity was less in the heel slide with dig condition than the heel slide condition ($p = 0.002$). Conversely, the activity of the medial hamstrings and lateral hamstring was higher in the heel slide with dig condition than without the dig ($p < 0.05$). The iliopsoas muscle activity was similar across all exercises and conditions. Knee extensor muscle activity was similar in all straight leg raise conditions.

DISCUSSION

Modifying the heel slide exercise to include digging the heel into the ground was successful in reducing the rectus femoris muscle activity while maintaining iliopsoas

activity. The hamstring muscles may have been inhibiting the rectus femoris activity as these muscles have antagonistic actions at the knee. In contrast, we did not find a difference in the muscle activity of the knee extensors during performance of the straight leg raise in three different rotation positions in this limited sample.

SUMMARY

Exercises thought to preferentially target specific muscles within a muscle synergy group should be carefully tested. Antagonistic muscle activity may be useful in reducing activation of one muscle while maintaining activation of another muscle which has a slightly different function.

REFERENCES

Cram, JR and Kasman, GS (1998). *Electrode Placement.* Gaithersburg, MD: Aspen.
Gottschall, JS and Kram, R (2005). *J Appl Physiol,* 99:23-30.

ACKNOWLEDGEMENTS

Exercise	Iliopsoas	Rectus Femoris	Vastus Lateralis	Vastus Medialis	Medial Hamstrings	Lateral Hamstring
Heel Slide	0.057	**0.007**	0.004	0.010	**0.008**	**0.008**
	(0.018)	**(0.001)**	(0.001)	(0.003)	**(0.002)**	**(0.002)**
Heel Slide w/ Dig	0.096	**0.005**	0.008	0.011	**0.035**	**0.032**
	(0.036)	**(0.001)**	(0.003)	(0.002)	**(0.010)**	**(0.012)**
SLR – Medial	0.036	0.024	0.016	0.020	0.005	0.004
	(0.014)	(0.003)	(0.006)	(0.003)	(0.001)	(0.001)
SLR – Neutral	0.057	0.024	0.015	0.018	0.004	0.004
	(0.031)	(0.003)	(0.005)	(0.003)	(0.001)	(0.001)
SLR – Lateral	0.066	0.027	0.011	0.016	0.005	0.005
	(0.029)	(0.003)	(0.003)	(0.003)	(0.001)	(0.001)

Table 1. Mean (and s.e.m.) root mean square (RMS) from the start of the movement to the end of movement. Bolded cells indicate significant difference between conditions.

HOW DIFFERENT MATERNAL VOLITIONAL PUSHING PROFILES AFFECT THE DURATION OF THE SECOND STAGE OF LABOR: A 3-D VISCO-HYPERELASTIC FINITE ELEMENT MODEL

Dejun Jing[1], James Ashton-Miller[1] and John O. DeLancey[2]

[1]Biomechanics Research Laboratory, Department of Mechanical Engineering, and
[2]Department of Obstetrics & Gynecology, University of Michigan, Ann Arbor, Michigan, USA
djing@umich.edu URL: http://me.engin.umich.edu/brl/

INTRODUCTION

During the second stage of labor the uterus contracts once every three minutes for about a minute. To deliver her baby a woman has to supplement this by 'bearing down' ('pushing') via volitional cocontractions of her diaphragm and abdominal wall muscles during each uterine contraction. This combined effort gradually helps drive the fetal head along the birth canal so that it passes through a 'ring' formed by the pubic symphysis and a 'U-shaped' ring of levator muscle. Medical professionals favor several different pushing styles to speed up the progress of labor (Thomson 1993). It would be useful to which pushing style maximizes the progress of labor while minimizing maternal effort (Sampselle 1999, Hudelist 2005). Lien (2006) has examined this question using a Matlab model and viscoelastic bands to represent the levator ani. We are unaware of any studies comparing the efficacy of different pushing profiles using finite element (FE) analysis.

METHODS AND PROCEDURES

A 3D finite element model of the birth process was developed (Figure 1). As a first order approximation, simplified geometries were used in which the pelvic floor muscles were simulated using a truncated cone-shaped deformable shell, while the fetal head was represented by a rigid sphere of average fetal head diameter reduced by 10% to
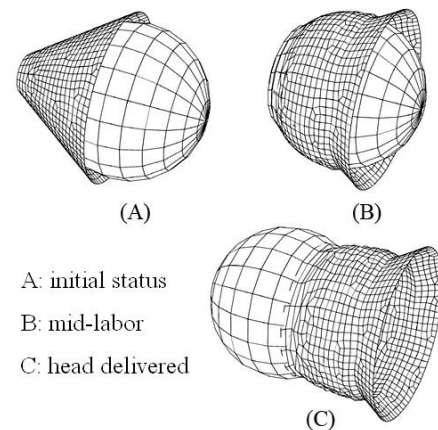

Figure 1. FE model of the second stage of labor at three stages. The fetal head moves along the 'birth canal' driven by a cyclic pushing pressure. Each pushing cycle lasts 3 minutes as shown in Figure 2.

A: initial status
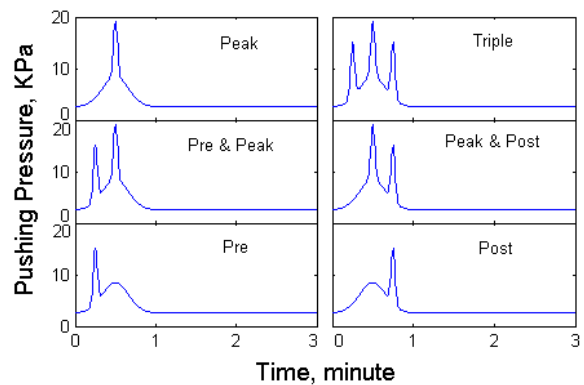B: mid-labor
C: head delivered

Figure 2. Six alternative pushing pressure profiles (10-s pushes) superimposed on one uterine contraction cycle.

account for molding (Lien 2006). A damping constraint, determined by trial-and-error, was applied to the fetal head to simulate its interaction with surrounding pelvic floor

structures and allow delivery of the head with the triple push pattern in a usual time of 90 minutes. Visco-hyperelastic muscle properties used in the model were taken from our own tissue tests on rat and human pelvic floor tissues, and the model was solved using ABAQUS Explicit code.

RESULTS

The descent of the fetal head exhibited a sigmoid displacement-time behaviour (Figure 3), descending rapidly at first (due to low muscle stiffness), then more slowly (as the muscle is stretched and becomes stiffer), then rapidly again once the mid-diameter is delivered at the end of the second stage. The total number of pushes and *length of labor* (*in minutes*) for the Triple, Peak, Pre & Peak, Peak & Post, Pre and Post pushing styles were 90 and *90*, 49 and *147*, 74 and *111*, 74 and *111*, 54 and *162*, 54 and *162*, respectively.
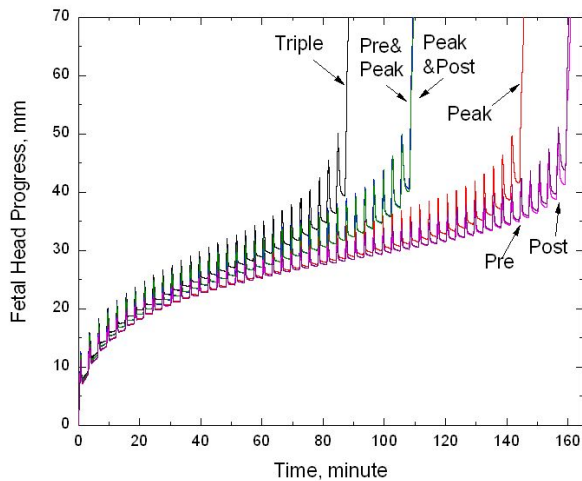

Figure 3. Simulated fetal head descent for each of the six pushing profiles.

DISCUSSION

It has been traditional in this country to use 'triple' pushing profile to shorten labor duration. However, our results suggest that the 'triple' style was less 'cost effective' than the 'peak' style because it costs significantly

increased maternal effort (total number of 10-s pushes) to gain the shorter labor duration (Fig. 4). Profiles involving a single volitional push timed near the peak uterine contraction were the most efficient.
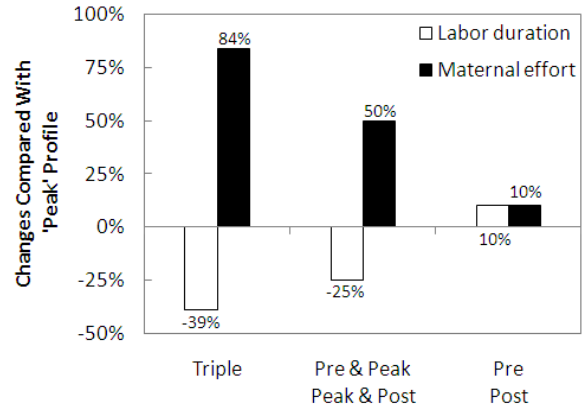

Figure 4. Effect of pushing style on change in labor duration and maternal effort compared with the 'peak' profile.

SUMMARY

The 'triple' and 'peak' pushing profiles were the most efficient in terms of duration and maternal effort, respectively. More pushes decrease the duration of labor, but at the expense of greater maternal effort, thereby increasing the risk of exhausting the mother, halting progress, and requiring instrumented delivery or C-section.

REFERENCES

Lien, KC (2006) Ph.D. Thesis, University of Michigan.

Hudelist GJ (2005). *Am J Obstet Gynecol, 192(3)*: 875-881.

Sampselle, CM et al. (1999). *J Nurse Midwif 44(1)*: 36-39.

Thomson, AM (1993). *J Adv Nurs,18(2)*: 171-177

ACKNOWLEDGEMENTS

MOTOR RESPONSE DURING UNEXPECTEDLY REDUCED PLANTAR FLEXOR TORQUE PROVIDED BY A POWERED ORTHOSIS DURING WALKING

Pei-Chun Kao[1], Cara L. Lewis[1], and Daniel P. Ferris[1]

[1]Human Neuromechanics Laboratory, University of Michigan, Ann Arbor, MI, USA
E-mail: kaop@umich.edu

INTRODUCTION

Timing a burst of ankle plantar flexion mechanical power during late stance is critical to producing an economical gait pattern. A powered walking model by Kuo (2002) indicates that push-off performed along the trailing leg immediately before heel strike of the leading leg is four times less costly than driving the stance leg with hip mechanical power at other time points over the gait cycle. In humans, the ankle mechanical power burst provides the majority of positive work required to restore the energy lost in redirecting the center of mass in step-to-step transitions (Kuo et al., 2005). In addition to the correct timing, adequate magnitude of ankle push-off is necessary to prevent energy loss due to collision in the leading leg. These two factors, timing and amplitude of ankle push-off, may explain why many pathological gaits exhibit high metabolic costs.

The purpose of this study was to investigate the effect of ankle plantar flexor mechanical power during human walking by taking it away. We hypothesized that decreasing plantar flexor mechanical power in stance by unexpectedly turning off a robotic ankle orthosis would result in changes to walking dynamics predicted by simple walking models (Kuo, 2002; Kuo et al., 2005).

METHODS

Two healthy subjects trained walking with a powered orthosis controlled by soleus EMG for two 30-minute treadmill sessions (Gordon & Ferris, 2007). A real-time computer controller modulated force in an artificial plantar flexor muscle proportional to soleus EMG amplitude via a pressure regulator. On a separate day after completing training, subjects walked with the orthosis without power for 5 minutes (**Passive**), with constant power for 15 minutes (**Powered**), and then with power but random unexpected steps when power was turned off at mid-stance (**Perturbed**).

We collected lower body kinematics, EMG, artificial muscle force, and ground reaction forces while subjects walked on a force-measuring treadmill at 1.25 m/s. We calculated joint kinetics and EMG linear envelopes using Visual 3D software.

RESULTS AND DISCUSSION

During steady state walking, the orthosis provided ~40% of the net ankle moment during push-off (0.71±0.08 Nm/kg) (Fig. 1). When orthosis power was turned off unexpectedly, subjects reacted quickly by increasing soleus activation for the second half of stance (Fig. 1). The soleus EMG pattern during perturbed steps deviated from the soleus EMG pattern during powered steps (mean +1 SD) with a time lag of 86.5±24.6 (mean±SD) milliseconds after the orthosis torque deviated from the powered step pattern. As a result of the rapid increase in soleus EMG, the ankle moment pattern during the perturbed steps was remarkably similar to the ankle moment pattern during

unperturbed powered steps (Fig. 1). There were noticeable differences in the ankle angle and power profiles during the perturbed steps compared to the powered steps (Fig. 1).
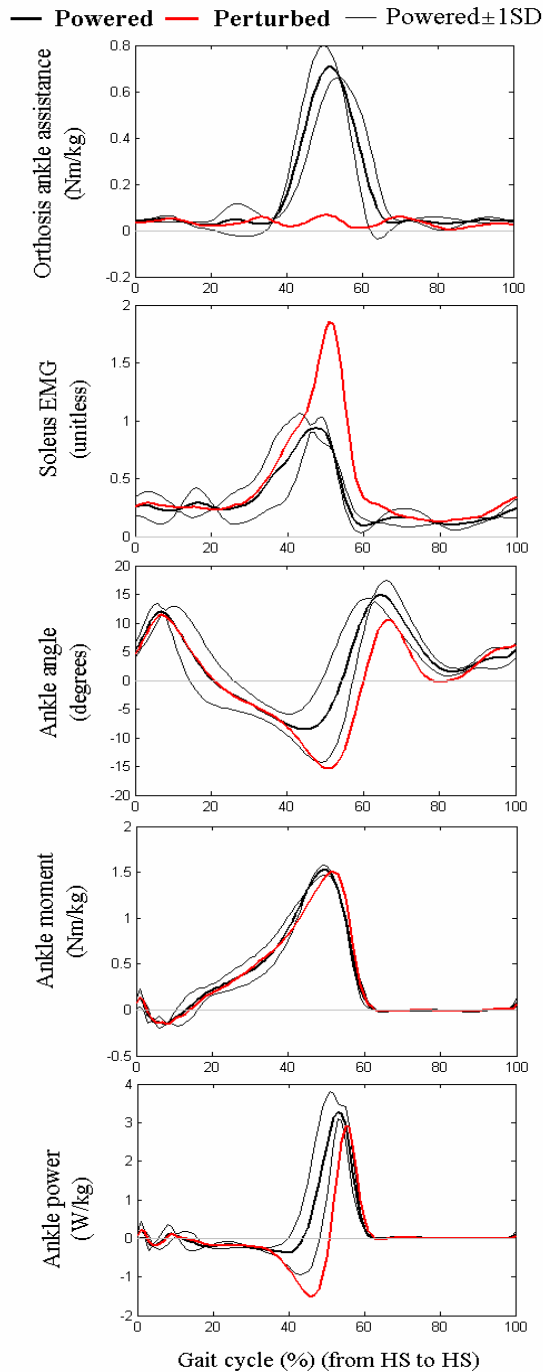

Figure 1. Gait dynamics during powered and perturbed walking trials (for ankle data, plantar flexion direction is positive).

Changes in the vertical ground reaction forces of the two legs were qualitatively consistent with predictions from simple walking models. The second peak of vertical ground reaction force was ~12% less for the perturbed steps compared to the powered steps (10.6 ± 0.4 N/kg vs. 12.1 ± 0.6 N/kg, respectively). The vertical ground reaction force in the contralateral leading leg was ~9% greater following the perturbed steps compared to following the powered steps (12.2 ± 0.8 N/kg vs. 11.2 ± 0.7 N/kg, respectively).

Previous studies have documented rapid increases in plantar flexor EMG following perturbed stretches due to stretch reflex activation (Sinkjaer et al., 1996). This is the first study to show that the reflex response results in remarkably normal ankle joint kinetics when encountering a gait perturbation.

SUMMARY/CONCLUSIONS

Although an unexpected decrease in mechanical assistance from a powered orthosis produced some changes in walking dynamics consistent with simple walking models, the rapid reflex response to the perturbation produced joint kinetics that were extremely similar to normal. This suggests that reflex gains are well modulated during gait to enhance stability to perturbations.

REFERENCES

Kuo, AD (2002) *J Biomech Eng*, 124:113-20.
Kuo, AD et al. (2005) *Exerc Sport Sci Rev*, 33:88-97.
Sinkjaer T et al. (1996) *J Neurophysiol*, 76:1112-20.

ACKNOWLEDGMENTS

A MODEL TO DETERMINE THE EFFECT OF MULTIPLE SUBCONCUSSIVE IMPACTS IN THE RAT

Erin Hanlon and Cynthia Bir

Wayne State University, Detroit, MI, USA
E-mail: cbir@wayne.edu, Web: www.bioengineeringcenter.org/home/labs/sports

INTRODUCTION

Many sports involve multiple impacts to the head during participation including soccer, football, and boxing. Research has determined tolerances for single concussive events however; the majority of these impacts are subconcussive (Stojsih Submitted). It remains unclear whether multiple subconcussive head impacts cause long-term damage.

The current study used a modification of the Marmarou (Marmarou 1994) weight drop model and Magnetic Resonance Imaging (MRI) techniques to detect small blood flow changes in the brain following single and repetitive subconcussive impacts.

METHODS AND PROCEDURES

A total of ten adult Sprague Dawley rats were tested; four 1 impact, four 10 impact and two shams. Prior to impact, preliminary MRI scans were performed using T1 weighted, T2 weighted, and arterial spin labeling (ASL) in all rats. These scans were used as intra-subject controls for each animal. Following baseline scans, rats were impacted using a modification of the Marmarou model (Marmarou 1994). The original model uses a

450 g mass dropped from 2 m to model traumatic brain injury. In order to model subconcussive events a reduction in mass and drop height was needed. Therefore, a 50 g weight was dropped from 40 cm. MRI scans were performed 24 hours post-impact.

RESULTS

The percentage change of blood flow was determined from the pre-impact scan with each animal serving as its own control (Figures 2-3). ASL revealed an average reduction in arterial cerebral blood flow (CBF) in the cortex and the hippocampus in the 10 impact group (Figure 3). While the 10 impact group showed decreases in blood flow, the one impact group showed increases in both the cortex and the hippocampus (Figure 2). In addition to CBF changes, one rat in the 10 impact group showed signs of hydrocephalus in the MRI post-impact (Figure 1).

Normalization of the data was necessary due to variability in the initial MRI scans. The pre-impact scan results were normalized to 100 mL/100g/min with the change in blood flow being calculated based on the normalized value (Figure 4). The ten impact group exhibited a statistically significant
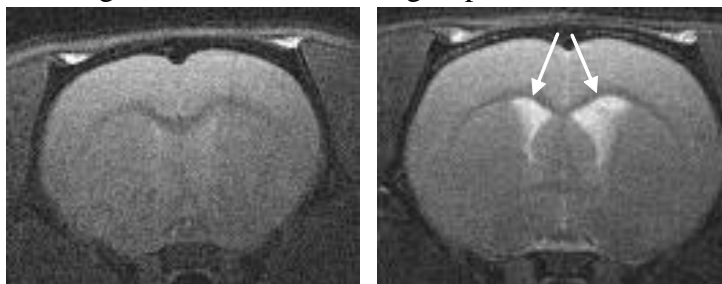
(a) pre-impact scan   (b) post-impact scan

Figure 1: Hydrocephalus, indicated by arrows, was present in one experimental specimen post-impact exposures.

decrease in CBF in comparison to the single impact group for both the cortex ($p=.026$) and the hippocampus ($p=.039$) regions.
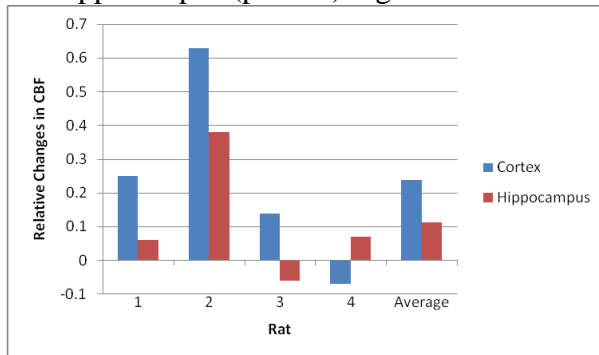

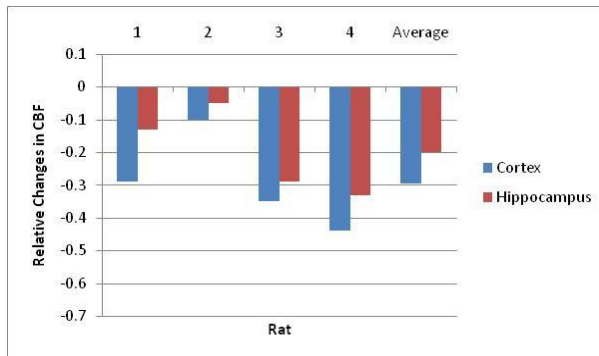**Figure 2: Changes in CBF measured by ASL in 1 impact group.**

Figure 3: Changes in CBF measured by ASL in 10 impact group.
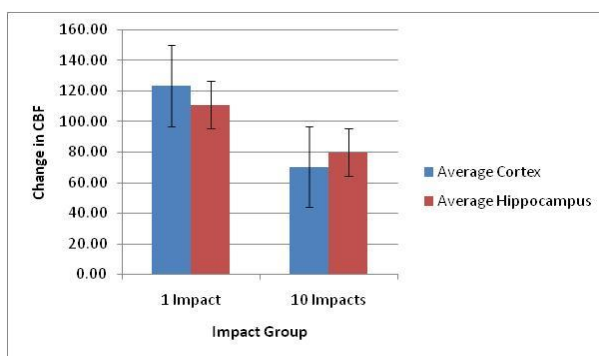

Figure 4: Normalized changes in CBF

DISCUSSION

One specimen (#2) in the one impact group had a high percentage increase in CBF post-impact (63% in the cortex and 38% in the hippocampus). These values appear to be outliers and are more likely due to the significant increase in heart rate exhibited by the specimen during the pre-impact scan (196 bpm) compared to the post-impact scan (263 bpm).

The current study was successful in reducing trauma level from the original Marmarou model. In the original model, there was a 44% mortality rate with 12.5% of non-survivors having a skull fracture using the 450 g mass and 2 m drop height. Using the current model, there were no fatalities and no skull fractures. Also, rats showed no signs of physical distress following impact.

SUMMARY

The current study provides preliminary justification for use of a modification of the Marmarou weight drop model as a model for testing the effects of multiple subconcussive events. The model demonstrates a subconcussive level of injury for a single impact, but an increase in the level of injury, as measured by decrease in CBF, for multiple subconcussive events. By using an animal model, variables such as previous head injury can be eliminated when studying the effects of multiple subconcussive head impacts.

REFERENCES

Marmarou, A., et al. (1994). *J Neurosurg* 802: 291-300.
Stojsih, S., et al. (Submitted). *Clin J Sport Med.*

ACKNOWLEDGEMENTS

EFFECT OF HIP PROTECTORS AND BODY MASS INDEX ON PRESSURE DISTRIBUTION DURING A FALL ON THE HIP

Woochol Joseph Choi[1] and Stephen N. Robinovitch[2]

[1]School of Kinesiology, Simon Fraser University, Burnaby, BC, Canada, woocholc@sfu.ca
[2]School of Kinesiology, Simon Fraser University, Burnaby, BC, Canada, stever@sfu.ca

INTRODUCTION

Hip fractures are a major health problem among the elderly, and 90% of fractures are caused by falls. Wearable hip protectors (Parker et al., 2006) represent a promising strategy for attenuating and redistributing the force applied to the hip region, and thereby reducing the risk for hip fracture during a fall. However, the protective effect of hip protectors should depend on the direction of the fall, and the amount of baseline soft tissue padding over the hip. In the current study, we tested these hypotheses through safe falling experiments in young adults.

METHODS AND PROCEDURES

Fourteen young women (aged 18-35) participated. Through initial screening, one-half of participants were selected to have a body mass index (BMI) greater than 25, and the other half had a BMI less than 18.5. Subsequent ultrasound measures confirmed that the high BMI group had considerably greater thickness of soft tissue over the greater trochanter (GT).

Sideways falls were simulated by releasing the participant (by means of a tether and electromagnet) from a height of 5 cm. Trials were acquired for pelvis orientations which produced direct lateral impact to the GT, with the pelvis tilted 20 degrees posterior to the lateral midline, and with the pelvis tilted 20 degrees anterior. For each configuration, three repeated measures were acquired in the unpadded condition, and while wearing a commercially available soft shell hip protector.

In each trial, an RSscan device (0.5 m model) mounted over the impact surface provided a measure of the pressure applied to the contact areas, at 500 Hz. The RSscan plate contains 4096 pressure sensors (each having a surface area of 7 mm x 5 mm) in a 64 by 64 cell array. The device has a measurement resolution of 1 kPa, range of 3 to 1270 kPa, and accuracy of 0.37 kPa based on in-house calibration.

The location of the greater trochanter (GT) and femoral diaphysis during impact were monitored at 250 Hz with an optical motion measurement system (Motion Analysis Corp, Eagle system), and custom routines were used to anatomically map the RSscan pressure record over the hip region (Figure 2).

Data were analyzed using RM ANOVA (with alpha=0.05), with BMI as a grouping factor, to determine whether the hip protector affected the magnitude and location of peak pressure over the hip region during impact.

RESULTS

ANOVA results indicated that normalized values of peak pressure associated significantly with hip protector condition (F=13.7, p=0.003), impact configuration (F=4.9, p=0.03), and BMI (F=6.7, p=0.024). Furthermore, there was a significant interaction between hip protector condition and BMI (F=7.8, p=0.016), reflecting a

greater protective effect for low BMI than high BMI participants. For example, in the lateral impact configuration, peak pressure decreased 77% (from 754 to 168 kPa) in low BMI participants, and 48% (from 369 to 180 kPa) in high BMI individuals (normalized pressures shown in Figure 1). Similar trends were observed in the posterio-lateral and anterior-lateral impact configurations.

The location of peak pressure (distance from the GT) also associated with hip protector condition (F=67.3, p<0.001 for absolute distance and F=7.3, p=0.02 for angle from the diaphysis), and with impact configuration (F=21.5, p<0.001 for angle). Furthermore, there was a significant interaction between protector and BMI (F=8.4, p=0.013 for distance and F=19.8, p=0.001 for angle), with the hip protector redirecting peak pressure, on average, from 53 mm to 71 mm away from the GT in low BMI individuals, and from 47 to 84 mm in high BMI individuals (Figure 2).
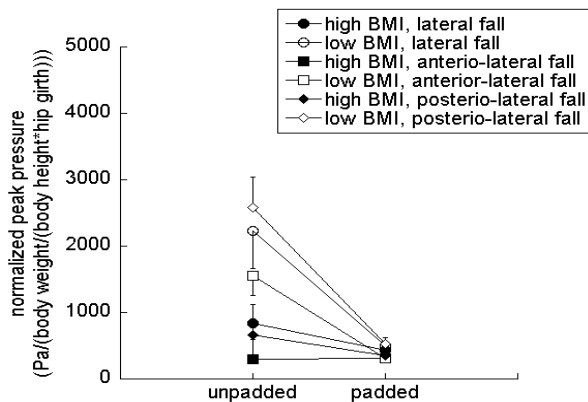

Figure 1. Mean values (with SE's) of normalized peak pressure in unpadded and padded conditions, for low and high BMI groups.

DISCUSSION

Previous studies indicate that peak force during a fall scales linearly with the thickness of soft tissues over the greater trochanter

(Robinovitch et al. 1995), and that such tissues typically reduce fall impact force by 50% (Bouxsein et al. 2007). In support of these observations, we found that peak pressures in the baseline, unpadded condition were much greater in low BMI than high BMI individuals. Furthermore, hip protectors substantially attenuate peak pressure in low BMI but not high BMI individuals, largely removing the variation in pressure between these groups.
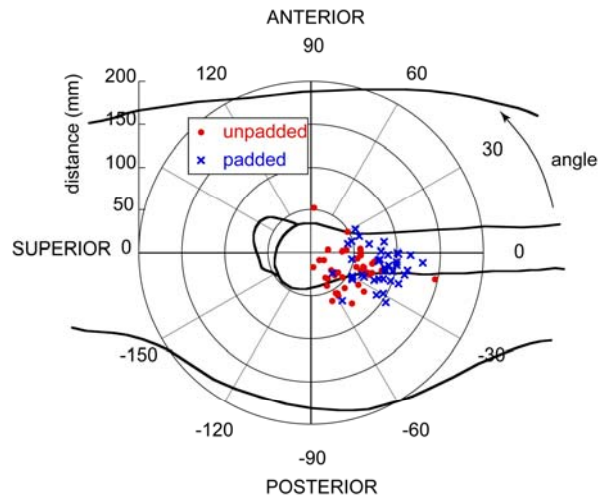
Figure 2. Location of peak pressure during lateral falls, unpadded and padded conditions.

SUMMARY

The soft shell hip protector we tested substantially reduced peak pressure over the hip for low BMI participants, but had less protective effect for high BMI individuals.

REFERENCES

Parker et al. (2006). BMJ 332(7541):571-4.
Bouxsein et al. (2007). JBMR 22:825-31.
Robinovitch et al. (1995). J Orthop Res. 13(6): 956-62.

ACKNOWLEDGEMENTS

AN EXPERIMENTAL MODEL OF DILATED CARDIOMYOPATY

Audrée McKenzie and Walter Herzog
Faculty of Kinesiology, University of Calgary, Calgary, AB, Canada
amckenzie@kin.ucalgary.ca

INTRODUCTION

Dilated cardiomyopahty (DCM) is a frequent heart disease characterized by cardiac dilation and reduced heart function. About one in three cases of congestive heart failure is due to dilated cardiomyopathy. Its triggers include gene mutations, as well as environmental factors (Seidman and Seidman, 2001). Inherited genetic defects are thought to account for 25% to 35% of all DCM cases (Franz WM et al., 2001; Fonarow, 2001). Mutations in dystrophin (Dys) and in certain Dys-associated proteins (DAPs) are known to cause DCM in human cases. Dys and DAPs form part of a system which links actin on the inside of cardiac muscle fibers to extracellular matrix proteins. This system is involved in transmitting the force developed by the actin-myosin cross-bridges to the extracellular matrix and provides mechanical resistance to the over-expansion of the sarcolemma (Kawada et al., 2005). The DAPs include two groups of proteins, the dystroglycans and the sarcoglycans (SGs).

The Bio TO-2 Syrian hamster strain is a valuable model of human hereditary DCM. It is missing the δ-SG gene and associated protein, and demonstrates a reduction of the α, β, and γ-SG proteins (Kawada et al., 2005; Nigro et al., 1997). It shows systolic and diastolic dysfunctions and a remarkable decrease of both the fractional shortening and the left ventricular ejection fraction, pathophysiological features very similar to human cases with DCM (Kawada et al., 2005).

Thus far, the sarcomere length distributions of experimental cardiac myofibrils from cardiomyopathic Syrian hamsters (Bio TO2) and of cardiac myofibrils from normal Syrian hamsters (Bio F1B) have been examined.

METHODS AND PROCEDURES

Male cardiomyopathic and normal hamsters were euthanized at 23 weeks of age. The hearts were rapidly excised and perfused with a Rigor solution at room temperature containing glucose and DDT. The hearts were then transferred to a relaxing solution at 0-4ºC containing an antiprotease cocktail. Cardiac papillary and trabeculea muscles were excised from the left ventricles and pinned in a relaxing solution at 0-4ºC containing an antiprotease cocktail and 1% v/v triton. After two hours, the muscles were washed with the relaxing solution containing an antiprotease cocktail but no triton and stored at 0-4ºC until the next day. Myofibrils were isolated from these muscle strips by homogenization in the same solution at a speed of 10 000 RPM for 7 to 14 seconds.

For sarcomere length determination, a few drops of the myofibril suspension were placed onto a cover slip chamber on top of an inverted microscope. Light was sent perpendicularly through the myofibrils and the associated dark/white (myosin/actin) striation patterns were captured with a high resolution photodiode array consisting of >10,000 individual elements providing a resolution of 6nm.

RESULTS

The length of sarcomeres isolated from cardiac papillary muscles of the Bio F1B hamster ranged from 2.2 to 2.7 µm (n = 3) averaging 2.5 µm (SD = 0.29). For the Bio TO2 hamster, they ranged from 2.3 to 2.7 µm (n = 10) also averaging 2.5 µm (SD = 0.16).
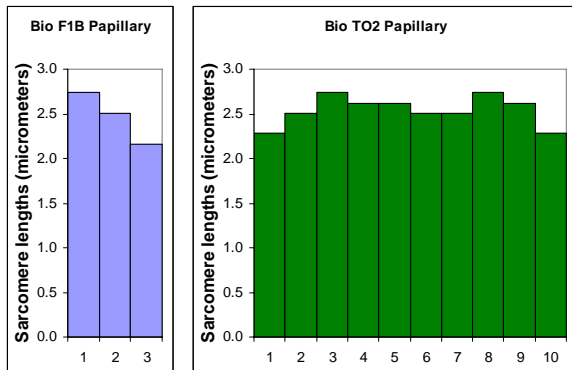

Figure 1: Sarcomere lengths of myofibrils isolated from cardiac papillary muscles of a Bio F1B hamster and of a Bio TO2 hamster. Each bar represents the length of one sarcomere from one myofibril.

The length of sarcomeres isolated from cardiac trabeculea muscles of the Bio F1B hamster ranged from 2.1 to 2.6 µm (n = 6) averaging 2.4 µm (SD = 0.26). For the Bio TO2 hamster, they ranged from 2.4 to 2.7 µm (n = 9) averaging 2.6 µm (SD = 0.13).
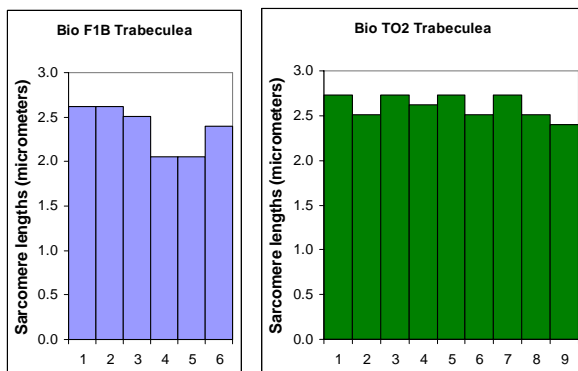

Figure 2: Sarcomere lengths of myofibrils isolated from cardiac trabeculea muscles of a

Bio F1B hamster and of a Bio TO2 hamster. Each bar represents the length of one sarcomere from one myofibril.

DISCUSSION

Dilatational cardiomyopathy is associated with structural and functional deficits of the heart. Here, we tested if gross sarcomere length non-uniformities of passive muscle might contribute to theses deficiencies, but the results from this study on papillary and trabeculae do not support this idea. This might be the case because cardiomyopathy has not progressed far enough in the 23 week old animals tested here, or because deficiencies are not visible in the passive state. Active sarcomere length distributions will be examined in future studies, as well as maximum active isometric forces at optimal sarcomere length, stiffness as a function of sarcomere lengths, titin and myosin isoforms, and stability of active sarcomeres on the descending limb of the force-length relationships.

SUMMARY

Passive sarcomere length distributions in papillary and trabecular muscles of hamsters with dilated cardiomyopathy and age-matched controls are similar and do not show the expected sarcomere length non-uniformities at 23 weeks of age.

REFERENCES

Fonarow GC. *Rev Cardiovasc Med* 2001;2:103-4.
Franz WM et al. *Lancet* 2001;358:1627-37.
Kawada T et al. *Pharm. & Therapeutics* 2005;107:31-43
Nigro et al. *Hum Mol Genet* 1997;6:601-607.
Seidman JG, Seidman C. *Cell* 2001:104:557-567.

ESTIMATING THE MOMENT OF INERTIA OF THE HUMAN BODY AS A SINGLE LINK INVERTED PENDULUM MODEL

Pilwon Hur and Elizabeth T. Hsiao-Wecksler

Mechanical Science & Engineering
University of Illinois at Urbana-Champaign, Urbana, IL, USA
E-mail: ethw@uiuc.edu   Web: www.mechse.uiuc.edu/research/hsiao-wecksler/

INTRODUCTION

Moment of inertia of the human body is a frequently used parameter to understand the human postural control system with control models that represent the upright body as a single link inverted pendulum. However, there is no unique way of calculating the moment of inertia. The most frequently used method is regarding the human body as a point mass. Then the moment of inertia can be easily computed as of $J=mh^2$, where m is mass of the body and h is height of the point mass from ankle. To obtain more accurate moment of inertia values, combining all moments of inertia of each segment based on anthropometric data can be used (Winter, 2005).

In this paper, a simple single link inverted pendulum model was used to derive equations of motion (EOM) relating center of mass (COM) and center of pressure (COP). COP was directly computed from forceplate data. COM was computed from the gravity line projection (GLP) method (Zatsiorsky and Duarte, 2000) which is robust and independent of standing conditions; furthermore, it only requires force plate data. By identifying the value of the moment of inertia, which best fits the COM from the EOM to the COM from GLP, the moment of inertia can be estimated.

METHODS
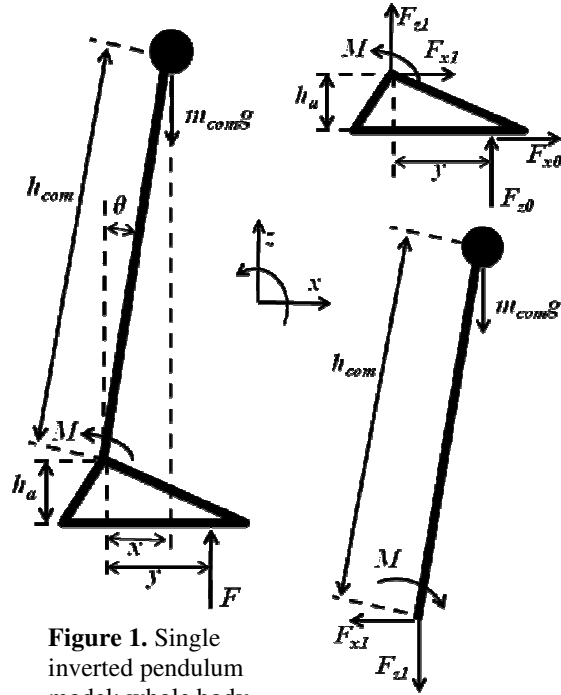
Figure 1. Single inverted pendulum model: whole body, and free body diagrams of foot and pendulum.

EOM of foot
By assuming that the foot is stationary,

$$\sum F_x = F_{x0} + F_{x1} = m_{foot}\ddot{x}_{foot} = 0 \tag{1}$$

$$\sum F_z = F_{z0} + F_{z1} = m_{foot}\ddot{z}_{foot} = 0 \tag{2}$$

$$\sum M_{ankle} = M + yF_{z0} + h_a F_{x0}$$
$$= J_{foot}\ddot{\theta}_{foot} = 0 \tag{3}$$

EOM of pendulum
By small angle approximation,

$$\sum F_x = -F_{x1} = m_{com}\ddot{x}_{com} \tag{4}$$

$$\sum F_z = -F_{z1} - m_{com}g = m_{com}\ddot{z}_{com} \tag{5}$$

$$\sum M_{ankle} = -M - m_{com}gh_{com}\sin\theta$$
$$= -M - m_{com}gh_{com}\theta = -J\ddot{\theta} \tag{6}$$

Since $x_{com} = -h_{com}\theta$ by small angle approximation, together with (1), (3), (4) and (6), the following equation can be derived.

$$x_{com} = \frac{1}{m_{com}g}\left(\frac{J}{m_{com}h_{com}} - h_a\right)F_{x0} \\ - y\frac{F_{z0}}{m_{com}g} \quad (7)$$

where, m_{com} is body mass without foot mass, g is gravity acceleration, h_{com} is length from ankle to COM and approximated from anthropometric data (0.559 of body height), h_a is ankle height from the ground, F_{x0} is anterior-posterior (AP) ground reaction force (GRF), F_{z0} is vertical GRF, and y is COP in AP direction. Both forces and y can be measured from the forceplate.

Parameter identification
COP in the AP direction can be computed from GLP method (Zatsiorsky and Duarte, 2000). The moment of inertia, J, in (7) can be therefore be identified by minimizing the following objective function.

$$\min F = \left\| x_{com,GLP} - x_{com,eq(7)} \right\|^2 \quad (8)$$

Experiment
Thirty healthy adult subjects were tested during a single session. Each conducted ten quiet standing trials, 30s in duration. The subject was instructed to maintain a quiet, upright posture throughout the recording. The subject stood on a force plate (AMTI, BP600900) with arms crossed at the chest and eyes open.

RESULTS

The results showed that the identified moments of inertia are not the same as the point mass configuration. It was found that there was relatively high correlation (r=0.85) between the point mass moment of inertia and the identified moment of inertia. Roughly, there was a constant ratio of 0.9 between the identified moment of inertia and point mass moment of inertia. However, this ratio changed as body mass index (BMI) changed with relatively weak correlation (r=0.43). It was hard to find a single equation that relates moment of inertia, body mass and body height.

SUMMARY/CONCLUSIONS

A simple way of estimating the moment of inertia was investigated. With a single link inverted pendulum model, the EOM was derived, and a relation between COM and COP was found. With parameter identification by minimizing the norm of errors of COM locations from the model and GLP, the moment of inertia can be estimated.

REFERENCES

Winter, D.A. (2005) *Biomechanics and motor control of human movement, Wiley 3rd ed.*
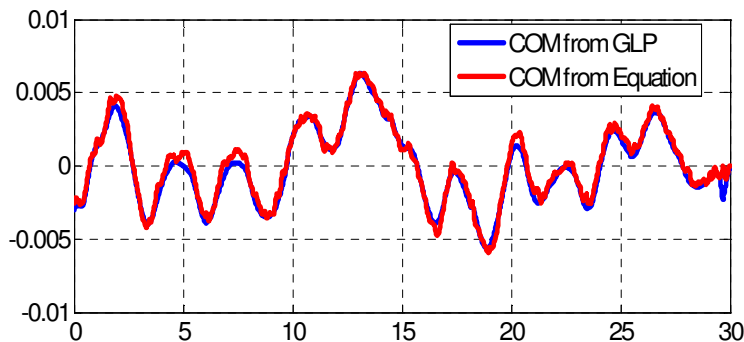Zatsiorsky, V.M. and Duarte, M, *Motor Control* 4, 185-200, 2000

Figure 2. Sample COM plots computed from GLP and equation (7) during quiet standing. This figure shows COM plots when the moment of inertia was optimized by minimizing the objective function (8).

TRUNK LEAN AS A MECHANISM TO REDUCE THE KNEE JOINT LOADING IN PATIENTS WITH KNEE OSTEOARTHRITIS

Heather Linley[1], Elizabeth Sled[2], Elsie Culham[2], and Kevin Deluzio[1]

[1]Department of Mechanical & Materials Engineering, Queen's University, Kingston, ON, Canada, http://me.queensu.ca
[2]School of Rehabilitation Therapy, Queen's University, Kingston, ON, Canada

INTRODUCTION

The adduction moment at the knee joint measured during gait analysis has received significant attention in the study of the pathomechanics of knee osteoarthritis. It has been shown to be a good surrogate for joint compartment loading, and has been shown to be related to both disease severity, and progression. Patients with knee osteoarthritis have been reported to alter their gait patterns in an effort to reduce the adduction moment at the knee (Mündermann et al., 2005). It was hypothesized that patients with osteoarthritis in the knee may display an increase in frontal plane thoracic tilt angle during the stance phase of gait in order to decrease the knee adduction moment in the affected limb.

METHODS AND PROCEDURES

Forty subjects were recruited for gait analyses, twenty of whom had knee osteoarthritis, verified clinically and radiographically. The other twenty subjects formed the control group and did not display, clinically or radiographically, any form of osteoarthritis, rheumatoid arthritis, or lower extremity joint pain. Gait analysis was performed for all subjects, and three-dimensional joint angles and net external moments at the hip, knee and ankle joints were calculated. Landmarks at the right and left superior acromions as well as the right and left anterior superior iliac spine were used with clusters of three markers on the thoracic trunk and sacral region to define coordinate systems in the trunk and pelvis. A standard for the calculation of thoracic tilt angle, or trunk lean, has not been previously established. In this study thoracic tilt angle was defined as the frontal plane angle between the coordinate system defined in the trunk in reference to the pelvis. Thoracic tilt angles were calculated across the stance phase of gait, with the affected leg being in stance for the osteoarthritic subjects. The mean thoracic tilt angle and the peak thoracic tilt angle were calculated for both subject groups across the stance phase. A Student's t-tests was performed to verify that the two means were distinct ($p < 0.05$).

RESULTS

Figure 1 shows the thoracic tilt angle in control (solid line) and osteoarthritic (dashed line) subjects across the stance phase of gait. The positive direction indicates trunk lean over the stance limb. Although both groups produce similarly shaped waveforms, the osteoarthritic subjects display a higher thoracic tilt angle throughout the entire stance phase of gait when compared with the control subjects. In other words, patients with osteoarthritis tend to lean farther over their stance leg during gait than control subjects. A mean angular difference of 2.9 degrees was found between the two groups during midstance (Table 1). A t-test performed showed a significant difference ($p < 0.05$) between the two means.
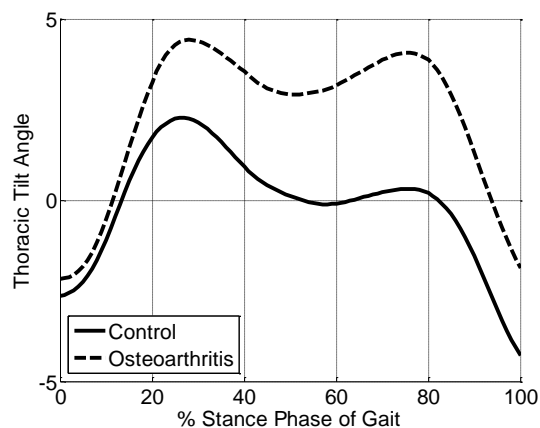
Figure 1. The thoracic tilt angles for both the control (solid line) and osteoarthritic (dashed line) groups displayed greater frontal plane trunk lean for subjects with knee osteoarthritis. A positive thoracic tilt angle refers to a lean over the stance leg.

Table 1. The mean thoracic tilt angles (standard deviations) for the control and osteoarthritic groups over midstance (20%-80% of Stance Phase), and the peak thoracic tilt angles (standard deviations) for the control and osteoarthritic groups over stance (0%-100% of Stance Phase).

Group	Mean Thoracic Tilt Angle (SD)	Peak Angle (degrees)
Control	0.7 (3.2)	2.9 (3.0)
Osteoarthritis	3.6 (4.3)	5.2 (4.5)

DISCUSSION

These results support our hypothesis that subjects with osteoarthritis have an increased trunk lean over their stance limb during gait compared to that of the control subjects. A previous study of healthy subjects reported that walking with an increased trunk sway significantly reduces the adduction moment at the knee (Mündermann et al., 2008). The increase in thoracic tilt angle displayed in the osteoarthritic group is thought to be a mechanism for lowering the adduction

moment at the knee during the stance phase of gait. This study examined trunk lean in the frontal plane only. It is expected that some unaccounted trunk sway also occurred in the sagittal plane. Further work is necessary to determine the effectiveness of this gait compensation as an intervention in treating knee osteoarthritis.

SUMMARY

Patients with osteoarthritis in the knee show a significant increase in thoracic tilt angle in the frontal plane over the stance phase of gait compared to control subjects. This gait strategy may be adopted to decrease pain by minimizing the knee adduction moment.

REFERENCES

Mündermann, A et al. (2005). *Arthritis and Rheumatism,* 52.9:2835-2844.
Mündermann, A et al. (2008). *Journal of Biomechanics,* 41:165-170.

ACKNOWLEDGEMENTS

LIMITED ASSISTANCE PRACTICE INCREASES ACTIVE DORSIFLEXION RANGE OF MOTION IN THE IMPAIRED ANKLE OF STROKE SUBJECTS

Kari A. Danek[1], R. Brent Gillespie[1], Daniel P. Ferris[2], Jessy W. Grizzle[3], and James L. Patton[4]

[1]Mechanical Engineering, [2]Kinesiology, [3]Electrical Engineering, University of Michigan,
Ann Arbor, MI, 48109, danekk@umich.edu
[2]Sensory Motor Performance Program, Rehabilitation Institute of Chicago, Chicago, IL 60611

INTRODUCTION

Drop-foot is an often chronic disability that accompanies hemiparesis in up to 20% of persons with history of stroke (Lyons, 2002). It is generally treated by prescribing an ankle-foot orthosis (AFO) to immobilize the foot or a portable peroneal stimulator to electrically stimulate active dorsiflexion (Granat, 1996). Therapeutic interventions addressing ankle mobility that employ robotic technology are also coming on-line (Girone, 2001), and could benefit a large number of patients if successful. We propose a mechanized exercise regime to rehabilitate ankle strength, range of motion, and coordination. We are particularly interested in developing robot-enabled therapies that feature self-assist modes. By engaging the patient to manually assist the movements of their impaired limb by means of a telerobot, we aim to increase patient involvement, motivation, and maximally facilitate neural activation of the impaired limb. Here we report on the results of a study in which we assessed range of motion by various means before and after a training bout involving telerobot-assisted ankle dorsiflexion.

METHODS AND PROCEDURES

We designed a motorized single foot cradle through which a subject could dorsiflex his ankle to increase the vertical displacement of a cursor on a monitor. Thirteen subjects with history of CVA and lasting hemiparetic effects participated in the study. The primary task during the experiment was to raise the cursor to clear the top of obstacles that were presented visually as bars moving from right to left on the monitor. Obstacle heights were

distributed randomly about each subject's own active range of motion (ROM) with a standard deviation of 5% of that ROM. Active ROM was determined during the initial assessments as described below. Each obstacle was previewed for 10 s with a duration width of 0.67 s.

Each subject completed an initial assessment, a training bout, and a final assessment. During the initial assessment, subjects attempted to complete 10 toe raises and three blocks of unassisted collision avoidance with 21 obstacles each. The training portion consisted of sixteen blocks of collision avoidance with 21 obstacles each. During training blocks, subjects completed the task using the motorized foot cradle in one of four possible settings: a) unaided, or with ankle assistive torque dictated b) by the experimenter through a hand-controlled teleoperator, c) by the subject through the same teleoperator, or d) by the computer based on the obstacle motion. The final assessment consisted of a single block of unaided collision avoidance and a repeat of the series of ten toe raises.

We compared initial and final ROMs for each subject as well as performance during the initial and final unaided obstacle avoidance blocks. Performance metrics included two position-based metrics for the toe raises: the absolute peak dorsiflexion angle and the range from the resting foot position to peak position. Performance metrics also included peak position achieved for each obstacle during the collision avoidance, and maximum EMG activity of the tibialis anterior. Subject

Table 1: Performance Summary

Active ROM	Number of Subjects			Group Change		Sig
	Inc	Unchg	Decr	(abs)	(%)	P
Peak Pos	9	2	2	1.95°	25%	0.05
Rest-Peak Range	6	6	1	2.03°	18%	0.05
EMG	6	5	2	0.08	21% *	0.04
Coll Avoid						
Peak Pos	3	6	4	0.07°	15%	0.35
EMG	4	6	3	0.02	9%	0.32

* One outlier was removed

performance means were analyzed using two-tailed paired t-tests with $\alpha = 0.05$.

RESULTS AND DISCUSSION

On average, subjects demonstrated improved active ROM following the obstacle avoidance training when compared to pre-training. The absolute peak position increased by 28% over the initial mean peak position, while the ROM measured between rest to peak increased by 18%. In addition, subjects demonstrated increased EMG activity in the final toe raises when compared to initial toe raises, with a mean increase in peak EMG of 21%. A break down of the number of subjects who increased, decreased, or remained unchanged for all performance metrics is summarized in Table 1. The group performance differences, in terms of absolute and percentage changes, are also presented in the table.

Subjects demonstrated improvement in the active dorsiflexion ROM of the impaired limb following assisted training in a task that required dorsiflexion; however, they did not demonstrate parallel performance improvements in the collision avoidance task itself. By including an evaluation not based on the task we were able to discern a change in the capabilities of our subjects which may otherwise have gone unnoticed. We feel the question of motivation plays an important role in detecting this change. During the toe raises, subjects were encouraged to push themselves

to their maximum ability. During the collision avoidance, the goal was very different: avoid hitting a presented obstacle. This task and its associated metrics were not able to capture the changes that occurred in subjects as a result of assisted practice and training on that task.

SUMMARY

Hemiparetic subjects that used a robotic device to practice ankle dorsiflexion with mechanical assistance were able to increase muscle recruitment and joint range of motion with short term practice. During the training, subjects were provided assistance in raising their toe to clear the obstacles, and in certain blocks this assistance was self-generated. The device allowed them to feel and understand successful activation of a muscle, potentially aiding them in motor relearning.

REFERENCES

Girone, M, et al, (2001). *Auto Robots,* 10: 203-212.

Granat, M. et al (1996) *Arc PM&R,* 77:19-24.

Lyons, GM, Sinkjaer, T, Burridge, JH, and Wilcox, DJ (2002). *IEEE Trans on Rehab Eng,* 10: 260-279.

ACKNOWLEDGEMENTS

OBJECTIVE EVALUATION OF ANKLE FOOT ORTHOTICS FOR AMBULATORY FUNCTION IN HEMIPLEGIC GAIT

Karen J. Nolan, PhD[1,2], Mathew Yarossi, BS[1], Krupa K. Savalia, BS[1], Howard J. Hillstrom, PhD[3], & Elie P. Elovic, MD[1,2]

[1]Kessler Medical Rehabilitation Research and Education Center, West Orange, NJ, USA
www.kmrrec.org; knolan@kmrrec.org
[2]University of Medicine and Dentistry, New Jersey-NJ Medical School, Newark, NJ, USA
[3]Hospital for Special Surgery, New York, NY USA

INTRODUCTION

Ankle foot orthotics (AFO) are often prescribed to patients with motor deficits due to stroke to address impairments, assist with ambulation, and lower the energy cost of walking. AFOs are designed to help compensate for common problems in hemiplegic gait such as foot drop (inadequate ankle dorsiflexion) or inappropriate foot strike due to spasticity or contracture (Gok et al. 2003). Currently, initial fit and subsequent improvements in AFOs are evaluated visually during gait by a clinician or corrected after patient feedback (Meyring et al. 1997). An objective study of the plantar pressure distribution within AFOs is needed to provide more quantifiable and functional information about the AFO's efficacy. The objective of this investigation was to use objective measureable gait parameters to evaluate the affect of a solid AFO for ambulatory function during walking in hemiplegic gait. The secondary objective was to use dynamic pedobarography to begin to understand how an AFO affects plantar pressure and loading during gait.

METHODS AND PROCEDURES

Participants (n=19) diagnosed with hemiplegia secondary to stroke currently using an AFO during ambulation were recruited for participation. All subjects were able to safely ambulate without their prescribed AFO for at least 25 feet. Subjects performed walking trials in two conditions: 1) with and 2) without the AFO. All subjects completed 10 walking trials, of a 4.5 meter walk at a self-selected walking speed on a level surface. The order of conditions was randomly assigned. During all walking trials, wireless pedobarography data was collected using the Pedar®-x Expert System (Novel Electronics Inc., St Paul, MN, USA) data included regional analysis of peak pressure, and maximum force on the plantar aspect of the foot. Selected temporal-spatial gait parameters: walking speed, double support, single support, stride length, and step width were used for analysis. A two-way mixed effect analysis of variance (ANOVA) was used to test for significant differences in outcome loading parameters.

RESULTS

While wearing the AFO there was a significant decrease in double support, and single support time remained significantly higher on the unaffected limb. Mean stride length increased with the AFO on both the affected and unaffected limb and step width remained unchanged regardless of condition or limb. While wearing the AFO, lateral and medial heel peak pressure, and maximum force at the lateral heel were significantly reduced. Maximum force at the medial heel showed a trend towards reduction. Maximum force in the medial arch significantly

increased. Trends for increases were observed in peak pressure at the medial arch and beneath the 2nd metatarsal head.

DISCUSSION

Temporal Spatial Outcomes: Walking speed increased with the AFO, due to the decrease in double support and increase in step length. Increased walking speed has been shown to positively correlate with a reduced energy cost ultimately improving gait efficiency. The decreased double support time may indicate a more stable gait when wearing the AFO. Single support on the unaffected side was more than the affected side regardless of condition. This increased swing time on the affected limb is likely utilized to ensure toe clearance. The subject spent more time on the unaffected limb in both conditions, even with the added support and stability afforded by the AFO. This compensatory gait deviation causes as asymmetrical gait and greater difficulty maintaining balance during gait. The AFO provided more stability but walking gait was still affected. Step length and step width contribute to balance during walking gait. An increase in step length with the AFO demonstrated that the subject improved the distance covered with each step, indicating improved balance. Step width remained unchanged suggesting that the brace effectively changed functional mobility to improve balance while the base of support remained unchanged.

Pedobarography Variables: The addition of an AFO significantly decreased peak heel pressure and caused an increase in medial peak pressure during gait. The decreased heel pressure is likely to be a direct result of the increased contact area afforded by the AFO. This may increase heel strike total contact area indicating a more stable foot strike during gait. The increase in medial pressure may indicate increased weight bearing on the affected limb and potentially a more effective rollover during gait. This may create a more efficient gait pattern increasing walking speed and decreasing energy cost. The addition of an AFO significantly decreased lateral heel forces and increased medial arch forces during gait. The increase in heel maximum medial force may indicate a more controlled foot strike when wearing the AFO. The increase in medial maximum force continues to indicate that the affected limb may support more bodyweight during gait causing an increase in balance.

SUMMARY

Quantitative assessment of gait parameters and plantar loading in hemiplegic gait can help identify which specific design characteristics of an AFO are functioning and which need improvement or correction to ultimately improve an individual's gait. Mechanically the brace can put the limb in the correct position but the individual may still be hesitant or not able to balance on their affected limb due to loss of sensation or motor control. Adding discrete pressure measurements to that region could further our ability to design a more effective AFO that minimizes stress and maximizes walking efficiency.

REFERENCES

Gok, H. et al., (2003) *Clinical Rehabil* 17:137-139
Meyring, S. et al., (1997) Clin Biomech 12:60-65

ACKNOWLEDGEMENTS

CHANGES IN KINETIC AND KINEMATIC GAIT PARAMETERS DUE TO FIREFIGHTING AIR BOTTLE CONFIGURATION

Kiwon Park[1], Pilwon Hur[1], K.S. Rosengren[2], Gavin P. Horn[1,3], and Elizabeth T. Hsiao-Wecksler[1]

[1] Mechanical Science & Engineering [2] Kinesiology [3] Illinois Fire Service Institute
University of Illinois at Urbana-Champaign, Urbana, IL, USA
E-mail: ethw@uiuc.edu   Web: www.mechse.uiuc.edu/research/hsiao-wecksler/

INTRODUCTION

Firefighters often use a self-contained breathing apparatus (SCBA) that includes a face mask and shoulder pack with air bottle, which may interfere with functional performance. Choice of air bottle is currently a controversial topic due to investment costs for lightweight, more compact, expensive bottles vs. heavier, larger but less expensive designs. Prior studies have examined the effect on balance of wearing protective clothing with SCBA packs for firefighters (Punakallio, 2003) and hazardous material workers (Kincl, 2002); however, no systematic gait assessments have investigated load carriage due to different bottle configurations (bottle weight and size). The goal of this study was to quantify changes in gait and obstacle crossing behaviors with different bottle configurations. We hypothesized that reduced weight and size would improve gait performance.

METHODS AND PROCEDURES

Twenty-one male firefighters (age 27±5 yrs) walked at either of two speeds ("normal, comfortable pace" or "as fast as possible without running"). Three obstacle conditions were tested (no obstacle, 10 cm, or 30cm obstacle). Three SCBA air bottles were tested: a low-budget, heavy aluminum (AL) bottle of 9.1kg; an expensive, light carbon fiber (CF) bottle of 5.4 kg; and a novel redesigned bottle (RD) constructed to provide a light, short design that was 5.4 kg and half the length of the others. Walking speeds and bottle configurations were randomized. Outcome parameters were averaged over two trials per condition.

Five kinetic parameters were obtained from the vertical ground reaction force (GRF) for the trailing foot when crossing the obstacle as measured by a force plate (BP600900, AMTI; sampled at 1000 Hz): time to 1st peak, peak force in early and late stance, and impulse in early and late stance. Early and late stance were defined as the breaking (heelstrike) and propulsion (toe-off) portions of the vertical GRF curve, respectively. Impulse was the integral of contact force with respect to time.

Six kinematic parameters were collected using a motion capture system (Datastation 460, Vicon; sampled at 100 Hz): overall gait speed (GS), time in single leg support while crossing the obstacle (SLST), minimum horizontal clearance from the obstacle of the trailing toe (HCT) and leading heel (HCL), and minimum vertical clearance of the trailing (VCT) and leading foot (VCL). Multivariate analysis of variance tests examined whether bottle configuration, obstacle height, and walking speed affected the kinetic and kinematic parameters.

RESULTS/DISCUSSION

Interesting observations were noted with bottle configuration. Six subjects (29%) hit

the 30 cm obstacle while wearing the heavier AL bottle and walking at normal speed. Four hit the obstacle during both trials. Two of these four also hit the obstacle during fast walking. Therefore, the 30 cm obstacle was contacted in 13 out of 84 trials (15%). No obstacle contacts were observed for lighter bottles (CF, RD). All obstacle contacts were due to trailing foot contact. Although not statistically significant ($p=0.076$), vertical clearance for the trailing foot VCT was less for the AL bottle than others (AL: 17.0 ± 1.4 cm (SE); CF: 17.8 ± 1.4; RD: 19.1 ± 1.0). A bottle $\times$ obstacle interaction effect for VCL ($p=0.076$) also suggested a trend for close vertical contact with the lead foot while wearing the AL bottle and crossing the 30 cm obstacle (12.1 ± 0.8 cm for AL-30 vs. 14.6 ± 0.7 for all others). Thus, it appears that the heavier bottle might pose a greater tripping risk.

Kinetic gait parameters suggest significant main effects in both early and late stance peak GRF associated with bottle configuration. No other kinetic or kinematic parameters had significant main or interaction effects due to bottle configuration. Peak GRFs were greater for the AL than CF/RD bottles during early stance ($p = 0.004$; AL: 1.66 ± 0.05 %BW vs. CF/RD: 1.60 ± 0.04) and late stance ($p < 0.001$, AL: 1.59 ± 0.03 %BW vs. CF/RD: 1.53 ± 0.03). No difference was found between CF and RD suggesting that only weight affects peak GRF. A recent study also found that peak vertical GRF increased with applied load during gait (Birrell et al., in press).

All kinetic parameters except time to 1st peak increased with the obstacle height ($p \le 0.007$). HCL, HCT and SLST ($p \le 0.010$) also increased, while VCL and GS decreased with the obstacle height ($p < 0.001$). High peak and impulse values suggest that greater effort

is required by the trailing leg as obstacle height increases.

Walking speed statistically affected ($p \le 0.001$) all gait parameters except, interestingly, vertical clearances. Peak GRF (early and late) and horizontal clearance (HCT and HCL) increased with walking speed, whereas time-related parameters of peak GRF time, GRF impulse (early and late), and SLST decreased, as might be expected. Thus, more challenging fast walking conditions appear to cause larger and more forceful steps around an obstacle.

SUMMARY

Increasing load weight with the heavier AL bottle resulted in 29% of the subjects contacting the challenging 30 cm obstacle while passing over it with the trailing limb. No subjects contacted either obstacle while wearing the lighter CF or RD bottles. Peak ground reaction forces were also significantly larger with the heavier bottle, but were the same for the other bottles. Thus, changing bottle length (and effectively lowering the bottle center of mass along the back) had no apparent effect on gait performance. Obstacle height and walking speed also influence gait behavior; therefore, firefighters need to cognizant of how gear and environment may affect their gait performance.

REFERENCES

Birrell, S.A. et al. *Gait Posture*, in press
Kincl, L.D. et al. (2002) *Appl Occup Environ Hyg,* **17**(4):256-66.
Punakallio, A. et al. (2003) *Aviat Space Environ Med*, **74**(11):1151-56

ACKNOWLEDGEMENTS

EFFECT OF AGE AND TARGET LENGTH ON THE SPEED-ACCURACY TRADE-OFF OF CENTER OF PRESSURE MOVEMENTS NEAR THE ANTERIOR MARGIN OF THE BASE OF SUPPORT IN STANDING

Manuel E. Hernandez MS[1,3], James Ashton-Miller PhD[1,2], and Neil B. Alexander MD[2-4]

[1]Biomechanics Research Laboratory, [2]Institute of Gerontology,[3]Mobility Research Center, The University of Michigan, [4]VA Ann Arbor Health Care System, Ann Arbor, Michigan.
manueleh@umich.edu   Web: www.med.umich.edu/geriatrics/moblab/

INTRODUCTION

Accurate control of the whole body center of mass is necessary when performing discrete tasks such as reaching or stooping. This will reduce the risk of losing balance, falling and/or suffering injury. Age-related differences observed on the variability of speed-accuracy tasks [1], and differences in speed-accuracy control between discrete and reciprocal movements [2] provide an impetus for examining the effect of age on the ability to control discrete foot center of pressure (COP) movement to target near the anterior edge of the base of support.

The overall goal of this study is to determine the effect of age on the COP speed-accuracy trade-off.   In this pilot study we tested the (null) hypothesis that neither target length nor age would affect COP movement time, number of submovements or variability in the sagittal plane. We tested the secondary (null) hypothesis that the results of the speed-accuracy tasks would not change when repeated on a second visit.

METHODS

Subjects. Three healthy young (mean±SD, age 18.3±0.6 years) and three healthy older females (age 74.3±7.4 years, were recruited from the local community (Table 1).

Protocol. Movement time was the time taken to move the COP, above 10% of the maximum COP speed, from a neutral upright stance (mid-foot) starting zone to the arrest of COP speed below 5% of the maximum, anywhere within the target 'length'. Submovements were defined as zero crossings in the trajectory of COP acceleration with a net change in speed above 10% of the maximum COP speed within a particular movement. Mean ΔCOP speed was defined as the average speed of corrected COP movements, which eliminated the contribution from volitional COP movements, as defined in previous work [3].

Participants performed whole body COP speed-accuracy tasks using visual feedback of their COP location starting from its location in neutral standing posture. Targets involved the anterior limit of their functional base of support. On average, 10 trials were conducted to each target length over a period of 60 seconds. Time-varying auditory cues (1-4 s) were used to signal the onset of the desired discrete, fast and accurate COP movement to target. Target lengths of 2, 4 and 6 cm were used in two balanced blocks. The first block included practice trials, so only results from the second block are reported here. Participants were also brought back for a second visit and the tests repeated in order to determine whether learning or practice effects were present. To control for maximal COP movement capacity, both the dimensions of the maximum functional base of support and COP movement velocity were also recorded.

A repeated measures ANOVA was used to examine the effect of target length, age, and learning with p<0.05 being considered significant.

RESULTS AND DISCUSSION

There was a significant trend for older women to have an increased ΔCOP speed across trials (p < .05). The mean ΔCOP speed for both young and older women was reduced from 4.5% to 3.1% as the target length was increased from 2 to 6 cm (Figure 1). There was also a trend for movement time to increase as the target length decreased (p=.115) (Figure 2). Other trends included older women demonstrating a decrease in submovements (p=.21) and a decrease in submovements as target length is increased (p=.37). Three older women completed the same tests on a second visit (secondary hypothesis). No significant learning effects were observed by the second visit, despite a trend toward decreased movement time (11% decrease, p =.36).

Characteristics	Young Women	Older Women
Weight (kg)	68.2±8.9	73.2±2.4
Shoe size	7.2±1.5	8.7±0.3
FBOS (cm)	19.2±1.7	17.1±3.7
Maximal COP velocity (cm/s)	70.6±10.4	71.8±4.8

Table 1: Characteristics of young and older women.

SUMMARY

These preliminary findings suggest that older women have increased ΔCOP speed over younger women and that movement time increases as the target length is reduced. At present no age differences were found, but these may appear with a larger sample size.
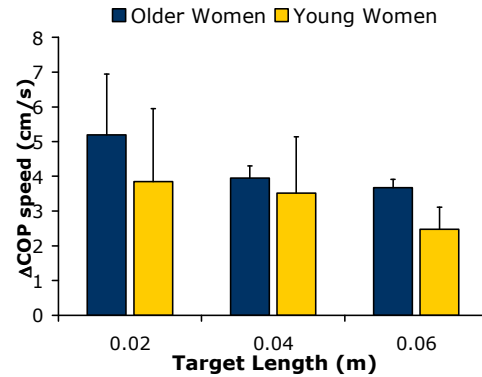

Figure 1: Mean (SD) ΔCOP speed during discrete COP control tasks at the anterior edge of the functional base of support.
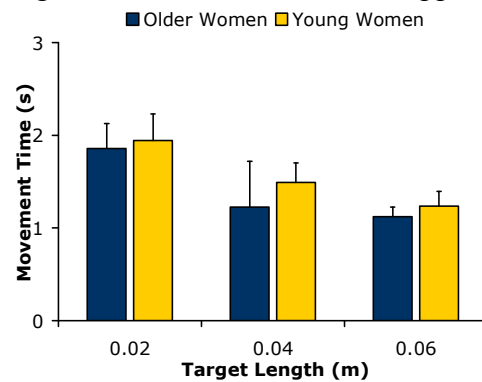

Figure 2: Mean (SD) COP movement time as a function of target length (m) at the anterior margin of the functional base of support.

REFERENCES

[1] Ketcham, CJ et al. (2002). *J Gerontol: Psychol Sci ,* **57**, P54-P64.
[2] Smits-Engelman, BC et al. (2002). *Exp Brain Res,* **145**, 222-230.
[3] Latash, ML (2003). *Exp Brain Res,* **150**, 314-324.

ACKNOWLEDGEMENTS

Selection of Double Support Duration In a Compliant Walking Model

Shawn M. O'Connor and Arthur D. Kuo

University of Michigan, Ann Arbor, MI, USA
E-mail: smoconno@umich.edu

INTRODUCTION

Humans walk with double support periods of about 20% of a step. Because many gait parameters such as step length and width appear to optimize energy expenditure (Kuo 2001), double support duration may also be optimized. It is unknown, however, what the consequences are for longer or shorter durations, and how it should vary with walking speed. Here we use an elastic locomotion model to demonstrate that very long or short double support periods may be disadvantageous because they require more work to perform the step-to-step transition. We also find that a strategy reducing collision loss at heel-strike explains the relative decrease in double support period with increased walking speed.

METHODS

The compliant locomotion model comprises a single point mass at the pelvis, two axially-compliant legs with very light arc feet, and a torsion spring acting between the legs (Figure 1). The model is a simplification of a passive bipedal running model (McGeer 1990) with the added capability of double support. We developed walking simulations for the model and searched for periodic gaits by varying the model parameters and initial conditions.

The model has only three physical parameters: the axial leg stiffness K, torsional hip stiffness, K_p, and the foot radius R. Gait parameters such as the double support period and step length, are set by

tuning the two stiffness parameters and selecting appropriate initial conditions for the simulation. Speed largely depends on the mechanical energy of the body center of mass and axial springs E, which is set by the initial conditions of the model states.
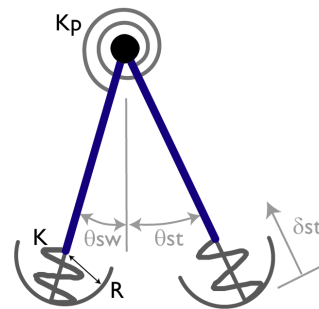

Figure 1: A two-dimensional elastic dynamic locomotion model with two stiffness parameters.

When searching for symmetric gaits with fixed arc radius, the three gait parameters of speed, step length, and double support period are determined by the two physical parameters, K and K_p, and the total energy E. The model can reproduce the ground reaction force and center of mass (COM) profiles of human gaits, simply by matching appropriate gait parameters. Interestingly, the model parameters can be varied to find an array of gaits with fixed speed and step length but a range of double support periods.

RESULTS AND DISCUSSION

We examined the consequences of changing double support period for a fixed speed and step length equivalent to normal human walking (1.25 m/s and 0.70 m). Variation of double support duration caused the model's heel-strike collision losses to vary by 18%, with an optimum for intermediate durations. This optimum is equivalent to a minimum amount of energy stored in the leading leg spring during the step-to-step transition,

which is a function of leg stiffness and leg compression ($E_{heelstrike} = \frac{1}{2} K \delta_{st}^2$). As double support increases, less positive work from push-off is performed on the COM before heel-strike, resulting in greater leading leg spring compressions. To decrease the double support and keep the step period constant, it is necessary to decrease the period of spring bounce, and thus increase the stiffness of the axial leg spring. Leg spring stiffness dominates the energy equation at low double support periods and leg spring compression dominates at high periods, resulting in a bowl shaped minimum in the energy stored in the spring.

If the amount of energy lost at heel-strike can be minimized for a given speed and step length, do humans use this criteria to optimize double support? To answer this question we varied leg stiffness, hip stiffness, and total energy and searched for model gaits over a range of speeds that minimized heel-strike collision work. We then compared the double support periods measured from the resultant gaits with corresponding human walking data. We used an empirical speed, step length relationship of V = SL^0.42 to further constrain possible gaits.

We also searched for gaits that maintained constant leg stiffness to see how this parameter might change as speed increases.

For these gaits, we fixed leg stiffness and varied hip stiffness and total energy to find an array of gaits that satisfied the speed step length relationship.

Model gait parameters produced from the gait searches are shown in Figure 2 and compared with human data. The three curves of constant leg stiffness demonstrate that this parameter likely increases for with walking speed. Three gaits are also shown that minimize heel-strike work at empirical speed and step lengths. These gaits clearly show a decrease in double support with speed that follows the human trend.

SUMMARY/CONCLUSIONS

An elastic walking model potentially explains how humans optimize double support. Humans increase the axial stiffness of the leg with faster speeds. They also decrease the double support period, perhaps to minimize energy loss at heel-strike.

REFERENCES

McGeer, T. (1990). *Proc. R Soc. London B*, **240**, 107-134.
Kuo, A.D. (2001). *J. Biomech. Eng.,* **123**, 264-269.
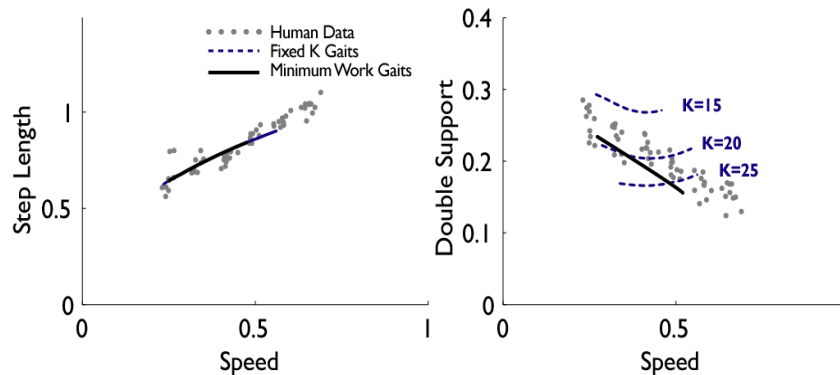
ACKNOWLEDGEMENTS

Figure 2: Comparison of non-dimensional gait parameters for two different methods of selecting double support. Constant leg stiffness gaits produce bowl shaped relationships between double support and speed whereas gaits that minimize heel-strike work show a decreasing trend that matches human results.

ARCHITECTURAL AND *IN VIVO* ANALYSES DEMONSTRATE THE UNIQUE STABILIZING FUNCTION OF THE LUMBAR MULTIFIDUS MUSCLE

Samuel R. Ward, Choll W. Kim, Carolyn M. Eng, Lionel J. Gottschalk, Akihito Tomiya, Steven R. Garfin, and Richard L. Lieber

Departments of Radiology, Orthopaedic Surgery, and Bioengineering, University of California, San Diego, La Jolla, CA 92093-9151 E-mail: srward@ucsd.edu

INTRODUCTION

The posterior paraspinal muscles control motion and provide dynamic stability to the multisegmented, multi-articular spinal column. Paradoxically, surgery designed to treat various spinal disorders actually disrupts these muscles, and in turn, may lead to significant functional deficits and various pain syndromes. However, the physical properties that govern function in many of the key lumbar spine muscles are relatively unknown. Therefore, the purpose of this study was to define the architecture and physiological operating range of the multifidus muscle.

METHODS AND PROCEDURES

In the cadaveric portion of the study, muscle architecture was determined according to previously defined methods (Sacks and Roy, 1982). Eight lumbar spines were harvested *en bloc*, stripped of superficial soft tissue and immersion fixed in 10% formalin for 72 hours. Specimens were positioned in supine at the time of fixation to maintain a neutral lumbar spine position. After fixation, the deep lumbar fascia was excised and longissimus and iliocostalis lumborum muscles were reflected to reveal the multifidus muscle. Half of the muscle was used for muscle fiber length measurements from predefined locations in the muscle. The remaining half was stored in PBS intact on the bony vertebral column from T11 to the sacrum for mass measurements. Comparisons to the remaining lumbar spine muscles were made using previously reported values (Delp et al., 2001) using one-way analyses of variance.

For the *in vivo* portion of the study, multifidus muscle specimens were obtained from patients undergoing spinal surgery (n = 16). After skin incision, the dorsolumbar fascia was incised and the multifidus muscle identified by its position adjacent to the spinous process and the cranial/medial-to-caudal/lateral projection of its fibers. A small segment of the multifidus on the posterior, lateral region of the muscle belly was isolated by blunt dissection along natural fascicular planes and a specialized clamp was slipped over the bundle and the biopsy immediately placed in Formalin for fixation. Laser diffraction was then used to measure sarcomere length (Lieber *et al.* 1984). Intraoperative lumbar spine position was quantified on fluoroscopic images by measuring the intraoperative L1-S1 angle (Fig. 1B) and comparing it to the preoperative standing flexion, neutral, and extension lateral plain film radiographs (Figs. 1A, 1C, and 1D).
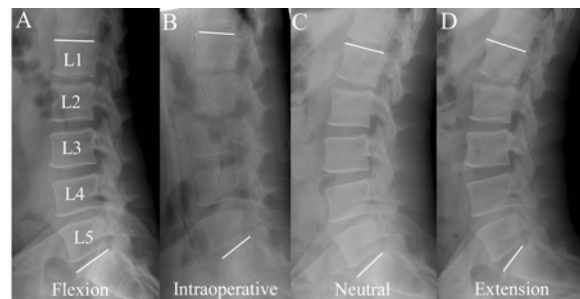

Figure 1: Radiographs of spine in (A) standing flexion, (B) Intraoperative, (C) standing neutral, and (D) standing extension.

RESULTS

Architecturally, the cadaveric mass data provided no unique insight into multifidus design relative to other lumbar muscles. However, physiological cross-sectional area (PCSA) was impressively large in the multifidus muscle (23.9 ± 3.0 cm^2). This value was over twice as large as any other muscle in the lumbar region ($p < 0.05$). In fact, the next closest muscle, the longissimus thoracis had a PCSA that was only about half of the multifidus (11.5 ± 1.1 cm^2) in spite of the fact that it's mass was greater.

In vivo muscle biopsies provided a unique opportunity to determine the *in vivo* sarcomere length operating range. In the neutral spine position sarcomere lengths were the shortest we have ever measured in human tissue (1.98 ± 0.15 μm, Fig. 2). When the spine was flexed ($41.4 \pm 3.5°$), significantly longer sarcomere lengths were observed (2.70 ± 0.11 μm; $p < 0.05$), as expected, since the muscle was "lengthened" with flexion.
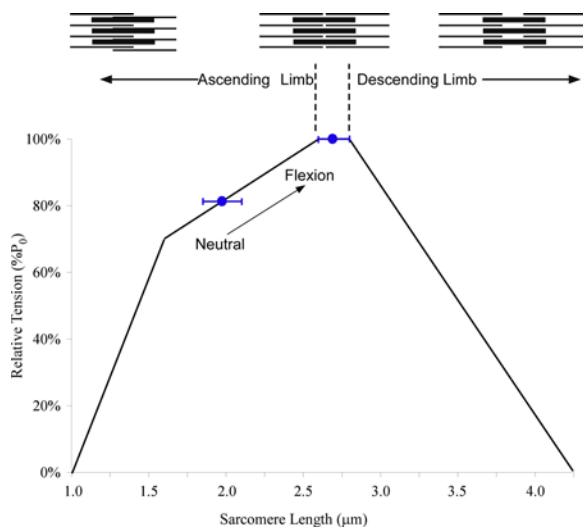

Figure 2: Sarcomere length operating range of the multifidus plotted on the human sarcomere length tension curve (black line). Blue circles represent average sarcomere length obtained via biopsy in prone (neutral, n=8) or lumbar flexion (n= 5).

DISCUSSION

Architecturally, the multifidus has an extremely large PCSA that results from the very short multifidus fibers which are arranged along its length, enabling very efficient packing of a large number of force generators into a small volume

In the biomechanical context of the length-tension curve, the extent of the sarcomere length increase was small. Therefore, throughout the range of motion that could be achieved intraoperatively, the muscle operated exclusively on its ascending limb. In the context of function, this indicates that the multifidus muscle becomes intrinsically stronger as the spine in flexed.

SUMMARY

This anatomical and intraoperative study clearly demonstrates the unique stabilizing design of the multifidus muscle. It's very high PCSA and unique operating range on the ascending limb of the length-tension curve indicate that the muscle is capable of producing extremely high forces and becomes stronger as the spine flexes, presumably becoming less stable.

REFERENCES

Delp, S L, *et al* (2001) *J Biomech,* 34, 371-375.
Lieber, Yeh and Baskin (1984). *Biophys. J.* 45, 1007-1016.
Sacks and Roy (1982). *J. Morphol.* 173, 185-195.

ACKNOWLEDGEMENTS

BIOMECHANICAL AND PHYSIOLOGIC COST OF BODY ARMOR

Leif Hasselquist, Carolyn K. Bensel, Brian Corner, Karen N. Gregorczyk, Jeffrey M. Schiffman

Natick Soldier Research, Development and Engineering Center, Natick, MA USA
E-mail: Leif.Hasselquist@us.army.mil

INTRODUCTION

Military and law enforcement personnel often wear armor vests to protect vital organs of the torso. There is also a need for ballistic protection of the arms and legs. Researchers have shown that added mass and the way the mass is distributed on the extremities affect the physiology and biomechanics of the individual. Miller and Stamford (1987) reported a 13% increase in energy expenditure during walking per 1.0 kg of weight added to the upper extremities and a 5 to 10% increase in energy expenditure during walking per 1.0 kg of weight added to the feet. Loading the lower extremities during running has similar physiologic effects (Martin, 1985). Martin also reported that adding a load to each foot produces small but significant changes in gait kinematics. Additionally, how the added mass is distributed on the extremities has been found to affect the metabolic cost of walking and running (Royer & Martin, 2005). We hypothesized that increases in body armor weight and body surface area covered would result in increases in energy cost of locomotion, changes in gait kinematics and kinetics, and detriments to maximal performance tasks. This knowledge of users' physical performance as affected by extremity armor may aid in designing these systems.

METHODS

Eleven Army enlisted men participated in the study (20 yrs; 1.8 m; 79.7 kg). Informed consent was obtained and the study was conducted in accordance with Army Regulation 70-25 (Use of Volunteers as Subjects in Research). Subjects performed treadmill (AMTI, Watertown, MA) walking (10 min at 1.39 m/s, 0% grade), and treadmill running (10 min at 2.34 m/s, 0% grade). During the fifth minute, 20 s of kinematic and kinetic data were collected (Qualisys, Gothenburg, Sweden). After six minutes, VO2 (ml/min) data were collected (COSMED, Rome, Italy). The following maximal effort performance tasks were also executed separate days: 5 continuous 30-m rushes, 5 minutes of repetitive box lifting (20.5 kg), and an obstacle course run consisting of: 4 hurdles (0.6 m), 9 cones zigzag oriented and equally spaced, 3.7 m crawl, 3.7-m horizontal shimmy pole, 1.4-m sheer wall, 27-m straight run, 1.4-m mantle, and 6.1 m ascension of stairs. Participants were tested in four conditions: no armor (NA), torso armor (Torso), torso + coverage of upper portion of extremities (Torso + Ext Up) and torso + coverage of full extremities (Torso + Ext Full). The weight and surface area of the ballistic coverage for each condition is shown in Table 1. One-way repeated measures ANOVAs (α=.05) were performed on kinematic, kinetic, VO2, and performance measures. Kinetic and VO2 variables were scaled to body mass.

	Torso	Torso + Ext Up	Torso + Ext Full
Coverage (m^2)	.411 (.033)	.628 (.049)	.717 (.052)
Weight (kg)	14.8	18.45	20.40

Table 1: Armor area coverage and mass.

RESULTS

Both the Torso + Ext Up and the Torso + Ext Full armor conditions significantly increased VO2 when compared with NA and Torso Armor alone, but the extremity coverage conditions did not differ from each other. VO2 was 15% higher during walking and 9% higher during running in both extremity armor conditions. There were significant physical performance decrements found with the armor conditions for the rushes, box lift, and obstacle course (Table 2).

Variable	NA	Torso	Torso + Ext Up	Torso + Ext Full
Rush (s)	48.18$_A$ (3.58)	52.39$_{AB}$ (7.14)	54.87$_B$ (4.17)	56.58$_B$ (4.05)
Box Lift (# Lifts)	63.36$_A$ (7.26)	59.55$_B$ (6.58)	57.55$_{BC}$ (7.20)	56.45$_C$ (7.90)
Obstacle Course (s)	54.97$_A$ (3.32)	58.63$_A$ (5.84)	63.67$_B$ (5.29)	67.59$_B$ (9.0)
Means that do not share the same subscript differed significantly in post-hoc tests (p< .05)				

Table 2: Mean (SD) for each armor condition of performance measures.

Kinematic and kinetic variables also significantly differed with the test conditions. Selected means (SDs) for kinematic and kinetic variables are shown in Table 3.

DISCUSSION/SUMMARY

There is an increased energy cost during locomotion when armor is worn on the torso, arms, and legs, rather than just on the torso. Changes in kinematics of gait were observed between the no armor condition and all armor conditions for running and walking. However changes were not significant between the armor conditions with the exception of stride width during running. Gait kinetics demonstrated a greater sensitivity to the armor conditions. The full coverage showed the greatest effects on the kinetics of the participants during walking and running. Even small masses located distally on the extremities will affect ground reaction forces in gait. The physical performance decrements increase when extremity armor coverage increases. The penalties associated with use of body armor highlight the importance of designing armor systems for maximum compatibility with the user's physical activities.

REFERENCES

Martin, PE (1985). *MSSE,* 17: 427-433.
Miller, JF and Stamford, BA (1987). *J Appl Physiol,* 62(4): 1497-1501.
Royer, TD and Martin, PE (2005). *MSSE,* 37(4): 649-656.

Walk Variable	NA	Torso	Torso + Ext Up	Torso + Ext Full
Double Supp. Time % Stride	30.54$_A$ (1.19)	31.75$_B$ (1.55)	32.27$_B$ (1.52)	32.75$_B$ (1.53)
Stance (s)	.71$_A$ (.03)	.73$_B$ (.02)	.72$_{AB}$ (.03)	.72$_{AB}$ (.03)
Swing (s)	.38$_A$ (.02)	.38$_{AB}$ (.02)	.37$_{AB}$ (.02)	.37$_B$ (.02)
Braking (N/kg)	-1.86$_A$ (.20)	-2.15$_B$ (.25)	-2.19$_B$ (.26)	-2.29$_B$ (.35)
Propulsion (N/kg)	1.90$_A$ (.22)	2.21$_B$ (.14)	2.31$_B$ (.15)	2.41$_C$ (.20)
Heel Strike (N/kg)	11.39$_A$ (.43)	12.54$_B$ (.54)	13.00$_C$ (.72)	13.35$_D$ (.78)
Toe Off (N/kg)	11.48$_A$ (.66)	12.59$_B$ (.67)	13.09$_C$ (.85)	13.47$_D$ (.86)
Run Variable	NA	Torso	Torso + Ext Up	Torso + Ext Full
Stance (s)	.34$_A$ (.01)	.35$_{AB}$ (.02)	.35$_{AB}$ (.02)	.35$_B$ (.02)
Swing (s)	.43$_A$ (.03)	.40$_B$ (.03)	.40$_B$ (.03)	.40$_B$ (.02)
Stride Width (m)	.10$_A$ (.02)	.10$_A$ (.02)	.11$_A$ (.02)	.12$_B$ (.02)
Braking (N/kg)	-2.16$_A$ (.31)	-2.44$_B$ (.23)	-2.53$_{BC}$ (.27)	-2.74$_C$ (.30)
Propulsion (N/kg)	1.62$_{AB}$ (.19)	1.58$_A$ (.31)	1.78$_{AB}$ (.33)	1.79$_{AB}$ (.37)
Heel Strike (N/kg)	22.35$_A$ (1.66)	23.42$_{AB}$ (2.28)	24.42$_{BC}$ (2.47)	24.87$_C$ (2.57)
Means that do not share the same subscript differed sig. in post-hoc tests (p< .05)				

Table 3: Mean (SD) for each armor condition of biomechanic variables.

HEAD AND NECK KINEMATICS DURING HORIZONTAL AND COMBINED HORIZONTAL/VERTICAL LOW VELOCITY WHIPLASH-LIKE PERTURBATIONS

Loriann M. Hynes[1] and James P. Dickey[1]

[1]Joint Biomechanics Laboratory, Human Health and Nutritional Sciences, University of Guelph, Guelph, Ontario, Canada, jdickey@uoguelph.ca

INTRODUCTION

Whiplash is a mechanism of injury that is commonly associated with rear-impact vehicle collisions. There is a large degree of variation in severity of symptoms between individuals for seemingly similar collisions. Rear-end collisions are responsible for most whiplash injuries (Berglund *et al.*, 2003).Some literature has reported vertical accelerations of both the occupant and vehicle during horizontal whiplash-like perturbations (Severy *et al.*, 1955) but no detailed studies of this phenomenon have been conducted. The purpose of this investigation was to compare the head accelerations and displacements, as well as sternocleidomastoid (SCM) activation (EMG), to horizontal acceleration whiplash-like perturbations and combined horizontal/vertical accelerations.

METHODS AND PROCEDURES

Permission for this study was obtained from the University of Guelph Research Ethics Board and written consent was obtained from all subjects. Twelve precisely controlled low-velocity rear impact whiplash-like perturbations were delivered to 8 subjects, 4 male and 4 female with an average age of 28.9 ± 7.7 years, using a robotic platform (PRSCO, NH, USA). Perturbations had a peak horizontal acceleration of either $9.7 \pm 0.5 \text{m/s}^2$ (High) or $5.6 \pm 0.2 \text{m/s}^2$ (Low). Rate of change of acceleration, or jerk; was 270m/s^3 (Mild) or 380m/s^3 (Severe). Perturbations were either strictly in the horizontal direction; or had an additional element of upward or downward acceleration which was half the magnitude of horizontal acceleration. Subjects were seated in a fully functional 1991 Honda Accord front passenger car seat mounted to the robot's platform. Subjects were instructed to adopt a comfortable seated posture facing forward and resting their forearms on their laps. A triaxial accelerometer (Crossbow CSL04LP3 ± 4g) was mounted on the robotic platform to determine the initial onset of the platform movement, which was defined zero time for the EMG onsets. Kinematic data of the head and thorax was collected using 3D motion capture (NDI Optotrak 3020), similarly to other researchers (Siegmund *et al.*, 2004). Surface electromyography was used to measure activity from the Sternocleidomastoid (SCM), Upper Trapezius (TRP), and Splenius Capitis (SCAP) muscles bilaterally. Resting bias and maximal contractions were collected for normalization of the EMG channels. EMG onsets were determined by visual inspection of the raw EMG data; EMG RMS amplitudes were quantified in adjacent 25 ms time windows.

RESULTS

Overall, high acceleration profiles caused significantly greater peak accelerations, displacements and EMG amplitudes than the low acceleration profiles. Perturbations that contained a vertical acceleration component caused different head kinematics than the strictly horizontal perturbations (Figure 1). For example, there was a statistically significant interaction between acceleration and perturbation direction. Follow-up tests

revealed statistically significant differences between the vertical head accelerations for the high and low acceleration conditions in the horizontal as well as the horizontal-up perturbation directions. (Figure 1). This trend was maintained in the horizontal-down perturbation direction, though it was not statistically significant.
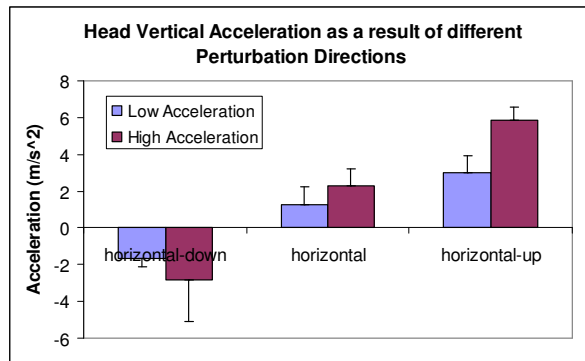

Figure 1. Vertical head acceleration for high and low accleration during each perturbation direction (Horizontal-down, Horizontal only, Horizontal-up).

DISCUSSION

Our results provide some biomechanical rationale for the epidemiological association between bumper height mismatch and patterns of injury. Researchers have shown increased severity of injuries in front-end collisions when bumpers vertical offsets (Siegel *et al.*, 2001). We believe that this may be caused by the vehicles having a downward component of the resulting perturbation pulse, similar to the horizontal-downward perturbation direction used in this study. Interestingly vertical components of acceleration have also been observed in collisions between test vehicles (Severy *et al.*, 1955), which are likely due to the vehicle suspensions.

SUMMARY

Although modelling studies are essential for investigating whiplash mechanisms of injury in automobile collisions, human studies are required to provide biologically relevant data. This study, enabled by the unique multi-directional capabilities of our robotic platform, illustrate that there appear to be systematic differences in head acceleration and muscle activation patterns between strict horizontal perturbations, and perturbations that include both horizontal and vertical accelerations. The differences that we observe shed light on the differences in patterns of injury that are observed in collisions between vehicles with offsets in bumper height, and illustrate that research studies that use sleds may not be capturing the meaningful vertical accelerations that occur in real vehicle collisions.

REFERENCES

Berglund, A et al., (2003). *Ann Epidemiol* 13: 66-72.
Severy, DM et al., (1955). *Can Serv Med J* 11: 727-759.
Siegel, JH et al., (2001). *J Trauma* 51: 975-990.
Siegmund, GP et al., (2004). *STAPP Car Crash Journal* 48: 419-430.

ACKNOWLEDGEMENTS

TRADE-OFF BETWEEN LIFT RATE AND BOX WEIGHT: A SPINE LOAD PERSPECTIVE

Susan E. Kotowski[1], Kermit G. Davis[1] and William S. Marras[2]

[1]Department of Environmental Health, University of Cincinnati, Cincinnati, OH, USA,
susan.kotowski@uc.edu, kermit.davis@uc.edu
[2]Deparment of Industrial, Welding and Systems Engineering, The Ohio State University,
Columbus, OH, USA, marras.1@osu.edu

INTRODUCTION

In many industries, workers are required to lift large amounts of material which leads to the age old question: "Is it better to lift heavy loads a few times or lift lighter loads many times?" While it is well known that load magnitude and lift rate influence the risk of developing a low back injury (Marras et al., 2006; Marras et al., 2003), there is little information about the interaction between these two factors, with even less information about the influence of gender on the choice of how the task is performed. Therefore, the aim of the study was to investigate spinal loads (peak and cumulative) and subjective ratings when lifting a specific magnitude of material weight, evaluating the trade-of between lift frequency and weight lifted. A secondary aim was to investigate whether gender influenced task performance.

METHODS AND PROCEDURES

Subjects: A total 3 males and 3 females who were inexperienced in manual material handling completed the study.

Experimental Design: A repeated measures design was utilized with two independent variables (load magnitude and lift frequency). All 9 combinations of three lift rates (4, 8, 12 lifts per minute) and three box weights (4.5 kg, 9.1 kg, 13.6 kg) were completed by each subject. For each condition, 364 kg of weight was lifted so the duration of each condition was dependent upon the lift rate and box weight.

The dependent measures consisted of three-dimensional spinal loads (compression, anterior-posterior shear, and lateral shear) predicted by an EMG-assisted biomechanical model, and two subjective ratings.

Experimental Task: All lifts were 90° asymmetric, alternating left and right. The lift origin was a conveyor at approximately knee height, sagittally symmetric to the subject, with the destination being a conveyor at approximately waist height. The lift frequency was projected through a computer generated tone. All boxes lifted were identical in size and color and did not have handles. Subjects were allowed to use a lifting style of their choice, but adopted the same technique for all nine trials.

Data Collection: Trunk kinematics were measured using the Lumbar Motion Monitor (LMM). A force plate and goniometers system was used to measure moment while an additional goniometer was used to measure pelvic angle. EMG data was collected on 10 muscles (right and left erector spinae, latissimus dorsi, external obliques, internal obliques, rectus abdominus) using biopolar surface electrodes. All EMG signals were normalized to MVC values collected prior to the lifting conditions. A subjective estimate of effort was recorded in the form of a rating of perceived exertion (RPE, Borg's 6-20 scale).

Analysis: Three-dimensional dynamic loads on the spine were calculated using an EMG-assisted biomechanical model with input including EMG, kinetic, and kinematic data

(Marras and Granata, 1997). Split-Plot Analysis of Variance was utilized to identify significant effects with standardized Tukey pairwise tests identifying the source of the significant differences

RESULTS
The results indicate that a trade-off between peak and cumulative loads occurred in all three-dimensions (See Figures 1 and 2 for examples of the loading patterns). In general, both the lift rate and the box weight influenced the three dimensional peak loads as well as the cumulative loads. Furthermore, males had higher compression and lateral shear loads but there were conditions where adaptations occurred that reversed the trends. Based on the results, the low loads being lifted at higher frequencies had the lowest peak loads but had higher cumulative loads.
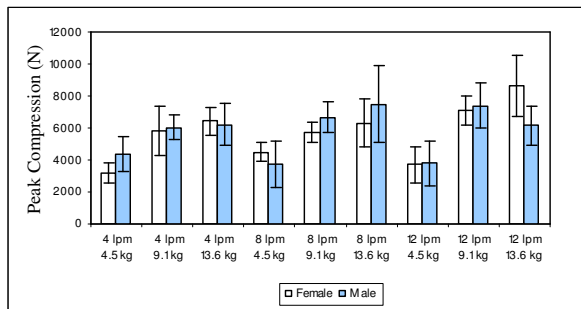

Figure 1: Peak Compression for males and females for different combinations of lift rate and load magnitude.
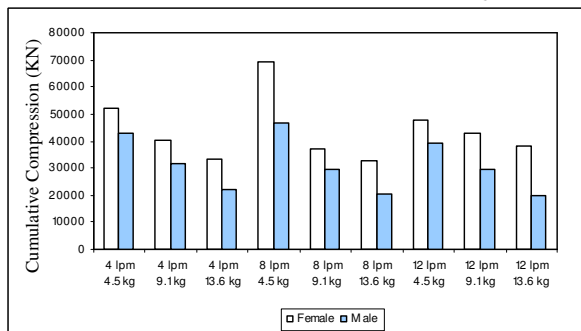

Figure 2: Cumulative Compression for males and females for different combinations of lift rate and load magnitude.

There were very few differences between males and females with regard to perceived exertions. The perceptions appeared to be driven by the weight rather than the lift rate.
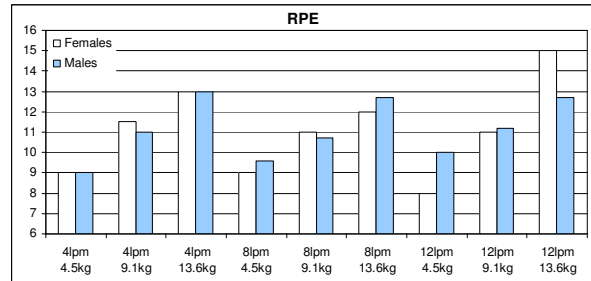

Figure 3: Perceived Exertion for males and females for different combinations of lift rate and load magnitude.

DISCUSSION
In all, the results indicate not a simple answer when determining which amount of weight at what lift rate is the best. There were trade-offs between the peak and cumulative loads that resulted from the changes in trunk kinematics and muscle activation patterns. Taking into account all the loading results (peak and cumulative three-dimensional loads), the most "optimal" combination is the 8 lifts per minute lift frequency and 9.1 kg box for both genders.

Other considerations: The study had a relatively low number of subjects which may influence the results. Also, a finite number of combinations of lift rate and weight magnitude were evaluated. Finally, a relatively low level of total load lifted which may limit the fatigue effects. The latter two issues were a result of limiting the exposure to the subjects.

REFERENCES
Marras, W.S., Parakkat, J., Chany, A.M., Yang, G, Burr, D. and Lavender S.A. (2006) "Spine Loading as a Function of Lift Frequency, Exposure Duration, and Work Experience" Clinical Biomechanics, 21(2) 345-352.

Marras, W.S., Davis, K.G., and Jorgensen, M. (2003) "Gender Influences on Spine Loads during Complex Lifting", The Spine Journal, 3(2), 93-99.

Marras, W.S., and Granata, K.P. (1997) "The Development Of An EMG-Assisted Model To Assess Spine Loading During Whole-body Free-Dynamic Lifting," Journal of Electromyography and Kinesiology, 7(4), 259-268.

A NOVEL AMBULATORY DEVICE FOR CONTINUOUS 24-H MONITORING OF PHYSICAL ACTIVITY IN DAILY LIFE

Bijan Najafi[1], James Wrobel[1], David G. Armstrong[1]

[1]Center for Lower Extremity Ambulatory Research (CLEAR), Rosalind Franklin University of Medicine and Science, North Chicago, USA, Bijan.Najafi@rosalindfranklin.edu
URL: http://diabeticfootonline.com

INTRODUCTION

A reliable measure of physical activity in daily life could contribute to improve our ability to assist in caring for our patients and helping them care for themselves. In the past, ambulatory measurements of physical activity were based on various motion sensors such as pedometers, actometers, accelerometers strapped on waist, wrist, or ankle. However, these methods provide no information on the type of activity. Recently new systems have been developed to identify the type of activity, but these methods are cumbersome because they use two or more different sites of attachment to the body and cable connection, reducing their applicability for long term monitoring of physical activity.

The system recently proposed by Najafi et al. (2003) can effectively overcome some of the key limitations of above-mentioned systems. The proposed system utilizes a combination of gyroscopes and accelerometers housed in a single portable kinematic sensor attached to the chest to detect the body posture and locomotion (sitting, standing, lying, and walking). The major drawback of this system is however its autonomy and calculation cost. The employment of gyroscope in the sensory module leads to high power consumption and therefore needs for battery recharge or exchange (maximum up to 12 hours). Although by adding more batteries, the autonomy might be increased, but it causes the device size that might hinder the subject activity. Here, we suggest a novel technology based on a single three-axial accelerometer sensor incorporated with a set of algorithms for overcoming the above limitations.

METHODS AND PROCEDURES

Our device consist a 3-axial accelerometer module integrated with a portable datalogger and attached to subject's chest using a pendant structure. Lying posture can be easily identified using the information from frontal and vertical accelerometer (Najafi et al. (2003)).

To identify sitting & standing posture, we used a similar approach suggested by Najafi et al. (2003, 2002), means first we identify postural transition (PT: the change of posture between sitting & standing), then the interval of PT is recognized and finally the pattern of the vertical accelerometer during the recognized interval is used to classify the detected PT into sit-stand or stand-sit (see Figure 1). However, here instead of using gyroscope to identify PT and its duration, we used only accelerometers information by developing a novel model integrated with a cascade filtering schemes. To estimate the true acceleration (i.e., that purely due to trunk movement), we used a time-frequency analysis, considering that gravitational acceleration has a lower frequency component as compared with translational (linear) acceleration, and that velocity does not have a DC component.

For validation of our method, three elderly subjects (older than 65 years) and three young healthy subjects carried the device, while

doing the classical test 'Timed-Up & GO'. The exact time of each postural transition as well as the duration of walking and number of taken steps were recorded by an observer using an embedded program integrated in a PDA.
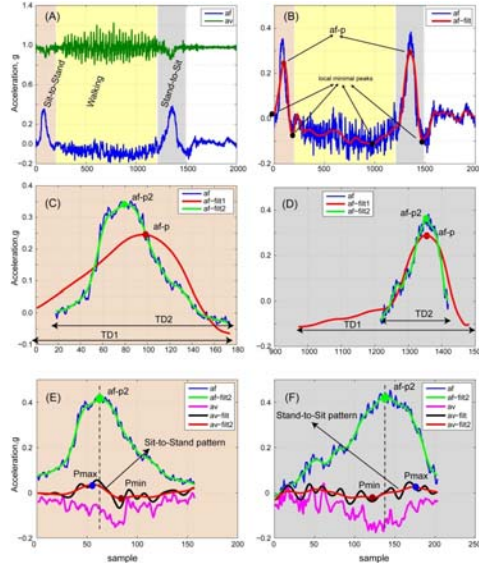

Figure 2. Walking identification results: (A) Original Signal (vertical acceleration), (B) Treated signal.

the pattern of the treated vertical acceleration during the postural transition period and using a simple peak detection algorithm (see Figure 1E&F).

Figure 1. Step by step results to identify the main motor tasks in a typical elderly subject data.

RESULTS

Figure 1 & 2 show step by step results of the applied procedures for postural transition identification and walking detection respectively. The obtained results demonstrate that the developed algorithm can identify accurately the period of walking, gait cycle time as well as cadence (see Figure 2).

Postural transition and its duration were also well estimated using a cascade filtering and local peak detection algorithm (see Figure 1 B). Postural transition duration was accurately identified using a peak matching algorithm (see Figure 1C & D). Trunk angle was estimated using a sinusoidal fitting algorithm during postural transition (see Figure 1E &F). True vertical acceleration was estimated using the estimated trunk angle and the information extracted from vertical and frontal accelerometers (see Figure 1 E&F). Finally, Sit-to-Stand and Stand-to-Sit postural transition were accurately recognized using
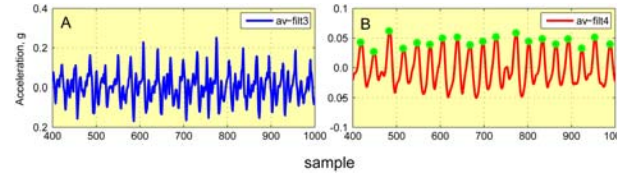
DISCUSSION & SUMMERY

This pilot study suggests that a simple, inexpensive portable device can quantify accurately the daily physical activity of a subject. Although, here we validated our approach in a short monitoring period, because of the used architecture, the autonomy of the system for recording the data can reach to several weeks. Since the device is based on a single portable module attached to subject's chest, it hinders minimally the user. The developed algorithm can identify and characterize one of the main and important motor tasks: postural transition during daily activity. Several studies demonstrated that the duration of postural transition and its characteristic are highly correlated with risk of falling as well as fear of falling in elderly population (Najafi et al. (2002), De Burin et al. (2007)). Quality of life, functional status, self-efficacy, satisfaction with care, and cost outcomes from this study will be addressed in future papers and in a larger sample size.

REFERENCES

Najafi et al. (2003). *IEEE Transactions on Biomedical Engineering*, 50(6): 711- 723,.
Najafi et al. (2002). *IEEE Transactions on Biomedical Engineering*, 49(8):843-851.
De Bruin et al (2007). *J Rehabil Res Dev*, 44:417-28.

TENNIS SERVE ANALYSIS USING ON-THE-FIELD MARKERLESS MOTION CAPTURE

Stefano Corazza[1], Alison Sheets[1], Geoff Abrams[1], Marc Safran[1] and Thomas P. Andriacchi[1,2]

[1] Stanford University, Stanford, CA, USA
[2] Bone and Joint Research Center, VA Palo Alto, Palo Alto, CA
E-mail: stefanoc@stanford.edu, Web: biomotion.stanford.edu

INTRODUCTION

Recent tennis studies (Elliot et al. 2003) have demonstrated how injuries are often related to the serve, in particular for the shoulder joint. Different types of serves, e.g. the *flat* and the *kick* types, may involve different kinematics and different musculoskeletal demands at the joints, that play an important role in the development of long term injuries (Reid et al. 2007). It has been difficult to study this problem because a rigorous analysis of the mechanics of the tennis serve has been encumbered by the need for placing markers or fixtures on the body to accurately capture the movement.

This study examines the application of a newly developed Markerless Motion Capture (MMC) (Corazza, 2006, Mundermann, 2006) method for performing a full-body 3D kinematic analysis on the tennis court. Differences between the *flat* and the *kick* serve are analyzed by comparing joint kinematics, and velocities of joint centers (JC) and the racket.

METHODS

In this pilot study the motion of two top players performing tennis serves was captured using eight ATV color cameras (resolution 640 by 480 pixels) at 200 Hz.
After performing background subtraction and silhouette extraction, a 3D representation of the athlete was generated for all frames. A subject specific model was then used to track the 3D representation and to extract joint angles and JC positions. Tracking was performed using exponential maps to describe the motion of the athlete's anatomical segments. Exponential maps were then converted into Cardan angles following the Grood and Suntay convention (Grood and Suntay, 1983). With respect to the protocol defined in (Cappozzo et al., 2005) the domain of the joint angles was expanded to [-180,180] using the local first derivative of the joint angles to solve for ambiguities.
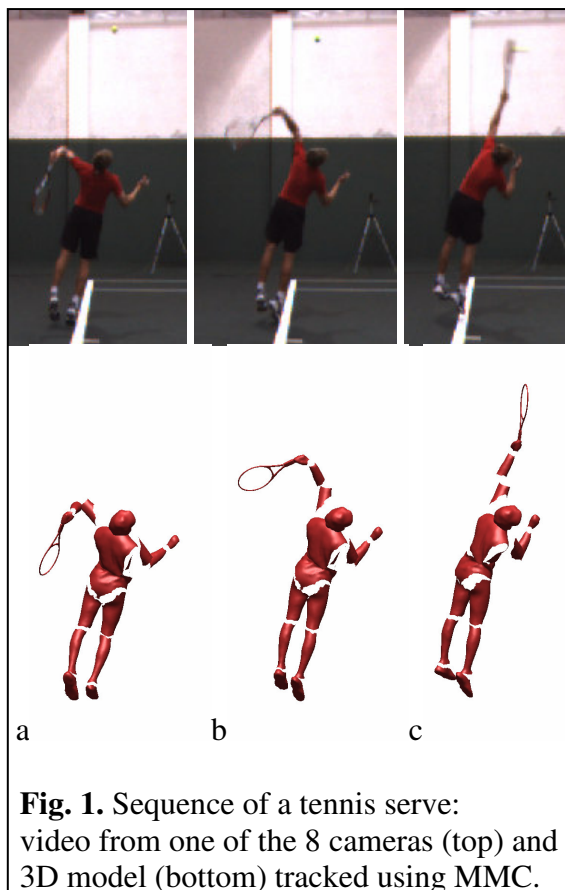

a   b   c

Fig. 1. Sequence of a tennis serve: video from one of the 8 cameras (top) and 3D model (bottom) tracked using MMC.

Each joint was allowed six degrees of freedom motion (three rotations and three translations) within the anatomical ranges. For a complete analysis of the serve the subject specific model included the tennis racket which was tracked in the 3D representation as a rigid segment attached to the hand of the player (Fig. 1).

RESULTS

The *kick* serve showed differences in the shoulder kinematics with respect to the flat serve (Fig.2 bottom). At the moment of ball impact during the *kick* serve both athletes showed, a less flexed (13.6° average) and more externally rotated (22.1° average) shoulder. Adduction did not show relevant differences (Fig.2 bottom).
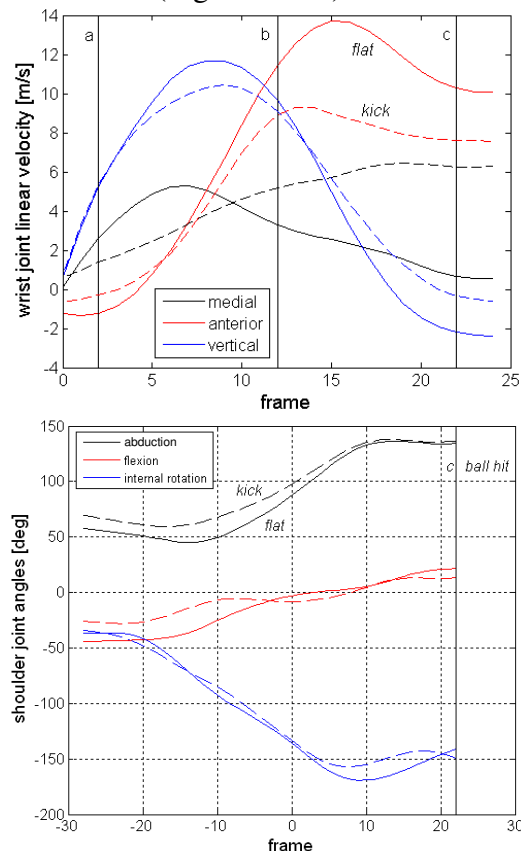

Fig 2. (top) Linear velocity at the wrist joint during *flat* (solid lines) and *kick* serve (dashed lines). (bottom) Joint angles at the shoulder in the 0.25 seconds before the impact with the ball (frame 22, marked with *c*).

More relevant differences were found in the velocities at the wrist joint (Figure 2 (top). Even if the magnitude of the linear velocity vector did not show large differences between the two types of serve (10.8 m/s for the *flat* serve and 9.9 m/s for the *kick* serve) the single components were substantially different.

DISCUSSION

This is the study first measure the motion of tennis top athletes directly on the tennis court and without the use of markers or fixtures that may affect the natural subject motion.

The analysis on two different styles of tennis serve showed some peculiar differences in the kinematics at the shoulder joint and in the linear velocities of the wrist joint. The *kick* serve is characterized by a much higher medial direction component of the velocity at the wrist and a lower value in the anterior direction. Both findings, when confirmed by a larger pool of athletes can provide more insight in the injury risk assessment of the two styles of serve. MMC also provides subject specific inertia model and full body six degrees of freedom motion of the anatomical segments which will allow accurate calculation of the inter-segmental forces and moments.

REFERENCES

Elliott B et al. (2003). *J Sci Med Sport*, 6, 76–87.
Reid M. et al. (2007). *Br J Sports Med*, 41, 884-889.
Corazza et al. (2006). *Annals Biomed Eng,* 34(6), 1019-1029.
Mündermann (2006). *J.Neur.Rehab.,* **3**(6).
Grood and Suntay (1983), *J Biomech Eng. 105(2):136-44.*
Cappozzo et al. (2005) *Gait & Posture*, 21(2), 186-196.

ACKNOWLEDGEMENTS

THE ADDUCTION MOMENT DURING WALKING IS CORRELATED WITH CARTILAGE THICKNESS RATIO IN YOUNGER MALE SUBJECTS

Chris Dyrby[1], Jessica Asay[2], Seungbum Koo[1], and Thomas Andriacchi[1,2]

[1]Stanford University, Stanford, CA, USA
[2]Bone and Joint Research Center, VA Palo Alto, Palo Alto, CA
E-mail: dyrby@stanford.edu web: biomotion.stanford.edu

INTRODUCTION

Osteoarthritis (OA) is a degenerative disease of cartilage that can be influenced by mechanical factors. Variations in thickness of tibial and femoral cartilage have been found to occur with the presence of OA. Hudelmaier found differences in absolute cartilage thickness in younger and older individuals when dividing men and women into separage groups (Hudelmaier, 2001). It has been suggested that loading during activities of daily living, such as walking, can influence the medial to lateral variations in cartilage thickness (Andriacchi, 2004, Koo, 2007). It is possible that there will be an adaptive response (increased thickness) to load in younger subjects and a degenerative response in older subjects.

The purpose of this study was to test the hypothesis that the magnitude of the adduction moment during walking is correlated with the ratio of medial to lateral articular cartilage thickness when comparing a younger and older population.

METHODS

Gait data and knee MR images were obtained for fourty-six healthy subjects after IRB approval and informed consent were obtained. The subjects were divided into two groups, older and younger: the younger group (Males (16): 30±4 yrs, BMI 24±2 kg/m^2, Females (8): 25±4 yrs BMI 21±2 kg/m^2) and an older group (Males (9): 59±5 yrs, BMI 25±5 kg/m^2, women (13): 59±4 yrs, BMI 25±4kg/m^2). In this study the data set includes both the left and right knee.

Gait data was obtained using a previously described Point Cluster Technique (Andriacchi, 1998). The external knee adduction moment was calculated (Andriacchi, 2004).

Three-dimensional models of the distal femoral cartilage were created from the knee MR images using custom software (Koo, 2005). The average thickness of each load bearing regions, found during activities of daily living, on the femur (Figure 1) and tibia was obtained.
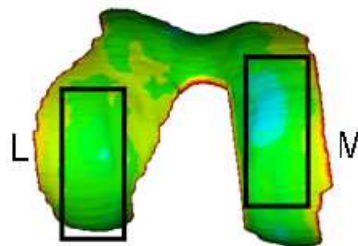

Figure 1: Load Bearing regions of the femoral cartilage were used to measure average cartilage thickness.

Average medial and lateral thickensses were calculated. Medial to lateral (ML) thickness ratios were then calculated. Regression analysis was used to correlate the ML ratios and the external adduction moment to determine the effect of load during walking on cartilage thickness.

RESULTS

The medial and lateral thicknesses were larger in the younger group when compared to the older group for the males. These differences were significant for both compartments in the femur and tibia. The women were equally matched, resulting in no significant difference in cartilage thicknees.

Regression analysis was used to determine the correlation between the ML thickness ratios (femur and tibia) and the external knee adduction moment. Results show that there were no correlations between ML thickness ratios and adduction moment for the women (younger or older). However, there was a positive correlation between ML thickness ratios for the younger males when compared to older males. This correlation was significant (femur: $p<0.04$, $r^2 = 0.14$, tibia: $p<0.001$, $r^2=0.39$, Figure 2, only tibia shown).
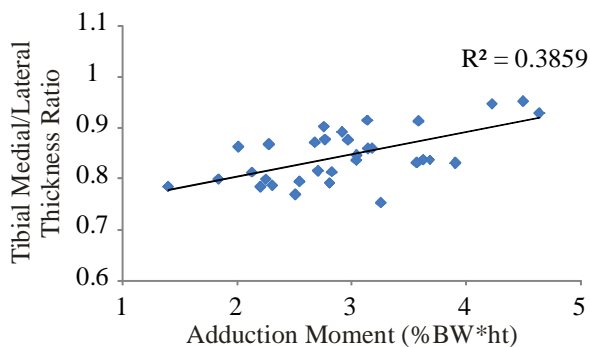

Figure 2: Adduction Moment vs. Tibial ML thickness ratio showing a significant correlation for the younger male group (shown alone for clarity) .

DISCUSSION

This study has shown that there was a correlation between the loading at the knee during walking and the medial to lateral cartilage thickness ratio in the younger male group. There was no such correlation for the older groups, possibly due to variations in cartilage health and the capability of cartilage to respond to mechanical stimulus.

The correlation could not be found in young female group. This could be due to the significantly lower BMI in this group could have lower levels of cartilage mechanical stress compared to the male counterparts.

In all groups, the lateral compartments cartilage thickness was greater than or equal to the medial. The absolute thickness was greater for the males but not the females.

REFERENCES

Andriacchi, T.P., et al. (1998). *J Biomech Eng*, **120**, 734-744.
Andriacchi, T.P. et al. (2004) *Ann Biomed Eng*, **32**: 447-457.
Hudelmaier, M., et al (2001). *Arthritis Rheum.,* **44**(11): 2556-2561.
Koo, S. et al. (2005). Osteoarthritis Cartilage, **13**, 782-789.

Table 1: Average femoral and tibial thickness normalize to height and their ratios. Data are means (SD).

	Medial	Latateral	ML Ratios	Medial	Lateral	ML Ratios
Female (younger)	1.12 (0.16)	1.19 (0.15)	0.94 (0.11)	1.07 (0.16)	1.41 (0.38)	0.78 (0.12)
Female (older)	1.17 (0.15)	1.16 (0.20)	1.04 (0.25)	1.08 (0.25)	1.34 (0.45)	0.90 (0.44)
Male (younger)	1.32 (0.31)	1.39 (0.15)	0.95 (0.21)	1.35 (0.19)	1.60 (0.21)	0.84 (0.05)
Male (older)	1.19 (0.23)	1.25 (0.19)	0.96 (0.15)	1.19 (0.24)	1.42 (0.29)	0.83 (0.05)

A PARAMETRIC APPROACH FOR ESTIMATING A RANGE OF PHYSIOLOGICAL TIBIOFEMORAL CONTACT FORCES DURING GAIT

Sean Scanlan[1], Darryl D'Lima[2], Clifford Colwell[2], and Tom Andriacchi [1,3]

[1] Stanford University, Stanford, CA, USA
[2] Shiley Center for Orthopaedic Research & Education, Scripps Clinic, La Jolla, CA, USA
[3] VA Palo Alto Health Care System, Palo Alto, CA, USA
E-mail: sscanlan@stanford.edu, Web: biomotion.stanford.edu

INTRODUCTION

The tibiofemoral contact force generated by muscular contraction at the knee during ambulation is an important component in understanding joint function, injury, and disease. However, determining the individual muscle forces required to balance the external joint loads remains a challenge due to the indeterminate nature of the joint. Various optimization techniques [Taylor 2004] are typically used to solve the muscle redundancy problem yet they often fail to elucidate potential antagonist muscle activity which may play an important role in pathologic, and even healthy, gait.

The purpose of this study was to apply a previously developed parametric hip model [Hurwitz 2003] to the knee joint. This model allows one to systematically study the effect of different levels of muscle force combinations on the tibiofemoral contact forces. The primary objective of this study was to compare the effect of antagonist muscle activity during walking with actual *in vivo* contact force measurements measured with an instrumented knee implant.

METHODS AND PROCEDURES

Experimental data were collected from a single patient with an instrumented knee implant (male, right knee, age 80, 68 kg, 1.7 m). The instrumented knee transmitted the tibiofemoral compressive load from 4 uniaxial load cells embedded in the tibial component at 70 Hz.

The subject performed walking trials at a self-selected normal speed (1.5 m/s). Kinematic and kinetic data were collected during walking using an optoelectronic system and force plate. The point cluster technique was used to calculate the kinematics of the lower limbs [Andriacchi 1998]. Inverse dynamics was used to calculate the 3-dimensional external joint moments.

The marker positions in the gait trials were used to scale and determine the kinematics of a lower-limb musculoskeletal model in SIMM (Musculographics, Inc., [Delp 1990]). The model was then used to determine the maximum isometric force, the moment arm (flexion-extension and varus-valgus), and orientation of each of the 13 muscles crossing the knee at every point in the gait cycle.

The parametric model predicts a range of knee contact forces at each time point by parametrically varying the combinations of physiologically feasible muscle forces for each muscle crossing the joint. The muscle force combinations that balance the external flexion-extension moment are collected and the medial contact force is calculated to balance the external knee ab/adduction moment and the sum of the frontal-plane muscle moments about the lateral compartment (the patient had a valgus knee angle during gait and thus the model assumed

a frontal-plane rotation about the lateral compartment). The lateral contact load is then the difference between the total and medial contact force. The maximum antagonist muscle activity was examined at a level of 5% for this study. The range of predicted tibiofemoral contact loads with the parametric model was then compared to the actual tibiofemoral compressive forces measured during the walking trials in the instrumented knee.
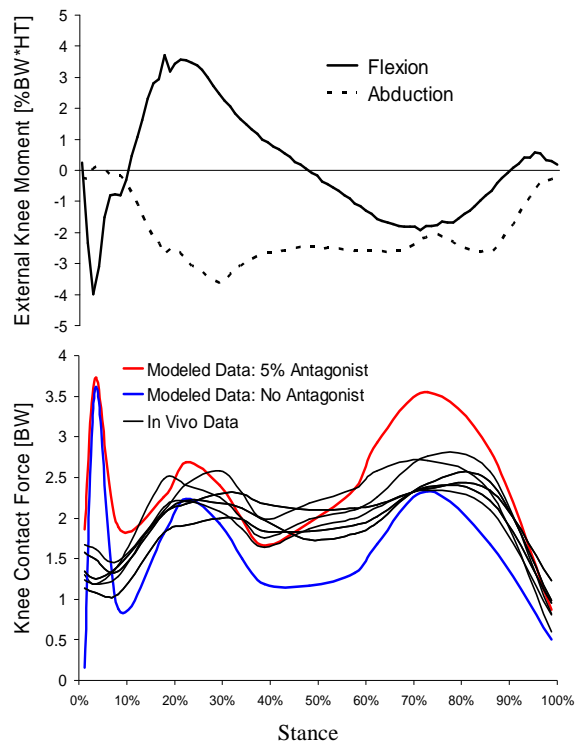
RESULTS

Figure 1. (Top) The pattern of external flexion and abduction moments during the stance phase of normal level walking. (Bottom) The range of parametrically estimated (colored lines) and *in vivo* (black lines) knee contact forces. The blue line represents the minimum possible contact force (no antagonist activity) and the red line represents maximum contact force with 5% antagonist activity.

The shape, magnitude, and timing of the contact force predicted by the parametric model were similar to those measured *in vivo* (Fig. 1). With antagonist activity set at 5%, the maximum parametric contact force (Fig. 1

red line) increased by an average of 0.78 BW from the minimum contact force possible (Fig. 1 blue line)

DISCUSSION

The parametric knee model allows one to fully explore the effect of all possible muscle force distributions on the tibiofemoral contact force subject only to physiological constraints and not predefined muscle activity patterns or optimization criterion. This model may be particularly valuable for examining pathologic gait, such as in the osteoarthritic knee or after ACL injury, in which it is suspected that antagonist muscle activity is present and significantly contributing to increased joint contact loads. Taking the subject in the current study as an example, the *in vivo* (instrumented knee) contact loading patterns appear to display antagonist activity, or non-optimal muscle recruitment, during walking thus supporting the use of the parametric model. While it appears that the model falsely predicted a spike in the contact load after heel-strike (corresponding to the large external extension moment), this could potentially be an artifact of differences in sampling rates between the two systems.

SUMMARY

A parametric knee model is presented that provides a method to study the sensitivity of the knee contact forces to specific agonist or antagonist activations patterns.

REFERENCES

Andriacchi TP, et al. (1998). *J Biomech Eng,* **120***,* 743-9.

Delp SL, et al. (1990). *IEEE Trans Biomed Eng,* **37,** 757-67.

Hurwitz DE, et al. (2003). *J Biomech,* **36,** 113-119.

Taylor WR, et al. (2004) *J Orthop Res,* **22,** 625-632.

MENISCAL MOTION DURING THE GAIT CYCLE

Nathan Netravali[1], Seungbum Koo[1], Brian Hargreaves[1], Nicholas Giori[2,3], Thomas Andriacchi[1,2,3]

[1] Stanford University, Stanford, CA, USA, nan4@stanford.edu
[2] Bone and Joint Center, VA Palo Alto Healthcare System, Palo Alto, CA, USA
[3] Department of Orthopedic Surgery, Stanford University, Stanford, CA, USA

INTRODUCTION

The menisci provide conforming surfaces between the femur and tibia that reduce the contact stresses between them during motions. (Mow et al. 1992). Loss or damage to the menisci results in an increased risk of cartilage degenerative disease (Roos et al. 1998 and Englund et al. 2003). The menisci help distribute load over an incongruent joint surface and are able to move to maintain congruency during knee motion (Vedi et al. 1999). The movement of the menisci during knee flexion and extension has been previously investigated (Thompson et al. 1991) but the mechanism by which the menisci may reduce tibiofemoral contact stresses is not yet well understood.

The purpose of this study was to develop and apply an image based *in vitro* test bed designed to investigate the movement of the menisci and tibiofemoral contact motion during simulated normal walking kinematics.

METHODS AND PROCEDURES

The test bed (Figure 1) was manufactured out of PVC, UHMWPE, and fiberglass to ensure compatibility with MRI. The device allows prescribed displacements (flexion angles, anterior-posterior (AP) displacements, and internal-external (IE)) to be applied to the tibia relative to a femoral reference frame.

The femur and tibia, harvested and kept frozen (-20°C) prior to imaging, were transacted approximately 15 cm from the knee, leaving the knee joint completely intact. Two ½" diameter holes were drilled through both the femur and tibia, through which threaded rods were placed, to attach them to a custom designed loading device.

The walking displacements (Andriacchi et al. 1998) were based on measurements of knee kinematics for 25 healthy normal subjects throughout the gait cycle. Three specific time points during the gait cycle were considered: heel-strike (HS), mid-stance (MS), and toe-off (TO) (Table 1).
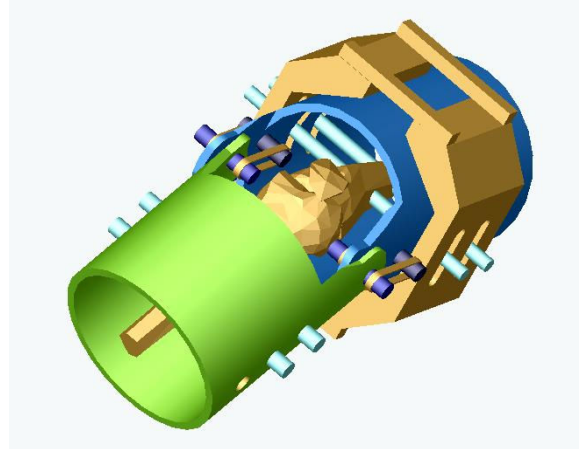

Figure 1. Loading device to fix the femur and prescribe motion on the tibia.

	HS	MS	TO
Flexion Angle°	-1	17.6	36
Tib. Ant. Disp.(mm)	13	-1	-5
Tib. Int. Rotation°	-6	-1	-1

Table 1. Flexion angles, tibial displacements, and rotations for tested instances during gait cycle tested.

A 1.5 T GE Signa MR scanner with a GE head coil were used. Fat-saturated 3D spoiled gradient recalled echo (SPGR) and a 3D balanced-steady state free precession (SSFP) scans were used to image the cartilage and meniscus, respectively. A 256 x 256 x 74 matrix with 0.5469 mm x 0.5469 mm pixel size and 1.5 mm slice thickness covered a 140 x 140 x 111 mm^3 volume of the knee for both MR scans. Three-dimensional models of the menisci, tibial and femoral cartilage were then created (Koo et al. 2005). The centroids of the contact areas between the femoral and tibial cartilage and the centroids of the lateral and medial menisci on the medial and lateral tibial plateaus were determined at each time point.

RESULTS

The change in location of cartilage contact medial plateau was substantially larger (11.7 mm) than movement of the medial meniscus 1.7mm). The lateral meniscus showed larger (5.98 mm) movement than the medial meniscus while the location of cartilage contact remained relatively small on the lateral plateau (1.8 mm) (Figure 2).
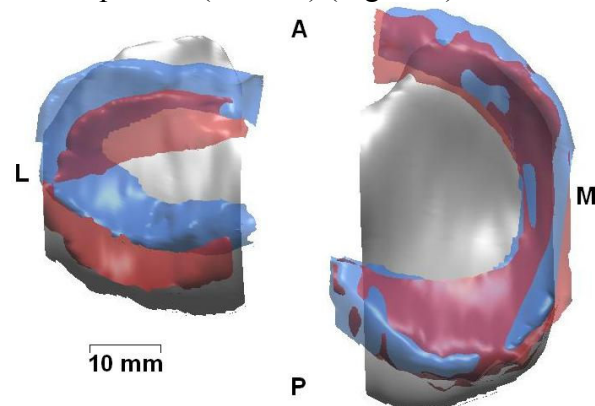

Figure 2. Displacement of the medial and lateral menisci on the respective tibial plateaus at HS (red) and TO (blue).

DISCUSSION

The results with this *in vitro* test bed are consistent with qualitative studies that suggest that the lateral meniscus is more mobile and provides better conforming surfaces than the medial meniscus (Rath et al. 2000).

The test bed provides for quantitive evaluation of the movement of the meniscus in positions representing the knee position during functional activities such as walking. The large movement of the lateral meniscus found using the test bed provides insight that helps to explain why damage to the lateral meniscus typically leads to earlier development of osteoarthritis (Covall et al. 1992). Specifically, the large movement of a healthy lateral meniscus during walking is required to maintain conformity in the lateral compartment where the articular tibiofemoral geometry is less comforming than in the medial side.

These results also provide insight as to why a rotational offset can lead to the chronic medial meniscal damage frequently observed following ACL rupture. This damage to the medial meniscus and the sensitivity of the medial compartment to shifts in contact location provide a functional explanation for the greater frequency of medial compartment relative to lateral compartment osteoarthritis following ACL injury. These results support the general hypothesis that rotational shifts in the locations of load bearing to regions of cartilage that cannot adapt to these loads (Andriacchi et al. 2004) result in degenerative changes that initiate the early stages of knee OA.

REFERENCES

Andriacchi, TP et al. (1998) *J Biomech Eng*, **120**: 743-749.
Andriacchi, TP et al. (2004). *Ann Biomed Eng,* **32,** 447-457.
Covall DJ and Wasilewski SK (1992). *Arthrosc*, **8,** 242-246.
Koo S et al. (2005), *Osteoarthritis Cartilage*, **13**: 782-789.
Englund M et al. (2003) *Arthritis Rheum*, **48(8):** 2178-2187.
Mow VC et al. (1992) *Knee Meniscus: Basic and Clinical Foundations*. New York, Raven Press.
Rath E et al. (2000) *Br J Sports Med*, **34**: 252-257.
Roos H et al. (1998) *Arthritis Rheum*, **41(4):** 687-693.
Thompson et al. (1991) *Am J Sports Med*, **19**: 210-216.
Vedi V et al. (1999) *J Bone Joint Surg,* **81-B**: 37-41.

MENISCAL MOTION DURING THE GAIT CYCLE

Nathan Netravali[1], Seungbum Koo[1], Brian Hargreaves[1], Nicholas Giori[2,3], Thomas Andriacchi[1,2,3]

[1] Stanford University, Stanford, CA, USA, nan4@stanford.edu
[2] Bone and Joint Center, VA Palo Alto Healthcare System, Palo Alto, CA, USA
[3] Department of Orthopedic Surgery, Stanford University, Stanford, CA, USA

INTRODUCTION

The menisci provide conforming surfaces between the femur and tibia that reduce the contact stresses between them during motions. (Mow et al. 1992). Loss or damage to the menisci results in an increased risk of cartilage degenerative disease (Roos et al. 1998 and Englund et al. 2003). The menisci help distribute load over an incongruent joint surface and are able to move to maintain congruency during knee motion (Vedi et al. 1999). The movement of the menisci during knee flexion and extension has been previously investigated (Thompson et al. 1991) but the mechanism by which the menisci may reduce tibiofemoral contact stresses is not yet well understood.

The purpose of this study was to develop and apply an image based *in vitro* test bed designed to investigate the movement of the menisci and tibiofemoral contact motion during simulated normal walking kinematics.

METHODS AND PROCEDURES

The test bed (Figure 1) was manufactured out of PVC, UHMWPE, and fiberglass to ensure compatibility with MRI. The device allows prescribed displacements (flexion angles, anterior-posterior (AP) displacements, and internal-external (IE)) to be applied to the tibia relative to a femoral reference frame.

The femur and tibia, harvested and kept frozen (-20°C) prior to imaging, were transacted approximately 15 cm from the knee, leaving the knee joint completely intact. Two ½" diameter holes were drilled through both the femur and tibia, through which threaded rods were placed, to attach them to a custom designed loading device.

The walking displacements (Andriacchi et al. 1998) were based on measurements of knee kinematics for 25 healthy normal subjects throughout the gait cycle. Three specific time points during the gait cycle were considered: heel-strike (HS), mid-stance (MS), and toe-off (TO) (Table 1).
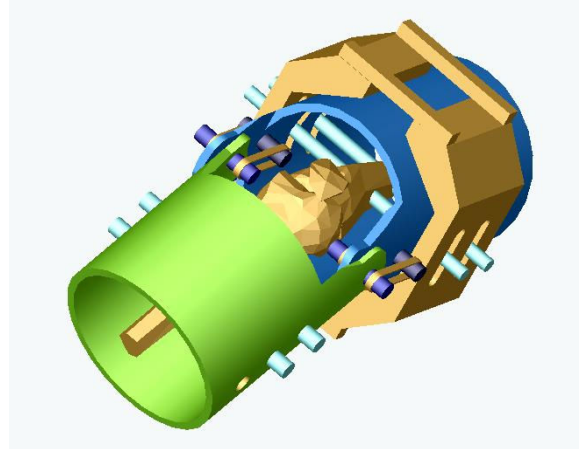

Figure 1. Loading device to fix the femur and prescribe motion on the tibia.

	HS	MS	TO
Flexion Angle°	-1	17.6	36
Tib. Ant. Disp.(mm)	13	-1	-5
Tib. Int. Rotation°	-6	-1	-1

Table 1. Flexion angles, tibial displacements, and rotations for tested instances during gait cycle tested.

A 1.5 T GE Signa MR scanner with a GE head coil were used. Fat-saturated 3D spoiled gradient recalled echo (SPGR) and a 3D balanced-steady state free precession (SSFP) scans were used to image the cartilage and meniscus, respectively. A 256 x 256 x 74 matrix with 0.5469 mm x 0.5469 mm pixel size and 1.5 mm slice thickness covered a 140 x 140 x 111 mm^3 volume of the knee for both MR scans. Three-dimensional models of the menisci, tibial and femoral cartilage were then created (Koo et al. 2005). The centroids of the contact areas between the femoral and tibial cartilage and the centroids of the lateral and medial menisci on the medial and lateral tibial plateaus were determined at each time point.

RESULTS
The change in location of cartilage contact medial plateau was substantially larger (11.7 mm) than movement of the medial meniscus 1.7mm). The lateral meniscus showed larger (5.98 mm) movement than the medial meniscus while the location of cartilage contact remained relatively small on the lateral plateau (1.8 mm) (Figure 2).
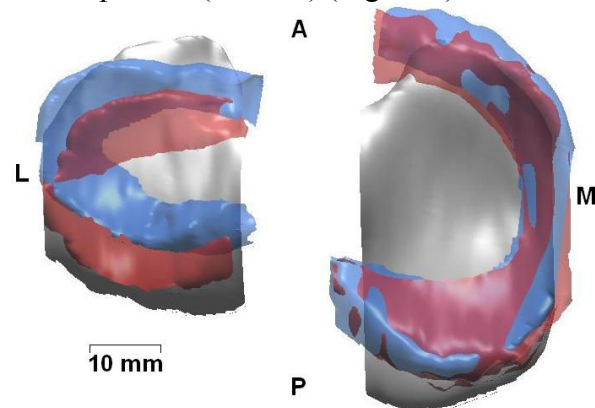

Figure 2. Displacement of the medial and lateral menisci on the respective tibial plateaus at HS (red) and TO (blue).

DISCUSSION

The results with this *in vitro* test bed are consistent with qualitative studies that suggest that the lateral meniscus is more mobile and provides better conforming surfaces than the medial meniscus (Rath et al. 2000).

The test bed provides for quantitive evaluation of the movement of the meniscus in positions representing the knee position during functional activities such as walking. The large movement of the lateral meniscus found using the test bed provides insight that helps to explain why damage to the lateral meniscus typically leads to earlier development of osteoarthritis (Covall et al. 1992). Specifically, the large movement of a healthy lateral meniscus during walking is required to maintain conformity in the lateral compartment where the articular tibiofemoral geometry is less comforming than in the medial side.

These results also provide insight as to why a rotational offset can lead to the chronic medial meniscal damage frequently observed following ACL rupture. This damage to the medial meniscus and the sensitivity of the medial compartment to shifts in contact location provide a functional explanation for the greater frequency of medial compartment relative to lateral compartment osteoarthritis following ACL injury. These results support the general hypothesis that rotational shifts in the locations of load bearing to regions of cartilage that cannot adapt to these loads (Andriacchi et al. 2004) result in degenerative changes that initiate the early stages of knee OA.

REFERENCES

Andriacchi, TP et al. (1998) *J Biomech Eng*, **120**: 743-749.
Andriacchi, TP et al. (2004). *Ann Biomed Eng,* **32,** 447-457.
Covall DJ and Wasilewski SK (1992). *Arthrosc*, **8,** 242-246.
Koo S et al. (2005), *Osteoarthritis Cartilage*, **13**: 782-789.
Englund M et al. (2003) *Arthritis Rheum*, **48(8):** 2178-2187.
Mow VC et al. (1992) *Knee Meniscus: Basic and Clinical Foundations*. New York, Raven Press.
Rath E et al. (2000) *Br J Sports Med*, **34**: 252-257.
Roos H et al. (1998) *Arthritis Rheum*, **41(4):** 687-693.
Thompson et al. (1991) *Am J Sports Med*, **19**: 210-216.
Vedi V et al. (1999) *J Bone Joint Surg,* **81-B**: 37-41.

MARKERLESS VERSUS MARKER-BASED MOTION CAPTURE: A COMPARISON OF MEASURED JOINT CENTERS

Katherine Steele[1], Stefano Corazza[1], Sean Scanlan[1], Alison Sheets[1] and Thomas P. Andriacchi [1,2]

[1] Stanford University, Stanford, CA, USA
[2] Bone and Joint Research Center, VA Palo Alto, Palo Alto, CA
E-mail: ksteele@stanford.edu, Web: biomotion.stanford.edu

INTRODUCTION

Markerless motion capture (MMC) techniques have recently been introduced as a viable alternative to traditional marker-based methods used for capturing motion and performing biomechanical analyses (Corazza, 2006, Mündermann, 2006). Since both methods attempt to measure underlying bone motion, calculated joint center (JC) locations should be similar. Traditional marker-based methods such as the point-cluster technique (PCT, Andriacchi, 1998) are the current standard for motion capture in biomechanical applications. Therefore, the purpose of this study was to compare JC locations during gait using markerless and marker-based motion capture techniques (Fig. 1).

METHODS

Markerless and marker-based motion capture were performed simultaneously for three subjects at the Stanford Biomotion Lab (2 female/1 male, height: 1.7(0.09) m, mass: 67.5(10.2) kg, age: 25.7(3.5)). Marker-based data was obtained using PCT protocol and an optoelectronic system (Qualisys Medical, Sweden) with eight infrared cameras. Eight ATV color cameras (resolution 640 by 480 pixels) were used to obtain each subject's 3D representation, or visual hull, for MMC. Both systems captured at 120 Hz and had their hardware synchronized.

The reference pose and JCs used for MMC and PCT were aligned by using a laser scan of the subject wearing markers. 3D digitization of the markers locations was achieved by fitting spheres to the markers' surface on the laser scan model. For PCT, transformation matrices correlating the technical and anatomical coordinate frames were calculated in the laser scan reference pose and used to track motion trials. The same laser scan and JC definitions were used to define the subject specific model used in MMC. This process ensured that deviations in JC locations were due to actual differences in motion capture techniques and not to differences in JC definition from the reference pose. Once the two reference poses were aligned, MMC data was tracked as previously described in (Corazza, 2006, Mündermann, 2006).
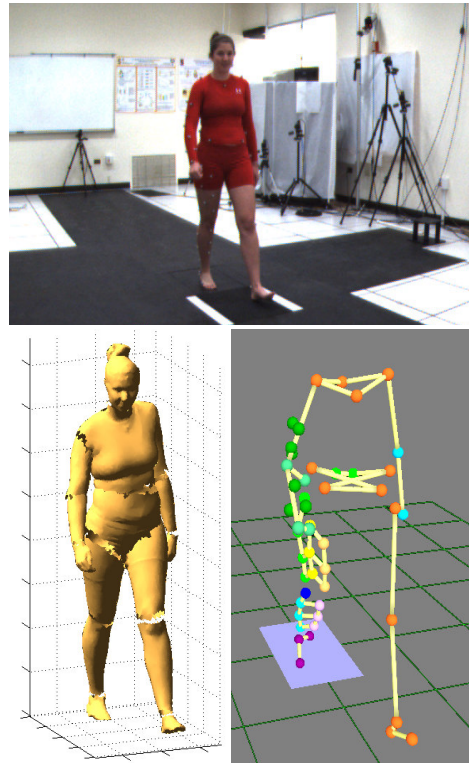

Fig 1. MMC and PCT models during gait.

Using the aligned reference pose, a total of nine walking trials were processed for each method to obtain the JC positions of the ankle, knee, hip, shoulder, and elbow. To eliminate systemic errors stemming from different anatomical reference frame and segment definitions, the average offset between JCs were subtracted to compare the differences between MMC and PCT for tracking motion.

RESULTS

The JC positions tracked with both MMC and PCT had average difference of 17.0(11.4) mm for the lower body joints and 15.0(10.2) mm for the upper body joints.
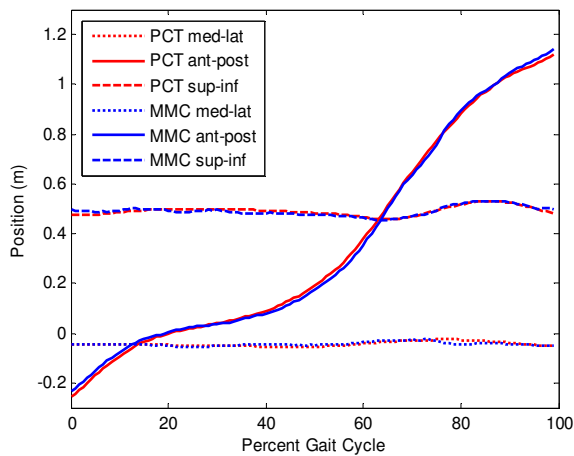

Fig 2. Knee joint position over a gait cycle

Measured JC positions in the medial-lateral direction had the smallest average differences: 5.6(4.7) mm and 7.3(4.9) mm in the in the lower and upper bodies, respectively. The average anterior-posterior and superior-inferior differences were 10.6(7.3) / 14.2(8.4) mm and 7.3(4.9) / 7.4(5.7) mm, respectively, for the upper/lower body.

	Ant-Post (mm)	Med-Lat (mm)	Sup-Inf (mm)
Hip	6.700	12.278	7.511
Knee	5.233	12.700	7.689
Ankle	4.867	17.489	6.933
Shoulder	6.311	9.333	5.844
Elbow	8.900	11.222	8.756

Table 1. Average difference in joint centers

DISCUSSION

Markerless and marker-based motion capture produced similar results for tracking JC positions. The small JC differences are most likely due to errors caused by skin artifacts, which affect the two methods differently. The differences in measured JC positions emphasizes the need for a gold standard that could justify which method, if either, best captures the motion of the underlying bones.

SUMMARY

Similar JC positions were calculated using both markerless motion capture and the PCT, marker-based technique. MMC has the advantages of reduced patient preparation time and greater flexibility in motion capture location. Further development of MMC, including higher resolution cameras and refining body-segment definitions could bring the results even closer to the PCT results in the future. However, for both methods, there is a strong need to develop a gold standard for in vivo joint motions to fully understand the accuracy of these methods.

REFERENCES

Andriacchi et al. (1998). *J Biomech Eng,* 120, 743-744.
Corazza et al. (2006). *Annals Biomed Eng,* 34(6), 1019-1029.
Mündermann (2006). *J.Neur.Rehab.,* **3**(6).

ACKNOWLEDGEMENTS